Euratom
European Commission

Nuclear fission safety programme 1992-94

Radiation protection research action

Final report

Volume 1

EUR 16769 DE/EN/FR

Comisión Europea
Europa-Kommissionen
Europäische Kommission
Ευρωπαϊκή Επιτροπή
European Commission
Commission européenne
Commissione europea
Europese Commissie
Comissão Europeia

Euratom

Programa
SEGURIDADDE LA FISIÓN NUCLEAR
Plan de «Investigación en materia de protección contra las radiaciones»

Program
SIKKERHED I FORBINDELSE MED KERNESPALTING
Programmet »Forskning vedrørende Strålingsbeskyttelse«

Programm
SICHERHEIT BEI DER KERNSPALTUNG
Aktion „Strahlenschutzforschung"

Πρόγραμμα
ΑΣΦΑΛΕΙΑ ΣΤΗΝ ΠΥΡΗΝΙΚΗ ΣΧΑΣΗ
Δράση «Έρευνα στον τομέα της Ακτινοσταυίας»

NUCLEAR FISSION SAFETY
programme
Action 'Radiation protection research'

Programme
« SÛRETÉ DE LA FISSION NUCLÉAIRE »
Action «Recherche en radioprotection»

Programma
SICUREZZA DELLA FISSIONE NUCLEARE
Azione «Ricerca sulla radioprotezione»

Programma
VEILIGHEID VAN KERNSPLIJTING
Actie „Onderzoek Stralingsbescherming"

Programa
SEGURANÇA DA CISÃO NUCLEAR
Acção «Investigação no domino da protecção contra radiações»

1992-1994
Final report

Volume 1

1997 EUR 16769 DE/EN/FR

Zahlreiche weitere Informationen zur Europäischen Union sind verfügbar über Internet, Server Europa (http://europa.eu.int).

A great deal of additional information on the European Union is available on the Internet. It can be accessed through the Europa server (http://europa.eu.int)

De nombreuses autres informations sur l'Union européenne sont disponibles sur Internet via le serveur Europa (http://europa.eu.int).

Bibliographische Daten befinden sich am Ende der Veröffentlichung.

Cataloguing data can be found at the end of this publication.

Une fiche bibliographique figure à la fin de l'ouvrage.

Luxembourg: Office des publications officielles des Communautés européennes, 1997

ISBN 92-827-7983-1

Printed in Belgium

INHALTSVERZEICHNIS

TABLE OF CONTENTS

TABLE DES MATIERES

VOLUME 1 Page

I. Einleitung/Introduction *1*

II. Mitglieder und Experten 1993-95
Beratender Verwaltungs und Koordinierungsausschuss "Strahlenschutz"
Members and Experts 1993-95
Management and Coordination Advisory Committee "Radiation Protection"
Membres et Experts 1993-95
Comité Consultatif en matière de Gestion et de Coordination "Radioprotection" *9*

III. Forschungstätigkeit Strahlenschutz
Research in Radiation Protection
Recherche en Radioprotection *13*

A EXPOSITION DES MENSCHEN DURCH STRAHLEN UND RADIOACTIVITÄT
HUMAN EXPOSURE TO RADIATION AND RADIOACTIVITY
EXPOSITION DE L'HOMME AUX RAYONNEMENTS ET À LA RADIOACTIVITÉ *15*

A1 Measurement of radiation dose and its interpretation.

A1A ICRU

FI3P-CT920054-A1A *17*
Radiation quantities units and measurement techniques for radiation protection.

1 Allisy BIPM

A1B EURADOS

FI3P-CT920001-A1B *25*
Collaboration on radiation dosimetry for radiation protection applications (EURADOS).

1 Dietze EURADOS
2 Golnik IAE-RPD

A11 Development and implementation of standards and procedures linked to the concepts of dose equivalent quantities for both external and internal exposure.

FI3P-CT920040-A11 . . . . . *55*
Accident dosimetry in populated areas: the use of solid-state dosimetry techniques with ceramics and other natural materials.

1 Bailiff Univ. Durham
2 Goeksu GSF
3 Stoneham Univ. Oxford
4 Bøtter-Jensen Lab. Risø
5 Nolte Univ. München - Technische
6 Hütt EAAS.IG *(PECO contract)*
7 Lippmaa ICPB

FI3P-CT920064h-A11 . . . . . *123*
The measurement of the spectral and angular distribution of external radiations in the workplace and implications for personal dosimetry.

1	Clark	NRPB
2	Spencer	UKAEA
3	Gualdrini	ENEA
4	Chartier	CEA - FAR

A12 Radiation measurement and instrumentation for individual and area dosimetry.

FI3P-CT920002-A12 . . . . . *161*
Realistic neutron calibration fields and related dosimetric quantities.

1	Klein	PTB
2	Thomas	NPL
3	Chartier	CEA - FAR
4	Schraube	GSF
5	Kralik	CSAS.IRD
6	Osmera	NRIRR
7	Grecescu	IRA

FI3P-CT920018-A12 . . . . . *219*
The measurement of environmental radiation doses and dose rates.

1	Bøtter-Jensen	Lab. Risø
2	Lauterbach	PTB
3	Delgado Martínez	CIEMAT
4	Pernicka	CSAS.IRD
5	Waligorski	INP. Krakow
6	Osvay	Il. Budapest

FI3P-CT920026-A12 . . . . . *283*
Detection and dosimetry of neutrons and charged particles at aviation altitudes in the earths's atmosphere.

1	McAulay	Univ. Dublin
2	Tommasino	ENEA
3	Schraube	GSF
4	O'Sullivan	DIAS
5	Grillmaier	Univ. Saarlandes
6	Hoefert	CERN
7	Spurný	CSAS.IRD

FI3P-CT920032-A12 . . . . . *339*
Dosimetry of beta and low-energy photon radiations.

1	Christensen	Lab. Risø
2	Chartier	CEA - FAR
3	Francis	NRPB
4	Herbaut	CEA - Grenoble
5	Spencer	UKAEA
6	Gasiot	Univ. Montpellier II
7	Scharmann	Univ. Giessen
8	Charles	Nuclear Electric
9	Olko	INP
10	Uchrin	MTA

FI3P-CT920039-A12 . . . . . *435*
Development of instruments and methods for radiation protection dosimetry with the variance-covariance method.

1	Kellerer	Univ. München
2	Lindborg	Inst. Nat. of Radiation Protection
3	Jessen	Univ. Århus - Hospital
4	Scendrö	Microvacuum Ltd. Budapest *(PECO contract)*

FI3P-CT920045-A12 . . . . . *467*
The use of microdosimetric methods for determination of dose equivalent quantities and of basic data for dosimetry.

1	Ségur	ADPA
2	Brede	PTB
3	Zoetelief	TNO - Delft
4	Schmitz	KFA
5	Grillmaier	Univ. Saarlandes
6	Bordy	IPSN - CEA - FAR
7	Morstin	CITEC *(PECO contract)*
8	Sabol	TECH.UNIV.CZ

FI3P-CT930072-A12 . . . . . *533*
Individual electronic neutron dosemeter.

1	Vareille	Univ. Limoges
2	Zamani-Valassiadou	Univ. Thessaloniki
3	Barthe	CEA - FAR
4	Fernández Moreno	Univ. Barcelona - Autónoma
5	Curzio	Univ. Pisa
6	Charvat	IRD
7	Moiseev	IFIN

A14 Assessment of internal exposure.

FI3P-CT920048-A14 . . . . . *605*
Assessment of internal dose from plutonium and other radionuclides using stable isotope tracer techniques in man.

1	Roth	GSF
2	Molho	Univ. Milano
3	Taylor	Univ. Wales, Cardiff
4	McAughey	UKAEA

FI3P-CT920060-A14 . . . . . *651*
Radionuclide dosimetry.

1	Nosske	BFS
2	Kendall	NRPB
3	Taylor	Univ. Wales, Cardiff
4	van Rotterdam	TNO - Delft
5	Andrási	KFKI
6	Toader	IHPH

FI3P-CT920064a-A14 . . . . . *703
Inhalation and ingestion of radionuclides.

1	Bailey	NRPB
2	Stahlhofen	GSF
3	Roy	CEA - FAR
4	Patrick	MRC
5	Stradling	NRPB
6	Iranzo	CIEMAT
7	Popplewell	NRPB
8	Strong	UKAEA
9	Jonhston	Inst. Occupational Medicine
10	Koblinger	HAS.RIAE
11	Gradón	ICH-MAW
12	Salowsky	UMP

A2 Transfer and behaviour of radionuclides in the environment.

A2A IUR

FI3P-CT920003-A2A 795
Promotion of formation, knowledge and exchange of information in radioecology.

1	Cigna	UIR

A21 Environmental behaviour of radionuclides in situations meriting particular attention for long-term behaviour or post-acident conditions.

FI3P-CT920029-A21 813
Towards a functional model of radionuclide transport in freshwaters.

1	Hilton	NERC
2	Ortins	Direcção-Geral do Ambiente
3	Cremers	Univ. Leuven (KUL)
4	Foulquier	CEA - FAR
6	Sansone	ENEA
7	Blust	Univ. Antwerpen
8	Fernández	Univ. Málaga
10	Comans	ECN
	Forset	NINA

FI3P-CT920046-A21 905
Mechanisms governing the behaviour and transport of transuranics (analogues) and other radionuclides in marine ecosystems.

1	Mitchell	Univ. Dublin - College
2	Gascó	CIEMAT
3	Guéguéniat	CEA - Cherbourg
4	Papucci	ENEA
5	Woodhead	MAFF
6	Holm	Univ. Lund
7	Sánchez-Cabeza	Univ. Barcelona - Autónoma
8	Dahlgaard	Lab. Risø
9	Salbu	Univ. Norway - Agricultural

A22 Natural radioactivity in the environment and its pathways to man.

FI3P-CT920035-A22 . . . . . *991*
Pathways of radionuclides emmited by non nuclear industries.

1	Lembrechts	RIVM
2	Germain	CEA - FAR
3	Travesi Jiménez	CIEMAT
4	Ortins	Direcção-Geral do Ambiente
5	García-León	Univ. Sevilla
6	McGarry	RPII
7	Ortins	Direcção-Geral do Ambiente
8	Dahlgaard	Lab. Risø
9	Heaton	Univ. Aberdeen
10	Zagyvai	TUBUD.INT

FI3P-CT930075-A22 . . . . . *1059*
Investigation on exposure to natural radionuclides in selected areas affected by U-processing.

1	Belot	CEA - FAR
2	Röhnsch	BFS
3	Massmeyer	GRS

A23 Influence of speciation, chemical modification, changes in physico-chemical properties and biological conversion.

FI3P-CT920010-A23 . . . . . *1085*
The bio-availability of long-lived radionuclides in relation to their physico-chemical form in soil systems.

1	Lembrechts	RIVM
2	Wilkins	NRPB
3	Cremers	Univ. Leuven (KUL)
4	Merckx	Univ. Leuven (KUL)
5	Staunton	INRA - Montpellier
6	Berthelin	CNRS
7	Mocanu	ROIAP
8	Szabó	NRIRR *(PECO contract)*

FI3P-CT920022-A23 . . . . . *1169*
Investigations and modelling of the dynamics of environmental HT/HTO/OBT levels resulting from tritium releases.

1	Bunnenberg	ZSR
2	Belot	CEA - FAR
3	Kim	Univ. München - Technische
4	Dertinger	KfK
5	Eikenberg	Inst. Paul Scherrer
6	Uchrin	HAS.II
7	Paunescu	IFIN

A24 The behaviour of accidentally released radionuclides, evaluation of the reliability of transfer parameters and experimental studies.

FI3P-CT920006-A24 . . . . . *1237*
Transfer of radionuclides in animal production systems.

1	Howard	ITE
2	Assimakopoulos	Univ. Ioannina
3	Crout	Univ. Nottingham
4	Mayes	Inst. MacAulay Land Use Research
5	Voigt	GSF
6	Vandecasteele	CEN/SCK Mol
7	Zelenka	UAB.FAGR
8	Hove	Univ. Norway - Agricultural
9	Hinton	Inst. Paul Scherrer

A25 The role of retention and release of radionuclides in natural ecosystems and in marginal agricultural areas.

FI3P-CT920016-A25 . . . . . *1327*
Deposition of radionuclides on tree canopies and their subsequent fate in forest ecosystems - Further studies.

1	Minski	IMPCOL
2	Rauret	Fundació "Bosch i Gimpera"
3	Ronneau	Univ. Louvain (UCL) - LLN

FI3P-CT920050-A25 . . . . . *1359*
Cycling of cesium 137 and strontium 90 in natural ecosystems.

1	Wirth	BFS
2	Moberg	Inst. Nat. of Radiation Protection
3	Bergman	Swedish Defense Research Establish.
4	Palo	Univ. Agricultural Sci. of Sweden
5	Impens	Faculté Sciences Agronom. Gembloux
6	Belli	ENEA
7	Feoli	CETA
8	Nimis	Univ. Trieste
9	Antonopoulus-Domis	Univ. Thessaloniki
10	Pietrzak-Flis	CLRP Warsaw

FI3P-CT920058-A25 . . . . . *1481*
Radiation doses and pathways to man from semi-natural ecosystems.

1	McGarry	RPII
2	Horrill	NERC
3	Nielsen	Lab. Risø
4	Johanson	Univ. Umeå - Agr.Sci. - Dep. Forestry
5	Veresoglou	Univ. Thessaloniki

A26 Development of countermeasures to reduce the contamination in the environment and to impede its transfer to man.

FI3P-CT920013a-A26 . . . . . *1533*
Studies of methods for the rehabilitation of soils and surfaces after a nuclear accident (RESSAC).

1	Foulquier	CEA - Cadarache
2	Sandalls	UKAEA
3	Vandecasteele	CEN/SCK Brussels
4	Vallejo	Fundació "Bosch i Gimpera"
5	Förstel	KFA
6	Gutierrez	CIEMAT
7	Arapis	Univ. Athens
8	Kirchmann	Faculté Sciences Agronom. Gembloux

FI3P-CT920049-A26 . . . . . *1617*
Transfer of accidentally released radionuclides in agricultural systems.

1	Cancio	CIEMAT
2	Real	IPSN
3	Rauret	Fundació "Bosch i Gimpera"

FI3P-CT930071-A26 . . . . . *1647*
Influence of the food-processing techniques on the level of radionuclides in foodstuffs.

1	Colle	CEA - FAR
2	Nicholson	UKAEA
3	Grandison	Univ. Reading

VOLUME 2

B FOLGEN DER STRAHLENEXPOSITION DES MENSCHEN; IHRE ABSCHÄTZUNG, VERHÜNTUNG UND BEHANDLUNG
CONSEQUENCES OF RADIATION EXPOSURE TO MAN; THEIR ASSESSMENT, PREVENTION AND TREATMENT
CONSEQUENCES POUR L'HOMME DE L'EXPOSITION AUX RAYONNEMENTS; EVALUATION, PREVENTION ET TRAITEMENT *1685*

B1 Stochastic effects of radiation.

B1A EULEP

FI3P-CT920030-B1A *1687*
Co-operative research on late somatic effects of ionizing radiation in the mammalian organism.

1	Maisin	EULEP

B11 Interpretation of low dose and low dose rate effects with the help of microdosimetry.

FI3P-CT920027-B11 . . . . . *1705
Biophysical models for the effectiveness of different radiations.

1	Paretzke	GSF
2	Goodhead	MRC
3	Terrissol	ADPA
4	Leenhouts	RIVM
5	Von Sonntag	Inst. Max-Planck
6	Smith	Univ. London
7	O'Neill	MRC

FI3P-CT920041-B11 1769
Specification of radiation quality at nanometre level.

1	Colautti	INFN - Legnaro
2	Watt	Univ. St. Andrews
3	Harder	Univ. Göttingen
4	Leuthold	GSF
5	Izzo	Univ. Roma - Tor Vergata
6	Kraft	GSI
7	Pszona	SINS.PL

B12 Repair and modification of genetic damage and individual radiosensitivity.

FI3P-CT920007-B12 1823
Molecular basis of radiosensitivty.

1	Lohman	Univ. Leiden
2	Bridges	MRC
3	Bootsma	Univ. Rotterdam - Erasmus
4	Moustacchi	CIR
5	Thacker	MRC
6	Backendorf	Univ. Leiden
7	Eckardt-Schupp	GSF
8	Szumiel	ICHTJ
9	Szymczyk-Wasiluk	WMS

FI3P-CT930080-B12 1889
Radiation ionduced mitotic aneuploidy.

1	Parry	Univ. Wales, Cardiff
2	Tanzarella	CNR
3	Kirsch Volders	Univ. Bruxelles (VUB)

B13 Cellular, molecular and animal studies to determine the risk of stochastic somatic effects of radiation with respect to low dose, low dose rate and radiation quality.

FI3P-CT920011-B13 1923
Cytogenetic and molecular mechanisms of radiation myeloid leukaemogenesis in the mouse.

1	Janowski	VITO
2	Cox	NRPB
3	Huiskamp	ECN

FI3P-CT920017-B13 . . . . . *1937*
Studies on radiation induced chromosomal aberrations.

1	Natarajan	Univ. Leiden
3	Ortins	Direcção-Geral do Ambiente
4	Bryant	Univ. St. Andrews
5	Pantelias	NCSR "Demokritos"
6	Benova	NCRRP

FI3P-CT920028-B13 . . . . . *1979*
Radiation-induced processes in mammalian cells: principles of response modification and involvement in carcinogenesis.

1	Van der Eb	Univ. Leiden
2	Sarasin	CNRS
3	Devoret	CNRS
4	Rommelaere	DKFZ
5	Bertazzoni	CNR
6	Thomou-Politi	NCSR "Demokritos"
7	Herrlich	KfK
8	Simons	Univ. Leiden
9	Russev	BAS

FI3P-CT920031-B13 . . . . . *2039*
Studies on radiation-induced chromosome aberrations in mammalian cells. 2) Applied aspects.

1	Olivieri	Univ. Roma "La Sapienza"
2	Cortés-Benavides	Univ. Sevilla
4	Palitti	Univ. Viterbo
5	Savage	MRC
6	Kalina	Univ. Safarikis

FI3P-CT920042-B13 . . . . . *2071*
Carcinogenic effects of low radiation doses and underlying mechanisms.

1	Davelaar	Univ. Leiden
2	Coppola	ENEA
3	Bentvelzen	TNO - Delft
4	Masse	CEA - Paris
5	Chmelevsky	GSF
6	Zurcher	TNO - Delft

FI3P-CT920043-B13 . . . . . *2107*
Measurement of oncogenic transformation of mammalian cells in-vitro by low doses of ionising radiation.

1	Mill	Nuclear Electric
2	Frankenberg	Univ. Göttingen
3	Roberts	UKAEA
4	Tallone Lombardi	Univ. Milano
5	Kellerer	Univ. München
6	Saran	ENEA

FI3P-CT920053-B13 . . . . . *2165*
Molecular and cellular effectiveness of charged particles (light and heavy ions) and neutrons.

1	Cherubini	INFN - Legnaro
2	Michael	Hosp. Mount Vernon
3	Goodhead	MRC
4	Belli	ISS
5	Sideris	NCSR "Demokritos"
6	Kiefer	Univ. Giessen
7	Reist	Inst. Paul Scherrer

FI3P-CT920063-B13 . . . . . *2231*
New technologies in the automated detection of radiation-induced cytometric effects.

1	Aten	Univ. Amsterdam
2	Nüsse	GSF
3	Bauchinger	GSF
5	Green	MRC

FI3P-CT920064i-B13 . . . . . *2275*
The induction of chromosomal changes in human lymphocytes by accelerated charged particles.

1	Edwards	NRPB
2	Natarajan	Univ. Leiden
3	Bimbot	CNRS
4	Dutrillaux	CIR
5	Kraft	GSI

FI3P-CT930067-B13 . . . . . *2317*
Development and investigation of systems for the quantification of radiation induced carcinogenesis in humans.

1	Mothersill	Inst. of Technology - Dublin
2	Riches	Univ. St. Andrews
5	Luccioni	CEA - Paris
6	Martin	CEA - IPSN
7	Arrand	Univ. Brunel
8	Franek	IMG-DFC

FI3P-CT930081-B13 . . . . . *2365*
Development and validation of an image analysis system for automated detection of micronuclei in cytokinesis-blocked lymphocytes. A tool for biological dosimetry in individuals or populations occupationally or accidentally exposed to ionizing radiation.

1	Tates	Univ. Leiden
2	Thierens	Univ. Gent
3	De Ridder	Univ. Gent

B14 Assessment of genetic risks in man.

FI3P-CT920005-B14 . . . . . *2389*
Radiation-induced genetic effects in mammals and the estimation of genetic risks in man: a concerted approach using theoretical, epidemiological, cytogenetic, biochemical and molecular methods.

1	Sankaranarayanan	Univ. Leiden
2	Tease	MRC
3	Jacquet	CEN/SCK Mol
4	Streffer	Univ. Essen
5	Czeizel	WHO

FI3P-CT920055-B14 . . . . . *2433*
Genetic risks associated with exposure to ionizing radiation.

1	Favor	GSF
2	Van Buul	Univ. Leiden
3	Cattanach	MRC
4	de Rooij	Univ. Utrecht
5	Miró Ametller	Univ. Barcelona - Autónoma
6	Eeken	Univ. Leiden
7	Hulten	EBHA

B15 Action of radionuclides on target cells in relation to radionuclide metabolism and studies on biological models for radionuclide-induced cancer.

FI3P-CT920021-B15 . . . . . *2487*
Dose assessment early cellular and late carcinogenic effects of exposure to radon and its progeny.

1	Fritsch	CEA - Paris
2	Collier	UKAEA

FI3P-CT920051-B15 . . . . . *2513*
Induction of osteosarcoma and leukaemia by bone-seeking alpha-emitting radionuclides.

1	Höfler	GSF
2	Harrison	NRPB
3	Wright	MRC
4	Erfle	GSF
5	Skou Pedersen	Univ. Århus
6	Höfler	Univ. München - Technische

B2 Non-stochastic Effects of Radiation.

B21 Radiation syndromes and their treatment after exposure of large parts of the body.

FI3P-CT920008-B21 . . . . . *2545*
Research on the management of accidentally radiation exposed persons.

1	Fliedner	Univ. Ulm
2	Wagemaker	Univ. Rotterdam - Erasmus
3	Covelli	ENEA
4	Jammet	CIR

FI3P-CT930069-B21 2605
Radiation effects and their treatment on the connective and vascular tissues in various organs.

1	Magdelenat	CIR
2	Van der Kogel	Univ. Nijmegen

B22 Irradiation and committed exposure from incorporated radionuclides.

FI3P-CT920064b-B22 2617
Reduction of risk of late effects from incorporated radionuclides.

1	Stradling	NRPB
2	Volf	KfK
3	Poncy	CEA - Bruyères-le-Châtel
4	Archimbaud	CEA - Pierrelatte
5	Burgada	ADFAC
6	Rencova	CHZ

B23 Radiation syndromes and their treatment after local exposure to skin and subcutaneous tissues.

FI3P-CT920059-B23 2661
Radiation effects and their treatment after local exposure of skin and sub-cutaneous tissues.

1	Masse	CEA - FAR
2	Hopewell	Univ. Oxford
3	Coggle	Hosp. St. Bartholomew
4	Di Carlo	IFO

B24 Radiation damage to lens, thyroid and other tissues of relevance in radiation protection.

FI3P-CT930076-B24 2719
Thyroid and its proximate tissues radiation dosimetry; stochastic and deterministic biological effects in humans and model systems.

1	Lamy	Univ. Bruxelles (ULB)
2	Malone	Hosp. Federated Dublin Voluntaries
3	Smyth	Univ. Dublin - College
4	Williams	Univ. Cambridge

B3 Radiation effects on the developing organism.

B31 Damage to the central nervous system and hematopoiesis.

FI3P-CT920015-B31 2763
Effects of protracted exposures to low doses of radiations during the prenatal development of the central nervous system.

1	Reyners	CEN/SCK Brussels
2	Coffigny	CEA - Bruyères-le-Châtel
3	Ferrer	Hosp. Principes de España
4	Saunders	NRPB
5	Janeczko	Univ. Jagiellonian

B33 Transfer of radionuclides in utero.

FI3P-CT920064c-B33 . . . . . *2805*
Dosimetry and effects of parental, fetal and neonatal exposure to incorporated radionuclides and external radiation.

1	Harrison	NRPB
2	Henshaw	Univ. Bristol
3	Van den Heuvel	VITO
4	Lord	Inst. Paterson
5	Visser	TNO - Delft
6	Tejero	Univ. Madrid - Complutense
7	Bueren	CIEMAT
8	Archimbaud	CEA - Bruyères-le-Châtel

VOLUME 3

C RISKEN DER STRAHLENEXPOSITION UND IHRE BEWÄLTIGUNG
RISKS AND MANAGEMENT OF RADIATION PROTECTION
RISQUES ET GESTION DE L'EXPOSITION AUX RAYONNEMENTS *2877*

C1 Assessment of human exposure and risks.

C12 Exposure to natural radioactivity and evaluation of parameters influencing these risks.

FI3P-CT920025-C12 . . . . . *2879*
Retrospective assessment of radon exposure from long-lived decay products.

1	Vanmarcke	CEN/SCK Mol
2	McLaughlin	Univ. Dublin - College
3	Falk	Inst. Nat. of Radiation Protection
4	Poffijn	Univ. Gent
5	Fehér	HAS.RIAE *(PECO contract)*
6	Samuelsson	Univ. Lund

FI3P-CT920034-C12 . . . . . *2921*
Characteristics of airborne radon and thoron decay products.

1	Porstendörfer	Univ. Göttingen
2	Poffijn	Univ. Gent
3	Vanmarcke	CEN/SCK Brussels
4	Akselsson	Univ. Lund
5	Falk	Inst. Nat. of Radiation Protection
6	Tymen	Univ. Brest
7	Ortega	Univ. Catalunya - Politécnica
8	Lebecka	CMI
9	Kobal	IJS
11	Schuler	Inst. Paul Scherrer

FI3P-CT920061-C12 3019
Study of the different techniques to mitigate high radon concentrations level disclosed in dwelling.

1	Sabroux	CEA - IPSN
2	Torri	ENEA
3	Ortins	Direcção-Geral do Ambiente
4	Quindós Poncela	Univ. Cantabria
5	Kritidis	NCSR "Demokritos"
6	Proukakis	Univ. Athens (Not yet submitted)

FI3P-CT920064d-C12 3069
Radon sources models and countermeasures.

1	Miles	NRPB
2	De Meijer	Univ. Groningen
3	Andersen	Lab. Risø
4	Wouters	CSTC-WTCB
5	Ball	NERC
6	De Meijer	Univ. Groningen
7	Hubbard	Inst. Nat. of Radiation Protection
8	Balek	BIJO
9	Cosma	NPL.RO

FI3P-CT930074-C12 3159
Evaluation of the combined helium/radon in soil gas mapping methodology as an indicator of areas in which elevated indoor radon concentrations may be found.

1	Madden	RPII
2	O'Connor	Geological Survey (Irish)
3	Van den Boom	ENMOTEC GmbH
4	Porstendörfer	Univ. Göttingen

C13 Comparative assessment of exposure and risks.

FI3P-CT920019-C13 3219
Comparative assessment and management of radiological and non-radiological risks assiciated with energy systems.

1	Dreicer	CEPN
2	Friedrich	Univ. Stuttgart
3	Uijt de Haag	RIVM

FI3P-CT920064e-C13 3249
Studies related to the expression of the detriment associated with radiation exposure.

1	Muirhead	NRPB
2	Schneider	CEPN

C14 Epidemiological studies in human populations.

FI3P-CT920047-C14 . . . . . *3271*
Investigation of late effects in humans after artificial irradiation (Thorotrast-patients) - Follow-up study.

1	van Kaick	DKFZ
2	Priest	UKAEA
3	Wallin	KBFOC
4	dos Santos Silva	School Hygie.and Tropic.Med. - London
5	Malveiro	Inst. Higiene e Medicina Tropical

FI3P-CT920056-C14 . . . . . *3303*
The risk assessment of indoor radon exposure.

1	Poffijn	Univ. Gent
2	Tirmarche	CEA - FAR
3	Kreienbrock	Univ. Wuppertal
4	Kayser	Dir. Santé Luxembourg
5	Darby	ICRF
6	Miles	NRPB
7	Kunz	NIPHE.CRH
8	Kunz	CHZ
9	Cosma	NPL.RO

FI3P-CT920062-C14 . . . . . *3341*
European childhood leukaemia/lymphoma incidence study.

1	Parkin	IARC
2	Gurevicius	LOC
3	Rahu	ECR
4	Tulbure	IISP

FI3P-CT920064f-C14 . . . . . *3351*
Epidemiological studies and tables.

1	Muirhead	NRPB
2	Kellerer	Univ. München
3	Chmelevsky	GSF
4	Oberhausen	Univ. Saarlandes
5	Holm	Inst. Karolinska
6	Becciolini	Univ. Firenze
7	Richardson	INSERM
8	Hill	Inst. Gustave Roussy
9	de Vathaire	INSERM
10	Wick	GSF
11	Spiess	Univ. München
12	Kellerer	Univ. München
13	Muirhead	NRPB
14	Kellerer	GSF
15	Kolb	Univ. München
16	Socie	Hosp. St. Louis

FI3P-CT930065-C14 . . . . . *3473*
Risk estimates of lung cancer from the follow-up of uranium miners.

1	Chmelevsky	GSF
2	Tirmarche	CEA - FAR
3	Muirhead	NRPB
4	Darby	ICRF
5	Kunz	NIPHE.CRH

FI3P-CT930066-C14 . . . . . *3529*
International collaborative study of cancer risk among nuclear industry workers.

1	Cardis	IARC
2	Sztanyik	NRIRR
3	Cesnek	SEP

C2 Optimisation and management of radiation protection.

C2A ICRP

FI3P-CT920004-C2A *3547*
Development of fundamental data for radiological protection.

1	Smith	ICRP

C21 Optimisation of radiological protection.

FI3P-CT920033-C21 . . . . . *3555*
Alara in installations.

1	Lefaure	CEPN
2	Zeevaert	CEN/SCK Mol
3	Pfeffer	GRS
4	Wrixon	NRPB

C22 Reduction of patient exposure in medical diagnostic radiology.

FI3P-CT920014-C22 . . . . . *3597*
Digital Medical Imaging: Optimization of the dose for the examination.

1	Malone	Hosp. Federated Dublin Voluntaries
2	Faulkner	Hosp. Newcastle
3	Busch	Univ. Heidelberg
4	Jankowski	IOM
5	Shehu	Inst. Onkologjise

FI3P-CT920020-C22 . . . . . *3653*
Quality assurance parameters and image quality criteria in computed thomography.

1	Jessen	Univ. Århus - Hospital
2	Ortins	Direcção-Geral do Ambiente
3	Schneider	Univ. München
4	Moores	IRS Ltd.

FI3P-CT920024-C22 . . . . . *3691*
Diagnosis related dose: an investigation on patient risk and image quality in european hospitals.

1	Van Loon	Univ. Bruxelles (VUB)
2	Thijssen	Univ. Nijmegen
3	Milu	IHPH
4	Karlinger	SUM

FI3P-CT920037-C22 . . . . . *3723*
Optimisation of image quality and reduction of patient exposure in medical diagnostic radiology.

1	Maccia	CAATS
2	Moores	IRS Ltd.
4	Dance	Hosp. Royal Marsden
5	Padovani	Unitá Sanitaria Locale - Udine
6	Vañó Carruana	Univ. Madrid - Complutense

FI3P-CT920052-C22 . . . . . *3759*
Patient dose from radiopharmaceuticals.

1	Smith	Hosp. Great Ormand Street
3	Petoussi	GSF
4	Evans	Univ. London

FI3P-CT920064g-C22 . . . . . *3797*
Medical dose assessment and evaluation of risk.

1	Wall	NRPB
2	Drexler	GSF
3	Fitzgerald	Hosp. St. Georges
4	Zoetelief	TNO - Delft

FI3P-CT930070-C22 . . . . . *3839*
Evaluation of dose and risk due to interventional radiology techniques.

1	Schmidt	Klinikum Nürnberg
2	Maccia	CAATS
3	Padovani	Unitá Sanitaria Locale - Udine
4	Vañó Carruana	Univ. Madrid - Complutense
5	Neofotistou	Hosp. General Athens

C23 Management of radiological protection in normal and accident situations.

FI3P-CT920013b-C23 . . . . . *3873*
Evaluation and management of post-accident situations. Project 1: Database and decision-aiding techniques.

1	Després	CEA - FAR
2	Alonso	Univ. Madrid Politéc. Fundación Gral.
3	French	Univ. Leeds
4	Vanderpooten	Univ. Paris IX

FI3P-CT930068-C23 . . . . . *3913*

Assessment and management of post accidental situations. Radiation detriment, risk perception and risk communication.

1	Brenot	CEA - FAR
2	Joussen	IFS
3	Sjoberg	CFR

C24 Probabalistic risk assessment and real-time models for assessing the consequences of accidental releases and for evaluating effectiveness and feasibility of countermeasures.

FI3P-CT920023-C24 . . . . . *3943*

CEC/USNRC joint project on uncertainty analysis of probabilistic accident consequence codes.

1	Goossens	Univ. Delft
2	Haywood	NRPB
3	Ehrhardt	KfK
4	Boardman	UKAEA
5	Roelofsen	ECN
6	Hofer	GRS

FI3P-CT920036-C24 . . . . . *3973*

Development of a comprehensive decision support system for nuclear emergencies in Europe following an accidental release to atmosphere.

1	Ehrhardt	KfK
2	Gland	EDF
3	Müller	GSF
4	French	Univ. Leeds
5	Sohier	CEN/SCK Mol
6	Haywood	NRPB
7	Bleasdale	Nuclear Electric
8	Zelanzy	IEA.CCC
9	Kanyar	OSSKI
10	Zelasny	Cyfronet
11	Mateescu	IFIN
12	Stubna	NPPRI

FI3P-CT920038-C24 . . . . . *4109*

Deposition of artificial radionuclides, their subsequent relocation in the environment and implications for radiation exposure.

1	Tschiersch	GSF
2	Roed	Lab. Risø
3	Brown	NRPB
4	Goddard	IMPCOL
5	Roed	Lab. Risø
6	Rybacek	CSAS.IRD
7	Jansta	Inst. Radioecology
8	Zomoori	KFKI

FI3P-CT920044-C24 . . . . . *4225*
Coordination of atmospheric dispersion activities for the real-time decision support system under development at KFK.

1	Mikkelsen	Lab. Risø
2	ApSimon	IMPCOL
4	Desiato	ENEA
5	Rasmussen	DMI
6	Thykier-Nielsen	Lab. Risø
7	Bartzis	NCSR "Demokritos"
8	Massmeyer	GRS
9	Deme	HAS.RIAE *(PECO contract)*

FI3P-CT920057-C24 . . . . . *4291*
Methodology for evaluating the radiological consequences of radioactive effluent released in accidents - the MARIA project.

1	Jones	NRPB
2	Ehrhardt	KfK
3	Alonso	Univ. Madrid Politéc. Fundación Gral.
4	Van der Steen	KEMA N.V.
5	Iordanov	BAS
6	Koblinger	AEKI

FI3P-CT930073-C24 . . . . . *4357*
Analysis and modelling of the migration of radionuclides deposited in catchment basins of fresh water systems.

1	Monte	ENEA
2	Van der Steen	KEMA N.V.
3	Boardman	UKAEA
4	Kozhoukharov	BAS
5	Bergström	Studivisk AB

FI3P-CT930077-C24 . . . . . *4411*
Multifractal analysis and simulation of Chernobyl radioctive fall-out in Europe.

1	Ratti	Univ. Pavia
2	Schertzer	CNRM

IV. Koordinierungstätigkeit
Coordination activities
Activités de coordination *4435*

V. - ERPET -
Europäische Aus-und Fortbildung auf dem Gebiet des Strahlenschutzes
European Radiation Protection Education and Training
Enseignement et formation européens en Radioprotection *4477*

VI. Auswahl einiger auf Veranlassung der Kommission erschienener Veröffentlichungen
Selection of publications issued on the initiative of the Commission
Choix des publications éditées à l'initiative de la Commission *4495*

VII. Liste des Acronyme und Abkürzungen
List of acronyms and abbreviations
Liste des acronymes et des abréviations *4541*

VIII. Verzeichnis der Forschungsgruppenleiter
List of research group leaders
Index des chefs de groupes de recherche *4545*

I

EINLEITUNG

INTRODUCTION

INTRODUCTION

VORWORT

Die vorliegenden 3 Bände enthalten einen umfassenden Bericht über den wissenschaftlichen Fortschritt während des achten mehrjährigen Forschungs- und Ausbildungsprogramms auf dem Gebiet des Strahlenschutzes, das die Kommission der Europäischen Gemeinschaften (KEG) in den Jahren 1992 bis 1995 im Rahmen des Euratom-Vertrags durchgeführt hat.

Für die europäische Strahlenschutzforschung ist dieses Programm nach wie vor wichtig, da es die Zusammenarbeit zwischen den nationalen Forschungseinrichtungen fördert. Dadurch sollen die Kenntnisse über die Risiken niedriger Strahlendosen erweitert und deren Quantifizierung ermöglicht werden. Die Strahlenschutzforschung wurde 1992 in das spezifische Programm über die Sicherheit bei der Kernspaltung des Dritten Rahmenprogramms integriert und in den Jahren 1992 bis 1994 als Strahlenschutzaktion geführt. Durch die Bereitstellung zusätzlicher Finanzmittel konnte die Laufzeit der Verträge bis Juli 1995 verlängert und so vermieden werden, daß bis zum Anlaufen der Projekte des Vierten Rahmenprogramms eine zu große Lücke bei den Grundlagenforschungsprojekten entstand. Das Programm 1992-1995 führte die multinationalen Mehrpartnerverträge fort, die klare Vorteile haben, da sie die Zusammenarbeit zwischen den einzelnen Forschungsgruppen vorantreiben und dazu beitragen, daß die Forschung auf spezielle Problembereiche konzentriert wird. Durch diese Art der Verträge können außerdem Doppelarbeiten vermieden und das Subsidiaritätsprinzip gewahrt werden. Trotz der Bedenken zu Beginn der Mehrpartnerprojekte waren sie dank des Einsatzes der Projektkoordinatoren und der Bereitschaft der Partner zu einer solch zwanglosen Zusammenarbeit im allgemeinen äußerst erfolgreich. Die Verträge haben den zusätzlichen Vorteil, daß sie den Aufbau des Forschungsprogramms transparenter und für die Programm-Manager überschaubarer machen. In dem Programm wurden 102 multinationale Mehrpartnervorschläge mit 385 Einzelprojekten finanziert, wofür von 1992 bis 1994 28,64 Millionen ECU zur Verfügung standen. Diese Verträge wurden durch eine Aufstockung der Mittel um 12,5 Millionen ECU bis Mitte 1995 verlängert. Norwegische, schwedische und schweizerische Wissenschaftler wurden im Rahmen einzelner Projekte an dem Programm beteiligt.

Beim Programm 1992-1995 wurde die 1990/91 eingeführte Dreiteilung beibehalten:

- Strahlen- und Radioaktivitätsexposition des Menschen:
  - Messungen der Strahlendosis und ihre Interpretation
  - Transfer und Verhalten von Radionukliden in der Umwelt

- Folgen der Strahlenexposition des Menschen; Abschätzung, Verhütung und Behandlung:
  - Stochastische Wirkungen von Strahlen
  - Nichtstochastische Wirkungen von Strahlen
  - Strahlenwirkungen auf den sich entwickelnden Organismus

- Risiken der Strahlenexposition und ihre Bewältigung:
  - Abschätzung der Strahlenexposition des Menschen und ihrer Risiken
  - Optimierung und Durchführung des Strahlenschutzes

Die Schlußberichte sind nach diesen Teilen gegliedert und enthalten über jeden multinationalen Mehrpartnervertrag einen eigenen Bericht, der einen Überblick über die geleistete Arbeit mit den Ergebnissen jedes einzelnen Gruppenmitglieds bietet. Dies soll deutlich machen, in welchem Verhältnis die Partner zueinander stehen und welcher Zusammenhang zwischen den einzelnen Verträgen jedes Programmteils besteht. Da die Berichte jedes Teils in numerischer Folge geordnet sind, ist der Gesamtaufbau jedes Bereichs zwar nicht direkt ersichtlich, letztlich aber doch zu erschließen.

Die bisherige Programmstrategie wurde beibehalten, den Informationsaustausch und die Zusammenarbeit zwischen Wissenschaftlern durch die Veranstaltung von 52 Studiengruppensitzungen mit Vertragspartnern und geladenen Sachverständigen und von 37 internationalen Seminaren und Workshops zu fördern. Die Berichte dieser Sitzungen und die aus den Vertragsarbeiten hervorgegangenen Veröffentlichungen beweisen, welch große Bedeutung der europäischen Forschung auf dem Gebiet des Strahlenschutzes zukommt.

Im Rahmen des Programms werden enge Kontakte mit den USA und Kanada, mit internationalen Organisationen wie der IAEO, WHO, OECD, ICRP und ICRU und mit anderen Ländern außerhalb der Gemeinschaft gepflegt.

Ein wichtiger Teil des Programms sind weiterhin die Maßnahmen im Bereich der Aus- und Fortbildung, die im Rahmen der europäischen Aus- und Fortbildung auf dem Gebiet des Strahlenschutzes (ERPET) koordiniert werden. Dadurch sollen das Fachwissen der älteren Mitarbeiter in der Industrie umfassend erhalten und die Aufstiegsmöglichkeiten für Nachwuchswissenschaftler auf dem Gebiet des Strahlenschutzes verbessert werden. 1993 unterstützte das Programm erstmalig die Teilnahme von vier europäischen Studenten an dem einjährigen Lehrgang über Strahlenbiologie am St. Bartholomew's Medical College, der zum Abschluß "Master of Science" an der Universität London befähigt. Bei dieser ersten Runde bestanden alle vier Stipendiaten. Studenten und Lehrkörper lobten das Experiment, das bis 1995 verlängert wurde. In den letzten 30 Monaten wurden 17 Lehrgänge über allgemeinen Strahlenschutz und über Spezialgebiete wie Dosimetrie, Radioökologie, Molekularbiologie, Behandlung von Unfallopfern, Qualitätssicherung und Strahlenschutz bei der medizinischen Diagnostik sowie Notfallbekämpfung veranstaltet.

E. Andreta
Direktor GD XII.F
Energie

S.Frigren
Direktor GD XI.C
Nukleare Sicherheit und
Katastrophenschutz

J. Sinnaeve
Referatsleiter GD XII.D.3
Strahlenschutzforschung

H. Eriskat
Referatsleiter GD XI. C.1
Strahlenschutz

PREFACE

These 3 volumes present a comprehensive account of the scientific progress achieved during the eighth multi-annual research and training programme on Radiation Protection which was carried out in the period from 1992 to 1995 under the Euratom Treaty of the Commission of the European Communities (CEC).

The programme continues an on-going role in European radiation protection research stimulating the collaboration between the different national research organisations to further the understanding and quantification of low dose radiation risks. In 1992 radiation protection research was incorporated into the Specific Programme on Nuclear Fission Safety in the Third Framework Programme as a Radiation Protection Action for the period 1992-1994. The contracts were extended through a "refuelling" of the budget to run up to July 1995 in an effort to avoid too large a gap in fundamental research projects before the start of the Fourth Framework Programme contracts. The 1992-1995 programme continued the multi-national, multi-partner contracts which have clear benefits, have fostered cooperation between the different research groups and helped to improve the focus of the research on specific problem areas. This type of contract helped to avoid duplication and ensured the principle of subsidiarity. In spite of some reservations at the inception of the multi-partner projects they have been, in general, most successful thanks to the input of the coordinators of the projects and also to the willingness of the partners to collaborate so freely. The contracts have also had the added advantage of making the structure of the research programme more visible and transparent for the programme managers. The programme funded 102 multi-national, multi-partner proposals involving 385 individual projects from a budget of 28.64 MEcu in the period 1992-1994 and these contracts were extended to mid-1995 by the refuelling budget of 12.50 MEcu. Norwegian, Swedish and Swiss scientists were involved in the programme on a project by project basis.

The 1992-1995 programme maintained the three main sections introduced in the 1990-1991 period, namely:

- Human Exposure to Radiation and Radioactivity, which includes
  - Measurement of Radiation Dose and its Interpretation
  - Transfer and Behaviour of Radionuclides in the Environment

- Consequences of Radiation Exposure to Man; Assessment, Prevention and Treatment, which includes:
  - Stochastic Effects of Radiation
  - Non-Stochastic Effects of Radiation
  - Radiation Effects on the Developing Organism

- Risks and Management of Exposure, which includes:
  - Assessment of Human Exposure and Risks
  - Optimization and Management of Radiation Protection

The Final Reports have been grouped into these sections and each multi-national multi-partner contract presents a single report giving an overview of the work carried out followed by the individual results from each member of the group. This should clarify the inter-relationship of the different partners in a contract and provide some indication of the association between the different contracts in each section of the programme. However, because the reports in each section are presented in numerical order the total structure of each sector is not totally clear although it can certainly be discerned.

The programme has continued its policy of promoting the exchange of information and cooperation between scientists by organising 52 study group meetings with contractors and invited experts and 37 international seminars and workshops. The proceedings of these meetings and the publications originating from the contract work testify to the important role played by European research in the field of radiation protection.

The programme maintains close contacts with the USA and Canada, with international organisations, such as the IAEA, WHO, OECD, ICRP and ICRU, and with other countries outside the Community.

Training and Education continue to be an important part of the programme's activities which are coordinated under ERPET (European Radiation Protection Education and Training) to preserve a cross-section of expertise in an aging industry and promote the career prospects of young scientists entering the field of radiation protection. A new venture started in 1993 when the programme supported four European students to participate in the year long course on Radiation Biology at St Bartholomew's Medical College which leads to the degree of Master of Science at London University. The first year produced four successful European students and was much appreciated both by the students and the course instructors and the exercise has been extended to 1995. 17 training courses have been organised during the past 30 months covering general radiation protection as well as more specialised areas such as dosimetry, radioecology, molecular biology, treatment of accident victims, quality assurance and radiation protection in medical diagnosis and nuclear emergency management.

E. Andreta
Director DG XII.F
Energy

S. Frigren
Director DG XI.C
Nuclear Safety and
Civil Protection

J.Sinnaeve
Head of Unit DG XII.D.3
Radiation Protection Research

H. Eriskat
Head of Unit DG XI.C.1
Radiation Protection

PREFACE

Ces 3 volumes présentent un compte complet des progrès scientifiques réalisés pendant les huitièmes recherche et programme de formation pluriannuels sur la radioprotection qui a été effectuée dans la période de 1992 à 1995 aux termes du Traité EURATOM de la Commission des Communautés européennes (CCE).

Le programme poursuit un rôle en cours dans la recherche en matière européenne de radioprotection stimulant la collaboration entre les différentes organisations de recherche nationales pour promouvoir la compréhension et la quantification des faibles risques de radiation de dose. En 1992 la recherche en matière de radioprotection a été incorporée dans le programme spécifique sur la sécurité de fission nucléaire dans le troisième programme-cadre comme action de radioprotection pour la période 1992-1994. Les contrats ont été avancés à travers un "réapprovisionnement en combustible" du budget à fonctionner jusqu'à juillet 1995 dans un effort pour éviter un écart trop grand dans les projets de recherche fondamentaux avant le commencement des quatrièmes contrats de programme-cadre. Le programme de 1992-1995 a poursuivi des contrats multinationaux et à partenaires multiples qui ont les bénéfices clairs, ont stimulé la coopération entre les différents groupes de recherche et ont aidé à améliorer le centre de la recherche sur les domaines problématiques spécifiques. Ce type de contrat aide à éviter la duplication et assurer le principe de subsidiarité. Malgré certaines réserves au commencement des projets à partenaires multiples ils ont été, en général, très réussis grâce à l'intervention des coordinateurs des projets et également à la volonté des partenaires de collaborer si librement. Les contrats ont également eu l'avantage ajouté de rendre la structure du programme de recherche plus visible et transparente pour les logiciels de gestion. Le programme a financé 102 propositions multinationales et à partenaires multiples impliquant 385 différents projets sur un budget de 28,64 MECU dans la période 1992-1994 et ces contrats ont été élargis le milieu de l'année 1995 par le budget de réapprovisionnement en combustible de 12,50 MECU. Des scientifiques norvégiens, suédois et suisses ont été impliqués dans le programme sur par projet une base le projet.

Le programme de 1992-1995 a maintenu les trois sections principales utilisées dans la période de 1990-1991, à savoir:

- Exposition humaine à la radiation et à la radioactivité, qui comprend
  - Mesure de dose de rayonnement et de son interprétation
  - Transfert et comportement des radionucléides dans l'environnement

- Conséquences d'exposition au rayonnement à l'homme; Évaluation, prévention et traitement, qui comprend:
  - Effets stochastiques de radiation
  - Effets non stochastiques de radiation
  - Effets de l'irradiation sur l'organisme en développement

- Risques et gestion d'exposition, qui comprend:
  - Évaluation d'exposition et des risques humains
  - Optimisation et gestion de radioprotection

Les rapports finaux ont été groupés dans ces sections et chaque contrat à partenaires multiples multinational présente un rapport unique donnant un aperçu des travaux effectués suivi des différents résultats de chaque membre du groupe. Cela devrait clarifier l'interdépendance des différents partenaires dans un contrat et fournir une indication de l'association entre les différents contrats dans chaque section du programme. Cependant, parce que les rapports dans chaque section sont présentés dans l'ordre numérique la structure totale de chaque secteur n'est pas totalement claire bien qu'elle puisse être certainement discernée.

Le programme a poursuivi sa politique de promouvoir l'échange d'informations et la coopération entre les scientifiques en organisant 52 réunions de groupe d'étude avec les contractants et les experts invités et 37 séminaires internationaux et les ateliers. Les travaux de ces réunions et des publications provenant des travaux sous contrat témoignent au rôle important joué par recherche européenne dans le domaine de la radioprotection.

Le programme maintient les contacts étroits avec les États-Unis et le Canada, avec les organisations internationales, telles que l'AIEA, l'OMS, l'OCDE, l'ICRP et l'ICRU, et avec d'autres pays en dehors de la Communauté.

La formation et l'enseignement restent une partie importante des activités du programme qui sont coordonnées sous ERPET (l'enseignement et la formation de radioprotection européens) pour préserver une section transversale de compétence dans une industrie de vieillissement et pour promouvoir les perspectives de carrière des jeunes scientifiques pénétrant le domaine de la radioprotection. Un nouveau projet a commencé en 1993 quand le programme a soutenu quatre étudiants européens pour participer au long cours d'année sur la biologie de radiation au collège médical de la WS du Bartholomew qui mène au degré de maître de science à l'université de Londres. La première année a produit quatre étudiants européens réussis et a été beaucoup appréciée à la fois par les étudiants et les instructeurs de cours et l'exercice a été élargi à 1995. 17 des cours de formation ont été organisés au cours des 30 derniers mois couvrant la radioprotection générale ainsi que des secteurs plus spécialisés tels que la dosimétrie, la radioecologie, la biologie moléculaire, le traitement des victimes des accidents, la garantie de la qualité et la radioprotection dans le diagnostic médical et la gestion nucléaire de situations d'urgence.

E. Andreta
DIRECTEUR DG XII.F
Energies

S. Frigren
DIRECTEUR DG XI.C
Sécurité nucléaire, Protection civile et Industrie

J. Sinnaeve
DG Chef d'unité DG XII.F.6
Action Recherche en Radioprotection

H. Eriskat
Chef d'Unité DG XI.C.1
Radioprotection

II

Mitglieder und Experten 1993-95

Beratender Verwaltungs- und Koordinierungsausschuss "STRAHLENSCHUTZ"

Members and Experts 1993-95

Management and Coordination Advisory Committee "RADIATION PROTECTION"

Membres et Experts 1993-95

Comité consultatif en matière de Gestion et de Coordination "RADIOPROTECTION"

Mitglieder und Experten 1993-95
Beratender Verwaltungs- und Koordinierungsausschuss "STRAHLENSCHUTZ"

Members and Experts 1993-95
Management and Coordination Advisory Committee "RADIATION PROTECTION"

Membres et Experts 1993-95
Comité consultatif en matière de Gestion et de Coordination "RADIOPROTECTION"

BELGIQUE - BELGIË

S. HALLEZ °
N. HENRY °

DANMARK

A. AARKROG °
K.A. JESSEN

DEUTSCHLAND

W. GÖSSNER °
H.H. LANDFERMANN °
Experts: W. BURKHART
G. DIETZE
A.M. KELLERER
SEIDEL

ELLINIKI DIMOKRATIA

S. DANALI-COTSAKI °
D. GLAROS °
Expert: A. KAPPAS

ESPAÑA

L. ARRÁNZ CARRILLO DE ALBORNÓZ °
F. MINGOT BUADES °
Experts: E. GIL
B. SÁNCHEZ FDEZ. MURIAS

FRANCE

Y. BELOT °
H. MÉTIVIER °
Experts: M. BLANC
F. DABURON
H. JAMMET

IRELAND

J.D. CUNNINGHAM °
C.P. O'TOOLE °

ITALIA

A. CIGNA °
F. MORSELLI °
Experts: V. COVELLI
F. DI MAURO

LUXEMBOURG

C. BACK °

NEDERLAND

H.R. LEENHOUTS °
J.P. TIJSSEN °
Expert: P.H. LOHMAN

PORTUGAL

J. CARVALHO PEDROSO DE LIMA
A. ORTINS DE BETTENCOURT °
Expert: I. GUEDES BRAVO

SWEDEN

U. BÄVERSTAM
M. RINGDAHL

UNITED KINGDOM

J.W. STATHER °
H. WALKER °

COMMISSION

H. ERISKAT (DG XI)

OBSERVANTS

FINLAND: R. MUSTONEN
NORGE: P.B. HAUGSØEN °
ØSTERREICH: E. HENRICH
SWITZERLAND: A. SCHENKER °

° Member of CGC

III

FORSCHUNGSTÄTIGKEIT STRAHLENSCHUTZ

RESEARCH IN RADIATION PROTECTION

RECHERCHE EN RADIOPROTECTION

III A

EXPOSITION DES MENSCHEN DURCH STRAHLEN UND RADIOACTIVITÄT

HUMAN EXPOSURE TO RADIATION AND RADIOACTIVITY

EXPOSITION DE L'HOMME AUX RAYONNEMENTS ET À LA RADIOACTIVITÉ

Final Report
1992 - 1994

Contract: FI3PCT920054 **Duration: 1.9.92 to 30.6.95** **Sector: A1A**

Title: Radiation quantities units and measurement techniques for radiation protection.

1) Allisy BIPM

I. Summary of Project Global Objectives and Achievements

Any determination of human exposure to radiation and radioactivity requires a fundamental set of quantities and units with which exposure can be specified and the means and ability to make measurements which yield results in terms of these quantities and units. Radiation protection, then, requires the capability to accurately quantify the characteristics and extent of radiation exposure so that appropriate and useful assessments of the potential health consequences and risks can be formulated. The work carried out via this project sought to meet these needs.

Important achievements related to these needs include the publication of seven new ICRU Reports, the completion of all but the printing of three other ICRU Reports, completion of ICRU review of two draft reports, the completion of the drafting work on four other reports.

Head of project 1: Prof. Allisy

II. Objectives for the reporting period

Publication of reports on

(1) interaction data
(2) measurement of dose equivalent
(3) phantoms
(4) stopping powers for protons and alpha particles
(5) quantities and units for radiation protection
(6) fundamental particle counting
(7) specification of therapy doses
(8) *in situ* gamma spectrometry

Preparation of printers manuscript for reports on

(1) performance assessment in diagnostic modalities
(2) beta-ray dosimetry for radiation protection
(3) secondary electron spectra from charged particle interactions.

(Objectives continue on Attachment No. 1)

III. Progress achieved including publications

Vital to radiation protection activities is information on the fundamental interaction of radiation with body tissues, including interaction data for photons, electrons, protons and neutrons. This has now been provided via ICRU Report 46, *Photon, Electron, Proton and Neutron Interaction Data for Body Tissues.*

To facilitate practical radiation protection activities, guidance is required on the implementation of measurement in terms of the defined operational quantities. This has been provided via ICRU Report 47, *Measurement of Dose Equivalents from External Photon and Electron Radiations.*

Phantoms constitute a key element in radiation protection measurements and work carried out via this project was aimed at specification of the vital properties of phantoms and the identification of phantoms that are appropriate for various uses. This work was brought to conclusion with the publication of ICRU Report 48, *Phantoms and Computational Models in Therapy, Diagnosis and Protection.*

(Progress continued on Attachment No. 2)

II. Continuation of objectives for the reporting period

Completion of drafting work on reports on

(1) conversion coefficients for use in radiological protection against external radiation
(2) absorbed dose standards for photon irradiation and their dissemination
(3) fundamental quantities and units
(4) dose specification for reporting interstitial therapy
(5) proton beam dosimetry
(6) ROC analysis

Initiation of new work on

(1) assessment of image quality in mammography
(2) determination of absorbed dose in patients from x-rays used in diagnostic and interventional radiology
(3) assessment of deposition of radionuclides in the body
(4) stopping powers for heavy ions
(5) radionuclide sampling in the environment
(6) image quality assessment in nuclear medicine, including dose to the patient
(7) radiobiological and beam quality aspects of proton dosimetry

(Attachment No. 1)

III. Continuation of progress achieved including publications

Among the physical data vital to radiation measurement is the stopping power for various radiation entities. Added to previously provided tabulations of stopping powers for electrons and photons is comparable information for protons and alpha particles, published in ICRU Report 49, *Stopping Powers and Ranges for Protons and Alpha Particles*.

Fundamental to radiation protection is a set of dose equivalent quantities, units and concepts that can be applied to practical determination of radiation exposures. These have been developed and were published in ICRU Report 51, *Quantities and Units in Radiation Protection Dosimetry*.

Radioactivity measurements are, of course, vital to many radiation protection activities. Work focused on the fundamentals of particle counting applied to radioactivity measurements has been carried out as part of this project. The report on this subject is (ICRU Report 52), *Particle Counting in Radioactivity Measurements*.

In the case of radionuclides released to the environment, radiation protection for the public requires an effective method for the determination of the radionuclides deposited and *in situ* gamma spectrometry provides this. ICRU Report 53 covers this subject.

The importance to radiation effects of the transport of energy by secondary electrons has long been recognized. Thus, a detailed knowledge of the energetics of ionized electrons is vital. Information on this important topic is compiled in a new report for which the printer's manuscript is now being prepared.

An important source of public exposure to radiation, and hence a concern of radiation protection, is medical application of radiation. Thus, dose reduction in medical application is important and a number of ICRU efforts have been focused on this area. Work on each of these has made important progress with a report on performance assessment for various diagnostic modalities (ICRU Report 54) now in press. A report on prescribing, recording and reporting therapy doses was published as ICRU Report 50. Work is underway on reports treating (1) assessment of image quality in mammography and (2) determination of absorbed dose in patients from x-rays used in diagnostic and interventional radiology .

Required for effective radiation protection are conversion factors for translation from calibration quantities to limiting quantities. A report on this subject, "Conversion Coefficients for Use in Radiological Protection Against External Radiation," has undergone preliminary review and final review is scheduled for the next ICRU meeting.

Protection against beta-ray exposure involves some special measurement problems. A report on this subject has been approved by the ICRU for publication as an ICRU report.

Also now undergoing ICRU review are reports on the following topics:

(1) fundamental quantities and units
(2) absorbed dose standards for photon irradiation and their dissemination
(3) dose specification for reporting interstitial therapy

(Attachment No. 2 page 1)

III. Continuation of progress achieved including publications

Plans are being formulated for work on:

(1) image quality assessment in nuclear medicine, including dose to the patient

(2) radiobiological and beam quality aspects of proton beam dosimetry

(Attachment No. 2 page 2)

International Commission on Radiation Units and Measurements
Financial Report
CEC Contract No. F13PCT 920054

For the Period 9/1/92 to 6/30/95

	9/1/92 To 12/31/92	1/1/93 To 12/31/93	1/1/94 To 12/31/94	1/1/95 To 6/30/95	Total
Personnel					
Operations	$39,250	$78,981	$106,602	$37,730	$262,563
Publications	7,505	22,918	15,625	1,587	47,635
Total Personnel	46,755	101,899	122,227	39,317	310,198
Travel					
Main Commission	26,018				26,018
Quantities & Units	1,306				1,306
Proton Beam Therapy	3,121				3,121
ICRU/ICRP Task Group	1,597				1,597
IN Situ Gamma Ray		5,890			5,890
Beta Ray Dosimetry		6,467			6,467
ICRU/ICRP Task Group		7,226			7,226
Main Commission		25,942			25,942
Secondary Electron Spectra		8,924			8,924
Electron Beam Therapy		3,069			3,069

Body Content of Radionulides		4,210			4,210
CEC Workshop		664			664
Proton Beam Therapy			4,996		4,996
Beta Ray Dosimetry			6,297		6,297
Dose Specifications			3,253		3,253
Proton Dosimetry			5,071		5,071
Electron Beam Therapy			4,063		4,063
Phantoms for Ultrasound			6,336		6,336
Interstitial Therapy			1,048		1,048
Main Commission			20,736		20,736
Body Content of Radionuclides			2,753		2,753
Stopping Powers			2,466		2,466
ICRU/ICRP Task Group				1,707	1,707
Fundamental Quantities				1,837	1,837
ICRU/ICRP Task Group				822	822
UNSCEAR				125	125
	32,042	62,392	57,019	4,491	155,944
Total	$78,797	$164,291	$179,246	$43,808	$466,142
37% of $466,142					$172,473

Final Report
1992 - 1994

Contract: FI3PCT920001 Duration: 1.9.92 to 30.6.95 Sector: A1B

Title: Collaboration on radiation dosimetry for radiation protection applications (EURADOS).

1) Dietze EURADOS
2) Golnik IAE-RPD

I. Summary of Project Global Objectives and Achievements

The European Radiation Dosimetry Group (EURADOS) is a European scientific society founded in 1981 with the main purpose of extending the co-operation in research in radiation dosimetry and related topics within Europe. About 200 scientists from about 65 laboratories in countries of the European Union participate in the work of EURADOS together with corresponding scientists from countries outside of the European Communities.

The main objectives of EURADOS in the running project were the stimulation of collaboration in research and technical development concerning the measurement and evaluation of exposure to ionising radiation and the harmonisation of methods for assessing radiation exposure. This has been achieved by collaboration in working groups, organisation of intercomparison measurements, preparation of reports on specific subjects of topical interest and performance of workshops.

Moreover, EURADOS is active in supporting the transfer of expertise and experience in radiation dosimetry from well-experienced laboratories to other sites and young scientists in Europe by organising seminars and tutorials.

A main part of the work has been carried out by EURADOS Working Groups (WG), each of which consists of 10 to 20 scientists from various European laboratories. During the project period 1992-1995, ten Working Groups performed various tasks related to following subjects:

WG 2: **Skin Dosimetry**
Intercomparison measurements with β-ray sources. β-dosimetry with extrapolation chambers. Dosimetry regarding hot particles.

WG 4: **Numerical Dosimetry**
Calculation and evaluation of conversion coefficients for the new radiation protection dose quantities in collaboration with the ICRP/ICRU Task Group. Study of radiation transport Monte Carlo codes.

WG 6: **Assessment of Internal Dose**
Stable isotope studies. Investigation of human lung models and their parameters. Study of internal dose assessment methods.

WG 7: **Radiation Spectrometry at Working Environments**
Intercomparison measurements of spectrometric systems at various sites with realistic neutron or mixed neutron-photon fields. Investigation of neutron spectrometers.

WG 8: **Development of Individual Dosemeters for External Penetrating Radiation**
Evaluation of intercomparison measurements of individual dosemeters. Study of etched-track detectors and electronic dosemeters.

WG 9: **Criticality Accident Dosimetry**
Performance of intercomparison measurements with accident dosimetry systems.

WG 10: **Basic Physical Data and Characteristics of Gas Ionization Devices**
Report on the design, the construction, the use and application of low-pressure proportional counters. Study of W-values for neutrons and characteristics of tissue equivalent proportional counters.

WG 11: **Radiation Exposure and Monitoring of Air Crews**
Preparation of a report on radiation in flight altitudes and monitoring of air crews.

WG 12: **Environmental Dose Measurements**
Intercomparision measurements with environmental dosemeters at various sites with well-specified radiation fields. Report on masurements of doses from external environmental radiation.

A detailed description of the objectives and of the progress and results achieved are given the sections due to the individual Working Groups.

Training Courses:

During the report period four training courses has been organised.

- A training course on "Modern Methods in Radiation Measurement and Dosimetry" has been organised and performed together with the GSF/Neuherberg and the CEC at Bad Honnef on November 23-27, 1992.
- A course on the "Assessment of Doses from Intake of Radionuclides" has been carried out in co-operation with CEA/France, EULEP and the CEC in Cadarache/France on April 18-22, 1994. The course with 37 participants includes lectures and training exercises and was judged by the participants to be well organised and very useful.
- A further training course on "Application of Modern Methods in Radiation Measurement and Dosimetry" has been organised together with the GSF/Neuherberg and the CEC. This course took place at the GSF/Neuherberg on September 5-9, 1994 and included in addition to lectures also 5 half-day exercises in various fields of radiation measurement.
- Most recently a training course for advanced scientists were again organised together with the GSF/Neuherberg and the CEC at Bad Honnef on April 24-28, 1995. The course with 36 participants deals with "Advanced Methods in Radiation Measurement and Dosimetry" presenting a very broad range of recent developments in the field of radiation detection.

Workshops:

A Workshop on "Individual Dosimetry" has been organised by WG 8 in co-operation with the Paul-Scherrer Institute/Würenlingen. The Workshop was held at the PSI on October 3-6, 1993 and the Proceedings were published in Radiation Protection Dosimetry (see WG 8).

A Workshop on "Advances in Radiation Measurements - Applications and Research Needs in Health Physics and Dosimetry" has been prepared and performed in October 1994 at Chalk River/Canada together with the AECL, Chalk River Laboratory (see WG 10).

During the period 1993-1995 partners from Middle and Eastern European countries participated in the Work of EURADOS via a co-operated contract (PECO). Scientists from various laboratories of Bulgaria, Croatia, Czech Republic, Hungary, Latvia, Poland, Romania, Russia and Slowakia became either members of one of the Working Groups of EURADOS or participated in training courses and Workshops. Knowledge transfer were also stimulated by Working Group meetings at laboratories in Krakow/Poland and Prague/Czech Republic.

WG 2: Skin Dosimetry — Chairman: M. Charles

Within the project period the Working Group concentrated its efforts on the following topics:

Study of the extrapolation chamber measurement method for standard beta dosimetry

The extrapolation chamber is used as a standard instrument for the measurement of dose rates from beta radiation fields. The aim of this project was to study the present state of the art of this dosimetry method as exercised in different laboratories, to identify parameters important for the accuracy of the method and to develop standardised operation and evaluation procedures which would facilitate the application of extrapolation chambers. The study has been centered on two intercomparison exercises using extended 4 cm x 4 cm, Pm-147 sources (NRPB type) and a circular, 1 cm diameter, Tl-204 source (PTB Beta Secondary Standard), respectively. Participants of the intercomparison were: PTB, NRPB, CEA Fontenay-aux-Roses, Riso National Laboratory and CEA Gif-sur-Yvette (participated only in the Tl-204 intercomparison).

Measurement results from the first intercomparison exercise (Pm-147) showed significant discrepancies which gave rise to detailed studies of operational parameters as well as specific evaluation procedures. As a result, standardised procedures have been developed for, e.g. determination of environmental influences (temperature, pressure, humidity) and for the evaluation of the measurement data obtained by the extrapolation chamber. Results from the Pm-147 intercomparison have been published [1] and a more comprehensive description of the experience from the intercomparison on measurement of dose rates from a Pm-147 source has been given in a draft report.

The second intercomparison exercise (TI-204) was initiated in order to test the extrapolation chamber method for a more energetic beta radiation field and thus avoid sources of uncertainty present for measurement of dose rates in beta fields of lower energies e.g. Pm-147. The absorbed dose rate to tissue at different depths should be evaluated from measured depth-dose curves. Unexpectedly high discrepancies observed for the initial results of the measured dose rates were found to be caused by different methods used by the participants for measuring depth dose curves. After follow-up experiments for the development of a consistent method for obtaining depth dose curves and applying this method for the intercomparison data the results of all participants agreed to within 2 %. The results from the TI-204 intercomparison exercise have been described in a report ready for submission for publication in Radiation Protection Dosimetry [6].

References

1. Francis, T.M., Böhm, J., Chartier, J.-L., and Christensen, P. Experience gained on extrapolation chamber measurement techniques from an intercomparison exercise conducted with a 147-Pm source. Radiat. Prot. Dosim. 39 (1/3), 109-114 (1991)

Progress report on the Tl-204 intercomparison

The retirement of T.M. Francis (NRPB) delayed the finalisation of the intercomparison by about half a year. A publication however is now almost ready, and one can draw the following conclusions from this intercomparison:

The intercomparison measurements with the Tl-204 beta source showed that the participants are able to measure $D'(d,\alpha)$ of the order of 1 mGy/h caused by beta radiation of mean energy of about 0.24 MeV for depths d between 0 and 0.07 mm and for $\alpha = 0°$ and 60° with relative combined standard uncertainties between 1.2 % and 1.6 %. Deviations of the individual results from the mean values of all the participants (regarded as "true" values) were less than about 2 %.

It turned out that one has to be cautious in deducing the dose rates for tissue depths between 0 mm and 0.07 mm from the dose rate $D'(d_{Win},\alpha)$ behind the entrance window of the chamber (thickness d_{Win}). A separate experiment revealed that for the chamber constructions used by participants, depth dose curves measured at a fixed chamber depth may cause additional errors. The depth dose curve turns out to be sufficiently accurate, if it is measured with a very small chamber depth, in this case 1 mm or smaller.

Progress report on the Sr-90/Y-90 benchmark study

Three reports have been exchanged between the participants of the benchmark experiment, CEA Grenoble, UPS Toulouse and PTB Braunschweig.

1. PTB source measurements with a PTW extrapolation chamber model 23391 with the results of measurements at CEA Grenoble (J.B. Leroux, Y. Herbaut, CEA Grenoble).
2. The UPS computer code for simulation of covered and titled beta sources (J.P. Patau, Université Paul Sabatier, Toulouse)
3. The benchmark problem with results of extrapolation chamber measurements on the source and of the calculations with the UPS computer code installed on a personal computer at PTB (P.Ambrosi, J. Böhm, K. Helmstädter, PTB).

Table 1 shows the comparison of some measured and calculated results at PTB. For a source-to-dosemeter distance of 300 cm, the discrepancies between measured and calculated values are less than 13 %.

Table 2 shows the measured results of CEA Grenoble. They agree well (within 2.5 %) for half of the measuring conditions. But there exist differences of up to 8.9 % for a source-to-chamber distance of 50 cm. These differences are not yet understood.

Some open questions still remains, e.g:
- Can the differences in the results between PTB and CEA be explained and/or should there be a third independent measurement?
- Can the program of Dr. Patau be improved and/or should another program be checked in addition?

Hot particle dosimetry

The overall aim of this project is to develop and validate methods for the measurements and calculation of doses from radioactive particles (hot particles). This is being achieved by constructing standard, well defined radioactive test sources of Co-60 and Tm-170 in order to allow parallel measurements and calculations to be compared. The initial measurement techniques of extrapolation chamber (EC) and radiochromic dye film (RDF) have been extended to include thermoluminescence dosimetry (TLD). The results of the various measuring laboratories (Berkeley, Grenoble & Montpellier) have been combined and compared with calculations based on a 'HOT' Monte Carlo code (Toulouse) or EGS4, and a semiempirical PC programme VARSKIN. High dose rate Co-60 particles have also been produced for dosimetry and radiobiological studies within a EULEP skin radiobiology programme. Because of interest in this subject in the USA the project has been extended to initiate a collaborative EU/US intercomparison/validation dosimetry programme including Brookhaven National Laboratory (BNL), the National Institute of Standards & Technology (NIST), Richland Battelle Laboratories and Yankee Atomic. The preparation of other radioactive test sources has also been initiated. The importance of this work has been underlined recently by the publication of reports from French and Spanish electricity utilities indicating severe radiological protection problems arising from hot particles on aging plant.

The measured values for EC and RDF are in reasonable agreement with the VARSKIN and EGS4 Code predictions for Tm-170. For Co-60 the EC and RDF measurements are in reasonable agreement, but the VARSKIN code provides significant under-estimates of the total dose. The 'HOT' Monte Carlo code provides significantly lower estimates than the VARSKIN values. TLD measurements have not yet provided satisfactory information for comparison with EC or RDF but have underlined problems with the Monte Carlo code calculations for Co-60 and have indicated considerable promise for rapid evaluation of isodose information using focused laser heating. Good agreement has been found for EC and RDF in a EU/US transatlantic intercomparison for a range of hot particle studies. Further work is necessary to achieve consistency in the results.

Publications

1. Charles, M.W. Dosimetry and biological effects of radioactive 'hot particles'. In: IAEA report of Kiev meeting of the CRP (Coordinated Research Project) on the radiobiological impact of hot beta particles from the Chernobyl fallout: risk assessment. IAEA J1-RC-478 (1992)
2. Darley, P.J., Charles, M.W. and Hart, C.D. Validation of theoretical models for calculating doses from hot particles. Proceedings of the 17th IRPA Regional Congress on Radiological Protection. Nuclear Technology Publishing. Pages 153-156 (1994)
3. Charles,M.W. Hot particles - are they still a problem? Meeting of the Association for Radiation Research, Dublin, June 1994. Abstract to appear in the International Journal of Radiation Biology.
4. Baum, J., Kaurin, D., Darley, P.J. and Charles, M.W. International hot-particle dosimetry intercomparison. Abstract submitted: International Congress on Radiation Protection, April 1996, Vienna.
5. Böhm, J., Charles, M.W., Cross, W.G., Piesch, E. and Seltzer, S. Beta Dosimetry for Radiation Protection. ICRU Report. ICRU Publications, Bethesda (1995, in press)
6. Helmstädter, K., Böhm, J., Chartier, J.-L., Cutarella, D., Chauvenet, B., Lecante, C., Christensen, P., Francis, T.M. Intercomparison of extrapolation chamber measurements of the directional absorbed dose rate for TI-204 beta radiation. To be submitted for publication.

Table 1: Comparison of measured and calculated results at PTB

Distance r in mm	Angle Θ in degree	$\frac{\dot{H}_t(x,y,0;\Theta)}{A_{nom}}$ **measured** in nGy/(MBq•s)	$\frac{\dot{H}_t(x,y,0;\Theta)}{A_{nom}}$ **calculated** in nGy/(MBq•s)	$\frac{\dot{H}_t(x,y,0.07;\Theta)}{A_{nom}}$ **measured** in nGy/(MBq•s)	$\frac{\dot{H}_t(x,y,0.07;\Theta)}{A_{nom}}$ **calculated** in nGy/(MBq•s)
300	0	40.50	38.9	43.05	42.2
300	60	48 56	51 9	48.90	55.2

Table 2: Results measured at CEA and PTB (reference date: 01.01.1990)

Distance r in mm	Angle Θ in degree	CEA $\dot{H}_t(0.07;\Theta)$ mGy/h	PTB $\dot{H}_t(0.07;\Theta)$ mGy/h	$\frac{\dot{H}_t(0.07;\Theta)_{CEA}}{\dot{H}_t(0.07;\Theta)_{PTB}}$
150	0	25.92	26.48	0.979
150	45	29.55	30.17	0.980
300	0	6.45	6.62	0.975
300	15	6.60	6.71	0.984
300	45	6.99	7.41	0.944
500	0	2.22	2.31	0.959
500	45	2.32	2.54	0.913

WG 4: Numerical Dosimetry

Chairman: B.R.L. Siebert

Objectives

For more than 20 years, in radiation protection dosimetry, theoretical calculations have increasingly gaind in importance. The Working Group has the important task of extending the exchange of information and the collaboration between all groups in Europe dealing with calculations in the field of radiation transport and radiation protection dosimetry. During the project period, the Group was additionally involved in a specific task concerning the evaluation of conversion coefficients for dosimetric quantities in co-operation with an ICRP/ICRU Task Group.

Progress achieved

The main topics and the progress achieved will be described in the following:

Calculation and evaluation of dose conversion coefficients

The work of the group was focused on the calculation and evaluation of fluence-to-dose equivalent conversion coefficients with the view of supporting the joint ICRP/ICRP Task Group in its efforts to collect data for the new radiation protection dose quantities, e.g. organ equivalent dose, effective dose, ambient dose equivalent and personal dose equivalent which have been defined in ICRP Publication 60 and ICRU Report 51, respectively. Two members of the Working Group were corresponding members of that task group. Several group members contributed calculations of conversion coefficients for electron, photon and neutron radiation (cf. Publications). Working Group members were also strongly involved in the evaluation of the data calculated by different groups. This was a very important task in order to obtain an evaluated set of mean data which can be accepted on the international level as reference data for use in practical applications. The recommendations published in ICRP Publication 60 refer especially to new data for neutrons. The situation for neutrons became even more complex, as in ICRU Report 49 the ICRU published new stopping power data for protons and alpha particles. This had a strong influence on the operational quantities, as the quality factor function Q(L) and hence the effective quality factor depend on the stopping power of charged particles. Figure 1 (lower curves) shows the values of $H^*(10)/\Phi$ as defined in ICRU Report 39 and ICRP Publication 51, the data resulting from ICRP 60 and the most recent data which take the new stopping power data into account. These data were finally accepted by the ICRP/ICRU Task Group. The ratio between the new and the old values is also shown in Figure 1. The changes seen are quite moderate, especially with respect to the most recent data obtained with the new stopping power values. However, a change in the shape can be clearly seen.

Study of Monte Carlo Transport Codes

Obviously, the use of computer codes in simulating processes has strongly increased. Numerical calculations which are of special interest for the Working Group engaged in dosimetric applications are often performed by the Monte Carlo method. Many of these calculations are carried out with the help of general transport programmes, e.g. the MCNP and EGS4 codes. But if these codes are more often used by researchers who are not experts but rather occasional users, additional guidance will be needed. To provide this guidance, the Working Group prepared a training course on the use of MCNP for solving dosimetric problems. This course is organised in co-operation with the ENEA/Italy and will be held in Bologna in May 1996.

Questionnaire on computer programmes used in dosimetry

The collection and distribution of information on the use of computer codes for dosimetric problems and the initiation of intercomparison calculations with different codes in order to ensure quality assurance remains an important task of the Working Group. After a first attempt with a questionnaire which has not met with sufficient response from users, the Working Group distributed a revised and extended questionnaire on the use and operation of radiation transport and dosimetric codes to many laboratories in Europe. The analysis of the answers is carried out by a subgroup chaired by M. Terrisol (Toulouse) and the results will be available and published in 1996.

Monte Carlo transport calculations with high energy radiation

Exposure of air crews in aeroplanes at high altitudes has attracted increasing attention (see WG 11). The study of the doses of air crew members by simulating the radiation fields at high altitudes and of the corresponding doses in human bodies makes it necessary to extend the common calculations to higher energies, mainly for neutrons and protons but to some extent also for photons. This extension is complex for two reasons. First, the cross section data needed for calculations for higher energies are not as readily available as they are for lower energies, e.g. neutron energies below 20 MeV. This is quite seriousvere in the case of neutrons and at very high energies also for protons. The principal method for obtaining such data consists in the use of generators in high energy codes such as for, instance, FLUKA or LAHET. The Working Group has started an activity with a view to providing a forum for the exchange of experiences gained in the application of these computer codes and for performing benchmark calculations with different codes. This task has not, however, yet been completed.

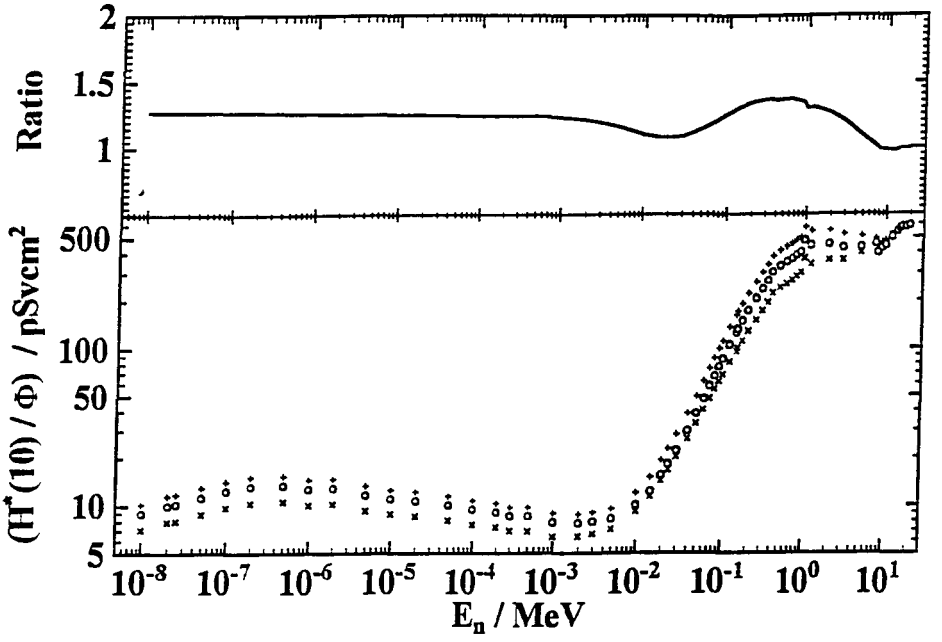

Figure 1: Bottom part: *$H^*(10)/\Phi$ calculated with the new (+) and old (x) stopping power data and using Q(L) as recommended by ICRP 60 and ICRU 51 and $H^*(10)/\Phi$* (o) *calculated with old stopping power data and the old Q(L) relation as recommended by ICRU 39 and ICRP 51 as a function of incident neutron energy E_n.*
Upper part: *Ratio between the new and the old neutron fluence-to-ambient dose equivalent conversion coefficients versus the energy of incident neutrons.*

Publications

1. Großwendt, B. and Chartier, J. L. Fluence-to-absorbed dose conversion coefficients and angular-dependence factors for 4-element ICRU tissue, water and PMMA slab phantoms irradiated by broad electron beams, PTB Report Dos-24, PTB, Braunschweig (1994).
2. Gualdrini, G.F., Monteventi, F., Morelli B., Padoani, F. and Sermenghi, I.: Field Parameters and Operational Quantities for the ICRU Sphere with Reference Photon Beams in 4 Parts:

2a Gualdrini, F. Part I: Monte Carlo Calculations of Angular Distribution of Backscatter Factors. Report RT/AMB/92/12, ENEA-Bologna (1992).

2b Gualdrini, G.F., Padoani, F., Morelli B. Part II: Monte Carlo Calculations of Backscattered Spectra and Backscattered Mean Energy Angular Distribution. RT/AMB/92/12, ENEA-Bologna (1992).

2c Gualdrini, G.F., Monteventi, F., Sermenghi, I. Part III: Experimental and Computational Analyses on the Tissue Substitute Material RS-1, Report RT/AMB/92/, ENEA-Bologna (1992).

2d Morelli, B., Gualdrini, G.F., Monteventi, F. Part IV: Monte Carlo and Experimental Evaluation of Angular Dependence of Dose Equivalent. Report RT/AMB/94/19, ENEA-Bologna (1994).

3. Gualdrini, G.F., Padoani, F. Monte Carlo Code Comparisons for the Calculation of Absorbed Dose per Unit Fluence in Slab Phantoms for Electron Energies from 50 keV to 10 MeV. Radiat. Prot. Dosim. 54 (1994) 203-207.
4. Leuthold, G., Mares, V., Schraube, H. Calculation of Neutron Ambient Dose Equivalent on the Basis of the ICRP Revised Quality Factor. Radiat. Prot. Dosim. 40 (1992) 77-84.
5. Marshall, M., Thomas, D.J., Perks, C.A., Naismith, O.F. Radiation Quantities: Significance of the Angular and Energy Distribution of the Radiation Field. Radiat. Prot. Dosim. 54 (1994).
6. Schuhmacher, H., Siebert, B.R.L. Quality Factors and Ambient Dose Equivalent for Neutrons Based on the New ICRP Recommendations, Radiat. Prot. Dosim. 40 (1992) 85-89.
7. Siebert, B.R.L. Radiation Quantities: Their Interrelationship. Radiat. Prot. Dosim. 54 (1994) 193-202.
8. Siebert, B.R.L., Grindborg, J.E., Großwendt, B., Schuhmacher, H. New analytical representation of W values for protons in methane-based tissue-equivalent gases. Radiat. Prot. Dosim. 52 (1994) 123-127.
9. Siebert, B.R.L., Schuhmacher, H. Calculated Fluence-to-Directional and Personal Dose Equivalent Conversion Coefficients for Neutrons. Radiat. Prot. Dosim. **54** (1994) 231-238.
10. Siebert, B.R.L., Schuhmacher, H. Quality Factors, Ambient and Personal Dose Equivalent for Neutrons, Based on the New ICRU Stopping Power Data for Protons and Alpha Particles. Radiat. Prot. Dosim. **58** (1995) 177-183.

WG 6: Assessment of Internal Dose

Chairman: J.A.B. Gibson

1. Objectives

The objectives of the Working Group within this project are:

- preparation of guidance on the interpretation of monitoring data relating to internal exposures of radiation workers and the implementation of ICRP recommendations on this topic within Europe.

The objective will be achieved by the pooling and exchange of information and by comparing operational experience. The programme of the actual work was:

- to develop computer models for excretion analysis;
- to interpret data from air sampling, bioassay and in-vivo monitoring;
- to establish availability of autopsy data;
- to consider compatibility of dose records and
- to organise training courses in internal dosimetry.

2. Progress achieved

The Working Group has continued to meet regularly to discuss the methodology of internal dosimetry including air sampling, bioassay techniques, in-vivo monitoring, and dose assessment. The purpose is to draw upon the experience within Western and Eastern Europe so that it can be pooled and benefited from by all members. The Working Group undertook the following activities during the project period:

1. The Working Group has participated in a very successful research programme of metabolic studies. This especially includes studies on the assessment of internal dose from plutonium and other radionuclides using stable isotope tracer techniques in man. While stable isotopes of strontium and tellurium have been chosen for first studies, the work has later been extended to other elements, e.g. cobalt. Work has been performed at Harwell investigating stable isotopes of the lanthanide series in order to find analogues for the transuranics.

2. The Working Group has organised two intercomparisons of assessment methods used in Europe, applying data from actual exposures, so that dose records of internal doses can be confidently used across national borders:
   The first intercomparison was already published by the CEC and in the open literature in 1992/1993. A second intercomparison has been performed by 14 laboratories. Ten cases have been included in the intercomparison, e.g. chronic exposure to uranium, intake of plutonium, intake of Am-241, inhalation of Co-60 and chronic intake of tritium. Preliminary results have been presented at the last WG meeting and a final publication is in progress.

3. The co-operation with EULEP through a joint EULEP-EURADOS task group on 'Deposition & Clearance of Inhaled Particles in the Human Respiratory Tract' has been continued. The Task Group strongly contributes to the development of the new Respiratory Tract Model which was adopted by the ICRP in 1993 and published by ICRP in 1995 (ICRP Publication 66). Further investigations have been performed in order to study the implications of the new ICRP and NCRP lung models for dose assessments including an assessment of variations in the predicted doses with model parameters. Details of the work have been described by Baily (1).

4. The Working Group initiates co-operation with the Committee on Interagency Radiation Research and Policy Co-ordination (CIRRPC) through discussions on Internal Dosimetry at a workshop in Atlanta, Georgia USA in April 1992. Some scientists from the USA act as corresponding members of the Working Group now.

5. The Working Group reviewed the internal dose assessment methods and record keeping within the CEC with a view to normalising such records within Europe through the establishment of a registry. Members of the Group participated in an IAEA Technical Committee set up to assess the feasibility of establishing such registries.

6. The Working Group organised a successful European Training Course within ERPET on "The Assessment of Doses from Intakes of Radionuclides". The course was organised in co-operation with CEA/Fontenay-aux-Roses and includes lectures and practical exercises. Scientists from Eastern European countries were also participating. A second course on "internal dosimetry" is in preparation and will take place at Mol in 1996.

Publications

1. Bailey, M.R. ICRP Respiratory Tract Dosimetric Model: Deposition and Clearance. EULEP Newsletters 73 (1993) 15.
2. Bailey, M.R. Report on the 6th Task Group Meeting. EULEP Newsletters 78 (1994) 15-18.
3. Bell, R.T., Bailey, M., Gibson, J.A.B., Henrichs, K., Menzel, H., et al. Proceedings of the Workshop on Internal Dosimetry Committee on Interagency Radiation Research and Policy Coordination (CIRRPC). Atlanta, Georgia, USA (1992).
4. Cantanone, M.C., Bartolo, D., Molho, N., Pirola, L. Gambarini, G., Hansen, Ch., Roth, P., Werner, E. Use of stable Ru clearance: experiments in animals. Phys. Med. 9, Supl. 1 (1993) 76-78.
5. Cantanone, M.C., Bartolo, D., Gambarini, G., Giussani, A., Molho, N., Pirola, Hansen, Ch., Roth, P., Werner, E. Stable and radioactive tracers in Ru biokinetic studies. J. Radioanal. Nucl. Chem. 178 (1994) 407-415.
6. Cox. et al. The determination of calcium isotope ratios in biological materials using high-resolution ICP-MS. Proc. of 5th Surrey Conf. on PSMS, July 1993, Durham, UK.
7. Gibson, J.A.B., Birchall, A., Bull, R.K., Henrichs, K., Iranzo, E., Lord, D.J., Piechowski, J., Sollett, E., Tancock, N.P. and Wernli, C. A European Intercomparison of Methods used for the Assessment of Intakes of Internally Deposited Radionuclides. Radiat. Prot. Dosim. 40 (1992) 247-257.
8. Gibson, J.A.B., Birchall, A., Bull; R.K. Henrichs, K., Iranzo, E., Lord, D.J., Piechowski, J., Sollett, E., Tancock, N.P. and Wernli, C.A. European Intercomparison of Methods used for the Assessment of Intakes of Internally Deposited Radionuclides. Commission of the European Communities. EUR 1419 EN (1992).
9. Gibson, J.A.B., Bull, R.K. and Carpenter, R.C. Models for the Assessment of Internal Dose and Implications for their Practical Application. 8th Int. Symposium of IRPA. Vol. 1, 297-300 (1992).
10. Gibson, J.A.B. EURADOS Working Group 6; the Assessment of Internal Dose. Radioprotection 28 (1993) 88-95.
11. Gibson, J.A.B. Internal Dose Measurement. Management and Control of Occupational Exposure to Ionising Radiation. IAEA/ANL Regional Training Course. Argonne National Laboratory, USA (1993).
12. Gibson, J.A.B. Interpretation of Whole Body Monitoring and Bioassay Data. Radiat. Prot. Dosim. 53 (1994) 87-93.
13. Gibson, J.A.B. Internal Dose Measurements. Management and Control of Occupational Exposure to Ionising Radiation. IAEA/ANL Regional Training Course, Argonne National Laboratory, USA (1993).
14. Gibson, J.A.B., Birchall, A., Bull, R.K., Henrichs, K., Iranzo, E., Lord, D.J., Piechowski, J., Sollett, E., Tancock, N.P. and Wernli, C. A European intercomparison of methods used for the assessment of intakes of internally deposited radionuclices. European Commission. Directorate-General, Science, Research and Development. EUR 14195 EN (1994).
15. Gibson, J.A.B. An introduction to internal dose measurements. ERPET Training Course on Assessment of Doses from Intakes of Radionuclides. Cadarache, France, (1994).
16. Gibson, J.A.B. Internal Dosimetry in Field Conditions. Presented at the 11th meeting of EURADOS Working Group 6 and submitted for publication (1995).
17. Gibson, J.A.B. et al. Second European Intercomparison of Methods used for the Assessment of Intakes of Internally Deposited Radionuclides (in preparation).
18. Hansen, Ch. et al. Assessment of intestinal absorption (f_1-values) of strontium for aqueous solutions and foodstuff. Proc. of the Workshop on health Effects of Internally Deposited Radionuclides: Emphasis on Radium and Thorium. CEC, Heidelberg 1994.
19. McAughey et al. Fractional gut absorption of strontium, barium and neodymium following administration of stable isotope tracers. Proc. 9th Intern. Conf. on Heavy Metals in the Environment, Vol. 1, Toronto 1993, 117-120.
20. Ramsden, D., Birchall, A., Bull, R.K., Foster, P.P., Hutton, C.F., Gibson, J.A.B., Philips, R.F., Roberts, G.A., Tancock, N.P., Tenwick, G.E., Wormold, S. and Wraight, J.C. Laboratory Intercomparison Dosimetry - Part II. Radiat. Prot. Dosim. 42 (1992) 97-102.
21. TARRONI, G. et al. An intercomparison among the whole body counter centres operating in Italy. Physica Medica (1995) (in press).

WG 7: Radiation Spectrometry at Working Environments

Chairman: H. Klein

Objectives

In neutron or mixed neutron-photon dosimetry the lack of information on the neutron spectrum at most workplaces results in both area and personal dosemeter readings being affected by major uncertainties. Further uncertainties will be introduced by the estimate of individual dosimetric quantities, for both neutrons and photons, if the directional dependence of the radiation incident on a human body is not known. Both problems were considered by the Working Group. The agreed objectives were:

- to discuss the properties of various (trans)portable neutron/photon spectrometers including their calibration procedures;
- to intercompare the various spectrometer systems by performing comparison measurements in working environments or well-specified radiation fields;
- to investigate the use of spectrometric measurements for the interpretation of individual dosemeter readings for the assessment of organ absorbed dose and dose equivalent.

Progress achieved

In May 1991 the Working Group and its objectives were approved by the EURADOS Council. During the period under review 6 Working Group meetings and 4 intercomparison exercises were held. The experience gained and major conclusions are reported.

1. Neutron spectrometry

A survey of neutron spectrometers used by WG7 members for radiation protection purposes showed that most groups have access to Bonner sphere systems (BSS). Their major advantages are a reasonably high sensitivity to neutrons with excellent discrimination with respect to photons (even if LiI crystals are used as thermal neutron detector), an almost isotropic response, high reliability and long-term stability. BSS cover a wide energy range (thermal to energies > 20 MeV) but the results are to some extent subjective because a few measured data are unfolded into a spectral fluence with up to 12 decades in energy and 3 to 5 channels per decade. Stable field conditions are required for sequential measurements in the point of reference, and the energy resolution is low. The latter drawback may cause major problems if the spectral fluence determined is to be folded with fluence-to-dose equivalent conversion coefficients or detector response functions in order to derive dose quantities or to predict readings, respectively.

For this reason, additional spectrometers are employed to complement the BS measurements and, in particular, to determine the spectral neutron fluence with improved resolution in the energy range > 10 keV where the conversion functions vary markedly. Recoil proton spectrometers (RPS) based on hydrogen- or methane-filled proportional counters or organic scintillation detectors proved to be best suited, because the response matrices can be reliably calculated on the basis of evaluated cross section data, and a unique solution can be achieved by multi-channel unfolding.

The groups participating used different response matrices, different detector calibration procedures and different unfolding codes for both few- and multi-channel data. Therefore, decisive verification tests were performed.

2. Photon spectrometry

Photon spectrometry in mixed fields is still a problem because the neutron response of commonly used spectrometers such as NaI- or BGO scintillators or Ge detectors has not been thoroughly investigated. Progress has, however, been achieved for NE213 liquid scintillators with n-γ discrimination techniques applied. The photon response function has been reliably calculated with the EGS4 Monte Carlo code. The neutron-induced photon events have been experimentally determined at selected neutron energies only and neutron/photon transport calculations combining

MCNP and EGS4 are being used to complete the response matrix, which is required for the determination of the photon spectrum in the mixed neutron-photon radiation field from the two simultaneously measured pulse-height spectra.

3. Comparison measurements

The Working Group directed most of its efforts at performing and evaluating four intercomparison exercises at workplaces in nuclear facilities and in calibration fields designed to replicate typical neutron spectra as encountered in the radiation protection practice. Table 7.1 summarises the various neutron spectrometers employed by different laboratories in these intercomparisons. Besides the neutron spectrometers the participants also irradiated different neutron and photon dosemeters. In close collaboration with WG 10, various tissue equivalent low pressure proportional counters (TEPC) - both high resolution laboratory systems and portable survey instruments - were also employed. The NE213 scintillators used allowed the spectral photon fluence to be determined. Most instruments employed are designed to have an isotropic response. Therefore, personal dosemeters symmetrically mounted on spherical or slab phantoms were additionally irradiated in these fields so that the directional distribution of the radiation fields could be investigated.

A first small-scale comparison exercise with only three laboratories was carried out at the 14 MeV neutron generator at CEA/Cadarache. The system included a hemispherical ^{238}U converter and the details of this and the associated moderator assembly were optimised by means of MCNP calculations such that thermal, intermediate (1/E) and fission neutrons were superimposed with certain fractions [2]. The spectrometric results obtained were consistent, and all dosimetric data obtained have been published in [3].

Six laboratories participated with different BSS and RPS in the second intercomparison carried out at AEA in Winfrith. Fission neutrons induced in a ^{235}U plate by thermal neutrons from the NESTOR reactor were moderated by water, iron and, optionally, a layer of polythene in order to

Table 7.1: Neutron spectrometers used in 4 intercomparisons by different laboratories (BS(x) = Bonner spheres with spherical (C) or cylindrical (F) ^{3}He-proportional counter, LiI-scintillator (L) or Au-activation foil (A); SC(y) = NE213 liquid (L) or stilben (S) organic scintillator; PC(z) = proportional counter with hydrogen (H) or ^{4}He (He) ; SDD = superheated drop detector; MC = Monte Carlo calculation)

Laboratory	**Comparison Exercise Location**			
	RNSF / 1 Cadarache	ASPIS Winfrith	PWR / CLAB Ringhals/ Oskarshamn	RNSF / 2 Cadarache
CEA, Fontenay -aux-Roses	BS(F),SC(L) PC(H),MC	-	-	BS(F),SC(L) PC(H),MC
CEA, Cadarache	-	-	-	BS(F)
GSF, Neuherberg	BS(L)	BS(L)	BS(L)	BS(L)
IAR, Lausanne	BS(F)*	BS(F)	BS(F)	BS(F)
NPL, Teddington	-	BS(C),SC(L)	BS(A)	BS(C),SC(L)
PTB, Braunschweig	BS(C,F),SC(L)	-	BS(C)	BS(C),SC(L) PC(H)
TU, Dresden	-	PC(H),SC(S)	PC(H),SC(S)	PC(H),SC(S)
CMI, Prague	-	-	-	BS(F)
NRI, Rez/ MA, Brno	-	-	-	PC(H),SC(S)
BfS, Berlin	BS(C)*	-	-	BS(C)
AEA, Harwell	-	PC(H,He)	-	-
AEA, Winfrith	-	PC(H),SC(L),MC	-	-
AECL, Chalk River	-	-	-BS(C)	

*measured in the course of the second exercise at Cadarache without the water moderator

simulate realistic neutron spectra. Neutrons backscattered from concrete walls completed the complex neutron spectrum in the point of measurement in the centre of the irradiation facility. The field properties were calculated with the MCBEND code developed at AEA. The NESTOR/ASPIS facility and a first comparison of the spectra and group fluence and dose equivalent values submitted by the participants are described by [7]. A detailed report is in progress.

The third and rather unique intercomparison was performed at workplaces in Swedish nuclear facilities, in the containment building of a pressurised water power reactor at Ringhals and in the vicinity of a transport cask filled with spent fuel elements at Oskarshamn. At the invitation of the Swedish Radiation Protection Institute (SSI) and in collaboration with the radiation protection officers of the Swedish facilities WG 7 and WG 10 carried out comprehensive measurements with neutron spectrometers (see Tab. 7.1), TEPCs and commonly used neutron and photon area and personal dosemeters in order to specify the mixed radiation field at workplaces. The reports of the participants have been compiled [4] and the final report on the evaluation is in progress [1]. A summary report will be published in the proceedings of the Chalk River workshop [6].

A total of 26 groups participated with neutron spectrometers (see Tab. 7.1), TEPCs and area and personal dosemeters in the fourth intercomparison again carried out at the 14 MeV neutron generator of CEA in Cadarache. An additional water absorber was used to modify the moderator assembly [2] such that the neutron spectrum became softer, replicating a type of spectrum encountered in practice. A new type of neutron spectrometer based on superheated emulsions and developed under the auspices of WG 7 was also employed for the first time during this exercise. The system, called BINS (Bubble Interactive Neutron Spectrometer) relies on the active control of the degree of superheat of two sensitive emulsions to generate detection thresholds in the 0.01-10 MeV range [10].

The evaluation based on the results submitted by the participants, and the detailed MCNP simulation of the directional spectral neutron and photon fluence will be discussed at the Neutron Dosimetry Symposium in Paris and summarised in a contribution by Thomas [9]. The reports of the participants will be compiled in a separate report, and a detailed description of the final evaluation will also be published [5].

The experience gained from these exercises can be summarised as follows:

- Detailed evaluations were necessary for the origin of discrepancies in the spectrometric results obtained by some participants to be determined. These problems could be solved with the aid of some improvements.
- Ambient dose equivalent values calculated from the evaluated spectral fluence may serve as reference values in intercomparisons with readings of survey instruments.
- If the energy-dependent response of an instrument is reliably known, spectral neutron fluences should be used to calculate the expected readings so that the consistency of both data sets measured can be checked.
- Irradiation of personal dosemeters on phantoms proved to be a useful tool for investigating the directional neutron fluence and for estimating the limiting dose quantities H_E or E.

The most important results and conclusions are:

- Bonner Sphere spectrometers are best suited for measurements at workplaces and allow the integral neutron fluence and the various operational dose equivalent quantities to be determined with uncertainties less than 10% to 15%, provided that the response matrix of the BS set has carefully been established by appropriate calculations and experimental calibration.
- Recoil proton spectrometers ideally complement the BSS for determining the spectral neutron fluence with a reasonable resolution for energies > 10 to 50 keV, provided properly calculated and experimentally verified response matrices are used.
- A comparison between integral dosimetric data measured and calculated on the basis of the (directional) spectral neutron fluence and the response function of the instrument used may either prove the consistency of all data involved or can indicate deficiencies in the

measurements, the response functions or the analysing procedures applied.

- The calculation of the radiation field properties also proved to be a very valuable tool. It is, however, recommended to simulate the radiation transport as realistically as possible utilising general purpose three-dimensional Monte Carlo code packages like MCNP, EGS4 or similar programmes.

- Response functions of area and individual dosemeters commonly used or just being developed should be carefully determined by calculation and experimental calibration and made available for predictions and consistency checks.
- Versatile calibration fields replicating the great variety of radiation fields encountered at workplaces should be made available for the testing of area and individual dosemeters and for calibration according to their application.

The procedures developed and the conclusions drawn from these intercomparisons will be discussed at the Neutron Dosimetry Symposium in Paris.

Publications

1. Bartlett, D., Drake, P., Lindborg, L., Klein, H., Schmitz, Th. and Tichy, M. Determination of the neutron and photon dose equivalent at workplaces in nuclear facilities of Sweden - An SSI-EURADOS comparison exercise, Part II: Evaluation. SSI-Report 95-16, Stockholm, 1995 (to be published).
2. Chartier, J.L., Posny, F. and Buxerolle, M. Experimental assembly for the simulation of realistic neutron spectra. Radiat. Prot. Dosim. 44 (1992) 125-130.
3. Klein, H., Thomas, D.J., Chartier, J.L. and Schraube, H. (Eds). Determination and realization of calibration fields for neutron protection dosimetry as derived from spectra encountered in routine surveillance, EUR Report 14927 DE/EN/FR, Luxembourg, 1993, 159-174.
4. Klein, H. and Lindborg, L. (Eds.). Determination of the neutron and photon dose equivalent at workplaces in nuclear facilities of Sweden - An SSI-EURADOS comparison exercise, Part I: Measurements and data analysis. SSI-Report 95-15, Stockholm, 1995.
5. Klein, H. Workplace radiation field analysis. Radiat. Prot. Dosim. 68 (1996) (to be published).
6. Lindborg, L., Bartlett, D., Drake, P., Klein, H., Schmitz, Th. and Tichy, M. Determination of the neutron and photon dose equivalent at workplaces in nuclear facilities of Sweden - A joint SSI-EURADOS comparison exercise. Radiat. Prot. Dosim. 61 (1995) (in print).
7. Murphy, M.F. A review of the neutron spectrometry measurements in the ASPIS reference fields. Laboratory report AEA-RS-5548, Winfrith, 1994.
8. Thomas, D.J., Klein, H. EURADOS Working Group 7: Radiation spectrometry in working environments. Radioprotection 28 (1993) 95-100.
9. Thomas, D.J., Chartier, J.L., Klein, H., Naismith, O.F., Posny, F. and Taylor, G.C. Results of a large scale neutron spectrometry and dosimetry comparison exercise at the Cadarache moderator assembly. Radiat. Prot. Dosim. 68 (1996) (to be published).
10. d'Errico, Alberts, W.G., Curzio, G., Guldbakke, S., Kluge, H. and Matzke, M. Active Neutron Spectrometry with Superheated Drop (Bubble) Detectors. Radiat. Prot. Dosim. 61 (1-3) (1995) 159-162.

WG 8: Development of Individual dosemeters for External Penetrating Radiations

Chairman: J. Harvey

Objectives

The general task of this Working Group was to develop and improve techniques for the individual dosimetry of ionising radiation. During the first project period the WG concentrated on investigation of individual dosemeters for neutron radiation, especially etched-track detectors. Investigations have been stimulated and co-ordinated regarding the response of such detectors with respect to the new operational quantity $H_p(10)$ and its directional dependence. Progress was achieved in five areas:

Progress achieved

One of the major contributions of this Working Group has been the number of studies into neutron dosimetry which have been made possible by the joint activities of the group including the provision of well-calibrated sources of neutrons. The extent and scope of the work in the project period under review is indicated by the number of reports published not only by members of the Working Group, but also by those who were able to take advantage of the joint activities organised by the Working Group. Some of these reports, to which the activities of the Working Group made a significant contribution, are listed below. Specific tasks are described in the following sections.

Joint irradiation and intercomparison of neutron dosemeters

A joint irradiation of neutron dosemeters from 17 European laboratories was organised by the Working Group in collaboration with the GSF/Neuherberg, PTB/Braunschweig and PSI/Villigen and carried out in 1992. The following laboratories took part, submitting between them 27 types of neutron dosemeter.

1. The Paul Scherrer Institute, Villigen, Switzerland
2. Karlsruhe Nuclear Research Centre, Karlsruhe, Germany
3. CRS - Dosimetry Laboratory, Algiers, Algeria
4. Dresden University of Technology, Dresden, Germany
5. Universidad Autonoma de Barcelona, Bellaterra, Spain
6. Institute of Naval Medicine, Alverstoke, England
7. University of Giessen, Giessen, Germany
8. CERN, Geneva
9. GSF-Forschungszentrum fur Umwelt and Gesundheit, Neuherberg, Germany
10. PTB, Braunschweig, Germany
11. Riso National Laboratory, Riso, Denmark
12. University of Thessaloniki, Thessaloniki, Greece
13. NRPB, Chilton, England
14. ANPA, Rome, Italy
15. ENEA-BO Institute, Bologna, Italy
16. Berkeley Technology Centre, Nuclear Electric plc, Berkeley, England
17. Universiy of Bristol, Bristol, England.

The dosemeters were irradiated at GSF/Neuherberg, PTB/Braunschweig and PSI/Villigen. This was the most comprehensive joint irradiation organised to date. In view of the growing realisation of the importance of the angular response of track-etch neutron dosemeters, irradiations were undertaken at 0^o , 30^o , 60^o and 85^o and at neutron energies of 0.144 MeV, 0.565 MeV, 1.2 MeV, 5.3 MeV, and 15.1 MeV and in a Cf-252 neutron field. Single-angle irradiations were also performed at 44 MeV and 66 MeV. In addition, linearity experiments were conducted over the range 0.4 mSv to 10 mSv at 1.2 MeV, 5.3 MeV, and 15.1 MeV. This major exercise, organised principally by H. Schraube of GSF/Neuherberg and W. G. Alberts of the PTB/Braunschweig, was greatly appreciated by the participants who valued access to well-calibrated sources of neutrons and the opportunity to compare the performance of their systems with those of other delegates. The large amount of work involved and the contribution made by the organisers cannot be overstated. The joint irradiation exercise has led to many publications and a significant improvement in

understanding of the performance of many neutron dosimetry systems as indicated by the reference list at the end of this report. The final report summarising the results from all participants will shortly be published (ref. 20).

Workshop on "Individual Monitoring of Ionising Radiation - The Impact of Recent ICRP and ICRU Publications" at PSI, Villigen, Switzerland in May 1993

Initiatives from the Working Group led to a Workshop held in Villigen, Switzerland, from May 5 - 7, 1993. The WG was strongly engaged in the organisation of the Workshop and was active in presenting many contributions dealing with various subjects of individual dosimetry (see Publications). An important task was the discussion of the new ICRP recommendations (ICRP Publication 60). The proceedings were published (ref. 15) in a form designed to give guidance to the radiation protection community on the practical consequences of recent publications of the ICRP and the ICRU; in addition, guidance for monitoring services and record keeping of dose data has also been included in the proceedings.

Exchange of Information on Track-Etch Neutron Dosimetry

This important function of the group continued over the period 1992-1995. During the meetings of the Working Group intense discussions on the quality of the different detector systems were performed. This includes topics of e.g. the quality of the different plastic materials, the different etching techniques and the track detection and evaluation procedures. Although not necessarily giving rise to an identifiable outcome, this activity has been recognised by the group members as of great value. The research programmes of many delegates have been significantly affected by discussions of the practical implementation of all aspects of neutron dosimetry and track-etch matters.

Status Report on Track-Etch Neutron Dosimetry

Working Group 8 was asked by the EURADOS Council to report on the present status of track-etch neutron dosimetry and to summarise the contribution made by Working Group 8 and its predecessor Working Group 5. A subgroup was set up and had preliminary discussions at the Strasbourg meeting of EURADOS in September 1994. The subgroup subsequently met at the NRPB, UK, in April 1995 to discuss a first draft. This draft is currently in its first revision. A condensed version of the report has been accepted for oral presentation at the 8th Symposium on Neutron Dosimetry, Paris, 13-17 November, 1995.

Electronic Neutron Personal Dosemeter

During the period under review it became clear that electronic personal dosemeters were likely to play a significant role in the future of personal dosimetry. Although photon sensitive electronic dosemeters are now becoming available, no neutron sensitive device is yet available in a form reliable and suitable for widespread application. Accordingly a small subgroup was formed to report on the present status of electronic neutron dosimetry, and to attempt to define the most promising lines of research. The group has a restricted reporting role and a defined lifetime. Preliminary discussions were held at the EURADOS meeting in Paris in November 1992 and a group met in February 1994 at the NRPB, UK, and subsequently, briefly, at the Strasbourg meeting of EURADOS in September 1994. It is hoped that this group will be able to continue to its final goal in the near future.

Publications

1. Alberts, W. G. (editor). Investigation of Individual Neutron Monitors on the Basis of Etched-Track Detectors; The 1990 EURADOS-CENDOS Exercise. EURADOS-CENDOS Report 1992-02. PTB-N-10, Braunschweig, May 1992.
2. Alberts, W. G. International Study of CR39 Etched Track Neutron Dosemeters (EURADOS-CENDOS 1990). Radiat. Prot. Dosim. 44 (1992) 323-324.
3. Azimi-Garakani, D., Langen, K. and Wernli, C. Further Studies of the Characteristics of Different Proton-Recoil Track Detectors at Various Neutron Energies. Radiat. Measure. 23 (1994) 241-245.
4. Barthe, J., Lahaye, T., Moiseev, T. and Portal, G. Personal Neutron Diode Dosemeter. Radiat. Prot. Dosim. 47 (1993) 397-399.

5. Barthe, J., Bordy, J. M., Lahaye, T. and Mourgues, M. New Principle of Single Diode Neutron Dosimeter Based on Time Resolution. Proc. 17th Congress of the IRPA, Portsmouth 1994, 97-100.
6. Bordy, J. M., Barthe, J., Boutruche, B. and Segur, P. Evaluation des Caractéristiques Dosimetriques d'un Nouveau Type de Compteur Equivalent au Tissu Destiné à la Dosimetrie Individuelle Neutronique en Radioprotection. Radioprotection. 29 (1994) 11-28.
7. Bordy, J. M., Lahaye, T., Flandre, F., Hofleck, C., Lequin, S. and Barthe, J. Single Diode Detector for Individual Neutron Dosimetry Using a Pulse Shape Analysis. To be published in the Proceedings of the 8th Synmposium on Neutron Dosimetry, Paris, 13-17 November, 1995.
8. Budzanowski, M., and Burgkhardt, B. Thin 6/7LiF;Mg,Cu,P and 6/7LiF;Mg,Ti Detectors for Automatic Albedo Neutron Dosimetry. Symp. on Luminescent Detectors and Transformers of Ionizing Radiation, Tallin, Estonia, Sept. 5-8, 1994.
9. Burgkhardt, B., Piesch, E. and Vilgis, M. Uncertainty of Measurement and Lower Detection Limit of Track Etched Detector Systems: Experimental Verification and Consequences for Intercomparison Experiments. Radiat. Prot. Dosim. 47 (1993) 617-622.
10. Jakes, J., Schraube, J. and Voigt, J. The Effect of Processing Conditions on the Track-size Distributions in CR-39 Detectors. Radiat. Measur. 25 (1995) 469-470.
11. Jakes, J., Voigt, J. and Schraube, H. Evaluation of the CR-39 Response on the Basis of Track-size Distributions. Radiat. Measur. 25 (1995) 437-440.
12. Lounis, Z., Cavaioli, M. and Tommasino, L. The Combined Use of Bubble Dosemeters and Electrochemical Etched Track Detectors. Radiat. Prot. Dosim. 59 (1995) 299-302.
13. Luszik-Bhadra, M., Alberts, W. G., Dietz, E. Guldbakke, S. and Matzke, M. A Wide-Range Neutron Dosemeter Based on a CR-39 Track Detector. Radiat. Measur. 22 (1993) 671-674.
14. Marshall, T. O., Wernli, C. and Tanner, R. J. Performance Requirements of Personal Dosemeters: Can These be Met by Future and Present Designs?. Radiat. Prot. Dosim. 54 (1993) 287-294.
15. Menzel, H. G., Marshall, T.O., Wernli, C. and Varma, M. (Eds.) Individual Monitoring of Ionising Radiation, the Impact of Recent ICRP and ICRU Publications. Radiat. Prot. Dosim. 54, 3/4 (1994).
16. Olko, P., Budzanowski, M., Bilski, P., Burgkhardt, B., Piesch, E. ^{6}Li Sandwich Type Detectors for Low Dose Individual Monitoring in Mixed Neutron-Photon Fields. Radiat. Prot. Dosim. 54 (1994) 349-352.
17. Savvidis, E., Alberts, W. G., Luszik-Bhadra, M. and Zamani, M. A Passive Neutron Dosemeter Based on a CR-39 Track Detector with Multi-Field Evaluation. Nucl. Instr. and Meth. B 94 (1994) 325-329.
18. Savvidis, E., Sampsonidis, D. and Zamani, M. Separation of Albedo Neutron Component of a CR-39 Neutron Dosemeter During on-Phantom Irradiation. Proc. of 11th. Int. Conf. on Solid State Dosimetry, Budapest, 10-14 July, 1995.
19. Schraube, H., Alberts, W. G. and Weeks, A. R. Fast and High-Energy Neutron Detection with Nuclear Track Detectors; Results of the European Joint Experiments 1992/93. GSF Report 15/95.
20. Spurny, F. Dosimetry of Neutrons and High Energy Particles with Nuclear Track Detectors. (Invited paper). Radiat. Measur. 25 (1995) 429-436.
21. Tanner, R. J., Bartlett, D. T. and Steele, J. D. NRPB PADC Neutron Personal Dosimetry after ICRP 60. Nucl. Tracks Radiat. Meas. 22 (1993) 703-706.
22. Tanner, R. J. and Bartlett, D. T. Low Dose Assessment with Track Etch Dosemeters. Radiological Protection Bulletin, 159 (1994) 18-21.
23. Tanner, R. J. and Bartlett, D. T. A New Criterion for Comparing Track Etch Dosimetry Systems. Radiat. Meas. 25 (1995) 445-448.
24. Tommasino, L. The Importance of Track Detectors in Radiation Protection Dosimetry. Nucl. Tracks Radiat. Meas. 22, 1-4 (1993) 707-717.
25. Tommasino, L. Torri, G., Cavaioli, M., Riccardi, M. and Trinh Van Giap. A Long Term Study of CR-39 Detectors for Neutron Dosimetry. Nucl. Tracks Radiat. Meas. 22, 1-4, (1993) 719-722.
26. Tommasino, L., Caggiati, F., Cavaioli, M, Notaro, M., Teodori, R., Torri, G. and Zhou, Z. From a Complex Cosmic Ray Stack to a Simple Dosimeter System for Aircrew Exposure. Presented at the VI Symposium on the Natural Radiation Environment (NRE-VI) 5-9 June, 1995, Montreal, Canada. 1995.
27. Turek, K. Universal Multidetector Etching Stand for Electrochemical Etched Plastic Track Detectors. Nucl. Tracks Radiat. Measur. 20 (1992) 601-604.
28. Turek, K., Spurny, F. and Alberts, W. G. On the Optimization of the Etching of CR39 as a Fast Neutron Dosimeter. Nucl. Tracks Radiat. Measur. 21 (1993) 299-301.
29. Turek, K., Piesch, E. and Bednar, J. Direct Measurements of the Critical Angle of Incidence in Electrochemical Etched CR39 and Makrofol Detectors. Radiat. Measur. 24 (1995) 43-51.
30. Turek, K., Bednar, J. and Piesch, E. Determination of the Neutron Angular Response Using a Single Etched Track Detector. Radiat. Prot. Dosim. 59 (1995) 205-211.
31. Weeks, A. R., Ford, D. T. and Harvey, J. R. An Assessment of Two Types of Personal Neutron Dosemeter which Utilise the AUTOSCAN 60 Automatic Etch-Track Reading System. UK Nuclear Electric plc., Technology Division Report TEPZ/REP/0084/93 (1993).

WG 9: Criticality Accident Dosimetry Chairman: R. Medioni

Objectives

The general task of the Working Group was

- to develop and to improve the techniques of measurement and the methods of interpretation in terms of dosimetric quantities relevant in cases of criticality accidents and
- to provide training of personnel in the operation of criticality accident dosimetry systems.

The Working Group started its work as early as 1989, and the main objectives during the project period were

- to carry out spectrometry measurements and establish reference dosimetry of the leakage radiation fields available around the Silène reactor. Two different fields were available - produced either by the bare core or by the core with a lead shield -, which resulted in different neutron spectra and different neutron-to-gamma-ray ratios. This characterisation was necessary as a prerequisite for the International Intercomparison performed later.
- to prepare arrangements for the intercomparison: a liaison with the CEC (DGXI), the IAEA and the CEA group operating the Silène reactor at Valduc.
- to propose a detailed protocol for such an intercomparison.
- to perform an International Intercomparison of criticality accident dosimetry systems on the Silène reactor at Valduc, France.

Framework

The Working Group and the studies were sponsored by EURADOS within the scope of this contract. As far as the characterisation of the fields and the feasibility studies at the reactor were concerned, these studies were additionally supported by two consecutive study-contracts (CEC/DG XII, No. BI7-0051-F and No. BI7-0076-F).

Later, the realisation of the International Intercomparison at the Silène reactor at Valduc, including the reactor running costs during the measurements, was also supported by CEC/DG XI (Luxembourg) by two contracts (No. 92-PR-007 and No. 92-PR-008). The intercomparison was further sponsored by the IAEA/Vienna and the DOE(USA).

Progress achieved

The objectives of the project were successfully achieved and a final report on this international intercomparison which was performed in three parts was published in June 1995. The following sections describe the work and the results achieved in more detail.

Experiments around the Silène reactor at Valduc/France

Co-ordinated measurements were performed at a reference location (in a direction of 90° to the main axis, a distance of 4 m from the reactor centre and a height of 1.20 m from the floor corresponding to the mid-level of the fuel in the reactor core) by various laboratories (IPSN/France, AEA/Harwell, NPL/Teddington and University of the Saarland/ Homburg/Saar). Various techniques were applied to determine neutron spectra, neutron doses and gamma-ray dose values. These techniques were :

- a high-resolution neutron spectrometry system based on recoil counters (in part with an NE213 scintillation detector) associated with a Bonner sphere detector system,
- activation detectors,
- GM counters,
- twin ionisation chambers (TE and Al),
- an LET spectrometer system based on a tissue equivalent proportional counter (TEPC),
- Si diodes and

- thermoluminescence detectors (TLDs, alumina).

The results of independent dose measurements agree well within ±10% (for neutrons and gamma-rays). These data have been used to provide 'reference values' of neutron and gamma-ray doses for the intercomparison.

An extensive study of the isotropy of the radiation field (horizontal and vertical) was performed on an arc around the source at a distance of 4 m from the reactor axis. By that way the arc range and area were determined which could be used for the intercomparison measurements. The uniformity over 6 m on the circumference was within ±5%. This area was then used for exposing dosimeters either free in air or in front of one of the two BOMAB phantoms. For this study the following detector systems were applied: Si diodes, activation foils and TLDs.

Two BOMAB phantoms were tested and prepared for sodium activation measurements.

Intercomparison measurements

The organisation, programme and timetable for this international intercomparison in the area of criticality accident dosimetry were defined at various meetings at IPSN, AEA, CEC/Luxembourg and IAEA/Vienna. The intercomparison was hosted by IPSN and in detail organised jointly by IPSN and AEA Technology.

A two-week intercomparison programme was proposed and successfully performed at the Silène reactor site at Valduc from 7-18 June 1993. Four intense radiation pulses were produced by the reactor; two pulses with the reactor shielded by lead with a thickness of 10 cm thick during the first week, followed by two pulses with the bare reactor core in the second week.

The intercomparison measurements and the procedure the participants had agreed to follow included:

- free-in-air and on-phantom exposure of dosimeters including Na-24 activation detectors,
- followed by dosimeter and sodium-24 activation measurements by the participants,
- assessment and reporting of preliminary results within 48 hours,
- analysis of preliminary results, lectures, informal discussion with presentation of papers on R&D and dosimetry systems used by participants at a later date.
- Participants were requested to send their final results together with a description of their accident dosimetry system to the coordinator.

16 laboratories from 14 countries of the European Communities, Russia, America and India participated in this intercomparison and checked their criticality dosimetry systems.
Some additional experimental studies like blood chromosome measurements, measurements using bubble detectors and electron spin resonance were also performed.

Conclusion of the Intercomparison

A set of three reports was published describing in detail the procedures, instruments used, measurements performed and results achieved (June 1995). The reports include:

- the reference dosimetry of the radiation fields,
- the description of the detector systems of the participants
- the description of the experiments and their results with analysis and conclusions.

For neutrons, the results of the measurements were very good; typically about 90 % of the results were within ±25 % compared with the reference dose values.
For gamma-rays, the results were, in general, good; typically about 80 % of the results were within ±25 % of the reference values, but for the lead-shielded radiation field, the free-in-air dose values agree only within ±50 %.

Publications

1. R. Médioni, H.J. Delafield. An International Intercomparison of Criticality Accident Dosimetry Systems at the SILENE Reactor. Invited Paper presented at the 8th Symposium on Neutron Dosimetry. Paris, 13-17 November 1995.
2. R. Médioni, H.J. Delafield. An International Intercomparison of Criticality Accident Dosimetry Systems at the SILENE Reactor, Valduc, Dijon, France, 7-18 June 1993. Part 1: Reactor and Reference Dosimetry of Radiation Fields. AEA Technology and IPSN Report HPS/TR/H/1(95).
3. H.J. Delafield, J.A.B. Gibson (Eds). An International Intercomparison of Criticality Accident Dosimetry Systems at the SILENE Reactor, Valduc, Dijon, France, 7-18 June 1993. Part 2 : Dosimetry Systems used by Participants at the Experiment. AEA Technology and IPSN Report HPS/TR/H/2 (1995).
4. H.J. Delafield, R. Médioni. An International Intercomparison of Criticality Accident Dosimetry Systems at the SILENE Reactor, Valduc, Dijon, France, 7-18 June 1993. Part 3 : Description of the Experiment and Participants' Results. AEA Technology and IPSN Report HPS/TR/H/3 (1995).
5. H.J. Delafield, C.A. Perks, D. Spencer, G.G. Gallacher. Harwell Spectrometry and Dosimetry Measurements made at the SILENE Reactor (Bare and with Lead Shield). AEA Environment and Energy Report HPS/TR/H/4 (1995).
6. J.L. Chartier, F. Posny, D. Paul, J. Kurkdjian, G. Audoin, C. Itié, G. Pelcot. Neutron Spectrum Measurements at the Silène Reactor. In: Final Report of EURADOS Contract CEC FI3P-CT92-0002. Report SDOS/95-273/JLC/lm. (1995).
7. B. Burgkhardt, M. Vilgis. Kritikalitäts-Personendosimetrie mit amtlichen Glas-und Albedodosimetern, Annual report, W. Koelzer (Ed.), FZK 5530 (1995) 151-153.
8. B. Burgkhardt. Aktuelle Entwicklungen im Forschungszentrum Karlsruhe; Kolloquium der Hauptabteilung Sicherheit, M. Urban (Ed.), to be published in FZK 5530 (1995).
9. D.J. Thomas, A.G. Bardell, G.C. Taylor. Neutron spectrometry measurements at SILENE reactor. (report in preparation).
10. F. Spurny, I. Votockova, O. Obraz, Z. Prouza. International Nuclear Accident Dosimetry Intercomparison. Results of Czech Participants. Nuclear Energy Safety, to be published (1995).
11. R. Médioni. Dosimetry and spectrometry measurements of the leakage radiation fields from the SILENE reactor with various shields. Report N° DPHD/SDOS/94-104-RM (1994).
12. P. Pihet, S. Gerdung, E. Arend, R. Médioni, H.G. Menzel. Neutron-photon dose radiation quality measurements with TEPCs at the reactor Silène, Valduc (France). Measurement report : Experiments June 1990 and December 1991. Report DPHD/SDOS 94/104/RM.
13. B. Tournier, F. Barbry, J. Rozain. Silène, a New Radiation Reference Source. In: Proceedings of the Topical Meeting on Physics, Safety and Applications of Pulse reactors. Washington DC, 1994. 72-79.
14. R. Médioni. Réunion du Groupe de Travail n°9 de l' Eurados "Dosimétrie des accidents de criticité". Radioprotection 28 (2) (1993) 209-213.
15. A. Rannou. Compte rendu de l' Intercomparaison Internationale de Dosimétrie de Criticité, Valduc, 7-18 Juin 1993. Radioprotection 28 (3) (1993) 333-334.
16. F. Spurny, I. Votockova, J. Beduar, O. Obraz, Z. Prouza. CEC Criticality Accident Dosimetry Intercomparison 1993. Review and Analysis of Results Obtained by Participants from Czech Republic. Report IRD AS CR 368/1993, Prague 1993
17. J.P. Rozain, F. Barbry, R. Médioni. Silène, a new radiation reference source. 8th ASTM Congress. Euratom Symposium on Reactor Dosimetry, Vail, Colorado, USA, September 1993.
20. K.W. Crase. Summary of the Savannah River Site Criticality Dosimetry Program. Westinghouse Savannah River Company Report WSRC-MS-93-148 (1993).
21. R. Médioni, F. Barbry. Silène, a Source of Reference Radiation Fields. Proceedings of the IRPA8 Congress. Montreal, Vol. 1 (1992) 108-111.
22. H.J. Delafield, C.A. Perks. Harwell Spectrometry and Dosimetry Measurements made at the SILENE Reactor with Lead Shield (June 1990). AEA Environment and Energy Report AEA-EE-0152 (1991).
23. D.J. Thomas, A.G. Bardell. Bonner sphere neutron spectrometry measurements performed at the SILENE reactor, Valduc, France (June 1990). NPL Report. RSA(RES) (1991).

WG 10: Basic Physical Data and Characteristics of Gas Ionization Devices

Chairman: P. Pihet

Objectives

The objective of the project was the assessment of basic physical data relevant to the biological effect of ionising radiations and the development of instrumentation for dosimetry in radiation protection and radiation biology.

The project consisted in increasing the collaboration between European laboratories, particularly universities and research institutes, in order to improve the knowledge of the basic information required for the development of operational instruments for radiation protection dosimetry and to extend their range of applicability. The suitability of low pressure gas detectors to provide experimental data (ionisation-, dose-, radial distributions) relevant to radiation biology experiments was investigated with emphasis laid upon the increasing performance in detection methods in correlation with the progress in computer calculations for micro- and nanodosimetry.

The current programme is aimed at co-ordinating the action of groups involved in the determination of basic data relevant to the measurement of ionising radiation (kerma, W, electron collision cross section in gases), and contributing towards the development and the implementation of low pressure proportional counters as operational and research instruments.

Progress achieved

The work performed during the contractual period included several specific actions such as :

- joint publications on the topics described below,
- the issue of a comprehensive report on the *Design, Construction and Use of Tissue Equivalent Proportional Counters* (TEPC) published in Radiation Protection Dosimetry,
- the organisation of a workshop held in Chalk River on *Advances in Radiation Measurements. Applications and Research Needs in Health Physics and Dosimetry* whose proceedings are published in Radiation Protection Dosimetry,
- experimental work using tissue equivalent proportional counters.

The activities were conducted and evaluated in six task group meetings organised by the participating laboratories (Homburg, Toulouse, Jülich, Krakow, New ork, Chalk River) and during satellites meeting held within international conferences (Berlin, Gatlinburg, Paris). Of special interest were the scientific contributions of various PhD students from the university groups. Several thesis works (C.Moutarde, J.M. Bordy, B. Boutruche, S. Gerdung, O. Schröder) could be discussed within the Working Group activities, some being already published. They led to direct exchanges between groups (e.g. Toulouse-Homburg-Legnaro-Jülich-Leeds).

The success of the activities in the Working Group was also due to the efficient co-operation of American and Canadian research institutes (Richland, New-York, Chalk River). Part of the work was accomplished with the direct collaboration of EURADOS Working Group 4 and Working Group 7 as represented in joint ublications included in the list below. The Working Group contributed to the ERPET training courses on Modern Methods in Radiation Measurements held in Bad Honnef and in Neuherberg. Specific subjects and achievements are summarised below.

W-values for neutrons

As the basic quantity required to convert the ionisation yield into energy deposition, the "average energy required to create an ion pair", W, is of fundamental interest for dosimetry and microdosimetry. W values for charged particles and averaged W values for the spectra of secondary particles are of practical relevance for the interpretation of ionisation spectra measured with PCs and for the determination of the accuracy achievable for mixed field dosimetry using gas detectors. A comprehensive study was performed to evaluate the consequences of recent W data for charged particles, especially protons, on the average W values for neutrons (W_n) as a function of

energy. The emphasis was placed upon the uncertainty of W_n with regard to the accuracy requirement of various types of application and the neutron energy range.

The work was based on the new ENDF/B VI nuclear data file, improved kerma data at high neutron energies (White et al, 1992, Taylor et al., 1992) and the compilation of most complete and recent set of W data for neutron charged secondaries. The investigations took into account a review of W values for charged particles by IAEA (IAEA TECDOC 799, 1995) and an earlier report on W_n prepared at the GSF, Neuherberg (1987).

The work presented in two publications (Siebert et al., 1992, Taylor et al., 1995) includes :

- a revision of W values for protons from 1 keV to 5 MeV, leading to a new analytical representation for W(E) in methane based TE gas; the variance analysis applied to the different data sets showed that the new fit allows W for protons to be represented with a relative standard deviation of 2.5 %;
- the re-evaluation on a similar basis of W(E) relationships for ^{4}He, ^{12}C, ^{14}N and ^{16}O ions;
- new neutron W_n values in methane based TE gas using improved W(E) fits for the secondaries.

In these investigations, the emphasis was placed upon the understanding of the shape of W(E) relationships and the critical influence of some scarce data whose poor accuracy limits the evaluation. The work also emphasises the need for comparable investigations in the propane based TE gas used in microdosimetric counters. Empirical approaches based on the results of kerma experiments with low pressure proportional counters were discussed (Pihet et al, 1992).

Electron discharge modelling data for gas proportional counters (PC)

Although low pressure proportional counters (PC) are widely applied in dosimetry and microdosimetry, the knowledge of their basic characteristics remained for a long time rather poor due to the lack of adequate understanding of the charge collection processes involved. This did not prevent successful applications of PCs as long as operation limits were not reached, e.g. for microdosimetric detectors operated at relatively high gas pressures commonly used to simulate sensitive volumes with several μm in diameter. Recently, however, research PCs operated at very low pressures to simulate nm volumes became technically operational, however their use requires precise knowledge of their gas gain properties.

Solutions to these problems could be approached since large progress was made in simulating the electron discharge combining new electron molecule cross sections for the full energy range of secondary electrons, macroscopic calculations of gas gain for high and intermediate pressures, and microscopic calculations for low pressures using Monte-Carlo methods. The original work in that regard was performed at Toulouse University based on its expertise in the field of electron discharge modelling (Ségur et al, 1989-1994).

The specific contribution of the working group was focused on two problems :

- the validation of gas gain calculations and electron collision cross section data : collaborations were initiated aimed at comparing experimental and theoretical determination of gas gain in microdosimetric counters and at verifying on this basis the accuracy of gas gain modelling calculations (Colautti et al 1995);
- the application of modelling techniques to simulate the response of different kinds of detectors in comparison with experimental results in order to better understand their behaviour and improve their design : operational instruments developed for radiation protection dosimetry (Verma et al 1992, Freyermuth et al. 1995) and PCs developed for research (Colautti et al 1995) including ultra-miniature counters developed at Columbia University in New York (Olko et al 1995).

The progress made is documented in a dedicated section of the TEPC report (see below).

Characteristics and implementation of tissue equivalent proportional counters

The suitability of TEPC techniques is well recognised for various applications in dosimetry and microdosimetry, e.g. for operational radiation protection instruments, investigation of radiation quality for radiobiology, neutron kerma measurements. The working group has intensively

discussed those applications and compared the experience gained by the members in particular in the implementation of TEPCs in radiation protection dosimetry. The following progress was achieved:

- Large size TEPCs for area monitoring (Varma et al 1992, Freyermuth et al 1995) and TEPCs with multi-element geometry for individual monitoring (Bordy et al 1995) have been developed.
- The TEPC dose equivalent response at low neutron energy has been optimised either by modifying operating characteristics (Gerdung, 1994) or quality factor algorithms (Taylor, 1995).
- More experience was gained in assessing the suitability of TEPC dose equivalent meters in different radiation protection environments or simulated realistic fields: five different TEPC systems developed at AECL, KFA, Homburg, CEA-Grenoble, CEA-Fontenay and SSI could be used in comparison with fluence spectrometry systems to measure the dose equivalent rates in the environments of a nuclear power plant and transport containers for spent fuel at Swedish nuclear facilities and in reference fields at CEA/Cadarache (see WG 7).

The work was also especially focused on increasing the reliability of TEPC design and construction. In that respect, it was decided to edit a dedicated report with the general aim to provide guidance to users of TEPC and to facilitate its technology transfer. It collects in a single volume basic information on TEPC principles, namely results of recent modelling studies, together with practical information on electrical and mechanical design. This comprehensive report wishes to contribute towards the implementation of TEPC in radiation protection practice as a powerful tool, as well as to make understandable its application in the field of dosimetry for radiation biology. The scope of the report includes 5 sections prepared by groups of two or three members of the Working Group dealing with :

- Principles of experimental microdosimetry
- Design of tissue equivalent proportional counters
- Physics of tissue equivalent proportional counter gain and response
- Practical considerations in the design and construction of tissue equivalent proportional counters
- Counter operation and application.

Workshop "Advances in Radiation Measurements. Applications and research needs in health physics and dosimetry"

The Workshop was jointly organised by the European Commission, AECL Research, CANDU Owners Group and EURADOS. It was held in Chalk River (Ontario) on 3-6 October 1994. The workshop was initiated by the Working Group and was organised by A.J. Waker. Twelve invited experts and about 80 participants from 16 different countries attended the Workshop. It was built as an interdisciplinary meeting to allow intensive interaction and discussion between scientists working in:

- radiation measurement and particle detection research;
- the practical implementation of radiation protection concepts and principles;
- experimental physics for radiation biology.

The objectives of the Workshop specified by the Programme Committee were framed within the context of three questions : Where is current research and development able to take us in solving radiation monitoring problems? How can physical measurements be made relevant to what is happening in the biological sciences? How can advantage be taken of advanced particle detection techniques developed in other areas of science such as astronomy and high energy physics? Proffered papers and discussions took place within height sessions dealing with :

- Need for improved measurement techniques in radiation protection
- Advanced particle detection techniques
- Dosimetry and spectrometry methods for radiation protection
- Physical measurements in modern radiation biology and their interpretation
- Implementation of active dosimeters and spectrometers in radiation protection

- Detector and electronic technology for active devices
- Particle interaction in tissue, cellular and subcellular targets
- Basic data and processes involved in gas and semi-conductor particle detectors.

Publications

1. Pihet, P. Données physiques de base et amélioration des détecteurs à gaz pour la mesure de l'ionisation et de l'énergie absorbée dans la matière. Radioprotection 27 (3) (1992) 320-323.
2. Pihet, P. Réunion du Groupe 10 de l'EURADOS. In Compte-rendu du Séminaire EURADOS, Montrouge et Fontenay-aux-Roses, November 1992. Radioprotection 28 (1993) 100-104.
3. Waker, A.J., Pihet, P. and Menzel, H.G. Advances in Radiation Measurements : Applications and Research Needs in Health Physics and Dosimetry. Proceedings of a Workshop held in Chalk River, October 1994. Radiat. Prot. Dosim. 61 (1-3) (1995).
4. Schmitz, Th., Waker, A.J., Kliauga, P. and Zoetelief, H. Design, Construction and Use of Tissue Equivalent Proportional Counters. EURADOS Report. Radiat. Prot. Dosim. 61 (4) (1995).
5. Pihet, P., Gerdung, S., Grillmaier, R.E., Kunz, A. and Menzel, H.G. Critical assessment of calibration techniques for low pressure proportional counters used in radiation dosimetry. Radiat. Prot. Dosim. 44 (1992) 115-120.
6. Schuhmacher, H. Tissue equivalent proportional counters in radiation protection dosimetry: expectations and present state. Radiat. Prot. Dosim. 44 (1992) 199-206.
7. Taylor, G.C. and Scott, M.C. A Monte-Carlo code for neutrons up to 60 MeV. Radiat. Prot. Dosim. 44 (1992) 53-66.
8. Verma, P.K. and Waker, A.J. Optimisation of the electric field distribution in a large volume tissue equivalent proportional counter. Phys. Med. Biol. 37 (1992) 1837-1846.
9. Gerdung, S., Grillmaier, R.E., Lim, T., Pihet, P., Schuhmacher, H.and Ségur, P. Performance of TEPCs at low pressures : some attempts to improve their dose equivalent response in the neutron energy range from 10 keV to 1 MeV. Radiat. Prot. Dosim. 52 (1-4) (1994) 57-59.
10. Ségur, P., Colautti, P., Moutarde, C., Conte, V., Talpo, G. and Tornelli, G. Comparison between experimental and theroretical determination of the space variation of the gas gain inside low pressure TEPCs. Radiat. Prot. Dosim. 52 (1-4) (1994) 65-71.
11. Siebert, B., Grindborg, J.E., Großwendt, B. and Schuhmacher, H. New analytical representation of W values for protons in methane based tissue-equivalent gas. Radiat. Prot. Dosim. 52 (1-4) (1994) 123-127.
12. Taylor, G.C. An analytical correction for the TEPC dose equivalent response problem. Radiat. Prot. Dosim. 61 (1-3) (1995) 67-70.
13. Lindborg, L., Bartlett, D., Drake, P., Klein, H., Schmitz, Th. and Tichy, M. Determination of neutron and photon dose equivalent at workplaces in nuclear facilities in Sweden. Radiat. Prot. Dosim. 61 (1-3) (1995) 89-100.
14. Feyermuth, M., Gerdung, S., Chouky, A., Grillmaier, R., Moutarde, C. and Ségur, P. Numerical simulation of a low pressure proportional counter used for area monitoring. Radiat. Prot. Dosim. 61 (1-3) (1995) 171-174.
15. Olko, P., Moutarde, C. and Ségur, P. Multi-level modelling of the response of the ultra-miniature proportional counter: gas gain phenomena and pulse height spectra. Radiat. Prot. Dosim. 61 (1-3) (1995) 205-210.
16. Colautti, P., Conte, V., Guli, M., Talpo, G., Tornielli, G., Boutruche, B., Moutarde, C. and Ségur, P. The electronic avalanche in proportional counters. Radiat. Prot. Dosim. 61 (1-3) (1995) 257-262.
17. Bordy, J.M., Barthe, J., Lahaye, T., Boutruche, B. and Ségur, P. Improving a multi-cellular tissue-equivalent proportional counter for personal neutron dosimetry. Radiat. Prot. Dosim. 61 (1-3) (1995) 175-178.
18. Taylor, G.C., Jansen, J.T.M., Zoetelief, J. and Schuhmacher, H. Neutron W values in methane based tissue equivalent gas up to 60 MeV. Radiat. Prot. Dosim. 61 (1-3) (1995) 285-290.

WG 11: Radiation Exposure and Monitoring of Air Crews

Chairman: I.R. McAuly

Objectives

In 1992, EURADOS has established a Working Group to be concerned with the exposure to cosmic radiation of air crew, and with the scientific and technical problems associated with radiation protection dosimetry for this occupational group. The Working Group was composed of fifteen scientist nominated by virtue of their involvement in this field of study and their knowledge of radiation measurement at the altitudes associated with aviation.

The primary reasons for the establishment of the Working Group were the ongoing revisions to the European Basic Safety Standards Directive and the recommendation by the International Commission on Radiological Protection in ICRP 60 that exposure to radiation in jet aircraft should explicitly be considered as occupational exposure for air crew and because of the overall reduction in dose limits recommended in the same publication.

The specific objective of the Working Group which has been supported also by DG XI/Luxembourg was to prepare a report collecting available information on radiation fields in flight height and describing measurement quantities and techniques for application in such radiation fields and to come out with practical recommendations with respect to air crew exposure.

Classification as a member of an occupationally exposed group should be made on the basis of dose rather than on other criteria and it was therefore agreed that the conclusions of the Working Group should apply to all air crew who were liable to receive equivalent doses in excess of the relevant annual limit of 1 mSv laid down for members of the public. Air crew on aircraft other than jet aircraft should therefore be considered to fall within the scope of the recommendations in this report in the event that their annual equivalent doses are liable to exceed 1 mSv.

Progress achieved

The Working Group held its first meeting in 1993 and, following extensive discussion of existing and prospective scientific understanding of the topic, three subgroups were set up to prepare draft reports on various aspects of the problem.

Subgroup 1 was to describe and assess the experimental studies carried out and reported on prior to 1993, to describe the radiation environment at altitudes relevant to civil aviation, and to survey the computational codes used to describe cosmic ray transport in the atmosphere.

Subgroup 2 was to survey measurement procedures and quantities and to consider appropriate instrumentation under three headings - active devices, tissue equivalent proportional counters and passive devices.

Subgroup 3 was to report on techniques and problems associated with calibration, reference instruments and reference fields.

The first draft reports of the sub-groups were considered at two plenary meetings of the Working Group and, following the necessary minor revisions to the three sections, the final draft of the report has been prepared in August 1995 and is planned to be published in near future.

The first section of the report assesses the existing data on radiation exposure, describes the radiation environment experienced at civil aviation altitudes, and summarises the computational approaches that have been developed to model the cosmic ray radiation field in the atmosphere.

The second section of the report describes the dose quantities which are used in the assessment of radiation dose and the relationship between the procedures which are used in the determination of the various quantities. It is clear from the nature of the radiation fields and from the particular circumstances associated with the working environment for air crew that conventional radiation protection dosimetry is not always applicable in the same terms as in the more usual fields encountered in occupational radiation exposure on the ground and that certain simplifications in

approach must be made. The strategies available for monitoring the doses of air crew in different categories are considered.

A summary of the conclusions reached by the Working Group as a result of the information detailed in this report and the recommendations which are based on these conclusions is then given. The Group was of the opinion that there are some areas relating to the assessment of the radiation exposure of air crew in which uncertainties remain. A brief account of these are included in this section of the report.

Appendix A gives an account of the principles of the various types of active and passive detectors which are appropriate for the measurement of the radiation fields due to cosmic radiation in the atmosphere.

Appendix B of the report deals with calibration, reference instruments and the use of reference fields to ensure the maintenance of consistency in field measurements which may have been carried out by different groups with different instrumentation. There was general agreement among all the participants in the Working Group that the availability of a suitable reference field for the comparison of instrumentation was extremely important in connection with measurements of the radiation doses received by air crew and this view has been reflected in the attention that has been paid to this topic.

Publications

1. McAuly, I.R. et al. Exposure of Air Crew to Cosmic Radiation. Report of Working Group 10 of EURADOS. To be published as a report of the CEC and EURADOS.
2. Bartlett, D.T., McAuly, I.R., Schrewe, U.J., Schnuer, K. and Menzel, H.G. Dosimetry for Occupational Exposure to Cosmic Radiation. Invited Paper presented at the 8th Symposium on Neutron Dosimetry. Paris, 13-17 November 1995.
3. Spurny, F. To the Air Crew Exposure to Cosmic Radiation. Paper presented at the 8th Symposium on Neutron Dosimetry. Paris, 13-17 November 1995.

WG 12: Environmental Dose Measurements

Chairman: I.M.G. Thompson

Objectives

The Working Group has been formed in February 1994. Its main objective is to harmonise the routine and emergency environmental radiation dose monitoring within Europe so that significant errors can be avoided and measurement results obtained in any country can be properly interpreted and accepted in other countries and adequate counter-measures can be implemented. It is aimed to prepare reports on this subject. Further tasks are the organisation of an intercomparison measurement during 1996 at both Riso, Denmark, and the PTB, Germany.

Progress achieved

The first meeting was held in Strasbourg from 5-7 September 1994, and the second in Krakow from 21-22 May 1995. The initial task undertaken by the Working Group was the drafting of a "Technical Recommendation on Measurement of External Environmental Radiation Doses" which can be used as a guide for persons involved in environmental monitoring. At the working group's first meeting the suggested contents for the recommendations was circulated, extensively discussed and modified.

It was decided not to include measurements of internal dose, however the environmental neutron dose will be included. Agreement was reached on who would contribute to the drafting of each section. Topics were grouped into proposed chapters and individuals were identified who would be responsible for combining the individual sections and production of the first drafts.

The sub-groups had prepared their chapters until February 1995 and prior to the working group's second meeting comments and revised versions of the first draft were circulated to the Working Group members.

At the second meeting in May 1995, each chapter was studied in detail and agreement was reached on the required revisions and on the additional technical issues that should be included. The participants agreed to complete the revisions of the different sections and chapters until September 1995. The chairman of the Working Group will act as the editor of this report, where the next draft is assumed to be prepared until November 1995.

The report will contain chapters on:

- the nature and variability of natural radiation in Europe;
- instrument characteristics of active and passive detectors;
- on-line systems;
- spectrometers;
- electronic dosemeters;
- calibration and type testing;
- traceability;
- uncertainties;
- intercomparisons and
- interpretation of measurements.

With authors from the USA, Europe and Eastern Europe the experience gained from the American and European intercomparison programmes will be used to provide advice to all those involved in such monitoring. These include nuclear operators, local government, governmental organisations, licensing authorities and environmentalists, the majority of whom have not been able to participate in intercomparisons.

Publications

1. L. Botter-Jensen et al. Technical Recommendations on Measurement of External Environmental Doses. Report of Working Group 12 of EURADOS. To be finished and published in 1996.

Head of project 2: Dr. Golnik

II. Objectives for the reporting period

The general aim of this project was to involve laboratories and scientists from Central and Eastern European countries in the work of EURADOS in order to increase their expertise in modern radiation protection measurement techniques and their knowledge of the work in Western European laboratories and to support the collaboration between laboratories in Eastern and Western Europe. This objective should be atteined by encouraging scientists either to become full or corresponding members of EURADOS Working Groups or to participate in training courses, seminars and workshops organised by EURADOS and other organisations.

III. Progress achieved:

During the report period from 1993 to 1995 scientists from Central and Eastern European countries participated in some of the Working Groups of EURADOS. They usually participated in their regular programme, e.g. in intercomparison measurements, in theoretical calculations or in writing reports. A more detailed description of the work can be found in the project reports of the Working Groups. Those reports include also the publications in which members from Eastern European countries were involved.

Most of those scientists who have actively contributed to the work of the Working Groups are from institutes in the Czech Republic, Poland and Hungary. In detail, the following scientists were involved:

WG 4:	K. Morstin	AGH, Krakow, Poland
WG 6:	A. Andrasi	KFKI, Budapest, Hungary
	Mrs. I. Malatowa	NRPI,Prague, Czech Republic
WG 7:	M. Tichy	IRD, Prague, Czech Republic
	M. Kralik	IIZ/CMI, Prague, Czech Republic
	T. Novotny	CMI, Prague, Czech Republic
	B.Osmera	NRPI, Prague, Czech Republic
WG 8:	F. Spurny	IRD, Prague, Czech Republic
WG 10:	P. Olko	INP, Krakow, Poland
	D. Srdoc	BNL, Zagreb, Croatia
	Mrs. Bronic	BNL, Zagreb, Croatia
WG 11:	F. Spurny	IRD, Prague, Czech Republic
WG 12:	S. Deme	KFKI, Budapest, Hungary
	P. Bilski	INP, Krakow, Poland
	M. Osvay	HAS, Budapest, Hungary
	F. Pernicka	IRD, Prague, Czech Republic
	M. Waligorski	INP, Krakow, Poland
	Mrs. Bronic	BNL, Zagreb, Croatia

Three Working Groups held meetings in Krakow and in Prague in order to improve the possibilities of collaboration by directly visiting laboratories in Central and Eastern European countries.

Many other institutes and scientists were invited to training courses and workshops and their participation was supported by EURADOS. This is especially the case for the courses organised by EURADOS itself. In the following, the number of scientists supported by EURADOS through the PECO contract is listed:

1. Training course on "Modern Methods in Radiation Measurement and Dosimetry" at Bad Honnef on November 23-27, 1992,
   6 participants from Eastern Europe
2. Training course on "Assessment of Doses from Intake of Radionuclides" in Cadarache/France on April 18-22, 1994,
   2 participants from Eastern Europe
3. Training course on "Application of Modern Methods in Radiation Measurement and Dosimetry" at the GSF/Neuherberg on September 5-9, 1994,
   8 participants from Eastern Europe
4. Training course on "Advanced Methods in Radiation Measurement and Dosimetry" at Bad Honnef on April 24-28, 1995,
   15 participants from Eastern Europe

Further support has been given to enable the participation in the Workshop at Chalk River/Canada (2 scientists) and about 10 scientists from Central and Eastern European countries are supported to enable them to participate in the Neutron Dosimetry Symposium in Paris in November 1995. This will provide a very good possibility of getting informed on recent developments in this field and of establishing further contacts with colleagues from laboratories in the European Community.

Final Report
1992-1994

Contract: F13P-CT920040 **Duration 1.9.92 to 30.6.95** **Sector: A11**

Title: Accident dosimetry in populated areas: the use of solid-state dosimetry techniques with ceramics and other natural materials.

1)	Bailiff	Univ. Durham	5)	Nolte	Univ. München-Technische
2)	Göksu	GSF	6)	Hütt	EAAS.IG (PECO Contract)
3)	Stoneham	Univ. Oxford	7)	Lippmaa	ICPB
4)	Bøtter-Jensen	Lab. Risø			

1. Summary of Project Global Objectives and Achievements

Project Objectives

1. To identify ceramic and other natural materials (such as teeth) which are suitable for retrospective accident dosimetry using solid-state techniques.
2. To ascertain appropriate experimental procedures for dose evaluation.
3. To evaluate transient fall-out dose in the sampled study areas down-wind of Chernobyl fall-out in the Ukraine and southern Belarus. To derive shielding factors by comparing dose determinations for interior and exterior samples.
4. To identify factors which affect minimum resolvable fall-out dose.
5. Integration of the results obtained to evaluate the capability of solid-state dosimetry techniques for retrospective accident dosimetry in populated areas.
6. To investigate the potential of the use of ^{36}Cl and ^{41}Ca for retrospective dosimetry and atmospheric transport modelling.

Achievements

Luminescence

- Establishment of a basic experimental framework for the application of luminescence methods to accident dosimetry within Europe which can serve as the basis for further development in specific areas of need.
- Investigation of the potential of the method in populated regions of Belarus and Ukraine which were contaminated by the Chernobyl accident. Surveys of settlements within these areas and the identification of potentially suitable samples for dose evaluations.
- Development of the method to a level where its use to provide benchmark dose evaluations for modelling calculations can be explored.
- Exploitation of the most recent advances in technique and the introduction of the use of optically stimulated luminescence and photo-transferred TL.
- Identification of dose-depth as an important adjunct to 'single' depth measurements and the introduction of new measurement techniques to enable surface scanning of cut ceramic samples.
- The investigation of the potential of a wide range of samples which are found in populated areas, including ceramic and other natural materials. The development of the use of porcelain for dose evaluations, particularly for well shielded interior locations.
- Detailed investigations of the luminescent properties of quartz and feldspar.

EPR of teeth

- Evaluation of dose levels of ca 100 mGy.
- Significant reduction in the background EPR signal associated with the presence of the organic component in teeth by the use of chemical treatments and by signal analysis.
- Identification of mechanical grinding of tooth enamel during preparation and after uv exposure as a source of potential background signal.
- A dose evaluation has been made using tooth enamel from an individual involved in the Kiisa incident.

AMS measurements of ^{36}Cl and ^{41}Ca

- Depth profiles of the radionuclides ^{36}Cl, ^{41}Ca, ^{60}Co, ^{152}Eu and ^{154}Eu have been measured with AMS and γ spectroscopy in a granite stone 106 m from the hypocenter of the Hiroshima A-bomb.
- For the first time the ^{41}Ca bomb peak has been measured in alpine glacier ice.
- It has been found that chlorine is gaseous in the stratosphere and that its fall-out to the earth is delayed by one year compared to the aerosol attached ^{90}Sr.

Project Summary

1. Introduction

This project brings together several experimental methods for the retrospective study of radiation dose estimation in populated areas following a radiation accident. The methods are applicable across a wide range of temporal scale, from the workplace to a geographic region. Since its inception the project has grown by the addition of new groups which have strengthened and extended the scope of application. There are three main areas of investigation which are reported here, each involving the application of :

i) Luminescence techniques with ceramic and a number of natural materials,
ii) Electron Paramagnetic Resonance (EPR) techniques with tooth enamel,
iii) Accelerator mass spectrometry with granite artefacts and atmospheric samples (argon).

All three, to varying degrees, are incorporating the results of computational modelling for comparisons and translation of dose determination for use in dose reconstruction.

By virtue of the nature of the materials sampled, the three experimental approaches have different roles to play in retrospective dosimetry. The luminescence method is based on the use of crystalline materials such as quartz, feldspar and certain carbonates extracted from ceramic materials which are natural solid-state dosemeters. This class of materials includes brick, tile and porcelain and consequently has specific application to buildings and their contents, but may also include, for example, porcelain artefacts from telegraphic and power distribution networks. From the point of view of dosimetry one of the key points concerning application of the method is that it provides evaluations of external gamma dose at various points in fixed structures within a populated area. The method determines integrated dose to the material sampled, and this includes sources of natural radiation; thus, resolution of cumulative dose above natural background is one of the issues raised in the study. The group has made use of the latest advances in measurement techniques, exploring the use of both thermoluminescence (TL) and optically stimulated luminescence (OSL) for dose evaluation, in addition to the use of photoluminescence (PL), x-luminescence and cathodoluminescence (CL) for more fundamental investigations.

In terms of dose assessment for people, a step closer to determining dose received by individuals is achieved by the use of EPR. Tooth enamel comprises predominantly a crystalline mineral (hydroxyapatite) which serves as a solid-state dosemeter material. EPR has been used in the past for such determinations, but only in cases of acute dose. The challenge of this area of the project has been to investigate means of extending the working range to levels of dose lower than ~300 mGy and to identify factors which may affect reliable evaluations of dose in typical tooth samples. The organic fraction within the enamel structure provides an intrinsic EPR signal with enamel samples which interferes with the dose-related signal and has been the subject of much investigation.

The assessment of dose at Hiroshima and Nagasaki provided the first impetus for the development of retrospective dosimetry methods. There has been considerable debate concerning the neutron and gamma ray transport calculations in the Dosimetry System 86 (DS86) and the resulting estimates of dose received by survivors. In particular there are discrepancies between the calculated and measured yields of neutron-induced radioactive isotopes of short (^{154}Eu, ^{152}Eu, ^{60}Co, $T_{1/2}$ < 20 years)) half lives. Such discrepancies are also reflected in the gamma-ray dose evaluations made using TL methods (at Hiroshima). The introduction of ultra-high sensitivity accelerator mass spectrometry (AMS) has meant that the long-lived isotopes (^{36}Cl and ^{41}Ca; $T_{1/2} >> 10^4$ years) can be measured.

2. Output of Project

2.1 Solid-state dosimetry - Luminescence methods

2.1.2 Organisation

The partners have divided the various elements of the work of the project to, on the one hand, capitalise on existing expertise within each laboratory and on the other to pool experimental resources in intercomparison and intercalibration experiments. The scope of this work can be divided into four main areas: Methodological Developments; Fieldwork and Dose Evaluation Measurements; New Techniques and Instrumentation Development. It is to be noted that the funding of the two PECO partners enabled participation at different stages in the project. 1993, the Palaeodosimetry Laboratory, Institute of Geology, Tallinn and 1994, the Institute of Chemical Physics and Biophysics, Tallinn. Two other laboratories also participated in the project as sub-contractors to Durham (University of Utah) and Risø (University of Helsinki).

2.1.3 Methodological developments

Investigation of new materials

An important element of this project has been the further development of the use of porcelain materials which can be found in a range of locations with various levels of shielding (see 2.1.4). The use of porcelain for dosimetry was pioneered by the Oxford Laboratory; in this project the exploitation of this material has been considerably advanced and porcelain in shielded interior locations has been of particular interest. Porcelain is a complex material and a number of detailed studies have been made of the (i) composition; (ii) luminescence processes by photoluminescence measurements (Risø); a combination of luminescence and EPR measurements (GSF and Durham) and (iii) dose evaluation procedures (GSF, Oxford and Risø) using TL and OSL with specially prepared slices from cored material (Oxford).

Porcelain has been found to be extremely sensitive when OSL is used for measurement. Measurements by Risø with ^{60}Co irradiated samples indicate that dose evaluations below 100 mGy are feasible, approaching the sensitivity of the pre-dose method. Porcelain is a translucent material and exposure of luminescent materials to light is a well known means of reducing the population of trapped charge. Illumination of porcelain samples with solar radiation has confirmed a penetration to ca 2 mm; it is therefore important to use material of at least 2-3 mm depth to avoid the underestimation of dose. It is to be noted, however, that the pre-dose technique has negligible light sensitivity under similar conditions.

The use of the TL from carbonates in ceramics is often overlooked. Durham reports the high sensitivity of carbonate in a field sample of brick manufactured in the FSU (Pripyat) and an example of dose evaluation based on the detection of orange TL emissions revealed by spectral measurements.

GSF has systematically investigated the potential for dosimetry of a number of natural and household materials which are known to be luminescent. Of a group of domestic materials including sugar, limescale, egg shells, chalk, baking powder and salt investigated using EPR and TL, the lower limits for dose evaluation are generally > 0.5 Gy; the phosphor coatings within fluorescent lamps are, perhaps not unsurprisingly, very sensitive and capable of registering dose > 1mGy. However, use in the field is problematic because of the sensitivity to light of the phosphors.

2.1.4 Fieldwork and Dose Evaluation Measurements

The Tallinn Institute of Geology's Palaeodosimetry Laboratory (IGPL) made vital contributions during the first half of this project by arranging fieldwork within Belarus and the Ukraine and the subsequent distribution of samples. During the period of the project 2 field expeditions were conducted to the Exclusion Zone. The aim of these fieldtrips was to examine the topography of settlements, building types, suitable ceramic materials and their locations, levels of contamination, etc. Links with dosimetrists working in the areas visited were also established, enabling evacuation details and the extent of monitoring data to be obtained.

Field expeditions (Durham, GSF, Oxford, Helsinki and IGPL, Tallinn) achieved the following:

i) sampling of a range of ceramic (and other materials as discussed above) materials in type and location from contaminated regions which had been subject to monitoring,
ii) monitoring of current levels of contamination (particularly within buildings),
iii) selection of samples from interior and exterior locations in buildings to examine the effects of shielding, during the later stages of the project this included the extraction of whole bricks within walls in order to examine dose as a function of depth in walls,
iv) the assessment in rural areas of the scope for obtaining samples from houses of mainly wood construction,
v) the development of appropriate strategies for sampling, ranging from detailed studies of building structures to investigations within a settlement or region.

An aspect of field sampling which needed to be addressed by the team was the ingress of radioactive contaminants for certain types of material and location. The material most susceptible is exposed brick (and mortar) at near ground level; for a number of samples GSF (also Oxford) has examined the degree of penetration, level and type of contamination. In a number of buildings, this problem was avoided by obtaining brick underlying less porous cladding tile. For many wooden houses brick is located within the foundations and is thus generally not a good sample location. On the other hand, glazed porcelain has the advantage of low retention of contaminants.

Once in the laboratory the experimental tasks performed included:

i) the identification of samples having luminescence properties suitable for reliable dose evaluation and if so, determination of the accrued dose,

ii) the determination of the natural background dose, based on field and laboratory measurements and building data, and the evaluation the transient field dose using the transient dose equation.

The transient gamma dose arising from exposure due to an accident, D_X, determined by luminescence techniques is given by

$$D_X = D_L - A(\dot{D}_\alpha + \dot{D}_\beta + \dot{D}_\gamma + \dot{D}_C)$$

where, D_L = accrued dose determined by luminescence; A = sample age; $\dot{D}_\alpha$, $\dot{D}_\beta$, $\dot{D}_\gamma$ & $\dot{D}_C$ = effective annual alpha, beta, gamma and cosmic dose respectively.

It is to be noted that for each dose evaluation appearing in this report there is a very high experimental overhead. Other than expecting samples to exhibit luminescence, the prior assumptions concerning dose response are minimal. Consequently many hours of instrumental time have been required first to characterise the properties of each sample and then to proceed with the accrued dose evaluation. Only as the data base of properties of ceramics increases, can the experimental time required be expected to reduce.

A joint paper on the assessment of preliminary dose evaluations obtained with samples from Pripyat has been published. A detailed study of the radioactivity of porcelain samples is reported by GSF, Oxford and Risø. Further testing of ceramics from Pripyat has been performed (Durham, GSF, Oxford and Risø) to examine both the transient dose and shielding factors for a particular building which has been the subject of modelling calculations at GSF. The results of this work are being prepared for publication. The integrated transient dose range from 1.5 to 2 Gy at external locations 1 m above ground level to ca 10 mGy for interior locations.

A large proportion of the survey testing of ceramics collected from contaminated regions was conducted by Oxford and Tallinn (IGPL); all the EU laboratories have contributed to the intercomparison locations and variously to other locations. All the laboratories have participated in an inter-laboratory calibration of laboratory radiation sources (a paper is in press).

2.1.5 New Techniques

Dose-depth profiles

The measurement of dose-depth profiles in brick and porcelain has led to the development of new experimental approaches. Both laboratory and field irradiated samples have been investigated using TL and OSL techniques. In addition to the use of extracted granular samples, it has been demonstrated (Risø) that OSL apparatus can be used to measure directly luminescence from the cut surface of a ceramic (brick or porcelain), using broad band green stimulation. Using calibrated gamma exposures of the sample following measurement of the emission due to the field dose, the equivalent dose as a function of depth can be evaluated. This provides a relatively rapid means of examining dose as a function of depth. An example of a 137 Cs irradiated brick is shown in the Risø report.

To complement this work, Durham, in collaboration with GSF, has used a slightly different approach to measure dose-depth in two composite ceramic blocks which were irradiated with ^{60}Co and ^{137}Cs photon beams at the secondary standard laboratories at GSF. The infra-red stimulated luminescence (IRSL) was measured using drilled powder samples; the ceramic used was of uniform composition and, with the homogenisation of drilling, enabled high precision to be obtained. A similar experimental approach has been used to measure the dose-depth profile in a sample from the Exclusion Zone. In both cases the experimental results show good agreement with Monte Carlo simulations of the dose-depth profile. The work is included in two publications.

Quartz for dosimetry

There is a large body of work on the use of OSL with sedimentary quartz for archaeological and geological dating applications, but considerably less on the study of fired quartz and feldspar. OSL measurements with quartz, feldspar and porcelain have shown high sensitivity to dose (tens of mGy lower detection limit reported by Risø in one case, but dependent on sample and thermal history).

Durham, in a detailed examination of TL peaks in the quartz glow curve and the effect of different annealing conditions has shown the importance of atmosphere during thermal treatment. One of the results of this work is the production of single crystal quartz specimens with a minimum resolvable dose in the region of 100 μGy, using the 210 °C TL peak - in a dose range which would enable a quartz dosemeter to be used in the field for ambient background measurements.

In addition to the investigations with porcelain discussed above, Durham and Risø describe the outcome of detailed investigations of the nature of luminescence processes in quartz and feldspar. The results provide important information on the nature of the trapping levels and recombination centres which are at the heart of the solid state mechanisms used for dosimetry in these minerals.

2.1.6 Instrumentation Development

Risø, in their report, describe the use of sophisticated equipment originally designed for the scanning of sediment cores and adapted for the OSL scanning of bricks. The University of Utah, under sub-contract to Durham, has developed experimental control software for use with the semi-automated luminescence readers used in the EU labs, specifically designed for use in retrospective dosimetry experiments. The report was received at the end of the contract period.

2.1.7 Role in Retrospective Dosimetry and Dose Assessment

Substantial progress has been made in terms of preparing dose evaluations obtained by luminescence for use in dose reconstruction. The work has proceeded in collaboration with GSF as part of a related EU funded dosimetry project. With the aid of Monte-Carlo calculations, the dose at reference points external to the building have been calculated for various source energies and fall-out patterns.

2.2 Solid-state dosimetry - EPR of teeth

2.2.1 Organisation

Three groups have contributed at various stages to the EPR work in this project: GSF, IGPL (Tallinn) and ICPB (Tallinn). This method is at a formative stage and efforts have been focused on the reduction of background and identification of sources of spurious signal. A number of advances have been made in understanding the origin of the unwanted background and preparation induced signals.

GSF have demonstrated that NaOH is an effective means of causing a three-fold reduction of the organic component in tooth enamel. While this does not completely remove the background signal, limiting the use of the method below ~0.3 Gy, mathematical methods (based on the representation of the measured signal by several Gaussian functions) have been developed to reduce the background EPR signal. This has enabled dose levels of ca 100 mGy (s.d. 15%) to be measured. (GSF, as part of the related EU project ECP10, has played a central role in organising the first EPR intercomparison with tooth enamel).

The IGPL (Tallinn) have investigated in detail the effect of mechanical grinding of tooth enamel during preparation which has been found to induce an EPR signal. The magnitude of the effect varies with the grain size of the prepared sample; for 250-850 μm grains the effect leads to an underestimation of absorbed dose. The group report the ability to be able to detect dose in the region of 250 mGy.

The ICPB (Tallinn) group have also been able to make advances in background reduction using signal averaging techniques and the resolution of the EPR signal into Gaussian components. The group have been able to detect doses in the region of 100 mGy as a result of these improvements. An important effect which potentially may affect dose evaluations has been revealed by ICPB (Tallinn) - it has been found that UV irradiation can stimulate an EPR signal indistinguishable form the dose-related signal - verification of this effect is currently being sought in other laboratories. Tooth enamel from a 14 y old boy involved in the Kiisa incident has been tested, giving a dose estimate of 2-2.5 Gy. As the minimum detectable dose is being lowered by these improvements, dental x-ray examination history will need to be considered.

2.3 AMS measurements of ^{36}Cl and ^{41}Ca

Two main subjects concerning dosimetry systems and atmospheric transport of radioactivities were studied by the Technical Univ., Munich (TUM), using an accelerator mass spectrometry (AMS) to detect ^{36}Cl and ^{41}Ca:

i) Depth profiles of the radionuclides ^{36}Cl, ^{41}Ca, ^{60}Co, ^{152}Eu and ^{154}Eu were measured with AMS and γ spectroscopy in a granite stone 106 m from the hypocenter of the Hiroshima A-bomb. MORSE neutron transport calculations were performed to calculate these neutron- produced radionuclides. The MORSE calculation gives 50 % more neutrons below 0.4 eV than DS 86. Neither MORSE nor DS 86 are able to describe these measured radionuclides. When averages of thermal neutron fluences are used, a bomb yield of 16 kt TNT is deduced.

ii) For the first time the ^{41}Ca bomb peak has been measured in alpine glacier ice. A general atmospheric transport model was developed which describes transport of gases and aerosols. For aerosols in addition to the exchange processes for all tracers, sedimentation has to be taken into account in the upper stratosphere. It was found that chlorine is gaseous in the stratosphere and that its fall-out to the earth is delayed by one year compared to the aerosol attached ^{90}Sr.

Head of Project 1 : I.K. Bailiff

II Objectives for the reporting period

1. Review of the experimental procedures for luminescence measurements.
2. Inter-laboratory calibration of laboratory radiation sources.
3. Experimental designs for dose-depth measurements in ceramic samples.
4. Characterization of the luminescence properties of minerals extracted from ceramics for dose evaluation. Investigation of the TL properties of quartz.
5. Measurement of TL emission spectra from field samples.
6. Improvement of software routines for semi-automated experimental control and data processing.
7. Coordination of fieldwork in regions contaminated by Chernobyl fallout and the development of sampling strategies.

III Progress achieved including publications

1. Optimizing luminescence detection systems

Because of the weakness of transient luminescence from samples of interest in this project and the rarity of ultra high sensitivity spectrometers, laboratories usually make assumptions concerning the emission spectrum from their samples. This often results in a detection system which is not optimized.

Two examples encountered with field samples of brick and porcelain illustrate how spectral measurements can improve sensitivity.

1.1 Brick

Tests of brick from various locations in Pripyat using the standard blue/uv pass detection filters had revealed problems of low luminescence sensitivity. XRD analysis of the brick indicated the presence of quartz, orthoclase, diopside and calcite. However, spectral measurements (Fig. 1) show that the TL emission from fine-grain material is in the orange/red region. With the use of suitable red-pass filters and special sample washing treatments, accrued doses in the region of 100 mGy could be evaluated (see discussion of roof brick below).

1.2 Porcelain

Porcelain has been found to be the main type of sample available from interior shielded locations for buildings within the Exclusion Zone. Since the levels of integrated dose are generally less than 50 mGy for such locations, the pre-dose method has played a central role in dose determinations. Since there has been no previous systematic study of the TL emission spectra from porcelain, measurements have been performed with field samples. In Fig. 2, the spectra reveal a result, important not only for optimization of detection sensitivity but also in terms of fundamental aspects of the physical mechanisms associated with the pre-dose effect (Paper 3). In the upper spectrum of the two shown, representing the sensitized sample

following thermal activation, two bands are present, at 360 nm and 420 nm. Whereas only the 360 nm band has been associated with the sensitization process, the 420 nm band is clearly involved. Pending an investigation of the behaviour of the 420 nm band, the use of an optical filter system passing both bands will significantly increase the strength of the detected signal.

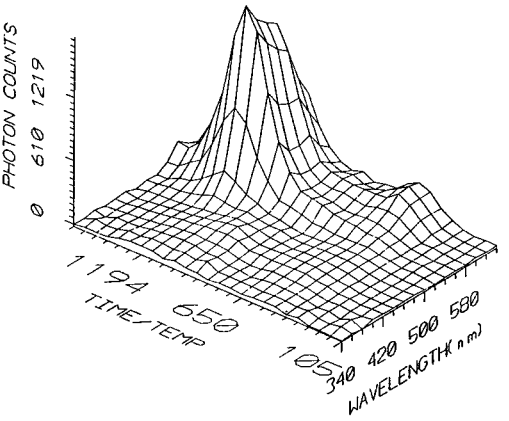

Figure 1.
TL emission spectrum obtained with fine-grain sample extracted from Polyclinic roof brick. To obtain the sample temperature in degrees Celcius, the TIME/TEMP axis should be divided by 4. The spectrum has been corrected for instrument response.

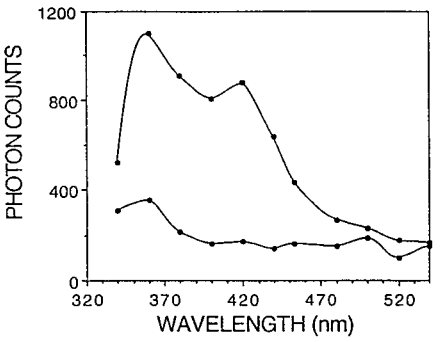

Figure 2.
TL emission spectra of a TL peak located at ~100°C and obtained with a porcelain slice (light fitting, Pripyat). The spectra represent the measurement of the initial sensitivity (lower curve), S_o, and the first activated sensitivity following thermal activation of the accrued dose. The test dose was 2 Gy. The spectra have been corrected for instrument response.

2. Dose-depth profiles

Dose-depth measurements made with ceramics which have received a transient field dose provide information concerning the time-averaged incident gamma spectrum. While the extent to which quantitative data concerning the incident spectrum can be extracted from such profiles has yet to be fully evaluated, they provide confirmation of the degree and form of attenuation within the wall (and may also indicate the existence of contributions from bremmstrahlung).

Studies have been conducted in parallel to investigate dose-depth profiles in photon irradiated ceramics in the laboratory and in the field (Fig. 3, Exclusion Zone).

Figure 3.
Cross section of typical wall showing external cladding tile, underlying mortar and bricks.

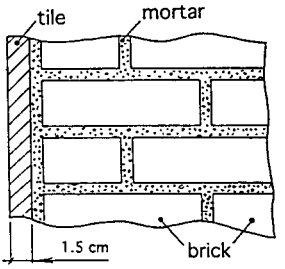

2.1 Control experiments

Modern terracotta tiles were selected for use in tests, providing the advantage over most bricks of a uniform ceramic matrix and the flexibility in assembling stacks of varying depth and irradiated area. Tests of the luminescence properties of the minerals within the ceramic used showed that stronger emission and better reproducibility could be obtained using IRSL rather than TL. Following a successful trial experiment using a single tile (25 mm thickness) that had been irradiated (dose at surface ~2 Gy) with a ^{137}Cs photon beam, multiple tile stacks were assembled and irradiated with ^{137}Cs and ^{60}Co photon beam facilities at GSF Neuherberg (Fig. 4).

Figure 4.
Brick stack subject to photon irradiation with cross sectional detail indicating sampling location.

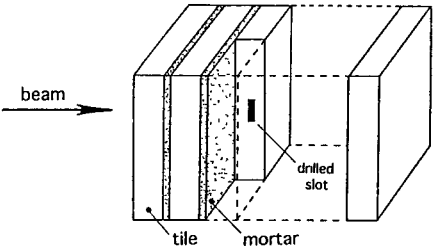

A simple sampling procedure was employed: powder samples were obtained by drilling slots into the tile using a 1.5 mm ø tungsten carbide drill. Material of 2-10 μm was extracted from the drilled sample using the fine-grain settling procedure. A typical IRSL decay curve is shown in Fig. 5; the equivalent dose (ED) for each sample location was evaluated using an additive dose procedure.

Figure 5.
IRSL decay curve obtained with a fine-grain sample extracted from brick. The sample was stimulated with broad-band i.r. radiation (840-920 nm) from an array of i.r.-emitting diodes and the recombination luminescence observed through an i.r.-rejecting filter (Schott BG39).

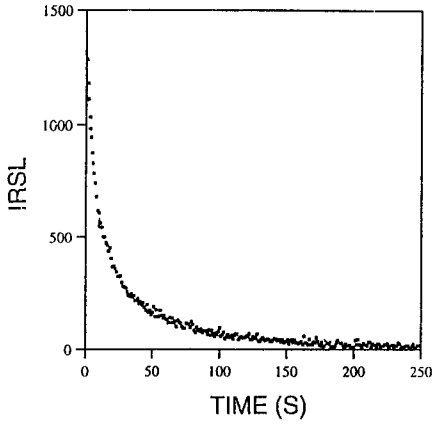

The measured relative absorbed dose determinations at various depths in the tile stacks are shown in the Fig. 6; they are to be compared with the relative kerma for each type of irradiation calculated by GSF using Monte Carlo methods (by Dr R. Meckbach, GSF).

Figure 6.
Open triangles: Monte Carlo calculation of relative kerma in terracotta tile due to parallel irradiation with a Cs photon beam. The average kerma is calculated for a volume element (1cm thickx2cm x2cm) at various depths located 1) along the central axis of the tile stack (upper symbols) and 2) along an axis parallel to the central axis located such that the volume element is located at the (same) corner of each tile (lower symbols).
Filled circles: Measured absorbed dose vs depth in stack measured using IRSL for a sampled volume as discussed in the main text. The stack was given a known incident photon dose from a Cs source at the GSF SSDL facility.

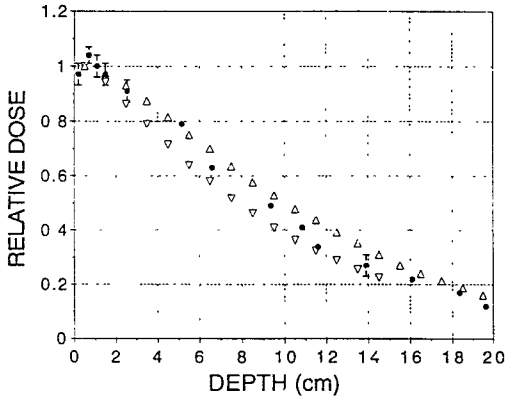

Two features of the experimental results are to be noted: i) good precision (generally better than ±5%) was obtained using drilled powder ii) general concordance of luminescence and calculated dose profile results. In the case of ^{60}Co irradiation, the luminescence evaluations appear to be systematically lower than the calculated values by several percent and will be the subject of further investigation. The experimental profiles for ^{137}Cs and ^{60}Co beams cannot be distinguished (within experimental error) until a depth of >15 cm - this is consisted with calculation (Paper 10).

While the relative dose profiles are encouraging, it should be noted that for the first cm of depth, the IRSL appears to give dose estimates which are lower than the calculated value by ~10%. The IRSL procedures are very sensitive to thermal treatments of the sample prior to measurement and the brick stacks are currently being subjected to long term storage (> 1year) to investigate whether delayed measurements are required to obtain better agreement. Nonetheless, the experiment is providing an important check for identifying sources of systematic error arising from the use of different procedures based on the use of optically stimulated luminescence.

2.2 Field Samples

As part of sampling strategies developed by the group, samples from ground and elevated locations have been sought. The results of tests with field samples underline the care which needs to be taken in sample selection and the limitations of sampling in the field.

2.2.1 Roof of Polyclinic, Pripyat

To test the variation of dose with height, samples from the upper regions of the 4-storey building had been sought. In the absence of full scaffolding or special working platforms, extraction of bricks from the walls of upper levels clear of the roof was not possible. Dose evaluations for the bricks obtained from the roof (using red TL emission as discussed above) indicate a substantial contribution from contamination on the roof (Fig. 7), while the dose in the outer brick is significantly lower. These results will be the subject of comparison with modelling calculations.

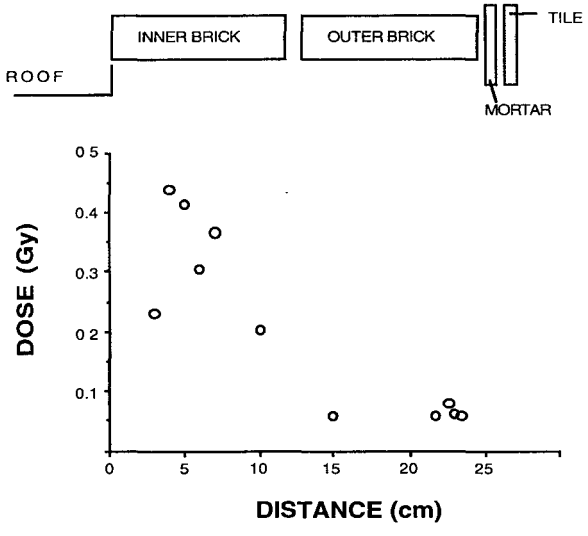

Figure 7.
Accrued dose, evaluated by TL, as a function of depth in bricks located on the roof of the polyclinic, Pripyat. The upper schematic diagram indicates the location of the bricks and tiles relative to the (flat) roof.

2.2.2 Masani, Belarus

Dosc-depth measurements were also made on brick from a house in the rural settlement of Masani, north of the reactor and on the southern border of Belarus. Measurements were performed using the fine-grain technique with a modified procedure based on the use of IRSL for sample normalisation because of strong thermally induced sensitization following first heating.

The dose-depth profile obtained is shown in Fig. 8 - it is consistent with a calculated profile obtained for isotropic irradiation of brick with 662 keV photons (Paper 10).

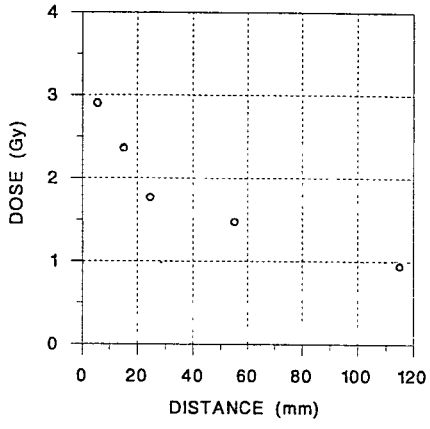

Figure 8.
Dose-depth measurements for brick from the village of Masani - based on TL measurements.

2.2.3 Lenin Prospect, Pripyat

In modern towns typical of those built in the 1970's, concrete is the most common building material and ceramics can be difficult to locate. Nearly all the multiple storey apartment blocks in Pripyat are of concrete construction (not so far suitable for dose evaluations using luminescence). The buildings in Lenin Prospect (Fig. 9) have been subject to modelling calculations by GSF Neuherberg and fortunately glazed tiles were used to decorate the outer walls to a height of 1-2 m.

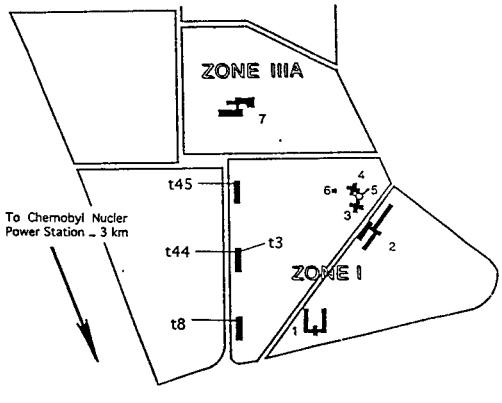

Figure 9.
Schematic plan of Pripyat showing the location of sampled buildings. Those labelled t8, t44 and t45 represent the buildings within Lenin Prospect.

Samples of these glazed tiles have been used for an interlaboratory comparison of accrued dose evaluation; the fine grain TL technique was used with material extracted from the body of the tile. A peak located at ~290°C in the TL glow curve (Fig 10) was used for dose evaluation.
Within the group both TL and OSL techniques were employed for dose evaluation; they will be compared with modelling calculations (GSF Neuherberg) of shielding factors and integrated dose. This work is the subject of a forthcoming group paper.

Figure 10.
Example of a TL glow curve obtained with fine-grain sample extracted from tiles which were located on the exterior of apartment blocks in Lenin Prospect.

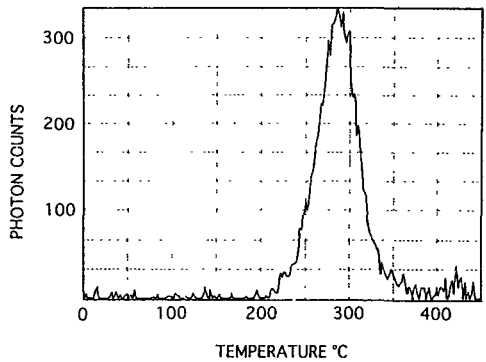

3. Properties of Quartz

Quartz is currently considered to be the most reliable dosimeter mineral in ceramics since it is not subject to significant loss of latent signal by athermal fading. There two peaks located at ~110°C and ~210 °C in the quartz TL glow curve which are of particular interest in retrospective measurements because thermal quenching mechanisms severely reduce the sensitivity of higher temperature peaks. Similar peaks are also found in glow curves obtained with porcelain.

3.1 '110°C TL Peak

Although the 110°C TL peak is not stable at room temperature over dosimetry timescales, sensitization of this peak provides the basis of the pre-dose technique, which is the most sensitive of the TL techniques. The 210°C TL peak, on the other hand, has a mean-life in excess of 1000 years and is potentially suitable - if of sufficient sensitivity. A detailed investigation of the TL properties of these two peaks has been performed .
Measurements performed with specimens of single crystals of synthetic and natural quartz, subjected to various thermal and radiation treatments, have shown that the TL in the 100°C region of the TL glow curve is considerably more complex than had previously been assumed (Fig. 11).

It has been noted previously that a high level of instrumental stability and regulation of measurement procedure is required to achieve good reproducibility in pre-dose measurements. Whereas the short half-life of the 100°C TL peak had been thought to be a major source of variability, our results indicate a significant dependence in both the sensitivity and the degree of sensitization on the sample temperature during laboratory

irradiation. Also, depending on the type of sample, up to three additional trapping levels have been identified in annealed quartz in the temperature region 0-200°C. These results are of importance in improving the performance of the pre-dose technique with quartz extracted from ceramic and with porcelain and provide valuable insights into the behaviour of the two types of material.

3.2 '210°C' TL Peak

The 210°C TL peak was studied using single crystal synthetic quartz which had been annealed at ~1200°C in controlled atmospheres for various periods (1-24h). The results indicate that oxygen vacancies play an important role in the luminescence properties of quartz. In a paper in preparation, we argue for the correlation of luminescence properties with sample impurity content and non stochiometric defects (intrinsic defects) in synthetic quartz.

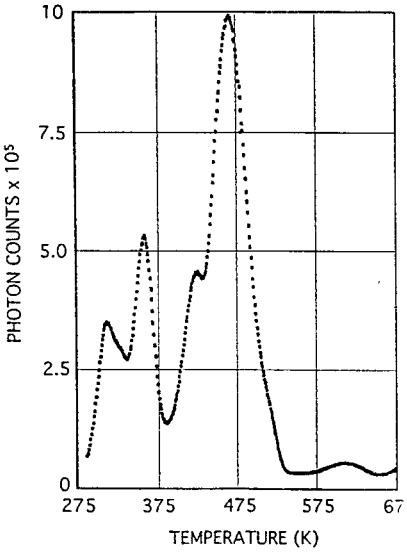

Figure 11.
TL glow curve obtained for a sample (cut slice from single crystal) of annealed natural quartz obtained following ß irradiation at 0°C. Sample heating rate was 1°/s.

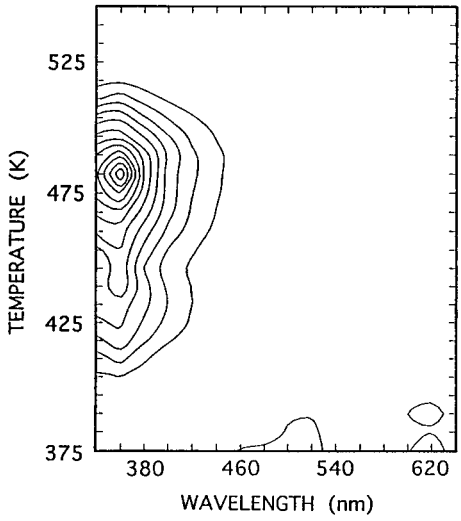

Figure 12.
TL emission spectra for a sample of quartz (as in Fig. 11) showing a uv band associated with the peak(s) in the 200°C region of the glow curve. The spectrum has been corrected for instrumental response.

As with the '110°C' TL peak, a detailed examination of the thermal trap depth has shown that the peak is not singular but comprises a complex of three component peaks (Fig. 11) which have emission bands in the uv region (Fig 12). Additionally we have shown that previous interpretations of the effect of thermal quenching on the evaluation of trap depth using the initial rise technique are incorrect and have proposed a method of calculation which circumvents this problem and allows the correct trap depth to be determined.

The high temperature annealing experiments have revealed that the sensitivity of TL peaks below 250°C show a strong dependence on the nature of the atmosphere during annealing (at 1200°C). this has both important implications on the mechanisms of luminescence in quartz and in understanding how to maximise sensitivity. So far we have been able to treat single crystal quartz such that the '210°C' TL peak can be used to register a dose of less than 100 μGy (Fig. 13). It is intended to use such samples for in-situ dosimetry in buildings to record the background dose (with energy dependence similar to that of the granular samples extracted from ceramic).

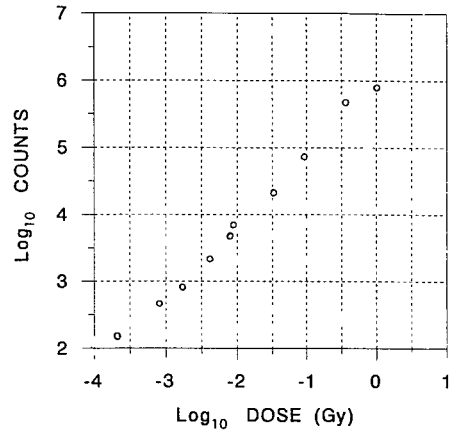

Figure 13.
TL growth characteristic obtained for the 210°C TL peak using treated single crystal quartz.

4. Development of new control system

Durham, in collaboration with the University of Utah (as sub-contractor) and Risø, has developed a new computer control system for luminescence measurements using the Risø semi-automated reader. The system has been design specifically for retrospective dosimetry measurements (Report 50pp including appendices).

Publications

1. Bailiff, I.K. (1992) Measurement of the stimulation spectrum (1.2-1.7 eV) for a specimen of potassium feldspar using a tunable solid state laser. *Radiat. Prot. Dosim.* **47**, 307-311.
2. Hütt G., Brodski, L., Bailiff, I.K., Göksu, Y., Haskell, E., Jungner, H. and Stoneham, D. (1993) Accident dosimetry using environmental materials collected from regions downwind of Chernobyl: A preliminary evaluation. *Radiat. Prot. Dosim.* **47**, 307-311.
3. Bailiff, I.K. (1994) The Pre-dose technique. *Radiation Measurements,* **23(2/3)**, 471-479.
4. Bailiff, I.K. (1995) The use of ceramics for retrospective dosimetry in the Chernobyl Exclusion Zone. *Radiation Measurements* accepted for publication.
5. Stoneham, D., Bailiff, I.K., Brodski, L., Göksu, H.Y., Haskell, E., Hütt, G., Jungner, H. and Nagatomo, T. (1993) TL Accident dosimetry measurements on samples from the town of Pripyat. *Nucl. Tracks Radiat. Meas.* **21**, 195-200.
6. Petrov, S. and Bailiff, I.K. (1995) The '110°C' TL peak in quartz. *Radiation Measurements*.. Accepted for publication.

7. Haskell, E.H., Bailiff, I.K., Kaipa, P.L. and Wrenn, M.E. (1994)Thermoluminescence measurements of gamma-ray doses attributable to fallout from the Nevada Test Site using building bricks as natural dosemeters. *Health Physics* **66(4)**, 380-391.
8. Göksu, H.Y., Bailiff, I.K., Bøtter-Jensen, L., Hütt, G, and Stoneham, D. (1995) Inter-laboratory beta source calibration using TL and OSL with natural quartz. *Radiation Measurements.* In Press.
9. Göksu, H.Y., Wieser, A., Stoneham, D., Bailiff, I.K. and Figel, M. EPR, OSL and TL spectral studies of porcelain. Int. Symposium on EPR Dosimetry and Applications, 15-19 May 1995, Munich. Submitted for publication.
10. Meckbach, R. Bailiff, I.K. Göksu, H.Y., Jacob, P. and Stoneham, D. Calculation and measurement of dose-depth distribution in bricks. 11th int. Symposium on Solid-state Dosimetry, Budapest 8-11 July, 1995. Submited for publication.
11. 6. Petrov, S. and Bailiff, I.K. Thermal quenching and the Initial Rise technique of trap depth evaluation. Submitted for publication.

Unpublished papers

12. Bailiff, I.K. The use of luminescence with ceramic materials. Workshop on Dose Reconstruction, Bad Honnef, Germany, June 1994.
13. Bailiff, I.K. Retrospective Dosimetry. Advanced Methods in Radiation Measurement and Dosimetry ERPET Course, Bad Honnef, Germany, April 1995.
14. Bailiff, I.K. Luminescence dosimetry measurements in the Chernobyl Exclusion Zone. UK TL and ESR Seminar, Royal Holloway and Bedford College, University of London, July 1994.
15. Petrov, S. The '110°C' TL peak in quartz. UK TL and ESR Seminar, Royal Holloway and Bedford College, University of London, July 1994.

Head of project 2: Dr. H.Y. Göksu

II. Objectives for the reporting period

1. Final evaluation of the potential of the TL and EPR methods for dose reconstruction using non-ceramic domestic material.
2. Optimisation of the individual dose assessment using EPR of tooth enamel.
3. Characterisation of luminescence properties of porcelain using EPR, OSL, TL and PTTL.
4. Dose assessment using porcelain from most shielded locations in Pripyat.
5. Measurement and assessment of surface contamination in bricks and other materials.
6. Compilation of in-situ gamma dose rate measurements. at indoor and outdoor locations.
7. Organisation and preparation of suitable material for interlaboratory beta source calibration
8. Interlaboratory beta source calibration using TL and OSL of quartz and porcelain.
9. Interlaboratory comparisons: alpha counting and depth dose studies.
10. Providing detailed documentation of materials, methods and procedures used during this project for future references.

III. Progress achieved including publications

1. Final evaluation of the potential TL and EPR methods for dose reconstruction using non-ceramic domestic material

The dose reconstruction after radiation accidents using natural material other than building material was found to be necessary especially in rural areas where most of the buildings are constructed using wood. The use of natural material, or household material has further advantages that they would not contain natural radionuclids that would have an appreciable contribution to the measured accumulated dose. The contribution from natural radionuclids sometime can hinder the dose reconstruction at shielded locations where accident doses approaches to the level of natural background radiation. This is especially important in the case of Chernobyl accidents where the dose reconstruction could be done only some years after accident.

The domestic materials like variety of medical pills, table salt, sugar, black board chalk, pot scale (main structure calcite), pearl buttons and sea shells (mainly aragonite), baking powder and many other plastic material were collected in 30 km zone during the field trip 1993 (complete documentation of the available material can be seen in Annex VIII). The radiation response of these material collected as well as commercial material similar to them were investigated by EPR and TL to select suitable materials for external gamma dose assessment in accident situations.

After the preliminary selection and elimination of the non suitable material, the dosimetric properties of the pot scale, table salt, fluorescence lamp coatings and blackboard chalk have been further investigated to establish the measurement and sample preparation procedures for retrospective dosimetry. The thermal and optical stability of the radiation induced centres have been measured. The other dosimetric properties such as linearity, reproducibility, homogeneity, self irradiation and environmental factors on the TL response have also been studied. The applicable time range of the method is assessed by determining the trap parameters for each material. The determination of lower limits are based on the precision required for dosimetry

being 20 %. The lowest detectable dose limit is assessed by taking three times the standard deviation of the zero dose reading. (The minimum detectable dose is variable in the way it depends not only on the sensitivity of the material, but also on the type of filter used in the readout equipment. In this case the values are quoted here for the use of only (HA 3) heat absorbing filters). All synthetic materials in this study were found not applicable for EPR dosimetry below 10 Gy. Cane sugar, boiler scale and egg shells were found to possess the most suitable properties for retrospective EPR dosimetry and all posses a lower dose limit of 0.5 Gy. The detection threshold for EPR dosimetry was found to be limited by the background signal. The most effective reduction of the background EPR spectrum would be achieved by chemical processing of the sample for certain materials. The details of TL and EPR methods of evaluation, sample preparation and experimental measuring conditions were already published in various journals (see pub. list 1, 4, 5). Materials found to be applicable for retrospective dosimetry are listed in table 1.

Table 1: List of the domestic material useful for retrospective dosimetry

Material	Method	Characteristics	Lowest Applicable Limits
Sugar	EPR	g = 2.0048	>0.5 Gy
Potscale	EPR	g = 2.005	>0.5 Gy
	TL	T_{max} = 180 °C	>0.3 Gy
Egg shells	EPR	g = 2.0018	
	TL	T_{max} = 260 °C	>1 Gy
Chalk	EPR	g = 2.0085	>1 Gy
	TL	T_{max} = 190 °C	>0.5 Gy
		T_{max} = 200 °C	
		T_{max} = 360 °C	
Baking Powder	EPR	g = 2.0075 g = 2.0025	>3 Gy
Salt (anhidrit)	TL	T_{max} = 220 °C	>0.5Gy
Fluorescent lamp	TL		>1mGy

1.1 Dose assessment using field samples

Most of the investigated domestic material were found at indoor locations at Pripyat. The black board chalk and pot scale and other material like medical pills were all tested and most of them were found to have doses below minimum detectable dose limits. The pot scale, however, found in Hostel 4 possessed doses almost twice as much as the threshold value (0.50±0.20 Gy). The lid of the pot was open and was heavily contaminated with ^{137}Cs. Chalk at the school was also measured to be in the order of minimum detectable dose (0.60±0.20 Gy). The other material like porcelain from indoor locations at Pripyat indicated doses in the order of 0.06±0.02 Gy. The materials listed in table 1 had limited applications in case of heavily shielded concrete buildings of Pripyat, but could be used in rural areas where shielding factors were comparatively smaller (see figs.2,3). On the other hand these material were shown to be very useful for reconstruction of doses in radiation accidents like Kiisa, where sugar and other medical pills could be used together with quartz containing ceramics and terracotta objects. (The dose reconstruction of Kiisa accident by use of building and domestic material is under preparation together with and other members of this project and PECO partners.)

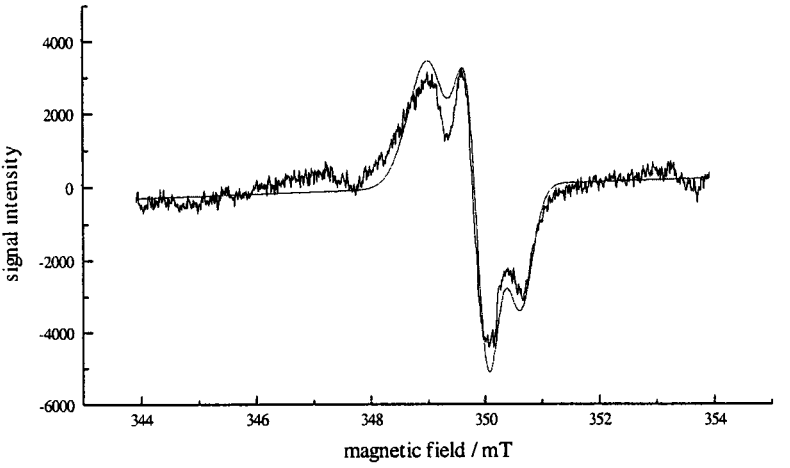

Figure 1: EPR spectrum of a tooth enamel sample irradiated with 400 mGy. The solid line is a fit of the spectrum using Gaussian functions.

2. Optimisation of the individual dose assessment using EPR of tooth enamel

In hydroxyapatite which is the main component of the inorganic tissue of teeth radicals are formed by ionising radiation. The EPR signal of the radiation induced CO_2^- radicals, which are located in hydroxyapatite, is however superimposed by a broad background signal. This background signal introduces problems in assessing absorbed dose below 1 Gy. The composition of dentine is similar to bone consequently the background signal is mainly due to organic components. The procedures developed for removing the organic fraction of bone was found to be less effective in the case of tooth enamel. The removal of the intrinsic EPR signals in tooth enamel requires different chemical treatment than bone or tooth dentine.

The treatment of bone in a Soxhlet apparatus with Diethyltriamine at 200°C was found to result in a 5-fold reduction of the organic EPR signal component (see pub. list 6). Similar results by the Soxhlet treatment were found also with tooth dentine. However, in the case of tooth enamel only little reduction of the intrinsic EPR signal was achieved after this kind of treatment. The reasons for the difference in behaviour of the intrinsic EPR signal in bone and tooth enamel by chemical treatment might be due to the very low organic content of tooth enamel. The most effective removal of the intrinsic EPR signal in tooth enamel was found by treatment with Sodium Hydroxide at room temperature in an ultra sonic bath. The treatment in sodium hydroxide for 40 hours was found to result in a 3-fold reduction of the intrinsic EPR signal.

The efforts in optimising the procedure for the chemical treatment of tooth enamel did not resulted a complete elimination of the background. Further reduction of the background is required to improve the precision at absorbed doses below 0.3 Gy. In addition to the development of chemical purifications of the samples, the mathematical methods were used for the evaluation of spectra for reduction of the background. The most promising procedure for spectrum evaluation was found by simulating the hydroxyapatite and the background spectrum

into Gaussian functions (see pub. list 15). The intensity of the radiation induced hydroxyapatite spectrum is determined in this procedure from the resulting amplitude of its principal Gaussian function. As an example, the measured and fitted spectrum of a irradiated tooth enamel sample (400 mGy) is shown in the figure 1. Dosimetry was found to be possible with a standard dev iation of 15% down to level of 100 mGy.

3. Characterisation of luminescence properties of porcelain using EPR, OSL, TL and PTTL

Porcelain is one of a group of promising building materials for reconstruction of dose from external gamma exposures. The type and lifetime of the recombination centres plays an important role in the accuracy of retrospective dose assessment, especially if the accident occurred many years before laboratory measurements. The properties of the recombination centres have been investigated by optically stimulated (green) luminescence (OSL), thermoluminescence (TL), phototransfered thermoluminescence (PTTL) and TL glow spectra. The investigations were carried out using (TL) read-out, following the green light exposures on the porcelain pre-heated at various temperatures. Photo-transfer peaks were recorded at 110°C, 170°C and 230°C. Among them, the PTTL peaks at 230°C and 110°C exhibited pre-dose sensitisation. The pre-dose and phototransfer (PTTL) techniques have been further used in conjunction with EPR measurements in order to obtain further information concerning the nature of the defects associated with these TL peaks. The effect of sensitisation associated with the two TL peaks has also been examined to check whether it is the same for the trapping of charge following the administration of either ionising radiation (TL) or optical radiation (PTTL).

Two types of porcelain obtained in 30 km zone were selected for the measurements. One type of porcelain, usually found in electrical fuses, lamp holders or electrical holders, was unglazed (type K). The other type from toilet cisterns and toilet basins was glazed (type E and TT). In both cases the outer surfaces were removed before sample extraction.

The relative Al and Ge contents in the E, K and TT type of porcelain were determined by the intensity of the corresponding radiation induced EPR spectrum. The Al and Ge spectrum were recorded at liquid nitrogen (77 K) and room temperature, respectively.

The sensitivities of the 110 °C and 230 °C TL peak differ for the two types of porcelain tested here and the Al concentration inferred by EPR was found to be lower for samples with low sensitivity. On the other hand the 130 °C peak, which was observed only on the E and TT type of porcelain, had no systematic relationship with the Al content. The amplitude of the Ge signal (single EPR line at g = 2.0005) was found to correlate to the sensitisation (that is S_N/S_0) of 110 °C and 230 °C TL peaks. As a result it is concluded that;

1. the 230 °C TL peak in porcelain appears to be related to Al content of the porcelain as measured by EPR.
2. the sensitisation of the PTTL and the TL peaks at 110°C and 230°C was found to be similar and both of them were found to be correlated with the amplitude of the Ge signal as observed by EPR.
3. the PTTL pre-dose sensitisation observed in porcelain offers the possibility of a new technique of dose assessment in retrospective dosimetry over 3 Gy, which is usually beyond the range of the pre-dose TL technique.

This investigation was completed in collaboration with Oxford and Durham University. The spectral measurements were performed by the Durham laboratory using a fast scanning interference filter spectrometer. EPR, TL and PTTL measurements performed at GSF and thermal activation and sample preparation was done by Oxford laboratories (see Pub.list 12).

4. Dose assessment using porcelain from most shielded locations in Pripyat

Some years after the Chernobyl accident, the experimental evaluation of shielding factors in Pripyat dwellings were rather difficult due to continuous indoor contamination after the evacuation of the people as windows and doors were broken. The toilets had no windows. As a result no contamination could be detected on the porcelain obtained in these locations. The samples were collected from various floors and levels at 9 story building at 15 Druzhby Narodov St. for possible discrimination of cloud shine from ground shine. The samples are labelled as N, S, W, E , to indicate the orientation, followed by an number, to indicate the floor level. The outer 2-3 mm of ceramics is removed while it contained glazed material, before the samples are crushed for TL measurements. Fine grains between 2-10 micron are deposited on stainless steel discs by suspending them in acetone. From each sample 24 discs are prepared for pre-dose additive dose measurements. All measurements were performed with a Chance Pilkington HA3 heat absorbing filter and Schott BG39.

The average accumulated dose of 12 samples is found to be 0.11 ± 0.05 Gy and the age dose to be 0.04 Gy (Table 3). There was not an obvious difference between various floors. The difference could be as well due to inhomogeneity of the material which can be seen in the values of U, Th contents (see Annex VII).

The age dose is assesses from natural radionuclid content of the samples. The uranium and thorium content of the samples were measured by using thick sample alpha counting. The homogenised powdered samples are counted more than 48 hours to obtain about 100 slow alpha pairs. Potassium content is measured by using atomic absorption spectrometer. The results are presented in Table 4. The annual dose rate is calculated from count rates by using "alpha" programme developed in our laboratory (table 2). The internal alpha dose rate were obtained by further multiplication with a value of 0.01. The external gamma dose rate before accident is assumed to be as low as the dose rate at Zylonmys which is 30 km away from the Pripyat. All the dose rate values multiplied with the age of the building which, in this case was 15 years. 28 mGy per year is also added to external dose rate due to cosmic ray contribution (Table 3).

Table 2: Internal annual dose calculated from U, Th and K content of ceramics

Sample	Dose rate β [mGy/a]	Dose rate α [mGy/a]
W 4	2.38	2.43
W 7	2.25	2.73
W 8	2.07	2.89
W 9	2.39	2.65
S 4	2.21	2.54
S 5	2.36	2.47
E 5	2.41	2.66
E 7	3.11	3.24
N 3	2.38	2.40
N 6	2.23	2.48
N 7	2.07	2.66
S9 t t	2.75	2.93

Table 3: Total accumulated dose measured by TL and Age dose from WC cistern tops from 15 Druzhby Narodov Street.

Sample	Accumulated Dose [Gy]	Age Dose [Gy]
W 4	0.11	0.046
W 7	0.08	0.044
W 8	0.12	0.041
W 9	0.20	0.046
S 4	0.18	0.043
S 5	0.08	0.046
E 5	0.11	0.046
E 7	0.09	0.056
N 3	0.09	0.046
N 6	0.18	0.045
N 7	0.09	0.041
S 9t t	0.10	0.051

Table 4: U, Th and K content of samples from 15 Druzhby Narodov Street

Sample	K_2O [%]	Th [ppm]	U [ppm]
W 4	1.25	11.59	7.76
W 7	1.01	19.51	6.82
W 8	1.77	20.56	10.11
W 9	1.24	17.76	6.99
S 4	1.40	18.74	5.84
S 5	1.11	20.59	5.86
E 5	1.23	15.88	7.56
E 7	1.81	22.43	8.29
N 3	1.58	22.06	4.54
N 6	1.32	20.68	5.34
N 7	0.85	22.05	5.79
S 9t t	1.54	19.72	7.66

5. Measurement and assessment surface contamination in bricks and other materials

It has been found that some samples, especially bricks collected within 30 km zone, are contaminated with various isotopes and mainly ^{137}C. Consequently it was agreed that the bricks collected in the zone should be measured before distribution to other laboratories for the TL dose assessment. The bricks were measured at GSF and then distributed to other laboratories . It is further calculated that the contribution of the internal contamination to the internal dose would be in the order of 0.1-10 mGy in 10 years. The bricks covered with tiles or glazed tiles were found to be free of contamination. The details of the measurements can be found in Annex VI.

6 Compilation of in-situ gamma dose rate measurements within 30 km zone at indoor and outdoor sample locations

The gamma dose rate at external and internal locations were measured during the field trip 1993. It is observed that the ratios of external dose rate and internal dose rate is not constant for even similar type of buildings in Pripyat. The degree of contamination depend on the number of windows and decontamination procedures applied in the area. The window sills were found to be highly contaminated. The location factors (shielding factors) in Cultural Palace, Milk kitchen, Technical school, 18 Lenin Prospect were found to be close to the

calculated value (f = 0.1). The green house on the other hand have higher dose rate at indoor than outdoor locations due to decontamination efforts around the area as well as the fall out material washed from the glass roof in to the green house. The summary of the results are presented in figures 2 and 3 (details can be found in Annex V).

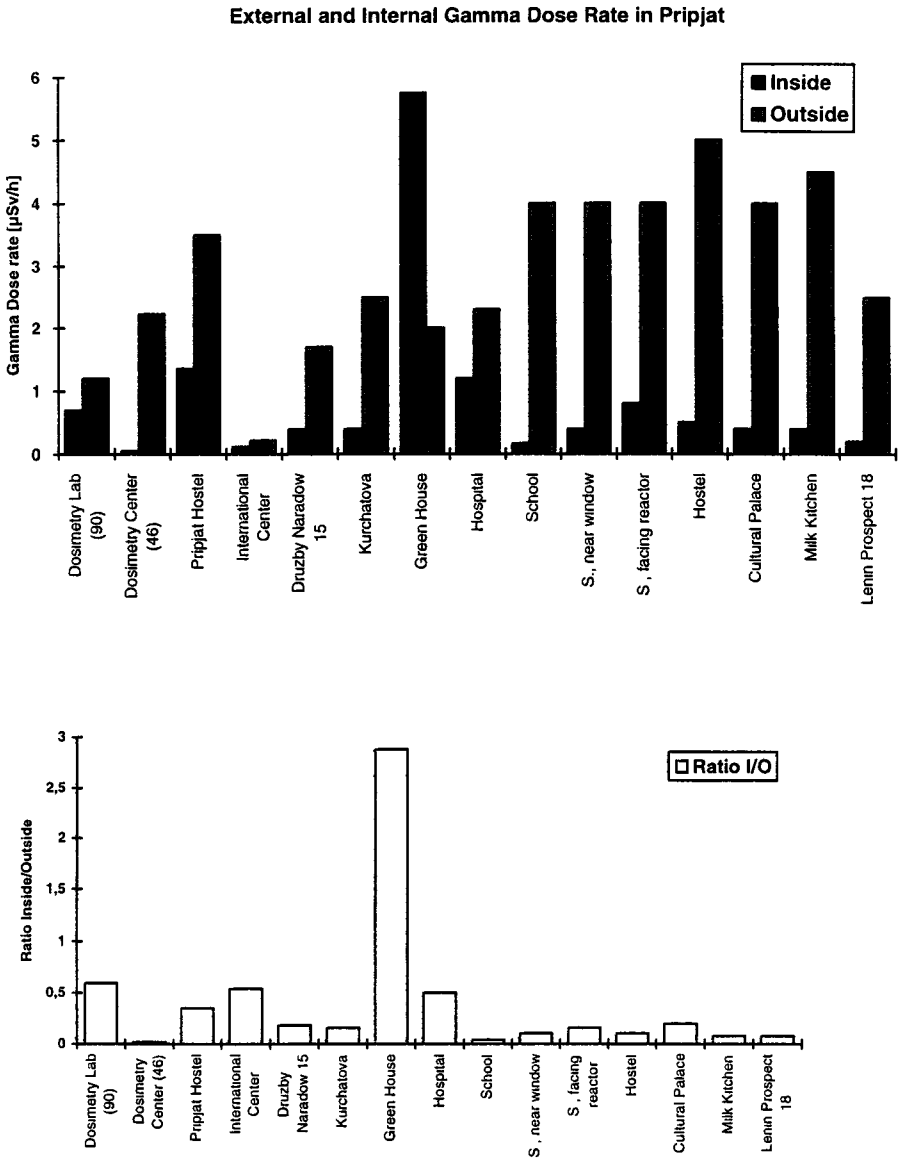

Figure 2: Gamma dose rates and their ratios measured at outdoor and indoor locations at Pripyat (August 1993 field trip)

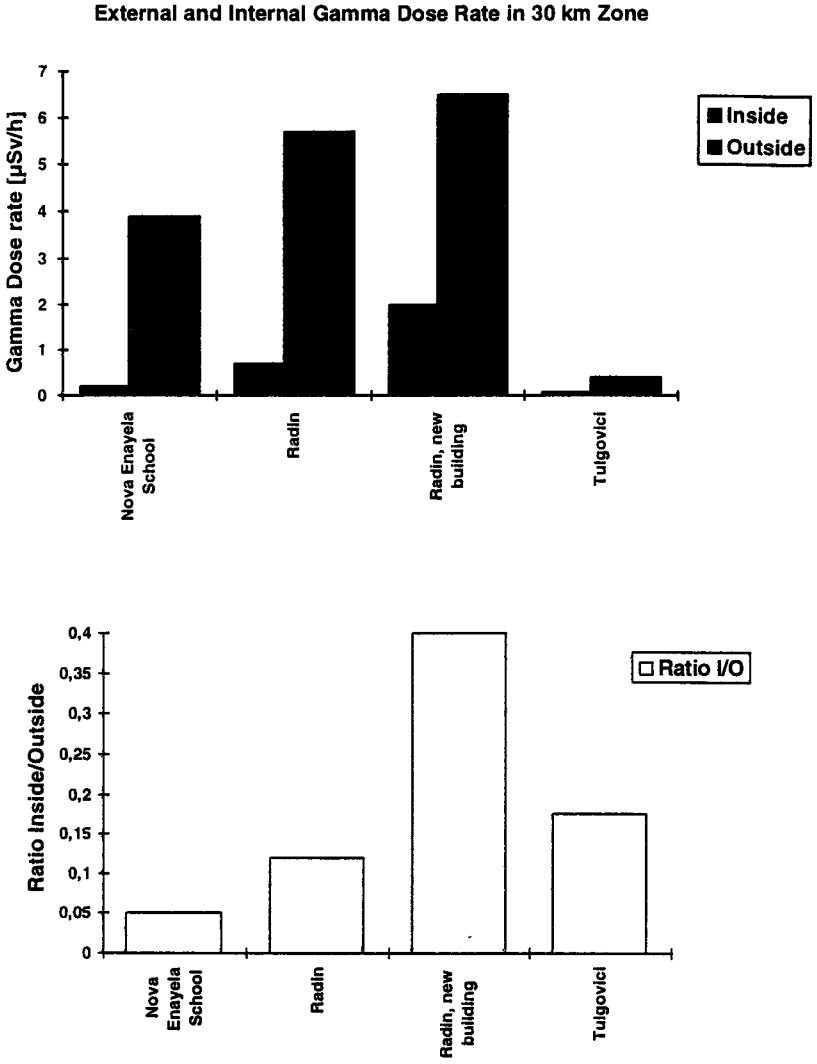

Figure 3: Gamma dose rates and their ratios measured at outdoor and indoor locations at 30 km zone (August 1993 field trip)

7. Organisation and preparation of suitable material for inter laboratory source calibration for all the participating laboratories

Number of material including various type of quartz is tested to organise an interlaboratory beta source calibration for the laboratories which are involved in this project as well as PECO partners. The reference material was selected after testing and stabilizing the dosimetric properties of the material (details can be seen in Annex 1). The sensitivity, linearity and stability of the 340°C peak of five different batches obtained from the Merck company were studied. The batch labelled as 1992 was found to be the most appropriate. The irradiation was performed at the Secondary Standard Dosimetry Laboratory at GSF using a ^{60}Co source as

well as the in-situ measurements with an ionisation chamber, calibrated with respect to the primary standards of PTB Braunschweig.

Quartz calibration programme using quartz is carried out as a first attempt to harmonise TL dose assessments produced by the various laboratories involved in retrospective dosimetry. Interlaboratory calibrations with porcelain and bricks were also performed (Further details are presented in Annex I and III). Apart from above intercalibration programme, the stacks of bricks and porcelain from Durham and Oxford, respectively, designed for intercomparison or dose depth distribution studies were irradiated at GSF, SSDL facilities.

8. Interlaboratory beta source calibration using TL and OSL of quartz and porcelain

Thermoluminescence and optically stimulated luminescence methods are used for source calibrations using quartz (Annex II). The results of the interlaboratory source calibration measured by different laboratories have been evaluated and published (See pub. list 9).

9. Interlaboratory comparison: U, Th, K content and depth dose studies

Dose reconstruction using building material is multiple stage process and contains independent components which has to be measured separately. This includes not only the luminescence methods of dose evaluation but also the content of the natural radionuclids inside the investigated material and as well as surrounding environment has to be measured.

U, Th content usually measured by most of the laboratories. Atomic absorption is used for K measurements. The Oxford University has organised the programme for the intercomarison of the U, Th and K content measurements.

9.1 Thick alpha counting

The samples distributed by Oxford Laboratory were measured by using thick sample alpha counting method. Alpha activity is measured by using commercial alpha counters with pair counting facility on a 42 mm ZnS screen. Counting was continued until at least 100 total pairs had been registered. Initially the equipment was calibrated by using US-Geological Standard known as G-2, GSP-1 and G2. Annual dose rate is calculated by using conversion factors and "TL alpha" program developed in GSF (Annex III). Furthermore, K content of 12 samples from 15 Druzhby Narodow St. were measured by atomic absorption method and compered with neutron activation measurements performed by Helsinki Laboratory. (see Table 4). The results sent to Oxford for evaluations.

Table 6: Uranium and Thorium content obtained by using thick alpha counting method

Ref. No.	α_{Total} [cpksec.]	Th [ppm]	U [ppm]	Annual Dose Rate [mGy/a]	
				α	β
[1]	18.8	17.3	5.9	2.41	1.38
[2]	23.5	17.4	8.8	3.03	1.79
[5]	19.6	19.9	5.6	2.51	1.40
[6]	15.5	18.3	3.8	1.98	1.07
[13]	14.6	13.1	4.8	1.87	1.08
[15]	11.93	12.06	3.4	1.51	0.85
[16]	22.03	15.9	8.2	2.82	1.67
[17]	23.01	17.7	8.3	2.96	1.74
[18]	23.58	16.5	7.1	3.01	1.80
[21]	22.49	20.8	7.1	2.88	1.64

9.2 Depth Dose Distribution:

Risø- National laboratory has provide cores irradiated with ^{137}Cs and ^{60}Co. The TL measurements were performed in both cores. It was found that the difference between ^{137}Cs and ^{60}Co measurements could only be distinguished after the depth of 6 cm.

A depth dose profile measured using thermoluminescence pre-dose method using a brick collected in 1993 field trip. The brick obtained from a settlement called Lomachi is found to be highly contaminated. At the surface of the brick the count level was 10^4 Bq/kg. The depth dose profile is shown in figure 5. (Annex III)

The depth dose profile obtained from the Lomachi brick was compared with the laboratory irradiated profiles. It is concluded that the depth dose profile is consistent with laboratory ^{137}Cs irradiation.

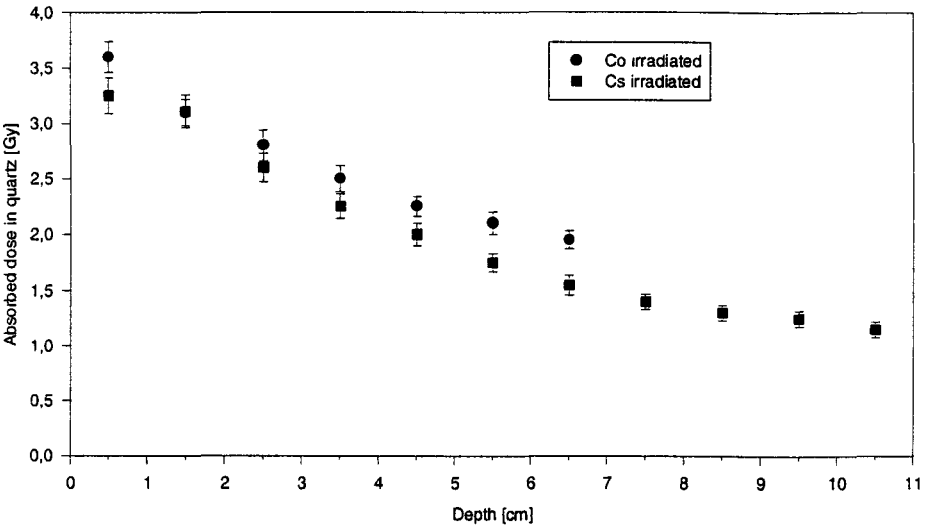

Figure 4: Depth dose obtained from two cores irradiated at Risø - National Lab.

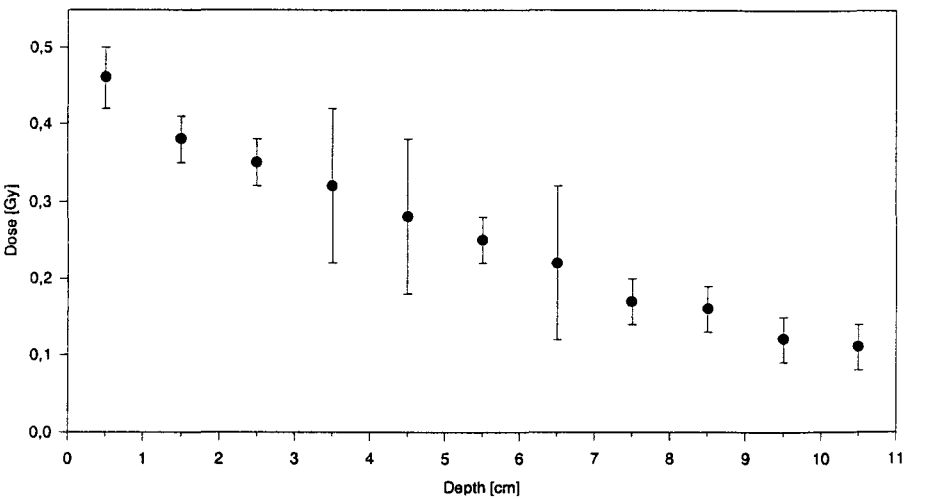

Figure 5: Depth dose profile of a brick from Lomachi (House 2).

10. Providing detailed documentation of methods and procedures for investigations of the survey and standard materials

The following documents containing the detailed methodology and measurements are submitted to co-ordinator and the other partners for future reference.

Annex I - Preparation of natural quartz for interlaboratory beta source calibration
Annex II - Calibration of ^{90}Sr beta source using quartz and porcelain.
Annex III - Interlaboratory comparison:
1. Alpha counting
2. Depth dose distribution
Annex IV - Excursion in 30 km zone: Survey of dosimetric material for retrospective dosimetry
Annex V - Environmental gamma dose measurement at 30 km zone and Pripyat
Annex VI - Radioactive contamination measurements from samples obtained in 30 km zone
Annex VII - The dose assessment from the most shielded locations at Pripyat
Annex VIII - The list of the samples at GSF

IV. Publications

a- Publications arising directly from the work of the contract

1. Hütt G., Brodski L., Bailiff I.K., Göksu H.Y., Haskell E., Jungner H. and Stoneham D. (1993) Accident dosimetry using environmental materials collected from regions downwind of Chernobyl: A preliminary evaluation. Radiat. Prot. Dosim. 47, 307-311.
2. Stoneham D., Bailiff I.K., Brodski L., Göksu H.Y., Haskell E., Hütt G., Jungner H. and Nagatomo T. (1993) TL Accident dosimetry measurements on samples from the town of Pripyat. Nucl. Tracks Radiat. Meas. 21, 195-200.
3. Wieser A., Göksu H.Y., Regulla D.F., Vogenauer A. (1994) Limits of Retrospective Dosimetry by EPR and TL with natural materials. Radiation Measurements Vol 23, Nos 2/3 509-514.
4. Göksu, H.Y. Bailiff, I, .Bötter Jensen, L, Hütt, G.: Interlaboratory beta source calibration using TL and OSL on natural quartz, in print Radiation Measurements (1995).
5. Bulur E., Göksu H.Y., Wieser A., Fiegel M.: Thermoluminescence properties of fluorescent material used in commercial lamps. Presented at 11th International Symposium on Solid State Dosimetry; Budapest 8-11 July 1995, submitted for publication.
6. Meckbach R., Bailiff I. K., Göksu H.Y., Jacob P., Stoneham D.: Calculation and Measurement of dose depth distribution in bricks. Presented at 11th International Symposium on Solid State Dosimetry; Budapest 8-11 July 1995, submitted for publication.
7. Göksu H.Y., Wieser A., Stoneham D., Bailiff I.K. and Figel M.: EPR, OSL, TL and spectral studies of Porcelain.; 4th International Symposium on EPR Dosimetry and Applications, 15-19 May 1995, München-Neuherberg , submitted for publication.
8. Göksu H.Y., Heide L.M., Bougrow N.G., Dalheimer A., Meckbach R. and Jacob P.: Depth dose distribution in bricks determined by thermoluminescence and by Monte Carlo calculation for dose reconstruction. Submitted for Publication in Applied Radiation and Isotopes(1995).
9. Egersdörfer S., Wieser A. and Müller A.: Tooth enamel as a detector material for retrospective EPR dosimetry. Submitted for Publication in Applied Radiation and Isotopes (1995).

b. Publications related to the work

1. Göksu H.Y., Regulla D. and Vogenauer A. (1993) Reconstruction of gamma dose distribution in salt at radioactive waste disposal site by the water insoluble fraction. Radiat. Prot. Dosim. 47, 331-333.
2. Regulla, D.F., Göksu, H.Y., Vogenauer, A. Wieser, A. (1994) Retrospective dosimetry based on egg shells. Appl. Radiat. Isot. Vol 45, No3, pp 371-373.
3. Wieser A., Haskell E., Kenner G., Bruenger F. (1994) EPR dosimetry of bone gains accuracy by isolation of calcified tissue. Appl. Radiat. Isot., Vol. 45, pp 525-526.
4. Wieser A., Göksu H.Y., Regulla D.: EPR Dosimetrie mit Knochen und Zähnen , Strahlenschutz: Physik und Messtechnik, Fachverband für Strahlenschutz e.V., pp 175-180, ISSN 1013-4506 Band II, 26. Jahrestagung Karlsruhe, 24-26 Mai 1994.
5. Fiegel M., Göksu H.Y. Wieser A., Regulla D.: Die Pre-Dose Thermolumineszenzmethode in der retrospektiven Dosimetrie., Strahlenschutz: Physik und Mess-technik, Fachverband für Strahlenschutz e.V., pp 629-633, ISSN 1013-4506 Band II, 26. Jahrestagung Karlsruhe, 24-26 Mai 1994.
6. Göksu H.Y., Wieser A., Stoneham D., Bailiff I.K. and Figel M.: EPR, OSL, TL and spectral studies of Porcelain.; 4th International Symposium on EPR Dosimetry and Applications, 15-19 May 1995, München-Neuherberg , submitted for publication.
7. Bulur E., Wieser A., Göksu H.Y.: Some Electron Spin Resonance Observation on Tooth Enamels, in print (1995).

Unpublished documents

1. Göksu H.Y. (1993) Application of thermoluminescence pre-dose method: From Hacilar to Chernobyl. Munich, LMU.
2. Wieser A.: Potentials and limitations of retrospective EPR dosimetry. Presented at workshop on Dose Reconstruction , Bad Honnef, June 6-9, (1994).
3. Göksu H.Y.: The limits of luminescence techniques with domestic materials for retrospective dosimetry. Presented at workshop on Dose Reconstruction , Bad Honnef, June 6-9, (1994),

Head of project 3: Doreen Stoneham

II Objectives for the reporting period

- The development of thermoluminescent routines for accident dose evaluation, using environmental materials
- The adaptation of porcelain testing procedures for accidental dose evaluation
- Investigation of TL properties of ceramic materials
- Preliminary dose evaluations using TL methods
- Comparison between standard methods of internal dose measurments
- Interlaboratory beta-source calibration using quartz grains irradiated at GSF
- Establishment of a protocol for interlaboratory calibration using porcelain slices

III Progress achieved

Introduction
The objectives were achieved using samples obtained on field trips to the contaminated regions of the Ukraine and Belarus. The achievements are summarised on the following pages and more detail may be found in the following Appendices

Appendix 1	Samples
Appendix 2	TL Normalisation of porcelain slices using Partial Activation
Appendix 3	Internal Dose-rate Data A comparison between laboratories and methods.
Appendix 4	Development of a protocol for an interlaboratory calibration of porcelain slices.
Appendix 5	Calibration of beta sources using the thermoluminescence (TL) of quartz.
Appendix 6	Dose determinations and TL data for samples collected 1990, 1991 and 1993.
Appendix 7	Radionuclide contamination found in two samples from Pripyat.

The samples
Almost 200 samples were collected from settlements in the exclusion zone. The major component of the collection came from a wide number locations, both internal and external, in the town of Pripyat. Two locations were studied in depth: 15 Druzhby Narodov- a 9 storey apartment block in Zone 1 and 18 Lenin Prospect, a 5 storey apartment block in Zone 1. A list of samples may be found in the Appendix. A small proportion of these was selected for study

The collection consists of low-fired terracotta objects such as brick and plantpots, and porcelain, principally light holders, insulators, and some fuse holders It was found that in heavily contaminated regions, such as the Red Forest, there was considerable penetration by particulate radionuclides into bricks presumably carried there by rainwater (See Appendix) The collection is dominated with porcelain samples because of the risk of absorbed particulate contamination, and also because in many locations, particularly relatively new settlements, there is a lack of

quartz/feldspar bearing building materials as concrete and mortar predominate and methods for dose evaluations in these materials have not yet been developed. However porcelain electrical fitting could be found in all locations.

Experimental

Dose evaluations were made using the fine-grain technique and quartz inclusion techniques for pottery and terracotta samples and pre-dose techniques for porcelain slices.

Fine-grain technique

Approximately 200mg of powder were drilled from the samples using a hand-held drill with a tungsten carbide bit. The powder was washed in dilute acetic acid to remove carbonates, the acid poured off and the sample washed in distilled water and centrifuged so that the washing water could be poured off easily. The washing procedure was repeated 3 times and a final washing/centrifuge carried out using acetone to remove the last traces of water. Grains between 4-10μm were selected by allowing the treated sample to settle in acetone between 2 and 20 minutes; after 2 minutes the grains larger than 10μm settled at the bottom of the test-tube and after 20 minutes only grains smaller than 4μm were still in suspension and were discarded. The required fraction was deposited onto 12-24 aluminium discs for TL measurement.

Measurements were made in a Riso automated reader using a photomultiplier fitted with a Corning 7-59 filter. Laboratory irradiations were performed with 40mCi Sr-90 beta sources and alpha irradiations with an off-plate 5μmCi Am-240 source. Preheat treatments were arbitrary - either 100°C for 5 minutes or 150°C for 100 seconds. Both pre-heats were satisfactory and the majority of plateaux started at 200°C and extended to 500°C.

Quartz Inclusion technique

Samples were crushed and sieved to obtain a size fraction between 90-150μm and soaked in 1 molar HCl to remove carbonates. Grains were then etched in concentrated HF for 40 minutes swirling every 5 minutes to ensure even etching. Samples were rinsed in distilled water and wet sieved to remove grains less than 90μm. The remaining samples were rinsed in acetone and dried. Heavy liquid separation (sodium polytungstate) was used to separate the quartz fraction, density <2.58>2.7g/cc. Grains were mounted on stainless steel using silicon oil for TL measurement. There were approximately 6mg of sample on each discs and 24 discs were prepared for each sample. A pre-heat of 150°C for 100 secs was used.

Porcelain

9mm diameter cores of porcelain were extracted using a diamond core drill cooled under running water. The cores were mounted in hollow Tuflon resin tubes using acrylic glue. When the glue had dried (several hours) the cores were cut into 200-300μm thick slices using a Buehler low speed saw fitted with a diamond impregnated wheel; cooling was by means of a waterbath. The remains of Tuflon and glue were removed by soaking the slices in acetone and several washings of acetone. After drying, the slices were supported on platinum cups for TL measurements. The preferred TL method for low doses (less than 1 Gy) is the pre-dose technique. For higher doses, certain high temperature peaks were utilised for additive dose methods but this has not been investigated systematically. All measurements were made using a Corning7-59 filter.

The pre-dose technique

Thermal activation characteristic (TAC) was the first part of the TL procedure to determine the temperature of maximum activation. The sensitivity of the 110°C peak was monitored as the sample was heated in steps to a maximum activation temperature of 670°C. Both Additive Dose (AD) and single aliquot multiple

activation (MA) methods were applied where possible but otherwise only the MA method was used: several single slice measurements being made with up to 8 activations for each slice.

TL Dose evaluations and characteristics

Fine-grain analysis
This method proved successful for most of the lower fired samples such as plantpots and bricks. Accrued doses ranged from 0.25-6Gy. Sensitivities were defined as the number of photons/channel/100mGy. Channel width was 2°C. Values ranged from 0.5 to 10. The lowest sensitivities were seen on a stoneware tile - high firing often reduces the sensitivity of high temperature peaks - and on some bricks which were later investigated for inclusion work and which proved to have very little quartz. The highest sensitivities recorded were for tiles where the 220°C peak dominated the glow-curve. This peak was used for analysis.

Quartz Inclusion measurements
Ten samples were selected for further study, based on their fine-grain properties. These samples had all exhibited a spurious signal and had an estimated dose of less than 0.5 Gy using this technique. All ten samples were bricks and came from various locations in the town of Pripyat and from the village of Berezhaki in the Krasnopolye region of Byelorus. An attempt was made to extract quartz inclusions from all samples and carry out a dose evaluation on these inclusions. The method has been described previously. The results are summarised below in Tables 1 and 2.

Results
Fine grain analysis proved to be a practical technique in most cases where the samples were relatively low-fired such as plant-pots, tiles and some bricks. The limiting factors were:

- the sensitivity of the sample (dependent on the concentration of TL minerals, mainly quartz and feldspars)
- the amount of spurious TL present in the glow-curve (affected by contaminants).

Quartz inclusion analysis of low dose/spurious samples brought about limited improvement in the results as a whole because although the spurious signal was removed, there was considerable scatter in results. This is probabably due to the contaminants still present in the etched samples. 91PT30 had marked improvement of the TL properties and the result 0.5±0.04Gy agreed well with the pre-dose results of 0.35 and 0.38Gy.

Points to notice are:
- The final overall yield of sample was very low - between 1-10% of quartz
- Unexpected contaminants such as pollen and asbestos as well as slag and clinker which would have been used to "grog" the clay.
- The variation in yield even within one brick - 91BZ49 was sampled in 5 locations and the quartz yield varied from 1-10%.

There was good agreement with results of 91BZ49; regardless of sampling location the quartz inclusion results were in the range 0.1-0.2Gy and these results agreed with a fine-grain results of 0.14-0.23Gy obtained previously.
In conclusion, fine-grain analysis of low-fired ceramics is feasible and practical with standard deviations usually less than 5%. However quartz inclusion measurements may be required in particular situations and despite the large random scatter this is a viable technique in certain cases, particularly where low sensitivity or spurious TL is present in fine-grains.

Porcelain
The first stage of the procedure is a single slice measurement for each sample to determine the temperature of maximum activation, known as a TAC. A typical TAC is shown in Fig. 1.

Although the samples were from different locations in the Ukraine and Belarus, and of several different types - external insulators from houses and electrical transformers and internal domestic fittings such as fuses, WC's, taps and lamp holders, all exhibited similar features in their TAC:

- The TAC rose to a plateau between 400°C and 500°C to above 600°C.
- There was a second plateau region above 600°C where maximum activation occurred.

For low dose samples (<0.2Gy) there was good agreement between MA and AD results where both methods were employed.

Points to note with the MA technique:

- Linearity was observed using the MA technique with up to 8 activations on each slice and a maximum laboratory applied dose of 2Gy.
- Virtually zero quenching was observed in the samples under study (all <200mGy) so no correction was applied.
- There was very little random scatter on each slice and between slices.

Points to note with the AD technique:

- This is the preferred technique as each slice is heated only once but because up to 24 slices were used to obtain each evaluation it is sometimes not possible to use this method.
- There is much greater random scatter in the build-up curve but this can be minimised by using the method of partial activation to normalise between slices. (see Appendix). Each slice is partially activated to 440°C and the sensitivity of the 110°C peak recorded (S_{440}). The sample is then activated to the maximum activating temperature and the values normalised by S_{440}. This is shown in Fig. 2 below.

Both Additive Dose (AD) and single aliquot multiple activation (MA) methods were applied where possible but otherwise only the MA method was used; several single slice measurements being made with up to 8 activations for each slice. For both methods it is important that the correct activating temperature is determined as dose evaluations will vary with activating temperature.

Although the pre-dose method is ideal for low dose samples, permitting routine dose evaluations of 100mGy or less, saturation effects limit its use for values above 1Gy. However it is of great value for porcelain from all internal locations, which for our field samples, yielded without exception, an accrued dose of less than 0.4Gy. It should be noted that this includes a large - up to 30% or more - internal component from naturally occurring radionuclides in the porcelain matrix, mainly uranium, thorium and K-40. The total internal component is proportional to the age of the object and one advantage of electrical fittings was that the date of manufacture was frequently stamped on the fitment. This eliminated a potential unknown quantity in the dose equation, which could be simplified to: Accident gamma dose = Accrued dose - Age x Internal dose.

A factor which can have a large effect on low dose evaluation is the value of S_0; this is the base-line value for measurement and in some cases can be elevated so that it is

a high proportion of the luminescence. One such case was investigated using the IPD (imaging photon detector) and it was found that the S_O luminescent signal emanated from a different region of the porcelain slice from that associated with luminescence after activation. In such a situation it may be argued that S_O should be taken as zero.

An effective and accurate method of evaluating high doses is currently under investigation and methods using the high temperature peak at 230°C, both as an additive dose method and as a pre-dosing peak appear promising. Phototransferred luminescence using green exciting light also appears as good alternative.

One application of pre-dose analysis of low dose porcelain samples was at 18 Lenin Prospect in the town of Pripyat as shown in Table 3. All samples were taken from internal locations. It should be noted that no account has been taken of the natural environmental gamma dose-rate from before the accident. It was assumed that this was small compared with the internal dose. Measurement in clean regions around the zone, such as Zeleni Mis, indicated a dose-rate of 0.06μSv/hr which would contribute less than 10mGy in 16 years.

Internal Dose measurements: a comparison between different methods.

From Table 3, it can be seen that the internal natural dose component is on average 30% of the accrued dose. Here we are looking at low dose samples (< 200mGy) from 16 year old samples. If the samples were older, the proportion would be even greater. In an attempt to improve the overall accuracy of the fallout dose estimates, the different methods of internal dose determination were compared to see if there were any large discrepancies. The methods currently used are thick-source alpha counting for U and Th determination combined with flame photometry for potassium analysis. The results from these two techniques were compared with the results obtained from NAA.

NAA measurements were carried out at Helsinki University, GSF and at an independent laboratory, XRAL. Alpha-counting and flame photometry were carried out at Oxford University. Samples were crushed to less than 37μm for alpha-counting and counted on 42mm zinc sulphide screens. They were measured first unsealed and then sealed for 2 weeks before recounting; the counting in each case continued until the total number of pairs was over 100 - this normally took about 1 week and around 3000 total counts were recorded. The data were broken into two main groups for comparison; potassium analysis and uranium/thorium analysis. These group were further subdivided so that the results from the different laboratories could be compared.

Potassium

Table 4 compares Oxford (OX), Helsinki (HU) and GSF laboratories. XRAL did not issue any potassium analyses. There was good agreement between the three laboratories and between the techniques; the ratios, OX/HU 1.01±0.21 and GSF/HU 0.93±0.16 lying within one standard deviation. It should be noted that Oxford and Helsinki shared the same aliquot of sample but GSF was independent. In addition, the samples in common between GSF and HU were all WC porcelain which came from one location but OX and HU had a mixture of bricks, stoneware tiles and porcelain from different locations in Pripyat and Belarus.
In conclusion it appears that either method is suitable and the standard deviation is ±20%.

Uranium and thorium

All results are shown in Table 4. Oxford (OX) used alpha-counting and flame photometry and Helsinki University (HU), GSF and XRAL used neutron activation.

Oxford and Helsinki and Oxford and XRAL used portions from the same aliquot of prepared sample. GSF prepared its samples independently.

1. There is a difference between two NAA laboratories, GSF and HU; the ratios GSF/HU being 1.15±0.23 and 1.26±0.23 for thorium and uranium respectively. However the degree of scatter is large and one standard deviation is approximately 20%.

2. Comparing alpha counting (OX) with NAA (HU and XRAL), there is good agreement with the thorium measurements but in the uranium measurements indicated that the ratio of OX with the other two laboratories is high. This applies to both sealed and unsealed alpha counts. This cannot be due to diseequilibrium as in that case the ratio would be less than unity as NAA measures the beginnng of the decay chain and alpha counting the end, and any radon loss would affect alpha counting but not NAA. Reasons could be (i) errors are introduced as the alpha counters are calibrated using a thorium sand; there was no corresponding calibration using a uranium sand (ii) there could be overcounting in the alpha counting procedure due to radon being trapped under the sample (iii) there could be undercounting by the NAA laboratories iv) in alpha-counting, pairs counting is used for calculations and fast pairs are only a small percentage of the total pairs - 100 pairs are allowed to accumulate and these are dominated by slow pairs. Statistically this may not be sufficient. Very recently there has been evidence to show that this may be the case and work is in progress to verify and if necessary, to rectify this problem.

3. Two samples were measured using the previous two techniques and also examined using gamma spectrometry (Table 6). Broadly speaking there is good agreement between the unsealed counts and the other two methods but for one sample (49) there is no agreement between the potassium content between any two methods. In this case the potassium content was high and it is possible that this could be a problem.

4. Comparing whole counts (rather than attempting to compute the Th and U contents separately) (Table 5), indicates that alpha counting predicts a 14% greater beta contribution and 16% greater alpha contribution than NAA regardless of whether the sample is sealed or not.

Based on the above it is recommended that any convenient form of potassium analysis may be used but that both alpha counting and NAA be used for the U/Th measurements. The mean of the two values should be used with an error limit of 7.5%. This means that in such cases as Lenin Prospect where the internal dose is 30% of the accrued dose, the error will be less than 2% when the potassium values are taken into consideration along with the alpha-counting.

Interlaboratory beta source calibration

1. Quartz grains.
Samples of quartz grains which had been irradiated at GSF, Munich, were used to calibrate the laboratory beta sources atttached to two Riso automated TL sets in operation at Oxford. These are designated sets II and III. The results (1 std.dev.) are as follows:

High temperature

Set	Grain Size	Dose Rate (Gy min-1)
II	90-150μm	1.94±0.095
II	150-200μm	2.03±0.055
III	90-150μm	1.88±0.088

The dose-rate from the laboratory calibration of Riso II for grain sizes 90-150μm was 1.93±0.06 Gy/min giving a ratio of OxfordGSF calibration = 0.996 - agreement to within less than 1%. The previous calibration of Riso III was 1.77 Gy/min giving a ratio of Lab/GSF of 0.94. The 6% discrepancy in this case is not surprising since original Riso III calibration had been derived by comparison with Riso II using quartz fine-grains instead of by direct measurement.

The dose-rate to 150-200μm grain size is predictably some 5% higher than for the 90-150μm grain size due to build-up as noted by Aitken and Wintle in earlier publications.

2. Porcelain slices

An interlaboratory calibration protocol for determining the dose-rate delivered from a Sr-90 source to slices of porcelain was established at Oxford. Full details are given in the Appendix. Porcelain slices between 200 and 300μm thick, were prepared by an irradiation and heating regime until no further sensitivity changes were observed. They were then packed into fused quartz containers and irradiated at GSF Munich with a Co60 source at a distance of one metre on both sides for equal lengths of time. The total dose was 29.66mGy at the centre. Measurements were made on both irradiated and zero-dose slices (to monitor any small sensitisation changes) as follows.

1. 28 slices are used for each calibration. 14 slices were irradiated with 29.66 mGy with a Co^{60} source at GSF and 14 slices are zero dosed, fully sensensitised slices for sensitivity monitoring.

2. For the first stage, 4 irradiated slices (measure thickness) and 4 monitor slices are arranged on the wheel alternately, with monitor slice first.

3. Calculate closest time to give monitors 30 mGy and irradiate them. Glow all discs to 500°C. Irradiate all discs with same dose as before, glow again and also glow blackbody.

4. Integrate under peak for 11 channels and calculate dose-rate compensating for thickness (in gamma irradiated discs only) and sensitivity changes.

5. Repeat using 10 slices of each type and new calibration.

6. Take 4 used slices and give 30mGy. Store for same length of time as has elapsed since irradiation.

7. Measure as before with alternate monitor slices. to determine degree of fading. Use to compensate in final calibration calculation.

Conclusions

Thermoluminescence is a viable method of dose evaluation in accident dosimetry. Analysis of both low-fired ceramics and porcelains from a variety of internal and external locations has been possible and dose evaluations from 0.1 to 6Gy made on samples downwind of the Chernobyl NPP. It is recommended that porcelain is less likely to have absorbed radionuclides in regions of high fallout in exterior locations and these samples should be collected in preference to bricks.

Fine-grain, quartz inclusions and pre-dose methods are all valid although for high dose porcelain samples other methods have to be developed as the pre-dose technique is non-linear above 1Gy.

Publications

Stoneham D., Bailiff I.K., Brodski L., Goksu H.Y., Haskell E., Hutt G., Jungner H. and Nagatomo T (1993) TL Accident dosimetry measurements on samples from the town of Pripyat. Nucl. Tracks Radiat. Meas. **21**, 195-200

Hutt G., Brodski L., Bailiff I.K., Goksu Y., Haskell E., Hutt G., Jungner H and Stoneham D. (1933) Accident dosimetry using environmental materials collected from regions downwind of Chernobyl: A preliminary evaluation. Radiat. prot. Dosim. **47**, 307-311

Stoncham, D. (1995) Accident dosimetry using porcelain: TL analysis of low dose samples. Radiation measurements.

Meckbach R., Bailiff I.K., Goeksu H.Y., Jacob P., Stoneham D. Calculation and Measurement of dose depth distribution in bricks. Presented at 11th International Symposium on Solid State Dosimetry: Budapest 8-11 July 1995. Submitted for publication.

Goeksu H.Y., Wieser A., Stoneham D., Bailiff I.K. and Figel M. EPR, OSL, TL and spectral studies of Porcelain. 4th International Symposium on EPR Dosimetry and Applications, 15-19 May 1995, Muenchen-Neuherberg, submitted for publication.

Table 1: Quartz inclusion results: yield and other constituents.

Sample Ref.	Sample section	Yield of 90-150μm grains (%)	Yield of etched from 90-150μm (%)	Overall yield from original sample (%)	Other constituents and TL Minerals
91PT4	whole	8	13.4	1	pollen, 85% matrix, 10-15% quartz
91PT27	whole	10	31	3	pollen asbestos slag and clinker 75% matrix 25% quartz
91PT28	front	11	34	3.7	90% matrix 10% quartz
91PT28	rear	12	35	4.2	<20% matrix 80% quartz 1-2% feldspars
91PT29	front	19			
91PT29	back	11			
91PT30	whole	12			
91PT31	whole	23	8	1.8	
91BZ48	whole			1	
91BZ49	surface 2mm	12	47 6	5.6	
91BZ49	top	7.5	38 3	2 9	
91BZ49	bottom	14.5	39	5.6	
91BZ49	rear	17.5	54 1	9.4	
91BZ49	side	13	42 7	5.6	
91BZ50	whole	19			
91BZ51	whole	10	47	4 7	95% quartz <5% matrix trace feldspars

Table 2: Quartz inclusion results: accrued doses

Sample	Q INC (GY)	AD (GY)	MA (GY)
91PT4	0.6±0.1	0.8±0.2	0.65±0.11
91BZ49 F	0.16±0.04		
91BZ49 B	0.13±0.07		
91BZ49 SIDE	O.11±0.03		
91PT30	0.5±0.1	0.35±0.06	0.38±0.11
91PT28	0.6±0.1		
91PT27	0		

Table 3: Dose evaluations of interior porcelain samples from 18 Lenin Prospect.

No.	Location	Sample	Act.Temp	MA (Gy)	AD (Gy)	Int. Dose (Gy)	Excess Dose (Gy)
1	1/F/Bed	Switch	657	0.15		0.05	0.1
6	5/F/Bed	Switch	657	0.17		0.062	0.11
7	5/B/Bed	Switch	657	0.13	0.18	0.059	0.11
14	1/R/Bed	Switch	636	0.16	0.15	0.05	0.11
15	5/F/Bed	Switch	625	0.11	0.14	0.04	0.09
16	1/F/Kit	Tap	657	0.17		0.049	0.12
17	1/B/Kit	Tap	657	0.14		0.052	0.09
18	1/B/Kit	Tap	636	0.13	0.15	0.052	0.09
21	5/B/WC	Top	657	0.18	0.14	0.048	0.11

Table 4: Internal dose measurements: Comparison between laboratories and methods

RATIO	TH unsealed	TH sealed	U unsealed	U sealed	K
OX/XRAL	1.02±0.12	1.11±0.13	1.29±0.12	1.22±0.1	
OX/HU	0.84±0.11	1.04±0 27	1.3±0.15	1.23±0.14	1 01±0.21
GSF/HU	1.15±0.23		1.26±0.23		0.93±0.16

Note: OX alpha-counting and flame photometry
HU/XRAL/GSF NAA

Table 5: Internal dose measurements: Alpha and beta dose-rate comparison

ALPHA unsealed	BETA unsealed	ALPHA sealed	BETA sealed
1.16 ±0.06	1.14±0.07	1.16±0.06	1.14±0.07

Table 6: Internal dose measurements: Comparison between three methods

SAMPLE	27			49		
	TH	U	K	TH	U	K
G-SPEC	6.47	3.62	1.54	7.8	1.96	2.95
A-US	4.96	5 55	1 59	7.9	2.57	4.4
A-S	5.78	5.9		12.4	1.87	
NAA	6.57	4 17	1 82	7.9	2.02	3 72

Fig.1

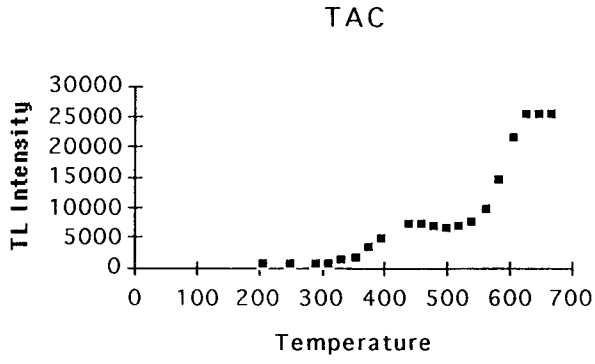

Fig 2. Normalisation using Partial Activation

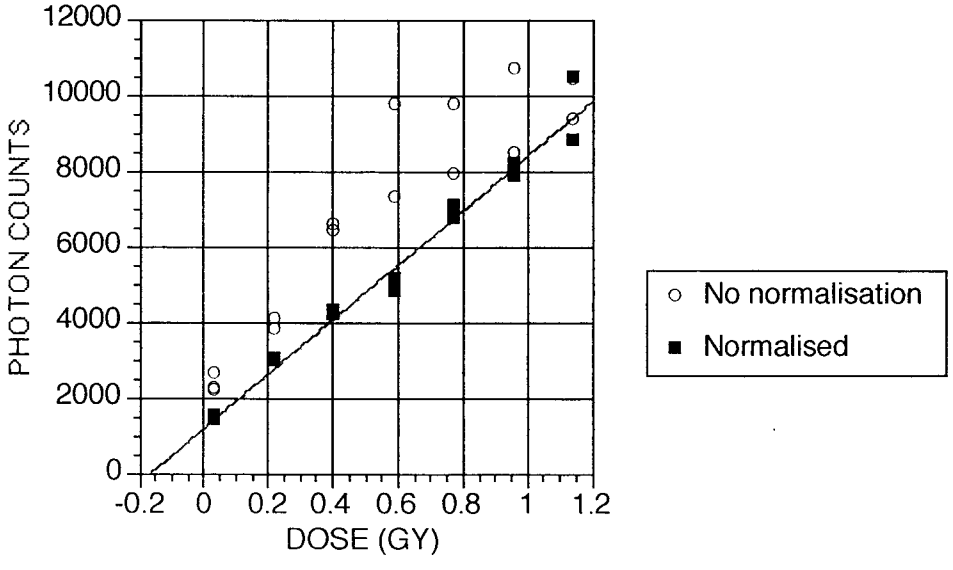

Head of Project 4: Dr. Bøtter-Jensen

II. Objectives for the reporting period

a) Development of OSL apparatus and techniques
b) OSL dosimetry characteristics of quartz
c) OSL sensitivity changes in quartz as a result of annealing
d) OSL dosimetry characteristics of feldspars
e) OSL dosimetry characteristics of unseparated brick materials
f) OSL dosimetry characteristics of porcelain

III. Progress achieved including publications

Optically stimulated luminescence (OSL) techniques especially aimed at using natural materials for retrospective reconstruction of accidental radiation doses in populated areas were developed and studied at Risø as part of this project. Quartz and feldspars separated from building materials, such as bricks and tiles, in addition to porcelain items had their OSL signals measured using different light sources for stimulation to assess radiation doses received by the material. Radiation doses were also evaluated from OSL measured directly on unseparated samples i.e. directly from the surface of brick and tile materials. Dr. H. Jungner, University of Helsinki, Finland, was assigned to the project under a subcontract with Risø.

a) Development of OSL apparatus and techniques

The apparatus used for the experimental work were mainly OSL units developed as attachments to the existing automated Risø TL reader and include monochromators for obtaining wavelength resolved luminescence measurements. An automatic OSL scanning instrument was also developed with the aim of being able to perform continuous OSL scanning measurements of brick cross-sections, allowing radiation depth dose profiles to be measured directly.

The basic OSL unit developed contains light sources for both green light and infrared stimulation, enabling measurements of OSL signals from both quartz and feldspar samples. Green light stimulated luminescence (GLSL) is achieved by illumination with a filtered light spectrum from a halogen lamp using exchangeable excitation and detection filter packs. The GLSL unit is designed to select a green light stimulation wavelength band using excitation filters extending to as low a wavelength as possible while still being sufficiently separated from the luminescence emission spectrum. The infrared stimulated luminescence (IRSL) is generated by an infrared diode array (peak emission of 875 Δ 80 nm) placed close to the sample. While GLSL can be used with both quartz and feldspars, IRSL seems only to work with feldspars.

Ideally, however, the spectral excitation and emission characteristics of quartz and feldspar materials prepared for dosimetric evaluation would be routinely scanned since this would also allow the possibility of choosing the most suitable energy windows in which to carry out the measurements. A compact module was developed that allows for the monochromatic illumination of samples in the wavelength range 380 to 1020 nm, enabling the measurement

of energy resolved OSL (Bøtter-Jensen et al. 1994). This unit can be directly coupled to the existing automated Risø TL/OSL system. The unit can also be used for recording wavelength resolved emission spectra, whether photo excited or thermally stimulated. A schematic diagram of the combined OSL attachment is shown in Fig. 1A.

A continuous OSL core scanner system was developed that allows the optical sensors to be moved across either sediment or brick cores. The optical sensor system consists of a photo-excitation and detector module together with lamps for bleaching and regenerating OSL. Photo excitation is made using a filtered halogen lamp generating a green wavelength band (420-550 nm) and the brick core is scanned using an excitation slit beam of 10 mm x 1 mm which determines the resolution of the system. OSL dose normalization is made either by using short wave UV light from a 20 W low pressure HG lamp or exposing the brick cores to a Cs-137 gamma field and afterwards scanning the OSL sensitivity across the brick profile. A schematic diagram of the OSL scanner system is shown in Fig. 1B.

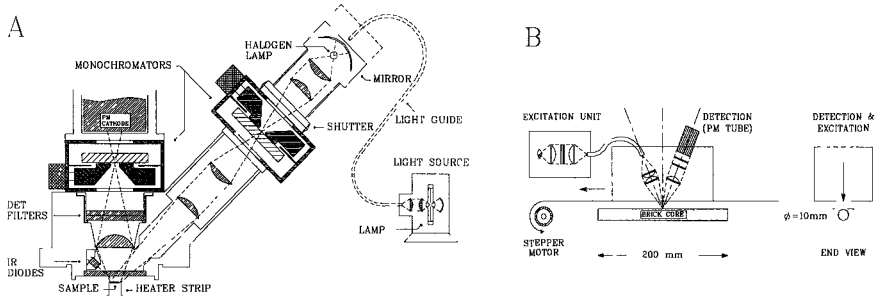

Fig.1.
(A) Schematic diagram of the OSL attachment showing the excitation lamp system with monochromators mounted on both the excitation side and the detection side.
(B) Schematic diagram of the automatic OSL brick core scanning system: the excitation beam is 1 mm wide.

b) OSL dosimetry characteristics of quartz

The OSL signal from quartz stimulated with green light is typified by a bright, rapidly decaying curve. The OSL sensitivity of quartz depends very much on the thermal history of the material, with annealed (or fired) samples giving up to an order of magnitude larger signals than unheated samples (e.g. sedimentary quartz). An attempt to determine the lower detection limit for OSL stimulated with green light on fired quartz was made by obtaining the dose response curves for a variety of quartz samples extracted from different specimens such as bricks, burnt stones and clay. An example of OSL versus dose for a sensitive quartz extracted from burnt clay obtained using the multiple aliquot method is shown in Fig. 2A. As seen, the lowest detectable dose for this material is well below 1 mGy.

The accumulated "natural" dose induced in quartz by radionuclides contained in brick materials and the environmental gamma radiation was measured using GLSL on extracted quartz samples. This experiment was aimed at determining the lower detection limit for an additional dose received by a typical building brick as a result of radioactive release from a nuclear accident taking into account the GLSL signal created by the natural background dose. A brick was chosen from an outer wall of a laboratory building at Risø which was known to be about 40 years old. The quartz grains were extracted from the material and the absorbed dose was determined by GLSL using the additive dose technique. As seen from the dose response curve in Fig. 2B the dose was estimated to be about 200 mGy which is in very good agreement with the expected value based on an annual dose rate of about 5 mGy/y from the environmental radiation and the natural radioactivity in a typical brick. For this particular brick the lower detection limit for an additional accidental dose would be of the order of 20 mGy (10% above the background).

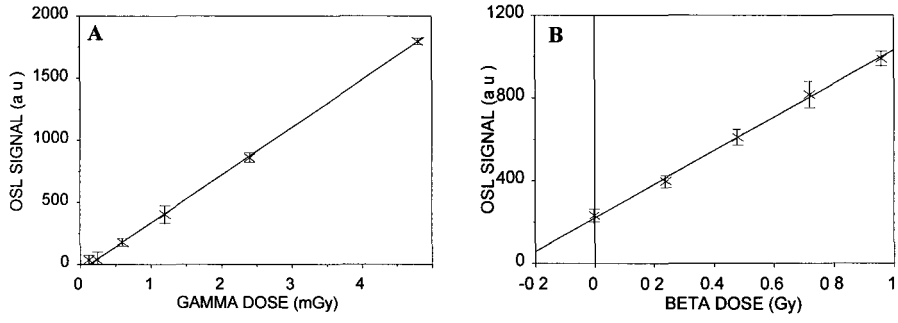

Fig.2.
(A) OSL versus ^{60}Co gamma dose (multiple sample technique) for quartz extracted from a burnt stone.
(B) OSL growth curve (multiple sample technique) for quartz extracted from a 40 years old brick.

A typical stimulation spectrum (OSL versus stimulation wavelength) for a sedimentary quartz annealed at 800°C obtained over the wavelength range 400 to 700 nm using the Risø developed monochromator and with detection using U-340 filters is shown in Fig. 3A. As seen there is a linear relationship between the logarithm of the intensity and the stimulation photon energy within the range 1.9-2.5 e.V. Essentially the same relationship of ln(I) vs E is found for both annealed and unannealed quartz.

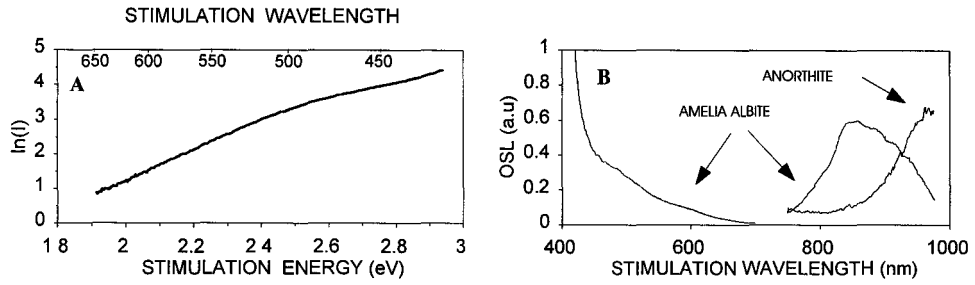

Fig.3.
(A) OSL stimulation spectrum for sedimentary quartz.
(B) OSL stimulation spectra for different feldspars.

c) OSL sensitivity changes in quartz as a result of annealing

Retrospective dosimetry using optically stimulated luminescence on quartz extracted from (for example) bricks needs to account for strong OSL sensitivity changes which are known to occur depending on the previous thermal treatment of the sample. Nonheated quartz exhibits orders of magnitude less OSL per unit radiation than that for heated material. The reason these temperature-induced sensitivity changes occur in quartz is presently not well understood.

At Risø we have studied the effect of high temperature annealing on the OSL and photo-transferred TL (PTTL) signals from natural sedimentary quartz, and from synthetic quartz. Sedimentary quartz was chosen for the study since it is thought unlikely to have undergone any high temperature annealing in nature. Likewise, synthetic quartz was examined since it is known not to have been subjected to any pre-dose, or high temperature annealing, prior to the study. The measurements indicate that the sensitivity enhancement observed can be satisfactorily explained by mechanisms involving alterations of the recombination centre concentrations. Computer simulations of the possible effects we made have shown to produce data which agree in all essential details with the experimental observations.

The intensities of OSL and PTTL (110°C TL peak created after green light illumination) are plotted as functions of the preirradiation annealing temperature for a typical sedimentary quartz sample in Fig. 4A. Nearly identical curves were obtained for other sedimentary quartz samples. As can be seen, the OSL and PTTL signals show nearly identical curves and it is noted that two distinct maxima of the OSL and PTTL sensitivities appear in temperature ranges which are coincident with the known phase changes of SiO_2, namely the α-ß quartz transition at 573°C and the ß quartz-$ß_2$ tridymit transition at 870°C.

To see whether the enhanced OSL sensitivity observed in sedimentary samples is an effect of the previous irradiation (pre-dose) to which the samples had been subjected in nature, synthetic quartz was also studied. OSL intensities versus annealing temperature for pre-irradiated (50 Gy ^{60}Co gamma radiation) and non-irradiated synthetic quartz samples are plotted in Fig. 4B. As can be seen, the two curves show a dramatically enhanced sensitivity at high temperatures similar to that for the sedimentary quartz, even for the sample that received no pre-dose. This observation, together with the fact that both curves in Fig. 4B are almost identical, suggests that the pre-dose effect, if present at all, is a minor, secondary effect and not the main cause of the large sensitivity enhancements observed with these materials.
Fig. 4

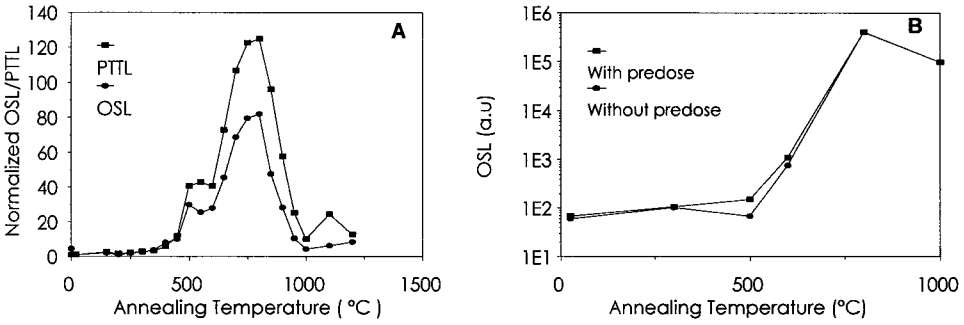

(A) OSL and PTTL sensitivity as a function of annealing temperature for a sedimentry quartz sample (test dose : 3 Gy).
(B) OSL versus annealing temperature for synthetic quartz. One curve is for samples that did not have a pre-dose, and the other for samples with a pre-dose (50 Gy). Test dose : 3 Gy.

d) OSL dosimetry characteristics of feldspars

The majority of feldspars show a wider dose response with higher saturation levels than that of quartz. However, certain feldspars suffer from "anomalous fading" and potassium-rich feldspars may also suffer from long term instability. For dosimetric measurements coarse-grained K-rich, N-rich and plagioclase components of feldspars are normally separated using heavy liquids and analysed independently, the reason being that the dosimetric properties of the three are significantly different. In addition to external radiation doses, the K-rich grains receive an internal dose due to the decay of ^{40} K, whereas certain plagioclase minerals are often unsuitable as dosemeters because of long term instability.

In contrast to quartz, the stimulation spectra for feldspars are much more complex. Fig. 3B shows the optical stimulation spectra we obtained from albite and anorthite feldspars using the Risø monochromator over the wavelength range 400 to 1000 nm with detection using U-340 filters. The characteristics obtained for the albite in the infrared range correspond well to previously reported spectra for alkali feldspars namely the appearance of an infrared resonance

at about 850 nm indicating the suitability of using infra red light emitting diodes (LED) as a stimulation light source.

e) OSL dosimetry characteristics of unseparated brick materials

Accident dosimetry requires rapid evaluation of doses received by the population, so attempts have been made at Risø to measure OSL signals directly from unseparated materials e.g. bricks, tiles and pottery, rather than producing samples using chemical separation techniques. Depth-dose profiles in bricks were determined by measuring the OSL signals directly from the unseparated material across the brick (Bøtter-Jensen et al., 1995). To simulate the effect of a nuclear accident, modern bricks were annealed at 500°C to remove any previously acquired TL/OSL signal and then exposed to 5 Gy ^{60}Co and ^{137}Cs photon radiation fields, respectively. After irradiation, 8 mm diameter cores were drilled out of the bricks and sliced into 1 mm thick circular discs using a diamond saw. Each disc, representing a particular depth in the brick, had its OSL measured directly from the surface of the unseparated material. An example of the normalized OSL as function of depth into the brick material is shown for a ^{137}Cs irradiated brick in Fig. 5A. The fitted exponential curve also shown, correspond well with the expected attenuation in brick material.

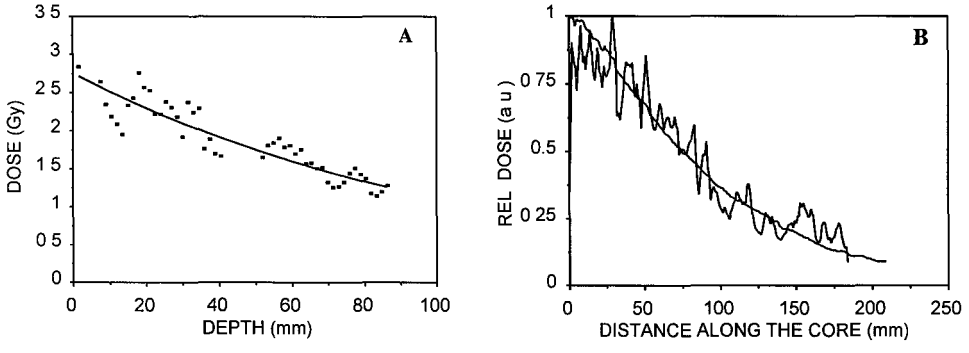

Fig.5.
(A) Dose versus depth into a brick irradiated with ^{137}Cs gamma radiation from one side. Measurements were made using green light OSL on 8 mm x 1 mm slices cut from a core through the brick.
(B) Relative depth dose profile into the same brick from ^{137}Cs gamma radiation exposed from one side and subsequently measured with the automatic OSL core scanner. The attenuation curve calculated by the Monte Carlo code MCNP is shown for comparison.

The automatic core scanner system was used to measure the depth dose profiles across the 200 mm length of a modern brick exposed in the laboratory to ^{60}Co and ^{137}Cs gamma radiation doses, respectively. 10 mm cores were drilled from the brick after irradiation and mounted directly under the light sensing head of the core scanner. Normalization was made after bleaching the cores by exposing the cores perpendicularly to a Cs-137 gamma field. Fig. 5B shows an example of a depth dose profile obtained from OSL scanning of a core taken from a brick that had been exposed from one direction in the laboratory to ^{137}Cs radiation (10 Gy). The Monte Carlo calculated (MCNP code) attenuation curve for the same irradiation geometry is shown as well and as seen it compares well with the experimentally obtained curve.

f) OSL dosimetry characteristics of porcelain

In view of the relevance of using OSL on porcelain in the field of retrospective dosimetry, we studied materials from a collection of mass produced ceramics that we consider would be representative of materials commonly found in many households. The materials are divided in: (i) common table ware; (ii) oven ware; (iii) sanitary ware, and (iv) wall/floor tiles. Both the glazing and main ceramic of these products were analysed.

It was examined whether signatures in the luminescence spectra of a particular sample can give ready information about the dose sensitivity, a method that might be used to ensure that, in a contaminated site, only highly sensitive materials are removed for retrospective dose evaluation.

In all experiments, the samples were drilled with a diamond-tipped tubular saw to create a short cylinder of material, diameter 8 mm, and this was subsequently cut into slices (thickness 1 mm) using a diamond edged, water cooled circular saw. All luminescence and dose measurements were carried out in the automated Risø TL/OSL reader equipped with compact scanning monochromators, usable in the wavelength range 380-1020 nm. UV stimulation for photoluminescence measurements was provided by a broad-band 75 W tungsten source, filtered with 6 mm standard Hoya U-340 (giving a narrow band centered at 340 nm).

The OSL excitation spectrum, i.e. OSL versus excitation wavelength, of typical porcelain samples were obtained using the Risø scanning monochromator (visible range 400-750 nm) attached to the stimulation light source. Typically, a smooth broad stimulation resonance was found peaking around 500 nm and thus very suitable for the Risø standard filtered halogen lamp system producing a broad stimulation wavelength band from 420 to 550 nm.

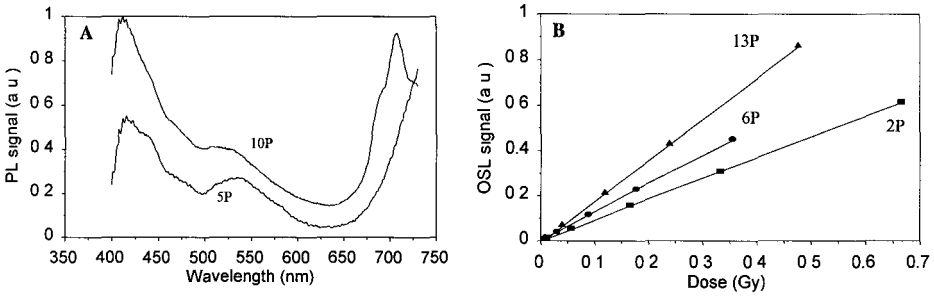

Fig.6.
(A) PL spectra (PL versus wavelength) for two bulk porcelain samples. The emission from Al_2O_3 is clearly demonstrated by the typical peaks at 410 and 700 nm.
(B) OSL versus ^{60}Co gamma dose for three different porcelain samples.

The time stable photoluminescence (PL) emission spectra were recorded with UV stimulation produced by a halogen lamp, filtered with U-340 filters (peak transmission at 340 nm). Fig. 6A shows PL spectra obtained from 2 different porcelain samples. From comparison with Al_2O_3:C TL material, which has been shown to be an extremely sensitive OSL dosemeter material (Poolton et al.,1995), the emission near 700 nm is almost certainly that arising from the internal transition of Cr^{3+}, a very common impurity in this material. The broader emission seen in this spectral region might also arise from Cr^{3+}, but from regions where the lattice sites are slightly distorted. The broad band peaking at 410 nm corresponds directly with the well know F-center emission in Al_2O_3.

Measured dose response curves, i.e. OSL versus ^{60}Co gamma dose, are shown for three porcelain samples in Fig 6B. For most porcelain samples the OSL signal increases linearly from 10 mGy up to 20 Gy and shows a further sublinear increase up to at least 200 Gy. Green light stimulation allowed doses lower than 50 mGy to be measured with a statistical uncertainty of 10% using the more sensitive porcelain samples. The fading examined over twenty days with successive OSL measurements of pre-irradiated samples every second day was found to be negligible.

A ceramic fuse collected from an accidentally contaminated area was analysed to determine the depth dose profile into the material. An 8 mm diameter core was drilled across the fuse and sliced into 1 mm discs. The normalized "accidental" OSL signals measured from the individual discs versus depth is shown in Fig. 7A. The curve shows a bleaching effect on the OSL signal in the outer layers of the material. From a depth of approximately 2 mm a decaying depth dose profile is clearly seen indicating the incident direction of the radiation.

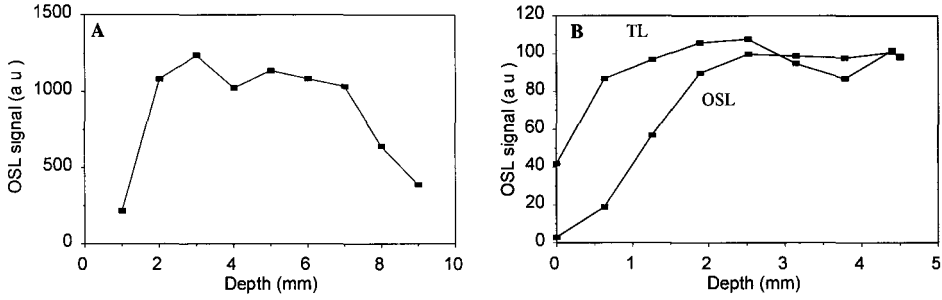

Fig.7.
(A) "Accidental" OSL versus depth into a ceramic fuse. Procedure: Slicing of an 8 mm diameter cross section core into 1 mm thick discs and subsequent measurement of the individual OSL signals.
(B) OSL and TL versus depth into the same porcelain material after exposing a cross section core uniformly to 2 Gy gamma radiation and subsequent placing the core in sunlight for 8 hours.

In order to examine the effect of the transparency of porcelain on the bleaching of the OSL signal caused by ambient daylight reaching into the material, OSL measurements were made on another cross section core drilled from the same ceramic fuse. The porcelain core was given a uniform ^{137}Cs gamma dose of 2 Gy and subsequently placed in sunlight for 8 hours. Discs (0.6 mm thick) sliced from the core had their individual OSL signals measured and the normalized OSL signals are plotted against the depth into the material in Fig. 7B. For comparison, TL measurements were also made on the same discs and TL versus depth is plotted as well. As seen, samples for both TL and OSL measurements must be taken at a depth of at least 2 mm into the porcelain in order to avoid bleaching caused by ambient daylight.

Publications

Bøtter-Jensen L., Poolton N.R.J., Willumsen F., and Christiansen H. (1994) "A compact design for monochromatic OSL measurements in the wavelength range 380-1020 nm". Radiat. Meas. 23, 2/3, 519-522.

Bøtter-Jensen L., Duller G.A.T., and Poolton N.R.J. (1994) "Excitation and emission spectrometry of stimulated luminescence from quartz and feldspars". Radiat. Meas. 23, 2/3, 613-616.

Jungner H. and Bøtter-Jensen L. (1994) "Study of sensitivity change of OSL signals from quartz and feldspars as a function of preheat temperature". Radiat. Meas. 23, 2/3, 621-624.

Bøtter-Jensen L., Agersnap Larsen N., Mejdahl V., Poolton N.R.J., Morris M.F., and McKeever S.W.S. (1995) "Luminescence sensitivity changes in quartz as a result of annealing". Radiat. Meas. (in press).

Bøtter-Jensen L., Jungner H. and Poolton N.R.J. (1995) "A continuous OSL scanning method for analysis of radiation depth dose profiles in bricks". Radiat. Meas. (in press)

Poolton N.R.J., Bøtter-Jensen, L., and Jungner H. (1995) "An optically stimulated luminescence study of porcelain related to radiation dosimetry". Radiat. Meas. (in press).

Poolton N.R.J., Bøtter-Jensen L., and Rink W.J. (1995) "An optically stimulated luminescence study of flint related to radiation dosimetry". Radiat. Meas. (in press).

Bluszcz A. and Bøtter-Jensen L. (1995) "Dosimetric properties of natural quartz grains extracted from fired materials". Radiat. Meas. (in press).

Bøtter-Jensen L. (1995) "Retrospective radiation dose reconstruction using optically stimulated luminescence on natural materials". In Proc. Int. Workshop on Scientific Bases for Decision Making after a Radioactive Contamination of an Urban Environment, Rio de Janeiro and Goiania, Brazil, 29 August-2 September 1994. IAEA TECDOC (in press).

Bøtter-Jensen L. and McKeever S.W.S. (1995) "Optically stimulated luminescence dosimetry using natural and synthetic materials". Radiat. Prot. Dosim. (Invited paper) (in press).

Bøtter-Jensen L, Markey B.G., Poolton N.R.J., and Jungner H. (1995) "Luminescence properties of porcelain ceramics relevant to retrospective radiation dosimetry". Submitted to Radiat. Prot. Dosim.

Markey B.G., Bøtter-Jensen L., Poolton N.R.J., Christiansen H.E., and Willumsen F. (1995) "A new sensitive system for measurement of thermally and optically stimulated luminescence". Submitted to Radiat. Prot. Dosim.

McKeever S.W.S., Bøtter-Jensen L., Agersnap Larsen N., Mejdahl V., and Poolton N.R.J. (1995) "Optically stimulated luminescence sensitivity changes in quartz due to repeated use in single aliquot readout: experiments and computer simulations". Submitted to Radiat. Prot.

CEC project PL 920 125

Project 5: Technical University of Munich, Prof. Dr. Eckehart Nolte

II. Objectives for the reporting period

1. Measurement and calculation of the neutron spectrum of the Hiroshima A-bomb: In order to test contents and predictions of the dosimetry system DS86, the neutron spectrum used in DS86 should be compared with own neutron transport calculations. The calculated neutron spectra should be used to calculate neutron produced radioactivities ^{36}Cl, ^{41}Ca, ^{60}Co, ^{152}Eu and ^{154}Eu which were measured by our group in a granite stone 106 m from the hypocenter. Because of different energy dependences of the neutron capture cross sections, the comparison between measurement and calculations allows the deduction of the neutron spectrum and fluence.
2. Measurement of the global ^{41}Ca bomb peak and development of a general atmospheric transport model: Concentrations of cosmogenic and nuclear weapon produced radionuclides should be measured in the past 60 years. These time profiles should be compared with atmospheric transport calculations for gases and for aerosols in order to deduce time constants for mixing and transport processes in the stratosphere and in the troposphere and to simulate fall-outs for all bomb produced radioactivities, gaseous or attached to aerosols.

III. Progress achieved including publications

1 Measurement and calculation of the neutron spectrum of the Hiroshima A-bomb

1.1 Introduction

Due to the improved Dosimetry System DS86, dose limits have been updated recently. In DS86, disease statistics of survivors of the two bombings of Hiroshima and Nagasaki are compared with doses which are estimated in neutron and gamma transport calculations. Our work was focussed on the comparison of measured and calculated concentrations of radionuclides which were produced by the Hiroshima bomb neutrons in order to deduce the neutron spectrum and the fluence of this bomb and to test the predictions of DS86 for the neutron spectra of the Hiroshima A-bomb.

Basis of our investigations is the measurement of several radionuclides in a granite stone 106 m from the hypocenter of the Hiroshima bomb and of radionuclides in a granite stone of simulation experiments with neutron irradiations at the Munich research reactor. The long-lived radionuclides ^{36}Cl and ^{41}Ca from the Hiroshima granite stone were detected with the high-sensitive technique of accelerator mass spectrometry (AMS) at Munich accelerator laboratory.

1.2 Measurement of depth profiles of radionuclides in a Hiroshima granite stone

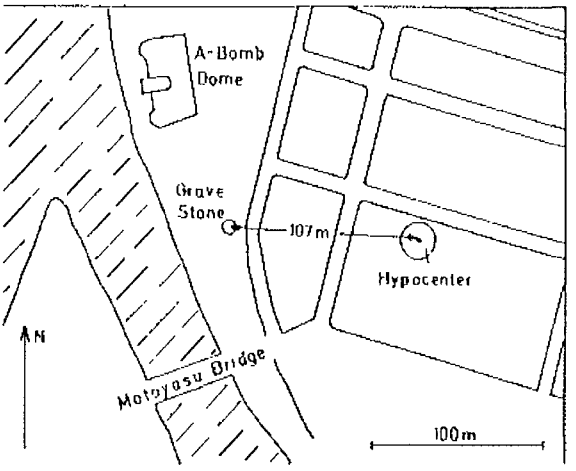

Fig. 1: Location of the gravestone

A granite grave stone in Hiroshima 106 m from the hypocenter was chosen for measurements of depth profiles of radionuclides produced by neutron capture reactions from the bomb neutrons. Fig. 1 shows the location of the graveyard and of the gravestone with respect to the hypocenter, Fig. 2 a photograph of the graveyard taken in October 1945. Fig. 3 shows a side-view of the gravestone. The goal of these measurements is to deduce at this location the neutron spectrum and the fluence since the capture cross sectons have because of nuclide specific resonances different neutron energy dependences. The measured radionuclides are ^{36}Cl, ^{41}Ca, ^{60}Co, ^{152}Eu and ^{154}Eu. The depth dependend results of these measurements for ^{36}Cl, ^{41}Ca and ^{152}Eu are shown as effective thermal neutron fluences in Fig. 4. The effective thermal neutron fluence $F_{th,eff}$ is defined as

$$F_{th,eff} = n(^{A+1}Z) / \{n(^{A}Z)\ \sigma_0)\},$$

where σ_0 is the thermal neutron capture cross section at 25.3 meV and n are the numbers of nuclei. The number n of produced nuclei ^{A+1}Z is given by

$$n(^{A+1}) = n(^{A}Z) \int dE\ \sigma(E)\ dF(E)/dE.$$

Deviations in $F_{th,eff}$ are due to contributions of non-thermal neutrons.

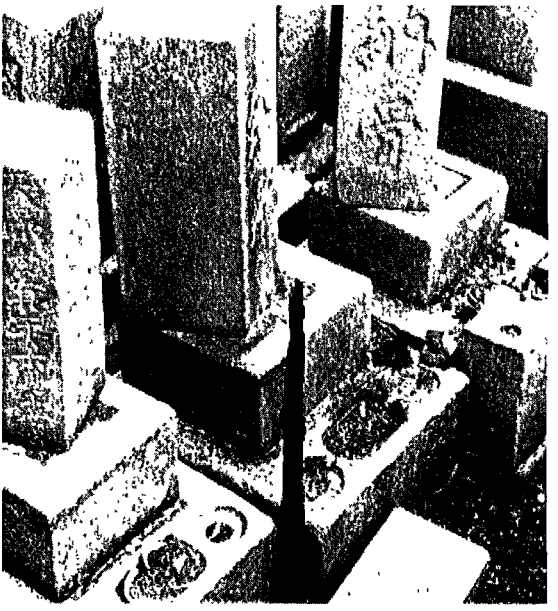

Fig. 2: Photograph of the graveyard taken in October 1945

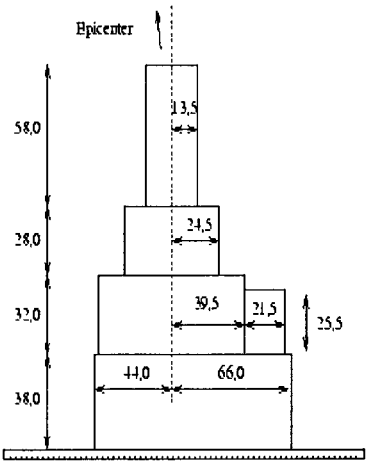

Fig. 3: Side view of the gravestone

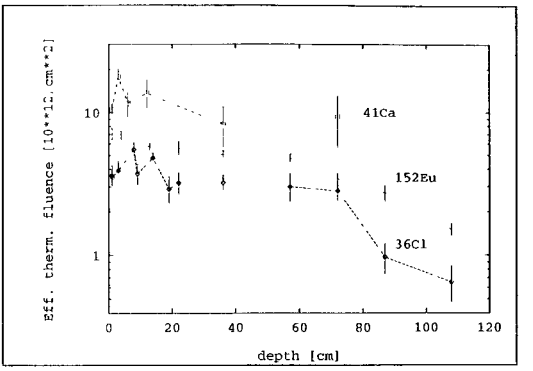

Fig.4: Effective thermal neutron fluences in the Hiroshima gravestone for ^{36}Cl, ^{41}Ca and ^{152}Eu as function of depth

1.3 Measurement of depth profiles of radionuclides in simulation experiments

A mock-up of the gravestone from the same quarry and with the same geometry was irradiated with thermal, epithermal and fast neutrons at the Munich research reactor. Gold foils and produced ^{198}Au radioactivities were used as monitors for thermal neutrons, nickel foils and ^{58}Co radioactivities as monitors for fast neutrons. Figs. 5 and 6 show the results for thermal and fast neutrons, respectively.

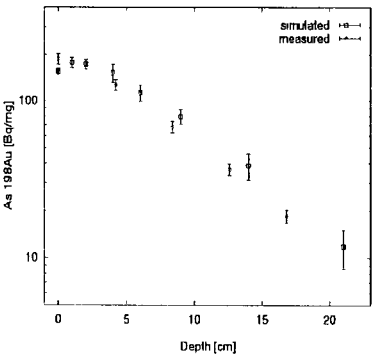

Fig. 5: Measured (rhombs) and simulated (squares) depth profile of the ^{198}Au activity in the granite mock-up.

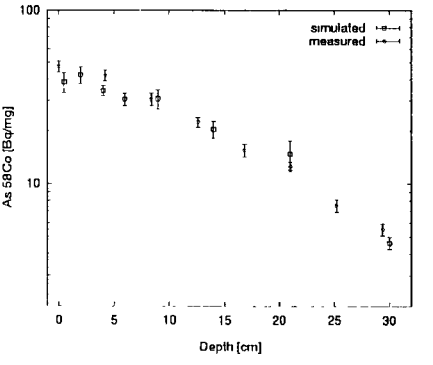

Fig. 6: Same as Fig. 5 for ^{58}Co

1.4 Neutron transport calculation

Neutron transport calculations were performed with the Monte Carlo code MORSE (Multigroup Oak Ridge Stochastic Experiment). MORSE contains 118 energy groups in contrast to 44 groups in DS86.

1.4.1 Simulation experiments

In order to test the MORSE transport calculations, the simulation experiments were calculated. As seen from Figs. 5 and 6, MORSE and experimental results agree within the error bars.

1.4.2 Hiroshima granite stone

In this application, the neutron spectra were calculated from the position of the bomb to the ground. The calculations were carried out for different ground compositions, for humid Hiroshima soil and for dry granite soil as in the graveyard. The DS86 calculations were performed for humid Hiroshima soil. Fig. 7 shows the neutron spectrum calculated with MORSE with the same parameters as in DS86 and for humid Hiroshima soil 1 m above ground in comparison to the DS86 spectrum. Above 0.4 eV, the agreement is good within error bars, below 0.4 eV MORSE yields about 50 % more neutrons. This difference is explained to be due to the finer energy binning of MORSE.

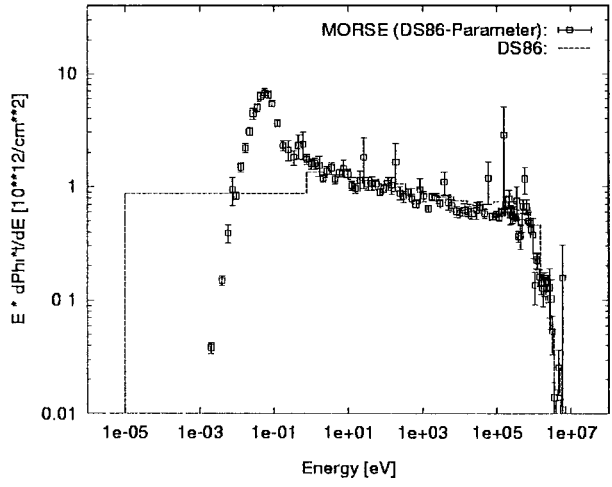

Fig. 7: MORSE neutron spectrum (with DS86 input parameters, 1 m above ground level and 106 m from the hypocenter) compared to the spectrum used in DS86

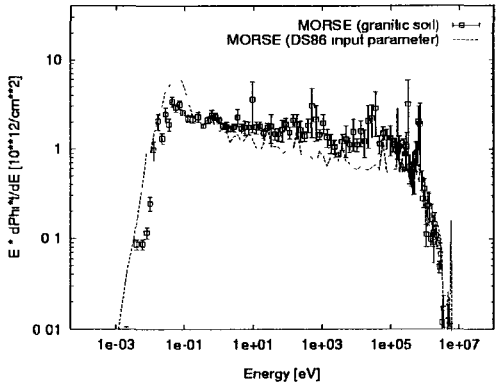

Fig. 8: MORSE spectrum with granite as soil compared to the neutron spectrum from Fig. 7 (dashed line).

The neutron spectrum obtained for the dry granite soil of the graveyard is shown in Fig. 8 in comparison to the MORSE spectrum for humid Hiroshima soil. With this neutron spectrum, the effective thermal neutron fluences were calculated in the first 2 cm of the granite stone and compared to the experimental ones (Fig. 9). Since ^{36}Cl, ^{41}Ca and ^{152}Eu are produced by neutron capture reactions with similar energy dependences of the cross sections, the effective thermal neutron fluences of these radionuclides were averaged. Using the bomb yield as fit parameter, a bomb energy yield of 16 kt TNT is obtained in full agreement with other observations.

If ^{36}Cl, ^{41}Ca and ^{152}Eu are considered individually, neither MORSE nor DS86 are able to explain the single effective thermal neutron fluences. This is an open question. Also other observations as the dependence of activations from the hypocenter cannot be explained by DS86. This means that at least two observations are not in full agreement with DS86 and comparable neutron transport calculations.

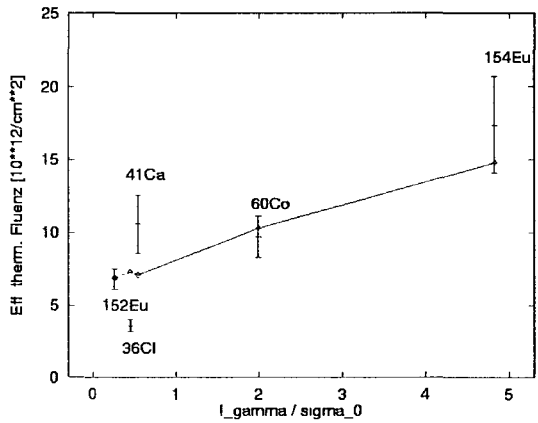

Fig. 9: Effective thermal neutron fluences calculated with the neutron spectrum from Fig. 8 (rhombs) in comparison with the measurements.

2 Measurement of the global ^{41}Ca bomb peak and development of a general atmospheric transport model

2.1 Introduction

For dosimetry applications, the atmospheric transport of radionuclides from bomb explosions or from accidents of nuclear power plants or reprocessing facilities has to be known in order to calculate global fall-out and global radiation doses. Because of the delta type input in time of nuclear weapon tests, the measurement of the so-called bomb peaks, i. e. of time dependences of concentrations of radionuclides, are an extremely powerful tool to study time constants for atmospheric mixing and transport. Bomb peaks of ^{14}C, ^{36}Cl, ^{90}Sr and ^{137}Cs are reported. In the present project, the bomb peak of ^{41}Ca was measured.

2.2 The ^{41}Ca bomb peak

Ice samples from the Fiescher Hörner glacier from 1950 to 1980 were provided from EAWAG Zürich. After chemical treatment of the ice samples, ^{41}Ca concentrations were measured in the final samples with AMS. The reults are shown in Fig. 10. It is for the first time that the ^{41}Ca bomb peak is observed. The occurrence of the peak in the early years of the nuclear weapon tests shows that ^{41}Ca is mainly produced by the atoll bombs. In order to understand the weak ^{41}Ca bomb peak, this peak was compared with bomb peaks of ^{14}C, ^{36}Cl and ^{90}Sr and atmospheric transport calculations were performed.

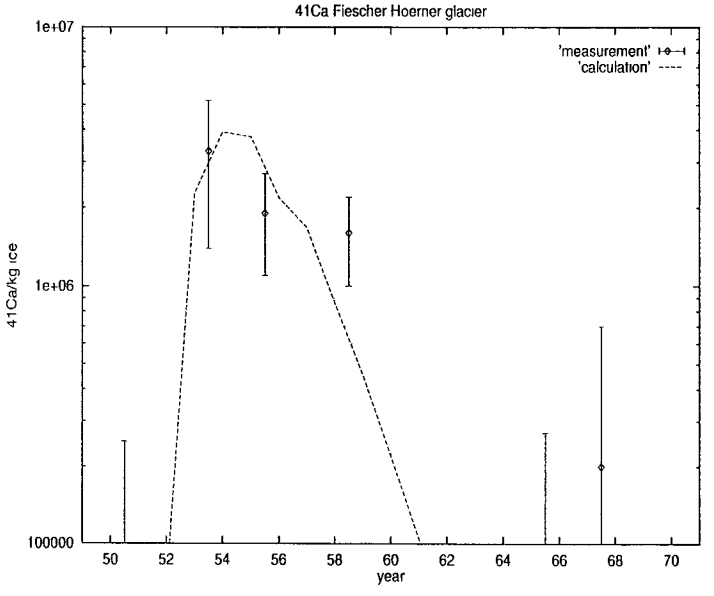

Fig. 10: ^{41}Ca concentrations in ice samples from the Fiescher Hörner glacier

2.3 Atmospheric transport box model

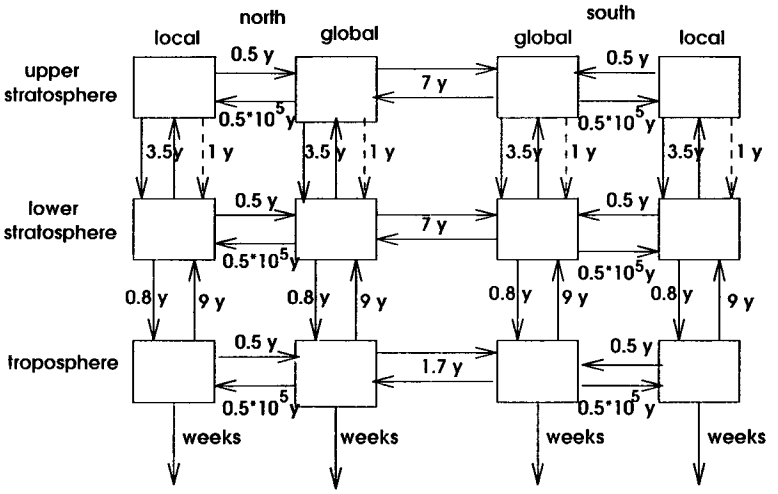

Fig. 11:Box model used for ^{36}Cl, ^{41}Ca and ^{90}Sr. Aerosols as ^{41}Ca and ^{90}Sr are also transported by sedimentation in the upper stratosphere (broken arrow).

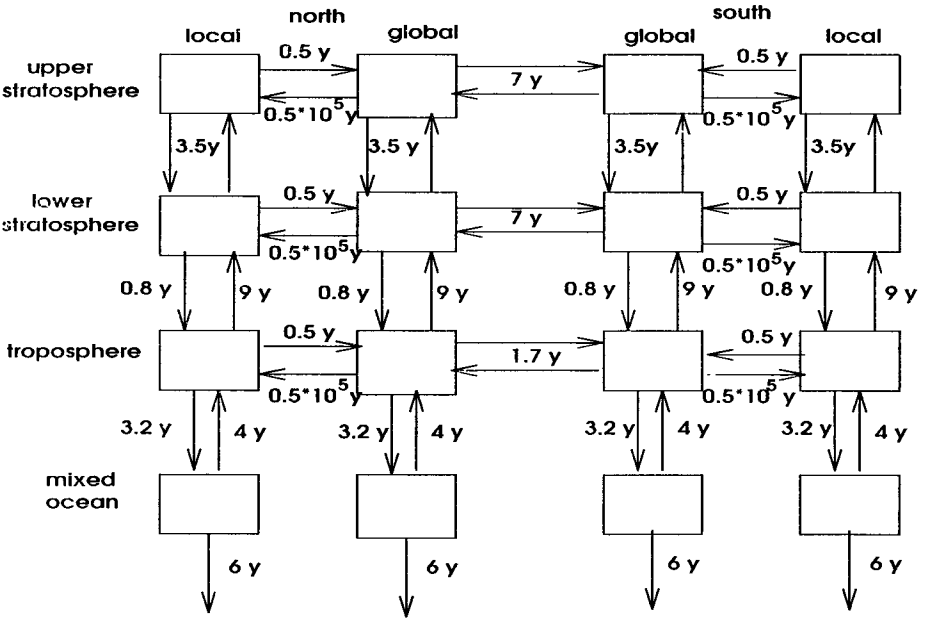

Fig. 12 :Box model used for ^{14}C

Vertically, the atmosphere was devided in three layers: upper stratosphere, lower stratosphere and troposphere. Horizontally, northern and southern hemisphere were distinguished. To take into account mixing processes in the hemispheres, local boxes were used for the input of the bomb explosions. ^{36}Cl, ^{41}Ca and ^{90}Sr were transported as fall-out into the

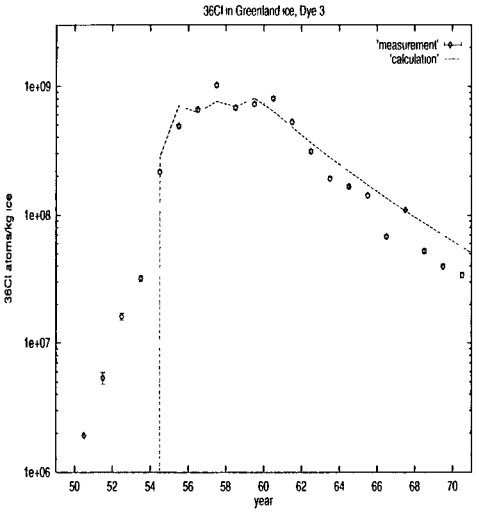

Fig. 13: ^{36}Cl bomb peak [1].

archives on the surface of the earth. For ^{14}C, additional reservoirs were used for the mixed ocean layer and the deep ocean. The used boxes and the transport processes between them are shown in Figs. 11 and 12.

Since aerosols in contrast to gases and small molecules are subject to sedimentation in non-turbulent regions of the atmosphere (in the upper stratosphere), for ^{41}Ca and ^{90}Sr an additional downward vertical transport was introduced in the upper stratosphere. The late appearance of the ^{36}Cl bomb peak [1] (Fig. 13) shows that ^{36}Cl is gaseous and not subject to sedimentation. ^{36}Cl is mainly produced by the explosions on the barges (1954-1958). The bomb peaks of ^{14}C [2] and of ^{90}Sr
[3] are shown in Figs. 14 and 15.

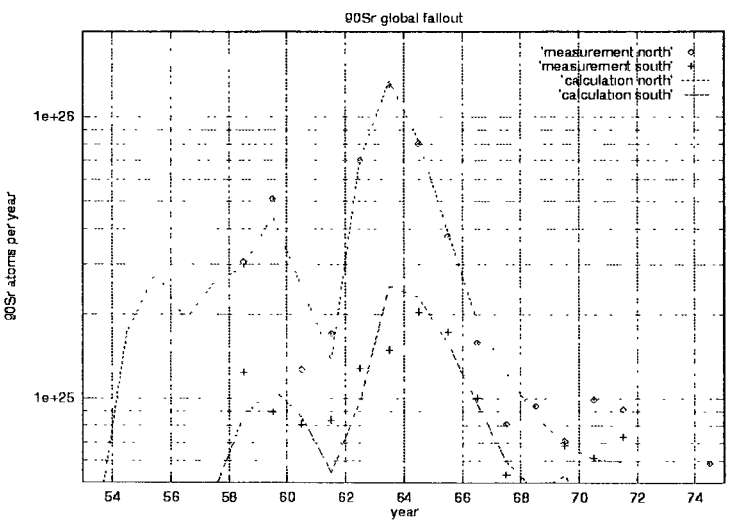

Fig. 14: ^{90}Sr bomb peaks in the northern and southern hemisphere [2].

Fig. 15: ^{14}C bomb peak [3].

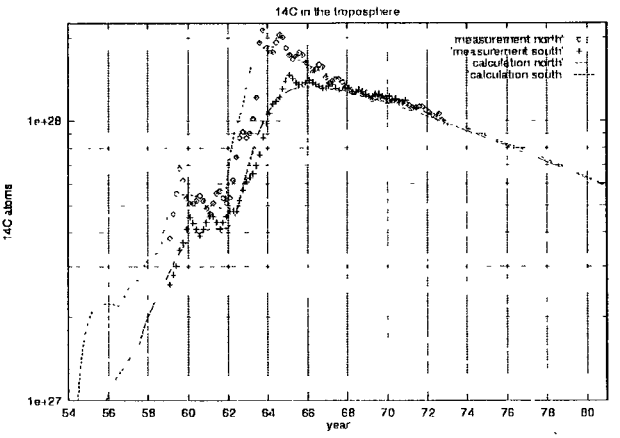

2.4 Obtained time constants

The boxes are connected by transport processes which are described by rate constants which are inverse time constants. The obtained time constants are also drawn in Figs. 10 and 11. The important results are:

a one universal model can be used for all bomb produced radionuclides so that predictions can be made also for other radionuclides and other catastrophic events.

b Chlorine is gaseous in the stratosphere

c Aerosols and radionuclides attached to aerosols as ^{10}Be, ^{41}Ca, ^{90}Sr and ^{137}Cs are additionally transported downward by sedimentation. Sedimentation is the main downward process for aerosols in the upper stratosphere.

d The main transport process between lower stratosphere and troposphere is not sedimentation but (turbulent) exchange.

References

1] H.-A. Synal, J. Beer , G. Bonani, M.Suter and W. Wölfli:
Atmospheric Transport of Bomb-produced ^{36}Cl . Dissertation ETH Zürich 1989
Nucl. Instr. and Meth. **B52** (1990) p. 483

[2] R. -L. Shia, Y.L. Yung, M. Allen, R.W. Zurek and D. Crisp: Sensitivity Study and Diffusion Coefficients in a two-dimensional Stratospheric Model Using Excess Carbon 14 Data.
Journal of Geophys. Res. **94**(1989) p. 18647

[3] UNSCEAR report: Ionizing Radiation: Sources and Biological Effects. Report to the General Assembly (1982)

Publications

K. Kato, M. Habara, T. Aoyama, Y. Yoshizawa , U. Biebel, G. Haberstock, J. Heinzl, G. Korschinek, H. Morinaga, U. Ratzinger and E. Nolte:
Measurements of Neutron Fluence from the Hiroshima bomb.
Journal of Radiation Research, **29** (1988) 261

H. Faestermann, K. Kato, G. Korschinek, P. Krauthan, E. Nolte, W. Rühm and L. Zerle:
Accelerator Mass Spectrometry with Fully Stripped ^{26}Al, ^{36}Cl, ^{41}Ca and ^{59}Ni Ions.
Nucl. Instr. and Meth. **B50** (1990) 275-279

W. Rühm , K. Kato, G. Korschinek, H. Morinaga, A. Urban, L. Zerle and E. Nolte:
The Neutron Spectrum of the Hiroshima A-bomb and the Dosimetry System 1986
Nucl. Instr. and Meth. **B52** (1990) 557-562

K. Kato, M. Habara, Y. Yoshizawa, U. Biebel, G. Haberstock, J. Heinzl, G. Korschinek, H. Morinaga and E. Nolte:
Accelerator Mass Spectrometry of ^{36}Cl produced by neutrons from the Hiroshima bomb
Int. J. Radiat.Biol. **58**,no.4,(1990)661

W. Rühm, K. Kato, G. Korschinek, H. Morinaga and E. Nolte:
^{36}Cl and ^{41}Ca depth profiles in a Hiroshima granite stone and the Dosimetry System 1986
Zeitschrift Physik, Hadrons and Nuclei , **A341**(1992) 235

D. Blamart, W. Rühm, W. Spiegel, K. Kato, G. Korschinek, H. Morinaga, G. Morteani and E. Nolte:
Oxygen stable isotope measurements on a gravestone exposed to Hiroshima A-Bomb explosion and the "Dosimetry System 1986".
Chemical Geology (Isotope Geoscience Section) **101**(1992)93

W. Rühm, K. Kato, G. Korschinek, H. Morinaga and E. Nolte:
The neutron spectrum of the Hiroshima A-bomb and the Dosimetrysystem 86.
accepted Int. Journal Rad. Biol.

Head of project 6: Dr. G. Hütt

II.Objectives for the reporting period

- Dose reconstruction by TL technique using the environmental dosimeters, collected during the field trips to Byelorussia and the town of Pripyat (Ukraine).
- Study of the influence of the background spectrum of the human tooth enamel on the dose assessment by EPR technique. Estimation of the systematic error in dose reconstruction introduced by the interference between the main radiation signal and spurious signals.
- Determination of the minimum detectable absorbed dose by EPR technique on the basis of tooth enamel.

III. Progress achieved including publications

A. Dose reconstruction using TL-technique

As a result of the accident in the Chernobyl Nuclear Power Plant on April 26, 1986 at 01:23 a.m., large densely populated areas were subject to radioactive pollution. First of all, this was the town of Pripyat with its 50,000 inhabitants, whose evacuation was started not until 36 hours had elapsed since the moment of accident. During the first days, the control over radiation situation was random or entirely absent. As a matter of fact, strict systematic monitoring at 80 points was set up only in 1987. It was of utmost consequence to reconstruct the doses received by the staff at the nuclear power station and local population during April 26-27, 1992.

It was attempted to reconstruct γ-doses since the moment of the accident until now. Both natural and widely available artificial materials served as study objects. Samples were taken from different kinds of constructions (dwelling houses, several institutions etc.) as well as from their surroundings. Accident doses were reconstructed for 32 samples using TL.

The data obtained allow the following conclusions to be drawn that support preliminary results:

1. Ceramic objects (bricks, wall tiles, flower pots) can be used in retrospective dosimetry.
2. The trend of considerable decrease in doses with height is revealed. It is proved by the fact that pollution of soil is considerably higher than the one of other surfaces.
3. Walls and windows of buildings have remarkable shielding properties. This conclusion is confirmed by numeric calculations.
4. The data obtained with TL method must be used in interlaboratory checking of results.
5. In the event of dose level observed in the town of Pripyat, retrospective EPR-dosimetry on the available materials proved ineffective due to low EPR dose sensitivity.

6. Results of the intercalibration proofed internal laboratory calibration of β-source. Determination of exact dose rate of the source will promote more reliable evaluation of accident doses.

It is necessary for laboratories involved in CEC dose reconstruction project to calibrate their β-sources and also be sure that they are using TL-signal measurement techniques that give correct equivalent dose value. These both objectives can be achieved simultaneously by using pre-irradiated quartz and TL technique usually used for accident dose reconstruction.

In order to perform such intercalibration, every laboratory obtained from GSF-Forschungszentrum, Germany two portions of granular quartz. One of the portions was irradiated at GSF, another portion had zero dose.

This quartz was irradiated and measured by routine TL technique at Institute of Geology. Dose rate obtained from these data is 1.0 rad/s (69 R/min), which is very close to the result of our last internal calibration - 67 R/min.

B. EPR study of tooth enamel as accident dosimeter

At present, a tooth enamel of different origin (human, mammoth etc.) is extensively used as a promising palaeodosimeter for dating of geological events by EPR technique. This natural material is also being probed for accident retrospective dosimetry purposes owing to its high sensitivity to radiation exposure and dose-response linearity in wide dose range. On one side, tooth enamel is a simple natural dosimeter, because of the relative simplicity of EPR spectrum, where the main radiation-induced signal with axial symmetry γ–tensor with principal values of $g_{\perp} = 2.0020$ and $g_{\parallel} = 1.9980$ is easily recognized. On the other side, a necessity of preliminary preparation of tooth enamel before EPR treatment causes definite complication upon interpretation of measurement results.

The role of mechanically-induced signal, generated during crushing and grinding of tooth enamel, still remains not elucidated in detail.

We performed a certain study of the influence of the preparation procedure (drilling of dentine and subsequent crushing and grinding of tooth enamel to obtain by sieving particular grain size fractions) on the results of the absorbed dose reconstruction by additive dose method.

The main results obtained may summarized as follows:

1. The mechanically-induced signal, superimposing the radiation signal at $g_{\perp} = 2.0020$, was found to be thermally stable and sensitive to radiation exposure.
2. The intensity of this mechanically-induced signal is increasing with time duration of mechanical grinding, that results, finally, in its dependence on the grain size of tooth enamel sample.
3. The contribution of the mechanically-induced signal to the radiation-induced signal at $g_{\perp} = 2.0020$ is considered as "negative" for the grain size d1 = 0.250 - 0.850 mm, that leads to the underestimation of the absorbed dose. However, the value of that systematic uncertainty depends on the grain size, lowering for finer grain size despite the total enhancement of the intensity of the mechanically-induced signal.

4. The more long-term mechanical stressing may result in a decrease of initial trap concentration and leads to a significant overestimation of absorbed dose.
5. The minimum detectable dose is estimated to about 20 - 25 rad under measurement conditions, used in the present study.

C. Publications

Hütt G., Brodski L., Bailiff I., Göksu Y., Haskell E., Jungner H., Stoneham D. Accident dosimetry using environmental materials collected from regions downwind of Chernobyl: a preliminary evaluation. *Radiation Protection Dosimetry,* 1993, Vol. 47, No. 1/4, 307-311.

Stoneham D., Bailiff I., Hütt G., Brodski L., Göksu Y., Haskell E., Jungner H. TL accident dosimetry measurements on samples from the town of Pripyat. *Nucl. Tracks & Radiat. Meas.,* 1993, Vol. 21, No. 1, 195-200.

Brodski L., Hütt G. The use of some vitreous materials in retrospective dosimetry, *Radiation Protection Dosimetry,* 1995, Vol. 59, No. 1, 55-57.

Polyakov V., Haskell E., Kenner G., Huett G., Hayes R. Effect of mechanically induced background signal on EPR dosimetry of tooth enamel. *Radiation Measurements,* 1995, Vol. 24, No. 3, 249-254.

Polyakov V., Brodski L., Hütt G. Absorbed gamma dose profiles for the radionuclide composition in Pripyat. *Radiation Measurements,* 1995, Vol. 00, No. 0, 000-000.

Hütt G., Brodski L., Polyakov V. Gamma-dose assessment after radiation accident in Kiisa (Estonia): preliminary results. *Applied. Radiat. & Isot.*, in press.

Göksu Y., Bailiff I., Bøtter-Jensen L., Brodski L., Hütt G., Stoneham D. Interlaboratory source calibration using natural quartz for retrospective dosimetry. *Radiation Measurements,* accepted for publication.

Contract F13PCT920040

Final Report

Head of project 7: Prof. E. Lippmaa

II. Objectives for the reporting period

1. To enhance the sensitivity and reliability of human tooth enamel dosimetry by using refined methods of electron spin resonance in the 35 Ghz frequency band (Q band) and to form a methodological basis of the individual dose assessment for people who can offer only small fragments of the teeth obtained by usual dental care procedures.

2. To measure samples collected from Chernobyl clean-up workers under epidemiological studies and to correlate the measured physical whole body gamma ray doses with those obtained by cytogenetic methods for the same persons.

III. Progress achieved including publications

1. High frequency (Q band) ESR measurement [1].

A comparision of tooth enamel electron spin resonance for gamma ray dosimetry in the usual X band (9.5 Ghz) and the Q band (35 Ghz) has been made in respect of sensitivity and spectral resolution. The main advantage of using Q band is better sensitivity for small samples: Q band is preferable if the quantity of enamel available from one person is less than 10 mg. Drawbacks of the Q band measurements are of technical nature: for correct quantitative measurements sample placing, phase adjustment etc. are to be made with great care; unwanted organic signal suppression by selective saturation is better in the X band due to more microwave power available. X and Q band ESR spectra for the same tooth material are presented in Fig. 2 (curve 1) and Fig. 4 (curve 1), respectively.

2. Sensitivity and reliability of the ESR method.

A practical measurement limit of 0.1 Gy dose increment in a 50 to 100 mg sample was achieved by using the signal averaging technique with 3 to 10 Hz longitudinal field modulation for suppression of the low frequency noise and by improved curve fitting procedure. Absorption spectrum in the actual g = 0.02 region was approximated with a sum of 4 Gaussians with 9 fixed and 5 free parameters using the GRAFIT program on a 90 Mhz GATEWAY2000 PC. Values for fixed parameters: linewidths, shifts between lines and relative intensities of components belonging to "carbonate" and "organic" radicals were determined from spectra of heavily irradiated and non-irradiated samples respectively. A tooth enamel spectrum decomposed accordingly is presented in Fig.1.

Chemical methods of sample handling aimed at suppressing the organic constituents in tooth enamel (collagenase and diethylenetriamine treatments) were found of little use; pretreatment in ultrasonic bath with sodium hydroxide was found useful for separating enamel from dentine.

The first international intercomparision of ESR dosimetry with teeth has given the same limits for selected laboratories [2]. The results obtained at the Institute of Chemical Physics and Biophysics (ICBP) are presented in Tab. 1.

3. UV irradiation effects in tooth enamel.

We have found that ultraviolet light from natural (e.g. Solar irradiation) or artificial (e.g. mercury lamp used in separating dentine from enamel) sources can create an ESR signal in tooth enamel which is almost indistinguishable from the signal created by radioactive sources in respect of its spectrum and thermal stability [3] (see Fig. 3). This effect (like the known effects of mechanical treatment or medical X-ray exposure) has to be considered when the baseline spectrum of an unirradiated tooth of a person is postulated for individual gamma ray dose assessment.

4. Case studies.

In October-November 1994 an irradiation accident has taken place in Kiisa, Estonia, resulting in death of one person involved and serious injuries to his family members living with a 100 Ci Cs-137 source in their kitchen drawer for more than 10 days. We measured the dose acquired by one of the above persons (R. T. aged 14) using his tooth enamel with the result of 2.0 to 2.5Gy (see Fig. 2). This corresponds to cytogenetic blood analyse data (chromosome aberrations detected with FISH) giving 2.8 to 3.4Gy and showing inhomogeneous body irradiation confirmed by burnings on his hands as the result of manipulations with the source.

A similar source was found later near a road junction at Valgejõe, Estonia. Fragments of milk teeth from children who had possibly visited the place where the source had been were examined by us with no positive findings: upper limit of the acquired dose less than 0.3Gy was measured. The small radiation sensitivity of teeth examined (revealed by reirradiadion experiments on a Co-60 source) was the reason for higher detection threshold.

The cohort of Estonian Chernobyl clean-up workers (nearly 2000 persons) with the mean recorded dose of 0.11Gy are under epidemiological (e.g. thyroid) and cytogenetic (GPA and FISH) studies in the Estonian Institute of Experimental and Clinical Medicine. Blood analyses made in Finnish Centre for Radiation and Nuclear Safety, University of California and Oak Ridge Institute for Science and Education have shown that for most members of this cohort individual doses are too low for cytogenetic assessments, therefore the odontodosimetric method is considered as the method of choice. Extraction of teeth is planned together with systematic teeth examination of the cohort by foreign dentists (for psychological reasons).

Publications relevant to the project

[1] T. Rõõm, G. Liidja and E. Lippmaa (1994). Temperature and frequency effects in tooth enamel electron spin resonance dosimetry. *Appl. Radiat. Isot.* **45**, 1061-1064.

[2] V. Chumak, ... G. Liidja, E. Lippmaa, ... J. Past, J. Puskar, ... (1996). The first international intercomparision of EPR-dosimetry with teeth: first results. *Appl Radiat. Isot.* **47** (in press); G. Liidja, E. Lippmaa, J. Past, J. Puskar, Annelie Meijer, Ü. Vaher (1995). ECP10 intercomparision of ESR techniques. Final Report (unpublished).

[3] G. Liidja, J. Past, J. Puskar & E. Lippmaa. Paramagnetic resonance in tooth enamel created by ultraviolet light (submitted to *Nature* on July 11, 1995).

Tab. 1. ICBP results for the First International Intercomparision of EPR Dosimetry with Teeth

Sample *) No.	Dose (in Gy) determined in ICBP **)	Dose (in Gy±5%) given in IAEA (Seibersdorf) ***)
86	0	0
91	0	
17	0.13±0.08	0.10
18	0.13±0.06	
22	0.16±0.14	
26	0.27±0.11	0.25
28	0.29±0.12	
34	0.41±0.16	
57	0.53±0.13	0.50
59	0.57±0.19	
72	0.52±0.18	
103	1.04±0.23	1.00
104	1.02±0.22	

*) 13 fine grained enamel samples weighting 100 mg, irradiated at each dose level at IAEA facilities in Seibersdorf, were sent to ICBP by dr. A. Wieser (GSF, Munich)

**) Relative doses were determined from 3 series of ESR measurements and converted into absolute doses after reirradiation of selected samples in the Co-60 source of the Institute of Experimental Biology (Harku, Estonia) and Cs-137 source of Swedish Radiation Protection Institute (Stockholm).

***) Those doses were unknown to the participants of the Intercalibration until presentation of their final results.

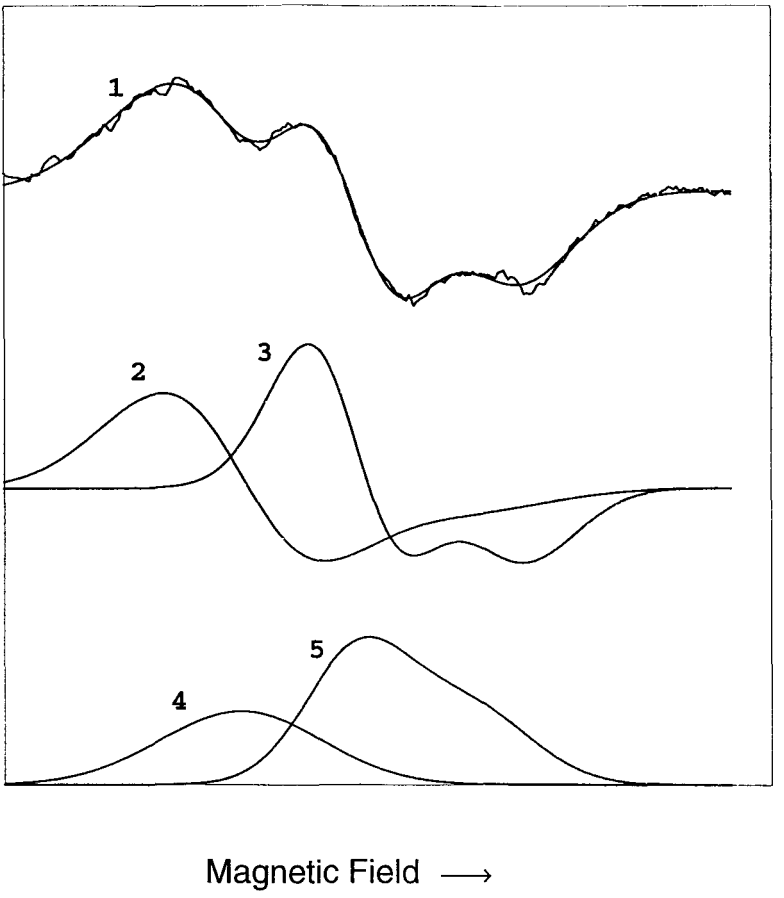

Fig. 1 Presentation of tooth enamel ESR as a sum of 4 Gaussian curves.

Upper part: Experimental 1-st derivative spectrum of grained enamel irradiated with gamma rays (1.5 Gy) and approximation curve (1) after least-square fitting.

Central part: Decomposition of (1) into two components representing organic radicals (2) and carbonate radicals (3), both consisting of two Gaussians.

Lower part: Integrated spectra representing absorption of organic (4) and carbonate (5) radicals. Curve (5) resembles approximately a powder spectrum with axially symmetrical centres which is strongly broadened by modulation (amplitude 4 G). The area under this curve is a measure of dose.

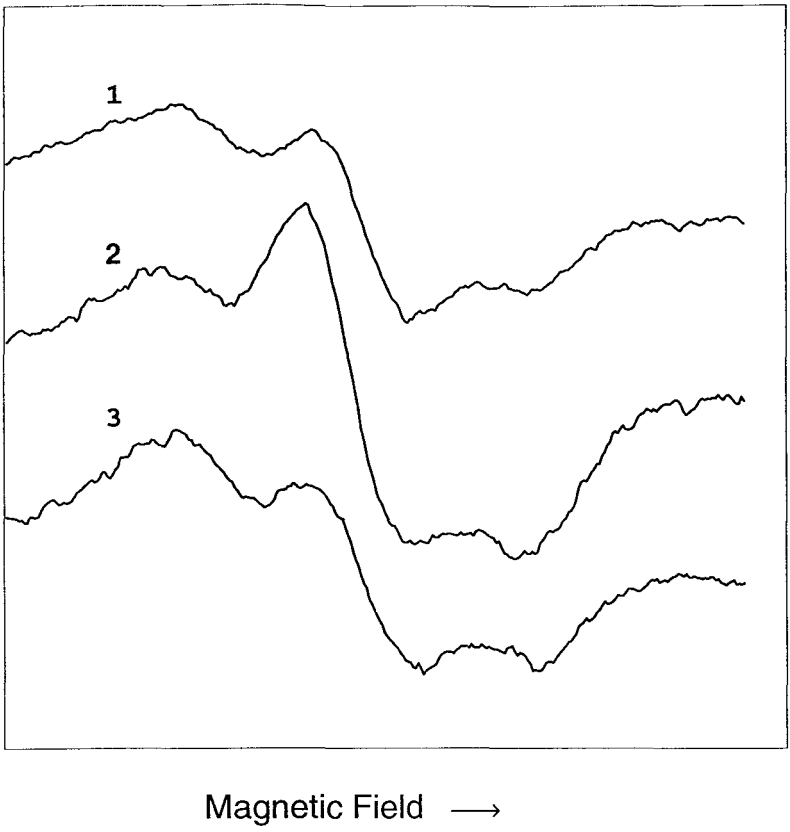

Fig. 2 X-band ESR spectra (1) of tooth enamel of a Kiisa irradiation victim (R. T.) and two samples of similar weight (50 mg) irradiated with Co-60 gamma rays with dose 4.5 Gy (2) and 1.5 Gy (3). Reirradiation experiments with a Cs-137 source at the Swedish Radiation Protection Institute have shown that sample (1) is less sensitive and its previous dose was 2.3±0.4 Gy.

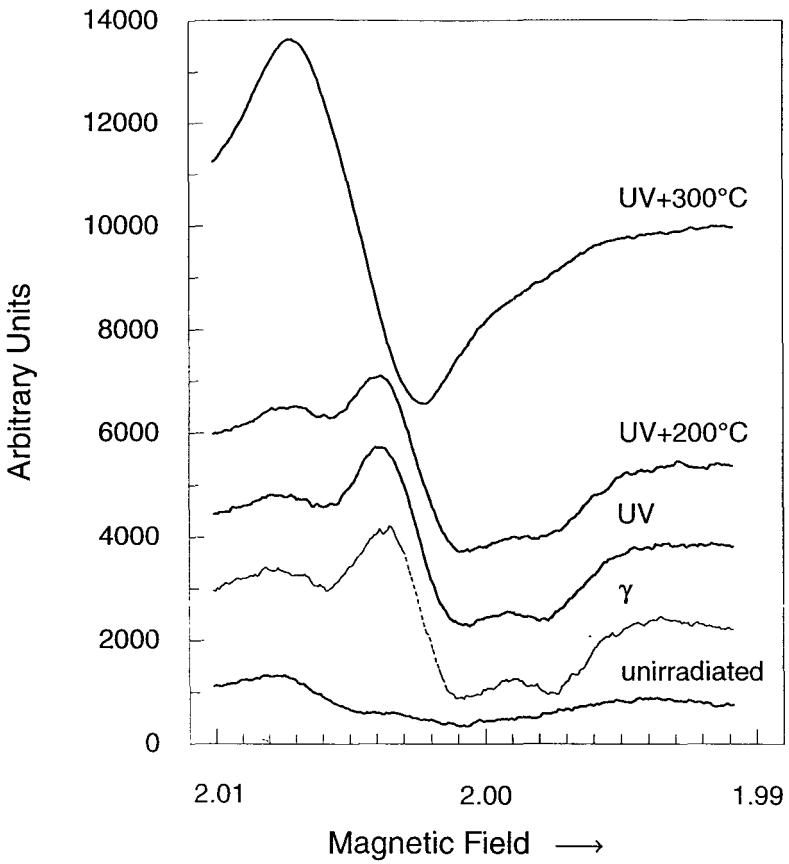

Fig. 3 X-band ESR spectra of tooth enamel showing the effect of ultraviolet irradiation.

A 31 mg grained enamel sample (previous gamma dose less than 300 mGy - "unirradiated") was irradiated with 1kW xenon lamp at various wavelengths between 240 and 330 nm through a grating monochromator (total energy about 20 Joules) and measured after 14 days at room temperature ("UV"). For comparision the spectrum of another sample after irradiation with Co-60 (4.5 Gy) is presented ("γ"). The UV irradiated sample was then heated for 20 min in steps of 50° C and measured at room temperature. Two upper spectra correspond to annealing temperatures just before (200° C) and after (300° C) major changes took place in the spectrum. Spectra are plotted against g factor values. Measurement conditions: microwave power 14 mW, 100 kHz field modulation amplitude 4 G, longitudinal field sweep frequency 10 Hz and amplitude 50 G, total acquisition time 819 s.

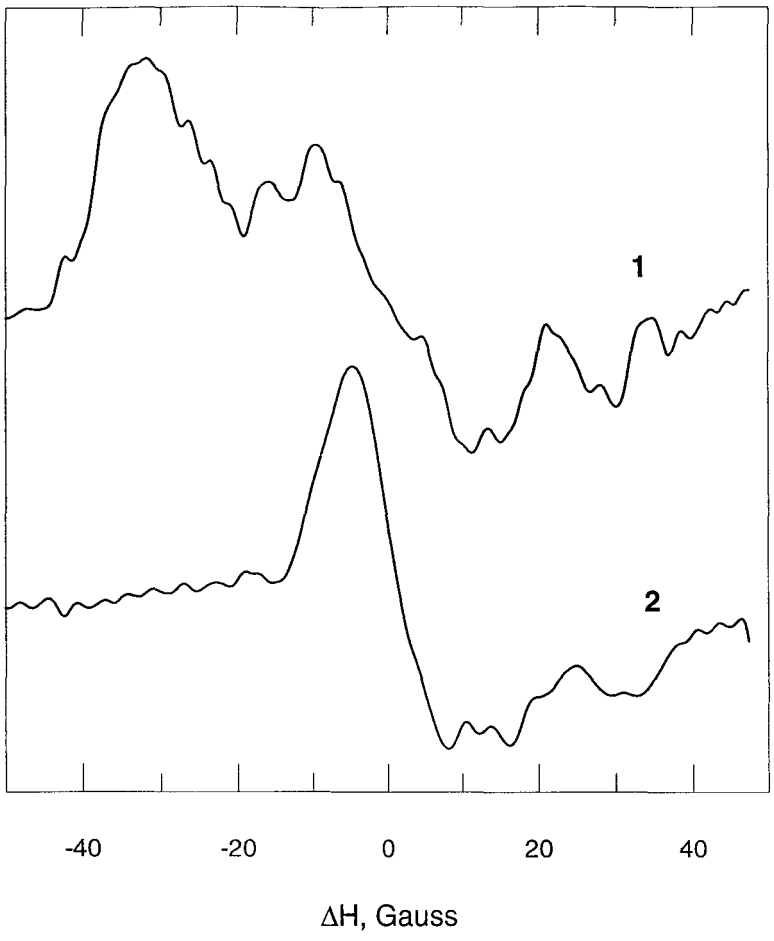

Fig. 4 Q-band ESR spectra of a 9.7 mg sample of grained tooth enamel of a Kiisa irradiation victim (R. T.) (1) and a similar sample irradiated with a γ dose of 500 Gy (2). Measurement conditions: microwave power below 1.5 mW, 100 kHz field modulation amplitude 12 G, longitudinal sweep frequency 3 Hz and amplitude (full) 120 G. Total acquisition time 1.5 hours (1) and 6 min (2). Central field value 12300 G. The width of spectral lines in (1) has a contribution from the magnetic field drift.

Final Report
1992-1994

Contract: **F13PCT920064h** **Duration: 1.1.93 to 30.6.95** **Sector:** **A11**

Title: The measurement of the spectral and angular distribution of external radiations in the workplace and implications for personal dosimetry.

1)	Clark	NRPB
2)	Spencer	UKAEA
3)	Gualdrini	ENEA
4)	Chartier	CEA - FAR

I. Summary of Project Global Objectives and Achievements

One of the main objectives of the project is to develop new methods for the measurement of external radiations in the workplace The emphasis has been on developing practical methods for measuring photon radiation fields because methods already exist for neutron radiations The aim has been to demonstrate a technique capable of measuring the spectral and angular characteristics of the photon field, which can be used in a variety of workplaces These measurements can then be used to calculate operational and protection dose quantities in the workplace Following a review of techniques available, the spectrometer has been developed by NRPB based on a portable sodium iodide detector system weighing less than 15 kg The design incorporates shielding and collimation so that angular can be measured The AEA have provided a computer programme to analyse the measured spectra. This programme uses the response function of the sodium iodide crystal to deconvolve the raw, measured spectrum into a photon energy and angle distribution This data is then used to calculate protection and operational dose quantities in the measured field, using a programme developed at NRPB. The objective of developing a new method of measuring workplace photon spectra has been achieved and measurements have been made in a number of workplaces to demonstrate the technique These results have been compiled for comparison with other measurements

In addition to being able to measure radiation fields, the calculation of dose quantities in such fields is important for both theoretical and practical studies A major objective of this project has been to improve the calculations of operational and protection quantities particularly the former. The ENEA has carried out a large programme of improvement to its numerical dosimetry capabilities and has installed and commissioned the MCNP and SABRINA codes The MCNP Monte Carlo code has been used to calculate photon fields and operational quantities for the calibration of personal dosemeters. Calculations of air kerma backscatter factors and directional dose equivalent have been made using a tissue equivalent sphere .Furthermore calculations of dose equivalent at a depth and backscatter factors have been calculated from 20 keV to 1 MeV for poly-methyl-methacrylate (PMMA) and water slab phantoms These phantoms are increasingly used for calibrating personal dosemeters for the measurement of the operational quantity personal dose equivalent In order to complete the numerical methodology,

conversion coefficients for fluence to effective dose have been calculated using the organ weighting factors given in ICRP Publication 60

Finally, it has been one of the major objectives of the project to look at the actual performance of personal dosemeters in measuring doses in practical radiation fields Dosemeters from various dosimetry services have been exposed to calibration and simulated workplace radiation fields. The services have then processed the dosemeters and provided their best estimates of dose The comparison of measured to delivered dose has been made by IPSN, to assess the ability to measure operational quantities in a variety of workplaces

Head of project 1: Dr Clark

II. Objectives for the reporting period

The main objectives for the reporting period were to commission the practical photon field spectrometer and to use it to make measurements in workplaces. In order to achieve this it was necessary to optimise the shield design for the spectrometer, primarily to optimise its directional characteristics while keeping within an acceptable weight. Furthermore, it was necessary to provide results for the development of the spectrometer unfolding programme by AEA, using calibration facilities at NRPB. Finally, a method was needed for using the deconvolved spectral results to calculate physical, protection and operational quantities in measured photon fields

III. Progress achieved including publications

A photon field spectrometer has been constructed at NRPB, using a 17 mm radius by 25 mm depth sodium iodide crystal with a photomultiplier tube surrounded by lead shielding and a collimator The detailed design of the spectrometer has been presented previously[1] and a schematic diagram is given in the report of Project 2 The size of crystal was chosen to minimise the lead shielding required, making the spectrometer portable The total weight of the spectrometer assembly is 15 kg. Such ergonomic factors are important in designing a spectrometer capable of obtaining directional and photon energy spectra in workplaces where there may be problems of access or contamination However, there is a price to pay because the size of crystal chosen precludes accurate measurements above 2 MeV or so

In order to commission the spectrometer and help the development of the unfolding programme by AEA, a series of measurements were carried out in calibration fields to characterise the following, backscatter peaks from the lead shielding, Compton scatter peaks, characteristic x-rays, annihilation and full energy photo-peaks. In particular the size of the lead shielding backscatter peak was characterised using a shadow shield technique to minimise the effect from changes in room scatter. The shadow shield was placed close to the source thereby attenuating the primary beam but having no significant effect on room scatter.

A series of test spectra were used to validate the unfolding programme and to improve the ability of the spectrometer to measure energy and angular distributions of photon radiations A set of ISO low and narrow x-ray spectra and γ-ray spectra from ^{137}Cs and ^{60}Co standard sources were obtained for the six orthogonal directions used for practical measurements In addition, a series of measurements were made with the end plug in place These measurements established the basic performance of the spectrometer for x-rays between 30 keV and 248 keV the measured spectra showed dominant photoelectric interactions and penetration of the lead shielding was insignificant; for ^{137}Cs and ^{60}Co radiations penetrations through the shielding were of the order of 5% and 10% respectively, and the photo-peak to Compton ratios were 25% and 10% respectively

During this phase of the work it was observed that the spectrometer had a poor (non-linear) energy response This was rectified by changing the configuration of the photomultiplier tube, and new results obtained for ISO low x-ray series and γ-rays from ^{137}Cs and ^{60}Co These measurements confirmed the satisfactory performance of the spectrometer and of the unfolding

programme for heavily filtered x-rays Some further measurements were carried out with the lightly filtered ISO wide x-ray series to test the unfolding programme more thoroughly Here, some undesirable features were observed, because the unfolding programme produced some discontinuities and spikes in the spectrum at low energies

Following the characterisation programme in the laboratory a series of measurements were made in various workplaces to test the operation and practicability of the instrument to measure the spectra and to make calculations of protection, physical and operational quantities

The following organisations were visited, BNFL Sellafield, BNFL Springfields, Nuclear Electric at Hinkley Point and Amersham International at Amersham In total, a set of 84 spectra were obtained at different locations at these plants, each with six measurements in orthogonal directions plus one measurement with the shield plug incorporated. The first direction, labelled "facing" was the one in which a worker was expected to face in normal circumstances, and the other 5 measurements, left, right, back, up and down are with reference to this direction. The seventh measurement was facing up with the plug in The other directional spectra were obtained by simply rotating the detector on the tripod at that point. In some cases, no one particular direction could be identified as the one in which people would normally face, and here the direction facing the maximum dose rate became the "facing" direction.

In order to calculate dose and dose rate in terms of ambient dose equivalent, effective dose equivalent and air kerma, the following formulation was adopted which uses conversion coefficients from ICRP Publication 51 (1987),

$$H = \sum_{e} \sum_{d} C_{e,d}\, k_{e,d}\, \phi_{e,d}$$

where $C_{e\,d}$ is the measured counts at energy, e, and direction, d (s^{-1})

$k_{e,d}$ is the characterisation constant for fluence at energy, e, and direction, d (cm^{-2} s)

$\phi_{e,d}$ is the conversion coefficient for a specified dose quantity or for air kerma (Sv cm^2 or Gy cm^2) at energy, e, and direction, d

$\sum_{e} \sum_{d}$ is the summation over all energies and directions.

A selection of measurements have been included (Figures 1 - 6 and associated tables) to illustrate the measurement capability and the results of dose calculations for chosen locations in the workplace The results demonstrate the ability to identify the dominant direction and energy of photon radiations in varied locations Because of the sensitivity, ease of use and size of the spectrometric system, these measurements can be carried out quickly and efficiently, even in areas where there may be problems of contamination The useful air kerma rate range is approximately 1 μSv h^{-1} to 100 μSv h^{-1}, for high energy radiation

A selection of results is given for each organisation and these include the measured ambient dose equivalent H*(10) rate, personal dose equivalent $H_p(10)$ rate, air kerma (K_a) rate

and the effective dose equivalent H_E rate at various locations The detailed spectral results for a particular location are given for the front, right, back, left, down and up directions, and these show some interesting features. For example, Figure 1 for location iv in Organisation A, shows that for the "front" direction the main component of dose is from relatively high energy photons, but there is also a significant low energy photon component from the "right" direction This would not have a significant effect on measured $H_p(10)$ doses as shown by the calculated ratio of $H_p(10)$ to effective dose equivalent H_E ratio. However, it has practical radiological protection implications and a subsequent review of procedures shows how this particular component of dose could be reduced.

Figure 2 for location ix at Organisation C, Site 2 shows a working environment where the photon spectra is dominated by low energy photons In contrast location ix at Site 4 (Figure 4) has significant contributions from high energy photons in all six directions.

Polar response measurements and calculations show that the detector used in the six orientations, can measure approximately 60% of the total (4π) field This value agrees with the ratio of measured to calculated dose rates observed at the various sites Provided that the areas viewed by the spectrometer are representative of the radiation field, this will not affect the calculated ratios of operational to protection quantities In most circumstances the worker is either close to an identifiable source and is relatively static, facing the source, or the worker is relatively distant from a large source and is relatively mobile in the field. However, it should be recognised that the technique used here could underestimate doses from narrow intense beams lying at 45° to the reference (Facing) axis in both horizontal and vertical planes. Hence the measurements using the spectrometer should always be accompanied by a measurement of ambient dose equivalent rate or air kerma rate using another instrument with a good polar response This should indicate a significant discrepancy in measured to calculated dose rates, but special care is still necessary to identify any intense narrow beams at 45° angles using this technique

This technique has demonstrated the ability to measure angular and directional photon spectra and to use this data for calculating operational and protection quantities in the workplace In the majority of cases, the spectrometric measurements showed that the operational quantity $H_p(10)$ was a suitable measure of the present legal quantity effective dose equivalent, H_E The $H_p(10)/H_E$ ratio was typically between 1 0 and 1.2 showing that $H_p(10)$ is a reasonably cautious overestimate of effective dose equivalent, in such cases For photon radiations, the difference between effective dose, E, and effective dose equivalent H_E is a few percent[3] so this general conclusion would not change with the implementation of recommendations in ICRP Publication 60[4] There are, of course, some exceptions to this as shown in Figures 1-6, where $H_p(10)$ is significantly higher than H_E (e.g location v at Organisation A) and also where $H_p(10)$ is an underestimate of H_E (e.g. location ix at Organisation C, Site 3). This technique clearly indicates where over- or under-estimates occur and how, in principle, suitable corrections can be made.

This research has identified a method of improving practical measurements of photon spectra in the workplace which should be an aid to reducing radiation exposures.

References

1. Clark, et al. The implementation of the operational dose quantities into radiation protection dosimetry. Final Report, BI6-347a (1992)

2. International Commission on Radiological Protection (ICRP). Data for use in protection against external radiation. ICRP Publication 51. Ann ICRP 17(2/3) (1987).

3. Zankl, M., Petoussi, N., and Drexler, G. Effective dose and effective dose equivalent - the impact of the new ICRP definition for external photon radiation. Health Physics 62(5), pp395-399 (1992).

4. International Commission on Radiological Protection (ICRP). Recommendations of the ICRP. ICRP Publication 60. Ann. ICRP 21(1-3) (1991).

Organisation A

Location	Dose Rate Hp(10) (μSv/h)	Dose Rate HE (μSv/h)	Air Kerma Rate, ka μGy/h	Dose Rate H*(10) (μSv/h)	Hp(10) HE	H*(10) Air Kerma
i	0.17	0.17	0.22	0.28	1 00	1 32
ii	7.64	7.84	8.35	10.35	0.97	1 24
iii	4.44	4.07	4.04	4.91	1.09	1.22
iv	4.92	4.48	4.50	5.24	1.10	1.16
v	21.18	12.61	14.89	21.32	1.68	1 43
vi	0.26	0.23	0.21	0.30	1.13	1 42
vii	0.38	0.38	0.40	0.49	1.00	1.23
viii	11.95	10.51	10.21	12.10	1.14	1 18
ix	10.00	8.87	8.66	10.60	1.13	1 22
x	1.53	1.41	1.36	1.98	1.09	1.45
xi	1.02	0.89	0.90	1.28	1.14	1.43
xii	0.64	0.49	0.64	0.95	1.29	1.48

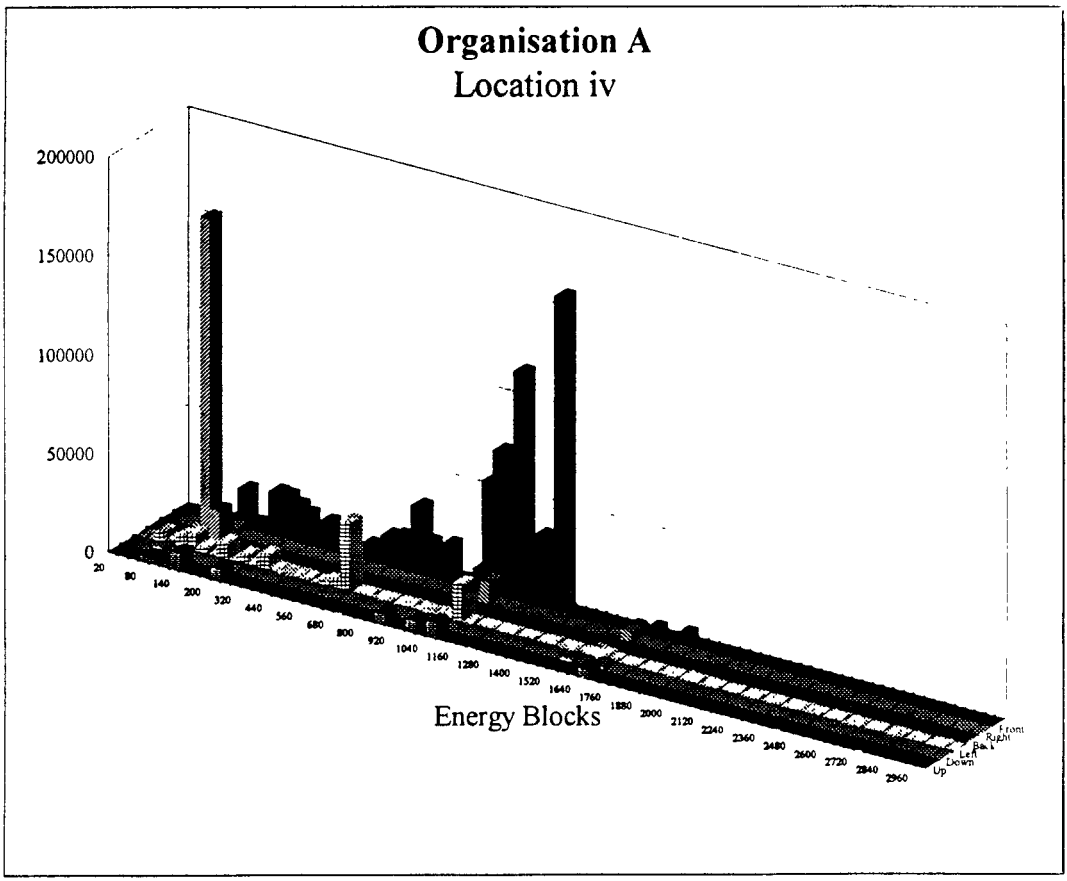

Figure 1 Photon spectra and dose quantities for location iv at Organisation A

Organisation B

Location	Dose Rate Hp(10) (μSv/h)	Dose Rate HE (μSv/h)	Air Kerma Rate, ka μGy/h	Dose Rate H*(10) (μSv/h)	Hp(10) HE	H*(10) Air Kerma
i	7.02	6.57	8.82	11.20	1.07	1.27
ii	7.00	5.42	7.07	8.85	1.29	1.25
iii	5.82	5.08	6.38	8.04	1.15	1.26
iv	1.01	0.92	1.13	1.32	1.10	1.16
v	12.75	10.78	13.73	15.74	1.18	1.15
vi	3.03	2.66	3.06	3.49	1.14	1.14
vii	5.99	5.74	7.38	8.69	1.04	1.18
viii	4.50	4.03	4.49	5.16	1.12	1.15
ix	2.15	2.01	2.42	2.89	1.07	1.19
x	9.08	7.20	9.73	11.12	1.26	1.14
xi	5.12	4.65	5.62	6.41	1.10	1.14
xii	0.62	0.58	0.71	0.83	1.06	1.16

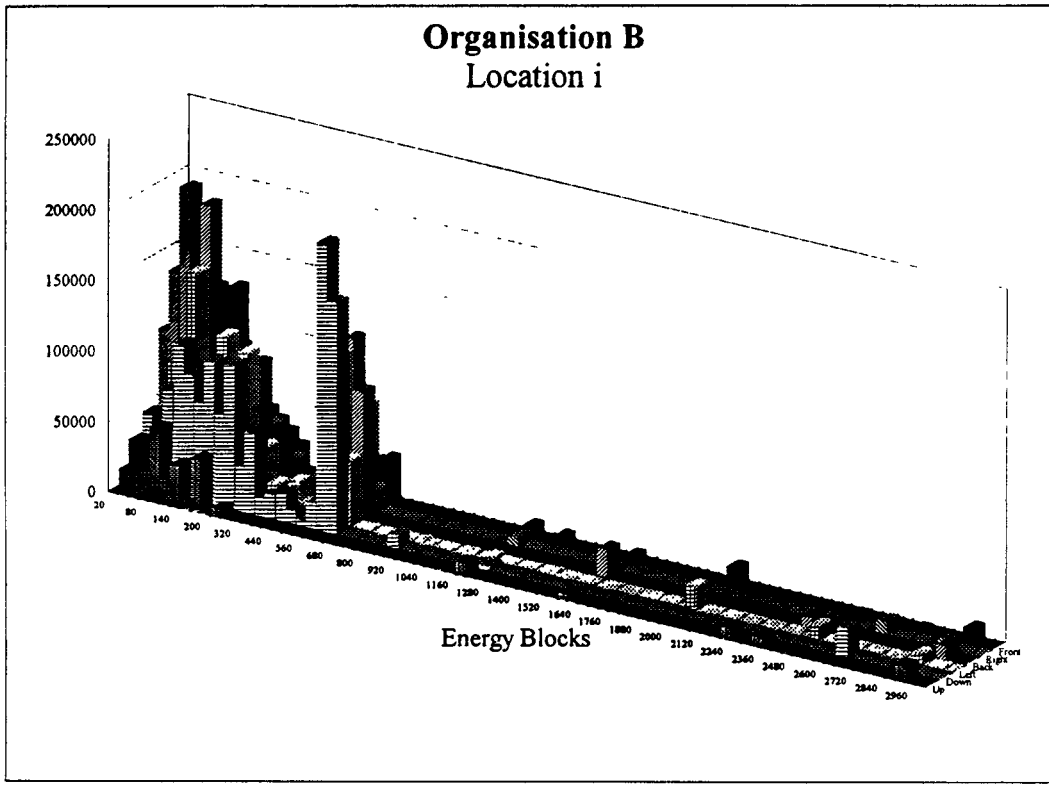

Figure 2 Photon spectra and dose quantities for location i at Organisation B.

Organisation C, Site 1

Location	Dose Rate Hp(10) (μSv/h)	Dose Rate HE (μSv/h)	Air Kerma Rate, ka μGy/h	Dose Rate H*(10) (μSv/h)	Hp(10) HE	H*(10) Air Kerma
i	2.77	2.36	2.63	3.31	1.18	1.26
ii	1.52	1.28	1.82	2.34	1.18	1.29
iii	1.21	1.10	1.20	1.54	1.10	1.28
iv	4.88	4.53	4.60	5.62	1.08	1.22
v	2.54	2.26	1.74	2.76	1.12	1.59
vi	3.25	2.54	3.63	4.61	1.28	1.27
vii	2.46	2.16	2.15	2.63	1.14	1.23

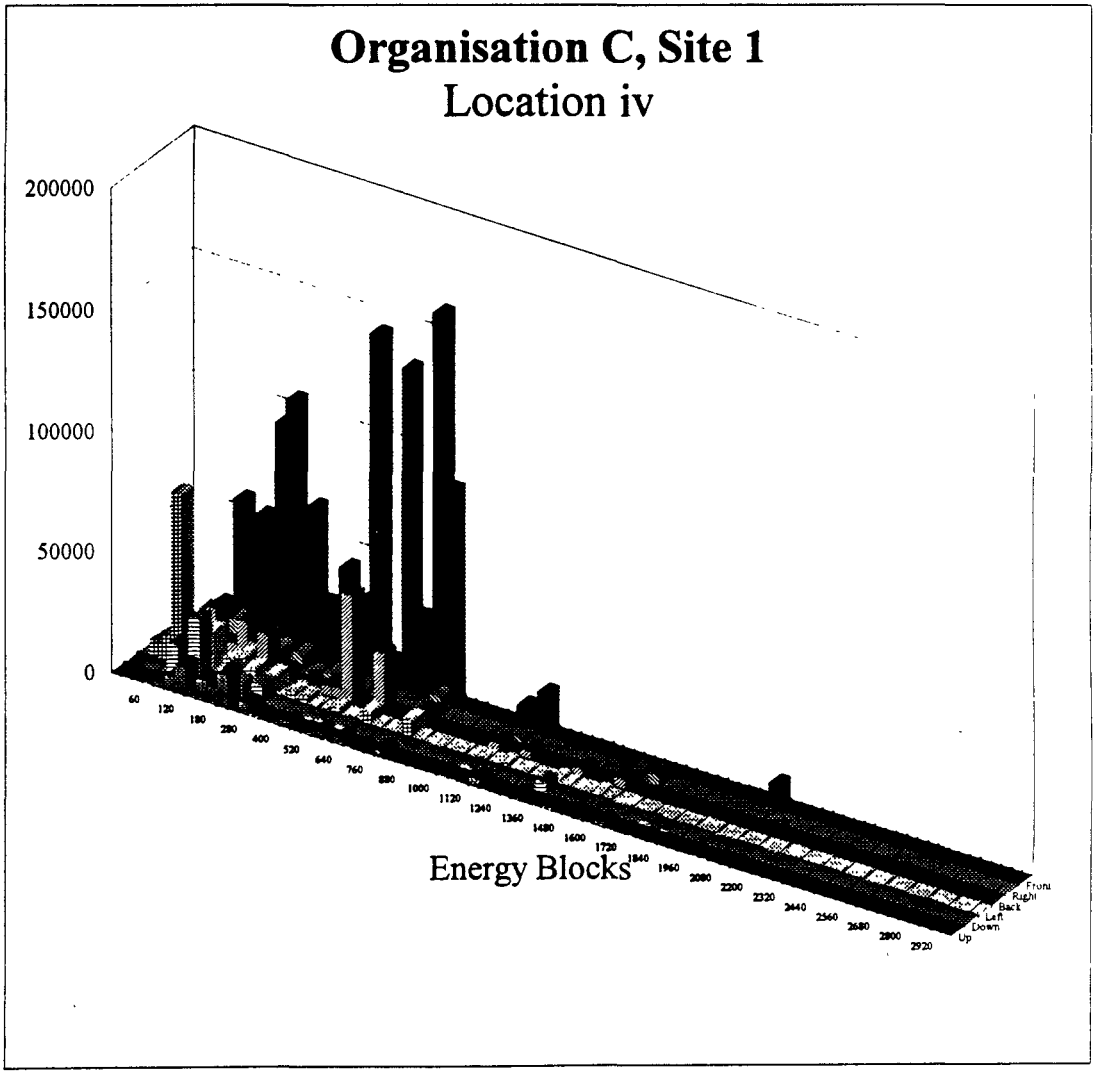

Figure 3 Photon spectra and dose quantities for location iv at Organisation C, Site 1

Organisation C, Site 2

Location	Dose Rate Hp(10) (μSv/h)	Dose Rate HE (μSv/h)	Air Kerma Rate, ka μGy/h	Dose Rate H*(10) (μSv/h)	Hp(10) / HE	H*(10) / Air Kerma
i	41.28	33.38	24.62	42.65	1.24	1.73
ii	1.50	1.34	1.16	1.72	1.12	1.49
iii	6.52	6.06	4.62	7.59	1.08	1.64
iv	5.86	5.05	5.01	6.49	1.16	1.29
v	1.94	1.78	2.02	2.34	1.09	1.16
vi	2.02	1.85	2.15	2.45	1.09	1.14
vii	0.84	0.81	0.84	1.01	1.05	1.21
viii	3.20	2.88	2.77	3.71	1.11	1.34
ix	1.81	1.47	2.01	2.67	1.24	1.32
x	17.55	15.13	17.07	20.40	1.16	1.20
xi	2.07	1.78	1.87	2.26	1.16	1.21

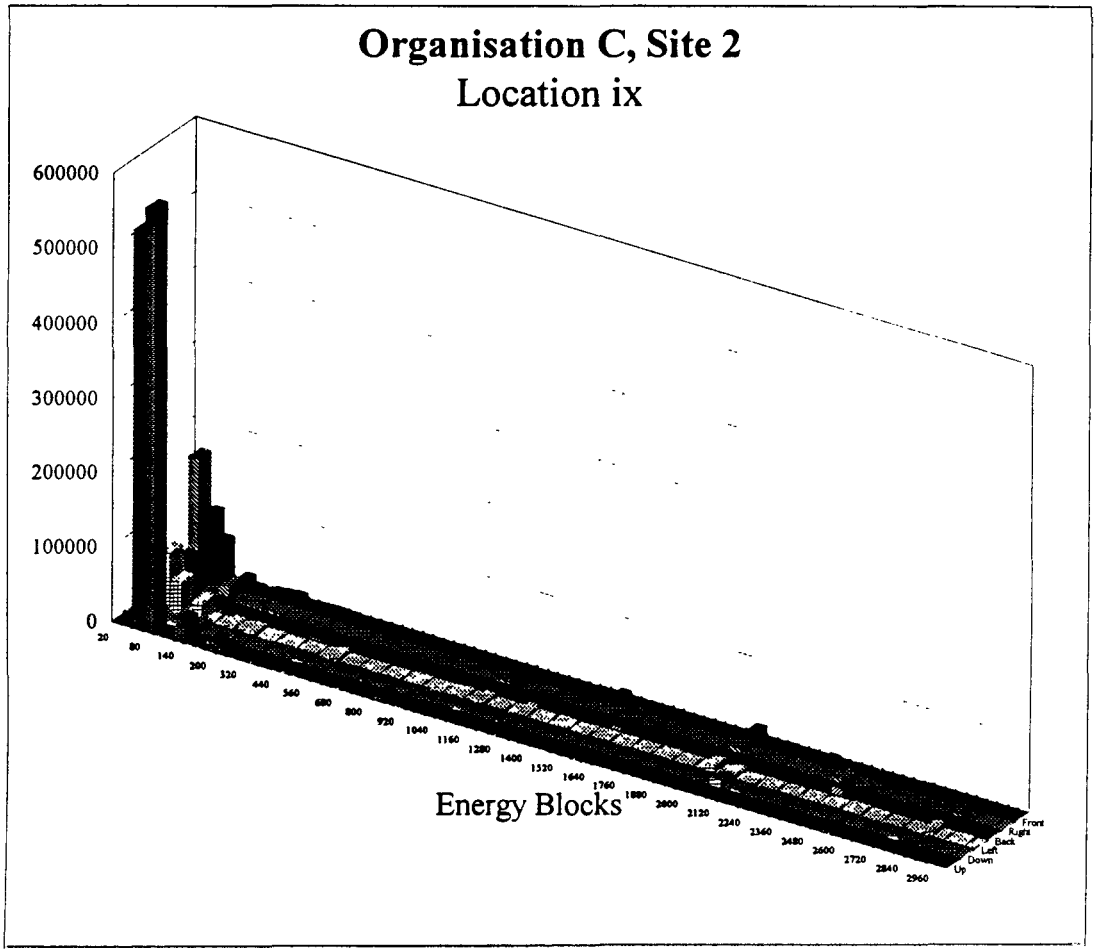

Figure 4 Photon spectra and dose quantities for location ix at Organisation C, Site 2

Organisation C, Site 3

Location	Dose Rate Hp(10) (μSv/h)	Dose Rate HE (μSv/h)	Air Kerma Rate, ka μGy/h	Dose Rate H*(10) (μSv/h)	Hp(10) / HE	H*(10) / Air Kerma
i	4.41	3.80	3.87	5.20	1 16	1 34
ii	1.81	1.76	2.59	3.49	1 03	1 35
iii	4.09	3.95	4.31	5.45	1.04	1 26
iv	3.25	2.63	3.70	4.91	1.23	1.33
v	15.28	15.41	17.40	21.99	0.99	1.26
vi	11.37	10.25	11.87	15.36	1.11	1.29
vii	3.80	3.02	3.85	5.16	1.26	1.34
viii	5.11	4.65	5.29	6.96	1.10	1.32
ix	2.37	3.51	5.15	6.88	0.68	1.33
x	6.41	6.56	7.90	10.09	0.98	1.28
xi	40.05	37.40	40.76	56.32	1.07	1.38
xii	3.29	2.87	3.59	4.68	1.15	1.31
xiii	2.91	2.44	2.53	3.36	1.19	1.33
xiv	19.51	17.28	17.68	22.13	1.13	1.25
xv	11.38	11 88	14 08	18.04	0.96	1 28

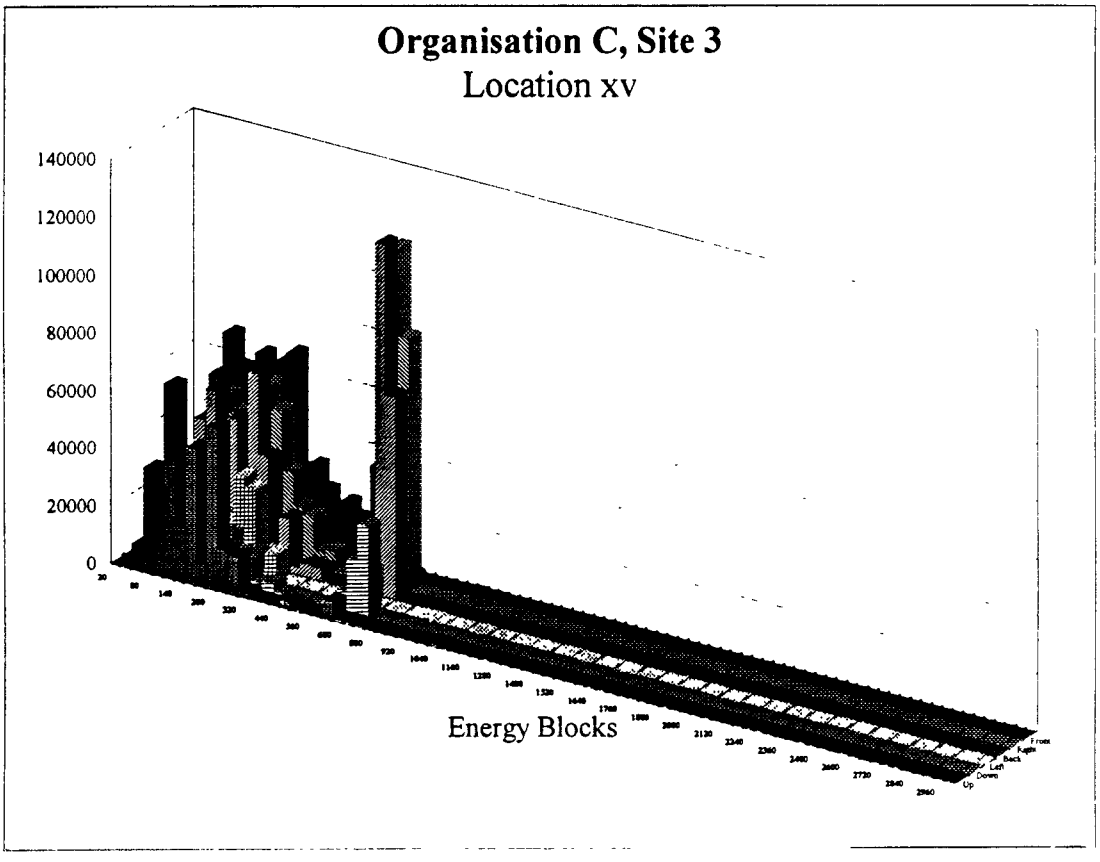

Figure 5 Photon spectra and dose quantities for location xv at Organisation C, Site 3

Organisation C, Site 4

Location	Dose Rate Hp(10) (μSv/h)	Dose Rate HE (μSv/h)	Air Kerma Rate, ka μGy/h	Dose Rate H*(10) (μSv/h)	Hp(10) HE	H*(10) Air Kerma
i	24.95	22.59	26.69	30.63	1.10	1.15
ii	6.43	5.91	6.58	7.71	1.09	1.17
iii	21.84	21.87	24.65	28.64	1.00	1.16
iv	3.91	3.48	4.35	5.07	1.12	1.16
v	1.27	1.13	1.30	1.49	1.12	1.15
vi	2.59	2.36	2.72	3.25	1.10	1.19
vii	11.67	10.27	12.50	14.28	1.14	1.14
viii	1.29	1.21	1.40	1.63	1.07	1.16
ix	6.34	5.44	6.96	8.13	1.17	1.17
x	2.25	2.06	2.32	2.79	1.09	1.20
xi	19.30	16.33	16.36	21.67	1.18	1.32
xii	24.00	20.69	22.63	26.28	1.16	1.16
xiii	0.50	0.47	0.56	0.66	1.07	1.17

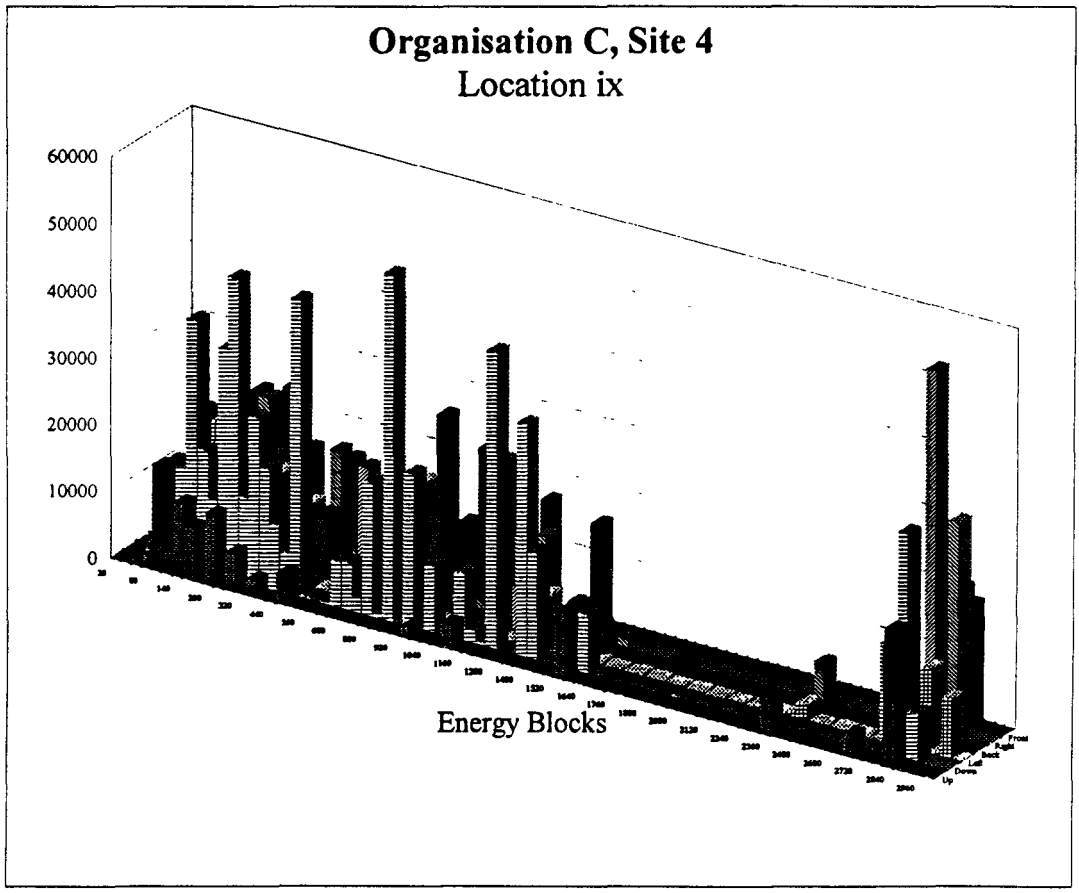

Figure 6 Photon spectra and dose quantities for location ix at Organisation C, Site 4.

Head of Project 2: Mr D Spencer

II. Objectives for the reporting period

1. To develop a Monte Carlo model for the calculation of the response of a photon spectrometer constructed by the NRPB .

2. To validate the Monte Carlo model by comparing calculated response functions with measured pulse height distributions (PHDs).

3. To generate an appropriate response function matrix for the spectrometer

4. To examine unfolding techniques developed for X-ray and neutron spectroscopy and adapt them to obtain energy and angular information from PHDs measured in the workplace.

5. To develop the chosen unfolding technique using response functions generated using the Monte Carlo Model.

6. To validate the unfolding technique using simple PHDs generated by the NRPB under laboratory conditions.

7. To test the unfolding of PHDs measured in workplace situations

8. To correct problems which arise with the unfolding technique.

9. To provide technical backup to NRPB as they carry out further pulse height measurements

10. To prepare a compilation of neutron spectra measured with the Harwell neutron spectrometry system and assess the implications of these spectra for the calibration of personal dosemeters used in the workplace

III. Progress achieved including publications

Development of Monte Carlo model

AEA Technology developed a Monte Carlo model of the collimated NaI spectrometer constructed by the NRPB. The model represented the geometry and construction materials, including the lead collimation, as closely as possible. A schematic diagram of the model is shown on figure 1.

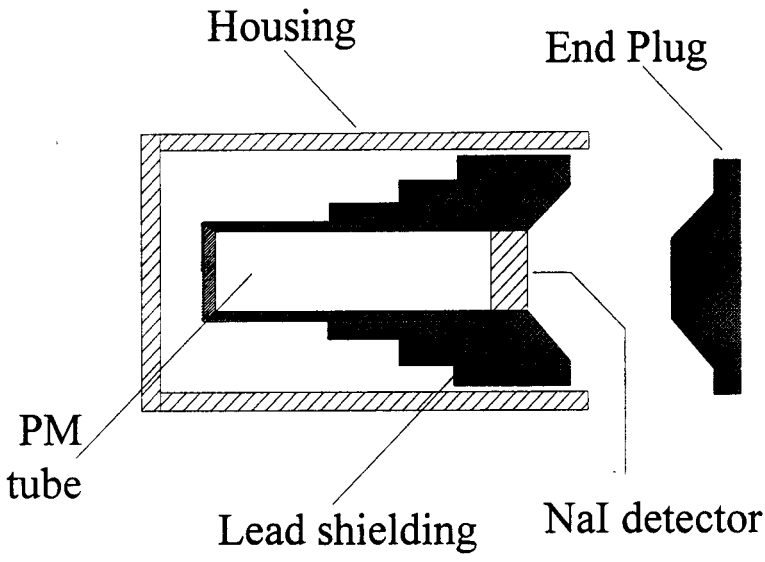

Figure 1. Schematic diagram of spectrometer

The model is based around the EGS4 suite of sub programs. EGS4 includes algorithms for representing both photon and electron interactions, including the photo electric effect. In order to represent the spectrometer, the modeller added routines to represent the geometry and further routines for physical aspects which were not accurately modelled. In order to reduce the required run times, the modeller implemented variance reduction techniques such as Russian roulette, particle biasing and particle splitting.

In order to validate the Monte Carlo model, a ^{137}Cs PHD was generated using the model. The model represented the source of photons as an infinite parallel field of photons. This was then compared with a PHD collected from a ^{137}Cs source by the NRPB using the spectrometer (figure 2). The main difference between the two PHDs is the backscatter peak, present in the measured PHD but not in the calculated PHD. In order to examine the backscatter peak further a model of the ^{137}Cs source was produced. This increased the size of the backscatter peak in the model, but it still remained smaller than the measured peak. It was concluded that the majority of the backscatter peak occurred due to scatter off the surroundings of the detector and source. This illustrates the advantage of using a model of the spectrometer, only the response of the spectrometer is measured and not the response of the detector and its surroundings.

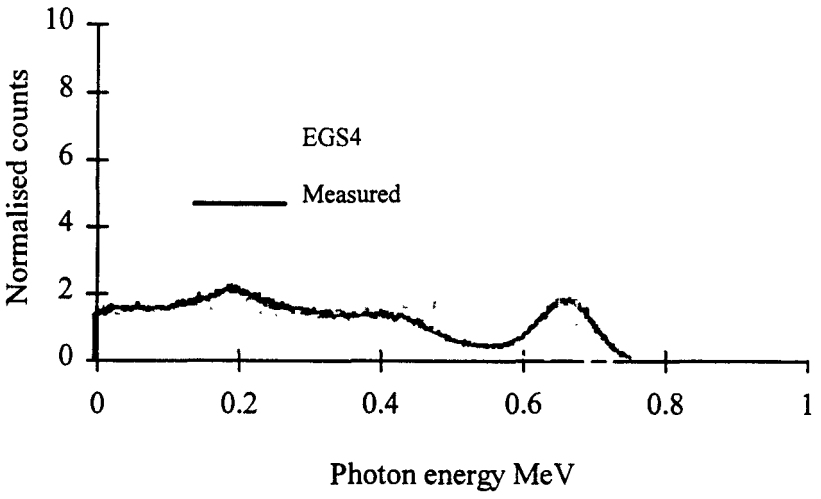

Figure 2. A comparison between an EGS4 generated PHD and a PHD measured using the spectrometer. Note that no resolution effects have been applied to the EGS4 PHD.

The EGS4 model was used to generate further PHDs at different energies to demonstrate that it represented all the appropriate electron and photon interactions. The different PHDs exhibited all the expected features, such as single escape and double escape peaks, Compton edges, electron annihilation peak, X-ray fluorescence peaks and the full energy peak.

Generation of response function matrix

The response of the spectrometer is also affected by random fluctuations in its signal. This introduces resolution effects. As resolution effects are not produced by the physical interactions of photons and electrons, the PHDs produced by the Monte Carlo model have perfect resolution. In order to include resolution effects, a program was written which applies a resolution function to the Monte Carlo generated PHDs. The parameters of the function were taken from spectrometer measurements made by the NRPB.

Response functions were generated at 40 keV intervals, above 200 keV and 20 keV intervals below 200 keV. The resolution effects were then applied to each response function. A matrix of response functions was then compiled.

Development of unfolding technique

A computer program for unfolding PHDs according to energy, which uses an iterative technique, was developed from a program previously developed at AEA Technology. Further programs where developed for rebinning data from the NRPB spectrometer.

We then considered different methods for unfolding PHDs according angle as well as energy. The chosen method uses the design of the collimation, which attenuates photons by same amount from all directions, including the front, when the lead plug is in place.

Six orthogonal measurements of PHDs are made without the plug in place. One additional measurement is made with the lead plug in place. By subtracting the PHD collected with the lead plug in place from each of the other PHDs, the contribution from photons penetrating the lead collimator to the PHD, for a particular direction, is accounted for. But some over compensation occurs, equivalent to the photons which would have penetrated the lead plug from the direction of measurement. The six individual PHDs are then each unfolded according to energy using the iterative technique.

Testing of unfolding technique

The unfolding technique was first tested using groups of PHDs, generated by the NRPB using one or two gamma-ray sources. This showed that the technique worked reasonably effectively.

Further testing was then carried out using PHDs collected by the NRPB from various nuclear sites within the UK. In some cases some unexpected spikes in the spectra were produced at low energies. Examples of a spectra with spikes are shown in figure 3.

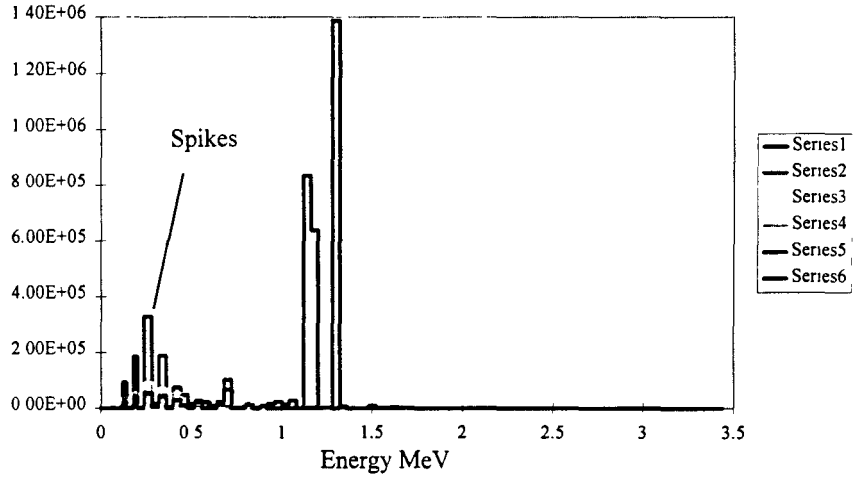

Figure 3. Unfolded spectra showing low energy spikes.

Corrections to unfolding technique

Problems with the unfolding process could arise due to incorrect binning of measured photons, instabilities in the unfolding process which cause oscillations between

adjacent channels, inaccuracies during the iterative stages of unfolding, or large uncertainties in the collected PHDs due to too few counts being collected.

Following examination of the unfolding process the following corrections were made:

- The response function matrix was adjusted to allow for the over compensation for attenuated photons;
- Error in binning program found and corrected;
- Minor errors in unfolding program found and corrected for.

The effect of counts oscillating between adjacent energy bins was not observed.

Figure 4 shows a group of spectra unfolded from a group of PHDs.

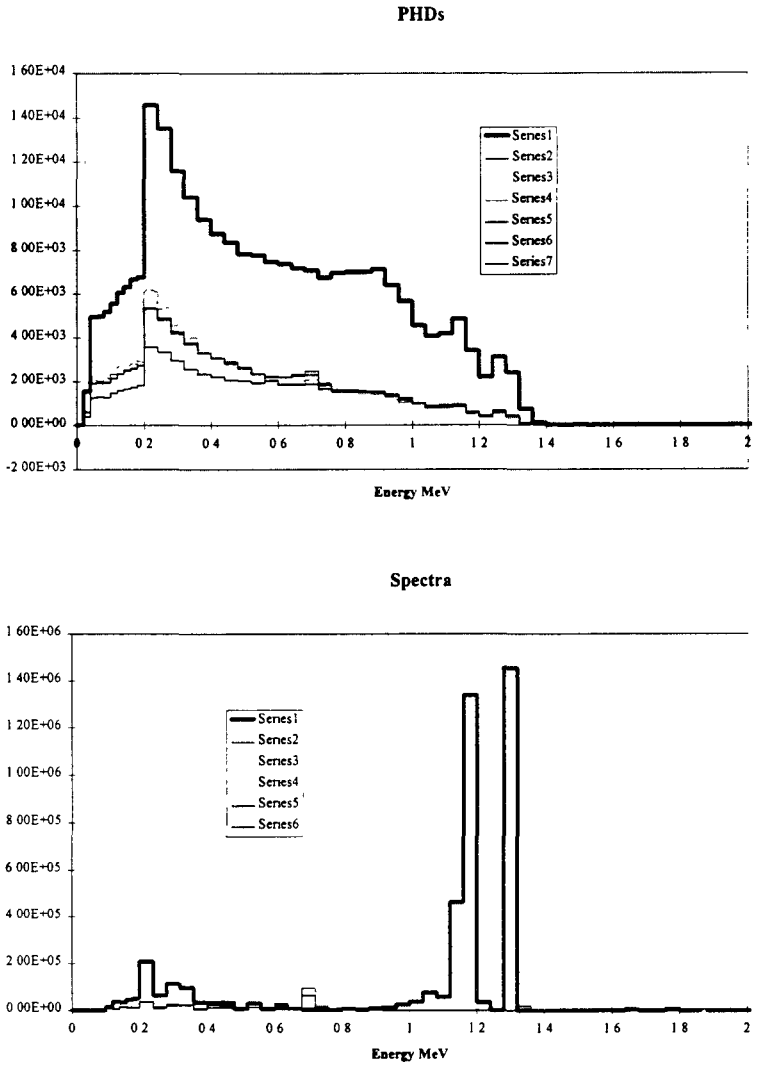

Figure 4. Six spectra unfolded from six PHDs.

Neutron spectrometry

Neutron energy spectra measured with a proton recoil counter spectrometry system and a multisphere spectrometry system have been passed on to the research group compiling a catalogue of neutron spectra under CEC contract number F13P-CT92-0002. During the contract period spectrometry measurements have been made at various locations and minor operational improvements made to the system.

PUBLICATIONS

Development of Energy and Angular Response Functions and an Unfolding Procedure for a Portable Gamma-ray Spectrometer. D Spencer, C A Perks, P Burgess and M Marshall. Proceedings of the 1994 IRPA Regional Congress on Radiological Protection. June 1994.

Head of project 3: Dr G-F Gualdrini

II. Objectives of the reporting period

II-a) Choice of most suitable practical phantom for photon dosimeter calibration

According to the most recent ICRU and ISO recommendations on calibration phantoms for photon radiation, the numerical investigations were addressed to the comparison of practical calibration phantoms (PMMA slab and water filled PMMA slab) with the ICRU theoretical one. The comparison was performed both on the air kerma backscatter factor and on the personal dose equivalent per unit air kerma (Hp/ka) at the various stated depths (0.07 mm, 3 mm and 10 mm).

II-b) Development of a methodology for the design of photon personal dosimeters

A methodology for the design of photon personal dosimeters was developed.

II-c) Assessment of the homogeneity limits on slab phantoms for contemporary calibration of photon personal dosimeters

Further investigations were devoted to the study of the homogeneity area on slab phantoms for contemporary calibration of several dosimeters.

II-d) Comparison of organ doses using ADAM phantom and MCNP

Finally detailed investigations were carried out on the ADAM phantom producing organ doses per unit fluence for various irradiation conditions.

III. Progress achieved including publications

III-a-1) Study of air kerma backscatter factors on the central axis of various tissue equivalent slabs for normally incident beams: Some comparisons with literature data have been carried out with satisfactory agreement. Figure 1 shows a comparison with values taken from Bartlett D. T., Dimbylow P. J. and Francis T. M..

III-a-2) Calculation of Hp/Ka conversion factors at the various stated depths within three tissue equivalent slab phantoms (ICRU 4-element material, PMMA and water in PMMA): These calculations allowed to confirm that water in PMMA phantom is a better substitute of the ICRU theoretical phantom if compared with the pure PMMA one (see figure 2). In tables I, II III and IV a complete study is presented of Hp/Ka values for the mentioned slabs. Monoenergetic normally incident photons were treated with photon energies ranging from 20 keV to 1 MeV. The same set of data was produced for the Narrow and Wide ISO X-ray series for various incident angles (0°, 45°, 60° and 75°)

III-b) Design of Photon Personal Dosimeters

The complete set of field parameters and operational quantities produced for the calibration phantoms were employed to develop a methodology for the design of personal dosimeters

It is possible to describe a dosimeter response through a semi-empirical formula based on a theoretical evaluation of photon interaction by employing both experimental data of the detector energy response R(E) and the numerical parameters obtained using the Monte Carlo method.

A dosimeter can be schematically described by three superposed layers: the radiation detecting layer packed as a "sandwich" between two usually metallic layers. The filtration, besides assuring with a proper thickness that the detector irradiation takes place in electron-photon equilibrium conditions, can be designed in a suitable way to optimise the dosimeter response versus energy and radiation incident angle. The dosimeter is supposed to be placed at a given distance from the phantom irradiated by a photon beam of known spectrum with incident angle ω . Figure 3 outlines the procedure that has been followed for the formulation of the dosimeter relative response function. The example is concerned with the ICRU sphere originally recommended as a suitable phantom, but it can be applied also to different shape phantoms like the slab ones, adopting the appropriate parameters.
In the mentioned example the reference operational quantity is the directional dose equivalent $H'(d,E,\omega)$ where d is the depth in the phantom, E the source energy and ω the incident angle. In the limits already explained $H'(d,E,\omega) = H_p(d,E,\omega)$.

Firstly the experimental energy response R(E) is determined for the bare detector irradiated with ISO reference beams (Wide and Narrow Spectrum Series) for energies ranging from about 20 keV to 1250 keV. Secondly the backscattered component of the field, due to the presence of the phantom, is characterised by means of the Monte Carlo calculations mentioned before.

For each value of equivalent energy E and direction ω of the incident radiation, the collision kerma backscatter factor and the backscattered radiation mean energy ($\bar{E}_B$) is computed and afterwards the $R(\bar{E}_B)$ is obtained by interpolating the R(E) curve.

In the formula the two contributions of the incoming and backscattered radiation components appear thereafter as separated terms and they are both corrected for the interaction process with the filtration. Thickness and material of the filtration can be varied in order to obtained the most possible constant relative response (H'/R'). So, for every reference ISO beam that is characterised by spectrum, or, more simply, by its equivalent energy (E), given the following parameters: incident angle (ω), distance (d') between the dosimeter and the phantom, matter (Z) and thickness (x) of the filtration, one can write the relative response function formula:

$$\frac{H'(d,\omega)}{R'} = \frac{\dfrac{H'(d,0)}{Ka}\,\dfrac{H'(d,\omega)}{H'(d,0)}}{R_{in}\,e^{-\mu_{in}(Z)\,x(\omega)} + (B(d',\omega)-1)\,R_B\,e^{-\mu_B(Z)\,x(\omega)}}$$

where *in* and *B* indicate that the values are related respectively to the incidence energy E and to the backscattered mean energy $\bar{E}_B(d',\omega)$ and the exponential terms represent the incident as well as backscattered beam attenuation through the front and back filters.

III-c) Studies on the homogeneity of photon fields for contemporary calibration of photon personal dosimeters on slab phantoms.

The most recent ICRU recommendations suggest to calibrate personal dosimeters under simplified conventional conditions on a phantom sufficiently representative of the average human trunk and with defined reference radiation beams. At the beginning ICRU-39 suggested the ICRU sphere as a suitable calibration phantom for individual monitoring. In this case to irradiate the sphere completely a field diameter of 30 cm is necessary.

The introduction of the already mentioned recently suggested slab phantoms implies that the field diameter that can guarantee an homogeneous phantom irradiation has to be increased to about 42-45 cm. Such large homogeneous field can be achieved in principle by larger distances from the source. For practical reasons however this is often not possible. The backscattering from the rear walls of the irradiation room has to be negligible and the air kerma rate of the primary radiation should be high enough to perform testing and calibration of dosimeters with very heavily filtered X-rays.

In Italy about 40 qualified Dosimetric Services are operating. It is foreseen that their number could be increased in the forthcoming years to about 80. This implies that the Secondary Standard Dosimetry Laboratory at ENEA in Bologna should in principle perform several different type tests of these dosimetric systems. It is therefore necessary to shorten as much as possible the irradiation time so that an high kerma rate X-ray Series has to be used. Notwithstanding the fact that ISO recommends the Narrow Spectrum Series for calibration purposes, the Wide Spectrum Series is foreseen to be adopted in the future for these purposes.
In order to characterise the X-ray fields in terms of their penumbra film slabs were used . A micro-densitometer was employed as a reader and the homogeneity of the field area was verified within ± 2.5% as stated by ISO 4037 (where an homogeneity of the calibration field within 5% is stated as permissible) . The high energy dependence of the film slab response was limited using adequate filtering .

A useful field of 15 cm. width at 1 meter from the source was in this way determined.

To enter in more detail in the study of the field homogeneity conditions on a slab phantom, two aspects are to be taken into account.
The first problem is that X-rays are emitted rather anisotropically from the tube especially when trying to obtain rather broad beams.
Secondly the backscattered radiation decreases from the central axis to the edges of the slab phantom.

The already mentioned experimental tests on field homogeneity in free air developed at the ENEA were carried out for a limited number of ISO reference beams. On the other hand the very accurate measurements by Shimizu and Minami and Will demonstrated that the non-homogeneity of the calibration field due to both the source X-ray beam anisotropy and the calibration phantom backscatter variation should be carefully taken into account during the calibration procedure.

The present numerical studies were therefore aimed at determining the homogeneity field limits in presence of the two proposed tissue equivalent slab phantoms. Some investigations on the effect of phantom rotation on the backscatter factor as a function of the position of the measurement point were also developed.

The first simplified study was carried out for PMMA and water in PMMA slab phantoms irradiated with the complete normally incident Narrow and Wide Spectrum Series. Figure 4 supplies an example of spatial air kerma backscatter factor (B) profile on the phantom front face: a set of figures like this can be used to state an homogeneity area (using again the ±2.5% criterion as mentioned above).

The effect of the phantom rotation was investigated for different angles in order to evaluate its influence on the backscattered component at various positions on the front surface of the phantom irradiated with a parallel homogeneous beam. The effect of rotation on the backscattered component can be significantly detected only at angles > 60°. At 75° angle the effect is quite evident . It has on the other hand to be pointed out the plotted backscatter factor values are referred to the air kerma value (ka free in air) as determined at the point corresponding to the centre of the phantom surface. This means that to determine the different air kerma backscatter factors from position to position on the phantom surface in realistic irradiation conditions an $(R_X/R_0)^2$ correction factor should be applied (where R_X is the distance from the anode to the "x" dosimeter and R_0 is the distance from the anode to the centre of the irradiated face that is also assumed as centre of rotation). Figure 5 supplies the corrected values for 3 m. source to phantom distance.

For the same reason when calibrating several dosimeters at a time with increasingly higher beam incident angles, each dosimeter is subject to different field rates, depending on its distance from the source: the higher the incident rate, the higher is also the backscatter component on the specific dosimeter. In order to achieve similar calibration conditions as compared with the central dosimeter, the measurement can be carried out in two equal time steps in two symmetric phantom positions.

Moreover very recently Kramer from PTB produced a complete mapping of air kerma measurements (free in air) for the ISO Narrow Series and for the ISO Wide Series, that allows a comprehensive analysis of the field homogeneity in realistic calibration conditions. The measurements were made at 1 meter from the source with a grid of 0.5 cm pitch. The size of the field corresponds to the largest divergence used at PTB Laboratory (a diameter of 15 cm. at 1 m.) that is in agreement with the largest field divergence adopted at ENEA . Figure 6 supplies a three dimensional profile of the air kerma free in air profile for a 300 kV beam of the Narrow Spectrum Series. The irradiation on the phantom is performed at PTB at 3 meters from the source: a preliminary check on the numerical values supplied by Kramer showed variations of about 3% from the maximum value in the area of interest: some studies were performed to evaluate the effect of this source azimuthal asymmetry. The spectrum was as a first approximation assumed as constant at every measurement point so that the source photon fluence profile could be taken as the same as the air kerma profile. A special source was prepared for MCNP to supply the probability density function depending on two spatial variables. The source was thereafter expanded to match with the irradiation area at 3 meters from the source. The slab surface was subdivided in little squares with dimensions very close to those of a dosimeter card (2.5x2.5 cm) for a total of 144 geometry cells. The air kerma values for every position were thereafter sampled tracking about 1.500.000 particles per run.

It has to be pointed out that the beam area that is used for the calibration is quite small as compared with the area where the air kerma free in air profile has been measured so that, as expected, the statistical fluctuations of the results can at some extent hide the effect of the small source field asymmetry.

The MCNP results are affected by a 1-1.5% standard deviation, so that the asymmetry in these two practical ISO beam series will not strongly affect the homogeneity limits on the slab surface as evaluated with the more simplified approach (see figure 7 for an example of comparison between the two modelling approaches). A quite significant asymmetry was experienced in the air kerma backscatter factor for the real spatial distribution of the 150 kV Wide Spectrum Series beam.

The discrepancies between the two approaches (homogeneous normally incident beam , and real beam) are normally within 2% with some cases reaching values > 4%.
Taking into account the two sensibly different spatial distributions of the source in the two cases, the results can be considered quite satisfactory.

To give some preliminary quantitative indication on the homogeneity areas on the slab phantom, we can say that for PMMA material variations of B within ± 1% (2% from the maximum central value) occur inside a 6x6 - 10x10 cm square, ± 2.5% variations (5% from the maximum central value) occur inside a 12x12 - 16x16 cm square, whilst variations within ± 5% (10% from the maximum central value) occur inside a 20x20 - 24x24 cm square. These conclusions , that are in substantial agreement with experimental results obtained by Mc Clure et al. (IRPA Meeting Portsmouth 1994) and Will (Rad Prot Dosim 1993), demonstrate that the useful area for contemporary calibration of individual dosimeters in slab phantoms has to be significantly reduced.

III-d) Effective dose and effective dose equivalent calculations

In the ICRP-60 recommendations, the International Commission for Radiological Protection substituted the effective dose equivalent, H_E , with a similar quantity - the "effective dose", E - changing both the set of organs considered and the respective weighting factors.
In a publication by Zankl et al on Health Physics 1992 a study of the impact of these new recommendations on the numerical values of E for various photon monoenergetic beams was carried out.

Some preliminary studies were developed also at ENEA with a previous version of the ADAM phantom . The investigations were carried out with MCNP for photon energies ranging from 100 keV to 10 MeV. General satisfactory agreement with organ doses as supplied by ICRP 51 document was obtained except for the thyroid for P/A irradiation, probably due to the different modelling of neck-head region as compared with the ICRP-51 based results (see figures 8-11). Some preliminary evaluations of E were carried out. The general trend of the results shows an underestimation of E as compared with H_E, confirming the conclusions of M. Zankl for photon energies > 15 keV .

At the moment a new phantom is available and a systematic study is about to be started both on ADAM (see figure 12) and EVA to evaluate organ doses as well as effective doses and supply an independent check of the already published data . It will be also worthwhile to examine in some detail the effect on the dose evaluations of the kerma approximation that have been used for all the previous calculations. The effect of taking into account secondary electron transport is expected to be significant for superficial organs of small dimensions (of the order of the secondary electron range) especially for higher energy incident photons.

The two available phantoms are also planned to be used for particular dose assessment situations with partial body irradiation.

Publications for the reporting period

/1/ Gualdrini G. F. and Morelli B. " Coefficienti di Conversione fra Kerma in Aria ed Equivalente di Dose su Fantocci Piani per il Monitoraggio Individuale di Fotoni da 20 keV a 1 MeV." XXIX Congresso AIRP (Trieste September 27- 30 1995)
/ 2/ Gualdrini G. F. and Morelli B. " Air Kerma to Personal Dose Equivalent Conversion Factors for the ICRU and ISO Recommended Slab Phantoms for Photons from 20 keV to 1 MeV." RT/ENEA/AMB in preparation
/3/ Gualdrini G. F. and Morelli B. " Studies on the Field Homogeneity Area on Tissue Equivalent Slab Phantoms for ISO X-Ray Reference Beams." RT/ENEA/AMB in preparation

References for the whole contract period

/1/ Gualdrini G.F. " Field Parameters and Operational Quantities for the ICRU sphere with Reference Photon Beams. PART 1° Monte Carlo calculation of angular distribution of backscatter factors. ENEA/RT/AMB/92/12
/2/ Gualdrini G.F., Padoani F. and Morelli B. " Field Parameters and Operational Quantities for the ICRU sphere with Reference Photon Beams. PART 2° Monte Carlo calculation of backscattered spectra and backscattered mean energy angular distribution." ENEA/RT/AMB/92/13
/3/ Gualdrini G.F., Monteventi F. and Sermenghi I. " Field Parameters and Operational Quantities for the ICRU sphere with Reference Photon Beams. PART 3° Experimental and computational analyses on the tissue substitute material RS-1" ENEA/RT/AMB/92/24
/4/ Gualdrini G. F., Lembo L., Monteventi F. and Padoani F. "Monte Calculations of Field Parameters for the ICRU Sphere with Reference Photon Beams." Rad. Prot. Dosim. 46, 5-13 (1993)
/5/ Morelli B. and Gualdrini G.F. Moteventi F." Field Parameters and Operational Quantities for the ICRU sphere with Reference Photon Beams. PART 4°. Monte Carlo and Experimental Evaluation of Angular Dependence of Dose Equivalent Quantities ENEA/RT/AMB/94/19.
/6/ Morelli B. "Valutazione di Dose da Irraggiamento Fotonico su Fantoccio Antropomorfo mediante Tecniche Monte Carlo" Heatlh Physisics Course Thesis - University of Bologna (1994)
/7/ Casalini L. "Applicazione dei Codici SABRINA e MCNP al Fantoccio Antropomorfo ADAMO." ENEA-ERG-RTI-CT WCD 00005, (1994)
/8/ Gualdrini G.F, Casalini L.and Morelli B., "Monte Carlo Technique Applications in the Field of Radiation Dosimetry at the ENEA Radiation Protection Institute: a Review.", Proceeding of the "Fourth Conference on Radiation Protection and Dosimetry " Orlando (Florida) October 23 - 27 1994.
/9/ Gualdrini G. F. and Morelli B. " Coefficienti di Conversione fra Kerma in Aria ed Equivalente di Dose su Fantocci Piani per il Monitoraggio Individuale di Fotoni da 20 keV a 1 MeV." XXIX Congresso AIRP (Trieste September 27- 30 1995)
/10/ Gualdrini G. F. and Morelli B. " Air Kerma to Personal Dose Equivalent Conversion Factors for the ICRU and ISO Recommended Slab Phantoms for Photons from 20 keV to 1 MeV." RT/ENEA/AMB in preparation
/11/ Gualdrini G. F. and Morelli B. " Studies on the Field Homogeneity Area on Tissue Equivalent Slab Phantoms for ISO X-Ray Reference Beams." RT/ENEA/AMB in preparation

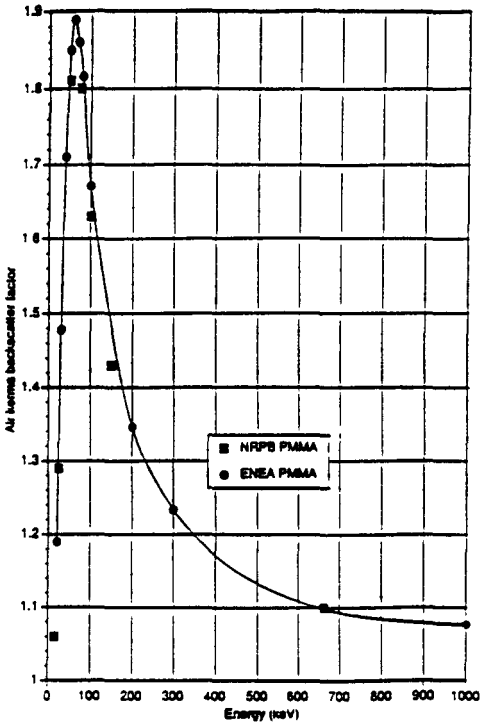

Fig. 1 Air Kerma Backscatter Factor per unit air Kerma (free in air) for normally incident monochromatic beams on a PMMA slab: comparison between NRPB and ENEA results.

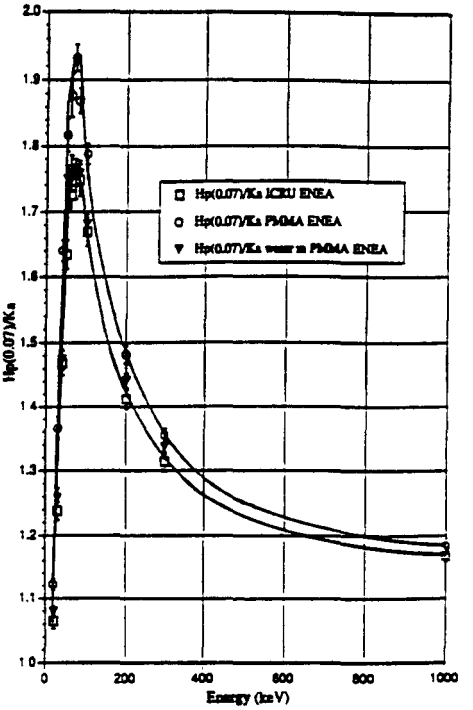

Fig. 2 Hp(0.07)/Ka comparison for the two practical slab phantoms (PMMA and water in PMMA) with the ICRU 4-element theoretical one.

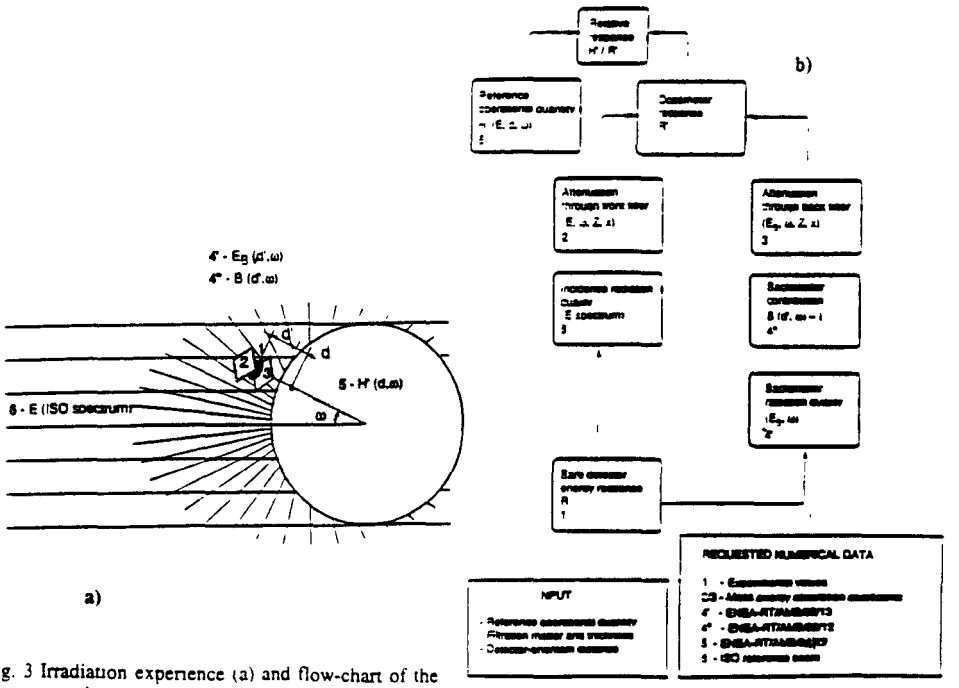

Fig. 3 Irradiation experience (a) and flow-chart of the dosemeter relative response function formulation (b).

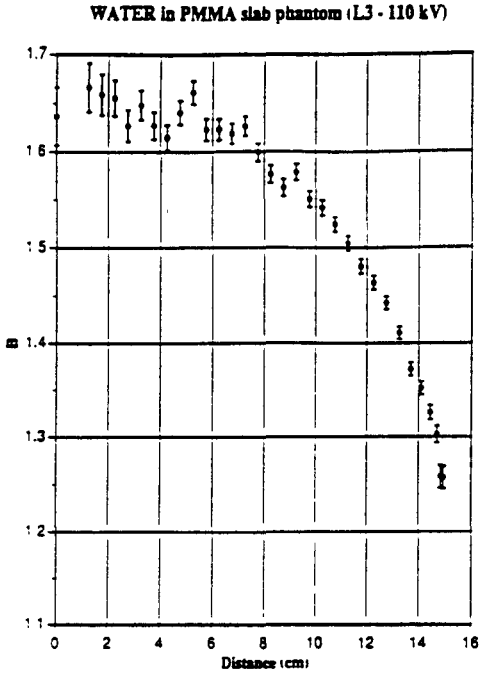

Fig. 4 Air Kerma Backscatter Factor per unit air Kerma (free in air) profile for a normally incident X-ray homogeneous beam of 110 kV (Wide Spectrum Series)

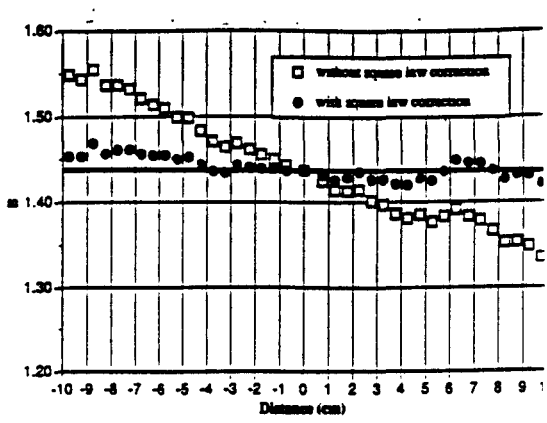

Fig. 5 Air Kerma Backscatter Factor per unit air Kerma (free in air) profile for a 110 kV (Wide Spectrum Series) X-ray beam incident at 75 degrees on a PMMA slab phantom and correction of the curve for the distance inverse square law.

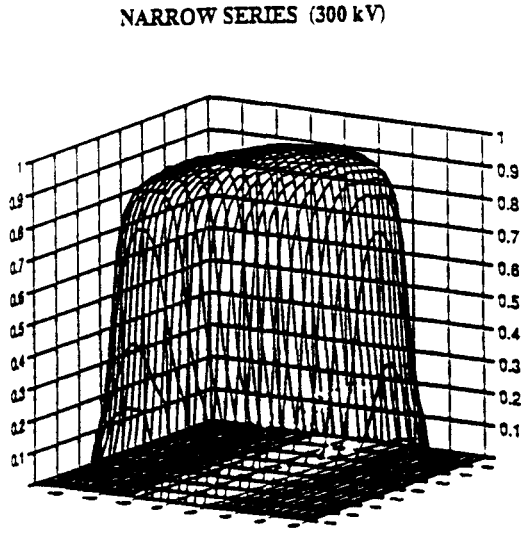

Fig. 6 Three dimensional shape of the Air Kerma distribution as measured by Kramer (300 kV of the Narrow Spectrum Series).

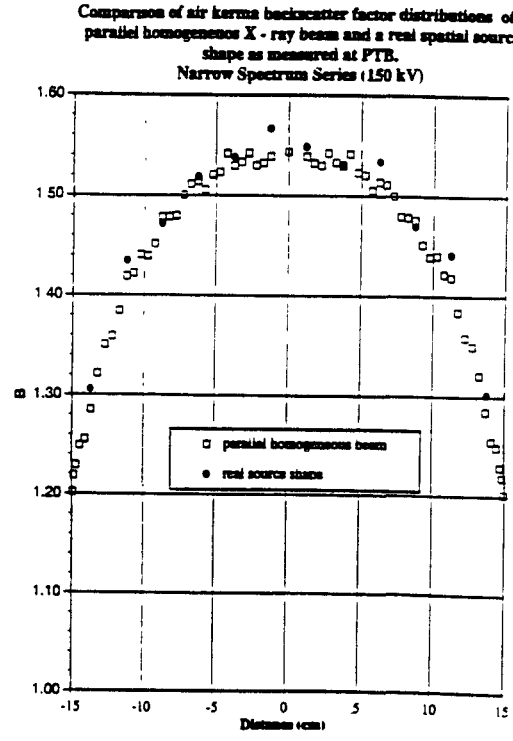

Fig. 7 Air Kerma Backscatter Factor per unit air Kerma (free in air) profile for a 150 kV X-ray beam of the Narrow Spectrum series: comparison between the two source models in MCNP

Fig. 8

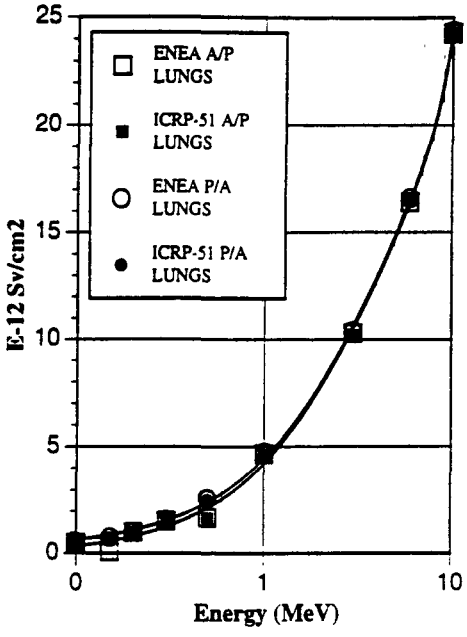

Fig. 9

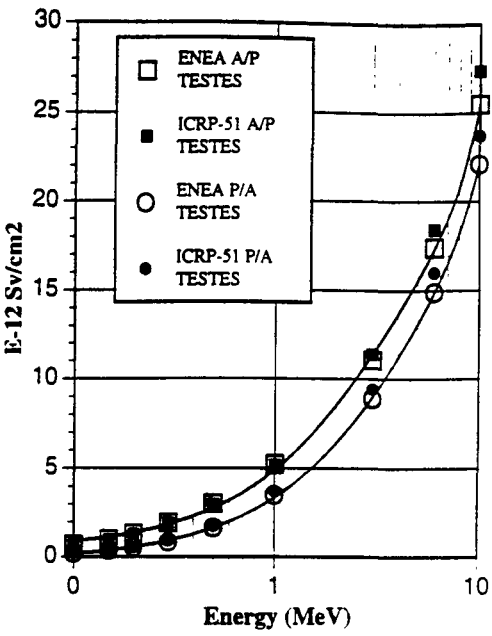

Fig.10

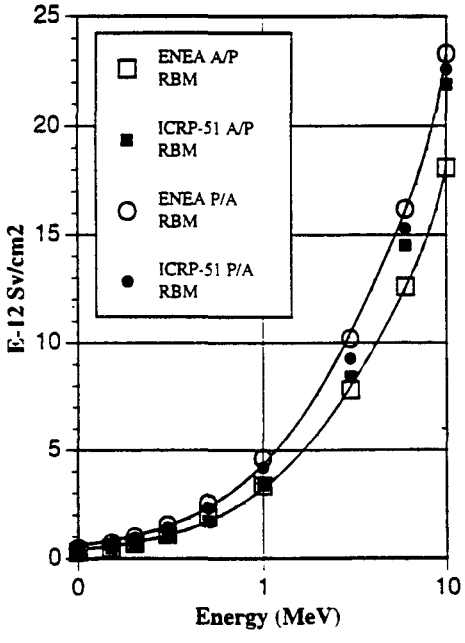

Fig. 11

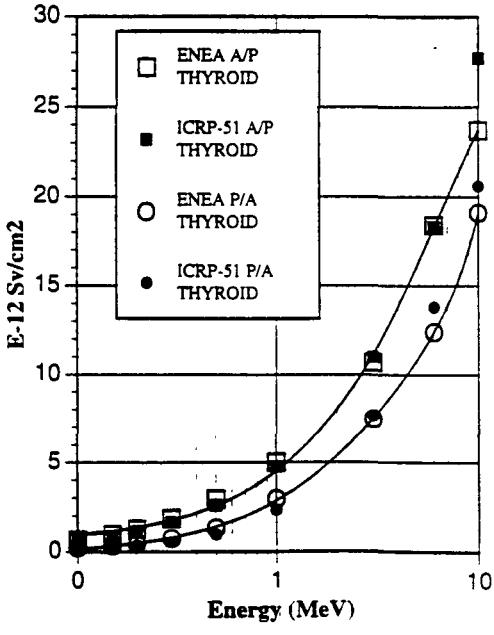

Tab. I: Hp/ka for three tissue equivalent slab phantoms.

Depth = 0.07 mm				
Energy	ICRU		PMMA	H_2O
(keV)	ENEA	PTB	ENEA	ENEA
20	1.065	1.040	1.122	1.079
30	1.238	1.227	1.366	1.258
40	1.469	1.441	1.641	1.474
50	1.635	1.629	1.817	1.749
60	1.725	1.720	1.877	1.758
70	1.746	1.741	1.932	1.761
80	1.748	1.719	1.869	1.758
100	1.670	1.670	1.788	1.681
200	1.412	1.424	1.482	1.441
300	1.314	1.338	1.355	1.336
1000	1.169	1.179	1.185	1.173

Tab. II: Hp/ka for three tissue equivalent slab phantoms.

Depth = 0.1 mm			
Energy	PMMA		H_2O
(keV)	ENEA	PTB	ENEA
20	1.120	1.087	1.0798
30	1.376	1.323	1.258
40	1.613	1.577	1.477
50	1.817	1.759	1.674
60	1.929	1.848	1.758
70	1.878	1.859	1.763
80	1.864	1.831	1.764
100	1.766	1.746	1.685
200	1.464	1.460	1.445
300	1.345	1.359	1.335
1000	1.182	1.179	1.178

Tab. III: Hp/ka for three tissue equivalent slab phantoms.

Depth =3 mm					
Energy	ICRU		PMMA		H_2O
(keV)	ENEA	PTB	ENEA	PTB	ENEA
20	0.939	0.909	1.061	0.984	0.959
30	1.250	1.223	1.398	1.348	1.252
40	1.545	1.496	1.707	1.657	1.523
50	1.707	1.713	1.934	1.880	1.718
60	1.796	1.807	2.010	1.976	1.864
70	1.783	1.823	1.981	1.994	1.855
80	1.805	1.809	1.968	1.941	1.812
100	1.726	1.743	1.842	1.831	1.740
200	1.460	1.463	1.527	1.499	1.474
300	1.347	1.354	1.394	1.383	1.367
1000	1.164	1.182	1.180	1.184	1.176

Tab. IV: Hp/ka for three tissue equivalent slab phantoms.

Depth =10 mm					
Energy	ICRU		PMMA		H_2O
(keV)	ENEA	PTB	ENEA	PTB	ENEA
20	0.644	0.613	0.758	0.718	0.631
30	1.155	1.105	1.346	1.254	1.129
40	1.529	1.495	1.742	1.683	1.516
50	1.778	1.769	1.982	1.979	1.783
60	1.921	1.890	2.110	2.095	1.949
70	1.921	1.911	2.105	2.109	1.956
80	1.916	1.891	2.100	2.051	1.943
100	1.832	1.812	1.978	1.926	1.831
200	1.483	1.489	1.543	1.531	1.495
300	1.342	1.370	1.403	1.396	1.369
1000	1.167	1.175	1.174	1.177	1.176

Head of project 4 : Dr. Chartier

II - Objectives for the reporting period.

The research programme of the IPSN-CEA/SDOS in the frame of this contract dealt with the calibration procedures of individual dosemeters taking into account the recommendations of ICRP[1] for risk (protection) quantities, those of ICRU[2] for operational quantities and also those of ISO/WG2[3] in charge of the preparation of international standards. This activity exhibits a clear complementarity with that of AEA Harwell - NRPB partners in charge of commissioning a spectrometric instrument to determine the angular and energy distributions of photon radiation fields at workplaces. Four french routine dosimetry services have contributed to this irradiation programme, providing different types of dosemeters currently in use for personnel monitoring. Several sets of irradiations were organised in order to study characteristics of dosemeters in terms of energy response, angular response and to clarify, in practical calibration conditions, the influence of phantom material and radiation incidence on the dosemeter. A further step was an attempt to simulate the movement of the dosemeter, when it is worn by a person moving in the radiation field encountered at workplace. In addition, based on spectrometric data provided by AEA Harwell - NRPB staffs, practical photon spectra were roughly replicated on the IPSN/SDOS calibration facility and used in irradiations.

III - Progress achieved including publications.

Irradiation programs :

In a first step, on-phantom irradiations of dosemeters were performed with X-ray qualities of the ISO narrow spectrum series : 23 keV (fluorescence), 48 keV, 83 keV, 118 keV, 205 keV (filtration) and ^{60}Co. Two incidence angles of the beam with respect to the phantom were considered, namely 0° and 30°. In addition, oscillating phantom conditions (- 30°, + 30°) were also applied. Then, in order to deal with the recent conclusions of the ISO/WG2[4], the influence of the phantom material was studied by performing a part of irradiations with a « reference » ISO phantom (water phantom with a 2 mm PMMA front face).

Each participating laboratory was asked to assess the « dose » value (« dose » stands for « dose for record-keeping ») by its usual procedure in order to quantify the deviation with respect to the $H_P(10)$ reference value, and, if necessary, to correct the algorithm enabling the « dose » determination.

For the last period of the contract, the objective was to replicate in the laboratory radiation fields encountered at workplaces, according to experimental data provided by other contractors (AEA Harwell and NRPB). In addition, routine dosimetry services proposed field characteristics (i. e. energy spectra) usually met in some nuclear installations, and in addition, the angular range of the oscillating calibration phantom was increased (- 45°, + 45°).

The irradiation programme is based on six spectral groups (SG) elaborated from different combinations of four photon radiation qualities : H-250, W-300, S-Co, F-Pb[3], as summarised in Table 1. Kerma-to-personal dose equivalent conversion coefficients are those given in references (3), (5), (6).

SG	S-Co		H-250		W-300		F-Pb		Total		Irradiation
	Ka	$H_p(10)$	Ka	$H_p(10)$	Ka	$H_p(10)$	Ka	$H_p(10)$	Ka	$H_p(10)$	Geometry *
1	2	2.30	-		-		-		2	**2.30**	F ; V
	5	5.75	-		-		-		5	**5.75**	F ; V
	10	11.50	-		-		-		10	**11.50**	F
2	2	2.25	-		-		-		2	**2.25**	F'
	5	5.60	-		-		-		5	**5.60**	F'
3	2	2.30	-		-		-		2	**2.30**	F
4	-		1	1.67	-		-		1	**1.67**	F ; V
	-		4	6.68	-		-		4	**6.68**	F
5 a	3	3.45	1	1.67	-		-		4	**5.12**	F ; V
5 b	2.5	2.875	2.5	4.175	-		-		5	**7.05**	F ; V
5 c	1	1.15	3	5.01	-		-		4	**6.16**	F
5 d	1	1.15	0.5	0.835	-		-		1.5	**1.985**	V
6 a	1	1.15	-		1	1.47	1	1.90	3	**4.52**	F
6 b	3	3.45	-		0.5	0.735	1	1.90	4.5	**6.085**	V

(*) **F** : stationary ISO phantom - **F'** : F + 5 mm thick PMMA slab - **V** : oscillating ISO phantom
K_a : air-kerma (mGy)
$H_p(10)$: Personal dose equivalent (mSv)

Table 1 : Personal dosemeters irradiation programme.

Realistic conditions are simulated by those different spectral configurations according to the following arrangements :

- SG 1, 2, 3 = Reference conditions (^{60}Co) including CPE conditions and applications.
- SG 4 = Energy range [40 keV - 250 keV] + W K lines [65 keV].
- SG 5 = Spectrum 4 + ^{60}Co.
- SG 6 = (^{60}Co) + energy range [40 keV - 300 keV] + Pb K lines [75 keV].

Four laboratories agreed to participate and provided 80 dosemeters.

Evaluation and comments on results :

1 - *Uncertainties* :

For each « point » (i. e. = energy, angle of incidence, phantom movement) a batch of four dosemeters has been tested. The uncertainty has been calculated according to the procedure recommended by WECC, with a value of 2 for k, applied to the distribution of 4 individual values.

Most results obtained by this method are generally below 10%, but a few values reach 15 and even 30% (Figure 1).

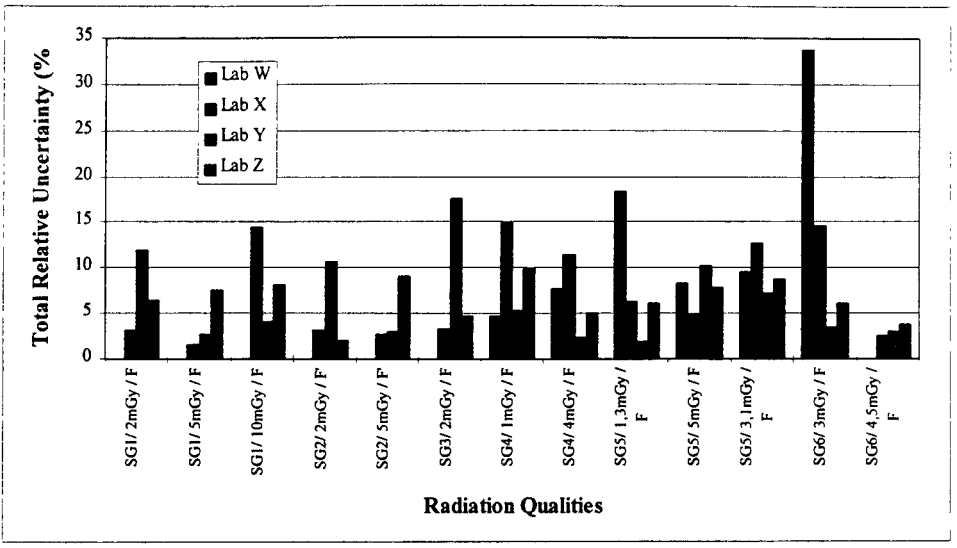

Figure 1 : Total uncertainty on dosemeters results.

2 - *Influence of phantom material and phantom movement* :

From previous measurements the influence of phantom material on the dosemeter response depends on the dosemeter construction (report IPSN/CEA - SDOS - june 1993-june 1994).

Concerning the effect of the phantom oscillation during irradiation, again it seems to be dosemeter construction and energy dependent. Those topics must be specifically dealt with, as shown on Figure 2 (Lab W - Sp. 1).

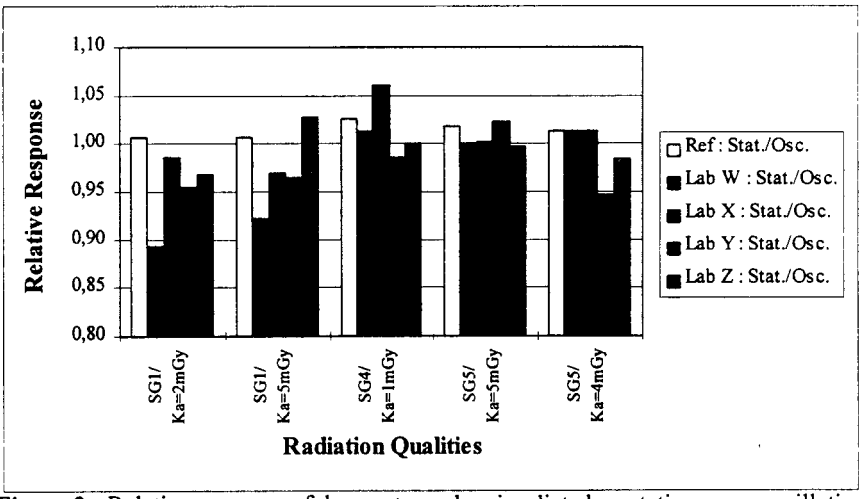

Figure 2 : Relative response of dosemeters when irradiated on stationary or oscillating phantom.

3 - *Relative deviations of results* :

An overall analysis of data provided by participating laboratories enables to derive some main trends. In order to simplify the final analysis, spectral configurations have been shared in two main parts :

- Part 1 includes SG 1, 2 and 3 refering to calibration conditions.
- Part 2 includes SG 4, 5 and 6 expected to simulate more realistic situations, for instance « wide » photon spectra exhibiting an additional low or/and high energy component.

Table 2 summarises the evaluation of results.

Lab.	Part 1	Part 2		
	SG 1, 2, 3	SG 4	SG 5	SG 6
X	+ 10% → + 20%	+ 10% → + 15%	≈ + 10%	+ 15% → + 20%
Y	+ 10% → + 20%	≈ + 30%	+ 15% → + 30%	+ 10% → + 20%
Z	- 4% → - 12%	+ 5% → + 8%	0% → + 8%	+ 3% → + 5%
W	+ 8% → + 12%	+ 8% → - 5%	0% → - 30%	0% → - 10%

Table 2 : Deviations of results in terms of $H_P(10)$.

Numerical results in column 2 give information on the calibration procedures as performed by each laboratory : i. e. systematic overestimation for Lab. X, Y and W, underestimation for Lab. Z. Due to the fact that irradiation conditions are very well defined, this behaviour denotes some inconsistency either in the experimental protocol or in the dosemeter construction.

In columns 3, 4, 5, a great similarity is observed for Lab. X and Y, i. e. a large overestimation of the dosemeters indications, reaching up to + 30% in some cases. Whereas Lab. Z gives generally satisfactory results (deviation below 8%), Lab. W results vary from + 8% down to - 30% when the photon spectrum is complex. A more detailed investigation about this point shows clearly the link with the relative kerma contributions of ^{60}Co and H-250 (or W-300) photon radiation (Figures 3, 4, 5, 6).

This experimental programme demonstrates the state of art of french routine dosimetry services faced to the implementation of ICRU operational quantities. Even if the « dose for record-keeping » does not deviate by more than ± 30% with respect to the $H_P(10)$ reference value, and just comply with the recommendations of ICRP Publication 35[7, 8], calibration techniques used by those laboratories need to be mastered and improved. In some cases, a « good » value derives rather from the compensation between two contradictory effects than from an accurate calibration and an optimised algorithm. Reminding the final objective of determining a calibration coefficient for a given photon spectrum measured at a specified workplace seems untimely before the routine laboratories modify their dose assessment methodology : i. e. a better knowledge of the energy and angular responses of the dosemeter and a unified calibration procedure according to ISO/WG2 recommendations.

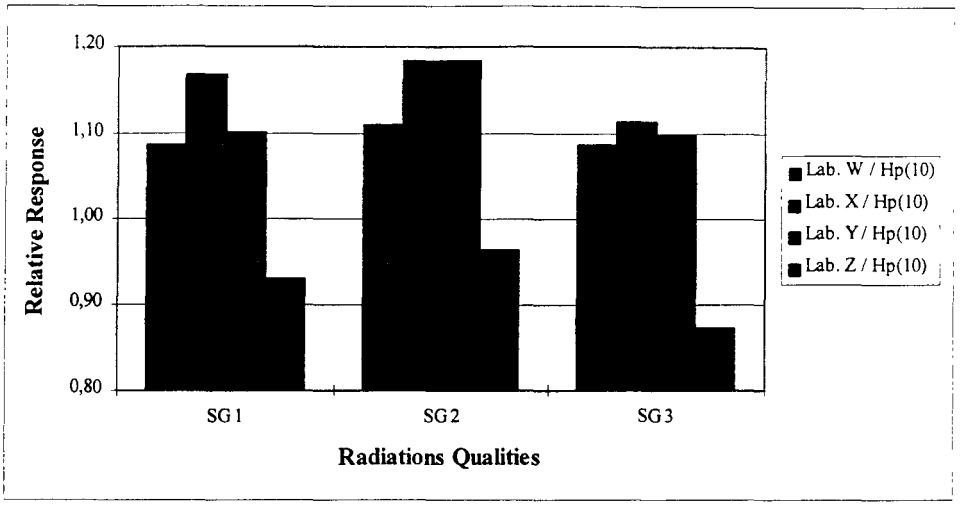

Figure 3 : Relative response in terms of $H_P(10)$ for dosemeters irradiated at Part 1 radiation qualities.

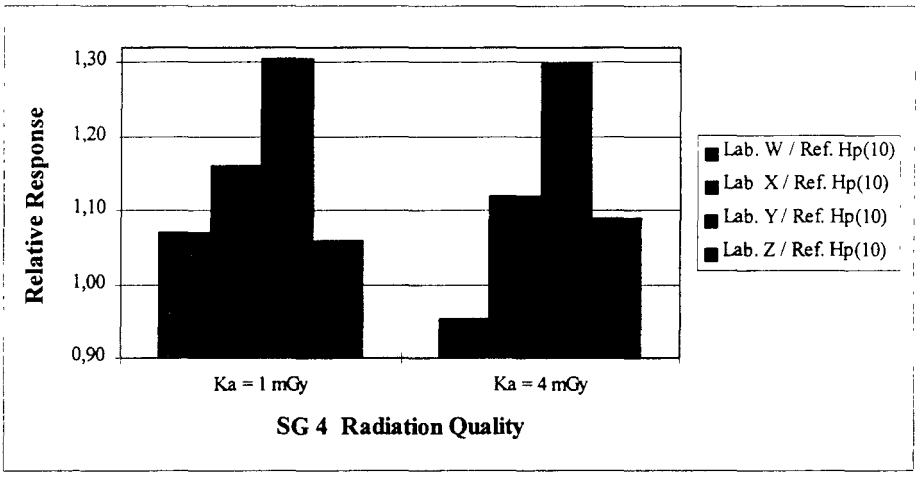

Figure 4 : Relative response in terms of $H_P(10)$ for dosemeters irradiated at SG 4 radiation quality.

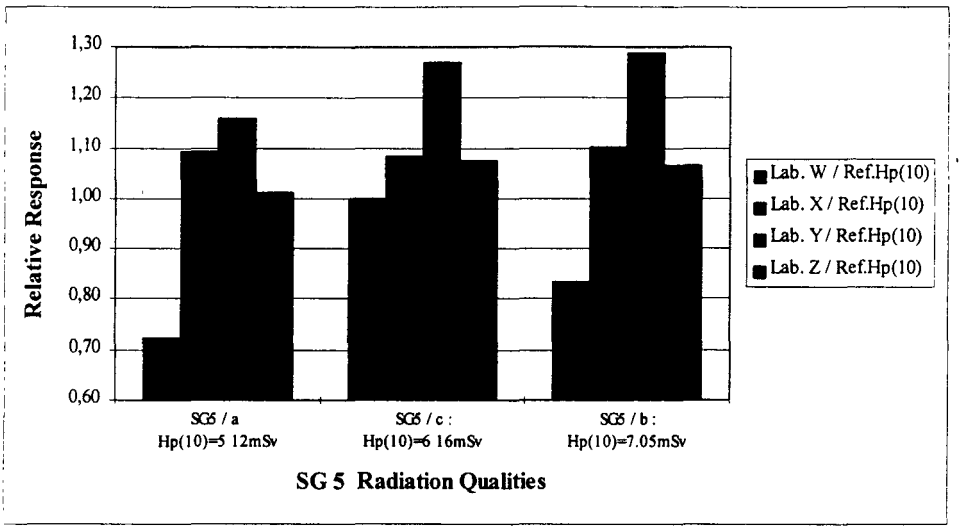

Figure 5 : Relative response in terms of $H_P(10)$ for dosemeters irradiated at SG 5 radiation quality.

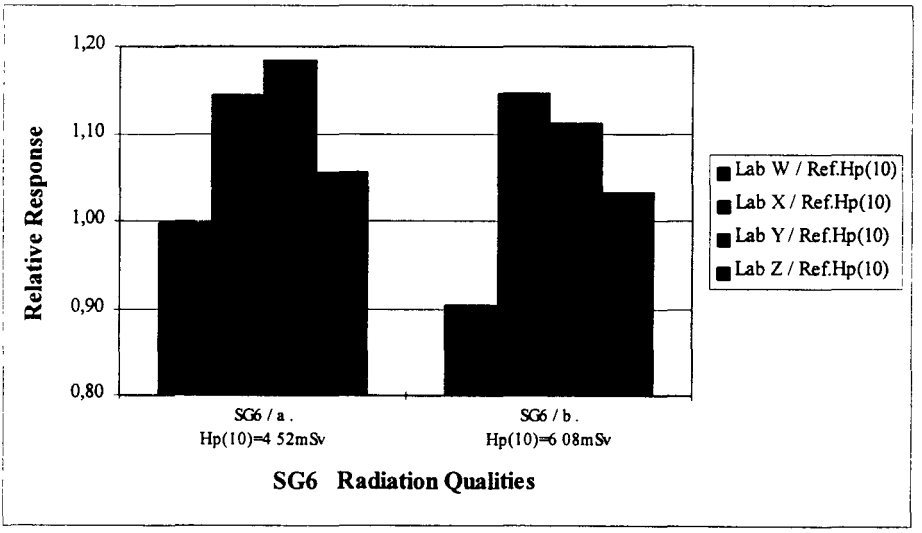

Figure 6 : Relative response in terms of $H_P(10)$ for dosemeters irradiated at SG 6 radiation quality.

References :

1. ICRP 1990 *Recommendations of the International Comission on Radiological Protection* - Publication 60 - Annals of the ICRP 21 N° 1-3 (Pergamon Press, New-York). (1991)

2. ICRU (International Commission on Radiation Units and Measurements) Report 47 *Measurements of Dose Equivalents from Photon and Electron Radiations.* Bethesda MD20814-3095. (1992)

3. ISO 4037 Part 3 *Reference Photon Radiations : Calibration of Area and Personal Dosemeters and the Determination of their Response as a Function of Photon Energy and Angle Incidence.* (1995)

4. W.G. Alberts, J. Böhm, H.M. Kramer, W.J. Iles, J.C. McDonald, R.B. Swartz, I.M.G. Thomson. *International Standardization for Reference Radiations and Calibration Procedures for Radiation Protection Instruments.* - Fachverband für strahlenschutz e.v. Publication Series : Progress in Radiation Protection - Band 1, 181-188. (1994).

5. B. Grosswendt. *The Angular Dependence and Irradiation Geometry for the Dose Equivalent for Photons in Slab Phantoms of Tissue Equivalent Material and PMMA.* Rad. Prot. Dosim., Vol. 35, N° 4, pp. 231-235. (1991)

6. B. Grosswendt. *Coefficients for the Conversion of Air Collision Kerma to Dose Equivalent for the Calibration of Individual Dosemeters in X-ray Fields.* Rad. Prot. Dosim., Vol. 40, N° 3, pp. 169-184. (1992)

7. J. Böhm, V. Lebedev, J.C. McDonald. *Performance Testing of Dosimetry Services and its Regulatory Aspects* - The Impact of Recent ICRP and ICRU Publications - Villigen (Switzerland) 5-7 May 1993.

8. P. Christensen, H.W. Julius, T.O. Marshall. *Technical Recommendations for Monitoring Individual Occupationnally Exposed to External Radiation.* EUR 14852EN. (1994)

Final Report

1992 - 1994

Contract: FI3PCT920002 **Duration: 1.7.92 to 30.6.95** **Sector A12**

Title: Realistic neutron calibration fields and related dosimetric quantities.

1)	Klein, H.	PTB	
2)	Thomas, D.J.	NPL	
3)	Chartier, J-L.	CEA	
4)	Schraube, H.	GSF	
5)	Kralik, M.	CMI	(01.10.93 - 30.06.95)
6)	Osmera, B.	NRI	(01.04.94 - 30.06.95)
7)	Grecescu, M.	IRA	(01.01.93 - 30.06.95)*

I. Summary of Project Global Objectives and Achievements

The main objective of this collaborative project was to produce in the laboratory a few well-characterized neutron fields that replicate typical spectral neutron fluence distributions encountered in radiation protection practice. The project consisted of four distinct parts, namely:

a) the measurement of typical spectral neutron fluences encountered in practice;
b) the preparation of a catalogue of measured neutron spectra, response functions of neutron detectors and dosemeters commonly used, and various fluence-to-dose conversion functions;
c) the development of a program system for using this catalogue, for example to calculate dosimetric quantities of the fields, to estimate the readings of detector systems and to derive the requirements for realistic calibration fields;
d) the computational prediction of configurations consisting of easily accessible neutron sources and appropriate moderators, and, on the basis of this, the realization of these basic fields in the laboratory for calibration purposes.

In July 1992 four laboratories of the Physikalisch-Technische Bundesanstalt (PTB) in Braunschweig, the National Physics Laboratory (NPL) in Teddington, the Commissariat à l'Energie Atomique (CEA) in Fontenay-aux-Roses and the GSF-Forschungszentrum für Umwelt und Gesundheit GmbH (GSF) in Neuherberg started this project. In October 1993 and April 1994 two Czech laboratories of the Czech Metrological Institute (CMI) in Prague and the Nuclear Research Institute in Řež near Prague respectively, joined the collaboration supported in the framework of the PECO program. Since January 1993, the Swiss group from the Institute de Radiophysique Appliquée (IRA) in Lausanne has investigated similar problems and received financial support directly from the Swiss government for close collaboration with the CEC contractors.

* supported by the Swiss Federal Office for Education and Science under contract No 94.0039

I.1 Neutron Spectrometry with Bonner Spheres

Well characterized detector systems are essentially for reliable neutron spectrometry at workplaces and in calibration fields. Considerable effort was therefore spent in determining the energy-dependent response of Bonner sphere (BS) and recoil proton (RP) spectrometers. Monte Carlo simulations of the response functions were compared with and adjusted to experimental data obtained in almost monoenergetic calibration fields. The instruments specified in this way were then successfully employed in comparison exercises performed by EURADOS (European Radiation Dosimetry Group) at workplaces in nuclear facilities [Ale95a, Aro95, Bar95a, Bar95b, Lin95, Sch95a], and in a "realistic" calibration field [Tho96].

The progress achieved in calculating the energy-dependent response of BS spectrometers is most remarkable. Previous calculations generally performed with the discrete ordinate code ANISN for spherically symmetric detector systems were not sufficient to explain experimental data available for neutron energies from thermal to 14.8 MeV [Ale92, Tho94]. The energy dependence was well reproduced for energies ≥ 1 keV, but the scaling factors varied by up to 40% with the diameter of the moderator. Moreover, the shape had to be adjusted for energies below 1 keV to fit the thermal data point which had been predicted too high by a factor of two.

Both problems were solved by means of three-dimensional Monte Carlo simulations using the MCNP code. Taking into account a realistic model of the central detector for thermal neutrons, either spherical [Wie94] or cylindrical [Kra95a] proportional counters filled with ^{3}He, or a ^{6}LiI scintillator [Mar94b], the calculations can be adjusted to the calibration data with a common factor independent of the neutron energy and the sphere diameter which finally accounts for the neutron detection efficiency of the central detector, e.g. for the ^{3}He content or the ^{6}Li isotope abundancy in the detector.

In addition, rules were developed to interpolate the existing response functions for intermediate sphere diameters or to correct for another density of the polyethylene commonly used for moderation. Taking also into consideration that the integral fluence and dose equivalent rates obtained within the framework of the comparison exercises were in excellent agreement for all BSS properly specified [Lin95, Tho96], it can be recommended that the calculated response be used for any system of similar design. The adjustment factor may then be obtained from measurements with standard calibration sources, e.g. Am/Be, ^{252}Cf, or D_2O mod. ^{252}Cf.

Further improvements were achieved by using special shieldings for the spheres [Gre96]. By means of covers made of natural boron with different areal density, the response functions of small spheres can be modified such that a selective sensitivity is obtained in the intermediate neutron energy range. Outer shells of copper considerably increase the response of the large spheres to neutrons with energies higher than 20 MeV; however, an optimization and experimental verification is still required.

The well-characterized BSS were the prefered instrument for measurements at workplaces and for specifying the various neutron fields developed and used for the calibration of personal and area dosemeters. The results were partially complemented by spectra obtained with recoil proton spectrometers. Most of the results were already submitted for inclusion in the new catalogue described below.

I.2 Database of Neutron Spectra, Instrument Response Functions and Dosimetric Conversion Factors

A database of neutron spectra, detector response functions and dosimetric conversion factors has been developed together with a suite of computer programs which assist the collection, interpretation and analysis of the spectra [Sie92]. The package can be installed on a personal computer.

There are now approximately 500 spectra in the catalogue. Half of these come from existing compendia of neutron spectra [Ing78,Gri90]; the rest are spectra measured or calculated more recently, from 10 countries across Europe, the USA, Canada, Japan and Russia. A large proportion of the new data were obtained by sending a questionnaire to colleagues worldwide, requesting spectra and information on the spectrometry techniques employed. The diversity of the data collected can be seen in Table 1. Approximately one third of the data are fission spectra encountered at the workplace, and most of these are new data compiled specifically for this project. Another third are spectra measured or calculated near charged particle accelerators, and the remainder are combinations of sources and moderators or experimental set-ups.

Table 1: Categories of neutron spectra included in the catalogue

Source type	New data	Gri90	Ing78
Neutron source preparation facility	4		
Nuclear fuel processing (incl. storage)	23	10	
Fuel transport containers	12		
PWR (inc. unspecified reactors)	56	22	
BWR	22	1	
GCR	10		
Accelerators	65	78	
Fusion 'reactor'	4	5	
Radionuclide sources: bare, moderated, scatter	20	24	
Cosmic rays	2	8	
Research reactors	3	28	3
Fission / monoenergetic through moderating sphere			49
Monoenergetic on-phantom		40	

There are some 40 personal dosemeter and area survey meter response functions in the database, half of which were extracted from an IAEA compendium [Gri90], and eight sets of Bonner sphere response functions, including the most up-to-date data from NPL, PTB and GSF. The catalogue also contains about 30 dosimetric conversion functions, both operational and limiting quantities, many of which have been determined following the recommendations of ICRP Report 60.

The spectra and response functions are initially standardised to a uniform format and normalised to facilitate entry of the new data into the catalogue. Two 'libraries' of spectra and response functions are produced, from which the data are subsequently accessed. Dosimetric quantities are contained in a separate file containing the most recent data available which can be altered or updated whenever necessary.

The main program of the package serves to manage the spectra in the catalogue. Its functions include plotting the data, storing sub-groups of spectra, and editing the contents of the library. Another important feature is the folding of spectra with detector response functions or dosimetric quantities. It is therefore a useful tool in investigating the influence which the choice of the calibration field has on the dosemeter response in realistic spectra. This program also provides the output for all the subsequent programs.

The effect of different bin structures on a spectrum and on various quantities (e.g. spectrum-averaged dose equivalent) derived from the spectrum can be studied with a separate program, e.g. the effect of imposing an unnaturally fine bin structure on a coarsely binned spectrum. This same program can also be used to sub-divide spectra into discrete energy intervals and to calculate the fraction of fluence, dose equivalent, dosemeter response etc. in each energy band. This may prove to be an important tool when the attempt is made to classify spectra. 'Calibration factors' can be calculated in a particular spectrum for all dosemeters with known energy dependence of the response.

Another program is used to compute combinations of detector responses which simulate a dosimetric quantity. It can also expand spectra encountered at the workplace in terms of a number of calibration spectra. In the case of fitting responses there are two possibilities. The response functions themselves can be fitted to the dosimetric curve (this method is similar to the procedure for combining spectra), or the response functions can first be folded with spectra and combined to fit the values of the spectrum-averaged dosimetric quantity. The code allows an over-determined system of linear equations to be solved by the method of least squares for any combination of up to eight parameters, e.g. fitting dosemeter responses to ambient dose equivalent. This program has proved very useful in both analysing methods for classifying spectra, using combinations or ratios of Bonner sphere response functions, and for investigating combinations of laboratory spectra which mimic a 'realistic' field.

The programs have been fully documented in an instruction manual which also includes several examples of their application [Nai95], and the whole package has been made available to all participants in the collaboration. Various applications have already been reported [Alb94, Mar94a, Sch95b, Tho95].

I.3 Design, Realisation and Specification of Realistic Neutron Calibration Fields

The inspection of the neutron spectra compiled in the catalogue, in particular those encountered at workplaces in nuclear facilities, indicates a great variety of spectra. Nevertheless, the majority of the spectra can be described as a superposition of three components, namely

- a fission spectrum, altered by scattering and absorption in the shielding , i.e. shifted in its mean energy,
- a down-scattered part proportional to $E^{-\alpha}$ with α ranging from 0.5 to 1.5, and
- a thermal distribution.

The relative contribution of these sub-spectra strongly depends on the particular neutron source and the materials involved. For most of the fields encountered in nuclear power plants and in the environment of transport and storage casks filled with spent fuel elements the mean ambient dose equivalent factor <h*> is smaller than 100 pSv cm^2 and the energy of the neutrons does not exceed about 1 MeV. In the intermediate energy region the readings of commonly used survey and personal dosemeters exhibit, however, significant deviations from the true values, e.g. remcounters of the moderator type may overread by up to 100% and tissue equivalent proportional counters may underread by 50%. Appropriate calibrations are therefore required, either in the particular field specified with a reference instrument, e.g. a BSS, or in realistic calibration fields replicating some typical spectra encountered in practice.

For this purpose, two different approaches have been investigated within the framework of this project in order to complement the standard calibration sources, e.g. radionuclide neutron sources, both bare and D_2O-moderated. The primary fission source was simply simulated by a ^{252}Cf source or by fission induced in a ^{238}U-shell covering a fast neutron sources, e.g. a T(d,n)- or a D(d,n)-neutron generator. Shielding and moderator assemblies were optimised by means of Monte Carlo simulations in order to realise different rather soft neutron fields [Jan94a, Jan94c, Cha92, Cha95, Pau96]. Alternatively, the $^{9}Be(d,n)^{10}B$ or $^{7}Li(p,n)^{7}Be$ reactions may serve as highly intense neutron source by using a thick target at a v.d.Graaff accelerator [Sch96, Wie95]. Even simple moderator assemblies can be sufficient to produce the desired neutron fields.

Most advanced are the calibration fields based on fission type neutron sources. The prototype assembly at the 14 MeV neutron generator of CEA in Cadarache [Cha92] was successfully used in two EURADOS comparison exercises [Kle93, Tho96]. MCNP calculations of the spectral neutron fluence were confirmed by spectrometry in absolute scale if the alpha particles of the n-producing reaction were measured at backward angles for normalisation. In future, a 3 MeV neutron generator may be employed as an alternative.

Rather strong Cf sources must be positioned in thick moderator assemblies in order to simulate the shielding of a reactor core. The leakage neutron spectra were also reliably specified by means of calculations and spectrometry [Jan94a, Jan94c].

The neutron fields to be produced with a v.d.Graaff accelerator must still be investigated in more detail, both by simulation and measurements, but their application seems to be very promising due to their flexibility as regards the softness of the spectra and the range of dose rates achievable.

I.4 Fluence-to-Dose Conversion Functions

Provided the angle-dependent spectral fluence of the neutron field is known from measurements and/or calculations, the operational and limiting dose quantities of the field are calculated by folding the spectra with the corresponding fluence-to-dose (equivalent) conversion functions. Comprehensive calculations became necessary as a result of recent recommendations of the ICRP (publication IRCP 60) concerning the new concept of radiation weighting factors, and of the ICRU (publication ICRU 49) concerning the stopping power and ranges of ions in tissue and other materials.

Considerable effort was spent at GSF and PTB to establish a complete set of conversion functions [Leu95, Sie95b]. Calculations were performed for the quantities ambient dose

equivalent H*(10) in the ICRU-sphere, personal dose equivalent $H_p(10)$ on an ICRU slab phantom and effective dose E in an anthropomorphic phantom. Furthermore, a joint proposal was made [Sie95a] which aims at a numerical consistency of radiation weighting factors, with the description of radiation quality using quality factors based on the Q(L) concept (see also the discussion in [Leu94] and [Sie94c]).

I.5. Summary and Conclusion

Considerable progress has been achieved in neutron dosimetry within the framework of this project.

Bonner sphere spectrometers proved to be very valuable instruments for specifying neutron fields at workplaces. Provided that the response functions are carefully determined by MCNP calculation and experimental calibration, the spectral neutron fluence and related dosimetric quantities can be determined for reference purposes, with uncertainties of less than 10% and 15% for the integral fluence and the ambient dose equivalent respectively.

A complete set of fluence-to-dose (equivalent) conversion functions has been calculated and evaluated taking into account recent recommendations of ICRP and ICRU. Application of these factors to neutron spectra encountered at workplaces in nuclear facilities results in an increase of about 30% if the ambient dose equivalent H*(10) is compared with the maximum dose equivalent H_{MADE} according to the former ICRP recommendation (publication 21).

This trend can easily be calculated using the new catalogue with the comprehensive set of neutron spectra and conversion functions. Versatile programs handling this catalogue allow the neutron fields to be categorised, for example according to their mean dosimetric quantities, and the properties of instruments in these fields to be inspected, provided the response functions are known. Since the program package requires only standard PC hardware the system should become a valuable tool for the practitioners in radiation protection service.

The imperfect response of the neutron survey meters most commonly used make a field calibration necessary if significant over- or underreadings are to be avoided. Since reference measurements at the workplace may be very difficult, for example due to safety regulations, it is advisable to perform routine calibrations in the laboratory. Besides standard neutron fields based on radionuclide neutron sources, various accelerator-based neutron fields may be used, in particular those replicating the rather soft neutron spectra encountered at workplaces in nuclear facilities. Standardisation, however, requires greater experience as regards the field properties and the calibration procedures applicable.

The most important results obtained within the framework of this project will be presented in 15 contributions at the 8th Neutron Dosimetry Symposium on November 13 - 17, 1995 in Paris.

References:

Ale92 A.V. Alevra, M. Cosack, J.B. Hunt and H. Schraube: *Experimental Determination of the Response of Four Bonner Sets to Monoenergetic Neutrons (II)*, Radiat. Prot. Dosim. **40** (1992) 91-102

Cha92 J.L. Chartier, F. Posny, M. Buxerolle: *Experimental assembly for the simulation of realistic neutron spectra*, Radiat. Prot. Dosim. **44** (1992) 125-130

Gri90 R.V.Griffith, J.Palfalvi and U.Madhvanath: *Compendium of Neutron Spectra and Detector Responses for Radiation Protection Purposes*, IAEA Technical Reports Series No.318. (Vienna: IAEA) (1990).

Ing78 H.Ing and S.Makra: *Compendium of Neutron Spectra in Criticality Accident Dosimetry*, IAEA Technical Reports Series No.180. (Vienna: IAEA) (1978).

Kle93 H. Klein, D. Thomas, J.L. Chartier, H. Schraube (Eds.): *Determination and realization of calibration fields for neutron protection dosimetry as derived from spectra encountered in routine surveillance*, EUR report 14927 DE/EN/FR, Luxembourg, 1993, p. 159-174

Sie92 B.R.L.Siebert, H.Schraube and D.J.Thomas: *A Computer Library of Neutron Spectra for Radiation Protection Environments*, Radiat. Prot. Dosim. 44 (1992) 135-137

Publications:

Alb94 W.G. Alberts, M. Luszik-Bhadra, R.R.L. Siebert: *Personal neutron dosimetry - conversion factors, calibration and dosimeter performance*. Proc. 4th Intern. Conf. on Radiation Protection and Dosimetry, report ORNL/TM-12817, Oak Ridge, 1994, 165-174

Ale94a A.V. Alevra, H. Klein, K. Knauf, J. Wittstock: *Neutron spectrometry for radiation protection purposes.* Strahlenschutz: Physik und Meßtechnik, Eds. W. Koelzer, R. Maushart, Verlag TÜV Rheinland, Köln 1994, Vol. II, 578-584

Ale94b A.V. Alevra, H. Klein, U.J. Schrewe: *Measurements with the PTB Bonner Sphere spectrometer in high-energy neutron calibration fields at CERN.* Report PTB-N-22, Braunschweig, 1994

Ale94c A.V. Alevra: *Accurate neutron fluence measurements using Bonner spheres.* Reactor Dosimetry ASTM STP 1228, Eds. H. Farrar IV, E.P. Lippincott, J.G. Williams and D.W. Vehar, ASTM, Philadelphia, 1994, 290-299

Ale95a A.V. Alevra: *Measurements with the PTB Bonner Sphere spectrometer and a Leake remcounter.* In: Determination of neutron and photon dose equivalent at workplaces in nuclear facilities of Sweden - An SSI-EURADOS comparison exercise Part I: Measurements and Data Analysis (Eds. L. Lindborg, H. Klein), SSI-report 95-15, Stockholm, 1995, 42-58

Ale95b A.V. Alevra, K. Knauf, J. Wittstock: *Measurements with the PTB Bonner Sphere spectrometer and various dosemeters around a model storage cask filled with a ^{252}Cf source both free in air and in a salt mine.* Laboratory report PTB-7.22-95-? (drafted)

Ale95c A.V. Alevra: *Spectrometric and dosimetric investigations of neutron fields at workplaces in a Czech nuclear power plant in Dukovany.* Laboratory report PTB-7.22-95-? (drafted)

Aro95 A. Aroua, M. Grecescu: *Measurements performed by the Institute of Applied Radiophysics (IAR) Lausanne.* In: Determination of neutron and photon dose equivalent at workplaces in nuclear facilities of Sweden - An SSI-EURADOS comparison exercise Part I: Measurements and Data Analysis, (Eds. L. Lindborg, H. Klein) SSI-report 95-15, Stockholm, 1995, 26-41

Bar95a A.G. Bardell, D.J. Thomas: *Spectrometry measurements by NPL at position A Ringhals reactor.* In: Determination of neutron and photon dose equivalent at workplaces in nuclear facilities of Sweden - An SSI-EURADOS comparison exercise, Part I: Measurements and Data Analysis, (Eds. L. Lindborg, H. Klein) SSI-report 95-15, Stockholm, 1995, 59-66

Bar95b D. Bartlett, P. Drake, L. Lindborg, H. Klein, T. Schmitz, M. Tichy: *Determination of neutron and photon dose equivalent at workplaces in nuclear facilities of Sweden - An SSI-EURADOS comparison exercise.* Part II: Evaluation SSI-report 95-16, Stockholm, to be published in 1995

Cha95 J.L. Chartier, J. Kurkdjian, D. Paul, G. Audion, G. Pelcot, F. Posny: *Considerations on calibration procedures with realistic neutron spectra.* Radiat. Prot. Dosim. **61** (1995) (in print)

Cva94 F. Cvachovec, P. Tiller, J. Kuchar, M. Komarek: *Measurements of Neutron Energetic Spectrum by Stilbene Scintillators.* Optic and Enhanced Mechanics, 3-4, 1994, 79

Cva95 F. Cvachovec et al.: *The measurement in a wide dynamical range with the stilbene scintillator.* to be submitted for publication in Nucl. Instrum. Meth. (drafted)

Jan94a B. Jansky, Z. Turzik, M. Kralik, J. Sauerova, T. Novotny: *Determination of basic dosimetric parameters of neutron reference fields at NRI in Rez.* NRI-report UJV 10315 R,D (in Czech), Rez, 1994

Jan94b B. Jansky, J. Kyncl, Z. Turzik: *Nuclear Research Institute Rez reference neutron field based on a ^{252}Cf source in a D_2O sphere of 30 cm diameter.* Nucleon (NRI, Rez, CZ) 2 (1994) 16

Jan 94c B. Jansky, Z. Turzik, M. Marek: *Reference Neutron Spectra Based on ^{252}Cf Sources used in NRI Rez (Assemblies Description, Results of Spectra Measurements).* NRI Report, UJV 10368 R.D. December 1994

Kra95a M. Kralik, T. Novotny: *Response functions of Bonner spheres with small cylindrical ^{3}He proportional counters determined by Monte Carlo calculations.* CMI-report GR2070/95, Prague, 1995

Kra95b M. Kralik, T. Novotny, A.V. Alevra, S. Guldbakke, D. Schlegel: *Determination of the response of a Bonner sphere spectrometer with cylindrical ^{3}He-proportional counters by experimental calibration and Monte Carlo simulation.* (in preparation)

Kra95c M. Kralik, A.V. Alevra, V. Kulich, T. Novotny: *Dosimetric characteristics of neutron-photon mixed fields at the nuclear power plant Dukovany.* (in preparation)

Leu94 G. Leuthold, H. Schraube: *Critical analysis of the ICRP60 proposals for neutron radiation and a possible solution.* Radiat. Prot. Dosim. 54 (1994) 217-220

Leu95 G. Leuthold, V. Mares, H. Schraube: *Monte Carlo calculations of dose equivalents for neutrons in anthropomorphic phantoms using the ICRP-60 recommendations.* GSF-report 15/95, Neuherberg, 1995

Lin95 L. Lindborg, D. Bartlett, P. Drake, H. Klein, T. Schmitz, M. Tichy: *Determination of neutron and photon dose equivalent at workplaces in nuclear facilities of Sweden - A joint SSI-EURADOS comparison exercise.* Radiat. Prot. Dosim. **61** (1995) (in print)

Mar94a M. Marshall, D.J. Thomas, C.A. Perks, O.F. Naismith: *Radiation quantities: significance of the angular and energy distribution of radiation fields.* Radiat. Prot. Dosim. 54 (1994) 239-248

Mar94b V. Mares, H. Schraube: *Evaluation of the response matrix of a Bonner sphere spectrometer with LiI detector from thermal energy to 100 MeV.* Nucl. Instrum. Meth. A337 (1994) 461-473

Nai95 O.F. Naismith, B.R.L. Siebert: *Manual for SPKTBIB: a PC-based catalogue of neutron spectra.* NPL report RSA(EXT)??, 1995

Sch94 H. Schuhmacher, R. Hollnagel, B.R.L. Siebert: *Sensitivity study of parameters influencing calculations of fluence-to-dose equivalent conversion coefficients for neutrons.* Radiat. Prot. Dosim. 54 (1994) 221-225

Sch95a H. Schraube, J. Jakes, G. Schraube, E.Weitzenegger: *Measurements with the GSF Bonner Sphere spectrometer and an Anderson & Braun type remcounter. In: Determination of neutron and photon dose equivalent at workplaces in nuclear facilities of Sweden - An SSI-EURADOS comparison exercise.* Part I: Measurements and Data Analysis (Eds. L. Lindborg, H. Klein), SSI-report 95-15, Stockholm, 1995, 12-25

Sch95b H. Schuhmacher, W.G. Alberts, A.V. Alevra, H. Klein, U.J. Schrewe, B.R.L. Siebert: *Characterization of photon-neutron radiation fields for radiation protection monitoring and optimization.* Radiat. Prot. Dosim. **61** (1995) (in print)

Sie94a B.R.L. Siebert: *Radiation quantities: their inter-relationship.* Radiat. Prot. Dosim. 54 (1994) 193-202

Sie94b B.R.L. Siebert, H. Schuhmacher: *Calculated fluence-to-directional and personal dose equivalent conversion coefficients for neutrons.* Radiat. Prot. Dosim. 54 (1994) 231-238

Sie94c B.R.L. Siebert, W.G. Alberts, R.A. Hollnagel, H. Schuhmacher: *Zur Konsistenz der Strahlenschutzgroßen für Neutronen nach ICRP 60.* Strahlenschutz: Physik und Meßtechnik, Eds. W. Koelzer, R. Maushart, Verlag TÜV Rheinland, Köln 1994, Vol. I, 195-200 (in German)

Sie94d B.R.L. Siebert, W.G. Alberts, R.A. Hollnagel, G. Leuthold, H. Schraube: *A proposal to revise the radiation weighting factors for neutrons on the basis of new calculations.* Radiat. Prot. Dosim. 58 (1994) 69-71

Sie95 B.R.L. Siebert, H. Schuhmacher: *Quality factors, ambient and personal dose equivalent for neutrons, based on the new ICRU stopping power data for protons and alpha particles.* Radiat. Prot. Dosim. 58 (1995) 177-183

Tho94 D.J. Thomas, A.V. Alevra, J.B. Hunt, H. Schraube: *Experimental determination of the response of four Bonner Sphere sets to thermal neutrons.* Radiat. Prot. Dosim. 54 (1994) 25-31

Tho95 D.J. Thomas, O.F. Naismith: *Developments in neutron spectrometry for radiation protection.* In: Neutrons and their Applications, G. Vourvopoulos, Th. Paradellis (Eds.), SPIE 2339, (1995) 261-266

Wie94 B. Wiegel, A.V. Alevra, B.R.L. Siebert: *Calculations of the response functions of Bonner Spheres with a spherical ^{3}He proportional counter using a realistic detector model.* Report PTB-N-21, Braunschweig, 1994

Wie95 B. Wiegel, B.R.L. Siebert: *Calculational optimisation of a moderator assembly around a $^{7}Li(p,n)$-neutron source for the production of realistic neutron calibration fields at PTB.* Laboratory report PTB-7.51-95-? (in preparation)

Accepted for oral or poster presentation at the 8th Symposium on Neutron Dosimetry, to be held on November 13-17, 1995 in Paris, and to be submitted for publication in the proceedings (Radiat. Prot. Dosim 68 (1996)):

Cha96 J.L. Chartier, B. Jansky, H. Kluge, H. Schraube, B. Wiegel: *Recent developments in the design, realisation and specification of realistic neutron calibration fields.*

Ale96 A.V. Alevra, U.J. Schrewe: *Measurements with the PTB „C" Bonner Sphere spectrometer in the PSI Villigen 55 MeV neutron field for spectrometry and calibration purposes.*

Aro96 A. Aroua, T. Buchillier, M. Grecescu, M. Höfert: *Neutron measurements around a high energy lead ion beam at CERN.*

Gre96 M. Grecescu, A. Aroua, S. Pretre, J.F. Valley: *Improved neutron spectrometer based on Bonner spheres.*

Jak96 J. Jakes, G. Schraube, E. Weitzenegger, H. Schraube: *Neutron spectrometry and microdosimetry at the nuclear power plant Dukovany.*

Kle96 H. Klein: *Workplace radiation field analysis.*

Klu96 H. Kluge, A.V. Alevra, S. Jetzke, K. Knauf, M. Matzke, K. Weise, J. Wittstock: *Scattered neutron reference fields produced by radionuclide sources.*

Kna96 K. Knauf, A.V. Alevra, J. Wittstock, H.J. Engelmann, M. Khamis, N. Niehues: *Neutron and photon spectra and dose rates around a shielding cask placed in a salt mine to simulate a nuclear waste package.*

Kra96b M. Kralik, A.V. Alevra, A. Aroua, M. Grecescu, V. Mares, T. Novotny, H. Schraube, B. Wiegel: *Specification of Bonner Sphere systems for neutron spectrometry.*

Leu96 G. Leuthold, V. Mares, H. Schraube: *On the conservativity of $H_p(10)$.*

Nai96a O.F. Naismith, B.R.L. Siebert: *A database of neutron spectra, instrument response functions, and dosimetric conversion factors for radiation protection applications.*

Nai96b O.F. Naismith, B.R.L. Siebert, D.J. Thomas: *Response of neutron dosemeters in radiation protection environments and investigation of techniques to improve estimates of dose equivalent.*

Pau96 D. Paul, J.L. Chartier, J. Kurkdjian, G. Pelcot, C. Itie: *Advances in realistic neutron spectra: progress in fluence monitoring of the DD reaction.*

Sch96 H. Schraube, B. Hietel, V. Mares, G. Schraube, E. Weitzenegger: *GRENF - the GSF-realistic neutron field facility.*

Tho96 D.J. Thomas, J.L. Chartier, H. Klein, O.F. Naismith, F. Posny, G.C. Taylor: *Results of a large scale neutron spectrometry and dosimetry comparison exercise at the Cadarache moderator assembly.*

Head of project 1: Dr. H. Klein

Scientific staff: A.V. Alevra, Dr. K. Knauf, Dr. B.R.L. Siebert, Dr. B. Wiegel, J. Wittstock

II. Objectives for the reporting period

The main objectives were:

- to calculate the response functions of the PTB Bonner sphere spectrometer using a realistic detector model,
- to carry out measurements at workplaces and in realistic calibration fields,
- to calculate fluence-to-dose equivalent conversion functions taking into consideration recent ICRP60 and ICRU49 recommendations,
- to update, inspect and apply the catalogue of neutron spectra, conversion functions and detector response functions and
- to optimize an accelerator-based neutron source and moderator assemblies assigned to replicate typical neutron fields encountered at workplaces.

III. Progress achieved including publications

III.1. MCNP calculations of the response functions of the PTB-C Bonner sphere spectrometer and comparison with calibration data

The Bonner sphere (BS) spectrometer used at PTB within the framework of this contract and referred to as PTB-C set consists of a spherical ^{3}He-filled proportional counter SP90 and 12 polyethylene (PE) moderator spheres with diameters d ranging from 7.62 cm (3") to 45.72 cm (18"). As the BS response function $R_d(E_n)$ can be experimentally determined at selected energies only, with a complete lack of data in the thermal to keV energy region, reliable calculations are required at least for the proper interpolation of the calibration data. The uncertainties of the calculations depend, among other factors, on the method of solving the neutron transport problem, on the accuracy of the cross sections used and on the adequacy of the geometry model. One goal of this work therefore was the establishment of an improved response matrix for the PTB-C BS system using a realistic detector model.

All results were published in detail in a PTB report [Wie94]: the description of the realistic geometry model, the calculated response values and investigations into the influence of the ^{3}He number density and the polyethylene mass density on the responses and the angular dependence. For the first time the interior structures of the proportional counter based on technical drawings provided by the manufacturer (Centronics) were used to calculate the response functions. The three-dimensional Monte Carlo Code MCNP [Bri93] was used to calculate the responses of the PTB-C system to monoenergetic neutrons in the energy range between 1 meV and 20 MeV. The calculated responses of each sphere diameter were compared with the results of calibration measurements performed in monoenergetic neutron fields (1.17 keV to 14.8 MeV) [Ale92] and in the thermal neutron field at NPL [Tho94]. It is shown in Fig. 1.1 that a common fit factor $f = 1.07$ is adequate to adjust the newly calculated responses (■) to the measurements. This figure also includes the fit factors deduced from a comparison of the measurements with response functions previously calculated by

D.J. Thomas [Tho92] with the ANISN code (◆) and by V. Mares et al. [Mar91] with the MCNP code (∗), both using a simple geometry model with spherical symmetry.

A critical parameter in the calculation of the response is the PE mass density ρ_{PE}. We clearly showed [Wie94] that a relative variation of the density, $\Delta\rho/\rho$, has the same effect on the response as has a relative variation of the wall thickness, $\Delta t/t$, of the PE sphere. This method allows our calculated response functions to be applied to BS systems for which the density of PE density differs slightly from the value used in the present calculations. As another example of our intensive calculations, Fig. 1.2 shows the influence of resonances in the carbon cross sections. At energies with maximum values of the cross section density $\Sigma_{PE}(E)$, the response shows a statistically significant minimum value due to outscattering or absorption on carbon.

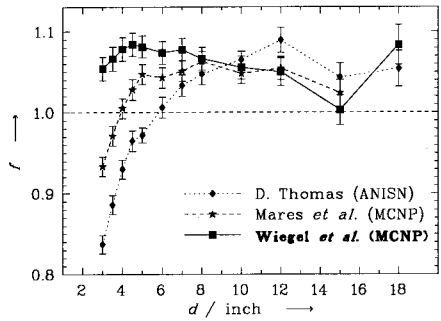

Figure 1.1 *Factors f fitting responses calculated by different authors to measured responses.*

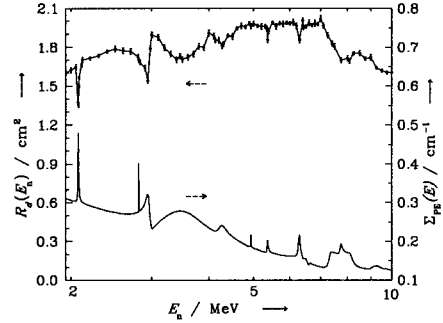

Figure 1.2 *The influence of resonances in the cross section density (lower curve, right axis) on the response function of the 12" BS (upper curve, left axis)*

III.2. Measurements at workplaces and in calibration fields

In addition to the very well specified Bonner sphere spectrometer (BSS), the PTB is running proton recoil spectrometers, i.e. hydrogen-filled spherical proportional counters and liquid organic scintillators. Although their response matrices are also well specified, these systems are only used to determine the spectral neutron fluence with considerably better energy resolution for neutron energies higher than 10 keV or, as a by-product, to investigate the spectral photon fluence of the mixed fields with the scintillation spectrometer. A combined unfolding procedure for all neutron spectrometers has not yet been established.

In the reporting period, the PTB-C BSS was preferably used in measurements at workplaces in nuclear facilities and in various calibration fields. The detector system has a sufficiently high neutron response, covers the entire energy range from thermal to hundreds of MeV and is very robust against extreme environmental conditions, for example in the containment building of a pressurized water reactor or in a salt mine. A remarkable number of measurements have been performed (Table 1.1).

Table 1.1: Measurements with the PTB Bonner sphere spectrometer in the period 1992 - 95

Time period month/year	Place where the measurements were performed	Kind of measured spectra	No of meas. sp.	No of diff. sp.*
FEB 1992	FZ-Karlsruhe Bunker - D	^{252}Cf, AmBe + room return	20	-
NOV 1992	CLAB - Oskarsham - S	Transport cask	3	-
NOV 1992	Ringhalsverket - S	1 GW reactor	2	-
JUL 1993	PSI - Villigen - CH	55.15 MeV "monoenergetic" & BG	2	1
JUL 1993	CERN - Genève - CH	High-energy calibration fields	4	-
JAN 1994	PTB Bunker - D	AmBe, with & without shadow object	2	1
JUL 1994	Cadarache - 2 - F	14 MeV + various materials	1	-
1994/95	PTB & Asse - D	^{252}Cf line source in model storage cask	43	-
MAY 1995	Dukovany power plant - CZ	440 MW reactor	3	-
AUG 1995	PTB Bunker - D	D_2O-mod. Cf+ ½-Cd sphere	4	2
Total number of measured spectra			84	4

* In the cases where background measurements were performed as well supplementary difference spectra (total - background) could be determined; their number is indicated in the last column of the table.

As the fluence response matrix of the PTB Bonner sphere spectrometer (BSS) is well specified in the whole energy range between 1 meV and 20 MeV [Ale92, Tho94, Wie94], the investigation of most of the neutron spectra encountered in practice can be done with an accuracy estimated to be ≈±4% in integral fluence and ≈±15% in dose equivalent [Ale94c].

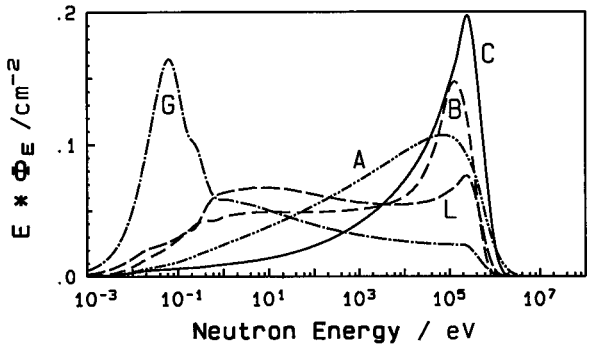

Fig. 1.3: *Neutron spectra measured at various locations in nuclear power plants in Dukovany (A,B,C) and Ringhals (G,L). All spectra are normalized to an integral fluence equal to unity.*

The most interesting series of measurements were performed inside the nuclear power plants at Ringhals/Sweden [Ale95a] and Dukovany/Czech Republic [Ale95c]. Results are illustrated in Fig. 1.3. Both the Ringhals and the Dukovany reactors are of the pressurized water type, however, their construction differs. The "Dukovany" spectra are harder than those of the Ringhals reactor, but the integral rates of fluence and dose equivalent (not shown in Fig. 1.3) are lower in Dukovany.

The largest series of measurements in which the BSS of PTB was ever involved was performed around a reduced model (a cylinder 135 cm long, 91 cm in diameter) with a ^{252}Cf line source simulating a storage cask with spent nuclear fuel. This was done in cooperation with the DBE (Deutsche Gesellschaft für Bau und Betrieb von Endlagern für Abfallstoffe mbH). Their AHE-project ('active handling experiment with neutron sources') aimed at studying the increase of the neutron fluence and dose equivalent rate around a storage cask when transported in a salt mine. The MCNP calculations [Ber95] and the measurements [Ale95b] were performed with the cask placed free in air and at various locations in a salt mine. One of the results obtained "free in air" is shown in Fig. 1.4. The "C" spectrum is the calculated one. The "E" spectrum was obtained with the BSS without using any external "a priori" information. The "U" spectrum was obtained using the calculated spectrum as "a priori" information in the unfolding of the BS measured counting rates. Except for a few details, the shapes of the spectra are very similar. At very low energies where the "U" and "E" results are nearly identical, the calculation fails to predict the thermal albedo neutrons from the ground. The values of the integral fluence rates obtained indicate an excellent agreement between the "E" and "U" results, but an overestimation of about 17% of the "C" result compared with that for "U". The "U" result was taken as a reference, bearing in mind that it combines the detailed description of the spectrum obtained from calculation with the good accuracy of the BSS in the determination of absolute values of the neutron fluence.

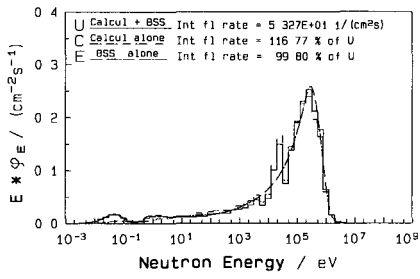

Fig. 1.4: *The neutron spectra obtained at a distance of 2 m from the bottom of the cask placed horizontally in "free" geometry, with its symmetry axis at only 150 cm from the ground. All the spectra are normalized to integral fluence equal to unity.*

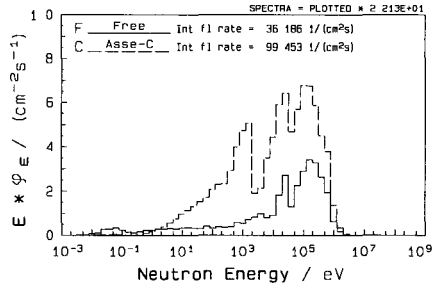

Fig. 1.5: *The two neutron spectra of type "U" measured at a distance of 2 m from the cover of the model cask "free in air" (F) and at the "Asse-C" the location (C) in the salt mine.*

The considerable contribution of the neutrons scattered by the salt is illustrated in Fig. 1.5. In the "Asse-C" spectrum the thermal albedo neutrons are no longer present. At a distance of 2 m from the cask, the contribution of the salt return neutrons is twice the contribution of the "direct" fluence. Also, the dose equivalent rate of $\dot{H}_{MADE}$ = 18.4 μSv/h obtained in "Asse-C" is more than twice the value of $\dot{H}_{MADE}$ = 8.8 μSv/h obtained in "free" geometry.

The increasing interest in the investigation of high-energy neutron fields (around high-energy accelerators, therapy installations, aircrafts at high altitude) induced us to extend the knowledge of the fluence response of our BSS to energies higher than 20 MeV. The small number of calculated high-energy response functions available from the literature exhibit different shapes. The various variants were compared with calibration measurements performed in the 55.15 MeV "quasi-monoenergetic" neutron beam at PSI/Villigen [Ale96].

The neutrons peaked at 55.15 MeV were collimated to a beam with a circular cross section about 8 cm in diameter at the place of measurement. The "in beam" neutron spectrum was measured for energies above 5 MeV using a scintillation detector in the time-of-flight method [Nol92]. The neutron fluence was determined in addition with a proton-recoil telescope for neutron energies above 48 MeV [Sch95]. The spectral neutron fluence of the "in beam" neutrons with energies below 5 MeV was unknown as was the spectral distribution of the background neutrons (room return).

As the cross section of the neutron beam was smaller than the diameters of most spheres, a scanning procedure was applied for these measurements (TOTAL spectrum). The BACKGROUND measurements were performed outside the scanned area. The result of these measurements is illustrated in Fig. 1.6. For neutron energies above 5 MeV, the DIRECT (TOTAL-BACKGROUND) spectrum was in complete agreement with the time-of-flight spectrum if the high-energy shapes of the responses from Aroua et al. [Aro92] were used to extend the response matrix. In this case the DIRECT neutron fluence determined with the BSS for energies above 48 MeV agrees with the telescope measurements within 8%.

The extended response matrix of the PTB BSS made possible the investigation of high-energy neutron fields produced at CERN-Geneve [Ale94b]. Three spectra behind concrete shieldings and one spectrum behind an iron shielding were measured and compared with calculations [Roe93]. Two examples are given in Fig. 1.7. Good agreement between calculations and measurements was obtained for all "concrete" spectra for energies above ≈10 keV. In the case of the "iron" shielding where the spectrum is considerably "softer" than the others, the calculations underestimate the absolute fluence values by ≈ 34%.

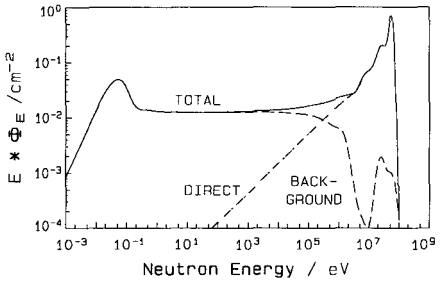

Fig. 1.6: *Neutron spectra obtained with the PTB BSS in the "quasi-monoenergetic" neutron beam at PSI-Villigen (see text for details).*

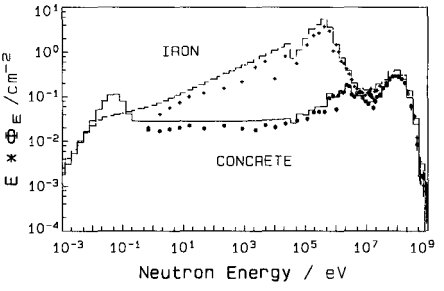

Fig. 1.7: *Spectral neutron fluence measured with the PTB BSS at CERN (histograms) compared with calculations (points). All data are given in absolute scale.*

An additional aim of most measurements reported here was to study the behaviour of various instruments used in practice as dosemeters. If the neutron spectrum is determined and the fluence response of the instrument is known as a function of energy, even on a relative basis, one can simulate its calibration in one of the calibration fields commonly used (bare ^{252}Cf, D_2O-moderatd ^{252}Cf, AmBe) and then "predict" its reading in the field investigated with the spectrometer.

The conclusions drawn from the investigation of a large number of neutron fields encountered in practice indicate that the moderator-type dosemeters normally used (e.g. Leake-type

remcounter) overestimate the dose equivalent in most cases, even if they have been calibrated with a moderated Cf source. The overestimation increases for calibrations with bare Cf, attaining even a factor of two for the calibration with an AmBe source. Otherwise, the measured values were always in good agreement with the "predicted" ones, thus indicating a reliable behaviour of the instruments even at extreme environmental conditions. In the case of a "tissue-equivalent proportional counter" (TEPC) calibrated in moderated Cf, the predictions were in very good agreement with the spectrometric results, but large fluctuations in the measured dose equivalent values indicated that the instrument suffered from "technical" problems in these environments (noise, high temperature). A moderator-type neutron survey meter recently developed and designed to meet the requirements of ICRP60 [Bur94] underestimates the dose equivalent by about 25-30%, independent of the reference field used (any of the three cited above).

From these results we conclude that the dosemeters used in practice should either be calibrated at the place where they are used, with reference to the results obtained with the spectrometer(s), or in realistic calibration fields replicating practical neutron fields in the laboratory.

III.3. Calculations of neutron fluence-to-dose equivalent conversion factors

Fluence-to-dose equivalent conversion factors are required to determine relevant dosimetric quantities from measured fluence spectra at workplaces. For routine radiation protection, the ICRU recommends in its reports 39 and 51 the quantities of ambient dose equivalent, $H^*(10)$, and personal dose equivalent, $H_p(10)$. The quantity $H'(10)$ is not used for neutrons.

The dose equivalent is the product of the absorbed dose, D, and the quality factor, Q_D. The quality factor is given as

$$Q_D = (1/D) \cdot \int Q(L) \cdot D_L \cdot \mathrm{d}L \qquad (1.1)$$

where L is the unrestricted linear energy transfer in water, $Q(L)$ is a weighting function and D_L the absorbed dose distribution in L. The unrestricted linear energy transfer is numerically equivalent to the stopping power. In 1991, the ICRP recommended in its publication 60 a revised weighting function Q(L) which differs in part considerably from that used previously. The fluence-to-dose equivalent conversion factors for neutrons were, therefore, recalculated [Sie94b and Sch94b]. Then, in 1993, the ICRU published in its report 49 revised stopping power values for protons and alpha particles for liquid water, taking account of the chemical binding.

These changes are demonstrated in Figures 1.8 and 1.9 [Sie95b]. Fig. 1.8 shows the old and new functions $Q(L)$ and the old and new values for the proton stopping power in water. The new values of $Q(L)$ are substantially higher than the old ones, especially in the vicinity of the Bragg peak. Furthermore, for protons the peak is shifted to lower values of L. Figure 1.9 shows the product of the dose distribution density and L, $L\,D_L(L)$, for an incident neutron energy $E_n = 19.9$ MeV in ICRU soft tissue as calculated using the new and the old values of the stopping power for protons and alpha particles. The product is used for the graphical representation in order that the same areas correspond to the same doses if plotting is made versus $\log(L)$. It is clearly seen that these changes influence the dose distribution in L. Use of the new $Q(L)$ function leads to higher contributions to Q_D for values of L up to about

200 keV/μm. However, the use of the new values for the stopping power reduces this enhancement.

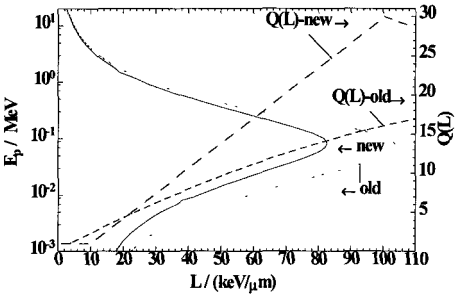

Figure 1.8: *The new (dotted curve) and the previously used values (solid curve) of stopping power for protons (energy scale: left ordinate) and the new and old Q(L) (right ordinate). For details see text.*

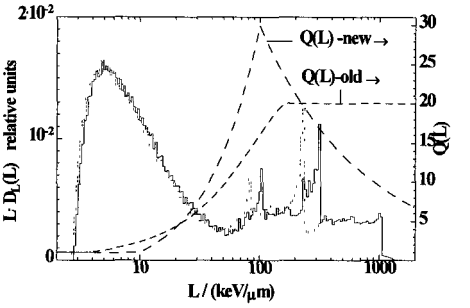

Figure 1.9: *Calculated dose distribution density $L\,D_L\,(L)$ (left ordinate) for a neutron energy E_n = 19.9 MeV using the new (dashed curve) and the old (solid curve) values of stopping power and old and new Q(L)*

The fluence-to-dose equivalent conversion factors for neutrons had, therefore, to be recalculated [Sie95b]. Fig. 1.10 shows the old, the intermediate and the latest values for $H^*(10)/\Phi$ and, in its upper part, the ratios of the intermediate and latest values to the old ones. Unfortunately, the new-to-old ratio depends on the incident neutron energy. This necessitates new designs of dosemeters and does not allow old dose equivalent values to be multiplied by a single constant factor. Furthermore, as a consequence of this, it will be necessary to recalibrate old instruments. Special problems are seen with tissue-equivalent proportional counters as they must take the new $Q(L)$ relation and the changes of the stopping power in liquid water into account.

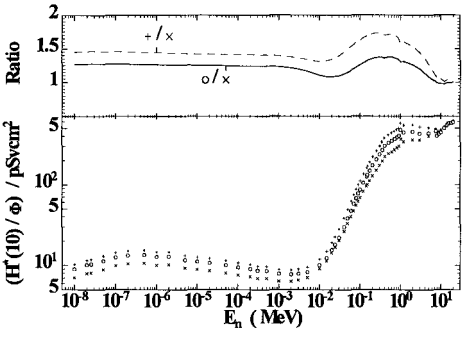

Figure 1.10: *Lower part: $H^*(10)/\Phi$ as a function of incident neutron energy calculated as recommended by ICRP 60 with the ICRU 49 (o) and old (+) stopping power data and (x) as recommended by ICRP 51. Upper part: Ratio of the latest to the old values*

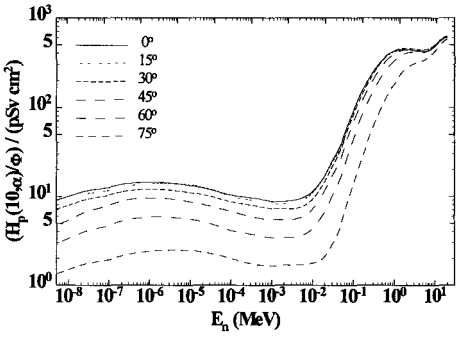

Figure 1.11: *Neutron fluence-to-personal dose equivalent conversion factors, $H_p(10,\alpha)/\Phi$, for various angles of incidence as a function of incident neutron energy E_n. Here, α denotes the angle of incidence of a broad undirectional neutron beam on the front surface of an ICRU slab phantom (ICRU47).*

Figure 1.11 shows the latest values for $H_p(10;\alpha)/\Phi$, for various angles of incidence α, for a

broad undirectional neutron beam impinging on the surface of an ICRU slab phantom (ICRU 47). These values are used for the calibration of personal dosemeters. Data for angles of incidence greater than 75^0 are not given, since the feasibility of the slab phantom at larger angles is doubtful.

It is expected that these new values of the neutron fluence-to-dose equivalent conversion factors for ambient dose equivalent, $H^*(10)$ and personal dose equivalent, $H_p(10;\alpha)$, will be recommended by the ICRP.

III.4. Routine use of SPKTBIB

The program package SPKTBIB has been developed by Naismith and Siebert [Nai95 and Nai96a] to determine dosimetric quantities in spectra found at workplaces. SPKTBIB serves as a database for those spectra and for the response functions of instruments used in dosimetry. The spectra and the response functions can be visualized, and numerical predictions of measurements with dosemeters in these spectra and the calculation of mean absorbed dose, mean absorbed dose equivalent and of quality factors are possible. A very special feature is the possibility of decomposing spectra found at workplaces into calibration spectra or of decomposing dose equivalent quantities in terms of the response functions of dosemeters. These features provide help in the search for appropriate calibration methods.

SPKTBIB was used routinely by several authors for studying the response of area and personal dosemeters at workplaces, for example [Alb94, Nai95b, Sch95b and Tho95]. Instead of performing actual measurements with dosemeters at these workplaces, the measured spectra and the response function of these dosemeters are used and their response is calculated. As an example, we show in Fig. 1.12 the ratios of calculated responses of a TEPC

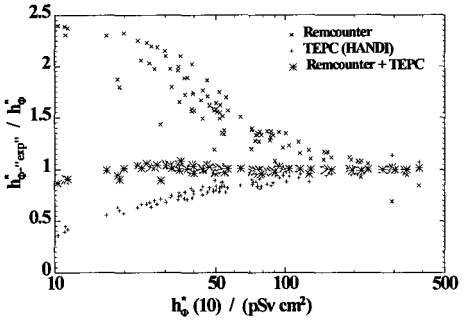

Figure 1.12: *Calculated ratios of „measured" and true values of $h^*_\Phi(10)$ for a TEPC, a remcounter and a combination of TEPC and remcounter in over 100 reactor spectra taken from the SPKTBIB catalogue as a function of the true mean neutron fluence-to-ambient dose equivalent conversion factor, $h^*_\Phi(10)$, in these spectra*

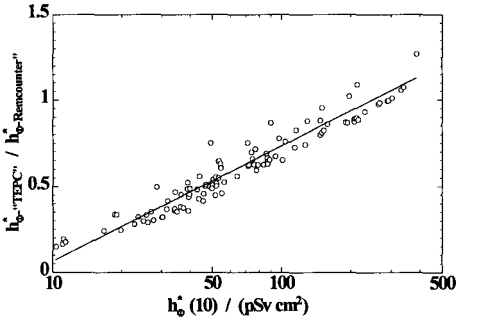

Figure 1.13: *Calculated ratios of „measured" values of $h^*_\Phi(10)$ in over 100 reactor spectra taken from the SPKTBIB catalogue for a TEPC and a remcounter and a linear fit to these ratios as a function of the true mean neutron fluence-to-ambient dose equivalent conversion factor, $h^*_\Phi(10)$, in these spectra.*

and a remcounter in over 100 reactor spectra taken from the SPKTBIB catalogue as a function of the true mean neutron fluence-to-ambient dose equivalent conversion factor, $h^*_\Phi(10)$, in

these spectra. Both dosemeters are numerically calibrated in a D_20-moderated Cf spectrum. The remcounter overresponds considerably for low values of $h^*_\Phi(10)$ and the TEPC underresponds. It is therefore reasonable to use a linear combination of both instruments as is also shown in Fig. 1.12 summing 75% of the TEPC and 25% of the remcounter response.

Instead of using linear combinations one could use a function of the responses to $h^*_\Phi(10)$ and derive dosimetric quantities. In Fig. 1.13 we have plotted the ratios of "measured" values of $h^*_\Phi(10)$ in over 100 reactor spectra taken from the SPKTBIB catalogue for a TEPC and a remcounter and a linear fit to these ratios as a function of the true mean neutron fluence-to-ambient dose equivalent conversion factor, $h^*_\Phi(10)$, in these spectra. The fit can be written as $R\,(h^*_\Phi(10)) = a + b \cdot \log(h^*_\Phi(10))$, and $h^*_\Phi(10)$ may then be obtained from the inverse function to within about 70% and 170% of the true value.

III.5. Accelerator-based calibration fields at PTB using the ^{7}Li(p,n)^{7}Be reaction

In order to get accelerator-based neutron fields with mean energies of a few keV and mean fluence-to-dose equivalent conversion factors <h*(10)> of less than 50 pSv cm^2 which are often encountered at nuclear facilities, it is advisable to start with primary neutron energies of 1 MeV or less. This can be achieved with the ^{7}Li(p,n)^{7}Be reaction and proton energies between 2 and 3.5 MeV. The target can be either a LiF target or a metallic Li target (in the following called LiM target), and it must be shielded by an appropriate moderator assembly. The calculations of neutron leakage spectra have been performed with the Monte Carlo code MCNP4A [Bri93]. To reduce the number of parameters of this problem, and with it the number of individual MCNP runs, a spherical geometry has been selected. The intention of this part of the project was to optimize the selection of the moderator material or combinations of materials, the thickness of the moderator and the required initial proton energy.

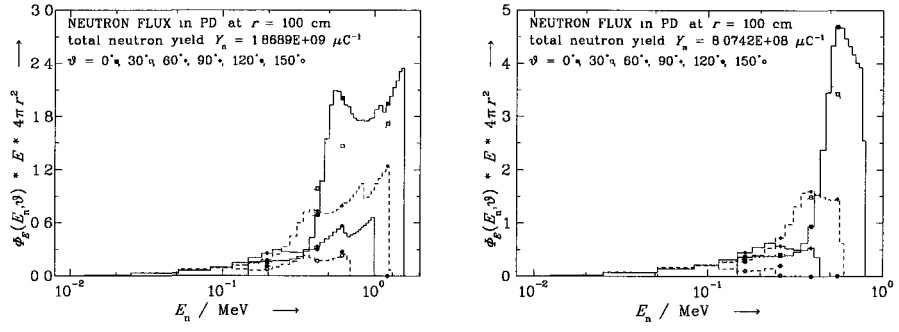

Figure 1.14: *Primary neutron spectra at different angles from 3.3 MeV protons (left) and 2.5 MeV protons (right) on a thick metallic Li target using the ^{7}Li(p,n)^{7}Be reaction.*

Although MCNP offers many possibilities of describing the spatial, directional and energy distribution of the starting neutrons we supplied, for reasons of flexibility, a user-defined neutron source. This FORTRAN subroutine simulates the (p,n) reaction in the target at the end of the beam pipe. To slow down the protons in the target, we used the stopping power data from the "TRIM95" code of Biersack and Ziegler [Bie95]. The angle-dependent n-production cross sections used to calculate the neutron yield were taken from Drosg and Schwerer [Dro87]. Fig. 1.14 (left) shows the primary neutron spectra for 3.3 MeV protons on

a thick LiM target (≥ 120 µm) at a distance of 1 m from the target, for 6 different emission angles $\vartheta = 0°, 30°, ..., 150°$. In this case the maximum neutron energy is $E_{n,max} = 1.614$ MeV, and the mean energy $\langle E_n(\vartheta)\rangle$ of the spectra varies from 884 keV (forward direction) to 312 keV (backwards), meaning that the spectra are rather hard. For 2.5 MeV protons, Fig. 1.14 (right), the ^{7}Li(p,n)^{7}Be* (1st excited state) reaction is kinematically not possible; $E_{n,max} = 808$ keV, and $\langle E_n(\vartheta)\rangle$ ranges from 560 to 110 keV.

As moderator material we used carbon (graphite with $\rho_C = 2.25$ g/cm^3), polyethylene ($\rho_{PE} = 0.95$ g/cm^3) and heavy water ($\rho_{HW} = 1.1044$ g/cm^3). We calculated the neutron and gamma energy spectra behind a shielding 5, 10 and 15 cm in thickness. The search for the optimal moderator assembly is guided by the following, to a certain extent conflicting conditions: mean neutron energies $\langle E_n\rangle$ below 80 keV, mean conversion factors $\langle h^*_\Phi\rangle$ below 50 pSv cm^2 and neutron fluxes φ_n greater than 10^4 cm^{-2} s^{-1} at 1 m distance. From the analysis of these parameters for the various calculated spectra it was concluded that a very promising assembly consists of an inner polyethylene shell with a wall thickness of 5 cm and a surrounding graphite shell 10 cm thick.

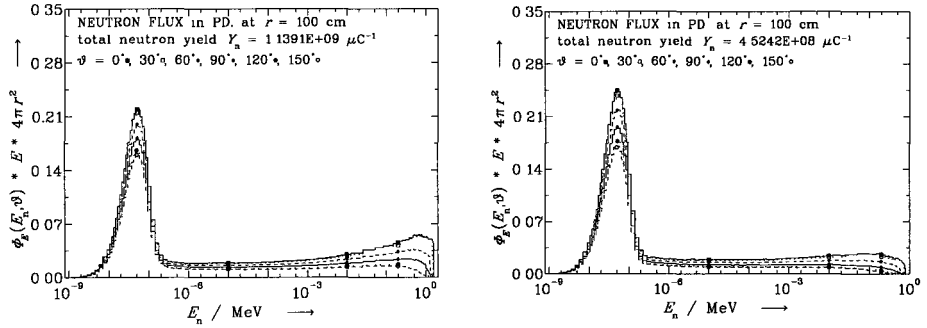

Figure 1.15: *Neutron spectra from ^{7}Li(p,n)^{7}Be and ^{7}Li(p,n)^{7}Be* reactions (the latter only on the left) for E_p = 3.3 MeV (left) and 2.5 MeV (right) placing an inner 5 cm polyethylene shell plus a 10 cm graphite shell around the target.*

For the higher proton energy, see Fig. 1.15 (left), the spectra have mean energies between 95 and 21 keV and mean conversion factors ranging between 46 and 20 pSv cm^2 for angles ϑ from 0° to 150°. In the forward direction, about 24 % of the neutrons have energies greater than 10 keV, which contribute significantly to the dose equivalent. At the lower end of reasonable proton energies, i.e. $E_p = 2.5$ MeV shown in Fig. 1.15 (right), these high-energy neutrons make a contribution of only 13 % to the total flux. In this case the spectra have mean energies between 22 and 4 keV whereas the mean conversion factors have values between 20 and 10 pSv cm^2. For a maximum proton current $J_{p,max} = 100$ µA we expect maximum neutron fluxes in the forward direction of $1.2 * 10^6$ cm^{-2} s^{-1} for 3.3 MeV protons and of $5 * 10^5$ cm^{-2} s^{-1} for 2.5 MeV protons at 1 m distance. All results of this work will be discussed in detail in a laboratory report [Wie95].

The use of proton beams with energies between 2 to 3.5 MeV from the Van-de-Graaff accelerator available at PTB and a thick metallic Li target will make it possible to produce neutron spectra with mean energies down to 4 keV, mean conversion factors of less than 20 pSv cm^2 and neutron fluxes of up to 10^6 cm^{-2} s^{-1}. The flexibility in the initial proton energy and the simple assembly geometry will allow neutron calibration fields with a wide range of

specifications to be produced. First investigations of neutron fields produced with the moderator assembly proposed here have been scheduled for 1995.

References

Ale92 A.V. Alevra, M. Cosack, J.B. Hunt, D.J. Thomas and H. Schraube,. *Experimental Determination of the Response of Four Bonner Sphere Sets to Monoenergetic Neutrons (II),* Radiat. Prot. Dosim. **40**, 91-102 (1992).

Aro92 A. Aroua, M. Grecescu, M. Lanfranchi, P. Lerch, S Prêtre and J.-F. Valley: *Evaluation and test of the response matrix of a multisphere neutron spectrometer in a wide energy range. Part II. Simulation,* Nucl. Instr. and Meth. **A231** (1992) 305-311

Ber95 W. Bernnat, M. Mattes, G. Pfister, *Bestimmung von Neutronen- und Gamma-spektren sowie der Dosis in der Umgebung des AHE-Versuchsbehälters auf dem PTB-Gelände*, IKE-report KE 6-FB-73, Stuttgart, 1995

Bie95 *TRIM-95 -- Ions in solids,* Computer Code by J.P. Biersack and J.F. Ziegler, 1995.

Bri93 J.F. Briesmeister (Editor), *MCNP - A general Monte Carlo N-particle transport code version 4A,* LA-12625-M, Los Alamos National Laboratory, 1993.

Bur94 B. Burgkhardt, G. Fieg, E. Piesch, A. Klett, R. Maushart, *Optimierung einer Neutronen-Äquivalentdosisleistungsmeßsonde,* In Strahlenschutz: Physik und Meßtechnik, Eds. W. Koelzer, R. Maushart, Verlag TÜV Rheinland, Köln 1994, Vol. II, 590 - 595.

Dro87 M. Drosg and O. Schwerer, *Production of monoenergetic neutrons between 0.1 and 23 MeV,* in Handbook on Nuclear Activation Data, IAEA-Tech. Reports Series No. 273, 1987, p. 83-162.

Mar91 V. Mares, H. Schraube, *Calculated neutron response of a Bonner sphere spectrometer with ^{3}He counter,* Nucl. Instrum. Meth. **A307** (1991) 398 - 412.

Nol92 R. Nolte, H. Schumacher, H.J. Brede, U.J. Schrewe, *Measurement of high-energy neutron fluence with scintillation detector and proton recoil telescope,* Radiat. Prot. Dosim. **44** (1992) 101-104.

Roe93 S. Roesler and G.R. Stevenson, *July 1993 CERN-CEC experiments: Calculation of hadron energy spectra from track-length distributions using FLUKA*, CERN/TIS-RP/IR/93-47 (November 1993).

Sch95 U.J.Schrewe, W.D. Newhauser, H.J.Brede, V. Dangendorf, P.M. DeLuca, Jr., S. Gerdung, R. Nolte, P. Schmelzbach, H. Schuhmacher and T. Lim, *Measurement of neutron kerma factors in C and O: neutron energy range of 20 MeV to 70 MeV,* Radiat. Prot. Dosim. **61** (1995) in press.

Tho92 D.J. Thomas, *Use of the program ANISN to calculate response functions for a Bonner sphere set with ^{3}He detector*, NPL report RSA (EXT) 31, Teddington, 1992

Publications (see part I):

[Alb94], [Ale94a], [Ale94b], [Ale94c], [Ale95a], [Ale95b], [Ale95c], [Bar95b], [Kra95b], [Lin95], [Nai95], [Sch94b], [Sie94a], [Sie94b], [Sie94c], [Sie95a], [Sie95b], [Tho94], [Wie94], [Wie95],
[Cha96], [Kle96], [Kln96], [Kna96], [Kra96], Nai96a], [Nai96b], [Tho96]

Head of project 2: Dr D.J. Thomas

Scientific staff: O.F. Naismith, A.G. Bardell, and Dr G.C. Taylor

II. Objectives for the reporting period

1. To develop an integrated set of validated neutron spectrometric instruments, including high resolution devices and a broad energy range device, for workplace measurements. Also, the development of techniques to combine results from the various devices into a single spectrum.

2. To measure spectra, both at workplaces and as part of international comparisons, and to include them in the database of realistic neutron spectra if appropriate.

3. To develop and improve the catalogue of realistic neutron fields and include in it all available spectra, instrument response functions, and conversion coefficients from fluence to dosimetric quantities.

4. To utilize the catalogue to investigate dosimetric quantities and dosemeter responses in workplace fields.

5. To categorise the spectra in terms of their features with a view to providing appropriate calibration facilities.

III. Progress achieved including publications

III.1 Development of the neutron spectrometry system

Much of the information on workplace spectra available in the literature, certainly the earlier data, must be treated with caution. Spectrometers were not well calibrated, and unfolding techniques tended not to have been validated with the result that the reliability of much of the data is questionable. One of the aims of this project was to develop at NPL a well calibrated and validated spectrometry system for making neutron field measurements. Evidence acquired from comparison exercises over the period of the contract[1][Lin95] has underlined the importance of good spectrometer calibration. {References to publications in the list in Part I of this report are shown as [Lin95], others by the convention [1] .}

Regardless of the number of spectrometric devices used when making a spectrum measurement the required final result is a single spectrum incorporating all the information from the instruments in a consistent way taking into account the uncertainties. A second aim was therefore to develop techniques for combining information from various spectrometers.

The first workplace spectrometer developed at NPL was a Bonner sphere set. It was based on a spherical ^{3}He proportional counter (Centronic SP9) used at the centre of nine spheres ranging in diameter from 7.62 cm to 38.1 cm. To use any Bonner sphere set for spectrometry the response function, i.e. the response as a function of neutron energy, must be known for each sphere of the set. This information is now available. It is based on: monoenergetic calibrations[2], a thermal measurement [Tho94], and two sets of calculations with neutron transport codes. The programs used were the discrete ordinates code ANISN[4] and the Monte Carlo code MCNP.

The response functions have been validated by measuring the well known spectrum from a ^{252}Cf source. Agreement was achieved, within the uncertainties, between the measured responses and the values predicted from the spectrum and the response functions. As a further improvement the ^{252}Cf data was used to refine the response functions. This was achieved by using the code normally used for spectrum unfolding to adjust the response functions while keeping the ^{252}Cf spectrum fixed, rather than the usual procedure which is to keep the response functions fixed and adjust the spectrum. In fact, this was the technique used to amalgamate all the response function data. The ANISN calculation, which provides the response function over the full energy range of interest, was taken as the *a priori* estimate of the shape, and this was adjusted using the measured data and the MCNP calculations. (This approach also allows the thermal calibration field to be represented by a realistic Maxwellian shape rather than making the approximation of treating it as occurring at a single energy).

Figure 2.1 illustrates the large amount of data which has been used to determining each response function, and also the good agreement between measurements and the MCNP calculation. It also highlights problems with the ANISN code in the thermal region and the importance of measurements in this area

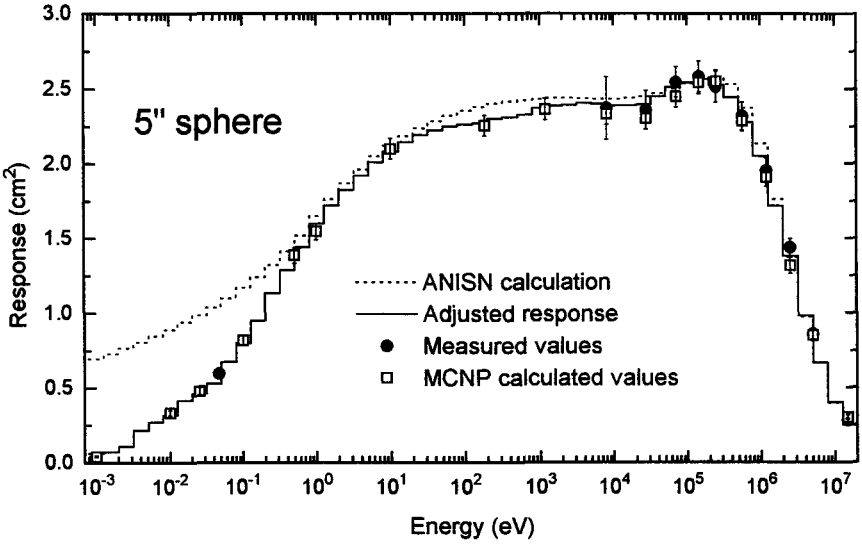

Figure 2.1. Data used for 5" Bonner sphere response function adjustment.

The system based on the SP9 ^{3}He counter is now well characterised and can be recommended as the Bonner sphere set of choice for any new user since the design and the validated response functions are freely available. This option has already been taken up by a Canadian group who have built a system based on the PTB/NPL design and used the NPL response functions after slight modifications for differences in polyethylene density[3].

Bonner sphere systems have the invaluable attribute of covering the whole energy range of interest in workplace dosimetry, i.e. thermal to about 20 MeV. They suffer, however, from poor resolution, especially at higher energies where the usual group structure of equal-width bins on a logarithmic scale results in very wide bins. For this reason additional instruments are often used to provide better resolution at higher energies and at NPL an NE213 scintillator

system has been developed for this purpose. Response functions have been derived from calculations backed up with measurements with monoenergetic neutrons over the energy range from 500 keV to 14 MeV[4]. Neutron/gamma discrimination is achieved by pulse rise time analysis using a dual-parameter data acquisition system, and, depending on the gamma contribution in a particular field, measurements can be made down to about 500 keV.

Although an NE213 scintillator may not cover a large fraction of the total fluence distribution in the majority of workplace spectra, it does provide extremely valuable information on the position of the upper energy edge of any neutron distribution. Despite the fact that the responses of a number of the spheres from a conventional Bonner sphere set peak in the region around 1 MeV, it can sometimes prove difficult with Bonner spheres alone to unfold the shape of the upper portion of a spectrum, and this can have significant implications for the derived dose equivalent. Combining data from an NE213 measurement with Bonner sphere results to give a combined spectrum is not, however, straightforward, it is in fact very spectrum dependent, and any approach to doing it needs to be flexible.

NE213 measurements were made by NPL at a number of sites including the international comparisons organised by Eurados Working Group 7 (WG7) at Winfrith and Cadarache II (see section III.2), and also at the SILENE reactor at Valduc, France. For the Winfrith and SILENE data the approach adopted for combining NE213 and Bonner sphere results was to perform an initial analysis of the data from both spectrometers completely separately, and then compare the unfolded spectra in the region of overlap. In both cases there was reasonable agreement, so the next step involved re-bining the NE213 results into the Bonner sphere energy group structure and using it to tie down, within the uncertainties, the spectrum in the overlap region. The Bonner sphere unfolding was then repeated resulting in a slightly revised shape outside the region of overlap, and some slight re-normalisation within the overlap region reflecting the slightly better absolute normalization of the Bonner sphere system. Finally the high resolution structure was re-introduced in the overlap region while maintaining the normalisation determined from the final Bonner sphere unfolding.

The final spectrum thus utilizes the detailed structure from the NE213 and the good overall normalization of the fluence as given by the Bonner spheres. It also gains from the fact that the NE213 data reduces the extent to which the Bonner sphere unfolding is under-determined since it restricts the freedom to alter the upper part of the spectrum. All this is possible because the unfolding code used, STAY'SL, allows *a priori* information, in this case the NE213 results, to be input with uncertainties.

Figure 2.2 shows a spectrum measured during the Winfrith intercomparison exercise and illustrates why *a priori* information from the NE213 measurement must be used with caution. Although it provides information in the region above 1 MeV it is not at all clear from the NE213 data alone whether the distribution peaks at 1 MeV or much lower.

For the Cadarache comparison there was very little fluence in the region of overlap between the two systems, but the NE213 results were still useful for tying down the very small 14 MeV peak in the spectrum and indicating the position of the upper energy edge of the broad neutron distribution which extended up to about 1 MeV. The flexibility needed to tailor the analysis to the particular spectrum being unfolded is only possible if good data handling programs are in place to transfer and re-bin data and to produce, in a quick and simple manner, a range of *a priori* spectra made up of various standard components.

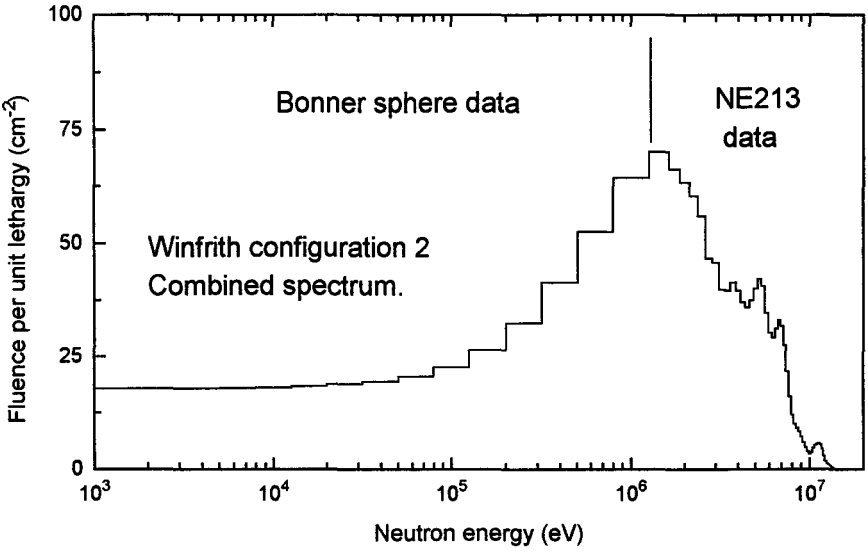

Figure 2.2. Upper energy part of spectrum measured at Winfrith showing the region covered by the NE213 scintillator measurement and the join point with the Bonner sphere data.

Ideally further high resolution instrumentation should be used to provide information on the region below that covered by the NE213 scintillator. Several groups have developed sets of proton recoil counters for this purpose, and these can measure down to 50 keV or even lower under favourable conditions. One instrument that had not been tried in Europe for this energy region, despite reports of its successful use at commercial nuclear plants in the USA[5], was a ^{3}He spectrometer. Such devices have the advantage that for energies up to 764 keV the measured pulse height distribution is a close approximation to the spectrum being measured which makes spectrum unfolding much easier than for proton recoil counters.

A ^{3}He spectrometer based on a cylindrical high-pressure gridded ionization chamber of the Shalev-Cuttler design[6] was developed for NPL at the University of Birmingham, and its performance investigated. The spectrometer worked well in the low-scatter area at NPL, but when tried in the realistic fields at Winfrith and Cadarache it proved impossible to derive any useful information. The problem was one of pulse pile-up from detection of low energy neutrons. The cross section for the ^{3}He(n,p)T reaction has a 1/v dependence at low energies, and to prevent detection of thermal neurons the counter has a cadmium sleeve. For the field measurements additional cadmium end-covers were used. This did not, however, prevent excessive pile-up from completely obscuring the spectrum. Since the cadmium absorbs all neutrons below about 0.5 eV, the problem must be due to detection of epi-cadmium neutrons. It may be possible by using additional absorbers, of samarium for example, and possibly further pulse shape analysis (pulse shape analysis is already used for n/γ discrimination), to use the device in fields where the spectrum does not contain excessively large numbers of low energy neutrons. At present, however, it would appear that a proton recoil counter set is still the instrument of choice for field measurements in the 50 keV to 1 MeV region.

One further area of instrument development has involved a Bonner sphere set with gold activation foils as the central thermal neutron detector. Despite low efficiency, a sphere set using activation foils has certain advantages. There are no electronic connections to the

spheres and so they are quick and very simple to set up. This can be an important advantage in high dose rate areas. Since there are no cables involved, the spheres can be enclosed in polyethylene bags and used in areas where contamination is a problem. They are sufficiently insensitive to γ rays that they can be used in intense photon fields, e.g. around hospital linear accelerators, and can be used equally as well in pulsed fields as in steady ones. NPL used a sphere set based on gold foils at the Eurados WG7 intercomparison at Ringhals in Sweden (see section III.2) at a site where dose rates were too high for the ^{3}He counter set [Bar95a].

Work to improving the gold foil Bonner sphere set has involved two aspects. To increase the efficiency the diameter of the gold foils was enlarged to give an increase of a factor of four in the efficiency. At the same time a new set of response functions were derived. Because of the low efficiency it is difficult to perform calibrations with monoenergetic neutrons. The response functions thus rely entirely on calculations with ANISN and MCNP backed up by validation and refinement using a ^{252}Cf source (c.f. validation of the ^{3}He system described above). As with the ^{3}He set the ANISN calculations provided the basic response function shapes, although they needed to be re-normalized by sphere-size dependent fit factors determined from the MCNP calculations and the ^{252}Cf measurements.

III.2 Spectroscopy measurements

Eurados WG7 has organized four comparisons of spectrometric measurements (Cadarache I in France, Winfrith in the UK, Ringhals and Oskarshamn in Sweden, and Cadarache II). NPL participated in three out of the four, the exception being the first Cadarache exercise which was a 'trial run' with only three participants. The results have shown good consistency with the measurements of others and with calculations of the spectra where available.

Measurements have also been performed at the SILENE experimental reactor at Valduc in France for two fields, the bare reactor and the reactor surrounded by 10 cm of lead[7]. This was in preparation for an international comparison of criticality accident dosimetry systems held in June 1993. To define neutron kerma values accurately the neutron spectra needed to be known. Measurements of the two fields were subsequently also performed by the CEA Fontenay team. Good agreement was achieved between the two sets of measurements with values for the total fluence agreeing to about 10% for both spectra[8].

Other field measurements have been performed, with the gold foil based sphere set to measure neutrons from a cyclotron, and with the ^{3}He based sphere set at various locations in the area outside a nuclear power reactor, see Figure 2.3. This latter set was unusual being measurements at levels near the limits applicable to members of the public, i.e. less than 1 mSv per annum. The high efficiency of the ^{3}He Bonner sphere set allowed these measurements to be made in reasonable time (about one day per site). They provided calibration figures for area survey instruments to be used for future measurements in this area. As expected the spectrum was very soft.

III.3 Developments and improvements to the catalogue

Much of the effort at NPL has involved developing and improving the catalogue of realistic neutron fields, including installing all available data for spectra, response functions, and conversion coefficients from fluence to dosimetric quantities. The computer program used to manipulate the data is complete and the whole package of data, program, and manual [Nai95] is available. Details are given in the special section in this report on the database.

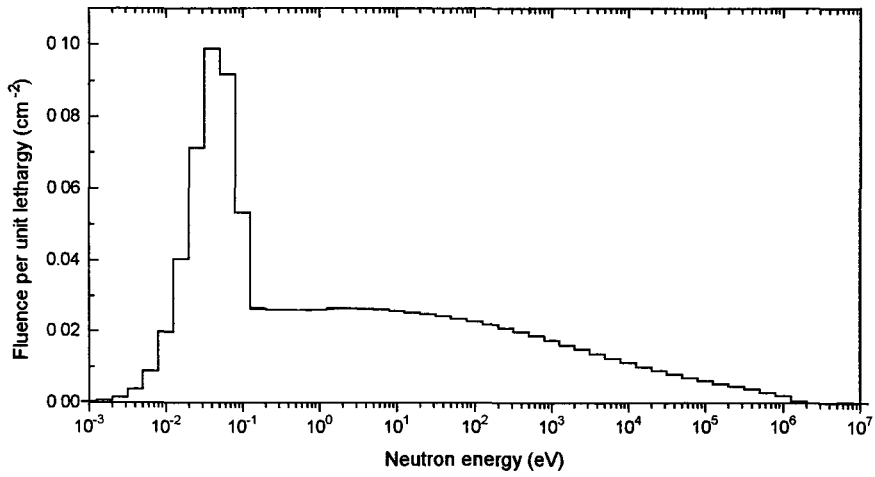

Figure 2.3. Neutron spectrum at a location outside a nuclear power reactor (data is normalized to unit fluence)

III.4 Use of the database to investigate dosemeter responses and relationships between dosimetric quantities

The database with its associated programs for handling the data provides an ideal tool for investigating dosemeter responses in realistic fields, and the implications of any changes to basic dosimetric quantities.

ICRP in their publication 60[9] propose radical changes to the quantities to be used in radiation protection dosimetry for neutrons. The operational quantities H*(10) and $H_p(10)$ change because the Q(L) relationship, used in calculating fluence to dose equivalent conversion coefficients, changes. More significantly, the ICRP propose a new limiting quantity, effective dose, E, to replace effective dose equivalent, H_E. It is derived from calculated organ doses by applying radiation weighting factors, w_R, which depend only on the nature of the incoming radiation rather than on the type of radiation actually delivering the dose. The net effect is an increase in the limiting quantity. This increase is, however, more than the increase in the operational quantities and with the new recommendations the operational quantities are no longer greater than the limiting quantity at all neutron energies, most noticeably at intermediate energies. The question then is whether the operational quantities are still, as they should be, conservative overestimates of the limiting quantities for workplace fields.

The database was used to investigate this problem. Spectra were grouped according to their locations (gas cooled reactors (GCR), pressurised and boiling water reactors (PWR and BWR), around fuel transport containers (Trans), fuel processing areas (Process), and radionuclide neutron source handling and fabrication areas (Sources)) and the ratios of E/H*(10) and $E/H_p(10)$ calculated for various directions of incidence. Data are shown in Figure 2.4 for E/H*(10) for anterior-posterior (AP), posterior-anterior (PA), radiation which is invariant around a vertical axis through an individual (ROT), and for irradiation from the sides (LAT). The results for $E/H_p(10)$ are similar although the ratios are a little larger.

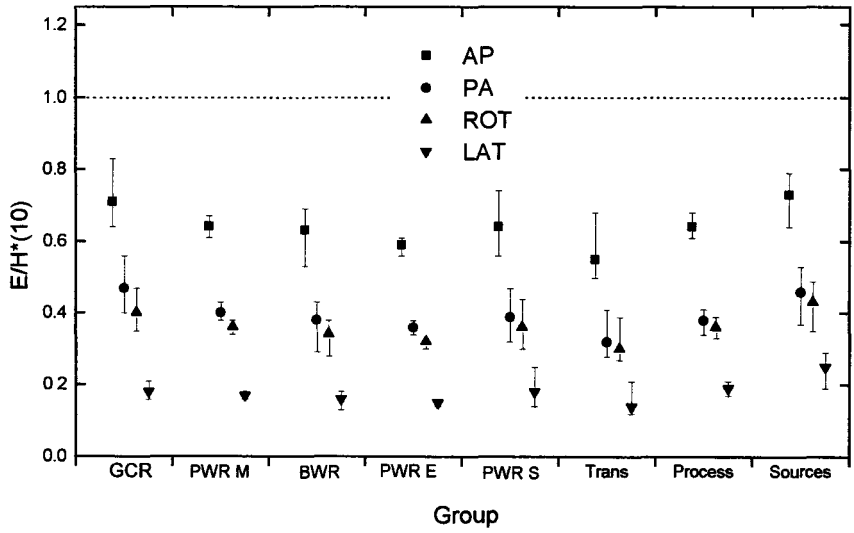

Figure 2.4. Ratio of effective dose, E, to ambient dose equivalent, H*(10). The data points represent the mean value of the ratio while the 'error bars' indicate the range of values.

Even for the softest spectra, the operational quantities remain overestimates of the limiting quantity except possibly for $E/H_p(10)$ for AP irradiation in the very softest fields. These results were presented at the topical workshop at Villigen in 1993 [Mar94] and used data available at that time. Since then further calculations of the conversion coefficients have been performed, including changes introduced by the new ICRU stopping power data published recently, and when a consistent set of evaluated conversion factors are published the analysis will be repeated.

Table 2.1. Responses of 3 area survey instruments as a ratio to ambient dose equivalent (calculated with ICRP 60 quality factors) after calibration in 3 different fields: Am-Be, ^{252}Cf, and D_2O-moderated ^{252}Cf.

Spectrum Group (data are mean values for group)	Effective Dose (pSv cm^2)	HARWELL 0949			ANDERSSON-BRAUN NM2			STUDSVIK		
		Calibration field			Calibration field			Calibration field		
		Am-Be	^{252}Cf	D_2O mod ^{252}Cf	Am-Be	^{252}Cf	D_2O-mod ^{252}Cf	Am-Be	^{252}Cf	D_2O-mod. ^{252}Cf
Gas-cooled reactors	20	2 37	2 17	1.66	1 16	1 14	1.07	0.90	0 93	0 89
PWRs in Europe and USA	32	1 80	1 65	1.26	1 04	1 02	0 96	0 84	0.86	0 83
PWRs (Endres and Schraube)	37	1.80	1.65	1 27	1.05	1 03	0 96	0 85	0.88	0 85
PWRs (Endres et al)	39	1.68	1.54	1.18	0 98	0 96	0.90	0 79	0.82	0 79
PWRs (Sanna et al)	51	1 54	1.41	1 08	0 95	0 94	0 88	0.83	0 85	0 82
Fuel transport containers	92	1 21	1.11	0 85	0.81	0 80	0.75	0 74	0 76	0 73
Fuel processing / storage	115	1 21	1.11	0 85	0 95	0 94	0.88	0 81	0 84	0.81
Source environments	187	1 15	1 05	0.81	1 02	1.01	0.94	0.93	0 96	0 92

Because neutron dosemeters do not have the required dose equivalent response over the full energy range of interest, the reliability of their readings in unknown neutron fields is open to question. Table 2.1 quantifies the extent of this problem for area survey instruments, and shows results for three commonly used devices for the groups of spectra described earlier. The table also illustrates how the dosemeter readings depend on the type of field used for calibration. The range of under- and over-read which can occur is large, however, the results have significant uncertainties, particularly for the Andersson-Braun and the Studsvik instruments because the data for their response functions are far from complete.

Personal dosemeters response functions tend to be less well defined than those for area survey instruments. Different dosimetry services, even when they use essentially the same neutron detecting element, e.g. CR-39 track-etch plastic, use different dosemeter configurations, materials from different suppliers, and different processing techniques. This makes it difficult to draw hard and fast conclusions about personal dosemeter under- and over-read in realistic fields. The problem has, however, been investigated using the catalogue [Tho95], and Table 2.2 gives some indications of typical values using response functions for a particular type of CR-39 dosemeter, and two somewhat different NTA film dosemeters. Film B has a cadmium cover to remove the inherent sensitivity to thermal neutrons, whereas film A does not.

Table 2.2. Responses of two types of personal dosemeter in three different neutron spectra after calibration in three different fields, namely Am-Be, ^{252}Cf, and D_2O moderated ^{252}Cf.

Spectrum type	CR39			NTA film A			NTA film B		
	Calibration field			Calibration field			Calibration field		
	Am-Be	^{252}Cf	D_2O mod. ^{252}Cf	Am-Be	^{252}Cf	D_2O mod. ^{252}Cf	Am-Be	^{252}Cf	D_2O mod ^{252}Cf
Spectrum (a) (soft)	1.35	1.14	1.22	0.30	0.50	0.57	0.01	0.02	0.02
Spectrum (b) (med)	1.25	1.05	1.13	0.27	0.45	0.52	0.24	0.35	0.42
Spectrum (c) (hard)	1.12	0.94	1.01	0.69	1.15	1.32	0.74	1.09	1.3

Only three spectra have been used as illustrations of (a) a very soft spectrum with a large thermal component, (b) a medium one, and (c) a hard one where the majority of the dose equivalent was in the fast neutron region. The table illustrates under- and over-read depending on the field in which the dosemeter is calibrated.

The particular type of CR-39 track etch plastic chosen gave very reasonable results in all three fields, particularly if calibrated with ^{252}Cf or heavy water moderated ^{252}Cf. Closer inspection revealed this to be a result of the good fast-neutron response of the dosemeter in case (c), and a combination of this and cancellation between over-response at thermal energy and under-response at intermediate energies for (a) and (b). Film A gave results that were low for the soft and medium spectra, regardless of calibration field, and film B gave very poor results in the two softer spectra highlighting the importance of the thermal response of NTA film both for responding to direct thermal neutrons, and also in providing a degree of albedo response.

III.5 Categorising and realizing realistic neutron fields

Efforts have been made to categorise the neutron spectra in the database. Unfortunately no simple method, such as measurement location, appears to work particularly well. Alternative methods are being investigated, such as ordering spectra according to their 9" to 3" Bonner sphere response ratio. This work will continue at NPL.

The facility at Winfrith in the UK, which was used for one of the Eurados WG7 comparisons, was based on moderation of neutrons from a fission plate irradiated by neutrons from a test reactor. A range of moderation configurations, and hence spectra, were possible, calculation of the spectra was easy because of the simplicity geometry, and dose rates could be varied over a wide range. It thus provided an excellent realistic field facility. Unfortunately, however, it has now been closed. As a result efforts will be made to set up realistic fields at NPL taking advantage of the experience already gained in the framework of this project.

References

[1] H. Klein, D.J. Thomas, J.L. Chartier, and H. Schraube (Eds.), *Calibration Fields for Neutron Protection Dosimetry as derived from Spectra Encountered in Routine Surveillance,* (final report on the CEC project B17-031), EUR report 14927 EN (1993) 159-174.

[2] A.V. Alevra, M. Cosak, J.B. Hunt, D.J. Thomas, and H. Schraube, *Experimental determination of the response of four Bonner sphere sets to monoenergetic neutrons (II),* Radiat. Prot. Dosim. **40**, 91-102, 1992.

[3] D.J. Thomas, *Use of the program ANISN to calculate response functions for a Bonner sphere set with a ^{3}He detector,* NPL Report RSA(EXT)31, March 1992.

[4] S. Green, M. Scott, and R. Koohi-Fayegh, *A User's Guide for the NPL NE-213 Neutron Spectrometry System,* University of Birmingham, report of work carried out under NPL research agreement 82/0462, September 1991.

[5] L.W. Brackenbush, W.D. Reece, and J.E. Tanner, *Neutron Dosimetry at Commercial Nuclear Plants, Final Report of Subtask C: ^{3}He Neutron Spectrometers,* Pacific Northwest Laboratory Report NUREG/CR-3610, PNL-4943, September 1984.

[6] S. Shalev and J.M. Cuttler, *The Energy Distribution of Delayed Fission Neutrons,* Nucl. Science and Eng. **51**, 52-66, 1973. (The instrument used, the FNS-1 is available from Common Sense, P.O. Box 123, Zippori 17910, Israel).

[7] D.J. Thomas, A.G. Bardell, and G.C. Taylor, *Neutron Spectrometry Measurements Performed at the SILENE Reactor, Valduc, France,* NPL Report RSA(RES)**, (in preparation).

[8] R. Medioni and H.J. Delafield, *An International Intercomparison of Criticality Accident Dosimetry Systems at the SILENE Reactor, Valduc, Dijon, France, 7-18 June 1993, Part I: Reactor and Reference Dosimetry of Radiation Fields,* AEA Technology and IPSN-CEA joint Report HPS/TR/H/1(95), April 1995.

[9] ICRP, *1990 Recommendations of the International Commission on Radiological Protection,* ICRP Publication 60, Annals of the ICRP **21**, No. 1-3, 1991.

Publications (see Part I):
Bar95a, Mar94, Nai95, Tho94, Nai96a, Nai96b, Tho96

Head of Project 3: Dr. J.L. Chartier

Scientific staff: Dr F. Posny, Dr D. Paul, J. Kurkdjian, G. Audoin, C. Itié, G. Pelcot.

II. Objectives for the reporting period

The contribution of IPSN-CEA to the joint contract is related to three main topics dealing with neutron dosimetry for radiation protection purposes:

1. Study and realisation of realistic neutron spectra facilities replicating in the laboratory some typical situations encountered at workplaces and enabling the calibration of dosimetric instruments in « practical » neutron fields.
2. Implementation of an operational neutron spectrometry involving proton-recoil counters and Bonner sphere systems. Measurements techniques and unfolding codes. Measurements at workplaces and in calibration facilities.
3. Transfer of neutron fluence references from PTB to a van de Graaff facility at CEA/Bruyères-le-Châtel in order to establish a reference beam line devoted to monoenergetic neutron applications in spectrometry and dosimetry.

III. Progress achieved including publications

III.1. Study and realisation of realistic neutron spectra facilities.

The IPSN-CEA laboratory has developed two facilities for the purpose of simulating realistic neutron spectra. Both are based on the same principle, i.e. a fission neutron source induced by monoenergetic neutrons irradiating a ^{238}U converter. They only differ by the values of the primary neutron energies (14.6 MeV and 3 MeV) and by the initial shielding of the assembly (with or without a 12 cm thick iron shell). Two configurations denoted « RNSF 14 MeV » and « RNSF 3 MeV » are described in the following paragraphs.

A - RNSF « 14 MeV »

The characterisation of the neutron field and the calibration of the monitoring system represent the bulk of the work. The modelling of the anisotropic 14.6 MeV source, as well as its spectral fluence and the detailed mechanical set-up were taken into account [Cha92]. Moreover, the detailed structure of the beam cross-section in terms of fluence and energy distribution was carefully analysed in the calibration zone (Fig. 3.1). The reference neutron

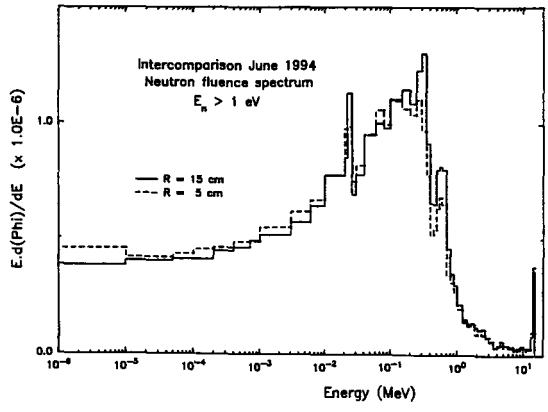

Figure 3.1: *Neutron Spectra at different distances R from the beam axis of the RNSF « 14 MeV » assembly*

fluence and spectrum were derived by an averaging procedure. In addition, an experimental validation has confirmed the reliability of MCNP calculations in absolute scale [Cha95] and should avoid the (PR + BS) spectrometry for characterising any radiation field produced by any combination of shielding materials and geometries. Instead, an integral measurement with one (or several) calibrated BS-like instrument can be carried out.

As to the monitoring system based on the associated particle method, a fluence measurement with an NE213 spectrometer calibrated at BIPM (Sèvres, France) enabled to check the calibration of Si detectors and the diaphragm arrangement.

The calibration of individual dosemeters need further refinements in the knowledge of the field specifications, in particular, its angular distribution, and eventually the corresponding spectral modifications (Fig. 3.2). Some changes in the assembly are suggested from calculations to realise an « almost parallel » broad beam which is quite appropriate to investigate the angular response of dosemeters in terms of $H_p(10,\alpha)$.

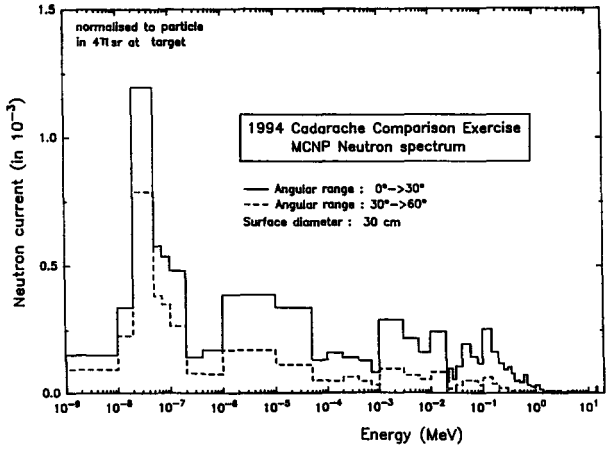

Figure 3.2: *Angle dependent energy distribution of the neutron beam in RNSF « 14 MeV »*

In 1994, a comparison exercise has been organised in the framework of EURADOS WG7 where several types of neutron spectrometers and dosimetric instruments have been tested. Three periods of two weeks each have been devoted to measurements and irradiations of neutron detectors involving more than 20 laboratories in charge of radiation protection tasks. The evaluation of the results of this large scale exercise is currently in progress [Tho96].

B - RNSF « 3 MeV »

In a previous progress report [Kle93] preliminary results have shown the interest of using the $D(d,n)^3He$ reaction as a primary neutron source yielding a « 3 MeV » neutron field. A facility based on a SAMES T400 type accelerator (max. H.V.400 kV) has been realized. In addition to the technical problems related to engineering (mechanics, vacuum techniques), a specific study (monitor program) has been undertaken to evaluate the characteristics of the monitoring system based on the competitive reaction D(d,p)T. By analogy with the $T(d,n)^4He$ reaction on the SAMES 150 kV J25 type accelerator currently in operation, the associated particle method using the proton count rate is deemed a satisfactory solution to monitor the neutron emission of the target. The protons are measured by 3 semiconductor detectors placed at an angle of

176° to the incident 330 keV deuteron beam. Special attention has been paid to optimise the proton count rate and to increase the solid angle of detection (diaphragm diameter : 4 mm). A check source (^{241}Am) has been also installed to test the 3 diodes and to control the reliability of the monitoring system based on the mean value of the 3 detector counts.

From the expression : $Y_n = (4\Pi/\Delta\Omega_p)K_p(\sigma_n/\sigma_p)$

the total neutron yield per measured proton can be derived. In this formula, the symbols have the following meanings :

- $\Delta\Omega_p$: mechanical solid-angle of measurement : 1.8 10^{-5}sr.
- K_p : anisotropy factor

Both reactions, $D(d,n)^3He$ and $D(d,p)T$, are markedly anisotropic in the CM system, and K_p is given by :

$$K_p = \left[\frac{\sigma_p}{4\Pi}\right] / \left[\left(\frac{d\sigma_p}{d\omega'}\right)\cdot\left(\frac{d\omega'}{d\omega}\right)\right]$$

where :

- $(d\omega'/d\omega)$: ratio of the differential solid angle $d\omega'$ in the CM system and the corresponding $d\omega$ in the LAB system

- $(d\sigma_p/d\varpi')$: differential cross section of proton yield in the CM system

- σ_n / σ_p : ratio of total neutron and proton production cross sections

For E_d = 330 keV we get Y_n : $6.97 \cdot 10^5$ neutrons in 4 Π sr/proton.

To validate this relation, fluence measurements have been carried out using a Ti-D target (thickness : 1300 μg/cm²) for 3 different versions of the set-up : i.e. without a moderator assembly surrounding the target (A), with the ^{238}U converter + $(CH_2)_n$ duct (B) and finally induding an additional 10 cm thick water shield (C). Combining Y_n with the MCNP calculated fluence spectrum, which is normalised to 1 neutron emitted in 4 Π sr, predicted and measured fluences at the calibration point in the beam are compared. Different instruments have been used : a calibrated Harwell N91 monitor and Bonner spheres. Results are presented hereafter for configurations (A), (B) and (C).

B - 1. Configuration (A)

The spectral neutron fluence distribution was calculated with the MCNP code for a distance of 100 cm from the target (Fig. 3.3). Taking into account the contribution of scattered neutrons (20% in fluence), the predicted monoenergetic 3.3 MeV neutron fluence was evaluated by applying the Y_n value previously determined and the absorption correction in the target backing (≅ 14% in fluence).

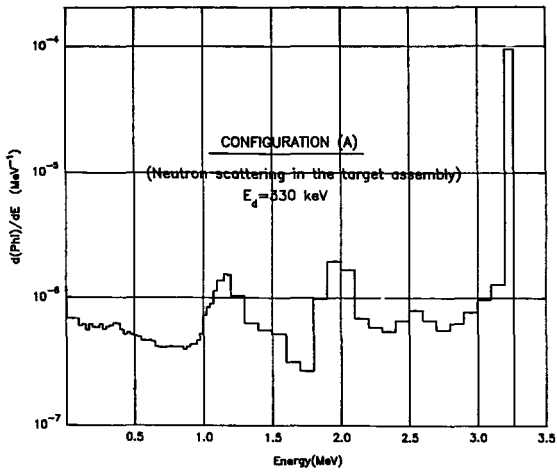

Figure 3.3: *Calculated neutron spectrum of the RNSF « 3 MeV » - configuration (A)*

The experiments were carried out with the Harwell N91 monitor as a reference. The calibration coefficient was calculated from the fluence response curve folded with the MCNP calculated spectrum. Additional spectrometric measurements were performed with a set of Bonner spheres. Results are presented in Table 3.1.

The discrepancy between predicted and experimental values has not yet been completely understood. Several reasons may be assumed, dealing with the modelling of interactions in the thick target and the evaluation of monoenergetic neutrons in the measured neutron field from the MCNP calculated spectrum.

Table 3.1

	Fluence (cm^{-2})	**H*(10) (nSv)**
Configuration (A)	Monoenergetic neutrons 3,3 MeV	
Calculation (MCNP) x Y_n	6.6 (*)	2.7 (*)
Harwell N91	8.4	3.4
Bonner spheres	9.7	3.8
Configuration (B)	[3.3 MeV + ^{238}U + PE duct]	
Calculation (MCNP) x Y_n	13.8	1.3
Harwell N91	12.7	1.2
Bonner spheres	12.3	0.9
Configuration (C)	[3.3 MeV + ^{238}U + PE duct + H_2O(10 cm)]	
Calculation (MCNP) x Y_n	8.1	0.3
Harwell N91	7.8	0.3

(*) normalised to 1 monitor count.

B - 2 Configurations (B) and (C)

Similar measurements and MCNP calculations were performed with configurations (B) and (C). A better agreement between both series of predicted and measured values is shown in Table 3.1. Furthermore, the main characteristics of neutron spectra shown in Figures 3. 4 and 3.5 are summarised in Table 3.2.

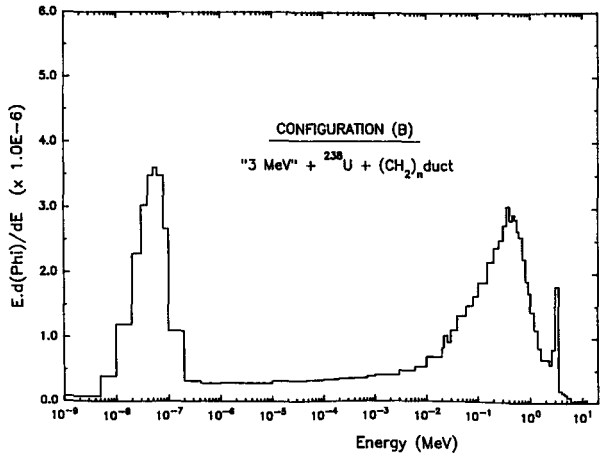

Figure 3.4: *Calculated neutron spectrum of the RNSF « 3 MeV » - configuration (B)*

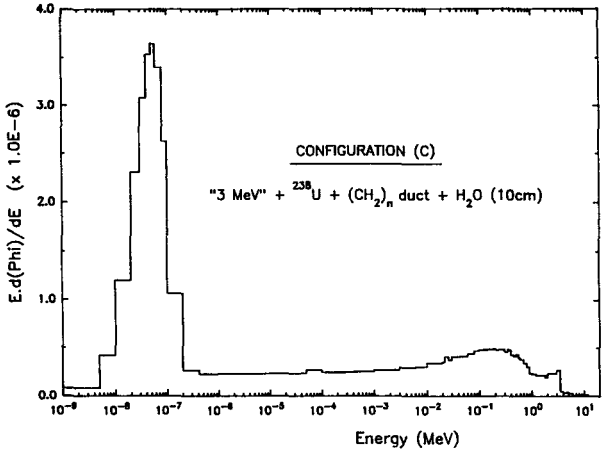

Figure 3.5: *Calculated neutron spectrum of the RNSF « 3 MeV » - configuration (C)*

Table 3.2

Configuration	E_{th} (MeV)	Th. (%)	Int. (%)	H_E (%)	h^*_{th} (pSv.cm²)
(B) : [3.3 MeV + ^{238}U + PE duct]	0.27	35.3	17.9	46.8	89
(C) : [(B) + H_2O(10 cm)]	0.10	59.8	21.4	18.8	35

III.2. Implementation of an operational neutron spectrometry and measurements at workplaces and at irradiation facilities

The operational neutron spectrometry developed at the IPSN/CEA laboratory takes advantage of the complementarity of PR and BS techniques. In the energy region where both techniques overlap, i.e. approximately above 100 keV, results derived from BS measurements are fitted to the PR spectrum which does not depend on an priori information. A difference between PR and BS integral fluences lower than 5% has been choosen as a criterion to select the most probable BS solution. This method has been applied at the SILENE reactor (CEA-Valduc) in the frame of an international criticality accident dosimetry intercomparison (7-18 june 1993). The IPSN-CEA laboratory was asked to contribute to the characterisation of the radiation field at the reference point in the reactor cell for 2 configurations : the « bare » reactor and the « lead shielded » reactor [Med95]. Similar measurements were performed by Harwell (AEA Technology) in collaboration with NPL. Results are presented in graphs of Figures 3.6 and 3.7.

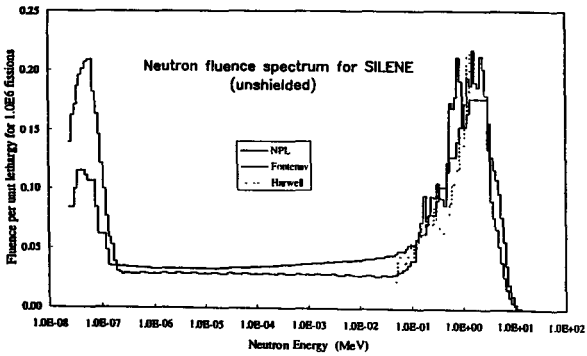

Figure 3.6: *Silene reactor (Unshielded)*

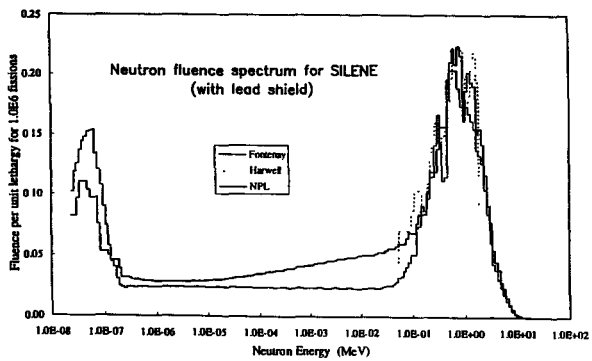

Figure 3.7: *Silene reactor (With lead shield)*

Other field spectra measurements have been carried out at the Venus research reactor (Mol Research Center, Belgium) at several locations in the reactor building. The Bonner sphere results (Fig. 3.8) are being evaluated and will be compared with Monte-Carlo calculations (Tripoli code) currently in progress. Finally, in the frame of the 1994 Spectrometry Comparison exercise organised at Cadarache, the spectrometric determination of the available neutron field was realised by the LRDE/FAR [Pos95] and LRDE/CAD [Kur95] groups. The evaluation of these data is in progress [Tho96].

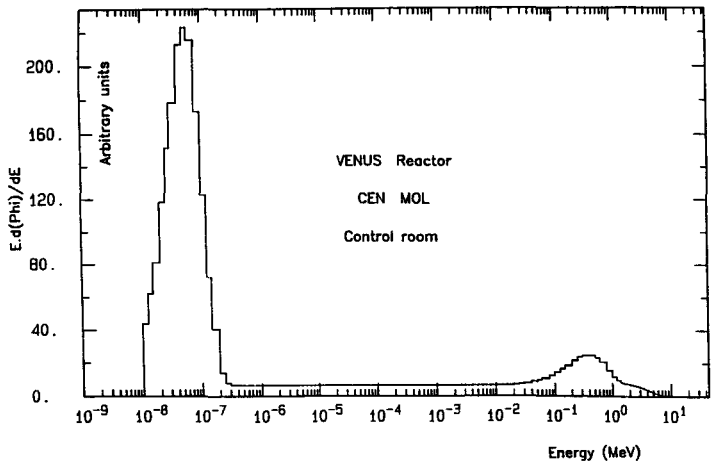

Figure 3.8: *Neutron spectrum at Venus reactor (Control room)*

III.3. Establishment of neutron fluence references at the Van de Graaff facility of CEA-Bruyères-le-Châtel

This study intends to realise reliable monoenergetic neutron fluence references in France by transfering the primary PTB references to the facility in CEA-Bruyères-le-Châtel, where a beam line has been devoted to neutron metrology and dosimetry since mid-august 1993. The current project is dealing with the neutron energies ranging from approximately 100 keV up to 3 MeV.

In the first part of the program, two SP2 spherical proportional counters were considered as transfer instruments (H_2 3 bars ; CH_4 5 bars). The experiments were performed at 6 neutron energies from 144 keV to 1.5 MeV at PTB in december 1992, and compared to previous measurements realised at CEA-Bruyères. Besides these fluence measurements, other problems had to be simultaneously studied, in particular the estimation and the influence of neutron scattering in the target assemblies. The presence of parasitic neutrons (and photons) could be observed when comparing the shapes of response functions measured at the PTB and the CEA facility, respectively. In addition, Monte-Carlo calculations using the MCNP code have been initiated to estimate the scattered contribution due to the target holder. The good agreement between MCNP results and those derived from the PTB TARGET code for the PTB target holder geometry gives confidence in the reliability of new calculations, currently in progress to optimise the CEA-Bruyères target construction. An example of calculated results is shown in Figure 3.9. This first part of the programme (EUROMET project) has demonstrated the satisfactory agreement of the energy calibration and the pulse height resolution of detectors when operated at both facilities, and discrepancies between values of the pulse height resolution appearing at low neutron energies (144 and 250 keV) are mainly due to the differences of the Li target realisation. The problem of the systematic underestimation of efficiency, which is clearly observed when experiments are carried out with SP2 counters at the CEA facility has not been explained yet and is currently under investigation. Additional measurements and calculations are planned for the neutron energy range extending from 1.2 MeV to 3 MeV at CEA-Bruyères in November 1995 and at PTB in December 1995. An NE213 spectrometer will be used as transfer instrument and again an SP2 proportional counter

(with CH_4 filling gas) for neutron energies below 2.5 MeV to check the reproducibility of detectors by repeating former measurements.

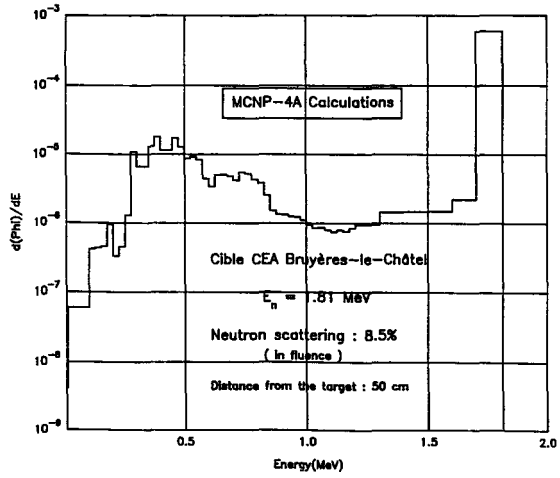

Figure 3.9: *Calculated neutron spectrum (CEA Bruyères target assembly).*

References

[Cha92] J.L. Chartier, F. Posny, M. Buxerolle, *Experimental assembly for the simulation of realistic neutron spectra*, Radiat. Prot. Dosim. **44** (1992) 125-130

[Kle93] H. Klein, D.J. Thomas, J.L. Chartier, H. Schraube, *Determination and realisation of calibration fields for neutron protection dosimetery as derived from spectra encountered in routine surveillance*, EUR report 14927 DE/EN/FR, Luxembourg, 1993, p. 159-174

[Med95] R. Médioni, H. Delafield, *An international Intercomparison of C.A.D. Systems at the Silène Reactor.* Valduc, Dijon, France 7-18 juin 1993. Part 1 Reactor and Reference Dosimetry of Radiation Fields. Report HPS/TR/H1 (95). April 1995.

[Pos95] F. Posny et al., Cadarache 1994 Intercomparison Exercise Provisional evaluation report by D. Thomas (1995).

[Kur95] J. Kurkdjian et al., Cadarache 1994 Intercomparison Exercise Provisional evaluation report by D. Thomas (1995).

Publications (see Part I):

[Cha95], [Cha96]

Head of Project 4: Dr.H.Schraube

Scientific technical staff: Dr.J.Jakes, Dr.G.Leuthold, V.Mares, G.Schraube, E.Weitzenegger

II. Objectives for the reporting period

The essential contribution of the GSF to the joint contract was the determination of basic radiological data, the measurement, evaluation and collection of neutron spectra as observed at places where workers and other people are exposed to neutrons, and to derive the relevant dosimetric integral quantities. The following objectives were treated:

1. Calculation of organ doses and other energy dependent dosimetric quantities in anthropomorphic phantoms, and considerations on a modified radiation weighting factor
2. Calculation of the response matrix to a BS system with ^{6}LiI detector
3. Evaluation of recent Bonner sphere experimental data for the spectral catalogue
4. Determination of integral quantities in realistic survey fields
5. Establishing of a simple slowing-down calibration field in the GSF neutron laboratory

III. Progress achieved including publications

Ad 1. Organ doses

Some differences of our previous phantom calculations to other findings motivated us to implement the ADAM and EVA anthropomorphic phantoms into the MCNP Monte-Carlo package and to calculate the organ dose equivalents and the other relevant quantities for these phantom models including the requirements of ICRP60 with respect to the revised organ list and weights. It appeared that the older SAM/CE code could not treat the neutron energy range below, say 10 eV, accurately enough due to a different treatment of the low energetic neutron transport.

This causes also changes in the production of secondary photons which may contribute up to 95% to the total energy dose in the depth of the phantom, and, herewith, to the effective dose after ICRP60. In Fig. 4.1 our results of fluence-to-effective dose conversion are compared with findings of others. Generally the MCNP-calculations (Morstin, 1992, and this work

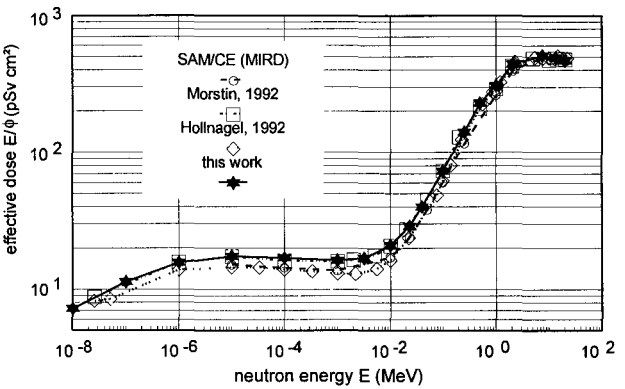

Figure 4.1: *Fluence-to-effective dose conversion E/Φ calculated for MIRD-phantom and for ADAM-phantom with three different MC-codes.*

[Leu 95]) agree well, but are approximately by 20% higher than the other calculations. This may be due to the different thermal neutron treatment but also due to the somewhat different organ modelling.

Our calculations of the organ doses in anthropomorphic phantoms led to the conclusion that the ICRP proposals on the introduction of the radiation weighting factor result in an considerable overestimation of the body doses, compared with the ICRP51/ICRU43 concept. Therefore, modifications were considered and determined, by altering the numerical values of the radiation weighting factor, but retaining the concept. The first modification (see Fig. 4.2 and 4.3) was chosen as a conservative envelope of all organ related quality factors, i.e. the ratio of dose equivalent to energy dose of the respective organ. The second one was done by defining the radiation weighting factor as the ratio of the whole body dose equivalent to the whole body dose for AP radiation incidence. Both modifications can, of course, not eliminate the assumption of ICRP60 that the high and low LET components inside the phantom do not change. By the modifications, the overestimation is reduced and, as a accompanying effect, the ICRU defined quantity ambient dose equivalent remains conservative up to 40 MeV.

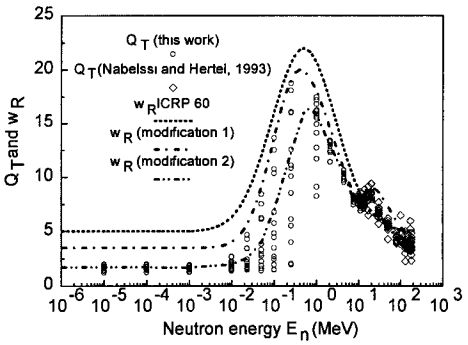

Figure 4.2: *Quality factors Q_T of seven important organs compared with the radiation weighting factor w_R and the two proposed modifications (each symbol depicts a certain organ and a certain irradiation incidence to the body. Here, the symbols are not referenced in order to keep clearness).*

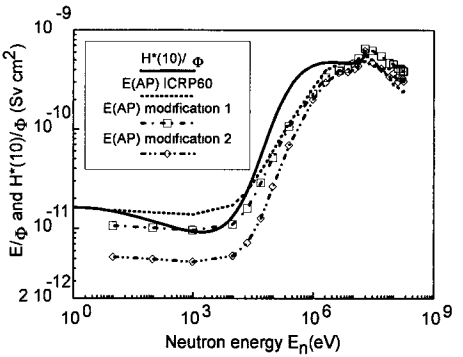

Figure 4.3: *Fluence-to-effective dose equivalent conversion function applying the ICRP radiation weighting factor and the two modifications. The operational quantity ambient dose equivalent H*(10)/Φ [Leuthold et al., 1992] is drawn for comparison.*

During earlier verification studies with Bonner spheres, it was already found that SAM/CE underestimated the thermal neutrons inside the moderator, while the MCNP calculations agreed well with experimental findings [Tho 94]. It is concluded that - besides the well known conceptual problems with the radiation weighting factor - the effective dose after ICRP60 depends sensitively on the treatment of the low energetic neutron transport, although low energetic neutrons and photons contribute only little to the dose equivalent in its basic definition.

Furthermore, the considerations were continued to reduce the impact of the application of the radiation weighting factor w_R due to the overweighing of neutron induced photons in the depth of a phantom or body. An improved proposal of a modified w_R was elaborated jointly with other colleagues of the contract [Sie 94d].

Ad 2. Bonner sphere responses

The unfolding and evaluation of the spectral neutron fluences collected or experimentally determined in the frame of this contract suffered from the imperfect knowledge of the response matrix of the Bonner sphere system with LiI(Eu) detector. Although a number of publications was dedicated to this problem in the past, the results were not in agreement with recent experimental findings. The reason is that most of them applied the multi-group transport code ANISN, which could not account for the chemical binding of the hydrogen in the polyethylene material of the spheres, could not model sufficiently precisely the thermal neutron detector assembly, and permitted only a course energy binning. Therefore, the total matrix was calculated for a LiI crystal of 4 mm diameter. x 4 mm height applying the Monte-Carlo code MCNP version 4. One result is shown in Fig. 4.4. For each of the available 86 experimental energy points [Alevra et al., 1992, Tho 94] the calculated response was divided by the experimental one. This resulted in a mean calibration factor of 0.72, with 9% standard deviation and 1% standard error of the mean. The calibration factor describes quantitatively the light event loss in the optical system, but also deviations of the crystal dimensions and the ^{6}Li content from the nominal values [Mar 94].

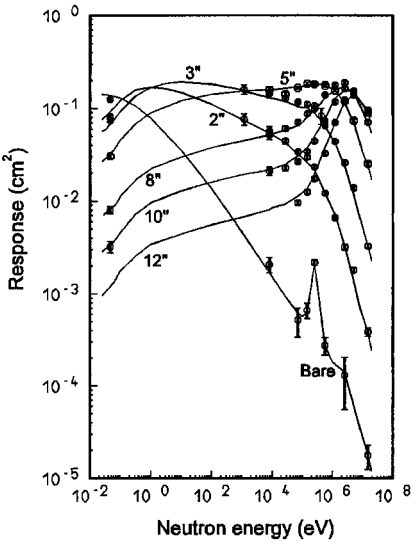

Figure 4.4: MCNP calculated and experimentally determined responses of Bonner spheres with 4 mm x 4 mm $^{6}LiI(Eu)$ detector. The error bars at the experimental data points depict the total (1σ) uncertainties, the lines connect the calculated data points.

Statistical checks indicated that no systematic deviations between calculated and experimental data were present, in contrast to comparisons with earlier calculations. Furthermore, it was found that a hybrid log-normal distribution versus the sphere mass (instead of the sphere diameter) gives an excellent possibility of interpolating the responses in the sphere size domain.

Ad 3. Evaluation of recent experimental data

The experiments which had been performed together with other members of the EURADOS group "Spectrometry" at the Ringhals reactors and the CLAB, Oskarsham, Sweden, were evaluated in order to receive the dosimetric informations for a typical part of the nuclear circle [Sch 95a].

The Bonner sphere (BS) data were unfolded applying the above mentioned matrix of the BS-responses for the system with LiI detector [Mar 94b]. The unfolding was done in a similar way as in a previous joint study using the unfolding SAND: A simple start spectrum was applied containing a fast and a thermal Maxwellian and a 1/E slowing down component. No attempt was made to influence the unfolding iterations by any additional informations.

Fig. 4.5 depicts as an example, the spectra obtained at CLAB at 3 different measuring positions of a spent fuel container, normalised to unit fluence. It is observed that the spectrum becomes harder with changing the position from the centre to the edge of the container.

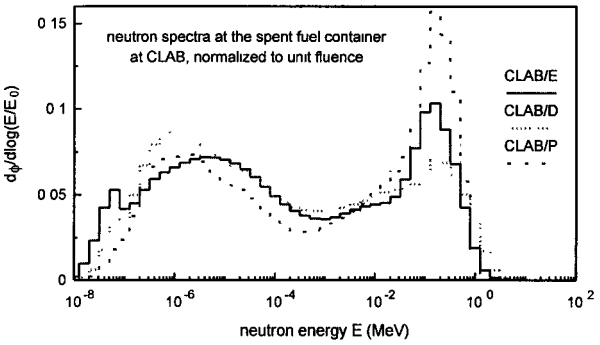

Figure 4.5: *Evaluated neutron spectra at the three positions of the spent fuel container at CLAB, Oskarsham*

The group participated also in a further joint experiment at the modified Cadarache facility. The results of the evaluated spectrum together with that of the earlier study is shown in Fig. 4.6.

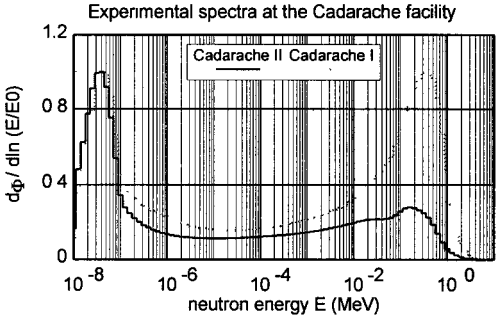

Figure 4.6: *Experimentally determined neutron spectra at the Cadarache facility with two different moderator arrangements.*

Further experiments were done near a container with unused MOX-elements, and at the Czech power-reactor in Dukovany. Fig. 4.7 demonstrates the build-up of the intermediate neutron component with increasing shielding from MOX element container with only back scatter from the floor, PWR V/1 above the pressure vessel with the shield effect of the vessel water and the iron, and PWR V/2 behind a thicker concrete shield.

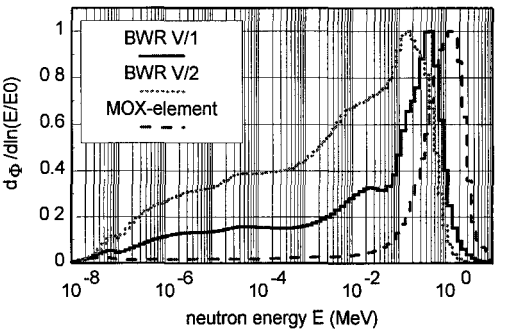

Figure 4.7: *Experimentally determined neutron spectra at the MOX element container and inside the power reactor at Dukovany (PWR).*

Ad 4. Determination of integral dosimetric quantities

For the spectra of the experiments in Sweden, in Fig. 4.8 three different quantities for an "ambient" dose are compared: H_{Made}, H*(10), and H*(10) with revised Q(L) after ICRP 60. The change from H_{Made} to H*(10) (Q(L) after ICRP 21) is approximately within ± 10 %, only due to the change of the reference phantom and of the reference point inside the phantom. The change in quality factor after ICRP60 gives rise to a factor between 1.5 and 1.7, the largest value observed at the relatively hardest spectrum (CLAB/P). Further effects on the operational quantities due to the changes in stopping power data by ICRU49 [Sie95b] were not considered here.

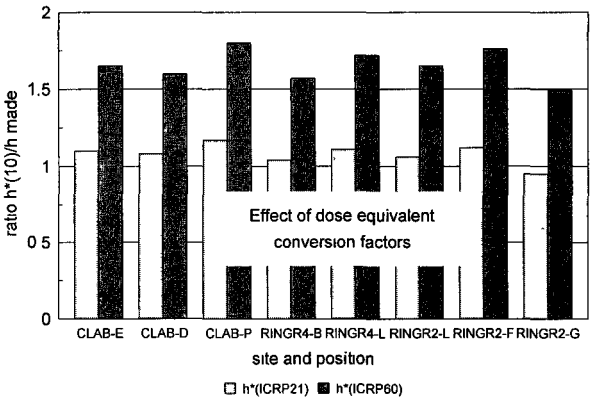

Figure 4.8 *Ratio of ambient dose equivalent H*(10) with Q(L) after ICRP21 and ICRP60, respectively, to maximum dose equivalent H_{MADE} after ICRP21: CLAB position E, D and P, and Ringhals reactors R2 and R4 at different positions.*

In Fig. 4.9 a summary is given for the effect of introducing the effective dose concept with the radiation weighting factor after ICRP60, for a selection of the experimental data gained by the GSF group throughout the course of the project.

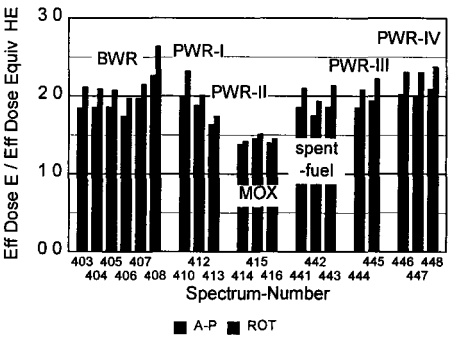

Figure 4.9: *Ratio of effective dose "E" to effective dose equivalent H_E for a series of spectra determined in the frame of the contract at different places of the nuclear fuel circle.*

Ad 5. Set-up of a realistic field facility

From Figs. 4.5 and 4.7 it is seen that the spectra at the facility (figure 4.6) at Cadarache do not yet cover certain fields found in practice. Recently, at the GSF a facility GRENF was established which consists of an igloo-type bunker with a d(2.8 MeV),Be-source and a variable moderator arrangement [Sch96]. In Fig. 4.10 the preliminary neutron spectra at three different positions along the beam axis are shown when a 30 cm thick spherical D_2O moderator is placed in front of the neutron producing target. The shape is generally well suited to simulate spectra of that type shown in Fig. 4.7.

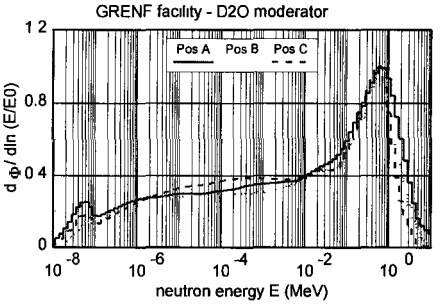

Figure 4.10: *Experimentally determined neutron spectra obtained at the GSF-realistic neutron field facility (GRENF) along the beam axis with a spherical D_2O moderator assembly.*

References

Leuthold, G., Mares, V. and Schraube, H.: Calculation of the neutron ambient dose equivalent on the basis of the ICRP revised quality factors. Radiat. Prot. Dosim. 40, 2 (1992) 77-84.

Alevra, A.V., Cosack, M., Hunt, J.B., Thomas, D.J. and Schraube, H.: Experimental determination of the response of four Bonner sphere sets to monoenergetic neutrons (II). Radiat.Prot.Dosim. 40,2 (1992) 91-102.

Hollnagel, R.A.: Calculated effective doses in anthropoid phantoms for broad neutron beams with energies from thermal to 19 MeV. Radiat.Prot.Dosim. 44, 1/4 (1992) 155-158.

Morstin, K., Kopec, M., Schmitz, Th.: Equivalent dose versus dose equivalent for neutrons based on new ICRP recommendations. Radiat. Prot. Dosim. 44, 1/4 (1992) 159-164.

Publications (see Part I) :

Cha 96, Jak 96, Kra 96b, Leu 94, Leu 95, Leu 96, Mar 94b, Sch 95a, Sch 96, Sie 94d, Tho 94

Head of project 5: Dr. M. Kralik

Scientific staff: T. Novotny, J. Sauerova

II. Objectives for the reporting period

1. Calculation of the response matrix for the PTB Bonner sphere spectrometer (BSS) with a small cylindrical ^{3}He proportional counter as a central detector of thermal neutrons (denoted "PTB-F" set) by means of the Monte Carlo neutron transport code MCNP and a realistic detector model.
2. Calculation of the response matrix of the CMI Bonner sphere spectrometer which differs from the PTB-F set by the polyethylene density only. Adjustment of the calculated response matrix to calibration data obtained in the monoenergetic neutron fields at PTB.
3. Measurement of neutron spectra in calibration fields to prove the reliability of the instrumentation and data processing.
4. Measurement of neutron spectra at work places to be included in the catalogue of neutron fields.
5. Taking part in the specification of realistic neutron calibration fields produced in the laboratory.

III Progress achieved including publications

III.1. Calculated responses of the PTB-F Bonner sphere system (BSS)

The responses of the PTB-F BSS, which consists of a cylindrical ^{3}He detector used either bare or Cd-covered, and polyethylene spheres with diameters from 5.08cm (2 inch) up to 45.72 cm (18 inch), were calculated by means of the Monte Carlo neutron-photon transport code MCNP [Bri93]. A detailed model of the polyethylene sphere and the detector assembly was used to avoid problems with the estimation of uncertainties due to neglecting details in the neutron transport. The responses were calculated for a specially selected set of neutron energies from thermal up to 20 MeV taking into account the occurrence of resonances in the carbon cross section. All calculations, except a few ones for the 18 inch sphere and lowest energies, were done with statistical uncertainties less than 1%.

The comparison of calculated with experimental responses obtained with monoenergetic neutrons at PTB [Ale92] revealed a very good agreement within experimental uncertainties as shown in Table 5.1. In Figs. 5.1 and 5.2 the mean ratios of the calculated to measured responses of the PTB-F set are shown along with the data for the PTB-C set taken from [Wie94]. From both figures it is evident that the responses for the two different systems, calculated with the code MCNP, are very similar. Only a common fit factor is needed to adjust the calculated responses to the calibration data.

The results are summarized in a CMI report [Kra95a]. On the Eight Symposium on Neutron Dosimetry, Paris, November 1995, these data will be presented in a broader context of investigations of Bonner sphere systems [Kra96].

III.2 The CMI Bonner sphere system

The BSS of CMI is of the same design as the PTB-F set, but the polyethylene density of the CMI set is lower. Therefore the same procedure was applied to calculate responses of the CMI

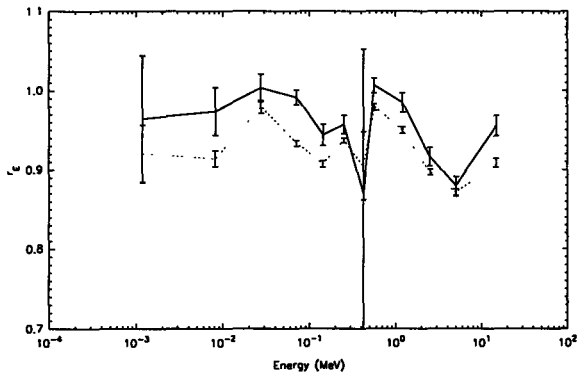

Figure 5.1: *Ratios r_E of calculated to measured responses for the PTB-F (full line) and the PTB-C BSS (dashed line) averaged for all sphere diameters at individual calibration energies. The error bars represent the total uncertainties.*

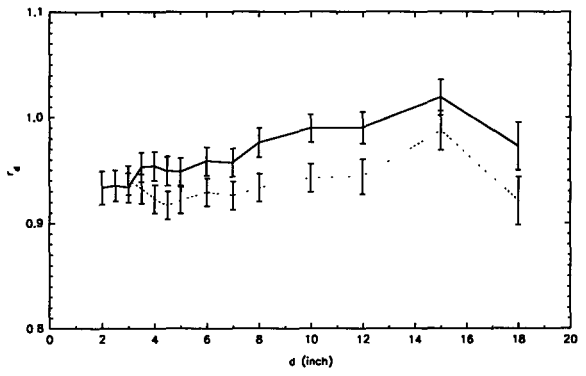

Figure 5.2: *Ratios r_d of calculated to measured responses for the PTB-F (full line) and the PTB-C BSS (dashed line) averaged for all energies at individual spheres. The error bars represent the total uncertainties.*

BSS. Two complete sets of responses calculated for the two BSS differing in polyethylene density allowed a thorough verification of the interpolation method suggested by Wiegel *et al* [Wie94]. This method enables to modify the response matrix if the polyethylene density is slightly different to the value used in the original calculation. The power of this method is illustrated in Fig. 5.3 showing data for the 15 inch sphere. The complete data are also summarized in the CMI report [Kra95a].

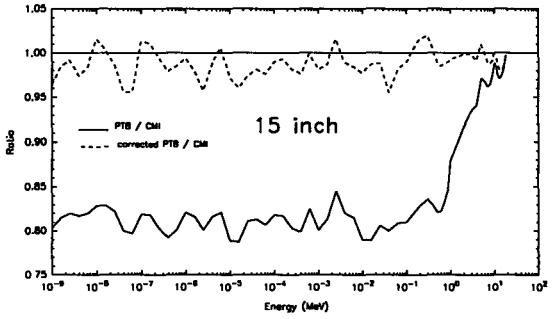

Figure 5.3: *Ratio of calculated PTB-F and CMI BSS response functions (full line). The dashed line represents the ratio of the PTB-F BSS response function corrected for the CMI polyethylene density to the CMI BSS response function.*

The CMI BSS was calibrated at PTB with monoenergetic neutrons. Preliminary results are shown for the neutron energy 2.5 MeV in Fig. 5.4. The final analysis of the experimental data including corrections for deadtime and target scattered neutrons and the evaluation of the uncertainties is in progress and the results will be documented in [Kra95b].

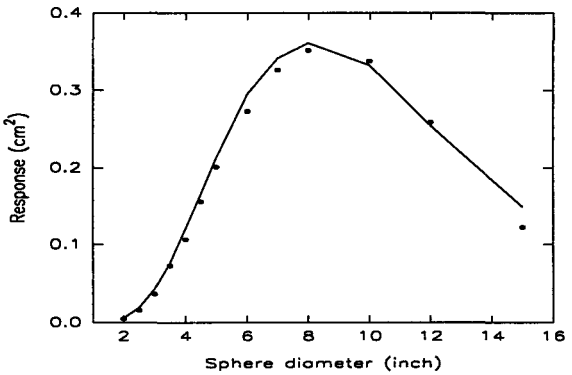

Fig. 5.4: *Calculated responses (curve) of the CMI BSS for 2.5 MeV neutrons compared with raw experimental data (points).*

III.3. Cadarache '94 intercomparison exercise

In 1994 the CMI group took part with the BSS in the EURADOS comparison exercise performed in the neutron calibration field realised at CEA Cadarache. The results were sent to the evaluator [Tho96] and will be published in a common report.

III.4. Measurements at work places

The dosimetric specification of mixed neutron-photon fields at the Czech nuclear power plant in Dukovany, equipped with four Russian VVER 440 type pressurized water reactors, were done by CMI and PTB groups at the end of May 1995. In these measurements CMI employed the BSS and an energy compensated Geiger-Mueller counter which is almost insensitive to neutrons. The results are being prepared to be submitted for publication in Radiat. Prot. Dosimetry [Kra95c]. Fig. 5.5 shows the neutron spectra as measured with the CMI BSS at the bottom of the reactor vessel and at the board of main circulation pumps.

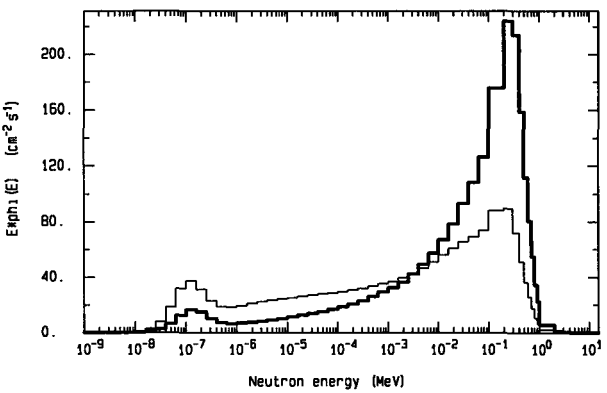

Figure 5.5: *Neutron spectra measured with the CMI BSS at workplaces in the Czech nuclear power plant Dukovany. The points of measurement are: the room A0065 below the reactor vessel (thick line), the board of the main circulation pumps (thin line).*

III.5. Specification of laboratory calibration fields

The BSS of CMI was also used to specify the neutron calibration fields built at the Nuclear Research Institute in Rez near Prague (NRI). These fields are realized by means of ^{252}Cf sources placed in a cylindrical shield made of the iron and polyethylene layers. The spectral fluence at the calibration point were measured for six different combinations of polyethylene and iron layers. Apriori neutron spectra needed for the evaluation of BSS measurements were calculated by means of the MCNP code. The measurements were completed in June 1994 and the results were published in an NRI report [Jan94a].

References:

[Bri93] J.F.Briesmeister, Editor, *MCNP - A General Monte Carlo N-Particle Transport Code, Version 4A*, LA-1265-M, Los Alamos 1993

[Ale92] A.V.Alevra, M.Cosack, J.B.Hunt, D.J.Thomas and H.Schraube, *Experimental determination of the response of four Bonner sphere sets to monoenergetic neutrons (II),* Rad. Prot. Dos. **40** (1992) 91-102

Publications (see part I):

[Jan94a], [Kra95a], [Kra95b], [Kra95c], [Kra96]

Head of project 6: Dr. B. Osmera

Scientific staff: Dr. B. Jansky, Z. Turzik, E. Novak, Dr. F. Cvachovec, Dr. P. Tiller

II. Objectives for the reporting period

1. Improvement of the spectrometer.
2. Participation in the "Cadarache comparison exercise".
3. Determination of the spectral neutron fluence of the reference fields by MCNP calculations and spectrometry - contribution to the catalogue of spectra.
4. Measurement in the containment of the VVER-440 nuclear power plant in Dukovany (in cooperation with Czech Metrological Institute - Bonner sphere spectrometer).
5. Calibration measurements at PTB.

III. Progress achieved including publications

III.1. Improvement of the spectrometer.

A new (2 dim + 1 dim) ADC/PC system was implemented at the NRI proton recoil counter spectrometer and some mechanical innovation were performed. Also the stilbene spectrometer [Cva94] of Military Academy (MA), Brno was improved. The dynamic range was extended such, that the neutron spectrum could be determined by one measurement in the energy interval 0.7 - 10 MeV [Cva95]. The stilbene spectrometer was tested in the NRI reference fields [Jan94c]. The direct deconvolution method and iterative unfolding were also tested. An important goal of these comparison and calibration experiments was the adjustment of the spectrometers for the Cadarache comparison exercise.

III.2. Intercomparison measurements in the realistic neutron calibration field, Cadarache (France).

The neutron spectrum measurement with the stilbene scintillator (Military Academy Brno) and proportional counters filled with hydrogen (NRI Rez) were carried out in September 21-23, 1994. The results were evaluated [Tho96] and will be reported. A new analysis will be performed when the calibration and response function measurements (see III.5) are evaluated.

III.3. Determination of the spectral neutron fluence of the reference fields by MCNP calculations and spectrometry

Eight ^{252}Cf driven reference fields were measured with the proton recoil spectrometers (MA Brno, NRI Rez) and the Bonner sphere spectrometer (M. Kralik, Czech Metrological Institute). The spectra of six disc shape slab assemblies (Fe, Fe + polyethylene), 50 cm diam. iron sphere and 30 cm diam. D_2O sphere with a ^{252}Cf source [Jan94a, Jan94b, Jan94c] were submitted for inclusion in the new catalogue [Nai96].

The leakage neutron spectra from the iron and heavy water spheres are presented in Figs. 6.1 and 6.4. The results of the differential spectrometer and Bonner sphere spectrometer measurements in the disc shape ^{252}Cf driven reference fields are illustrated in Figs. 6.2, 6.3.

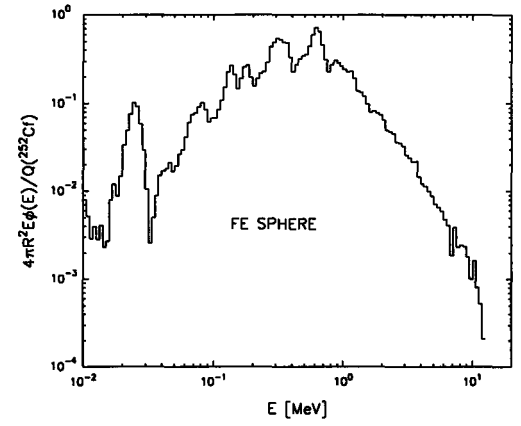

Figure 6.1: *The leakage neutron spectrum of a ^{252}Cf source in an iron sphere (50 cm diameter) as measured with the proton recoil spectrometer [Jan94c].*

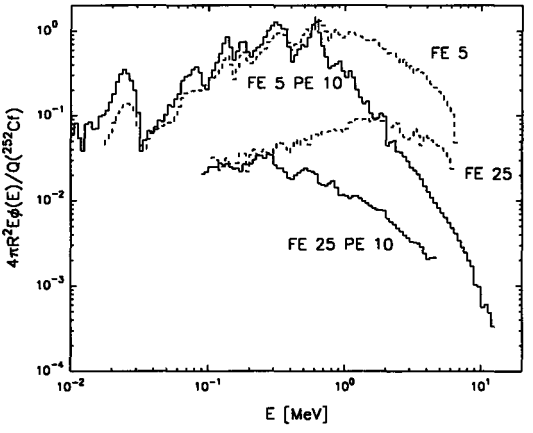

Figure 6.2: *The leakage neutron spectra of a ^{252}Cf source in disc-shaped iron-polyethylene (PE) slabs (FE x cm, PE y cm) as measured with the proton recoil spectrometer [Jan94c].*

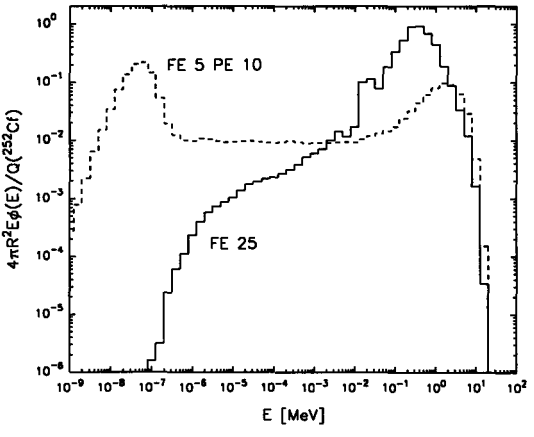

Figure 6.3: *The leakage neutron spectra of a ^{252}Cf source in disc-shaped iron-polyethylene slabs measured with Bonner spectrometer in the same geometry as in Fig. 2 [Jan94a, Jan94c].*

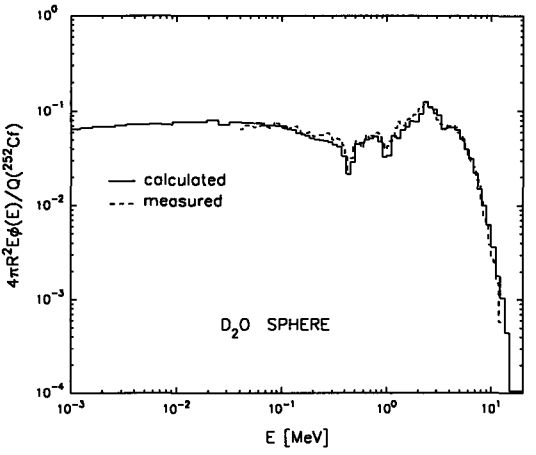

Figure 6.4: *The calculated and measured leakage neutron spectra from the D_2O spherical (30 cm diameter) assembly with a ^{252}Cf source [Jan94b].*

The results of MCNP heavy water sphere leakage spectrum calculation [Jan94b, Fig. 6.4] are relatively in good agreement with measured ones.

The NRI reference neutron field assemblies are situated in a suitable hall of the experimental reactor. Several ^{252}Cf sources of different strength and a flexo rabbit source transport system are used. The reproducibility of the reference fields and experimental conditions are well established.

III.4. Measurements in the containment of the VVER-440 NPP in Dukovany

After the preliminary measurement of Czech Metrological Institute with the Bonner spheres it was found that the neutron flux density at the point of interest was unmeasurable with the differential spectrometers of MA and NRI. The measurement in the technological area, prohibited for persons during the operation could be hardly interpreted physically and has no meaning for radiation protection.

III.5 Calibration measurements at PTB.

The calibration and response function measurements have been performed in June 12-16, in PTB Braunschweig. The accelerator produced monoenergetic neutrons 0.144, 0.250, 0.565, 1.2 MeV and Fe and Si filtered reactor beams were used for PRC, the accelerator based monoenergetic neutrons with energies of 1.2, 2.5, 5.0, 14.8, 19.0 MeV were used to investigate the angle dependent response of the stilbene scintillator. The first evaluated results are expected by the end of 1995. According to the preliminary analysis the results seem to be promising, in particular for the stilbene scintillator.

Publications (see Part I):

[Cva94], [Cva95], [Jan94a], [Jan94b], [Jan94c], [Cha96]

Head of project 7*: Dr. M. Grecescu

Scientific staff : Dr. A. Aroua, J.-P. Laedermann, Dr. J.-F. Valley

II. Objectives for the reporting period (01.01.93 - 30.06.95)

1. Improvement of the performance of the Bonner spheres neutron spectrometer with respect to the following characteristics :
   - energy resolution in the low and intermediate energy range;
   - sensitivity in the high energy region.
2. Measurement of neutron fluence spectra and associated dosimetric quantities in neutron calibration fields during intercomparisons organized by EURADOS WG7.
3. Contribution to the catalogue of neutron spectra with the results of measurements performed in Swiss nuclear facilities.

III. Progress achieved including publications

III. 1 Improvement of the Bonner spheres neutron spectrometer

1.a) The energy resolution at low and intermediate energies of the Bonner spheres system of the Institut de Radiophysique Appliquée (IRA) has been improved by introducing an absorber around the small spheres and thus implementing a new set of response functions with the maxima evenly distributed in the range 1 eV - 100 keV (one per decade) and with reduced width.

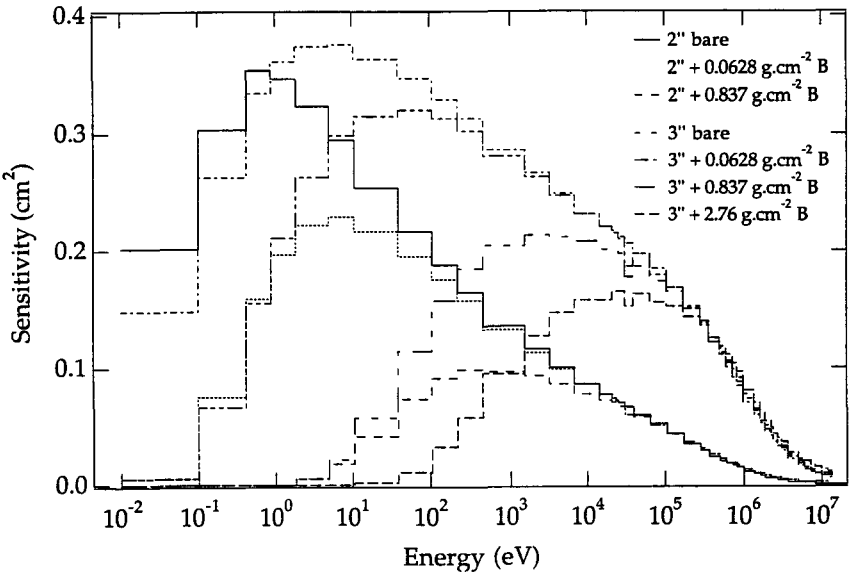

Figure 7.1: *Response matrix of the modified spectrometer*

* Supported by the Swiss Federal Office for Education and Science under contract No. 94.0039

The improvement has been studied at first by numerical simulation by means of the neutron transport code ANISN. The influence of absorbing layers with different compositions and thicknesses on the response functions of the small Bonner spheres (diameters up to 6") and the effect of metallic containers for the absorbing material was also investigated. On basis of the simulations a compromise was found between the improved resolution, the sensitivity and the cost. Three aluminium boxes containing natural boron powder with mass thicknesses 0.063, 0.837 and 2.76 $g.cm^{-2}$ were used together with the 2" and 3" spheres. An experimental calibration of the response of these combinations was performed at the PTB reactor with monoenergetic neutron beams of 0.186, 2, 24 and 144 keV. The computed response functions were adjusted to the experimental calibration points. A single normalization factor is valid (within ±1%) for the whole set. The normalized response functions are represented in Fig. 7.1.

Computer simulations with numeric neutron spectra containing a peak in the intermediate energy range confirmed the improved resolution of the new system.

1.b) A major limitation of the Bonner spheres spectrometer for the qualification of high energy neutron fields is the reduced response beyond 20 MeV, even for the large spheres. The possibility of increasing the response in the high-energy region has been studied by computer simulation. Monte Carlo calculations have been performed up to 1 GeV with the GCALOR code developed at CERN. Alternative calculations with the ANISN neutron transport code and the HILO library have been performed up to 400 MeV. The response function of the 12" sphere has been particularly investigated and it turned out that the response beyond the peak sensitivity can be increased by introducing a 3 cm layer of copper around the sphere (Fig. 7.2). Both calculations yielded similar results.

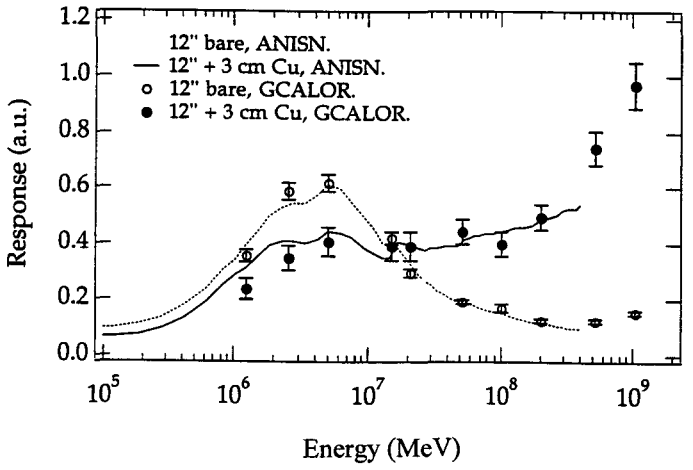

Figure 7.2: *Calculations of the high-energy response of a 3 cm Cu covered 12" Bonner sphere.*

III.2 Comparison of experimental and calculated response of Bonner spheres

Until now, the response functions of the IRA Bonner spheres system were based on calculations with the ANISN transport code and experimental calibrations in monoenergetic

neutron fields [1]. Recently a new set of response functions has been calculated at CMI (Prague) for a system similar to that of IRA (proportional counter LCC type 0.5NH10, polyethylene density 0.921 g.cm^{-3}) using the MCNP code [2]. A comparison has been performed between the new set of response functions and the experimental calibration, employing a procedure used for similar comparisons [3]. The calculated response functions have been adjusted to the experimental data by a least squares fit and individual adjustment factors have been determined.

A detailed investigation of the measured to adjusted response ratio versus energy and versus sphere diameter allowed to identify some doubtful experimental points. By eliminating them, a coherent set of individual adjustment factors were obtained, suggesting the use of a unique value with reasonable accuracy (Fig. 7.3).

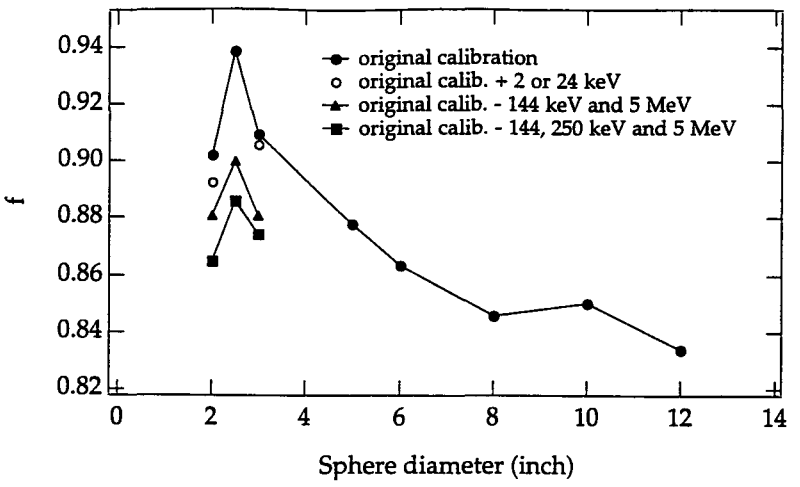

Figure 7.3: *Individual adjustment factors with the various considerations mentioned on the plot.*

III.3 Neutron measurements in the field

3.a) Calibration neutron fields

The neutron fields for the calibration of neutron dosimetric equipment are usually qualified both by Monte Carlo calculations and by experimental measurements involving several types of instruments. Such measurements were performed during intercomparisons organised by EURADOS involving the participation of several groups. The IRA participated in the following intercomparisons:

- At AEA Technology - Winfrith Technology Centre (Dorchester, Great Britain) two reference neutron fields were produced in the ASPIS facility of the NESTOR reactor [4]. The IRA performed measurements with the Bonner spheres system, a GM counter and a neutron monitor. The results of the neutron fluence spectra are represented in Fig. 7.4.

- At CEA - Centre d'Études Nucléaires (Cadarache, France) one reference neutron field was produced with a 14 MeV neutron generator and a suitable set of converters and moderators

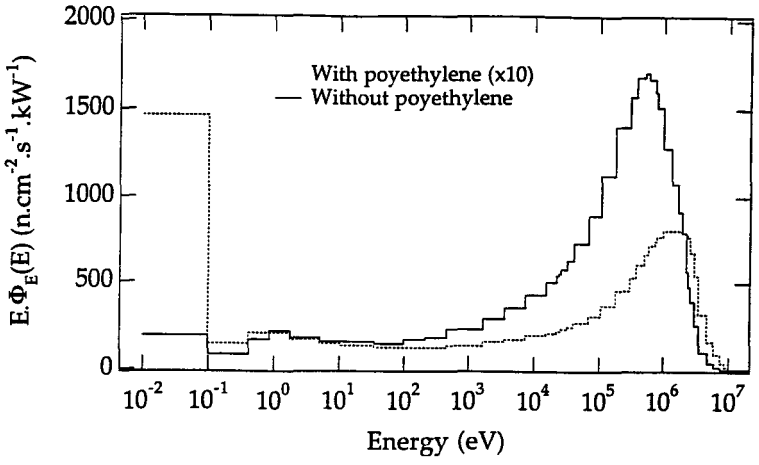

Figure 7.4: *Neutron fluence spectra measured in Winfrith*

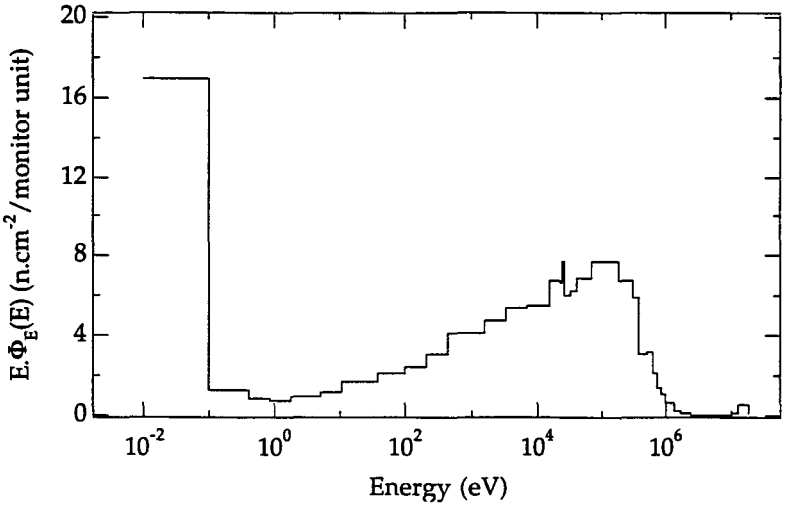

Figure 7.5: *Neutron fluence spectrum measured in Cadarache*

[5]. The IRA performed the measurements with the same instruments and with TEPCs. The measured neutron fluence spectrum is represented in Fig. 7.5.

- At CERN (Geneva, Switzerland) two reference neutron fields were produced with a 205 GeV positive hadron beam hitting a thick copper target surrounded by concrete and iron shields. The IRA performed the measurements with the same instruments and with TEPCS. The measured neutron fluence spectra are represented in Fig. 7.6.

These results were included in the evaluations prepared by the coordinators of each intercomparison.

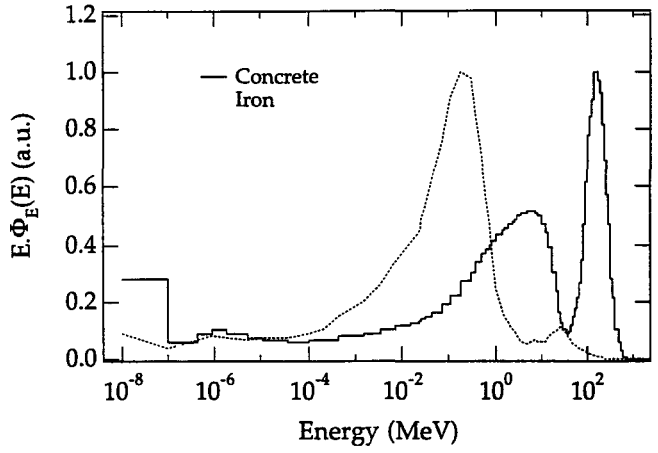

Figure 7.6: *Neutron fluence spectra measured at CERN*

3.b) Neutron fields around high-energy accelerators

The spectrum of a new neutron field has been measured at CERN. The neutrons are produced in the collision of 35 TeV lead ions hitting a lead target which is heavily shielded. The neutron fluence spectrum is represented in Fig. 7.7.

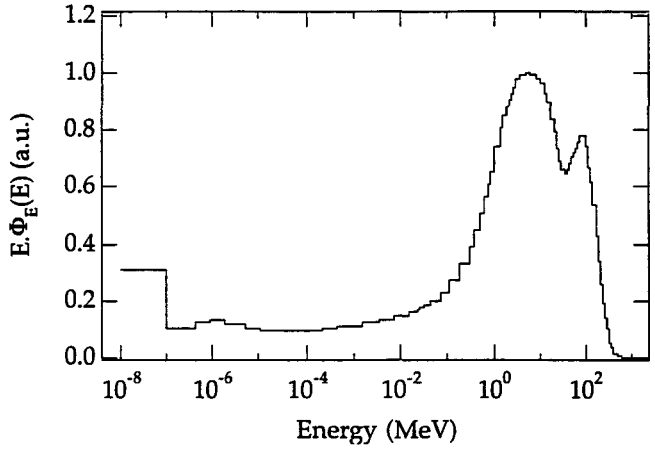

Figure 7.7: *Neutron fluence spectrum measured around the shielded lead ion beam*

3.c) Neutron fields at nuclear facilities

The experimental data obtained in an EURADOS intercomparison exercise performed in November 1992 at the Ringhals nuclear power plant and the CLAB fuel storage facility (Sweden) have been processed [Aro95]. A detailed comparison of the results of all participants suggested a modification of the response matrix of the IRA Bonner spheres set. It has been implemented by introducing individual adjustment factors of the calculated response

functions to the experimental calibration points. The modification improved the agreement with the other participants' results.

III.4 Contribution to the catalogue of neutron spectra

The IRA had previously measured several neutron spectra in the Swiss nuclear facilities [6, 7] (inside reactor confinements, in a fuel storage, around spent fuel transport casks and around neutron sources). A selection of 28 spectra, reevaluated using an improved version of the Bonner spheres response matrix, were documented according to the request of the catalogue editors and included in the catalogue.

References:

[1] A. Aroua, M. Grecescu, M. Lanfranchi, P. Lerch, S. Prêtre, J.-F. Valley, V. Vylet, *Evaluation and test of the response matrix of a multisphere neutron spectrometer in a wide energy range.* Part I and II. Nucl. Instr. Meth. **A321** (1992) 304-311.

[2] see [Kra95a] in Part I.

[3] see [Wie95] in Part I.

[4] M.F. Murphy, *A review of neutron spectrometry measurements in the ASPIS reference fields.* Report AEA-RS-5548 (1994).

[5] J.L. Chartier, F. Posny, M. Buxerolle, *Experimental assembly for the simulation of realistic neutron spectra.* Radiat. Prot. Dosim. **44**, (1992) 125-130.

[6] A. Aroua, D. Azimi, M. Boschung, F. Cartier, M. Grecescu, S. Pretre, J.F. Valley, Ch. Wernli, *Rapport sur la campagne de mesure des neutrons effectuee dans les centrales nucleaires suisses,* Joint IRA,PSI,DPSN-report, Lausanne, October 1991 (ISBN-2-88444-001-1).

[7] A. Aroua, D. Azimi, M. Boschung, F. Cartier, M. Grecescu, S. Pretre, J.F. Valley, Ch. Wernli, *Characterisation of the mixed neutron-gamma fields inside the Swiss nuclear power plants by different active systems,* Radiat. Prot. Dosim. **51** (1994) 17-25.

Publications (see Part I):

[Aro95], [Gre96], [Aro96], [Kra96]

Final Report
1992 - 1994

Contract: FI3PCT920018 Duration: 1.9.92 to 30.6.95 Sector: A12

Title: The Measurement of Environmental Radiation Doses and Dose Rates.

1)	Bøtter-Jensen	Lab. Risø
2)	Lauterbach	PTB
3)	Delgado Martínez	CIEMAT
4)	Pernicka	CSAS.IRD
5)	Waligorski	INP. Krakow
6)	Osvay	II. Budapest

I. Summary of Project Global Objectives and Achievements

The measurement of changes in the level of ambient photon radiation requires instruments and dosemeters which have both adequate sensitivity and sufficient accuracy to record small variations. To ensure that such measuring devices, which are typically ionisation chambers, scintillators, GM counters and integrating electronic and TL dosemeters, provide reliable measurement data, it is necessary to determine the responses of the detectors to both cosmic and terrestrial radiations.

Based on the collaboration between Risø, PTB and CIEMAT in 1990-92 on the evaluation of practical calibration methods for environmental monitoring and testing of new types of sensitive detectors for the measurement of ambient photon radiation, work was continued by an extended group in 1992/95 that further studied demanding aspects of environmental radiation measurements. The incorporation of the Institute of Radiation Dosimetry (IRD), Prague, as an associated PECO partner in 1993 and two other PECO partners in 1994, namely the Institute of Nuclear Physics (INP) in Krakow and the Institute of Isotopes (I.I.)/Atomic Energy Research Institute (AERI) in Budapest, have strengthened the group and extended the scope of application. I.M.G. Thompson, UK, contributed to the project under a sub-contract with Risø.

The present project brings together several experimental methods for the measurement of environmental doses and dose-rates and the main objectives studied by the group in the period 1992-95 are:

1) Determination of scattered gamma radiation in the calibration of environmental dose rate meters (Monte Carlo calculations).
2) The assessment of external photon dose rates in the vicinity of nuclear power stations.
3) Establishment and commissioning of standard calibration facilities for environmental radiation detectors.
4) International intercomparisons of dose-rate meters, TL dosemeters and electronic dosemeters in relation to environmental radiation monitoring.
5) Investigation of instrument and dosemeter characteristics at ultra low dose rates (Asse mine).
6) Determination of detector responses to high energy photons (6 MeV).
7) Development of computerized glow-curve analysis for different TLD materials.
8) Study of self dose and long term stability of TLD materials (Asse mine).

9) Development of new highly sensitive TL materials for environmental radiation measurements and investigation of their properties.
10) TL measurements of environmental photon dose rates over ultra short periods (few hours).
11) Development of new compact and computerized portable TL readers for environmental radiation measurements.
12) OSL properties of materials for environmental radiation measurements.

The free-field and shadow-shield calibration facilities established at **Risø** during a previous phase of the EC project were commissioned in the present programme by determining the scattered gamma photon contribution to the detector responses in different calibration geometries by Monte Carlo calculations.

Measurement data obtained from experiments carried out at the Hinkley Point Nuclear Power Station in the UK with the aim of comparing the responses from different types of dose rate meters and TL dosemeters were further evaluated and analysed. An attempt was made to determine the separate dose rate contributions from the different ambient radiation components present at this special location including that from the periodic release of Ar-41.

Two natural environment measurement stations were established and commissioned at Risø in 1994-95. A terrestrial measurement station was established at a field site inside the Risø grounds, and a cosmic measurement station was established at a wooden pier extending into the Roskilde Fjord directly from the Risø grounds. The measurement stations were commissioned by long-term measurements of the ambient photon radiation using different types of detectors.

Several manufacturers provided a variety of electronic dosemeters to be tested under environmental conditions. The dosemeters were exposed to the natural radiation at the terrestrial measurement site at Risø over prolonged periods as well as to the additional radiation from calibrated gamma sources. Also the responses of the electronic dosemeters to cosmic radiation were determined at the new cosmic measurement platform at Risø.

In the week 12-18 June 1994 an international intercalibration experiment was performed at Risø with participants from USA, Eastern Europe (PECO), and EU. One aim of the meeting was to intercompare the home calibrations of detectors and dosemeter responses of environmental radiation measurement systems used in the USA, Eastern Europe, and EU and to try to make a link between the different reference standards used. Details and results are presented in the Risø report.

Finally, the optically stimulated luminescence (OSL) properties of the highly sensitive TL material Al_2O_3:C were investigated at Risø in relation to environmental radiation dosimetry.

The **PTB** mainly used their underground laboratory (UDO) in the Asse mine for investigations of detector characteristics at ultra-low radiation dose rates. In the present phase emphasis has been put on 1) Accurate determination of background dose-rate levels, 2) Experimental determination of the scattered radiation from different calibration set-ups, 3) Investigation of the inherent background and of the linearity of newly developed electronic dosemeters and dose rate meters, 4) Determination of the inherent radioactivity of the

construction materials, e.g. batteries, of electronic dosemeters.

As a prerequisite for the experiments during the contract period the remaining environmental radiation level in the ultra-low background laboratory UDO in 925 m depth in a pure rock salt area of the Asse salt mine was determined more accurately by applying and comparing dosimetric and spectrometric methods. Additionally the contribution of the scattered radiation in the radiation fields of the collimated beam facility in UDO was measured by gamma spectrometric methods and compared with Monte Carlo calculations carried out by Risø. Based on these data the inherent background and the linearity of dose rate meters and especially newly developed electronic dosemeters were investigated. Spectrometric measurements and the operation of the electronic dosemeters with a remote power supply instead of the built-in batteries revealed that the inherent background is partly generated by the natural K-40 in the batteries. In the 6 MeV facility of the PTB the responses of the electronic dosemeters, the dose rate meters and of TLD's were determined and their build-up effects were investigated. The investigation of the self-dose contribution to the readings of various TL-dosemeters in the UDO laboratory was continued in cooperation with CIEMAT as a service for this partner.

At **CIEMAT** the main achievement of the project has been the demonstration of practical measurement capabilities of new hypersensitive TL materials, especially LiF:Mg,Cu,P, for environmental radiation dosimetry. This was possible after an intensive study of the TL material characteristics and by proposing innovative solutions for the problems that these materials present when evaluated by conventional procedures.

A further refinement achieved as a result of the analysis was the implementation of a system that controls the maximum temperature reached during heating. This system has been shown to have practical advantages in permitting operations at high heating rates in the order of 10°C/s. In addition, it has been shown that temperatures higher than 240°C can be favourably used over short times for annealing to remove high residual signals of LiF:Mg,Cu,P.

Experiments to determine the self dosing and long-term stability of TLDs were carried out inside the UDO laboratory in the Asse salt mine where detectors were stored for six months. In particular the two LiF varieties, TLD-100 and GR-200, showed a negligible self dosing (<0.8 nGy.h^{-1}). The results of the long term stability experiments showed that the LiF:Mg,Cu,P has a substantially better stability than that for TLD-100.

To check the ultra short term environmental monitoring capability of LiF:Mg,Cu,P, calibration exercises were performed for three types of hypersensitive TL phosphors: Al_2O_3:C from Russia and LiF:Mg,Cu,P from China (GR-200A) and from Poland (MCP-N). The estimated dose rates determined from the TLD measurements were compared with the reference values calculated by the Monte Carlo code (MCNP) at Risø. A very good agreement was found for the Cu doped lithium fluoride (better than 10% in all cases), but noticeable bias ($>20\%$) were obtained for the Al_2O_3:C material when the source-detector distance increased.

The study of TLD responses to high energy photons included the determination of the energy dependence of the two types of copper-doped lithium fluoride (GR-200A from China and MCP-N from Poland) and one type of carbon-doped aluminium oxide (TLD-500K from Russia) in the range 0.6 - 6.0 MeV. Both the air kerma and dose responses of the

hypersensitive phosphors LiF:Mg,Cu,P and AL_2O_3:C to high energy photons showed to be close to those from ^{137}Cs photons.

The Institute of Radiation Dosimetry (**IRD**), Prague, started as an associated PECO partner of the project in November 1993 and the main items of IRD's research work has been 1) implementation of computerized glow curve analysis methods of TLD systems for environmental radiation measurements at IRD, 2) theoretical and experimental studies of environmental radiation fields and their variations and 3) unfolding of NaI photon spectra obtained from measurements of environmental photon radiation.

Environmental studies included Monte Carlo calculations of spectral distributions of the air kerma from different natural and man made radiation fields. The results were used to determine the responses of a number of active and passive detectors to the ambient radiation at different field sites. A major achievement was the spectral characterization of ten test field sites in the Czech Republic, the UDO underground laboratory, and the Risø Natural Environment Measurement Stations. IRD further put much effort in determining the environmental radiation air kerma rates by developing a reliable unfolding technique for photon spectra obtained with NaI detectors of both the terrestrial and the cosmic components of the natural environmental radiation and of the additional radiation from radionuclides used for field calibrations.

IRD participated in the intercomparison experiments organised by Risø and by PTB with several different active detectors and the results obtained contributed significantly to the statistical evaluation of the overall intercomparisons. Especially the unfolded spectra from NaI detector measurements compared remarkably well with measurements carried out with dose rate meters and with calculated values.

The Institute of Nuclear Physics (**INP**) Krakow, joined the project in January 1994 as an associated PECO partner with a formal agreement signed in April 1994. The main objective of INPs contribution to the project was to improve the accuracy and sensitivity of TL-based methods of assessing environmental dose rates. To this end, over the period April 94 - May 95, ultra-sensitive LiF:Mg,Cu,P detectors of different Mg, Cu, and P compositions were synthesized, developed, investigated, and optimised at INP. Furthermore, a new model of a compact TL reader-analyzer was designed and tested at INP. Intercomparison measurements and field measurements have demonstrated the suitability of the INP developed LiF material, TLD equipment and readout techniques for environmental monitoring with superior sensitivity, permitting daily or even hourly dose assessment. Work in progress at INP concerns a systematic survey of the dosimetric properties of LiF:Mg,Cu,P phosphor with respect to dopant concentration, in which a new promising LiF:Mg,Cu,P phosphor may have been discovered. Also in progress is the development of an automatic TL system (TL cards and reader) designed specifically for large-scale environmental monitoring using LiF:Mg,Cu,P. These tasks are described in the INP report under the following headings: 1) Development of an optimum procedure for producing sintered MCP detectors, 2) development of a new model of a compact computerized TL reader-analyzer, 3) field tests of detectors, readout system and measurement techniques, 4) a systematic multi-parameter survey of the effect of dopant composition on the dosimetric properties of LiF:Mg,Cu,P phosphor and 5) design and development of an automatic reader specially suited for monitoring environmental dose rates.

Both the Institute of Isotopes (**I.I.**) and the Atomic Energy Research Institute (**AERI**), Budapest, joined the project under one PECO contract (with I.I. as principal investigator) in January 1994 with a formal agreement signed in April 1994. The main objectives of the I.I./AERI contribution to the project were: 1) Determination of TL properties of new, highly sensitive Al_2O_3:C single crystal dosemeters for environmental monitoring including handling and readout parameters, reproducibility, lowest detectable dose, UV-sensitivity and fading. 2) Development of a microprocessor controlled portable TLD reader for in situ environmental dose measurements.

Much effort has been devoted to studying the TL properties of the newly developed Al_2O_3 single crystal doped with carbon prepared in Russia. One of the important properties of this material is that it exhibits an increased sensitivity compared with common TL dosemeters (e.g. TLD-100).

The following TL properties were investigated: 1) Annealing procedure in order to optimise reproducibility, 2) inherent background of dosemeters during long term storage, 3) fading characteristics at various temperatures, and 4) light and UV sensitivities of dosemeters.

A portable TL reader capable of reading TL dosemeters at the place of exposure ("in situ TLD reader") eliminates the errors caused by the transit doses normally received by TL dosemeters during their transport to and from the measurement site. Since no such sensitive portable reader was commercially available, AERI decided to develop a microprocessor based portable TLD reader for monitoring environmental gamma radiation doses and for on-board reading of doses in space stations.

Based on the experience gained at AERI since 1982 in the development of portable TL readers a new microprocessor version of the battery operated portable reader was developed in 1994-95. The main features of the new system are: 1) Increased sensitivity by one order of magnitude, 2) improvement of the precision of the measurements using automatic corrections of the individual dosemeter sensitivity and of the temperature dependence, 3) providing automatic data processing and subsequent storage of data and 4) enabling programmed automatic continuous readout of a dosemeter placed in the reader to measure the temporal distribution of the dose rate.

Conclusions

New detectors and methods for the measurement and determination of environmental photon dose rates and doses have been intensively studied by the extended group of partners in 1992-95. All the three PECO partners contributed significantly to the results achieved in the last phase. It is the hope and intention that the broad field of investigations carried out as a collaborative work between the partners of the project and the results obtained will be useful for European laboratories involved in environmental radiation measurements.

Head of project 1: Dr. Bøtter-Jensen

II. Objectives for the reporting period

a) Determination of scattered gamma radiation in the calibration of environmental dose rate meters.

b) The assessment of external photon dose rates in the vicinity of nuclear power stations.

c) Establishment and commissioning of the Risø Natural Environment Measurement Stations.

d) An international intercomparison of detectors used for environmental radiation monitoring.

e) OSL properties of Al_2O_3:C in relation to environmental radiation dosimetry.

III. Progress achieved including publications

To ensure the accuracy of environmental photon radiation measurements, it is necessary to determine the responses of the monitoring detectors to cosmic and terrestrial radiation. Instrument calibrations often encounter severe problems as gamma calibration facilities for which the photon exposures are low enough to permit calibration of the instruments in the actual range of the ambient background radiation are usually not available. Ground- or room scattered photons from a calibration set-up have to be taken into account as they each contribute significantly to the total dose. Such problems were intensively studied by Risø as one of the main tasks of the present project. I.M.G. Thomsen, UK, contributed to the work under a sub-contract with Risø.

a) Determination of scattered gamma radiation in the calibration of environmental dose rate meters.

In recent years, free-field and shadow-shield calibration techniques have been intensively studied at Risø and several intercalibration experiments using these techniques were carried out among EU Member States.

Previous free-field calibration experiments were based on determining the contribution from ground scattered photons to the air kerma rate at the detector position using the Chilton-Huddleston empirical formula from the differential gamma dose albedo for concrete.

Recently, within the present EC project, Monte Carlo (MC) calculations using the MCNP (Monte Carlo Neutron Photon) code were made at Risø to determine the air kerma rates produced by scattered photons from ^{137}Cs, ^{60}Co and ^{226}Ra sources as a result of surrounding media in different free-field and shadow shield calibration geometries (Bøtter-Jensen and Hedemann Jensen, 1992). These MC calculations include scattered photons with energies ranging from 10 keV up to the primary energies. This energy distribution of the total calculated air kerma rate is suitable for interpreting the responses of detectors normally considered for measuring the ambient dose rate. Air kerma rates measured with a variety of environmental

dose rate meters in European intercomparison programmes have been compared with the MC calculated total air kerma rates.

For a given radionuclide the energy distribution of the air kerma rate from scattered photons at the detector point will depend on the measurement geometry, viz. the source-to-detector distance and the height of the source and detector above the ground.

In Fig.1A the MC calculated ratios of total scattered to uncollided air kerma rate is shown for the three sources ^{137}Cs, ^{60}Co and ^{226}Ra as a function of the source to detector distance (D) and with the source and detector elevated 1 m above ground.

It is concluded from both calculations and experiments that the scattered radiation from obstructions farther away than 15 m from a free-field set-up contributes negligibly to the detector response relative to the contribution from ground and air. Calculations have further shown that the dose rate measured by a detector at a source-to-detector distance of 5 m in a shadow-shield set-up typically has a scattered radiation component of the order of 60%.

As part of the collaborative work between Risø and PTB, Risø also used the MCNP Monte Carlo code to calculate the scattered radiation produced in addition to the primary beam in the detector position of a ^{137}Cs collimated beam calibration set-up in the Asse underground laboratory. Based on detailed information about the collimator construction and the structure of materials and obstructions surrounding the calibration set-up the total scatter contribution at the detector position was found to be about 10%, see Fig.1B, which corresponds very well with the experimental data obtained from dose rate meter and spectrometer measurements.

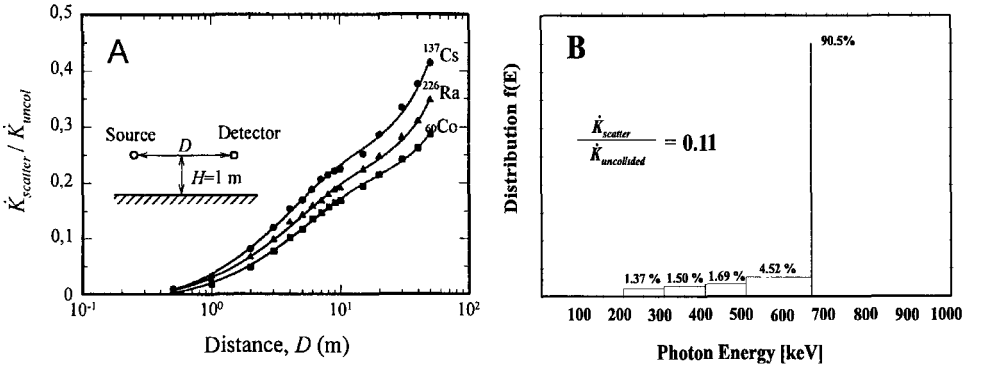

Fig. 1
A) Relative scattered free-field air kerma rates from ^{137} Cs, ^{60} Co and ^{226} Ra sources at 1 m height above ground as a function of distance.
B) Schematic diagram showing the Monte Carlo calculated (MCNP) distribution of scattered radiation from the collimated beam calibration set-up in the UDO underground laboratory (Asse). Gamma radiation source: ^{137}Cs

b) The assessment of external photon dose rates in the vicinity of nuclear power stations.

In 1991 experiments were carried out to investigate the responses of instruments to additional exposures above normal environmental levels. Four environmental dose rate instruments having different detectors, a high pressure ionisation chamber, a geiger-Muller counter, a proportional counter, and a scintillation counter, were used to make continuous measurements over a four month period of the air kerma rate at a location close the the Hinkley Point Nuclear Power Plant in the UK. Three types of TL dosimeters normally used for monitoring environmental radiation were also used to compare the responses of solid state passive dosemeters with those of the active dose rate meters.

As part of the present EC project measurement results from these experiments have been further evaluated and analysed (Thompson et al., 1993).

At the measurement location the dominant sources of gamma air kerma rate originating from the power station's magnox reactors are the ^{41}Ar in the plume discharge, when the wind takes it over the detectors, and the ^{16}N direct radiation the latter producing 6 MeV photons.

The instrument air kerma rate reading, R_{total}, at any instant of time is given by the following equation:

$$R_{total} = [r_c(K_c) + r_t(K_t) + r_{Ar}(K_{Ar}) + r_{dir}(K_{dir})] + R_i$$

where r_c, r_t, r_{Ar} and r_{dir} are the responses of the detectors to cosmic radiation, terrestrial gamma radiation, ^{41}Ar and the power station's direct radiation, respectively, K_c, K_t, K_{Ar} and K_{dir} are the "true" air kerma rates from the cosmic radiation, terrestrial gamma radiation, ^{41}Ar and the power station's direct radiation, respectively, and R_i is the inherent instrument background. Table 1 gives the air kerma rate responses to the radiation components of the above equation for the four dose rate instruments and for the TLDs.

Table 1. Air kerma rate responses of dose rate instruments and TLDs to different radiation fields.

Dose rate instruments or TLD	Response*				R_i** (nGy·h^{-1})
	r_c	r_t	r_{Ar}	r_{dir} 6 MeV	
Proportional counter	1.49	1.19	1.26	1.64	12.4
Scintillation detector	0.95	0.95	0.95	0.95	<5
High Pressure ionisation chamber	1.08	1.00	1.00	1.20	1.0
Geiger-Müller counter	1.61	0.83	1.06	1.76	10.0
LiF TLD-100	0.97	0.83	1.10	1.04	<1.0
$CaSO_4$:Tm	0.97	0.83	0.86	1.04	2.3

* r_c, r_t, r_{Ar}, and r_{dir} are the responses of the detectors to cosmic radiation, terrestrial gamma radiation, ^{41}Ar and the power station's direct radiation, respectively.
** R_i is the contribution to the reading of the instrument from internal radioactive contamination and/or non-radiation reading.

All the detector responses to the 6 MeV photon radiation were determined from calibration experiments at PTB. The measured uncorrected variations in air kerma rate for the four dose rate meters over a four month measurement period are shown in Fig.2. The variation in total power levels for the reactors over the same period are shown as well. Constant dose rates of different magnitudes are caused by the natural background and the high energy ^{16}N radiation at different power steps of the reactor. The peak shaped variations riding on the constant dose rates have their origin in the changes of the wind direction blowing the ^{41}Ar plume above the dose rate meters.

A detailed analysis was made of the results over a two month period of time (period B in Fig.2). By comparing the power levels and the measured air kerma rates for each system sample period it is possible to separate the contribution to the readings of the instruments from the various components of the radiation field. From this information the integrated air kerma rate for these radiation components were calculated. The corrected estimates of the air kerma over the two month period for the different radiation components and for the total air kerma are given in Table 2.

Table 2. Values of integrated air kerma for period B, 11 January to 7 March 1991, for different radiation components corrected for each dose rate instrument and TLD response to the different components.

Dose rate instruments or TLD	Air kerma (μGy)			
	Cosmic + Terr. K_c+K_t	^{41}Ar K_{Ar}	Direct (6 MeV) K_{dir}	Total K_{Total}
Proportional counter	110.5	28.9	302	441.4
High Pressure ionisation chamber	113.7	31.4	283	428.1
Geiger-Müller counter	112.8	26.4	253	392.5
LiF TLD-100*	126	27	269	423
$CaSO_4$:Tm*	111	33	263	406
Mean value for dose rate instruments and TLDs	114.8	29.3	274	423.8
Standard deviation (% of mean value)	6.4 (6%)	2.8 (10%)	19.1 (7%)	22.0 (5%)

* To estimate the TLD values corresponding to the different radiation components the percentage of the total dose as estimated by the active dose rate instruments was used for each component.

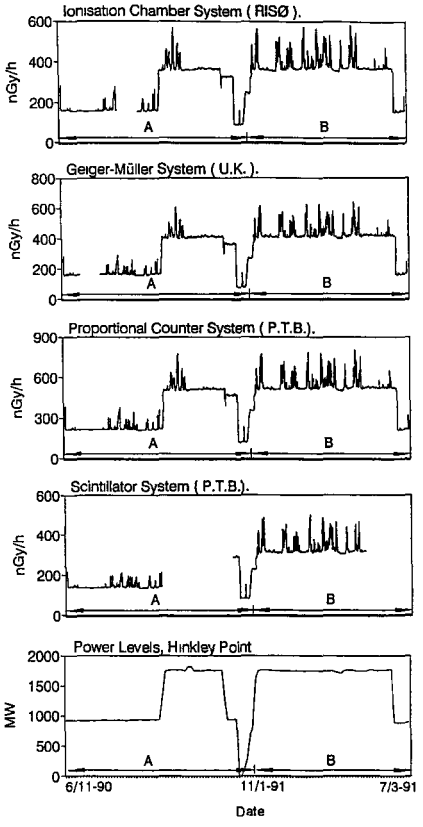

Fig. 2
The uncorrected variations in air kerma rate as measured by the four active detector systems as well as the reactor power levels over a four month period.

c) Establishment and commissioning of the Risø Natural Environment Measurement Stations.

The Risø Natural Terrestrial Radiation Measurement Station, partly funded by the CEC, was established in 1994 at a field site at Risø with the aim of being able to make reference measurements of a well determined natural environmental photon spectrum. 6000 m^2 (60 m x 100 m) of flat agricultural land sown with grass inside the fence of Risø National Laboratory was kindly offered by the Risø management especially for this particular purpose. The test site is situated far from other laboratory buildings, and the detectors tested there are thus unaffected by the nuclear installations at Risø.

An instrument control hut made of wood was designed and built at the field site and contains data loggers and controlling computers. Power lines, telephone and data net are installed which permit the on-line transfer of data to any place in the world. Precipitation, air pressure and temperature gauges are also installed, which are continuously monitored by a computer.

A Reuter Stokes high pressure ionisation chamber and a 3" x 3" NaI detector connected to a multi-channel analyser for continuous measurements of the total photon dose rate and gamma spectra, respectively, are permanently installed at the test station. Computer software was developed to allow one PC to control a number of environmental dose rate meters over a prolonged time. The computer screen displays real time dose rates measured by the different detectors as a function of time together with precipitation, air pressure and temperature data, and the results are automatically stored so that any event can be recalled and analysed. The software also provides the display of real time gamma spectra obtained by the NaI detector, and the spectra are continuously stored. Special emphasis has been placed on the evaluation of the contribution to the ambient radiation from radon daughters. These disturbing "radon peaks" play an important role in assessing action levels in connection with national early warning systems installed in many countries. For this particular task special curve-fitting software was developed and incorporated with the aim of being able to distinguish between ^{40}K and Rn-daughter gamma peaks by comparing them with two standard spectra. The result is a response curve representing the Rn-daughter concentration only as a function of time. Figure 3A shows an example of measurement results obtained over 48 hours at the Risø Measurement Station from (i) a Reuter Stokes high pressure ionisation chamber, (ii) a NaI gamma spectrometer (radon daughter window)

and (iii) a precipitation gauge. The "radon peak" associated with the rain fall is clearly seen. Figure 3B shows two gamma spectra obtained in the same period. One spectrum is strongly affected by radon daughters and the other is the "normal" environmental spectrum.

A cosmic measurement station was also established at a wooden pier extending into the Roskilde Fjord directly from the Risø grounds.

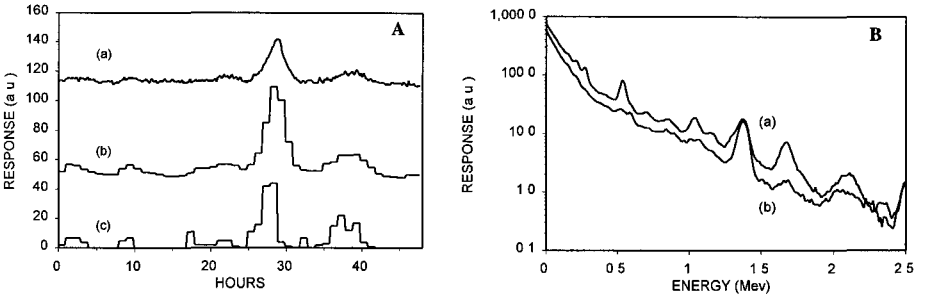

Fig. 3
A) Measurement results obtained over 48 hours at the Risø Measurement Station from (a) a Reuter Stokes high pressure ionisation chamber, (b) a NaI gamma spectrometer (radon window) and (c) a precipitation gauge.
B) Two gamma spectra obtained in the same period as for Fig. 3. Spectrum (a) is affected by radon daughters and (b) is the "normal" environmental spectrum.

d) An international intercomparison of active and passive detectors used for environmental radiation measurements.

During June 1994 an EC sponsored international intercalibration experiment was performed at Risø National Laboratory with participants from the USA, Eastern and Central Europe and the EU member countries. One aim of the experiment was to intercompare the "home" calibration of detectors and dosemeter responses of environmental radiation monitors used in the above countries and to try to make a link between the different reference standards used. A special feature of this recent intercomparison was the testing of a variety of recent designs of electronic dosemeters to see how they respond to environmental radiation. Another important feature was the use of highly sensitive TLD materials over ultra short integration periods (e.g. 3 hours) to determine the natural background air kerma rate. A total of 12 active dose rate meters, 21 electronic dosemeters and 8 different TL materials were used in the experiments which included (i) free-field calibrations using certificated ^{137}Cs, ^{60}Co and ^{226} Ra gamma sources, (ii) measurement of the natural radiation at the terrestrial field site at Risø, (iii) measurement of the cosmic ray component both on a platform at sea and on a boat at sea and (iv) shadow shield calibration experiments using a certificated ^{137}Cs source. Comprehensive evaluation and analysis of the measurement results obtained during the intercomparison have been carried out and presented in a paper that has been accepted for publication (invited paper) in the journal Radiation Protection Dosimetry (Bøtter-Jensen and Thompson, 1995).

Participants, instruments and detectors

The USA was represented by the Environmental Measurements Laboratory (EML), New York, who participated in the experiments with two of their new high pressure ionisation chambers (PICs) and one Ge. gamma spectrometer.

Eastern Europe was represented by 1) The Institute of Nuclear Physics in Krakow who participated with their own developed highly sensitive LiF:Mg,Cu,P (MCP-N) TL material, 2) The Institute of Isotopes/Atomic Energy Research Institute in Budapest who participated with LiF:Mg,Cu,P (Polish MCP-N) and Al_2O_3:C (TLD-500) TL materials, and 3) The Institute of Radiation Dosimetry in Prague who participated with i) a Reuter Stokes RSS-112 high pressure ionisation chamber, ii) two plastic scintillators.

The EU was represented by 1) The PTB who participated with two new plastic scintillator systems, 2) The UK (I.M.G. Thompson) participated with an energy compensated GM environmental monitoring system and different types of electronic dosemeters, 3) CIEMAT, Madrid, who participated with a variety of electronic dosemeters and new TL materials [LiF:Mg,Cu,P (Chinese GR-200), LiF:Mg,Cu,P (Polish MCP-N) and Al_2O_3:C] and finally 4) RISØ, as the host, who participated with the Risø environmental radiation monitor (Reuter Stokes RSS-111) and TL materials.

Source calibrations

A summary of the results of the free-field and shadow shield calibrations are shown in Table 3 for the dose rate meters, spectrometers and TLDs. The results are presented as the ratios of the participants' measured values to the calculated reference values. For the free-field calibrations the reference values include the air and ground scatter contributions calculated by Monte Carlo calculations whereas for the shadow-shield calibrations the reference values are for the direct radiation field only. It should be noted that most of the TL data were obtained over very short integration times, typically 3 to 16 hours, indicating a completely new scope of short term evaluation of environmental radiation levels using TL techniques (Bilski et al., 1995).

In all cases the calibrations agree to better than $\pm 5\%$ but there is an indication that the American calibrations have a systematic bias of 3% to 4% lower than the EU calibrations.

Table 3. Results of source calibrations expressed as measured-to-MCNP calculated values obtained by the dose rate instruments,spectrometers and TLDs

Detector Type	Free Field[1]			Shadow Shield[2]
	Ra-226	Co-60	Cs-137	Cs-137
HPI				
EML/Spicer	0.955*	0.956	0.974	0.960
EML/PIC	0.975*	0.976	0.974	0.985
IRD/RS PIC	0.971	0.981	0.991*	1.000
Risø/RS	0.983	0.992	0.994*	0.990
Scintillators				
PTB/Pl.Sc	1.016	1.021	0.992*	0.968
PTB/Pl.Sc	0.987	1.030	0.974*	1.000
IRD.Pl.Sc	1.023	1.049	1.008*	1.023
IRD/Pl.Sc	0.993	1.016	0.991*	0.977
GM				
UK/GEC	0.972*	1.033	0.839	0.822
Spectrometer				
EML/Ge	-*	-	-	0.959
IRD/NaI	0.994	1.002	1.012*	0.978
IRD/NaI (diff. response)	0.964	0.949	0.931*	0.862
TLDs				
Krak/MCPN	0.921	0.940*	0.947	-
CIEMAT/MCP-n	0.957	0.993*	0.963	-
CIEMAT/GR-200	0.995	1.048*	1.008	-
BUD/Al_2O_3	1.032	0.996*	0.892	-
CIEMAT/Al_2O_3	1.153	1.056*	1.093	-
BUD/$CaSO_4$	0.995	0.964*	1.017	-

1) Mean response of calibration at 3, 5 and 10 m.

2) Mean response of calibration at 3, 4 and 5 m.

* Radionuclide source used for "home" calibration.

Field intercomparison

The dose rate meters were exposed for different periods of time from 6 to 16 hours to the natural radiation at the terrestrial field station and at the cosmic platform station. The dose rate meters were then exposed to cosmic radiation during a two hour cruise on the Roskilde Fjord. The measured air kerma rates at the cosmic platform are on average 12% higher (approximately 3.9 nGy h^{-1}) than the air kerma from cosmic radiation as measured at sea on the boat. Figure 4A gives histograms of the air kerma rates for the field location, for the cosmic measurements at sea and for the terrestrial component taken as the difference between the field measurements and the cosmic (sea) measurements.

Figure 4B shows histograms for the TLDs of the air kerma rates for the field, estimated cosmic (sea) and the terrestrial air kerma rates. Except for the Al_2O_3:C TLDs, excellent overall agreement was found between most of the participating TL detectors.

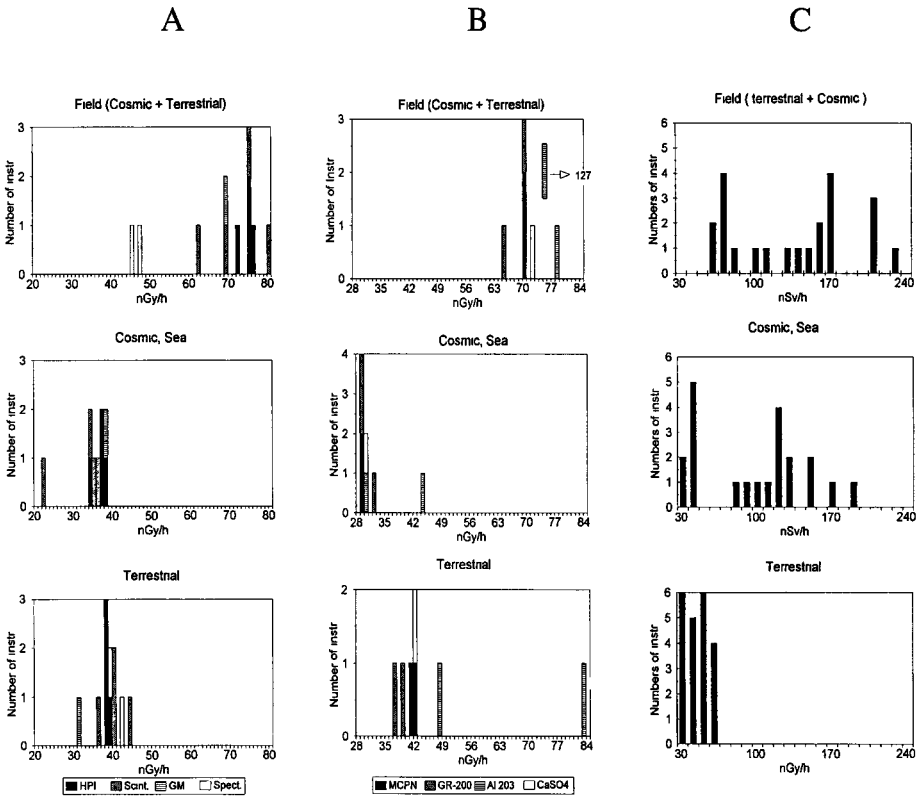

Fig. 4
A) Field, cosmic and terrestrial radiation results for the dose rate meters and spectrometers obtained at the Risø Environmental Radiation Measurement Stations.
B) Field, cosmic and terrestrial radiation results for the TLDs obtained at the Risø Environmental Radiation Measurement Stations.
C) Field, cosmic and terrestrial radiation results for the electronic dosemeters obtained at the Risø Environmental Radiation Measurement Stations.

As with the TLDs, the electronic dosemeters were not exposed to cosmic radiation at sea. The exposure time at the field station was 336 hours and the exposure time at the cosmic platform station was 840 hours. Their response to cosmic radiation was estimated by reducing their measured air kerma rate at the cosmic platform by 12%. Figure 4C shows the histograms for the electronic dosemeters of the air kerma rates for the field measurements, the estimated cosmic (sea) and terrestrial air kerma rates.

Conclusions

The intercomparison of the source calibrations demonstrated that the participants' home calibrations were, with one exception, within approximately 2.5% of the Risø standard values for the corresponding radionuclides. There seems to be a systematic difference of about 3% between the Risø calibration and the US high pressure ionisation chamber calibration. This should be investigated in a possible further intercomparison.

The active dose rate meters were the only instruments used to measure the air kerma rate from cosmic radiation at sea. The high pressure ionisation chambers and the GM detector gave readings up to 4 nGy h^{-1} higher than the previously measured value of 33.7 nGy h^{-1}. The spectrometer measurements at sea also indicated the presence of a contribution of about the same magnitude from photon radiation.

There was an excellent agreement for the TLD results with only the Al_2O_3:C material presenting any problems.

The TLD results show good agreement with the active dosemeter results. The cosmic results for the sea exposure, estimated from measurements made on the pier, indicate that the TLDs underestimate the cosmic radiation air kerma rate. Estimating the shortest exposure period required to evaluate the natural gamma-ray dose rate with MCP-N, GR-200 and TLD-500 detectors, we found that they were all capable of reliably measuring natural doses after exposure times of a few hours. Clearly there are problems with the Al_2O_3:C dosemeters and these should be further investigated in future intercomparisons.

No significance should be attached to the variations of the calibrations observed for the group of electronic dosemeters. These were received directly from the manufacturers and had not been calibrated at a secondary laboratory prior to the intercomparison.

Electronic dosemeter measurements of environmental radiation obviously require careful interpretation due to either the dosemeters' high cosmic responses or to their high inherent responses. Nevertheless it is most encouraging that the estimates of the terrestrial air kerma rate are in close agreement with that measured by active dose rate meters and TLDs.

e) OSL properties of Al_2O_3:C in relation to environmental radiation dosimetry.

The introduction of the highly sensitive Al_2O_3:C TL dosemeter material indicates that this material possesses a TL sensitivity some 40-60 times greater than that of LiF TLD-100. However, potential limitations in the use of Al_2O_3:C are the thermal quenching processes in the material and the light induced fading. As an alternative to TL the optically stimulated luminescence (OSL) properties of Al_2O_3:C were investigated at RISØ in relation to environmental radiation dosimetry (Bøtter-Jensen and McKeever, 1995). Experimental comparisons of the total light sum for OSL with that for TL showed that the OSL sensitivity is a factor of 2-4 times higher than the TL sensitivity. Preliminary measurements of the OSL sensitivity using green light stimulation (16 $mW.cm^{-2}$ at the sample) have shown that a dose of 0.5 μGy (5 hours of exposure to the natural background) can easily be detected. No measurable fading was observed over 80 days.

Publications

(1) Bøtter-Jensen, L. and Hedemann Jensen, P. Determination of Scattered Gamma Radiation in the Calibration of Environmental Dose Rate Meters. Radiat. Prot. Dosim. 42, 291-299, (1992).

(2) Thompson, I.M.G., Bøtter-Jensen, L., Lauterbach, U., Peßara, W., Sáez-Vergara, J.C. and Delgado, A. The Assessment of External Photon Dose Rate in the Vicinity of Nuclear Power Stations: An Intercomparison of Different Monitoring Systems. Radiat. Prot. Dosim. 48, 325-332, (1993).

(3) Gomez Ros, J.M. Muniz J.L., Delgado A., Bøtter-Jensen, L., and Jørgensen F. A glow curve analysis method for non-linear heating hot gas readers. Radiat. Prot. Dosim. 47, 483-488, (1993).

(4) Prokic M. and Bøtter-Jensen L., Comparison of main thermoluminescent properties of some TL dosemeters. Radiat. Prot. Dosim. 47, 195-199 (1993).

(5) Bøtter-Jensen, L. The Risø Natural Radiation Environment Test Station. 110 PTB Seminar "Ortsdosisleistungsmessungen Ionisierender Strahlung im Bereich der natürlichen Umgebungsstrahlung (30 Nov-1 Dec. 1993). PTB Report (in press).

(6) Thompson I.M.G. Measurement results of specially calibrated different dosemeters in the vicinity of a nuclear power station. 110. PTB seminar "Ortsdosisleistungsmessungen Ionisierender Strahlung im Bereich der natürlichen Umgebungsstrahlung". (30 Nov - 1 Dec, 1993). PTB Report (in press).

(7) Bøtter-Jensen, L. and Thompson I.M.G. An international intercomparison of passive dose meters, electronic dose meters, and dose-rate meters used for environmental radiation measurements. Radiat. Prot. Dosim. Invited paper (in press), (1995).

(8) Bilski P., Bøtter-Jensen L., Budzanowski M., Delgado A., Saez-Vergara J.C. and Waligorski M. Comparison of Short Term Dose Rate Measurements of the Terrestrial and Cosmic-Ray Background Components Using MCP-N and GR-200 Ultrasensitive TL Detectors. Presented at the 11th Solid State Dosimetry Conference, Budapest, July 1995. Submitted to Rad. Prot. Dosim. (1995).

(9) Bøtter-Jensen L. and McKeever S.W.S. Optically stimulated luminescence dosimetry using natural and synthetic materials. Rad. Prot. Dosim. (1995) (in press).

Head of project 2: Dr. Lauterbach

II. Objectives for the reporting period

A. INVESTIGATION OF ELECTRONIC DOSEMETERS

1. Introduction

2. The radiation environment in the extreme low background facility UDO

a) Improved dosimetric determination of the background radiation level in UDO and comparison with spectrometric measurements

b) Monte Carlo calculations of the radiation fields in the collimated beam facility of UDO and comparison with the measurements in co-operation with the Risø National Laboratory

3. Investigation of the inherent background and of the linearity of newly developed electronic dosemeters

a) Measurement of the inherent background by storing the devices in UDO

b) Measurement of the inherent background and of the linearity using radiation fields of weak ^{137}Cs sources in UDO

c) Determination of the inherent radioactivity of the construction material of dose meters

4. Determination of the response of electronic dose meters to 6 MeV - photons

5. Conclusions

B. INVESTIGATION OF GAMMA DOSE RATE METERS

1. Introduction

2. Linearity, inherent background and calibration of the dose rate meters

a) Determination of the linearity, of the inherent background and comparison of the calibrations

b) Determination of the response of dose rate meters to 6 MeV - photons

3. Conclusions

C. SERVICES FOR OTHER PARTNERS OF THE PROJECT "THE MEASUREMENT OF ENVIRONMENTAL RADIATION DOSES AND DOSE RATES"

Self-dose contribution to the readings of TL-dosemeters in co-operation with the Ciemat

D. PUBLICATIONS

III Progress achieved including publications

A. INVESTIGATION OF ELECTRONIC DOSEMETERS

1. Introduction

Electronic dosemeters developed as personal dosemeters could be also used as integrating monitoring instruments for long term measurements of the environmental radiation level. In the case of taking into account the natural environmental radiation in personal dosimetry it is also important to know the instrument's properties to be investigated in the course of this project. Besides their responses to the natural and artificial radiation fields to be measured the knowledge of their inherent background and the linearity of their readings at very low dose rates are important for this special application. In the course of this project the inherent background and the linearity of the reading of newly developed dosemeters were investigated. Instruments with two different construction principles (solid state diodes or GM tubes as detectors) were incorporated in this study. More details will be given below.

The knowledge of the composition and the dose rate of the background radiation level in the extreme low background "Underground Laboratory for Dosimetry and Spectrometry" (UDO) in the Asse salt mine is essential for the investigation of the inherent background of electronic dosemeters or for the determination of the self-dose contribution of TL-dosemeters. Of the same importance is the exact knowledge of the composition and the air kerma rates of the used weak photon fields. The reference dose rates in the order of 8 nGy/h up to 135 nGy/h for five ^{137}Cs sources are published in the CEC report EUR 11665 EN.
These investigations were to be carried out before the measurements of the inherent background and of the linearity could be performed.

2. The radiation environment in the extreme low background facility UDO

a) Improved determination of the background radiation level in UDO and comparison with spectrometric measurements

Earlier measurements of the gamma ray spectra in the laboratory had shown that the predominant sources of the background radiation are ^{40}K in the surrounding rock salt, natural radionuclides of the Uranium-Radium-series and a low contamination of the wooden framework below the building by ^{137}Cs and ^{134}Cs. But the contamination of the framework is negligible.
As a follow up of the earlier research work long term measurements of the dose rate of the background radiation in UDO were performed combined with dose rate measurements inside the special 5 cm thick lead shielded box in the laboratory.
The dose rate meter FHZ 600A of the manufacturer Kugelfischer was used for these measurements. The reading R_{TOTAL1} of this instrument is given by the following equation (1):

$$R_{TOTAL1} = r_K \cdot \dot{K}_K + r_{Ra} \cdot \dot{K}_{Ra} + R_i \qquad (1)$$

where r_K, r_{Ra} are the responses of the detector to ^{40}K-radiation and to the radiation from radionuclides of the Uranium-Radium-series respectively.
$\dot{K}_K$ and $\dot{K}_{Ra}$ are the "true" air kerma rates from the mentioned radionuclides respectively, and R_i is the contribution to the reading of the instrument from internal radioactive contamination and/or non-radiation reading, such as leakage current or electrical noise.

For the reading inside the lead shield the attenuation of each component of the background radiation has to be taken into account. In equation (2) F_K and F_{Ra} are the dose attenuation rates for the considered radiations. The reading R_{TOTAL2} is given by

$$R_{TOTAL2} = (1/F_K) \cdot r_K \cdot \dot{K}_K + (1/F_{Ra}) \cdot r_{Ra} \cdot \dot{K}_{Ra} + R_i \qquad (2)$$

Values for the air kerma rate of the background radiation $\dot{K}_B$ and for the inherent instrumental background reading R_i can be calculated from the equations (1) and (2) under the assumption that the background radiation is caused only by the two radiation sources mentioned above and their air kerma contributions $\dot{K}_K$ and $\dot{K}_{Ra}$ have the given composition

$$\dot{K}_B = a \cdot \dot{K}_K + b \cdot \dot{K}_{Ra} \qquad (3)$$

with a + b = 1. The result for the air kerma rate $\dot{K}_B$ of the environmental radiation in UDO is not very sensitiv against the choose of a and b. For the values of $\dot{K}_B$ in Table 2 is a=b=0.5. In the case of a=1 and b=0 $\dot{K}_B$ yields 0.62 nGy/h respectively 0.071 nGy/h.
The equivalent air kerma rate of R_i is 12.39 0.15 nGy/h.

Table 1 shows the responses of the used detector FHZ 600 A for the environmental radiation in UDO and the dose attenuation rates for the lead shielded box.

Table 1

	^{40}K	Uranium-Radium-series
Response *r*	**1.42**	**1,12**
Dose attenuation rates *F*	**12.5**	**16.7**

The readings R_{TOTAL} and the calculated total air kerma rates $\dot{K}_B$ are presented in Table 2.

Table 2

	R_{TOTAL} nGy/h	$\dot{K}_B$ nGy/h
UDO	**13.27 0.15**	**0.69 0.15**
Lead shield	**12.45 0.15**	**0.063 0.12**

The measurements by the dose rate meter were supplemented by spectrometric measurements. Two types of scintillation spectrometers were used for these investigations in co-operation with the Institute of Radiation Dosimetry, Prague, Czech Republic. The photon fluence rate of the gamma spectrum was converted into the corresponding air kerma rate. The agreement between the spectrometric determination of the background radiation level in UDO and the determination by a doserate meter is satisfactory. The values in Table 2 can be taken as a good basis for the evaluation of measurements of the inherent background of dosemeters and dose rate meters.

b) Monte Carlo calculations of the radiation fields in the collimated beam facility of UDO and comparison with the measurements in co-operation with the Risø National Laboratory

A collimated beam irradiation facility with a set of radioactive sources is provided in UDO for the generation of weak photon fields which are required for the investigations during this project. The determination of scattered radiation in the calibration fields of the collimated beam facility was initiated to assess the composition and quality of the photon fields. Scattered

photons with lower energies contribute to the air kerma rate at the reference point This contribution depends on the amount of the scattered radiation.
It seemed to be worth-while to perform Monte Carlo (MC) calculations to get information on the energy distribution and on the amount of the contribution of the scattered photons in the calibration field at the reference point. The Risø National Laboratory performed the calculations by a Monte Carlo code.

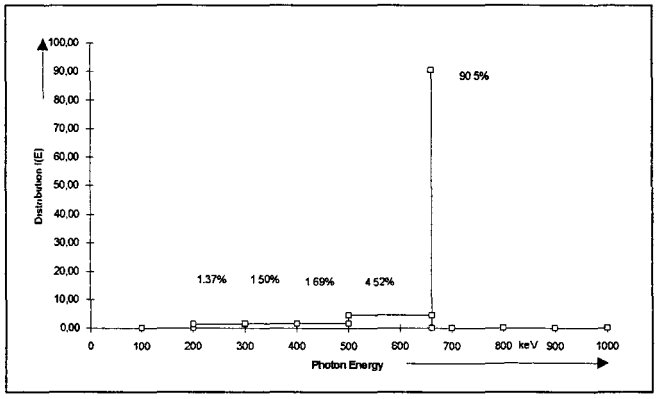

Figure 1. Calculated energy distribution of the photon field at the reference point in UDO.

Figure 1 presents the calculated energy distribution of the scattered photons separated in energy bands of 100 keV at the reference point which has 2 m distance from the source. These calculations are based on the geometrical design of a ^{137}Cs source, of the collimated beam facility and on the construction of the UDO building.
From this distribution the contribution of the scattered photons to the air kerma rate was calculated. This value is given in the last column of Table 3 as the ratio of the contribution from scattered and from uncollided photons. $\dot{K}_{Total}$ is the total air kerma rate generated by uncollided and scattered photons and $\dot{K}_{Uncollided}$ is the contribution from uncollided photons. The difference of both values yields the air kerma rate from the scattered photons. The measured air kerma rate $\dot{K}_{Meas.}$ at the reference point comprises all contributions and should be equal to $\dot{K}_{Total}$.
The air kerma rate generated by the uncollided photons can be calculated ($\dot{K}_{Calc}$)from the uncollided photon fluence rate Φ of the source on the design of which the MC calculations were based. The value of the fluence rate was measured by a germanium spectrometer.

Table 3. Measured and calculated air kerma rates at the collimated beam facility.

Measured Photon fluence rate Φ $s^{-1}sr^{-1}$	Calculated air kerma rate $\dot{K}_{Calc.}$ nGy/h	Measured air kerma rate $\dot{K}_{Meas.}$ nGy/h	$\frac{\dot{K}_{Meas.} - \dot{K}_{Calc}}{\dot{K}_{Calc.}}$	$\frac{\dot{K}_{Total} - \dot{K}_{Uncollided}}{\dot{K}_{Uncollided}}$
$5.016\ 10^5$	137.3	140 84	0.026	0.11

The difference ($\dot{K}_{Meas.} - \dot{K}_{Calc}$) of both air kerma rate values should also give the air kerma rate from the scattered photons The ratio of scattered to uncollided photons calculated from measured values is given in the fourth column of Table 3. There is less agreement between the ratio of the MC calculations and the ratio of the measured values.

3. Investigation of the inherent background and of the linearity of newly developed electronic dosemeters

a) Measurement of the inherent background by storing the devices in UDO

The inherent background of dosemeters and dose rate meters is generated by radioactive contamination of the construction material of the devices and by electrical noise of the electronics. Both sources cause an indication which is not due to an external radiation field. The magnitude of this effect must be known if these instruments are used for measurements of environmental radiation levels.
For these investigations a total of 12 different models of electronic dosemeters were available. In Table 4 the models, the type of detectors (GM tube or solid state diode) and the used battery types are presented in the first three columns. This overview makes obvious that there are mainly two groups of instruments with GM tubes or solid state diodes as detectors. As power supplies for instruments with GM-tubes only alkaline batteries are used. In contrary the dosemeters with solid state diodes are equipped with Lithium batteries having a longer life time.
The inherent background can easily be determined by storing the devices at a place with a negligible environmental radiation level. This supposition is fulfilled in UDO and in the special lead shield in UDO where the air kerma rates of the background radiation are 0.69 nGy/h respectively 0.063 nGy/h.

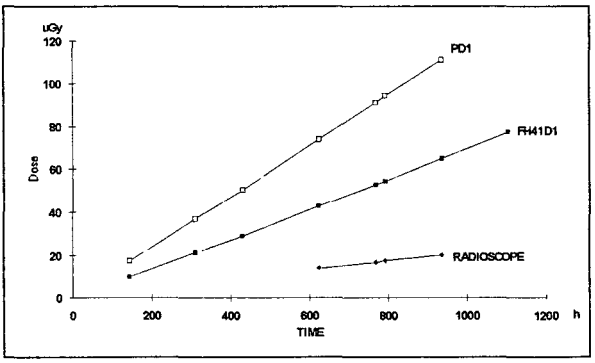

Figure 2. Accumulated doses of electronic dosemeters stored in UDO.

Three models of electronic dosemeters were stored for more than 1000 hours in UDO. Figure 2 shows the readings of the accumulated doses in µGy during this period. The measurements demonstrate considerable differences of the indicated inherent backgrounds. The slopes of the straight lines are equivalent to the inherent backgrounds and yield dose rate values which vary between 20 nGy/h and 120 nGy/h. The real background in UDO does not affect significantly the indicated accumulated doses of the three instruments. These values are in the order of the natural environmental radiation level. In Table 4 the dose rate equivalents of the inherent background of these instruments are given in the 10th column.
In the course of these investigations five other models of electronic dosemeters were also stored in the special lead shielded box in UDO for more than 70 hours. These results are given

in the 11th column of Table 4 and are of the same magnitude as the results of the first experiment.

b) Measurement of the inherent background and of the linearity using radiation fields of weak ^{137}Cs sources in UDO

In several types of electronic dosemeters the indication of the environmental background radiation is often used as a test for the correct operation of the instruments. Several dosemeters seemed to have a threshold at a fixed count rate below which they are internally switched off stating an error. Nevertheless, they may have an inherent background but it is not directly measurable by storing them in a nearly radiation free environment.
To solve this problem these measurements were performed by irradiating the dosemeters for several days with 3 different ^{137}Cs sources of suited source strengths. The doses accumulated by the instruments can be converted into a dose rate by the well known time interval for the irradiation.
The dependence of the reading R_{Tot} of an instrument on the air kerma rate $\dot{K}_{ref}$ in the photon field of the collimated beam facility is given by equation (1) where r_{ref} is the response to the photons of the reference field and B is given by equation (2).

$$R_{Tot} = r_{ref}\dot{K}_{ref} + B \qquad (1)$$

$$B = r_B\dot{K}_B + R_i \qquad (2)$$

R_i is the indicated inherent background and r_B the response to the photons of the background radiation field in UDO with the air kerma rate $\dot{K}_B$.
Applying the linear relationship of equation (1) on calibration measurements with the collimated beam facility using different reference dose rates the slope yields the response r_{ref}. If the response to the background radiation field is known the inherent background reading R_i can be derived from B.
The responses r_{ref} of the dosemeters for ^{137}Cs photons are given in the 4th column of Table 4. R_i was determined with the batteries installed in the dosemeters and with a remote power supply to clear up if the reading for the inherent background is influenced by the batteries. The values of R_i are shown in the columns 12 and 13 of Table 4.

c) Determination of the inherent radioactivity of the construction material of dosemeters

The relative high inherent background is supposed to be caused mainly by the inherent radioactivity of the instruments. Preliminary measurements of the gamma radiation of the dosemeters with a high purity germanium spectrometer showed that the 1461 keV -line of ^{40}K is increased by a factor of two compared with the environmental spectrum in UDO. Removing the battery from the instrument the pulse rate in the 1461 keV -line is considerably reduced.

In the course of these investigations the high purity germanium spectrometer system was used for an estimation of the inherent radioactivity of the dosemeters. The instruments were placed at the middle on the top of the cylindrical detector .The spectra of the dosemeters were measured with and without batteries. The spectra show that ^{40}K is the main radionuclide of the inherent radioactive contamination. This radionuclide is also a component of the potassium of the electrolyte in alkaline batteries.
The results of these qualitative determinations are also presented in Table 4. The count rate with the batteries installed is given in the 7th column, with remote power supply in the 8th

column and the difference of both values which is proportional to the inherent radioactivity of the construction material in the 9th column.
There are two groups of instruments as mentioned above. Devices with alkaline batteries show clearly a reduction of the ^{40}K gamma line with the batteries removed. This effect is significantly lower or not measurable within the statistical uncertainty with other kinds of batteries.
The measured inherent backgrounds and the results of the qualitative determination of the internal contamination with the natural radionuclide ^{40}K for the instruments with alkaline batteries are given in the histogram Figure 3 .

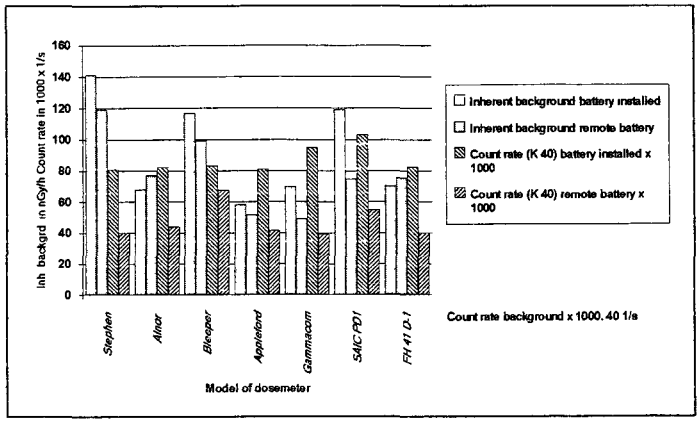

Figure 3. Inherent background and estimation of the internal contamination with ^{40}K.

This histogram clearly demonstrates that in each case the count rate of the ^{40}K line is reduced mostly to the background level after removing the batteries. But the readings of the inherent backgrounds are not reduced to the same extent. It can be assumed that sources for the inherent background can also be the contamination of the construction material by other radionuclides and/or electrical noise, especially in the case of the GM-tubes. It seems impossible to identify the various sources for the background readings from this qualitative measurements because the construction designs of these dosemeters are not known.
Three of the four dosemeters with diodes show a negative background reading. The reason can be an electronic overcompensation of indications not to be considered in the readings (e.g. an estimated internal or a mean natural environmental background) which then yields negative values in the ultra low external background in UDO.
These special features must be taken into account for the use of these instruments for monitoring radiation levels in the order of the natural environmental radiation level.
With respect to the linearity of the indication on the air kerma rate the correlation coefficients of the linear regression analysis given in column 6 of Table 4 clearly show that there is a good linear relationship between the reading and the air kerma rate of the radiation field at very low air kerma rates.

Table 4. Calibration - Estimation of Inherent Radioactivity - Determination of Inherent Background.

Instrument	Detector	Batteries	Response r_{ref}	Interception B nGy/h	Correlation coefficient r	Count rate *) power supply installed s^{-1}	Count rate *) remote power supply s^{-1}	Difference of count rates with and without batteries s^{-1}	Bckgrd reading by storing in the UDO lab nGy/h	Bckgrd reading by storing in the lead shield nGy/h	Inherent bckgrd. power supply installed by using phot.field nGy/h	Inherent bckgrd. remote power supply by using phot.field nGy/h
1	2	3	4	5	6	7	8	9	10	11	12	13
STEPHEN	GM	1 x Alkaline Size AA	1.14	142	0.9999	0.0811 ± 0.007	0.0400 ± 0.006	0.0411 ± 0.009	-	133	141 ~ ± 1	119 ~ ± 1
ALNOR	GM	3 x Alkaline Size AAA	1.03	69	0.9985	0.0822 ± 0.007	0.0439 ± 0.005	0.0383 ± 0.008	-	73	68 ~ ± 10	77 ~ ± 10
BLEEPER SV	GM	3 x Alkaline Size AAA	1.02	118	0.9996	0.0833 ± 0.007	0.0675 ± 0.008	0.0158 ± 0.01	-	110	117 ~ ± 10	99 ~ ± 10
APPLEFORD	GM	2 x Alkaline Size AA	0.86	59	1.0000	0.0809 ± 0.008	0.0417 ± 0.006	0.0392 ± 0.01	-	49	58 ~ ± 10	52 ~ ± 10
GAMMACOM	GM	1 x Alkaline Size 522	0.88	71	1.0000	0.0950 ± 0.009	0.0393 ± 0.006	0.0558 ± 0.01	-	73	70 ~ ± 10	49 ~ ± 10
SAIC PD1	GM	1 x Alkaline Size AA	-	-	-	0.1033 ± 0.013	0.0550 ± 0.001	0.0483 ± 0.013	119	-	-	75 ~ ± 1
FH 41 D-1	GM	1 x Alkaline Size 522	-	-	-	0.0825 ± 0.008	0.0400 ± 0.006	0.0425 ± 0.01	70	-	-	76 ~ ± 10
RADIOSCOPE	GM	1 x Alkaline Size 522	-	-	-	-	-	-	20	-	-	-
MERLIN GERIN	DIODES	Lithium Size AA	1.10	2	0.9985	0.0517 ± 0.007	0.0350 ± 0.005	0.0167 ± 0.009	-	-	1	-
MYDOSE ADM-102	DIODES	DL 2450 u. LR 44	1.00	(-8)	0.9998	-	-	-	-	-	(-9)	-
MYDOSE PDM-102	DIODES	DL 2450	1.08	(-10)	0.9994	0.0483 ± 0.006	0.0417 ± 0.006	0.0066 ± 0.008	-	-	(-11)	-
SIEMENS PLESSY	DIODES	Lithium	1.06	(-19)	0.9978	0.0399 ± 0.0005	-	-	-	-	(-20)	-

*) Background count rate : 0.0400 ± 0.001 s^{-1}

4. Determination of the response of electronic dose meters to 6 MeV - photons

The 6 MeV facility in the PTB generates a beam of 6 MeV photons using a nuclear reaction with accelerated protons. The air kerma at the measuring points was well known for the period of each measurement. The experiments comprised measurements at various distances for the determination of the response to the 6 MeV photons as well as measurements with build-up material (perspex) in order to discover if the secondary electron equilibrium is already achieved by the instrument's material around the detector itself or not.
Table 5 shows the results of the responses for the electronic dosemeters. All electronic dosemeters have an over-response between 15 % and 69 % with the exception of one probe which has a response of 1. The probes with the GM-tubes show the highest responses.

Table 5. Response of Electronic Dose Meters to 6 MeV Photons.

Instrument	EPD (1)	EPD (2)	EPD (3)	FH 41 D1	PD-1	PD-2	
Manufacturer	Siemens Plessy	Siemens PLessy	Siemens Plessy	FAG	SAIC	SAIC	Merlin
Detector	Solid state diode	Solid state diode	Solid state diode	GM-tube	GM-tube	GM-tube	Solid state diode
Response to 6 MeV photons without build-up material related to the response to 0,661 MeV photons	1,22	1,28	1,15	1,69	1,39	1,40	1,00

The results of build-up experiments with the electronic dosemeters presented in Fig. 4 exhibit that the relative values of the air kerma readings related to the value at zero thickness of the perspex plates have partly a contrary dependence on the thickness of the perspex plates even for instruments of identical model.

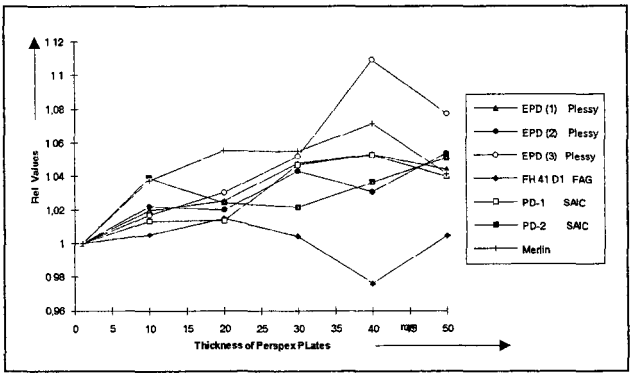

Figure 4. Build-up experiments with the electronic dose meters in the 6 MeV photon field.

5. Conclusions

These investigations exhibit to which extent the monitoring of low level radiation fields by these instruments can be influenced by the investigated properties of electronic dosemeters. In each case the reading of the inherent background due to various sources must be considered evaluating measurements of very low radiation levels.

In the neighbourhood of nuclear power plants 6 MeV photons can contribute to the radiation field. For the evaluation of measurements at such sites the dependence of the response on this photon energy must be taken into account.
The linearity of the indication of low air kerma rates is satisfactory for all investigated models of electronic dosemeters. But the resolution of the digital display is mostly only 1 μGy. Using these instruments for measurements of levels in the order of the natural environmental background an integration time of at least 5 days is necessary to get an uncertainty in the order of 10% due to the resolution.
In the course of these investigations there were problems with the short life time of alkaline batteries as power supply during experiments with storage times of several weeks also in fields of low air kerma rates. Models with Lithium batteries were more suited for this application due to the longer life time.

B. INVESTIGATION OF DOSE RATE METERS

1. Introduction

The radiation fields of the collimated beam set up at UDO were used for the calibration and investigation of instruments at several intercomparison and intercalibration programmes in the course of the various EU projects. These fields were calibrated by a secondary standard instrument of the PTB. By this measure the traceability to the national primary standard was established.
During this reported programme the consistency of calibrations performed in UDO and at other institutes was checked by the measurements in UDO based on the home calibration of the participants and comparison with the results based on the PTB calibration. The Environmental Measurements Laboratory, New York and the Institute of Radiation Dosimetry, Prague were involved in this intercomparison with their dose rate meters.

2. Linearity, inherent background and calibration of the dose rate meters

a) Determination of the linearity, of the inherent background and comparison of the calibrations

The procedure described in section **A.3.b)** using weak ^{137}Cs sources for the determination of the response to 661 keV photons and of the inherent background was also applied to dose rate meters. The results of these measurements are summarised in Table 6.
Besides the determination of the responses r_{ref} and their evaluation by applying equation (1) in section 3. b) the reading B_m of each instrument achieved by storing the instruments in the lead shielded box is given in the last column. The inherent background R_i derived from the interception B is presented in the 7th column. The correlation coefficient r in the 6th column is a measure for the goodness of the linear fit.
The ionisation chambers of the EML were calibrated by ^{226}Ra sources and that of the IRD by the manufacturer of the instrument. The determined responses for all ionisation chambers agree very well within the stated uncertainties with the home calibration of the participants. These results confirm the consistency of the calibrations performed by the different institutes.

The scintillation dose rate meters used by the PTB were calibrated by the manufacturers. Their responses in the order of 0.85 up to 0.91 show the difficulty of a reliable calibration for air kerma rates of this order.
The correlation coefficients in the order of 1 confirm a good linear relationship for all investigated instruments between the air kerma rate and their readings.

The interception B should be comparable with the background radiation levels measured by each instrument. The negative value for R_i of the ionisation chamber RS-112 indicates that there are measures to compensate the inherent background comparable with the results discussed in section **A.3.b)**.

Table 6. Results of Calibration Measurements for Dose Rate Meters with ^{137}Cs Sources.

Instrument	Detector	Institute	Response r_{ref}	Interception B nGy/h	Corr. coefficient r	Inherent bckgrd R_i nGy/h	Bckgrd reading B_m nGy/h
Spicer	Ionisation chamber	EML[1]	1.00*)	1.82	1.000	1.13	-
Rs-111	Ionisation chamber	EML[1]	0.96**)	1.17	1.000	0.48	1.58
RS-112	Ionisation chamber	IRD[2]	0.99***)	0.52	1.000	(-0.17)	1.25
MAB 500 (1)	Scintillator	PTB[3]	0.90+)	11.2	0.999	10.5	12.5
MAB 500 (2)	Scintillator	PTB[3]	0.85+)	5.74	0.999	5.04	5.39
DLM 7908	Scintillator	PTB[3]	0.91+)	1.86	0.999	1.17	0.88

1) US Dept. of Energy, Environmental Measurements Laboratory, 376 Hudson Street New York, New York 10014, USA
2) Institute of Radiation Dosimetry, Na Truhlarce 39/64, 180 86 Prague, Czech Republic
3) Physikalisch-Technische Bundesanstalt, Bundesallee 100, 38116 Braunschweig, Germany

*)Statistical uncertainty at 2 σ is ± 8% (± estimated systematic uncertainty 5%)

**)Statistical uncertainty at 1 σ is ± 6%

***)Statistical uncertainty at 1 σ is ± 5%

+)Statistical uncertainty at 1 σ is ± 5%

b) Determination of the response to 6 MeV - photons

The 6 MeV facility in the PTB generating a beam of 6 MeV photons with accelerated protons by a nuclear reaction was also used for the investigation of the response of the dose rate meters to 6 MeV - photons. The experiments comprised measurements at various distances for the determination of the response as well as measurements with build-up material (perspex) in front of the detector in order to discover if the secondary electron equilibrium is already achieved by the instrument's material around the detector itself or not. The detectors of the dose rate meters were GM-tubes, scintillators and ionisation chambers.
Table 7 shows the results of the responses for the dose rate meters. The probe with the GM-tube shows the highest value of the response. The probes with a scintillator as detector have a response near 1

Table 7. Response of Dose Rate Meters to 6 MeV Photons.

Instrument	Radioscope	MAB 500	NB 3201	RS-111	RS-112
Manufacturer	MAB	MAB	TESLA	REUTER-STOKES	REUTER-STOKES
Detector	GM-tube	Scintillator	Scintillator	Ionisation-chamber	Ionisation-chamber
Response to 6 MeV photons without build-up material related to the response to 0,661 MeV photons	1,71	1,05	1,04	1,26	0,94

The two ionisation chambers were expected to have nearly the same response, but they differ by 32 %. May be, they have a different design inside with respect to the used construction material. These two instruments indicate also a rather different behaviour in the build-up experiments as seen in Figure 5 where the responses are related to zero thickness of the perspex plates. The dose rate meters with the GM-tube and with the scintillators do not point out any significant build-up effect.

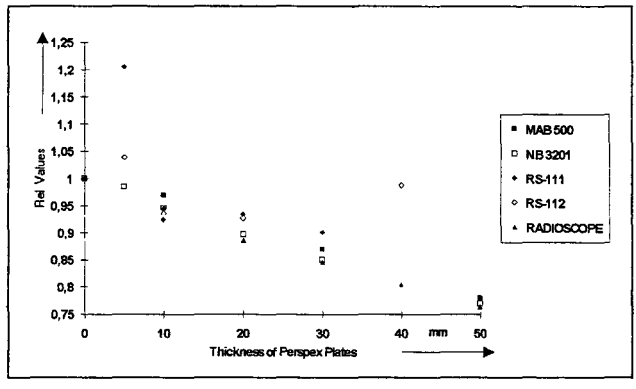

Figure 5. Build-up experiments with the dose rate meters in the 6 MeV photon field.

3. Conclusions

The behaviour of the dose rate meters of the design incorporated in this programme agrees well with the results of earlier EU intercomparisons. A detailed and comprehensive analysis of the earlier results is published in the CEC reports EUR 11665 EN and EUR 12731 EN.
But an outstanding outcome of this reported intercomparison is the consistency of calibrations performed in Europe and the USA. This result confirms that measurements of air kerma rates of this order can be made comparable and reliable in any case.

C. SERVICES FOR OTHER PARTNERS OF THE PROJECT "THE MEASUREMENT OF ENVIRONMENTAL RADIATION DOSES AND DOSE RATES"

Self-dose contribution to the readings of TL-dosemeters in co-operation with the Ciemat

TL-dosemeters of the Ciemat were stored for longer periods in the low level facility in the Asse salt mine and evaluated in UDO in order to avoid uncertainties due to any transport doses. The results of these investigations are reported by the Ciemat.

D. PUBLICATIONS

1. Peßara, W. and Lauterbach. U. *Ein strahlungsarmes Untergrundlaboratorium für Dosimetrie und Spektrometrie (UDO)*. Tagung des Fachverbandes für Strahlenschutz in Binz auf Rügen, FS-93-67-T, 455-460 (1993).

2. Lauterbach, U. and Peßara, W. *Investigation of Environmental Dosemeters in the Ultra Low Background Facility "UDO"*. Radiat. Prot. Dosim. (in press 1995)

3. Peßara, W. and Lauterbach. U. *The Inherent Background of Electronic Dosemeters* (in preparation)

Head of project 3: Dr. Delgado

II. Objectives for the reporting period

a) Refinement of the computerized evaluation methods for LiF:Mg,Cu,P (CIEMAT).

b) Selfdosing and long term stabililty experiments (CIEMAT-PTB, ASSE mine).

c) Check of the very short term environmental capability of LiF:Mg,Cu,P (CIEMAT-RISO).

d) Study of TLDs response at high energy photons (CIEMAT-PTB).

e) Comparison of the response of HPIC and TLDs response.

f) Reliability of environmental TLD systems based on the new highly sensitivity phosphors.

III. Progress achieved including publications

a) Refinement of the computerized evaluation methods for LiF:Mg,Cu,P (CIEMAT)

The main achievement of the project has been the demonstration of the practical measurement capability of the new hypersensitive TL materials, specially LiF:Mg,Cu,P, for environmental dosimetry. This has been possible after an intensive study of its characteristics, proposing innovative solutions for the problems that these materials present when evaluated by conventional procedures.

For LiF:Mg,Cu,P in particular the problem caused by the high residual signals induced by high doses that badly affect the low dose measurement capability, has been practically solved by a new and simple glow curve analysis. This analysis method has been developed during the project and permit the material reutilization after only reader anneal,i.e. the simplest working procedure. An article describing the main features of the analysis method and the dosimetric results obtained by its application has been accepted for publication in Radiation Protection Dosimetry.

During the reporting period a further refinement of that analysis method has been implemented permitting to take control of the maximum temperature reached during heating. The maximum temperature at which LiF:Mg,Cu,P dosemeters can be heated is known to be the most severe limitation of this material. Very often the maximum readout temperature cannot be fixed in commercial readers with the reliability and reproducibility required by LiF: Mg,Cu,P. This causes irreproducibilities is the TL response.

In our laboratory we have efficiently solved this problem by fixing the maximum readout temperature with respect to the

position of the glow curve maximum (peak 4). On every measurement the peak position is detected during readout allowing heating to continue during a time according to the "temperature beyond the maximum" selected for that measurement.

The system has shown to have practical advantages permitting to work at high heating rates, of the order of 10ºC/s. In addition temperatures higher than 240ºC are permitted during short times favouring the annealing of the high residual signals characteristic of LiF:Mg,Cu,P.

b) Self-dose experiments in the ASSE mine

A relevant activity developed during the project in cooperation with PTB was on the measurement of seldosing and long term stability of different TLDs. The experiment was carried out inside the UDO laboratory in the ASSE salt mine. detectors were stored there for six months. In particular for the two LiF dosimetric varieties TLD-100 and GR-200 self dosing was found similar and practically negligible (<0.8nGy/h). The results of the long term stability experiments showed that liF GR-200 has a substantially better stability than the traditional TLD-100. After six months storage at 22 °C, GR-200 experienced a sensitivity decrease of the order of 5-8 % that compares very well with the 25-30 % decrease detected for TLD-100. This is another excellent characteristic in favour of the use of the more sensitive LiF GR-200 for environmental dosimetry, an activity in which GR-200 can replace with clear advantages the old LiF TLD-100. A paper with a description of the ASSE experiment and the results obtained has been publishen in RPD.

c) Check of the very short term environmental capability of LiF:Mg,CU,P (CIEMAT-RISO)

CIEMAT participated in the Intercomparison carried out at the Riso environmental field station in June 94. A calibration exercise was performed for three types of hypersensitive phosphors: Al_2O_3:C from Russia, LiF:Mg,Cu,P from China (GR-200A) and Poland (MCP-N). The TLDs were exposed to three different low dose-rate certified sources (^{137}Cs, ^{60}Co and ^{226}Ra) and four distances to the detectors (1, 3, 5 and 10 m) were tested. Detectors were irradiated overnight and the imparted dose ranged 1-250 µGy.

The estimated dose rates from the TLDs measurements were compared with the reference values calculated by the Monte-Carlo codes developed at Riso (Figure 1). A good agreement was found for the lithium fluoride copper-doped (better than 10% in all cases), but noticeable bias (>20%) were obtained for aluminium oxide when the distance to source increased. Degradation of spectra (scatter photon component can reach 20%) and the expected over-response of this phosphor to low energy photons seem to be the reason for this behaviour.

LiF:Mg,Cu,P (GR-200A)

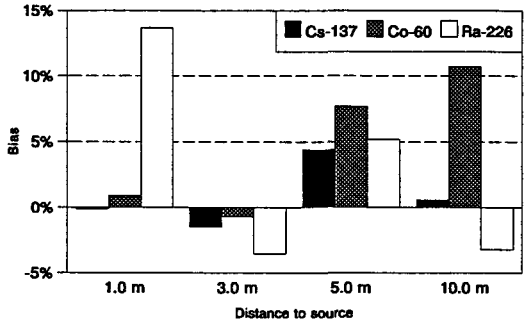

LiF:Mg,Cu,P (MCP-N)

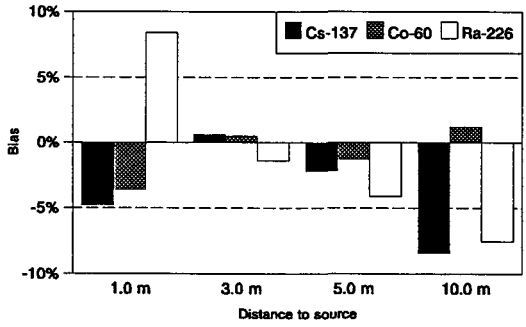

Al_2O_3:C (TLD-500K)

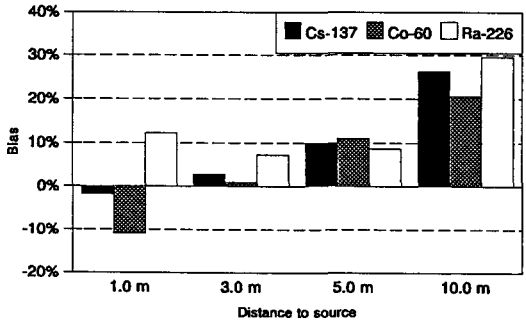

In addition, controlled exposures to environmental cosmic and cosmic plus terrestrial components were developed. The hypersensitive phosphors demonstrated their capabilities to determine environmental doses in ultrashort periods (< 5 hours). Particular attention was given to cosmic TLD response. After three days of exposure on a wooden pier at Roskilde fiord, TLDs under 1 $g \cdot cm^{-2}$ measured a 20% lower dose than the reference HPIC Reuter-Stokes. This result confirmed previous suggestions made on the possible under-response of TLDs to cosmic radiation when placed at the recommended depth of tissue equivalent material for the estimation of the ambient dose.

d) Study of TLDs response at high energy photons (CIEMAT-PTB)

The energy dependence of two types of Copper-doped Lithium Fluoride (GR-200A from China, MCP-N from Poland) and one type of Carbon-doped Aluminium Oxide (TLD-500K from Russia) has been studied in the range 0.6-6.0 MeV. For completion, standard LiF:Mg,Ti (TLD-100 from USA) was also tested with the same methods. All the irradiations were carried out in Metrological Facilities in Spain (CIEMAT) and Germany (PTB).

A build-up experiment was performed using different thicknesses of PMMA placed at the front and back of detectors (Figure 2). Corrections from photon attenuation, build-up factor and dose enhancement have been calculated and compared in evaluation of the absorbed dose in TL detector.

Both air kerma and dose TLD response of hypersensitive phosphors LiF:Mg,Cu,P and Al_2O_3:C to high energy photons are close to the response to ^{137}Cs calibration photons. Only a slight bias (5%) in TL results can be expected if the presence of 6 MeV photons is noticeable (small over-response for the lithium fluoride and small under-response for the aluminium oxide).

Therefore, these materials employed in routine TLD environmental monitoring are useful in providing valid dose measurements in the presence of high energy photons (1.00±0.05 relative to ^{137}Cs). This feature improves the value 1.0±0.1 for the standard LiF:Mg,Ti which is currently the most employed phosphor in environmental monitoring.

Furthermore, the four studied phosphors (TLD-100, GR-200, MCP-N and TLD-500K) also exhibit an unexpected good energy response, even when the wall thickness is not enough to reach charge particle equilibrium conditions.

Abnormal decrease in TLD response to ^{60}Co has been found for standard LiF:Mg,Ti irrespective of the wall thickness. This effect could be observed in two separate experiments using different irradiation facilities in Germany and Spain.

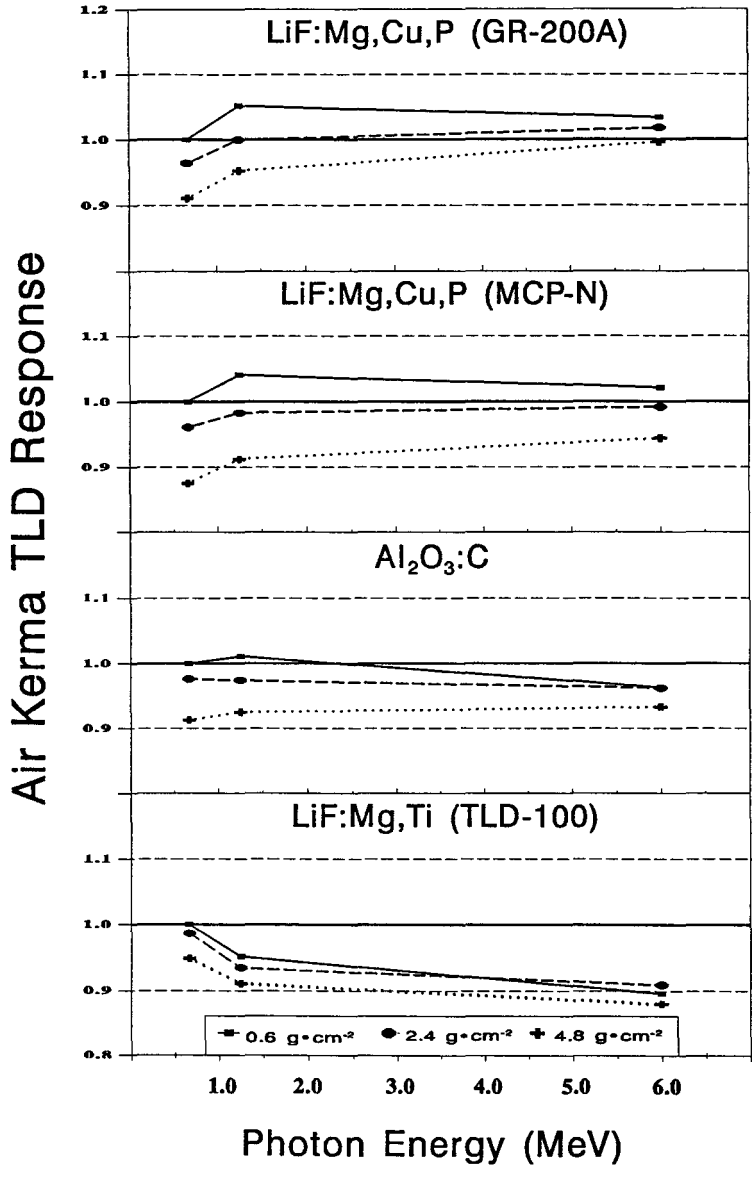
LiF:Mg,Cu,P (GR-200A)
LiF:Mg,Cu,P (MCP-N)
Al2O3:C
LiF:Mg,Ti (TLD-100)
1.2
1.1
1.0
0.9
0.8
0.6 g•cm-2
2.4 g•cm-2
4.8 g•cm-2
1.0
2.0
3.0
4.0
5.0
6.0
Air Kerma TLD Response
Photon Energy (MeV)

e) Comparison of the response of HPIC and TLDs response

Lower detection limits below 1 μGy have been reported for the new hypersensitive thermoluminescence phosphors such as LiF:Mg,P,Cu and Al_2O_3:C. Considering that usual environmental daily doses are in the range of 1-5 μGy, the CIEMAT has designed an experiment to examine the real capability of these phosphors to assess extremely low doses.

Three types of these phosphors (GR-200A from China, MCP-N from Poland, TLD-500K from Russia) have been studied.

The experiment consists of the determination of the integrated dose after one-three days of exposure to environmental radiation. These measurements were carried out with each one of the passive systems using a high pressure ionization chamber as the reference instrument. The study also compares the results from two different sites: indoor (air conditioned room) and outdoor (ambient temperatures from 0°C to 40°C).

Additional badges were exposed in order to study the additivity and stability of the doses for different exposure periods ranging from one week to six months.

Figure 3 presents a comparison of the daily results obtained from an active instrument (HPIC) and three hypersensitive passive detectors:GR-200A, MCP-N and TLD-500K. The results in the figure show that the new TL materials are capable to estimate very low doses in very good agreement with the active instrument. In general, TLDs show slight under-response when compare with HPIC, reaching 15% for MCP-N in the indoor station.

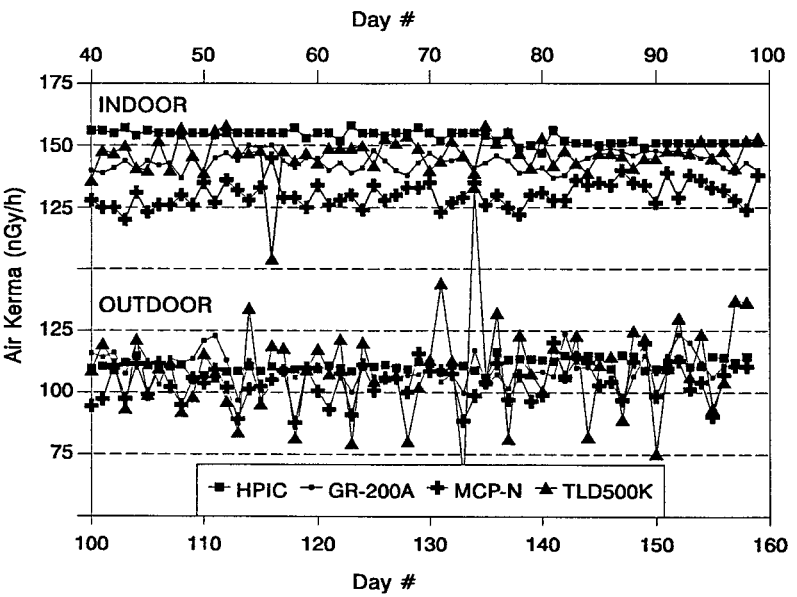

Significant difficulties on stability have been found for the aluminium oxide in the outdoor measurements. Due to its high sensitivity to UV and visible light, special efforts were paid to avoid any influence of this factor. However, noticeable decrease in response (up to 50%) were measured when the exposure period was longer than 48 hours. Similar results were obtained in the separate tests on additivity and stability.

f) Reliability of environmental TLD systems based on the new highly sensitivity phosphors.

In order to implement the use of hypersensitive phosphors in routine environmental TLD systems, some efforts have been paid at CIEMAT to analyze some practical aspects. Because of its increasing popularity, the study was focused on the LiF:Mg,P,Cu (GR-200) manufactured in China. In addition, this phosphor present an unusual and critical behaviour very dependent on the practical heating conditions. Dramatic loss of stability and important changes in sensitivity have been reported when these aspects were not well considered.

The following operative procedures have been considered: heating system (planchet and hot nitrogen), readout cycles, anneal and thermal initialization methods.

Several groups of ten completely new detectors were formed. Each group was intended to characterize one parameter, i.e., reader vs oven anneal. The groups were correspondingly prepared and irradiated to 80 μGy, which is the usual environmental monthly dose. This scheme was repeated up to fifty readouts for every different group.

The CIEMAT software codes to analyze the obtained glow curves has been employed and a comparison between the results from conventional and simplified glow curve analysis was also examined. To investigate the effect of the functional aspects on the TL features the following properties were studied: sensitivity, repeatability, stability of glow curve shape and residual dose.

One of the most discussed topic related to GR-200A is the maximum readout temperature. It seems to be well established that this temperature is the most critical point for that material. The limitation refers to the real detector temperature. Unfourtunately, commercial TLD readers cannot provide any accurate estimation of the "true" temperature in the detector. These instruments usually monitor the planchet or gas temperature. This creates practical difficulties to LiF:Mg,Cu,P.

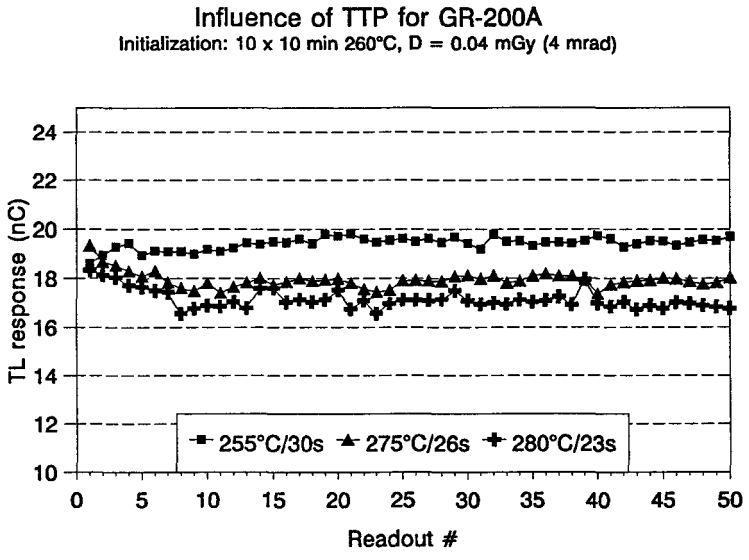

Figure 4 shows a stability study for several readout cycles. These data were obtained in an automatic loose chips TLD reader using hot gas heating and a "plateau" heating profile. When maximum temperature is greater than 260°C (as indicated by the reader), a decrease of 5% is noticed in the first five readouts. From this point a very stable sensitivity is maintained up to the end of experiment.

As a brief conclusion, the GR-200A phosphor can be successfully used as a routine environmental dosemeter employing the existing readers and ancillary equipment without any special requirement. However, some cautions concerning the maximum temperature in the reader and the oven anneal should be taken, preliminary tests are recommended in order to procure the best practical conditions, which are strongly dependent on the particular equipment.

References

1.- Glow Curve Analysis: A method Improving TTD Reliability. A.Delgado and J.M. Gomez Ros. Radiat. Prot. Dosim. 43, 143-146 (1992).

2.- Temperature Effects in LiF TLD-100 Based Environmental Dosimetry. A.Delgado, J.M. Gomez Ros and J.L. Muñiz. Radiat. Prot. Dosim. 45, 101-105 (1992).

3.- Confirmation of the Evolution of TLD-100 Glow Peaks 4 and 5 During Storage at Ambient Temperatures. A. Delgado, J.M. Gómez Ros , J.L. Muñiz, A.J.J. Bos and T.M. Piters. Radiat. Prot. Dosim. 47, 231-234 (1993).

4.- High Energy Response of Different Environmental TLDs. J.C. Saez Vergara, J.M. Gómez Ros and A. Delgado. Radiat. Prot. Dosim. 47, 327-330 (1993).

5.- A Glow Curve Analysis Method for Non-Linear Heating Hot Gas Readers. J.M. Gómez Ros, J.L. Muñiz, A. Delgado, L. Botter-Jensen and F. Jorgensen. Radiat. Prot. Dosim. 47, 483-488 (1993).

6.- An Intercomparison of Glow Curve Analysis Programs:I. Synthetic Glow curves. A.J.J. Bos, T. M. piters, J.M. Gómez Ros and A. Delgado. Radiat. Prot. Dosim. 47, 473-477 (1993).

7.- An Intercomparison of Glow Curve Analysis Programs:II. Measured Glow Curves. A. J. J: Bos, T.M. piters, J.M. Gómez Ros and A. Delgado. Radiat. Prot. Dosim. 51, 257-264 (1994).

8.- Medida de Dosis Absorbidas en el Rango del uGy con LiF:Mg,Cu,P (GR-200). A. Delgado, J. M. Gómez Ros and J.L. Muñiz. Radioprotección 1, 5-13 (1994).

9.- On the Peculiarities of Peak 4 in LiF TLD-100. A. Delgado, J.L. Muñiz and J.M. Gómez Ros. Radiat. Measurements 23, 693-701 (1994).

10.- Intrinsic Self-Dosing and Long Term Stability of LiF TLD-100 and GR-200 detectors. A. Delgado, J.C. Saez Vergara, J.M. Gómez Ros and A. Romero. Radiat. Prot. Dosim. 58, 211-216 (1995).

11.- Computerised analysis of LiF GR-200 TL Signals. Application to Dose Measurements in the uGy range. A. Delgado, J.M. Gómez Ros and J.L. Muñiz. To be published in Radiat. Prot. Dosim. (1995).

12.- Recent Advances in LiF:Mg,Ti and LiF:Mg,Cu,P Environmental Dosimetry. A. Delgado. Invited talk, 11th Solid State Dosimetry Conference (Budapest July 1995).

Other six communications were presented in the 11th SSD Conference and one more in the Conference on Radiation Protection and Dosimetry (Orlando, USA October 1994).

Head of project 4: Dr.Pernička

II. Objectives for the reporting period

1. Installation of the CIEMAT's computerized evaluation method on the Solaro TLD Processor and a software development for the TL glow curve analysis. The software testing on reference TL glow curves.

2. Theoretical and experimental studies of environmental radiation fields and their variations using Monte Carlo modeling and measurements with active detectors including a NaI(Tl) spectrometer. Response calculations for different detectors in these fields.

3. Participation in intercomparison activities organized by PTB and Risoe groups. Organization of intercomparison experiments in the Czech Republic.

III. Progress achieved including publications

1.1. CSOL - a software package for the Solaro TLD Processor

In a first phase, a package DEKO was developed for deconvolution of TL glow curves (Pernička and Šlachta, 1994). The main program is written in Fortran and besides a minimization system MINUIT (from CERN) it is also using a program CONV. This was written to convert data stored in the Solaro's output files *solinfo.dat* and *solindx.dat* into an ASCII format so that they can be handled by a number of commercial as well as user written packages. The software allows analysis of even very complicated TL models. Unfortunately, it is relatively slow for practical applications. In the next step, the whole concept of a TL glow curve analysis by the Solaro TLD processor was thus changed.

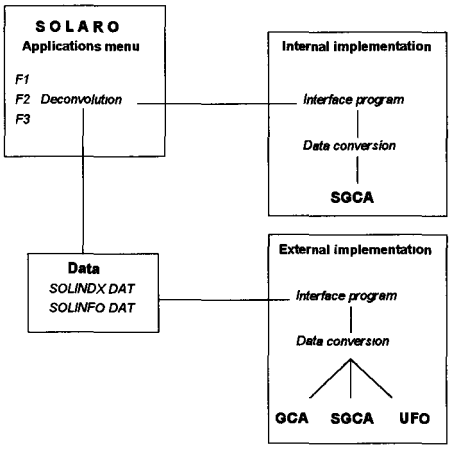

Fig.1. Flow diagram of software arrangement for the Solaro system

A software package CSOL was written (Linh and Pernička, 1994; Linh and Pernička, 1995) which can be used to analyze data from the Solaro. It is based on two main procedures SGCA and GCA developed at CIEMAT and an optimization procedure UFO. A flow diagram of software arrangement for the Solaro system is given in Fig.1. Two different solutions of a glow curve evaluation were designed. One is intended for application on low efficiency computer systems and it is using a simple SGCA procedure (*internal implementation*). Second solution was designed for systems with a higher computing efficiency, quite often for use on external computers (*external implementation*). Communication between the Solaro system output and the glow curve analysis programs are realized by means of an interface procedure which is designed according to a pull down menu concept. It enables an easy and straightforward manipulation with all operations through a short introduction in the HELP menu and complete prompts accompanying each action. A program itself displays two autoexplicative screens consisting of different menus to select glow curves for a data

conversion into ASCII data files or to evaluate them with the aid of other programs for glow curve analysis. The CSOL was designed to run on IBM PC/AT and true compatibles. A math coprocessor, respectively a virtual RAM disk, are certainly useful for acceleration of calculations but they are not essential.

1.2. Use of UFO procedure

The Universal Functional Optimization (UFO) procedure used in CSOL is an application of the UFO system that was originally written in NPI Prague. A TL glow curve analysis is based on minimization of the sum of squares for a selected model of the thermoluminescence process. An optimization method used for this purpose is the *hybrid Gauss-Newton method* and *variable metric method with a trust region realization.*

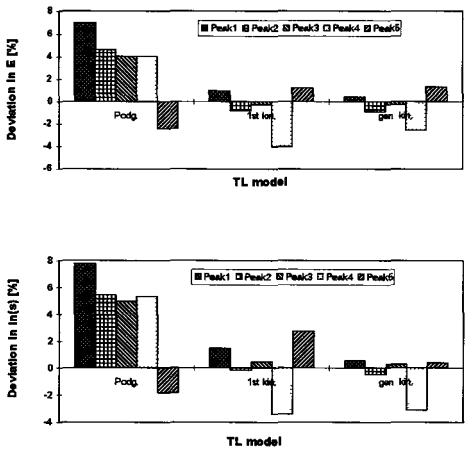

Fig.2. Deviation in activation energy, E, and frequency factor, ln(s), for different peaks and models used

For evaluation of single peak glow curves three well known models of a TL kinetics (Podgorsak model and the models of first-order and general-order kinetics) are used. The multiple peak glow curves are analyzed using a linear combination of the single peak glow curves. Synthetic as well as experimental test glow curves have been analyzed.

A relative deviation of the activation energy, E, and the frequency factor, ln(s), obtained by the UFO procedure from "true" values of these parameters for the experimental glow curve with 5 peaks are given in Fig.2. One can see a good agreement between the UFO and the true values especially for the first-order and general-order kinetic models. An analysis of other test glow curves (Pernička and Linh, 1995) gives results similar to the results from the GLOCANIN project. The main advantage of the UFO is its modularity which enables an easy definition of a new model and/or a new optimization method.

2.1. Theoretical and experimental studies of environmental radiation fields

Spectral distributions of the air kerma and the ambient dose equivalent at a standard height of 1 m above the soil were calculated for homogeneously distributed ^{40}K and radionuclides from the Uranium and Thorium series, ^{222}Rn and daughters homogeneously distributed in the open air, on the ground and in the soil air, ^{137}Cs deposited on the ground and ^{131}I distributed homogeneously in air. The Monte Carlo code MCNP, version 4A, was used for that purpose. The spectra for naturally occurring radionuclides were further used for calculation of different spectral distributions for a soil composition corresponding to different bedrock. Examples of the calculated differential air kerma for the soil with a limestone composition is given in Fig.3. One can see contributions from different gamma lines of naturally occurring radioisotopes as well as from the scattered radiation. The cumulative distribution gives an immediate indication about the relative contributions for different parts of the energy spectrum thus enabling rough

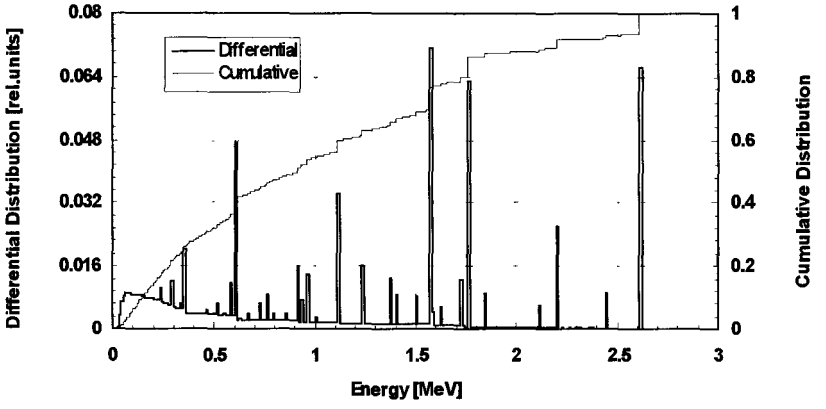

Fig.3. Calculated differential and cumulative kerma distribution at 1 m height above the ground for limestone

judgment of the effect on the response of a particular detector. A slightly higher low energy part for the ambient dose equivalent was obtained (Pernička and Klusoň, 1995).

Spectral measurements of a photon fluence were done at 10 test sites using a 3"x3" NaI(Tl) spectrometer (Klusoň *et al*, 1994; Klusoň and Pernička, 1994). The test fields were given code names TF1-10 and they correspond to different kinds of the environmental photon fields. The fields TF1, TF2 and TF5 are the remedied places with waste from the uranium industry, fields TF3 and TF4 are on the site of a former radium factory. Typical natural radiation fields in the Czech Republic are represented by the fields TF6 and TF7. Finally, the radiation field created by Rn and daughters in the air is represented by the test fields TF8, TF9 and TF10.

An example of the measured kerma distribution for the test field at the site remedied after

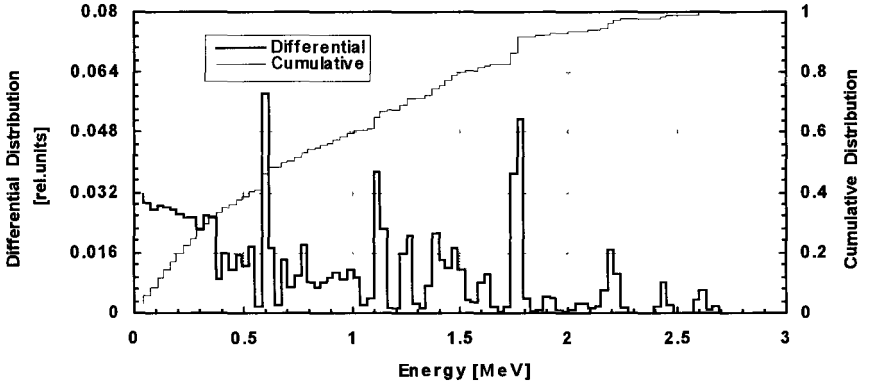

Fig.4. Measured kerma distributions for the test field TF5

uranium industry is given in Fig. 4. Measurements did show a high degree of inhomogeneity

with respect to the air kerma. They also indicated that the main source of the air kerma comes from Rn and daughters supplied to a top layer of the soil from larger depths rich of the gas.

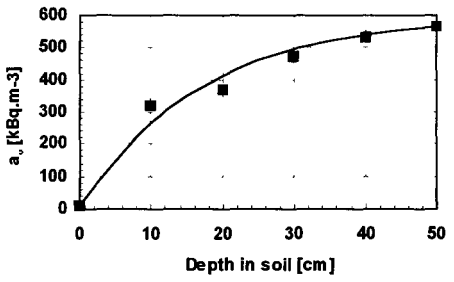

Fig.5. Depth profile of ^{222}Rn in soil

Depth profiles of the soil Rn were measured using Lucas cells and standard sampling procedure between January and April, 1995 (total 7 samplings). During this time period weather conditions varied with temperatures ranging from -12°C to +10°C, occasional rain and snow together with a different wind velocity. Samples were taken from depths between 10-50 cm at different sampling sites. A standard deviation of a single measurement was typically 5-10%. Measurements did not show any influence of weather parameters. This was less than or comparable with uncertainties of the measurements. A depth profile of the soil Rn averaged over the sampling period is given in Fig.5. Experimental points were fitted by a model curve. This was used to describe a probability density function of the activity distribution for modeling the radiation field TF5.

2.2. Detector responses to the environmental photon radiation

Theoretical and experimental spectral distributions were used to predict behavior of different instruments in these fields. Detector responses to photon radiation relative to the response to the ^{137}Cs radiation were calculated for a set of detectors (Pernička and Klusoň, 1995). The high pressure ionization chamber RSS-112 was considered together with the plastic scintillator NB 3201, the proportional counter FHZ 600A, a GM system with two tubes ZP 1221/01 and ZP 1313 and the thermoluminescence detector LiF:Mg,Cu,P. The results for different photon

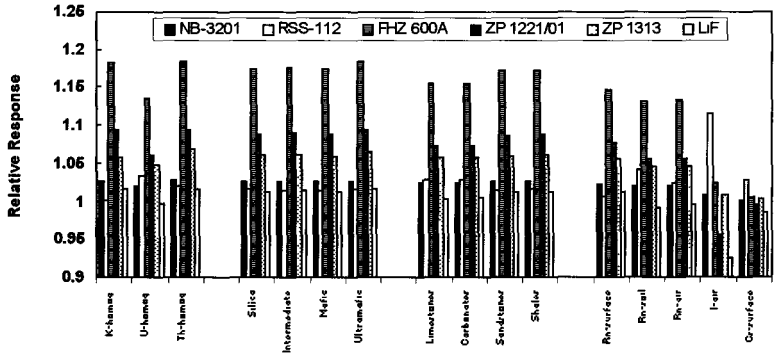

Fig.6. Relative response of detectors calibrated in air kerma

fields are given in Fig.6. One can see a smoothing effect of a wide photon spectrum on the resulting responses and the fact that a major part of the air kerma is due to photons with relatively high energies. The small differences in the response for naturally occurring

radionuclides are further smoothed in the case of the soil from different bedrock. One of the conclusions we can make from these calculations is that any of these instruments can be used for measurement of the air kerma from the natural radiation once its relative response to one of the natural radiation fields is established. The situation is slightly different for the fields with a narrow energy spectrum and/or special source geometry. This is seen for example from the values of the response obtained for ^{131}I distributed in air. The detectors with larger response variations are more likely to under or overresponse in these fields.

Calculated responses of the detectors to the ambient dose equivalent show similar trends as in the case of the response to the air kerma. The best compensation is achieved for the RSS-112 ionization chamber. It is natural as the response per unit air kerma for this detector matches a H^*/K_a - dependence better than other systems.

The detector responses calculated from measured differential distributions of the air kerma for discussed test fields are given in Fig.7. The results are slightly different than those expected

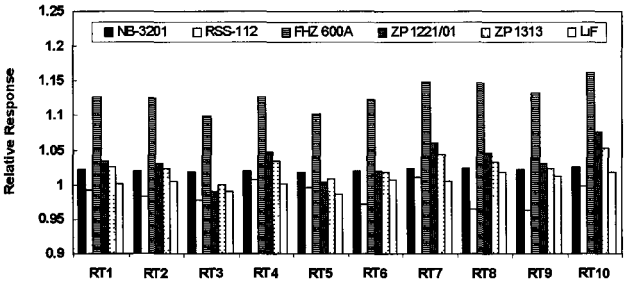

Fig.7. Relative response of detectors from spectral measurements

from theoretical calculations. Further analysis has revealed this is mainly due to more averaged experimental spectra with wider energy bins (in our case 30 keV). Other conclusions are the same as in the case of results for the theoretical spectra. This supports ideas about the detector's behavior derived from the theoretical analysis of the natural environmental fields.

2.3. Response of detectors to cosmic radiation

Theoretical and experimental studies were done on a response of detectors at cruising altitudes of commercial aircraft. An attempt was also made to establish a conversion factor between the measured absorbed dose in air and the ambient dose equivalent. Two systems, a high pressure ionization chamber (HPIC) and a plastic scintillation detector (PSD) were studied. Our experiments in a radiation field behind the shielding of a 600 MeV proton accelerator indicate negligible sensitivity of HPIC and PSD to neutrons with energy distribution such that about 40% of the dose equivalent comes from neutrons with energies between 20-350 MeV. This supports the idea that these instruments measure just the ionizing part of cosmic radiation.

The main contribution into air ionization at investigated flight levels comes mainly from electrons and protons. Contributions from other types of radiation were neglected in a calculation of relative responses for the HPIC and PSD to the ionizing part of cosmic radiation. The results obtained with consideration of theoretical charged particle spectra, show that the relative response (normalized to the response for Cs-137) to ionizing part of cosmic

radiation of these detectors is R(HPIC) = 1.091 and R(PSD) = 0.882. The 20% enhancement due to the transition effect for the HPIC and particle fluxes and spectral distributions for middle latitudes were considered during calculations. The ratio of these figures largely agrees with our experimental findings. Further, the value of 1.25 $Sv.Gy^{-1}$ for a conversion factor between the measured absorbed dose to air and the ambient dose equivalent for an ionizing component of cosmic radiation was established (Michalik *et al*, 1994). This was used during an analysis of experiments to establish a dose to aircrew members (Spurný *et al*, 1993). Beside this application, the results can be partly used for predictions of the instrument's behavior and the dose equivalent due to cosmic radiation to populations at higher living altitudes.

3.1. Participation in intercomparison activities organized by PTB and Risoe groups

A high pressure ionization chamber RSS-112 made by Reuter Stokes (USA), plastic scintillators NB3201 and NB3202 made by Tesla (CR) and NaI(Tl) spectrometry systems with detectors from SM&D (CR) and Bicron (USA) were used during intercomparison measurements organized by PTB and Risoe groups. An evaluation of the results from these joint experiments show a good agreement with the results achieved by other participants (Pernička and Klusoň, 1994; Klusoň and Pernička; 1994; see also reports of PTB and Risoe groups).

Measurements at the UDO laboratory enabled the establishment of an inherent background of our NaI spectrometer. A spectral distribution of the kerma rate (measured inside a shielding box) from the inherent background and a possible low component from the natural radiation shows that a large part of the air kerma rate comes from ^{40}K. This can be due to the radionuclide imbedded in construction material of the detector (glass of a PMT) or it can be the effect of stray radiation from the radionuclide distributed in the surrounding salt. Before a final decision, further experiments and theoretical considerations are needed. At present, this measurement clearly indicates that the background inside a shielding at the UDO laboratory is of the order of 0.5 $nGy.h^{-1}$ or less.

If we accept a hypothesis that a signal measured by the spectrometer at UDO is the inherent background itself we can probably explain higher values of measured responses to cosmic radiation on lake Orlík (Pernička *et al*, 1995). Preliminary analysis of measurements shows that about 12-15% of the measured signal was from ^{222}Rn and daughters distributed in the air. A similar effect was observed during experiments at Risoe.

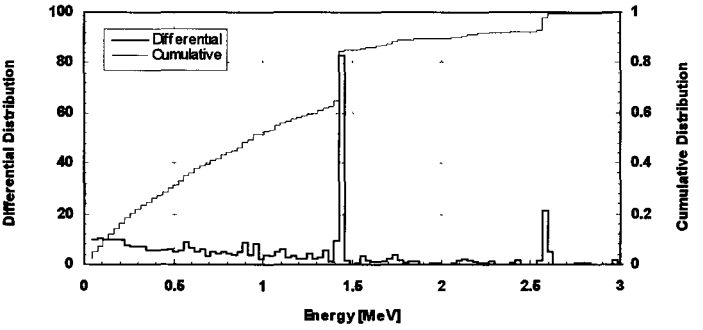

Fig.8. Measured differential and cumulative kerma distribution at 1 m height above the ground at the NEMS station

The spectrometry method enabled measurement of spectral distribution of kerma rates for source to detector geometry used during the shadow-shield and free-field calibrations at Risoe. This information can be used for spectral adjustments of the energy response in the case of detectors with larger response variations. Additionally, the spectral distribution of the background radiation at the NEMS station was established. The differential as well as cumulative distribution of the background kerma rate at this place is given in Fig.8. One can see that a substantial part of the kerma rate comes also from potassium.

Generally, these experiments have helped to improve the standard of measurements in the NPI Prague (Pernička and Klusoň, 1994). They also contributed to a better understanding of general characteristics of the radiation fields at calibration facilities of other countries, namely the UDO laboratory at the Asse salt mines and the NEMS station at Risoe.

3.1. Organization of intercomparison experiments in the Czech Republic

Selected sites with varying terrestrial and cosmic components of the environmental radiation field have been measured using different instruments. A ratio of the terrestrial to cosmic component was established (Pernička *et al*, 1995) and all the sites were characterized by a spectral distribution of the terrestrial radiation (Pernička and Klusoň, 1995). The sites have been prepared for the planned intercomparison measurements. The intercomparison was not undertaken which had been a joint decision of the group made during the coordinating meeting in Prague.

Publications

Klusoň J., Čechák T., Pernička F. *Dosimetry of External Photon Fields.* In Proc. of the CTU Seminar 94, CTU Prague, January 3-4, (1994)

Klusoň, J., Pernička, F. *Using of the Spectral Information in Environmental Photon Fields* Measurements. Presented at the XVIII. Radiohygienic Days, Jáchymov (Czech Republic), November 20-22 (1994), (in Czech; an English abstract available)

Linh H.Q., Pernička F. *** *TLD-Deconvolution* ***. *An Improved Software Package for Solaro TLD Reader.* Report IRD AS CR, IRD-379/94, Prague, (1994)

Linh H.Q., Pernička F. *CSOL-An Improved Software Package for The Solaro TLD Processor.* Radiat. Meas. (submitted for publication in 1995)

Michalik V., Pernička F., Spurný F. Nguyen V.D. *Some Aspects of the Exposure of Aircraft Crew Members to Cosmic Radiation*, Workshop on Individual Monitoring of Ionizing Radiation: The Impact of Recent ICRP and ICRU Publications, Villigen, May 5-7, 1993, published at Radiat.Prot.Dosim., **54**, pp.255-258 (1994)

Pernička F. *Intercomparison of Environmental Gamma Dose and Dose Rate Meters in the ČSSR 1990.* Presented at the 110.PTB Seminar, Braunschweig, November 30-December 01, (1993) (submitted for Proceedings)

Pernička F., Šlachta V. *DEKO-Program for Deconvolution of TL Glow Curves.* Report IRD AS CR, IRD-378/94, Prague, January 10, (1994)

Pernička F. *Dosimetry of Cosmic Radiation in the Earth Atmosphere.* A Final Report of AS CR Grant No.33551, IRD AS CR, Prague (1994), (in Czech)

Pernička, F., Klusoň, J., Prouza, Z. *Calibration of Instruments Used for Measurements of Doses of External Radiation in Environment.* Presented at the XVIII. Radiohygienic Days, Jáchymov (Czech Republic), November 20-22 (1994), (in Czech; an English abstract available)

Pernička, F., Spurný, Z., Lauterbach, U., Peßara, W., Strachotinsky, C., .Kažimír, D. *Sázava Intercomparison of Environmental Gamma Dose and Dose Rate Meters.* Radiat.Prot.Dosim. (submitted for publication in 1995)

Pernička, F., Klusoň, J. *Variations of Natural Radiation Background and Their Effect on Detector Response.* Presented at the International Symposium on the Natural Radiation Environment, Montreal (Canada), June 5-9 (1995), (full paper will be published in Proceedings - journal: Environment International)

Pernička, F., Linh, H.Q. *Use of UFO for TL Glow Curve Analysis.* Presented at The 11th International Conference on Solid State Dosimetry, Budapest (Hungary), July 10-14 (1995), (full paper will be published in Proceedings - journal: Radiat. Prot. Dosim.)

Spurný F., Obraz O., Pernička F., Votočková I. (1993) Dosimetric Characteristics of Radiation Fields on Board of CSA Aircraft as Measured with Different Active and Passive Detectors. Radiat. Prot.Dosim. **48,** pp. 73-77

Head of project 5: Dr. Michael P. R. Waligórski

II. Objectives for the reporting period

In the frame of contract following tasks were undertaken:

1. Development of an optimum procedure for producing sintered MCP detectors
2. Development of a new model of a compact computerized TL reader-analyzer
3. Field tests of detectors, readout system and measurement techniques
4. A systematic multi-parameter survey of the effect of dopant composition on the dosimetric properties of LiF:Mg,Cu,P phosphor (work in progress).
5. Design and development of an automatic reader specially suited for monitoring environmental dose rates (work in progress).

III. Progress achieved including publications

The Institute of Nuclear Physics INP joined CEC Contract F13PC920018 in January 1994, with a formal agreement signed in April 1994. The main objective of INP's contribution to the project was to improve the accuracy and sensitivity of TL-based methods of assessing environmental dose rates. To this end, over the period April'94 - July'95, ultra-sensitive LiF:Mg,Cu,P detectors of different Mg, Cu, and P composition were synthesized, developed, investigated and optimised at INP. Batches of INP material were distributed to all collaborators. A new model of a compact TL reader-analyzer was designed and tested at INP. Intercomparison measurements and field measurements have demonstrated the suitability of INP material and measuring equipment and techniques for environmental monitoring with superior sensitivity, permitting daily or even hourly dose assessment. Work in progress at INP concerns a systematic survey of dosimetric properties of LiF:Mg,Cu,P phosphor with respect to dopant concentration, in which a promising LiF:Mg,Cu,P phosphor may have been discovered, and development of an automatic TL system (TL cards and reader) designed specifically for large-scale environmental monitoring using LiF:Mg,Cu,P.

1. Development of an optimum procedure for producing sintered MCP detectors

A sintered TL detector of type MCP (LiF:Mg,Cu,P) is obtained as a result of the following production stages:
- synthesis of LiCl or LiOH into LiF
- activation of Mg, Cu and P at high temperature
- mechanical operations on activated LiF powder (washing, sieving, pill pressing)
- sintering pressed pills at an elevated temperature

Over the reporting period the two most important stages: activation and sintering have been improved and optimised. Special high-temperature furnaces with exchangeable platinum crucibles were constructed. The process of activation takes place at a high temperature, whereby Mg, Cu and P activators enter the volume of liquid LiF, and is highly sensitive to many factors, such as temperature, period of activation and neutral gas (argon) flow rate. Special stands allowing these parameters to be carefully and reproducibly controlled, were constructed. Using the present manufacturing technique, uniform batches of up to 2000 LiF:Mg,Cu,P detectors (of 1 SD sensitivity spread in the range 2.5-3.5 % per batch) can be obtained in a consistently repeatable manner. Each participant received 50 pellets of MCP-N (natural LiF:Mg,Cu,P) of dopant composition 0.05 mol% Cu, 0.2 mol% Mg and 1.25 mol% P.

2. Development of a new model of a compact computerized TL reader-analyzer

The design of a compact TL reader-analyzer suitable for field measurements was laid out and construction of the prototype completed in April 1994, preceding the field intercomparison at Riso. The reader, RA'95, exploits the heated planchet principle, well-tested in previous INP reader designs, a Peltier-cooled PM system (thus obviating the need for tap water supply for cooling) and is fully microprocessor-controlled, enabling digital internal and external control and data transfer via any IBM/PC DOS - standard computer. Combined with a lap-top computer, the reader is light, compact and can readily be used in field conditions where mains supply (220V) is available.

In order to accommodate for the extreme temperature sensitivity of LiF:Mg,Cu,P detectors, it was found necessary to design special digital control and temperature compensation of the heater temperature control. Software was implemented to perform simple analysis of glow-curves, exporting data in ASCII format, etc. The mechanical and electronics parts of the RA'95 reader were manufactured under contract by a daughter company of INP, Microlab.

3. Field tests of detectors, readout system and measurement techniques

Participation in the international intercalibration experiment, Riso 1994

In the period 12-16 June 1994 Mr.P. Bilski and Mr. M. Budzanowski took part in the EU intercalibration experiment organized by the Riso National Laboratory at Roskilde, Denmark. The INP team participated in two experiments using passive TL detectors to measure natural doses. In the first experiment the cosmic component of natural background radiation was determined. Eight detectors packed in mini-phantoms (5mm PMMA) were placed inside a plastic chamber located at the end of a wooden pier at Roskilde Fjord (Riso Cosmic Station) and exposed for three days The actual dose rate was monitored over this time by an ionization chamber. The dose rate evaluated by the ionization chamber was about 40 nGy/h. Results

obtained with MCP-N and GR-200 detectors are presented in Table 1. The difference between values measured by LiF detectors and by the ionization chambers is expected and confirms results of earlier experiments.

Detector type	Measured dose rate [nGy/h]	Uncertainty (1SD) [nGy/h]
MCP-N	32.1	1.8
GR-200	32.7	2.4

Table 1. Dose rates of the cosmic component of natural background evaluated by MCP-N (INP) and GR-200 detectors (8 detectors of each type exposed)

The second experiment was performed in order to evaluate the shortest time required to measure natural background radiation dose-rates. In this case detectors were located on the test field and suspended 1m above ground level. Results obtained after 3.5 and 16 hours of exposure (8 detectors exposed at one time) and uncertainties are shown in Table 2. The results show that exposure times of a few hours are sufficient to measure natural background dose-rates using ultra-sensitive LiF:Mg,Cu,P (MCP-N) detectors. The glow-curve for MCP-N detector after 1 day exposure in environment is shown in Fig. 1.

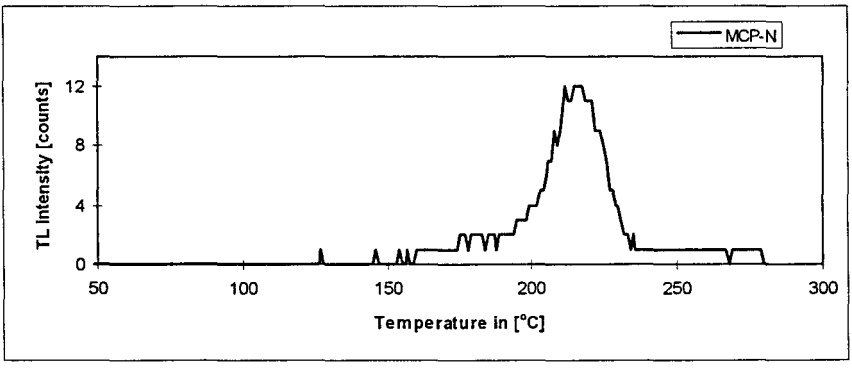

Fig. 1. Typical glow-curve for LiF:Mg, Cu, P after 24 h exposure to cosmic and terrestrial radiation.

Total time of exposure [h]	Measured dose rate [nGy/h]	Uncertainty (1SD) [nGy/h]
3.5	68.5	13.8
16	71.1	6.8

Table 2. Natural background dose rates measured using MCP-N detectors after short-term exposures (8 detectors exposed together).

Results of this intercomparison confirm that GR-200 and MCP-N detectors can be well applied for a short term monitoring of environmental doses.

Measurements of terrestrial and cosmic ray gamma dose rates at the INP

The aims of this experiment, performed outdoors at the INP over a period of 3 months in 1995 were as follows:
- to measure environmental air-kerma rates in field conditions and compare daily, weekly and monthly readouts
- to compare results obtained using MCP-N and GR-200 detectors;
- to test the stability of detectors after multiple use
- to control self-background stability after multiple readout
- to test detector response after post-readout annealing in TL reader against oven annealing.

A batch of 700 MCP-N detectors was produced (dispersion of sensitivity better than 3.5% at 1 SD), individually calibrated and divided into several groups. Chinese GR-200 detectors were also used. Detectors, placed in 5 mm-thick mini-phantom PMMA holders, were exposed 1 m above ground at two outdoor grass sites on INP premises. Detectors were collected daily, weekly and monthly. Detectors in each time-group were either only read out in the reader or read out in the reader and annealed in an oven (240 deg. C over 10 mins.). A 3 step heating was applied for the readout: (Stage I): 5 sec at 150 deg. C, followed by 15 (Stage II) and 3 sec (Stage III). at 240 deg. C. Calibration of detectors was performed with a Co-60 source.

Results show that doses measured with MCP-N detectors over a longer exposure periods as a one week or a one month agree well with the sum of the obtained daily doses. It was also demonstrated that both MCP-N and GR-200 detectors could be successfully applied in environmental monitoring for such exposure periods. However, using identical handling procedures, terrestrial doses measured with GR-200 were systematically about 8% higher than those obtained with MCP-N (see Fig.2). This effect needs some further investigation. No significant difference in results for oven and reader annealing was observed with the exception of an 9% increase of MCP-N self-dose for reader annealing. The present investigations also demonstrated the need for a precise control of readout parameters (temperature readout 240 ±5 C) in order to maintain LiF:Mg, Cu,P stability and sensitivity

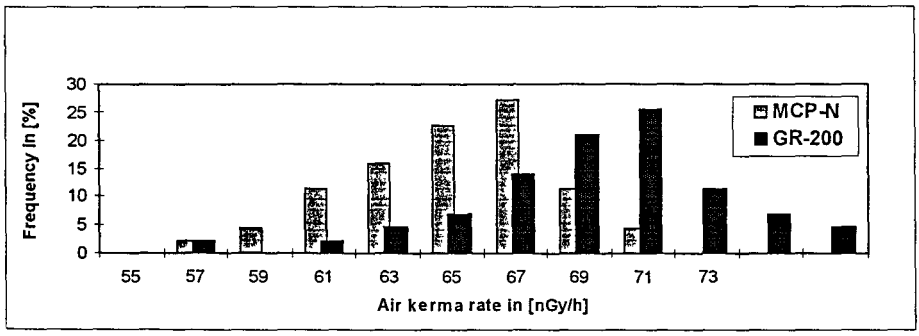

Fig. 2. The air kerma frequency distribution measured with MCP-N and GR-200 detectors annealed in reader.

4. A systematic multi-parameter survey of the effect of dopant composition on the dosimetric properties of LiF:Mg,Cu,P phosphor (work in progress).

Aims

The aims of this experiment which will be completed later in 1995/96, are

a) to find, in a systematic manner, Mg, Cu and P dopant concentrations at which the glow curve of the LiF:Mg,Cu,P phosphor shows optimum properties, i.e.:

- high sensitivity (to photon)
- low contribution of high-temperature peaks in the glow-curve

b) to study the role of individual activators in the thermoluminescence of LiF:Mg,Cu,P

Sample preparation

Using high-purity chemical reagents, a large (800 g) uniform portion of LiF was synthesized. Doping was carried out by melting LiF in the presence of activators in the atmosphere of argon in a furnace specially constructed for this purpose. In all, 120 sample of activated LiF were prepared at about 80 different concentrations of magnesium, copper and phosphorus. Samples with dopant concentrations believed to be more promising were prepared twice. All LiF compositions were turned into sintered pellets using another furnace specially constructed for this purpose.

Measurement procedure

Detectors were tested after annealing at 240 or 270 °C. TL glow curves were measured at a heating rate of 5 °C/sec, maximum temperature 350 °C, after 2 mGy irradiation with a Cs-137 source. To study the influence of the sintering process on the TL signal, identical measurements were performed using non-sintered material in powder form.

Preliminary results

Among many parameters determined for each measured glow-curve, particular attention is devoted to the amplitude of peak 4 (main dosimetric peak) and to the integrated area of high-temperature peaks, defined as the sum of TL pulses over the temperature range T4+30 °C to 350 °C, where T4 is the temperature at which the maximum of peak 4 occurs.

A particularly interesting result of this investigation is the discovery of a new range of activator concentration, distant from that used so far, at which LiF appears to demonstrate clearly enhanced properties (at least, with respect to glow curve parameters). The concentrations in the new region are between five and ten times less for copper (0.01÷0.005 mol% against 0.05 mol%) and two times less for magnesium (0.1 mol% against 0.2 mol%) ; at the same time all parameters of the glow curve appear to be better in the new region (higher sensitivity for peak 4, smaller high-temperature peak contribution). The results of optimization investigations are schematically presented in Fig. 3.

This material appears to be extremely promising, but requires further investigations, with respect to temperature stability, background, etc.

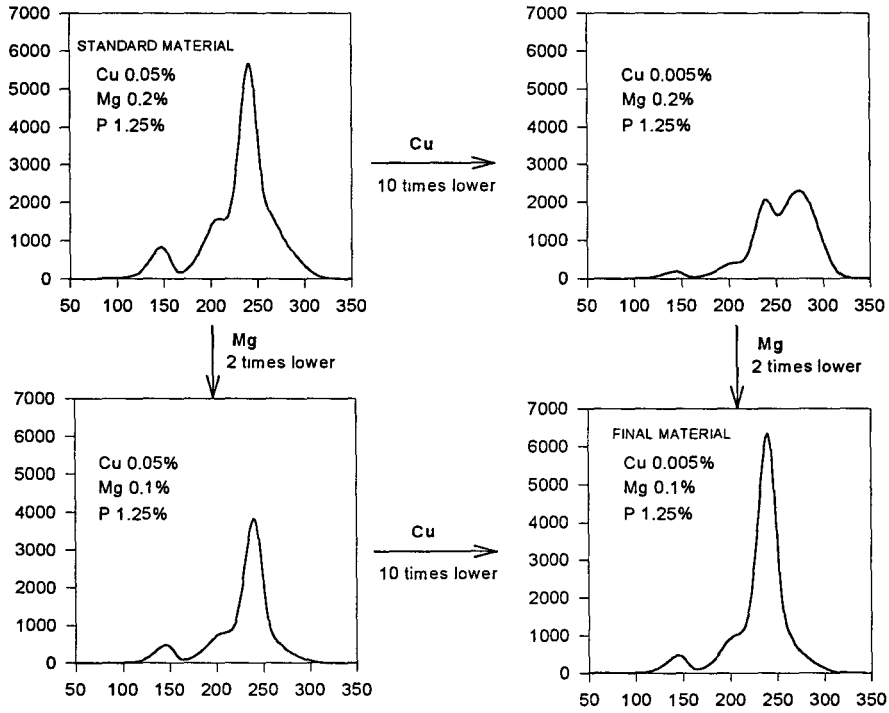

Fig. 3. Schematic presentation of the final results of dopant composition investigations.

As for the general role of the three different activators in LiF:Mg,Cu,P, it appears that:
- Mg is the main activator. At zero Mg concentration only trace luminescence is observed, unlike the case for samples with zero Cu and P concentrations.
- The dependence of TL intensity on P concentration is a step function; rising by an order of magnitude as the concentration of P exceeds 0.15 mol%.
- Cu and Mg act together, where Cu appears to act as a mediator, reducing the high-temperature peaks caused by overabundance of Mg.

5. Design and development of an automatic reader specially suited for monitoring environmental dose rates (work in progress)

Basing on our experience gathered with the prototype of the portable RA'95 TL reader-analyser and on our past experience in developing large-scale environment monitoring using MTS (LiF:Mg,Ti) detectors placed in automatic reader cards, we are designing an automatic TL reader specifically for reading MCP (LiF:Mg,Cu,P) detectors placed in reader cards. As we have learned from the RA'95 experience, particular attention must be paid to careful temperature control within readout cycles and post-readout annealing. According to our designs, the automatic reader should be capable of reading up to 500 3-detector cards per day,

should be fully computer-controlled and software-interfaced to standard data management programs, such as e.g. MS EXCEL or MS ACCESS in the WINDOWS environment. A suitable object-oriented data base interface for the automatic reader is currently under development.

PUBLICATIONS

M. Budzanowski (1), B. Burgkhardt (2), P.Olko (1), W. Pessara (3), and M.P.R. Waligorski(1,4) *LONG-TERM INVESTIGATION OF SELF-IRRADIATION AND SENSITIVITY TO COSMIC RAYS OF TL DETECTOR OF TYPESTLD-200,TLD-700, MCP-N, AND NEW PHOSPHATE GLASS DOSEMETERS.* (submitted to Radiat. Prot. Dosim. 1995)

M. Budzanowski (1), P. Bilski (1), L. Boetter-Jensen (2), M. Delgado (3), P. Olko (1), J.C. Saez-Vergara(3) and M.P.R. Waligorski (1,4) *COMPARISON OF LiF:Mg, Cu, P (MCP-N, GR-200) AND Al203 (TLD500) TL DETECTORS IN SHORT-TERM MEASUREMENTSOF NATURAL RADIATION* (submitted to Radiat. Prot. Dosim. 1995)

P. Bilski, M. Budzanowski and P. Olko *A SYSTEMATIC EVALUATION OF THE DEPENDENCE OF SENSITIVITY AND GLOW-CURVE STRUCTURE ON DOPANT CONCENTRATION AND THERMAL TREATMENT IN LiF:Mg,Cu,P* (submitted to Radiat. Prot. Dosim. 1995)

P. Olko *MICRODOSIMETRIC INTERPRETATION OF THERMOLUMINESCENCE EFFICIENCY OF LiF:Mg,Cu,P (MCP-N) DETECTORS FOR WEAKLY AND DENSELY IONIZING RADIATIONS* (submitted to Radiat. Prot. Dosim. 1995)

M.P.R. Waligórski(1,2), K. Skarzyńska (3), E. Zawisza (3), E. Ryba (1), M. Jasińska (1) and K. Kozak (1), *ENVIRONMENTAL RADIOMETRY AROUND COAL MINING WASTES USING MCP (LIF:Mg,Cu,P) DETECTORS AND GAMMA-RAY SPECTROMETRY* (submitted to Radiat. Prot. Dosim. 1995)

J.C. Saez-Vergara, A.M. Romero, P. Olko and M. Budzanowski THE RESPONSE OF THE NEW HYPERSENSITIVE THERMOLUMINESCENCE MATERIALS TO HIGH ENERGY PHOTONS (0.6-6.0 MeV) (submitted to Radiat. Prot. Dosim. 1995)

INSTYTUT FIZYKI JĄDROWEJ
im. Henryka Niewodniczańskiego
SAMODZIELNA PRACOWNIA
OCHRONY PRZED PROMIENIOWANIEM
ul. Radzikowskiego 152
31-342 Kraków

Principal Investigator for INP Michael P.R. Waligorski, Ph.D.
Head, Health Physics Laboratory,
The Henryk Niewodniczański
Institute of Nuclear Physics, Kraków, Poland

Head of project 6: Dr. M. Osvay

II. Objectives for the reporting period

1. Determination of TL properties of new, high sensitive Al_2O_3:C single crystal dosemeters for environmental monitoring purposes (handling and read out parameters, reproducibility, lowest detectable dose, UV-sensitivity, fading at combined heat cycles, self dose). Participation in CEC intercomparison at the Risø Natural Environmental Monitoring Station.
2. Development of a microprocessor controlled portable TLD reader for in situ environmental dose measurement.

III. Progress achieved including publications

1. Application of Al_2O_3:C TL dosemeters for environmental dosimetry (Margit Osvay, Institute of Isotopes)

1.1 Introduction

Much effort is devoted to studying the TL properties of the newly developed Al_2O_3 single crystal doped with C and prepared in Russia (1-2).

One of the important parameters of this material is that it exhibit an increased sensitivity compared with common TL dosemeters (eg. TLD-100).

The aim of this work was to investigate the handling and read out parameters of this high sensitive aluminium oxide TL dosemeters suitable for environmental radiation measurements and to prepare the dosemeters for participation at the Natural Environmental Monitoring Station on the intercomparison experiments at Risø.

The following TL properties were investigated:
- annealing procedure in order to optimization of reproducibility
- background of dosemeters during long term store to get the lowest detection limit
- fading characteristics at various temperature and in case of combined heat cycle
- linearity of dosemeters as a function of dose
- light and UV sensitivity of dosemeters
- self dose during store at a low background place

1.2 Experimental

Measurements were carried out on Harshaw 2000 AB and TLD-04 (developed and produced by Central Research Institute for Physics, Hungary) TL readers at a heating rate of 10°C/s.The intercomparison experiments were made by the TL reader developed for TL dating at Risø. The dosemeters were linearly heated to 300°C, the dosimetry peak was integrated within the interval of 120°C to 250°C.

Fading properties were studied using an ultrathermostat at various temperature as: -25, 0, 20 and 40°C.

All measured data were calculated as the average of 5 dosemeters reading. During irradiation and handling the

dosemeters were kept in dark polyethylene foil to exclude undesirable light exposure.

Self dose measurements and room temperature fading investigations were performed at a low background place, in an iron shield, 20 cm thick (internal dimensions: 2m x 1m x o.6m). The dose rate within the shield is 20 nGy/h as measured with a high pressure ionisation chamber.

For TL measurements the dosemeters were exposed using a calibrated ^{90}Sr-^{90}Y source.

The UV source for the PITL measurements was a Swiss Camag type low pressure UV lamp (0.25W) with filters to give 254 nm and 366 nm monochromatic light.

1.3 Results and Discussion

Reproducibility of Al_2O_3:C dosemeters on the basis of repeated (5 times) irradiation and evaluation are shown in the Figure 1. The standard deviation was found within 5 %. The reproducibility could be satisfactory using no annealing between irradiations and the optimal read out cycle for dosemeters consist of heating up to 300°C.

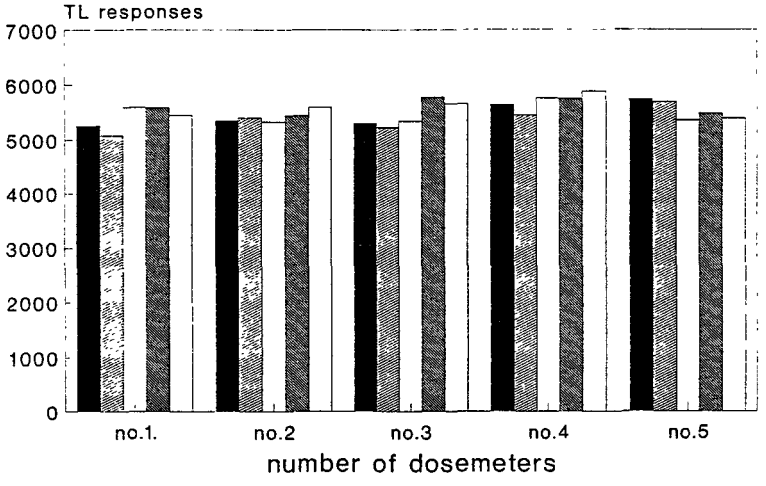

Fig.1. Reproducibility of Al_2O_3:C dosemeters (D=1.75 mGy)

The result of long term store can be seen in the Figure 2. The dosemeters were placed in an iron shield (dose rate is 20 Ngy/h) in order to get the background and the lowest detectable dose. We also stored dosemeters in a laboratory, where the dose rate is 120 nGy/h. It can be stated, that the lowest detectable dose is about 100 Ngy.

We did not get any effect of the self dose on the dose responses of the dosemeters storing them for 2 months in the iron shield place.

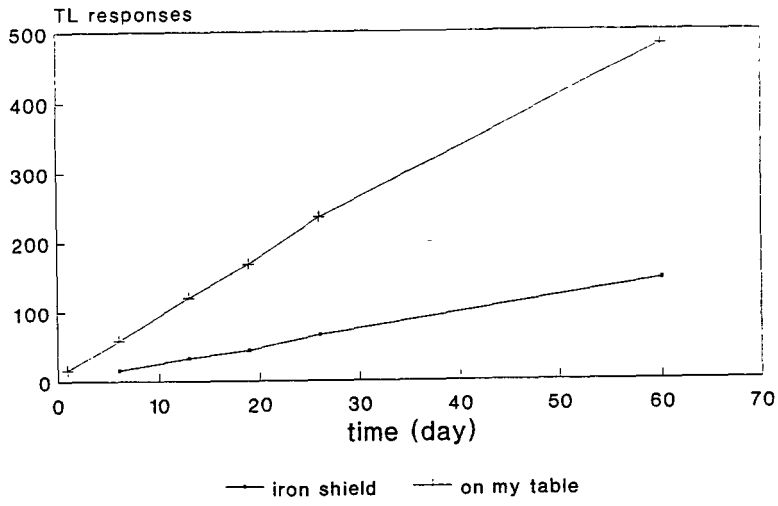

Fig.2. TL responses of Al_2O_3:C as a function of store time at a low background place and in a laboratory

The fading was found negligible storing the dosemeters four weeks at room temperature in an iron shield. Results on fading properties are shown in Fig. 3, storing the dosemeters at room temperature in the laboratory, at 40°C in the ultrathermostat and at low background place, separately. We also investigated the fading of dosemeters in case of combined heat cycle: 2 weeks at 0°C, 2 weeks at room temperature and 2 weeks at -10°C. The TL responses of dosemeters did not changed.

The UV sensitivity of dosemeters is selective to the wavelength of 254 nm UV light.The 254 nm UV light results in more than one magnitude higher PITL response than the 366 nm light at the same condition. The UV light induced glow curves are shown in the Figure 4.

Participation in reference measurements at the Natural Environmental Monitoring Station at Risø showed that aluminium oxide single crystal have enough sensitivity to measure cosmic radiation dose. The result of cosmic and terrestrial radiation measurements at Roskilde Fjord and on the field was found 34 nGy/h and 78 nGy/h, respectively. The time of irradiation was 3 days.

The glow curves of Al_2O_3:C dosemeters irradiated at various distances from a calibrated ^{60}Co source at the Risø National Environmental Monitoring Station is shown in the Fig.5.

The result of intercomparison experiments at Risø, eg. the comparison of calculated and measured data made on Al_2O_3 TL dosemeters using various radionuclides and dose rates can be seen in Fig.6. The standard deviation of aluminium oxide dosemeters was found lower than 10 % which can be improved using individual calibration.

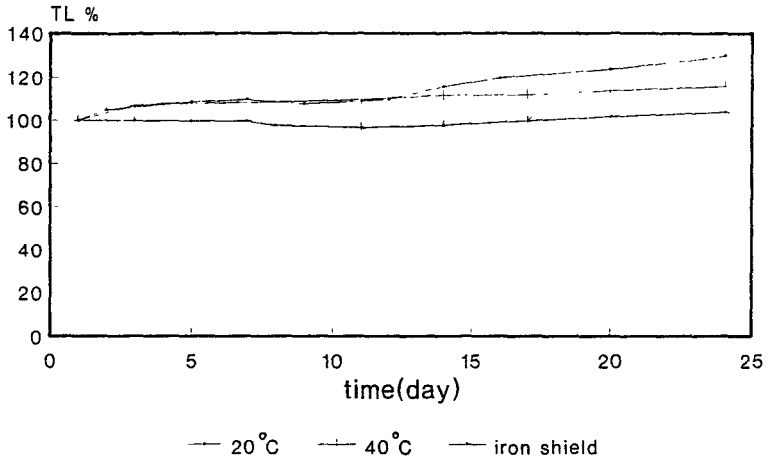

Fig.3. Fading of Al_2O_3:C at various temperature and in an iron shield facility

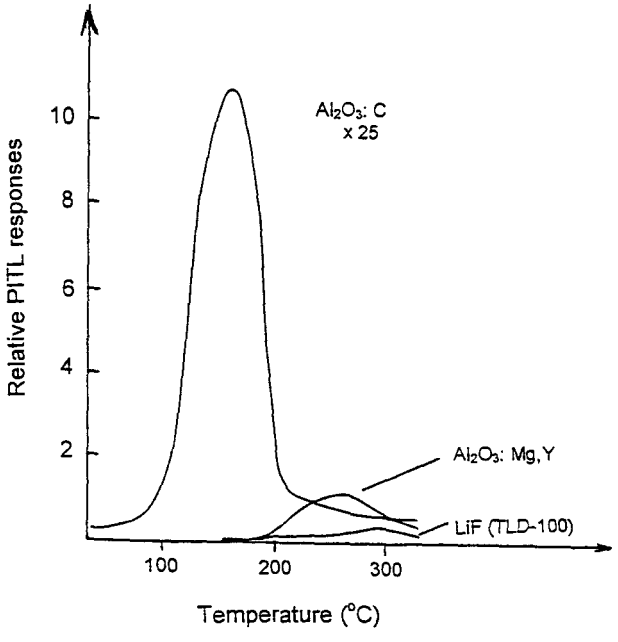

Fig.4. UV light induced glow curves of Al_2O_3:C compared with those of Al_2O_3:Mg,Y ceramic detectors and with LiF(TLD-100)

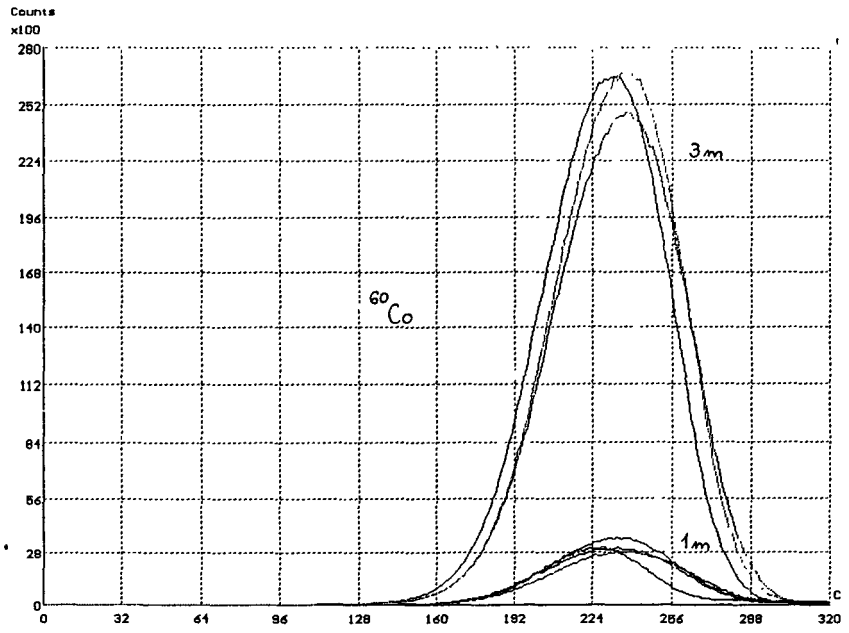

Fig.5. Glow curves of Al_2O_3:C dosemeters irradiated at various distances from a calibrated ^{60}Co source

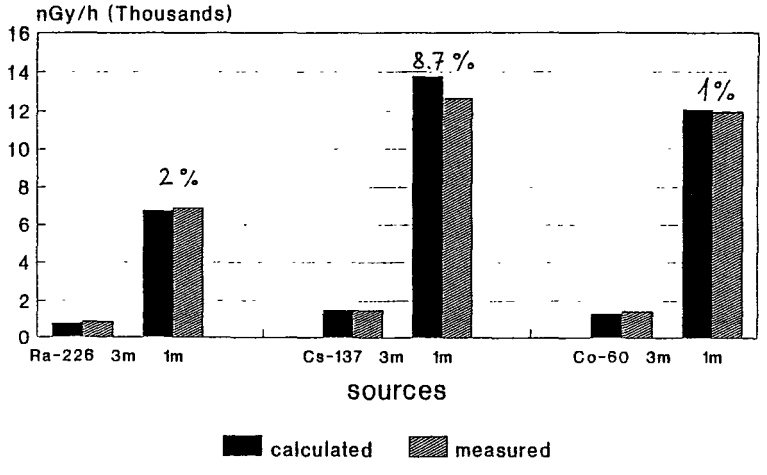

Fig.6. Comparison of calculated and measured data made on Al_2O_3:C using various radionuclides and dose rates

1.4 Conclusions

Results obtained suggest that the Al_2O_3:C dosemeters are promising for environmental monitoring. Its TL sensitivity is 40 times higher compared with TLD-100 dosemeters, other TL properties such as reproducibility and fading are excellent for long-term environmental radiation measurements. Encapsulation needed to exclude the light exposure.

2. Development of a microprocessor controlled portable TLD system for environmental monitoring (S. Deme, KFKI Atomic Energy Research Institute)

2.1 Introduction

Environmental gamma-radiation dosimetry is mainly based on TL (thermoluminescent) dosimetry. This method offers considerable advantages because of its high precision, low cost, wide range, etc. At the same time its application involves uncertainty caused by the dose collected during the transport from the point of annealing to the place of exposure and back to the place of evaluation. Should an accident occur read out is delayed due to the need to transport to a laboratory equipped with a TLD reader.

A portable reader capable of reading out the TL dosemeter at the place of exposure ("in situ TLD reader") eliminates the above mentioned disadvantages. Because no sufficiently high enough sensitive portable reader is available on the market, we have developed a microprocessor based portable TLD reader for monitoring environmental gamma-radiation doses and for on board reading out of doses on space stations.

At the beginning of the 80th our laboratory produced a great number of portable, battery operated TLD readers (named Pille - "Butterfly") (3,4). These devices used $CaSO_4$ bulb dosemeters and the evaluation technique was based on analogue timing circuits and analogue to digital conversion of the photomultiplier current with a read out precision of 1 μGy and a measuring range up to 10 Gy. The measured values were displayed and manually recorded. The version with an external power supply was used for space dosimetry as an onboard TLD reader.

2.2. Goals of development

Based on a microprocessor an up to date version of the battery operated portable reader was developed in 1994-95 at the Atomic Energy Research Institute. The main goals of the development were:

1. To increase the sensitivity of the reader by one order of magnitude.
2. To improve the precision of the measurement using automatic correction of the individual dosemeter sensitivity and of the temperature dependence.
3. To obtain a programmable heating current profile, e.g. to product a quasilinear temperature increase up the bulb heating plate.
4. To provide automatic data processing and subsequent

storage on a memory card of the processed data, date, time, dosemeter number, dose, and the digital glow data.

5. To enable the programmed automatic read out of a dosemeter placed in the reader to measure the time distribution of the dose rate.

2.3 Characteristics

The new system consists of a set of TL bulb dosemeters with built in memory chips,and the microprocessor based reader. The $CaSO_4$:Dy bulb dosemeter is the same as the earlier one (3).

A block diagram of the reader is given in Fig.7. The TLD bulb has a common case with the memory chip containing the identification number of the bulb. The DC/DC converter type heating supply as well the Cockroft-Walton type high voltage supply are controlled via digital-analogue converters by the microprocessor thereby providing the possibility to program the time dependence both of the heating current (e.g. to obtain quasilinear or steplike temperature profiles) and of the high voltage (to change the sensitivity of the photomultiplier tube in autorange mode). The light output of the bulb dosemeter is measured by a photomultiplier, a wide range I/U converter, and a digital voltmeter. (The range of the light detecting system exceeds 8 orders of magnitude.) The built in, stabilized LED light source controls the light sensitivity of the reader in each measuring cycle.

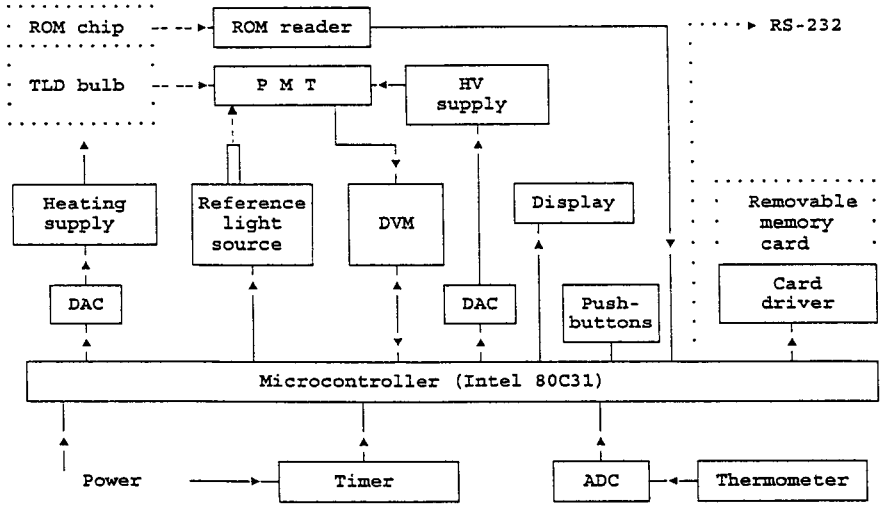

Fig. 7. Simplified block diagram of the Pille'95 TLD reader

The four digit alphanumeric LED display indicates the measured dose in exponential form, the possible error codes and the menu/submenu points of the setup. The removable memory card can store up to 4000 measured data (dose, identification number, date and time, and digital glow curves).

The mass of the battery operated version of the reader is about 2 kg, its dimensions are 190 x 155 x 70 mm. The rechargeable battery (9.6 V) provides capacity for about 200 read-outs. The reader also works from a 12 V or 24 V car battery in buffer mode. The space version is supplied by 27 V d.c.

The glow curve of a $CaSO_4$:Dy bulb irradiated with 0.5 mGy dose of gamma-radiation is given in Fig.8. At higher doses the glow curve is distorted by high temperature peaks. This effect requires nonlinearity correction, performed by the software of the reader.

The environmental temperature influences both the position and the area of the glow curve (Fig. 9). Using the built in digital thermometer this effect can be taken into account.

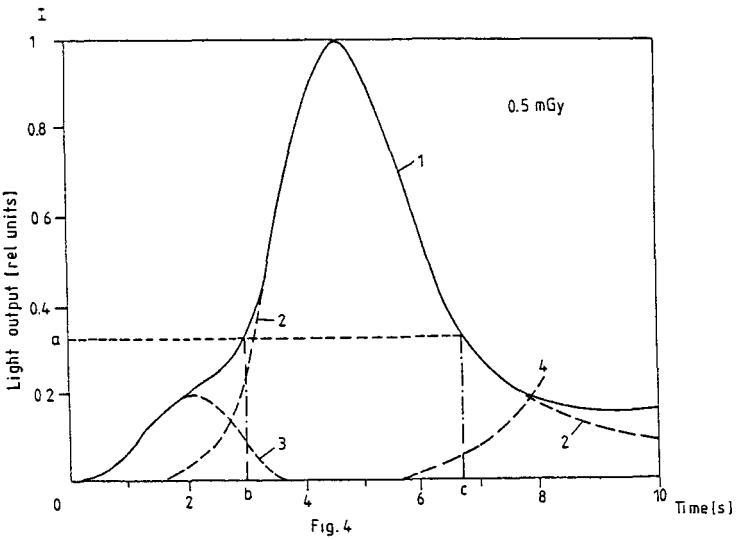

Fig. 8. Glow curve of a $CaSO_4$:Dy bulb irradiated with 0.5 mGy dose of gamma-radiation. The measured curve (1) is decomposed to main dosimetric peak (2), low temperature peak (3) and thermal background (4)

Figure 10 shows the stochastic error (σ) as a function of dose. The lower limit of the dose measurement with σ = 10% is equal to 3 μGy, i.e. an environmental dose of one or two days.

The dosemeter has low light sensitivity: it can be evaluated in a room having moderate illumination from filament lamps, or in scattered daylight of low intensity.

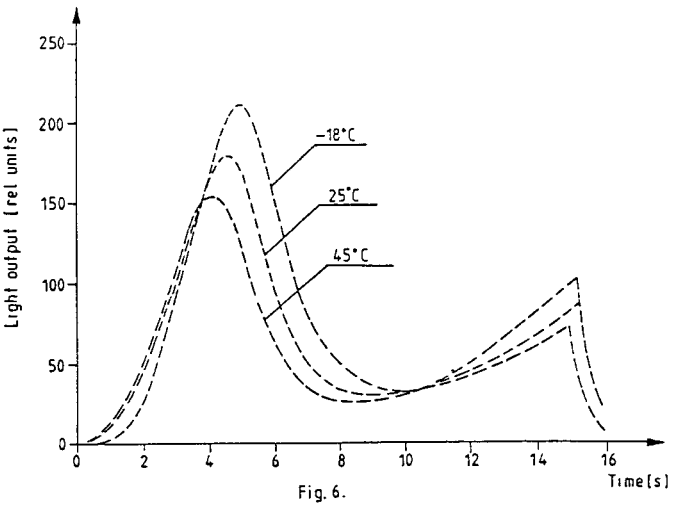

Fig. 9. Glow curves measured at different environmental temperatures

2.4 Applications

The system is utilizable both for environmental monitoring and measurement of doses on board of space vehicles.

Environmental doses can be measured using in situ read out of the dosemeters. The wide measuring range of the system (3 μGy - 10 Gy) provides the possibility to measure dose values from natural background up to very large accidental doses. The in situ measurement makes it possible to avoid the transit dose when monitoring the normal environmental gamma radiation and to obtain the dose values immediately in case of an accident.

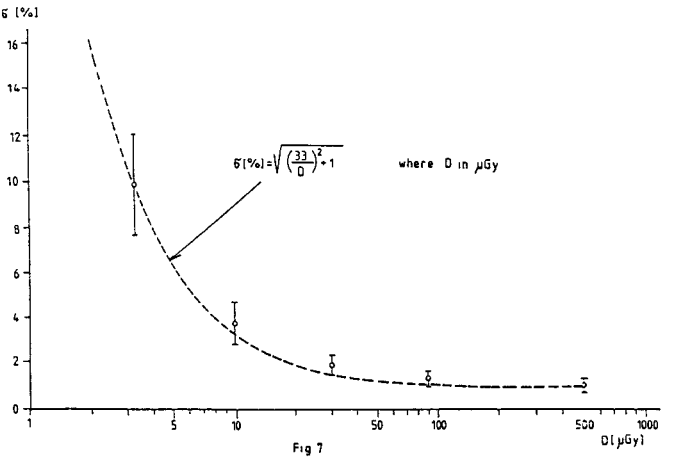

Fig. 10. Stochastic error (σ) versus dose; the dashed line gives a mathematical approximation

The use of the system in space dosimetry gives an opportunity to get separate dose values for time periods having different flight height, sun activity, etc. In automatic mode the measured dose is obtained from a dosemeter that is left permanently in the reader, using preprogrammed time periods without assistance of the astronauts. This mode can be used on non permanently manned space stations, as well.

2.5. Conclusions

The development of an up to date microprocessor based portable battery operated reader was completed during 1994-1995. The lower limit of measurement with σ = 10% is equal to 3 μGy, at higher doses up to 10 Gy, the reproducibility is in the range of 1-2%. The measured data together with digital glow curves are stored in the removable memory card of the reader. With a portable TLD system the transport dose - that normally gives a systematic error during environmental dosimetry - is avoided and the data availability accelerated in the event of a nuclear accident.

References

(1) Akselrod, M.S.,Kortov,V.S.,Kravetsky,D.J.and Gotlib, V.I. Highly Sensitive Thermoluminescent Anion-Defective Al_2O_3:C Single Crystal Detectors. Radiat. Prot. Dosim. 32,15-20(1990)

(2) Osvay, M., M.Ranogajec-Komor, F.Golder: Light sensitivity of LiF:Mg,Ti, CaF_2:Mn and various Al_2O_3 Thermoluminescent Detectors. Kernenergie 34,116-118(1991)

(3) Szabó, P.P., Fehér, I., Deme, S., Szabó, B., Vágvölgyi, J., Germán, E., Environmental monitoring with a portable TLD system. Radiat.Prot. Dosim. 6/1-4:100, 1983.

(4) Szabó, P.P., Fehér, I., Deme, S., Szabó, B., Vágvölgyi, J., Dosimetrical properties of the portable wide dose range TLD reader "PILLE". Radiation Protection Dosimetry. 17/1-4:279, 1986.

Publications

1. Osvay, M., F. Golder, M. Ranogajec-Komor: Reproducibility of the New High Sensitive TL Materials Proc. Second Symp. Croatian Rad. Prot. Assoc. Nov. 1994. p.195
2. Deme, S., M. Osvay, I. Apáthy, I. Fehér: Comparison of Laboratory and in Situ Evaluation of Environmental TL Dosemeters 1996 International Congress on Rad. Prot. April 14, Vienna (submitted)
3. Apáthy, I., Deme, S. and Fehér,I. Microprocessor controlled portable TLD system. Radiat. Prot. Dosim. (to be published)
4. Deme, S., I. Apáthy, I. Fehér: Environmental dose measurement with microprocessor based portable TLD reader, Proc. Symp. on Rad. Prot. in Central Europe, Portoroz Sept. 4-8, 1995 (to be published)

Final Report
1992 - 1994

Contact: F13PCT920026 **Duration: 1.9.92 to 30.6.95** **Sector: A12**

Title: Detection and dosimetry of neutrons and charged particles at aviation altitudes in the earth's atmosphere.

1)	McAulay	Univ. Dublin
2)	Tommasino	ENEA
3)	Schraube	GSF
4)	O'Sullivan	DIAS
5)	Grillmaier	Univ. Saarlandes
6)	Hoefert	CERN
7)	Spurný	CSAS.IRD

I. Summary of Project Global Objectives and Achievements.

The global objectives of the project as set out in the Contract proposal and prolongation proposal were:

(1) To obtain detailed information on flux and energy spectrum of neutrons at aviation altitudes.

(2) To obtain charge spectra and flux for high Z and high energy particles at aviation altitudes.

(3) To use data obtained during flights on a number of civil aviation routes to calculate doses received by air crew as a result of their occupation.

(4) To validate and modify computer programs for the computation of doses on the basis of the impinging external radiation fields.

(5) To make intercomparisons of instrumentation and develop calibration procedures using standard reproducible radiation fields provided by the high energy particle accelerator at CERN.

(6) To suggest procedures for the estimation and minimisation of doses experienced by civil aviation air crew as a result of their duties.

Most of these global objectives have been substantially achieved by the Contractors, although in one or two respects a complete fulfilment of the proposal has not been possible for reasons which will be detailed below. The overall results of the Contract can best be described by considering first the development of the instrumentation and the measurements made. The theoretical work on the computer modelling of the fields and the response calculations are then briefly discussed. This overview concludes with a description of the calibration and intercomparison procedures and the implications of the results for the assessment of doses and their minimisation in the field of civil aviation.

Different systems of detectors for the measurement of high and low energy neutrons were set up and calibrated as part of Project 2 of the Contract. As a result of this work, it was concluded that a passive multidetector stack would provide a simple method for measurement of the different components of the radiation field experienced at aviation altitudes. This had the advantage that it would provide average exposure data if left on an aircraft over an extended period of time.

As the Contract work proceeded, a large amount of co-operative effort developed and this is well exemplified by the joint approach adopted by Projects 2 and 4 in the production and testing of the passive multidetector system. The study of HZE particles in the radiation flux at aviation altitudes was the primary aim of Project 4 and this was carried out using track etch detectors, which were incorporated into the multidetector package. The track etch detectors were utilised on flights carried out at a number of different altitudes and have confirmed the presence of particles with Z values up to and including magnesium (Z = 12) at the highest altitudes relevant to civil aviation.

The main objectives in respect of active instrumentation were the use of the extended rem counter (LINUS) at aviation altitudes and the development of the HANDI (Homburg Area Neutron Dosimeter). Calibration and testing of both these instruments has proceeded in accordance with the plans set out in the proposal. The HANDI instrument was studied under the heading of Project 5 and it has been calibrated in a high energy neutron field and its response to heavy ions studied in different configurations. It has been used for the measurement of absorbed doses and lineal energy distribution at an altitude of 3777 metres in ground based measurements.

However, at the conclusion date of the Contract, very little has been achieved by the use of these active instruments in terms of in-flight measurement. The failure to make such measurements has been due to the difficulty of obtaining certification to enable such instruments to be carried on passenger flights. The inability to complete this section of the Contract was not due to any lack of effort on the part of the Contractors and could probably not have been foreseen without advice from someone very familiar with the requirements for electrical instrumentation on board aircraft. It should be added that the necessary certification was obtained towards the end of the Contract period and measurements with these instruments began in September 1995, although no results from such measurements could be made available for this report.

The most successful source of new in-flight measurements using active instrumentation was Contract Project 7 , which provided measurements on some 20 return commercial flights to various destinations during the course of the Contract. These measurements were made with both active and passive instrumentation and have studied altitude and latitude effects, the influence of the solar cycle, and other factors which may affect doses associated with particular routes. This Project has also investigated extensively the calibration of the various instruments in a number of different radiation fields at various ground based facilities.

The general objectives of Project 3 were to compare and refine existing models for the production of the cosmic radiation field at aviation altitudes and to investigate

the response calculations for dosimetric devices and the calculation of dosimetric quantities. These calculations were to be followed by validation experiments in high energy radiation fields.

Differences in the results obtained using the LUIN and FLUKA codes were studied and it was generally found that the latter predicted higher fluxes. Discrepancies remain between expected and observed results and it is concluded that the LUIN code needs improvement with respect to the neutron contribution to dose. Codes used in the calculation of the response of dosimetric devices were also found to yield inconsistent results and it is clear that this area will need further study.

The calculation of dosimetric quantities concludes that ambient dose equivalent is a conservative estimate of the quantities effective dose and effective dose equivalent for the fields encountered at aviation altitudes. The conservativity has been quantified in a number of different spectral distributions. The necessary validation measurements were carried out in appropriate artificial and natural high energy fields.

Contract Project 6 was primarily concerned with the establishment of reference radiation fields at the high energy proton accelerator facility at CERN. These reference fields proved to be most valuable in enabling comparisons to be made of the instruments used by the various Contractors. Six experimental runs were provided during the period of the Contract at the CERN facility and the field provided was considered to be very similar to the fields encountered at aviation altitudes. One of the more important results established using these experimental fields was that the dose limit of 2 mSv recommended in ICRP 60 at the surface of the abdomen for a pregnant woman does not assure a dose limit to the foetus of 1 mSv.

Much of the work in this Contract was carried out during the period when a report by the European Dosimetry Group (EURADOS) on Exposure of Air Crew to Cosmic Radiation was in course of preparation. This coincidence provided a great deal of useful discussion of value both to EURADOS and to the Contractors involved in the work detailed here. Conclusions resulting from work within the Contract have been utilised in the preparation of the EURADOS report and this is perhaps most noteworthy in the results of Project 1, which was to co-ordinate the Contract and make recommendations for the assessment and minimisation of doses to air crew resulting from cosmic radiation.

The results obtained within this Contract confirm the view that air crew normally employed on medium and long haul flight duties are likely to receive doses in excess of the annual dose limit of 1mSv for members of the public. This conclusion implies that such workers fall within the classification of Category B radiation workers and requires that an assessment of their doses should be made. Project 1 considers a number of options for assessing the dose and concludes that a route dose can be allocated for each flight, the total of such doses providing a satisfactory estimate of total dose in compliance with the European Radiation protection Directive.

In the case of pregnant female air crew, the possibility exists that continuing flight duties for the first trimester of pregnancy could result in exceeding the relevant dose limit. This must not be permitted to occur and appropriate legislative steps will need

to be considered in the near future to obviate the possibility. The results obtained within the Contract suggest that normal flight duties within the aviation industry should not result in any air crew falling into the Category A for radiation workers. It is therefore not likely that elaborate procedures require to be introduced for minimisation of doses.

The detailed aims set out in the Contract proposal have been substantially achieved. The failure to carry out the number of flights planned with active instrumentation resulted from administrative difficulties which could not have been foreseen at the start of the Contract. All of the Contractors co-operated extremely well in the detailed research and one of the best consequences of the collaboration was the free and valuable exchange of information that developed rapidly between individuals during the period. It is clear that there remain a number of problems to be solved within this research area, but a good start has been made and it is likely that those involved in this Contract will continue to work together in the future towards the solution of these problems.

Head of project 1: Dr. McAulay

II. Objectives for the reporting period

The following were the objectives of Project 1 within the Contract:

(1) To assess the implications of the doses due to cosmic radiation fields experienced at aviation altitudes.

(2) To consider methods available for assessing the occupational radiation doses to air crew.

(3) To suggest procedures for minimisation of doses where appropriate.

III. Progress achieved including publications

At the beginning of the Contract period it was recognised that, in the course of their work, civil air crew and frequent flyers are exposed to elevated levels of natural background radiation, namely cosmic radiation of galactic and solar origin and secondary radiation produced in the atmosphere, aircraft structure, etc.

The proposals of the International Commission on Radiological Protection (ICRP) in Publication 60 recommend a decrease in the average annual limits on occupational radiation exposure and this implies that anyone exposed to doses which exceed the dose limit for public exposure (1 mSv per annum) should be considered to be occupationally exposed. In this context, exposure to cosmic radiation in the operation of jet aircraft is mentioned specifically. However, ICRP states that whereas, in general, individual monitoring should be used for all those who are occupationally exposed, it may not be required if it is clear that "doses will be consistently low, or, as in the case of air crew, it is clear that the circumstances prevent the doses from exceeding an identified value".

Additional controls which may be necessary to protect the conceptus where a woman is, or maybe, pregnant must also be considered. ICRP policy is that `the methods of protection at work for women who may be pregnant should provide a standard of protection for any conceptus broadly comparable with that provided for members of the general public' and that this policy objective will be met, if a woman is exposed prior to declaration of pregnancy, by following the standard system of protection they recommend. Following declaration of pregnancy, ICRP has recommended a supplementary limit to the surface of the woman's abdomen of 2 mSv for the remainder of the pregnancy.

The proposed revised CEC (Commission of the European Communities) Directive on Basic Standards for the Protection of the Health of Workers and the General Public Against the Dangers Arising from Ionising Radiations considers exposure in jet aircraft in flight to constitute exposure to natural radiation sources at work and proposes that "each member state shall make arrangements for the assessment of

exposure of air crew involved in the operation of jet aircraft by their employers and shall, where appropriate, classify air crew as exposed workers".

The draft Basic Safety Standards propose classification and delineation of areas for all workplaces where there is a risk of exposure to ionising radiation in excess of the relevant dose limit for members of the public. In essence controlled areas are defined as those where there can and should be management controls in place. Supervised areas are classified areas not further delineated as controlled areas. The categorisation of workers is then, in part, based on whether they work in controlled or supervised areas. Category A workers are those who work in controlled areas and who are liable to receive an effective dose greater than 6 mSv per year or an equivalent dose greater than three-tenths of the dose limits as laid down for the lens of the eye, skin and extremities. Category B workers are those exposed workers not classified as workers of category A, routinely working in supervised areas or occasionally in controlled areas. From the measurements carried out within the Contract and also from other reported measurements, it is clear that, in general, aircraft need not be classified as controlled areas. However, air crew flying routinely at altitudes over 8,000 m on long and medium haul flights must be deemed to be category B workers, it is therefore important that the measures taken to record, control and, where necessary, to limit doses should be adequate for the desired purposes, but should not be UN-necessarily restrictive on individuals in the course of their occupations. The requirement of the European Directive in relation to the recording of occupational doses is that effective dose is the appropriate quantity for entry into dose records. The procedure by which this figure is determined is not specified in detail. Effective dose may be calculated or ambient dose equivalent may be used as an operational quantity derived from instrumental measurements and used in turn to produce a figure for effective dose to be recorded as laid down in the Directive.

A number of methods are available for assessing the doses experienced by air crew. These may be summarised:

(i) Assess Personal Dose Equivalent: This quantity can to a fair degree of approximation be measured by practical devices (personal dosemeters attached to the person) and the magnitude of the quantity is a direct estimate of dose equivalent in that part of the individual's body on which it is attached and can, in theory, be related, with assumptions about the radiation field, to effective dose and organ equivalent doses.

(ii) Assess Ambient Dose Equivalent: Where area monitoring is made of radiation fields mainly comprised of penetrating radiation and for which control of `stochastic' risk (as estimated by effective dose) is required, the operational quantity to be measured is ambient dose equivalent H*(10). Where dose assessment is to be based on combining the results of area monitoring measurement and staff roster information, the approach would be to estimate total ambient dose equivalent. The results of this estimation could be entered directly into records or readings of instruments combined with occupancy could be entered directly in terms of effective dose (and organ equivalent dose).

(iii) Assess effective dose (and/or organ equivalent dose): Where area monitoring of fields is carried out, the results of measurements, that is the readings of the instruments, may be related to effective dose. This may be done directly or by the application of a modifying factor to the interpretation of the instrument reading as ambient dose equivalent (or other quantity).

(iv) Calculate effective dose and organ equivalent dose: The results of measurements and calculations of the radiation fields at functions of aircraft altitude and latitude and solar cycle phase can be used to calculate a figure for effective dose. Occupational doses can be derived from the results of these calculations, staff roster information and the flight log kept by airlines of altitude, latitude and time.

For the fields experienced at aviation altitudes, the data obtained within this Contract indicate that ambient dose equivalent is a very conservative estimator for effective dose. The direct use of ambient dose equivalent for entry into records would therefore be inappropriate.

Routine monitoring using active instrumentation on all flights would be a cumbersome and unreliable procedure for assessment of occupational doses and this possibility is not further considered here. However, a number of alternatives remain.

(a) No dose estimates: For short flights with little time spent at altitude above 8,000 m, for combinations of specific flight altitudes and latitudes and limited staff flying hours, total annual doses will not exceed 1 mSv. Staff would not be considered to be exposed workers. Some measurements may be required to verify the assessment.

(b) Route doses and occupancy: In the case of exposed workers for whom records are required, estimates of individual doses could be obtained from route doses (for whatever quantity is selected) and records of staff rostering. The route doses may be based on measured values preferably with a reference instrument system or from dose rates calculated from flight parameters and solar cycle phase. Confirmation by measurement of the calculated dose rates should be made periodically (not more frequently than annually) for representative routes. This option would be the most generally applicable.

(c) On-board monitoring in special cases: Commercial aircraft designed to fly above 15,000 m already carry monitoring devices but these are primarily intended as warning devices in case of steep increase in dose rates due to solar flares. The increase in cruising altitudes in some aircraft of recent design results in dose rates in such aircraft approaching 10 $\mu Sv\ h^{-1}$. On-board radiation monitoring equipment should be carried by all aircraft which routinely fly at altitudes in excess of 15,000 m.

(d) Partial or full use of personal dosemeters: Simple designs of thermoluminescence dosemeter to measure the photon plus directly ionising component, and a track-etch neutron dosemeter are sufficient for these purposes, subject to corrections applied to their readings to take account of their energy and directional dependence of response. There are considerable difficulties in

measuring low doses to the crew of aircraft on a routine basis with existing personal dosemeters.

Of the options considered above, the preferred procedure in order to estimate doses to air crew in appropriate cases is to determine route doses and fold these with data on staff rostering. Route doses are likely to be obtained from calculations of the radiation field as a function of aircraft altitude and latitude (and solar cycle phase).

Air crew are one of the most highly exposed occupational groups. It is considered desirable that, where there is a prior knowledge of the radiation field, this should be applied to obtain the best estimate of the protection (limit) quantity. Dose estimation procedures will not be necessary for persons for whom total annual doses will not exceed 1 mSv and therefore, in general, for aircraft not routinely flying above 8,000 m. Where doses may exceed 6 mSv per year on-board monitoring of dose may be necessary.

Minimisation of doses will clearly be appropriate for the protection of the embryo/foetus in cases where female crew may be pregnant. This appears to be the only circumstance in which a dose limit could be exceeded in occupational exposure at aviation altitudes. It would be prudent to withdraw pregnant crew from all flying duties immediately following the declaration of pregnancy.

Publications: A report on Exposure of Air Crew to Cosmic Radiation has been prepared and submitted to the EURADOS Committee. This will be published after approval.

Head of project 2: Dr. Tommasino

II. Objectives for the reporting period

The initial objectives were to set up and calibrate different detectors such as the bubble detector, the bismuth fission track detector and the extended rem-counter for the measurement of low and high energy neutrons at civil aviation altitudes.
As a result of strong cooperative efforts with other participants of the contract, these preliminary objectives have been expanded to include the set up of a passive multidetector system for the measurement and spectrometry of neutrons and HZE particles.

III. Progress achieved including publications

Following the approval of the contract, it was soon decided to set up the detectors for the measurement of high energy neutrons, such as the damage track detectors (for the registration of neutron-induced fission fragments in bismuth) and the extended rem counter (hereafter referred to as the Linus). Since the fission track detectors will be described later together with the other passive detectors of the stack, the progress achieved with the Linus will be first reported.

The Linus rem-counter. The extended rem-counter-(Linus), first developed at the Italian National Institute of Nuclear Physics-INFN, remains the only real-time dosemeter capable of measuring both low and high energy neutrons. Since the beginning of the contract, a close cooperation was initiated with the INFN from Frascati-Rome with the specific mission goal in mind to use this active dosemeter for the assessment of the aircrew exposure at civil aviation altitudes.The first requirement for the use of Linus on long-haul flights was to have a self-powered system

with long battery life. This system, once set up, has been calibrated by the INFN group from Frascati in different neutron fields. Within this contract, it was possible to test the Linus together with a conventional rem counter at different high energy fields made available at CERN. The response of the Linus has been twice of that of the conventional rem-counter in the field characterized by high energy neutrons. For the spectrum with low energy neutrons the response of the two rem counters has resulted the same.
The detection principle of the extended rem-counter has been also applied to spherical moderators formed by polyethylene, boron plastics and lead, in which moderators thermoluminescent dosimeters (TLD-600 and TLD 700) have been placed. The responses of these rem balls have been consistent with those of Linus-types of counters. However when compared with Linus, these passive energy-extended spherical moderators have resulted not sufficiently sensitive for in-flight measurements.

Multidetector stack. A multidetector system has been developed within this contract, which is formed by two substacks for the measurement of neutrons and HZE particles respectively. While the substack for neutrons has been developed at ANPA (Rome) with the support of other participants of the contract, the substack for HZE particles has been developed at DIAS (Dublin) with a limited support from ANPA.
The entire stack is formed by many replicates of different passive detectors such as:
-Bubble detectors for neutron measurements,
-Several types of damage track detectors for the registration of both neutrons and HZE particles.
When compared with the bubble devices, damage track detectors are relatively much less sensitive to neutrons. The strategy adopted to increase the sensitivity of damage track detectors was to increase both the exposure time and the detector area.This can be easily achieved with the registration characteristics of track etch detectors, such as the absence of fading and the possibility to rapidly scan large detector areas with simple automatic or semiautomatic systems.
Stack for long-term exposures. It was soon clear that sufficiently long times of exposure resulted in hundreds of flight hours. To facilitate these long-term exposures, the stack should not contain passive detectors which are sensitive to low-LET radiations (such as the x-rays from the security scanner and the terrestrial radiation) and thermal neutrons because of their abundance at sea level. In this case, the stack does not require any particular assistance after landing and/or between flights, since it is sensitive to the type of radiation present mainly at high altitudes (typically low-energy and high-energy neutrons and HZE particles).Because of these characteristics, the substack can be used by different operators such as pilots, couriers,etc. In particular it can be flown just by special courier service by sending the stack to any laboratory which is willing to send it back on its arrival.

Rapid scanning of many large area detectors. About one hundred track detectors (each having an area of 225 cm2) have been used in the stack resulting in a total area of 2 square meters. Even though this multidetector system presents the complexity typical of cosmic ray stacks, the scanning of many different types of track detectors has been made relatively simple and rapid as required for dosimetric applications. These successful achievements have been made possible through the appropriate choices of the detectors adopted in the stack. For all these techniques, the detector principle is based on avalanche processes induced at high- LET particle-tracks, which greatly facilitate the registration of the tracks. These avalanche processes are based on bubble formation, spark and/or electrochemical breakdown induced at track sites. In spite of the different registration techniques used, the manual and/or automatic counting procedures for damage tracks and bubbles are just the same. Furthermore the detection principle of coincidence counting (highly exploited for cosmic ray measurements) has been also applied for the scanning of the track detectors even for short-range particles such as fission fragments.

The neutron substack. The only possible way to measure neutrons over a wide energy range is to use detectors with different neutron energy responses, each of which covers a fairly wide segment of the total energy range. The detectors, which have been used, are:

-Bubble detectors;
-Electrochemically etched polycarbonate bottles;
-Large area etched-track detectors (polycarbonate, CR-39, LR-115)for the registration of neutron-induced recoils;
-Large area track detectors for the registration of neutron-induced fission-fragments in bismuth.

The only detector which has its principal response at energies above 50 MeV is based on the neutron-induced fission of bismuth. The Bi-fission track detector is made of a 25-micron-thick bismuth radiator (deposited on a plastic backing) and 6-microns thick mylar film for the registration etched-trough holes induced by fission fragments.Two different radiator-detector geometries have been used, where track holes in single film and coincident holes in paired films are counted.The overall Bi-section of the stack was formed by 25 large area detectors resulting in a registration area of about half square meter and a total weight of about 200 g.

The neutron substack has been developed with the ambitious project in mind to evaluate the neutron spectra. The requirement of this method of neutron spectrometry (based on the unfolding procedures) is to irradiate a number of detectors, which have a precisely known response as a function of the neutron energy and chosen in such a way that all the parts of the expected energy range are included. While the evaluation of the response of most of the detectors has been carried out with neutron beams, the response of the Bi-detector was obtained by using high energy proton beams from DUBNA. Unfortunately, the

response of almost all the detectors to high energy neutrons is typically a blend of neutron data for energies below 20 MeV, with proton data for all higher energies. Few neutron data exist for energies above 20 MeV. The two kinds of data are often joined with a smooth curve. For nearly 40 years it was assumed that the value of the Bi fission cross section of neutrons is equal to that of protons. Both theoretical and sperimental new data indicate that the fission cross sections for neutrons are 2 to 3 times smaller than those for protons. According to these new data there are probably considerable errors in the cosmic-ray neutron spectrum measured by Hess at energy above 50 MeV.
Fig. 1 shows the neutron spectrum evaluated by unfolding the data, obtained from the stack esposed to the high-energy radiation field at CERN. The spectrum obtained by Roesler and Stevenson for the same beam, using the Fluka Monte-Carlo code, is also reported in Fig.1 for comparison.
The low energy part of the experimental spectrum is limited to about 200 keV, since no detector has been used to cover the very low-energy range of the spectrum.
Fig. 2 shows the response per unit of fluence of three different types of neutron detectors formed respectively by the bubble detectors, the polycarbonate bottles (i.e.the container of the bubble detectors) and the Bi-fission track detectors. Since the spectrum of cosmic rays is formed by low energy neutrons (evaporation spectrum) and high energy neutrons (knock-on spectrum), the most convenient detector combination is formed by bubble detector and the Bi-track detector. In this case, the response of bubble detectors covers the evaporation part of the spectrum, while that of Bi-fission track detectors covers the remaining high energy part.
The limitations of bubble detectors (such as small linearity range and the effects of both wide temperature excursions and mechanical shocks) can be overcome by using the bottle (containing the bubble sensitive material) as back-up detector, based on track registration on its polycarbonate walls.In particular, the counting procedure, whether it is manual and/or automatic can be the same for bubble detectors and for the polycarbonate bottle detectors.
Table 1 compares the results obtained with the bubble detector with those from the bottle detector irradiated at CERN to neutrons having the spectrum reported in Fig.1. The dose equivalents are reported using the fluence-to-dose conversion factors from ICRP 21.

Table 1

Bubble Detectors	Bottle Detectors
(0.60 $\pm$ 0.17)mSv	(0.59 $\pm$ 0.23)mSv

The responses of the bubble detectors and polycarbonate bottles

are very similar for CERN high energy fields, thus justifying the use of polycarbonate bottles as back-up detectors in cosmic ray fields. Table 2 reports the data of both low-energy and high-energy neutrons for the same CERN exposure. For the high energy neutrons (measured with the Bi-detector) the dose conversion factors are again from ICRP 21.

Table 2

Low Energy Neutrons	High Energy Neutrons
(0.60 ± 0.17)mSv	(0.80 ± 0.28)mSv

The possibility to measure both the low-energy and the high-energy neutron components (or even the cosmic ray neutron spectrum) is highly valuable for the assessment of the aircrew exposure. The data available so far, specially for what concerns the high energy neutrons, are scanty and conflicting. Unfortunately the Bi-detectors have been calibrated only with high energy protons. The calibration with high energy neutrons is urgently needed.

Substack for the measurement of HZE particles. The set-up and/or calibration of the substack for HZE particles have been carried essentially from the School of Cosmic Ray Physics (DIAS-Dublin). Through the cooperation between ANPA and DIAS a particular substack has been designed, which facilitates the scanning of large detector areas. As shown in Fig. 3, the distinguishing features of HZE particles are that they cross several different track detectors. The only way to identify HZE particle tracks is to search for pair of etch pits at the top and bottom surfaces of one or more thick track detectors.
For dosimetric applications, rapid scanning procedures of large-area detectors are needed. To achieve rapid scanning, thin film detectors have been used, which are made respectively of 12-microns-thick cellulose nitrate (LR-115 from Kodak) and 20-microns-thick polycarbonate films. These films are placed between thick detectors of CR-39 and polycarbonate. After exposure, the thin films are etched and spark counted.
Coincidence counting in several different thin-film detectors can be easily carried out by shining light through the stack of properly matched large area replicas, induced on the sparked thin-aluminum electrodes.
While the complete stack for balloon or space experiment is very complex and is formed by a large variety of track detectors with different thicknesses and sensitivities, Fig. 3 shows the section of the stack made of the most sensitive track detectors. This section is formed by 10 different thin-films of LR-115

sandwiched between CR-39 detectors. Thanks to the DIAS cooperation the substack for the spectrometry of HZE particles has been flown on a high altitude balloon in North Canada in August 1993 and was exposed at a maximum floating altitude of about 129000 feets for 50 hours. The thin LR-115 films, once etched, have been spark counted to locate the position of each etched-through track. Coincidences have been then sought between selected pair of plates.The number of coincidences decreases with depth in the stack and levels off at about 100 microns.The events below 100 microns are tracks due to neutron recoils and star particles. The number of coincidences between the first and the last plate, which represents a vertical range of 120 microns, can therefore be assumed to represent tracks of cosmic ray nuclei which have traversed the stack as far as, and beyond, this section.

Achievements, present and future activities.

The progress achieved in this contract is by far exceeding what was initially planned. At the time when the project started, the most important problem to be tackled was to set up the appropriate strumentation for the measurement of the high energy neutrons at civil aviation altitudes. The Linus extended rem-counter and the neutron substack assembled in this contract make it possible to obtain both short-term and long-term measurements of neutrons in the entire energy range.

At present more detector-calibrations are needed, specially for high energy neutrons. However, even at this stage of knowledge all the systems described above are now being extensively used to measure the cosmic ray neutrons at mountain altitudes (such as in Cervino-Italy and Chacaltaya) and on board supersonic and subsonic flights.

List of Publications

L. Tommasino, G. Torri, M. Cavaioli, M. Riccardi and Trinh Van Giap (1994). A long-term study of CR-39 detectors for neutron dosimetry. Nuclear Tracks and Radiation Measurements.Vol.22, 719-724.

Z. Lounis, M. Cavaioli, and L. Tommasino (1995). The combined use of bubble detectors and damage track detectors for neutron dosimetry. Rad. Prot. Dos. Vol. 59, 299-302.

J. Byrne, D. O'Sullivan, L. Tommasino, and D. Zhou (1995). A new method for the rapid evaluation of cosmic ray particles. Results from a balloon borne experiment. Rad. Meas. Vol. 25, 471-474.

L. Tommasino, F. Caggiati, M. Cavaioli, M. Notaro, R. Teodori, G. Torri, D. Zhou, J. Byrne, and D. O'Sullivan. From a complex cosmic ray stack to a simple dosimeter system for aircerw exposure. Paper presented at the International Conference of Natural Radiation Environment. NRE VI, Montreal-Quebec, June 5-9, 1995.

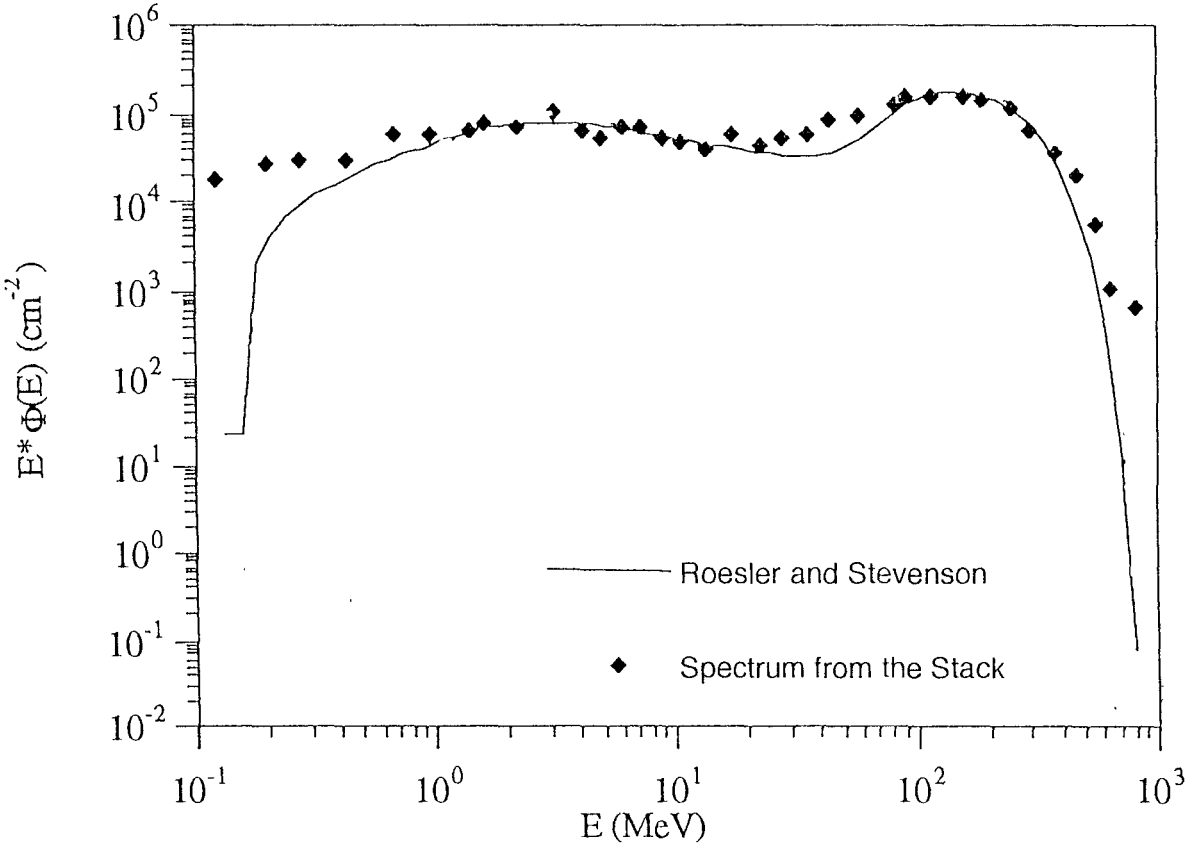
10^6
10^5
10^4
10^3
10^2
10^1
10^0
10^{-1}
10^{-2}
E*Φ(E) (cm^{-2})
Roesler and Stevenson
Spectrum from the Stack
10^{-1}
10^0
10^1
10^2
10^3
E (MeV)

Fig. 1

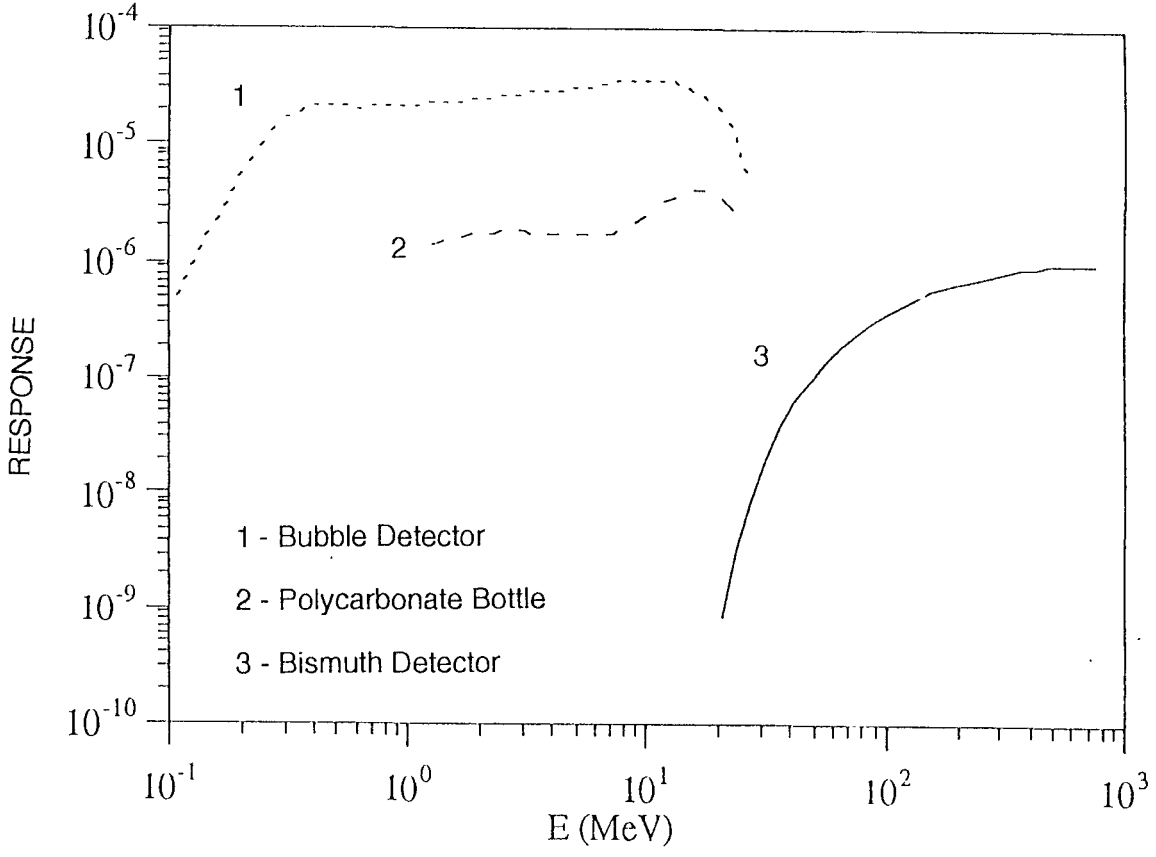
RESPONSE
10^{-4}
10^{-5}
10^{-6}
10^{-7}
10^{-8}
10^{-9}
10^{-10}
1
2
3
1 - Bubble Detector
2 - Polycarbonate Bottle
3 - Bismuth Detector
10^{-1}
10^{0}
10^{1}
10^{2}
10^{3}
E (MeV)

Fig. 2

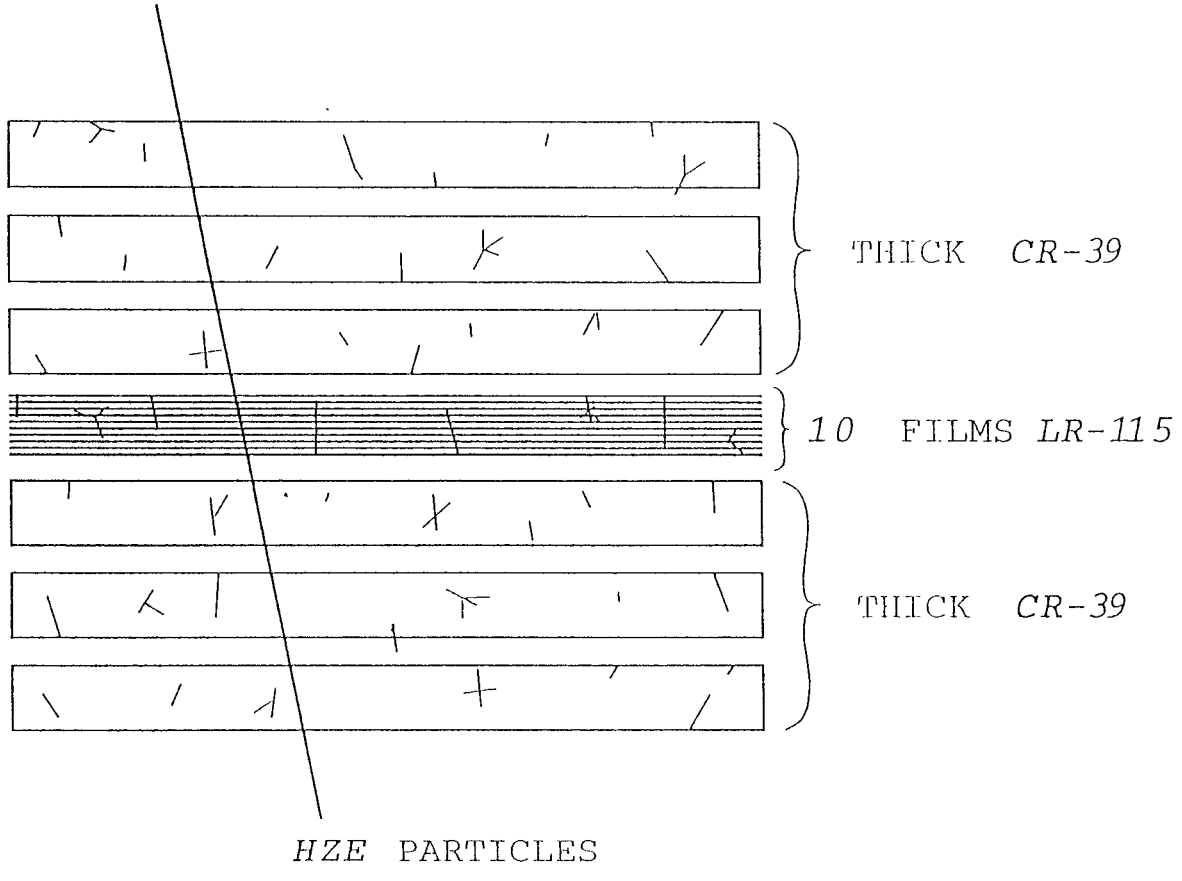

Fig. 3

Head of Project 3: Dr.H.Schraube
Scientific technical staff: Prof Dr W.Heinrich, S.Roesler (subcontractors), Dr.J.Jakes, Dr.G.Leuthold, V.Mares, A.Sannikov, G Schraube, E Weitzenegger.
Consultant: Prof.K.O'Brien

II. Objectives for the reporting period

The general objective of the project was to provide a data basis for the determination of the radiation fields to which air crews and other frequently flying individuals are exposed. The project was subdivided roughly into the following four parts.

1. Calculation of cosmic secondaries which included
   - study of predictions of different models and comparison with experimental data,
   - investigation of systematical dependence of dose measurement on position on earth (geomagnetic cut-off), on time (solar modulation), and on flight altitude,
   - modelling of the cosmic ray nuclear component in the atmosphere and comparison to data measured by the DIAS group in Concorde flights.
2. Response calculations of dosimetric devices.
3. Calculation of dosimetric quantities and set-up of a computer program to calculate flight route doses.
4. Accompanying validation experiments in high energy radiation fields

Strong emphasis was placed upon the neutron component as it contributes considerably to the radiation exposure but is, on the other hand, currently subject to changes with respect to the risk estimates. Consequently it seemed necessary to obtain basic informations on spectral distributions as a sound basis for other considerations. Strong emphasis was also put to the mutual encouragement of calculation and experiments in artificial and natural high energetic fields, as well within the reporting group, as in co-operation with the other members of the contract.

III. Progress achieved including publications

Ad 1. Calculation of cosmic secondaries

Two different models have been used, the code LUIN, which is based on a fast analytic solution of the transport equations and the Monte-Carlo code FLUKA-CR. The code LUIN was developed more than 20 years ago (O'Brien et al , 1972) and has been continuously updated Particle fluxes in the atmosphere are obtained based on the Boltzmann equation. The approximation used in this code limits the calculation of particle spectra to energies above 100 MeV. For neutrons the spectrum is extrapolated towards lower energies by patching the spectrum measured by Hess et al (1959) at 100 MeV. The code FLUKA has been developed to describe hadronic and electromagnetic cascades. This code was applied and extended to calculate radiation fields in the atmosphere based on primary cosmic ray spectra considering effects of solar modulation and geomagnetic shielding. We note that the primary cosmic ray spectrum, which is implemented in LUIN, is different and simplified in comparison to the spectra we use together with FLUKA. Since results of the calculations depend on our extension of the code with respect to the primary spectra and on further assumptions like the idealised model of the atmosphere, we will call the model consisting of the original FLUKA code, together with our modifications and input, FLUKA-CR.

Differences between the results of these two models may be caused by the different descriptions of particle interactions and, additionally, also by differences within the primary cosmic ray spectra. A comparison of calculated proton and neutron spectra in the atmosphere

has shown the general tendency that FLUKA-CR predicts higher fluxes than LUIN, especially for larger atmospheric depths. It is difficult to draw further conclusions on which model might be able to describe the measurements more realistically based on the data of older cosmic ray experiments, alone

Neutron spectra have been calculated for an atmospheric depth of 700 g/cm² air, which corresponds to conditions at the Zugspitze where recently verification measurements were performed (see chapter 4). Results of FLUKA-CR (solar minimum, location 47° northern

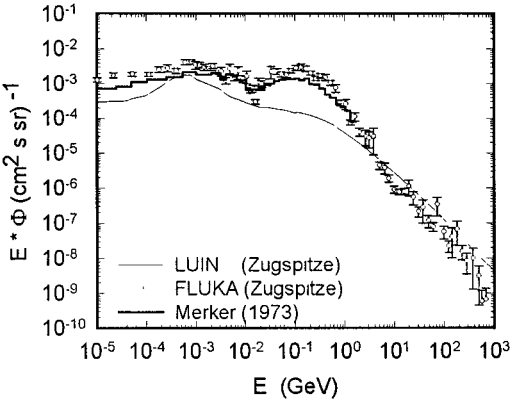

Figure 1.1: *Neutron fluence rate per logarithmic energy interval calculated with the codes FLUKA and LUIN for the conditions of the top of the mountain Zugspitze (3000m) and compared with data of Merker (1972).*

latitude and 11° eastern longitude) and the LUIN code (heliocentric potential: 500 MV, same location) are shown Additionally shown are results of a calculation by Merker (1973). The calculated fluxes using FLUKA-CR are significantly higher than those calculated with LUIN. The LUIN results do not show the nuclear cascade peak which is expected at about 100 MeV. There is fairly good agreement in the shape of the Merker spectrum in comparison to the FLUKA-CR spectrum. However the evaporation and nuclear cascade peaks at 1 MeV and 100 MeV, respectively, are less pronounced in the Merker spectrum.

In Figure 1.2 the neutron spectra in the atmosphere were integrated for different atmospheric depths. The integral neutron flux density for energies between 10^{-14} GeV and 1300 GeV for neutrons coming from the upper hemisphere only (2π) and for omnidirectional neutrons (4π) are shown. The lines show exponential fits to the results at depths above 400 g/cm². The ratio of the omnidirectional flux to the flux coming from the upper hemisphere does not change significantly for depths larger than 100 g/cm² Again the flux calculated by FLUKA-CR seems to be too high.

Apparently, the FLUKA-CR calculations support the assumption made in the LUIN code that differential neutron spectra for energies below 100 MeV show no significant change in shape for different geomagnetic shielding (i.e. position on earth) and different depths in the atmosphere below 200 g/cm². However, the shape of the calculated FLUKA-CR spectra differs significantly from the Hess spectrum, especially in the region from 1 to 100 MeV, which is relevant for the dose equivalent quantities. The slope of the neutron spectrum calculated with FLUKA-CR agrees with the predictions by Merker. The measurements at the Zugspitze show a characteristic cascade peak at 100 MeV which is predicted by FLUKA-CR calculations and by the model of Merker, but not seen by Hess et al.. The absolute fluxes of the FLUKA-CR spectra exceed those predicted by the LUIN calculations and those of the Merker spectrum

and the values measured at sea level and during the mountain experiment. This needs further investigation. It can be concluded that the LUIN code, which is the basis for dose predictions

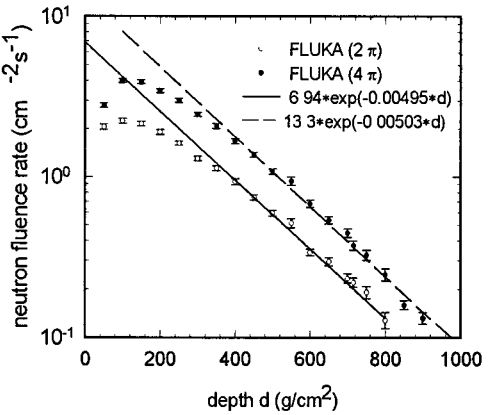

Figure 1.2: *Integral neutron fluence rate versus the atmospheric depth determined with the code FLUKA-CR (solar minimum, location like Zugspitze)*

by the widely used CARI program, needs improvement with respect to contributions from neutrons.

Besides protons and their secondaries, cosmic ray nuclei contribute to the aircraft radiation exposure, especially at higher flight altitudes. Measurements of these particles are performed within this project with CR-39 nuclear track detectors by the Dublin group. We have extended a model of heavy ion propagation through matter, which was developed at the University of Siegen, to cover this problem at air craft altitudes.

In table 1 the number N_{calc} of predicted particles is compared to the number N_{exp} of particles seen in the experiment for nuclei with charges from 2 to 26. The experimental data which have been supported by the DIAS group are first preliminary results There is a reasonable agreement within a factor of about two between the predictions and the data for He-nuclei. For heavier nuclei with charges 3 and 4 the excess of nuclei detected in the experiment is much higher. Furthermore there is a significant disagreement between the measurements and the predictions for Z=8. However, these discrepancies are expected to disappear after corrections for scanning efficiencies for large charges and after a more detailed investigation of detector sensitivity.

Table 1: *Heavy ions observed during Concorde flights. comparison of predicted and experimental results (scanning area 23 cm²)*

charge	Ncalc	Nexp
2	33 7	77
3	3.5	23
4	3.1	16
5	6.7	13
6	17.9	26
7	13.1	13
8	69.7	13
9	13.8	16
10	15.3	13
11	9.2	
12	9.7	
13	4 2	
14	4.6	
15-19	6 2	
20-26	2 4	

Ad 2. Response calculations of dosimetric devices

Based on the experiences gained during the experiments in the high energy fields at the CERN facility (see Chapter 4), it appeared that the determination of the neutron component employing a device with TEPC is not very promising, because of the low LET of charged particles created by high energetic neutrons. Therefore, the effort of the response calculation was shifted to the determination of the response of the Bonner sphere device which permits to evaluate the neutron fluence distributions from measurements from which all other required dosimetric quantities can be derived.

There were two additional motivations to study numerically the responses of the Bonner sphere spectrometer in the energy range above 15 MeV: Some findings in the frame of the co-operative experiments at CERN indicated that the recently calculated responses (Mares and Schraube, 1994) were too low in the high energy range. The second one was the recent opportunity of using the library LA100 Evaluated Nuclear Data Library for transport calculations involving incident neutrons and protons of energies up to 100 MeV, which became available in the meantime through the NEA Data Bank at Issy-les Moulineaux in France. This library is based on nuclear theory/model calculations with parametrisations obtained by matching calculations with experimental data, mainly the PSR-125/GNASH statistical/preequilibrium/fission theory code. The library includes neutron- and proton-induced reactions for nine targets and specifies the production cross sections, and energy-angle correlated spectra of emitted neutrons, protons, alpha-particles, photons, and other significant charged particles. The library LA100 is written in format ENDF/B-6 and must be processed through the NJOY 89 Nuclear Data Processing System, which is designed to handle the new ENDF-6 formats. The MCNP code was modified with a special patch to properly handle the new pointwise libraries up to 100 MeV.

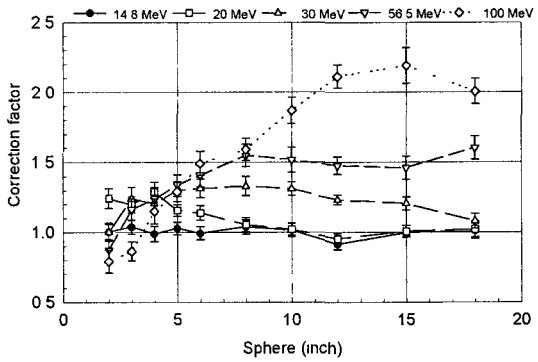

Figure 2.1: *Correction factors to be applied to the responses of the Bonner spheres with 6Li(EU) neutron detector based on recently available carbon cross section data in the MCNP format*

The responses of 10 spheres with diameters between 2 and 18 inch were re-calculated for incident neutrons in the energy range from 14.8 MeV to 100 MeV using the carbon cross sections from LA100 In the past, when the carbon cross section data above 20 MeV in the MCNP format were not available, MCNP code was permitted to extrapolate automatically by using the constant cross section value at 20 MeV. However, the carbon total cross section decreases slowly from the value of about 1500 mb at 20 MeV to the value of about 500 mb at 100 MeV.

In figure 2.1, the response correction factors calculated as the ratio of the recalculated responses using the LA100 libraries and the responses calculated with constant carbon cross section approximation are shown It can be seen that at 14.8 MeV neutron energy there are no

considerable changes in the responses of all sphere diameters within the statistical uncertainty. In the case of neutron energies higher than 14 8 MeV the correction factor increases with increasing energy. Its maximum is shifting toward the larger spheres reaching the absolute maximum of 2.2 for the 15 inch sphere at 100 MeV neutron energy The lithium cross section data for energies over 20 MeV are not yet available in suitable MCNP format and therefore the constant extrapolation of cross section value given at 20 MeV was still used to cover the energy range up to 100 MeV.

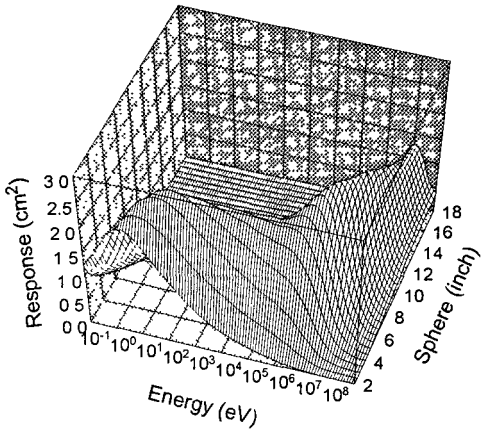

Figure 2.2: *Three dimensional representation of the response matrix of the Bonner-sphere spectrometer with ^{3}He-proportional counter up to 100 MeV (Mares and Schraube, 1995)*

Further effort was posed to study the response of the high sensitive Bonner sphere spectrometer with ^{3}He-detector in the very interesting energy range above 20 MeV up to 1 GeV from which finally the high energy contribution of the neutron dose at flight levels may be derived. Two different approaches were used. The MCNP-4A code in the above mentioned energy range up to 100 MeV, and the cosmic particle cascade code HADRON in the energy range 40 MeV to 1 GeV. It appeared that between 40 and 100 MeV the results of both codes were in rather good agreement, despite their different approach to the physical processes. The combined responses is labelled with MCNP/HADRON in figure 2.3. A comparison with data in the recent literature (Hsu et al., 1994) , however, shows an increasing difference with increasing energy. Furthermore the response data are not consistent for the different sphere diameters, i.e. they do not exhibit an unique relative calibration factor even not for energies below 20 MeV, which could account for differences in the sensitivity of the thermal neutron detector.

The HADRON code developed at IHEP (Protvino, Russia) is based on the cascade-exciton model of nuclear reactions This model includes cascade stage (modified version of the Dubna cascade model), pre-equilibrium stage (exciton model) and equilibrium evaporation stage. Low energy neutrons below 20 MeV are transported in the HADRON code by the Monte-Carlo code ANEUT.

LAHET is the Monte Carlo code developed at LANL based on the HETC code for transport of nucleons, pions, and muons, originally developed at ORNL. In contrast to the original HETC code which uses cascade-evaporation model with Bertini intranuclear cascade code, LAHET has different options. There are Bertini and ISABEL cascade models, the last one is based on the VEGAS code developed at BNL. At the de excitation stage the pre-equilibrium exciton model or Fermi break-up model (for light nuclei) may be used The philosophy behind

the LAHET is to treat all interactions by protons, pions and muons within LAHET, but to treat neutron interactions only above a cut-off energy 20 MeV. Any neutron appearing from a reaction with energy below the cut-off energy is recorded with its kinematic parameters on neutron file for subsequent transport by the Monte Carlo code HMCNP (modified version of MCNP) utilising ENDF/B-based neutron cross section libraries.

It is not easy to draw any conclusion from these comparison because it is not well known what options were used in LAHET calculations performed by Hsu et al The present benchmark calculations document the effect of the different philosophy behind the both codes and different versions of Dubna and Oak Ridge physical models. The possible reason of discrepancies is among others that inelastic cross sections are calculated by LAHET code itself whereas MCNP and HADRON use evaluation of experimental data.

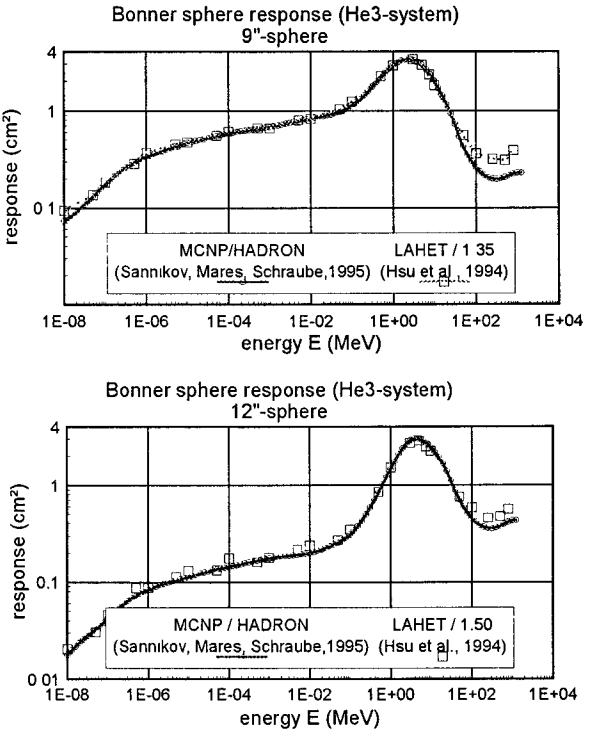

Figure 2.3: *Fluence response of the 9"-**(top)** and the 12"- Bonner-sphere **(bottom)** with ^{3}He-proportional counter from thermal up to 1 GeV neutron energy.*

Ad 3. Calculation of dosimetric quantities

The calculations of the organ doses in the MIRD phantom were extended from 20 MeV (Leuthold et al., 1995) to the energy range up to 100 MeV (Mares et al., 1995) using the MCNP code in the configuration described in chapter 2. In figure 3.2 as an example the fluence-to-effective dose conversion function is shown calculated for different angles of incidence (from 0 degree = A-P to 75 degree) to the left side of the ADAM-phantom in the neutron energy range from 0.01 eV up to 100 MeV For the calculation of absorbed dose the kerma approximation was used, i e., it is assumed that the dose is absorbed at the place where the secondaries are generated. This may lead to an overestimation of the doses in organs close

to the body surface to some extent. Above 10 MeV the recommended kerma values of White et al. were taken. For the calculation of effective dose the smooth radiation weighting factor of ICRP 60 was applied.

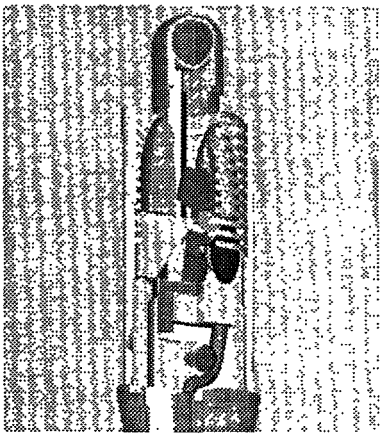

Figure 3.1: MIRD-phantom ADAM implemented into the MCNP code and used for the calculation of the organ doses and derived limiting radiation protection quantities.

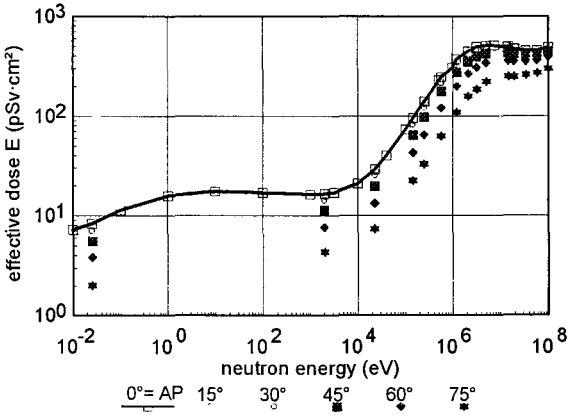

Figure 3.2: Effective dose calculated for 6 angles of incidence to the surface of the MIRD-phantom ADAM

Considering the radiation to which air crews are exposed the question raised which operational quantity is appropriate for an upper estimate of the risk related and primary limiting quantities. A series of broad neutron spectra was extracted from the literature and used to calculate the integral operational and limiting quantities Figure 3.3 exhibits the ratio H*(10)/E for 19 spectra of artificial and natural sources which were calculated or experimentally determined. The integration was extended to 1 GeV neutron energy although the data base for the conversion function is partly still weak

It is concluded that even for the hardest spectral distributions considered, ambient dose equivalent remains a conservative estimator for the phantom defined quantities effective dose and effective dose equivalent. The conservativity is better for rotational irradiation than for frontal irradiation and should be slightly better for isotropic irradiation. It is reasonable to

assume that air crew members are exposed isotropically (or isotropically from above) rather than from front.

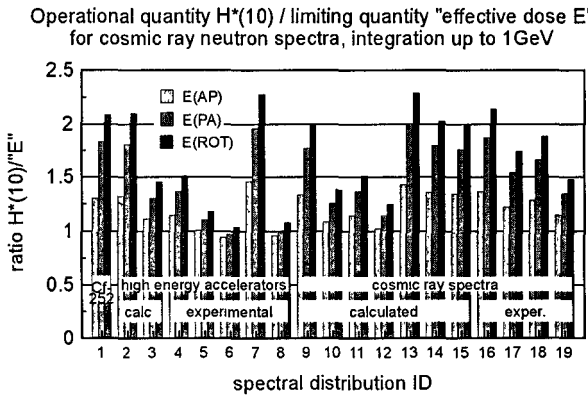

Figure 3.3: Ratios of the operational quantity H(10) to the risk related quantity effective dose "E" after ICRP60 for a series of neutron spectra from cosmic origin and around high energy accelerators with essential high energetic neutron components.*

4. Accompanying validation experiments in artificial and natural high energy radiation fields

The group participated in the joint experiments conducted by CEU and CERN for a better understanding of air borne experiments. In the 120 GeV/c proton produced radiation field, measurements were done with a 2" spherical tissue equivalent proportional counter (TEPC) simulating 2µm tissue using a series of build-up caps. This should give the possibility of an additional analysis of the radiation field components. Figure 4.1 presents measuring results of the bare counter and those obtained with three different PE-caps applied. The high LET part between 10 keV/µm and the proton edge at around 120 keV/µm was analysed to derive the attenuation characteristics for the specific field condition.

The result is shown in figure 4.2, where the attenuation coefficient $\beta_{(120GeVp \rightarrow Cu)}$ = 0.39 and 0.72 (1/cm) for the fields behind iron and concrete shields, respectively. The data are compared with those derived from measurements with the TEPC and an ionisation chamber in monoenergetic neutron fields. It can be seen that the specific coefficient fits the other data well

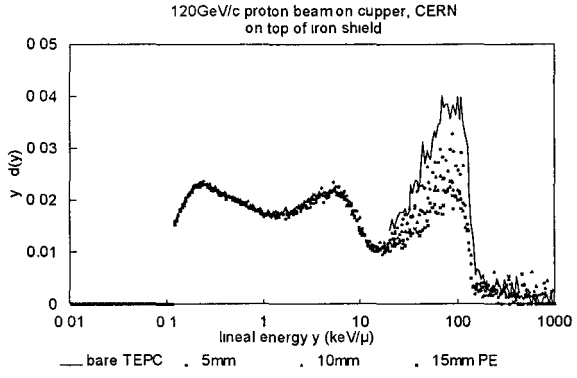

Figure 4.1: Relative dose distribution y·d(y) versus lineal energy as measured at the CERN relativistic stray radiation field behind iron shielding with a TEPC with and without PE build-up caps.

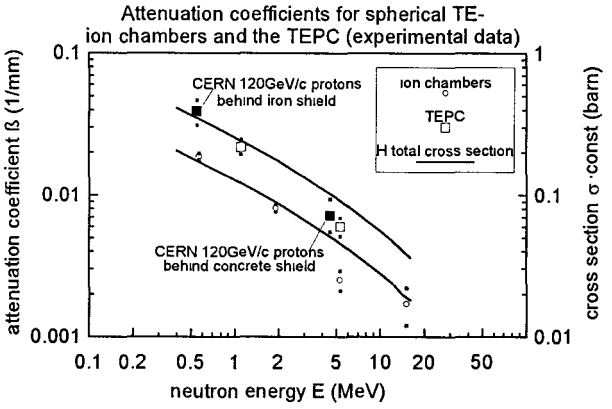

Figure 4.2: Attenuation characteristics as measured at the CERN relativistic stray radiation field behind iron and concrete shieldings and monoenergetic neutrons with a TEPC with and without PE build-up caps. Ion chamber measurements are included for comparison reasons, the cross section curves should only indicate the physical tendency.

when an (dose averaged) energy of approximately 0.55 MeV and 4 MeV are assumed for the both fields. Apparently, the attenuation characteristic is essentially determined by neutrons below roughly 20 MeV, while higher energetic neutrons deliberate charged particles essentially with lineal energies below 10 keV/µm. In this range of lineal energies they can no more be distinguished from electrons and muons. This fact limits the merit of a TEPC based device to high energetic neutron fields

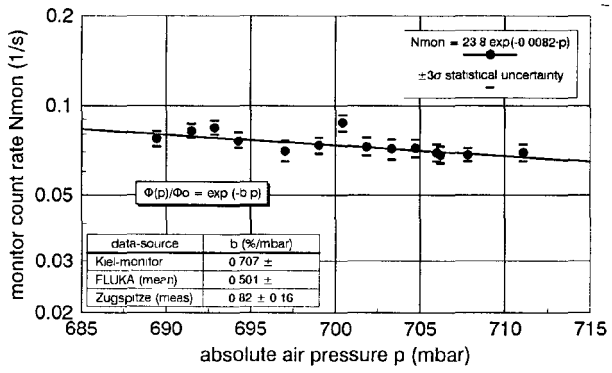

Figure 4.3: Count rate of the 5" sphere used as monitor of the neutron fluence rate as a function of air pressure

Further experiments were done with the Bonner sphere spectrometer (chapter 3) with ^{3}He-detector on top of the mountain Zugspitze (3000m) for which the calculations are presented in chapter 1. The 5" sphere was used to monitor the neutron fluence rate as a function of air pressure. The result is shown in figure 4.3. An exponential fit delivers a coefficient of (0.82± 0.16) %/mbar which is in agreement with the data of the University of Kiel observatory within the statistical uncertainty, but significantly higher than the FLUKA data described in figure 1.2. This means that the attenuation in the earth atmosphere calculated by FLUKA is somewhat too small. In the figures 4.4 the measured Bonner sphere data are compared with data which were gained by scalar multiplication of two calculated neutron spectra with the response matrix,. The data are normalised here to the 5"-sphere measurements. They indicate that the thermal

neutron contribution obtained from the transport calculations is considerably too low. At high energies (large spheres) the agreement between calculation and measurement is better with a tendency of a higher component for the FLUKA calculation.

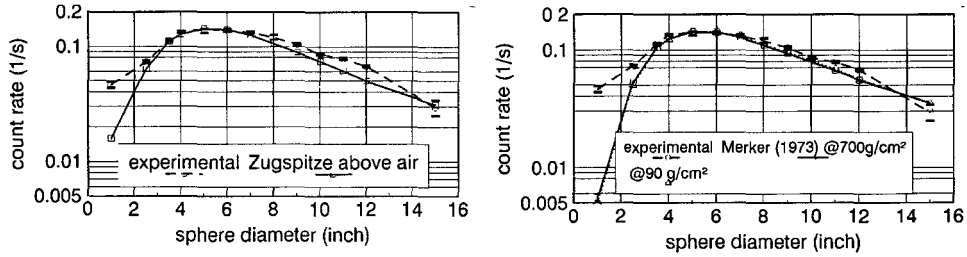

Figure 4.4: Experimental count rates of the BS-Spectrometer compared with calculated date on the basis of FLUKA spectra (left) and of the spectra after Merker (1973) (right). The calculated data are normalised to the 5" point.

References

Hess, W.N., Patterson, H.W., Wallace, R., Chupp, E.L.: Cosmic-ray neutron energy spectrum. Physical Review 116, 2 (1959) 445-457

Hsu, H.H., Alvar, K R , Vasilik, D.G.. A New Bonner-Sphere Set for High Energy Neutron Measurements - Monte-Carlo Simulation. IEEE Transactions on Nuclear Science 41, 4 Part 1(1994) 938-940

Leuthold, G., Mares, V., Schraube, H.. Calculation of the neutron ambient dose equivalent on the basis of the ICRP revised quality factors Radiat.Prot.Dosim. 40 (1992) 77-84

Leuthold, G., Mares, V., Schraube, H.: Monte-Carlo calculations of dose equivalents for neutrons in anthropomorphic phantoms using the ICRP-60 recommendations and the recent stopping power data of ICRU49. GSF-Bericht, in print (1995)

Merker, M.: The contribution of galactic cosmic rays to the atmospheric neutron maximum dose equivalent as a function of neutron energy and altitude. Health Physics 25 (1973) 524-527

O'Brien, K.: Cosmic-ray propagation in the atmosphere. Il Nuovo Cimento 3a, 3 (1971) 521

White, R.M., Broerse, J.J., DeLua Jr., P.M , Dietze, G , Haight, R.C., Kawashima, K., Menzel, H.G., Olsson, H., Wambersie, A.. Status of Nuclear Data for Use in Neutron Therapy. Radiat. Prot. Dosim. 44(1/4), 11-20 (1992).

Publications

Mares, V., Schraube, H.: Evaluation of the response matrix of a Bonner sphere spectrometer with LiI detector from thermal energy to 100 MeV. Nucl Instrum.Meth. A 337, 461-473 (1994)

Mares, V., Schraube, H.: Improved response matrices of Bonner sphere spectrometers with 6Li scintillation detectors and 3He proportional counter between 15 MeV and 100 MeV neutron energy. Nucl.Instrum.Meth. A (1995) (in print)

Contributions to the 8th Symposium on Neutron Dosimetry, Paris, 13-17 November 1995:

Leuthold, G., Mares, V , Schraube, H : On the conservativity of Hp(10).

Mares, V., Leuthold G., Schraube, H. Organ doses and dose equivalents for neutrons above 20 MeV.

Sannikov, A., Mares, V , Schraube, H.: High energy response functions of Bonner spectrometers.

Schraube, H., Jakes, J , Sannikov, A.., Weitzenegger, E , Roesler S., Heinrich, W.: The cosmic ray neutron spectrum on top of the Zugspitze (3000 m)

Head of Project 4: Dr. O'Sullivan

II. Objectives for the reporting period

The main objectives were to investigate methods suitable for the study of charged particles heavier than protons at aircraft altitudes and to carry out exposures of detectors on a variety of commercial airline routes. As a result of these exposures it was hoped that the presence or otherwise of helium and heavier nuclei would be confirmed at aircraft altitudes and that some preliminary knowledge of the flux and relative abundance of $Z \geq 2$ nuclei would be obtained. Finally, a comparison of the experimental values with those predicted by radiation propagation models calculated by the Siegen Group, would be undertaken.

III. Progress achieved including publications

In a joint experiment on a high altitude balloon with the ANPA (Rome) group the combination of DIAS and ANPA techniques of particle location and identification was successfully executed and provided useful information for future projects at aircraft altitudes.
Negotiations with several airlines were successful and DIAS detector stacks were exposed on flight routes varying from 10.6km to 17.6km in altitude. The data confirmed the presence of particles with Z values up to and including magnesium (Z=12) at the highest altitude (Concorde) and mainly helium nuclei at the lower altitudes (Boeing 747 and Gulfstream-4 Jet). Comparison of the preliminary helium flux measured on the Concorde route with that predicted by a theoretical propagation model showed reasonably good agreement.

Dublin Institute for Advanced Studies (DIAS) GROUP FINAL REPORT

D. O'Sullivan and J. Byrne
Dublin Institute for Advanced Studies
Dublin, Ireland.

The presence of cosmic ray particles in the Earth's atmosphere presents a source of ionising radiation at high altitudes, and concern has arisen regarding the possible hazardous effects of prolonged exposure to this radiation. To date, investigations of cosmic radiation at altitude in the atmosphere have employed techniques to determine, mainly, the total dose delivered by the radiation.
For the purposes of radiation protection, cosmic radiation may be separated into the neutron component, the photon component and the charged particle component. In the work described here, we are investigating those charged particles in the atmosphere with charge $Z \geq 2$. The primary objective of this study was to determine the presence of helium and heavier particles at the altitudes at which commercial aircraft operate. In the execution of this task, the high resolution techniques usually undertaken for the investigation of heavy cosmic ray nuclei in cosmic ray physics were employed.
Solid state nuclear track detectors (mainly CR-39) were exposed on board various aircraft for periods of several months. A sample of detector material exposed on each aircraft was calibrated with 85 MeV/nucleon carbon ions at GSI, Darmstadt in January 1995.

Balloon Flight Experiment

The investigation of the flux and charge spectrum of high energy ($E > 10$ Mev/nucleon) nuclear particles with charge $Z \geq 2$ for dosimetry purposes requires a different approach to that used in the field of cosmic ray astrophysics. Measurements undertaken for astrophysical purposes require high resolution techniques, which are typically time consuming. For dosimetry purposes, the introduction of rapid evaluation procedures could be advantageous, and less stringent resolution requirements necessary.
While preparing a detailed programme for the investigation of cosmic ray particles and their secondaries at aircraft altitudes, approaches were made to the US National Scientific Balloon Facility (NSBF) requesting facilities to expose a combined detector stack to investigate the combination of techniques used by Tommasino and co-workers at ANPA, and by the DIAS group. This preliminary study of the combined techniques was carried out in an effort to provide an improved method for the study of neutrons, protons and heavier nuclei in the Earth's atmosphere. The main aim was to apply any potential advantages found in the joint investigation to the experiments planned in aircraft at high altitude.
The stack, illustrated in figure 1, contained many sections, and was designed to investigate neutron and proton spectra as

well as the spectra of heavier cosmic ray nuclei. It was flown as part of the payload on a high altitude balloon launched in August 1993 in northern Canada. The maximum floating altitude of the balloon was approximately 129,000 feet (39.1 km), and the minimum was approximately 106,000 feet (32.1 km). The total exposure time was 50 hours.

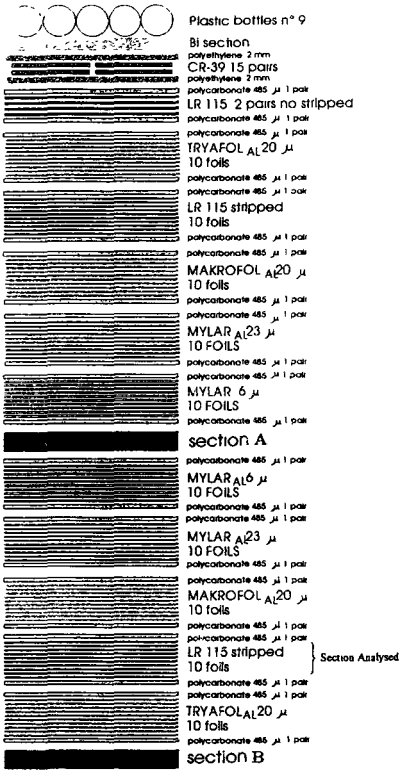

Figure 1: Cross Section of Detector Indicating Section Analysed

Following exposure and retrieval of the detector stack, that section indicated in figure 1 was removed and investigated. The thick polycarbonate plates (485µm), adjacent to the top and bottom of the ten sheet LR-115 layer, were removed and chemically etched in a solution of NaOH (6.25N) at 40°C for 168 hours. The plates were subsequently scanned using an optical microscope to locate particles. The thin sheets (12µm) of LR-115 were processed by our colleagues at ANPA. The sheets were etched in a solution of NaOH (10%) at 60°C for one hour. The position of each etched track was located using the spark-replica technique.

Of primary interest in this investigation are those particles which are observed above threshold over the entire section. Eleven such events were located, and identified as having charge $Z \geq 20$, as indicated in figure 2.

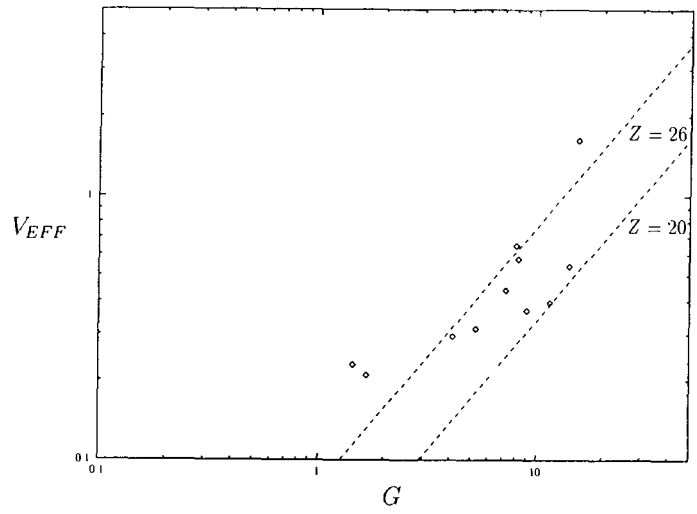

Figure 2: The Effective Etch Rate versus Gradient for the eleven events which penetrated the Section under investigation and remained above threshold

The number of coincidences in the LR-115 is seen, in figure 3, to decrease with depth, or range, in the layer and levels off above approximately 100μm.

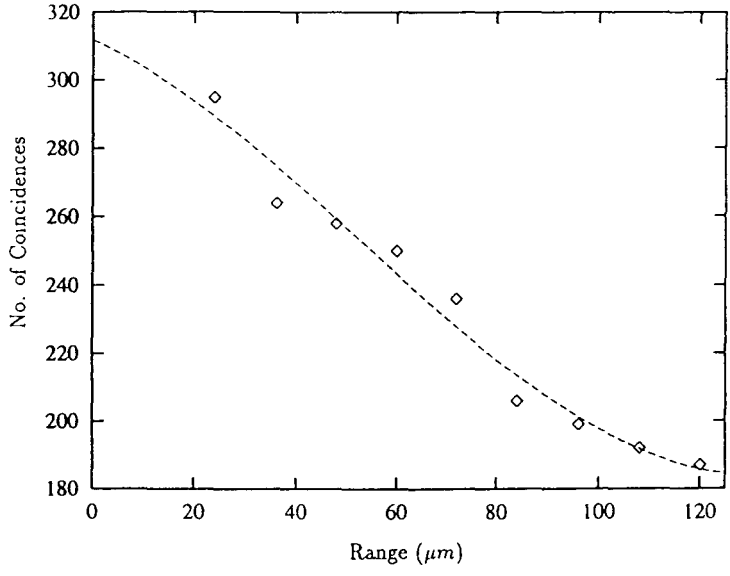

Figure 3: Number of Coincidences versus Range in thin LR-115 stack

The range at which the track density levels off is equivalent to carbon and nitrogen nuclei of energy $E \leq 5MeV/nucleon$, which is consistent with the expected energy for these recoils. Thus the number of coincidences between the top and bottom sheets of the LR-115 (vertical range of 120μm) represents approximately the number of cosmic ray nuclei (or secondaries) which have traversed the stack as far as this section and remained above threshold.

Given the number of cosmic ray nuclei (with $Z \geq 20$) observed in the thick polycarbonate plates, the expected number of coincidences was determined, taking into account the charge and energy spectra of galactic cosmic rays, and the registration threshold for the polycarbonate and LR-115 materials. The calculated value was consistent with the observed value to within 10%. The results indicate that the system operates satisfactorily, separating low energy recoil events from the main cosmic ray flux.

By extending the system to several sets of LR-115 layers, thick CR-39 and polycarbonate plates, it could be applied to the rapid location of track enders using the thin films, and accurate identification of particles using the thick plates. Charge identification could also be determined using the total range registration method. Further investigation of this combined system is necessary to determine the best possible combination of these detector materials for particular requirements.

The Aircraft Exposures

Following negotiations with various aircraft operators, high altitude exposure facilities were secured on board an Aer Lingus Boeing 747, the Irish Government Gulfstream 4 jet and a British Airways Concorde. These exposures facilitated data acquisition in the altitude region 35,000 feet (10.6km) up to approximately 58,000 feet (17.6km), and are presented here in order of decreasing altitude.

Concorde

The supersonic Concorde is currently the highest flying commercial aircraft in operation, operating at a cruising altitude of up to 58,000 feet. Following approaches to British Airways, agreement was reached to place three DIAS detector stacks on board a Concorde aircraft operating primarily on the London-New York route. Arrangements were also made for our colleagues at ANPA to expose some material on this aircraft.

The three stacks each contained CR-39 and Lexan polycarbonate, and each had an exposure area of approximately $0.02m^2$. The material was installed on the aircraft early in October 1993

and was removed in March 1994, after a total flying time of approximately 325 hours.

Subsequently, CR-39 material from one of the stacks was chemically etched in a solution of NaOH (6.25N) at 60°C for 30 hours. Optical scanning revealed particle tracks. The scanning procedure was based on selecting those particles which penetrated at least one detector plate. Thus, in order to be selected, the particle had to have a minimum observable range of approximately 500μm, and the background of shorter tracks on the surface of the plate was excluded.

A total of 115 events was recorded in a total area of 20cm^2. Each event was labelled and followed from its starting point to its stopping point in the stack, or to the point where it exited the stack. Of the total number of events located, approximately 30% were found to penetrate the entire stack thickness of ~1.5cm.

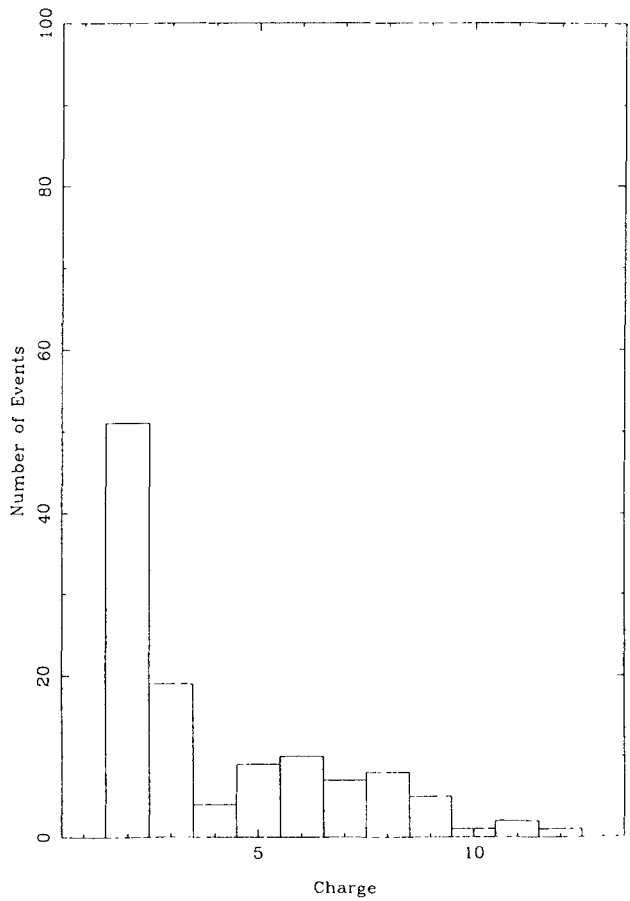

Figure 4: Observed Charge Distribution for Concorde Exposure

In the case of particles which penetrated more than one plate of detector material, the directional characteristics of the event were verified along the trajectory of the particle. In the case of particles passing through the entire detector stack, a continuous set of data was obtained for each particle, and all chance coincidences were eliminated.

Each nucleus was identified and the observed charge distribution is illustrated in figure 4. The charge resolution, ΔZ, is approximately $\pm 0.5e$.

With the benefit of our knowledge from this first investigation on board Concorde, we have recently deployed newly designed stacks on the aircraft and these exposures will form part of future studies in this area.

Irish Government Jet

Approaches were made to the Irish Air Corps requesting exposure facilities on board the Irish Government Gulfstream 4 jet. Two detector stacks, with a total area of $0.07m^2$, were installed on the aircraft in May 1993. They were removed in December 1993, by which time a total of 600 hours flying time had elapsed. During this exposure period, the aircraft operated on a variety of routes and at altitudes ranging from 39,000 feet (11.8km) up to 43,000 feet (13.0km).

Following exposure, one of the stacks was chemically processed, and subsequent optical scanning revealed 19 particle tracks in an area of $26cm^2$. In contrast to findings on Concorde, all particles located, so far, stop in the stack and are of short range($2000\mu m$), and each one was followed from its starting point to its stopping point in the stack and etch rate and residual range measured. The charge distribution is illustrated in figure 5.

In February 1994 a second set of four detectors was installed on the aircraft. By this time very preliminary results from the balloon flight experiment were available, and it was decided to further investigate the use of a combined system of thick and thin detectors on this exposure. Four detector stacks, which were comprised of layers of LR-115, CR-39 and Lexan polycarbonate were deployed. This material will form part of future studies.

Aer Lingus Boeing 747

Negotiations with Aer Lingus resulted in an agreement to place six detector stacks on board a Boeing 747 aircraft operating primarily on the Dublin-New York and Dublin-Boston routes. The stacks were comprised of CR-39 and Lexan polycarbonate. The total detector area exposed was approximately 0.2m. Between May and December 1993, the stacks were exposed for a total of 2054

hours. During this time the average cruising altitude of the aircraft was between 35,000 feet (10.6km) and 37,000 feet (11.2km).

Following chemical processing, optical scanning revealed 86 particle tracks in an area of 16cm^2. All of these were of short range (< 3000μm) and the charge distribution is illustrated in figure 5.

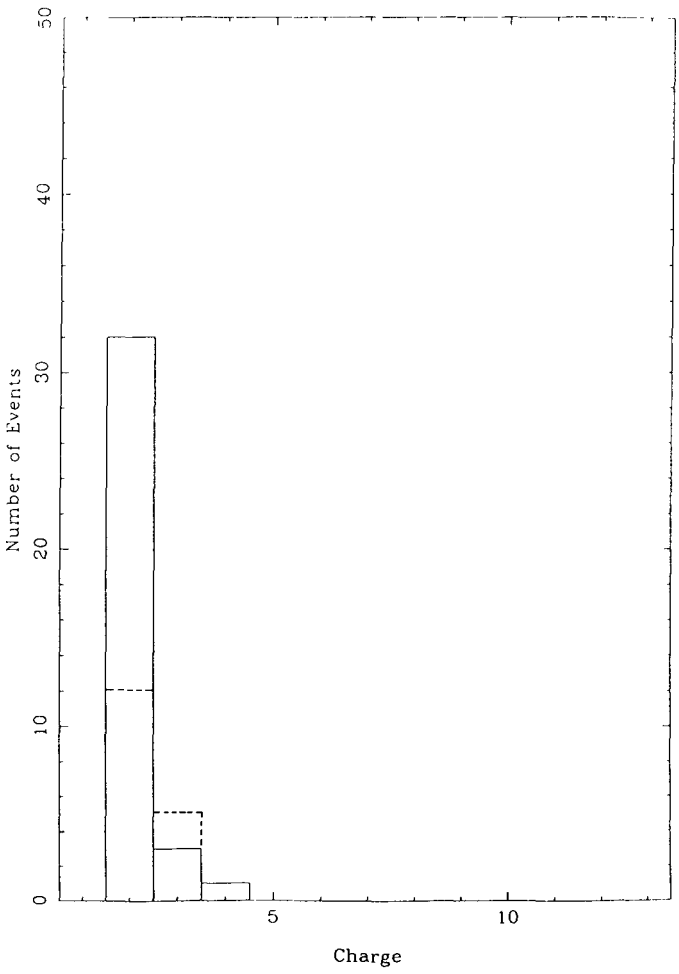

Figure 5: Charge Distribution for Boeing 747 Exposure (solid line) and Gulfstream 4 Jet (Dotted line). See Table 1 for details of area-time factors.

Initial examination of material from each of the aircraft exposures revealed a significant increase in track density per unit time with altitude, as expected (see Table 1).

Altitude (feet)	Total Area (cm^2)	Time at Altitude (Hours)	Track Density (No./cm^2)	Density per Unit Time (No./cm^2/hr)
37,000	80	2054	0.5	$2.4 \pm 0.4 \times 10^{-4}$
42,000	26	600	0.7	$1.3 \pm 0.3 \times 10^{-3}$
58,000	20	325	5.8	$1.8 \pm 0.2 \times 10^{-2}$

Table 1: Track Densities

Preliminary Charge Spectra

The measured charge spectra of Z>1 particles on the Concorde aircraft demonstrates the presence of charged nuclei all the way from helium up to magnesium (Z=12). Work on the determination of the abundances of the Z>2 nuclei relative to He is still in progress and will be reported later. This involves further investigation of the energy intervals of registration and scanning efficiency for each charge value. For instance although oxygen nuclei register in our CR-39 in principle right up to relativistic velocities the particular scanning technique employed to separate the cosmic ray primaries and secondaries from the large background of recoil nuclei limited the upper energy values to E≤800 MeV/nucleon.

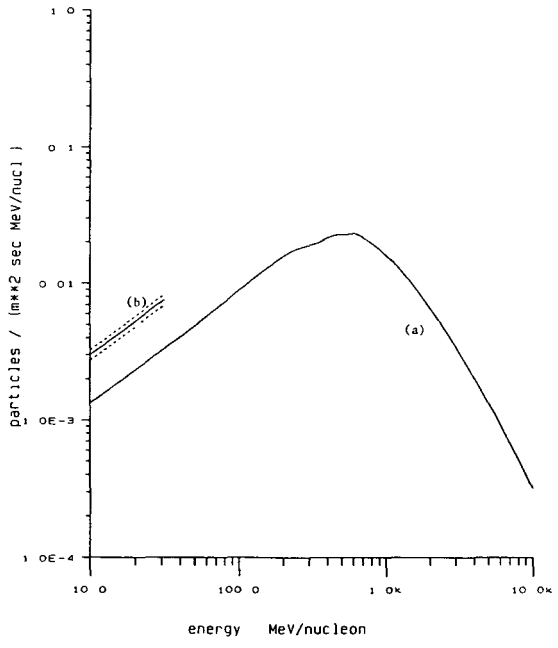

Figure 6:(a) Calculated He spectrum for a London-New York trip on Concorde Route (Private Communication from Prof. Wolfgang Heinrich, Univ. of Siegen). (b) He spectrum measured on Concorde

Figure 6 shows the flux of helium nuclei observed in the Concorde exposure compared with that predicted by the calculations of the group at Universitat Gesamthochschule Siegen (private communication from Prof. Wolfgang Heinrich - see this report). The spectra are calculated for a London-New York journey. Similar comparisons for spectra of Z>2 nuclei will form part of the continuing investigations.

The preliminary spectra observed on the Boeing 747 and the Gulfstream 4 jet (Fig. 5) extend only to $Z \leq 4$ reflecting the lower probability of survival of heavier nuclei at these lower altitudes in the atmosphere. Indeed, those nuclei above Z=2 are likely to represent a spill over from the He peak. The detectors exposed in the Boeing aircraft have been calibrated using the 80 MeV/nucleon Carbon ions from GSI Darmstadt. However the Gulfstream data has yet to be calibrated and it has been assumed for the present purposes that the peak in the Z>1 data represents helium. Investigations at these lower altitudes are continuing.

Acknowledgements

This work was supported under the Radiation Protection Research Contract: F13P-CJ92-0026 of the Commission of the European Community. We wish to thank Mrs Eileen Flood for technical and administrative assistance throughout the project; Dr. Dieter Schardt of GSI for arranging the calibration exposures; Mr. Don Dixon of British Airways; Mr Stuart Dobbyn of Aer Lingus; Col. O'Malley and the staff of the Irish Air Corps at Baldonnel; Mr. D. Grouse of Trinity College Dublin and finally, Mr. D Ball at the NSBF(USA) who arranged the high altitude balloon exposure in Northern Canada.

Publications

1. D. O'Sullivan. "Results from the Investigation of Cosmic Rays using SSNTD at Dublin". Rad. Meas. **25**, 295-300, (1995).

2. J. Byrne, D. O'Sullivan, L. Tommasino, D. Zhou. "A New Method for the Rapid Evaluation of $Z \geq 1$ Cosmic Ray Particles - Results from a Balloon Borne Experiment", Rad. Meas, **25**, 471-474, (1995)

3. L. Tommasino, F. Caggiati, M. Notaro, R. Teodori, G. Torri, D. Zhou, J. Byrne, D. O'Sullivan. "From a Complex Cosmic Ray Stack to a Simple Dosimeter System for Aircrew Exposure".

4. J. Byrne. "A Study of Cosmic Ray Nuclei with $Z \geq 2$ at Civil Aviation Altitudes in the Earth's Atmosphere", MSc Thesis, Dublin University, (1995).

5. D. O'Sullivan, J. Byrne. "The Spectrum of $Z \geq 2$ Nuclei Observed at Altitudes frequented by Concorde Aircraft", in preparation

Head of Project 5: Prof. Dr. R E. Grillmaier

II. Objectives for the reporting period

1. Calibration of HANDI (**H**omburg **A**rea **N**eutron **D**os**I**meter) equipped with a cylindrical tissue equivalent proportional counter (TEPC) in the radiation field at the SPS facility in CERN, Geneva/Switzerland :

   A Influence of wall thickness and simulated diameter on the dose equivalent response (R_H).
   B. Investigation of the contribution of muon background in the stray radiation field.
   C. Investigation of pile-up effects.

2 Investigation of the dose equivalent response of HANDI to heavy ions at the SIS facility in GSI, Darmstadt/Germany.

3 Measurements of absorbed dose and lineal energy distribution on the mountain Mont Blanc, France at the altitude of 3777 m.

4 Measurements of absorbed dose and lineal energy distribution in civil aircraft at aviation altitudes in collaboration with ENEA and Alitalia

III. Results achieved including publications

The portable ambient dose equivalent dosimeter HANDI has been developed for radiation protection measurements in mixed gamma-neutron radiation fields. The battery powered HANDI system with a resolution of 16 channels is equipped with a low pressure **T**issue **E**quivalent **P**roportional **C**ounter (TEPC) simulating small volumes of human tissue. The sensitivity of the new developed cylindrical TEPC (physical diameter d = 8 cm) with A-150 wall in our laboratory is about 3 times bigger than that of a commercial TEPC, type LET-2 (physical diameter d = 5.7 cm) The measurements with HANDI in the radiation field at the SPS facility in CERN which is similar to that found at civil aviation altitudes were carried out in July 1993 (Ep = 205 GeV/c positive), in September 1993 (Ep = 120 GeV/c positive), in May 1994 (Ep = 205 GeV/c positive) and in August 1994 (Ep = 120 GeV/c negative). The SPS facility of CERN has provided the mixed gamma-neutron radiation field which is produced by high energetic hadrons of about 2/3 protons and 1/3 positive or negative pions bombarding a copper target.

Table 1. Summary of measurements in CERN. *ds: simulated diameter

Time	Energy of primary beam	Shielding	TEPC
July 1993	205 GeV/c	concrete	cylindrical, ds=2 μm
September 1993	120 GeV/c	concrete, iron	cylindrical, ds=2 μm spherical, ds=1 μm
May 1994	205 GeV/c	concrete, iron	cylindrical, ds=2 μm spherical, ds=1 μm
August 1994	120 GeV/c	concrete, iron	cylindrical, ds=2 μm spherical, ds=1 μm

A Precision Ionisation Chamber (PIC) provided a beam monitoring value as reference One PIC-count is equivalent to about $2x10^4$ incident particles to the copper target. The radiation field in CERN is

characterised by a grid system on two different shieldings (iron and concrete) In order to vary the beam intensity a series of collimators were used.

1. Calibration of HANDI in high energetic neutron field at CERN.

1.A Investigations of influence of wall thickness and simulated diameter on the dose equivalent response R_H of HANDI to high energetic neutrons.

In May 1994 measurements using the cylindrical TEPC and a commercial spherical TEPC, type LET-1/2 (physical diameter d = 1,3 cm) with a 5,5 mm thick A-150 cap were performed. Additionally in August 1994 the influence of wall thickness on the R_H of HANDI to neutrons using the cylindrical TEPC (wall thickness of A-150 = 3 mm) with polyethylene caps of 5, 10, 15 and 20 mm thickness were also investigated on the top position of concrete shielding. In order to increase the resolution our laboratory system (BIO) was used The results of measurements in May showed no difference of absorbed dose within the statistical uncertainty when increasing the wall thickness. This can be explained by the relatively small difference of wall thickness (3,8 mm) for such high energetic neutrons. However, measurements in August indicate an increase of the R_H with increasing wall thickness (13 % increase of absorbed dose between 3 mm and 18 mm wall thickness) (table 2).

Table 2. Results of measurements varying the wall thickness on the top of concrete shielding, grid number 1 in May and August 1994.

Measurement	wall thickness (mm)	PIC rate (counts/sec)	D / PIC (nGy/PIC)
May 1994	3	950	0,112
May 1994	6,8	820	0,106
August 1994	3	201	0,132
August 1994	8	230	0,132
August 1994	13	219	0,144
August 1994	18	163	0,149
August 1994	23	258	0,147

These investigations show that the secondary charged particle equilibrium is not achieved with standard wall thickness at these high energies and therefore the absorbed dose was underestimated.

Measurements with two simulated diameters were performed in May 1994 using BIO on the top position of iron shielding For this analysis two types of TEPC (cylindrical and spherical, type LET-1/2) were used Both counters were filled with propane based tissue equivalent gas mixture The cylindrical and spherical LET-1/2 TEPCs simulated diameters of 2 and 1 micron, respectively The values of absorbed dose (1 µm: 0,249 nGy/PIC, 2 µm: 0,246 nGy/PIC) are in good agreement which is confirmed by calculations of other contractors This implies that on the iron shielding there are very few low energetic neutrons contributing only small part to the total dose. Therefore the simulated diameter has no influence on the measurement on the iron shielding.

1.B Investigations of the contribution of muon background in the stray radiation field

The primary radiation field at SPS facility in CERN consists of 2/3 protons and 1/3 pions. The muon background which originates from pion decay in the primary beam is present during the whole measurements. In order to estimate the contribution of muon background to total absorbed dose measurements were carried out using HANDI and BIO In May 1994 the muon background was

measured only with HANDI on the top position of concrete and of iron shielding (figure 1) The shape of the two spectra is in good agreement But the absorbed dose measured on the iron shielding (D=1,5 nGy/s) is 50 % higher than that on the concrete shielding (D=1,0 nGy/s).

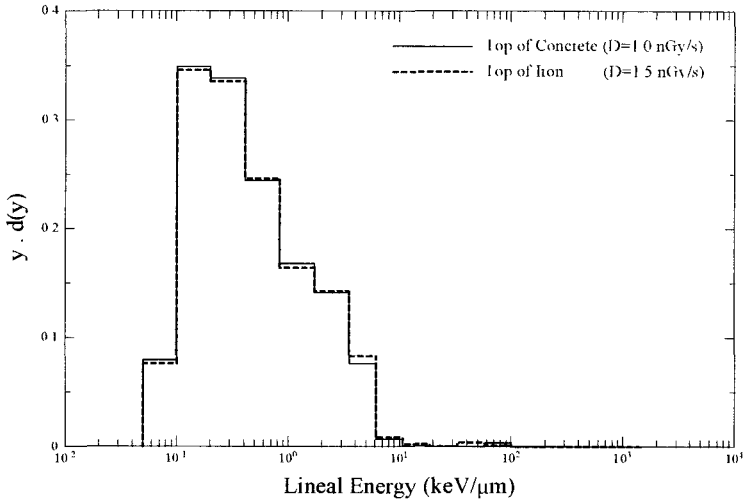

Figure 1. Muon background measured with HANDI on the top position of concrete shielding and of iron shielding in May 1994.

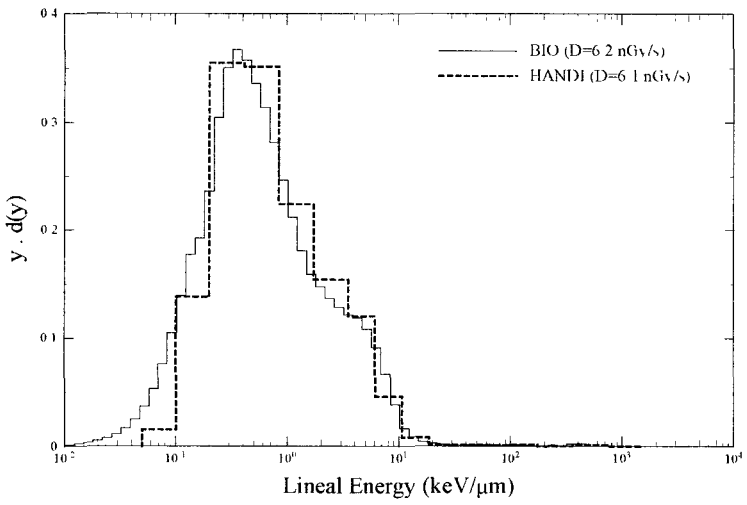

Figure 2. Measurements of muons on the top position of iron shielding using HANDI and BIO in August 1994

In August 1994 the muon background was analysed using both systems on the top position of iron shielding (figure 2). Not only the spectrum of both systems, but also the values of absorbed dose are in very good agreement (BIO: D=6,2 nGy/s, HANDI: D=6,1 nGy/s). The comparison with investigations of May and of August shows that the muon background strongly depends on the characteristics of the

radiation, for instance energy of primary beam or type of shielding Additionally the intensity of the primary beam can be another reason, because during the investigations the intensity could not be measured.

1.C. Investigation of pile-up effects.

Since in September 1993 the pile-up effects were observed, the influence of the beam intensity on measurements with HANDI has been investigated on the top position of concrete shielding in September 1993, in May 1994 and on both shieldings in August 1994 Various beam intensities were used and the results were normalised to the effective time of beam extraction (2,48 sec) The high sensitivity of the cylindrical counter caused pile-up with increasing PIC counting rate In September 1993 pile-up leaded to a decrease of HANDI counting rate and an underestimation of absorbed dose up to 35% The influence of pile-up on the dose equivalent rate is smaller (15%) than that on absorbed dose rate, because pile-up occurs mainly in the low lineal energy region (< 10 keV/μm) In May 1994 the dose underestimation observed was larger than that in September 1993 (48%). It implies that the underestimation of dose depends on the energy of the primary beam (Sep. 93. Ep=120 GeV/c, May 94: Ep=205 GeV/c) (table 3).

Table 3 The pile-up effects measured on the top of concrete shielding

Measurement	PIC rate (PIC/s)	Absorbed dose rate (nGy/s)	Absorbed dose (nGy/PIC)
September 1993	335	76,35	0,23
	525	113,81	0,22
	1158	169,80	0,15
May 1994	134	3,89	0,29
	499	8,46	0,17
	1054	15,01	0,14

In August 1994 the investigations of pile-up were repeated on both shieldings. The energy of primary beam (Ep=120 GeV/c) was lower than that of in May 1994 but it was similar to that in September 1993 Specially the low beam intensities were used and varied in small steps. The absorbed dose underestimation was larger than that in September (44%), although the energy of primary beam is similar to that of in September The results indicate that pile-up is a severe problem in such high energetic field (table 4).

Table 4. Investigation of pile-up varying the PIC rate on the position of concrete and of iron shielding in August 1994

Shielding	PIC rate (PIC/s)	Absorbed dose rate (nGy/s)	Absorbed dose (nGy/PIC)
concrete	78	33,17	0,43
concrete	83	42,57	0,51
concrete	134	45,91	0,34
concrete	152	45,38	0,30
concrete	261	63,55	0,24
iron	85	57,97	0,68
iron	116	59,79	0,52
iron	140	61,97	0,44
iron	171	69,43	0,41
iron	207	72,70	0,35

2. Investigation of the dose equivalent response of HANDI to heavy ions at the SIS facility in GSI, Darmstadt.

At aviation altitudes 1,5 % heavy ions of the incident particles contribute about 10 % to total absorbed dose For the calibration purposes R_H of HANDI to heavy ions was investigated in neon ion field with energy of 400 MeV/u using HANDI with the cylindrical TEPC in July 1993 and in carbon ion field with energy of 195 MeV/u in March 1995 using BIO with the spherical LET-1/2 to avoid pile-up. These experiments were carried out with bare counter, a 1,5 mm thick A-150 cap and 4 cm thick water phantom Homogenous irradiation was ensured by a scansystem. The measurements show a sharp peak which corresponds to the energy loss of the primary radiation in the counting gas The peak shifts to high lineal energy region with increasing wall thickness (figure 3).

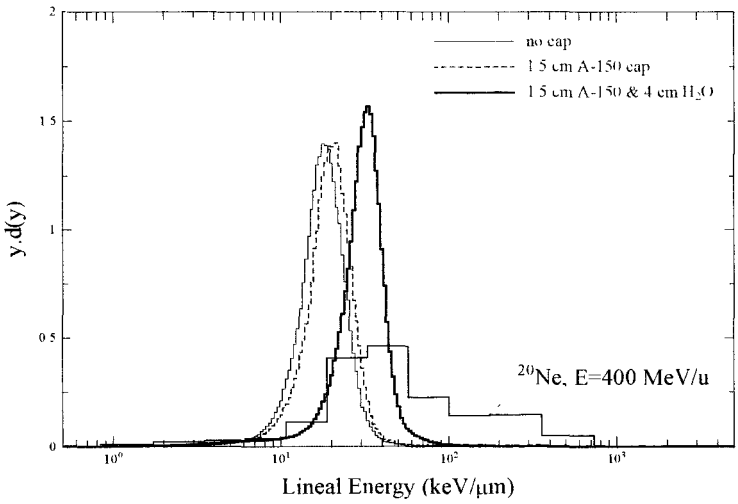

Figure 3. Measurements with BIO in carbon ion beam with energy of 195 MeV/u using a spherical LET-1/2 TEPC. Spectrums show the effect of increase of wall thickness.

This is also reflected by an increasing absorbed dose with thicker wall (table 5). In contrast to the measurements of ^{20}Ne the results in ^{12}C field don't show any other peaks The broad spectrum of ^{20}Ne measurements are due to fragmentation, which is not visible in the ^{12}C experiments because of its small atomic weight.

Table 5. Results of BIO measurements using the small TEPC with a A-150 cap and 4 cm water phantom in ^{12}C field with energy of 195 MeV/u

particles [1/scan/cm^2]	D / Particles [µGy/particle]	Remarks
2030	0,26	no cap
2030	0,28	1,5 cm A-150
2030	1,46	1,5 cm A-150 + 4 cm H_2O

Quantitative information on absorbed dose and dose equivalent could not be given by the host institute The position of peak which corresponds to the mean energy loss of ^{12}C is not in agreement with the calculated values, except measurement with the bare counter.

1 dE/dx = about 15 keV/μm with no cap
2. dE/dx = about 17 keV/μm with 1,5 cm A-150 cap.
3 dE/dx = about 22 keV/μm with 1,5 cm A-150 cap and 4 cm water phantom

These deviation attribute to the rough calculation of the mean energy loss.

3. Measurements of absorbed dose and lineal energy distribution on the mountain Mont Blanc at the altitude of 3777 m.

The absorbed dose and dose equivalent at the altitude of 3777 m were measured on the Mont Blanc in August 1994 The lineal energy spectra in August 1994 show that high LET particles (> 6 keV/μm) contribute about 40 % to total dose equivalent while they contribute only 7 % to total absorbed dose (figure 4). From these measurement an annual dose equivalent of 4 mSv can be estimated (table 6).

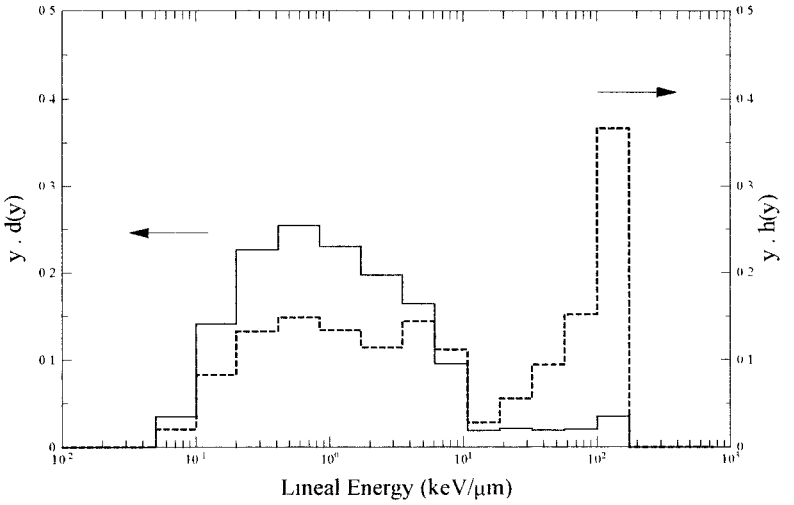

Figure 4. Measurements at the altitude of 3777 m.
The continued line indicates the spectrum of absorbed dose and the dotted line is the spectrum of dose equivalent

Table 6 Results of measurement on the mountain Mont Blanc at the altitude of 3777m

Measurement time	9000 sec
Total Counts	84737 cts
Total absorbed dose rate	0,272 μGy / h
Total annual absorbed dose	2,383 mGy
Total dose equivalent rate	0.467 μSv/ h
Total annual dose equivalent rate	4,091 mSv

4. Measurements of in civil aircraft at aviation altitudes in collaboration with ENEA and Alitalia.

The measurements in civil aircraft are performed in collaboration with ENEA and Alitalia. A series of measurements are foreseen on the route from Rome to Los Angeles and to Rio de Janeiro, respectively. Besides HANDI several active and passive detectors are used. For these investigations two HANDI systems are equipped with the cylindrical TEPC and a spherical TEPC, type LET-2 Extensive preparations of instrumentation were necessary, for instance fixation on board, proof of the electro - magnetic community The inflight measurements have been started in September 1995 and will be continued presumably until end of November.

Scientific staff :

M. Freyermuth, S Gerdung, T Lim

Publications :

Exposure of Air Crew to Cosmic Radiation, A report of EURADOS Working Group 11, Eds. I.R.McAulay, K Schnuer, H.G Menzel, in preparation, 1995.

Homburg Area Neutron Dosimeter and its applications T Lim, E.Arend, S.Gerdung, R Grillmaier, In : Proc. Annual Symp. of Korean Association of Radiation Protection, submitted, 1995

Head of project 6 : Dr. Höfert

II. Objectives for the reporting period :

Establish reference radiation fields for the fellow contractors at a high-energy proton accelerator facility which are similar to those encountered by aircrews due to the galactic cosmic radiation.

Provide these reference fields for use by contractors for the test and intercomparison of measurement techniques designed to establish the doses received by aircrews.

Provide information on beam energy and intensity of this test facility such that all data can be normalised and comparisons between results of different users and for various experimental periods become possible.

Expose as an additional service passive detectors frequently sent to CERN by participants and expose them in fixed positions at the facility with defined doses. These reference doses are based on the result of a HANDI TEPC measurement and are used to normalise the results of passive detectors.

Participate as CERN in these experimental intercomparisons and provide theoretical data on the spectra reference radiation fields.

Study the behaviour of the HANDI and REM-500 TEPCs in these reference radiation fields that are of pulses nature and compare the response of the two instruments.

Study a possible build-up effect in high-energy hadron fields with the help of the HANDI using caps of plastic material of various thickness.

III. Progress achieved including publications :

In the reporting period (September 93 to August 95) reference radiation fields were provided for contractors during six experimental runs:

Period	Beam momentum	Participation of Contractors
Sept. 23 to 29, 1993	120 GeV/c, negative	CERN, GSF, USAAR
May 10 to 17, 1994	205 GeV/c, positive	CERN, ENEA, USAAR
July 7 to 10, 1994	50 to 120 GeV/c, negative 75 to 120 GeV/c, positive	CERN, GSF
Aug. 24 to 29, 1994	120 GeV/c, negative	CERN, USAAR
April 21 to 30, 1995	205 GeV/c, positive	CERN, DIAS,USAAR
Aug. 16 to 18, 1995	120 GeV/c, positive	CERN

Using a high-energy hadron beam, the H6 beam in the North experimental hall interacting with a copper target of 50 cm length and 7 cm diameter, the stray radiation fields behind iron and concrete shields of 40 and 80 cm thickness

respectively were established at about 90 degrees with the beam direction [Aro94c, Hoe94a]. The composition of the radiation field over the concrete shielding resembles rather closely the one encountered at altitudes above 10 000 metres except that the low LET radiation component in the former case is identified as being muons while at flight heights electrons are present [Hoe93].

The running periods of the beam facility were subdivided in shifts of four hours each. In most cases CERN staff acted as shift leaders until some of the more frequent participants had acquired sufficient experience such that they could deal with the beam facility including contacts with the machine control room and hence serve as their own shift leaders. Running periods were attributed to a main user who decided on the position of the target (below the iron or the concrete shielding) and occupied generally the central position on the shielding while other participants could still place their detectors in other irradiation positions without disturbing the main user.

During all these experimental runs CERN assured the beam monitoring using a precision ionisation chamber with a digitizer. Hence all users could and were asked to normalise for the sake of a direct comparison of their results to the number of counts (PICs) where one count corresponds to a beam intensity of $2 \cdot 10^4$ particles with an uncertainty of $\pm 10\%$ [Ste94]. During all these runs the CERN made rem-counter and ^{11}C measurements in addition to specify furthermore the stray radiation field. In the case of passive detectors the participants received information on reference doses and dose equivalents based on the result of HANDI-TEPC measurements and the total number of PICs accumulated during the exposure. All users carried individual neutron monitors and CERN's Dosimetry Service transmitted the accumulated personal doses to all the participants.

In the geometry of the experimental conditions particle spectra were calculated for defined reference positions using Monte Carlo programme FLUKA and the results were made available to the participants [Roe93]. All estimates of ambient dose equivalent are based on standard fluence to dose equivalent conversion factors [San93].

The results of HANDI and REM-500 TEPC measurements confirmed the presence of various radiation components in the stray field. In order to separate these components the existing program for the evaluation of dosimetric values and microdosimetric distributions for this instrument was analysed and completely rewritten [San94]. In particular a method was developed for the HANDI to subtract the muon "background" that is independent on the beam intensity on the target of the H6 beam [Hoe94b]. The response of the HANDI and the REM-500 TEPCs were compared and their usability in mixed radiation fields around high-energy accelerators shown [Aro94a, Aro95a]. Further analysis of the data confirmed that these instruments can be used in pulsed radiation fields [Aro94b].

Finally the build-up of both absorbed dose and dose equivalent in the stray radiation field was studied in view of the protection of the foetus. It was shown that a dose limit of 2 mSv at the surface of a pregnant woman does not assure a limitation to the foetus of 1 mSv. In fact, the decrease of dose equivalent behind 10 cm of tissue

equivalent material is only of the order of 10 % in the case of a high-energy stray field [Aro95b].

References:

Aro94a A.Aroua, M. Höfert and A. V. Sannikov, Comparison of the Response of the HANDI and the REM-500 TEPCs in High-energy Radiation Fields, CERN/TIS-RP/IR/94-12 (1994).

Aro94b A.Aroua, M. Höfert and A. V. Sannikov, Study of the Effects of High Intensity and Pulsed Radiation on the Response of the HANDI TEPC, CERN/TIS-RP/TM/94-19 (1994), Presented at the Workshop on Advances in Radiation Measurements, Chalk River, Ontario, Canada.

Aro94c A.Aroua, M. Höfert, A. V. Sannikov and G. R. Stevenson, Reference High-energy Radiation Fields at CERN, Accepted for publication in Applied Radiation and Isotopes Journal

Aro95a A.Aroua, M. Höfert and A. V. Sannikov, On the Use of Tissue-equivalent Proportional Counters in High-energy Stray Radiation Fields, Rad. Prot. Dosim. **59**, 49 (1995).

Aro95b A.Aroua, M. Höfert, A. V. Sannikov, G. R. Stevenson and C. Vaerman, An Investigation of Build-up Effects in High-energy Radiation Fields, Accepted for publication in Rad. Prot. Dosim.

Hoe93 M. Höfert, G. R. Stevenson and W. G. Alberts, Measurement of Radiation Fields and Dosimetry in the Stratosphere (in German), Proc. 26. Jahrestagung des FS, p. 541, Karlsruhe 1994.

Hoe94a M. Höfert and G. R. Stevenson, The CERN-CEC High-energy Reference Field Facility, Proc. 8th Int. Conf. on Radiation Shielding, Arlington, Texas, USA, [American Nuclear Society] pp 635--642 (1994).

Hoe94b M. Höfert, A. V. Sannikov and G. R. Stevenson, Muon Background Subtraction from the HANDI TEPC Measurement Data, CERN/TIS-RP/IR/94-13 (1994).

Roe93 S. Roesler and G. R. Stevenson, July 1993 CERN-CEC Experiments: Calculation of Hadron Energy Spectra from Track-Length Distributions using FLUKA, CERN/TIS-RP/IR/93-47 (1993).

San93 A. V. Sannikov and E. N. Savitskaya, Ambient Dose and Ambient Dose Equivalent Conversion Factors for High-energy Neutrons, CERN/TIS-RP/94-14/PP (1993).

San94 A. V. Sannikov, HAN93 Program for Evaluation of Dosimetric Values and Microdosimetric Distributions from HANDI TEPC Measurement Data, CERN/TIS-RP/IR/94-03 (1994).

Ste94 G. R. Stevenson, J. C. Liu, K. O'Brien and J. Williams, Beam Intensity Measurements using ^{11}C Activation for the CERN-CEC Experiments, CERN/TIS-RP/TM/94-15 (1994).

I. **HEAD OF PROJECT 7:** dr. F. Spurný

Scientific staff : dr. V.P. Bamblevski, dr. J. Bednář, dr. M. Běgusová, dr. J. Charvát, dr. V. Michalik, dr. A.G. Molokanov, dr. F. Pernička, dr. K. Turek, B. Vlček, I. Votočková

II. OBJECTIVES FOR THE REPORTING PERIOD

The main objectives of the contribution had been defined as the following:

1. To contribute to the calibration of TLDs', SSNTDs', bubble detectors, ionization chambers, remmeters, environmental radiation dose-rate meters, etc., in the beams of high energy particles and behind their shielding;
2. To obtain new data during in-flight measurements on directly ionizing radiation (low LET) and neutron (high LET) contribution to the equivalent dose.
3. To contribute to the microdosimetry and radiation protection interpretation of data using appropriate theories.

The studies had been started at the end of 1992. The objectives have been slightly enlarged and modified, following the development of common studies on the project and some other factors.

III. PROGRESS ACHIEVED INCLUDING PUBLICATIONS

1. On-Earths' calibrations

1.1. Calibration in high energy proton beams

Several series of calibration of TLD, SSNTDs' and some other equipments have been performed in high energy proton beams available at the JINR Dubna. In the same beams SSNTDs' with spallation fragments radiators (Au, Bi, Ta) and without them have been exposed for other contractors' on the project. Monitoring and proton fluence determination were ensured by means of ionisation chambers and/or activation detectors [R2].

1.2. Calibration in mixed neutron-gamma reference fields

Several series of calibration have been realized in mixed neutron-gamma radiation fields available in the IRD AS CR Prague and in the Nuclear Research Centers at Fontenay-aux-Roses and Cadarache. Equipments and detectors used for in-flight measurements have been tested to get more precise their responses to neutrons (high LET radiation) as well as to photons. Particular attention has been paid to the comparison of these responses with the data available from our own measurements with tissue equivalent proportional counter. Some of these results have been already published [R3].

1.3. Calibration and measurements in reference fields behind shielding of high energy particle accelerators

1.3.1. CERN high energy reference fields [P5,10,13,14; R4]

We have participated at four runs of studies organized at CERN-CEC high energy reference fields (07/93; 09/93; 05/94; 04/95). Several active instruments and passive detectors have been used to determine dosimetric characteristics of both low as well as high LET components of radiation fields. They are presented in Table 1. The results obtained during all runs were quite homogeneous and they can be summarized in the following way:

Table 1: Measuring instruments and detectors used to characterize radiation fields in CERN-CEC high energy reference field.

Type of detector	Used to characterize radiation with	
	low LET	high LET
active	TEPC-NAUSICAA; scintillator-based dose-rate meter; GM-based individual dosemeter; Si-diode based individual dosemeter	TEPC-NAUSICAA; rem-counter NM2; survey meter based on superheated drop detectors
passive	thermoluminiscent detectors (TLDs')	track etch detectors (TEDs')`bubble damage neutron detectors (BDNDs')

1. As far as low LET radiation is concerned, the actually read values measured on the top positions (iron or concrete shielding) depends on the relative contribution of muon background. Nevertheless, at sufficiently high intensity (number of monitor counts higher than about 3000 per burst), this factor is practically negligible. At such conditions some slight differences appeared: scintillator based equipment readings are slightly higher due to the sensibility to neutrons; Si-diode based electronic personal dosemeter readings are systematically lower due to their underestimation of muons.
2. The spread of readings of high LET (neutron) radiation instruments has been much larger as compared to low LET radiation. Besides the reading ratios were quite different for top concrete, resp. top iron positions. If TEPC is taken as reference instruments, moderator-type remcounter NM2 overestimate the dose equivalent behind iron shielding, underestimate it behind concrete (in both cases by a factor about 1.5). Bubble detectors also underestimate the dose equivalent behind concrete, TED CR39 underestimate it in both cases.
3. All these variations can be well explained when neutron spectra in both positions are taken into account [R4]. While neutron spectrum behind iron is dominated by neutrons with energies below 1 MeV, the peak of high energy neutrons (about 80 MeV) is very pronounced in the spectrum behind concrete. It was also stated that the second type of spectra would be typical also for the board of an aircraft.
4. Taking into account the actual shape of spectra the values of dosimetric characteristics have been estimated from all our results. They are presented in Tab.2.

Table 2: Dosimetric characteristics of CERN-CEC high energy reference fields (E~205 GeV/c; ≥3000 PIC/burst; central positions).

Dosimetric characteristics		Value[1], per 1 hour at 7.5×10^5 PIC	
		top concrete	top iron
Thermal neutron fluence	[cm^{-2}]	8.25 05	4.72 06
Low LET H* (10)	[μSv]	68	60
High LET H* (10)	[μSv]	375	1350

[1] The accuracy estimated ± 10% ($1\sigma_{rel}$)

1.3.2. JINR high energy reference fields [R1; P9,15]

We have participated at three runs of studies in reference fields at JINR, Dubna, Russia (04/93; 04/94; 06/95). Passive detectors have been also irradiated in the meantime by our russian colleagues. The same detectors have been used as given in Table 1 for CERN, with the exception of TEPC. As reference values we have therefore taken the results of studies performed with combined Bonner and activation ($^{12}C \rightarrow {}^{11}C$; $^{27}Al \rightarrow {}^{24}Na$) spectrometer. It would be reminded that JINR hard reference field is formed by leakage neutrons from a thick concrete shield bombarded by secondary radiation from accelerator chamber. The soft reference field has been created in the basement of the phasotron, in the shielded labyrinth.

The results obtained during all runs mentioned were reasonably homogeneous, some problems were revealed at the hard field when the accelerator mode is very different from the standard one. Generally, they followed the same tendencies as mentioned above for CERN fields, at soft JINR field the thermal neutrons modified in some cases the readings of low LET radiation equipments. We were also able to estimate the dosimetric characteristics of both these fields. They are presented in Tab.3.

Table 3: Dosimetric characteristics of JINR reference fields.

Dosimetric characteristic		Value[1], per 1 hour, at I_p~1 μA	
		hard field	soft field
Thermal neutron fluence	[cm^{-2}]	4.2 06	1.1 08
Low LET H* (10)	[μSv]	130	790
High LET H* (10)	[μSv]	1200	4600

[1] The accuracy estimated ± 10% for soft field, ± 15% for hard field (1 σ_{rel})

2. In-flight measurements

2.1. In-flight measurements on the board of commercial aircraft [P1-4,7,11,12,14]

Since the beginning of the contract up to the end of July, 1995, in-flight measurements on the board of commercial aircraft have been performed during about 20 return commercial flights. Flight routes extended from the equator (Singapore - 1.3 °N) up to rather northern region (Umea - 66 °N; flights from Europe to New York (Montreal) - up to 65 °N). The seven of these flights were typical long-haul ones. Flying altitudes varied from 8.2 km (27000 feet) to 12.5 km (41000 feet). To enlarge the analysis, we have also included the results obtained previously, at the middle of 1991, in the period a little after the last sun maximum (see paragraph 2.2).

All equipments and detectors mentioned in the Table 1 were used during in-flight measurements; additionally, Reuter Stokes chamber RSS 112 was used to characterize low LET radiation on the board. Only in few of flights (the most of long-haul) it was possible to use more complete sets, in four of them the TEPC-NAUSICAA [R5] has been installed on the board. Typical examples of direct readings during some of flights are shown in Figures 1 and 2. One can see there important influence of flight altitude and also the geographical latitude for the flights between Prague (50 °N), resp. Abu Dhabi (24 °N). Generally, a good agreement has been observed between the integral values calculated from the dependencies presented in Figs 1 and 2 and the integral values measured with TLDs', BDNDs'and individual dosemeters except Si-based dosemeter for which the reading on H*(10) of ^{60}Co has been systematically lower

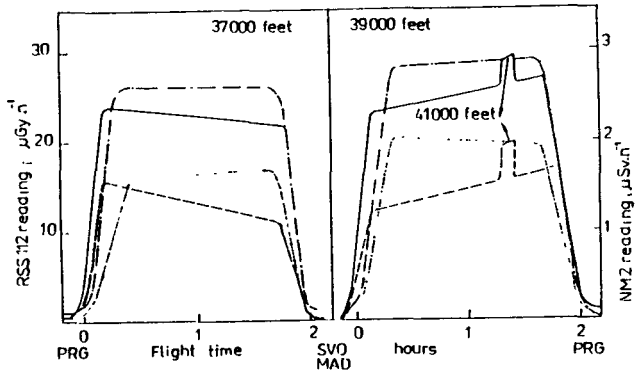

Fig.1: Readings of RSS 112 and NM2 during some return flights.
—— RSS 112 PRG-MAD-PRG —·—· RSS 112 PRG-SVO-PRG
– – – NM2 PRG-MAD-PRG ····· NM2 PRG-SVO-PRG

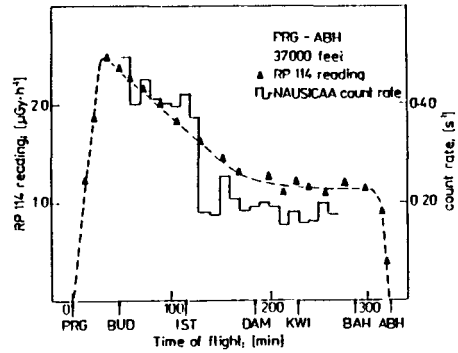

Fig 2: Readings of a GM-based low LET radiation dose meter and TEPC-NAUSICAA (t_{int} = 10 min) during the flight Prague - Abu Dhabi.

(0.6 - 0.7), as itwas already mentioned for on-Earths' high energy reference fields.

Direct readings of instruments used exhibited following rules:

1. They do not depend on the position in the aircraft within the precision of measurements (± 10%).
2. They depend on the geographical latitudes mostly between 50 °N and 25 °N. Close to the equator their values are, when compared to the region above 50 °N, about two to three times lower for directly ionizing component (electrons, protons), more than four times lower for neutron component.
3. They increase regularly with flight altitude, the average increase for each 600 m (2000 feet) is for northern (> 50 °N) region and both components about 15%.
4. Following the actual conditions of flight (altitude, the wind, etc.), the integral value of dose equivalent can differ for the same route up to the factor of 1.5.

Direct readings (in H* (10) of ^{60}Co, resp. ^{252}Cf neutrons) are not explicitly equal to H* (10) for the radiation on the board because of different spectrum particles' composition. We have tried to find appropriate correction factors through the analysis of available spectral data. We have found out that, in the case of low LET radiation, the direct readings should be multiplied by a factor of 1.25 to obtain H*(10) values on the board. For high LET (neutron) component, we have tried to obtain the correction factor

on the base of our previous measurements in the fields behind the shielding of JINR high energy accelerators. The multiplication by a factor of 2 has been found as realistic for NM2 remcounter, closely the same value has been found for BDNDs' [R6]. This correction factor has been directly confirmed in our last direct measurements with reference instrument - TEPC - as can be seen in Table 4.

Table 4: Comparison of direct readings of high LET component measuring instruments.

Radiation field		Directly read value of H* (10)[1], μSv by		
		NAUSICAA-TEPC	NM2	BDND
Prague -	9.5 km	2.24 ± 0.32	1.0 ± 0.1	1.3 ± 0.2[2]
- Montreal -	10.1 km	2.38 ± 0.25	1.3 ± 0.1	1.4 ± 0.2[3]
- Prague,	10.7 km	3.98 ± 0.42	1.6 ± 0.2	1.3 ± 0.2[2]
February 1995	11.3 km	3.35 ± 0.42	1.8 ± 0.2	1.4 ± 0.2[3]
CERN - top	T6	524 ± 25	267 ± 7	270 ± 20
concrete position	S2	644 ± 60	303 ± 7	310 ± 20

[1] per hour on the board, per 10^8 counts of PIC monitor at CERN
[2] Average value for 9.5 and 10.7 km [3] Average value for altitudes 10.1 and 11.3 km

One can see there also that the same ratios of readings is observed in CERN top concrete field, it proves that this reference field is suitable for the calibration of on-board high-LET radiation measuring devices.

When these correction factors are applied, the level of aircrew members exposure can be estimated at ≥ 50 °N to about 6 to 8 μSv per hour at flight altitudes about 11 km, roughly half due each component.

2.2. Solar cycle influence on the exposure level

It is known that the exposure level due to galactic cosmic radiation (predominant contribution for the most of time) is inversely proportional to the solar activity. As an example, the curves in Fig.3 confront the sunspot index with the countings of cosmic radiation monitor situated at Lomnický štít, The High Tatras, Slovakia (height 2653 m, geomagnetic rigidity 4 GV). For comparison, the Fig.4 shows countings of cosmic radiation monitor situated at Calgary (height 1128 m, geomagnetic rigidity 1.09 GV). What is important is that our measurements were generally performed after the end of 1992. Since that time, the variation of cosmic radiation monitors counting is low (see Figs 3 and 4). Only measurements performed earlier were realized the end of April - the beginning of May,1991 just before the deep minimum of the middle of June. The relative ratios of monitors countings for periods since the end of 1992 to the April/May 1991 is about 1.14 ± 0.2, the relative readings of RSS 112 are equal to 1.16 ± 0.02. Nevertheless it should be mentioned that these ratios are comparable with the uncertainies of experimental results themselves. The studies of the type and complexness presented in this report have to be continued to confirm the influence of solar cycle on the exposure level more clearly.

Besides, there are another important features following from Figs 3 and 4. First, daily variations can be important.. The second, it is not excluded that solar eruptions can reach the Earths' surface. It is clearly demonstrated by the peak corresponding to the flare at 29th September 1989. It is important even at the rigidity 4 GV (Lomnický štít) - +20%, much more at the rigidity 1.1 GV (Calgary) - +80%; both for daily average values.

In the case of hour average values it is even more (+100%, resp. +500%). It could reinitiate the question of on-board monitoring.

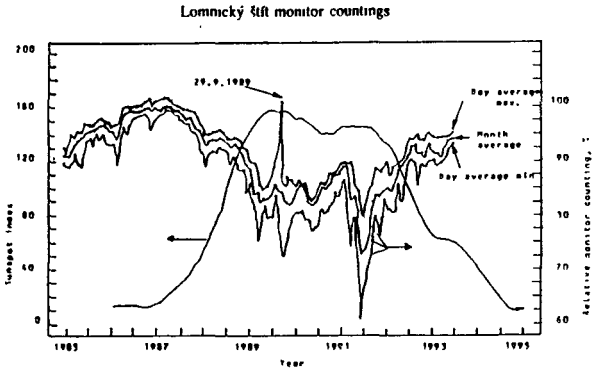

Fig. 3: Sunspot smooth index and Lomnický štít relative monitor countings during the last (22nd) solar cycle.

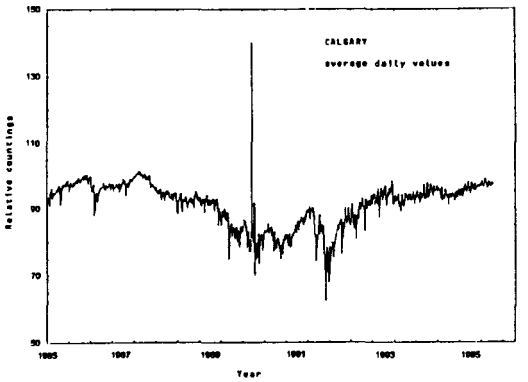

Fig. 4: Calgary relative monitor countings during the last (22nd) solar cycle.

3. Microdosimetry and radiation protection aspects

Measurements with TEPC-Nausicaa performed at February 1995 permitted also to determine the most important microdosimetric characteristics of the field on board of a subsonic aircraft. We have observed that LET spectra at different flight altitudes are the same, when statistical reliabilities are taken into account. The average values of global microdosimetric characteristics are presented in Table 5, the dose and dose equivalent microdosimetric distributions for the return flight to Montreal are presented in Fig.5.

Table 5: Global microdosimetric characteristics during long-haul flights measured by means of TEPC, February 1995.

Flight	Q_{high} [1,2]	Q	$\bar{Y}$	$\bar{Y}_D$
			keV/μm	
Prague-Montreal-Prague	6.16 ± 0.38	1.83 ± 0.07	0.438 ± 0.006	7.39 ± 0.82
Prague-Bangkok-Prague	6.26 ± 0.33	1.75 ± 0.06	0.411 ± 0.010	6.73 ± 0.62

[1] High: $Y \geq 3.5$ keV/μm [2] ICRP 26 conversion factors

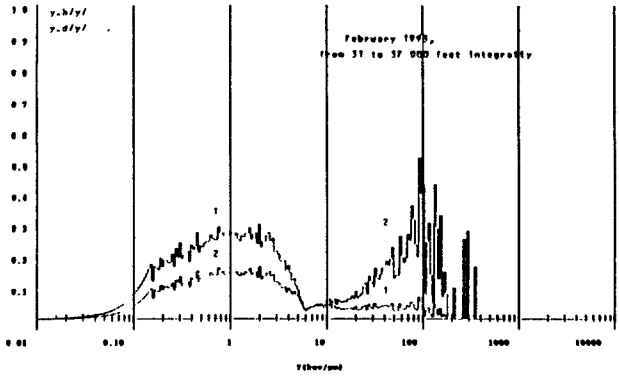

Fig. 5: Dose (1) and dose equivalent (2) distributions of linear energy Y.

One can see there that:

a) There is only slight difference of these characteristics for typical northern-route flight and to-equator flight. It consists in a little more important contribution of low LET radiation during to-equator flight (see Q and Y).
b) As far as high LET part is concerned, the value of Q_{high} is a little less than published before. The most probable reason is that usual threshold for high LET region is about 10 keV/μm, we have chosen 3.5 keV/μm. And, the proportion of the part between these two thresholds is rather important (see Fig. 5).

As far as radiation protection aspects of the results of our measurements are concerned, they can be summarized as follows:

a) The usual limits of annual aircrew flight hours correspond to about 500 hours of flights above 10 km. It corresponds at 11.3 km to about 4 mSv per year, with ICRP 60 conversion factors to about 5 mSv per year.
b) It is well below the limit, however, much higher than for other groups of occupationally exposed persons (bellow 1 mSv in medicine, below 1.6 mSv in industry [R7].
c) Monthly flight hours limit (~ 100 hours) does not exclude that the exposure of a pregnant women can exceed 1 mSv, particularly in the period of sun minimum.
d) The aircrew exposure should, therefore, be checked, controlled and administered as conscientiously as for any other group of occupationally exposed persons.

LIST OF PUBLICATIONS:

1, F. Spurný et al.: „Dosimetric characteristics of radiation fields on board of CSA aircraft as measured with different active and passive detectors." Radiat. Prot. Dosim. 48, (1993), p. 73-78.
2, F. Spurný, O. Obraz, F. Pernička, I. Votočková: „Dosimetry on board of subsonic aircraft. CSA flight route data and their new interpretation". Proc. 24th Inter. Symp. Radiat. Prot. Physics, TU Dresden Report 1993, p. 52-57.
3, F. Spurný et al.: „Exposure of aircrew and passengers on some CSA flight routes". Nuclear Energy Safety (in Czech) 1(39), (1993), p. 137-143.
4, F. Spurný, V. Michalik, F. Pernička, I. Votočková: „Aircrew exposure measured during CSA commercial flights". Proc. 1st Inter. Symp. Radiat. Biol. Space Research, Brno 1993, p. 23-31.
5, F. Spurný, V.D. Nguyen, J.-F. Bottolier-Depois: „Response of SDOS-DPHD measuring equipment in CERN high energy reference fields". Report SDOS/93-471, Fontenay-aux-Roses, October 1993.

6, V. Michalik, F. Spurný, F. Pernička, V.D. Nguyen: „Some aspects of the exposure of aircraft crew members to cosmic radiation". Radiat. Prot. Dosim. 54, (1994), p. 255-258.

7, F. Spurný, I. Votočková: „Radiation exposure of aircrew and passengers during some CSA commercial flights". Proc. 26. Jahrestagung des Fachverbaudes für Strahlenschutz, Karlsruhe 1994, vol. II., p. 549-553.

8, D. Zhou, L. Tommasino, F. Spurný: „Registration of high energy neutrons by Bi-fission track detectors". Radiation Measurements, submitted for publication.

9, F. Spurný: „Dosimetry of neutrons and high energy particles with nuclear track detectors" (invited paper). Radiation Measur. 25, (1995), p. 429-436.

10,F. Spurný, V.D. Nguyen, J.-F. Bottolier-Depois, I. Votočková, K. Turek: „Responses of different dosimetry systems in high energy calibration fields at SPS accelerator at CERN". Nuclear Energy Safety, accepted for publication.

11,F. Spurný, I. Votočková: „To the aircrew exposure to cosmic radiation. Field characteristics and radiation protection aspects". Proc. 2nd Inter Symp. Radiat. Biol. Space Research, Brno 1995.

12,F. Spurný, I. Votočková: „Aircrew members exposure to cosmic radiation". Presented at the NRE VI, Montreal, June 1995; will be published in „The Science of the Total Environment".

13,F. Spurný, I. Votočková, K. Turek: „Equipments and detectors calibration behind shielding of CERN high energy particle accelerator SPS. III. April 1995". Report DRD NPI AS CR 405/95, Prague, June 1995.

14,F. Spurný, I. Votočková, J.-F. Bottolier-Depois: „Aircrew exposure on board of a subsonic aircraft studied with complex dosimetric set". Radioprotection, accepted for publication.

15,F. Spurný, I. Votočková, K. Turek, V.P. Bamblevski: „Response of different dosimeters in high energy reference fields behind the shielding of the phasotron at Dubna". Nuclear Energy Safety, accepted for publication.

REFERENCES

1. V.E. Alejnikov et al.: „Reference neutron fields for metrology of radiation monitoring". Radiat. Prot. Dosim. 54, (1994), p. 57-59.
2. I. Votočková, V.P. Zorin, A.G. Molokanov, F. Spurný: „Dosimetry of medical proton beams at the JINR phasotron in Dubna". Report JINR P16-93-310 (in Russian), Dubna, September 1993.
3. F. Spurný, I. Votočková, J. Kurkdjian, D. Paul, D. Nikodémová: „Dosimetric characteristics of some reference neutron fields". Nuclear Energy Safety 3(41), (1995) p. 000.
4. M. Höffert, G.R. Stevenson: „The CERN-CEC high energy reference field facility". Presented at the 8th Inter. Conf. on Radiat. Shielding, Arlington, Texas, April 1994.
5. P. Boussef, V.D. Nguyen et al.: „Description de l'instrument NAUSICAA concu pour effecteur des mesures instantanées de H, D, et du spéctre de T.E.L. en champs complexes". IRPA8, Montréal, May 1992, Acte du Congrés, p. 463-466.
6. F. Spurný, I. Votočková, V.P. Bamblevski: „To the energetical dependence of bubble damage neutron detectors". Radiat. Measur. 23, (1994), p. 247-249.
7. Z. Prouza, F. Spurný et al.: „Occupational radiation exposure in the Czech and Slovak Republic". Radiat. Prot. Dosim. 54, (1994), p. 255-258.

Final Report
1992 - 1994

Contract: FI3PCT920032 **Duration: 1.9.92 to 30.6.95** **Sector: A12**

Title: Dosimetry of beta and low-energy photon radiations.

1)	Christensen	Lab. Risø
2)	Chartier	CEA - FAR
3)	Francis	NRPB
4)	Herbaut	CEA - Grenoble
5)	Spencer	UKAEA
6)	Gasiot	Univ. Montpellier II
7)	Scharmann	Univ. Giessen
8)	Charles	Nuclear Electric
9)	Olko	INP
10)	Uchrin	MTA

I. Summary of Project Global Objectives and Achievements

Objectives

The main objectives of the project were to develop standard calibration facilities and to establish standardised measurement and calculation procedures for dosimetry of beta and low-energy photon radiation, thereby achieving a more consistent and reproducible dosimetric practice for determining exposures to individuals from weakly penetrating radiation. Results were to be obtained through a number of specific studies, i.e.:

- identification and evaluation of influencing parameters important for achieving optimal dosimetric characteristics of the radiation fields in designing standard beta calibration beams, e.g. source design and beam-flattening filters.
- characterisation of beta radiation and the accompanying photon radiation fields (bremsstrahlung and characteristic X rays) in terms of dosimetric quantities as well as in terms of energy and angular spectra.
- investigation and development of measurement techniques and procedures for characterising beta radiation fields (with the accompanying photon radiations) and for individual monitoring for doses from these fields.
- establishment and characterisation of low-energy photon radiation calibration beams and characterisation of individual dosemeters for dosimetry of these fields.
- development and validation of methods for the measurement and calculation of doses from radioactive particulates ("hot particles").

The results of this study were expected to lead to the realisation of well-characterised beta calibration facilities which conform to the specifications of ISO Series 2 references as well as low-energy photon calibration facilities and thereby facilitate calibration of personal dosemeters and monitoring instruments for weakly penetrating radiations. Furthermore, improvements were expected to be achieved on dosimetry techniques and procedures applicable for characterising weakly penetrating radiations and for personal dosimetry in such fields, as well as for measurement of doses from radioactive particulates ("hot particles"). Such techniques and procedures would comprise extrapolation chambers, beta spectrometers, TL, TSEE, and radiochromic dye systems as well as computer models, in particular those based on the EGS4 system.

Achievements

Beta calibration facilities

A major aim of the project was to identify and evaluate influencing parameters important for the dosimetric characteristics of the beta radiation fields and using this information to define optimal designs of the irradiation facilities. The work would focus on the ISO Series 2 type sources which can yield higher dose rates than the ISO Series 1 type sources and therefore provide calibration beams that are more generally applicable for calibrating routine monitoring instruments.

The characterisation of beta radiation fields in terms $\dot{D}_t(d;\alpha^o)$ where d is tissue depth and α angle of radiation incidence have been performed for different source constructions with radionuclides covering a broad variety of beta energies, i.e. $^{106}Ru/^{106}Rh$ (E_{max} = 3.54 MeV), $^{90}Sr/^{90}Y$ (E_{max} = 2.27 MeV), ^{204}Tl (E_{max} = 0.76 MeV), ^{147}Pm (E_{max}= 0.225 MeV), ^{14}C (E_{max} = 0.156 MeV, and ^{63}Ni (E_{max} = 0.067 MeV). The dose rate values were obtained from measurements by extrapolation chambers. The characterised beta radiation fields have been used in this project for a number of studies of energy and angular responses of dose ratemeters and dosemeters. For the $^{106}Ru/^{106}Rh$, $^{90}Sr/^{90}Y$, ^{204}Tl and ^{147}Pm two types of source constructions were studied, the sources produced by the Amersham Company with the radionuclides encapsulated in silver and another type of sources (OMH type) produced at the Hungarian Institute of Isotopes (HII) with backing materials of PMMA and only covered with thin foils of aluminised mylar and therefore expected to produce minimal bremsstrahlung. Studies of the $^{106}Ru/^{106}Rh$ obtained from the Amersham Company showed that the source contained a significant amount of radioactivity from a different radioisotope. The Amersham Company was not able to deliver a replacement source; so for this radionuclide only the HII type source have been available for this project. The ^{14}C source was obtained from the Amersham Company as 0.9 mm thick PMMA sheets with the ^{14}C radionuclide contained in the source as part of the PMMA material. The ^{63}Ni was also produced by the Amersham Company with the ^{63}Ni radioactivity electro-deposited on siver and without any further protective cover. Due to the strong absorption in air of beta particles from ^{63}Ni, implying a significant degradation of the spectrum at short distances from the source, a special container, of diameter 50 cm and length 35 cm, enabling irradiation under reduced air-pressure conditions was constructed at Risø for this source. In this way it was possible to achieve a dose rate of 235 $mGy.h^{-1}$ at a distance of 20 cm from the source. The ^{63}Ni source is not catagorised as an ISO Series 2 type source; however it was found useful to extend the range of energies to the low energy of ^{63}Ni, in particular for studies of energy and angular responses of thin solid state detectors.

The dose rate homogeneity of the established beta radiation fields were studied by using different methods: TLD laser heating scanning using $CaSO_4$:Dy foils (Montpellier), GM counters and radiochromic dye foils (HII in collaboration with NIST,USA), graphite-mixed thin MgB_4O_7:Dy TL detectors (Risø) and beta spectrometer scanning (CEA-FAR). The results showed that the ISO requirements of variation in dose rates being within $\pm$ 5% for the ^{204}Tl source and sources with higher energies and $\pm$ 10% for the ^{147}Pm source and sources with lower energies can be fulfilled for all the established sources for beam diameters ranging between 5 and 10 cm.

The ISO have set a lower limit for the residual maximum energy, E_{res}, present at the calibration position to ensure against excessive degradation of the beta spectrum taking place in the source itself and/or in the absorber between source and calibration point. E_{res} values have been determined for different beta sources by use of GM counter (CEA-Grenoble, NRPB and Risø), by use of beta spectrometer (HII and CEA-FAR) and by calculation (AEA-Harwell). The beta spectra obtained for the HII type sources show E_{max} energies for these sources very close to the theoretical E_{max} values. The results of the E_{res} measurements for other sources showed that the ISO requirements could be fulfilled for all the established ISO Series 2 type sources.

A serious problem of beta calibration fields is the presence of bremsstrahlung. Although the contribution from bremsstrahlung in terms of dose rate is small compared to that from the beta particles (less than 0.04% measured for an extended Amersham type $^{90}Sr/^{90}Y$ source at NRPB) it may

become a significant error source for the determination of beta responses of dose ratemeters and dosemeters, in particular for low-energy beta radiation. Photon spectra of beta sources have been obtained at NRPB and HII and the problem has been intensively analysed by Monte Carlo calculations (EGS4) performed at AEA, Harwell. The results of the study show that an important factor for the production of bremsstrahlung is the source material itself, and they emphasise the importance of performing separate analyses of the bremsstrahlung spectrum and dose contribution for each beta source.

Techniques and methods for characterising beta radiation fields and for individual monitoring for beta radiation doses.

A major part of the work of the project has been devoted to development and study of different dosimetry techniques and procedures for use for characterisation of beta radiation fields and for use for individual dosimetry of beta radiation doses. Techniques that have been involved in the study are: extrapolation chambers, GM counters, beta spectrometers and solid state detectors. Furthermore computer programs have been developed for analyses of the radiation fields and for validation of the experimental results.

Extrapolation chamber

The extrapolation chamber measurement method is the basic standard dosimetry measurement method applied to beta dosimetry. Extrapolation chambers have been established in six of the laboratories participating in the project and most of them are being operated through computerised automated measurement procedures.
Important aims of studying the extrapolation chamber measurement method were to optimise the evaluation procedure and the accuracy of measurement of the method. Joint results have been obtained through comparative measurements of $\dot{H}'(d;\alpha^{o})$ and the collected data have been used as basis for further refinement of the measurement method and evaluation procedure. Specific computer programs developed at CEA-FAR have lead to standardised procedures for evaluation of the measurement data, and in particular for estimation of the total uncertainty for the measured dose rate value. Measurements of dose rates in inhomogene radiation fields, e.g. around hot particles and from low-energy beta sources have required operation with extrapolation chambers with very small electrode areas of diameters ranging from 1 to 10 mm (Birmingham, CEA-Grenoble, Risø).
The joint study of the characteristics of extrapolation chambers have focussed on two intercomparison exercises. The first one was initiated under the previous contract period and was performed with an extended area circular ^{204}Tl source with a diameter of the active part of 42 mm. The second one using an extended area ^{147}Pm source with the same dimensions as the ^{204}Tl source was started in 1993. Participants of both intercomparisons were NRPB,CEA-FAR, CEA-Grenoble and Risø. Parallel with these intercomparisons three of the participants also joint two similar exercises being performed within the framework of EURADOS. The exercises were carried out by circulating the sources between the participating laboratories where measurements of absorbed dose rates to tissue for different tissue depths, angles of incidence of the radiation and at different distances from the sources were made according to an agreed measurement programme. The collaborative work from these intercomparisons have clarified a variety of problems connected to the extrapolation chamber measurement method and as a result standardised measurement procedures, in particular for low-energy beta radiation have been developed.
Results of the intercomparisons have been reported in individual reports from CEA-Grenoble and CEA-FAR and parts of the results have also been reported in previous EC progress reports. A joint report summarising the results of the two intercomparisons is in preparation.
Table 1 presents some of the measurement data obtained from the two intercomparisons illustrating that all results are within $\pm 5\%$ from the average value and in most cases within $\pm 3\%$.

Table 1. Ratio: $\dot{D}_t(0.07;\alpha^o)/(\dot{D}_t(0.07;\alpha^o))_{average}$ and$(\dot{D}_t(0.07;\alpha^o))_{average}$ values for the results from the four laboratories for the ^{204}Tl source and the ^{147}Pm source presented for different irradiation distances and different angles of incidence of the radiation.
(Reference dates: 1. January 1991 for the ^{204}Tl source and 1. January 1993 for the ^{147}Pm source)

Laboratory	$\dot{D}_t(0.07;\alpha^o)/(\dot{D}_t(0.07;\alpha^o))_{average}$							
	^{204}Tl source				^{147}Pm source			
	20 cm distance		30 cm distance		15 cm distance		20 cm distance	
	$\alpha=0°$	$\alpha=45°$	$\alpha=0°$	$\alpha=45°$	$\alpha=0°$	$\alpha=45°$	$\alpha=0°$	$\alpha=45°$
RISØ	1.000	0.980	0.986	0.976	1.015	1.028	1.046	1.018
CEA/FAR	0.981	1.025	1.028	1.039	0.997	0.956	1.003	0.983
NRPB	0.986	1.000	0.988	1.027	0.992	0.983	0.953	0.991
CEA/Grenoble	1.033	0.990	0.995	0.958	0.995	1.034	0.999	1.008
Average ($mGy.h^{-1}$)	211	202	85.5	78.5	79.01	54.65	16.16	11.40

Geiger Müller counter

Studies of GM counters for beta dose rate measurements were initiated at Risø with the aim of utilising the extremely high sensitivity of particle detectors, e.g. GM tubes, for exposures in beta radiation fields where ionisation chambers have some shortcomings. Due to high energy dependence of the GM detector for beta dose rate measurements some information on the energy of the beta radiation must be provided by the measurement. Such information can be obtained by measurement with different absorbers in front of the GM tube and it was found that even with use of only one extra absorber in addition to the absorber represented by the window it was possible to obtain useful measurements of dose rates in unknown beta radiation fields by use of the GM counter.
The high sensitivity of GM tubes to photon radiation also makes the instrument useful for a fast estimation of the magnitude of the photon radiation accompanying the beta particle emission.

Beta spectrometry

The characteristics of the beta reference radiations used for calibration and type testing of radiation protection dosemeters generally rely on data derived from dosimetric techniques implying either extrapolation chamber measurements or passive detector irradiations. Those devices enable the determination of several parameters of the calibration fields : absorbed dose at reference tissue depth, depth-dose curves, evaluation of the field homogeneity and residual range. But generally they provide an integral information concerning the radiation field. In order to get a more detailed knowledge of the radiation field characteristics, a beta spectrometer has been considered as a complementary and efficient tool, being able to quantify the alterations of the primary spectrum of the radionuclide. Modifications resulting from radiation scattering by the surroundings: source holder, protective metallic layer, flattening filters, have to be clearly identified in terms of energy and spatial distributions. Different instruments have been developed over the last years. A beta telescope spectrometer, previously used by J.Böhm, PTB for comparing beta secondary standards, has been assembled at CEA-FAR. It consists of 2 coaxial Si detectors Intertechnique D_1 : IPT 150-300-16 and D_2: LEC 200-5000, inserted in a metallic housing.
The Si thicknesses are 300 μm and 5000 μm, respectively. By combining those 2 types of detectors, a satisfactory compromise of low energy threshold (IPT type) and a good efficiency (LEC type) can be obtained. Both detectors are operated at room temperature.
Details about the electronic circuitry and the measurement procedure will be given in the individual laboratory report, and currently available results will be presented and commented.

Thin solid state detectors

Solid state dosemeters intended for characterisation of beta radiation fields and for individual monitoring for skin doses from beta radiation should contain detectors with a small effective thickness capable of measuring $H'(d;\alpha^{\circ})$ nearly independently of energy and angle of incidence of the radiation. Studies of dosimetric characteristics of thin detectors for dosimetry of beta radiations have taken place in seven of the ten participating laboratories. New highly sensitive detectors have been developed and studied (LiF:Mg,Cu,P detectors at INP Krakow, and $CaSO_4$:Dy foils for laser heating scanning at Montpellier). With a sensitivity of the new materials that is 20-40 times higher than that for normal LiF, the thin detectors show detection thresholds well below 50 μSv. The TSEE technique has been intensively studied at Giessen University showing that BeO TSEE detectors present ideal dosimetric characteristics for beta dosimetry in mixed beta/gamma fields. For thin TL detectors the efficiency for the measurement of beta doses from ^{147}Pm varied from about 40% to 90%. For the measurement of $H_p(0.07;\alpha^{\circ})$ this lower efficiency can be compensated for by using a cover with a thickness lower than 0.07 mm tissue-equivalent material. Thin solid state detectors have proven to be useful for a number of applications for beta dosimetry e.g. personal dosimetry (HII,Risø), dose homogeneity measurements of large beta radiation areas (Montpellier, Risø), and dose measurements and distributions close to small radioactive particulates ("hot particles") (University of Birmingham, CEA-Grenoble, Montpellier).

Calculations

At AEA, Harwell, Monte Carlo codes based on the EGS4 system were developed for characterisation of beta radiation fields. Models were developed for the two types of sources (Amersham and OHM type) used in the project and a number of electron and photon energy spectra and energy flux data have been generated for studies of influencing parameters in the design of beta calibration fields. The results of the work show that Monte Carlo models are powerful tools for exploring the behaviour of radiation fields, but for the models to be useful the composition of the beta source holders and particularly the matrix containing the beta emitter must be well known.

Low energy photon dosimetry

Low energy photons, i.e. below 20 keV, are dosimetrically considered as low penetrating radiations and calibration of radiation protection dosemeters has to be performed in terms of $H_p(0.07)$ or $H'(0.07)$. Therefore reference radiations involved in the calibration or type testing of such devices must be thoroughly characterised. Within the framework of this contract, an action has been initiated at CEA-FAR to realise a X-ray facility devoted to that purpose, enabling the availability of quasi-monoenergetic filtered photon beams at 3 energies: 6.5, 8.5 and 12.2 keV. For each radiation quality, the reference quantity $H_p(0.07;\alpha°)$ has been determined by a technique involving measurements with an extrapolation chamber. Measurements were performed for different angles of incidence of the radiation up to 45° and kerma-to-directional dose equivalent coefficients have been experimentally determined. Due to the energy range of the photon radiation involved in that measurements, $H'(0.07;\alpha°)$ can be considered as a satisfactory approximation of H_p $(0.07;\alpha°)$ dose equivalent at depth 0.07 mm in a ICRU tissue slab. At Risø a 6 keV, 37 GBq ^{55}Fe, photon irradiation facility has been established and characterised in terms of absorbed dose rate to air and to tissue at different tissue depths by use of the extrapolation chamber.
From a metrological point of view, measurements of K_{air} with 2 different devices, e.g. a free air chamber and an extrapolation chamber, represent an interesting crosscheck of dosimetric references.

Hot particle dosimetry.

The overall aim of the project was to develop and validate methods for the measurement and calculation of doses from radioactive particulates ("hot particles").
A number of test sources (^{60}Co, ^{170}Tm, ^{46}Sc, ^{175}Yb) with well-defined source designs have been produced for the project. Comparative measurements of doses from a ^{60}Co source using different measurement techniques have been performed at different laboratories: University of Birmingham (extrapolation chamber and radiochromic dye films), CEA-Grenoble (extrapolation chamber and TLD), University of Montpellier (TLD and OSL) and NIST, USA (radiochromic dye films). Recently, an intercomparison involving two more US laboratories, Brookhaven National Laboratory and Richland Battell Laboratories and Yankee Atomic has been initiated.
Four calculational codes have been used in the study: VARSKIN MOD 2 a semi-empirical code developed at Battelle labs, USA; a PC-based Monte Carlo code developed by Dr. Patau; an adapted version of EGS4 for ^{170}Tm and the HOT series of codes specially developed for ^{60}Co.
The results obtained for the ^{170}Tm source showed a reasonable agreement between the experimental values measured with extrapolation chamber and radiochromic dye foils and VARSKIN MOD 2 and EGS4 code predictions. Results for the ^{60}Co source showed also reasonable agreement between the two experimental methods but disagreed with predictions from the VARSKIN MOD 2 code and the HOT code. Good agreement between the extrapolation chamber results and those of the radiochromic dye was also found for the measurements performed within the new EU/US intercomparison programme. The TLD measurements showed good agreement with measurements obtained with the radiochromic dye films if a correction factor calculated by the VARSKIN MOD 2 code was applied for the TLD results.

Head of project 1 : Dr. Christensen

II. Objectives for the reporting period

The main objectives of the project were:
- establishment and characterisation of standard beta calibration fields.
- analyses of important parameters of the extrapolation chamber measurement method, e.g., by participating in intercomparison exercises on measurements of beta dose rates using extrapolation chambers.
- development and characterisation of solid state dosemeters with small effective detector thicknesses for dosimetry in radiation fields from weakly penetrating radiations.
- establishment and characterisation of a standard low-energy photon calibration field using a ^{55}Fe source (6 keV).

III. Progress achieved including publications

1. Establishment and characterisation of standard beta calibration fields

During the period of the project a number of beta calibration fields representing a broad spectrum of beta energies have been established and characterised for application for radiation protection dosimetry purposes. The beta sources have been setup in arrangements allowing irradiations at different angles of incidence of the radiation as well as at different distances from the sources. Due to the strong absorption in air of beta particles from ^{63}Ni (E_{max}= 67 keV) with the result of a significant degradation of the spectrum at short distances from the source, a special container, of diameter 50 cm and length 35 cm, enabling irradiation under reduced air-pressure conditions was constructed for this source. The established beta calibration facilities have been utilised for a number of studies of responses of dosemeters and dose rate meters performed by participants of the project [1,2,3,4]. Some important characteristics of the beta calibration fields established at Risø National Laboratory are given in Table 1.

1.1 Dose rate, $\dot{D}_t(0.0061;0^o)$

The beta dose rates, at a tissue depth of 0.0061 mm and for normal incidence of the radiation, $\dot{D}_t(0.0061;0^o)$, shown in Table 1, were determined by use of extrapolation chambers. The two $^{90}Y/^{90}Sr$ sources have originally been calibrated at PTB when they were purchased from the Büchler Company in 1978 and calibration certificates for these are available for use. Measured dose rates at Risø were in agreement with the data of the PTB certificate to within $\pm 1\%$. Two PTW, type 23392 extrapolation chambers with different electrode diameter, 30 mm and 4 mm, respectively, were used for the measurement of $\dot{D}_t(d;\alpha^o)$. The chamber with the small electrode area was used for radiation fields for which a homogene radiation field was only present over small areas, e.g. those from ^{63}Ni. Both chambers have a window thickness equivalent to 0.61 mgcm^{-2} tissue. The measurements of dose rates from the ^{63}Ni source under reduced air-pressure conditions were made with thin MgB_4O_7:Dy TL detectors which had previously been inter-calibrated with measurements with the extrapolation chamber of dose rates at 1 cm distance from the ^{63}Ni source under normal air-pressure conditions.

1.2 Depth dose profiles

Knowledge of depth dose profiles of beta calibration beams is important for studies of responses of dosemeters and dose rate meters, e.g. for the measurement of doses to the skin at a certain depth. Depth dose profiles can be obtained by measurement of dose rates behind plastic absorbers of increasing thickness and converting the absorber thicknesses to equivalent thicknesses of tissue by

Table 1. Characteristics of beta calibration fields established at Risø National Laboratory. Reference date for source strengths (nominal) and dose rates is 1. July 1995. Dose rates are expressed in terms of absorbed dose rate to tissue at a depth of 0.61 mg.cm^{-2}, i.e. $\dot{D}_t(0.0061;0^o)$. The shown uncertainty values indicate ± 2 S.D.

Radio-nuclide	Source Strength (MBq)	Max.beta energy unmodified (MeV)	Source design	Calibrat. distance (cm)	Res. max. beta energy, (MeV)	Dose rate $\dot{D}_t(0.0061;0^o)$ (mGyh^{-1})
$^{90}Sr/^{90}Y$	1231	2.26	PTB-Buchler standard[a]	30	1.87 (Herbaut)[i]	194±2%
$^{90}Sr/^{90}Y$	49	2.26	PTB-Buchler standard[b]	30	1.89 (Herbaut)[i]	6.27±2%
^{204}Tl	16.4	0.77	PTB-Buchler standard[c]	30	0.52 (Herbaut)[i]	0.84±2%
^{204}Tl	352	0.77	Amersham 42mm diam.[d]	30	0.62	40.1±2%
^{147}Pm	388	0.22	PTB-Buchler standard[e]	20	0.11 (Herbaut)[i]	1.39±3%
^{147}Pm	84	0.22	Amersham (NRPB)[f]	20	0.142	1.56±3%
^{14}C	2 x 10^4 s^{-1}.cm^{-2} (2π geom)	0.155	Amersham PMMA 10 cm diameter[g]	1	0.130	107± 3 %
				5	0.117	17.3 ± 3%
				10	0.103	1.72 ± 3%
^{63}Ni	203 MBq.cm^{-2}	0.067	Amersham 1 cm diameter[h]	1	0.062	15382± 3%
				2	0.055	1246± 3%
				3	0.052	151 ± 3%
				20; (100Pa)	-	235 ± 4%

a.No beam flattening filter. Cover of source: 50 mgcm^{-2} silver+80 mgcm^{-2} stainless steel.
b.With beam flattening filter. Cover of source: 50 mgcm^{-2}silver+10 mgcm^{-2} gold flashing.
c.With beam flattening filter. Cover of source: 20 mgcm^{-2} silver + 5 mgcm^{-2} gold flashing.
d.No beam flattening filter. Cover of source: 20 mgcm^{-2} silver + 10 mgcm^{-2} gold flashing.
e.With beam flattening filter. Cover of source: 5 mgcm^{-2} silver + 0.5 mgcm^{-2} nickel plating.
f.No beam flattening filter. Cover of source: 5 mgcm^{-2} silver+ 0.5 mgcm^{-2} nickel plating (see ref.[7]).
g.One mm thick perspex sheet fabricated with the ^{14}C radionuclide as a component of the acrylic mass.
h.The ^{63}Ni radionuclide electro-deposited in silver. No protective cover.
i.See individual report from CEA-Grenoble of this final report

using the scaling factors reported by Cross [5]. Transmission factors for obtaining depth dose curves were measured in a simple way using only one fixed setting of the chamber depth (1000 μm) for each absorber thickness. Results from an intercomparison concerned with measurement of dose rates from a ^{204}Tl source organised within the framework of EURADOS have shown that transmission factors can be obtained with satisfactory accuracy in this way if a chamber depth not greater than about 1000 μm is used [6]. From the transmission factors depth dose curves were obtained by 3rd degree polynomial fits of either the measured data (^{90}Y/^{90}Sr and ^{204}Tl) or of their logarithmic values (^{63}Ni, ^{14}C and ^{147}Pm) [7].

The characterisation of a calibration beam in terms of $D_t(d;\alpha°)$ requires the determination of depth dose profiles for a number of angles of incidence of the radiation. Figure 1 shows an example of depth dose profiles obtained for the, 4cm x 4 cm, ^{147}Pm calibration source listed in Table 1.

In Figure 2 depth dose curves are shown for different beta sources, listed in Table 1, and which all (except for ^{63}Ni) belong to the ISO series 2 type sources.

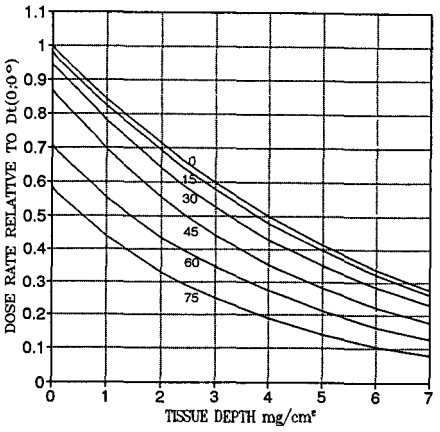

Figure 1. Dept dose profiles for irradiation of tissue at a distance of 20 cm from a 4cm x 4cm, ^{147}Pm source for different angles of incidence of the radiation as indicated in the figure. The curves have been obtained from fitting of experimental data using the expression: $\ln I = a + bx + cx^3$ where I is dose rate and x tissue depth.

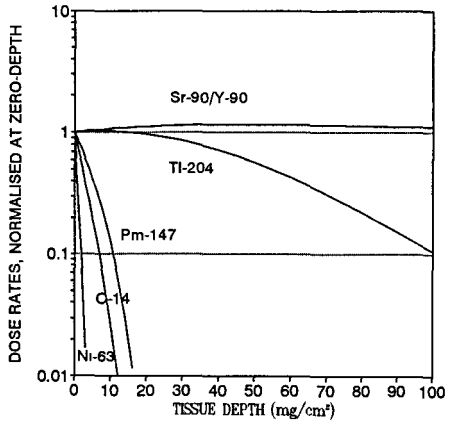

Figure 2. Depth dose curves measured for some of the beta sources listed in Table 1. The curves are obtained by polynomial fits of experimental values. Calibration distances were: ^{90}Sr/^{90}Y and ^{204}Tl: 30 cm, ^{147}Pm: 20 cm, ^{14}C: 5 cm, and ^{63}Ni: 1 cm. All data are given for normal incidence of the radiation.

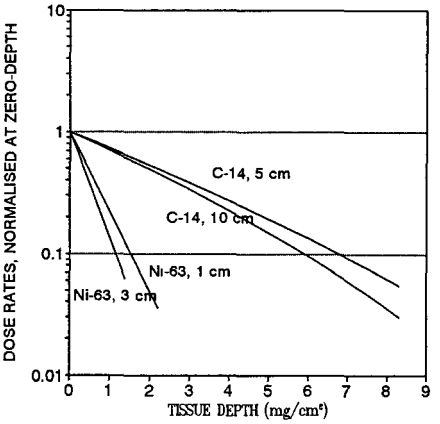

Figure 3. Depth dose curves measured for beta radiation fields at different distances from the source as indicated in the figure. The curves are obtained by polynomial fits of experimental data. All data are given for normal incidence of radiation.

Figure 3 shows depth dose curves for some low-energy beta radiation fields obtained for different distances from the sources illustrating that a significant degradation of the beta spectrum occurs during the penetration through a few cm of air and that it is important to specify calibration distance when, e.g. the response of a dosemeter have been determined for a certain beta source.

The possibility of combining absorbers of air with plastic absorbers by using the scaling factors defined by Cross was confirmed by some preliminary measurements of dose rates from the ^{63}Ni source at a distance of 20 cm under different air-pressure conditions and comparing these with results obtained with mylar absorbers. Figure 4 illustrates the agreement obtained by using the two types of absorbers.

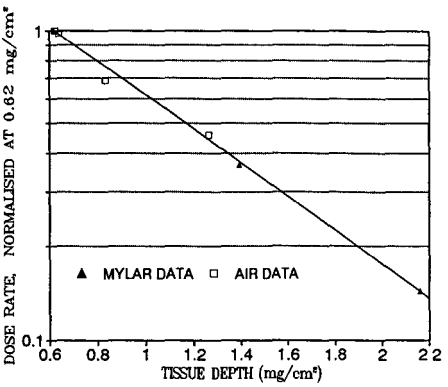

Figure 4. Transmission data for ^{63}Ni beta radiation measured with thin MgB_4O_7:Dy TL detectors at 20 cm distance from the source under reduced air pressure. ▲: Mylar absorbers at air pressure 100Pa. □: Air pressures 100Pa, 1kPa, 10kPa and 30kPa, all with additional 0.66 mgcm^{-2} Mylar absorber.

1.3 Mass absorption coefficients $(\mu/\rho)_{abs}$

For low energy beta radiation, e.g. from ^{147}Pm, ^{14}C and ^{63}Ni the absorption curves have no pronounced build-up region as observed for beta emitters with higher energies (see Figure 2). A suitable fit of absorption curves for low-energy beta fields can be obtained from the expression: Ln D = a + bx + cx^3, where D

Table 2. Mass absorption coefficients, $(\mu/\rho)_{abs,air}$, measured for radiation fields from low-energy beta sources.

Radionuclide	Source type	Calibration distance	$(\mu/\rho)_{ab,air}$ (cm^2.mg^{-1})
^{147}Pm	PTB-Büchler, standard	20	0.217
	4cm x 4 cm, area source	15	0.123
		20	0.148
^{14}C	PMMA 10 cm diameter	5	0.255
		10	0.320
^{63}Ni	1 cm diameter	1	1.232
		3	0.321

is measured absorbed dose rate for absorber thickness x, expressed in units of mass per area [7]. A value of the mass absorption coefficient can now be obtained from: $(\mu/\rho)_{abs} = (d(\ln D)/dx)_{x=0} = b$. Table 2 presents values of $(\mu/\rho)_{abs,air}$ for the low-energy beta calibration fields listed in Table 1. The mass absorption are important for evaluating the correction factor, Kad, correcting for variation of the air mass between source and detector caused by changes of environmental conditions, i.e. pressure, temperature, and relative humidity [7]. They are also valuable for predicting beta-dose responses of thin solid state detectors.

1.4 Residual maximum beta energy, E_{res}

The ISO have setup requirements on minimum values of the residual maximum beta energy, E_{res} for ISO Series 2 sources, to ensure against unacceptable degradation of the beta-spectrum [8]. E_{res} values for the beta fields used at Risø are presented in Table 1. The values for the PTB-Büchler standard sources have been taken from the individual report from CEA-Grenoble of this final report. All other values were obtained by use of a geiger tube with an end window thickness of 1.60 mgcm^{-2} using mylar foils as absorbers and converting to tissue-equivalent thicknesses by use of the scaling factors given by Cross [5]. The great difference observed between the theoretical maximum beta energies and the measured E_{res} values (see table 1) indicates that a significant degradation of the beta spectra have taken place. However, all E_{res} values measured for the ISO Series 2 type sources fulfill the ISO requirements.

1.5 Dose rate homogeneity

The PTB-Büchler standard sources are provided with beam flattening filters that ensure a satisfactorily homogene radiation field at the calibration distance over an area with a diameter of about 10 cm [9]. The ISO Series 2 sources are not expected to use beam flattening filters; however the ISO have set limits for allowable maximum variation of the dose rate over the area of the calibration beam to be used [8]. At Risø the homogeneity of radiation fields from extended area sources of ^{147}Pm and ^{14}C were studied by using graphite-mixed MgB_4O_7:Dy TL detectors. These detectors have an effective thickness equivalent to a mass per area of 2-3 mgcm^{-2} and show good energy- and angular responses for measurement of doses from beta radiation [10]. During the irradiation, 15 x 17 detectors (1mm thick, 4.5 mm diameter) were arranged in depressions in a perspex plate in form of a matrix covering an area of 8.82 cm x 9.6 cm. By using average values of three repeated measurements the uncertainty for each measurement point was estimated to be below $\pm$ 1.5% ($\pm$1 S.D.). In Figures 4 and 5, examples of measured dose rate distributions for different irradiation geometries are
presented for the two sources where the results are given as curves obtained from polynomial fits of the experimental data. It can be seen that the ISO requirement of a variation in the dose rates lower than $\pm$ 10% can be fulfilled in all cases for beam areas with a diameter of about 80 mm. However, corrections of a few percent for this inhomogeneity must be applied in standard measurements with extrapolation chambers with an electrode diameter of 30 mm.
The method used at Risø for dose rate homogeneity studies was compared with the laser heating TLD scanning method used at Montpellier University by performing identical irradiations with ^{147}Pm beta rays of the $CaSO_4$:Dy foils used at Montpellier and the MgB_4O_7:Dy used at Risø. The two methods agreed with a variation less than 3.5% (see also the individual report from Montpellier of this final report)

2. Beta dose rate measurements

2.1 Extrapolation chamber standard beta dosimetry

The extrapolation chamber is the standard instrument for measurement of absorbed dose rate to tissue $\dot{D}_t(d;\alpha^o)$ from beta radiations. Risø has collaborated with other participants in joint studies of the

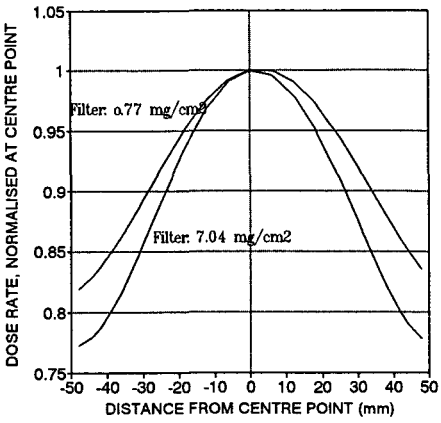

Figure 5. Dose rate homogeneity measurement results for a, 4 cm x 4 cm, ^{147}Pm source at 20 cm distance. Results are presented for two different absorbers.

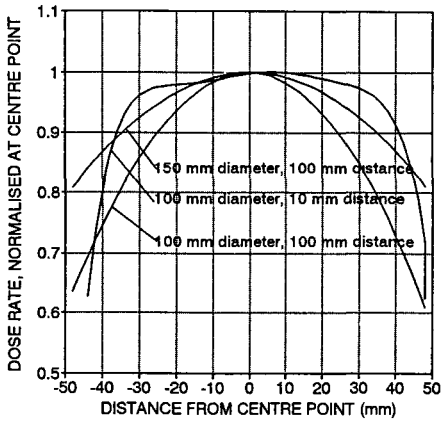

Figure 6. Dose rate homogeneity measurement results for a ^{14}C source, shown for distances 100 mm and 10 mm from a 100 mm diameter source and 100 mm from a 150 mm diameter source.

extrapolation chamber measurement method through participation in intercomparison exercises using ^{204}Tl and ^{147}Pm sources. Important aims of the intercomparison exercises were to identify significant uncertainty sources of the method as well as to facilitate the use of extrapolation chambers by introducing automated computer controlled procedures for the operation of the chamber and standard procedures for the evalution of the measurement results. At Risø two PTW type 23392 extrapolation chambers with different electrode diameter (30 mm and 4 mm, respectively) have been established. Two types of Keithly electrometers, type 642 and 6517, both operating in charge mode have been applied for the current measurements. The Keithly 6517 type is a newer and cheaper model than type 642; however both models are suitable for low-current measurements with a lower range of measurement of $10^{-17}A$ and no significant difference in accuracy between the two electrometer types was seen for measurement of currents in the range 1-10 fA. Computer programs have been developed enabling a fully automatic operation of the extrapolation chamber and handling of the measurement data including influencing environmental parametre (air pressure, temperature and humidity). Specific computer programs developed at CEA-FAR for dose evaluations of the measurement results, i.e. fitting programs for evaluating extrapolation curves and depth dose data (see individual report from CEA-FAR of this final report), have been adopted as standard evaluation procedures. The two extrapolation chambers have been used for characterising a number of beta calibration fields in terms of $D_t(d;\alpha^o)$(see Section 1).

2.2 Use of GM counters for beta dosimetry

GM counters were studied with the aim of utilising the extremely high sensitivity of particle detectors, e.g. GM counters, for dose rate measurements in beta radiation fields where ionisation chambers have some shortcomings. As the conversion factor K_{Beta} for converting measured count rate to dose rate is

highly dependent on beta energy, some information on the energy of the beta radiation must also be provided by the measurement. In this work the possibility of using two different absorbers to provide useful information on the beta energy for obtaining a value of K_{Beta} was studied [2].
The measurements were carried out with a LND-type GM tube (30 mm in diameter, and approximately 1 cm deep) with an end-window thickness equivalent to 1.60 mgcm^{-2}. By using a number of absorbers in front of the GM detector, absortion curves were obtained for some of the beta radiation fields that have been calibrated by use of the extrapolation chamber. Figure 7 presents beta dose GM responses as a function of absorber thickness for different beta sources showing that the response of the GM detector for beta dose measurement is highly dependent on beta energy. In Figure 8, the K_{Beta}values for the measurement of skin dose rates, i.e. dose rates to tissue at a depth of 0.07 mm, are presented as a function of the ratio of the GM count rates measured with two absorbers, one without additional absorber to the end-window thickness of 1.6 mgcm^{-2} and the other one with a total absorber thickness(window+filter) of 7 mgcm^{-2}. The figure clearly illustrates that for unknown beta radiation fields the ratio of GM measurements with two absorbers can be used to obtain a value of K_{Beta}.

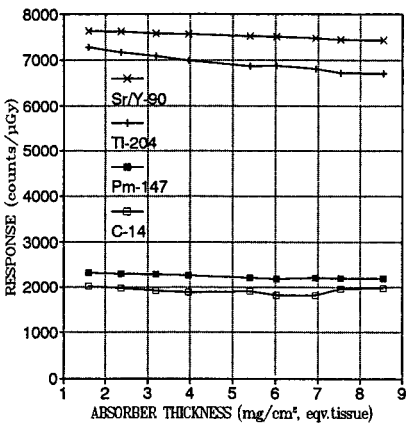

Figure 7. GM responses to beta-ray doses as a function of thickness of total absorber (widow+filter) measured for four different beta sources. Reference dose for each absorber thickness is the dose measured with extrapolation chamber using the same total absorber mass.

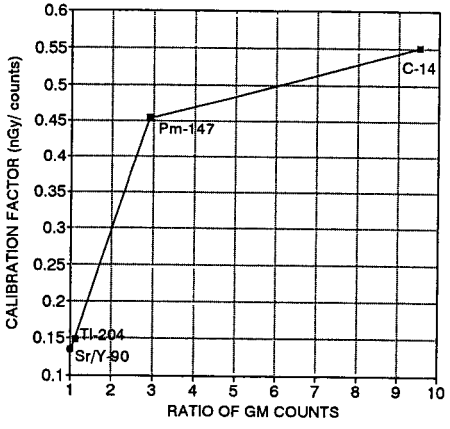

Figure 8. Beta dose calculation factor $K_{beta}(0.07,0°)$ for GM detector provided with 7 mg.cm^{-2} total absorber, as a function of ratio of measured GM counts for the two total absorbers, 1.6 and 7.3 mgcm^{-2}.

Study of solid state detectors for beta dosimetry.

Dosimetric characteristics important for beta dosimetry were studied for a number of thin TL detectors prepared from the highly sensitive TL materials, LiF:Mg,Cu,P (INP-Krakow and SSDL-Beijing), $CaSO_4$:Dy (Montpellier) and MgB_4O_7:Dy (Boris Kidric). The detectors from INP-Krakow consist of a 8.5 mgcm^{-2} LiF:Mg,Cu,P sintered on an 4.5 diameter inactive LiF pellet. The detectors from SSDL-Beijing and Montpellier were received as kapton foils with thin layers of TL material fixed on one

side. In order to obtain a detector design suitable for the TLD reader used at Risø, circular samples of 4.5 mm diameter were cut from the foils and fixed by heat-resistant silicone-based glue onto Al supports, 0.7 mm thich and 4.5 mm diameter. The samples from the Boris Kidric Institute were sintered, 4.5 mm diameter, 0.9 mm thick, MgB_4O_7:Dy detectors mixed with 3% graphite. Also BeO TSEE detectors from the Battelle Institute, Frankfurt were studied for application for beta dosimetry. It was expected that these detectors with a detector thickness below 100 nm combined with a high sensitivity would be useful for accurate beta dosimetry in beta radiation fields, in particular for fields with beta rays of low energies. The TSEE measurements were performed with an ENDOS type ENDOVA-50 reader using a GM counter equipped with a point anode.
In Table 4 dosimetric characteristics of the four types of thin TL detectors and the BeO TSEE detector are presented together with those of the well-known 0.9 mm thick LiF TLD-700 chip for comparison. It can be seen that all detectors show a detection threshold below 60 μGy ^{60}Co dose and that the threshold found for the TSEE detector is significantly lower than that observed for the TL detectors. The beta-ray response of the thin TL detectors for the measurement of doses from a low-energy beta radiation field (^{147}Pm) is in the range from 0.40 to 0.90. If the detectors are used for measuring $\dot{H}'(0.07;\alpha^{\circ})$ the lower efficiency can be compensated for by using an absorber thickness for the detector that is smaller than 7 mgcm^{-2}. All the thin detectors showed a response near one for measurement of beta doses from the ^{204}Tl and the ^{90}Sr/^{90}Y sources. Results from studies of angular responses for angles up to 60° confirmed previous observations that the responses of thin detectors for beta dose measurements are only slightly dependent on radiation incidence. It can be seen from Table 4 that the response of TSEE detectors for measurement of beta doses from ^{147}Pm is only 0.78. These results are unexpected considering the small detector thickness and they disagree with the results obtained with the same detector type at Giessen University showing responses of one for the measurement of $H_p(0.07)$ from exposures in beta radiation fields from both ^{90}Sr/^{90}Y, ^{204}Tl and ^{147}Pm (see the individual report from Giessen University of this final report). Different absorber foils were used for the two experiments which may explain some of the discrepancy.

Table 3. Dosimetric characteristics of four types of thin TL detectors, a TSEE detector and a LiF-TLD-700 chip.

Detector	Effective detector thickness	γ-ray (^{60}Co) sensitivity	Background [eqv.μGy^{60}Co]	*)Detection threshold [eq.μGy^{60}Co]	**) ^{147}Pm beta-ray response
LiF TLD-700 (Harshaw)	240 mgcm^{-2}	100	28	11	0.03
MgB_4O_7:Dy (3% graphite) (Boris Kidric)	2 mgcm^{-2}	6	370	50	0.89
LiF:Mg,Cu,P (INP-Krakow)	8.5 mgcm^{-2}	100	38	7	0.40
LiF:Mg,Cu,P (SSDL,China)	5 mgcm^{-2}	24	100	25	0.54
$CaSO_4$:Dy (Montpellier)	Grain size $<35\mu$m	48	51	14	0.54
BEO-TSEE (Battelle)	<100nm	-	2	2	0.78

*) The detection threshold defined as three standard deviations of the background reading.
**) Beta ray response is the response per unit absorbed dose to tissue given to the surface of the bare detector, normalised to the response per unit dose to tissue from ^{60}Co γ-radiation.

4. Low-energy photon dosimetry

A 37 GBq ^{55}Fe source purchased from the Amersham Company has been arranged in an irradiation setup. The ^{55}Fe activity is plated on one face of a 13 mm diameter copper disk and covered by a 0.25 mm thick protective beryllium window. ^{55}Fe decays by electron capture to the ground state of ^{55}Mn, with emission of manganese K x-rays (5.9 and 6.5 keV), its half life being 2.68 y. A photon energy spectrum measured from the source by use of a cooled silicon-lithium drifted detector showed two peaks at 5.9 and 6.3 keV with a ratio of counts of 4:1. The source was obtained with the aim of establishing a 6-keV photon calibration beam to be used for calibration in terms of air kerma rate as well as absorbed dose rate to tissue.

It has been shown that the extrapolation chamber is suited for measurement of absorbed dose rate to tissue if only that part of the chamber where electronic equilibrium exists is used [11] (see also the individual report from CEA-FAR of this final report). The maximum range of electrons produced by a 6 keV photon is about 1 mm in air which means that electronic equilibrium exists at chamber depths greater than 1 mm. In this case the differentiated value of the extrapolation curve, extrapolated from 1mm depth to zero depth should be used for the dose evaluation. An example of an extrapolation curve obtained for ^{55}Fe is shown in Figure 9.

The figure presents values of current, I (corrected for deviations from standard air conditions) for chamber depths ≥ 1 mm together with a 2. degree polynomial fit and its derative dI/dl. The value of dI/dl, 42.33 fA/mm, obtained by extrapolating to I = 0 is the figure used for dose rate evaluation.

The absorbed dose rate to air is obtained from:

$$D_{air}(0.0061_{mylar},0°) = \frac{(W/e).(dI/dl)}{a.\rho_0}$$

where W/e = 33.87 eV, a = area of electrode = 7.16 x 10^{-4}m^2 and ρ_0 = 1.1995 kg.m^{-3} (air density under standard conditions).

The dose rate to tissue is now obtained by multiplying the value for air by the ratio of mass energy absorption coefficients $(\mu_{en}/\rho)_{tissue}$ to $(\mu_{en}/\rho)_{air}$ = 0.975.

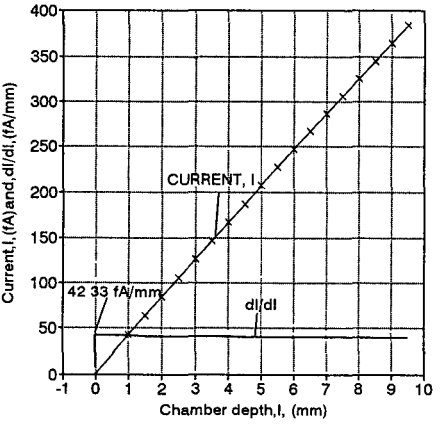

Figure 9. Extrapolation curve and its derative, dI/dl, measured for a, ^{55}Fe source at a distance of 30 cm. All I values refer to standard air conditions.

Transmission factors obtained from measurements with different mylar absorbers showed good agreement (within 0.1%) with calculations using the absorption coefficient for a 6 keV photon beam. The following results were obtained for a radiation distance of 30 cm:

$D_{air}(0;0°)$ = 5.87 mGy.h^{-1}; $D_t(0.07;0°)$= 4.91 mGy.h^{-1} ; $D_t(0.07;45°)$ = 4.62 mGy.h^{-1}. This gives a value for the ratio $D_t(0.07;\alpha°)/D_{air}(0;0°)$ of 0.84 for α = 0° and 0.79 for α = 45°. The value 0.84 found for 0° is in good agreement with a reported calculated value of 0.83 [12]. Results from dose rate measurements at different distances from the source showed that the dose rates (corrected for attenuation by the air) follow the inverse square law with good agreement for distances between 30 and 50 cm.

Responses of thin TL detectors to ^{55}Fe photons were measured for a distance of 30 cm from the source. The following responses in terms of TL signal per unit dose to tissue to the bare detector/ TL signal per unit dose to tissue from ^{60}Co, were found: MgB_4O_7:(Dy)(3%C) (Boris Kidric) : 1.39; LiF:Mg,Cu,P (China): 0.52 and LiF-TLD-700 (0.9 mm thick): 0.21.

References

1.Christensen, P., Study of LiF:Mg,Cu,P TL Detectors for Individual Monitoring for Weakly Penetrating Radiations. Radiat. Prot. Dosim., 47, 1/4 pp. 425-430 (1993).
2. Borg, J. and Christensen, P., Determination of Dose Rates in Beta Radiation Fields Using Extrapolation Chamber and GM Counter, Radiat. Prot. Dosim. (1995). In press.
3. Setzkorn, R., Prévost, H., Gasiot, J. and Christensen, P., Laser Heating ofThermoluminescent Films: Dose Mapping Applied to Beta Dosimetry. Presented at 11th International Conference on Solid State Dosimetry, July 10-14, 1995, Budapest, Hungary, (1995).
4. Bilski, P., Budzanowski, M., Olko, P. and Christensen, P., Properties of Different Thin-Layer LiF:Mg,Cu,P TL Detectors for Beta Dosimetry. Submitted to Radiat. Prot. Dosim. (1995)
5. Cross, W.G.,Variation of Beta Dose Attenuation in Different Media. Phys. Med. Biol.,13, 611-618 (1968).
6. Helmstädter, K., Böhm, J., Chartier, J.-L., Cutarella, D., Chauvenet, B., Lecante, C., Christensen, P., and Francis, T.M., Intercomparison of Extrapolation Chamber Measurements of the Directional Absorbed Dose Rate for ^{204}Tl Beta Radiation. Submitted for publication in Radiat. Prot. Dosim. (1995).
7. Francis, T.M., Böhm, J.L., Chartier, J.-L. Christensen, P., Experience gained on extrapolation chamber measurement techniques from an intercomparison exercise conducted with a ^{147}Pm source. Radiat. Prot. Dosim. 39, 109-114 (1991).
8. ISO. Reference Beta Radiations for Calibrating Dosemeters and Doserate Meters and determining their Response as a Function of Beta Radiation Energy. ISO 6980. First Revision, 1990-11-01.
9. Helmstädter, K., and Böhm, J., The PTB Beta Secondary Standard for Absorbed Dose to Tissue, Proceed. 24th Intern. Symp. on Radiation Protection Physics, Gaussig, Germany (1992)
10. Christensen, P., and Prokic, M.,Energy and Angular Response of TL Dosemeters for Beta Ray Dosimetry. Radiat. Prot. Dosim. 17 pp. 83-87 (1986).
11. Böhm, J., Hohlfeld, K., and Reich, H., A Primary Standard for Determination of Absorbed Dose in a Phantom for X-Rays Generated at Potentials of 7.5 tp 30 kV: PTB Mitteilungen 89, 3/79.
12. British Committee on Radiation Units and Measurements, Conversion from Air Kerma to Directional Dose Equivalent for Photons Below 10 keV. Radiat. Prot. Dosim. 27, pp. 267-269 (1989).

Publications

Christensen, P., Study of LiF:Mg,Cu,P TL Detectors for Individual Monitoring for Weakly Penetrating Radiations. Radiat. Prot. Dosim., 47, 1/4 pp. 425-430 (1993).

Borg, J. and Christensen, P., Determination of Dose Rates in Beta Radiation Fields Using Extrapolation Chamber and GM Counter, Radiat. Prot. Dosim.(1995). In press.

Setzkorn, R., Prévost, H., Gasiot, J. and Christensen, P., Laser Heating of Thermoluminescent Films: Dose Mapping Applied to Beta Dosimetry. Presented at 11th International Conference on Solid State Dosimetry, July 10-14, 1995, Budapest, Hungary, (1995).

Bilski, P., Budzanowski, M., Olko, P. and Christensen, P., Properties of Different Thin-Layer LiF:Mg,Cu,P TL Detectors for Beta Dosimetry. Submitted for publication in Radiat. Prot. Dosim. (1995).

Helmstädter, K., Böhm, J., Chartier, J.-L., Cutarella, D., Chauvenet, B., Lecante, C., Christensen, P., and Francis, T.M., Intercomparison of Extrapolation Chamber Measurements of the Directional Absorbed Dose Rate for ^{204}Tl Beta Radiation. Submitted for publication in Radiat. Prot. Dosim. (1995).

Head of project 2 : Dr. Chartier

II. Objectives for the reporting period

For the reporting period, the main actions included in the work programme of the CEA-FAR/SDOS have dealt with the 3 following topics

-dosimetry of beta reference radiations used for the calibration and typetest of radiation protection dosemeters. Metrological problems involved in extrapolation chamber measurements have been investigated together with an analysis of individual uncertainties.

-spectrometry of beta radiation fields as those available in high dose rate ISO secondary standards developed by french calibration laboratories.

-dosimetry of low energy photons (6 keV-20keV), with the objectives of realising a calibration facility and measuring the kerma-to-directional dose equivalent conversion coefficients which are needed for the determination of energy and angular responses of radiation protection dosemeters.

III. Progress achieved including publications

Beta dosimetry

The CEA-FAR/SDOS laboratory has participated in 1993 to an intercomparison exercise based on the calibration of an extended area ^{147} Pm source (active diameter · 42 mm) circulating through 4 laboratories. All the results have been transmitted to the coordinator in order to prepare a compilation from which mean values of angular conversion factors and associated uncertainties for ^{147} Pm should be derived.

During the contract period, the contractors have agreed on the interest of including mathematical protocols at different steps of the evaluation of measurements performed with extrapolation chambers In particular, fitting procedures involving generally weighted least square techniques have been applied for extrapolation curves and depth-dose curves using a software distributed by CEA-FAR.[3]

By referring to the experimental results and associated uncertainties, efforts have focused on the methodology to evaluate the overall uncertainties on extrapolation chamber measurements Starting from a previous publication [4], several versions of a paper entitled " Proposal for a simplified procedure to evaluate the uncertainties in extrapolation chamber measurements " have been released taking into consideration the WECC recommendations.

In the last issue, a procedure has been developed to assign an uncertainty to the dose at any depth x on the fitted depth-dose curve

From the relation

$$D_t(x) = k_{wi}(x) \quad D_t(x_{wi})$$

where

$D_t(x_{wi})$ dose-to-tissue at depth x_{wi} derived from the "extrapolated to zero chamber depth " corrected current

x_{wi} thickness of the extrapolation chamber entrance window

$k_{wi}(x)$ correction factor taking into account the absorption and scattering in the additional filter placed in front of the entrance window of the chamber

Knowing that $k_{wi}(x) = I_f(x)/ I_f(x_{wi})$= ratio of the fitted values of the ionisation current (measured with the same chamber depth =1mm) [and applying specific procedures for the determination of uncertainties respectively on $k_{wi}(x)$ and $D_t(x_{wi})$] , it has been considered that the confidence interval for the polynomial regression fitting the depth dose curve, should provide a good estimation of uncertainty on $I_f(x)$ and $I_f(x_{wi})$.
A software devoted to this task has been elaborated and is available at CEA-FAR.[5]

Beta spectrometry

The principle of the spectrometer can be described as follows · low energy electrons in the range from 40 keV up to 200 keV are measured by D1. For higher energy electrons crossing D1 with an energy loss ΔE, the residual energy is absorbed by D2, and both detectors pulses are used to yield the spectrometric data. Such a spectrometer is usable in the energy range below 2.3 MeV, as shown by Monte Carlo calculations with EGS 4 code.[6]

The data acquisition is a two-step procedure which enables to reconstruct the total pulse height distribution When D1 and D2 are operated in an anticoincidence mode, D1 pulses are produced by low energy electrons stopping in D1, i.e. this corresponds to the low energy part of the beta spectrum. When D1 and D2 are operated in coincidence and if D1 and D2 pulses are summed up, the high energy part of the spectrum is obtained Both contributions overlap approximately at 150 keV without any correction. Energy calibrations of D1 and D2 must be quite similar Photon energies of ^{207}Bi, ^{137}Cs and ^{57}Co sources have been used for that purpose. The advantage of the room temperature operation is counterbalanced by technical problems such as detector sensitivity to daylight, atmospherics and instabilities of power supply The spectrometer with the irradiation set-up and mechanical devices, must be installed in a dark and ground-shielded cell

In addition, scanning of the spectrometer in a radiation field are servo-controlled by linear guides and step motor. An application software achieves a sequential movement along different paths and the data acquisitionby a MCA/PC. Unfolding techniques to derive the beta spectrum from the pulse height distributions have been investigated but not implemented in a software.

Many series of preliminary measurements with ^{204}Tl point source has been necessary to optimise the characteristics of the electronic circuitries connected to the detectors. The field of an extended area ^{204}Tl source (wilthout flattening filters) installed on a CEA Secondary Standard has been investigated at a 20 cm distance By moving the spectrometer in a cross section of the radiation "beam", several sites have been considered for spectral and fluence analysis. Some results are shown in Figure 1 (PHD on the "beam" axis) and on Figure 2 (PHDs at 25 mm and 50 mm).

In Figure 1, contributions of each detector are indicated on each side of 150 keV energy threshold. According to the energy calibration, the maximum energy is only about 610 keV, due to absorption in the protective metallic foil covering the radioactive material and in the 20 cm air path
Shape differences exhibited in the PHD graphs of Figure 2 measured at distances of 25 mm and 50 mm from the beam center are representative of beam inhomogeneities in terms of spectral distribution and total fluence. Numerical values of mean energy and fluence variations are summarised in Table 1.

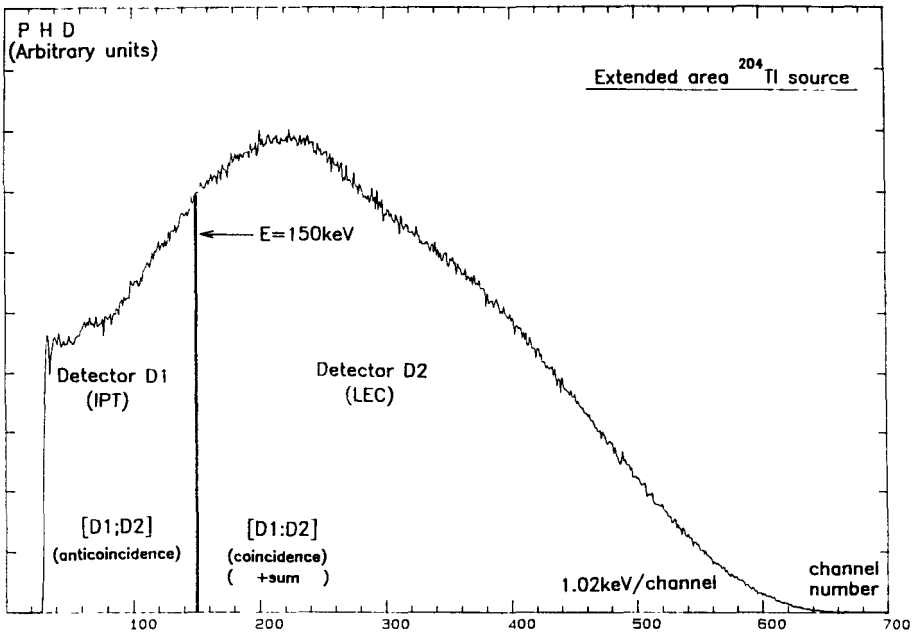

Figure 1 ^{204}Tl source (beam axis PHD)

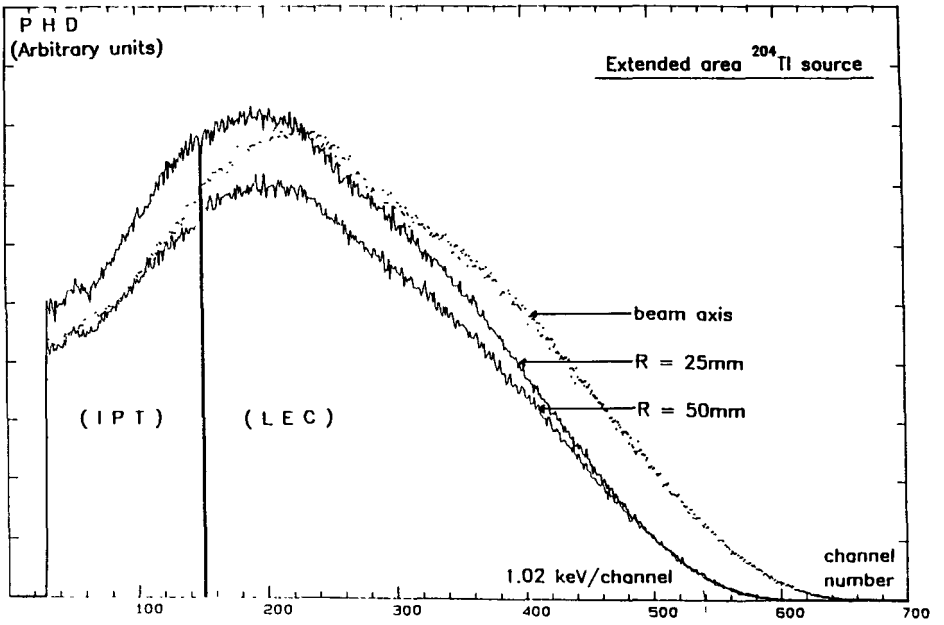

Figure 2 Spectral modifications of a ^{204}Tl source radiation field in terms of R = off axis distance

Distance off-axis (mm)	Maximum energy (keV)	Mean energy (keV)	Relative fluence
0	610	≈260	1
25	≈550	≈235	0.95
50	≈550	≈230	0.83

Table 1 Homogeneity of the radiation field

Although technical difficulties have delayed the progress of this research work on beta spectrometry, the measurements results currently available appear very promising and will be completed by additional data in order to investigate the influence of flattening filters

Low-energy photon dosimetry

The objective of the CEA-FAR/SDOS was to realise a photon calibration facility in the energy range 6 keV-20 keV, characterised in terms of H'(0.07; α°) , operational quantity recommended by ICRU to calibrate radiation protection dosemeters. Due to specific approximations for low penetrating radiations, H_p (0 07;α°) defined in the ICRU slab is numerically very close to H'(0.07,α°).

J.Boehm [1,2] has demonstrated that an extrapolation chamber, generally involved in beta dosimetry, could be satisfactorily used to define an absorbed dose primary standard in a dosimetric medium (water,tissue). When an extrapolation chamber is irradiated by low-energy photons, the ionisation current in the cavity is produced by 3 main contributions. Electrons are created in the entrance window, in the cavity gas and backscattered by the collecting electrode. Instead of the extrapolation curve I (x), where x is the chamber depth, the differentiated curve [dI/dx]=f(x) is the interesting element which enables to consider the extrapolation chamber as a "wall less free-air chamber" verifying the CPE conditions.

By applying the relation (1)

$$K_m = D_m = \frac{(\overline{\mu_{en}/\rho})_m}{(\overline{\mu_{en}/\rho})_{air}} D_{air} \qquad (1)$$

the dose to material m can be derived, the ratio (μ_{en} / ρ) being determined for the photon spectrum in the ionisation cavity. If d stands for the thickness of the entrance window, made of material m , D_m refers to a dose at that specified depth

The determination of the required conversion coefficient h_{pk} (0 07;α°) requires the determination of 2 quantities . H_p (0.07,α°) and K_{air} . H_p (0.07;α°) is the dose equivalent at depth 0.07mm and K_{air} is the kerma in air derived from free-air chamber measurements

The procedures involved in the evaluation of data from measurements performed with an extrapolation chamber require a reliable extrapolation curve and consequently a high stability radiation source.

A high performance X-ray unit (PHILIPS MG 105) has been purchased by CEA-FAR/SDOS in collaboration with the LCIE Institute.The characteristics (high voltage and current stabilities) have been

checked with an ionisation chamber measuring the radiation output at 10 and 20 kV over 8 hour-periods Satisfactory results have been obtained (maximum of ionisation current deviations below 0.35%) making unnecessary an additional monitoring of the radiation beam.
The extrapolation chamber PTW type 23382 is automatically operated through a software implemented on a COMPAQ 386 microcomputer. Different sets of filters and diaphragms define a collimated radiation beam. Measurements have been performed for 3 X-ray qualities, as given in Table 2

Tube voltage kV	Tube current mA	Additional filtration * mm Al	E keV	Electron range air mm
7 5	6		6 5 ± 0.5	1.12 ± 0 15
10	6.5	0 1	8.5 ± 0.5	1 9 ± 0.2
15	7	0.5	12 2 ± 0 7	3.3 ± 0.3

* Inherent filtration . 1 mm Be

Table 2 X-ray qualities involved in measurements

For each radiation quality, a series of measurements have been performed according to the following sequence

-determination of K_{air} with a free-air chamber

-determination of $H_p(0.07,\alpha°)$ for $\alpha = 0°,15°,30°,45°$ with an extrapolation chamber. An example of differential extrapolation curve is shown in Figure 3.

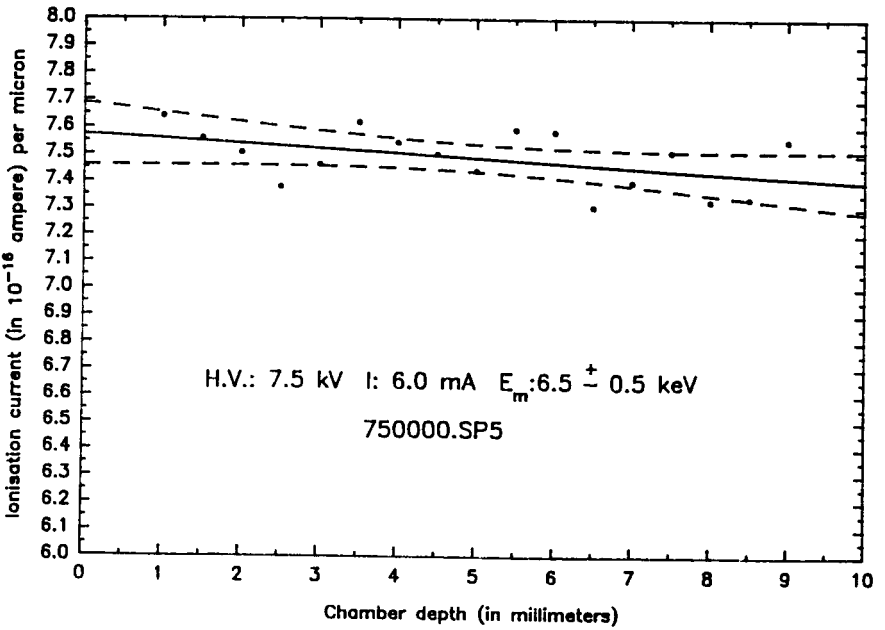

Figure 3 Differential extrapolation curve for irradiation conditions: 7 5 kV/without filtration/6 mA

Results are presented in Table 3

	h_{pk} (0.07; α°)			
	α = 0°	α = 15°	α = 30°	α = 45°
7.5 kV without filtration 6 mA	0 89	0 88	0 86	0 86
10 kV 0.1 mm Al 6.5 mA	0 90	0.89	0 88	0 88
15 kV 0.5 mm Al 7 mA	0 92	0 91	0.90	0.90

Table 3 · Conversion coefficients h_{pk} (0.07,α°)

References :

1- J Boehm, K. Hohlfeld and H. Reich -PTB- Mitteilun-gen 89 3/7
2- J. Boehm, K. Hohlfeld and H Reich -IAEA/SM/222/30- National and International Standardization of Radiation Dosimetry -Vol 1- IAEA (Vienna, 1978)
3- Fortran software DDCREGR FOR and XTCREGR.FOR
4- J. Boehm PTB-Report Dos 13 (APRIL 1986)
5- Fortran software DDCREGR4 FOR
6- D. Paul Private communication (1994)

Head of Project 3: Mr T M Francis

II Objectives for the reporting period

1 To take part in the intercomparison exercises conducted among the participating laboratories with a view to standardising measurements of beta and low-energy photon radiations.

2 To carry out further measurements and analyses of photon spectra from the $^{90}Sr/^{90}Y$ source and make the data obtained available to the group concerned with the computational aspects of this programme.

3 To formulate and carry out experiments that would serve as benchmark for the development of computational models.

III Progress achieved including publications

As part of the agreed procedure for standardising the extrapolation chamber measurements among the participating laboratories, a measurement intercomparison was carried out using an extended area ^{204}Tl foil source. Measurements of $\dot{H}'(0.07;\alpha)$ due to beta radiation at 15 and 20 cm with α at 0° and 45° and depth dose at these distances and orientations were undertaken. The results of this will be reported jointly elsewhere.

Measurements of dose rates, depth-dose at different angles and distances not covered (0.15 and 0.4 m) under the previous contract and the measurement of residual maximum beta particle energy, E_{res}, at these distances were completed. The details of the source construction and the design of the holder as well as the methodology used for these measurements were given previously[1]. Table 1 gives all the results obtained so far. For completeness, some of the results obtained and reported under the previous contract[1] are also included in the table. The results show that at this range of distances, variation in dose rates with distance (approximately an order of magnitude from 0.15 to 0.4 m) is more or less consistent with that predicted by the inverse square law. This gives a certain degree of flexibility in the choice of dose rates by the variation of distance as may be required for some experimental applications. As the source to detector distance is increased the maximum value of "build up" and its dependence with orientation gradually decreases. As would be expected, the value of E_{res} decreases with distance and at 0.4 m it is just below the minimum specified[2] value.

Work on estimating mean energy of dose and dose rate due to bremsstrahlung and characteristic x rays that generally accompany beta rays from a practical source ($^{90}Sr/^{90}Y$ extended area source) has been carried out. For studying photon spectra exclusive of beta radiation from the source, special primary shields were used: one made of polymethyl methacrylate (PMMA) with thickness (10 mm) just sufficient to stop the most energetic beta radiation from the source and the other a composite of 10 mm thick PMMA layer and 1 mm thick lead layer. With the source placed beneath a primary shield, the radiation emerging from the surface of the shield will be totally free from beta radiation, and will be a photon spectrum composed of bremsstrahlung and characteristic x rays from the source itself, generated in its

holder and the primary shield in use A GM counter (Mini Instruments GM Probe Type E) in conjunction with a Mini Instrument Scaler ratemeter Type 6-90 was used to measure the count rate due to these photons. The count rate as a function of absorber (lead) thickness was measured at distances of interest. The dose equivalent rate due to the photon spectra at these distances from the special source holder (with the source placed in it) was measured with an ion chamber (Eberline Ion Chamber, Model RO-10). Simple analyses of the measured transmission curves based on attenuation coefficients for photons in lead indicate that the photon spectrum consists of two distinct components, one of low energy ($\approx$85 keV) and the other of moderately high energy (700-800 keV) This is shown by the rapid fall of the transmission curve initially which is followed by a tail that decreases relatively slowly with absorber thickness Figure 2 shows measured transmission curves at three source to detector distances (0.2, 0.3, 0.4 m). Transmission curves obtained at these distances have almost an identical shape with the result they are not distinguishable from each other This indicates that the composite photon spectrum has not undergone significant change in shape with distance at least in this range of distances. The last column in Table 1 gives $\dot{H}'(0.07;0^\circ)$ due to photons (bremsstrahlung and characteristic x rays) from the source at three distances as measured by a typical monitoring instrument (Eberline Ion Chamber, Model RO-10). These are less than 0.05% of the total $\dot{H}'(0.07;0^\circ)$ at these distances

From purely theoretical considerations, PMMA is made of elements with a relatively low atomic number therefore production and attenuation of bremsstrahlung in the primary shield utilising only PMMA will be small Furthermore, the spectrum emerging from its surface may be considered to a first approximation as that emerging from the surface of the source Depending on the mode in use, either with lead layer immediately above the source followed by PMMA layer or PMMA layer immediately above the source followed by lead layer, the spectra emerging form its surface will be different. The study of the variation in spectral shapes and dose rates ($\dot{H}'(0.07;0^\circ)$) at 1 m for different thicknesses of two materials, one of a low atomic number (PMMA) and the other of a relatively high atomic number (lead), was the main objective of this work A spectrometer consisting of a thallium activated sodium iodide crystal (Bicron Model No. 6H 4Q/5L-SS) with the associated electronics was used to measure the photon spectra. The sodium iodide crystal was cylindrical in shape and measured 13 cm in diameter x 10 cm in thickness. The detector was placed behind a lead shielding (5 cm thick) with an aperture of 3 mm diameter with its centre concentric with the aperture. The bremsstrahlung source was held with its face parallel to the detector face and its centre aligned with the centres of detector and aperture on the shielding a distance of 1 m from the detector face Spectra transmitted through various thicknesses of absorber (PMMA) were measured at 1 m The dose equivalent rate due to the photon spectra at these distances from the source-holder combination was measured with an ion chamber (Eberline Ion Chamber, Model RO-10) Measurements were repeated with lead absorbers under the same conditions.

Results are presented in tables 2 and 3 Table 2 gives mean energy of photon spectra corresponding to different thicknesses of PMMA absorber placed on primary shielding (for three configurations). The table also gives values of personal dose equivalent rate, $H'(0.07; 0^\circ)$, measured for some of the absorber thicknesses. Additional PMMA absorbers on the PMMA primary shield have brought about very little change in the calculated mean energy which indicates that spectral shapes have not undergone significant changes having traversed a relatively thick (2609 mg/cm^2) PMMA layer. An interpolation of data given under PMMA primary shield yields a value of 3 26 μSv/h for $\dot{H}'(0.07;0^\circ)$ corresponding to an absorber thickness of 1000 mg/cm^2 which indicates that the dose rate has only attenuated by about 12% for an additional 10 mm PMMA absorber. Therefore it can be inferred that the PMMA primary shield has had only negligible effect on the photon spectrum emerging from the source

surface and that the measured spectrum can be considered as that emerging from the source surface. The results obtained for two modes of composite primary shield show significant variation in the values of $\dot{H}'(0.07;0^{\circ})$. The dose rate measured under mode 2 (PMMA layer adjacent to source) is only 50% of that measured under mode 1 (lead layer adjacent to source) This indicates that a considerable amount of bremsstrahlung is generated in the lead layer by the interaction of beta radiation from the source which has not yet been attenuated significantly by the PMMA layer following it. Reduction in the value of mean energy for mode 2 further indicates bremsstrahlung generated in lead is on average of relatively high energy Further PMMA absorbers have not made significant difference to the relative values of mean energy or $\dot{H}_P(0.07;0^{\circ})$ for two modes. Table 3 gives similar data obtained for lead absorbers. Additional thicknesses of lead absorbers have brought about increase in the calculated values of mean energy. This is as would be expected, because lead being of high atomic number would preferentially absorb low energy component of the photon spectrum Figure 3 shows measured number-energy spectra for two modes of the composite primary shield. Overall uncertainties are estimated to be about 10% and 12% on the values of mean energy and $\dot{H}'(0.07;0^{\circ})$ respectively.

The results of this work have been used by another contractor (AEA, UK) to develop computational models for the emission of beta and bremsstrahlung radiations from standard sources. This has required collaboration on the exchange of data. bilateral meetings and discussions on the detail of the results and on the precise designs of the beta sources

References

1 Final Report for Contract No Bi7-028, 1992.

2 ISO Reference Beta Radiations for Calibrating Dosemeters and Doserate Meters and for Determining their Response as a Function of Beta Radiation Energy ISO 6980. (Geneva: International Organisation for Standardisation) (1984)

Figure 1: Schematic diagram of the special holder used for the studies of photon spectra from a $^{90}Sr/^{90}Y$ foil source.

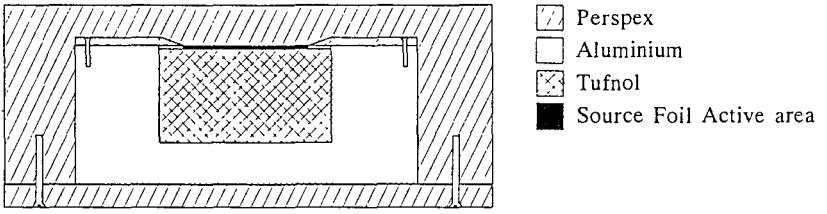

Figure 2: Transmission (normalised to unity at zero thickness) of photon spectra from a $^{90}Sr/^{90}Y$ foil source through lead at three source to detector distances (0.2, 0.3 and 0.4 m).

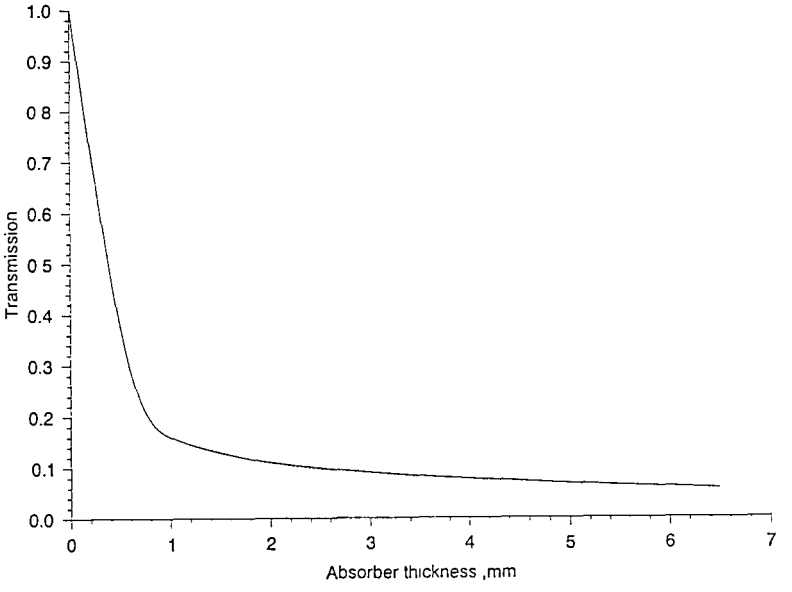

Table 1: Directional dose equivalent rates, $\dot{H}'(0.07;0°)$ for four distances and their variation with orientation (normalised at 0°), residual maximum beta particle energy, E_{res} and directional dose equivalent rate (only due to photons), $\dot{H}'(0.07;0°)$ obtained for a $^{90}Sr/^{90}Y$ foil source of nominal activity of 370 MBq.

Distance m	Tissue depth,d kg/m²	$\dot{H}'(d;0°)$ mSv/h	$\dot{H}'(d;\alpha)/\dot{H}'(d;0°)$					Residual Emax MeV	$\dot{H}'(0.07;0°)$ photons only mSv/h
			α=0°	α=15°	α=30°	α=45°	α=60°		
0.15	0.07	421	1.00	1.02	1.07	1.13	1.15	1.98	--
0.2	0.07	239	1.00	1.02	1.06	1.12	1.12	1.95	0.08
0.3	0.07	104	1.00	1.02	1.07	1.09	1.08	1.86	0.04
0.4	0.07	56	1.00	1.03	1.05	1.10	1.07	1.76	0.02

Table 2: Variation with absorber (PMMA) thickness of mean energy of and dose rate at 1 m due to photon spectrum from a Sr-90/Y-90 foil source for three primary shield configurations.

Thickness of additional absorber on primary shield (mg/cm²)	Primary shield= PMMA(10 mm)		Primary shield= Lead(1mm)+PMMA(10mm)		Primary shield= PMMA(10mm)+Lead(1mm)	
	Mean energy (keV)	$\dot{H}_p(0.07;0°)$ (μSv/h)	Mean energy (keV)	$\dot{H}_p(0.07;0°)$ (μSv/h)	Mean energy (keV)	$\dot{H}_p(0.07;0°)$ (μSv/h)
0	237	3.7	382	2.4	344	1.2
335	236	3.6	384		339	
451	239	3.5	373		342	
675	237	3.4	380		343	
787	236	3.3	374		334	
1243	237	3.1	374	2.2	335	1.1
1919	236	2.9	369		329	
2609	237	2.7	376	2.0	337	1.0

Table 3: Variation with absorber (Lead) thickness of mean energy of and dose rate at 1 m due to photon spectrum from a Sr-90/Y-90 foil source for three primary shield configurations.

Thickness of additional absorber on primary shield (mg/cm²)	Primary shield= PMMA(10 mm)		Primary shield= Lead(1mm)+PMMA(10mm)		Primary shield= PMMA(10mm)+Lead(1mm)	
	Mean energy (keV)	$\dot{H}_p(0.07;0°)$ (μSv/h)	Mean energy (keV)	$\dot{H}_p(0.07;0°)$ (μSv/h)	Mean energy (keV)	$\dot{H}_p(0.07;0°)$ (μSv/h)
0	237	3.7	382	2.4	344	1.2
646	301		406		368	
1134	328		411		368	
1781	347		416		378	
2212	358		430		383	
2858	362	0.7	434	1.5	390	0.7
3346	376		440		394	
3992	386		446		394	
4446	385		446		403	
5093	391	0.5	452	1.1	397	0.6
5580	391		454		399	
6227	401		458		406	
6714	401		454		400	
7361	404	0.4	479	1.0	428	0.5

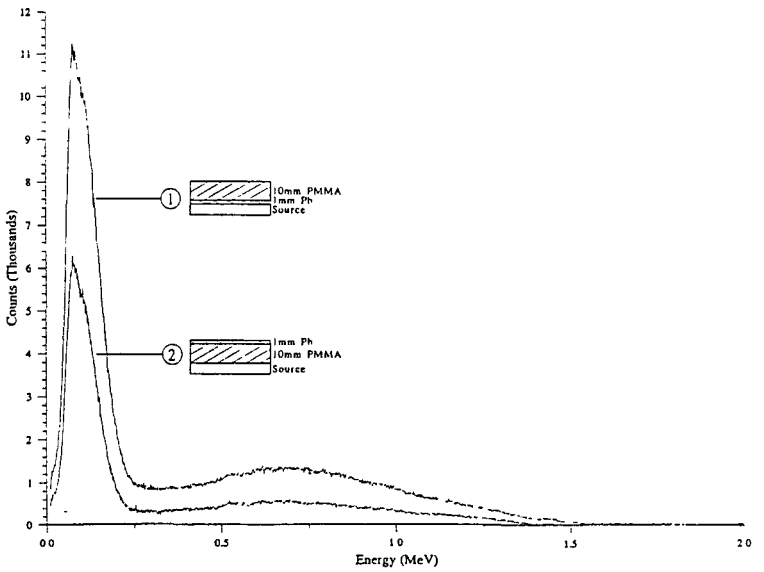

Figure 3: Number-energy spectra (as measured with a NaI detector & uncorrected) at 1 m due to photons from a Sr-90/Y-90 foil source after traversing a Pb-PMMA composite shield. 1. Pb layer immediately above source. 2. PMMA layer immediately above source.

Head of project 4 : Dr Y. HERBAUT

II - Objectives for the reporting period.

1 - Control of reliability of extrapolation chambers for the measurement of absorbed dose rates to tissue by participating in comparative measurements in the frame of two intercomparisons organised by the coordinator of the project. The first one would be concerned with an extended 42 mm diameter ^{204}Tl beta source (belonging to Dr J-L CHARTIER) and the measurements would be carried out with a PTW model 23391 extrapolation chamber. A ^{147}Pm beta source with an identical geometrical form would be used for the second one and the experiments would be performed with a PTW model 23392 chamber operated essentially manually.

2 - Development of computer-controlled automated extrapolation chamber measurement set-up.

3 - Determination of the residual maximum energy for the beta sources of the Buchler secondary standard Grenoble facility .

4 - Study of the main characteristics of carbon loaded LiF dosemeters for measurement of doses from weakly penetrating radiations.

5 - Collaboration with Dr CHARLES concerning hot particle dosimetry. A spherical ^{60}Co sample (ϕ=200 μm) would be used for this study.

III - Progress achieved including publications.

1 - ^{204}Tl and ^{147}Pm intercomparisons [1][2].

1.1 - Main characteristics of the PTW model 23391 extrapolation chamber (^{204}Tl intercomparison).

The main characteristics are summarised up in **Table 1**. The collecting electrode areas were determined according to Dr BÖHM's method [3] ; a weighted linear regression leads to the following relationship :

$$D_{exp}(mm) = 1{,}004\ D_{mech}\ (mm) + 0{,}64$$

where D_{exp} and D_{mech} indicate the experimental and mechanical electrode diameter, respectively.

1.2 - Main characteristics of the PTW model 23392 extrapolation chamber. (^{147}Pm intercomparison).

The main characteristics are presented in **Table 2**. The collecting electrode area is 7.072 cm^2 (± 0.05% for 2 standard deviations) ; the field strength was maintained at a value of 150 V/cm to provide a good collection efficiency.

The beta detector (extrapolation chamber either model 23391 or 23392) is associated with a KEITHLEY model 642 electrometer which measures the ionisation current ; it uses an acquisition software program including the knowledge of ambient parameters P,T,H and correction factors,

according to Reference 4, have been applied. So, for beta rays of low energies, the attenuation factor k_{ac} [4] has been calculated with the following formula :

$$k_{ac} = \left[1 + \frac{L}{d}\right] \times \left[1 + 0{,}5\,\frac{\mu}{\rho}\,\rho\,L\right]$$

where :

- L is the chamber depth,
- d is the distance from the source,
- μ/ρ (cm^2/g) is the mass absorption coefficient,
- ρ (g/cm^3) is the air density.

Moreover, remote operation of the 23392 chamber (electrode separation, sign and value of the chamber bias voltage) controlled by a HP E2 microcomputer, can be totally automatic ; however, control problems still remain.

Table 1 - Main characteristics of PTW model 23391 extrapolation chamber.

Entrance window Material Thickness (mg/cm^2) Density (g/cm^3)	 Kapton 4 5,8 5,12.5 1.42
Movable Electrode Range (mm) Precision (mm)	Manually 0 6-25 0.01
Collecting Electrode Material Mechanical Diameter D_{mech} (mm) Experimental Diameter D_{exp} (mm)*	 A 150 5 - 10 - 15 - 20 - 30 - 40 5 72(0.3)-10.70(0 3)-15.52(0 15) 20.65(0.05)-30.78(0.05)-40.81(0.02)
Field Strength (V/mm)	50
* Estimated relative uncertainties in % (± 1 S. D.) are indicated in brackets.	

Table 2 - Main characteristics of PTW model 23392 extrapolation chamber

Entrance window Material Thickness (mg/cm2)	 Hostaphan 0.75
Movable Electrode Range (mm) Precision (mm)	Manually or Automatically 0.2 - 11 0.005
Collecting Electrode Material Mechanical diameter D_{mech} (mm) Experimental diameter D_{exp} (mm) *	 Perspex 30 30.01 (0.013)
Field strength (V/mm)	15
* Estimated relative uncertainty in % (± 1 S D.) is indicated in brackets.	

1.3 - ^{204}Tl intercomparison [5].

An extended area ^{204}Tl source (active diameter 42 mm) with the standard French holder was used for this exercise ; the laboratory at CEA/CENG has contributed to this exercise with a

PTW Model 23391 extrapolation chamber using the following parameters:

- Kapton entrance window thickness.
  - 8.5 mg/cm^2 for dose measurements,
  - 4.5 mg/cm^2 for depth-dose profiles.
- Collecting electrode diameter : 30.8 mm (1SD = 0.05%),
- Feedback capacitor : 98.3 pF (1SD = 0.005%).

The measurements of $D_t(0.07,\alpha)$ were performed at three distances (15,20 and 30 cm) from the source and two irradiating angles (0°, 45°). **Table 3** presents our results.

Moreover, depth-dose profile measurements with a 4.5 mg/cm^2 thick entrance window (equivalent to a 4.14 mg/cm^2 tissue thickness), for the same geometrical conditions, were carried out. **Figure 1** shows 20 cm depth-dose curves.

Table 3 - Measured dose rates $D_t(0.07,\alpha°)$ in mGy/h delivered by the ^{204}Tl source at three distances (15, 20, 30 cm and two irradiating angles α (0°, 45°). Reference date : 01 01.1991

d=15 cm		d=20 cm		d=30 cm	
α = 0°	α = 45°	α = 0°	α = 45°	α = 0°	α = 45°
411 6 (1.7 %)	383.3 (1.7 %)	218 0 (1 7 %)	200 0 (1 7 %)	85.1 (1 6 %)	75.2 (1 6 %)

Relative estimated uncertainties (± 1 S.D.) are indicated in brackets.

1.4 - ^{147}Pm intercomparison.

An extended area ^{147}Pm beta source (42 mm active diameter) with the standard French holder was sent to the participants ; the CEA/CENG laboratory has contributed to this exercise with the Model 23392 PTW chamber associated with a 30.056 pF (± 0.01 %) feedback capacitor. The measurement programme comprised the determination of tissue dose rates at two distances from the source (15 and 20 cm), for two irradiating angles α (0°, 45°), under two tissue depths (0.02 and 0.07 mm). The results should be given in terms of $D_t(0.02,\alpha)$ and $D_t(0.07,\alpha)$. **Tables 4 and 5** give the CEA/CENG results. Furthermore, depth-dose data, for the same geometrical conditions, should be acquired for the range from the entrance window thickness (0.75 mg/cm^2 of mylar which is equivalent to 0.69 mg/cm^2 of tissue [6]) up to 9 mg/cm^2. **Figure 2** shows an example of results for d=20 cm and for the two irradiating angles. The depth-dose curves (DDC) [7] have been fitted by a (1+3) degree polynomial function as given in the following relationship for d=20 cm and α=0°.

$$\mathrm{Ln}\left[D_t\,(\,k\,x, 0^0\,)\,\right] = 4{,}09 - 0{,}16\,x - 5{,}4.10^{-4}\,x^3$$

where :

- x is the tissue layer thickness in mg/cm^2,
- $D_t(\,k\,x,0°)$ is the tissue dose rate in mGy/h at depth x for α=0°,
- k = 0,01 mm / (mg./cm^2).

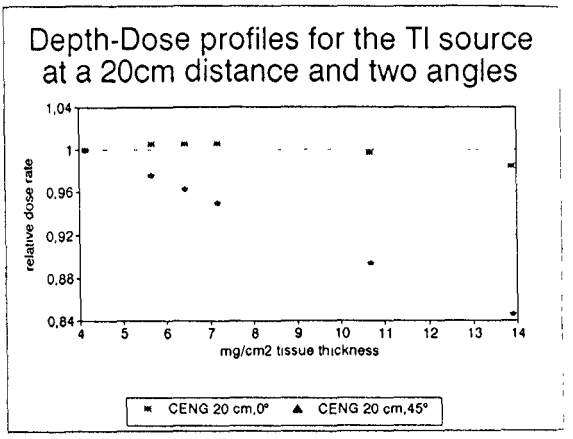

Figure 1

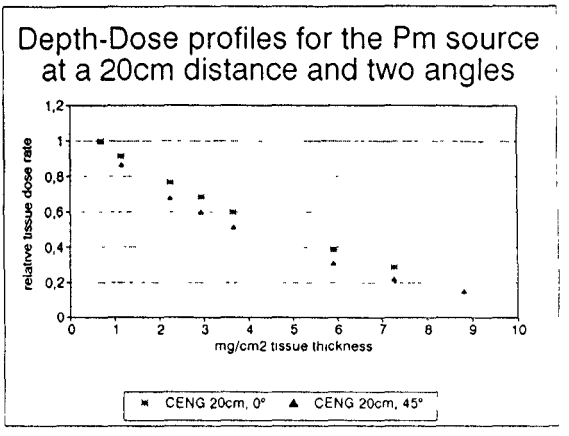

Figure 2

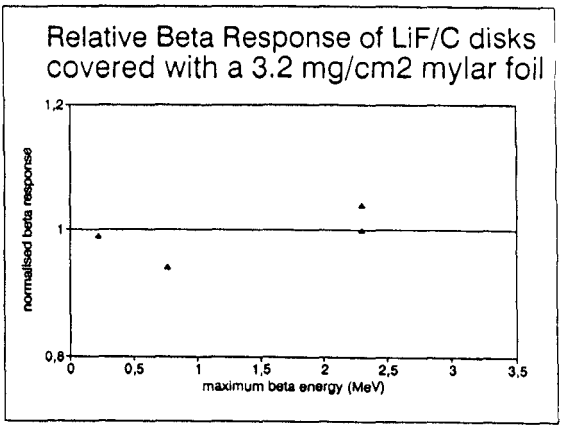

Figure 3

Table 4 - Measured tissue dose rates $D_t(0.02, \alpha)$ and $D_t(0.07, \alpha)$ in mGy/h delivered by the ^{147}Pm beta source at d = 15 cm . Reference Date · 01 01 93

$D_t(0.02,\alpha)$ mGy/h		$D_t(0.07,\alpha)$ mGy/h	
$\alpha = 0°$	$\alpha = 45°$	$\alpha = 0°$	$\alpha = 45°$
175.25 (2.8 %)	152 40 (2.8 %)	78.65 (2.8 %)	56.50 (2.8 %)

Relative estimated uncertainties (± 1 S.D.) are indicated in brackets

Table 5 - Measured tissue dose rates $D_t(0.02, \alpha)$ and $D_t(0.07, \alpha)$ in mGy/h delivered by the ^{147}Pm beta source at d = 20 cm . Reference Date : 01.01.93

$D_t(0.02,\alpha)$ mGy/h		$D_t(0.07,\alpha)$ mGy/h	
$\alpha = 0°$	$\alpha = 45°$	$\alpha = 0°$	$\alpha = 45°$
43.12 (2.7 %)	37.16 (2.7 %)	16 15 (2.7 %)	11 98 (2.7 %)

Relative estimated uncertainties (± 1 S.D) are indicated in brackets

2 - Residual maximum beta energy.

Residual maximum beta particle energy E_{res} was determined for the beta sources of the CENG Büchler facility. The measurements were carried out either with a scintillator protected by an 0.7 mg/cm^2 thick aluminium film (SMIB70 probe) for the most energetic beta rays or with a Geiger - Mûller tube having an end 1.8 mg/cm^2 thick mica window (SMIBM probe) for the ^{204}Tl and ^{147}Pm radionuclides ; they were positioned at the calibration distance and connected to a MIP10 scaler. Mylar foils and perpex slabs were used as absorbers and scaling factors given by CROSS [6] permit to convert to tissue-equivalent thicknesses. The computation of E_{res} and R_{res} (residual maximum beta particle range) from the measured depth-dose data was made according to the procedure described in Reference 8. From the results presented in **Table 6** it can be seen that the E_{res} values obtained are close to the lowest limits recommended in the 6980 ISO Standard [8].

Table 6 - Residual Maximum Beta Range (R_{res}) and Residual Maximum Beta Energy (E_{res}) for the CENG beta sources of the Büchler Secondary Standard

Nuclide	Calibration Distance (cm)	Flattening Filter	R_{res} (mg/cm^2)	E_{res} (MeV)	E_{res} (ISO) [8] (MeV)
$^{90}Sr/^{90}Y$	30	without	868	1 87	1,80
$^{90}Sr/^{90}Y$	50	without	844	1.82	1,80
$^{90}Sr/^{90}Y$	30	with	882	1.89	1,80
^{204}Tl	30	with	183	0.52	0,53
^{147}Pm	20	with	14	0.11	0,13

3 - Carbon loaded LiF TL dosemeter properties [2].

During recent years, the importance of beta dosimetry for skin and extremities has increased, at least in part due to an awareness of the beta problem in nuclear plants [9]. The directional dose equivalent H'(0.07) recommended by ICRU [10] for use with environmental monitoring of weakly penetrating radiation is an appropriate quantity for the purpose of calibrating dosemeters designed to indicate the individual dose equivalent, $H_p(0.07)$. This quantity is defined in the ICRU sphere .However, because of the limited range of beta particles in dense media, a slab phantom in tissue équivalent material, of dimensions greater than the maximum range of the most energetic of the beta radiations used is considered appropriate.

The sensitivity of thick detectors decreases at low beta radiation energies; thin detectors can solve this problem but are not sufficiently robust especially for routine applications ; one method for satisfying these opposite requirements is to use a thick TL device made effectively thin by adding to the TL material carbon which stops luminescence emission from deep layers.

Therefore we have performed studies of the dosimetric properties of carbon loaded LiF detectors [11] 400μm thick, 12.7 mm in diameter, manufactured by the NE Technology (Vinten) Company [12], whose composition by weight is : LiF^7 30%, C 7.5%, PTFE 62.5%.

They were positioned on a flat cylindrical perspex phantom, which can be tilted (20 mm in depth and 150 mm in diameter) and irradiated by the punctual beta sources of a Büchler secondary standard facility with or without a flattening filter. The beta radiation beams have been calibrated by PTB at fixed distances in terms of tissue absorbed dose rates at a 7 mg/cm^2 depth and for an irradiating angle $\alpha=0°$ [$D_t(0.07,0°)$].

3.1 - The LiF/C beta energy relative response.

The TL detectors were covered by a mylar foil 3.2 mg/cm^2 ; **Table 7 and Figure 3** present the results for the three nuclides and $\alpha = 0°$; R_β is the relative beta response normalised to the response for the $^{90}Sr/^{90}Y$ source without filter. We can observe that R_β is independent of the beta energy, even in the lowest range.

Table 7. Relative beta response R_β for measurement of $D_t(0,07,0°)$ and total uncertainty Δ of LiF/C TL dosemeters

Radionuclide	Filter	R_β	Δ (k=2)
$^{90}Sr/^{90}Y$	without	1.00	
$^{90}Sr/^{90}Y$	with	1.04	11%
^{204}Tl	with	0.94	25%
^{147}Pm	with	0.99	10%

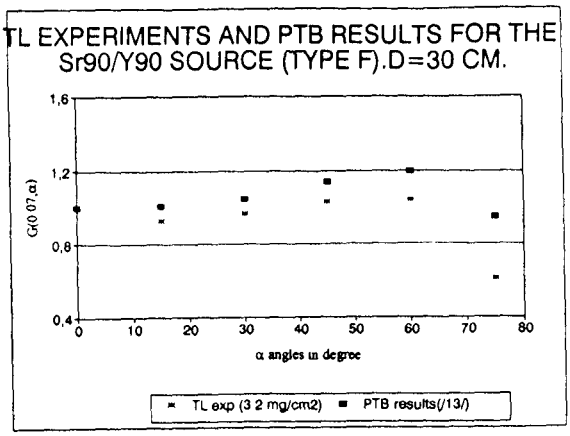

Figure 4

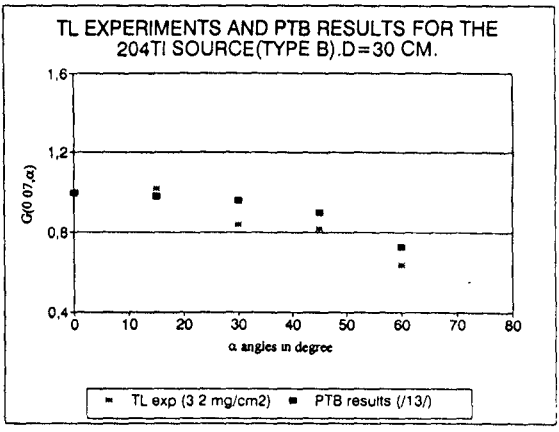

Figure 5

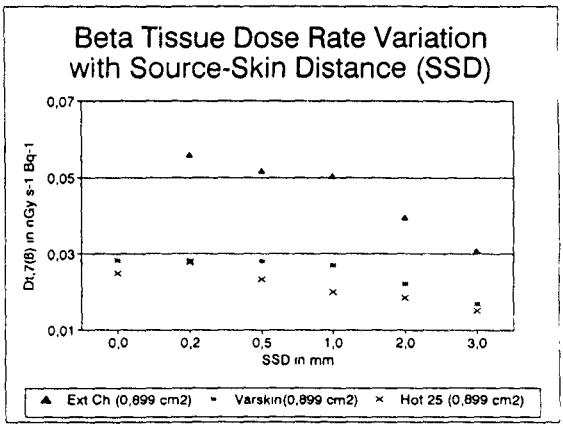

Figure 6

3.2 - Conversion factors measured with TL detectors and comparison with the values obtained by extrapolation chamber [14].

Determination of the conversion factor $G(0.07,\alpha)$ at the irradiating angle α defined as :

$$G\ (\ 0{,}07,\ \alpha\ ) = \frac{D_t\ (\ 0{,}07,\ \alpha)}{D_t\ (\ 0{,}07,\ \alpha\ =\ 0°\ )}$$

would facilitate the knowledge of absorbed dose to tissue for beta radiation incident at various angles on a phantom. These factors were determined with the thermoluminescent detectors irradiated by the beta sources of the BÜCHLER secondary standard facility at 30 cm ($^{90}Sr/^{90}Y$, ^{204}Tl) or 20 cm (^{147}Pm) and covered with a 3.2 mg/cm^2 (23 μm) thick mylar foil ; the results were compared with values deduced from extrapolation chamber (type 23392) measurements performed at PTB [13]. This is shown in **Figure 4** for the $^{90}Sr/^{90}Y$ without filter source (type F of Reference 13) and in **Figure 5** for the ^{204}Tl source (type B of Reference 13) : we can observe the build-up phenomen for the most energetic beta source and the attenuation for the ^{204}Tl source (because of smaller penetrating power, the build-up is smaller and it occurs at depths less than 0.07 mm). Results obtained look similar to those measured at RISO laboratory with graphite-mixed sintered MgB_4O_7 : Dy pellets [13] ; this reinforces the view that very thin detectors are needed for measuring absorbed dose from weakly penetrating low energy radiations.

4 - Hot Particle Dosimetry [15].

Highly radioactive particles named "hot particles" were simulated by a ^{60}Co spherical source (193 μm in diameter, 0.7 MBq in activity) provided by Dr CHARLES (University of BIRMINGHAM, UK) ; ^{60}Co was chosen as the radionuclide best suited for an initial investigation, despite its gamma emission.

Tissue doses at a tissue depth of 7 mg/cm^2, averaged over a 1cm^2 area, for several air gap distances, have been evaluated by two dosimetric methods :

- the extrapolation chamber method (the PTW model 23391 detector has a 10.7 mm diameter movable collecting electrode),
- the LiF/C thermoluminescent dosemeters, at a 2 mm skin-source distance, for measuring the depth-dose profile up to 130 mg/cm^2,

Moreover calculations have been performed and compared with the experiments ; two computer codes were run : Varskin Mod 2 from J. S. DURHAM [16] which calculates eventually the gamma contribution and Dr PATAU's Monte Carlo code [17] for the beta component only.
The following conclusions can be drawn :

- There is an agreement within a factor 1.9 for the beta component between the PTW experiments and the Varskin calculations **(Table 8 and Figure 6).**
- The total dose (beta + gamma contributions) measured by thermoluminescent dosemeters overestimates the Varskin code computations by a factor of 3.7 ; actually, no explanation for this discrepancy has been found.
- The computer code results agree well for similar input data **(Table 8).**

Table 8 - ^{60}Co source - Comparison between PTW extrapolation chamber beta measurements and beta calculations issued from Dr. PATAU'S code and Varskin program for the same irradiated area (0.899 cm^2).

Distance from the source. (mm)	Extrapolation Chamber ($nGy\ s^{-1}\ Bq^{-1}$) B	HOT25 (100000 primaries) ($nGy.s^{-1}\ Bq^{-1}$) C	VARSKIN ($nGy.s^{-1}.Bq^{-1}$) A	Ratio B / A	Ratio A / C
0	no measurement	$2.48.10^{-2}$	$2.82.10^{-2}$	-	1.14
0.2	$5.59.10^{-2}$	$2.76.10^{-2}$	$2.81.10^{-2}$	1 99	1.02
0.5	5 18 10^{-2}	$2.32.10^{-2}$	$2.80.10^{-2}$	1 85	1.21
1	5 04 10^{-2}	1.99 10^{-2}	$2.69.10^{-2}$	1.87	1.35
2	$3.95.10^{-2}$	$1.84.10^{-2}$	$2.19.10^{-2}$	1.80	1.19
3	$3.09.10^{-2}$	1 505.10^{-2}	1.68 10^{-2}	1.84	1 12

B, C and A (in $nGy.s^{-1}.Bq^{-1}$) are dose rates for the beta component only.

5 - References and Publications.

[1] Progress Report, CEC Contract F13P-CT920032(1993).

[2] Progress Report, CEC Contract F13P-CT920032(1994).

[3] Instruction Manual : Extrapolation Chamber for the measurement of the absorbed dose rate to tissue for beta radiation, type 23392. PTW-Freiburg (1986)

[4] BÖHM J. The National Primary Standard of the PTB for Realizing the Unit of the Absorbed Dose Rate to Tissue for Beta Radiation. PTB-Dos-13 (1986).

[5] LEROUX J.B., HERBAUT Y. ^{204}Tl Intercomparison with an Extrapolation Chamber. SPR/SMI/LDI - Note d'Etude n°93-03 (1993).

[6] CROSS W.G. Variation of Beta Dose Attenuation in Different Media. Phys. Med. Biol. 13 - 4 - 611 - 618 (1986).

[7] CHARTIER J-L. Private Communication.

[8] ISO. Reference Beta Radiations for Calibrating Dosemeters and Doserate Meters and determining their Response as a Function of Beta Radiation Energy. Draft International Standard. ISO / DIS 6980. (1993).

[9] CHRISTENSEN P., JULIUS H.W., MARSHALL T.O. Implications of New CEC Recommendations for Individual Monitoring for External Radiation Doses to the Skin and the Extremities. Rad. Prot. Dosim. 39 (1/3) 91-94 (1991).

[10] ICRU. Determination of Dose Equivalents Resulting from External Radiation Sources ICRU Report 39 (1985).

[11] FRANCIS T.M. and al. Response Characteristics of Carbon-loaded TL Detectors to Beta Radiation. Rad. Prot. Dosim. 28(3) 201-205 (1989).

[12] VINTEN TLD. Technical Data Sheet 1. Dosimetrically Thin Dosemeters for the Measurement of Low Penetrating Radiation.
[13] CHRISTENSEN P., BÖHM J., FRANCIS T.M. Beta dosimetry. Fifth information seminar on the radiation protection dosemeter intercomparison programme. EUR 11363(1987).
[14] GARREL F. Etude de la sensibilité des dosimètres LiF/C en fonction de la variation de l'angle d'orientation. Rapport de stage. INT/SPR 94.677 (1994).
[15] LEROUX J.B., HERBAUT Y. Mesures et Calculs des Doses délivrées par des particules radioactives. Note d'Etude SPR/SMI n°94-04 (1994).
[16] DURHAM J. S. Varskin Mod 2 and Sadde Mod 2 : Computer codes for assessing skin dose from skin contamination. NUREG/CR 5873 (1992).
[17] PATAU J. P. Monte-Carlo calculations of the depth-dose distribution in skin contaminated by hot particles. Radiat. Prot. Dosim. 39 (1/3) 71-74 (1991).

Head of Project 5: Mr D Spencer

II. Objectives for the reporting period

1. To model the beta source holder which is used by the National Radiological Protection Board (NRPB) using a Monte Carlo program based around the EGS4 system.
2. To validate the model by comparing the calculated results with measurements made at the NRPB.
3. To examine any problems which arise from the validation.
4. To model the energy and angular distributions of electrons and photons produced by selected sources. To model factors affecting the source spectrum such as source imhomgeneity and holder design.
5. To study the effects of beam flattening filters on radiation fields and to optimise the filters.
6. To calculate the dose under the window of the extrapolation chamber used at the NRPB.

III. Progress achieved including publications

Initial modelling

We identified a function for the representation of beta decay spectra. A computer program was written which uses the function to generate cumulative probability distribution functions (CPDFs) for beta decay spectra. The Monte Carlo models sample the CPDFs to create beta spectra.

Two simple Monte Carlo models of source holders were created using the EGS4 system of sub programs. The EGS4 system consists of sub programs containing algorithms representing the physical behaviour of photons and electrons. The user adds his own geometry and scoring routines. In addition the user is able to modify the algorithms if the physical representation needs to be changed. The first model consists of a square shaped source, representing the geometry of sources belonging to NRPB, and the second has a circular geometry, which reflects the geometry of sources used by participants in the project.

Routines were written to store information on particles leaving the source. The stored data may be used to produce identical source spectra for the study of perturbations to the radiation field caused by objects in the radiation beam. This includes charge, energy, position and direction of motion for each particle. As information for millions of particles are stored, the data are saved as single bytes.

Modelling of the NRPB source

A schematic diagram of the NRPB source model is shown in figure 1. Initially we chose Thallium 204 as the beta emitter.

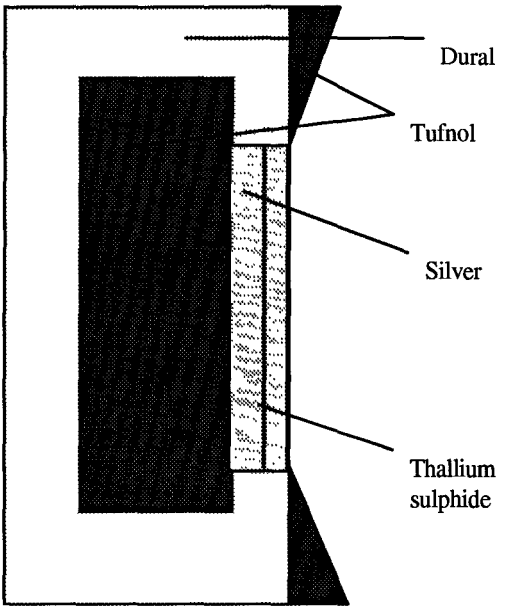

Figure 1: Thallium beta source holder.

Except for the source matrix itself, the geometry and material composition of the source holder is well known. The NRPB were unable to supply accurate details, and the manufacturers of the source were unwilling to give further details. An estimate of the source matrix composition was used and the spectra shown in figures 2 and 3 were generated using the model.

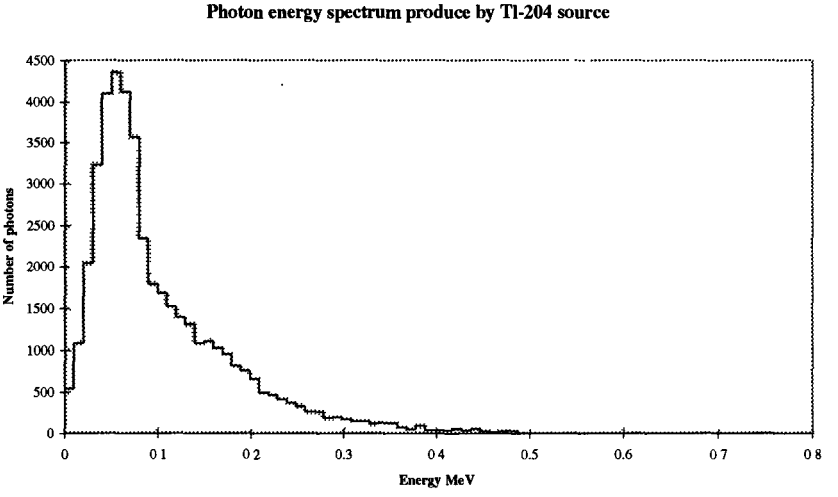

Figure 2

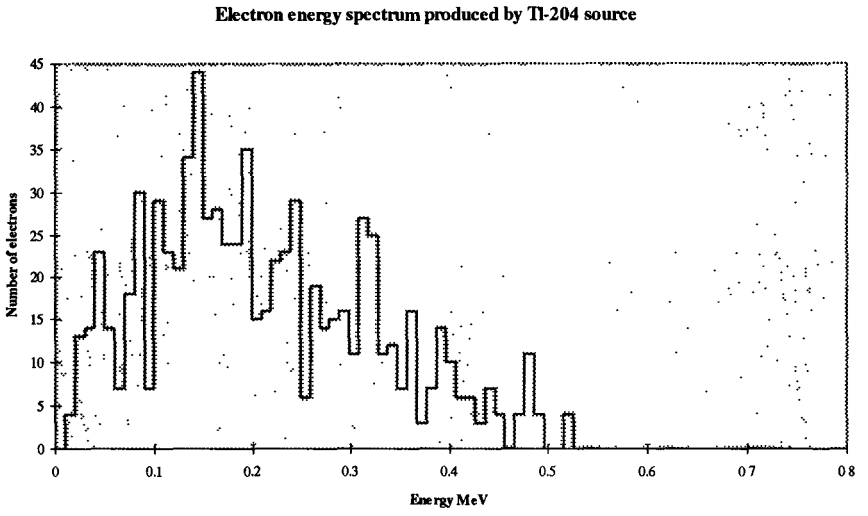

Figure 3

The spectra show that the number of beta particles leaving the source is far less than the number of photons. Further examination of the model demonstrated that the majority of bremsstrahlung photons were generated within the source matrix itself. This suggests that an incorrect source matrix was being used.

A simple model, shown in figure 4, was used to study the effect of changing the properties of the source matrix.

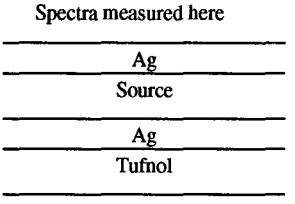

Figure 4: Simple model for assessing the effect of source matrix properties on emitted spectra.

Three versions of the source matrix were modelled. The first contained the same materials as those used in the Thallium 204 source holder. In the second case, the density of the source matrix was reduced by a factor of 10. In the third version, the number density of Thallium atoms was reduced by a factor of 10. Spectra generated using the three models are shown in figures 5 and 6.

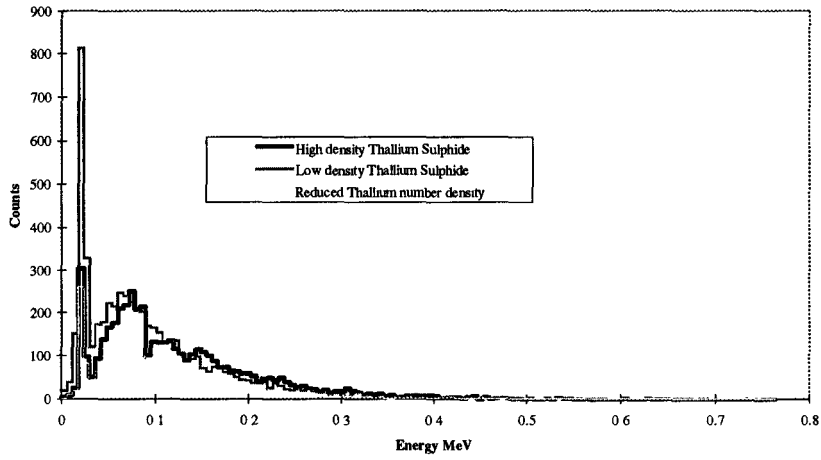

Figure 5: Bremsstrahlung spectra using three different source matrices.

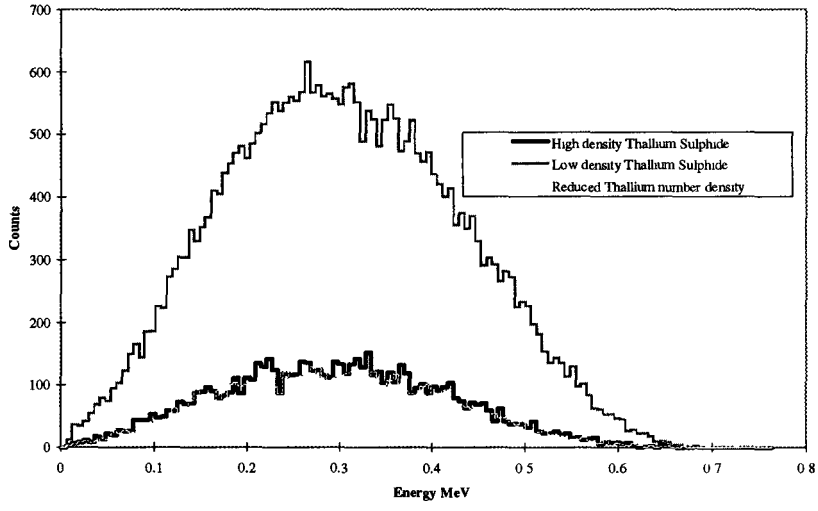

Figure 6: Beta spectra using three different source matrices.

It can be seen from figure 6 that reducing the source matrix density increases beta particle output due to reduced absorption in the source matrix. However the bremsstrahlung output is significantly decreased by reducing the number of Thallium atoms present (figure 5). Reducing the Thallium present reduces the average atomic number of the source matrix. Therefore a decrease in bremsstrahlung photons would be expected. The peak at the start of the bremsstrahlung spectra is due to fluorescence photons from the silver window.

Further tests using simple models

In order to check the physical behaviour of electrons and photons within EGS4, two simple models were constructed and compared with other methods of collecting results. The first model consisted of studying the transmission of bremsstrahlung photons, produced by electrons from a ^{90}Sr-^{90}Y source, through the two combinations of PMMA and lead absorber. Figure 7 shows a schematic diagram of the experiment.

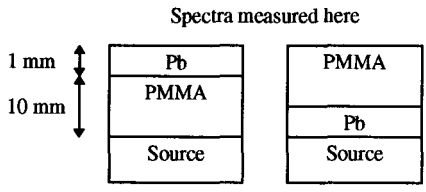

Figure 7. Experiment to study the transmission of bremsstrahlung photons.

Figure 8 shows pulse height distributions measured at the NRPB and figure 9 shows the EGS4 generated spectra. It can be seen that the shapes of the curves are different. This is due to lack of detail for both the composition of the source matrix and the detector configuration; and no account being taken of the response function of the detector. The comparison does show a similar ratio of heights between each pair of curves produced by measurement and the model. This indicates that the transmission of the bremsstrahlung photons through the sources is accurate in the model.

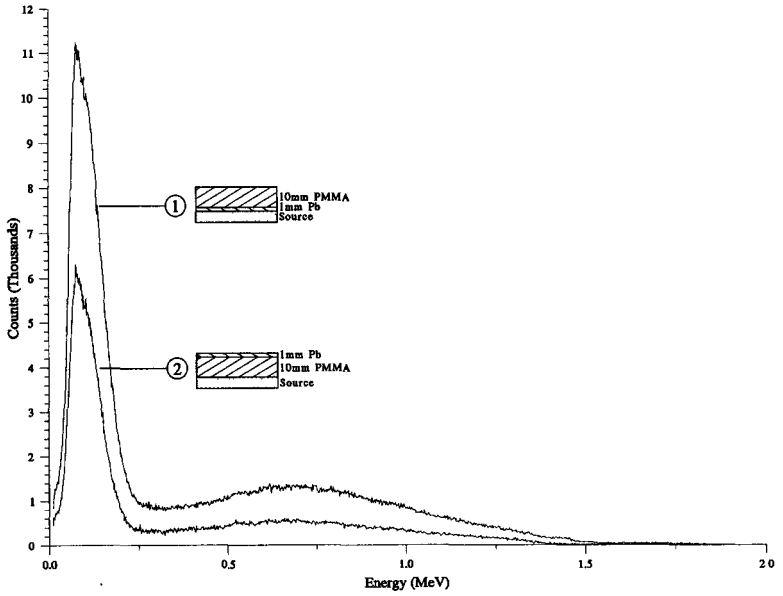

Figure 8: Pulse height distribution of bremsstrahlung photons from ^{90}Sr-^{90}Y source after transmission through lead and PMMA absorbers. Measured by NRPB.

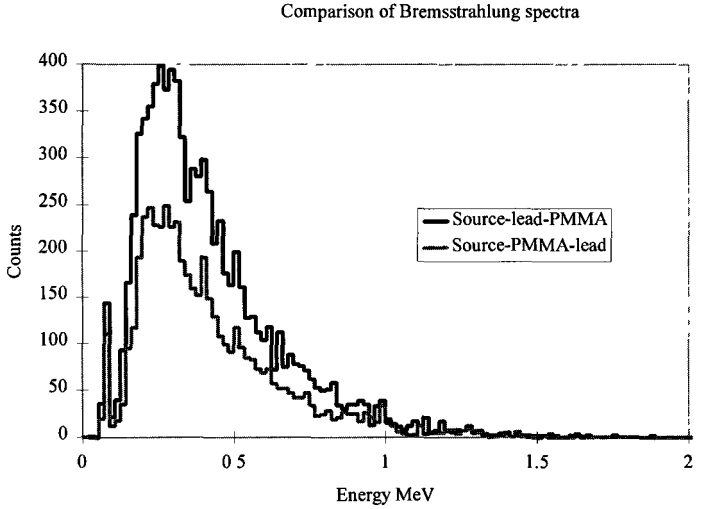

Figure 9: Spectra of bremsstrahlung photons from ^{90}Sr-^{90}Y source after transmission through lead and PMMA absorbers. Generated using Monte Carlo model.

A second test consisted of modelling the impact of mono-energtic electrons on a tungsten target. The shape of the resulting spectrum was then compared with that generated using a semi-empirical model (Birch and Marshall, 1979) As can be seen in figure 10, the two spectra match well except for the L-edge X-rays. Modelling of the L-edge fluorescence is not included in this EGS4 model.

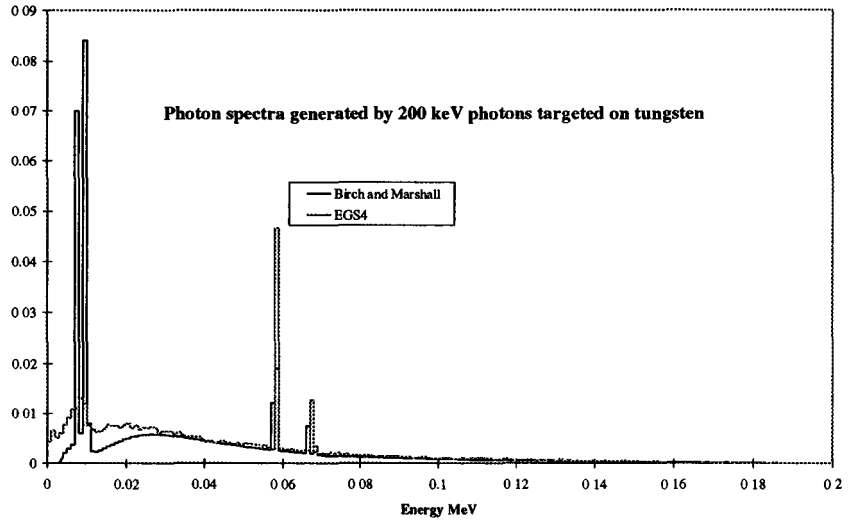

Figure 10: Comparison of bremsstrahlung spectra generated using two different methods.

Model of source manufactured at Hungarian Institute of Isotopes

The Hungarian Institute of Isotopes has manufactured a number of its own beta sources and therefore are able to define all the source geometry and source materials accurately. AEA Technology used data provided by the Hungarian Institute to model the Hungarian sources. The sources are of circular geometry and have been designed to minimise bremsstrahlung photons. Results for a $^{106}Ru/^{106}Rh$ are shown throughout this text.

The first model saved information for each particle leaving the source as individual bytes and measured the energy spectra of photons and electrons leaving the front face of the source. Figures 11 and 12 show spectra generated using the model.

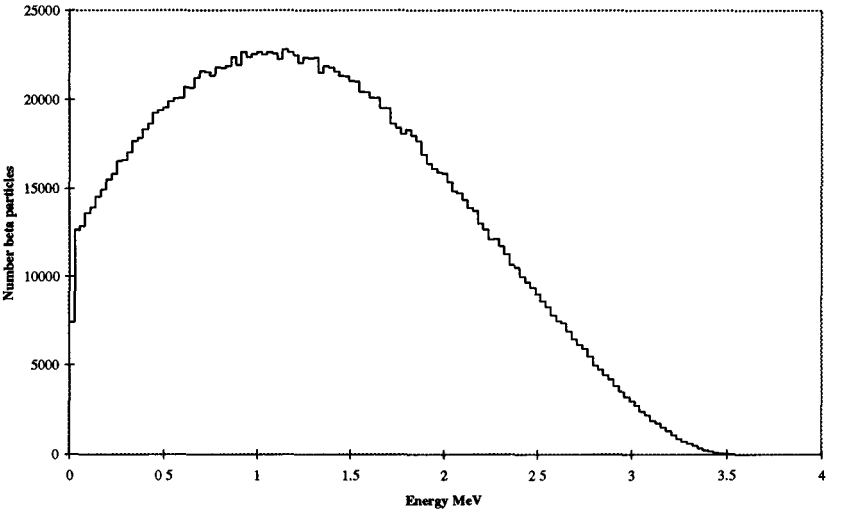

Figure 11: Beta spectrum generated by Monte Carlo model for Hungarian $^{106}Ru/^{106}Rh$ source.

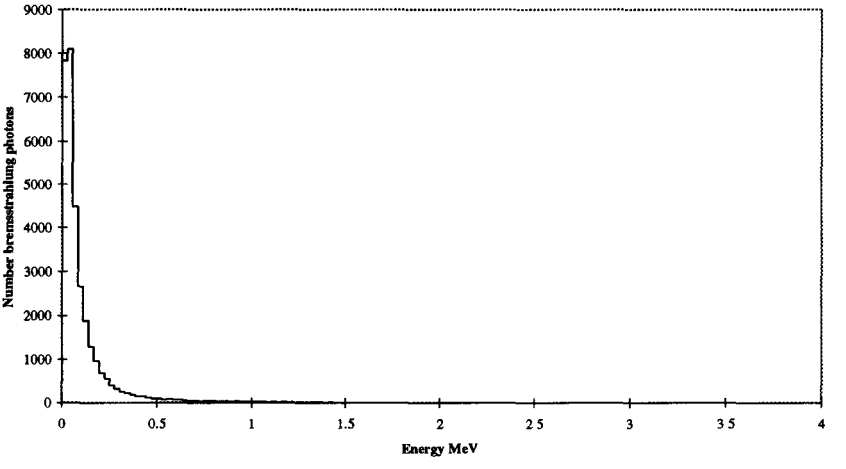

Figure 12: Bremsstrahlung spectrum generated by Monte Carlo model for Hungarian $^{106}Ru/^{106}Rh$ source.

Figures 11 and 12 show that the bremsstrahlung component produced by the source is small compared with the number of betas leaving the source. This indicates that that the representation of the source matrix is likely to be good.

In order to examine the homogeneity of the radiation field produced by beta sources, a second circular source model was constructed. A layer of air was added to the front of the source. The model includes planes perpendicular to the axis through the source. As the electrons and photons cross the planes their

properties are scored according to energy and distance from the source axis passing through the centre of the source. A schematic diagram of the source and scoring planes are shown in figure 13.

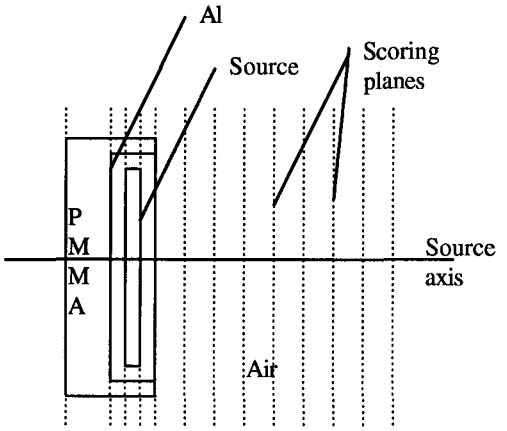

Figure 13: Schematic diagram of model for examining the homogeneity of the radiation field produced by a beta source.

Examples of the variation of energy flux and electron and photon fluences are shown in figures 14 to 18 for the $^{106}Ru/^{106}Rh$ source.

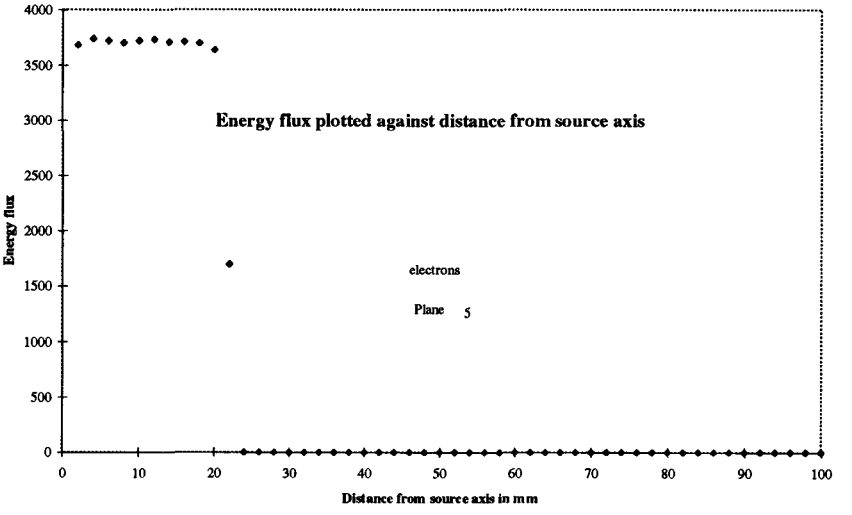

Figure 14: Electron energy flux on $^{106}Ru/^{106}Rh$ source surface

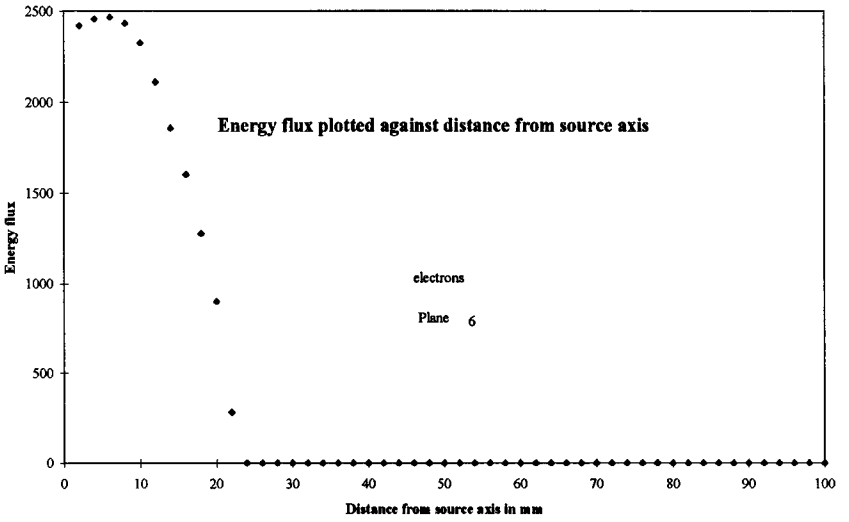

Figure 15: Electron energy flux 10 mm from $^{106}Ru/^{106}Rh$ source surface.

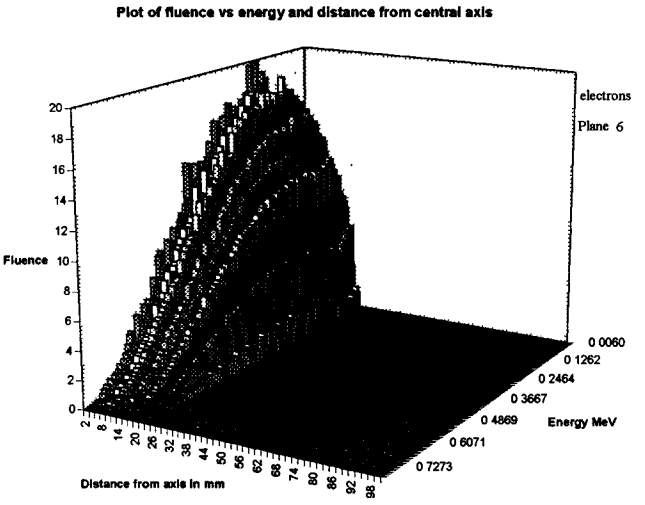

Figure 16: Three dimensional plot of electron fluence 10 mm from the $^{106}Ru/^{106}Rh$ source surface.

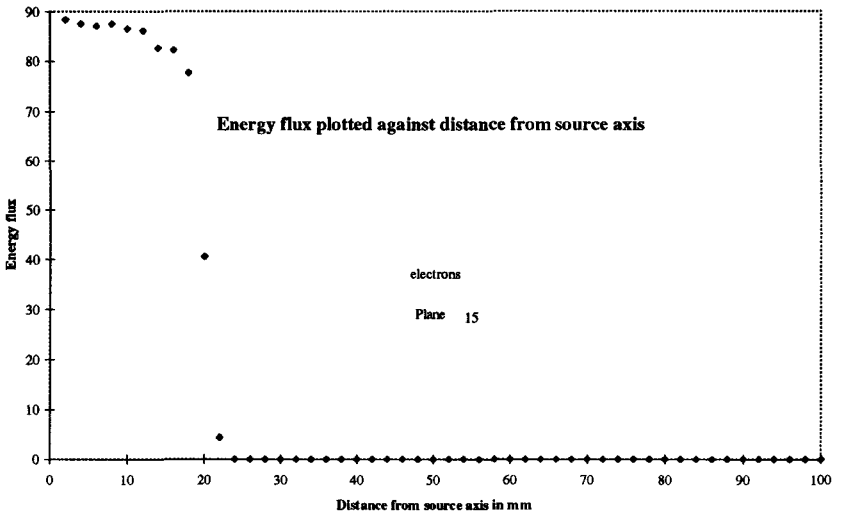

Figure 17: Electron energy flux 100 mm from $^{106}Ru/^{106}Rh$ source surface.

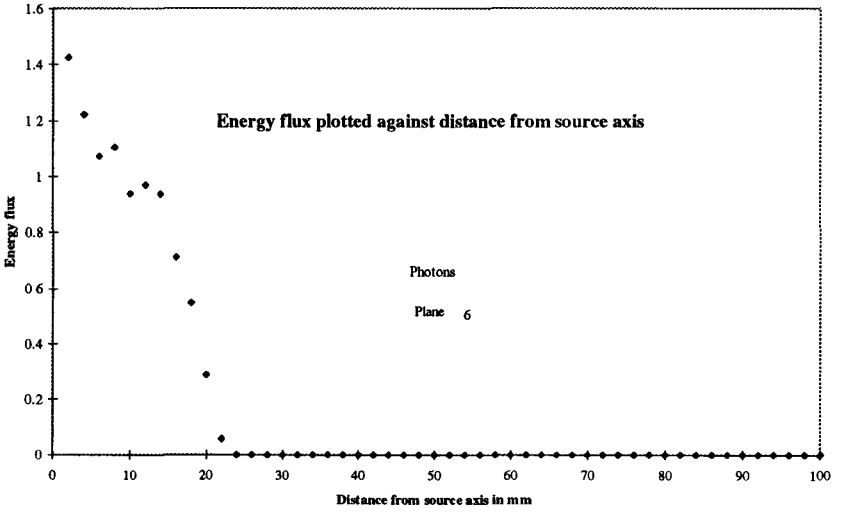

Figure 18: Photon energy flux 10 mm $^{106}Ru/^{106}Rh$ from source surface.

The above plots show how detailed information may be obtained about the behaviour of the radiation field at different distances from the front surface of the source.

During the development of the above model a similar calculation was carried out for the same geometry but with no aluminium at the edge of the beta emitting material. A schematic diagram of this model is shown in figure 19.

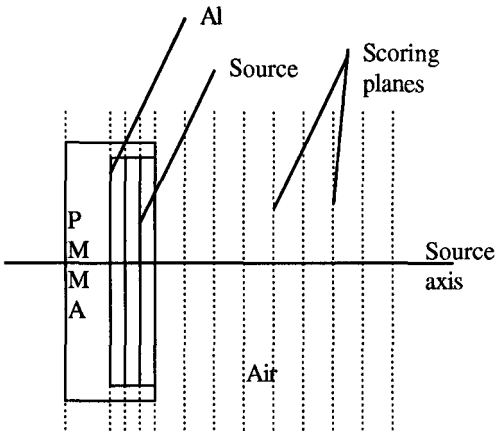

Figure 19: Early version of model of Hungarian source holder.

As there is no aluminium at the edge of the source matrix, more electrons were able to penetrate the PMMA ,and escape into air, than in the later model. The effect of this is shown on figures 20 and 21.

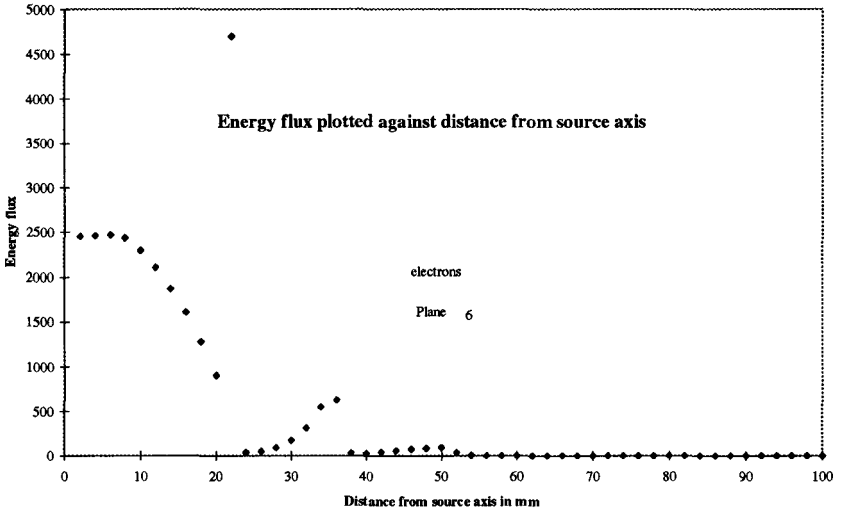

Figure 20: Electron energy flux 10 mm from $^{106}Ru/^{106}Rh$ source surface, no aluminium at edge of beta emitter.

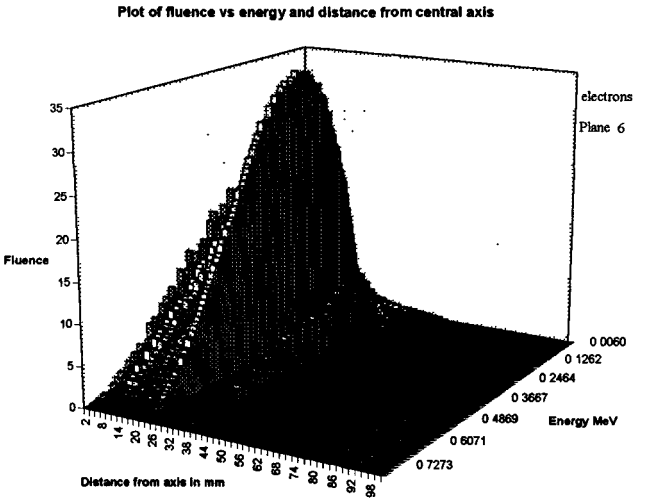

Figure 21: Three dimensional plot of electron fluence 10 mm from the $^{106}Ru/^{106}Rh$ source surface, no aluminium at edge of beta emitter.

The above figures, which may be directly compared with figures 15 and 16, show how a source imhomogeity may affect the homogeneity of its radiation field. The above models could be used to further examine the effect of likely imhomogeities.

The study of beam flattening filters and extrapolation chambers

Unfortunately due to difficulties obtaining data to validate the Monte Carlo Model at the early stages of the project, it proved impossible to move on to the creation of models for the examination of beam flattening filters and extrapolation chambers. But the models described in the above text may easily be extended to carry out Monte Carlo experiments with both beam flattening filters and extrapolation chambers.

Summary

Monte Carlo models are powerful tools for exploring the behaviour of radiation fields near beta sources. but to be useful the composition of the beta source holders and particularly the matrix containing the beta emitter must be well known.

References

Birch R and Marshall M, Computation of bremsstrahlung x-ray spectra and comparison with a Ge(Li) detector, Med. Phys. Biol. 24, 505-517 (1979).

Head of project 6: Prof. Gasiot

II. Objectives for the reporting period

The overall objectives of the project were to investigate and develop the TLD laser heating technique, using a computer controlled scanning laser heated TLD reader, and to construct and characterize thin solid state detectors (TLD), for dosimetry of weakly penetrating radiations. The laser heating technique offers the possibility of using detectors with a small effective thickness which is important for characterization of beta radiation fields and for individual monitoring of skin doses from beta radiation [1-6].
In particular, the work for the reporting period would concentrate on:
- Dosimetric characteristics of thin TLD detectors suited for laser heating for characterizing beta radiation fields in terms of H' (d;α°).
- Radiation field homogeneity measurements using large-size $CaSO_4$:Dy foils and laser heating (Montpellier) as well as carbon loaded MgB_4O_7:Dy detectors and conventional reader (RISØ National Laboratory).
- "Hot particle" dosimetry using the laser heated TLD reader and an OSL (optical stimulated luminescence) imaging system. The dose distribution originating from a small radioactive particulate would be evaluated and compared with results obtained using radiochromic dye films (Dr. M. Charles, University of Birmingham).

III. Progress achieved including publications

III.1. Development of thin TLD detectors for beta dosimetry

The initial activity was concentrated on material synthesis and dosemeter optimisation. The work is related to the conception, simulation and finally the test of dosemeters adapted to our TLD reader and to radiation dosimetry of low energy radiations. Dosemeters have been developed to measure doses, in particular, from $^{90}Sr/^{90}Y$, ^{147}Pm, ^{204}Tl. Improvement of the dosemeters has been achieved by varying both the kind of support and the TL material. Methods for the preparation of rare earth activated $CaSO_4$ have been developed at Montpellier [7, 8].
For $CaSO_4$:Dy, seven TL peaks are observed at temperatures ranging from 80-100°C for peak one, to 580-620°C for peak seven. Peak three, at about 220-240°C, is called the "dosimetric peak". Dosimetric characteristics have been studied as a function of dopant concentration, annealing temperature and grain size, using a conventional reader. Samples with nine different concentrations of Dy were prepared and irradiated to 3 mGy from a $^{90}Sr/^{90}Y$ source [9, 10]. The characteristic low temperature peaks of $CaSO_4$:Dy (80-100 and 120-140 °C) and the high temperature peak 3 (220-240 °C) are strongly dependent on the dopant concentration. The criteria for selecting the most sensitive material with respect to dopant concentration, is that the low temperature peak is separated from the high temperature peak and that the ratio of the low temperature peak height to the high temperature one is small. Under these conditions, $CaSO_4$ with 0.1% and 0.25% Dy appeared to be the best material. Glow curves were studied for annealing temperatures ranging from 400 to 900 °C. The ratio of low temperature peak height to high temperature peak height is minimum for an annealing temperature of 600 °C. However subsequent fading studies indicated a lower loss of TL signal, i.e. less than 3% fading on storage at room temperature over a month, could be obtained for 0.1% Dy and an annealing temperature of 700 °C. This TLD material was therefore selected for all our studies. Performance tests using $CaSO_4$:0.1% Dy pellets (60 $mg.cm^{-2}$) deposited on an aluminium holder (80 $mg.cm^{-2}$ thick) indicated a detection treshold of 0.02 mGy for a confidence level of 95 % and linearity of the dosemeter in the dose range from 0 to 30 mGy [10, 11].

III.2. Dosimetric characteristics of thin TLD films based on laser heating

Thin TLD films based on $CaSO_4$:0.1% Dy deposited on kapton and suited for laser heating have been developed. A programme for studying the dosimetric characteristics of these thin TLD detectors has been set up in collaboration with RISØ National Laboratory who did the irradiations at different beta energies and angles of the incident radiation.

III.2.1 Characterization of thin detectors for measurement of H'(d; α°) from beta radiation fields

For characterizing beta radiation fields in terms of H'(d,a°), TLD films with three different grain sizes (<36 μm, 25<g<50 μm and 36<g<63 μm) have been developed and tested. Dosemeter responses have been measured for energies originating from three beta sources ($^{90}Sr/^{90}Y$, ^{147}Pm, ^{204}Tl), at four different doses (between 10 and 100 mGy) and for different irradiation angles (from 0 to 75°).
For sensitivity and homogeneity tests, the TLD films were annealed and irradiated with a dose of 200 mGy delivered by a calibrated homogeneous ^{60}Co radiation field. The detectors (2 cm x 2 cm) used for these experiments had about the same sensitivity to ^{60}Co-γ radiation (within 3% for grain size g<36 μm and 5% for grain size 36<g<63 μm.).

Irradiation: All beta irradiations were done with the dosemeters placed on a 2 cm thick, 20x20 cm2, perspex plate and covered with a 0.77 mg/cm^2 mylar foil. The beta doses quoted by RISØ are absorbed dose to tissue to the surface of the dosemeter, i.e. the dose just below the mylar foil.The dose determinations were made with an extrapolation chamber. The source-detector geometry was:
^{147}Pm: 4x4 cm^2 source. Irradiation distance: 15 cm. No beam flattening filter used.
^{204}Tl: PTB-Buchler standard (1 cm diam.). Irradiation distance: 30 cm. With beam- flattening filter placed at 10 cm from the source.
$^{90}Sr/^{90}Y$: PTB-Buchler standard (1 cm diam.). Irradiation distance: 30 cm. No beam flattening filter used.
Different irradiation angles were obtained by turning the dosemeter together with the perpex plate (support) around an axis equal to the midline of the dosemeter surface.
For statistical reasons, three dosemeters were irradiated in the same conditions. For calibration purpose, three detectors were irradiated with a dose of 20 mGy delivered by a calibrated homogeneous ^{60}Co field, and all results were normalised to the ^{60}Co-readings.

Reading: The dosemeters were divided into groups according to grain size and irradiation conditions. All irradiated dosemeters were read with our new TLD reader [12] with the following setting: laser power 6W; laser beam diameter 0.8 mm; spacing between reading points 2 mm; heating time 12 ms.

Dose dependencies: Figure 1 presents, for grain size g<36 μm, mean values of the measured doses from three detectors, D_{exp}(beta), vs quoted beta doses, measured by extrapolation chamber, for the three beta sources ^{147}Pm, ^{204}Tl and $^{90}Sr/^{90}Y$. The measured dose is calculated as:

$$D_{exp}(beta) = [TL\,signal\,(beta) / TLsignal\,(^{60}Co\text{-}\gamma)]\,.\,D(^{60}Co\text{-}\gamma);\; with D(^{60}Co\text{-}\gamma) = 20mGy.$$

Ideally ratio $D_{exp}/D = 1$. Linear regression curves have been calculated through the experimental dose values. The slope indicates the efficiency of the dosemeter to the corresponding beta energy. Results are summerized in table 1, indicating also the average thickness of the detector material for each grain size.

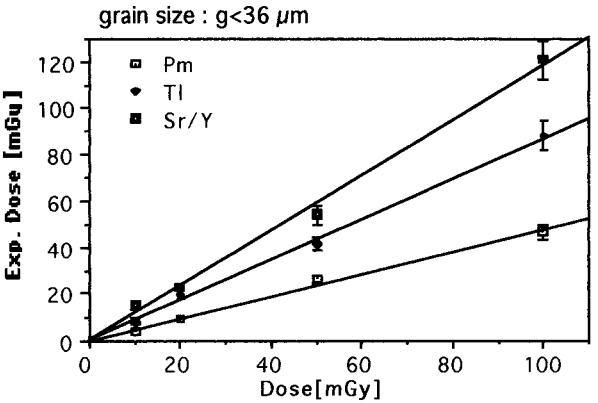

Figure 1 : Measured doses vs quoted beta doses for ^{147}Pm, ^{204}TL and $^{90}(Sr/Y)$ with $CaSO_4$:Dy detectors (g<36μm)

The efficiency to $^{90}Sr/^{90}Y$ is approximately 1 for grain sizes 25<g<50 μm and >1 for g<36 μm and 36<g<63 μm. Ratio D_{exp}/D is ranging between 0.8 and 0.87 for ^{204}Tl and between 0.44 and 0.52 for ^{147}Pm [13]. These values are lower than those observed for carbon loaded MgB_4O_7 detectors [3]. Measurements for the efficiency of $CaSO_4$:Dy TLD foils to ^{147}Pm beta doses (TL signal per unit beta dose / TL signal per unit ^{60}Co dose) were performed at RISØ with an Alnor Dosacus type reader operating with hot nitrogen heating. The measured efficiencies were respectively 0.51, 0.43 and 0.45 for grain sizes g<36 μm, 25<g<50 μm and 36<g<63 μm.

grain size	g < 36 μm	25 < g < 50 μm	36 < g < 63 μm
thickness of layer	≈50 μm	≈ 70 μm	≈ 80 μm
^{147}Pm	0,48	0,52	0,44
^{204}Tl	0,87	0,80	0,80
$^{90}(Sr/Y)$	1,18	0,98	1,10

Table 1 : Measured efficiencies of dosemeters

Angular dependencies of the dosemeter response are presented in figures 2a, b, c. All response values are mean values from measurements with three detectors and they are expressed as the ratio of measured, dose D_{exp}(beta), to the quoted dose.

For ^{147}Pm the dosemeter response is almost independant of the angle of irradiation for all grain sizes. For irradiations with $^{90}Sr/^{90}Y$ and ^{204}Tl, the observed response is close to 1 for angles between 0 and 40°, and decreases for higher irradiation angles. However, for 75° the low response to $^{90}Sr/^{90}Y$ cannot be explained; for irradiations with ^{204}Tl, an underresponse is observed at 60° for grain size g<36 μm and an overresponse for grain size 36μm<g<63 μm at 0° and 20°.

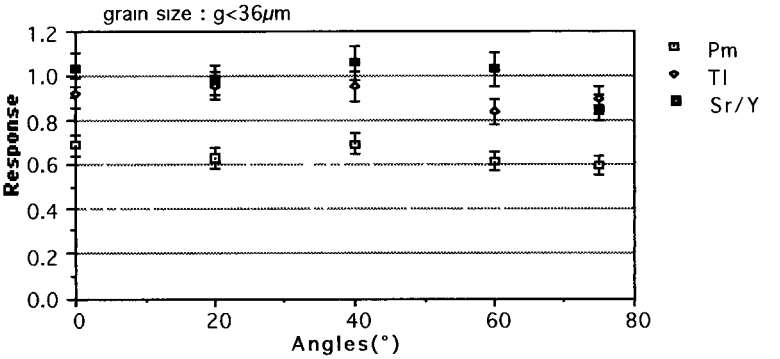

Figure 2a : Angular dependencies for ^{147}Pm, ^{204}TL and ^{90}(Sr/Y) with CaSO4 : Dy detectors (g<36μm),

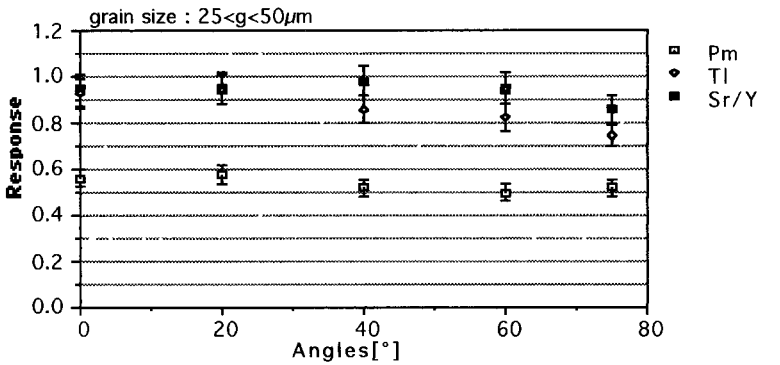

Figure 2b : Angular dependencies for ^{147}Pm, ^{204}TL and ^{90}(Sr/Y) with CaSO4 : Dy detectors (25<g<50μm),

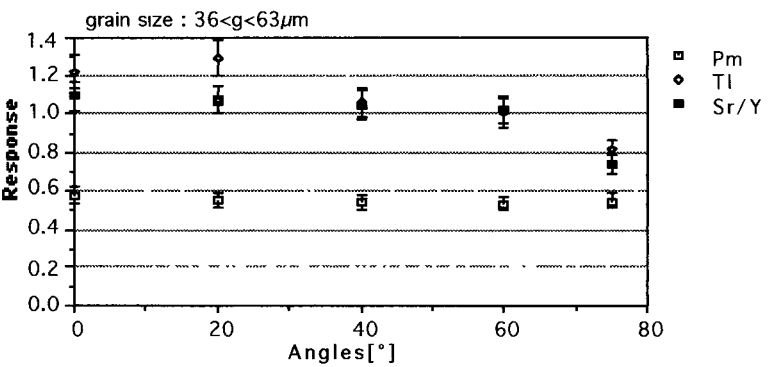

Figure 2c : Angular dependencies for ^{147}Pm, ^{204}TL and ^{90}(Sr/Y) with CaSO4 : Dy detectors (36<g<63μm),

III.2.2 Depth dose profile

A TLD film of size 4 cm x 10 cm was placed between two perpex plates and irradiated against the edge at 30 cm with a $^{90}Sr/^{90}Y$ source, so that the irradiation axis was parallel to the detector surface (radiation incidence 0°). The dosemap in 3D is presented in figure 3. The TL signal (a.u.) is presented in z direction. The x direction indicates the size of the dosemeter and the y direction the depth of penetration. The mean depth dose profile deduced from the dosemap is presented in figure 4. It can be seen that the maximum of the dose is located at a depth of about 0.5 mm and that the maximum depth of penetration for the $^{90}Sr/^{90}Y$ source is about 6 to 7 mm. These results are in good agreement with those given in the calibration certificate for the irradiation source and measured by PTB (figure 5). This experiment shows the capability of dose mapping to characterize a beta source with a good accuracy [13].

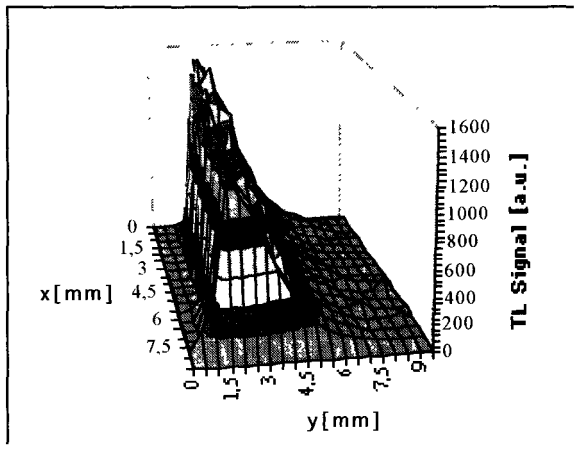

Figure 3 : Dose map from ^{90}(Sr/Y) source

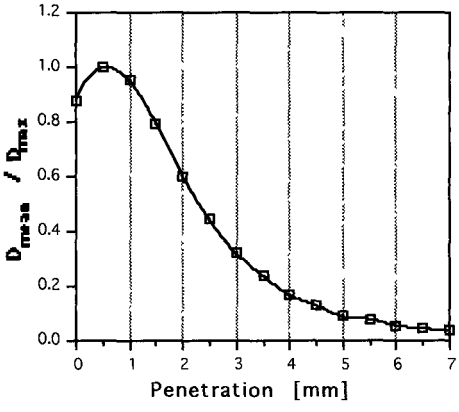

Figure 4: Depth dose profile measured at Montpellier (spacing betwen points : 0.05mm)

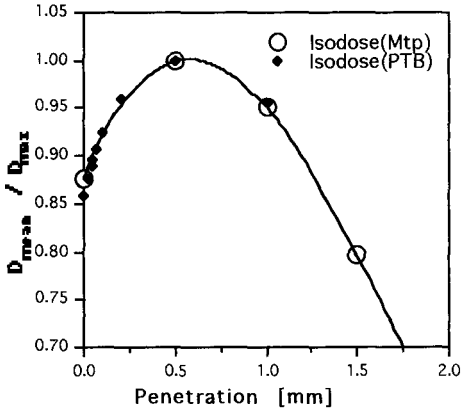

Figure 5: Superposition of depth dose profiles obtained with TLD foil (Mtp) and measured at PTB

III.2.3 Characterization of large beta radiation fields

The accuracy of large size (15 cm x 20 cm) dosemeter foils of CaSO4:Dy for measuring the dose homogeneity of beta radiation fields has been analyzed. A large size TL dosemeter was irradiated with the ^{147}Pm extended area source (20 cm, filter 0.77 mg.cm^{-2}) in order to measure the radiation field homogeneity. A similar experiment was conducted at RISØ using

very thin graphite-mixed MgB_4O_7:Dy TL detectors (1 mm thick, 4.5 mm diameter). 15 x 17 of these detectors were arranged in form of a matrix on an area of 8.82 cm x 9.6 cm. The detectors were read out with an Alnor Dosacus type reader. Dose profiles were calculated from the dose maps by averaging the values respectively over 3 rows of detectors (RISØ) and 6 rows, of measurement points (Mtp), in x and y direction. Regression curves were calculated through the experimental points, obtained from 4^{th} degree polynomial fits of experimental data. In order to intercompare the two measuring methods, experimental and calculated curves, for both methods, are presented in figures 6 and 7 respectively. There is a good agreement between both dose profiles, within a variation less than 3.5%. A good agreement of the calculated curves is observed for distances between -5 cm and +5 cm from the centrepoint. The same experiment has been repeated using a filter of 7.04 mg/cm^2 for the irradiation, as it is used to measure H'(0.07). The measured data and calculated dose distributions obtained from 4^{th} degree (RISØ) and 8^{th} degree (Mtp) polynomial fits of experimental data are presented respectively in figures 8 and 9.

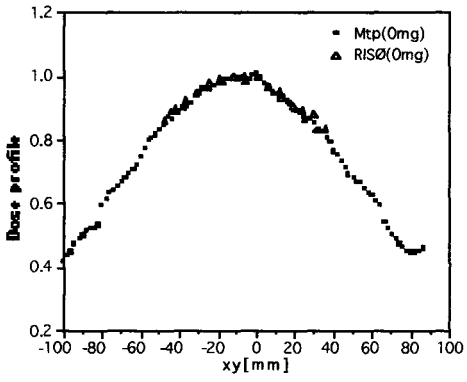

Figure 6: Dose profile data of Montpellier and RISØ (filter 0.77 mg/cm^2)

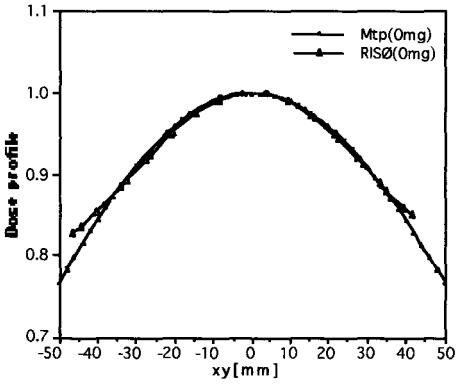

Figure 7: Dose profile regression curves of Montpellier and RISØ (filter 0.77 mg/cm^2)

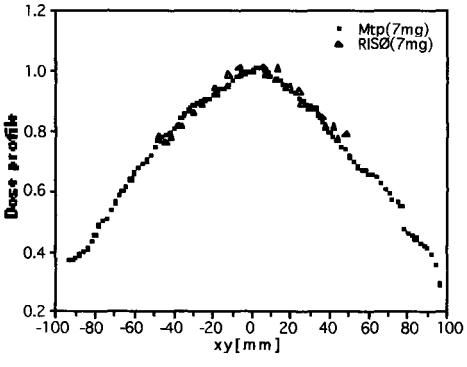

Figure 8: Dose profile data of Montpellier and RISØ (filter 7.04 mg/cm^2)

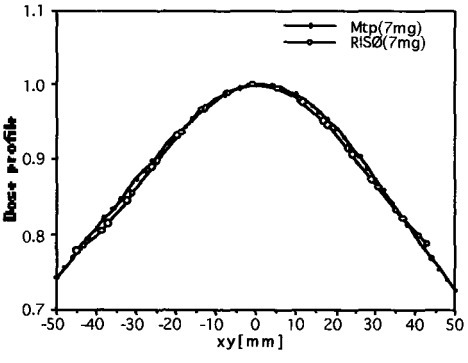

Figure 9: Dose profile regression curves of Montpellier and RISØ (filter 7.04 mg/cm^2)

The experimental results show that thin laser heated TLD foils based on CaSO4:Dy are a good alternative to conventionally heated thin TL detectors (graphite mixed LiF or MgB4O7). Laser heating of large TLD foils offers an efficient and easy method to visualize large size radiation fields or depth dose profiles in form of 2 dimensional dosemaps with a good resolution.

III.4. "Hot particle" dosimetry.

The most relevant point in our work on hot particle dosimetry, has been to study the feasability of dose mapping in the mm scale for hot particle dosimetry using the laser TLD system or OSL (Optically Stimulated Luminescence) [14, 15]. These methods are attractive compared to other possible techniques used to evaluate the dose, like extrapolation chambers (complex and time-consuming method, limited spatial resolution) or radiochromic dye films, which have the disadvantage of limited dynamic range and very long exposure times due to low sensitivity.

4.1.The source

The "hot particle" was a spherical 200 μm diameter ^{60}Co source provided by Dr. Charles (Univ. of Birmingham). We received the source from Dr. Herbaut (CEN Grenoble) who had performed dose rate measurements using an extrapolation chamber. The activity of the source at the date of our irradiations (17/07/94) was 0.486 MBq (13.11 μCi). The cobalt sphere was glued on an aluminium support and covered by a 15 μm thick aluminium foil. Between the support and the cover was air.

4.2. Detector and irradiation

For the laser heating TLD measurements, our detector was a 50μm thick layer of $CaSO_4$:Dy, grain size < 36μm, deposited on a 50μm thick kapton support. To check the linearity of the dose response of the detector, pellets of $CaSO_4$:Dy were irradiated for various times: 5, 10, 15, 30 and 60 min. and read with a conventional reader. The results confirmed a linear relationship of TL signal vs time of irradiation [14]. To measure essentially the energy deposited by the beta radiation in the TL material, the source must be in close contact with the detector. Therefore, our TLD detectors were not covered by any metallic or tissue-equivalent filter. To measure the lateral dose distribution, it would only be necessary to irradiate one detector. For the depth dose profile we built a stack of 4 detectors (12 x 12 mm^2) [15]. Their sensitivity to gamma radiation from a calibrated ^{60}Co source was found to be within a standard deviation < 5%. In order to improve the dynamic range of the reading and resolution, we needed two identical stacks. Each stack was sticked on a plexiglass plate and irradiated separately for 10 minutes by the source, placed in close contact on top of the stack, in the center of the first detector. The center of the source was close to the point where the laser beam hits the detector (within 20 μm).In this configuration, we estimate that the gamma radiation dose from the source deposited in the detector can be neglected compared with the beta dose and that we mainly see the contribution of the beta peak to the TL signal. For calibration purpose, we irradiated the 9th dosemeter with a dose of 200 mGy from a calibrated ^{60}Co source.

4.3. Reading

Reading conditions were: spacing between reading points: 0.4 mm; diameter of the laser beam: 0.8 mm; laser power: 4W; heating time of each point: 18 millisecs. Under these conditions, the reading points overlap in such a way that the effective average area per point was about 0.16 mm^2. The intrinsic dynamic range of our reading system allows to detect TL signals corresponding to doses ranging approximately between 1 and 1000 mGy. By attenuation of the TL signal (placing gray filters in front of the PMT), signals corresponding to higher dose values can be detected.

4.4. Results

Dose mapping of the radiation received on each dosemeter indicate that the TL signal decreases over several decades from dosemeter 1 (in contact with the "hot particle") to dosemeter 4, at a distance of 300 μm from the source. The TL signal was expressed as dose rate values (Gy/h), relative to ^{60}Co-γ calibration. Dose maps were transformed into radial coordinates relative to the center point in contact with the source.Radial dose distribution and calculated regression curve for the dosemeter in contact with the source are presented in figure 10. A maximal dose rate of 79 Gy/h was measured in the center of the detector. The dose rate is decreasing rapidly with the radial distance (5.5 Gy/h at r=0.5 mm; 0.02 Gy/h for r>5 mm). Regression curves obtained from dose mapping for the hole stack of four dosemetrs is presented in figure 11. The dose deposited in the center of each detector is decreasing by a factor of about 10 from one detector to the next deeper one.

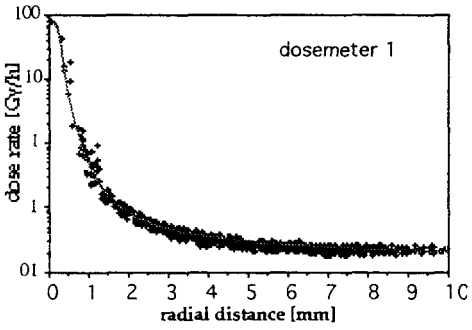

Figure 10: Experimental values and regression curve for the 1st dosemeter

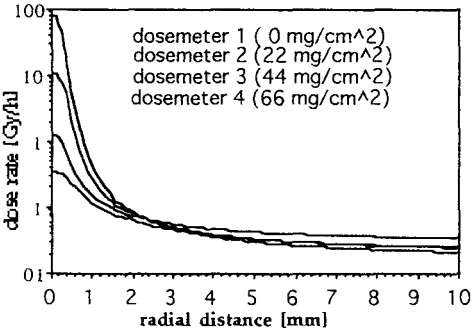

Figure 11: Calculated regression curves for the four dosemeters

4.5. Comparison with radiochromic dye films

We compared our TLD laser heating results with those reported by Dr. Charles (Birmingham), using radiochromic dye films. After correcting the results obtained using dye films for source activity decrease, both radial dose distribution curves are presented in figure 12, showing a fairly good agreement between the two techniques. The lower dose rate measured by TLD in the center of the dose map (79.0 Gy/h compared to 153.5 Gy/h by dye films giving a ratio of 1.94), is mainly related to the different irradiation conditions (we did not use an aluminized film on top of the first dosemeter) and reading geometries. Using Varskin Mod2 code, taking into account the respective depth of penetration and the average area per reading point, the calculated value of the mean dose ratio, D_m (Bir) / D_m (Mtp) = D_m(5.37mg/cm^2, 0.008 mm^2) / Dm(4.05 mg/cm^2, 0.16 mm^2), was 2.3 which is close to the experimental value of 1.94. The advantages of TLD films over radiochromic dye films are high sensitivity and therefore short

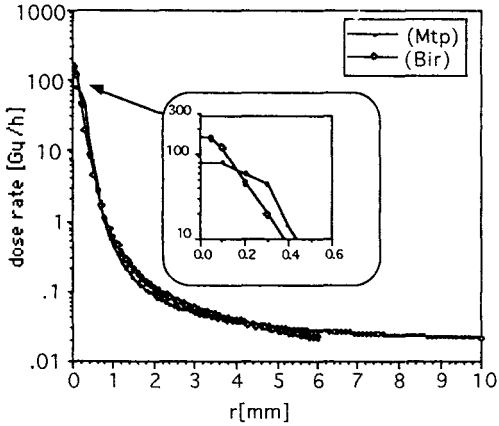

Figure 12 : Dose rate curves of Birmingham and Montpellier

irradiation times (10 min.) and large dynamic range (6-7 decades for the detector, 2.5 decades for the reading system, compared to 1 decade for dye films). The disadvantage of laser heating is limited lateral resolution. The advantages of dye films are higher lateral resolution and thinner dosimetric layer (about 7μm), but their low sensitivity needs irradiation times up to 1 week.

4.6. OSL measurements

To picture the spatial dose distribution we also performed OSL measurements. The reader, initially built for imaging, was equiped with a CCD (charge coupled device) camera to measure the OSL signal [16]. In this case, the irradiated luminescent material was stimulated by infrared light. Electrons leaving traps recombine, producing an emission of visible light. Only a few milliseconds of stimulation are necessary and a bright visible light is observed. This represents a real advantage for dose evaluation over radiochromic dye films [9]. Three radial dose distributions corresponding to irradiations of 1 min., 1h and 16.5 h have been measured and results for three different radial regions are presented in the same figure in figure 13. A regression curve has been calculated through the experimental points.

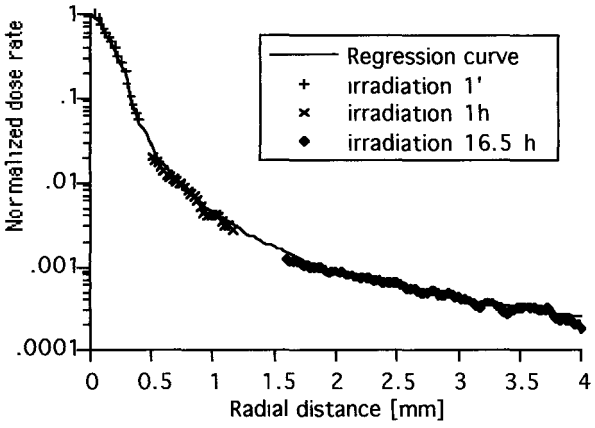

Figure 13 : Dose rate curves of Birmingham and Montpellier

Bibliography

1. Gasiot, J., Fillard, J. P. and Bräunlich, P. Laser Heating in Thermoluminescent Dosimetry. J. Appl. Phys. 53, 5200-5208 (1982).
2. Bräunlich, P., Tetzlaff, W., Gasiot, J. and Jones, S. C. Development of a Laser Heating TLD Reader. In: Proc. Int. Beta Dosimetry Symp. Washington DC. February 15-18, 293-305 (1983).
3. Christensen, P. and Prokic, M. S. Energy and Angular Response of TL Dosemeters for beta ray Dosimetry. Radiat. Prot. Dosim. 17, 83-87 (1986).
4. Christensen, P., Herbaut, Y. and Marshall, T. O. Personal Monitoring for external sources of beta and low Energy Photon Radiations. Radiat. Prot. Dosim. 18, 241-260 (1987).
5. Gasiot, J. CEC Contract N° Bi7-028 Report August 1992.
6. Servière, H., Vignolo, C. Prévost, H. and Gasiot, J. Laser Heating of TL dosemeters: Application to beta dose mapping. Radiat. Prot. Dosim. 39, 145-148 (1991).

Publications

7. V. Gérôme, P. Iacconi, D. Lapraz A. Baumer and H. Prévost, Thermoluminescence of undoped and Dy doped $CaSO_4$. Influence of the preparation methods. 11th International Conference on Solid State Dosimetry (SSD), July 10-14, Budapest, Hungary, 1995.
8. Goyet, D. Lapraz, D., Iacconi, P., Portal, G., Barthe, J., Prévost, H. and Gasiot, J. UV Emission in the TL Peaks of $CaSO_4$:Dy; Origin and Application to High Temperature Dosimetry. Radiat.Prot. Dosim. 47, 147-150 (1993).
9. Gasiot, J. and Prévost, H. Progress Report on CEC Contract FI3P-CT920032, Sept.15, 1993.
10. Luguera, E. Estudio y caracterizacion de un Dosimetro Termoluminiscente para Radiacion Beta de Baja Energia. Ph.D. Thesis, UAB, Barcelona, July, 1994.

11. Luguera, E., Fernandez, F. Paucar, R., Prévost, H. and Gasiot, J. Preparation and Dosimetric Properties of $CaSO_4$:Dy thermoluminescent dosemeter. Radiat. Prot. Dosim. (to be published).
12. Servière, H. Cartographie de dose gamma en champ mixte neutron-gamma en milieu modérateur, Thesis, Montpellier, Dec. 1993.
13. Setzkorn, R., Prévost, H., Gasiot, J. and Christensen, P. Laser heating of thermoluminescent films: dose mapping applied to beta dosimetry. 11th International Conference on Solid State Dosimetry (SSD), July 10-14, Budapest, Hungary, 1995.
14. Gasiot, J. and Prévost H. Progress Report on CEC Contract FI3P-CT920032, August 15, 1994.
15. Prévost, H., Setzkorn, R.and Gasiot, J. Draft Report on Hot Particle Dosimetry using laser heated thermoluminescence, November, 1994
16. Setzkorn, R., Béteille, D., Dusseau, L., Prévost, H., Fesquet, J., and Gasiot, J. Dosimétrie des particules "chaudes" utilisant la thermoluminescence par chauffage laser et la luminescence par stimulation optique. accepted in Radioprotection (SFRP), July 1994.

Head of Project 7: Prof. Dr. A. Scharmann

II. Objectives for the reporting period

The overall objectives of the project were to study, develop and apply the TSEE technique for dosimetry of weakly penetrating radiations, making use of the extremely thin effective thickness and high sensitivity of BeO thin film detectors. Dosemeters were to be developed for applications in mixed fields of photon and beta radiation. They had to be opimized with regard to dose sensitivity, dose range, short- and long-term reproducibility after storage in atmospheres of different humidity, dependence of the response on radiation energy, angle of radiation incidence and composition of window materials. These studies comprised the construction and test of an extremity dosemeter. The smaller size of the detectors for this purpose afforded an adjustment to the heating system of the read-out instrument. Another aim was to optimize the readout accuracy and reliability.

III. Progress achieved including publications

Improvement of TSEE readout

For TSEE detection a self-constructed computer controlled reader was used which allows automatic readout of up to 48 samples. In this instrument the samples are linearly heated up to 590 °C with a halogen lamp. The temperature is determined by means of the heat radiation emitted from the graphite substrate of the detectors. This method of temperature measurement and heating avoids problems associated with therrmal contacts. It was initially designed for detectors of more than 10 mm diameter. The light beam of the halogen lamp cannot completely be focused on the small size of the detectors needed for an extremity dosemeter. For this reason the standard geometry for the heating process was established by placing the smaller detectors in special graphite frames.

Exoelectron counting was performed with a cylindrical methane gas flow counter operated in the proportional range. This mode of operation provides superior pulse resolution at high counting rates in comparison to Geiger-Müller needle counters and therefore enables fast readout cycles over a wide linear range of more than 5 orders of magnitude. However, because of the low energy of emitted exoelectrons of less than 1 eV one obtains a Polya pulse height distribution which inevitably overlaps with the noise level. The detection sensitivity is therefore affected by variations of the gas gain of the counting tube with the counting voltage or temperature and pressure of the counting gas. These parameters are stabilized in the instrument used in Giessen, but as yet there existed no adequate reference electron emitter by which the correctness of the gas gain could easily be verified. Beta sources are unsuited for this purpose, because the pulse height distributions of even low energy beta radiation and of exoelectrons are different, and correspondingly the portions of pulses beyond the discriminator level. The electron emission from sources based on the photoelectric effect or thermionic emission is affected by variations of the work function. Therefore a two-channel method was developed which uses the exoelectron emission during dose readout as an inherent reference source.

In the case of TSEE the portion of the Polya distribution beyond the electronic noise level exhibits an exponential shape with a slope depending on the gas gain. The scheme in Fig. 1 shows two distributions for the cases of high and low gas gain. For pulses higher than the discriminator level x_1 the areas below these distribution curves are corresponding to the total TSEE pulse number, denoted by $TSEE_1$. Beyond an additional higher discriminator level at the pulse height position x_2 one obtains the additional pulse number $TSEE_2$ The ratio Q of $TSEE_1$ and $TSEE_2$ is independent of the absolute number of pulses but strongly affected by variations of the gas gain, as can be seen from Fig. 1. Q is a very convenient control parameter for the counting tube operation because $TSEE_1$ and $TSEE_2$ can simultaneously be determined without the requirement of an additional measurement.

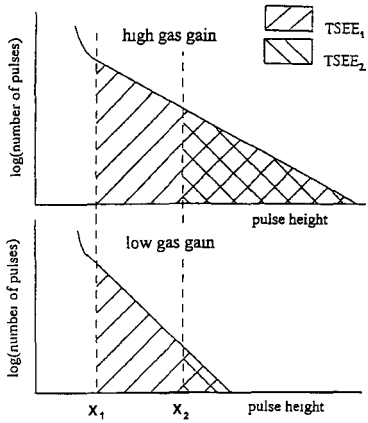

Figure 1. Logarithmic plot of the exponential portion of the Polya distribution for high and low gas gain, and pulse numbers $TSEE_1$ and $TSEE_2$ detectable beyond discriminator levels x_1 and x_2.

From the plot of the TSEE sensitivity S_n and the pulse ratio Q_n (both normalized to the values of the standard conditions) versus counting voltage, gas pressure and gas temperature (Fig. 2) can be seen that Q_n is more sensitive to variations of the operational parameters of the counting tube than S_n. This result is corresponding to the relationship $S_n = Q_n^{-x1/\Delta x}$ derived for the exponential portion of the Polya distribution, where x_1 denotes the lower discriminator level and Δx the difference between x_1 and the upper discrimator level x_2. Computed and experimentally determined data are in good agreement (Fig. 3). This relationship enables corrections of erratic dose readout after the TSEE measurement in the case of gas gain variations.

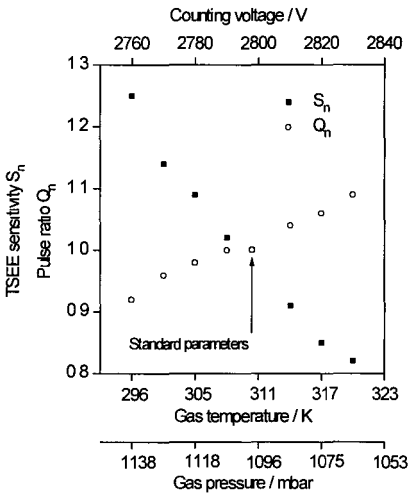

Figure 2. Dependence of normalized TSEE sensitivity S_n and normalized ratio Q_n on the operational parameters of the counting tube. Mean values of TSEE results from 10 BeO thin film detectors (σ <2.5 %). Corresponding values of counting voltage, gas pressure and temperature computed for equivalent gas gain by means of Diethorn formula [1,2].

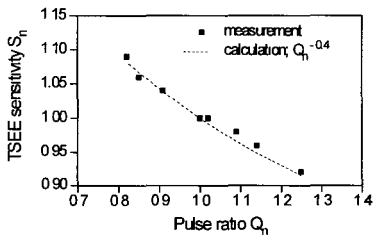

Figure 3. Computed and experimentally determined relationship between S_n and Q_n for $x_1/\Delta x = 0.4$.

2. Response of BeO thin films to photon and beta readiation

TSEE dosemeters are mainly intended for individual monitoring of weakly penetrating radiation. During such an application additional exposures to strongly penetrating photons cannot be excluded. This affords a correct measurement of $H_P(0.07,\alpha)$ for beta radiation, X-rays and gamma radiation. Sudies were performed with detectors of 12.5 mm diameter, prepared by the Battelle Institute, Frankfurt, and with detectors of 6.5 mm diameter produced by MPA, Dortmund. Battelle detectors covered a dose range of about 5 μSv - 2 Sv (lower limit corresponding to a reading of about twice the background level). For 1 mSv and 0.5 Sv they showed standard deviations of the dose response of 2 - 3 %, at 2 Sv of 6 - 7 %. Detectors of 6.5 mm diameter had a dose range of about 20 μSv - 5 Sv and at 1 mSv and 2 Sv standard deviations of 6 - 7 %.

2.1. Response to photons

2.1.1. Influence of window materials on the TSEE

The TSEE sensitivity to X-rays is strongly dependend on the atomic number Z of the window materials above the exoelectron emitting layer. With increasing Z it becomes almost proportional to the mass energy transfer coefficient of the window (Fig. 4). The data of Fig. 4 were obtained with window foils of atomic numbers ranging from 4 (Be) to 73 (Ta) and mean photon energies of 33 and 65 keV. Each foil had a thickness of more than the range of photoelectrons in order to enable secondary electron equilibrium, but was kept as thin as possible to avoid photon attenuation. All TSEE results were corrected for attenuation and normalized to the response obtained with Be window. It can be concluded that secondary electrons originating from photon interactions in the material above the TSEE sensitive layer are decisively contributing to the occupation of TSEE traps. Because of their very thin sensitive layer TSEE detectors approach the behaviour of Bragg-Gray detectors. Complete linearity between TSEE response and μ_{tr}/ρ would be corresponding to the dotted lines in Fig. 4. At lower photon energy the deviation from linearity becomes stronger because the contribution of photon interactions in the window to TSEE excitation decreases due to the smaller photoelectron range. Correspondingly interactions in the BeO layer itself are dominating.

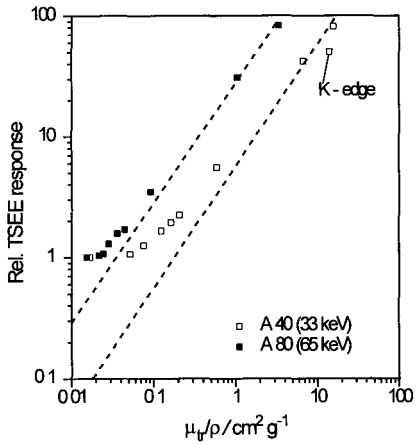

Figure 4. Relationship between TSEE response and mass energy transfer coefficient μ_{tr}/ρ of window materials of different atomic number Z on BeO thin film detectors, for constant exposures to heavily filtered A40 and A80 X-rays.

2.1.2. Energy dependence

For the choice of an appropriate window material suitable for the detection of $H_P(0.07)$ the dependence of the TSEE response on photon energy was determined for 4 plastic foils of 7 mg·cm^{-2}

thickness, whose effective atomic number ranged from 6.7 to 9.7. In a first series of measurements at the CEA institute in Fontenay-aus-Roses the detectors were irradiated under secondary electron equilibrium at constant air kerma on a 30×30×15 cm PMMA phantom by ^{60}Co, X-rays according to the ISO narrow spectrum conditions and monoenergetic X-rays from fluorescence sources. The TSEE response data (Fig.5a) were normalized to constant $H_P(0.07,0^\circ)$ by applying the conversion coefficients for the PMMA phantom [3]. The maximum values of the response at photon energies of 30 - 40 keV differed by almost the same factors as the mass energy transfer coefficient of the foils. Similar results were obtained for irradiations free in air and normalization of the TSEE response to constant air kerma (Fig. 5b). These measurements were carried out with photon sources of the GSF, Neuherberg.

The best approach to energy independence was achieved with detectors covered by Lutamer. In the range from 15 keV - 1.25 MeV the maximum deviations of the response from the mean value was ±13 %. Lutamer is a black intrinsically counducting polypyrrole material ($N_3C_{18}H_{14}SO_3$). It is mechanically and chemically stable and protects against optical fading. The electric conductivity prevents charging effects at the BeO surface by which the TSEE dose readout could be disturbed.

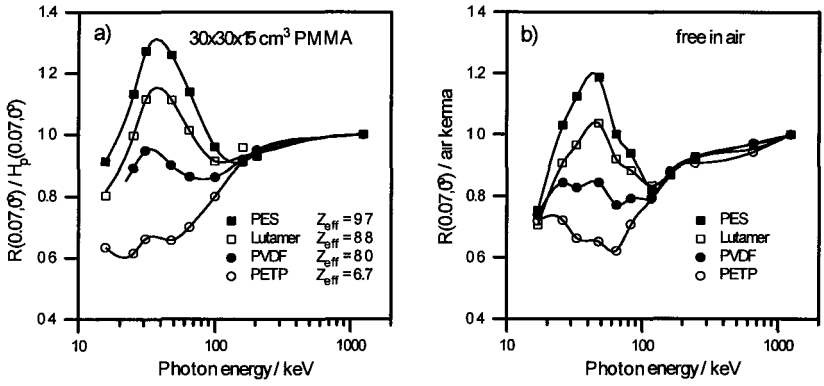

Figure 5. Photon energy dependence of BeO thin film detectors with 7 mg·cm^{-2} windows consisting of polyethersulfone (PES), Lutamer, polyvinylidenfluoride (PVDF) or polyethylene terephthalate (PETP). The TSEE data are mean values from 9 detectors. *Left:* Irradiations on 30×30×15 cm PMMA phantom, TSEE normalized to constant $H_P(0.07)$ and corrected for differences of backscatter factor between PMMA phantom and ICRU sphere. *Right:* Irradiation free in air, normalization to constant air kerma.

Skin dosimetry is mainly carried out with finger ring dosemeters. Working group 2 'Reference Radiations' of the ISO committee TC85/SC2 suggested for the calibration of such dosemeters in terms of $H_P(0.07)$ a rod phantom consisting of a PMMA cylinder of 19 mm diameter and 300 mm length [4]. The energy and angular response of BeO thin film detectors on this phantom to photons were determined at the GSF, Neuherberg. Detectors of 6.5 mm diameter of origin MPA Dortmund, were used, which were designed for finger dosemeters and put to our disposal by Dr. Chartier, CEA, Fontenay-aux-Roses. They were covered with a Lutamer foil of 6.7 mg·cm^{-2} thickness. Again the photon irradiations occured under secondary electron equilibrium with X-rays of the ISO narrow spectrum series and gamma radiation from ^{137}Cs and ^{60}Co. The relative TSEE response $R(0.07,0^\circ)/H_P(0.07,0^\circ)$ was determined from the response per air kerma by applying the kerma-to-dose-equivalent conversion coefficients calculated for the rod phantom by Grosswendt [6]. These factors are close to 1. For this reason $R(0.07,0^\circ)/H_P(0.07,0^\circ)$ of detectors irradiated on the rod phantom is very similar to the response of detectors irradiated at constant kerma free in air (Fig. 6).

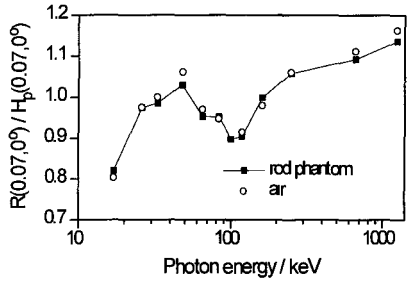

Figure 6. Photon energy response $R(0.07,0^0)/H_p(0.07,0^0)$ of detectors of 6.5 mm diameter irradiated on the PMMA rod phantom (■) and of 12.5 mm diameter irradiated free in air (o), both covered with 6.7 mg·cm^{-2} Lutamer.

BeO thin films habe been undersensitive to photons for all tested plastic window materials and phantoms at photon energies of less than 25 keV. In this energy range TSEE excitation is no longer mainly due to photon interactions in the window material but to interactions in the exoelectron emitting BeO layer. The mass energy transfer coefficient μ_{tr}/ρ of BeO is by about 20 % smaller than of tissue. Compensation of the resulting deficiency of sensitivity by a window material of significantly higher atomic number would cause an unwanted overproportional increase of the response at photon energies in the range between 30 - 50 keV. A better energy response can therefore only be achieved by windows composed of layers of different materials. Windows of this kind were tested. The compositions of the regarded combinations are listed in Table 1, the results are depicted in Fig. 7.

Name	Material and thickness in mg·cm^{-2}			Total thickness mg·cm^{-2}
	inner layer	middle layer	outer layer	
Lut / Al		Lutamer 4.96	Al 1.62	6.58
Al / PETP / Lut	Al 0.14	PETP 1.68	Lutamer 4.96	6.78
Al / PETP / Al-1	Al 0.14	PETP 4.20	Al 2.43	6.77
Al / PETP / Al-2	Al 0.54	PETP 2.10	Al 4.05	6.69

Table 1. Composition and layer thickness of studied window combinations. The inner layer was facing the detector.

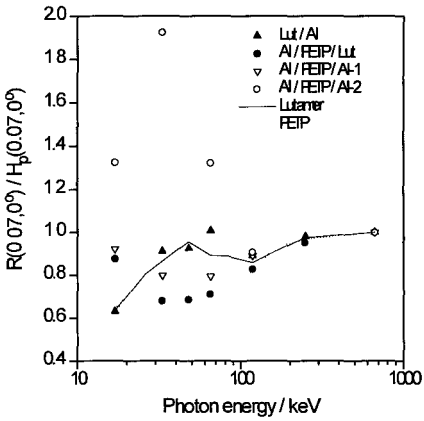

Figure 7. Photon energy response of BeO thin films covered with the window material combinations listed in Table 1. Irradiations free in air at constant air kerma, experimental conditions like in Fig. 5b.

Favourable would be a window composed of three layers. The middle layer should consist of Lutamer or another material of the same effective atomic number. With outer layers of aluminium the response to photons of low energy and of the range around 100 keV can be raised. A flat response behaviour at low energy photons can be achieved with an aluminium layer of 0.14 $mg \cdot cm^{-2}$ adjacent to the detector, corresponding to a thickness of 500 nm. An aluminium thickness of 0.54 $mg \cdot cm^{-2}$ already causes significant oversensitivity in the energy range of prevailing photoelectric effect. Plastic foils of the effective atomic number of Lutamer coated with an aluminium layer of the desired thickness were not available. Therefore corresponding polyethylene terephthalate (PETP) foils, known under the tradename Hostaphan, were tested. However, the effective atomic number of this material is too low, as can be seen from Fig. 5 and Fig. 7. Because of this difficulty a mono-layer Lutamer window was used for the further dosemeter development, and no attempt was made to extend the measurements into the photon energy range below 17 keV.

2.1.3. Angular dependence

The response ratio $R(0.07,\alpha)/R(0.07,0^o)$ corresponding to $H_P(0.07,\alpha)/ H_P(0.07,0^o)$ was determined for ^{60}Co and the ISO narrow spectrum radiation qualities A20, A30, A40, A120 for angles α ranging from 0^o - 180^o. Detectors of 6.5 mm diameter with Lutamer window were irradiated on the PMMA rod phantom. The results in Fig. 8 are compared with angular dependence factors calculated by Grosswendt [6] for monoenergetic electrons. There is a rather good agreement at low and high photon energies. At mean photon energies the response is too low at angles $>90^o$. In the case of A40 radiation with a mean energy of 33 keV a maximum deviation of 15% was observed for $\alpha = 180^o$. Under these reverse incidence conditions photon interactions in the window material are no longer the origin of exoelectron excitation, but interactions in the graphite substrate of the detectors. The response becomes lower because the energy transfer coefficient of graphite is smaller than of Lutamer.

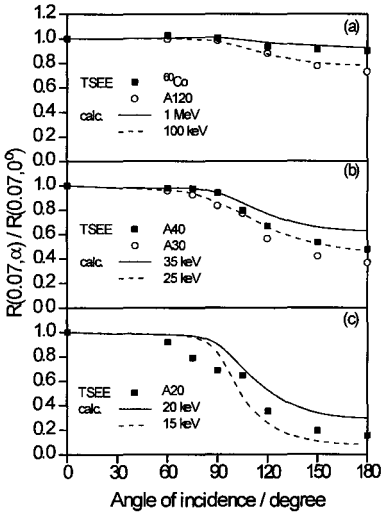

Figure 8. Photon angular response $R(0.07,\alpha)/R(0.07,0^o)$ of detectors of 6.5 mm diameter for irradiations on the PMMA rod phantom.
a: ^{60}Co (1.25 MeV) and A120 (mean energy 100 keV),
b: A40 (33 keV) and A30 (26 keV),
c: A20 (17 keV),
compared with angular dependence factors $H_P(0.07,\alpha)/H_P(0.07,0^o)$ calculated by Grosswendt [6] for monoenergetic photons (lines).

2.2. Response to beta radiation

2.2.1 Energy dependence

The relative response $R(0.07,0^o)/H_P(0.07,0^o)$ of BeO thin films to beta radiation was determined with the point sources of the Buchler secondary standard in Fontenay-aux-Roses and at the GSF,

Neuherberg. Detectors of 12.5 and 6.5 mm diameter were exposed on a PMMA slab and on the PMMA rod phantom, respectively. For the series of exposures on the PMMA slab the detectors were again covered with 7 mg·cm^{-2} foils of PETP, PVD, Lutamer or PES. With Lutamer windows the TSEE sensitivity was independent of beta radiation energy (Table 2). The composition of the window foils was not as important as in the case of photon irradiations, because the mass stopping power for electrons is less depending on atomic number than the mass energy transfer coefficient in the photon energy range of prevailing photoelectric effect. However, the sensitivity to beta radiation from ^{147}Pm (mean energy 60 keV) is strongly influenced by small variations of the window thickness. The PETP foil was 10 % thicker than assumed and declared by the manufactorer. This caused a decrease of the response of about 20 %. One has to keep in mind that only beta particles of the uppermost energies of the beta spectrum of ^{147}Pm have a range sufficient to penetrate 24 mg·cm^{-2} of air, corresponding to the irradiation distance of 20 cm, and the additional 7 mg·cm^{-2} of the detector window. The response to ^{147}Pm can be raised by a window thickness of slightly less than 7 mg·cm^{-2}.

The sensitivity of BeO thin films for beta particles is the same as for gamma radiation from ^{60}Co (Table 3).

Nuclide	Mean Energy keV	$R(0.07,0^\circ)/H_P(0.07,0^\circ)$			
		PETP	PVDF	Lutamer	PES
^{90}Sr/^{90}Y	800	1.02	1.04	1.00	1.02
^{204}Tl	240	0.95	1.00	0.96	0.98
^{147}Pm	60	0.78	0.93	0.98	0.93

Table 2. Relative response of BeO thin films to beta radiation for the same four plastic foil windows as in Fig. 5. Data normalized to Lutamer window and ^{90}Sr/^{90}Y (mean values from 8 detectors). Detectors irradiated on PMMA slab.

PETP	PVDF	Lutamer	PES
1.00	1.06	1.02	1.04

Table 3. Response $R(0.07,0^\circ)/H_P(0.07,0^\circ)$ to ^{90}Sr/^{90}Y relative to ^{60}Co (mean values of 9 detectors). Exposures to ^{60}Co on 30×30×15 cm PMMA phantom, exposures to ^{90}Sr/^{90}Y on PMMA slab.

2.2.2 Angular dependence

The angular response $R(0.07,\alpha)/R(0.07,0^\circ)$ of BeO thin films covered with 6.7 mg·cm^{-2} Lutamer to beta radiation was studied for detectors of 12.5 mm and 6.5 mm diameter on a PMMA slab and the PMMA rod phantom, respectively. The results obtained with the larger detectors (Fig. 9) are in almost full agreement with $H_P(0.07,\alpha)/H_P(0.07,0^\circ)$. For the rod phantom such reference values are as yet not available. One can assume that the different shapes of the two phantoms are of only minor importance for the response to beta radiation. It is therefore reasonable to compare the rod phantom results with the conventional data of $H_P(0.07,\alpha)/H_P(0.07,0^\circ)$ for the PMMA slab (Fig. 10). For ^{90}Sr/^{90}Y the measured response was lower than these reference data. The deviations are not due to phantom parameters, but caused by the inner side wall of the graphite substrate of the BeO thin film detectors, which is partly shading the sensitive BeO area. The response of 6.5 mm detectors is affected stronger, because the BeO area extends to the side wall, while there is a gap of 1 mm in the case of 12.5 mm detectors. At lower beta energies multiple scattering expands the directional distribution of the beta radiation striking the detector and thus reduces the influence of shading.

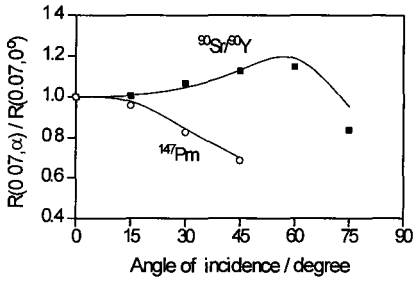

Figure 9. Beta radiation angular response $R(0.07,\alpha)/R(0.07,0^{\circ})$ of detectors of 12.5 mm diameter with Lutamer window for irradiations on semi-infinite PMMA slab, compared with the conventional angular dependence factors $H_P(0.07,\alpha)/H_P(0.07,0^{\circ})$ [7] (lines).

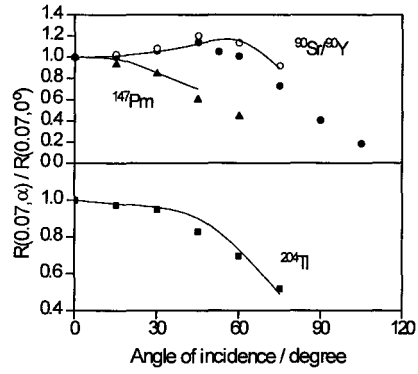

Figure 10. Beta radiation angular response $R(0.07,\alpha)/R(0.07,0^{\circ})$ of detectors of 6.5 mm diameter with Lutamer window for irradiations on the PMMA rod phantom, compared with the conventional angular dependence factors for slab phantom conditions.

2.2.3. Depth dose

The depth dose response $R(d,0^{\circ})/R(0,0^{\circ})$ of detectors covered with Lutamer foils of different thickness d agreed exactly with the transmission factors T(d) of tissue (Fig. 11).

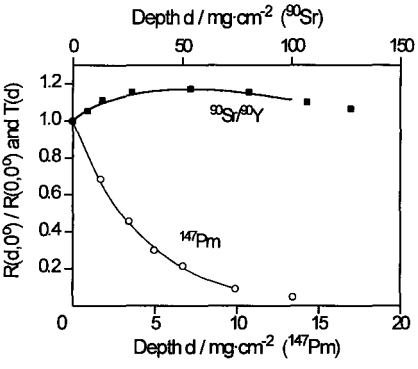

Figure 11. R(d)/R(0) of BeO thin films covered with Lutamer of different thickness d for beta radiation from $^{90}Sr/^{90}Y$ and ^{147}Pm in comparison to tissue transmission factor T(d), given in the PTB report of the Buchler standard.

3. Reproducibility and long-term stability of the dose response

BeO thin film detectors were formerly prepared by the Battelle Institute, Frankfurt, and in recent years by MPA, Dortmund. A reliability test was carried out with 60 detectors (12.5 mm diameter) of different charges from both origins, which after exposure to $^{90}Sr/^{90}Y$ were stored up to 4 weeks in normal laboratory air and saturated water vapour. Battelle detectors produced mean standard deviations of 2 - 3 % of the dose response and were hardly affected by the change from normal to

humid storage conditions. MPA detectors were less sensitive by a factor of about 3. They produced higher standard deviations of up to 7 - 10 % and showed fading of up to 20 % within 4 weeks in humid air. It was attempted to improve the behaviour of MPA detectors by wash procedures and chemical treatments. The experiments were combined with surface analysis measurements (SIMS, XPS). Additionally the MPA institute provided detectors produced at different oxidation temperature and flow of the oxidation gas. In spite of these efforts no essential improvement of the long-term dose reliability could be achieved. It is assumed that presently the detector oxidation occurs too slowly because of an insufficient flow of water vapour.

4. Badges for reference irradiations and extremity dosemeters

Badges (Fig. 12 and Fig. 13) were designed for detectors of 12.5 mm and 6.5 mm diameter, respectively. In both cases the entrance window of 6.7 mg·cm^{-2} Lutamer is larger than the size of the detectors, in order to avoid disturbing scattering effects, particularly at larger angles of radiation incidence. The badge for 12.5 mm detectors consits of black plexiglass. The badge for the extremity dosemeter is made of a 150 µm thick plastic strip of coloured high density polyethylene (HDPE), which can be wrapped around a finger and be fixed by an adhesive pad. Here the detector is placed in a bag of HDPE which can be sealed by welding for the application in individual monitoring. The Lutamer foil is sticked together with the cover part of the bag. Sealed badges cannot be re-used, because they are destroyed when the detector is removed.. The response characteristics of the detectors are not affected by these badges. Only the badge for 12.5 diameters causes a slight reduction of the sensitivity at angles of radiation incidence > 60°.

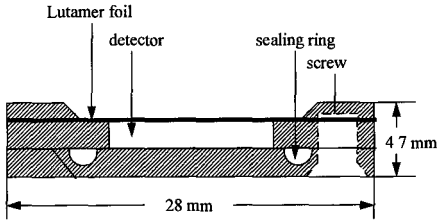

Figure 12. Badge for detectors of 12.5 mm diameter.

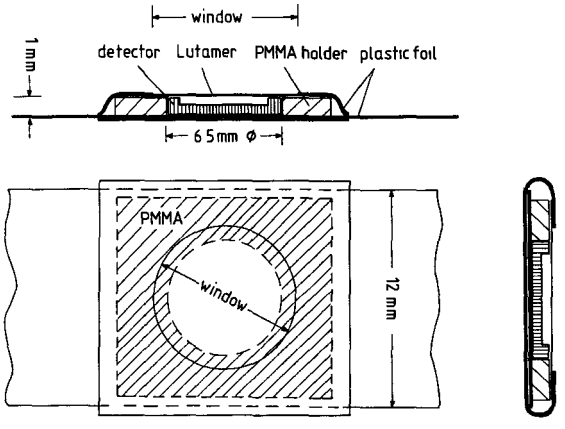

Figure 13. Scheme of extremity dosemeter with detector of 6.5 mm diameter.

References

[1] W. Kriegseis, A. Scharmann, W. Senger and B. Woerner. *Equipment for Fast Automatic Readout of TSEE Dosemeters Employing a Wide-Range Proportional Counter.* Japan. J. Appl. Phys. **24** Suppl. **24-4**, 60-64 (1985).

[2] H.-E. Habermehl, W. Kriegseis and A. Scharmann. *Calculation of the time dependence of the pulse shape in a cylindrical proportional counter using the Diethorn assumptions.* Nucl. Instr. Methods **A303**, 370-373 (1991).

[3] W. Kriegseis, K. Rauber, A. Scharmann, K.-H. Ritzenhoff, J.L. Chartier, D. Cutarella, C. Itié, M. Petel. *Dependence of the TSEE response of BeO thin films on photon energy and composition of cover materials.* Radiat. Prot. Dosim. **47**, 143-146 (1993).

[4] Alberts, W.G., Böhm, J., Kramer, K.-M., Iles, W.J., McDonald, J. Schwartz, R.B. and Thompson, I.M.G. *International Standardization of Reference Radiations and Calibration Procedures for Radiation Protection Instruments.* In: Strahlenschutz: Physik und Meßtechnik, Vol. 1, Ed. W. Kölzer, R. Maushart, ISSN 1013-4506, TÜV Rheinland GmbH, Köln, 181-188 (1994).

[5] Burkhardt, W., Kriegseis, W., Petel, M., Regulla, D., Schäm, M. and A. Scharmann. *TSEE response of BeO thin film detectors irradiated on ISO rod phantom to photons and beta radiation.* Forthcoming publication in Radiat. Prot. Dosim.

[6] Grosswendt, B. *Angular Dependence Factors and Kerma-to-Dose-Equivalent Conversion Coefficients for 1.9 cm Rod and 7.3 cm Pillar Phantoms Irradiated by extended Monodirectional X-Ray Beam.* Data reprinted in: Alberts, W.G., Ambrosi, P., Böhm, J., Dietze, G., Hohlfeld, K. and Will, W. *Neue Dosis-Meßgrößen im Strahlenschutz.* PTB-Report Dos-23, ISSN 0172-7095, Braunschweig (1994).

[7] Christensen, P., Böhm, J. and Francis, T.M. *Measurement of Absorbed Dose in Tissue in a Slab Phantom for Beta Radiation Incident at Various Angles.* In: Proc. Fifth Information Seminar on the Radiation Protection Dosemeter Intercomparison Programme. CEC Report EUR 11363, 39-75 (1988).

Publications derived from the contractual work

W. Kriegseis, K. Rauber, A. Scharmann, K.-H. Ritzenhoff, J.L. Chartier, D. Cutarella, C. Itié, M. Petel. *Dependence of the TSEE response of BeO thin films on photon energy and composition of cover materials.* **47**, 143-146 (1993).

W. Kriegseis, K. Rauber, D. Regulla, A. Scharmann. *Properties of TSEE active BeO thin film detectors for beta-ray and photon dosimetry* (in German). In: Strahlenschutz: Physik und Meßtechnik, Vol. 2, Ed. W. Kölzer, R. Maushart, ISSN 1013-4506, TÜV Rheinland GmbH, Köln, 487-492 (1994).

Burkhardt, W., Kriegseis, W., Petel, M., Regulla, D., Schäm, M. and A. Scharmann. *TSEE response of BeO thin film detectors irradiated on ISO rod phantom to photons and beta radiation.* Forthcoming publication in Radiat. Prot. Dosim.

Burkhardt, W. Kriegseis, W., Scharmann, A., Senger, W. *Improved exoelectron detection with proportional counters by two-channel analysis of the pulse height distribution.* To be published in Nucl. Instr. Methods.

Head of Project 8: Dr M W Charles

II. Objectives for the reporting period

The overall aim of the project was to develop and validate methods for the measurement and calculation of doses from radioactive particulates (hot particles). This was to be achieved by constructing standard, well defined radioactive test sources of Co-60 and Tm-170 in order to allow parallel measurements and calculations to be compared. The initial measurement techniques of extrapolation chamber (EC) and radiochromic dye film (RDF) were extended to include thermoluminescence dosimetry (TLD). The results of the various measuring laboratories (Berkeley, Grenoble & Montpellier) were to be combined and compared with calculations based on a Monte Carlo code (Tolouse) and a semi empirical PC programme VARSKIN. A high dose rate Co-60 particle was to be produced for dosimetry and radiobiological studies. A high resolution micro-densitometer was to be computer automated at Berkeley/Birmingham to utilise radiochromic dye films for hot particle dosimetry. Because of interest in this subject in the USA the project was extended to initiate a collaborative EU/US intercomparison/validation dosimetry programme including Brookhaven National Laboratory (BNL), the National Institute of Standards & Technology (Washington DC), Richland Battelle Laboratories and Yankee Atomic. The preparation of other radioactive test sources was also initiated.

III. Progress achieved including publications

PRODUCTION OF HOT PARTICLE TEST SOURCES

A series of test hot particle sources has been produced by neutron activation of spherical cobalt containing particles and pure thulium cylindrical discs individually mounted on an aluminium support and covered by a 15 μm thick aluminium window. Initial cobalt sources were 200 µm diameter with a ^{60}Co activity of 8 x 10^5 Bq. The ^{170}Tm cylinders, 400 µm diameter and 100 µm thick, had an activity of 10^6 Bq. The cobalt sources were surrounded by air, and secured with a thin layer of glue. For some calculations the surrounding air was replaced with unit density material to investigate the effect of thicker glue layers and potential problems arising from deviations from the ideal design. Higher activity (8 x 10^6 Bq) ^{60} Co sources have also recently been produced for future dosimetry and radiobiology experiments. For the US/CEC intercomparison particles of Sc-46, Yb-175, Tm-170 and Co-60 were produced in collaboration with BNL. All these sources had linear dimensions between 200 and 400 µm and activities of the order of 10^8Bq.

EXTRAPOLATION CHAMBER (EC) MEASUREMENTS

Contact dose rates for both the ^{170}Tm and ^{60} Co sources were measured at Birmingham using an automated Loevinger type extrapolation chamber with interchangeable electrodes of 1, 3, 10 and 30 mm nominal diameter. The chamber was operated in a mode employing seven electrode spacings (at 50 μm intervals for Co and 100 μm intervals for Tm) with the physical starting separation adjusted so that the final electrode spacing was just greater than that at which instability was observed (typically 40-50 μm). The positioning of the sources was critically adjusted and repeat determinations (>5) of the variation in ionisation current with separation were routinely performed. Average values of the current at each separation were fitted to a set of possible extrapolation curves and the most appropriate model selected on the basis of closest conformity with the current best estimate of the instrument scale intercept to correct for the non-linear chamber response observed in such measurements. The EC measurements at CEA Grenoble are described separately in another part of this report. The EC measurements made by Yankee Atomic were carried out with a portable automated chamber with a 1 cm^2 area electrode.

RADIOCHROMIC DYE FILM (RDF) MEASUREMENTS

Contact and depth dose rates have been measured from the various hot particle sources using GAFCHROMIC(TM) type DM1260 dosimetry media which consists of a 6-8 μm thick radiochromic dye layer on a 100 μm thick polyester substrate. When irradiated the colourless monomer undergoes polymerisation yielding a blue coloured polymer exhibiting peak optical absorption near 650 and 600 nm wavelengths. The change in absorbance with absorbed dose is nearly linear over a range from 0.05 to 1.0 kGy. The exposure conditions of the extrapolation chamber measurements were emulated by placing the source in contact with stacks of GAFCHROMIC oriented with the radiation sensitive layer towards the source and covered by a layer of the same aluminised melinex (1.32 mg cm^{-2}) as used for the extrapolation chamber window. The limited dynamic range of the GAFCHROMIC was extended by exposing a number of stacks for different time periods.

Samples of GAFCHROMIC from the same batch were calibrated using ^{60}Co gamma rays and $^{90}Sr/^{90}Y$ beta particles at the National Institute of Standards and Technology (NIST), an ionometrically calibrated 420 kVp X-ray beam at Berkeley Technology Centre and a Co-60 radiotherapy facility at the Churchill Hospital, Oxford. Films were read out at NIST using a Scanning Laser Densitometer and at Birmingham using a Joyce-Loebl MDM 6 scanning microdensitometer (an object plane flat bed scanner using focussed tungsten halogen illumination). Absorbance values in each film were converted to absorbed dose rate using the exposure time and calibration curves, and manipulated to provide estimates of the mean dose rates averaged over various areas including those corresponding to the extrapolation chamber electrodes as previously described.

THERMOLUMINESCENCE DOSIMETRY (TLD)

TLD measurements of dose rates from a Co-60 hot particle source were made at CEA Grenoble using 0.4 mm thick carbon loaded LiF/teflon dosemeters and at Montpellier using scanning laser heating of 50 µm thick $CaSO_4$ on 50 µm kapton tape. The detailed results are described separately in another part of this report. At Birmingham TLD was used to measure depth doses from an extended plane source of ^{147}Pm using ultra thin LiF/teflon discs (utTLD) 70 µm thick of mass thickness 13 $mgcm^{-2}$.

COMPARISON BETWEEN MEASUREMENTS AND CODE PREDICTIONS

The measured doses to date have been compared with the predictions of the latest version of the analytic VARSKIN code (VARSKIN MOD2, developed at Battelle labs by Durham) and the Monte Carlo codes developed by Patau *viz;* an adapted version of EGS4 for ^{170}Tm and the HOT series of codes specially developed for ^{60}Co.

Comparisons of measurements and calculations for ^{60}Co are shown in Figure 1a. Direct comparison between the measurements and predictions for the ^{60}Co source is complicated by the gamma component which has not as yet been incorporated into HOT and is only normally evaluated for 1 cm^2 averaging area by VARSKIN MOD2. The latter uses the model of Lantz and Lambert which simply postulates a point source separated from the target region by tissue equivalent material and incorporates a correction for lack of charged particle equilibrium. Extension of this model to averaging areas other than 1 cm^2 has been made and the results incorporated in Figure 1a together with beta dose estimates predicted by VARSKIN and the HOT Monte Carlo codes.

The total dose predictions from VARSKIN MOD2 generally fall significantly below the measured values, underestimating by 60% to 80%, except for the small extrapolation chamber and large GAFCHROMIC averaging areas where the largest measurement uncertainties would be expected. Some underestimation might be expected from VARSKIN in view of the potentially increased contribution of

backscatter from the aluminium mounting relative to the tissue postulated in the VARSKIN model. This should however have been correctly taken into account in the Monte Carlo code and the large discrepancy between the HOT and VARSKIN beta dose estimates for the small averaging areas presently remains unresolved. The sensitivity of the HOT code to modifications in source design are show in Figure 1b. Calculations which vary the density of the material in which the particle is embedded and which vary the thickness of elemental volumes over which the dose is calculated (1 µm or 10 µm) produce only minor changes in calculated doses. It is now considered that the problem arises from the inability of current Monte Carlo codes to satisfactorily transport low energy electrons below 30 keV. Such electrons form a significant part of the low energy spectrum for low energy beta emitters such as Co-60. The development of improved codes and their validation is to be the subject of a further collaborative EU research project.

TLD measurements of dose distributions from the Co-60 hot particle source have been made at Grenoble using carbon loaded LiF/teflon and at Montpellier using Laser heating of 50 µm thick $CaSO_4$ on 50 µm kapton tape. These measurements are described in more detail in the report of the relevant groups in another part of this report. The HOT code, which simulates the carbon loaded TL dosemeters, considerably under-estimates the measured doses (a factor of 7 at depths of 70 µm). Earlier measurements by the Birmingham group had found indications of unresolved differences between extrapolation chamber and TL measurements for ^{147}Pm so it was decided to carry out a comparison of the different dosimetric techniques for a simpler plane geometry. Figure 2 shows excellent agreement between the depth doses for EC, RDF and utTLD for a large area plane ^{147}Pm source. The significant difference between carbon loaded TLD measurements and the HOT code calculations may thus arise from code limitations or from problems of calibration for the highly non-uniform exposure from hot particle measurements. The laser heating measurements were extremely successful in that they provided good agreement with the two dimensional (radial) dose distributions from RDF, to within a factor of 2. The high sensitivity makes this an important potential method of hot particle dosimetry. However, the relatively thick and non-tissue equivalent dosimetric materials which are currently used make it difficult to derive detailed depth dose data for comparison with other dosimetric techniques and with calculations.

Comparisons of measurements and calculations for ^{170}Tm are shown in figure 1c. The agreement between the VARSKIN MOD2 and the EGS4 beta dose estimates is good, with the ratio EGS4/VARSKIN ranging from about 0.87 to 1.03 as the averaging area is increased. The extrapolation chamber values increase from 72% of the predicted value for the 1 mm electrode to approximately 150% of the predicted values for the 10 mm and 30 mm electrodes. Inclusion of the Auger and internal conversion electrons in VARSKIN MOD2 using the method recommended however seems to merely scale the predicted dose rates by the energy emission ratio of approximately 1.6. This is obviously incorrect since the contribution, in view of the low energies involved, will be small. This problem can be overcome by using the individual Auger electron energies and intensities and treating them as monoenergetic sources within VARSKIN.

EU/US INTERCOMPARISON

This intercomparison programme was only initiated during the final contract phase but has shown very good agreement between RDF and EC measurements made at 3 laboratories for all hot particle sources (figure3). The measurements generated considerable isodose data, giving radial doses, depth doses and doses averaged over various areas and depths. This will provide a useful test of calculational methods in due course. Some TLD and exoelectron measurements were made but the data is still preliminary at this stage.

CONCLUSIONS

Validation of computer codes used to predict beta doses from hot particles has been attempted by the direct measurement of doses from model sources, using

both automated extrapolation chambers (EC), radiochromic dye film (RDF) and thermoluminescence dosimetry (TLD). The measured values for EC and RDF are in reasonable agreement with the VARSKIN MOD 2 and EGS4 Code predictions for ^{170}Tm. For ^{60}Co the EC and RDF measurements are in reasonable agreement but the VARSKIN MOD 2 code provides significant under-estimates of the total dose. The 'HOT' Monte Carlo code provides significantly lower estimates than the VARSKIN values. TLD measurements have not yet provided satisfactory information for comparison with EC or RDF but have underlined problems with the Monte Carlo code calculations for ^{60}Co and have indicated considerable promise for rapid evaluation of isodose information using focused laser heating. Good agreement has been found for EC and RDF in a EU/US trans-atlantic intercomparison for a range of hot particle studies. Future Work should

1. Extend the intercomparison and validation programme from the currently achieved Co-60 study to include other sources such as Tm-170, and Ru/Rh-106 to cover the whole energy range relevant to radiobiolgy, medicine and the nuclear industry.
2. Develop improved Monte Carlo codes for the transport of low energy electrons relevant to beta emitters such as Co-60 which are of importance in the nuclear industry.
3. Further develop rapid, sensitive TLD techniques, such as scanning laser heating, for hot particle and related dosimetry applications.

PUBLICATIONS

Darley, P. J., Charles, M. W., Hart, C. D., Wells, J., and Coleby, M. S. E. Dosimetry of planar and punctiform beta sources using an automated extrapolation chamber and radiochromic dye films. Radiat. Prot. Dosim. 39(1/3), 61-66, 1991.

Patau, J. P. Monte Carlo calculations of the depth-dose distribution in skin contaminated by hot particles. Radiat. Prot. Dosim., 39(1/3), 71-74, 1991.

Darley P. J, Charles M. W, & Hart C. D. Validation of theoretical models for calculating doses from Hot particles. Proceedings of the 17th IRPA Regional Congress on Radiological Protection, June 1994. Nuclear Technology Publishing. Pages 153-156.

Charles M. W, Hot particles - are they still a problem? Meeting of the Association for Radiation research, Dublin, June 1994. Abstract to appear in the International Journal of Radiation Biology.

150. International hot-particle dosimetry intercomparison. J. Baum, D. Kaurin, P.J. Darley, M.W. Charles et al. International Congress on Radiation Protection, April 1996, Vienna.

133. Beta Dosimetry for Radiation Protection, 1995 (In press)
J. Bohm, M. W. Charles, W. G.. Cross, E. Piesch & S. Seltzer. Report of the International Commission on Radiation Quantities and Units (ICRU)

Figure 1a

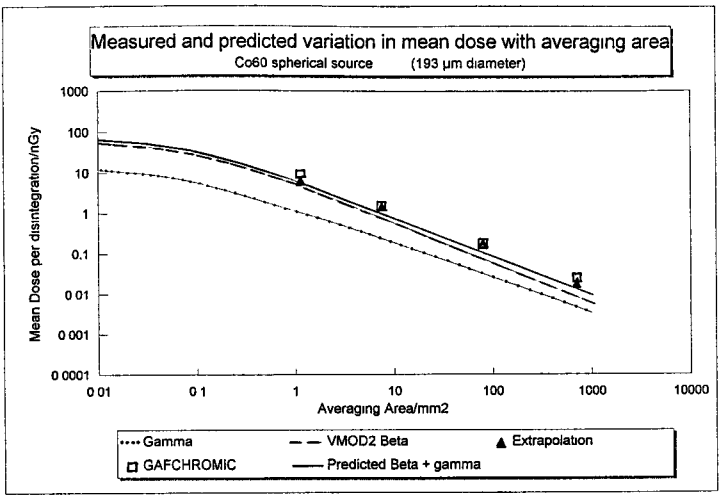

Figure 1b

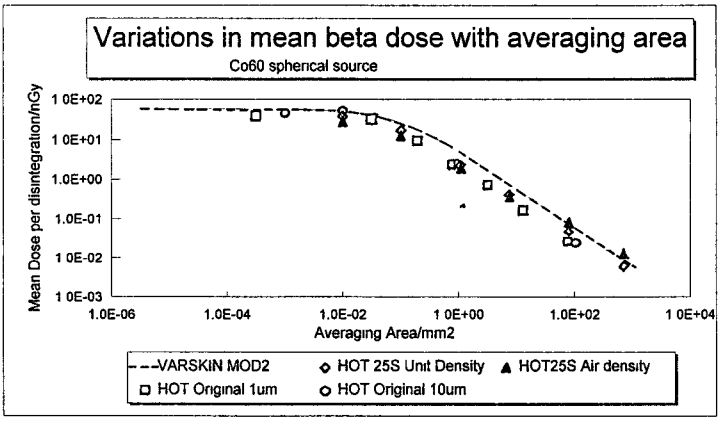

Figure 1c

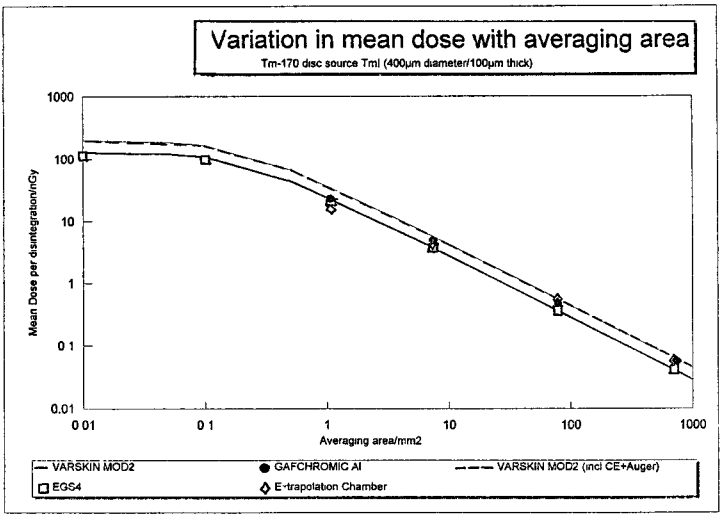

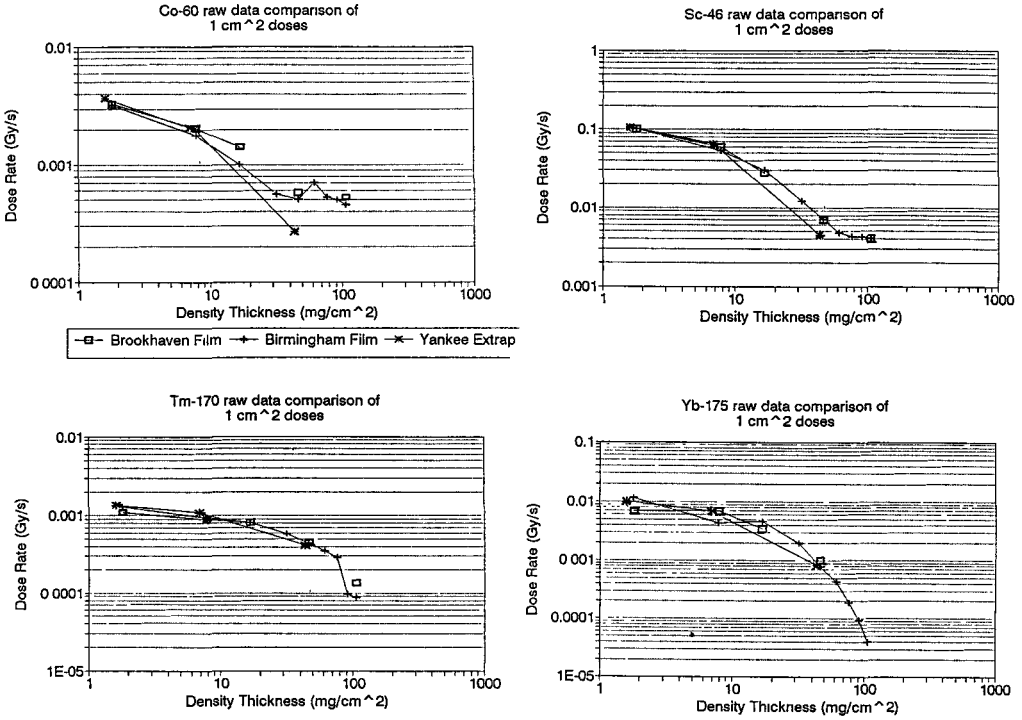

Figure 3

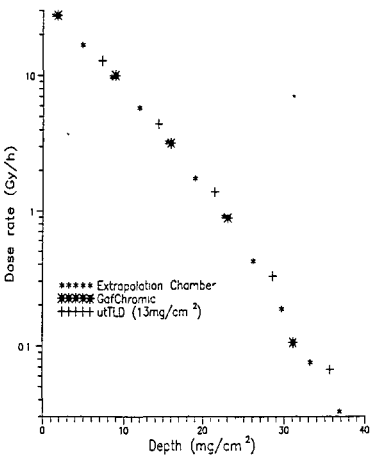

Depth dose distribution from ^{147}Pm in Kapton using extrapolation, chamber, GafChromic™ and utTLD (13mg/cm²)

Figure 2

Head of project 9: Dr. Olko

II. Objectives for the reporting period

The general scope of our project was to investigate and optimize properties of the self-developed high-sensitive LiF:Mg,Cu,P thermoluminescent material and to apply this phosphor to construct ultra-thin TL detectors for beta-electrons and low-energy X-rays. In the frame of this goal the following tasks were undertaken:

- development of TL detectors with a thin active layer of LiF:Mg,Cu,P for skin dosimetry
- testing the dosimetric properties of thin layer detectors
- investigation of relative TL efficiency of LiF:Mg,Cu, P for low and high-LET radiations
- development of microdosimetric model to explain the LiF:Mg,Cu,P TL detector response for radiations of different LET

III. Progress achieved including publications

Ultra-sensitive lithium fluoride activated with magnesium, copper and phosphor is particularly useful for dosimetry of photon and electron fields: it is over 30 times more sensitive than conventional TLD-100 and it is tissue-equivalent with regard to photons showing flat photon energy response (-15% +5% for energy range 20-2000 keV). An original technology for production of sintered LiF:Mg,Cu,P pellets with standard thickness of 0.9 mm was developed at the Institute of Nuclear Physics in Kraków, Poland at the end of the 'eighties. However, such thick detectors are not suitable for skin dosimetry as they underestimate skin doses in mixed radiation fields with a contribution of low-penetrating radiations. In addition, the variation of the response of LiF:Mg,Cu,P detectors for radiations with different LET is much stronger than that for LiF:Mg,Ti (TLD-100) detectors, which had not been yet explained theoretically.

In the following sections of this report results of theoretical and experimental investigation of LiF:Mg,Cu,P TL detectors will be presented which fulfill the main scopes proposed in the project:

1. Development of TL detectors with a thin active layer of LiF:Mg,Cu,P for skin dosimetry.

LiF:Mg,Cu,P thermoluminescent phosphor is obtained in form of solid pellets as a result of the following production stages:

- synthesis of LiCl or LiOH and HF into LiF
- activation with Mg, Cu and P at high temperature (1050°C)
- mechanical operations on activated LiF powder (crushing, sieving)
- pill pressing
- sintering pressed pills at an elevated temperature

During the project the two most important stages: activation and sintering have been improved and optimized. Special high-temperature furnaces with exchangeable platinum crucibles were constructed. The process of activation takes place at a high temperature, whereby Mg, Cu and P activators enter the volume of liquid LiF, and is highly sensitive to many factors, such as temperature, period of activation and neutral gas (argon) flow rate. Special stands allowing these parameters to be carefully and reproducibly controlled, were constructed.

Thermoluminescent detectors with a standard thickness of 0.9 mm may seriously underestimate personal skin doses which are defined at the depth of 7 mg cm^{-2}. Solid, sintered detectors thinner than 0.5 mm are mechanically unstable. Therefore, a new type of detector (named MCP-Ns) has been developed at INP to fulfill simultaneously the requirements of mechanical stability, flat energy response for beta-rays and the ability to measure low beta-ray doses. 8.5 mg/cm^2 active layer of LiF:Mg,Cu,P phosphor was bonded with a 0.8 mm-thick base of undoped lithium fluoride. This pure LiF was mixed with 4% graphite (by weight) to eliminate any spurious luminescence. MCP-Ns detectors are mechanically stable and the non-thermoluminescent base does not change their photon-energy response.

Using the present manufacturing technique, uniform batches of up to 500 MCP-Ns detectors (of 1 SD sensitivity spread in the range 4-6 % per batch) can be obtained in a consistently repeatable manner. Each participant of the CEC contract received free 30 (or more, if requested) pellets of MCP-Ns detectors.

For production of thick pellets applied e.g. for gamma-ray dosimetry a standard dopant composition is usually applied (1.25 % of P, 0.05% of Cu and 0.2% of Mg). This composition was applied in INP since 1988, relaying on results of preliminary experiments and literature studies. However, it was found that the same TL active phosphor with the dopant composition specified above when applied to thin layer detectors yielded much lower sensitivity than that predicted from the layer thickness. In addition, high-temperature peaks in TL glow-curves occur, which disturb the proper dose evaluation. Therefore, systematic studies of LiF:Mg,Cu,P glow curve structure and sensitivity were undertaken with regard to dopant composition. More than 100 samples with different dopant composition were prepared and investigated. It was possible to improve the glow-curve structure by increasing the concentration of Cu to 0.2% in the LiF:Mg,Cu,P phosphor applied in the thin layer (see Fig. 1). The reason for this is probably a high-temperature diffusion of Cu ions from the thin layer to the non-thermoluminescent LiF base.

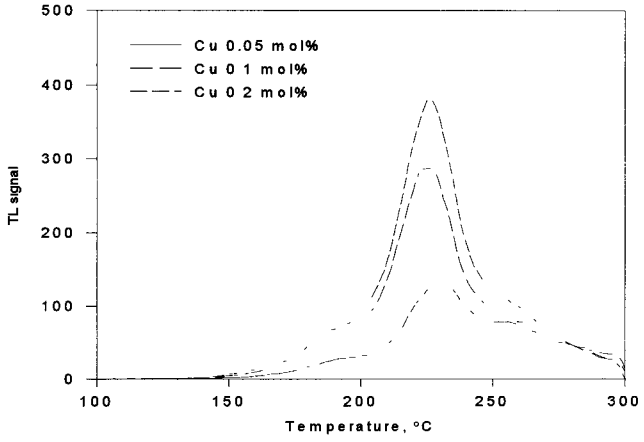

Fig. 1.
Comparison of TL glow curves of MCP-Ns detectors with different Cu concentration in the active layer.

2. Testing of dosimetric properties of thin layer detectors

The advantages of thin layer LiF:Mg,Cu,P detectors (MCP-Ns) for dosimetry of beta and low-energy photon radiations has been fully confirmed during experimental investigations:

2.1 Dose limits and sensitivity

Due to the high-sensitivity of LiF:Mg,Cu,P phosphor, MCP-Ns detectors were found to be suitable for measuring radiation doses at the μSv range. The main properties of the detector, obtained after investigations with Cs-137 gamma-rays, are listed in Table 1.

Table 1
Basic dosimetric properties of thin-layer MCP-Ns detectors

Photon response relative to TLD-700		1.28
Detection threshold [μSv]		3
Zero-dose signal [μSv]		4
Standard deviation % at doses:	10μSv	4.8
	50μSv	5.4
	1mSv	0.5

2.2. Energy response for beta electrons

The energy response of MCP-Ns detectors was investigated for ^{147}Pm, ^{204}Tl and $^{90}Sr/^{90}Y$ beta-electrons and ^{137}Cs photons. Thin detectors were exposed together with

standard TLD-700 pellets of 0.9 mm thickness. Detector response to beta-electron doses was studied after covering the detector with polyethylene foils of thickness: 1.1, 2.1, 3.7, 6.9 and 7.7 mg cm^{-2}. MCP-Ns demonstrates a much flatter energy response than TLD-700. MCP-Ns detectors measure accurately doses for $^{90}Sr/^{90}Y$ and ^{204}Tl beta-rays independently of foil thickness. For ^{147}Pm beta electrons the detector response depends strongly on foil thickness. Our results indicate that the optimum cover foil thickness is about 2 mg cm^{-2}. The overresponse without covering foil is intentional, as in practice a detector is never used without covering foil in a dosimeter holder.

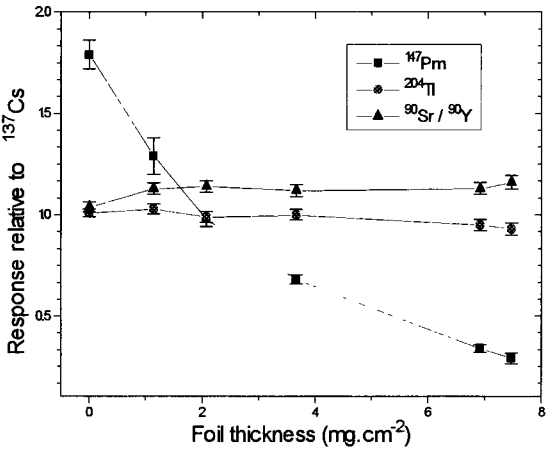

Fig.2.
Beta response relative to ^{137}Cs of thin LiF:Mg,Cu,P as a function of thickness of covering foil.

2.3 Angular response

Measurements of angular dependence of the detector response were performed at angles of incidence of 0°, 20°, 40° and 60° without and with 2.1 mg cm-2 covering foil. The angular response of the MCP-Ns detectors, characterized as the ratio of response for beta and Cs-137 radiations, averaged over incident angles between 0° and 60°, is lower than the required 15%.

Table 2
Values of relative beta/^{137}Cs response ratio $R_{\beta\gamma}$ for thin LiF:Mg,Cu,P averaged over incident radiation angles of 0°, 20°, 40° and 60° for ^{147}Pm, ^{204}Tl and $^{90}Sr/^{90}Y$ beta sources.

Irradiation conditions	$^{90}Sr/^{90}Y$	^{204}TL	^{147}Pm
bare detectors	1.00±0.02	1.00±0.03	1.02±0.07
detectors covered with 2.1 mg.cm^{-2} foil	0.98±0.01	0.97±0.02	1.01±0.05

2.4 Comparison of thin layer detectors from Risoe National Laboratory and INP

At Riso National Laboratory beta-electron detectors were prepared by bonding LiF:Mg,Cu,P powder onto a Kapton tape, fixed to 0.7 mm thick Al pieces. Two types of LiF:Mg,Cu,P powders were used in preparation: GR-200 from China and a standard MCP-N dosimetric powder (grain below 20 μm) from the Institute of Nuclear Physics. Similar detector devices were also prepared from the thin GR-200 kapton detectors developed at Solid State Detector Laboratory, Beijing , China. Dosimetric properties of these detectors have been compared with MCP-Ns sintered pellets such as reproducibility (see Fig.4), energy response and angular response.

To test the stability of the response after series of annealing/reading cycles the following experiment was performed at INP and Riso. Groups of detectors were annealed, irradiated with gamma rays and read out. The test dose used was 5 mGy at INP and 10 mGy at Riso. The same procedure was repeated 15 times. Results are showed in Fig.3 in terms of relative response normalised to that of the first read-out. It should be mentioned that between each measurement at Riso the detectors were used for an other measurement, so these results cover in total 30 consecutive re-uses. Both detector types exhibit a small decrease of the response, specially in first 5÷7 cycles, but all results lay within an interval of 6% around average value.

Results of all experiments demonstrate that both type of detectors could be well applied in personal beta-dosimetry.

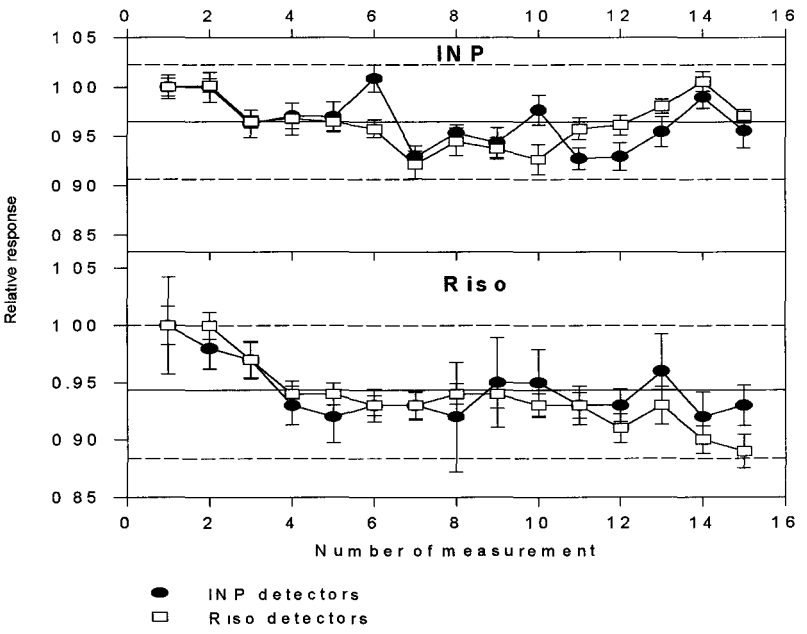

Fig. 4
Photon response in series of re-use cycles, measured at INP and Riso. Values are normalised to that of the first readout. (●) MCP-N, (□) GR-200.

3. Investigation of relative TL efficiency of LiF:Mg,Cu, P for low and high-LET radiations

LiF:Mg,Cu,P detectors show an anomalously low photon energy response for photons with energies lower than 150 keV, as compared with LiF:Mg,Ti (see Fig.3).

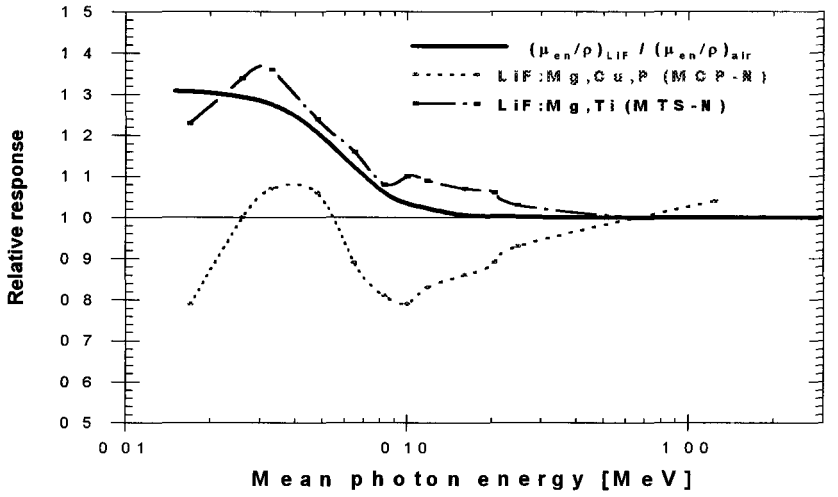

Fig.3.
Comparison of photon energy response of standard LiF:Mg,Ti and high-sensitive LiF:Mg,Cu,P TL detectors.

This phenomenon has been explained as a microdosimetric effect. The thermoluminescence efficiency of LiF:Mg,Cu,P shows such a strong dependence on radiation ionization density (LET) that even a slight change of photon LET results in a clear change of the detector response. Thus, a local minimum of TL efficiency observed for 100 keV photons corresponds to the local maximum of photon LET. A similar photon energy response with a local minimum in photon energy response for 100 keV was measured for BeO TSEE detectors. Both examples tend to show that the photon energy response of TL detectors is determined not only by the effective atomic number of a detector, Z_{eff}, but also by the intrisinic efficiency of this detector to convert energy of radiations with different LET.

Therefore, systematic investigations of LiF:Mg,Cu,P TL efficiency were performed in order to gather experimental data over a broad spectrum on radiations. The thermoluminescence efficiency, η, of LiF:Mg,Cu,P (MCP-N) detectors), relative to 662 keV Cs-137 gamma rays, has been measured for (i) 1250 keV Co-60 gamma-rays, (ii) filtered X-ray beams of average energies in the range 15 - 300 kVp , (iii) Pm-147 beta-electrons, (iv) thermal neutrons and (v) stopping alpha-particles of initial energies in the range 0.5 - 5 MeV. A rapid decrease of TL efficiency with decreasing mean photon energy from $\eta=1.04 \pm 0.02$ for Co-60, $\eta=0.93 \pm 0.02$ for 300 kVp X-rays to $\eta=0.59 \pm 0.016$ for 15 kVp X-rays was observed. The measured value of relative efficiency for Pm-147 beta-electrons was $\eta=0.90 \pm$

0.02. The relative efficiency for alpha particles decreased from $\eta=0.06 \pm 0.004$ to $\eta=0.03 \pm 0.007$ for particles of initial energies of 5 MeV and 1 MeV, respectively. The measured response of MCP-N detectors after doses of thermal neutrons was equal to $0.72\ 10^{10}$ Gy $n^{-1}cm^2$, which corresponds to $\eta=0.10 \pm 0.01$. The efficiency for 2.73 MeV ^3H tritons was found to be $\eta = 0.155 \pm 0.02$.

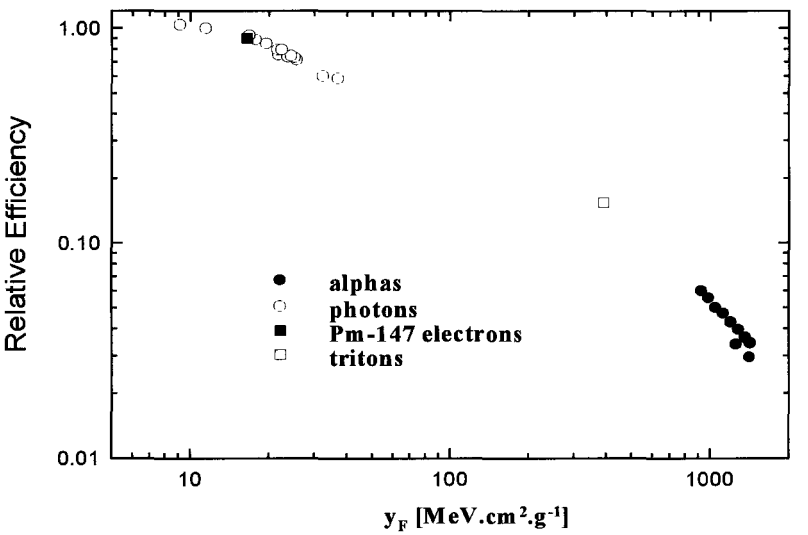

Fig.5.
Relative TL efficiency of alphas, photons, electrons and tritons versus mean lineal energy.

4. Development of a microdosimetric model to explain the response of LiF:Mg,Cu,P TL detectors to radiations of different LET

Several models of thermoluminescence (TL) have been proposed in the last 30 years to explain the phenomena of supralinearity, saturation of TL response or the dependence of TL efficiency of LiF:Mg,Ti (TLD-100) detectors on LET. A new generation of lithium fluoride TL detectors, activated with magnesium, copper and phosphor (LiF:Mg,Cu,P), show quite different dosimetric properties: they saturate at high doses with no supralinearity and their TL efficiency decreases even more rapidly with ionization density, showing an anomalously low response for photon energies below 100 keV. In all presently applied models no explanation is offered for the observed variation of TL efficiency of LiF:Mg,Cu,P one-hit detector for photons or electrons of different energies

Experimental data, obtained at INP, Kraków, Poland (see Section 3) were analyzed using a one-hit microdosimetric model which allows the value of relative TL efficiency, η, to be interpreted for a broad spectrum of radiations, including weakly ionizing modalities. Microdosimetric distributions applied in model calculations were obtained for photons, beta-electrons, tritons and alpha-particles from calculations using MOCA-8, MOCA-14 and TRION Monte Carlo track structure codes (see Fig. 5). of thermoluminescence where it is assumed that distribution of ionization due to a low-LET radiation can be treated as uniform. The marked decrease of η for weakly ionizing radiations is still explained by the saturation of TL response in a small (24 nm diameter) sensitive site in LiF:Mg,Cu,P. This target size cannot be directly connected to any particular structure in the detector and should rather be treated as an indication of the dimensions of the volume over which the entire TL mechanism takes place.

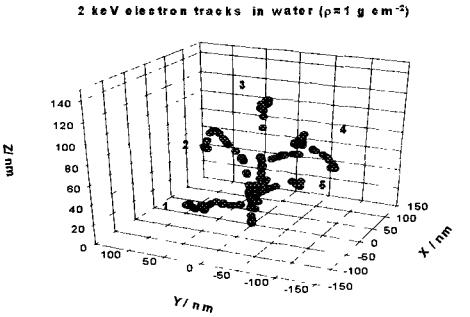

Fig. 5
2 keV electron tracks in water simulated with MOCA-8 electron code

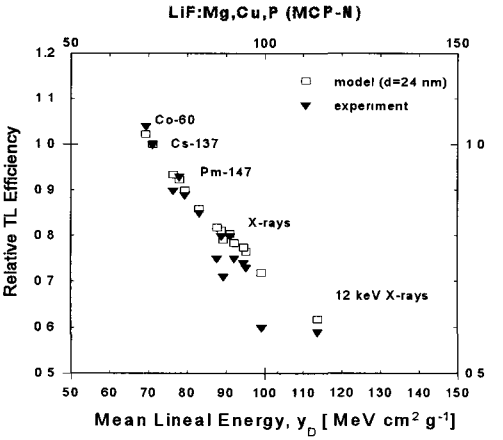

Fig. 6.
Comparison of measured and calculated, with one-hit microdosimetric model, relative TL efficiency of LiF:Mg,Cu,P detectors

PUBLICATIONS RESULTING FROM THE PROJECT

1. Bilski, P., Olko,P., Burgkhardt, B., Piesch, E. and Waligórski, M.P.R. *Thermoluminescence Efficiency of LiF:Mg,Cu,P (MCP-N) Detectors to Photons, Beta Electrons, Alpha Particles and Thermal Neutrons.* Radiat. Prot. Dosim. **55**, 31-38 (1994)

2. Bilski, B., Olko, P., Burgkhardt, B., and Piesch, E. *Ultra-Thin LiF:Mg,Cu,P Detectors for Beta Dosimetry.* accepted to publication in Radiat. Measur. (1995)

3. A.J.J. Bos, K. Meijvogel, P. Bilski and P. Olko *Thermoluminescent Properties of LiF:Mg,Cu,P with Different Cu Concentrations.* submitted to Radiat. Prot. Dosim. (1995)

4. Bilski, P., Budzanowski, M., Olko, P. *A Systematic Evaluation of the Dependence of Glow-Curve Structure on Dopant Concentration in LiF:Mg,Cu,P.* submitted to Radiat. Prot. Dosim. (1995)

5. Bilski, P., Budzanowski M., Olko P. and Christensen, P. *Properties of Different Thin -Layer LiF:Mg,Cu,P TL detectors for Beta Dosimetry.* submitted to Radiat. Prot. Dosim. (1995)

6. Olko, P. *Microdosimetric Interpretation of Thermoluminecsent Efficiency of LiF:Mg,Cu,P (MCP-N) Detectors for Weakly and Densely Ionizing Radiation.* submitted to Radiat. Prot. Dosim. (1995)

Head of project 10: Dr. Uchrin

II. Objectives for the reporting period

The main objectives of the work were: investigation and development techniques and procedures used for measurements of beta radiation fields and to study solid state detectors for skin dosimetry. Works were focused on design and production of new extended area beta sources having nearly tissue equivalent conditions, investigation of the main characteristics of beta sources such as radiation field homogeneity, beta and bremsstrahlung spectra and dose-rates. An extrapolation ionization chamber has been constructed and used for dose-rate determination. An experimental set-up for TSEE measurements has been performed utilizing proportional counter. TL and TSEE characteristics of different dosimetric materials have been investigated in order to use them for skin dosimetry purposes.

III. Progress achieved including publications.

1. Beta sources commonly used for calibration in most cases consist of radioactive materials mounted into or rolled into metal surfaces. In order to simulate conditions existing in case of skin surface contaminations or contaminations on low atomic number materials extended area beta sources were designed and constructed. The series of generally used calibration sources, ^{147}Pm, ^{204}Tl and $^{90}Sr/^{90}Y$, were extended with a $^{106}Ru/^{106}Rh$ source of which maximum beta energy is 3.5 MeV allowing to investigate the energy dependence of TL detectors at higher energy which might have significance in practical situations such as monitoring radiation fields within nuclear reactors.

The active diameter of new beta sources are identical to that of the Amersham produced extended area beta sources allowing investigation sources being different only in their encapsulation. The main features of these sources are: active spots 3-4 mm in diameter are deposited and dryed on a 0.2 mm thick tissue equivalent adhesive material (tesaprint) and this is mounted on a PMMA holder. The number of active spots are approximately 70 and the weight of inactive carrier is kept low in the case of $^{106}Ru/^{106}Rh$ these values were: Fe 15.4 μg, Ni 0.44 μg, Cu 0.05 μg and Pb 0.15 μg.

The main parameters of new beta sources together with Amersham extended sources are given in Table 1. The protective cover of the new beta sources are aluminized Mylar, they are very thin, 1.3-3 mg·c,$^{-2}$ and their activity was selected in such a way that dose-rate measurements at 30 cm and 20 cm and irradiation of solid state detectors in 'contact' geometry could be carried out.

Table 1. Main parameters of newly designed and 'old' Amersham extended area beta sources

Radio-nuclide	Type, producer	Holder material	Holder dimensions (mm)	Source dimensions (mm)	Protective cover	Activity 01.07.95 MBq·cm
$^{90}Sr/^{90}Y$	SIC 106 Amersham	silver	ϕ 58 *d 2-3	ϕ 42	Ag foil 50 mg·cm^{-2}	144.5
^{204}Tl	TEC 23 Amersham	silver	ϕ 58 d 2-3	ϕ 42	Ag foil 50 mg·cm^{-2}	39.6
^{147}Pm	PHC 26 Amersham	silver	ϕ 58 d 2-3	ϕ 42	Ag 3 μm+ Pa 2 μm	799.4
$^{106}Ru/^{106}Rh$	OMH-Hungary	PMMA	ϕ 62 d 10	ϕ 42	Al-Mylar 3.0 mg·cm^{-2}	24.5
$^{90}Sr/^{90}Y$	OMH-Hungary	PMMA	ϕ 62 d 10	ϕ 42	Al-Mylar 1.3 mg·cm^{-2}	15.1
^{204}Tl	OMH-Hungary	PMMA	ϕ 62 d 10	ϕ 42	Al-Mylar 1.3 mg·cm^{-2}	31.4
^{147}Pm	OMH-Hungary	PMMA	ϕ 62 d 10	ϕ 42	Al-Mylar 1.3 mg·cm^{-2}	128.0

*d = thickness

2. Homogeneity measurements

Dose-rate homogeneity measurements were carried out with a specially designed scanner in which below an end window GM tube, of diameter 2 mm the source is moved step by step, and row by row automatically. The scale of scanning is 5 mm x 5 mm. The measuring time was selected in such a way that approximately 10^4 pulses were collected for each point. Figure 1 show the homogeneity diagrams of $^{90}Sr/^{90}Y$ and $^{106}Ru/^{106}Rh$ (OMH)

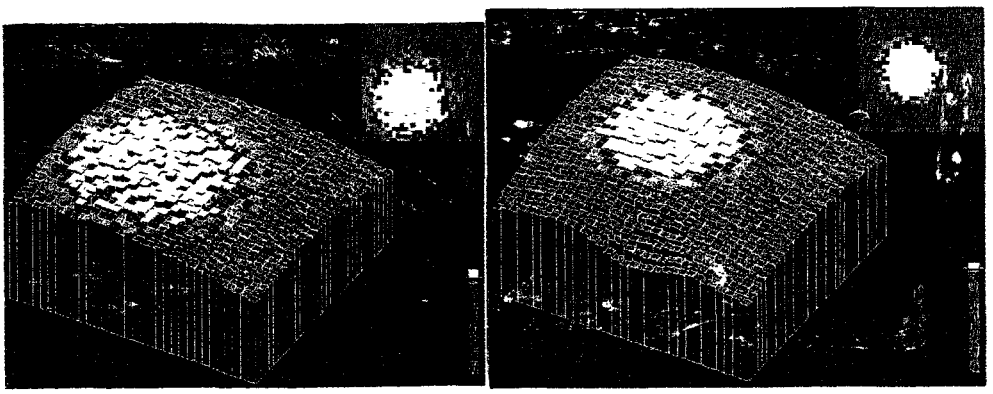

Fig.1. Field homogeneity diagrams

sources. The source-detector distance was 20 cm for ^{147}Pm and 30 cm for the other sources. Measurements have shown that the homogeneity of beta radiation field is letter than ±5 % for a circle of which is diameter 7 cm centered around the vertical axis of the source and for a source to detector distance of 30 cm. The inhomogeneity of radiation field in the case of ^{147}Pm reaches ±10 % for the same circle. The dose rates on a plane facing the source parallel and 30 cm from it drop by 10-12 % if the circle diameter is 10 cm on the plane from the source axis. No beam flattening filters were used during the measurements. Dose-rate homogeneity of Amersham extended beta sources was investigated by Gaf-Chomic foils, in cooperation with W. McLaughlin.

3. Extrapolation ionization chamber

All parts of the chamber are made of materials are in good approximation equivalent to tissue with respect to the transmission and backscattering of beta rays. The chamber consists of a perspex block with graphite surface divided into collecting electrode and guard ring by a groove which is 0.3 mm in width and depth. The main characteristics of extrapolation chamber developed at Institute of Isotopes given in Table 2.

Table 2. Main characteristics of extrapolation chamber

Entrance window	
material	Aluminized Mylar
thickness	1.3 $mg \cdot cm^{-2}$
Collecting electrode	
material	perspex
diameter	16.5 mm
Movable electrode	
between	0-15 mm manually
Filling gas	air
Field strength	20 V/mm

The collecting electrode is surrounded by a PMMA disc 12 cm in diameter and 8 mm thick.

Table 3. Main parameters of flat ionization chambers type ND-1009, OMH

Material of electrodes	perspex and graphite
diameter of limiting diaphragm	12.2 cm
entrance window	
material	Hostaphan
thickness	1 $mg \cdot cm^{-2}$ or 7 $mg \cdot cm^{-2}$
diameter of collecting electrode, variable	1, 3 and 8 cm
volume of collecting electrode, variable	0.15-55 cm^3
electrode separation variable	0.2, 0.4, 0.8 and 1.1. cm

4. Dose-rates measurements

Dose-rates determined by extrapolation chamber and flat ionization chambers were intercalibrated with PTB Beta Secondary Standard $^{90}Sr/^{90}Y$ sources.

The dose-rates determined by extrapolation agreed within ± 2.5 % with the dose-rates of PTB Secondary Beta Standards ($^{90}Sr/^{90}Y$). Dose-rates determined by extrapolation chamber and with appropriate flat ionization chamber did not differ more than ± 3 %, except for the 'contact' geometry where dose-rate from $^{106}Ru/^{106}Rh$ was 6 % less than the value measured by extrapolation chamber.

Absorbed dose rates to tissue at a tissue depth of 1.3 $mg \cdot cm^{-2}$ and 7.8 $mg \cdot cm^{-2}$ $D_t(0.013; 0°)$, $D_t(0.078; 0°)$ were measured at distances 0.7 cm, 5, 10, 15, 20, 30 cm from the sources. Absorbed dose rates to tissue $D_t(0.078; 0°)$ from the new beta sources are given in Table 4.

Table 4. Absorbed dose-rate to tissue at a tissue depth of 7.8 $mg \cdot cm^{-2}$, $D_t(0.078; 0°)$ measured at a distance of 0.7 cm from the source

Source	Dose-rate		Relative dose-rate %	
	$\mu Sv \cdot s^{-1}$	$Sv \cdot s^{-1} \cdot Bq^{-1} \cdot cm^2$	(1)	(2)
^{147}Pm-OMH	842	$9.1 \cdot 10^{-11}$	174	174
^{204}Tl-OMH	577	$2.53 \cdot 10^{-10}$	119	117
^{90}Sr-^{90}Y-OMH	484	$2.22 \cdot 10^{-10}$	100	100
$^{106}Ru/^{106}Rh$-OMH	358	$2.03 \cdot 10^{-10}$	74	70

note: measurements with extrapolation chamber (1) and flat ionization chamber with collecting electrode ϕ10 mm (2)

5. Beta spectra measurements

Energy spectra measurements of the new (OMH) and Amersham extended area beta sources were carried out by a HPGe detector the main parameters of which are:

detector model: GLP 1619S/ID-P, EG and ORTEC
detector active diameter: 16 mm
detector sensitive depth: 10 mm
absorbing layers: Beryllium 0.127 mm
Germanium 0.3 μm
resolution: (FWHM) at 122 keV, ^{57}Co, 482 eV

Beta spectra, unfolded, of ^{204}Tl (OMH), $^{90}Sr/^{90}Y$ (OMH) and $^{106}Ru/^{106}Rh$ (OMH) are given in Fig.5 and Fig.6. Source-detector distance for all cases is 30 cm.

The spectra indicate that due to very thin absorber layer the measured maximum beta energies nearly exactly match the theoretical values of $E_{\beta max}$.

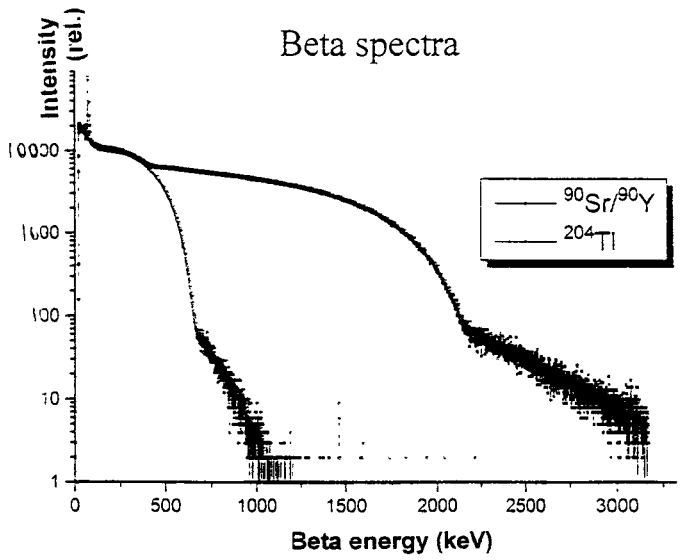

Fig.2. Beta spectra of ^{204}Tl and $^{90}Sr/^{90}Y$ (OMH) sources

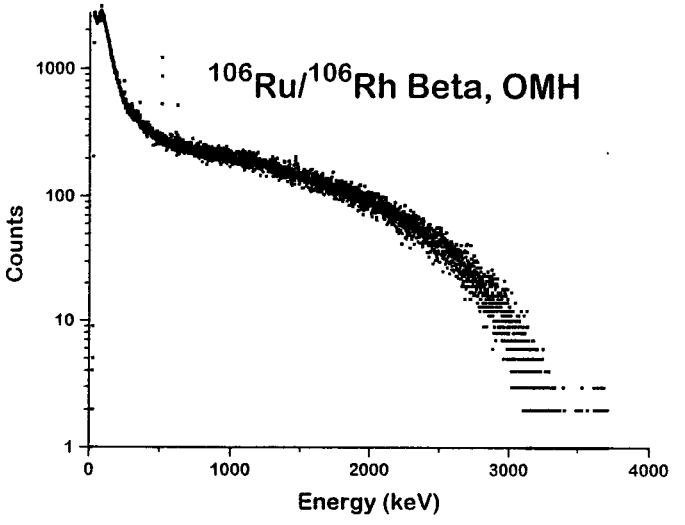

Fig.3.Beta spectrum of $^{106}Ru/^{106}Rh$ (OMH) sources

6. Bremsstrahlung spectra measurements

Bremsstrahlung of all sources listed in Table 1 were recorded using a HPGe detector with the following main parameters:

HPGe model 7229 N	
relative efficiency	10 %
resolution	1.8 keV (FWHM) at 1.33 MeV
detector diameter	46 mm
length	33 mm
active area facing window	16.6 cm^2
window material	Beryllium
thickness	0.5 mm

Bremsstrahlung spectra were recorded in two different geometries. Geometry 1 meant that the source was covered with PMMA thick enough for the full absorption of the beta radiation e.g. 10 mm for ^{147}Pm, ^{204}Tl and $^{90}Sr/^{90}Y$ and 20 mm for $^{106}Ru/^{106}Rh$, respectively. Geometry 2 meant that the sources were covered additionally directly by a lead foil 1 mm thick for all sources except $^{106}Ru/^{106}Rh$ for which the Pb foil is 2 mm thick. Bremsstrahlung unfolded spectra for OMH and Amersham source are shown in Fig.4. Bremsstrahlung spectra were calculated using Monte Carlo method by David Spencer AEA, Harwell for $^{90}Sr/^{90}Y$ and $^{106}Ru/^{106}Rh$ OMH sources which are show in Fig.4. and Fig.5. together with the corresponding measured spectra. Further studies are needed unfolding the measured spectra, calculation and measurement of dose contributions in order to evaluate the significance of bremsstrahlung component.

7. TL and TSEE techniques for skin dose measurements

Different solid state detectors were applied for skin dose measurements. Some parameters of detectors used are given in Table 5.

Table 5. Parameters of solid state detectors used for skin dose measurements

Type	Origin	Size (mm)	Area (cm^2)	Mass per area unit ($mg \cdot cm^2$)
LiF:Mg,Ti	INP Krakow Poland	ϕ4.5x0.6	0.16	135
LiF-MCP-Ns	INP Krakow Poland	ϕ4.5x0.6	0.16	183*
TLD-100 hot pressed chip	Harshaw Bicron	3x3x0.9	0.09	255
LiF+0.85%C cold pressed	Inst.of Isotopes Hungary	ϕ6x0.8	0.28	214

*Of this only 8.5 $mg \cdot cm^{-2}$ surface layer is TL active material

Cold pressed LiF (TLD-100 powder) mixed with graphite, 0.85 % in weight, and BeO, Battelle Institute, Frankfurt were used for TSEE measurements. TL readings were carried out by a Daybreak system utilizing photon counting while for TSEE records a multineedle counter aided with PC, Fontenay-aux-Roses, France, was utilized.

A new TSEE reader were set up modifying the VAZ-530 type WEB Vakutronik proportional counter and using the Daybreak system for heating and data evaluation. Deconculated glow curve of LiF (TLD-100) taken by this reader is shown in Fig.7.

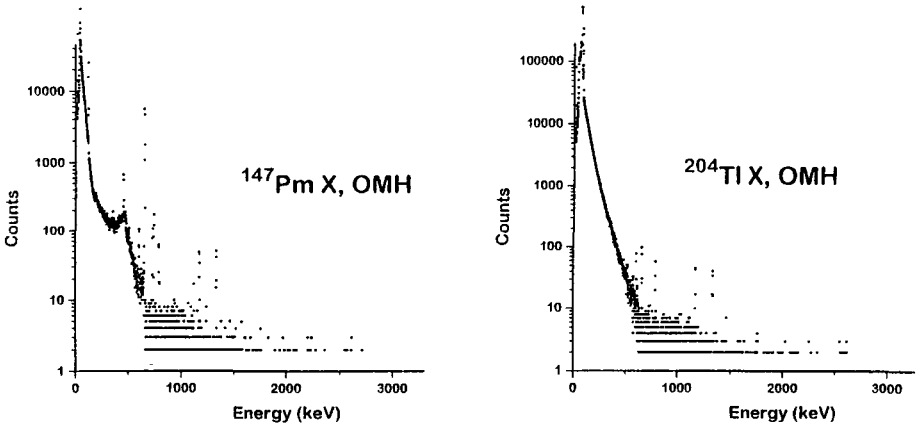

Fig.4. Bremsstrahlung spectra of ^{147}Pm and ^{204}Tl sources

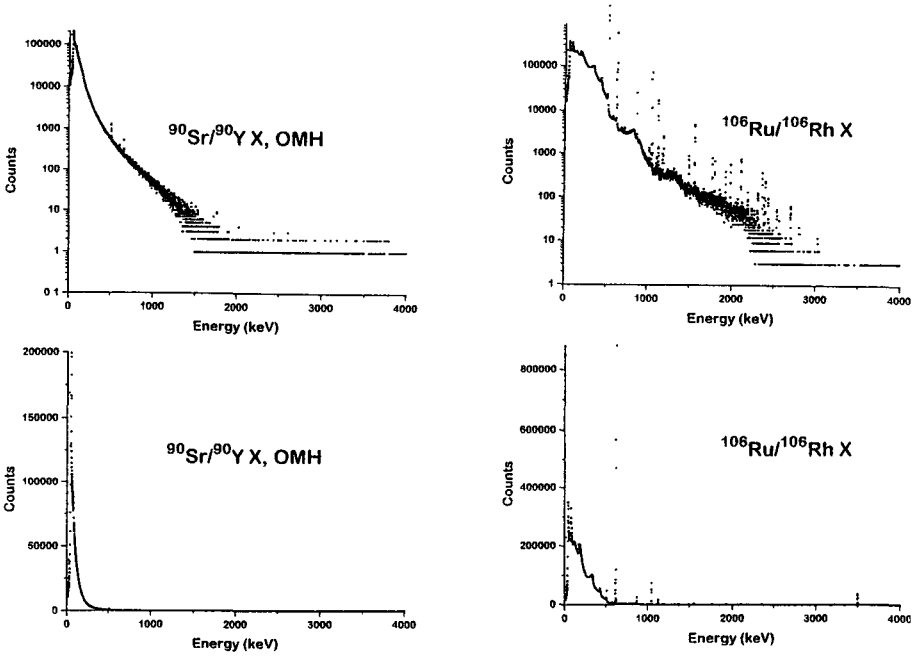

Fig.5. Bremsstrahlung spectra of $^{90}Sr/^{90}Y$ and $^{106}Ru/^{106}Rh$

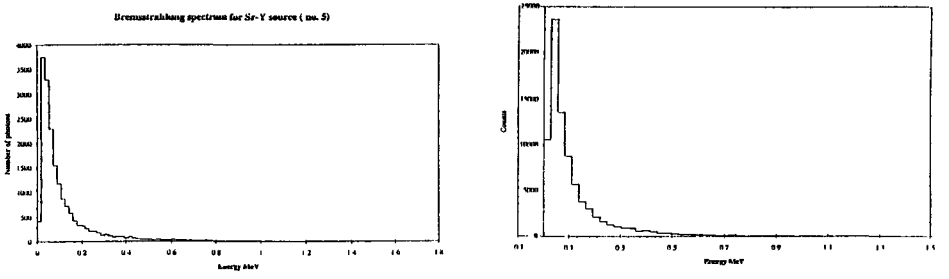

Fig.6. Calculated bremsstrahlung spectra of $^{90}Sr/^{90}Y$ and $^{106}Ru/^{106}Rh$

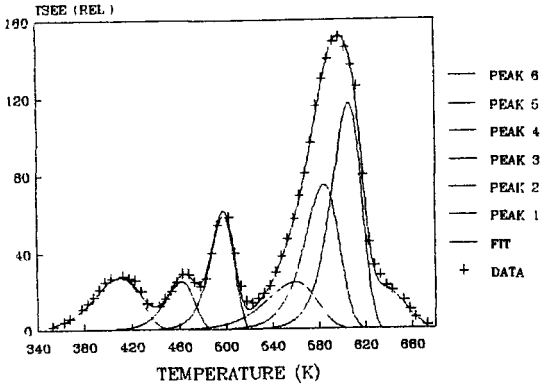

Fig.7. TSEE spectrum of TLD-100 taken by experimental TSEE reader

Detectors were selected such that the batch homogeneity was better than ±3 %. Six dosemeters were irradiated at each time and then read out. Different geometries were used such as 'contact' irradiation (source to detector distance is 0.7 cm). and geometry corresponding to calibration distances i.e. 30 cm

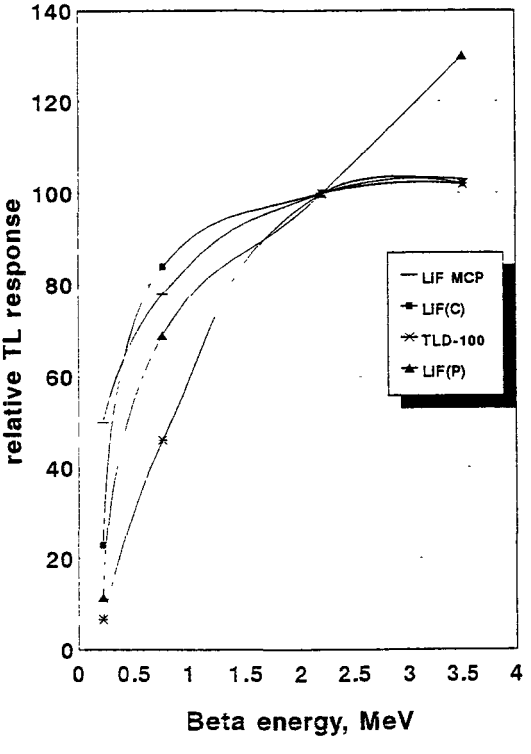

Fig.8. Energy dependence of TL responses-sources OMH

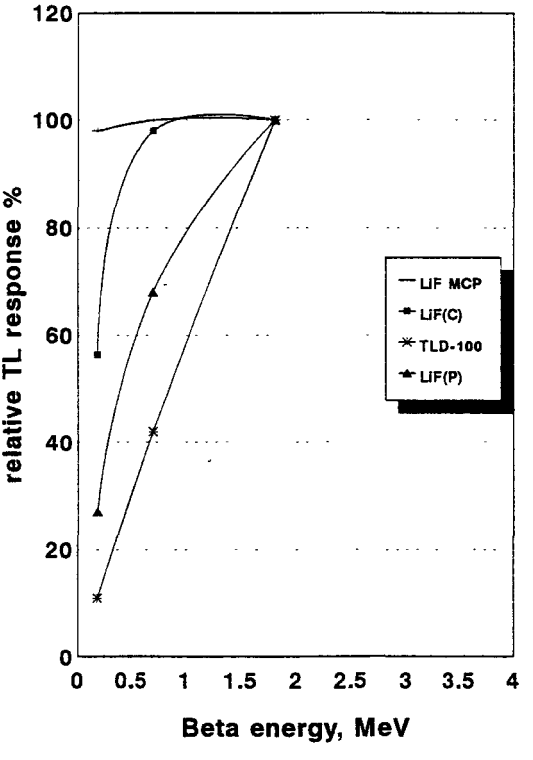

Fig.9. Energy dependence of TL responses-sources Amersham

for $^{90}Sr/^{90}Y$, ^{204}Tl and $^{106}Ru/^{106}Rh$ and 20 cm for ^{147}Pm. Irradiations were repeated ten times and the average responses were calculated. The energy dependence of TL responses for the 'contact' irradiation geometry of the materials listed in Table 5. is illustrated in Fig.8. when the new beta sources were used. Similar data are shown in Fig.9. for the same materials but for irradiations done with Amersham large area extended sources. Nearly energy independent skin dose measurement is achievable if LiF MCP-Ns or LiF(C) is used and proper entrance window thicknesses are selected.

A sandwich type configuration was tested in order to yield information on beta energy of the radiation. Two detectors in a stack geometry were exposed and then evaluated. Only LiF MCP-Ns and LiF(C) were applied. The relative TL response ratios vs beta maximum energy are shown in Fig.10. If a sandwich type configuration is used to construct the dosemeter not only $D_t(0.07, \alpha)$ can be measured nearly energy independently but also the energy of the radiation is easily estimated.

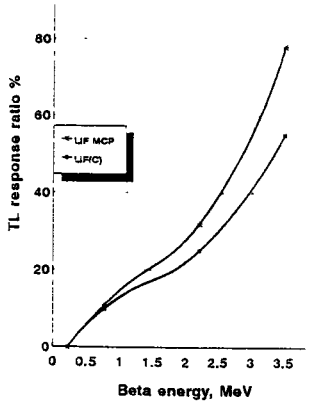

Fig.9. Energy dependence of TL responses ratios of a sandwich type detector arrangement

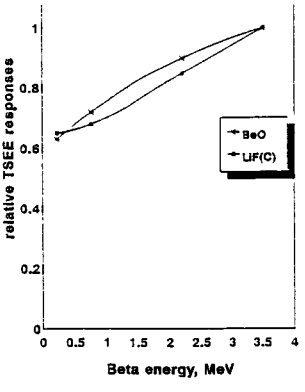

Fig.10. Energy dependence of two TSEE detectors

TSEE measurements

BeO and LiF(C) irradiated with new beta sources were red out and TSEE responses evaluated. The energy dependence of TSEE responses of these two detectors is shown in Fig.11.

TL and TSEE measurements carried out showed that real dosemeters for skin dose determination are available and

sensitivities offered by different techniques are high enough to follow up easily and fast a skin surface contamination. Sensitivities of methods applied are given in Table 6.

Table 6. Sensitivities of TL and TSEE method to follow up surface contamination

Method	Detector	Dose-rate	Surface contamination
TSEE	BeO	4 $nSv \cdot s^{-1}$	20 $Bq \cdot cm^{-2}$
	LiF(C)	5 $\mu Sv \cdot s^{-1}$	22 $kBq.cm^{-2}$
TL	LiF MCPN-S	10 $nSv \cdot s^{-1}$	50 $Bq \cdot cm^{-2}$
	LiF(C)	150 $nSv \cdot s^{-1}$	750 $Bq \cdot cm^{-2}$
	LiF(P)*	40 $nSv \cdot s^{-1}$	200 $Bq \cdot cm^{-2}$
	TLD-100*	75 $nSv \cdot s^{-1}$	360 $Bq \cdot cm^{-2}$

Conditions: irradiation time 10 mins; LDL is set to 3 σ of the 2nd reading; integration: the main dosimetr

*sensitivities are valid only for higher, $E_{\beta} \geq 0.5$ MeV radiations due to strong energy dependence of TL detector responses

TL and TSEE characteristics dependence on thermal treatment of LiF MCP-Ns and LiF MCP type GR-200 (Chinese) detectors has been investigated. Subsequent readings up to 500°C were carried our after irradiations with a given dose. The glow curves are given in Fig.12. and Fig.13. The TL sensitivity after 10 cycles decreased to approximately 10 % of its original value than remained nearly uncharged the TSEE sensitivity decreased to 30 % of the first reading and approximately decreases by 6 %/cycle. Both TL and TSEE glow peaks are shifted to higher temperature.

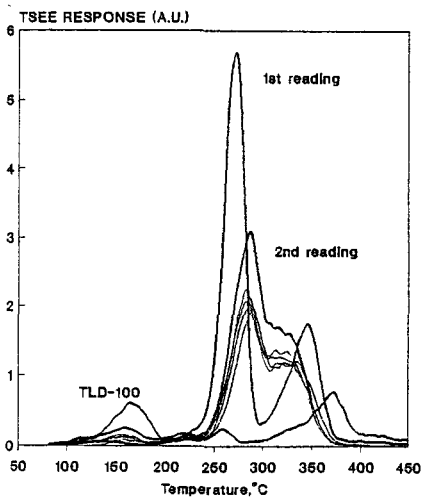

Fig.12. TL glow curves of LiF MCP-Ns detectors heated up 500°C. Heating rate is $3°C \cdot s^{-1}$.

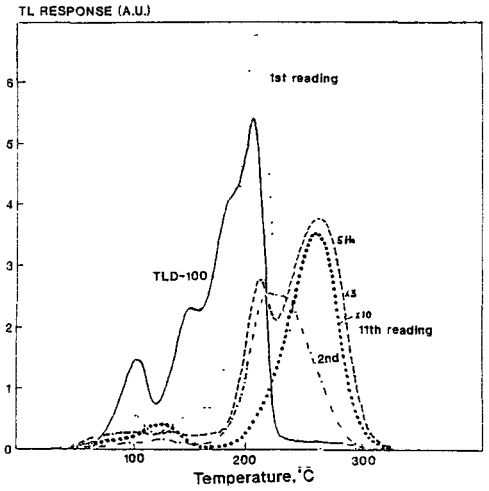

Fig.13. TSEE glow cuves of LiF MCP-Ns detectors heated up 500°C. Heating rate is $3°C \cdot s^{-1}$.

Publications

G. Uchrin, Exoelectron Emission, Thermoluminescence and Optical Properties of LiF crystals of Different Origin, Proc. 11th Int. Symp. Exoemission and its application, Sept. 11-17, 1994, Part I. p.427, Scientific Rep.Techn.Univ. Opole, No.207.
G. Uchrin, TL and TSEE measurements of skin doses due to surface contamination with beta emitters paper presented at 11th Solid State Dosimetry Conference, 10-14 July, 1995, Budapest, Hungary
G. Uchrin, TL and TSEE characteristics of LiF:Mg,Cu,P detectors, paper presented at Symp.Radiat.Prot.in Neighbouring Countries in Central Europe - 1995, Portoroz, Slovenia, Sept. 4-8, 1995.

Final Report

Contract: **FI3P-CT920039** **Sector A12**

Title: Development of instruments and methods for radiation protection dosimetry with the variance-covariance method.

1)	Kellerer	University of Munich
2)	Lindborg	Swedish Radiation Protection Institute, Stockholm
3)	Jessen	University of Aarhus-Hospital
4)	Szendrö	MicroVacuum Ltd, Budapest (PECO)

I. Summary of the Project Global Objectives and Achievements.

With the extension of the rules of radiation protection to new professional areas, the tightening of dose limits, and the increase of the quality factors for densely ionising radiation, tissue equivalent microdosimetric detectors have become increasingly important in radiation protection practice. In typical applications single event distributions of energy imparted are determined. However single event measurements are often time consuming or impracticable, especially in high dose rate fields or in pulsed radiation fields.

An alternative technique to perform microdosimetric measurements is the variance method. With this technique microdosimetric parameters, such as dose average lineal energy or dose average specific energy, are determined from the fluctuations of energy imparted in a microdosimetric detector. While the variance method requires constant dose rate the variance-covariance method is applicable in time varying fields. Two detectors are applied to perform simultaneous measurements. By subtracting the covariance of the signals of the two detectors from the variance of the signal of one detector the influences of the dose rate fluctuations are eliminated.

The efforts of the groups participating in the contract have been directed towards:

1) further development of the variance-covariance technique,

2) the construction of improved twin- and multiple proportional counters and of twin ionization chambers and,

3) the design of suitable electronics for the detectors in their various operational modes.

- ***Further development of the variance-covariance method and extension of its applicability limits.***

A new approach for the evaluation of microdosimetric parameters in time varying fields has been proposed at the University of Munich. The new algorithm obviates the restriction of constant dose-rate ratio at the locations of two simultaneously working detectors. The variance-covariance measurements in the new form can be applied under very general circumstances, including, for example, measurements in moving objects in non-uniform radiation fields, for example on aircrafts and in satellites.

- ***Design and fabrication of tissue equivalent detectors for variance-covariance measurements.***

The need for more sensitivity and for more precise measurements require changes in detector dimensions and construction, including multi-detector assemblages with miniaturised elements, as proposed by Rossi. The efforts of the group at the University of Munich have been directed toward design and fabrication of multi-element detectors with high neutron sensitivity. A test and calibration method, applicable for small proportional counters and especially for multi-element detectors that utilises ^{37}Ar, has been developed. The influence of the eccentricity of the multiplication wire which is assumed to be critical in multi-element systems, was theoretically and experimentally investigated. A multi-element detector consisting of 54 individual elements has been designed and fabricated.

The activities of the Aarhus group are directed mainly towards the application of the method in measurements in diagnostic and therapeutic beams. Because of the high dose rate in such fields no gas multiplication is applied and the detectors are operated as ionization chambers. Twin ionization chambers have therefore been developed.

- ***Development of electronic equipment for signal processing.***

While the conventional pulse technique is applicable to single event measurements the variance-covariance method requires high precision direct current measurements. To perform simultaneous measurements in two detectors, or in two groups of detectors, two independent working channels of signal processing are required.

Electronic equipment has been developed, with emphasis on different applications, by the Aarhus and Stockholm groups and by the PECO partner Micro Vacuum Ltd.

The Stockholm group developed low noise electrometers which are central components in the electronic systems. Two electrometers based on charge integrating technique and current measurement technique have been designed, investigated and compared at the Radiation Protection Institute in Stockholm.

The next important step in the signal processing is the analog to digital conversion of the electrometer signal. Different ADCs have been tested by the group in Aarhus to find the converters that satisfy best the requirements of high accuracy and high speed of the conversion.

The task of Micro Vacuum Ltd was the development of a portable instrument for variance-covariance measurements. Low noise and low offset electrometers were designed and adjusted to the parameters of tissue equivalent proportional counters of the Munich group. Analog to digital converters with high resolution (20 bit) were implemented, and suitable high voltage supply was developed. The unit can work as a battery powered stand-alone device. To adjust the instrument for different applications the unit can be re-programmed via RS232 interface.

- ***Application of the variance-covariance method in radiation protection practice.***

Within this contract the variance-covariance method has been successfully applied in measurements in pulsed neutron fields, therapeutic electron and x-rays beams, in diagnostic x-rays fields, and on board of aircraft (see References).

Variance-covariance measurements at smallest simulated diameter of 6 nm were performed at the Swedish Radiation Protection Institute. The dose mean lineal energy, y_d, has been evaluated for two low LET-beams (^{60}Co gamma ray beam and 100 kV x-ray beam). It was seen that the y_d-values of the two beams tend to become roughly equal at diminishing object diameter. At the simulated diameter of 6 nm the y_d-value of the x-rays beam exceeds that of the cobalt beam by 25%.

In addition the Stockholm group has applied the variance-covariance technique to determine absorbed dose in x-ray beams. In the dosimetry of high energy photons the Bragg-Gray relation is successfully applied. To account for the deviations that occur if the Bragg-Gray conditions are not exactly met, for instance in the dosimetry of x-rays, the IAEA suggested a correction factor. With the measurements in small simulated volumes that are attainable with the variance-covariance technique it is possible to meet the Bragg-Gray conditions in x-rays fields and to check the IAEA corrections. It was found that if the revised IAEA procedure is applied, the deviations are preliminary less than 3%.

Head of project 1: Prof.Dr.A.M.Kellerer

II. Objectives for the reporting period.

- Development of-multi-element proportional counter of moderate size with high neutron sensitivity.
- Investigation of the influence of wire eccentricity on the performance of cylindrical proportional counters.
- Development of a test and calibration method applicable for small proportional counters and especially for multi-element detectors.
- Design and implementation of portable electronics for radiation-protection measurements with the variance-covariance method.
- Further development of the variance-covariance method for measurements in time varying fields.

III. Progress achieved including publications.

1. Design and fabrication of multi-element detector.

Two types of prototype detector elements, the CC-detector (continuous cylinder) and the SC-detector (segmented cylinder) have been produced and tested. The sensitive volume of each of the detectors is cylindrical with diameter 3 mm. The walls are made of A-150 tissue equivalent plastic material. All prototype elements are operated in a gas tight aluminium housing connected to a gas flow system. Methane based tissue equivalent gas has been used in all experiments. A gold plated tungsten wire with diameter 20 μm serves as central electrode in all cases.

The CC-detector has uninterrupted sensitive volume as shown in Fig. 1.

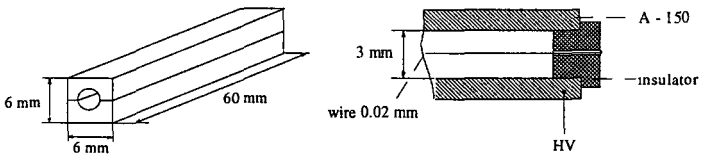

Fig. 1 A-150 body of the CC-detector (left panel); insulator which supports the multiplication wire of the prototype detector (right panel).

The second type of detector elements has interrupted, separate sensitive regions. Its design is indicated in Fig.2. The gas filled volume is subdivided by separator discs that are 0.5 mm thick and are made from isolating material. Near the separators the gas multiplication can be affected by charges on the isolators. A special shape of the central electrode as shown in Fig.2b,c was, therefore, used. With this design, gas multiplication is suppressed by increase of the diameter of the central wire in the proximity of the separator discs. The fabrication of the electrode begins with a gold plated tungsten wire of diameter 20 μm. By galvanic coating the diameter is increased to about 100μm. With the use of a photolitographic process (coating with photoresist, UV exposure through a structured mask, development followed by etching) parts of the wire are reduced to their original diameter of 20 μm. In this way 9 sensitive regions of

height 3 mm (right cylinders) are created. The "functional" parts of the central electrode work accurately, and through optimisation of the etching process good quality of the transition structures between coated and uncoated wire has been achieved, as presented in Fig.2c.

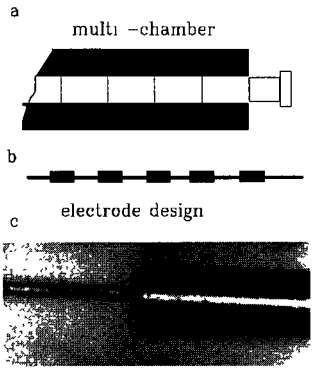

Fig.2. Schematic diagram of one 'channel' in prototype II with 5 separate sensitive regions (a) and the central electrode with segmented shape (b). Example of the realisation of the central electrode after photolitographic processing (c).

The two prototype detectors have been tested in photon and neutron fields. No substantial differences in the shape of single event spectra were seen. However the determination of the microdosimetric spectra in photon and neutron fields is not sufficient for reliable quantification of the detector resolution. This was the reason to develop a sophisticated calibration technique that utilises ^{37}Ar. This technique is discussed in detail in Chapter 2. With the new calibration technique it was established that the CC-detector element provides better resolution (see Fig.5) and more electrical stability. In addition, the preparation of this detector type is easier. The deviation of the chord length distribution for a long cylinder from that of a regular right cylinder is of minor influence. Due to the small diameter of the central wire, i.e. low mass per unit length, and its high tension no difficulties with microphonic noise were encountered. The CC-detector prototype was chosen, therefore, as the basic element for the multi-element detector.

After extensive tests with various techniques the injection molding has been chosen to produce the multi-element detector bodies. Suitable molding equipment was designed to mold A-150-bodies consisting of 54 cylindrical elements , each, with a cylinder radius 1.5 mm and with length 58 mm arranged in a hexagonal pattern, the diameter of entire cylindrical detector body is 40 mm.

With the injection molding technique it turned out to be a complex task to achieve both precise shape and good conductivity of the A-150 plastics. In a series of experiments, therefore, parameters such as the temperature and pressure of the A-150-material during injection, the temperature of the mold during injection, and the time profile of the temperature after injection, had to be optimised. The necessary procedures have been developed in cooperation with the group of Prof.H.Menning at the Technical University of Chemnitz. After a series of tests the technique was sufficiently improved to the point that detector bodies with precise shape and sufficient conductivity can now be molded. The injection molding has thus been demonstrated to be suitable for the production of a large number of A-150 detector bodies. Once the equipment is available, to control the various critical parameters, the detector production is fast and efficient.

The small radius of the single detector channel as well as the large number of channels are critical aspects in the fabrication of multi-element detectors. It is normally assumed that the precise centering of the multiplication wire is particularly critical for the proper performance of the counter, and this is then evidently a critical point in detectors with small dimensions. Furthermore, the resultant errors, are expected to be increasingly important in detector systems that contain a multiplicity of small counters. Theoretical and experimental investigations of the effect of wire eccentricity were, therefore, carried out. The results of this investigation (Ch.3)

have shown that systems of small detectors are useable without undue constructional effort, to achieve high precision of wire centering. Thus the conditions can be met that allow adequate neutron sensitivity at moderate detector sizes with acceptable resolution.

Different techniques for supporting the central wire at the detector ends have been tested. Apart from good centering of the wire, attention must be paid to avoid leakage currents and to achieve stable function of the detector at high voltage. The construction that is shown in Fig.3 was selected as a suitable compromise between simplicity in construction, good resolution, and stable function of the multi-element detector.

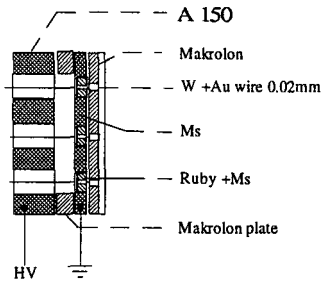

Fig.3. Part of the detector end.

2. Calibrating and testing TEPC by ^{37}Ar.

The conventional methods for energy calibration of TEPC (low energy characteristic x-rays or collimated α-ray beam) are impracticable in the case of very small counters and multi-element counters. We have, therefore, reestablished and technically improved a calibration procedure using ^{37}Ar. This method has been used much earlier in the development of proportional counters and it was also briefly employed in earlier microdosimetric studies by Rossi, Srdoc, Booz, Menzel and Lindborg. To implement this important calibration technique a method for production of ^{37}Ar by activation of argon, in its normal isotope composition was used. This obviates the need for chemical separation and purification and the resultant radiation protection problems that arise with other production methods.

The potential of the use of ^{37}Ar for calibrating and testing was illustrated by studies of the performance of the prototype elements. The calibration with ^{37}Ar provides two peaks of approximately 0.2 and 2.6 keV mean energy that can be readily observed in order to determine calibration factor and resolution of the counter (Fig.5). It was demonstrated in these studies

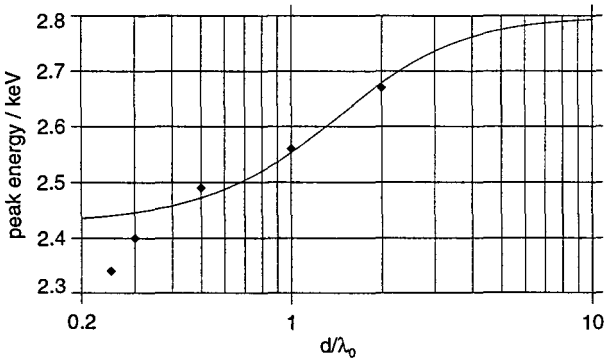

Fig.4. Dependence of the position of the K-peak on the ratio simulated diameter to mean free path of the photon. The line gives the computed values that do not account for an escape of electron energy, the points give measured values derived by means of intercalibration with α-rays.

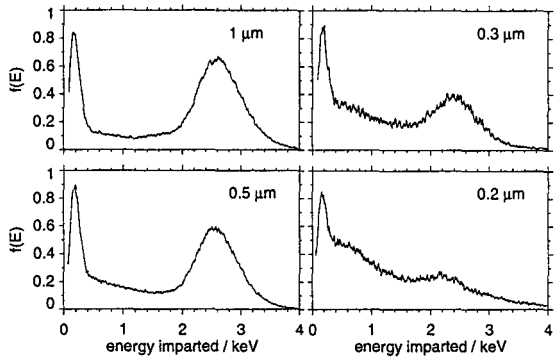

Fig.5. Examples of calibration spectra obtained with the CC-prototype detector.

that even simple detector constructions without electric field tubes can achieve a resolution nearly equal to that of a counter with uniform response and with the optimal distribution $\sim x \cdot \exp(-2x/x_0)$ of pulse heights for single ions. The full width at half maximum (FWHM) was found to be 26% - 32% at the energy of the K-peak (2.4 - 2.6 keV) at simulated diameters 2 - 0.3 µm and high voltages 800 - 1100 V for the CC-prototype detector.

For smaller simulated diameters, the calibration in terms of the K-peak is more complicated, as one needs to account for incomplete energy deposition by some of the Auger electrons. The K-peak broadens and shifts to lower energies, and the contribution of L-shell electrons becomes correspondingly more prominent. The observation of L-peak, which is close to the noise, requires high gas gain and low noise at corresponding high voltage. With the CC-prototype detector calibration in terms of the L-peak of ^{37}Ar was possible for simulated diameters down to 0.1 µm.

The method of testing and calibrating TEPC with ^{37}Ar which has been developed in the project is now an important tool. It is a major step in microdosimetric technique, because it is actual a precondition, to achieve objective comparisons of the performance of novel detector constructions, and to select the best suitable configurations, especially for multi-element detectors. The measurements performed with the CC-prototype, in neutron fields, have confirmed the findings in the calibration studies and have shown additional advantages of this detector. Single event spectra for neutrons that were produced by the $D^2(d,n)He^3$ reaction, were obtained at reasonably small simulated diameters with well resolved spectral features (Fig.6). The high energy peak due to heavy particle recoils and the proton edge are clearly seen in the spectra at simulated diameter 100 - 30 nm.

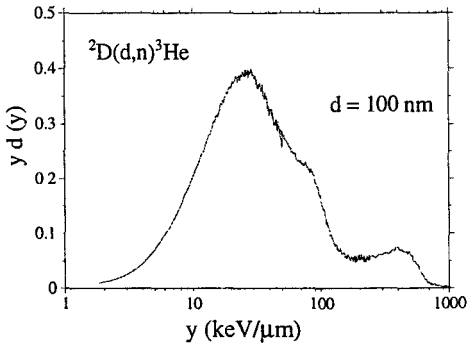

Fig.6. Dose distribution of lineal energy, yd(y), for 5 MeV neutrons, measured with the CC-prototype detector.

At these sizes the pulse height spectra were calibrated in terms of the proton edge. The observed broadening of the main peak is in good accordance with the calculations of Coyne and Caswell.

3. Effect of wire eccentricity on the performance of cylindrical proportional counter.

There are technical limitations to the precise positioning of central electrode in detectors with small dimensions. The resulting eccentricity is usually considered as a main source of error, and it is taken to be of increasing importance in detector systems that contain a multiplicity of small cylindrical counters. A theoretical and experimental investigation of the influence of eccentricity of the central electrode on detector performance was, therefore, carried out.

The electric field in an eccentric cylindrical detector was computed by the method of images. The gas multiplication factor for electrons originating from different positions in the detector volume, was calculated in terms of the Townsend formalism. The curves in Fig 7 give the results of the calculations for the two directions of maximal gain and minimal gain. For different simulated diameters and for different voltages, the two values are derived in their dependence on eccentricity.

The experimental investigations were carried out with the CC-detector element with a cylinder length of 65 mm, interior radius R = 1.5 mm and a multiplication wire of radius r = 0.01 mm. The wall mounting was constructed to allow positioning with variable eccentricity. The precision of wire positioning was 0.01 mm. The measurements were performed with the ^{37}Ar calibration technique. To show the general trend of the results, Fig.7 gives the pulse height spectra for the 2.6-keV peak of ^{37}Ar that are obtained with different eccentricities. With increasing eccentricity one observes a shift of the peak to higher average gains, but also a broadening of the spectra, which is in line with the differences of the electric field in different directions. The effective gas gain under different operating conditions is represented by the data points in Fig.7. The diamonds give the gain values that correspond to the K-peaks of the observed spectra, i.e. they present the most probable values of the gain. The dots give the average gain, as determined from the mean values of the spectra. The mean values lie well between the computed curves.

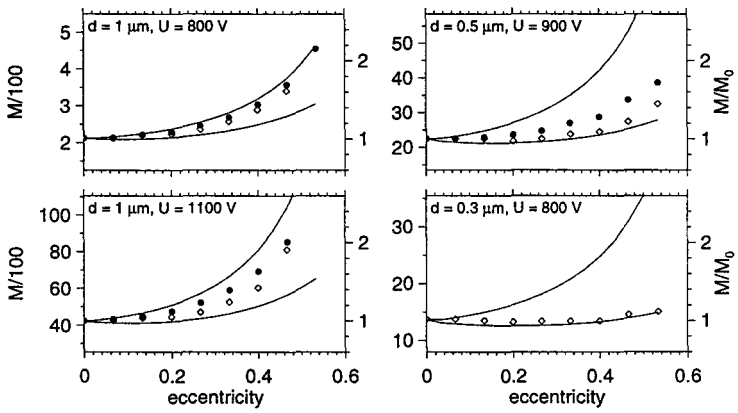

Fig.7. Dependence of the gas multiplication, M, on the eccentricity (left ordinate: absolute values; right ordinate: values relative to eccentricity zero). The curves are calculated for positions with minimal and maximal gain, the diamonds and the dots give the relative gas multiplication factors, M/M_0, determined from the K-peak position and from the mean values of the measured spectra.

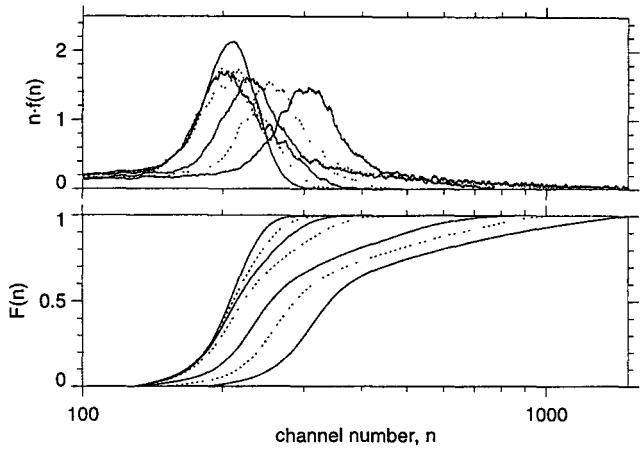

Fig.8. Pulse height spectra in the region of the K-peak of ^{37}Ar at 0.5 μm simulated diameter and different eccentricity. From left to right the eccentricities are 0, 0.20, 0.27, 0.33, 0.40, 0.47, 0.53. Lower panel: The corresponding sum distributions, F(n), i.e. the fraction of pulses up to the specified channel. The parts of the distributions, that lie more than two standard deviations below the K-peak have been disregarded.

Increased eccentricity causes a decrease of detector resolution, which is illustrated in terms of the dependence of the relative variance on the eccentricity (Fig.9). The argon K-peak has a very small relative variance ($V_r = 0.015$), and its broadening at larger eccentricities appears, therefore, as a considerable distortion. Usual energy deposition spectra in mixed photon neutron fields, on the other hand, have relative variances that are substantially larger than 2. The increase, due to the eccentricity are then fairly inconsequential and the detector resolution is, therefore, not highly critical. One concludes that eccentricities up to 0.2 will be entirely tolerable in TEPCs for measurements in common photon or neutron fields.

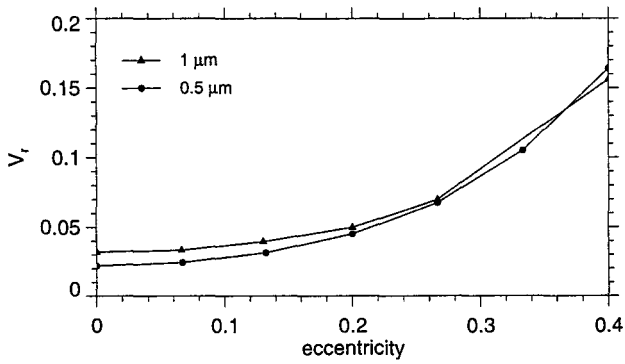

Fig.9. Dependence of the relative variance, V_r, of the ^{37}Ar K-peak on eccentricity at simulated diameters 1 and 0.5 μm.

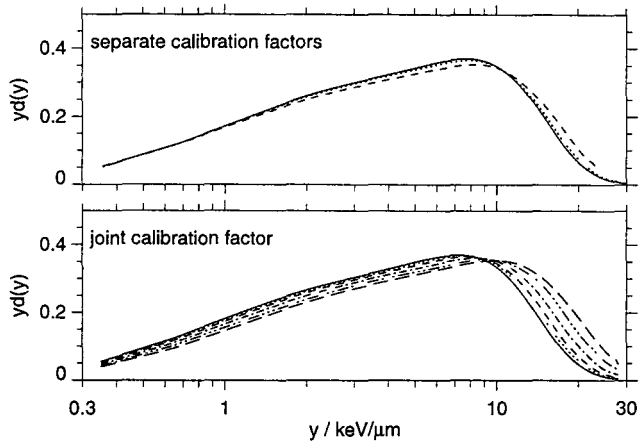

Fig.10. The microdosimetric distribution yd(y) vs. lineal energy, y, for ^{137}Cs radiation at 1µm simulated diameter and different eccentricity. Upper panel: each spectrum is calculated with the calibration factor determined at the corresponding eccentricity: e = 0, 0.2, and 0.4. Lower panel: the spectra at eccentricities 0, 0.13, 0.20, 0.27, 0.33, and 0.40, all calculated with joint calibration factor for eccentricity 0.2.

Measurements in a ^{137}Cs field are presented in the top panel of Fig.10. Eccentricities up to 0.2 were found to be tolerable. The situation is more complicated for an assembly of several counters. In such systems average calibrating factors need to be employed and differences in effective gain of individual detector elements are then the determinant influence on the resolution of the spectra (see lower panel of Fig.10).

The result of the investigation of eccentricity facilitates the design and production of small cylindrical proportional counters for microdosimetric measurements. The analysis was here related to a system of cylindrical proportional counters with an interior radius 1.5 mm, as the radius of our prototype detector. In this case it is not difficult to ensure a centering of the multiplication wires that is better than ±0.3 mm, i.e. better than eccentricity 0.2, and considerably more precision can actually be achieved. The results of this investigation show that systems of small detectors are feasible without undue constructional constraints and that they can achieve adequate neutron sensitivity at moderate detector sizes with acceptable resolution.

3. New approach for the evaluation of the microdosimetric parameters in time-varying fields. Comparison with the conventional variance-covariance method.

The variance-covariance method was developed by Kellerer and Rossi (1984) as a method for the determination of microdosimetric parameters from the fluctuations of the energy deposition in time varying radiation fields. It has been successfully used to obtain microdosimetric parameters in different pulsed radiation fields of neutrons, electron beams from pulsed linear accelerators, and x-rays from medical linear accelerators. Developed as a method suitable for high dose rates the variance-covariance method was shown to work in time varying low-dose rate fields and recently Lindborg applied it in radiation-protection measurements on board aircraft. The principal limitation of the method is the requirement that the doses at the detectors location differ at most by a constant factor. However in practice it is quite possible that the requirement of constant dose ratio is not fulfilled and some slow deviations do take place.

If $\varepsilon_{A,i}$ and $\varepsilon_{B,i}$ are the energies imparted in the sensitive volumes of the detectors A and B in the i-th sampling interval, the dose average of energy imparted per energy deposition event $\bar{\varepsilon}_{D,A}$ and $\bar{\varepsilon}_{D,B}$ can be expressed by following equations:

$$\bar{\varepsilon}_{D,A} = \frac{\sum_{i=1}^{N} \varepsilon_{A_i}^2}{\sum_{i=1}^{N} \varepsilon_{A_i}} - \frac{\sum_{i=1}^{N} \varepsilon_{A_i} \cdot \varepsilon_{B_i}}{\sum_{i=1}^{N} \varepsilon_{B_i}} \qquad \bar{\varepsilon}_{D,B} = \frac{\sum_{i=1}^{N} \varepsilon_{B_i}^2}{\sum_{i=1}^{N} \varepsilon_{B_i}} - \frac{\sum_{i=1}^{N} \varepsilon_{A_i} \cdot \varepsilon_{B_i}}{\sum_{i=1}^{N} \varepsilon_{A_i}} \quad (1)$$

The best correction for the additive disturbances can be achieved if one uses the averaged result from the two detectors:

$$\bar{\varepsilon}_D = (\bar{\varepsilon}_{D,A} + \bar{\varepsilon}_{D,B}) / 2 \quad (2)$$

The other microscopic parameters that characterise the radiation quality, dose average lineal energy $\bar{y}_D$ and dose average specific energy $\bar{z}_D$, can be easily obtained as follows:

$$\bar{y}_D = \bar{\varepsilon}_D / \bar{l} \quad \text{and} \quad \bar{z}_D = \bar{\varepsilon}_D / m \quad (3)$$

where $\bar{l}$ is the mean chord length and m is the mass of the simulated sensitive volume. As pointed out in the original presentation of the variance-covariance method, these considerations are valid, provided the dose rates at the detectors locations differ at most by a constant factor.

If the two-detector system for variance-covariance measurements moves through a radiation field, it may often not be practicable to ensure a constant intensity ratio at the locations of the two detectors. An improved method is then required and it has been developed within the project. Although the somewhat sophisticated underlying statistical theory has not yet been published, the new analysis technique has been experimentally tested. Because it is practically important, this procedure and its potential will in the following be indicated in preliminary form, without an attempt to present the somewhat demanding theoretical basis.

Assume that the change of dose rate ratio is sufficiently slow to be effectively constant over two sampling time intervals. A suitable estimator for the microdosimetric parameter dose mean event size can then be constructed out of successive signals $\varepsilon_{A,i}$ and $\varepsilon_{B,i}$ in the two detectors A and B:

$$\bar{\varepsilon}_{D,A} = \frac{1}{2}\left\{ \frac{\sum_{i=1}^{N-1} (\varepsilon_{A_i} - \varepsilon_{A_{i+1}})^2}{\sum_{i=1}^{N-1} \varepsilon_{A_i}} + \frac{\sum_{i=1}^{N-1} (\varepsilon_{A_i} - \varepsilon_{B_i})^2}{\sum_{i=1}^{N-1} \varepsilon_{B_i}} - \frac{\sum_{i=1}^{N-1} (\varepsilon_{B_i} - \varepsilon_{A_{i+1}})^2}{\sum_{i=1}^{N-1} \varepsilon_{B_i}} \right\}$$

$$\bar{\varepsilon}_{D,B} = \frac{1}{2}\left\{ \frac{\sum_{i=1}^{N-1} (\varepsilon_{B_i} - \varepsilon_{B_{i+1}})^2}{\sum_{i=1}^{N-1} \varepsilon_{B_i}} + \frac{\sum_{i=1}^{N-1} (\varepsilon_{A_i} - \varepsilon_{B_i})^2}{\sum_{i=1}^{N-1} \varepsilon_{A_i}} - \frac{\sum_{i=1}^{N-1} (\varepsilon_{A_i} - \varepsilon_{B_{i+1}})^2}{\sum_{i=1}^{N-1} \varepsilon_{A_i}} \right\} \quad (4)$$

These seemingly complex relations are in practice numerically evaluated by the electronics of the detector system without problem; they are here given without proof. As in the conventional variance-covariance estimation it is best to use the average of the values for the two detectors.

The practical determination of the applicability and the limitations of the new evaluation algorithm was the aim of two series of experiments performed in the photon field of ^{137}Cs. Two quite different sources were used: a small one with an activity of 185 MBq and a medical source with an activity of 130 TBq. In the first series of measurements (low dose measurements) a small Cs-capsule was mounted on a mechanical arm connected to a step motor. A circular motion with a frequency of 5 - 20 Hz or a nearly stochastic motion with varying frequency were realised. The dose rate at the detector locations varied between 1400 μGy/h and 20 μGy/h, the ratio, ρ, of dose rates in the two detectors varied between 0.2 and 5. The second series of measurement was performed at a high dose rate of about 1 Gy/h. The variation of the dose-rate ratio at the detectors locations was achieved by moving a segmented circular plate (4 mm lead), between the detectors and the source, with a frequency of 2 Hz. The lead segment decreased the dose rate by about 15%.

The inferred values of the dose mean lineal energy, $\bar{y}_d$, illustrate the effect of the new algorithm when ρ is variable. Every set of obtained data was evaluated in three different ways: with conventional variance-covariance algorithm and with the new algorithm. Before the start of the measurements in the time-varying field, measurements were made in constant radiation fields, to determine the value $\bar{y}_d(c)$. The values $\bar{y}_d(c)$ for ^{137}Cs at simulated diameters of 1 μm and 2 μm which are obtained with the different algorithms are in good agreement with each other and with the values reported from other authors. The conditions were quite different in the cases of high and low dose rate, and therefore the results are discussed separately.

Low dose rate: At constant ρ the fluctuations of the measured voltage increments (proportional to the energy imparted) are large and the ratio of voltage increments in measurement intervals varies between 0.01 and 100. Because of the wide range of the fluctuation of ΔU, it was difficult to see any influence of the change of ρ when the source was moved around the detectors. An effect was seen only when the signal was averaged over longer time intervals. The y_d values, obtained at constant dose-rate ratio by the two evaluation algorithms, did not show differences. When the dose-rate ratio was variable the values obtained with conventional variance-covariance algorithm are too large by a factor of two at lower sampling frequencies. The new technique is thus essential.

High dose rate: The fluctuations of measured voltage increments at constant dose rate were of the order of 10% of the average signal as can be seen in the upper panel of Fig. (11). The observed changes of $\bar{y}_d$ - values at constant ρ were very small when the sampling frequency was changed. The largest deviation was less than 10%, the standard deviation was independent of the algorithm used in the calculation of $\bar{y}_d$.

When the segmented circular shielding was moved, the readings of detectors changed with time, in accordance with the motion of the shield (Fig.11), the change amounted to about ±8% In this case the inferred values $\bar{y}_d$ increased drastically and depended strongly on the evaluation algorithm. In Fig.11, where a logarithmic scale is required to cover the range of $\bar{y}_d$ values by factor of ten the conventional variance-covariance algorithm can no longer be applied for obtaining microdosimetric parameters, but the new approach shows acceptable stability of $\bar{y}_d$ values.

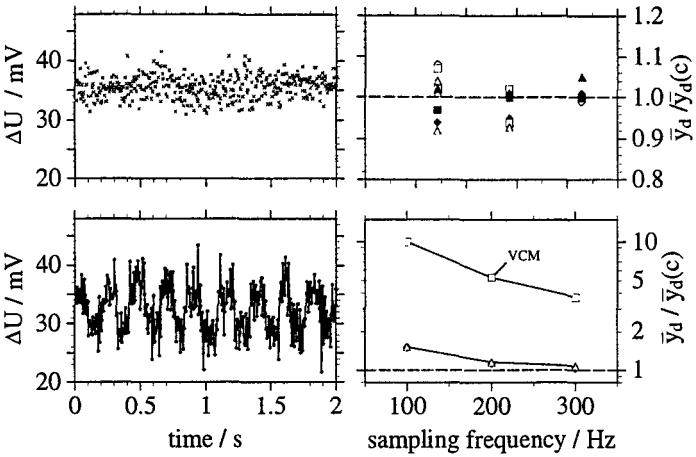

Fig.11: Left: Time dependencies of voltage increments at high dose rate. Upper panel: constant dose rate. Lower panel: lead shield moving with circular frequency of 2 Hz. Right: Comparison of the different evaluation algorithms for the determination of $\bar{y}_d$. Upper panel: constant dose-rate ratio. The transparent symbols correspond to ρ =1, the filled ones to ρ = 1.18. Lower panel: time varying ρ. The squares correspond to conventional VC algorithm, the triangles represent results obtained with the new approach.

The investigation has shown that at high dose rate, even a small change of the dose-rate ratio of the order of some percents, causes a considerable bias in the microdosimetric parameters if the conventional algorithm is used. The new approach eliminates most of the error. One concludes that the variance-covariance measurements, can in this form be applied under very general circumstances, including, for example, measurements in moving objects exposed to non-uniform radiation fields, examples are radiation measurements in aircrafts or satellites.

References:

1. J. Chen, H.Roos and A.M.Kellerer, Microdosimetry of diagnostic x-rays: Applications of the variance-covariance method. Radiat. Res.**132**, 271-276 (1992).

2 E.Anachkova, A.M.Kellerer and H.Roos, Calibrating and testing tissue equivalent proportional counters with ^{37}Ar. Radiat. Environ. Biophys. **33**, 353-364, (1994).

3. J.Chen, K.Hahn, H.Roos and A.M.Kellerer, Microdosimetry of therapy electron beams - measurements and Monte-Carlo simulations. Radiat. Prot. Dosim. **52**, 435-438 (1994).

4 E.Anachkova, H.Roos, E.Nekolla and A.M.Kellerer, Effect of wire eccentricity on the performance of cylindrical proportional counters. Radiat. Environ. Biophys.**34** 4 (1995).

5. E.Anachkova, A.M.Kellerer and H.Roos, Neutron energy deposition spectra at simulated diameter 50 - 500 nm. 8th Symposium on Neutron Dosimetry, 13 - 17 November 1995, Paris (France).

6. E.Anachkova, A.M.Kellerer and H.Roos, New approaches for the evaluation of the microdosimetric parameters in time-varying fields. Comparison with the convenient variance-covariance method. (in preparation)

Head of project 2: Prof. Dr. L.Lindborg

II. Objectives for the reporting period.

The objectives have been

to investigate different electrometer types for applications with the variance-covariance method

to investigate the dependence of y_D with radiation quality and with object size

to investigate the accuracy of absorbed dose measurements in water in x-ray beams

III. Progress achieved including publications.

Two different types of electrometers have been designed based on charge integrating technique and current measuring technique. The initially expected advantage of lower electronic noise with charge integrating electrometers was never found in practice. To us the current measuring technique turned out to be the simpler one to use and most measurements were made in this way. However, both techniques have been used and the value of y_D was not depending on the electrometer design. A more detailed analysis of the electronic noise components have been in the earlier progress report and is summarised in Ref. 1.

The dose mean value of the lineal energy, y_D . has been evaluated for two low-LET beams (ref. 1). A ^{60}Co gamma ray beam and a conventional x-ray beam, 100 kV and HVL 0.14 mm Cu. Results down to a diameter of 6 nm are reported in Ref. 1. In the cobalt beam the agreement between results obtained with the variance method and the variance-covariance method agree within 10 % down to 18 nm. A slightly larger difference was seen below that. (The variance-covariance method gave consequently a lower results) In the x-ray beam a similar agreement was found down to about 20 nm, below which the variance-covariance method results were very much below those from the variance method, leading to y_D values even smaller than at larger object diameters, Figure 1. This unrealistic result is believed to be due to a covariance component of the background signal. Its value was not possible to determine accurately, because of the low values of the current. This component is also present during irradiation and is affecting the values of both the variance and the covariance term. However, as y_D was calculated from the background corrected signal, the lack of correction for the covariance component of the background, will lead to a too small y_D. This turned out to be the limiting factor in the analysis of the experimental results. If instead the results obtained with the variance-method are used, this problem is avoided. However, then for instance the covariance component of the radiation field will not become corrected for, and those results will represent overestimates.

An interesting observation is that the y_D-values of the two beams tend to come closer together at diminishing object diameter. For instance at about 6 nm the y_D-value for the x-ray beam is 25 % larger than for the cobalt beam. At a diameter of about 1 µm the difference is a factor two. The small difference at 6 nm happens to be very close to the difference in total absorbed dose given to patients undergoing radiation therapy with the two different types of beams. Whether or not this interesting observation has any deeper meaning will be looked into.

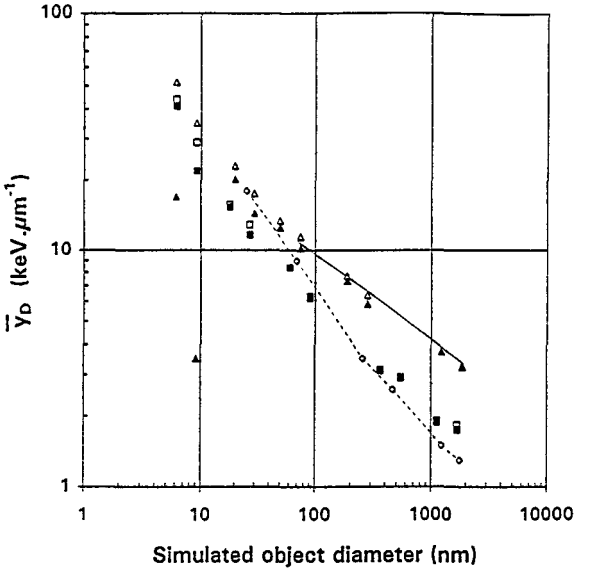

Figure 1. Dose mean lineal energy as a function of simulated object diameter. For all data points both $\bar{y}_{Db}$ and $\bar{y}_{Dbc}$ are given but in some cases only $\bar{y}_{Dbc}$ is seen because of overlapping. For the measurements in the x-ray beam: (Δ) $\bar{y}_{Db}$; (▲)$\bar{y}_{Dbc}$; The solid line is the best fit, made by the authors, for data given by Forsberg et al.. For the measurements in the ^{60}Co gamma beam: (□) $\bar{y}_{Db}$; (■) $\bar{y}_{Dbc}$; (◊) from Forsberg and Lindborg. The data points from Forsberg and Lindborg are connected with a dashed line as a guideline for the eyes.

The determination of absorbed dose in conventional x-ray beams has during the last years been discussed. The IAEA suggested a few years ago new correction factors, which gave quite large differences in absorbed dose values as compared to the same measurement, but using a procedure suggested by the ICRU several years ago. The IAEA has since then modified there correction factors. The difficulty in this energy region is that the Bragg-Gray relation, used succesfully at high photon energies, is not applicable. The secondary electron ranges are too short. However, at the reduced pressure we have used, most secondary electrons created by the x-rays will cross the gas cavity and the Bragg-Gray conditions will be fulfilled. A determination of the absorbed dose based on Bragg-Gray principles and on the method suggested by the IAEA with the two different correction factors will then show which set of factors is the more likely. Figure 2 shows the ratio of the absorbed dose values based on the Bragg-Gray principles to the values obtained using the IAEA modified code. Preliminary the two methods agree within 3 % . If the original IAEA correction factors had been used a larger difference had been seen. What still remains to be examined is the influence of the insulator material on the ionisation current. The results have been reported in reference 3.

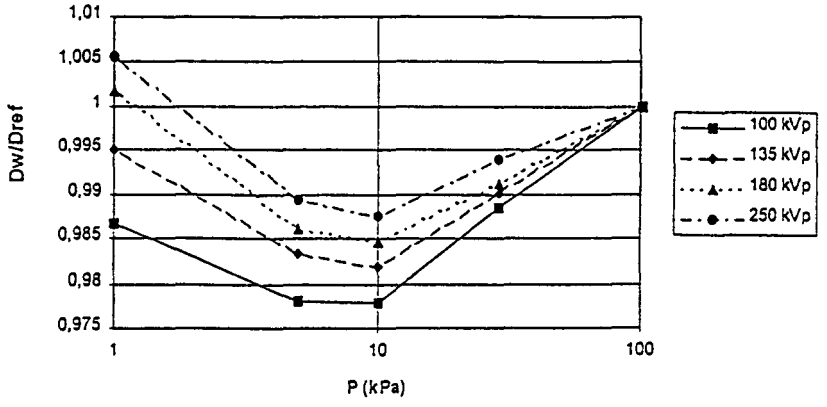

Figure 2. Results of measurements at different gas pressures in the x-ray beams. Diamonds are 100 kV, squares are 135 kV, triangles are 180 kV and circles are 250 kV.

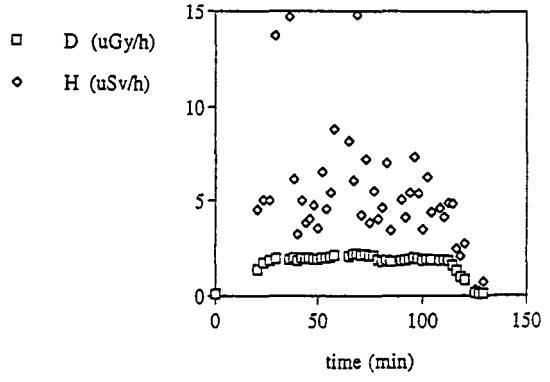

Figure 3. The results of dose(squares) and dose equivalent measurements on board an aircraft between Geneva and Stockholm in July 1993. Each experimental point is the result of 400 integrations over 2 min. The decrease in dose rate after about 80 min was caused by a decrease in flight level from FL350 to FL330.

During the course of this project a growing interest in dose measurement on board aircraft appeared and we took the opportunity to test an area monitor based on the variance-covariance method. The instrument, which is called the Sievert instrument, was calibrated at CERN for high neutron energies and then used on board aircraft for two flights. While the variance-covariance method was necessary for evaluation of the calibration measurements, the variance mathod was sufficient for the measurement on board the aircraft. Figure 3 (from Ref.2) shows an example of the results. The measured dose equivalent rate was in good agreement with results reported by other groups. The quick evaluation possible with the variance method made it possible to observe results after only two minutes of measurement. However, the relevance of this information is questioned because of the large fluctuation in dose equivalent. A more likely measurement interval seems to be 10 minutes. On the basis of the measurements a modified instrument will be constructed, Reference 4.

During the period we have published the following reports:

1. Grindborg, J.E., Samuelson, G. and Lindborg, L.: Variance-Covariance Measurements in Photon Beams for Simulated Nanometer Objects. Accepted for pupblication in Radiat. Prot. Dosim., 1996.

2. Lindborg, L. Grindborg, J.E., Gullberg, O., Nilsson, U., Samuelson, G. and Uotila, P.: TEPC Measurements with the Variance-Covariance Method on Board Aircraft. Accepted for publication in Radiat. Prot. Dosim., 1996.

3. Grindborg. J.E., Kyllönen, J.E. and Lindborg, L.:Absorbed Dose Measurements in x-ray Beams at Different Gas Pressures, in the progress report, 1995 from the Swedish National Dosimetry Laboratory, presented at the 12th meeting of the Section 1 of CCEMRI, Bureau International des Poids et Measures, 1995, (figure 2 revised on the 14th of August).

4. Kyllönen, J.E. A Theoretical Study of a Proportional Counter Suitable for Microdosimetry Work in Neutron Fields. M.Sc. Degree Project, Department of Technology, Uppsala University. 1994.

Head of project 3: Dr. K.A. Jessen

II. Objectives for the reporting period.

- Developing an improved twin - ionization chamber designed to perform measurements of dose averaged lineal energy in diagnostic and therapeutic radiations beams.
- Optimization of integration time and noise reduction to improve the quality of the data.
- Adjustment and extension of computer programs for data processing.
- Finally test of the experimental arrangement.

III. Progress achieved including publications.

The variance-covariance measurements are based on simultaneous detecting of current or pulses generated in the same time period in the two independent detectors placed in a radiation beam.
The work has been concentrated on measurements of microdosimetric quantities as the lineal energy in a continuous beam.

The project started with designing and manufacturing a vacuumchamber, suitable for the tissue-equivalent detectors. The chamber was cylindrical and made of aluminium (Figure 1).

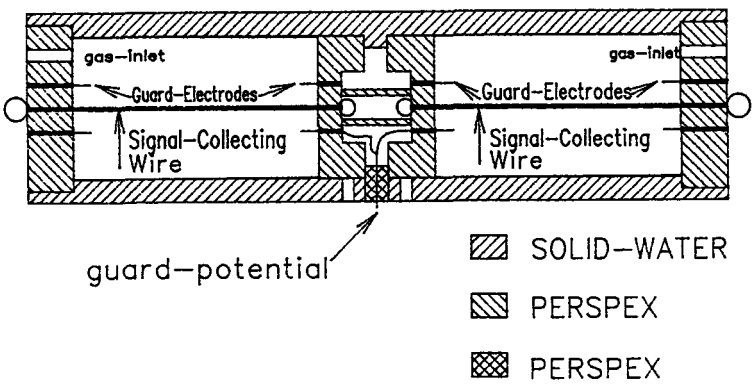

Figure 1. Principle of the cylinder-shaped detector pair.

The conclusion of the tests performed with this first manufactured cylinder-shaped detector was that a charge accumulation take place inside the wall-material (Solid-water) and in the connecting wire to the collecting-electrodes, especially at low dose-rate and low chamber-voltage (under about 100 Volt).

After these results it was decided to redesign and manufacture a new cylindrical detector - designed on the experience, gained from the first cylinder-shaped detector.

This new cylinder-shaped detector is made of A-150 tissue equivalent conducting plastic. The sensitive volume is of a cylindrical shape with a diameter of 12 mm. The collecting electrode is made of steel wire with a diameter of 0.7 mm. The guard electrode has a 4.5 m diameter. The detector is mounted in the vacuumhousing, using shielded wire-connections, shielded at ground potential to prevent charge pile-up in the wires (Figure 2).

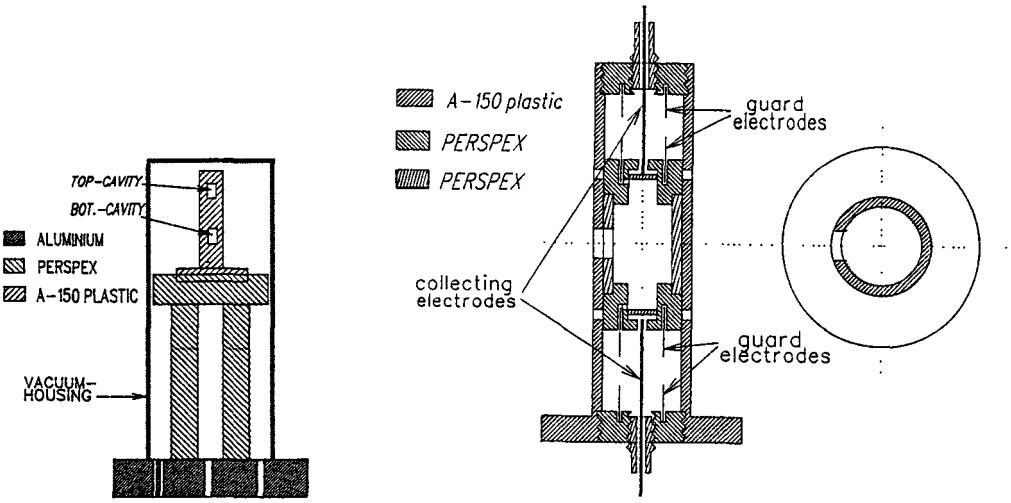

Figure 2. Principle design of the new detector pair, mouted in the vacuum-housing.

The detector was tested as the former in to kinds of therapeutic, continuously beams: ^{60}Co γ -rays and 250 KV conventional X-rays. Figure 3 shows the experimental arrangement in the ^{60}Co beam.

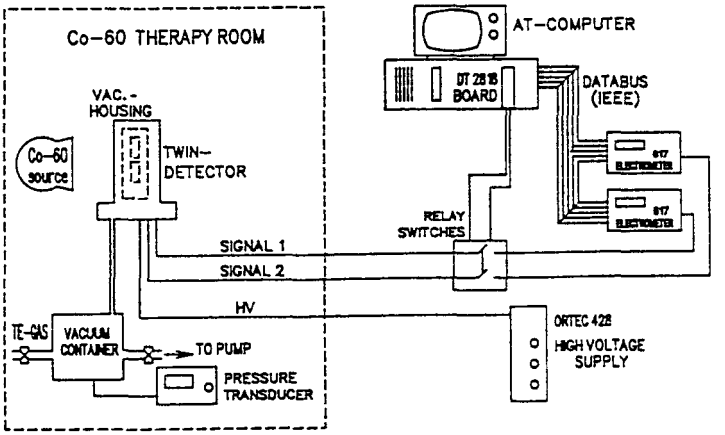

Figure 3. The experimental arrangement for measurements in the Co^{60}-beam.

It was not possible to measure reproducible values of the dose average lineal energy y_D, and the values of y_D was to high.

First, the signal size has been checked via the measuring system and it has been concluded that the charge was measured correctly and the calculations was correct.

The signal generated in the detectors is in the range of 10^{-12} A, and the variance is on 3. digit of that. In order to obtain a charge high enough to exceed the sensitivity of the electrometer, charge have been collected for more than 2 second per pulse.
The test-measurements show also that the resolution of the converted signal must be better than 12 bit.

To overcome difficulties with integration time and signal size, amplifiers near the detectors has been considered. Therefore it was decided to manufacture an amplifier - ADC converter.
The experimental arrangement has been retained, only the A/D converter has been changed and the amplifier has been introduced as close as possible to the detector (Figure 4).

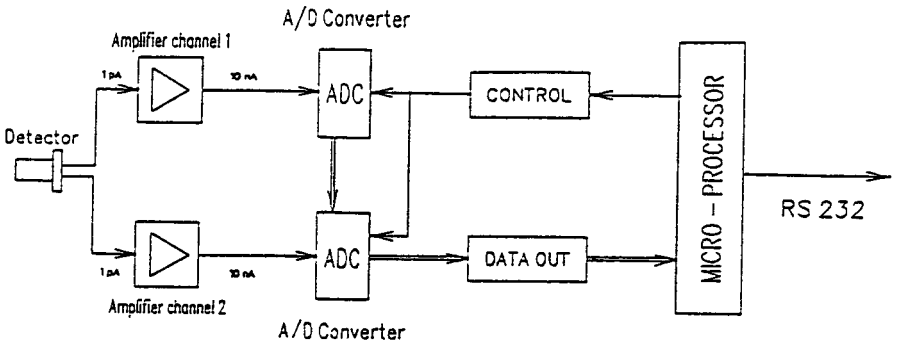

Figure 4. The new experimental arrangement.

The produced amplifier is made as a current converter based on two OPA 128 amplifiers from Burr & Brown, and have a current amplification on 80 dB (10.000 times).
The ADC (DDC101) is a so-called charge (current) input ADC, and can therefore be coupled directly on the output from the amplifier through a long cable. The ADC have the resolution of 20 bit.

Before the detectors high voltage became connected, the AC-noise on the amplifier

has been measured to 6 nA. After connecting the detectors high - voltage, it was possible to measure the AC-noise on output to the amplifier. The noise was about 12 nA output current. The double noise on output of the amplifier means that, the detector make a noise. If this noise-increase is computed backward to the output of the detector, it gives 0.6 pA, it means, that the detectors own signal to noise ratio exceed the detectors own noise highly.

The detectors have between the terminals, on each output, a very high isolated resistance. This means that even if the detector is not irradiated, it will give some 'white noise'. The signal to noise ratio is calculated at the most noisy point, with the assumption that the smallest variation which must be detected is 1 fA.

Noise calculations assume also that the maximum bandwidth which the whole circuit will receive is 1 kHz.

$$i_{noise}R_i = \frac{U_{noise} \cdot R_i}{R_i} = 0.927\,fA$$

$$S/N_{det.} = 20 \cdot \log\frac{i_g}{i_{noise} \cdot R_i} = 0.652dB$$

In this calculation, it must also be cosidered, that the detector will possibly supply more noise than calculated. The detector must have a high potential of about 300 V to operate. Since this voltage comes from a conventional powersupply, it will not be possible to avoid noise from this supply.

As it appears from the calculations it will be impossible to detect a variation of 1 fA from the detector, as the noise is at the same level as the signal.
This is valid naturally for a 1 kHz bandwidth. If the bandwidth falls, the signal to noise ratio will be greater.

It is possible based on the calculation to conclude that the following amplifier step may not add any noise, if a level of 1 fA is to be kept.

For that reason, a usable method to amplify the extremly low current, which came from the detector should be found.

In various application notes some current to voltage converters are described for conversion of a very smal current for example from photodiodes. It was decided to test one of these arrangement.The test arrangement is configured as in Figure 5.

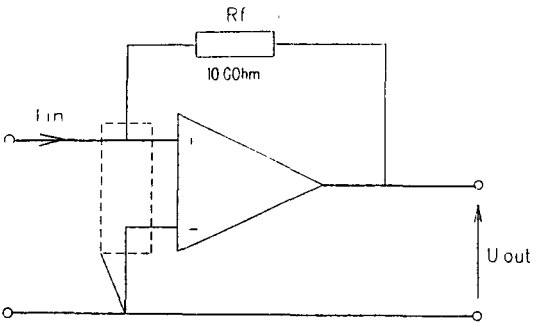

The arrangement will give 10 mV/pA, which is sufficient as a theoretical basis. If this voltage again is converted to a current, there is a considerable current amplification from input to output.
In the arrangement a resistance of 10 GOhm is placed as a feed-back resistance. The flow in R_f is needed to provide i u-conversion (current to voltage conversion).

Figure 5. The current to voltage converter.

To obtain high isolation, the input terminal to the amplifier and the resistance are mounted on a teflon tower.

This arrangement was used for the measurements.

The tests show that the arrangement was so sensitive to the mains frequency of 50 Hz, that it together with a connection to the detector simply started to work at 50 Hz ± supply current.
The arrangement has also other very essential defects. The recent test of the 10 GOhm resistance shows, that between terminals, on this resistance, there was a capacity on about 0.5 pF. This condition results in a very low upper frequency limit of about 40 Hz.

As earlier mention, the A/D converters circuit is bild up arroud a new A/D converter from Burr & Brown. The ADC's have been controled by one micro-processor. It has been decided that communication between ADC circuit and micro-proccesor have to be serial form. The micro communication with the PC is via an serial link (RS 232C). The test measurrements on the digital parts have been made in blocks.

It was expected that the A/D converters will be ready on december 1994. But, it was impossible to finish the A/D converter circuits for technical reasons. Therefore another solution has been considered.

The idea with this solution is to amplify the current as close as possible to the detector. Accordingly the current, after being conducted through the 4 m long cable, has to be amplified again. After a second amplification stage the signal should be integrated and A/D converted (Figure 6). The signal integration should be variable.

It was the intention that the product of that last amplification should result in a signal

size of about 100 mV. With the reference voltage of the A/D converter of the same size, it should be possible to exploit the full resolution of the converter.

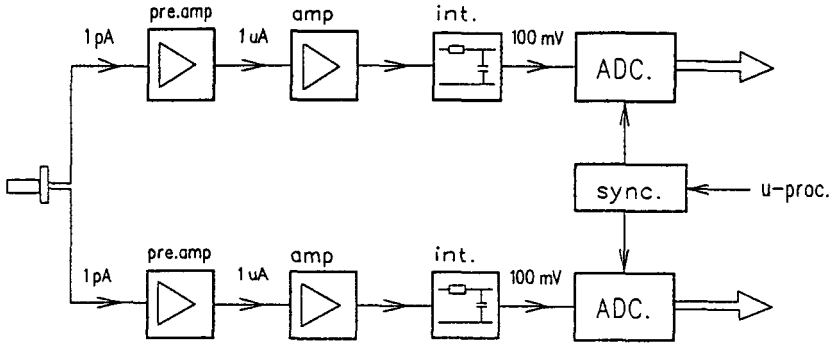

Figure 6 The experimental arrangement.

In the experimental arrangement an A/D converter from Analog Devices was chosen. The A/D converter is a 16 bit converter with the type number AD 1382.

The reason that it is necessary to exploit the A/D converters resolution fully, is because, as the Figure 7a shows, the information is of a high DC level. One idea could be to filter the DC signal, with the help of a capacitor, then the signal can be amplified additionally, so it look like Figure 7b. It will mean that, it will not be necessary to use an A/D converter with 20 or 16 bit resolution.

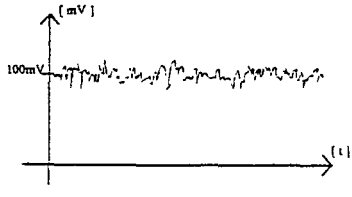

Figure 7a. The amplifiers 2 output.

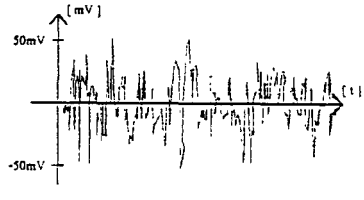

Figure 7b. The amplifiers 2 output. After DC filtration and amplifcation.

Unfortunately there was no time to apply this solution in practice.

Conclusion.

The conclusion must be that the signal size on the output from the detectors must be increased and the signal to noise ratio must be improved. The detectors must be better isolated and screened from the electric noise.

Generally, the biggest problem is the thermic noise from the resistors and semiconductors.

Publications:

1 .H.B. Honorè, K.A. Jessen and H.H. Nielsen, *Variance-Covariance Measurements of the Dose Mean Lineal Energy in Beams for Radiotherapy.* Rad. Prot. Dosim., 31, 453-455 (1990).

2. H.B. Honorè, L.C. Jensen, K.A. Jessen and H.H. Nielsen. *Variance-Covariance Measurements in Radiation Beams of Different Qualities.* 9 th. International Congress of Radiation Research, Toronto 1991. Congress Abstract.

3. H.B. Honorè, L.C. Jensen, K.A. Jessen and H.H. Nielsen. *Variance-Covariance Measurements in Therapeutic and DiagnositcRadiation Beams* . Rad. Prot. Dosim., 52, 387-390 (1994).

4. J.Hansen, H.Honoré, L.Jensen, K.A.Jessen and H.H Nielsen. *Variance-Covariance measurements in medical radiations beams of different qualities.* The World Congress on Medical Physics and Biomedical Engineering. Rio de Janerio, 1994.

Head of project 4: Dr. István Szendrõ

II. Objectives for the reporting period

In order to implement the variance-covariance method into radiation protection practice the development of specialised compact electronics was required, and this is the objective of the present project.

The electronics had to be specifically designed for variance-covariance measurements with multi-element tissue equivalent proportional counters as they were developed within the main project FI3P-CT92-0039..

III. Progress achieved:

1. A battery powered high voltage supply with high operational stability was developed.

2. A low noise, low offset current electrometer was developed, and it was adjusted to the parameters of the multi-element tissue equivalent proportional counters.

3. The main amplifier, the ADC, and the signal processor were integrated in such a way that simultaneous measurements in two channels can be performed and the measured signals can be processed to evaluate the dosimetric quantities of interest.

The electronics consists of the following parts:

1. High Voltage Power Supply
2. 2-channel electrometer unit with reset switch
3. 2-channel A/D converter

4.1. Controller
4.2. LCD display + buttons
4.3. Power supply

1. High voltage power supply unit

The high voltage power supply unit provides output of voltage negative polarity of 400 to 1300 V. The full range of output voltage can be controlled by an external reference voltage in the range of 0 to 5 V dc furnished by the microcontroller panel (D/A converter). This input is protected by a nominal 5.1 V Zener diode. The high voltage power supply is based on a tuned-circuit oscillator in push-pull configuration with a sinusoidal frequency oscillation between 40 to 44 kHz. This frequency is determined by the primary inductance LR and the parallel capacitor CR. The collector voltage is coupled by the first secondary winding of the transformer to the basis of the transistor to achieve positive feedback. The second secondary winding is associated with a voltage doubling circuit and delivers the required DC output voltage, ranging from -400 to -1300 V.

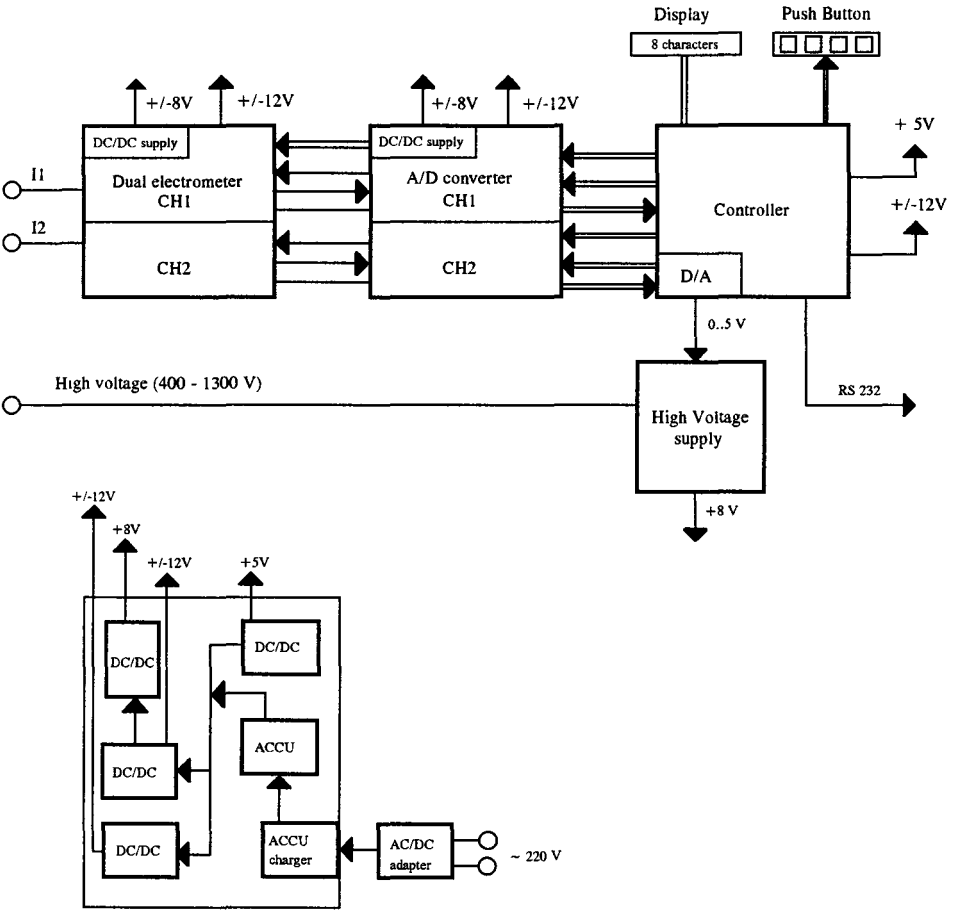

Fig.1. Block scheme of the integrated electronics

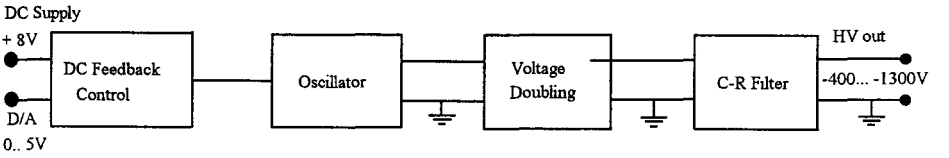

Fig. 2. Block-scheme of the high voltage power supply unit.

The feedback control voltage (1-5V) regulates the high voltage output linearly. The high voltage increases slowly, in 50 V steps with delay time of 5 s. Ripple voltage lower than 3 mV with no line distortion was achieved by using a simple Π-filter circuit at the output.

Specifications:

Input Voltage range:	0...10 Vdc
Power Supply:	+ 8V
Input Current (with no load):	max.13 mA
Output Voltage (with full load):	max. 40 mA
Variable output voltage range:	- 400V... -1300 V
Output current:	0.12 mA
Ripple/Noise (p-p):	1 mV_{ppm}

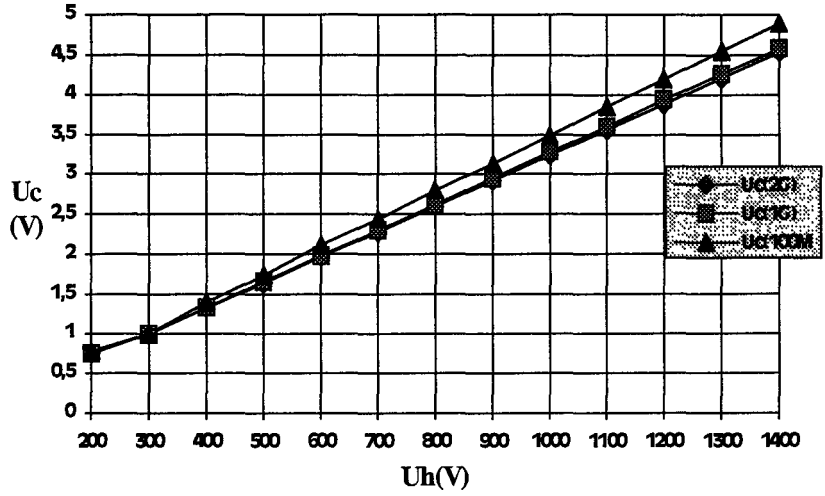

Fig.3 High voltage controlling characteristics

2. Two-channel electrometer unit with reset switch.

The electrometer unit is based on the ultra-low bias-current operational amplifier AD549, which is specially designed for electrometer amplifier application. The input offset voltage and output offset voltage drifts are laser-trimmed for precision performance. The offset voltage of each channel can be adjusted by a potentiometer.

Each channnel can convert an input current to an output voltage by integration using a high precision (270 pF ± 1 %) integration capacitor. The discharge of the integration capacitor is achieved by controlled p-channel MOSFET (Type: 3N163). The inverting input of AD549 is protected against over-voltage by special diodes with pA reverse current. (Type: BAV45) The transferred charge due to the discharging system is compensated and minimized by using a reverse-cycled MOSFET.

The small current parts of the electrometer circuit are mounted on teflon isolated solder-pads, which are surrounded by grounded guard-ring. The entire electrometer unit is enclosed in special shielding box.

Measurements were performed to investigate the offset + drift characteristics of the electrometer unit, and the results are given below. The droop is the change in the output voltage over time as a result of the bias current of the amplifier, leakage of the RESET switch, or other external leakage currents.

The measured droop in our present electrometer was:
Droop1 = 1 mV/s → with C_{int} =270 pF it corresponds to 279 fA input current,
Droop2 = 0,27 mV/s → with C_{int} = 270 pF it corresponds to 72 fA input current.
According to the theory this droop increases by a factor of 2 for each 10°C increase of ambient temperature.

Specification

Analog input		
input voltage range	-1500 + 1500	V
Input resistor	10^{13}	Ω
Input bias current	100 1000	fA
Output		
Integration mode droop	1	nV/μs
Current output (direct)	± 10	mA
Output voltage off-set	-200	μV
Output resistance	100	Ω
Output	short-circuit protected	
Power supply	± 12	V
Integration capacitance	270	pF
accuracy	1	%
temperature coefficient	-50	ppm/°C

3. Two -channel A/D converter

The two-channel-A/D conversion is achieved by using the 20 bit resolution DDC101 A/D converter (Burr-Brown). The task is to measure the output voltage of the 2-channel electrometer with high precision. As the electrometer circuit output supplies positive voltage, the DDC101 is configured in unipolar mode with input series resistors. The DDC101 operates as integrator, the integration (sampling) time is programmed. (The adjustable shortest integration time is 64 μs). In this instrument we chose integration time of 216 μs as the lowest limit, i.e. 4,6296 kHz sampling frequency. The input resistor (2,5M Ω) and the integration time 216 μs result in a measurable voltage range of 6,25V (current range 2,5 μA). This means that the total voltage range of the current integrator output is covered. The resolution of the voltage measurement is 5,96 μV. One can convert this to get the measurable charge resolution by using the parameters of the electrometer. In our case the integration capacitance in electrometer circuit C=270 pF; the output voltage range U= 6,25V gives total charge Q = 1,6875 Cb, with theoretical resolution of 1.609×10^{-15} Cb.

The DDC101 is programmed in CDS (Correlated Double Sampling) mode, which allows to compensate the inner errors of the DDC101 (like charge-injections, thermal noise, offset error). The adjusted CDS parameters are: K (acquisition periods) 16; M (oversamples) 32.

The -2,5V reference voltage is supplied by LM136 reference source IC. The exact value of the reference voltage can be adjusted by a potentiometer.
The potentiometer on each input allows the adjustment of the exact input voltage range.
The A/D converter panel is connected to the electrometer panel by a 10-pole connector, and to the microcontroller panel by a 34-pole connector.
The control signals of the DDC101 and the reset switch signal of the electrometers are supplied by Schmitt-trigger IC-s.

The DDC101 panel was designed in a way that it can also be connected and programmed as current meter although in the present construction we do not use the current mode.

Actual programming of the DDC101 panel is described in the controller chapter.

4. Controller unit and program

Specification of the controller hardware

Microcontroller:	80C537 16MHz clock signal 32Kbyte EPROM 32 Kbyte RAM 8Kbyte EEPROM
Display:	1 x 8 character LCD display
Controls:	4 push-buttons (RESET, STEP, ENTER, START)
Serial communication :	RS232 port, Set-up: 9600,8,N,1 No Handshake
Power supply:	4 x 1.2V=4.8V/2200mAh NiCd accumulator power consumption from the accu max. 1 A Operation time from charged accu min 2,5 hours Accu-charger unit: - MAX 713 controller - max. 1A charging current - output voltage limit: 6 V, adjustable - adapter can be connected continuously - adapted input is guarded against reverse polarity - charging indication with LED - adapter specification: 220V AC/ 8-9 VDC, 1A - automatic charging control - charging time: min. 3 hours - the instrument can be switched on with adapter Supply voltages made of accu voltage by DC/DC converters + 5VDC, 400 mA +12VDC/-12VDC, 80 mA for DDC101 and electrometer + 12VDCF/-12VDCF , 80mA ill. 8VDCF , 50mA for the DA and high voltage supply

DA converter: 12-bit serial
control signal isolated with opto-coupler
output voltage: 0-10 V
DA slew rate: max 50 V/sec

AD converter: built-in to the microcontoller, resolution 8 bit, that is 20 mV
applied for measurement of accu voltage with accuracy 50 mV

Control of DDC101: with microcontroller and surrounding IC's.
each signal is accepted and driven by 74HC14 Schmitt-trigger
SYSTEM CLOCK= 2 MHz

Sampling cycle time:

5kHz	- 216µs	=4630Hz
1kHz	- 1008µs	=992Hz
100Hz	- 10008µs	~100Hz
10Hz	- 100008µs	~10Hz
2Hz	- 500016µs	~2Hz

Operation mode: continuous at 5 kHz
not continuous at other frequencies
Acquisition time control:
K: 01, that is 1 CLK RESET and 15 CLK

A.Time Samples/Integration - M: 0101
that is 32 Samples/Integration
Integration/Conversion -L: 0000 ,
that is 1 Integration/Conversion
Input Range: 0 , that is Unipolar
Output Format: 0 , that is Straight Binary
-deltaU calculation:
dU=R x I=2.5MOhm x 500pC(DDC out/1048576)/Tmeas
Tmeas=Tint-K clock period -M clock period
Tmeas=216-8-16=192usec

Control program description

RESET procedure

- after Switch on or **RESET** a **HELLO** message appears on the LCD
- Accu voltage is measured and displayed: e.g. **UB=5.34 V**
- **EEPROM** message EEPROM test
- **EXTRAM** message external RAM test
- **HV=200V** offers high voltage set in 50 V steps up to 1300 V the required voltage can be accepted by **ENTER** button
- **f=5 kHz** offers sampling frequency set. The required frequency can be set in the following steps 5 kHz, 1 kHz, 100 Hz, 10 Hz and 2 Hz.
- **N=500** offers sampling number set. The following values can be chosen: 500, 1000, 2000
- **DA SET** when this message is on the High voltage is going up to the adjusted value.
- The inic. procedure evaluates the 2 MHz and the FDS signals
- **READY** message indicates that the instrument is ready for sampling

Measurement and calculation procedure

- After the **START** button is pushed the **SAMPLE** message appears and the two channel sampling and data storage is started
- As soon as the sampling ended the **COMPUTE** message appears and the data evaluation is started
- At the end of the calculation

  Yd = □□□,□ dose mean lineal energy (Yd dimension: **keV/μm)** or

  H = □□□,□ dose equivalent rate (H dimension: **μSv/h)**

  calculated results are displayed. The STEP button is used to choose between the two parameters
- **ERROR-1** and **ERROR-2** messages indicate that the signal on the corresponding channel is too high,
- The sampling starts again after pushing the **START** button

The calculations are made according to the given Block scheme. In the first version the parameters for calculation are fixed except the sampling frequency.

In a improved version the instrument will be able to communicate with the PC through RS232 port in READY state, the new parameters can be transferred from the PC to the EEPROM of the instrument. The last parameter set will be stored in the EEPROM. The PC will be able to read the measured results of the last sampling with the corresponding parameter set.

Final Report

1992-1995

Contract : FI3PCT920045 Duration : 1.9.92 to 30.6.95 Sector: A12

Title: The use of microdosimetric methods for the determination of dose equivalent quantities and of basic data for dosimetry.

1)	**Ségur**	**ADPA**
2)	**Brede**	**PTB**
3)	**Zoetelief**	**TNO-DELFT**
4)	**Schmitz**	**KFA Jülich GmbH**
5)	**Grillmaier**	**Univ. Saarlandes**
6)	**Bordy**	**IPSN-CEA-FAR**
7)	**Morstin**	**CITEC (PECO contract)**
8)	**Sabol**	**TECH. UNIV. CZ (PECO contract)**

I. Summary of Project, Global Objectives and Achievement:

As there is an increasing number of people who are exposed to high-energy neutrons ($E_n > 20$ MeV), it is necessary to develop new detectors for use in radiation protection dosimetry for this energy region. Most of these detectors can be ambient detectors, but individual detectors, for the purpose of accident dosimetry, are also necessary.

This project was mainly devoted to the improvement and also the design of various detector systems for radiation protection dosimetry in neutron-photon fields. The techniques investigated are based on the measurement of absorbed dose and LET in order to determine the dose equivalent. Depending on the type of application, TEPCs working at very low pressures and personal dosemeters have been investigated. The dose equivalent response of these TEPCs was determined in calibration fields with realistic spectra Furthermore, to improve the calibration of individual dosemeters according to the new recommendations of ICRP, a transfer device for the determination of dose equivalent quantity was studied.

Finally, since the understanding and the usefulness of microdosimetric devices strongly depends on the basic knowledge of many microscopic physical quantities, special emphasis was devoted to the determination of basic data such as W values for neutrons and heavy charged particles, electron-molecule cross-sections in organic vapours, Kerma factors, etc

a) Basic data for dosimetry :

a 1 Determination of W values in methane based TE gas (TNO):

In the case of heavy charged particles, simple analytical relationships were used to fit measured data W values for different particles (Proton, He, C, N, O) in methane based TE gas have been analysed in terms of this relationship

Using the analysis of W of charged particles as a function of specific energy, W values were calculated for neutrons as a function of energy with the Caswell/Coyne code for calculation of energy deposition and ion yield

a.2 Determination of electron-molecule cross-sections in organic vapours (ADPA).

The knowledge of electron-molecule cross-sections in organic vapours is of paramount importance not only for the theoretical study of the transport of electrons through TE gas but also for the numerical modelling of the motion of electrons in the various counters investigated in this project Cross-sections of isobutane and ethane were determined using a technique based on the unfolding of swarm parameters in gases. Furthermore a semi-analytical formula was developed to give the total ionisation cross-sections in various alkanes. It is now possible to predict, using these cross-sections in available codes, gas gain in isobutane or ethane based TE gas mixtures

a.3 Determination of gas-to-wall absorbed dose conversion factors (PTB, Univ Saarlandes, CITEC):

When using cavity detectors the gas-to-wall absorbed dose conversion factor, $r_{m,g}$, is needed to interpret the measured ion yield spectra and to relate the measured spectra in the cavity to the absorbed dose in the PC wall material. Calculational studies were performed in order to account for the differences in the transport of directly and indirectly ionising radiation in the various detector materials, including effects such as attenuation of primary fluence, buildup of secondary particle fluences and to obtain the charged particle spectral fluences from neutrons in the energy range from 25 to 250 MeV. The Los Alamos High Energy Transport Code was used to generate the initial charged particle spectra for neutrons.

a 4 Determination of oxygen Kerma factors (PTB):

Kerma factors, necessary to convert neutron fluence to dose or dose equivalent quantities that are based on measurements, are scarcely known for neutron energies above 15 MeV and often only based on theoretical modelling. In particular, experimental data for the kerma factors of carbon, oxygen and nitrogen are needed to determine kerma in tissue or in biological systems. In addition, most of the radiation protection instruments use these nuclei in their sensitive volumes.

Experiments were performed at PSI (Switzerland) in order to determine carbon, oxygen and nitrogen kerma factors. Special cavity chambers with walls made of Al, Al_2O_3, AlN, C, Zr and ZrO_2 were used.

a 5 Calculational optimisation of a transfer device for dose equivalent (PTB).

Calculational optimisation of size and materials of a phantom to be used in connection with a TEPC was made (PTB). These calculations show that the response of a transfer device is influenced by differences in atomic composition of ICRU phantom and TEPC material and, in particular for low energy neutrons, the quality of approximating L by y

a 6 Radiation transport calculations in anthropoid phantoms (KFA, TNO)

The aim of these calculations was to investigate the effect of the recommendations of ICRP in Report 60 on limiting quantities in radiation protection through the determination of dose equivalents and of microdosimetric spectra in a male and female phantom The investigations show that microdosimetric distributions are useful for characterising radiation quality variations within complex biological systems and that they can be applied for predicting radiological risks, i e the probabilities of specific low level radiation effects in particular organs There is however

an obvious need for response functions derived from radioepidemiology and from in vivo animal experiments, such as leukaemia induction

b) Improvement and developement of dosemeters based on microdosimetric principles:

b 1 Development of a low pressure tissue equivalent proportional counter (Univ Saarlandes, ADPA, TECH UNIV CZ))

The work in this contract was also focused on the development of a low pressure proportional counter (TEPC) for area dose monitoring. To fulfil the requirements of area monitoring the detector should have a constant dose equivalent response over the relevant neutron energy range, a sensitivity high enough to ensure a sufficient accuracy and a robustness to allow routine use These requirements led to a cylindrical single wire detector (named HTEPC) with a 3 mm thick wall of tissue equivalent material A 150 and a sensitive volume of 400 cm^3. The improvement of the geometry of this detector was made in strong collaboration with ADPA

The investigation of the characteristics of HTEPC in fields of practical relevance was necessary. In the frame of an intercomparison of dosimetric and spectrometric methods co-ordinated by WG 7 of EURADOS, measurements have been performed in the mixed neutron photon field in the Cadarache facility where radiation fields encountered in working environments of nuclear industries are simulated. To confirm the theoretically predicted improvement of the dose response R_H to moderated neutrons by reducing the simulated diameter, the measurements have been performed with 2, 1 and 0.5 µm simulated diameter in the configuration canel+ with 10 cm water as moderator. The dose equivalent readings increase about 12% from 2 to 1 µm and 10% from 1 to 0 5 µm

Measured (Univ. Saarlandes) and calculated (ADPA) single electron spectra were also obtained in order to improve the understanding of the counter response Furthermore, new Monte Carlo calculations of avalanche growth in cylindrical proportional counter was undertaken by TECH UNIV CZ.

b 2 Determination of the neutron response of GM counters and Mg/Ar ionisation chambers for energies above 20 MeV (TNO, PTB)

Measurements were made at the University of Louvain-la-Neuve to determine the neutron sensitivities of tissue equivalent (TE/TE), Magnesium/argon (Mg/Ar) ionisation chambers and a Geiger-Müller (GM) counters However the analysis is not yet completed.

b 3 Individual dosemeters (KFA, CEA, ADPA)

b 3 1 Semi-conductor Detector (SCD):

Experimental investigation of various SCD was performed using SRAM (Static Random Access Memory) and GaAs (Galliumarsenid) detectors and the respective performances of these detectors were carefully compared to conventional results given by proportional counters (KFA) The comparison of dose values measured with the SRAM chips and with proportional counters in the same field differ by about a factor of ten. The DRAM chips were also studied but they do not allow the measurement of microdosimetric spectra.

An alternative concept for a personal dosemeter was established The basic idea of this concept is to build up a detector system with an answer proportional to the individual dose equivalent $H_p(10)$ and a principle layout has been developed. Experiments with GaAs diodes have been performed and also with diodes based on silicon technology

b 3 2 Multi-cellular low pressure tissue equivalent proportional counter (MCPC)

The application of TEPC's to personal dosemeters meets large difficulties mainly due to a low sensitivity for small devices and to the long term behaviours of gas in sealed counters. This leads to investigate completely new design based on a multi-cellular geometry The multi-cellular geometry is aimed to increase the inner surface of the cathode to obtain a higher sensitivity. This is obtained by using two identical flat cathodes in which multiple cylindrical cavities (channels) are machined In order to approach the multi-cellular geometry, a single channel and a five channel prototypes have been designed and tested

The results show that the multi-cellular counter is able to perform microdosimetric measurement above 1 keV/µm for radiation protection purpose The multi-cellular geometry may be suitable to ensure the neutron sensitivity and partially the isodirectional response required for personal dosimetry Nevertheless, the MC TEPC has to be improved. Thus, by reducing the long chord length probability and modifying the Q(L) function used in the microdosimetric calculation, it seems possible to achieve a nearly flat energy response.

Head of Project 1 : Dr. P. Ségur

II Objectives for the reporting period

Determination of electron-molecule cross-sections in organic vapours

Determination of the limit of operation of proportional counters

Numerical modelling of real counters.

III Progress achieved including publications

1-Determination of electron-molecule cross-sections in organic vapours

The knowledge of electron-molecule cross-sections is of paramount importance to carry out not only the numerical modelling of the motion of electrons in a particular detector, but, also, to calculate the energy deposited by high and low energy electrons in a given tissue equivalent gas during the slowing down process.

As a few number of cross-sections were available in organic vapours, it was our first task, under the frame of this contract, to improve their knowledge. To do that we used the techniques based upon the unfolding of swarm parameters.

In the following, we will distinguish between the low energy case (electron energies lower than 1000 eV) and the high energy case

At low energy, we studied isobutane (i-C_4H_{10}) and ethane (C_2H_6) cross-sections. At high energy, we investigated the whole series of alkanes.

Figures 1 and 2 show the two sets of cross-sections obtained in isobutane and ethane for electron energies lower than 1000 eV. The cross sections given correspond to elastic processes, vibrations, dissociation, total excitation and total ionisation of the molecules We note that, for very low energy (before 10 eV), the structure of the various cross-sections become very complex indicating the strong interaction between the electron and the molecule Obviously, these cross-sections can now be used to calculate many quantities necessary to improve our understanding of the working properties of some detectors.

The determination of low-energy electron-molecule cross-section was made using the knowledge of available experimental swarm parameters For high energy, the situation is completely different and the unfolding of swarm parameters cannot be used In this case, however, the most important cross-sections to determine are total ionisation cross-sections and asymptotic formula based on quantum mechanical calculations are available together with some experimental results. We then used the experimental results available, together with the following semi-empirical relationship for the ionisation cross-sections $\sigma_{ion,n}$:

$$\sigma_{ion,n}(\varepsilon) = A_n \frac{4\pi a_0^2 R}{\varepsilon} Log(1 + 0.08(\varepsilon - I_n))\phi_n(\varepsilon)$$

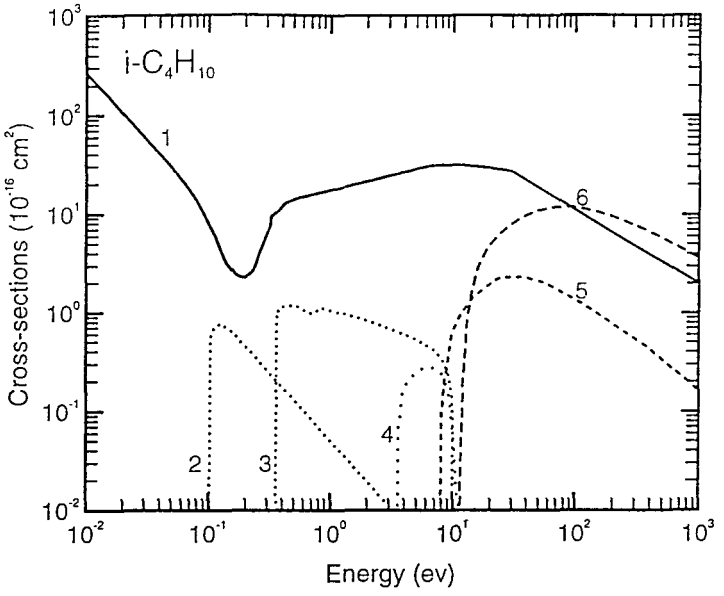

Figure 1 : *Electron-molecule cross-sections in isobutane*
(1), Elastic momentum transfer cross-section, (2,3), Vibrations (4) Dissociation (5) Excitation (6) Ionisation

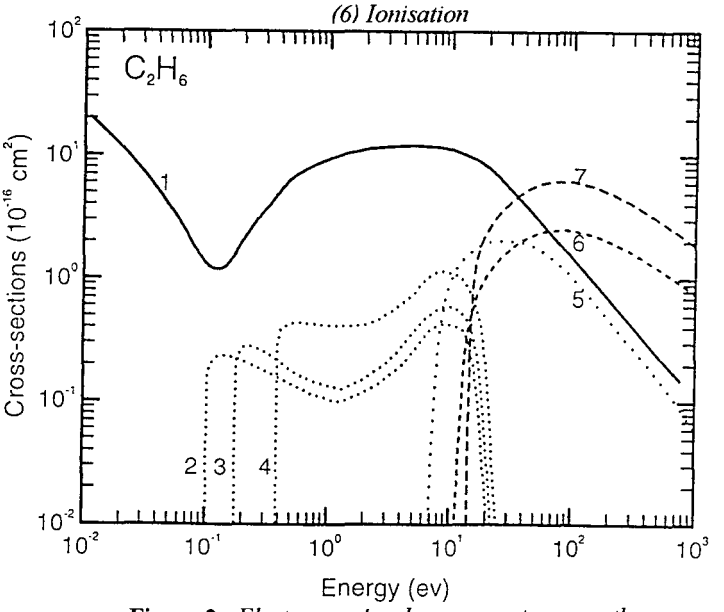

Figure 2 . *Electron-molecule cross-sections in ethane*
(1), Elastic momentum transfer cross-section, (2-4), Vibrations (5) Dissociation (6) Excitation (7) Ionisation

FI3PCT920045 Final Report

which is valid for the whole series of alkanes

In the above relationship, ε is the kinetic energy of electrons and I_n is the ionisation threshold of the molecule. $\phi_n(\varepsilon)$ function and constant A_n are specific to a given gas. A_n is determined using the high energy data available for ionisation cross-section and, furthermore, is directly connected to the oscillator strength. Table I shows the values of A_n obtained for the various alkanes.

Alkanes	A_n	M_i^2	I
CH_4	4.37	4.28	12.98
C_2H_6	9.02	8 63	11.65
C_3H_8	13.33	13.08	11.08
n-C_4H_{10}	17.57	17 80	10 5
i-C_4H_{10}	17.62	17.40	10.5
n-C_5H_{12}	24.61	24.40	10.33
i-C_5H_{12}	23.65	25.00	10.33
neo-C5H12	22.06	23.00	10.33
n-C_6H_{14}	34.23	34 80	10.17

Table I

constants	$\phi_1(\varepsilon)$	$\phi_2(\varepsilon)$.
a	5.21	4.02
b	9.51	27.22
a'	-13.66	14.10
b'	23.48	-22.75
a"	9.50	-17.09
b"	-2.34	3.94

Table II

Function $\phi_n(\varepsilon)$ must be determined from low energy experimental results for total ionisation cross-sections. Looking at the various experimental results, it appeared that only two different $\phi_n(\varepsilon)$ functions are necessary. The first one ($\phi_1(\varepsilon)$) must be introduced in the case of methane. The second one ($\phi_2(\varepsilon)$) is valid for all other alkanes. The following relationship shows the general analytical expression for the $\phi_n(\varepsilon)$ functions and the values of the corresponding constants are given in Table II.

$$\phi_n(\varepsilon) = a\exp(-b/\varepsilon) + a'\exp(-b'/\varepsilon^2) + a''\exp(-b''(\varepsilon - I_n)/\varepsilon^2)$$

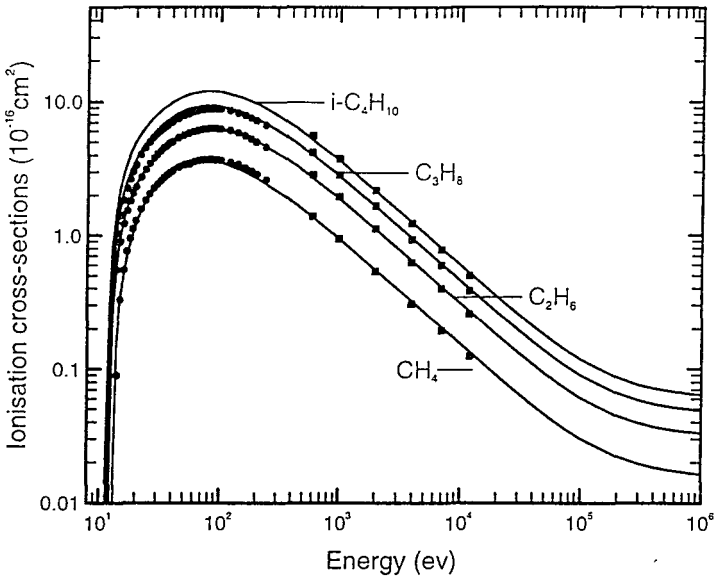

Figure 3a · *Total ionisation in alkanes*
(Symbols) experimental results (lines) calculations

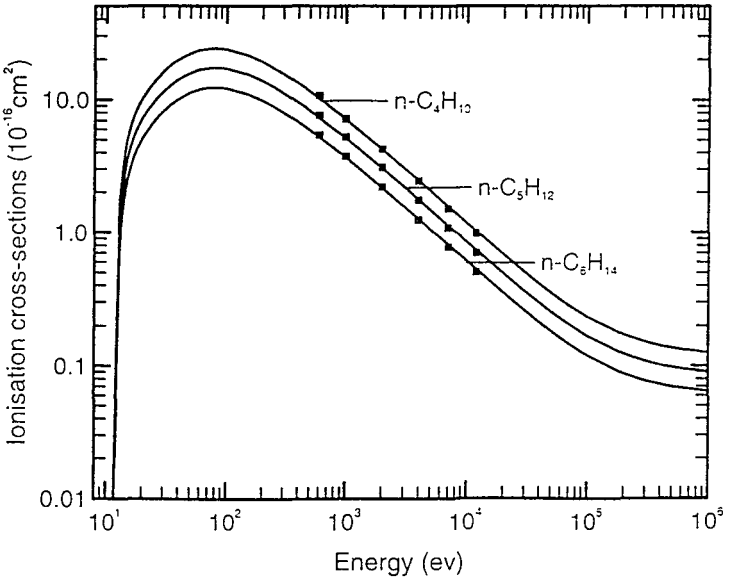

Figure 3b : *Total ionisation in alkanes*
(Symbols) experimental results (lines) calculations

Figure 3 shows the results obtained using our formula compared with experimental data Once the A_n constant is known for a given alkane, our formula allows the calculation of total ionisation cross-sections for the whole energy range (including relativistic effects) For example, this formula allowed the calculation, in isobutane, of low energy values of ionisation cross-sections which were missing in the literature and which were included in the low energy determination of cross-sections shown above

2-Determination of the limit of operation of proportional counters :

In connection with experiments made in Saarlande University (S. Gerdung, Pr. Grillmaier) and Legnaro (Dr. Colautti), the limit of operation of proportional counter was determined for propane tissue equivalent gas and pure isobutane. These calculations were based on Monte Carlo methods and the cross-sections determined in the first part of our work were used. Figure 4 shows the variation of the reduced gas gain lnG/K versus the reduced electric field at the anode *((E/N)a)* The gas is propane TE. In this figure, comparisons between equilibrium and non-equilibrium values are given As expected, the gas gain is lower than equilibrium values at low fields and higher at high fields. These results can be explained in term of electric fields gradients (low fields part) and in term of rotating effect of electrons (high fields part). Data in figure 4 are obtained for different voltage V (corresponding to different values of the ratio $K=V/log(rc/ra)$ where r_c and r_a are respectively the cathode and anode radius.) and different anode radius. Thin anodes (2.5 mm) correspond to the highest maximum and other anodes (5 mm) to the first maximum. The existence of a maximum followed by a decrease in the reduced gas gain, corresponds to the situation where the counter is no more proportional, the multiplication region filling up completely the counter volume Results in figure 4 show that the choice of a very thin anode allow, for a given pressure and gas, to extend the limit of operation of a proportional counter.

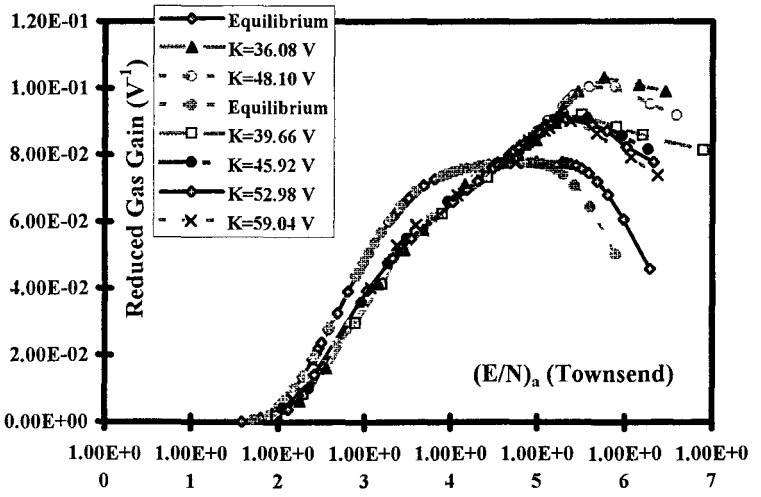

Figure 4 *Comparisons between equilibrium and non equilibrium values of the reduced gas gain in propane based TE.*

The above results show a slight dependence of the reduced gas gain with the factor K which is known to be a measure of the field gradient effect inside the counter. Normally, in most works devoted to the determination of the gas gain in a proportional counter, it is assumed that there is no gradient effect and that the reduced gas gain is only a function of $(E/N)_a$. Experimental and theoretical evidence shows that gradient effect can be very important Figure 5 shows experimental results obtained by A Waker (following some EURADOS Working group X discussions) The results, obtained at different pressures, for the same range of voltage and for methane based tissue equivalent gas, show that the reduced gas gain is a function of the K factor It is then clear that the reduced gas gain can no more be considered to be a unique function of $(E/N)_a$. Figure 6 shows the reduced gas gain obtained from Monte Carlo calculations, in pure methane and for different values of the K factor. Instead of a unique curve we now have a set of curves each curve corresponding to a different value of K. We must note that the biggest reduced gas gain correspond to equilibrium values. The equilibrium values (and consequently the Campion formula) can be considered as the limit when K becomes infinite of the reduced gas gain. The set of curves given in figure 6 generalises the usual results of the literature and allows a quick determination, for a given value of K, of the best value of the gas gain.

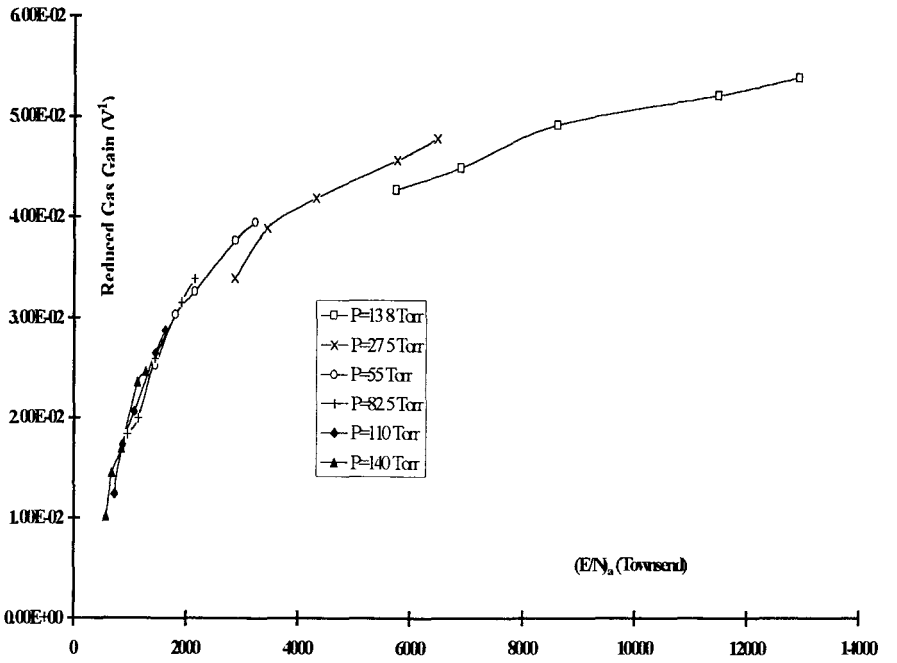

Figure 5 : *Experimental determination of the reduced gas gain as a function of the reduced electric field at the anode for different pressures ; gas : methane based TE, cathode radius, 0.75 cm, anode radius 25 μm*

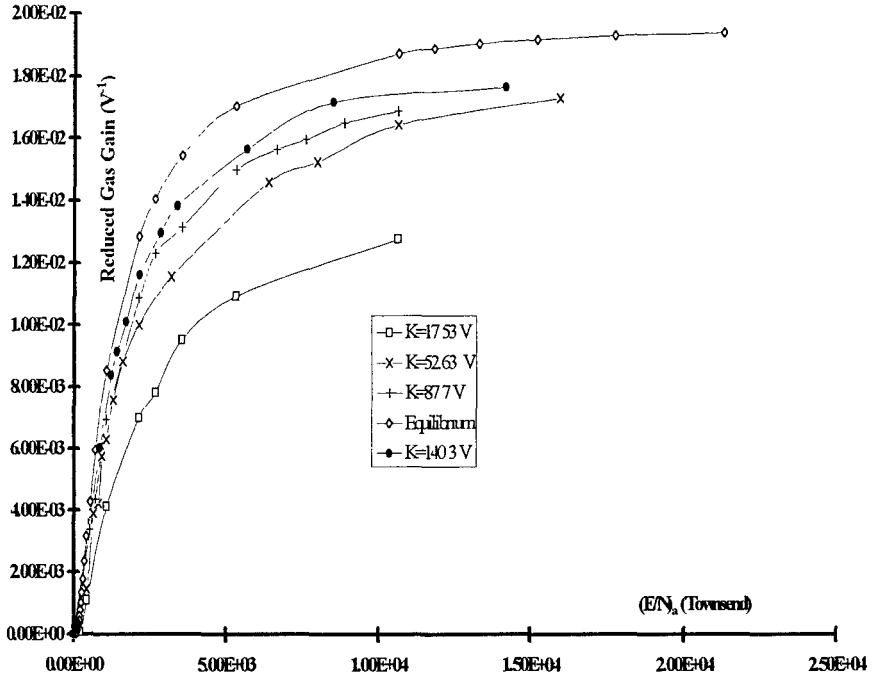

Figure 6 : *Monte Carlo calculations of the reduced gas gain in pure methane for different K values, cathode radius, 1.5 cm, anode radius, 50 μm.*

3-Numerical modelling of real counters

3.1 University of Saarlandes and S-DOS experiment:

In most works, the numerical modelling of a proportional counter is limited to the calculation of the gas gain through the integration of the ionisation coefficient over the radial distance from the wire The accuracy of this calculation can only be improved through a better knowledge of the ionisation coefficient. Although this procedure is usually well suited to give an order of magnitude of the gas gain in an 'ideal' proportional counter, it does not allow calculation of this gas gain in real situations since a counter is never perfect and strong field gradients may occur at the extremity of the anode wire (due to the existence of dielectric and metallic rings needed to fix the wire)

To calculate the gas gain in these conditions, it is necessary to determine first the real electric field inside the counter. The determination of the electric field is made numerically solving the Laplace equation When there is a cylindrical symmetry (as in the Homburg counter), the space is assumed to be two dimensional The main drawback in solving this problem is taking account the exact geometry of the counters including dielectric ring, guard rings, etc

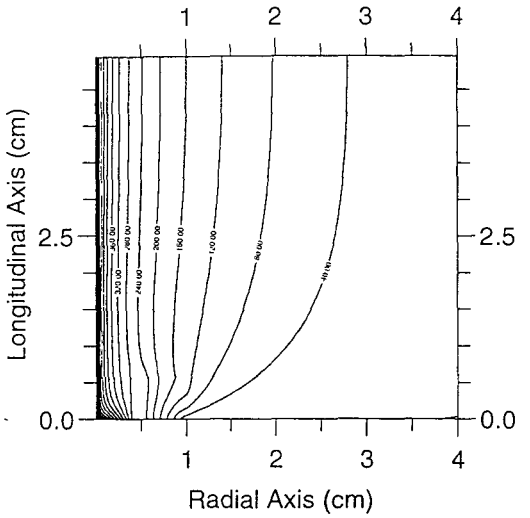

Figure 7 : *Equipotential lines, Voltage applied, 800 Volts, radius of the anode, 0.005 μm, radius of the cathode, 2.53 cm.*

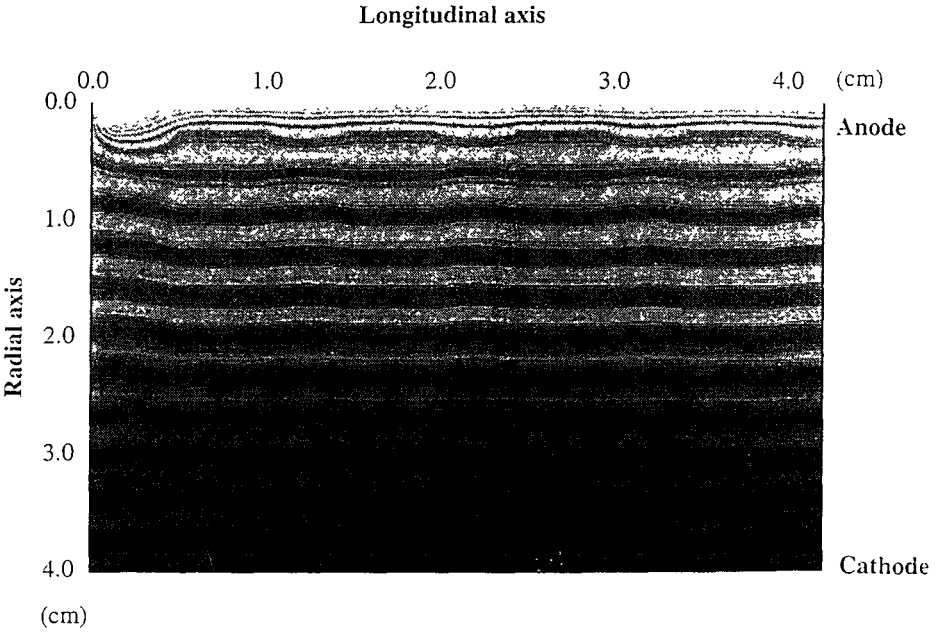

Figure 8 : *Equipotential lines in pentacellular counter.*

A numerical code was then developed which gives the two dimensional variation of the electric field for the Homburg counter and for some simplificated versions of S/DOS Multicellular Chamber

Once the electric field is obtained, it is necessary to calculate the gas gain The gas gain is then defined as the ratio between the total number of electrons collected at the anode to the initial number of electrons released in the gas. To determine the total number of electrons collected we solved, using the swarm parameters calculated with our electron-molecule cross-sections, the continuity equation We then obtain the space and time variation of the number of electrons inside the counter from the time when they were created inside the gas to the time when they completely disappear at the anode

It is then possible to calculate the variation of the gas gain versus some parameters such as, voltage applied, size and shape of guard and dielectric rings, nature and pressure of the filling gas, position of the initial particles, etc. and, consequently, to optimise the geometry of the detector

3.1.1 Homburg counter.

Figure 7 gives the 'optimum' electric field obtained for the Homburg counter.

To improve the knowledge of the response of the HANDI counter, measurements and calculations of single electron spectra were undertaken in Homburg. Results are given in the University of Saarlande report..

3 1.2 Multicellular Drift Chamber·

Different simplified versions of this counter were considered Figure 8 shows the spatial distribution of electric field in a cylindrical prototype The counter geometry is very close to that of the Homburg counter except that now a Shonka plastic bored with channels is located inside the counter.

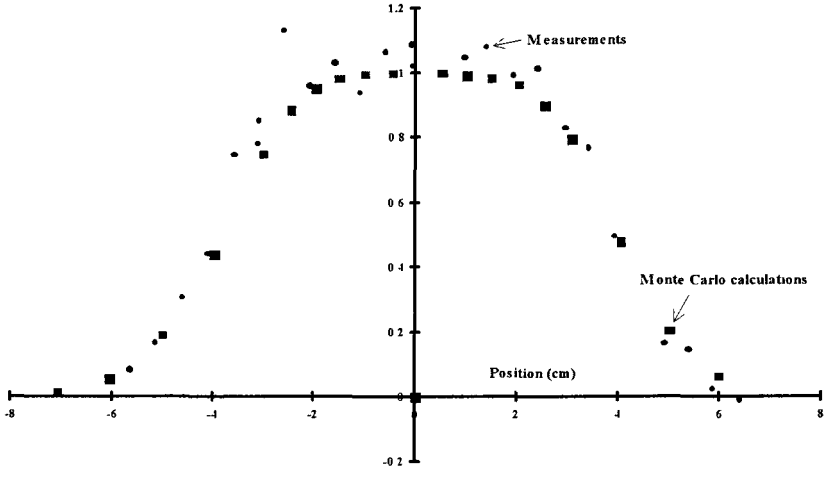

Figure 9 . *Transmission efficiency of electrons to cross a slit according to their initial position with respect to the center of the slit.*

3.2 Legnaro experiment.

Some Monte Carlo calculations were undertaken in connection with Legnaro experiment (see final report of contract FI3P-CT920041). One of the goal of this experiment is to allow the measurement of secondary ionisation created by the passage of a single charged particle in small organic gas volumes simulating nanometric dimensions. For this experiment to be efficient, electrons created inside a drift region must cross at the end a 2 mm hole which defines a sensitive volume of 10 nm diameter Obviously, the transmission power of this hole must be maximum.

To estimate the efficiency of the hole transmission, we developed a two dimensional code. In this code, a certain number of electrons are released inside the drift region, in front of a hole, and they move under the effect of applied electric field and collisions Figure 9 shows experimental and calculated values of the transmission efficiency of the hole depending of the location of the initial source of electrons Calculations were made in pure propane using our set of cross-sections The figure shows a very good agreement between experiment and calculations

Publications

J Barthe, M. Mourgues, J.M Bordy, P. Segur, B. Boutruche et G. Portal *Etude de compteurs miniatures pour la dosimétrie des neutrons.* Congrès IRPA Montréal 17-22 mai 1992.Vol. 1, pp. 479-482, Montréal.

D. Blanc, P. Segur P., J. Barthe, J. M. Bordy, *Les compteurs proportionnels à milieu équivalent au tissu, en radioprotection.* Congres IRPA Montréal 17-22 mai 1992 Vol 1, pp 459-462, Montréal

C. Bordage, J. Y. Gosselin, A. Chouki, P Ségur, *molecule collision cross sections in Propane. Swarm parameters in propane and argon-propane mixtures*, ESCAMPIG, St Petersbourg, (Aout 1992)

J. M Bordy, J. Barthe, T. Lahaye, B Boutruche, P. Ségur *Improving a multicellular tissue equivalent proportional counter for personal neutron dosimetry* Workshop in Chalk River, Canada, Radiat. Prot Dosim. 61(1-3), pp 175-178, (1995)

B Boutruche, J M Bordy, J. Barthe, P. Segur and G. Portal, *New concept of a high sensitive tissue equivalent proportional counter for individual neutron dosimetry.* 11th Symposium on microdosimetry, Gatlinburg, Tennessee USA, September 1992

A. Chouki, M. C Bordage, P Ségur, *Determination of electron-molecule cross-sections in alkanes*, ESCAMPIG, August 1994

A. Chouki , *Determination des sections efficaces de collision électron-molécule dans l'éthane, le propane et l'isobutane,* thèse d'Université, Toulouse, 1994, n° 1801.

Chouki , P. Ségur P., M. C. Bordage, *Analytical formula for ionisation cross-sections in alkanes and alkenes,* ESCAMPIG, August 1994

P Colautti, V Comte, M Guli, G. Talp, G Tornielli, B. Boutruche, C Moutarde, P Ségur, *The electronic avalanche in proportional counter* Workshop in Chalk River, Canada, Radiat Prot. Dosim 61(1-3), pp 257-262 (1995).

M Freyermuth, S Gerdung, A Chouki, R E. Grillmaier, C. Moutarde, P. Pihet, P. Ségur *Numerical Simulation of a Real Low Pressure Proportional Counter for Use in Radiation Protection* Workshop in Chalk River, Canada, Radiat Prot Dosim. 61(1-3), pp 171-174 (1995)

S. Gerdung, M. Freyermuth., R G. Grillmaier, P Pihet, P. Ségur *Entwicklung eines gewebeäquivalenten Niederdruck-Proprtionalzählers fur den Einsatz im Strahlenschutz* Fachverband fur Strahlenschutz 26 Jahrestagung, Köln, Verlag TÜV Rheinland, 1994, pp.572-577

Gerdung S , Grillmaier R.G., Lim T., Pihet P., Schuhmacher H. and Ségur P *Performance of TEPCs at low pressures: Some attempts to improve their dose equivalent response in the neutron energy range from 10 keV to 1 MeV*, Radiat. Prot Dosim 52(1-4), 1994, pp.57-59

S Lafont, Etude du non équilibre des électrons engendré par une forte variation spatiale du champ électrique, Thèse d'Université, Toulouse, 1995

C. Moutarde, Détermination numérique de l'amplification d'un compteur proportionnel cylindrique fonctionnant à basse pression ; application à la nanodosimétrie, Thèse d'Université, Toulouse, 1994, n° 1821

P. Olko, C Moutarde, P. Ségur *Multi-level modelling of the response of the ultraminiature proportional counter : gas gain phenomena and pulse height spectra* Workshop in Chalk River, Canada, Radiat. Prot. Dosim. 61(1-3), pp 205-210 (1995).

P Ségur, A. Chouki, M C. Bordage, J. Y. Gosselin, *Determination of electron-molecule cross sections in propane and calculation of swarm parameters in propane based mixtures,* XI Symp Microdos. Gatlinburg, Ten , USA (Sept. 1992)

P Ségur, *Kinetic description of electrons in inhomogeneous electric fields*, invited paper at theTwelfth European Sectional Conference on the Atomic and Molecular Physics of Ionized Gases (ESCAMPIG), August 1994

Scientific staff:

A. Alkaa, M C Bordage, A Chouki, S. Lafont, A Rabehi, P. Ségur

Other research groups collaborating actively in this project:

Legnaro Laboratories (Italia), Dr Colautti

Krakow University (Poland), Dr. P Olko

Members of WG 10 of EURADOS

Head of Project 2: Dr. H.J. Brede

II Objectives for the reporting period

i) Setup of a novel facility for reference fields in the neutron energy range above 20 MeV and the improvement of neutron spectroscopy and monitoring

ii) Calculations of gas-to-wall absorbed dose conversion factors

iii) Determination of oxygen kerma factors

iv) Calculational optimisation of a dose equivalent transfer device

III. Progress achieved including publications

i) Setup of a novel facility for reference fields in the neutron energy range above 20 MeV and the improvement of neutron spectrometry and monitoring

There is an increasing number of people who are exposed to high-energy neutrons ($E_n > 20$ MeV) in the environment of accelerators, radiotherapy facilities or aircraft at high flight altitudes In order to develop new detectors for use in radiation protection dosimetry for this energy region, a facility that provides neutron reference fields is a prerequisite The new detectors are to be experimentally studied, calibrated and intercompared with respect to the energy dependence of their response

In 1994 a unique facility in the European Community for high-energy neutron beams came into operation at the Université Catholique de Louvain-la-Neuve (UCL), Belgium. A cyclotron with an external pulsing system can produce beam bursts of 1 ns duration with a beam repetition time of 500 ns A flight path of up to 9 m between the neutron source and detector allows time-of-flight (TOF) spectroscopy to be applied in order to specify the properties of the neutron reference fields

In cooperation with UCL a series of measurements were performed to determine the properties of the neutron beams produced by the p + Li reactions. As an example, Fig 1 shows the spectral neutron fluence corresponding to a proton energy of 26,5 MeV which are available at UCL and the Paul Scherrer Institue (PSI), Switzerland Both spectra were determined with an NE213 liquid scintillation detector by applying pulse-shape discrimination techniques for photon - neutron separation and TOF techniques for neutron energy determination.

In addition, a new proton recoil telescope (PRT) was tested and used to determine the absolute neutron fluence This device has an efficiency which is about a factor of 10 larger than that of the previously used PRT and extends the measurement of neutron fluence to the energy region from about 20 to 100 MeV.

The consistency of spectral neutron fluence determination with hydrocarbon scintillation detectors using TOF techniques and fluence measurements with a PRT was investigated for neutron energies of 44 MeV and 65 MeV (see publ. 1,3). If the full response of the scintillation detector including contributions from neutron reactions with carbon is used for the fluence determination, the results differ up to 15 % from the measurement made with a PRT The

deviations depend on the threshold of the scintillation detector and the neutron energy. An explanation of this deviation may be an inadequate description of the n-C reaction channels and the cross section data sets available in the Monte Carlo Code SCINFUL [DI 91] that has been used to calculate the response and the efficiency of the scintillator

Neutron monitoring in the reference beams was improved by using several systems. An NE102 liquid scintillator of 2 mm thickness as a transmission detector, a fission chamber with a ^{238}U layer, and a 1 mm thick silver disc as an activation detector. The energy dependence of the $^{238}U(n,f)$ and $^{107/109}Ag(n,3/5n)^{105}Ag$ cross sections, however, have to be taken into account [LI 91, RA 87, SC 92].

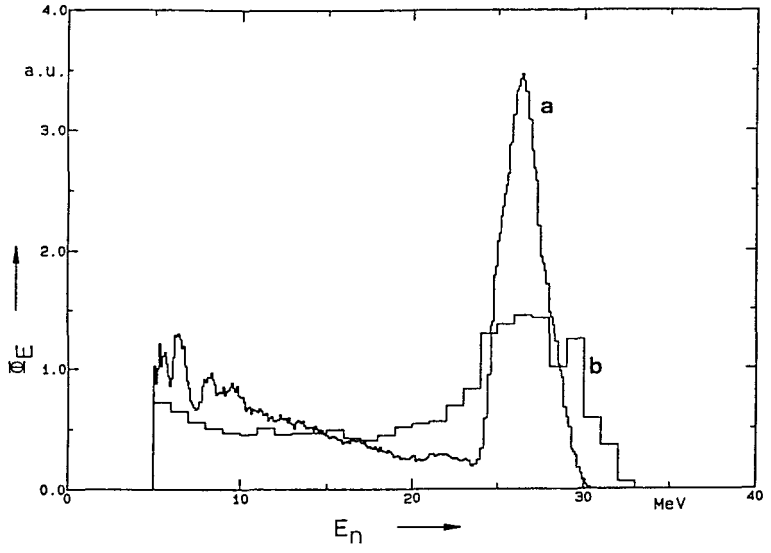

Fig. 1. Spectral fluence of the p+Li collimated neutron source at a distance of 5 m from the target measured with an NE213 scintillation detector with pulse-shape and TOF techniques at UCL (a) compared to the p + Be neutron source at PSI (b).

ii) Calculations of gas-to-wall absorbed dose conversion factors

Special proportional counters (PCs) with walls of Al, Al_2O_3 and AlN developed at the University of Birmingham, U.K. and of Zr and ZrO_2 at the University of Wisconsin-Madison, USA, were used in the high-energy neutron fields at PSI in order to determine absorbed dose. When using cavity detectors the gas-to-wall absorbed dose conversion factor, $r_{m,g}$, is needed to interpret the measured ion yield spectra and to relate the measured spectra in the cavity to the absorbed dose in the PC wall material. Calculational studies were performed in order to account for the differences in the transport of directly and indirectly ionising radiation in the various detector materials, including effects such as attenuation of primary fluence, buildup of secondary particle fluences and to obtain the charged particle spectral fluences from neutrons in the energy range

from 25 to 250 MeV. The Los Alamos High Energy Transport (LAHET) Code System (LCS) [PR 89] was used to generate the initial charged particle spectral fluences of protons, deuterons, tritons, ^{3}He, and α-particles produced in C, ZrO_2, Zr, Al, Al_2O_3, AlN and A 150 plastic

For the present purposes, $r_{m,g}$ includes differences in stopping powers and atomic compositions, but does not explicitly account for attenuation of the primary neutron fluence Energy deposition is only considered for coulombic interactions of protons and heavier ions Energy deposition in the form of nuclear excitation is excluded, as are radiative processes

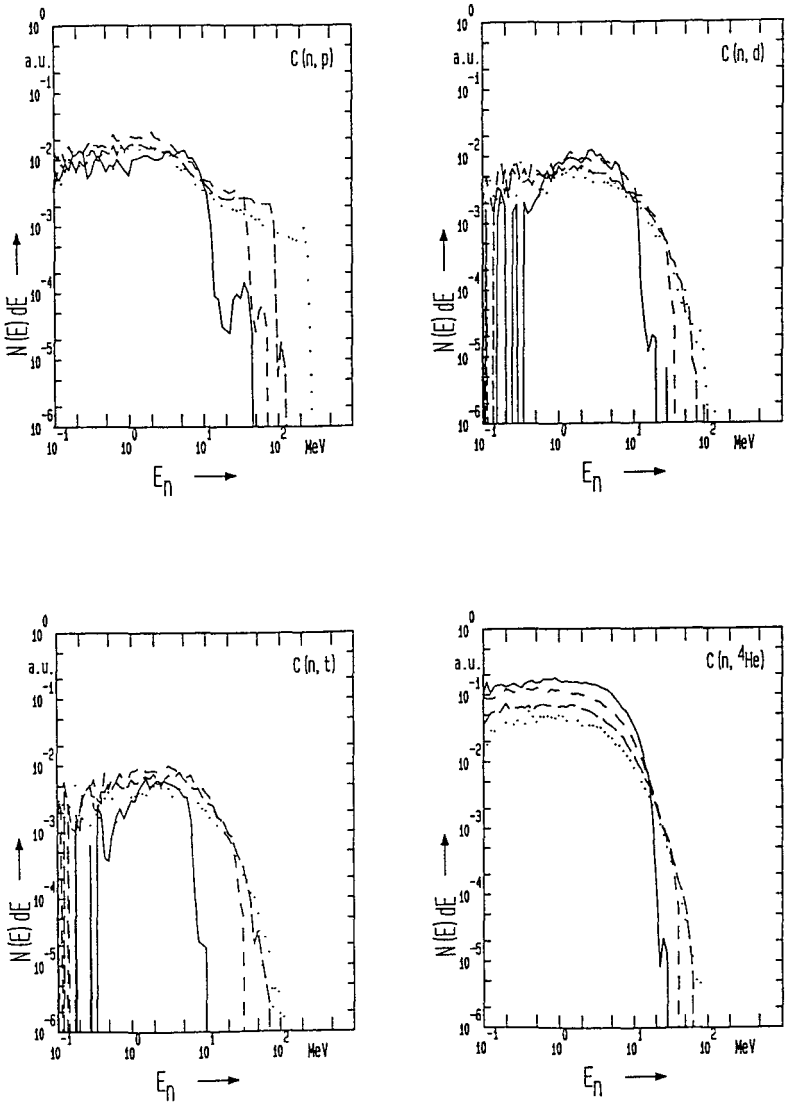

Fig. 2: Calculated initial secondary particle spectral fluences from neutrons incident on ^{nat}C Shown are production spectra from monoenergetic neutrons of 25 MeV (—), 50 MeV (— —), 100 MeV (---), and 250 MeV (· · ·), of protons, deuterons, tritons, and α-particles (see publ 6)

Since measured double-differential, single-differential, or integral charged particle production cross sections at higher neutron energies are scarce, LAHET's intranuclear cascade (INC) model was used to generate the initial charged particle spectral fluences. At lower neutron energies, a statistical model is used to describe the evaporated particles from compound nuclei In the intermediate neutron energy range a single-stage preequilibrium model was used.

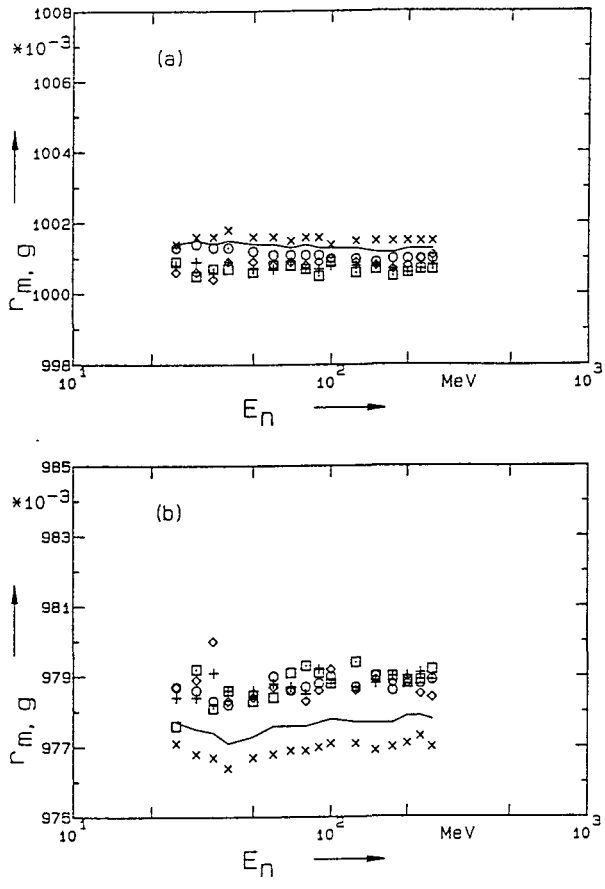

Fig. 3: Calculated gas-to-wall absorbed dose conversion factors, $r_{m,g}$, versus neutron energy for monoenergetic neutrons incident on A150 plastic with a propane-based tissue equivalent gas cavity Absorbed dose weighted average values (solid line). Only considering (o) protons, (◊) deuterons, (+) tritons, (□) ^{3}He, and (×) α-particles (see publ. 6). (a) Calculations using stopping power data of Ziegler and Biersack for A150 plastic and PTE gas [ZI 85] (b) Calculations using the stopping power data of ICRU [IC 93].

As an example, Fig. 2 shows the initial secondary particle spectral fluences from neutrons incident on ^{nat}C The charged particle spectra of O, C, H, Ca, and N calculated with the LAHET Code are used to derive the gas-to-wall absorbed dose conversion factor for an A150 plastic detector with a propane based tissue equivalent (PTE) gas cavity (see publ 6), (Fig 3).

iii) Determination of oxygen kerma factors

Kerma factors, necessary to convert neutron fluence to dose or dose equivalent quantities that are based on measurements, are scarcely known for neutron energies above 15 MeV and often only based on theoretical modelling. In particular, experimental data for the kerma factors of carbon, oxygen and nitrogen are needed to determine kerma in tissue or in biological systems In addition, most of the radiation protection instruments use these nuclei in their sensitive volumes

Experiments were performed at PSI in order to determine carbon, oxygen and nitrogen kerma factors. Special cavity chambers with walls made of Al, Al_2O_3, AlN, C, Zr and ZrO_2 were used.

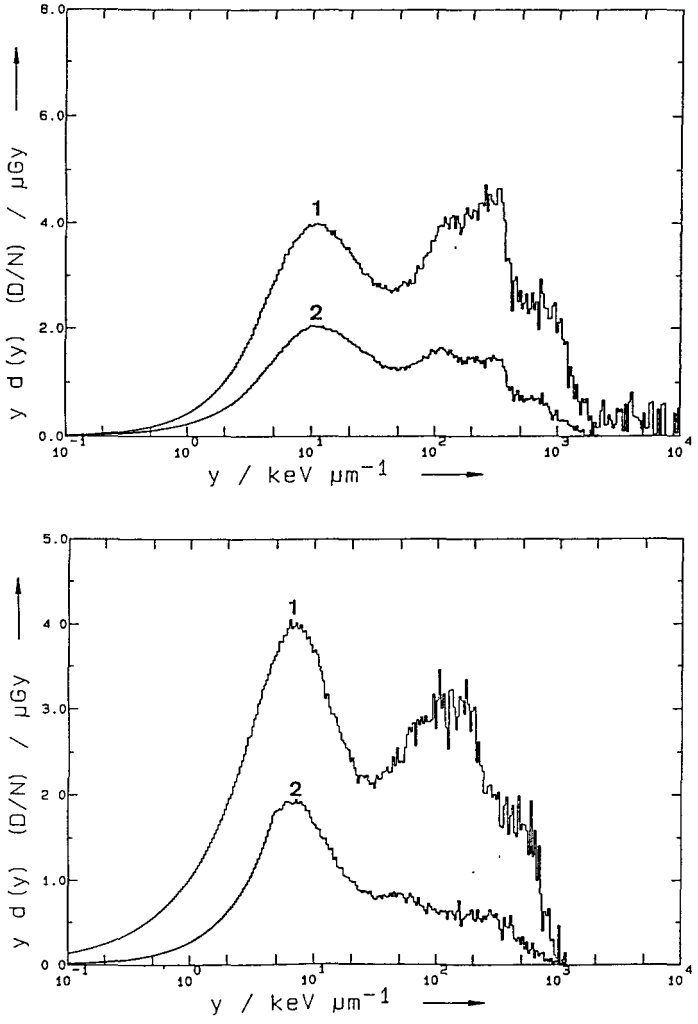

Fig 4 (top) Ion yield spectra in Al_2O_3(1) and Al (2). Both spectra were normalised to the counts of the neutron fluence monitor and to equal numbers of Al atoms in the detector walls (bottom). Normalised ion yield spectra of ZrO_2 (1) and Zr (2).

Fig. 4 shows the results of an analysis for $E_n = 45$ MeV. The difference in the spectra in each figure corresponds to the contribution of oxygen for both detector systems. These different spectra (i.e oxygen ion yield spectra) from Al/Al_2O_3 measured with PTE gas differ from those from Zr/ZrO_2 measured with $Ar+CO_2$ gas. From a comparison of the ion yield spectra of carbon-walled PCs measured with the respective gases, it can be concluded that this difference is almost exclusively due to the different gas-to-wall dose conversion factors The oxygen kerma was calculated from the ion yield spectra of 'pure' oxygen using the absorbed dose to the gas in the ZrO_2 and Zr PCs, using the gas-to-wall conversion factors calculated by Newhauser [NE 95] and the charged particle stopping power data from Ziegler and Biersack [ZI 85]. The summary of the analysis of the oxygen and carbon kerma data is shown in Fig. 5 together with a least square fit (see publ. 7).

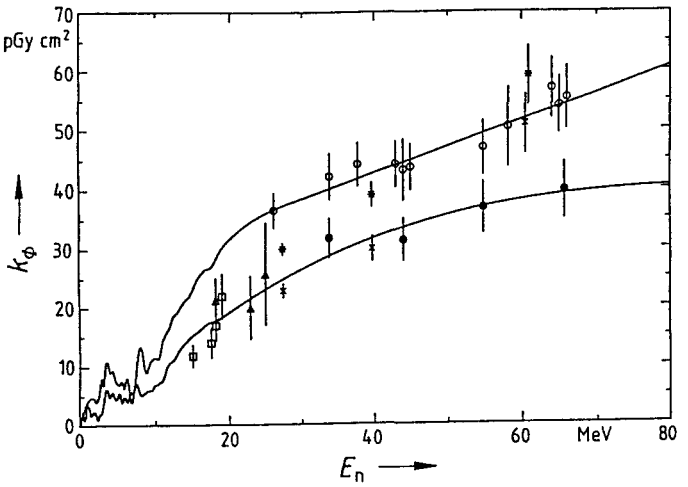

Fig. 5· Neutron kerma factors for carbon and oxygen The circles indicate the results of the present experiments, open circles are for carbon, the filled circles for oxygen, and the lines represent the least square fit. Experimental oxygen kerma factors of other authors are given for comparison (□) DeLuca et al [DE 88], (×) Brady and Romero [BR 79], (*) Romero et al [RO 85] and (Δ) Hartmann et al [HA 92].

iv) Calculational optimisation of a transfer device for dose equivalent

Calculational studies of a suitable combination of a tissue equivalent proportional counter (TEPC) and a phantom for use as a transfer device for dose equivalent were performed for a TEPC positioned at 10 mm depth in slab phantoms of various materials and sizes.

The operational dose equivalent quantities H*(10) and $H_p(10)$ [IC 85] are determined by the absorbed dose and its distribution in linear energy transfer, L, at the reference position in the ICRU sphere and slab, respectively The reading of the dose equivalent transfer device, on the other hand, is determined by the absorbed dose and its distribution in lineal energy, y, in the gas cavity of the TEPC. Fig. 6 compares these distributions for two neutron energies.

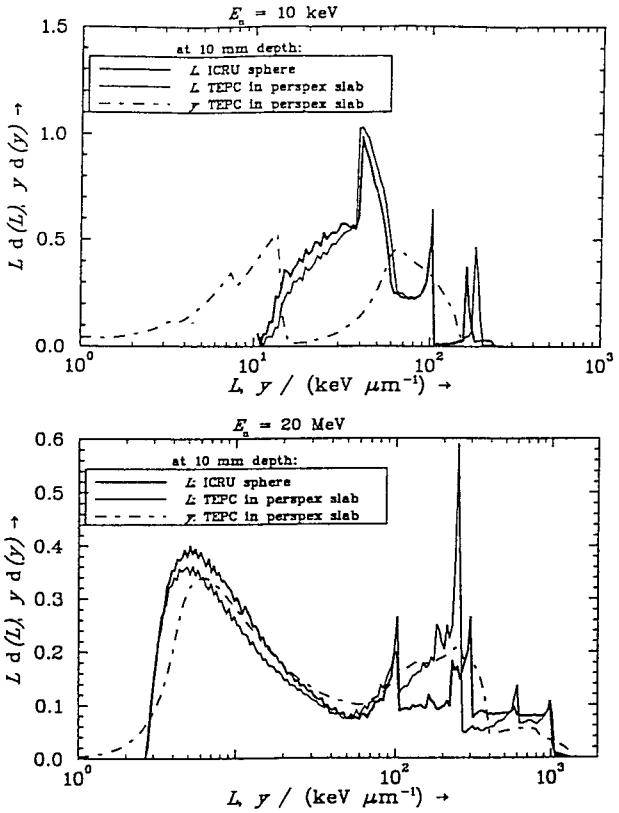

Fig 6 Absorbed dose as function of lineal energy, y, and as function of linear energy transfer, L, calculated for ICRU sphere and transfer instrument. Incident neutron energies are 10 keV (top) and 20 MeV (bottom).

For 10 keV neutrons the L·d(L) spectra in the ICRU sphere and of TEPC material (A150) are very similar They show contributions from recoil protons, protons from the N(n,p)C reaction and carbon ions from N(n,p)C (peaks from left to right in Fig 6). This reaction is induced by neutrons that are thermalized in the phantom. The slight differences reflect the different stopping powers in water and tissue-equivalent gas, respectively The y·d(y) spectrum consists of two peaks The peak from recoil protons is shifted to lower values compared to the L·d(L) spectra because the protons are stopped inside the TEPC cavity The two secondaries from the N(n,p)C reaction show up as one peak because they are detected as a single event

For 20 MeV, the L d(L) spectra show small differences because of the difference in atomic composition of ICRU tissue and tissue-equivalent plastic (A150) and in stopping powers as mentioned above. The y d(y) spectrum is very similar because of the long ranges of the secondaries.

These two examples show that the response of a transfer device is influenced by differences in atomic composition of ICRU phantom and TEPC material and, in particular for low-energy neutrons, the quality of approximating L by y (see publ 8)

References

[BR 79] F.P Brady and J L. Romero. 1979: Neutron Induced Reactions in Tissue Resident Elements Final Report to the National Cancer Institute, Grant No 1r01 CA16261 Technical Report (University of California-Davis, Davis, CA).

[DE 88] P M. DeLuca, H H Barschall, Y. Sun, and R C. Haight. 1988 Kerma Factors of Oxygen, Aluminium, and Silicon for 15 to 20 MeV Neutrons Radiat Prot. Dosim. 23, p 27-30

[DI 91] J K. Dickens. 1991: SCINFUL: A Monte Carlo Based Computer Program Oak Ridge National Laboratory, Report ORNL/TM-11812

[HA 92] C.L Hartmann, P.M. DeLuca, Jr , and D.W Pearson 1992 Measurement of Neutron Kerma Factors in C, O, and Si at 18, 23, and 25 MeV. Radiat. Prot. Dosim. **44**, p 25-30.

[IC 85] International Commission on Radiation Units and Measurements. 1985: Determination of Dose Equivalent for External Radiation Sources ICRU Report 39, Bethesda, MD, USA

[IC 93] International Commission on Radiation Units and Measurements. 1993: Stopping powers and ranges for protons and alpha particles ICRU Report 49, Bethesda, MD, USA

[LI 91]P.W. Lisowski, A. Gavron, W.E. Parker, J.L. Ullmann, S J. Balestrini, A.D Carlson, O.A. Wasson, and N.W. Hill. 1991: Fission Cross Section in the Intermediate Energy Region, Proc of a Specialist's Meeting on Neutron Cross Section Standards for the Energy Range above 20 MeV, Uppsala, Sweden, Report NEANDC-305 "U", Paris, p 177-186.

[NE 95] W. D Newhauser. 1995 Neutron Kerma Factor Measurements in the 25 MeV to 85 MeV Neutron Energy Range Ph.D Thesis, University of Wisconsin - Madison.

[PR 89] R.E. Prael and H. Lichtenstein. 1989: Users guide to LCS The LAHET Code System. Report LA-Ur-89-3014, Los Alamos National Laboratory, NM, USA

[RA 87] J. Rappaport, J. Ullmann, R.O Nelson, S. Seestrom-Morris, S A Wender, and R C Haight. 1987 Preliminary measurement of the $^{235}U(n,f)$ cross section up to 750 MeV LANL Report UC-34C LA-11078-MS, Los Alamos National Laboratory, NM, USA

[RO 85] J.L. Romero , F.P. Brady, and T S Subramanian 1985 Neutron Induced Charged Particle Spectra and Kerma from 25 to 60 MeV. In Proc Int Conf. on Nuclear Data for Basic and Applied Science, Santa Fee, NM, USA (New York Gordon and Breach Science Publishers), p 687-699

[SC 92] U J Schrewe, H.J. Brede, M. Matzke, R. Nolte, J P Meulders, H Schuhmacher, and I Slypen 1992. $^{107/109}Ag(n,3/5n)^{105}Ag$ reaction cross section for $20 < E_n < 70$ MeV. Proc Int Conf on Nuclear Data for Science and Technology, Jülich, Germany, 1991. (Ed S.M. Qaim, Springer Verlag, Berlin, 1992), p 669-671.

[ZI 85]Ziegler and Biersack 1985 The Stopping and Ranges of Ions in Solids Vol 1 of the Stopping and Ranges of Ions in Matter. Pergamon, New York

Publications

1 R Nolte, H Schuhmacher, .H.J. Brede, and U.J. Schrewe 1992 Measurement of High-Energy Neutron Fluence with Scintillation Detector and Proton Recoil Telescope Radiat Prot. Dosim **44**, p 101-104

2 U J Schrewe, H.J Brede, S Gerdung, R Nolte, P. Pihet, P. Schmelzbach, and H Schuhmacher. 1992 Determination of Kerma Factors of A-150 Plastic and Carbon at Neutron Energies between 45 and 66 MeV. Radiat. Prot. Dosim **44**, p 21-24

3 R Nolte. H J. Brede, U J Schrewe, and H. Schuhmacher. 1993. Neutron Spectrometry with Liquid Scintillation Detectors at Neutron Energies between 20 MeV and 70 MeV. A Status Report. Physikalisch-Technische Bundesanstalt· PTB-N-9 (June 93) ISSN 0936-0492

4 H Schuhmacher, R.A. Hollnagel, and B.R.L. Siebert. 1994: Sensitivity Study of Parameters Influencing Calculations of Fluence-to-Dose Equivalent Conversion Coefficients for Neutrons. Radiat Prot. Dosim. **54**, p 221-225

5 B.R.L. Siebert and H. Schuhmacher. Calculated Fluence-to-Directional and Personal Dose Equivalent Conversion Coefficients for Neutrons Radiat Prot. Dosim. in press

6 W.D. Newhauser, U.J. Schrewe, and B. Wiegel. Gas-to-Wall Absorbed Dose Conversion Factors for 25 to 250 MeV Monoenergetic Neutrons Radiat Prot.Dosim. in press.

7 U.J Schrewe, W.D. Newhauser, H J. Brede, V. Dangendorf, P M. Deluca, Jr., S. Gerdung, R. Nolte, P. Schmelzbach, H Schuhmacher, and T Lim. Measurement of neutron kerma factors in C and O: Neutron energy range of 20 MeV to 70 MeV. Radiat Prot. Dosim. in press

8 H. Schuhmacher. On the Operational Radiation Protection Quantities for Mixed Photon-Neutron Radiation Fields, Radiat. Prot Dosim. in press.

Scientific staff:

H.J Brede, V Dangendorf, O. Hecker, W D Newhauser, R Nolte, U J Schrewe, H Schuhmacher, and B.R.L. Siebert

Other research groups collaborating actively in this project:

Université Catholique de Louvain-la-Neuve (UCL), Belgium (Prof J P. Meulders)

Paul Scherrer Institute (PSI), Villigen, Switzerland (Dr P Schmelzbach)

University of Madison, Wisconsin, U S A (Prof P DeLuca, Jr.)

University of Birmingham, U K (Prof M Scott)

Members of EURADOS Working Group 10

Head of project 3: Dr J. Zoetelief

II. Objectives for the reporting period

The irradiation facilities at the University of Louvain-la-Neuve (UCL) are essential to explore basic data and detector characteristics at neutron energies in excess of 20 MeV Trough the characterisation of these neutron fields as planned for by PTB, the sensitivities of Geiger-Muler (GM) and magnesium/argon (Mg/Ar) and tissue-equivalent (TE/TE) ionisation chambers for neutrons at energies in excess of 20 MeV will be determined The measurements will be made in close collaboration between PTB, UCL and TNO Calculations will be made using the Monte Carlo Neutron and Photon transport code (MCNP-4) and using the Caswell/Coyne (NIST) analytical code for energy deposition and ion yield gaseous detectors These calculations will be performed complementary to the experimental investigations Finally, TNO will contribute to the activities of EURADOS Working Group 10, collaborating on improvement of basic data for neutron dosimetry. Emphasis will be placed on improvement of W-values for neutron dosimetry.

III. Progress achieved including publications

Measurement of relative neutron sensitivities of detectors at high (>20MeV) neutron energies
Measurement were performed at the University of Louvain-la-Neuve (UCL) with tissue equivalent (TE/TE) and Magnesium/Argon (Mg/Ar) ionisation chambers and Geiger-Müler (GM)-counter for neutrons with an energy of 26 MeV produced by the p(28)+Li reaction. For the Exradin model T2 (serial number 224) TE ionisation chamber both the TNO Keithley 617 and the PTB Keithley 642 electrometer were used for charge measurements. For the measurements with the Exradin model MG2 (serial number 159) Mg/Ar Chamber, due to the low current, the Keithley 617 electrometer was not sensitive enough to perform accurate charge measurements and only the Keithley 642 electrometer was used. The GM tube (Philips 18529) was operated at+550 V, surrounded by an energy compensating lead-in shield according to Wagner and Hurst and connected to the PTB counter

The T2 (number 224) chamber was positioned at the reference position (5.215 m distance from the target) and a 6 mm build-up cap was used The chamber was operated at a collecting voltage of 250 V When connected to the Keithley 617 electrometer a relative reading normalised to the target charge of (2 25 ± 0 08) 10^{-17} Gy/MC resulted when k_T and h_T values of 1 00 were applied

The MG2 (number 159) chamber was positioned at the reference position with a 6 mm build-up cap added The chamber was operated at various collecting potentials (-250 V, + 150 V, +250V, +350 V and +500 V) since previous results (Schlegel-Bickmann et al , 1990) showed differences in k_U values at different polarities of up to about 15 per cent

A detailed analysis of the results has to be completed in close collaboration with PTB.

Analysis of W-values of charged particles in methane based TE gas

FI3PCT920045 Final Report

Concerning basic physical data, emphasis has been placed in the present contract on the improvement of W_n-values, i e the mean energy expended by neutrons per ion pair formed. For proportional counters or ionisation chambers used in neutron dosimetry, the ion yield or specific ionisation may be converted into energy loss or absorbed dose in the gas by means of an average W-value This average concerns a variety of charged particles generated in the wall and the gas of the detectors.

At the start of the project, various general reports on W-values are available or in preparation including ICRU-31 (1979), Goodman and Coyne (1980), Rubach and Bichsel (1982), Burger and Makarewicz (1984), Burger et al (1985), Coyne et al. (1990) and IAEA (1995). In ICRU-31 emphasis is placed on W-values of charged particles and various gases. Goodman and Coyne (1980) calculated W_n for neutron energies between 0.1 and 20 MeV for A-150 plastic ionisation chambers with infinite cavities for methane based tissue equivalent (TE) gas using evaluated published information on W-values for charged particles. Rubach and Bichsel (1982) performed calculations of W_n in the neutron energy region from 0 4 to 14 MeV for different cavity sizes and A-150/methane based TE-gas and C/CO_2 chambers. The activities at GSF (Burger and Makarewicz, 1984, Burger et al., 1985) concerned an evaluation of W for charged particles and calculation of W, for neutrons with energies from thermal to 20 MeV in A-150/methane based TE-gas and C/CO_2 ionisation chambers with various cavity sizes Coyne et al. (1990) employed information from Huber et al (1985) and Waibel and Willens (1985) on W-values of charged particles for calculation of microdosimetric spectra for low energy neutrons. The IAEA co-ordinated research programme on atomic and molecular data for radiotherapy focused on providing more recent information on W-values for charged particles including validity of additivity rules for mixtures of gases (IAEA, 1995)

The present work is aimed at providing an update of existing information on W_n As a first step, an analysis is made of W-values for charged particles based on more recent information, e g Huber et al , 1985

Concerning W-values for protons in methane-based TE-gas, recently a new analytical representation was presented by Siebert et al (Radiat Prot Dosim. 52 123-127, 1994) They proposed the following analytical expression for the W-values of protons as a function of energy ($W_f(Ep)$)

$$W_f(Ep) = A\{\ln(Ep + B)\}^{-D} + CEpE_b/(Ep^2 + E_b^2) + W_\infty \qquad (1)$$

Where Ep is the proton energy, W_∞ the W-values at infinite proton energy, the parameters A, B, and D are similar to those used in an older expression suggested by Coyne et al (Read Prot Dosim 31,217-221, 1990) and the constant C and co-factor are used to model a "bump" at a proton energy near E_b. The subscript *f* was introduced to have a value of 1 for a model without a bump, i e., C=0 and a value of 2 for a model with a bump The parameters and uncertainties (one standard deviation) are given in Table 1 for the model with bump

For the analysis of W-values for α, C, N and O particles, equation (1) has been rewritten

$$W_R(E_R) = A\{\ln(E_R + B)\}^{-D} + C\,E_R\,E_b / (E_R^2 + E_b^2) + W_\infty \qquad (2)$$

Where E_R is the specific energy in keV per nucleon for the particle (R) under consideration.

Edwards (Phys Med. Biol 28, 367-374, 1983), Thomas and Burke (Phys Med Biol., 30, 1215-1223, 1985), Rohrig and Colvett (Rad. Res., 76, 225-240,1978), Varma and Baum (Phys Med Biol 23,1162-1172,1978), Kemmochi (Health Phys 30, 439-446, 1976) and Krieger et al. (Phys Med Biol 24, 286-298, 1979) The uncertainties stated by the authors vary from 0 3 percent (e g , Rohrig and Colvett) to approximately 3 per cent (e.g Nguyen et al) The error discussion by the various authors differs greatly in detail Some authors only include statistical uncertainties whereas others give an estimate and error propagation of statistical as well as systematic errors Some of the results were obtained relative to other gases whereas other investigators performed absolute measurements The smaller uncertainties quoted seem not be realistic. Fits to all data according to equation (2) employing a relative uncertainty of 1 6 per cent results in a p-values in a p-values of 0 48. The resulting value of B of 1 14 is not significantly different from 1 The value of one minus the parameter B might be physically interpreted as the specific energy at which the production of ion pairs is no longer possible. Since charged particles without energy cannot form ion pairs a value of B greater than one seems unrealistic Therefore B was fixed to one. With this fixed values of B the p-values of the fit reduces only slightly to 040. A fit without a "bump" i.e C=O results in a p-value of $6\ 10^{-3}$ This suggest that similar to the situation for protons a bump around a specific energy of about 200 keV/nucleon is realistic.

Experimental data on W-values of C-, N- and O-particles in methane based TE-gas are less abundant than for protons or α-particles. Data for W-value of carbon were obtained from Huber et al (1985), Rohrig and Colvett (1978) and Chemtob et al. (Phys. Med. Biol. 23, 1197-1199, 1978) W-values for nitrogen were taken from Huber et al (1985) and Chemtob et al (1978) For W-values for oxygen, data were used from Huber et al. (1985), Nguyen et al (1980) and Varma et al. (Radiat. Res. 70, 511-518, 1977) The uncertainties quoted by the authors vary from about 1 to 3 per cent Fits to the data allowing for a "bump" result in negative W-values for nitrogen and oxygen and a C-value not significantly different from zero for carbon. Therefore fits were made for the model without bump (i e , C=O) and a fixed value for B equal to one and a relative uncertainty of 3 per cent for the data. Resulting p-values for C, N and O were 0.40, 0.995 and 0 69 respectively This might lead to the conclusion that errors for N are estimated too large However, W_∞ -values were quite different, i.e , 27 7±1 8 eV for C, 15.5±1 5 eV for O The largest specific energies investigated are quite different, i e. for oxygen by far the largest value was included in the measurements, i.e. 2569 keV/nucleon, whereas the maximum values for C- and N-particles are only 53 and 27 keV/nucleon, respectively Since the W_∞ -values for (α-particles and O-particles) were not significantly different, it was decided to fix W_α for all particles to 23 eV.

The results of fits of W-values for protons (Siebert et al), α-, C- N- and O-particles (present work) are summarised in Table 1 for methane-based TE-gas as a function of specific energy. An indication of the uncertainties is given in Table 2,

To improve the existing information experimental studies might be conducted at larger specific energies for C-and N-particles. In addition, measurement could be performed to provide some explanation for the bump in the proton and α-particle data

Table 1. *Analytical fits for W-values of charged particles as a function of specific energy in methane based TE-gas according to equation (2).*

particle	A (eV)	B	C (eV)	D	E_b(keV)	W_∞ (eV)
p	16 56 ± 0.39	1 043 ± 0 034	2 01 ± 0 19	1 653 ± 0 054	400	29 10 ± 0 11
He	36 2 ± 0 3	1	4 1 ± 0 6	0 817 ± 0 010	201 ± 2	23
C	44 1 ± 0 6	1	0	0 799 ± 0 015	-	23
N	43 3 ± 0 4	1	0	0 715 ± 0 006	-	23
O	46 3 ± 0 5	1	0	0737 ± 0 012	-	23

Table 2. *Uncertainties in the fits presented in Table 1.*

particle	relative standard deviation (%)	p-value
p	2 5	-
α	1 6	0.40
C	3	0 21
N	3	0 18
O	3	0 75

Calculation of W_H-values for neutron energies up to 60 MeV in methane-based TE-gas

Using the analysis of W-values of charged particles as function of specific energy (see previous section) W-values were calculated for neutrons as a function of energy with the Caswell/Coyne code for calculation of energy deposition and ion yield A comparison was made with results obtained using different sets of W-values of charged particles, i e , of Goodman and Coyne (1980) and Siebert et al. (1990) and Siebert et al. (1994) In addition, in the version of the Caswell/Coyne code supplied by Schuhmacher (PTB) also ENDF/B-VI data for carbon are available. Differences obtained between the use of ENDF/B V and ENDF/B VI data for carbon are negligible W-values for neutrons derived from charged data according to various authors are shown in Figure 1 for the energy range 0.1 to 20 MeV Maximum differences occur between values based upon Goodman and Coyne (1980) and Coyne et al (1990) of about 0 9 eV It should be borne in mind, however, that the values of Coyne et al. were intended to be used only at low neutron energies. Compared to the values based on Goodman and Coyne, the W-values of Siebert et al (with bump) and the new (draft) data show differences below 0.3 MeV and above about 3 MeV and are at maximum about 0 8 eV, i e., approximately 2 5 per cent

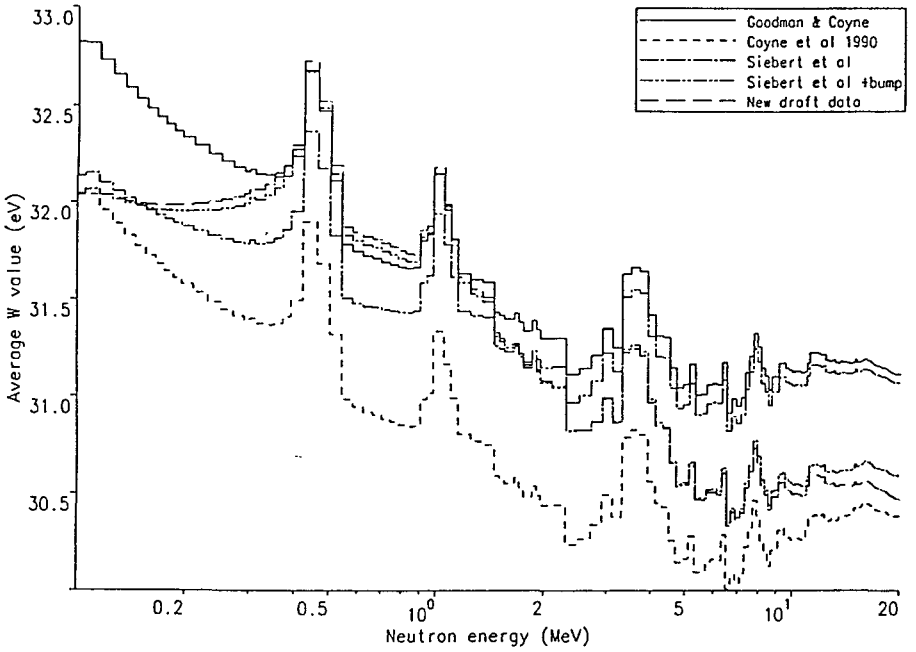

Figure1 *W_n in TE gas as a function of neutron energy calculated from W-values for charged particles according to various authors. The W_n-values were calculated employing the Caswell/Coyne and ENDF/B V cross sections.*

Using the new evaluation of W-values for charged particles calculation of W_n-values in excess of 20 MeV were performed in a joint enterprise of PNL (National Physical Laboratory), PTB and TNO (Taylor et al., in press) The results were calculated using different sets of cross-sections, i e., ENDF/B VI data for hydrogen, data of Brenner and Prael (Atomic Data and Nuclear Data, Tables 41, 71-130, 1989) for non elastic cross sections with carbon and oxygen, with elastic cross-sections for carbon and oxygen being taken from Dimbylow (NRPB-R78,1978) up to 50 MeV, and from Meigooni et al (Phys Med Biol 29, 643-659, 1984) and Islam et al. (Phys Med. Biol 33, 315-328,1988) beyond 50 MeV, for simplicity this diverse set is termed "the HX set"; the ENDF/B VI cross-sections (EB6) and the recommended kerma factors of White et al (K_{rec}, Radiat. Prot. Dosim 44, 11-20, 1992) The results for W_n using different combinations of cross sections are shown in Table 3.

It is concluded that above 20 MeV, the W-values decrease smoothly with neutron energy, enabling the use of a simple interpolation routine for the calculation of intermediate values. The re-evaluation highlights the lack of experimental data for higher energy heavy recoils, with only one datum point above 60 keV a.m u $^{-1}$ for ^{16}O and none at all for either ^{12}C or ^{14}N Furthermore, with different gases (e.g propane-based TE-gas) being used increasingly often because of their superior gas gain properties, there is a demonstrable need for equivalent investigations into the W-values properties of other counting gases.

Table 3. *W_n-values for high energy neutrons in methane-based TE-gas employing kerma factors from various sources.*

1 HX kerma factors for H, C and O, 2 HX kerma factors for H and O and EB6 for C: 3 K_{REC} FOR H, C and O, and 4 K_{rec} for H and O and EB6 for C (Taylor et al , 1995)

E_n	$W_n(1)$	$W_n(2)$	$W_n(3)$	$W_n(4)$
20	30.43	30.51	30 46	30.44
25	30.33	30 43	30 35	30.35
30	30 24	30.37	30.22	30.25
35	30.19	-	30.18	-
40	30.12	-	30.12	-
45	30.08	-	30 08	-
50	30.04	-	30 03	-
55	30 01	-	30.01	-
60	29.98	-	29.99	-

Calculation of organ and effective dose per unit fluence for exposure of ADAM to broad neutron beams in AP direction

Until recently, the use of the MCNP code at TNO had been restricted to calculations of organ and effective doses in case of external photon and electron beams employing anthropomorphic phantoms developed by GSF for adult male (ADAM) and adult female (EVA) (Kramer et al , GSF Bericht S-885, 1982). To obtain confidence in the use of the MCNP-code for calculation of neutron transport, organ and effective doses were calculated for ADAM exposed in Antherior-Posterior (AP) direction with broad beams of mono-energetic neutrons (Figure 2). MCNP version 4.2 was used employing cross-sections from ENDL85 except for nitrogen where the ENDF/B IV data were used

Compared to the results of Hollnagel (Radiat Prot. Dosim 44, 155-158, 1992) for energies between 10^{-6} and 3 10^{-1} MeV the results agree between about -7 per cent and +20 per cent (our values generally being 10 to 20 per cent higher). For the lowest two energies our values are about 50 per cent higher and, at 3 MeV, 35 per cent lower, at 10 MeV, 30 per cent and, at 20 MeV, 80 per cent higher This might be due to the use of different radiation transport codes (MCNP versus in-house developed cod) or due to different cross section data (Hollnagel employed ENDF/B V data). With the exception of the values below 10^{-6} and 20 MeV the differences are acceptable for radiation protection purposes

Relative neutron sensitivity of TE-ionisation chambers in an epithermal neutron beam

In the framework of optimisation of the use of radiation detectors for dosimetry, calculations have been performed of the relative neutron sensitivity (k_T) of TE-ionisation chambers in beams of epithermal neutrons at the facility of the High Flux Reactor in Petten in close collaboration with the Antoni van Leeuwenhoek Hospital Amsterdam Calculations have also been performed for the chamber shielded by ^{6}Li containing cap to shield the detector from thermal neutrons Information on neutron sensitivity in this energy range is important for boron-neutron-capture therapy as well as for radiation protection purposes e.g. around reactors. For the latter situation, it has been reported by e.g. Bartlett et al. (Radiat. Prot. Dosim. 44, 233-238, 1992) that the contributions from thermal and epithermal neutrons to the ambient dose equivalent (H*(10)) can amount to 75 per cent.

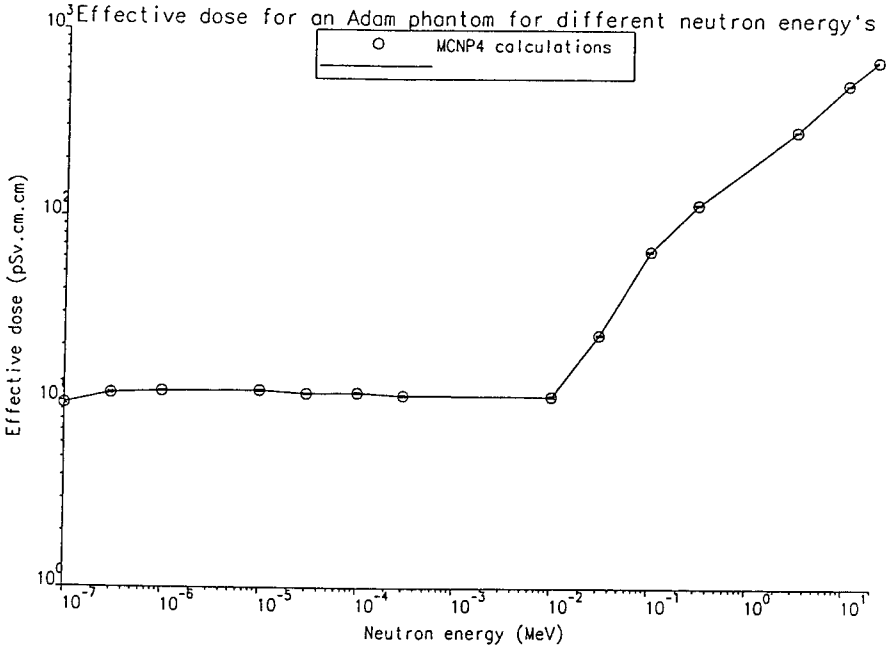

***Figure 2** : Effective dose E per unit neutron fluence plotted as a function of neutron energy for AP incidence of broad parallel neutron beams.*

The energy dependence of k_T of TE-ionisation chambers depends on the W-value as well as the ratio of kerma factors between muscle tissue and A-150 plastic. The epithermal neutron beams cover a wide energy range i e. from 2 5 10^{-8} to 20 MeV. Therefore in first instance k_T was calculated for mono-energetic neutrons in this range W_n values calculated in this energy show a distinct peak in the energy range from 10 eV to 10 keV with a maximum at around 0.4 keV, similar to data published by Makarevicz and Burger (Proc. Fifth Symp on Neutron Dosimetry

Makarevicz and Burger (Proc. Fifth Symp. on Neutron Dosimetry 275-283, 1985). The largest difference in W_n-values between the present calculations and those of Makarevicz and Burger (1985) amounts about 20 per cent and occurs at the maximum W_n-values This difference is most likely due to the different fit functions used for W of charged particles as a function of energy i.e equations 1 and 2 versus the relation of W as a function of particle energy

$$W \propto 1/(1-U/\varepsilon^1)$$

Where U is a constant, representing an ionisation threshold and ε^1 the kinetic energy of the charged particle in question.

Using the kerma factors of Caswell et al (Radiat. res 83, 217-254, 1980) and assuming a gas to wall conversion factor of 1.0, k_T has been calculated (Figure 3). The highest k_T value (at about 18.5 MeV) is about 1.042, the lowest k_T (at about 5 10^{-4} MeV) is about 0.193 For thermal neutrons k_T is approximately 0.94. These results are quite different from the values published by Rogus et al. (Med Phys. 21, 1611-1625, 1994) as shown in Figure 4. The differences are due to the approximations used for W_n values of Goodman and Coyne (Radiat Res 82, 13-26, 1980) linearly to neutrons energies below 0.1 MeV or applied W_p-data of Leonard and Boring (Radiat Res. 55,1-9, 1973) which results in infinite W-values below about 10^{-3} MeV. More recent information. of Huber et al. 1985 (see previous sections) showed that W_p does not increase as rapidly as found by Leonard and Bohring. linear extrapolation of W_n below 0.1 MeV is not valid (previous paragraph).

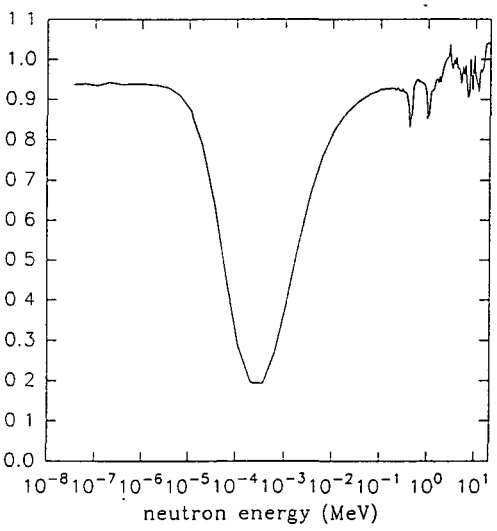

Figure 3 :*Relative neutron sensitivity of a TE-ionisation chamber as a function of neutron energy*

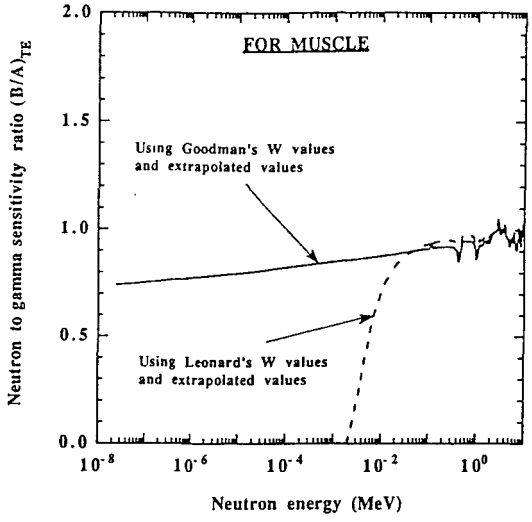

Figure 4 : *Relative neutron sensitivity of a TE-ionisation chamber as a function of neutron energy (Rogus et al , 1994).*

Neutron spectra were determined free-in-air and at different depths in a polythene phantom at the HB11 epithermal neutron beam facility of the High Flux Reactor in Petten. Spectral data will be presented elsewhere (Jansen et al , 1995). Originally, W_n-values and resulting k_T-values were calculated using the Caswell/Coyne code for energy deposition and ion yield. However, due to the wide range of neutron energies (about 10 decades) and the limited number of linear energy bins, erroneous results were obtained due to the fact that the important low energy parts of the spectrum were all in one too large energy bin Therefore, an in-house computer code was developed for the calculations of k_T The results were compared to those obtained with the Caswell/Coyne code when the spectrum was subdivided to achieve a reasonable number of energy bins in each region The results of this comparison were good (differences less than 93 per cent). Table 4 shows the results of k_T at different irradiation conditions in the presence and absence of a ^{6}Li containing cap.

Table 4. *Relative neutrons sensitivity of a tissue equivalent ionisation chamber in the absence and presence of a ^{6}Li containing cap at various conditions in the HB 11 epithermal neutrons beam facility at Petten*

conditions	k_T	k_T (with ^{6}Li containing cap)
free-in-air	0.905	0 877
polythene-phantom, 0 cm	0 870	0 861
polythene-phantom, 1 cm	0 866	0 857
polythene-phantom, 2 cm	0 900	0 858
polythene-phantom, 3 cm	0 913	0 868

It can be seen from the table that the variation in k_T is somewhat larger (4 per cent) without the ^{6}Li containing cap than that in the presence of the ^{6}Li containing cap (2per cent) In absence of spectral data, k_T-values of 0.89 and 0.86 could be applied in the absence and presence of a ^{6}Li containing cap, respectively These values are smaller than the value of 0 95 proposed by Rogus et al , 1994.

Publications

- G.C Taylor, J. Th.M. Jansen, J. Zoetelief, H Schuhmacher. Neutron W-values in methane-based tissue-equivalent gas up to 60 MeV (in press, Radiat. Prot. Dosim.).

- J.Th M. Jansen, C.P.J. Raaijmakers, B.J. Mijnheer, J Zoetelief. W-values and relative neutron sensitivity of tissue-equivalent ionisation chambers in an epithermal neutron beam for boron neutron capture therapy (in preparation).

Scientific staff

- Dr. F.W. Schultz, Dr. J.Th M Jansen, Dr. J. Zoetelief.

Other research groups collaborating activity in this project

- EURADOS Working Group 10 (mainly Prof. J.P. Meulders (UCL) and Dr. G.C. Taylor (NPL)) and Drs Raaijmakers and Mijnheer from the Netherlands Cancer Institute.

II Objectives for the reporting period

- investigation of semiconductor devices (Static Random Access Memory (SRAM), Dynamic Random Aqccess Memory (DRAM), and Diodes) for the application as individual dosemeters in mixed neutron and photon radiation fields

- radiation transport calculations in anthropoid phantoms to investigate the effect of the recommendations of ICRP in Report 60 on limiting quantities in radiation protection

III Progress achieved including publications

The initial goal of the project was to investigate, wether commercially available semiconductor devices are applicable as detector elements for a dosemeter to be used in mixed neutron gamma radiation fields, which is based on microdosimetric principles. Two basic requirements for such a detector are that a single sensitive volume of such a detector has micrometer dimensions (so that ideally it is small in comparison to the range of secondary charged particles produced by the radiation) and that the secondary charged particle spectrum produced by the radiation in the detector is similar to the one that would be produced in tissue.

The second requirement can be fullfilled, if the detector is covered with an equilibrium thickness of tissue equivalent material. However, neutrons incident on the detector will also interact with the semiconductor matrial. Charged particles produced in those interactions will contribute to the charged particles spectrum detected by the device. This influence has been studied (Fig.1).

The first requirement can be fullfilled if integrated circuits are used, since the depletion zones (the sensitive volumes) of single transistors or diodes in those circuits have microscopic dimensions. Memory chips were considered as most promising and therefore SRAMs (Static Random Access Memory) were studied initially. Important parameters required to judge the suitability of these devices are tabulated in table 1. In particular the geometrical dimensions, which are important parameters for the evaluation of measured pulse height distributions in terms of lineal energy y had to be determined experimentally, since no reliable manufacturer data were available. Figure 2 displays microdosimetric spectra measured with the SRAM chips and compares them to the spectrum derived with a Tissue Equivalent Proportional Counter (TEPC) in the same field. Differences in the spectra measured with the SRAMs can be explained on the basis of the different geometrical parameters of the chips and the fact that the 64kBit chip in contrast to the 4kBit chip was directly covered with a thin ployamid layer and has a thinner inactive top layer (dead layer). The consequence of the latter is that alpha particles and heavier ions produced by fast neutrons in the polyamid layer (contribution above100keV/μm for the 64kBit chip) are detected by the 64kBit chip. In case of the 4kBit chip charged particles heavier than protons.

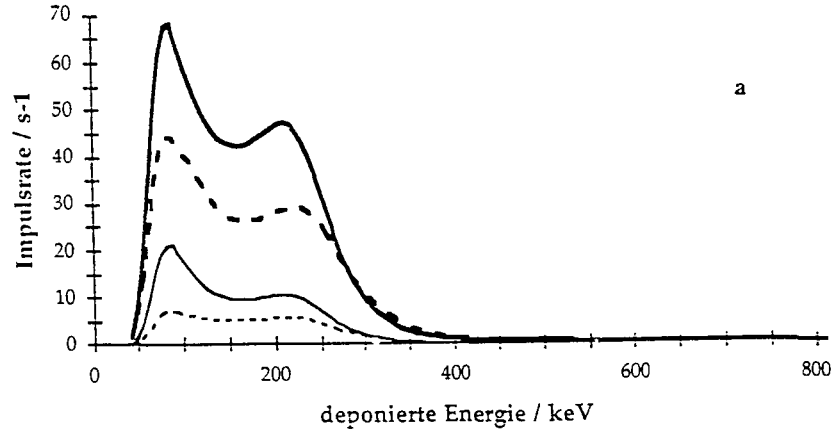

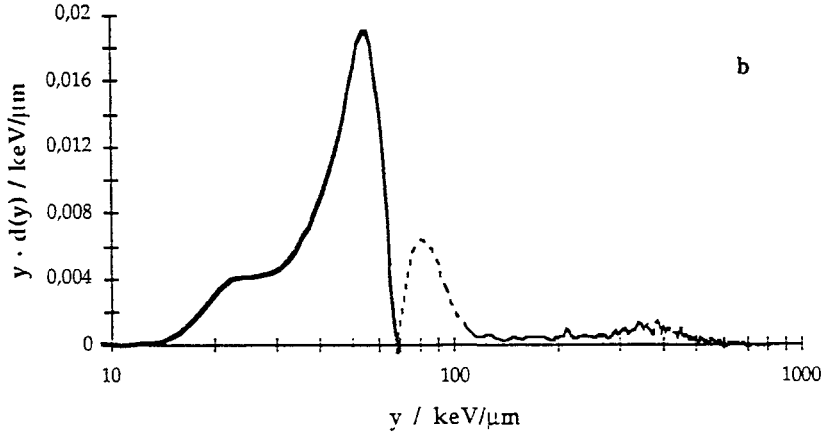

Figure 1: a. Measurement using a 64kBit SRAM chip in a neutron field produced by bombarding a thick beryllium target with 14MeV deuterons. The heavy lines indicate the measurement directly in front of the collimator, the thin lines the measurement in 1m distance from the collimator. In the experiments depicted by the solid lines the memory chip was covered by 2mm A150 tissue equivalent plastic, whereas the broken lines depict experiments without the A150 cover. In the latter case, the chip was still covered by a 100μm polyamid layer. b. Microdosimetric spectrum derived from the difference of the pulse height spectra measured directly in front of the collimator with and without A150 cover (a). The dotted part of the distribution is due to heavy charged particles produced in the polyamid layer.

	SRAM		DRAM	GaAs-diodes	
dimension / memory size	4kBit	64kBit	1MBit	320·320μm	80·160μm
active volume thickness/μm	2.36±0.17	3.4±0.3	5.8±0.2	1.5	1.5
mean chord length/μm	4.1±0.4	3.9±0.7	3.95±0.05	2.9	3.0
mean chord / longest chord	12	3.3	2.5	156	60
aktive area/mm	4.8	5.5	36	0.10	0.013
detection threshold/keV	5	10	900	10	10
efficiency for γ-radiation (^{137}Cs)	(2.6±0.2)· 10^{-8}	(5.7±0.7)· 10^{-9}	(1.7±0.7)· 10^{-8}	(6.6 ± 0.1) · 10^{-6}	
efficiency for neutrons	(3.31 ± 0.9) · 10^{-4}	(4.0±0.3)· 10^{-3}	(6.8±0.1)· 10^{-5}	(7.0±0.1)· 10^{-3}	(1.3±0.1)· 10^{-2}
typical frequency- and dose mean value for the used neutron source with $< E_n >= 5.3$MeV					
simulated diameter in tissue[1] / μm	14.4	13.6	13.7	24.0	24.6
$\bar{y}_F / \frac{\mu m}{keV}$	25.0	47.7	-	56.5	74.2
$\bar{y}_D / \frac{\mu m}{keV}$	42.4	58.4	-	279	217

Table 1: Geometrical, physical and microdosimetric parameters of the investigated detector devices. The ratio *mean chord / longest chord* describes the distortion of the microdosimetric spectra.

which are produced in the tissue equivalent layer are stopped in the dead layer and are consequently not detected. The differences of the memory spectra in comparison to the TEPC result can qualitatively be understood in terms of the different simulated diameters (table 1). A detailed discussion however, has to be guided by computer simulations, which could not be performed during the contract period.

Alternatively to the SRAM chips, single GaAs (Galliumarsenid) diodes were studied. Their characteristics are also tabulated in table 1. The advantage of these elements is that their geometrical parameters are well known, since they

[1] In the calculation the density of the semiconductor materials and the ratio *(mean chord length / diameter of a spherical proportional counter)* have been considered

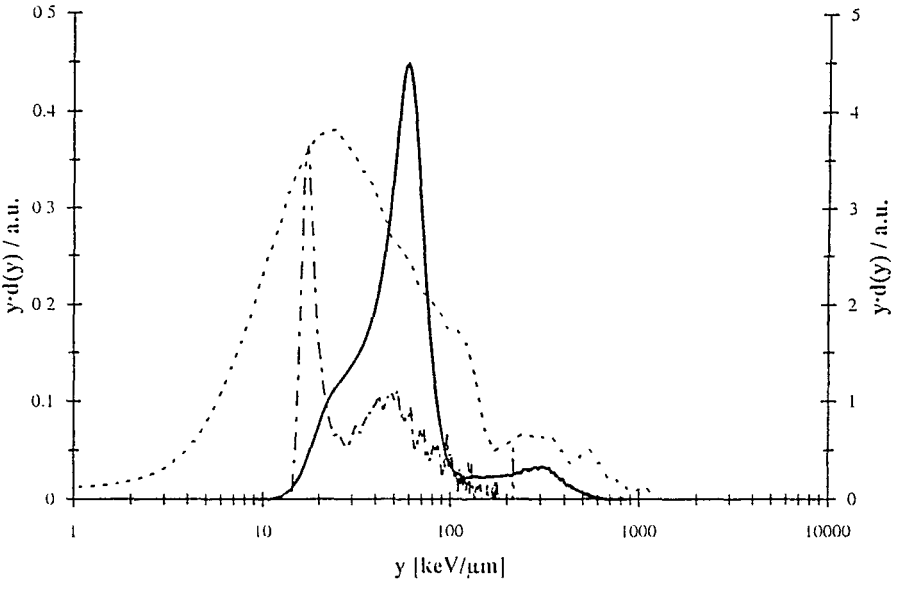

Figure 2: Microdosimetric spectra measured with two different SRAM chips (64kBit (——), 4kBit (– · –) in a fast neutron field produced by bombarding a thick beryllium target with 14MeV deuterons. For comparison the spectrum measured with a TEPC operating at a simulated site size of 2 μm is also given (– –).

were produced within KFA. A further potential advantage is that these devices show a carrier multiplication effect, which would promise a lower detection threshold. Also these devices were found suitable to measure microdosimetric distributions in neutron fields.

For the SRAM chips and the GaAs diodes it could be shown that they are in principle suitable as detectors for a dosemeter based on microdosimetric principles. The devices studied, however, do not have the optimal parameters an optimised designs must be developed to apply them for a personal dosemeter.

The DRAM chips listed in table 1 do not allow the measurement of microdosimetric spectra. They are counting devices and their detection threshold can be adjusted by the thickness of the counting elements. In principle, therefore, DRAM chips with sensitivities to different neutron energy ranges can be produced and used in parallel to form a dosemeter which is sensitive in a large neutron energy range. Investigations in this direction are beeing performed.

During the contract period an alternative concept for a personal dosemeter was established. The basic idea of this concept is to build up a detector system with an answer proportional to the individual dose equivalent $H_p(10)$. A principle layout based on the counting of secondary charged particles produced by neutrons in converter materials has been developed. Figure 3 shows the principle layout of this detection system.

Two converter materials have to be used, that the answer even for a broad range of neutron energies (from meV and MeV) is proportional to dose equivalent.

Experiments with GaAs diodes have been performed. The surface of the diodes was covered with a photo resist layer (containing hydrogen atoms). Recoil protons due to elastic scattering of the neutrons in the photo resist could be detected by the GaAs diodes It can be shown that the answer of such a detector system per unit neutron fluence is proportional to dose equivalent for neutron

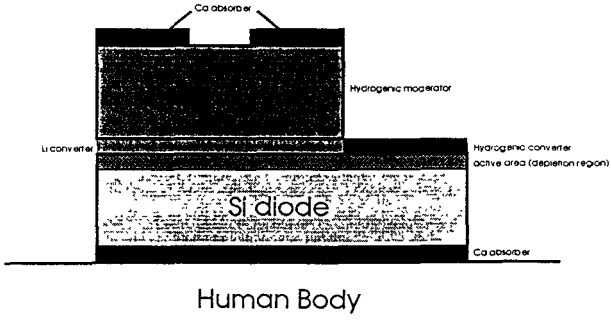

Figure 3: Principle layout of the neutron detector system with an answer proportional to $H_p(10)$

energies $E_n > 100$keV.

Beside hydrogenic layers Lithium Fluoride (LiF) is used as a second converter material. Low energy neutrons ($E_n < 100$keV) interact in LiF via the nuclear reaction ^{6}Li(n,α)^{3}H.

Thin layers of both converter materials cover the surface of a semiconductor detector. Although first experimental results have been achieved with GaAs devices, it was decided to use diodes based on silicon technology (the interaction cross section for γ-radiation in Si is about 25 times lower than in GaAs. The semiconductor detector has to have a very thin dead layer (less than 1micron) to detect as many as possible of the secondary particles leaving the converting layers. A thickness of the active area of the detector of about ten microns is sufficient for the use of the device as a counter. Two types of diodes have been choosen to fulfill these requirements, pn-diodes (pn-junction) and Schottky-diodes (semiconductor-metal-junction).

Two elements are used to establish the wanted answer of the detector system. In a hydrogenic moderator neutrons with energies in the range from eV to keV and subthermal neutrons are thermalized in order to increase their reaction rate in the LiF-converter. A Cd-absorber is used to decrease the number of detected thermal neutrons.

Processes to produce Si-pn and Schottky-diodes have been elaborated in the Institut für Schicht- und Ionentechnik (KFA). First test diodes have been produced. The covering of silicon-wafers with thin LiF-layers has already been tested.

With respect to the second objective of the contract, the Monte Carlo transport code MNCP has been used for the necessary transport calculations. Two phantoms have been developed for this code, a male phantom on the basis of the ADAM phantom and a female phantom on the basis of the EVA phantom. Both phantoms (ADAM and EVA) were modified in the sense that they contain all organs, for which weighting factors are given in the last ICRP (ICRP 60, 1990) recommendations, i.e. gonads, red bone marrow, colon, lung, stomach, bladder, liver, oesophagus, thyroid, skin, bone surface, and remainder. The tissues and their material composition follow exactly the MIRD-5 specifications, except for some trace elements which have been neglected.

Effective dose equivalents H_e using the quality factor definition of ICRP 60, and equivalent doses E have been calculated for both phantoms for 33 incident neutron energies and different geometries, e.g. AP, PA etc... The concept of weighting factors used to calculate effective dose E and organ dose equivalents is seen by the ICRP as a simplification against the concept of using a LET dependent quality factor, which is characteristic for the radiation at the location of the organ. The achieved results indicate that the simplified concept of assigning radiation weighting factors to an undisturbed field, and thus of neglecting quality variations within the human body, is highly incompatible with the LET-based quality factor concept. The discrepancy between the effective dose equivalent and

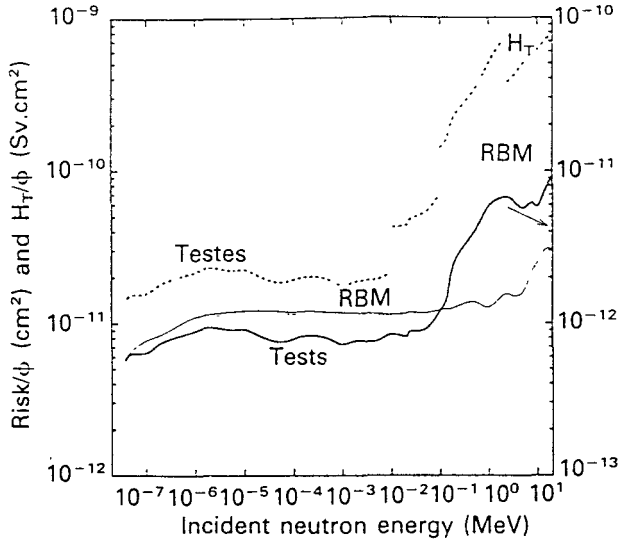

Figure 4: Probabilities of chromatid exchange in testes and of abnormal chromosomal metaphase in red bone marrow (solid lines) compared with corresponding equivalent doses (dashed lines), calculated for the ADAM phantom relative to incident neutron energy (AP exposure).

the effective dose depends on the energy of the incident neutrons. For energies below 10keV both quantities differ by a factor of 2, while between 10keV and 100keV this factor changes between 7 and 2. Generally the new quantity gives the higher values, with exception of the region 2 to 4MeV, where it is slightly lower than H_e.

The results of our calculations of organ doses, organ dose equivalents, effective dose equivalents and effective doses have been transferred to the PTB to include them into the data set, which was used by a joint ICRP-ICRU committee to determine amongst other things fluence to equivalent dose conversion functions.

The results of the MCNP calculations were in addition used to calculate microdosimetric distributions in different organs of the phantoms. The size of the assumed sensitive sites were 1μm, 8μm and 20nm. In order to evaluate the radiological risk in such organs, the microdosimetric spectra were folded with biological response functions for some selected endpoints. E g., for red bone marrow (RBM), the response function for abnormal metaphases determined on the basis of biological data from Skarsgard et. al. (1967) was applied. The resulting risk estimates per unit incident fluence can be compared to conventional measures of the radiological hazard, such as dose equivalents in particular organs.

HT. (Fig.4). The dependence of the ICRP defined equivalent doses on neutron energy cannot be justified on the basis of these phenomenologically derived risk estimates.

The investigations showed that microdosimetric distributions are useful for characterising radiation quality variations within complex biological systems and that they can be applied for predicting radiological risks, i.e. the probabilities of specific low level radiation effects in particular organs. There is however an obvious need for response functions derived from radioepidemiology and from in vivo animal experiments, such as leukaemia induction.

IV Scientific staff

Michael Balzhäuser, Diemo Barthmann, H.-W. Müller-Gärtner, Th. Schmitz, O. Schröder

V Other research group(s) collaborating on this project

- Members of EURADOS working committee 10
- Institut für Schicht- und Ionentechnik, Forschungszentrum Jülich GmbH
- Fraunhofer-Institut für mikroelektronische Schaltungen und Systeme, Institutsteil Dresden

VI Publications

Olko, P., Morstin, K., Schmitz, Th.
Simulation of the Response of a Ultraminiature Microdosimetric Counter for Fast Neutrons. Rad. Prot. Dos. **44**, 73–6 (1992)

Morstin, K., Kopec, M., Olko, P., Schmitz, Th., Feinendegen, L. E.
Microdosimetry of Tritium. Health Physics **65**, 648–56 (1993

Morstin, K., Olko, P.
Calculation of Neutron Energy deposition in Nanometric Sites. Rad. Prot. Dos. **52**, 447–52 (1994)

Morstin, K., Kopec, M., Schmitz, Th.
Equivalent Dose versus Dose Equivalent for Neutrons based on New ICRP Recommendations. Rad. Prot. Dos. **44**, 159–64 (1992)

Pierschel, M., Ehwahld, K.-E., Heinemann, B., Januschewski, F., Schmitz, Th., Schröder, O.
A BCCD-based Dosimeter for mixed Radiation Fields Proceedings of the Sixth European Symposium on Semiconductor Detectors. Nuclear Instruments & Methods in Physics Research, **A326**, No. 1,2, 304–09 (1993)

Schröder, O., Schmitz, Th., Pierschel, M.
Microdosimetric Dosemeters for Individual Monitoring based on Semiconductor Detectors. Rad. Prot. Dos. **52**(1–4), 431–4 (1994)

Schröder, O., Schmitz, Th.
Can a Personal Dosemeter for Neutron Radiation based on a Semiconductor Chip match the new ICRP Recommendations. Rad. Prot. Dos. **54**(3/4), 361–4 (1994)

Schröder, O.
Halbleiterdetektor für ein mokrodosimetrisches Personendosimeter zur Anwendung in gemischten Neutronen-Gamma-strahlenfeldern; Vergleich möglicher Prototypen. Dissertation, RWTH Aachen(1995)

Schröder, O., Schmitz, Th.
The Application of Commercial semiconductor Chips for Personal Neutron Dosimetry. Rad. Prot. Dos. (in press)

Schröder, O.
Counting Protons with Semiconductors — A Simple Approach to a Personal Neutron Dosemeter. Rad. Prot. Dos. (in press)

Head of Project 5. Prof Dr R E Grillmaier

II. Objectives for the reporting period

1. Development of a low pressure tissue-equivalent proportional counter (TEPC) for routine area monitoring including calibration and investigation of long term stability and reproducibility Adaptation of the detector to the laboratory system 'BIO' and the portable system 'HANDI'

2 Gas gain studies in collaboration with ADPA, Toulouse, (i) to optimise the design of the TEPC developed for monitoring and (ii) to study the gas gain properties of the detector with special regard to the improvement of the gas gain when simulating tissue diameters below 2 μm.

3. Optimisation of the dose equivalent response to neutrons with energies ranging from 10 keV to 1 MeV and application to the n-γ field at CEN, Cadarache, which simulates distributions encountered in working environments

4 Contribution to Kerma measurements of oxygen and nitrogen at high neutron energies performed by the PTB-group at PSI, Switzerland. Collaboration in EURADOS Working-group 10.

III. Progress achieved including publications

1.Development of a low pressure tissue-equivalent proportional counter

After the development of the ambient dose equivalent meter HANDI in the previous contract the work in this contract was focused on the development of a low pressure proportional counter (TEPC) for area dose monitoring. To fulfil the requirements of area monitoring the detector should have a constant dose equivalent response over the relevant neutron energy range, a sensitivity high enough to ensure a sufficient accuracy and a robustness to allow routine use These requirements led to a cylindrical single wire detector (named HTEPC) with a 3 mm thick wall of tissue equivalent material A 150 and a sensitive volume of 400 cm^3 (Figure 1)

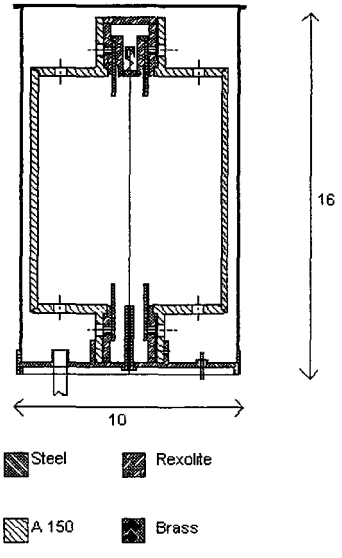

Figure 1: *Cross section of HTEPC*

The detector housing which maintains the vacuum is made of steel with a thickness of 0 1 mm The field shaping tubes with outer diameter of 15 mm are made of brass whereas the anode is made of a gold plated tungsten wire with 100 μm diameter. The insulation material separating the anode voltage of about 800 Volt from ground potential is Rexolite. The anode is tightened by a spring and electrically contacted directly through the outer housing support. The potential of the field shaping tubes is 25% of the anode voltage

The sensitive volume is defined by the detector wall and the height of the field shaping tubes resulting in 8 cm

diameter and 8 cm height The equality of diameter and height ensures a sufficient isotropy of the response

The calibration of the HTEPC in a ^{60}Co γ field and in a ^{252}Cf n-γ field at PTB has shown a good agreement in the shape of the microdosimetric distributions compared to measurements with spherical detectors but a difference in the dose values of 18% compared to the expected value. This result has been confirmed in the mixed n-γ field at Cadarache, France (Tab.1). The overestimation of the dose by the cylindrical detector is a consequence of the fact that the sensitive volume is larger than assumed. As this difference is constant a factor of 0 82 can be applied to correct the dose values

Table 1: *Comparison of the response of HTEPC and expected values in various radiation fields.*

radiation field	Response R		ratio HTEPC / expected R
	HTEPC	expected value	
^{60}Co γ	1,18	1,00	1,18
^{252}Cf n-γ	0,98	0,83	1,18
n-γ	0,84	0,72	1,17

The detector has been adapted successfully to the HANDI and it was used in practical applications (see EU project Nr FI3P-CT920026). The HTEPC is in use for nearly 3 years without modification except the refilling of counting gas. During the first 2 years of this period no ageing effects have been observed. Since about half a year the performance of the detector is decreasing The reproducibility of the detector design has been verified by the assembly of five identical detectors which show very similar characteristics.

The ageing effect is correlated to the general problem of spurious pulses that could not be solved in the contract period. The spurious pulses in the high region of lineal energy contribute between 1-5 nGy/pulse to the absorbed dose and 7-60 nSv/pulse to the dose equivalent. Whereas the rate of these pulses during the first 2 years was constant with 2 pulses/h it has increased to 7 pulses/h during the last half year. Because of the high sensitivity of the detector the deviation due to the spurious pulses decreases rapidly with the dose rate of the radiation field (allowing shorter measurement time) and can be neglected in most applications

The reason for these pulses is not fully understood but tests varying the design and the material of insulation excluded this part as a possible reason. The pulserate decreases when the height of the field shaping electrodes is enlarged or when the gas pressure is increased However, these solutions are not suitable because of the resulting much larger detector volume when keeping the sensitivity constant and the increase of the simulated diameter with the gas pressure

2 Gas gain studies

In collaboration with ADPA, Toulouse, the gas gain properties of the HTEPC have been studied theoretically and experimentally. Two experimental approaches have been applied (i) the use of an internal alpha source emitting particles which cross the detector volume on a defined path and (ii) a photo electron source In case of the alpha source the mean energy loss of the alpha particles in the sensitive volume was converted to primary electrons and the measured charge to

the number of collected electrons. The ratio of electrons collected to primary electrons is the gas gain In case of the photo electron source the evaluation is more complex because of the fact that a part of the spectrum is cut by the electronic noise

The simulation of gas gain starts with the numerical determination of the electrical field under consideration of the real geometry. The electrical field, the swarm parameters of the filling gas and its pressure are used as input to the iterative solution of the transport equation which gives as result the gas gain Measurements and calculations have been performed for the same detector configurations The filling gases considered have been methane-based TE, propane-based TE and isobutane. The comparison of simulation and experiment shows good agreement over a large range of configurations which corresponds approximately to electrical field strengths at the anode ranging from 8000 $V.cm^{-1}$ to 40000 $V.cm^{-1}$ and simulated diameters between 0.5 µm and 2 µm.

The investigations prove the suitability of the simulation to define the gas gain for a wide range of configurations by calculations. In practice the simulation can identify the optimum configuration of a TEPC without testing experimentally the gas gain. In the case of HTEPC the simulation has been used to optimise the detector for the simulation of very low diameters. The calculations also confirmed the assumption that the sensitive volume is not exactly limited by the field shaping electrodes which explains the 18% overestimation in dose in the calibration measurements.

The photo electron source experiment has been set-up to approach the conditions of the calculation of single electrons because of the very low energy of the photo electrons and the fact that they are all produced at the same place inside the detector. The calculation of single electrons is based on the 'history' of low energy single electrons simulated by Monte Carlo methods (whereas the solution of the transport equation above is always performed for an entity of electrons) Figure 2 shows a calculated and a measured distribution of electron avalanche sizes with good agreement in the shape Nevertheless the differences in the gas gain calculated and experimentally deduced are too large to allow a straight forward interpretation.

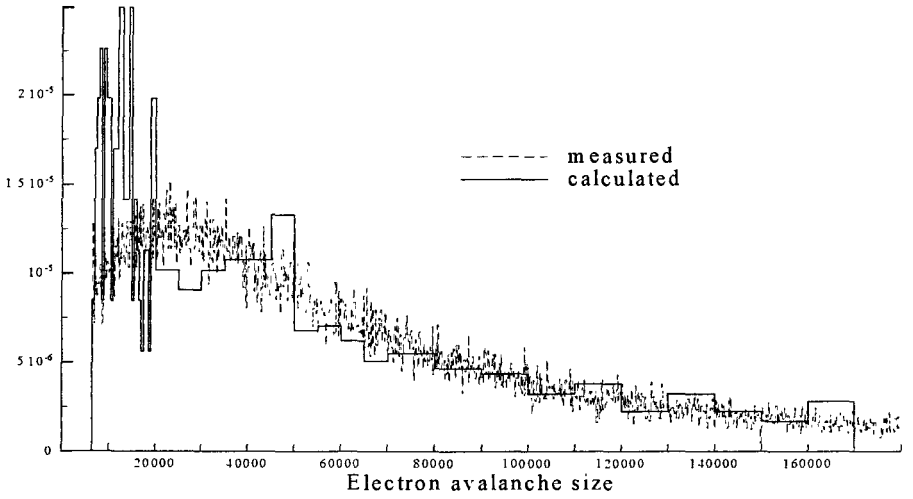

Figure 2 : *Electron avalanche size spectra of measured photo electrons and of calculated single electrons for 0.5 µm simulated diameter (isobutane, 263 Pa)*

3 Optimisation of the dose equivalent response to neutrons with energies ranging from 10 keV to 1 MeV.

Theoretical and experimental investigations of the TEPC dose equivalent response to neutrons in the past (see previous EU-contract) have shown that in the energy range from 10 keV to 1 MeV the decrease of the simulated diameter below the commonly used 2 µm is required to increase the detector response The optimisation of the detector response has been continued by investigation of the TEPC response in radiation fields as they are typically encountered in realistic environments. The facility at CEN, Cadarache, provides a radiation field with such neutron energy spectra. Measurements with TEPCs simulating diameters of 2, 1 and 0.5 µm have been performed (partly in the frame of the intercomparison organised by WG7 of EURADOS) The neutron fluence spectra provided by the groups of CEA and PTB have been used to derive the TEPC response theoretically with the Caswell-Coyne code. Table 2 summarises the results of measurements and calculations and indicates the ratio of dose equivalent values to the results derived at 2 µm simulated diameter.

Table 2: *Comparison of measured and calculated dose equivalent as a function of simulated diameter and the ratio to the results derived at 2 µm simulated diameter.*

	Simulated diameter (µm)	H (Sv/monitor)	ratio to H at 2 µm simulated diameter
Measurement	2	$2.26\ 10^{-9}$	1
	1	$2\ 72\ 10^{-9}$	1.20
	0 5	$3.22\ 10^{-9}$	1.42
		(Sv/neutron/cm^2)	
Calculation	2	$2\ 13\ 10^{-11}$	1
(Caswell-Coyne)	0.5	$2.64\ 10^{-11}$	1.24

The improvement of the detector response when decreasing the simulated diameter from 2 to 0.5 µm is due to the large fraction of low energy neutrons in that field The difference between measurement and calculation is most probably due to the influence of the detector wall which has not been taken into account in the calculation The investigations show that it is recommended to simulate smaller diameters than 2 µm when using the TEPC in environments with a large contribution of low energy neutrons

The HTEPC which has been developed for routine work has therefore been optimised to operate at very low gas pressures (some hundred Pa) Applying the calculation of gas gain it was shown that a thicker anode wire leads to better gas gain This result which inverts the situation at higher pressures where the gas gain increases with a thinner anode wire has been confirmed experimentally In addition the simulation shows that the extension of the multiplication region in the detector volume is acceptable when using a thicker wire diameter

Beside the work described above the group was engaged in the Kerma measurements using PCs with walls of pure metal and its compounds with oxygen or nitrogen The measurements have

been performed in collaboration with the PTB group at PSI, Switzerland, for neutron energies ranging from 30 up to 70 MeV

Additionally the group contributed to the work of WG10 of EURADOS

Other research group(s) collaborating actively in this project

Commissariat à l'Energie Atomique, CEA Fontenay Aux Roses (Dr J L Chartier, F.Posny, F)

Centre d'Etudes Nucléaires, CEN Cadarache (Dr J Kurkdjean) (F)

Batelle Pacific Northwest Laboratories, Richland (Dr. J. McDonald, USA)

Members of EURADOS WG 10

Publications

Gerdung, S , Grillmaier, R.E , Lim, T., Pihet, P , Schuhmacher, H. and Ségur, P. *Performance of TEPCs at Low Pressures: Some Attempts to improve their Dose Equivalent Response in the Neutron Energy Range from 10 keV to 1 MeV*, Proc. Eleventh Symp. on Microdosimetry, Gatlinburg, Radiat. Prot. Dosim. 52(1-4), 57-59 (1994).

Gerdung, S., Freyermuth, M , Grillmaier, R.E , Pihet, P and Ségur, P *Entwicklung eines gewebeäquivalenten Niederdruck-Proprtionalzählers für den Einsatz im Strahlenschutz* Fachverband für Strahlenschutz 26 Jahrestagung, Köln, Verlag TÜV Rheinland, 572-577 (1994)

Freyermuth, M.,
Gerdung, S., Chouki, A., Grillmaier, R E , Moutarde, C , Pihet, P. and Ségur, P. *Numerical Simulation of a Real Low Pressure Proportional Counter for Use in Radiation Protection* Workshop in Chalk River, Canada, Radiat Prot Dosim. 61(1-3) (1995).

Gerdung, S , Pihet, P., Grindborg, J.E , Roos, H., Schrewe, U.J and Schuhmacher, H *Operation and Application of Tissue Equivalent Proportional Counters.* in *Design, Construction and Use of Tissue Equivalent Proportional Counters.* Editors· Kliauga, P., Schmitz, T , Waker, A and Zoetelief, H., Radiat. Prot Dosim 61(4) (1995)

Schrewe, U J , Newhauser, W D , Brede, H J., Dangendorf, V , DeLuca, P.M Jr , Gerdung, S , Nolte, R , Schmelzbach, P., Schuhmacher, H and Lim, T. *Measurement of Neutron Kerma Factors in C and O: Neutron Energy Range of 20 MeV to 70 MeV.* Workshop in Chalk River, Canada, Radiat. Prot Dosim 61(1-3) (1995)

McDonald, J C , Posny, F , Gerdung-List, S., Chartier, J L., Kurkdjian, J *Dosimetric Measurements Using Simulated Practical Neutron Energy Spectra.* Radiat Prot. Dosim. (submitted) 1995

Head of project 6 : J.M. BORDY
Scientific staff : T LAHAYE

II Objectives for the reporting period

The SDOS objectives in the contract were to design electronic sensor for individual neutron dosimetry. Within this frame the SDOS studied the design and the optimisation of a special shaped tissue equivalent proportional counter made of two flat multi-channel cathodes and a set of anode wire. This counter is called MC TEPC.

The studies were carry out in three steps:

- Design of the MC TEPC.
- Design, realisation and experimentation of a single channel and a five channel prototypes associated to a wire anode.
- Study of the dosimetric characteristics of the multi-cellular counter. Angular and energy responses in reference mono energetic neutron beams according to the ICRP 60 recommendations

Additionally, calculation codes on the electric field configuration were developed in collaboration with the CPAT research team headed by P. SEGUR and reported in his contract.

IV Progress achieved including publications.

1 - Design of the multi cellular counter.

1.1 Geometry

The application of TEPC's to personal dosemeters meets large difficulties mainly due to a low sensitivity for small devices and to the long term behaviours of gas in sealed counters. This leads to investigate completely new design based on a multi-cellular geometry.

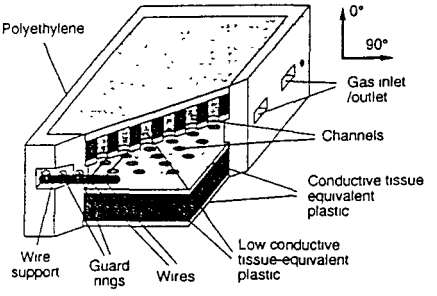

Figure 1 : Conceptual design of the MC TEPC (the drawing is not to scale).

The multi-cellular geometry is intended to increase the inner surface of the cathode to obtain a higher sensitivity. This is obtained by using two identical flat cathodes in which multiple cylindrical cavities (channels) are machined (figure 1). Cathodes face each other Each cathode is made of three tissue equivalent plastic plates. A thick plate of high resistivity plastic (few Gohm/cm) is sandwiched between two thin A150 conductive plastic plates. Channels are polarised using a 50 V positive voltage applied to the punched face of the cathodes Thus, the

electric field generated inside the channels drifts the electrons to the anode wires These are tightened in front of each hole row. The anode wire set is fixed at the centre of the gas cavity between the two cathodes A 700 V high voltage is applied to the anodes. A polyethylene plate keeps the cathodes and wire supports in position. The smallest distance between two neighbouring channels is 2 mm Eight and four millimetres are respectively the height and the diameter of the channel Four millimetres is the distance between the two cathodes. The external dimensions of the counter are 5 6 x 5.6 x 2.8 cm.

The following gives the increase of the internal surface ratio, between the multi-cellular TEPC and ortho-cylindrical or spherical counters.

Internal diameter (cm) (sphere or ortho-cylinder)	1.0	2.0	3.0
Surface area ratio w.r.t. a sphere	87	22	10
Surface area ratio w.r.t. an ortho-cylinder	58	15	7

Chord length distribution

A Monte-Carlo code was written to assess the chord length distribution of different counters. The code was checked for spherical and cylindrical counters and good agreement with the theoretical values (less than 0.1% difference) was found. Figure 2 shows the chord length distribution obtained for multi-cellular and ortho-cylindrical counters. The reduced standard deviations are respectively 47% and 51% The chord length distribution of the MC TEPC looks like a DIRAC distribution; the mean value and the most probable chord length are about identical (difference less than 1%). Thus, whether the mean or the most probable chord length is used in microdosimetric calculation, their results are better in the case of the MC TEPC because 71% of the chord length distribution is within −/- 40% of the most probable chord length instead of 59% for an ortho-cylinder. It has to be mentioned that long chord length can introduce errors into the microdosimetric calculations.

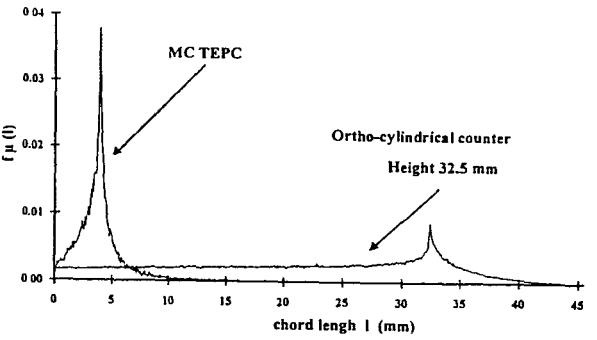

Figure 2: Chord length distribution in the multi-cellular and the ortho-cylindrical counters.

Estimation of the simulated volume

As can be understood from figure 1, the gas volume is not convex. Let us consider the interaction of a neutron or a photon with the counter; the probability of obtaining more than one interaction is less than 0.01%. Moreover, due to the thickness of the cathode between two neighbouring channels, the recoil proton and the electron (E<1MeV), cannot interact consecutively in two different channels. So, the multi-cellular counter volume can be considered as a convex volume, because it can be crossed through only once by the same secondary charged particle.

The simulated volume is calculated, by applying the Kellerer criteria for the convex volume, 0 65 µm diameter at 6 7 kPa pressure is found. The total volume of the gas has been taken into account. This diameter is compatible with the lineal energy measurement.

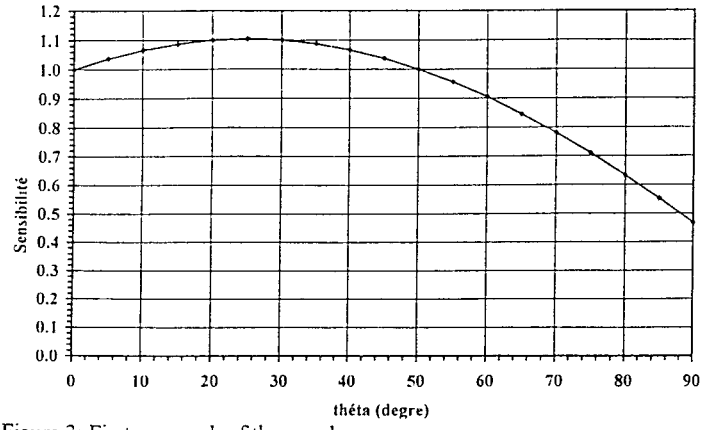

Figure 3: First approach of the angular response.

Angular response

A first approach of the angular response has been made using only geome-trical assumptions (figure 3). The calculations shown that the « flat » geometry is suitable to achieve the isodirectional response required for individual dosemeters.

1.2 Gas mixture used to fill the counter.

One of the aspects of TEPCs ageing is correlated to the gas behaviour and its chemical interactions with cathodes and anode. In order to reduce the ageing effect, It has been decided to add argon to the classical tissue equivalent gas mixture based on propane Because argon is a noble gas, it is assumed that the ageing effects will be less for a gas mixture including argon than for a gas mixture without argon To approximate the tissue equivalence conditions, a gas mixture containing 35 3 % argon, 56.2% propane, 5% carbon dioxide and 3.5% nitrogen was used.

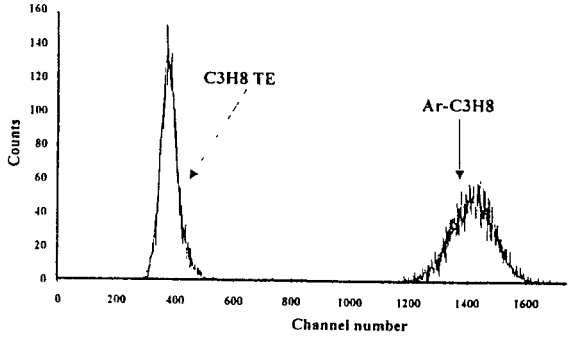

Figure 4: Spectra obtained with the alpha source of the CIRCE counter with C3H8 TE and Ar-C3H8 mixtures.

To date, no ageing tests have been performed to confirm our assumptions but the gas gains of Ar-C3H8 and C3H8-TE have been compared using the CIRCE counter. As shown in figure 4, amplification with Ar-C3H8 is about 3.5 times higher than with C3H8-TE.

2 - Study of the operating conditions.

2.1 - Description of the single and five channel prototypes.

In order to approach the multi-cellular geometry, a single channel and a five channel prototypes have been designed and tested. The prototype (figure 5) employs a stack of epoxy resin plates covered with a thin tin-copper layer and provided with a central hole or a row of five holes To create a constant electric field in the drift region inside the channel, a biased resistance bridge is used. The counter is filled with methane at a 13.4 kPa pressure. An alpha source (^{238}Pu) induces ionisation in the gas volume between the cathode and the first electrode. The electrons generated are subjected to the electric field inside the channel, and drift through the channel towards the multiplication region. A 25 µm diameter anode wire made of tungsten and a channel height of 1 cm have been used for both prototypes.

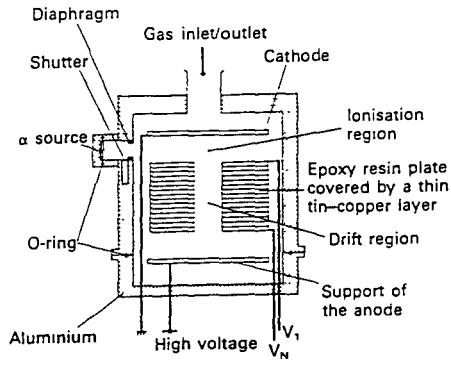

Figure 5: Cut view of the single channel prototype

2.2- Experimental setup

The experimental setup consists of the counter prototypes, a Canberra 2006 preamplifier, two siléna 7611 linear amplifiers and a two way Inel Cicero 4K multi-channel analyser (2 x 2048).

2.3 - Experimental results

Two sets of experiments have been carried out to study the effect of channel diameter (0.5 and 1 cm) and the effect of the number of channels (1 and 5).
For each experiment, drift and multiplication regions have been investigated. When the drift region is investigated, the potential in the multiplication region is maintained constant and the difference in potential applied between the channel extremities varies and vice versa when the multiplication region is investigated.
Figure 6 shows the variation of the collected charge for the two different channel diameters on the drift and multiplication regions. For the drift region (a and b curves), it is observed that the amount of charge collected increases with drift efficiency when the anode voltage is below 450 V (100 volt difference in potential for the drift region). This can be explained by the enhanced focusing effect of the electrons coming from the ionisation region towards the channel. Above 700 V (350 volt difference in potential in the drift

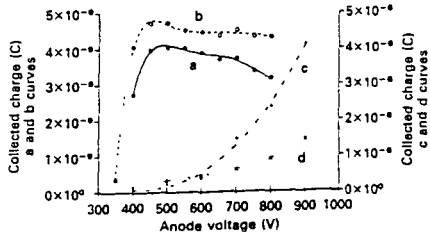

Figure 6: Amount of charge collected versus anode voltage for drift region: (a) 1 cm diameter. (b) 0 5 cm diameter; and for multiplication region (c) 1 cm diameter, (d) 0.5 cm diameter.

region) for the 0 5 cm diameter channel, a light decrease in charge collection is observed with increasing drift efficiency This might be explained by a greater number of electrons being collected by the first electrode. In the case of the multiplication region (c and d curves) an increase in the amount of charge collected with the applied potential is observed The collected charge is more increased in the case of the smallest diameter, this could be attribute to a greater field in the drift region.

Figure 7 shows for two different numbers of channels, how the charge collected varies in the drift and multiplication regions. In the drift region (a and b curves), the observations are close to those for figure 2 a and b curves. The amount of charge collected is greater for the largest number of channels but the respective ratio is not proportional to the number of channel. This paradoxical behaviour can be explained by the assumption of overlapping effects in the ionisation region. In the case of the multiplication region (c and d curves), an increase in the amount of charge collected with applied voltage is observed, but the lowest amount of collected charge corresponding to the largest number of channels. This seems to be due to the alpha beam collimator in the experimental setup.

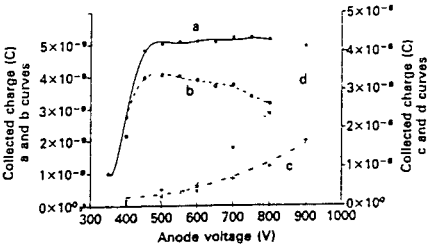

Figure 7: Amount of charge collected versus anode voltage for the drift region: (a) single-channel prototype, (b) five channel prototype; and for multiplication region: (c) single-channel prototype, (d) five channel prototype.

3 - Experimental results achieved with the MC TEPC.

The counter is filled (6 7 kPa pressure) with the Ar-C3H8 gas mixture. The instrument has been calibrated using external references, mainly neutron sources. In this case, the micro-dosimetric spectra could be calibrated in terms of lineal energy using the proton edge as a reference (y = 125 keV/µm). This lineal energy calibration has been defined for 0.565 keV neutron energy and then applied to the other spectra. The multi-event calibration in terms of dose equivalent was also used. The dosemeter response is the ratio $R_H/H_p(10)$ R_H is the instrument reading, in terms of dose equivalent obtained by integrating the function q(y) y n(y).

$$R_H = k \Sigma q(y) \, y \, n(y) \, \Delta y$$

where n(y) is the pulse height distribution as a function of y and q(y) approximates the quality factor Q(L) (ICRP 60 values) by setting y= L∞. k takes into account the conversion of lineal energy to dose units the effective quality factor has been derived by the ratio of the reading in term of dose {k Σ y n(y) Δy} by the reading in terms of dose equivalent R_H

3 1 - Response to mono energetic neutrons

The MC TEPC has been exposed on a slab phantom of polymethyl methacrylate with mono energetic neutron beams within the energy range from 144 keV up to 2 5 MeV

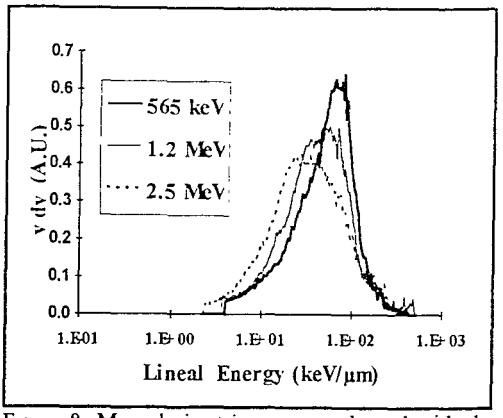

Figure 8: Microdosimetric spectra achieved with the MC TEPC.

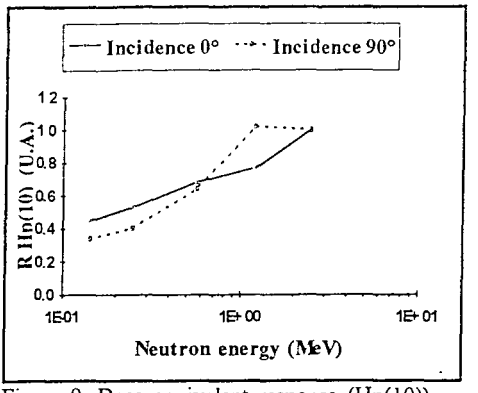

Figure 9. Dose equivalent response (Hp(10)) , normalised to 2.5 MeV, against neutron energy for 0° and 90° of incidence.

Figure 8 shows a few representative spectra; The spectra are cut off for low lineal energies below 1 keV/µm.. This threshold is due to the electronic background. Improvements of the associated electronic are necessary to obtain a lower lineal energy threshold. In all measured spectra, some large size events can be seen above the proton edge, even for low neutron energies. Some of these may be due to protons having long path length in the counter. It would be able to reduce this phenomenon by modifying the layout of the channel in the counter in such a way that the long chord length probability decreases

The decrease of dose equivalent response for low neutron energies is observed similarly as when using a conventional TEPC (figure 9). It would be able to achieved a nearly flat response by modifying the q(y) function.

3.2 - Dose equivalent response as a function of counter orientation. (First experimental approach of the angular response).

As a preliminary investigation of the angular response of the prototype MC TEPC, the influence of its orientation (90° and 0°) on the shape of the microdosimetric spectra and on the derived dosimetric quantities was assessed. The counter orientation was modified, the phantom remaining perpendicular to the incident beam axis Spectra measured for neutrons at 0° and 90° orientations are shown in figure 10.

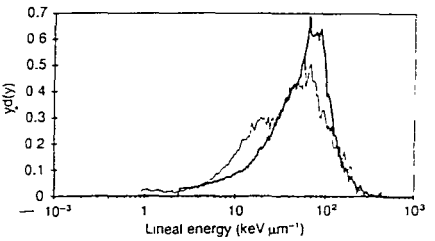

Figure 10: Microdosimetric spectra achieved for 0° (thick line) and 90° (thin line) counter orientation. Neutron energy : 500 keV.

As can be seen from table 2 and figure 9, the decrease of dose equivalent response is slightly greater at 90° than at 0° The variation of the response with orientation may be attributed to two main causes First, the ratio of the counter cross-section for the two orientations S90°/S0° is 0 45. Therefore, the better response ratio has to be, at least, of this order of magnitude, it is the case for 1.2 MeV Second, the y spectrum measured at 90° shows a higher contribution of events with low lineal energy(figure 10).

Table 2. Variation of the ratio of the 90° orientation response in term of individual dose equivalent Hp(10) to the 0° one and of the quality factor

Energy (MeV)	0.144	0 250	0.565	1 2	2.5
R90°/R0°	0.28	0 28	0.25	0.49	0 37
Quality factor (0°)	13.7	13.5	16 0	13.0	11 6

Further experiments are necessary to characterise the angular response of the MC TEPC. These preliminary results, however, indicate that the MC TEPC geometry is suitable to meet the isodirectional response requirements of personal dosemeter.

3 3 - Silène reactor and ^{60}Co gamma ray spectra.

The MC TEPC has been irradiated in front of the Silene reactor (a solution-fuelled reactor) in lead shield and bare source configurations (figure 11). The measured spectra show a larger photon component (below 10 keV/µm) for the bare source configuration as expected. Above this limit, the neutron spectrum component is shifted to lower lineal energy values that can be due to harder neutron energy spectrum for the bare source compared with the lead shield geometry. This assumption is confirmed by spectrometry measurements.

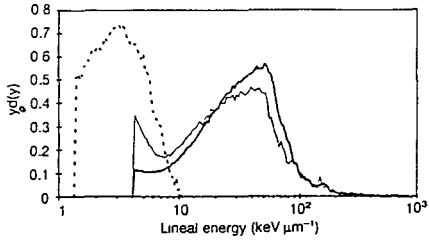

Figure 11: Microdosimetric spectra achieved for the two Silene reactor configurations, ^{60}Co gamma ray is added for comparison. Cobalt (dashed line), bare source (thin line), lead shield (thick line).

4 - Conclusion.

The results show that the multi-cellular counter is able to perform microdosimetric measurement above 1 keV/µm for radiation protection purpose. The multi-cellular geometry may be suitable to ensure the neutron sensitivity and partially the isodirectional response required for personal dosimetry. Nevertheless, the MC TEPC has to be improved. Thus, by reducing the long chord length probability and modifying the Q(L) function used in the microdosimetric calculation, it seems possible to achieve a nearly flat energy response
Three problems must be solved : i) the associated electronic has to be improved to decrease the lineal energy threshold, ii) a better air tightness is necessary to study the behaviour of the counter during long irradiation to choose the filling gas, iii) the set of anode wire must be replaced by microstrip anode or a set of needle shaped anode to avoid microphonic effects. These improvements will be the next step of the MC TEPC development.

5 - References.

J. Barthe, M Mourgues, J.M. Bordy, P. Segur, B Boutruche et G. Portal.
Etude de compteurs miniatures pour la dosimétrie des neutrons
Congrès IRPA, Montréal, 17-22 mai 1992
Actes du congrés, Vol 1, pp 479-482, Montréal

D Blanc, P. Segur, J. Barthe et J.M Bordy
Les compteurs proportionnels a milieu équivalent au tissu en radioprotection
Congres IRPA, Montréal, 17-22 mai 1992.
Actes du congrès, Vol. 1, pp 459-462, Montréal

B. Boutruche, J.M Bordy, J. Barthe, P. Segur and G. Portal.
New concept of a high sensitive tissue equivalent proportional counter for individual neutron dosimetry.
11th Symposium on microdosimetry, Gatlinburg, Tennessee USA, September 1992
Radiation Protection Dosimetry, Vol 52, No. 1-4, pp 335-338, 1994

J.M. Bordy.
Contribution à la réalisation d'un compteur proportionnel à dérive équivalent au tissue destiné à la dosimétrie individuelle en radioprotection.
Rapport CEA -R-5603, Service de documentation, CE Saclay 91191 Gif sur Yvette Cedex France, July 1992.

J.M. Bordy, J. Barthe, B. Boutruche et P. Segur.
Evaluation des caratéristiques dosimétriques d'un nouveau type de compteur équivalent tissu destiné à la dosimétrie individuelle neutronique en radioprotection.
Radioprotection, Vol 29, n° 1, pages 11 à 28, 1994.

J.M. Bordy, J. Barthe, B. Boutruche and P. Segur.
Characteristics of a new proportional counter for individual neutron dosimetry
International Workshop on Individual Monitoring, may 5-7 1993 Villigen, Switzerland.
Radiation Protection Dosimetry, Vol. 54, No 3-4, 369-372, 1994.

B. Boutruche.
Etude d'un compteur proportionnel multicellulaire à dérive pour la dosimetrie individuelle des neutrons.
PhD thesis, Paul SABATIER University, Toulouse, 30-10-1994

J.M. Bordy, J. Barthe, T. Lahaye, B. Boutruche and P. Segur.
Improving multi-cellular tissue equivalent proportional counter for personal neutron dosimetry.
Workshop "Advances in radiation measurement", Chalk River, Ontario (Canada), 3-5 October 1994

J.M Bordy
Dosimétrie individuelle des neutrons : étude de capteur électroniques et des méthodes associées
PhD Thesis Paul SABATIER University, Toulouse, 03-07-1995

Head of Project 7: Dr Morstin

II. Objectives for the reporting period

Adaptation of the mathematical description of humanoidal phantoms used for quantification of radiological hazards in view of their allowance for high-energy particle transport (long mean free paths of neutrons and long ranges of charged secondaries)

Calculation of charged-particle production data for reactions of neutrons with main tissue constituents in the incident energy range up to several hundred MeV. Compilation of the results in the form of cross-section and reaction-rate library, enabling further evaluations of energy deposition patterns induced indirectly by high-energy neutrons in humanoidal phantoms.

III. Progress achieved including publications

In spite of what we expected, the humanoidal phantoms developed previously (and described roughly in the Project 4) appeared inadequate in energies higher than, say, 50 MeV. This is so at least with the use of the Monte Carlo transport codes selected for further calculations, i e. LAHET and HMCNP, both using the same geometrical description as we applied below 20 MeV (as described in Project 4 in 1994) This description is build out of the second order surfaces with the radii of curvature frequently comparable with ranges of high-energy particles. The use of the SABRINA program as the graphical interface for the MCNP-type geometry allowed to detect and, consequently, to remove several cross-over of particular organs, disturbing random walk of long-range particles in Monte Carlo simulations The lay-outs of some organs in the corrected geometrical set-up of the male (ADAM) and female (EVA) phantoms are given in the enclosed Figures. They are only of illustrative value. The phantoms themselves are defined by algorithms (several hundred of instructions each) which may be available for the potential cooperants.

Charged-particle production cross-sections for main tissue constituents (H, C, N, O, P, Ca) generated with the Bertini approach (intra-nuclear cascade model + evaporation for residual nuclei) have been compiled in the energy range 20 - 400 MeV, as well as the derived reaction rates and kerma factors. This will allow to avoid in further radiation transport and energy deposition simulations unnecessary repeating of nuclear-model calculations for each tissue composition (varying from organ to organ)

Completion of high-energy radiation-transport and energy-deposition calculations in the developed humanoidal phantoms ADAM and EVA will allow to quantify according to ICRU and ICRP specifications the radiological hazards due to external high-energy neutron exposures, for each of the organs separately as well as for the whole phantoms. Up to now, no publishable results have been obtained (except for the phantoms themselves, which may be of interest far beyond the radiation protection applications).

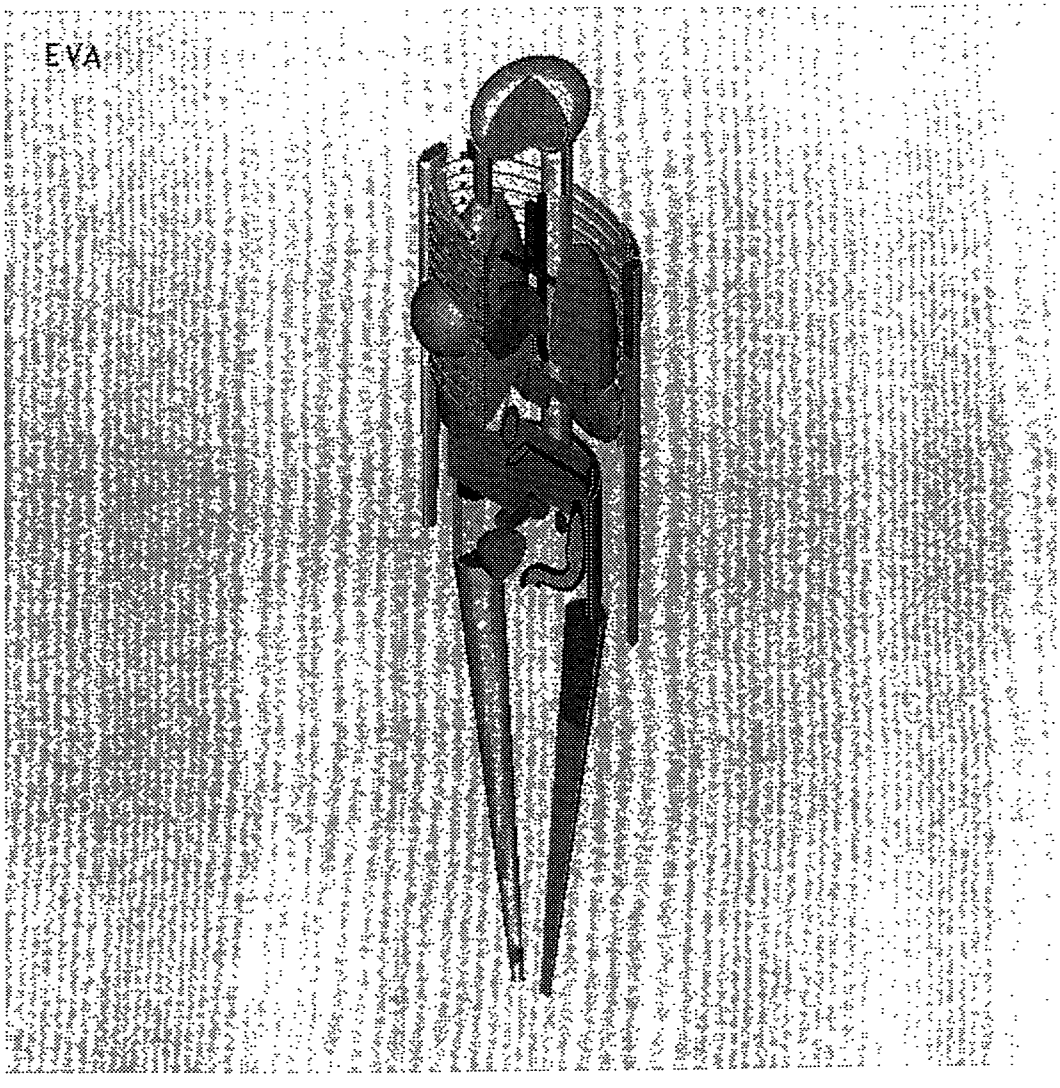
EVA

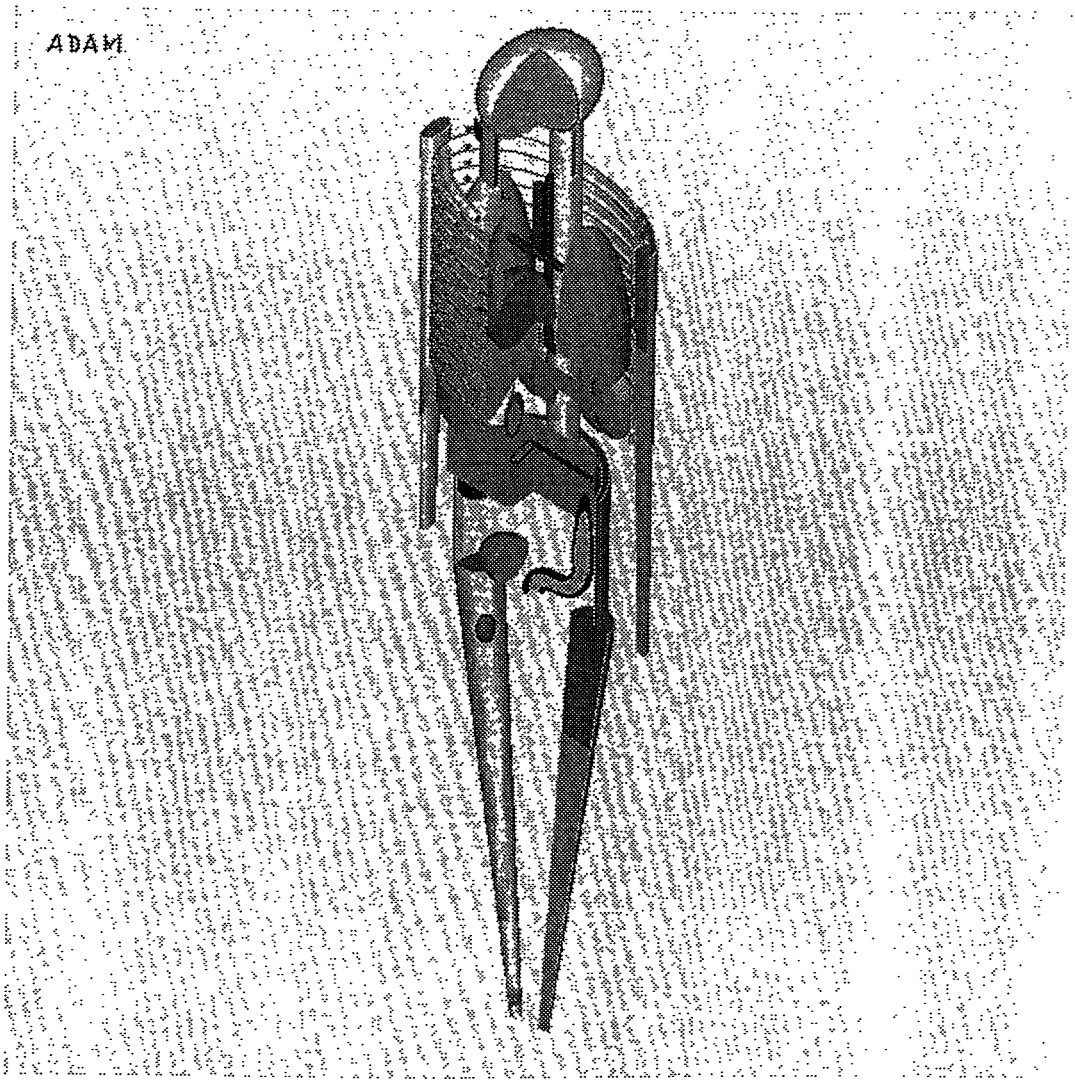
ADAM

I. Head of the project: *Dr. Jozef Sabol*

II. Objectives for the reported period

The main objectives of this PECO project included such topics as *Monte Carlo Studies of Electron Avalanches in Low Pressure Tissue Equivalent Proportional Counters, Microdosimetric Approach to the Radiation Weighting Factor, Selected Aspects of Relation between the TEPC Microdosimetry and Radiation Protection* as well as *Calculations of Secondary Electron Spectra Originating in Tissue Equivalent Materials Based on the Code EGS4.* The principal aims of these individual parts of the project have already been described in our previous Progress Report. Therefore, here only some additional aspects will be summarized.

One of the the primary goal of the work carried out during the last period was concentrated on the study of electron avalanches in a low pressure proportional counter of a cylindrical shape. In order to analyze all the relevant processes involved a Monte Carlo code for modelling the electron interactions with gas molecules in electric field had to be developed. The technique should be based on the simulation of the motion of electrons in electric field and their interactions with the tissue equivalent gas. The objectives also included the analysis of the gas amplification process under typical conditions encountered in low pressure microdosimetric counters.

The other task has been addressing the selected problems regarding the microdosimetric approach to the radiation weighting factor. It is well known that the ICRP introduced recently the quantity radiation weighting factor accounting for the fact that the biological effect of a given absorbed dose of ionising radiation depends on the microscopic energy deposition in the irradiated tissue. For mixed radiations the appropriate value of radiation weighting factor (w_R) is derived from the quality factor (Q). The definition of the quality factor according to the ICRP 60 is, however, based on the linear energy transfer (LET) instead of the lineal energy (y) whose advantage over the concept of LET are undisputed. The ICRU 40 recommended the quality factor in terms of the lineal energy, but there is certain difference in values Q calculated according to the above mentioned publications. It is therefore desirable to modify the function

Q(y) defined in ICRU 40 with respect to the function Q(L) introduced in ICRU 60 to obtain comparable values of qualityfactors in cases where both quantities LET and y are meaningful. In this way, the radiation weighting factor could be derived directly from microdosimetric spectra without necessity of their conversion to the required LET spectra.

The calculation of the quality factor based on the lineal energy is sometimes considered to be laborious because of the necessity to perform the numerical integartion. Consequently, an attempt has been made to calculate the quality factor from lineal energy averages y_F, and y_D.

Since the TEPC microdosimetry can successfully be applied in radiation protection, some work has also been carried in this direction. In the microdosimetry based radiation protection the measured (or calculated) physical microdosimetric quantities are related to radiation induced biological effects. Because DNA macromolecule is of a primary importance for the assessment of the biological effects, the quantities reflecting the energy deposition (in the best case its spatial distribution) at nanometer scale are important for radiation protection and quantitative radiation biology.

The microdosimetry concept is not directly transferable to biological studies at nanometer scale because of the inadequacy of the W-value concept, the influence of target heterogeneity and the phase effect. The objectives for the reporting period were mainly focused on the last two of the above mentioned factors. Specifically, we have performed a systematic comparison of energy deposition characteristics in simple and heterogeneous targets irradiated by electrons, protons and alpha particles and we have studied the phase effect on the microdosimetric characteristics for electrons, protons and alpha particles.

III. Progress achieved including publications

Various important electron avalanche parameters for a low pressure microdosimetric counter with the cathode diameter of 1.27 cm and the anode diameter of 7 μm, filled with methane have been studied and calculated. Using the applied simulation method it was possible to investigate all relevant space and temporal aspects of electron avalanche development. In this case all electrons are traced simultaneously in time and their co-ordinates and velocities were recorded. The approach depends only on the experimentally obtained electron-molecule cross sections. From the results several important characteristics of the electron avalanche behaviour, especially the existence of the seeding region in the avalanche (where a relatively small number of secondary electrons are created) can be concluded. On the basis of these results, the dependence of gain and the time extent of electron avalanche on gas pressure as well as the

distance from the anode where the primary electron was released can be documented and explained.

The operational limits of the TEPCs at low pressures are mainly due to the fact that with decreasing pressure the size of the seeding region is increasing and consequently the counter is becoming less and less proportional. Another negative effect contributing to the loss of proportionality is the avalanche spreading along the anode wire. The present technique makes it possible to establish these operational limits and to study possible improvements in the construction and optimisation of tissue equivalent proportional counters.

The applied methods, which can be easily extended to other geometries, proved to be reliable and correct since they could bring some new data required for better understanding all relevant processes taking place in TEPCs.

In practical radiation protection the simplified procedures for the conversion of dose distributions in LET into corresponding distribuutions in y are often very useful since they can easily be applied. It was assumed that particles of a given LET produce a triangular pulse height spectrum in a spherical volume. The relationships for the function Q(y) can be obtained ffrom the definition expression for the mean quality factor in ICRU 40, i.e. by solving the inherent Fredholm integral equation. In the case analyzed the exact solution would be as follows: $Q(y) = 1$ for $y < 15$, $Q(y) = 0.284\ y - 2.2$ for $15 < y < 150$, and $Q(y) = 306.2 / \sqrt{y}$ for lineal energy $y > 150$, where y is expressed in keV/μm. The mean quality factor at given LET calculated with the above function Q(y) coonformably to the definition in ICRU 40 corresponds to the quality factor according to ICRP 60.

To study the influence of target non-homogeneity we have performed calculations for two different models of a biological target. As a target we have used the basic unit of the chromatin structure, the nucleosome particle. The first model realistically reflects the complex geometry as well as the heterogeneity of the nucleosome particle. It takes into account different densities of the histone core, DNA molecule and primary hydration shell layer. In this model the DNA molecule is represented by its atomic structure. To evaluate the energy deposition events in nanometer sized structured nonhomogeneous targets we have used a method based on the random volume sampling.

The second model represents a classical microdosimetric approach. The target is a water sphere of unit density with the mean chord length equal to the mean chord length of the complex geometry target (the density effect is taken into account in the calculations of the mean chord length for the complex target). The microdosimetric characteristics for the sphere were calculated using the method of fluctuation detector.

The frequency- and dose-averaged mean energies imparted, ε_F and ε_D, to the volumes with the same effective mean chord length irradiated by a given radiation were calculated for low energy electrons (up to 5 keV), protons in the energy range 0.5 MeV - 10 MeV and for alpha particles in the energy range 2 MeV - 50 MeV. The results are summarized in Tables 1-3.

Table 1: The frequency- and dose-averaged mean energies, ε_F and ε_D, imparted by electrons to the complex geometry non-homogeneous target and a homogeneous sphere with the same effective mean chord lengths.

	Complex target of nucleosome		**Simple sphere**	
Energy (keV)	ε_F	ε_D	ε_F	ε_D
0.5	129.8	226.5	128.8	203.2
1.0	118.1	230.1	106.6	177.7
2.0	90.7	190.3	83.9	147.0
5.0	70.2	151.3	65.6	123.2

Table 2: The frequency- and dose-averaged mean energies ε_F and ε_D, imparted by protons to the complex geometry non-homogeneous target and a homogeneous sphere with the same effective mean chord lengths.

	Complex target of nucleosome		**Simple sphere**	
Energy (MeV)	ε_F	ε_D	ε_F	ε_D
0.5	180.5	320.2	152.3	234.5
1.0	120.4	222.6	105.1	167.5
2.0	85.5	166.2	81.8	137.7
5.0	67.2	157.2	62.2	114.1
10.0	57.5	134.8	54.6	109.0

Table 3: The frequency- and dose-averaged mean energies ε_F and ε_D, imparted by alpha particles to the complex geometry non-homogeneous target and a homogeneous sphere with the same effective mean chord lengths.

	Complex target of nucleosome		**Simple sphere**	
Energy (MeV)	ε_F	ε_D	ε_F	ε_D
2.0	401.3	979.1	329.4	673.6
5.0	241.5	499.7	204.8	351.3
10.0	180.5	335.7	145.6	234.9
20.0	122.9	238.1	106.3	171.5
50.0	80.8	153.3	78.5	137.2

For high energy particles the differences between the two models are within 10% for ε_F and within 20% for ε_D. The results for low energies, especially for charged particles, exhibit larger differences of about 20% in the case of ε_F and up to 30% for ε_D. The differences between the two targets are a function of ionization density. With increasing ionization density increases the difference in the single event distributions of the energy imparted to the given target. Even if both targets have the same mean chord length remarkable differences exist for high-LET particles. For particles with high ionization density the simple geometry model considerably underestimates high energy depositions and therefore the ε_D values are underestimated.

Publications:

J. Sabol: Microdosimetric Quantities in Radiation Protection. In: J. Sabol and P.S. Weng: *Introduction to Radiation Protection Dosimetry*. World Scientific Publishing Co., Singapore 1995.

H. Průchová and B. Franěk: Monte Carlo Studies of Electron Avalanches in Microdosimetric Proportional Counters. Submitted for publication in Nuclear Instruments and Methods, 1995).

H. Průchová and B. Franěk: Influence of the Space Charge Effects on Electron Avalanche Development in Microdosimetric Proportional Counters. Prepared for publication in Nuclear Instruments and Methods, 1995).

H.Q. Linh: Code MTMICRO for the Monte Carlo Calculation of Photon Transport in Tissue Equivalent Proportional Counter of Spherical Shape. CTU FNSPE 27(1994), Report of the Czech Technical University, Prague 1994.

A. Sedlák and J. Sabol: The Microdosimetric approach to the Raddiation Weighting Factor. To be submitted for publication in Radiation Protection Dosimetry.

E.A. Bigildeev and V. Michalik: Charged Particle Tracks in Water of Different Phases - Monte Carlo Simulation of Light Ions. Submitted for publication in *Radiation Physics and Chemistry.*

Scientific Staff :

J Sabol, T Cechak, A Sedlak, V Michalik, H. Pruchova, M. Smejkalova.

Final Report
1992 - 1994

Contract : FI3PCT930072 **Duration 1.1.93 to 30.6.95** **Sector : A12**
Title : Individual electronic neutron dosemeter.

1)	Vareille and Decossas	Univ. Limoges
2)	Zamani-Valassiadou	Univ. Thessaloniki
3)	Barthe and Bordy	CEA - FAR
4)	Fernandez Moreno	Univ. Barcelona - Autonoma
5)	Curzio	Univ. Pisa
6)	Charvat and Spurny	IRD
7)	Moiseev	IFIN

Summary of Project Global Objectives and Achievements

The contract began in 1993 with five laboratories (Univ. Limoges, Univ. Thessaloniki, IPSN-SDOS, Univ. Autonoma Barcelona, DCMN Pisa), then in June 1994 the Institute of Radiation Dosimetry (Prague) and the Institute for Physic and Nuclear Engineering - IPNE- (Bucarest) have joined the project.

In spite of a considerable progress in neutron dosimetry there is no dosemeter which is capable to measure neutron doses indepently of the neutron spectrum with adequate accuracy and no real time dosemeter exists.

Different options for the development of an individual electronic neutron dosemeter were investigated within this contract. Original proposal concerned two families of detection principles which were studied in order to improve the methods and the devices :

- silicon diodes sensor
- superheated emulsions

And the question was : is it possible to improve one of the devices or the two devices for personal neutron radioprotection ? It is the framework within which the different laboratories worked during this contract, trying to point out various solutions as complementary as possible.
The intrisic nature of the two different neutron detectors is quite different, still the two systems appear suitable for an optimised approach to practical neutron dosimetry. The two approaches have been investigated aiming at the development of dosemeters optimised for various environments differing in terms of radiation field quality and strengh, as well as condition of noise, vibration and temperature. Detectors were first individually studied with monoenergetic neutron beams, at the IPSN Bruyeres le Chatel for silicon diodes and PTB Braunschweig for bubble detectors. The resulting devices were finally tested thanks joint to irradiations for all contractors carried out in IPSN Cadarache with radionucleides sources, thermal beams and realistic benchmark fields.

Superheated emulsions were mainly studied by DCMN Pisa and later one by IRD Pragua.
Over the two years of research, the activities of DCMN were divided into an initial investigation into the physics of these detectors followed by the exploitation of the previous findings for the development of a neutron survey meter and a spectrometer of new conception.

Detection principle :
Superheated drop detectors (SDD), also known as bubble detectors, consist of uniform emulsions of over-expanded halocarbon and/or hydrocarbon droplets dispersed in a compliant material such as gel or a polymer.Nuclear interactions nucleate the phase transition of the superheated liquid therein generating macroscopic bubbles. These are counted acoustically by means of piezo-electric transducers in contact with the detector vials.

The experimental work of DCMN Pisa carried out at the PTB Braunschweig indicates that bubble nucleation is primarily due to charged recoils generated through fast neutron collisions inside or next to the superheated drops. The microscopic vapor cavities these ions induce along their path grow to form macroscopic bubbles if sufficient energy is deposited within a critical volume.

It was demonstrated that the higher the degree of superheat of the liquid, the lower the minimum energy secondary charged particles, and therefore primary neutrons, must impart to the drops in order to nucleate their evaporation. For this reason, these detectors present a temperature-dependent (i.e. superheat-dependent) threshold response, like activation detectors, and a fairly flat response for higher energies.

Neutron dosimetry :

If the halocarbon droplets are sufficiently superheated and contain chlorine, they may be nucleated by the products of the 35Cl(n,p)35S neutron capture reaction. Through this mechanism, fast neutron sensitive halocarbon-12 emulsions also respond to thermal and intermediate neutrons, as required for a neutron dosemeter.

A prototype neutron area monitor was developed which improves the performance of these emulsions. The detectors are thermally controlled: this removes external temperature effects while ensuring a dose equivalent response optimised with respect to its energy dependence. The system was first characterized through calibrations with monoenergetic neutron beams. In the intermediate energy range, where experimental investigations were not possible, Monte Carlo response calculations were carried out. The device was extensively tested by means of numerical and in-field tests of the response to broad neutron spectra: from benchmark fields, through nuclear power plants and spent fuel storage sites, to relativistic stray radiation areas. All these indicated a remarkably constant dose equivalent response regardless of the neutron energy distributions.

The prototype DCMN developed within this research offers a virtually complete gamma discrimination and a neutron sensitivity of 5 bubbles per μSv. It is a fairly delicate system, though, and can be operated reliably when environmental conditions are not extreme. Nevertheless, when it was possible to employ it, the monitor demonstrated an accuracy far superior to that of conventional meters used in routine surveillance.

Neutron spectrometry :

The approach is analogous to the one employed in the optimisation of SDDs for ambient dosimetry and relies on the active control of the degree of superheat of two types of sensitive emulsions. These are insensitive to thermal neutrons and present very different response thresholds at room temperature.

A system was designed allowing temperature regulation within 0.2°C by means of thin heating strips operated by a time proportioning controller and monitored by a platinum resistance sensor. By varying the operating temperature of the emulsions, accurately defined detection thresholds are correspondingly generated : virtually any desired one between 0.01 and 10 MeV. This range is of the greatest importance in radiation protection dosimetry, as neutron exposures are most commonly received in this interval.

With the response curves of the system it is possible to scan the neutron spectra: the two detectors are first irradiated at a temperature of 25°C, and their temperature then successively increased in 5°C steps after adequate counting statistics--typically based on almost a thousand bubbles--has been accumulated at each step. The prototype has been tested with radionuclide neutron sources: analysed results confirm the potential of this original approach. Unfolding by means of adjustment codes shows that measurements are consistent with the source spectra: fluence values agree well within the calculated uncertainties. Monte Carlo unfolding without any pre-information on the spectrum generates fluence integrals from the detector readings with an uncertainty of about 10% in the relevant energy range.

The contribution of IRD Pragua, with scientific relations with DCMN Pisa, can be summarized as follows. Two types of bubble detectors were tested : bubble neutron damage detectors (BDNDs') and superheated drop detectors (SDDs'). Their response have been studied in several

polyenergetic reference neuton sources, particularly in the case of BDNDs'. It was proved that both these detectors are energetically independent to neutrons with energies between several tens of keV and 10 MeV, their response decreases for neutrons with energies approaching to 100 MeV. It was also proved that both types of detectord can be used as a neutron spectroscometers with the satisfactory resolution for radiation protection purposes. The lowest limit of detection for samples tested has been 10 μSv (± 30%). Detectors based on several supeheated halocarbons were realized and studied in terms of variable thermodynamic conditions.

Different steps can be pointed out for studies of diode sensor, they mainly came out of setting up between Limoges University, Thessaloniki University, IPSN-SDOS, Barcelona University, then IAP Bucarest.

***Diode sensor* 1st step :**

Differential method has been proposed by Limoges University within the frame of a collaboration between Limoges and IPSN SDOS (French patent n° 89 04469).
Thanks to results already obtained on a device using this method (in particular during the contract BI07020) some simple improvements in order to increase the signal to background ratio, principally by reducing gamma contribution were tested ; mainly they were :

- reducing of the metallic part of the device (cases realised in Limoges and used in Thessaloniki and Limoges)
- reducing of the thickness of the depleted zone (until 10μm in IPSN-SDOS)
- reducing of the detection area (until 19,6 mm^2 in Bucarest)

Studies (calculations and experiments) were also done on phantom contribution (Limoges)
It appeared that the results obtained are not satisfactory. Briefly, with a classical converter (i.e. 35 μm polyethylene implanted with boron 10) an energy threshold is necessary which does not allow to detect neutons with energies under 600 keV ; up to 4 MeV the sensitity lies between 0,5 and 1 pulse/μ Sv. Thermal neutrons are well detected by this device, the sensitivity depends on the density of boron atoms. At this step we can say that the device fails to realize a good personal dosemeter because the energy range around several hundred keV is an important contribution in usual neutron fields.

In these conditions, it was decided by the partners to undertake two tasks :

**** An improvement of the device using differential method (refered as 2nd step by :***
- back to back detector
- new converters and moderators
**** The study of new proposals of electronic devices (refered as 3rd step) :***
- pulse shape analysis
- coïncidence detection

***Diode sensor* 2nd step :**

Mainly two ways were studied in order to improve the devices using the classical method.

- ***First one :*** To avoid any discrepancy between the two diodes, a double diode on the same silicon substract located in the opposite side was designed. It is necessary that the wafer has homogeneous electrical characteristics. This device was proposed by IPSN-SDOS and CANBERRA.It has been tested and used in Barcelona University.

Barcelona used a dosemeter arrangement composed of a 40μm thick layer of polyethylene converter followed by a double diode detector The latter (CD-NEUT- 200-DBL) consists of two Canberra diodes, with an effective area of 2 cm^2 located on the opposite sides of a single silicon wafer the bulk resistivity of which is about 500 Ω.cm. The diodes have in their actual configuration a depleted layer of 35 μm for a polarisation of 10 V, separated by 222 μm of Si. With this configuration,the results can be summarized as follows :

* The dosemeter displays a low response value for low energy neutrons and a high response for photons. These effects required to introduce an energy threshold around 250 keV for neutron registration.

* A detection limit of 10 μSv was obtained for 1,2 MeV neutron energy

* The neutron dosse equivalent response may be obtained with an error of about ± 50% in the energy range from 570 keV up to 15 MeV.

* Simulation of the response of this dosemeter using a Monte Carlo code confirms the experimental results obtained and the value around 250 keV of the energy threshold.

It was shown that it is difficult to obtain the same photon sensitivity on both diodes, then in conclusion, it seems that the differential method is only slightly improved by this device.

- ***Second one :*** A special converter and various moderators were especially adapted to electronic device. Thessaloniki University mainly worked on this subject. And after joining the contract Bucarest Institute also studied a special moderator.

Thessaloniki's converter configuration is as follows : ^{6}LiF (thickness around 3 μm) is evaporated on polyethylene foil (0.5 cm). Two types of PIP diodes were used. One of them was delivered by Limoges University : it used a special 30 μm depleted silicon diodes inserted in a PMMA mount. The other used commercial available PIP diodes with 100 μm depleted zone in a metalic mount.

The results of this work appear very interesting for the realization of a real time dosemeter based on a single PIP diode. They can be summarised as follows :

* In the spectra α particle and ^{3}H regions are clearly distinguished. This permit to set a threshold in order to separate the γ ray contribution,

* The response varies from 100 pulses/μSv to 10 pulses/μSv when neutron energy increases from thermal up to 14 MeV. The flatness of the energy response curve was improved by controlling albedo contribution from the phantom.

* Concerning angular dependance, the system follows Hp(10) and isodirectional stantards.

* Experiments were also made in order to estimate γ ray contribution to higher channels than that of electronic noise which was estimated by separate experiments.

* There is no significant difference in the γ ray contribution for the two diodes ; in both cases it is restricted to low chanels, well below the interesting part of the spectum and so does not influence the dose measurement.

Thanks a complementary study, IPNE Bucarest relied a moderator for this application on the "Bonner spheres" principle, with the new approach of a "selected" energy range for moderation instead of the "full moderation" of neutrons over the whole energy range required by the Bonner spheres principle. Two silicon diodes with and without converter (polyethylene foil with 40 μm thickness and a high concentration layer of Boron 10) are used through differential method. This detection assembly (the two diodes covered by an Al shielding) is positioned inside a small size polyethylene moderator having a hemispherical shape (50 mm diameter)with a central cylindrical opening (10 mm diameter). We can point out :

* This device has a sensitivity from 10 to 40 times higher than the "classical device (i.e. without moderator), for realistic neutron fields,

* Compared to its response to fast neutrons, it shows an over response for the realistic neutron fields and also for on phantom measurements.

During steps 1 and 2, and concerning also colleagues working on bubble detectors, some calculations were done concerning the converter, the moderator, the phantom influence, device sensitivity (EGS4, MCNP), and they were an opportunity to have large exchanges and discussions between the seven contractors. The phantom influence was also studied through experiments, particularly during joint irradiations.

***Diode sensor* 3rd step :**

At the same time new principles were also studied in order to propose various solutions to problems appearing in the "classical electronic device". The aim was to eliminate γ contribution.

- IPSN - SDOS proposed a new method using only one diode covered with an hydrogenous boron 10 loaded converter. It is based on pulse shape analysis to discriminate the photon to neutron signal. Protons and alpha particles generated in the converter interact essentially in the depleted layer of the silicon diode and not noticeably in the wafer, whereas photons interact in both depleted layer and wafer.Due to the difference in electric field the charge velocities are different in these two regions. It leads to a faster rise time time for heavy charged particle pulses. Magnitude and rise time pulses depend on the geometric and electric characteristics of the diode. Moreover, the rise time of pulses depends on the associated electronic characteristics.

Two devices made of NIM standard electronic boards or using a specially designed board have been studied. Better results were obtained with NIM standard associated electronic.The rise time analysis allows to reduce drastically the photon sensitivity. The maximum deposited energy of the photon spectra is about 225 keV instead of 650 keV previously with the classical differential method . Additionaly, using a photon correction factor, there is almost no photon sensitivity left. The detection threshold in term of fast neutron energy usually met with semi conductor does not exist any more. At the very most, it can bee seen a low response around 0.25 MeV.

IPSN-SDOS proposed to use lead shield to reduce the photon sensitivity and a special shaped moderator to increase the neutron sensitivity for energies around 250 keV. Using a 6 mm shield the photon sensitivity is reduced by a factor of 2. The hydrogenous moderator placed at the top of the detector, increases the neutron sensitivity by a factor of 2 for 250 keV neutron energy.

- IRD Prague tested the possibility to distinguuish neutrons and photons on the base of position sensitive charge collection. Preliminary results are promising.

- Limoges University proposed to use a coïncidence method thanks to a sandwich device "Diode-Reactive Layer -Diode" realized by microelectronic techniques. The reactive layer can be Boron 10 or Lithium 6. The aim is to realized a multi aera dosemeter as a simple spectrometer wich separates different neutron energy ranges. The main problem is to obtain a correct sensitivity for intermediate neutrons.

The principle consists in analysing the total energy deposited by $^{6}Li\ (n,\alpha)^{3}H$ or $^{10}Bo(n,\alpha)^{7}Li$ reactions in silcon detectors working in coïncidence. The first step of this work was to calculate the response, thanks to codes developped in the laboratory, as a function of the characteristics of the reactive layer (nature and thickness from 10 nm to 500 nm) and the dead layer thickness (from 10 nm to 500 nm) of the diode. The excited state in nuclear reaction on Boron 10 gives complex spectra leading to some difficulties for analysis. Lithium 6 leads to better spectra for two reasons: no excited state exists and emitted particles are lighter and more energetic.

In the second step of this work, first experiments were done thanks to a device, which was conceived in the laboratory, composed of commercially available low cost diodes (Hamamatsu diodes) including a Boron layer and associated electronic for analysis. Results obtained with Am-Be and paraffin shielding show the feasability of the method in spite of the complexity of the spectra.

In order to use Lithium 6 as reactive layer some technical problems must be solved, the major of them being the diffusion of Lithium inside silicon. Technical solutions are in foreseen, in particular the use of LiF layers.

As said above the prototypes of different devices were finally tested through intercomparisons organised by IPSN-SDOS. Furthermore IRD Pragua used many different instruments (TLDs' - track etch detectors - remcounter - scintillator, GM device - tissue equivalent counter which was lend out by SDOS) to get more precise dosimetric and microdosimetric characteristics of reference fields. Particular attention has been concentrated to the gamma

component. Full microdosimetric event size spectra have been also established. All these data are available to all contractors to use them for the interpretation of their measurements.

This report can only be a summary of the work realized in the frame of the contract. More detailed results, comprising numerous values of tresholds, sensitivities, and their varations as a function of the parameters of the studies which have been shortly presented in this report are available in the final report of each participant to the contract. For the conclusion we must consider separately the SDDs and diode based dosemeters.

Superheated emulsions constitute delicate systems but allow for the development of high sensitivity neutron detectors with an almost constant dose équivalent response as a function of neutron energy and a complete photon rejection.

Research on diodes did not lead to the development of a simple single structure usable as a neutron dosemeter.However important conclusions can be drawn for the future. (i) It appears impossible to find among commercially available diodes or chips the solution of the problem. It means that the development of a specific chip will be necessary. (ii) The probability of designing a single chip suitable for the whole energy range is very low. More probably, the various components of usual neutron spectra will have to be treated by separate areas possibly on a single wafer. (iii) The main problem is still the 10-500 kev range.Even if important improvements have been proposed (use of nuclear reactions associated with a slowing down of neutrons, rise time analysis) the problem is not totally solved. (iiii) The sensor which will be developped in the future will perhaps borrow solutions from this study, that is : optimization of the surrounding materials, use of nuclear reactions, moderation of the incident spectra, reduction of the depleted zone thickness, pulse rise time analysis.

Head of project 1 : Prof. J.C. Vareille – Prof. J.L. Decossas

II. Objectives for the reporting period

The main objectives of this contract were :

– to improve the double diode device using differential method already proposed by LEPOFI. To do that a special device has been realized, which takes into account the results already obtained, reducing the metal parts of the device. The aim is to increase the signal to background ratio, principally by reducing gamma contribution.

– to study the response of this device, particularly the phantom influence thanks to calculations and experiments with monoenergetic neutron beams and realistic fields.

– to propose a new device in order to obtain multi area detector. The first step is to obtain a system capable to eliminate (if possible) the gamma contribution. In these conditions a "sandwich device" is proposed which uses coïncidence method. It is composed of Boron 10 layer between two diodes; Modelisation (thanks to codes developped in the laboratory) of the system must permit to obtain theoritical response and to study the influence of different parameters. A prototype is to be realized.

III. Progress achieved including publications

During this contract the scientific staff was composed of : C. BARRAUD, B. BARELAUD, J.L. DECOSSAS, F NEXON, J.C. VAREILLE.

DIFFERENTIAL METHOD

At the end of 1992 some conclusions had been drawn concerning the studies on a diode based neutron dosemeter ; It had been shown that for its improvement, further studies were necessary, concerning :

– the reduction of the depth of the depleted layer to reduce the sensitivity to photons,

– the adjonction of a silica layer on the detector (differential method) to get a more symetric sensor and obtain a better rejection of the photon signal,

– the need of a front aluminium sheet,

– the replacement of the metal parts around the sensor by organic ones in order to reduce Compton electrons.

The results which are now presented and analysed correspond to the study of these items.

Concerning the depleted layer, the effect of the bias voltage has been studied on diodes having a depleted layer of 35 μm for 10 volts which is necessary for the secondary particle spectrometry. For a reduced bias voltage, an increase of the electronic noise is observed as the thickness of the depleted layer is reduced. This is not compensated by the corresponding reduction of the γ background. The exhaustive study of this parameter would have need the manufacturing of specific diodes or chips ; this was not possible in the frame of this contrat.

A new case has been realized using polyethylene as discribed in figure 1. As proposed, the front aluminium sheet was removed and a silica layer used to protect both diodes from protons emerging from the surrounding polymeric materials. Irradiations have been realized with this sensor during several experiments at Bruyères le Chatel (CEA), Montrouge (ETCA), Limoges (University), Cadarache (CEA).

Monoenergetic beams (144 keV, 250 keV, 575 keV, 788 keV, 1 MeV, 1.2 MeV, 1.5 MeV, 2.5 MeV), an AmBe source, realistic spectra realized thanks to an appropriate shielding of a 14.8 MeV beam in Cadarache, (Canel+), and thermal neutrons have been used.

Most experiments were made with and without a slab (30 x 30 x 15 cm^3) PMMA phantom in order to study the albedo contribution to the response (it must be kept in mind that PE convertors are ^{10}boron implanted). The results presented in this report comprises tables and spectra. Sensitivities were calculated using fluence to dose conversion coefficient taken either from ICRP 21 in order to compare the results obtained with the new sensor to that of the old one, or from ICRP 60.

MONOENERGETIC FIELDS - RESULTS AND ANALYSIS

For practical reasons only 575 keV, 780 keV, 1 MeV and 5 MeV beams were used to study the phantom influence. Irradiations at 144 keV, 250 keV, 1.2 MeV, 2.5 MeV were on phantom. Angle influence was studied at 1.2 MeV. Table 1 summarizes the experimental conditions.

				With phantom				Without phantom			
Energy	Signal	Q*eff		H(mSv/h)		H(mSv)		H(mSv/h)		H(mSv)	
(MeV)		ICRP21	ICRP60	ICRP21	ICRP60	ICRP21	ICRP60	ICRP21	ICRP60	ICRP21	ICRP60
0.144	neutron	N.D.	N.D.	9	15	6	10	N.D.	N.D.	N.D.	N.D.
0.250	neutron	N.D.	N.D.	8.7	14.3	1.3	2.1	N.D.	N.D.	N.D.	N.D.
0.575	neutron	13.1	20.4	17.8	27.6	7.2	11.3	18.5	28.8	6.5	10.1
	photon	1	1	14 e -3		5.5 e - 3		14 e - 3		4.9 e - 3	
0.788	neutron	12.4	18.7	24	37	6	9	24.6	37	6	9
	photon	1	1	15.8 e - 3		3.9 e - 3		16.1 e - 3		3.9 e - 3	
1.000	neutron	11.7	17.2	25.5	36	5.6	8.2	27.7	40.6	5.9	8.6
	photon	1	1	19 e - 3		4.4 e - 3		21.6 e - 3		4.6 e - 3	
1.200	neutron	N.D.	N.D.	32	43.6	3.1	4 3	N.D.	N.D.	N.D.	N.D.
1.500	neutron	10.2	14.7	29	40	3.8	5.4	31.2	43.8	5.2	7.3
	photon	1	1	29 e - 3		3.8 e - 3		31.3 e - 3		5.2 e - 3	
2.500	neutron	N.D.	N.D.	36 3	46.7	3.3	4.3	N.D.	N.D.	N.D.	N.D.

Table 1 :Experimentals conditions used in monoenergetic neutrons fields -N.D. : No Data

For all experiments the symetry of the two channels (differential measurements) was not perfectly realized ; this is especially important for the very low energy channels of the analyser for which the differential methods leads to important fluctuations. A threshold must then be introduced when integrating spectra. The choice of this threshold from which the response can be taken as valid is a compromise between several needs :

- (i) a high sensitivity,
- (ii) a low uncertainty,
- (iii) a flat response versus energy,
- (iiii) a good photon rejection.

The results are quite different when the threshold is determined with or without phantom as it will be analysed. The thresholds are : 120 keV without phantom, 500 keV for phantom measurements.

MEASUREMENTS WITHOUT PHANTOM

Figure 2 shows the spectra for 788 keV neutrons. The corresponding sensitivities and uncertainties are given in table 2. Figure 3 gives the sensitivity as a function of neutron energy for the old and new device. Figure 4 gives the sensitivity as a function of the neutron angle of incidence.

Energy (keV)	S_n (Pulses.mSv^{-1}.cm^{-2})		σ_n	
	ICRP21	ICRP60	ICRP21	ICRP60
575	215	138	9	6
788	465	313	10	7
1000	650	443	12	8
1500	1000	712	15	11

Table 2 : Sensitivity of the dosemeter irradiated without phantom versus neutron energy (energy threshold : 120 keV)

ON PHANTOM TESTS

An example of the spectra which were measured (see table 1) is given in figure 5 (575 keV). Several conclusions can be drawn from this figure :

- an increase of the number of pulses in the 1.4 MeV region is visible
- an increase of the background pulses on both diodes up to 600 keV also occurs.

		Without phantom		With phantom	
		ICRP21	ICRP60	ICRP21	ICRP60
Energy (keV)	Seuil (keV)	$S_n \pm \sigma$	$S_n \pm \sigma$	$S_n \pm \sigma$	$S_n \pm \sigma$
575	120	215 ± 9	138 ± 6	N.D.	N.D.
*570 **	*125*	*550*			
	500	0.3 ± 1	0.2 ± 1	14 ± 3	9 ± 2
788	120	465 ± 10	313 ± 7	N.D.	N.D.
	500	51 ± 3	34 ± 2	60 ± 3	40 ± 3
1000	120	650 ± 12	443 ± 8	N.D.	N.D.
*1200**	*125*	*750*			
	500	229 ± 5	156 ± 4	239 ± 5	163 ± 3
1500	120	1000 ± 15	712 ± 11	N.D.	N.D.
	500	638 ± 10	455 ± 7	692 ± 8	493 ± 6
*2500**	*1075*				

Table 3 : Sensitivity S_n versus neutron energy obtained with and without phantom.
(N.D. = No Data ; * = results from previous experiments)

These modifications of the spectra are explained by the interactions of the neutron beam with the phantom : the first peak (1.4 MeV region) corresponds to the intermediate and thermal albedo neutrons from the phantom interacting with the ^{10}B atoms implanted in the converter. The extra pulses in the background region can be attributed to the γ photons from the capture reaction on hydrogen atoms of the phantom. This gamma background explains the need of a rather high threshold (500 keV) which has a strong influence on the sensitivity of the device. Sensitivity results are presented in table 3 and plotted on figure 6. It can be seem that the sensitivity drops down as the neutron energy decreases. Below 500 keV it is only due to the detection of albedo neutrons through ^{10}B.

The sensitivity increase due to albedo neutron can be evaluated from mesaurements with and without phantom by taking into account the pulses due to the reactions on ^{10}B by an appropriate integration of spectra. The corresponding results are given in table 4.

Energy (keV)	ICRP21		ICRP60	
	$S_A \pm \sigma$	Ratio	$S_A \pm \sigma$	Ratio
575	10 • 1	100 %	6 • 1	100 %
788	9.5 • 1	32 %	5.5 • 1	28 %
1000	6.5 • 1	5.4 %	4.5 • 1	5.5 %

Table 4 : Albebo sensitivity S_A in pulses/mSv.cm^2 as a function of energy and ratio of albedo sensitivity/total sensitivity

RESPONSE IN NEUTRON SPECTRA

AmBe source

Figure 7 gives the spectra for an irradiation with an AmBe source, with and without phantom. The two spectra seems to be similar. This is mainly due to the wide energy range in which recoil protons are found. Furthermore, the photon component in the incident field is important and the number of thermal albedo neutrons is lower for an incident AmBe spectrum than for an incident 550 keV beam.

		Without phantom		With phantom	
		ICRP21	ICRP60	ICRP21	ICRP60
Energy (MeV)	Seuil (keV)	$S_n \pm \sigma$	$S_n \pm \sigma$	$S_n \pm \sigma$	$S_n \pm \sigma$
to 0 from 11	500	615 ± 12	488 ± 10	686 ± 11	541 ± 9

Table 5 : Neutron sensitivity S_n in pulses/mSv.cm^2 obtained with an AmBe source (energy threshold : 500 keV).

The difference in sensitivity between the two experiments is not very important (about 11 %) and a little variation of some experimental parameters (distance between the source and the detector, ...) can lead to greater diffrences.

Some pulses above 2.5 MeV can be seen on figure 7. They cannot correspond to recoil protons since the depleted layer was not thick enough to detect a proton energy above 2.5 MeV. They must be probally caused by direct interactions of neutron on the silicon atoms of the diodes through two possible reactions : $^{28}Si(n,p)^{28}Al$ et $^{28}Si(n,\alpha)^{25}Mg$.

Realistic spectra

They have been used in the frame of joint irradiations at CANEL+ (Cadarache). These spectra are obtained thanks to a 14.8 MeV primary beam, an Uranium converter and various shieldings. Two spectra (fig. 8) have been used :

- the first (CANEL+, Fe shielding) is centered at 300 keV with a thermal and epithermal component,
- the second (CANEL+, Fe + water shieldings) has a stronger low energy (thermal, epithermal) component.

Spectra plotted on figure 9 were obtained with and without phantom. A peak centered at about 1.4 MeV can be seen, corresponding to the α particles from ^{10}B. the attached Lithium peak at 800 keV cannot be discriminated from background pulses. The alpha peak and the number of background pulses are greater if the phantom is used. This phenomenon increases as the thermal component of the incident beam increases. Sensitivities are given in the table 6.

	CANEL+ with Fe		CANEL+ with Fe and H_2O	
	Without phantom	With phantom	Without phantom	With phantom
ICRP21	176 ± 4	221 ± 6	244 ± 7	363 ± 10
ICRP60	120 ± 3	150 ± 4	170 ± 5	253 ± 7

Table 6 : Sensitivity S_n (pulses/mSv.cm^2) (energy threshold : 550 keV).

The rather low values of the sensitivity are explained by the high threshold (550 keV) which does not allow to take into account the recoil protons so that the response is only due to thermal neutrons either from the direct beam or from the albedo when a phantom is used.

Conclusion on the use of a phantom

From the results which have been presented it clearly appears that a phantom modifies the behaviour of the electronic dosemeter.

Albedo neutrons play a role which is more and more important as the thermal componant of the incident beam is high.

The second and cumbersome effect concerns the increase of the number of pulses in low energy channels. The threshold which is then necessary is very high. For the same field, the use of a phantom moves the threshold from 120 to 500 keV, leading consequently to a decrease in sensitivity and to a system which cannot operate in most of neutron fields of interest. All the possible reactions on the phantom (photon interactions, nuclear reactions, ...) have been analyzed in order to explain the increase of the background. From this analysis it appears that the main phenomenon responsible is the capture reaction of neutrons on hydrogen atoms of the PMMA phantom. An approximate evaluation using the reaction cross sections leads to the results of table 6.

From the characteristics of the phantom and cross sections of the various reactions and taking into account the albedo, the contributions of each reaction to the background has been approximatively calculated. It clearly appears that the capture reaction of neutrons on H atoms of PMMA is mainly responsible of the extra background pulses. So, one of the major conclusion is that the system, whatever its structure, must be studied and calibrated on a phantom.

DETECTION BY COÏNCIDENCE : FIRST STEP OF THE STUDY OF A MULTIAREA DOSEMETER

From results already obtained it appears clearly that the energy range 10 keV – 500 keV is generally not correctly monitored. In these conditions, a microelectronic structure designed for neutron spectrometry (multi area device) was studied. The studied device works as a spectrometer based on $^{10}B(n, \alpha)^7Li$ or $^6Li(n, \alpha)^3H$ reactions. A diagram of the sensor is given on fig. 10. The reactions products are detected in coïncidence ; the coïncidence detection is combined with an electronic threshold to eliminate the gamma background of realistic fields.

The main part of our study presented here consists in the modeling of the device through Monte-Carlo calculations to show that the device is feasible and could work properly. Preliminary results on the first experimental device realized in our laboratory are also presented.

MODELISATION OF THE REPONSE

Principle

The parameters influencing the response of the structure proposed fig. 10 are the following :

* The amount of reactive product which defines the sensitivity of the sensor. An increase of layer thickness produces an absorption of the particles from nuclear reactions occuring inside the layer. Spectrometric properties need a layer as thin as possible not compatible with the need of high sensitivity necessary for dosimetry.

* The thickness of the dead layer of the detecting diodes must be minimized since it always acts as an absorber of the energy of recoils.

* The thickness of the depleted layer must be adapted to the range of the most energetic particles crossing normally the various layers.

* The bulk of the wafer is supposed not to have any influence on the response of the sensor.

The sensor response has been modeled thanks to calculation codes developped in our laboratory. The response has been first calculated for thermal neutrons : the problem is rather simple, the reaction being isotropic. The spectra presented are the distributions of the energy which is deposited in depleted layers. The resolution of the electronic measuring device has not been taken into account. We shall examine in turn the role of the dead layer and the reactive layer. A catalogue of spectra have been calculated but only few are presented here.

The dead layer

The nuclear reactions are supposed occuring in an infinitely thin layer on the common surface of the two facing diodes. The reaction being isotropic, an emission angle is chosen at random. The particles are followed and the energy which is lost in the dead layer deduced from the initial energy. The distribution of the remaining energy is calculated. 10^5 interactions have been simulated, and 10 , 50, 100, 200, 500 thich dead zones have been considered. On spectra, we note that peaks of the two particles ^4_2He and ^7_3Li of fundamental and excited states of the reaction appear clearly. As the thickness increases, two effects can be noted : on one hand, low energy pulses appear due to particle having had a long path in the dead layer, and, on the other hand, the maximum energy of the peak is modified.

The distribution of the total energy deposited in coïncidence by one nuclear reaction has also been calculated : an example is given figure 11. The two possible values of the reaction energy (Q = 2,31 MaV and Q = 2,79 MeV) appear clearly.

As for ^{10}B the results with ^6Li illustrate the role of the dead layer thickness on the two peaks (the reaction has no excited state) detected by one of the diodes. The comments on ^{10}B remain for ^6Li, but spectra are less disturbed. The differences in the modifications can be explained by the nature and energy of the particles : being lighter and more energetic than the ^7Li, the ^3H has a lower LET.

3 – The reactive layer

Its thickness effect appears on figure 12 and 13 for ^{10}B and for ^6Li. The calculations have taken into account the roles of the dead zone and fo the reactive layer. The flattening of the peaks is explained by nuclear reactions occuring at random inside the reactive layer. We can note that spectra are less disturbed in the case of ^6Li than in the case of ^{10}B.

The global analysis of the results shows that the thicknesses of the reactive layer and of the dead layer give the spectrometric properties of the device ; in these conditions, the device must be realized with diodes having an as thin as possible dead layer. For neutron dosimetry, the condition of a thin reactive layer could lead to a too low sensitivity.

EXPERIMENTAL DEVICE

First boron coating experiments on silicon wafer show a great fragility of wafers due to the stess induced by the ^{10}B layer ; so it was very difficult to obtain diodes with a boron layer. Studies of boron deposition were made in order to solve this problem. But, it was rapidly decided to realize the feasability tests thanks to the following device : It is composed of commercially available low cost diodes including boron 10 layer as described by figure 10. Some technological problems had to be solved to realize this device. Electronic tests on the "diodes-sandwich" were performed. The electronic system was realized and tested. Thanks to an AmBe source and paraffin shielding a neutron field was obtained in order to expose the device. The result is presented on figure 14 which shows the spectrum of particles which were detected in coïncidence. Thanks to this first experiment, and even if it is a preliminary one, we have shown that the sandwich structure is feasible.

conclusion on the sandwich device

From theoritical results it appears that ^{6}Li layers give better results than ^{10}B layers. But on the technological point of view some difficulties exist in realizing Li layers on silicon wafer without any modification of the electronic properties of the silicon diodes on which the Li is deposited. These technological problems should be solved in the first step of a future work which is planned.

REFERENCES

1 - D. PAUL, Perturbation γ dans un dosimètre neutronique à diodes. - Limoges - Thesis n° 14-92, (1992).

2 - B. DUBARRY, Contribution à l'étude d'un capteur électronique pour la dosimétrie personnelle des neutrons. - Toulouse - Thesis n° 1254, (1992).

3 - B. BARELAUD, B. DUBARRY-CHABANAIS, D. PAUL, L. MAKOVICKA, J.L. DECOSSAS, J.C. VAREILLE - Evolution du capteur électronique pour la dosimétrie des neutrons développés au LEPOFI. Radioprotection, Vol. 28, n° 4, 387-409, (1993).

4 - D. PAUL, B. CHABANAIS, B. BARELAUD, L. MAKOVICKA, J.C. VAREILLE, J.L. DECOSSAS - Capteur à semi-conducteur pour la dosimétrie neutronique des personnels. - XXXII^{ème} Congrés de la Société Française des Physiciens d'Hôpital - Poitiers, (1993).

5 - B. BARELAUD, J.L. DECOSSAS, J.C. VAREILLE - Dosimètrie électronique des neutrons. Journée d'étude et de reflexion sur la dosimétrie dans le cadre des études de défense. D.G.A. - D.R.E.T. - C.E.B., Arcueil, (1993).

6 - B. BARELAUD, F. NEXON, J.L. DECOSSAS, J.C. VAREILLE, G. SARRABAYROUSSE - Study of an integrated monitor for neutrons fields. Rad. Prot. Dos., Vol. 61,n° 1-3, (1995).

7 - F. MOKHTARI, B. BARELAUD, J.L. DECOSSAS, J.C. VAREILLE - Etude d'un détecteur électronique intégré pour les champs de neutrons. - XXXIII^{ème} Congrés de la Société Française des Physiciens d'Hôpital - Strasbourg, (1995).

8 - B. BARELAUD, J.L. DECOSSAS, G. SARRABAYROUSSE, J.C. VAREILLE - Perpestives pour la détection des neutrons par un système électronique multiplage.- Congrés S.F.R.P. « L'instrumentation en radioprotection des travailleurs ». C.E.N. Saclay (INSTN), (1995).

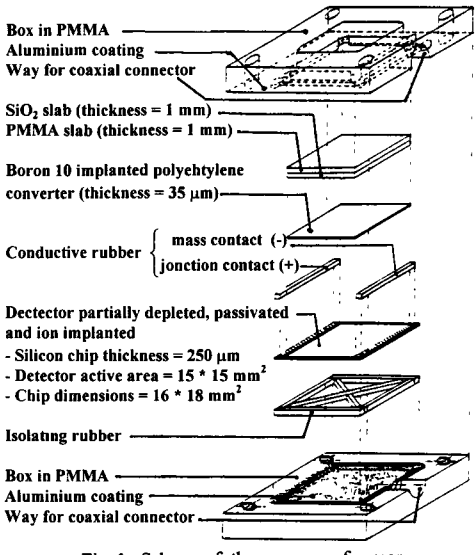

Fig. 1 : Schema of the new case of sensor

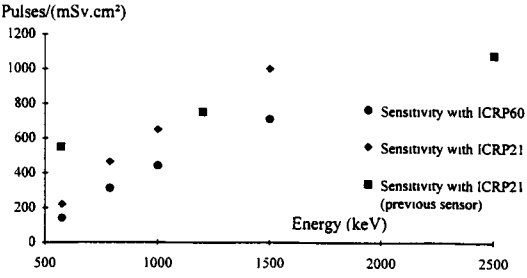

Fig. 3 : Sensitivity S_n versus neutron energy.

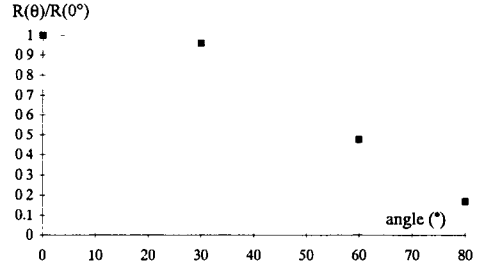

Fig. 4 · Relative sensitivity versus incidence angle with an 1.2 MeV neutron energy.

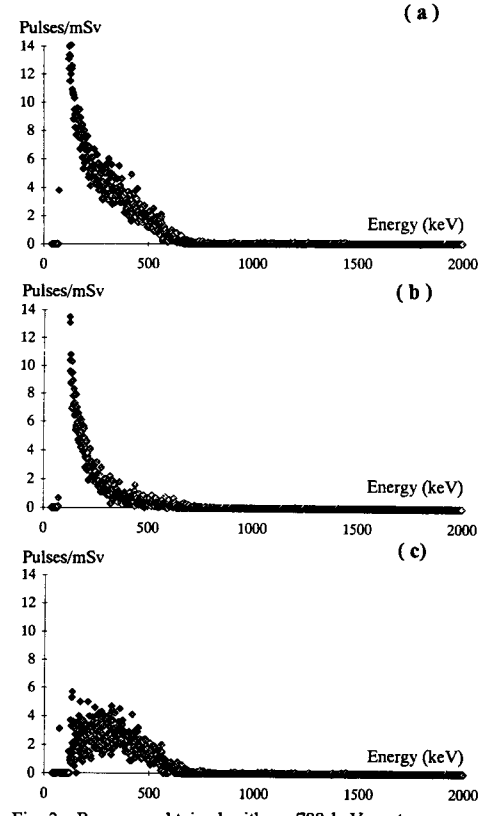

Fig. 2 . Response obtained with an 788 keV neutron energy without phantom ; a - with $(CH_2)_n$ converter ; b - without converter ; c - differential spectrum.

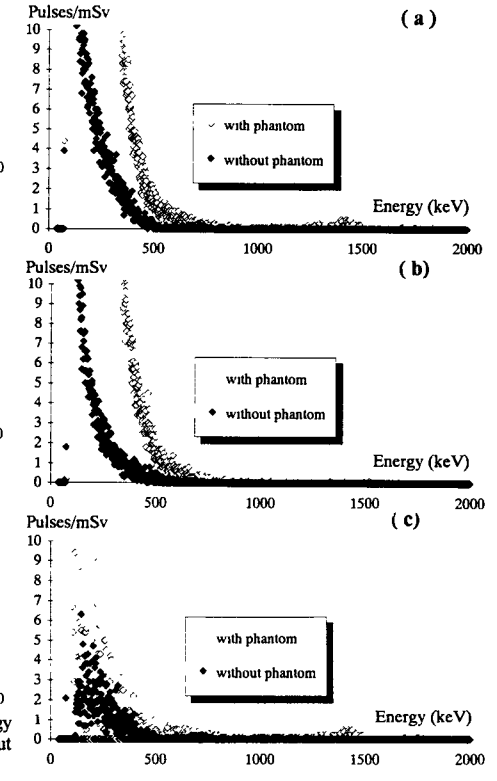

Fig. 5 : Response obtained with an 575 keV neutron energy with and without phantom ; a - with $(CH_2)_n$ converter , b - without converter ; c - differential spectrum.

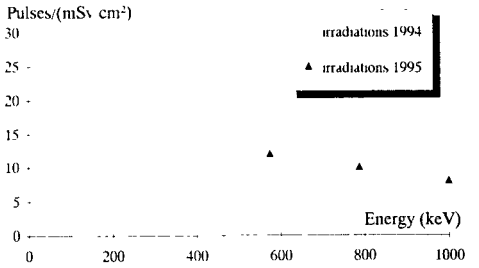

Fig 6 Albedo sensitivity as a function of energy (on phantom) in accordance with ICRP60

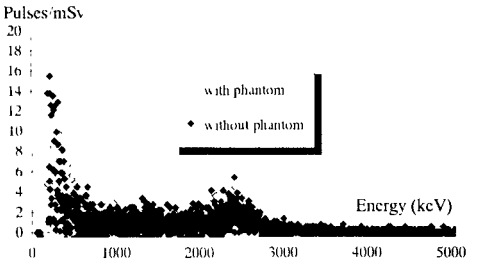

Fig 7 · Differential spectrum due to an AmBe source Comparison of spectra obtained with and without phantom

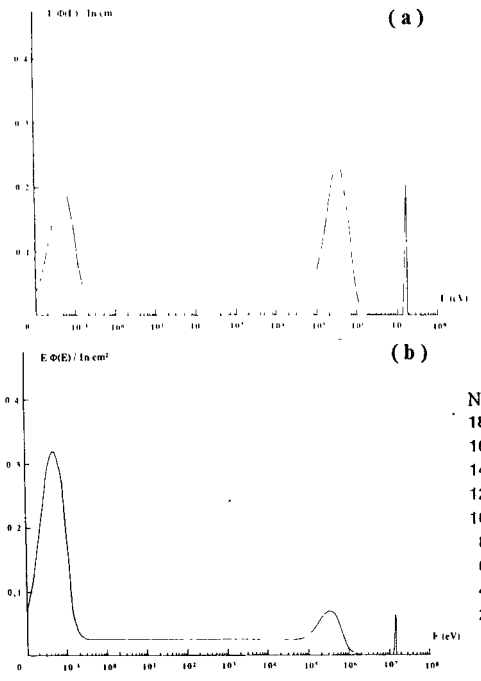

Fig 8 · Canel+ neutrons spectra : a - Canel+ with Fe shield , b - Canel+ with (Fe + H_2O) shields

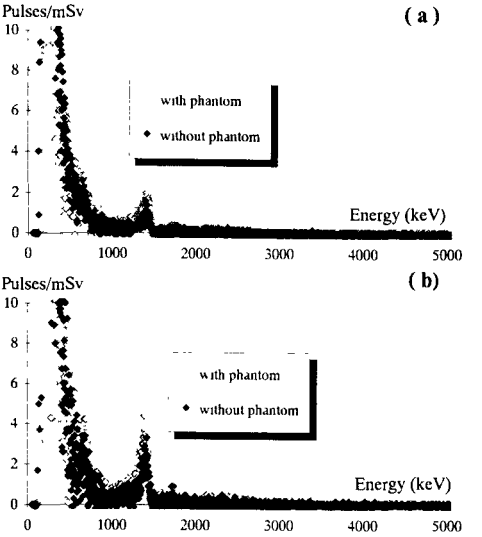

Fig 9 . Comparison of differential spectra obtained with and without phantom a - Canel+ with Fe screen , b - Canel+ with (Fe + H_2O) screens

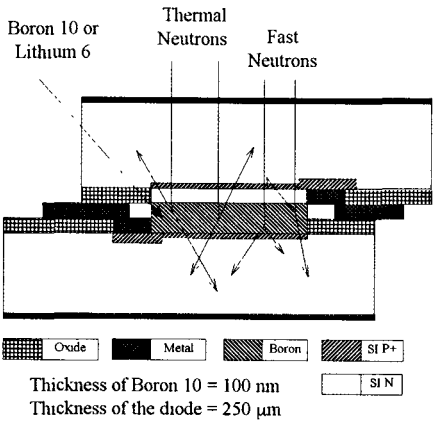

Fig 10 Schematized view of the sensor

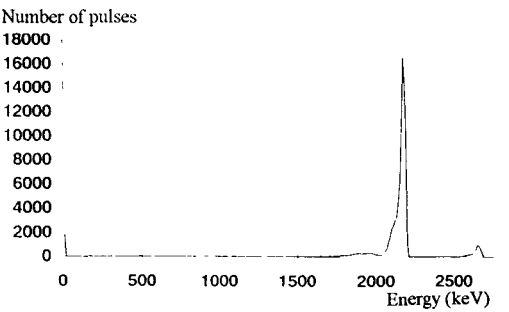

Fig 11 Distribution of the total energy deposited in the diode (dead zone 100 nm ; boron layer 100 nm)

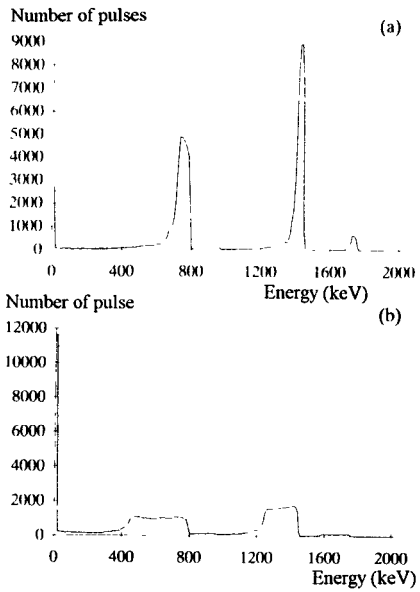

Fig 12 : Spectrum from one diode with a boron reactive layer . Dead zone thickness : 100 nm
a- boron thickness : 100 nm
b- boron thickness : 500 nm

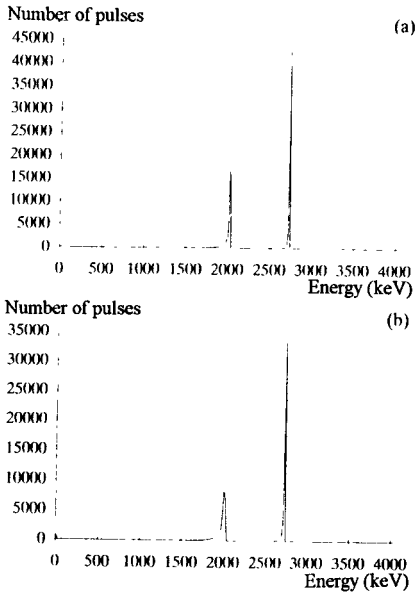

Fig 13 . Spectrum from one diode with a lithium reactive layer Dead zone thickness · 100 nm
a- Lithium thickness . 100 nm
b- Lithium thickness 500 nm

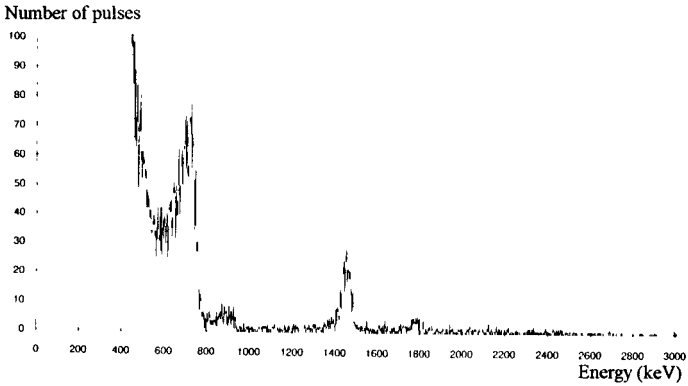

Fig. 14 · Experimental spectrum obained with an AmBe source and paraffin shielding

Project 2:

Head of project: M. Zamani-Valassiadou

Objectives of the reporting period:

The programme of the work was focused to the study of the response characteristics of of an electronic neutron dosemeter based on PIP diodes with a new (n,α) (n,p) converter.

The work can be splitted in to two main parts: 1)Study of the system response and as final product the calibration of the system diode-converter under monoenergetic neutron beams 2) Study of the system behavior under realistic neutron fields. Both experiments include investigation of separate components contributing to the spectrum obtained with diodes i.e.: moderation of the incomming beam b) albedo contribution c) fast neutron component. The knowlege of each component can be used to the control of the energy response curve of the dosemeter.

Progress achieved including publications.

Last years a new converter was developed from our group. The development includes study of the converter in order to be used with passive as well as real time systems.

Converter configuration: The converter consists from ^{6}LiF (1-3 μm) evaporated on polyethylene foil (0.5 - 1.0 cm). The study of the converter characteristics is given in refs [1-3] and can be summarized as follows:

1) Continuous response from thermal neutrons up to 14 MeV (in fact several decades MeV).

2) High response, higher than the usual systems based on proton recoils for whole energy range of neutrons. However the modification of the energy response curve, i.e. to be more flat (which is mostly important for individual dosimetry) lowers the response mainly in the low energy neutrons but it remains higher than the commonly used systems .

Diodes: Two types of PIP diodes were tested: The one of them was delivered from the LEPOFI Lab. and was of special design as it was developed in the frame of this project. The other diode tested was a commercial PIP diode with 100 μm depletion zone and metalic mount. In both type of diodes the γ-ray contribution and the background were separately examined.

Results.

1. Method.

The results were taken from analysis of the spectrum obtained with diodes. A typical spectrum of the system diode with the discussed converter is given in fig. 1. The spectrum can be analysed in three parts: 1) Low channels in which the γ-ray contribution is mainly appeared but

also electronic noise 2) Intermediate region where a large peak can be seen. This peak corresponds to the alpha particles with maximum energy of 2 MeV and they are produced from $^{6}Li(n,\alpha)^{3}H$ reaction with thermal and low energy neutrons. However according kinematics of the reaction alpha particles of higher energies are produced from fast neutrons which are distributed in the whole spectrum but they are of minor importance because of their poor crossectional contribution 3) The ^{3}H peak dominates the spectrum been a sharp clear peak. The energy of ^{3}H particles is 2.7 MeV for thermal neutron reaction with ^{6}Li. In this case higher energies are also produced from fast neutrons but their contribution is also small. Proton recoils coming from the moderator give an almost continuous distribution up to the enegry of the incoming neutrons. From the spectrum is resulted that proton contribution is lower than those of alpha and ^{3}H particles.

The shape of the neutron spectrum permits to use electronic thresholds in order to work with particle spectrum only and avoid γ-ray component. For this reason it is possible to work with one diode against differencial method.

2. Test and calibration in monoenergetic neutron fields.

The system diode - converter was tested for individual neutron dosimetry purposes. So the tests of the system were programmed for the study of the required characteristics of individual neutron dosimetry (ICRP60). All irradiations were performed on a polyethylene phantom 15x15x30 cm^3. Monoenergetic beams of neutrons were provided from CEN-Bruyeres le Chatel organized by the CEA group. During these experiments the γ-ray contribution was also studied as well as the proper background of the system. The irradiations were made for 75 KeV, 144 KeV, 250 KeV, 570 KeV, 1.2 MeV and 2.5 MeV neutrons [4]. Tests at 14 MeV neutrons were also made in CEA Cadarache neutron facility in the frame of this project. The response of the system to thermal neutron fluxes was studied during separate experiments performed in the Nuclear Research Center "Democritos" of Athens.

The results can be summarized as follows:

a) Energy response continuous from thermal neutrons up to 14 MeV. From fig. 2 is resulted a reponse of 10^5 pulses/mSv up to 10^4 pulses/mSv respectively. It is of importance to remark that the system respond very well at 14 MeV equally to the lower neutron energies. The flatness of the energy response curve was improved by controlling albedo neutron contribution arising from the phantom [5]. The curves presented in fig. 2 labelled as (a) (b) (c) are refered to integration of the various parts of the neutron spectrum [6]. Curve (a) concerns integration over the whole spectrum. Curve (b) is taken by setting a threshold to the lower part of alpha particle peak and (c)

with a threshold between alpha and ^3H peak. It can be seen that the response decreases when integration is made on a part only of the spectrum. However it is not of importance the absolute value of the response but the ratio of the net events to the γ-ray component. The last one diminishes for higher channels [see below].

b) Angular dependence. The system follow $H_p(10)$ and isodirectional standards, fig.3, [6].

c) Linearity. The linearity of the system was examined at 1.2 MeV neutrons with dose equivalents from 0.2 mSv - 10 mSv. Identical linearity is resulted, fig.4, [6]. Curve (a) corresponds to results taken from alpha particles + ^3H peak while curve (b) to the ^3H peak only.

d) Estimation of the γ-ray contibution and background. Separate experiments were performed at CEN Bruyeres le Chatel in order to estimate γ-ray contribution. For this purpose an equivalent diode without LiF converter is used. The results are given as integrgrals above a threshold, fig. 5 . For the comparison with spectrum of fig.1 the two systems have the same channel-energy calibration.

For background estimation the two systems (with LiF converter and with Teflon) were exposed in the same ambient out of run for about 10h.. The results are summarized in Table I.

Table I. Background results for diodes with (^{6}LiF) and Teflon converter out of neutron field.

	Pulses / h				
Channel threshold:	0	100	200	300	900
Diode with CR-39(LiF)	157	9	1.5	0.4	0
Diode with Teflon	990	13	1.7	0.6	0.1

Finally comparison of the two types of diodes shows the same dosemeter characteristics. There is no significant difference in the γ-ray contribution which in both cases is restricted to low channels, well below the spectrum of interest and so does not influence neutron dose estimation.

e) Lowest detectable dose. Concerning the lowest detectable dose we have found that depends slighly on the part of spectrum used for integration. The most sensitive and accurate value is that estimated from the ^3H peak. For this case H_{LD} is of the order of 0.5 μSv [6].

3. **Realistic neutron fields.**

a. Measurements at realistic neutron fields were performed in the frame of this project at CEA-Cadarache. Intercomparison with the other dosimetric systems were made.

Our experiment concerns dosemeter readout at the given fields but also the albedo component coming from the phantom. The study was made for each part of the spectrum separately in order to test the sensitivity of the response. The results are given in Table II.

Table II. Dose equivalent response at realistic neutron fields.

Facility	Reference Dose equivalent $H^*(10)$ mSv	Dose equivalent response, α-part.+^3H	Dose equivalent response ^3H
CANEL$^+$ H_2O	1	$4.8 \cdot 10^5$	$2.6 \cdot 10^5$
SIGMA	0.075	$1.2 \cdot 10^6$	$6.4 \cdot 10^5$
14 MeV	2.2	$2.3 \cdot 10^4$	$5.0 \cdot 10^3$

Publications.

1. Fast neutron detection using (n,p), (n,α) converter.
   E.Savvidis, M.Zamani, D.Sampsonidis and S.Charalambous
   Nucl. Tracks Rad. Meas. 19, 527-530, 1991.

2. A CR-39 fast neutron dosemeter based on an (n,α) converter.
   E.Savvidis, D.Sampsonidis and M. Zamani
   Rad. Prot. Dos. 44, 341-342, 1992.

3. An individual neutron dosemeter with (n,α) and (n,p) converters.
   M.Zamani, D.Sampsonidis and E.Savvidis
   To be appeared in Rad. Meas.

4. Eurados - Cendos meeting, Strasbourg, Sept. 1994

5. Separation of the albedo neutron component of a CR-39 neutron dosemeter during on phantom irradiations.
E.Savvidis, D.Sampsonidis and M. Zamani
(11th IC on Solid State Dosimetry, Budapest 1995, abstr T7)

6. A real time personal neutron dosemeter with a single PIP diode and (n,p), (n,α) converter.
M.Zamani and E.Savvidis
Submmited to Rad. Prot. Dos.

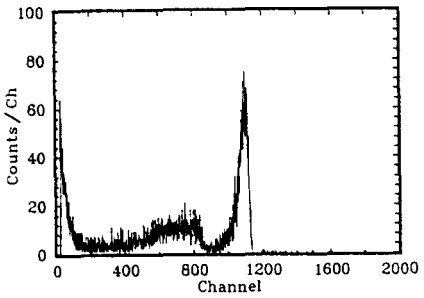

Figure 1. Spectrum taken by Si diode with PE-LiF converter. On Phantom irradiation. E_n = 1.2 MeV.

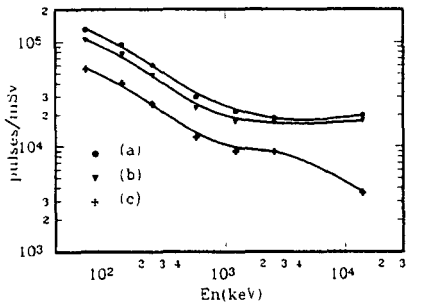

Figure 2. Energy response of the system for different channel thresholds.

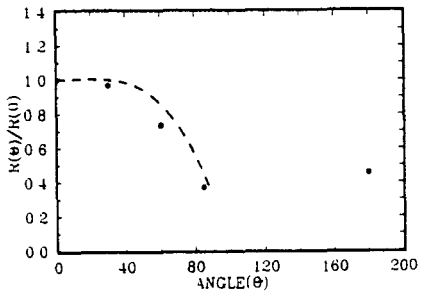

Figure 3. Angular dependence of the system response.

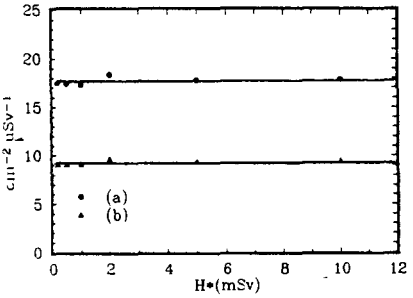

Figure 4. Linearity of the system. E_n = 1.2 MeV.

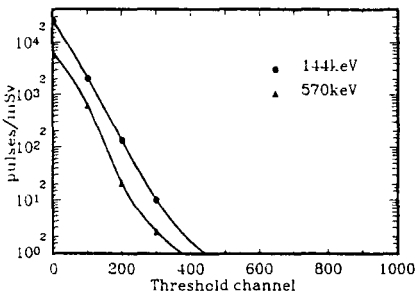

Figure 5. The γ- ray component. Each point represents intergral above the indicated channel.

Head of project 3 : J.M. BORDY
Scientific staff · T. LAHAYE

II - Objectives for the reporting period.

The SDOS objectives in the contract were to design electronic sensor for individual neutron dosimetry and to improve its associated methods (electronic signal treatments and dose equivalent calculation)

The SDOS studies were carry out in two steps :

- First step (1993-1994) : Improvement of the differential method
- Second step (1994-1995) · Set up and development of the pulse shape analysis method.

Additionally the SDOS organised intercomparisons for monoenergetic neutron beams and realistic spectra which simulate those observed at different power plant location

III - Progress achieved including publications.

1 Neutron sources and irradiation conditions

Monoenergetic neutron beams (0 073, 0 144, 0 250, 0 570, 1.2 and 2.5 MeV) were obtained from a Van de Graaf accelerator using (p,n) reaction on Lithium or Tritium target. 14 8 MeV neutrons were obtained from a SAMES accelerator using (d,n) reaction on Tritium target

Broad energy spectra such as AmBe and ^{252}Cf neutron sources, Silene reactor and realistic fields were used too. Realistic fields simulate those observed at different power plant locations. They were obtained from the well-known CANEL and CANEL+ facilities - a 14 8 MeV neutron source (see above) is covered with polyethylene, light water and iron shield.

The reactor Silène is a solution-fuelled reactor made of a stainless steel cylinder filled with a uranium solution. It can be surrounded with a cylindrical lead shield (10 cm thick)

Thermal neutrons were obtained in front of the SIGMA source assembly It is composed of 6 AmBe neutron sources placed at the centre of a graphite cube The measurement point is located outside the graphite cube, 88 % of the fluence is due to thermal neutrons, the remainder is due to fast neutrons

Detectors have been irradiated on phantom according to the requirements of the calibration procedure for individual dosimeters A slab phantom (30 cm X 30 cm X 15 cm) made of Polymethyle methacrylate has been used Dosemeters have been placed at the centre of its front side.

2 - Differential method

2.1 - Principle.

Neutrons are detected indirectly through elastic scattering (n,p) reactions and (n,α) reactions in a hydrogenous material (polyethylene) boron 10 loaded. Protons and alpha particles emitted by the converter are detected by a semiconducting diode. The detector is made of two diodes : the first diode, in contact with the hydrogenous converter, detect not

only protons and alpha particles but also every particles interacting in the diode (electrons, neutrons, photons). The second diode is not covered with a converter, thus it detects only particles interacting in the diode. Therefore the signal subtraction between the two diode is mainly due to protons and alpha particles created in the converter. Thermal neutrons are detected through (n,alpha) reaction on Boron-10

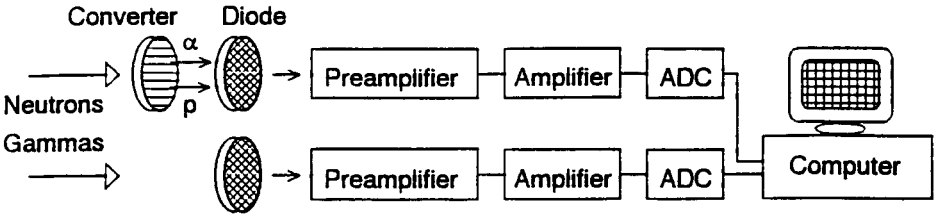

Figure 1 · Block diagram of the two-diode dosemeter using the differential method.

2.2 Method

The dosemeter response in term of personal dose equivalent in the phantom R_H is given by the following formulae.

$$R_H = Hp(10,0°)ref / Hp(10,0°)meas \qquad (1)$$

Where Hp(10,0°)ref is the reference personal dose equivalent at 10 mm depth in phantom and for 0° of incidence and Hp(10,0°)meas is the measured personal dose equivalent at 10 mm depth in phantom and for 0° of incidence.

with $$Hp(10,0°)meas = K\,N \qquad (2)$$

Where K is an experimental calibration coefficient and N is the number of pulses due to neutrons.

Calculation of N.

Let $\frac{d(N(E))}{dE}$ the « deposited energy spectrum » , where N(E) is the number of pulses as a function of the deposited energy (E) in the diode.

Let $\frac{d(N\gamma n(E))}{dE}$ the spectrum obtained with the diode covered with the converter and $\frac{d(Nn(E))}{dE}$ the spectrum obtained with the bare diode.

$$N = \int_{E=200keV}^{E=\infty} \frac{d(N\gamma n(E))}{d(E)} d(E) - \int_{E=200keV}^{E=\infty} \frac{d(N\gamma(E))}{d(E)} d(E)$$

Theoretically it is possible to detect thermal and fast neutrons using two identical diodes. The main problems encountered are the differences in background and in photon sensitivity between the two diodes. The aims of the SDOS studies were ·

- to decrease the photon sensitivity by reducing the size of the depleted layer.
- to reduce the difference in electric properties between the diodes using two P.N. junctions implanted back to back on the same wafer

2 2 Experimental set-up

The two diode detector consists of two Canberra diodes (sensitive area : 1.5 cm^2, bulk resistivity of about 600 Ω.cm). Intertechnique preamplifiers (PSC762) and amplifiers were used; two PC compatible multichanel analyser boards (Ortec) were used.

2.4 Results.

The dose equivalent response has been studied for monoenergetic neutrons, from 144 keV up to 2 5 MeV, and broad neutron energy spectra such as SIGMA , Silène and ^{252}Cf sources.

Figure 2a and 2b shows the spectra obtained with the "Silène" reactor and the ^{252}Cf source. As expected, these spectra are similar because both sources present fission spectra. It can be seen two components: i) below 0 5 MeV, the pulses are assumed to be mainly due to photons, they mask in its entirety the neutron component, ii) above this limit the « flat » components of the spectrum are assumed to be due to neutrons

Figure 3 shows the spectra obtained with the SIGMA source One can see a peak at 1.3 MeV It is due to alpha particles created by nuclear reactions between thermal neutrons and boron-10. As previously, the first part of the spectra (below 0.5 MeV) is assumed to be due to the photon component.

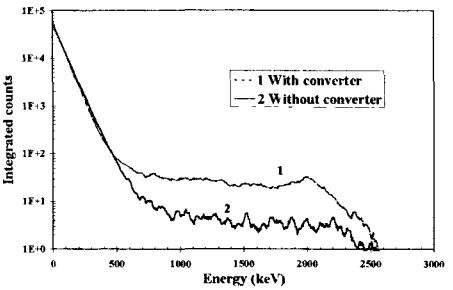

Figure 2a Spectrum obtained for Silène reactor

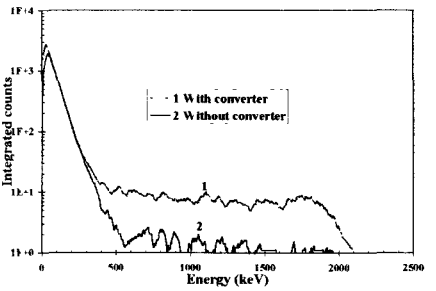

Figure 2b Spectrum obtained for ^{252}Cf.

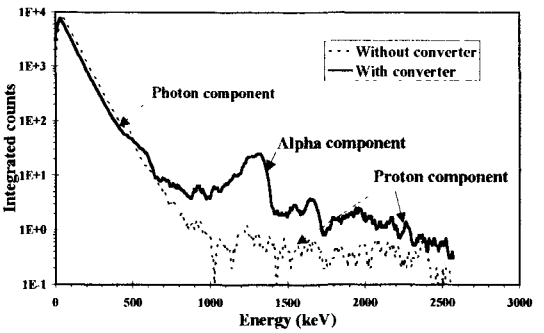

Figure 3 Spectra obtained with SIGMA neutron source.

In spite of the depleted layer thickness decreasing (10 µm was used), the photon component of the spectra is still very important - its maximum deposited energy is about 650 keV Thus the detection threshold in term of neutron energy is about 500 keV

Table 1 . Dose equivalent response as a function of neutron energy for the two-diode detector (converter thickness 35 µm).

Energy	0.57 MeV	1 2 MeV	2 5 MeV
Calibration coefficient (Pulses Sv^{-1} cm^{-2})	$2.44\ 10^5$	$5\ 63\ 10^5$	$7.25\ 10^5$

A decrease in response versus neutron energy is found (table 1). This effect is due to the reduction of the secondary proton emission that reaches the depleted layer of the diode. Indeed the mean path length of secondary protons decreases with initial neutron energy and only protons produced from a thin layer close to the converter surface can be counted

The sensitivity remains too low for energies below 800 keV to fulfil the ICRP 60 requirements for individual dosemeters. The difference in photon sensitivity between the 2 diodes must be reduced to decrease this threshold

To avoid any discrepancy between the two diodes, a detector (called the back-to-back diodes) was designed with Canberra It is composed of two diodes located in the opposite sides of the same silicon subtract (called wafer) The wafer thickness is about 250 µm. The depth of the depleted layer is the same below each point of the surface for the two P N. junctions.

Advantages and disadvantages of the "back-to-back diode" detector

- Similar electronic background and better symmetry between the two diodes,
- Difference in back scattering for photons between the two diodes.

The "back-to-back diodes" were made The Barcelona University tested them

2.5 Conclusions

The two-diode dosemeter has a high photon sensitivity below 0 5 MeV. The differential method cannot obviate this problem because it is very sensitive to the difference in photon sensitivity between the two diodes This difference leads, mainly for low neutron energies either to an over-estimation of the neutron dose equivalent (if the most sensitive diode is associated with the converter), or to an under-estimation of the neutron dose equivalent (if the most sensitive diode is the bare one) Therefore, such a dosemeter does not record intermediate energy neutrons between 10 keV and 500 keV Below 10 keV the neutron sensitivity is due to (n,alpha) reactions combined with the albedo effect. Even if the « back-to-back diode » should improve the photon rejection, the sensitivity will remain very low for intermediate neutrons. The differential method cannot fit the requirements of individual dosimetry. Also, the SDOS developed a new method based on pulse shape analysis to discriminate the photon pulses.

3 - Pulse shape analysis method.

3 1 - Principle.

This method is based on only one P.N. junction covered, as previously, with a polyethylene boron 10 loaded converter. Neutron dose equivalents are calculated through recoil nuclei counting (mainly protons and alpha particles). The photon rejection is based on a pulse shape analysis.

The P N. junction can be roughly divided into two parts· the depleted layer and the remainder of the silicon detector called « wafer » in this paper.

In our case, proton and alpha particles, generated in the converter, interact essentially in and close to the depleted layer and not noticeably in the wafer, while photons interact on either in both. Charge carrier velocities are different in these two regions, they are faster in the depleted layer because electric field are higher in this region For this reason, rise times of heavy charge particle pulses are faster than those of photon pulses.

Two devices have been studied, the first one was made of NIM standard boards, the second one used a specially designed board.

3 2 Device made of NIM standard boards.

3.2.1 Experimental setup.

The device (fig 5) is composed of 3 parts i) the detector and the preamplifier (Intertechnique PSC762) ii) The amplifier stages and the pulse shape analyser, all of them made of commercial NIM standard boards iii) three multichanel analysers to record the spectra corresponding to SO1, SO2 and SO3

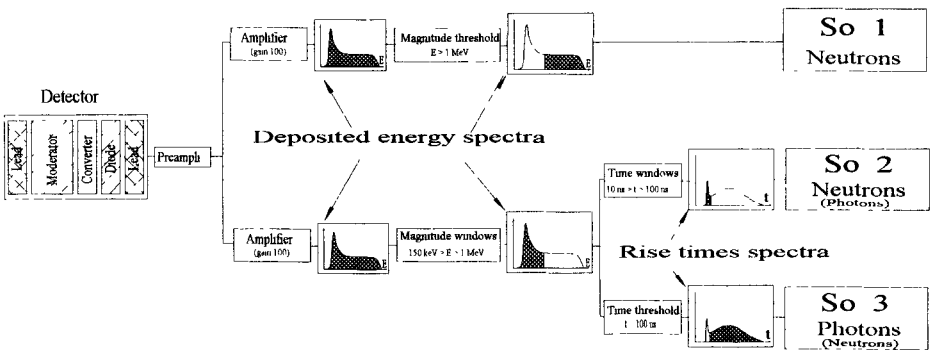

Figure 5 : scheme of principle of the device.

The detector consists of a Canberra PIPS diode (Passivated Implanted Planar Silicon) - 300 µm thick and , 1 cm² of sensitive area. It is covered with a polyethylene converter boron 10 loaded (5 10^{15} Bore, 30 µm thick). Conductive plastic joints are used to apply a reverse bias - applying 12 V, the depleted layer is about 30 µm thickness. An aluminium plate (0.2 mm thick) protects against external electric and magnetic fields. Two printed circuits keep the different pieces in position. A polyethylene moderator (1 cm thick) bored of holes covers the detector. The total sensitive area of the diode covered by holes is 0.75 cm². Lead shield (6 mm thick) covers both sides of the detector.

3 2.2 Method

The dosemeter response in term of personal dose equivalent in the phantom R_H is always given by the formulae (1).

Calculation of N.

Let N(E,t) the number of pulses as a function of the deposited energy in the detector (E) and the rise time of the pulses (t).

It can be defined two kinds of spectra

- The « deposited energy spectrum » $\frac{d(N(E))}{dE}$ with $N(E) = \int_{t=0}^{t=\infty} \frac{\partial(N(E,t))}{\partial t} dt$
- The « rise time spectrum » $\frac{d(N(t))}{dt}$ with $N(t) = \int_{E=0}^{E=\infty} \frac{\partial(N(E,t))}{\partial E} dE$

The deposited energy spectrum is calibrated using alpha particle sources such as Cm244 ($E\alpha$=5.8 MeV) Am241 ($E\alpha$=5.3 MeV), photoelectric peak of Am 241 gamma ray ($E\gamma$= 60 keV) and monoenergetic neutron between 250 keV and 2.5 MeV In this last case, the maximum deposited energy corresponds to the neutron energy according to the (n,p) elastic scattering theory. Thus a wide range of energy in covered

Rise time measurement requires time and electric consumption To accelerate the pulse treatment and to reduce the electric consumption, the deposited energy spectrum is divided into three parts

- Due to electronic background, superposed on pulses, a good accuracy in rise time measurement is obtained if the pulse magnitude is greater than 3 times the electronic background magnitude (50 keV) Also, below 150 keV, pulses are not taken into account.
- Above 1 MeV, the rise time is not measured because the higher magnitude of photon pulses is about 650 keV Thus using 1 MeV as threshold value, one can be sure that pulses are exclusively due to neutrons The total number of pulses above 1 MeV is

$$SO1 = \int_{E=1MeV}^{E=\infty} \frac{d(N(E))}{dE} dE$$

- Between 150 keV and 1 MeV, pulses are due to photons or to neutrons. Also rise time is measured for each pulses. The rise time spectrum is divided into two parts
- Below 100 ns, pulses are considered as pulses due to neutrons.

$$SO2 = \int_{E=0\,15MeV}^{E=1MeV} \int_{t=0}^{t=100ns} \frac{d(N(E,t))}{d(E,t)} d(E,t)$$

- Above 100 ns, pulses are considered as pulses due to photons.

$$SO3 = \int_{E=0\,15MeV}^{E=1MeV} \int_{t=100ns}^{t=\infty} \frac{d(N(E,t))}{d(E,t)} d(E,t)$$

The rise time threshold (100 ns) has been chosen experimentally. It is a compromise solution, a small number of pulses having lower rise time than 100 ns are due to photons. In

mixed n,γ radiation fields, one must subtract them from the total number of pulses To estimate the number of photon pulses counted as neutron pulses, the detector is exposed to pure photon radiation. Thus a « gamma correction factor » kγ = SO2 / SO3 is found. Table 2 gives the kγ values for different photon radiation fields. The ratios are in the same order of magnitude, the greater value (Cobalt-60) is used in this paper, thus it is assumed that the residual photon component is not under estimated.

Table 2 · Gamma correction factor for different photon sources.
The detector is covered with 6 mm lead shield.

Sources	^{137}Cs	^{60}Co	^{226}Ra
Energie (MeV)	0,66	1,25	2,5
kγ	$9,9\ 10^{-3}$	$1,29\ 10^{-2}$	$1,24\ 10^{-2}$

Then the formulae to calculate the number of neutron pulses is : N = SO1 + SO2 - kγ SO3 (3)

One has to take into account the photon spectrum seen by the P.N. junction. Because everything around the junction (lead, aluminium, converter, plastic case, phantom, etc.) modifies this spectrum, it is obvious that the kγ factor is found not only for a given source but for a given environment too The shape of the rise time spectrum depends mainly on the detector and preamplifier characteristics. The integration time of the amplifier - corresponding to the SO2 and SO3 outputs - has, at least, to be greater than the highest rise time achieved for neutron pulses at the preamplifier output.

3 2 3 Results.

3 2 3 1 Photon sensitivity

As mentioned previously lead shields have been added on both sides of the detector to decrease the photon sensitivity. Table 3 gives the relative photon sensitivity as a function of the shield thickness. The values are normalised to the bare detector configuration. A 6 mm thick shield reduces by a factor of two the photon sensitivity.

Table 3. Photon sensitivity as a function of the lead shield thickness Colbalt 60 source
Sensitivities are normalised to the bare detector

Thickness (mm)	0	2	4	6	8	10
Relative sensitivity	1,00	0,72	0,60	0,54	0,46	0,46

3.2.3.2 Response as a function of neutron energy.

Figure 6 shows a spectrum plotted from the SO1 and SO2 outputs for 2,5 MeV monoenergetic neutrons. It is compared with a spectrum achieved without photon rejection. It can be seen that the photon component is drastically reduced Only a few photon pulses between 0.15 and 0.25 MeV are still recorded. It can be observed that the number of pulses decreases between 0.25 and 0.5 MeV This could mean that some neutron pulses are eliminated together with photon pulses. This assumption will have to be confirmed in the future It is possible to correct this by applying a weighting factor k_w. Thus the formulae (3) is modified as follows .

$$N = SO1 + k_w (SO2 - k\gamma\ SO3)$$

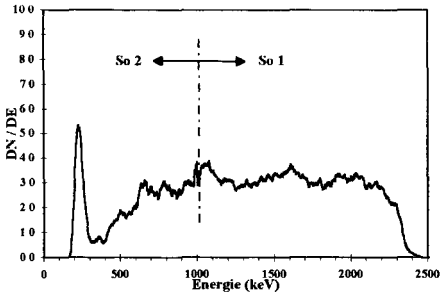

Figure 6 Spectrum obtained for 2.5 MeV neutron

The dip in neutron sensitivity around 0 25 MeV can be filled in, at least partially, by increasing the value of the weighting factor (figure 7). For k_w values up to 5, the increasing in sensitivity below 1 MeV is faster than above 1 MeV thus the variation in neutron sensitivity is reduced. With $k_w > 5$, the ratio between the minimum and the maximum sensitivities is not noticeably reduced because the sensitivity around 1 2 MeV becomes greater than the 2 5 MeV one.

As mentioned previously a hydrogenous moderator has been added. It allows to increase the sensitivity around 0 25 MeV (figure 7) but the sensitivity remains low. Additionally the standard deviation for this energy is very large (50 %) instead of 10 % for 0 144 MeV and 5% for the upper energies. Also, a better knowledge of the sensitivity for 0.25 MeV is necessary and needs extra measurements.

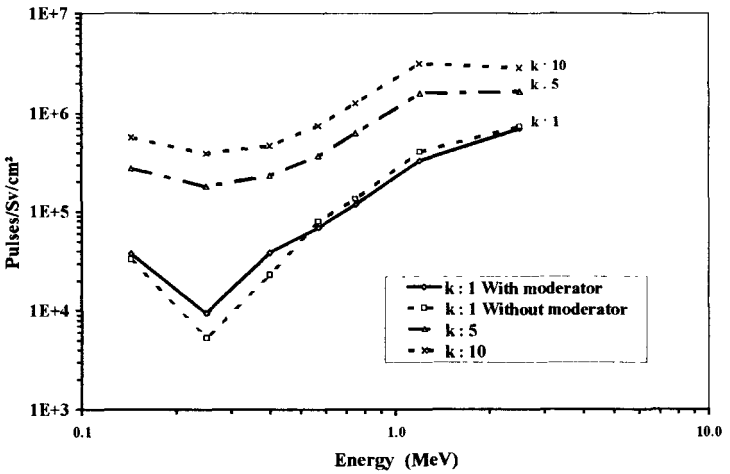

Figure 7 : Dose equivalent response of the NIM standard device

3.3 Device using a specially designed board.

A first attempt has been made to reduce the size of the device A specially designed board has been manufactured to provide photon rejection through measurement of pulse rise time.

3 3.1 Experimental setup

The device is composed of three parts i) The detector and the preamplifier (Hamamastu H4083), ii) The amplifier and the specially designed electronic board, iii) A counting scale The electronic board ensures two thresholds, one on the pulse magnitude, Tm, and a second one on the rise time, Tt. Pulses having a rise time greater than the Tt threshold and pulses having a magnitude lower than the Tm threshold are not counted.

The detector is the same as previously but the converter thickness is 10 μm The electronic characteristics of the device are different than those of the NIM standard electronic Thus, the background magnitude is 100 keV instead of 50 keV with the previous device. The first part of the devices is put in a thick aluminium case providing electromagnetic shielding. The specially designed electronic board measures rise times using the second order derivated of the amplifier output signal The SO2 and SO1 part of the response are not registered separately. The limit between SO2 and SO1 is 600 keV As for the first device, the pulse magnitude threshold is 150 keV.

3.3.2 Results

Monoenergetic neutron beams within the energy range from 73 keV up to 2 5 MeV have been investigated.

Figure 8 (4) shows the dose equivalent response as a function of the rise time threshold for neutrons and photons. As Tm decreases, the dip in sensitivity around 0.25 MeV increases Finally, there is no neutron sensitivity below 0 25 MeV when Tm = 1.6 μs. The photon sensitivity is still very important even for Tm = 1 6 μs.

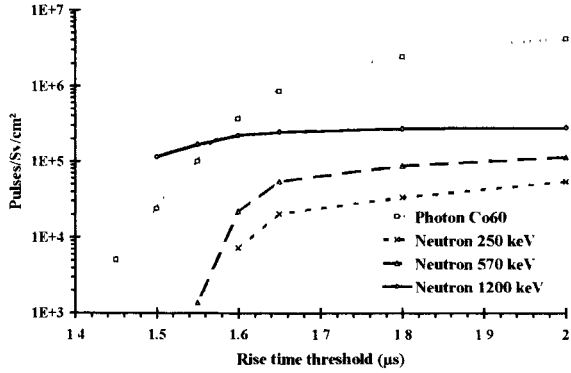

Figure 8 : the dose equivalent response as a function of the rise time threshold for neutrons and photons

3.4 Discussion and conclusion

Results achieved with the specially designed board were less good compared to the NIM standard device are due to the principle of the rise time measurement It seems to be too much simple compared to the NIM standard one Thus, it is very sensitive to the electronic background. This principle has to be improved to find closer results to those of the NIM standard device.

In spite of this problem, the pulse shape analysis allows to reduce drastically the photon response of the semi-conductor detector Using the photon correction coefficient, k_γ, this response can be reduced to a very low level. Thus, the detection threshold in term of fast neutron energy usually met with semi conductor detector does not exist any more. At the very most, it can be seen a low response around 0 25 MeV. To fill this dip in sensitivity, a weighting function, decreasing as the deposited energy increases, could be used up to 1 MeV instead of the single weighting factor, k_w. This requires a better knowledge of the deposited energy spectrum under 0.25 MeV. It could be obtained thanks to a decrease of the electronic background level. In this case, the accuracy of the rise time measurement and therefore the photon pulses rejection would be better. Thus, the number of recorded photon pulses under 0.25 MeV would decrease

References

J BARTHE, T. LAHAYE, T. MOISEEV and G PORTAL.
"Personal neutron diode dosemeter",
Rad Prot. Dos., Vol 47, Nos 1/4, (1993), pp 397-399

J. BARTHE, J M. BORDY, M. MOURGUES, T LAHAYE, B. BOUTRUCHE and P. SEGUR
New devises for individual neutron dosemeters,
Rad Prot. Dos., Vol 54, Nos 3/4, (1994), pp 365-368.

J. BARTHE, J M. BORDY, T LAHAYE and M MOURGUES.
New principle of single diode neutron dosemeter based on time resolution.
IRPA Regional congress on Radiological protection. Porstmouth 1994
Proceeding of the 17th Congress. pp. 97 - 100.

J.M. BORDY, T. LAHAYE, F LANDRE, C HOFLACK, S LEQUIN, J BARTHE
Single diode detector for individual neutron dosimetry using a pulse shape analysis.
8th Symposium on neutron dosimetry, Paris, 13-17 November 1995

Head of the project 4: Prof. Francisco Fernández Moreno

II. Objectives for the reporting period

1. **Setting up of an electronic detection system based on the usage of a PN diode real time neutron dosimeter.**

2. **Monte-Carlo optimisation of the neutron response as a function of neutron energy.**

3. **Results of the Bruyère-le-Chatel irradiations.**

III. Progress achieved including publications

1. Electronic detection system

Principle

Many devices based on silicon diodes have been extensively developed last year in order to perform photon and neutron dose measurements for individual as well as for area monitoring. Specially designed dosemeters have been applied to individual neutron dosimetry[1-7] with the aim of fulfilling the ICRP 60 requirements on their implementation. The main problem of such dosemeters is to separate the neutron component from the gamma one, as in practice they coexist in real fields

Among the procedures used in order to fulfil this separation, the differential method[8] has been often employed. This method is based on the usage of two diodes. The first of these diodes is placed behind and in contact with a converter, and detects not only the charged particles produced in the converter as a result of interaction of neutrons, but also all particles (electrons, photons) originated by interactions in the depleted zone, as well as those created in the sensor's surrounding. The second diode is not covered by any converter, and therefore it detects only particles (electrons, neutrons, photons) that are originated by interactions in the diode itself and in the sensor's surrounding. The difference between the response of the two diodes used is, thus, mainly due to particles originated by interaction of neutrons in the converter.

Although it is theoretically possible to detect thermal and fast neutrons using two identical diodes, the existence in practice of differences in their electronic background and their photon sensitivity makes necessary to introduce an energy cut-off, large enough in order to reduce the signal due to the presence of radiation background, mainly originated from the gamma contribution. This energy cut-off increases the dosemeter detection threshold and, at the same time, reduces its field of application to fast neutrons.

Experimental set-up

We have used a dosemeter arrangement composed of a 40 μm thick layer of polyethylene converter followed by a double diode detector. The double diode detector (CD-NEUT-200-DBL) consists of two Canberra diodes, with an effective area of 2 cm^2 and a bulk resistivity of about 500 Ω/cm, located on the opposite sides of a single Silicon block. The diodes have in their actual configuration a depleted zone of 35 μm each for a polarisation tension of 10 V, separated by 222 μm of Si. Ortec preamplifiers and a Canberra multichannel analyser with amplifier are used and connected to a Toshiba T-180 portable computer, as indicated in figure1. Data analysis is performed using the Ortec Maestro II software.

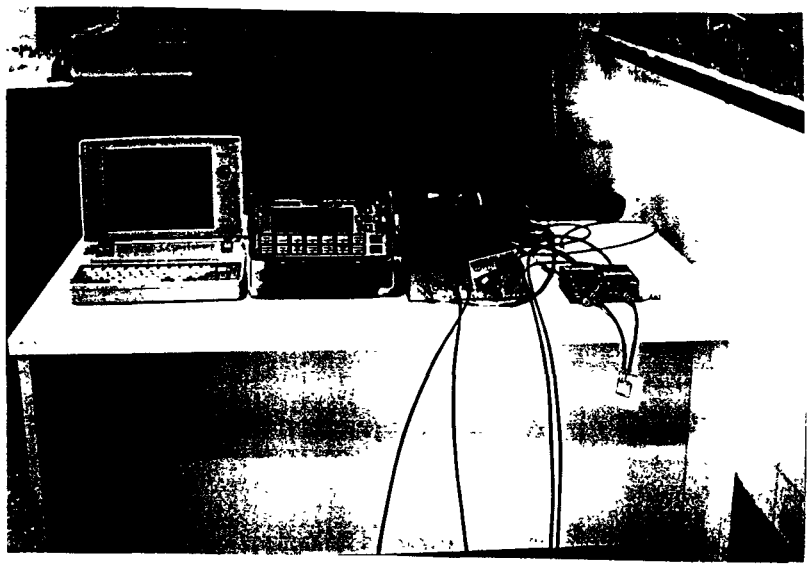

Figure 1. Experimental set-up

Two types of irradiation were used in order to calibrate the personal electronic dosemeter: photons of about 1 MeV from a ^{60}Co source for low energy loss rates, and alpha particles of about 5 MeV from a ^{231}Am, ^{239}Pu, ^{244}Cm combined source for high energy loss rates. It has been obtained that the energy in keV is given by the channel number divided by 1.6.

The dosemeter was irradiated, once calibrated, during a joint irradiation experiment in March 1994 at the Bruyère-le-Chatel nuclear research center, to a range of dose equivalent doses ($H^*(10)$, according to the ICRP 60) comprised between 0.3 and 5.7 mSv of monoenergetic neutron beams of 73 keV, 144 keV, 250 keV, 570 keV, 1.2 MeV and 2.5 MeV. The dosemeter was fixed for irradiation on the center of the front face of a (30x30x15) cm^3 PMMA slab phantom, as recommended by the ICRU[11] for calibration purposes, and irradiated to normally incident neutrons. The net spectrum, that correspond to protons originated in the converter, is calculated by subtracting the integrated spectra obtained from the two diodes.

2. Neutron Response Calculation

A code based on the Monte Carlo method, written in Fortran77 language, has been used in a personal computer to simulate the passage of a normally incident neutron beam through a polyethylene converter plus a (30+222+30) μm Si detector. The transport of the gamma and the electron components that are present, originated in the sensor's surrounding, has not been taken into account as the contribution of such components to the recorded response may be neglected if the differential method is used.

The Monte Carlo procedure employed is based on the general principles outlined elsewhere[11,12]. The dosemeter equivalent response in terms of $H^*(10)$ ($cm^{-2} \cdot mSv^{-1}$), which equals the ambient dose equivalent $H^*(10)$ for normally incident protons, is obtained for each incidence energy from the net spectrum, taking into account the area of the diode surface and using the ICRP 60 conversion factors[13].

3. Results and Discussion

Analysed spectra

The spectra for each diode (front and back) of the detector are presented in figure 2, together with the net spectra, for neutron incidence energies of 0.073, 0.144, 0.250 and 0.570 MeV. This figure evidences the existence of a shift between the spectra obtained in both diodes, due probably to differences between their

capacities. This fact prevents us from applying the differential method to proton energies below 239 keV (corresponding to channel number 383), and therefore a neutron energy cut-off of greater than this value.

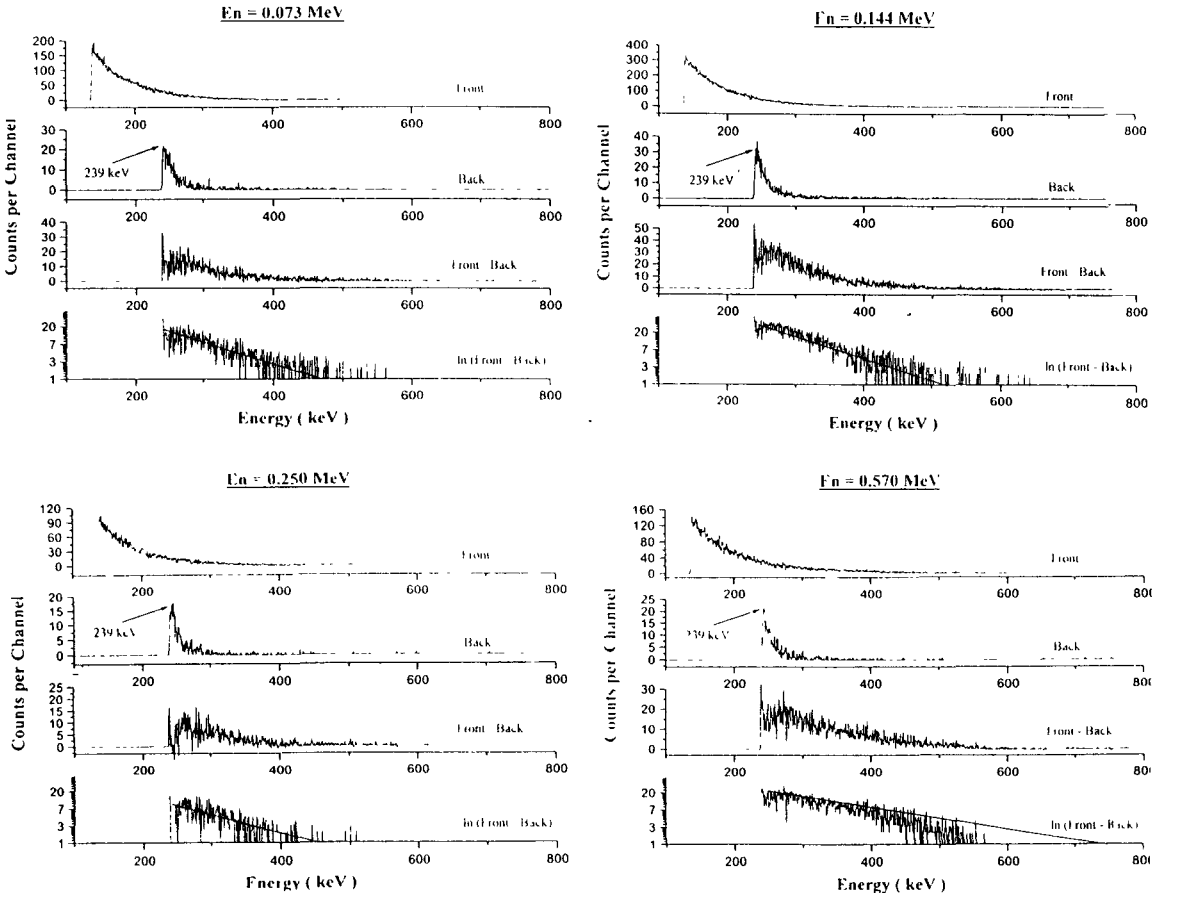

Figure 2. Spectra obtained for each diode together with the net spectra for neutron energies of 0.073, 0.144, 0.250 and 0.570 MeV.

At the same time, as observed in the figure, for the energies of 0.073, 0.144 and 0.250 MeV, the exponential behaviour of the net spectra suggest a contribution originated from electromagnetic radiation. It is observed, for the 0.570 MeV neutron net spectra, that a small deviation from the exponential behaviour appears. This deviation suggest the presence of signal in the detector, due to recoil protons with energy greater than 239 keV, having a maximum energy of the spectrum comparable to that of the incoming neutrons (the maximum possible energy of recoil protons). These results confirms the necessity of introducing the above mentioned energy cut off.

Figure 3 displays the net spectra obtained for neutrons of energies greater then the cut off. In the case of 1.2 MeV neutrons the non-exponential form of the net spectrum evidences the presence of recoil protons with a maximum energy that equals the incidence neutron energy. For 2.5 MeV neutrons it is observed, although in a non conclusive way due to lack of statistics, the presence of a maximum of the number of recorded protons around channel number 3000, that corresponds to a proton energy of 1.6 MeV. This value agrees with that obtained by Monte Carlo simulation for neutrons of this energy. The presence of a peak of the number of recorded protons that corresponds to the most probable proton energy, originated from a given neutron energy, is not observed clearly in all cases, fact which is probably due to the small number of recorded events.

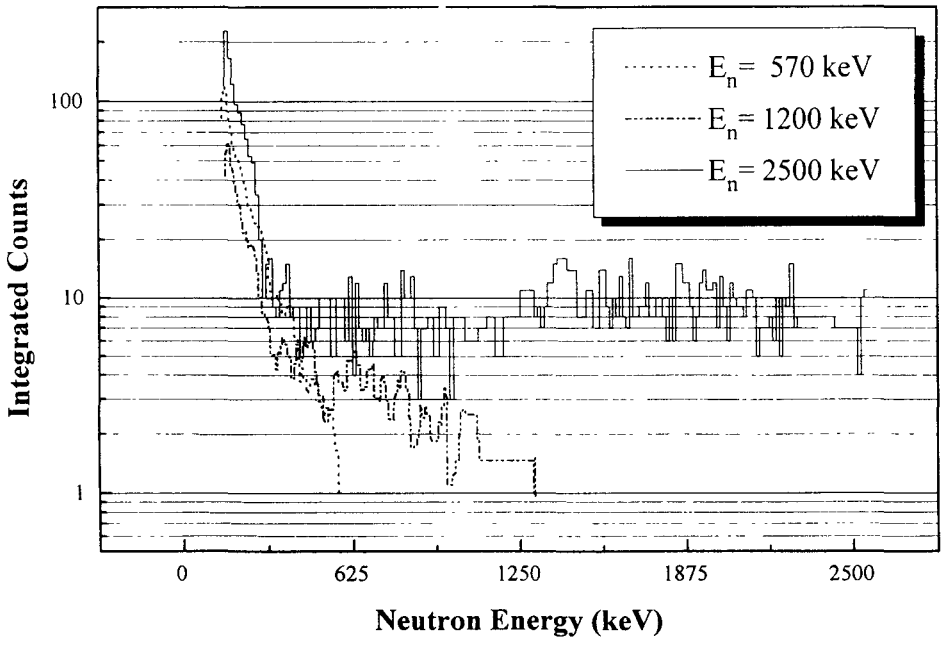

Figure 3. Net spectra obtained for neutron energies of 0.570, 1,2 and 2.5 MeV.

Linearity

A fit of the integrated counts of the net spectrum at 1.2 MeV versus reference dose equivalent ($H'(10)$) is shown in figure 4. The intercept value obtained of 0.010mSv may be considered as the dosemeter detection limit for this energy and for our energy cut off. On the other hand, taking into account the slope (1105 counts/mSv) and the area of the diode surface, a value of 553 $cm^{-2} \cdot mSv^{-1}$ is obtained for the mean equivalent dose response value for this energy and for our energy cut off. This value is a factor of eight greater than that obtained for a SSNTD dosemeter[14] for the same energy and agrees with that obtained by Barthe[6], using a dosemeter configuration very similar to ours.

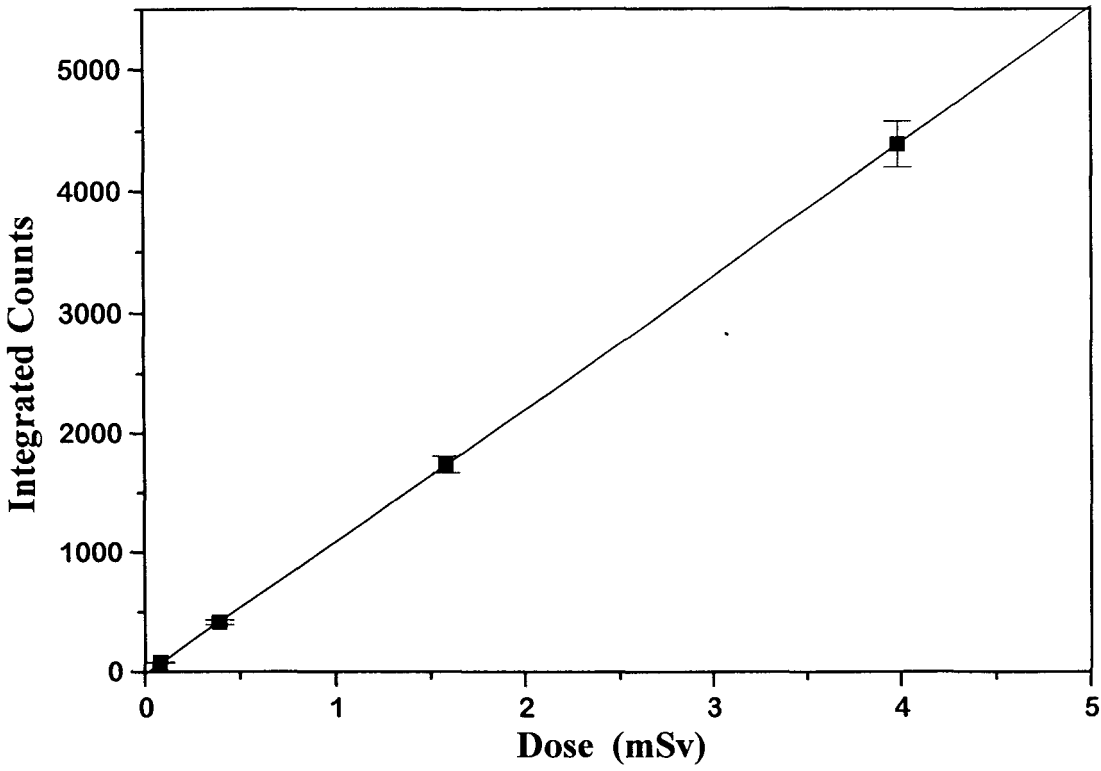

Figure 4. Integrated counts as a function of the directional dose equivalent ($H'(10)$) for 1,2 MeV neutrons.

Energy dependence

Figure 5 shows the simulated dose equivalent response $R_{H'}$ for normally incident neutrons as a function of neutron energy for our dosemeter configuration and several polyethylene converter thicknesses, as well as the experimental values obtained. The excellent agreement between the simulated and the experimental results is to be emphasized. The dosemeter response may become flatter if the polyethylene converter thickness is reduced, as deduced from the figure. Nevertheless, a converter thickness around 30 μm is the most adequate, as the fluence rate of emerging protons is roughly proportional to the neutron dose rate, although its response is not flat. Once this thickness is selected, it is obvious from the results obtained that it is necessary to reduce as much as possible the energy cut off introduced in order to increase the response to 144, 250 and 570 keV neutrons. It seems not to be probable to have net signal for neutrons below 250 keV, using the actual technology. This fact would imply that it is not possible to improve much the response flatness in the energy range studied.

Conclusions

The characteristics of our real time personal neutron dosemeter gathered from the results of the present study can be summarized as follows:

1) The dosemeter displays, on its actual configuration, a low response value for low energy neutrons and a high response value for photons. These effects make necessary to introduce an energy threshold of the order of 250 keV for neutron registration.

2) It is possible to obtain, with this dosemeter and using a 20 mm thick polyethylene radiator, the neutron dose equivalent with an error of about ±50% in the energy range from 570 keV to 15 MeV.

3) The usage of ^{10}B in the polyethylene converter would allow to record thermal neutrons, as the energy of the alpha particle originated in the $n + {}^{10}B$ reaction is over the energy cut off that has been introduced in order to eliminate the gamma contribution.

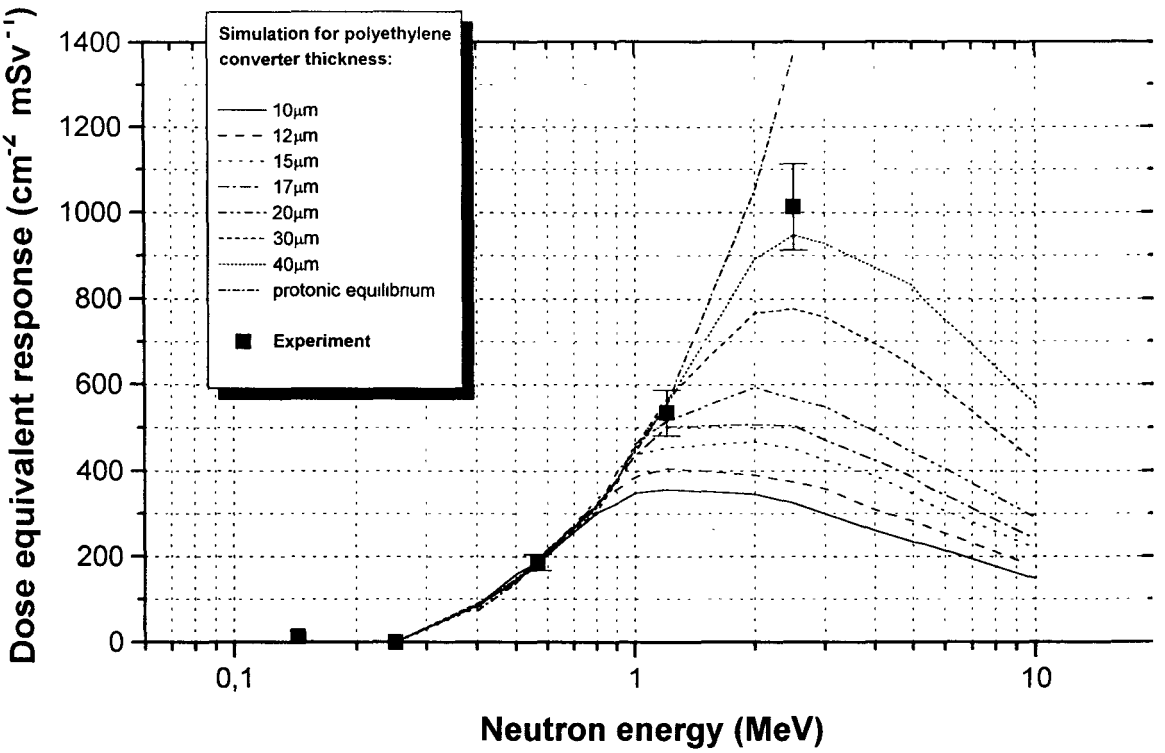

Figure 5. Experimental and calculated dose equivalent response R_H' for normally incident neutrons as a function of neutron energy.

References

1. Eisen, Y., Engler, G., Ovadia, E., Shamai, Y., Baum, Z. and Levi, Y. *Single Silicon Surface Barrier Detector.* Workshop on Personal Neutron Dosimetry held jointly with CENDOS. Acapulco (Mexico) (1983).

2. Eisen, Y., Engler, G., Ovadia, E. and Shamai, Y. *Combined Real Time Wide Energy Range Neutron Dosemeter and Survey Meter for High Neutron Dose Rates with Si Surface Barrier Detectors.* Nucl. Instr. And Meth. **211,** 171–178 (1983).

3. Fasasi, M., Jung, M. and Siffert, P. *Thermal Neutron Dosimetry with Cadmium Telluride Detectors.* Radiat. Prot. Dosim. **23**(4) 429–431 (1988).

4. Nakamura, T., Horiguchiond, M. and Yamano, T. *A real Time Wide Energy Range Personal Neutron Dosemeter with Two Silicon Detectors.* Radiat. Prot. Dosim. **20**(3) 149–156 (1989).

5. Matsumoto, T. *Pin Diode for Real Time Dosimetry in a Mixed Field of Neutron and Gamma rays.* Radiat. Prot. Dosim. **35**(3) 193–197 (1991).

6. Barthe, J., Lahaye, T:, Moisseev, T. and Portal, G. *Personal Neutron Diode Dosemeter.* Radiat. Prot. Dosim. **47**(1-4) 397–399 (1993).

7. Jung, M., Teissier, C., Siffert, P. and Raffasoe, C. *Fast Neutron Monitoring with Silicon Detectors.* Strahlenschutz: Physik und Messlechnik, **1**, 151–158. Karlsruhe (1994).

8. Paul, D., Barelaud, B., Dubarry, B., Makovicka, L., Vareille, J.C. and Decossas, J.L.. *γ-interference on an electronic dosemeter response in a neutron field.* 7th Symposium on Neutron Dosimetry. Berlin (1991).

9. Makovicka, L. *Contribution à la Dosimétrie Neutron-Gamma: Étude d'un Ensemble Radiateur-Detecteur Type CR-39.* Thèse d'Etat. Université de Limoges. France. (1987).

10. ICRU. *Measurements of Dose Equivalents from Extermal Photon and Electronic Radiations.* Report 47 (Bethesda: ICRU Publications) (1992).

11. Fernández, F., Domingo, C., Luguera, E. and Baixeras, C. *Experimental and theoretical determination of the fast neutron response using CR-39 plastic detectors and polyethylene radiators.* Radiat. Prot. Dosim. **44**(1-4), 337–340 (1992).

12. Fernández, F, Bouassoule, T., Domingo, C.; Luguera, E. and Baixeras, C. *Response of a CR-39 Fast Neutron Dosemeter with a Polyethylene Radiator*

Improved with Makrofol. 11th Solid State Dosimetry Conference, Budapest, July 1995 (submitted for publication in Radiat. Prot. Dosim.).

13. ICRP. *1990 recommendations of the International Commission on Radiological Protection.* Report 60 (Oxford: Pergamon Press) (1991).

14. Fernández, F., Baixeras, C., Domingo, C. and Luguera, E. *EURADOS-CENDOS Joint Neutron Irradiation, 1990. Results from Grup de Física de les Radiacions.* EURADOS-CENDOS Report 1992-02 (1992).

Publications

F. Fernández, E. Luguera, C. Domingo and C. Baixeras. *Separation of the neutron signal from the gamma component in (n-γ) fields usingdifferential pulse analysis techniques with a double silicon diode.* Radiat. Prot. Dosim.(accepted for publication).

CEC CONTRACT FI3P-CT93-0072 FINAL REPORT - Contractor nr 5: DCMN Pisa
Work-project: SUPERHEATED EMULSIONS, Francesco d'Errico and Giorgio Curzio

OBJECTIVES

Objectives of DCMN Pisa within the CEC contract were to study, develop and test neutron sensors based on superheated emulsions (superheated drop or bubble detectors) for radiation protection dosimetry applications. Over the two years of research, the activities were divided into an initial investigation into the physics of these detectors followed by the exploitation of the previous findings for the development of a neutron survey meter (sub-project 1) and a spectrometer of new conception (sub-project 2).

STATE OF THE ART

Superheated drop detectors (SDD)[1], also known as bubble detectors[2], consist of uniform emulsions of over-expanded halocarbon and/or hydrocarbon droplets dispersed in a compliant material such as a gel or a polymer. Nuclear interactions nucleate the phase transition of the superheated drops therein generating macroscopic bubbles.

These detectors were presented to the radiation protection community over fifteen years ago[1], but only recently have they reached a level of development that makes them suitable for practical applications. Despite their delicacy, SDDs are often addressed as the only devices currently meeting the increased sensitivity requirements for neutron personal dosimetry.

Several devices based on this technology have been designed[3]. Some are active counters acoustically detecting the pulses radiated when drops vaporise (Figure 1): recent versions discriminate true counts from external noise on the basis of pulse shape analysis; they can record the exposure time-history and provide dose-rate estimates. Others are passive, integrating meters typically employed in personal monitoring Two versions of the latter exist: some are based on the optical—manual or automated—counting of the bubbles which are permanently trapped in a stiff matrix (Figure 2a), others rely on the measurement of the total volume of the bubbles which is correlated to the expansion of the soft gel they are dispersed in (Figures 2b, 2c).

The sensitivity of these detectors depends on the composition, number and volume of the drops in suspension, and can be varied to meet the requirements of various applications. Threshold response SDDs are employed in spectrometric investigations Those responding from thermal to fast neutrons are instead employed in individual and area monitoring: a typical SDD dosemeter response is in the order of a few bubbles per μSv.

Since the density of the energy deposition from photons is too low for bubble nucleation, most SDDs are insensitive to γ and x-rays, at least below the energy thresholds for photo-nuclear reactions—generally in the range 10-15 MeV for the low-Z detector constituents As a result, these detectors are virtually zero noise systems, the background vaporisations corresponding to "true" events induced by cosmic radiation. Extreme heating, though, or violent mechanical shocks can cause large scale bubble nucleation.

The response of an SDD depends on its degree of superheat, in turn defined by the temperature and pressure of its droplets, therefore environmental variations of these two quantities inherently affect the sensitivity. The temperature dependence, in particular, has long been considered a serious limitation of these devices, until techniques to correct or compensate for this effect have been developed. In the attempt to render them robust beyond their intrinsic nature, though, the unique response properties of the SDDs have been neglected in commercial instrumentation.

The predominant effect on the response as temperature increases is a threshold shift towards lower energies. This parallels the decrease in the minimum energy deposition which is necessary to nucleate bubble formation. The threshold shift is accompanied by an overall increase in fast neutron sensitivity.

Currently available electronic devices correct for this with a factor of 0.055 K^{-1}, derived from the variation of response to Am-Be neutrons[4] This way, the overall variation in sensitivity is

roughly accounted for, but not the energy dependence of the response. In passive personal dosemeters, volatile liquids are introduced atop the sensitive composition to compensate for temperature changes through the variation of their vapour tension[5]. Low boiling point liquids are used for the purpose[6], and keep the detector constantly under pressure: this lowers the temperature dependence from 0 055 to 0.012 K^{-1}. This approach reduces the degree of superheat, and lowers the response to neutrons as well, particularly in the 0.1-1 MeV range[7].

The analysis of the physics of these detectors[8,9] combined with extensive experimental work on their response to neutrons[10] and other radiations[11] led us to utilise the inherent temperature dependence of the sensitivity as a means to control the characteristics of the SDDs, i.e. generate desired detection thresholds[12] or match recommended response shapes[13].

SUB-PROJECT 1) NEUTRON DOSIMETRY

Characterisation of Dosimetric Emulsions

First goal was the analysis of detectors with dosimetric capabilities, i.e. those based on halocarbon-12, which are sensitive from thermal to fast neutrons. The fluence response as a combined function of operating temperature and neutron energy was thoroughly investigated. The detectors we employed were vials containing 4 cm^3 of sensitive composition, a suspension of about 20000 superheated drops of ~100 µm diameter dispersed in an aqueous gel

Bubbles were counted acoustically, detecting the pressure wave that accompanies each vaporisation event. For this purpose, a meter similar to the one described by Apfel and Roy[14] was used This scaler counts the pulses picked up by a piezo-electric transducer placed in contact with the vial. The pulses are damped sinusoids and fade in 10-15 ms; the dead time of the counter is set accordingly to have a duration of 20 ms.

Temperature regulation of the detectors was achieved by means of thin, flexible etched-foil heating elements wrapped around the vials along with a ribbon of platinum resistance-temperature-sensor. Heaters and thermometer were surrounded by a light-weight latex-foam thermal insulator and were operated by a time proportioning controller (Figure 3).

Due to the progressive depletion of superheated drops, the integrated response of the detectors, i.e. the total number of counts (bubbles), as a function of fluence exponentially approaches an asymptote corresponding to the initial number of drops (Figure 4) For this reason, SDDs were always used up to a maximum of about 3000 counts, so that their response would still be close to linear and only minor corrections necessary.

The experimental investigations were mainly carried out at the PTB, in Braunschweig For the free-in-air response determinations, monoenergetic neutron fields in the thermal to 19 MeV energy range were produced at the 1 MW research and measurement reactor (FMRB) and at the 3.75 MV Van de Graaff accelerator[15].

At the FMRB, collimated filtered neutron beams of 144 keV and thermal neutrons—the latter using a Cadmium filter difference method to eliminate contaminating fast neutrons—were employed for this study. The beam cross sections are large enough to cover the detector vial entirely—diameters are 13 3 and 4.2 cm, respectively, at half maximum flux density. Neutron fluences were measured using standard methods (precision long counter, gold foil activation) and monitored during the measurements by proportional counters and fission chambers. The reactor operating power was reduced to about 50 kW, so that the count rate would not conflict with the counter dead-time setting.

Irradiations with monoenergetic neutron fields of 0.024, 0.07, 0.144, 0.57, 1.2, 2.5, 4 0, 5.0, 14 8, and 19 MeV were carried out in the low-scatter hall of the PTB Van de Graaff accelerator. Fluence calculations were based on recoil proton proportional counter or telescope measurements, and the uncertainties were assessed to be in the order of 3% (relative standard deviation). The contribution to dose equivalent from the low-energy neutron background due to scattering on target backing, air, walls, and equipment, estimated to be

always less than 5%[16], was neglected. The maximum energy of the γ components in all fields is less than 15 MeV[17], below which SDDs are known to be virtually insensitive to photons[18]. Therefore, this contamination was disregarded as well. Given the aforementioned considerations on count rate, irradiations were performed at different distances from the target, depending on the neutron yield of the various reactions we employed.

Tests with higher energy neutrons were performed at the 590 MeV proton accelerator of the Paul Scherrer Institut (PSI), Switzerland, where the DCMN informally participated in the 1992 EURADOS intercomparison of nuclear-track detectors. The fields were produced bombarding a ^{9}Be target with 50.3 and 71.8 MeV protons This generates broad energy distributions with about a third of the neutron fluence in peaks at 44.5 and 66.1 MeV, respectively[19].

The free-in-air fluence response of the halocarbon-12 detector as a combined function of energy and temperature is illustrated in Figure 5. Plot symbols include the error bars; measured relative standard deviations are in the range 2-8%, consistent with an expected 3-4% based on Poisson statistics. At 25°C, the two high energy points from the PSI tests are reported: average values of 25 and 30 MeV are used to represent the observed response to the whole energy range Error bars along the energy axis approximate the width of the two broad neutron spectra

The predominant effect on the response as the degree of superheat increases is a threshold shift towards lower energies. This parallels the decrease in the minimum energy deposition which is necessary to nucleate bubble formation. The threshold shift is accompanied by an overall increase in fast neutron sensitivity. Moreover, the detector becomes sensitive to recoil protons entering the drops from the surrounding gel—superheated drops contain no hydrogen. This is confirmed by tests performed at the INFN-LNL 7 MV Van de Graaff accelerator in Legnaro (Italy), where a detector vial with a 6.5 μm mylar-window was irradiated with 5.5 MeV protons, and bubbles began to appear at temperatures between 25 and 30°C

The response to thermal neutrons, finally, appears to increase between 25 and 30°C and then to become fairly constant (up to 40°C), consistently with the arising detection efficiency for both particles—i.e., protons, too—from the exo-ergic ^{35}Cl(n,p)^{35}S reaction responsible for the sensitivity to low energy neutrons.

Monte Carlo Simulations

Various quasi-monoenergetic reactor-based filtered beams of intermediate energies are available at the PTB. However, it was not possible to calibrate the SDD with these epithermal beams because of their fast neutron contamination which was detected with much higher efficiency. Therefore, in this energy region we performed a Monte Carlo simulation of the detector's response[20]. The choice of a Monte Carlo method (MCNP 4.2) resulted from the need to treat explicitly neutron transport and slowing down phenomena when evaluating the collision rates in the detector volume.

Since the exo-ergic neutron capture reaction on the ^{35}Cl nuclei is the only mechanism behind the detector's low-energy response, modelling the phenomenon was relatively straightforward. Two concentric cylinders were used to describe the SDD. The outer one represented the glass vial containing the emulsion, the inner one represented the homogenised sensitive volume, where the droplet material was assumed as uniformly distributed throughout the emulsifier gel matrix.

Broad parallel beams of monoenergetic neutrons were employed in the simulation. All capture reactions on chlorine were assumed to take place in the superheated droplets (Cl is absent from the gel-matrix) and to yield a bubble in the detector. Under these hypotheses, the agreement between our calculated fluence response at $2.53 \cdot 10^{-8}$ MeV and that measured at the PTB thermal beam was within 30%. The discrepancy appeared acceptable given the inevitable uncertainties in the description of the SDD (which does not present a rigid geometry) and, more importantly, the fact that the thermal beam employed in the experimental calibrations consists of a broad spectrum

A comparison between the shape of the calculated response and that of the cross section for the detected reaction shows the relevance of neutron transport processes inside the SDD (Figure 6): neutrons are slowed down interacting with the hydrogenated gel-matrix, therefore when they encounter a chlorine nucleus the capture cross section is higher than that corresponding to their initial energy. This is confirmed by Figure 7 indicating that about 50% of primary neutrons below 100 keV interact somewhere in the detector volume, while the average number of collisions increases from about two below 10 keV to three at thermal energies.

Dosemeter Numerical Testing

It was found that by stabilising the superheated emulsions at 31.5 °C a close agreement is attained with the fluence to ambient dose equivalent conversion factor based on the new ICRP Q(L) relationship and the new ICRU stopping power data for protons and alpha particles[21] (Figure 8). While the fluence response matches quite closely the fluence to ambient dose equivalent conversion factor for thermal and fast neutrons, it deviates downwards at intermediate energies

Neutron spectra encountered in radiation protection practice (typically around nuclear power plants) usually present a high energy (fission) peak and a thermal peak separated by an "1/E" region with a relatively scarce neutron population. Therefore, the underestimation in this region does not imply a severe hindrance on the dosemeter performance. This was first theoretically checked by folding the detector fluence response over more than 150 neutron energy distributions from catalogues of measured and realistic spectra[22,23,24].

The results are presented in Figure 9 where data are plotted as a function of spectral hardness, i.e of the fluence to ambient dose equivalent conversion factor averaged over each neutron spectrum. All data are normalised to the response to bare ^{252}Cf neutrons. Results for heavy-water moderated-californium and for americium-beryllium neutrons are marked differently and compared to the experimental values. The scatterplot indicates that by choosing the response to ^{252}Cf as a normalisation value, over 95% of the points fall within 20% of the norm and 70% fall within 10%. This confirmed the expectations for an excellent performance of this neutron dosemeter despite the under-reading in the intermediate energy region.

Experimental Testing

These conclusions were verified experimentally through the participation in a series of measurements carried out during several neutron dosimetry intercomparison exercises. The experiments took place in a variety of environments: from benchmark fields (CEA Cadarache, F), through nuclear power plants and spent fuel storage sites (SSI Ringhals and Oskarshamn, S), to relativistic stray radiation areas (CERN Geneva, CH).

Tests were mostly performed on a "blind" basis, i.e. data were measured and provided to the intercomparison organisers who later released the reference dose rate values. These were usually based on multisphere spectrometry data folded with the appropriate conversion factors.

The instrument we employed in the intercomparisons was the prototype monitor we had previously used in the energy response determinations[10]. Prior to the experiments, the detector vials were calibrated at DCMN Pisa with an Am-Be source. Figure 9 indicates that the response to Am-Be is about 90% of the response to bare Cf. Since the latter provides a preferable calibration, we accordingly increased our measured response (number of bubbles per unit dose equivalent) by a factor 1.11. For the intercomparisons, data were requested in terms of the operational dose equivalent quantities defined by ICRU Report 39[25] When expressed in these quantities, the average response of the SDDs was about 5 bubbles per μSv

Table I summarises the results of our measurements in the fields described hereafter.

Table I Results of tests of the SDD monitor in various neutron fields[13]

Neutron fields		Dose Units	SDD	BS (TEPC)	Reference
EA-Cadarache	Bloc Sigma	μSv h^{-1}	128	131	—
	Canel+	nSv MU^{-1}	13.8	13.0	—
	Canel+ with water	"	4.2	4.0	—
wedish xercise	Containment Lock "L"	μSv h^{-1}	220	223	27
	CLAB "D"	"	38	42	"
	CLAB "E"	"	38	35	"
	CLAB "P"	"	40	43	"
PS-CERN	Iron Top	nSv MU^{-1}	2.25	2.67 (1.85)	29 (30)
	Concrete Top	"	0.28	0.52 (0.39)	"

Legend: MU = Monitor Unit (of the local monitoring system), BS = Bonner Spheres, TEPC = Tissue Equivalent Proportional Counter.

In Cadarache, the Bloc Sigma consists of a large graphite moderator cube (1.5 m x 1.5 m x 1.5 m) containing six Am-Be sources of 6 10^{11} Bq each: the measurement position in front of the assembly corresponds to a leakage thermal neutron spectrum. Canel+ is a realistic neutron field realised by placing thick uranium-238 and iron shells in front of a 14 8 MeV neutron generator· it reproduces the environment of a nuclear reactor containment; by adding water shields the neutron energy distribution is degraded to simulate the spectrum behind the biological shielding[26].

During the "Swedish exercise"[27], measurements were carried out around and inside the containment building of a 900 MW_e PWR plant in Ringhals. Here, we could only measure properly in the air-lock access to the containment: temperature and noise levels inside were too high for our prototype (above 45°C and 100 dB, respectively). At CLAB-Oskarshamn, test points were in the proximity of spent-fuel transport casks where spectral distributions were much harder than at the nuclear power plant.

Finally, at CERN measurements were carried out in two high energy fields generated at the Super Proton Synchrotron by bombarding a thick copper target with a beam of 205 GeV/c protons and pions[28]. Either concrete or iron slabs were used to shield the nuclear interaction products, giving rise to neutron transmission spectra with different high energy component. The higher energy one (Concrete Top) was meant to reproduce the cosmic radiation fields encountered on-board aircraft in the stratosphere.

Results reported in Table I amply validated the positive indications of the dosemeter simulated testing by spectral folding The SDD reading was generally within 10% of the reference dose values[27,29,30], which confirmed the adequate energy response of the system An exception was the under-response registered at the highest-energy field of CERN Although definitive reference data for this field are not available yet, the result appeared qualitatively consistent with the discrepancy between the SDD response and the fluence to dose equivalent conversion factor for energies above 10 MeV (cf. Figure 8).

SUB-PROJECT 2) NEUTRON SPECTROMETRY

Variable Threshold Device

The technique we devised relies on the combination of two different superheated emulsions for the continuous generation of any detection threshold between 0.01 and 10 MeV. This energy range is of the greatest importance in radiation protection as neutron exposures are most commonly received in this interval. Assessment is rendered complex by the variation of the dose equivalent per unit fluence by over a factor of 40.

The approach is analogous to the previous one being still based on the active control of the degree of superheat of the emulsions In the previous case, a single temperature had been found corresponding to the flattest dose equivalent response of halocarbon-12 emulsions In

this case, by varying the operating temperature of two different detectors, accurately defined detection thresholds are correspondingly selected.

The two kinds of detectors we employed are suspensions of either octafluorocyclobutane (C-318) or dichlorotetrafluoroethane (R-114). Since the two emulsions have different levels of superheat their detection thresholds are quite different: at room temperature, the threshold of C-318 arises for neutrons above 1 MeV, that of R-114 above 8 MeV.

For different reasons, neither emulsion is sensitive to thermal neutrons in the temperature range of interest—as was verified at the PTB research reactor. In fact, octafluorocyclobutane (C_4F_8) contains no chlorine. As mentioned before, this element allows some superheated halocarbons to detect low energy neutrons *via* the exo-ergic reaction $^{35}Cl(n,p)^{35}S$ Dichlorotetrafluoroethane ($C_2Cl_2F_4$) does contain chlorine but is not superheated enough to be nucleated by the energy deposition pattern of the reaction products. In fact, while the sulphur ion is not energetic enough to trigger the vaporisation of this emulsion, the proton receives most of the 615 keV released in the neutron capture but its ionisation density of is too low. This was verified experimentally by direct tests with protons up to 65 MeV[11].

Moreover, both emulsions are insensitive to low LET radiation, as was confirmed by intense irradiations with ^{137}Cs γ rays yielding no bubbles while detector temperatures were increased up to 50°C

Response Matrix

The responses of the two detectors as a function of neutron energy and temperature, i.e. degree of superheat, were thoroughly investigated at the PTB. Here, the complete series of monoenergetic ISO recommended beams were employed along with other monoenergetic neutron fields including, in particular, the recently set up 8 MeV neutron field produced with a deuterium gas-target at the compact cyclotron[15]. For all detector temperatures and neutron energies, measurements were carried out until counting statistics ensured an accuracy better than 10% on each data point.

The free-in-air fluence responses of the two detectors as a combined function of energy and temperature are reported in Figures 10 and 11 (plotted symbols include error bars) These curves document that the higher the degree of superheat of the liquid, the lower the minimum energy secondary charged particles—and therefore primary neutrons—must impart to the drops in order to nucleate their evaporation.

An interesting feature is that the threshold variation associated with a given temperature increment progressively decreases as the degree of superheat increases. In fact, the same 5°C step corresponds to variations in the order of some MeV for the lower superheat detector (R-114), and to fractions of an MeV for the higher superheat one (C-318). Therefore, the resulting sets of curves are spaced in quasi-isolethargic intervals which is advantageous for neutron spectrometry purposes.

An upper limit of 40°C was set for the operating temperature of the detectors. In fact, at higher temperatures (~50°C) the emulsions become unstable and radiation induced vaporisation may spuriously nucleate adjacent drops. Furthermore, an undesirable broad maximum appears in the C-318 response (cf. Figure 10) that may be ascribed to an increasing detection efficiency for the recoil protons entering the drops from the surrounding hydrogenated gel. This is consistent with the Bragg-peak structures that were observed in extremely superheated emulsions irradiated with protons[11]. Finally, at 40°C the R-114 threshold virtually coincides with that of C-318 at 25°C, which allows for a continuous transition between the families of curves offered by the two detectors

Spectrometry Tests

The applicability of these nested threshold curves to neutron spectrometry was verified through tests with two radionuclide neutron sources having well known spectra, californium-252 and americium-beryllium.

Measurements were carried out as for the monoenergetic neutron response determinations. The two detectors were first irradiated at 25°C, and their temperature then

successively increased in 5°C steps after adequate counting statistics—typically based on almost a thousand bubbles—had been accumulated at each step. Repeated irradiation cycles indicated that the relative response of the detectors is reproducible.

A simplified approach was first adopted for the analysis of these measurements. The fluence response curves were approximated by means of step functions based on "effective-fluence-responses", given by the average response plateaux, and "effective-energy-thresholds", E_{eff}, in turn defined as the energies corresponding to 70% of the plateaux. For both sources, the reading at each temperature, i.e. at each effective-energy-threshold, was divided by the respective effective-fluence-response values, and these ratios were compared to the corresponding integrals, $I_{E_{eff}}$, of the spectral fluence, $\Phi_E(E)$:

$$I_{E_{eff}} = \int_{E_{eff}}^{\infty} \Phi_E(E)dE$$

The remarkable agreement shown in Figure 12 was achieved through minor simultaneous adjustments on the effective-energy-threshold and effective-fluence-response values—the double error bars reflect these adjustments combined with the experimental uncertainties. This confirmed the suitability of the SDD response matrix for the determination of fluence integrals.

More stringent consistency tests on the neutron source results—including uncertainty estimates—were then performed by "few channel" unfolding with a modified STAY'SL code[31] named MSITER and with the Monte Carlo code MIEKEB[32]. MSITER applies the least-squares method. the weighted absolute differences between measured and calculated counting rates are minimised with respect to the fluence The program requires a-priori information on the spectrum, i.e. fluence values and their co-variance matrix. MIEKEB, instead, performs a sampling of possible spectra by calculating the average of the fluence in a suitably chosen probability distribution.

For these runs, the measured response matrix of the detectors was double-logarithmically spline-interpolated and converted to an energy structure of fifty isolethargic groups in the 0 028-20 MeV range. An uncorrelated uncertainty of 10% on the scaling factor of each response function was assumed and added quadratically to the 10% uncertainties on each measured data point.

The adjustment runs with MSITER were performed using numerical data available from the literature[33,34] as a-priori information on the californium-252 and americium-beryllium spectra.

As a first step, consistency of all measured data was checked for both spectra. Uncorrelated relative uncertainties of 2% were associated with each energy group of the a-priori spectra Running MSITER with these assumptions, virtually no differences resulted between input and output spectra. The χ^2 values per degree of freedom were 0.6 and 0.7, respectively, for californium-252 and americium-beryllium, proving consistency of all data.

In a second adjustment run, a "blind" unfolding was performed for both spectra using constant fluence values and a 100% relative uncertainty in each energy group as a-priori information. χ^2 values after the adjustment were again less than 1 in both cases.

Finally, the spectra unfolded with MIEKEB, without any pre-information, presented large uncertainties in the single energy groups. However, due to the negative correlations in adjacent groups, fluence integrals over broader intervals were assessed with much smaller errors

Results obtained by "blind" adjustment with MSITER and by unfolding with MIEKEB are reported in Table II, compared with the values calculated from the reference spectra.

Table II Fluence integrals for the reference source spectra compared with the values calculated unfolding the SDD readings with MSITER and MIEKEB codes[12]. All data are normalised to the fluence above 0.2 MeV.

Energy	Californium-252			Americium-Beryllium		
(MeV)	Ref. (33)	MSITER*	MIEKEB*	Ref. (34)	MSITER*	MIEKEB
0.2-20	1	1	1	1	1	1
0 3-20	0.970	0 97 (10)	0.93 (7)	0.984	0.99 (7)	0.96 (5)
0.5-20	0 901	0.90 (10)	0 84 (7)	0.954	0 96 (7)	0.91 (5)
1.0-20	0.727	0.72 (13)	0.69 (8)	0 892	0.90 (7)	0.85 (5)
2 0-20	0.434	0 41 (22)	0.42 (10)	0.797	0.79 (6)	0 75 (6)
3 0-20	0.245	0 20 (64)	0.21 (16)	0.678	0.63 (12)	0.59 (11)
4 0-20	0.133	0.14 (109	0.12 (22)	0.521	0.49 (18)	0.44 (16)
5.0-20	0.071	0.10 (165	0.07 (29)	0.378	0.36 (25)	0.34 (17)

* In parentheses: relative uncertainty in %.

SUMMARY OF CONTRACT RESULTS

Neutron Dosimetry

A prototype neutron area monitor was developed which improves the performance of superheated drop detectors based on halocarbon-12. The detectors are thermally controlled this removes external temperature effects while ensuring a dose equivalent response optimised with respect to its energy dependence The system was first characterised through calibrations with monoenergetic neutron beams. In the intermediate energy range, where experimental investigations were not possible, Monte Carlo response calculations were carried out. The prototype was then extensively tested by means of simulated and in-field irradiations with broad neutron spectra All these tests indicated an extremely constant dose equivalent response regardless of the neutron energy distributions. The current device is a fairly delicate system which can be operated reliably when environmental conditions are not extreme. Nevertheless, when it was possible to employ it, the monitor demonstrated an accuracy far superior to that of conventional meters used in routine surveillance.

Neutron Spectrometry

A new method for neutron spectrometry was also proposed which is based on the intrinsic temperature dependence of superheated drop detectors. By controlling the temperature of the detectors, accurately defined detection thresholds, virtually any desired one, can be generated in the 0.01-10 MeV neutron energy range. A prototype device operating on this principle was developed and tested with radionuclide neutron sources. Analysed results demonstrated the potential of this original approach Unfolding by means of adjustment codes shows that measurements are consistent with the source spectra. Fluence values agree well within the calculated uncertainties. Monte Carlo unfolding without any pre-information on the spectrum generates fluence integrals from the detector readings with an uncertainty of about 10% in the relevant energy range.

REFERENCES

1 Apfel, R E *The Superheated Drop Detector* Nucl. Instrum. Methods **162** 603-608 (1979)

2 Ing, H and Birnboim, H C *A Bubble-Damage Polymer Detector for Neutrons.* Nucl. Tracks **8**, 285-288 (1984)

3 d'Errico, F *Superheated Drop (Bubble) Detectors.* Lecture notes of the ERPET/EURADOS training course "Modern Methods in Radiation Measurement and Dosimetry", April 1995, Bad Honnef, D. Report DCMN 001(95)

[4] Apfel, R E., Martin, J D and d'Errico, F *Characteristics of an Electronic Neutron Dosemeter Based on Superheated Drops.* Health Phys , Supplement to **64**(6) S49 (1993)
[5] d'Errico, F *Advances in Individual Neutron Dosimetry.* Physica Medica**10**(Suppl1) 32-33 (1994).
[6] Apfel, R.E. *Characterisation of New Passive Superheated Drop (Bubble) Dosemeters.* Radiat. Prot. Dosim **44**(1-4) 343-346 (1992)
[7] d'Errico, F., Alberts, W.G., Apfel, R E., Curzio, G., and Guldbakke, S. *Applicability of Superheated Drop (Bubble) Detectors to Reactor Dosimetry.* Reactor Dosimetry ASTM STP 1228 (Farrar, H., Lippincott, E.P., Williams, J G. and Vehar, D.W. eds) pp. 225-232 (Philadelphia: ASTM) (1994)
[8] Lo, Y C and Apfel, R.E. *Prediction and Experimental Confirmation of the Response Functions for Neutron Detection Using Superheated Drops.* Phys. Rev A **38**(10) 5260-5266 (1988)
[9] Sun, Y.Y , Chu, B T and Apfel, R E *Radiation-Induced Cavitation Process in a Metastable Superheated Liquid* J. Comp. Physics **103**(1) 116-140 (1992)
[10] d'Errico, F and Alberts, W.G. *Superheated Drop (Bubble) Detectors and Their Compliance with ICRP 60* Radiat Prot Dosim **54**(3/4) 357-360 (1994)
[11] d'Errico, F and Egger, E *Proton Beam Dosimetry with Superheated Drop (Bubble) Detectors* In: Hadrontherapy in Oncology (Amaldi, U and Larsson, B eds) Excerpta Medica, International Congress Series 1077, pp 488-494 (Amsterdam: Elsevier Science) (1994)
[12] d'Errico, F., Alberts, W G , Curzio, G , Guldbakke, S , Kluge, H and Matzke, M *Active Neutron Spectrometry with Superheated Drop Detectors.* Rad Prot Dosim **61**(1-3) 159-162 (1995)
[13] d'Errico, F , Alberts, W.G , Dietz, E., Gualdrini, G F , Kurkdjian, J., Noccioni, P. and Siebert, B.R.L. *Neutron Ambient Dosimetry with Superheated Drop Detectors* Radiat. Prot. Dosim. (1996)
[14] Apfel, R E and Roy, S C. *Instrument to Detect Vapor Nucleation of Superheated Drops.* Rev Sci. Instrum. **54**(10) 1397-1400 (1983)
[15] Guldbakke, S , Dietz, E., Kluge, H. and Schlegel, D *PTB Neutron Fields for the Calibration of Neutron Sensitive Devices* In Strahlenschutz. Physik und Messtechnik (Kölzer, W. and Maushart, R eds) pp. 240-247 (Rheinland, Köln Verlag TÜV) (1994)
[16] Alberts, W G , Dietz, E., Guldbakke, S., Kluge, H. and Schuhmacher, H. *International Intercomparison of TEPC Systems Used for Radiation Protection.* Radiat Prot Dosim **29** (1-2) 47-53 (1989)
[17] Guldbakke, S PTB-Braunschweig, private communication (1993)
[18] Nath, R , Meigooni, A S., King, C R , Smolen, S. and d'Errico, F *Superheated Drop Detector for Determination of Neutron Dose Equivalent to Patients Undergoing High-Energy X-Ray and Electron Radiotherapy*, Medical Phys., **20**(3) 781-787 (1993)
[19] Schuhmacher, H and Alberts, W G *Reference Neutron Fields with Energies up to 70 MeV for the Calibration of Radiation Protection Instruments* Radiat. Prot. Dosim., **42**(4) 287-290 (1992).
[20] Gualdrini, G.F , d'Errico, F and Noccioni, P *Monte Carlo Evaluation of the Detection Efficiency of a Superheated Drop Detector* ENEA Report RT/AMB/95 In press
[21] Siebert, B R L and Schuhmacher, H. *Quality Factors, Ambient and Personal Dose Equivalent for Neutrons, Based on the New ICRU Stopping Power Data for Protons and Alpha Particles* Radiat Prot Dosim **58**(3) 177-183 (1995).
[22] Ing, H and Makra, S. *Compendium of Neutron Spectra in Criticality Accident Dosimetry* Technical Report Series 180 (Vienna IAEA) (1978)
[23] Griffith, R.V , Palfalvi, J. and Madhvanath, U. *Compendium of Neutron Spectra and Detector Responses for Radiation Protection Purposes.* Technical Series 318 (Vienna: IAEA) (1990)
[24] Aroua, A , Boschung, M , Cartier, F., Grecescu, M., Pretre, S., Velley, J F and Wernli, C *Characterisation of the Mixed Neutron Gamma Fields inside the Swiss Nuclear Power Plants by Different Active Systems.* Radiat Prot Dosim. **51**, 17-25 (1994)
[25] ICRU *Determination of Dose Equivalents Resulting from External Radiation Sources.* Report 39 (Bethesda, MD: ICRU Publications) (1985).
[26] Chartier, J.L , Posny, F. and Buxerolle, M. *Experimental Assembly for the Simulation of Realistic Neutron Spectra* Rad Prot Dosim **44**(1/4) 125-130 (1992)
[27] Lindborg, L , Bartlett, D , Drake, P., Klein, H , Schmitz, T and Tichy, M. *Determination of Neutron and Photon Dose Equivalent at Work-Places in Nuclear Facilities in Sweden* Rad Prot Dosim **61**(1-3) 89-100 (1995)
[28] Höfert, M and Stevenson, G.R *The CERN-CEC High-energy Reference Field Facility.* In Proc 8th Int Conf on Radiation Shielding, Arlington, Texas (1994)

[29] Alevra, A V , Klein, H and Schrewe, U.J. *Measurements with the PTB - Bonner Sphere Spectrometer in High-energy Neutron Calibration Fields at CERN* PTB-Report N-22 (1994).

[30] Aroua, A , Höfert, M. and Sannikov, A V. *On the Use of Tissue Equivalent Proportional Counters in High Energy Stray Radiation Fields.* Rad Prot Dosim. **59**(1) 49-53 (1995).

[31] Perey, F G *Least-Squares Dosimetry Unfolding: The Program STAY'SL.* Report ORNL/TM-6062, (Oak Ridge, TN Oak Ridge National Laboratories) (1977)

[32] Matzke, M. and Weise, K. *Neutron Spectrum Unfolding by Monte Carlo Methods.* Nucl Instr Methods **A234**, 324-330 (1985)

[33] Grundl, J.A and Eisenhauer, C.M. *Fission Rate Measurements for Materials Neutron Dosimetry in Reactor Environments.* In Proc of First ASTM-EURATOM Symposium on Reactor Dosimetry, EUR 5667 e/f, Part I, 425-454 (Luxembourg· Commission of the European Communities) (1977)

[34] Kluge, H and Weise, K *The Neutron Energy Spectrum of a ^{241}Am-Be(α,n) Source and Resulting Mean Fluence to Dose Equivalent Conversion Factors.* Rad. Prot Dosim. **2**, 85-93 (1982).

PUBLICATIONS DERIVING FROM THE CONTRACTUAL WORK

1 d'Errico, F and Alberts, W.G *Superheated Drop (Bubble) Detectors and Their Compliance with ICRP 60* Radiat Prot Dosim **54**(3/4) 357-360 (1994)

2 d'Errico, F and Egger, E. *Proton Beam Dosimetry with Superheated Drop (Bubble) Detectors* In. Hadrontherapy in Oncology; eds U Amaldi and B. Larsson. Excerpta Medica, International Congress Series 1077, pp. 488-494 (Amsterdam· Elsevier Science) (1994)

3 d'Errico, F , Alberts, W G., Apfel, R.E , Curzio, G., and Guldbakke, S *Applicability of Superheated Drop (Bubble) Detectors to Reactor Dosimetry.* In. Reactor Dosimetry; eds H.Farrar, E.P. Lippincott, J G.Williams and D.W.Vehar. ASTM STP1228, 225-232 (Philadelphia: ASTM) (1994)

4 d'Errico, F *Superheated Drop (Bubble) Detectors.* Lecture notes of the ERPET/EURADOS training course "Modern Methods in Radiation Measurement and Dosimetry", April 1995, Bad Honnef, D. Report DCMN 001(95).

5 d'Errico, F., Alberts, W G , Curzio, G , Guldbakke, S., Kluge, H. and Matzke, M *Active Neutron Spectrometry with Superheated Drop Detectors* Rad Prot. Dosim **61**(1-3) 159-162 (1995)

6 Gualdrini, G F , d'Errico, F. and Noccioni, P *Monte Carlo Evaluation of the Detection Efficiency of a Superheated Drop Detector* ENEA Report RT/AMB/95 In press

7 d'Errico, F , Alberts, W G , Dietz, E., Gualdrini, G F , Kurkdjian, J., Noccioni, P and Siebert, B.R.L. *Neutron Ambient Dosimetry with Superheated Drop Detectors* Radiat. Prot. Dosim. (1996)

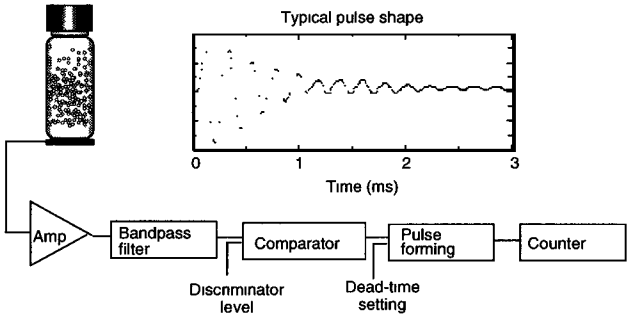

Figure 1 Superheated drop (bubble) detectors vial and pulse counting electronics.

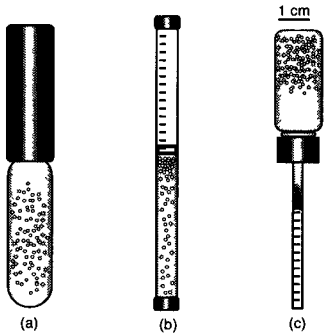

Figure 2. Passive, integrating superheated drop (bubble) detectors. (a) optical couting device, (b,c) volumetric counting devices for low and high doses.

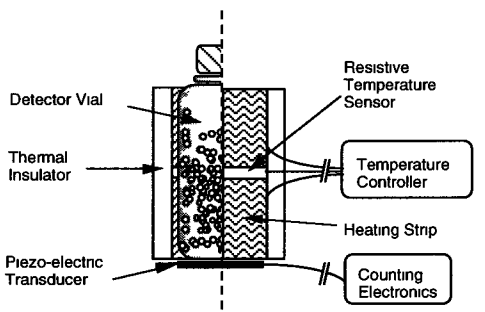

Figure 3 Superheated-drop detector probe for the determination of response as a combined function of temperature and energy.

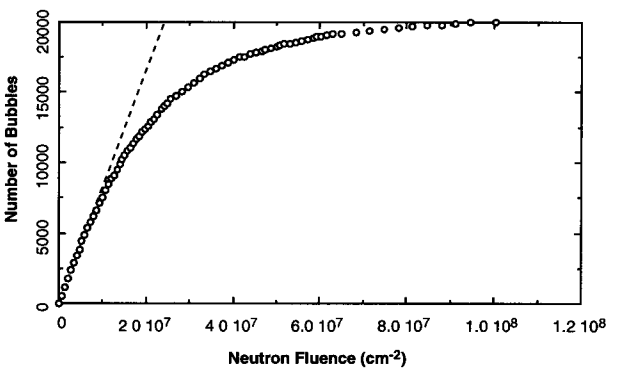

Figure 4. Integrated SDD response as a function of neutron fluence.

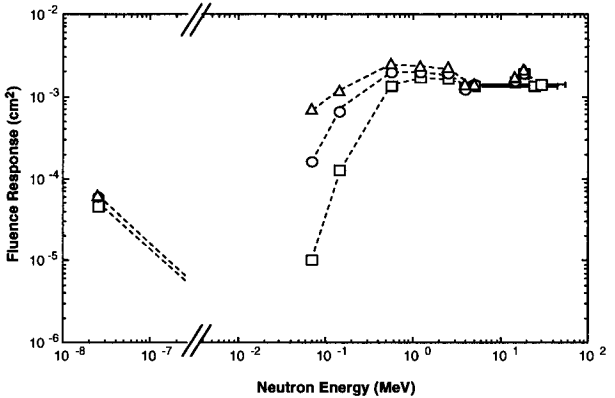

Figure 5. Fluence response of a halocarbon-12 emulsion as a function of neutron energy, measured at 25(□), 30 (O), and 35 (Δ) degrees Celsius. Dashed lines are eye guides only

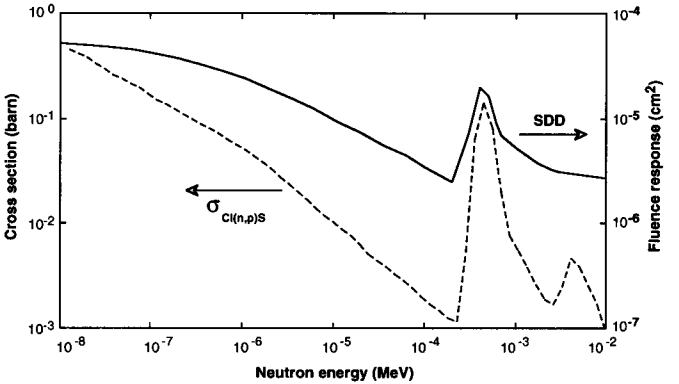

Figure 6 MCNP calculated response of a halocarbon-12 SDD in the epithermal region (---) and microscopic cross section of the $^{35}Cl(n,p)^{35}S$ capture reaction (---) versus neutron energy

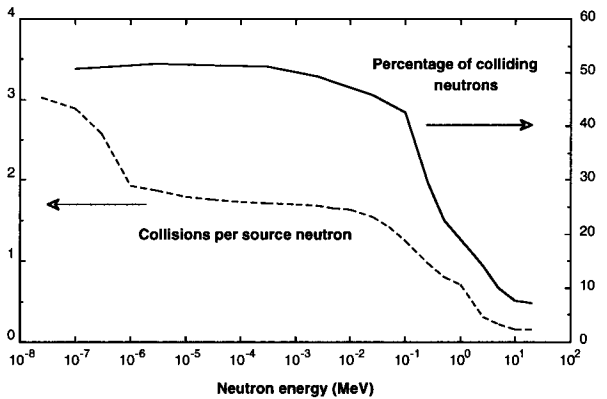

Figure 7. MCNP calculated percentage of colliding primary neutrons (—) and average number of collisions inside an SDD vial (---) versus neutron energy

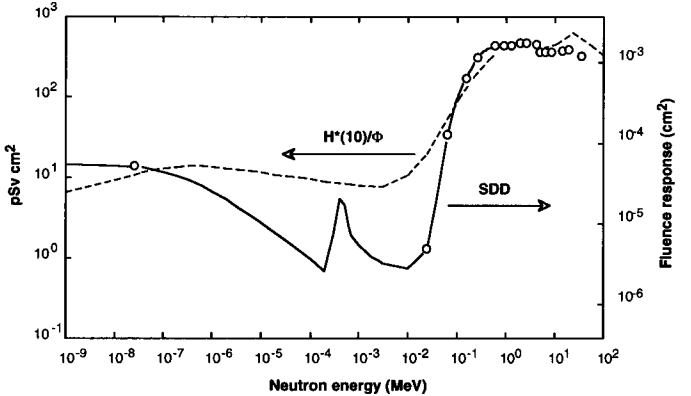

Figure 8 Fluence response of a halocarbon-12 SDD stabilised at 31.5 °C (— MCNP calculation and, above 10^{-2} MeV, lagrange interpolation of experimental points O) and fluence to ambient dose equivalent conversion factor (---) versus neutron energy.

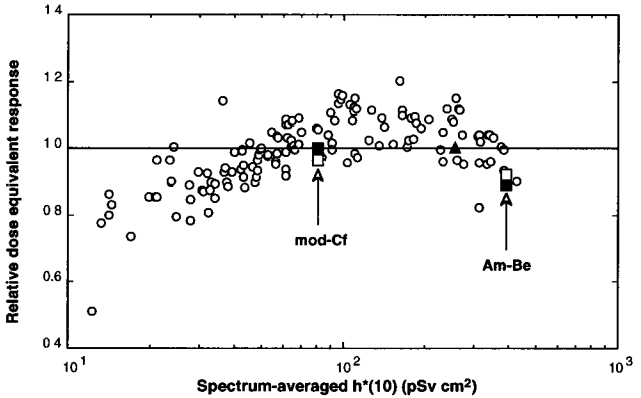

Figure 9. Relative dose equivalent responses of the SDD monitor to practical neutron fields: spectra catalogue (O), calculated (❑) and measured (■) response to radionuclide sources, bare californium normalisation (▲).

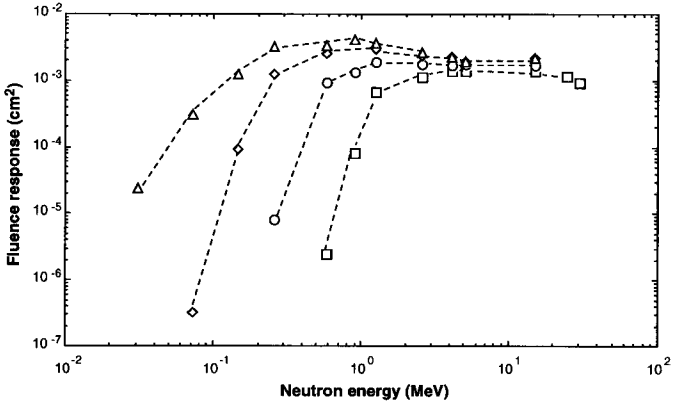

Figure 10. Fluence response of an octafluorocyclobutane detector as a function of neutron energy, measured at 25 (❑), 30 (O), 35 (◊), and 40 (Δ) degrees Celsius. Dashed lines are eye guides only

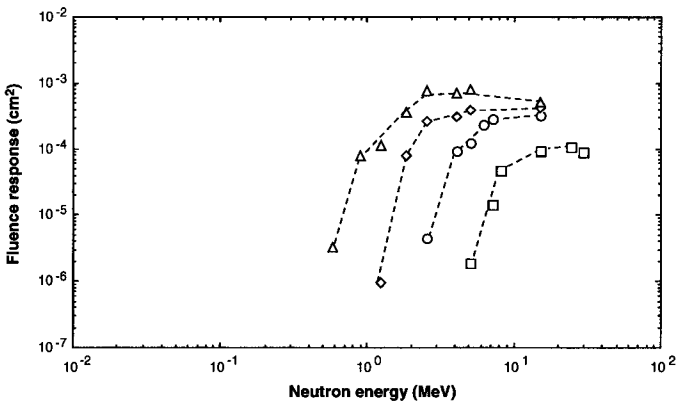

Figure 11 Fluence response of a dichlorotetrafluoroethane detector as a function of neutron energy, measured at 25 (❑), 30 (O), 35 (◊), and 40 (Δ) degrees Celsius. Dashed lines are eye guides only.

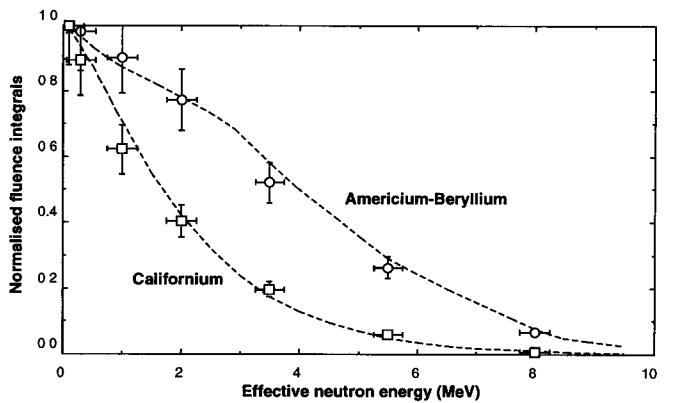

Figure 12. Fluence integrals measured by the active SDD spectrometer with californium-252 (❑) and americium-beryllium (O) sources versus effective neutron energy, E_{eff}, compared with the corresponding integrals deduced from the reference source spectra (dashed lines). Data are normalised to the fluence above 0.2 MeV

I. **HEAD OF PROJECT 6:** dr. J. Charvát (since July 1, 1994, dr. F. Spurný)
Scientific Staff: dr. V. P. Bamblevski, dr. J. Bednář, dr. M. Běgusová, dr. J. Bouček, dr. J. Charvát, dr. K. Turek, B. Vlček, I. Votočková

II. OBJECTIVES FOR THE REPORTING PERIOD

The main objectives formulated in the proposal to join, since the end of 1993 the project, were formulated in the following way:

a) the development of an electronic sensor: to perform some additional transport calculations (MCNP) with the goal to optimize the radiator - sensor combination; to test the possibility to use a Si-diode as position sensitive device for neutron detection;
b) the testing of bubble damage and superheated drop neutron detectors in various neutron beams and fields: to verify their basic dosimetric characteristics (linearity, energetic dependence of the response, the lowest limit of detection, longer term stability, etc.);
c) the determination of dosimetric and microdosimetric characteristics of reference and other neutron fields: to improve the knowledge of basic dosimetric characteristics of different fields (reference fields, radionuclide neutron sources, fields behind shielding of high energy accelerators, etc.); to determine microdosimetric characteristics in these fields, all with the goal to improve the conditions of testing of sensors developed by other contractors.

III. PROGRESS ACHIEVED INCLUDING PUBLICATIONS

1. Development of electronic neutron sensor

Neutron transport through the combination radiator-sensor have been realized (MCNP) to compare programs available in Prague and Limoges. A good agreement has been stated, i.e. optimum polyethylene radiator thickness would be for neutron with energies between 100 keV and 3 MeV about 20 to 30 μm.

Four electrodes have been connected to a large surface Si-diodes acquired from Poland before the official beginning of the participation on the contract. Preliminary tests have been performed to distinguish neutrons and photons on the base of position sensitive charge collection. It was found out that such solution would be principally possible. The first version of software permitting such application has been developed.

2. Bubble detectors' testing

Two types of bubble detectors were tested: bubble damage neutron detectors (BDNDs') and superheated drop detectors (SDDs'). The main characteristics studied were: the energetical dependence of response, statistics of the counting with the respect to the lowest limit of detection, and the possibilities of neutron spectrometry with them. The principal results obtained are briefly presented in next paragraphs.

2.1. Counting statistics of BDNDs'

Multiple irradiation of several pieces of BDNDs' (type PND, compensated for the temperature, threshold 0.1 MeV) has been realized using AmBe radionuclide neutron source. The standard deviation of a single reading was found to be regularly close to the $\sqrt{N}/N$, where N is number of counted bubbles. It seems therefore that the bubbles appearance with dose follows the normal distribution. It signifies also that the precision ±30% claimed for a personal dosemeter is achieved when total number of

bubbles is a little above 10. The BDNDs' tested had the nominal sensitivity to AmBe neutrons at least 1 bubble per μSv. At such sensitivity, 10 μSv is measurable with the relative uncertainty ±31%. When the sensitivity is double, the lowest limit of detection decreases twice.

2.2 Energetical dependence of BDNDs'.

Energetical dependencies of BDNDs' have been studied in neutron beams and fields characterized in the Table 1. One can see there that the choice of these fields is very large, going from the practically thermal neutron source (SIGMA) up to the reference field behind the shielding (80 cm of concrete) of very high energy accelerator (205 GeV) c protons and pions impinging on thick Cu-target as primary radiation - CERN top concrete). Studies of energetical dependencies of BDNDs' had

Table 1: Reference and other neutron fields used for energetical dependencies studies of BDNDs' [1/5].

Neutron source	E_N [MeV]	H*(10) conversion factor [Sv.cm^2]	Neutron source	E_N [MeV]	H*(10) conversion factor [Sv.cm^2]
SIGMA	< 0.1	2.29 - 11	AmBe	4.4	3.80 - 10
Canel +(H_2O)	0.096	3.47 - 11	PuBe	4.2	3.80 - 10
CANEL +	0.19	7.26 - 11	JDNR soft field	0.25	2.90 - 11
^{252}Cf/D_2O/Cd	0.54	9.10 - 11	CERN top iron	1.9	1.60 - 10
AmF	1.5	3.4 - 10	JDNR hard field	12.5	1.05 - 10
^{252}Cf	2.1	3.4 - 10	CERN top concrete	49.8	2.80 - 10

been performed in two runs. First one was realized at 1994, the type BD-100R (threshold 0.1 MeV, not compensated for temperature) has been tested. Two different nominal sensitivities of BD-100R were available, 0.8 and 2.2 bubbles per 1 μSv of H*(10) of AmBe neutrons. Results obtained expressed in the relative responses to H*(10) of reference AmBe neutrons are presented in Table 2.

At the end of 1994 we were able to purchase a new lots of BDNDs' of two types: BD-100R and PND (threshold ~ 100 keV, compensated for temperature). We repeated the most of energetical dependence studies. Their results are presented in Table 3, the most important was the participation at the intercomparison organized in the frame of contract at Cadarache, April 1995.

Table 2: Relative responses of BDNDs' (BD-100R, 0.8 or 2.2 bubbles per μSv of H*(10) of AmBe neutrons to neutrons of different sources.

Neutron source	Relative response[1)]	Neutron source	Relative response
SIGMA	0.48 ± 0.06[2)]	AmBe	0.99 ± 0.03
CANEL + (H_2O)	0.89 ± 0.11	PuBe	0.97 ± 0.06
CANEL +	1.06 ± 0.07	JINR - soft field	0.95 ± 0.09
^{252}Cf/D_2O/Cd	1.01 ± 0.06	CERN - top iron	0.98 ± 0.05
AmF	1.06 ± 0.07	JINR - hard field	0.69 ± 0.08
^{252}Cf	1.11 ± 0.08	CERN - top concrete	0.60 ± 0.04

[1)] Relatively to H*(10) of AmBe neutrons

[2)] 50% of H*(10) comes from thermal neutrons

Table 3: Relative responses of BDNDs' (BD-100R, PND-60th with nominal sensitivities about 1 bubble per μSv of H*(10) of AmBe neutrons) to neutrons of different sources.

Neutron source	Relative response[1]		Neutron source	Relative response	
	BD-100R	PND		BD-100R	PND
SIGMA[2]	0.52±0.04	0.54±0.04	AmBe	1.00±0.06	0.94±0.07
CANEL + (H_2O)	1.13 ±0.09	1.06±0.08	PuBe	1.05±0.07	1.03±0.07
CANEL +	1.22 ±0.09	1.06±0.08	JINR - soft field	-	1.13±0.13
$^{252}Cf/D_2O/Cd$	-	-	CERN - top iron	1.28±0.13	1.17±0.10
AmF	1.10 ±0.08	1.16±0.08	JINR - hard field	-	0.70±0.07
^{252}Cf	1.34 ±0.14	1.38±0.15	CERN - top concrete	0.63±0.04	0.62±0.04

[1] Relatively to H*(10) from AmBe neutrons
[2] 50% of H*(10) comes from thermal neutrons

General conclusions from both Tables can be formulated in the following way:

a) With the exception of very high energy fields there is a reasonable agreement of data measured with BDNDs' and reference values.
b) Nevertheless, it should be mentioned, that new lots of BDNDs' seem to have a little different energetic dependence. The relative responses for „soft" fields (both CANEL +, AmF, ^{252}Cf, JINR and CERN soft fields) are for them systematically higher (compare Tables 2 and 3). Apparently, the response to lower energy neutrons is for these new lots relatively higher than to reference AmBe neutrons.
c) As far as „hard" fields are concerned, the response of BDNDs' is systematically lower. Such behaviour is typical for any LET-threshold type detector [6]. Such tendency has to be kept in mind when BDNDs' are used as individual neutron dosemeters in high energy neutron fields (high energy accelerator radiation environment, board of subsonic or supersonic aircraft).

2.3. Energetical dependence of SDDs'

The results of first run of studies of the energetical dependence of SDDs' are presented in the Table 4. One can see there, that:

Table 4: Relative responses of SDDs' to neutron of different sources.

Neutron source	Relative response at the threshold		
	0.1 MeV	1 MeV	6 MeV
AmBe	1.00[1]	0.48 ± 0.06	0.16 ± 0.02
AmF	1.03 ± 0.15	0.028 ± 0.004	0.028 ± 0.005
Cf	1.20 ± 0.15	0.20 ± 0.03	0.09 ± 0.01
PuBe	0.94 ± 0.08	0.40 ± 0.05	0.16 ± 0.02
CERN - top iron	0.70 ± 0.10	0.09 ± 0.02	0.17 ± 0.03
CERN - top concrete	0.50 ± 0.05	-	-

[1] Reference value

a) The energetical dependence of SDD 100 (Threshold 0.1 MeV) is comparable with the dependencies of BD-100R and PND (compare Tables 2, 3 and 4), the underestimation of high energy neutrons included (CERN - top concrete).

b) The use of SDD with different energy threshold can provide very interesting spectrometric information. The sources like ^{252}Cf or AmF can be clearly distinguished from AmBe sources when comparing the responses of SDD 100 and SDD 6000 (1000).

2 4. Neutron spectrometry with BDNDs'

BDNDs' are also available with different energy thresholds, the neutron contribution in several energy bands can be therefore established. We have tested such spectrometer in reference fields behind the shielding of Dubna phasotron [4]. The results of these tests, relatively to the spectrum determined by means of combined Bonner and activation ($^{12}C \rightarrow {}^{11}C$; $^{27}Al \rightarrow {}^{24}Na$) spectrometer, are presented in Table 5. One can see there, that the agreement of BDNDs' spectrometer data is

Table 5: Results of the tests of neutron spectrometer based on BDNDs'in JINR reference fields.

Energy threshold [MeV]	H*(10) measured by a BDND, relatively to reference values	
	soft field	hard field
0.01	0.87 ± 0.11	0.92 ± 0.07
0.10	0.86 ± 0.12	0.92 ± 0.08
0.60	0.75 ± 0.08	0.88 ± 0.09
1.00	0.36 ± 0.04	0.57 ± 0.07
2.50	0.91 ± 0.11	1.24 ± 0.12
10.00	1.2 ± 0.5	0.92 ± 0.08

quite good, taking into account that no normalization was undertaken. Only the results with detectors having threshold 1 MeV are too low. Probably their nominal sensitivities were not established correctly.

3. Determination of dose characteristics of some neutron fields

Many different instruments and detectors (TLDs', track etch detectors, a remcounter, scintillator and GM-based dose-rate meters, a tissue equivalent proportional counter, individual electronic dosemeters, etc.) have been used to get more precise dosimetric and microdosimetric characteristics of fields used to test direct reading potential neutron personal dosimetrics (electronic sensors, bubble detector). Particular attention has been concentrated to the gamma component for which the data available were only scarce and incomplete. The studies were performed at all sources mentioned in the Table 1, for some of them with several of the same type (Cf, AmBe, PuBe) at Prague, Fontenay-aux-Roses and Cadarache. The many results have been already published (see the list of publication). As an example, the relative dose equivalent of photons in studied fields is presented in Table 6, some examples of microdosimetric event size spectra are given in Figs 1 and 2. One can see in the Table 6, that the photon (low LET) contribution to the H*(10) is generally low. Nevertheless, in some cases (Am sources without Pb shield) and for some instruments (not compensated for photon energy, sensitive to both neutrons and low LET component, etc.) the photons can complicate seriously the interpretation of readings. It should be also mentioned that our results are in comparable cases about 20% lower than these presented in ISO 8529 [5]. Perhaps, a more profound analysis of photon contribution should be undertaken for all recommended reference neutron sources.

Table 6: Relative dose equivalent H*(10) of photons in studied reference and other neutron fields.

Neutron source	Relative H*(10) of photons (low LET)	Neutron source	Relative H*(10) of photons (low LET)
SIGMA	0.060 ± 0.009	AmBe[1)]	0.033 ± 0.005
CANEL + (H_2O)	0.14 ± 0.03	PuBe	0.030 ± 0.004
CANEL +	0.038 ± 0.005	JINR - soft field	0.15 ± 0.02
$^{252}Cf/D_2O/Cd$	0.12 ± 0.02	CERN - top iron	0.059 ± 0.007
AmF[1)]	0.087 ± 0.015	JINR - hard field	0.10 ± 0.02
^{252}Cf	0.038 ± 0.007	CERN - top concrete	0.28 ± 0.03

[1)] Covered by 1.5 mm of Pb; without Pb the relative contribution can be up to 0.8 for AmF, resp. 0.3 for AmBe.

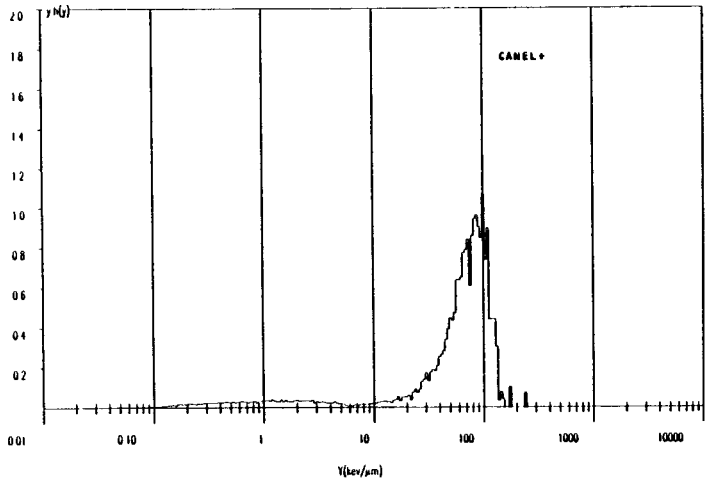

Fig. 1: Microdosimetric dose equivalent distributions at CANEL +

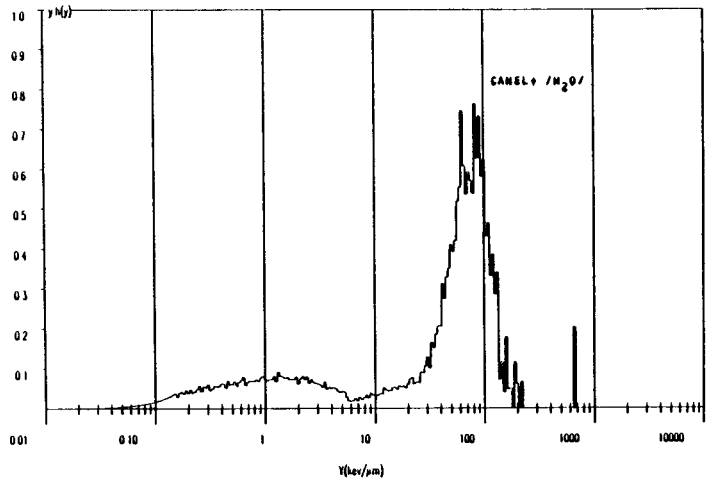

Fig. 2: Microdosimetric dose equivalent distributions at CANEL + (H_2O)

REFERENCES

1, J.-L. Chartier, F. Posny, M. Buxerolle: „Experimental assembly for the simulation of realistic neutron spectra." Radiat. Prot. Dosim. 54, (1994), p. 125-130.

2, P. Candes: „Moyens et dispositifs d'irradiation et d'étalonnage." Radioprotection 5, (1970), p. 323-328.

3, M. Höfert, G. Stevenson, W.G. Alberts: „The CERN - CEC High Energy Reference Field Facility." Presented at the 8th Inter. Conf. Radiat. Shielding, Arlington, Texas, April 1994.

4, V.E. Aleinikov et al.: „Reference neutron fields for metrology of radiation monitoring." Radiat. Prot. Dosim. 54, (1994), p. 57-59.

5, ISO 8529: „Rayonnement neutroniques de réference déstinés a l'étalonnage ...". M60-516, Décembre 1989.

6, F. Spurný: „Response of different SSNTD to protons with energies betweeen 0.01 and 10 GeV." Nucl. Tracks Radiat. Measur. 19, (1991), p. 125-127.

LIST OF PUBLICATIONS

1, F. Spurný, I. Votočková, V.P. Bamblevskyi: „To the energetical dependence of bubble damage neutron detectors". Radiat. Measur. 23, (1994), p. 247-249.

2, F. Spurný, I. Votočková, J.-F. Bottollier-Depois, J.-L. Chartier, J. Kurkdjian, D. Paul: „Caractéristiques dosimétriques de certains champs mixtes disposibles au SDOS-DPHD-IPSN". Rapport IRD AS RTch. 381/94, Prague, Janvier 1994.

3, F. Spurný, K. Turek, I. Votočková, V.P. Bamblevskyi: „Dosimetry measurements in reference fields behind the shielding of the phasotron of the LNP JINR at Dubna". Report IRD AS CR 387/94, Prague, May 1994.

4, F. Spurný, I. Votočková, K.. Turek: „Equipment and detectors calibration behind shielding of CERN high energy particle accelerator SPS-II; May 1994. Report IRD AS CR 391/94, Prague, June 1994.

5, F. Spurný, I. Votočková, J.-F. Bottolier-Depois, J. Kurkdjian: „Résultats des mesures dans les champs mixtes du CEIR au moyen du CPET - NAUSICAA". Rapport DDR IPN AS Ré. Tch. 392/94; Prague, Octobre 1994.

6, F. Spurný, I. Votočková, J.-F. Bottollier-Depois: „Microdosimetric characteristics of some reference and other radiation fields". Presented at the 2nd Symp. Radiat. Biol. and its Application in Space Research, Brno, November 1994.

7, F. Spurný et al.: „Individual electronic neutron dosimeter: Research activities and results up to XI/94". Presented at Contractor's Meeting, Pisa, December 1994, (Report DRD NPI AS CR, 394/94; November 1994).

8, F. Spurný, I. Votočková: „WG7 EURADOS Intercomparison of the methods of dosimetry and spectrometry in neutron-gamma fields". Report DRD NPI AS CR 399/95, Prague, January 1995.

9, F. Spurný, I. Votočková, J. Kurkdjian, R. Médioni, D. Nikodémová: „Dosimetric characteristics of radiation fields at radionuclide neutron sources". Nuclear Energy Safety (in Czech), 3(41), 1995, 000.

10,F. Spurný, I. Votočková, K. Turek, J. Kurkdjian, D. Paul, D. Nikodémová: „Dosimetric characteristics of some neutron reference fields" Nuclear Energy Safety (in Czech), accepted for publication.

11,F. Spurný, I. Votočková, K. Turek: „Equipments and detectors calibration behind shielding of CERN high energy particle accelerator SPS. IV. April 1995". Report DRD NPI AS CR 405/95, Prague, June 1995.

12 F. Spurny, I. Votočková, J. Bednář, K. Turek: „Intercomarison of methods studied in the frame of the CEC Project FI3P-CT93-0072". Report DRD NPI AS CR 407/95, Prague, July 1995.
13.F. Spurný, I. Votočková: „Bubble damage neutron detectors responses in some reference neutron fields". Presented at the 11th SSD Conf., Budapest, July 1995, will be published in the journal Radiat. Prot. Dosim.
14,V.V. Bamblevskyi, F. Spurný, V.E. Dudkin: „Neutron spectrometry with bubble damage detectors". Radiat. Prot. Dosim., submitted for publication.
15,F. Spurný, J. Kurkdjian, D. Paul et al.: „Radiation field characteristics at some radionuclide radiation sources". Will be presented at the 8th Symp. Neutr. Dosim., Paris, November 1995 and published in the journal Radiat. Prot. Dosim.
16,F. Spurný, B. Vlček: „To the use of bubbles detectors in the individual neutron dosimetry". XIX Radiohygienic days, Jasna pod Chopkom, Slovakia, November 1995.

Head of project 7 : Dr. Moiseev

II. Objectives for the reporting period

1- To design the detection assembly (the small-size moderator and the radiator-diode system) in order to improve the dosemeter's response in the intermediate neutron energy range.
This includes the choice of the moderator, its size, geometry and position with respect to the silicon detectors ; as well as the choice for the B10 concentration in the radiator.

2- To test the proposed design of the dosemeter in various neutron fields in order to determine its energy response.

3- To study the improvements and the drawbacks brought by the use of large area PIN silicon detectors.

III. Progress achieved including publications

1- As known from the response of the "Bonner Spheres", a polyethylene sphere of 2" in diameter will moderate neutrons in the energy range from near thermal up to 1 keV (3), while higher energy neutrons will have fewer interactions, as their mean free path increases with energy as shown in Fig. 1.

The detection assembly (moderator + diodes) shown in Fig. 2 consists of two implanted silicon diodes, having an active area of 19.6 mm^2, one of the diode being provided with a convertor deposed with a 2μm layer of B_2O_3 (96% B10 enriched).

The pulses from the diodes are fed through two acquisition chains and then treated by a differential method.

Each diode is covered with an Aluminium shielding cover (0.3mm thick) and both diodes are included in an hemispherical polyethylene moderator provided with a cylindrical front opening (Fig.2).

The cylindrical opening in the moderator was invented to provide a direct detection for fast neutrons at normal and near normal incidence.

The low amplitude threshold of the acquisition chains is at 100 keV and an informatic cut was imposed at 290 keV, in order to discriminate all gamma ray generated pulses.

With these settings, the gamma ray sensitivity oi the detection assembly is of about 15 pulses/mSv for the Co60 radiation, and lower for lower energy gamma rays. Tests for the detection system with and without a moderator, performed in gamma ray fields, proved that the presence of the moderator does not affect the sensitivity to gamma rays of the detection assembly (Fig.8).

2- <u>The irradiation tests in neutron fields</u>

The irradiation tests have been performed using the "realistic neutron fields" from CEA/CEN Cadarache - France.

The main parameters characterizing thes fields are indicated in table n°1, data being provided by CEA/CEN Cadarache and CEA/IPSN/DPHD Fontenay-aux-Roses (2). The following parameters are indicated :

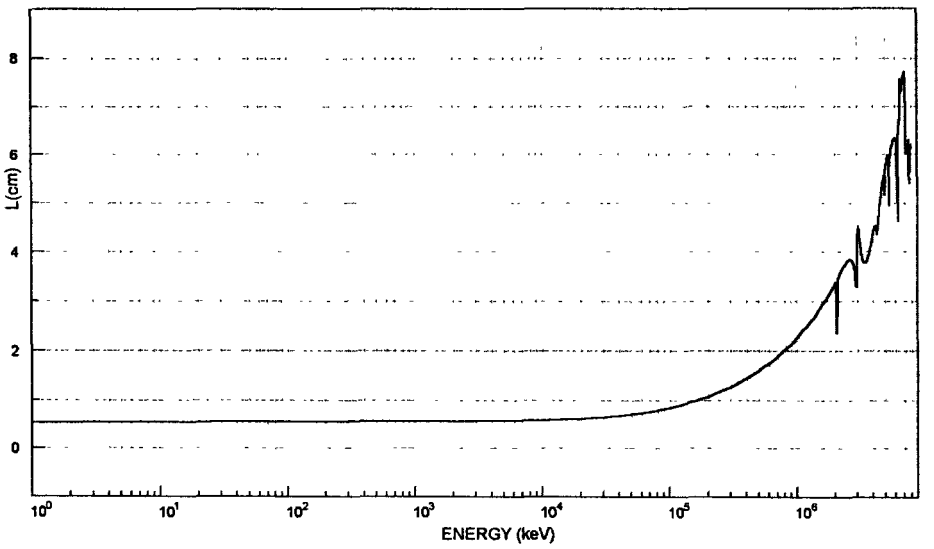

Fig.1. The Mean Free Path of neutrons in polyethylene.

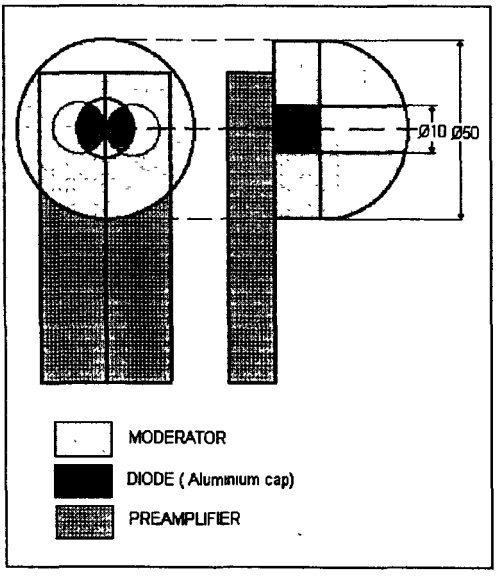

Fig.2.: The detection assemby with two Silicon diodes (implanted).

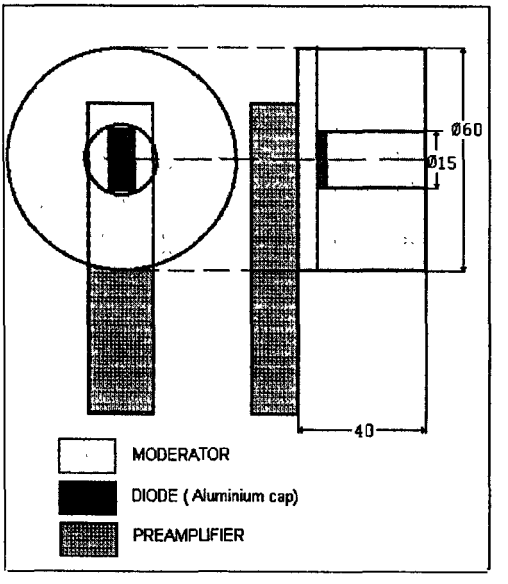

Fig.3.: The detection assemby with one PIN diode.

- the spectral distribution of the neutron fluence Φ and the neutron dose equivalent H for three neutron energy ranges : thermal (0.025 eV - 1eV), intermediate (1eV - 10 keV) and fast neutrons (10 keV - 14 MeV)

- the mean energy E (keV) and the effective energy E_H (keV).

For each field, there have been performed the following irradiation tests :

- "free air" irradiations of the detection system with and without moderator

- "on phantom" irradiations using a PMMA phantom (30 × 30 × 15 cm), the detection system with and without moderator being placed at the center front face of the PMMA phantom.

All irradiations have been performed at normal incidence.

The dosemeter's response for the above tests is shown in table n°2, and compared to the response of a differential detection system with two PIPS detectors (provided only with a radiator and no moderator), developed in previous work during an I.A.E.A. fellowship at CEA/ Fontenay-aux-Roses, France (1, 4). For comparison purposes, the silicon diodes active area has been normalised to 19.6 mm^2.

The typical charged particles spectra are shown in Fig.4, Fig.5 and Fig.6.

Irradiation tests in fast neutron fields have been performed using Cf252 and Am-Be sources and the fast neutron beam from the U120 cyclotron facility (Bucharest). The results are shown in table n°3.

Discussion and Conclusions

The proposed moderator type neutron dosemeter shows a decrease in the sensitivity for fast neutrons due to the small active area of the detector and also to the slowing down of the generated protons in the B_2O_3 layer.

For thermal neutrons it was obtained an over response with and without moderator, which is due to the high B10 concentration on the radiator.

In the intermediate neutron energy range (neutron fields : CANEL+ and CANEL+ with water shield) the sensitivity of the moderator system is higher than that obtained with the "classical system" using only a convertor.

Although necessary in order to decrease the sensitivity to gamma rays, the small active area of the diodes has the disadvantage of providing a low sensitivity to fast neutrons.

The moderator type neutron dosemeter investigated has a high sensitivity to the intermediate neutron energy range, where other detection systems using silicon diodes proved to have a gap in response.

3- An improved design using silicon diodes

In order to increase the dosemeter sensitivity for fast neutrons, the detection system was re-designed using large area PIN silicon detectors (150 mm^2 active area).

As the gamma ray sensitivity was kept low (about 15 pulses/mSv for Co60 radiation) by the use of a detection threshold at 300 keV, it was used only one diode provided with a 40 μm polyethylene radiator having a 20 mm central circular area deposed with a layer of B_2O_3 (2μm thick).

The moderator has been changed as shown in Fig.3. A hemispherical moderator of 60 mm diameter has also been tested and its effect compared with the one of the cylindrical moderator.

This detection system has been tested to thermal neutrons (Cf252 field moderated inside a 30 cm polyethylene sphere) and in fast neutron fields : Cf252 and Am-Be souces, and the fast beam from the U120 Cyclotron facility. All irradiations have been performed at normal incidence.

TABEL No.1.

Neutron Field	CANEL+	CANEL+ with H2O	SIGMA
Ø thermal	36 %	43 %	97 %
Ø intermediate	20 %	26 %	1 %
Ø fast neutrons	44 %	31 %	2 %
Mean Energy	150 keV	80 keV	72 keV
H thermal	6 %	10 %	46 %
H intermediate	3 %	7 %	4 %
H fast neutrons	92 %	83 %	50 %
Effective Energy	610 keV	68 keV	1323 keV

TABEL No.3.

Neutron Source	SENSITIVITY (imp /mSv) No Moderator	With moderator
Am-Be	135	196
^{252}Cf	137	199
Cyclotron (E=5 4 MeV)	92	116

(For a detector active area of 19.6 mm^2)

TABEL No.2.

Free air irradiations	MODERATOR TYPE DOSEMETER No Moderator	with Moderator	CLASSICAL TYPE DOSEMETER
SENSTIVITY (counts/ mSv) for a detector active area of 19.6mm^2			
CANEL +	337.3	397.3	48.4
CANEL + WITH H2O	773.9	720.1	18.4
SIGMA	1353	2766	170 4

On Phantom Irradiations	MODERATOR TYPE DOSEMETER No Moderator	with Moderator	CLASSICAL TYPE DOSEMETER
SENSTIVITY (counts/ mSv) for a detector active area of 19.6mm^2			
CANEL+	631.5	763.5	data not available
CANEL+ WITH H2O	1489.4	2785.5	data not available

TABEL No.4.

Neutron Source	SENSITIVITY (imp./mSv) No Moderator	With Moderator
Am-Be	935,4	967.7
252Cf	879.3	930.5
Cyclotron (E=5.4 MeV)	917.5	956 6
Thermal	1280	1981.5

(For a detector active area of 150 mm^2)

The corresponding sensitivities are shown in table n°4.

Discussion and conclusions

The proposed detection assembly using PIN diodes has an improved energy response, much closer to the ICRP60 recommendations than the previous design.

A drawback when using PIN silicon diodes for this application is the fast neutron interactions with the silicon atoms inside the diode.

This "background" signal is about 460 pulses/mSv for fast neutrons at 5.4 MeV and consists of high amplitude pulses which cannot be discriminated by amplitude treshold (Fig.7)

General Conclusions

The results from the irradiations tests in realistic neutron fields, prove that this "moderator type neutron dosemeter" has a sensitivity from 10 to 40 times higher for this neutron energy range than the "classical" individual neutron dosemeter (provided only with a 35 µm polyethylene radiator implanted with B10, and no moderator), for the same active area of the silicon detector.

The moderator type neutron dosemeter described shows an over response for the "realistic neutron fields", compared to its response to fast neutrons ; and also an over response (up to double) for "on phantom" measurements.

An improved version of this dosemeter (using PIN silicon detectors having 150 mm^2 active area and a different radiator and moderator) has been tested, proving an energy response closer to the ICRP60 requirements than the previous one.

As the duration of this contract has been short, delivery delays did not allow us to complete the moderator study using the PIN diodes.

Although extremely important for the design of the moderator, it was not possible to perform the Monte Carlo calculations using the MCNP code , as the MCNP code has not been provided to us, in spite of all our efforts to obtain it.

In the frame of this collaboration we had the opportunity to perform irradiation tests at the CEA/CEN Cadarache - France

REFERENCES

1- Barthe J., Lahaye T., Moiseev T and Portal G.
"Personal neutron dosemeter" Radiat. Prot. Dosim. 47 (1-4), 397-399, 1993
2- Buxerolle M., Massoutie M., Kurdjian J.
"Catalogue de spectres de neutrons" DPT/SIDR/GDN C.E.N. Cadarache, Mars 1986
3- Knoll, Glenn F., "Radiation Protection and Measurement"
4- Moiseev T.
"The final fellowship report" - Private communication to I.A.E.A. - Wien.
5- Langner I., Schmidt J., Woll D.
"Tables of evaluated neutron cross sections for fast reactor materials" - Kernforschungsztrum - Karlsruhe.

Fig. No.4.: IRRADIATIONS ON CANEL+

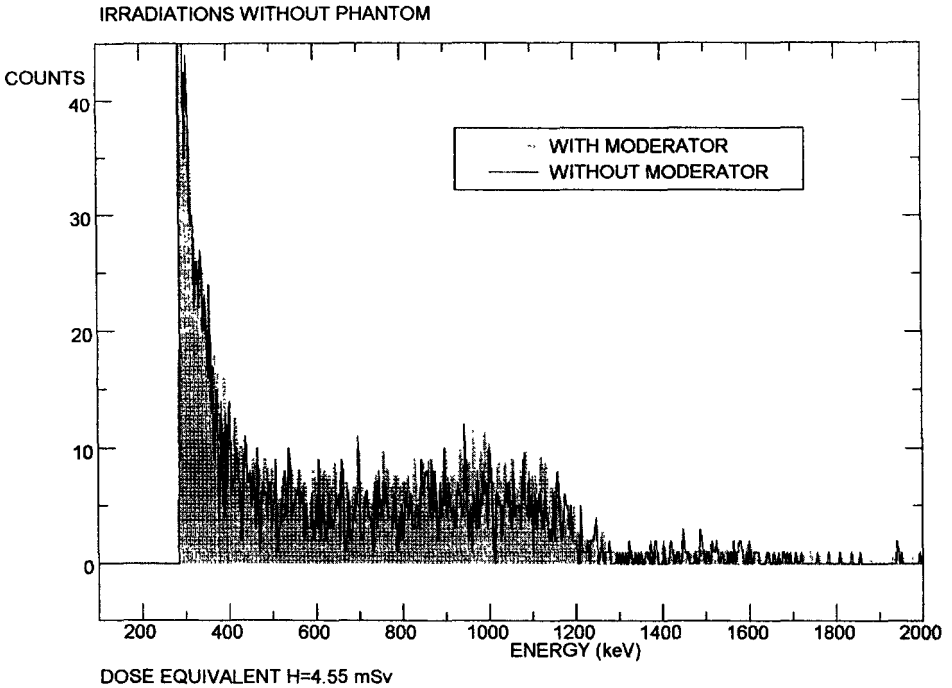

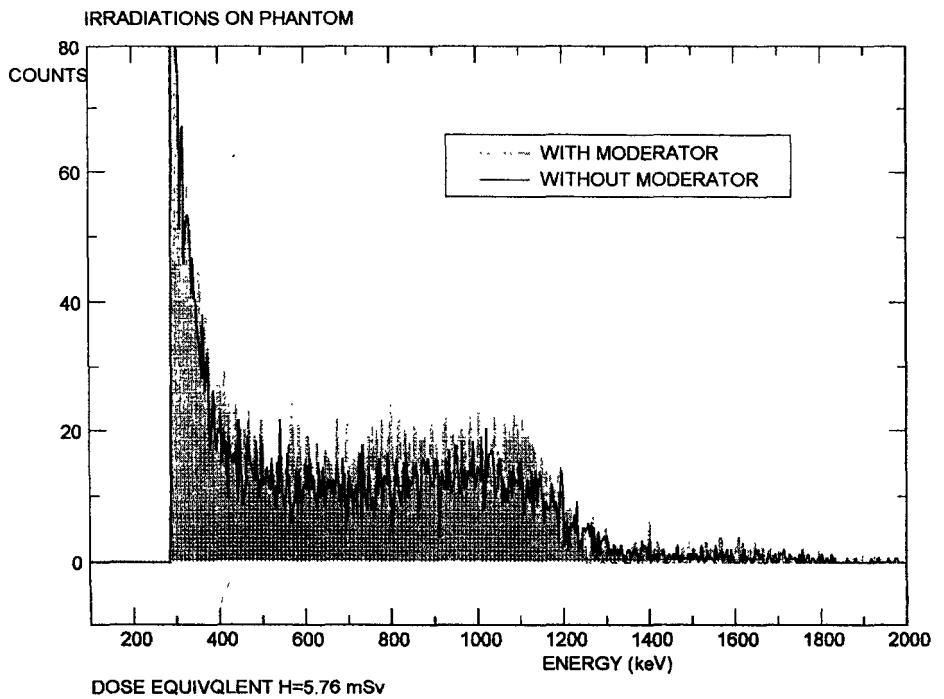

Fig. No.5.: IRRADIATIONS ON CANEL+ WITH WATER

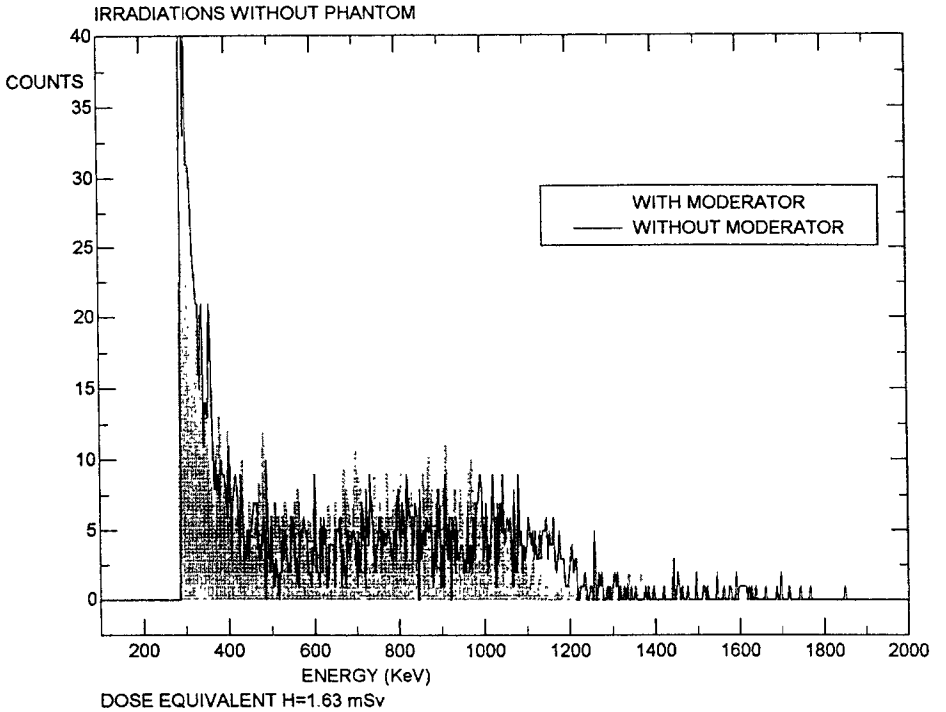

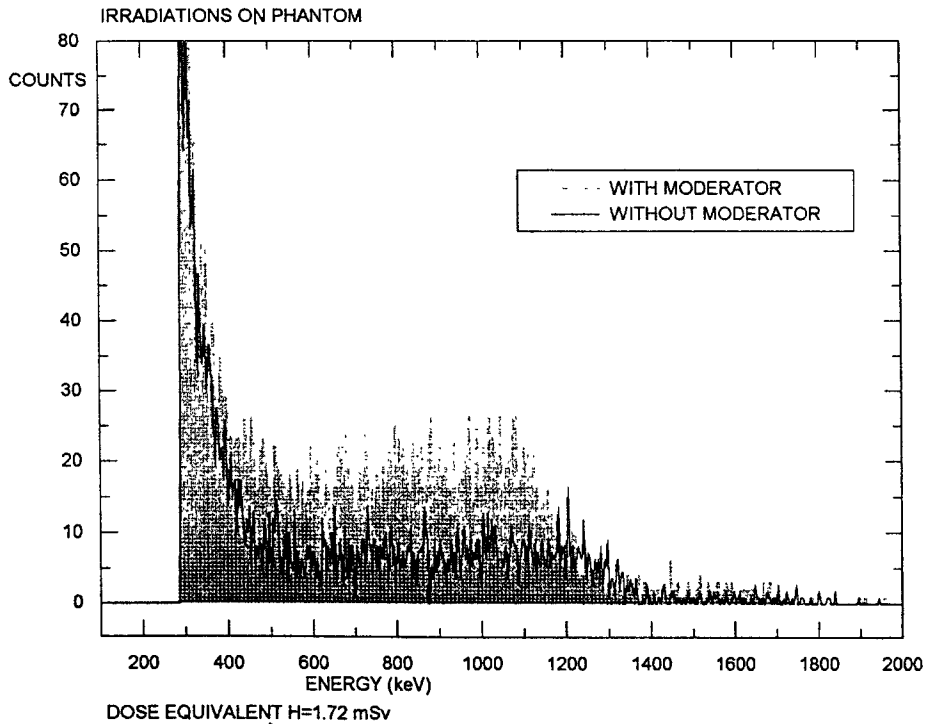

Fig. No.6.

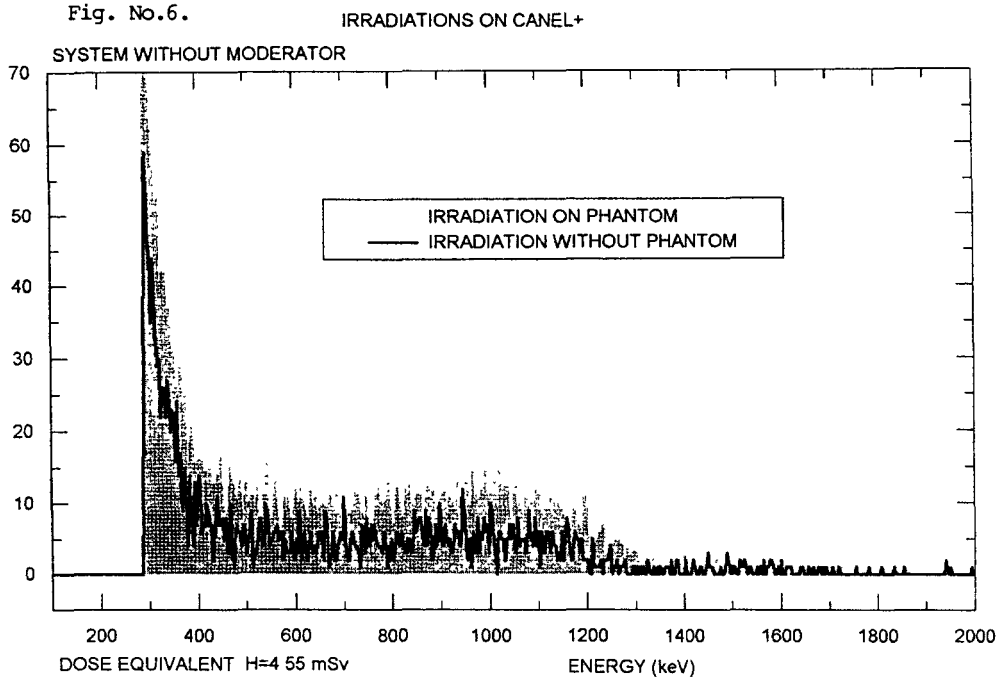
IRRADIATIONS ON CANEL+
SYSTEM WITHOUT MODERATOR
IRRADIATION ON PHANTOM
IRRADIATION WITHOUT PHANTOM
70
60
50
40
30
20
10
0
200
400
600
800
1000
1200
1400
1600
1800
2000
DOSE EQUIVALENT H=4 55 mSv
ENERGY (keV)

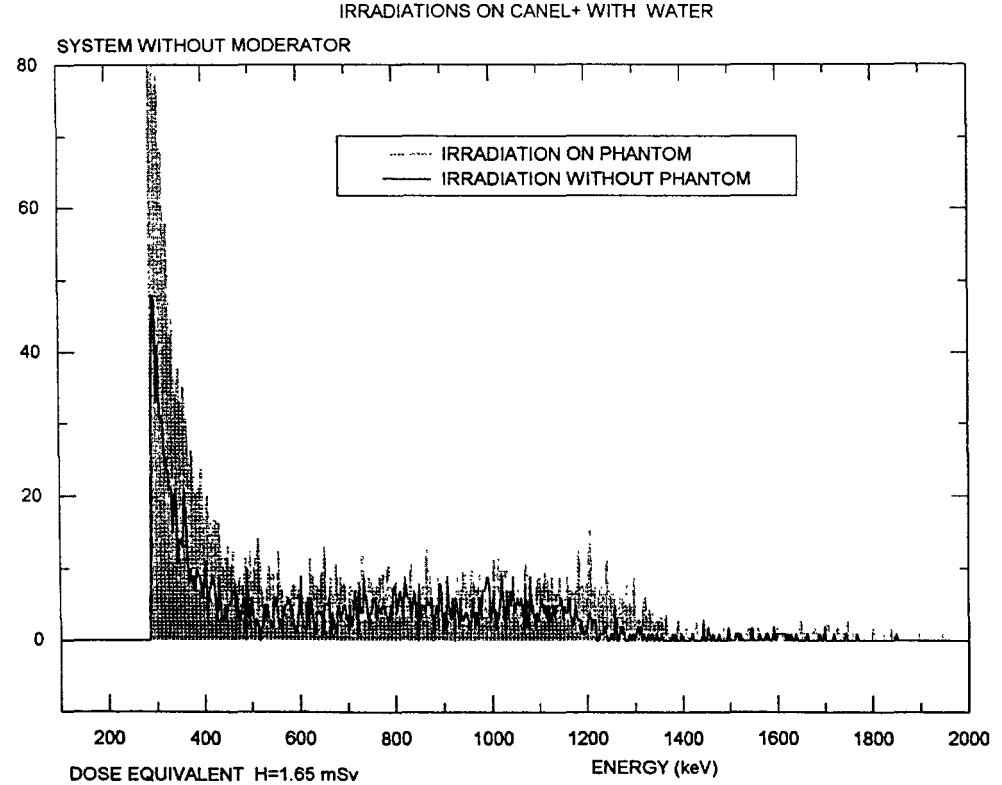
IRRADIATIONS ON CANEL+ WITH WATER
SYSTEM WITHOUT MODERATOR
IRRADIATION ON PHANTOM
IRRADIATION WITHOUT PHANTOM
80
60
40
20
0
200
400
600
800
1000
1200
1400
1600
1800
2000
DOSE EQUIVALENT H=1.65 mSv
ENERGY (keV)

Fig. No.7.: IRRADIATIONS ON CYCLOTRON BEAM (E=5.4 MeV)

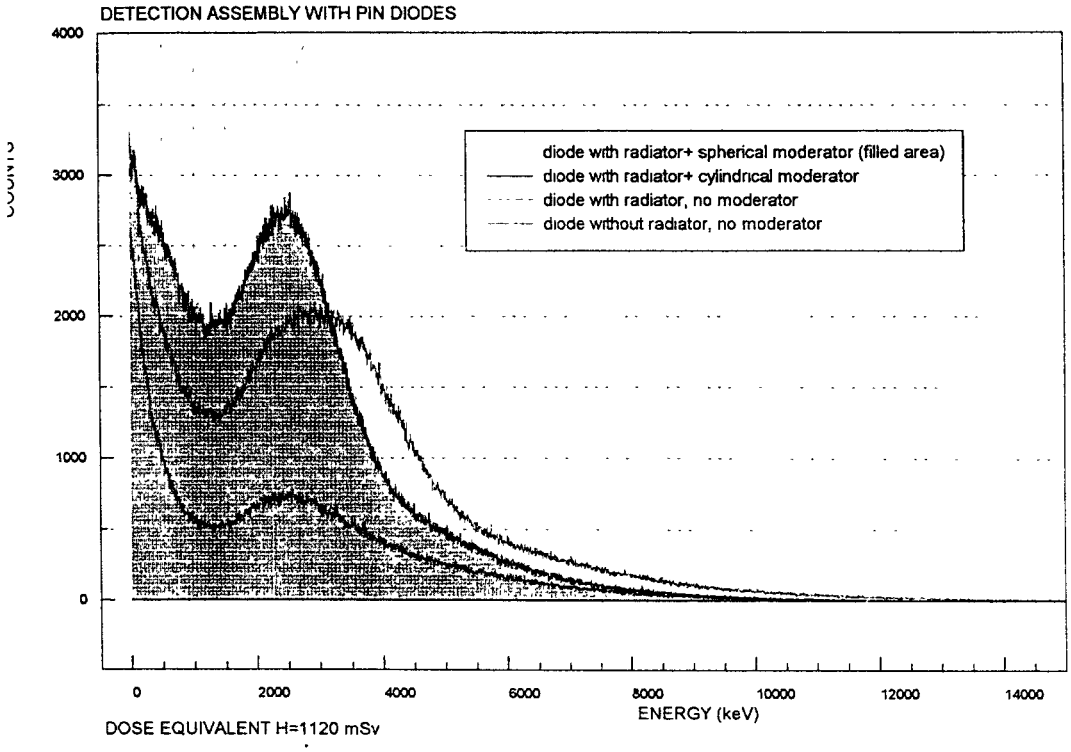

Fig. No.8.: IRRADIATIONS WITH 60Co SOURCE

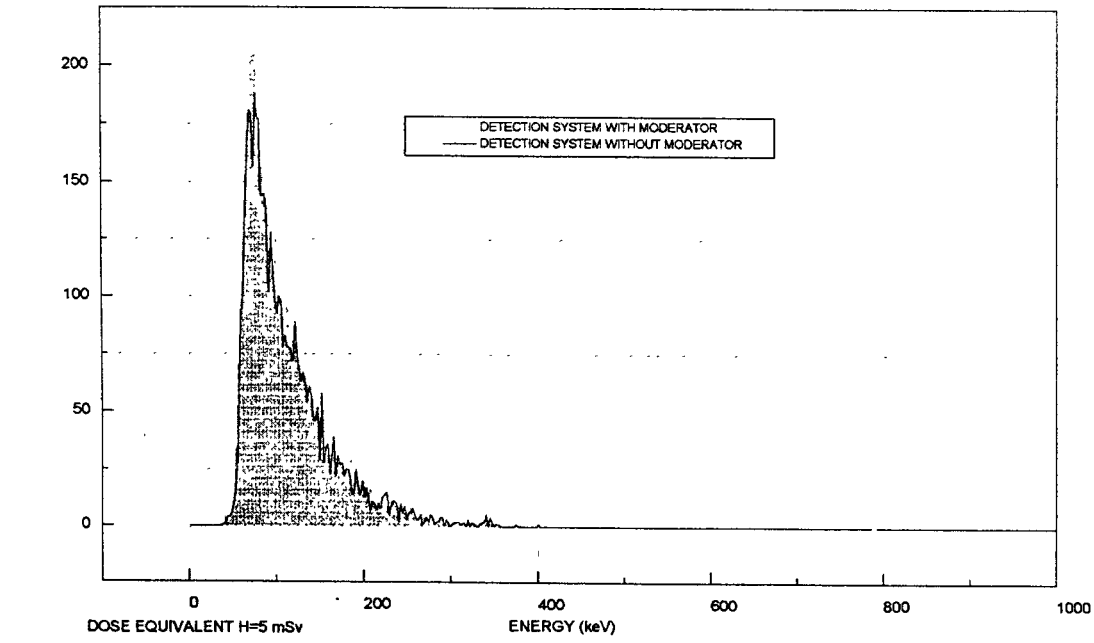

Final Report
1992 - 1994

Contract: FI3P-CT920048 Duration: 1.9.92 to 30.6.95 Sector: A14

Title: Assessment of internal dose from plutonium and other radionuclides using stable isotope tracer techniques in man.

1)	Roth	GSF Frankfurt
2)	Molho (Cantone)	Università degli Studi di Milano
3)	Taylor	University of Wales, Cardiff
4)	McAughey	AEA Technology Harwell Laboratory

I. Summary of Project Global Objectives and Achievements

A) Global objectives of the project

This coordinated project continues the work carried out under contract BI7-0029 "Assessment of internal dose from radionuclides using stable isotope tracer techniques in man", CEC Radiation Protection Research Programme 1990 - 1992.

The global objective of this project was to provide human biokinetic data for some radionuclides of relevance in radiation protection by use of stable isotopes as tracers in metabolic investigations. The transfer of radionuclides into the human body via the food chain was investigated by experimental studies in man, with particular attention to the reliability and variability of transfer parameters under realistic conditions. Additional investigations on the internal distribution and excretion patterns should improve the metabolic and dosimetric models and consequently the dose assessments of internal exposure.

The metabolic behaviour of some radionuclides can be studied by substituting the radioactive isotopes by stable isotopes of the same element as tracers. For plutonium and other highly toxic radioelements, where no stable isotopes exist, it should be evaluated if stable analogues can be used in metabolic studies.

The goals of this project require the close collaboration of several laboratories to contribute with their special expertise and experience in the different aspects involved. The work of each of the laboratories depends largely on the results obtained by the other ones. The cooperation among the participating laboratories was succesfully established during the previous contract. Several analytical techniques for the measurement of the stable isotopes in tissue and excretion samples have already been developed and optimised for a number of elements. Based on these results, these experiences guided the development of analytical techniques for the measurement of hafnium, barium, neodymium, zirconium and other elements in samples of biological materials. Exchange of samples among the laboratories for measurements helps in defining the most suitable methods.

B) Summary of achievements

B1 Validation of potential surrogates for actinides

In this part of the work (*Project 3*), the validity of using stable isotopes of the low-toxicity elements Eu, Gd and Hf as surrogates for the highly radiotoxic actinides Am, Cm and Pu, respectively, for studies of their biokinetics in human subjects of all ages was established. The technique of computer simulation of chemical speciation was used to investigate the chemical interactions of Hf, Eu and Gd with the biologically important ligands acetate, lactate, tartrate, citrate and oxalate, and to compare them with those of Pu, Am and Cm. The speciation data, together with published information on the biochemical and physiological behaviour of these elements in animals were compared in order to assess the validity of using Hf, Eu, and Gd as surrogates for Pu, Am and Cm, respectively.

The speciation studies suggest that Eu can be used as an analogue for Am, although Gd could be a better choice. However, the differences between Gd^{3+} and Cm^{3+} indicate that the former is not a very suitable analogue for Cm.

The original assumption that Hf could act as a surrogate for Pu was based on the similarity of their ionic charge and radius, rather than on true chemical similarities. Early biochemical studies showed that both Pu and Hf in plasma were bound to transferrin and that the patterns of subcellular distribution and protein binding in liver were also similar, however *in vivo* studies in rats and hamsters revealed that there were quantitative differences between the two metals. Consideration of all the information now available indicates that Hf could, with caution, be used as a surrogate for Pu for studies of the absorption from the gastrointestinal tract. However, the observed differences in the tissue distributions of the two elements in animals, and in their *in vitro* speciation profiles, show that Hf does not mimic the behaviour of Pu *in vivo* sufficiently accurately for it to be regarded as a reliable general surrogate for Pu in human studies.

The hypothesis that certain lanthanide elements could be used as surrogates for corresponding members of the actinide series is based on the well-known general chemical similarities between the two families of elements. The results obtained show that while there are some, relatively small differences in the magnitude of the uptake of the two actinides and the two lanthanides in liver and skeleton, the retention pattern is generally similar. This reinforces the conclusions drawn from the speciation studies that Eu and Gd could be used as reasonable surrogates for Am and Cm for biokinetic studies in humans. However, the speciation studies do indicate that there are some variations between Gd and Cm which, although these do not appear to influence their general pattern of biological distribution and clearance *in vivo*, might possibly be reflected in non-trivial differences in the detailed molecular interactions of Gd and Am with the components of cells and tissues. It appears most likely that the four elements do exhibit essentially similar behaviour in the gastrointestinal tract and in their transfer from there to blood. Thus Eu or Gd can be considered, to a first approximation, to mimic the behaviour of Am and Cm sufficiently well for stable isotopes of these elements to be used as surrogates in human studies.

B 2 Experimental studies

Molybdenum

The intestinal absorption of molybdenum in man and its variabilities were evaluated. (*Project 1, Project 2*). Gut uptake from aqeous solutions was determined for different oral loads in six healthy volunteers. The results show that for small oral doses intestinal absorption is almost complete, with f_1-values between 0.9 and 1.0. For an oral dose of 5 mg the uptake decreases to 0.73. Additional studies were carried out with labelled foodstuffs which resemble more the reality in emergency situations. Cress, intrinsically as well as extrinsically labelled with different stable Mo isotopes were administered to 3 volunteers. There was a significantly higher uptake of Mo from the extrinsic label than from the intrinsically bound Mo. A further reduction in gut uptake was observed when Mo was administered together with a commercially available mashed meal, possibly due to inhibitory ligands in the meal. This is of significance in both occupational and environmental radiological protection in that maintaining food intake can be a useful way of reducing systemic uptake of radionuclides from ingestion.

Two stable Mo isotopes were administered simultaneously (orally and intravenously) to a healthy volunteer to evaluate internal Mo distribution (*Project 2*). Blood half time was 1 hour, which is considerably shorter than the adopted ICRP value of 6 hours. Also the urinary Mo excretion shows a pattern which differs considerably from the ICRP model.

Zirconium

Proton nuclear activation analysis (PNA) appears to be a suitable analytical method for determination of stable zirconium isotopes ^{90}Zr and ^{96}Zr. As a feasibilty test for zirconium biokinetic studies in humans, animal experiments were carried out in 3 rabbits to evaluate Zr plasma clearance and intestinal absorption (*Project 2, Project 1*). The plasma clearance can be described by a two-exponential function with half times of 30 min and 365 min respectively. The fractional intestinal absorption was found to be less than 1×10^{-3}.

Strontium and Calcium uptake in neonates

Continuing previous investigations on Sr uptake in man, stable ^{43}Ca (500 µg) and stable ^{84}Sr (50µg) were administered to a neonate (*Project 4*). Neonates form a critical group in the assessment of ^{90}Sr dosimetry, as they have a high rate of Ca uptake and Sr is incorporated with Ca into bone. Results from this investigation indicate that Ca absorption (f_1 = 0 98) and Sr absorption (f_1 = 0.72) are rapid with significant fractions absorbed. Currently, data are being collected for up to another 4 male neonates (*Project 4*).

Collaborative work has been undertaken to compare calcium and strontium analyses from the neonate samples using ICP-MS, High Resolution ICP-MS (*Project 4*) and Thermal Ionization Mass Spectrometry (*Project 1*). The data show no significant differences between these 3 techniques.

Neodymium and Barium

Neodymium and barium isotopes were administered orally under differing dietary regimes to determine the influence of diet on radionuclide uptake from the gut in four male and four female healthy volunteers (*Project 4*). For Ba, as for earlier Sr data, is has been shown that fractional gut uptake for the fasted state is significantly higher than the adopted ICRP value of 0.1. Also for Nd, fractional absorption in the fasted state exceeds the adopted ICRP value of 3×10^{-4}, with consequent implications for dosimetry. Uptake values for Ba and Nd are decreased in the presence of citrate relative to fasting, but not significantly at the 95% confidence level. A preliminary study has been initiated to determine neodymium absorption following inhalation.

Whole body retention of injected Ba after 7 days shows large variability between individuals. Excretion of Nd was principally via urine with whole body retention found to be 0.94 ± 0.03 after 7 days (*Project 4*).

Bone samples have been collected from one of the subjects (*Project 4*). It will be determined whether translocation of lanthanides after ingestion is consistent with existing data and models.

Hafnium (as surrogate for Plutonium)

Results reported in *Project 3* of this contract indicate that hafnium may serve as a surrogate for Pu for studies of the absorption from the gastrointestinal tract. Analytical methods for the measurement of stable Hf isotopes in biological samples have been developed. Results of PNA measurements indicate that the sensitivity for Hf in plasma is of the order of 10 ng/ml for ^{176}Hf and ^{178}Hf (*Project 2*).

^{175}Hf and ^{237}Pu have been administered orally to rats and the distribution of both Pu and Hf between liver and bone was measured (*Project 4*). The results confirm the findings of the validation studies (*Project 3*), showing similarities and differences for Pu and Hf behaviour after systemic uptake.

A pilot volunteer study was conducted in 2 male volunteers for simultaneous injection and ingestion of enriched stable hafnium isotopes (*Project 4*). Analysis of the data is currently in progress.

C) Conclusions

The work carried out under this contract confirmes the usefulness of the stable isotope technique for measuring uptake and kinetic behaviour of elements of radiological relevance. The use of stable isotopes in tracer investigations can provide valuable human metabolic data which is not otherwise obtainable. The results of this co-ordinated project indicate that for a number of elements the currently adopted dosimetric factors must be revised, whereas others could be verified.

A close and fruitful collaboration has been established among the participating laboratories from Germany, the United Kingdom and Italy. To a large extent, it is this cooperation that enabled the progress achieved which in turn provides the basis for the development and success of these studies.

Head of project 1: Dr. Roth

II. Objectives for the reporting period

- Development of analytical techniques for the measurement of molybdenum concentrations in biological materials.
- Optimization of mass spectrometric analysis of stable molybdenum isotopes in aqueous solutions and in biological materials.
- Double tracer studies in human volunteers on molybdenum metabolism.
- Determination of f_1-values for molybdenum in humans regarding aqueous solutions and foodstuffs with internal or external contamination.
- Evaluation of renal excretion pattern following ingestion of molybdenum.
- Exchange of samples from in vivo studies for intercomparison of results with the Milan and the Harwell groups.

III. Progress achieved including publications

Analytical

The radionuclide ^{99}Mo is one of the isotopes with the highest abundance in nuclear reactors and may be released in very high quantities in a nuclear accident. Moreover, ^{99}Mo is used in large quantities in nuclear medicine departments as the mother nuclide in ^{99m}Tc generators. Although its physical half life is only 2.8 days, accidental uptake may result in significant internal radiation exposure.

The element molybdenum has been proved to be essential for human life, although Mo concentrations are reported to be low in human blood plasma. Due to severe matrix effects direct measurements of Mo concentrations in human blood plasma and urine by means of atomic absorption spectrometry proved not to be possible. Consequently, different methods for the extraction of Mo from biological samples were tested. Nearly quantitative extraction of Mo was achieved with liquid-liquid extraction of Mo from wet ashed samples applying di(2ethylhexyl)phosphoric acid (HDEHP). Up to 1 ml of blood plasma or urine were wet ashed under pressure with 0.8 ml of concentrated nitric acid. Mo is than extracted in 2 ml of a 0.03molar HDEHP solution. The organic solution can be measured directly by means of atomic absorption spectrometry, applying the standard addition technique.

The human requirements for molybdenum are met mainly by ingestion with foodstuffs of vegetable origin. Data on molybdenum concentrations in a series of vegetables as evaluated by the above described technique are given in table 1. The data obtained are in general agreement with values published in the literature.

Table 1: Mo concentrations in various vegetables

Vegetable	Mo concentration (ng/g)
Stock beet	150 ± 30
French bean	150 ± 40
Tomatoe	90 ± 35
Spinach	75 ± 20
Fennel	50 ± 15
Broad beans	45 ± 20
Basil	40 ± 10
Mushrooms	40 ± 20
Zucchini	35 ± 15
Radish	30 ± 10
Cucumber	30 ± 10

In a group of 18 healthy male volunteers (age: 45 - 62 years) a mean Mo concentration in plasma of 4 µg/l (range: 0.3 to 12 µg/l) and a mean Mo excretion in 24 hours urine of 50 µg (range: 1 - 129 µg) was found. These values are in accordance with the limited data found in literature.

For the tracerkinetic investigations on healthy volunteers, solutions of two highly enriched stable isotopes of molybdenum were prepared. The isotopes ^{95}Mo and ^{96}Mo were obtained as metallic powder. The abundances of the isotopes are given in table 2 in comparison to those of natural molybdenum. An aliquot of 150 mg of each isotope was dissolved in 5 ml of aqua-regia and heated to dryness. The residue was dissolved in 5 ml conc. hydrochloric acid and diluted to 50 ml with sterile deionized water. Molybdenum concentrations were measured in nine samples of each solution by graphite furnace atomic absorption spectrometry and found to be:

^{95}Mo-solution: 1.96 ± 0.03 g Mo · l^{-1}

^{96}Mo-solution: 1.91 ± 0.03 g Mo · l^{-1}

For the applications, the solutions were adequately diluted so that the administered amounts could be determined by weighing with sufficient accuracy, i.e. less than 3 % uncertainty. Solutions prepared for injections were diluted with sterile isotonic saline and the solutions were always injected through a sterile membrane filter (0.2 µm pores).

Table 2: Isotopic composition of the enriched stable molybdenum solutions

	92	94	95	96	97	98	100
^{95}Mo (enriched)	.0031	.0069	.9540	.0224	.0051	.0065	.0020
^{96}Mo (enriched)	.0023	.0024	.0133	.9590	.0097	.0112	.0021
natural molybdenum	.1422	.0905	.1575	.1668	.0965	.2463	.1003

Studies on healthy volunteers were carried out according to a standardized protocol (Fig. 1). After overnight fast subjects were given at the same time the oral test dose or test meal labelled with ^{96}Mo and the intravenous injection of ^{95}Mo. Urine was collected for 24 hours after the administration; aliquots of 1 ml each were taken from every 24 h pool and processed in addition to blank urine samples collected before the application of the enriched isotopes. Samples were heated to dryness within 3 to 5 hours in Teflon vessels. After addition of 800 µl of conc. HNO_3 , samples are digested for about 7 hours using a pressure digestion system. It consists of a heating block and a series of stainless steel bombs in which the Teflon vessels are inserted. Thereafter, the sample is evaporated for 12 hours and after addition of 1 ml of conc. HNO_3 to the dried residue mixed with an equal volume of 0.2 mol · l^{-1} HDEHP (di(2-ethylhexyl)phosphoric acid) dissolved in toluene. The mixture is shaken vigorously for 3 minutes. The upper, clear phase is removed and an equal volume of ammonia added. After shaking again for 3 minutes the upper, aqueous phase is discarded and after heating to dryness for 7 hours the residue is digested again after addition of 800 µl of conc. HNO_3. The solution is heated once again for 12 hours to dryness and the residue is dissolved in 4 µl of deionized water. This solution is used as sample for the mass spectrometric analysis of the isotope ratios of molybdenum isotopes.

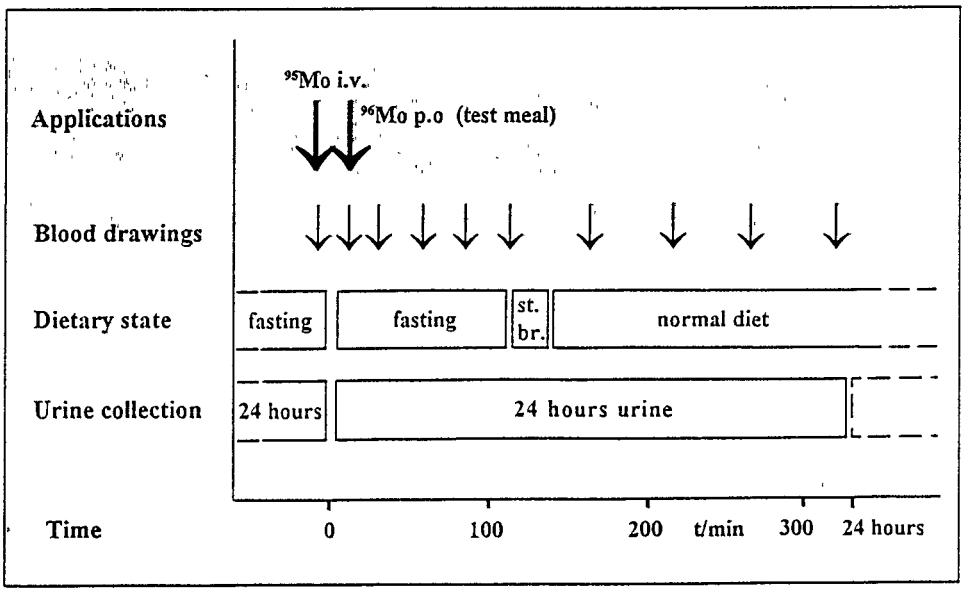

Figure 1: Scheme of study protocol for evaluation of f_1 - values in humans

Mass spectrometry is carried out applying thermal ionization, quadrupole-focusing and detection of ions by a secondary electron multiplier. At double rhenium filament technique is used for the detection of molybdenum isotopes. Since a much higher ion yield was obtained for MoO_3^- than for Mo^+ ions, the instrument was operated in the negative mode. The yield of negative ions was further enhanced by loading a calcium nitrate solution of 1 µg Ca as $Ca(NO_3)$ onto the ionization filament in order to depress the work function of rhenium. All the rhenium filaments were previously degassed at 4.8 A in a vacuum of 10^{-6} mbar or better in order to minimize possible interferences due to traces of molybdenum contained in the filament itself.

For the measurement of molybdenum 4 µl of the aqueous solution prepared from the biological samples are loaded onto the evaporation filament and heated to dryness by letting a current of 1 A flow in the filament. The evaporation and the ionization filament are then stepwise and alternately heated so that finally a steady ionization current of about 10^5 counts $\cdot$ s^{-1} for m/z=146 ($^{98}MoO_3^-$ ions) is obtained. Three blocks of 11 scans are performed in each run and the ratios are measured with reference to the ions with m/z=146. Since oxygen has its own isotopic composition, a correction of the measured ratios must be performed in order to obtain the ratios between the molybdenum isotopes expressed with reference to ^{98}Mo. This correction is carried out after each block, and the weighed mean of the three blocks is taken as a result of the measurements.

When samples of aqueous solution of natural molybdenum were loaded onto the filament, the deviations of the measured values from the expected values for the isotopes ratios 92/98, 94/98, 95/98, 96/98, 97/98, and 100/98 were all less than 0.25 %. For the samples processed from biological material, accuracy and precision were only marginally less than for aqueous solutions. An amount of 10 ng of molybdenum loaded onto the filament was sufficient to obtain a steady ion current of at least $5 \cdot 10^4$ counts $\cdot$ s^{-1} for m/z=146.

Human studies

The series of uptake studies from aqueous solutions was supplemented so that now data of a total of six investigations are available. Doses administered were 0.5 mg Mo (twice), 1.0 mg Mo (thrice) and 5 mg Mo. As already stated, amounts of up to 20 µg Mo per kg of body weight are nearly completely absorbed in the gastro-intestinal tract (Fig. 2). This finding is in accordance with recent data of Turnland et al. (Am.J.Clin.Nutr., in press).

Additional studies were carried out on labelled foodstuffs. For the assessment of f_i-values from contaminated whole meals it is necessary to use the extrinsic tag technique. For the trace element iron it has been shown by several authors that differences in intestinal absorption between intrinsically and extrinsically labelled foodstuffs are rather small. But for other trace metals like cobalt it is significant. Since for molybdenum no data are available, a group of three subjects was investigated. The volunteers were given cress grown on a solution enriched by ^{95}Mo (2 mg $\cdot$ l^{-1}) which was additionally tagged extrinsically before the administration by ^{96}Mo. Amounts administered simultaneously to the subjects were 0.5 mg ^{95}Mo and 0.3 mg ^{96}Mo. The results show a significantly higher uptake of molybdenum from the extrinsic label in all three subjects (Fig. 3) but the ratio between the two values seems to be quite constant.

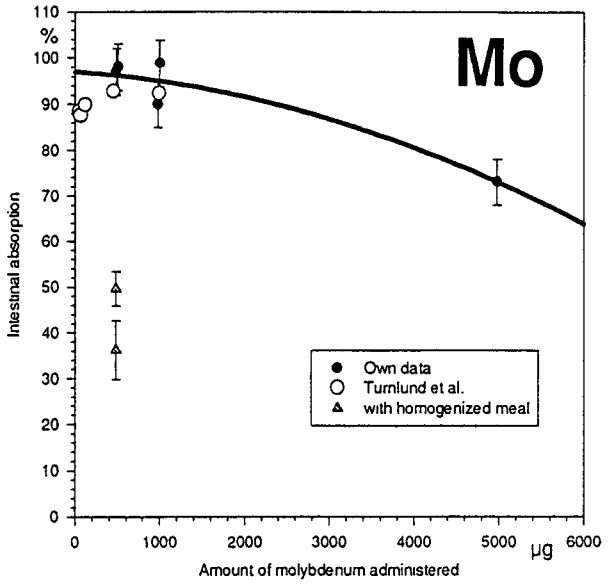

Fig.2: Relationship between intestinal Mo absorption and amount administered

In another study, two volunteers were given a commercially available mashed meal (beef, vegetables, potatoes) which was extrinsically labelled with 0.5 mg ^{96}Mo. The results of gut uptake are somewhat lower than for the extrinsically labelled cress (Fig. 2). This could possibly be due to inhibitory ligands in the mashed meal.

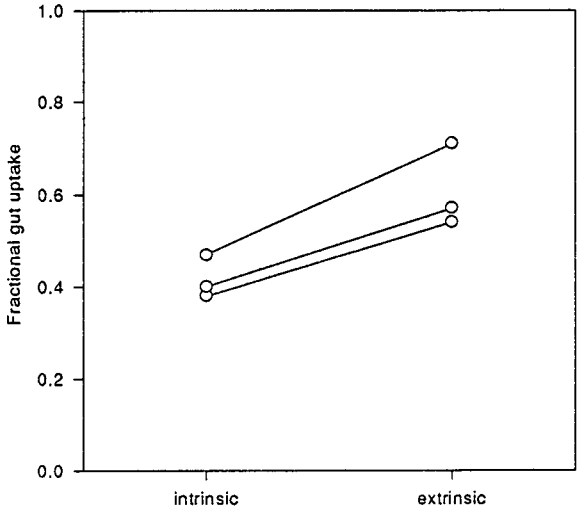

Fig 3. Intraindividual intercomparison of f_1-values obtained for molybdenum uptake from intrinsically and extrinsically labelled cress

Part of the samples from these investigations were also analyzed by proton nuclear activation analysis by the Milan group (see report of Dr. Cantone). A close agreement was obtained for the assessed f_1-values as evaluated at both places, although the applied methods differ not only with respect to the analytical technique used, but also in their method for assessing intestinal absorption from the tracer data. Therefore, a sufficient accuracy of the evaluated biokinetic data of human molybdenum metabolism can be reasonably assumed. These data obtained by investigations on healthy volunteers fit with the average f_1-value of 1 for salts of molybdic acid adopted by the ICRP (ICRP Publication 67) and may be used as basis for the assessment of measures to inhibit or reduce intestinal uptake of molybdenum isotopes.

Table 3: Fractional intestinal absorption (f_1-values) of molybdenum in human volunteers

	subject	f_1-value	
		intrinsic tag	extrinsic tag
Aqueous			
0.5 mg Mo	A	0.95	
	B	0.99	
1 mg Mo	A	0.94	
	A	0.88	
	B	0.83	
5 mg Mo	A	0.73	
Cress	A	0.47	0.71
	B	0.38	0.54
	C	0.40	0.57
Mashed meal	A		0.50
	B		0.33

Following ingestion of the labelled cress, the renal excretion of natural molybdenum and tracer molybdenum were measured for two days. It shows a rapid excretion of the ingested tracers: The excretion is maximum in the first 12 hours (Fig. 4). There was no difference between the excretion pattern of the extrinsic and intrinsic label. Of the amount excreted within 2 days, between 85 % and 90 % are excreted in the first 12 hours. Concomitant to the renal loss of the tracer molybdenum, an increased excretion of natural molybdenum is observed but with a slightly different pattern. These excretion patterns require more detailed investigations in further human experiments.

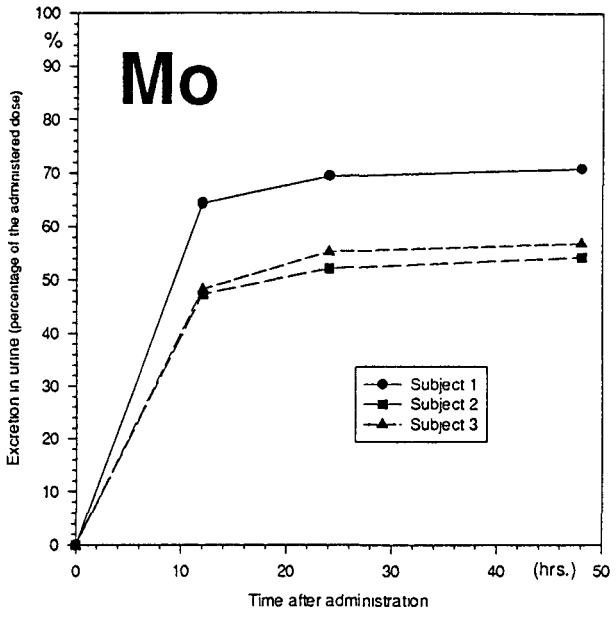

Fig.4 Urinary excretion of tracer molybdenum after oral administration of 0.3 mg ^{96}Mo

Exchange of samples

Since in many procedures only the reproducibility of the results can be checked but not the accuracy, it is of substantial significance especially in such scientific investigations to develop a measure of accuracy by evaluation of results applying independent methods. Similarly to the evaluation of f_1-values for molybdenum by the Milan group and the GSF group, samples of ashed faeces and neonate urine were supplied by the AEA Harwell group to GSF. These samples had been investigated for their content of enriched ^{43}Ca and ^{84}Sr by ICP-MS in Harwell. At GSF, they were prepared for thermal ionization MS. The enrichments in the ratios of ^{43}Ca/^{42}Ca and ^{84}Sr/^{88}Sr were in good agreement with the AEA results. Therefore it was possible to pool data on f_1-values of strontium from aqueous solutions from both laboratories (see joint publication) which show a considerably higher gut uptake especially for low strontium doses (f_1 almost 1) than the value adopted by ICRP ($f_1 = 0.3$).

Publications

Cantone, M.C., de Bartolo, D., Molho, N., Pirola, L., Gambarini, G., Hansen, Ch., Roth, P., Werner, E.: Molybdenum metabolism studied by means of stable tracers. Med. Phys. 19., 439-444 (1992)

Hansen, Ch., Kron, T., Werner, E.: Renal excretion after peroral administration of tellurium to humans. Phosphorus, Sulfur and Silicone 67, 429-434 (1992)

Hansen, Ch., Roth, P., Werner, E., Cantone, M.C., de Bartolo, D., Gambarini, G., Molho, N., Pirola, L.: Physiological and pharmacokinetic modelling of trace element metabolism. Proc. VI Mediterranean Conference on Medical and Biological Engineering (Eds. M. Bracale, F. Denoth) Area de Ricerca NCR di Pisa I, 93-96 (1992)

Cantone, M.C., de Bartolo, D., Gambarini, G., Giussani, A., Molho, N., Pirola, L., Hansen, C., Werner, E., Roth, P., Nüsslin, F.: Intestinal absorption of tellurium studied with stable isotopes. J. Radioanal. Nucl. Chem. 170, 433-442 (1993)

Cantone, M.C., de Bartolo, D., Molho, N., Pirola, L., Gambarini, G., Hansen, C., Roth, P., Werner, E.: Response to a single test of molybdenum stable isotopes for absorption studies in humans. Physiol. Meas.14, 217-225 (1993)

Kron, T., Roth, P., Hansen, C., Ewald, U., Werner, E.: A metabolism model for tellurite and tellurate. Trace Elements in Medicine 10, 71-76 (1993)

Molho, N., Cantone, M.C., de Bartolo, D., Gambarini, G., Giussani, A., Pirola, L., Hansen, C., Roth, P., Werner, E.: Use of cyclotrons for trace element analysis in biological samples and related metabolism studies. Nucl. Instr. Meth. in Physics Research B 79, 560-563 (1993)

Cantone, M.C., de Bartolo, D., Giussani, A., Molho, N., Pirola, L., Gambarini, G., Hansen, Ch., Roth, P., Werner, E.: Stable and radioactive tracers in Ru biokinetic studies. J. Radioan. Nucl. Ch. 178, 407-415 (1994)

Cantone, M.C., de Bartolo, D., Gambarini, G., Giussani, A., Ottolenghi, A., Pirola, L., Hansen, Ch., Roth, P., Werner, E.: Proton activation analysis of stable isotopes for a molybdenum metabolism study in humans, Med. Phys. (in press) (1995)

Cantone, M.C., de Bartolo, D., Giussani, A., Ottolenghi, A., Nüsslin, F., Hansen, Ch. , Roth, P., Werner, E.: Influence of the administered mass of tellurium on plasma clearance in rabbits. Appl. Radiat. Isotopes (in press) (1995)

Giussani, A., Hansen, Ch., Nüsslin, F., Werner, E.: Application of thermal ionization mass spectrometry to investigations on molybdenum absorption in humans. Int. J. Mass Spec. Ion Proc. (in press) (1995)

Werner, E., Hansen, Ch., Roth, P., McAughey, J., Haines, J.: Assessment of intestinal absorption (f_1-values) of strontium for aqueous solutions and foodstuffs. In: Health Effects of Internally Deposited Radionuclides: Emphasis on Radium and Thorium (Eds.: G.van Kaick et al.) Singapore: World Scientific Publisher, 113-116 (1995)

Roth, P., Werner, E., Hansen, Ch.: Comparative biokinetic behaviour of Sr and Ca in man. In: Health Effects of Internally Deposited Radionuclides: Emphasis on Radium and Thorium (Eds.: G.van Kaick et al.) Singapore: World Scientific Publisher, 125-128 (1995)

Head of project 2: Prof. Molho (Dr. Cantone)

II. Objectives for the reporting period

- Optimization of proton activation analysis for quantitative determination of stable isotopes of Mo and Zr in biological samples.
- Evaluation of intestinal absorption of Mo and of Zr in animals, as feasibility test.
- Determination of biokinetics parameters of interest in Mo metabolism in humans.
- Evaluation of Mo absorption in humans after oral administration of different tracer amounts and after labelled meal intake.

III. Progress achieved including publications

Molybdenum biokinetics

In previous works we developed a tracer method based on the simultaneous use of two stable isotopes of the element under study and on proton activation analysis (PNA), that has proved to be a promising tool for undertaking studies on biokinetics of essential and of non essential elements, without undue radiation exposure to the investigated subjects. During the reporting period the methodology was implemented and optimized in order to study Mo metabolism. In a pilot study Mo intestinal absorption was evaluated in two rabbits, thereafter two volunteer subjects were investigated and moreover repeated investigations on the same subjects were performed.

Optimization of PNA for measuring Mo isotopes

The optimization of proton activation analysis showed that ^{95}Mo and ^{96}Mo are the most suitable to be used as tracers.

Two enriched solutions were prepared from metallic ^{95}Mo and ^{96}Mo (A. Hempel Düsseldorf - Germany) by dissolving the enriched powders in aqua regia, heating the solutions to dryness, dissolving again the residual and finally making up to a final concentration of 2 mg/ml with deionized water. The isotopic enrichment were 95.4 % for ^{95}Mo powder and 95.9 % for ^{96}Mo powder. The impurity of ^{96}Mo in the ^{95}Mo enriched solution was 2.24 % of the total weight whereas the impurity of ^{95}Mo in the ^{96}Mo enriched solution was 1.33 %.

Proton energy corresponding to the maximum yield of the chosen reactions was determined by irradiating with a 20.5 MeV proton beam two stacks of isotopically enriched thin targets (5 mg/cm^2) obtained by means of a gelling procedure. In Fig. 1 the intensities of the 765.8 keV gamma line from ^{95}Tc decay and of the 812.5 keV gamma line from ^{96}Tc decay, measured using the same geometry and the same collecting time for each target, are plotted as a function of the corresponding proton energy. From these data an incident proton energy in order to have 11 MeV in the median plane of the

plasma sample was chosen. The possible proton induced interfering reactions ascribable to the contiguity of the chosen isotopes were considered. An evaluation of their contribution together with the effect of impurities was easily obtained by preparing, irradiating and measuring two standard samples, each one containing a known amount of one of the enriched solutions.

The minimum detectable quantity was determined for each isotope used as tracer, as that quantity corresponding to a signal equal to 4 65 $\sqrt{\mu_B}$ counts where μ_B is the background signal. In our experimental conditions (6 h irradiation time, 48 h cooling time and 10 h collection time, detector relative efficiency 70 %) detection limits were found to be 2 ng/ml of plasma for both isotopes.

To test the response linearity for both Mo isotopes considered, two series of plasma samples were analysed. The samples of the two series were added with different, accurately measured, quantities of ^{95}Mo and ^{96}Mo. Moreover as a test we applied proton activation analysis to Mo determination in the reference material bovine liver NBS 1577 and we found a value in good agreement with the values reported in literature.

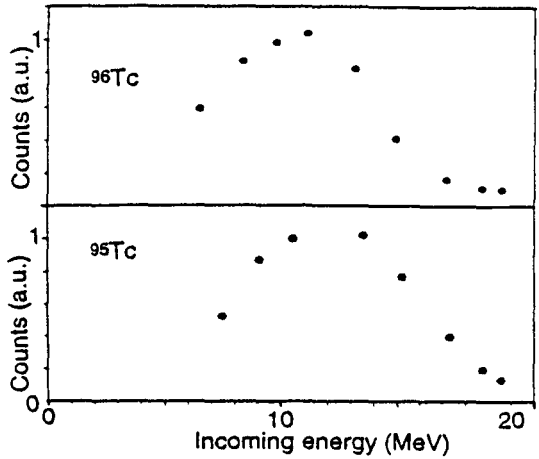

Fig. 1 ^{95}Tc and ^{96}Tc intensities (arbitrary units) as a function of incoming proton energy in targets doped with ^{95}Mo and ^{96}Mo respectively.

Animal studies

Two male rabbits (about 3.0 kg body weight) were given 2.74 and 2.90 mg of ^{96}Mo, respectively, using an intragastric tube. After 7 and 3 min, respectively, 75 and 73 μg of ^{95}Mo were administered intravenously. A known dose (400 kBq) of the radioactive isotope ^{99}Mo was intravenously administered together with the stable ^{95}Mo to one rabbit. Seven blood samples were drawn from each rabbit within 360 min after the oral test. Plasma samples were prepared and irradiated. For irradiation a properly designed multitarget chamber with a rotating disc supporting up to 30 samples was utilized. Each sample remained in front of the beam for the time resulting from the rotation speed (20 ms each turn, 1 turn per second). The concentrations of the tracers ^{95}Mo and ^{96}Mo in the plasma samples were determined by analysing the gamma spectra.

The agreement between the behaviours of radioactive and of stable tracers confirms the reliability of the analysis performed by proton activation analysis Convolution integral technique was utilized for determining fractional intestinal absorption. Values of 0.034± 0.002 and 0.033±0.002 were obtained respectively for the two rabbits as intestinal Mo absorption within 360 min from the oral administration.

Human studies

Two healthy volunteers were investigated for intestinal absorption of molybdenum: subject A, male, age 51 years, weigh 90 kg, and subject B, female, age 36 years, weight 60 kg. Plasma volumes were evaluated on the basis of the body weights and of the haematocrit, and resulted to be 3.86 L for subject A and 2.36 L for subject B. After an overnight fast, the two volunteers were injected with 442 μg and 209 μg of ^{95}Mo respectively. Thereafter they were given orally 940 μg and 484 μg of ^{96}Mo respectively. Blood samples were withdrawn into heparinized syringes at different times post injection. Plasma samples were irradiated to a total charge of approximately 4 mC per sample.

To determine the biokinetics parameters of interest, the metabolic model described by Fig. 2 and based on ICRP Pubbl. 30, was adopted. It is a four compartment catenary system, where translocation between compartments or to excretion is assumed to be governed by first order kinetics. The transfer compartment consists of the fluids where the tracers are distributed, that is mainly plasma and interstitial fluids. Its total volume actually depends on the chemical properties of the tracer. We studied this model in the case of analysis of output signals from compartment 3 following impulse test signals in compartment 1 and 3. In studies with tracers, these signals correspond to a bolus oral administration and a bolus intravenous injection, respectively. The oral administration of a tracer is generally described as equivalent to a continuous intravenous infusion at variable rate into the vascular system and the tracer's behaviour is considered as independent of the administration modality. Under these conditions the volume of transfer compartment and the parameters governing the tracer dynamics assume common values. Therefore it is possible to fit the functions describing the model to the whole set of data, for both injection and ingestion, and optimize all the model parameters simultaneously.

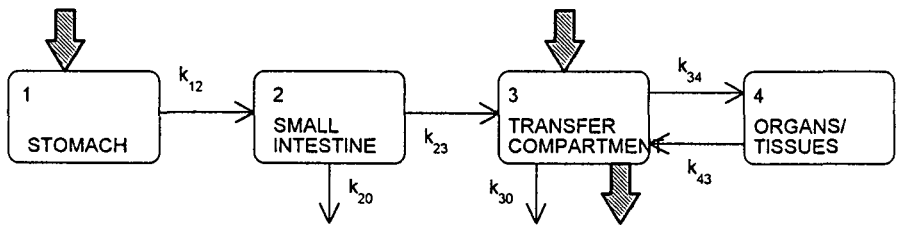

Fig. 2 Schematic representation of the adopted model. k_{ij} is the transfer rate from compartment i to compartment j (0 stands for excretion).

According to the specific aims of the study, the compartmental model shown in Fig. 2 was applied to describe molybdenum kinetics in the two volunteer subjects. The parameters k_{12}, k_{23}, k_{34}, k_{43}, k_{30} are the fractional transfer rates between the compartments; V_3 is the volume of the transfer compartment and f_1 is the fractional intestinal absorption, which with the assumed model can be expressed as $k_{23}/(k_{20}+k_{23})$. It can be shown that the model is identifiable although k_{23} and k_{12} cannot be uniquely determined. Anyway, a restriction of the k_{12} value to a physiological meaningful region enables a unique determination of all the parameters.

Fig. 3 shows the measured concentration in plasma for both isotopes as a function of time, relative to subjects A and B respectively. Error bars represent standard deviations, and take into account errors mainly due to sample preparation, counting statistic and interference and impurity phenomena.

Table 1 shows the parameters obtained from the weighed fits relative to individuals A and B respectively. The volume of transfer compartment is 2.2 ± 0.5 times the plasma volume for subject A and 1.6 ± 0.6 for subject B, consistent with the fact that the total volume of extracellular fluids is about 4 times the plasma volume, and that the effective transfer volume may depend on the chemical form of the tracer

Repeated Mo investigations in humans

In the course of about three years repeated investigations were performed on the two volunteers considered in the previous paragraph, following the plan reported in Table 2.
In the first three experiments absorption studies with different amounts of tracers were performed. With the aim to evaluate the modification in Mo absorption caused by a meal, the last two experiments for each subject, consisted in a single oral administration of ^{96}Mo from enriched aqueous solution and of a single oral administration of ^{96}Mo mixed with an infant formula. Administrations were always performed after an overnight fast.

For ingestion of amounts up to 1 mg Mo the uptake to blood is fast, but the data corresponding to Exp. 1 (ca. 5 mg) show a completely different pattern. In order to assess a different behaviour for high levels of ingested molybdenum and/or high Mo concentrations in blood plasma more experiments are recommended.

The plasma concentrations of the injected tracer show a good reproducibility. The cumulative data of Exp. 2 and 4 have been fitted with a two exponential function, corresponding to 60% of the injected tracer cleared from blood plasma with half-time $T_{1/2}$=10 min. and the remaining 40% with half-time of approx. 3 hours. The data of Exp. 1 may seem to slightly deviate from such behaviour, but as already pointed out the effect of high Mo concentration in plasma should be better studied.
The average pattern of the injected tracer was used to assess intestinal absorption in Exp. 3 and 5.

The results are summarised in Table 2. The absorption from aqueous solution for administrations up to 10 μg Mo/kg body weight is very high. The absorption of Mo mixed with semisolid food occurs later than with aqueous solutions, and is also significantly reduced.

Similar results are obtained for subject B.

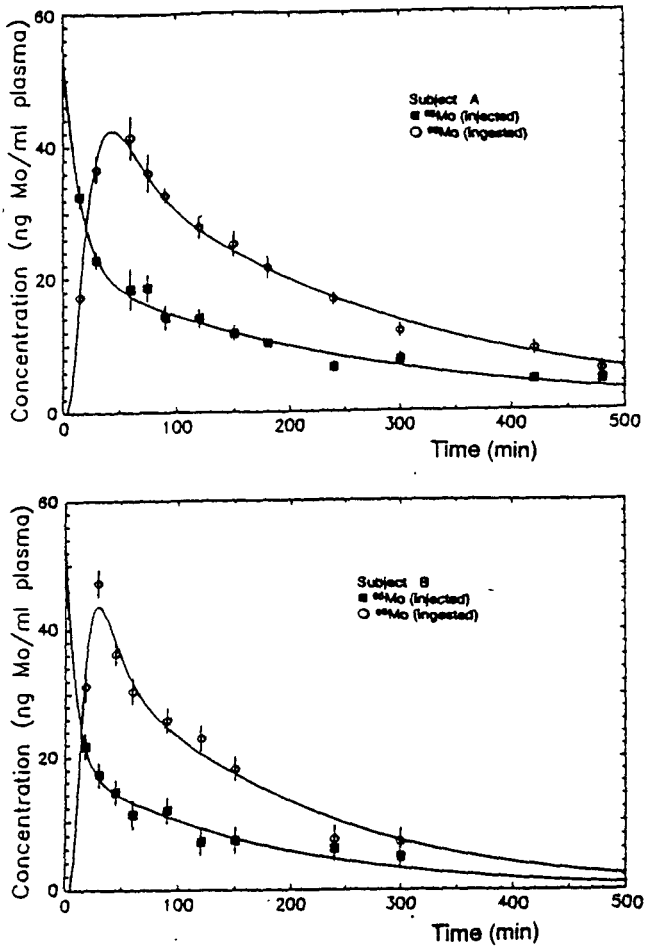

Fig. 3 Concentration of injected and ingested tracers versus time, for subjects A and B. Full lines correspond to the best fit curves obtained with employment of the proposed model.

Table I
Best fitted model parameters
(errors correspond to a chi-square change of unity)

subject	f_1 absorbed fraction	V_3 (l)	k_{23} (min^{-1})	k_{34} (min^{-1})	k_{30} (min^{-1})	k_{43} (min^{-1})	χ^2	probability
A	.84 ± .03	8.0 ± 2.4	.048 ± .012	.033 ± .020	.009 ± .003	.027 ± .006	17.2	.51
B	.86 ± .07	3.8 ± 1.5	.109 ± .049	.058 ± .033	.016 ± .006	.039 ± .008	12.0	.44

Table 2 Amounts of stable isotopes used in the experiments and obtained intestinal Mo absorption.

Exp.	Subject	Ingested ^{96}Mo (μg)	Injected ^{95}Mo (μg)	Mo absorbed fraction
1	A	4776	446	n.c.
2	A	940	442	0.84 ± 0.03
3	A	990	-	0.95 ± 0.04
4	A	465	296	$0.98 \pm {}^{0.02}_{0.04}$
5	A	480*	-	0.51 ± 0.03
6	B	484	209	0.86 ± 0.03
7	B	1000	-	0.83 ± 0.06
8	B	478*	-	0.31 ± 0.03

* administered together with an infant formula

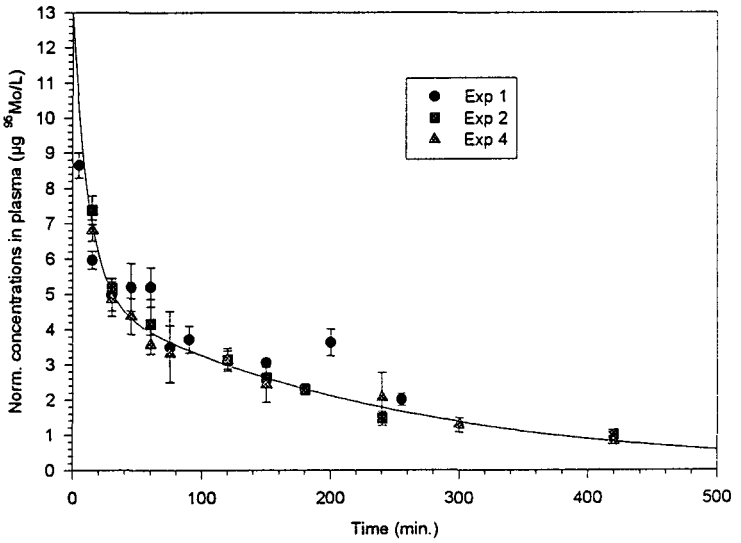

Fig. 4 Concentrations in plasma of the injected tracer vs. time for subject A. The values are normalized to an injection of 100 μg ^{95}Mo. The line is the result of the best fit to the set of data corresponding to Exp. 2 and 4.

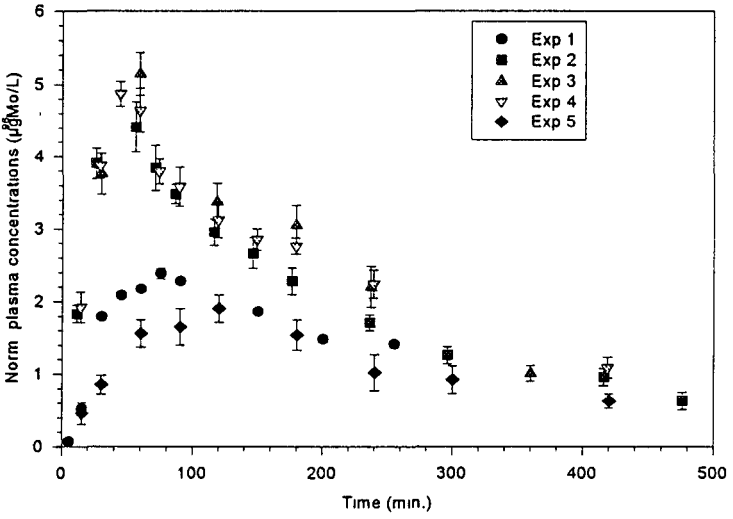

Fig. 5 Concentrations in plasma of ingested tracer vs. time for subject A. The values are normalized to an ingestion of 100 μg ^{96}Mo.

Zirconium biokinetics

On the basis of natural isotopic composition of Zr and of the possible nuclear reactions induced by protons, ^{90}Zr and ^{96}Zr resulted to be the most appropriate for simultaneous determination. Indeed (p,n) reactions produce Nb radioisotopes which have convenient half lives and decay characteristics for an off line detection.

Two enriched solutions were prepared from ^{90}Zr and ^{96}Zr oxides (Chemotrade Düsseldorf, Germany) by fusion (1:25 zirconium oxide/potassium bisulphate) followed by dissolution in sulphuric acid and dilution with bidistilled water to a final concentration of 0.75 mg/ml and 1 mg/ml respectively. The isotopic enrichments were 97.2% for ^{90}Zr solution and 91.4.% for ^{96}Zr solution. The impurity of ^{96}Zr in the ^{90}Zr solution was 0 16 % of the total weight whereas the impurity of ^{90}Zr in the ^{96}Zr enriched solution was 3.95 %.

Fig. 6 shows the intensities of 141.1 keV gamma line from ^{90}Nb decay and of 778.2 keV gamma line from ^{96}Nb decay, measured in a series of targets doped with natural Zr. From these data an incident proton energy in order to have 11.5 MeV in the median plane of the plasma sample seems a good choice when both isotopes have to be determined simultaneously.

The minimum detectable concentrations in plasma were found to be 2 ng/ml in our experimental conditions (6 h irradiation time, 6 h cooling time and 4 h collecting time, detector relative efficiency 30 %).

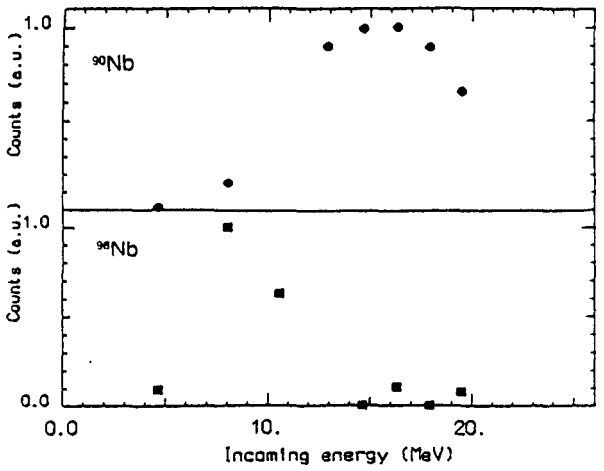

Fig. 6 ^{90}Nb and ^{96}Nb intensities (arbitrary units) as a function of incoming proton energy in targets doped with ^{90}Zr and ^{96}Zr respectively.

In literature, data on Zr biokinetics obtained with radiotracers suggest an intestinal absorption of less than 2‰. With the future aim to study Zr biokinetics by double tracer technique (^{90}Zr and ^{96}Zr) a feasibility test was carried out by single isotope administration to evaluate separately plasma disappearance time and response to single oral dose test.

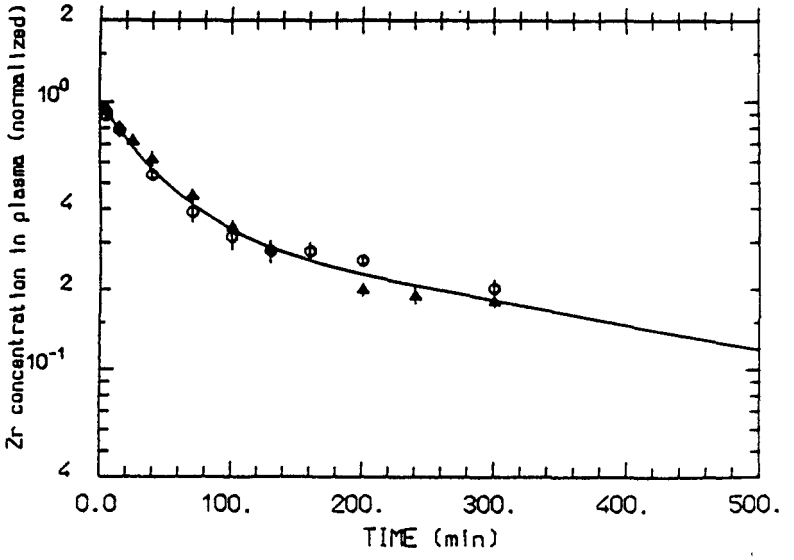

Fig. 7 Normalized concentration in plasma of the injected tracer versus time relative to the two investigated animals. The line is the result of the best fit to the two sets of data simultaneously.

Two rabbits (about 2.5 kg body weight) were intravenously injected with 50 μg of ^{90}Zr. Ten and nine blood samples respectively for the two rabbits were withdrawn within 300 min after test. Fig. 7 shows for the two rabbits the measured tracer concentration in plasma (normalized with respect to the initial concentration) as a function of post injection time. The functions describing the model of Fig. 2 when tracer is administered directly in compartment 3 were fitted to the two sets of data simultaneously, and the following values of the biokinetics parameters were obtained: $k_{30} = (5.30 \pm 0.80) \times 10^{-3}$ min^{-1}; $k_{34} = (1.13 \pm 0.13) \times 10^{-2}$ min^{-1}; $k_{43} = (0.95 \pm 0.23) \times 10^{-2}$ min^{-1}.

A two-exponential function ($A\ e^{-k_1 t} + (1-A)\ e^{-k_2 t}$) was obtained from compartmental approach, for describing the clearance process. The injection data from the three experiments were fitted simultaneously. The best fitted parameters were :
$k_1 = (1.9. \pm 0.5) \times 10^{-3}$ min^{-1}, $k_2 = (2.3 \pm 0.3) \times 10^{-2}$ min^{-1} and $A = 0.32 \pm 0.04$.

One rabbit was orally given 2.5 mg of ^{90}Zr. Due to the low intestinal absorption, as expected, tracer concentrations close to the detection limits (between two and six time the minimum detectable quantity) were found in plasma samples withdrawn at different times after oral test.
Even if the determination of intestinal absorption by double tracer technique is obviously based on the injection and ingestion data relative to the same subject, an evaluation of Zr intestinal absorption was attempted from the data obtained in this work. The two sets of data obtained after the tracer injection in two rabbits were fitted together with the data obtained after the tracer ingestion in another rabbit and a Zr intestinal absorption less than 0.001 was found.

List of publications

M.C.Cantone, N.Molho, L.Pirola, G.Gambarini, Ch.Hansen, P.Roth, E.Werner: Molybdenum metabolism studied by means of stable tracers, Medical Physics, 19, 439-444 (1992).

M.C.Cantone, D.de Bartolo, G.Gambarini, A.Giussani, N.Molho, L.Pirola, Ch.Hansen, P.Roth, E.Werner: Intestinal absorption of tellurium studied with stable tracers, J.Radioanal. Nucl. Chem., 170, 433-442 (1993).

M.C.Cantone, D.de Bartolo, N.Molho, L.Pirola, G.Gambarini, Ch.Hansen, P.Roth, E.Werner: Response to a single oral test of molybdenum stable isotopes for absorption studies in humans, Physiol. Meas., 14, 217-225 (1993).

N.Molho, M.C.Cantone, D.de Bartolo, G.Gambarini, A.Giussani, L.Pirola, Ch.Hansen, P.Roth, E.Werner: Use of cyclotron for trace element analysis in biological samples and related metabolism studies, Nucl. Instr. Meth. Phys.Res. B79, 560-563 (1993).

M.C.Cantone, D.de Bartolo, N.Molho, L.Pirola,G.Gambarini, Ch.Hansen, P.Roth, E.Werner: Use of stable Ru in assessing Ru clearance: experiments in animals, Phys. Med. 9, (Suppl.1), 76-78 (1993).

M.C.Cantone, D.de Bartolo, A.Giussani, G.Gambarini, N.Molho, L.Pirola, Ch.Hansen, P.Roth, E.Werner: Molybdenum stable isotopes for absorption studies in humans, in:'Trace Elements in Man and animals' (M.Anke, D.Meissner, C.F.Mills Eds.) - Verlag Media Touristik, Gersdorf (Germany), p.431-434, (1993).

M.C.Cantone, D.de Bartolo, G.Gambarini, A.Giussani, N.Molho, L.Pirola: Irradiation chamber for the simultaneous nuclear activation of several targets, Nucl. Instr. Meth. Phys.Res. A 337, 274-279 (1994)

M.C.Cantone, D.de Bartolo, G.Gambarini, A Giussani, N.Molho, L.Pirola, Ch.Hansen, P.Roth, E.Werner: Stable and radioactive tracers in Ru biokinetic studies, J.Radioanal Nucl. Chem., 178, 407-415 (1994).

M.C.Cantone, D.deBartolo, G.Gambarini, A.Giussani, A.Ottolenghi, L.Pirola, Ch.Hansen, P.Roth, E.Werner: Proton nuclear activation in stable tracer technique for ruthenium metabolism studies, Nucl. Instr. Meth. Phys. Res.A 353, 440-443 (1994).

M.C.Cantone, D.de Bartolo, G.Gambarini, A.Giussani, A.Ottolenghi, L.Pirola, Ch.Hansen, P.Roth, E.Werner: Proton activation analysis of stable isotopes for molybdenum metabolism study in humans, Medical Physics , in press (1995).

M.C.Cantone, D.de Bartolo, A.Giussani, A.Ottolenghi, F.Nüsslin, Ch.Hansen, P.Roth, E.Werner: Influence of the administered mass of tellurium on plasma clearance in rabbits, Applied Radiation and Isotopes, in press (1995).

Head of Project 3: Prof. Taylor

II. Objectives for the reporting period

The objective of this project was to establish the validity of using stable isotopes of the low-toxicity elements Eu, Gd and Hf as surrogates for the highly radiotoxic actinides Am, Cm and Pu, respectively, for studies of their biokinetics in human subjects of all ages.

The technique of computer simulation of chemical speciation was used to investigate the chemical interactions of Hf, Eu and Gd with the biologically important ligands acetate, lactate, tartrate, citrate and oxalate, and to compare them with those of Pu, Am and Cm.

The speciation data, together with published information on the biochemical and physiological behaviour of these elements in animals were compared in order to assess the validity of using Hf, Eu, and Gd as surrogates for Pu, Am and Cm, respectively.

III. Progress achieved and publications

The work carried out falls into three parts: computer simulation studies with Eu, Gd, Am, and Cm; the experimental measurement of formation constants for Hf- oxalate and Hf-citrate, as an essential preliminary to comparing the speciation behaviour of Hf and Pu; the validation of Hf, Eu and Gd as surrogates for Pu, Am and Cm by comparison of the results of the speciation studies with published information on the biodistribution and biochemical behaviour of these elements in experimental animals.

Computer simulation studies

Computer simulation methods were used to model the chemical speciation profiles for the interactions of Hf, Eu and Gd with the five physiological, low molecular mass ligands citrate, oxalate, tartrate and acetate in order to assess their suitability as analogues for the actinides Pu, Am and Cm.

The term chemical speciation is used to describe the state in which a metal is present in solution, i.e. its valence, whether it is present as a free aquated ion, or as a metal-ligand complex, or complexes. The relative concentrations of each species depend on the parameters applied to the system, for example the pH at equilibrium, the presence of complexing ligands and the total dissolved concentration of each component. In addition to these parameters the input data for the computer speciation programme must include information about the component metals and ligands, such as mass, charge and the thermodynamic formation constants describing all the possible interactions of the components.

The computer code used in this work was MINTEQA2. This is primarily, a geochemical equilibrium speciation model which is capable of calculating the chemical equilibrium distribution of the various species present in dilute aqueous systems, once total component concentrations and the relevant formation constants are known. MINTEQA2 includes in its own database many thermodynamic formation constants, but few were directly relevant to this work. Thus an extensive literature search was needed to expand and update the MINTEQA2 database; using the best validated formation constants which were available.

Constants measured at temperatures of 20°C or 25°C were used and all constants were corrected to zero ionic strength , $I = 0$. Wherever possible all the data for a particular chemical complex were taken from the work of the same author in order to minimise errors.

Protonation constants for the organic acids, the anions of which were to be considered as ligands, were also included in the database.

The five physiologically important ligands studied were citrate, lactate, oxalate, tartrate and acetate. The speciation behaviour of each element in the presence of each ligand was modelled For initial runs, the total concentrations for both metal and ligand were set at 0.1 M and the system was allowed to equilibrate from pH 2 to pH 10 This enabled the speciation profile to be presented graphically as a plot of species concentration against pH, which showed clearly the speciation pattern over the pH region of greatest physiological interest, namely ~ pH 5.0 to 7.4.

Actinide and lanthanide speciation

The number of different species which can be assumed to be present in any system at equilibrium is limited by the availability and the quality of the experimental data. For example, the data available for Am^{3+} and $citrate^{3-}$ included $AmOH^{2+}$, $Am(OH)_2^{+}$, $Am(OH)_3$, AmCit, $Am(Cit)_2^{3-}$, $AmHCit^{+}$ and $AmCitOH^{-}$, thus allowing the possibility of seven different species to be formed when the system equilibrates: in contrast, the published data for Eu^{3+} and Cit^{3-} were limited to $EuOH^{2+}$ and EuCit, thus the formation of only two species could be considered. This posed a problem with respect to obtaining a fair comparison of the manner in which Am and Eu behaved in the presence of citrate, since only "*like*" species should be compared. To remedy this, the initial run included all the data for Am, in order to give an accurate and informative profile of its behaviour. Then, to compare the profile with Eu, a run was carried out including only $AmOH^{2+}$ and AmCit since these were the only species for which data were available for Eu. In most cases this meant omission of the higher complexes and higher hydroxides, e.g. $M(L)_3$ and also the omission of the protonated and higher hydroxy complexes, e.g. $ML(OH)_X$ The results for these "*like with like*" speciation runs are shown in Table 1, which, for simplicity, records only the percentages of the dominant species present when the system equilibrated at pH 7.4.

Table 1. The percentage of the dominant species present at pH 7.4

Metal / Ligand	Eu(III)	Am(III)	Gd(III)	Cm(III)
Citrate–3	EuCit 100%	AmCit 100%	GdCit 100%	CmCit 100%
Lactate–1	EuLact+2 90%	AmLact+2 90%	GdLact+2, 80%	CmOH+2 83%
Oxalate–2	EuOx+ 95%	AmOx+ 45%	GdOx+ 90%	$Cm(Ox)_2$ /CmOH+ 40% $Cm(Ox)_2$ /Cm(OH)+2 50%
Tartrate–2	EuTart+ 95%	AmTart+ 95%	GdTart+ 95%	No data
Acetate–1	EuAc+2 50%	AmAc+2 40%	GdAc+2 38%	CmOH+2 92% Cm(OH)+2 100%

Comparison of the simplified Am speciation model with that for Eu showed that, for citrate at pH 7.4, all (100%) of the Am and Eu in the system was present as the monocitrate complex. This indicates very good agreement. However, when the entire speciation graph for all the Am species was considered $AmCitOH^-$ appeared as the dominant species, accounting for 95% of the total Am. This was quite different from the simple Eu model and suggested that the two metals may behave differently. However, since in the simple systems, both metals showed the same speciation, it has been assumed that the Eu profile would in fact be similar to that for Am if the formation constants for the other Eu species had been available.

For Am and Eu, comparison of the profiles for the "*like with like*" studies generally indicated very good agreement for most of the ligands studied, for example with citrate 100% complexing of both metals was achieved at about pH 4; the acetate profiles showed a similar pattern, but the Eu hydrolysed less rapidly than Am, as demonstrated by the smaller percentage of $AmAc^{2+}$ shown in Table 1. The only noticeably different profiles were seen with oxalate and this was echoed by the values listed in Table 1. In both profiles the monooxalate is dominant over most of the considered pH range, however, this species accounted for a maximum of 76% of Eu(III) as compared to only 52% with Am(III).

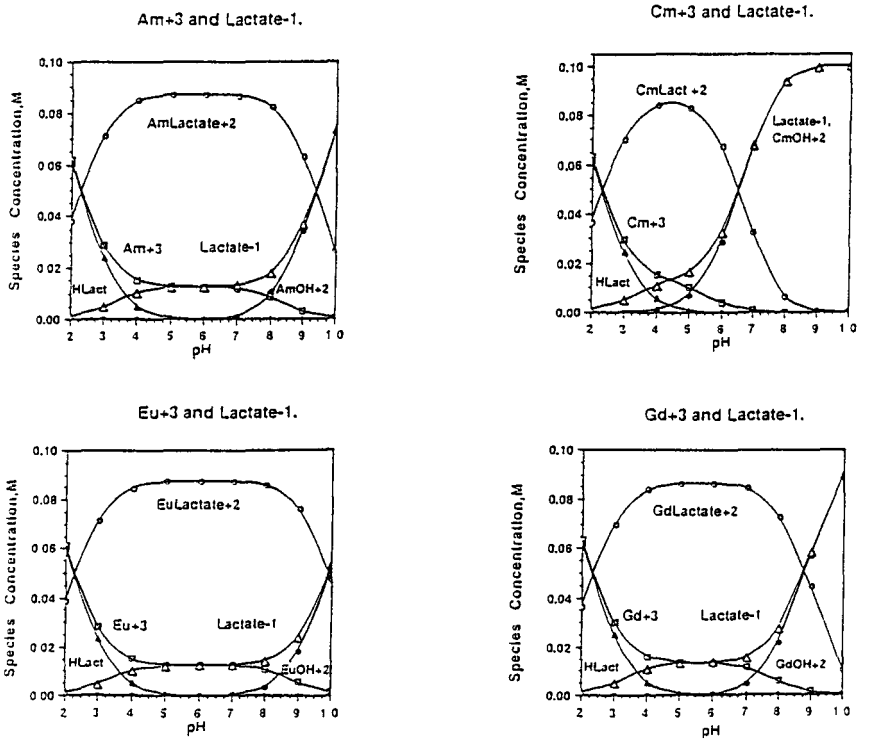

Figure 1. Speciation profiles for Am(III), Cm(III), Eu(III) and Gd(III) with lactate obtained with MINTEQA2 at equi-molar, 0.1 M, concentrations of metal and ligand.

In contrast, with Gd(III) and Cm(III) only the citrate profiles showed any real agreement, even though 95% of the Cm was complexed to citrate at pH 2, compared to only 10% of Gd. For both lactate and acetate the Cm and Gd profiles were similar up to about pH 4, but thereafter the proportions of the various species began to diverge with the $CmLact^{+2}$ species beginning to dissociate at about pH 5 while the $Gd\text{-}Lact^{+2}$ species remained stable up to pH 7 Further, in the presence of lactate or citrate, Cm begins to hydrolyse at about pH 3 - 4 so that by pH 8 $CmOH^{+2}$ has become the predominant species, in contrast Gd does not begin to hydrolyse appreciably below pH 7. The lactate profiles for all four elements are shown in Figure 1, these data show that the speciation behaviour of Cm(III) is significantly different from that of Eu(III), Gd(III) or Am(III). Further studies are needed to elucidate the reasons for these observed differences.

No data are available for Cm and tartrate, thus the Gd tartrate profile had to be compared to that of Am tartrate. The profiles were very similar and Gd appeared to mimic Am more closely than Eu; this was also observed with lactate and acetate. Since in blood plasma the ligand concentration is about 10^{-5} M, the Am, Gd and Cm citrate systems were remodelled at this total concentration. The effect of reducing the concentration was to increase hydroxide formation at lower pH values, and to increase the percentage of free cation at higher pH. The Gd system was also studied at a metal:ligand ratio of 1:5, a situation closer to that found in plasma, this increased the formation of $Gd(Cit)_2^{-3}$, which, at pH 7.4, reduced the total percentage of the dominant hydroxy-citrate species.

Conclusion — These speciation studies suggest that Eu can be used as an analogue for Am, although Gd could be a better choice. However, the differences between Gd^{3+} and Cm^{3+} indicate that the former is not a very suitable analogue for Cm.

Hafnium speciation

To investigate the chemical speciation of Hf, an extensive literature search was necessary to construct a database containing good formation constant data. This search revealed that most previous studies of Hf interactions with various ligands had been hampered by the tendency of the metal to undergo rapid hydrolysis, with the consequence that very few reliable formation constants were available. The problem of hydrolysis was confirmed by speciation studies using MINTEQA2. In order to make experimental measurements of the formation constants for Hf with at least one ligand of biological interest it was necessary to select an appropriate system that would minimise the problems of hydrolysis. Oxalate was selected for the initial study and experiments were performed in the presence of fluoride ions, on the assumption that these would act as competitive ions against the strongly binding hydroxide ligand, and, thus, suppress the hydrolysis of hafnium. In the experimental system an acidified Hf solution was titrated into an alkaline mixture of ligand and fluoride ions, using a fluoride selective electrode to measure the fluoride ion displacement; measurements were made at oxalate concentrations of 0, 5, 10 and 100 mM. The results led to the following conclusions:

- that there was significant competition between the various hydroxide and oxalate species present.
- that in all cases the hydroxide ion, rather than the oxalate, was responsible for the initial displacement of fluoride ions.
- that the fluoride complex formed in solution was of comparable stability to that of the *bis*-oxalate.

- that some of the fluoride ions released in the initial stages of the titration recombined with other Hf fluoride species to form the $[HfF_5]^{-1}$ complex which predominated in the solution.

Despite these problems it was possible, using the ESTA (Equilibrium Simulation for Titration Analysis) computer code, to optimise the calculations to yield an estimate for the $Hf(Ox)_2$ formation constant. The calculated average value was log β = 19.42 ± 0 23 (standard deviation) at I = 0.15 M, and this was comparable to the literature value of 19.4 (I = 2 M), measured using a phase distribution method. If both values are extrapolated to zero I, a difference in values is observed, but this is probably due to the use of different techniques. The $Hf(Ox)^{2+}$ complex was not considered in the optimisation because at all times oxalate was present in huge excess compared to Hf^{4+}. However, it was possible to determine formation constants for some of the mixed ligand species present in the solution. The value for the complex $HfOx_2F_2$ was 23.9 ± 2.0 and that for the species HfF_2OH_2 was 11.89 ± 0.6. These last two constants were obtained by separate, as opposed to group, optimisations and so should be regarded as estimates.

A second series of experiments was designed to investigate the Hf-oxalate interaction, this time using the classic glass and reference electrode method. This allowed Hf to be studied under more acidic conditions than were possible with the fluoride system. The stock Hf solution now contained no fluoride, so that the percentage of hydroxide was higher than before, however, the amount of free Hf^{4+} in solution was increased greatly, to around 80%. Both the metal and ligand stock solutions were prepared in dilute hydrochloric acid, using sodium chloride to bring the ionic strength to 150 $nmol.dm^{-3}$ with respect to chloride ions. The metal-ligand interaction was investigated using molar oxalate:Hf ratios of 3:1; 2:1 and 1:1 The first two titration ratios posed no problems, but an unexpected precipitate appeared on mixing the two stock solutions for the 1:1 titration. This precipitate was prevented by raising the acid concentration of the vessel solution by 0.1 M. This change in ionic strength meant that it was necessary to repeat the other ratios under the same conditions; this was achieved by working at I = 0.28 M.

Finally, an investigation of the same system was performed at I = 1.0 M, to determine whether the higher concentration would affect the accuracy of the results. The formation constants for the Hf-oxalate system yielded by each study are listed in Table 2

Table 2. Results predicted from the hafnium-oxalate studies; formation constants converted to I = 0 for comparison

Species	Study			Literature value (I = 2M)
	Fluoride I = 0.15M	Glass I = 0.28M	Glass I = 1M	
ML_2	22.28 ± 0.23	22.27 ± 0.16	21.92 ± 0.09	19.23
ML_2OH		18.16 ± 0.24	19.45 ± 0.06	
ML_2OH_2		12.89 ± 0.16	13.14 ± 0.07	
Goodness of fit	$5.1.\ 10^3$	$4.7.\ 10^2$	$2.9.\ 10^2$	

Conclusions:

- All three studies yielded very close values for the complex $Hf(OX)_2$, the average value being 22.16 at I = 0.
- The fluoride electrode study produced a good constant, but the statistics are poorer than are usually acceptable. Also, the presence of three ligands (fluoride, oxalate and

hydroxide) complicated the system, and necessitated many inconvenient data calculations before the basic refinement could be performed.

- The glass electrode method proved more suitable, since higher acidity could be used, only two ligands were present and data could be analysed without prior correction. The hydrolysis of Hf proved to be a problem only in the latter part of the titration, so that the advantages of using fluoride as a competing ligand proved to be limited.
- These studies have produced formation constants, which are in good agreement, and which provide the first reported data for ternary hafnium-oxalate-hydroxide species.
- Working at higher ionic strength appears, as shown by the improved statistics for all constants, to decrease the errors associated with the precipitate formation which is characteristic of this system.

Validation of potential surrogates

The ideal validation of the ability of one element to mimic the biological behaviour of another would require simultaneous comparison of the biokinetics and biodistribution of the two elements in the same animal or human subject, however, such information is rarely available or easily obtainable. The validity of the assumption that Hf, Eu and Gd would be suitable analogues for Pu, Am and Cm, respectively, for use in human biokinetic studies has been examined by comparing the results of the computer speciation studies discussed above and published information on the biokinetics and biodistribution of the elements in experimental animals.

Hf as a surrogate for Pu — The original assumption that Hf could act as a surrogate for Pu was based on the similarity of their ionic charge [+4] and radius [76 & 86 pm, respectively], rather than on true chemical similarities; in fact, Pu lies in Group IIIB of the Periodic Table, while Hf is a IVB element. Early biochemical studies showed that both Pu and Hf in plasma were bound to transferrin and that the patterns of subcellular distribution and protein binding in liver were also similar, however *in vivo* studies in rats and hamsters revealed that there were quantitative differences between the two metals. Some tissue distribution data for Hf and Pu in rats are compared in Table 3.

Table 3. Comparison of the tissue deposition/retention of Hf and Pu in *Sprague-Dawley* rats 1 and 14 days after i.v. injection of the citrate complexes.

	Liver	Kidney	Spleen	Testes	Lungs	Bone	Muscle	Skin	Plasma	*n*
1 d.										
Hf	5.6	1.5	0.36	1.0	0.6	16	18	19	9.6	9
Pu	3.8	0.73	0.13	0.29	0.20	46	3	*[~2]*	4.3	8
14 d.										
Hf	4.1	1.5	0.37	0.95	0.44	29	13	10	0.24	8
Pu	5.4	0.38	0.12	0.10	0.08	72	1	*[~2]*	0.19	7

These data, as well as those for later time intervals show that the rates of clearance from the liver, skeleton and plasma are broadly similar for both elements up to ~120 days However, the uptake of Hf in testes, skin and muscle is greater than that of Pu, while in the skeleton the deposition of Pu is almost three times greater than that of Hf. The mean fractional absorption of Hf from the gastrointestinal tract of rats or hamsters is shown in Table 4, together with the 90% confidence limits (CL) of the observations, these values are of a similar magnitude to those measured for Pu.

Table 4. The fractional absorption (f_1) of Hf and Pu in hamsters.

Element	No of hamsters	Administered mass [ng]	Fractional absorption [x E4]	
			Mean ± 1 SD	90% CL
Hafnium	51	100 as nitrate	7 ± 3	4 - 11
Plutonium	6	32 x 50 in 75d as nitrate.	1.3 ± 0..6	0.7 - 2.3
	6	17 as citrate	0.6 ± 0.2	0.4 - 0.9
	4	~0.5 in sediment	0.7 ± 0.4	0.4 - 1.4
	5	~20 as ferritin	0.6 ± 0.2	0.4 - 0.9
Plutonium in Humans			*3*	*1 - 8*

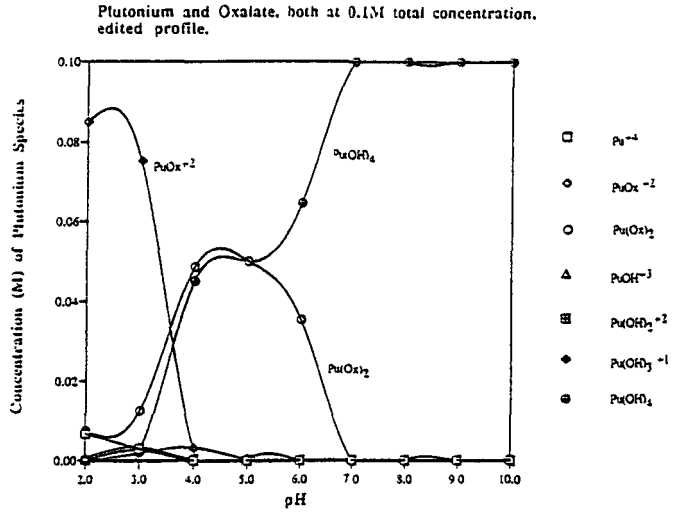

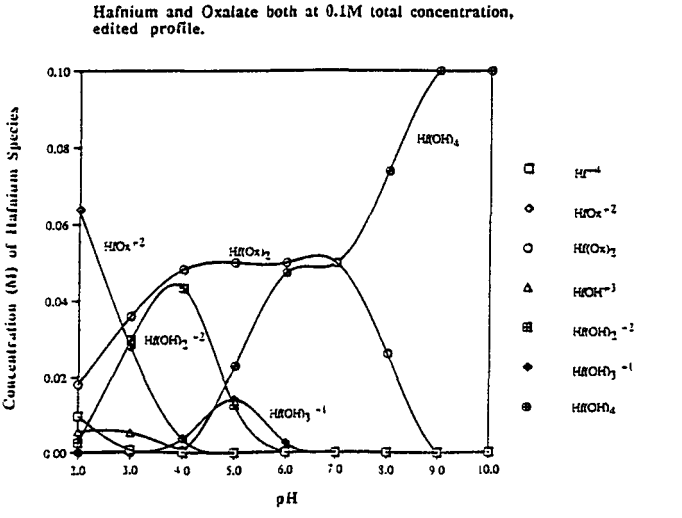

Figure 2. — Speciation profiles for Hf-citrate and Pu-citrate.

Speciation profiles were produced to compare the interactions of Hf and Pu with oxalate at low concentrations. Since only analogous species could be compared; this required the omission of the mixed ligand species. The $Pu(OH)_4$ species was dominant over the pH range 4 to 10, whereas $Hf(OH)_4$ became predominant only above pH 7. Also, around 40% of the Hf was present as an oxalate complex at physiological pH, while 100% of the Pu was present as hydroxide. Although, overall, the two elements exhibit broadly similar speciation profiles, the similarities are not sufficiently close for Hf to be described with confidence as being generally analogous to Pu. The speciation studies also indicate some differences between Hf and Pu Most noticeably, Pu undergoes hydrolysis at lower pH than Hf, resulting in a hydroxide or hydroxy-ligand species predominating in most Pu profiles at pH values above ~ 5-6. This can be seen in the edited citrate profiles for each metal, that are shown in Figure 2. The formation constants used in producing the Hf-citrate profile were measured as a part of this project, and they provide the most complete set of values available for this system.

Only the EDTA and DTPA profiles of Hf and Pu were very similar; Hf remaining complexed at all pH values, whereas Pu became hydrolysed above pH 8.

Conclusion — Consideration of all the information now available indicates that Hf could, with caution, be used as a surrogate for Pu for studies of the absorption from the gastrointestinal tract. However, the observed differences in the tissue distributions of the two elements in animals, and in their *in vitro* speciation profiles, show that Hf does not mimic the behaviour of Pu *in vivo* sufficiently accurately for it to be regarded as a reliable general surrogate for Pu in human studies.

Lanthanides as surrogates for actinides — The hypothesis that certain lanthanide elements could be used as surrogates for corresponding members of the actinide series is based on the well-known general chemical similarities between the two families of elements. The trivalent actinide and lanthanide elements all exhibit a high ionic charge/radius ratio and this leads to a marked tendency to undergo hydrolysis and complex formation, which is reflected in a very low absorption of the elements from the gastrointestinal tract, see report of Contract F13PCT920060. *In vitro* studies suggest that the interactions of the trivalent actinides and lanthanides with the blood serum protein transferrin are also broadly similar.

The biodistribution and clearance of Eu, Gd, Am and Cm in rat liver and skeleton is summarised in Table 5. The data for Eu and Gd were obtained from a study, carried out under EU Contract BT17-029-A-14, in which ^{152}Eu and ^{153} Gd were injected intravenously and simultaneously into *Sprague-Dawley* rats; the data for Am and Cm are taken from other studies, in *Marshall-August f_1 hybrid* rats, which matched, as closely as possible, the experimental conditions of the lanthanide study.

Table 5. Comparison of the retention of Eu, Gd, Am and Cm in rat liver and skeleton following intravenous injection.

Time	Liver				Skeleton			
Days	Eu	Gd	Am	Cm	Eu	Gd	Am	Cm
4	10.9	10.7	18.4	21.8	62	61	46	44
16	3.2	4.2			54	58		
21			3.4	5.3			48	42
28			3.6	2.5				
32	2.6	2.5			54	60	51	47
64	0,4	1.6	1.7	2.5	47	51	45	48

The values given are the mean % of the injected dose in the tissue [3 - 9 rats/group].

Conclusions —These data show that while there are some, relatively small differences in the magnitude of the uptake of the two actinides and the two lanthanides in liver and skeleton, the retention pattern is generally similar. This reinforces the conclusions drawn from the speciation studies that Eu and Gd could be used as reasonable surrogates for Am and Cm for biokinetic studies in humans. However, the speciation studies do indicate that there are some variations between Gd and Cm which, although these do not appear to influence their general pattern of biological distribution and clearance *in vivo*, might possibly be reflected in non-trivial differences in the detailed molecular interactions of Gd and Am with the components of cells and tissues. It appears most likely that the four elements do exhibit essentially similar behaviour in the gastrointestinal tract and in their transfer from there to blood. Thus Eu or Gd can be considered, to a first approximation, to mimic the behaviour of Am and Cm sufficiently well for stable isotopes of these elements to be used as surrogates in human studies.

Publications:

Taylor, D. M. and Gillis, T. M., Attempts to correlate biokinetic behaviour with specific physico-chemical parameters within chemical families: Alkali metals and lanthanides. *Radiation Protection Dosimetry*, **53**, 183-186, 1994.

Taylor, D. M., Transferrin Complexes with non-physiological and toxic Metals. in *Perspectives on Bioinorganic Chemistry*, JAI Press Ltd, London, pp 140-159 (1993) ISBN 1-55938-272-4.

Taylor, D. M. and Gillis, T. M., Is hafnium a valid surrogate for plutonium for biokinetic studies *in vivo*? *In preparation.*

Gillis, T. M. and Taylor, D. M., The interactions of europium, gadolinium, americium and curium with biologically important ligands: A computer speciation study. *In preparation.*

Gillis, T. M., Taylor, D. M. and Williams, D. R., Formation constants for complexes of hafnium with oxalate and citrate. *In preparation.*

Head of project 4: John McAughey

II. Objectives for the reporting period

The objectives of the study related to a series of sub-studies aiming to better define the behaviour of enriched stable isotopes in human volunteers as analogues for elements of radiological significance, to expand the database of excretion levels of these elements with respect to age and gender, including variation within the population, and to validate analytical results between participating laboratories.

Individual studies include:

1. Neodymium, barium

   The effect of speciation and fasting on fractional gut uptake of barium and neodymium in man, as analogues of radium and the actinides respectively. An assessment of their metabolism by administration of stable isotopes by ingestion or inhalation, and by intravenous injection.

2. Hafnium

   An animal study involving injection and ingestion of ^{237}Pu, and ^{175}Hf, both γ-emitting radiotracers. This was designed to yield information on the relative metabolic behaviour of hafnium and plutonium to assess the usefulness of stable isotopes of hafnium as a plutonium analogue in humans.

   Volunteer study to determine the fractional gut absorption of ingested Hf as a Pu analogue

3. Calcium and strontium

   Fractional gut absorption of stable isotopes of radiological significance in neonates to determine risk in critical groups.

   Exchange of biological samples for the optimisation of analytical methods and of samples from in vivo studies for comparison of results between GSF and AEA.

4. Age-related excretion of elements of radiological significance with respect to bone turnover to allow the design of studies to extend the use of tracers to obtain biokinetic and dosimetric data from critical sub-population groups (especially with respect to age-related dosimetry and nutritional status)

Project background (UK)

The principal objectives of this work in the UK stem from the recommendations of the report by Sir Douglas Black on "Investigation of the possible increased incidence of cancer in West Cumbria" particularly with respect to increased leukaemia and lymphoma diagnosed in young people. This was centred principally around the areas of the UK's nuclear fuel reprocessing plants. Included under the heading of health implications of radioactive discharges were recommendations that more work should be carried out on :-

a) the gut transfer factors at present used, especially for children, with special attention being paid to radionuclides, where this factor is believed to be low, and to organic forms of radionuclides.

b) the metabolic differences between adults and children with a view to improving the models used.

The lanthanide series of elements are of interest as they show similar chemical properties to the actinide series. Relative retention in bone and liver has been shown to be related to ionic radius for the actinide and lanthanide series of elements (from the data of PW Durbin, in Uranium Plutonium Transplutonic Elements, HC Hodge et al., Eds., Springer-Verlag, Berlin (1973)). Thus, the lanthanides offer potential for use as actinide analogues, to better quantify model source terms.

A number of lanthanide materials have been evaluated for use as actinide analogues in both animals and man, with this work concentrating on.the measurement of fractional absorption following oral and intravenous administration, as well as information on relative routes and rates of excretion. This has been carried out for neodymium and dysprosium, each of which has two suitable isotopes. The uptake of samarium, gadolinium and europium has previously been measured following oral administration alone. In addition, work has been carried out using strontium and barium, which are also of significance in environmental radiological protection, especially in critical population groups such as children and pregnant women.

The objective of this work period has been to extend available data on the use of lanthanide stable isotopes (in this case, neodymium) as analogues of actinide element behaviour, as well as the use of strontium and barium stable isotopes as direct measures of behaviour. Work to date has demonstrated that fractional gut absorption values of the various elements may exceed ICRP adopted values, and vary with mass administered and nutritional status. In addition, early data from neonate studies indicate that strontium absorption is very closely linked to calcium absorption.

The relevance of age-related factors to elements of interest, such as Sr, Ca, Ba, Nd, Hf, Th., U relative to elements of nutritional importance will help determine the importance of the pubertal growth spurt with respect to the dosimetry of bone-seeking radionuclides, and the appropriateness of current adopted values. The excretion of each element determined in 24 hour urine samples from groups of pre-pubertal, pubertal and post-pubertal children, relative to markers of bone turnover (e.g. pyrolidine cross links) will allow subsequent study design for real-life uptake studies in critical populations.

Progress achieved

1. Barium and Neodymium

Studies of fractional gut absorption in a group of 4 male and 4 female volunteers were completed:

a) after an overnight fast,
b) after a standard meal,
c) in the presence of citrate following an overnight fast.

These experiments have been designed to demonstrate whether fractional gut absorption is enhanced after fasting, and whether simple ligands present in the diet, such as citrate, could further enhance uptake. Results are shown in Tables 1 and 2 for Ba and Nd respectively.

Table 1 - Barium Uptake

Subject	f_1 Fasted	f_1 + Citrate	f_1 Fed	Mean F/U	Mean Retention
Male					
A	0.20	0.12	0.04	14	-
B	0.43	0.24	-	19	0.11
C	0.29	0.08	0.01	11	0.59
D	0.41	0.32	0.08	10	0.52
Female					
E	0.55	-	0.65	5	0.46
F	-	0.13	-	9	<0
G	0.36	0.17	0.03	21	0.10
H	0.10	0.33	0.13	17	0.12

For Ba, as for earlier Sr data, it has been shown that fractional gut uptake is significantly higher than the adopted ICRP value of 0.1 when subjects have fasted prior to administration. Whole body retention of injected Ba after 7 days showed large variability between individuals. For Nd, fractional gut uptake is also enhanced in individuals who have fasted prior to ingestion, relative to those who had eaten a "standard breakfast" with a number of the fasted uptake values exceeding the adopted ICRP value of 3×10^{-4}. Excretion of Nd was principally via urine with whole body retention found to be 0.94 ± 0.03 after 7 days. Uptake values for Ba and Nd are decreased in the presence of citrate relative to fasting, but not significantly at the 95% confidence level.

Table 2 - Neodymium Uptake

Subject	f_1 Fasted	f_1 + Citrate	f_1 Fed	Mean F/U	Mean Retention
Male					
A	6.3×10^{-3}	1.7×10^{-4}	$<1 \times 10^{-7}$	0.145	0.93
B	2.1×10^{-4}	5.7×10^{-4}	-	0.138	0.93
C	1.4×10^{-4}	6.5×10^{-4}	9×10^{-5}	0.216	0.92
D	3.0×10^{-3}	4.3×10^{-4}	6×10^{-5}	0.043	0.92
Female					
E	5.3×10^{-4}	-	2.3×10^{-3}	0.096	0.94
F	-	2.3×10^{-4}	-	0.083	0.93
G	3.6×10^{-3}	8.7×10^{-5}	$<1 \times 10^{-7}$	0.068	0 95
H	4.8×10^{-4}	5.1×10^{-4}	5.8×10^{-4}	0.081	0.92

AEA Technology are currently in the process of commissioning a High-Resolution ICP-MS instrument. It is hoped that this will allow analysis of neodymium and barium isotope ratios in blood samples taken during the course of these experiments to improve uncertainties associated with uptake coefficients and excretion biokinetics.

In addition, a small sample of bone has been collected from one of the male volunteers who participated in the lanthanide ingestion studies following dental surgery work. Isotope ratios will be measured to determine whether translocation to bone is consistent with existing data and models.

After completion of studies of fractional gut absorption in groups of 4 male and 4 female volunteers, a preliminary study to determine fractional absorption of neodymium following inhalation has been initiated with a a view to investigating 2 male volunteers. The intention of the experiment is to expose two male volunteers to sub-micron particles of $NdCl_3$, generated using a condensation process. $NdCl_3$ was chosen rather than Nd_2O_3 as its reported toxicity is lower and that the initial use of $NdCl_3$ would set up an upper limit of absorption for soluble lanthanide series compounds.

Ethical permission to conduct this study has been delayed for both this study and another using radioactive Tb_4O_7 due to concerns over the pulmonary toxicity of the lanthanides with a preliminary administration of Tb_4O_7 to rodents. Data from this study have now been evaluated by a series of independent experts on inhalation toxicology and confirmed that the chemical doses proposed are acceptable, allowing ethical permission to proceed to be re-sought.

2. Hafnium

^{175}Hf and ^{237}Pu (both γ-emitting isotopes) have been administered orally to rats and the distribution of both Pu and Hf between liver and bone were measured by γ-spectrometry After 7 days the fraction of ingested Pu in the liver was a factor of 3.7 greater than the fraction of ingested Hf and the fraction of ingested Pu in the femora exceeded the Hf fraction by a factor of 2.0. The ratios observed were consistent with literature data available.

A pilot volunteer study was conducted in 2 male volunteers for simultaneous injection and ingestion of enriched hafnium stable isotopeswith levels administered based on background Hf concentrations, determined in urine and faecal samples from 8 subjects from the Ba/Nd uptake study. Samples for 3 consecutive days for each subject were analysed for hafnium content and it isotope ratios were measurable in faecal and urine samples.

The dual administration of enriched hafnium isotopes was given to 2 male volunteers and excreta collections carried out for a week after administration. However, in contrast to feasibility studies, analytical recovery of Hf from faeces as monitored by a ^{175}Hf radiotracer has been variable with 50% of samples giving 80-100% recovery but the other 50% showing 0-20% recoveries. Further work is required to investigate this phenomenon before any analytical work is carried out on the urine samples collected, as these are both limited and critical for the f_1 determinations.

3. Calcium and strontium uptake in neonates

Following strontium uptake studies in adults, 500 μg enriched ^{43}Ca and 50 μg enriched ^{84}Sr were administered to a single neonate (by ingestion). Preliminary data from this study indicate that Ca absorption (f_1 = 0.98) and Sr absorption (f_1 = 0 72) is rapid with a significant fraction absorbed, and that excretion to urine, for both, follow a similar pattern, as shown in Figure 1 Excretion to urine and faeces has been measured over a period of 5 days but results suggest that urine collection for 3 days will collect the majority of the Ca and Sr excretion. These measurements effectively formed a pilot study, the results of which have been used to validate the experimental design for a larger group of neonates. Data are being collected for up to another 4 male neonates in conjunction with the Child Health Unit at St. Georges Hospital, London as clinical committments and resources allow.

Analytical

Collaborative work has been undertaken to compare calcium and strontium analyses from the neonate samples above using ICP-MS, High Resolution ICP-MS and Thermal Ionisation Mass Spectrometry (TIMS). The data show no significant differences between the 3 techniques, as shown from isotope ratio measurements in Figure 2.

The results obtained to date confirm the usefulness of the stable isotope technique for measuring uptake and early kinetic behaviour of these elements. The experiment has yielded

Figure 1

Calcium and Strontium Isotope Ratios in Human Neonate Urine Following Oral Administration of 500 µg ^{43}Ca and 50 µg ^{84}Sr

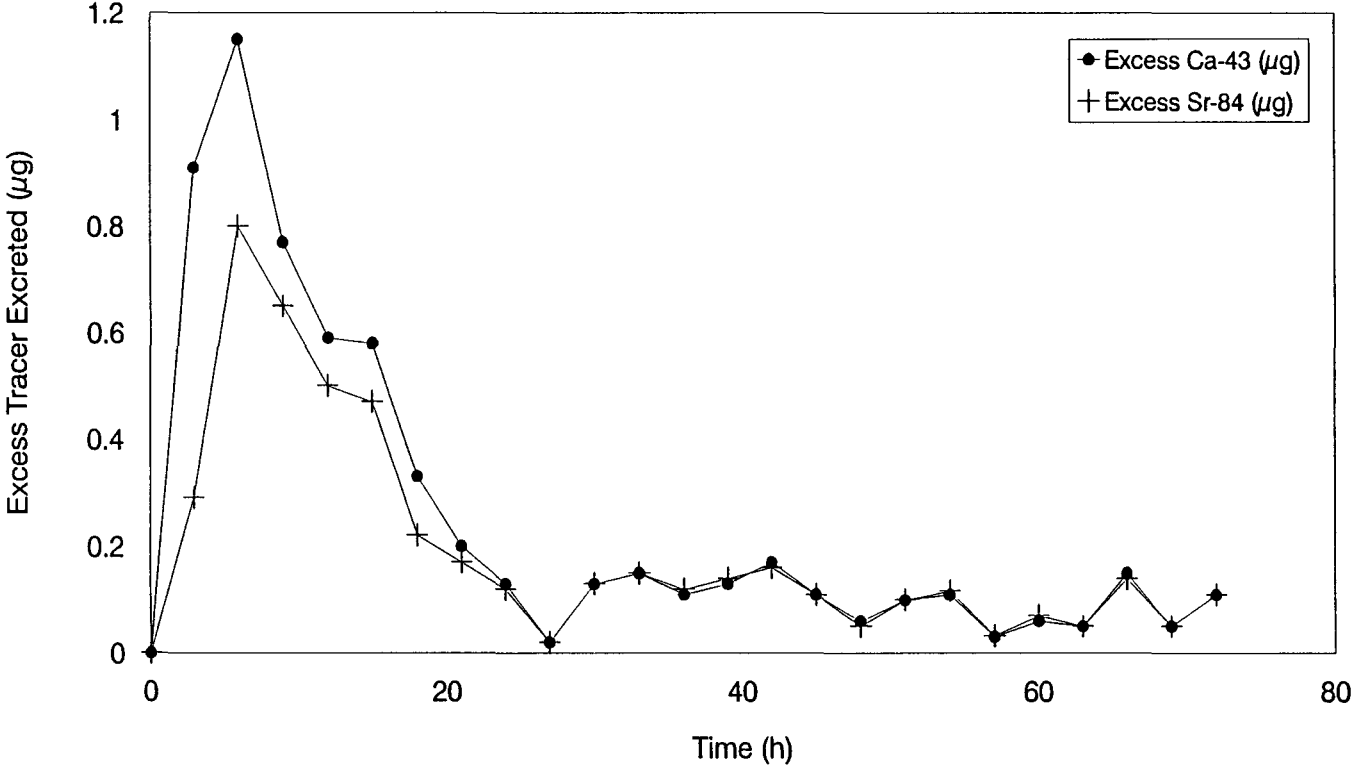

Figure 2

Analytical Intercomparison of Calcium Isotope Ratios in Neonatal Urine Following Oral Administration of 500 µg ^{43}Ca and 50 µg ^{84}Sr Intercomparison of ICP-MS, ICP-High Resolution MS and TIMS

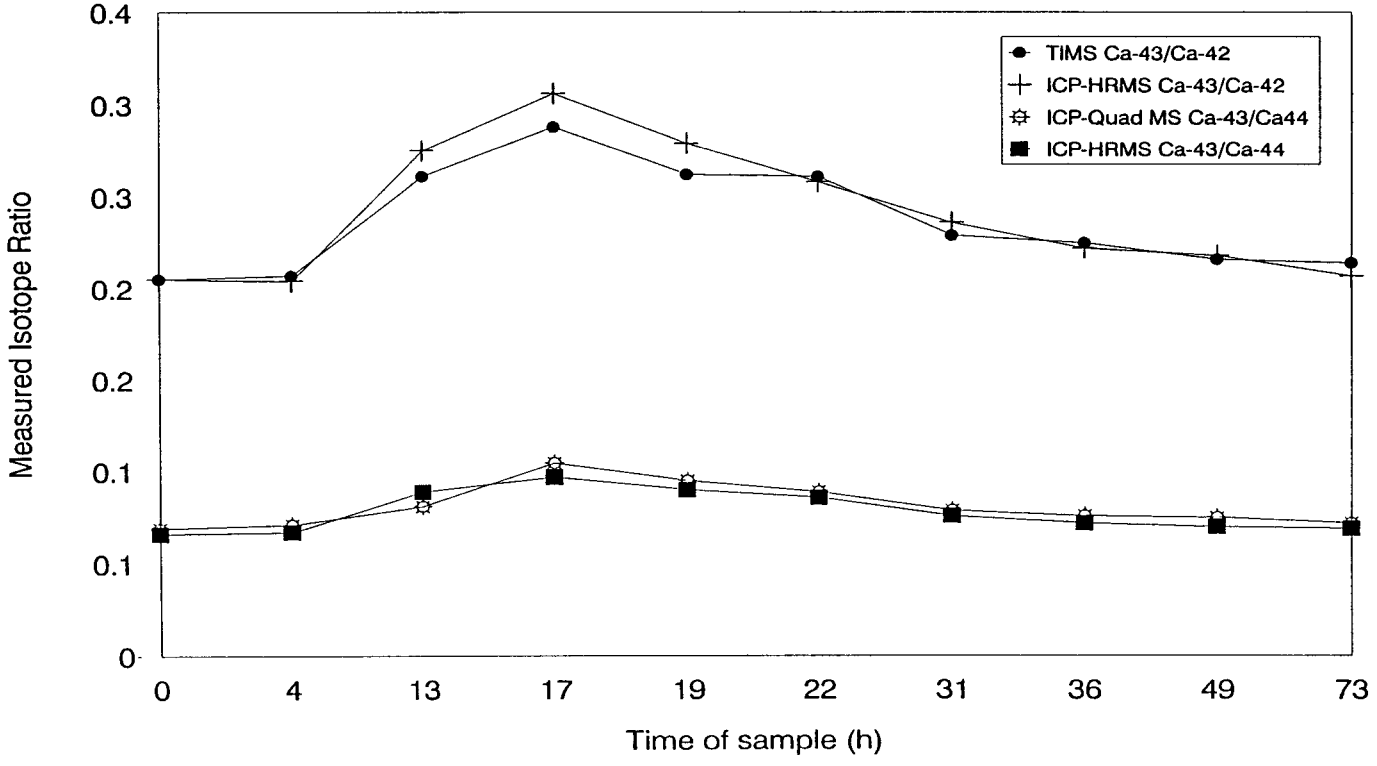

information on potential gender and age differences but principally on the effect of dietary status (fasted or fed) on fractional gut absorption, and hence dosimetry. This has confirmed observations in earlier work for elements such as lead, that enhanced uptake of metals can result from their ingestion in the fasted state. This is of significance in both occupational and environmental radiological protection and that maintaining food intake can be a useful way of reducing systemic uptake of radionuclides from ingestion.

4. Age Related Dosimetry

In extending the techniques used to determine isotope absorption to critical groups such as children, it is important to develop non-invasive, non radiometric techniques, where possible. As part of this process, further data are required on the variation of elemental excretion within and between subects and at different ages.

A total of 60 samples were planned for the study, to be obtained as duplicate samples on different occasions from 30 volunteers, comprising a cohort of young people of both sexes, spanning the age of puberty. A local school was approached to obtain their co-operation in recruiting volunteers to provide samples. The group considered most accessible was First Year 6th Form, which corresponds to a typical age of 17 years. After discussion of the best approach with science teachers, the group was addressed, the purpose of the study explained to them, and their co-operation requested in providing samples. The size of the group was approximately 150, with slightly more than 50% girls. From this initial contact, 5 volunteers came forward. Subsequently, a further 3 came forward and offered samples (2 male, 6 female).

Samples were also provided by 12 young people who were children of members of staff (4 male, 8 female). Two adults were included in the study who had taken part in previous studies involving rare earths, and for whom excretion data were already available. Parameters recorded for each volunteer were age, sex and urine volume. Each sample was assigned a serial code, and the identity of volunteers was known only to the organiser of the study. It had been intended to record the weight of each volunteer; however, advice was obtained from the Head of Year at the co-operating school that this information would only be obtained with difficulty, and that it would be undesirable to ask for it.

Overall, the success rate in obtaining samples was disappointing. Of those who actually promised samples, only about 50% actually provided them, of which the majority were female. This difficulty in obtaining samples appeared to be caused by embarrassment, particularly with peer group.

Collection of Samples

Volunteers were provided with two cleaned, 2 litre bottles which were numbered, and asked to collect total samples from rising in the morning through to the same time the next morning. Samples were transported rapidly to the laboratory as rapidly as possible, typically within 24 hours. Sub-samples were taken for creatinine and bone turnover (deep frozen) and minor element analysis (2.5 % nitric acid added), and the rest dry-ashed and processed for rare earth analysis using the previously-developed and tested column separation method

Analysis

Minor elements (Ca, Cu, Fe, Sr, Zn) were measured quantitatively against aqueous standards using ICP-AES, with an ARL/Fisons 3560 simultaneous spectrometer. The total uncertainty of these measurements is probably better than ±10% at levels significantly above the detection limit.

The same sub-samples were also analysed semi-quantiatively by ICP-AES for a wider range (45) of trace elements. At levels significantly above the detection limit, overall uncertainty of ±50% can be expected from this kind of measurement, although the sample-to-sample precision would be of the order of 10% or better. As expected, the only elements detected at levels above the detection limits of the method used were B, K, Mg, Na, P, S & Si. These samples were also analysed by ICP-MS for U and Th, using standard additions calibration. Only one value above the detection limit was recorded for these elements.

Data for the rare earths (La, Ce, Pr, Nd, Sm, Gd & Tb) were obtained for the processed urine samples by ICP-MS using standard additions calibration. Results were corrected for yield using a radiotracer. Yields were generally all greater than 60%, with most greater than 80%. Blanks were measured at the same time to assess the contamination introduced during the (extensive) sample preparation, so that the significance of data could be estimated. Data for La, Ce, Pr and were in most cases less than blank levels, and have been reported as "<". A higher proportion of Sm, Gd and Tb measurements were positively detected at levels above the blanks.

All measured "concentrations" have been converted to "24-Hour Totals" by multiplying levels measured with the total excreted volume, as measured in the laboratory on receipt of samples. Rare earth data have additionally been corrected for yield of the separation process used.

Results

Details of subjects in each age group are shown in Table 3. Values for the common elements are shown in Tables 4 and 5 for gender and age respectively. A summary of all data is given as Table 6; excretion is given in the indicated units, and has been rounded to the appropriate level of significance. The blank level quoted for rare earths corresponds to a 1.5 l sample, and a recovery of 80%. For comparison, values quoted by Iyengaar for 24 Hour Urine are also included, as are data from an EU survey for Italian volunteers published by Sabbioni et al corrected to allow for the average 24 Hour urine volume.

For most elements, there is a close agreement between literature data quoted and the range of values found in this survey. For the rare earths, values found are much lower than the sparse data available from Iyengaar, but are in reasonably good agreement with the lowest values of the range quoted by Sabbioni. True mean values found in the current study are less than the values given, as "less than" values have not been included in calculating the mean.

The rare earth levels found indicate that there may be a dietary source of these elements; most of the samples elevated above the background occur as duplicates (1, 7, 11, 14, 15, 22), with several (1&15, 7&17, 8 & 18) within the same family. If contamination is ruled out, a shared dietary source is the most likely explanation. The one Th level measurable above the background (Volunteer 20) was also associated with a high Sm (and perhaps Tb) level. These data, taken together, suggest that dietary sources (unrecognised) may exist which could be used for uptake studies, but clearly more analytical data on dietary items is required.

Table 3 - Urine samples collected by age and sex

Volunteer	Age	Sex	UVol 1 (ml)	UVol 2 (ml)
1	11	F	2114	1220
2	13	F	1580	870
3	17	F	1220	1640
4	10	F	1430	1180
5	14	F	640	860
6	16	F	820	1370
7	11	F	700	1030
8	9	F	560	
9	8	F	1180	1280
10	17	F	820	1660
11	17	F	500	640
12	17	F	1140	1080
13	17	F	960	600
14	17	F	1740	2090
15	48	M	2700	2169
16	7	M	860	1000
17	10	M	1260	1400
18	7	M	700	
19	9	M	1200	1400
20	35	M	1130	1470
21	17	M	860	680
22	17	M	720	1700
F Mean	±SD		1145	±449
M Mean	±SD		1283	±568

For the majority of trace elements, although no significant difference exists between mean values for boys and those for girls, the girls levels are approximately 60-70% of those of the boys. This difference is greater than the difference in mean urine volume, but may be related to

diet and body weight. For zinc, there is interestingly no difference. Data for iron may be skewed by a few values contaminated with blood (girls).

Table 4 - Mean values of all elements (excluding '<') by sex

Element	Male (Mean ± SD)	Female (Mean ± SD)	CEC (per 1.21)	Iyengaar
Ca (mg)	144 ± 91	166 ± 50.8		145 - 460
Cu (mg)	0.022 ± 0.025	0.017 ± 0.007	0.028	0.011 - 0.325
Fe (mg)	0.012 ± 0.009	0.023 ± 0.027		0.131 - 1.2
Sr (mg)	0.19 ± 0.123	0.139 ± 0.054		0.11 - 0.39
Zn (mg)	0.344 ± 0.166	0.358 ± 0.122	0.46	0.04 - 1.25
B (mg)	1.135 ± 0.616	0.76 ± 0.28	2.27	~1
K (g)	2.3 ± 1.3	1.5 ± 0.76		1.8 - 3.0
Li (mg)	0.01 ± 0.004	0.009 ± 0.005		0.6 - 0 8?
Mg (mg)	104.2 ± 43.4	79.5 ± 24.3		60 - 154
Na (g)	2.61 ± 1.09	2.06 ± 0.75		2.9 - 4.6
P (mg)	932.8 ± 320.1	595 ± 201		500 - 1200
S (mg)	870.1 ± 329.7	553 ± 192		800 - 1300
Si (mg)	15.14 ± 9.72	12.1 ± 5.0	9	
La (ng)	22.1 ± 21.4	19.0 ± 19.6	16 - 3900	
Ce (ng)	97.8 ± 101.5	52.1 ± 68.4	120 - 12400	
Pr (ng)	9.6 ± 10.7	6.6 ± 10.1		
Nd (ng)	38.1 ± 50.7	21.0 ± 24.4	220 - 12000	
Sm (ng)	10.8 ± 17.5	3.2 ± 1.7	1 - 250	
Gd (ng)	4.3 ± 7.0	2.5 ± 2.7	< 1000	
Tb (ng)	0.75 ± 1.17	0.32 ± 0.29		
Th (ng)	1 100 (n=1)			

Markers of bone turnover and resorption, such as pyrolidine cross-links are in the process of analysis. These data will then be used to determine degrees of intra-subject and inter-subject variation, the importance of the pubertal growth spurt with respect to the dosimetry of bone-seeking radio nuclides, and to determine the appropriateness of current adopted values.

Table 5 - Elemental urinary excretion (≤ 16 y versus >16 y)

Element	≤16y excretion (mg/day)	>16 y excretion (mg/day)
B	0.6 ± 0.5	1.2 ± 1.3
Ca	89 ± 81	136 ± 121
Cu	0.006 ± 0.012	0.005 ± 0.021
Fe	0.010 ± 0.029	0.009 ± 0.017
K	1260 ± 1180	2070 ± 2110
Mg	66 ± 48	92 ± 78
Na	1580 ± 1110	2650 ± 2220
P	470 ± 380	810 ± 660
S	460 ± 370	760 ± 680
Si	10 ± 7	12 ± 9
Sr	0.11 ± 0.09	0.16 ± 0.13
Zn	0.28 ± 0.24	0.38 ± 0.33

Publications

BG Dalgarno, RM Brown and CJ Pickford (1988) Potential of inductively coupled plasma-mass spectrometry for trace element metabolism studies in man. Biomed. & Env. Mass Spectrometry 16 377-380.

BG Dalgarno (1989) The distribution and uptake of rare earth elements in the food chain and their use as analogues for the Transuranic elements. AERE-R 13220, HMSO.

BG Dalgarno, RM Brown and CJ Pickford (1989) Strontium metabolism - a study of uptake using the stable isotope 86Sr as a tracer. Journal of Trace Elements In Experimental Medicine.

JJ McAughey, L Vernon, J Haines, T Sanders and R Clark, Fractional gut absorption of strontium, barium and neodymium following administration of stable isotope tracers. Proceedings of the 9th International Conference on Heavy Metals in the Environment, Toronto, 1993 1 117-120.

PJ Roth, N Molho, DM Taylor and JJ McAughey, Assessment of internal dose from radionuclides using stable isotope tracer techniques in man. CEC Radiation Protection Programme. Contract No. B17-0029, CEC, Brussels (1993).

Ch. Hansen, P Roth, E Werner, JJ McAughey and J Haines, Assessment of intestinal absorption (f1-values) of strontium for aqueous solutions and foodstuff. Proceedings of the Workshop on Health Effects of Internally Deposited Radionuclides : Emphasis on Radium and Thorium. CEC, Heidelberg, 1994

RJ Cox, C J Pickford, N M Reed and M Thompson. The determination of calcium isotope ratios in biological materials using high resolution ICP-MS. Proceedings, 5th Surrey Conference on PSMS, July 1993, Durham, UK

R J Cox, C J Pickford and M Thompson. The determination of isotope ratios of lanthanide elements in biological materials using ETV-ICP-MS. Proceedings, 1994 Winter Conference on Plasma Spectrochemistry, January 1994, San Diego, CA

R J Cox. ICP-MS in stable isotope uptake studies. Ronald Belcher Memorial Lecture, RSC Analytical Division R & D Topics Meeting, July 1993, Bradford

Final Report
1992 - 1994

Contract: FI3PCT920060 **Duration: 1.9.92 to 30.6.95** **Sector: A14**

Title: Radionuclide dosimetry

1)	Noßke	BfS
2)	Kendall	NRPB
3)	Taylor	Univ. Wales, Cardiff
4)	van Rotterdam	TNO - Delft
5)	Andrási	KFKI
6)	Toader	IHPH

I. Summary of Project Global Objectives and Achievements

The objectives of the project were:
- to develop and implement more realistic models for dose estimation following intakes of radionuclides by workers and the general public (including doses to the embryo and fetus from maternal intakes)
- to address the more important uncertainties in the biokinetic and dosimetric models used in radiation protection.

To achieve these objectives a broad programme of research has been conducted including:
- the determination of biokinetic data by measurement and literature review
- the assessment of uncertainties in these parameters
- the formulation of new biokinetic models
- the development of computer codes for dose calculations.

This work was performed in close collaboration with the ICRP Task Group on Internal Dosimetry, INDOS (formerly Age-dependent Dosimetry, AGDOS), and the ICRP Task Group on Dose Calculations.

Determination of biokinetic data

There has been extensive work to determine biokinetic data
- for caesium and strontium by various measurements for a long period after the Chernobyl accident including measurements of caesium transfer from the mother to the embryo;
- by literature review
  - to characterise the systemic behaviour of various elements
  - to describe the kinetics of the gastrointestinal tract and their dosimetric implications.

Measurements to determine the biokinetic behaviour of caesium and strontium following the Chernobyl accident have been performed in the Eastern European countries Hungary and Romania. KFKI performed whole body mesurements to investigate the variation of caesium retention with age and sex. IHPH performed measurements of intake and urinary excretion of caesium and strontium for adults and children of different ages as well as caesium

concentration in aborted embryos giving a basis for obtaining reliable biokinetic and dosimetric models.

The caesium retention determined by KFKI showed good agreement with the ICRP models. There was no significant variation in adult retention with age and sex, in contrast to results reported by some other groups.

IHPH determined urinary excretion functions for caesium and strontium. They made many measurements of caesium concentration in aborted embryos together with the corresponding maternal intakes. These data are important for the derivation of dose coefficients to the embryo.

Literature review of the gastrointestinal absorption and systemic behaviour (including excretion) of various elements has been performed by the University of Wales, College of Cardiff (UWC). This work has been incorporated in ICRP Publications 67 and 69 to which BfS and NRPB also contributed. For the forthcoming revisions of ICRP Publications 30 and 54 work has started to review the biokinetic behaviour of further elements, considering the effect of different chemical compounds as well as the suitability of the models for dose assessments and bioassay.

As an initial step in the development of a new model for the gastrointestinal tract, BfS performed a literature review to identify biokinetic and dosimetric items to be included in a new model.

A rigorous method of estimating more reliable model parameters using the Kalman filtering technique has been investigated by TNO.

Assessment of uncertainties

It is important to identify the sources of uncertainties of models and parameters in order to estimate the reliability of calculated doses. This important topic will also be covered by a forthcoming ICRP Publication prepared by the INDOS Task Group.

Implicitly this uncertainty is also a result of the experimental studies by KFKI and IHPH showing the variability within the measurement data. UWC performed an analysis to determine the uncertainties of f_1 values giving the fraction of activity transferred from the gastrointestinal tract to the systemic circulation for several elements. This work included also the determination of the possibilities of extrapolation of results from animal to man.

TNO has implemented into its COMPART code (see below) the option of performing stochastic calculations (assuming that biokinetics are governed by stochastic processes) as an alternative to the usual deterministic assumptions.

Formulation of biokinetic models

On the basis of data obtained by literature review and experimental studies, biokinetic models for dose calculations have been formulated which also consider dosimetric aspects. Because of the new tissue weighting factors of ICRP Publication 60 the gastrointestinal tract and urinary bladder have become more important. Therefore INDOS (with members of UWC, BfS and NRPB) included excretion pathways in the biokinetic models. These models have been published and applied in ICRP Publications 67 and 69.

For the lanthanide elements UWC formulated a new generic physiologically based biokinetic model for workers which is also suitable for dose assessments.

The new tissue weighting factors make it necessary to develop a new gastrointesintal tract model. On the basis of literature review (see above) BfS formulated a first version of such a model taking into account knowledge of biokinetic processes and the sensitivity of target cells. The influence of more realistic non-linear biokinetic processes within the gastrointestinal tract has been examined by TNO.

Establishment of new computer codes

The final step on the way from observation of biokinetic processes via the formulation of models to doses is the implementation of the biokinetic and dosimetric models in computer codes.

Oak Ridge National Laboratory (ORNL) was the only institution performing dose calculations for ICRP Publications 30. Now European groups - especially NRPB and BfS have joined this task and intercomparisons can now be conducted. The advantage of this is to provide quality assurance for the results of these complex calculations which is essential for the Radiation Protection Community using these values. Not only computational quality assurance is achieved by this but also quality assurance of the model formulation because by the implementation of the models independently by several groups it can be checked if the models have been interpreted in the same way by different groups. These intercomparisons revealed, for example, that the implementation of independent daughter kinetics is not completely unambiguous. Therefore ICRP Publication 74 will contain an addendum to clarify this. It was also recognised that the method of caclulating the effective dose described in ICRP Publication 60 is not clear for age-dependent calculations.

NRPB and BfS independently developed codes to compute age-dependent dose coefficients using the latest biokinetic and dosimetric models of ICRP. There have been extensive intercomparisons between these groups including exchanges of scientists each year between organisations. Additionally there was much intercomparison work in the ICRP Task Group on Dose Calculations with ORNL and the Ukraine Scientific Centre for Radiological Medicine, Kiev. In this way the dose coefficients published in ICRP Publications 67, 68, 69, and 74 have been checked independently by several groups. The values of ICRP Publication 68 have been originated by NRPB as the first European institution producing dose coefficients published by ICRP. NRPB and BfS also perform calculations of effective dose

coefficients for the Basic Safety Standards of EU and IAEA which will also be a basis of numerous national radiation protection standards.

NRPB also implemented procedures to calculate doses to embryo and fetus due to activity intake by the mother. For these calculations compartmental models are being developed and a simplified standard model for those elements for which sufficient knowledge is not available has been implemented. For drafts of a forthcoming ICRP Publication various calculations have been performed assuming several time-dependent intake patterns by the mother, and the doses to embryo and fetus have been compared to those to the mother. These methods and results also have been discussed with other members of INDOS such as UWC and BfS.

KFKI and TNO were engaged in the development of computer codes for dose calculations. KFKI has developed a PC code considering not only single intakes but also continuous and interrupted intake functions. The new ICRP respiratory tract model and the new physiologically based systemic models necessitated an extension of the number of compartments the code can handle.

TNO has developed COMPART, a computer code for dose calculations, based on the solution of difference equations which is a useful alternative approach to demonstrate that the same results can be obtained by different methods. The aim of this code is to be more flexible in the types of retention functions. For example, with this code non-linear aspects in the kinetics of the gastrointestinal tract can be assessed which is necessary in the formulation of a new gastrointestinal tract model.

Conclusions

Internal dosimetry is currently a rapidly developing field in radiation protection. This can be seen in numerous ICRP Publications (56, 66, 67, 68, 69, 74) issued in the last few years or in press. Further publications on reliability of dose coefficients, doses to embryo and foetus and revisions of Publications 30 and 54 are in preparation. These new developments have to be considered in new national and internation regulations. The work performed within this contract has made valuable contributions to this development.

Head of project 1: Dr. Noßke

II. Objectives for the reporting period

The main objectives of this project were

- the design of the structure of a biokinetic gastro-intestinal (GI) tract model including the identification of radiosensitive cells and tissues of the GI tract as a basis of the revision of the present GI tract model;
- the implementation of age-dependent dose calculations with regard to all present biokinetic and dosimetric models of ICRP into our computer code DOSAGE;
- to perform dose calculations for ICRP, EU and IAEA including quality assurance procedures with other computaitonal groups, especially with the co-contractor NRPB.

III. Progress achieved including publications

Development of a gastro-intestinal tract model

The current model of the gastrointestinal tract is described in ICRP Publication 30 as a four-compartment model, including the stomach (ST), small intestine (SI), upper large intestine (ULI) and the lower large intestine (LLI) and gives only allowance to an absorption to the body fluids from the SI. This model is intended for a reference man which is a 70 kg healthy adult caucasian male and does not allow the variation of conditions such as age, gender and the element considered including its physical and chemical form. On the other hand, it has become more important to assess realistic doses to the GI tract, because explicit weighting factors have been assigned to the oesophagus, the stomach and the colon. The ICRP 30 GI-tract model therefore needs to be revised in view of the results from recent studies and experiments, also considering the greater importance of the GI-tract in calculating the effective dose according to ICRP 60. Within this project different models recommended for the GI-tract and various morphological and structural aspects were summarized and evaluated in order to give a basis for the development of a new and expanded GI-tract model.

The human gastro-intestinal (GI) tract consists of the oral cavity including the radiation sensitive salivary glands, the oesophagus, the stomach, the bowel separated into duodenum, jejunum, ileum, and the colon. The colon is also separated into three segments, the ascending, the transverse and the descending colon, followed by the rectosigmoid part. This rather complex morphological stucture was described by ICRP Publication 30 as a four compartment model (see above). All transfer processes between the four compartments are described as first order processes independent of age, gender and health status of the persons considered.

There is a basic similarity of structure in all parts of the GI tract, with differences in arrangement and differentiation of the basic structures in different parts of the GI tract. The reasons for different radiosensitivities of cells and organs are based on the different development of cells in the tissues. From the innermost to the outermost layers the GI-tract

consists of the mucosa, the submucosa and the muscularis. The radiation sensitivity of the different parts varies with the type of epithelium in the mucosa and glands, with the degree of vascularization and other variables, such as turnover rate. Turnover is supported by marked mitotic activity. The various regions of the GI tract in the order of decreasing radiosensivity are duodenum, jejunum, ileum, oesophagus, stomach, colon and rectum (Casarett, *Radiation Histopathology*, CRC Press, Boca Raton, Florida, 107-135, 1980). These theoretical considerations partly contradict the epidemiologically based statements of ICRP Publication 60. The mouth is until now not included.

Summarizing and evaluating the results lead us to an expanded GI model, see Figure 1.

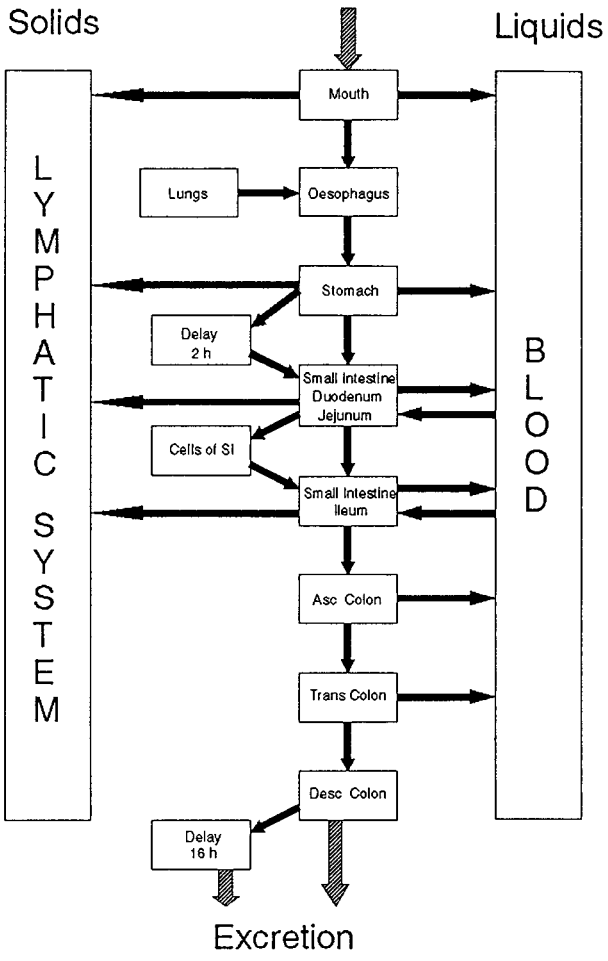

Fig. 1: The proposed GI tract model

In general, ingestion starts by material entering the oral cavity. The residence time of particles of different sizes could be remarkably prolonged there up to some hours by attachment of small fractions of the ingested material to the teeth mainly if the particles are deposited in the gaps between teeth resulting in a dose to the gum. Additionally, very small molecules can be resorbed directly via the oral mucosa, entering the blood stream. This may be important by e.g. smoking of contaminated cigarettes, but also by intake of alcoholics or other small molecules. Also small unsoluble particles can be resorbed to the lymphatic stream. They have a longer transit time because the lymphatic stream is slower than the blood stream.

The oesophagus, as the second compartment, is covered with epithelial cells which are much more radiosensitive than those lining the stomach, for example. The tissue weighting factor for the oesophagus is 0.05 (ICRP Publication 60) and therefore it is relevant in dosimetrical aspects. The transit time through the oesophagus is considered to be very short. However, radionuclides from the lung can be transferred via the oesophagus to the GI-tract, thereby considerably increasing the dose to that compartment because of the possibility of deposition of the mucin from the respiratory tract.

After passing the oesophagus nutrients enter the stomach. From the stomach there will be a resorption of special elements, such as iron and cobalt, into the blood stream. Indigestible components of the nutrients stay for about 2 h in the stomach and are only transported during the "fasting phase", leading to a delay of 2 h in this model (Stubbs, *Rad. Prot. Dosim.* **41** 63-69, 1992).

Corpuscular substances about 50-100 μm in size enter the lymphatic system by so-called paracellular mechanisms. In current systemic models this separation to lymphatic system and blood is not taken into consideration.

The time given for the stomach to be completely emptied ranges from 10 minutes up to 4 hours. In ICRP Publication 30 the transit time in the stomach was assumed to be 1 hour and assigned to a first order kinetic. The times for soluble and insoluble substances which show quite different retention times were not distinguished.

The SI compartment of the ICRP 30 model should be split into two compartments, according to the different absorption rates of the different parts of the SI. The main part of absorption takes place in the duodenum and jejunum which are suggested in the model shown above as one compartment but for this region also a splitting into up to 3 compartments might be considered reflecting the different absorption sites for different kinds of foodstuff. The ileum, with a significantly lower absorption, is described as an own compartment. Corpuscular substances of sizes of about 50-100 μm may enter the lymphatic system by so-called paracellular mechanisms.

The residence times in the small intestine reported in literature are varying for adults. The most results are within the range of 3-4 hours. Also Stubbs (1992) is reporting a 4 hour transit time in the small intestine and is referring to the scintigraphically determined data by Bailey et al. (*Gastroenterology* **98** A324, 1990). For the transport within the SI partly a linear food transport is described whereas others determined that portions of food are transported in the large intestine in 30 minute intervals.

In that section of the GI-tract the major portion of substances is absorbed, with absorption primarily progressing in one direction ie by active transport. By way of diffusion, the substances can be reabsorbed from blood into the small intestine and thus lead to additional doses from radioactive material. There is a discrepancy between ICRP 53 and ICRP 67 regarding the passive backflow from blood to the bowel. The ICRP 30 recommendations for workers don't mention this mechanism at all, whereas the ICRP 53 model for patients in nuclear medicine contains the backflow from the blood via the liver and the gallbladder into the small intestine. The ICRP 67 model for members of the public describes this backflow to the upper large intestine which is under the anatomical view not correct but reflects that in many cases the recommended f_1-values describing the gastro-intestinal absorption are no realistic but "apparent" absorption coefficients which also include the re-absorption of systemic material transferred to the GI-tract. Only potassium ions and hydrogencarbonite ions can be resorbed into the ULI.

The stem cells are the most important cells. A genetic change can lead to transformed cells and give rise to malignancy. Also the goblet cells are very radiosensitive and have importance by possible transformations after exposure. The macrophages are able to take up particles and transport them to other tissues and organs, comparable to the respiratory tract model in ICRP 66 where the macrophages give a significant dose to the lymph nodes. The entrocytes and the cells of the wall of the SI are very radiation sensitive, and should therefore be regarded separately in the dosimetry as well as in formulating more precisely the biokinetics of the absorption processes.

The ICRP 30 recommendation separates the large intestine into two compartments, the ULI and the LLI. Stubbs proposed three compartments, namly the ascending colon, the transverse colon and the descending colon including the rectosigmoid part. This separation has been adopted for the following reasons: First of all the residence time of the faeces in different parts of the large intestine are substantially different and this can lead to different radiation exposures to organs like spleen and liver. Moreover, the important resorption of electrolytes takes place in the ascending and transverse colon but not in the descending colon.

The residence time of faeces in the large intestine is reported to be differently long from 16-120 hours with significant individual differences. A delay of 16 h describes the defaecation in boli which means the partial defaecation.

ICRP 30 assumes that all transfer processes are first order processes. To a better understanding of biological processes, this assumption should be reconcidered.

Development of the DOSAGE code

The aim of our first computer code for dose calculations - developed in the 80s - was to give the capability to perform calculations according to the models of ICRP Publication 30 for workers. During the last few years - with the development of more sophisticated age-dependent models by ICRP for the general public - it became necessary also to perform calculations for infants, children and adolescents with age-dependent biokinetic and dosimetric parameters. Furtheron the models, especially the new physiologically based

systemic models for alkaline earths and actinides, became more sophisticated and could not be handled by our former code.

The aim of the work within this project was to implement the possibility to calculate age-dependent doses using very general first-order kinetics - including recycling models - and the new dosimetric models of ICRP.

Especially the recycling models required much implementation effort because - especially in the case of independent daughter kinetics - operations of extremely large matrices (up to more than 750×750 matices) have to be performed.

The biokinetic input files define the retention of material within and its movement between compartments. Therefore it was very easy for us - due to the design of our DOSAGE code only by creating an appropriate input file - to implement the biokinetics of the new ICRP respiratory tract model of Publication 60, especially because this model can be formulated as a non-recycling model.

There was, however, some work to implement the dosimetric items of the new ICRP respiratory tract model. DOSAGE does not calculate SEE values but uses the dosimetric data calculated by the SEECAL code of M. Cristy (Oak Ridge National Laboratory, ORNL) as an input file. The new ICRP respiratory tract model, however, needs many additional SEE values of various recently defined source/target regions. Because these SEE values for a prolonged period were not available by ORNL, the calculations of these values have been implemented by us in an additional code. For the calculation of SEE values for β-radiation not the values calculated by using the mean β-energy have been used but those SEE values have been calculated using the β-spectrum and absorbed fraction values for monoenergetic elctrons.

For age-dependent calculations a continuous change of biokinetic and dosimetric parameters is assumed. This is approximated within the DOSAGE code by stepwise constant biokinetic and dosimetric parameters. The optimal number of steps - enough steps to get results close enough to those calculated by consideration of a continuous change of parameters, but as few steps as possible to save computational time - has been determined by various test calculations. These test calculations could also show that the results really were converging with an increasing number of steps, i.e. that the code is stable. The numbers of steps used for calculations can be determined for each run of DOSAGE individually, but generally the default values mentioned above are used. Table 1 shows these default numbers of steps used in our age-dependent calculations.

For the biokinetic models for lead, the alkaline earths and the actinides which assume adult parameters starting with age 25 years the values of the last column are doubled.

Age at intake	3m - 1y	1y - 5y	5y - 10y	10y - 15y	15y - 20y
3 months	30	25	25	20	5
1 year	-	35	30	25	8
5 years	-	-	35	35	8
10 years	-	-	-	35	8
15 years	-	-	-	-	10

Tab. 1: Number of steps used by DOSAGE for age-dependent calculations

Dose calculations and quality assurance

Dose coefficients published in ICRP Publications 56, 67, 68 and 69 have been calculated with DOSAGE and the results served for quality assurance by intercomparison procedures with results obtained by NRPB and ORNL.

Additionally, age-dependent calculations for about 800 radionuclides have been performed by BfS for the CEC Basic Safety Standards. These values have been compared with values calculated by NRPB for the IAEA Basic Safety Standards to assure that all international bodies recommend the same dose coefficients. For these intercomparison procedures there has been a scientist exchange between BfS and NRPB for many years. At the end of these intercomparison procedures the effective doses computed by different groups agree within the range of rounding errors.

These intercomparison procedures, however, do not only assure the correctness of numerical computations but serve also as a quality assurance for the formulation of models because several groups implement these models independently and in some cases different results are obtained because of different interpretation of the model descriptions. Also inconsistencies in the models are easier detected by these procedures.

As a result of these intercomparisons, for example, the treatment of the rest of body compartments of daughter nuclides with biokinetics independently from the biokinetics of the parent nuclide has been extensively discussed within the groups and has been reformulated in the ICRP Publication series.

At the moment NRPB uses the approach proposed by ORNL which uses some simplifications leading to an expected slight underestimation of source sorgans and to a slight overestimation of non-source organs. On the other hand, our calculations with DOSAGE use a more exact approach which, however, needs much more compartments. First comparisons suggest that the differences in organ doses are less than 5% and the differences in effectiv dose even less. In this way the BfS calculations serve as a control that the slight simplifications in the implementations by NRPB and ORNL do not result in significant over- or underestimation of doses.

Publications

Simkó, M. and Noßke, D. Grundlagen zur Revision des Mage-Darm-Trakt-Modells. ISH-IB 5. Bundesamt für Strahlenschutz, Salzgitter, 1995

Simkó, M. and Noßke, D. Basis for a revision of the gastrointestinal tract model. Accepted by Rad.Prot.Dosim.

Head of project 2: Dr. Kendall

II. Objectives for the reporting period

In broad terms the objectives for the period of contract have been to improve estimates of dose per unit intake values (dose coefficients), to provide quality assurance for these estimates and to make them available to the radiation protection community. Improvements have been achieved by implementing new ICRP models for the lung and element-specific systemic models. The calculation of dose coefficients for non-adults has been greatly improved including the development of a calculation method for the embryo/fetus.

Revised dose coefficients for the CEC Basic Safety Standards are currently being prepared and quality assured through intercomparisons with co-contractors ISH. Consistent values have already been published in the IAEA BSS (interim).

III. Progress achieved including publications

New method of calculation

The introduction of the new generation of physiologically-based recycling biokinetic models in Publications such as ICRP 67 and 69 necessitated the development of a new method of solution to replace a previous method based on an iterative approach. The new method uses a standard eigenvalue technique to solve the system of first order differential equations which represents the biokinetics of activity in the body.

The new method proved to be much faster than the previous approach which means that results can be quickly revised if there are changes in recommended models at a late stage in the development of a publication.

Implementing the new ICRP model for the respiratory tract

Much work went into the implementation of the new ICRP model for the respiratory tract. The model constitutes an update of that recommended in ICRP Publication 30 and is published as ICRP Publication 66. There are some similarities with the ICRP Publication 30 model: the respiratory tract is represented by a compartmental model with first order kinetics; deposition fractions for different regions are given which are dependent on particle AMAD. The main change in method is in the dosimetry of the lung. The ICRP Publication 30 model calculated the average dose to lung tissue. The new model allows for the calculation of doses to specific groups of cells at risk. It thus takes into account differing radiosensitivity within the lung.

Functions are given for absorbed fractions (AF) which describe energy deposition patterns for mean beta (and positron) energies as well as for discrete electron energies. There are thus two ways of dealing with beta dosimetry: one could either use the mean energy with the AF for mean beta energy or else represent the beta spectrum by a series of discrete

emissions and then use the AF functions for electrons for each emission. It was agreed with co-contractors ISH that the latter is the preferred method. This change necessitated regenerating the radiation database used by the code to include the data for beta spectra. For all tissues other than those within the lung, mean beta energies continue to be used. The inclusion of beta spectra data in our radiation records will be useful in future when it is likely that dosimetry for bone and the GI tract will be revised to include more detailed modelling of beta doses.

Work on investigating the changes in dose coefficients caused by introducing the new models was essentially completed during the contract period and it is hoped to publish a summary of results very soon. Preliminary results show that lung doses are usually lower than those of the ICRP 30 model for types F and S (Fast and Slow, respectively); this results mainly from lower depositions. There are substantial increases for some type M (Moderate) materials; these result from longer overall retention in the lung. The recommended default value for particle size in the workplace is now 5 μm rather 1 μm; this further reduces depositions in the thoracic regions and consequently lung doses. The activity transferred to blood for type F materials is about 75% of that for the corresponding class in the previous model. A similar picture emerges for type M materials. In the case of type S, the fraction is much less, around 10%, and this can lead to lower doses for many tissues. The effects on effective doses are complicated by the introduction of substantial changes in systemic models. Some examples are given in Table 1.

Table 1 Comparison of lung doses and committed effective doses for some important nuclides using the ICRP 66 (AMAD = 5 μm) and ICRP 30 (AMAD = 1 μm) models

Nuclide	Class / type	f_1	ICRP 30 lung dose	New lung dose	ratio	ICRP 30 CED	New CED	ratio
Co-60	Y/S	0.05	3.4E-07	9.6E-08	0.28	5.6E-08	1.7E-08	0.30
Ni-63	D/F	0.05	8.8E-10	5.1E-10	0.58	8.5E-10	5.2E-10	0.61
Zr-95	W/M	0.002	1.8E-08	2.2E-08	1.22	3.9E-09	3.6E-09	0.92
Mo-99	D/F	0.8	1.2E-09	1.5E-10	0.13	4.8E-10	3.6E-10	0.75
Tc-99	W/M	0.8	1.7E-08	2.4E-08	1.41	2.4E-09	3.2E-09	1.33
I-131	D/F	1.0	6.5E-10	8.1E-11	0.12	1.3E-08	1.1E-08	0.85
Pu-239	Y/S	1E-5	3.2E-04	4.7E-05	0.15	6.4E-05	8.3E-06	0.13

Age-dependent dosimetry

Dose coefficients are calculated as the sum over all source organs of the product of the number of decays in the source organ and the specific effective energy, or contribution to the dose in the target tissue per decay in the source organ:

$$H_T = \sum_s U_s \, SEE\ (T \leftarrow S)$$

H_T = dose to target tissue T

U_s = number of disintegrations in source organ S

SEE (T←S) = specific effective energy.

In the past, the NRPB internal dosimetry code had been constrained to use constant parameters in biokinetics models (variation with time of Specific Effective Energy (SEE) values had been allowed for, but in an approximate manner). This situation had arisen because internal dose calculations were originally only concerned with adult workers. During the contract period there has been an increasing interest within the EC in doses to members of the public, including children. Substantial modifications have been made to the code to allow for age-dependent biokinetic parameters and SEE values.

Biokinetic models are specified by ICRP for six standard ages, 3-month-old, 1, 5, 10, 15-year-old, and 20-year-old adult. These models specify the rate at which material is transferred between the different parts of the body. Rate constants at intermediate ages are derived using linear interpolation. In the new NRPB code, the continuous variation of transfer rates is modelled discretely using a time-stepping method. Starting at the age of intake, the calculation is advanced by a time-step small enough for the interpolated rates to be considered constant. The computed activities at the end of the preceding time-step are then used as the initial conditions for the next step. In this way the number of transformation within each step or interval is computed.

Absorbed fraction data for photons and charged particles are available for six standard ages enabling full sets of SEE values to be generated for newborn, 1, 5, 10, 15-year-olds and the adult. At intermediate ages, SEEs can be derived using a linear interpolation scheme based on inverse total body mass. As described above, calculations proceed by breaking down the time period into a series of steps or intervals. SEE values calculated at the beginning of a step are assumed to be constant within the interval. Having calculated SEEs and the number of transformations for a step, the dose received in that step can be calculated and these can be summed over all steps to give the committed dose.

This new code, PLEIADES (**P**rogram for Lin**E**ar **I**nternal **A**ge-dependent **DosES**), enabled NRPB and co-contractors ISH to carry out a valuable QA exercise for the dose coefficients published in ICRP Publication 67 and Publication 69. Consistent results will also be included in the CEC Basic Safety Standards.

Calculations for ICRP Publication 68

ICRP published Annual Limits on Intakes for workers in Publication 30. These calculations were updated to take account of the ICRP 60 tissue weighting factors in Publication 61. Many developments then took place after the release of Publication 61. In particular, the introduction of the new respiratory tract model. Physiologically based recycling models were also been introduced for some important elements in ICRP Publications 67 and 69. A generic model for calculating doses from activity in excretion pathways was introduced in Publication 67, and all ICRP Publication 30 models were updated in the NRPB code to take

this into account. For some elements, new information is available on absorption from the GI tract; in these cases f_1 values have been revised accordingly.

A complete set of dose coefficients for adults for over 800 radionuclides by ingestion and inhalation of both 1 μm and 5 μm AMAD particle sizes based on the above changes were issued by ICRP in Publication 68. Quality assurance was provided by intercomparisons with co-contractors ISH and ORNL, USA. Again, consistent results will also be included in the CEC Basic Safety Standards.

Independent biokinetics for decay products

In the models of ICRP Publication 30 it was recommended, with only a few exceptions, that decay products produced in the body should be taken to share the biokinetics of the parent nuclide. In contrast, in the recent ICRP Publications 67 and 69 special models are described for dealing with decay products. PLEIADES has therefore been further improved to allow daughter radionuclides which in-grow in the body to be treated using a biokinetic model specific to each daughter nuclide. This applies to isotopes of Te, Sb, Pb, Ra, Th and U. Some of these decay chains are long (eg, Th-232) thus many special models have to be derived and evaluated. Much effort was devoted to the implementation of this work in co-operation with the co-contractors ISH.

Fig. 1:

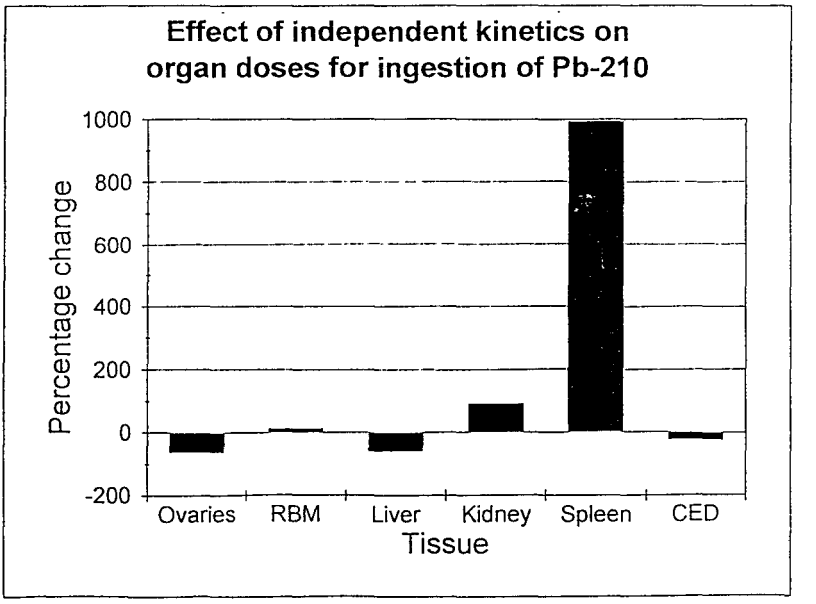

This new treatment has important consequences for cases such as Pb-210/Po-210 and Ra-226/Rn-222. In the former case total doses are dominated by the alpha emission of the Po-210 grand-daughter, with the new treatment uptake of Po-210 in the spleen is explicitly modelled leading to spleen doses which are higher by an order of magnitude (figure 1). In previous calculations about 75% of the Rn-222 daughter of Ra-226 was taken to be lost instantaneously from all tissues. In the new models, Rn-222 is taken to be cleared rapidly from soft tissues leading to reduction in doses by around a factor of two. Retention of Rn-222 in bone is, however, greater and red bone marrow doses are increased by 50%.

Calculations for the IAEA Basic Safety Standards

The new computer code, PLEIADES, was used to calculate dose coefficients for inclusions in the IAEA Basic Safety Standards (Interim). This comprehensive set of values addresses intakes by both inhalation and ingestion of over 800 nuclides for six age groups of the public (3-month-olds, 1,5,10 and 15 year-olds, and adults) as well as workers. The results for workers are consistent with the results issued by ICRP in Publication 68. This marks a major step towards harmonisation of dose coefficients throughout the world. A consistent set of results will be supplied to CEC for publication in the Euratom Directive.

Results for the final issue of the BSS are currently being quality assured by cross-checking with results generated by ISH.

Quality Assurance

The quality assurance (QA) of dose coefficients for publications by international bodies such as CEC, ICRP and IAEA is of utmost importance. The computer codes used to calculate these values are large and complicated, reflecting the complexity of the underlying problem. Although great care is taken, and software QA procedures are followed, during the development of these codes, some errors inevitably arise. Probably the most efficient method for finding and correcting these errors is to compare the results calculated by different groups, using codes which have been developed independently.

Committee 2 of ICRP has set up a Task Group on Dose Calculations, NRPB and ISH are strongly involved in this group. Other groups represented are Oak Ridge National Laboratories (ORNL), USA and the Ukraine Scientific Centre for Radiological Medicine (USCRM). One of the main roles of the Task Group is to allow detailed cross-checking of results generated by different groups. This has proved very successful with many problems located and resolved. As well as the above, NRPB and ISH have fostered a particularly close working relationship and have established a procedure of exchanges of personnel during each summer, these exchanges have proved extremely fruitful.

During the contract period NRPB and ISH provided QA for ingestion dose coefficients published in ICRP 56, 67, 68 and 69. The calculations for ICRP 74, although not yet published have also recently been quality assured. As noted above, a large set of results for inclusion in the IAEA Basic Safety Standards in the final stages of approval, and future publications by CEC will benefit from this high level of QA.

Embryo/fetal dose calculations

In most cases there is insufficient data available to enable the development of full compartment models for the calculation of doses to the embryo/fetus. Thus a generic method for calculating these doses, based on a scaling of maternal tissue doses, was developed. Doses to the embryo (taken to be the first 8 weeks after conception) are calculated using results generated using a 3-month pregnant phantom. After organogenesis is complete (8 weeks), doses to fetal tissues are estimated using information on experimentally observed ratios of the concentration of activity in maternal and fetal tissues.

Effective doses for the embryo/fetus are calculated using ICRP 60 tissue weighting factors. It is recognised that these weighting factors may not be appropriate for the embryo/fetus, but, in the absence of better information, they do enable the calculation of a single quantity which can be compared with the effective dose to the mother. In most cases, this effective dose is much less than that to the mother. A set of representative calculations was discussed with co-contractors ISH and submitted to ICRP Committee 2 and later to the Main Commission for comments. It is anticipated that the method, and further updated results, will be adopted by ICRP in the future.

In future calculations parameters will be allowed to vary in a step-wise manner throughout gestation so as to model the continuous growth of the fetus. In some cases element-specific compartmental models will be developed.

Simplification of recycling models

Biokinetic models which involve recycling, such as that recommended for plutonium in ICRP Publication 67, require considerably more effort to implement than their predecessors. Work was carried out which shows that such models may be conveniently represented by a set of simplified organ retention functions compatible with the simple non-recycling models of ICRP Publication 30.

The method uses an analytical approach to solve the biokinetic model, yielding exact organ retention expressions. These expressions are then reduced, by curve fitting, to functions consisting of the sum of only a few exponential terms. It is shown that errors introduced by the use of the simplified expressions are small in the context of the overall dose calculation, less than 5% in committed doses and 10% in activities. Illustrative fitted functions of two and three terms for plutonium in liver using the new ICRP model are shown in figure 2, the three-term fit is very close to the full expression.

Simplified retention expressions have been published in an NRPB report for all recycling models of ICRP 67 and a paper giving details of the method, as well as the fitted functions for plutonium has been submitted to Health Physics. It is hoped that these representations of the new models will be of value to RP practitioners in situations where implementing the full models would be impractical or inappropriate.

Fig. 2:

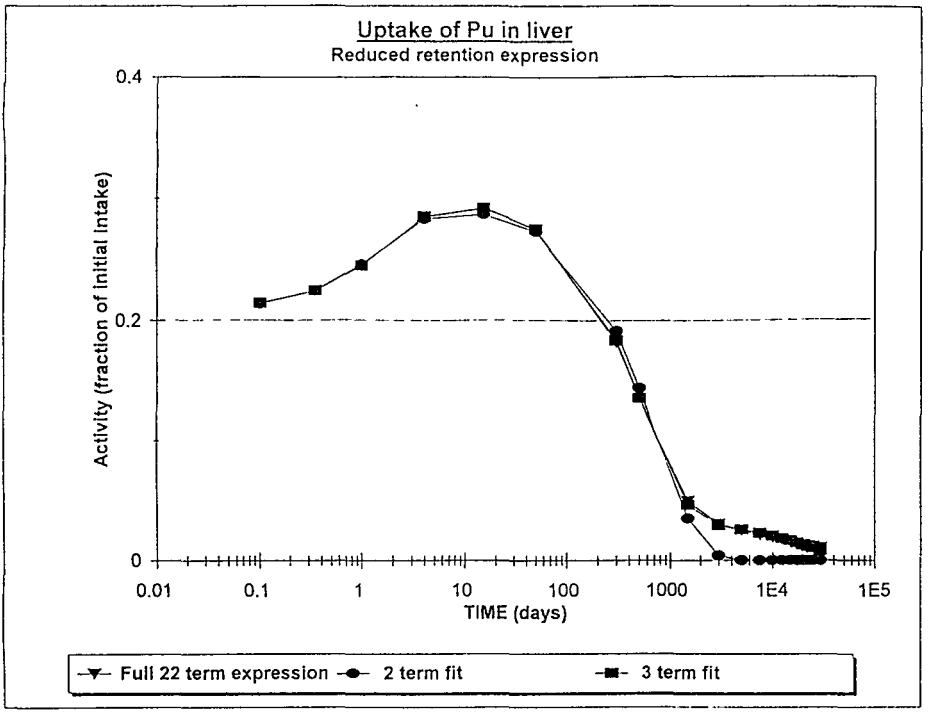

Dose coefficients for Ores and Mineral Sands

The implications of the new ICRP respiratory tract and systemic models for doses from naturally occurring uranium, radium and thorium was investigated with particular reference to the mining and milling industries. Generally doses are substantially lower (by a factor of two to four, but possibly by as much as a factor of ten) using the new models as a results of lower total deposition, a larger default particle size, and more realistic modelling of bone doses.

Publications

Kendall, G M, Bailey, M R, and Stather, J W. Developments in internal dosimetry. Radiol. Prot. Bull., 158, pp 8-17 (1994).

Khursheed, A. Simplified organ retention functions for actinide and alkaline earth biokinetics recycling models. Chilton, NRPB-M564 (1995).

Silk, T J, Kendall, G M, and Phipps, A W. Revised estimates of dose from ores and mineral sands. J. Radiol. Prot., (1995, in press).

Stather, J W, Harrison, J D, and Kendall, G M. Uptake and distribution of radionuclides in the embryo and fetus - implications for dosimetry. Radiation Research: A Twentieth-Century Perspective. Volume II: Congress Proceedings (eds. Dewey, W C, Edington, M, Fry, R J M, Hall, E J, and Whitmore, G F), pp 306-311. Academic Press (1992).

Haines, J W, Harrison, J D, Pottinger, D E, and Phipps, A W. Transfer of polonium to the embryo and foetus of rat and guinea pig. Int. J. Radiat. Biol., Vol 67, 3, pp 381-390 (1995).

Moody, J C, Stradling, G N, Wilson, I M, Pearce, M J, Phipps, A W, Gray, S A, and Hodgson, A. Biokinetics of plutonium in the rat after the pulmonary deposition of three nitrate bearing materials from B.205: Implications for human exposure. Chilton, NRPB-M427, (London, HMSO) (1993).

Head of project 3: Prof. Dr. Taylor

II. Objectives for the reporting period

- To review and re-evaluate all the available literature on the biokinetics and distribution of the elements of major radiological significance, particularly H, C, S, Mn, Fe, Co, Ni, Zn, Se, Sr, Zr, Nb, Mo, Tc, Ru, Ag, I, Cs, Ba, Ce, Pb, Po, Th, U, Np, Pu, Am and Cm.
- To complete the general, age-dependent models for the above elements and to add excretion functions so that they become suitable for the calculation of body contents from bioassay (urinary or faecal excretion) data.
- To formulate and validate a generic model for the lanthanide series of elements.
- To critically review the validity of extrapolating to humans data derived from animal studies either with the specific element of interest or with a chemical analogue of that element.
- To start assessing the uncertainties in the biokinetic parameters proposed.

III. Progress achieved including publications

The principal aim of this project is to develop internationally acceptable, human biokinetic models for use in calculating radiation doses to workers and the general public from radionuclide intakes. Ideally, these new models should be based on human physiology, be computationally simple and, also, permit the assessment of exposure from measurements of the excretion of the relevant radionuclides in urine and/or faeces. The formulation of state of the art, physiologically-based, biokinetic models requires critical evaluation or re-evaluation, of all available data on the biological behaviour of the individual radionuclides and their most important compounds. Since, frequently very few direct human biokinetic data are available, many models must be derived using data obtained in experimental animals. In the work described here, there has been a much greater emphasis than previously on examining the biological and chemical validity of the extrapolation to humans of data derived from animal studies with the element of interest, or a chemically related element.

In the last year of the project, work was begun on the assessment of the uncertainties inherent in the selected biokinetic parameters.

During this reporting period the collaborative work on the formulation and validation of general, age-dependent biokinetic models for the 30 elements of greatest radiological significance has been largely completed and published in ICRP Publications 67 and 69. Work was begun on the further development of some of these models to cover occupational exposures to radionuclides and to specific radionuclide-labelled compounds, and on the revision of models for the remaining elements of radiological interest, including the proposal of a generic biokinetic model for the lanthanide elements.

A Generic Biokinetic Model for the Lanthanide Elements

The fifteen elements from $_{57}$La to $_{71}$Lu form the lanthanide, or rare earth, series and many radionuclides of these elements are important in industry, medicine and research. For all the elements in the series the M^{3+} state is the most stable, or only known, oxidation state; the elements possess broadly similar chemical properties and also exhibit many similarities to the corresponding members of the actinide series. Human data on the biodistribution and kinetics of individual lanthanide elements is fragmentary and experimental animal data are far from complete. Thus it has been important to establish the validity of using the limited information available either for individual lanthanides or for actinide elements in order to formulate a generic biokinetic model for the complete lanthanide series.

This generic lanthanide model is outlined in Figure 1 below together with a summary of the chemical, biochemical and physiological considerations used in its formulation.

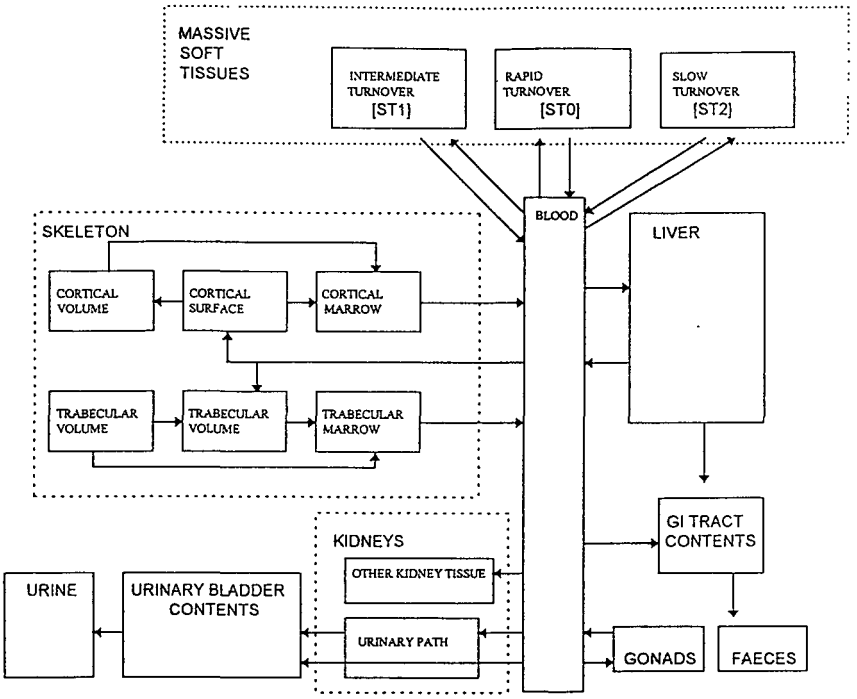

Figure 1. The proposed generic biokinetic model for lanthanides.

Transfer of lanthanides from the gastrointestinal tract to blood — Information on the gastrointestinal absorption of lanthanide elements in humans or animals is sparse. Human data are limited to only two elements. Studies in 2 adult volunteers indicated that the fractional absorption (f_1) of ^{143}Pm was ~1 E-5 and <5 E-6, respectively (Palmer, H. E. *et al. Hlth. Phys.*18,53-61,1970) A dual, stable isotope study of neodymium absorption in four volunteers yielded f_1 values of ~2E-4 to ~4E-3 (McAughey, J. *et al.* Fractional gut

absorption of strontium, barium and neodymium following administration of stable isotope tracers. *Proc 9th. Int. Conf. Heavy Metals in the Environment, Toronto, 1993*). In rats the f_1 of ^{147}Pm ranged from ~1E-4 in fed to 7E-4 in fasting animals. The few direct human measurements suggest that the f_1 for lanthanides is very low and probably lies in a similar range, 1 E-5 to 1 E-3, to that observed in studies of the absorption of the actinides Th, Np, Pu, Am and Cm in a small number of adult human volunteers (Popplewell, D. S., *Appl.Radiat.Isotopes* 46, 279-286, 1995). For this reason, it has been considered reasonable to apply the ICRP Publication 67 recommended general f_1 value of 5 E-4 for unknown forms of Pu, Am and Np to all lanthanides.

The validity of assuming a single f_1 value for all chemically unknown forms of the lanthanides, was examined by a critical review of the relevant chemical properties of the actinides and lanthanides. The absorption of most metallic elements takes place in the duodenal and ileal regions of the human small intestine, where the pH lies in the range ~6 to ~8. Because of their strong tendencies towards hydrolysis and complex formation, free ionic lanthanide-, or actinide-species are unlikely to exist in this pH range and the elements will be present predominantly as unabsorbable hydroxy- or oxo-species, or as insoluble complexes with food residues. An important indicator of this hydrolytic tendency is the ionic charge/ionic radius ratio (*e/r*), which for those lanthanides and actinides whose f_1 values have been measured, is high, e/r = ~25 to ~29. The solubility of the lanthanide and actinide hydroxides is very low, ~0.1 — ~1 mg/dm^3. These considerations give no grounds for expecting physiologically significant variations in the absorption of individual lanthanides from the gastrointestinal tract and they serve to validate the assumption of a single value for f_1 for all lanthanides. The same considerations may be applied to other elements exhibiting similarly pronounced hydrolytic tendencies at pH values > ~3, thus an f_1 value of 5 E-4 can also be proposed for Y, Sc, In and Hf.

The biokinetics of lanthanides following entry into the systemic circulation — Human data on lanthanide biokinetics and deposition are limited to two studies, each in two subjects, of the retention, over a period of about 1 year of intravenously injected ^{143}Pm (Palmer *et al.*, 1970) or ^{88}Y (Etherington, G., *et al.*, In *Radiation Protection–Theory and Practice*, Malvern June 1989,445-448). No very detailed systematic study of the biokinetics of actinides and lanthanides in animals has been published. Animal studies showed deposition in liver and skeleton to account for ~80% of the lanthanide entering the blood, and that uptake in both tissues exhibited approximately linear relationships to ionic radius, *r*, (Durbin, P. W., *Hlth.Phys.***8**, 665-671, 1962). These relationships may be described by the equations:

$$\text{Skeletal uptake (\%)} = -2.3\,r + 260$$

$$\text{Liver uptake (\%)} = 3.0\,r - 250$$

where *r* is measured in picometres (pm).

Analyses of the retention patterns in rats indicates that in rats, at least, the rates of clearance of trivalent lanthanides and actinides from both liver and skeleton are similar. Comparison of the calculated and observed values for the uptake of Pm and Y in human liver and skeleton suggests that these equations are valid for humans, Table 1.

Table 1. Comparison of observed and calculated deposition of Pm and Y in humans.

ELEMENT	SKELETON		LIVER	
	Calculated	Observed	Calculated	Observed
Promethium	43%	40-50%	14	30-40%
Yttrium	13%	~11	11	~65%

Assuming the same uptake–ionic radius relationships to apply to all lanthanides in humans the liver:skeleton deposition ratios shown in Table 2 were calculated.

Table 2.

LANTHANIDE	LIVER:SKELETON RATIO
Lanthanum	60:20
Cerium, Praseodymium, Neodymium, Promethium	45:35
Europium, Gadolinium, Terbium	35:45
Dysprosium, Holmium, Erbium	25:55
Thulium, Ytterbium, Lutetium + Yttrium	15:65

Table 3. Transfer rates for europium, gadolinium and terbium in adults.

GI absorption fraction	0.0005
blood to Liver 1	11.6
blood to cortical surface	3.49
blood to trabecular surface	3.49
blood to urinary bladder content	1.63
blood to kidney (urinary pathway)	0.466
blood to other kidney tissue	0.116
blood to ULI contents	0.303
blood to testes	0.0082
blood to ovaries	0.0026
blood to ST0	10.0
blood to ST!	1.67
blood to ST2	0.466
ST0 to blood	1.386
kidneys (urinary pathway to bladder)	0.099
other kidney tissue to blood	0.00139
ST1 to blood	0.0139
ST2 to blood	0.000019
trabecular surface to volume	0.000247
trabecular surface to marrow	0.000493
cortical surface to volume	0.0000411
cortical surface to marrow	0.0000821
trabecular volume to marrow	0.000493
cortical volume to marrow	0.0000821
cortical/trabecular bone marrow to blood	0.0076
Liver 1 to blood	0.00185
Liver 1 to small intestine	0.000049
gonads to blood	0.00019

Comparison of data for the plasma clearance of Ce, Eu, Tb, Tm, Ac, Am and Cm in rats over the first 24 hours after injection suggests that, to a first approximation, the clearance of the elements from the plasma may be described by the general equation:

$$P(\%) = 70\, e^{-0.03t} + 20\, e^{-0.003t} + 10\, e^{-0.0003t}$$

where t is measured in hours and the coefficients of variation on each constant is ~20%.

In view of these general similarities in the chemical and biological behaviour of the trivalent lanthanides and actinides the development of a generic model for lanthanides, based on that recommended for americium in ICRP Publication 67 [1993], appeared justifiable. The proposed generic model for lanthanides is shown in diagrammatic form in Figure 1; the transfer rate values for europium, gadolinium and terbium are listed in Table 3 above.

This model, which is now being further developed, will be required mainly for the calculation of doses to workers from intakes of radionuclides, therefore no age-dependent parameters are proposed at this time.

Biokinetic models for individual elements

In collaboration with the ICRP Task Group INDOS (formerly AGDOS) work on the age-dependent biokinetic models for the general public for the elements: H, C, S, Mn, Fe, Co, Ni, Zn, Se, Sr, Zr, Nb, Mo, Tc, Ru, Ag, I, Cs, Ba, Ce, Pb, Po, Th, U, Np, Pu, and Am, and these models, together with the dose coefficients for their most important radionuclides have been completed and published. Work has begun on the further refinement of these models, as well as the revision of the biokinetic models for other radiologically important elements, in order to make them suitable for use in assessing internal exposure to radionuclides in workers. This requires an new evaluation of the available information of the effects of the chemical form on the biokinetic behaviour of the element of interest, as well as the extension of the models so that, as far as is possible, they are also appropriate for the assessment of exposure on the basis of measurements of the excretion of the radionuclide of concern in urine and/or faeces.

During the period under review, the first drafts of new proposals for the biokinetic and excretion models for workers for the elements H, C, Co, Zr, Nb, Ru, I, Hf, Pu, Am and Cm were prepared and, in part, discussed with the ICRP INDOS Task Group.

In the model for hydrogen as tritiated water (HTO), the need to be able to use the model to interpret bioassay (excretion) data obtained at long periods after intake, will necessitate the inclusion of a second, long-term, retention function in the model, even though this compartment accounts for only a few percent of the HTO that entered the systemic circulation. Thus the whole body retention function for HTO in adults will be:

$$R(t) = 0.97e^{-0.693t/10} + 0.03e^{-0.693\,t/\,40}$$

where t is measured in days. For organically bound tritium (OBT) the validity of the default retention equation used in ICRP Publication 56 (1989), which assumed that 50% of the incorporated activity entered the body water pool and was lost with an average half-time of 10 days, while the other 50% entered the carbon pool and was lost with an average half-time of 40 days, is not adequate to describe the metabolic fate of the tritium in the wide variety of tritiated organic compounds that may be encountered by workers. Compound-specific models will need to be developed for both hydrogen and carbon and work is in hand to

identify and classify the compounds of most importance in order to define two or three generic models for tritium/carbon compounds.

The age-dependent biokinetic model for cobalt, published in ICRP Publication 67, incorporated the results of a re-evaluation of all the available human data, including some not previously reviewed. For workers, the routes of intake and the range of cobalt compounds to which they may be exposed is larger than for the general public. Thus the influence of the chemical form in which cobalt enters the systemic circulation on its organ and tissue distribution and biokinetics needs to be critically re-evaluated.

Limited human data on the plasma clearance of cobalt injected intravenously as the chloride, the relatively weak glycine complex or as an apparently strong complex with the cytotoxic drug bleomycin, are available for periods up to 24 hours post injection. These suggest, Figure 2, that the Co-bleomycin complex (Co-BLM) is cleared more rapidly than either the chloride or the glycine complex, This conclusion is supported by the more rapid urinary excretion of the unchanged Co-bleomycin complex during the first 24 hours, 88±11%, compared to 34±7% for the chloride and glycinate complexes. A similar pattern is also found for the same three compounds in rats.

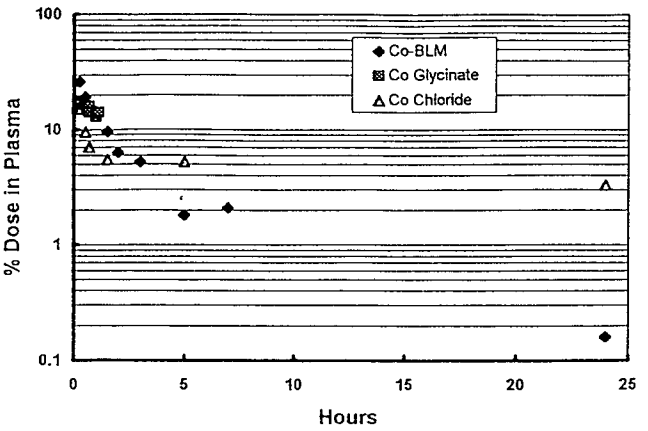

Figure 2. The comparative plasma clearance of $^{57,58}Co$ in human volunteers after intravenous injection of cobalt as chloride, or as the glycine or bleomycin (BLM) complexes.

As mentioned in the discussion of the generic biokinetic model for lanthanides, a re-evaluation of the quite extensive information on the behaviour of americium and curium in experimental animals and of the far fewer human data is also in progress in order to assess the validity of using the biokinetic model developed for americium to describe the behaviour of curium. Based on comparative analyses of the plasma clearance, uptake and retention in liver and skeleton and the excretion of americium and curium, it appears that, to a first approximation, the biokinetic model for americium can also be adopted for curium for the purposes of radiation protection.

Uncertainties in biokinetic parameters

For radiological protection purposes, it is necessary to assume single values for the biokinetic parameters used in the dosimetric models for each element, or for specified chemical compounds of that element. However, these single values can give no indication of the uncertainties in the assignment of the specific value, these uncertainties arise from many sources. For example, the methodological validity, experimental errors; variations between the individuals, animal or human, in the study groups; and, where data from several species have been used to derive a parameter, inter-species variations; in addition further uncertainties may arise from operator bias in the selection of the data from which the parameter is derived. Because the complete range of uncertainties may often be unidentifiable and/or unquantifiable, the validity of applying formal statistical methods for parameter uncertainty analysis to biokinetic parameters used in radiological protection, such as fractional absorption (f_1) from the human gastrointestinal tract, may be questionable. Nevertheless, it is necessary to address the question of the uncertainties underlying such parameters.

The sources of information used to derive biokinetic models for humans have been categorised [A. Bouville and R. W. Leggett - Private communication - *Reliability of the ICRP's dose coefficients for intake of radionuclides*, ICRP/94/C2-6, 1994] as follows:

- H1: direct information based on quantitative studies of the element of interest in humans.
- H2: chemical analogy, that is information derived from quantitative studies of a chemically related element in humans.
- A1: animal analogy, quantitative studies of the element of interest in laboratory animals.
- A2: animal/chemical analogy, information from studies with chemically-related elements in laboratory animals.

Of these categories, H1 and H2 are seen as the most important. Bouville and Leggett proposed that the reliability of biokinetic parameters could be indicated by the assignment of confidence intervals [A,B] such that the central value for adults would be expected with reasonably high confidence (say, 90%) to lie between A and B. Since the available data are often limited the assignment of such confidence intervals may have to be subjective, rather than truly statistical. Six categories were suggested, according to the likely reliability of the specific biokinetic parameter.

An attempt has been made to address the uncertainties in inherent in the assignment of f_1 values for the actinide and some other elements. For the elements which are to be considered here, the most recent assignment of f_1s has been based predominantly on H1 and H2 information with some contributions from A1 data.

The actual value of the absorbed fraction will be *unique* to each intake of the element and may be influenced by such factors as the concentrations of the various complexing ligands in the upper gastrointestinal tract at the time of the intake, which in turn will be influenced by the type of food consumed and the time since the last food intake.

For elements which are very poorly absorbed it must be anticipated that the uncertainties attached to the assumption of any single f_1 value will be quite large, because of both the

errors in the experimental measurement of very low absorption values and the intra- and inter-individual variations must be expected to be relatively large.

In order to attempt to assess the likely variability of the values assumed for the fractional absorption [f_1] of actinides, lanthanides and barium, both human and animal data, have been examined and an attempt has been made to estimate likely values of A and B. Table 4 summarises the human data for Pu, Am, Cm, Np, Th, Nd, Pm and Ba together with the coefficients of variation and 90% confidence limits for each set of observations.

The very much larger body of data from animal studies, which is not listed here, indicate that the median value for the coefficients of variation actinide elements is ~ 35%: this corresponds to 90% confidence limits of 45% and 155% of the mean fractional absorption; this yields a B/A value of ~3.

Comparing the human data for actinides and lanthanides, presented in Table 1, the currently assigned value of 5E-4 for the fractional absorption of soluble, or unknown, assumed to be soluble, compounds lies reasonably close to the mean values observed in the human studies. The uncertainties of the observed data support Bouville and Leggett's assignment of the actinides to uncertainty category IV for which $3 \leq B/A \leq 5$. Thus, the actual values which would be observed in the majority of individuals would probably lie within a factor of ~3 on either side of the assigned value, namely between ~1E-4 and 1.5E-3.

A preliminary analysis of the data for the fractional absorption of barium indicate that the uncertainty is probably less than that estimated for the actinides and lanthanides, perhaps falling into the Bouville and Leggett Category III $2 \leq B/A \leq 3$,_with the values observed in the majority of individuals lying 0.05 and 0.30, the f_1 value presently assigned for the general public being 0.20.

Table 4 - Summary of human data for the fractional absorption of some actinide and lanthanide elements and barium.

Element	*n*	Range	Median	mean ± SD	90% CL A	90% CL B	B/A
			Fractional absorption x E4				
Pu	2	8 - 10	9	9			
Pu	8	02 - 4.9	1	2	0.8	4	5
Pu	5	2 - 9	8	6 ± 4	3	12	4
Am	8	0.4 - 3	1	1	0.4	2	5
Cm	5	0.9 - 3	2	1.6 ± 0.8	1	3	3
Np	5	1 - 3	2	2 ± 0.6	1	3	3
Th	4	1 - 6	2	3 ± 2	1	6	6
Nd	15	0.6 - 6	2	3 ± 2	2	4	2
Pm	2	0.5 - 1					
			Fractional absorption x E0				
Ba	20	0.01 - 0.64	0.18	0.23 ± 0.18	0.15	0.30	2

Comparing the human data for actinides and lanthanides, presented in Table 1, the currently assigned value of 5E-4 for the fractional absorption of soluble, or unknown, assumed to be

soluble, compounds lies reasonably close to the mean values observed in the human studies. The uncertainties of the observed data support Bouville and Leggett's assignment of the actinides to uncertainty category IV for which $3 \leq B/A \leq 5$. Thus, the actual values which would be observed in the majority of individuals would probably lie within a factor of ~ 3 on either side of the assigned value, namely between $\sim$ 1E-4 and 1.5E-3.

A preliminary analysis of the data for the fractional absorption of barium indicate that the uncertainty is probably less than that estimated for the actinides and lanthanides, perhaps falling into the Bouville and Leggett Category III $2 \leq B/A \leq 3$, with the values observed in the majority of individuals lying 0.05 and 0.30, the f_1 value presently assigned for the general public being 0.20.

In collaboration with other members of the INDOS Task Group of ICRP this type of uncertainty analysis is being extended to cover the fractional absorption of all radionuclides of radiological importance.

Publications

Taylor, D. M. and Gillis, T. M. (1994) Attempts to correlate biokinetic behaviour with specific physico-chemical parameters within chemical families: Alkali metals and lanthanides. *Radiation Protection Dosimetry*, **53**, 183-186.

International Commission on Radiological Protection* (1993) ICRP Publication 67. Age-dependent Doses to Members of the Public from Intakes of Radionuclides: Part 2 Ingestion Dose Coefficients. *Annals of the ICRP*, **23**(3/4).

International Commission on Radiological Protection* (1995) ICRP Publication 69. Age-dependent Doses to Members of the Public from Intakes of Radionuclides: Part 3 Ingestion Dose Coefficients. *Annals of the ICRP*, **25**(1).

Taylor, D. M., The influence of the chemical form injected on the biokinetics and distribution of cobalt in animals and humans: A review. *In preparation.*

Taylor, D. M and Leggett, R. W., A generic biokinetic model for the lanthanide elements. *In preparation.*

[*ICRP Publications are published only in the name of the Commission. The two publications cited were prepared by a task group of which the following European Union scientists were members — J. D. Harrison (GB), A. Kaul (D), G. M. Kendall (GB), H. Metivier (F), D. Noßke (D), M. Roy (F), J. W. Stather (GB) and D. M. Taylor (GB).]

Head of project 4: Dr. van Rotterdam

II. Objectives for the reporting period

The first objective of the project was to develop general models for the biokinetic behaviour of ingested radionuclides. These compartmental models should be suited to describe systems with residence times of widely different magnitude, in order to properly study the influence of newly obtained experimental data and to evaluate, among others, the effect of different gastro-intestinal properties on the cumulated activity. Also the effect of possible non-linear aspects of digestion on the cumulated activities should be incorporated in the models.

Problems concerning the modelling of biokinetic behaviour of radionuclides are, for instance, the justification of the models and the verifiability. These aspects are of major importance for the dosimetry because poorly modelled biokinetics may easily lead to serious over- or underestimation of the deposition of radionuclides in the body and, hence, to uncertain dose estimates. It was therefore an objective to investigate these problems.

III. Progress achieved including publications

The development of general compartmental models

Based on the assumption that the processes underlying the deposition and clearance of radionuclides in the organs of the body can only be specified in discrete time steps, we reformulated the biokinetic processes by means of difference equations. We, hence, refrained from the use of redundant differential equations which, anyhow, have to be replaced by discrete approximations because only the latter can be manipulated numerically.

A straight-forward algorithm for the solution of coupled difference equations has been developed and has been incorporated in a computer system COMPART. This system enables the evaluation of outputs of linear multi-compartmental models of arbitrary complexity (including recycling) which can be excited instantaneously or by means of time-varying forcing functions.

The program is menu directed and can be operated in an interactive way. It runs on any personal computer with a MS-DOS operating system and a hard disk with a capacity of, at least, 20 MB. Input, output and system information is stored in files and can be easily manipulated by means of simple spreadsheet techniques. Input, output and computation sampling intervals as well as the time span of the output signals can be chosen. Simple plotting routines enable the representation of the different signals as a function of time.

With COMPART a number of simulations of well known metabolic processes have been performed. The time behaviour of the activities and cumulated activities could be accurately estimated. Hence, it can be concluded that COMPART can be a valuable tool for the computation of retention and clearance of radioactive compounds.

Until to date, the question of model uncertainty has not been answered. One aspect of this problem concerns the physiological relevance of the model parameters and the answer can only be obtained by further physiological experimentation. Another aspect, however, concerns the intrinsic stochastic behaviour of the radioactive compounds in the body.

We therefore developed a stochastic algorithm and implemented this in COMPART as a second computational mode. The algorithm is based on the assumption that residence times of elementary amounts of a radioactivity in an organ or part of an organ, have no fixed value but are governed by a stochastic process.

In the first order description of biokinetics the distributions of the residence times will be negative exponential. A second probability, determined by the coupling between the compartments, describes the transport of the activity from one to another compartment.

In the stochastic mode of COMPART it is therefore possible to simulate different realisations of the same biokinetic process. These simulations allow the user to judge whether measured activities have only an accidental character or are caused by significant kinetic properties of the organs under study.

Finally it has to be mentioned that these stochastic simulations can be performed with integer numbers so that the computation does not introduce any additional inaccuracies.

Parameter estimation of compartmental models

Until to date, the question whether linear compartmental models rightly describe the retention, deposition and clearance in the different organs after inhalation or ingestion of radionuclides has not yet been satisfactory answered.

We succeeded in mimicking the intrinsic stochastic behaviour of radioactive compounds in an organ by means of models simulating negative exponentially distributed residence times and randomly varying coupling coefficients between the different compartments.

The attention has also been focused on the reliability of the model parameters which, in general, are obtained from physiological experimentation. To that end we simulated deposition, retention and excretion in biokinetic models of increasing complexity and tried to estimate the model parameters by means of an advanced recursive parameter estimation technique which is known as Kalman filtering. This maximum likelihood estimation not only makes an optimal use of the available data but also allows the estimation of the covariance matrix of the parameter vector. This information on the confidence intervals of the parameter vector is needed to decide whether one model differs significantly from another one.

From the Kalman estimation on computer generated excretion of models with two, three and four compartments with residence times in the order of magnitude of one, ten, hundred and thousend days we can state the following:

The number of parameters representing the compartmental model is twice the number of first order compartments constituting the model.

If parameters can be properly estimated, i.e. their variances are small in relation to the expected values, the parameter vector forms a sufficient description of the model. This does not mean, however, that the parameters can be identified as representing real physiological mechanisms, because a given transfer function between in- and output can be realized by a multitude of equivalent systems which cannot be discriminated.

The updated estimates converge to limit values in the course of the recursion. However, the question whether these limits constitute proper unbiased estimates is not easily answered in models with more than three compartments.

In these multiparametric models a proper convergence can only be reached if the recursion starts from initial values for parameters and covariance matrix which are not too far away from the true values. In many estimation trials only false local limits could be reached.

Several modifications of the original Kalman algorithm have been developed and implemented such as a forget function and the selective skipping of samples. However the performance of the estimation for models with parameters of widely different magnitude could not be improved.

It is well known that Kalman filtering is one of the most efficient and accurate methods for the estimation of the system parameters and their spreads. It can, therefore, be safely concluded that the various other estimation methods which have been applied and described in the literature on dosimetry do not show a better performance than Kalman filtering. Consequently, biokinetic parameters published until to date should be re-evaluated.

In the field of radiological protection and dosimetry there is a tendency to develop models with increasing complexity. The question, however, remains whether these multicompartmental models can be identified as realistic models of the deposition and transport of radionuclides.

From the above it seems reasonable to state that complex models with parameters of widely different magnitude do not contribute to better estimates of cumulated activity and hence to more precise dose estimates.

Non-linear aspects of gut transport

For the gastrointestinal-(GI-)tract it has been investigated whether simple non-linear models could explain the time course of activities and cumulated activities (CA's) in the different regions of the GI-tract in a better way than the the conventional linear ones. For instance, the ICRP-30 model assumes a continuous excretion of faeces. This is certainly not a realistic assumption since the large intestine (LI) is regularly, typically once a day, emptied via the sphincter.

Hence in a preliminary model study, the lower large intestine (LLI) compartment of the ICRP-30 model was adapted as follows. Over one day the contents of the LLI was simply accumulated (average wash-out rate zero) and the compartment was emptied once a day instantly by resetting the cumulated activity to zero level.

Simulation results indicated that, in comparison to the linear model, the activity in the LLI reaches a higher peak but that the cumulated activity as function of time was only slightly influenced. It might be that the original four compartmental representation of the GI-tract masks the effect of emptying but that a more sophisticated chain model of both the small and large intestines would show an outspoken effect of instant emptying.

Therefore the original small intestine (SI) compartment was subdivided in four compartments with an average residence time of one hour each. Also the upper large intestine (ULI) compartment as well as the LLI compartments were subdivided in 12 and 24 equal compartments respectively.

In doing so, it appeared that the cumulated activities in the intestines were 10-20 per cent higher than in the conventional model. A regular emptying in this chain model caused the CA's to become lower than in the conventional model. The CA in the blood compartment connected to the GI-tract model by means of an absorbtion coefficient, however, increased considerably as a consequence of instantaneous emptying.

It has to be noted here that saturation non-linearities were introduced in every compartment of the chain in order to avoid accumulation in the 24'th compartment of the LLI only. As a consequence of this saturation mechanism accumulation in the LLI accumulation is propagated backwards from the sphincter on.

From a dosimetric point of view, the above simulation results indicate that CA's in the GI-tract can only indicatively be modelled. More precise estimations of dosimetric quantities in the GI-tract can only be made if reliable physiological data on gut transport become available.

Publications

van Rotterdam, A., Schultz, F.W., Hummel, W.A., Zoetelief, J., Broerse, J.J. and Nyqvist, C., PCDOSE: An Interactive Software System to Calculate Internal Radiation Dose on a Personal Computer, Comput. Biol. Med. 21:43-59 (1994).

van Rotterdam, A. and Schultz, F.W., Stralingsbescherming van patienten by toepassing van nucleaire geneeskunde, WVC proj. RST90-06 (1993). (Radiological protection of patients in nuclear medicin, report of the dutch ministry of health)

Beekhuis, H., Broerse, J.J., Claessens, R.A.M.J., Delhez, H, Noteboom, J.L., van Rotterdam, A. and Zoetelief, J., Stralingsbelasting van leden van de bevolking als gevolg van medische toepassing van radiofarmaca: consequenties for ontslagcriteria, VROM rapport 1992/55 (1992). (Radiological burden of members of the population caused by the administration of radiopharmaceuticals, report of the dutch ministry of housing, planning and environmental research).

Battermann, J.J., Broerse, J.J., van Kleffens, H.J., Koedooder, C., Mijnheer, B.J., van't Riet, A., van Rotterdam, A., Visser, A.G. and Zoetelief, J., Stralingsbelasting van leden van de bevolking als gevolg van permament geimplanteerde radioactieve bronnen voor radiotherapie, VROM rapport (1993). (Radiological burden of members of the population cuased by permenently implanted closed radioactive sources for radiotherapy, report of the dutch ministry of housing, planning and environmental research).

van Rotterdam, A. COMPART: An Algorithm for the Evaluation of Large Compartmental Models with Residence Times of Widely Different Magnitude (submitted for publication in Computers in Biology and Medicine).

Head of project 5: Dr. Andrási

II. Objectives for the reporting period

Since the main objectives of the project were directed to improve the knowledge on internal dose assessment considering new findings on more realistic biokinetic models and model parameter values, the specific objectives of our participation were selected accordingly to be able to contribute to the main aim of the project. These are the followings:

- We planned to investigate the frequency distribution of whole-body retention parameters of caesium in humans based on large number of whole-body counter measurements and assuming close correlation between potassium content in the body and caesium retention parameter values. The study was intended to be extended to investigate also the sex and age dependence as well as the various influencing factors which are contributing to the final frequency distribution patterns.
- New versions of a general computer code for biokinetic model calculations was planned to be developed for the model structures given in the ICRP Publications 30,56 and 67 as well as considering also the new respiratory tract model recommended in ICRP Publication 66. The computer code is based on a quasi-analytical procedure which has been developed to handle arbitrarily chosen multi-compartment models providing several advantages compare to other numerical methods. The calculated results on selected radionuclides was intended to be compared with those obtained by other participating contractors.

III. Progress achieved including publications

According to our planned working programme and after the discussions with the co-ordinator the following investigations have been carried out and results achieved in the relatively short period of time.

Distribution parameters of caesium in humans

The fission product caesium radionuclides, ^{137}Cs and ^{134}Cs, play an important rule in internal dose received by members of the population as the consequence of reactor accidents or nuclear weapon tests. Better knowledge on the biokinetic parameters of these radionuclides leads to more realistic dose estimate. Since these parameters, apart from their age and sex dependence have also individual variability, it is worth to investigate quantitatively and characterize statistically these variations.

In this study the individual variability of the parameters of the systemic retention function were investigated which has the following form according to the ICRP Publ. 30 and 56 recommendations;

$$R(t) = a \exp [- 0.693\ t/T_1] + (1-a) \exp [- 0.693\ t/T_2]$$

where the coefficient a and the half lives T_1 and T_2 are independent parameters to be investigated.

The study was based on whole-body potassium measurements assuming the validity of close correlation between potassium content and the above given retention parameters of caesium according to a predicting model suggested by R.W. Leggett [Health Physics 50/6, 747 (1986)]. The basic investigated data set was obtained by measurements of the whole-body counter of our institute. Altogether the whole-body counting results of 286 adult male and 84 adult female subjects were investigated together and separately in two age groups, namely from 20 to 40 and above 40 years of age. The frequency distribution of the three independent parameters of the given two-exponential function was studied by fitting normal and log-normal distributions. According to the goodness-of-fit in most cases slightly better fit were obtained when log-normal distribution was assumed, however the differences were not significant.

The most characteristic results of these statistical investigations obtained for the three parameters as mean values and for their standard deviations assuming normal distribution together with the ICRP recommended parameter values are shown in the following table:

Table 1

Sex	Age-group [year]	a	σ_a [%]	T_1 [day]	σ_{T1} [%]	T_2 [day]	σ_{T2} [%]
m	20-40	0.091	25	1.5	29	113	12
m	40-	0.104	25	1.7	29	106	12
f	20-40	0.160	24	4.8	15	102	16
f	40-	0.160	18	4.8	12	101	13
ICRP	adults	0.1	-	2	-	110	-

As it is seen the calculated mean values of the three parameters are quite close to the ICRP recommended values and their standard deviations varied from 12% to 25% depending on the investigated age and sex groups.

For better illustration the frequency distributions of the potassium content and the three parameters for males between 20 and 40 years are shown in Fig. 1.

The investigated data sets represented the final results of whole-body counter measurements which contained the spread of data of different origin. To consider the contribution due to the applied scanning WBC technique (reproducibility, geometry, counting statistics, body size, etc.) and of the short term variation of whole-body potassium to the total frequency distribution pattern, the data obtained by repeated measurements on selected individuals were also investigated. The measurements of 5 male and 10 female subjects have been repeated 15-27 times within a relatively short time period in which no significant age and weight variation could be expected. The frequency distributions were investigated and spread of retention parameters was characterized by their standard deviations. The averaged standard deviations are shown in Table 2:

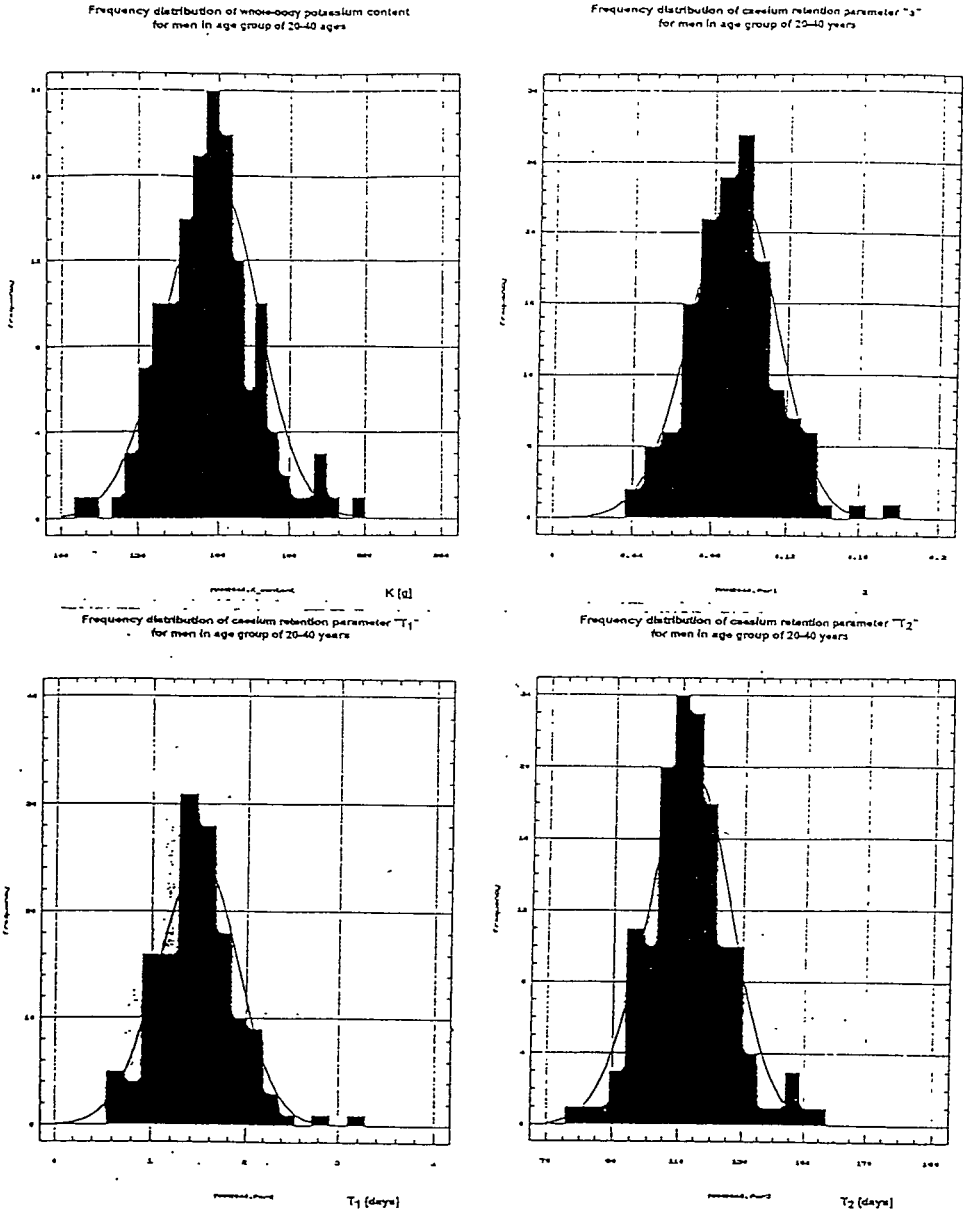
Frequency distribution of whole-body potassium content
for men in age group of 20-40 ages
K [g]
Frequency distribution of caesium retention parameter "a"
for men in age group of 20-40 years
Frequency distribution of caesium retention parameter "T1"
for men in age group of 20-40 years
T1 [days]
Frequency distribution of caesium retention parameter "T2"
for men in age group of 20-40 years
T2 [days]

Fig. 1

Table 2

Sex	σ_a [%]	σ_{T1} [%]	σ_{T2} [%]
m	13	14	6
f	13	8	9

These figures are characteristics to our measuring conditions (scanning bed technique, least squares spectrum resolution, etc.), while another whole-body counting method can provide another feature of these data. For instance the data measured by a four detector stretcher arrangement on selected individuals show about half of the values of the above given Table 2 [H. Doerfel, Personal communication]. However considering even our data this source of error is reducing the parameter total uncertainties (see Table 1) by 2-5% only. On this reason due to the biological variability the data given in Table 3 are more realistic figures for adults disregarding age dependence:

Table 3

Sex	σ_a [%]	σ_{T1} [%]	σ_{T2} [%]
m	21	25	10
f	16	11	12

For comparison we investigated data sets measured on adult subjects from the territory of the previous Soviet Union measured by a German WBC laboratory using single detector chair technique [E. Werner, Personal communication] The standard deviations of the caesium retention parameters derived by the given method are shown in the next table.

Table 4

Sex	σ_a [%]	σ_{T1} [%]	σ_{T2} [%]
m	21	23	12
f	21	13	16

The figures in Table 4 are quite close to the values obtained by using our measurements, which confirm the validity of the outcome of our investigations. It is to be mentioned that G. Schwarz and D.E. Dunning found much larger values for these distribution parameters that is 40, 32 and 27 percent for a, T_1 and T_2 respectively [Health Phys. 43/5, 631 (1982)]

Development of mathematical method in model calculation and application for internal dosimetry

The ICRP has recently published new recommendations for internal dose calculation to be applied to workers and all members of the public, namely

- ICRP Publication 56: Age dependent doses to members of the public from intake of radionuclides: Part 1 (1990),

- ICRP Publication 67: Age dependent doses to members of the public from intake of radionuclides: Part 2 (1993),

- ICRP Publication 69: Age dependent doses to members of the public from intake of radionuclides: Part 3 Ingestion dose coefficients (1995),

- ICRP Publication 66: Human respiratory tract model for radiological protection (1994).

These new recommendations summarize the increased knowledge on human anatomy and physiology and give a revision of ICRP 30 (1979). Both the age-dependency of internal dose and the more exact information on human respiratory system have resulted more complexity in biokinetic models and calculation methods.

In our whole body counting laboratory a quasi-analytical mathematical method was applied to solve linear compartmental models [Beleznay and Beleznay, Vienna: IAEA; IAEA-SM-276/48; 1985: 475-488]. This method use an exact numerical solution of the linear compartmental model based on matrix exponentials and its main advantage in comparison with other numerical solution of the coupled differential equation systems is that it is very fast and numerically stable even in cases when the transfer constants (and rates) differ many orders of magnitudes ($\sim 10^8$). In addition, retention curves are obtained in closed analytical form as a sum of exponentials. This gives the possibility to evaluate the total number of transformations of the radionuclide in any compartment by simple integration and any type of excretion (urine, faces, milk, saliva,...) as a function of time.

Based on this method the following essential extensions have been finished in frame of the present project:

- maximum number of compartments is 70 (based on a 32 bits extension of the standard PC programming tools);
- retention and excretion can be obtained in cases of single, continuous and interrupted intakes (which is more realistic for an occupational contamination);
- any possible intake pattern can be handled for a given radionuclide (inhalation, ingestion, injection, wound deposition, in any body region).

The program was tested by comparison of the calculated integrals for organs and tissues applying the new biokinetic data from ICRP Publ. 56 and 67 with those given in ICRP Publ. 30 (in Supplements). The total number of nuclear transformation over 50 years in different organs and tissues were computed for ^{134}Cs, ^{137}Cs, ^{103}Ru, ^{106}Ru, ^{95}Zn and ^{95}Nb in age group 'adults'.

To calculate age-dependent doses correctly, the age-dependency of the Specific Effective Energy (SEE(T←S);t) is also required besides of biokinetic parameters. We plan to follow our effort in this direction.

Model calculation was carried out by studying the features of the new lung model proposed in ICRP 66.

The thoracic retention was investigated in the case of poorly dissolving materials (Type S) assuming different aerosol sizes in the range of AMAD = 0.1-20 μm. As it was expected, the activity integral of the lung basically determined by the deposition in the alveolar interstitial (AI) region. The fractional deposition in AI is a function of the aerosol particle size. Normalizing the retention data to the time over the early rapid clearance period (t_{ref} = 5 -10d), the slope of the retention curves will be very similar and almost independent from the inhaled particle size (Fig. 2). If the initial lung deposition is extrapolated from the actual lung deposition on the reference (normalization) day, the activity integral over 50y will differ less than 15% in the range of particle size 0.1-20 μm.

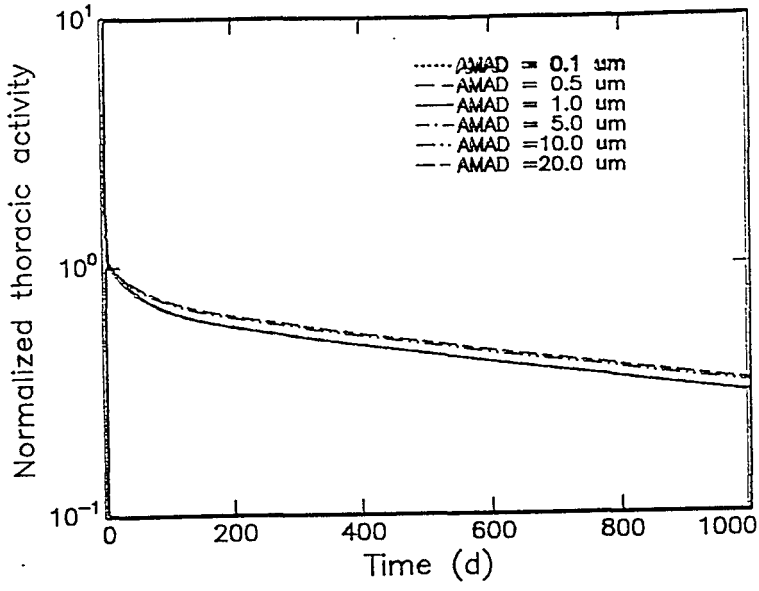

Fig. 2 Calculated thoracic retention in case of poorly dissolving materials (Type S); $s_p = s_{pt} = s_t = 0$

Whole body retention data after accidental inhalation of ^{60}Co aerosols were compared with model prediction applying the new lung model for Type M materials. [Beleznay, É.; Osvay, M. Health Phys. 66: 392-399; 1994] Measured data and the model-calculations are presented on Fig. 3 a-b.

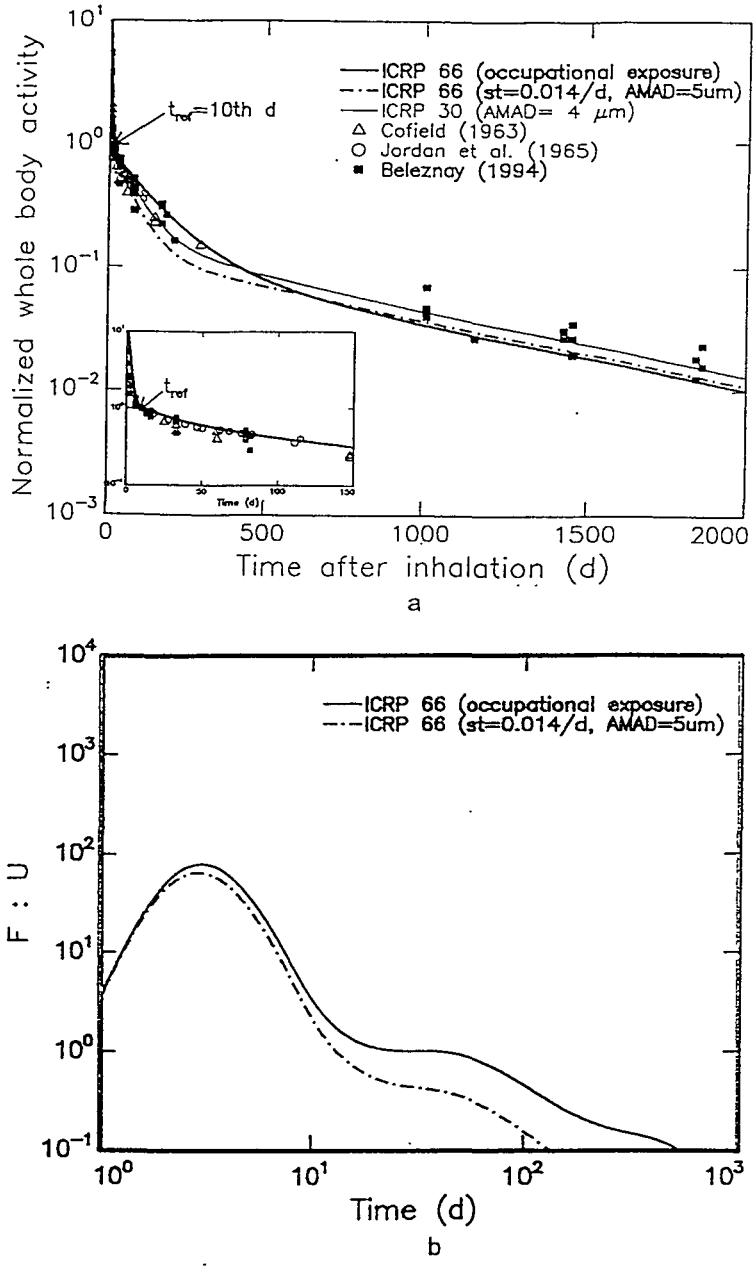

Fig. 3 Comparison of measured and calculated retention of ^{60}Co aerosols (Type M).
a) Whole body retention
b) Ratio of faecal to urinary excretion

Publication

A. Andrási, Investigations on frequency distribution of whole-body retention parameters of caesium in humans. (Submitted as a paper for the IRPA 9 Congress on Radiation Protection to be held in Vienna, (1996)

Head of project 6: Dr. Toader

II. Objectives for the reporting period

The accident from the Chernobyl nuclear power plant allowed us to perform an experiment in which large population groups have ingested continuously, during nine years after Chernobyl, variable amounts of Cs^{137} and Sr^{90}. The measurements we have made gave us the possibility to:

- estimate caesium and strontium dietary intake and urinary excretion, as well as the accumulation, equilibrium and elimination periods for adults and children of different ages;
- asses the internal doses due to the continuous ingestion of variable amounts of caesium and strontium, for adults as well as for children;
- estimate the excedentary cancer risk due to internally deposited caesium and strontium
- characterise the transfer of Cs^{137} from mother to 5-11 weeks embryos, when the mother ingested continuously different amounts of caesium, and to compare the results with the transfer process from mother to embryos in the case of a prolonged but constant intake of the mother.

III. Progress achieved including publications

Source of samples

All the samples were prelevated since April 1986 until April 1995, during nine years after the Chernobyl accident, in the Bucharest area.

The first population group, selected for this study, was a group of adult men, aged between 25 and 40 years, without any health problems, hard labourers. The food samples were prelevated from the restaurant of the factory, where their were all taking their meals. Usually, the food was prelevated in the second part of every month. The urine samples were prelevated two days after prelevating the food samples. The urine was prelevated for minimum 24 hours.

A second group of study consisted in children, separated in three age subgroups: 4-6 years old, 7-9 years old and 10-12 years old. These children were living in the kindergartens and schools hostels. The data for the dietary intake and urinary excretion for the children were then compared with similar data for the adult women working as teachers and educators at the same schools, and taking their meals together with the children. The food samples were prelevated from restaurants of the schools. The 24 hour urine samples were prelevated the next day after the prelevation of food samples.

The embryos used to determine Cs^{137} content in embryos were prelevated from the Obstetrics and Gynaecology Department of the Military Hospital from Bucharest.

Radiochemical and chemical analysis

Caesium-137
The method applied is presented largely in HASL-300 EML Procedures Manual. After digesting the samples in nitric acid, caesium, rubidium and potassium are extracted from solution with ammonium phosphomolybdate (APM). Finally, caesium is collected as caesium chloroplatinate.

Strontium-90
The method presented in HASL-300 EML Manual is used to separate strontium-90. The samples are prepared by dry ashing and then digested in nitric acid. Separations with fuming HNO_3 remove the calcium and most other interfering ions. Radium, lead and barium are removed with barium chromate. Traces of other fission products are scavenged with yttrium hydroxide. After attaining Sr^{90}-Y^{90} equilibrium, Y^{90} is precipitated as yttrium hydroxide and converted to yttrium oxalate for counting.

After the radiochemical separation of caesium and strontium, the radiometric measurement was performed with a low-level anticoincidence beta counting system, with high efficiency.

Caesium-137 dietary intake and urinary excretion data for adults

During the nine years of our study, the quantity of ingested Cs^{137} varied a lot from one year to another. As expected, the caesium-137 intake had the highest value in the first year after the accident. The peak of the caesium-137 intake was reached in May 1986, when the average daily ingested quantity was 408.5 Bq. Beyond this date, the ingested quantity of caesium is continuously decreasing, until October 1986, when a new peak occurs in the intake plot. This new increase was an artificial fact, due to some local conditions, and was presented in previous papers.

Beginning with October 1986, the quantity of Cs^{137} intake by diet was continuously decreasing. However, a very small peak occurs again, at about 700 days after the accident. This is possible to be due to Cs^{137} migration in soil. The experimental data are very well fitted by the following "dietary intake function":

$$I(t) = 1.8410^{-2} \cdot t^{4.31} \cdot \exp(-0.16t) + 184\exp\left[-\left(\frac{t-220.52}{186.56}\right)^2\right] + 23.27\exp\left[-\left(\frac{t-683.4}{193.5}\right)^2\right]$$

with t - the time elapsed after the accident, in days. As it can be seen, the three peaks presented above are present in the equation, too. The continuous (and fast) decrease of Cs^{137} intake lead to an average daily value of 0.102 Bq in March 1995.

After the Chernobyl accident, Cs^{137} amount in urine was increasing every month, until it reaches its highest value in October 1986 (38 Bq/day). To begin with November 1986, Cs^{137} urinary excretion is slowly decreasing, until it reaches an average daily value of 0.088 Bq, in March 1995. The shoulder that occurs at 500 days is probably due to the second intake

peak, from October 1986. The measured values were fitted with an "urinary excretion function", presented below:

$$E(t) = 29.951\left[\exp\left[-\left(\frac{t-234.73}{111.84}\right)^2\right] + \exp\left[-\left(\frac{t-470}{376.79}\right)^2\right]\right]$$

where t - the time elapsed from the accident, in days.

The experimental results were compared with the results predicted by ICRP 10A, and the conclusion was that there is a good agreement between the theoretical predictions and the measured values, as presented in a previous paper.

Some conclusions concerning the metabolism of caesium in human organism, were drawn using the "observed ratio" - OR - during these nine years. The observed ratio was defined as:

$$V = \left(\frac{Cs\text{-}137_{urine}}{K_{urine}}\right) / \left(\frac{Cs\text{-}137_{intake}}{K_{intake}}\right)$$

In the nine years elapsed from the accident, the OR took values ranged between 0.017 and 1.456. The distribution of these values was the following:

- immediately after the accident there was a continuous increase of the OR, since t=0 days (April 1986) until t=600 days after the accident; this was the accumulation period, when most of the ingested Cs^{137} was assimilated by the organism;
- in the time interval from 600 days to 2800 days, the OR values were spread around 1, which would mean that an equilibrium was reached among Cs^{137} intake and Cs^{137} excretion;
- after 2800 days, the OR tends to increase to values above 1, which would mean that the de-assimilation process of caesium has began. This last period could last a few years.

Caesium-137 dietary intake and urinary excretion data for children

During 1986 - 1995, we have selected four time periods in which we have studied the dietary intake and urinary excretion of Cs^{137} at children, for three age groups: 4-6 years, 7-9 years and 10-12 years. In order to make a comparison, we have also studied a group of women, with ages between 24 and 49 years.

The first period was September 1986 - December 1987. From the point of vue of the ingestion and excretion processes, this was the most complex period. During this period, an intake peak occurred in October 1986 at all the age groups, including the women. This is probably due to the same reasons presented above. After this date, Cs^{137} dietary intake is continuously decreasing, but the slope of the decrease is age-dependent.

A general characteristic for this time period is the continuous increase of the OR values, for all the age groups, including women. The differences between the age groups are given by

the times at which the "quasi-equilibrium" occurs (the plateau of the OR versus time plot), as well as the value of the plateau.

At 4-6 years and 7-9 years children, the OR reaches the plateau (the "quasi-equilibrium state") in April 1987 while at 10-12 years old children the plateau occurs in May 1987. The values of the OR, in the plateau zone, are also different, as it follows: the quasi-equilibrium value of the OR varies around 1.6 for 4-6 years old children, around 1.3 for 7-9 years old children and around 1.2 for 10-12 years old children.

The data about Cs^{137} dietary intake and urinary excretion at children and women, in the next three periods (May 1988 - August 1989, January 1991 - December 1991 and April 1994 - March 1995) confirmed and completed the conclusions drawn from the data collected in the first period.

During all these three periods, caesium intake and excretion decreased at all age groups. During the ninth year after the accident, the average caesium intake by children was 0.046 Bq/(gK.day), while the average for excretion was 0.056 Bq/(gK.day). It is worth to mention that, during May 1988 - March 1995, the amount of excreted caesium was higher then the amount of ingested caesium.

The OR analysis for this long period (1988 -1995) leads to the following conclusions:

- within the same age group, the OR tends to decrease as the time goes by; for example, at the 4-6 years old children, the OR decreased from an average value of 1.643 in 1988 - 1989 to 1.544 in 1991, then to 1.256, nine years after the accident.
- if we are considering the same time interval, the OR is decreasing as the age of the children is increasing; for example, during May 1988 - August 1989, the average OR was 1.643 for 4-6 years children, 1.486 for 7-9 years children and 1.289 for 10-12 years children. During the ninth year elapsed from the accident, 4-6 years children still have the highest average for OR values.

This experimental findings seem to indicate that caesium is as faster eliminated from the organism, as the organism is younger.

We have also studied the correlation between the Cs^{137} dietary intake and the Cs^{137} urinary excretion. The equations obtained are the following:

$$E_u = -0.0635 I_d^2 + 1.90 I_d - 0.107 \text{ (for 4-6 years)}$$
$$E_u = -0.0727 I_d^2 + 1.66 I_d - 0.047 \text{ (for 7-9 years)}$$
$$E_u = -0.0342 I_d^2 + 1.46 I_d - 0.109 \text{ (for 10-12 years)}$$
$$E_u = -0.0282 I_d^2 + 1.10 I_d - 0.036 \text{ (for adult women)}$$

where E_u stands for Cs^{137} urinary excretion, and I_d stands for Cs^{137} dietary intake.

As it can be seen, the values are correlated by quadratic equations, but the coefficient of the quadratic term is much smaller than the coefficient of the linear term (there is a difference of two magnitude orders), which mean that the correlation could be very well approximated by linear equations.

Sr^{90} dietary intake and urinary excretion data for adults

The study effectuated after the Chernobyl accident lead to the conclusions that there was a continuous Sr^{90} dietary intake, in different amounts.

It could be seen that there is a strong variation of strontium intake during April 1986 - March 1995. To begin with May 1986, Sr^{90} dietary intake increased continuously, until it reached 1.48 Bq/(gCa.day) in October 1986 Strontium intake remains at high values until April 1987, then it decreases continuously. The highest value of strontium intake occurred in the first year after the accident, when an average daily value of 1.07 Bq/gCa was reached. That value decreased to an average daily value of 0.36 Bq/gCa in the fifth year, then to 0.086 Bq/gCa in the ninth year after the accident.

Before the Chernobyl accident, Sr^{90} urinary excretion, for the Bucharest population, had very low values (it was practically unexistent). After the accident, strontium urinary excretion increases continuously, until it reaches its peak value of 1.52 Bq/(gCa.day), in December 1986.

Strontium excretion maintains high values until April 1987, then decreases continuously. In the first year after the accident the average Sr^{90} daily excretion was 0.088 Bq/gCa, then it decreases to an daily average of 0.067 Bq/gCa, in the ninth year after the accident.

The intake-to-excretion balance for strontium is reflected by the "observed ratio" (OR), defined here as:

$$V=\left(\frac{Sr\text{-}90_{urine}}{Ca_{urine}}\right)/\left(\frac{Sr\text{-}90_{intake}}{Ca_{intake}}\right)$$

The plot of the OR values evidenced two distinct periods:

- since April 1986 until September 1987, the OR has sub-unitary values, which mean we are still in the assimilation period;
- after September 1987, the OR values are varying around 1, meaning that an equilibrium was reached between strontium intake and excretion.

We could not detect any de-assimilation period.

All these data are now studied in order to obtain a mathematical model of these metabolic processes.

Sr^{90} dietary intake and urinary excretion data for children

During 1986 - 1994, we have selected three time periods in which we have studied strontium-90 dietary intake and urinary excretion for three groups of children: 4-6 years children, 7-9 years children and 10 -12 years children. In order to compare their metabolism with the metabolism of the adults, we have performed the same measurements for a group of adult women.

The first interval of study was September 1986 - September 1988. During this time, Sr^{90} dietary intake and urinary excretion was studied for a group of 4-6 years children and for group of adult women, aged between 24 and 49 years. The maximum strontium intake in children was 1.198 Bq/(gCa.day), reached in October 1986. Strontium dietary intake in 4-6 years children remained at values higher than 1 Bq/(gCa.day) until March 1987, then decreased quite fast, and reached 0.326 Bq/(gCa.day) in September 1988.

Since September 1986 until September 1988, strontium intake in adult women had constantly higher values than the values measured for children. Therefore, the average strontium intake during this period was 0.927 Bq/(gCa.day) for adult women, while the average for children was 0.614 Bq/(gCa.day).

Maximum strontium intake in women was reached in October 1986 (1.594 Bq/(gCa.day)). The values remained high until June 1987, then decreased to 0.560 Bq/(gCa.day), in September 1988.

The excretion curves for women and children generally have the same shape, which means they increase until a maximum value is reached, then exhibit a continuous decrease. The amount of excreted strontium differs from women to children: strontium urinary excretion has higher values for children than for women, during the entire interval. The maximum value of strontium excretion of children was 2.48 Bq/(gCa.day), while for women it was 1.39 Bq/(gCa.day).

The observed ratio has different values for the two age groups. The OR values for children cover a range between 0.899 and 2.338, with an average value of 1.828, while the OR values for women cover a range between 0.660 and 1.070, with an average of 0.882.

These data seem to point out that the Sr^{90} accumulation period in 4-6 years children lasts until July 1987, reaching by then a quasiequilibrium state (the OR plateau), while the accumulation period for women lasts until February 1988, when the OR values reach the plateau.

The second period of study was January 1991 - December 1991. During this interval we have determined strontium intake and urinary excretion for 3 groups of children (4-6 years, 7-9 years, and 10-12 years), and a group of adult women.

The amount of ingested Sr^{90} decreased a lot, compared to the first period of study. The average amount of ingested strontium, in this period, by the children, has values between 0.182 Bq/(gCa.day) and 0.218 Bq/(gCa.day) - depending of the age of the children - while the average strontium daily intake in women was 0.269 Bq/(gCa.day).

In 1991, the average strontium urinary excretion was higher than the amount of ingested strontium for all children groups (the lower the age, the higher the difference), while the women had similar values for strontium intake and urinary excretion.

This is reflected very well by the OR versus time plots. The OR decreases as the age increases: the average values for 1991 are 1.662 for 4-6 years children, 1.529 for 7-9 years

children and 1.352 for 10-12 years children, while the average OR for women was 0.959. These values show that, the younger the organism, the quicker is the removal of Sr^{90} by Ca. We have also determined the equations which describe the OR versus urinary calcium plot, for every age group, in 1991, by means of least-squares method. The equations are the following:

$$OR = -16.6U_{Ca} + 2.76 \text{ (for 4-6 years)}$$
$$OR = -10.1U_{Ca} + 2.26 \text{ (for 7-9 years)}$$
$$OR = -120U_{Ca}^2 + 19.4U_{Ca} + 0.581 \text{ (for 10-12 years)}$$
$$OR = -0.960U_{Ca} + 1.07 \text{ (for adult women)}$$

where U_{Ca} stands for urinary calcium.

It could be seen that all curves intersect in the same point, of approximate co-ordinates $U_{Ca}=0.13$ and $OR=0.95$. There is interesting to notice the very small slope of the curve for adult women, compared to the slopes of the curves for children.

The last period of study - since January 1993 until December 1994 - included measurements of Sr^{90} dietary intake and urinary excretion for two children groups - 4-6 years and 10-12 years - and a group of adult women.

This period is characterised by low values of Sr^{90} dietary intake and urinary excretion. The average amount of ingested strontium for this period was 0.073 Bq/(gCa.day) for 4-6 years children and 0.102 Bq/(gCa.day) for 10-12 years children. As during the other periods, Sr^{90} urinary excretion had higher values, for both children groups, than the intake values.

The OR keeps its age-dependence exhibited during the other periods: the smaller the age, the higher the OR value. The OR for women has values varying around 1. The analysis of the OR values, for the whole 1986 - 1995 period, leads to the following conclusions:

- within the same time interval, the OR increases as the age decreases, indicating a higher removal rate of strontium from the organism at small ages;
- within the same age group, the OR decreases as the time from the accident goes by.

Radionuclides transfer from mother to embryo

We have studied the radionuclide transfer from mother to embryo, as well as the role of the placenta, since 1973, beginning with experiences on animals. After 1986, we have studied the radionuclide transfer from human organism to embryos, as a consequence of the ingestion of contaminated foods, in two cases:

- a continuous, prolonged, variable intake, and
- a continuous, prolonged, but rather constant intake.

The accident from Chernobyl allowed us to study the transfer of Cs^{137} from mother to embryo, considering that the mother was continuously ingesting variable amounts of caesium. The study was carried on for a period of three years after the accident.
During April 1986 - September 1989 we have determined caesium content in 96 human embryos, aged between 5 and 11 weeks at the moment of prelevation, as well as caesium

dietary intake and urinary excretion of the mother, while they were in hospital for the abortion. All the subject mothers were living in Bucharest, and were aged between 17 and 44 years. Within this period, caesium content in embryos increased from 97.3 mBq/g tissue in 1986, to 137.9 mBq/g tissue in 1987, then it decreased to 10.3 mBq/g tissue in 1988. In 1989, the caesium content in embryos was very small; in many cases the content was bellow the minimum detectable activity (MDA). During these three years, caesium intake and urinary excretion of the mothers varied a lot.

Since April 1986 until December 1986, embryos of different ages were prelevated monthly, as well as dietary intake and urine samples from their mothers, in order to measure caesium content. The percentage distribution of caesium content in embryos was as follows: 16% had less than 75 mBq/g tissue, 34% had between 75 and 100 mBq/g tissue and 50% had more than 100 mBq/g tissue. In most cases, caesium content in embryos was between 100 and 120 mBq/g tissue. Among the 44 embryos studied, 16 were 7 weeks old, 11 were 6 weeks old, and the other covered the other ages from 5 to 11 weeks. The percentage distribution of caesium content in embryos for the two age groups was:

Embryo age (weeks)	Cs^{137} content in embryos (mBq/g tissue)		
	50 - 75	75 - 100	> 100
6	18%	36%	45%
7	6%	38%	56%

It seems that there is a tendency of increased caesium content for 7 weeks embryos. The average value of the caesium content in the embryos analysed in 1986 was 97.3 mBq/g tissue (for all the ages). Considering this value as reference value for that period, we have separated the caesium content in embryos in two groups: "high caesium content", when it exceeds the average value, and "low caesium content" when it is lower than the average. The percentage distribution of the caesium content in embryos, considering the reference value and the age of the embryos, is listed bellow:

Caesium content in embryos (mBq/g tissue)	Age of the embryos (in weeks)					
	6	7	8	9	10	11
> 97.3	45.45%	56.25%	60%	-	66.66%	100%
< 97.3	54.55%	43.75%	40%	100%	33%	-

It appears that, the older the embryos are, the higher the number of cases with increased caesium content (with one exception: 9 weeks embryos). As it can be seen, the percentage of embryos with "high caesium content" increased from 45.45% at 6 weeks embryos to 100% at 11 weeks embryos. This indicates that caesium content tends to increase as the age of the embryo increases.

Cs^{137} intake of the mothers took values between 61.5 and 127.2 Bq/day, in 1986, with an average value of 90.16 Bq/day. The percentage distribution of embryos with caesium content higher than 97.3 mBq/g tissue, with respect to caesium intake of the mother, is as follows:

Cs^{137} content in embryos	Cs^{137} intake of the mother (Bq/day)							
(mBq/g tissue)	40.3	61.5	70.4	93.8	103.5	105.6	119.0	127.2
> 97.3	20%	75%	-	-	80%	66.6%	80%	85.7%
< 97.3	80%	25%	100%	100%	20%	33.4%	20%	14.3%

The table above seems to point out that there is a step value for the mother intake (103.5 Bq/day, which is more than the average of the considered period) above which the percentage of embryos with "high caesium content" is directly dependent of the quantity of Cs^{137} ingested by the mother, no matter how old is the embryo.

Caesium content in embryos prelevated during January 1987 - April 1987 was the highest among all the considered periods. The average value of the caesium content in embryos for this period was 137.9 mBq/g tissue. The highest value was reached in March 1987, when the caesium content in studied embryos was in the range of 138 - 171 mBq/g tissue, with a monthly average of 159.6 mBq/g tissue. The percentage distribution of the caesium content in embryos shows that only 6% of the embryos had caesium content smaller than 100 mBq/g tissue, the other 94% having more than 10 mBq/g tissue caesium content.

The 16 embryos studied in 1987 had ages between 6 and 10 weeks, the number of embryos of a certain age being variable (from one 10 weeks old embryo, to 6 embryos aged 7 weeks). This imposed an overall discussion of the values for all the embryos. In 1987, the percentage distribution of embryos with caesium content higher than the annual average was the following:

Cs^{137} content in embryos	Age of the embryo (weeks)				
(mBq/g tissue)	6	7	8	9	10
> 137.9	25%	83.3%	50%	100%	100%
< 137.9	75%	16.7%	50%	-	-

It can be seen that, while only 25% of the 6 weeks embryos have caesium content higher than the average, all the 9 weeks and 10 weeks embryos have higher caesium content than the average.

Caesium intake of the mothers during January 1987 - April 1987 ranged between 92.6 and 134 Bq/day. The percentage distribution of embryos with "high caesium content", with respect to caesium intake of the mother, is given bellow:

Cs^{137} content in embryos (mBq/g tissue)	Cs^{137} intake of the mother (Bq/day)			
	92.6	101.8	120.5	134.0
> 137.9	25%	66.6%	25%	100%
< 137.9	75%	33.3%	75%	-

This is possible to have the meaning that the caesium content in embryos increases as the caesium intake of the mother increases, no matter what age has the embryo. Caesium

content of the 17 embryos studied in 1988 was lower than in the precedent years, and ranged between 6.7 and 15.8 mBq/g tissue, with an annual average of 10.3 mBq/g tissue.

Performing the same analysis as before, we have obtained the following data for the percentage distributions of "high caesium content" with respect to the age of embryos:

Cs^{137} content in embryos (mBq/g tissue)	Age of the embryo (weeks)					
	5	6	7	8	9	10
> 10.3	50%	50%	66.66%	66.66%	33.3%	100%
< 10.3	50%	50%	33.3%	33.3%	66.6%	-

In this case too, the caesium content seems to be higher in older embryos than in younger embryos.

Caesium intake of the mother during January 1988 - August 1988 took values between 6.5 Bq/day and 11.5 Bq/day. The frequency of embryos with caesium content higher than the annual average, with respect to mother intake, is in this case the following:

Cs^{137} content in embryos (mBq/g tissue)	Cs^{137} intake of the mother (Bq/day)		
	6.5	7.9	11.5
> 10.3	40%	37.5%	100%
< 10.3	60%	62.5%	-

Although the data are not sufficient, if we take into account the previous results we could conclude that higher intake leads to higher caesium content in embryos.

In 1989 caesium content in embryos was extremely low, 32% of the embryos having caesium content bellow MDA, and the average caesium content in embryos was 3.35 mBq/g tissue (for all the embryos analysed), and 6.31 mBq/g tissue (for the embryos with caesium content above MDA).

Because of the low caesium content in embryos, any attempt of correlating the caesium content with the age of the embryos is very difficult.

Cs^{137} intake of the mothers decreased in 1989 to values between 3.5 and 5.1 Bq/day, and the average value was 4.24 Bq/day. The percentage distribution of embryos with caesium content higher than 3.35 mBq/g tissue, with respect to the intake of the mother, is given in the table below:

Cs^{137} content in embryos (mBq/g tissue)	Cs^{137} intake of the mother (Bq/day)			
	3.5	4.2	5.1	4.9
> 3.35	25%	75%	66.6%	100%
< 3.35	75%	25%	33.3%	-

As it can be seen, there is a clear increase of the caesium content in embryos, as the intake of the mother increases.

As for the caesium urinary excretion of the mother, it was not possible to find any correlation between the level of caesium urinary excretion and caesium content in embryos.

The transfer from the mother to the human embryo, when the mother is subject to prolonged continuous intake with constant amounts of radionuclides was studied only for natural radionuclides. The nuclides selected for this study were Ra^{226} and Po^{210}, because of their relative constant concentration in the dietary intake of the population from a chosen area. The embryo, dietary intake and urine samples were prelevated directly from a town situated in the area of interest, which is an uranium mining area. The period of prelevation was February - March 1995.

The intake and urine samples were prelevated from the mothers while they were in hospital for abortion. It is worth telling that the natural radioactive content in various environmental factors around within the chosen area was under monitoring, and was determined at defined intervals, during 1978 - 1995. This survey lead us to the conclusion that the variation of Ra^{226} and Po^{210} dietary intake of the population from the chosen town was no higher than 22%.

Publications

M. Toader, R. A. Vasilache, "The evolution of the effective doses committed annually by adults and children, due to caesium intake, in the first three years after the Chernobyl accident", Proceedings of the XXXth Scientific Symposium of the IISPSSC, 28 March 1995.

M. Toader, R. A. Vasilache, "Estimate of the internal doses due to Cs^{137} and Sr^{90} in the population of Bucharest, in the first five years after the Chernobyl accident", Rom. J. Biophys., **5**, (2), 214, April - June 1995.

M. Toader, R. A. Vasilache, V. Tomulescu, M. Rusu, "Population contamination monitoring after the Chernobyl accident", Rom. J. Phys. (in press).

M. Toader, R. A. Vasilache, "Internal contamination with caesium and stronitium of a population goup from Bucharest, in the first 7 years aftr the Chernobyl accident", Rom. J. Byophys., **6**, (1), January -March 1996 (in press).

Final Report
1992-1994

Contract: FI3P-CT920064a Duration: 1.7.92 to 30.6.95 **Sector: A14**

Title: Inhalation and ingestion of radionuclides.

1)	Bailey	NRPB
2)	Stahlhofen	GSF
3)	Roy	CEA - FAR
4)	Patrick	MRC
5)	Stradling	NRPB
6)	Iranzo	CIEMAT
7)	Popplewell	NRPB
8)	Strong	UKAEA
9)	Johnston	Inst. Occupational Medicine
10)	Koblinger	HAS.RIAE
11)	Gradoń	ICH-MAW
12)	Salowsky	UMP

I. Summary of Project Global Objectives and Achievements

1. Objectives

The objectives of the Contract are to address the more important uncertainties in the models used in radiation protection for evaluating doses to internal organs from intakes of radionuclides; to develop and implement more comprehensive and realistic models for relating exposures and intakes to organ doses and monitoring results for workers, and for calculating the distribution of doses among the general population. The emphasis is on inhalation, the main route of intake for workers, and for this the Contract includes experimental and theoretical studies to provide basic data required to improve models.

An important part of the work is linked to the development of ICRP models and recommendations relating to the dosimetry of internally deposited radionuclides. This is a particularly active area at present and will continue to be so for the next several years, with the revision of the respiratory tract and GI tract models, reference man, and age-dependent biokinetic models for individual elements. These will be used to calculate inhalation dose coefficients for members of the public with the new ICRP respiratory tract model, and to revise ICRP Publications 30, 54 and 61, which apply to workers.

3. Achievements

Superscript numbers are used below to identify participants by Project number above. It should be noted that the programme was formed from several proposals[5&6,9,10,11,12] in addition to the original, and that participants started at various times: two[5,6] joined in 1992-3, four[7-10] in 1993-4, and two[11,12] in 1994-5. Three[10-12] were supported by PECO.

2.1 Dosimetric modelling - support for ICRP Committee 2 Task Groups

Much effort went to support the ICRP Task Group on Human Respiratory Tract Models for Radiological Protection, of which three participants: Bailey[1], Roy[3], Stahlhofen[2] were members. Final changes were made to the model, which was adopted by ICRP in April

1993: in particular, deposition was re-structured, to treat each region explicitly during both inhalation and exhalation; and the slow clearance of particles deposited in the bronchial tree was made size-dependent. The documentation was revised and updated, and issued as ICRP Publication 66 in 1994. Emphasis then shifted to implementing it: selection of parameter values for various situations, and development of personal computer (PC) software.

The ICRP Internal Dosimetry Task Group (INDOS), formed in 1993, is applying the new model to calculate dose coefficients (effective dose per unit intake) for both workers and members of the public. Considerable support was provided towards the work of this Task Group, of which two participants (Bailey and Roy) are members. Reference values of breathing parameters, time budgets, regional deposition fractions and target tissue masses were specified for workers, and for members of the public at each of the six reference ages.

For Publication 68, issued in 1995, guidance was also given on the treatment of gases and vapours. A review of the literature on the particle size characteristics of radioactive aerosols in workplaces was carried out at NRPB[1]. The results support the use of a default Activity Median Aerodynamic Diameter (AMAD) for occupational exposure of 5 μm.

A draft of Publication 74 (inhalation dose coefficients for members of the public), was prepared for submission to ICRP at its September 1995 meeting. For each of the 30 elements included, a review was conducted of studies of the biokinetics of compounds following deposition in the respiratory tract. NRPB[1] and CEA[3] were responsible for about half of them. For each element the information is summarised, and guidance given on the choice of absorption Types: fast (F), moderate (M) or slow (S), which describe the rate of transfer from the respiratory tract to the blood, and hence determine the dose coefficient. A PC program (SOLTY) was written to assist in application of the criteria to the results of experiments.

For the revision of Publication 30, it is intended to apply material-specific absorption parameters for important compounds. Work began at NRPB[1] on development of methodology to derive absorption parameters for use in the model, from experimental results.

A first version of the PC program LUDEP (LUng Dose Evaluation Program) which applies the new model to calculation of organ doses, was published by NRPB[1]. In collaboration with colleagues at CEA[3], a French language version was produced and issued.

2.2 Physiological parameters for respiratory tract modelling

In order to evaluate exposures and intakes of inhaled radionuclides by the general population, CEA[3] measured important parameters of ventilation and breathing modes, and their individual ranges of variability. Apparatus was constructed to measure physiological parameters and the partition between nose and mouth breathing during graded exercise. Measurements made in healthy adults and children indicate that in children there is greater variability than in adults and that mouth-breathing at rest is more common. Complete ventilation parameters at both breathing modes were also measured in children. Ventilation parameters (oral and nasal airflows, maximal inspiratory and expiratory flowrates; airway resistances and flow-volume curves) were measured in groups of healthy subjects to evaluate the physiological variabilities. Measurements were made in children, (males and females 5-17 years old) to investigate correlations between the parameters and with body height; and adults, (males and females) of different ethnic origins: Caucasians, Africans and Asiatics. Results indicate lower nasal resistance in Africans than in Caucasians.

2.3 Deposition of inhaled radionuclides in the respiratory tract

Research in this area involves both experimental work and mechanistic theoretical studies of the behaviour of inhaled particles. Phenomenological deposition modelling is included in Section 2.1. Measurements focused on areas where basic information is needed (subjects different from healthy men; ultrafine and hygroscopic particles). Respiratory tract

deposition of monodisperse (1, 2 and 3 μm) particles inhaled by children, healthy adults (male and female), and adults with impaired lung function was measured at CEA[3]. The aerosols were inhaled under the same, controlled, conditions to investigate the effect of airway dimensions. Initial measurements of deposition of ultrafine particles (30 nm) inhaled by healthy adults were made at GSF[2].

Controversy over the extent of slow bronchial clearance (Section 3.4) has drawn attention to the limitations of current models to predict the deposition of particles inhaled as a bolus. To investigated this directly, GSF[2] measured the deposition of aerosol boluses in hollow casts of human and dog lung airways. The results support the view that boluses administered at the end of a breath ('shallow boluses') do not penetrate to the alveolar region.

Preparations were made at AEA[8] to measure total and regional deposition of hygroscopic aerosols in female volunteers, as functions of particle size and breathing pattern, using radio-labelled salt particles. Ethical approval for the study has been given in principle. Effort has concentrated on commissioning the apparatus. A new PC-controlled inhalation valve system allows volunteers to breathe to a pre-programmed regime, and records the actual breathing pattern. A system for administering aerosol boluses was combined with a laser Doppler anemometer, allowing real-time measurements of particle size on both inhalation and exhalation, and thus enabling better quantification of hygroscopic particle growth. Aerosols in the range 0.5-3 μm can be generated, and inhaled by a subject to various lung depths.

At KFKI[10] a comparison was made of deposition in rat and human lungs, to determine appropriate scaling factors, since the rat is the most frequently used experimental model in studies of inhalation biokinetics and toxicology. A dynamic model of an alveolus was also developed. A fluid dynamics program was used to study the deposition of particles inhaled into an alveolus, modelled as three-quarters of a sphere, the diameter of which changes, taking account of expansion and contraction during the breathing cycle.

2.4 Clearance of radioactive material deposited in the respiratory tract

Experimental work within the Contract continues to address areas of uncertainty highlighted by the new ICRP model. A sensitivity analysis carried out by NRPB[1] demonstrated that including slow bronchial (and bronchiolar) clearance in the ICRP model significantly affects both the equivalent lung dose and effective dose, for many radionuclides.

Investigations of particle retention in these regions were the main themes of two Projects[2,4]. GSF[2] conducted further studies in which subjects inhaled radiolabelled particles as boluses. Experiments using particles of various sizes and densities, indicated that the slow-cleared fraction decreases with increasing particle geometric size, and this relationship was included in the ICRP model. A study in which boluses of 7 μm diameter polystyrene particles (PSL) were inhaled to different lung depths, supported the views that shallow boluses can be deposited exclusively in the bronchial tree, and that a size-dependent fraction is cleared slowly. In collaboration with the Karolinska Institute Stockholm, shallow boluses were inhaled by 12 healthy volunteers. About 30% of the deposited particles were not cleared rapidly, confirming slow clearance of a substantial fraction of particles administered as a shallow bolus. The retained particles were cleared with half times of 7-12 days, which is faster than expected for alveolar deposition.

MRC[4] carried out studies to investigate the slow clearance mechanisms. The study of the clearance of gold particles deposited in rats by alveolar microinjection was extended. The biokinetics of intravenously injected gold in the rat were determined and used to assess the contributions of dissolution and particle transport to alveolar clearance. A study was carried out of the proportion of non-ciliated tracheal epithelium. Detailed measurements on tracheas from 12 F-344 rats indicated that ~60% of the surface is non-ciliated, and that marked inter-individual differences occur. Measurements on 6 HMT rats, 7 CBA mice and 6 guinea pigs

showed marked differences between species. Longitudinal sections from rats and guinea pigs showed similar distributions of non-ciliated lengths to the transverse sections, indicating that the non-ciliated regions are not long and narrow. The size-dependence of the clearance kinetics of particles deposited in the rat trachea was studied. For 1.4 μm diameter $^{133}BaSO_4$ and 0.03 μm ^{195}Au-labelled colloidal gold, the slow-cleared fraction and the rate constant for the fast component were similar, but for the slow phase the rate constant was lower for colloidal gold. These results differ from those inferred for man from the studies at GSF[2].

At KFKI[10] a model of mucociliary clearance in the bronchial tree, linked to the stochastic lung model has been developed. Residence times of particles in different bifurcation units were calculated and numbers of nuclear transformations during the transit times of the particles were determined for radioaerosols, including ^{131}I and ^{99m}Tc. Cellular doses were calculated on the basis of surface activities.

Substantial effort was applied to the study at NRPB[1] to determine the effects of particle size and breathing pattern on particle deposition and retention in the human nose. Monodisperse ^{99m}Tc-labelled PSL in the size range 1-15 μm were produced using spinning top and vibrating orifice aerosol generators. Work is well advanced on commissioning the equipment needed to administer the aerosols to subjects under closely controlled and monitored conditions; and to measure respiratory tract deposition and retention.

Alveolar retention of inhaled Fe_3O_4 was found to be greater in smokers than non-smokers by GSF[2], using magnetopneumography. The change in rotational behaviour of particles in a magnetic field after phagocytosis by alveolar macrophages was used to study the cell microenvironment, and to monitor the time course of uptake *in vivo* in humans.

At Warsaw[11], a theoretical model has been developed of clearance of material deposited in the alveolar region of the human respiratory tract. The influence of assumed effects of radiation exposure on the local alveolar deposition pattern, on the transmembrane transport of deposited matter, and on chemotactic movement of alveolar macrophages were considered. Complementary experiments were conducted on the behaviour of lung surfactant exposed to gases and particulate material in the inhaled air. The influence of various substances on the activity of the lung surfactant monolayer was investigated *in vitro*.

A collaborative study was conducted between CIEMAT[6] and NRPB[5] on the inhalation of plutonium isotopes and ^{241}Am in soil contaminated by the nuclear weapons accident at Palomares, Spain in 1966. At CIEMAT[6], the chemical, radiochemical and mineralogical characteristics of soil samples were determined, *in vitro* simulated pulmonary dissolution studies performed, and samples selected for *in vivo* biokinetic studies. *In vitro* dissolution studies were conducted on respirable fractions of three samples. In the first few weeks similar fractions of $^{239+240}$Pu and ^{241}Am dissolved, but that of ^{238}Pu was several times greater. Samples were removed from the solvent after 6 or 12 months, and subjected to sequential leaching to identify the geochemical associations of the radionuclides that had not already been extracted. *In vitro* dissolution studies were completed on three further dust samples: total soil; and the 20-40 μm and 125-250 μm fractions. For each sample, similar fractions of ^{238}Pu, $^{239+240}$Pu and ^{241}Am dissolved each week, during the first six weeks. On the basis of the results obtained, the Palomares dust was classified into a combination of ICRP Publication 30 inhalation Classes W and Y, and doses per unit intake were estimated.

At NRPB[5], two *in vivo* studies were conducted of the biokinetics of ^{239}Pu and ^{241}Am present in four soil fractions. The respirable fraction (<5 μm aerodynamic diameter) derived from each was administered by intratracheal instillation to the lungs of rats, groups of which were killed for analysis at intervals up to 12 months later. In the first study the respirable fractions derived from two soil fractions (<5 μm and 125-250 μm) were administered. An initial assessment was made of the implications for human exposure and individual monitoring of persons exposed to such dusts. The second study was conducted on two further

samples: total soil and the 20-40 μm fraction. The results of both studies are being used with the new ICRP respiratory tract model to predict the biokinetics in humans of the actinides present, and hence the dose coefficients for the inhaled contaminated dusts.

A collaborative study is being conducted between NRPB[5] and the University of Pleven, Bulgaria[12] on the characteristics, biokinetics and toxicology of radionuclide bearing dusts formed in a nuclear power plant (NPP), and on uranium tri-n-butyl phosphate (UTBP). The NPP dust contains a range of radionuclides, including actinides, fission and activation products. Experiments are in progress at NRPB[5] on the biokinetics of the dust after deposition in the rat lung. About 80% of the ^{137}Cs and 40% of the ^{60}Co present cleared from the lung in the first day, mainly to blood. *In vitro* dissolution experiments on the dust conducted in Bulgaria[12] gave consistent results.

The biokinetics of UTBP were examined at NRPB[5] after instilling two different masses into the lungs of rats. Within the first day, ~75% of the instilled activity was absorbed into blood, and after one week ~2.5% of the uranium remained in the lung. In supplementary experiments, the f_1 for uranium was calculated to be 0.025. Toxicity studies are being undertaken at Pleven[12]. Following intratracheal instillation of the materials into rats, groups were killed on days 1, 3, 7, 14 and 28 after treatment, for electron microscopy and lung lavage to examine biochemical markers in bronchoalveolar lavage fluid.

2.5 Development of improved methods of assessing intakes of radionuclides

A prototype high volume personal air sampler, based on electrostatic precipitation, and suitable for use in nuclear industries has been developed at IOM[9]. A first model, with a back-up filter to permit determination of the collection efficiency of the sampling stage, was designed, constructed and tested. On the basis of the results and further theoretical considerations, a second version was designed and constructed. A series of tests has been carried out to determine the collection efficiency of the device for a number of different configurations, including different types of discharge electrodes, collection electrodes made from different metals, and varying electrode spacings. Tests were carried out to determine the the rates of production of noxious gases, particularly ozone, to ensure that the device does not produce harmful levels. Tests to determine the most energy-efficient air mover showed that there are suitable centrifugal fans commercially available.

A human volunteer study is being conducted at NRPB[7] of the gastro-intestinal absorption and long term urinary excretion of plutonium, using the long-lived isotope ^{244}Pu. Measurements of urinary excretion from three healthy adult male volunteers following intravenous injection of Pu(IV) in a citrated saline solution have continued, now reaching 3 years after administration for one subject, and 2 years for the other two. The oral intake phase of the experiment has been completed for the two final volunteers. Preliminary estimates of their gut transfer (f_1) factors are consistent with those of the first three subjects. Their intravenous injections are planned for the near future.

Participants (CEA[3], NRPB[1]) were involved in the organisation of the CEC-EURADOS First Training Course on "Assessment of Doses from Intakes of Radionuclides" held in Cadarache, France, April 1994, as part of the CEC ERPET programme. Several scientists involved in this Contract lectured on this course, and also lectured on internal dosimetry on ERPET courses held in September, 1994 and April 1995.

2.6 Meetings

Contractors' meetings were held in Bath UK, 13 September 1993, and Neuherberg, FRG, 28/29 March 1994 and 16/17 January 1995. All were joint meetings with the Contracts "Radionuclide dosimetry" and "Assessment of internal dose from plutonium and other radionuclides using stable isotope tracer techniques in man".

Head of project 1: Dr M R Bailey

II. Objectives for the reporting period

i. Implementation of the ICRP Publication 66 Respiratory Tract Model (IRTM), including treatment of radioactive decay products, age dependence, radon progeny, and development of mathematical modelling techniques.
ii. Measurement of particle clearance from the human respiratory tract.

III. Progress achieved including publications

i. Model implementation

Collaboration with the ICRP Task Group on Human Respiratory Tract Models for Radiological Protection continued into the early part of this reporting period. The main changes made to the ICRP Respiratory Tract Model (IRTM) were:

- deposition in each respiratory tract region is now treated explicitly as a series of filters in which deposition occurs during inhalation and during exhalation.
- the slow clearance of particles from the bronchial and bronchiolar regions was made particle-size dependent, as indicated by the recent studies at GSF (Project 2).
- the fraction of material deposited in the alveolar region subject to very long-term retention was decreased from 33% to 10%.
- the fractions of energy absorbed in the target tissues in the respiratory tract from transformations in each source within the respiratory tract ('absorbed fractions', AFs) for each important type of radiation, were re-calculated.

In collaboration with colleagues at Battelle Pacific Northwest Laboratories, AFs were re-calculated for alpha particles, mono-energetic electrons, beta and positron emissions, for each of the 22 source-target combinations specified in the IRTM. Most AFs are energy dependent, and so algebraic expressions were determined to express them as functions of energy, enabling interpolation between values calculated at specific energies. As an example, Figure 1 compares the re-calculated AFs ("EGS4" calculations) with the previous values and the corresponding fitted algebraic function, for monoenergetic electrons and one source-target combination.

Staff contributed to the completion of the Task Group report, which was approved by the ICRP Main Commission in 1993, and issued as ICRP Publication 66 in 1994. The emphasis of modelling work then shifted to application of the IRTM. Considerable support was given to the ICRP Internal Dosimetry Task Group (INDOS), which is advising on the IRTM's use for calculation of inhalation dose coefficients (effective dose per unit intake) for members of the public and for workers. In collaboration with other members of ICRP Task Groups, reference values of breathing parameters, time budgets, regional deposition fractions and target tissue masses were specified for workers, and for members of the public at each of the six reference ages.

Contributions were made to ICRP Publication 68, which provides dose coefficients for workers using the IRTM. These dose coefficients are also required for revision of the Euratom Directive. In particular, the treatment of gases and vapours in ICRP Publication 30 was reviewed and guidance given on the use of the IRTM to represent the behaviour described. Internal and external doses from submersion in noble gases were calculated to confirm that, following implementation of Publications 60 and 66, external radiation from the

cloud would still dominate exposure for all isotopes of Ar, Kr and Xe, except ^{37}Ar.

The Activity Median Aerodynamic Diameter (AMAD) of an aerosol can have a marked effect on dose per unit intake (Figure 2), but in practice its value is often not known, making it necessary to use a default value. A review of the literature on the particle size characteristics of radioactive aerosols in workplaces was carried out. Results were compiled from 52 publications covering a wide variety of industries and workplaces. Reported values ranged from 0.12 μm to 25 μm, and most were well fitted by a log-normal distribution with a median value of 4.4 μm (Figure 3). This supports the choice by ICRP of a 5 μm default AMAD as a realistic rounded value for occupational exposures. Median values for both the nuclear power and nuclear fuel handling industries were ~4 μm, but for uranium mills ~7μm (Figure 4).

A review of the literature on particle size distributions of radioactive aerosols in the environment is in progress. Results have been compiled from 15 papers reporting 114 measurements. Reported AMADs for aerosols from anthropogenic sources ranged from 0.3 to 18 μm, with a median of 1.5 μm; aerosols from the Chernobyl accident gave a median of 0.9 μm. These results support the choice of a 1 μm general default AMAD for public exposures. However, the few (14) measured AMADs for aerosols generated by resuspension were all greater than 1 μm, with a median of ~6 μm. Measurements of natural radioactive aerosols (excluding radon, ie. ^{7}Be) gave a median value of 0.4 μm.

The main task relating to model implementation is to review studies of the biokinetics of compounds of each element following deposition in the respiratory tract. The first stage is to review information on the 31 elements for which ICRP will provide inhalation dose coefficients for the public, in order to give guidance on which of the three default absorption Types: F (fast), M (moderate) or S (slow) in the IRTM should be assumed for environmental exposure, in the absence of specific information. Criteria were developed by INDOS for assigning compounds to each Type. A personal computer (PC) program (SOLTY) was written to assist in applying the criteria to the results of experiments. Reviews of the literature were conducted at NRPB on 12 elements (Ag, Ce, I, Nb, Pu, Ru, S, Sr, Th, Zn and Zr).

The revision of ICRP Publication 30 will recommend rates of absorption to blood for compounds for which information is available, and for others a default Type. This will require a much more extensive review of the literature, with more detailed analysis of the information. Figure 5 shows a compartment model representing absorption as in the IRTM: there are two phases of dissolution, rapid and slow, and dissolved material may be retained in the respiratory tract following dissolution in the form of a bound state. A methodology is being developed to determine the model parameters (ie. fractions and rate constants for the rapid, slow, and bound states) from experimental data, and has been implemented for the trial case of plutonium nitrate.

The method assumes that clearance from the respiratory tract results from competition between absorption to blood and particle transport to the gastro-intestinal tract; that absorption, which depends on the material, is independent of mammalian species; and that particle transport is independent of the material. For plutonium nitrate, suitable experiments on rats have previously been carried out. A biokinetic model describing respiratory tract clearance in the rat was developed. The representation of absorption is the same as in the IRTM, while that of particle transport is a simplified version of it, with parameter values appropriate to the rat. Absorption parameter values for plutonium nitrate were then determined by fitting model predictions simultaneously to data sets of activity in the lungs and activity absorbed from the lungs to the carcass. Figure 6 shows one of these fits, obtained in this example by allowing deposition parameters, the fast dissolution fraction and the slow dissolution rate to vary.

Inhalation of radon decay products is the dominant source of radiation exposure at

home and at work, and the predictions of the IRTM for doses from such exposures are therefore of great interest. The effective dose per unit exposure was calculated, using the IRTM and ICRP Publication 60 risk-weighting factors (eg. the tissue weighting factor for the lung), to be ~15 mSv/WLM (Working Level Month). However, comparison of the results of epidemiological studies of miners and Japanese atom bomb survivors suggest a lower value, ~5 mSv/WLM. In an attempt to reconcile these, an uncertainty analysis was carried out. Probability distributions were constructed for each of the IRTM parameters which most affect dose per unit exposure, reflecting the estimated accuracy with which each parameter value is known. A frequency distribution of dose per unit exposure values was then generated using the Latin Hypercube sampling method (Figure 7). This indicated that the two estimates are unlikely to be reconciled by changes in IRTM parameter values.

An analysis was carried out of the sensitivity of the equivalent lung dose, and effective dose, to assumptions made in the IRTM about the extent of slow bronchial clearance. This was identified by the Task Group as a major model uncertainty, and is a main theme of two other Projects: No. 2 (GSF) and No. 4 (MRC). Results (eg. Table 1) showed that inclusion of slow clearance of material deposited in the bronchial tree has a significant effect on both equivalent lung dose and effective dose (of the order of 10-50%) for a wide range of radionuclides. For some alpha-emitters, its inclusion increases doses by up to a factor of three, so that it makes the dominant contribution to the calculated dose. The IRTM assumes that material in transit through the bronchial tree, having initially deposited in the alveolar region, is not subject to slow clearance. Including retention of this material would typically increase doses by a further factor similar to that resulting from the slow clearance of the bronchial deposit.

Table 1. Ratio between effective dose calculated using the ICRP Publication 66 model and that calculated using the same model, but excluding airway retention

Radio nuclide	Absorption Type	AMAD (μm) 1	5	Radio nuclide	Absorption Type	AMAD (μm) 1	5
^{111}In	F	1.0	1.0	^{210}Po	F	1.0	1.0
	M	1.3	1.2		M	4.7	3.9
	S	1.3	1.2		S	4.0	3.1
^{106}Ru-Rh	F	1.0	1.0	^{234}U	F	1.0	1.0
	M	1.1	1.1		M	3.7	2.8
	S	1.0	1.1		S	1.5	1.5
^{60}Co	F	1.0	1.0	^{238}Pu	F	1.0	1.0
	M	1.3	1.3		M	1.1	1.1
	S	1.1	1.0		S	1.4	1.5

The PC program LUDEP (LUng Dose Evaluation Program) which applies the IRTM to calculate organ doses, was published as a software package (LUDEP 1.1). This version is appropriate for adults, and for single radionuclides or radionuclides with simple decay chains. The user can calculate doses or dose-rates to each region of the respiratory tract at any time after intake. All the biokinetic models from ICRP Publication 30 have been incorporated,

allowing doses to other organs to be calculated. Parameter values recommended by ICRP are installed as defaults, but the user can change many of them for specific situations. In collaboration with colleagues at CEA/IPSN (Project No. 3) a French language version of LUDEP (1.1F) has been published. A module to calculate excretion rates following intake by inhalation, for bioassay calculations, has been completed and will be included in version 2.0. A method was developed to represent the new ICRP recycling biokinetic models in terms of independent organ retention functions, which are then used to calculate organ doses. Work also began on the development of software for the calculation of doses from radioactive decay chains, with a view to inclusion in a future version of LUDEP.

ii. Experimental studies

After an extended period during which little effort had been available, substantial effort is now being expended on this experimental programme. (Additional effort was required for the modelling programme above to meet new tasks and deadlines agreed internationally). Our objective had been to commence the human volunteer studies of deposition and clearance in the nasal airways during this period. The need to seek ethical re-approval has meant that they cannot now start until February 1996. Effort is therefore mainly being directed towards further development of techniques for aerosol generation, labelling and administration to volunteers for the nasal clearance study. Effort will focus on development of proposals for studies of bronchial clearance once ethical approval for the current study is received.

The objectives of the nasal clearance study are to investigate the effect on particle clearance of particle size and breathing pattern, to investigate the degree of inter-subject variation in clearance, and to determine the fraction of material deposited under various conditions which can be removed by nose-blow sampling. Figure 8 shows the apparatus which is being set up to administer controlled amounts of insoluble radio-labelled aerosol particles to subjects under controlled conditions for this study. A wide range of sizes (aerodynamic diameter, d_{ae}, from <1 to >30 μm) will be administered. For the smaller particles, a laser aerosol photometer will be used to monitor inhaled and exhaled aerosol concentrations. For the larger particles, which deposit completely in the respiratory tract, and for which losses due to gravitational settling and impaction in any pipework would be high, subjects will inhale directly from the chamber into which the labelled particles are resuspended. Deposition fractions and clearance rates will be measured for various breathing patterns and work rates using direct *in vivo* techniques. Gamma-ray detectors positioned around the body will measure activity as a function of time in the nasal airways, lungs, and gastro-intestinal tract, the last being one of the main clearance pathways.

As with all volunteer studies, doses must be kept as low as possible, and below the relevant limit. Calculations were performed to determine the minimum initial nasal deposit (IND) to provide adequate measurement sensitivity for the determination of clearance parameters. The maximum committed effective dose a volunteer could receive from administrations giving this IND was shown to be well below the WHO and ICRP limits.

Monodisperse polystyrene aerosols (PSL) for the study have been produced using a spinning top aerosol generator (STAG) in the size range 1 - 8 μm, with efficiencies of over 25% for particles up to 5 μm. A Mark 2 version of the STAG was purchased to facilitate generation of the smaller particles required (ie. down to d_{ae} ~ 0.6 μm). For sizes above a few μm, a vibrating orifice aerosol generator (VOAG) can produce aerosols with narrower size distributions. The VOAG has been used to make monodisperse aerosols from 2 - 15 μm with satisfactory efficiency. Work is in progress on generating larger particles.

Aerosols produced using both the STAG and VOAG have been successfully labelled

with ^{99m}Tc. The aerosols are collected on filters and must be resuspended for administration to subjects; equipment to achieve this has been set up. The problem of leaching of activity from ^{99m}Tc-labelled particles during resuspension, has now been overcome for sizes ≥3 μm. The first experiment will use 3 μm particles, and it has been confirmed that this size can be resuspended and administered at an adequate concentration. Work is progressing on the calibration of measurements of flow rates and aerosol concentrations with the laser aerosol photometer, and software is being developed to use these to monitor and control administration of the aerosols to subjects.

Clearance will be followed by *in vivo* measurements with gamma ray detectors. A calibration phantom based on the BOMAB type (Bottle-Mannikin-Absorption) has been constructed to calibrate measurements of activity in the head, thorax and abdomen. The required calibrations have been performed for both ^{99m}Tc (for the pilot study) and ^{111}In (for the main study). A feasibility study into the use of small NaI(Tl) detectors for measurements of regional deposition and clearance in the nasal airways is progressing, and is yielding favourable results. Work continued on upgrading the low background *in vivo* measurement facilities. Although their development is not carried out under this contract, they will be used for the inhalation studies. In particular, measurements made with an array of n-type Ge detectors may well prove useful for measurements of retention in the nasal airways

Publications

Bailey, M.R. *New ICRP Human Respiratory Tract Model.* Radiol. Prot. Bull. 144 22-29 (1993).

Bailey, M R. The new ICRP model for the respiratory tract. Proceedings of the Workshop on Intakes of Radionuclides: Detection, Assessment and Limitation of Occupational Exposure. Bath, UK. 13-17 September 1993. Radiat. Prot. Dosim. 53 (1-4) 107-114 (1994).

Birchall, A, and James, A C. Uncertainty analysis of the effective dose per unit exposure from radon progeny using the new ICRP lung model. *ibid.* 133-140.

Jarvis, N S, and Birchall, A. LUDEP 1.0, a personal computer program to implement the new ICRP respiratory tract model. *ibid.* 191-193.

Smith, J R H, Marsh, J W, Etherington, G, Shutt, A L and Youngman, M J. Evaluation of a high purity germanium detector body monitor. *ibid.* 73-75.

Bailey, M R, Dorrian, M-D and Birchall, A. Implications of airway retention for radiation doses from inhaled radionuclides. Presented at the Symposium on the Fate of Aerosol Particles in the Airways, Frankfurt am Main, FRG, 25-26 March 1994. J. Aerosol. Med (in press).

Birchall, A, and James, A C. A rapid method for modelling the kinetics of radioactive progeny applied to thorium in the lungs. Health Phys. 67, 162-169 (1994).

Birchall A , Jarvis N S, James A C and Akabani G. Algebraic functions to approximate the fractions of energy absorbed by target tissues in the 1994 ICRP Respiratory Tract Model. NRPB-M573 (1995).

Dorrian, M-D, Jarvis, N S and Birchall, A. LUDEP: Past, Present and Future. Radiol. Prot.

Bull. 159, 14 (1994).

Dorrian, M-D, and Bailey, M R. Particle size distributions of radioactive aerosols measured in workplaces. NRPB-M528 (1995).

Dorrian, M-D, and Bailey, M R. Particle size distributions of radioactive aerosols measured in workplaces. Radiat. Prot. Dosim. 60, 119-133 (1995).

International Commission on Radiological Protection (ICRP). Human Respiratory Tract Model for Radiological Protection. Publication 66 (Oxford: Pergamon) Ann. ICRP., 24, (1/4) (1994).

James, A C, Stahlhofen, W, Rudolf, G, Kobrich, R, Briant, J K, Egan, M J, Nixon, W and Birchall, A. *ibid.* Annex D: Deposition of Inhaled Particles.

Bailey, M R and Roy, M. *ibid.* Annex E: Clearance of Particles from the Respiratory Tract.

James, A C, Roy, M and Birchall, A. *ibid.* Annex F: Reference Values for Regional Deposition.

James, A C, Akabani, G, Birchall, A, Jarvis, N S, Briant, J K and Durham, J S. *ibid.* Annex H: Absorbed Fractions for Alpha, Beta, Positron and Electron Emissions.

James, A C, Birchall, A, Thrall, K D, Hui, T E, Briant J K, Hopke, P K and Wasiolek, P T. Dosimetry and Aerosol Technology of Radon Progeny. IN: Pacific Northwest Laboratory Annual Report for 1993 to the DOE Office of Energy Research. Part 1, Biomedical Sciences, February, 1994. PNL-9000 Pt.1, UC408., pp 69-76 (1994).

Jarvis, N S, Birchall, A, James, A C, Bailey, M R, and Dorrian, M-D. LUDEP 1.1 Personal computer program for calculating internal doses using the new ICRP respiratory tract model. NRPB-SR264 (1994).

Jarvis, N S and Birchall, A. LUDEP 1.0, un logiciel pour ordinateur personnel qui applique le nouveau modele pulmonaire de la CIPR. Radioprotection 29, 81-86 (1994).

Jarvis, N S, Birchall, A, James, A C, Bailey, M R et Dorrian, M-D. LUDEP 1.1F logiciel de dosimétrie interne utilisant le nouveau modèle pulmonaire de la CIPR. NRPB-SR264(F) (1994).

Kaul, A and Bailey, M R. Application of the new ICRP human respiratory tract model to the assessment of secondary limits. Presented at the Symposium on Radiobiology of Inhaled Nuclides. Richland, WA, USA. 9-10 November 1993. Radiat. Prot. Dosim. (in press).

Stahlhofen, W, Scheuch, G and Bailey, M R. Investigations of retention of inhaled particles in the human bronchial tree. *ibid.*

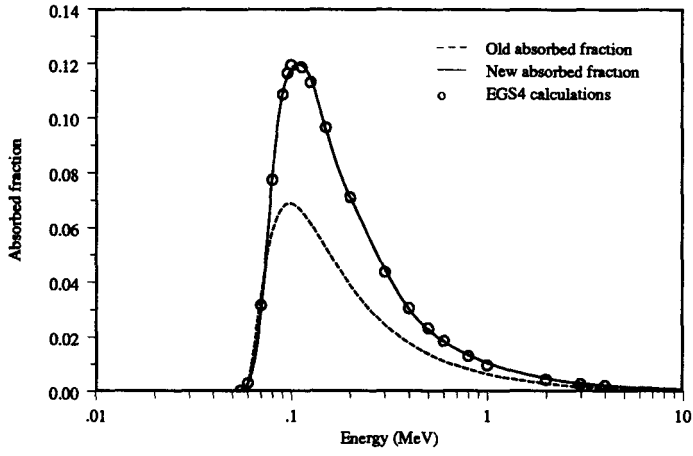

Figure 1 **Absorbed fraction in bronchial basal cells for mono-energetic electrons emitted from rapidly cleared material in mucus**

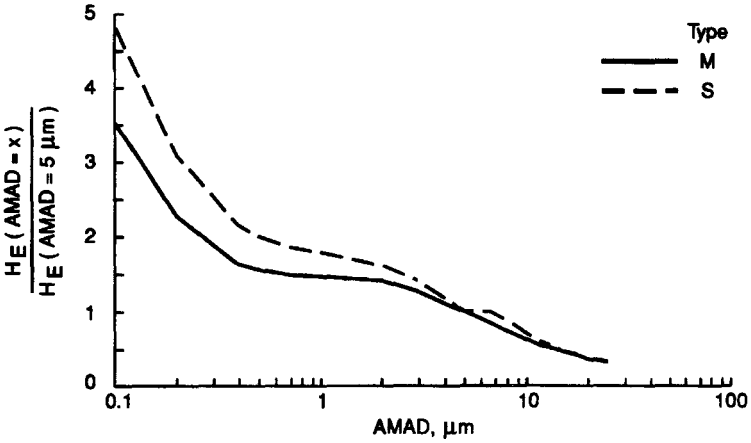

Figure 2 **Effect of AMAD on committed effective dose, H_E, for ^{239}Pu**

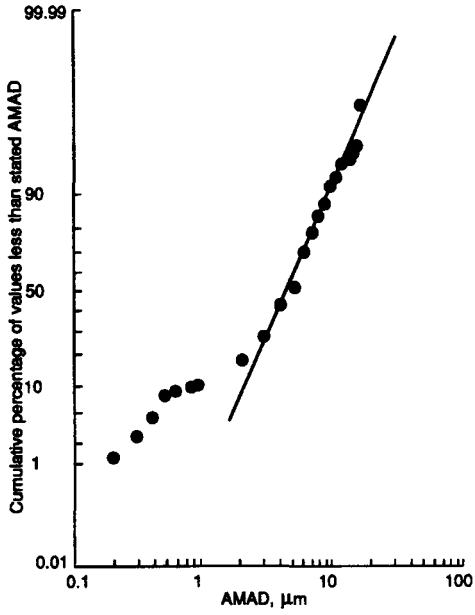

Figure 3 **Distribution of AMADs in all workplaces**

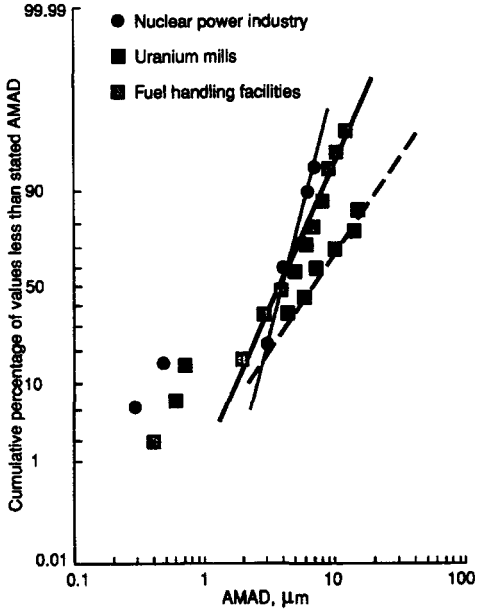

Figure 4 **Distribution of AMADs in different nuclear industries**

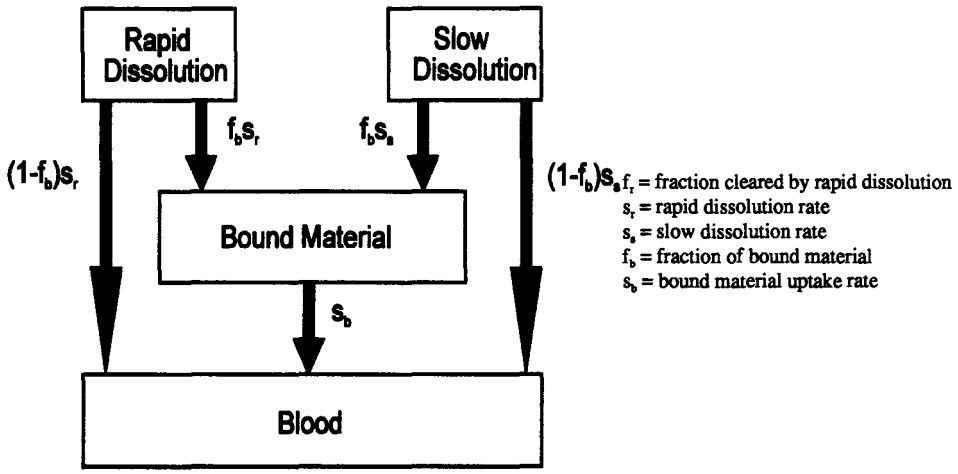

Figure 5 **Compartment model representation of absorption to blood**

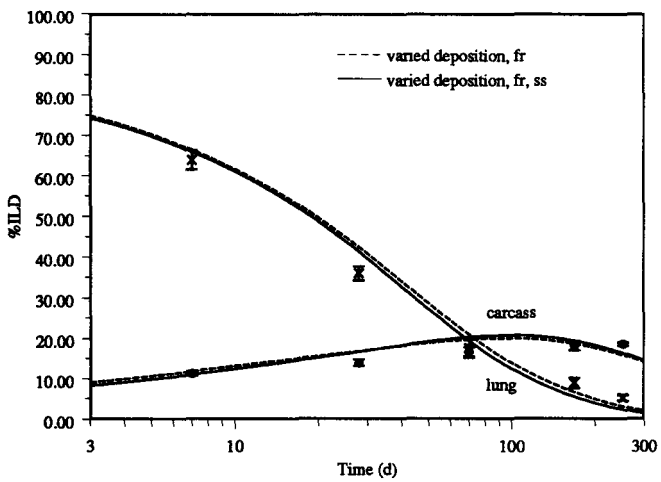

Figure 6 **Fit of model predictions to experimental data on retention in rat lung and carcass, for plutonium nitrate (ILD - initial lung deposit)**

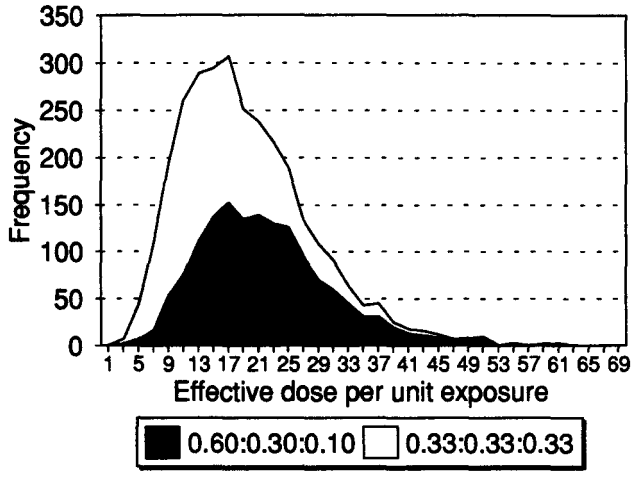

Figure 7 **Frequency distribution of the calculated effective dose per unit exposure to radon (mSv/WLM), for two sets of risk apportionment factors between the three lung regions: bronchial (BB), bronchiolar (bb), and alveolar-interstitial (AI). The values 0.6:0.3:0.1 were proposed by the Task Group; 0.33:0.33:0.33 were adopted by ICRP.**

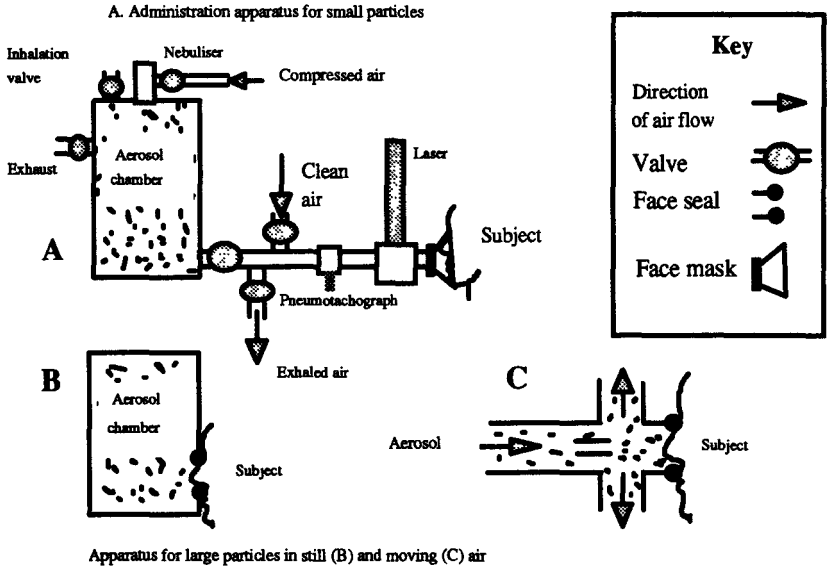

Apparatus for large particles in still (B) and moving (C) air

Figure 8 **Aerosol administration apparatus**

Head of project 2: Dr. Stahlhofen

II. Objectives for the reporting period

- Aerosol bolus studies in casts and human lungs (dispersion and retention of particles).
- Mucociliary clearance measurements in humans after bolus inhalations.
- Production and inhalation studies with ultrafine particles.
- Studies with magnetic particles to investigate phagocytosis *in vivo* and *in vitro*.

III. Progress achieved including publications

Aerosol bolus dispersion and retention

Aerosol bolus dispersion and retention of particles in the human airways were measured while varying particle size (0.8-6 µm) and penetration into the lungs (volumetric depth, VL). The movement of the heart increased the dispersion of inhaled aerosol particles during a breath-hold for particles smaller than 2 µm. Larger particles were deposited more efficiently in the airways by sedimentation during breathholding periods (Scheuch and Stahlhofen, 1992).

Comparing the experimental results from recovery measurements in healthy human subjects with theoretical model calculations, it could clearly be shown that only a small fraction (<2-3%) of shallow inhaled boluses could have reached the alveolar space during inhalation (Scheuch, 1994).

The aerosol bolus dispersion and retention of particles in hollow human and dog airway casts was measured. The hollow casts (made available from New York University Medical Center) were complete from the trachea to the 1 mm airways. The inner volumes were about 150 ml. The casts were ventilated with a piston pump and they were connected to the bolus inhalation device. It could be shown that the oropharyngeal region in the human has a significant influence on the aerosol dispersion in the first 100 ml of the respiratory system. For the dog it could be shown that dispersion measurements in the cast were in excellent agreement with data measured on living beagle dogs under similar conditions (intubated with a 10 mm intubation tube) (Scheuch et al., 1995).

Aerosol was injected as 15 ml boluses at different (VL) into both casts. Particles which penetrated through the entire airways of the cast left the open ended 1 mm airways, and were lost in the ventilation chamber. Hence the recovery of particles in the inhalation device after a breathing cycle was a measure of particles located in the conducting airways at the end of the inhalation. In Figure 1 the results for the human airway cast are given. Aerosol boluses injected in VL < 100 ml were recovered by more than 95%. Less than 5% were lost in the airways or had left the 1 mm airways into the ventilation chamber.

With these experiments it was shown that aerosol inhaled near the end of an inhalation only reaches conducting airways and that this technique enables us to inhale aerosol only into the tracheobronchial region.

The effect of a sympathomimetic drug was tested with an aerosol method. It could be shown that the deposition in the airways was reduced for various breathholding periods after the application of ß2-Sympathomimetico. Thus the aerosol derived airway diameter in the central lung region was enlarged after the inhalation of the drug (Siekmeier et al., 1994a).

Mucociliary clearance measurements

After aerosol bolus inhalations the clearance of inhaled radiolabelled particles was measured by following the radioactivity over the lung region with a sensitive collimated scintillation counter. Aerosol particles of polystyrene (PSL) labelled with ^{111}In, with particle diameters between 2.1 and 6.7 µm were produced with a vibrating orifice generator. After the production of the PSL particles they were washed several times and nebulized in a 7 l container. These aerosols were inhaled to different lung depths by 6 healthy volunteers with a bolus inhalation device. (The volumetric lung depth, VL, represents the average penetration, and the front depth,VF, the maximum penetration of the bolus). The aerosol boluses were produced with a fast operating valve system injecting small volumes of aerosol into an inhalation of particle free air. Inhaled and exhaled particles could be detected and quantified with a laser aerosol photometer directly in front of the mouth. The subjects in this study inhaled boluses of about 30 ml aerosol at a constant 250 cm³/s flow rate. At the end of the inhalation, particles were deposited in the airways by sedimentation during a breathholding period. The retention of the particles in the lungs was measured for 3 days after inhalation with the collimated scintillation counter.

Clearance from the airways was found to be complete within one day when 6.7 µm particles were inhaled into VL of about 55 ml. Even when boluses with these larger particles were inhaled intoVL of about 100 ml, more than 90% of the aerosol that was deposited in the lungs was cleared within one day. A substantial fraction of these particles was also cleared within the following two days. These particles were probably located in small airways where the mucociliary clearance rate is low.

All investigations with PSL particles are listed in Table 1. It can be seen that the fraction of particles found after one day increased with decreasing particle size. For particles of 2 µm diameter, a fraction of about 60 % of the particles deposited in the lungs were not cleared within one day.

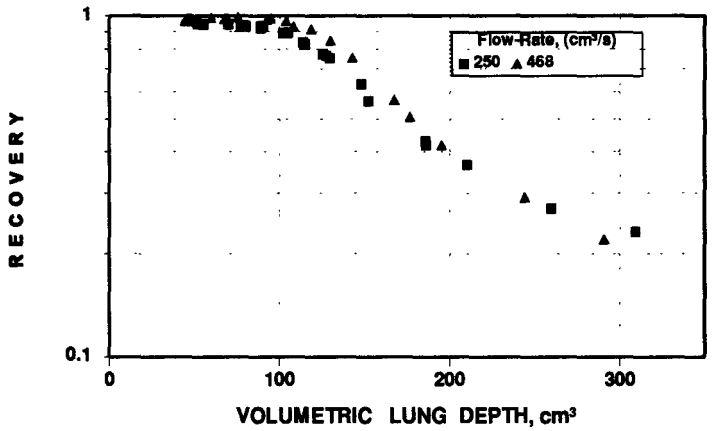

Figure 1: Recovery of 1µm particles injected as boluses into different volumes of a human airway cast. The ventilation flow rate was varied.

Particles of different materials and sizes were inhaled into shallow volumetric lung depths (VL), so that they were deposited in the conducting airways, exclusively. The following particles were used in this study :

- Polystyrene labelled with ^{111}In
- Iron oxide labelled with ^{99m}Tc
- Fused aluminium silicate labelled with ^{111}In
- Teflon labelled with ^{111}In

It was found that the effectiveness of mucociliary clearance is particle size dependent. Large particles were cleared more efficiently than smaller particles. In Figure 2 the fraction of slowly cleared particles (Ret24h) as function of the aerodynamic particle diameter is given. One can see that Ret24h decreased with increasing particle size.

Table 1

Subject	VF (ml)	dae (µm)	tp (s)	Ret24h	± SD
25	60	2.1	20.1	**0.61**	±0.06
2	82	2.1	20.1	**0.62**	±0.04
25	48	3.74	10	**0.33**	±0.06
1	60	3.74	10	**0.29**	±0.05
4	75	3.74	10	**0.25**	±0.10
4	76	3.74	8	**0.23**	±0.10
1	100	3.74	8	**0.37**	±0.05
2	120	3.74	8	**0.43**	±0.04
25	55	3.9	0.6	**0.32**	±0.06
33	48	4.3	8.1	**0.16**	±0.07
2	70	4.3	10.1	**0.29**	±0.03
31	73	4.3	0.7	**0.25**	±0.06
4	58	6.15	0.71	**0.05**	±0.05
1	55	6.7	8	**0**	±0.04
2	92	6.7	8	**0.08**	±0.03
1	104	6.7	8	**0.1**	±0.10
4	121	6.7	6	**0.12**	±0.03
4	653	6.7	4	**0.85**	±0.10

VF = volumetric front depth of the inhaled bolus; dae = aerodynamic particle diameter; tp = period of breathholding, A = retention of particles in the lungs after 24h; S.D. = Standard deviation.

In Fig. 2 it can also be seen that the Ret24h values for PSL were significantly lower than for the other materials. Aerosol particles with similar aerodynamic diameters, d_{ae}, but of

different materials with different densities, have different geometric diameters, d_g. To test the influence of d_g on Ret24h the results were plotted as a function of d_g (Fig.3), which resulted in a much better correlation between Ret24h and size. From these results it was assumed that d_g might play an important role in the mucociliary clearance kinetics of inhaled aerosol particles. These preliminary results must be confirmed by investigation of more subjects (smoker vs. non-smoker, healthy subjects vs. subjects with particular lung diseases) and extended particle size range.

The particles which were cleared rapidly were eliminated from the tracheobronchial tree with a mean half time of 2.4 hours. The half time of the slowly cleared particles ranged between 6 and 30 days.

In collaboration with colleagues at the Karolinska Institute (KI) Stockholm ^{111}In-labelled Teflon particles were tested for bolus inhalation studies at the GSF in Frankfurt. The particles were produced with a spinning top generator and were sampled and washed. For the inhalation study the particles were nebulised into a storage vessel of about 40 l.

At KI 12 healthy volunteers inhaled shallow boluses (VL = 50 - 60 ml) of ^{111}In-labelled Teflon particles (d_{ae} = 3.5 µm, flow rates = 300 ml/s). Six subjects inhaled a broncho-constrictor before the bolus inhalation. It could be shown that a bronchoconstrictor did accelerate the mucociliary clearance. In no case was complete clearance after 24 h found. A fraction of 23% (6 - 56) % of the inhaled particles, 35% (11 - 65 %)of the deposited particles, were not cleared within one day. The slowly cleared particles were cleared with half times of 7 - 12 days (Scheuch et al., 1995).

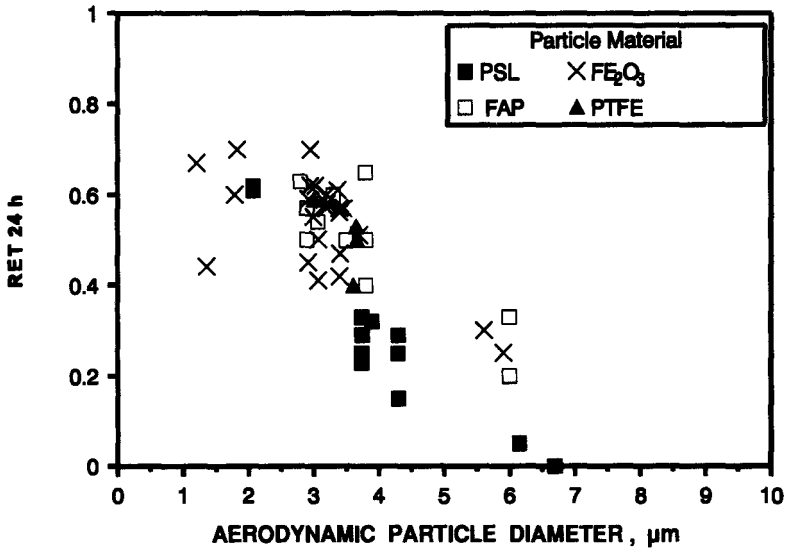

Fig. 2 : Slow cleared fraction of particles inhaled with the bolus inhalation technique (VF between 35 and 85 ml) as function of the aerodynamic particle diameter (d_{ae}).

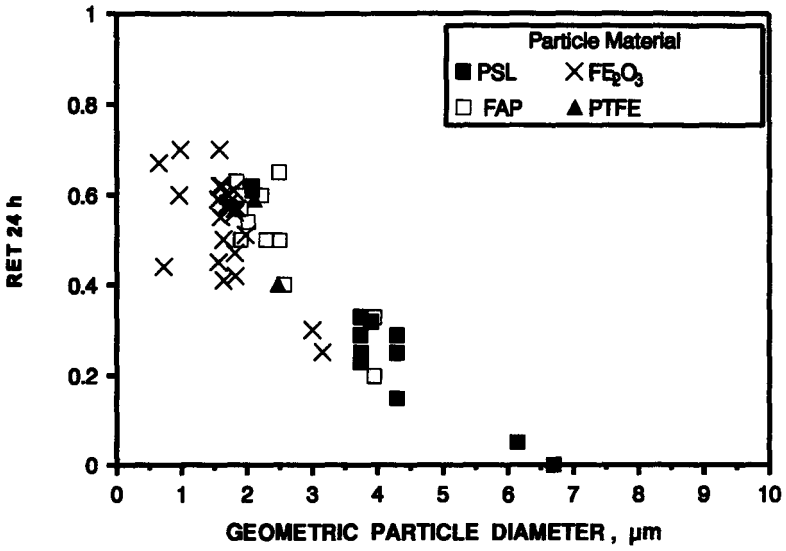

Fig. 3 : Slow cleared fraction of particles inhaled with the bolus inhalation technique (VF between 35 and 85 ml) as function of the geometric particle diameter (d_g).

Ultrafine particles

Aerosols of ultrafine, monodisperse, inert ^{111}In-oxide particles were produced for inhalation studies. In this method indium chelate is vaporised at 300°C and converted into indium oxide in a high temperature furnace (1100°C). In a condensation chimney behind the furnace a quasi-monodisperse aerosol is produced by controlled condensation. This aerosol is lead through a differential mobility analyser (DMA) to obtain a monodisperse aerosol fraction, which is stored in a 7 l container for the inhalation. (Roth et al., 1994).

In a first pilot study three healthy subjects inhaled, during steady state breathing, particles with a diameter of 30 nm. The chosen tidal volume was 1 l and the flow rate was 250 cm³/s. Only about 4-7% of the deposited particles were cleared within the first few hours. More than 90% were cleared slowly (Roth et al., 1994).

In another pilot study the ultrafine particles were inhaled as very shallow boluses (VF = 42 ml). A breathholding period of 10 s was performed after inhalation to allow particle deposition by diffusion (brownian motion). The expired particles were sampled on an absolute filter and the activity on the filter was measured. From the known activities on the filter and in the subject the total deposition was found to be DE = 7%. The retention curve is given in Figure 4. Only about 20% of the deposited aerosol was cleared within the first day, the other particles remained longer in the airways (Roth et al., 1993b). From this preliminary results it seems that ultrafine particles deposited in shallow volumetric lung depths are not very efficiently cleared via the mucociliary escalator and remain much longer in the airways than expected.

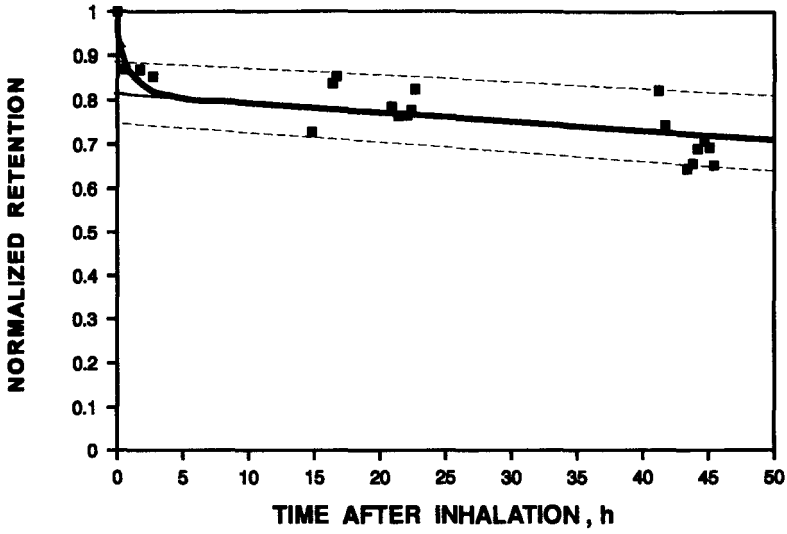

Figure 4 : Retention of 30 nm particles inhaled with the bolus inhalation technique into a volumetric front depth of 42 ml as a function of the time after inhalation.

Magnetopneumographic (MPG) Measurements

Magnetic microparticles were used to investigate long term particle retention in the human lungs, particle relaxation, alveolar macrophage mobility and intracellular viscoelasticity by magnetopneumography (MPG). For this purpose, ferrimagnetic particles (Fe_3O_4) were produced with a spinning top aerosol generator. About 0.5 mg of the particles were deposited in the lungs by inhalation. The particles are monodisperse with d_{ae} between 2 - 3 µm. The particle size was chosen to have $d_{ae} < 3\mu m$ in order to obtain deposition mainly in the alveolar region. After deposition in the lungs the particles were magnetised by an external field. The magnetic field of all particles in the lungs can then be detected with a SQUID-system (superconducting quantum interference device).

A younger (A, age 31.5 ± 5 years) and an older (B, 55 ±15) group of healthy subjects were investigated. Both groups were subdivided into smokers (S) and never-smokers (NS). Cigarette consumption was 10 pack years (P-Y) in group A-S and 45 P-Y in group B-S. The MPG measurements were performed directly after inhalation, and after 2 days, 1 week, 1, 5 and 9 months. All subjects were free of any lung disease and had normal values of conventional lung function tests.

Table 2

Group	Number of subjects	Cigarette Consumption (Pack-Years)	Half time ± SD of long term retention (days)
A - NS	10	0	126 ± 55
A - S	9	10	198 ±85
B - NS	11	0	174 ±107
B - S	9	45	570±509

Table 2 shows that cigarette consumption has a significant ($p < 0.05$) influence on particle clearance from the alveolar region. Even a relative low cigarette consumption of 10 P-Y induced an impairment of alveolar clearance in man (Möller et al. 1995).

After the inhalation of the ferrimagnetic particles they are phagocytized rapidly by alveolar macrophages. Thereby, the particles come under their influence and should show a rotational behaviour different from that when free on the lung surface. By applying weak magnetic fields the particles can rotated into certain directions. *In vitro* investigations in J774 macrophage cells have shown that phagocytized particles are rotatable in the cells. The *in vivo* investigations in humans show directly (about 1 hour) after particle inhalation a large amount of non-rotatable particles (about 50%). This amount decreases rapidly, within hours, after particle inhalation. It is concluded that this change reflects the process of uptake of the particles by the macrophage cells in the human lungs. The non-rotatable particles represent the fraction of particles still free on the lung surface. The method has the capability to monitor the time course and the effectiveness of the phagocytosis process. First studies have shown that there might be differences in the time course and probably also in the effectiveness between healthy non-smokers and smokers, and patients with particular lung diseases.

In vitro experiments of particle rotation in J774 macrophage cells were done in order to obtain a deeper understanding of the mechanical properties of the cytoskeleton of macrophages. Subsequently shear experiments were performed with increasing shear stress. These experiments showed that the cytoskeleton has very complex viscous and elastic properties. With increasing applied stress the cytoskeleton increases its stiffness. There is a linear relation between stiffness and stress, which is uncommon in man-made materials. This very characteristic behaviour is, however, found in other living tissues, for example the volumetric expansion characteristic of the human lung. The magnetic particle method provides a novel opportunity to perform cytoskeletal studies on a basic cell biological level.

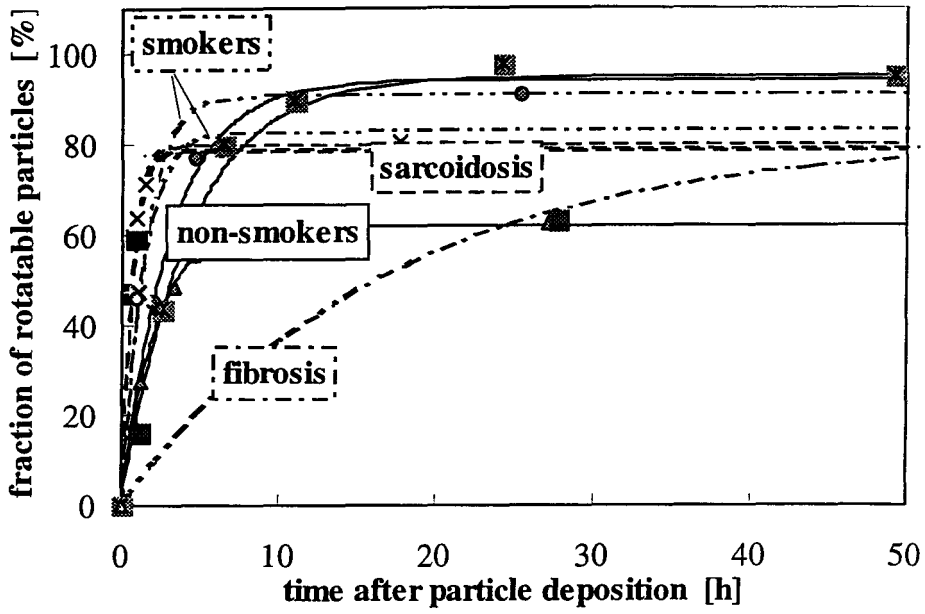

Fig. 5: Process of particle uptake by alveolar macrophages by investigation of the fraction of rotatable and non-rotatable particles.

The apparent viscosity with respect to shear rate could be modelled by a power law with a power near -1. For high shear rates of 0.1 rad/s, viscosity was near 50 Pa.s, while for shear rates below 0.001 rad/s apparent viscosity increased to above 1000 Pa.s. This was characteristic *in vivo* and *in vitro*. Model calculations with a hydrodynamic object have been performed. In these calculations a viscosity and an elasticity was connected in parallel. These calculations yielded also the characteristic power law behaviour with a power of -1, see Figure 6, independent of the applied shear stress (twisting field). When using a Newtonian viscosity (NV) no shear-rate dependence is present. The shear-rate analysis can be used to obtain information about the viscous properties. For every applied shear stress (twisting field B_M) the apparent viscosity with the highest shear-rate is close to the Newton-viscous behaviour. No information could be obtained about elasticity.

Therefore, MPG - twisting experiments were modified. Stress was applied only for a short duration (10 s). If the particles in the cells rotate in an elastic environment an elastic recoil should occur. This elastic recoil was recorded with this technique in the macrophages. From the time course of the recoil, we obtained a direct estimate of the elastic properties. The elastic recoil came back to the initial orientation (detected before stress application) only for small applied stresses. For a higher stress a nonrecoverable strain occurred. This indicates deformation of the cytoskeleton. Cell deformation might occur only above a certain value of the applied stress, indicating plastic properties. This MPG method in this way gives information about very characteristic and complex mechanical properties of living cells *in vivo*.

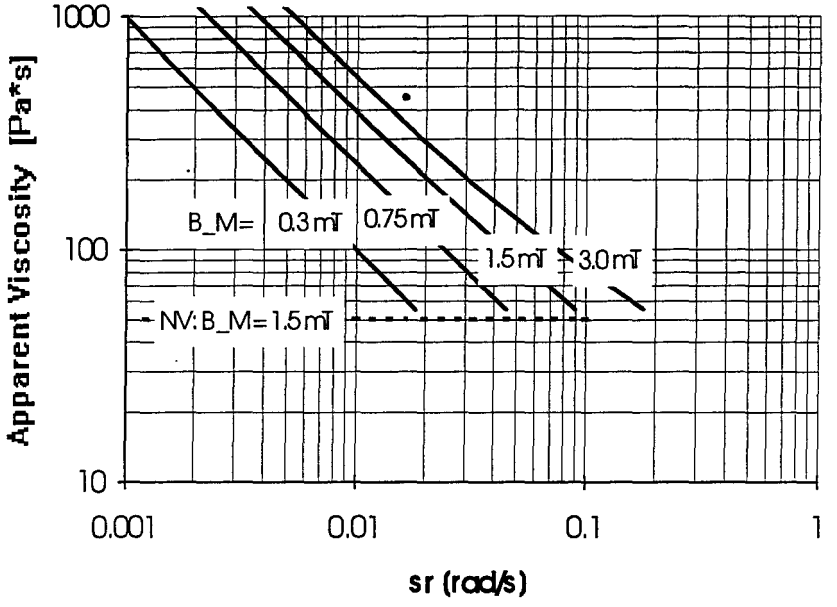

Fig. 6: Calculated apparent viscosity of a viscoelastic body for increasing applied magnetic field (rotational shear stress).

Publications

Barth, W., Möller, W., Pohlit, W., Stahlhofen, W., Wiegand, W. (1994) Magnetopneumographic estimation of particle phagocytosis in the human lungs, *Journal of Aerosol Science*, **25**, Suppl. 1, S491-492

Köbrich, R., Rudolf, G., and Stahlhofen, W. (1994) A mathematical model of mass deposition in man. *Ann. occup. Hyg.* **38**, 15 - 23.

Möller, W., Guzijan, V., Stahlhofen, W. and Wiegand, J. (1993) Using cytomagnetometry to measure intracellular viscosity in a macrophage like cell line J774. J. Aerosol Med. **6**, Suppl., 30

Möller, W. and Stahlhofen, W. (1994) Cytomagnetometry with J774-macrophage cells - influence of shear-stress on the rheology of the cytoplasm. *Journal of Aerosol Science*, **25**, Suppl. 1, S503-S504

Möller, W., Wiegand, J., Stahlhofen, W., Barth, W., Pohlit, W. and Rust, M. (1995) Impairment of Long-Term Particle-Clearance of the Lungs by Cigarette Smoke and by Age in Man. J. Aerosol Med. **8**,.84

Roth, C., Scheuch, G. and Stahlhofen, W. (1994) Radioactively labelled ultrafine particles for clearance measurements. *Ann. occup. Hyg.* **38**, 101-106

Roth, C., Scheuch, G. and Stahlhofen, W. (1993a) Clearance measurements with ultrafine particles. *J. Aerosol Med.* **6**, Suppl., 47

Roth, C., Scheuch, G. and Stahlhofen, W. (1993b) Clearance of the human lungs for ultrafine particles. *J. Aerosol Sci.* **24**, S95-S96.

Rudolf, G., Köbrich, R., Stahlhofen, W., and James, A. C. (1994) Regional aerosol deposition in man - A statistical and algebraic model. *Ann. occup. Hyg.* **38**, 1-14

Scheuch, G. (1994) Particle Recovery from Human Conducting Airways after Shallow Aerosol Bolus Inhalation. *J. Aerosol Sci.* **25**, 957-973

Scheuch, G. and Stahlhofen, W. (1992) Deposition and Dispersion of Aerosol Particles in the Airways of the Human Respiratory Tract: The Effect of Particle Size. *Exp. Lung Res.* **18**, 343-358.

Scheuch, G. and Stahlhofen, W. (1994) Effect of settling velocity on particle recovery from human conducting airways after breath holding. *Ann. occup. Hyg.*, **38**, 101-106

Scheuch, G., and Stahlhofen, W. (1994) Aerosol Disperion in Human Airways During one Breathing Cycle: The Dependence of the Aerosol Penetration. *J. Aerosol Sci.* **25**, S553-S554.

Scheuch, G., Kreyling, W., Haas, F. and Stahlhofen, W. (1993) The clearance of Polystyrene particles from human intrathoracic airways. *J. Aerosol Med.*, **6**, Suppl., 47.

Scheuch, G., Stahlhofen, W., Fang, C.P. and Lippmann, M. (1993) Aerosol Recovery after Bolus Inhalations into an Airway Cast. *J. Aerosol Sci.* 24, S355-S356.

Scheuch, G. and Stahlhofen, W. (1994) Effect of settling velocity on particle recovery from human conducting airways after breath holding. *Ann. occup. Hyg.*, **38**, 159-166.

Scheuch, G., Stahlhofen, W. Fang, C.P. and Lippmann, M. (1995a) Dispersion of Aerosol Particles in an Airway Cast. *Exp. Lung Res.* **21**, 519-534.

Scheuch, G., Philipson, K., Falk, R., Anderson, M., Svartengren, M., Stahlhofen, W. and Camner, P. (1995b) Retention of particles inhaled in boli with and without bronchoconstriction. *Exp. Lung Res.*, in press.

Schiller-Scotland, CH.F. and Siekmeier, R. (1993) Correlation between aerosol derived airspace dimensions and airway resistance in the case of pharmacon induced bronchoconstriction. *Aerosol Sci.* **24**: 475-476.

Schiller-Scotland, CH.F., and Siekmeier, R. (1993) The effect of inhaled terbutaline sulfate powder on aerosol derived airspace dimensions. *J.Aerosol Sci.* **24**: 465-466.

Siekmeier, R., Schiller-Scotland, CH.F. Stahlhofen, W. and Kronenberger, H. (1994a) Langzeitwirkung des ß2-Sympathomimetikums Formoterol bei jungen Rauchern-Untersuchung von Wirkdauer und Wirkort der Bronchodilatation mittels konventioneller Lungenfunktionsmethoden und monodisperser Modellaerosole. *Pneumologie.* **48**, 225-230.

Siekmeier, R., Schiller-Scotland, CH.F. Gebhart, J. and Kronenberger, H. (1994b) Dose-dependent changes of airway resistance and aerosol pulse dispersion in cases of pharmacologically induced airway obstruction. *Ann. occup. Hyg.*, **38**, 175-180

Siekmeier, R., Schiller-Scotland, CH.F. and Gebhart, J. (1993) Influence of experimental changes of lung inflation on pulmonary convective gas transport. *J.Aerosol Sci.* **25**: 447-448.

Siekmeier, R., Schiller-Scotland, CH.F. and Stahlhofen, W. (1994) Influence of asthma bronchiale on convective gas transport in patients with asthma bronchiale. *J.Aerosol Sci.* **25**: 447-448.

Siekmeier, R., Scheuch, G. and Stahlhofen, W. (1994) Effect of Heart Rate and Lung Inflation on Aerosol Derived Effective Airway Dimensions. *J.Aerosol Sci.* **25**: 479-480.

Stahlhofen, W. and Möller, W. (1993) Behaviour of magnetic micro-particles in the human lungs *Radiation and Environmental Biophysics*, **32**, 221-238.

Stahlhofen, W. and Möller, W. (1994) In vivo and in vitro studies of the cellular defense system of the human lung, *Toxicology Letters*, **72**, 127-136.

Stahlhofen, W., Scheuch, G. and Bailey, M.R. (1994) Measurements of the tracheobronchial clearance of particles after aerosol bolus inhalation. *Ann. occup. Hyg.*, **38**, 189-196

Stahlhofen, W., Wiegand, J. and Möller, W. (1993) In vivo investigations of shear-rate dependence of intracellular viscosity of alveolar macrophages in healthy persons. *J. Aerosol Med.* **6**, Suppl., 65.

Head of project 3: Dr Roy

II. Objectives for the reporting period

Assessment of doses from intakes of radionuclides by inhalation of gases and aerosols is an important task for the radiological protection of workers and members of the general population. Predictive models of intake by inhalation relate particle deposition of exposed subjects, for a large part, to their respiratory physiology, ventilation rates and pattern of airflows inhaled through extra-thoracic airways, nose and mouth. These parameters depend upon age and exertion levels. In models, reference values for adult Caucasians have been derived from the experimental published studies, for mouth and nose breathing; in children, mouth breathing data existed, but nose breathing had to be scaled from adults. Moreover, these models were to apply to all the various population groups, but very few data on oral airflows, and none on nasal ones were available for the various ethnic groups. An important objective to meet was to validate the necessary extrapolations by measuring directly these parameters in healthy volunteers, without allergic history, adults and children, with their parents consent, and to evaluate the potential range of uncertainty. Another one was to contribute experimental data on particle deposition in the respiratory tract for some critical groups of the population, such as children of a defined range of age, and adults with impaired lung function, patients with restrictive and obstructive lung diseases.

III. Progress achieved including publications

Ventilation parameters and breathing modes

This study was aimed at measuring:

- In healthy children of various ages, while breathing through the nose and through the mouth, the ventilation airflows and airway resistances, comparing the data obtained by the two modes and looking for possible relationships with age.
- In adults of various ethnic groups, Caucasians, Asiatics, and Africans, for whom standard respiratory volumes and flow rates are known to show differences, but for whom little is known about possible differences in oro-nasal breathing patterns, ventilation airflows and airway resistances.
- In healthy subjects, adults and children, performing graded exercise, the distribution of ventilation through nose and mouth, looking for possible relationships with individual characteristics of breathing modes and respiratory physiology.

1. Measurements of oral and nasal airflows in children

1.1 **In a group of 62 healthy children**, 31 males and 31 females, aged 4 to 17 years, oral expiratory peakflows were measured by spirometry, during forced vital capacity manoeuvres, and nasal inspiratory peakflows by a calibrated Youlten flowmeter. Individual data showed that lower values were obtained for oral than for nasal airways. (Figure No 1). However, this could be partly explained by a possible difference between inspiratory and expiratory routes. In order to look for possible age dependency, these data were plotted, not directly against age but against body size, and the logarithms of values were fitted to linear regression functions. The data of both genders gave very similar coefficients, and were therefore not separated in the following equation:

Oral peakflow: log PEF or. (l. s^{-1}) = 2.39 log H (cm) - 4.545 (r = 0.82 ; RSD = 0.082).

This regression is close to the one published by Solymar L., Aronsson P. H., Bake B., Bjure J. 1980, Nitrogen single breath test, flow volume curves and spirometry in healthy children, 7-17 years of age Eur. J. Respir Dis., 61, 275-286.

Nasal peakflow: log PIF nas. (l. s^{-1}) = 2.1 log H (cm) - 4.52 (r = 0.42 ; RSD = 0.22)

Like the oral peakflows, nasal peakflows are dependent upon body height but a lower correlation coefficient and a higher residual standard deviation are observed. This might be an effect of nasal features, explained only partly by body size. In order to better understand these relationships, more complete studies were necessary:

1.2 **Another group of 24 healthy children**, aged 4 to 17 years, were asked to perform more complete measurements of oral and nasal flow rates, by various techniques: spirometer, Fleisch pneumotachographs (PNT), inspiratory peakflowmeter (Youlten), and of airways resistance to airflows, through mouth, and through nose, by posterior rhinomanometry.

Data obtained by the various methods were compared: Forced Expiratory Volume in one Second, (FEV1), through mouth and through nose, Peak Inspiratory Flow rate (PIF), through mouth and through nose, nasal and oral Resistances to airflows, (**Table 1**).
Good correlations were found between:

- *Data from different devices*:

Oral inspiratory peakflow, (PIF or) measured by Youlten and by PNT, (r=0.82), and Nasal inspiratory peakflow, (PIF na) measured by Youlten and by PNT, (r=0.57), indicating that the data given by the two instruments were in agreement.

- *Various measured parameters*:

Oral inspiratory (PIF or), and expiratory (PEF or) peakflows, measured by PNT (r=0.65) showing the agreement between inspiratory and expiratory routes. Oral inspiratory peakflow, (PIF or) and oral resistance, (r=0.57), Nasal inspiratory peakflow, (PIF na) and airway resistance, (Raw, including resistance of the nose itself, plus those of the thoracic airways) (r=0.72).

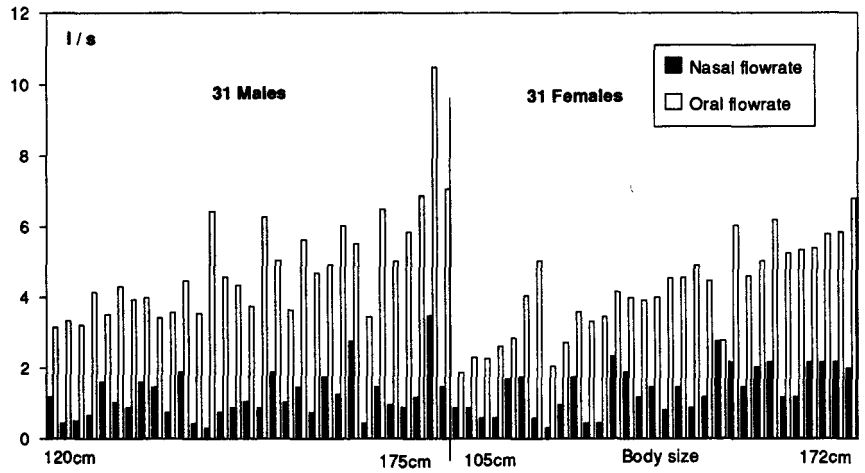

Figure No 1 : Maximal oral and nasal flow rates in 62 healthy children aged 4 to 17 years

The latter led us to think that the nose data could be fitted by linear regression, and the following equation gave a better correlation than the one above with body height in the group of 62 children:

Nasal peakflow:

log PIF nas. (l. s^{-1}) = - 0.94 log Raw (hPa. $l^{-1}s$) +0.95 (r = 0.60 ; RSD = 0.17)

This relationship shows that nasal inspiratory flow rate is better explained by airway resistance, Raw, to airflow breathed through the nose. It is thus still indirectly explained by body size because nose resistance decreases with age in children.

2. Measurements of breathing flow rates and airways resistance in ethnic groups

In three groups of healthy adults of both genders:

- **20 Caucasians**, 11 males and 9 females, aged 18 to 59 years;
- **22 Africans**, 14 males and 8 females, aged 22 to 61 years;
- **21 Asiatics**, 15 males and 6 females, aged 20 to 77 years,

various ventilation parameters, that could influence intake of radionuclides were measured:

Forced Expiratory Volume in one Second, FEV1, through mouth and through nose, Peak Inspiratory Flow rate through mouth and through nose, oral and nasal resistances to airflows.

Sex	Age	Height	Weight	FEV1 Oral PNT	FEV1 Nasal PNT	Insp. Flow rate Oral (Youlten)	Insp. Flow rate Nasal (Youlten)	Total Resistance Oral at 0.250 l.s⁻¹	Total Resistance Raw at 0.250 l.s⁻¹	PIF Oral PNT	PEF Oral PNT	PIF Nasal PNT	PEF Nasal PNT
	y	cm	kg	l.s⁻¹	l.s⁻¹	l.s⁻¹	l.s⁻¹	hPa		l.s⁻¹	l.s⁻¹	l.s⁻¹	l.s⁻¹
1	7	120	22	1.35	1.32	2.46	1.16	2.35	8.51	2.14	3.14	2 47	3.15
1	7	134	41	1.80	0.92	3.76	1.02	2.71	8.63	4 14	4.31	0.88	1.61
1	10	143	37	1.70	0 95	3.62	0.73	2.62	6 63	2.59	3.57	1.37	0.97
1	11	149	42	2 27	1.12	3.75	1.03	2 03	5.30	3 91	3.29	1.46	1.24
1	12	158	48	2.55	2.22	4.15	2.15	1.70	4.33	4.41	3 35	2.86	2.81
1	14	157	45	2.80	2.75	4.70	2.75	1.38	4.60	3.75	5.52	2.41	4.77
1	15	170	67	3.30	1.02	3 76	0.95	1.22	5.43	4.76	5 02	1.46	1.12
1	15	176	57	4 12	2.30	5.22	1.88	2 41	7.03	6 46	7.90	3.42	2 58
2	4	105	16	0.70	0.67	0.73		2.44	10.54	0.68	1.87	0.86	1.61
2	6	115	18	1.07	0.92	1.88	0.87	1.34	4 75	2.49	2 29	1.92	1.75
2	7	123	24	1.25	0.47	2 90	1.67	2.40	8 95	1.95	2.84	1 00	0 68
2	8	130	31	1.65	1 40	3.48	0.72	1 86	7.16	3.51	4.32	1.61	1.75
2	9	141	25	1 47	1.32	3 33	2.32	2.58	7.83	2.17	4.16	1 46	3.61
2	10	150	46	2.12	1.62	4.35	1.15	1.02	5 18	3.80	5.18	1.00	2.57
2	11	135	30	1.85	0.95	2.03	1.74	1.80	6.58	2.59	3.58	1.30	1.20
2	11	144	41	1.67	1.07	3.18	1.45	2 03	8.26	3.23	4.00	1.3	1.24
2	12	152	34	2 12	0.62	3.33	0.86	1.86	7.56	4.47	5.71	0.49	1.26
2	12	155	35	1.85	1.97	4.34	2.75	1.52	5.05	4.21	2.77	2.7	2.31
2	13	147	45	2.15	1.22	4.78	2.46	3 39	9 14	5.89	5.59	1.38	3.15
2	14	172	57	2.37	1 57			1.98	6.45	5.00	6.81	1.99	1.68
2	14	162	45	3 32	2.17	4.20	2.17	1.43	4.33	3.78	6 19	1.92	3.51
2	16	167	45	3.42	2.47	4.93	2.75	1.69	4.59	7.39	7 46	3.36	3.51
2	16	163	59	2.17	1.6	4.15	2 10	2.00	4.92	3.06	5.11	1.97	1.93
2	17	169	51	2.60	1.37	4.63	2.17	1.06	2 79	5.35	5.85	3.42	1.71

PNT = Fleisch pneumotachograph FEV1 = Forced Expiratory Volume in 1 second
PIF = Peak Inspiratory Flow rate PEF = Peak Expiratory Flow rate
Raw = Airway resistances measured through nose

Table 1 : Individual measured respiratory parameters in 24 healthy children aged 4 to 17 years

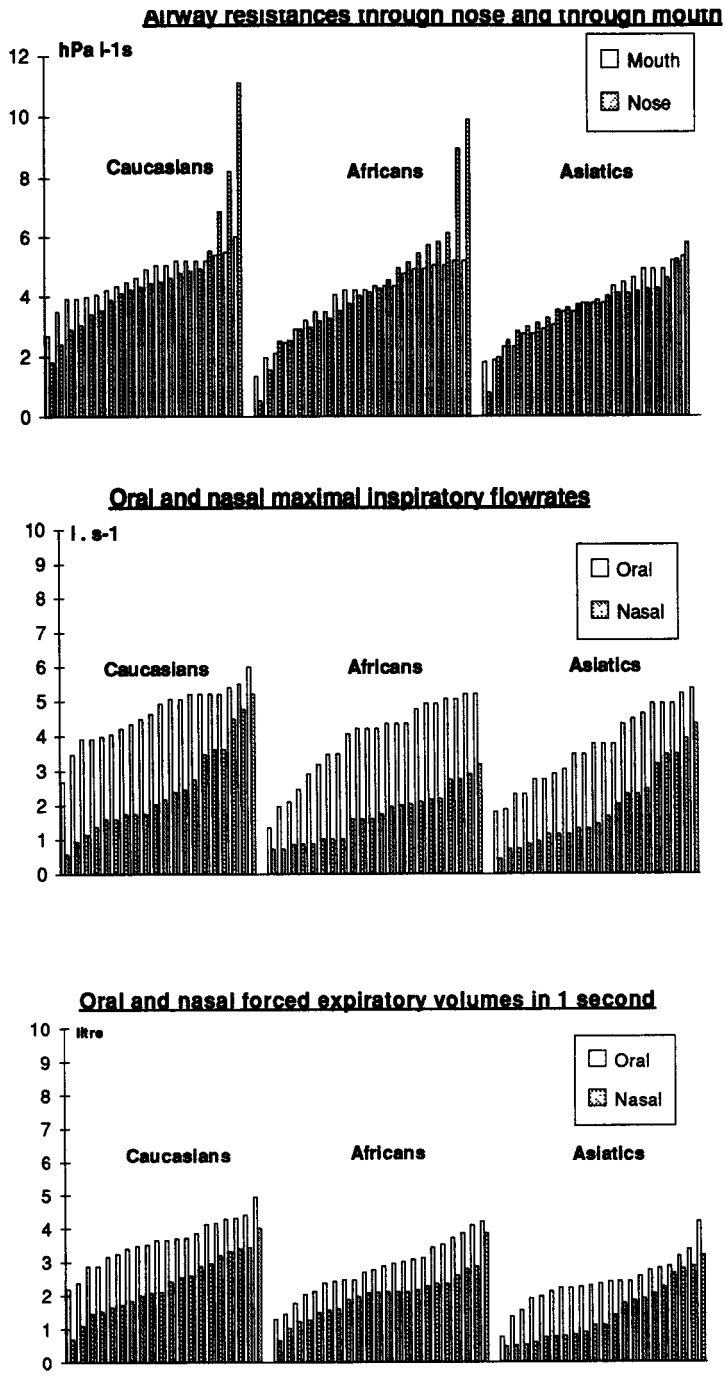

Figure No 2 : Measured ventilation parameters in 3 ethnic groups

Individual data showed that the values measured in Africans and Asiatics were lower than those of the Caucasians. (**Figure No 2**). In Africans, the Wilcoxon non parametric test showed that the differences were very significant for FEV1 oral, and fairly significant for maximal inspiratory flow rate through mouth and through nose. For Asiatics, the differences were significant for all the data (**Table 2**). The ethnic differences in FEV1 through mouth have already been established in relevant published studies, but those of the nasal parameters are less familiar and thus more interesting. They indicate that the nasal airflows differ from one ethnic group to another, and that this should be taken into account especially for modelling deposition by nose breathing. However the number of subjects is small, and further studies on this subject would help ascertain these data.

Measurements of the distribution of ventilation through nose and mouth during graded exercise in healthy subjects

1. A group of ten Caucasian adult volunteers (7 men and 3 women) performed incrementally graded exercise with a special device, set up to record separately oral and nasal flow rates during exercise on an ergometer bicycle automatically incrementing the workload by 25 W every minute. (**Figure No 3**). Two Fleisch No 2 pneumotachographs (PTG), one in the nasal mask, the other in the mouthpiece, connected to pressure transducers, measured flow rates and tidal volumes, through analog/time integration. During the test, ventilation was recorded continuously. Cardiovascular parameter values were recorded at the end of each step. During maximal vital capacity manoeuvres by oral and by nasal breathing total nasal resistances and flow/volume curves were measured in every subject.

In all subjects, oral breathing supplemented airflow through the nose at levels of ventilation rate which varied among individuals. (**Table 3**). The oral fraction of airflow was dependent upon the total ventilation required. At the maximal work it ranged from **30 to 67%.** Among the ten subjects, we observed two kinds of behaviour: in six breathing was entirely nasal at rest and became abruptly oro-nasal at ventilatory rates ranging from **38 to 65 L. min^{-1}** (switching point); their maximum mouth-breathed fractions ranged from **45 to 67%**. In the four other subjects, the oral breathing fraction was already important at rest, ranging from **10 to 30%** (mean value 50%) for the maximum level of exercise, for which ventilation reached **22 to 90 l.min^{-1}**. In these subjects, the ratios of oral / nasal flow volume curve areas were generally higher in the four latter subjects, (except **No** 9), than in the six former ones. This suggested an impaired permeability of the nasal airways of those subjects who already breathed spontaneously by mouth at rest.

Parameters	FEV1 oral (l)	FEV1 nasal (l)	Airway resistances through nose (hPa l^{-1} s)	Maximal inspiratory flowrate	
				Oral l s^{-1}	Nasal l s^{-1}
Caucasians n = 20	3.59 (0.15)	2.34 (0.19)	4.67 (0.35)	4.62 (0.18)	2.47 (0.29)
Africans n = 22	2.80 *** (0.17)	2.02 (0.15)	4.35 (0.39)	3.90 * (0.24)	1.71 * (0.16)
Asiatics n = 21	2.38 *** (0.16)	1.48 *** (0.19)	3.64 *** (0.14)	3.66 *** (0.24)	1.93 * (0.25)

Significantly lower than Caucasians by Wilcoxon non parametric test : *p≤0.10, ***p≤0.02

Table 2: Mean values and standard errors on means (SEM) of measured ventilation parameters in 3 groups of healthy adults

2. A group of 10 Caucasian children, of both genders, aged 7 to 17 years, performed the test. They were healthy and free of any nasal disease, infection or allergy. The device was used with a Fleisch No1 PTG. The ergometer bicycle was adapted to children, incrementing the workload by 10 W every minute.

In all of the subjects, (except No 8), the oral breathing fraction was already important at rest, ranging from **20 to 84%** of total ventilation. It increased steadily with ventilation rate and ranged from **32 to 99%**, (mean value 80%), for the maximum level of exercise, for which ventilation reached **18 to 92 l.min^{-1}**. Subject No 8, aged 14 years, was the only one who breathed entirely through the nose at rest, and like adults, switched abruptly to oro-nasal breathing at a ventilatory rate of **59 l.min^{-1}** with the maximum mouth breathed fraction of **45% (Table 4).** The children generally had difficulties to perform the test correctly and several attempts were necessary to provide reliable values. It seemed clear, however, that most of them currently have oronasal breathing at rest. This would be of interest to verify on a larger number of subjects.

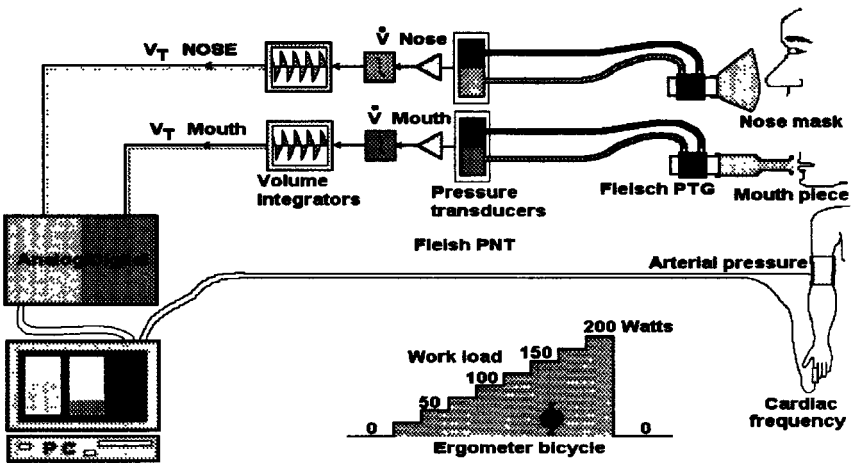

Figure No 3: Facilities for breathing pattern and cardiovascular variable measurements during graded exercise.

Subjects	Height	TR	$\dot{V}_{/V}$	Max.		Minute ventilation				
Age		o/n	o/n	Exercise		Rest		Max. Exercise		S. P
(sex)	cm			Watts	C. F.	l	Oral %	l	Oral %	l
43 (M)	175	0.64	2 24	225	145	10 0	0	71 4	49.9	50
46 (M)	185	0 63	1.47	175	133	12.7	0	72.4	67	40
55 (M)	180	0.30	1.68	200	124	13 9	0	71.7	63.6	65
43 (F)	167	0.45	1 18	175	157	10.0	0	84.0	51	60
56 (F)	156	0.68	1.29	125	145	12.0	0	44.2	47	40
27 (M)	175		2.16	225	158	11 6	0	56.8	45 4	38
39 (M)	165	0.45	3 00	225	157	15.4	23	90.8	55	
35 (M)	175	0.13	3 33	175	136	8 3	10	50 4	57	
27 (F)	175		1.00	150	164	9.6	30	24 7	30	
28 (M)	190		2 30	125	121	12 2	17	22.1	34	

TR o/n = Total resistance oral / nasal
$\dot{V}$ / V o/n = Flow / volume curve oral / nasal
C. F. = Cardiac frequency (min^{-1})
S. P = Nasal to oronasal ventilation switching point

Table 3 : Individual biometry of 10 healthy adults; observed cardiac frequency at maximum exercise completed and ventilatory data at rest and at maximum exercise

Experimental total deposition of inert particles in the airways of 4 groups of subjects

This study was aimed at measuring total respiratory tract deposition of inhaled inert particles in subjects for whom model predictions established from data of healthy adult subjects, should eventually be modified with specific experimental values. Looking for possible relationships between individual deposition data and measured respiratory function volumes and airflows should help to explain the role of airway dimensions in deposition efficiency.

Four groups of subjects with various airway sizes and physiopathological states, were studied:

- **healthy non smokers adults**, of both genders, (18);
- **children, aged 8 to 15 years**, (13);
- **adults** with impaired lung function, **restrictive**, (15) and **obstructive**, (15).

Total deposition fractions of an aerosol inhaled through the mouth and containing three sizes of monodisperse particles (**1.2, 2.3, and 3.3 µm** aerodynamic diameter) were measured with controlled respiratory parameters. **(Figure No 4)**

All the subjects were required to perform the test with the same tidal volume, **VT = 0.5 litre,** and inspiratory times, **t_i = 1.5 seconds**, because meaningful observations of variations in aerosol deposition among subjects with various lung dimensions would be possible only if the breathing pattern was kept constant for all of them. This test was performed by four groups of volunteers with the aim of studying the influence of the size of lung volumes and flow rates, and therefore of body size, and of age and eventually of pathology. The required parameters, VT and t_i, were correctly completed by almost all of them, and their deviations were smaller than **10%**; the highest were observed in obstructive subjects.

Subjects	Height	TR	$\dot{V}$ /V	Max		Minute ventilation				
Age (sex)		o/n	o/n	Exercise		Rest		Max. Exercise		S.P.
	cm			Watts	C.F	1	Oral %	1	Oral %	1
8 (M)	120	0 38	1.0	75	180	3.9	30.2	17.6	89.7	
8 (M)	120	0 38	1.0	50	156	4.9	24.2	27.1	90.6	
8 (F)	130	0.35	1.9	75	99	4.0	83 7	28.7	99.4	
10 (F)	150	0.25	1.7	100	186	9 6	20.4	36 0	95.8	
12 (M)	158	0 64	2.0	150	170	10 4	53 6	54.7	56.7	
12 (F)	155	0.43	1.0	125	170	8.9	21.7	48.7	32.0	
13 (F)	147	0.59	1.9	100	156	6.8	42.6	34.4	92.0	
14 (M)	157	0.43	1.0	175	160	8.7	4.0	59.1	45.0	25
15 (M)	176	0.52	2.1	150	151	7.4	30.9	92.3	51.4	
16 (F)	167	0.58	1.8	150	124	7.9	49.1	51.3	73.8	
16 (F)	163	0.68	1.4	175	170	6.1	37.6	48.1	42.2	

TR o/n = Total resistance oral / nasal
C. F. = Cardiac frequency (min^{-1})
$\dot{V}$ / V o/n = Flow / volume curve oral / nasal
S. P = Nasal to oronasal ventilation switching point

Table 4: Individual biometry of 10 healthy children; observed cardiac frequency at maximum exercise completed and ventilatory data at rest and at maximum exercise

The differences in deposition data obtained in **11 men and 7 women, out of 18** healthy adult non smokers were not found to be significant by the Wilcoxon non parametric test between the two genders, possibly because the numbers of subjects were too small. Men and women had similar values of Functional Residual Capacity, **FRC**, but women who had smaller values of Forced Expiratory Volume in one second, $\mathbf{FEV_1}$, also had higher deposition of **3.3 µm** particles (**47%** against **44.1%**). These differences being non significant, data of both genders were treated as a whole in all groups: healthy adults and children, restrictive and obstructive adult patients, without separating them into gender sub-groups.

Mean deposition values and standard errors on means, along with ventilation parameters of the four studied groups are summarised in **Table 5**. All the deposition data are lower in the healthy non smoker adults, and most of the differences are significant by the Wilcoxon non parametric test, except for obstructive patients, whose data are the most dispersed; this is probably related to their disability to keep their breathing pattern quite consistent with the required parameters. It also could be a consequence of their high and irregular tobacco consumption that is missing in the other groups

In order to examine whether aerosol deposition could be dependent on lung volumes and flow rates, individual deposition data for each particle size were plotted against the different lung function parameters, and by intuitive modelling, fitted by simple linear regression by the least squares method. Inverse linear correlation was found between all deposition data and lung function data, Total Lung Capacity, **TLC**, Functional Residual Capacity, **FRC**, and Forced Expiratory Volume in one second, $\mathbf{FEV_1}$.

As an example, in the three groups, healthy adults, children and restrictive patients, **TLC**, presented significant inverse correlation coefficients with deposition, especially for **2.3 µm** particles, that was linearly increased in lungs with reduced volumes.

$$\mathbf{DE_{,\,2.3\mu m}\,(\%) = -\,3.85\ TLC\ (l) + 59} \qquad \mathbf{r = 0.46}$$

In obstructive patients, inverse correlations of deposition of the three particle sizes were only observed with $\mathbf{FEV_1}$. Multiple correlations with FEV_1 and FRC or TLC did not improve the significance of the correlation coefficient, probably indicating the predominant effect of airway obstruction over lung dimensions in these subjects.

In our subjects, the children and the two groups of patients had greater deposition rates than did the healthy adults. In children and in restrictive patients this could be related to small lung volumes, while in obstructive patients, it could rather be related to impaired flow rates

These few experimental data show that healthy children have specific nose flow rate values, that can be estimated from their body size. At exercise, they increase their ventilation more through the mouth than adults do, and total deposition at rest through the mouth is higher than in adults for the same breathing pattern.

Persons of three different ethnic groups have shown variations in their inhalation flow rates, the lowest values being found in Asiatics.

In adults with impaired lung function, in whom all the lung volumes and flow rates are reduced, total deposition data are higher than in healthy subjects, for the same breathing pattern.

In order to apply to the largest possible number of persons in the population, predictive models of intake from inhalation of radionuclides should include those ranges of uncertainty upon respiratory tract features and breathing parameters, and recommend modifying factors related to specific groups of persons.

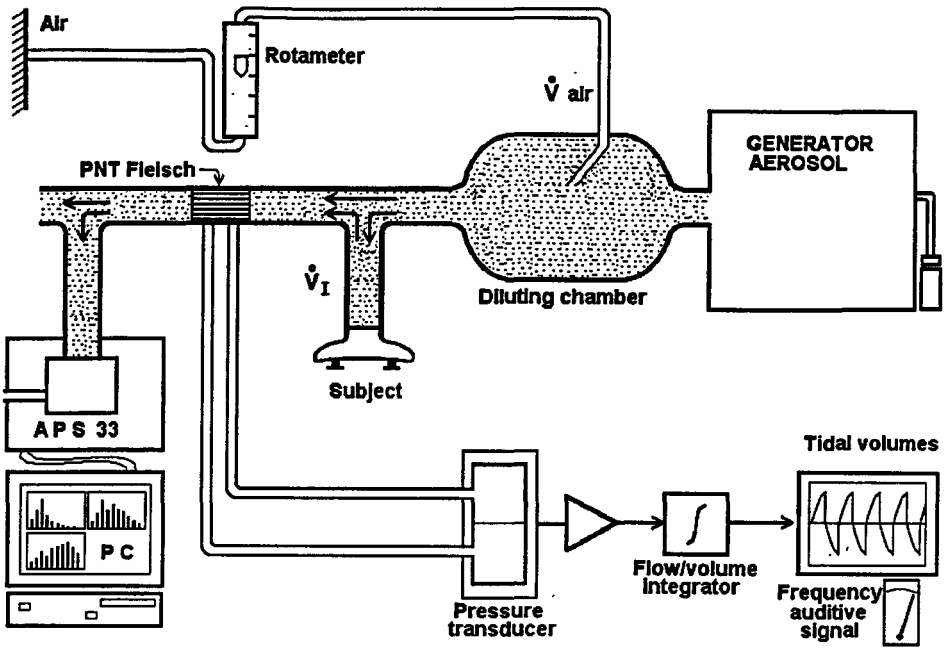

Figure 4: Facilities for particle total deposition measurements during controlled breathing.

Particle Size / Deposition	1.2µm %	2.3µm %	3.3µm %	Ventilation Parameters Vt (l)	ti (s)
Healthy Non Smokers n = 18	26.1 (2 9)	34.2 (2.5)	45 2 (2 3)	0.53 (0.01)	1.59 (0.06)
Obstructives n = 15	39.2 *** (5.4)	47.7 *** (5.3)	56.7 (5.2)	0.52 (0.01)	1.66 (0 06)
Restrictives n = 15	37.7** (2.8)	46.3** (3.1)	56 6 ** (3.3)	0.52 (0.03)	1.61 (0.06)
Children (8 - 15 y) n = 13	20.6 (5.2)	47.1 ** (3.8)	60.3** (2.9)	0.48 (0.01)	1.38 (0.06)

Significantly higher than healthy non-smokers by Wilcoxon non parametric test : **p ≤ 0.05, ***p ≤ 0.02

Table 5: Mean per cent total depositions and standard errors on mean (sem) values of inhaled particles in the airways of 4 groups of subjects.

IV. Publications during the reporting period.

Yu C. P., Zhang L., Becquemin, M. H.,, Bouchikhi, Roy M. (1992) *Semi-empirical algebraic modelling of total and regional deposition of inhaled particles in the human lung of various ages.* J. Aerosol Sci., **23**, No 1, 73-79.

Roy M. *Age - related aspects of physiology in respiratory tract modelling. In : Age -dependent factors in the biokinetics and dosimetry of radionuclides.* (1992) Radiat. Prot. Dosim., **41**, No 2-4, 93-98.

Masse R. and Roy M. *Vie des groupes de travail de la Commission Internationale de Protection*

Radiologique. Le modèle pulmonaire du Comité 2. Etat de la question. (1992) Radioprotection , **27**, No 4. 459-467.

Landman R., Roy M., Bouchikhi A., Becquemin M. H. *Aerosol de pentamidine.* (1992) Rev. Mal. Resp. , **9**, 651-652.

Bouchikhi A., Becquemin M. H., Roy M., Bertholon J. F., Malarbet J. L. (1993) *Importance de la morphologie des voies aériennes sur le dépôt des particules chez l'homme.* Rev. Mal. Resp., **10**, supp. 2, R123.

Roy M., Malarbet J. L., and Courtay C. *Débits respiratoires et activités quotidiennes : paramètres de l'exposition aux substances inhalées.*(1993) Radioprotection, **28**, No 3. 279-290.

Becquemin M. H., Bouchikhi A., Bertholon J. F., Roy M., Malarbet J. L. (1993) *Inhaled particle deposition in the airways of adults and children.* Eur. Respir. J., **6**, Supp. 17, 214S.

Bertholon J. F., Becquemin M. H., Taieb G., Bouchikhi A., Malarbet J. L., Roy M. (1993) *Distribution of ventilation through nose and mouth in healthy subjects performing graded exercise.* Eur. Respir. J., **6**, Supp. 17, 492S.

Roy M. *Circumstances of contamination and intake routes.* in : Assessment of Doses from Intakes of Radionuclides ; ERPET Cadarache, France, 17-22 April 1994.

Bertholon J. F., and Roy M. *Metabolically consistent breathing rates are irrelevant to assess airborne contamination, and prone to large errors.* (1994) Letter to the Editor, Health Phys., **66**, 1,. p. 89.

Becquemin M. H., Bouchikhi A., Plagnieux N., Bertholon J. F., Taieb G., Roy M., Malarbet J. L. (1994) *Oronasal ventilation partitioning in healthy adults and children performing graded exercise.* Aerosol Sci. Technol., **2**, p. 751.

Becquemin M. H., Bouchikhi A., Bertholon J. F., Roy M., Harpey C., Stahlhofen W., Nizar Z. (1994) *Granulométrie et mesure du dépôt d'un aérosol médicamenteux (fusafungine) dans les voies aériennes normales et pathologiques.* Rev. Pneumol. Clin., **50**, 309-315.

Feretti Pire P., Versari A., Becquemin M. H., Bouchikhi A., Roy M., Malarbet J. L, Barchi E., Gafa S. (1994) *Pulmonary deposition of aerosolized pentamidine using a new nebulizer : efficiency measurement in vitro and in vivo.* Eur. J. Nucl. Med., **21**, 299-406.

Ansoborlo E., Henge-Napoli M. H., Donnadieu-Claraz M., Roy M., Pihet P. (1994) *Industrial exposure to uranium aerosols at laser enrichment processing facilities.* Radiat. Prot. Dosim. **53**, No 1-4, 163-169.

Roy M., Malarbet J. L., Becquemin M. H., Bouchikhi A., and Bertholon J. F. (1994) *Airway deposition of inhaled particles in healthy and pathological subjects.* Radiat. Prot. Dosim., **53**, No 1-4, 115-117.

Malarbet J. L., Bertholon J. F., Becquemin M. H., Taieb G., Bouchikhi A and Roy M. (1994) . *Oral and nasal flow rate partitioning in healthy subjects performing graded exercise.* Radiat. Prot. Dosim. 1994, **53**, No 1-4, 179 - 182.

INTERNATIONAL COMMISSION ON RADIOLOGICAL PROTECTION (ICRP) 1994 *Human Respiratory Tract Model for Radiological Protection* ; ICRP Publication 66. Annals of the ICRP **24** (1-3) Elsevier Science Ltd, Oxford.

INTERNATIONAL COMMISSION ON RADIOLOGICAL PROTECTION (ICRP) 1994 *Dose Coefficients for Intakes of Radionuclides by Workers.* ICRP Publication 68. Annals of the ICRP **24** (4) Elsevier Science Ltd, Oxford.

Bouchikhi A., Becquemin M. H., Malarbet J. L., Roy M., Bertholon J. F., Becquemin M. H., Taieb G. (1995) *Experimental measurements of oral and nasal flow rates in chidren for lung deposition modeling.* J. Aerosol Medicine, Suppl., (in press).

Head of project 4: Dr. Patrick

II. Objectives for the reporting period

The overall aim was to explore the mechanisms underlying the clearance of particles in the respiratory tract. The specific objectives were:

(A) To investigate the clearance of gold colloid test particles deposited in rat lung by alveolar microinjection, especially the contribution of particle dissolution to alveolar clearance.

(B) To measure the extent to which slow tracheo-bronchial clearance, measured using the rat tracheal model, depends on particle size in the same way as in humans.

(C) By studying the functional morphology of the large airways, to explore the possibility that slow clearance might be related to discontinuities in the muco-ciliary clearance process; and to determine whether this might explain the difference between humans and other species in the extent of slow clearance. To meet these objectives, morphometric studies on the F-344 rat would be extended to other strains and species, including human subjects.

III. Progress achieved including publications

(A) *Alveolar Clearance*

The technique of intra-alveolar microinjection has been used to study the mechanisms underlying the clearance of particles from the alveoli of rat lung. By this method particles were deposited only in the alveolar region, and not at all on the conducting airways, so avoiding the complication of long-term retention of particles that is now known to occur after deposition on the airways. ^{195}Au-labelled colloidal gold particles were used as a non-toxic, inert test material; the median physical diameter was in the range 10-21 nm, which allowed the particles to pass readily through the glass micro-pipette, whose outside tip diameter was 10-14 μm. The clearance kinetics from the alveolar region of the rat were determined over 462 days. The overall clearance of ^{195}Au was found to be well described by two exponential terms, with 22% being cleared with a half-time of 14 days and the remainder with a half-time of 583 days. At 4 time-points during this study, the urinary and faecal excretion of ^{195}Au was measured, with the aim of analysing the overall rate of lung clearance into (i) particle transport up the conducting airways, and (ii) the absorption to blood of dissolved gold. The last two time-points (273 and 462 days) were chosen such that only the very slow clearance term was still significant.

In order to provide necessary information about the excretion of dissolved gold from the blood circulation, an ancillary study was undertaken in which ionic gold chloride ($H^{195}AuCl_4$) was injected intravenously into 5 rats. Excretion was monitored over 3 weeks. Over this period some 30% of the ^{195}Au was cleared from the body, 16.8 $\pm$ 0.9% appearing in the urine and 13.3 $\pm$ 0.7% in the faeces.

Assuming that, in the microinjection study, the ^{195}Au which appeared in the blood from dissolved gold colloid was similarly partitioned between urine and faeces, then the overall clearance in that study could be analysed as shown in Table 1.

Table 1. Clearance of colloidal gold from the alveoli

Days after microinjection	Proportion of overall clearance (%)	
	Particle transport	Absorption to blood
28	75.6	24.4
56	93.6	6.4
273	31.5	68.5
462	22.7	77.3

Thus at the later times, when only the slow phase of clearance remained, more ^{195}Au was cleared by dissolution than by particle transport up the bronchial tree. As expected, particle transport was more prominent at the earlier times.

After the injection of gold chloride, 42% of the amount injected was retained in the liver, with lesser amounts in the kidney and spleen, and only 0.25% in the lung. The extent of liver uptake raised the possibility that at least some of the gold chloride had been converted into metallic gold in the blood. Before injection, the solution was at pH 3.5 and did not precipitate. In contrast, in the intra-alveolar microinjection study with colloidal gold, the mean uptake of ^{195}Au by the liver had never exceeded 1.2% of the initial lung content.

Clearly caution needs to be exercised in applying the gold chloride excretion data to the excretion rates in the colloidal gold study. Nevertheless it appears that, even for such an insoluble material as metallic gold, long-term clearance from the alveolar region of the lung is at least partly the result of dissolution and absorption to blood. It was concluded that the rate of particle transport from the alveoli is known only approximately.

(B) *Slow Clearance in Experimental Animals*

Scheuch *et al* (project 2; *J Aerosol Med.* 6 [suppl.], 47, 1993) have shown that the extent of slow tracheo-bronchial clearance in humans depends on the geometrical particle diameter. Because of certain quantitative differences in slow clearance which had already been observed between humans and experimental animals, it was of great importance to see if the same relationship with particle size obtained in the rat model.

Studies have therefore been carried out on the kinetics of clearance of particles deposited locally in the trachea of the F-344 rat by intra-tracheal instillation. The volume instilled was 2.5 μl, which is known to result in local deposition confined to the distal trachea.

A comparison was made between $^{133}BaSO_4$ particles, used as a reference for comparison with earlier work, and ^{195}Au-labelled colloidal gold. The median particle diameters were 1.4 μm and 22-30 nm respectively. As before, for $^{133}BaSO_4$ particles, the retention (R) in the deposition region could be described over 48 hours by two exponential terms:

$$R = Pe^{-at} + (1 - P)e^{-bt}$$

where P is the fraction of particles subject to fast mucociliary clearance and (1 - P) represents slow clearance as previously defined for this model; a and b are rate constants

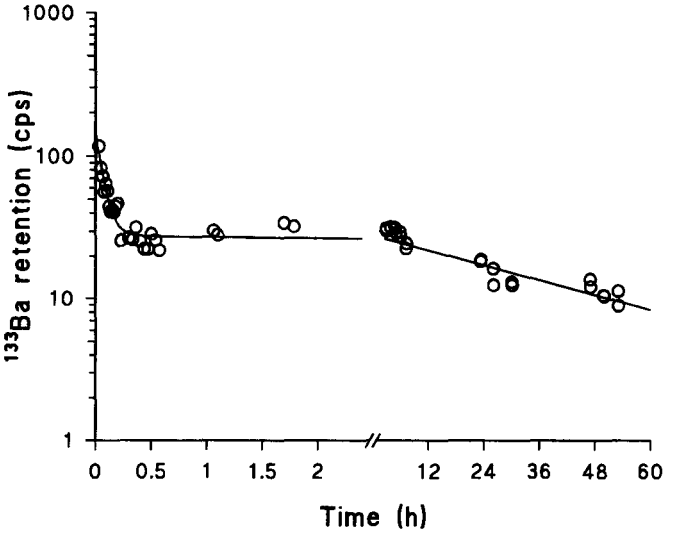

Fig. 1. Kinetics of tracheal clearance of $^{133}BaSO_4$ particles. Retention given in counts per second. Typical data for one animal. Note break in time axis.

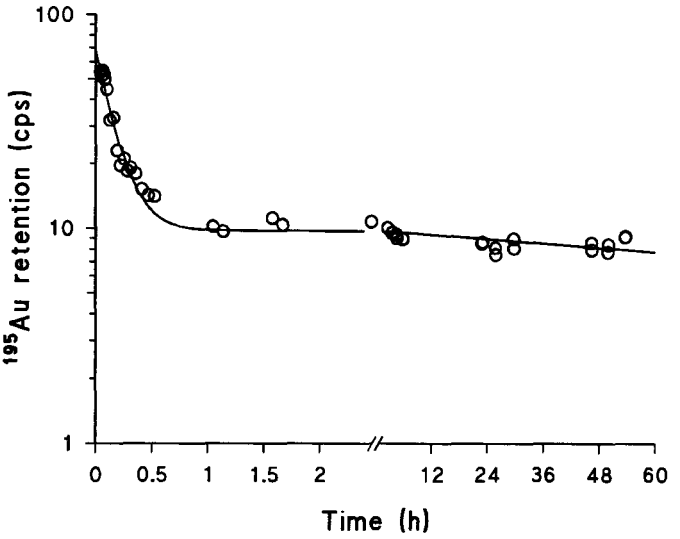

Fig. 2. Kinetics of tracheal clearance of ^{195}Au-labelled colloidal gold particles. Typical data for one animal; other details as in Fig. 1.

and t = time. The results for a typical animal are given in Fig. 1. With the colloidal gold particles, it was again found that the clearance kinetics conformed to the two-exponential expression (Fig. 2).

As shown in Table 2, the average fraction of particles subject to slow clearance (1 - P) was essentially the same for the two particle sizes. Also the rate constant for the fast component (a) was not significantly different in the two cases, but for the slow phase the rate constant (b) was lower for colloidal gold than for the $BaSO_4$ particles.

Table 2. Kinetic parameters for tracheal clearance (means ± SEM)

	$BaSO_4$ particles	Colloidal gold particles
Median physical diameter (μm)	1.4	0.022 - 0.030
No. of animals	7	7
(1 - P)	0.286 ± 0.078	0.319 ± 0.095
a (h^{-1})	14.6 ± 6.1	8.6 ± 2.7
b (h^{-1})	0.0224 ± 0.0073	0.0039 ± 0.0011

The results for $BaSO_4$ particles are in good agreement with those obtained previously (with HMT rats). The fraction cleared slowly was also similar to the values obtained in an earlier study for 1.1- and 5.7-μm fused alumino-silicate particles, as well as for 1.0-μm $BaSO_4$ particles. Thus it can be concluded that in the rat tracheal model the magnitude of the slow-cleared fraction does not vary with particle size. This differs from the results in humans for particles of widely differing sizes, as defined by Scheuch *et al.* A paper describing this study is in preparation.

(C) *Functional Morphology of the Conducting Airways*

This part of the project was designed to see whether slow tracheo-bronchial clearance, and in particular the apparent differences in the extent of slow clearance between animals and humans, can be explained in terms of the functional morphology of the mucociliary clearance apparatus of the large airways.

The approach chosen for this purpose was to measure the proportion of the epithelium of the trachea which is not covered by cilia. The method is based on histological and image analysis procedures to measure the sum of the lengths of segments which are devoid of cilia in transverse and also in longitudinal sections, together with the total lengths of epithelium in the same sections. From this an estimate can be made of the fraction of the epithelial surface of the trachea which is not ciliated. For 12 Fischer F-344 rats, which were studied first, sections from each animal were taken from 3 levels: proximal, middle and distal trachea. Each section was divided into 4 quadrants: dorsal, ventral, and left and right lateral.

A statistical analysis of the F-344 rat data for transverse sections showed that there were no significant differences in the fraction of non-ciliated epithelium between the 4

quadrants, nor between the 3 levels. The overall proportion of epithelium devoid of cilia was 54.3 ± 1.5%. There were however differences between individual animals. On the basis of these findings, only the middle portion of the tracheas from other strains and species was studied.

The F-344 rat data have been analysed in terms of the distribution of lengths of non-ciliated sections of tracheal epithelium. Here the working hypothesis is that if discontinuities in the ciliary cover of the epithelium do affect the rate of mucociliary clearance, and conceivably the extent of slow clearance, then larger gaps between ciliated areas will have more significance for mucus flow than shorter intervals. In transverse sections, up to 20% of the epithelium corresponded to non-ciliated lengths of 50 μm or more, and even lengths of over 100 μm have been recorded (Fig. 3).

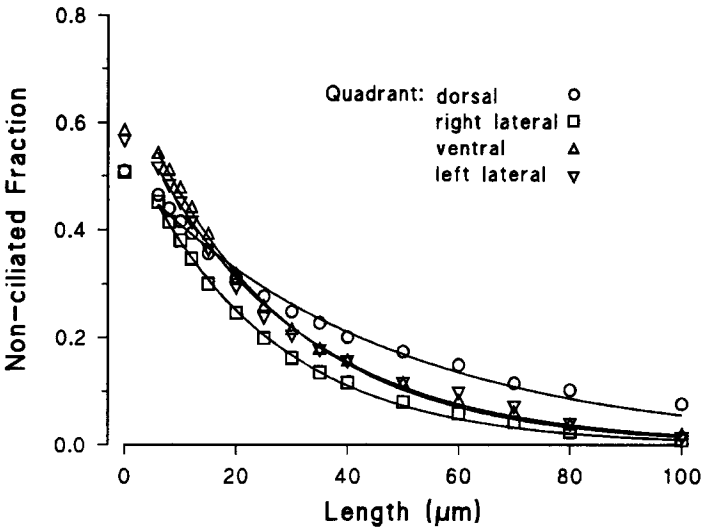

Fig. 3. Length distribution of non-ciliated epithelial regions in *transverse* sections of trachea of the F-344 rat. Each point represents the non-ciliated fraction including only segments equal to or longer than the given length (abscissa). Fitted curves are single exponentials. Mean results for each quadrant, averaged over 12 rats and all 3 levels.

Differences in length distribution were noticed between individual animals, averaged over all 3 levels and 4 quadrants: this could be attributed to a greater proportion of longer non-ciliated regions in just two of the rats. Distribution curves averaged over all 12 animals had suggested a greater proportion of longer non-ciliated regions in the dorsal quadrant (Fig. 3), and also for the middle level (data not shown). These various differences were eventually isolated to dorsal and lateral specimens from the middle level of these two animals. Fresh sections were prepared from the appropriate tissue blocks. Repeat measurements ruled out the possibility that the differences in length distribution were due to errors in the original analysis, i.e. these are real differences.

For longitudinal sections, taken from two different animals, the overall length distribution of non-ciliated epithelium (Fig. 4) was similar to that observed in transverse sections, demonstrating that the discontinuities in ciliary cover were not markedly different in the two dimensions. It may be concluded therefore, in the F-344 rat, that the non-ciliated regions of tracheal epithelium are not composed of long narrow areas, which might have been possible bearing in mind the widely-observed phenomenon of mucus streaming.

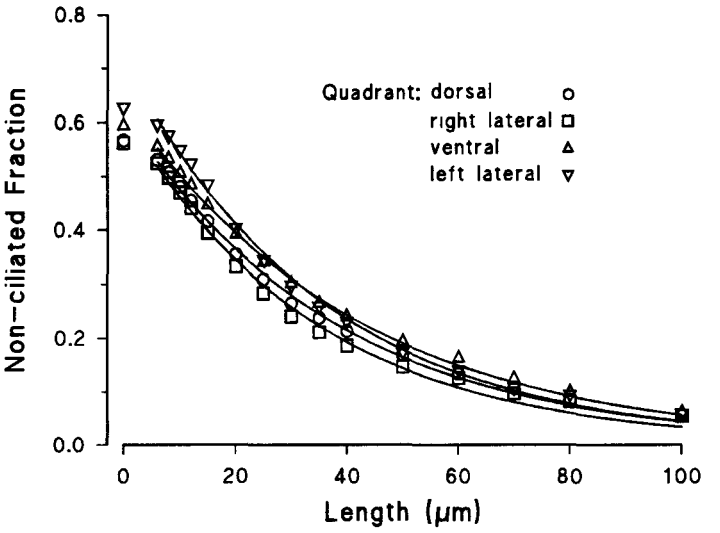

Fig. 4. Length distribution of non-ciliated epithelial regions in *longitudinal* sections of trachea of the F-344 rat. Mean results for each quadrant, averaged over 2 rats and all 3 levels.

Measurements have also been made on tracheas from other strains and species besides the F-344 rat. At present data are available for transverse sections from 6 HMT rats, 7 CBA mice and 6 guinea pigs, and also for longitudinal sections from 2 guinea pigs. Contrary to expectations from studies elsewhere on the relative abundance of different cell types in the airway epithelium, the overall proportion of epithelium which is non-ciliated does differ among these species, as shown in Table 3. This shows data for transverse sections, as mean values for all 4 quadrants, and, where studied, for all 3 levels.

Table 3. Overall proportion of non-ciliated epithelium

	No. of animals	Non-ciliated fraction
F-344 rat	12	0.543
HMT rat	6	0.667
CBA mouse	7	0.617
Guinea pig	6	0.150

Efforts are continuing to complete this study by the analysis of specimens of human tissue. To date, tracheal and bronchial samples from several post mortem cases have been provided by the John Radcliffe Hospital, Oxford. However, only two of these proved to have sufficient intact epithelium for useful measurements to be made. Further human specimens are now being actively sought from this and other sources. It is intended that this part of the project will be completed in the near future and a final report prepared.

Publications

Patrick G & Stirling C (1992). The transport of particles of colloidal gold within and from rat lung following local deposition by alveolar microinjection. *Environmental Health Perspectives* 97, 47-51.

Im Hof V & Patrick G (1994). Particle retention and clearance. *Journal of Aerosol Medicine* 7, 39-47.

Patrick G & Stirling C (1994). The redistribution of colloidal gold particles in rat lung following local deposition by alveolar microinjection. *Annals of Occupational Hygiene* 38 (suppl 1), 225-234.

Patrick G, Batchelor A L & Stirling C (in press). Long-term retention of inhaled fused alumino-silicate particles in the trachea and first bifurcation of the rat. *Journal of Aerosol Science.*

Head of project 5: Dr. Stradling

II. Objectives for the reporting period

(i) To undertake studies on the biokinetics of uranium after deposition in the rat lung as the tributylphosphate complex.
(Studies on the toxicity of tributylphosphate are being undertaken by the University of Medicine, Pleven).

(ii) To undertake studies on the biokinetics of ^{137}Cs and ^{60}Co present in dust obtained from the Kozloduy Nuclear Power Plant Bulgaria to examine the viability of using these radionuclides for assessing intakes of actinides present in the dust.
(Studies on the toxicity of the dust and *in vitro* solubility measurements are being undertaken by the University of Medicine, Pleven and the Institute for Nuclear Research and Nuclear Energy, Sofia).

(iii) To continue studies on the biokinetics of ^{239}Pu and ^{241}Am present in dust samples derived from contaminated soil at Palomares, Spain.
(*In vitro* solubility studies are being undertaken by CIEMAT Madrid).

III. Progress achieved including publications

(i) Biokinetic studies with uranium tributylphosphate

Tri-n-butyl phosphate (TBP) is used for the extraction of uranium from its ores and from mixtures of fission products. Uranium is both chemically and radiologically toxic to man and TBP is chemically toxic to man. There is also a small but real risk of explosion during the processing of uranium using TBP and several accidents have already occurred. The major health risk to the workforce is probably from inhalation of these materials. There is, however surprisingly little information on the biokinetics or effects of TBP after inhalation and no information at all on the biokinetics of uranium after uranium TBP (UTBP) inhalation. This study was therefore designed to examine the absorption and distribution of uranium after UTBP inhalation and a concurrent study was set up by our collaborators in Bulgaria to investigate TBP toxicity after inhalation.

The biokinetics of uranium were examined after instilling 5 µl UTBP (20% (v/v) TBP in n-dodecane containing 1.2 µg or 7.7 µg of uranium) into the lungs of female HMT strain rats and are summarised in Tables 1 and 2. The mass concentrations of uranium in the rat lung represent overexposures by workers not greatly in excess of the daily limit based on chemical toxicity, namely 2.5 mg. At the lower mass concentration (Table 1) the initial clearance of uranium from the lungs was very rapid with 93% of the instilled activity being removed within the first day. In fact the results from both experiments gave similar results except that slightly more uranium was excreted in the faeces and slightly less in the urine in the higher dose experiment (Table 2) than with the lower dose one. Since this discrepancy is probably due to slightly different deposition patterns of the UTBP in the lungs from now on the experiments will be described together except where it is considered appropriate to give individual values for each experiment. The majority of the uranium, 70-80% was absorbed into the blood by 1 day, 79.6% after the low dose administration and 70.4% after the high dose administration. The remaining uranium was cleared by particle transport and excreted in the faeces. Most of the uranium translocated to the blood was rapidly transferred via the kidneys to the urine, about 70% by the first day after exposure. About 16% of the instilled activity was, however, initially deposited in the carcass, mainly the skeleton and 0.35% in the liver. These tissue deposition and excretion characteristics are typical of U(VI).

There was a gradual loss of activity from the carcass and all of the measured organs, including the lungs, to the urine from day 1 onwards. In both cases, by day 84 the carcass

Table 1. Tissue distribution and excretion of ^{233}U after instillation of ^{233}U-tri-n-butyl phosphate into the lungs.
5 µl of ^{233}U-tri-n-butyl phosphate (20% (v/v) in dodecane) was instilled into the lungs of each of a group of female, HMT strain, rats.
Each animal received 1.2 µg, 414 Bq ^{233}U.

Time (Days)	No. of rats	Percentage of Instilled Activity (Mean ± Standard Error)						
		Lungs	Liver	Kidney	Carcass	Urine	Faeces[a]	Blood[b]
0.125	4	15.0 ± 3.4	0.63 ± 0.08	12.5 ± 3.0	30.6 ± 2.7	na[c]	na[c]	na[c]
1	5	6.74 ± 1.42	0.34 ± 0.03	7.72 ± 1.17	16.7 ± 0.8	54.8 ± 4.7	13.7 ± 4.2	79.6 ± 4.9
3	3	2.24 ± 0.34	0.30 ± 0.04	6.66 ± 0.74	16.6 ± 0.5	60.4 ± 1.7	13.8 ± 1.4	84.0 ± 1.9
7	5	2.24 ± 0.58	0.22 ± 0.02	4.06 ± 1.02	14.3 ± 0.9	65.3 ± 4.3	13.9 ± 3.4	83.9 ± 4.5
14	4	2.05 ± 0.20	0.15 ± 0.03	1.38 ± 0.22	11.0 ± 0.6	71.5 ± 2.6	13.9 ± 2.4	84.0 ± 2.7
28	5	1.64 ± 0.13	0.10 ± 0.00	0.80 ± 0.08	10.5 ± 0.4	73.0 ± 3.3	14.0 ± 3.1	84.4 ± 3.3
84	5	0.82 ± 0.23	0.10 ± 0.00	0.18 ± 0.02	8.78 ± 0.24	76.1 ± 1.1	14.2 ± 1.1	85.2 ± 1.1

[a] Faeces + gastrointestinal tract
[b] Provisional values based on ^{233}U in liver, kidney, carcass and urine
[c] na Data not available. Total of Faeces + Urine + Gastrointestinal tract at 0.125 days is 41.2 ± 2.1 %

Table 2. Tissue distribution and excretion of ^{233}U after instillation of a mixture of ^{233}U- and natural uranium tri-n-butyl phosphate into the lungs. 5 µl of tri-n-butyl phosphate (20% (v/v) in dodecane) containing ^{233}U plus natural uranium was instilled into the lungs of each of a group of female, HMT strain, rats. Each animal received 7.7 µg uranium.

Time (Days)	No. of Rats	Percentage of Instilled Activity (Mean ± Standard Error)						
		Lungs	Liver	Kidney	Carcass	Urine	Faeces[a]	Blood[b]
0.125	4	13.0 ±3.8	0.75 ± 0.11	20.8 ± 4.7	29.9 ± 3.0	na[c]	na[c]	na[c]
1	4	6.90 ± 1.55	0.38 ± 0.03	12.0 ± 3.0	15.4 ± 0.8	42.6 ± 4.6	22.8 ± 2.6	70.4 ± 6.0
3	3	2.43 ± 0.87	0.30 ± 0.00	9.03 ± 3.72	12.3 ± 0.7	53.2 ± 13.3	22.9 ±12.7	74.8 ± 13.8
7	4	2.55 ± 0.24	0.25 ± 0.03	3.93 ± 0.31	11.8 ± 1.4	58.0 ± 3.0	23.5 ± 2.6	74.0 ± 3.3
14	5	1.82 ± 0.52	0.28 ± 0.06	1.26 ± 0.18	10.6 ± 0.3	63.3 ± 7.2	22.8 ± 7.2	75.4 ± 7.2
28	5	1.92 ± 0.47	0.22 ± 0.02	0.60 ± 0.06	8.20 ± 0.18	66.2 ± 3.9	22.9 ± 3.9	75.2 ± 3.9
84	5	0.52 ± 0.14	0.14 ± 0.03	0.28 ± 0.08	8.92 ± 1.17	67.2 ± 3.4	23.0 ± 3.1	76.5 ± 3.6

[a] Faeces + gastrointestinal tract

[b] Provisional values based on ^{233}U in liver, kidney, carcass and urine

[c] na Data not available. Total of Faeces + Urine + Gastrointestinal tract at 0.125 days is 35.6 ± 10.2 %

content had dropped below 10%, the lung below 1% and the liver and kidneys below 0.5% of the initial instilled activity.

Experiments were also performed to examine the distribution of uranium over a 3 day period after intravenous injection (IV) or gavage of 5 µl UTBP (IV, 1.5 µg uranium; gavage, 1.3 µg uranium per rat).

After gavage, the uptake of uranium was very low. At 1 day only 2.4% of the instilled activity had crossed the gut wall and the majority of this was deposited in the carcass or excreted in the urine (1.42 and 0.84% of the instilled activity respectively). Liver and lung uptake were both very low, 0.06% and 0.02% of the injected uranium respectively. The low liver content indicates that the uranium was no longer complexed with the TBP. By day 3 the uranium in the carcass had reduced to 0.82%. Using the results from both the gavage and IV data from the observations at 1 day and 3 days the average gut uptake factor (f_1) was calculated to be 0.022 ± 0.008.

One hour after IV injection of UTBP 7.6% of the uranium activity was detectable in the lung. This is an effect which is not seen after IV injection of uranium nitrate and is probably due to uptake of the UTBP complex some of which may form micelles in the blood stream and remain transiently stable for a short period of time. (The stability of the UTBP complex would be very short lived, however, because when aliquots of UTBP were mixed with 0.01M phosphate buffered saline, pH 7.4, during this study over 99% of the uranium transferred to the aqueous phase within 5 minutes.) This lung uptake may explain observation by other researchers that 0.1 ml of TBP injected intraperitoneally or intramuscularly causes respiratory distress within 3 minutes of injection. Respiratory distress was not observed in our animals when using 5 µl UTBP. By 1 day 77.7% of the injected activity had been excreted (66% via the urine and 11.7% via the faeces), 11.4 % was retained by the carcass, presumably the skeleton, and 7.9% was present in the kidney. The activity in the lungs and liver was 1.5% and 1.4% respectively. Between day 1 and day 3 there was a slow loss of uranium from all the organs measured, which was excreted almost exclusively in the urine.

The remainder of the contract will be used to compare these data with those on the behaviour of different uranium compounds and plutonium TBP in animals after inhalation, to extrapolate this data to humans, and to calculate the dose coefficient for UTBP, though based on the criteria above intake limits for uranium should be based on chemical toxicity. The report will be completed by the end of 1995.

(ii) Biokinetics of dust from Kozloduy Nuclear Power Plant

The dust obtained from the reactor hall (see report of University of Medicine, Pleven) contains a mixture of actinides and fission products. Though present in low concentrations the inhalation dose will result predominantly from alpha emitting actinides and ^{241}Pu. The radionuclides ^{137}Cs and ^{60}Co are present at relatively high concentrations and the objectives of the experiments undertaken here are to assess the dose coefficient for the dust and to evaluate whether intakes of the actinides in workers can be assessed from whole body measurements of ^{137}Cs and ^{60}Co. To attain the latter objective the biokinetics and absorption characteristics of these latter radionuclides are being investigated in rats. The amounts of the actinides that can be administered are too low for this purpose and subsequent advice will be based on default characteristics for type M and S materials as defined in the ICRP human respiratory tract model, and the results of the *in vitro* experiments.

The biokinetic data for ^{137}Cs and ^{60}Co available so far are given in Tables 3 and 4. For ^{137}Cs, 81.2% is cleared from the lung by 1 day, the majority of which (51.7%) is absorbed by the carcass, presumably in the muscle tissue. Most of the remaining activity is excreted through the urine, 11.8%, and through the faeces/gastrointestinal tract (GIT), 13.4%, with a small amount,

3.6%, being present in the liver. After 7 days, 52.6% has been excreted (33.9% in urine and 18.7% via faeces/GIT. The majority of the material excreted between day 1 and day 7 (27.5%) is lost from the carcass (17.9%) with only 7% being cleared from the lungs.

For ^{60}Co the picture is somewhat different. Only 39% of the activity is cleared from the lungs after 1 day and the total removed after 7 days is 47.8%. Unlike ^{137}Cs the ^{60}Co absorbed by the blood undergoes rapid excretion with very little retention of activity in the carcass (only 1.86% after 1 day to 0.55% after 7 days). After 1 day 15.1% of the instilled ^{60}Co is excreted via the urine and 20.7% via the faeces/GIT, rising to 22.3% and 27.3% respectively after 28 days.

Provisional values (the absolute values will be revised upwards on completion of supplementary iv experiments) for the percentage of ^{137}Cs and ^{60}Co absorbed into blood after 28 days, 62% and 24% of the initial lung deposit are consistent with the results of *in vitro* studies carried out in Bulgaria. In these experiments 82% and 23% of these radionuclides were leached from the dust by 22 days.

Table 3. Tissue retention and excretion data for ^{137}Cs

Time	Percentage of instilled ^{137}Cs ($\bar{x}$ ± SE)[a]					
d	Lungs	Liver	Kidneys	Carcass	Urine	Faeces[b]
1	18.8±0.9	3.62±0.47	0.71±0.21	51.7±1.1	11.8±1.6	13.4±2.3
3	16.3±1.1	2.00±0.15	0.33±0.03	48.1±1.0	21.9±2.7	11.4±1.5
7	11.8±1.1	1.56±0.12	0.18±0.17	33.8±2.3	33.9±4.2	18.7±3.1
28	13.6±1.4	0.33±0.03	0.13±0.02	11.4±0.6	50.3±3.8	24.2±3.1

Table 4. Tissue retention and excretion data for ^{60}Co

Time	Percentage of instilled ^{60}Co ($\bar{x}$ ± SE)[a]					
d	Lungs	Liver	Kidneys	Carcass	Urine	Faeces[b]
1	61.0±2.1	1.40±0.06	0.33±0.02	1.68±0.11	15.1±2.1	20.5±3.0
3	57.3±0.3	0.76±0.03	0.18±0.02	0.77±0.08	18.9±2.6	22.1±2.7
7	52.3±3.3	0.39±0.11	0.10±0.02	0.55±0.08	20.6±2.6	26.1±3.8
28	49.7±2.9	0.09±0.03	0.02±0.01	0.49±0.06	22.3±1.9	27.4±3.2

Initial lung deposit 2.9 mg dust.
a: mean ± standard error, 4 rats per group.
b: faeces + gastrointestinal tract.

The remaining time on the contract will be utilised to complete the lung deposition experiments and the supplementary experiments on the uptake of the dust from the GIT and on the distribution of the material within the body after intravenous injection which are at present underway. The data will be examined to establish whether or not the incorporation of ^{60}Co and ^{137}Cs within the dust alters the biokinetic behaviour of these isotopes than when present as simple inorganic forms. A gut uptake factor (f_1) will be evaluated for each isotope from the supplementary experiments. ^{137}Cs and ^{60}Co will then be assessed to see if they can be used as markers for actinide detection and assessment after inhalation of this dust. A dose coefficient for the dust will be calculated and the data will be extrapolated to humans for the assessment of intake using the new ICRP model for the respiratory tract and associated computer software. The report will be completed by the end of 1995.

(iii) Biokinetics of ^{239}Pu and ^{241}Am in dust obtained from Palomares

On 17th January 1966 an aviation accident occurred in the airspace over Palomares in southern Spain which resulted in the contamination of about 226 hectares of farmland. The radionuclides of most concern were ^{239}Pu and ^{241}Am. Despite extensive clean-up operations contamination persists. Since the accident comprehensive studies have been undertaken by CIEMAT on the correlation between ^{239}Pu and ^{241}Am concentrations in the soils and their granulometric, mineralogical and chemical composition. The resuspension characteristics of these actinides have also been determined.

Until recently no information was available on the biokinetic behaviour of ^{239}Pu and ^{241}Am after their deposition in the lungs. A major study is being undertaken by NRPB on the behaviour of ^{239}Pu and ^{241}Am after their deposition of the respirable component (nominally <5 μm aerodynamic diameter) observed from the total soil and three particle size fractions, namely 250-125 μm, 20-40 μm and <5 μm. These fractions were considered important since the ^{239}Pu concentrations in the fractions <5 μm and 250-125 μm are the lowest and highest respectively of all those characterised below 1000 μm, namely 1000-250-125-63-40-20-10-5-<5 whilst the 20-40 fraction contains the highest abundance of ^{239}Pu.

The aims of the work reported here were to evaluate the difference in behaviour of ^{239}Pu and ^{241}Am present in the total soil and the three fractions identified, to derive a representative dose coefficient for the dust and to provide guidance for the interpretation of chest monitoring and urine data after accidental inhalation. In the latter case the predicted behaviour of ^{239}Pu and ^{241}Am in humans will utilise absorption data obtained from rats and the new ICRP respiratory tract model and associated software.

The biokinetics of the fractions 250-125 μm and <5 μm have been reported previously although these data now need to be re-interpreted in the light of recent ICRP recommendations and models. The work in progress involves biokinetic studies with the total soil and 20-40 μm fractions. To date the ^{238}Pu data is complete up to 252 days after exposure (Tables 5 and 6).

Table 5. Lung retention and tissue distribution of ^{239}Pu after intratracheal instillation of respirable component of total soil

Days	Actinide	Lungs	Liver	Carcass	Total to blood %
7	Pu	67.6 ± 5.6	0.32 ± 0.05	0.92 ± 0.10	1.22 ± 0.15
28	Pu	5.5 ± 4.0	0.52 ± 0.08	1.28 ± 0.17	1.70 ± 0.21
84	Pu	47.3 ± 4.9	0.72 ± 0.09	2.00 ± 0.19	2.66 ± 0.30
168	Pu	35.7 ± 3.8	0.78 ± 0.07	2.63 ± 0.22	3.50 ± 0.36
252	Pu	27.9 ± 3.3	0.81 ± 0.07	2.89 ± 0.18	3.84 ± 0.33

ILD ^{239}Pu 6.85 ± 0.61 Bq

Notes

(a) Mean ± standard error, number of animals per group = 6
(b) Calculated value, carcass content x 1.33 ± 0.08

Table 6. Lung retention and tissue distribution of ^{239}Pu after intratracheal instillation of respirable component of soil initially 20-40 µm.

Days	Actinide	%ILD of Pu ($\bar{x}$ ± SE)[a]			Total to blood %
		Lungs	Liver	Carcass	
7	Pu	71.3 ± 6.4	0.34 ± 0.04	0.99 ± 0.13	1.32 ± 0.19
28	Pu	64.6 ± 5.7	0.61 ± 0.13	1.86 ± 0.22	2.47 ± 0.32
84	Pu	54.8 ± 6.3	0.97 ± 0.12	2.80 ± 0.34	3.72 ± 0.50
168	Pu	42.2 ± 5.5	1.15 ± 0.13	3.52 ± 0.40	4.68 ± 0.60
252	Pu	31.9 ± 4.8	1.08 ± 0.11	3.77 ± 0.38	5.02 ± 0.59

ILD ^{239}Pu 4.77 ± 0.45 Bq

Notes

(a) Mean ± standard error, number of animals per group = 5
(b) Calculated value, carcass content x 1.33 ± 0.08

For the purpose of this report, the absorption rates for ^{239}Pu into blood are averaged over 0-28 days and 28-168 days after exposure. The data given in Table 7 show that apart from the early clearance of the <5 μm fraction, the other rates are reasonably similar.

The final report will include more precise absorption functions which are currently being evaluated using the NRPB computer code GIGAFIT.

A comprehensive report will be finalised in the autumn of 1995 which will include the biokinetic data from all four studies, the predicted behaviour of ^{239}Pu and ^{241}Am in humans, recommended dose coefficients for the dust and advice on the interpretation of human data.

Table 7. Average absorption rates for ^{239}Pu

Initial dust fraction (μm)	Absorption rate $10^{-3}d^{-1}$	
	0-28d	28-168d
< 5	2.2	0.18
125-250	0.37	0.22
Total soil	0.80	0.28
20-40	1.1	0.30

Head of project 6: Dr. Iranzo

II. Objectives for the reporting period

The objectives of the CIEMAT contribution are:

(i) Analysis of various fractions of contaminated dusts, to provide information about their chemical and mineralogical composition, and correlation of these characteristics with the Pu and Am concentrations and the physico-chemical forms of these actinides.

(ii) *In vitro* simulated pulmonary leaching experiments with different soil fractions to assess the physiological dissolution characteristics of plutonium isotopes and americium present in the dust samples.
After the end of the *in vitro* simulated pulmonary leaching experiments, sequential leaching of the remaining sample material with specific reagents, to determine the geochemical associations of radionuclides extracted by the physiological solution.

(iii) Assessment according to ICRP Publication 30 methods, of the biological behaviour of plutonium isotopes and americium associated with soil, using data from the *in vitro* simulated pulmonary leaching experiments.

(iv) Comparison of the results obtained in the *in vitro* experiments with those obtained in the *in vivo* experiments at NRPB, to assess the doses per unit intake and specific ALI's for members of the public exposed to Palomares dust in a contaminated environment.

III. Progress achieved including publications

The main objective of this work has been to determine the biokinetic parameters of plutonium and americium inhaled in the state in which they are found in the environment as a result of their deposition in the soil, from an aviation accident that generated different plutonium oxides. The studies carried out have three different parts.

- Studies of the geochemical and mineralogical properties of Palomares soil and their associations with plutonium present in the soil 28 years after the nuclear accident.
- Preparation of respirable dust for animal experiments (conducted at NRPB) and performing *in vitro* simulated pulmonary leaching studies.
- Assessment of internal doses to humans resulting from intake of plutonium and americium bearing dusts present in this area and establishment of ALIs for inhalation.

Soil sampling was performed in 1986 in an area close to the impact point of one of the damaged thermonuclear bombs at regular points distributed along diagonals of a square area (50 m x 50 m). Samples were taken from the surface and at depths of 15 cm.

Granulometry.

A separation of the different soil particle fractions was obtained by maceration and ultrasonic dispersion. Nine size fractions were obtained with the following size intervals:

$$\Phi \geq 1000\text{-}250\text{-}125\text{-}63\text{-}40\text{-}20\text{-}10\text{-}5 \geq \mu m.$$

Fractional division of particles greater than 63 μm, after leaching with water over a mesh of a prescribed size, was carried out by screening according to NLT 104/72 standards. Particles smaller than 63 μm were fractionated by the "British Rema" air classifier (mean density was considered to be 2.7 g/cm^3). "Coulter TA II" particle counter, Sherard methodology was used to determine the dispersion index.

For these studies four soil fractions were selected:

Sample 1: $\Phi < 5$ µm.

Sample 2: $125 < \Phi < 250$ µm.

Sample 3: $20 < \Phi < 40$ µm.

Sample 4: Total soil.

The first fraction represents the natural respirable fraction of the soil; the other fractions were ground until over 90% of the particles were less than 5 µm and known to contain the highest concentration of plutonium.

The mineralogical analyses were carried out by optical microscopy and X-ray diffraction. The second technique was used to analyse each of the granulometric fractions. The quantitative analysis of the mineral species was based on the intensity of the most important reflections. The values of the intensity, Y, are represented in arbitrary units, 100 being the Y value for the highest reflection intensity in the different granulometric fractions. The soil is composed of silty sand.

The soil is composed of silty sand (ref. 1), and the activity is fairly uniformly distributed between the silt and sand fractions, with rather less in the clay (Table 1).

TABLE 1. COMPONENTS OF THE SOIL AND DISTRIBUTION OF ACTIVITY BETWEEN THEM

Component	Clay <5 µm	Silt 5 - 63 µm	Sand >63 µm
Mass %	8.7	54.6	36.5
Activity %	2.32	63.1	34.5
Relative specific activity (Activity%/Mass%)	0.26	1.15	0.94

Chemical composition and physico-chemical parameters (cationic and anionic macroconstituents) were determined on solid samples and in water obtained from maceration and leaching of each of the samples by spectrometry emission with plasma source, ionic chromatography and specific ion electrode, turbidimetry, C-S analyser and fluorimetry. The Eh, pH and conductivity were determined from soil elutriation waters.

Chemical and mineralogic studies showed that each fraction consisted mainly of SiO_2, Al_2O_3, CaO, Fe_2O_3 and CO_3^{-2}. The main mineralogical components are quartz, calcite, dolomite, chlorite and muscovite-illite.

Plutonium and americium activity concentrations in each sample were determined by performing 40 radiochemical analyses on aliquots of different sizes taken from extractions carried out on soil samples of 10 g each, which had first been homogenized. Plutonium analyses were performed, based on the HASL-72 procedures manual. All the samples were ashed before determination of the plutonium and americium contents. The actinide elements were extracted with 1M HF and 12M HNO_3. The plutonium was taken up in 8M HNO_3. Final purification was accomplished by adsorbing the Pu(IV) onto an anion-exchange column. The Pu(IV) was reduced to Pu(III) and eluted from the column with 0.5N HCl. After purification, the plutonium was electrodeposited on stainless-steel plates, and the amount of Pu^{238} and $Pu^{239+240}$ were determined by alpha spectrometry with low-background high-

resolution surface barrier detectors. Counting times ranged from 2 to 7 days, depending on the plutonium concentration of the sample. An internal standard of Pu^{236} or Pu^{242} was used to determine recovery efficiencies.

TABLE 2. MINERALOGICAL COMPOSITION OF SIZE FRACTIONS

Size μm	Chlorite d(Å)-14	Muscovite-Illite d(Å)-10	Quartz d(Å)-4.24	Calcite d(Å)-3.03	Dolomite d(Å)-2.88
< 5 μm	67.39	46.48	6.65	100.00	5.42
5 < Φ > 10	58.70	72.24	11.97	76.78	10.54
10< Φ > 20	58.70	59.62	21.51	61.30	7.53
20< Φ > 40	84.78	97.18	55.43	65.33	24.90
40 < Φ > 63	62.22	100.00	58.09	39.00	100.00
63 < Φ >250	80.43	93.43	84.92	49.54	54.81
250< Φ>1000	41.30	33.80	100.00	73.99	19.58

Plutonium activity concentration was determined in the size fraction between 125 and 250 μm. This fraction showed a value of 6389 ± 315 Bq/g. Because of its high value, this fraction was selected for administration to rats. It was first ground to obtain a size fraction < 5 μm. The specific activity of this respirable component of the soil fraction was 2420 Bq/g, lower than the activity of the parent material.

The dust representing the natural respirable fraction of the soil, (< 5 μm) was also selected for administration to animals. The plutonium content of this fraction was 504 ± 140 Bq/g. Autoradiography studies showed that both fractions contained dispersed forms and particulates. It appears that each form represents about half of the total activity present.

***In vitro* pulmonary leaching studies.**

The purpose of these experiments is to study the pulmonary biokinetics (by means of simulation) of plutonium and americium associated with contaminated soil. The methodology used takes into account different fractions of soil: Φ < 5 μm (respirable fraction), 20-40 μm, 125-250 μm and total soil. For pulmonary simulation small amounts of each dust sample were placed in a tube-shaped, semipermeable membrane closed at both ends. Each membrane was placed in a plastic bottle with 400 ml of pH 7.3 physiological solution. Every bottle was kept at 37°C and was shaken for half an hour every three hours so as to simulate the physiological conditions of the lung. Each week the bottle was replaced by another with fresh physiological solution, and the solution was analysed using radiochemical techniques.

The chemical composition of the physiological solution used contained mineral salts (NaCl, NH_4Cl, NaH_2PO_4, $CaCl_2$), amino acids (glycine, Na_3Cit) and H_2SO_4.

The first stage of the experiment was maintained for 3 months, and during this time it was observed that the amount leached did not exceeded 0.5% of the total plutonium contained in the sample (see figure 1). Another simulation experiment was performed with two other aliquots of the fraction below 5 μm. During the first weeks of this experiment similar percentages of $Pu^{239+240}$ and Am^{241} were dissolved, but the percentage of Pu^{238} was several times higher (see figures 2 and 3). The total amounts of $Pu^{239+240}$ and Am^{241} extracted during the first 140 days were less than 0.58% and 0.32% of the total $Pu^{239+240}$ and Am^{241} contained in the respirable fraction of soil. For Pu^{238} the values were about 2%.

Six months after the start of the experiment, the physiological solution used in one sample was replaced by specific reagents for sequential leaching, in order to establish the

geochemical associations of the radionuclides not extracted in the simulated pulmonary leaching experiment. The method employed is basically that of McLaren and Crawford. The reagents and fractions extracted are shown in the following table:

TABLE 3. SEQUENTIAL LEACHING EXPERIMENT

FRACTION EXTRACTED	REAGENT
Specifically adsorbed	0.05M Acetic acid
Organically bound	0.01M $Na_4 P_2 O_7$
Oxide bound	0.175M $(CO_2NH_4)2$/0.1M $(CO_2H_2)_2$
Residual	7.8M HNO_3
Residual (strongly bound)	HF + HNO_3

The sequential leaching in two samples (6 months and 1 year after pulmonary experiment) with acetic acid and sodium pyrophosphates showed that the specifically-adsorbed and organically bound fractions had been reduced, or even disappeared in the case of the 1-year pulmonary leaching experiment. This result shows that the radionuclides in exchangeable, specifically-adsorbed and organically bound forms are the most readily leached by the physiological solution (see figure 7). These fractions represent less than 4% of the total activity for $Pu^{239+240}$ and 8% for Pu^{238} in the total soil sample.

It is important to underline that in the pulmonary simulation experiments with the respirable fraction sample (employing 3 aliquots), the Pu^{238} extraction, especially during the first four weeks, was higher that the $Pu^{239+240}$ extraction obtained. This phenomenon did not take place in the simulation experiments with the other soil fractions (see figures 4, 5 and 6). The reason could be, following refs. 2 and 3, due to the presence of plutonium nitrate in this soil fraction. According to Garland *et al.*, Pu^{238} added as the nitrate to soil was consistently a factor of 2 to 3 times more soluble than $Pu^{239+240}$ initially added as the nitrate. This difference is explained as probably resulting from the formation of larger hydrated oxide particles at the higher plutonium concentration (Pu^{239}). The water solubility of Pu^{238}, when incorporated in relatively large plutonium oxide particles (>1 μm), would be expected to be greater than the solubility of $Pu^{239+240}$ oxide particles of similar size as a result of crystal damage and radiolysis arising from the greater specific activity of the Pu^{238} (an approximate factor of 270).

The activity percentage leached in the respirable fraction experiment, during the first six weeks, is similar for Pu^{239} and Am^{241}. The Pu^{238} activity percentage leached is about 4 times higher than that of the Pu^{239}, the difference being greater during the three first weeks.

Figures 4, 5 and 6 show the results obtained in the pulmonary leaching experiments performed with 20-40 μm and 125-250 μm granulometric soil fractions, and total soil. In all cases the similar behaviour of the plutonium isotopes and Am^{241} can be noted, with the Am^{241} leached fraction being higher than $Pu^{239+240}$ and Pu^{238} leached fractions. This is contrary to the observation in the experiment performed with the respirable fraction, where the most soluble form was Pu^{238}. The different behaviour of the respirable fraction of the Palomares soil, in the simulation experiments, can be explained by its different mineralogical composition (see table 2). Correlation factors between the plutonium activity concentration in each granulometric fraction and the abundance of the minerals present in each fraction were calculated for some samples of the Palomares area and are shown in table 4. These factors show the correlation that exists between the plutonium activity concentration and the abundance of minerals like chlorite and illite-muscovite. Both of them are phyllosilicates formed as sheets, respectively

14 and 10 Ångströms wide, fixed to one another by cations like K, Na, Fe, Mg. Plutonium and americium can be principally adsorbed onto the surface of these minerals. Some amounts of these radionuclides could also be occluded or trapped into the structure of the crystals, according to the extraction with HF-HNO_3 mixture realized during the sequential extraction procedure.

TABLE 4. MULTIPLICATIVE COEFFICIENTS OF CORRELATION BETWEEN THE ACTIVITY CONCENTRATION OF Pu-239+240 AND THE MINERALS.

SAMPLE	CHLORITE	MUSCOVITE	QUARTZ	CALCITE	DOLOMITE
1	0.82	0.90	-0.03	-0.56	0.45
2	0.85	0.90	0.31	-0.49	0.50
3	0.87	0.88	0.03	-0.55	0.50
4	0.97	0.74	-0.08	-0.15	0.21
5	0.75	0.41	-0.13	0.03	-0.07

After the *in vitro* experiment with the respirable fraction of the soil, we can classify this Palomares dust in relation to internal contamination by inhalation, for different plutonium isotopes and also for americium, according to ICRP (30) in the following way:

TABLE 5.

ICRP 30 inhalation class	$Pu^{239+240}$	Pu^{238}	Am^{241}
Y	87%	93%	92%
W	13%	7%	8%

The committed effective dose (CED) per unit intake after inhalation of such an aerosol, based on the ICRP-30 and 1990 ICRP recommendations and this classification for the Palomares dusts, is 0.0645 mSv/Bq for $Pu^{239+240}$. We have considered that any americium detected in urine was formed by the decay of Pu^{241}. The CED factor estimated is 0.0008 mSv/Bq.

Annual limits on intake

The annual limit on intake for workers, considering the committed effective dose (CED) limit recommended by ICRP Publication 60 of 20 mSv y^{-1} is 312 Bq y^{-1} for $Pu^{239+240}$. Thus for members of the public exposed to Palomares dust an annual intake of 15.5 Bq y^{-1} corresponds to a CED of 1 mSv y^{-1}. The following table shows different values of CED derived for aerosols of 1 μm AMAD for Palomares people, taking into account different ages.

Considering the new lung model (ICRP 66) for $Pu^{239+240}$, the effective dose is 1.08 x 10^{-2} mSv/Bq. The annual limit on intake for workers is around 900 Bq, and for members of the public an intake of 45 Bq corresponds to a CED of 1 mSv.

TABLE 6. COMMITTED EFFECTIVE DOSE FOR PALOMARES PEOPLE

Committed effective dose mSv/Bq inhaled			
isotope	infants	children	adults
$Pu^{239+240}$	0.15	0.09	0.06
Am^{241}		7.4×10^{-3}	8.6×10^{-4}

References

1. E. Iranzo, *et al.* Distribution and migration of plutonium in soils of accidentally contaminated environment. Radiochemical Acta 52/53, 249-256 (1991).

2. T.R. Garland, R.E. Wildung and R.C. Routson. The chemistry of plutonium in soils. I. Plutonium solubility. In Pacific Northwest Laboratory Annual Report for 1975 to the USERDA Division of Biomedical and Environmental Research ERDA report BNWL-2000.

3. T.R. Garland and R.E. Wildung. (1977) Physiochemical characterisation of mobile plutonium species in soils. In Biological implications of metals in the environment. REDA Symposium CONF-750929, NTIS.

List of publications

J.A.B. Gibson, A. Birchall, R.K. Bull, K. Henrich, E. Iranzo, D.J. Lord, J. Piechowski, E. Sollet, N.P. Tancock and C. Wernli. A European intercomparation of methods used for the assessment of intakes of internally deposited radionuclides. Rad. Prot. Dosim., 40, 245-257 (1992).

G.N. Stradling, S.A. Gray, J.C. Moody, A. Hodgson, M. Ellender, A. Phipps, M. Pearce, I. Wilson, C.E. Iranzo, P. Rivas, A. Espinosa, A, Aragón and E. Iranzo. Biokinetics of Plutonium-239 and Americium-241 in the Rat after the Pulmonary Deposition of Contaminated Dust Obtained from Soil Samples at Palomares: Implications for Human Exposure. Report NRPB M-444 (November, 1993)

J. Gutierrez, C.E. Iranzo, A. Espinosa and E. Iranzo. Spanish experience in intervention at an accidentally contaminated site. International Symposium "Remediation and Restoration of Radiactive - contaminated high in Europe. Antwerp. - Belgium. (October,1993).

C.E. Iranzo, A. Espinosa and J. Martinez. Resuspension in the Palomares area of Spain. A sumary of experimental studies. Journal of Aerosol Sciences. Vol.25,No. 5,pp 833-841, 1994.

A. Espinosa, A. Aragón, J. Martinez and C.E. Iranzo. Pulmonary biokinetic of Pu associated with soil particles.The first research coordination meeting of participants in the coordinated research programme on "dose per unit intake factors for members of the public" Vienna IAEA tecdoc (in press)

C.E. Iranzo, A. Espinosa, J. Martinez and A. Aragón. Estudio de la contaminación ambiental de suelos y aire en distintos escenarios como consecuencia de la liberación a la atmosfera de radionucleidos por accidentes nucleares. Implicaciones a la población. "Vº Congreso de la Sociedad Española de Protección Radiológica" Abril 1994.

Fig 1 Percentage of activity extracted as a function of time Respirable fraction of soil 0

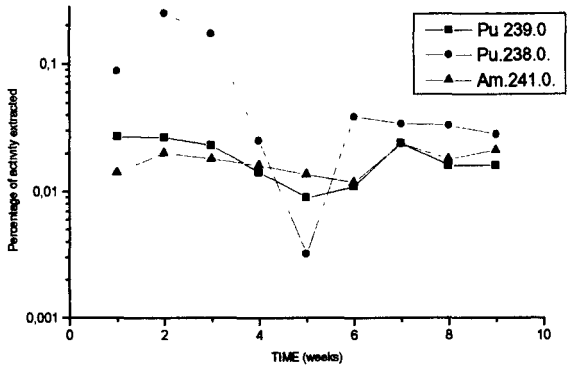

Fig 2 Percentage of activity extracted as a function of time Respirable fraction of soil 1

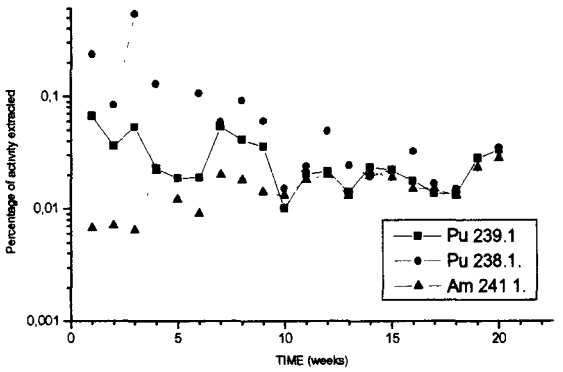

Fig 3 Percentage of activity extracted as a function of time Respirable fraction of soil 2

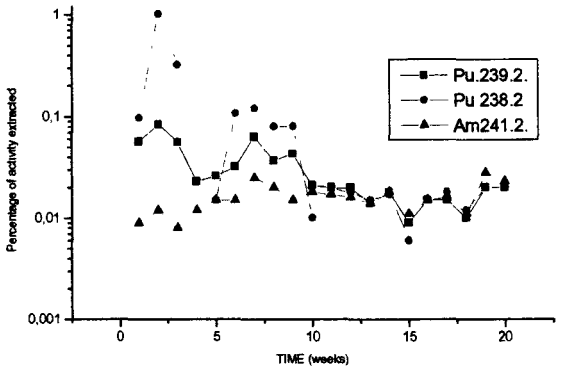

Fig. 4 Percentage of activity extracted as a function of time Fraction 20-40 microns

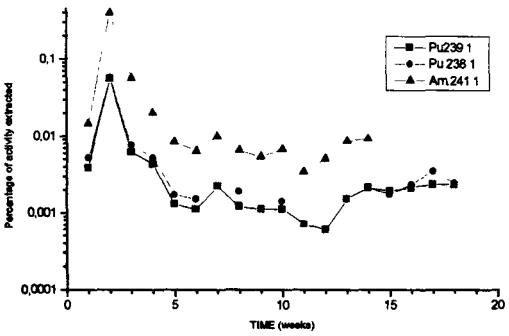

Fig 5 Percentage of activity extracted as a function of time Fraction 125-250 microns

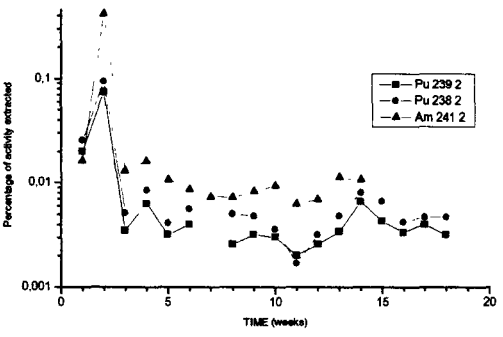

Fig 6 Percentage of activity extracted as a function of time Total soil fraction

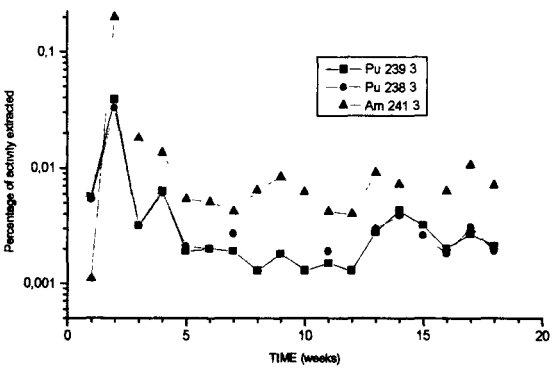

Figure 7. Percentage of activity extracted by each reagent during the sequential extraction, performed after six months (S1) and one year (S2) of pulmonary leaching simulation

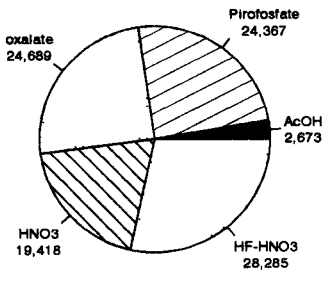

fig 7a Pu-239 percentage extracted (S1)

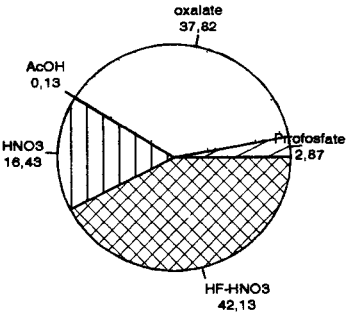

Fig 7b Pu-239 percentage extracted (S2)

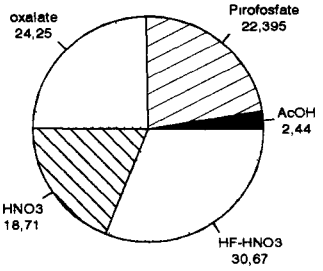

Fig 7c Pu-238 percentage extracted (S1)

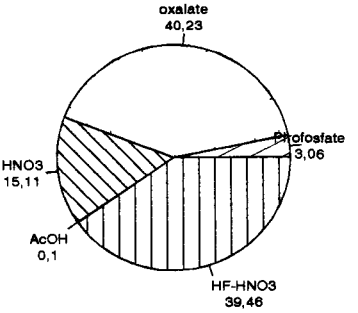

Fig 7d Pu-238 percentage extracted (S2)

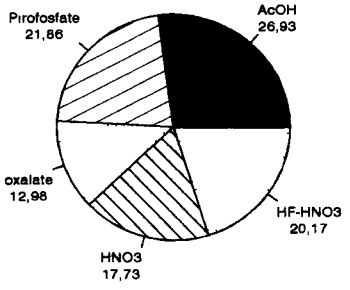

Fig 7e Am-241 percentage extracted (S1)

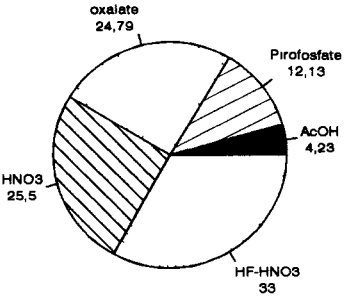

Fig 7f Am-241 percentage extracted (S2)

Head of project 7: Dr Popplewell

II. Objectives for the reporting period

The overall objectives of the work were to measure, in healthy adult male volunteers, the gut transfer of plutonium (f_1) following its ingestion, and the urinary excretion following intravenous injection. Objectives for this period were:

i) to prepare the results from three subjects for publication at a Workshop co-sponsored by the CEC, held in September 1993.
ii) to measure the excretion after oral intake of plutonium for two additional volunteers.
iii) to prepare for the injection phase on the two additional volunteers.
iv) to continue to measure the urinary excretion from the three original volunteers.

III. Progress achieved including publications

Introduction

This work was planned to provide human data for the urinary excretion of plutonium over as long a period as possible, and for the gut transfer of plutonium, two areas where human data are notably scarce. The principle of the work is that of Maletskos *et al* [1] and is as follows. The subject has an oral intake of plutonium, and the urinary output of plutonium is measured over several days. After an interval of several months, when the urinary excretion has become too low to measure, the subject receives an intravenous injection of plutonium, and the urinary output is measured over the same period as in the oral phase of the experiment. This second phase gives the portion of the systemic plutonium that passed to the urine. This enables the amount of systemic plutonium that resulted from the oral intake to be calculated, and hence the fractional gut transfer. The urinary output following the injection should be measurable throughout the life of the subject, giving valuable data on the long term excretion of plutonium in humans.

In order to limit the radiation dose to the volunteers to acceptable levels, the isotope used was ^{244}Pu, $t_{½} \approx 8 \times 10^7$ year. The estimated radiation dose to each subject was about 130 μSv, mainly due to the impurities ^{238}Pu, ^{240}Pu, and ^{241}Pu. The ^{244}Pu was measured by mass spectrometry, the only technique available to us that was sufficiently sensitive to measure the plutonium excretion at this level.

Experimental

An oral intake of 10^{14} atoms (40 ng) of ^{244}Pu was contained in a mixture of about 2 ml of 0.1 M hydrochloric acid and 20 ml of 2% trisodium citrate at pH 6.4. Small aliquots were self administered by the volunteers to the back of the throat from dropper bottles, part-way through the mid-day meal of sandwiches and tea or coffee. Complete collection of urine commenced immediately, and continued for eight or nine days. The samples were combined before analysis. A known amount of ^{242}Pu was added to the urine samples and validated radiochemical methods were used to isolate the plutonium. At the Atomic Weapons Establishment, Aldermaston, the plutonium was adsorbed on to anion exchange beads from 8 M nitric acid solution. The beads were then subjected individually or severally to thermal ionisation mass spectrometry. The ^{244}Pu contents of the urine samples were calculated from the mass spectrometric $^{244}Pu/^{242}Pu$ ratios, and the amounts of ^{242}Pu tracer that were used.

The intravenous injection part of the experiment was started about six months after the oral intake, by which time the plutonium excreted in the urine from the oral stage was below the limit of detection. Sterile, pyrogen-free solutions were used for the intravenous

injections. The injection solution was ^{244}Pu in essentially a 0.9% saline solution with traces of hydrochloric acid and sodium citrate, sterilised by filtering through a 0.2 μm pore diameter sterile membrane. Intravenous injections were carried out by a physician immediately after the midday meal. Collection of consecutive 24 hours urine samples commenced at once. Individual 24 hours samples were collected and analysed for the first eight or nine days. Then multiple 24 hours samples were collected at progressively longer intervals. The further the sampling time was from the time of injection, the longer the interval and the longer the collection period. The later samples have been bulked from 7 days collection and are being taken at about six monthly intervals.

Results

The first three volunteers have undergone both phases of the experiment. One was injected with plutonium in July 1991 and two in September 1992, giving elapsed times to the end of June 1995 of 1,447 days and 1,009 days respectively. Analytical results have been obtained up to 1,155 days for the first volunteer and 650 days for the other two. Two further volunteers have completed the oral phase of the experiment; they ingested the plutonium in September 1994 and the urinary output has been measured.

The f_1 has been calculated for the first three volunteers as 2×10^{-4}, 8×10^{-4} and 9×10^{-4}. It is not possible to determine accurately the f_1 of the two further volunteers since their injection phase is not yet complete and so their individual blood:urine factors are not yet available. However if the median blood to urine factor from the three previous volunteers is used, the gut transfer factors of the two new volunteers would be 1.8×10^{-4} and 11.7×10^{-4}. The age at ingestion of volunteers covers the range from 37 to 65 years. If the estimates for the two most recent volunteers are combined with the earlier data, then over the age range studied there appears to be a linear relationship between f_1 and age at ingestion (Figure 1). The overall variability was a factor of about six. The uncertainties in the analyses were approximately 1 - 5% of the measured values. However the variability of an individual's gut uptake is unknown and has not been investigated in this work. This observation deserves further study once the results of the injection phase are available for the two most recent volunteers.

The measured data for urinary excretion following injection of plutonium is shown in Figure 2 along with that predicted by the plutonium biokinetic model in ICRP Publication 67. The agreement is encouraging. Figure 3 compares the NRPB data with the predictions of the Jones[2] and Durbin[3] excretion functions. With the exception of the higher day one excretion, the results are close to the Durbin function for the early period, and closer to the Jones function thereafter. The results are also similar to those obtained in a recent study by AEA Technology, Harwell[4] (Figure 4), which involved two volunteers and made use of ^{237}Pu. However, the comparison between the two studies is limited because the short half-life of ^{237}Pu (45.6 days) meant that excretion data could only be obtained for 21 days.

References

1. Maletskos C.J., Keane A.T., Telles N.C. and Evans R.D. (1969) Retention and absorption of ^{224}Ra and ^{234}Th and some dosimetric considerations of ^{234}Th in human beings. In Delayed Effects of Bone-seeking Radionuclides, p. 29 (Mays C.W., Jee W.S.S., Lloyd R.D., Stover B.J., Dougherty J.H. and Taylor G.N., Eds). University of Utah Press, Salt Lake City.

2. Jones S.R. (1985) Derivation and validation of a urinary excretion function for plutonium applicable over tens of years post uptake. Radiat. Prot. Dosim. **11**, 19.

3. Durbin P.W. Plutonium in man: a new look at the old data. In Radiobiology of plutonium, p. 469 (Stover B.J., Jee W.S.S. Eds). J. W. Press, Salt Lake City.

4. Talbot R.J., Newton D. And Warner A.J. (1993) Metabolism of injected plutonium in two healthy men. Health Phys. **65**, 41.

Publications

Popplewell, D S, Ham, G J, McCarthy, W, and Lands, C. Plutonium biokinetics in humans. Radiol. Prot. Bull. No. 150, (1994).

Popplewell, D S, Ham, G J, McCarthy, W and Lands, C. Transfer of plutonium across the human gut and its urinary excretion. IN Proceedings of the Workshop on Intakes of Radionuclides: Detection, Assessment and Limitation of Occupational Exposure. Bath, September 1993. Radiat. Prot. Dosim. 53, 241 (1994).

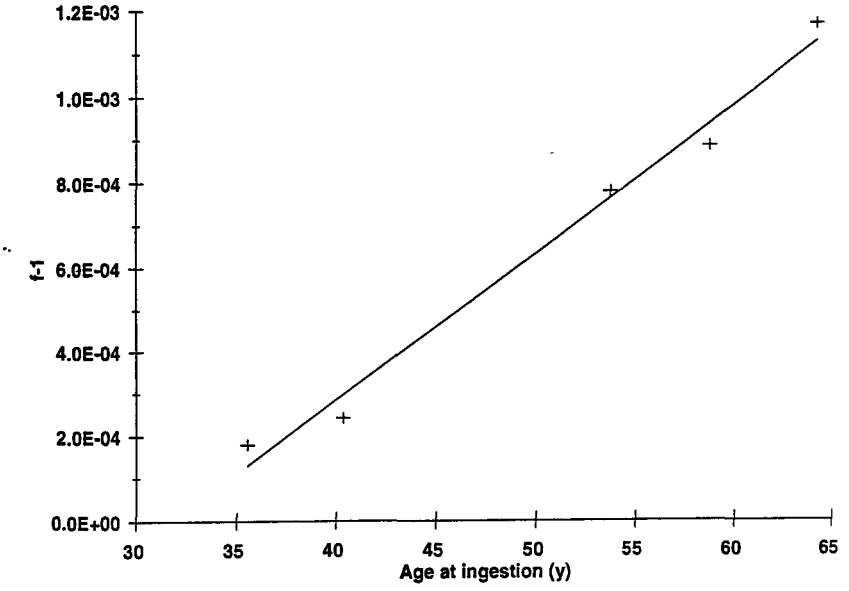

Figure 1 **Relationship between f_1 and age at ingestion**

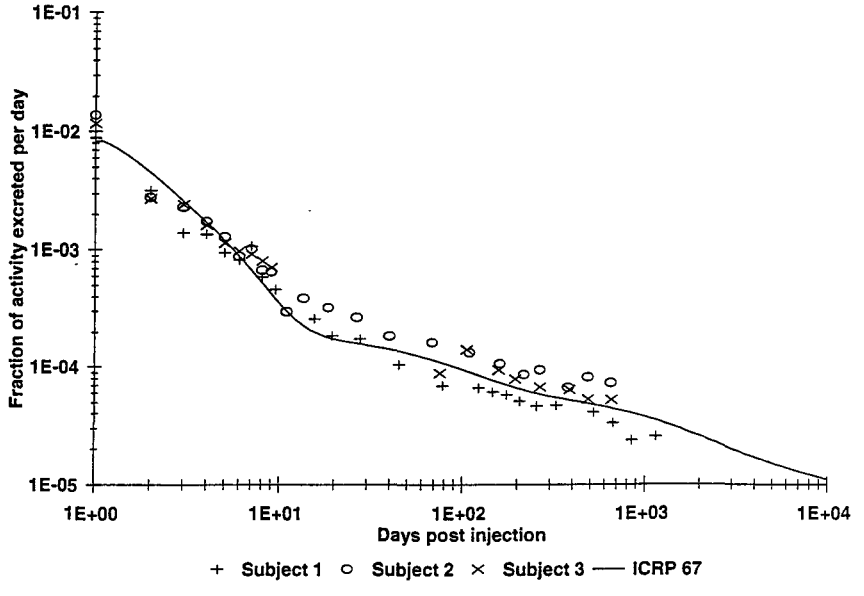

Figure 2 **Comparison of NRPB data and ICRP Publication 67 model**

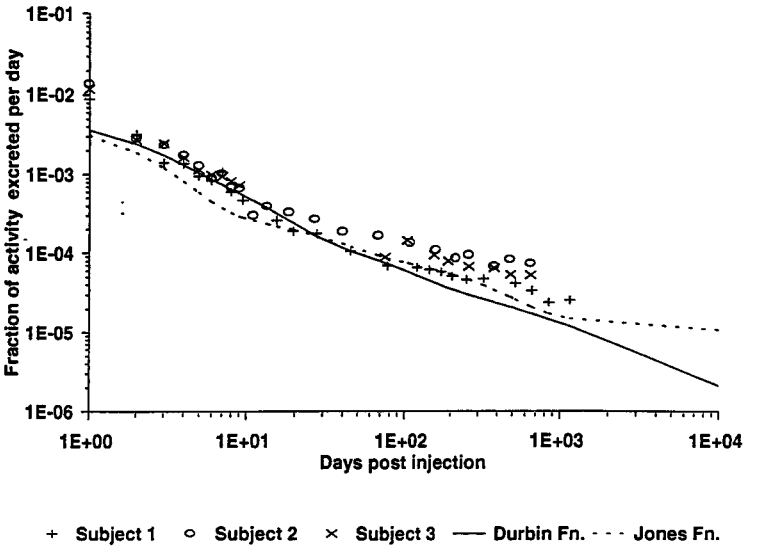

Figure 3 **Comparison of NRPB data and the Jones and Durbin functions**

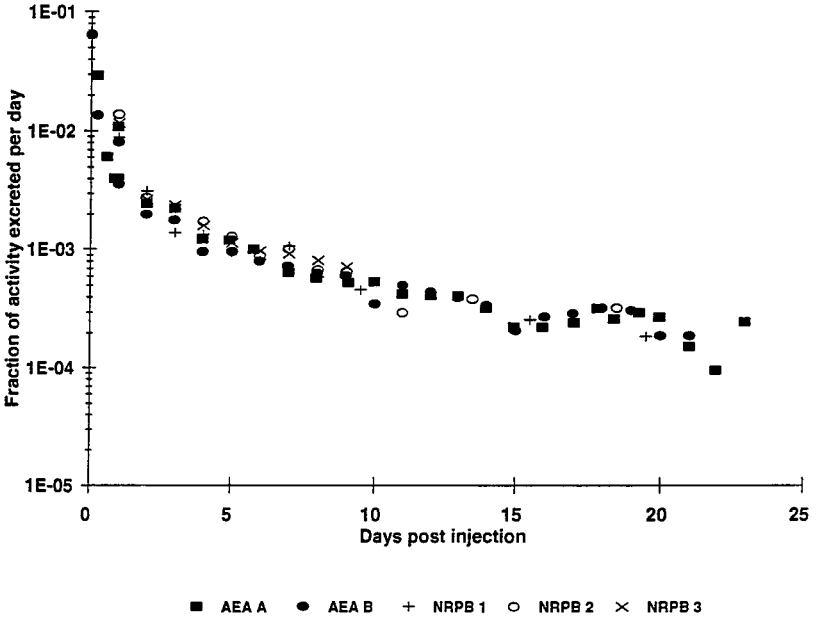

Figure 4 **Comparison of NRPB and AEA data**

Head of Project 8: Mr. Strong

II. Objectives for the reporting period

In order to improve the understanding of the deposition of inhaled radionuclides in the human respiratory tract we proposed to study the deposition of hygroscopic aerosols. Two approaches were to be used:

a. Measure the deposition in female volunteers of salt aerosol particles labelled with ^{123}I.
b. In the same volunteers measure the deposition of inert salt particles using a bolus technique interfaced with a phase Doppler particle measuring system.

III. Progress achieved including publications

a. Tests of the system to provide the aerosols were made by dissolving ^{123}I-labelled 1-iodohexadecane in ethanol prior to mixing with a dilute solution of NaCl such that, on evaporation, the NaCl particulates contained less than 2% by mass of label. Output of ^{123}I tagged aerosol was measured by collecting the aerosol on a filter at the outlet of an electrostatic classifier coupled to an ultrasonic nebuliser. The ^{123}I content of the filter deposit was measured using a twin crystal sodium iodide system. Initial measurements indicated the output efficiency to be low, however, modifications were made to the ultrasonic nebuliser by decreasing the reservoir volume thus increasing the concentration of ^{123}I available for nebulisation. This improved the output efficiency to about 3% compared to the concentration of ^{123}I in the nebuliser. On deposition in the lung, the sodium chloride will rapidly dissolve but the iodohexadecane will clear with a similar pattern to that of an insoluble material, permitting regional deposition information to be obtained. ^{123}I will be added to the iodohexadecane in sufficient quantity to achieve a lung deposit of approximately 15 kBq per administration this being adequate to follow the clearance over the two days of an experiment using an array of six sodium iodide detectors.

The system used for the exposure of subjects to test aerosols has been modified and is shown in the figure below.

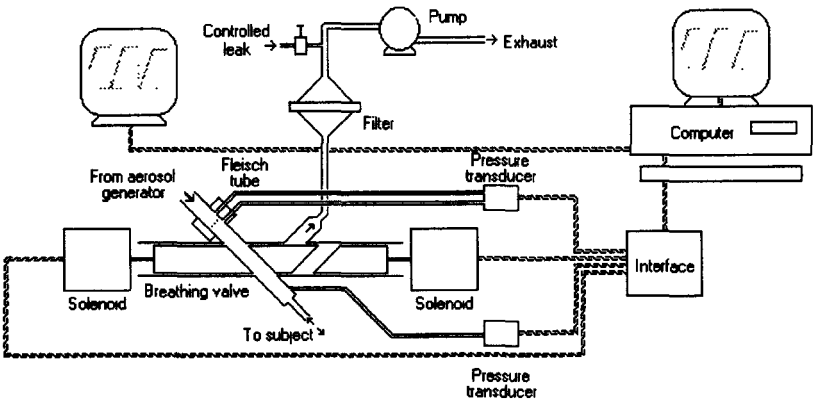

The valves which direct the aerosol laden air to the subject and divert the exhaled air through a filter have been improved and a PC is now used to measure and display flow and to switch the valves. A visual display unit mounted in front of the subject displays the required breathing pattern together with that achieved by the subject. The collection of particles in the expired breath has been improved by providing a suction on the rear of the filter to aid the subject in breathing through it. Thus better assessments of the total lung deposition can be made and compared with similar data provided by subsequent whole body counting.

Ethical approval for the volunteer study has been given in principle.

b. In parallel progress has been achieved on combining a valving system for the introduction of boluses of particles to known depths within the lung with a laser Doppler anemometer, allowing real-time measurements of particle size and velocity on both inhalation and exhalation. Use of this apparatus offers the opportunity to better quantify the degree of hygroscopic particle growth in real-time without the use of radionuclide tracers.

It has been demonstrated that with the bolus system, aerosols in the size range 0.5 to 3 μm can be generated and inhaled by a subject to various lung depths. Using non hygroscopic particles of polystyrene latex a slight increase in particle size was observed and measured in the exhaled breath using the system. At first this was thought to be due to condensation onto the surfaces of the polystyrene particles but further investigations by drying the air passing between the subject and the laser measuring volume still produced a shift in the size of the exhaled particles compared with that of the inhaled air. This size shift has been found to be due to the way in which raw data from the laser Doppler anemometer is interpreted by the data handling software, corrections have been made to the software to overcome the problem. Deposition fractions measured in a single male subject (as shown in the table below) were found to be consistent with those predicted using the ICRP-66 lung model.

	Deposition, %		
Depth, ml	Breath hold duration, seconds		
	0	2.5	5
1μm particles			
700	54	58	50
500	46	65	77
300	80	77	84
100	82	86	91
3μm particles			
700	77	84	90
500	88	96	98
300	93	97	98
100	97	99	99

Head of Project 9: Dr Johnston

II. Objectives for reporting period:

Accurate assessment of committed internal doses of radioactivity from inhaled radionuclides involves two vital elements, (i) determination of the amount of activity which enters the body, and (ii) determination of the resultant dose to the various body tissues. This part of the project relates to the first of these. The most commonly used method of assessing the airborne concentration of radioactive material is to sample the air in the breathing zone of the worker. This is normally done using an open faced filter holder carrying a suitable filter through which air is drawn at a flow rate of 2 l min^{-1}. However, this flow rate has been shown to be too low for α-emitters of high specific activities for which Derived Air Concentrations are low. The aims of this project have, therefore been to design, produce and carry out preliminary testing on a personal air sampling device capable of operating at a flow rate of 15 l min^{-1}.

III. Progress achieved including publications:

1. Introduction

This project is based on the premises that there is a clear need for exposure assessments to be based on the use of personal rather that static (or area) samplers, and that the sampling flow rates for currently-available instruments (normally in the region of 2 l min^{-1}) are too low.

There are two possible reasons for the difficulties which arise from low flow rates. These are, (i) possible problems associated with the detection and quantification of α-particle emissions from very small amounts of collected material against any background counts, and (ii) statistical problems associated with assessment of low concentrations on the basis of small samples (Birchall et al 1988).

In an earlier feasibility study, Johnston et al (1993) considered the possible options for a personal air sampling device. The principal contenders were considered to be (i) an uprated version of the currently available "pump-and-filter" systems, and (ii) a system based on electrostatic precipitation of aspirated material. In relation to (i) there are no technical barriers to the production of a battery operated sampling system capable of operating at an air flow rate of greater that 15 l min^{-1} for a full 8 hour shift. The problem here is an ergonomic one in that higher flow rates mean greater energy requirements and bigger pumps. It was considered that, even with a strong design emphasis in this area. the outcome was likely to be the production of a system which would be unacceptable to the wearer.

An electrostatic precipitation (ESP) system comprises an initial section in which incoming particles are charged by contact with air ions produced by a corona discharge. These charged particles are then forced by a d.c. electric field to move in a direction perpendicular to the air flow such that they are deposited on an earthed collecting surface. This (ESP) option was considered to offer better promise. The reasons for this relate to the inherently low pressure drops associated with the absence of a collecting filter. This, it was believed, would allow the use of a fan-based air mover rather than a pump.

The form of the ESP device that was recommended by Johnston et al (1993) was similar to that described by Wilkening (1952), wherein the aerosol passes through a rectangular channel formed from brass shim stock to be deposited on a moving aluminium foil.

2 Design considerations for the initial prototype.

2.1 Introduction

The aims of this particular design exercise may be summarised as follows:

1. Sample collection efficiency : The collection efficiency of the device must be appropriate for particles over the whole size range of interest.
2. Wearer acceptability : The device must be sufficiently comfortable as to be acceptable to the wearer.
3. Safety: possible problems arising from high voltage "nuisance shocks" and from possible production of noxious gases must be addressed.
4. Sample analysis: The nature of the deposit collected by the sampler must be such as to allow for accurate and convenient counting.

These aims are considered in the following sub-sections.

2.2 Collection efficiency.

2.2.1 *Definition*

The elements which determine the actual collection efficiency (ξ_c) of an aerosol sampler are, (i) the efficiency with which particles cross the plane of the inlet - the *aspiration efficiency, (ii)* the efficiency with which they are transported to the deposition region - the *transport efficiency,* and (iii) the efficiency with which they are deposited on the collecting substrate - the *deposition efficiency.*

In this device the options were that the instrument should aim to collect either:

(i) the total airborne dust concentration to which the respiratory tract is potentially exposed ("total dust" sampling);

(ii) the fraction of the total airborne dust which enters the region of the respiratory tract of interest (the potential regional dose);

(iii) the fraction of the total airborne dust which enters the region of the respiratory tract of interest and deposits there (the actual regional dose).

Detailed consideration of these alternatives in relation to the ICRP 66 (1994) dose assessment model led to the conclusions that; (i) the particle size dependent aspiration efficiency should aim to match the inhalability definition given in ICRP 66 (1994), (ii) the internal deposition efficiency of the sampler should aim to be 100% of the aspirated particles across the whole particle size range.

2.2.2 *Particle deposition within the sampler*

The basis of electrostatic precipitation is that an aerosol particle carrying a charge q in an electric field E will experience a ("Coulomb") force defined as;

$$F_e = qE \qquad 2.1$$

As a result, the particle is accelerated until it (rapidly) reaches a terminal velocity v_s where;

$$v_s = \frac{qEC}{3\pi\eta d} \qquad 2.2$$

and where C is the Cunningham slip correction (which is significant only for small particles where collisions with air molecules can be regarded as discrete events), η is the air viscosity, and d the particle diameter.

Individual particle velocities depend on individual particle electrical mobilities (B) defined as:

$$B = \frac{v_s}{E} \qquad 2.3$$

So from Equation 2.2:

$$B = \frac{qC}{3\pi\eta d} \qquad 2.4$$

The critical factor in determining the efficiency of particle collection is the relationship between particle electrical mobility and the time spent in the collection zone (t_z). For particles of electrical mobility (B), the collection efficiency ξ, (in the case of laminar flow, and for $\xi <$ 100%), may be expressed as:

$$\xi = \frac{BEt_z}{y} \times 100\% \qquad 2.5$$

where y is the distance between the collecting electrodes.

To attain 100% collection efficiency demands that B, E, and t_z be maximised and y minimised within the constraints imposed by other considerations. In practice, E is limited by the need to avoid electrical breakdown of the air between the electrodes, and by the need to minimise the rates of production of noxious gases. The treatment time (t_z), for a given sampler geometry, is inversely proportional to the flow rate and is, therefore, limited by the need for a flow rate of at least 15 l min^{-1}. Also, reduction of the inter-electrode spacing, on its own, serves only to reduce the treatment time proportionally (by increasing the internal air velocity), and is, therefore, of no advantage. The only parameter on the right hand side of Equation 2.14 that can be maximised with no consequent decrement in other areas is therefore the particle electrical mobility. This requires that particle charge be maximised.

2.2.3 *Particle charging*

Particle charging is by contact with air ions produced in the corona discharge region of the device. Two charging processes are involved, **diffusion charging** (Arendt and Kallmann 1926) where charged air ions arrive at the particle surface as a result of their thermal motion, and **field charging** (Pauthenier and Moreau-Hanot 1932) where air ions are driven on to the particle surface by the electric field. In practice both processes operate together, the relative magnitudes of the resultant charge depending on such parameters as the size of the particle.

Comparison of the relative magnitudes of the charge arising from these two processes shows that field charging dominates for the larger particles, and diffusion charging for the smaller particles.

In either case, rapid and efficient charging depends on a high air ion concentration. This can be achieved by ensuring that the corona discharge electrode is so designed as to give as high an air ion current as possible for a given applied voltage. However, high current demands mean large batteries, so the relative importance of these conflicting needs must be carefully balanced.

2.3 Wearer acceptability

Optimisation of the ergonomic aspects of design was not within the scope of this project. However, due consideration, particularly of the need to keep the size and weight of

the device to acceptable levels has been given.

2.4 Safety

2.4.1 *Electrical safety*

It is anticipated that the high voltage charging and deposition electrode in this device will operate at a voltage between 5 and 10 kV. The electrocution threat arising from devices incorporating voltages of this magnitude only applies where the charge storage, or current delivery capability of the device is sufficiently high. Neither of these conditions apply in this case.

A second potential hazard and certain discomfort, arises where "nuisance shocks" may occur. Due consideration has been given to the need to avoid such occurrences, but the likelihood of these can only be assessed in wearer trials.

2.4.2 *Production of noxious gases*

In addition to potential safety problems accompanying the use of high voltages, high voltage corona discharges are known to produce the noxious gases ozone and oxides of nitrogen. In terms of occupational health criteria, previous measurements on devices of this nature (Johnston *et al,* 1988) have shown ozone production to be the greater problem. For this reason, consideration of minimising the rate of ozone production has been included in the design of the discharge electrodes. Ozone production rates for the prototype device have also been measured in the laboratory (Section 5).

2.5 Sample analysis by α-counting

For the Personal Electrostatic Precipitator (PEP) sampler described here, analysis of the sample will be by α-particle counting. An important feature of the design of the PEP will, therefore, be the compatibility of the deposition substrate with conventional α-particle counters.

3. Specification and construction of the initial prototype sampling head

3.1 Introduction

The principal design considerations referred to in Chapter 2 may be summarised as:

(i) The particle size dependent aspiration efficiency should aim to match the inhalability definition given in ICRP 66 (1994).

(ii) The internal deposition efficiency of the sampler should aim to be 100% of the aspirated particles across the whole particle size range, and hence (a) the time spent by particles in the charging region should be as large as possible, (b) the rate of air ion production at the charging electrode should be high.

(iii) The device should be as light and as compact as possible.

(iv) The pressure drop through the device should be as low as possible.

(v) The sampling head should be connected to the air moving device via a flexible tube.

(vi) The possibility of "nuisance shocks" arising from the device should be minimised.

(vii) The rate of production of ozone should be such that the concentration in the exhausted air does not give rise to exposures that exceed the current Occupational Exposure Standard.

(viii) The collection substrate should be compatible with conventional counting techniques.

In the following section, details are given of how these requirements have been incorporated in the prototype instrument.

3.2 The design of the prototype instruments

The actual device which was constructed on the basis of these considerations is shown in Figure 1a. Following a fairly short period of initial testing, however, it became apparent that a device of this design and of the required size would have difficulty in attaining the required collection efficiency. This was because the time spent by particles in the charging region was too short for efficient charging. Therefore, a second prototype of the form shown in Figure 1b was constructed. In this case, the back-up collecting filter was replaced with an optical particle counter (which gives faster results) because of the perceived need to carry out an extensive programme of efficiency testing over a range of conditions.

Further discussion in this Section relates entirely to measurements carried out with this second prototype instrument.

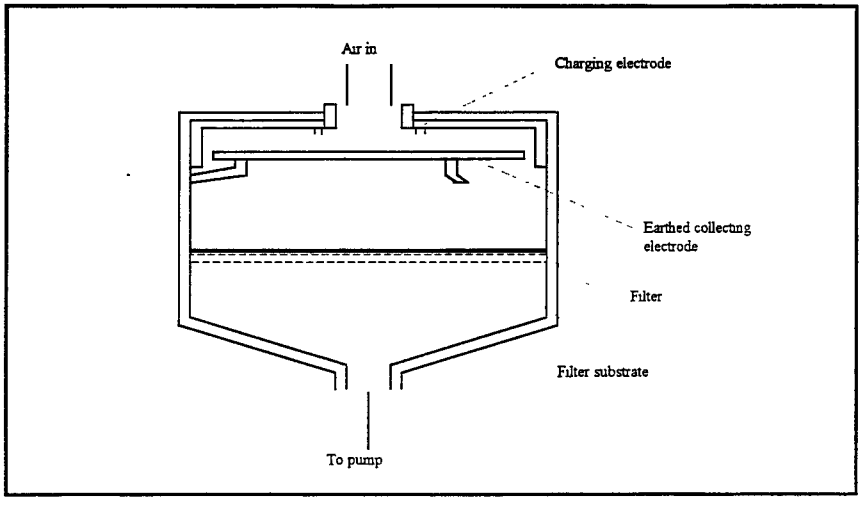

Figure 1a; An outline diagram of the original prototype device which is similar to that described by Wilkening (1952) in that it incorporates a central collection orifice from which air flows radially outwards.

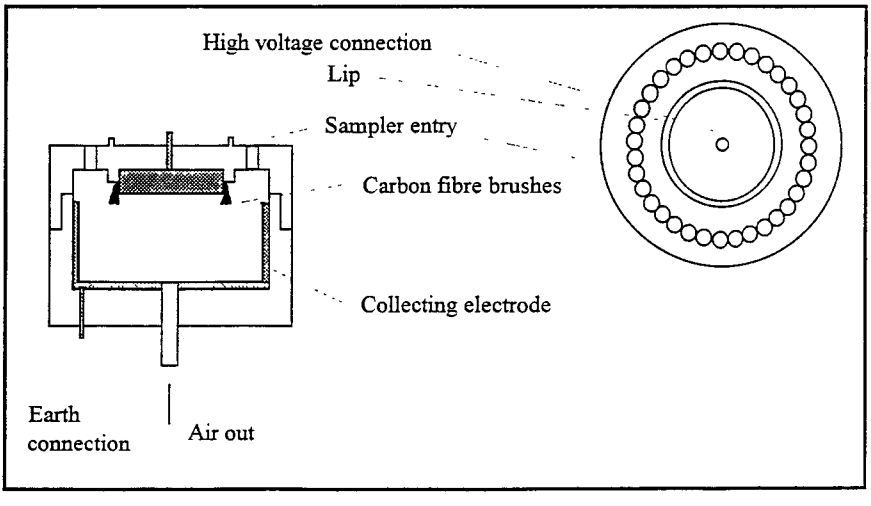

Figure 1b; Outline diagram of the second protype device. This design incorporates a peripheral collection orifice from which air flows radially invwards.

3.2.1 *Aspiration efficiency*

The only personal air sampling devices which have been shown empirically to have an aspiration efficiency which approximates to that of an accepted definition of the particle size dependence of inhalability are the "7-hole sampler" (HSE 1993), and the "IOM Personal Air Sampler" (Mark et al 1986). The entry on the former comprises 7 holes each of diameter 4mm giving an entry velocity of 0.375 m s^{-1}, whereas that on the IOM sampler comprises a single hole of diameter 15 mm, giving an entry velocity of 0.19 m s^{-1}.

The entry on the high volume PAS described here was designed as a ring of 24 holes each of diameter 6.5 mm giving an entry velocity of 0.31 m s^{-1}, when operated at a flow rate of 15 l min^{-1}. Thus the inlet velocity is within the range covered by the two experimentally verified devices.

The IOM PAS device incorporates a lip to attempt to alleviate the problem of "particle bounce" where (particularly the larger) particles initially impact on the surface of the sampler and then bounce into the inlet. Particle bounce changes the aspiration efficiency of the device by "oversampling" of the larger particles. A similar lip has been incorporated in the device considered here.

3.2.2 *Deposition efficiency*

In order to achieve maximum deposition efficiency in the PEP sampler particles must be (i) charged to as high a level as possible, and (ii) spend as long a time as possible in the collection zone.

In relation to (i), several types of discharge electrodes were tried but the two that performed best were carbon fibre and frayed steel mesh. Both of these types were carried through to the final prototype (Section 6).

In relation to (ii), to balance the conflicting needs of this requirement with the need for compact design, a collection substrate diameter of 60 mm was chosen.

3.2.3 *Wearer acceptability*

Consideration of the need for the device to be as light and compact as possible has been included in the initial design. All components of the device have been designed to be as light as possible within the constraints of operational efficiency and safety.

4. Specification and selection of a suitable air mover.

The sampling head is designed for use with a centrifugal fan. The performance requirements for such a fan depend on the flow rate and resulting pressure drop across the proposed system. The largest pressure drop in the system is likely to be that associated with the tubing. This was measured and found to be 3 mbar m^{-1} and 4 mbar m^{-1} for flow rates of 15 l min^{-1} and 20 l min^{-1} respectively. Several commercially available fans were then tested. Some of these were able to achieve the required performance for the maximum anticipated hose length of 1 metre.

None of the commercially available fans were optimally designed for the performance required here. However, one of the potential suppliers contacted, Racal Health and Safety Limited, Bognor Regis, England, has a computer package which provides the capability of producing centrifugal fans to customers specifications. It was decided, however, to proceed with laboratory testing using the best available device or a mains operated pump as appropriate and leave specification of such a device to a later date.

5 Laboratory investigations using the second prototype sampling head

5.1 Introduction.

The principal design criteria for this device are (i) high particle collection efficiency across the range of particle sizes, and (ii) a low level of production of the potentially hazardous gases ozone and oxides of nitrogen. The performance of the second prototype in these respects has been tested in a series of laboratory trials, details of which are given in the following Sections.

Early trials using collection electrodes of different metals indicated a preference for aluminium. The reason for this is that the current/voltage relations for the alternative brass and stainless steel electrodes tried proved to be highly variable. The reason for this was not clear at this stage in the project, so all of the results quoted in this Chapter are for the aluminium electrode. This matter is considered again in Section 6.1.

5.2 Measurement of the dust particle collection efficiency.

Particle charging efficiency, (and hence collection efficiency) depends to some extent on the nature (specifically the dielectric constant) of the particulate material. However, charging mechanisms are the same for all materials, so laboratory investigations involving the actual radioactive materials themselves can be avoided at this stage. Particle collection efficiency measurements have, therefore, been based on the most conveniently available aerosol, i.e. on the ambient material within the laboratory.

The basic experimental system is outlined in Figure 2.

Both the pump and optical particle counter contribute to the total air flowrate (15 l min^{-1}) through the sampler, the pump sampling rate being controlled by the valve on the flowmeter, while the sampling rate of the optical particle counter is fixed at 2.8 l min^{-1}.

The optical particle counter (OPC) (Royco Instruments Model 4100, Menlo Park, California) has two analogue outputs each giving a d.c. voltage proportional to the particle count rate in a selected particle size channel. This allows the count rates of particles in different size ranges from 0.3 μm diameter upwards to be displayed simultaneously.

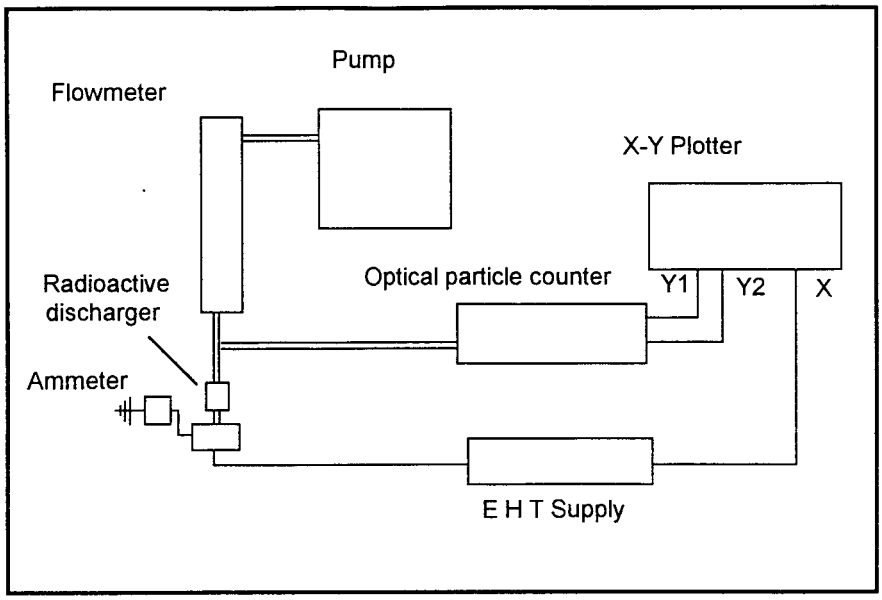

Figure 2; Outline diagram of the laboratory experimental system used to determine the collection efficiency of the protoype PAS device.

With the air flow rates set at an appropriate level, the voltage supplied to the high voltage electrode may be increased from zero and the rate of decrease in the number of particles *penetrating* to the OPC determined as a function of applied voltage. Any decrease in particle penetration is associated with an increase in particle collection rate. The X axis of the X-Y plotter is supplied with a voltage proportional to the output voltage of the EHT supply.

Several different types of discharge electrode have been tested for this prototype. The best of these was one formed by fraying a strip of stainless steel mesh of a length equal to that of the electrode circumference and a width of about 5 mm, and another formed by gluing strips of carbon fibre "tow" to one of the flat surfaces of the electrode disc in a radial pattern, then trimming all of the projecting fibres to the same length in a purpose built jig.

Tests carried out on this second prototype device indicated that this configuration was capable of giving the required collection efficiency at an operating potential of around 6kV, but ozone production rates, particularly for the steel discharge electrode, were higher than that which may be considered acceptable for the final prototype. Some problems also arose with breakages of the carbon fibres. However, these tests gave a good indication of the design requirements for the final prototype. Design, construction and testing of this device is described in the Section 6.

6 Design, construction and testing of the final prototype device.

6.1 Design considerations

The final prototype (Figure 3) retained the main features of the second prototype, but with a few structural changes to improve wearer acceptability. The entry was changed from a ring of holes to four annular slots, and the tube and wires changed to a more convenient position. The body of the sampler was designed to split in such a way that the collecting electrode could be easily accessed for counting.

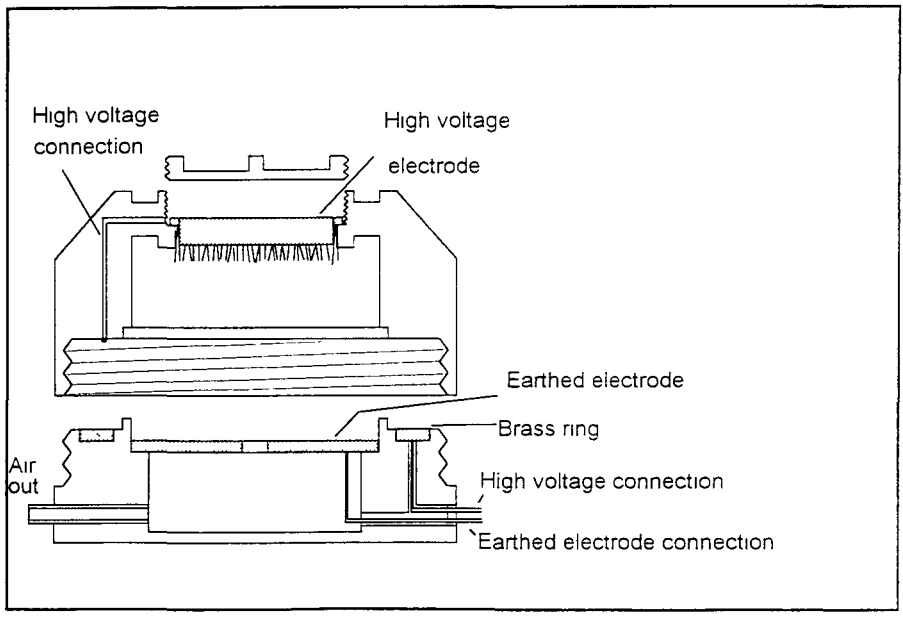

Figure 3; A section through all components of the third protype sampler (with the electrode retaiing cap unscrewed). For clarity the electrical and tube connections are shown as being on opposite sides of the base, whereas in practice they are close together.

Two problems that occurred with earlier prototypes were sparkover, and discharge instability. To solve these, a high voltage resistor was incorporated in the line connecting the collecting electrode to earth. The principal here is that in normal mode of operation the resistance across the gap between the discharge and collecting electrodes is much higher than that (1.6MΩ) of the resistor. However, when sparkover is initiated, the resistance of the inter-electrode gap drops and hence the voltage appears across the resistor. This immediately lowers the potential difference between the electrodes and prevents continuation of the spark.

6.2 Test Results

A series of tests similar to those described Section 5 have been carried out to determine the optimum operating conditions for this device and to determine whether it is capable of operating within the required constraints on collection efficiency and ozone production rate. Again, both carbon fibre and steel mesh electrodes, have again been investigated.

The outcome of these test was that carbon fibre electrodes operated at negative polarity were capable of giving the required combination of high collection efficiency and a low rate of ozone production. For the alternative combinations; (i) steel electrodes operated at negative polarity produced too much ozone, (ii) steel electrodes operated at positive polarity gave very poor collection efficiency than the same system operated at negative polarity, and (iii) carbon fibre electrodes operated at positive polarity gave poorer collection efficiency,

However, efficiency testing to this point in development had been based on short term measurements. At this point the negative polarity carbon fibre electrode system was tested for long term stability. Results were poor, the efficiency of collection falling over a period of around 10 minutes to unacceptably low levels. This problem was investigated and found to be associated with oxidisation of the carbon fibre electrodes. Several possible solutions were tried including changing the electrode gap, gold coating the carbon fibre electrode, and reverting back to steel electrodes operated at negative polarity with the introduction of activated charcoal filtration into the exhaust air. On the basis of these trials none of these was considered to offer a viable alternative. (Steel electrodes did not suffer from long term degradation of performance.)

Measurements of long term stability were then carried out for the carbon fibre electrodes operated at positive polarity. When tested, the problem of electrode oxidisation was found to be less severe for this system, and ozone production rates were generally low. However, for a newly produced electrode, air ion current was seen to fall to the extent that the operating efficiency of the system became unacceptably low in a period of some 30 minutes from switch-on. Following an extended period of operation, however, the rate of degradation of performance was considerably reduced to the extent that satisfactory operation over a period of several hours was possible.

Clearly a satisfactory solution to this problem of long term instability is required before proceeding further. The obvious requirement is for an electrode material having a similar physical form to carbon fibre, but with greater resistance to oxidisation. One possibility is the use of boron fibre.

7. General conclusions

Referring back to Section 3.1, the outcomes of this design, production, testing and development programme are as follows:

(i) The device has been designed in accordance with the general features of other personal sampling devices whose particle size dependent aspiration efficiency matches the inhalability definition accepted in the non-nuclear industries. This definition closely

matches the inhalability definition given in ICRP 66 (1994).
However, problems associated with long term performance stability have precluded laboratory wind tunnel testing to this point in time.

(ii) Laboratory measurements have demonstrated that, in short term tests internal deposition efficiencies of over 90% are achievable within the constraints imposed by considerations of sampler size and weight and of safe operation.

(iii) The weight of the sampling head is currently 150 grams. On the basis of the electrical power requirements of the current system the anticipated weight of the fan and the power pack is approximately 800 grams.

(iv) The pressure drop through the device at the operating flow rate is less than 4 mbar.

(v) The sampling head is connected to the air moving device via a 6.5 mm diameter plastic tube.

(vi) In limited "wearer" tests with the device operated from a high voltage power supply, no "nuisance shocks" occurred.

(vii) The rate of production of ozone has been shown to be strongly dependent on the choice of discharge electrode and operating polarity. In short term tests, with the device operating in its most satisfactory configuration (carbon fibre electrodes operated at positive polarity), the concentration in the air that is exhausted from the fan was less than the current short term Occupational Exposure Limit.

(viii) The collection substrate is the "top" surface of a flat metal disc which is the highest point of the bottom half of the sampler. When the sampler is split, this section may be pushed under the α-particle counter as would a conventional filter.

To the extent to which performance can be currently assessed, the sampling device in its current form is capable of fulfilling all of the design requirements over a period of up to about 30 minutes. The critical immediate requirement is that a durable discharge electrode material be found to greatly extend this period of operation.

8. References

Arendt, P., and Kallmann, H., (1926). Z Phys. 35: 421-441.

Birchall A, Muirhead C R and James A C. (1988) . Ann. Occup. Hyg., 32, Supplement 1. 851-863.

Health and Safety Executive (1993), Methods for the determination of hazardous substances. (MDHS 14). HMSO. London.

Johnston A M, Dempsey S, Richardson G (1993) Investigation of the feasibility of developing suitable 'high volume' personal sampling devices for assessment of exposures to airborne particulate radionuclides. IOM Report to Client.

Mark D, Vincent J H. (1986). Annals of Occupational Hygiene; 30: 89-102.

Moore, A D.(1973). Electrostatics and its Applications. Wiley & Son N.Y..

Pauthenier, M. M., and Moreau-Hanot, M. (1932) J. Phys. Radium 3: 590-613.

Wilkening M H (1952) A monitor for natural atmospheric radioactivity. Nucleonics. 10. No.6 36-39.

Head of projeect 10: Dr. Koblinger

II. Objectives for the reporting period

(I) Study of particle random walk in the stochastic lung model. Analysis of the effects of differences between human and rat lung structures on aerosol particle deposition patterns.

(ii) Extension of the stochastic program developed for aerosol particle deposition and exhalation simulation, with a clearance model. Study of doses from radioaerosols of various decay constants.

(iii) Replacement of the former (basically static) alveolus model by a new, dynamic model which describes the deposition in and exhalation from an expanding and shrinking alveolus.

III. Progress achieved including publications

The intension of all works described below was the further development and refinement of the stochastic morphometric lung model constructed earlier at the KFKI Atomic Energy Research Institute (Budapest, Hungary) and at the University of Salzburg (Austria).

(i) Comparison of aerosol particle deposition in human and rat lungs

The human bronchial tree is approximately dichotomous, and thus tubes and bifurcations are generally classified by their generation (bifurcation) numbers. The rat lung is more monopodial and asymmetric, therefore generation numbers have no real physical meaning, and tubes are most reasonably classified by their diameters.

Rat lung is often used as a surrogate to human lung. The question is how the data obtained from rats can be converted to humans in deposition studies, *ie.* what quantities are to be used for comparison, and how should rat parameters be scaled to humans? Three types of comparisons were carried out: deposition probabilities for both species were plotted vs. generation numbers, tube diameters and cumulative tube lengths. The rat lung diameters were scaled down according to the ratio of the human and rat tracheas: a factor of 6, whereas an analysis of penetration showed that the application of a factor of 4 transforms the cumulative tube lengths properly (Fig. 1).

The comparison of the three sets of curves shows that very similar deposition patterns are obtained for humans and rats if deposition probabilities are plotted vs. diameter (Fig. 2). (Breathing conditions. human: tidal volume 1000 cm^3, total lung volume 3000 cm^3, cycle time 4 s; rat: tidal volume 2 cm^3, total lung volume 8 cm^3, cycle time 0.512 s)

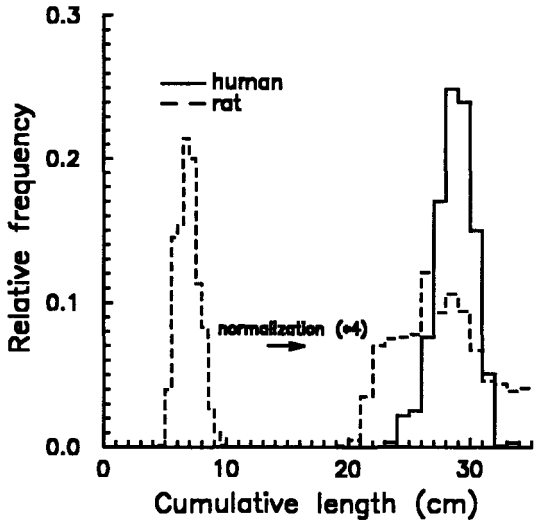

Fig. 1: Cumulative length distributions for human and rat lungs.

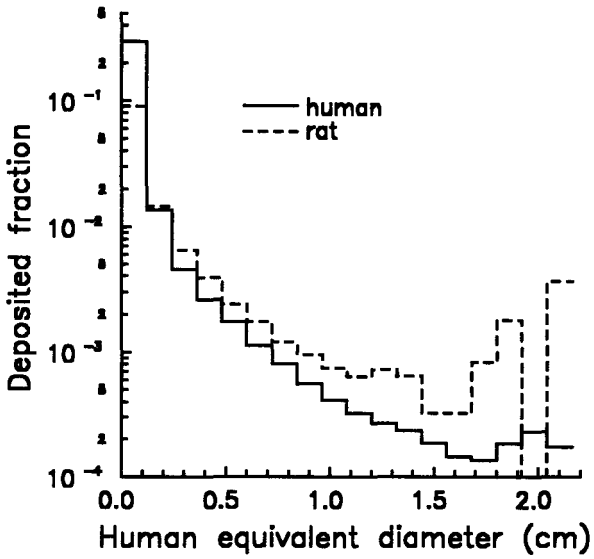

Fig. 2: Deposition fractions of 0.1 μm particles vs. human equivalent diameter.

The agreements are much worse if comparisons are based on generation numbers or cumulative tube lengths.

While interspecies modelling of particle deposition is presently based on the generations concept, our computations suggest that the effects of inhaled particles on the functional properties of the lung may better be expressed as functions of the tube diameter.

(ii) Bronchial mucociliary clearance

Bronchial mucociliary clearance has been implemented into the stochastic lung model. In this clearance model the transport time from the most distal terminal bronchioles up to the trachea is assumed to be constant: τ, and the mucuciliary clearance velocity in each airway, v_i, is assumed to be proportional to the diameter of that airway, d_i, *ie,* $v_i = \alpha d_i$. The proportionality constant for a random pathway composed of airways of diameters d_i and lengths l_i is given by

$$\alpha = \frac{\sum \frac{l_i}{d_i}}{\tau}.$$

An average parameter α can be derived from the simulation of many individual random paths. This value allows us to compute the residence times of initially deposited and subsequently cleared particles in different airway bifurcations. In the stochastic lung model morphometry the average of $\sum(l_i / d_i)$ is 36.3. The maximum transport time found in literature is 24 hours, a more realistic value is about 10 hours.

For illustration, two radionuclides (both with an activity of 1 Bq) with long and short half-lives relative to the total transport time τ have been selected, ^{131}I (half-life = 8 days) and ^{99m}Tc (half-life = 0.25 days).

Deposition patterns are computed for resting breathing conditions (tidal volume 1000 ml, cycle time 4 s). The initial bronchial deposition patterns, the residence times of the deposited particles on their way to the trachea (displaying the effect of mucociliary clearance), the retained activities (illustrating the combined effect of clearance and radioactive decay) and surface activities (which are proportional to radiation dose) are given.

Results for 0.5 µm ^{131}I particles are given in Fig. 3. Here, the activity pattern is proportional to the distribution of the residence time, because of the relatively long half-life of 8 days as compared to the total transport time τ.

In case of the 1 µm ^{99m}Tc particles (Fig. 4.) there is a clear distinction between residenc times and radioactivity patterns, since the radioactive half-life of 0.25 days is in the same order as the total transit time τ.

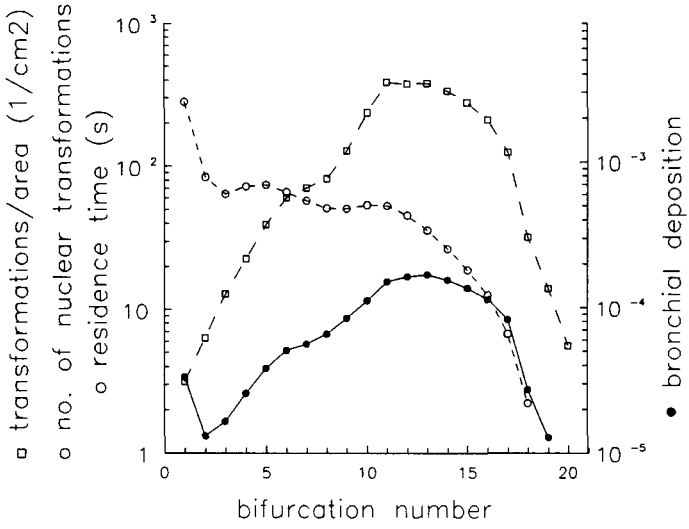

Fig. 3. Initial bronchial deposition, residence time and number of nuclear transformations, as well as number of decays per unit bifurcation surface area for ^{131}I.

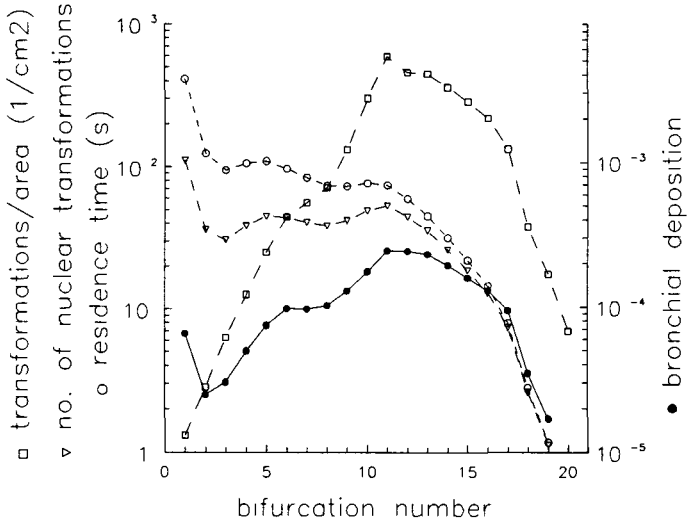

Fig. 4. Initial bronchial deposition, residence time and number of nuclear transformations, as well as number of decays per unit bifurcation surface area for ^{99m}Tc.

(iii) Dynamic alveolus model

Works on the stochastic lung model have revealed that deposition of aerosol particles is highly sensitive to alveolar processes. Especially the lack of information about the dynamic behavior of the alveolated lung regions leads to uncertainties in lung deposition modeling. For this reason we developed a new numerical model for the characterization of airflow and particle trajectories in alveoli.

In current lung deposition models (i) the alveoli are described by a fixed geometry (spheres), (ii) a highly idealized airflow is assumed, and (iii) the various deposition mechanisms are treated independently.

In the numerical alveolus model presented in this study the geometry of the alveolus is described by three-quarters of a sphere. This shape is the most likely in the human respiratory system (Hansen J.E. and Ampaya E.P., J. Appl. Physiol. 38, 990, 1975). Within the model, the alveolar geometry, the breathing pattern, and all particle characteristics are described by a number of input parameters. For this study, we have chosen an alveolus of average size with breathing conditions which are typical for normal working activity in man. The volume of the alveolus is assumed to increase linearly during inhalation (two seconds), decreasing in the same manner during exhalation (two seconds), and there is no pause between them. The tidal volume is one liter. The depth and the radius of the inflated alveolus are 174 μm and 129 μm, respectively, the corresponding values for the deflated alveolus are 152 μm and 113 μm.

Since it is not possible to assign realistic velocity values at the orifice of an isolated alveolus, a tubular duct has to be introduced for the calculation of the flow field. The radius of this tube in the present study is constant in time and its value is 125 μm, which corresponds to an average size of an alveolar duct. The alveolus opens in the middle of the length of the tube.

The flow field is computed by the FIRE commercial fluid dynamics program package which uses a finite volume approach. The Navier-Stokes and continuity equations are solved for the non-stationary case with moving boundaries for laminar compressible flow. The inlet boundary conditions for both inspiration and expiration are either parabolic or uniform flows. The outlet boundary condition ensures a uniform pressure distribution at the end of the tube. The average air velocity during inhalation and exhalation is set to 10 cm/s. This value is typical for alveolar ducts located at intermediate generations of the pulmonary region during light activity.

The points of entrance of the particles are randomly selected at the orifice of the alveolus. The velocity of a selected particle is equal to that of the air at the same location of the orifice. Single particle trajectories are used for the characterization of particle deposition.

Deposition of inhaled particles in the human lung is basically governed by four physical mechanisms, having different relative efficiencies in different flow rate and particle size regimes: inertial impaction, gravitational sedimentation, Brownian motion, and interception. The air velocity in an arbitrary point is computed with a weighted interpolation technique from the values presented in the node points of the distorted computational elementary cells of the FIRE code output. For the calculation of impaction not the air velocity but the air velocity gradient is considered to be constant during the elementary time step of the numerical procedure (Δt). The

movement of particles by Brownian motion is selected from the Fokker-Plank equation or from the Maxwell's velocity distribution by a Monte Carlo selection technique depending on the relation between the relaxation time of the particle and Δt.

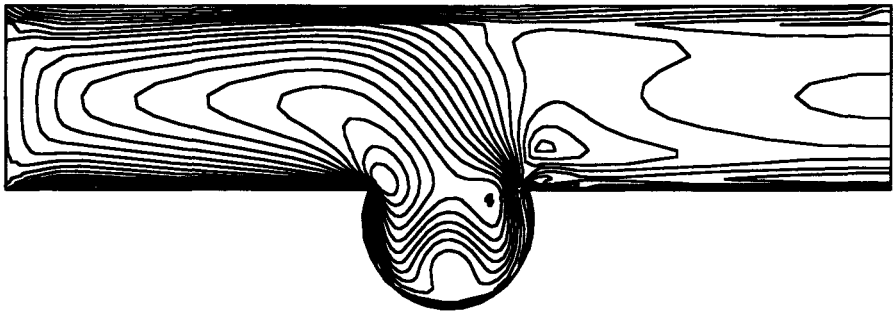

Fig. 5. Isoline representation of the velocity field for a moving geometry, 20 isolines and 0.1m/s uniform inspiratory flow in the tube, 15% of inhalation cycle passed.

When selecting a large number of particles the model can provide for the following information: (i) the deposition efficiency during one breathing cycle (T); (ii) the probability of exhalation during T and the time distribution of particle transit from the alveolus to the alveolar duct; (iii) the probability that the particle remains within the alveolus till the end of the breathing cycle; and (iv) the history of the particle after T. These parameters are naturally depending on the properties of the particles, the airflow, and all geometrical parameters. The role of the position of the alveolus relative to the direction of gravity and the significance of the individual deposition mechanisms can also be examined with this model.

Here, several representative results are given about the structure of the computational mesh, the computed stationary and non-stationary velocity fields, and the deposition patterns for both large and ultrafine particle sizes.

In Fig. 5. a calculated velocity field in the case of moving geometry is presented. The figure clearly demonstrates that the air velocity field is quite complex in the case of an inflating geometry.

Particle deposition densities are presented in Fig. 6. for ultrafine and for large particle sizes along the symmetry plane of the alveolus. Comparing the two panels of the figure the role of impaction and gravitation is clearly demonstrated, the deposition is enhanced at the bottom and at the right side of the alveolus in the case of large particles.

Both the flow and the deposition patterns are highly sensitive to the assumption whether the geometry is fixed or time-dependent. In the case of moving geometry, results are also sensitive to the time behavior of inflation and deflation.

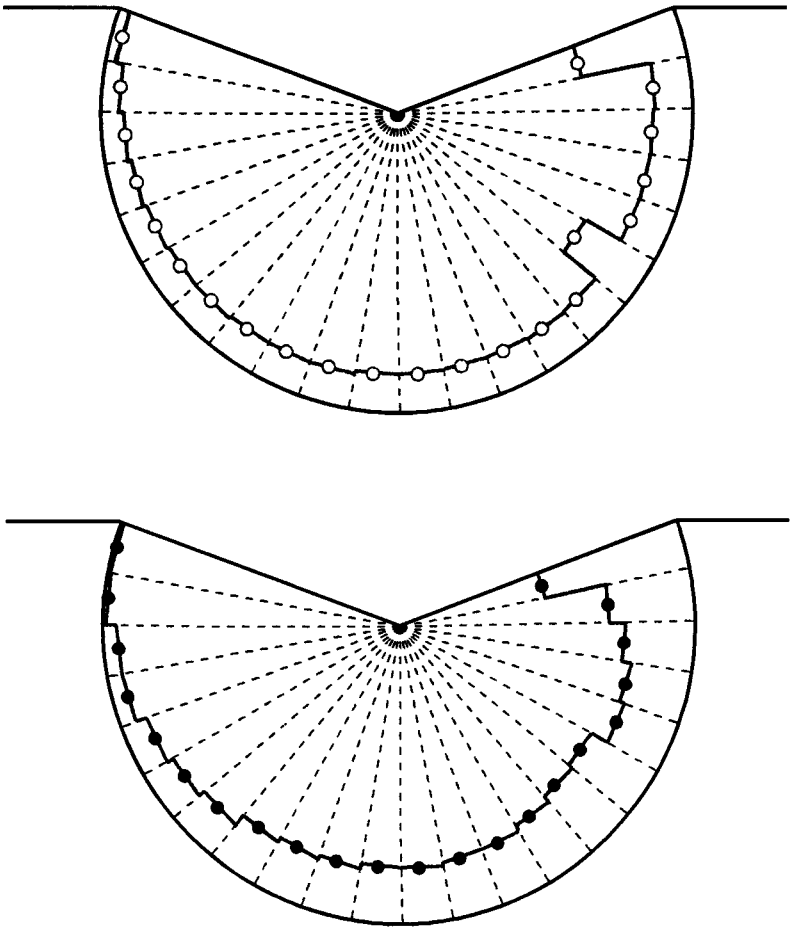

Fig. 6. Distribution of deposition sites of unit density, spherical particles along the symmetry plain of the alveolus (minute volume 15 l/min, breathing cycle time 4 s, particle diameter 0.01 μm (upper panel), and 10 μm (lower panel)).

Publications

I. Balásházy and W. Hofmann: Particle Deposition in Airway Bifurcations. - I. Inspiratory Flow. *J. Aerosol Sci.*, **24**, 745, 1993.

I. Balásházy and W. Hofmann: Particle Deposition in Airway Bifurcations. - II. Exspiratory Flow. *J. Aerosol Sci.*, **24**, 773, 1993.

W. Hofmann and L. Koblinger: Comparison of particle deposition patterns in human and rat lungs. *J. Aerosol Sci.*, **25**, S505, 1994.

L. Koblinger, W. Hofmann, R.C. Graham and R.R. Mercer: Aerosol Inhalation in the Rat Lung. Part I: Analysis of the Rat Acinus Morphometry and Construction of a Stochastic Rat Lung Model. *J. Aerosol. Med.*, **8**, 7, 1995

L. Koblinger and W. Hofmann: Aerosol Inhalation in the Rat Lung. Part II: Theoretical Predictions of Particle Deposition Patterns. *J. Aerosol. Med.*, **8**, 21, 1995

Hofmann, W., Koblinger, L.: The effect of mucociliary clearance on bronchial doses from inhaled radioactive aerosols. Int. Soc. Aerosols in Medicine, 10th Biennial Congress, Hamilton, Canada, May 15-19, 1995.

Balásházy, I., Hofmann, W.: Distribution of deposition sites in airway bifurcations computed by different numerical models. Int. Soc. Aerosols in Medicine, 10th Biennial Congress, Hamilton, Canada, May 15-19, 1995.

Hofmann, W., Heistracher T., Balásházy, I.: Deposition patterns of inhaled radon decay products in human bronchial airway bifurcations. Int. Symp. Natural Radiation Environment, Montreal, Canada, June 5-9, 1995.

Hofmann, W., Koblinger, L., Mohamed, A.: Incorporation of biological variability into lung dosimetry by stochastic modeling techniques. Int. Symp. Natural Radiation Environment, Montreal, Canada, June 5-9, 1995.

Head of project 11: Prof. Gradoń

II. Objectives for the reporting period

(i) Development of a theoretical model of retention of material deposited in the alveolar region of the human respiratory tract.
(ii) Experimental analysis of the behaviour of lung surfactant exposed to gases and particulate material in the inhaled air.

III. Progress achieved including publications

1. Theoretical model of retention of material deposited in the human respiratory tract.

A mathematical model of retention of aerosol particles penetrating the lungs during inhalation has been developed. Based on calcualtions of the number of particles deposited per unit area and per unit time, and their residence time in each generation of the respiratory system - due to different mechanisms of clearance - the retention dynamics of deposits has been determined. Our attention was focused on the pulmonary region of the lungs. The particles deposited in that region exist as "free" or/and phagocytosed matter at any given instant. Both forms of deposits may either be withdrawn by the mucociliary escalator or alternatively propelled into the lung's interstitium, the lymph nodes, and finally towards the blood system.

The estimation of the residence times of both forms of particles in the pulmonary region of the lung is uncertain. Two general mechanisms of translocation of alveolar macrophages (AM) are suggested. The first is that of directed migration through airways to the mucociliary escalator. In this case AM migration is presumed to be due either to a directed motion of the alveolar lining layer, on which AM as well as "free" deposited particles are passively transported by hydrodynamic effects, or to a surface tension gradient in the surfactant monolayer adsorbed on the hypophase. This theoretical hypothesis was examined experimentally, as described below. Motion may also arise from the chemoattractant gradient which directly polarises and facilitates AM migration along the alveolar epithelium surface.

There is a second proposed pathway for deposits to leave the pulmonary region. It is the slow phase of displacement of deposits into the lung parenchyma, followed by entrance into the lymphatic system. In our model, we assume that this slow phase is composed of two stages. In the first stage, part of the deposited material that is contained in the alveoli and terminal bronchiole of a given generation is transferred to the wall of the tissue at a constant rate K. The material is then transported to the lymphatics and blood system at the rate Λ. Estimation of both parameters, and rates of transport mentioned above allows us to make calculations of the retention process.

The influences of the composition of the inhaled particles and of the carrier gas on transport rates were examined theoretically and experimentally. In particular, we have analysed the influence of long-term exposure of the lung to different types of radiation on the transport rate. We found that most sensitive to that effect, in the whole structure of the model, is the change of transport rate K due to ultrastructural changes of lung tissue. Some quantitative description of the phenomena is proposed.

2. Experimental analysis of the behaviour of lung surfactant exposed to gases and particulate material in the inhaled air

The activity of the lung surfactant (LS) monolayer was investigated *in vitro* using a Langmuir Film Balance, LFB, (LAUDA, Germany). The device allows for cyclic variation of

the air/water interfacial area, A, on which a monolayer of surfactant phospholipids is adsorbed. In this way dynamic oscillations similar to those of the alveolar area during the breathing cycle may be simulated under laboratory conditions. Continuous measurements of surface pressure, π, which are conducted by means of the LFB during each experiment, may be regarded as a quantitative criterion for evaluation of surfactant quality and performance. A characteristic π-A hysteresis loop may be observed during a compression-expansion (expiration-inspiration) cycle simulated on the LFB, and it is directly related to dynamic phenomena taking place at the interface and in the liquid hypophase.

Our experiments were focused mainly on the influence of various gases inhaled with air on the dynamic properties of LS. Lung surfactant, being an essential compartment of healthy lungs, also plays an important role in clearance processes. Hydrodynamic phenomena occurring in pulsating alveoli are responsible for translocation of "free" or phagocytosed aerosol deposits. In this sense the surface properties of LS under dynamic conditions mediate the rate of alveolar clearance.

In order to assess the influence of a toxic atmosphere on the hydrodynamics of the system, the LFB was supplemented by video equipment (SONY, Japan) - Fig.1. This set-up allowed for continuous observation of fine solid tracers at the interface. In this way it was possible to investigate relationships between the shapes of π-A curves and patterns of displacement of solid deposits. The influence of very low concentrations (~ ppm) of ozone or sulphur dioxide was examined. In all experiments synthetic dipalmitoyl phosphatidylcholine (DPPC - the main constituent of LS) was used instead of natural LS in order to avoid dispersion resulting from variability of extracts from lung lavage. All measurements were carried out under conditions close to physiological ones (temperature, pH, compression ratio, etc.).

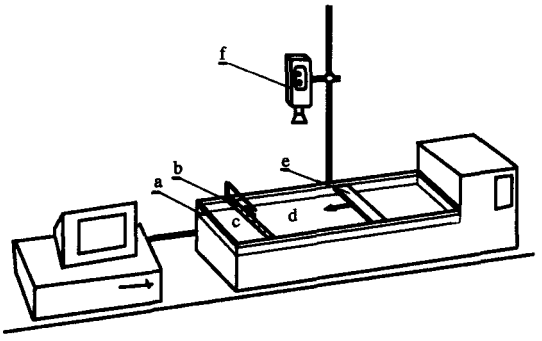

Fig.1. Experimental set-up:
a - Langmuir Film Balance, b - measuring PTFE float, c - reference pool,
d - measuring pool (DPPC monolayer), e - moving PTFE barrier, f - video camera

The experiments supported our assumptions of strong correlations existing between surfactant quality and its transport properties during oscillations of interfacial area. Due to specific interactions at the interfacial region after exposure of the monolayer to toxic gases, surfactant loses its stability on the interface, which in turn has effects both in change of the shape of the π-A curve and in an alteration of the displacement pattern of solid tracers. The velocity profile at the interface was disturbed in that case, which suggests that a synergistic harmful effect of dust inhalation in the presence of toxic gases (i.e. possible impairment of clearance rate) may occur in the alveolar region.

3. Mathematical model of hydrodynamical phenomena in a Langmuir Film Balance (LFB)

The LFB is often used for investigation of surface phenomena in a gas/liquid system which contains a monolayer of a surface-active substance. We employed this device to analysis of the dynamic behaviour of a monolayer of DPPC (as a model compound of lung surfactant). In order to understand the hydrodynamic processes taking place in the system and to find its most important parameters, a mathematical description of the system is needed. Our model being elaborated is based on general equations for a two-phase fluid system containing an active monolayer. It takes into account the specific properties of the surfactant under consideration. A system of differential equations derived from the equation of continuity and balances of momentum and mass, is adapted for real geometry and supplemented by proper boundary conditions.

The model is being solved numerically to obtain: velocity profiles in the liquid sublayer and on the interface, surface concentration, and surface tension distribution under dynamical compression and expansion (simulation of breathing cycle).

The results of the computations are being compared with experiments on the displacement of solid tracers at the interface in the LFB. Verification, if successful, should support our hypothesis of a special role of LS for alveolar transport of solid deposits.

4. Pulsating Bubble Surfactometer (PBS) experiments

In the last stage of the project preliminary experiments of bubble dynamics in the presence of LS are being conducted using a Pulsating Bubble Surfactometer, PBS, (Electronetics Corp., USA). The device allows for continuous measurement of the surface tension-area (π-A) relationship for a small (d = 0.4 mm) air bubble pulsating in a surfactant suspension at various rates (up to 100 cycles per minute). In this way more physiologically realistic experiments in an air/water/surfactant system may be performed. We plan to compare the results of the PBS studies with our previous investigations of LS dynamics conducted with the LFB.

5. Publications

Gradoń, L., Podgórski, A., *(Invited Paper)* Discussion of Present Modelling Techniques (a Modeller's Point of View)., *10th ISAM Congress*, May 15-19, Hamilton, Canada. Abstract in: *J. Aerosol. Med.*, **8**, 63.

Gradoń, L., Podgórski, A., Sosnowski, T.R., Experimental and Theoretical Investigations of Transport Properties of DPPC Monolayer., *10th ISAM Congress*, May 15-19, Hamilton, Canada. Abstract in: *J. Aerosol. Med.*, **8**, 66.

Orlicki, D., Gradoń, L., Gas Flow and Particulate Deposition in the Model of Human Alveolus. Pathological Cases., *10th ISAM Congress*, May 15-19, Hamilton, Canada. Abstract in: *J. Aerosol. Med.*, **8**, 69.

Sosnowski, T.R., Gradoń, L., Influence of Toxic Gases on Alveolar Surface Transport. *10th ISAM Congress*, May 15-19, Hamilton, Canada. Abstract in: *J. Aerosol. Med.*, **8**, 113.

Gradoń, L., Podgórski, A., The Retention of Inhaled Particles in the Human Respiratory System. Cytotoxic Effects. *Proceedings of the Workshop*, Sept. 19-20, 1995, Warsaw, Poland - in preparation.

Head of project 12: Professor Salowsky

II. Objectives for the reporting period

(i) To obtain a suitable sample of dust from the Bulgarian nuclear industry and to determine characteristics of the respirable fraction of the dust sample.
(ii) To carry out *in vitro* dissolution measurements on the dust sample obtained.
(iii) To investigate the early pneumotoxic effects of the Bulgarian radioactive dust and Tri-n-butyl phosphate (TBP), using sensitive biochemical markers in bronchoalveolar lavage fluid (BALF); histological examination (antioxidant protective systems); light and electron microscopy of lung tissue.

III. Progress achieved including publications

1. Obtaining a dust sample from the Bulgarian nuclear industry, preparation and characterisation of a respirable dust fraction[1].

The sample was obtained from one of the ventilation grids of the reactor hall of Units 1 and 2 of Kozlodoui Nuclear Power Plant (NPP). This plant is the Bulgarian nuclear industry's largest facility. It was built by Russian organistions and started to operate in 1974. All reactors (four 440 MW and two 1000 MW) are of the VVER type.

The radioactive sample is formed by sedimentation of the dust particles in the reactor hall air on ventilation grids. A similar dust can be obtained from other reactor halls of Units 3, 4, 5 and 6 of the Kozlodoui NPP. Furthermore, it is possible to find similar dust in other nuclear power plants of the same type.

The dust from Kozlodoui NPP poses a potential risk to the health of staff working in the Reactor Hall. It can enter the human body mainly by inhalation, and the lung is the first target organ. Therefore, the studies on the biokinetics of the radionuclides present in the dust, assessment of the committed doses, and the toxicological effects on the lung are an important part of the radiological protection of workers at the Kozlodoui NPP.

The colour of an ethanol suspension of the radioactive material was yellowish, probably due to lubricants. For this reason a portion of about 60 g was washed by five extractions as follows: methanol+CCl_4 (once), methanol (twice) and ethanol (twice). The grease-free sample was used to separate the respirable size particle fraction (nominally < 5 μm aerodynamic diameter) by sedimentation in absolute ethanol.

The respirable fraction obtained was collected in a 250 ml measuring flask and a 100 ml aliquot was transferred to a vial and identified as BGID. After evaporation of the ethanol the weight of the residue in the vial was 0.2496 g.

The elemental content of the material was as follows: silicon (Si) ~ 30%, Calcium (Ca) ~ 8%, Aluminium (Al) ~ 8%, Potassium (K) ~ 4%, Magnesium (Mg) ~ 2%, Iron (Fe) ~ 2%, Lead (Pb) ~ 1%, Titanium (Ti) ~ 1%, Sodium (Na) ~ 1%, Manganese (Mn) ~ 0.2%, Barium (Ba) ~ 0.3% etc.

For radiochemical analysis, a second aliquot of BGID was dried to remove the ethanol. The residue was spiked with ^{234}Th and ^{236}Pu tracers and dissolved in a hot solution of 8 M HNO_3 + concentrated HF (1:1) + 1 ml concentrated $HClO_4$. The solution was fumed and the residue finally dissolved in 3 M HNO_3. It was transferred to a 50 ml vessel with standard

[1]The preparation of a respirable fraction of the dust sample, and the *in vitro* dissolution measurements were carried out by The Institute for Nuclear Research and Nuclear Energy, Sofia, Bulgaria

geometry and counted for 50,000 s on a low background γ-spectrometer with a HPGe detector. Afterwards, the sample was loaded in TEVA.SPEC® and Th and Pu strips separated. Samples for α-spectrometry were prepared by coprecipitation with NdF_3.

The γ-spectrometric analysis of the BGID shows the following specific activities:

Radionuclide	Specific activity, Bq/mg
^{60}Co	43.7
^{137}Cs	11.3
^{54}Mn	1.34
^{134}Cs	1.19
^{144}Ce	0.27
^{241}Am	0.11
^{65}Zn	0.08
^{58}Co	0.07
^{110m}Ag	0.04
^{155}Eu	0.03

The data from α-spectrometric analysis in mBq/mg are: ^{238}Pu-47, $^{239/240}$Pu-82, ^{230}Th-7.6. The ^{90}Sr content obtained by β-spectrometry was 2090 mBq/mg.

2 Measurement of the *in vitro* dissolution of BGID

An aliquot of BGID was dried. Lung fluid simulant (LFS) (2 ml) was added to the dried BGID, sonicated for 2 minutes and transferred to Visking tubing (Medical International plc, London), using a syringe. The sample was sealed by knotting and suspended in 100 ml LFS contained in a closed flask secured in a water bath maintained at 37±0.5°C. The suspension was agitated for 30 min every 3 hours using a magnetic stirrer. The amount of BGID used in the *in vitro* dissolution experiments was 82.2 mg.

The LFS was removed and measured by γ-spectrometry according to the following schedule:

first day - every 6 hours,
second day - every 8 hours,
third and fourth days - every 12 hours,
fifth and sixth days - every 24 hours,
seventh to tenth days - every 48 hours,
eleventh to twentieth days - every 120 hours,
twenty-first to fifty-fifth days - every 168 hours.

Samples were bulked and analysed for plutonium according to the following scheme: first and second days - samples 1 to 7, third to sixth days - samples 8 to 13, seventh to twentieth days - samples 14 to 17, twenty-first to fifty-fifth days - samples 18 to 22.

Gamma-spectrometry. After contact with the BGID, the LFS was transferred to a beaker, evaporated almost to dryness, dissolved in 50 ml 1M HNO_3, and transferred to a standardised 50 ml measuring vial. The samples were analysed using a low-background high

resolution γ-spectrometer with a 21% efficiency HPGe detector. Measuring times were between 70,000 and 200,000 s.

Plutonium determination. Plutonium was determined in the bulked samples after γ-spectrometry. Tetravalent plutonium was separated using a column packed with TEVA.SPEC® (80-160 μ) from Eichrom Industries, Inc. U.S.A. The plutonium source was prepared by coprecipitation with NdF_3 according to the method of Hindman (Anal. Chem., 1238-1241, 1986). Plutonium-236, 3.5 dpm was used as the chemical yield tracer in each determination.

Of all the isotopes registered in the γ-spectrometric analysis the following appeared to be of interest: ^{60}Co, ^{137}Cs, ^{54}Mn, ^{134}Cs and ^{110m}Ag.

The results for ^{60}Co, ^{137}Cs, ^{134}Cs and ^{54}Mn are consistent with those expected. The dissolution rates decrease according to the linear function:

$$\log(ATR)=B*\log(T)+A$$

where ATR is the activity transfer rate expressed as % of initial activity per day, T is time andA and B are constants. The data for ^{110m}Ag are near to the detection limit of the procedure and a function could not be derived.

The cumulative dissolution for ^{60}Co, ^{137}Cs and ^{239}Pu for some selected times are given below.

Radionuclide	% dissolved			
Time	1d	8d	27d	55d
^{60}Co	16.4	21.2	22.8	23.6
^{137}Cs	74.8	80.0	81.4	83.5
Time	2d	6d	20d	
^{239}Pu	0.57	0.78	0.90	

3. Investigation of the toxicological effects of BGID and TBP

Material and methods

The experiment was carried out with 135 male Wistar rats (weight 280-300 g) 4 months old, divided into 3 groups (Group 1 - controls, Group 2 - treated with BGID and Group 3 - treated with TBP).

Each animal of Group 2 received 0.15 ml of aqueous suspension of BGID (0.1997 g of BGID in 10.7 ml saline) intratracheally through a metal probe (0.15 ml = 2.9 mg of BGID). The animals of Group 3 were also treated intratracheally with 5 ml TBP (20% v/v in n-dodecane, equivalent to 1 ml TBP and 4 ml dodecane). For TBP intubation into the lungs a polythene tube (external diameter 1.6 mm, internal diameter 0.6 mm, Portex Ltd, Hythe, Kent) was used.

Six animals from each group (control and both treatment groups) were sacrificed on post-treatment days 1, 3, 7, 14 and 28.

Under sodium pentobarbital anaesthesia the abdominal aorta was sectioned, the chest opened and intracapillary perfusion of the lung was carried out with 40 ml saline. The right lung was homogenised in 1:10 ratio with ice-cold 0.25 M sucrose solution, containing 50 mM Tris-HCl, pH=7.4. The lung homogenate obtained was centrifuged at 6000 g for 10 minutes to collect the supernatate for biochemical studies.

Triple lavage of the left lung through the trachea with a total of 5 ml saline was

performed. One aliquot of the bronchoalveolar lavage fluid (BALF) was used for counting the total number of cells. Then the cells were removed by centrifugation at 300 g for 10 minutes and the cell pellet was resuspended in 1 ml saline. A cytospin preparation of the cells was performed. The supernate obtained from the centrifugation was used for biochemical analysis.

The following measurements were made:

a) Lung weight coefficient (organ weight in mg to 100 g body weight)
b) Blood - leukocyte number, haemoglobin content
c) Serum - cholinesterase activity (to day 7 only)
d) BALF - total cell number; differential cell counting, including alveolar macrophages (AM), lymphocytes and granulocytes (PMN); activity of the enzymes lactate dehydrogenase (LDH), alkaline phosphase, acid phosphatase and γ-glutamyl transferase; content of the total protein and the glucose.
e) Lung homogenate - activity of the enzymes superoxide dismutase, catalase, glutathione peroxides, glutathione reductase, glucose-6-phosphate dehydrogenase and cholinesterase; content of the non-protein sulphydril (NPSH) groups, malondialdehyde and protein.
f) Light and electron microscopically examinations - the lung material was fixed in 10% formol and thereafter processed according to routine methods. The staining by hemaloun eosin, according to van Gieson, PAS reaction, toluidin blue and according to Gomory (for reticular fibres), was carried out. Ultrathin sections were examined in electron microscope Hitachi.

The obtained experimental results were statistically analysed by Student's t test ($p < 0.005$). The arithmetical mean of each variable was obtained from six animals in each group.

Results from the toxicological examinations

Toxicological effects of BGID

The intratracheally administration of an aqueous suspension of BGID (0.15 ml = 2.9 mg) into rats increases the total cell number, the PMN, the LDH and alkaline phosphatase activities and the protein and glucose contents in BALF up to day three after the treatment. These findings suggest an acute transitory toxic response of lung tissue to BGID. The results of the microscopy examination on rat lungs support this conclusion, namely: interstitial oedema, blood vessel congestion and single neutrophils around the blood vessels and bronchioles on day one. The electron microscopy on days one and three shows a destruction of type 2 pneumocytes (Pn2), cellular debris mixed with secreted laminar bodies (LB) in the alveolar spaces, an impairment of the bronchiolar epithelium with inclusion of dust particles.

The alkaline phosphase activity is higher in comparison to the LDH activity until day seven. These biochemical data suggest a more toxic lesion of the Pn2 compared to the other pulmonary cells. The electron microscopy examination also shows marked damage to this pneumocyte type in an earlier stage.

An increase of the acid phosphatase activity in BALF is established after day three. This sign of intensive phagocytosis is in conformity with the cytological and electron microscopy data for dust particle inclusions in the AM.

The BGID changes the correlation between the links of the pulmonary antioxidative defence - it decreases the superoxide dismutase and catalase activities until day seven, but increases the activities of the glutathion peroxidase, glutathione reductase and NPSH content during the same period. Probably that is the reason why the antioxidant protective capacity of

the lung remains unchanged. An evidence of this phenomenon is the normal content of the malondialdehyde during the studied period.

Toxicological effects of TBP

As a result of intratracheal application of 5 ml TBP (20% v/v in n-dodecane) into rats the following are increased mainly on day one: the total cell number, the PMN, LDH and alkaline phosphatase activities and the protein content of the BALF. Blood congestion of the lung and single perivasal infiltrates of lymphocytes were observed by light microscopy on days one and three after the treatment. The electron microscopy examination of the same period shows an increased number of AM in the alveolar spaces, containing many excreted LB. Type 2 pneumocytes had swollen mithochodria and single LB. These changes have a quite moderate character and suggest a low toxic response of the lung to this agent.

The tendency to increase the total cell count, LDH activity and protein content on days fourteen and twenty-eight, probably reflects another slight inflammatory process during this later period. The electron microscopy examination demonstrates degenerative changes on Pn2 and AM during the above mentioned stage.

TBP decreases the activities of the superoxide dismutase and catalase until day seven as well as the enzyme activities of the glutathione peroxide system on day one and after day fourteen. This depression in the pulmonary antioxidative capacity leads to increase of the lipid per oxidation in the lung tissue. Some evidence of this process is the tendency to increase of the malondialdehyde content from day three to day fourteen.

Similar to all organophosphoric compounds TBP inactivates the cholinesterase in serum on day one. This finding confirms the already known fact that TBP has a slight inhibitory influence on the cholinesterase.

The establishment of an acute toxic damage caused by TBP and particularly BGID requires further investigation on some later effects in the lungs, including pulmonary fibrosis. Therefore an assessment of the local immunity in the lung would be of great interest. Furthermore, the presence of a high amount of silicon in the primary radioactive material requires a more detailed chemical and mineralogical analyses of BGID.

Measurements are in progress on additional control groups: one negative and two positive (with n-dodecane and inert dust respectively), and light and electron microscopy of the liver and kidney. Papers are being prepared for publication. The present results of the studies emphasise the need for investigations of the toxicological aspects of radioactive materials which are potential human health hazards to be investigated. Such toxicological data could become an important part of the assessment of the limits on intake.

Final Report

Contract: FI3P-CT920003 Duration: 1.9.92 to 30.6.95 Sector: A2A

Title: Promotion of formation, knowledge and exchange of information in radioecology.

1) Cigna UIR

I. Summary of Project Global Objectives and Achievements

The primary objective of UIR over the contract period was the exchange of information in the field of radioecology particularly in relation to major (accidental) releases of radioactive materials. This objective is not restricted to information on the transfer of important radionuclides in the environment but includes information which can aid in understanding the impact of radiation exposure on populations of living organisms and ecosystems.

The objective was met by a series of Task Forces which aimed to collate available information on specific topics and to provide syntheses which could be applied to the design of new research programmes and for assessing overall priorities in radioecology. These Task Forces included:

- TF1: Priorities in Radioecology
- TF2: Assessment of the Relative Dose Contribution of Various Pathways Under Different Environmental Conditions, Including Semi-Natural Environments
- TF3: Assessment of the Relative Importance of Various Freshwater Exposure Pathways and the Major Parameters Influencing Pathways
- TF4: Behaviour of Less Commonly Considered Radionuclides
- TF5. The Effects of Radiation on Organisms in their Natural Environment

A further Task Force on the application of biotechnology to restoration of areas affected by radioactive contamination was also initiated during the contract period.

At the same time, UIR continued to provide a mechanism for the training of young scientists and for maintaining links with radioecologists in non-EC countries via a series of Steering Committees including the following.

- SC1: Training
- SC2. Publications
- SC3: Co-operation with Central and Eastern Countries

UIR also initiated an Advisory Panel to provide an interface between scientists, politicians and the public on radioecological topics.

Over the last three years UIR has provided an effective mechanism for promoting the development and understanding of radioecology, and the European Commission has benefited from UIR initiatives, especially as concerns the exchange of information with countries outside the European Community. UIR is a non-governmental organisation and all of its administrative and scientific activities are fulfilled by volunteer staff. Membership

subscriptions provide only a very small contribution to the overall running costs of the Union and therefore the financial contribution of the European Commission and other bodies is much appreciated. These contributions allow the Union to complete individual scientific projects to the benefit of the contributor and the Union alike.

Over the reporting period UIR has provided advice to the European Commission on priorities for radioecological studies with specific reference to aquatic ecosystems, semi-natural ecosystems, the effects of radiation on natural populations, and less-commonly considered radionuclides. The study on priorities for radioecology has addressed other topic areas worthy of potential future study, especially in relation to problems of the nuclear industry associated with radioactive waste disposal. The UIR Newsletter has succeeded in keeping radioecologists and other interested parties informed about developments in radioecology. The various Steering Committees have continued to provide a mechanism for generating and motivating networks for the exchange of information, especially as regards countries of the former Soviet Union.

At the same time, UIR has attempted to take a more pro-active role than previously by generating agreements for the development and financing of future studies, the most important of which are the current agreement with the Chernobyl Zone Administration to assist with the development of a management strategy for the Chernobyl Exclusion Zone, and for the development of an independent centre for radioecological studies in the Urals (one of the founding regions of modern radioecology). At the request of the European Commission, UIR has attempted to forge links with other organisations having a bearing on radiation protection such as EURADOS and EULEP. The well-developed administrative structure of UIR will assist with the development of these links and the existing Newsletter and Advisory Panel will help to ensure that activities in radiation protection are brought to the attention of public, administrative and scientific organisations alike.

The positive activities of UIR described in the following pages have been reflected in an almost linear growth of the Union over the last few years with the current membership of over 500 persons representing more than 250 organisations from 37 different countries. UIR will continue to offer its resources to the European Commission and to other bodies as an independent non-governmental organisation providing expert advice on radioecological matters and as an organisation able to undertake individual research studies and to prepare state-of-the-art reviews under contract to appropriate sponsors. At the same time UIR will continue to promote networks for the exchange of information in countries such as those of the former Soviet Union and the far East in an attempt to provide an unbiased source of information for decision-making purposes.

Project 1: Priorities in Radioecology (Acting Chairman: P.J. Coughtrey)

Objectives

The objective of this Task Force was to prepare a state-of-the-art overview of radioecology and to identify priorities for future research which could be used by the European Commission as a basis for preparing a programme of research on radioecology.

Progress

Progress on this project was delayed by the unfortunate death of Constant Myttenaere, Chairman of the Task Force and previously President of UIR.

Following several drafts, a final version of the report was submitted to the European Commission in May 1995 [1]. This report has the following structure:

- Introduction
- Sources of radioactivity
- Pathways for radionuclide transport
- Accidental conditions, countermeasures and rehabilitation
- Mechanisms involved in radionuclide transport
- Assessment models
- Conclusions and priorities
- Acknowledgements

It is concluded that the priorities and recommendations for further radioecological research are as follows.

Sources of radionuclides

- The sources and extent of contamination in various ecosystems should be identified
- Methods used for data collection should be evaluated and new methods recommended
- A computerised database of appropriate data should be established

Pathways for radionuclide transport

Temperate zones

- A centralised databank should be created for predictive purposes
- Case studies should be undertaken at specific sites
- Specific studies should be undertaken on water movement and radionuclide fluxes
- Specific studies should be undertaken on synergistic effects between radionuclides and conventional pollutants
- A databank should be created on waste processing techniques and on ameliorative techniques for sites contaminated by accidents
- Studies should be undertaken on radionuclides produced from medical applications

Tropical and subtropical zones

- Food production and consumption patterns should be identified
- Differences between transfer mechanisms in temperate and tropical or subtropical zones should be studied
- Studies should be undertaken on radionuclide interactions with different soil fractions

Arctic zone

- Radioactivity deposited as a result of tests at Novaya Zemlya should be evaluated
- The potential runoff of radionuclides with Siberian rivers should be studied
- The impact of radioactive waste disposal at Novaya Zemlya should be studied
- Inventories should be produced for key radionuclides in the Arctic Ocean
- The significance of the Arctic Basin and Siberian Rivers for fishing grounds in the North Atlantic should be defined

Accidental conditions, countermeasures and rehabilitation

Realistic estimates of the effectiveness of countermeasures should be obtained with respect to:

- Accident type
- Release characteristics
- Pathways
- Meteorology
- Season
- Persons likely to be involved
- Availability of alternative food supplies
- Provision of information
- Procedures for monitoring economic, social and health implications

Mechanisms involved in radionuclide transport

- Mechanisms for fixing radionuclides in different ecosystems need to be identified
- The effects of readily measurable parameters which affect radionuclide transport in soils need to be quantified
- Understanding of biogeochemical and physiological pathways for radionuclide cycling should be improved
- Basic parameters used in the study of transfer mechanisms should be harmonised
- The role of microflora should be studied, particularly in environments which favour their activity
- The cycling and interactions of radiocaesium and radiostrontium with the balance of Sr, Ca, Cs, K and N in ecosystems should be studied
- The mechanisms underlying procedures which can be used to block radionuclide transfers should be studied

Assessment models

- Information on the behaviour of Ca and K in semi-natural ecosystems should be collated and models developed for that behaviour based on biological principles
- Further information should be obtained on the discrimination between Cs and K or Sr and Ca in sensitive semi-natural ecosystems

- New models should be developed and tested on the basis of homeostatic principles
- Understanding of dietary pathways and methods for identifying critical pathways needs to be improved
- Models should be based on the measurement and control of biological variables

Future conditions

- The effects of sea level rise on past and future discharges of radionuclides need to be determined
- The effects of changes in mean water temperature and salinity on fixation and mobilisation of radionuclides need to be determined
- The effects of low frequency high magnitude effects such as storms, floods and drought need to be determined
- The effects of radionuclide contamination of soils via irrigation waters need to be determined
- The effects of fire on radionuclide retention in semi-natural ecosystems need to be determined
- More information is required on radionuclide cycling in urban environments via waste water treatment and disposal
- Methods need to be developed for assessing radionuclide transport from landfill sites
- The effects of novel food production and processing technology need to be determined
- Studies are required on the consequences to man and his environment from fusion technology
- Studies are required on radionuclides of particular interest as a consequence of radioactive waste disposal
- Studies are required on biogeochemical mechanisms which control the cycling of long-lived radionuclides

Publications

1. Priorities in Radioecology. Final Report of UIR Task Force 1. Submitted for publication. May 1995

The work of the Task Force has also been presented and discussed at a number of meetings and conferences.

Project 2: Semi-Natural Ecosystems (Chairman: C. Bunnenburg)

Objectives

The objective of this Task Force was to collate information in order to evaluate and quantify the relative contributions of different pathways to the total dose of the population and critical groups and to define research activities to fill knowledge gaps.

Progress

Progress was made during the UIR October 1993 meeting in Udine, Italy, and preliminary conclusions were presented at a European Commission contractors meeting in Brussels during the first part of 1994. Work continued on the identification of processes and parameters which are important in radionuclide transfer in different types of semi-natural ecosystems. Participants were requested to list:

- relevant radionuclides;
- natural and semi-natural ecosystems;
- animal and plant products;
- components of animal diet; and
- transfer processes.

By combining qualitative and quantitative assessments of the importance and state of knowledge for individual parameters, a tentative ranking of priorities for future research was derived. An overview of the results was presented at the Brussels meeting and the comments received were discussed at a nucleus meeting of the Task Force in April 1994. The lists were then revised and formulated into a two-dimensional matrix for further circulation to participants and interested parties. Participants were requested to rank individual radionuclide transfer processes according to the following scheme.

Importance (I):	Never	0
	Sometimes	1
	Always	2
Knowledge (K):	Well defined	0
	Reasonable estimate	1
	Poor estimate	2
	No values	3

Ranking of research priorities (P) could then be determined from:

$$P = I \times K$$

Evaluation of results from the first stage of the work provides the following example results for importance of different factors (*I*) given in brackets.

Radionuclide:	Most important	Cs	(2.0)
	Least important	Ce	(0.9)
Ecosystem	Most important	Lowland grassland	(2.0)
	Least important	Montane (alpine)	(0.3)
Animal/ plant product	Most important	Cow meat & milk	(2.0)
	Least important	Pheasant, beech nut	(0.5)
Animal diet	Most important	Grass	(2.0)
	Least important	Nuts	(0.5)

Combination of such results with estimates of knowledge gives a preliminary ranking for research priorities ranging from P=5 6 for abiotic/biotic sorption processes in the top layer of soil to 0.6 for the effects of pH.

The work has therefore demonstrated the application of a method to evaluate the importance and knowledge of different factors involved in radionuclide transfer in semi-natural ecosystems in order to identify the priorities for future research. The combination of information from a number of experts in the field has resulted in some surprising results. A further circulation of the questionnaires and evaluation of the results will indicate the extent to which the preliminary results can be confirmed. It will also be necessary to consider statistical evaluations of the results to ensure that mean P values are a useful indication of real research requirements.

Another result of the work is the identification of the critical group associated with natural and semi-natural ecosystems as that group of persons leading a life-style of self-subsistence because of tradition, lack of alternatives or by individual decision. This group is characterised by the consumption of self-produced and self-collected foodstuffs. Enhanced intake of radioactivity results from the limited choice of dietary components, high rates of recycling of organic matter, limited processing of food products, lack of dilution of drinking and irrigation water, and the fact that the application of countermeasures to natural and semi-natural ecosystems is problematic. It has also been concluded that the level of knowledge of ecosystems not affected by the Chernobyl accident is precariously low. Special attention has been and will be paid to the parameters affecting ecological half-lives and biological availability of radionuclides in semi-natural ecosystems

For the results of the Task Force to be of real value in identifying the importance of semi-natural ecosystems in contributing to dose to man it is essential that there is sufficient input from those persons having real experience with the effects of the Chernobyl accident and of accidents or incidents which occurred at MAYAK.

In order to ensure sufficient input to the work from the former Soviet Union, a supplementary agreement under the PECO programme was sought but was not successful. This agreement would have allowed the following issues to have been addressed.

- Ecological characterisation of ecosystems affected by the Chernobyl and Urals accidents.
- Transfer processes of some radionuclides in extensively used semi-natural ecosystems.
- Time-dependence of bioavailability in semi-natural ecosystems of the CIS.

Publications

A draft report on the activities of the Task Force is in preparation.

Project 3 Freshwater Ecosystems (Chairmen: L. Foulquier & U. Sansone)

Objectives

The objective of this Task Force is to identify the important exposure pathways and the parameters controlling radionuclide transport in freshwater ecosystems by reference to different areas in Europe.

Progress

The main activities within this Task Force were initiated during a meeting on freshwater radioecology organised by the European Commission in Lisbon during March 1994. Prior to that meeting work had concentrated on the production of a list of all laboratories working in the field of aquatic radioecology and the development of a network for correspondence between selected laboratories.

Pathways under consideration include internal exposure from drinking water, freshwater fish and irrigation of agricultural products, and external exposure from swimming, boating, contact with fishing equipment, and the use of beaches. The study considers the relative importance of materials deposited directly on to water surfaces and run-off from the catchment area, seasonal factors (including the importance of snow cover), and inputs associated with organic materials. Consideration has been given to the partition between fixed and soluble forms and the processes associated with deposition and suspension of sediments. The appropriateness of using concentration factors to determine uptake by flora and fauna is questioned given inputs from a variety of sources.

The influence of such factors is being examined taking examples from a range of situations in different areas of Europe.

The meeting in Lisbon in 1994 involved contributions from twenty five scientists representing some sixteen countries. One area given particular attention was the role of micro-organisms, especially bacteria, in the cycling of radionuclides in aquatic systems by the solubilisation of radionuclide complexes and the immobilisation of radionuclides in organic matter or mineral salts. It was concluded that:

- there is a need for parallel development of practical and fundamental studies;
- *in situ* studies are fundamental for ecological understanding;
- kinetic studies on transfer between water and suspended materials should be continued;
- studies on biodegradation should be advanced; and
- knowledge on less well studied radionuclides (e.g. transuranics) should be improved.

Agreement was reached on the content of the final report of the Task Force. This report will include (but will not be limited to) the following items.

- Sources of radionuclide contamination of aquatic ecosystems
- Physical and chemical processes of radionuclide behaviour in aquatic ecosystems
- The role of living components in dispersion of radionuclides in aquatic ecosystems

- Interaction between biological and physical or chemical processes
- Methods of research

The Chernobyl accident and recently released information on radioactive contaminated sites in the former Soviet Union and the USA provide opportunities to highlight sensitive processes and parameters and to determine those for which further understanding and data are required.

Publications

A draft final report has been prepared for submission to the European Commission.

Project 4: Less commonly considered radionuclides (Chairman: A. Aarkrog)

Objectives

The objective of this Task Force was to determine the potential significance of less commonly considered radionuclides, particularly pure beta and alpha emitters.

Progress

Radioecological research has generally concentrated on those radionuclides which have been of most environmental concern from a radiological protection point of view, especially those radionuclides considered of importance as a consequence of fallout from testing of nuclear weapons. In local situations other radionuclides may play a role (e.g. as a consequence of ingestion pathways from fuel reprocessing). Further radionuclides may be of significance in the long term future as consequence of releases from radioactive waste disposal sites.

The Task Force met at Riso National Laboratory in 1992 and again during the UIR General Assembly in Udine in 1993. The Task Force collated radioecological data on some 48 radionuclides which had been given little attention in previous studies For each radionuclide, a table was developed including information such as physical characteristics (e.g. half-life, decay scheme), environmental characteristics (e.g. reported environmental concentrations, concentration factors, K_d) , radiobiological characteristics (e.g. ALI) and specific properties or problems.

A semi-quantitative scheme was developed to rank the identified radionuclides in terms of their potential importance to man This included the development of a number of radioecological indices based on ratios of environmental parameters to the ALI.

The following radionuclides were identified as requiring the first priority for further radioecological study: Be-7, Be-10, Na-22, Si-32, S-35, Cl-36, Ni-63, Se-75, Se-79, Rb-87, Mo-93, Ru-103, Ru-106, Ag-110m, Cd-109, Sn-126, I-125, I-129, Sm-147, Lu-176, Pb-210, Po-210, Ac-227, Pa-231, Np-237 and Cf-252.

A final report [1] containing Tables for each radionuclide and a breakdown of results for terrestrial, marine and freshwater ecosystems was submitted for publication in June 1994.

Publications

1. The Behaviour of Less Commonly Considered Radionuclides. Final Report of UIR Task Force 4. Submitted for publication. June 1994.

Project 5: Radiation Effects (Chairman: D. Woodhead)

Objectives

The objective of this Task Force was to further collate and analyse information on the effects of ionising radiation on native organisms with special attention to information available from the former Soviet Union.

Progress

In recent years it has become apparent that there is a substantial body of information in the Russian literature concerning the effects of increased radiation exposure on organisms in their natural environment. These data have been collected both from controlled experiments employing large, scaled gamma-ray sources and from contaminated areas following serious accidents in the Urals in 1957 and at Chernobyl in 1986.

Intensive work has been undertaken to identify information in the former Soviet Union on the effects of radiation on native organisms. Subsequently the identified information was collated, translated and analysed by a joint team of Western and former Soviet Union scientists. Key subject areas addressed in this analysis were:

- Environmental dosimetry
- The effects of increased radiation exposure on the processes of gametogenesis, embryonic development, mutation, morbidity and mortality in all classes of plants and animals in:
    - areas of high natural radiation background;
    - areas contaminated by controlled radioactive waste disposal;
    - areas contaminated by accidental releases;
    - biological communities experimentally exposed to radiation fields from either sealed gamma-ray sources or deliberate, but controlled contamination with radionuclides; and
    - laboratory studies under carefully controlled conditions.

The importance of the information available from former Soviet Union countries is that: it extends the range of dose rates at which environmental effects have not been observed beyond the limit previously available from studies of controlled waste disposal situations; and that because dose rates and total doses in some areas were sufficiently high for effects to be observed in wild animals under natural conditions, it provides an improved basis for determining threshold dose rates at which the impact of increased radiation exposure is likely to be of significance for natural populations.

In the context of protecting the environment from increased radiation exposure it is generally accepted that the population should be the object of protection. It follows, therefore, that there should be no effects of radiation exposure on those attributes of individuals which

combine to ensure the maintenance of the population within its normal range of variability. These attributes include morbidity and mortality, fertility, fecundity, and genetic effects.

Preliminary conclusions of the review were discussed at a meeting in Budapest in April 1994 and indicated the need for an even more-searching examination of the available literature and a requirement for the study of all relevant attributes for populations of single species at a range of dose rates.

As a consequence of the above, an extension to the work of this Task Force was sought with financial assistance from PECO. The objective of this extension was to identify plants and animals which exist as discrete populations at a range of dose rates at both contaminated and control areas and to study all attributes of the selected populations. A proposal was submitted to this effect in 1994 and an extension granted in November 1994. Technical work is being undertaken in collaboration with the Institute for Biology of the Southern Seas in Sevastopol (Ukraine), the Experimental Research Station at MAYAK, Cheliabinsk (Russia), the Institute of General Genetics in Moscow (Russia), and the Institute of Agricultural Radiology at Obninsk (Russia).

Publications

The results of this Task Force will be presented in a final report to the European Commission on conclusion of the work currently being financed by PECO It is anticipated that the work will result in a number of publications in peer reviewed journals in collaboration with UIR's partner organisations.

Project 6: Steering Committees

SC1: Training (Chairman: U. Sansone, previously J. Van den Hoek)

The objective of this Steering Committee remains the organisation of meetings and training courses to attract and develop young scientists in the field of radioecology.

In addition to maintaining UIR's reputation for organising and implementing successful summer schools in radioecology, this Steering Committee continued its activities in seeking additional finances for a workshop in radioecology sponsored by the European Commission in Sevastopol during autumn 1994, and for an advanced training course sponsored by NATO in the Urals during summer 1995.

The meeting at Sevastopol provided an opportunity for radioecologists from many former Soviet Union countries to renew and strengthen their contacts. Many aspects of radioecology were discussed and the meeting allowed for discussion on the scientific basis for decision-making in the newly independent States. It also allowed for discussions on related problems such as those caused by exposure to chemical contaminants and the interactions with radiation exposure.

The advanced training course at Zarechny was intended for all those professionally involved in radioecology and nuclear site restoration. The main emphasis of the course was on specific radioecological problems in severely contaminated areas such as the Southern Urals trace from the Kyshtym accident of 1957, the rivers Techa-Isert-Tobol-Irtish-Ob contaminated from discharges at MAYAK from the late 1940s, and the 30 km zone at Chernobyl. Major problem areas were identified as forests and aquatic ecosystems and attention was focused on the special problems encountered in heavily contaminated areas as a consequence of extreme heterogeneity of contamination and the presence of 'hot particles' as experienced after the Chernobyl accident.

Over the contract period, UIR also organised a workshop on microbial aspects in radioecological research at Udine in Italy during September 1993. This meeting resulted in the development of a Task Force to assess the use of biotechnological methods in environmental restoration

The UIR Summer School on Radioecology held in Budapest during July/August 1993 attracted 25 students, 8 of which were local and 17 of which came from other countries including five from Eastern Europe. A questionnaire indicated that the course was much appreciated by the students.

The success of training courses organised by UIR is further demonstrated by a number of requests from countries of Central and Eastern Europe, Asia and South America to host future courses and to attempt to provide funding from national sources for this purpose.

SC2: Publications (Chairman P J. Coughtrey, previously N. Pattenden)

The objective of this Steering Committee is to maintain awareness amongst radioecologists by means of a periodical Newsletter and by the preparation of a textbook in radioecology.

In addition to the preparation and circulation of a periodic Newsletter providing up to date information on radioecological issues, this Steering Committee has also investigated the potential for producing a Journal of Radioecology targeted at central and eastern European countries and the publication of a textbook on radioecology. During the reporting period the size of the Newsletter has been increased considerably to allow for the inclusion of additional information such as forthcoming meetings of relevance to radioecologists and articles on topical issues. The Newsletter is received by all paid-up members of UIR and is available for a small charge to libraries, funding bodies, research organisations etc.

Work on the textbook was temporarily halted due to the unfortunate and unexpected death of Norman Pattenden, the editor in chief. Arrangements were therefore put in hand to continue the work via an editorial committee.

In addition to the Newsletter, the following relevant publications have been produced during the reporting period with assistance from UIR.

The Journal of Radioecology (Edition 1 and 2).

'Handbook of Parameter Values for the Prediction of Radionuclide Transfer in Temperate Environments' IAEA Technical Report Series No. 364. Produced in collaboration with the International Union of Radioecologists, Vienna 1994.

'Radioecology After Chernobyl' (SCOPE 50).

The Steering Committee has also overseen the editing and publication of the UIR Technical Reports referred to in preceding Sections.

SC3: Co-operation with Central and Eastern Countries (Chairman: R. Kirchmann)

The objective of this Steering Committee was to promote co-operation and exchange of information between radioecologists, in particular from Eastern European countries and other countries outside the European Community, in order to stimulate interactions that would increase our understanding of radioecological problems.

A delegation of UIR members visited the MAYAK Production Association during June 1993 stimulating the production of a protocol stressing the need for development of bilateral and multilateral co-operation in applied and general radioecology for the restoration of nuclear sites in Europe. A number of proposals for joint work were elaborated and it was agreed that there is a need to establish an international centre for environmental restoration. UIR has subsequently worked to bring the resulting agreement to the attention of the scientific community and to potential funding organisations.

UIR has continued to co-operate closely with representatives of Russia, Belarus and Ukraine responsible for areas affected by the Chernobyl accident. During late 1994 and early 1995, UIR has been responsible for obtaining an agreement signed by representatives of all three States requesting assistance with the development of a programme for an independent assessment of current conditions and environmental safety in the Chernobyl Exclusion Zone. This agreement recognises that there are potential impacts of the Exclusion Zone on nearby territories and that there is a need for a long term management strategy for the zone based on sound scientific principles. UIR is continuing to work with representatives of all three States to prepare a detailed programme for the work and to identify potential mechanisms for its financing.

During the NATO ASI at Zarechny in June 1995, UIR prepared a statement to the effect that there is a serious radioecological situation in the Urals as a consequence of the operation of military and civilian nuclear installations from the late 1940s. This statement called for the development of an independent centre of radioecological expertise in the Urals Region. Subsequently an agreement was prepared between UIR, representatives of the Russian Ministry of Science and Technology, the Russian Academy of Sciences, and the Zarechny Technopolis, in which the need for the aforementioned independent centre was confirmed. This agreement also sets out the arrangements for developing the proposal with the support of UIR through its Advisory Panel.

Other activities

Advisory Panel
The objective of the Advisory Panel (chaired by R. Kirchmann) is to provide a link between political and scientific bodies and a source of information on radioecological matters to the public. Since its inception in 1994, the Panel has met three times and has discussed a number of key issues in radioecology. The Panel comprises a broad spectrum of persons representing the UIR Bureau, former UIR Presidents, and other persons chosen according to their official functions in their respective countries. Meetings have included representatives of the Ministry of Extreme Situations in Russia and the Ministry of Chernobyl in Ukraine.

Advisory Panel members have also participated in a number of meetings organised by authorities in Russia, Belarus and Ukraine, including the recent meeting at Golitsino, near Moscow, which was organised to prepare for the tenth anniversary of the Chernobyl accident, and a meeting in Kiev on International Co-operation in Nuclear Development.

SCOPE-RADPATH
The aim of this project under the auspices of the Scientific Committee on Problems of the Environment (SCOPE) was to collate information on biogeochemical pathways for the transport of artificial radionuclides in the environment. The results of SCOPE-RADPATH have been published in SCOPE 50 (above). This publication recognises the considerable contribution of UIR to the activities of SCOPE-RADPATH and contains a number of contributions by UIR members

SCOPE-RADTEST
The aim of this project is to determine the local effects of radiation exposure from nuclear weapons-testing. UIR has assisted with the organisation of three workshops (in Vienna,

Barnaul and Liege) and has provided an important mechanism for drawing together scientists from former Soviet Union countries, Europe and the USA for the exchange of information, much of which is unpublished or which has not been discussed in 'open' conditions.

UNESCO-CESN

UIR has continued to maintain contact with UNESCO during the development and implementation of the Chernobyl Ecological Sciences Network (CESN). CESN acts as a decentralised network of scientists and research institutions for the sharing of information, research facilities and training activities UIR members have participated in a number of meetings organised by UNESCO CESN and are playing an active role in stimulating the contacts and exchange of information necessary to fulfil the objectives of CESN.

BIOMOVS/VAMP

UIR members have participated actively in both the VAMP and BIOMOVS II projects, the aim of which are to provide opportunities for the testing and validation of models used to describe the transport of radionuclides through ecosystems from source to man. BIOMOVSII has continued to investigate the use of real data extracted from existing contamination situations or small scale experiments, often as a result of the activities of UIR scientists.

Final Report

Contract: FI3P-CT92-0029

Title: Towards a functional model of radionuclide transport in freshwaters.

1)	Hilton	NERC
2)	Vaz Carreiro	DGA
3)	Cremers	Univ. Leuven (KUL)
4)	Foulquier	CEA
6)	Sansone	ANPA
7)	Blust	Univ. Antwerpen (RUCA)
8)	Fernandez	Univ. Malaga (UMAG)
10)	Comans	ECN
	Forseth	NINA

Summary

Measurement and Prediction of radiocaesium distribution coefficient (K_d)

The distribution coefficient (K_d) is a fundamental parameter in mathematical models of radionuclide transport in aquatic systems. Measured values in the literature range from 10^2 to 10^5. Because of this wide range the use of an estimated K_d is very prone to error. The ion-exchange theory of sorption suggests that in the presence of a major competitor the K_d is given by:

$$K_d = \frac{K_c\,[\text{sites}]}{[M^{a+}]}$$

where K_c is the selectivity coefficient, [sites] is the number of sites in terms of equivalents per gramme of solid and $[M^{a+}]$ is the concentration in solution of the major competitor (with the same charge as the material of interest) for sites on the solid. For radiocaesium, previous work has shown that the selectivity of the so-called frayed edge sites (FES) on illite particles is so high that these sites define the sorption of caesium, even in mixed mineral systems. Under aerobic conditions K^+ is the major competing ion for these specific sites and under anaerobic conditions NH_4 competes. Studies in the present programme have focused on the extension of our understanding of the parameters defining K_d.

Because of the high selectivity of FES for Cs, it is necessary to know the FES if the K_d in any chemical scenario is to be predicted. In a previous study a complex masking technique using silver thiourea was developed. As a result of new work by KUL this method has been replaced by a single measurement of K_d in a defined medium (Ca^{2+}: 100 mM; K^+: 5 mM). Under these chemical conditions all the potassium and caesium will be confined to the FES. Hence, knowing the K^+ concentration in solution and the K_d it is possible to calculate the product K_c.[FES]. By measuring this in a series of similar, mixed Ca: K: NH_4 or Na solutions, it is possible to measure K_c.[FES] for the ammonium and sodium systems, respectively. From these constants and a knowledge of the in situ [K], NH_4] and [Na] it

was possible to predict the K_d for a range of soils and sediments to within a factor of 3 in laboratory experiments where K_d covered the range 50 - 50000 l kg^{-1}. Using the same approach, DGA/DPSR were able to predict K_d's of suspended solids and bottom sediments in field samples to within a factor of 2.

A detailed set of measurements of K_d's in sediment cores taken from a number of locations has confirmed that the ion-exchange equation is valid over a wide range of ammonia concentrations: a very good relationship is seen between log ammonium concentration and log total K_d. A similar plot of exchangeable (i.e. ammonium extractable) K_d, however, which should according to the fixation theory (see later) be a better estimate of the field K_d , gives a much lower correlation. This suggests that, contrary to expectation, over the time scale of years, the total K_d is a better predictor of Cs mobility than the exchangeable K_d.

For caesium there is a general assumption that the concentrations in natural waters are so low that it is possible to assume the simplifying conditions of trace levels, compared to the major competitor, potassium. Previously there were very few measurements of stable Cs in the literature to confirm this assumption. A study by IFE of stable Cs concentrations in 21 lakes covering a wide range of K and Ca concentrations showed that concentrations range between 1 -13 ng l^{-1} ($\equiv$0.01 - 0.1 nM) and, unlike Sr, are independent of major ion concentrations. At these levels, the assumption of trace concentrations is valid. Measurements of K_d made in the laboratory by the addition of radionuclide containing carrier Cs, however, are likely to be biased underestimates. The bias will increase with increasing amounts of carrier.

From a study of the properties of sediments taken from rivers in France, CEA showed that the Cs concentration on the solid was a linear function of the proportion of fine silt and the percentage organic matter, i.e. the K_d increased with increasing fractions of fine silts and organic matter. This is a result of a combination of the increased area available for sorption, relative to the sample weight, for fine silts and the presence of higher concentrations of illites in the smaller size ranges. The relationship with organic matter is probably a result of a co-correlation between fine silt deposition and organic matter deposition, since both need slow flowing waters to deposit. A detailed study of a single river by ENEA suggested that the total K_d can be predicted from a weighted mean of the K_d's measured on individual size fractions.

Reversibility of caesium and strontium sorption

On the basis of frayed edge site studies it appears to be possible to predict values of radiocaesium K_d after short equilibration times (24 hours). Following a fallout event, however, caesium slowly moves to less available sites on the solid phase, a process commonly known as "fixation". Desorption studies were carried out by DGA/DPSR on sediments spiked with ^{90}Sr and ^{137}Cs and then left for a period of three days. After this time, it was found that all of the strontium could be removed from the solid by a concentrated solution of a competing ion (Ca^{2+}), but that only 40-50% of the caesium was removed by one of its competitors (K^+), implying "fixation" of 50-60% of the caesium. Further studies showed that after 4 days adsorption in solutions containing different competing ions, fractions of ^{137}Cs in the fixed phase were 20-35% in K^+ solution, 40-55% in Na^+, and 60-75% in Ca^{2+} solution. It appears that the poorly hydrated ions competing with Cs for the FES (K^+, NH_4^+) also inhibit transfers to fixed sites.

Measurements of radiocaesium in the environment, mainly resulting from the Chernobyl accident and thus aged for around 7 years, were carried out by ECN and IFE. It was found that in freshwater sediments only 1-10% of the ^{137}Cs could be desorbed by an ammonium acetate extraction. After removal of all of the exchangeable ^{137}Cs, two of the sediments were then left in ammonium acetate solution for one year. After this period it was found that a further 1-2% of the ^{137}Cs was de-sorbed from the solid, implying that there is a slow transfer of activity from the so-called "fixed" phase back into solution. An approximate rate constant for the reverse reaction was calculated from these data, giving a half-life for the transfer of around 80 years.

It appears, then, that the "fixation" of ^{137}Cs is not a truly irreversible process. Short term (timescale days) laboratory desorption experiments can give a measurement of that fraction of the radiocaesium which is available for transport and uptake by biota on a similar timescale. On longer timescales (years-decades), however, it is necessary to take account of the slow movement of ^{137}Cs to and from "fixed" sites.

Transfers of radiocaesium across the sediment-water interface

A model based on the advection-diffusion equation has been developed by IFE and ECN to determine the mobility of radiocaesium in the bottom sediments of lakes and rivers. In many freshwater systems the bottom sediments act as an important sink for radionuclides since activity in the water column accumulates in the sediments via the settling of suspended particles or direct diffusion across the sediment-water interface. Settling of contaminated particles is relatively simple to measure using sediment traps, or calculating mass accumulation of bottom sediments. The direct diffusion process, however, is controlled by the thickness of the benthic boundary layer, a thin layer of laminar flow water overlying the sediment. To our knowledge, few measurements of this boundary layer have been made in lakes. A method has been developed to measure this layer both *in situ* using gypsum plates, and by studying the diffusion of ions to sediments in an experimental flow chamber. *In situ* measurements in Esthwaite Water, UK gave a value of 0.43 mm for the boundary layer thickness, of the same order as suggested from a model of radiocaesium removal from Devoke Water. In the experimental chamber it was shown that boundary layer thickness varied between 0.27-0.56 mm, and was inversely proportional to the mean velocity of the overlying water.

Previous work has shown that radiocaesium may be remobilised from bed sediments, particularly when sediments become anoxic, resulting in high ammonium concentrations. The model takes account of changes in short-term K_d as ammonium concentrations change down the sediment profile, and of long term movement of activity to and from "fixed" sites. Model predictions showed that remobilisation of activity from Hollands Diep and Ketelmeer sediments resulted in loss rates of around 2.5% of the sediment inventory per year shortly after the Chernobyl accident, and around 0.15% per year 30 years after the accident. In agreement with the experimental studies, it was found that in order to fit the observed field data, it was necessary to include a rate constant for transfers of activity from the fixed phase. The model fitted value of this constant gave a half-life for this process of around 10 years, lower than, but of the same order as the experimentally determined value.

Mechanisms and models of radionuclide transfer in aquatic food chains

The objective of this part of the project was the study of the kinetics and mechanisms of radionuclide uptake and accumulation in aquatic plants and animals. Special attention was given to the effects of environmental conditions on these processes. The results have been used to construct mechanistic models for the accumulation of radionuclides by aquatic organisms which can account for the effects of chemical speciation and ionic composition on the accumulation of the radionuclides in aquatic organisms. The results reported here are based upon the complementary work performed by the five groups participating in the biological part of the project. The work consisted of three work packages which together provided new insights into the mechanisms of radionuclide uptake and transfer in aquatic ecoystems. Most studies were performed with caesium or cobalt as model radionuclides. The information provides the basis for the development of a new generation of models for the prediction of the transfer of radionuclides in aquatic food chains. Briefly, the work packages dealt with the following:

1 Development of mechanistic models for the uptake of radionuclides in plants and animals.Experimental characterisation of the transport systems involved in the translocation of radionuclides across biological interfaces (RUCA/UMAG)..

2.Determination of the effects of environmental and metabolic factors on the accumulation of radionuclides by aquatic plants and animals. Special attention was paid to key factors such as ion composition, complexation capacity and temperature (DGA/NINA/RUCA/UMAG)..

3. Determination of the transfer of radionuclides in model food chains to determine the relative importance of water and food in different environments. Effect of metabolic activity and growth rate on radionuclide accumulation in top level predators (CEA/DGA/NINA)..

Radionuclide uptake depends on the biological availability of the radionuclides in the environment and the systems involved in the uptake of the radionuclide by the organisms. To model the effects of environmental conditions on the chemical speciation of radionuclides a model was developed which allows the calculation of the activities of radionuclide species in aquatic environments taking into account the effects of changes in ionic compositin and complexation capacity on the behaviour of the radionuclides in the environment. The model has been used to predict the effect of changes in water composition on the biological availability of radionuclides. In general only the free metal ion appears to be taken up by aquatic organisms. Much of the variation observed in radionuclide uptake from water is explained when uptake is expressed on a free metal ion activity scale rather than a total metal activity scale.

Radionuclides do not permeate biological interfaces by simple permeation but require gating systems which facilitate their uptake. For caesium, potassium channels and for strontium and cobalt, calcium channels have been implicated to be the major pathways for uptake of the radionuclides. Within the framework of this project it has been shown that indeed these channels are involved in the uptake of these radionuclides by a variety of aquatic organisms. Based upon a fundametal appreciation of the processes being

involved. a model has been developed to account for the effect of environemtal conditions on the accumulation of caesium and cobalt.

The effects of key environmental conditions on the uptake of caesium was studied in *Riccia fluitans* as a model plant and *Cyprinus carpio* as model animal. As expected caesium was taken up by a potassium transport system. The results of the experimental work were used to construct a mechanistic model from which radiocaesium concentration factors in freshwater plants can be predicted as function of the potassium concentration in the water. The models considers two systems for the uptake of potassium. One is opperative under potassium limitation and one when potassium supply is not a constraint. In the latter case, radiocaesium is accumulated by plants through potassium channnels. The concentration of caesium in plants reached at equilibrium is determined by the electrochemical potential gradient which exists across the membrane interface and can be predicted from the Nernst equation. The cellular caesium concentration reaches equilibrium when the Nernst potential for caesium equals the membrane potential. Thus, the concentration factor of caesium in plants can be predicted from the membrane potential which in turn depends on the concentration of potassium in the environment. When potassium concentrations in the environment are limiting, an active system is invoked which has a higher affinity for caesium then the channel system. In this case, uptake displays saturation kinetics which can be described by a Michaelis-Menten type transport model. The same approach has been used to describe the uptake of caesium and other radionuclides by fish, which present the highest trophic level. In fish the situation is somewhat more complex since radionuclides are accumulated from both water and food sources but the principals remain the same. To model the accumulation of radionuclides by aquatic plants and animals a clearance constant based pharmacokinetic model has been developed which uses membrane transport kinetics to describe the fluxes of the radionuclides in an out of the organisms. The model accounts for the effect of changes in chemical speciation on the biological availability of the radionuclides and the selectivity of the transport systems involved in the uptake of the radionuclides.

The effect of environmental conditions such as dissolved organic carbon, water ion composition and temperature have been determined under a variety of conditions in experimental food chains. These experiments provided essential information on the long term accumulation kinetics and relative importance of water and food at different trophic levels. These food chains include a variety of plant and animal species, i.e. unicellular algae, insects, crustaceans and bivalves and different fish. The results of the uptake and accumulation experiments have been combined to construct mechanistic models from which the effect of environmental conditions on the accumulation kinetics can be predicted. For each trophic level information is required on the absorption efficiencies, feeding rates, growth rates and excretion rates. Effects of environmental conditions on absorption efficiencies from water and food are described by membrane transport models. As such these models provide truely mechanitic descriptions that can be used to model the long term fate of radionuclides in aquatic food chains under combinations of conditions that have not been studied experimentally.

For example, experiments conducted concerning the uptake of caesium by *Chondrostoma* under different potassium and caesium regimes showed that the model developed for the interaction between potassium and caesium almost perfectly

described the observed variation in Cs accumulation under the different exposures regimes. Similar results were obtained for the interaction between calcium and cobalt to explain the variation in cobalt accumulation by *Cyprinus*.

In conclusion, this project has cumulated in the development and experimental validation of a set of mechanistic models for the uptake and accumulation of radionuclides in aquatic organisms of distinct structural and functional organisation. The results obtained prove that it is possible to integrate the different models into one robust system that can be used to predict the fate of radionuclides in entire food chains. Although it has been shown that the approach works for some plants and fish under a variety of conditions, essential information is still lacking concerning the kinetics of radionuclide uptake at intermediate trophic levels to allow the construction whole food chain pharmacokinetic models.

Head of project 1: Dr. J. Hilton

II. Objectives

(a) To measure the rates of diffusional transport of radionuclides from water to bottom sediments and the mobility within, and remobilization from, contaminated sediments.

(b) To assess the influence of stable Sr and Cs concentrations on the solids/aqueous distribution of their radioactive isotopes, and to relate these to the concentrations of competing ions.

III. Progress achieved including publications

(a) Studies on the sediment/water interface

The transfer of radioactive pollutants into and out of the bottom sediments of lakes and rivers occurs both in the solid phase by the sedimentation and resuspension of particles, and in the aqueous phase, by the diffusion of ions across the sediment/water interface. The importance of diffusive transfers, however, is not yet well understood. The aim of our work was to quantify this latter process by measuring the thickness of the benthic boundary layer, a thin layer in which the flow is laminar or stagnant, so that vertical transport within the layer occurs only by molecular diffusion. Based on these measurements, a model has been developed (in collaboration with ECN) for the remobilisation of ^{137}Cs from freshwater sediments.

The boundary layer has been measured in two ways: the first using the rate of dissolution of gypsum plates to make an *in situ* estimate in Esthwaite Water, Cumbria, and the second using a flow chamber to assess the effects of flow rate on the boundary layer thickness.

Gypsum Plate Method

The gypsum plates were made by heating gypsum ($CaSO_4.2H_2O$) at 130 °C for 5 hr to form $CaSO_4.(1/2H_2O)$. This was then mixed with water at a ratio of 5 parts $CaSO_4.(1/2H_2O)$ to 3 parts water (by weight) forming a smooth paste. Small (5.2 cm diameter) petri dishes were then filled with the paste until a clear meniscus was seen over the rim of the dish. The dishes were then dried at 40 °C for 24 hr, then smoothed to a flat surface with coarse sandpaper. Residual dust was removed by blowing compressed air over the surface of the plates, before returning them to the oven for a further 24 hr. Apparatus holding 7 plates was constructed to lower the plates to the sediment surface, a moveable lid being used to protect the plates during deployment and retrieval of the apparatus. This apparatus was deployed in Esthwaite Water, Cumbria, the boundary layer thickness being calculated from the rate of dissolution of the plates over a 50 hour period. Results showed that the mean boundary layer thickness was 430μm, within the range 370-2000μm obtained by other workers using both this method and benthic flux chambers (Santschi *et al.* 1983; Hesslein 1987; Devol 1987).

Flow chamber studies

An experimental flow chamber (see Fig. 1) has also been used to study chemical fluxes across the sediment/water interface under controlled conditions (House *et al.* 1995). Because of radiation safety regulations, it was not, at that time, possible to use a radioactive element in this experimental setup, so a stable isotope, the phosphate (HPO_4^{2-}) ion was used. A spike of phosphorus was added to the water overlying the sediment, and aqueous phosphorus concentrations were measured as the phosphorus was absorbed by the sediment over a 24 hr period. The experiment was carried out for different flow rates of the overlying water.

The diffusive flux, *F*, across a boundary layer of thickness z is proportional to the concentration gradient across the boundary, leading to the following equation for the change in water concentration over time (House *et al.* 1995):

$$C_w = C_w(0)\,e^{-kt} + C_i(1 - e^{-kt}) \qquad (1)$$

where

$$k = \frac{D_0}{z\bar{d}} \qquad (2)$$

and C_w is the water concentration, z the boundary layer thickness, $\bar{d}$ the mean depth of water, and D_0 the diffusion coefficient of the HPO_4^{2-} ion.

Equation (1) was fitted to the measurements of C_w vs time by varying the unknown boundary layer thickness, z to give the best least squares fit to the data (Fig. 2). It is clear from Fig. 2 that the flux to the sediments is increased at higher water flow velocities. Fig. 3 shows a clear linear proportionality (correlation coefficient $R^2 = 93.1$ %) between the best fit boundary layer thickness and the inverse of the flow velocity. The intercept of the regression line is not significantly different to zero, so we can write:

$$z \approx \frac{2500}{v} \qquad (3)$$

where z is measured in μm and v is the mean flow velocity in cm/s.

A further experiment was carried out in order to compare boundary layer estimates from the phosphorus flux model with those obtained using gypsum plates. Four gypsum plates were placed in the flow chamber so that their surfaces were level with the surface of the sediment. The plates were left to dissolve into the flowing water for a period of 98 hrs, then removed and the loss of gypsum calculated to give a boundary layer estimate of 380 μm, in reasonable agreement with the phosphorus flux measurements.

FIGURE1.
Fluvarium channel for bed-sediment flux studies.

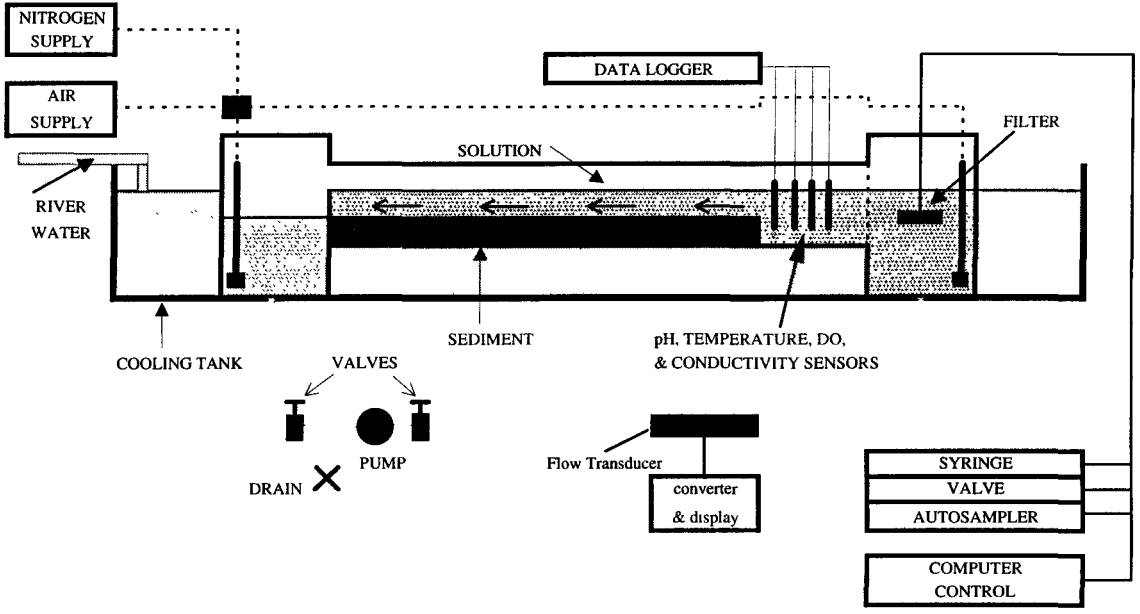

FIGURE 2

FIGURE 3

Modelling diffusional removal to bottom sediments.

A simple box-type model has been used to analyse data on aqueous ^{137}Cs concentrations in Devoke Water, Cumbria for several years following the Chernobyl accident. It was found that, in the long term (90 days - 6 years) after the accident, the concentrations of ^{137}Cs in the water column can be explained by measurements of inputs from the catchment (Hilton *et al.* 1993), and by flushing of the lake. In the initial period, however, there is a significant loss of dissolved activity to the sediments which cannot be explained by particulate settling alone. The results suggest that this is due to diffusional uptake by the bottom sediments across a boundary layer of thickness around 1000 μm, of the same order as that obtained in the experimental studies.

Modelling remobilisation from contaminated sediments.

Clearly, diffusional fluxes across the boundary layer are not constant with time, but will change as the concentration gradient across the boundary changes. As ^{137}Cs builds up in the sediment pore waters, the diffusional uptake will reduce, and this may lead to remobilization of activity from sediments back into the water column, particularly during periods where sediments become anoxic. In collaboration with ECN a model has been developed to predict changes in ^{137}Cs concentration in aqueous, exchangeable and fixed phases within the sediment, and rates of remobilisation to the water column.

Let C_w ($Bqcm^{-3}$) represent the radiocaesium activity in the aqueous phase, C_s (Bqg^{-1}) the exchangeably sorbed activity and C_f (Bqg^{-1}) the activity which is "fixed" in the mineral lattice (see Fig.). The aqueous $\Leftrightarrow$ exchangeable reaction is believed to be of order minutes, so that these two phases can be assumed to be in instantaneous equilibrium with distribution coefficient

$$K_d^e = \frac{C_s}{C_w}. \qquad (4)$$

It has been shown that the ammonium ion directly competes with ^{137}Cs for exchange sites on clay minerals. We have therefore assumed that the K_d^e varies with depth in inverse proportion to the ammonium concentration, C_{NH4}:

$$K_d^e(x) = K_d^e(0)\frac{C_{NH4}(0)}{C_{NH4}(x)}. \qquad (5)$$

Transfers of activity to and from the "fixed" phase are modelled by first-order rate constants k_f, k_b (s^{-1}). The final phase is termed "fixed" since on the timescale of most laboratory sorption/desorption experiments (weeks-months) no reverse reaction has been determined, although it will be shown that there is evidence to suggest that the reaction is reversible on a timescale of several years.

The equations describing the transport of trace elements in sediments have been described

elsewhere (Berner 1980). Full details of modelling methods and assumptions can be found in Smith & Comans (1995), so a brief outline only will be given.

In the coupled aqueous/exchangeable phase, transport occurs both by diffusion in the sediment pore waters, and by advection as sediment layers accumulate. These processes are described by:

$$\frac{\partial C_e}{\partial t} = \frac{\partial}{\partial x}\left[\phi\psi D_0 \frac{\partial}{\partial x}\left(\frac{C_e}{\phi + sK_d^e(x)}\right) - rC_e\right] - k_f C_e + k_b s C_i - \lambda C_e. \quad (6)$$

where D_0 is the diffusion coefficient of the free ion in water ($1.45 \times 10^{-5} cm^2 s^{-1}$ at $10\,^0C$), ϕ is the porosity of the sediment and r the (constant) mean sedimentation rate (cms^{-1}). ψ is a dimensionless factor (< 1) to take account of the tortuosity of path an ion must follow in diffusing through the sediment. Tortuosity is estimated by

$$\psi \approx \phi^2. \quad (7)$$

The transport of activity in the fixed phase is described by:

$$s\frac{\partial C_i}{\partial t} = -sr\frac{\partial C_i}{\partial x} + k_f C_e - k_b s C_i - \lambda s C_i. \quad (8)$$

For the case of diffusion across the upper boundary, the boundary condition is:

$$F_e(0,t) = -\phi\psi D_0 \frac{\partial}{\partial x}\left(\frac{C_e}{\phi + sK_d^e}\right) + rC_e(0,t) - \frac{D_0}{z}\left(\frac{C_e}{\phi + sK_d^e} - C_a\right) \quad (9)$$

where z is the thickness of the non- turbulent flow "boundary layer" and C_a the concentration in the water column. For the fixed phase the condition is

$$F_i(0,t) = rsC_i(0,t) \quad (10)$$

where $F_e(0,t)$ is the flux of activity to the sediment in the aqueous/exchangeable phase, and $F_i(0,t)$ the flux in the "fixed" phase. The above equations are solved by a simple explicit finite-difference method. Computer codes were written in FORTRAN and run on a SUN workstation. Inputs to the sediment from the Chernobyl event were modeled using a smoothed short duration spike, those from the weapons fallout followed the history of atmospheric depositions, a smoothed spike corresponding to the relative deposition (corrected for decay) being input each year. Activities were scaled to the total inventory of each profile.

Fig. 4 Ketelmeer Cs-137. Model fits shown as solid lines.

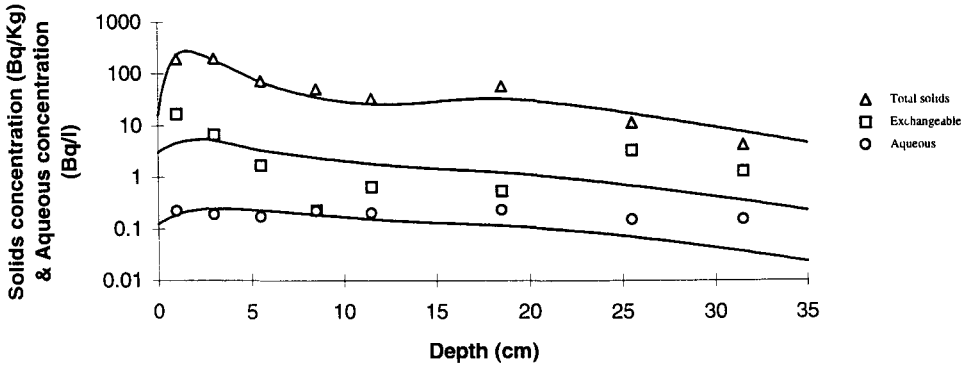

Model results

The above model was applied to measurements of ^{137}Cs concentrations in the aqueous, exchangeable, and fixed phases of the sediments of two Dutch lakes, Ketelmeer and Hollands Diep. Parameter values were varied to get the best chi-squared fit to the data. Fig. 4 shows the best model fit to the measurements from Ketelmeer.

The transport of activity to less-exchangeable sites on illites has been demonstrated in many ^{137}Cs sorption experiments and the forward rate constants, k_f, estimated by the model fits ($T_{1/2}$= 50 and 125 d) are in good agreement with experimental observations of 35-150 d (Comans & Hockley 1992) and with an estimate of 100d made by Comans & Hockley (1992) from data obtained by Evans and co-workers (Evans *et al.* 1983). Because of the very long timescale on which it operates, a reverse rate constant for this reaction has not been established experimentally, although exchangeable ^{137}Cs has been found in sediments more than 15 years after the contamination event (Evans *et al.* 1983). Using the exchangeability measurements made by Evans & co-workers (85% "fixed", 15% exchangeable), and a forward rate constant of half-time 100d, we calculate a reverse rate constant, k_b, of half-time around 600 days. This is lower than, but of the same order as, our model estimates of 3000 and 4000 days for Ketelmeer and Hollands Diep respectively.

Values of the boundary layer thickness, z we have measured and obtained from a literature survey range between 0.37 and 2.0 mm (Santschi *et al.* 1983; Hesslein 1987; Devol 1987). Within this range, the remobilisation flux did not vary significantly since, on the timescales of interest here, remobilisation is limited by diffusion rates within the sediment rather than across the boundary layer. Using the best-fit parameters, and assuming that $C_a = 0$ (ie giving a maximum estimate) we have made tentative predictions for remobilization rates resulting from the Chernobyl fallout event for times between 1 and 30 years after the time (1.5y after the accident) at which the cores were taken. Remobilization rates, quoted as a percentage of the core inventory at the time of coring, for Hollands Diep changed from 2.8% per year after 1 year to 0.2% per year after 30 years, and for Ketelmeer from 2.4% per year after 1 year to 0.1% per year after 30 years.

(b) Stable Cs and Sr concentrations in freshwaters in Northern England and their effect on estimates of sorption coefficients (K_d).

When simple ion exchange is the dominant mechanism of sorption, the K_d can be incorporated into the standard ion exchange equation by making the simplifying assumption that the concentration of the sorbing material of interest is very small compared to the competing major ion concentration, (see Comans et al, in press, for the derivation), so that:

$$K_d = \frac{K_c[sites]}{[M^{a+}]} \qquad (11)$$

where K_c is the selectivity coefficient, [sites] is the number of sites in terms of equivalents per gramme of solid and $[M^{a+}]$ is the concentration in solution of the major competitor (with

the same charge as the material of interest) for sites on the solid. A number of studies have found results in agreement with this equation. For example, Comans et al. (1989) confirmed an inverse linear relationship between log K_d^{Cs} and log ammonium ion concentrations in anaerobic sediments.

If radionuclides in the natural environment were carrier free the assumption of trace status would be irrefutable. However, almost all radionuclides have stable analogues, naturally occurring in the environment. Since the concentration of these stable isotopes is considerably higher than the radionuclide concentration, it is possible that the assumption of trace status is not entirely valid. Concentrations of stable caesium and stable strontium were measured in lake waters covering a range of major ion chemistries and the concentrations were compared with the major ions and with measured K_d .

Surface water samples and sediment cores were taken from twenty lakes in the North of England. The lakes were chosen to give as wide a range of potassium and calcium concentrations as possible, in fresh waters. A sub sample of filtrate was analysed for major cations by atomic absorption spectroscopy using a Perkin Elmer instrument. Further subsamples of filtrate were acidified and analysed by ICPMS for stable strontium caesium.

Sediment samples were taken using a Jenkin corer (Ohnstad and Jones, 1982). The core was extruded in the field and the top 1 cm slice was stored in a plastic bag for transport to the laboratory. A sub sample of each sediment was dried at 60°C and the percentage dry weight detemined. K_d measurements were performed as follows: 10 mg of wet sediment was conditioned for 24 hours in 15 ml (≡650 mg/l wet suspended solids) filtered surface water from the same lake. The samples were centrifuged and the pellet dispersed in clean lake water containing a spike of 25 kBq Cs-134 and 25 kBq Sr-85. Samples were agitated for 24 hour. The solid and liquid were then separated by filtration through a 0.45 um membrane filter and the activity on the solid and in the liquid was determined by gamma spectoscopy on a Canberra Packard spectrometer. It was not possible to obtain carrier free samples of these isotopes. Specific activities of the two radioactive isotopes were 431 MBq / mg for Cs-134 and 278 MBq / mg for Sr-85. With the additions used in these experiments, the resulting additional stable isotope concentrations were 3.87 ug/l (29 nM) and 6 ug/l (67 nM) for Cs and Sr repectively.

Stable Cs and Sr concentrations.
Stable strontium concentrations range from 8 - 214 ug/l, which are consistent with values in the literature. A good linear relationship was observed between stable strontium concentrations and the sum of Mg and Ca (stable Sr v (Ca + Mg), i.e. Sr = 0.1166 + 0.6438 (Ca + Mg), (R^2 = 0.825) where the concentrations of (Ca + Mg) and Sr are in mM and uM respectively.

Stable Cs levels in the Northern English lakes varied from 1.3 to 13.5 ng/l. The authors could only locate one publication reporting a value for stable caesium in freshwaters. Seelye (1975) measured concentrations in one lake using activation analysis and reported values of a few ng/l. This is consistent with our data. Unlike the situation for Sr, there appears to be no relationship between stable Cs and any of the major ions or ammonium. A plot of stable caesium versus potassium is given in figure 5.

The effect of stable isotope concentrations on the K_d.
If the assumption of trace radionuclide is not made, i.e. Cs or Sr atoms cover a significant proportion of the exchange sites, then the following equation can be derived (a similar equation holds for Ca^{2+} competition for Sr^{2+}:

$$K_d^{Cs} = \frac{K_c(Cs/K) \cdot FES}{([K^+] + K_c(Cs/K)\,[Cs^+])} \qquad (12)$$

From direct measurement De Preter (1990) reported K_c - Cs^+/K^+ = 1000 for illite. For the sampled sites, K_c (Cs/K) $[Cs^+]$ has been calculated as a proportion of the potassium concentration. Over the range of ionic concentrations observed in this study stable caesium contributes no more than about 1% to the variation in K_d. Hence it is reasonable to assume trace levels in their effect on K_d. Equivalent calculations for Sr^{2+} using K_c (Sr / Ca) = K_c (Sr / Mg) = 1 from a compilation of selectivity coeficients presented by Burggenwert and Kamphorst (1982) show that the maximum value of K_c (Sr/Ca). $[Sr^{2+}]$ is 0.26%. Hence, the trace assumption for stable Sr in natural waters is also reasonable. However, it is worthy of note that, because of the high selectivity of the frayed edge sites for caesium, nanomolar concentrations of caesium are comparable with millimolar concentrations of potassium. In comparison, uM concentrations of Sr have much less effect as a result of its low selectivity coefficient with respect to mM Ca concentrations.

Under the laboratory conditions created by the presence of extra stable Sr due to the carrier (equivalent to 6 ug/l = 67nM) in the determination of K_d , the addition is relatively small compared to the naturally occuring conditions (see above) and the trace assumption still holds. For Cs the high selectivity coefficient relative to K extenuates the effect of carrier Cs (an addition equivalent to 3.87 ug/l = 29 nM) in the laboratory conditions of K_d measurement. This additional concentration of Cs in solution {average = 15nM: $[Cs]_{soln} = [Cs]_{added} / (1 + K_d$ SS), where SS is the suspended solids in the laboratory measurement in kg dry solid l^{-1}} is orders of magnitude greater than the natural concentrations (1-14 ng/l = 0.01-0.102 nM). When the dissolved Cs concentration is multiplied by the selectivity coefficient a factor results which, in many cases, is several times greater than the potassium concentration. As expected from theory there is a reasonable negative relationship between log [K] and log K_d^{Cs} (figure 6a) with an R^2 value of 0.55. However, inclusion of the stable Cs term at a total additional concentration of 29 nM raises the R^2 for the plot of log K_d versus log {[K] + K_c (Cs/K). $[carrier\ Cs]_{soln}$}to 0.67 (figure 6b). There is an accompanying increase in slope, from -0.69 for potassium alone to -0.87, which is very close to the theoretical slope of -1. About 8% of the total variability is accounted for by the inclusion of K_d into the right hand side of the equation, 2% is due to differences in the water content of the wet sediment used in the laboratory measurements. The other 2% is due to either or both effects and indicates a small co-varience between the K_d and dry solids content.

In order to assess the influence of any ion, other than the primary competitor, on the K_d it is necessary to define the K_d in terms of both the primary and the secondary competitors. Sweeck et al. (1990) proposed a method for achieving this for homovalent competition. An alternative, simpler, derivation was used to obtain a similar equation to (12) for homovalent competition and the method was extended to include divalent - monovalent competition.

Manipulation of data from Brouwer et al., (1983) gives: K_c-(M^{2+}/K^+) = 2.445 x 10^{-10}; K_c-(Na^+/K^+) = 0.015. From De Preter (1990) K_c -NH_4^+/K^+ = 5.85. The bivalent cation - potassium selectivity is so low that bivalent cations have no effect on the K_d for caesium. The concentrations of the secondary competing ions multiplied by the selectivity coefficient with respect to potassium were calculated as a proportion of the potassium concentration. Over the range of chemical conditions found in this study, sodium ions should be as important as potassium in determining the K_d and, even under aerobic conditions, ammonium ions can be dominant. As shown above log-log plot of K_d^{Cs} versus potassium has R^2 = 0.55. Regressions of log ammonium concentration and log sodium concentration versus log K_d separately show weak correlations with R^2= 0.21 and 0.26 respectively. When combined with the potassium concentrations using an extension of equation 1 the regression shows only a marginal improvement (R^2 = 0.57). If the equation includes the additional stable Cs present in the K_d measurement R^2 reduces from 0.67 to 0.63. The implication is that the cumulative errors attained, at this level of complexity in the model, are larger than the effect itself over the relative narrow range of secondary competitor concentrations observed here.

In a review of K_c values for standard ion exchange sites on soils, Bruggenwert and Kamphorst (1979) quoted: K_c (K^+/Ca^{2+}) = 2.04 ; K_c (Na^+/Ca^{2+}) = 0.40 ; K_c (NH_4^+/Ca^{2+}) = 2.04 ; K_c (Mg^{2+}/Ca^{2+}) = 1.01. The coefficients show a much narrower range than those compared to K on frayed edge sites and are within about a factor of 2 above and below 1. As a secondary competitor, Mg follows the simple homovalent equation and contributes about 30% to the total K_d , and, since K_c (Mg/Ca) = 1, the sum (Ca + Mg) can be considered as a single ion. A plot of log K_d^{Sr} v log (Ca + Mg) shows (figure 7) a very high correlation (R^2 = 0.83) with a slope of 0.59. The slope is a little lower than the predicted slope of 1. All three monovalent competitor ions show much lower contributions than would have been the case if the homovalent equation had been valid. Ammonia contributes less than 1% to the K_d compared to Ca. The contribution of K is normally less than 2% and Na is normally contributes less than 50 % compared to Ca. Na, K and NH_4 all show lower correlations with K_d^{Sr} when plotted on log-log form (R^2 = 0.52, 0.32 and 0.26 respectively). Because of the heterovalent form of the competition between Ca and the three monovalent ions (NH_4 , K and Na) it is not possible to develop a simple, single equation to combine all three effects in the same way as is possible for homovalent competition. However, NH_4 and K are likely to have very little effect on the K_d. A plot of the heterovalent combination of (Ca + Mg) and Na has much lower R^2 (=0.529) than the R^2 for (Ca + Mg) alone. This probably results from the cumulative errors outweighing the effect of Na.

It is clear from this study that the nanogram per litre stable Cs concentrations measured in the natural environment are 3 - 4 orders of magnitude lower than the microgram per litre concentrations of stable Sr measured in the same samples. However, because of the large selectivity of Cs with respect to potassium at the FES, very small quantities of stable Cs can affect the value of the K_d . Although no effect was observed in the natural environment, up to 12% in the variability of the measured K_d could be due to this effect under the measurement conditions used in our experiments, where stable carrier was added with the radio-isotope. Conversely, stable Sr carrier showed no such effect due to its much lower selectivity coefficient with respect to Ca at normal ion exchange sites. These data suggest that, for Cs but not for Sr, the use of non-carrier free isotopes in laboratory measurements can result in both increased variability and under-estimation of the K_d. In addition, it appears that, for the range of secondary competitor concentrations covered in this study, the variability of measured K_d's is much greater than the effect of secondary competition in aerobic samples.

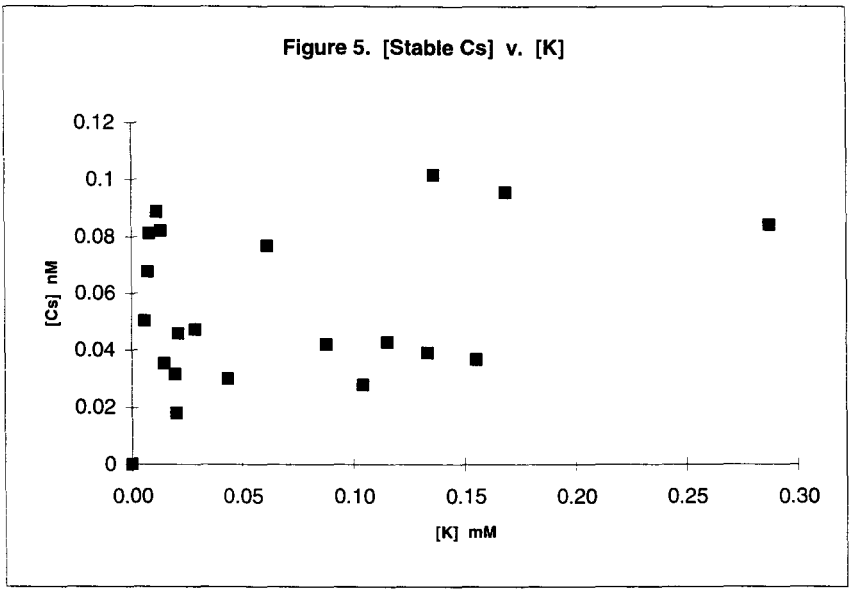
Figure 5. [Stable Cs] v. [K]
0.12
0.1
0.08
0.06
0.04
0.02
0
[Cs] nM
0.00
0.05
0.10
0.15
0.20
0.25
0.30
[K] mM

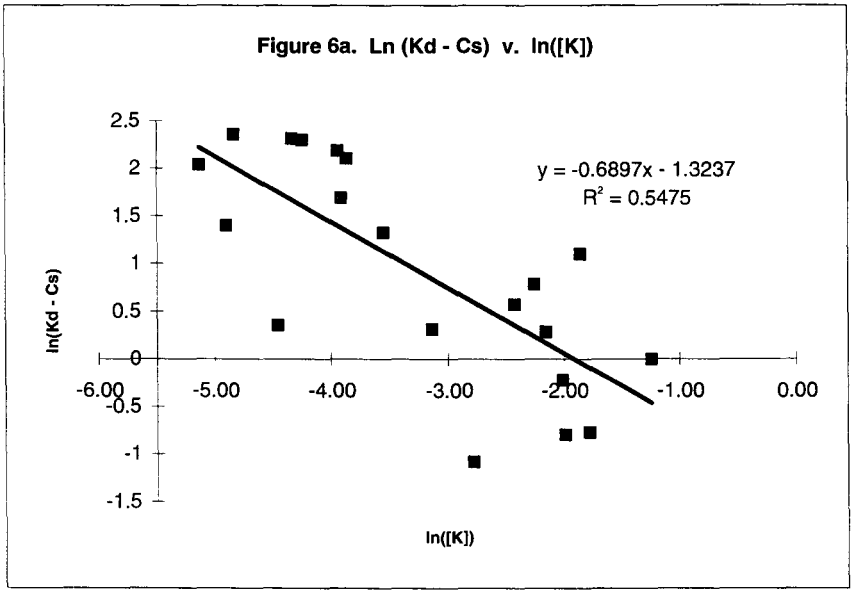
Figure 6a. Ln (Kd - Cs) v. ln([K])
y = -0.6897x - 1.3237
R² = 0.5475
2.5
2
1.5
1
0.5
0
-0.5
-1
-1.5
ln(Kd - Cs)
-6.00
-5.00
-4.00
-3.00
-2.00
-1.00
0.00
ln([K])

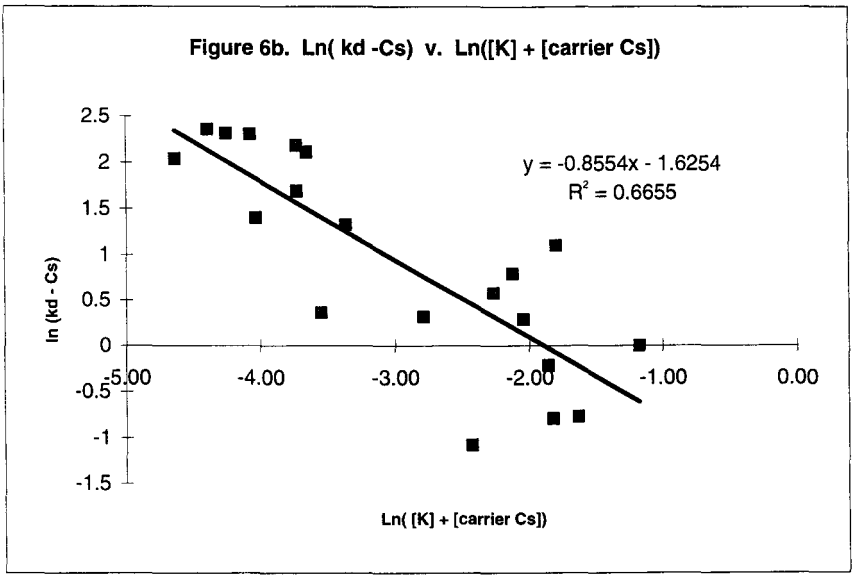
Figure 6b. Ln(kd -Cs) v. Ln([K] + [carrier Cs])
y = -0.8554x - 1.6254
R² = 0.6655
ln (kd - Cs)
Ln([K] + [carrier Cs])
2.5
2
1.5
1
0.5
0
-0.5
-1
-1.5
-5.00
-4.00
-3.00
-2.00
-1.00
0.00

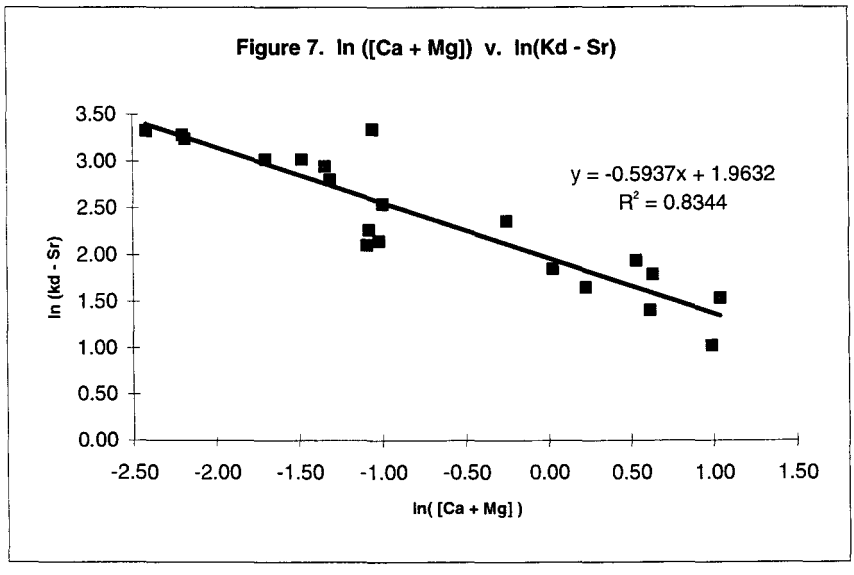
Figure 7. ln ([Ca + Mg]) v. ln(Kd - Sr)
y = -0.5937x + 1.9632
R² = 0.8344
ln (kd - Sr)
ln([Ca + Mg])
3.50
3.00
2.50
2.00
1.50
1.00
0.50
0.00
-2.50
-2.00
-1.50
-1.00
-0.50
0.00
0.50
1.00
1.50

References

Berner R.A. (1980) *Early diagenesis.* Princeton University Press.

Brouwer E., Baeyens B., Maes A., and Cremers A. (1983) Cesium and rubidium ion equilibria in illite clay. *J. Phys. Chem.* **87,** 1213-1219.

Bruggenwert, M.G.M and A.Kamphorst. (1979) Survey of experimental information on cation exchange in soil systems. in "Soil Chemistry, B. Physico-chemical models" Ed. G.H.Bolt. Developments in soil Science. Elsevier, Amsterdam, New York.

Comans R.N.J., Middelburg J.J., Zonderhuis J., Woittiez J.R.W., De Lange G.J., Das H.A., Van Der Weijden C.H. (1989) Mobilization of radiocaesium in pore water of lake sediments. *Nature* **339,** 367-369.

Comans R.N.J. and Hockley D.E. (1992) Kinetics of cesium sorption on illite. *Geochim. Cosmochim. Acta* **56,** 1157-1164.

Comans R.N.J., Hilton J., Cremers A, Geelhoed-Bonouvrie P.A., Smith J.T. (1995) Predicting radiocaesium ion-exchange behaviour in freshwater sediments. *Submitted for publication.*

Devol A.H. (1987) 'Verification of flux measurements made with in situ benthic chambers' Deep-Sea Res. 34 Nos. 5/6, 1007-1026.

Evans D.W., Alberts J.J., Clark R.A. (1983) Reversible ion-exchange fixation of cesium-137 leading to mobilization from reservoir sediments. *Geochim. Cosmochim. Acta* **47,** 1041-1049.

Hesslein R.H. (1987) 'Whole-lake Radiotracer Movement in Fertilized Lake Basins' Can. J. Fish. Aquat. Sci. 44 (suppl. 1), 74-82.

Hilton J., F.R. Livens, P. Spezzano and D.R.P. Leonard, (1993) 'Retention of radioactive caesium by different soils in the catchment of a small lake.' Sci. Tot. Env., 129 253-226.

House W.A., Denison F.H., Smith J.T., Armitage P.D. (1994) 'An investigation of the effects of water velocity on inorganic phosphorus influx to a sediment' (in press, J. Environ. Pollut.)

Ohnstad, F.R. and J.G.Jones (1982) The Jenkin surface mud sampler (a users manual). Freshwater Biol. Assoc. Occ. Publ. no.15.

de Preter, P. (1990) Radiocaesium retention in the aquatic, terrestrial and urban environment: a quantitative and unifying analysis. Ph.D thesis. Katholieke Universiteit, Leuven.

Santschi P.H., Bower P., Nyffeler U.P., Azuedo A., Broecker W.S. (1983) 'Estimates of the resistance to chemical transport posed by the deep sea boundary layer' Limnol. Oceanogr. 28 No. 5, 899-912.

Seelye, J.G. (1971) A measurement of low level caesium isotope concnetrations in a freshwater lake. U.S. Atomic Energy Commission Report Coo-1975-7, 38p.

Smith J.T. & Comans R.N.J. (1995) 'Modelling the diffusive transport and remobilisation of ^{137}Cs in sediments: the effects of sorption kinetics and reversibility' Geochim. et Cosmochim. Acta (accepted for publication).

Sweeck, L., J.Wauters, E.Valcke and A.Cremers. (1990) The specific interception potential of soils for radiocaesium, in: "Transfer of radionuclides in Natural and Semi-natural environments." 249-258. Ed. G.Desmet, P.Nassimbeni and M.Belli. Elsevier Applied Science.

List of publications

Hilton J., F.R. Livens, P. Spezzano and D.R.P. Leonard, (1993) 'Retention of radioactive caesium by different soils in the catchment of a small lake.' Sci. Tot. Env., 129 253-226.

Davison, W., Hilton J., Hamilton-Taylor, J., Livens F., Kelly M. (1993) 'Measurement, interpretation and modelling of Cs-137 transport through two freshwater lakes after Chernobyl. *J. Environmen. Radioactivity* **19**, 213-232.

Spezzano, P., Hilton, J., Lishman, J.P. and Carrick, T.R. (1993) The variability of Chernobyl

Cs retention in the water column of lakes in the English Lake District, two years and four years after deposition. *J. Environ. Radioactivity* **19**, 213-232.
Hilton, J. and Spezzano, P. (1994) An investigation of possible processes of radiocaesium release from organic upland soils to water bodies. *Wat. Res.* **25**, 975-983. publication.
Hilton, J. (1993) Vulnerable aquatic systems and the location of nuclear power stations. Proceedings of the Workship: Hydrological Impact of Nuclear Power Plant systems. UNESCO, Paris, Sept. 23-25. 1992. UNESCO SC-93/WS.
Hilton, J., Davison, W., Hamilton-Taylor, J., Kelly, M., Livens, F., Rigg, E. and Singleton, D.L. (1994) Similarities in the the behaviour of Chernobyl derived Ru-103 and Ru-106 in two freshwater lakes. *Aquatic Sciences.* **56(2)**, 133-144.
Hilton, J. Dispersion of radionuclides in aquatic systems. Chapter for book by IUR request. IUR Radioecology text book. Submitted for publication.
Hilton, J., Rigg, E., Davison, W., Hamilton-Taylor, J., Kelly, M., Livens, F.R., and Singleton, D.L. (in press) Modelling and interpreting element ratios in water and sediments: a sensitivity analysis of post-Chernobyl Ru, Cs ratios. *Limnol. Oceanogr.*
Hilton, J. (Submitted, 1994) Aquatic radioecology post Chernobyl - a review of the past and a look to the future. *Sci. Tot. Environ.*
Smith J.T. & Comans R.N.J. (1995) 'Modelling the diffusive transport and remobilisation of ^{137}Cs in sediments: the effects of sorption kinetics and reversibility' Geochim. et Cosmochim. Acta (accepted for publication).

Scientist Responsible of Project 2: A.Ortins de Bettencourt

Head of Project 2: Maria Carolina Vaz Carreiro

Research Team: Maria Carolina Vaz Carreiro
Maria José B. Madruga
José Alberto G. Corisco

1) PHYSICO-CHEMICAL BEHAVIOUR OF RADIONUCLIDES IN FRESHWATER SEDIMENTS

II. Objectives

1. Study of the effect of ionic composition, sediment drying and temperature on radiocaesium fixation in sediments;

2. Study of the solid-phase speciation of radiocaesium and radiostrontium in sediments;

3. Characterization of suspended matter (Fratel dam) in terms of relevant parameters for the short-term prediction of solid/liquid partitioning of radiocaesium.

III. Progress achieved including publications

1. Factors influencing the radiocaesium fixation in sediments

Ionic composition

On the basis of a rather consistent and coherent caesium selectivity pattern in the frayed edge sites (FES) of the sediments, it was accepted that the FES in the various sediment systems are essentially similar structures, although this is an oversimplification considering the erratic and unpredictable irreversibility pattern of radiocaesium sorption in various systems. Such diversity in behaviour could eventually be connected, with weathering effects. In the protocols followed before to radiocaesium irreversibility studies, the radiocaesium contamination of the systems was carried out on the system as such (i.e. in the ionic state as sampled) without pretreatment. However, it should be considered the effect of the sediment ionic composition and that of the overlying water column.

Two scenarios were considered:

a) Sediments homoionically saturated with various ions

A comparison was made between the potassium, sodium, and calcium forms of the sediment, Tejo river (T1<63μm, T2<500μm) and Tejo estuary (A<212μm, S<212μm) and their natural conditions. Homoionic systems (1g/10ml) (K $2x10^{-3}$M; Na $2x10^{-3}$M; Ca 10^{-3}M) were labelled with radiocaesium in a 10^{-5} M KCl ^{137}Cs labelled solution and allowed to age for 4 and 52 days. They were subsequently dispersed in 200ml of 10^{-3}M NH_4Cl containing a dialysis membrane with giese (ammonium copper

hexacyanoferrate) granulate ("Infinite Bath" method). Desorption progress was monitored by counting the adsorbent (fresh adsorbent is used after each sampling).

Fig.1.1 summarizes the results obtained in terms of a comparison of plateau fixation levels in the various systems studied for the natural, potassium, sodium and calcium states and for 4 days aging time. In spite of some minor differences, a very consistent pattern in the behaviour of all systems is observed. It is seen that, fixation levels decrease from the natural conditions to the K-state; fixation levels increase in the sodium state; the highest fixation being found in the Ca-state. It appears that the action of strongly hydrated ions (Na, Mg, Ca) leads to (structural) configurations unfavorable for radiocaesium desorption within a very short time scale (days). Possibly, the presence of strongly hydrated ions in the FES pool may lead to a wedge-effect, allowing for a deeper penetration of radiocaesium into the solid, resulting in a dramatic drop in subsequent desorption levels. This may be confirmed by the difference in fixation behaviour between the freshwater (T1 and T2) and estuarine sediments (A and S), showing a higher fixation level in the systems with the lower FES capacity. However, the higher fixation levels are very likely related to differences in ionic composition. When the various sediments were submitted to an aging time process (52 days) the differences in fixation behaviour become less pronounced and the Ca-saturated sediments scarcely show any aging effects.

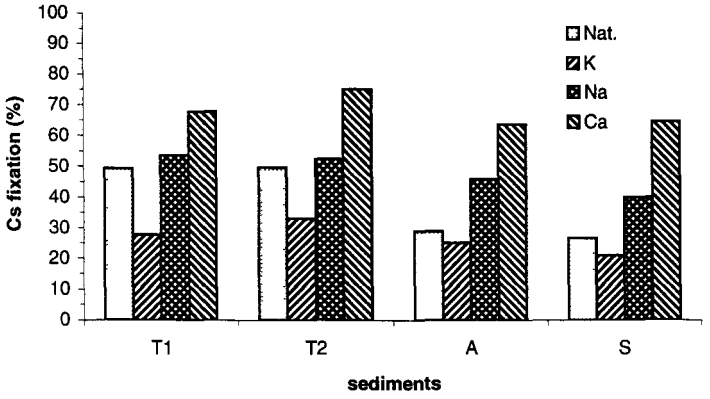

Fig. 1.1 - Effect of K, Na and Ca ions on radiocaesium fixation for Tejo river sediments (T1, T2, A, S) and 4 days aging time.

b) Mixed potassium-calcium solutions

The possible effect of ionic concentration was investigated in a homoionic (K) and a mixed (K-Ca) scenario. For the first case, sediment samples (T2) were preconditioned homoionically at 4 different potassium concentrations (0.1, 0.5, 1 and 2 meq.l^{-1}), ^{137}Cs labelled in the same solutions and aged for 2 and 165 days. They were subsequently dispersed in 200ml of 10^{-3}M NH_4Cl containing a dialysis membrane with giese granulate ("Infinite Bath" method). Desorption progress was monitored by counting the adsorbent (fresh adsorbent is used after each sampling).

For the K-Ca scenario, sediment samples (T2) were preconditioned with three solutions at the same potassium adsorption ratio (0.08) but increasing total concentrations. The compositions studied were (in meq.l^{-1}): K=0.1, Ca=3; K=0.5, Ca=75; K=1, Ca=300. The systems were ^{137}Cs labelled in these conditions, aged for 2, 129 and 165 days and submitted to the same desorption protocol.

Results are shown in Fig. 1.2 and Fig. 1.3 for the homoionic and mixed scenarios respectively.

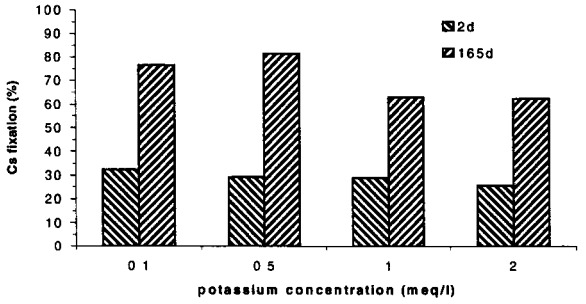

Fig. 1.2 - Effect of potassium concentrations on radiocaesium fixation for T2 sediment, at different aging times (2 and 165 days).

For the potassium scenario (Fig.1.2), there are only a very small trend towards fixation promotion at lower concentration. The fixation levels increase by a factor of about two up to 165 days aging, for all potassium concentrations. In the case of the K-Ca system, the effect of total concentration is more pronounced, particularly at longer aging times (a factor of about 1.5).

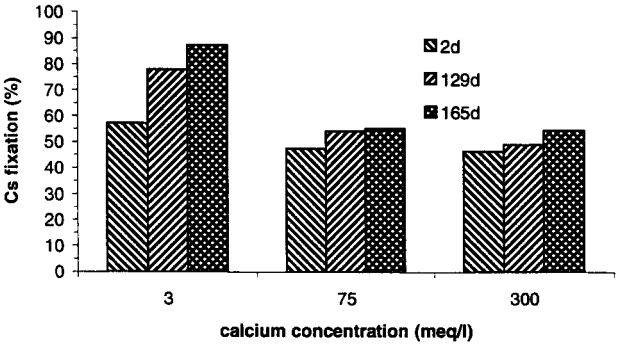

Fig.1.3 - Effect of potassium-calcium concentrations on radiocaesium fixation for T2 sediment, at different aging times (2, 129 and 165 days).

It is concluded that the cationic composition of the liquid phase (and therefore the solid) plays a key role in the radiocaesium fixation behaviour: strongly hydrated cations (Ca, Mg, Na) lead to a pronounced enhancement of radiocaesium fixation in the solid phases; poorly hydrated ions (K, NH_4) have the opposite effect and promote sorption reversibility.

Sediment drying and temperature

In sediment sampling methodology is important to know if a sediment should be dried and, if so, at what temperature and what is the possible effect on the desorption behaviour of radiocaesium. Another question which raises to soils sampling is how important are aging effects in dry conditions. These issues are being addressed here.

Sediment samples (≈1g) were weighted in aluminium plates and contaminated using 2.5ml 10^{-5}M KCl ^{137}Cs labelled solution. These systems were submitted to 5 drying-wetting cycles at 25°C using 2.5ml bidistilled water. The entire procedure took 4 days.

Another set of samples were labelled with ^{137}Cs, using the same procedure, dried at 25°C and left to age for 48 days. The effect of temperature was studied by oven-drying the ^{137}Cs contaminated samples at 110°C and left to age for 4 and 48 days.

In parallel, reference samples were contaminated with ^{137}Cs and left to age at room temperature (25°C) in wet conditions for 4 and 48 days.

For the desorption protocol all the samples were dispersed in 200ml 10^{-3}M NH_4Cl using the giese granulate in a dialysis membrane.

These procedures were carried out to Tejo river (T1, T2) and Tejo estuary (A) sediments.

The results obtained are summarized in Table 1.1 in terms of fixation levels as obtained from the desorption plateaus, for 4 and 48 days aging times.

From Table 1.1 it is seen that, for short aging times (4 days) the wetting/drying cycles have a limited effect on radiocaesium fixation, except for sediment A, as compared with the reference samples left to age for 4 days under wet conditions. Submitting the systems to a drying procedure at 110°C leads to a significant increase in fixation levels.

In what concerns the aging effects, an increase in fixation levels by a factor of about 2, for wet systems, was observed. However, the most important is the finding that in the dried systems, aging leads to minimal changes in fixation levels. It means that, when sediments (or soils) are air-dried after sampling, aging effects are interrupted and, if one is interested in studying radiocaesium desorption yields, the picture obtained relates in fact to the date of sampling. Moroever, these data show very clearly that drying the system at high temperature should in any case be avoided.

It is concluded that, drying a sediment at room temperature has a very limited effect on fixation but appears to put a brake on the aging effects.

Table 1.1 - Effect of sediment drying and temperature on radiocaesium fixation for 4 and 48 days aging times.

Aging time days	Sediments	Wet	Dry (25°C)	Dry (110°C)
4	T1	41.5	44.6 *	66.7
	T2	41.4	54.3 *	-
	A	26	47.8 *	59.6
48	T1	75.9	49.3	63
	T2	74.7	50.7	-
	A	39.7	33.1	55.5

* 5 wetting/drying cycles

2. Solid-phase speciation of radiocaesium and radiostrontium in sediments

It is commonly thought that the fraction of sediment-bound radiostrontium and radiocaesium, dispersed in 1M ammonium solutions -the ion exchangeable pool- is associated with the "regular" part of the ion exchange complex (the planar and easily exchangeable sites). A study on radiostrontium and radiocaesium sorption reversibility, covering a range of sediments and desorption agents (complex ions, KCl, NH_4Cl, $MgCl_2$, $CaCl_2$, $Sr(NO_3)_2$), demonstrated that radiostrontium and radiocaesium are associated with different exchange sites in the solid. On the basis of this different behaviour a sequential ion exchange displacement protocol was developed which allows the quantitative separation of the ion exchangeable fractions of the two radionuclides.

Sediment samples (≈1g) inside dialysis membranes were thoroughly equilibrated with mixed K-Ca solutions (10^{-5} M KCl, 10^{-5} M $CaCl_2$) which were double labelled with ^{137}Cs and ^{90}Sr. After three days equilibration ^{137}Cs radioactivity in the dialysate was counted by gamma spectrometry and the amount of ^{137}Cs adsorbed was calculated. For ^{90}Sr, dialysate samples were counted by beta spectrometry after 16 days (allowing a stationary state of the ^{90}Y daughter nuclide), and ^{90}Sr radioactivity adsorbed on the sediments was calculated. Appropriate corrections were made for the ^{137}Cs interference (maximum energy of 0.51 MeV) in the liquid scintillation counting assays of ^{90}Sr (maximum energy of 0.54 MeV).

Radiostrontium desorption was carried out by transferring the dialysis membranes to 50ml 1N $SrCl_2$ (end-over-end shaking, 24 hours); ^{90}Sr and ^{137}Cs activities were monitored in the dialysate (taking appropriate time delays and corrections as described). From such measurements, desorption levels of both radiostrontium and radiocaesium could be calculated. Finally, dialysis membranes were transferred to a

vessel containing 12g (dry) giese granulate in 200ml 10^{-3}M NH_4Cl, and the radiocaesium desorption was monitored by regular gamma counting of the adsorbent.

In addition, reference desorption experiments were carried out on the various sediments (using single labelling), applying the 1N $SrCl_2$ and the "Infinite Bath" protocol (10^{-3}M NH_4Cl, giese granulate).

The results are summarized in Table 1.2 for the studied sediments. Five data series are shown: the ^{90}Sr desorption levels obtained with 1N $SrCl_2$ (double labelled systems), ^{137}Cs desorption levels in 1N $SrCl_2$ (double labelled), cumulative ^{137}Cs desorption levels (obtained as the plateau values after 11 days of desorption) using the "Infinite Bath" technique (double labelled), ^{90}Sr desorption levels in 1N $SrCl_2$ (single labelled) and ^{137}Cs desorption levels (single labelled) with the "Infinite Bath" technique.

It is seen that in all systems (double and single labelled), ^{90}Sr desorption is nearly quantitative (96-100%), clearly demonstrating complete reversibility. The ^{137}Cs displacements in the 1N $SrCl_2$ treatment are quite low (1-3%) showing that ^{137}Cs is not at all present in sites accessible to strontium. The desorption levels obtained for ^{137}Cs, after having been submitted to a 1N $SrCl_2$ treatment are seen to be significantly lower (a factor of about 1.5) than the values obtained in the single labelled systems (no 1N $SrCl_2$ treatment). This effect should be due to the enhancement of fixation, resulting from the effect of concentrated solutions of strontium, as shown before to calcium.

Table 1.2 - Radiostrontium and radiocaesium desorption yields (%) for T1, T2, A and S sediments, in the presence of 1N $SrCl_2$ and 10^{-3}M NH_4Cl giese ("Infinite Bath" protocol). Standard deviations are given in parenthesis.

	Mixed "Infinite Bath"				
	^{90}Sr	^{137}Cs	^{137}Cs	^{90}Sr	^{137}Cs
Sed.	1N $SrCl_2$		10^{-3} M NH_4 giese	1N $SrCl_2$	10^{-3} M NH_4 giese
T1	98.4 (±0.3)	2.7 (±0)	33.4 (±0.5)	95.6 (±0.1)	49.3 (±0.5)
T2	99.3 (±0.2)	3.3 (±0.1)	28.2 (±0.8)	97.3 (±0.6)	46.5 (±0.1)
A	96.4 (±0.2)	1.3 (±0)	39.6 (±0)	96.8 (±0.1)	61.9 (±0.2)
S	97.1 (±0.4)	1.3 (±0.1)	40.2 (±0.2)	97.3 (±0.1)	67.5 (±0)

It is concluded that the ion exchangeable fractions of ^{90}Sr and ^{137}Cs can be rather well separated, the procedure making use of the fact that the radionuclides are associated with different sites of the solid phase. Radiocaesium is quantitatively associated with the FES and its desorption is only partially reversible; radiostrontium is quantitatively associated with the regular ion exchange complex and its adsorption is completely reversible.

3. Short-term prediction of radiocaesium solid/liquid partitioning to suspended matter (Fratel dam)

Suspended matter samples (grain size <106μm) from Fratel dam (Tejo river) collected at 1m (FU) and 10m (FL) depth, were characterized in terms of cation exchange capacity (CEC), organic matter content (OM) and potassium and ammonium radiocaesium interception potential, K_dm_K and K_dm_{NH4} respectively (Table 1.3). The results obtained for the various parameters are in good agreement with those obtained to other freshwater sediments (Madruga, 1993) and show that the two suspended matter samples have very similar properties.

Table 1.3 - Relevant parameters for the suspended matter samples.

Suspended matter	CEC meq.100g^{-1}	OM %	K_dm_K meq.g^{-1}	K_dm_{NH4} meq.g^{-1}	K_c (NH_4/K)
FU	39.4	22.8	2.8 ± 0.3	0.73 ± 0.04	3.8
FL	37.8	18.2	3.0 ± 0.1	0.81 ± 0.05	3.7

The solid phase characteristics relevant for the specific sorption of radiocaesium (K_dm_K and K_dm_{NH4}) have been determined in the presence of a masking agent (silver thiourea). However, it is of interest to test if the radiocaesium adsorption is exclusively confined to the FES. Such predictions could be confirmed by experimental data for scenarios in which the entire ion exchange complex is accessible to radiocaesium.

Predictions of the radiocaesium partitioning for field scenarios can be made using the following equation:

$$K_d(Cs) = \frac{[K_d(Cs).m_K]}{K_c(NH_4 / K).m_{NH4} + m_K}$$

where the denominator expresses the total competitive effect of K and NH_4 ions, multiplied by its weight factor, obtained from $[K_dm_K]$ /$[K_dm_{NH4}]$ ratios. Taking into account the values in Table 1.3 and the water column composition (Fratel dam) in terms of K (69 μeq.l^{-1}) and NH_4 (17 μeq.l^{-1}) concentrations, the distribution coefficients obtained are $2.1x10^4$ and $2.3x10^4$ ml.g^{-1} for FU and FL respectively. These values are higher by a factor of two than those obtained "in situ" ($1.1x10^4$ ml.g^{-1}). The same calculations were made to bottom sediments and also based on the predictions, a higher K_d ($6.3x10^3$ ml.g^{-1}) than "in situ" K_d ($2.8x10^3$ ml.g^{-1}) was obtained. Consequently, it may be concluded that in spite of the higher K_d values the solid/liquid partitioning of radiocaesium in field scenarios can reliably be predicted on the basis of sediment laboratory characterizations and column water composition.

The radiocaesium fixation levels at short time period, for the suspended matter were also evaluated. Suspended matter samples (FU, FL) (solid/liquid ratio=1g/25ml) were first preequilibrated (three times) with water from Fratel dam. The radiocaesium

adsorbed on the suspended matter was determined after the samples equilibration (one day, end-over-end shaking) with the same water ^{137}Cs labelled. The labelled suspended matter samples were dispersed in 1M NH_4Cl shaken and centrifuged at each sampling time. The procedure was repeated four times and desorption yields expressed in cumulative terms. The results obtained show fixation levels of about 22%. These values are lower than those obtained for bottom sediments (about 50%). It can be concluded that for the same aquatic environment and short aging times the suspended matter plays a more important role than the bottom sediments in what concerns the radiocaesium desorption.

Publications

- Madruga, M.J. Adsorption-desorption behaviour of radiocaesium and radiostrontium in sediments. PhD thesis, K.U. Leuven, Belgium, October 1993.
- Madruga, M.J. On the differential binding mechanisms of radiostrontium and radiocaesium in sediments. Presented on the "International Seminar on Freshwater and Estuarine Radioecology", Lisbon 21-25 March 1994. In publication on the journal "Science of the Total Environment".
- Wauters, J, Madruga, M.J., Vidal, M., Cremers, A. Solid phase speciation of radiocaesium in freshwater sediments. Presented on the "International Seminar on Freshwater and Estuarine Radioecology", Lisbon 21-25 March 1994. In publication on the journal "Science of the Total Environment".

2) BIOLOGICAL PROCESSES

II. Objectives

Radiocaesium bioaccumulation shows a large variability in nature, being higher in oligotrophic lakes, with low potassium concentration, and lower in freshwaters with high potassium content. More recently, after the Chernobyl accident, very high ^{137}Cs concentrations in freshwater fishes were found, mainly in lakes in Northern Europe, with large differences from lake to lake.Temperature is another environmental factor, which is referred in literature as affecting the bioaccumulation of radionuclides by fish.

The objective is the evaluation of the effects of changing environmental parameters which affect the variability of concentrations and transfer factors.
a) Under the assumption that it is not only the K^+ concentration in water that affects the radiocaesium accumulation by fish, but also the K^+-Cs^+ balance, series of experiments were programmed to study the effect of the K^+-Cs^+ in water, on radiocaesium accumulation and retention by the Cyprinid fish *Chondrostoma polypepis polylepis.*
b) To study the combined effect of different K^+ concentrations and different temperatures in water on radiocaesium accumulation by the same fish species.

III. Progress achieved including publications

MATERIALS AND METHODS

All the experiments were performed in small aquaria with 5 liters of an artificial freshwater medium, without water filtration system, but with aeration and artificial light during 8 hours a day, except for weekends (continous lighting). Artificial medium was composed of distilled water to which some salts were added, in order to get a basic cationic composition similar to the one found in Tejo River at the site of Fratel dam. Ca^{2+}, Mg^{2+}, Na^{+} and K^{+} concentrations were, respectively, 36, 11, 25 and 3.3 mg l^{-1}. Only K^{+} concentration was changed and the values used were 0.35, 3.5 and 35 mg l^{-1}. ^{134}Cs was in the chloride form, in a solution 0.1 M of chloridric acid, with a massic concentration of 2 µg $Cs^{+}ml^{-1}$. Water was changed once a week and the contaminated feccal pelets were daily separated by screening, to prevent their ingestion by fish.

Small specimens of the cyprinid fish *Chondrostoma polylepis polylepis*, aged of about 1 year and weighing about 2g, were used and fed 5 days a week with milled soft parts of bivalves (containing 0.9 mg K^{+} per gramme), each meal representing about 5% of the total fish weigth. Each group was previously acclimated to the artificial medium, for 2 weeks, before contamination with radiocaesium.

During the uptake phase fishes were fed in separated aquaria, with uncontaminated media, to avoid fish contamination from the food pathway.

Radioactivity measurements were made on pre-weighed living fishes, anaesthetized in an aqueous solution of 0.3 $g.l^{-1}$ of MS-222 (Sandoz). To measure ^{134}Cs concentration in the liquid phase during the uptake, 5 ml samples of labelled water were filtered through membranes (0.45 µm).

The measuring equipment was based on a well-type NaI(Tl) detector, associated with a multi-channel analyser.

The first set of experiments at the temperature of 20° ± 2°C had the objective of studying the balance of potassium-stable caesium. Table 2.1 shows the concentrations of stable Cs^{+}, K^{+} and also of $^{134}Cs^{+}$ added during the uptake phase.

Table 2.1 Concentrations of K^{+}, stable Cs^{+} and radioactive Cs^{+} in the artificial medium, at 20°C

(ppm)

	K^{+}	stable Cs^{+}	radio Cs^{+} **
group 1	0.35	5.8E-04	6.16E-04 to 6.28E-04
group 2	3.5	5.8E-04	6.16E-04 to 6.28E-04
group 3	35	5.8E-04	6.16E-04 to 6.28E-04
group 4	5.8E-04	0.35	6.56E-04 to 6.64E-04
group 5	5.8E-04	3.5	6.56E-04 to 6.64E-04
group 6	5.8E-04	35	6.88E-04 to 7.04E-04

** only for uptake phase

The second and third sets of experiments were carried out at the temperatures of 12° ±2°C and 5°±1°C, but being the temperature effect the aim of the experiment, the same three different K^+ concentrations were used and stable caesium was kept constant, 5.8 x 10^{-4} mg l^{-1}. Very similar conditions as described in Table 2.1 for groups 1,2 and 3, were settled.

RESULTS AND DISCUSSION

Data expressed in Bq g^{-1} of fish (fresh weight) are affected by a confidence interval of 0.95. Concentration Factor, CF_t , the ratio Bq g^{-1} (fish) / Bq ml^{-1} (water), was computed considering the mean value of water radioactivity for all the uptake period. Retention, R_t, was computed considering the mean total radioactivity of fishes, so that data would not be affected by the biological dillution of radiocaesium, due to the weight increase of fishes. Retention data represent the percentage of the initial radioactivity of fishes during the elimination phase and is based upon a multicompartmental analysis. Biological half-life, T_b, means the time needed for a retention compartment to loose 50% of its radioactive content.

In order to be comparable, all the uptake kinetic curves are fitted to power functions, because for the lowest temperature retention analysis could not yet be completed, but for those already completed the results are also presented according to the treatment described by Garnier-Laplace (1991) and Badie *et al.* (1985), where the elimination rate is taken into account.

Potassium-stable caesium effect

^{134}Cs concentration in fishes during 4 weeks of direct uptake, has increased in all six groups without reaching a steady state. Figs. 2.1 and 2.2 show the CF_t experimental data and the adjusted uptake functions for groups 1, 2, 3 and 4, 5, 6, respectively.

Keeping a low stable Cs^+ concentration of 5.8 E-04 mg l^{-1} in the artificial medium (groups 1, 2 and 3), it can be easily verified that the higher the K^+ concentration in water the lower the radioactive contamination of fishes, Figure 2.1. The same happens when, on the contrary, there is a low K^+ concentration of 5.8 E-04 mg l^{-1} and stable Cs^+ is present as a major cation (groups 4,5, and 6) Fig. 2.2.

Analysis of variance reveals that, for CF_t experimental data, variances for groups 2 and 3 are not significantly different at the significance level of 0.95, but both are different of group 1, while groups 4, 5 and 6 are significantly different. The same analysis applied to the retention data reveals that groups 1, 2 and 3 are not significantly different, and the same for groups 4, 5 and 6.

The $[K^+]/[Cs^+]$ balance appears to be determinant on the ^{134}Cs uptake by fishes, and there seems to be a resemblance of Cs^+ and K^+ behaviour when their relative concentrations in medium are inversed.

It is important to enhance that at K^+ concentration of 3.5 ppm and at the same concentration of Cs^+, CFs are quite similar.

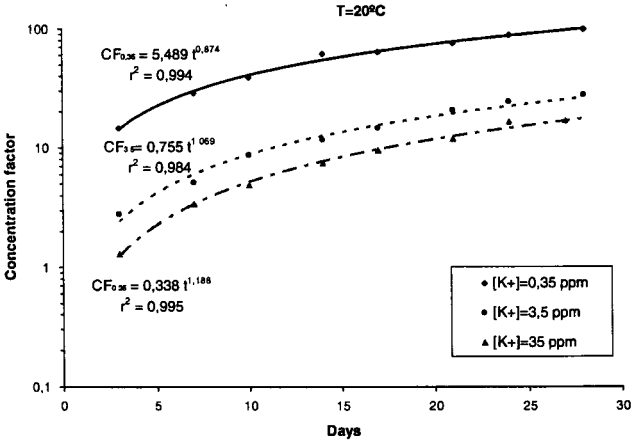

Fig. 2.1 ^{134}Cs uptake by a freshwater fish from water with different K^+ concentrations, at 20°C

Uptake curves based on the treatment used by Garnier- Laplace (1991) and Badie *et al.* (1985):

$$0.35 \text{ ppm: } CF_t = 419\,(1-e^{-0.009\,t}) + 7\,(1-e^{-0.183\,t})$$

$$3.5 \text{ ppm: } CF_t = 96\,(1-e^{-0.011\,t}) + 0.15\,(1-e^{-0.161\,t})$$

$$35 \text{ ppm: } CF_t = 50\,(1-e^{-0.013\,t}) + 1.3\,(1-e^{-0.114\,t})$$

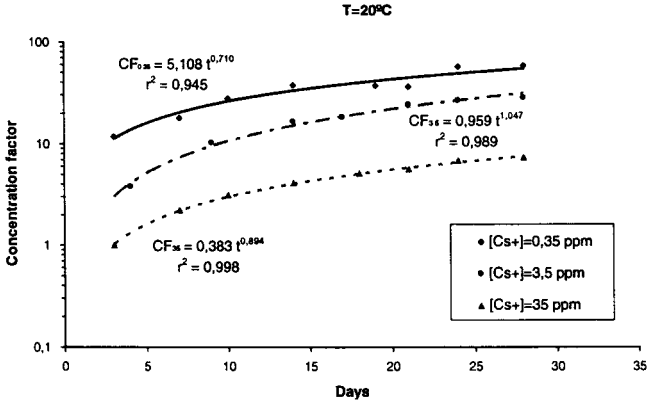

Fig. 2.2 ^{134}Cs uptake by a freshwater fish from water with different Cs^+ concentrations, at 20°C

Uptake curves based on the treatment used by Garnier- Laplace (1991) and Badie *et al.* (1985):

$$0.35\ ppm: CF_t = 653\ (1-e^{-0.003\ t})$$
$$3.5\ ppm: CF_t = 227\ (1-e^{-0.005\ t}) + 0.24\ (1-e^{-9.61\ t})$$
$$35\ ppm: CF_t = 232\ (1-e^{-0.001\ t}) + 1.1\ (1-e^{-0.126\ t})$$

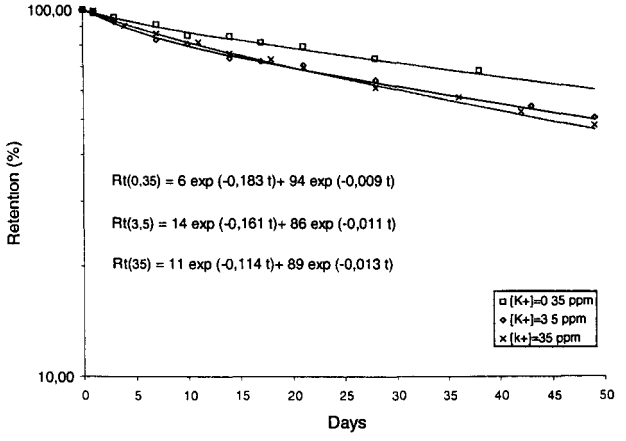

Fig. 2.3 ^{134}Cs retention by a freshwater fish at different K^+ concentrations in water

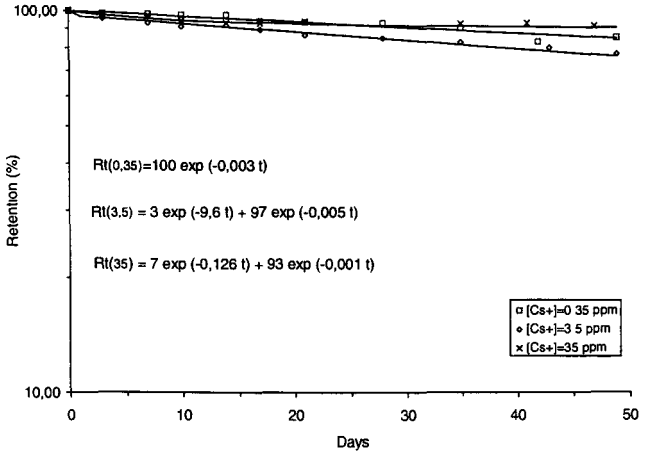

Fig. 2.4 ^{134}Cs retention by a freshwater fish at different Cs^+ concentrations in water

However, the retention curves show that the removal of radioactive caesium by stable caesium is not as efficient as it is by potassium (Figures 2.3 and 2.4). In fact, comparing retention functions, all the long term retention components of groups 4, 5 and 6, exhibit longer biological half-lives than their respective pairs, ranging from 139 to 693 days. While at the three K^+ concentrations used in water the longer biological half-life varies from 53 days (at 35 ppm) to 77 days (at 0.35 ppm).

One possible explanation is that practicaly no more exchange is possible between the radiocaesium in fish and the potassium in water, as in this case it is only in a tracer amount, and fish must keep constant the internal K^+ concentration (homeostatic regulation).

Potassium concentration and temperature effect

An interesting point to enhance is that the K^+ concentration effect remains approximately the same, at the temperatures of 20° and 12°C, Figs. 2.1 and 2.5. Variance analysis does not reveal for both temperatures (see page 11) significant difference on radiocaesium uptake kinetics for K^+ concentations of 3.5 and 35 ppm, although at 12° C it was observed that these uptake kinetics curves are "inverted", Fig.25. In fact following the treatment used by Garnier-Laplace (1991) and Badie *et al.* (1985), they are superposed, which for the moment can not be explained.

However the elimination at 12° C is much different than at 20°C. Not only the biological half-lives are longer, what could be expectable (0.35ppm K^+: Tb_1=17 days, Tb_2=305 days; 3.5ppm K^+: Tb_1=14 days, Tb_2=167 days; 35ppm K^+: Tb_1=16 days, Tb_2=105 days), but the elimination at 35ppm K^+ is faster. This fact seems to mean that the higher K^+ concentation favorizes radiocaesium elimination.

At the temperature of 5°C, Fig. 2.6, the different K^+ concentations did not affect differently the radiocaesium accumulation. The three uptake kinetics curves of ^{134}Cs are not significantly different. (Fishes are not very active and they feed at a very low rate).

So, it is noticed that at the temperatures of 20° and 12° C, there is actually an inverse relation between K^+ concentation in water and radiocaesium concentration factor (CF). Based on the values at the end of each experiment, the three different values of CF obtained according to the three potassium concentrations in water, at the temperature of 20°C, show the following trend:

$$CF = 70.33\ [K^+]^{-0.368} \qquad R^2 = 0.92 \qquad (1)$$

At the temperature of 12°C the trend is similar, although the correlation is not so good:

$$CF = 21.15\ [K^+]^{-0.444} \qquad R^2 = 0.67 \qquad (2)$$

At the temperature of 5°C it is not possible to establish such kind of relation.

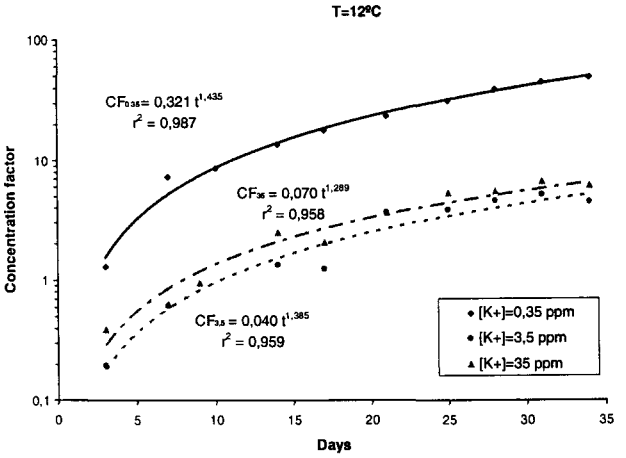

Fig. 2.5 ^{134} Cs uptake by a freshwater fish from water with different K^+ concentrations at 12 °C

Uptake curves based on the treatment used by Garnier- Laplace (1991) and Badie *et al.* (1985):

$$0.35 \text{ ppm: } CF_t = 313\ (1\text{-}e^{-0.005\ t})$$
$$3.5 \text{ ppm: } CF_t = 24.4(1\text{-}e^{-0.006\ t})$$
$$35 \text{ ppm: } CF_t = 24.3\ (1\text{-}e^{-0.009\ t})$$

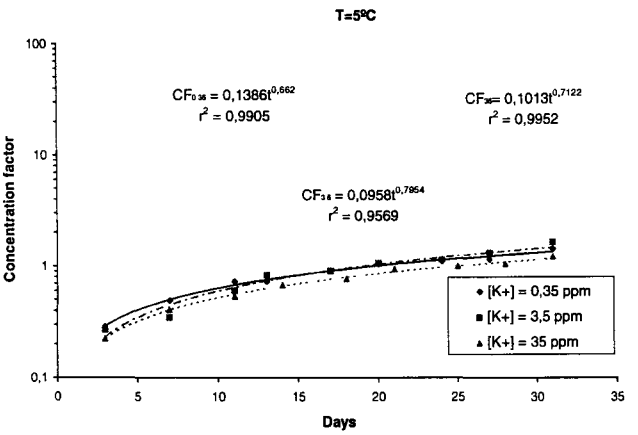

Fig. 2.6 ^{134} Cs uptake by a freshwater fish from water with different K^+ concentrations at 5 °C

These adjusted exponential functions, with only one term, mean very likely that the accumulation was still far from the equilibrium, in a phase of steep slope, when the process is very well described by a power function (coefficient correlations are about 0.99), and that might respond to the fast component of the elimination curve. So, when adjusting the uptake function, according to the retention study (> 250 days), that first part of the uptake is meaningless and only one exponential term is obtained.

Comparing Figs. 2.1., 2.5 and 2.6 and Cfs equations, it may be seen that: Cfs at equilibrium, at the lower K^+ concentration, represent 73% and 2.2% of the CF at 20°C, at 12°C and 5°C respectively. For the "normal" K^+ concentration, 3.5 ppm, they are reduced to 25% and 8%, at 12° and 5°C respectively, and at the higher K^+ concentration they represent 47% and 11% at the same temperatures respectively.

It must be stressed that the retention experiment was stopped at the 35th day because some deaths occurred and the number of remaining fish was not enough to continue the experiment.

CONCLUSIONS

Potassium-stable caesium effect

According to the proposed objective, it appears that $[K^+]$ / $[Cs^+]$ balance is determinant on the ^{134} Cs uptake by fishes, and there seems to be a resemblance of Cs^+ and K^+ behaviour when their relative concentrations in medium are inverted.

The high stable caesium concentrations in the medium cause a decrease in radiocaesium concentration factor, but at long term the decrease brought about by potassium is stronger. These results suggest a stable caesium descrimination by fish physiology.

The elimination of radiocaesium by fish seems to be independent of the external K^+ concentration (conclusion from an only 50 days experiment).

Potassium concentration and temperature effect

Decreasing temperatures at different K^+ concentrations in water decreases the radiocaesium accumulation, the pattern being almost the same at 20° and 12° C. At 5°C it is completely different, and it seems possible to say that there is no influence of the K^+ concentration in water on the radiocaesium uptake. CF equations show that the highest K^+ concentration influence on radiocaesium accumulation is at 20°C, where the Cf_{eq} at 35 ppm K^+ is 53% of the CF_{eq} at "normal" K^+ concentrations (3.5 ppm).

It was previously concluded, at 20° C, that different K^+ concentrations in water did not seem to affect the radiocaesium elimination rate, as well as at 5°C, but these former experiments lasted only 50 and 35 days respectively, while those ones at 12° C lasted for 250 days. In this case, at higher K^+ concentration in water, the elimination is faster, the exchange rate is higher, and the longer biological half-life is lower. Therefore, it

raises the question as to whether a long time experiment influences the goodness of results.

Publications

- Corisco, J.A.G.; Carreiro, M.C.V.
  Potassium- stable caesium effect on the radiocaesium uptake and loss by the Cyprinid fish *Chondrostoma polylepis polylepis* Steindachner. Presented on the "International Seminar on Freshwater and Estuarine Radioecology", Lisbon 21-25 March 1994. In publication on the journal "Science of the Total Environment".

- Corisco, J.A.G.; Carreiro, M.C.V.
  ^{60}Co transfer in a freshwater simplified trophic chain. III Accumulation and retention by the fish *Chondrostoma polylepis polylepis* Steindachner (to be published)

- Fernandez, J. A.; Heredia, M. A.; Garcia-Sanchez, M. J.; Corisco, J. A .G.; Carreiro, M.C.V.; Rios, A. D. de los
  Mechanisms of radiocesium uptake and accumulation in *Riccia fluitans* (to be published)

Head of Project 3: A. CREMERS

II. Objectives for the reporting period

1. Speciation of radiocaesium in freshwater sediments
2. A simplified procedure of specific site characterization for radiocesium sorption
3. Prediction of K_D for radiocaesium in sediments and soils
4. Radiocaesium uptake in microalgae: effect of K concentration
5. Characterization of sapropell sediments

III. Progress achieved including publications

1. Speciation of radiocaesium in freshwater sediments

In earlier reports, various approaches have been presented for assessing the solid-phase speciation of radiocaesium in sediments. One of these methods is based on the difference in caesium sorption selectivity in the Regular Exchange Complex (REC) and the illitic Frayed Edge Sites (FES) responsible for the very selective sorption of radiocaesium. In particular, it is well known that the K and NH_4 ions are equally competitive with radiocaesium in the REC; in contrast, NH_4 is about 4-7 times more competitive than K for Cs sorption in the FES. Theoretical basis and experimental procedure have been described earlier. In short, the method is based on the measurement of the K_D(Cs) response to NH_4 injection in systems preequilibrated with a mixed Ca-K solution (Ca: 100mM; K: 10 mM). If radiocaesium is intercepted in the REC, then K_D(Cs) should remain invariant to the increase in NH_4 concentration. If it is present in the FES, then K_D should decrease according to the equation

$$\frac{K_D\ (Ca/K)}{K_D\ (Ca/K/N)} = 1 + K_c\ (N/K)\ \frac{m_N}{m_K}$$

in whick K_D(Ca/K) and K_D(Ca/K/N) refer to K_D(Cs) in the Ca/K and Ca/K/NH_4 scenarios, K_c(N/K) to the N/K selectivity coefficient in the FES and m_N/m_K to the ratio of N/K concentrations in the liquid phase. This procedure has been applied to a set of 19 sediments originating from various sources in Europe (Rhône, Moselle, Loire, Vienne, Meuse, Rhine, Garonne, Seine, Tejo, Po, Ravenglass, Lake Devoke and Zoete Waters Lake (Belgium). Systems cover a very wide range in textural properties (% clay + fine silt 5-80%), cation exchange capacities (1-26 meq/100g) and specific sorption potentials. The results are summarized in figure 1 in terms of the averages of K_D(Cs) ratios (and standard deviations) in the two scenarios, K_D(Ca/K) / K_D(Ca/K/N) versus m_N/m_K. Data can be described in terms of the linear regression equation:

$$\frac{K_D\ (Ca/K)}{K_D\ (Ca/K/N)} = 1.12 + 7.17\ \frac{m_N}{m_K}$$

All individual systems show slopes in the range of 6-8, i.e. the K_D(Cs) response for all systems to increasing NH_4 levels is identical to what is found for illite clay, thus demonstrating quantitative interception of radiocaesium in the FES. This means that reliable predictions of K_D(Cs) can be made on the basis of FES specific sorption potentials and water composition (see below).

2. A simplified procedure of specific sorption potential for radiocaesium sorption

The fact that radiocaesium is, in the very large majority of field scenarios, quantitatively intercepted in the FES group, makes the quantitative assessment of this sorption pool of paramount importance if we wish to make K_D predictions. In the early stages, the specific sorption potential, defined as the product of FES capacity and trace Cs to K selectivity coefficient (formally represented by the symbol $[K_D.m_K]$ was measured on the basis of an elaborate silver-thiourea masking procedure. The principle of a new and simple protocol, eligible for routine applications was introduced in the K_D workshop at the 1984 Lisbon freshwater ecology meeting. It was presented in our 1984 progress report and applied to a limited number of systems. In short, it is based on a single K_D(Cs) measurement in systems preequilibrated with a Ca/K mixed solution (Ca:100mM); K:.5mM) i.e. a PAR (Potassium Adsorption Ratio $m_K/\sqrt{m_{Ca}}$) of 0.05. At this low PAR value, K ions are (nearly) exclusively confined to the FES. This procedure has now been extended to over one hundred sediment (and soil) samples of a wide range in textural properties, cation exchange capacity and organic matter content. Figure 2 shows the correspondance between results obtained by the masking procedure and the simplified PAR protocol. The agreement is essentially perfect: the linear regression yields

$$[K_D.m_K]^{PAR} = -0.083 + 1.01\,[K_D.m_K]^{AgTU} \qquad R^2 = 0.85$$

An additional demonstration of the nature of the agreement between the elaborate masking technique and the PAR protocol is based on a comparison of $[K_D.m_K]$ and $[K_D.m_N]$ values. Figure 3 shows the results.
Both procedures are in excellent agreement in demonstrating the highe competitivity of NH4 as compared to K. The linear regressions are:

$$[K_D.m_K]^{PAR} = -0.11 + 5.12\,[K_D.m_K]^{PAR} \qquad R^2 = 0.90$$
n=105

$$[K_D.m_K]^{AgTU} = -0.065 + 5.70\,[K_D.m_K]^{AgTU} \qquad R^2 = 0.92 \qquad n = 116$$

$$[K_D.m_K]^{All} = -0.046 + 5.28\,[K_D.m_K]^{All} \qquad R^2 = 0.91$$
n= 221

It thus appears that the sorption characteristic, necessary for making K_D predictions is obtainable from a single measurement using simple laboratory procedures readily available.

The reliability of predictions based on such characterizations is demonstrated in the section below.

3. Prediction of K_D(Cs) in sediments and soils

Predictive capabilities were tested on a broad range of systems using the following equation

$$K_D\ (Cs) = \frac{[K_D\ m_K]}{m_K + 5.3\ m_N + 0.02\ m_{Na}}$$

in which 5.3 and 0.2 refer to the N/K and Na/K selectivity coefficients in the FES. The following tests were carried out:(1) fifty freshwater sediments were thoroughly preequilibrated with a (modal) synthetic river water (m_K = 0.15 mM; m_N = 0.1 mM, m_{Ca} = 2 mM, m_{Mg} = 0.5 mM m_{Na} = 1 mM) and K_D(Cs) measured; (2) twenty-five freshwater sediments were equilibrated with the (Cs^{137} labelled) water described in (a) and K_D(Cs) measured; liquid phase compositions were measured after equilibration; (3) five estuarine sediments were submitted to tests 1 and to equilibration with synthetic seawater; (4) six widely different soils (texturally) were subjected to 8 different cationic scenarios (Ca = 3.5 mM; Mg = 1.5 mM) varying the K and NH_4 concentration in the range of 0.3 - 2 mM. In total, some 133 systems (combinations of sediments/soils and water compositions) were included in the study. Figure 4 shows the nature of the agreement between predicted K_D(Cs) values (K_D-pred) and experimental findings (K_D-exp). It is seen that K_D values cover a range of three orders of magnitude (50 to 50000 L/Kg) and that the agreement is reasonably good. In general, predictions somewhat overestimate experimental values but 90% of all observations deviate by less than a factor 3 from predictions. On the average it is found that

$$\frac{K_D(\exp)}{K_D(pred)} = 1.61 \pm 0.75$$

It may thus be concluded that reasonably reliable predictions of K_D(Cs) can be made on the basis of [$K_D.m_K$] values (obtainable by routine procedures) and liquid phase compositions (K and NH_4, and in saline scenarios, Na ion concentrations).

4. Radiocaesium uptake in algae: effect of K concentrations

The main aim of this study was to assess the nature of the competitive effect of K (covering a range of 0.1 to 10 mM) on TF values for radiocaesium uptake in microalgae (Dunalliella viridis). In a preliminary stage, efforts were directed at: (a) setting up a chemostat cultural system; (b) testing the ability of Dunaliella to grow in media of large differences in K concentration; (c) optimizing counting procedures for TF measurement in microalgae for marine (high conc.) conditions. It was found that the organism could be grown in a K conc. range of 10^{-4} to 10^{-2} M without significant loss in growth rate and photosynthetic activity. Ca concentrations could be varied in a range of 2.10^{-4} to 2.10^{-2}M but growth rate and photosynthetic activity were affected. Cs^{137} contents of algae were measured, using glass-fiber filtration for cell harvesting.

K effects on TF were measured in a standard simplified Johnson & Johnson medium labelled with Cs^{137}. Algae were grown (batch culture) for one week in a growth chamber at constant temperature and ligth intensity at 10^{-2}, 10^{-3} and 10^{-4} in K. No significant differences in growth rate were observed. Cs^{137} activity was measured on filters (100 ml suspension for 0.1 g of algae d.w.). The results (averages of three runs) are TF = 0.9(± 0.15) at 10^{-2} M K, 1.1 (± 0.3) at 10^{-3} M and 28.5 (± 1.3) at 10^{-4} M. These data, which are relevant for scenarios of low K concentration in freshwaters, clearly show that, at low K concentrations, TF values increase more than proportionally with decreasing K levels. These findings are in agreement with unpublished data (E. Smolders, K.U.Leuven) for higher plants indicating high sensitivity of TF (Cs) below K concentration of 0.25 mM.

5. Characterization of Sapropell sediments

Sapropell refers to sediments containing indigested vegetal and animal residues and which is available in large quantities in lakes in the CIS, particularly in Belarus and the Ukraine. Sapropell has been used in recent years as a countermeasure in radiocontaminated soils. A set of six samples, originating from various lakes in Belarus were characterized in terms of organic matter (OM) content, CEC, ionic composition of the exchange complex, specific sorption potential and fixations properties for radiocaesium.
OM content covers a range of 23 to 73% and CEC values range from 27 to 105 meq/100g. Normalizing CEC values to OM content leads to an average value of 1.24 (±0.23)meq/g, showing that exchange capacity is nearly exclusively associated with OM. In all samples (except one) NH_4 levels exceed those of K, sometimes by a factor of 10, as could be expected from the anoxic conditons of the sediments. $[K_D.m_K]$ values cover a range of 0.1 to 1 meq/g. This is the range commonly found for the soils in the Chernobyl contaminated area. It follows that the beneficial effect, if any, is not connected with the sorption properties of those materials. In contrast, its use as a countermeasure for radiostrontium is predictable, particularly in case of high OM content.
As an experimental test, a series of K_D measurements were carried out on sandy soils originating from the contaminated area with and without sapropell for both radiocaesium and radiostrontium. The effects observed were completely consistent with the relative sorption properties of soils and sapropell amendment for both radiocaesium and radiostrontium.

6. Publications

Submitted (Applied Geochemistry)
Prediction of solid/liquid distribution coefficients of radiocaesium in soils and sediments
- Part one: a simplified procedure for the solid phase characterization
J. Wauters, A. Elsen, A. Cremers, A.V. Konoplev, A.A. Bulgakov and R.N.J.Comans
- Part two: a new procedure for solid phase speciation of radiocaesium
J. Wauters, M. Vidal, A. Elsen and A. Cremers
- Part Three: a quantitative test of a K_D predictive equation
J. Wauters, A. Elsen and A. Cremers

To be submitted

- The use of sapropell as amendment in radio-contaminated soils (Applied Geochemistry)
E. Valcke, L. Moskaltchuk and A. Cremers
- The influence of particle concentration and fixation on radiocaesium sorption (Env.Chem.)
J. Wauters and A. Cremers
- Caesium-specific sorption sites on illite-bearing substrates (Env. Chem)
J. Wauters, A. Dierickx and A. Cremers
- Adsorption Kinetics of radiocaesium in aquatic sediments (Env. Chem.-)
J. Wauters, S. Rampelberg and A. Cremers

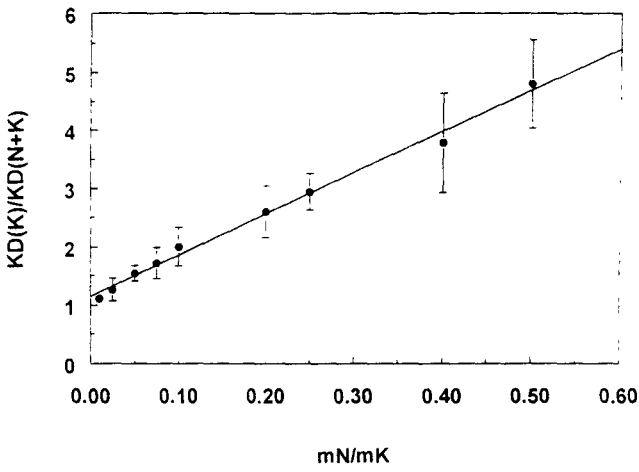

Figure 1. Effect of increasing NH_4 concentration on the K_D ratios (K-Ca/K-N-Ca scenarios) for freshwater sediments

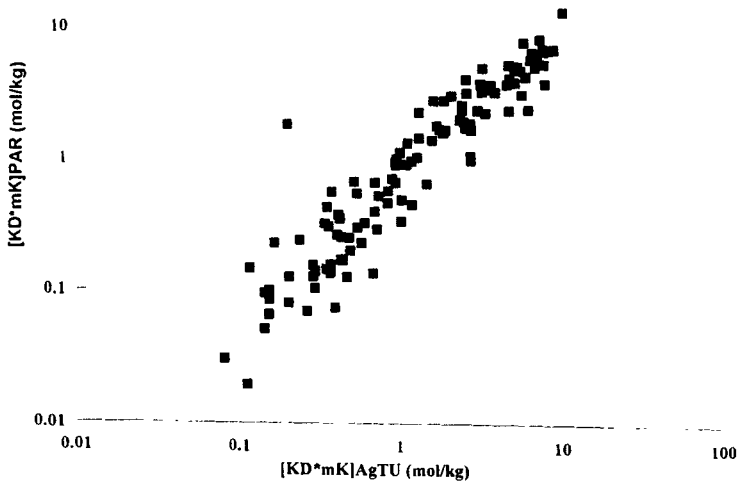

Figure 2. Comparison of $[K_D.m_K]$ values obtained by the AgTU masking technique and the simplified PAR protocol.

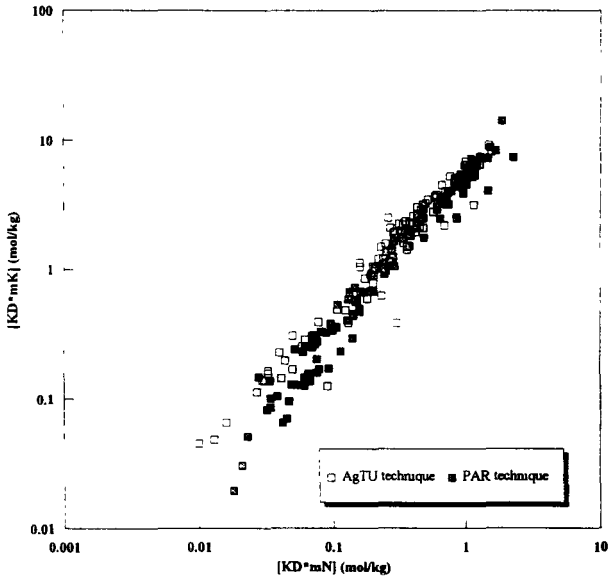

Figure 3. $[K_D.m_K]$ versus $[K_D.m_N]$ for the AgTU masking technique and the simplified PAR protocol.

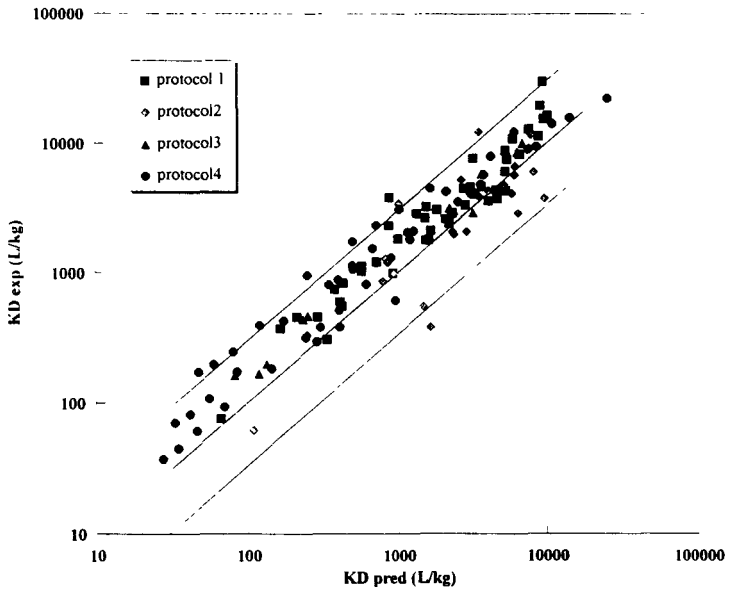

Figure 4. Experimental versus predicted K_D values: upper and lower lines refer to K_D(exp) / K_D(pred) values of 3 and 0.33.

I. head of project 4: Dr. FOULQUIER

II. Objectives.

- The Chernobyl accident showed the importance of cesium 137 in aquatic ecosystems and its fixation in the sediments. In relation with the different source terms (fallout from the atmospheric weapon tests and the Chernobyl accident, liquid wastes from nuclear plants), a review of our knowledge about cesium 137 fixation in the sediment of main french rivers is done.

- The importance of radioruthenium was shown in Chernobyl fallout and in the liquid wastes of reprocessing fuel plants. An experimental work studies the fixation of ruthenium 106 in an aquatic ecosystem.

III. Progress achieved including publications

1) CESIUM IN THE FRENCH RIVERS.

French rivers are an intereting investigation field to study the behaviour of cesium in aquatic ecosystems. Seven rivers are fitted with nuclear power stations (Figure 1): the Rhône with 5 stations (Creys, Bugey, St Alban, Cruas, Tricastin) and the fuel reprocessing plant of Marcoule), the Garonne with 1 station (Golfech), the Loire with 4 stations (Belleville, Dampierre, Saint Laurent, Chinon), the Seine with 1 station (Nogent), the Rhine with 1 station in France (Fessenheim) but under the influence of other stations upstream (Gosgen, Beznau, Liebstat, Muhleberg), the Moselle with Cattenom, the Meuse with Chooz.

Roughly, differences exist between the granulometric composition of the river sediments. Some like Rhône, Meuse, Rhine rivers have silty sediment, others like Moselle, Garonne, Loire have sandy sediments. The percentage of thin particles (lower than 50µm) and the organic matter are given in table 1:

Table 1. Percentage of thin particles, and composition of organic matter in sediments of french rivers.

River	particles < 50µm	organic matter (g/kg DW)
Rhône	30-70%	2.6 - 17.5
Meuse	72-75%	7.1 - 7.7
Rhin	50-54%	3.2 - 3.5
Seine	48-57%	2.9 - 9.1
Moselle	11-36%	5.6 - 6.5
Garonne	21-32%	1.7 - 2.1
Loire	18-37%	4.2 - 9.3

The radiocesium concentrations were studied upstream and downstream from every nuclear plants. The concentrations of these nuclides in the different rivers sediments from 1989 to 1993 are given in table 2.

Differences exist between eastern and western rivers which are the consequences of several factors:

-first is that the Chernobyl plume flew mainly over the eastern parts of France.

-other reasons are related with the type of reactors and the hydroelectric equipment of the rivers.

The lowest values of ^{137}Cs concentration are found in the Garonne river sediments ; ^{134}Cs was not detected. The effluents of the Golfech 1300 MWe PWR have a very low radioactive level.

In the Loire and the Seine rivers concentrations of ^{137}Cs are higher because the presence of 900 MWe PWR (which did not retreat their effluents as well as 1300 Mwe power stations) and the graphit-gaz reactors (St Laurent and Chinon).

In the eastern rivers like Meuse, Moselle, Rhin, the concentration of radiocesium in the sediments is higher, showing the effect of the Chernobyl fallouts and of the liquid effluents from the old reactors (from 1970 in Chooz, 1977 in Fessenheim).

Table 2. Concentrations of ^{134}Cs and ^{137}Cs in the different sections of the french rivers. ($Bq.kg^{-1}$ D.W.)

Rivers	sections	^{134}Cs	^{137}Cs
Garonne	upstream Golfech	-	3.9 ± 3.1
	downstream Golfech	-	2.8 ± 3.2
Loire	upstream Belleville	1.1 ± 0.9	13.5 ± 13.3
	Belleville-Dampierre	2.1 ± 1.5	7.8 ± 5.2
	Dampierre St.Laurent	1.8 ±1.1	13.4 ± 7.5
	St-Laurent-Chinon	2.2 ± 1.2	12.7 ± 6.5
	downstream Chinon	9.4 ± 7.0	23.3 ± 21.0
Meuse	upstream Chooz	1.7	31
	downstream Chooz	5.9 ± 1.0	79.5 ± 53.0
Moselle	upstream Cattenom	-	5.5 ± 39.6
	downstream Cattenom	4.8 ± 3.3	16.6 ± 39.6
Rhine	upstream Fessenheim	10.9 ± 5.0	64.7 ± 22.9
	downstream Fessenheim	9.0 ± 6.5	56.0 ± 28.4
Rhône	Geneva lake	8.0 ± 5.8	66.5 ± 40.5
	Geneva-Creys	1.7 ± 1.6	16.6 ± 15.8
	Creys-Bugey	2.1 ± 2.2	24.0 ± 16.2
	Bugey-St.Alban	2.8 ± 1.9	19.0 ± 17.9
	St.Alban-Cruas	3.5 ± 1.6	31.1 ± 12.5
	Cruas-Tricastin	5.6 ± 5.3	36.8 ± 25.3
	Tricastin-Marcoule	3.1 ± 2.5	32.0 ± 21.7
	Marcoule-Camargue	28.6 ± 13.7	253 ± 72
	Grand Rhône	8.5 ± 5.2	75 ± 33
	Petit Rhône	11.5 ± 3.9	195 ± 91
	Camargue delta	1.3 ± 0.4	16.1 ± 7.3
Seine	uptream Nogent	1.1 ± 0.7	13.3 ± 6.0
	downstream Nogent	3.7 ± 4.1	16.0 ± 18.9

The Rhône river presents several aspects. In the lake of Geneva the sediments have 66 Bq/kg DW of ^{137}Cs showing the characteristic of lakes with large catchment area and slow renewal flux.

In the upper Rhone, the sandy sediments have a concentration of around 20 Bq/.kg^{-1} DW. From Lyon to Marcoule the ^{137}Cs activity is about 30 Bq.kg^{-1} and 250 downstream from the reprocessing fuel plant of Marcoule and less in the two arms of the river (Grand-Rhône and Petit-Rhône) surrounding the delta of Camargue.

The same comments could be made for ^{134}Cs which shows concentrations 10 times lower than ^{137}Cs.

Radiocesium concentrations are well correlated with sediment thin particles and organic matter.

Multivariated analysis were done on these field data. For example figure 2 shows a graphical representation of a Principal Component Analysis (PCA) done with 9 parameters on 26 samples of sediment of upper Rhône.

The first graph shows the projection of the parameters on the factorial plan constructed with the first two axis that represent 70% of the total variability.
The correlation circle shows that the best correlated parameters in the principal plan are ^{137}Cs (-0,94), thin silts (-0,89), thick silts (-0,84) and thick sands (+0,79)

The parameters having correlations close to the circle (-1, +1) are the best variables represented on the principle plan. Axis 1 explains 50% of the variability, it could, roughly represent the sediment granulometry.

When two variables are in the same direction, their evolutions are correlated. So 137Cs is a function of the percentage of thin particles, and specially silts (and it is in opposite with percentage of sands).

Axis 2 explains 20% of the variability and it does not give interesting informations.

The second graph shows the projection of the different samples on the factorial plan. One could see different populations:

- on the left are the samples characterised by a high percentage of thin particles ; they are the sediments on the dam reservoirs, and two samples downstream from Lyon.
- on the upper part of the diagram are the samples from Bugey area, where sandy sediment is found. - the last population is composed by the sediments sampled between the Geneva lake and the area of Creys, with sandy sediments.

When several parameters are in the same direction it is possible to draw the regression graph between them. For example figure 3 shows the relation between the percentage of thin particles and the cesium concentration in the sediments from upper Rhône.

In conclusion, this study shows that the concentration of radiocesium in river sediment can be related whith the different source terms and with the granulometric characteristics of the sediments.

2) RUTHENIUM 106 EXPERIMENTAL TRANSFER MODEL.

A research program was undertaken on evaluation, modeling and analysis of ^{106}Ru transfer in a fresh water trophic net. The reason was that ^{106}Ru was found in Tchernobyl fallout and constituted 95% of liquid wastes of the reprocessing fuel plant of Marcoule. It was the subject of Françoise Vray PhD. Her thesis defence occured on november 24th 1994. 72 experimentations

studying the transfer of ^{106}Ru in a freshwater ecosystem including 2 abiotic compartments and 10 species from 3 trophic levels were done.

The CEC-DG XII cofinanced a part of the experimentations concerning the following components:

- Water sampled in the Rhône river, upstream from the Cruas power station.
- Primary productors, which are two species of algae abundant in freshwater ecosystems (*Scenedesmus, Chlorella*). These two species present differences in morphology, size, and digestibility by their consumers.
- First order consumers, (*Daphnia magna)* which is a planctonic crustacea important in fish diets.
- Second order consumers (*Gambusia*) which is chosen because its small size, used as a food for young trouts.
- Third order consumer (*Salmo trutta)* which is a ichtyophagus fish.

Experiments are done in plastic tanks (1 to 10 liters, according to the size of the organisms), temperature is fixed at 18°C, oxygenation is made with air pumps. For the direct transfers from water, contamination with ^{106}Ru ($RuCl_3$, in HCl) is realized in a single time, one or two days before introducing organisms. For the trophic transfers, food is previously contaminated and rinced in inactive water before it is given to predators. Sampling and radioactive measuring is done regularly. For water, samples of 5 and 10 ml are taken, part is measured non filtered, an other one after filtration at 0.45 µm.
Algae are sampled by filtration on 0.45 µm membrane, biomass is evaluated in a Malassez cell.
Daphnids are sampled by filtering the water on a nylon sieve. They are rinced in inactive water then dried on blotting paper.
Fish are sampled with a spoon net, they are anesthetized, then put in plastic tubes. Radioactivity is measured by gamma spectrometry on a NaI cristal.

2.1 TRANSFER FROM WATER TO ALGAE.

The contamination of the two species was done at several ages of the population (0, 6, 13, 26 days).
Figure 4 shows the simulation of the concentration factor evolution for a constant concentration of water and without cellular divisions.

The transfer of ^{106}Ru to phytoplancton is characterized by an intensive accumulation (FC#800). It is influenced by the morphology of the cells, or by physiological characteristics (mucus). ^{106}Ru does not seem to go inside the cell but only adsorbed on the membrane. Depuration is slow in relation with the biological dilution. So, algae are an important vector of contamination for their predators.

2.2 TRANSFER FROM WATER TO DAPHNID

Uptake and depuration were realised for two different levels of contamination (70 and 370 $Bq.ml^{-1}$). Figure 5 shows accumulation and depuration curves of daphnids concentrations. The CF is 120 to 140 at the steady state (11 days). Elimination is characterized by two biological half-lives : 4 hours and 48 hours.

2.3. TRANSFER FROM ALGAE TO DAPHNIDS.

After 14 days of culture, algae were contaminated with 500 $Bq.ml^{-1}$ of ^{106}Ru. After 3 to 5 days, algal cells were filtered and given to daphnids as one meal a day. The radioactivity of food was estimated by comparison of filtered and unfiltered culture medium and numeration of algae.

The parameters computed were the trophic transfer factor (TTF) which measures the bioaccumulation of ruthenium during accumulation phase (concentration in daphnia/concentration in algae) and the retention factor (R) in depuration phase (C_t/C_0).

Figure 6 shows the transfer of ruthenium to daphnids via *Scenedesmus* and *Chlorella*. The growth of daphnids and the transfer of ruthenium are higher with *Scenedesmus* than *Chlorella*. In fact the concentration of ^{106}Ru in daphnids is in relation with the concentration in algae and with the number of cells absorbed.

The elimination curve is similar with the two species of algae (figure 7). The transfer factor is 0.21 with Chlorella and 0.23 with Scenedesmus.

2.4. TRANSFER FROM WATER TO GAMBUSIA.

14 fish were put in the contamination tank for 40 days. No weight growth was observed as they were adult fish, in spite they were fed. Figure 8 shows the ^{106}Ru concentration in the water and in the fish. The medium was renewed twice (12 and 26 days). The activity of ^{106}Ru was between 500 and 300 Bq/ml. Figure 9 shows the depuration : gambusia lost 58% of their ^{106}Ru concentration after 14 days.

Figure 10 shows simulations for adult gambusiae in a steady water concentration and the retention of the nuclide when contamination stops. The concentration factor reaches 1.1 after 120 days ; 2 biological half lives exist in depuration phase, respectively 16 hours and 21 days .

2.5. TRANSFER FROM WATER TO TROUTS.

Trouts were fed with midge larvae ; the fish weight increased from 5 to 8 g during the 49 days of experimentation. Figure 11 shows the ^{106}Ru concentration in filtered water -which was renewed every week- and in the fish. Figure 12 shows the simulation of the trout concentration factor for a steady water concentration and the nuclide retention when contamination stops. The concentration factor reaches a value of 1.4 at 140 days. Depuration shows 2 biological half lives of 2 and 36 days.

2.6. TRANSFER FROM GAMBUSIA TO TROUTS.

Trouts were fed with *Gambusiae* in order to have a rapid growth. The concentration of ^{106}Ru in the food shows very important variations. The concentration in predators is proportional to this of preys. The depuration of the ^{106}Ru from trout is going through 14 days. The simulation of the trophic transfers from food to trouts for a constant feeding rate and a steady concentration in food is shown on figure 13. The trophic transfer factor at a steady state is $4.1.10^{-3}$. The retention factor after 60 days is less than 0.5%.

2.7. CONCLUSION.

This table shows the values of all the ^{106}Ru transfer parameters obtained from the several experimentations :

Experimentation	FC	FTT	Tb1	Tb2
water-chlorella	710	-	220 j	-
water-Scenedesmus	830	-	100 j	-
water-daphnia	170	-	4 h	2 j
algae-daphnia	-	0.2	15 h	-
water-Gambusia	1	-	16 h	21 j
water-Salmo	1.3	-	2 j	36 j
Gambusia-Salmo	-	0.004	6 h	24 h

Experimental results were expressed mathematically so they could be included in a global model which was tested in two different situations with the shell-fish called *Dreissena* and the carp. The comparison of the available data concerning the *in situ* measured concentrations to the corresponding computed values validated the procedure (Vray, 1994).

IV. Papers published or in press resulting from this work

FOULQUIER L. & BAUDIN-JAULENT Y. (1992). Impact radioécologique de l'accident de Tchernobyl sur les écosystèmes aquatiques continentaux. *C.C.E. RADIATION - PROTECTION-58* : 392 p.

FOULQUIER L., GARNIER-LAPLACE J., LAMBRECHTS A., CHARMASSON S. & PALLY M. (1993). The impact of nuclear power stations and of a fuel reprocessing plant on the Rhone river and its prodelta. In: *Environmental impact of nuclear installations. Proceedings of the joint seminary from september 15th to 18th 1992 at the university of Fribourg (Suisse), organised by the Société Française de Radioprotection and the German-Swiss Fachverband für Strahlenschutz.* : 263-270.

FOULQUIER L., LAMBRECHTS A. (1994). Radioecology assessment in waterways in France with nuclear facilities (1989-1993). *International seminar on freshwater and estuarine radioecology, Lisbon, Portugal, 21-25 march 1994 : 7p.*

LAMBRECHTS A., FOULQUIER L. & PALLY M. (1992). Synthèse des connaissances sur la radioéologie du Rhône. *Comité de bassin Rhône Méditerranée Corse. Groupe de travail "Qualité des eaux du Rhône" sous groupe "Micropollution toxique"* : 172 p.

VRAY F., SVADLENKOVA M. & BAUDIN J.P. (1993). Accumulation et élimination du ^{106}Ru par *Daphnia magna* Strauss. Etude des voies directe et trophique. *Annls. Limnol.* **29** (3-4) : 281-293.

VRAY F. (1994) Evaluation, modélisation et analyse des transferts expérimentaux du ^{106}Ru au sein d'un réseau trophique d'eau douce. Université se Montpellier II, Sciences et techniques du Languedoc, Thèse de doctorat (spécialité Biologie des populations et écologie) 24/11/94 : 377p

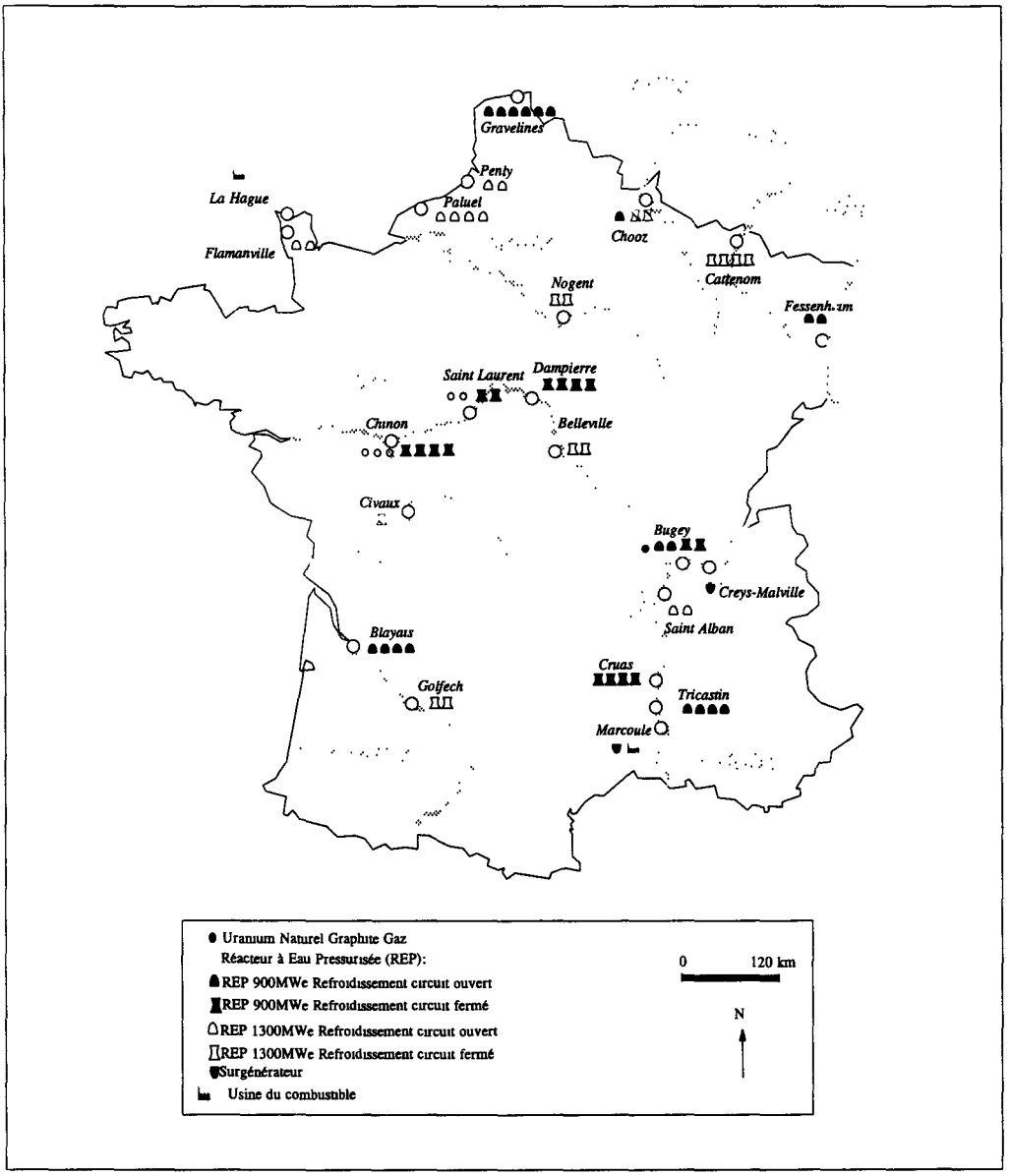

Fig 1. Installations nucléaires françaises

Fig. 1. French nuclear facilities

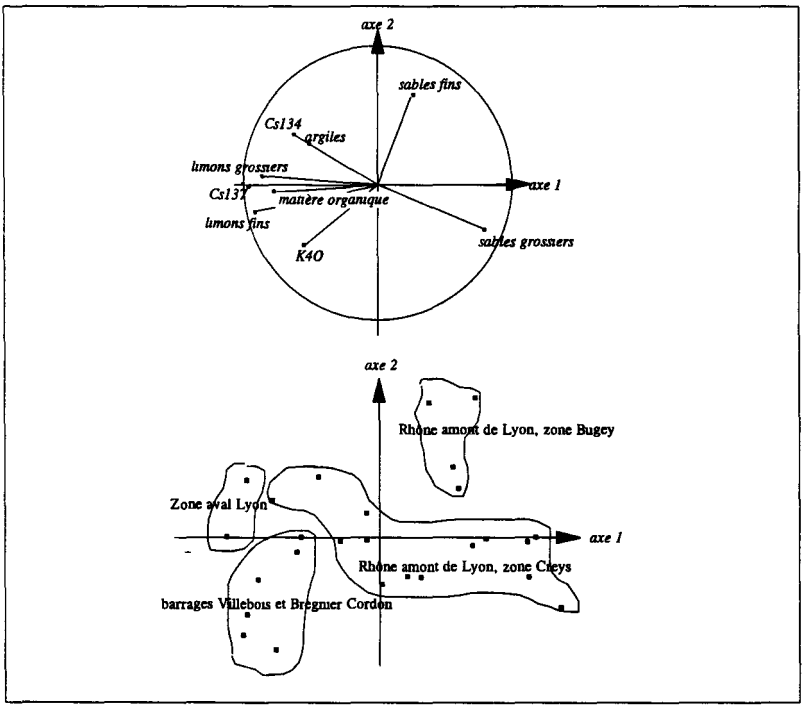

Fig.2: A.C.P. sur les sédiments du Haut-Rhône Français
Fig.2 : P.C.A. on french upper Rhone sediments

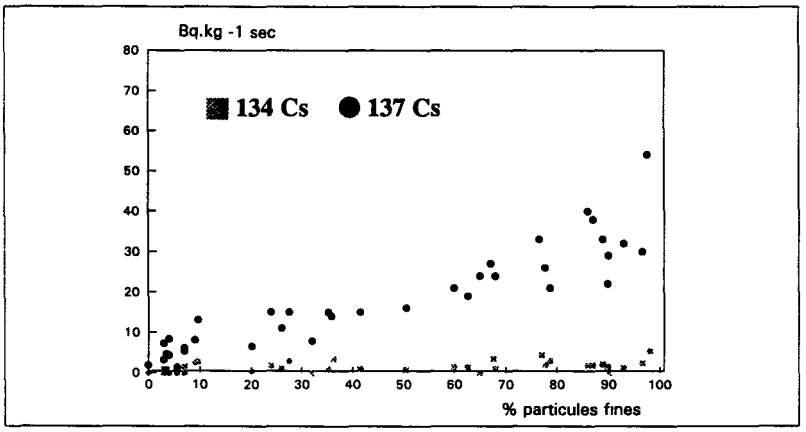

Fig.3: Relations entre radiocésium et particules < 50μm dans les sédiments du Haut-Rhône Français
Fig.3: relations between radiocesium and particles < 50 μm in french upper Rhone sediments

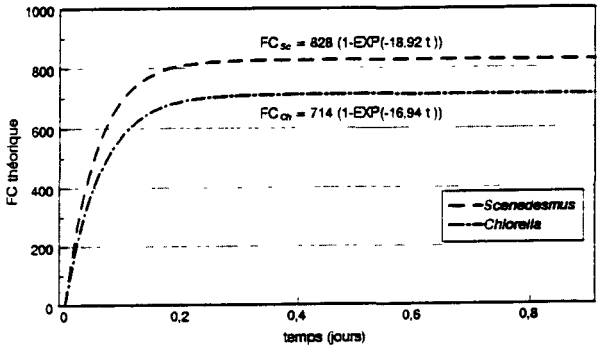

Fig. 4 : Simulation de l'évolution du facteur de concentration (FC) du ^{106}Ru par les algues en l'absence de divisions cellulaires et pour une concentration du radionucléide dans l'eau constante.

Fig.4 : simulation of algae ^{106}Ru concentration factor evolution for a constant water concentration and without cellular divisions

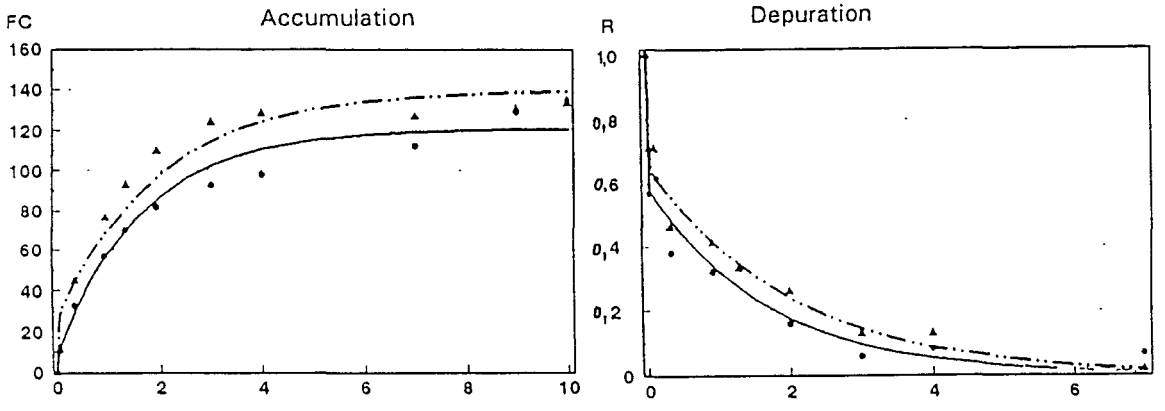

Fig. 5 : transfert du ^{106}Ru de l'eau aux daphnies (accumulation et élimination)

Fig 5 : transfer of ^{106}Ru from water to daphnids (accumulation and depuration).

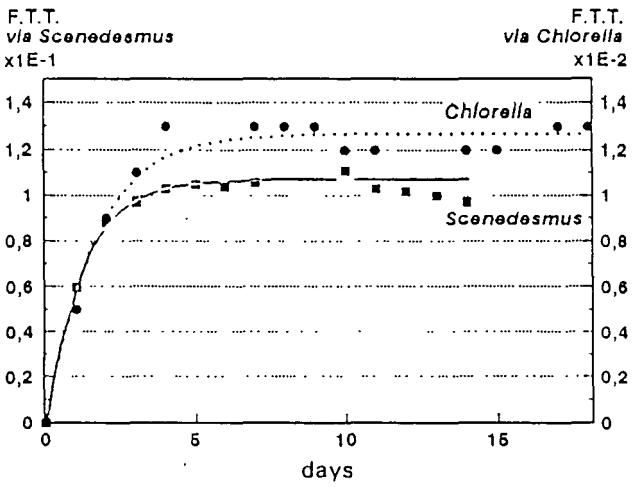

Fig 6 : transfert du ^{106}Ru des algues contaminées aux daphnies

Fig 6 : transfer of ^{106}Ru from algae to daphnids

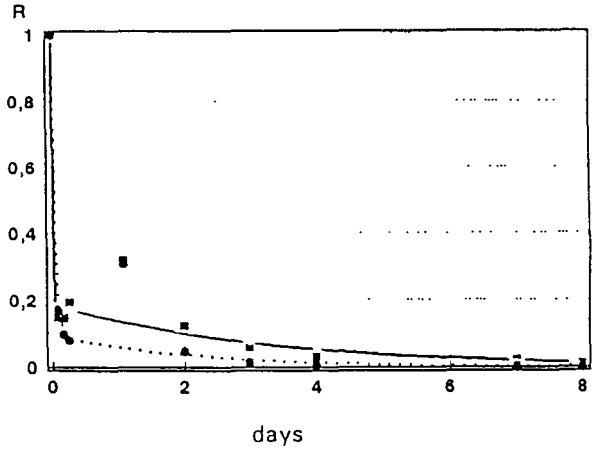

Fig 7 : élimination du ^{106}Ru des daphies aprés leur contamination par la nourriture

Fig 7 : depuration of daphnids after their contamination with food

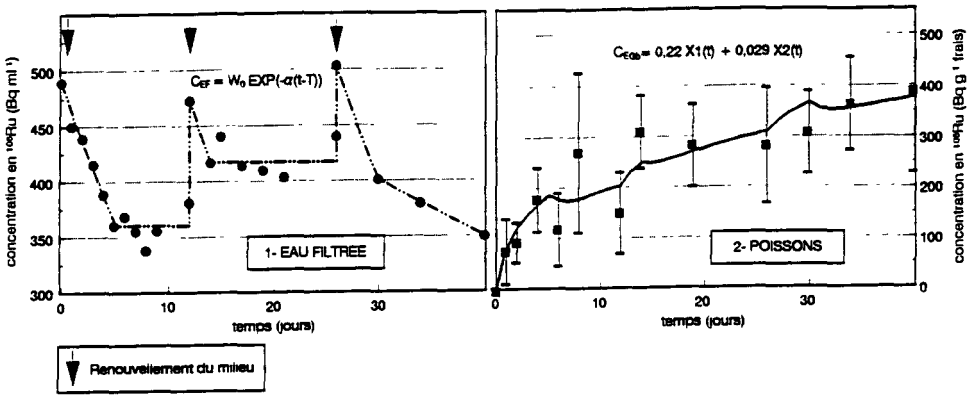

Fig 8 : transfert du ^{106}Ru de l'eau aux gambusies

Fig 8 : transfer of ^{106}Ru from water to gambusiae

Fig 9.: élimination du ^{106}Ru par les gambusies

Fig 9 : depuration of ^{106}Ru from gambusiae

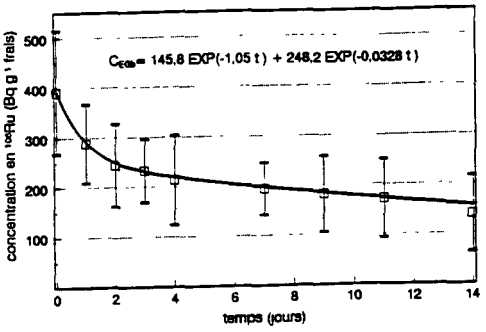

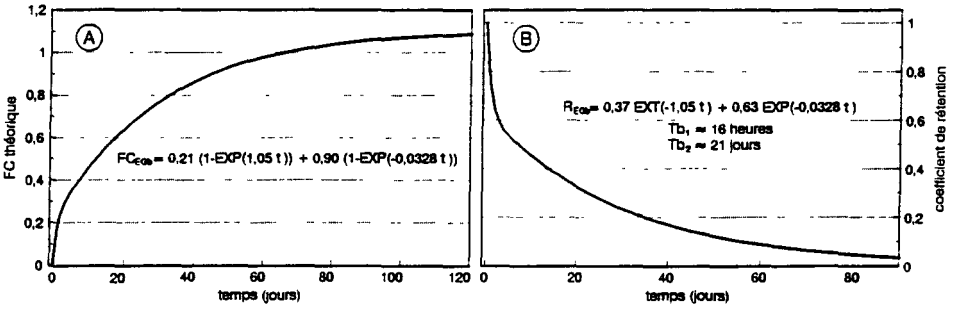

Fig 10 : simulation de l'évolution du facteur de concentration (FC) du ^{106}Ru par des gambusies pour une concentration dans l'eau stable (A) et rétention du radionucléide à l'arrêt de la contamination (B).

Fig 10 : simulation of gambusiae ^{106}Ru concentration factor evolution for a constant water concentration (A) and retention of nuclide in fish after contamination (B)

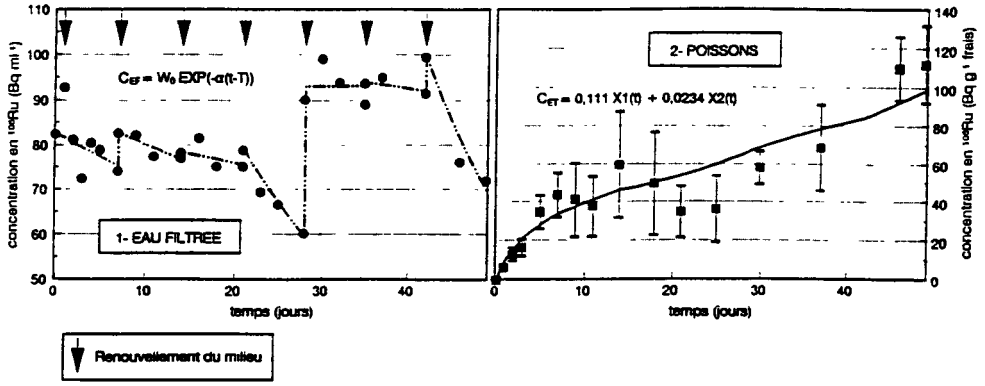

Fig. 11 : transfert du ^{106}Ru de l'eau aux truites

Fig. 11 : transfert of ^{106}Ru from water to trouts

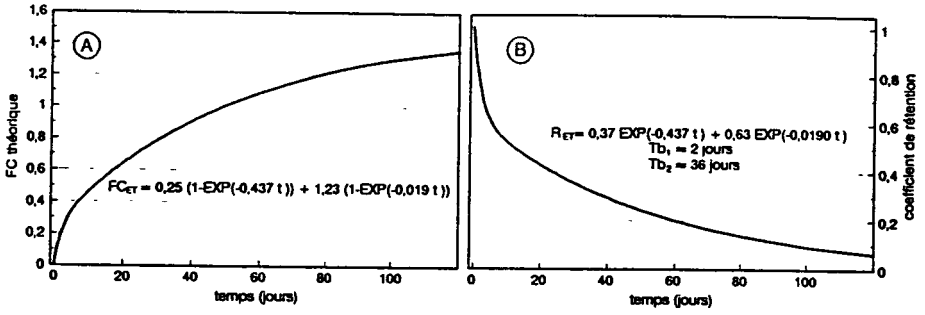

Fig. 12 : Simulation de l'évolution du facteur de concentration (FC) du ^{106}Ru par la truite pour une concentration dans l'eau constante (A) Rétention du radionucléide à l'arrêt de la contamination (B)

Fig. 12 : Simulation of ^{106}Ru concentration factor (CF) evolution for trout in a steady water concentration (A). Retention of the nuclide when contamination stops (B)..

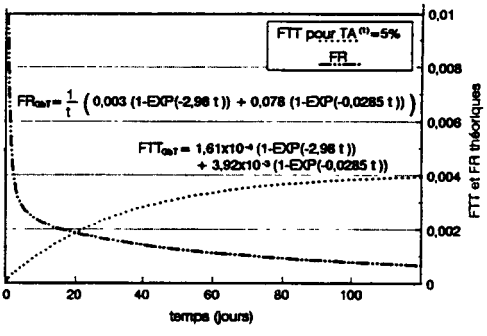

Fig. 13. Simulation de l'évolution du facteur de transfert trophique (FTT) et de rétention (FR) du ^{106}Ru à la truite liés à l'ingestion de gambusies contaminées.

Fig. 13. Simulation of trophic transfer factor (TTF) and retention factor (RF) of ^{106}Ru for trout ingesting contaminated gambusiae.

Head of project 6: Dr. Umberto Sansone, ANPA, Italy

II. Objectives

The main objective of this project is to study the role of particulate phase of a spring river in the transport of radiocaesium. In particular the study was focused on the distribution of radionuclides between solid and liquid phases because this is one of the most important parameters involved in the migration and fate of radionuclides in surface waters.

The experimental activities were carried out on a spring river (Stella river) located in the Friuli-Venezia Giulia region (north-eastern part of Italy). This site was selected because during our researches in the earlier EC contract, relatively high caesium concentration was observed in the sediments at the Stella mouth and this fact seemed to be in contrast with the regimen of the river (spring river) [1]. In fact the solid solid flow of this river has been always considered scarce owing to its spring characteristics. For this reason time series of solid measurement are lacking.

III. Progress achieved including publications

In the Friuli Plain, all the rivers with a mountain drainage basin loose their water discharge after a few kilometres due to the gravelly deposits of the high plain. Downwards the spring-line, in low plain characterized by sandy and silty deposits, rivers receive waters from ground-water table. Only during main floods, particularly in spring and autumn, waters flow all along the river-bed, from mountain area to the sea.
The Stella river (47 Km length) is the most important river flowing into the Lignano basin, the westernmost basin of the Marano lagoon. Its source is formed by a large number of springs located southward the spring-line.
The Stella river slighty erodes the silty-clayed soils of the plain, producing a wide and flat depression, recognizable as far as the lagoon border.
From 1926 until 1950, an average annual discharge of 33.6 $m^3 s^{-1}$, was calculated. A similar value (32.6 $m^3 s^{-1}$) was provided during the 1966-1974 period. The monthly average discharge of Stella is quite regular through the year: the minimum value seldom falls under 25 $m^3 s^{-1}$, while the maximum value is about three folds the average discharge.
By examining and comparing the daily discharge with the rainfall data, it can be noted that the former increases for one or two days after heavy rains (over 25 mm), owing to a rapid drainage.

In order to provide a complete set of enviromental data to characterize such a complex environment, different field activities where carried out from 1992 to 1994.
To assess the exchange processes between river and lagoon environment, the total suspended matter concentrations were measured by filtering 1 dm^3 of water, sampled by means of a Niskin bottle, on a Whatman GF/F fibreglass filter (0.8 µm pore size, 47 mm filter diameter). Elemental particulate organic carbon and nitrogen analyses were performed by combustion in pure oxigen atmosphere, using helium as entrainer by means of a Perkin Elmer 2400 CHN Elemental Analyzer.

The grain-size analyses of the suspended matter were performed by means of a Coulter Multisizer Analyzer, with an orifice tube of 140 µm.
The mineralogical composition was performed on a Siemens D 500 diffractometer, using CuKα radiation; scanning interval ranged between 2° and 35° of 2 Θ, pitch 0.1°, 2 seconds of computation per pitch. Quali-quantitative computation of the mineralogical phases were done using the diffractogram height of peaks.
Samplings of water and suspended matter for radiocaesium determination were carried out at the same depth (about 1 m from water surface) using two device capable of performing size fractionation of suspended solids using cartridge filters of 40, 10 and 0.45 µm porosity and filtering large amount of water (more than 500 dm^3). Each system was equipped with resin columns (ammonium exocyanocobaltferrate, NCFN) to fix radiocaesium dissolved in water. To determine the efficiency of the resins, two resins columns (diameter of 20 mm and height of 160 and 80 mm respectively) connected in series were used. ^{137}Cs concentrations were determined in samples by gamma-spectrometry using high purity Germanium detectors (HPGe).

Results

The mean grain size distribution of the total suspended material concentrations in the Stella river, from 1985 to 1993, show that the most frequent concentrations range between 5-10 mg dm^{-3}; whereas concentrations between 10 and 30 mg dm^{-3} are observed in more than one third of cases. Concentrations higher than 60 mg dm^{-3}, measured only during flood tide, can be considered exceptional.

The following table reports the mean elemental particulate organic carbon and nitrogen content on suspended particles performed by means of a Perkin Elmer 2400 CHN Elemental Analyzer on samples collected during the contract period.

	µg/l	sd
C (n=5)	436	43
N (n=5)	43	12
C/N (mol) (n=5)	12.4	3

The average mineralogical composition of the Stella river suspended material results as follows (in percent): calcite (14 ± 3), dolomite (50 ± 9), quartz (18 ± 10), feldspar (3 ± 1), illite (7 ± 4), kaolinite (2 ± 2), clorite (6 ± 3).
Dolomite is the most important mineral, followed by quartz and calcite. The sum of clay mineral percentages can reach 15 %; illite and chlorite content are almost equal, kaolinite is lower. Montmorillonite or other expandable clay minerals were not detected.

Following are reported the values of the main ions measued in the water of the Stella river.

Ca (mg/l)	Mg (mg/l)	K (mg/l)
70.3	24.6	0.94

In the following table are given the mean "in situ" Kd values for suspended material from the Stella river measured from 1992 to 1994. The partitioning of ^{137}Cs between soluble and particulate phases is here defined as the ratio of ^{137}Cs sorbed in the particulate phase to the concentration of this radionuclide in solution.

The table reports the mean ^{137}Cs Kd evaluated for the the different grain size of suspended particles and the totat Kd (40+10+0.45 μm) assessed considering the ^{137}Cs concentrations in the different fractions of suspended particles as follows:

$$\text{Total } Kd_{(40+10+0.45\mu m)} = [(\Sigma\, C_i\, a_i) \cdot (\Sigma a_i)^{-1}] - C^{-1}_{water}$$

where C_i is the ^{137}Cs concentration in suspended particles with size i;
a_i is the concentration of this size of particles in water and
C_{water} represents the ^{137}Cs dissolved in water.

Filter Size μm	Mean ^{137}Cs Kd l/g	Coefficient of Variation %
40 (n=5)	151±29	19
10 (n=5)	169±51	30
0.45 (n=5)	243±73	30
(40+10+0.45)	**166±36**	**22**
0.45 (n=12)	**151±51**	**34**

In the same table is reported the mean value of the total ^{137}Cs "in situ" Kd evaluated filtering the water only with 0.45 μm size filter.

Discussion and conclusions

The data of elemental particulate organic carbon and nitrogen content on suspended particles allow to define the relations between the suspended material and the surrounding environment (predominance of the detrital component over the living one).
Molar ratios of C/N less than 5 indicate that metabolic phenomena are established due to the presence of bacteria responsible of a more rapid degradation of the organic carbon. Values ranging around 6 are characteristics of living phytoplanktonic communities. Higher C/N values are found when the organic detrital component are prevailing over the living component, or when there is a remarkable contribution of eroded material. The suspended material collected in the Stella river shows a C/N mean value of 12.4±3 and indicates the presence of material derived from erosion processes.

The ^{137}Cs concentration in the water of the Stella river was quite uniform from 1992 to 1994, since it ranged between 4.1 x 10^{-4} and 12.0 x 10^{-4} with a mean of 8 x 10^{-4} Bq l^{-1}. A low variability it is also observed in the ^{137}Cs concentrations measured in the suspended material collected in the same period.

The ^{137}Cs "in situ" Kd values evaluated for the different grain size of suspended particles show higher values for the grain collected on filter of 0.45μm size. The values are higher (about one order of magnitude) if compared with measurements carried out by other Authors [2] in laboratory experiments. Our values could be explained considering the presence of significant concentrations of clay minerals (about 15 %) in particles transported by the Stella river. The Stella river in fact slighty erodes the silty-clayed soils of the plain located southward the spring-line. The high Kd values could be attributable to the aging effect of Chernobyl caesium. In this case, the long time elapsed from deposition has as result a partially irreversible binding of radiocaesium in the clay minerals. The high ^{137}Cs Kd values are also in agreement with the low amount of K^+ found in the water of the Stella river (0.94 mg/l).

The total ^{137}Cs Kd (40+10+0.45 μm) assessed considering the ^{137}Cs concentrations in the different fractions of suspended particles (166±36 l/g) and the mean value of the total "in situ" ^{137}Cs Kd evaluated filtering the water only with 0.45 μm size filter (151±51l/g) are in agreement. This confirm, that the devices developed by ANPA to perform size fractionation of suspended particles on large amount of water, do not influence, with regards to radiocaesium, the distribution between liquid and solid phases.

Finally, combining the average suspended matter concentration with the average annual discharge of the Stella river, it is possible to evaluate the amount of suspended material and ^{137}Cs transported into the lagoon. Assuming a mean concentration of suspended matter of 10 mg dm^{-3}, the corresponding annual amount cannot be lower than 10000 ton y^{-1}, leading to an input of 10^8 Bq y^{-1} of ^{137}Cs discharged into the lagoon. In contrast with the regimen of the Stella river (spring river), the transport of suspended material cannot be considered negligible. The relatively high radiocaesium concentration found in the sediments at the mouth of the river is attributable to the continuous deposition of materials eroded from the silty-clayed soils of the plain.

References

M. Belli, E. Colizza, G.P. Fanzutti, F. Finocchiaro, R. Melis, R. Piani, U. Sansone (1994). The role of a spring river as source of radiocaesium in a lagoonal environment: the case of Stella river (Marano lagoon, Northern Adriatic Sea). Presented at the "International Seminar on Freshwater and Estuarine Radioecology", Lisbon, 21-25 March 1994.

.

P. Benes, M. Cernik, P. Lam Ramos. (1992). Factors affecting interaction of radiocaesium with freshwater solids. Jour. of radioch. and nuclear chem., 159, 2. 201-218.

Head of project 7: Dr. Blust

II. Objectives:

Development of mechanistic concepts and models for radionuclide uptake in aquatic organisms based upon a fundamental appreciation of chemical and biological processes. The research focused on the effect of environmental conditions on the uptake of radiocaesium and cobalt using the carp, *Cyprinus carpio* as a model organism. The results obtained have been used to construct a pharmacokinetic model for radionuclide uptake by aquatic organisms that can be used to predict the effect of changes in water composition and radionuclide speciation on accumulation kinetics.

III. Progress achieved including publications:

Radionuclide speciation analysis and modelling

In aquatic systems, radionuclides do not occur as single entities, but as a set of different chemical species distributed among soluble, colloidal and solid reservoirs. The biological availability of a radionuclide is largely determined by the chemical speciation of the metal in the environment. Since the speciation of a radionuclide is one of the most important factors to consider when assessing the environmental impact of a radionuclide, it is evident that accurate assessment requires knowledge of both its concentration and speciation. While methods to measure concentrations are well established, methods for speciation analysis are still being developed. .

The speciation of radionuclides in solutions strongly depends on the composition of the water. Inorganic species such as chloride, carbonate and phosphate that can interact with metals are easily measured and their interactions with the metals characterised. Organic ligands, however, present a different situation. They occur in an almost infinite variety and can interact with the metals in a multitude of fashions. Natural sources contribute the bulk of the organic matter present in most surface waters. Humic and fulvic acids, which are important complexing agents for metals, constitute the majority of the organic matter.

The speciation of a metal in solution is represented most simply by a set of equilibrium expressions, ($M+nL=ML_n$ and $K=[ML_n]/[M][L]^n$). A number of values are needed to characterise these relationships. The concentration of the metal ions, the concentrations of the ligand, the stoichiometry of the reactions and the corresponding stability constant. The concentration of the free ligand in the solution is referred to as the complexation capacity. For multi-ligand systems the measured stability constant will not be that for a single ligand but an average value which is the result of the overall extent of complexation. The measured stability constant is actually a conditional stability constant. That is, the constant is measured under a set of limiting conditions (hardness, temperature, hydrogen ion activity), which makes the value different from the thermodynamic stability constant. The thermodynamic stability constant can be calculated provided that the dependence of the equilibria on the conditions are known.

One of the most promising methods for chemical speciation are metal-ligand competition solvent extraction equilibration procedures. The extent of complexation of the metal depends on the concentration of the ligands normally present in the system and an added ligand used as a competitor. The competitor forms complexes with the radionuclides which partition between the aqueous and organic phase. If the partitioning of the radionuclide between the aqueous and organic phase is measured at different metal and competitor concentrations, then the stability constants and concentrations of the natural ligand can be calculated. The technique is based on the thermodynamic rather than the kinetic properties of the reactions considered. The method is thermodynamically well characterised and involves a minimum of operationally defined conditions. The results of these measurements have been used as input in a newly developed chemical speciation model to calculate the chemical speciation of radionuclides in aquatic systems (SOLUTION).

Pharmacokinetics of radionuclide uptake by fish

The design of most radionuclide uptake and elimination experiments with aquatic organisms assumes constant exposure regimes. Constancy of exposure greatly simplifies analysis of uptake kinetics and enables simple estimation of steady state concentrations. However, constant exposures are rare in the real world and often difficult to realise in the laboratory. Clearance constant-based pharmacokinetic models are unique in that model parameters represent discrete physiological processes, i.e. absorption, metabolism, excretion, whereas model parameters in the more conventional rate constant-based models can be a function of more than one physiological process. Thus, it is possible to gain insight into absorption rate-limiting processes from the magnitude of the absorption clearance constant. Additionally, the model-predicted pharmacokinetic parameters can be used to make predictions regarding the bioconcentration factor and the expected concentration in the fish at steady state.
Pharamacokinetic analysis indicated that in the most simple form the fish could be treated as a one-compartment open model for uptake of radionuclides with changes in the rate of radionuclide uptake by complexation and loss to container walls (see appendix). The models developed can be used to analyse data involving non-constant exposure to radionuclides in natural environments. In more complex situations a two compartment model should be used but the principals are the same. The clearance of radionuclides depends on a number of factors which can be related to 1) the concentration and chemical speciation of the radionuclide in the water and other sources and 2) the kinetics and selectivity of the transport systems involved in the uptake and elimination of the radionuclide by the organism. A convenient model to describe these effects and incorporate them in the pharmacokinetic model is the Michaelis-Menten model for enzyme kinetics. Instead of a single parameter describing clearance two parameters are required, Clearance=$V_{max}/(K_m+S)$ in which S is the concentration of the radionuclide in the environment and V_{max} and K_m are the maximal uptake rate and K_m is the dissociation constant.

The uptake of radionuclides is a mediated process in which the radionuclide interacts with the transport systems to form a temporary association. In its most simple form this process can be presented by the following model:

$$S_{out} + T \underset{k_{-1}}{\overset{k_1}{<====>}} ST \xrightarrow{k_2} T + S_{in}$$

Where k_1 and k_{-1} are the rate constant for the forward and reverse complex formation reactions and k_2 the rate constant of the irreversible translocation reaction. The kinetics of the uptake process can be described by the Michaelis-Menten equation:

$$V=V_{max}*S/(K_M+S) \text{ with } K_M=(k_{-1}+k_2)/k_1$$

where Vmax is the maximum uptake rate, S the radionuclide concentration, and K_M the half-saturation constant. This is the concentration of the radionuclide at which V=1/2Vmax. When the concentration of the radionuclide is small relative to K_M then the transport kinetics are first order:

$$V=V_{max}*S/K_M$$

Values of Vmax and K_M have been determined by measuring uptake rate for carps exposed to a wide range of caesium and cobalt concentrations. The concentration of potassium in freshwater environments is a critical factor determining the uptake of ^{137}Cs by aquatic organisms. The uptake of caesium decreases with increasing potassium concentration in the water, which results from the competition of potassium and caesium for the same transport system. Similar interactions account for the effect of calcium on cobalt uptake. These interactions can be described by a competitive inhibition model:

$$V=V_{max}*S/(K_M*(1+i/K_i(+S))$$

where K_M is the Michaelis constant of the uninhibited process and K_i is the dissociation constant of the inhibitor-transporter complex. The effect of a competitive inhibitor is therefore to decrease the apparent affinity of the radionuclide for the transporter. The latter equation substitutes for the uptake rate (k_1) in the kinetic model for radionuclide accumulation. This results in a new model that accounts for changes in water composition on radionuclide uptake.

The effect of organic complexation on the uptake of cobalt by carps has been studied in chemically defined environments with ligands of different thermodynamic stability. Complexation decreases the uptake of the radionuclide which is in agreement with the general view that the availability of metals to aquatic organisms depends on the activity of the free metal ion in the solution. There is no evidence that the direct uptake of complexes is of any significance. This means that the effect of chemical speciation on the uptake of cobalt from the water can be described by one single variable, the free metal ion activity in the solution. This means that radionuclide uptake does not depend on the concentration of the radionuclide in the water but on the activity of the radionulide species that are taken up by the organisms, i.e. the free metal ion.

A clear decrease in cobalt uptake was also observed with increasing calcium concentrations, but not with magnesium concentrations is observed. The effect of calcium in the water of acclimation is significant but much less than the direct effect of calcium in the exposure water. Since uptake kinetics of both cobalt and calcium show similar results for influx in body, gills and blood, and both elements inhibit each others uptake, the effect of calcium on cobalt uptake is due to a direct interaction at the membrane translocation system. An increase in ionic strength reduces cobalt uptake and this effect is fully explained by the effect of ionic strength on the activity coefficient of the free metal ion.

As an illustration the pharmacokinetic model for the uptake of radionuclides by carp has been used to model the accumulation of caesium and cobalt by carp in different potassium and calcium regimes, respectively (Fig 1-4). In the examples given the concentrations of the radionuclides in food have been fixed to better show the effect of water composition on the relative importance of water and food in radionuclide uptake. In the natural environment however this will not be the case and food contamination will also change with exposure conditions. As expected the model for caesium predicts that the uptake of caesium from water is of minor importance and only becomes a potential concern in very low potassium regimes. For cobalt the situation is more complex, since both water and food are important sources of the radionuclide, water being the main source in soft waters and food the main source in hard waters. In general these models explain more than 90 % of the variation observed under experimental conditions.

Conclusions

The research on the effects of environmental conditions on the uptake of radionuclides by carp has cumulated in the construction of a general mechanistic model for the accumulation of radionuclides in aquatic organisms. The key feature is the linkage of a chemical speciation model to a model for the transport of radionuclides across biological interfaces. As such it has been proved possible to model the effect of changes in the ionic composition and complexation capacity of the environment on the accumulation of radionuclides by biota. The models are much more robust than the ones being used today to predict the fate of radionuclides in aquatic ecosystems since processes are described in terms of mechanisms rather than correlations. The research has also identified many major gaps in the fundamental understanding of radionuclide accumulation in food chains. In general there is a lack of good quality data which can be used to construct mechanistic models for the effect of environmental conditons on radionuclide transfer. The major problem which remains is the lack of information on the uptake of radionuclides at lower trophic levels, especially invertebrates, which make it difficult to model the concentration of radionuclides in the food of predators in a variable environment.

Publications

Comhaire, S., Blust, R., Van Ginneken, L., Vanderborght, O. 1994. Cobalt uptake across the gills of the common carp, *Cyprinus carpio*, as a function of calcium concentration in the water of acclimation and exposure. Comparative Biochemistry and Physiology, 1, 63-76.

Van Ginneken, L. and Blust, R. 1995. Sequential determination of a combined gamma/beta and pure beta emitter by gamma and liquid scintillation counting: application to the transport of metals across fish gills. Analytical Biochemistry, 224, 92-99.

Comhaire, S. Blust, R. Van Ginneken, L., D'Haeseleer, F., Vanderborght, O. Environmental calcium influences radio-cobalt uptake by the common carp, *Cyprinus carpio*. Science of the Total Environment, In Press.

Blust, R., Van Ginneken, L., Comhaire, S. Vanderborght, O. Uptake of radio-cobalt by the common carp, *Cyprinus carpio* in complexing environments. Science of the Total Environment, In Press.

Comhaire, S., Blust, R., Van Ginneken, L., Verbost, P., Vanderborght, O. Branchial uptake by the carp, *Cyprinus carpio*: Partial involvement of the calcium uptake system. Journal of Experimental Biology, Submitted.

Comhaire, S., Blust, R., Vanderborght, O. Branchial cobalt uptake is competitively inhibited by waterborne calcium in carp. Journal of Experimental Biology, Submitted.

Blust, R., Comhaire, S, Van Ginneken, L.. A Michaelis-Menten pharmacokinetic model for the accumulation of cobalt by carp. Environmental Chemistry and Toxicology, Submitted

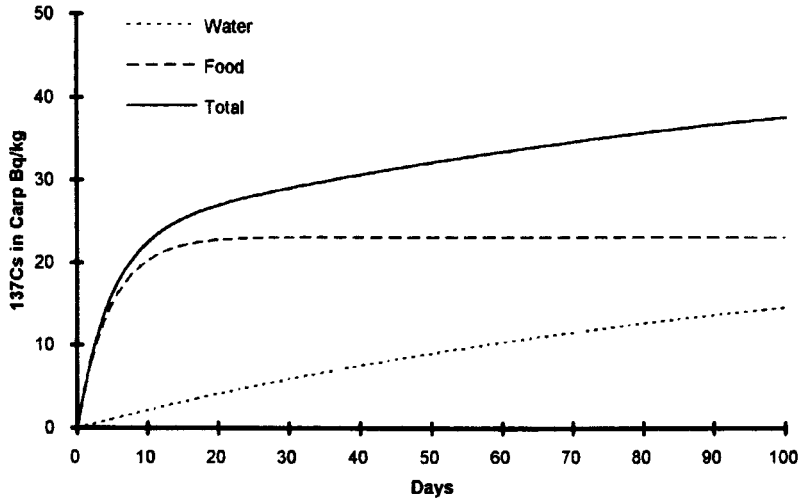

Fig 1: Accumulation of ^{137}Cs by carp from solution and food in a 0 01 mM K^+ environent. The water contains 1Bq.l^{-1} and the food 100 Bq kg^{-1} of ^{137}Cs. The food ration equals 5 % of the body weight per day.

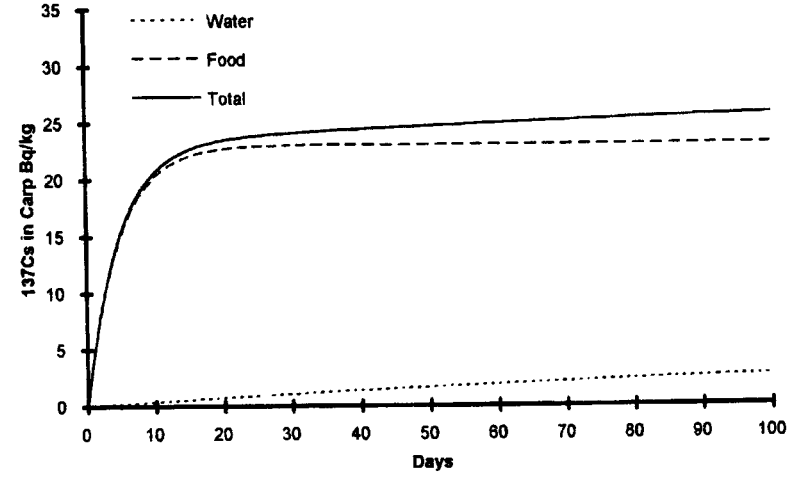

Fig 2: Accumulation of ^{137}Cs by carp from solution and food in a 0 1 mM K^+ environent. The water contains 1Bq.l^{-1} and the food 100 Bq.kg^{-1} of ^{137}Cs. The food ration equals 5 % of the body weight per day.

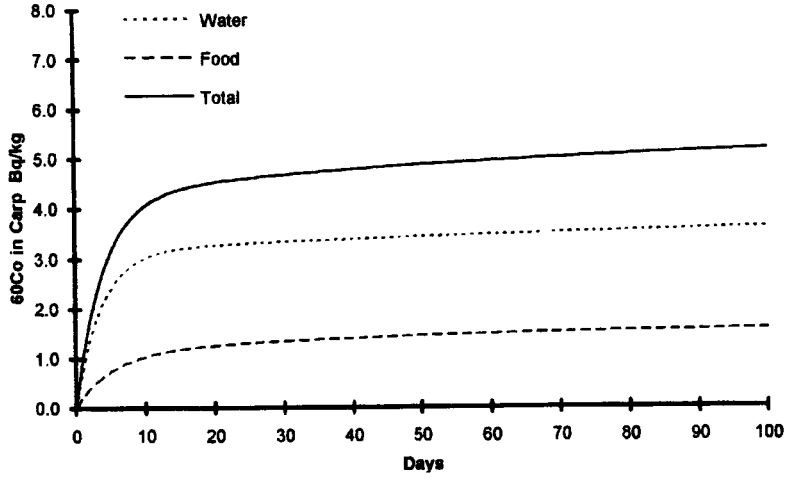

Fig 3: Accumulation of ^{60}Co by carp from solution and food in a 0.1 mM Ca^{2+} environent. The water contains 0.1Bq.l^{-1} and the food 100 Bq.kg^{-1} of ^{137}Cs. The food ration equals 5 % of the body weight per day.

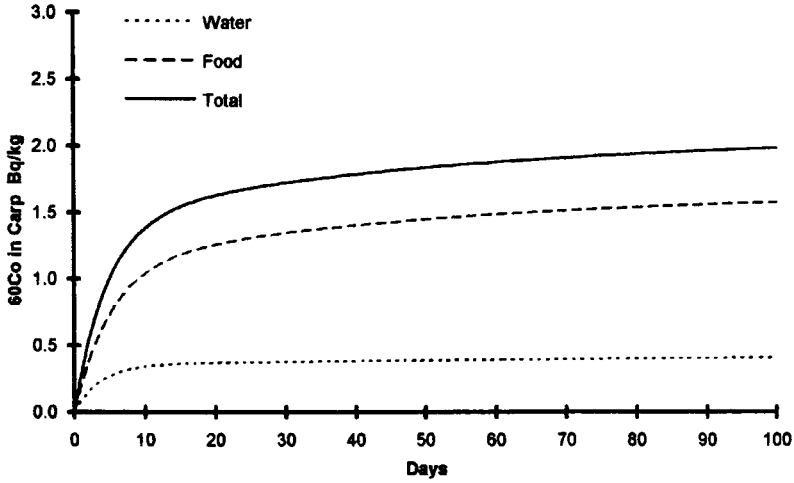

Fig 4: Accumulation of ^{60}Co by carp from solution and food in a 1 mM Ca^{2+} environent. The water contains 0 1Bq.l^{-1} and the food 100 Bq.kg^{-1} of ^{137}Cs. The food ration equals 5 % of the body weight per day.

Appendix:

One-compartment open model for uptake of radionuclide by fish with loss to container walls.

Rate of change in the amount of radionuclide in the fish

$$dX_f/dt=CL_a(C_w-C_f) \quad (1)$$

CL_a=absorption clearance constant

C_w=concentration of radionuclide in water

C_f=concentration of radionuclide in body water of the fish

The apparent volume of distribution (V_d), is the proportionality constant that relates the amount of radionuclide in the body to its concentration in the body water of the fish.

$$dX_f/dt=CL_a(C_w-X_f/V_d) \quad (2)$$

Rate of change in the concentration of radionuclide in water:

$$dC_w/dt=(CL_a\ FW/V_0)\cdot[(X_f/V_d)-C_w]-(k_l\cdot C_w) \quad (3)$$

FW=mean fish weight

V_0=volume of water in tank.

Integration of (2) and (3) gives:

$$X_f=[(CL_a.C_w^0)/(\beta-\alpha)]e^{-\alpha t}+[(CL_a.C_w^0/(\alpha-\beta)]e^{-\beta t} \quad (4)$$

$$C_w=[C_w^0((CL_a/V_d)-\alpha)/(\beta-\alpha)]e^{-\alpha t}+[C_w^0((CL_a/V_d)-\beta)/(\alpha-\beta)]e^{-\beta t} \quad (5)$$

C_w^0 is the initial concentration in water.

α and β are hybrid rate constants that are defined in terms of model parameters.

$$\alpha+\beta=CL_a/V_d+(CL_a.FW)/V_0+k_l=x \quad (6)$$

$$\alpha.\beta=(CL_a.k_l)/V_d=y \quad (7)$$

Equations (4) and (5) are fitted simultaneously to the experimental data to obtain values for the model parameters CL_a,, V_d and k_l. Estimates for the hybrid rate constants were obtained as secundary parameters by using the quadratic solution to: $\alpha^2-x\alpha+y=0$

Input required to model the system:

C_w^0 is the initial concentration of radionuclide in water.

C_w is concentration of radionuclide in water at time t.

FW is mean fish weight

V_0 is volume of water in tank.

X_f amount of radionuclide in fish.

t is time of incubation.

Head of project 8: Dr. Fernández

II. Objectives

The objective of this project was to study the mechanisms of uptake and accumulation of radiocesium in freshwater plants, taking *Riccia fluitans* as plant type. The initial hypothesis was to consider the mechanisms of transport and accumulation of potassium as the possible ways for transport and accumulation of radiocaesium in aquatic plants. Once these mechanisms were investigated, the influence of some selected environmental variables was studied in order to define the major control variables influencing the mentioned processes. The data obtained were used to define a mechanistic kinetic model that could be of general application in the most conspicuous freshwater plants. Finally the kinetic parameters obtained were integrated in a general mathematical model to predict the flow of radiocaesium through freshwater ecosystems.

III. Progress achieved including publications

Depending on the concentration of potassium in the environment, freshwater plants incorporate potassium in two different ways (Fernández et al., in press; Sanders et al, in prep.). Under potassium sufficiency (plants growing at an overall external potassium concentration around 0.1 mM), potassium is transported at plasmalemma level through potassium channels. This transport system is diffusive, the driving force being the electrochemical potential gradient for potassium at both sides of the membrane:

$$\Delta\mu_{K+}/F = z\,(Em - E_N^{K+}) \qquad \text{Eqn. 1}$$

where z is the charge of potassium, Em is the membrane potential, and E_N^{K+} is the Nernst potential for potassium.

The diffusive constant for such a transport is defined by the membrane permeability for potassium. This intrinsic membrane characteristic is roughly uniform for most freshwater plants, and is accounted for the abundance, activity and conductivity of the potassium channels in the plasmalemma. Potassium channels in plants are not perfectly selective for potassium (Bentrup, 1990). There is a series of positive monovalent ions that enters the cells through potassium channels. Ordered from the most permeable ion i.e. potassium, to the less permeable one, caesium, a general series for freshwater plants could be: $K^+ > Rb^+ > NH_4^+ > Na^+ > Li^+ > Cs^+$. Being the relative permeability of Cs^+ with respect to K^+ around 0.6 in the case of *R. fluitans* (Fernández et al. in press).

Under potassium deficiency (plants growing at an overall potassium concentration around 0.01 mM), *R. fluitans*, and probably most freshwater plants exhibit an active transport system for potassium (Sanders et al. in prep.). This system has higher affinity for potassium (k_s=25 μM) and exhibits a Michaelis-Menten type uptake kinetic, compared with channel transport that exhibit, over the concentration range assayed, a lower affinity and a linear uptake kinetic. Cytoplasmic pH (pHc) measurements performed by using pH sensitive microelectrodes (for a complete description of this technic see Felle and Bertl, 1986), indicate that a transient acidification of pHc takes

place upon the addition of micromolar amounts of potassium or caesium (figure 1). These results suggest that potassium and caesium enter the cells in a proton cotransport, the driving force being the electrochemical gradient for protons. Such a gradient being generated by the operation of a proton pump present in the plasmalemma of green plants. As expected, this system does not work in the presence of inhibitors of dark respiration as CCCP, azide, cyanide, or in the presence of inhibitors of the proton pump as vanadate or eritrosine b.
Radiocaesium is transported by means of both mechanism. In the figure 2, the uptake kinetics for caesium in *R. fluitans* plants, submitted to potassium sufficiency (linear kinetic) and deficiency (Michaelis-Menten kinetic). The transport efficiency of the active system being ten times higher than the efficiency of the passive (diffusive) system. In addition both system exhibit a different capacity for radiocesium accumulation (figure 3). Channel transport, in plants submitted to potassium sufficiency, yields a CF for radiocesium of 51±2 (n=8), in contrast, active system for potassium yields a CF for radiocesium of 1329±128 (n=5).

Plants submodel.
Kinetic data obtained in the experiments mentioned above were used for building up a tentative mathematical model, to predict the CF for radiocesium in freshwater plant as a function of the most conspicuous variable affecting to the processes of radiocesium uptake and accumulation. Since caesium uses the same transport systems than potassium for entering the cells, uptake rate and CF for caesium are dramatically affected by the external concentration of potassium at two levels: instantaneous, because potassium compete with caesium for the transport system and the integrated effect of the overall external potassium concentration during the life of the plant.
For modelling purposes we assumed a threshold of 0.1 mM of external potassium concentration to define plants submitted to potassium sufficiency (plants living at potassium concentration equal or higher than 0.1 mM) and plants submitted to potassium deficiency (plants living at external potassium concentrations below 0.1 mM). This figure can be used as the threshold to predicting CF from the kinetic parameters obtained for the diffusive transport or from those obtained for the active transport of radiocaesium.
Potassium sufficiency
Under potassium sufficiency, radiocesium is accumulated in plants through potassium channels. The amount of caesium accumulated in the equilibrium, can be expressed as a millivoltage by using the Nernst equation,

$$E_N^{Cs} = RT/zF \cdot \ln Cs^+_o/Cs^+_i \qquad \text{Eqn 2.}$$

where R is the gas constant, T the absolute temperature, z the electrical charge of caesium, F the Faraday constant, Cs^+_o is the concentration of caesium in the water and Cs^+_i is the concentration of caesium inside the cells. Since Cs^+_i/Cs^+_o is the concentration factor (CF), equation 1 can be expressed as

$$E_N^{Cs} = RT/zF \cdot \ln CF^{-1} \qquad \text{Eqn 3.}$$

Caesium reaches equilibrium when the Nernst potential for caesium (E_N^{Cs}) equals the membrane potential (Em) thus, by knowing Em, and additionally the response of Em to some fundamental environmental variable, as the potassium concentration in the

water, it is possible to predict CF as a function of Em and additionally as a function of potassium concentration in the water.
For a well known freshwater green plant as *Riccia fluitans*, the relationship between Em and the external potassium concentration has been determined. This relationship can be defined by the equation,

$$Em = E_0 + p\ RT/F\ .\ \ln K^+_w \qquad \text{Eqn 4.}$$

where E_0 is the membrane potential for a potassium concentration in the water of 1 mM, p is the selectivity of potassium channels for caesium over potassium, and for this plants takes the value 0.73, and K^+_w is the concentration of potassium in the water. The fitting of this equation to experimental data is $Em = -105 + 18.45 \ln K^+_w$ (r=0.98, n=23).
Since CF can be predicted from Em,

$$CF = 1 / EXP [\ EmzF / RT\ ] \qquad \text{Eqn 5.}$$

and Em can be predicted, according to Eqn 4, from the potassium concentration in the water, it is possible to predict CF as a function of the concentration of potassium in the water,

$$CF = 1 / EXP [\ (E_0zF / RT) + p \ln K^+_w \qquad \text{Eqn 6.}$$

In the model, CF is assessed by equation 6 when plants are not under potassium deficiency, i.e. when plants grow at a potassium concentration in the water of 0.1 mM or higher. This equation reflects that under these conditions, the only transport mechanism operating in the membranes are potassium channels. Figure 4 shows the agreement between experimental figures (closed circles) for CF obtained for plants submitted to potassium sufficiency at different external potassium concentrations and the prediction of the model (line) based in the Nernst equation approach.

Potassium deficiency.
It is generally accepted that green freshwater plants are submitted to potassium deficiency when they grow under potassium concentrations in the water clearly below 0.1 mM. In these cases, potassium is incorporated actively by plant cells. The uptake mechanism proposed is a cotransport, in which the driving ions are either protons or sodium. These transport systems are also sensitive to caesium, but they exhibit an higher affinity and produce an higher CF than potassium channels. In this case, the uptake kinetic is a Michaelis-Menten type and the selectivity of the transport system is a function of the relative affinity of caesium over potassium for the carrier. Uptake rate (V) can be computed from

$$V = Vmax\ .\ Cs_w / [\ Ks_{Cs}\ .\ (1 + K^+_w / Ks_K)] + Cs_w \qquad \text{Eqn. 7}$$

where Vmax is the maximum rate of transport for caesium, Cs_w is the concentration (total) of caesium in the water, Ks_{Cs} is the half saturation constant for Cs^+ transport and Ks_K is the half saturation constant for potassium.
Elimination has been defined as a function of an average biological half life (BHL) for phytoplankton,

k elimination = ln 2 / BHL Eqn 8

In the model, the change of the concentration of caesium in the plants (dC/dt) is,

$dC/dt = k\ uptake\ .\ Cs_w - k\ elimin\ .\ Cs_p$ Eqn. 9

where k uptake is V times Cs_w and k elimin times Cs_p (the concentration of Cs^+ in the plants) is the elimination rate.
Concentration factor of these plants is computed as the concentration of caesium in the plants divided by the concentration of caesium in the water when the model reaches equilibrium. In the figure 5, it is shown a good agreement between experimental data obtained with plants submitted to potassium deficiency (closed circles) and the predicted values of CF as a function of the external potassium concentration (line) by using the kinetic parameters from the Michaelis-Menten approach.

Plants submodel has been developed in collaboration with Dr. Rudie Heling (KEMA, Holland) and integrated in more complex mathematical models used to predict the fate of radiocaesium in lakes of Europe in the VAMP program framework.

References

F.W. Bentrup.1990. Potassium ion channels in the plasmalemma. *Physiologia Plantarum*, 79:705-711.

Felle H. and A Bertl. 1986. The fabrication and use of H^+-selective liquid-membrane micro-electrodes for use in plant cells. *Journal of Experimental Botany*. 37(52): 1416-1428.

Fernández J.A., Heredia M.A., García-Sanchez M.J., Gil J.A., Vaz Carreiro M.C. and Diez de los Rios A. (1994). Mechanisms of radiocesium uptake and accumulation in *Riccia fluitans*. Proceedings of the International Seminar on Freshwater and Estuarine Radioecology. Lisbon. Portugal.

Sanders D., Corzo A. and Fernández J.A. Mechanism of potassium uptake in *Riccia fluitans* submitted to potassium deficiency. Submitted.

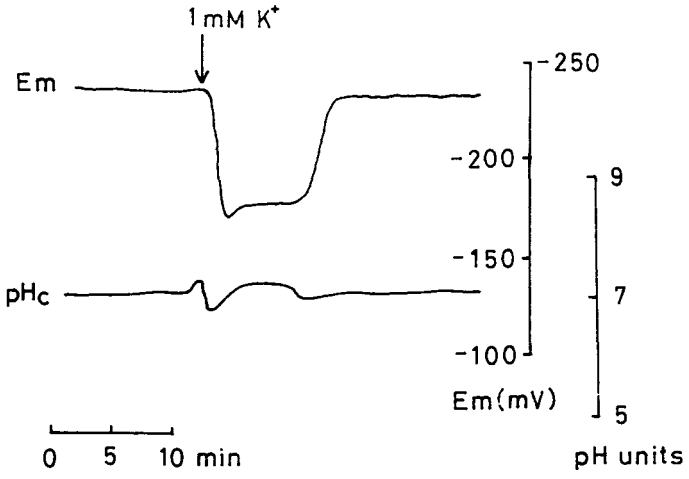

Figure 1.- Continuous recording of membrane potential (Em) and cytoplasmic pH (pHc) in cells of the aquatic liverwort *Riccia fluitans* submitted to potassium deficiency. Addition of 1 mM of KCl is marked by an arrow.

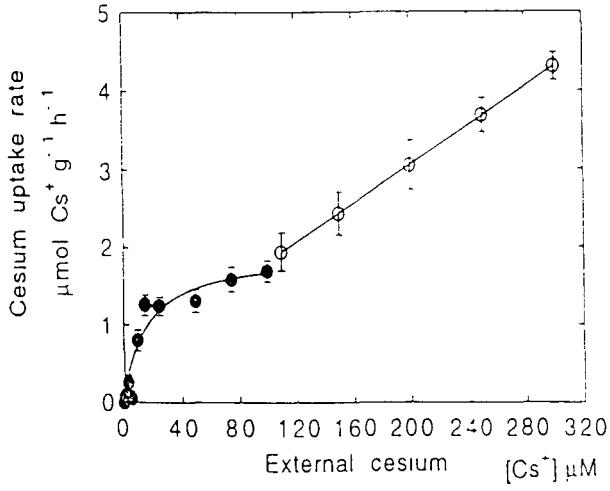

Figure 2.-Dual uptake kinetic of caesium as a function of the external total caesium concentration in *Riccia fluitans*, submitted to potassium deficiency (closed circles) and potassium sufficiency (open circles).

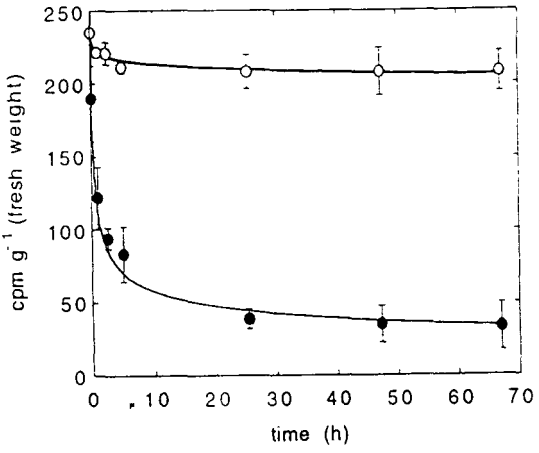

Figure 3.- Time course of the variation of radiocaesium activity in the water, corrected by the biomass of *Riccia fluitans* used in the experiments. Open and closed circles denote plants submitted to potassium sufficiency and deficiency respectively.

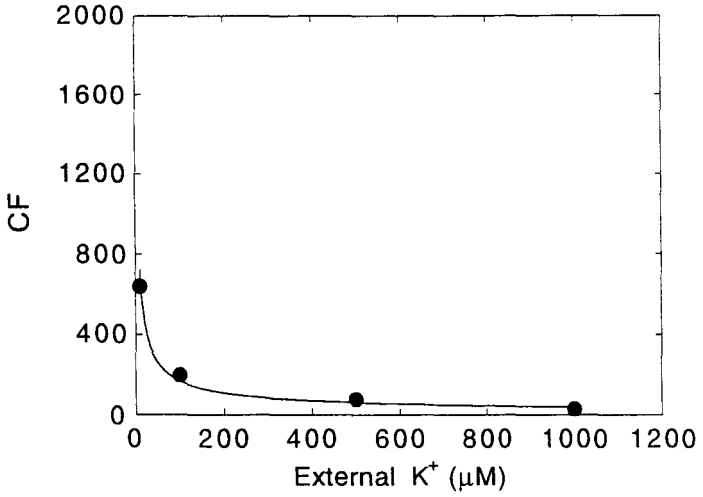

Figure 4.- Comparison between the values of concentration factor for radiocaesium (CF) obtained experimentally in plants submitted to potassium sufficiency (closed circles) with the values predicted by the Nernst equation as a function of the external potassium concentration (line).

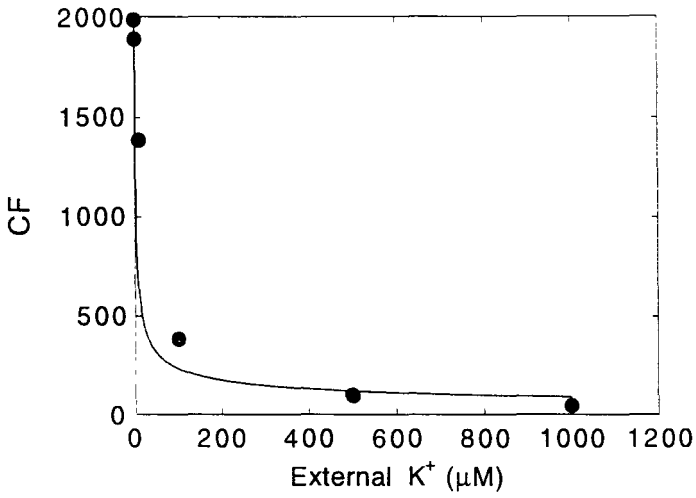

Figure 5.- Comparison between the values of concentration factor for radiocaesium (CF) obtained experimentally in plants submitted to potassium deficiency (closed circles) with the values predicted by the Michaelis-Menten kinetic approach as a function of the external potassium concentration (line).

Head of project 10: Dr. R.N.J. Comans

II. Objectives for the reporting period

1. To test the general validity of the *in-situ* $K_D(^{137}Cs)/NH_4^+$ ion-exchange relationship and its power to predict radiocaesium mobility in (and remobilisation from) freshwater sediments.
2. Determination of "exchangeable" *in-situ* radiocaesium-K_D's, in addition to "total" *in-situ* radiocaesium-K_D's, by multiple extraction of the sediment with NH_4^+-solutions and subsequent preconcentration/low-background measurement of the extracted-^{137}Cs.
3. Search for possibilities (method) to measure the reverse rate constants of radiocaesium sorption (remobilisation) on natural samples, to be included in kinetic models for radiocaesium sorption

III. Progress achieved including publications

Investigation of in-situ K_D-values for radiocaesium

Since the Chernobyl accident, it has become clear that the mobility of radiocaesium is controlled by a highly selective interaction with the frayed particle edges of illitic clay minerals (Cremers et al., 1988), and that competition for these binding sites by the high levels of ammonium in anoxic sediments may partly remobilise sediment-bound ^{137}Cs (Comans et al., 1989). Within the framework of this project, we have investigated a number of widely different W. European freshwater sediments, both in the laboratory and *in-situ*, focusing on the two major factors controlling radiocaesium mobility: the quantity of selective binding sites and the competition for these sites by other cations.

Five sediment profiles from four different freshwater lakes in The Netherlands and the UK (Table 1), which differ widely in their chemical and mineralogical properties, have been carefully sampled and analysed in our laboratories. Sediments were collected in October 1987 (Hollands Diep), November 1987 (Ketelmeer; both prior to the programme), April 1991 and August 1992 (Esthwaite), and February 1992 (Devoke). Sediment collection, slicing at different depths, pore-water extraction, and ultra-low-background ^{137}Cs-counting were done following the strategy outlined in Comans et al. (1989). The treatment of Esthwaite and Devoke sediments was slightly different in that a Mackereth type corer was used and that pore water was separated using high-speed (20,000 x g; 30 min.) refrigerated centrifugation. The *in-situ* distribution of radiocaesium between the sediment particles and the pore water was measured, together with the pore water concentrations of potentially competing major cations as described in Comans et al. (1989). The highly selective binding sites for radiocaesium were measured on the same sediments by Wauters (1994).

Compilation of all *in-situ* K_D-values, measured within the framework of this project to date in Figure 1 (Comans *et al.* 1994), reveals a single relationship between the radiocaesium K_D and the pore-water ammonium concentration. This observation is in agreement with ion-exchange theory in that, among the major ions that compete with caesium for binding sites on illite clays, NH_4^+ outcompetes K^+ in anoxic sediments as it reaches higher concentrations and is about five times more selectively bound. Hence radiocaesium in sediments binds to frayed edge sites (FES) on illite according to the ion-exchange reaction:

$$FES\text{-}NH_4^+ + Cs^+ \quad \overset{K_c^{Cs/NH4}}{\leftrightarrow} \quad FES\text{-}Cs^+ + NH_4^+$$

It can be shown that under natural freshwater conditions, with negligible stable caesium concentrations, the radiocaesium K_D (= $[FES\text{-}Cs^+]/[Cs^+]$) is related to the dissolved NH_4^+ concentration, on a log-log basis, according to the linear relationship:

$$\log K_D = - \log[NH_4^+] + \log (K_c^{Cs/NH4}[FES])$$

in which [FES] is the frayed edge site capacity of the sediment (meq/g) and $K_c^{Cs/NH4}$ the selectivity coefficient that describes the preference of the FES for Cs^+ relative to NH_4^+. Figure 1 shows the $\log K_D$ - $\log NH4^+$ plot of the *in-situ* data for the sediments which have been studied in this programme (Table 1; Comans *et al.*, 1994), which clearly indicates that the data follow a straight line with a slope close to (but significantly steeper than) -1. The vertical variation in the plot is about one order of magnitude or less in K_D and suggests that the product of the selectivity coefficient and the concentration of the caesium selective (frayed edge) sites in all of these European sediments would also show a limited variation.

Table 1. *Sediments studied for in-situ radiocaesium mobility, with sampling dates and values for the product of the selectivity coefficient and the concentration of caesium-specific sites, i.e. the "radiocaesium interception potential"*

Sediment	**Sampling date**	**$K_c^{Cs/NH4}$[FES], meq/g**
Hollands Diep, NL	21 October 1987	0.65
Ketelmeer, NL	12 November 1987	0.23
Esthwaite, UK	10 April 1991 & 17 August 1992	0.64
Devoke, UK	28 February 1992	0.24

The intercept $K_c^{Cs/NH4}$[FES] can be independently measured when the FES are "isolated" by blocking all other exchange sites in sediments with AgTU. Using this procedure, Wauters (1994; KU-Leuven) has measured $K_c^{Cs/NH4}$[FES] for all sediments in Figure 1. The results of these measurements are included in Table 1 and show that the values vary indeed by no more than a factor of 3.

We conclude from the above that ^{137}Cs obeys ion-exchange theory and thus allows its solid-liquid distribution coefficient (K_D) in radiological assessment models to be predicted from environmental variables, rather than to be erroneously treated as a constant. The radiocaesium K_D in freshwater sediments can be predicted, within acceptable limits, on the basis of the quantity of highly selective exchange sites and the pore-water NH_4^+ concentration. Figure 1 and Table 1 show that the variation in the former property is limited for widely different W. European sediments indicating that, in situations directly following a nuclear accident, a first estimate of the radiocaesium K_D can be deduced solely from the pore-water ammonium concentration.

Exchangeability of sediment-bound radiocaesium

We have shown earlier (Comans *et al.*, 1991; Comans & Hockley, 1992) that radiocaesium migrates slowly into the interlayers of illite from which it is difficult to displace. This apparent fixation proceeds faster at low levels of competing cations, i.e. at high K_D-values. The same process effectively increases [FES] over time. The effect of this process is apparent in the $\log K_D$ - $\log NH_4^+$ plot of the *in-situ* data (Comans *et al.*, 1994) in that the *in-situ* K_D-values are generally higher than the values predicted on the basis of (short-term) laboratory measurements of $K_c^{Cs/NH4}$[FES]. Moreover, the faster migration into clay interlayers in high-K_D (i.e. low-NH_4) environments may also be reflected in the slope of the data in Fig. 1, which is significantly steeper than -1 (~ -1.4). We also note that the Esthwaite and Devoke sediments, which have relatively low ammonium in their pore waters, deviate more from the predicted K_D-values than the Hollands Diep and Ketelmeer sediments, which have pore-water NH_4 concentrations in the millimolar range and have *in-situ* K_D's which are quite close to the predicted values.

The exchangeability of sediment-bound radiocaesium has been investigated by extraction of the sediments with 0.1 M NH_4-acetate. These extractions have been performed on all sediment cores that have been studied to date within the framework of this project (Table 1). The sediment samples have been stored frozen (-20 °C) since the pore water separation directly after sampling. Each sediment slice was extracted three times sequentially, each step for 24 hours, with 0.1 M NH_4-acetate at a liquid/solid ratio of 10 L/kg. For each sample the NH_4-acetate from the three extractions was combined. It appeared necessary to remove the ammonium ion from the solution prior to the preconcentration of the radiocaesium on ammoniummolybdophosphate (AMP) as only low recoveries (< 20%) were reached when radiocaesium was preconcentrated directly from the 0.1 M NH_4-acetate solution. Therefore, the extracts were boiled at pH > 10, to remove ammonium as $NH_3(g)$ and the volumes reduced to about 100 mL by evaporation. Radiocaesium preconcentration and measurement by ultra-low background γ-spectrometry was performed as described in Comans *et al.*, 1989).

Results of the exchangeable ^{137}Cs measurements are given in Table 2. The amount of ^{137}Cs that can be released by the three sequential NH_4-extractions from the more mineral sediments of Hollands Diep, Ketelmeer and Esthwaite is very low; on average 2, 3, and 7%, respectively. The more organic-rich sediments of Devoke show a much higher exchangeability of 16%. The values for the three mineral sediments are low if we compare them, for instance, with those of Evans et al. (1983), who have measured ^{137}Cs exchangeabilities (also in 0.1 M NH_4^+) of 10-20% in the sediments of the Par Pond reservoir, 15-20 years after contamination. These

authors attribute their relatively high exchangeabilities to the high kaolinite content of the Par Pond sediments. Western European sediments generally contain illite as the major clay mineral, which likely causes the strong fixation of radiocaesium that has been observed in the Hollands Diep, Ketelmeer and Esthwaite sediments. Devoke apparently behaves more like the Par Pond sediments in that similar amounts of ^{137}Cs are exchangeable.

If we accept that radiocaesium in all four of the above sediments is bound solely to frayed edge sites on illitic clays in the sediments, the up to one order of magnitude differences between the exchangeable fractions of radiocaesium in these sediments is unexpected. The differences are clearly not related to the different contact times of radiocaesium with the sediments, as the lowest values are found for the sediments sampled only 1.5 years after the Chernobyl accident (Hollands Diep and Ketelmeer). Admittedly, the latter sediments have only recently been extracted, but the cores had been stored frozen at -20 °C since the pore water separation directly after sampling. We do not expect caesium migration into the clay interlayers to have progressed much further under those storage conditions.

"Exchangeable" K_D-values for radiocaesium in the sediments, calculated from the exchangeable rather than total amount of ^{137}Cs in the sediments, are included in Figure 1. We would expect "exchangeable" K_D's to correspond better with values predicted on the basis of (short-term) laboratory measurements of $K_c^{Cs,NH4}$[FES] than the total K_D's. Although this may be the case for the Devoke sediments, total and exchangeable K_D-values for Esthwaite correspond about equally with the predictions, whereas the "exchangeable" K_D's for Hollands Diep and Ketelmeer deviate much more from the predicted values than the total K_D's. These observations strongly suggest that the short-term exchangeability measurements of radiocaesium, especially in the more mineral sediments, underestimate the amount of the radionuclide that is actually taking part in ion-exchange with the pore waters and, hence, is available for remobilisation by high concentrations of ammonium.

The low overall activities of ^{137}Cs in the Hollands Diep and Ketelmeer sediments and in the extractions in particular, have led to large counting errors on the exchangeability data. These sediments contain high levels of NH_4 in their pore waters. The kinetic ion-exchange model (Comans & Hockley, 1992) would predict radiocaesium to be taken up more slowly by clay mineral interlayers under these conditions of high competition, which is inconsistent with the findings above. New measurements on fresh (non-frozen) and larger samples (higher absolute activities) from sediments with high pore-water NH_4 are needed to investigate whether there are significant differences in the long-term exchangeability of radiocaesium in sediments with high and low levels of competing ions. It is also still uncertain what role (the high content of) organic material plays in the relatively high exchangeability of radiocaesium in de sediments of Devoke. This issue clearly needs further investigation because the kinetics of interlayer migration controls the amount of sediment-bound radiocaesium that may be remobilised on the long term. Moreover, knowledge of this process may provide "tools" that allow us to influence the "availability" of particle-bound radiocaesium in order to reduce the bioavailability and risk of remobilisation from sediments.

Table 2. Total and exchangeable radiocaesium in the different sediment cores.

Sediment	Depth [cm]	total ^{137}Cs [Bq/kg]	exchangeable ^{137}Cs [Bq/kg]	exchangeable ^{137}Cs [fraction of the total]
Hollands Diep	0.5	249.15	0.85	0.003
	1.5	269.79	0.69	0.003
	3.5	83.05	0.55	0.007
	6.5	5.00	0.50	0.100
	9.5	17.90	-	-
	16.5	46.31	0.51	0.011
	24.5	47.96	1.36	0.028
	31.5	21.31	5.01	*0.235*
	40.4	21.70	-	-
				***average** ± s.d.: 0.022 ± 0.038**
Ketelmeer	1	115.46	10.06	0.087
	3	124.73	4.33	0.035
	5.5	224.23	5.33	0.024
	8.5	59.07	0.27	0.005
	11.5	37.466	0.76	0.020
	18.5	64.41	0.61	0.009
	25.5	51.79	14.89	*0.288*
	31.5	9.44	2.94	*0.312*
				***average** ± s.d.: 0.030 ± 0.030**
Esthwaite	0.5	214.80	13.60	0.063
	2.5	330.73	22.12	0.067
	4.5	545.61	32.31	0.059
	6.5	474.14	38.44	0.081
	8.5	353.43	24.93	0.071
	10.5	345.36	18.06	0.052
	12.5	325.69	21.99	0.068
	14.5	266.41	20.31	0.076
	16.5	164.03	15.03	0.092
	18.5	42.73	9.329	*0.218*
	20.5	21.59	4.791	*0.222*
				***average** ± s.d.: 0.070 ± 0.012**
Devoke	0.5	1813	343.78	0.190
	1.5	1860	401.78	0.216
	2.5	2142	345.69	0.161
	3.5	2598	375.72	0.145
	4.5	3096	363.83	0.118
	5.5	2579	270.93	0.105
	6.5	1524	208.66	0.137
	7.5	1023	237.20	0.232
	8.5	848	174.72	0.206
	9.5	727	181.78	0.250
	10.5	644	140.63	0.218
	11.5	653	44.73	0.068
	12.5	719	108.70	0.151
	13.5	685	94.97	0.139
	14.5	588	81.80	0.139
	15.5	392	58.42	0.149
	16.5	244	103.70	*0.426*
	17.5	146	81.32	*0.558*
	18.5	130	68.18	*0.523*
	19.5	106	56.20	*0.531*
				***average** ± s.d.: 0.164 ± 0.050**

*average and s.d. values exclude the (unexplained) high exchangeabilities in the bottom sections of each core (indicated in italics)

Slow (reverse) migration of radiocaesium from clay-mineral interlayers into solution

In the kinetic model we have developed previously on the basis of laboratory sorption experiments of radiocaesium on illite (Comans & Hockley, 1992), we were unable to consider a reverse process of radiocaesium remobilisation from interlayer sites. The equilibration times of up to 4-weeks were too short for the reverse process to become apparent. Nevertheless, the fact that radiocaesium in sediments is still exchangeable to a certain extent after more than 20 years of contact with sediments (Evans et al., 1983), indicates that such a reverse process must exist.

Because of its relevance for the long-term availability of sediment-bound radiocaesium, we have investigated the long-term release of particle-bound radiocaesium in more detail. The primary objective of this part of our study is to estimate the existence and magnitude of a slow remobilisation (reverse rate) of radiocaesium from clay mineral interlayers during contact with a high concentration of competing ions. After the three sequential 0.1 M NH_4-acetate extractions, the sediments have been resuspended for a fourth time in a fresh 0.1 M NH_4-acetate solution and have been allowed to equilibrate for more than one year (400-560 days). Ammonium has been removed from the solution and radiocaesium preconcentrated on AMP and counted on the ultra-low background γ-spectrometer as described above.

Table 3: *Average fraction of exchangeable-^{137}Cs in sediments after 3 sequential 24-hr NH_4-extractions and the additional fraction mobilised after a 4th 400/560-d extraction. A reverse rate constant and halve-life for the slow remobilisation of ^{137}Cs from the sediments has been calculated on the basis of the 4th extraction, assuming a first order process.*

Sediment	**exch. ^{137}Cs after 3x 24-hr extraction [fraction of the total]**	**additional exch. ^{137}Cs after 400/560-d extraction* [fraction of the total]**	**reverse rate constant [y^{-1}]**	**$t_{1/2}$ [y]**
Hollands Diep	0.022 ± 0.038	0.0089 ± 0.0050	0.0082	85
Ketelmeer	0.030 ± 0.030	0.0095 ± 0.0030	0.0087	79
Esthwaite	0.070 ± 0.012	(still equilibrating)	-	-
Devoke	0.164 ± 0.050	0.0380 ± 0.0355	0.0220	31

*equilibration time 4th extraction = 400 days for Hollands Diep & Ketelmeer; 560 days for Devoke.

Table 3 shows the average fraction of exchangeable-^{137}Cs in sediments after 3 sequential 24-hr NH_4-extractions and the additional fraction mobilised after the 4th, long-term (400/560-days) extraction. Assuming that (1) all (rapidly) "exchangeable" radiocaesium had been removed by the three prior extractions, and (2) a first order remobilisation process, we can roughly calculate the reverse rate constant that describes the slow remobilisation of ^{137}Cs from the sediments, which we interpret as the slow release of radiocaesium from the interlayer sites (see Comans & Hockley, 1992). Table 3 indicates that the half-life of this reaction is of order 30-80 y^{-1}. Independently, and using a model that includes radiocaesium sorption kinetics to simulate radiocaesium in each of three phases in sediment profiles: aqueous, exchangeably bound and slowly reversible (often termed "fixed"), Smith & Comans (1995) have found evidence for a reverse reaction from the slowly reversible sites of order 10 years. These findings are in fairly close agreement and suggest that radiocaesium on interlayer sites, which

is generally referred to as being "fixed", is not truly immobilised but can, at least partly, be very slowly remobilised.

General conclusions from this study

The *in-situ* K_D-values that have been measured in this study have successfully been related to fundamental properties of the sediments: the concentration of highly selective binding sites for radiocaesium —frayed edge sites on illite— and the concentration of the major ion competing with radiocaesium for these sites —the ammonium ion—. Our results show that the mobility of radiocaesium in sediments follows ion-exchange theory and allow the *in-situ* radiocaesium distribution coefficient to be predicted beyond the conditions under which the measurements were made.

The exchangeability of radiocaesium, measured by 3 sequential rapid (24-hr) extractions is low for the more mineral sediments of Hollands Diep, Ketelmeer and Esthwaite; 2-7% of the total amount in the sediment. For the more organic sediments from Devoke, the exchangeability is significantly higher; 16%. These results would imply "exchangeable" K_D-values for radiocaesium to be down to almost two orders of magnitude lower than the total K_D-values.

Long-term extractions with NH_4, after having first removed the rapidly exchangeable amount, have given evidence for a slow remobilisation of radiocaesium from clay mineral interlayers and indicate that the term "fixed" is not truly appropriate for that particular pool of radiocaesium in sediments. We have been able to estimate a half-live for the slow remobilisation of radiocaesium of 30-80 years. "Exchangeable" K_D-values for radiocaesium in environments where the radionuclide is in contact with (high concentrations of) competing (NH_4) ions for many years would, therefore, be higher than the values measured by short-term extractions.

The good correspondence between total *in-situ* K_D's and values predicted on the basis of ion-exchange theory and the observation that radiocaesium can, after removal of the rapidly-exchangeable amount, still be slowly released from sediments that have been in contact with this radionuclide for up to 6 years, suggest that the amount of radiocaesium in sediments which is available on the long-term is, therefore, likely to be larger than is generally believed.

References

Comans, R.N.J., Middelburg, J.J., Zonderhuis, J., Woittiez, J.R.W., De Lange, G.J., Das, H.A. & Van Der Weijden, C.H. (1989) Mobilization of radiocaesium in pore water of lake sediments. *Nature* **339,** 367-369.

Comans, R.N.J., Haller, M. & De Preter, P. (1991) Sorption of cesium on illite: non-equilibrium behaviour and reversibility. *Geochim. Cosmochim. Acta* **55,** 433-440.

Comans, R.N.J. & Hockley, D.E. (1992) Kinetics of cesium sorption on illite. *Geochim. Cosmochim. Acta* **56,** 1157-1164.

Comans, R.N.J., Hilton, J., Cremers, A., Bonouvrie, P.A. & Smith, J.T. (1994) Predicting radiocaesium ion-exchange behaviour in freshwater sediments. *Report- ECN-RX--93-108. (also submitted for publication).*

Cremers, A., Elsen, A., De Preter, P. & Maes, A. (1988) Quantitative analysis of radiocaesium retention in soils. *Nature* **335,** 247-249.

Evans, D.W., Alberts, J.J. & Clark, R.A. (1983) Reversible ion-exchange fixation of cesium-137 leading to mobilization from reservoir sediments. *Geochim. Cosmochim. Acta* **47,** 1041-1049.

Smith, J.T. & Comans, R.N.J. (1995) Modelling the diffusive transport and remobilisation of ^{137}Cs in sediments: the effects of sorption kinetics and reversibility. *Geochim. Cosmochim. Acta (accepted for publication)*

Wauters, J. (1994) *Radiocaesium in aquatic sediments: sorption, remobilization and fixation.* Ph.D. thesis No. 246, Faculteit Landbouwkundige en Toegepaste Biologische Wetenschappen, Katholieke Universiteit Leuven.

Figure 1. Total (closed symbols), exchangeable (open symbols), and predicted (lines) *in-situ* K_D-values for different w-European lake sediments.

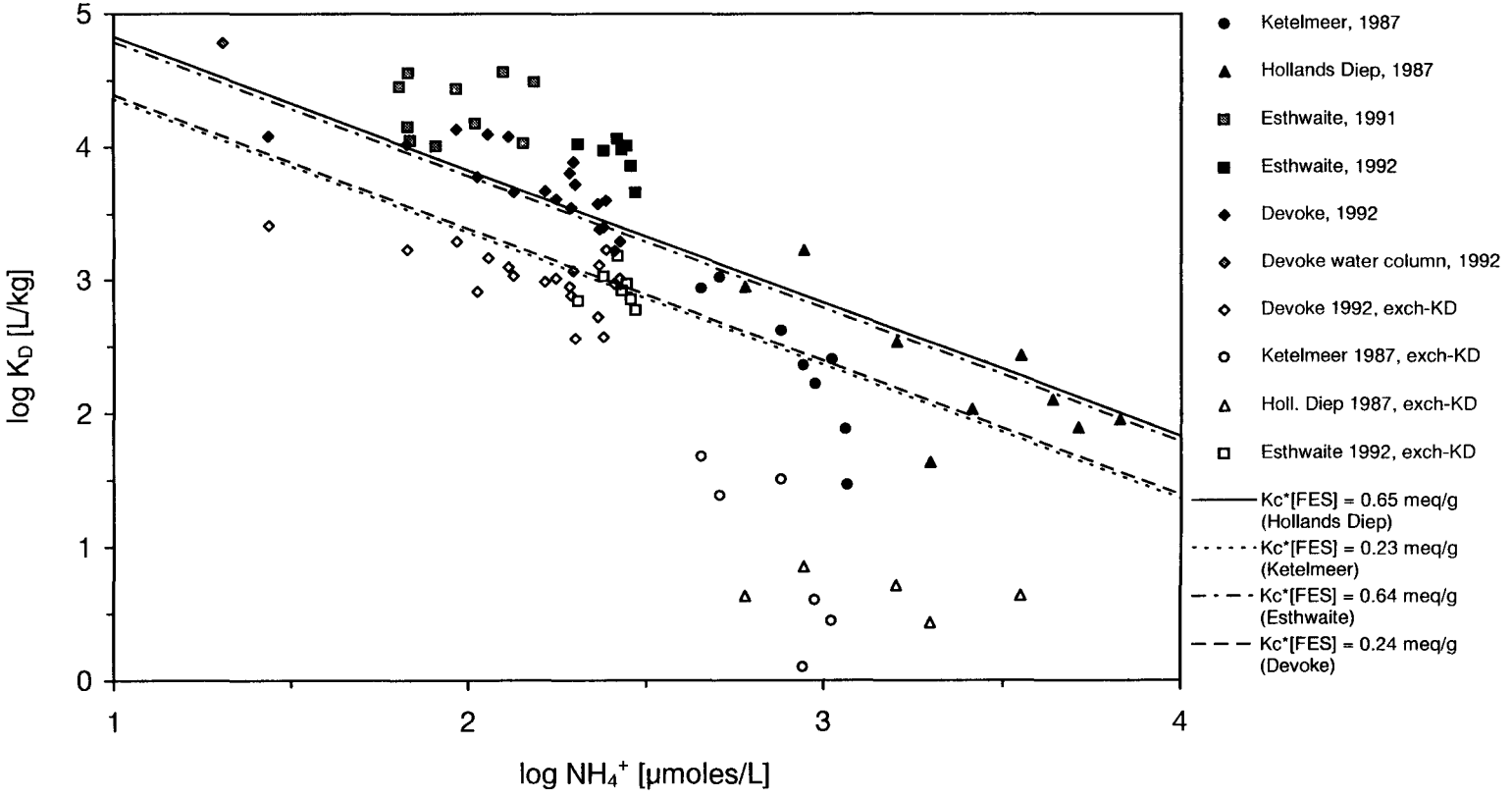

Dynamics of radiocaesium turnover in brown trout: model predictions

NINA, Norway

Aim: To model how environmental and metabolic variables determine radioactivity in brown trout.

The Model

The model is structured by five tiers of equations, each feeding parameters into above levels (Fig. 1). The core equation describes the changes in fish radiocaesium body burden with time. At the level below, equations for radiocaesium excretion and intake provides the input parameters to this equation. Next, a series of equations is given for radioactivity of prey animals and absorption efficiency, feeding rates and growth rates of brown trout that provide parameters for the radiocaesium intake equations. Growth rates determine the body size of brown trout which is an important parameter for feeding rates and radiocaesium excretion. Growth rates are used to quantify feeding rates at levels below maximum feeding. At the lowest level, equations for ambient temperature in lakes provides data necessary for estimating growth rates, feeding rates and radiocaesium excretion rates.

To test the model predictions in a natural setting we compared predicted and measured 137Cs-radioactivity from age-2 to age-4 for the 1985, 1986 and 1989 year-classes of brown trout from the Norwegian Lake Høysjøen. Model performance was evaluated for the period 1987-90, shortly after the Chernobyl fallout when radioactivity in fish and prey declined quite rapidly, and for the period 1991-3 under steady-state-like conditions without major changes in fish and prey radioactivity. Model predictions were made for the dynamic conditions during the first two years after a fallout, and for the subsequent steady-state-like conditions. Predictions for three different lakes with different temperature regimes (data source: temperate: Lake Liavatnet, 59°N, 6°E, 40 m above sea level; boreal: Lake Høysjøen: 63°N, 11°E, 222 m above sea level; and sub-Alpine: Lake Aursjø: 61°N, 8°E, 1085 m above sea level) were made.

Model predictions

Maximum radioactivity attained in brown trout after a fallout is influenced by lake type, time of fallout, fish growth and feeding rates, and fish size. Peak radioactivity is predicted to be considerably higher in the temperate and boreal lakes than in the sub-Alpine lake (Fig. 2). Peak radioactivity increases with increasing feeding and growth rates of the fish. The effects of high feeding rates on caesium accumulation is especially pronounced in the temperate lake where an increase in growth rate, and the accompanying feeding rate, from 80 to100 % of the maximum nearly doubled peak radioactivity. In all lakes a fallout during spring when water temperature is increasing, gives the highest peak radioactivity. In the temperate and boreal lakes a much higher peak radioactivity is predicted for a spring than a summer fallout. Although fallout date is important for peak radioactivity, its influence on the long term development in fish radioactivity for different fallout dates is within 20% of each other.

The relationship between specific radioactivity (S, Bq g^{-1}) and fish size (W, g), $S = aW^b$, changes with time. Shortly after the fallout, the caesium accumulation rate is highest in the small fish with

b-values at approximately -0.2 in all three lake types. After peak radioactivity is reached, the b-values gradually approaches zero. Finally, the relationship between specific radioactivity and fish size became positive with b-values at 0.10-0.15. For the temperate and boreal lakes the relationship changes from negative to positive in the spring one year after the fallout, whereas for the sub-Alpine lake the model predicts that positive b-values occur later during the second summer. Thus, irrespective of lake type radioactivity should increase with fish size in the second year, not decrease as in the year of contamination.

At steady state the model predicts a seasonal variation in biomagnification, with minimum values in late spring and maximum in the autumn. In the temperate and boreal lakes the predicted biomagnification is higher and the seasonal variation more pronounced than in the cold lake. The biomagnification (B_m) at steady state depends on fish size (W, g): $B_m=aW^b$. For the three temperature regimes modelled, there is a negative relationship between fish size and the biomagnification factor at the autumn maximum. The relationship is the most negative in the warmest lake. On the other hand, this relationship is slightly positive at the late spring minimum in the temperate and boreal, but not the sub-Alpine lake.

The model (Fig. 1) where used to develope a quantitative model for biomagnification of radiocaesium in brown trout under steady state conditions. Due to non-linear relationships between maximum biomagnification, body size and growth rate (G, % of maximum growth), we used a polynomial model: $Bm = A\ (b_0 + b_1W + b_2W^2 + b_3G + b_4G^2 + b_5G^4)$ where A is the absorption efficiency of radiocaesium. Coefficients were estimated for the three different lake types by multiple regressions for brown trout weighing from 5 to 500 g, growing at rates between 20 and 100 % of the maximum at 100% absorption efficiency (A=1).

Biomagnification is highest for small fish in the temperate lake growing and feeding at maximum rates (Fig. 3). At growth and feeding rates below this maximum, the maximum biomagnification is reduced. This reduction is most pronounced in the temperate and boreal lakes, and when the growth rate decreases from 100 to 80% of the maximum.

Model generality

The present model gave reasonable predictions for the radioactivity of brown trout in the Lake Høysjøen, Norway. This holds true both during a period with declining radioactivity after the fallout, and in a period with steady-state-like conditions. Different absorption factors were used, however, in the two situations. To be general, the model should be applicable for brown trout in a wide range of ecological systems, as this species have a wide geographical range. The model application depends strongly upon the generality of the sub-models, which in this case is chiefly based on established, bioenergetic knowledge about brown trout. Experiments have been performed to establish absorption efficenecy and excretion rate (including the size and temperature dependecy) for Arctic charr (*Salvelinus alpinus*, two poulations), bream (*Abramis brama*), whitefish (*Coregonus lavaretus*) and Atlantic salmon (*Salmo salar*, two populations), and the present model may be further developed to be valid for freshwater fishes in general.

There is a growing appreciation for bioenergetically based models in eco-toxicology, as they describe the actual mechanism at work in contaminant accumulation. This approach is most valuable for radiocaesium contamination, and we feel that it is applicable for other cantaminants

as well, given that the rates of intake and excretion can be defined.

List of Figures

Fig 1. Model structure: five tiers of equations (A-D), each feeding parameters into above levels: A: The core equation describing the changes in radiocaesium body burden with time. B: equations for radiocaesium excretion and intake which provides the input parameters to the core equation. C: equations for radioactivity of prey and the brown trout feeding rates, providing parameters for the radiocaesium intake equations. D: the equation for brown trout growth rates. Growth rates determine the body size of the fish which is an important parameter for feeding rates and radiocaesium excretion (at level B). Growth rate are used to quantify feeding rates at levels below maximum feeding. E: equations for ambient water temperature in lakes providing parameters for estimating growth at level D, feeding rates at C and radiocaesium excretion rates at level B.

Fig. 2. Predicted effects of fallout date (from 1 May to 1 August) and fish growth and feedingrates on peak radioactivity of brown trout in different lake types. Results are shown for brown trout weighing 100 g 1 May.

Fig. 3. Predicted biomagnification of ^{137}Cs in brown trout at different growth rates and body sizes, in a situation with stable radioactivity in prey animals. Results are shown for three different lake types and an absorption efficiency at 0.45.

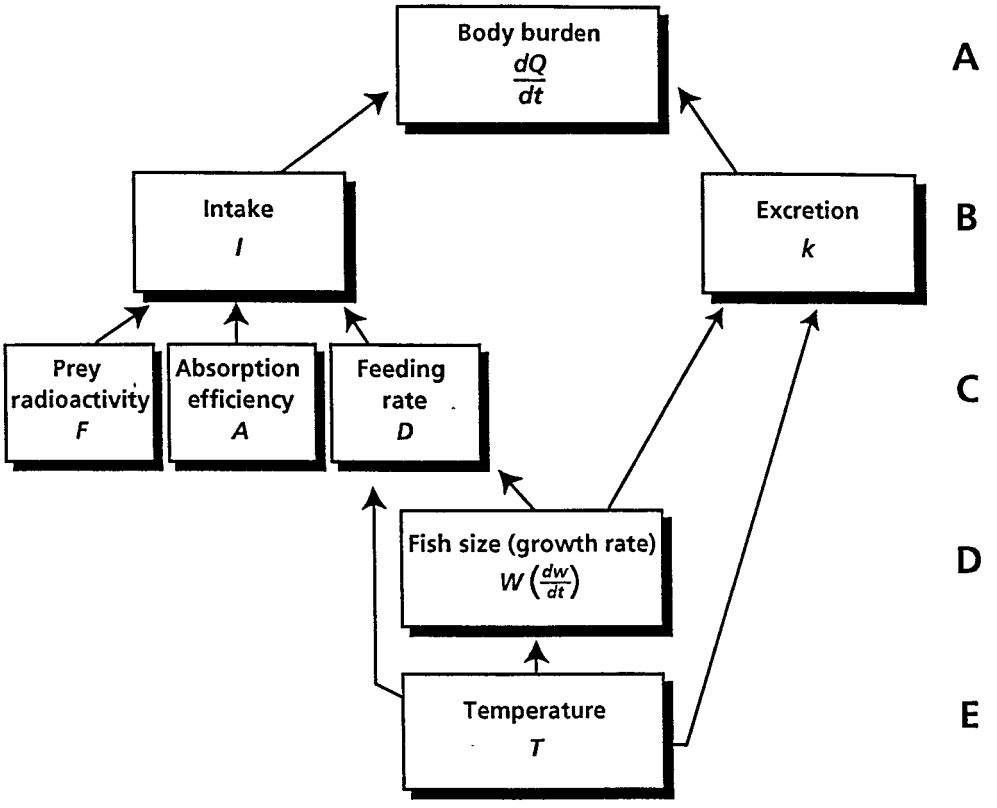
Body burden
dQ/dt
A
Intake
I
Excretion
k
B
Prey radioactivity
F
Absorption efficiency
A
Feeding rate
D
C
Fish size (growth rate)
W (dw/dt)
D
Temperature
T
E

Figure 1.

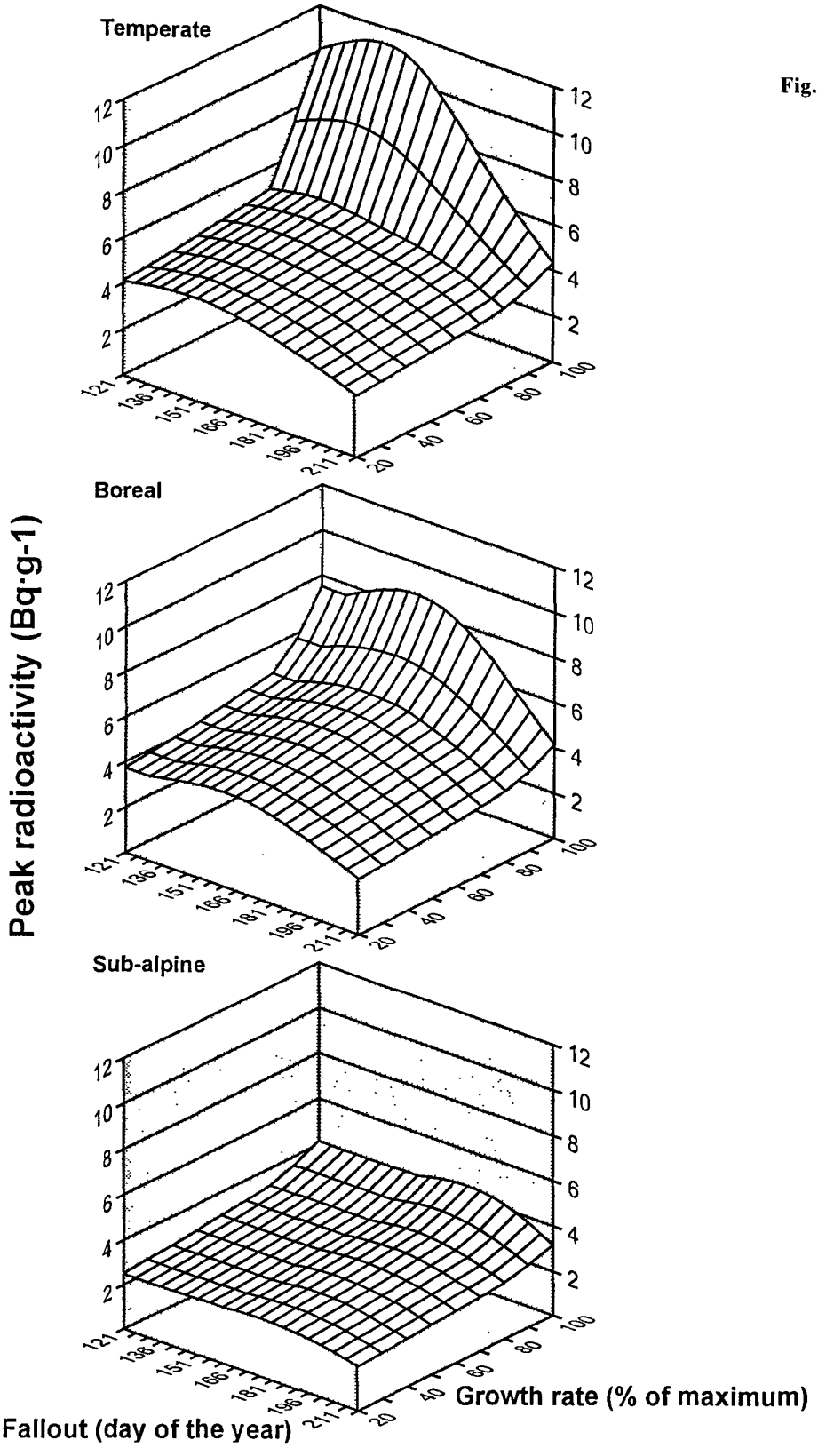
Temperate
Boreal
Sub-alpine
Peak radioactivity (Bq·g-1)
12
10
8
6
4
2
121
136
151
166
181
196
211
20
40
60
80
100
Fallout (day of the year)
Growth rate (% of maximum)

Fig. 2

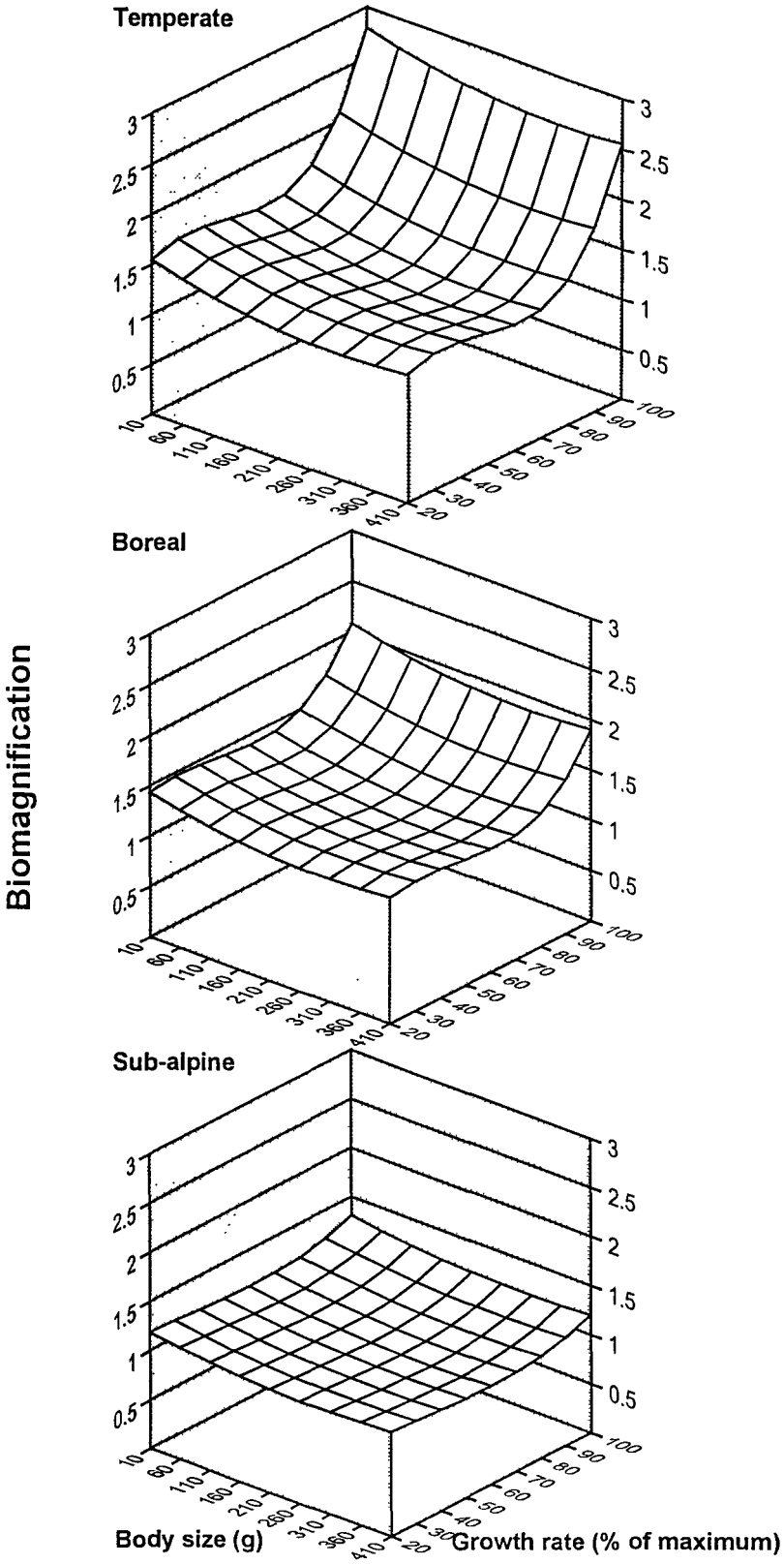
Temperate
Boreal
Sub-alpine
Biomagnification
Body size (g)
Growth rate (% of maximum)
3
2.5
2
1.5
1
0.5
10
60
110
160
210
260
310
360
410
20
30
40
50
60
70
80
90
100

Fig. 3

Final Report
1992 - 1994

Contract: F13P-CT920046 **Duration: 1.9.92 to 30.6.95** **Sector: A21**

Title: Mechanisms governing the behaviour and transport of transuranics (analogues) and other radionuclides in marine ecosystems.

1)	Mitchell	Univ. Dublin - College (UCD)
2)	Gascó	CIEMAT
3)	Guegueniat	CEA - IPSN - LRM Cherbourg
4)	Papucci	ENEA
5)	Woodhead	MAFF
6)	Holm	Univ. Lund
7)	Sánchez-Cabeza	Univ. Barcelona - Autónoma (UAB)
8)	Dahlgaard	Lab. Risø
9)	Salbu	Univ. Agricultural - Norway (AUN)

I. Summary of Project Global Objectives and Achievements

The overall objective of this project was to identify the basic mechanisms and define the key parameters governing the physico-chemical speciation, vertical and horizontal mobility, biological magnification, incorporation to seabed sediments and ultimate fate of transuranium and other long-lived radionuclides in the marine environment, with a view to providing high-quality data of a universal character for use in the development and validation of predictive models based on fundamental mechanisms rather than the simpler box-model approach. It is considered that such models are more likely to yield realistic predictions upon which sound decisions can be made, particularly when applied to situations involving accidental releases under unforseen conditions.

The project addressed a number of diverse marine environments where radionuclides have become concentrated and where they pose potential problems in environmental protection. This diversity proved to be important, for by studying the behaviour of particular radioelements under distinctly different conditions, we were more easily able to identify a number of the key parameters which regulate their migration in the hydrosphere.

At the outset, the project was divided into a set of major research tasks (or studies), each supported by a comprehensive and integrated work package of collaborative character. These included (i) the characterisation of important source terms, (ii) the chemical modification of radionuclides following release to the marine environment, (iii) the presence and persistence of hot particles, (iv) the influence of physical and chemical speciation (including organics) on horizontal and vertical mobility, as well as on biological availability, (v) the importance of colloids, (vi) behaviour in estuarine and deep environments, (vii) transfer from land to sea, (viii) transfer *via* particles in shallow environments, (ix) transfer from shelf waters to deep-sea, (x) transfer through the primary producer route to man, (xi) modelling the long-term bioavailability of transuranics and other radionuclides in seabed sediments, and (xii) the development of new (relevant) radioanalytical techniques. In our opinion, the successful completion of these work packages has led to a significant improvement in our overall understanding of radionuclide behaviour in the marine environment. It has also yielded much

invaluable data; data which are now available to modellers and other professionals tasked with assessing the risks of human exposure associated with the transfer of radionuclides through the marine food-chain to man.

As discharges of radionuclides from the spent nuclear fuel reprocessing plant at Sellafield (UK) are one of the major sources to the shelf seas of north-west Europe, it was considered essential to characterize the physico-chemical form of the more important radionuclides in the main effluent streams. To this end, MAFF successfully carried out experiments on source-term effluents (SIXEP and Seatank) to determine the proportions of different radionuclides present in colloidal form. Nuclides examined included ^{99}Tc, ^{90}Sr, ^{137}Cs, ^{239,240}Pu(IV), ^{239,240}Pu(VI) and ^{241}Am. In certain cases, significant fractions were found to be colloidal. However, the radio-colloid distributions in pre- and post-EARP effluents proved to be indistinguishable.

Although MAFF identified small amounts of ^{99}Tc, ^{90}Sr, ^{137}Cs, and ^{239,240}Pu(V) colloidal species in SIXEP effluents, their studies indicated that these forms did not persist in sea water. In contrast, they found evidence that ^{239,240}Pu(IV) and ^{241}Am colloidal species, originating mainly from Seatank effluent, do persist at least in the short term. It is suggested that the disaggregation of iron floc upon dilution in sea water gives rise to measurable amounts of radio-colloids. Studies carried out by UCD in collaboration with MAFF have confirmed the presence of colloidal species of ^{239,240}Pu(IV) and ^{241}Am in sea water near the Sellafield outlet and further afield in the western Irish Sea. Other measurements by UCD and UAB in the western Mediterranean have shown the presence of similar proportions of ^{239,240}Pu(IV) and ^{241}Am in colloidal form. These issues are discussed in more detail below.

The presence of hot particles in Sellafield effluents is well established, as is the fact that they persist in the marine environment for some months before dissolving. A previous study by MAFF showed that up to 10% of the plutonium in surface sediments close to Sellafield was in the form of these particles. In the course of this project, both CIEMAT and UAB detected anomalously high concentrations of plutonium and americium in some samples of seabed sediment from Palomares (Spain), site of a mid-air collision (1966) between two military aircraft, one of which was carrying thermonuclear weapons. Analysis by UCD of the ^{240}Pu/^{239}Pu atom ratio in a few of these samples, as well as in some samples of terrestrial soil from the same zone, gave a mean of 0.056 ± 0.003, confirming the presence of weapons-grade plutonium. Attempts by AUN to isolate and characterise hot particles from these samples using autoradiography, alpha-track radiography and SEM with XRM have not yet proved successful, although some progress has been reported.

IPSN and UCD, in the course of the GEDYMAC '94 expedition in the English Channel, examined the oxidation state distribution of plutonium in filtered sea water close to the La Hague source-term and in mid-Channel, some 100 km to the east. The data show that the percentages of plutonium in an oxidised form at both stations were identical, indicating that any transformations which may have occurred upon release to sea water were rapid.

UCD, in collaboration with ENEA and UAB, have successfully completed a detailed examination of the physico-chemical speciation of plutonium and americium in the western Mediterranean water column and in coastal waters near the site of the Palomares accident. This was a major undertaking, as the logistics of the operation were, to say the least, considerable. Besides confirming the presence of the classic sub-surface maximum in the plutonium concentration profile at depths between 250 and 500 m, the dominance of the

plutonium(V) oxidation state in the soluble phase, in what are well-oxygenated waters, was found to be reversed at ~50 m. This reversal in oxidation-state characterisation has been attributed to the reduction of oxidised plutonium by phytoplankton forming in a biologically productive layer near the surface.

In addition to being invaluable in the elucidation of the basic mechanisms governing the behaviour of plutonium and americium in the western Mediterranean, these data represented an important addition to the database of radionuclide concentrations in this zone which, when combined with other data (see below) and conventional oceanographic data, have been used to determine radionuclide residence times and inventories, and to characterise the different water masses in the western Mediterranean.

In the broad context of physico-chemical speciation, experiments carried out by UCD appear to show that little if any of the plutonium and americium present in sea water is in the form of neutral organic complexes. Other studies by LUND have shown exceptionally high concentrations of dissolved actinides in waters containing significant concentrations of high molecular weight humics. Complementary laboratory studies by IPSN on the behaviour of plutonium under simulated estuarine conditions have demonstrated the reduction of plutonium(V) to plutonium(III, IV) by humic acids, particularly under conditions of reduced salinity. A preliminary evaluation by UCD of the role of the sea-surface microlayer in the retention of transuranium has highlighted the difficulties of sampling less than the top 150 μm layer in quantities sufficient for radiochemical analyses. Nevertheless, plutonium enrichment factors of 10^2 - 10^3 in solutions of partial sea water containing high concentrations of humic material and monolayers of oleic acid have been demonstrated in laboratory experiments.

Sequential extraction experiments by AUN on sediment sampled near the Sellafield effluent outlet and at the adjacent mud-patch demonstrated that all of the ^{137}Cs is strongly fixed to inert sediment components. Consequently, the transfer of ^{137}Cs from sediments to the water phase can not be attributed to reversible exchange processes but, more likely, to the resuspension of particles. In contrast, AUN found that between 70 and 90% of the ^{90}Sr in these sediments is present in an easily exchangeable form, which would suggest that contaminated Irish Sea sediments represent a potential (diffuse) source of ^{90}Sr. Similar results were obtained with sediments from Stepovogo Fjord, sampled in the course of joint Russian-Norwegian expeditions to the Kara Sea in 1993 and 1994. The interaction of radionuclides with sediments was also studied by AUN in model experiments using labelled ($^{134}Cs^+$ and $^{85}Sr^{++}$ ions) sea water added to fresh Stepovogo sediments at 4°C. The results confirmed that the retention of ionic strontium would be low, while these sediments could act as a sink for released ionic caesium.

CIEMAT has examined the geochemical association of plutonium and americium in sediments sampled on the continental shelf near Palomares. Significant findings include the observation that while fallout plutonium from weapons tests is mainly associated with organic matter and sesquioxides, refractory plutonium and americium from the Palomares accident appear in the residual fraction. Americium from weapons tests is mainly associated with the organic and exchangeable fractions.

Careful analyses by AUN, MAFF and UCD, using *in-situ* ultrafiltration, on samples of water from the north-eastern Irish Sea have identified the presence of small quantities of ^{90}Sr, ^{137}Cs, $^{239,240}Pu$ and ^{241}Am in colloidal form. Further measurements by MAFF and UCD suggest that

most of the colloidal plutonium (and americium) fraction is associated with very small particles (< 10 kD). Examination of the oxidation state distribution of plutonium in the different size fractions upon ultrafiltration showed no evidence of significant plutonium(V) retention, even by a 1 kD ultrafilter. Clearly, plutonium present in sea water in an oxidised form is genuinely soluble. In contrast, the data show that some of the plutonium in a reduced chemical form, i.e. plutonium(IV), is retained by a 1 kD ultrafilter. Similar measurements by UCD and UAB on surface sea water from the western Mediterranean indicated that, in this zone, the colloidal plutonium fraction is mainly associated with larger particles (100 kD - 0.45 μm). Although various suggestions have been advanced to explain this difference, further measurements are indicated before firm conclusions can been drawn.

IPSN has examined the pathways of plutonium associated with deposited sediments in the English Channel and has successfully estimated the transit times of plutonium-bearing particles throughout the Channel. The results indicate average velocities ranging from some kilometres per year to some tens of kilometres per year, in contrast to residual currents of *ca.* 1,000 km y^{-1} in the same zone. Evidently, seabed sediments are transported very slowly and are only efficiently mobilized during paroxystic events. Further, the study suggests that the transit times for permanently suspended particles are likely to be considerably higher. IPSN has also examined the distribution of plutonium in the waters of the Channel and confirmed that it is generally consistent with the now well-established pattern of water circulation in the Channel.

Field studies in the Seine Estuary by IPSN have highlighted the non-conservative behaviour of plutonium during estuarine mixing. Specifically, plots of plutonium activities versus salinity display excess dissolved plutonium at low salinity and depletion at intermediate salinity. Other studies by LUND in the Kalix River Estuary in northern Sweden have determined how the dissolved and particulate concentrations of ^{137}Cs and $^{239,240}Pu$ change during spring discharge. These studies indicated that flocculated plutonium does not sediment within the estuary but, instead, is exported to the open Baltic Sea.

ENEA, in collaboration with UCD, CIEMAT and UAB, have undertaken a detailed and wide-ranging study of the general mechanisms governing the long-term behaviour and mass balance of long-lived radionuclides in the western Mediterranean. Subjects addressed included time trends of vertical profiles in the water column, partitioning between soluble and particulate forms, vertical transport in the water column in relation to both water mixing and sinking particles, accumulation in sediments, and fluxes through the Sicily and Gibraltar Straits. As a result, an extensive database on radiocaesium, plutonium and americium concentrations in the western Mediterranean water column and the seabed sediments has been assembled. Analysis of this database in conjunction with earlier measurements has enabled the determination of a number of important parameters including vertical fluxes, residence times, total inventories (including the contribution from the Chernobyl accident) and present inputs, including fluxes at the Gibraltar and Sicily Straits. Further, it has facilitated the elucidation of some of the key processes controlling the vertical distributions of these radioelements in the water column and the role of different water masses in their physical tranport. By way of example, ENEA and UCD have shown that while there is a small net input of ^{137}Cs ($\sim$6 MBq y^{-1}) to the western Mediterranean through the Strait of Gibraltar, the reverse is true for $^{239,240}Pu$ and ^{241}Am, with net outputs of 630 and 30 MBq y^{-1}, respectively.

CIEMAT, with support from ENEA and UAB, has examined the influence of orography in the relocation of transuranium nuclides and, specifically, the role played by submarine

canyons. At least two mechanisms of transuranic transport, one physical and the other chemical have been identified in the canyon system off Palomares. In addition, the study has highlighted the importance of the land-to-sea transfer of transuranics and, in particular, terrigenous input *via* fluvial transport.

UAB has completed an important study on the transfer of transuranics through the primary producer route in the marine food-chain leading to man. Specifically, plutonium and americium concentrations were determined in samples of phyto- and zooplankton from the western Mediterranean shelf, together with matching samples of seabed sediments and overlying water. Concentration factors and transfer factors were derived from these data, and it was shown that roughly 50% of the plutonium present in particulate form in the water column was associated with phytoplankton species. Evidence was found of elevated concentrations of both nuclides in plankton and seabed sediment sampled in the Palomares/Garrucha zone, leading to the conclusion that plankton may have an important role in the cycling of sediment-associated transuranics in shallow coastal waters.

RISØ, in a key study to identify and quantify some of the main processes controlling the behaviour of transuranic and other radionuclides in sediments, found that a two-layer bio-diffusion model adequately simulated unsupported ^{210}Pb, weapons fallout ^{137}Cs and pulsed (1968) Thule $^{239,240}Pu$ concentration profiles in a set of ten seabed cores retrieved in 1991 from the Thule accident area (north-western Greenland). Significantly, this study demonstrated that the mixing parameters used in the model could not be correctly identified from an interpretation of the unsupported ^{210}Pb profile alone, but that data from the $^{239,240}Pu$ profile were also necessary. RISØ's study has provided new information on processes which influence the time scale and the extent to which contaminated sediment remains in contact with sea water and, thus, is available for further dispersion.

UCD has successfully modelled time-series data on radiocaesium and plutonium concentrations in the surficial sediments of the western Irish Sea mud-patch using a semi-empirical model which assumes that the environmental material (in this case sediment) is in equilibrium with its environs. The model not only predicts future concentrations but also those in years prior to the initiation of sampling. Predicted mean availability times for ^{137}Cs are in the range 7-17 years, while for $^{239,240}Pu$ they are in the order of several hundred years.

In addition to these achievements, the Group can report the development and application of various technical and analytical innovations. For example, a practical and relatively inexpensive technique to measure the $^{240}Pu/^{239}Pu$ ratio in environmental samples was developed at UCD, which has been used to label various source-terms in collaboration with CIEMAT, MAFF, RISØ and UAB. Further, a substantial and on-going exchange of scientific and technical expertise has taken place between the partners, facilitated by both multilateral and bilateral meetings at which progress achieved and problems encountered have been reviewed and discussed, complemented by research visits to one another's facilities.

The Group held five formal meetings (Madrid 3/93, Lund 10/93, Cherbourg 6/94, Barcelona 1/95 and Roskilde 6/95) in the course of the reporting period, at which the development of a well-integrated research programme and the advancement of the various work packages were discussed in depth. A number of collaborative research campaigns aboard dedicated marine research vessels were also undertaken by the participants during the same period. Here, it is appropriate to recognise the roles of ENEA, IPSN-LRM and MAFF, who organised the various sea-going campaigns and, most importantly, provided vital berths and

onboard facilities for other members of the collaboration.

Some of the more obvious benefits and deliverables which have accrued from this project include (a) a very significant improvement in our understanding of the processes governing radionuclide behaviour in marine ecosystems, (b) a concomitant improvement in the scientific foundation of those aspects of Radiation Protection that relate to source definition and pathway identification, (c) the training of young researchers who, in the future, will provide the Community with continuity of expertise in this important field, (d) the direct dissemination of practical expertise amongst the participants *via* collaborative interaction in both the laboratory and the field, and (e) the broader dissemination of results and data to the international community through the significant number of quality research publications and reports which have arisen directly from the project. Many of these publications were collaborative in character, having been jointly prepared by two or more of the participating laboratories (see, for example, the contributions of the Group at the EC-sponsored MARINA-MED *Seminar on the Radiological Exposure of the Population of the European Community from Radioactivity in the Mediterranean Sea*, Rome, June 1994, and at the *International Symposium on Plutonium in the Environment*, Ottawa, July 1994).

Head of project 1: Dr. P.I. Mitchell

II. Objectives for the reporting period

UCD's overall objective was to examine the physical and chemical speciation of transuranic and other radionuclides in the marine environment, in order to better understand at a more fundamental level the basic mechanisms and defining parameters governing the transport, dispersion and accumulation of these radionuclides in marine zones of interest. These included (i) a deep, enclosed sea (the western Mediterranean), (ii) a shallow, open, high energy marine channel (the English Channel), (iii) a shallow, semi-enclosed shelf sea (the Irish Sea including Carlingford Lough and Dublin Bay) and (iv) a typical lough (Foyle) on the north coast of Ireland.

Specific objectives included:

(1) A detailed examination of the physico-chemical speciation of plutonium and americium (a) at geographically well-separated deep water stations (vertical profiles) in the western Mediterranean, (b) in coastal waters near the site of the 'Palomares' nuclear accident (Gulf of Vera, January 1966), (c) in the English Channel, at stations close to and down-stream of the spent nuclear fuel reprocessing plant at Cap de La Hague (France), and (d) in the inner environs of Dublin Bay, near the interface where fresh water from the River Liffey meets the saline environment of the Bay, as well as in Lough Foyle;

(2) An estimation (including size classification) of the proportions of plutonium (and americium) in colloidal form in filtered (<0.45 μm) water in (a) the Irish Sea and (b) the Catalan-Balearic Sea, using the technique of tangential-flow ultrafiltration (separation on the basis of physical size), supported by chemical speciation analysis and/or differential sorption analysis;

(3) The development of a continuous-flow, solvent-based, extractor for the separation of non-polar organic matter from natural waters, with a view to establishing whether significant fractions of plutonium and americium are present in the form of neutral organic complexes in sea water;

(4) A preliminary evaluation of the role of the sea surface microlayer in the retention and transport of transuranium nuclides;

(5) The measurement of plutonium and americium concentrations at various stations in the western Mediterranean water column, with a view to determining radionuclide inventories, vertical fluxes and mean residence times;

(6) An evaluation of plutonium and americium input and output fluxes at the Strait of Gibraltar and assessment of their impact on the mass-balances of both radionuclides in the western Mediterranean water column;

(7) The development of a practical and reliable technique, based on high-resolution alpha spectrometry and spectral deconvolution, to measure the $^{240}Pu/^{239}Pu$ ratio in environmental materials, and its application to samples gathered near the spent nuclear fuel reprocessing plant at Sellafield (UK) and at Palomares (Spain) for the purpose of labelling plutonium from these 'historic' sites;

(8) The modelling of time-series data, gathered in the course of this project (and previously), on plutonium and radiocaesium concentrations in the seabed sediments in the western Irish Sea, with a view to assessing the long-term bioavailability and ultimate fate of both elements.

III. Progress achieved including publications

The data presented here derive from an extensive series of analyses carried out by our laboratory during the reporting period. Most of the samples analysed were collected in the course of collaborative research expeditions with our partner laboratories (CIEMAT, ENEA, IPSN, MAFF and UAB). In all, eleven separate research expeditions were undertaken by our team to the Irish Sea, the western Mediterranean and the English Channel.

Results

(1) Physico-chemical speciation of the transuranics in the water column

Western Mediterranean and the Gulf of Vera

Our study of the oxidation state distribution of plutonium in the western Mediterranean Sea has been successfully completed, as has our examination of the partition of ^{241}Am between the particulate and soluble (<0.45 μm) phases in surface sea water in the same zone.

^{239,240}Pu concentrations in filtered sea water sampled at various locations and depths in the western Mediterranean, together with the percentages of plutonium on suspended particulate and the percentages of plutonium(V) in the filtered fraction, are summarised in Table 1.

There is clear evidence of a sub-surface maximum in the total plutonium concentration profile at depths of some few hundred metres in the western Mediterranean. Similar sub-surface maxima have been observed at approximately the same depth in the Ligurian Sea and in open ocean waters by other researchers. It is suggested that these maxima are related to vertical transport and the dissolution/remineralisation of biogenic debris and organic matter, with the return of plutonium into solution.

The mean ^{238}Pu/^{239,240}Pu activity ratio in (filtered) open waters was found to be 0.039 ± 0.016 ($n = 9$), and is statistically consistent with that reported for the western Mediterranean zone by other workers. It is also indistinguishable from the ratio measured in coastal waters in the Gulf of Vera, namely 0.042 ± 0.020 ($n = 5$). The mean ^{241}Am/^{239,240}Pu ratio in (filtered) surface water in the vicinity of Palomares, at 0.038 ± 0.020 ($n = 3$), was also found to be similar to that observed in open waters, namely, 0.031 ± 0.016 ($n = 4$).

The percentage of plutonium in particulate form (>0.45 μm) in sea water throughout the western Mediterranean and the Gulf of Vera was found to lie in the range 1-14%. Plutonium levels on suspended particulate matter in Gulf waters were not substantially different from those measured in open waters, suggesting little input of a riverine or 'land run-off' character in this zone. In contrast to plutonium, approximately 50% of the ^{241}Am in the water column was associated with particulate matter.

It is also evident from the data (Table 1) that there is a pronounced sub-surface maximum in the plutonium(V) concentration profile at some few hundred metres depth. This maximum is also apparent in the case of the plutonium(IV) concentration, though it appears to occur nearer to the surface. It is noteworthy that the percentage of plutonium associated with particulate matter at a depth of 50 m is also maximum. Below a few hundred metres, the concentration of reduced plutonium diminishes significantly. In fact, the percentage of plutonium in a reduced chemical form in the water column was found to increase from a

Table 1. Partition of plutonium between suspended particulate and filtered (<0.45 μm) sea water, and percentage of plutonium(V) in filtered water sampled throughout the western Mediterranean (July-August, 1991 and 1992).

Depth (m)	^{239,240}Pu (filtrate) (mBq m^{-3})	% ^{239,240}Pu (particulate)	% ^{239,240}Pu(V) (filtrate)
Alboran Sea:			
	***Station 03** (37°49'N, 02°32'E; 2770 m);*		
15	12.6 ± 0.5	7.0 ± 0.9	70.7 ± 1.6
515	29.1 ± 0.8	2.4 ± 0.3	87.0 ± 0.8
1200	21.3 ± 1.8	1.4 ± 0.3	92.2 ± 0.9
2745	24.8 ± 1.2	3.0 ± 0.6	94.8 ± 0.6
Catalan-Balearic Sea:			
	***Station 05** (42°00'N, 03°40'E; 931 m);*		
3.5	16.1 ± 0.7	4.2 ± 0.8	62.8 ± 1.9
50	14.8 ± 0.6	10.6 ± 0.9	28.2 ± 1.8
250	33.4 ± 1.3	2.4 ± 0.4	80.3 ± 1.0
911	24.3 ± 0.9	1.9 ± 0.5	88.0 ± 0.8
	***Station 06B** (41°22'N, 02°15'E; 46 m);*		
5	11.7 ± 0.5	13.5 ± 1.4	91.7 ± 1.0
Gulf of Vera:			
	***Station 04** (36°59'N, 01°32'W; 1620 m);*		
3	15.7 ± 0.6	-	68.2 ± 1.1
	***Station 10** (37°10'N, 01°40'W; 773 m);*		
30	17.8 ± 0.6	6.4 ± 1.1	52.7 ± 1.7
697	27.0 ± 1.2	3.9 ± 0.8	95.4 ± 0.5
	***Station 13** (37°11'N, 01°48'W; 57 m);*		
5	12.0 ± 0.5	4.7 ± 0.6	63.4 ± 1.8

minimum of 5-12% close to the seabed, to a maximum of over 70% at a depth of about 50 m, most if not all of this increase taking place in the upper half of the water column. Further, the percentage of plutonium in a reduced form near the seabed appeared to be independent of depth.

The percentages of reduced plutonium in (filtered) surface waters at Stations 10 and 13 in the vicinity of the Palomares offshore zone were 47% and 37%, respectively. Thus, with the exception of the heavily polluted zone (Station 6B) close to the port of Barcelona, the proportion of plutonium(IV) in coastal surface waters was only marginally higher than in the more open waters of the western Mediterranean where it was typically 30-40%.

In contrast to surface waters, the percentage of plutonium(IV) in near-bottom waters was found to be less than 12% in all cases. This is an important observation. The presence of a higher proportion of plutonium(V) in near-bottom waters has also been observed in the Pacific Ocean. While the mechanism responsible for maintaining this distribution is unknown, its uniformity in samples collected near the sediment-water interface in the Pacific, the Mediterranean and shallower coastal environments such as the Gulf of Vera and the Irish Sea, suggests that some component of bottom sediments is involved either as a catalyst or as an active agent in the plutonium redox reactions. The increased stability of oxidised plutonium near the bottom could be a mechanism for the return of plutonium from the sediment surface into solution. Loss of plutonium from particles at the seabed has previously been postulated to explain the low inventories of plutonium in deep-sea sediments relative to the fluxes calculated from sediment trap data.

Representative sediment - water distribution coefficients (K_d) for plutonium in the western Mediterranean water column were also determined in the course of this programme. Our overall mean K_d-values for total plutonium and plutonium(IV) were $(1.6 \pm 1.8) \times 10^5$ l kg^{-1} (n = 10) and $(1.1 \pm 1.2) \times 10^6$ l kg^{-1} (n = 11), respectively.

English Channel

The oxidation state distribution of plutonium in filtered sea water from the English Channel was examined in the course of the GEDYMAC '94 expedition aboard the R.V. *Noroit*. Two sampling stations were chosen, one (St. 125) close to the La Hague source term and the second (St. 146) in mid-Channel some 100 km to the east. The data are given in Table 2 and show clearly that the percentages of plutonium in an oxidised form at both stations are identical. They are also similar to the percentages observed in the open waters of the Irish Sea. The absolute activity concentrations are at least an order of magnitude lower than those observed in the open waters of the Irish Sea, being close to those found in surface waters in the south-western Mediterranean in 1994. However, the $^{238}Pu/^{239,240}Pu$ ratio, at ~0.8, is clearly indicative of releases from La Hague.

Table 2. Plutonium concentrations and oxidation state distribution in filtered sea water in the English Channel (September, 1994)

Location	$^{239,240}Pu$ (mBq m^{-3})	$^{238}Pu/^{239,240}Pu$	% $^{239,240}Pu$(V)
Station 125 49.47°N 1.56°W	16.9 ± 1.3	0.83 ± 0.12	76 ± 3
Station 146 50.15°N 0.10°W	14.9 ± 1.8	0.72 ± 0.10	79 ± 3

Lough Foyle and Dublin Bay

An examination of the levels of plutonium and americium in sea water sampled in Lough Foyle in 1992 showed that between 40 and 70% of the plutonium and 75% of the americium were associated with the suspended particulate fraction. In the filtered fraction, most of the plutonium was in an oxidised form, with only ~10% in a reduced form, more than likely colloidal (see below). In Dublin Bay, a similar proportion of the plutonium in the filtered fraction was found to be in an oxidised form. The relevant data are summarized in Table 3.

Table 3. Physico-chemical speciation of plutonium and americium in sea water in Lough Foyle (June, 1992) and Dublin Bay (August, 1993)

Location	Conc. (mBq m^{-3})		% on susp. particulate		% Pu(V) (filtrate)
	$^{239,240}Pu$	^{241}Am	$^{239,240}Pu$	^{241}Am	
Culmore Pt.	116 ± 3	87 ± 5	70 ± 3	76 ± 7	87 ± 18
Redcastle	51 ± 2	32 ± 3	50 ± 3	78 ± 12	93 ± 14
Magilligan Pt.	37 ± 1	18 ± 3	37 ± 4	74 ± 13	-
Mean (n=3)	*68 ± 42*	*46 ± 36*	*52 ± 17*	*76 ± 2*	*90 ± 4*
Dublin Bay	126 ± 5	11 ± 1	7 ± 3	46 ± 4	90 ± 1

(2) Partition of plutonium and americium between colloidal and dissolved phases

Irish Sea

We have examined the distribution of plutonium and americium between the colloidal and dissolved phases in the filtered (<0.45 μm) fraction at a number of stations in the Irish Sea, Carlingford Lough and Lough Foyle using the technique of differential sorption on aluminium oxide. Certain reproducible features are evident from the data. Firstly, it is clear that a proportion of the plutonium and most of the americium in filtered sea water are subject to enhanced sorption. Secondly, there is a certain correspondence, albeit qualitative, between the proportion of plutonium in (operationally defined) colloidal form and that determined to be in a chemically reduced form. At low colloidal concentrations (5-20%), the correspondence is almost quantitative.

In the case of americium, it is well established that the dominant oxidation state in aqueous solution is Am(III). Indeed, measurements on the chemical speciation of americium in filtered water from the north-eastern Irish Sea appear to confirm that americium is present almost exclusively as Am(III). Thus, a much greater proportion of americium than plutonium can be expected to be in a highly insoluble, hydrolysed form, leading to a stronger affinity for suspended particulate matter, colloids and sedimentary deposits. Pu(IV), similarly, has a strong tendency to hydrolyse in alkaline media such as sea water. As the percentage of reduced plutonium in open waters in the Irish Sea seldom exceeds 20%, one does not expect the colloidal fraction to be any greater. Our data broadly confirm this to be the case. In contrast, essentially all of the americium in the microfiltered phase appears to be hydrolysed.

Within Carlingford Lough, about 30% of the plutonium and, apparently, most of the americium in filtered water (i.e., the colloidal plus soluble fractions) were found to be in colloidal form (as defined by sorption). Given that 70 ± 18% of the plutonium and the totality of americium in filtered sea water from the Lough were in a reduced chemical form (Table 4), it is not unreasonable to infer that, in Lough waters, about 50% of the plutonium(IV) and most of the americium in the filtered fraction are colloidally-bound.

Table 4. Percentage of colloidally-bound plutonium compared with the percentage of plutonium(IV) in filtered sea water sampled in the Irish Sea and Lough Foyle

Location	% colloidal Pu	% Pu(IV)
Carlingford Lough	31 ± 6	70 ± 18
Lough Foyle	16 ± 11	10 ± 4
Dublin Bay	9 ± 4	10 ± 1
Western Irish Sea	15 ± 3	17 ± 7
Eastern Irish Sea (<0.45 μm)	13 ± 3	8.9 ± 0.9
Eastern Irish Sea (<1 kD)	4 ± 1	5.4 ± 0.3

Outside the Lough, about 15% of the plutonium and almost all of the americium in filtered water were found, on average, to be associated with the colloidal fraction. The fact that the proportion of colloidal ^{239,240}Pu in open waters in the western Irish Sea is significantly lower than in Carlingford Lough, while the proportion of colloidal ^{241}Am in both ecosystems appears to remain constant, is undoubtedly related to the significantly lower presence of plutonium(IV) in open waters relative to the waters of the Lough. In fact, our mean value for colloidally-bound ^{239,240}Pu in the western Irish Sea is statistically identical to the mean percentage of plutonium(IV) in (filtered) surface and bottom waters from the same zone, namely 17 ± 7% (Table 4). In contrast, the proportions in colloidal form in Lough Foyle are similar to those in open waters.

In a complementary study, carried out in collaboration with MAFF, large volumes of water were collected in the north-eastern Irish Sea near Sellafield and filtered *in situ* using a selection of tangential flow ultrafiltration membranes with a view to (a) comparing both the oxidation state distribution and the colloidal component of plutonium in the different size fractions, and (b) determining the physical size of the colloidal particles or aggregates in question.

Our data show that the percentage of colloidal plutonium (as defined by sorption) in the (nominal) 1 kD permeate is lower than in the 3 kD, 10 kD or 0.45 μm fractions. The retention of colloidal plutonium by a 1 kD filter (defined as the relative difference in the colloidal ^{239,240}Pu concentrations in the <0.45 μm and <1 kD fractions) was found to be significant, while that of a 3 kD filter was less so. Indeed, it would seem as if the onset of this reduction occurs in the size range 10 - 1 kD. In other words, much of the plutonium in a colloidal form in these waters is associated with particles in the size range <10 kD.

Careful analysis of the oxidation state distribution of plutonium in the different size fractions upon ultrafiltration showed no evidence of significant plutonium(V) retention, even by a 1 kD filter. Clearly, plutonium present in sea water in an oxidised form is genuinely soluble. In contrast, our data provide convincing evidence that plutonium in a reduced chemical form is retained in increasingly significant quantities by progressively lower NMWL ultrafilters. In fact, from 20 to 50% of the reduced plutonium present in filtered water appears to be retained by 1 kD filters. Moreover, the percentage of plutonium(IV) in the 1 kD retentate shows a significant rise, as it should if the percentage in the permeate has fallen. Further, we have

observed that the proportion of ^{210}Po retained by a 1 kD membrane (~30%) is not dissimilar to that of Pu(IV). In general, these observations are not inconsistent with the results of our sorption experiments, provided it is recognised that the colloidal phase has been defined operationally in two distinct ways, and suggest that most of the plutonium(IV) in sea water is also associated with particles in the size range < 10 kD. In this regard, we should caution that because fractionation by ultrafiltration is achieved on the basis of molecular size rather than mass, the nominal pore size of the ultrafilter does not necessarily correspond to the actual molecular weight of, for example, naturally occurring organic material.

Western Mediterranean

The partition of plutonium between the particulate, colloidal and soluble fractions in surface waters has been examined in the Gulf of Vera and at a station close to the port of Barcelona. In the Gulf of Vera, the mean percentage of plutonium in colloidal form, as operationally defined by differential sorption on aluminium oxide, was found to be 10 ± 4%. This is considerably smaller than the percentage of plutonium(IV) in filtered water from the same zone (*ca.* 30 - 50%), and would indicate that, in relatively unpolluted Mediterranean waters, much of the reduced plutonium is in a non-colloidal form. This contrasts with the open waters of the Irish Sea, where the percentages of reduced and colloidal plutonium appear to be similar. Interestingly, the percentage of plutonium in a colloidal form in filtered water from the Gulf of Vera was similar to that observed in the open waters of the Irish Sea. In contrast, near Barcelona, little or no plutonium was detected in colloidal form (<3%). A similar observation has been reported by UAB, who also attempted to measure the colloidal fraction at this location. Chemical speciation analysis by our laboratory has shown that almost all of the plutonium in filtered surface water at this station is in an oxidised form (95%), unlike surface waters sampled elsewhere in the western Mediterranean (Table 1). It, thus, seems likely that biological or, indeed, chemical pollution is responsible for this anomaly.

We have also carried out experiments (based on tangential-flow ultrafiltration and chemical speciation measurements) to determine whether the size fractionation of the colloidal plutonium component in the western Mediterranean is similar to that observed in the Irish Sea. Our results confirm our earlier findings that approximately 30% of the plutonium(IV) in filtered surface water is in a colloidal form. However, our analyses show clearly that, in the western Mediterranean, this plutonium is associated with particles in the size range 100 kD - 0.45 μm, in contrast to the Irish Sea, where it appears to be associated with very much smaller particles (< 10 kD).

(3) Development of a continuous-flow, solvent based, extractor for the separation of non-polar organic matter from natural waters

A double-chamber solvent extraction system, based on a design originally conceived by Ahnoff and Joseffson (1976) for the separation of non-polar organic matter from natural waters, was constructed in our laboratory for the purpose of determining whether significant fractions of the plutonium and americium present in sea water are associated with neutral organic complexes. The system was calibrated using divalent ^{210}Pb as metal and 1-pyrrolininecarbodithioic acid (APDC) as complexing agent. The bulk of the ^{210}Pb in a 50 ml solution of partial sea water 10^{-3}M in APDC was found to be readily extractable using cyclohexane as solvent. The extraction efficiency was determined by passing sea water solutions of ^{210}Pb-labelled APDC sequentially through two extraction chambers at a flow-rate of ~5 l h^{-1}. Under these conditions, the mean extraction efficiency was 92 ± 1%.

Preliminary experiments have been carried out with samples of sea water from the Irish Sea. However, no measurable extraction of either plutonium or americium has been observed. This would suggest that little if any plutonium or americium is present in sea water in the form of neutral organic complexes. Interestingly, some researchers have suggested that many of the apparently conflicting results from studies on dissolved organometallic complexes in sea water could be reconciled if it were assumed that the concentration of molecular organic complexes was negligible, and that all metal-organic interaction takes place between metals and organic colloids. Since colloids, by definition, are charged, they are not extractable with a non-polar solvent. That much of the organic matter present in natural waters is in colloidal form is indisputable. Whether there is a significant fraction in the form of molecular complexes seems very doubtful.

(4) Plutonium and americium enrichment in the sea surface microlayer

The retention of metals within the sea-surface microlayer is well known, various studies having demonstrated substantial trace-metal enrichment in the top 100 μm relative to the bulk water beneath. Mindful of these facts, we have carried out a set of experiments under laboratory conditions in which we have been able to demonstrate plutonium enrichment factors of 10^2 - 10^3 in solutions of partial sea water containing high concentrations of humic material and monolayers formed with oleic acid. However, under field conditions, we found it difficult to sample less than the top 150 μm layer in any quantity. The feasibility of detecting measurable enrichment is thus problematic, given that the bulk of the sample is drawn from beneath the microlayer. A simple example illustrates the difficulty: with a microlayer of 20 Å and an enrichment factor of 1.5 x 10^3, sampling the top 120 μm will yield an effective enrichment factor of just 1.02. Accordingly, under these sampling conditions, enrichment factors as large as 10^3 may not be detected.

(5) Plutonium and americium inventories, vertical fluxes and mean residence times in the western Mediterranean water column

Mean residence times for plutonium and americium in Mediterranean surface waters

In the course of this project, we have developed an extensive database on plutonium and americium concentrations in surface sea water throughout the western Mediterranean (Catalan-Balearic Sea, Gulf of Vera, Alboran Sea and Algerian Basin). In general, these concentrations (corresponding to the period 1991-94), were lower than those recorded in previous studies carried out by other workers in the same zones.

By 1994, the mean ^{239,240}Pu concentration in the Algerian Basin was found to be 7.8 $\pm$ 0.3 mBq m^{-3} and was indistinguishable from the mean of 8 $\pm$ 3 mBq m^{-3} obtained for surface waters in the vicinity of the Strait of Gibraltar and the Alboran Sea. It can thus be taken as representative of the ^{239,240}Pu concentration in surface waters. When our data for the period 1991-94 is combined with previously published ^{239,240}Pu concentrations spanning the period 1970-90, an exponential decrease in concentrations with time is apparent. From the best fit to the data a mean residence time for plutonium in the surface layer of 14.5 years is derived, in good agreement with values estimated by other workers. An examination of similar data for ^{241}Am gives a mean residence time of $\sim$3 years.

From the isotopic composition of the plutonium, i.e., the ^{238}Pu/^{239,240}Pu activity ratio, it is clear that the concentrations measured in our study were representative of global fallout. This

is further confirmed by the fact that the mean ratio was almost identical to that reported in open oceans. In contrast, the $^{241}Am/^{239,240}Pu$ ratio in surface sea water was approximately an order of magnitude lower than the value of 0.30 ± 0.06 reported for the integrated global fallout (derived from soil measurement data) in the mid-1980s. Since the $^{241}Am/^{239,240}Pu$ activity ratio should, if anything, increase with time due to ingrowth following the decay of ^{241}Pu, it is evident that ^{241}Am must be removed from the water column more rapidly than $^{239,240}Pu$. This is supported by the observed increase in the $^{241}Am/^{239,240}Pu$ ratio in seabed sediments over the past decade (having allowed for ^{241}Am ingrowth). For example, surface sediment sampled in the Alboran Sea in 1994 showed an $^{241}Am/^{239,240}Pu$ ratio of 0.28 ± 0.01 which is at least an order of magnitude greater than that observed in surface waters.

Inventories

The inventories of $^{239,240}Pu$ and ^{241}Am were calculated at each of our stations by integration of the concentrations profiles, assuming a linear variation in concentration between sampling depths. A linear increase in the inventories with depth was observed. Using mean depths and the known areas of each of the western Mediterranean sub-basins (as defined in the ATOMED-3 regional model), best estimates of 20 TBq($^{239,240}Pu$) and 1.2 TBq(^{241}Am) were derived for the total inventories in the water column of the western Mediterranean. When compared with estimates of the total deposition, it is clear that approximately 30% of the plutonium and only 5% of the americium still reside in the water column, confirming the considerably lower americium residence time.

An examination of previously published vertical profile data shows that since 1974 the $^{239,240}Pu$ inventory in the western Mediterranean has been falling more or less linearly at a rate of about 1.1 TBq y^{-1}. IAEA-MEL data on vertical fluxes obtained from sediment trap experiments in the north-western Mediterranean indicate that a representative value for the plutonium loss from the water column in association with sinking particles is ~ 0.25 Bq m^{-2} y^{-1}. This is equivalent to a loss of ~ 0.21 TBq y^{-1} and is clearly lower than the figure of 1.1 TBq y^{-1} estimated on the basis of inventory data.

From an analysis of plutonium and americium concentration profiles in the vicinity of the Strait of Gibraltar it is clear that inflowing Atlantic water has lower transuranic concentrations than outflowing Mediterranean water. If comparable quantities of water are exchanged through the Strait, this will result in a net loss of transuranium nuclides from the western Mediterranean water column. The significance of this mechanism for the plutonium and americium mass-balance in the western Mediterranean is discussed below.

(6) Plutonium and americium input and output fluxes through the Strait of Gibraltar

A two-layer exchange of water takes place through the Strait of Gibraltar, with a surface inflow of less dense Atlantic water (salinity <36.5‰), a bottom outflow of denser Mediterranean water (salinity >37.5‰) and a strong vertical salinity gradient layer separating the inflowing and outflowing masses. In order to determine the plutonium and americium input and output fluxes through the Strait, the concentrations of these radionuclides were determined in sea water sampled at various stations and depths in the vicinity of the Strait and in the Alboran Sea in October 1994. The sampling depths were selected with the aid of detailed hydrological data to ensure that the samples collected were fully representative of the distinct water masses exchanging through the Strait.

The mean $^{239,240}Pu$ concentration in the inflowing Atlantic water was found to be 5.7 ± 1.2 mBq m^{-3}. The equivalent figure for the outflowing Mediterranean water was 20.5 ± 2.8 mBq m^{-3}. The exact amount of water flowing through the Strait of Gibraltar is difficult to estimate, as the net flow represents only about 5% of the total flow in each direction. In our calculations, values of 1.39 x 10^6 m^3 s^{-1} and 1.32 x 10^6 m^3 s^{-1} were used for the inflowing and outflowing fluxes, respectively. The resulting net flow, at 7 x 10^4 m^3 s^{-1}, is compatible with a number of other values reported in the literature and, further, is consistent with the deficit which results from a combination of evaporation, precipitation and runoff. On this basis, an annual inflow of 0.22 TBq($^{239,240}Pu$) from the Atlantic and an outflow of 0.85 TBq($^{239,240}Pu$) from the Mediterranean gives rise to an annual net outward flux of 0.63 TBq($^{239,240}Pu$), representing ~3% of the present inventory in the western Mediterranean water column and ~60% of the total annual loss in the basin. The same calculation for ^{241}Am, taking the inflowing and outflowing concentrations to be 0.11 and 0.8 mBq m-3, respectively, gives an annual net outward flux of about 0.03 TBq(^{241}Am), also representing ~3% of the present inventory in the water column.

If the net annual flux through the Strait and the loss *via* particle scavenging are taken together, the total annual loss from the water column can, in fact, be accounted for. It is clear from the above that, at present, the loss of plutonium through the Strait is comparable to, if not more important than, the loss *via* removal by sinking particles, and that the horizontal and vertical transport of the different water masses play a key role in the evolution of transuranium concentrations in the western Mediterranean basin.

(7) Development of a technique for measuring the $^{240}Pu/^{239}Pu$ ratio in environmental samples

Accurate measurement of the $^{240}Pu/^{239}Pu$ ratio in environmental samples is of importance as it may provide evidence for the definitive identification of a particular source-term. Usually, the measurement is performed by mass spectrometry, unless the activities involved are relatively high. In such cases, as the published literature shows, it is feasible to determine this ratio using high resolution alpha spectrometry and appropriate algorithms to deconvolute the partially resolved $^{239,240}Pu$ multiplet. In the course of the present programme, a practical technique, based on commercially-available software developed for gamma spectra analysis, has been developed by which this complex multiplet can be resolved at the much lower activities typical of many environmental samples. In our approach, it is not necessary to make any alterations to the normal alpha spectrometric set-up (including energy dispersion), other than to improve collimation. The instrumental function is defined for each spectrum by fitting a modified gaussian with exponential tails to the comparatively well-resolved ^{242}Pu 'doublet' (used as tracer) and, if present, the ^{238}Pu 'doublet'. The fitted peaks are used to create an energy calibration file with which, using published energy data, the positions (in channels) of the component peaks of the multiplet are predicted. These positions are not altered subsequently when an interactive multiplet analysis facility is used to quantify the relative spectral intensities of the components. Before calculating the $^{240}Pu/^{239}Pu$ ratio, it is advisable to correct for coincidence summing of alpha particles and conversion electrons. The technique has been applied to the determination of the $^{240}Pu/^{239}Pu$ ratio in a set of environmental samples, some of which were supplied by IAEA-MEL under their laboratory intercomparison programme. Subsequently, replicate samples were analysed independently using thermal ionisation mass spectrometry. The agreement between the two sets of data was most satisfactory. Further validation of this deconvolution technique was provided by the good agreement between the measured alpha-emission probabilities for the component peaks in the

$^{239,240}Pu$ multiplet and published values.

Table 6. $^{240}Pu/^{239}Pu$ atom ratios in selected samples determined by spectral deconvolution (AS) and mass spectrometry (TIMS)

Sample	Description	Measured $^{240}Pu/^{239}Pu$ atom ratio	
		AS	TIMS†
IAEA-134	Cockle flesh, Cumbria, UK, 1991	0.226 ± 0.011	0.2104 ± 0.0007
IAEA-135	Intertidal sediment, Cumbria, UK, 1991	0.198 ± 0.005	0.2083 ± 0.0004
Mayo Peat	Blanket-bog peat, Ireland, 1990	0.171 ± 0.002	0.1820 ± 0.0003
IAEA-367	Marine sediment, Enewetak Atoll, 1982	0.289 ± 0.007	0.296 ± 0.003
EN-5011	Marine sediment, Enewetak Atoll, 1975	0.33 ± 0.04	0.295 ± 0.002
IAEA-368	Marine sediment, Mururoa Atoll, 1989	0.032 ± 0.004	0.0315 ± 0.0004

† Mean of 4 separate determinations
[Uncertainties quoted to 1 standard deviation (S.D.)]

The technique has also been applied with success to the determination of variations in the $^{240}Pu/^{239}Pu$ atom ratio in sediment cores from the western Irish Sea and to the measurement of the same ratio in samples of sediment and soil containing hot particles from the Palomares zone. In the western Irish Sea, the ratio was found to be considerably lower in the deeper sediments, varying from ~0.17 near the surface to ~0.07 at some few tens of centimetres depth, reflecting changes in the isotopic composition of the plutonium discharge over the decades. The Palomares samples, which were provided by CIEMAT and UAB, showed a mean ratio of 0.056 ± 0.003 (n = 4), entirely consistent with weapons-grade plutonium of the period (1960s).

(8) Modelling of time-series data on plutonium and radiocaesium concentrations in the sediments of the western Irish Sea

Plutonium, americium and radiocaesium concentrations in seabed sediments have been determined by our laboratory at defined stations in the western Irish Sea since the mid-1980s. The experimental data confirm that, while caesium levels have been falling continuously in the course of this study, plutonium concentrations have not changed significantly in the same period. This is in sharp contrast to the pattern observed in the vicinity of Sellafield, where both caesium and plutonium concentrations have fallen steadily as a result of successive reductions in annual discharges and dispersion.

$^{238}Pu/^{239,240}Pu$ activity ratios and pre-depositional mixing

Two features are evident from an examination of the annual $^{238}Pu/^{239,240}Pu$ activity ratios: firstly, the ratios have remained almost constant since 1982 and, secondly, they are consistently lower than those reported for recent discharges (>0.3 since 1980). In fact, over the period for which we have experimental data, measured ratios clearly reflect those of the

time-integrated Sellafield discharge. This observation can best be explained by 'pre-depositional' mixing of contemporary and past discharges, rather than 'post-depositional' mixing *in situ*. Additional evidence in support of this hypothesis is discussed below.

Mixing is believed to take place mainly in the muddy sediments close to the Sellafield outfall, where a combination of bioturbation (the physical disturbance of the sediment by benthos), erosion and very low sedimentation rates (<0.1 mm y^{-1}) leads to extensive vertical mixing. If, as now believed, these sediments have become the dominant source of the plutonium transported further afield, radionuclide activity ratios throughout the latter must reflect cumulative rather than annual discharges.

The particle transport of contaminated sediment to locations far removed from Sellafield has been identified by several authors as the main mechanism controlling radionuclide concentrations. Dispersion of plutonium reworked from a mixed pool of contaminated sediment, either by resolubilisation and subsequent soluble transport or by direct suspended particulate transport, appears to be the most probable mechanism controlling the transfer of this element from the eastern to the western Irish Sea.

Modelling and estimation of mean availability times

A semi-empirical model developed by Nicholson and Hunt (1995) has been applied to the ^{239,240}Pu and ^{137}Cs time-series data with a view to predicting trends and estimating mean availability times. The model considers the environmental material, in our case sediment, to be in equilibrium with its environs. This assumption means that the time-span over which a particular nuclide is available to the material depends only on the rate of loss of the nuclide from the environment and its physical decay. Two parameters, estimated by a maximum likelihood process, are derived from the experimental time-series data: the mean availability time (i.e., the time for which the nuclide will effectively be available to the material, defined as the time in which the original concentration will decrease by a factor of *e*) and a constant incorporating the concentration factor (the equilibrium activity in the material per unit activity in the environment) and any scaling effects such as distance from the discharge point. The values obtained are then used to calculate the nuclide concentration in the material for a particular year, taking into account the contribution of contemporary and historic discharges. In the model, the activity *A(i)* for a particular year *i* is given by the expression

$$A(i) = \alpha \sum_{j=0}^{\infty} D(i-j)\ e^{-\lambda_e j}$$

where *D(i-j)* is the radioactivity discharged *j* years prior to *i*, λ_e is the inverse of the mean availability time and α is the constant that accounts for the concentration factor and scaling effects. Predicted ^{137}Cs and ^{239,240}Pu concentrations for each of the three stations are shown in Figure 3, together with the experimental data. The model not only predicts future concentrations but also those in years prior to the initiation of our sampling.

In the case of ^{137}Cs, the predicted evolution at each of the three stations follows a similar pattern. Concentrations increase from the mid-1950s, reach a maximum at about 1981 and from then on decrease. This is consistent with the known evolution of ^{137}Cs concentrations in western Irish Sea waters in the same period. The rate of decrease varies depending on the station. Mean availability time estimates for Stations #7, #8 and #9 are 16.5, 9.0 and 6.9 years, respectively. Variations between the three stations most likely reflect differences in

physical dispersion and dilution processes which, in turn, are dependent on local hydrological conditions such as currents and depth. These availability times are considerably higher than the estimate of 3.1 years reported by Nicholson and Hunt (1995) for sediments close to the Sellafield outfall and the value of ~ 5 years reported by MacKenzie *et al.* (1994) for sediments in the Solway Firth. This is not surprising, as the eastern Irish Sea is shallower than the western Irish Sea and the probability of sediment resuspension is higher in shallower waters.

In the case of $^{239,240}Pu$, the estimation of the mean availability time is more difficult. The constancy of the plutonium concentrations during the period of this study implies an availability time which, at the very least, is considerably greater than that of ^{137}Cs. Predicted concentrations, using a range of availability times, τ, indicate that a mean availability time of at least 800 years best satisfies our, admittedly limited, data. Model predictions (based on this assumption) for each of the stations are shown in Figure 1. Concentrations at all three stations begin to increase in the mid-1950s and continue to do so until the early 1980s, from which point they level off. Monitoring of the plutonium concentrations for at least another decade should enable us to make a better estimate of the actual mean availability time. Nevertheless, it is clear that plutonium will remain biologically available within western Irish Sea sediments for many decades, if not hundreds of years, to come.

Summary

Our studies confirm that most of the plutonium in open (oxygenated) waters is in a highly soluble, oxidised form, with a smaller fraction in a reduced form and an even smaller fraction associated with suspended particulate matter. These observations apply to open oceans, semi-enclosed seas and shallow continental shelf waters. However, in zones where there is a significant increase in, for example, the levels of DOC, there is a redistribution of the plutonium between the dissolved and particulate (>0.45 μm) phases with the percentage of plutonium on particulate increasing due to the reduction of plutonium(V) to plutonium(IV). Further, our results indicate that a significant proportion of the plutonium in a reduced state in the so-called dissolved phase is in a colloidal form. Both speciation analyses and enhanced sorption measurements on samples of ultrafiltered sea water from the north-eastern Irish Sea and the western Mediterranean, indicate a significant difference in the physical size of the colloidal particles with which plutonium is associated in the two zones. Clearly, it will not be possible to develop a reliable model of the dispersion of plutonium in the marine environment unless these key observations are taken fully into account.

Acknowledgements

The support and co-operation afforded the co-ordinating laboratory by each of the participants in this collaboration and by the staff of the Commission throughout the reporting period is gratefully acknowledged.

References

Nicholson, M.D. and Hunt, G.J. (1995), 'Measuring the availability to sediments and biota of radionuclides in wastes discharged to the sea', *J. Environ. Radioactivity* **28**, 43-56.

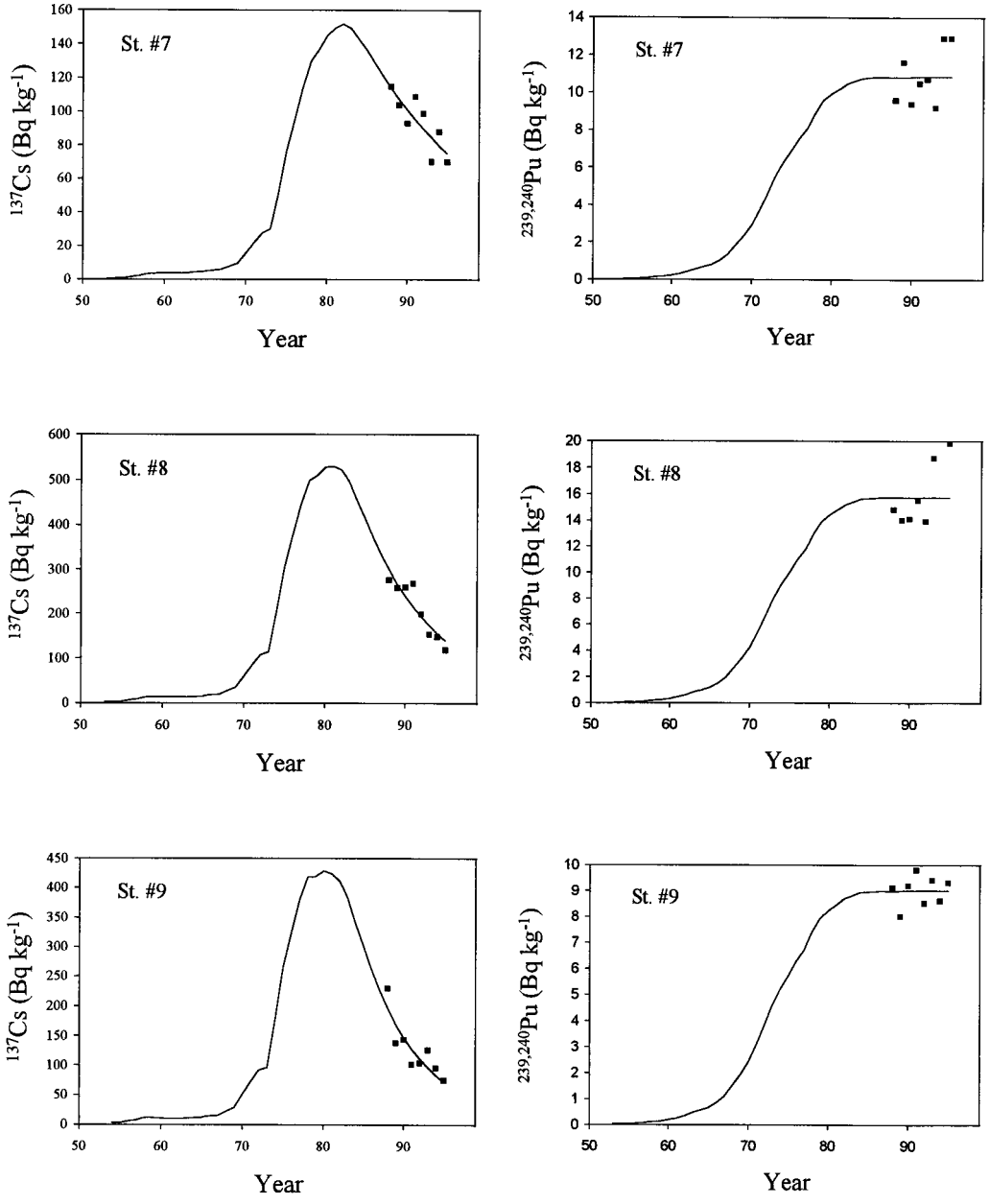

Figure 1. Temporal evolution of measured (■) and model-predicted (—) concentrations of ^{137}Cs and ^{239,240}Pu in surficial sediments at Stations #7, #8 and #9 in the western Irish Sea

Publications

Articles

Boust, D., Mitchell, P.I., García, K., Condren, O.M. and León Vintró, L. (Submitted), 'A comparative study of the speciation and behaviour of plutonium in the marine environment of two reprocessing plants', In: 5th International Conference on the Chemistry and Migration Behaviour of Actinides and Fission Products in the Geosphere (MIGRATION '95), Saint-Malo (France), 10-15 September, 1995, *J. Contaminant Hydrology*.

Condren, O.M., Mitchell, P.I., Downes, A.B. and León Vintró, L. (Submitted), 'Plutonium in western Irish Sea sediments: origin, bio-availability and ultimate fate', In: Symposium on Irish Marine Science '95, Galway (Ireland), 6-9 September, 1995, *Proc. Royal Irish Academy (Special Edition)*.

Ryan, T.P., McGarry, A.T., Lyons, S., Smith, V., Cunningham, J.D, Mitchell, P.I., León Vintró, L., Larmour, R.A. and Ledgerwood, F.K., (Submitted), 'Plutonium, americium and radiocaesium in biota, sea water and sediment in Lough Foyle', In: Symposium on Irish Marine Science '95, Galway (Ireland), 6-9 September, 1995, *Proc. Royal Irish Academy (Special Edition)*.

Mitchell, P.I., León Vintró, L., Dahlgaard, H., Gascó, C. and Sánchez-Cabeza, J.A. (Submitted), 'Perturbation in the $^{240}Pu/^{239}Pu$ global fallout ratio in local sediments following the nuclear accidents at Thule (Greenland) and Palomares (Spain)', In: International Conference on Environmental Radioactivity in the Arctic, Oslo, 21-26 August, 1995, *Sci. Tot. Environ.*

León Vintró, L., Mitchell, P.I., Condren, O.M., Moran, M., Vives i Batlle, J. and Sánchez-Cabeza, J.A. (In Press), 'Determination of the $^{240}Pu/^{239}Pu$ atom ratio in low activity environmental samples by alpha spectrometry and spectral deconvolution', In: ICRM '95 Conference and International Symposium on Radionuclide Metrology and its Applications, Paris, 15-19 May, 1995, *Nucl. Instr. Meth. Phys. Res.*

Mitchell, P.I., Vives i Batlle, J., Downes, A.B., Condren, O.M., León Vintró, L. and Sánchez-Cabeza, J.A. (1995), 'Recent observations on the physico-chemical speciation of plutonium in the Irish Sea and the western Mediterranean', *J. Appl. Rad. Isot.* **46**(11), 1175-1190.

Sánchez-Cabeza, J.A., Molero, J., Merino, J., Pujol, Ll. and Mitchell, P.I. (1995), '^{137}Cs as a tracer of the Catalan current', *Oceanologica Acta* **18**(2), 221-226.

Molero, J., Sánchez-Cabeza, J.A., Merino, J., Vives i Batlle, J., Mitchell, P.I. and Vidal-Quadras, A. (1995), 'Particulate distribution of plutonium and americium in surface waters from the Spanish Mediterranean coast', *J. Environ. Radioactivity* **28**, 271-283.

Sánchez-Cabeza, J.A., Merino, J., Schell, W.R. and Mitchell, P.I. (1995), 'Transuranic accumulation in plankton from the Spanish Mediterranean coastal environment', In: Proc. XXXIVe Congres Commission Internationale pour l'Exploration Scientifique de la Mer Mediterranee, La Valette (Malte), 27-31 March, 1995. *Rapp. Comm. int. Mer Médit.* **34**, p. 231.

Molero, J., Sánchez-Cabeza, J.A., Merino, J., Pujol, Ll., Mitchell, P.I. and Vidal-Quadras, A. (1995), 'Vertical distribution of radiocaesium, plutonium and americium in the Catalan Sea (Northwestern Mediterranean)', *J. Environ. Radioactivity* **26**, 205-216.

Mitchell, P.I., Vives i Batlle, J., Downes, A.B., Sánchez-Cabeza, J.A., Merino Pareja, J., Delfanti, R. and Papucci, C. (1994), 'Chemical speciation and colloidal association of plutonium in the western Mediterranean water column and in the Gulf of Vera', In: *Proc. MARINA-MED Seminar on the Radiological Exposure of the Population of the European Community from Radioactivity in the Mediterranean Sea*, Cigna *et al.* (Eds.), Rome, 7-19 June, 1994, EUR-Report 15564 EN, pp. 441-457.

Delfanti, R., Papucci, C., Salvi, S., Vives i Batlle, J., Downes, A. and Mitchell, P.I. (1994), 'Distribution of Cs-137 and transuranic elements in seawater of the Western Mediterranean Sea (Algerian Basin, Balearic Sea)', *In: Proc. MARINA-MED Seminar on the Radiological Exposure of the Population of the European Community from Radioactivity in the Mediterranean Sea*, Cigna *et al.* (Eds.), Rome, 7-19 June, 1994, EUR-Report 15564 EN, pp. 427-439.

Sánchez-Cabeza, J.A., Merino, J., Molero, J., Pujol, Ll. and Mitchell, P.I. (1994), 'On the use of

Cs-137 as a tracer of the Liguro-Provençal-Catalan Current', In: *Proc. MARINA-MED Seminar on the Radiological Exposure of the Population of the European Community from Radioactivity in the Mediterranean Sea*, Cigna *et al.* (Eds.), Rome, 7-19 June, 1994, EUR-Report 15564 EN, pp. 459-467.

Mitchell, P.I. with SCOPE RADPATH Collaboration (1993), 'Radionuclide Aquatic Pathways', In: *Radioecology After Chernobyl*, Sir Frederick Warner and Roy M. Harrison (Eds.), John Wiley and Sons, Chichester, Chapter 5, pp. 177-274.

Ryan, T.P., Mitchell, P.I., Vives i Batlle, J., Sánchez-Cabeza, J.A. and McGarry, A. (1993), 'Low-level ^{241}Pu analysis by supported-disc liquid scintillation counting', In: *Liquid Scintillation Spectrometry 1992*, J.E. Noakes, F. Schönhofer and H.A. Pollack (Eds.), *Radiocarbon*, pp. 75-82.

Molero, J., Morán, A., Sánchez-Cabeza, J.A., Blanco, M., Mitchell, P.I. and Vidal-Quadras, A. (1993), 'Efficiency of radiocaesium concentration from large volume natural water samples by scavenging with ammonium molybdophosphate', *Radiochimica Acta* **62**, 159-162.

Mitchell, P.I. and Vives i Batlle, J. (1992), 'The behaviour of plutonium and americium in the western Irish Sea', In: *Proc. AIB Conference on Environment and Development in Ireland*, Dublin, 9-13 December 1991, J. Feehan and F.J. Convery (Eds.), Publ. by The Environmental Institute, University College, Dublin, pp. 435-443.

Doctoral Theses

Downes, A.B. (In Preparation), 'Physico-chemical Speciation and Colloidal Association of Transuranium Nuclides in the Marine Environment', PhD Thesis, National University of Ireland, Dublin.

Vives i Batlle, J (1993), 'Speciation and Bioavailability of Plutonium and Americium in the Irish Sea and Other Marine Ecosystems', PhD Thesis, National University of Ireland, Dublin, 347 pp.

Reports / Abstracts

Mitchell, P.I., León Vintró, L. and Downes, A.B. (In Press), 'MED'94 Campaign: plutonium and americium concentrations (and concentration ratios) in different water masses in the vicinity of the Strait of Gibraltar and the open western Mediterranean', In: MED'94 Cruise Report, R. Delfanti and C. Papucci (Eds.), Ente per le Nuove Tecnologie, l'Energia e l'Ambiente (ENEA), La Spezia.

Condren, O.M., Downes, A.B., León, L. and Mitchell, P.I. (1995), 'Radioecological studies of the behaviour and long fate of plutonium in the marine environment', *The Irish Scientist* **3**, p. 41.

Vives i Batlle, J., Mitchell, P.I., Linkov, I. and Schell, W.R. (1995), 'Characterisation of radionuclide species in the environment', In: Proc. Workshop on Radionuclide Speciation in Soils and Sediments, National Institute of Standards and Technology, Gaithersburg, MD, 13-15 June, 1995.

Delfanti, R., Papucci, C., Salvi, S., Lorenzelli, R., Mitchell, P.I., Downes, A.B. and Vives i Batlle, J. (1995), 'Time evolution of the vertical profiles of artificial radionuclides in the Western Mediterranean water column', In: *Proc. International Conference on Chemistry and the Mediterranean Sea*, Taranto (Italy), 23-27 May, 1995, pp. 236-237.

Mitchell, P.I. and Vives i Batlle, J. (1993), 'Studies of the physical and chemical speciation of plutonium and americium in the western Mediterranean Sea zone', In: *MED'92 Cruise Report*, R. Delfanti and C. Papucci (Eds.), Ente per le Nuove Tecnologie, l'Energia e l'Ambiente (ENEA), La Spezia, 147 pp.

Mitchell, P.I., Vives Batlle, J., Ryan, T.P., McEnri, C., Long, S., O'Colmain, M., Cunningham, J., Caulfield, J.J., Larmour, R.A. and Ledgerwood, F.K. (1992), 'Artificial Radioactivity in Carlingford Lough', Published (jointly) by The Radiological Protection Institute of Ireland and the Department of the Environment, Northern Ireland, September 1992, 37 pp.

Mitchell, P.I. and Vives i Batlle, J. (1992), 'Plutonium speciation in the western Mediterranean Sea', In: MED'91 Cruise Report, R. Delfanti and C. Papucci (Eds.), ENEA, La Spezia, 63 pp.

Head of project 2: Dra. C. Gascó

II. Objectives for the reporting period

In this final report the sampling campaigns and analyses carried out, the analytical methodologies developed, and the main conclusions obtained are described in some detail. CIEMAT's objectives were detailed in the annex to the contract. Briefly, these were:

(A) To study the influence of orography in the relocation of transuranics and, specifically, the role played by submarine canyons;
(B) To study the geochemical association of transuranics and other long-lived radionuclides to marine sediments;
(C) To analyze the post-depositional migration of transuranium nuclides in the accident area of Palomares;
(D) To study terrigenous input from rivers and transuranic translocations in the continental shelf;
(E) To characterize hot particles;
(F) To determine the maximum vertical penetration of americium in marine sediments near Palomares;
(G) To participate in international intercalibration exercises.

III. Progress achieved including publications

(A) It is important to have detailed knowledge of the submarine floor orography of a contaminated area in order to predict the relocation of radionuclides associated to marine sediments. The bottom topography strongly influences deep sea flow and enhances vertical exchange. The redistribution of radionuclides can occur as a result of both erosion from local hills and slopes, and particular mesoscale events that give rise to the resuspension of sediment. The area where highest transuranic concentrations are found extends from Palomares to Garrucha on the continental shelf (water depth 0-50 m). This area is know to have a complex topography.

A bathymetric study covering the area of interest was carried out with a 3.5 kHz seismic profiler aboard the N/O *Urania* in 1992. The study corroborated that of 'Carte Bathymetrique' (carried out by SEGANO), and revealed few differences close to Garrucha. The presence of a deep canyon surrounded by a complex chain of sub-tributaries close to the coast was confirmed. Two of these sub-tributaries are located off Palomares and Garrucha, very close to the continental shelf. When the main flood occurred in 1973, these could have acted like a trap for the sedimentary particles and transuranics associated with them.

To achieve this objective, an extensive set of depth profiles (obtained in 1992) were analysed and compared with existing bathymetric records.

(B) The high values of the K_d factors for plutonium and americium reflect their preferential accumulation in marine sediments. Thus, the transuranics are found mainly in continental shelf sediments in zones where the sedimentation rates are comparatively high (0.3 to 0.5 cm y^{-1}). After deposition, the transuranics associated with marine sediments can be translocated by several mechanisms. Some useful predictions about their recycling can be made by analysing their geochemical association to marine sediments in zones such as Palomares. Sequential leaching experiments performed in the course of this project have shown (Figure 1):

- The effect of different source terms on plutonium and americium geochemical distribution, in that fallout plutonium from weapons tests in the 1960s is mainly associated with organic matter and sesquioxides, whereas refractory plutonium from the Palomares terrestrial accident appears in the residual fraction. Americium from weapons tests is mainly associated with the exchangeable and organic matter fractions, while americium from the Palomares accident appears in the residual fraction

- Plutonium and americium from the accident seem to be relatively immobile and not readily available to bottom feeding biota. Accordingly, plutonium and americium mobility is largely restricted to physical dispersion by currents or slumping phenomena

- Americium is associated with the more 'soluble' fractions and, theoretically, is more 'transportable' from a chemical point of view. In sediments where transuranic heterogeneities were observed, americium appeared to be present in a more 'soluble' form than plutonium

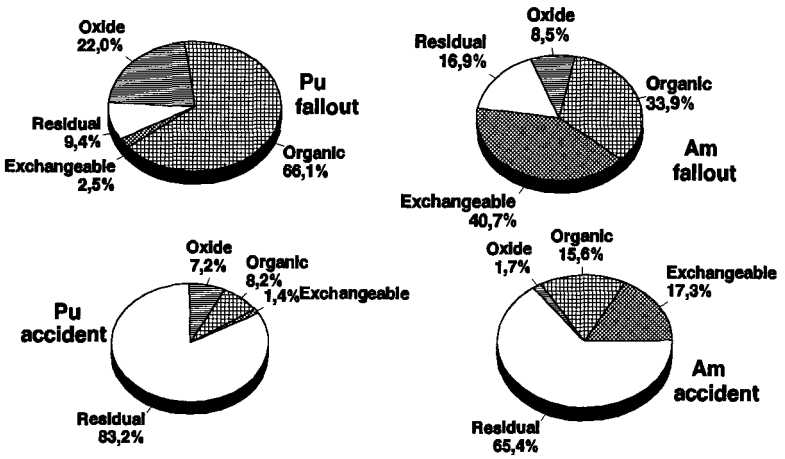

Figure 1. Sequential leaching of plutonium and americium from marine sediments sampled on the continental shelf near Palomares

One point should be highlighted: the sequential leaching of soil samples from Palomares using the same procedure showed a smaller percentage of plutonium in the residual fraction (Figure 2)[1] than in marine sediments. This observation would appear to suggest that accident plutonium is less soluble in the marine environment. More experiments on the extraction of transuranics from soils and marine sediments should be carried out to test this hypothesis.

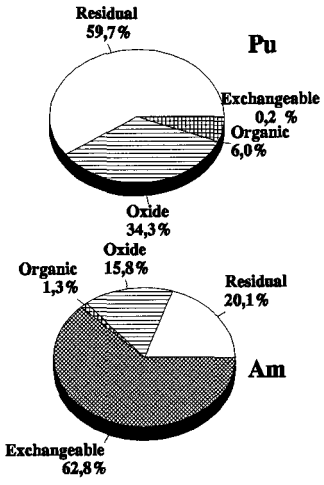

Figure 2. Sequential leaching of plutonium and americium from Palomares soil

Radiocaesium showed a preferential association for the residual fraction. The relevant data were presented in the course of the XXXIV CIESM Congress (Malta, March 1995).

The achievement of this objective required us to (a) implement a technique for americium extraction and purification in our laboratory and (b) develop a new technique for the sequential leaching of transuranics.

(C) At least two mechanisms of transuranic transport, one physical and the other chemical, are possible given the particular bathymetry of the submarine canyons off Palomares and the association of these radionuclides with the several phases of marine sediments:

(a) Physical transport of sediments and the radionuclides fixed to them

The settling material will escape the shelf, go to the continental slope and fall further into the

[1]Data obtained from Aragón A, Canal, A et al. (1992) Study of specifity in the sequential leaching of Pu and Am in low contaminated soils . Proceedings of the International Symposium of Radioecology . Chemical Speciation.Hot particles.Znojmo. Checoslovaquia. Octubre 12-16.

deep sea. Much of this escape will probably be along the bottom through a bottom turbidity layer, *via* mass movements, slumping and sliding along the edge and slope, and by turbidity currents through the tributaries of the Palomares submarine canyon.

Other well known mechanisms will contribute to the dispersion of the transuranics that have settled: suspended sediment on the shelf will be moved by surface waves and by a complex of currents, wind forcing and density gradients. The effects of surface waves decrease with water depth. Storm waves, however, may affect the entire shelf. In the Palomares area, twenty-eight years post-accident, it is clear that a combination of bioturbation and some or all of the above-mentioned mechanisms have contributed to the distribution now observed.

(b) Chemical transport

The decomposition of organic matter and other inorganic complexes can occur with the return of the associated transuranics to the overlying water. The fine particles of plutonium and americium oxide formed in the accident and originally present in marine sediments can be dissolved by sea water and, finally, can appear several years after as dissolved cations.

Fallout plutonium and americium settled onto the sediment (associated with sesquioxides and organic matter) may again be recycled into overlying water if: there is a dissolution of inorganic Fe-Mn-OH-P complexes or a microbial remineralization of organic-rich material

Residual plutonium and americium may be recycled if there are microorganisms or benthic infauna that solubilize refractory plutonium or that can feed with the whole particle changing its coating *via* ingestion.

An extensive bibliography was assembled on the subject of the dissolution of plutonium oxides and the corrosion of plutonium alloys in marine waters, as well as on the organic and inorganic species that complex plutonium cations. In certain cases, this information is available only for high plutonium concentrations.

(D) The tranfer of transuranics and other long-lived radionuclides from land to sea can be carried out *via* fluvial or aerial transport. Studies of the continental shelf off Palomares indicate that the fluvial mechanism may have been predominant after the Palomares accident (1966). The highest concentrations of transuranics in sediment profiles and their maximum depth penetration were found in the area of terrigenous input of the Almanzora river, while the lowest concentrations were located in areas of carbonate formation far removed from the terrigenous zone. This is true not only of transuranics from the accident, but also of fallout.

In general, Mediterranean areas subject to riverine input, albeit of a seasonal nature, present highest values of fallout transuranics and other radionuclides. Some of these areas were studied in this project and show similar sediment profiles to those obtained from the continental shelf off Palomares. Barcelona and Tarragona (50-90 m depth) are representative of areas of terrigenous input *via* Spanish Mediterranean rivers (marine sediments enriched in illites), while Valencia and Alicante are representative of non-terrigenous input (carbonate-enriched sediments). From the data given in Table 1 below, it is clear that radionuclide inventories are significantly higher in the Palomares zone compared to other zones, such as Barcelona and Tarragona, well removed from the accident site.

A distortion in the $^{238}Pu/\ ^{239,240}Pu$ ratio in sediments from the Palomares zone was observed. This departure from the global fallout ratio of ~0.03 was used to estimate the percentage of plutonium from the accident in the different sediment layers. This percentage ranged from 10 to 90%.

Table 1. Seabed sediment inventories (Bq m^{-2}) along the Spanish Mediterranean shelf

Area	Station	$^{239,240}Pu$	^{238}Pu	^{241}Am	^{137}Cs
Barcelona	Urbar	116 ± 4	3.0 ± 0.1	44 ± 4†	NM
Tarragona	Urtar	59 ± 2	3.0 ± 0.6	22 ± 4†	427 ± 23
Valencia	Urval	21 ± 2	0.80 ± 0.03	15 ± 2†	NM
Alicante	Urali	25 ± 2	1.7 ± 0.5	19 ± 2†	NM
Almería	St. 12	128 ± 32	6 ± 2	60 ± 16†	440 ± 100
	St. 05	295 ± 14	5.2 ± 0.9	42 ± 6† 43 ± 16‡	344 ± 28
	St. 13	674 ± 36	13.0 ± 1.8	190 ± 24‡	383 ± 29
	St. 17	1402 ± 42	25 ± 1	170 ±12† 1445 ± 53‡	1460 ± 46

NM: Not measured
† measured by alpha spectrometry (10 g aliquot)
‡ measured by gamma spectrometry (45 g aliquot)

This part of CIEMAT's study involved the analysis of a large number of sediment samples for plutonium, americium and radiocaesium, as well as the determination of the geochemical composition of the sediments. Some of the data on radionuclide inventories derived from the radiometric measurements were presented at the MARINA-MED Symposium (Rome, June 1994).

(E) An aerosol comprised of plutonium and americium oxides was formed after the accident occurred in Palomares. The conditions for transuranic fixation to metal alloys from the bomb, the later spread and deposition of the aerosol, and the transuranic association to atmospheric dust and to soil-sediment components, are very different to the conditions which prevail immediately following a nuclear explosion, where much higher temperatures are attained and fission products are formed. Particle sizes, types of oxides formed, coatings and associations are different for each event. For this reason, the Palomares and Thule accidents offer new perspectives to determine the behaviour of transuranic oxides in the environment. A comparative study of the structure of the transuranic particles in soil and marine sediment was proposed in order to improve our knowledge of the behaviour of these particles. The main questions to be answered were: (a) what is the coating of these particles in soils?, (b) what is the coating of these particles in marine sediments?, (c) are they absorbed onto the surface

of big particles or are they covered by minerals up to bigger sizes?, (d) are they more 'soluble' in aquatic conditions?, and (e) are there differences between transuranic association in soil compared to that in marine sediments?

The determination of the structure, shape, thickness and mineralogical composition of the coating is seen as essential to an understanding of the solubility of these particles in the marine environment and to an evaluation of their transfer *via* the marine food-chain, remineralization or mechanical transport. An attempt by AUN to characterise some of these particles using state-of-the-art technology has, to date, been only partially successful due to the scarcity of the particles, their low activity and their very small size.

The $^{239}Pu/^{240}Pu$ ratio in two samples of soil from Palomares was measured separately by alpha spectrum deconvolution and ICP-MS. The results confirmed that almost all of the plutonium in these samples was of weapons-grade quality. There was good agreement between these measurements and those carried out previously by UCD on samples of soil and sediment from Palomares.

(F) On the basis of the analysis of more than 1,000 data obtained in the Palomares marine zone, it is clear that deposited transuranics have a tendency to be incorporated into the deeper sediments. Significant concentrations appear in layers of sediments not predicted by the sedimentation rate. There is little doubt that the orography of the zone encourages physical processes which modify the manner in which sediment accumulates in certain areas.

However, a number of the sediment cores taken in the general vicinity of Palomares were found not to contain any accident plutonium. The plutonium and americium inventories in these cores were typical of global fallout, with no plutonium or americium detectable below the 30 cm horizon.

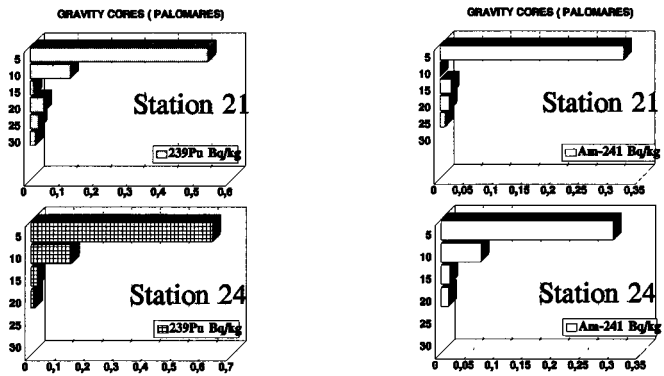

Figure 3. $^{239,240}Pu$ and ^{241}Am concentrations in marine sediments

(G) Intercomparisons

Annually, during this project, 20 analyses of plutonium and 22 of americium were conducted on IAEA Intercomparison materials (IAEA-373, IAEA-134, IAEA-135, IAEA-368, IAEA-300, IAEA-315, IAEA-326, IAEA-327) as part of our QA/QC programme.

Publications

Gascó, C., Antón, MªP. and Romero, L. (1994), 'Radioecología de transuránidos en el Mediterráneo Español', *Radioprotección* **1**, 21-29.

Antón, MªP., Gascó, C. and Romero, L. (1994), 'Global inventory of radionuclides along the Mediterranean continental shelf of Spain', In: *Proc. MARINA-MED Seminar on the Radiological Exposure of the Population of the European Community from Radioactivity in the Mediterranean Sea*, Cigna et al. (Eds.), Rome, 7-19 June, 1994, EUR-Report 15564 EN.

Antón, MªP., Gascó, C., Sánchez-Cabeza, J.A. and Pujol, Ll. (1994), 'Geochemical association of plutonium in marine sediments from Palomares (Spain)', *Radiochimica Acta* **66/67**, 443-446.

Gascó, C. (1994), 'Procedimiento para la determinación radioquímica de Am-241 en sedimentos (nivel poso radiactivo) utilizando extracción cromatográfica', Analytical Method, CIEMAT PR-X3-06, Madrid.

Scientific Team

Principal researchers: MªPaz Antón Mateos (CIEMAT-UGIA), Juan Palomares López and Milagro Pozuelo.
Technicians: José Meral Carrillo, Alberto Ortiz and Francisco Santos

Acknowledgments

We sincerely thank ENEA (St. Teresa) and, in particular, C. Papucci and R. Delfanti for their excellent organisation of the scientific campaigns on board the oceanographic vessel *Urania* (MED'92, 93, 94) and the participants and crew of the ship for their cooperation and assistance during the expedition.

Head of project 3: Dr. P. Guéguéniat

II. Objectives for the reporting period

(1) Pathways of plutonium associated with deposited sediments.
(2) Behaviour of plutonium isotopes in seawater of the Channel and in the Seine Estuary.

III. Progress achieved including publications

1. Pathways of plutonium associated with deposited sediments

One of the main objectives of the work undertaken in the past years in this field of investigation was to estimate transit times of plutonium-bearing particles throughout the Channel. This goal has been achieved and we will focus here on this point with reference to data presented in the previous progress reports.

In the Roads of Cherbourg, ^{238}Pu and $^{239,240}Pu$ isotopes have been measured on more than 40 sediment samples taken from 3 sediment cores collected in 1988, 1990 and 1993, and dated by the ^{210}Pb(excess) method. Vertical distribution of these isotopes have been described in the '94 Progress Report. The most striking pattern of this data set is that Pu isotopic ratios continuously increase from the early seventies (0.05) up to 1990 (*ca.* 0.9; Figure 1). This is consistent with the increase of the Pu isotopic ratios in the release of the La Hague reprocessing plant since it started. Nevertheless, the values observed in sediments are always lower than those measured in the release because they record an integrated signal originating from the plant. This is a consequence of complex mixing processes taking place in the vicinity of the release point (30 km west of Cherbourg). As earlier mentioned ('93 Progress Report), the Roads of Cherbourg acts as a natural sediment trap: therefore, sediment cores collected in this area display a record of the particulate Pu fluxes passing off Cherbourg. From the synthetic graph presented in Figure 1, one can derive a relationship between the time and the Pu isotopic ratio:

$$t = \left[10^4 R - 400\ (\pm 100)\right]^{0.360(\pm 0.008)} + 64$$

in which t is the number of years after 1900 and R, the isotopic ratio. From this equation, the date (t_0) at which any surficial sediment collected in the Channel has passed the meridian of Cherbourg, can be calculated. As the date of sampling (t_s) at any location is known, the average velocity, v, can be derived from the expression:

$$v = \frac{d}{t_s - t_0}$$

where d is the distance from Cherbourg to sampling location. We assumed here that medium to coarse grained sediment pathways can be well approximated by straight lines: this is indeed consistent with linear sediment structures observed especially in the Central and Eastern Channel by bottom sonar imagery. When applied to surficial sediments collected in 1992-94, from the Golfe Normand-Breton to the Straits of Dover, this relation yields average velocities ranging from some kilometres per year to some tens of kilometres per year (Figure 2). This is orders of magnitude lower than residual tide currents (*ca.* 1000 km y^{-1}) and means that seabed deposits move very slowly or are only efficiently mobilized during paroxystic events.

In Figure 2, average velocities are plotted versus distance from Cherbourg (distances and velocities are arbitrarily taken negative westwards). We observed that the faster the sediments are moving the further from Cherbourg they are found. The data are more scattered for samples collected to the West of Cherbourg, mainly in the Golfe Normand-Breton, probably due to Channel Islands perturbation and specific coastal geometry (right angle facing northwest).

The general pattern obtained here is consistent with the broad features of bottom sediment distribution in the Channel and the seabed dynamics mainly driven by the energy of tidal currents: gravels and sandy gravels are essentially located in the Central Channel while the proportion of sand gradually increases eastwards and westwards together with the occurrence of more or less muddy sediments in sheltered areas. It also strongly suggests that a certain grain-size sorting occurs during the transit of sediment pools. If such a process does exist, the fine-grained fraction of any sediment should be representative of more recent particulate Pu fluxes. Such a fractionation was not evidenced in a site located 20 km east of Cherbourg ('94 Progress Report): aggregation processes taking place in deposited sediment can account for this observation. As a matter of fact, upon resuspension, only a small fraction of a muddy sand is liable to escape short-term sedimentation. Consequently, the isotopic signature of the sediment admixture is only poorly affected by sedimentation-erosion cycles.

Although Pu-carrier particles yield to the general sediment dynamics, no significant correlation is observed between average velocity (estimated from isotopic Pu ratios) and clay abundance (estimated from Al, Si and ^{40}K contents). This can be easily accounted for by the fact that local sediment inputs (sands to clays) free of any industrial Pu influence may occur.

The reliability of this transfer model was tested on a core collected in the Seine Estuary (near Le Havre) in October 1992 ('94 Progress Report). The $^{60}Co/^{137}Cs$ ratios continuously increase throughout the core to reach 0.4 $\pm$ 0.1 in the topmost samples, i.e., in 1992 $\pm$ 1. The same

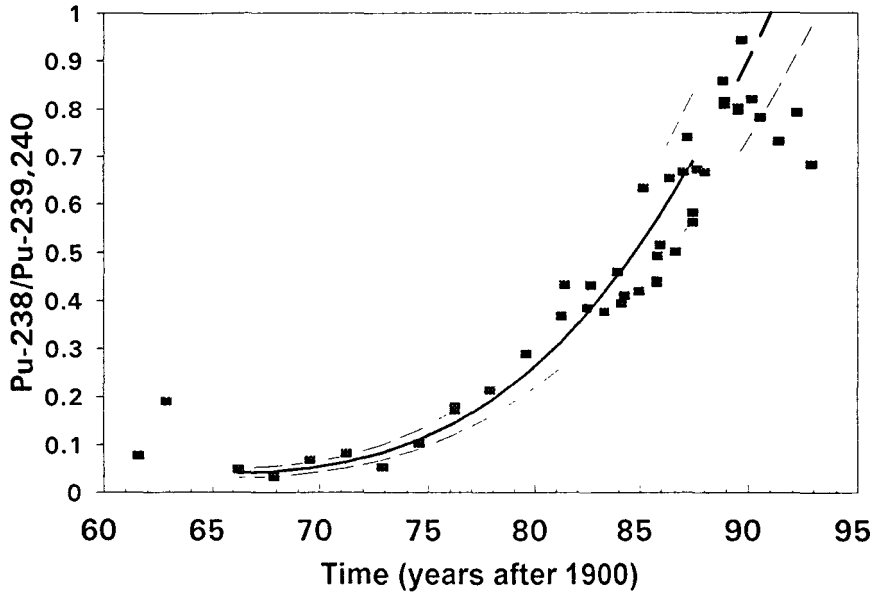

Figure 1. Plot of plutonium isotopic ratio versus time established on 3 sediment cores collected in the Roads of Cherbourg

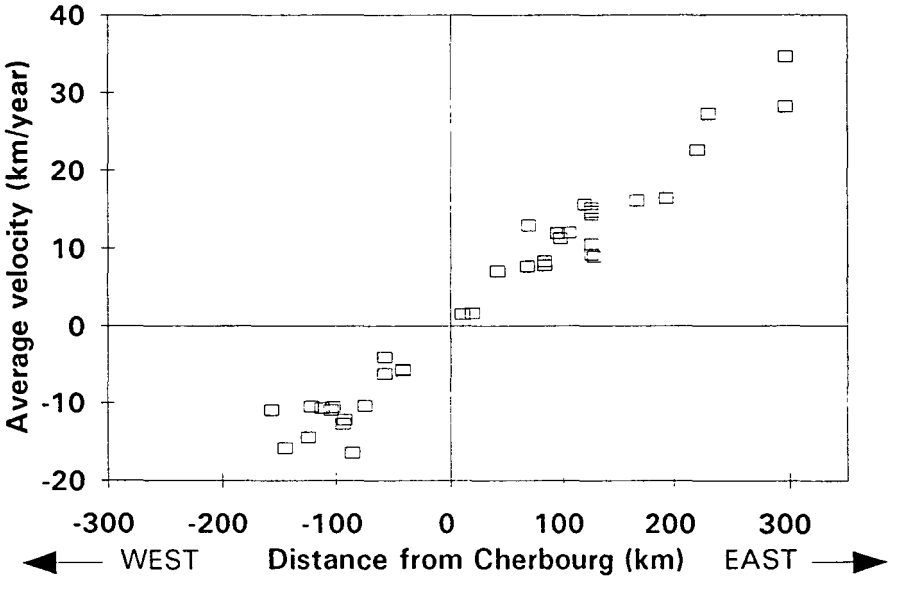

Figure 2. Average velocity (as determined from the relation presented in Figure 1) versus distance from Cherbourg for sediments collected in the Channel ; westwards distances and velocities are arbitrarily taken negative

evolution is observed in our reference cores in Cherbourg in which this value is reached much earlier (1984 ± 1), giving a transit time of *ca.* 8 ± 2 years. This estimation is fully confirmed by the model as the Pu isotopic ratios (0.45 ± 0.06) measured in topmost samples in Le Havre yield 1984.0 ± 1.5.

When compared to the transit times of water masses from Cherbourg to Dover Straits (4-8 months), those of sediments are considerably lower, ranging 10-50 years. This means that either the major part of the sediment masses remains deposited most of the time and/or that sediment transport is dominantly influenced by the strongest instantaneous tide currents ($3x10^4$ km y^{-1}), allowing backward and forward motions. Nevertheless, it is highly probable that greater transit times are to be found for permanently suspended particles.

2. Behaviour of Pu isotopes in seawater of the Channel and in the Seine Estuary

2.1. The distribution of plutonium in the waters of the Channel

The inputs of plutonium to the waters of the Channel originate from nuclear reprocessing plants and fallout of atmospheric nuclear weapon testing. The isotopic ratios $^{238}Pu/^{239,240}Pu$ (IR) are indicative of the source of plutonium: nowadays, the IR of the La Hague reprocessing plant discharge is about 2, that of Sellafield about 0.2, while those reported for atmospheric fallout are *ca.* 0.05 in the Northern Hemisphere. The latter should characterize the Atlantic waters and most of the river waters.

Most of the effluent from the La Hague reprocessing plant is spread eastwards to the North Sea and partially in the Golfe Normand-Breton and the Bay of Seine. Data obtained during 4 cruises and coastline sampling missions are presented in Figure 3. The RADECO'93 campaign provided information on the distribution of plutonium isotopes near the release point of the La Hague plant. The IRs measured were about 1 with the same values for Pu as on the coastline.

The distribution of plutonium isotopes is generally consistent with what we know of water circulation in the Channel (Salomon's model ; Guéguéniat *et al.*, 1993). The central part of the Channel was investigated during the VALDIVIA'93 and the GEDYMAC'94 campaigns. Decreasing values are observed when moving from Cap La Hague to Southern England where ^{238}Pu values are about 2.2 mBq m^{-3} with an IR of 0.2-0.3 at the West of the Isle of Wight and 5 mBq m^{-3} with an IR of 0.7-0.8 at the East. The model reveals that when easterly winds are blowing, the English coast can be marked by the La Hague discharges from the Isle of Wight to the North Sea; the western coast of England may only be marked by the Atlantic waters and, eventually, by the Sellafield discharges. An IR of 0.2 suggests a Sellafield influence but further investigation in the Atlantic waters is necessary before drawning any firm conclusions. The only values available are at the west of the Golfe Normand-Breton: the ^{238}Pu levels were about 1.8 mBq m^{-3} with an IR about 0.2 in 1993 and 5 mBq m^{-3} with an IR about 0.5 in 1994.

During PUMA'94 campaigns, the distribution of plutonium originating from the La Hague plant was investigated in the Golf Normand-Breton and in the Bay of Seine where the residence times of the waters are longer than in the central part of the Channel; a water mass was distinguishable by the IR in the North-West Cotentin (0.5-1.9), which does not mix with the waters of the Golfe Normand-Breton where low IRs (0.3-0.4) were observed. However,

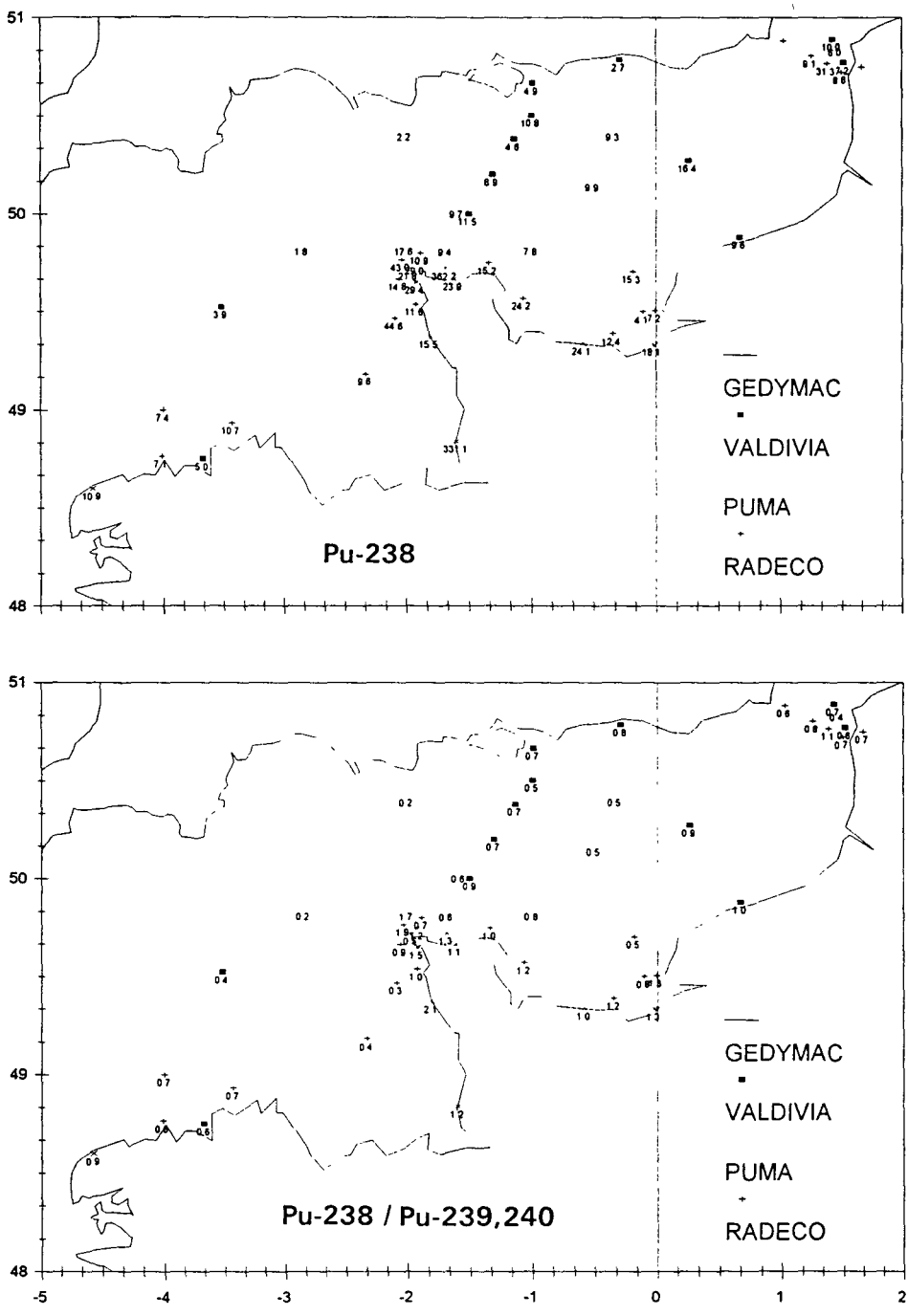

Figure 3. Distribution of ^{238}Pu concentrations (mBq l^{-1}) and $^{238}Pu/^{239,240}Pu$ activity ratios in the waters of the Channel as measured during the cruises GEDYMAC, VALDIVIA, PUMA and RADECO

plutonium values in the Golfe (10-40 mBq m^{-3}) are indicative of the La Hague influence which is not clearly accounted for by the model.

In the waters of the Bay of Seine, little mixing was observed in regards of the mixing occurring in the central part of the Channel. The values and IR are similar to the ones measured near Cap La Hague. The IR range 1-2 in the Golfe Normand-Breton and 0.6-0.9 in the coastal waters of Brittany which could be representative of a 'coastal current' not predicted by Salomon's model.

2.2. Distribution of plutonium in the waters of the Seine Estuary

Several sampling campaigns were carried out in the Seine Estuary (ESTRA; March and October '93) to observe the behaviour of plutonium isotopes (^{238}Pu and $^{239,240}Pu$) versus salinity (30, 15, 8, 4, 1,5 and 0,5 g l^{-1}), in 0.45 μm filtered waters.

Some samples were collected upstream (160 km from the mouth) to measure the amount of plutonium brought by the Seine river: 2.6 ± 0.1 and 6.7 ± 0.2 mBq m^{-3} for ^{238}Pu and $^{239,240}Pu$, respectively. The values for $^{239,240}Pu$ obtained in 1993 are similar to those reported by Jeandel *et al.* (1979), but ^{238}Pu was not measurable in 1979. The IRs measured nowadays evidence an unknown source of ^{238}Pu in the Seine river. Unexplained ^{238}Pu excesses (IR=25.3 and 1.05) were earlier occasionally observed in 1982 and 1983 over Paris by Martin *et al.* (1988). In open waters off the Seine Estuary, Pu concentrations of *ca.* 18 and 14 mBq m^{-3} for ^{238}Pu and $^{239,240}Pu$, respectively, are observed, indicating the influence of discharges from the La Hague reprocessing plant.

The distribution of plutonium in the estuary shows that the levels are higher than those measured in 1979: 5-20 mBq m^{-3} with an IR between 1 and 2 at present, versus 0.74-6.29 mBq m^{-3} in 1979 with an IR of *ca* 0.4. The IR evidences the influence of the La Hague discharges in the estuary. During estuarine mixing, the plutonium behaves non-conservatively: plots of Pu activities versus salinity display excess dissolved Pu (50% of total dissolved Pu) in low salinity waters (0.5 and 1.5 g l^{-1}) and depletion (35-40%) in the zone of intermediate salinities (8 to 15 g l^{-1}), with respect to conservative dilution. In the Esk Estuary, near the Sellafield reprocessing plant, the same Pu excesses were observed at low salinity by Kelly *et al.* (1987) which originated in desorption of Pu from sediments. The determination of 'dissolved' Pu excesses in low salinity waters shows that the contribution of only 1% of the plutonium associated to the suspended matter is necessary to account for the data. As a consequence, in 1993, the sediments appear as a significant source of dissolved plutonium in the estuary. The activity ratios $^{238}Pu/^{239,240}Pu$ in the Seine Estuary are in the range 1.1-1.3 except at intermediate salinities (1.5 to 8 g l^{-1}) at which lower values are observed (0.67 - 0.86). At lower salinities, the IR of the plutonium associated with suspended matter is about 0.4 while the IR of the Pu excess in the filtered fraction is above 1.3. The dissolved+colloidal Pu arriving from seawater has an IR between 1 and 2 and must contribute to the plutonium excess in low salinity waters. That is why the estuarine reactivity of dissolved and colloidal plutonium arriving from seawater was further investigated.

2.3. Laboratory studies on the behaviour of plutonium in estuarine conditions

In order to decipher the mechanisms liable to account for these field observations, the colloid formation of marine plutonium and its evolution under estuarine mixing were studied in laboratory simulated conditions using $^{236}Pu(V)$. Mixtures of seawater + Pu(V) with Seine

water at different salinities show that Pu(V) is reduced to Pu(III,IV) by Seine river components such as humic acids and sorbed on particles larger than 0.45 μm; these phenomena increase when salinity decreases. This could explain the depletion observed at intermediate salinity in the Seine Estuary (Garcia *et al.*, 1995).

These particles are likely to be in contact with water masses of different salinities due to macrotidal conditions. Analyses performed before and after 24 hours of contact between estuarine sediments and Seine river water showed a desorption of plutonium from the particulate phase. The loss of plutonium in the particulate fraction (mainly controlled by Fe-Mn coatings) is balanced by the gain in the dissolved one. The scenario should be the following : marine dissolved and colloidal plutonium is reduced and sorbed on particles in the estuary ; in anoxic conditions, when deposited on the river bed, iron and manganese together with Pu can desorb from mineral coatings. All the phenomena described above occur repeatedly due to erosion-sedimentation cycles taking place in a macrotidal estuary.

References

Garcia K., Boust D., Moulin V., Fourest B. and Guillaumont R. (In Press), 'Multiparametric investigation of the reactivity of plutonium in estuarine conditions', *Radiochimica Acta.*

Guéguéniat, P., Salomon, J.C., Wartel, M., Cabioch, L. and Frazier, A. (1993), 'Transfer pathways and transit time of dissolved matter in the Eastern English Channel indicated by space-time radiotracers measurement and hydrodynamic modeling', *Est. Coast. Shelf Sci.* **36**, 477.

Jeandel, C., Martin, J.M. and Thomas, A.J. (1981), 'Plutonium and other artificial radionuclides in the Seine Estuary and adjacent Seas', In: *Techniques for Identifying Transuranic Speciation in Aquatic Environments* (IAEA), Vienna, p. 89.

Kelly, M., Mudge, S. and Hamilton-Taylor, J. (1987), 'The behaviour of dissolved plutonium in the Esk estuary', In: *Radionuclides, a Tool for Oceanography*, Guary, Guéguéniat and Pentreath (Eds.), Cherbourg, p. 321.

Martin, J.M. and Thomas, A.J. (1981), 'Anomalous concentrations of atmospheric plutonium-238 over Paris', *J. Environ. Radioactivity* **7**, 1.

Publications

Boust, D., Mitchell, P.I., García, K., Condren, O.M. and León Vintró, L. (Submitted), 'A comparative study of the speciation and behaviour of plutonium in the marine environment of two reprocessing plants', In: 5th International Conference on the Chemistry and Migration Behaviour of Actinides and Fission Products in the Geosphere (MIGRATION '95), Saint-Malo (France), 10-15 September, 1995, *J. Contaminant Hydrology.*

Garcia, K. (In Preparation), 'Mesure et Spéciation du Plutonium dans les Eaux de la Manche et des Embouchures de la Seine et du Rhône', Thèse Univ. Paris XI.

Garcia, K., Boust, D., Moulin, V., Fourest, B. and Guillaumont, R. (In Press), 'Multiparametric investigation of the reactivity of dissolved and colloidal plutonium in estuarine conditions', *Radiochimica Acta.*

Head of project 4: Dr. C. Papucci

II. Objectives for the reporting period

To study the main oceanographic processes controlling the long-term behaviour of long-lived radionuclides in the Mediterranean Sea and their time scales.

Specific objectives were:

- to define the present characteristics of the vertical profiles of ^{137}Cs in the water column of the open Western Mediterranean;
- to calculate the global inventory of ^{137}Cs in the Mediterranean water column after the Chernobyl accident;
- to identify the most important mechanisms governing the re-distribution of this radionuclide in the whole basin;
- to evaluate fluxes at Sicily and Gibraltar Straits;
- to study the time trend of ^{137}Cs inventory in the Mediterranean Basin.

III. Progress achieved including publications

The Mediterranean is a mid-latitude semi-enclosed sea, an almost isolated oceanic system. Many processes which are fundamental to the general circulation of the world's oceans also occur within the Mediterranean, either identically or analogously, but the relatively small size of the Mediterranean facilitates research logistics and minimises resources required for field experimental and modelling research. For these reasons, the Mediterranean can be considered a laboratory basin for general circulation research and provides an ideal opportunity for the development and assessment of observational monitoring systems and operational forecast models. Rapid progress has been made in recent years in describing the physical structure of Mediterranean currents and circulation and identifying associated space-time variabilities.

The Mediterranean is a concentration basin, i.e., the total evaporation exceeds precipitation and runoff, and the conservation of mass and salinity are maintained by the balance of the flow through the Strait of Gibraltar. The strait is characterized by a two layer flow regime: in the upper layer Atlantic water enters the Mediterranean Sea with a salinity of about 36.15 psu and a temperature of about 15° C; in the lower layer, below 150 m, Mediterranean water (salinity up to 38.4 psu and temperature of about 13° C) flows toward the Atlantic, carrying out the excess water mass and salts. The water leaving the Mediterranean is a mixture of Levantine Intermediate Water (LIW) and Western Mediterranean Deep Water (WMDW). The LIW originates in the Eastern Basin, where, during the winter there are appropriate conditions for limited thermohaline convection. The WMDW is formed in the NW Mediterranean by deep convection.

From a radiological point of view, a first attempt to calculate doses to man from Mediterranean marine radioactivity was made in 1994, using different methodologies, within the EC MARINA-MED programme. Radionuclide concentrations and dose to the population of the European Community were calculated, at different time scales, by a dispersion model and the results obtained were compared to measured values. Although the model can be considered an adequate tool for the prediction of the dispersion of ^{137}Cs with respect to radiological risk assessment, some uncertainties still exist, mainly related to sedimentation processes, vertical mixing and fluxes between basins.

In strict relation to these studies, a research programme has been initiated in 1991, in collaboration with UCD, CIEMAT and UAB, for the study of the general mechanisms governing the long-term behaviour and mass-balance of long-lived radionuclides in the Western Mediterranean Sea and their time scales. Specific fields of interest were:

- time trends of vertical profiles in the water column;
- partitioning of radionuclides between soluble and particulate forms;
- vertical transport in the water column in relation to both water mixing and sinking particles;
- accumulation in sediments;
- accumulation by plankton;
- fluxes through Sicily and Gibraltar Straits.

In this general framework, ENEA's specific objectives were mainly related to the behaviour of ^{137}Cs in the water column and in sediments, as reported above.

Methodology

In the period 1991-94, five sampling campaigns have been carried out in the Western Mediterranean and at the Strait of Gibraltar. Sampling points were selected for a complete spatial coverage of the Western Mediterranean at water depths ranging from 1,000 to 3,000 m. Preliminary studies have also been carried out at Gibraltar and Sicily Straits.

Water samples for the determination of the vertical profiles of radionuclides were collected by 30 l *Go-Flo* bottles mounted on a 'Rosette' sampler, after CTD casts that allowed a precise identification of the water masses at each sampling station.

^{137}Cs was pre-concentrated onboard from 100 l of seawater by co-precipitation with ammonium molybdo-phosphate (AMP). ^{137}Cs concentrations were measured by gamma spectrometry. Chemical recoveries were calculated for each sample by addition of a known amount of ^{134}Cs.

Sediment samples were collected by a modified Reineck box-corer and samples were sectioned in 1 cm thick intervals directly onboard. ^{137}Cs was determined by gamma spectrometry.

The accuracy of gamma measurements was checked by the analysis of standard reference materials and by participation in international intercalibration exercises.

Results and discussion

Prior to the present study, the bulk of the ^{137}Cs data available for the Mediterranean were mainly related to coastal, surface waters, while the coverage with profile stations was most uneven and very few data existed for stations at water depths greater than 2,000 m.

Sources, distribution and inventory of ^{137}Cs in the Mediterranean Sea before the Chernobyl accident have been summarized by Holm *et al.* (1988). ^{137}Cs concentrations decreased from a surface value of about 3 mBq l^{-1} to bottom values usually lower than 1 mBq l^{-1}. The global inventory of the Mediterranean was estimated to be 10.7 PBq, 5% of which resided in sediments. The major source of ^{137}Cs was bomb fallout with minor contributions coming from river runoff (3%) and from a net influx *via* the Strait of Gibraltar.

The deposition of Chernobyl fallout over the Mediterranean region was quite uneven. In May 1986, the deposition of ^{137}Cs was about 15-20 kBq m^{-2} in the N Adriatic Sea and about 1.5 kBq m^{-2} in the Ligurian Sea. It has been estimated that the accident produced in the Aegean Sea an additional input of about 800 TBq and that the inventory in the Black Sea was doubled.

In the framework of this programme a complete data set has been produced, describing in detail the horizontal and vertical distributions of ^{137}Cs in the Western Mediterranean after the Chernobyl accident, in relation to the hydrographic characteristics. Twenty-two vertical profiles of ^{137}Cs in the water column have been determined, characterizing the whole Western Mediterranean Basin, including the areas of dense water formation and the Sicily and Gibraltar Straits. Sampling locations are shown in Figure 1.

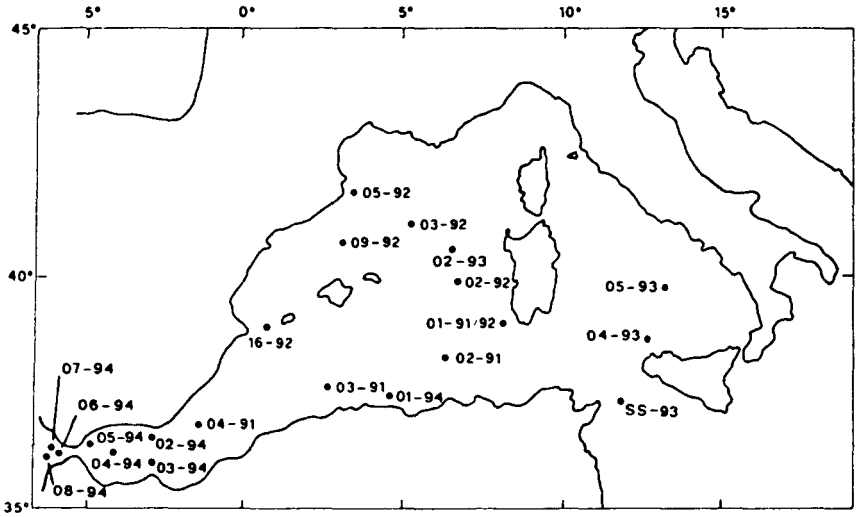

Figure 1. Sampling stations for ^{137}Cs vertical profiles, 1991-94

The results obtained have been analyzed to define:

(1) the removal of ^{137}Cs from surface waters;
(2) the processes controlling the vertical distribution of ^{137}Cs in the water column and the role of different water masses in the physical transport of this radionuclide;
(3) the contribution of the Chernobyl accident to the global inventory of the Mediterranean;
(4) present input of ^{137}Cs to the Mediterranean Sea, including fluxes at the straits;
(5) future evolution of the ^{137}Cs inventory in the whole basin.

1. Removal of ^{137}Cs from surface waters

The time trend of ^{137}Cs concentration in surface water of the open Western Mediterranean in the period 1970-94 has been analyzed (Figure 2). The data reported are mean concentrations in the layer 0-100 m, derived by studies conducted by ENEA in 1991-94 in the framework of the present programme and, DHI Hamburg, IAEA MEL Monaco, CEA IPSN Toulon for the period 1970-1988.

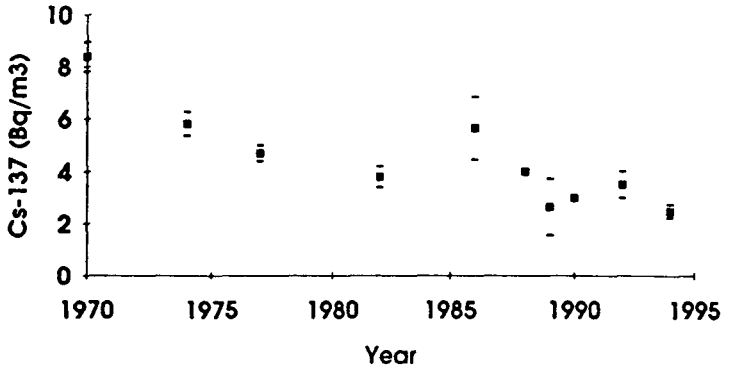

Figure 2. Time trend of ^{137}Cs concentration in open water of the Western Mediterranean

In the pre-Chernobyl period, the concentration of ^{137}Cs in surface waters decreased from an average value of 8.4 ± 0.4 mBq l^{-1} to 5.8 ± 0.4 in 1974, 4.7 ± 0.3 in 1977 and 3.8 ± 0.4 mBq l^{-1} in 1982. The rapid decrease in this period is related to physical and biological processes and to the decrease in ^{137}Cs input from atmospheric fallout.

In the period 1986-88 an increase in ^{137}Cs concentration with respect to previous levels was observed, due to the input of Chernobyl caesium. The concentration in the top layer of water reached in May 1986 in some cases very high levels (up to 500 mBq l^{-1}), but the studies carried out at the end of the year in the open NW Mediterranean, indicate concentrations of ^{137}Cs in the range 6 - 8 mBq l^{-1}. Starting from 1990 the values reported are very similar to pre-Chernobyl ones (3 mBq l^{-1}), with no significant variability between different years or sub-basins.

The decrease in ^{137}Cs concentration after the Chernobyl accident has been much faster than in the previous period: in fact Chernobyl contamination was highest in the NW Mediterranean and lateral advection of less contaminated water coming from the southern part of the basin produced rapid dilution of the radionuclides present in the surface layer.

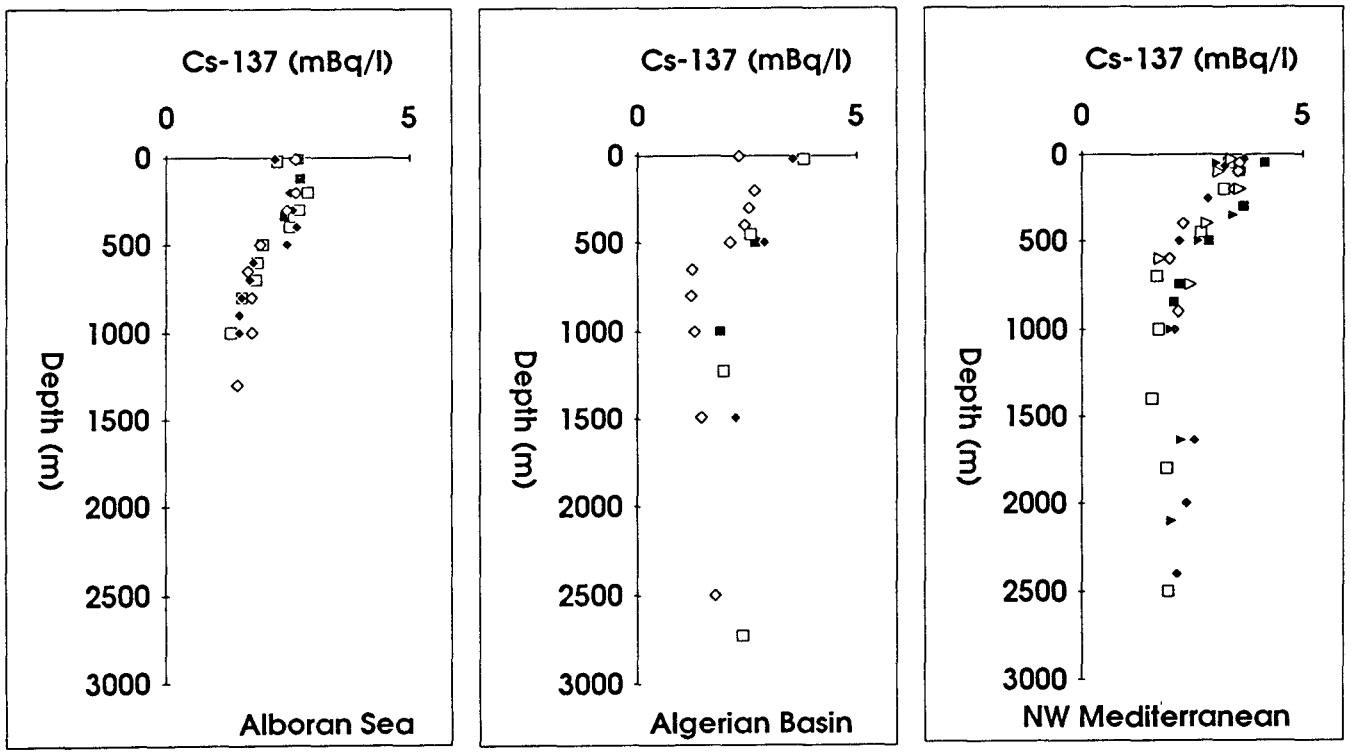

Figure 3. Vertical profiles of ^{137}Cs in the water column of the Western Mediterranean Sea

2. ^{137}Cs vertical profiles in the water column

In Figure 3 are shown the vertical profiles of ^{137}Cs determined in the period 1991-94 in different basins of the Western Mediterranean. The ^{137}Cs concentration decreases from the surface (3.1 ± 0.6 mBq l^{-1}) to the bottom (1.7 ± 0.4 mBq l^{-1}). There are not relevant differences in the profiles measured in different areas.

^{137}Cs surface concentrations are slightly lower (2.5 ± 0.2 mBq l^{-1}) in the Alboran Sea, which is strongly influenced by the inflow of low-salinity Atlantic water. In this area, ^{137}Cs concentrations are almost constant in the first 300 m, corresponding to intense mixing of Atlantic and Mediterranean waters.

In a vertical profile determined in 1991 SW of Sardinia, a pronounced subsurface maximum (4.7 mBq l^{-1} against 3.8 mBq l^{-1} measured in the overlying water) was found in the Levantine Intermediate Water. This supports data obtained by IAEA-MEL in 1989 and 1990 and indicates that Chernobyl caesium removed from contaminated surface water of the Eastern Mediterranean by intermediate water formation has been transferred to the Western Mediterranean. None of the profiles obtained in the following years (even at the same station) shows similar anomalies: the LIW presently leaving the Eastern Mediteranean is characterized by radionuclide concentrations very similar to those found in the Western Basin (see below, point 4.).

If compared to typical vertical profiles of the pre-Chernobyl period, present ones show higher values in Western Mediterranean Deep Waters: this implies that ^{137}Cs input to deep waters exceeds the loss due to physical decay. Deep convection appears to be an efficient mechanism in removing radionuclides from the surface layer.

3. Inventories

The inventory of ^{137}Cs was calculated at each profile station, assuming that the concentration varied linearly between sample points.

The inventories range between 1.9 (1,000 m water column) and 6.8 kBq m^{-2} (3,000 m). There is an almost linear relationship between caesium inventory and water depth (Figure 4). In the layer 0-600 m, corresponding to MAW and LIW, where horizontal water motions are dominant, ^{137}Cs inventory is rather homogeneous all over the basin (1.7 ± 0.3 kBq m^{-2}).

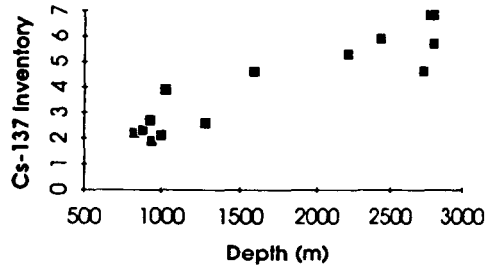

Figure 4. ^{137}Cs inventory (kBq/m^2) vs. water depth in the Western Mediterranean

From the vertical profiles determined in the present study an average vertical profile of ^{137}Cs in the water column has been calculated, which can be assumed as representative of the whole Mediterranean Basin. From this profile, the global inventory of ^{137}Cs in the water column of the Mediterranean, excluding Black Sea, is estimated to be 13.1 $\pm$ 1.5 PBq, showing an increase of about 35% with respect to the pre-Chernobyl situation (Holm *et al.,* 1988). However, for an accurate estimate of the consequences of the Chernobyl accident it is necessary to obtain data also for the Eastern Mediterranean. Preliminary data, obtained in 1995 on the deepest part of the Ionian Sea and the Levantine Basin indicate that the vertical distribution of ^{137}Cs is very similar to that found in the Western Basin, with an increase in concentrations in the deep water layers (below 2,000 m) with respect to those measured in the pre-Chernobyl period.

^{137}Cs inventory in sediments has been determined at two stations, at water depths of about 1,000 m, in the Sardinian and Balearic Basin: in both cases the inventory is 0.2 kBq m^{-2}, corresponding to 6-9% of the water-sediment inventory at the sampling point.

Caesium sediment inventories show a considerable increase with respect to pre-Chernobyl ones in some restricted coastal areas, in particular near the mouths of rivers flowing through regions that have been heavily contaminated after the accident (e.g. NE Italy - N Adriatic Sea). The fate of radiocaesium transported by rivers to the sea and accumulated in sediments was investigated in the N. Adriatic coastal area. Concentrations and inventories obtained for the areas of influence of the most important rivers (Tagliamento, Isonzo, Piave, Adige and Po) were compared. Radiocaesium preferentially accumulates in the prodelta areas. In 1987 ^{137}Cs maximum inventories in these zones ranged between 12 and 64 kBq m^{-2}, respectively. The temporal dynamics in selected zones was studied until 1991 by sampling at the same site in different years. Temporal differences in the radionuclide inventories show that some areas are unstable on the time scale of one year due to sediment resuspension processes. Outside the prodelta areas ^{137}Cs inventories were much lower (0.5 - 1 kBq m^{-2}).

4. Fluxes at the straits

Measurements have been carried out at the Sicily and Gibraltar Straits to give a first estimate of fluxes of radionuclides between Mediterranean and Atlantic and Eastern and Western Mediterranean. One vertical profile of ^{137}Cs has been measured at the Strait of Sicily. Hydrological characterization of the sampling area by CTD casts allowed us to collect samples of surface MAW and of the underlying LIW. In 1993, the concentrations of ^{137}Cs were very similar in the two water masses: 3.1 mBq l^{-1} in MAW flowing from West to East and 3.4 mBq l^{-1} in LIW. The last value was still slightly higher than the average concentration in LIW sampled in the Western Basin (2.6 mBq l^{-1}). As the fluxes of water at the strait in the two directions differ by no more than 5%, we can conclude that the quantities of ^{137}Cs entering and leaving the Western Mediterranean are roughly the same.

In October 1994 a detailed study has been carried out in the Alboran Sea and in the Atlantic Ocean near the Gibraltar Straits. The overall hydrological features of the Alboran - Gibraltar - Atlantic system have been investigated by CTD casts along three N-S transects. Based on these data and on the available literature, the sampling stations have been selected in order to characterize the main path of the Atlantic water entering the Mediterranean and the Mediterranean water leaving Gibraltar. CTD profiles were also used to precisely define sampling depths along the water column. The mean ^{137}Cs concentration in the water entering

the Mediterranean is 2.56 ± 0.19 mBq l^{-1} and 2.57 ± 0.40 mBq l^{-1} is the mean activity in the water mass entering the Atlantic Ocean. Based on literature data on water fluxes at Gibraltar (Bethoux, 1980) we can estimate a maximum input of ^{137}Cs from the Atlantic to the Mediterranean of 6 MBq y^{-1}, negligible with respect to the global inventory.

5. Evolution of the global inventory of ^{137}Cs in the Mediterranean Sea

Based on literature data and on the present study, the inputs of ^{137}Cs to the Mediterranean Sea can be summarized as follows:

Atmospheric fallout: 30 TBq y^{-1}
River runoff : 1.2 TBq y^{-1}
Discharges to rivers from nuclear industry: 5 TBq y^{-1}
Input from Black Sea: 30 TBq y^{-1}
Net input at Gibraltar: 6 MBq y^{-1}
Total: 66 TBq y^{-1}

These inputs are much less than the loss by radioactive decay of the ^{137}Cs presently in the Mediterranean Sea and we can expect, in the future, a possible decrease of the ^{137}Cs global inventory in the overall Mediterranean Basin.

Publications

Delfanti, R., Papucci, C., Salvi, S., Vives i Batlle, J., Downes, A. and Mitchell, P.I. (1994), 'Distribution of ^{137}Cs and transuranic elements in seawater of the Western Mediterranean Sea (Algerian Basin, Balearic Sea)', *In: Proc. MARINA-MED Seminar on the Radiological Exposure of the Population of the European Community from Radioactivity in the Mediterranean Sea*, Cigna *et al.* (Eds.), Rome, 7-19 June, 1994, EUR-Report 15564 EN, pp. 427-439.

Mitchell, P.I., Vives i Batlle, J., Downes, A.B., Sánchez-Cabeza, J.A., Merino Pareja, J., Delfanti, R. and Papucci, C. (1994), 'Chemical speciation and colloidal association of plutonium in the western Mediterranean water column and in the Gulf of Vera', *Ibid.*, pp. 441-457.

Delfanti, R., Frignani, M., Langone, L., Papucci, C. and Ravaioli, M.A. (In Press), 'The role of the rivers in Chernobyl radiocaesium delivery, distribution and accumulation in coastal sediments of the Northern Adriatic Sea', *Sci. Total Environ.*

Delfanti, R., Papucci, C., Fiore, V., Bassano, E., Salvi, S., Lorenzelli, R. and Alboni, M. (1995), 'Distribuzione del ^{137}Cs nelle acque superficiali del Mediterraneo Occidentale (1991-93)', In: *Proc. Meeting La radioattivita ambientale nell'area del Mar Mediterraneo*, Triulzi and Nonnis-Marzano (Eds.), Isola del Giglio, May 1994, University of Parma, pp. 13-18.

Delfanti, R., Papucci, C., Testa, C., Desideri, D., Meli, M.A. and Roselli, C. (1995), 'Distribuzione verticale di $^{239,240}Pu$ in sedimenti di mare profondo del Mediterraneo (Bacino Algerino, Mar Ionio)', *Ibid.*, pp. 97-103.

Delfanti, R. and Papucci, C. (1995), 'Inventories of $^{239,240}Pu$ in slope and deep-sea sediments from the Ionian Sea and the Algerian Basin', In: Proc. XXXIVe Congres Commission Internationale pour l'Exploration Scientifique de la Mer Mediterranee, La Valette (Malte), 27-31 March, 1995. *Rapp. Comm. int. Mer Médit.*, No. 34, p. 225.

Delfanti, R., Papucci, C., Alboni, M., Lorenzelli, R. and Salvi, S. (1995), '^{137}Cs inventories in the water column and in sediments of the Western Mediterranean Sea', *Ibid.*, 226.

Arnaud, M., Charmasson, S., Delfanti, R. and Papucci, C. (1995), 'Caesium inventories in sediment cores in areas under the influence of the Po river (Italy) and the Rhone river (France)', *Ibid.*, 223.

Delfanti, R., Papucci, C., Salvi, S., Lorenzelli, R., Mitchell, P.I., Downes, A.B. and Vives i Batlle, J. (1995), 'Time evolution of the vertical profiles of artificial radionuclides in the water column of the Western Mediterranean', In: Proc. Int. Conf. MEDITERRANEANCHEM, Taranto, 23-27 May, 1995, pp. 236-237.

Delfanti, R., Desideri, D., Martinotti, W., Meli, M.A., Papucci, C., Queirazza, G., Testa, C. and Triulzi, C. (In Press), 'Plutonium concentration in sediment cores collected in the Mediterranean Sea', *Sci. Total Environ.*

MED 91 Cruise Report (1992), R. Delfanti and Carlo Papucci (Eds.), ENEA, La Spezia, 63 pp.

MED 92 Cruise Report (1993), R. Delfanti and Carlo Papucci (Eds.), ENEA, La Spezia, 121 pp.

MED 94 Research Expedition Report (In Press), R. Delfanti and Carlo Papucci (Eds.), ENEA, La Spezia.

Head of project 5: Dr. D. Woodhead

II. Objectives for the reporting period

To determine the physico-chemical speciation of radionuclides in the Irish Sea prior to, and post, the introduction of additional reprocessing operations at the BNFL plant at Sellafield.

The specific aims were:

(1) Characterisation of radionuclides in individual waste streams at Sellafield (SIXEP and Seatank) by size distribution;
(2) To study the transformation of radionuclide species following dilution of effluents into seawater;
(3) To determine the distribution, stability and persistence of radiocolloidal forms around the Sellafield outfall, in the vicinity of the contaminated mud patch located in the eastern Irish Sea, and further afield;
(4) To study the stability of radiocolloids in relation to the techniques employed for fractionation, and the influence of fine grained sediments upon the production and removal of radiocolloids;
(5) To examine the far field dispersion and distribution of radionuclides into the north-western European Shelf and beyond.

III. Progress achieved including publications

As discharges of radionuclides from Sellafield are one of the major sources to the shelf seas of north-west Europe it is essential that their physico-chemical behaviour is fully understood. In recent years discharges from Sellafield have decreased significantly as a result of improvements in waste treatment. However, commissioning of the Enhanced Actinide Removal Plant (EARP) in 1994, to assist in the reduction of discharges to sea of α-emitting radionuclides, enabled previously stored medium active wastes to be reprocessed. Consequently, as a result of the additional operations carried out using the EARP plant, certain radionuclides (e.g., ^{99}Tc) were discharged at elevated levels. In addition, because of a general trend of decreased discharges, the sediments of the Irish Sea are now considered as a significant source-term for other radionuclides (e.g., ^{137}Cs, ^{239,240}Pu and ^{241}Am). Therefore, the overall aim of this project was to provide information concerning the physico-chemical speciation (including colloidal and dissolved distributions) of a number of radionuclides in the Irish sea following the introduction of EARP.

(1) ***Characterisation of source term effluents.*** Laboratory experiments, carried out to determine the extent of radionuclides present in the colloidal size region in a number of source term SIXEP and Seatank effluents, have been successfully completed. The range of percentages of radiocolloids (size range $<0.45\mu$m, >3kDa) found in pre-EARP effluents are given in Table 1. ^{99}Tc existed almost entirely as low molecular weight species (<3kDa) in both effluents. Although not apparent in Seatank effluents, small amounts of ^{90}Sr, ^{137}Cs and ^{239,240}Pu(V) colloid species were identified in SIXEP effluents. ^{239,240}Pu(IV) and ^{241}Am, which are more particle reactive species, were observed to be colloidally-bound in both effluent

streams. The majority of these nuclides were present as radiocolloids in the SIXEP effluents. The radiocolloid distributions found in post-EARP effluent were typical of pre-EARP results and no further evaluation of their behaviour has been carried out.

Table 1. Range of colloidal distributions observed in Seatank and SIXEP effluents

Radionuclide	Range of colloidal distributions %	
	Seatank	SIXEP
^{99}Tc	0.0 - 0.1	0.0 - 0.1
^{137}Cs	0.0 - 0.6	9.9 - 29.2
^{90}Sr	0.7 - 1.1	21.2 - 38.4
^{239,240}Pu(IV)	2.8 - 15.4	88.3 - 98.2
^{239,240}Pu(VI)	0.0 - 1.7	14.9 - 18.1
^{241}Am	3.1 - 14.1	53.5 - 84.1

(2) ***Dilution of effluents into seawater.*** The following conclusions were drawn concerning the possible transformations of colloidal species upon discharge into the marine environment. Although small amounts of ^{99}Tc, ^{90}Sr, ^{137}Cs and ^{239,240}Pu(V) colloids species have been identified in SIXEP effluents, these forms did not appear to persist in seawater. Moreover, in the solution phase, the Seatank effluents contained appreciably more activity than in SIXEP effluents. Since it has been shown that these radionuclides were in the form of simple ions in Seatank effluent, it is concluded that the presence of colloids from discharges was not significant. During the period of investigation, by far the largest concentrations of ^{239,240}Pu(IV) and ^{241}Am discharged into seawater were derived from the particulate material (iron floc) in Seatank effluents. Moreover, upon dilution some disaggregation of iron floc occurs giving rise to measurable amounts of radiocolloids. Consequently, it is apparent colloidal forms of ^{239,240}Pu(IV) and ^{241}Am do originate from Sellafield effluents and may persist in seawater, at least for small time scales.

In addition to characterising the individual physico-chemical forms in Sellafield effluents, it has been possible to crudely quantify the percentages of radiocolloid forms (following immediate discharge) originating from each effluent stream. The initial assessment (as given in Table 2) shows that approximately 1 and 3% of the total activities of ^{239,240}Pu(IV) and ^{241}Am, respectively, were likely to be present as colloidal forms in seawater from the discharge of Seatank effluent. This compares with 0.2 and 32% of ^{239,240}Pu(IV) and ^{241}Am, respectively, from the discharge of SIXEP effluent (Table 3).

The estimated percentages of radiocolloids from the combined effluent discharge (SIXEP and Seatank) are given in Table 4. Since the total concentrations in SIXEP effluent are at least an order of magnitude less than corresponding Seatank effluent, it is concluded that the discharge of these radionuclides (including ^{239,240}Pu(IV) and ^{241}Am) associated with colloidal material was relatively small.

Table 2. Estimated colloidal component in seawater from Seatank effluent

Radionuclide	Total discharge (TBq) {A}	Dissolved fraction (%) {B}	Dissolved speciation (%) {C}	Retention coefficient {D}	Colloidal discharge (TBq) {E}†	Colloidal component (%) {F}‡
^{239,240}Pu total	0.0284	2.87	-	-	-	-
^{239,240}Pu(IV)	-	-	96.7	0.500	3.9×10^{-4}	1.4
^{239,240}Pu(V)	-	-	3.3	0.000	0.0000	0.0
^{241}Am	0.0246	5.17	-	0.576	7.3×10^{-4}	3.0

† {E} = {A} ({B}/100) ({C}/100) {D}
‡ {F} = ({E}/{A}) 100

Table 3. Estimated colloidal component in seawater from SIXEP effluent

Radionuclide	Total discharge (TBq) {A}	Dissolved fraction (%) {B}	Dissolved speciation (%) {C}	Retention coefficient {D}	Colloidal discharge (TBq) {E}†	Colloidal component (%) {F}‡
^{137}Cs	0.413	99.7	-	0.000	0.0000	0.0
^{90}Sr	0.0164	97.7	-	0.000	0.0000	0.0
^{239,240}Pu total	0.0043	98.9	-	-	-	-
^{239,240}Pu(IV)	-	-	0.4	0.469	7.98×10^{-6}	0.2
^{239,240}Pu(V)	-	-	99.6	0.000	0.0000	0.0
^{241}Am	7.1×10^{-5}	83.9	-	0.380	2.26×10^{-5}	31.9

† {E} = {A} ({B}/100) ({C}/100) {D}
‡ {F} = ({E}/{A}) 100

(3) ***Marine distribution, stability and persistence of radiocolloidal forms.*** In all, five sampling locations were chosen in the immediate vicinity of the Sellafield discharge pipeline (PLZ) to study the environmental distribution of radiocolloids in seawater. This included a south-west transect (incorporating the area of contaminated muddy sediment) away from PLZ, and locations north and west of PLZ. The results, in Figure 1, indicate that the contribution of radiocolloidal forms of Pu(IV) and Am in surface waters of the Irish Sea, prior to EARP, were fairly low (< 10%). There appeared to be no large variation between sample locations. Although these values are similar to the colloidal contribution estimated to arise from the source effluents it is also possible their origin is from radionuclide remobilisation from contaminated sediment. Colloidal distributions in surrounding UK waters are awaiting radiochemical analysis.

Table 4. Estimated colloidal component in seawater from Sellafield effluents

Radionuclide	Total discharge-SIXEP and Seatank (TBq)	Colloidal discharge-SIXEP and Seatank (TBq)	Total colloidal component (%)
^{137}Cs	1.222	0.0010†	<0.1†
^{90}Sr	0.2194	0.0011†	0.5†
^{99}Tc	0.0220	0.0000	0.0
$^{239,240}Pu$ total	0.0327	-	-
$^{239,240}Pu(IV)$	-	0.0004	1.2
$^{239,240}Pu(V)$	-	0.0000	0.0
^{241}Am	0.0247	7.5x10-4	3.1

† No account taken for dilution of Seatank effluent in seawater

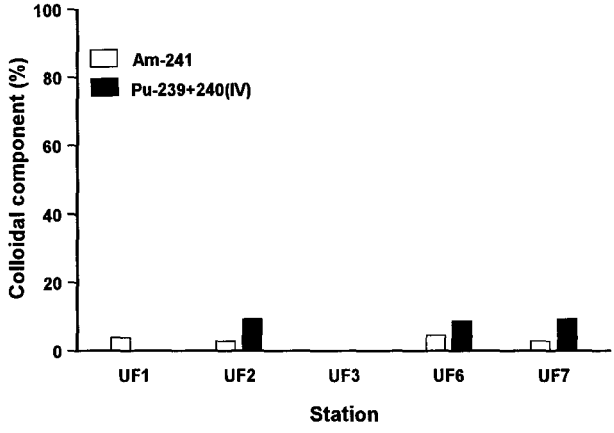

Figure 1. Estimated colloidal component of dissolved Pu(IV) and Am in surface waters of the Irish Sea.

(4) ***Stability of radiocolloids in relation to methodology and fine grained sediments.*** Supporting field ultrafiltration trials to investigate the stability of radiocolloids in seawater due to applied pressure conditions (20-25 psi - transmembrane pressure) indicated that deformation of radiocolloids did not occur under these chosen operating conditions.

Table 5. Ultrafiltration methodology experiments

Transmembrane pressure (psi)†	Colloidal component of Pu(IV) (%)
10	10
11	10
17	14
26	9
31	13

† Pressure = (inlet pressure - back pressure)/2 - permeate pressure

The results given in Table 5, using replicate samples from a single site (UF1, close to the Sellafield pipeline), show that the colloidal content of Pu(IV) was reasonably consistent over a wide range of transmembrane pressures (10-26 psi) and unlikely to introduce artifacts from the separation procedure. Experiments involving the dilution of whole seawater into large volumes of deionised water, prior to the ultrafiltering, have recently been carried out (CIR 10/94) to determine the stability and degree of association of actinide colloids with fine grained Irish Sea particles. At the time of reporting, radiochemical assay of these samples has not been completed.

(5) ***Far field dispersion and distribution of radionuclides.*** The assessment of physico-chemical forms of radionuclides in seawater, pre and post EARP, was made from the results of four research expeditions. Prior to the EARP releases two cruises (CIR 12/92 and CIR 11/93) were completed, involving surveys of the Irish Sea and UK coastal waters. A short period (three months) after the first release, a comprehensive survey of the Irish Sea (CIR 6/94) was carried out to establish the increase in key radionuclides in nearby coastal waters. After a further six months another expedition to the Irish Sea and other UK coastal waters (CIR 10/94) was conducted to assess the extent of effluent migration into more distant waters. Radionuclides considered were ^{99}Tc, ^{137}Cs, ^{241}Am and $^{239+240}$Pu (including oxidation state distributions). The work has resulted in a large database and the initial findings have been summarised below. Prior to any releases from EARP the concentration of ^{99}Tc (and other radionuclides) decreased with distance from the point of discharge (as shown for ^{99}Tc in Figure 2) and the data for all three transects fit a single biexponential decay curve. Consequently, the spatial distribution was not dependant upon the direction of dispersion.

Shortly following the first EARP releases the transport of the ^{99}Tc pulse in a northerly direction was clearly observed, as shown by the peak in concentration $\approx$50 km in distance from the point of discharge (Figure 3). Along the southern coastline and a west-south-west transect offshore, the levels of ^{99}Tc with distance from Sellafield were very similar to those observed on the previous CIR 12/92 expedition (Figure 2). Therefore, the initial migration of the first EARP releases was predominantly round the northern coastline before leaving the Irish Sea *via* the North Channel.

A comparison of two surveys (CIR 12/92 and CIR 6/94, i.e. pre and immediately post EARP) of the migration north along the coastline is given in Figure 4. Using these data it has been possible to conclude that the time for conservative radionuclides leaving the North Channel has been underestimated in the past, with a transit time of 2-3 months. By extrapolation it has also been possible to determine the distance of dispersion over the time

elapsing after the initial discharge (3 months), which is in the region of 170 km.

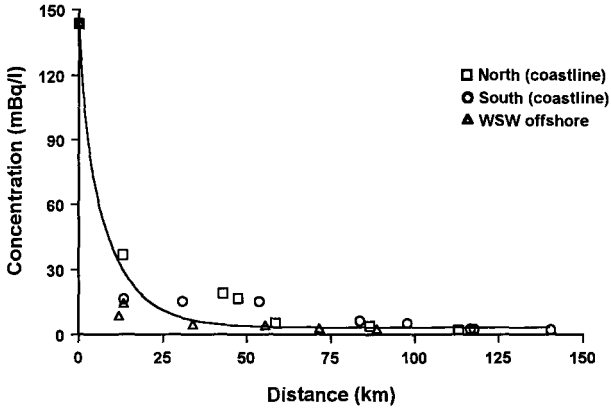

Figure 2. Concentration of ^{99}Tc with distance from Sellafield pre-EARP (CIR 12/92)

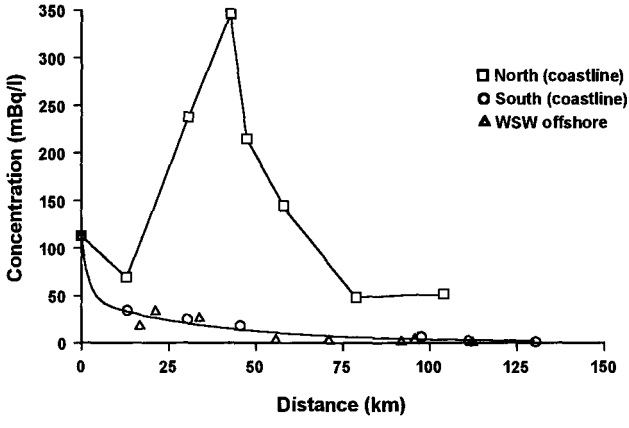

Figure 3. Concentration of ^{99}Tc with distance from Sellafield following the first EARP releases (CIR 6/94)

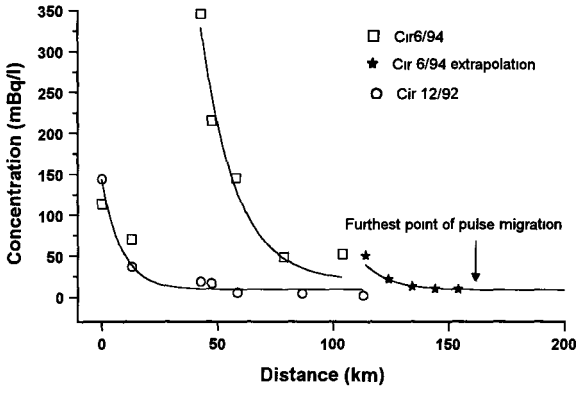

Figure 4. Estimated distance of migration of first EARP discharge from Sellafield after 3 months (round northern coastline)

Following subsequent releases prior to the next expedition, a somewhat different distribution of ^{99}Tc was observed on the CIR 10/94 survey (Figure 5). The migration of ^{99}Tc along the northern coastline was similar to that observed on the preceding expedition (CIR 6/94), although the maximum $\approx$ 50 km distant from Sellafield was much less pronounced. However, on this occasion there was a marked difference between levels of ^{99}Tc along the coastline to the south of Sellafield and a west-south-west transect offshore. An exponential decrease in concentration was observed along the offshore transect whereas the falloff along the southern coastline was approaching that of the northern coastline trend, indicating more uniform mixing from coastal currents with time. Levels throughout the whole of the eastern Irish Sea were notably greater than those observed 6 months previously with a minimum concentration $\approx$ 5 mBq/l compared to $\approx$ 2 mBq/l.

Complementary ^{137}Cs data have been used to determine ^{137}Cs/^{99}Tc ratios pre and post EARP releases and the results are given in Figure 6. Clearly, prior to EARP releases, an increase in the ratios with distance from the source was observed, presumably as a consequence of the greater mobility of ^{99}Tc which decreases more rapidly with distance from Sellafield. As a result of the increases in ^{99}Tc following the EARP discharges the ^{137}Cs/^{99}Tc ratios are observed to be fairly constant ($\approx$ 1.5) and provide a clear isotopic signal of water transport for study of the migrational behaviour further afield.

The introduction of EARP had no significant effect on the overall quantities of $^{239+240}$Pu discharged into the Irish Sea and it is likely that remobilisation from contaminated sediment now provides a significant contribution to overlying water. The behaviour of Pu radionuclides in the marine environment is dependant upon the distribution between oxidation states and the percentages of $^{239+240}$Pu(V) in seawater, was observed to be somewhat variable. Results from two expeditions (CIR 11/93 and CIR 6/94) are given in Figure 7 and it is evident more of the reduced form was present close to Sellafield in the later survey.

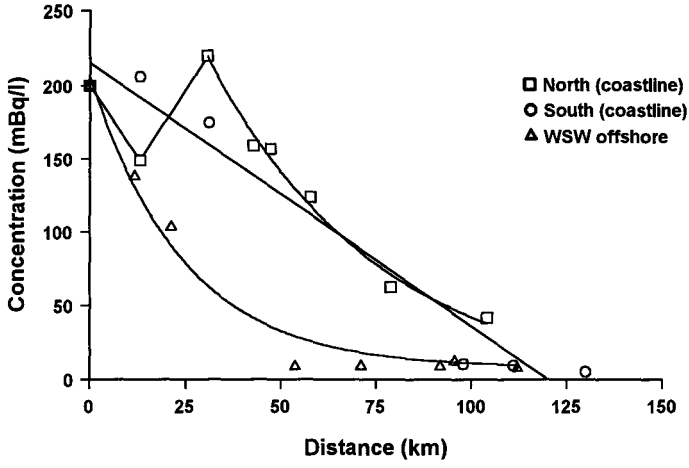

Figure 5. Concentration of ^{99}Tc with distance from Sellafield following 9 months of releases from EARP (CIR 10/94)

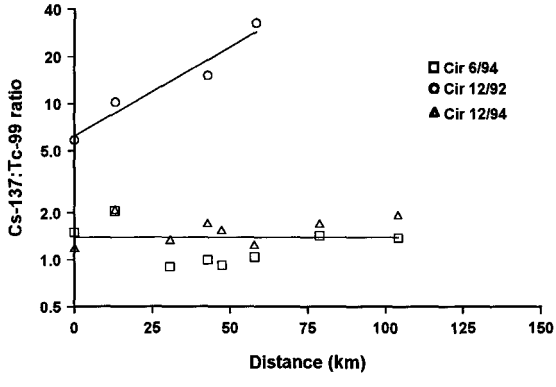

Figure 6. Variation of $^{137}Cs/^{99}Tc$ ratio with distance from Sellafield along northern coastline

However, the concentration of dissolved Pu(IV) then decreased with distance from Sellafield, most likely as a result of sorption and redox reactions. It is likely that dispersion of $^{239+240}Pu$ in seawater would have been slower due to less particulate resuspension in calmer sea conditions, particularly in the immediate vicinity of the pipeline, during the latter survey.

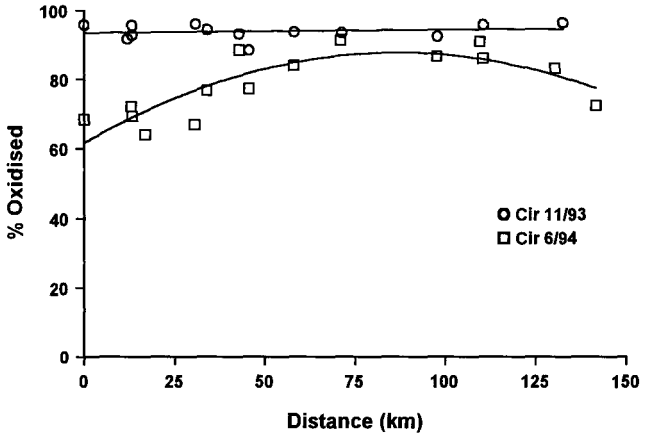

Figure 7. Variation in redox distribution of Pu with distance from Sellafield along northern coastline

Publications

McCubbin D. and Leonard K. S. (1993), 'A preliminary study to assess the effect of some seawater components on the speciation of plutonium', *J. Radioanal. Nucl. Chem. Articles* **172**, 363-370.

Leonard K. S., Harvey B. R., Woodhead R. J., Brooks T. and McCubbin D. (1994), 'Assessment of an ultrafiltration technique for the fractionation of radionuclides associated with humic material', *J. Radioanal. Nucl. Chem. Articles* **181**, 309-320.

Kershaw P.J., Woodhead D.S., Leonard, K. S. and Lovett M. B. (1995), 'Plutonium from European reprocessing operations - its behaviour in the marine environment', *J. Appl. Radiat. Isot.* **46**(11), 1121-1134.

Leonard K. S., McCubbin D. and Lovett M. B. (In Press), 'Physico-chemical characterisation of radionuclides discharged from a nuclear establishment', *Sci. Tot. Environ.*

McCubbin D. and Leonard K. S. (In Press), 'Use of radiotracers for studies of metal sorption behaviour', *Sci. Tot. Environ.*

Leonard K. S., McCubbin D., Brown J., Bonfield R. and. Fernand L. (Submitted), 'Distribution of ^{99}Tc in UK Coastal Waters', *Marine Pollution Bulletin.*

Head of project 6: Dr. E. Holm

II. Objectives for the reporting period

The Kalix River in north Sweden is one of the last major unregulated rivers in the boreal zone. Much of the catchment is situated above the Arctic Circle. The total drainage basin for the Kalix River is 23,600 km^2. The Kalix River has its source in the Caledonian mountains and roughly 5% of the drainage area is situated within this region. The remaining drainage area is divided between coniferous forest (55-65%) and peatland (17-20%). Four percent of the area is covered by lakes and less than 1% is farmed land. The water flow situation in the river over a year is characterized by a very intensive spring discharge in May increasing the water flow by a factor of 10-20 compared to winter base flow. Often a second flow peak is present in mid-June due to snow melt in the mountains.

The main objectives of this study were to determine how the dissolved and particulate concentrations of radiocaesium and plutonium in the river water are changed during spring discharge and if flocculation (mainly for Pu) can be detected in the low salinity gradient (end point 3 permille) in the estuary. The reason for this interest lies in the fact that high-molecular weight humics are known to start flocculating at salinities around 5 permille. During spring discharge the mires in the drainage area becomes flooded and may contribute substantially with dissolved Pu to the river water. In other studies where we have sampled mire waters, we have found exceptionally high concentrations of dissolved actinides in these waters.

III. Progress achieved including publications

Sampling

Sampling of river water has been done after the last rapid before the river reaches the Bothnian Bay archipelago. Due to the very low concentrations of Pu in the river water, it was necessary to process volumes of 500 l. For suspended matter analysis volumes between 1,000 and 3,000 l were pumped through 1 micrometer polypropylene cartridge filters. Radiocesium were either collected on a copper ferrocyanide precipitate after adding yield tracer or adsorbed from large volumes by passing the water through two copper ferrocyanide impregnated filters arranged in series.

In the estuary, sampling were done at three stations with depths around 15 m and salinities from 0.4 to 2.8 g l^{-1}. Sediments were taken with a gravity corer as well as with a freeze corer in order to be able to analyze the different sediment layers in the laminated sediments.

Results

The radiocesium concentration in the water as a function of time during one year is shown in Figure 1 together with the river water flow. Corresponding results for plutonium (only during the spring flood) are plotted in Figure 2. In spite of the more than tenfold increase in water flow during the spring discharge, radiocesium concentrations are not lowered but instead are slightly enhanced as compared to concentrations before and after the spring flood.

This implies that roughly 50-60% of the annual ^{137}Cs discharge comes during 3-4 weeks in May-June. Tributaries draining mires during spring discharge have ^{137}Cs concentrations of 10-15 mBq l^{-1} which may partly explain the increased levels in the river during spring flood.

Although the suspended load during spring flood is increased by a factor of about 5-10, the fraction of radiocesium on particles only increases from about 15 to 30% during this time.

Information from radiocesium depth profiles in laminated estuarine sediments (see Figure 3) shows that the concentration of ^{137}Cs in the river water from nuclear bomb test fall-out has declined with a half-life of 12 years when corrected for radioactive decay. About 5 TBq, or 15% of total bomb test fall-out in the drainage area, has to this date been discharged.

As seen from Figure 2 concentrations of plutonium are only slightly (about 25%) lowered during spring flood, which means that 30-40% of the annual discharge of plutonium comes during May-June. Only 10-20% of this plutonium is associated with particles larger than 1 μm. From estuarine sediment data (Figure 4) the half-life decline in plutonium concentrations in the discharging river water has been estimated to be about 4 years. Less than 0.2% of the plutonium deposited in the drainage area from nuclear test fall-out is estimated to reach the sea.

When trying to evaluate possible flocculation in the estuary it was important to separate resuspended sediments from coagulated material. In this study this was done by 'normalising' to ^{232}Th. It was found from several (n=6) measurements of top sediments at different sites in the estuary that the $^{239,240}Pu/^{232}Th$ ratio was 0.026 $\pm$ 0.003 while the particulate material collected on the 1 μm filters had significantly different ratios as seen from the table below. This is not surprising as ^{232}Th is more likely to be associated to the coarser sediment fraction than is plutonium.

Table 1.

Salinity (g l^{-1})	$^{239,240}Pu/^{232}Th$ particulate fraction	$^{239,240}Pu/^{232}Th$ total
0.4	0.067	0.09
0.8	0.073	0.08
1.7	0.081	0.26
2.6	0.072	0.17

The third column has been roughly corrected for the contribution from resuspended surface sediments by assuming that resuspended material has a $^{239,240}Pu/^{232}Th$ ratio similar to the ratio in surface sediments. Comparing $^{239,240}Pu/^{232}Th$ ratios in suspended matter with surface sediments it seems obvious that plutonium belongs to a finer particulate fraction which to a larger degree is not trapped in the estuary (not sedimenting). It has been shown (Pettersson, 1992; Widerlund, 1995) that river dissolved iron and DOC to a large extent escape the estuary. The increase in particulate to total plutonium indicates, however, that some coagulation may occur even at these low salinities, possibly as an effect of flocculation of the

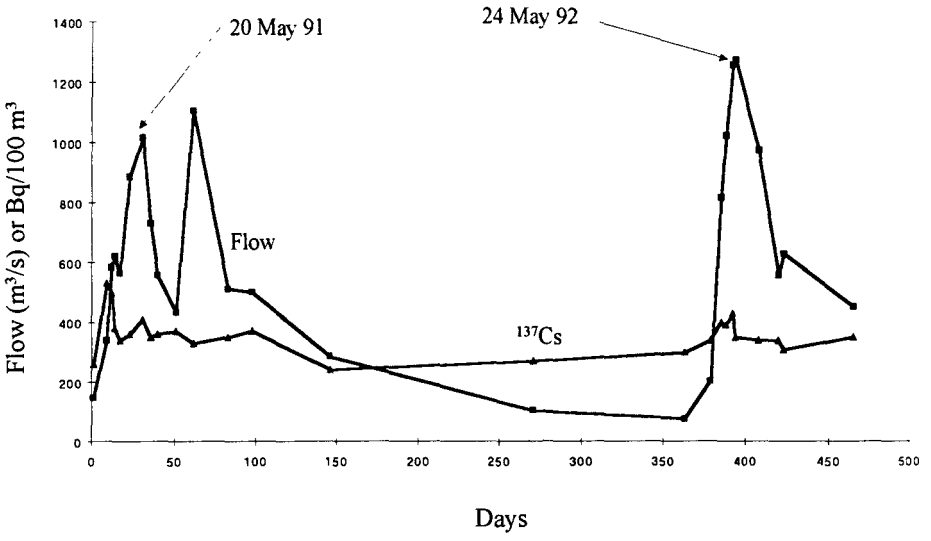

Figure 1. ^{137}Cs in the Kalix River

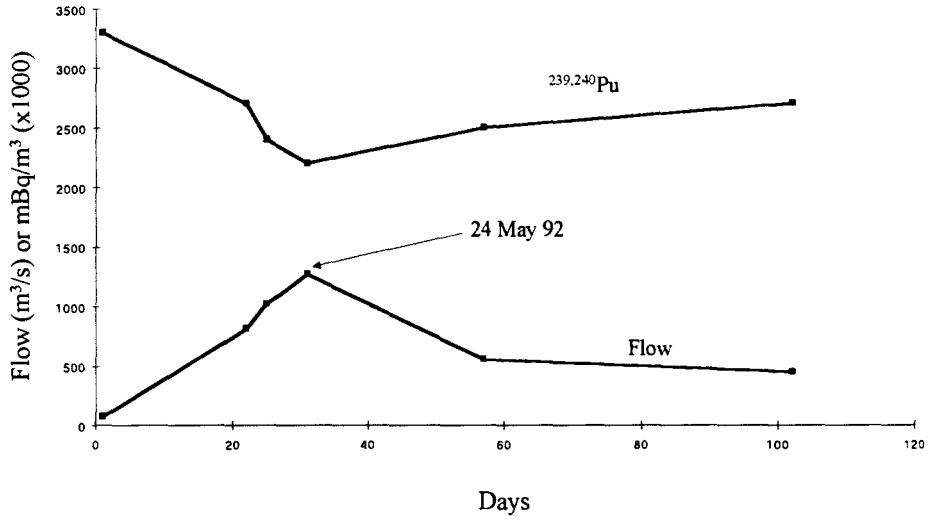

Figure 2. $^{239,240}Pu$ in the Kalix River during spring discharge

high molecular fraction of humics (which is the only fraction of DOC which has been observed to slowly coagulate at low salinities).

Comparing $^{239,240}Pu/^{232}Th$ ratios and concentrations in several layers of a freeze-core showed insignificant differences between typical spring discharge sediments (grey) and late summer/autumn sediments (brown), which further points to the fact that flocculated plutonium does not sediment within the estuary but is instead exported to the open Baltic Sea.

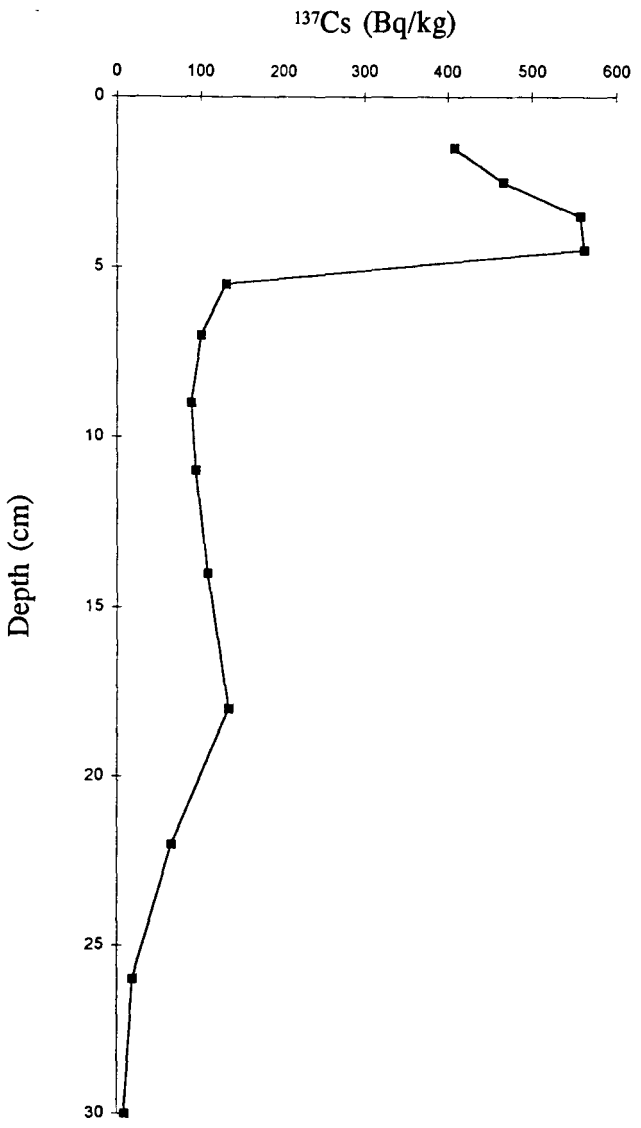

Figure 3. ^{137}Cs vertical profile in laminated estuarine sediments

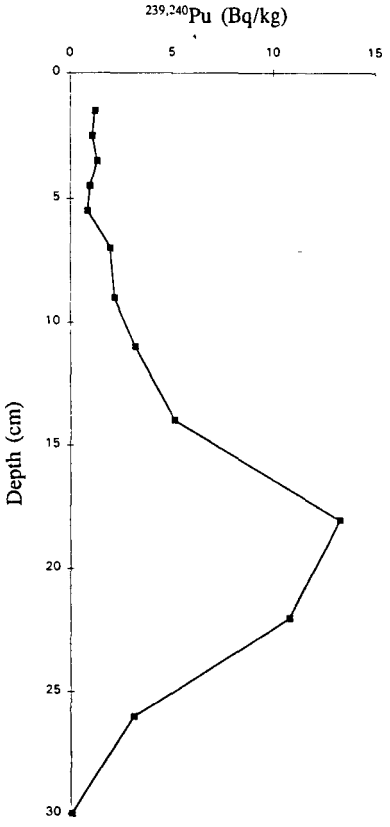

Figure 4. $^{239,240}Pu$ vertical profile in laminated estuarine sediments

References

Pettersson C. (1992), 'Properties of Humic Substances from Groundwater and Surface Waters', Thesis, University of Linköping, Sweden.

Widerlund A. (Submitted), 'Early diagenesis of iron, manganese and trace metals in sediments of the Kalix River Estuary, Bothnian Bay', *Chem. Geol.*

Publications

Widerlund A. and Roos P. (In Press), 'Varved sediments in the Kalix River Estuary, Bothnian Bay', *Aqua Fennica.*

Roos P. and Holm E. (In Preparation), 'Plutonium, americium, thorium and radiocesium behaviour in the Kalix River and its estuary during spring discharge'.

Head of project 7: Dr. Sánchez-Cabeza

II. Objectives for the reporting period

The distribution and fate of transuranics (and other key radionuclides) in the marine environment can be understood in terms of the nature of the source term and their biogeochemistry, transport with water masses and sedimentation processes. However, relatively little is known about the role of plankton in the mobility of radionuclides in the marine environment.

The key subject addressed in this project was the transfer of transuranics (TU) and other radionuclides through the primary producer route in the food-chain leading to man (sediment-water-plankton-fish-man). As the processes that govern this transfer may depend on water and sediment geochemistry, work on the water column (including physico-chemical speciation) and sediments was also carried out. This study was conducted in different environments such as the western Mediterranean Sea, mostly affected by global fallout contamination, and the Irish Sea, contaminated with low-level liquid radioactive waste from Sellafield. In the Mediterranean Sea special attention was paid to the contaminated area of Palomares. Though more work had been originally planned in the Ebro Delta area, it was subsequently recognised by the participants that more relevant data would be acquired by expanding our study in the Irish Sea.

The specific questions addressed were:

- The concentration process of TU and other radionuclides in zooplankton and phytoplankton from surface waters of the western Mediterranean and the Irish Sea.
- The physico-chemical speciation (oxidation states and colloidal association) of TU in the western Mediterranean area.
- The vertical transport of TU and radiocaesium in the Catalan Sea, including water column and sediment traps.
- The distribution and inventory of TU and radiocaesium in sediments in relevant areas of the Mediterranean Sea, such as Palomares and the Catalan Sea.

III. Progress achieved including publications

1. Sampling campaigns

Most of the information gained on the concentration processes of radionuclides in plankton was derived from samples obtained during the MED'92 (onboard N.O. *Urania*, ENEA) and CIROLANA 6/94 (onboard R.V. *Cirolana*, MAFF) research expeditions. Other objectives were accomplished in the course of sampling campaigns such as FE'91 (Institut de Ciències del Mar-ICM, CSIC), MED'91 (ENEA), VARIMED'93 (ICM, CSIC), FLUBAL'93 (Univ. Barcelona-UB), CONCENTRA 1,2 & 3 (ICM, CSIC) and EUROSWAP (Univ. Perpignan-UP).

2. Plankton

The transfer of radionuclides through the primary producer route of the marine food-chain

leading to man was studied in field experiments in the Mediterranean and the Irish Seas. Broadly speaking, zooplankton and phytoplankton include mobile and immobile microbial marine species, respectively. In general, phytoplankton are photosynthetic organisms and zooplankton are phytoplankton consumers, thereby representing the first and second levels of the classical marine trophic chain. However, real food-chains may be very complex, depending on the species involved.

A widely accepted cut-off between phytoplankton and adult zooplankton is 200 μm, though some zooplankton species may have smaller sizes (microzooplankton). Furthermore, most phytoplankton species have dimensions larger than 20 μm, though some species may also be smaller (picoplankton). These represent the adopted plankton cut-offs used in our work. Zooplankton is collected by towing during 30-60 minutes a large conical net (diameter: 1 m, length: 5 m) immersed in surface waters and provided with a flow-meter. When the net saturates, some phytoplankton species of smaller dimensions may also be collected. Phytoplankton was collected by filtering large volumes of water through 20 μm cellulose filters. In addition, other size fractions were obtained using 8 and 0.2 μm membrane filters.

2.1. Plankton in the Mediterranean Sea

Phytoplankton

Large volume (*ca.* 1000 l) water samples were sequentially passed through 20 μm, 8 μm and 0.2 μm filters, and analyzed for plutonium (Table 1) and americium. In the Palomares area, three sampling locations were chosen: Palomares, Garrucha and Golfo de Vera. Excluding the Garrucha sample, phytoplankton fractions (>20 μm) showed activities ranging from 50-364 μBq m^{-3}. The concentrations observed in the medium-sized particles (8-20 μm), mostly constituted by small plankton species, were small (28-119 μBq m^{-3}), though the smallest particles (0.2-8 μm), mostly inorganic, showed concentrations of the same order as phytoplankton (46-225 μBq m^{-3}). Thus, about 50% of the particulate plutonium in the Mediterranean Sea was associated to phytoplankton.

The Garrucha phytoplankton sample was collected from 50 m below the water surface, near the thermocline and within a submarine canyon. It showed ^{239,240}Pu concentrations about 30 times higher than the observed mean phytoplankton concentration (Table 1).

Table 1. Plutonium concentrations in phytoplankton (> 20 μm) and suspended particles from the Mediterranean Sea, August 1992

Station	^{239,240}Pu (μBq m^{-3})		
	>20 μm	8-20 μm	0.2-8 μm
Barcelona	168 ± 23	28 ± 24	149 ± 56
Golf de St. Jordi	364 ± 158	119 ± 63	225 ± 84
Garrucha (-50 m)	1912 ± 113	135 ± 43	1232 ± 208
Palomares	59 ± 20	-	46 ± 27
Golfo de Vera	49.6 ± 7.9	-	-

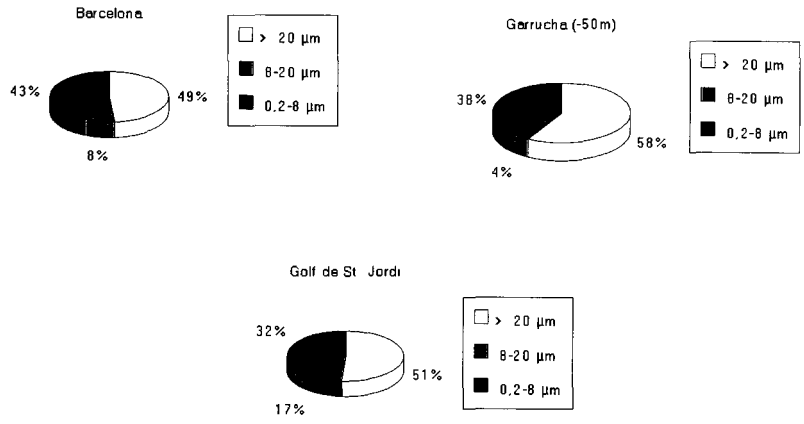

Figure 1. Plutonium distribution amongst different size fractions in the Mediterranean Sea

Zooplankton

Zooplankton from the western Mediterranean Sea was collected and measured for TU (Tables 2 and 3) and γ-emitters (Table 4). This is the first time that such an experiment has been carried out in the Mediterranean Sea. The Mediterranean Sea is highly oligotrophic and, therefore, zooplankton biomass was, in general, very small. Higher productivity was observed in the northernmost stations (Barcelona and Golf de St. Jordi, mean 18 $\pm$ 2 mg(dw) m^{-3}), indicating higher productivity due to higher nutrients inputs (from urban waste and riverine input, respectively). Biomass in the Palomares area (5 $\pm$ 2 mg(dw) m^{-3}), which included samples from Palomares, Garrucha and Playa Macenas, was much smaller.

Table 2. $^{239,240}Pu$ concentrations in zooplankton from the Mediterranean Sea, August 1992

Location	$^{239,240}Pu$		C.F.	$^{238}Pu/$
	(mBq kg^{-1}, dw)	(μBq m^{-3})	(l kg^{-1}) x10^3	$^{239,240}Pu$
Barcelona	418 $\pm$ 27	8.4 $\pm$ 0.6	36 $\pm$ 3	0.065 $\pm$ 0.014
Golf de St. Jordi	589 $\pm$ 23	9.5 $\pm$ 0.4	99 $\pm$ 10	0.099 $\pm$ 0.011
Palomares	2046 $\pm$ 61	6.5 $\pm$ 0.2	164 $\pm$ 14	0.018 $\pm$ 0.005
Garrucha	383 $\pm$ 15	3.13 $\pm$ 0.14	31 $\pm$ 2	0.026 $\pm$ 0.007
P. Macenas	612 $\pm$ 23	2.90 $\pm$ 0.12	49 $\pm$ 4	0.024 $\pm$ 0.008

Zooplankton efficiently concentrates TU and other radionuclides. Excluding the sample from Palomares, TU concentrations ranged from 383-612 Bq kg^{-1} and 27-168 Bq kg^{-1} for $^{239,240}Pu$ and ^{241}Am, respectively. Mean concentrations were 474 ± 60 Bq kg^{-1} and 52 ± 21 Bq kg^{-1} for $^{239,240}Pu$ and ^{241}Am, respectively. These results cannot be compared to others as no data on TU concentrations in Mediterranean zooplankton are known.

The observed concentration factors, on a dry weight basis, ranged from 30-164 x 10^3 l kg^{-1} for Pu and 47-375 x 10^3 l kg^{-1} for Am. The highest TU concentrations per unit mass and concentration factors (CF) were found in Palomares and showed isotopic ratios typical of bomb material from the Palomares accident.

Table 3. ^{241}Am concentrations in zooplankton from the Mediterranean Sea, August 1992

Location	^{241}Am		C.F.	$^{238}Pu/$
	(mBq kg^{-1}, dw)	(μBq m^{-3})	(l kg^{-1}) x10^3	$^{239,240}Pu$
Barcelona	27 ± 5	0.54 ± 0.11	23 ± 6	0.064 ± 0.013
Golf de St. Jordi	56 ± 20	0.9 ± 0.3	47 ± 18	0.10 ± 0.03
Palomares	449 ± 27	1.42 ± 0.09	375 ± 66	0.220 ± 0.015
Garrucha	74 ± 7	0.61 ± 0.06	62 ± 12	0.19 ± 0.02
P. Macenas	168 ± 17	0.80 ± 0.08	140 ± 27	0.27 ± 0.03

In the Palomares sample, both $^{239,240}Pu$ and ^{241}Am showed activities 4 and 9 times higher, respectively, than the mean values observed in the other samples. The $^{238}Pu/^{239,240}Pu$ ratio in the zooplankton (0.018 ± 0.005) fraction showed a value close to that of weapons-grade plutonium, and similar to that found in contaminated sediments from the area. Consequently, it was concluded that both phytoplankton and zooplankton from some stations near Palomares were contaminated with plutonium from the accident. As no bomb TU was found in the soluble fraction, it was concluded that the origin of Palomares TU was contaminated surface sediments. A similar effect was observed in Golf de St. Jordi, were surface sediments show plutonium traces from a nearby nuclear power plant. These observations suggest that plankton may play an important role in the cycling of sediment-associated TU in shallow waters. Other radionuclides were observed and are discussed below.

The remobilisation of TU from sediments can be explained on the basis of the following mechanism: during summer, phytoplankton in the Mediterranean Sea is mostly found below the thermocline, at about 50 m depth. In relatively shallow waters, such as those sampled in Palomares, phytoplankton, as well as zooplankton, may feed directly from the sediment-water interface, thereby being exposed to higher plutonium concentrations. As water concentrations observed during the same sampling campaign did not reflect the presence of bomb plutonium, phytoplankton could only obtain plutonium from the contaminated sediments. On the other hand, zooplankton might have obtained plutonium from both the phytoplankton and/or the sediments. Therefore, our results show that sediments act as a source of plutonium for plankton in this area.

If one defines biomagnification from one trophic-chain level to the next as the inverse quotient of their respective mass concentrations, biomagnification factors of 2 and 0.5 can be estimated for plutonium and americium, respectively.

In regard to the actual plankton species involved, the phytoplankton contaminated sample showed a distinct signal of dynoflagellates, whilst the zooplankton contaminated sample was rich in copepods.

Among the detected γ-emitters, the data on ^{137}Cs and ^{60}Co are too few to draw conclusions. It is possible that the ^{60}Co detected off the Barcelona coastline is attributable to nuclear industry waste. However, we are unable to explain the presence of ^{60}Co in the Palomares area. ^{40}K concentrations showed little variability (mean value 188 $\pm$ 44 Bq kg^{-1}, dw), but the contrary was observed for ^{226}Ra (range 7.5-31.2 Bq kg^{-1}, dw), where the highest activity was observed in Golf de St. Jordi. This is related to ^{226}Ra input to the area from the Ebro River. Due to its short half-life, ^{7}Be was not detected in some of the samples. The highest excess ^{210}Pb concentration, which ranged from 151-494 Bq kg^{-1}, was also detected in Golf de St. Jordi.

Table 4. Various γ-emitter concentrations (Bq kg^{-1}) in zooplankton from the Mediterranean Sea, 1992.

Location	^{7}Be	^{40}K	^{60}Co	^{137}Cs	^{210}Pb	$^{210}Pb_{ex}$	^{226}Ra
Barcelona	835 $\pm$ 36	288 $\pm$ 13	5.5 $\pm$ 0.9	<3	416 $\pm$ 19	398 $\pm$ 19	18.3 $\pm$ 1.2
G. St. Jordi	1090 $\pm$ 180	219 $\pm$ 6	<5	7.3 $\pm$ 0.7	525 $\pm$ 15	494 $\pm$ 15	31 2 $\pm$ 1.8
Palomares	340 $\pm$ 140	209 $\pm$ 6	<7	<6	350 $\pm$ 12	342 $\pm$ 12	7.70 $\pm$ 0.08
Garrucha	<380	131 $\pm$ 6	5 73 $\pm$ 0.14	<3	159 $\pm$ 8	151 $\pm$ 8	7.5 $\pm$ 0.6
P. Macenas	<620	177 $\pm$ 5	<6	<6	236 $\pm$ 14	222 $\pm$ 14	14.0 $\pm$ 1.2

2.2 Plankton in the Irish Sea

During the CIROLANA 6/94 research expedition, phytoplankton and zooplankton samples were collected from 16 stations in the Irish Sea, using the methods described above. Samples were measured by γ-spectrometry and the concentrations of ^{137}Cs were determined. Though caesium is more conservative than TU in the water column, a small fraction is also tightly bound to the clay fraction in sediments.

Plankton biomass in the Irish Sea was, as expected, higher than in the Mediterranean, due to the higher productivity of its waters, and ranged from 0.1-3.3 mg l^{-1} and 5.7-203 mg m^{-3} for phyto- and zooplankton, respectively. Highest biomass was usually found near coastal stations.

Phytoplankton

^{137}Cs concentrations in phytoplankton ranged from 0.7-4.2 Bq kg^{-1} and showed highest values

both near Sellafield and south-west Scotland. In general, the observed concentration distribution (Figure 2) compared well with the distribution observed in sea water by MAFF. This would indicate that the main source of caesium to phytoplankton in this area is sea water. It is interesting to point out that highest phytoplankton biomass was found close to Sellafield and, therefore, a maximum in ^{137}Cs budget was found in this region.

Zooplankton

^{137}Cs concentrations in zooplankton ranged from 10-366 Bq kg^{-1}, one to two orders of magnitude higher than in phytoplankton. Though this observation would suggest biomagnification in the trophic chain, it should be realised that highest concentrations were found near the Cumbrian coast, closely matching the well known distribution of radionuclides in eastern Irish Sea surface sediments. This clearly showed that the main source of radionuclides to zooplankton in the Irish Sea is sediments rather than sea water. As zooplankton is mobile, it vertically migrates to the nutrient-rich surface sediments to graze, where it becomes contaminated with radionuclides. This represents, therefore, a remobilisation mechanism for radionuclides from surface sediments in this area.

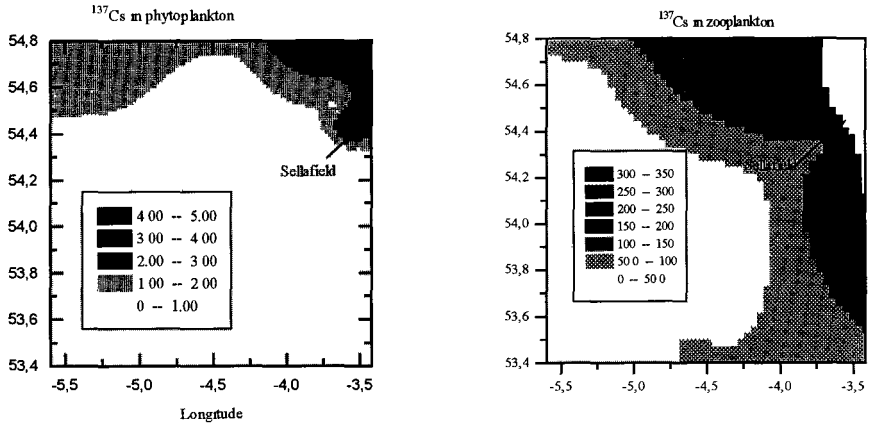

Figure 2. ^{137}Cs concentrations (Bq kg^{-1}, dw) in phytoplankton and zooplankton in the Irish Sea (land mask not shown)

3. Physico-chemical speciation of plutonium and americium

3.1. Soluble and particulate plutonium

Soluble plutonium concentrations were determined in 3 surface water samples from the

Mediterranean Sea and another sample from -50 m near the canyon mouth close to Garrucha (Table 5). In two cases the total activity was derived from alumina adsorption experiments. As observed in previous experiments, and also by other partners in this project, mean soluble plutonium activities were close to 12 mBq m^{-3}, including the Garrucha sample. However, soluble activities in Golf de St. Jordi were only 6.0 ± 0.6 mBq m^{-3}, indicating scavenging from the water column either by biological activity or by flocculation processes in the estuarine area. This sample also showed the highest particulate plutonium concentration, representing up to 10% of the total concentration. Finally, the Garrucha sample showed a particulate plutonium activity 3.27 ± 0.24 Bq m^{-3}, which represented 21% of the total activity. This high concentration may be attributed to nepheloid layer formation and downward transport of contaminated particles in the canyon.

Table 5. Plutonium concentrations in the soluble and particulate fractions in the western Mediterranean coastal zone, August 1992

Location	Depth	Particulate		Soluble	K_d
		(μBq m^{-3})	%	(mBq m^{-3})	(l kg^{-1}) x10^3
Barcelona	surface	339 ± 65	3	11.5 ± 0.4	30 ± 6
G. St. Jordi	surface	701 ± 190	11	6.0 ± 0.6	118 ± 34
Garrucha	surface	102 ± 33	0.8	12.5 ± 0.6	8 ± 3
Garrucha	50 m	3272 ± 240	21	12.5 ± 1.0	262 ± 28

3.2. Plutonium oxidation states

The NdF_3 selective co-precipitation technique to separate reduced (III,IV) and oxidised (V,VI) plutonium was successfully implemented in our laboratory with the help of UCD, and was used to determine the oxidation states of plutonium in two surface water samples from the western Mediterranean (Catalan Sea and the Palomares zone; Table 6). At both stations, most of the plutonium in filtered sea water was present in an oxidised form, though a significant fraction (*ca.* 30%) was present in the more insoluble, reduced form. These results are in excellent agreement with those reported by UCD in their more extensive database for the Mediterranean Sea. Interestingly, the amount of plutonium present in the particulate phase was relatively large in the case of the Palomares sample.

3.3. TU colloidally-bound fraction

The association of TU with colloids using the preferential sorption on aluminium oxide technique, optimised at UCD in collaboration with UAB, was examined by our laboratory in two samples, one from the Palomares coastal area and the other from the Barcelona coastal area (MED'92). The sample from Palomares showed a plutonium colloidal fraction of 23 ± 9%, which is in good agreement with results reported by UCD for the same zone. However, the sample from the Barcelona area showed no detectable colloidal plutonium, probably because of competition with complexing agents arising from urban and industrial wastes (see Section 2 of UCD's report).

Table 6. ^{239,240}Plutonium (mBq m^{-3}) oxidation states in the NW Mediterranean Sea

Fraction	Catalan Sea	Palomares
Reduced (III,IV)	4.7 ± 0.3	5.0 ± 0.3
% Reduced	31 ± 2	32 ± 2
Oxidized (V, VI)	10.4 ± 0.5	10.7 ± 0.5
% Oxidized	69 ± 4	68 ± 4
Total soluble	15.1 ± 0.6	15.7 ± 0.6
Particulate	1.58 ± 0.09	6.0 ± 0.2
Total soluble + particulate	16.7 ± 0.6	21.7 ± 0.6
% Particulate	9 ± 1	28 ± 1
Apparent K_d (l kg^{-1}) x 10^5	3.5	13

As discussed above, the observed plutonium speciation deduced from two Mediterranean Sea surface water samples showed that near 30% of the soluble plutonium was in a reduced from. On the other hand, about 20% of the 'soluble' plutonium in a surface water sample from Palomares was found to be in a colloidal form (as defined by differential sorption on alumina). This may explain, in part, the presence of reduced plutonium, a highly insoluble species, in the soluble fraction. Interestingly, 16% of plutonium and 98% of americium passed without adsorption in the Palomares alumina adsorption experiment. The soluble americium concentration was 2.26 ± 0.50 Bq m^{-3}, corresponding to a ^{241}Am/^{239,240}Pu ratio of 0.18. The ^{238}Pu/^{239,240}Pu ratios in the Barcelona and Palomares alumina adsorption experiment were 0.040 ± 0.013 and 0.030 ± 0.007 respectively, in good agreement with fallout ratios.

4. Vertical transport

As plankton may play an important role in the vertical transport of radionuclides in the marine environment, an experiment was carried out in the Catalan Sea, involving the measurement of high-resolution, large-volume, ^{137}Cs and ^{239,240}Pu vertical profiles in the water column, sediment traps and a sediment core.

4.1. High-resolution vertical profile

^{137}Cs concentrations (Figure 3) showed a maximum surface activity of 5.34 ± 0.31 Bq m^{-3}. Levels decreased to a minimum value of 1.28 ± 0.38 Bq m^{-3} at 700 m depth, but rose again to 3.82 ± 0.37 Bq m^{-3} at 1,000 m depth. It is suggested that the presence of this sub-surface maximum may be related to deep water formation in the Gulf of Lyons. The total ^{137}Cs inventory in the water column was estimated to be 3.4 kBq m^{-2}.

In contrast to ^{137}Cs, ^{239,240}Pu concentrations (Figure 3) showed a broad sub-surface maximum centered at about 400 m depth. This observation is in good agreement with the sub-surface maxima observed for plutonium in the western Mediterranean by UCD in 1991 and 1992, as well as that reported by other authors for open ocean waters of the Atlantic and Pacific Oceans. The total soluble ^{239,240}Pu inventory was 17 Bq m^{-2} at this station (1,200 m depth).

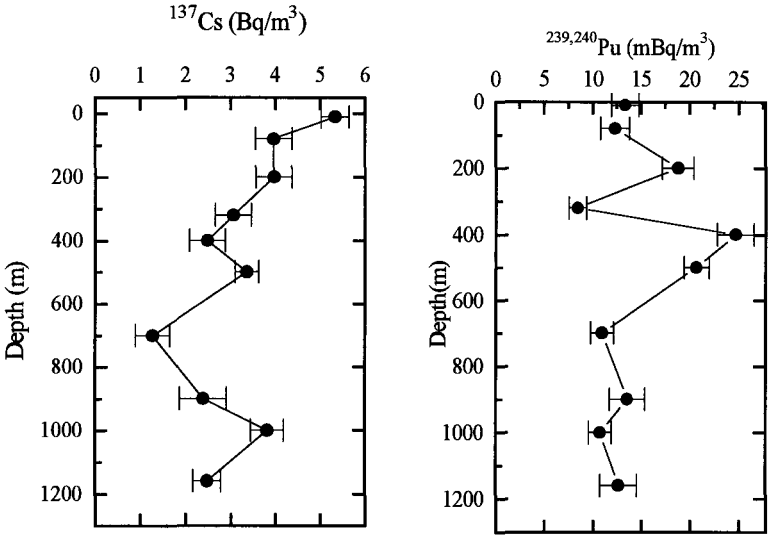

Figure 3. ^{137}Cs and soluble ^{239,240}Pu concentration profiles in the Catalan Sea, June 1993

4.2. Flux to sediment traps

Sediment traps were deployed in the Catalan Sea by ICM (CSIC) to study the transfer of particles from shelf to ocean. One sample, collected during a fortnight with a sediment trap located at the bottom of a canyon (1,200 m depth), was analyzed in order to determine the feasibility of using such sampling devices to study TU (and other radionuclide) fluxes to surface sediments in the Catalan Sea (Table 7). The analyses gave a ^{239,240}Pu flux of 13.1 ± 0.9 mBq m^{-2} d^{-1} and showed the ^{238}Pu/^{239,240}Pu ratio to be indicative of fallout plutonium. The ^{241}Am flux was of the same order of magnitude as that of plutonium. Though ^{137}Cs sea water concentrations are about three orders of magnitude higher than plutonium, the observed flux was only one order of magnitude higher, reflecting the relative solubility of caesium in sea water. In the course of a one-year long experiment, the ^{137}Cs flux was found to be in the range 7.3-10.2 Bq m^{-2} y^{-1}.

Table 7. TU and ^{137}Cs vertical fluxes (mBq m^{-2} d^{-1}) and ratios in the Catalan Sea determined using a sediment trap

^{239,240}Pu	^{241}Am	^{137}Cs	^{238}Pu/ ^{239,240}Pu	^{241}Am/ ^{239,240}Pu	^{239,240}Pu/ ^{137}Cs
13.1 ± 0.9	8.9 ± 1.1	172 ± 25	0.034 ± 0.018	0.68 ± 0.10	0.076 ± 0.012

5. Sediments

5.1 Catalan Sea core

From the same location as that where the sediment trap was deployed, a sediment core was retrieved and analyzed for γ-emitters. The ^{137}Cs profile (Figure 4) showed the presence of two maxima, which may be related to the Chernobyl accident in 1986 and the peak in global fallout deposition in 1963. If this is confirmed to be the case by ^{210}Pb dating, the sedimentation rate is high, *ca.* 3 mm y^{-1}, which would suggest that the canyon is both active and very effectively as a natural trap for particles transported by currents.

5.2. Palomares cores

Two cores from the Palomares area were also retrieved. A sediment core from the Garrucha canyon, collected from a depth of 1,290 m, was analyzed for TU and γ-emitters (Figure 5). The core had a sandy layer between the 6 and 10 cm horizons, as confirmed by granulometry analyses. Excess ^{210}Pb measurements indicated high sedimentation rates in sections 6-10 cm, causing some ^{137}Cs dilution. The plutonium isotopic ratios indicated the presence of bomb plutonium in the top sections. Estimated radionuclide inventories were 109 $\pm$ 2 Bq($^{239,240}Pu$) m^{-2}, 36.5 $\pm$ 1.1 Bq(^{241}Am) m^{-2} and 623 $\pm$ 16 Bq(^{137}Cs) m^{-2}. Thus, it can be concluded that the canyon may be actively transporting particulate-associated radionuclides, a point already made above in the context of uptake by plankton.

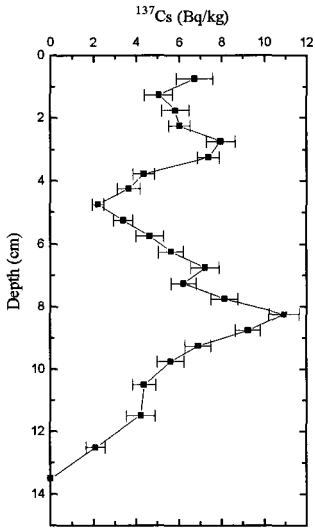

Figure 4. ^{137}Cs in a sediment core from the Catalan Sea

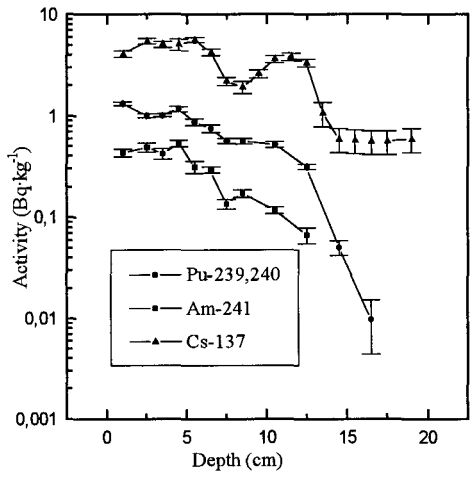

Figure 5. Artificial radionuclide profiles in a sediment core from the Palomares area

The second core from the Palomares area was collected near the coast from 50 m depth and analyzed for TU and γ-emitters. Again, the plutonium isotopic ratios indicated the presence of bomb plutonium along the core, as the ratio was close to 0.02 rather than the fallout value of 0.04. This was confirmed by the relatively high value of the $^{239,240}Pu/^{137}Cs$ ratio. The inventories in this core were 274 $\pm$ 3 Bq($^{239,240}Pu$) m^{-2}, 63 $\pm$ 2 Bq(^{241}Am) m^{-2} and 465 $\pm$ 15 Bq(^{137}Cs) m^{-2}, all of them higher than those observed in the 'canyon' core.

At least one hot particle was found in this core, with an activity in the order of 1 Bq(Pu). Though detection by Scanning Electron Microscopy / X-Ray fluorescence analysis has been attempted, the particle has not yet been characterised.

Acknowledgements

We wish to acknowledge the invitations received from ENEA, ICM, UB, UP and MAFF to participate in various research expeditions. We also are grateful to UCD, CIEMAT, ENEA, MAFF and AUN for the technical and scientific support received in the development of various collaborations within this programme. We thank ICM for carrying out the plankton identification and granulometry analyses.

Publications

Sanchez-Cabeza, J.A., Merino, J., Mitchell, P.I. and Schell, W.R. (In Preparation), 'Plutonium contamination of marine plankton from Palomares (Spain)'.

León Vintró L., Mitchell P.I., Condren O.M., Moran M., Vives i Batlle J. and Sanchez-Cabeza J.A. (In Press), 'Determination of the $^{239}Pu/^{240}Pu$ atom ratio in low activity environmental samples by alpha spectrometry and spectral deconvolution', In: ICRM '95 Conference and International Symposium on Radionuclide Metrology and its Applications, Paris, 15-19 May, *Nucl. Inst. Meth. Phys. Res.*

Sanchez-Cabeza J.A., Molero J., Merino J., Pujol Ll. and Mitchell P.I. (1995), '^{137}Cs as a tracer of the Catalan current', *Oceanologica Acta* **18**(2), 221-226.

Mitchell P.I., Vives i Batlle J., Downes A.B., Condren O.M., León Vintró O.M. and Sanchez-Cabeza J.A. (1995), 'Recent observations on the physico-chemical speciation of plutonium in the Irish Sea and the western Mediterranean', *J. Appl. Rad. Isot.* **46**(11), 1175-1190.

Molero J., Sanchez-Cabeza J.A., Merino J., Vives Batlle J., Mitchell P.I. and Vidal-Quadras A. (1995), 'Particulate distribution of plutonium and americium in surface waters from the Spanish Mediterranean coast', *J. Environ. Radioactivity* **28**, 271-283.

Molero J., Sanchez-Cabeza J.A., Merino J., Pujol Ll., Mitchell P.I. and Vidal-Quadras A. (1995), 'Vertical distribution of radiocaesium, plutonium and americium in the Catalan Sea (Northwestern Mediterranean)', *J. Environ. Radioactivity* **26**, 205-216.

Sanchez-Cabeza J.A., Merino J., Schell W.R. and Mitchell P.I. (1995), 'Transuranic accumulation in plankton from the Spanish Mediterranean coastal environment', *Rapp. Comm. int. Mer Médit.* **34**, 231.

Antón M.P., Gascó C., Sanchez-Cabeza J.A. and Pujol, Ll. (1994), 'Geochemical association of plutonium in marine sediments from Palomares (Spain)', *Radiochimica Acta* **66/67**, 443-446.

Mitchell P.I., Vives i Batlle J., Downes A.B., Sanchez-Cabeza J.A., Merino Pareja J., Delfanti R and Papucci C. (1994), 'Chemical speciation and colloidal association of plutonium in the western Mediterranean water column and the Gulf of Vera', In: *Proc. MARINA-MED Seminar on the Radiological Exposure of the Population of the European Community from Radioactivity in the Mediterranean Sea*, Cigna *et al.* (Eds.), Rome, 7-19 June, 1994, EUR-Report 15564 EN, pp. 441-457.

Sanchez-Cabeza J.A., Merino J., Molero J., Pujol Ll. and Mitchell P.I. (1994), 'On the use of Cs-137 as a tracer of the Liguro-Provençal-Catalan current', In: *Proc. MARINA-MED Seminar on the Radiological Exposure of the Population of the European Community from Radioactivity in the Mediterranean Sea*, Cigna *et al.* (Eds.), Rome, 7-19 June, 1994, EUR-Report 15564 EN, pp. 597-610.

Sanchez-Cabeza J.A., and Merino J. (1994), 'Radiactividad artificial en el medio marino (Océano Atlántico Nororiental y Mar Mediterráneo Occidental)', In: *Actas del 5º Congreso Nacional de la Sociedad Española de Protección Radiológica,* Santiago de Compostela, 26-29 April 1994, pp. 298-307.

Merino J. (1993), 'Especiación Físico-Química del Plutonio en Aguas del Mar Mediterráneo', MSc Thesis, Universitat Autònoma de Barcelona, 180 pp.

Molero J., Morán A., Sanchez-Cabeza J.A., Blanco M., Mitchell P.I. and Vidal-Quadras A. (1993), 'Efficiency of radiocaesium concentration from large volume natural water samples by scavenging with ammonium molybdophosphate', *Radiochimica Acta* **62,** 159-162.

Ryan T.P., Mitchell P.I., Vives i Batlle J., Sanchez-Cabeza J.A., McGarry A. and Schell W.R. (1993), 'Low-level Pu-241 analysis by supported disc liquid scintillation counting', In: *Liquid Scintillation Spectrometry 1992*, J.E. Noakes, F. Schönhoffer and H.A. Polach (Eds.), *Radiocarbon*, pp. 75-82.

Molero J. (1992), 'Comportamiento y Distribución de los Radionúclidos de Vida Larga en Ecosistemas Marinos. Estudio Relativo a Radiocesio y a los Transuránidos Plutonio y Americio en el Entorno Ambiental de la Costa Mediterránea Española', PhD Thesis, Universitat Autònoma de Barcelona, 353 pp.

Head of project 8: Dr. H. Dahlgaard

II. Objectives for the reporting period

In the case of RISØ, the reporting period corresponds to the final 13 months of the programme (May 1994 - June 1995).

A number of unique sediments cores taken in 1991 in the Thule accident area (north-west Greenland) became available in collaboration with the Bedford Institute of Oceanography, Canada. The cores were sectioned in 1-cm slices. The work reported here is based on these and earlier samples from the Thule accident area.

The objectives for the reporting period were:

- to analyze the cores for ^{210}Pb;
- to analyze the cores for ^{239,240}Pu by alpha spectrometry;
- to compare ^{210}Pb and transuranics as tracers for sedimentation and bioturbation processes;
- to determine sedimentation rates and bioturbation parameters of interest in connection with radiological assessments in the Arctic.

III. Progress achieved including publications

Materials and methods

Samples of marine sediments were collected in 1991 from Greenland by the Bedford Institute of Oceanography, Canada, and shared with Risø National Laboratory. The sampling covered the plutonium contamination of the Thule area where a US military aircraft carrying nuclear weapons crashed on the ice in January 1968. Sediment cores (0-50 cm) were sampled and sliced in 1-cm sections. Risø carried out radiometric analyses on 10 cores from the near-zone (within 10 km) of the point of impact (Figure 1) and on 5 cores from the northern part of Baffin Bay. The analyses comprised gamma-spectrometric determinations of natural radionuclides including ^{210}Pb and the fallout radionuclide ^{137}Cs, and radiochemical isolation of the plutonium isotopes followed by the detection of ^{239,240}Pu by alpha spectrometry.

The vertical profiles of the radionuclide concentrations were interpreted in order to obtain information on sediment characteristics of importance for the evolution with time of the plutonium contamination in the Arctic marine environment. ^{210}Pb in the sediment originates from the natural content of ^{226}Ra and decay products (supported fraction), and from the flux of ^{210}Pb on particles settling from the water column on surface sediments (unsupported fraction). The excess ^{210}Pb in the surface sediments thus represents a historical record of sedimentation within about two hundred years, limited only by the physical half life of ^{210}Pb (22 y). An undisturbed sediment profile will show an exponentially decreasing concentration of ^{210}Pb where the rate of decrease is determined by the rate of sedimentation and the ^{210}Pb

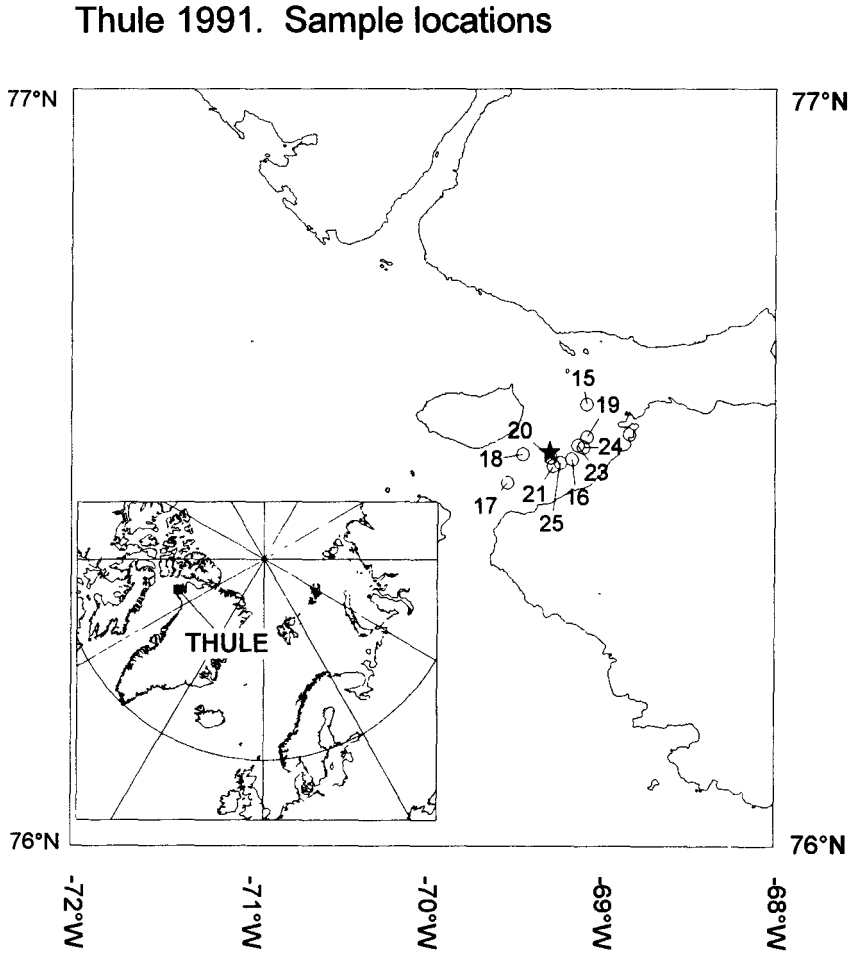

Figure 1. Locations (Station #) for the Thule 1991 sediment samples. ★: point of impact

half-life. Deviations from the exponential decrease of ^{210}Pb in the surface sediments may be interpreted in terms of mechanical mixing due to biological activity and water flow generated by wind and tidal forces. It is important to understand and quantify the mixing processes because they speed-up and enhance the transfer of radionuclides from the sediment back to the water column, from where they may more readily enter into human food chains.

A mathematical compartmental model for the activity of radionuclides in sediments was set up considering sedimentation and mixing. The model was based on the work by Christensen (1982). The model assumes that mixing may be expressed as a diffusive process with gaussian mixing in the upper layer. The diffusion coefficient is thus assumed to decrease with depth from a maximum value at the water-sediment interface following a gaussian function:

$$D = D_0 \cdot e^{-\frac{z^2}{2\sigma^2}}$$

where D_0 ($cm^2\ y^{-1}$) is the diffusion coefficient (mixing rate) at the sediment surface, z (cm) the depth, and σ (cm) the effective mixing depth. There are biological reasons for choosing a gaussian diffusion coefficient, since deposit-feeding animals, like worms, are mainly found in the top sediments and their distributions with depth are close to gaussian. Furthermore, physical mixing generated by water movement also declines rapidly with depth.

For unsupported ^{210}Pb, the model simulates continuous deposition for about two hundred years until 1991, and for plutonium the model starts with a single input of $^{239,240}Pu$ in 1968 followed by a 23-year simulation without input until 1991. The depth profiles calculated with the model are compared with the observed profiles and the model parameters are selected to minimise the differences.

The parameters used by the model for each sediment core include the sedimentation rate (cm y^{-1}), the mixing depth (cm), the mixing rate ($cm^2\ y^{-1}$), the continuous ^{210}Pb input rate (Bq m^{-2} y^{-1}) and the single $^{239,240}Pu$ input (Bq m^{-2}) in 1968.

Results and discussion

The concentration profiles of ^{210}Pb and $^{239,240}Pu$ were analyzed with the model for each core. The availability of the $^{239,240}Pu$ profiles proved to be important for the determination of mixing rates. If ^{210}Pb profiles were analyzed separately, best fits would often result in mixing rates that were very high (above 10 $cm^2\ y^{-1}$). Such high mixing rates effectively remove any structure in the $^{239,240}Pu$ sediment profile above the mixing depth, and the comparison between predicted and observed $^{239,240}Pu$ data thus proved very valuable. It was thus not possible to select values for mixing depths and mixing rates directly from computer optimisation due to the variable and unreliable results produced by this approach. Instead, these values were selected on the basis of best judgement and visual inspection of the agreement between observations and model predictions.

Figure 2 illustrates the result of the analysis of unsupported ^{210}Pb and $^{239,240}Pu$ concentration profiles from one of the sediment cores, Station No. 20, collected in the near-zone of the Thule accident area. For this core the sedimentation rate is determined at a value of 0.26 cm

y^{-1} ± 9% (1 S.D.), the mixing depth at a value of 5 cm, the mixing rate at a value of 1 cm^2 y^{-1}, the ^{210}Pb input rate at a value of 220 Bq m^{-2} y^{-1}, and the single $^{239,240}Pu$ input in 1968 at a value of 71 kBq m^{-2}. Furthermore, the observed ^{137}Cs profile for the core is included for comparison.

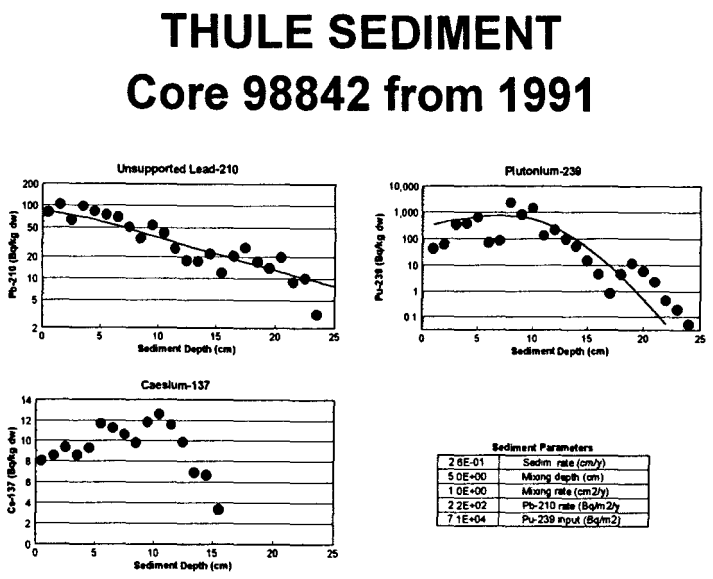

Figure 2. Observed and calculated radionuclide concentration profiles for sediment core No. 98842 including estimated parameter values (Station No. 20, coordinates: 76° 30.79´N, 69° 17.18´W)

The sediment parameters estimated from the 10 cores from the Thule accident area are shown in Table 1 listing the mixing depths and mixing rates, the sedimentation rates and the corresponding uncertainties (1 S.D.), the ^{210}Pb input rates, the $^{239,240}Pu$ inventories and the ^{137}Cs inventories. The mixing parameters are generally consistent across all sediment cores with a mixing depth of 5 cm and a mixing rate of 1 $cm^{-2}y^{-1}$. The mean sedimentation rate is 0.3 cm y^{-1}, varying from 0.2 to 0.4 cm y^{-1}. The ^{210}Pb input rate varies from 74 to 460 Bq m^{-2} y^{-1}, with a mean value of 261 Bq m^{-2} y^{-1}. This value agrees with the average deposition flux of ^{210}Pb of about 1 dpm cm^{-1} y^{-1} (= 170 Bq m^{-2} y^{-1}) found in sediments at temperate latitudes. The atmospheric flux of ^{210}Pb is lower at northern latitudes, but at the Thule area sedimentation is high due to particle transport from land by run off. The ^{137}Cs inventories are closely associated with the ^{210}Pb input rates for the ten sediment cores: the two sets of data show a strong correlation of 0.9 ($P<0.001$). Actually, both data sets are highly correlated with the rates of sedimentation (correlation coefficients of 0.8, $P<0.01$). These data are

presented in Figure 3 showing the ^{137}Cs inventories and the ^{210}Pb input rates versus the sedimentation rates. The $^{239,240}Pu$ inventories vary significantly from 2 to 71 kBq m^{-2}, with a mean value of 15 kBq m^{-2}.

Table 1. Parameter values from sediment samples collected from the Thule area

Station No Sample No	Mix. depth (cm)	Mix. rate (cm^2 y^{-1})	Sed. rate (cm y^{-1})	Uncertainty (1 SD, %)	^{210}Pb rate Bq m^{-2} y^{-1}	^{239}Pu Bq m^{-2}	^{137}Cs Bq m^{-2}
15-98832	3	1	0.20	18	140	4400	650
16-98834	5	1	0.40	8	460	21000	1720
17-98836	5	1	0.18	20	74	2200	80
18-98838	5	1	0.18	29	110	2600	320
19-98840	5	1	0.22	10	280	5700	1030
20-98842	5	1	0.26	9	220	71000	1050
21-98844	5	1	0.28	12	350	16000	960
23-98848	5	1	0.21	14	330	7600	980
24-98850	5	1	0.38	15	370	7300	1130
25-98852	5	1	0.34	10	280	12000	1290
Mean	4.8	1	0.27	15	261	14980	921
SD (%)	13	0	31	44	48	137	51

Conclusions

Analyses of radionuclide profiles in sediment cores collected in 1991 at Thule in Greenland have provided information on processes that occur in the sediments. The radionuclides include the naturally occurring ^{210}Pb, $^{239,240}Pu$ originating from the aircraft accident in 1968, and ^{137}Cs originating from nuclear weapons testing. The processes include mixing of the surface sediments mainly from biological activity and burial of sediments due to particle scavenging. These processes influence the time scale and the extent to which the plutonium contamination is in contact with seawater and thus available for further dispersion. The quantified description of these processes is necessary for numerical modelling of the impact of radioactive contamination of the marine environment. These processes are of particular importance for the transuranic elements due to their relatively high radiotoxicity, their long physical half-lives and the sediment-reactive properties of these elements.

The radionuclide profiles have been analyzed with a numerical model to identify values of parameters describing the sediment processes. The average parameter values for the Thule area are: 0.3 cm y^{-1} for the sedimentation rate, 5 cm for the mixing depth and 1 cm^2 y^{-1} for the mixing rate. It was found that the mixing parameters were not correctly identified from interpretation of the unsupported ^{210}Pb profile alone but that information from the $^{239,240}Pu$ profile was necessary. This stresses the need for caution when interpreting ^{210}Pb profiles where no other information is available.

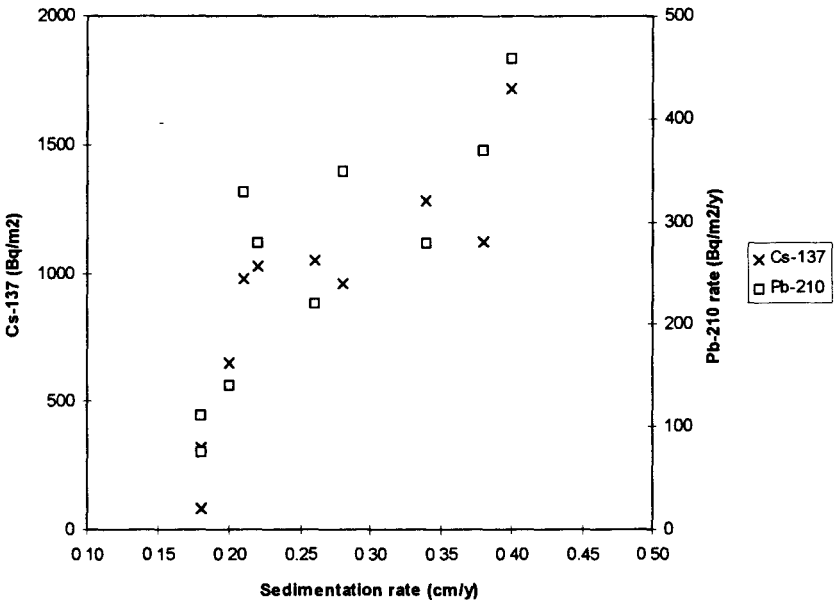

Figure 3. Caesium-137 depositions and ^{210}Pb input rates shown versus sedimentation rates for the ten sediment cores from the Thule accident area. The correlation coefficient for both of the two data sets is 0.8

References

Christensen, E. (1992), 'A model for radionuclides in sediments influenced by mixing and compaction', *J. Geophys. Res.* **87**, 566-572.

Publications

Smith, J.N., Ellis, K.M., Aarkrog, A., Dahlgaard, H. and Holm, E. (1994), 'Sediment mixing and burial of the $^{239,240}Pu$ pulse from the 1968 Thule, Greenland nuclear weapons accident', *J. Environ. Radioactivity* **25**, 135-159.

Head of project 9: Prof. B. Salbu

II. Objectives for the reporting period

To study:

(1) Mobility of radionuclides in Irish Sea sediments
(2) Mobility of radionuclides in the Kara Sea (Stepovogo Fjord)
(3) Analytical techniques for characterising radioactive particles

The work includes:

(1) Collection of samples during expeditions to the Irish Sea near the discharging point of effluent from Sellafield and at the mud patch, and the Kara Sea, Stepovogo Fjord east of Novaya Zemlya, where radioactive waste has been dumped
(2) Analysis of samples with special emphasis on ^{90}Sr using low level liquid scintillation spectrometry (Quantulus)
(3) Mobility studies based on sequential extraction of radionuclides in sediments
(4) Study of sediment-water interactions (sorption - desorption experiments) using tracers
(5) Testing analytical techniques for characterization of radioactive particles in sediments (Irish Sea, Kara Sea as well as samples from Palomares (Spain) and Thule (Greenland)

III. Progress achieved including publications

Mobility of radionuclides in Irish Sea sediments

The Sellafield reprocessing plant, UK, is one of the major sources contributing to fission products in the Arctic Seas. According to recent assessments, a total of 41 PBq of ^{137}Cs and 6.2 PBq of ^{90}Sr have been discharged into the Irish Sea since the 1960s. The maximum releases occurred during 1974-78 and has declined since then. The transit time from Sellafield to the Barents and Kara Seas is estimated to be 4-6 years for mobile radionuclide species. The Cs-signal from Sellafield was recognised in the Kara Sea in 1992 (JRNC, 1993).

Based on previous investigations (Salbu *et al.*, 1993) radionuclides in the Sellafield effluent are to a certain extent associated with particles and colloids. Furthermore, sorption of reactive radioactive species to sediment surfaces will take place. Thus, Irish Sea sediments may act as a sink for radionuclides in the Sellafield effluent. When the releases from a point source are reduced, the mobilisation of radionuclides from previously contaminated sediments may become increasingly important. Thus, contaminated Irish Sea sediments may act as a diffuse source contributing to transfer of radionuclides to the water phase.

The expedition to the Irish Sea took place in December 1992, together with MAFF (Ministry of Agriculture, Fisheries and Food), UK, onboard the *R.V. Cirolana*. Sampling of waters and sediments took place at the Sellafield effluent outlet and at the sedimentation 'mud patch' area. Additional samples were collected in December 1994 by MAFF.

Distribution of radionuclides

The concentrations of radionuclides in waters and sediments were highest close to the Sellafield effluent outlet (Fjelldal *et al.*, 1995). The concentrations in surface water (203 ± 5 Bq m^{-3} for ^{137}Cs, 113 ± 2 Bq m^{-3} for ^{90}Sr) were somewhat higher than in near bottom waters. Based on tangential flow ultrafiltration, about 30% of Cs-isotopes and 10% of ^{90}Sr were associated with colloids (> 10 KDa).

Similarly, the concentrations of radionuclides in sediments were higher at the effluent outlet than at the mud patch. The highest concentrations of ^{137}Cs and ^{90}Sr observed at 10-20 cm depth (Figures 1 and 2) may reflect high deposition in sediments decades ago. The $^{134}Cs/^{137}Cs$ isotopic ratio (0.17 ± 0.01 in 0-5 cm sediment) decreased to 0.018 at 25 cm depth. As ^{134}Cs is a short-lived radionuclide (~2 years), the recent contribution is also of relevance.

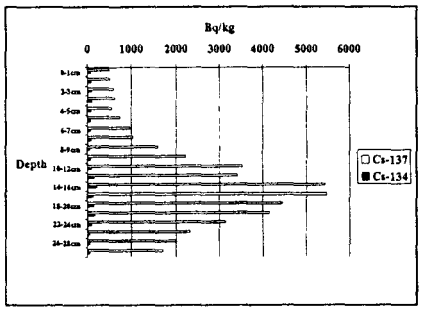

Figure 1. Vertical distribution of ^{134}Cs and ^{137}Cs in Irish Sea sediment collected close to the Sellafield effluent outlet

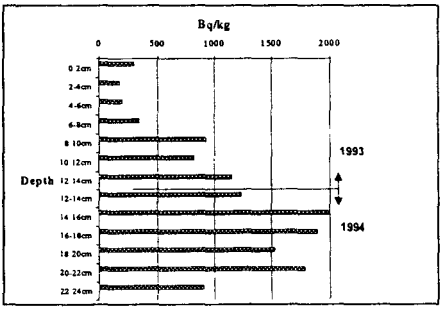

Figure 2. Vertical distribution of ^{90}Sr in Irish Sea sediments collected in 1993 and 1994 close to the Sellafield effluent outlet

Mobility and interactions

Sequential extractions of sediments demonstrated that all of the ^{137}Cs is strongly fixed to inert sediment components, i.e., dissolved in 7M HNO_3. Thus, transfer of ^{137}Cs from sediments to the water phase can hardly be attributed to reversible exchange processes, but more likely to resuspension of particles. About 80-90% of ^{90}Sr in sediments collected close to the effluent outlet is, however, mobile, i.e., present as easily exchangeable forms (Figure 3). As similar results (70% mobility) are obtained for ^{90}Sr in mud patch sediments, the contaminated Irish Sea sediments seem to represent a potential diffuse source for releasing ^{90}Sr.

To obtain information on the interaction of radionuclides with sediments, model experiments using labelled sea water (^{134}Cs + ^{85}Sr) added to Irish Sea sediment systems have been performed at 4°C. By withdrawing samples of water, information on the distribution coefficients, K_d, is attained. Using sequential extraction, kinetic information on the interaction of the tracers with the mobile or inert sediment fraction can be achieved (Oughton *et al.*, 1995). By implementing these data in the compartment model Modelmaker, information on time dependant interactions is attained (Figure 4).

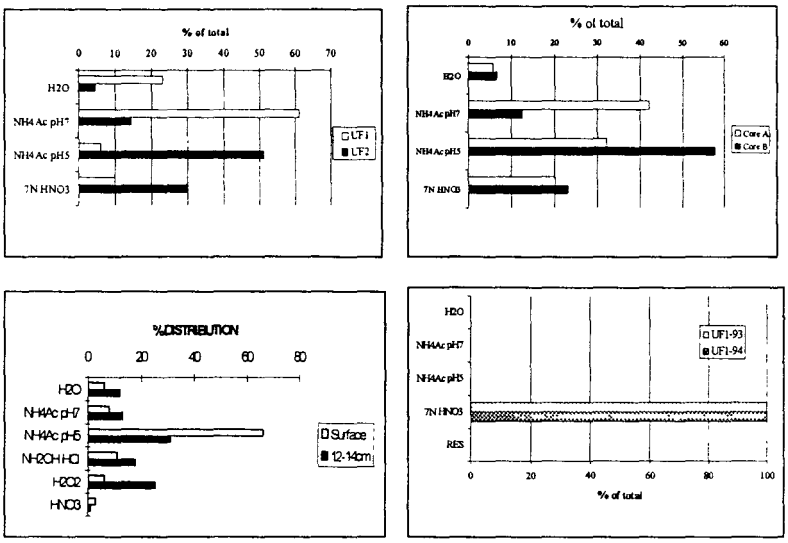

Figure 3. Sequential extractions of ^{90}Sr in Irish Sea sediments collected close to the effluent outlet in 1993 (UF1), at the mud patch in 1993 (UF2) and close to the effluent outlet in 1994 (Cores A and B)

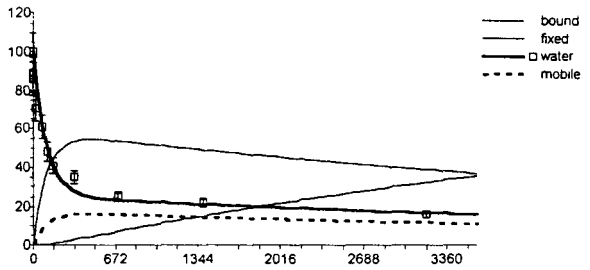

Figure 4. Interaction of $^{134}Cs^{+}$ ions with mobile and inert Irish Sea sediment fraction

The results demonstrate a rapid interaction of $^{134}Cs^{+}$ ions with sediments while the interaction of $^{85}Sr^{++}$ ions is extremely weak. Thus, Irish Sea sediment could act as sorbent for ionic ^{137}Cs species in the Sellafield effluent, while ^{90}Sr should be considered mobile. The high deposition of ^{90}Sr in Irish Sea sediments may, therefore, reflect the presence of ^{90}Sr species other than ionic in the previous effluent. $^{134}Cs^{+}$ ions in the sediment is initially rapidly associated with mobile sediment fractions (Figure 4). With time, however, the ions are strongly fixed to inert sediment fractions (7M HNO_3).

Mobility of radionuclides in the Kara Sea (Stepovogo Fjord)

According to the White Book No. 3 (1993) provided by the Russian Authorities, radioactive waste including 7 reactors with spent fuel, 11 reactors without fuel, several barges and more than 5,000 containers have been dumped in the Kara Sea since the early 1960s. In order to obtain information on the actual radionuclide contamination in the area and to assess long-term consequences of dumped waste, joint Russian-Norwegian expeditions to the open Kara Sea and to the dumping sites at Novaya Zemlya have taken place annually since 1992 (JRNC, 1993; JRNC, 1994; Strand *et al.*, 1994).

The joint Russian-Norwegian expedition to dumping sites in the Stepovogo Fjord took place during August/September 1993 and 1994 (Nikitin *et al.*, 1995; Salbu *et al.*, 1995). The objectives of the expedition were to localise and visually inspect dumped objects in the areas and to collect samples of water, sediments and biota for radionuclide analysis at institutes in Russia and Norway. In the Stepovogo Fjord, a submarine was located in the outer fjord, while a large number of containers were located in the inner part of the fjord.

Selected sediment samples, subjected to mobility studies,were included in the present CEC project.

Distribution of radionuclides

The concentration of ^{137}Cs in surface and near-bottom waters varied within the range 7-8 Bq m^{-3} and 10-20 Bq m^{-3}, respectively. ^{90}Sr varied within 2-3 Bq m^{-3} in surface water and 3-6 Bq m^{-3} in the near bottom water. Thus, the general level of radionuclides in waters and sediments in the Stepovogo Fjord was similar to that obtained in the open Kara Sea in 1992 (Salbu *et al.*, 1995). The concentrations of radionuclides in waters were somewhat higher in bottom water close to localised containers.

Similarly, the concentrations of radionuclides in sediments were highest close to the dumped containers, showing activity levels of ^{137}Cs up to 110 kBq kg^{-1}, of ^{60}Co up to 3.2 kBq kg^{-1}, and ^{90}Sr up to 0.3 kBq kg^{-1}. In most cases the contamination was associated with the upper 5 cm sediment layer (Figure 5). However, large variations were observed in the activity levels and in the vertical distribution of radionuclides in sediment profiles from the same site.

Mobility and interaction

Autoradiography demonstrated the presence of radioactive particles in the sediments. Thus, the contamination in the vicinity of dumped containers was rather inhomogenously distributed. Sequential extraction of sediments demonstrated that most of the ^{137}Cs is strongly fixed to inert sediment components, while ^{90}Sr in sediments is rather mobile, i.e., present in exchangeable forms (Børretzen *et al.*, 1995).

Interaction of radionuclides with sediments was studied by model experiments using labelled sea water ($^{134}Cs^{+}$ ions, $^{85}Sr^{++}$ ions) added to fresh Stepovogo sediments at 4°C (Oughton *et al.*, 1995). Information on the distribution coefficients, K_d, and time-dependant mobility (sequential extraction) demonstrated that the retention of ionic Sr would be low while the sediment could act as a sink for released ionic Cs-species (Børretzen *et al.*, 1995). Thus, the physico-chemical forms of radionuclides released from the dumped waste in the future are crucial for retention in sediments or transport by the water mass.

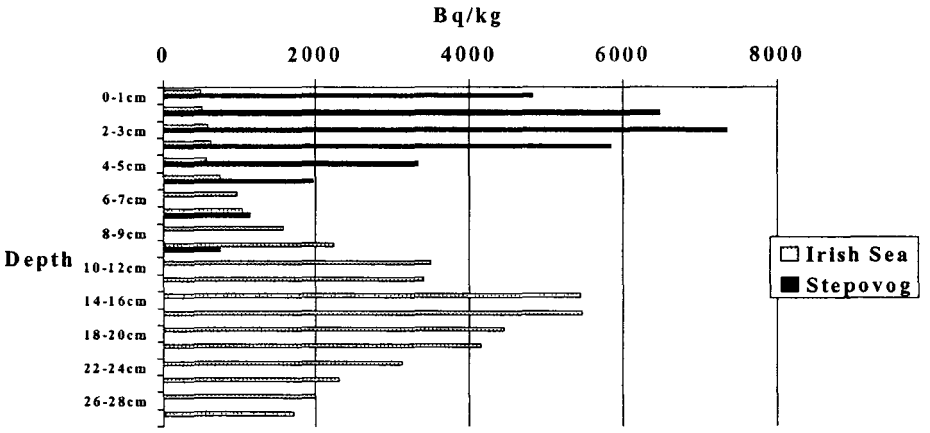

Figure 5. Vertical distribution of ^{137}Cs in Stepovogo Fjord sediments collected in 1994. Data from Irish Sea are also included

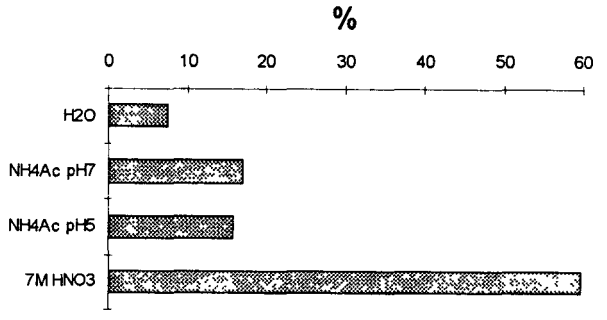

Figure 6. Sequential extraction of ^{90}Sr in Stepovogo Fjord sediments collected in 1994 (n=2)

Analytical techniques for characterising radioactive particles

Different techniques have been applied for separation of radioactive particles in waters and sediments collected from the Irish Sea (high activity levels of fission products), Stepovogo Fjord (high activity level of fission products), Palomares in Spain (very low activity level of

^{239}Pu) and Thule in Greenland (very low activity level of ^{239}Pu).

On-site tangential flow ultrafiltration of waters

Water from the Irish Sea were ultrafiltered *in situ* using a tangential flow system. About 30% of the ^{137}Cs and 10% of the ^{90}Sr were retained by the 10 kDa membrane. Similar experiments in the Kara Sea indicated that a small fraction of ^{239,240}Pu could be retained.

Scanning Electron Microscopy with XRM

Carbon coated stubs were analyzed at different magnification in scanning electron microscopy (SEM) with X-ray microanalysis. Using backscattered electrons to identify particles having surfaces covered with high atomic number elements (SEM in BEI-mode), particles with an unusual composition were identified (Figure 7). The activity levels of ^{239}Pu are believed to be low and, so far, no positive signals from plutonium have been recognised.

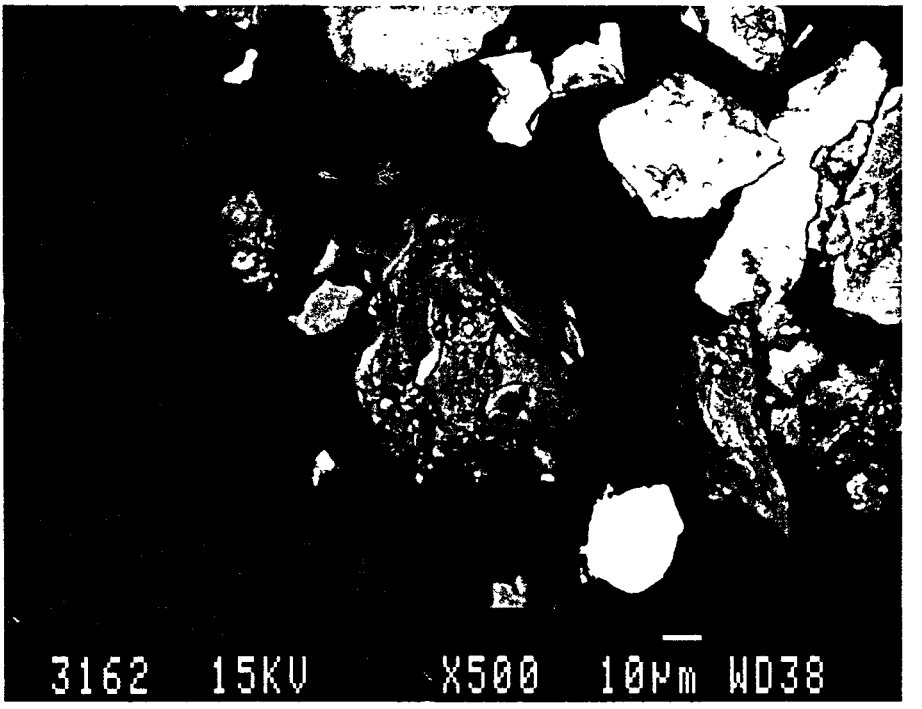

Figure 7. Scanning electron micrograph using back-scattered electrons (BEI-mode). Light areas reflects high atomic number elements. XRM of the α-emitting sub-sample reveals the presence of Pb-particles, Ti-particles and Ba-particles, respectively

Autoradiography

Using X-ray films and varying time of exposure, sediment samples from the Irish Sea, Stepovogo Fjord, Palomares (soil and sediments delivered by CIEMAT and UAB) and Thule (soil and sediments delivered by RISØ) were subjected to autoradiography. Distinct hot spots were obtained in samples from Stepovogo Fjord and Palomares, while diffuse contamination was seen in samples from the Irish Sea. For the remaining samples the time of exposure should exceed 2 weeks.

Alpha-spectrometry and alpha-track

Sediment sub-samples (hot-spots) mounted on electron microscopy (EM) stubs were subjected to alpha spectrometry. Sub-samples from Palomares revealed positive perturbated signals. These stubs were subjected to alpha track radiography. However, the time of exposure needed seems to be relatively long (more than one month).

Conclusions

The concentrations of ^{137}Cs and ^{90}Sr in water and sediment collected close to the Sellafield effluent outlet is very high compared to other marine systems. ^{137}Cs is strongly fixed to inert sediment fractions while ^{90}Sr is mobile. The Irish Sea sediment may act as a sink for $^{137}Cs^{+}$ ions released from Sellafield today. The Irish Sea sediments represent also a potential diffuse source for the release of ^{90}Sr present as mobile exchangeable species.

The general level of radionuclide in waters and sediment in the Stepovogo Fjords is similar to that of the open Kara Sea, i.e., significantly lower than in other marine systems (e.g., Irish Sea, Baltic Sea, North Sea). In the inner Stepovogo Fjord the contamination of ^{137}Cs and ^{90}Sr (as well as ^{60}Co, $^{239,240}Pu$) in sediments collected at the near vicinity of dumped containers demonstrate that leaching from dumped material has taken place. The contamination is inhomogeneously distributed and radioactive particles are present. ^{137}Cs is strongly fixed to sediment components, while ^{90}Sr is to a large extent mobile (exchangeable).

Tangential flow ultrafiltration is useful for the fractionation of radionuclides associated with colloidal material in waters, even when large volumes are involved. Sequential extractions seem useful for assessing potential mobility, while model tracer experiments are well suited for studying sediment-water interactions and binding mechanisms (sorption/desorption experiments). Characterization of radioactive particles using autoradiography, alpha-track and SEM with XRM is useful if the particles have a surface cover with sufficient activities. For low level samples, more sensitive techniques are needed.

References

Børretzen, P., Fjelldal, H., Lien, H., Oughton, D.H. and Salbu, B. (In Press), 'Mobility of radionuclides in sediments from Abrosimov and Stopovogo Fjords', In: *Proc. Second International Conference on Environmental Radioactivity in the Arctic*, 21-25 August, 1995, Oslo, Norway.

Fjelldal, H., Lien, H., Oughton, D.H. and Salbu, B. (In Press), 'Mobility of radionuclides in Irish Sea sediments', In: *Proc. Second International Conference on Environmental Radioactivity in the Arctic*, 21-25 August, 1995, Oslo, Norway.

JRNC (1993), 'A survey of artificial radionuclides in the Kara Sea. Results from the Russian-Norwegian 1992 expedition to the Barents and Kara Seas', Report ISBN 82-993079-0-2, Norwegian Radiation Protection Authority, Norway.

JRNC (1994), 'Radioactive contamination at dumping sites for nuclear waste in the Kara Sea. Results from the Russian-Norwegian 1993 expedition to the Kara Sea', Report ISBN 82-993079-2-9. Norwegian Radiation Protection Authority, Norway.

Nikitin, A.I., Salbu, B., Strand, P., Christensen, G.C., Chumichev, V.B., Lind, B., Fjelldal, H., Bjerk, T.O., Selnæs, T.D., Rudjord, A.L., Sickel, M., Valetova, N.K. and Føyn, L. (In Press), 'Joint Russian-Norwegian collaboration on radioactive contamination from dumped nuclear waste in the Kara Sea - 3 years with expeditions to the dumping sites: goals and investigations', In: *Proc. Second International Conference on Environmental Radioactivity in the Arctic*, 21-25 August, 1995, Oslo, Norway.

Oughton, D.H., Børretzen, P., Mathisen, B., Tronstad, T. and Salbu, B. (In Press), 'Mobilization of radionuclides from sediments: potential sources to Arctic waters', In: *Proc. Second International Conference on Environmental Radioactivity in the Arctic*, 21-25 August, 1995, Oslo, Norway.

Salbu, B., Bjørnstad, H.E., Sværen, I., Prosser, L.S., Bulman, R.A., Harvey, B.R. and Lovett, M.B. (1993), 'Size distribution of radionuclides in nuclear fuel reprocessing liquids after mixing with sea water', *Sci. Tot. Environ.* **130/131**, 53-63.

Salbu, B. (In Press), 'Sources, mobility and biological uptake of radionuclides in aquatic systems', In: *Proc. Int. Conf. Kongsvoll*, Norway, 1994.

Salbu, B., Nikitin, A.I., Strand, P., Christensen, G.C., Chumichev, V.B., Lind, B., Fjelldal, H., Selnæs, T.D., Rudjord, A.L., Sickel, M., Valetova, N.K. and Føyn, L. (In Press), 'Joint Russian-Norwegian collaboration on radioactive contamination from dumped nuclear waste in the Kara Sea - results from the 1994 expedition to Abrosimov and Stepovogo Fjords', In: *Proc. Second International Conference on Environmental Radioactivity in the Arctic*, 21-25 August, 1995, Oslo, Norway.

Yablokov, A.V., Karasev, V.K., Rumyantsev, V.M., Kokeev, M.E. and Petrov, O.J. (1993), 'Facts and problems related to radioactive waste disposal in seas adjacent to the territory of the Russian Federation', Whitebook No. 3 (Materials from Report by the Govermental Commission on Matters related to Radioactive Waste Disposal at Sea, created by decree No. 613 of the Russian Federation President, October 24, 1992). Small World Publisher, Moscow.

Publications

Børretzen, P., Fjelldal, H., Lien, H., Oughton, D.H. and Salbu, B. (In Press), 'Mobility of radionuclides in sediments from Abrosimov and Stopovogo Fjords', In: *Proc. Second International Conference on Environmental Radioactivity in the Arctic*, 21-25 August, 1995, Oslo, Norway.

Fjelldal, H., Lien, H., Oughton, D.H. and Salbu, B. (In Press), 'Mobility of radionuclides in Irish Sea sediments', In: *Proc. Second International Conference on Environmental Radioactivity in the Arctic*, 21-25 August, 1995, Oslo, Norway.

Oughton, D.H., Børretzen, P., Mathisen, B., Tronstad, T. and Salbu, B. (In Press), 'Mobilization of radionuclides from sediments: potential sources to Arctic waters', In: *Proc. Second International Conference on Environmental Radioactivity in the Arctic*, 21-25 August, 1995, Oslo, Norway.

Salbu, B. (In Press), 'Sources, mobility and biological uptake of radionuclides in aquatic systems', In: *Proc. Int. Conf. Kongsvoll,* Norway, 1994.

Final Report
1992 - 1995

Contract: FI3P-CT920035 **Duration: 1.9.92 to 30.6.95** **Sector : A22**

Title: Pathways of radionuclides emitted by non nuclear industries.

1)	Dahlgaard	Risø, DK	
2)	Lembrechts	RIVM, NL	
3)	Germain	IPSN, FR	
4)	Travesi	CIEMAT, SP	
5)	Bettencourt / Carvalho	DGA, PT	
6)	García-León	U. Sevilla, SP	
7)	Pollard / Ryan	RPII, IR	
8)	Heaton	U. Aberdeen, UK	
9)	Zagyvai	T.U. Budapest, HU, (PECO)	
	Germain / Ryan	IPSN, FR / RPII, IR	Intercomparison

I. Summary of Project Global Objectives and Achievements

Introduction

The main emphasis has gradually changed from quantifying the radiological consequences of the aquatic discharges of ^{210}Po and other radionuclides emitted from the phosphate industry, towards gaining a deeper understanding of natural fluctuations in ^{210}Po concentrations and bio-geo-chemical behaviour in selected parts of the marine / estuarine environment. The reason for this shift in main emphasis was that natural variability was masking the effect of industrial discharges on environmental ^{210}Po levels at the studied sites.

The work reported here concerns the emissions of ^{210}Po and ^{210}Pb by various European phosphorous industries, field studies including use of the marine bioindicators *Mytilus edulis* & *Mytilus galloprovincialis* (mussels) in several estuarine and marine environments around active and former phosphate industries as well as in background areas, laboratory studies with *Mytilus edulis*, intensive studies in an inter-tidal marsh environment in Spain directly influenced by a large phosphate industry, dose assessments and modelling.

1. Emission of ^{210}Po and ^{210}Pb by phosphorous industries

The emissions from the phosphate industries were characterised under a previous contract, Bi7-006. In extension of results reported there, it is suggested, that the procedure of decanting and stockpiling the phosphogypsum on land before discharging the waste waters - a procedure being used at most of the active industrial sites studied under this project - seems to have been effective to reduce the enhancement of natural radioactivity levels in the recipient estuarine environments. This is in contrast to the procedure used at the Spanish phosphate industry in Huelva discharging phosphogypsum suspension directly to the Odiel river leading to clear enhancements of environmental radioactivity levels in the river as well as in an intertidal marsh environment. A similar procedure has been used at a now closed plant in NW England - not included in the present project - where a clear enhancement of natural levels in various parts of the marine environment has been reported in the literature.

Head of project 3: Dr. P. Germain

II. Objectives for the reporting period

The studies presented were aimed at evaluating the possible influence of industrial releases on levels of ^{210}Po in bioindicator species (mussels and fucus seaweed). The area under consideration includes the Seine estuary and the adjoining Channel coast of France. Various industrial producers of phosphate fertilizer have released phosphatic gypsum waste into the Seine river and estuary, while the last factory to release waste of this type stopped releases at the end of 1992. In order to explain the distribution of this radionuclide, measurements were also carried out on samples of seawater,suspended particulate matter and sediments.
In order to know the level of ^{210}Po in other species involved in the marine food chain so as to allow an estimation of the amount of this radionuclide ingested by consumers of food products of marine origin, shrimps (crustaceans) and flat-fish caught in the Seine estuary and the Baie du Mont Saint Michel were analysed for ^{210}Po activity.

Progress achieved including publications

I- Polonium-210 activity in *Fucus vesiculosus, Mytilus edulis*,filtered seawater, suspended matter (cf. references of LRM)

The distribution ^{210}Po in *Fucus vesiculosus* and *Mytilus edulis* was investigated in the Seine estuary and along the adjoining Channel coast of France (Fig. 1). The Seine estuary has been subjected to industrial releases of phosphatic gypsum waste which represents a potential source for increased levels of ^{210}Po in the environment.During the reporting period, mussel flesh samples yielded ^{210}Po activities in the range 90-700 Bq kg^{-1} dry weight, while *F. vesiculosus* yielded values between 3 and 22 Bq kg^{-1} dry weight. Variations in ^{210}Po are apparently controlled by the geographical location of the sample, the highest levels being recorded in the southeastern part of the Golfe Normand-Breton. Seasonal fluctuations are observed in the mussel samples, with maximum activities at the end of winter and the beginning of spring.
The factors controlling polonium distribution in mussels were studied, leading to the conclusion that suspended matter has an influence in the southeastern Golfe Normand-Breton. Moreover, physiological (gametogenesis) and physico-chemical factors intervene in the bioavailability of this radionuclide, thus accounting for the observed seasonal variations. Generally speaking, no significant correlation can be seen between the activities measured in mussels and the activities of filtered seawater (0.45 μm), these latter samples giving values between 0.2 and 4.6 mBq l^{-1}. Samples of suspended matter show ^{210}Po activities ranging between 20 and 180 Bq kg^{-1} dry weight. Values in sediments from the bed of the Seine river are lower than 290 Bq kg^{-1} dry weight. By contrast, values are higher - ca 1.000 Bq kg^{-1} dry weight - in sediments sampled near the effluent outlet pipe.

II - Polonium-210 distribution in sediments of the Seine estuary and along the Channel coast

The analytical data obtained from the 33 surficial sediment samples collected along the French coast of the Channel (Fig. 1) are reported in table 1. All analyses have been carried out on bulk sediments..
Major elements.
Al, Ca and Si have been analysed as representative of the main components of the sediment admixture and allow further comparison to shale reference . The Al concentrations (expressed as Al_2O_3) display a wide range of variations (0-10% wt). Nevertheless, they are likely to be related to aluminosilicate abondances. They are still far from shale concentration (Al_2O_3 = 16,6%) due to a strong dilution effect by quartz and carbonates.
Phosphates.
Phosphorus analyses are expressed as P_2O_5 (%wt. ; Tab.1). Special attention has been drawn to phosphates because they are known to be potential carrier-phases of uranium decay-chain nuclides. The concentrations range 0.03-0.242 %wt. and no seasonal variations are observed. Phosphate concentrations are not correlated to Al_2O_3 contents and all display an excess when compared to shale-type material. This excess concentration can be quantified as a P_2O_5 anomaly :

$$P_2O_5\ \text{anomaly} = \left[\left(P_2O_5 / Al_2O_3\right)_{\text{sample}} / \left(P_2O_5 / Al_2O_3\right)_{\text{shale}}\right] - 1$$

and is plotted versus sample references on figure 2. The most striking pattern is that 3 (out of 4) samples collected at Digue Nord, in the mouth of the Seine river display strong P_2O_5 anomalies (9-15) which is interpreted as the impact of the nearby industrial release of phosphogypsums.

Lead-210.

^{210}Pb activities display wide variations from site to site (10-75 Bq kg^{-1}) but not in a given site (except for Aber Wrach - 22/03/93 and Saint-Laurent - 22/06/93) nor with seasons. Relationships between ^{210}Pb activities and Al_2O_3 (Fig.3) is poorly significant, yielding the idea that only a weak amount of total ^{210}Pb is bound to the aluminosilicate fraction (45 Bq kg^{-1} of uranium for 16.6% Al_2O_3 in shale-type material). The excess ^{210}Pb thus evidenced can be due to either anthropogenic inputs or to natural fallout (radon degasing) the integration of which in the sediment column depends on local hydrosedimentary processes and on sedimentation rates, as well as the sampling depth.

We have demonstrated that, assuming there is no specific enrichment process before release into the sea, the ^{210}Pb excesses observed in most of the sites is unlikely to be accounted for by the phosphate phase. Nevertheless, further investigation would be necessary to explain the observed correlations between excess ^{210}Pb and P_2O_5 excess. We can conclude that, from this data set, industrial influence, if any, cannot be demonstrated, with the possible exception of Digue Nord in the Seine estuary. Therefore ^{210}Pb excess mainly originates from natural atmosphoric fallout.

Polonium-210.

To a first approximation, the general features observed for the ^{210}Pb spatial distribution and seasonal variations apply for ^{210}Po. We will then focus the attention on the significance and interpretation of ^{210}Po excesses or depletions.Figure 4 shows that no significant ^{210}Po depletion at any site (within the error bars). Most of ^{210}Po excesses fall in the interval 10-30Bq kg^{-1}. In the sites with a ^{210}Po excesses higher than 10Bq kg^{-1}, ^{210}Po excess can represent up to 50% of the ^{210}Po activity at equilibrium with ^{210}Pb. This suggests very active processes (because of short decay period of ^{210}Po) depending on both particle surface properties and local hydrodynamics. Unfortunately, no significant relation has been found with available parameters, so the ^{210}Po excess significance is still to be decypher.

III- Polonium-210 activity in crustaceans and fish from Channel waters

^{210}Po activities were measured in edible species fished in the estuary of the Seine. The sampled species comprise a crustacean (the shrimp, *Crangon crangon*) and a fish (the flounder, *Platichthys flesus*). Some further samples were also collected in the southern part of the Golfe Normand-Breton, in view of the fact that another member of the food web - the mussel - shows enhanced levels of polonium along this stretch of the Channel coast. A number of results concerning other fish species (the plaice, *Pleuronectes platessa*, and the sole, *Solea solea*) are given by way of comparison. The samples of sole were taken in the Golfe Normand-Breton and the Strait of Dover areas.

The results of ^{210}Po activity measurements on the shrimp *Crangon crangon* are presented in Table 2. With the exception of the smaller specimens collected on 1st July 1993, all the sampled shrimps have closely similar lengths and weights. For the whole dataset, ^{210}Po levels are situated between 180 and 450 Bq kg^{-1} dry weight of the whole organism. The cephalothorax shows levels of polonium (260-780 Bq kg^{-1} dry weight) that are higher than values measured in the muscles or the carapace. It is noteworthy that the cephalothorax includes the hepatopancreas, thus explaining the enhanced levels of polonium in this part of the animal.

Table 3 reports the ^{210}Po results obtained for the different fish species. The flounders caught on 18th November 1993 in the estuary are small compared with specimens from other catches. For the whole set of flounders, the intestine and liver display the highest specific activities (in Bq kg^{-1} dry weight): intestine,80-300; liver, 60-180; gills, 30-80; skin, 10-40; muscles,7-25.The specific activity of ^{210}Po in the intestine depends on the intestinal contents. With respect to the other studied organs, the liver posesses the highest capacity to fix polonium, showing homogeneous activities in both the plaice and flounder (140-180 Bq kg^{-1} dry weight), apart from flounders caught in the estuary on 18th November 1993. In each catch, the muscle tissue displayed the lowest specific activities.

The levels appear to be closely similar in the Golfe Normand-Breton and the estuary of the Seine.

IV- Polonium-210 transfer mechanism into studied bioindicators

The results obtained in the course of this study point out the dominant role of digestive organs in the absorption of ^{210}Po by crustaceans and fish. Polonium is seen to follow the metabolic pathways of the digestive system, which provides evidence for a major transfer mechanism via food intake. This supports the conclusions of numerous other workers. Germain *et al.* (1995) have also mentioned the importance of the digestive system in the mussel, especially with regard to the contribution of the visceral mass to the absorption of ^{210}Po.

There is a large difference between ^{210}Po levels in mussels and *Fucus* sp., while another mollusc species - *Patella* sp., which feeds on algae - shows generally lower levels compared with mussels (i.e. 120 Bq kg^{-1} dry weight in the Seine estuary and 70 Bq kg^{-1} dry weight in the Golfe Normand-Breton, samples collected in 1991). The nutrition system of mussels (suspension feeders) has an effect on the uptake rate, thus explaining why the bioavailability of polonium in mussels is much greater than that observed for *Patella* sp. or *Fucus* sp.

V - Conclusions

Industrial activities in the Seine estuary do not affect levels of ^{210}Po in any of the studied boxes of the estuarine or adjoining coastal environments, except in the vicinity of the effluent outlet.

Although the mussel proves to be a good bioindicator, polonium is also strongly taken up by fish species and especially the crustaceans. The importance of the trophic pathway is demonstrated and, in the case of mussels, fluctuations in ^{210}Po activity are observed as a function of time (physiological factors and bioavailability varying with seasonal changes in ecological parameters) and geographical location (role of the suspended matter).

Publications of LRM:

Germain P., Leclerc G., Simon S.,1992, Distribution of ^{210}Po in *Mytilus edulis* and *Fucus vesiculosus* along the Channel coast of France; influence of industrial releases in the Seine river and estuary. Radiation Protection Dosimetry, 45, 257-260.

Germain P., Leclerc G., Simon S., 1995, Transfer of polonium-210 into *Mytilus edulis* (L.) and *Fucus vesiculosus* (L.) from the baie de Seine (Channel coast of France), Sci. Total Environ., 164, 109-123.

Germain P., Leclerc G., Study of ^{210}Po behaviour in *Mytilus edulis* in the Seine estuary (Channel coast of France), in preparation.

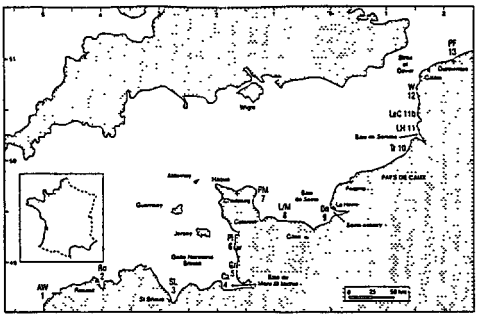

Figure 1. Location of sampling stations: 1 - Aber Wrach, AW ; 2 - Roscoff, Ro ; 3 - St Laurent, SL , 4 - Cancale, Ca , 5 - Granville, Gr , 6 - Pirou, Pi , 7 - Pointe de Moulard, PM , 8 - Luc sur Mer, L/M , 9 - Digue nord Le Havre, Dn ; 10 - Le Tréport, Tr ; 11 - Baie de Somme, Le Hourdel, LH , 11b - Le Crotoy, LeC , 12 - Wimereux, W , 13 - Gravelines, Pont Fort Philippe, PF.

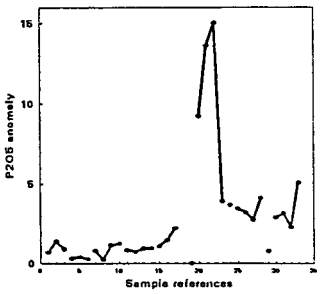

Figure 2. P2O5 anomalies calculated for each sediment sample ; numbers refer to references quoted in table 1.

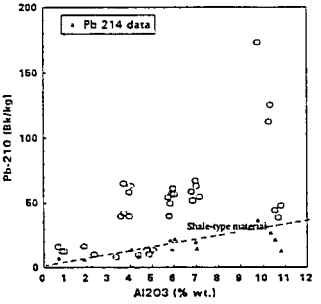

Figure 3. Pb 210 activities versus Al2O3 contents in surficial sediments triangles indicate Pb 214 data fitting well the shale-supported activities.

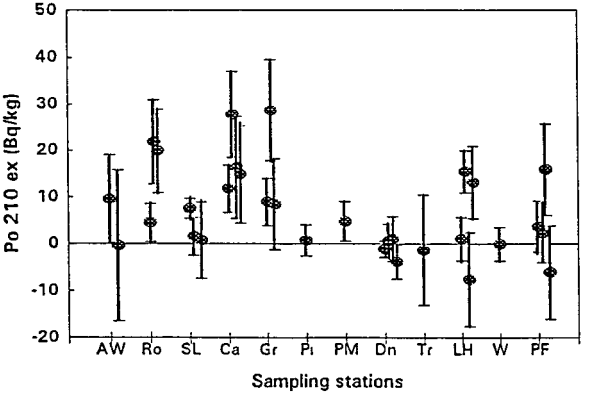

Figure 4. Po 210 excess in surficial sediments , data are pooled at each station , error bars are ± 1sigma.

Table 1. Radionuclide activities and major element concentrations determined in sediment samples.

Stations Dates	Ref.	Pb 210 Bq/kg	Po 210 Bq/kg	Pb 214 Bq/kg	Th 234 Bq/kg	Al2O3 % wt.	CaCO3 % wt.	SiO2 % wt.	P2O5 % wt.
Aber Wrach									
07/07/92	1	112.4 ± 5.2	122.0 ± 8.0	n.m.	n.m.	10.29	0.9	57.55	0.169
22/03/93	2	173.4 ± 23.0	n.m.	37 ± 8	55 ± 22	9.79	3.0	48.46	0.226
21/06/93	3	125.1 ± 14.7	124.8 ± 6.6	27 ± 5	37 ± 15	10.36	1.7	50.82	0.192
Roscoff									
06/07/92	4	38.4 ± 2.7	43.0 ± 3.0	n.m.	n.m.	10.71	2.6	62.74	0.138
22/03/93	5	44.2 ± 7.8	66.1 ± 4.7	22 ± 4	27 ± 11	10.55	3.4	61.76	0.145
21/06/93	6	47.7 ± 8.1	67.6 ± 3.9	13 ± 4	30 ± 13	10.82	2.6	62.34	0.134
Saint-Laurent									
17/06/92	7	13.7 ± 1.8	21.3 ± 1.2	n.m.	n.m.	4.76	33.6	51.62	0.083
14/10/92	8	9.9 ± 3.9	11.5 ± 1.0	n.m.	n.m.	4.88	30.6	56.60	0.060
23/03/93	9	13.5 (*)	59.0 ± 4.4	n.m.	n.m.	5.09	30.0	52.35	0.106
22/06/93	10	39.7 ± 7.6	40.5 ± 2.9	n.m.	n.m.	5.81	25.1	50.26	0.127
Cancale									
17/06/92	11	58.4 ± 3.5	70.2 ± 3.6	n.m.	n.m.	6.81	38.8	32.84	0.122
14/10/92	12	51.7 ± 7.2	79.5 ± 5.9	n.m.	n.m.	6.88	37.0	37.04	0.116
23/03/93	13	66.9 ± 9.7	83.3 ± 5.1	20 ± 4	27 ± 11	7.00	39.3	34.54	0.132
22/06/93	14	63.0 ± 9.5	77.9 ± 4.3	15 ± 4	22 ± 10	7.04	33.8	32.31	0.134
Granville									
15/06/92	15	54.5 ± 3.5	63.5 ± 3.6	n.m.		7.17	38.8	36.63	0.146
24/03/93	16	56.7 ± 9.1	85.4 ± 5.9	22 ± 4	28 ± 12	6.04	41.0	37.26	0.145
23/06/93	17	57.1 ± 8.9	65.6 ± 3.9	15 ± 4	34 ± 13	5.94	36 4	37.38	0.185
Pirou									
23/06/93	18	8.2 ± 3.3	9.0 ± 0.5	n.m.	n.m.	3.37	24.7	65.21	0.032
Pointe du Moulard									
14/06/93		9.6 ± 4.1	14.4 ± 0.8	9 ± 2	14 ± 6	4.39	49.8	38.54	0.044
Digue nord									
30/06/92	19	12.4 ± 1.5	11.3 ± 0.8	n.m.	n.m.	0.95	12.5	80.58	0.094
12/10/92	20	12.6 ± 3.3	13.3 ± 1.3	n.m.	n.m.	0.85	5.2	85.27	0.120
08/03/93	21	16.1 ± 4.6	17.2 ± 1.3	8 ± 2	n.m.	0.68	8.5	81.38	0.105
07/06/93	22	16.3 ± 3.5	12.5 ± 0.9	6 ± 2	n.m.	1.87	7.4	81.88	0.089
Le Tréport									
08/06/93		58.2 ± 11.4	56.9 ± 3.0	n.m.	38 ± 15	3.99	55.4	22.52	0.181
Le Hourdel									
15/07/92	23	42.2 ± 3.1	43.3 ± 3.4	n.m.	n.m.	3.74	38.3	42.51	0.161
16/09/92	24	39.8 ± 2.9	55.3 ± 3.5	n.m.	n.m.	3.60	46.5	37.76	0.146
09/03/93	25	63.2 ± 9.0	55.7 ± 4.3	14 ± 4	25 ± 11	4.06	46.5	35.49	0.148
09/06/93	26	39.8 ± 7.0	53.0 ± 3.4	n.m.	n.m.	3.99	46.8	32.40	0.197
Wimereux									
10/06/93	27	10.0 ± 3.5	10.0 ± 0.8	n.m.	n.m.	2.35	4.8	88.12	0.041
Petit Fort Philippe									
16/07/92	28	54.0 ± 3.4	57.7 ± 4.2	n.m.	n.m.	5.76	32.7	42.26	0.218
15/09/92	29	60.9 ± 3.8	63.3 ± 5.1	n.m.	n.m.	5.99	35.3	40.27	0.242
10/03/93	30	49.2 ± 8.5	65.1 ± 4.9	21 ± 4	n.m.	5.84	32.1	42.37	0.186
10/06/93	31	65.1 ± 9.5	59.1 ± 2.9	n.m.	n.m.	3.72	30.8	39.73	0.219

(*) lower value estimated from shale composition
Error bars are ± 1 sigma.
n.m. : not measured.

Table 2
210-Po activities measured in shrimps, Bq/kg dry weight ± 1 s.d.

- *shrimp, Crangon crangon* Seine estuary

	05/11/92	01/07/93	18/11/93	04/03/94
complete specimens	449 ± 27 (0 25)	185 ± 10 (0 25)	177 ± 9 (0 26)	212 ± 10 (0 27)
cephalothorax	781 ± 69 (0.37)	267 ± 15 (0 30)	258 ± 11 (0.32)	339 ± 18 (0 29)
abdomen flesh	86.3 ± 6 7 (0.27)	77 0 ± 4.5 (0 24)	60.1 ± 4.3 (0 25)	80.6 ± 5.2 (0.23)
abdomen carapace	97.4 ± 7.6 (0 48)	73.0 ± 4 5 (0 33)	55.9 ± 3.1 (0 36)	79.7 ± 5.0 (0.35)
xl=	6 9 ± 0.4 cm	5.6 ± 0 6 cm	6.3 ± 0.5 cm	6 6 ± 0.7 cm
xp=	2 7 ± 0.4 g ww	1.5 ± 0 6 g ww	2.2 ± 0.5 g ww	2.7 ± 1.0 g ww
(n=30)		(n=30)	(n=30)	(n=30)

- *shrimp, Crangon crangon* Golfe Normand Breton

	08/04/94
complete specimens	173 ± 10 (0.27)
cephalothorax	416 ± 23 (0 30)
abdomen flesh	22.2 ± 1.1 (0 24)
abdomen carapace	25.2 ± 1.3 (0 33)
xl=	6.3 ± 0 6 cm
xp=	2.2 ± 0.7 g ww
	(n=30)

( ) = dry weight/wet weight
xl= average length
xp= average wet weight
ww= wet weight

Table 3
210-Po activities measured in fish, Bq/kg dry weight ± 1 s d

- *fish, Platichthys flesus* Seine estuary
(flounder)

	05/11/92	01/07/93	18/11/93	04/03/94
intestine	297 ± 18 (0 16)	139 ± 7 (0 24)	77 5 ± 4 5 (0 21)	294 ± 17 (0 14)
gills	79 1 ± 5 3 (0.24)	52.1 ± 3 1 (0 23)	34 3 ± 1 8 (0 26)	47.2 ± 2 3 (0.18)
muscles	18 1 ± 1 5 (0 20)	14 2 ± 0 9 (0 19)	7 2 ± 0 4 (0 21)	21 2 ± 1 2 (0 17)
skin	39 1 ± 2 6 (0 29)	32 6 ± 1 9 (0 25)	12 3 ± 0 8 (0 30)	28 3 ± 1 5 (0 22)
liver	144 ± 9 0 (0 35)	179 ± 10 (0 27)	57 0 ± 3 8 (0 39)	158 ± 11 (0 20)
xl=	33 0 ± 1 4 cm	30 0 ± 4 6 cm	18 8 ± 2 0 cm	35 3 ± 1 2 cm
xp=	350 ± 49 g ww	383 ± 61 g ww	83 8 ± 26 4 g ww	600 ± 37 g ww
	(n=2)	(n=3)	(n=27)	(n=3)

- *fish Platichthys flesus* Golfe Normand Breton
(flounder)

	08/04/94
intestine	81 5 ± 3 5 (0 31)
gills	53 3 ± 4 0 (0 20)
muscles	25 1 ± 1 2 (0 15)
skin	30 1 ± 1 5 (0 27)
liver	182 ± 11 (0 19)
xl=	36 0 cm
xp=	408 g ww
	(n=1)

-*fish, Pleuronectes platessa* Golfe Normand Breton
(plaice)

	30/03/94
intestine	67 7 ± 4 7 (0 12)
gills	23 5 ± 1 9 (0 21)
muscles	6 3 ± 0 5 (0 16)
skin	12 2 ± 0 8 (0 21)
liver	177 ± 10 (0 18)
xl=	35 5 ± 2 5 cm
xp=	413 ± 66 g ww
	(n=4)

- *fish, Solea solea* Pas de Calais
(sole)

	21/06/93
flesh	9 9 ± 0 9 (0 20)
xl=	28 6 ± 1.3 cm
xp=	217 ± 33 g ww
	(n=7)

- *fish, Solea solea* Golfe Normand Breton
(sole)

	02/07/93
flesh	1.7 ± 0 3 (0 23)
xl=	35 3 ± 1 7 cm
xp=	451 ± 77 g ww
	(n=4)

( )= dry weight/ wet weight
xl= average length
xp= average wet weight
ww= wet weight

2. Marine environment

Intercomparisons

In the start of the project, two IAEA intercomparison samples were analysed by all laboratories then participating with satisfactory results.

A further intercomparison was performed between two laboratories, IPSN, France and RPII, Ireland, comprising sampling as well as ^{210}Po analysis of mussels, seaweed, filtered seawater and suspended particles > 0.45 μm. The mussel data were virtually identical, whereas the seaweed data deviated a factor of 4. The difference was explained as inhomogeneity between the two sets of sampled material. For filtered seawater and suspended particles > 0.45 μm, significant differences should probably be explained by differences in applied filtration techniques. This last observation in combination with the observed reproducibility problems for ^{210}Po and ^{210}Pb in filtered seawater observed at Risø, leads to the conclusion, that sampling and analysis methodologies for ^{210}Po and ^{210}Pb in filtered seawater and suspended particles probably needs to be reassessed.

Field studies

Marine and estuarine environments close to active and former phosphate industrial sites as well as sites considered to represent natural background levels, have been studied in Spain, Portugal, France, Ireland, The Netherlands and Denmark. In Scotland, a bay influenced by de-scaling offshore oil rigs, has been studied.

At several locations, ^{210}Po was measured in filtered water and in particles > 0.45 μm. Levels in water varied generally in the range 0.2 - 2 Bq m^{-3} with extreme results up to 19 Bq m^{-3} (Scotland). The division between dissolved and particulate activity varied with site, time and particulate load. In general, 50 - 98% of the total ^{210}Po activity was found in particles.

Polonium is accumulated to high levels in mussels, *Mytilus edulis* & *Mytilus galloprovincialis*. Generally 100 - 1000 Bq ^{210}Po kg^{-1} dry soft parts were recorded. The digestive organs play a major role for the ^{210}Po concentration pointing to food chain transfer as the major route of ^{210}Po accumulation. The highest concentrations of ^{210}Po have been observed in mussels from exposed seashores, whereas mussels taken in the industrially influenced estuaries (Portugal, France, Ireland, Netherlands) generally display lower concentrations. Variations between sampling sites are thus not correlated to industrial discharges, nor are they readily correlated to a single environmental factor.

Repeated sampling at the same sites has shown a high degree of variability with time. At one intensively sampled site (Portugal), a seasonal fluctuation in ^{210}Po concentrations in mussels was observed, whereas the ^{210}Pb level seemed to be more constant. From other sites with repeated samplings (Denmark, Scotland, Ireland) distinct fluctuations have been recorded without a clear correlation to season. It has been observed that smaller mussels generally show higher concentrations than larger specimens from the same location. There is furthermore a tendency towards higher concentrations with low condition index. Although the correlation of ^{210}Po and ^{210}Pb concentrations with condition index is significant in the Danish data, this is not generally the case. It is concluded, that ^{210}Po concentration in mussels is related to the annual production cycle and probably to the condition of the mussels. However, a significant proportion of the observed fluctuations may be considered unexplained.

Significant differences between sites were observed. This may be due to food availability and growth, which is reflected in the condition index: high food availability, fast growth and thereby high condition index probably correlates with low ^{210}Po concentration. This may be the explanation

for the observed higher concentrations in exposed mussels compared to mussels from estuaries with better food conditions. Salinity did not correlate with the ^{210}Po levels.

The phosphate industries at most of the studied sites have ceased the production of phosphoric acid and thereby the by-product phosphogypsum. This is the case for Portugal (1991), France (1992), Ireland and Denmark. It has not been possible to establish any late environmental effects of the former industrial discharges at any of the sites. This may partly be caused by the reduction in radionuclide discharges by stockpiling on land. Furthermore, the discharge areas tend to be estuarine sites with good living conditions for mussels. In general, this leads to good conditioned and fast growing mussels with relatively lower levels of natural radionuclides than mussels from harsher - and cleaner -- environments. In addition, the environmental conditions in various estuaries may influence the physico-chemical forms of ^{210}Po and ^{210}Pb and thereby their bio-availability. Thus, variability of ^{210}Po concentrations in mussel caused by variation in natural parameters such as, for example, food availability, growth rates and physico-chemical forms, is apparently greater than any possible effect of present or past discharges from the studied industrial sites.

Seaweed, *Fucus vesiculosus,* has been analysed for ^{210}Po at several sites. Concentrations in the range 3 - 22 Bq ^{210}Po kg^{-1} dry weight was recorded. Seaweeds appears to react differently than mussels, presumably because it does not systematically filter off suspended particles, as mussels do. In seaweed, the ^{210}Po / ^{210}Pb ratio is generally close to unity, whereas it is high, 10-70, in mussels. This indicates, that the ^{210}Po level in seaweed originates from ^{210}Pb, whereas mussels accumulate excess ^{210}Po.

The concentration of ^{210}Po in fish varies with species, but apparently not with salinity. Concentrations fall generally in the range 0.1 - 5 Bq ^{210}Po kg^{-1} fresh weight for muscle tissue. Guts, liver and kidney show higher concentrations. The concentration in whole shrimp is dominated by high levels in the digestive gland, the hepatopancreas. In tail muscle, level of 5 - 30 Bq ^{210}Po kg^{-1} fresh weight has been measured.

By comparing excess ^{210}Pb and P_2O_5 in sediments sampled in the Seine estuary and at the French Channel coast, it was concluded that effects of industrial effluents could hardly be demonstrated there; that is, the observed ^{210}Pb excess could entirely be explained by natural atmospheric fallout. The $^{210}Po/^{210}Pb$ ratio was close to unity or slightly above.

Laboratory studies

The RIVM performed a series of mussel experiments aiming at studying the bioavailability of ^{210}Po in different effluent types. Effluent from the wet "phosphogypsum" process (PT) showed a much higher uptake in mussels than effluents from the thermal process (HT). The uptake from the PT effluents is connected to particles: after filtration, the bioavailability of the remaining "dissolved" fraction was very low. In contrast, ^{210}Po added as dissolved nitrate was more bioavailable than any other fraction. Two sets of experiments, winter and summer, gave different results. The accumulation in mussels over one month was linear indicating long biological half lives. It may be concluded, that the availability of ^{210}Po for mussels is depending on the type of effluent, the physico-chemical form and possibly the season.

3. Inter-tidal marsh environment: the Huelva estuary

The environment of the Huelva estuary is different from the other sites studied in this project: it is an inter-tidal marsh dominated by two rivers: the Odiel and the Tinto. Also the discharge procedure is different: although part of the phosphogypsum is piled on the river banks, a significant part is

discharged with the acid liquid wastes into the river. As an effect, enhanced levels of the radionuclides ^{210}Po, ^{210}Pb and ^{226}Ra is recorded in several parts of the environment including river water and sediments. In river water, 3.7 - 289 mBq L^{-1} of ^{210}Pb was found compared to an assumed background of only 1 mBq L^{-1} and in river sediments <63 μm ^{210}Pb levels up to 800 mBq g^{-1} were found against an assumed background level below 10 mBq g^{-1}. For 1993 it was estimated that a total of 0.5 TBq of the 3 radionuclides was released to the Huelva environment from the fertiliser industries, and an inventory of 1 TBq was found mainly in the river bed. Polonium is more easily adsorbed onto suspended particulate matter than ^{210}Pb. This results in an increase in the ^{210}Po / ^{210}Pb ratio in the sediments as compared to discharge values. Also inter-tidal marsh soils and plants are affected by the discharges. The levels of ^{210}Po, ^{210}Pb and ^{226}Ra are increased by an order of magnitude in several soil samples as compared to a background marsh. The varying level of radionuclides in the soils affected the concentrations in two marsh grasses, *Spartina densiflora* and *Spartina maritima.* Concentration factors for ^{210}Po, defined as the ratio between radioactivity concentrations in plant and in soil, were in the range 0.01 - 0.5 - apparently with lower values for higher soil concentrations. The same was found for ^{238}U in the concentration factor range 0.02 - 0.2.
The activity distribution in the marsh environment has been influenced by tidal movements.

4. Dose assessment

Based on analyses of the Portuguese diet, the individual intake of ^{210}Po and ^{210}Pb for the average population was estimated at 1.2 and 0.47 Bq d^{-1}, respectively. Sea food contributes to 70% of the ^{210}Po ingestion, whereas 79% of the ^{210}Pb ingestion is caused by cereals, vegetables and meat. The concentration of ^{210}Po was furthermore measured in fish caught at various times and locations in France, Ireland and Denmark. A species difference has been observed (plaice > herring > cod) - probably due to different food habits.

Due to the absence of any observations of enhanced levels of industrially related radionuclides in edible species taken in the vicinity of the industries compared to more remote areas, it is not possible to estimate the excess radiation dose to the public arising from industrial discharges. It can only be assumed that the industrially enhanced doses are relatively low compared to natural levels.

5. Modelling

A mathematical model to study the dispersion of ^{226}Ra and ^{210}Pb in the Odiel river has been developed. As a first approach, these radionuclides have been considered as conservative substances, remaining in solution. Thus, their dispersion is governed by advection and diffusion processes. Resolutions of the model are 100 m and 6 s. The model has been applied to study the experimental activity concentrations measured along the river for two sampling campaigns performed during 1990 and 1991. The general behaviour of ^{226}Ra and ^{210}Pb is reproduced by the model, both for the samples collected during high and low water at each sampling campaign. Nevertheless, all substances interact with the solid phases (suspended matter and sediments) showing, to a reasonable degree, a non-conservative behaviour. Thus, the ionic exchanges among the phases must be taken into account. Four phases are considered in the model: water, suspended matter and two grain size fractions of sediments, a small and a large grain size fraction. Only the small grain size fraction can be resuspended and incorporated to the water column as suspended matter. In a first stage the model has been applied to study the dispersion of ^{226}Ra. The general behaviour of ^{226}Ra activity concentrations in water and

suspended matter is in good agreement with experimental measurements. The computed sorption of radionuclides by the sediments all over the river is in good agreement with observations as well.

6. PECO

The Technical University of Budapest's PECO contract was associated with the project. The studied Hungarian phosphate industry does not produce phosphogypsum as a by-product. As an effect, there is no enrichment of ^{210}Pb in the effluents. This was confirmed in the environmental analysis, where no industrially related excess activity could be detected. Observed excess ^{210}Pb relative to ^{226}Ra could be explained by natural atmospheric deposition. A new advanced method for separation of ^{210}Pb from ^{210}Po using a crown ether and thereby avoiding the lengthy in-growth method has been developed and published.

The PECO project was extended till end of November 1995 due to a late start. A separate final report therefore appears later.

7. Conclusions

Marine and estuarine environments around various European phosphate industries have been studied to evaluate the level of technologically enhanced natural radionuclides. Several industries have ceased the production of phosphoric acid and the by-product phosphogypsum, where enhanced levels of natural radionuclides are found. No residual effects could be detected in the environments around former industry sites. Other industries studied when the phosphogypsum process was still active, showed no clear environmental enhancement maybe because the discharges were limited by stockpiling phosphogypsum on land. Finally one industry discharging suspended phosphogypsum directly into the environment of the Odiel river and the Huelva estuary was found clearly to enhance natural levels of ^{210}Po, ^{210}Pb and ^{226}Ra.

Polonium is accumulated to high levels in mussels, *Mytilus edulis & Mytilus galloprovincialis.* Generally 100 - 1000 Bq ^{210}Po kg^{-1} dry soft parts were recorded with 10-70 times lower levels for ^{210}Pb. The digestive organs play a major role for the ^{210}Po concentration pointing to food chain transfer as the major route of ^{210}Po accumulation. It is concluded, that ^{210}Po concentration in mussels is related to the annual production cycle and probably to the condition of the mussels. However, a significant proportion of the observed fluctuations may be considered unexplained.

The detection of possible minor enhancements of ^{210}Po and ^{210}Pb has been hampered by variations in environmental levels caused by natural geo-chemical processes in the estuarine transition zones and by natural ecological differences - for example food availability, growth rates and condition - affecting concentrations in the bioindicators *Mytilus edulis & Mytilus galloprovincialis.* It is therefore recommended to further quantify the variation in levels of natural radionuclides in selected components of estuarine and marine environments and to further study the causes of this variation. Finally it was concluded, that sampling and analysis methodologies for ^{210}Po and ^{210}Pb in filtered seawater and suspended particles probably needs to be reassessed.

Head of project 1: Dr. Dahlgaard

II. Objectives for the reporting period

- to survey the concentration of ^{210}Po and ^{210}Pb in marine fish and mussels (Mytilus edulis) from Danish waters,
- to study the function of Mytilus edulis as a bioindicator for ^{210}Po and ^{210}Pb based on a field program .
- Mytilus edulis from one location will be sampled approximately monthly to study the variation with time.
- Mytilus will be repeatedly sampled from 10 locations throughout Denmark aiming at studying the variation with time as well as salinity and location.
- three fish species will be sampled from 3 different locations repeatedly
- The above mentioned samples will be measured for ^{210}Po by α spectrometry. ^{210}Pb will be measured by the ^{210}Po ingrowth method.
- In the program extension, effort will be laid on evaluation of mechanisms causing the observed variation of "background" ^{210}Po concentrations in mussels, *Mytilus edulis,* based on the field results.
- We will aim at introducing methodology to measure ^{210}Po and ^{210}Pb in water and suspended particles from the Mytilus locations.

III. Progress achieved including publications

Abstract

Polonium-210 has been measured in Danish fish meat caught in the North Sea, the Kattegat and the Baltic in 1991 - 1994. Average values of 0.35, 0.65 and 0.96 Bq ^{210}Po kg^{-1} fresh weight were observed for cod, herring and plaice fillets, respectively. The difference between species is statistically significant, whereas no effect of salinity or location could be observed. There is a high variation giving SD values in the range 70 - 100%.

Mytilus edulis soft parts were analysed for ^{210}Po and ^{210}Pb from 11 Danish locations ranging from full North Sea salinity to Baltic 8‰ water. Significantly increasing concentrations with decreasing "condition index" was observed for ^{210}Po as well as for ^{210}Pb. Two former phosphate industry sites were not statistically different from the other locations. The average ^{210}Po concentration in the Mytilus soft parts was 156 Bq kg^{-1} dry ± 51% SD (n=62). On average, the ^{210}Pb concentration was 5.5% ± 60% SD (n=34) of the ^{210}Po concentration in Mytilus soft parts.

A method for measuring ^{210}Po and ^{210}Pb in suspended particles and filtered seawater has been introduced. An average level around 1.5 Bq m^{-3} in total water with approximately 40% in the particulate (> 0.45 μm) fraction was observed.

The present levels of ^{210}Po and ^{210}Pb may represent a natural baseline.

Polonium-210 in Danish fish.

The important commercial fish species cod (Gadus morruha), herring (Clupea harengus) and plaice (Pleuronectus platessa) were sampled from the North Sea (Ringkøbing), the Kattegat (Hundested) and the Baltic (Bornholm) during 1991 - 1994 (Figure 1) . From each catch several fish were filleted, and two separate sub-samples of fish muscle were taken. Average values of the measured ^{210}Po concentrations in fish are given in Table 1. In 35 cases two independent samples were taken from the same catch and analysed separately. A χ^2 test

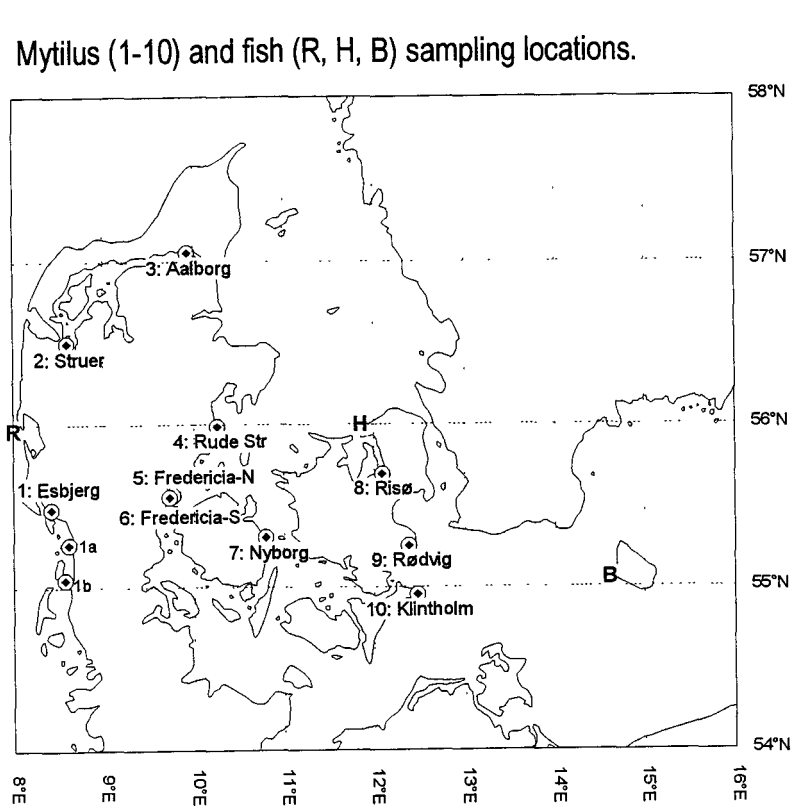

Figure 1. Sampling locations for fish and for Mytilus edulis. The 3 fishing areas are Ringkøbing (R), Hundested (H) and Bornholm (B). The Mytilus locations are numbered 1-10

Table 1. Polonium-210 in fish meat. Average ± SD% of n independent catches 1991 - 1994 from 3 different Danish water areas (Figure 1).

	Bq kg^{-1} fw	± SD%	n	Bq kg^{-1} dry
Cod	0.35	± 101%	13	1.81
Herring	0.65	± 70%	14	2.03
Plaice	0.96	± 88%	14	4.26

showed a 26% variance between double determinations, which is more than ascribed to analytical errors. This indicates a large individual variation of the ^{210}Po concentration in fish meat, which is also shown by the high SD values (70-100 %) in Table 1. An analysis of variance showed a significant effect of fish species on the ^{210}Po concentration, whereas no significant differences could be demonstrated between the 3 catch areas in spite of their large environmental difference: the Baltic location Bornholm has a stable salinity of 7-8 ‰, whereas the North Sea location Ringkøbing show around 30 ‰. Given the observed high variability, the

measured ^{210}Po concentrations in fish including the observed species differences are comparable with other observations from the same area (Skwarzec, 1988; Holm, 1994). Cherry et al. (1994) suggest, that part of the observed variation in the ^{210}Po concentration in fish should be explained by size differences, and reports furthermore that the family Clupeidae is high in polonium. In the present study Clupeidae is represented by herring. As polonium is accumulated in fish via the diet (Carvalho & Fowler, 1994), the high levels in plaice is probably caused by its preference for bivalves, that are relatively high in ^{210}Po.

Polonium-210 and lead-210 in Mytilus edulis from Danish waters

In June/July 1993, September 1993, May 1994 and December 1994, Mytilus edulis samples were taken from 10 locations covering different hydrological regions in Denmark from the North Sea, the Fjords, Kattegat, the Belts and the western Baltic (Figure 1). From Risø (location 8), monthly samples were taken. In each case the soft parts were isolated from 30-60 individuals and homogenised, before two sub-samples were taken for separate analysis.

A χ^2 test indicated a variation between double determinations of mussel samples of 11% (n=41). As these double determinations were taken from homogenated samples, they indicate the total analytical error.

Figure 2 shows average ±SE values of ^{210}Po and ^{210}Pb concentrations in Mytilus edulis soft parts. All values are averaged for the Waddensea (loc. 1, 1a, 1b), the fjords and straits (loc. 2 - 7), Risø (loc. 8) and for the Baltic (loc. 9 - 10). An analysis of variance showed that the ^{210}Po value for the fjords & straits are significantly lower than the Waddensea and Baltic values. For ^{210}Pb, the differences are barely significant.

A condition index was calculated as the ratio between the average individual soft parts dry weight multiplied by 10^6 and the cubed length, g dry * 10^6 /(mm)^3 (Bodoy et al., 1986). Differences between the above mentioned areas were weakly significant (P > 95%) with a low tendency at Risø and the Baltic sites (Figure 4). Significantly increasing concentrations with decreasing "condition index" was observed for ^{210}Po as well as for ^{210}Pb (Figure 3). A linear regression analysis of ^{210}Po concentrations versus the condition index showed a significant negative correlation: $C_{Po} = 240 \pm 23 - (19.7 \pm 4.9) * CI$, where C_{Po} is the ^{210}Po concentration and CI the condition index defined above. The similar line for ^{210}Pb is $C_{Pb} = 12.9 \pm 2.4 - (1.05 \pm 0.48) * CI$.

Figure 4 shows ^{210}Pb as a percentage of ^{210}Po in Mytilus edulis soft parts from different areas compared with the condition index. The Waddensea samples shows significantly lower fraction of ^{210}Pb supported ^{210}Po than the other areas. Figure 4 seems to indicate, that this is not correlated with the condition index.

Figure 5 shows the time series of Mytilus edulis data from location 8, Risø. There is a clear peak in the ^{210}Po data for mussels sampled June 29, 1994 falling off to normal levels during the next two months. Comparing the concentration of ^{210}Po with the condition index does not explain the phenomenon. Individual ^{210}Po loads indicates, that the mussels have actually accumulated unusually much ^{210}Po since the previous sampling June 1st. At present, we have no explanation for the phenomenon, but it indicates that ^{210}Po loads may change rapidly.

The average ^{210}Po concentration in Mytilus soft parts was 156 Bq kg^{-1} dry ± 51% SD (n=62). On average, the ^{210}Pb concentration was 5.5% ± 60% SD (n=34) of the ^{210}Po concentration in Mytilus soft parts. This is in accordance with published bivalve data (Yamamoto et al., 1994; Heyraud et al., 1994). The two locations close to former phosphate industries (Fredericia and Aalborg, locations 5-6 and 3) were not statistically different from the other fjords & straits values.

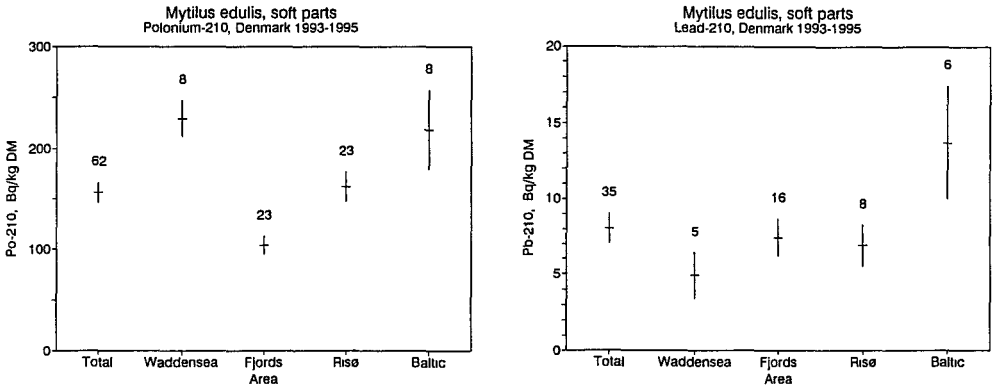

Figure 2. Concentration of ^{210}Po and ^{210}Pb in Mytilus edulis soft parts sampled 1993 - 1995 in different areas of Denmark. Average ± SE. Number of samples indicated.

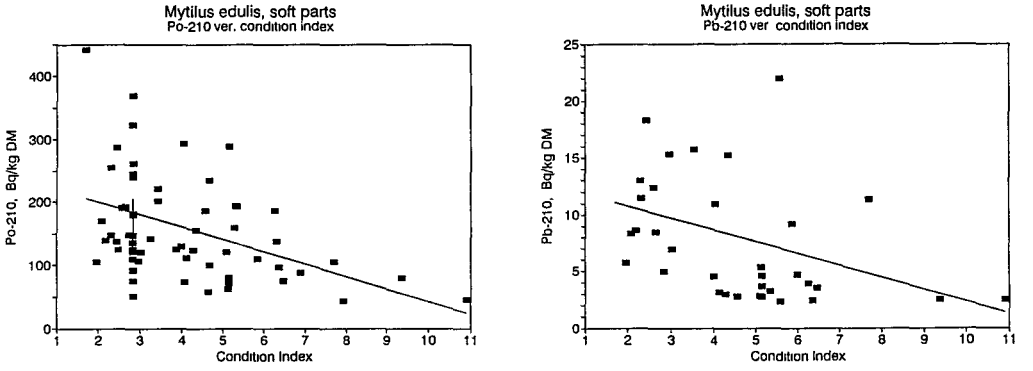

Figure 3. Concentration of ^{210}Po and ^{210}Pb in Mytilus edulis versus condition index. Regression lines: see text.

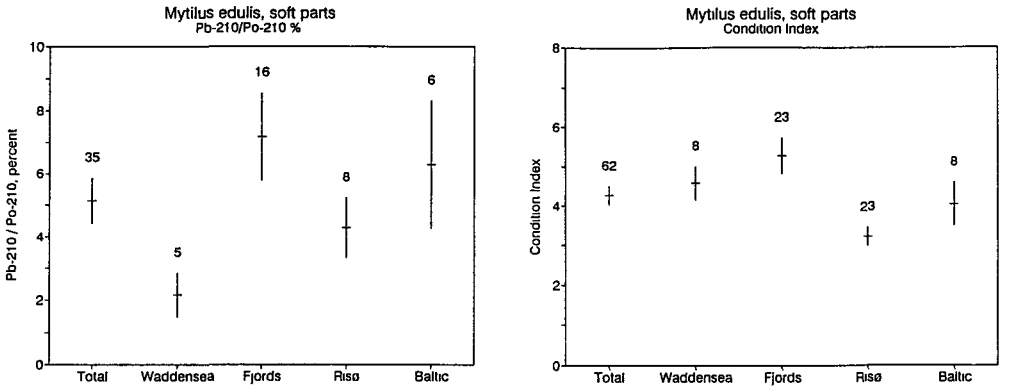

Figure 4. ^{210}Pb as a percentage of ^{210}Po in Mytilus edulis soft parts from different areas. Right graph shows condition index (cf. text). Average ± SE and n.

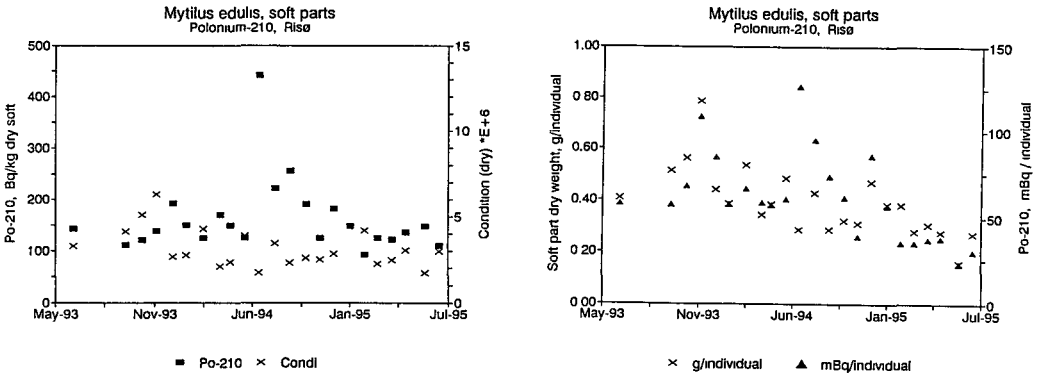

Figure 5. Mytilus edulis soft parts sampled 1993 - 1995 at location 5, Risø. Concentration of ^{210}Po compared with the condition index, and the individual load of ^{210}Po compared with he individual soft parts weight.

Polonium-210 and lead-210 in water and suspended particles.

A method for measuring ^{210}Po and ^{210}Pb in suspended particles and filtered seawater has been adapted from Fleer and Bacon, 1984. Whole seawater is separated in a "particulate" fraction and a "dissolved" fraction by pressure filtration through 0.45 μm Millipore filters. The dissolved fraction is acidified, spiked with ^{208}Po and coprecipitated on cobalt ammonium pyrrolidine dithiocarbamate (Co-APDC). Triple determinations on the same batch of water indicates, that the method may have a problem with lacking isotopic equilibrium between the spike and the sample polonium, as the variation in ^{210}Po values is much larger for the dissolved fraction than for the particulate fraction and for the ^{208}Po spike. For future work it is recommended to alter the method, e.g. by oxidising the dissolved fraction before polonium is coprecipitated on Co-APDC, and further verify the reproducibility.

Average data from 3 triple-samples taken in Roskilde Fjord at Risø (location 8) are given in Tables 2 and 3. On average, 40% of the total ^{210}Po and ^{210}Pb is found in the particulate fraction. The data obtained on water samples are too few to explain variations in the Mytilus samples.

Table 2. Polonium-210 in filtered water (<0.45 μm) and in particulate material (>0.45 μm). Triple determinations, three times, Roskilde Fjord at Risø.

	Particles g m^{-3} ± SD	^{210}Po, water Bq m^{-3} ± SD%	^{210}Po, Particles Bq m^{-3} ± SD%	^{210}Po, Particles % of total
Oct. 94	0.83 ± 0.27	0.75 ± 49%	0.50 ± 10 %	40.1
Nov. 94	1.50 ± 1.01	0.91 ± 69%	0.68 ± 8%	42.7
Dec. 94	1.12 ± 0.04	0.60 ± 22%	0.36 ± 2%	37.4
Average	1.15 ± 0.34	0.75± 21%	0.51± 31%	40.1± 2.7

Table 3. Lead-210 data for samples in table 2.

	^{210}Pb, water Bq m^{-3}±SD%	^{210}Pb, Particles Bq m^{-3} ± SD%	^{210}Pb, part. % of total	$^{210}Pb/^{210}Po$ % water	$^{210}Pb/^{210}Po$ % particles
Oct. 94	0.83 ± 38%	0.39 ± 13 %	32	119	80
Nov. 94	1.14 ± 51%	0.90 ± 4%	44	146	133
Dec. 94	0.99 ± 34%	0.48 ± 7%	32	163	133
Average	0.99± 16%	0.59 ± 46%	36 ± 7	143 ± 22	115 ± 31

Publications

Dahlgaard, H. Polonium-210 in mussels and fish from the Baltic - North Sea Estuary. International Seminar on Freshwater and Estuarine Radioecology, Lisbon, 21 - 25 March 1994.

References

Bodoy, A., Prou, J. & Berthome, J.-P., Etude comparative de differents indices de condition chez l'huitre creuse (Crassostrea gigas). Haliotis 15 (1986) 173-182.

Carvalho, F.P. & Fowler, S.W., A double-tracer technique to determine the relative importance of water and food as sources of polonium-210 to marine prawns and fish. Mar.Ecol.Prog.Ser. 103 (1994) 251-264.

Cherry, R.D., Heyraud, M. & Rindfuss, R., Polonium-210 in teleost fish and in marine mammals: interfamily differences and a possible association between polonium-210 and red muscle content. J. Environ. Radioactivity, 24 (1994) 273-291.

Fleer, A.P. & Bacon, M.P., Determination of ^{210}Pb and ^{210}Po in seawater and marine particulate matter. Nuclear Instruments and Methods in Physics Research, 223 (1984), 243-249.

Heyraud, M., Cherry, R.D., Oschadleus, H.-D., Augustyn, C.J., Cherry, M.I. & Sealy, J.C., Polonium-210 and lead-210 in edible molluscs from near the Cape of Good Hope: sources of variability in polonium-210 concentrations. J. Environ. Radioactivity, 24 (1994) 253-272.

Holm, E., Polonium-210 and radiocaesium in muscle tissue of fish from different Nordic marine areas. In: Dahlgaard, H. (Ed.), Nordic Radioecology, The Transfer of Radionuclides through Nordic Ecosystems to Man. Elsevier Science Publishers, Amsterdam, 1994, pp. 119-126.

Skwarzec, B., Accumulation of ^{210}Po in selected species of Baltic fish. J. Environ. Radioactivity, 8 (1988) 111-118.

Yamamoto, M., Abe, T., Kuwabara, J., Komura, K., Ueno, K. & Takizawa, Y., Polonium-210 and lead-210 in marine organisms: intake levels for Japanese. Journal of Radioanalytical and Nuclear Chemistry, Articles, 178 (1994) 81-90.

Head of project 2: Dr. J. Lembrechts

II. Objectives for the reporting period.

Technical and administrative coordination of the CEC "Pathways" project.
Laboratory studies under controlled conditions of the actual uptake by mussels (*Mytilus edulis*) of ^{210}Po present in the effluents of wet (i.e. phosphogypsum) and of thermal phosphorous plants, to check the influence on uptake of the matrix in which the nuclides are embedded.
The relative importance of the physiological condition of the animals forms a second point of interest as earlier investigations showed considerable fluctuations in the concentration of ^{210}Po in mussels collected at the same site throughout time. As a result, the experiments discussed in the previous progress report have been repeated in another season.

III. Progress achieved including publications.

1. Materials and methods.

Experiments with mussels were carried out in February (at 6°C) and in September (at 15°C) in estuarine water to which different effluents were added as well as fresh algae for food. In winter experiments were carried out with effluent from a thermal process plant (HT), phosphogypsum effluent (PT), filtered (0.45μm) phosphogypsum effluent (PD) and without an additional ^{210}Po source (CONT). In summer the filtered effluent was replaced by a treatment in which a $^{210}Po(NO_3)_2$ solution (DIS) was used. All effluents were diluted to obtain a feasible solution which still contained a reasonable ^{210}Po concentration.

Groups of 12 mussels of the same length were exposed in continuous flow systems, the total volume (15 L) of which was refreshed each day. Aquaria were sampled after one month and for some of the treatments after 10 and 20 days of exposure. Samples taken at the start were used to quantify background concentrations.

^{210}Po was measured in effluent samples, in the freeze-dried soft parts of the mussels, in suspended matter and faeces, and in the filtered water of the aquaria. Losses during sample preparation were traced back by adding ^{208}Po as an internal standard.

2. Observations.

2.1 How does the uptake of ^{210}Po change as a function of time?

No significant change in the ^{210}Po content of the mussels was observed in the control and PD treatments as ^{210}Po exposure levels were very low. A significant increase in the concentration of ^{210}Po throughout the experiment was observed in the PT and HT treatments in both experimental periods, and when ^{210}Po was added as $Po(NO_3)_2$, a treatment which was solely tested in summer. The increase in the ^{210}Po concentration in mussels was linear throughout time (Figure 1), which indicates that excretion is low and consequently that biological half-life is long. Biological half-lives reported in literature vary between 3 and 11 days for some fish species and between 7 and 28 days for a shrimp. These differences in accumulation strategies should be considered when interpreting data from the field.

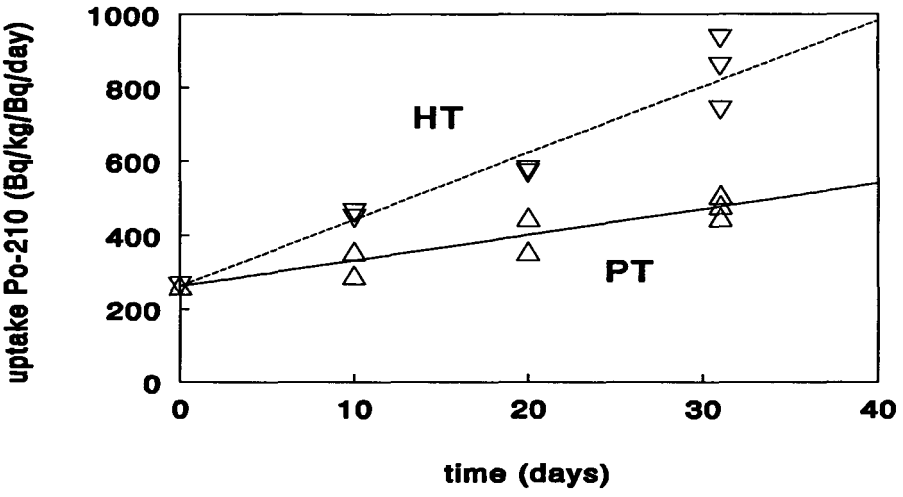

Figure 1: Uptake of ^{210}Po by mussels as a function of time when exposed to estuarine water mixed with phosphogypsum (PT) and effluent from a thermal process plant (HT)

2.2 Does the origin of the effluent affect the availability of ^{210}Po?

The results of our study show that differences in uptake of ^{210}Po from the various effluents within each of the experiments can partly be attributed to differences in concentration and partly to matrix effects.

Mussels exposed to HT showed a much higher uptake than those exposed to PT, uptake from DIS was even higher than from HT. Correction for load (data expressed as $Bq.kg^{-1}/Bq.day^{-1}$) showed that these differences could partly be attributed to matrix effects (Figure 2). This representation of data showed uptake from HT and PT to be significantly higher compared to PD and to be lower compared to DIS. In winter and in summer all treatments differed significantly from each other (Tukey-Kramer method).

Although it is not yet clear which characteristics of the effluent may affect the uptake by biota and to what extent, concentrations in field samples seem to be mainly determined by the overall concentration. Further research on the effect of the matrix on uptake is recommended.

Table 1: Weight of soft parts of mussels, which were not treated with industrial effluents, and their ^{210}Po content in winter and summer

Mussels	Dry weight per individual		^{210}Po content ($Bq.kg^{-1}$)	
	Winter	Summer	Winter	Summer
Start	0.65±0.15	1.32±0.29	255-272	111-139
Control	0.70±0.23	1.30±0.28	196-279	108-117

2.3 Does accumulation of ^{210}Po vary throughout the year?

We observed a two-fold difference in ^{210}Po concentration in reference mussels and the control samples in winter and summer (Table 1). Comparable changes have been found in France (Germain, *this report*) and Portugal (Carvalho, *this report*). In the other treatments higher values were observed in winter as well (Figure 2). Seasonal differences in concentrations of various elements, a.o. ^{210}Po, have been described for a number of marine organisms. Our data on ^{210}Po seem to fit in the overall pattern of high concentrations in winter and low ones in summer which has been reported in literature. The reproductive cycle, temperature, food availability and other environmental factors can be important factors in determining the observed seasonal variation in element concentrations. In calculating mean dose to man due to consumption of mussels, season thus should be taken in account.

For the samples taken from the continuous flow system seasonal differences in uptake rate could be explained by differences in weight. After correction for weight, seasonal differences in the reference samples, the PT and HT samples, and in the control samples were not significant.

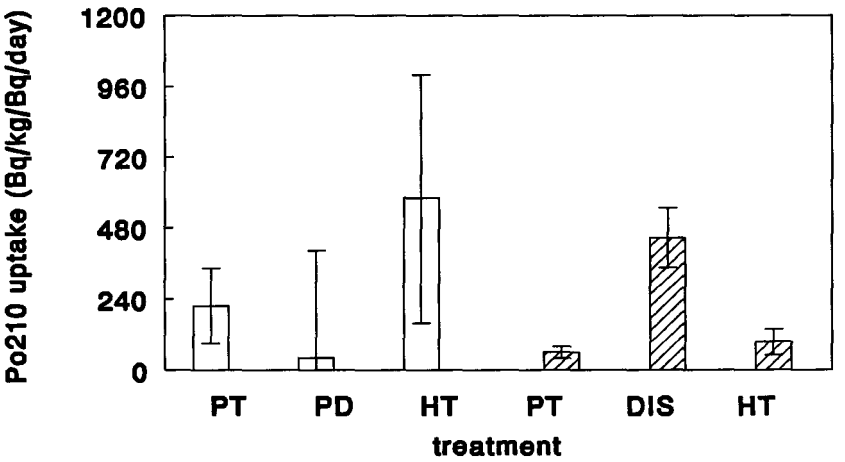

Figure 2: Comparison of the availability of ^{210}Po from different sources, i.e. a soluble ^{210}Po-salt (DIS) and effluents from phosphorous industries (PT, PD, HT), in winter (blank) and in summer (shaded).

References.

Köster H, Berger G, Carvalho F, Germain P, Heling R, Pennders R. Polonium-210 in effluents of phosphorous industries and in European estuaries. Sci. Total Environ., submitted

Pennders R, Janssen M, Köster H, Lembrechts J, Hummel H, Schout P, Timmermans B. Uptake of ^{210}Po by mussels from effluent emitted by different phosphorous industries. Int. Seminar on Freshwater and estuarine radioecology, Lisbon, 940321

Head of project 4: Dr. A. Travesi

I. Introduction

In Spain a large phosphate ore processing complex is located at Huelva, close to the estuary formed by the rivers Tinto and Odiel. The "phosphogypsum" produced as a waste product of the industrial process is, in part directly dumped in suspension into the Odiel River near its confluence with the Tinto river before it reaches the sea. Approximately 8 millions cubic meters of liquid effluents are discharged into the Odiel every year, containing around 4 10^8 Kg of phosphogypsum. The major fraction of phosphogypsum is not directly dumped, but carried out in suspension and deposited over the tidal flats on the eastern side of the Tinto river forming large deposits of phosphogypsum which have resulted in the near total sterility of the tidal flats. These deposits are made through dikes that are formed from the gypsum itself which are successively covered by new flows of the suspension. The overlying liquid drains away through fissures, after the deposition of the solids, into the Tinto river. The gypsum deposits reach a thickness of 4 to 6 m and their total surface covers approximately 4.25 10^6 m^2. It is estimated that, to the present, more than 10^{10} Kg of phosphogypsum has been deposited in this area. The industrial effluents produced in such treatment are discarded in big amounts to both rivers and transported away till the estuary and further to the Atlantic Ocean.

Those effluents contain more than 400000 tons of solid materials, mainly phosphogypsum, and are contaminated with the radioactive nuclides. Also it has been estimated that the radioactivity released in the last years has reached about 2 x 10^{12} Bq in total.

Some characteristics of this ecosystem makes it an unique scenery with several differentials parameters from other estuaries. a) It has a large influence area in the marine environment of about 16 x 23 Km. b) It has a high intensity tide movements with an average of about 730 big tides annually. c) Its waters has an elevated concentration of suspension particles (an average of about 0.16 g/l). d) Also normally the water has a very acid pH, produced by the effluents discarded by the nearby industrial plants. This elevated acidity can affect the radionuclides transportation mechanisms, and to transports some radionuclides till deeper waters than usually.

Preliminary studies have shown an Uranium activity up 800 mBq/l in waters and up to 1000 mBq/g in sediments in some spots in the estuary. This figures are very high compared with the reference values from non contaminated areas of 20 mBq/l in waters and 10 mBq/ g in sediments (1).

II. Objectives for the reporting period.(1992-1995)

A) Characterization and evaluation of effluents from industrial Plants.

To characterize the chemical parameters and radioactive compositions of the effluents discharged from the phosphate factories to the Odiel river, and to the phosphogympsum piles.

B) Bottom sediments sampling.

To collect bottom sediments samples to be analyzed in the sampling sites already selected along both rivers Tinto y Odiel and along the common mouth of the estuary formed by them till the Atlantic Ocean.

C) Determine Radioactive nuclides in sediments samples.

To determine the ^{210}Pb, ^{210}Po and ^{226}Ra activities in a two series of 16 sediments samples by radiochemical separations, alfa spectrometry and gamma ray spectrometry respectively in the small grain size ($< 62,5\ \mu m$) sediments particles.

D) Intercomparison test

To determine ^{210}Pb,^{210}Po in OIEA intercomparison samples

E). Distribution and Inventory of natural radionuclides at the estuary

To carried out a preliminary inventory of ^{210}Pb,^{210}Po and ^{226}Ra activities at the Huelva estuary.

F) Scientific Publications.

To present the research results in scientific publications and specialized congress.

III- Progress achieved including publications.

Summary

The radiological impact of phosphate factories on the environment is easily detectable in the area of Huelva estuary. Higher levels of natural radioactivity are observed in the rivers Tinto and Odiel than in others not affected by such industries (ten to fifteen times the content of a non-polluted Spanish river) .

The releases of 0.5 TBq from the factories are preferentially transferred to the river-bed which has a present inventory approximately 1 TBq for the three radionuclides considered in this study. The $^{210}Po/^{210}Pb$, $^{226}Ra/^{210}Pb$ and $^{226}Ra/^{210}Po$ activity ratios manifest disequilibria in the natural radioactive series after the acid treatment of the mineral and as a consequence of differential behaviour in the estuarine ecosystem.

The particles less than 2 μm in diameter contain a small percentage of radionuclides (5-15%), but this has to be considered in models of radiological hazard assessment as this is the fraction which is easily resuspended and transported.

Publications

The following papers has been written:

(1) A. Travesí, C. Gascó Leonarte, J. Palomares, M. Pozuelo.
Lead-210, Polonium 210, and Radium 226 Activities in bottom sediments samples at the Huelva Stuary. Presented a poster on the International Seminar on Fresh Water and Sturine Radioecology. Lisbon, Portugal 21-25 March 1994.

(2) A. Travesí, C. Gascó, J. Palomares, M.R. García and L.P. Villas.
Distribution of natural Radioactivity within and stuary affected by releases form the phosphate industries submitted for publication to the Journal of Environmental Sciences.

(3) A. Travesí, M. Pozuelo Cuervo, C. Gascó Leonarte, J. Palomares y M.R. García Sanz. Impacto radiactivo ambiental de industrias no nucleares. Niveles de radiactividad en sedimentos de la Ría de Huelva. Presented at the XX Reunión Annual de la Sociedad Nuclear Española. Cordoba, España 26-28 Octubre 1994.

(4) A. Travesi, C. Gascó Leonarte, J. Palomares, M. Pozuelo y R. Garcia Sanz Readioactive Impact of Fertilizer Industries at the Huelva Estuary. International Conference on Fluxes and Technological Enhancement of Radionuclides in and around large-scale non-nuclear industries. Khon Kaen, Thailand, January 9-13, 1995

Detailed account of activities and findings.

Radioactivity of Factory Effluents

The most significant discharges from the phosphate works were the direct discharges from the factory to the Odiel and the supernatant and the indirect erosion of phosphogypsum stockpiles on riverbanks outflowing to the Tinto River. The activities concentrations of range from 2-12 Bq/l for ^{210}Pb, 2-5 Bq/l for ^{210}Po and from 2.9 to 19 for ^{226}Ra. The activity ratios between the different radionuclides from the discharge pipes illustrate the disequilibrium existing after the treatment of the phosphate minerals. The estimated quantity of radionuclides released during 1993 in the whole area is 0.52 $\pm$ 0.04 TBq, which is comparable with the total inventory in the sediments of 0.92 $\pm$ 0.20 TBq present during that year.(2)

Sediments Samples collection

Sampling sites have been selected along both rivers **Tinto y Odiel** and along the common mouth of the estuary formed by them till the Ocean. The sampling sites start at the industrial plants FORET and FOSFORICO in the **Odiel** river and at the phosphogypsum piles in the **Tinto** river. Some samples have been collected upstream these sites in both rivers for control purposes. Other samples have been collected at the Atlantic Ocean Coast near the estuary mouth. Figure 1 shows a map of the area with the sampling stations location.

Two series of 16 samples each of bottom sediments has been collected at these selected sites (February and November 1993) by an University of Seville team, since their geographic proximity, wide knowledge and previous experience in this scenery for similar research.

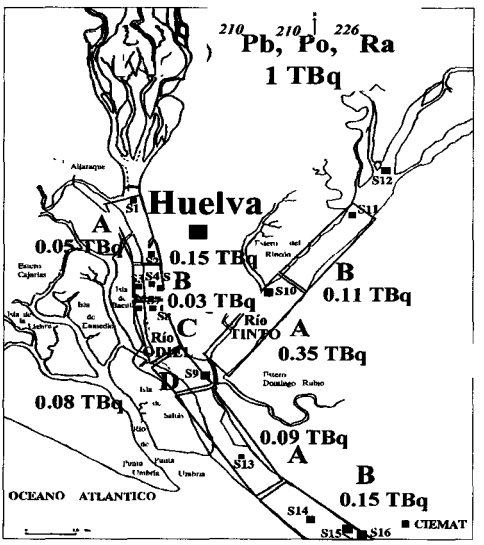

Figure 1: Sampling Stations

Determination of radioactive nuclides in sediments samples.

The measurement of ^{210}Pb,^{210}Po and ^{226}Ra activities in both bottom sediments samples series (dry and wet station) carried out by radiochemical separations, alfa

spectrometry and gamma ray spectrometry respectively in the small grain size (< 62,5 μm) sediments particles for standardization. The results shown a wide range of variation from 15 to 5000 Bq/kg for the February and November series respectively. The results of ^{210}Pb,^{210}Po and ^{226}Ra concentration activities (1993) along the river shows a considerable increase in radionuclide activity close to the discharge point of the effluent pipes and a decrease of activity in the stations located close to the estuary, as expected. The $^{210}Pb/^{210}Po$ activity ratio upstream is close to unity as expected in an area not influenced by the discharge. The stations downstream of the pipes in both rivers and close to the estuary, show $^{210}Pb/^{210}Po$ activity ratios between 0.36 ± 0.27 and 0.86 ± 0.05, significally lower than in the discharge pipe and the phosphogypsum piles. This reduction in the activity ratio of these radionuclides in the riverine sediments can be attributed to their different geochemical behaviour. Because ^{210}Po is more easily adsorbed onto the suspended particulate matter than ^{210}Pb , this results in a rapid removal of the polonium and a higher accumulation rate for this element than lead, and consequently a higher polonium concentration in the sediments and a decrease in the $^{210}Pb/^{210}Po$ activity ratio. A similar behaviour can be observed in the Tagus estuary which is also influenced by the releases of phosphate industries.

Grain size distribution and carbon concentration.

Grain size distribution studies, total carbon concentration, carbon associated to organic-matter and carbon associated to carbonates. have been carried out in four bottom sediments samples have been selected at the effluents discard sites and at the spills of phosphogypsum piles. The grain size distribution in percentage for grain size interval (μm) for this samples ranges from 2 -10 %. The percentage in total carbon, carbon associated to organic-matter and carbon associated to carbonates determined in these samples does not shows meaningful differences. (2,3)

E) Activity concentration in the fraction less than 2μm

For separation of the < 2μm fraction, the dry sample was stirred in distilled water. The fraction remaining in suspension after 24 hours, was collected with the Stokes law being particles remaining in dissolution are those with a diameter < 2μm . The process was repeated until a quantity of these particles was sufficient for analysis.

The activity concentration in the sediment fraction less than 2μm at selected stations ranges from 0.12 to 7.7 Bq/g.(1,3). These stations were selected as representatives of maximum and minimum values of activities. The percentage of activity associated with the size less than 2μm was calculated comparing the activity of 1 g of the fraction less than 2μm of each station with the activity calculated for 1 g of the bulk sample considering an homogenous distribution of activity in each grain size. As is shown, the fraction of radioactivity present in these particles is between 5 and 15%. This fraction is "theoretically" resuspendible, and can be transported and collected by the organisms that live in the estuary. This is an important factor that must be taken into account when models are applied in the context of radiological hazard.

Intercomparison test

Intercomparison test for Pb-210 and Po-210 in OIEA standards OIEA-134 and OIEA-135 has shown good agreements with other participants laboratories in sediment samples

Inventory estimation

The determination of inventory was made using the following formula

$$I_i = A_i \cdot D_i$$

where:
I_i = inventory of radionuclide i expressed in $Bq.m^{-2}$
A_i = concentration activity of radionuclide i expressed in $Bq.kg^{-1}$ (dry weight)
D_i = Surface density of sediment expressed in $kg.m^{-2}$

To calculate the inventories, D_i was assumed constant along the river, with an average value of 43 $\pm$16 $kg.m^{-2}$ (6 stations) .

The determination of inventory was made in three areas identified for the purposes of this study. The area of the Odiel river, about 3 km^2 was divided into four sectors, The areas of the Tinto river and the Estuary were both divided in two sectors, The estimated total inventory of ^{210}Pb, ^{210}Po and ^{226}Ra in sediments is estimated approximately in 1 TBq for the three radionuclides.

The estimated quantity of radionuclides released during 1993 in the whole area is 0.52 $\pm$ 0.04 TBq, which is comparable with the total inventory in the sediments of 0.92 $\pm$ 0.20 TBq present during that year.

Head of project 5: Dr. O. Bettencourt

Report by F. P. Carvalho

II. Objectives for the reporting period

1. Dispersal of radionuclides from the phosphogypsum stockpiles at the south river bank of the Tagus estuary
2. ^{210}Po and ^{210}Pb in biological indicators in the Tagus estuary and seasonal concentrations in marine mussels
3. ^{210}Po and ^{210}Pb in sea food
4. Review of results and conclusions of the project

III. Progress achieved including publications

Summary - The concentrations of ^{210}Po and ^{210}Pb were measured in soils, intertidal sediments, salt-marsh plants and edible vegetables collected in the surroundings of the phosphogypsum piles and in reference zones around the Tagus estuary. Enhanced levels of those radionuclides were detected in soils and sediments close to the gypsum piles but no enhanced levels could be detected in the nearest agricultured soils and vegetable produces. Following rainfalls, radionuclides in the gypsum piles are seeped into the estuary both in dissolved forms and associated with the insoluble residue of phosphated gypsum. In the Tagus estuary, the concentrations of ^{210}Po and ^{210}Pb in bottom sediments and suspended matter indicate that the enhancement of radioactivity is restricted to the close vicinity of the phosphate plant waste water discharge pipe. Concentrations of ^{210}Po and ^{210}Pb in biological indicators (*Fucus vesiculosus, Balanus spp, Mytilus galloprovincialis*) collected throughout the estuary and at the seashore generally did not display enhanced levels. Measurements of ^{210}Po and ^{210}Pb in samples of mussels collected monthly at the coast, displayed marked seasonal fluctuation of ^{210}Po concentration. This seasonal fluctuation may render results from environmental surveys difficult to interpret and enhancement of radioactivity levels caused by industrial discharges difficult to detect. Taking into consideration the levels of ^{210}Po and ^{210}Pb measured in estuarine biota, it is unlikely that consumption of sea food from the Tagus estuary would rise the human intake of those radionuclides in comparison with the intake through consumption of sea food from the coastal sea.

Detailed report- A survey was made to monitor ^{210}Po and ^{210}Pb concentrations in the terrestrial and shoreline environments near the phosphogypsum stockpiles at the south bank of the Tagus estuary. Soil samples collected in the very near vicinity of the gypsum piles, and clearly containing some admixture of gypsum, displayed concentrations ranging from 800 to 1085 Bq kg^{-1} (dry wt). However, soil samples

collected at the nearest agricultured land (200-300 m distance) contained ^{210}Po concentrations ranging from 49 to 65 Bq kg^{-1} (dry wt, <63 μm fraction) and were identical to concentrations measured in soils at reference sites both in the north and south river banks. Salt-marsh plants collected in the zone near the gypsum piles contained ^{210}Po at concentrations ranging from 3 to 20 Bq kg^{-1} (dry wt) and were comparable to concentrations measured in reference sites. Edible vegetables (potato, cabbage, lettuce) collected in the surroundings (200-300 m) of the gypsum piles, displayed also ^{210}Po concentrations similar to those measured in reference sites, ranging from to 0.2-5.6 Bq kg^{-1} (dry wt) depending on plant species. These results indicate that dispersal of radionuclides by runoff, wind, and anthropogenic actions, from the gypsum stockpiles into the terrestrial environment, has been minor.

The production of phosphoric acid, and therefore the release of the by-product phosphogypsum, was discontinued in 1991. Stockpiles of phosphogypsum accumulated on the river bank are surrounded by drains which collect the rainfall into the estuary. Water samples collected in the drains contained dissolved concentrations of ^{210}Po at 20-48 Bq/m^3, whereas ^{210}Po concentrations in suspended particles attained about 1 x 10^4 Bq kg^{-1} (dry wt). Laboratory experiments on the dissolution of phosphogypsum indicated that up to about 1.3 g L^{-1} of gypsum may dissolve in distilled water and leave an insoluble residue of about 2% (dry wt: dry wt) which contains more elevated concentrations of ^{210}Po (23 times higher than in gypsum). The concentrations of ^{210}Po in this insoluble residue were at about 1.2 x 10^4 Bq kg^{-1} (dry wt) and were, therefore, comparable to suspended particulates sampled in the drains. Furthermore, the concentration of ^{210}Po dissolved by the distilled water attained 32 Bq m^{-3}, which is also comparable to concentrations measured in the water of the drains. These results indicate that radionuclides in gypsum piles are gradually leached by rain water and seeped into the estuary. Following mixing with the estuary water, those radionuclides are rapidly scavenged by the suspended matter and bottom-sediments and may enhance the environmental concentrations in this zone of the estuary.

Concentrations of ^{210}Po and ^{210}Pb were measured in bottom sediments and suspended matter sampled throughout the estuary. A method was set up to standardize radionuclide analyses in sediments. Baseline levels of naturally-occurring ^{210}Po and ^{210}Pb in sediments (grain-size fraction $< 63\mu m$) were determined at 68 $\pm$ 19 Bq kg^{-1} (dry wt). Enhanced levels related with the discharge of phosphated wastes, could be measured near the outlet of the waste water discharge and attained a maximum of 1580 Bq kg-1 (dry) (Fig. 1). However, elevated radionuclide concentrations related with phosphatic wastes could not be detected in sediments and suspended matter in other

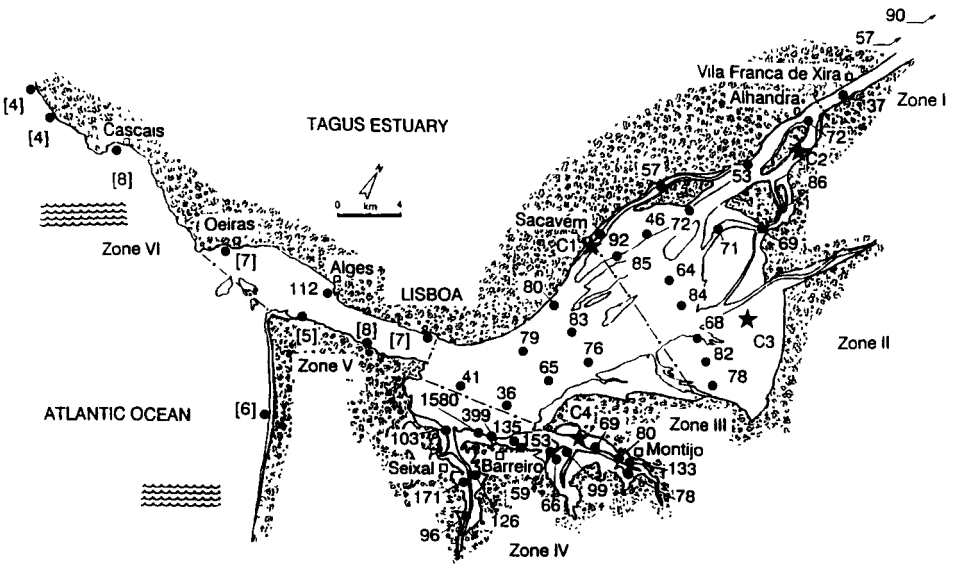

Fig. 1. *^{210}Pb concentrations (Bq kg^{-1} dry weight) in surface sediments (size fraction < 63 μm) of the Tagus estuary. Enhanced levels are restricted to the zone near the outlet of phosphate discharges at the south bank (Carvalho, 1995).*

zones of the estuary (Carvalho 1995). The distribution of ^{210}Po and ^{210}Pb elevated levels in some sediment spots around the Barreiro peninsula, suggests that most of this radioactivity may have been introduced in the past by direct releases of gypsum into the estuary. Nevertheless, the decantation of gypsum in ponds prior to the discharge of waste waters was the procedure followed, most of the time, by the manufacturing company. This procedure was effective to the retention of the radionuclides.

Concentrations of ^{210}Po and ^{210}Pb were measured in the seaweed *Fucus vesiculosus*, the barnacle *Balanus spp.*, and the mussel *Mytilus galloprovincialis* collected throughout the estuary. Several surveys were made from 1991 to 1994. ^{210}Po in *Fucus* ranged from 4 to 37 Bq kg^{-1} (dry wt). ^{210}Po concentrations in *Balanus* ranged from 23 to 360 Bq kg^{-1} (dry wt). Concentrations of ^{210}Po in *Mytilus* ranged from 88 to 945 Bq kg^{-1} (dry wt). In general, in these three species no elevated concentrations could systematically be detected in the zone of the estuary receiving the phosphate plant releases. Moreover, the spatial distribution of ^{210}Po concentrations in mussels clearly indicated that higher concentrations were consistently displayed by mussel samples collected at the seashore, outside the estuary. These higher concentrations were not in relationship with any discharges of industrial wastes. Furthermore, similar samples of mussels collected in different months showed varying concentrations and suggested important temporal fluctuations of ^{210}Po in mussels.

Therefore, a research programme was implemented in order to define the baseline levels and seasonal fluctuation of ^{210}Po and ^{210}Pb in mussels. Results of ^{210}Po and ^{210}Pb in monthly samples of mussels collected always at the same site on the coast (outside the estuary) indicate that ^{210}Po concentrations fluctuate seasonally whereas ^{210}Pb concentrations are relatively constant throughout the year (Carvalho et al, in prep) (Fig. 2). Simultaneous measurements of the radionuclides in sea water, suspended matter, plankton biomass, particulate organic carbon, etc, at the same station allowed the conclusion that ^{210}Po concentration in mussels is related to the annual reproductive cycle of mussels. Among sites, ^{210}Po concentrations in mussels may also differ substantially due to food availability and growth of mussels as reflected in the condition index of mussels (Carvalho et al, in prep.). Taking this into consideration, ^{210}Po concentrations measured in mussels from the Tagus estuary were lower than in coastal mussels, and are interpreted as a result of faster growth and accumulation of reserve lipids by estuarine mussels. These results have important implications to environmental monitoring programmes based on the analyses of mussels, namely on sampling procedures, selection of individual specimens, and relationship between

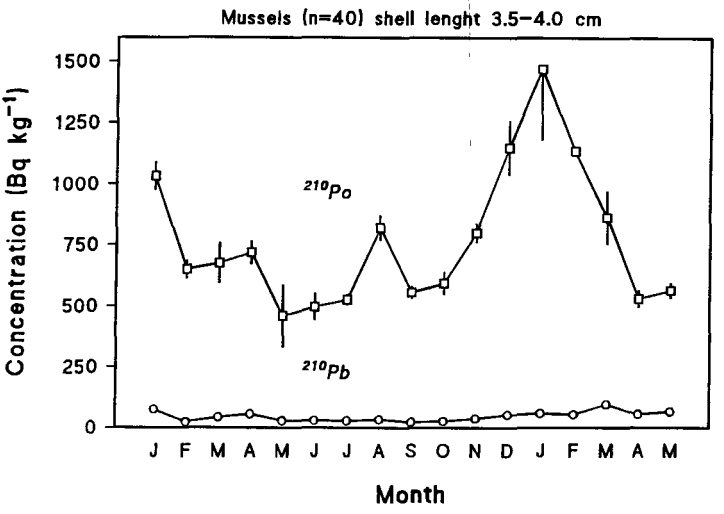

Fig. 2. Concentrations of ^{210}Po and ^{210}Pb (Bq kg^{-1} dry weight) in the soft tissues of mussels collected at the Atlantic coast of Portugal.

radionuclide concentrations and the condition index of mussels (Carvalho et al, in prep.).

Based on analyses of the Portuguese diet, the average individual intake of ^{210}Po and ^{210}Pb in the Portuguese population was estimated respectively at 1.2 and 0.47 Bq d^{-1}. Sea food contributes to about 70% of the ^{210}Po ingested with the diet, whereas cereals, vegetables and meat contribute to 79% of the ^{210}Pb ingestion (Carvalho, in press). Concentrations of ^{210}Po and ^{210}Pb were determined in shrimp, crabs, mussels and fish collected in the estuary of the Tagus (Carvalho et al, 1992). The concentrations of these radionuclides vary significantly with the species analyzed, but do not differ from concentrations determined in similar marine species from coastal zones. Therefore, the consumption of sea food from the Tagus estuary would hardly contribute to elevate the intake of ^{210}Po and ^{210}Pb in comparison to sea food from coastal areas.

Based on the results of this project several conclusions can be made:

1. Wastes from the production of phosphoric acid contain natural radionuclides (^{226}Ra, ^{210}Pb, ^{210}Po) in concentrations of about 0.6-1 kBq kg^{-1}. In the case of the industry located at the south bank of the Tagus estuary, most of the phosphogypsum was, in general, decanted and stockpiled on the river bank before the discharge of waste waters into the estuary. This procedure seems to have been effective to prevent the enhancement of the natural radioactivity levels in the estuary. Enhanced radioactivity levels were detected only in sediments collected near the waste water discharge.
2. Although the production of phosphoric acid in this plant has been discontinued in 1991, the stockpiles of phosphogypsum at the river bank continuously release radionuclides which are transported by surface runoff into the estuary. Radionuclides dissolved by rain water, in particular ^{210}Po and ^{210}Pb, are however rapidly scavenged by suspended particles and accumulate with the bottom sediments.
3. After the shut down of phosphoric acid plant, no enhancement of ^{210}Po and ^{210}Pb levels could be detected in seaweeds, barnacles, mussels, shrimp and fish, that could be attributed to discharges of phosphated wastes. Marked seasonal fluctuation of ^{210}Po in mussels and different concentrations of ^{210}Po in mussels collected at different sites in the estuary and at the coast, were found to relate with the condition index of mussels rather than to radionuclides in industrial waste discharges. The seasonal fluctuation of ^{210}Po and ^{210}Pb concentrations in bioindicators may render difficult the evaluation of any enhancement due to industrial wastes.
4. The biogeochemistry of polonium and lead in the estuarine environment and in particular in estuaries with extended salt-marshes, such as the Tagus, is poorly known.

Radionuclides added by wastes from industrial activities will distribute and cycle in this environment likely in the same manner as naturally-occurring nuclides do. However, sound predictions to the fate and behaviour of those radionuclides on the long term can not be made.

References

Carvalho, F.P., Alberto, G. and Oliveira, J.M., ^{210}Po, ^{210}Pb and uranium in the estuaries of Tagus and Mira rivers (Portugal). Impact of releases from phosphate industry. LNETI/DPSR-A-No.4, III SERIE, 1992.

Carvalho, F.P., ^{210}Pb and ^{210}Po in sediments and suspended matter in the Tagus estuary, Portugal. Local enhancement of natural levels by wastes from phosphate ore processing industry. *Sci. Total Environ.* 159 (1995) 201-214.

Carvalho, F.P. (in press). Polonium-210 and Lead-210 intake by the Portuguese population. The contribution of sea food in the dietary intake of ^{210}Po and ^{210}Pb. *Health Physics*.

Carvalho, F.P., Oliveira, J.M., Alberto, G. (in prep). Seasonal fluctuation of ^{210}Po and ^{210}Pb in marine mussels.

Head of project 6: Dr. M. García-León

I. Introduction

It is well known that the operation of phosphoric acid industries provokes, in some cases, a clear contamination of natural radionuclides, at least, in their close environment. These industries use phosphate mineral as raw material which due to geological reasons can contain large amounts of U. The fertilizer complex located at the Southwestern Spain (Huelva) uses phosphate rock imported for some north Africanian countries (Marroco, Togo, and Senegal). This rock has a sedimentary origin which, in contrast to igneous rocks, can contain U concentrations ranging from 50 to 300 ppm.

Processing of this mineral to obtain phosphoric acid, produce a large amount of liquid and solid wastes (phosphogypsum) which are, in general, released to the close environment. The south spanish fertilizer complex is located near an estuarine system compounded by two rivers (Odiel and Tinto rivers) which have a common mouth into the Atlantic Ocean and an important biologically wet Marshland affected by the income of the Odiel waters. A large amount of solid wastes are stored in uncover piles at the border of the Tinto river (see Fig. 1), while the liquid wastes (very acid) and part of the phosphogypsum are directly released into the Odiel river channel nearby the industries. These wastes, with high amounts of natural radionuclides, provoke the distribution of the contaminants along the river. The scenario has been studied by the University of Sevilla group since the last 8 years. We present here the results obtained according to the objectives planned within the project FI3P-CT92-0035 developed during the last three years.

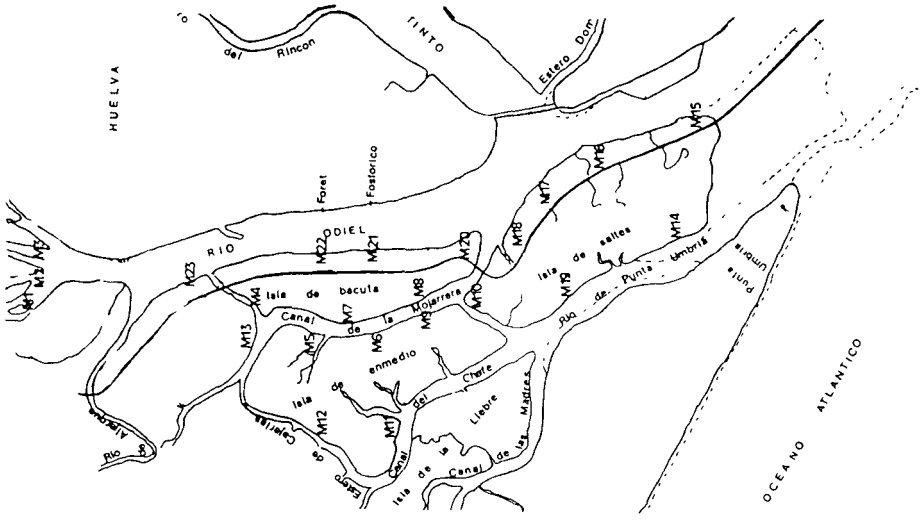

Fig. 1; Map of the studied area located near the city of Huelva at the south of spain

II. Objectives of the project

1. - To extend previous works on the presence of natural radionuclides in the Odiel and Tinto river channels to the case of $^{210}Pb(^{210}Po)$. Within this objective a mathematical model has been developed which simulate the dissemination of ^{226}Ra and ^{210}Pb along the Odiel river.

2. - To evaluate the influence of the phosphoric acid factories operation on the Odiel wet

marshland (see Fig. 1). Being such area a natural reservation, has a high environmental relevance. The following task were undertaken to carry out this objective

- to determine natural radionuclides in surface soil samples collected in the marsh during two sampling campaigns. A similar work was carried out at the Guadalquivir marsh, not affected by radioactive contamination, for the sake of comparison.
- to measure the depth distribution of natural radionuclides in soils from the Odiel marsh, as a first step to study the temporal distribution of the radioactive contamination.
- to measure selected metals in soil samples. Such metals are known to be clearly associated to the phosphate rock mineral. Their presence in the environment should represent a fingerprint of the impact of the phosphoric acid production.
- to determine natural radionuclides in plant estuarine species, so as start studies on pathways in the biosphere.

III. Progress achieved including publications

Summary to accomplish the above mentioned objectives three sampling campaigns were performed. Surface soil samples from the Odiel marsh were collected in March 1993 (13 soils) and November 1993 (23 samples). Additionaly Spartina Densiflora and Spartina Maritima species were collected in the same locations. The latter specie could not be collected in all stations. Moreover, 7 soil surface samples from the Guadalquivir marsh were collected in December 1994 for comparison with data obtained in the Odiel marsh. Finally, 10 cores from the Odiel marsh were collected at the same campaign. The cores were separated into 8 layers of 3.3 cm thickness. Determinations of density and water and organic content were performed in all soil samples.

^{210}Po was determined in all samples by α-spectrometry with ion-implanted detectors. ^{210}Pb, ^{226}Ra and other natural radionuclides were determined by γ-spectrometry. For this sake, a reverse biased Germanium (REGE) detector was used. Finally, heavy metals in soil samples were determined by PIXE.

1. Odiel and Tinto rivers

Samples collected in 1990 and 1991 were analyzed for ^{210}Pb. In each campaign 7 stations at the Odiel river and 4 at the Tinto river were sampled for water and sediments.

Water samples

The levels of ^{210}Pb in the Odiel river area under study range from 3.7±0.5 to 289±22 mBq/l with the maxima, in summer and in winter, in front of one of the fertilizer industries. The levels decrease quickly downstream from such a point. This activity pattern is similar to those obtained for other radionuclides in previous works and identifies the presence of a local source of activity. The levels found in summer are clearly higher than those found in winter, probably due to a lower water stream flow of the river in the dry season. A non constant input of radioactivity from the source can also explain such a differences. In the case of the Tinto river the levels along the channel are quite constant, ranging from 17.0±1.5 to 26.6±3.0 mBq/l, with a slight decrease downstream the channel. All data seem to be higher than 1 mBq/l given as the background level, reflecting either an enhanced along all the area or that a different background level for South Spain should be considered.

Sediment samples

7 bottom sediments from the Odiel river of each year were separated into four different fractions. The small fraction ($\leq$63 μm) was analyzed for ^{210}Pb determinations in both set of samples. Additionally another fraction (size between 63μm and 355 μm) was analyzed for ^{210}Pb in the 1991 set of samples. The activity levels in the $\leq$63 μm fractions range from 8.0±0.7 to

799±49 mBq/g in the Odiel river, without differences between seasons. Only in two sampling points (upstream from the industries) the level of ^{210}Pb falls in the non enhanced range (100 mBq/g) with 8.0±0.7 and 40.9±2.7 mBq/g respectively. The rest of sampling points are clearly enhanced during both seasons. Comparing both fractions analyzed for ^{210}Pb in the campaign of 1991, the same conclusions are extracted as with the analysis of the complete samples, the levels being quite similar.

In the Tinto river the levels range from 33.1±3.3 to 233±9 mBq/g in the $\leq$63 μm fraction for both years. Again, no differences between fractions were found.

In general, no correlations between ^{210}Pb content and organics were found for both rivers, and the activity pattern obtained is similar to those obtained for other nuclides in previous years.

Modelling radionuclides dispersion in the Odiel river

A mathematical model to study the dispersion of ^{226}Ra and ^{210}Pb in the Odiel river has been developed. As a first approach, these radionuclides have been considered as conservatives substances, remaining in solution. Thus, their dispersion is governed by advection and diffusion processes. To solve the advective-diffusive dispersion equation the instantaneous water state (water velocities and water displacements from the mean level) must be known. The water state is obtained by solving the depth-averaged hydrodynamic equations. A spatial and temporal discretization of the Odiel river has been carried out so as to solve the equations by using a finite differences technique. Resolutions of the model are 100 m and 6 s. The model has been applied to study the experimental activity concentrations measured along the river for two sampling campaigns performed during 1990 and 1991. The general behaviour of ^{226}Ra and ^{210}Pb is reproduced by the model, both for the samples collected during high and low water each sampling campaign.

Nevertheless, all substances interact with the solid phases (suspended matter and sediments) showing, to a more or less degree, a non-conservative behaviour. Thus, the ionic exchanges among the phases must be taken into account in order to improve the model predictions when studying the dispersion of radionuclides in aquatic environments more realistically.

Four phases are considered in our model: water, suspended matter and two grain size fractions of sediments, a small and a large grain size fraction. Only the small grain size fraction can be resuspended and incorporated to the water column as suspended matter, then the resuspension and deposition processes produce an exchange of radionuclides between suspended matter and the small grain size fraction of the sediment. On the other hand, radionuclides in water and suspended matter can be transported along the river by advection and diffusion processes. Finally, the water is in contact with the other three phases, thus an ionic exchange takes place between them. Of course, external sources of radionuclides are introduced in the point where they exist.

2. The Odiel Marsh

Surficial soils

Two sampling campaigns were performed across the Odiel marsh. During the first one, February 1993, 13 soil samples were collected. The samples were taken during the low tide in areas covered by water during high tide. The complete sample was analyzed for ^{210}Po, ^{210}Pb and ^{226}Ra. The distribution of activities across the marsh was found to be the same for all the above mentioned radionuclides and globally reflects the tidal pattern intrusion of Odiel river waters into the marsh. Its shows a clear radioactive impact of the factories operation into the marsh as well. It was found samples with levels below 50, 100 and 20 mBq/g for ^{210}Po, ^{210}Pb and ^{226}Ra respectively, but the majority presented higher concentrations and an important group

even above 260, 480 and 300 mBq/g for such radionuclides. The former were located along the Chate channel and the Punta Umbria river whereas those enhanced are mainly located along the Mojarrera channel and east of the Saltés island (see Fig. 1). All that supporting the previous conclusion.

A second sampling campaign was performed in November 1993. Now, 20 surface soil samples were collected as well as 3 additional samples from the Northern marsh in the Odiel river, upstream the industries. The general conclusions obtained with the previous results apply here, confirming the impact of the factories on the marsh, which can be clearly observed in Fig. 2, which shows the ^{210}Po and ^{210}Pb concentrations in mBq/g in all stations. It is interesting to notice, however, that samples from the Northern marsh contained levels well above 600, 700 and 600 mBq/g for ^{210}Po, ^{210}Pb and ^{226}Ra respectively. The reason for a such clear enhancement resides on the influence of the Odiel river which distributes radioactivity according to tidal movements.

For the sake of comparison we collected some soil samples from the Guadalquivir marsh area, which is supposed not to be affected by any local source of radioactivity contamination. There are no special variations in the radioactivity concentrations for several radionuclides. For instance, the mean activities found for ^{210}Po, ^{238}U, ^{232}Th and ^{230}Th are respectively 24.4, 9.5, 21.5 and 27.8 mBq/g similar to the world mean average given by UNSCEAR 1988. Being that marsh close to that of the Odiel and of similar characteristics it is concluded that the operation of the phosphoric acid production factories clearly affect also the Odiel marsh area.

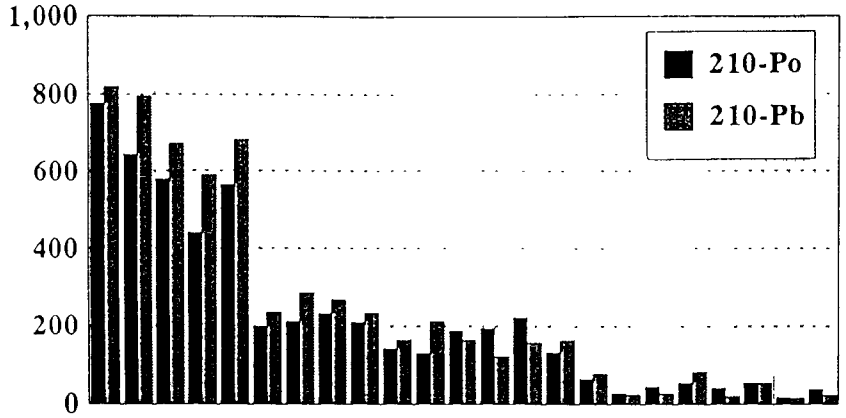

Fig. 2; Concentration in mBq/g of ^{210}Po and ^{210}Pb in soil samples from the Odiel marsh

Radioactivity depth distribution

It is interesting to study the radionuclide concentration distribution in depth as a preliminary step to assessing the time evolution of the contamination found at the marsh. For that, 10 soil cores, 26 cm depth, were collected during December 1994.

They were splited into 8 layest 3.3 cm thick. ^{210}Po was determined in the different layers. The activity profile varies depending on the location. Thus, it is possible to get profiles where ^{210}Po activity resides essentially on the first layer decreasing steadily with depth until reaching values similar to those obtained in the Guadalquivir marsh. Besides that, it is posible to obtain profiles where high ^{210}Po activities, up to 400 mBq/g, are found until the first 20 cm, reflecting that the contamination affects the soil also in depth. On the other hand, it appears uniform profiles

where ^{210}Po activities in all layers are well consistent with those found in the Guadalquivir marsh soils.

It is clear that effects such a differents sedimentation rates, underwater intrusion of radioactivity from the Odiel river, compacity, etc, affect the form of the activity profiles. Consequently, it is not easy at the present stage of the work to extract definitive conclusions. Nevertheless the obtained results address to a very interesting research work. They provide with a first tool to help assessing the temporal evolution of the radiological impact from the industries.

Heavy metals

The PIXE method was used to determine the presence of selected elements in soils from the Odiel marsh. They are all known to be present at high concentrations in the phosphate rock. Consequently, they should be redistributed along the studied environment as the radionuclides are.

In general, it is clear that the analyzed soils contain important amounts of some relevant elements. Thus, up to 30000 ppm and 2500 ppm of P and As respectively was found with a pattern distribution very similar to that of radionuclides shows in Fig. 2. Furthermore, most soils were found to be contaminated by Pb, Fe, Zn and Cu. The case of S is also interesting with concentrations in the Northern marsh of around 40000 ppm.

Correlations studies among the different elements and radionuclides concentrations have been carried out. The results reveal that P and As are well correlated between them and at the same time with natural radionuclides and stable Pb. The results for Cu, Fe, Zn and S are not so clear.

It seems, therefore, that phosphate industries are also sources of environmentally relevant elements to their, at least, close environment, as P, As and stable Pb.

In addition, the obtained results confirm all our conclusions on the range and extent of the radioactive impact from the phosphate industries, since heavy metal concentrations provide with clear fingerprint of such impact.

^{210}Po and U isotopes in Spartina Densiflora and Maritima

23 Spartina Densiflora plants were taken from the same sampling stations as the surficial soil samples (November 1993). The roots of the plants were separated as soon as posible and ^{210}Po and U isotopes were determined in the rest of the plant. The activities range, in general, from 5.58 ± 0.41 to 55.1 ± 2.8 mBq/g for ^{210}Po and from 2.16 ± 0.23 to 42.6 ± 2.7 mBq/g for ^{238}U. The pattern distribution of radioactivity concentrations in the plants follows that of the soils. However, there is not a clear separations in activity concentrations between areas as was found in the case of soils. The $^{234}U/^{238}U$ activity ratio reveals, in general, the existence of secular equilibrium or a slight excess of the daughter isotope. Spartina Maritima could be sampled only from 9 stations. The levels range from 5.86 ± 0.45 to 43.4 ± 2.1 mBq/g for ^{210}Po and from 3.01 ± 0.42 to 49.6 ± 3.1 mBq/g for ^{238}U. From the obtained results it is concluded that again the radioactivity concentrations in the plants seems to reflect that of the soils. Again, the $^{234}U/^{238}U$ activity ratios reflect the secular equilibrium or excess of the daughter isotope.

The concentration factors, defined as the quotient between radioactivity concentration in plant and soils, for ^{210}Po and ^{238}U were calculated. Concentration factors for ^{210}Po ranging from 0.013 to 0.460, with a mean value of 0.130 were found. However, it is interesting to notice that considering the three different areas, different concentration factors can be found. Thus, the highest values appear in stations with the lowest concentrations in soils, and the lowest in stations with the highest concentrations in soils. If we consider each zone separately, the mean concentration factors is 0.27 in the non enhanced area, 0.057 in the intermediate levels area and 0.047 in the enhanced area. In the case of ^{238}U the experimental concentration factor range from 0.017 to 0.160, with a mean value of 0.066. We also find different values in each zone, with mean values of 0.094 in the non enhanced area, 0.055 in the intermediate levels area and 0.029 in the

enhanced area. Thus, it seems that the concentration factor is a non constant parameter and depends on the concentration of the radionuclide in the soil. This effect can be clearly observed in Fig. 3 which shows the CF for ^{210}Po in Spartina Densiflora versus the concentration of ^{210}Po in mBq/g in the underlying soil.

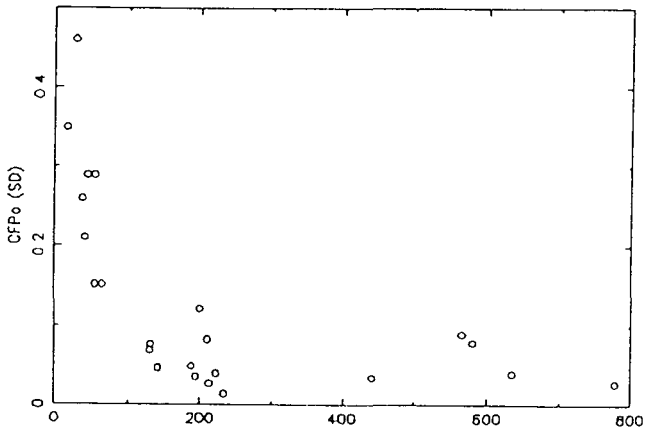

Fig. 3; Concentration factors versus ^{210}Po (mBq/g) in soil for S. Densiflora

Publications

-A. Martínez-Aguirre, M. García-León and M. Ivanovich. "The distribution of U, Th and ^{226}Ra derived from Phosphate fertilizer industries on an estuarine system in Southwest Spain". J. Environm. Radioactivity 22 (1994) 155-177.

-A. Martínez-Aguirre, M. García-León and M. Ivanovich. "Identification and effects of anthropogenic emissions of U and Th on the composition of sediments in a river/estuarine system in Southern Spain". J. Environm. Radioactivity 23 (1994) 231-248.

-A. Martínez-Aguirre, M. García-León and M. Ivanovich. "U and Th distribution in solution and suspended matter from rivers affected by the phosphate rock processing in Southwest Spain". Nucl. Instrum. Methods Phys. Research A 339 (1994) 287-293.

-M. García-León, A. Martínez-Aguirre, R. Periañez, J.P. Bolivar and R. García-Tenorio. "Levels and behaviour of natural radioactivity in the vecinity of phosphate fertilizer plants". Fifth International Conference on Low-Level Measurements of Actinides and Long-Lived Radionuclides in Environmental and Biological Samples, Aomori (Japan), July 1994.

-A. Martínez-Aguirre and M. García-León. "^{210}Pb enhancements in rivers affected by the phosphate rock processing at the South of Spain". International seminar on Freshwater and estuarine radioecology, Lisbon, March 1994. It will appear in Science of the Total Environment.

-R. Periañez and M. García-León, 1993. "Ra-isotopes around a phosphate fertilizer complex in an estuarine system at the southwest of Spain". J. Radioanal. Nucl. Chem. 172, 71-79.

-R. Periañez, J.M. Abril and M. García-León, 1994. "A modelling study of ^{226}Ra dispersion in an estuarine system in South-West Spain". J. Environ. Radioactivity 24, 159-179.

-A. Martínez-Aguirre and M. García-León. "Distribution of ^{210}Pb in water and sediments enhanced by the phosphate fertilizer production". Submitted to J. Applied Radiation and Isotopes.

-A. Martínez-Aguirre and M. García-León. "Radioactive impact of the phosphate ore processing in a marshland in southwest Spain". Submitted to J. Environ. Radioactivity.

-A. Martínez-Aguirre and M. García-León. "Transference of natural radionuclides from soils to plants in a wet marshland". It will be presented at the ICRM'95 Conference on Low Level Measurement Techniques, Seville, Spain, 2-6 October 1995.

-I. García-Orellana, A. Martínez-Aguirre and M. García-León. "Enhanced levels of U and Th in soils from a marshland at the Southwestern Spain". It will be presented at the ICRM'95 Conference on Low Level Measurement Techniques, Seville, Spain, 2-6 October 1995.

-A. Martínez-Aguirre, M. García-León, C. Gascó and A. Travesí. "Anthropogenic emissions of ^{210}Po, ^{210}Pb and ^{226}Ra in an Estuarine Environment". In preparation.

Head of project 7: Mr. D. Pollard
Reporting scientist: Dr. T.P. Ryan

II Objectives for the Reporting Period

(a) to examine the spatial distribution of ^{210}Po in mussels around the Irish coast paying particular attention to areas with an historic involvement in phosphate ore processing industries;
(b) to characterise the Irish coastal environment in terms of concentration of ^{210}Po in water, suspended material, seaweed and sediment;
(c) to determine temporal fluctuations in ^{210}Po concentrations in mussels at a selected number of sites;
(d) to assess, where appropriate, the effects of the fertiliser industry on ^{210}Po concentrations in environmental compartments;
(e) to assess the dose due to ^{210}Po arising from the consumption of fish and shellfish produce caught in Irish waters;
(f) to determine the concentration of ^{210}Pb in air at a selected number of sites on the island of Ireland and
(g) to examine, if possible, the historical pattern of releases of phosphogypsum by studying ^{210}Pb and ^{226}Ra profiles in sediment cores.

III Progress Achieved

^{210}Po in Mussels and Sea Water

Mussels were collected from 27 locations around the island of Ireland between March 1993 and February 1995 (Figure 1). Where possible, mussels in the size range 5.5 - 6.5 cm were taken. A subset of the 27 locations were sampled more than once with the site at Sutton being sampled some 21 times providing a high resolution time series data set.

^{210}Po concentrations in mussels were found to range between 80 ± 9 Bqkg^{-1} at Seapark near Belfast to 459 ± 26 Bqkg^{-1} at Dunquin on the Dingle Peninsula. The mean concentration throughout the Island over the sampling period was found to be 196 ± 81 (1 S.D.) Bqkg^{-1}. Expressing ^{210}Po activities in terms of body content (Bq/mussel), the concentrations were found to range between 0.052 Bq mussel^{-1} at Arklow to 0.336 Bq mussel^{-1} at Achill. The mean $^{210}Pb/^{210}Po$ ratio in mussels was 0.06 over the sampling period with 94% of the polonium unsupported.

^{210}Po was measured in sea water and suspended particulate taken from 10 locations around the country. Concentrations in filtered sea water (excluding the Sutton site) ranged between 0.21 ± 0.08 mBql^{-1} at Carlingford to 1.05 ± 0.13 mBql^{-1} at Ringaskiddy (Table 1). Concentrations on suspended material ranged between 2.8 ± 0.2 mBql^{-1} at Carlingford to 43.5 ± 1.7 mBql^{-1} at Ringaskiddy. However, the correlation between ^{210}Po concentration in filtered water and on suspended load was poor ($R^2 = 0.29$). Considering the 9 sites where water samples were taken, excluding Sutton, the correlations between ^{210}Po concentration in mussels and ^{210}Po in filtered sea water and suspended material were poor with R^2 values of 0.24 and 0.19 respectively. Between 2 and 10% of ^{210}Po was found in the filtered fraction (< 0.45 μm).

Water samples were taken monthly from Sutton between October 1993 and February 1995. ^{210}Po concentrations in the filtered fraction were found to range between 0.19 mBql^{-1} and 1.96 mBql^{-1}. The concentration on suspended material ranged between 0.95 mBq/l and 4.33 mBql^{-1}. No obvious temporal trends were observed (Figure 2). The correlation between ^{210}Po concentration in the filtered sea water and on the suspended material was weak (R^2 = 0.003, n= 10). Interestingly, the ^{210}Po concentration on suspended material, expressed in mBql^{-1}, correlated well with the mass of material in suspension (Fig. 3).

The difficulties surrounding the analysis of ^{210}Po in filtered water are non-trivial and some of these are explored in an intercomparison exercise between the RPII and the laboratories of the IPSN, a report of which is appended to the final report.

^{210}Po in Seaweed, Sediment, Sediment Cores and Fish

Seaweed (predominantly *Fucus vesiculosus*) was sampled at 21 sites around the coast of Ireland (Table 1). ^{210}Po concentrations in the seaweed varied between 3.8 ± 1.1 Bqkg^{-1} at Seapark near Belfast to 75 ± 12 Bqkg^{-1} at Glenbrook near Cork, the latter being a significant outlier. With some notable exceptions, the ^{210}Pb/^{210}Po ratio approximated unity. ^{210}Po concentrations in sediment varied between 3 Bqkg^{-1} at Arklow to 59 Bqkg^{-1} at Fota Bridge near Cork. In general, the Cork area had higher concentrations of ^{210}Po in sediment than any other.

It was proposed to collect a sediment core from a site which was used for the disposal of phosphogypsum to build an historic record of the discharges. However, due to the nature of the areas into which the gypsum had been discharged and the frequency of dredging activities in these areas, it was not possible to find a suitable sampling location in the time allotted.

A total of six fish and crustacea species were sampled from the main Irish landing ports in the coarse of the study. ^{210}Po concentrations tended to be an order of magnitude lower than for mussels with the concentration in prawns, on average elevated above the rest (Table 2). Plaice tended to have higher concentrations than cod, whiting, ray or mackerel and this may reflect a particular dietary preference.

Where possible, additional measurements were made at each sampling location for the purpose of testing correlations. These measurements included: pH, salinity, suspended material, dissolved material, nutrient phosphate, nitrate, silicate and particle fractionation. In the case of mussels, biometric data such as shell length, shell weight together with fresh and dry weights were recorded. ^{210}Pb concentrations in air were recorded at a number of locations throughout the country and were found to range between 0.14 mBqm^{-3} and 0.36 mBqm^{-3} with a mean concentration of 0.22 mBqm^{-3}.

IV DISCUSSION

An index of mussel condition was estimated for each sample reflecting the biological activity of the animal. When all sites were considered together, little correlation was found between condition index and ^{210}Po concentration (R^2 = 0.16) or body content (R^2 = 0.21). The correlation coefficient for mean mussel dry flesh weight versus polonium body content (Bq mussel^{-1}) was found to be R^2 = 0.63. While there are many perturbing factors such as differences in ^{210}Po water concentrations at different locations, there is a general trend in evidence of increasing body content with increasing body size. This reflects the simple fact that bigger mussels generally contain more polonium than smaller ones.

Little correlation was found between ^{210}Po concentration and: (i) shell length (R^2 = 0.21); (ii) shell weight (R^2 = 0.22) and mean dry flesh weight (R^2 = 0.30). Correlations with

physical parameters pertaining to sampling sites such as salinity, pH and nutrient content (phosphates, nitrates and silicates) proved to be insignificant. Similar tests were performed for the data at Sutton and the only significant correlation found was between mean ^{210}Po body content and mean dry flesh weight (R^2 = 0.76, Figure 4). Removing one outlier increased the R^2 value to 0.93. This relationship was observed at a second site (Carlingford) and underlines the observation that larger mussels contain more polonium than smaller ones. The correlation between polonium concentration (Bq/kg) and mussel sizes was found to be poor both in the general study and in the study at Sutton when all of the data is considered. But when a number of mussel size classes were sampled at the same time, then smaller mussels tended to have higher concentrations (Bq/kg) than larger ones.

Temporal Trends in Mussels and the Impact of the Phosphate Industry

Mussels were sampled on two occasions separated in time by 8 to 10 months from Creadan Head, Arthurstown, Fota Bridge, Ringaskiddy, Dunquin and Cultra. The second sampling at Creadan Head and Arthurstown had lower concentrations than on the previous occasion with Cultra slightly elevated and the remaining indistinguishable from the original analysis. Mussels were sampled on three occasions from Carlingford and concentrations varied between 120 ± 10 Bqkg^{-1} in June 1993 to 206 ± 17 Bqkg^{-1} in April 1994.

The ^{210}Po in mussels sampled monthly from Sutton between June 1993 and February 1995 in the size range 5.5 - 6.5 cm, varied from a minimum of 156 ± 11 Bqkg^{-1} in February 1994 to a maximum of 378 ± 20 Bqkg^{-1} in June 1994 (Figure 5). The high June 1994 value contrasts with the June 1993 concentration of 172 ± 15 Bqkg^{-1} and is not explained by loss of mussel body weight. No obvious cyclical effects were observed at Sutton which might be correlated to the mussels reproductive cycle. This may be due to the specific nature of the mussel bed at Sutton and the complexity of perturbing environmental factors.

The concentrations of ^{210}Po found in Belfast Lough ranged between 80 ± 9 and 136 ± 10 Bqkg^{-1}. Although there was a history of phosphogypsum discharges into the Lough, the ^{210}Po concentrations in mussels are lower than in most of the other sites examined in the study. This seems to suggest that the phosphogypsum discharges have had little residual effect on the concentration of ^{210}Po in mussels in the Lough. Similarly, six mussel beds were sampled in Cork Harbour and the concentrations in these mussels ranged between 139 ± 14 and 235 ± 14 Bqkg^{-1}. A seventh site was sampled at Myrtleville which is outside the Harbour and further down the coast and mussels had a concentration of 406 ± 31 Bqkg^{-1}. On average, the concentrations found in Cork mussels are higher than those found in Belfast. There was a three month difference in sampling times and this may account for some of the variation. The mean concentration in mussels from Cork at 215 Bqkg^{-1} compared well with the mean concentration in mussels from Waterford at 198 Bqkg^{-1}. The latter site had no history of phosphogypsum discharges. Indeed, much higher concentrations were observed in Dunquin on the Dingle peninsula (459 ± 26 Bqkg^{-1}) which is devoid of heavy industrial activity. While nutrient phosphate gradients were observed both in Belfast Lough and Cork Harbour, correlations with ^{210}Po concentrations in mussels were not significant. It is concluded therefore that given the natural variation of ^{210}Po concentrations in mussels and the absence of any significant correlating parameter, it was not possible to identify any residual effects from the phosphate industry.

Dose to Man

Radiation doses due to the consumption of seafood are estimated by converting the ingested activity using standard conversion factors (Phipps et al. 1991). The activity ingested was obtained from assumed fish and shellfish consumption rates in Ireland. The assumed intake rates of the Irish consumer are for the *typical consumer* - 40g of fish and 5g of shellfish daily and for the *heavy consumer* - 200g of fish and 20 g of shellfish daily. The doses to the typical and heavy consumer were found to be 13 and 58 μSv y^{-1} respectively.

IV CONCLUSIONS

(i) there is a factor of six variation in ^{210}Po concentration in mussels collected around Ireland;
(ii) on average, 94% of the ^{210}Po found in mussels was unsupported;
(iii) the residual influence of phosphate ore producing industries on the concentration of ^{210}Po in mussels and in other environmental compartments such as sediment and seaweed was not detected;
(iv) monthly measurements of concentrations of ^{210}Po in mussels, sea water and suspended material at Sutton did not display any specific cyclical pattern over period of observation with one significantly high concentration occurring in June 1994;
(v) there is a significant relationship between ^{210}Po content and mussel dry weight at a mussel bed at Sutton and Carlingford;
(vi) an estimate of dose from ^{210}Po to the typical and heavy Irish fish and shell fish consumer was made and found to be 13 and 58 μSv y^{-1} respectively;
(vii) between 2 and 10% of the polonium was found to be in the filtered fraction of sea water but this may primarily be a function of turbidity at a given site and
(viii) the mean ^{210}Pb concentration in air over Dublin for the calender year 1994 was 0.22 $mBqm^{-3}$.

REFERENCES

Phipps, A.W., Kendall, G.M., Stather, J.W. and Fell, T.P. (1991). Committed Equivalent Organ Doses and Committed Effective Doses from Intakes of Radionuclides. NRPB-R245.

RPII PUBLICATIONS

Ryan, T.P., Dowdall A.M. and McGarry, A.T. *Mytilus edulis* (L.) as a Bio-Indicator of ^{210}Po in the Irish Marine Environment. Submitted to the Proceedings of Fifth International Conference on Low Level Measurements of Actinides and Long-Lived Radionuclides In Biological and Environmental Samples, Aomori, Japan, July 10-15, 1994.

Ryan. T.P., Dowdall. A.M. and McGarry, A.T. Submitted to the proceedings of International Seminar on Freshwater and Estuarine Radioecology, Lisbon, Portugal, 21-25 March, 1994.

Ryan, T.P., Dowdall, A.M. and Pollard, D. Dose to the Irish Population from ^{210}Po due to the Consumption of Seafood. In preparation.

FIGURE 1: Sampling Locations around Ireland

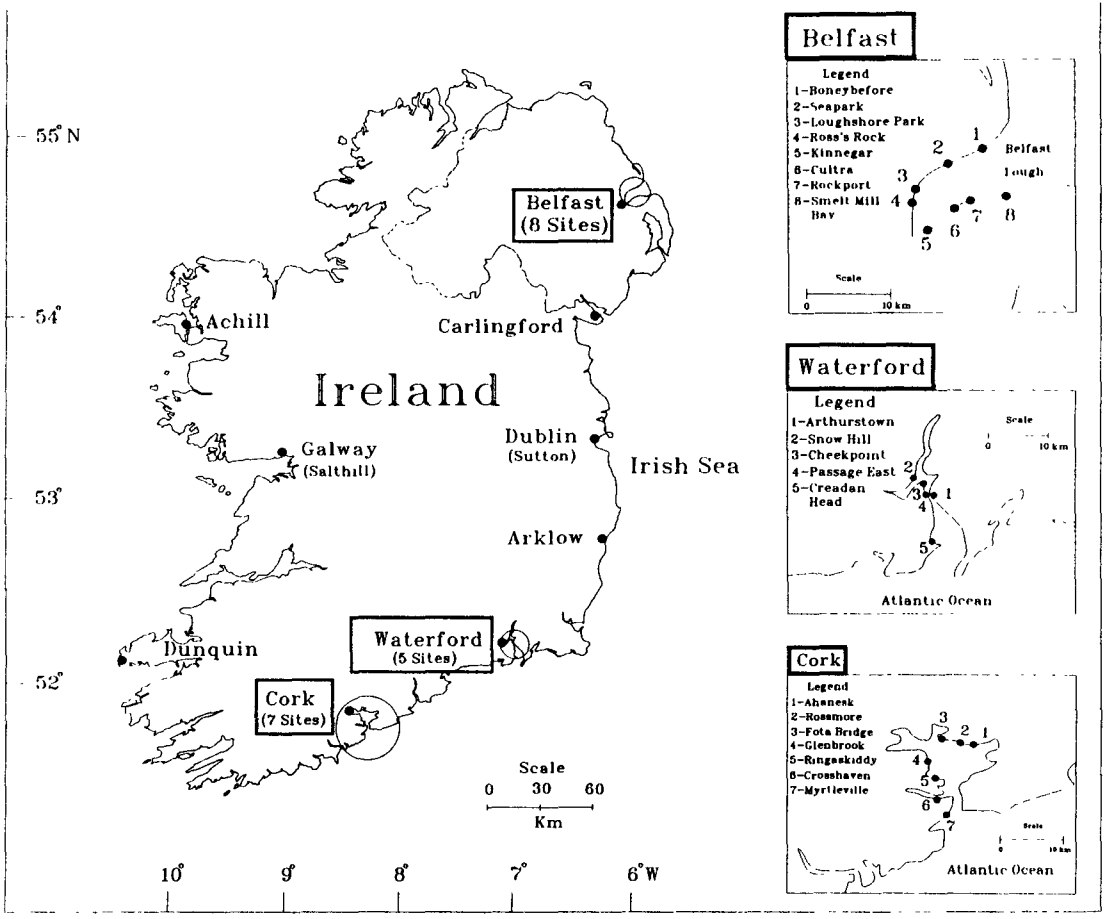

FIGURE 2: Variation of ^{210}Po in Filtered Sea Water ($<0.45\ \mu m$) and on Suspended Material with Time at Sutton

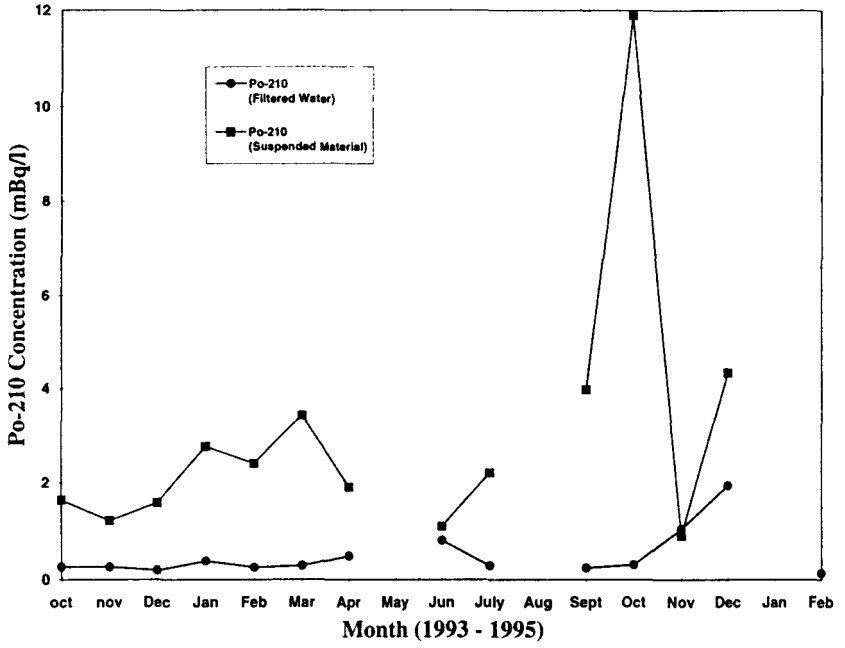

FIGURE 3: ^{210}Po on Suspended Material as a Function of the Quantity of Suspended Material Present at Sutton

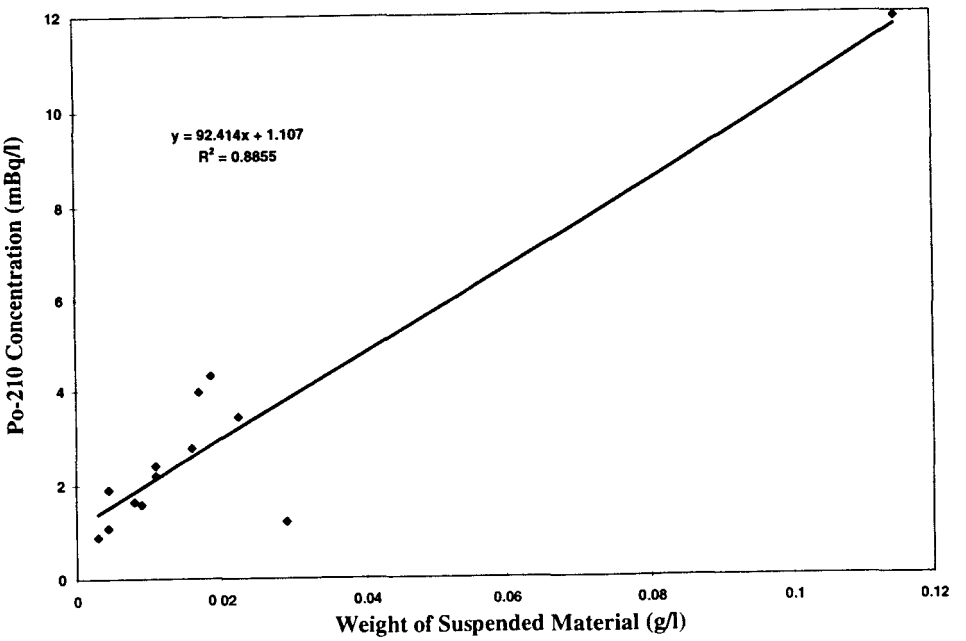

FIGURE 4: ^{210}Po Body Content of Mussels as a Function of Mean Dry Weight at Sutton

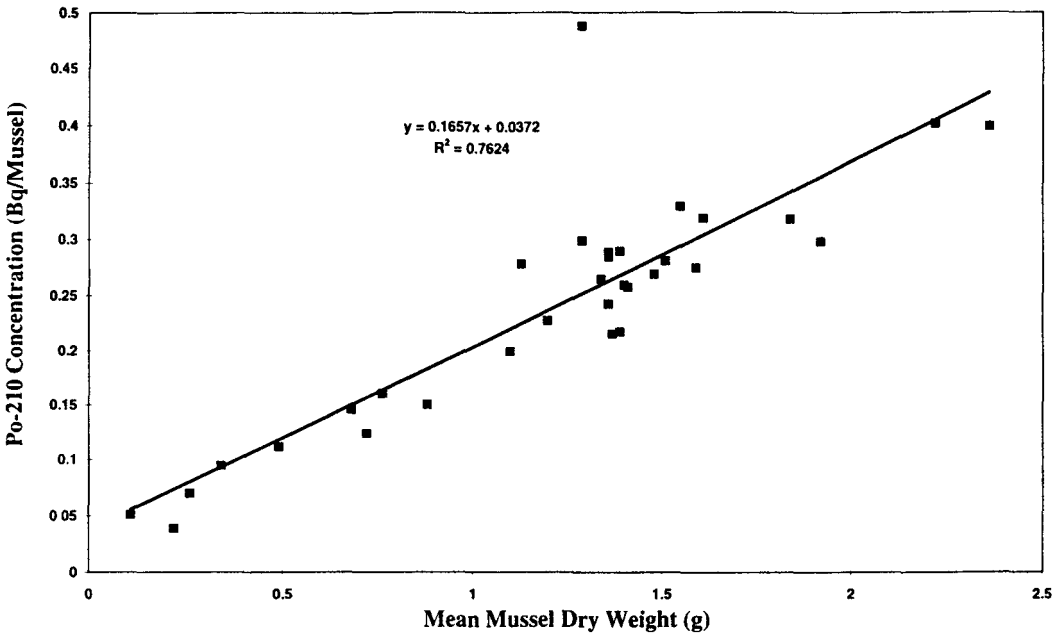

FIGURE 5: Variation in ^{210}Po Concentration in Mussels with Time at Sutton

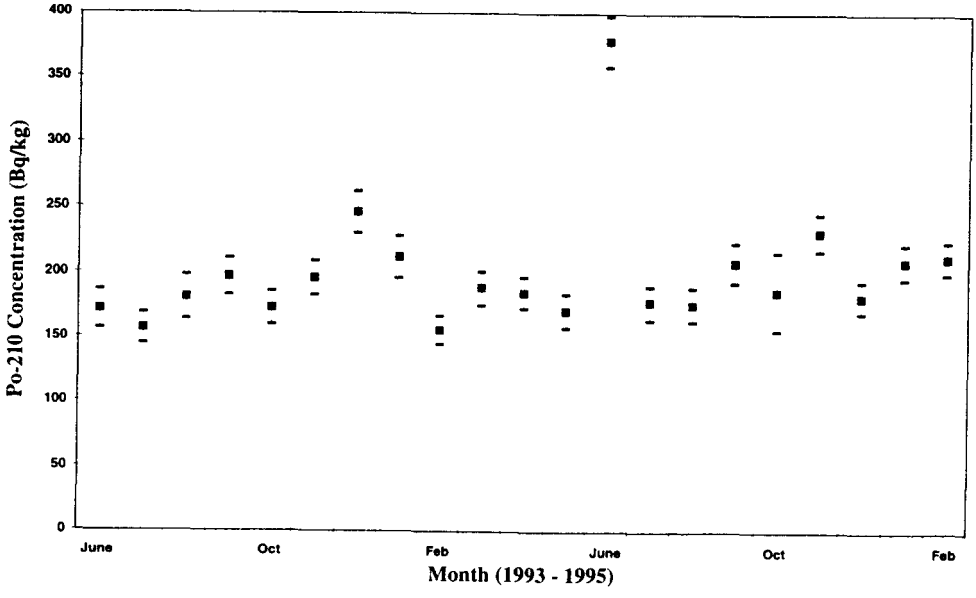

TABLE 1: Polonium-210 Concentrations in Environmental Samples Collected from around Ireland (dry weight).

Location	Date Sampled	Mussel length (cm)	Mussels (Bq/kg)	Seaweed (Bq/kg)	Sediment (Bq/kg)	Water (mBq/l)	S. Load (mBq/l)
WATERFORD							
Cheekpoint	22/3/93	6 1	175±10	10.5±1 4	21.6		
Passage East	22/3/93	6 0	169±11		15.8		
Creadon Head	22/3/93	5 6	226±19	6.7±1 9	16.7		
	25/1/94	5 9	150±9			0 47±0 17	4.5±0 2
Snow Hill	23/3/93	5 8	233±14	6 7±1 4	36 2		
Arthurstown	23/3/93	5.5	187±13	6 2±1.1	13 4		
	25/1/94	5 5	107±16			0.64±012	6.5±0 2
CORK							
Fota Bridge	24/3/93	5.8	148±9	18 8±2.4	58 7		
	26/1/94	6 4	121±20			0.38±0 10	3.4±0.2
Ahanesk	24/3/93	6.3	235±14	12.3±2.0	42.7		
Rossmore	24/3/93	6 0	185±12	9.9±1 6	53.5		
Ringaskiddy	24/3/93	6 4	233±19	15 5±2 3	50 9		
	26/1/94	6 5	211±16			1 05±0 13	43.5±1 7
Glenbrook	24/3/93	6 0	162±12	75±12	46 0		
Crosshaven	25/3/93	6 1	139±14	19.1±2 3	17 6		
Myrtleville	25/3/93	4 7	406±31	28±8	54 3		
DUNQUIN	26/3/93	4 5	459±26	10 8±1.9			
	27/1/94	3 2	446±34				
ARKLOW	17/6/93	3.3	191±13	39±11	2.7		
CARLINGFORD	17/6/93	6.4	120±10	10.4±1 9	25 5		
	10/1/94	6 2	130±9			0.41±0 15	8 0±0 4
	22/4/94	6.3	206±17			0.21±0 08	2 8±0 2
ACHILL	3/3/93	7 1	168±18				
SALTHILL	28/1/94	6 1	157±12	18.5±2 3	14 7	0.50±0 07	12.4±0 4
LOUGH FOYLE	30/6/94	5.6	235±19				
BELFAST							
Ross's Rock	30/6/93	6 2	91±8		9 5		
Boneybefore	30/6/93	6 4	136±10	9.1±1 6	10.4		
Seapark	30/6/93	5 8	80±9	3.8±1.1	17 2		
Loughshore	30/6/93	5 7	124±11	5.5±1.2	12.7		
Kinnegar	30/6/93	6 0	126±12		20.0		
	24/2/94	5 5				0 46±0 23	10 51±
Cultra	30/6/93	5 9	81±9		9 5		
	24/2/94	5 8	123±15			0 16±0 32	5 3±0 2
Rockport	1/7/93	5 8	115±10	5 4±1 4			
Smelt Mill	1/7/93	5 4	132±17	5 2±1 2	5 6		

Table 2: Polonium-210 Concentration in Fish (fresh weight).

Location	Species	Sampling Date	Po-210 (Bq/kg)	Location	Species	Sampling Date	Po-210 (Bq/kg)
HOWTH				**DUNMORE EAST**	Prawns	15/6/94	28 7±3.2
	Whiting	9/11/94	1.1±0 4		Whiting	15/6/94	3 6±0 9
	Cod	9/11/94	10±1		Cod	15/6/94	4 6±1.0
	Plaice	9/11/94	7.5±1 1		Plaice	15/6/94	11 8±2 1
	Ray	9/11/94	0.64±0 43		Ray	15/6/94	2 9±0 7
	Mackerel	9/11/94	3.8±0 7				
	Prawns	9/11/94	12.3±1.5				
GALWAY				**KILLYBEGS**			
	Plaice	9/8/94			Whiting	30/6/94	11 3±1 7
	Whiting	9/8/94	5 5±1 3		Plaice	30/6/94	27 3±2.7
	Cod	9/8/94	4.5±1 0		Ray	30/6/94	1 4±0 5
	Ray	9/8/94	4 3±1 0				
	Prawns	9/8/94	61.5±4 3				

I. Head of project 8: Dr. B. Heaton

II. Objectives for the reporting period.

The main aim of this project concerned the quantification of the levels of Po-210 and Pb-210 in various shellfish species and other environmental samples taken from around the coast of Scotland, with particular emphasis on the seasonal variation in *Mytilus edulis* at one site. As virtually no technologically enhanced natural radionuclides are being emitted from specific sites in Scotland, the shellfish would be used as bio-indicators for assessing the levels and the input into the environment of these radionuclides from purely natural sources

There was a supplementary programme undertaken to realise the levels of Po-210 and Pb-210 within specific tissue parts of shellfish and also some dose assessment work relevant to human consumption of shellfish.

III. Progress achieved including publications.

1) LEVELS OF Po-210 IN SHELLFISH FROM AROUND SCOTLAND

A number of sites around Scotland were selected and shellfish samples taken from them The main sampling site chosen was on the Ythan estuary, approximately 20km North of Aberdeen. Five other sampling sites were chosen, two on the Scottish mainland, two on islands off the mainland and one site approximately 15km offshore.

After the shellfish were sampled, they were held in a seawater aquarium for a period of 48 hours in order for the gut to be purged of any residual matter. This ensured that all measurements reflected the concentration of radionuclides within the animal tissue rather than in food in the gut. The tissue was removed from the shell, weighed, dried at 65°C for 48 hours, homogenised and then two or three aliquots sampled and analysed for Po-210 The resulting solution was stored for at least six months so that Pb-210 could be analysed by way of the in-growth of Po-210 from Pb-210. All activity results for shellfish are for tissue dry weights. Water was analysed after filtration through 0.45μm membrane filters to remove particulate matter which was also separately analysed.

The site at Culbin bar was chosen primarily as a coastal site as no local freshwater outlets existed. This meant that the mussels were only coming into contact with seawater at high tide. It is approximately 100km north-west of Aberdeen and was sampled on two occasions, in May and June of 1994. On the first occasion two batches of mussels were sampled, one containing mussels measuring between 3-4 cm and the other between 6-7 cm in length. The small mussels gave a reading of 228.1 Bq/kg for Po-210 dry weight and the larger mussels, 406.6 Bq/kg dry weight. Filtered water gave a result of 18.9 mBq/l and particulate matter a result of 64.8 Bq/kg. On the second sampling occasion, approximately 70 mussels were sampled so as to get a size stratified sample. The mussels were then divided up into size categories and analysed (results in Table I). The results were for 3-4 cm mussels - 280.4 Bq/kg, 4-5 cm mussels - 342.0 Bq/kg, 5-6 cm mussels -

346 9 Bq/kg and 6-7 cm mussels - 259.0 Bq/kg. Levels of Po-210 in filtered water and particulate matter were 1.76 mBq/l and 35.74 Bq/kg respectively. These results show a steady increase in Po-210 activity corresponding to increasing mussel size except for the activity in the largest group which has the lowest activity of all. One explanation for this may be that as only a small number of mussels were pooled into this group a significant error in the Po-210 activity arose. However it is more probable that the difference is due to seasonal variations, climatic change, tidal variations, etc. It should be noted that the levels of Po-210 in pre-filtered water and particulate matter also decrease from May to June and this variation may have also been caused by the above changes.

Mussels were also sampled from a coastal site on Arran, a small island off the West coast of Scotland, in June 1994. Thirty mussels, between 3-4 cm in length, gave a result of 99.6 Bq/kg which was the lowest result recorded for Po-210 in shellfish in Scotland However these mussels were taken from a relatively high point on the shore so they probably only spent a short amount of time submersed by the tide.

Another site, picked in order to obtain shellfish from all around Scotland, was the river Eden which is situated just north of St. Andrews. Thirteen cockles were sampled from near the mouth of this river in October of 1994 and analysed for Po-210, the result being 103.6 Bq/kg. No water or particulate matter samples were taken. These samples were actually left in an aquarium for over 30 days in which time their guts would have been completely purged. This long period of starvation would also have resulted in a general decrease in tissue wet and dry weights as well as a change in the amount of Po-210 present due to its decay and in-growth from Pb-210 present

A further site at Finstown, Orkney in the North of Scotland was chosen so that a number of different shellfish could be obtained. Oyster and cockle samples were taken in late September 1994 and in January 1995 some scallops and mussels were also sampled. Twenty-four oysters were sampled giving a result of 102.5 Bq/kg and 21 cockles were sampled with an activity of 138.8 Bq/kg of Po-210. The scallops sampled at the later date contained 166.0 Bq/kg of Po-210 and the mussels, which were all between 7-8 cm in length, had an activity of 277.2 Bq/kg. No relevant environmental samples were taken from here as these were commercial samples..

The largest sampling programme was carried out at the Ythan estuary, approximately 20km North of Aberdeen. No TENORM sites exist near here although large amounts of nitrate fertilisers are added to the surrounding farmland causing the area to be classified as being nitrate sensitive. It is not known if a large amounts of phosphate fertilisers are also being applied.

Sampling was carried out at the end of each month from April 1994 to March 1995 inclusive. On each occasion, thirty mussels were sampled from a similar site at low tide, all between 6-7 cm in length. This size was chosen as mussels between 6-7 cm in length were most abundant. Filtered water and particulate matter samples were also taken in addition to two sediment samples, one from the top 1 cm of the sediment surface and the second being sediment from below the top 1 cm layer.

The mean shell length varied from a minimum of 62.2 mm up to 66.9 mm with the dry weight varying from 1.0 up to 1.84 grams. The condition index (relationship between dry weight of tissue and shell length) of these mussels varied from 3.7 up to 7.2. The activity of Po-210 varied from a minimum of 276.8 Bq/kg in June up to a maximum of

472.7 Bq/kg in August (results in figure I). The activity of Po-210 per mussel varied from 0.38 Bq per mussel in May up to a maximum of 0.84 Bq per mussel in August (figure II). The level of Po-210 in filtered water varied from 0.77 mBq/l in July to 5 7 mBq/l in April (figure III) and levels for particulate matter varied from 41.7 Bq/kg in October to 398.6 Bq/kg in August (figure IV). Sediment samples also displayed variations (figure V). The sediment sample taken from the top 1 cm showed levels between 7.6 Bq/kg in July to 46.8 Bq/kg in February. The deeper sediment samples showed levels between 7.8 Bq/kg and 68.0 Bq/kg.

The results clearly show that levels of Po-210 in shellfish do not remain constant from month to month. Many of these variations can be attributed to changes in the tissue wet weight of the sample or the increased activity of Po-210 in particulate matter but other parameters such as climate or water flow may be important in causing levels in the shellfish to change. It is noteworthy that mussels 6-7 cm in length at the Culbin and Ythan sites both display drops in the level of Po-210 between May and June yet live in different habitats in different areas, one coastal the other estuarine. The minimum and maximum value for Po-210 per kg in July and August respectively can also be found for the level of Po-210 in filtered water and particulate matter suggesting some correlation between levels here and in the shellfish. The peak of Po-210 per mussel in August can be explained partly by the fact that the wet and dry tissue weights were also at a maximum here due to the greater abundance of food in the summer containing higher levels of Po-210.

In order to gain some information regarding where Po-210 accumulates in shellfish tissue a batch of scallops were sampled, dissected into their constituent parts and analysed for levels of the radionuclide.

Fifteen scallops were sampled from the sea bed approximately 15 km off the coast of Aberdeen. After being caught they were held in the aquarium for 12 hours so that the gut could purge. After their length and breadth were measured, their tissue was then removed and pooled into one of the following six groups; Mantle, gills, male gonad, female gonad, abductor muscle and digestive tissue. Wet and dry weights were measured for each tissue type and then the sample was analysed for Po-210. Over 54% of the dry weight of scallops is made up of the abductor muscle followed by the digestive tissue (16.5%), mantle (14%), gill (7.2%), male gonad (4 7%) and female gonad (2.8%) (Results in Table II) The digestive tissue, being made up of certain lipids and fats, does not have the appearance of dry tissue after drying at 65°C for 48 hours although it readily dissolves in concentrated Hydrochloric and Perchloric acids. Activity levels for Po-210 in the different tissue types vary widely, the actual results being: abductor muscle - 21.6 Bq/kg, gill - 73.3 Bq/kg, mantle - 31.5 Bq/kg, male gonad - 116.4 Bq/kg, female gonad - 101.7 Bq/kg and finally digestive tissue - 1076.2 Bq/kg. The Po-210 activity for the scallops, if all the tissue had been pooled together, gave an average value of 207.2 Bq/kg. These results clearly indicate that Po-210 is accumulated to quite a high degree by the digestive tissues of the scallop. Although these scallops were sampled from the seabed where they are constantly immersed and hence constantly feeding, they were taken from an area far from any river outlet or TENORM site, thus suggesting that shellfish living in most areas around the coast can accumulate high levels of radionuclides.

2) LEVELS OF Pb-210 IN SHELLFISH AROUND SCOTLAND

Using the in-growth method, it was possible to analyse the samples for levels of Pb-210. As this method requires a waiting period of at least six months between sample preparation and analysis, only a small number of samples have been analysed for Pb-210. These include the first three months worth of samples from the Ythan estuary plus the samples taken from Culbin in May 1994. Levels of Pb-210 in mussels sampled at the Ythan vary from 5.6 Bq/kg in June up to 58.6 Bq/kg in April. In water, levels vary from 1.7 mBq/l in May to 4.7 mBq/l in April. For particulate matter, levels varied from 20.2 up to 132.2 Bq/kg between April and June. For the samples taken from Culbin, Pb-210 activity varied from 5.9 to 37.3 Bq/kg for mussels between 3-4 cm and from 13.5 to 20.0 Bq/kg for the 6-7 cm mussels. The value for Pb-210 in the filtered water sampled at Culbin was 5.29 mBq/l.

Overall in all the shellfish samples there is between 7 and 70 times as much 210-Po as there is Pb-210 but in the water samples the ratio between the two is much closer to unity

3) PRELIMINARY DOSE ASSESSMENT

A small amount of work was carried out regarding the dose received from Po-210 in shellfish. Using the ICRP 60 recommendations, it was assumed that the annual limit of intake for Po-210 is $9*10^4$ Bq which will give a CEDE of 20 mSv. The maximum yearly dose for a member of the public is 1 mSv with the proviso that only 0.5 mSv is received from any one source. A constraint dose would typically be 0.3 mSv per year. If this dose is compared to the ICRP recommendations then 0.3 mSv would equal an intake of 1350 Bq of Po-210. If we consider mussels sampled from the Ythan estuary contain between 0.38 and 0.8 Bq per mussel, then between 1687 and 3550 mussels would have to be consumed in a year to exceed the constraint dose, or 33 to 68 mussels per week. An average value of 0.59 Bq per mussel would mean that 2288 mussels per year or 44 per week would have to be consumed in order to exceed the constraint dose Similarly for scallops, assuming an average activity for Po-210 of 2.8 Bq per scallop and also that the whole animal was consumed, then 482 scallops would have to be consumed in a year or 10 per week. The addition of the Pb-210 dose would reduce these numbers slightly. Clearly certain groups will consume these amounts of shellfish and therefore exceed the constraint dose.

CONCLUSIONS

The results obtained show that levels of Po-210 are well in excess of the levels of Pb-210 in shellfish tissue, with the activity of the two nuclides comparable in water and particulate matter samples. This suggests that preferential uptake of Po-210 is taking place by shellfish around Scotland with sometimes as much as seventy times the concentration of Po-210 as there is Pb-210. The disequilibrium conditions which exist between the two nuclides in shellfish result in a significant dose from Po-210 to any animal

which may consume them. It is therefore apparent that certain groups who eat large numbers of shellfish are at risk from increased radiation doses.

With regard to the variation in levels of Po-210 in shellfish from differing sites around Scotland, it can be seen that no great differences exist in levels of these radionuclides from site to site. Mussels sampled from Culbin bar and the Ythan estuary display comparable Po-210 results although the sites are rather different environments. The estuarine site receives a constant influx of water which has passed over granite rock and therefore contains elevated levels of dissolved Uranium and Thorium decay progeny, whilst the coastal site receives tidal seawater from the North sea. Scallops taken off the coast of Aberdeen and from Orkney also show comparable activities of Po-210 as do cockles from Orkney and St. Andrews. This evidence suggests that even without the presence of TENORM sites the background level of Po-210 in shellfish sampled from around Scotland is relatively high with little variation between estuarine and non-estuarine sites. This would make any advice on the preferential placement of any future shellfish farms difficult as the data from this research indicates that there are no areas where shellfish can grow without taking up significant amounts of Po-210.

Dose rate work indicates that the variation in the activity of Po-210 per mussel leads to large variations in the numbers of shellfish that would have to be consumed in order to exceed certain constraint doses. Although only a small percentage of the population may consume these quantities of shellfish, these critical groups will exist and receive large doses of radiation from Po-210 found in shellfish. Clearly before any future fish-farms are sited around Scotland, some preliminary work should be carried out regarding the levels of Po-210 in the shellfish in the area and the radiation dose that these animals may deliver to the human population.

PUBLICATIONS

One paper has now been prepared and is about to be submitted for publication. A second paper is planned when al the Pb-210 results have been obtained.

Table I
Mussels sampled from Culbin bar, June 1994.

Size of mussels	**3-4 cm**	**4-5 cm**	**5-6 cm**	**6-7 cm**
No. of mussels sampled	22	16	27	5
Mean shell length (mm)	36.1	44.6	54.4	64.2
Mean Dry Wt. (g)	0.23	0.37	0.53	0.65
Po-210 (Bq kg-1)	280.39	342.0	346.87	259.17
Po-210 per mussel	0.06	0.12	0.184	0.201

Table II
Scallops sampled 15km off Aberdeen Coast.

	Mantle	**Gill**	**M. Gonad**	**F. Gonad**	**Digestive**	**Muscle**
Wet Wt. (%)	21.4	12.7	4.8	3.7	12.8	44.6
Dry Wt. (%)	14	7.2	4.7	2.8	16.5	54
Po-210 (Bq kg-1 Dry Wt.)	31.5	73.3	116.4	101.7	1076.2	21.6

Figure I

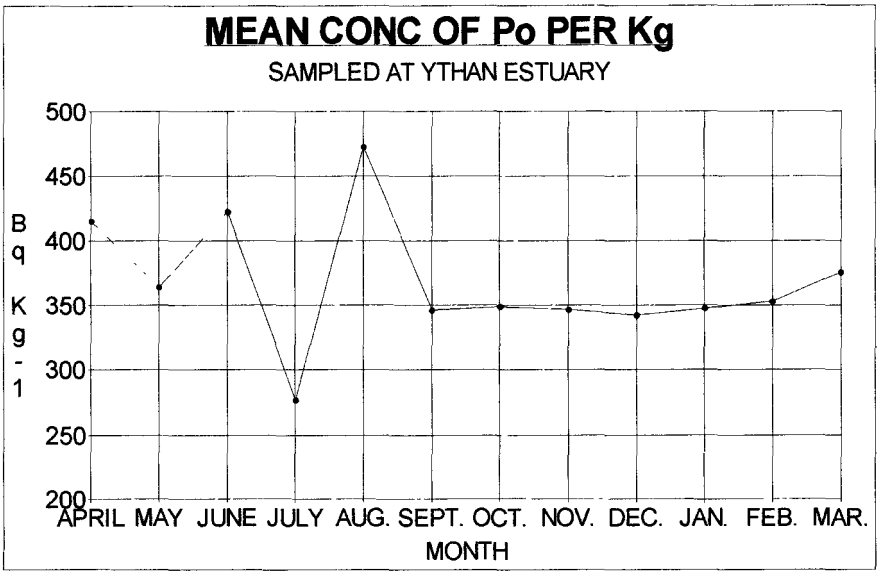

Figure II

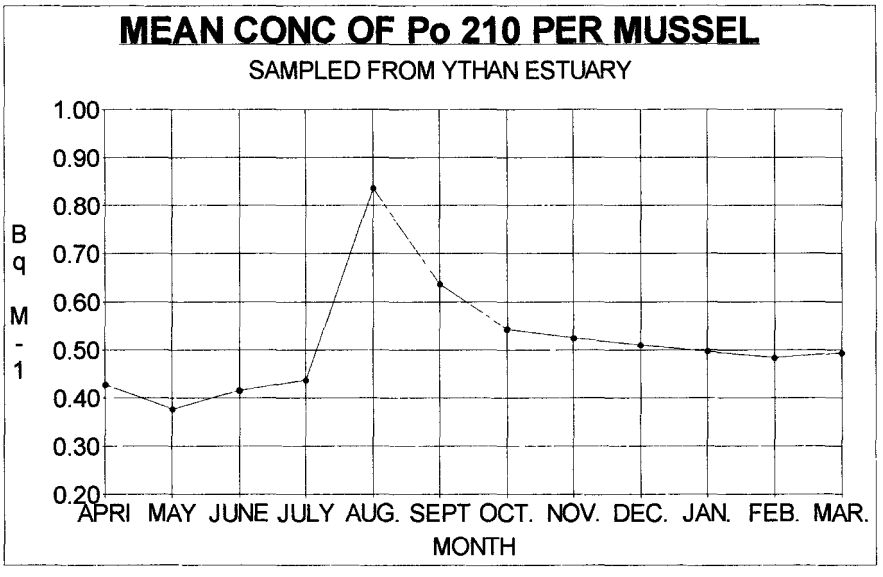

Figure III

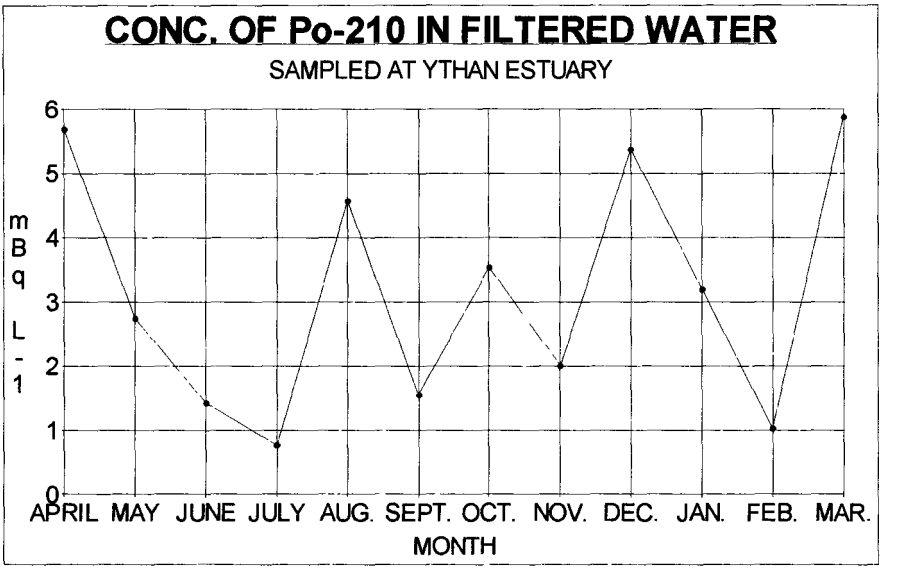

Figure IV

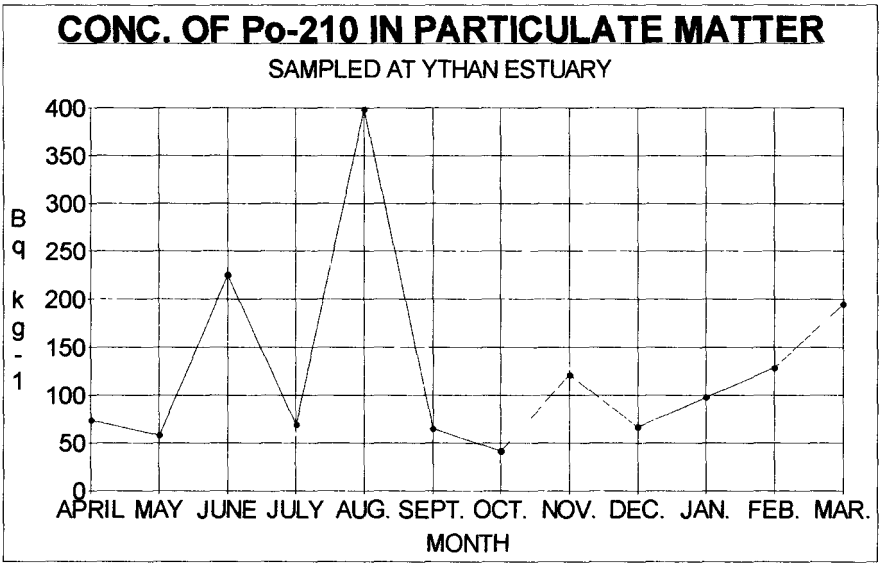

Figure V

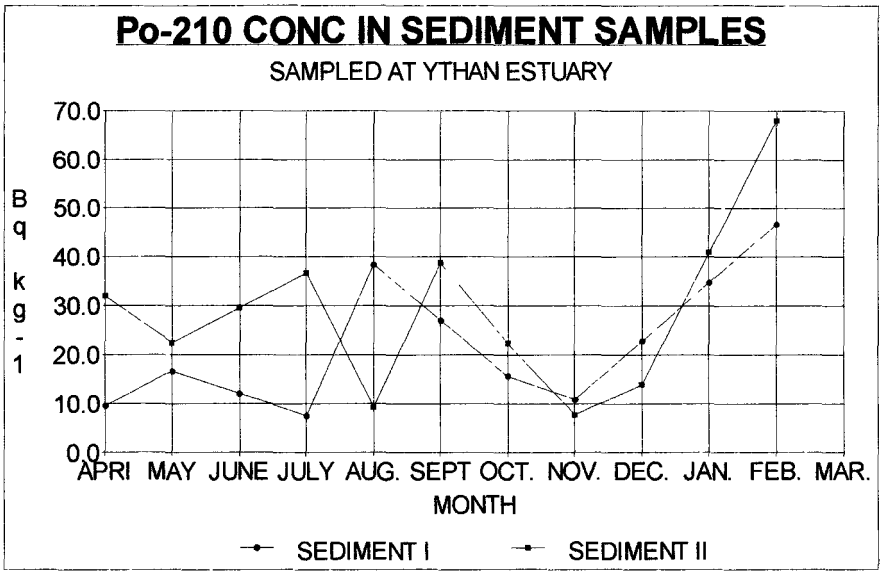
Po-210 CONC IN SEDIMENT SAMPLES
SAMPLED AT YTHAN ESTUARY
Bq kg-1
70.0
60.0
50.0
40.0
30.0
20.0
10.0
0.0
APRI MAY JUNE JULY AUG. SEPT OCT. NOV. DEC. JAN. FEB. MAR.
MONTH
SEDIMENT I
SEDIMENT II

Head of project 9: Dr. P. Zagyvai

1. Objectives

The following research objectives were specified:
- analysis of products, by-products and wastes of the phosphate fertiliser industry as well as samples from the affected environment;
- establishment of "background" levels for long-lived natural radionuclides;
- assessment of emission from other industrial sources;
- in case of a confirmed discharge of ^{210}Pb, ^{210}Po or other natural radionuclides from the phosphate fertiliser production to the environment, its contribution to radiation dose exposure of the population should be assessed.

2. Phosphate fertiliser technology in Hungary

Phosphate fertiliser is manufactured at TVM works in Szolnok, an East Hungarian town by the Tisza river. Phosphate ore (mainly of igneous origin) is transported mainly from mines of the Kola peninsula, Northern Russia. According to the technology pursued at TVM phosphogypsum is not separated from the phosphate slurry. Instead, it is contained in the end-product fertiliser, that is, the ^{210}Pb and ^{210}Po content is not expected to be enriched significantly in any product or waste.

3. Methods of analysis

3.1. Measurements

Gamma spectrometry (GS), alpha spectrometry (AS), liquid scintillation (LSC), neutron activation analysis (NAA) and X-ray fluorescence analysis (XRFA) were applied.

3.2. Radiochemical separation

A/ Separation of ^{210}Pb

A new method was recently developed by experts of I.N.T. in order to achieve the rapid, selective and efficient separation of lead from other elements present in the sample. The procedure is presented in Refs. [2] -[4]. The sensitivity of the separation combined with LSC beta analysis is about 0.05 Bq/sample with a chemical yield of >70 %.

B/ Separation of ^{210}Po

A method taken from the literature was improved and modified. Recovery rates are 45 - 70 % for Po and 50 - 95 % for ^{210}Pb in a combined procedure. (LSC was used for ^{210}Pb and AS for ^{210}Po, respectively.)

C/ Separation of ^{226}Ra

A modified method of Sill [6] was applied. Detection limit: 1-2 mBq/sample.

4. Results

4.1. Analysis of standard reference materials

Seven standard reference materials (phosphate ores, seaweed and sediment samples) were analysed by direct gamma spectrometry and by radiochemical processing according to the method of Refs. [2] - [4]. The procedure proved accurate and reliable.

4.2. Analysis of samples from the phosphate fertiliser plant

The inactive trace element composition (determined by NAA, GS and XRFA) of the phosphate ore samples showed significantly high concentrations of rare earth metals compared to the findings quoted in the literature.

The results of radioanalysis of various samples related to phosphate fertiliser production are summarised in Table 1.

Table 1.
Radioactive concentrations of phosphate samples

Sample	Pb-210	Th-234	Ra-226	Pb-214	Bi-214	Pb-212	Ac-228	Tl-208	Bi-212	K-40	Cs-137
Phosphate ore (Kola)	55 7 ±1 8	76 5 ±2	81 ±1 5	74 ±2	75.2 ±1	82 ±1 1	79 ±1	82 ±1 5	76 ±2	87 ±2	N D
Phosphate end-product	15.8 ±1.3	60 ±2	67 ±1.1	35 ±2	34 ±0.8	43.1 ±0.6	41 ±1	39.5 ±1.4	38.6 ±1.5	321 ±2	N D
Sodium poly-phosphate	N D	N D	0 6 ±0.4	0 4 ±0.3	0.7 ±0 3	N D	N D	N D	N D	N D	N D
Potassium fertiliser	N D	N D	N D	N D	N D	1.1 ±0 5	1.3 ±0.5	N D	N D	1 55E4 ±2	N D
Mono-ammonium-phosphate	10.4 ±1 8	43 ±2	39 ±0 8	36 ±0 8	39 ±1	39 ±0.6	41.1 ±1	40.5 ±1.3	36.2 ±1.4	30 3 ±1.6	N D

N.D. : Not detected
Three replicates were prepared and analysed. Aggregate errors are given.

Various on-site environmental samples were collected and analysed. The ratio of activity concentration in these samples over that in off-site reference ("background") samples were determined. The range of these "site enhancement ratios" are shown in Table 2.

Table 2.
Site enhancement ratios (on-site/off-site activity concentrations) for soil samples from the site of the TVM chemical works, Szolnok

	Pb-210	Th-234	Ra-226	Pb-214	Bi-214	Pb-212	Ac-228	Tl-208	Bi-212	K-40	Cs-137
Range of enhance-ment ratios	0.73-2.0	0.25-2.2	0.60-2.3	0.37-1.8	0.63-2.3	0.19-1 0	0.20-1 0	0.23-1.1	0.27-1.2	0.29-0.86	0.076-2.0
Off-site soil (Bq/kg)	13.1 ±1.4	25.2 ±2	31.1 ±1.6	26.4 ±1.8	23 5 ±1.2	42.8 ±1 3	42.0 ±1 4	36 7 ±1.5	40.5 ±1.4	661 ±3	11 9 ±2

4.3. Natural radionuclides released from other non-nuclear sources in Hungary

Electricity generated in coal-fired power plants has an approximate 20 % share in Hungarian power production. A detailed study of the radioactive emission of coal-fired power plants was reported by Bódizs et al. [7]. Emission of natural radioactivity with the fly ash is more pronounced than in the case of phosphate fertiliser industry.

4.4. Natural radionuclides in environmental samples

Environmental samples of various origin and nature were analysed for the same natural radionuclides as in industrial samples. The presence of "unsupported" (excessive) ^{210}Pb was confirmed in the majority of samples of cattle fodder, grass and various harvested plants, due to airborne sedimentation rather than the use of ^{210}Pb-rich fertilisers.

A series of soil samples of very specific nature was obtained at Mátraderecske, north-east Hungary, where enormously high radon emission values were reported in recent years. Activity concentration of ^{238}U-series descendants were 5 -10 times higher than that of the reference soil.

Atmospheric discharges (wet fallout and active aerosol sampling) were collected and analysed. Tables 3. and 4. show the main components of airborne radioactive discharge in the Budapest region.

Table 3.
Radioactive concentration of wet fallout samples
[Bq/m^2/month]

Isotope	Median	Range
^{210}Pb	2.64	2.1 - 2.9
^{7}Be	8.1	0.4 - 15
^{137}Cs	0.36	0.2 - 0.5
^{40}K	3.4	2.4 - 6.3

Samples were collected in the period January 1994 - March 1995.

Table 4.
Radioactive concentration [μBq/m³ air] of a long-term aerosol sample
(October 1994 - March 1995)

Radionuclide	Concentration
^{7}Be	362 ± 15
^{137}Cs	4.8 ± 1.7
^{210}Pb	154 ± 8
^{226}Ra	2.7 ± 1.2

5. Conclusions

5.1. Analytical methods

The procedure described in Refs.[2] - [4] proved to be swift, effective and reliable for the radiochemical separation of ^{210}Pb and ^{210}Po. Alpha spectrometry and liquid scintillation counting were applied for processed samples. Participation in intercomparisons, analysis of reference materials confirmed the accuracy of the analyses.

5.2. Environmental samples

Biological and soil samples from farmlands treated with phosphate fertiliser were collected and analysed. The sensitivity of gamma spectrometry was often insufficient for ^{210}Pb. The "unsupported" (probably airborne) ^{210}Pb content significantly exceeds the "supported" part ascribed to ^{226}Ra. Compared to concentrations of ^{7}Be or ^{40}K, that of ^{210}Pb showed less fluctuation within replicate samples of the same type. Values associated directly with airborne particles showed the same features.

5.3. Discharges from the phosphate fertiliser technology

The difference from the phosphate products of Western Europe in origin (igneous vs. sedimentary rocks) and in chemical technology (inclusion vs. exclusion of phosphogypsum in the end-product) clearly explain the relatively low concentrations of ^{210}Pb in the studied samples. As phosphogypsum is not separated, enrichment and segregation of ^{210}Pb cannot occur. Secular equilibrium in the ^{238}U chain was confirmed in all cases, so the whole amount of ^{210}Pb is considered "supported". No significant unsupported ^{210}Pb content could be found in the associated soil samples either. The inactive trace element analysis of the igneous phosphate ore showed high levels of rare earth metals.

References

[1] Zs.Molnár, G.Keömley, D.Bódizs, Z.Lengyel:
Application of neutron activation analysis in the Institute of Nuclear Techniques of the Budapest Technical University
Periodica Polytechnica Ser. Physics, **1** (1) 45. (1993)

[2] N.Vajda, Gy.Kis-Benedek, D.Bódizs, M.Vodicska:
Radiochemical determination of ^{210}Pb by the use of crown ether
Izotóptechnika és Diagnosztika **37** (1), 25. (1994)
[In Hungarian]

[3] N.Vajda:
Determination of ^{210}Pb in Brazilian soil using a crown ether
IAEA Report CU-94-012 (1994.05.03)

[4] N.Vajda, J. LaRosa, R. Zeisler et al.:
A novel technique for the simultaneous determination of ^{210}Pb and ^{210}Po using a crown ether
Journal of Environmental Radioactivity (in press)

[5] I. Kádár:
Investigations in natural and environmental protection - Studies on the heavy metal content of soils and plants
Internal Report of the Ministry of Environmental Protection 1991.
[In Hungarian]

[6] C.W. Sill:
Nuclear and Chemical Waste Management **7**, 239.(1987)

[7] D. Bódizs, L.Gáspár, G.Keömley:
Radioactive emission from coal-fired power plants
Periodica Polytechnica Ser. Physics, **1** (1) 87. (1993)

Report on French/Irish Polonium-210 Intercomparison Exercise

Personnel:

IPSN: Dr. P. Germain and Mr. G. Leclerc
RPII: Dr. T.P. Ryan and Ms. A.M. Dowdall

INTRODUCTION

The laboratories of the IPSN (France) and the RPII (Ireland) have undertaken, as part of the EU contract N. F13P-CT92-0035, the analysis of sea water, suspended material, mussels and seaweed. In keeping with an internal quality control programme, the participating laboratories took part in analytical intercomparison exercises using IAEA intercomparison samples. These included cockle flesh and sediment samples. No sea water intercomparison samples were available at the time and this was identified as a potential weakness in the quality control process.

In this context, the laboratories of the IPSN and the RPII planned and executed a joint sampling campaign in October 1994 at Sutton in Dublin, Ireland. The sampling and analysis strategy was designed in order to compare both sampling and analytical techniques. Priority was given to sea water, but samples of suspended material, mussels and seaweed were also collected.

SAMPLING HANDLING

LABORATORY A (IPSN):

Water

Each water sample (20 l) was filtered through 0.45 μm filter papers with frequent filter paper changes. The water was acidified with concentrated HNO_3 (100 ml) before a known quantity of ^{208}Po spike was added. Samples were stirred for 4.5 h. The pH of the filtered samples was raised to between 8 and 9 with concentrated ammonia solution and 1.6 g of $KMnO_4$ (in solution) were added together with H_2O_2 to induce the precipitation of MnO_2. The sample was stirred for 5.5 h. After stirring, the supernatant was decanted and the precipitate dissolved in 1.2 M HCl (100 ml) containing 2 ml H_2O_2. The solution was evaporated and 5 ml of concentrated HCl were added to the residue and evaporated to remove any remaining H_2O_2. A final addition of HCl was made to obtain a 0.3 M solution and ascorbic acid and hydroxylamine hydrochloride (30%) were added. The polonium was deposited onto a silver disc at 90° C for 4 h with stirring.

Suspended Material

Suspended material samples were recovered by filtering 60 l of sea water using 0.45 μm papers. The samples were dried at 80° C and placed in a teflon bomb together with a ^{208}Po spike. The samples were dissolved with a HF/HCl solution and digested with HNO_3 for 48 h. The solution was filtered, evaporated, retaken in HCl and made up to 0.3 M. Ascorbic acid and hydroxylamine hydrochloride were added to the solution and polonium was spontaneously deposited onto a silver disc.

Mussels (*Mytilus edulis*)

The mussels were collected by hand from a large surface area on the shore and the sedimentary material was removed before drying at 80° C and then grinding. Mussels were not depurated of their faecal and pseudo faecal material prior to analysis. After drying, grinding and homogenisation, aliquots were placed in teflon bombs together with a know quantity of ^{208}Po spike. Sample dissolution was carried out with 10 ml of HNO_3 at 80° C for 48 h. After evaporation, the residue was retaken in HCl and plated as before. A condition index was estimated for 30 mussels randomly selected from the size range 4.66 cm to 7.34 cm. The mean value of the condition index was found to be: 5.616.

Seaweed (*Fucus vesiculosus*)

The *Fucus vesiculosus* was collected by hand from the low water mark on the shore to the high water mark. The sedimentary material, epiphytes and epifauna were removed before drying at 80° C and then grinding. The chemical analysis proceeded as for mussels.

LABORATORY B (RPII):

Water

Each water sample (20 l) was filtered through a single pair of 0.45 μm filter papers. The filtered water was acidified with HCl, spiked with ^{209}Po and 200 mg of $FeCl_3$ were added. The sample was stirred for 4 hours. The polonium was co-precipitated with iron as an hydroxide and the precipitate was allowed to settle. It was filtered through a 0.45 μm paper and was subsequently redissolved off the paper with HCl. The Iron was again precipitated and the precipitate was collected by centrifugation. A plating solution was made up to 200 ml by dissolving the precipitate in 5 ml concentrated HCl together with hydroxylamine hydrochloride, ascorbic acid and water. The polonium was deposited onto a silver disc over 4 hours with moderate stirring and heating ($< 90°$ C).

Suspended Material

Each water sample was filtered through two pre-weighted 0.45 μm papers. After drying the suspended material in an oven at 80° C to a constant weight they were digested in 200 ml of Aqua Regia for 4 h and spiked with ^{209}Po. The mixture was filtered and the filtrate was evaporated and retaken in 5 ml concentrated HCl and the polonium was deposited onto a silver disc over 4 hours with moderate stirring and heat ($<90°$ C).

Mussels (*Mytilus edulis*)

Mussels within the range 5.5 cm and 6.5 cm were selected for analysis (127

specimen). Ten specimen were randomly selected to determine mean mussel length, dry weight and shell weight values for the sample together with an estimation of the condition index. The mean value of the condition index was found to be: 6.50. The remaining sample was dried to a constant weight at 80° C, pulverised and sieved through a 0.22 mm mesh. A 1 g aliquot was sub-sampled, spiked with ^{209}Po and digested with nitric acid and hydrogen peroxide in a microwave digester. The sample was evaporated and retaken in concentrated HCl and was digested for a second period before being filtered through a 0.45 μm filter paper. The solution was made up to 200 ml with 5 ml hydroxylamine hydrochloride, 5 ml ascorbic acid and de-ionised water. The polonium was plated onto a silver disc with moderate stirring and heating (< 90° C) for 4 h.

Seaweed (*Fucus vesiculosus*)

Fucus vesiculosus was collected from a localised area close to the high water mark. When it was returned to the laboratory it was thoroughly washed and dried to a constant weight at 80° C. It was then pulverised and the chemical analysis proceeded as for mussels.

RESULTS

The following is the table of results derived from the joint sampling and analysis programme (Results given in $Bqkg^{-1}$ are in dry weight).

Filtered Sea water ($mBql^{-1}$)		Suspended Material ($Bqkg^{-1}$)		Mussels ($Bqkg^{-1}$)		Seaweed ($Bqkg^{-1}$)	
IPSN	**RPII**	**IPSN**	**RPII**	**IPSN**	**RPII**	**IPSN**	**RPII**
0.76±0.02	0.42±0.07	71.9±5.1	117±9	181±12	174±11	7.5±0.5	27±6
0.92±0.05	0.26±0.06	62.3±4.1	100±10	179±13	203±19	6.6±0.5	26±5
	0.25±0.05	71.9±4.8	96±11	181±12	182±15	7.0±0.5	27±6
MEAN							
0.84	0.31	68.7	104	180	186	7.0	27

DISCUSSION

Comparing the data for filtered sea water acquired by both laboratories, it is immediately obvious that there is a significant divergence with the IPSN presenting a higher mean value of 0.84 $mBql^{-1}$ in the filtered fraction than the RPII at 0.31 $mBql^{-1}$. Significantly, when comparing the results for suspended material, the trend is in the opposite direction with the IPSN presenting a mean value of 68.7 $Bqkg^{-1}$ which is lower than the mean value presented by the RPII at 104 $Bqkg^{-1}$. These differences and the order in which they appear, may reflect

differences in the modalities of filtration as practised by both laboratories. The turbidity of the water was high (0.1 gl^{-1}) and IPSN changed their filter papers regularly where as, in contrast, the RPII forced their water samples through a single pairing of filter papers. The different modalities in filtration may have resulted in differences in exchange between the polonium in the filtered fraction and that on suspended material. It is possible also that the different methods resulted in different actual filter pore sizes as the amount of material collected on the filter papers increased. Furthermore, the total polonium found in the samples by the two laboratories was not equal with the RPII finding a mean of 12.2 $mBql^{-1}$ and the IPSN with 7.7 $mBql^{-1}$. This may again reflect the differences in modalities of filtration as the RPII collected and analyzed as part of the suspended material the coarser material which the IPSN allowed to settle out. Other considerations such as differences arising from the use of disparate chemical schemes cannot be fully ruled out.

The agreement between the two laboratories in terms of the ^{210}Po analysis of mussels was excellent with the IPSN finding a mean activity of 180 $Bqkg^{-1}$ and the RPII finding a mean of 186 $Bqkg^{-1}$.

There is a significant difference between the two laboratories on the values arrived at for *Fucus vesiculosus* with the IPSN presenting a mean value of 7 $Bqkg^{-1}$ and the RPII presenting a higher value of 27 $Bqkg^{-1}$. In an attempt to pin point the source of this discrepancy, samples were exchanged between laboratories and subsequent analysis confirmed the original results. It was concluded therefore that the difference was not an artifact of the chemistry but must have something to do with sampling and preparation procedures. However the only difference recorded was in the sample collection where the IPSN collected along a line from the low water mark to the high water mark and the RPII collecting in a localised area close to the high water mark.

In conclusion, the present work points towards the necessity to standardise filtration procedures and also towards the need for further work to fully explore the processes involved.

Final Report
1992-1994

Contract: F13PCT930075 **Duration: 1.1.93 to 30.6.95** **Sector: A22**

Title: Investigation on exposure to natural radionuclides in selected areas affected by U-processing.

1)	Belot	CEA-FAR
2)	Roehnsch	BfS
3)	Massmeyer	GRS

I. Summary of Project, Global Objectives and Achievements

Introduction

Solid wastes from uranium mining and milling have the potential to release radionuclides into air and surface waters. These radionuclides contribute to the radiation dose that can be delivered to the population living in the vicinity of the disposal site. The most recent radiation safety recommendations of the ICRP raise the pressure towards determining the impact of the wastes from uranium industry and investigating appropriate countermeasures.

Given the international interest in these topics, a cooperative approach was estimated to be beneficial. Possible opportunities for collaborative research were discussed between IPSN, France; BfS and GRS, Germany. The three parties decided to join their efforts in a multidisciplinary approach, based on modelling and experimentations on typical test sites. The program is composed of two distinct studies. The first study is devoted to the atmospheric pathway and deals with the atmospheric dispersion of radon and the behaviour of its progeny in the vicinity of emanating tailings piles (Part I). The second study is focussed on the aquatic pathway, and investigates the hydrological and geochemical aspects of the uranium and radium transport through the layers of radioactive and non-radioactive materials that have been deposited in a settling pond (Part II). The three organisms that are associated in this joint program have participated to both studies.

Part I: Atmospheric pathway

Dispersion of radon from tailings piles

The dispersion of radon from tailings piles was studied on a specific site, by acquiring experimental data on the sources of radon and the observed air concentrations, trying to describe the dispersion of radon by different models and comparing the measured and predicted data. The selected test site situated at Lengenfeld in Saxony was composed of two main tailings piles backed against a natural hill, covered with a 0.5 m layer of soil and partially planted with small trees (epiceas) of about 3 m high, and also of another zone in the bottom of the site where some tailings had been accidentally spilled away due to the rupture of the earthen dike of a settling pond. The geographical distribution of the radon source strength was measured on this site by a team of IPSN (cf. project 1) during one week in September 1993, and further on assumed, for modelling purpose, to be in a first approximation constant throughout the year. The meteorological conditions of wind speed and wind direction were derived from previous measurements made on the site and estimated also from regional data. Long-term (annual) concentrations of radon in air were obtained from systematic measurements made by BfS with track detectors placed at fixed points on and around the site (cf. Project 2).

The modelling of the radon atmospheric dispersion could be envisaged as the modelling of any other pollutant, radioactive or not. In the last decades, with the advent of regulatory air pollution programs came the need for practical tools for estimating transport and diffusion of pollutants

from continuously emitting sources and different types of models were developed to reach this objective. In the specific case of radon emission from tailings piles, there are several complications that make the task less easier than in other fields of industrial pollution. First the area-sources are at the ground level itself instead of being at some height above this level as this is the case in many other situations. Secondly, the terrain where the tailings piles is situated is not generally a flat nude land as in the case of many industrial lands, but rather a terrain of more or less complex orography with a patchy natural vegetation of grass, bushes and woods.

The first step of the modelling approach made in the present work was to try to use very simple old models such as the standard Gaussian models which are still in wide use despite their age and limitations (flat land, relatively large distance between source and receptor...). The second step was to apply more sophisticated models that can handle details on the site orography, calculate the airflow field and superimpose atmospheric dispersion. A third step, somewhat apart from the others, was to focus attention on the near-field dispersion in that region nearby the source(s) where the microstructure of the lower boundary layer and its influence on the vertical dispersion of radon can no longer be ignored. All these existing or tentative models were applied to the site of Lengenfeld (Saxony) on which data had been acquired.

The concentrations of radon in air at distances from the sources greater than 1 km can be approximated by the MILDOS model. The more complex WITRAK model gives similar concentrations but shows the influence of orography on the shape of the isoconcentration lines (cf. GRS: project 3). Both models show a fast decrease of concentration as the distance from the sources increases, which is qualitatively in full accordance with the field observations. At smaller distances from the sources these models cannot give safe predictions because they do not consider the variation of wind speed with height above groung level. To overcome this limitation, the Lagrangian model LASAT and the Eulerian model FLURAD were tentatively used by GRS (project 3) and IPSN (project 1) respectively. These models consider a realistic wind speed verical profile instead of assuming a constant wind speed profile. The predicted values obtained by the two models are very similar and not very different from the measured ones, but the main difficulty in using such models is to define the microstructure of the boundary layer close to the ground, particularly in the case of a soil covered by patchy vegetation.

Characteristics of radon progeny above or nearby a waste pile

Many observations have been made on the characteristics of radon progeny on sites of infinite extension that are supposed to release radon at an uniform fluence rate. By contrast, very little information exists on the radon progeny above or nearby a strong source of limited area such as a tailings pile. This information would be needed for evaluating the doses related to a certain radon concentration, and also to investigate if one can discriminate between the contribution of the industial source (tailings pile) and the contribution of the surrounding natural environment (background).

Initial investigations were made at the Crossen waste-rock pile (Saxony) in August 1994 in short-term experiments (IPSN: project 1) and long-term experiments (BfS: project 2). The short-term experiments consisted of sampling the radon and its progeny during 5-min periods, measuring the radon by an ionisation chamber and the radon daughters by the Thomas' method. It was shown that the activity concentrations of the radon daughters were much lower than the radon concentrations and that the equilibrium factor was around 0.1 under unstable weather and 0.2 under stable weather conditions. The long-term experiments were made by measuring the on-pile equilibrium factor over periods of one-month duration with the Megarad 04 device. Average values of 0.14, 0.11 and 0.06 were found in September, October and December respectively. These values are to be compared with the value of 0.7 usually found as a background value for the undisturbed terrestrial environment. This research will be continued in another framework.

Part II: Aquatic pathway

Experimental site and joint program

The uranium, radium and lead aquatic pathway was studied for an industrial dry settling pond situated at Lengenfeld (Saxony). The dry settling pond on study had been formed by diverting a small river from its bed, closing the original bed by an earthen dike, depositing uranium mill tailings in the bottom of the reservoir so formed, and finally covering the contaminated layer with a non-radioactive layer of baryte-sand.

The preliminary study reported hereafter has implied the cooperation of the three organisms that are associated in the contract. BfS and GRS have had a prominent contribution in the management of the field study and the acquisition of hydraulic and chemical data; IPSN has focused on geochemical aspects through the characterization of samples and the modelling of processes by a geochemical code.

Hydrology and chemical characteristics of the pond

In Summer 1994, sampling wells have been drilled at different points on the pond as described in the GRS report (cf. project 3, Part II). Observations have been made of material sequences and water level in the different wells in order to generate an hydrogeological cross-section of the deposited layers. At the basis there is a granite formation, followed by an aquifer of river sediments, then a layer of fine-grained tailings material whose thickness increases in the downstream direction, and finally a cover layer made of several meters of baryte-sand on the top.

Determinations have been made of the hydraulic conductivity, grain size distribution and pore water composition at different levels (cf GRS: project 3). On another hand, ^{238}U, ^{226}Ra and ^{210}Pb and their distribution between the solid phase and the pore waters have also been determined by BfS (cf project 2). All these measured data are to be used to run the geochemical and hydraulic models PHREEQE and NAMMU.

Geochemical study of the source term
Preliminary modelling

Pore water from RKS1 samples have been analyzed for major and minor elements. The solid phases of the samples have been submitted to chemical and mineralogical analyses to determine their composition. Waters and solids compositions are given in the report of IPSN (project 1, part II) for the materials of surface layer, tailings and underlying soil. The surface-layer cover is characterized by the predominance of alkaline-earth carbonate and sulfate, a neutral pH and weakly reducing conditions. The tailings layer is characterized by a noticeable proportion of sodium carbonate and an akaline pH ($\approx$ 10.2) that probably result from an alkaline treatment of the ore, and shows a greenish colour which is indicative of strongly reducing conditions. The underlying soil consists of river sediments, it has a low alkaline pH ($\approx$ 8.3) and is probably in reducing conditions.

Preliminary data have been obtained from the geochemical code CHIMERE. It was shown that the solution composition was fixed in the surface layer by calcite and dolomite; in the tailings by the dolomite. A further modelling effort would be necessary to precise the medium and long-term probable behaviour of the source term. It would then be beneficial to understand the behaviour of radium and uranium in the zone where waters from the tailings are mixed with waters from the cover. One would also need to precise the migration-retention mechanisms of Ra and U in the underlying soil and particularly the role of the Al-Fe oxides.

Head of project 1: Dr. Belot

PART I: Atmospheric pathway (contributors: M.C. Robé, S. Raviart)

II. Objectives for the reporting period

During the reporting period, IPSN has concentrated in acquiring field data on the radon flux distribution and radon daughters characteristics over two waste disposal sites (Lengenfeld and Crossen; Saxony). The knowledge of the radon flux data was required to drive some models of radon dispersion on an around the site, and try to validate the models by comparing experimental data and theoretical predictions. The characterisation of the radon daughters in the vicinity of a waste disposal site or even above the site itself was carried out with the objective to discriminate between the contribution of an artificial source and the contribution of the regional background. The experiments carried out within this contract are only initial ones. They will be continued during the following years within another framework.

Besides these field measurements, some theoretical work has also been devoted to the estimation of long-term radon concentrations over a well-characterized site. The idea was to calculate the radon air concentrations in the near-field of the area-sources, just where the classical Gaussian models are questionable.

III. Progress achieved including publications

Measurement of the radon flux at the Lengenfeld site (M.C. Robé)

The radon flux was measured at a number of sampling points selected, when possible, at the nodes of a preestablished sampling grid whose mesh depends for practical reasons on the total surface area to be explored. Each sampling point consists of a small plot of ground area of about 1 m in diameter on which the vegetation has been cut as short as possible; the point is marked with a peg and precisely identified on a map. The fluxes at the different points are measured nearly simultaneoulsy by allowing radon to accumulate in closed chambers (accumulator device) resting on the surface for three hours. At a few selected emplacements, the measurement has been replicated at different times during a week's period to have an idea of the variability of the radon flux for different soil and weather conditions.

An accumulator device is an open bottom small chamber made of a simple 30 L-cylindrical bucket. It simply collects radon atoms originating below the surface and prevents them being mixed through the atmosphere. The accumulation time (2 h) has been chosen to have a simple relationship between the flux and the concentration of radon at the end of the accumulation period, since the presence of the accumulator during that time would not seriously disturb the exhalation process. When the accumulation time is elapsed, the chamber is connected to an evacuated 125-ml scintillation flask through a sampling orifice on the top of the chamber. The samples are counted on a radon alpha counting system after three hours to insure daughter product equilibrium. The uncertainty on flux measurement has been estimated to be ± 25 per cent.

The radon source strength was determined during one week's period in September 1993 by measuring the radon flux at 81 points over a presumed area-source of roughly 25 ha situated on the site of Lengenfeld in Saxony. We found two distinct areas (~ 2 ha each) (Lenkteich and West of Nordhalde) of a relatively high flux density of 3.5 Bq m^{-2} s^{-1} on average. Besides, we recognized two other areas (~ 7ha) of medium flux density with an average value of 0.8 Bq m^{-2} s^{-1}. The remaining part of the explored zone (~ 15 ha) was characterized by an average value of 0.2 Bq m^{-2} s^{-1}. Replications of measurements were made at a few selected points during the one week's period. The distribution of the values obtained at the same points was rather narrow in spite of some variation in soil moisture due to light rains occurring at night. The measured fluxes were used as input to the predictive models implemented in the joint work, as-

suming that the values of radon flux determined during a limited period of time is valid for a one year's period.

Field determination of the time-varying equilibrium factor between radon-222 and its short-lived decay products in the atmosphere above a waste-rock pile (S. Raviart)

The aims of this preliminary study were to measure the variations in the concentration of radon and its decay products on a waste-rock pile and to relate the resulting equilibrium factor to the concomitant weather characteristics. To achieve these preliminary objectives, short-term measurements (5-min sampling) of radon-222 and its decay products, and the simultaneous determination of weather characteristics were carried out at sampling points situated on a waste-rock pile (Crossen, Saxony) during the week 17-21 August 1994.

During 5-min intervals, the radon-222 concentration was measured at different heights above ground level, using a 120 L-differential ionization chamber. At the same heights, the radon daughters were determined by the classical Thomas' method. It consisted of sampling the in-air particles on a 47-mm filter at a flowrate of 30 L min^{-1} and counting the filter on a ZnS scintillator during three preselected time intervals, 2-5, 6-20, 21-30 min after end of the sampling. From the counts in the three intervals, the number of atoms of each of the three nuclides ^{218}Po, ^{214}Pb and ^{214}Bi is calculated by solving three simultaneous equations. From these determinations, the potential alpha energy concentration and the equilibrium factor can be readily obtained.

The meteorological parameters measured during the sampling intervals were the wind direction (10 m), the wind speed with cup anemometers (2 and 8 m), the temperature with ventilated air temperature sensors (1, 2, 4 and 8 m). The cloud cover data was directly observed. The Pasquill stability class was determined from the date, hour, cloud cover and wind velocity using the method of Luna and Church. Another method, based on the determination of the Monin-Obukhov length from heat flux, friction velocity and temperature lapse rate, was used in parallel for purpose of comparison.

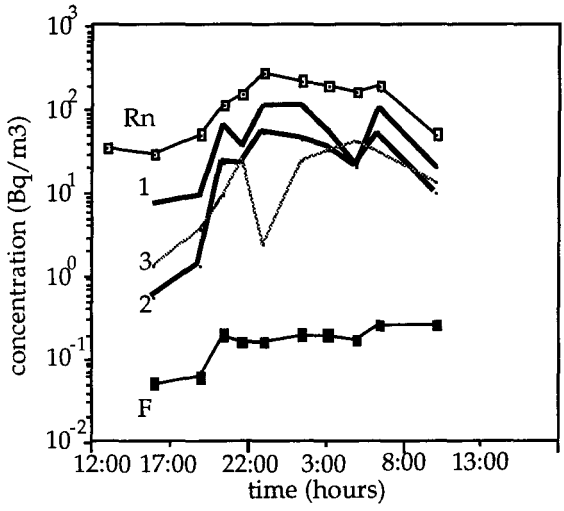

Fig.1: Variation of activity concentrations of ^{222}Rn, ^{218}Po (1), ^{214}Pb (2) and ^{214}Bi (3) at 1.5 m above ground level from August 20th at 16:00 to August 21th at 11:00, on the Crossen waste-rock pile. The bottom line represents the corresponding equilibrium factor F (without dimension).

Fig.1 gives an example of the evolution of the activity concentrations of ^{222}Rn and its three short-lived daughters, from the beginning of afternoon to the next morning. There is a significant increase of radon concentration from from 30 Bq m^{-3} at 16:00 to 267 Bq m^{-3} at 23:00, which corresponds to the passage of an unstable atmosphere to a stable atmosphere characterized by a positive gradient of temperature and a low wind speed. The concentrations of the radon daughters are generally much lower that those of the parent. The equilibrium factor, which is calculated as a linear combination of the activity concentrations of the three decay products divided by the activity concentration of the parent, increases from 0.05 to roughly 0.20. It must be remembered that these results of concentrations and equilibrium factor include the contribution of the regional background.

These initial results indicate that the equilibrium factor measured above a waste disposal pile could be much lower than known for an undisturbed homogeneous environment where the equilibrium factor is generally around 0.6. This is not surprising since the values measured on a pile are mainly influenced by the radon emissions issued from the pile itself. The radon atoms that emanate from the pile do not travel a long time before reaching any receptor situated on the source itself or even in its immediate vicinity. So the equilibrium factor of the radon exhaled from the pile is expected to be relatively low compared to the equilibrium factor of the radon from regional background which originates from more remote places and has travelled for a longer time before reaching the detector. Nevertheless, the equilibrium factor is certainly influenced also by the contribution of the radon background, which is substantiated by the presence of an appreciable proportion of ^{214}Bi. The last radionuclide might probably derive entirely from the contribution of the regional background. If so, this would allow to reconstruct the natural and the industrial part of the air contamination measured on a pile. The validation of this approach will necessitate further studies on the proportion of radon short-lived daughters above and far from waste piles. These studies would only be feasible after having improved the radon daughter measurement technique to get a better precision under the conditions of low radon levels and frequent changes in wind direction commonly met in the open environment. Further investigations will be performed accordingly.

A tentative model of radon dispersion above waste piles (Y. Belot)

While our colleagues from GRS (cf. project 3) have concentrated their efforts on the modelling of the radon dispersion at a relatively large scale (a few km from the sources), and on the study of the influence of a complex orography on the radon transport, we tried in the present work to model the dispersion of radon at a very close distance from the sources or even above the sources themselves. The interest of this research was raised by the observation that the highest radon concentrations are found above the sources and that the supplement of concentration due to the source rapidly vanishes as the distance from the sources increases.

The particularity of radon emission resides in the fact that the sources of this element are strictly situated at ground level. In consequence, the transport of radon atoms initially occurs in the region adjacent to the ground where the vertical gradient of horizontal wind speed is very large compared to the other levels in the atmosphere. It can then be inferred that the dispersion at close distances from the sources will be greatly influenced by the presence of vegetation and various obstacles that determine the structure of the surface boundary layer and particularly the structure of wind speed and turbulence profiles in the first meters above ground level. A first attempt was done to incorporate this influence in the classical models of a Gaussian type that are widely accepted as practical tools for estimating the long-term average concentrations due to multiple sources emissions.

The classical models to determine the average annual air concentrations that result from area-sources are based on the geographical distribution of the source strength and the distribution of specific meteorological data. The concentration at a given point is obtained by summing up the contributions of the elementary point sources over the different categories of wind direction, wind speed and atmospheric stability. The contribution of an elementary point-source to the

total concentration at a specified point is calculated by cross-wind integration of the classical Gaussian formula and given by the following formula:

$$C(V, S; r) = [0.798\ Q / (r\ \omega\ u_m\ s_z)] \exp [- 0.5\ (h/s_z)^2]$$

where C is the long-term average radon air concentration for a given weather situation; V and S are integers that denote respectively the wind speed and stability classes; Q the radon source strength; r the distance between the source and the receptor; ω the angle enclosed by a wind direction sector (in radians); h the sampling height above the source level; u_m the average wind speed representative of the wind speed class considered ; s_z the standard deviation of the vertical concentration distribution, which is function of distance and stability.

In the classical model u_m is defined as the wind speed at a standard height above ground level (usually 10 m) and kept constant throughout computation. We propose, following the suggestion already made by a few investigators, to replace this constant wind speed by an average advective speed that increases with downwind distance from the source. This variable speed is intended to characterize in a more realistic way the average horizontal speed of pollutant transport in each vertical section of the plume. This speed will be very low close to the source and will increase gradually with the vertical extension of the plume that occurs downwind the source. It was shown that the best estimate of this variable advective speed should be $u_m = u(0.6\ s_z)$, the function u(z) describing the average vertical profile of wind speed.

In the case of a woody landcape such as the Lengenfeld site, the presence of trees results in a dampening of wind speed close to the ground surface. The wind speed profile can be described as linear-logarithmic above the top of the trees and exponential below. If such a profile is used in the calculation, as precedently shown, and if the flux measured on the site is used to characterize the distribution of source strength, the predicted yearly average concentrations are respectively 300 and 359 Bq m^{-3} at the center of the main sources of Lenkteich and W. Nordhade respectively. These values do not differ very much from the values actually measured on the site at the same places. Nevertheless, this should not dissimulate some difficulties. It is for instance particularly difficult to characterize the boundary layer over a terrain of variable roughness. The boundary layer properties and particularly the vertical wind speed profiles given in the literature as representative of low level boundary-layer properties over the land are those observed over fairly extensive flat plains with no more cover than homogeneous forest or low vegetation. In general, and specially on the site which was studied in the present work, the relevant surface properties are affected by the patchiness of the vegetation cover and the presence of individual obstacles ranging from bushes and hedges to woods and buildings, and also to some degree by the natural topography of the landscape. While this spatial inhomogeneity does not affect very much the dispersion of pollutants from a high stack, it becomes of greater importance when the source is at ground level and the receptor very close to the ground at a short distance from the source.

Publications

S. Raviart, P. Richon, D. Haristoy, M.C. Robé and Y. Belot (IPSN); M. Kümmel, C. Düshe and W. Ullmann (BfS) "Field determination of the time-varying equilibrium factor between radon-222 and its short-lived decay products in the atmosphere above a waste-rock pile" *6th International Symposium on the Natural Radiation Environment*, NRE VI, June 5-9, 1995, Montreal (to be published in *Environment International*)

Y. Belot, H. Camus, S. Raviart, D. Haristoy, P. Richon and M.C. Robé (IPSN); R. Martens, K. Maßmeyer, M. Kümmel and C. Dushe (GRS/BfS) "Atmospheric dispersion of radon from uranium mining and milling wastes: tentative model and field data" *6th International Symposium on the Natural Radiation Environment*, NRE VI, June 5-9, 1995, Montreal (to be revised).

Part II : Aquatic pathway (contributors : D. Stammose, S. Bassot, G. Biton)

II. Objectives for the reporting period

The aim of this study is to improve our knowledge on the mobility of the radionuclides in an uranium mill tailing site. During this period, field experiments have been conducted on a german site (located in Lengenfeld) which contains 300 000 m^3 of tailings covered by a sandy soil. The drillings of observation wells have allowed to obtain several cores. The analysis of different samples of these cores (solids and solutions) have allowed to precise the geochemistry of the residues.

III. Progress achieved including publications

a) field experiments

The description of the site and the location of the drillings are detailed in the part III (J.LARUE). During the field investigation period (11-22 of July), drillings have given samples of surface layer, uranium mill tailings and underlying soil. An evolution of the color of the samples (greenish to redish) has led us to assume a reducing medium. Some differences in the tailings textures obtained in the cores RKS1(clayeous) and GWP5 (sandy) have been observed. Immediately after the drilling, a part of the samples have been squezzed in order to obtain the solutions in contact with the solids. For the tailings, the volume of solution obtained was low because of their high plasticity.

b) laboratory experiments

The chemical composition of the solutions have been determined as precisely as possible considering the low volume of solution obtained in some cases (tailings). The chemical composition (both major and minor elements) of the solids have been determined and their mineralogical compositions have been obtained through X Ray diffraction patterns. In this report, we will present the main data concerning the RKS1 cores.

c) results and modelling

Surface layer

The particles size is less than 150μm. The solid is mainly constituted with quartz (65 %), micas (7.5 %) and fluorite (9.5%). The amount of carbonate is relatively low (see Table 1). The high content of baryum (up to 10000 ppm) is in agreement with the nature of this sand (see GRS contribution). The pH of the solution is closed to 8, and slightly increases with depth (7 to 8.2). The concentrations of calcium and magnesium in the solution decrease with depth while the concentrations of sodium and potassium increase. At least no trace of uranium and radium were detected in the solid or in the solution.

Although only 3 samples have been analysed, their composition have been used in a geochemical code , CHIMERE, in order to precise the nature of the solid phase controlling the solution composition. In this layer, the solution composition is fixed by the carbonate phases, calcite ($CaCO_3$) and dolomite ($(CaMg)(CO_3)_2$). This result has to be confirmed by complementary analysis.

Tailings

The granulometry of the tailings particles is very low (less than 10μm). The mineralogical composition of the solid is given in Table 2. The content of quartz is lower than in the surface layer, and the carbonate phase is mainly dolomite (or magnesian calcite). The solution obtained by squeezing is basic (10.2) and contain an important amount of sodium arising probably from the chemical treatment. These results have led us to assume that the ore has a sedimentary origin, and the applied chemical treatment is a basic one. The contents of radionuclides has been measured (see Table 2).

According to litterature data and to chemical results (basic pH and reducing medium), a modelling has allowed to define the speciation of the different components and the nature of the phase controlling the chemical composition. The dolomite controls the solution composition. According to thermodynamic data, uranium is present as an anionic species, $UO_2(CO_3)_3^{4-}$. The retention of this species is very low. But the stability range of this carbonate complexe is very narrow and as soon as the pH decreases until pH 8 (with Eh<0), uranium carbonate precipitates. Therefore its mobility decreases significantly.

At least, complementary studies on the mineralogical composition of samples obtained at different depths will allow to point out a possible weathering of the solids.

Underlying soil

As it is mentionned in the GRS contribution, this layer is constituted by the sediment of the river. A high heterogeneity of the particle size is observed. No sample of the RKS1 core have been available for our experiments. Therefore, we discuss here the data obtained on the RKS4 cores. The solid and solution compositions are present in Table 3. The granulometry, the particles shape and the chemical composition of the solids are quite representative of river sediments. Uranium, radium and lead have been easily measured in solids and solution samples (see Table 3).These radionuclides have migrate from the tailings to the first 50 cm of the soil. Measurements of the content of uranium at different depths will confirm this mobility.

The study of others samples of the different components of the cores will allow to elucidate the processes responsible of the chemical behaviour of the contaminants. Moreover, detailed observations of the solid phases will allow to point out a possible weathering of the mineralogical phases present.

Publications :

S.BASSOT, D.STAMMOSE and C.DUBOIS : Study of the uranium mill tailing source term : First results of modelling, presented at Migration-95, St Malo, 10-15 September 1995

L. De WINDT and S.BASSOT : Preliminary modelling of 226-Ra and U speciation and transfer in weathering waters and underlying soil within the Lengenfeld uranium mill tailings presented at Migration-95, St Malo, 10-15 September 1995

Solid phase	Solution
particles size less than 100µm	Eh < 0, pH = 8.2
SiO_2 73 %	[Ca] = $1.5\ 10^{-4}$ M
Al_2O_3 4 %	[Mg] = $8.6\ 10^{-5}$ M
CaO 8 %	[Na] = $2.7\ 10^{-3}$ M
Fe_2O_3 8 %	[K] = $5.9\ 10^{-4}$ M
$Na_2O + K_2O$ 1 %	[Al] = $1.1\ 10^{-3}$ M
Quartz 65 %	
Micas 7.5 %	
Feldspars 1.5 %	[Sulfate] = 10^{-6} M
Carbonate 3.5 %	
Kaolinite 2.5 %	
Fluorite 9.5 % Clorite 2.5 %	

Table 1 : Characteristics of the surface layer

Solid phase	Solution
particles size < 10µm	Eh < 0, pH =10.2
SiO_2 51 %	[Ca] = $1.1\ 10^{-4}$ M
Al_2O_3 16 %	[Mg] = $2.1\ 10^{-5}$ M
Fe_2O_3 8 %	[Na] = $6.2\ 10^{-2}$ M
$Na_2O + K_2O$ 5 % ; MgO 3 %	[K] = $3\ 10^{-4}$ M
Quartz 25 %	[Al] = $3.1\ 10^{-3}$ M
Micas 35 %	
Feldspars 7.5 %	
Dolomite 7.5 %	
Kaolinite 9 %	
Swelling clays 2.5 %	
[U-238] = 2.7 Bq/g	Ut = 7.7mg/l
[Pb-210] = 14.5 Bq/g	[Ra-226] = 1 Bq/l
[Ra-226] = 16.9 Bq/g	

Table 2 : Characteristics of the tailings

Solid phase	Solution
wide range of particles size 25µm to 5 cm	Eh < 0, pH = 8.3
SiO_2 70 %	[Ca] = $8.7\ 10^{-4}$ M
Al_2O_3 15 %	[Mg] = $6.7\ 10^{-5}$ M
Fe_2O_3 3 %	[Na] = $5.5\ 10^{-3}$ M
$Na_2O + K_2O$ 8 %	[K] = $1.4\ 10^{-4}$ M
Quartz 33 %	[Al] = $2.6\ 10^{-4}$ M
Micas 20 %	
Feldspars 22 %	[Sulfate] = $3.8\ 10^{-4}$ M
Dolomite 3 %	
Kaolinite 9 %	
Swelling clays 3 %, Chlorite 3 %	
[U-238] = 5.2 Bq/g	
[Pb-210] = 6.7 Bq/g	[Ra-226] = 0.3 Bq/l
[Ra-226] = 5.9 Bq/g	

Table 3 : Characteristics of the underlying soil

Head of project 2: Prof. Röhnsch

II. Objectives for the reporting period

During the reporting time period the objectives were:

(1) investigation of the aquatic pathway at the Lengenfeld site (Saxony, Germany)

- assistance in the field experiments to investigate the hydraulic system of the tailings pond and the transport of radionuclides (mobilisation from the tailings pond and retardation within the geosphere),
- measurement of the concentration of U-238, Ra-226 and Pb-210 in samples of water and solids taken at the tailings pond and its geological ground and,
- measurement of the U-238, Ra-226 and Pb-210 concentration of liquid and solid samples from batch- and column experiments carried out by a sub-contractor in order to calculate k_D-values and

(2) investigation of the equilibrium factor of radon in the atmosphere

- additional investigations to measure short-term equilibrium factors of radon on, and close to, a large waste rock pile in Crossen (Saxony, Germany), and,
- measurements of long-term equilibrium factors of radon on a large waste rock pile in Crossen, and,
- during short-term and long-term investigations, simultaneous measurements of meteorological parameters.

III. Progress achieved

1. Aquatic pathway

1.1. Assistence in the field experiments

From 11 till 22 of July 1994 a joint field experiment at the Lengenfeld site was carried out by IPSN, GRS and BfS in order to investigate the hydrological and geological conditions of the site and to take samples from materials required for special measurements by the laboratories of IPSN, BfS and the sub-contractor. During that time five boreholes were drilled into the tailings pond by a drilling company.

Apart from the organisation of good prevailing conditions for a successful course, it was the task of the BfS to

- measure the gamma-dose-rate at the drilling locations and at the drilling cores,

- take and prepare the sample materials from the drilling cores which were designated for following investigations and
- take samples from groundwater also designated for following investigations.

1.2. Measurement of the concentration of U-238, Ra-226 and Pb-210 in solid samples

As a result of the drilling the following solid samples were taken from the tailings pond:

drilling point	total number of samples	number of samples from cover material	number of samples from tailings	number of samples from sediments
GWP 5	17	0	10	7
RKS 1	4	1	3	0
RKS 2	4	1	2	1
RKS 3	3	0	3	0
RKS 5	8	1	3	4
total	36	3	21	12

After preparation the concentrations of U-238, Ra-226, Pb-210 and other nuclides of the U/Ra decay-chain were measured by using a GMX (n-type, high purity germanium) detector. Following ranges of concentration were determined:

kind of material	concentration in Bq/kg	concentration in Bq/kg	concentration in Bq/kg
	U-238	Ra-226	Pb-210
cover material (barite)	88 - 350	54 - 3 100	< 30- 3 000
tailings	540 - 5 000	2 030 -19 700	1 460- 17 300
sediments	95 - 490	77 - 250	50 - 220

The measurements were finished.

1.3. Measurement of U-238, Ra-226 and Pb-210 in samples of groundwater

Along the longitudinal axis of the tailings pond five groundwater observation wells are placed. During the field experiment nine samples of groundwater from different depths were taken and the concentration of U-238, Ra-226 and Pb-210 were measured using radiochemical methods. The following ranges of concentration were determined:

nuclide	range of concentration in mBq/l
U-238	222.6 - 25750
Ra-226	15.59 - 2172
Pb-210	39 - 8180

The measurements were also finished.

1.4. Measurement of U-238 and Ra-226 in liquids of batch and column experiments

In order to calculate the specific k_D-values for U-238, Ra-226 and Pb-210 batch and column experiments were carried out by a sub-contractor. For the experiments sixteen tailings samples and three sediment samples were choosen. The liqiud samples from these experiments were investigated by using laserinduced phosphorescence to measure the U-238 concentration and the emanometry to measure the concentration of Ra-226. The concentration of Pb-210 could not be measured (low sample volume and concentration) . The following ranges of concentration were determined:

kind of material	kind of experiment	concentration in mBq/l U-238	concentration in mBq/l Ra-226
tailings	batch	0,375 - 97 500	77 - 2 155
sediment	column	15 000 - 67 625	

Because of the time-consuming method the measurements of the Ra-226 concentration in liquid samples from the column experiments are not finished yet.

All results of the measurements are used for modelling the amount of radioactivity present in the tailings pond (inventory).

2. Atmospheric pathway

2.1 Organization of the field experiments

The joint field investigations to determine the short-term equilibrium factor between radon and its short-lived progeny and the meteorological parameters were organized by BfS and carried out 17-21 August 1994 at Crossen (Saxony, Germany).

Additional BfS made the field experiments to determine as well as the long-term equilibrium factors and the meteorological parameters at Crossen until 10 January 1995.

2.2 Measurement of meteorological parameters

Investigations of the correlation between equilibrium factor and the state of the atmospheric stability require simultaneous measurements of meteorological and radiological data.
BfS installed a meteorological mast on the waste rock pile Crossen.

During the field experiments the following data were measured in a 10 s interval and saved as a 5 min average in a datalogger:

* wind direction (10 m above ground)
* wind speed (8 m and 2 m above ground)
* air temperature (1 m, 2 m, 4 m and 8 m above ground)
* relative air humidity (2 m above ground)
* precipitation

The collected data were prepared and sent to the IPSN for further evaluation.

2.3 Investigations to determine short-term equilibrium factor

During the short-term experiment BfS carried out the following investigations on the waste rock pile (close to the BfS mast):

2.3.1 Measurement of the equilibrium factor

The continuous determination of the equilibrium factor by one equipment ("Megarad 04") was carried out from 16/8/94 to 18/8/94 (0.4 m above ground, measurement interval: 2h).

For the time period a mean value of equilibrium factor of 0.20 was obtained (mean value of Rn-222 concentration: 48.5 Bq/m^3).

The continuous determination of the equilibrium factor by simultaneous measurement of the Rn-222 gas concentration ("alphaguard", measurement interval: 10 min) and the short-lived daughters ("AMZ 200", measurement interval: 1 h) was carried out from 16/8/94 to 7/9/94 (0.4 m above ground) with the following results:

	mean value	minimum	maximum
Rn-222 concentration in Bq/m^3	104	2	3200
Rn daughters concentration in WL	0.0034	0.0003	0.0196

2.3.2 Measurement of the unattached fraction of Rn daughters

In addition to the measurements of the equilibrium factor BfS investigated the unattached fraction of Rn daughters in the atmosphere. For the period from 17/08/94 to 21/08/94 six measurements were carried out with the device "RGR-11". All results show a unattached fraction of potential alpha energy concentration of short-lived Rn daughters in a range of 4 to 6 % .

2.3.3 Measurement of size distribution of aerosols

The size characteristics of the aerosols in the atmosphere are important parameters for estimation of radiation exposure due to inhalation of short-lived Rn decay products.
From 16/8 - 17/8/94 (24 h) BfS has measured the dust concentration in the atmosphere on the waste rock pile for classes of diameters of aerosols. The size ditribution measurements were performed using two cascade impactors (Berner- and SIERRA-impactor).

The results of the measurements were prepared and sent to, and subsequently discussed with, the IPSN.

2.4 Investigations to determine the long-term equilibrium factor

The following investigations were carried out till 10/01/1995:

* Continuous determination of the equilibrium factor by "Megarad 04" on the waste rock pile (location: close to BfS mast and 0.4 m above ground, measurement interval: 2h).

  Following means of the equlibrium factor and Rn-222 concentration were obtained:

Time period	equilibrium factor	Rn-222 concentration in Bq/m^3
06/09/94-06/10/94	0.14	150
11/10/94-07/11/94	0.11	370
01/12/94-10/01/95	0.06	530

* Additional measurements of long-term Rn-222 concentration by E-PERM-System. During the long-term experiment, five E-PERMs were exposed. Three measurement points were located on the waste rock pile (close to BfS mast and 1.5 m, 1.2 and 0.65 m above ground) and two points adjacent to the waste rock pile (Niederhohndorf and Berthelsdorf). The measurement intervals of E-PERM-System and ALGADE-System (IPSN) were the same (about four weeks).

Following Rn-222 concentrations in Bq/m^3 were obtained:

Exposure time	Nr.1	Nr.2	Nr.3	Nr.4	Nr.5
16/08/94-21/08/94	109	30	47		
21/08/94-07/09/94	56	37	51	28	22
07/09/94-05/10/94	64	46	66	23	17
05/10/94-07/11/94	91	126	138	26	21
07/11/94-01/12/94	80	97	96	16	15
01/12/94-15/12/94	113	101	161	14	14
15/12/94-10/01/95	17	78	81	20	15

Measurement point number	location
1	waste rock pile, BfS mast, 1.5 m above ground
2	waste rock pile, BfS mast, 1.2 m above ground
3	waste rock pile, BfS mast, 0.6 m above ground
4	Niederhohndorf, garden Uhlig, 1.5 m above ground
5	Berthelsdorf, garden Müller, 0.60 m above ground

The results of the measurements were prepared and sent to, and subsequently discussed with, the IPSN.

Head of Project 3: Prof. Dr. Maßmeyer

PART I: Atmospheric pathway (contributors: K. Maßmeyer, R. Martens)

II. Objectives for the reporting period

In the context of uranium mining and milling activities large waste disposal sites which serve as area sources for airborne radon and radon progeny concentration often can be found. Radon emanating from these irregular shaped areas is continuously transported to the neighbouring regions, possibly leading to enhanced radiation exposure. In order to assess the environmental effects of radon, different approaches to model atmospheric dispersion can be applied. Simple graphical schemes (nomograms) display the decrcease of radon concentration with increasing distance from a homogeneous area source. Using Gaussian type models (for area sources) the long term areal radon distribution in flat terrain can be evaluated including inhomogeneous source conditions. These calculations are based on frequency distributions of specific meteorological data and the geographical distribution of the source strength. In orographically structured terrain additional data like orography and land use information have to be taken into account and a numerical flow model has to be applied coupled with a threedimensional dispersion model.

Within the reporting period GRS has concentrated on modelling atmospheric dispersion of radon from large area sources with models of different complexity. Data concerning source term and meteorological information have been sampled by IPSN and BfS, focussed at the site of Lengenfeld (Saxony). In Lengenfeld a field experiment has been carried out during one week in September 1993. Horizontal variability and time dependence of radon exhalation rates, radon concentration in the ambient air and meteorological parameters have been measured. To describe long term radon dispersion in the environment of Lengenfeld meteorological and radon concentration data sampled over a one year period have been used for model intercomparisons and validation studies.

III. Progress achived including publications

Within the last decade a multitude of new dispersion codes have been developed (attributable to the different types of models i.e. Lagrangean particle models, Gaussian puff models, Eulerian models). These models are capable of handling threedimensional and time dependent meteorological data and inhomogeneous source conditions in space. Already in simple conditions (flat terrain, stationary meteorology) the use of such models is attractive due to their ability of handling wind and turbulence data varying with height. Today these models are operational on a PC. With a normalized source strength and specified meteorological conditions these models can be used for preparation of nomograms displaying the decrcease of radon concentration with increasing distance from a homogeneous area source. In case that no detailed meteorological information and/or source term data are/is available these nomograms can be used for a first guess concerning the environmental situation (e.g. worst case scenarios). Based on more detailed input data complex models can be used.

Within the project three different models have been compared. The Lagrangean particle model LASAT has been used to construct the above mentioned nomograms which can be used to assess maximum radiation exposure for specified meteorological conditions as well as long term exposure if the statistical distribution of meteorological conditions is known. Such statistical

kind of input can also be used to drive the dispersion model MILDOS (Gaussian plume model for level terrain and area sources with adapted dispersion parameters for near surface release) distributed by NEA. Whereas the use of nomograms for long term calculations only neccessitates a pocket calculator, for a MILDOS run a PC has to be started. In a orographically structured terrain the use of MILDOS is no longer appropriate because this model does not encounter any orographical influence on atmospheric dispersion. This can be achieved by running a coupled flow and dispersion model namely the model system WITRAK developed at the Meteorological Institute of the University of Cologne.

Within the reporting period it has been shown that all three modelling approaches give a similar source distance dependance of the airborne radon concentration. This result enables the implemantation of a three step procedure to assess the radiological impact of waste disposals originating from milling and mining activities:

1. Use the nomograms calculated with LASAT for a first guess of the radon concentration on and in the neighbourhood of an area source. Wind speed data and source strength can be handled as normalizing parameters. As an example in fig. 1 such a nomogram is shown for diffusion category D, a wind speed of 5 m/s and a source strength of 1 Bq/(m²s).

2. In case of an irregular shaped area source with inhomogeneous source strength but approximately level terrain use MILDOS to calculate the radon concentration in space. In the limit of homogeneous source strength method 1 and 2 give comparable results.

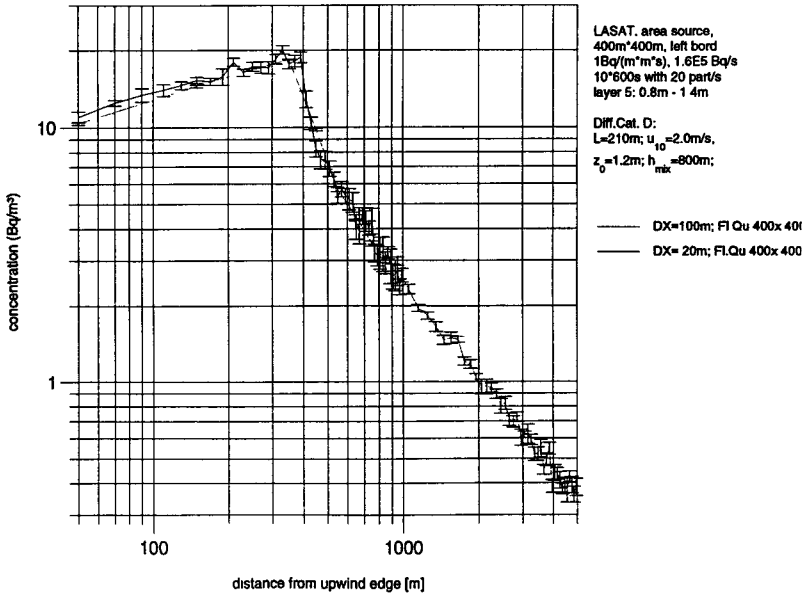

Fig. 1: Dependance of the near surface radon concentration following the centerline of a square shaped area source (400 m x 400 m). The concentration first is built up as long as the atmospheric radon transport takes place over the source (0 - 400 m), the concentration falls off leeside the source (400 - 1000m). In a former report it has been shown that LASAT-nomograms and MILDOS-calculations give similar results.

3. If the calculational domain is no longer flat, in addition to step 1 (as a first guess) a complex flow and dispersion model has to be used. Similar to the MILDOS code inhomogeneous source term data can be handled with such a model but in addition the influence of the orography on atmospheric dispersion can be displayed. In fig. 2 the additional radon impact (mean value) in the Lengenfeld area (in Bq/(m³)) as calculated with the models MILDOS and WITRAK is shown . The results of both models show similar concentrations near by and far away of the source. But orographical influences on the isoconcentration lines (due to channeling of the flow during a certain percentage of the year within the valley regions) are only present in the results of WITRAK. However the source strength in this area is so low that a significant enhancement of the background concentration of radon (30 Bq/m³) can only be found within 500 m distance from the source.

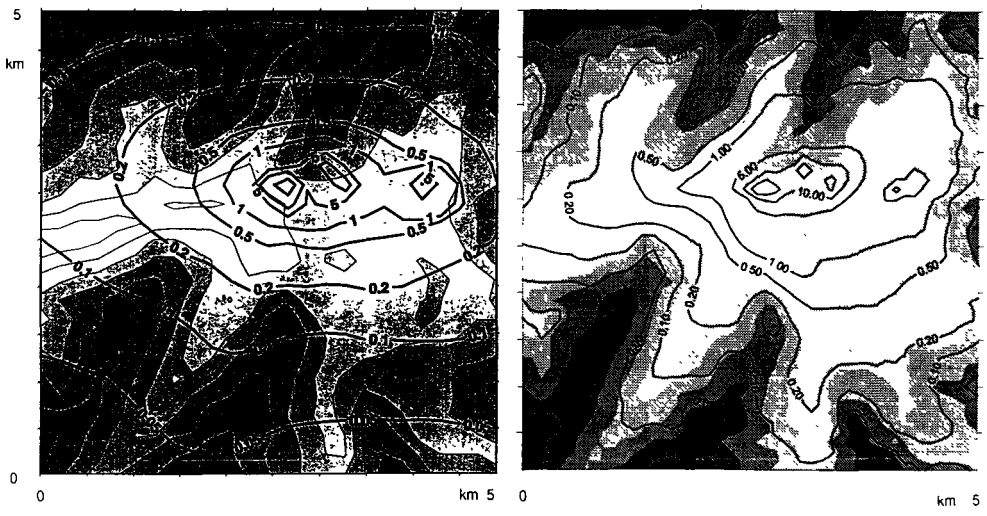

Fig. 2: Additional radon concentration (yearly mean vaue in Bq/m³) in the Lengenfeld area calculated with the models MILDOS (left) and WITRAK (right).

Publications:

K. Maßmeyer, R. Martens, R. Bendick, M. Kümmel, C. Dushe and Y. Belot; Modellierung der Langzeitausbreitung von Radon aus Flächenquellen in der Umgebung von Uranbergbau- und Aufbereitungsanlagen; 9. Fachgespräch zur Überwachung der Umweltradioaktivität, München-Neuherberg, 25. - 27. April 1995.

PART II: Aquatic pathway (contributor J. Larue)

II. Objectives for the reporting period

Objective is the identification of specific natural conditions with favour high mobility or strong fixation of natural uranium. The contribution of the GRS in the joint project 'Migration- and Fixation Study of Natural Uranium under Exogenic Conditions' consist of:
(i) planning and managing the field studies and laboratory experiments for the investigations of the industrial settling pond (IAA) of the Lengenfeld site.
(ii) acquiring hydrogeological field data from investigations at the Lengenfeld site,
(iii) organising hydrochemical and laboratory experiments on water and soil samples of the industrial settling pond (IAA) at the Lengenfeld site,
(iv) hydrochemical and hydraulic modelling of the groundwater content and groundwater movement out of the settling pond (IAA).
During the first reporting period field investigations had been done for two weeks (11 - 22 of July) during drillings of observation wells. The aim of the drillings was to get soil samples and to install groundwater observation wells. In the time period of 15 - 19 August hydrogeological investigations (pumping tests, hydraulic head measurements and sampling of groundwater) had followed. The period up to December 31st, consisted in geotechnical and hydrochemical laboratory experiments on the soil and water samples. In the last period (until 31st of April) laboratory experiments (column and batch-test) were carried out to get data for the modelling of the radionuclide transport out of the settling pond. Therefore a hydrogeological model was generated to simulate the groundwater movement out of the settling pond.

II. Progress achieved

1) Field experiments in Lengenfeld (Saxony)

The experimental devices and method including a hydrogeological site description are described in a GRS - report. The full data obtained will be written in a Technical Report entitled: **"Investigations on the Aquatic Pathway Releases at the Lengenfeld Site** (Industrial Settling Pond)" (in preparation).

Figure1: Map of the IAA Lengenfeld

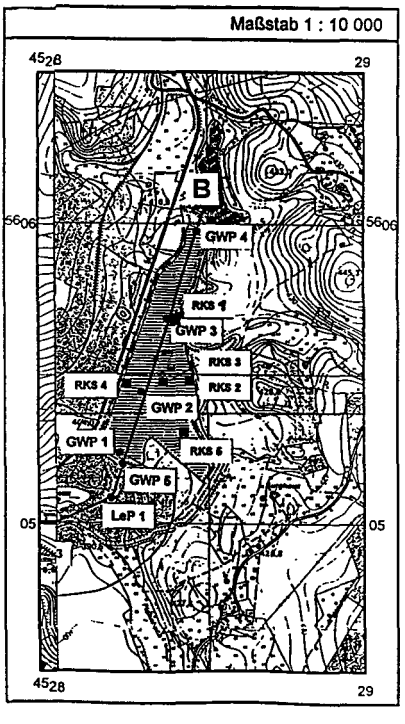

Detailed knowledge about the hydrogeological behaviour of the settling pond and its radionuclide soil inventory are essential for the determination of source terms and locality-dependent transport phenomena of radionuclides. Therefore 5 observation wells (RKS1-5, see figure1) had been drilled to get samples of the contaminated (tailings) and uncontaminated (barytesand) soil of the settling pond. Furthermore a groundwater observation well (GWP5) was installed in the aquifer (weathered zone of granite) below the tailings. The geological investigations on the samples are used to generate a hydrogeological cross section through the settling pond (see figure1). Hydraulic and hydrochemical data had been collected by using the five groundwater observation wells shown in figure1. They are filtered in the tailings and the sand layer above (GWP1-4) or in the weathered zone downstream the settling pond (GWP5, LeP1). The measured average groundwater level of the settling pond is shown in figure1.

The sequence of the layers filling the settling pond can be described as follows: Basis of the sequence is a granite formation with low permeability. In the interface between the granite and tailings an aquifer build by riversediments and weathered zone (" Verwitterungszone des Grundgebirges" is situated. The thickness differs between 3 and 5 meters. At its top a sequence of tailings material with different sediment behaviour is the situated. The thickness follows the former valley slope, the biggest tailing sequence is 25 meters in front of the dam. The tailings are covered by baryt-sands ("Fluß-/ Schwerspatsande) up to a thickness of 10 meters.
A hydraulic pumping test had been made by pumping and measuring GWP5. During this test and over a period of a year groundwater samples were taken and analysed in laboratory.

Figure2: Hydrogeological cross section through the IAA Lengenfeld.

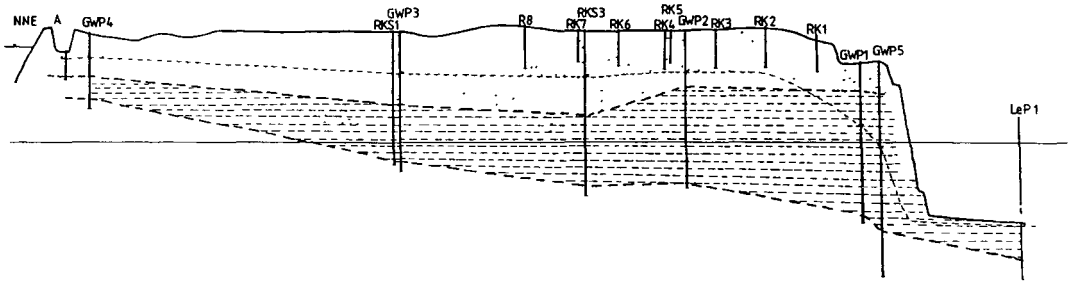

For bilancing the hydrological system of the Lengenfeld site measurements on rainfalls and surfacewater-flow of the small rivers situated near the site had been carried out. Moreover discharge tests in observation wells (slug test) had been performed to get hydraulic data for the different layer of the IAA. Together with the pumping test and geotechnical laboratory tests they lead to the hydraulic data used in the simulation of the NAMMU-model (see table 2).

Figure3: Geochemical and soil-geological results from GWP 5

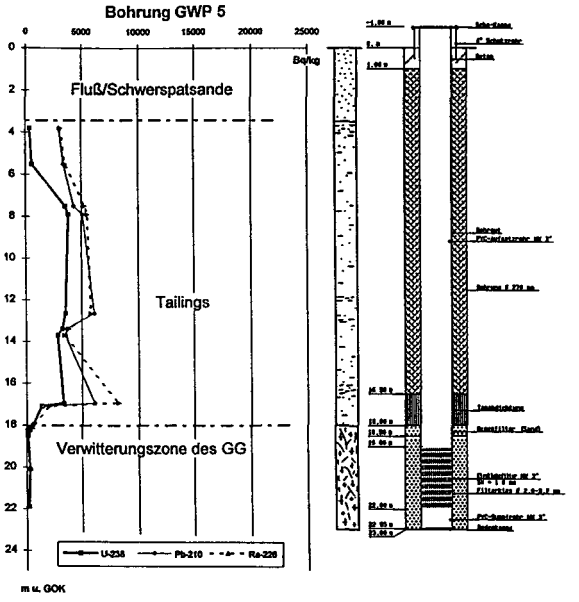

2) Hydrochemical and Geotechnical laboratory experiments

Field investigations had been performed on the settling pond (IAA) of a former uranium processing plant in Lengenfeld by probing and analysing soil profiles and groundwater. According to our present knowledge soils and contaminated water in this industrial drainage basin (IAA) have different geochemical and soil-geological qualities (see figure3).
The experimental devices and methods used in these determinations are described in detail in a special GRS-report. Table 1 shows the different types of groundwater in the groundwater body IAA (first three columns) and some typical groundwater components of the granite Aquifer passing the IAA.

Table 1: Average concentration of uranium in the different layer

Components (mg/l)	weathered granite upstream IAA	baryte sand	tailings	weathered granite below IAA	weathered granite downstream IAA
uranium	0.0004	0.0050	1.3200	0.1440	0.8700
HCO_3^-	33.1000	132.2000	378.7000	362.0000	213.7000
SO_4^{2-}	151.0000	416.5000	97.5000	223.0000	198.3000
Cl^-	12.7000	15.2300	53.0000	51.8300	50.8600

The average concentration of main components of the ground- and pore water in the different observation wells (anions and uranium) are shown in figure 5.

Figure4: Development of the kation concentrations in groundwater and ground water level of the observation well LeP1 downstream the IAA

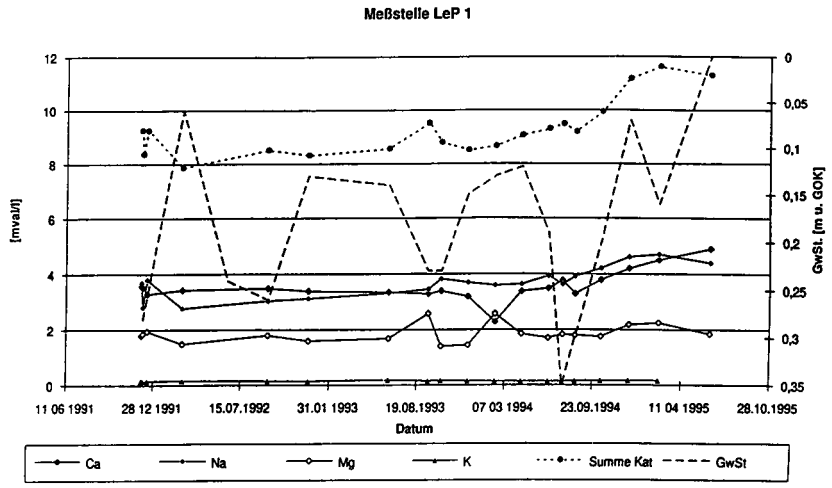

The long-term observation (Period 1991 -1995, see figure4) of groundwater-components and head-measurements downstream the settling pond shows a nearly constant source term independent from rainfall (piecometric head). Comparing the uranium - radium content of the groundwater below the drainage basin (GWP5) and 100 meters downstream (LeP1) shows that there is high influence of drainage water, which infiltrate into the aquifer after passing the dam (see figure5).

Figure5: Concentration of anions and uranium along the cross section

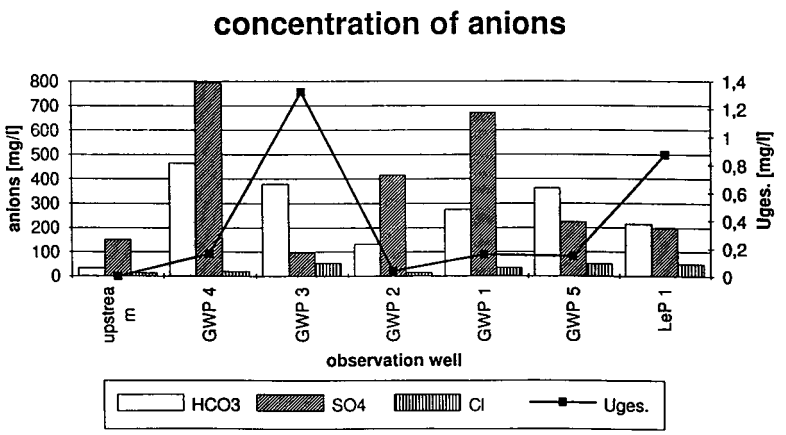

To get a better knowledge of the hydrogeological situation of the settling pond geotechnical investigations and sedimentological analyses of the cores sampled in liners were carried out. Samples from the three different layers (baryte-sand, tailings and sand of weathered zone)

were analysed. The typical grain size distribution of these layers is shown in granulometric curve in figure6.

Figure6: Typical particle-size distribution of the sediments building the 3 layers of the IAA

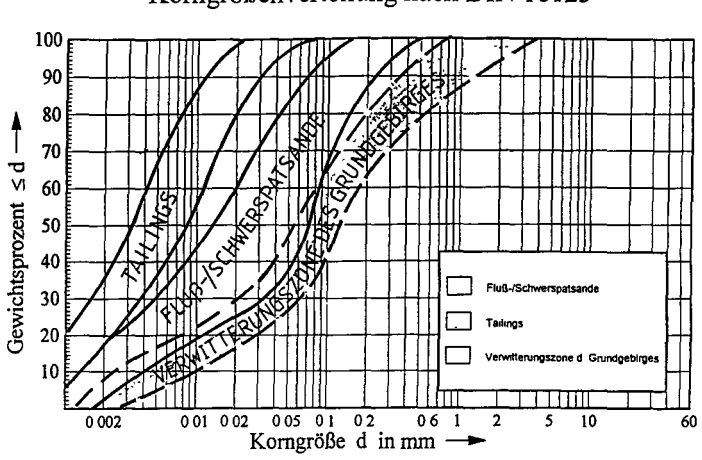

Determination of uranium mobilisation by seepage from associated materials is the most essential factor contributing to future spreading of toxic material. Therefore the tailings sampled by observation wells in liner were studied by leaching experiments in columns and batch tests, furthermore percolation studies were adjusted to natural conditions.

3)Physicochemical and Hydraulic Modelling

Elution studies were complemented by theoretical considerations of mobile uranium species stability fields in aqueous solutions as well as solubility characteristics of stable uranium species. Hydraulic and geochemical modelling of the IAA are done with the codes PHREEQE and NAMMU. They allow simulations of various factors which govern uranium solubility. They calculations will be closed after getting all results from the batch tests. Thus in combination with the experimental study key answers will be obtained for construction of "natural" geochemical barriers and for transport of radionuclides in the geosphere. The two-dimensional FE-model grid used for the NAMMU-code is shown in figure7. The input-data used for the first groundwater simulations are shown in table 2.

Table 2: Input-data for the simulation of Groundwater with the NAMMU-code

hydraulic conductivity (m/s)	pumping-test	slug-test	granulometric analysis
weathered granite below IAA (GWP5)	$2 \cdot 10^{-5}$ - $3 \cdot 10^{-6}$	$2 \cdot 10^{-5}$ - $3 \cdot 10^{-6}$	10^{-6} - 10^{-7}
baryte sand			10^{-6} - 10^{-8}
tailings		$3 \cdot 10^{-7}$	10^{-7} - 10^{-8}
weathered granite downstream (LeP1)	10^{-5}		

Figure7: NAMMU 2D-model grid , generated by using the cross section of figure2

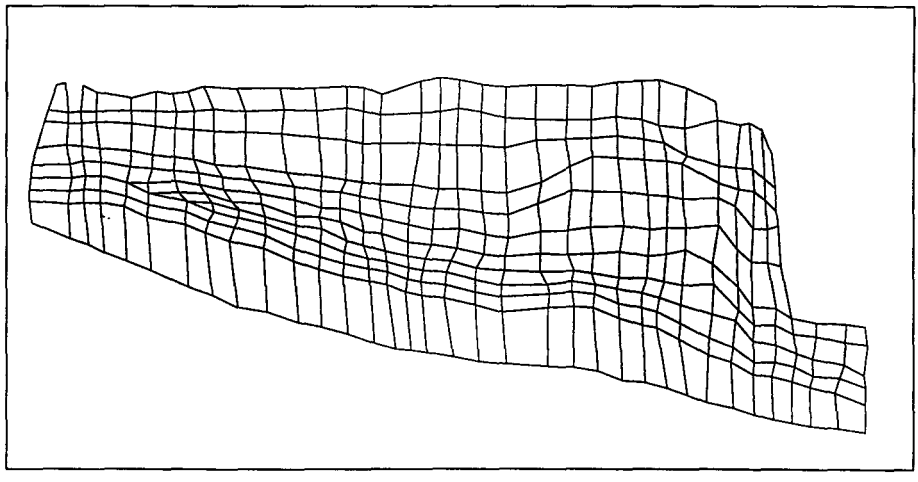

Puplications:

J. Larue;
Bewertung der Grundwassergefährdung durch radioaktive Altablagerungengen (Fallbeispiel Lengenfeld)
17. GRS-Fachgespräch, Köln, 6. und 7. Oktober 1993

J. Larue, G. Henze, I. Schall
Standortanalyse Lengenfeld
18. GRS-Fachgespräch, München, 6. und 7. Oktober 1994

Final Report
1992-1995

Contract: FI3P-CT920010 **Duration: 1.9.92 to 30.6.95** **Sector: A23**

Title: The bio-availability of long-lived radionuclides in relation to their physico-chemical form in soil systems.

1)	Lembrechts	RIVM
2)	Wilkins	NRPB
3)	Cremers	Univ. Leuven (KUL)
4)	Merckx	Univ. Leuven (KUL)
5)	Staunton	INRA - Montpellier
6)	Berthelin	CNRS
7)	Mocanu	ROIAP (PECO-contract)
8)	Szabó	NRIRR (PECO-contract)

I. Summary of Project Global Objectives and Achievements

The project concentrates on the processes governing the availability to biota of long-lived radionuclides present in soil. An analysis of the distribution of radionuclides between solid and liquid phase and of their accumulation from the liquid phase by biota is of special interest to predict the leaching of radionuclides from the soil as time passes by and to interpret effects of remedial measures against transfer into the foodchain (see figure 1).

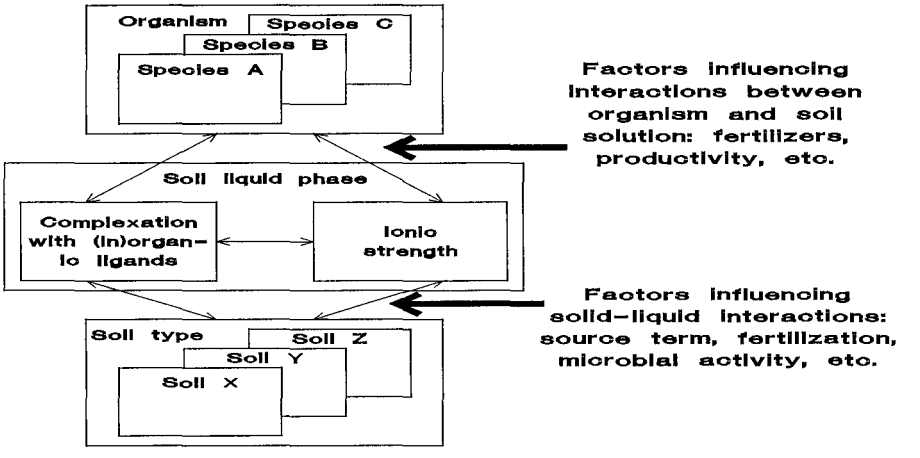

1. Studied interactions between soil, soil solution and organism

In this project the availability of radionuclides is studied in artificial as well as in natural systems at different levels of organization. The study includes the chemical characterization of binding properties of the soil, the determination of distribution functions and the description of the uptake and release processes by different organisms (plants, microorganisms and soil invertebrates). Integration of the results and a mathematical description of

the processes studied are part of the project. Most of the subprojects have been carried out with the radionuclides $^{134}Cs/^{137}Cs$ and ^{90}Sr. A variety of techniques is presented to quantify and interpret the solid-liquid distribution and a number of practical advises are given to evaluate the effectiveness of countermeasures.

Between September 1994 and June 1995 the various participating institutes essentially finalized experiments and tasks which have been announced and initiated in the course of previous reporting periods. As a result this final report largely is an update and extension of the foregoing reports. Although each of the participating organisations worked on different aspects of soil-to-organism interactions, they accentuated specific topics because of their experience, equipment and facilities (figure 2).

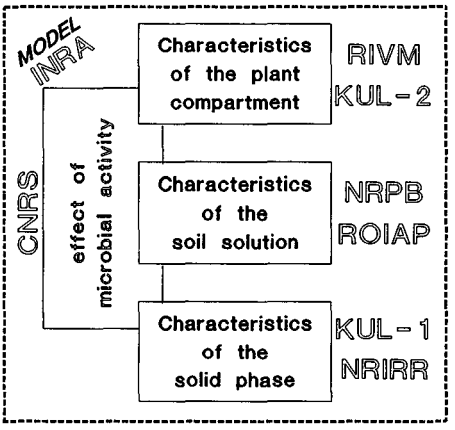

2. Schematic overview of the specific contribution from each of the participants

Binding of radionuclides to soil and the effects of amendments

It is generally assumed that radionuclide levels in soil solution are an indication of the quantity that can be absorbed by animals or plants. It is thus important to identify the key factors that determine the equilibrium between the solid phase and the liquid phase of various soils, the effects of measures on this equilibrium and the time-dependent changes of this distribution. The variability of the $^{134}Cs/^{137}Cs$ concentration in the liquid phase of the soil has been determined for various soil types by NRPB, IFIN, KUL and NRIRR. The aim of the first two institutes has been the development of practical recommendations on agricultural countermeasures. The latter two participants mainly focused on the chemical aspects of amendments to reveal the characteristics of fixation mechanisms.

The frayed edge sites (FES) are characterised as the main long term sink for radiocaesium. In most cases the regular exchange complex (REC), i.e. organic matter and planar sites of mineral compounds, contributes less than 5% to the radiocaesium interception potential. For the bigger part of the soils the K_D can thus be described as a function of its FES-concentration and the selectivity and level of the major competitors for Cs-binding (K and NH_4^+):

$$K_D = \frac{RIP^{FES}}{m_K + K_c^{FES}(N/K).m_N}$$

The release of radiocaesium in response to amendments as a function of age of the deposit has been quantified as well as its dependence on soil type. Pronounced effects of ageing have been observed for mineral soil. Negligible effects have been seen for some organic soils, where practically all radiocaesium becomes reversibly associated with the REC. The

dominant factors in the kinetics of long term fixation and release remain, however, unclear, which means that diagnostic tools and a mechanistic mathematical description of the exchange kinetics are not within reach at the moment. For ^{90}Sr no ageing could be observed.

Determination by KUL of the specific radiocaesium interception potential at low potassium adsorption ratios (PAR) for more than one hundred soils and sediments provided results comparable to determinations based on the masking technique with silver-thiourea:

$$[K_D.m_K]^{PAR} = -0.083 + 1.01.[K_D.m_K]^{AgTU} \qquad R^2 = 0.85$$

As such a simplified and inexpensive alternative method for the quantification of FES has been developed. It was furthermore demonstrated that a comparison of the K_D-values and the K and NH_4 selectivity of contaminated soils and substances added to the soil (such as zeolites) is shown to be a good basis to identify useful substances in countermeasure strategies.

Experiments by NRPB and IAP in which different amendments have been added to five distinct soil types, have shown remarkable differences in the reduction of the ^{134}Cs:K ratio in soil solution between organic soils and mineral soils. These results indicate that addition of potassium and organic matter reduces the ratio in organic soils. A potassium treatment, however, is hardly effective or may even increase the ratio in mineral soils. Ammonium-based fertilisers are also detrimental in loam and sand soils by increasing Cs:K quotients in the liquid phase. All treatments, however, had adverse effects in terms of absolute Cs level in the soil solution. Smaller changes in absolute Cs-concentrations and thus larger effects on the Cs:K ratio could be observed in aged soils, because of the more pronounced Cs fixation. Whether the observed changes in Cs:K ratio reduce the Cs level in e.g. plants depends on the potassium status of the system, as has been demonstrated by the contractors studying uptake by biota.

Moderate K-treatments had no effect on ^{90}Sr:Ca quotients. Phosphate and calcium treatments reduced the latter ratio for all soils, but had no effect on the Cs:K ratio. These treatments thus can be applied in case of mixed deposits.

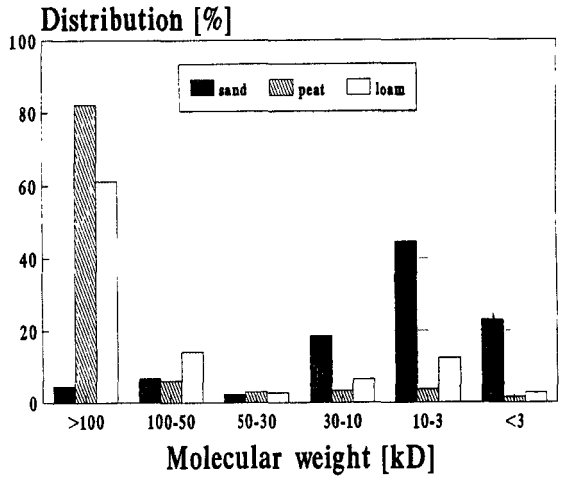

3. Distribution of ^{241}Am in different humin fractions

NRIRR not only studied ^{137}Cs and ^{90}Sr, but did batch experiments on the sorption of ^{110m}Ag, ^{241}Am and ^{239}Pu with model substrate and Hungarian soils. Experiments with radiosilver demonstrated that artificial particles can be used as a model for the different constituents of the soil. Organic matter appeared to determine the speciation of the latter three nuclides. In the absence of humic

materials or at pH > 8 the sorption properties of Fe/Mn oxide become more important for fixation of radiosilver. As transuranic elements and radiosilver are predominantly associated with organic matter, the molecular weight distribution of the labeled complexes is highly dependent on the soil type, i.e. the composition of the organic matter (figure 3).

Accumulation in biota

The relation between soil chemistry and uptake of radionuclides by organisms needed investigation as considerable species differences in uptake and transfer factors are found. These differences can only be explained when incorporating organism characteristics, such as growth rate and root surface area of a plant, in the uptake models in combination with the dynamics of other key ions at the absorption sites. Influx/efflux studies have been carried out for different plant species and for different earthworm species in order to characterize the uptake process.

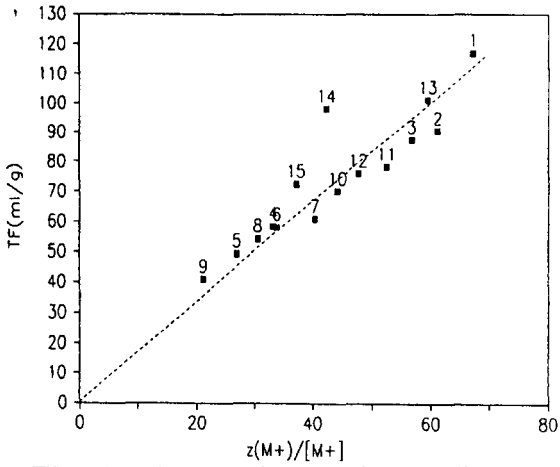

4. TF against the ratio of the fractional loading of the root exchange complex by monovalent ions and their solution concentration

Experiments by KUL in which spinach and wheat are exposed to a varying ratio of mono- and divalent cations demonstrated the importance of the role of the Cs-loading of the root exchange complex for the uptake of radiocaesium (figure 4). As exchange capacity is highly species-dependent, the effect of changes in composition of the nutrient medium varies among species. A shortage in K supply, even locally, was demonstrated to distinctly increase Cs uptake. In the K-concentration range which is representative for many soil solutions, Cs uptake has been found to depend more than proportionally on the reciprocal of the K-concentration. This explains why K-fertilization, which, however, mobilizes Cs in soils by ion-exchange reactions generally reduces Cs availability in soil. Cs uptake per unit root surface appeared not depend on the number of roots exposed. The root:shoot ratio of radiocaesium was observed to be controlled by xylem transport and the K supply. The importance of readily available K and of the Cs:K ratio in solution was confirmed by the study of IAP in which results of batch equilibrium experiments were compared with transfer experiments using the plantlet method of Neubauer and Schneider in which K resources are limited. These experiments demonstrated a treatment with K-salts to be effective even in normally supplied soils and at later stages of contamination.

Experiments by RIVM showed that changes in individual environmental parameters altered the uptake of ^{134}Cs by earthworms up to a factor of 3. A maximum difference in uptake of a factor of 15 was observed between combinations of parameters. A change in pH did not result in a different uptake, but addition of potassium and stable caesium resulted in a lower ^{134}Cs concentration in both earthworm species. Ammonium and calcium did not

Eisenia sp. was three times higher than the TF to *Lumbricus rubellus*. This difference could not be reproduced for soil. An increase in temperature from 10 °C to 20 °C led to a longer biological half life and an average increase in activity with a factor 1.5. The earthworms had a distinct effect on the water soluble and ammonium-acetate extractable Cs fraction in the soil.

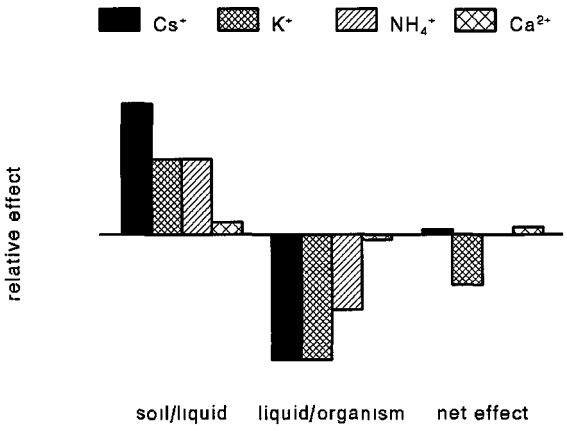

5. Relative effect of four cations on Cs partitioning and on its accumulation by earthworms

The relation between potassium and caesium at cellular level may reveal some of the observed differences between plant species and between species of invertebrates, but is not yet fully understood. It appears that high potassium concentrations are observed in the plant vacuole compared to caesium. Potassium concentrations in earthworms remained remarkably stable along a range of external potassium concentrations. This may indicate that the low caesium concentrations are the result of higher turnover at high external potassium concentrations.

The effects of organisms on radionuclide release

Organisms may affect the release of radionuclides from the solid phase of the soil e.g. by the release of exudates or by the process of bioturbation. Addition of earthworms to soil resulted in increased K^+ concentrations, conductivity and activity in soil solution. Leaching experiments by CNRS with soil columns filled with Rendzina and brown soil from France showed that microorganisms enhanced leaching of caesium, especially during the first month after addition of glucose as substrate. Leaching differed a factor 2 between the soils. Experiments with the fungus *Trichoderma viride* showed that the fungus may fix a considerable amount of caesium indicating that fungi can enter efficiently into competition with clay minerals for caesium fixation.

The experiments suggest both direct (accumulation, translocation to plant roots) and indirect effects of microorganisms (weathering, agent of plant growth) on the Cs-cycle. The relative importance of each of the processes under field conditions, however, still has to be quantified.

Modelling bioavailability

The model of INRA describing plant uptake of radionuclides includes the usual soil and plant characteristics e.g. K_D values, diffusion coefficients, moisture content of soil, slow reaction rate, root uptake rate, rooting density, radius and length. It also takes into account variable root density with depth, root turnover, redistribution between roots and shoots and recycling from roots and shoots to the soil. From the results of the experiments described above as well as from the model simulations it can be deduced that species-specific characteristics, such as rooting pattern and root turnover, are important parame-

ters in describing/modelling the uptake of radionuclides. For a large part such information is gathered from the literature. The model simulations furthermore clearly reveal the potential effect of recycling of absorbed Cs on the depth distribution of Cs in soil. Root uptake from the soil solution is described by Michaelis Menten kinetics which approximates to a linear uptake when trace levels of Cs are considered. Simulations showed that although Cs availability is not sensitive to root uptake characteristics in mineral soils, it may become iportant in soils with low potassium content en low K_d. At the end of the project period the predictive value of the model was felt to be limited because information on root architecture and turnover and Cs distribution within the whole plant remains scanty. However, it provides very useful indications for the efficient planning of further research.

In order to make an adequate description of the availability of radiocaesium in soils it was thought essential to differentiate between agricultural/mineral soils and semi-natural/organic soils. In agricultural/mineral soils clay mineralogy and the growth characteristics active root length and depth distribution will have a dominant influence, whereas in semi-natural/organic soils the potassium status and the root uptake characteristics, root and shoot turnover and effective root length (a.o. influence by mycorrhiza), are important parameters. More data on redistribution of absorbed Cs within the plant is required.

Head of the project 1 : Dr. Lembrechts
Reporting scientist : Dr. Janssen

IIa. Objectives for the reporting period

1. Study the transfer of ^{134}Cs along the soil - soil solution - organism interfaces under different environmental conditions. At first experiments were carried out on the equilibrium between solution and organism.
2. Study of the kinetics of ^{134}Cs uptake from solution for different earthworm species in order to describe the speed of uptake and release at different temperatures, and the relative importance of intra-species differences.
3. Execute experiments with earthworms in solution in which key factors such as pH, calcium concentration and potassium concentration are varied, in order to quantify their influence on the ^{134}Cs concentration in organisms.
4. Describe the uptake of ^{134}Cs by earthworms from soil and the effect of temperature on the uptake process.
5. To describe the effect of the temperature and of the presence of earthworms on the distribution of ^{134}Cs between soil and soil solution.

III. Progress achieved including publications

1. Effect of K, stable Cs, Ca, NH_4 and pH on the uptake of ^{134}Cs from liquid medium.

1.1. Materials & methods

Earthworms (*Eisenia foetida, Lumbricus rubellus*) were kept at 15 °C in 50 ml of liquid medium with a ^{134}Cs concentration of 50 Bq l^{-1}. The K/stable Cs experiments consisted of six different treatments for *E. foetida* and fifteen different treatments for *L. rubellus*. The concentration ranges of both elements (K: 0-10 mM, Cs: 0-0.075 mM) reflect those observed in the soil solution under field conditions. The earthworms were sampled and analyzed individually after two weeks. The effects of K and stable caesium on the ^{134}Cs concentration in the earthworms was described by multiple regression for both species.
The Ca/NH_4 experiments consisted of twelve different treatments: 4 Ca concentrations (0, 0.3, 2.6 and 26.0 mM) and 3 NH_4 concentrations (0 and 0.3 en 3.0 mM). The concentration ranges of both elements reflect those observed in the soil solution under field conditions. The experiment was carried out with *E. foetida* only.
For the pH experiment the amount of liquid per pot which was enlarged to 100 ml. pH's were set at 4, 6 and 8 by adding HCl or NaOH. The liquid medium of the treatments for which the shift in pH was biggest (pH 4 and 6), was refreshed every 100 hour. Samples were collected after two weeks.

1.2. Observations

It was expected that both K and Cs compete for binding sites at the solution-earthworm interface and thus reduce uptake of the radionuclide. Addition of K lead to a significantly lower activity in the earthworms, whereas the effect of Cs was not significant. No interactions between both ions were observed in this experiment. The non significance for stable Cs may partly be attributed to the much smaller concentration range compared to that of K. It is obvious from the results that the effect decreases with increasing K concentration. The experiments showed no effect of the K or stable Cs concentration in the solution on the internal K concentration in both species. The ^{134}Cs and K

concentrations in *E. foetida* at different external K concentrations are given in Table 1. The activity in both species could be described by multiple regression:
E. foetida: [Cs-134] = 676 - 63.9ln[K] - 29.8ln[Cs]
L. rubellus: [Cs-134] = 229 - 19.9ln[K] - 6.59ln[Cs]
in which the ^{134}Cs concentrations are expressed in Bq/g and the K and Cs concentrations in mM.

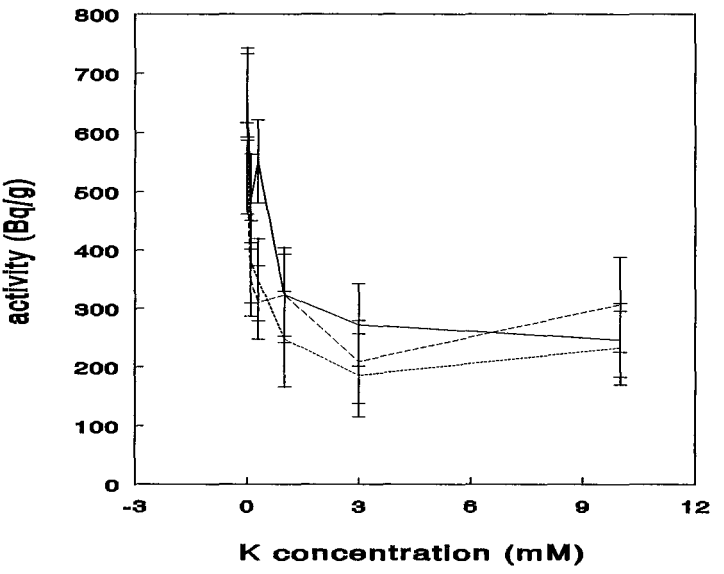

Figure 1. The effect of K and Cs on the uptake of ^{134}Cs by the earthworm *L. rubellus* in solution, continuous line = 0.0 mM Cs, small stripes = 0.0075 mM Cs and large stripes = 0.075 mM Cs.

The results show a small significant effect of the addition of NH_4 in the solution resulting in a lower activity in the earthworm. No significant effect of Ca was observed. NH_4 and Ca are expected to have a larger effect on the solid-liquid interface. The addition of Ca in solution led to a significant increase in Ca in the earthworms, whereas increasing the level of K in solution has no effect on its concentration in the earthworms.

Table 1. Concentrations of K and ^{134}Cs in *Eisenia foetida* after two weeks of exposure in liquid medium with a stable Cs concentration of 0 mM. Standard errors are given in brackets.

Concentrations in medium		Concentrations in *E. foetida*	
^{134}Cs (Bq ml^{-1})	K (mM)	^{134}Cs (Bq g^{-1})	K (μmol g^{-1})
50	0	2220 (90)	169 (16)
50	1	1160 (220)	175 (6)
50	10	980 (90)	160 (13)

In our experiments no significant effect of pH on the ^{134}Cs uptake by *E. foetida* or *L. rubellus* from solution was observed although uptake was increased a little in *E. foetida* at pH 6. The difference between the two species, however, was significant at all pH's. No interaction between pH and species was observed.

2. Effect of temperature on the uptake kinetics.

2.1. Materials & methods

Two earthworm species *E. foetida* and *L. rubellus* were kept individually in solution for two weeks at different temperatures (10, 15 and 20 °C). Five individuals from each species were sampled at different time intervals and the ^{134}Cs activity was measured. The uptake and release process was described by parameters which were calculated using a one compartment model described by the formula $C_t = A/k_*(1-e^{-kt})$ in which C_t is the concentration at a given time (t) in Bq/g dry weight, A is the assimilation in Bq/g/hr, k = the excretion constant in hours^{-1} and t is time in hours. A two compartment model was also applied to describe the uptake of ^{134}Cs by both species. However, this model did not give a good description of the uptake by *L. rubellus*. Equilibrium concentrations were calculated from the uptake (A) and elimination parameters (k) of the one compartment model through the formula: equilibrium concentration = A/k.

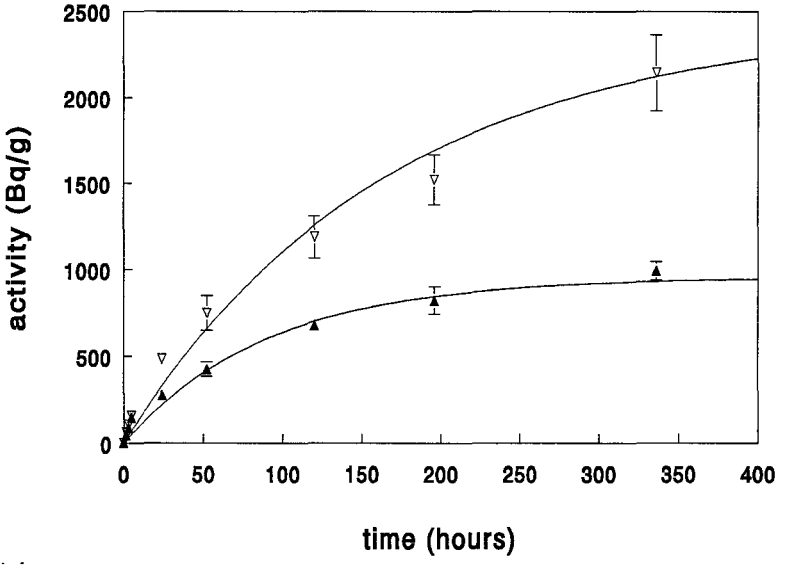

Figure 2. Uptake of ^{134}Cs by the earthworm *E. foetida* at 10 °C (△) and 20 °C (▽).

2.2. Observations.

The kinetics of ^{134}Cs showed to be different in both species. Uptake showed to be much higher in *E. foetida* than in *L. rubellus* (see progress report 1993). The effect of temperature on the uptake process was also different in both species. Uptake increased with temperature in *E. foetida*, but was similar for *L. rubellus* at different temperatures. Elimination was constant in *E. foetida*, but peaked at 15 °C in *L. rubellus*. As a result ^{134}Cs at equilibrium increased with temperature in *E. foetida* and peaked at 15 °C in *L.*

rubellus.

and *L. rubellus* (see table 1). Concentration factors from solution to earthworm at each temperature, calculated from the equilibrium concentrations, were 18.4 and 37.9 for *E. foetida* and 13.8 and 19.3 for *L. rubellus* respectively. Biological half life ranged between 52 and 119 hours in both species. The results show that equilibrium of ^{134}Cs in earthworms is reached quite rapidly compared to some other elements.

Table 2. Uptake and release parameters of ^{134}Cs kinetics in two earthworm species by using a one compartment model.

	temp. °C	A (Bq/g/hr)	k (hrs^{-1})	activity at equilibrium (Bq/g dw)	T½ (hrs)
E. foetida	10	12.4	0.013	920	52
	15	20.1	0.011	1797	62
	20	20.5	0.011	1893	64
L. rubellus	10	5.62	0.008	688	85
	15	4.55	0.012	367	56
	20	5.59	0.006	963	119

3. Concentration factors of caesium in the earthworms *E. foetida* and *L. rubellus*.

3.1. Materials and methods

Data from the experiments with varying levels of stable Cs were used to calculate concentration factors (Table 3). The data from the different experiments were used to calculate maximum difference in ^{134}Cs concentration for each species (Table 4).

3.2. Observations

The data show considerable differences in concentration factors between *E. foetida* and *L. rubellus*, concentration factors in the first species being about 4 fold that of the latter. The concentration factors decrease only slightly. The results indicate that under field circumstances no large variation in ^{134}Cs concentration can be expected due to variation in the stable Cs concentration.

Table 3. Caesium concentrations in solution and concentration factors (CF) for the earthworms *E. foetida* and *L. rubellus* at 15 °C in absence of potassium after two weeks exposure. Standard errors are given in brackets. - = not studied.

concentration in solution		*E. foetida*		*L. rubellus*	
^{134}Cs (Bq ml^{-1})	Stable Cs (mM)	^{134}Cs (Bq g^{-1})	CF	^{134}Cs (Bq g^{-1})	CF
1.8	0	103 (-)	57.2	25 (4)	13.9
50	0	2220 (90)	44.4	820 (110)	16.5
50	0.0075	1820 (310)	36.4	780 (90)	15.5
50	0.075	-	-	620 (130)	12.4

Highest and lowest concentration within each species differed about a factor of five, differences between the species was about a factor of three to four (Table 4). The maximum difference between the lowest and highest concentrations in all experiments is about a factor of 15.

Table 4. The impact of several environmental parameters (concentrations are in mM) on the uptake of ^{134}Cs from liquid medium by the earthworms *E. foetida* and *L. rubellus*. Given are highest and lowest ^{134}Cs concentrations and their quotient. (1) 621 Bq g^{-1} dry weight at 0.075 mM, (2) - = not studied, (3) 367 Bq g^{-1} at 15°C.

Parameter	Range	Highest and lowest values observed plus quotient					
		E. foetida			*L. rubellus*		
		Bq g^{-1}	Bq g^{-1}		Bq g^{-1}	Bq g^{-1}	
[K]	0 > 10	2220	980	2.3	820	280	2.9
[Cs]	0 > 0.0075	2220	1820	1.2	820	780	1.1(1)
pH	6 > 8	3400	2650	1.3	1210	1160	1.0
	6 > 4	3400	2440	1.4	1210	1070	1.1
[Ca]	2.6 > 0.26	1810	1650	1.1			-(2)
	0 > 0.26	1700	1650	1.0			-(2)
[NH_4]	3 > 0.3	1950	1480	1.3			-(2)
	0 > 0.3	1700	1480	1.2			-(2)
temp.	20 > 10	1890	920	2.1	960	690	1.4(3)

4. Uptake of caesium by earthworms from soil

4.1. Material & methods

Two earthworm species *E. andrei* and *L. rubellus* were kept in a sandy soil for two and three weeks respectively at three different temperatures (10, 15 and 20 °C). Five individuals from each species were sampled at different time intervals and the ^{134}Cs activity in the earthworms was measured. Soil solution characteristics were monitored throughout the experiment. Stable Cs concentrations were measured in soil and earthworms.

The uptake and release process was described by parameters which were calculated using a one compartment model described by the formula $C_t = q + A/k_e(1-e^{-kt})$ in which C_t is the concentration at a given time (t) in Bq/g dry weight, q is the start concentration, A is the assimilation in Bq/g/hr, k = the excretion constant in $hours^{-1}$ and t is time in hours. Equilibrium concentrations were calculated from the start concentration (q), uptake (A) and elimination parameters (k) of the one compartment model through the formula: equilibrium concentration = q + A/k.

4.2. Observations

Concentration factors for stable Cs in earthworms ranged from 0.06 to 0.08. For ^{134}Cs concentration factors between 0.23 and 0.41 were measured (Table 5). Concentration factors based on ^{134}Cs concentration in the soil solution are much higher and vary between 6.24 and 22.23. The concentration factor was comparable for *E. andrei*, but was much higher in soil solution than in liquid medium for *L. rubellus*.

Table 5. ^{134}Cs concentrations in the soil, the soil solution and the earthworms *E. andrei* and *L. rubellus*. Data are calculated after 14 and 21 days for *E. andrei* and L. rubellus respectively. The partitioning coefficient (K_d), and the concentration factors (CF) relative to soil concentration and soil solution concentration are given as well.

Species	temp. °C	Conc. in soil Bq g^{-1}	conc. soil sol. Bq ml^{-1}	K_d	conc. in earthworms Bq g^{-1}	CF soil	CF solut.
E. andrei	10	52.3	1.7	31	11.8	0.23	7.1
	15	52.1	1.2	32	13.4	0.26	8.3
	20	52.6	1.3	41	19.3	0.37	15.1
L. rubellus	10	31.8	1.5	21	9.4	0.30	6.2
	15	30.9	0.8	37	11.3	0.37	14.2
	20	31.8	0.6	53	12.9	0.41	22.2

A 10 °C rise in temperature resulted in a 1.6 fold increase in ^{134}Cs concentration in *E. andrei* and a 2.1 fold increase in *L. rubellus*. Maximum difference between the two species was 2.4. The increase in internal ^{134}Cs concentration with increasing temperature could mainly be explained by earthworm-related factors such as increased metabolism or feeding rate as ^{134}Cs concentrations in solution did not increase with temperature. The data showed that earthworms enhanced the ^{134}Cs concentration in soil solution compared to pots without earthworms. K, Ca, and ^{134}Cs concentration and conductivity in soil solution increased with time in most treatments.
The parameter estimations are given in Table 6 plus biological half life times and equilibrium concentrations.

Table 6. Parameter estimates (q, A, k) for the uptake of ^{134}Cs from soil by the earthworms *E. andrei* and *L. rubellus* at different temperatures. Equilibrium concentration (Eq., in Bq g^{-1} dw), biological half life times ($T_{1/2}$, in hours) and concentration factors (CF, no dimensions) are calculated from these parameters. A in Bq $hour^{-1}$, k in $hours^{-1}$. The CF is based on the calculated equilibrium concentration and the ^{134}Cs concentration in soil at the end of the experiments.

	E. andrei			*L. rubellus*		
	10	15	20	10	15[1]	20[1]
q	2.12	2.11	1.99	2.29	3.63	2.58
A	0.041	0.074	0.153	0.029	0.036	0.108
k	0.0025	0.0057	0.0083	0.0031	0.0042	0.0100
Eq.	18.7	15.1	20.4	11.5	12.1	13.4
$T_{1/2}$	270	120	84	223	164	69
CF	0.36	0.29	0.39	0.36	0.39	0.42

Publications

Janssen MPM, Glastra P & J.F.M.M. Lembrechts. 1993. Waardoor wordt de opname van caesium-134 door regenwormen bepaald? Symposium Netherlands Integrated Soil Research Programme, Lunteren, The Netherlands.

Janssen MPM, Glastra P & Lembrechts J. 1994. The effects of environmental parameters on the availability of caesium. Abstract 3rd European Conf. Ecotoxicology, Zürich.

Janssen MPM, Glastra P & Lembrechts J. 1994. De effecten van omgevingsfactoren op de opname van ^{134}Cs door regenwormen. Nat. Symp. Bodemonderzoek, Lunteren, 941206.

Janssen MPM, Glastra P & Lembrechts J. (1995a) Uptake of caesium-134 by the earthworm species *Eisenia foetida* and *Lumbricus rubellus*. Env. Toxicol. Chem. submitted.

Janssen MPM, Glastra P & Lembrechts J. (1995b) The effects of environmental parameters on the uptake of Caesium-134 by earthworms. J. Environm. Radioact. submitted.

Janssen MPM, Glastra P & Lembrechts J. The effects of temperature on ^{134}Cs uptake from a sandy soil by two earthworm species. in preparation

Lembrechts J. 1993. A review of literature on the effectiveness of chemical amendments in reducing the soil-to-plant transfer of radiocaesium and radiostrontium. EG Workshop on the relative effectiveness of agricultural countermeasure techniques. Brussel, 911001. Science of the Total Environment 137, 81-98.

Nisbet AF, Konoplev AV, Shaw G, Lembrechts J, Merckx R, Smolders E, Vandecasteele CM, Lönsjö H, Carini F, Burton O. 1993. Application of fertilisers and ameliorants to reduce soil to plant transfer of radionuclides in the medium to long term. A summary. EG Workshop on the relative effectiveness of agricultural countermeasure techniques. Brussel, 911001. Science of the Total Environment 137, 173-182

Head of Project 2: Dr B Wilkins/Dr A Nisbet

Objectives for reporting period

1. Evaluation of clinoptilolite as a countermeasure using the batch equilibrium technique.

2 The validation of the batch equilibrium technique using published data on soil-plant uptake.

Progress achieved including publications

1. The development of the batch equilibrium procedure

1.1 Experimental methodology

The underlying objective of this project was to evaluate whether a small scale batch equilibrium technique could be used to predict the effectiveness of soil-based countermeasures. The experimental protocols are described in detail in reference 1. Briefly, five diverse soil types were used in this study. Their detailed characteristics are given in reference 1, but the general classifications were a Hamble loam, a Fifield sand, an Adventurers peat, a peat ranker and a raw oligofibrous peat (referred to in the remainder of this report as a deep peat). These soils had been collected from the field in November 1992. They were allowed to dry at room temperature until friable and then contaminated artificially with a solution of caesium-134 and strontium-90 The homogeneity of the contamination was checked by determining the caesium-134 content in 10 aliquots of each soil In all cases the standard deviation about the mean was less than 10% All soils were then kept at field moist conditions using distilled water until required For the batch equilibrium experiments, *in situ* conditions were replicated in the laboratory by using these field moist soils and their associated soil solutions The solutions had been collected from the field using the porous cup sampler technique and stored at 4°C until required

Soil treatments can reduce the transfer of radionuclides to plants by

(i) increasing the fixation of the radionuclide in a non-available or less available form within the solid phase of the soil, eg, application of clay minerals, chelates, or by co-precipitation with insoluble salts such as phosphates, silicates and sulphates;
(ii) modifying the solid-liquid equilibrium of various ions in the soil to reduce the quotient of radioelement nutrient analogue in the soil solution, eg, Cs K and Sr Ca

In this study, changes in the solid-liquid distribution of radiocaesium, radiostrontium, potassium and calcium were determined following the application of a range of common agricultural treatments The main part of the study, described in reference 1, considered the application of potassium, ammonium, phosphate and lime, as well as organic matter, which in these experiments was in the form of pelletised chicken manure In the present phase of the project, the potential effectiveness of clinoptilolite has been evaluated Throughout the study, the application rates used were based on those in common use in the field, those employed in the main phase of the study are given in reference 1

The assessment of the potential effectiveness of a given treatment was based on the resultant changes in the quotient of the radionuclide : stable nutrient analogue in the soil solution. A treatment was considered potentially effective if this quotient was reduced compared to a control sample to which no treatment had been applied. In all of the experiments, the effects of a given treatment were evaluated for both radiostrontium and radiocaesium, because in the case of a mixed deposit, it is essential to know whether a beneficial effect on one radionuclide could be ofset by detrimental effects on the other.

1.2 The extension of the study to clinoptilolite

Clinoptilolite is a natural zeolite with a very high specificity for the sorption of caesium ions. However, sorption is not irreversible and so the application of zeolite as a countermeasure to reduce radiocaesium uptake by plants is likely to be most effective in soils having a low caesium fixation potential. Field research in semi-natural systems in the UK has indicated that the application of clinoptilolite resulted in a 50% reduction in the transfer to bulk vegetation[2]. Moreover, the effect increased with time as the clinoptilolite became more incorporated into the rootmat Two application rates were employed in the evaluation of clinoptilolite using the batch equilibrium procedure. These corresponded to rates in the field of 5 and 10 tonnes ha^{-1}, which were within the range reported in reference 2 and which might reasonably be considered in practice. The first series of experiments utilised clinoptilolite in its native Na form. However, since there was published evidence that this form might induce toxicity effects due to high Na concentrations in the rooting zone, a second series was performed in which the clinoptilolite had been converted predominantly to the Ca form. For each individual treatment, the experiments were carried out in duplicate, and in each case two control samples to which no ameliorant had been added were also included

1.2.1 Results

All the results tabulated in this section represent the mean of two determinations

(i) Caesium-134

The batch equilibrium experiments were carried out about 18 months after the soils had been contaminated Consequently, the activity concentrations of caesium-134 had decreased and uncertainties in some of the measurements were in the range 20-50% When this factor was taken into account, changes in the $^{134}Cs{\cdot}K$ quotient were not significant for those experiments involving agricultural soils Consequently, results for the poor-quality peat soils only are shown in Tables 1 and 2, although the full results are given in reference 3 For the peat ranker, changes were not significant for either form of clinoptilolite because of the large associated counting uncertainties For the deep peat, activity concentrations in the soil solution were higher than in the other soils and so counting uncertainties were lower The results for the two forms of clinoptilolite were similar. changes in the quotient were due to both a decrease in the ^{134}Cs concentrations and an increase in the corresponding values for K These results suggest that clinoptilolite could be an effective countermeasure in reducing radiocaesium uptake to vegetation in some poor quality peat soils. Reduction factors of up to 3 might be expected, which is in reasonable agreement with observations from field studies[2]

(ii) Strontium-90

For the three agricultural soils, the results for the Na form of clinoptilolite were generally similar to those for the Ca form: the addition of clinoptilolite at either application rate produced commensurate changes in both the ^{90}Sr and Ca concentrations in the soil solution and so changes to the ^{90}Sr:Ca quotient were not significant. The results are set out in reference 3. Some effects were observed in the poor quality peat soils, and the results are shown in Tables 1 and 2. For the Na form, a decrease in the quotient was observed only in the deep peat, and this was due to a decrease in the concentrations of ^{90}Sr in the soil solution. This was an unexpected result, since clinoptilolite was not considered to be highly selective for strontium ion, and any effect should have been observable in similar soils such as the peat ranker. This finding deserves further attention. For the Ca form of clinoptilolite, increases in the Ca concentrations in the soil solution resulted in decreases in the ^{90}Sr:Ca quotients. The exchangeable calcium in these soils is much lower than those in the mineral soils studied, and 2-10 times lower than that in the agricultural peat soil[1]. Consequently, an increase in the Ca concentrations in the soil solution is to be expected; any decrease in the ^{90}Sr:Ca quotient would be due to the effect of the added calcium and not to the clinoptilolite itself.

The full results for clinoptilolite will be discussed in a forthcoming publication[3], but the overall conclusions are that clinoptilolite would not be a useful countermeasure in the reduction of ^{90}Sr uptake into plants No field data were available for comparison.

TABLE 1: Effect of clinoptilolite (Na-form) treatment on ^{134}Cs, K, ^{90}Sr, Ca, ^{134}Cs:K, ^{90}Sr:Ca quotients in the liquid phase

	^{134}Cs[a]	K[b]	^{134}Cs:K	^{90}Sr[a]	Ca	^{90}Sr:Ca[b]
PEAT[c] control	9	7	1.3	25	1	25
5 T	10	6	1 7	26	1	26
10 T	7	6	1.2	22	1	22
PEAT[d] control	27	9	3 0	109	10	11
5 T	19	12	1 6	61	7	8 7
10 T	15	15	1.0	61	10	6.1

a Bq l^{-1}
b mg l^{-1}
c peat ranker
d deep peat

TABLE 2: Effect of clinoptilolite (Ca-form) treatment on ^{134}Cs, K, ^{90}Sr, Ca, ^{134}Cs:K, ^{90}Sr:Ca quotients in the liquid phase

	^{134}Cs[a]	K[b]	^{134}Cs:K	^{90}Sr[a]	Ca[b]	^{90}Sr:Ca
PEAT[c] control	5	7	0.71	74	2	37
10 T	3	10	0.3	85	4	21
PEAT[d] control	25	8	3.1	135	7	19
5 T	19	13	1.5	132	10	13
10 T	13	15	0.9	116	12	9.7

a Bq l^{-1}
b mg l^{-1}
c peat ranker
d deep peat

1.3 Validation of the batch equilibrium approach

The literature has been searched to find any field or lysimeter studies of plant uptake that can be used to validate the laboratory scale batch equilibrium approach The results are shown in Tables 3-7 No appropriate field data were located for radiostrontium For radiocaesium, there was generally a reasonable agreement between the values observed in the field and those implied from the batch equilibrium technique It was noticeable that the effectiveness of K on radiocaesium uptake under field conditions was usually at the lower end of the range of values implied by the laboratory studies (Tables 3 and 4) The results from the batch equilibrium studies indicated that the observed effectiveness factor will depend on the potassium status of the soil This is consistent with observations made in collaborative studies with the former Soviet Union within JSP1, although in this case a direct comparison has not so far carried out because of the changing composition of the fertiliser applied[4]

TABLE 3: Validation of batch equilibrium results with published data for uptake of Cs into grass from peat soils: potassium treatment

K application kg ha^{-1}	Reduction factors for soil-plant uptake of ^{137}Cs (grass)	Reduction factors for ^{134}Cs:K quotients in soil solution
100	2-4 (Cumbria and N Wales[2])	3-6
	3 (Sweden[5])	
200	4-10 (Sweden[6])	7-10
500	6, 35, 36 (Sweden[7])	16-45

TABLE 4: Validation of batch equilibrium results with published data for uptake of Cs into grass from mineral soils: potassium treatment

K application kg ha^{-1}	Reduction factors for soil-plant uptake of ^{137}Cs (grass)	Reduction factors for ^{134}Cs:K quotients in soil solution
75	1.5 Norway[8]	1
100	1.7 Italy[9]	
150 - 300	3-5 Norway[8]	1 - 13 (depending on K status of soil)
525 +	6 Norway[8]	1 - 30 (depending on K status of soil)

TABLE 5: Validation of batch equilibrium results with published data for uptake of Cs into crops from mineral soils: potassium treatment

K application kg ha^{-1}	Reduction factors for soil-plant uptake of ^{137}Cs (crops)	Reduction factors for ^{134}Cs:K quotients in soil solution
156 + 31	2 Sweden (oats, peas, mustard)[10]	no data
625 + 156	6-30 Sweden (oats, peas, mustard)[10]	1 - 13 (depending on K status of soil)

TABLE 6: Validation of batch equilibrium results with published data for uptake of Cs into grass from peat soils : clinoptilolite treatment

Clinoptilolite application T ha^{-1}	Reduction factors for soil-plant uptake of ^{137}Cs (grass)	Reduction factors for ^{134}Cs:K quotients in soil solution
5	1.5-2 Cumbria and N Wales[2]	2
15	2-4 Cumbria and N Wales[2]	3 (10 T ha^{-1})

TABLE 7: Validation of batch equilibrium results with published data for uptake of Cs into grass from mineral soils: ammonium treatment

NH_4 application kg ha^{-1}	Enhancement factors for soil-plant uptake of ^{137}Cs (grass)	Enhancement factors for ^{134}Cs:K quotients in soil solution
50	2-3 Cumbria[11]	4-7
60	2.9 Austria[12]	

TABLE 8: Summary of effects of soil treatments on a mixed deposit of ^{134}Cs and ^{90}Sr six months and one year after contamination

Treatment	Soil type	Response	
		^{134}Cs:K	^{90}Sr:Ca
Potassium (100-2000 kg ha^{-1})	Mineral	No response	No response
	Organic	**Beneficial** effect increasing with treatment rate	Small increase in peat ranker at 1000-2000 kg ha^{-1}
Ammonium (50-500 kg ha^{-1})	Mineral	**Deleterious** effect increasing with treatment rate	No response
	Organic	Small increase in deep peat at 500 kg ha^{-1}	Small increase in peat ranker at 500 kg ha^{-1}
Potassium (100-500 kg ha^{-1}) + Ammonium (100 kg ha^{-1})	Mineral	**Deleterious** effect of NH_4 decreasing with increasing K	No response
	Organic	**Beneficial** effect of K increasing with increasing K	Small increase in peat ranker, irrespective of K NH_4 ratio
Organic (1-10 T ha^{-1})	Mineral	**Deleterious** effect increasing with treatment rate (NH_4-effect)	No response
	Organic	**Beneficial** effect increasing with treatment rate (K-effect)	Small increase in peat ranker and deep peat at 5-10 T ha^{-1}
Calcium (2-10 T ha^{-1})	Mineral	No response	No response
	Organic	Small decrease in deep peat at 10 T ha^{-1}	**Beneficial** in peat ranker and deep peat
Phosphate (150-300 kg ha^{-1})	Mineral	No response	No response
	Organic	No response	**Beneficial** in peat ranker and deep peat (Ca-effect)

1.4 Conclusions

The earlier studies are described in full in reference 1 The overall results are summarised in Table 8, and the conclusions may be summarised as follows.

(i) Throughout the experimental programme, the results from the control experiments demonstrated that the reproducibility of the technique was high.

(ii) The validation exercise was confined to radioaesium, since no published information could be located on the effects of soil treatments on the uptake of radiostrontium by plants. For radiocaesium at least, the exercise indicated that the technique can be used as a screening procedure to determine the immediate effects of soil treatments on the solid-liquid distribution of radionuclides and their stable analogues: potentially detrimental treatments can be identified and eliminated immediately, and for beneficial treatments a reasonable estimate of effectiveness in the field can be obtained. More specific information can then if necessary be obtained from more protracted plant uptake experiments.

(iii) The results demonstrate that, for radiocaesium, potassium can be a useful ameliorant in low fertility soils, whereas ammonium has a detrimental effect in all soils The diverse nature of organic fertilisers makes generalisations about their use impossible. The results obtained in this study were explained by the presence of K and Ca in the material used

(iv) Both lime and superphosphate could be useful in reducing the uptake of radiostrontium from peat soils

(v) In the case of mixed deposits, those treatments considered so far that were aimed at one radioelement would be unlikely to induce significant detrimental effects in the other

References

1 Nisbet A F Effectiveness of soil-based countermeasures six months and one year after contamination with of five diverse soil types with caesium-134 and strontium-90 NRPB-M546 (1995)

2 Paul L Field investigation of the effects of chemical treatments on the soil-to-plant transfer of radiocaesium 1990-1993 Contract report to MAFF WS Atkins Report No WSA-E5232-R1 (1995)

3 Nisbet A F and Wilkins B T Effectiveness of soil-based countermeasures applicability of experimental and modelling approaches for use in the UK. NRPB Memorandum (in preparation)

4 Paul M, Wilkins B T, Nisbet A F, Perepelyatnikova L V, Ivanov Y, Fesenko S V, Sanzharova N and Bouzdalkin C N The development of countermeasure strategies at selected settlements in the areas affected by the Chernobyl accident (in preparation)

5. Rosen K. Effects of potassium fertilisation on caesium transfer to grass, barley and vegetables after Chernobyl. In 'The Chernobyl fallout in Sweden' Ed L Moberg Swedish Radiation Protection Institute (1991)

6. Rosen K. Effects of potassium on the caesium transfer to the crops after Chernobyl. In proceedings of XVth regional congress of IRPA entitled: The Radioecology of natural and artificial radionuclides. Ed. W Feldt. Verlag TUV Rheinland GmbH, Koln, pp232-237 (1989).

7 Fawaris B H and Johanson K J. Uptake of ^{137}Cs from coniferous forest soil by sheep's fescue in pot experiments. In proceedings of the XXIVth Annual ESNA/IUR Meeting, Varna, Bulgaria, pp (1994)

8 Haugen and Uhlen, (1992).

9. Belli M, Sansone U, Ardianii R, Feoli E, Scimone M, Menegon S and Parente G. The effect of fertiliser applications on ^{137}Cs uptake by different plant species and vegetation types. J. Environ Radioactivity 27. 75-89 (1995)

10 Lonsjo H E, Haak E and Rosen K Effects of remedial measures on long term transfer of radiocaesium from soil to agricultural products as calculated from Swedish field experimental data. In Environmental contamination following a major nuclear accident International symposium Vienna, Austria. Vol 2: IAEA-SM-306/32, Vienna, pp151-162 (1990).

11 Cawse P. Influence of organic and inorganic fertiliser on the soil-to-plant transfer of radioactive Cs and K-40 to ryegrass in west Cumbria (post Chernobyl) In EC Workshop on the Transfer of Radionuclides in Natural and Semi-natural Environments. Udine, Italy. Elsevier Applied Science, pp411-418 (1990)

12 Schechtner G and Henrich E Influence of fertilisation, utilisation and plant species on Cs-137 content of grassland growth In Environmental contamination following a major nuclear accident International symposium Vienna, Austria Vol 2: IAEA-SM-306/17, Vienna, pp (1989)

Head of Project 3: A. CREMERS

II Objectives for the reporting period

1. A simplified procedure for the specific site characterization in radiocesium sorption in soils and sediments
2. A predictive equation of K_D^{Cs} in soils and sediments: a comprehensive test
3. Kinetics of radiocesium sorption in soils
4. Coutermeasure strategy: a soil chemical approach

III Progress achieved including publications

1. A simplified procedure of specific sorption potential for radiocaesium sorption

The fact that radiocaesium is, in the very large majority of field scenarios, quantitatively intercepted in the FES group, makes the quantitative assessment of this sorption pool of paramount importance if we wish to make K_D predictions. In the early stages, the specific sorption potential, defined as the product of FES capacity and trace Cs to K selectivity coefficient (formally represented by the symbol $[K_D.m_K]$ was measured on the basis of an elaborate silver-thiourea masking procedure. The principle of a new and simple protocol, eligible for routine applications was introduced in the K_D workshop at the 1984 Lisbon freshwater ecology meeting. It was presented in our 1984 progress report and applied to a limited number of systems. In short, it is based on a single $K_D(Cs)$ measurement in systems preequilibrated with a Ca/K mixed solution (Ca:100mM); K:.5mM) i.e. a PAR (Potassium Adsorption Ratio $m_K/\sqrt{m_{Ca}}$) of 0.05. At this low PAR value, K ions are (nearly) exclusively confined to the FES. This procedure has now been extended to over one hundred sediment (and soil) samples of a wide range in textural properties, cation exchange capacity and organic matter content. Figure 2 shows the correspondance between results obtained by the masking procedure and the simplified PAR protocol. The agreement is essentially perfect: the linear regression yields

$$[K_D.m_K]^{PAR} = -0.083 + 1.01\ [K_D.m_K]^{AgTU} \qquad R^2 = 0.85$$

An additional demonstration of the nature of the agreement between the elaborate masking technique and the PAR protocol is based on a comparison of $[K_D.m_K]$ and $[K_D.m_N]$ values. Figure 2 shows the results.
Both procedures are in excellent agreement in demonstrating the high competitivity of NH_4 as compared to K. The linear regressions are:

$$[K_D.m_K]^{PAR} = -0.11 + 5.12\ [K_D.m_N]^{PAR} \qquad R^2 = 0.90 \qquad n=105$$

$$[K_D.m_K]^{AgTU} = -0.065 + 5.70\ [K_D.m_N]^{AgTU} \qquad R^2 = 0.92 \qquad n=116$$

$$[K_D.m_K]^{All} = -0.046 + 5.28\ [K_D.m_N]^{All} \qquad R^2 = 0.91 \qquad n=221$$

It thus appears that the sorption characteristic, necessary for making K_D predictions is obtainable from a single measurement using simple laboratory procedures readily available. The reliability of predictions based on such characterizations is demonstrated in the section below.

2. Prediction of KD(Cs) in sediments and soils

Predictive capabilities were tested on a broad range of systems using the following equation

$$K_D\ (Cs) = \frac{[K_D\ m_K]}{m_K + 5.3\ m_N + 0.02\ m_{Na}}$$

in which 5.3 and 0.2 refer to the N/K and Na/K selectivity coefficients in the FES. The following tests were carried out:(1) fifty freshwater sediments were thoroughly preequilibrated with a (modal) synthetic river water (m_K = 0.15 mM; m_N = 0.1 mM, m_{Ca} = 2 mM, m_{Mg} = 0.5 mM m_{Na} = 1 mM) and K_D(Cs) measured; (2) twenty-five freshwater sediments were equilibrated with the (Cs^{137} labelled) water described in (a) and K_D(Cs) measured; liquid phase compositions were measured after equilibration; (3) five estuarine sediments were submitted to tests 1 and to equilibration with synthetic seawater; (4) six widely different soils (texturally) were subjected to 8 different cationic scenarios (Ca = 3.5 mM; Mg = 1.5 mM) varying the K and NH_4 concentration in the range of 0.3 - 2 mM. In total, some 133 systems (combinations of sediments/soils and water compositions) were included in the study. Figure 4 shows the nature of the agreement between predicted K_D(Cs) values (K_D-pred) and experimental findings (K_D-exp). It is seen that K_D values cover a range of three orders of magnitude (50 to 50000 L/Kg) and that the agreement is reasonably good. In general, predictions somewhat overestimate experimental values but 90% of all observations deviate by less than a factor 3 from predictions. On the average it is found that

$$\frac{K_D(\exp)}{K_D(pred)} = 1.61 \pm 0.75$$

It may thus be concluded that reasonably reliable predictions of K_D(Cs) can be made on the basis of [$K_D.m_K$] values (obtainable by routine procedures) and liquid phase compositions (K and NH_4, and in saline scenarios, Na ion concentrations).

3. Kinetics

The specific sorption properties of soils are usually assessed by masking techniques involving 24 hours equilibrations. Whether such procedures lead to reasonable approximations was assessed by a comprehensive study on radiocaesium kinetics in soils, covering a very wide range in organic matter content. The results obtained can be briefly summarized as follows. The sorption of radiocaesium in systems containing micaceous minerals is governed by kinetic effects. The initial rapid sorption on organic matter and planar clay surface sites is followed by a moderately fast sorption reaction on interlayer edge sites in the FES. For high organic matter soils, with low FES content, kinetic effects are marginal while for low organic matter soils, with low FES content, kinetic effects are marginal while for low organic matter soils, with high FES content, the moderately fast

sorption takes two to three weeks (for well-mixed conditions), leading to an increase in K_D(Cs) values by a factor of 2 to 3. Consequently, characterizations based on 24 hrs equilibration, when used as a predictive tool for K_D values can be expected to lead to a slight underestimate of long term K_D values.

4. Countermeasure strategy: a soil chemical approach

The potential effect of a countermeasure agent on the soil-plant transfer of a radionuclide depends on the relative values of the Interception Potentials (I.P.'s) i.e. n° of sorption sites and RN sorption selectivity, and the dose. The beneficial effect is related to a RN shift from soil to amendment and a corresponding decrease of the RN levels, confronted by the plant root. The RN partitioning between soil (s) and amendment (a) can be written:

$$\frac{f_a}{f_s} = \frac{IP_a.m_a}{IP_s.m_s}$$

where f and m refer to the fractions and amounts. The ratio of IP_a/IP_s can be identified with the K_D ratios of amendment and soil and the in-situ soil solution composition. Alternatively, we may write :

$$f_s = \frac{IP_s.m_s}{IP_s.m_s + IP_a.m_a}$$

It is seen that, if we wish to obtain a significant effect, say a factor of 2, we require a two order of magnitude difference in IP's for a 1% dose (or some 40-50 Ton/ha). In the case of radiostronti um, effects are essentially related to ion exchange capacity and we may write:

Sr: $$\frac{f_a}{f_s} = \frac{CEC_a.m_a.p}{CEC_s.m_s}$$

in which p refers to the K_c(Sr/Ca) ratio in amendment and soil. In general, p differs very little from unity except in some zeolites. Therefore, the scenarios in which we may obtain favourable effects are combinations of low soil CEC and high CEC of amendment, combined with a high Sr-to-Ca selectivity.

In the case of radiocesium, the conditions appear more favourable since some materials (synthetic, natural) show specific sorption potentials of very high values as compared to those commonly found for soils. In the case of radiocesium, we may write:

Cs: $$\frac{f_a}{f_s} = \frac{\left[K_D.m_K\right]_a.m_a}{\left[K_D.m_K\right]_s.m_s}$$

If we wish to make predictions on expected beneficial effects, thus providing a rationale for the selection of countermeasure amendments, then it is mandatory to quantify their trace sorption characteristics. This issue is addressed in this section: firstly a thorough study was carried out of Cs and Sr in a set of zeolites; secondly, their beneficial effect was measured through a phytotronic uptake study and the results confronted with expectations.

a. Cesium exchange sorption in zeolites

Three types of zeolites were included in the study: a reference clinoptilotite (Hector, California) CLI, a natural mordenite (Karpats) MOR, and a synthetic (commercial)

mordenite zeolon, ZEO (Akzo Nobel Comp. Sweden). CEC values for the samples, as measured in the homoionic K, resp. Cs form are, in meq/g, 1.60-1.82 (CLI), 1.03-1.24 (MOR) and 1.90-1.96 (ZEO). The experimental study focused on the following issues: (a) characterisation in terms of radiocesium sorption potential in the K-saturated zeolite samples; (b) the K/NH_4 selectivity pattern; (c) a complete Cs/K ion exchange study; (d) radiocesium sorption pattern as a function of the Ca level in the system. The main results, and practical consequences can be summarised as follows:

(1) *Specific sorption potentials* [$K_D.m_K$] are extremely high: the values are 34.4 (±0.7) for CLI, 64.9 (±1.5) for MOR and 66.9 (±0.9) meq/g for ZEO. The corresponding parameters for peat and sandy soils are in the range of 0.05 to 0.5 meq/g, i.e. we notice a difference of two to three orders of magnitude. Therefore, such materials are potentially effective countermeasure agents.

(2) *K and NH_4* are about equally sorption competitive; consequently, the sorption efficiency for radiocesium will not be adversely affected by NH_4 ions, as is the case in soils.

(3) *The Cs sorption* in the samples is describable in terms of a *model* comprising four groups of sites each of which are characterised by some K_c(Cs/K) value. The two sites, exhibiting the high Cs/K selectivity represent some 10% of the overall CEC; these are the sites which in a soil chemical scenario remain K saturated and, as could be expected on the results presented in (a), their effect exceeds the one for sands and peats by two order of magnitude at least.

(4) *Effect of Ca*: Ca is only partially exchangeable in the zeolites and the sites in the lattice responsible for the selective Cs sorption are inaccessible to Ca (and Mg). The most interesting observation however is that the Cs/K selectivity coefficient in the most selective sites is enhanced by introducing Ca in the lattice, i.e. a synergistic effect. This amounts in practice to a doubling of the sorption efficiency of the specific sites. As a consequence, it can be expected that these materials are potentially very interesting countermeasure materials for radiocesium.

b. Strontium exchange sorption in zeolites

A sorption study was carried out along the same lines as described above using the Hector clinoptilotite CLI, the Karpate mordenite MOR, and a synthetic zeolite 5A from Union Carbide. Ca, respectively Sr CEC values were, in meq/g, 1.07-0.72 (CLI), 0.42-0.31 (MOR) and 5.7-1.3(5A). The following issues were addressed: (a) the overall sorption potential of the zeolites; (b) a complete Sr sorption isotherm; (c) effect of the presence of Mg. The results can be summarised as follows:

(a) *Sorption potentials*: The Sr sorption potentials as obtained through trace-Sr K_D measurements on Ca saturated samples are, in meq/g, 5 (MOR), 20.3 (CLI) and 27 (5A). These values are quite high as compared to sandy soils (≅ 0.02meq/g).

(b) *Sorption isotherm of Sr*: The sorption is characterised, as for cesium, by a pronounced site heterogeneity. Sorption can accurately be described in terms of a two or three site model comprising sites of a characteristic selectivity coefficient. Zeolite 5A and clinoptilotite are the most interesting cases. The most selective sites show a K_c(Sr/Ca) value of about 130 (5A) and 460 (CLI), and the site populations amount to 15% (5A) and 1.5% (CLI) of the overall capacity. Such exceedingly high Sr/Ca selectivity coefficients are in sharp contrast with what is known for soils ($K_c \cong 1.5$-2) a fact which makes these materials, particularly zeolite 5A, quite promising materials in countermeasure practice.

(c) The sorption of radiostrontium is not significantly affected when Ca is gradually replaced by *Mg*.

c. The measurement of TF values.

The soil used in the study is a podzol (Mol): CEC = 1.73 meq/100g; $[K_D.m_K]$ = 0.21 meq/g. In the case of cesium three amendments were tested: synthetic Na-mordenite (1%), natural clinoptilotite (1%) and vermiculite (2%); for strontium, tests were performed on zeolite 5A (1%), and two organic high CEC materials: a peat soil (Bragin) of CEC 1.14 meq/g and a sapropell (Belarus) of CEC 0.85 meq/g, both at a dose of 2%.

Experimental procedure

8 Soil samples (about 6 kg) were thoroughly mixed with 1L non-active 1/2 diluted Steiner solution using a kitchen mixer, followed by further mixing with 200ml of the same solution labelled with either Cs-137 (4 samples) or Sr-85 (4 samples). For both cases, activities were about 300 Bq/g soil. Systems were left to age for 2 weeks, applying two drying-wetting cycles (from 80% of field capacity (26ml/100g) to about 35% of F.C.). Soil amendments were added at a soil water content of 35% of F.C., using again vigorous mixing; soils were again allowed to age for two weeks (2 drying wetting cycles) and finally divided over 5 one-litre pots for TF measurement. Labelling homogeneity was tested by counting 5 g. samples (variation <2%).

Spinach seeds were germinated for two days on moist paper and transferred to the pots (one/pot). Soil surface was covered with 40g. polyethylene beads (evaporation reduction) and plants were grown in a walk-in growth chamber, using a 12hrs/12hrs day-night cycle. Soil moisture was adjusted twice a day, daily alternating deionized water or 1/2 diluted Steiner solution. After three weeks of growth, shoots were removed and stored in scintillation vials for counting and oven-drying (70°C). In addition, from each pot, a 20 ml core was taken for measuring soil water content and soil solution characterisation using immiscible displacement. TF values are expressed in terms of TF (plant content oven dried/dry soil) values (average of 5 observations). Plant weight at harvest was in the range of 0.3 to 0.5g (dry-shoot).

Results and discussion

The results for Cs-137 are summarised in Table 1. It is seen that the reproducibility of TF values is reasonably good (20% on average) and that significant effects are obtained. The overall effect is in good agreement with what could be expected on the basis of $K_D.m_K$

values: a factor of about 2 difference between the synthetic mordenite and clinoptilotite. The overall effect of vermiculite appears to be similar to the one obtained for clinoptilotite. It is apparent that the reduction in TF is accompanied by a - not proportional - decrease in the interstitial Cs-137 levels. Of course, the overall effect may be a combined result of some reduction of interstitial concentration of K and a plant response to that effect.

The results obtained for Sr-85 are shown in Table 2. Again, the reproducibility is good (12% on average) and somewhat better as compared to Cs-137. The effect obtained in the case of zeolite A is quite high as expected on the basis of the difference in sorption potential (3 orders of magnitude). It is particularly striking that the decrease in TF is accompanied by a nearly identical decrease in Sr-85 concentration in the soil solution. In the case of the peat and the sapropell, the decrease in TF is also accompanied by a decrease in Sr-85 concentration. Moreover, the effect on TF is also consistent with the resulting increase in CEC (a factor of 2.31 and 1.99 respectively).

Table 1: Effect of amendment on Cs-137 uptake in spinach. TF values are averages of 5 observations. Cs-137 ratios refer to values in the soil solution (control-amendment)

	TF	TF-effect	Cs-137 ratio
control	0.75 (0.09)		
1% Na-Mordenite	0.164 (0.042)	4.57	12.3
1% Clinoptilotite	0.25 (0.04)	2.99	7.1
2% Vermiculite	0.124 (0.042)	6.08	3.6

Table 2: Effect of amendment on Sr-85 uptake in spinach. TF values are averages of 5 observations. Sr-85 ratios refer to values in the soil solution (control-amendment)

	TF	TF-effect	Sr-85 ratio
control	35.1 (6.4)		
1% Zeolite A	1.41 (0.1)	25	29.9
2% Peat	12.8 (1.5)	2.75	1.72
2% Sapropell	17.0 (2.1)	2.06	1.28

5. Publications

Accepted (Applied Geochemistry)

Prediction of solid/liquid distribution coefficients of radiocesium in soils and sediments

- Part One: A Simplified Procedure for the Solid Phase Characterization
  J. Wauters, A. Elsen, A. Cremers, A. V. Konoplev, A. A. Bulgakov and R.N.J.Comans
- Part Two: A New Procedure for Solid Phase Speciation of Radiocesium
  J. Wauters, M. Vidal, A. Elsen and A. Cremers
- Part Three: A Quantitative Test of a K_D Predictive Equation
  J. Wauters, A. Elsen and A. Cremers

To be submitted

The use of zeolites as amendments in radiocesium and radiostrontium contaminated soils: a soil chemical approach

- Part One: Cs-K exchange in clinoptilotite and mordenite and the influence of Ca
  E. Valcke, B. Engels and A. Cremers
- Part Two: Sr-Ca exchange in clinoptilotite, mordenite and 5A
  E. Valcke, B. Engels and A. Cremers
- Part Three: A simple soil chemical test of the potential effect of zeolite amendments
  E. Valcke, A. Cremers, J. Ivanow and G. Perepelyatnikov
- Part Four: A plant growth test of the predicted effect
  E. Valcke, A. Elsen and A. Cremers

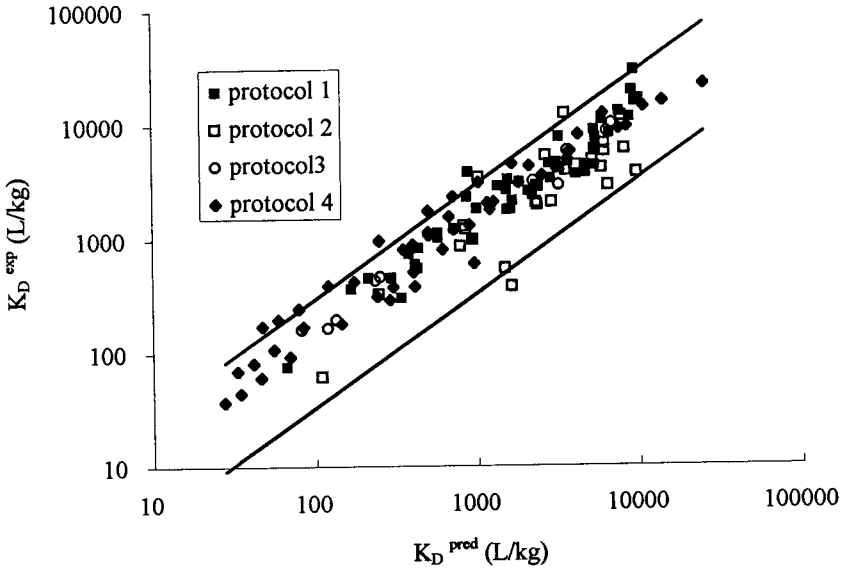

Figure 3: Experimental versus predicted K_D values: upper and lower lines refer to K_D(exp)/K_D(pred) values of 3 and 0.33.

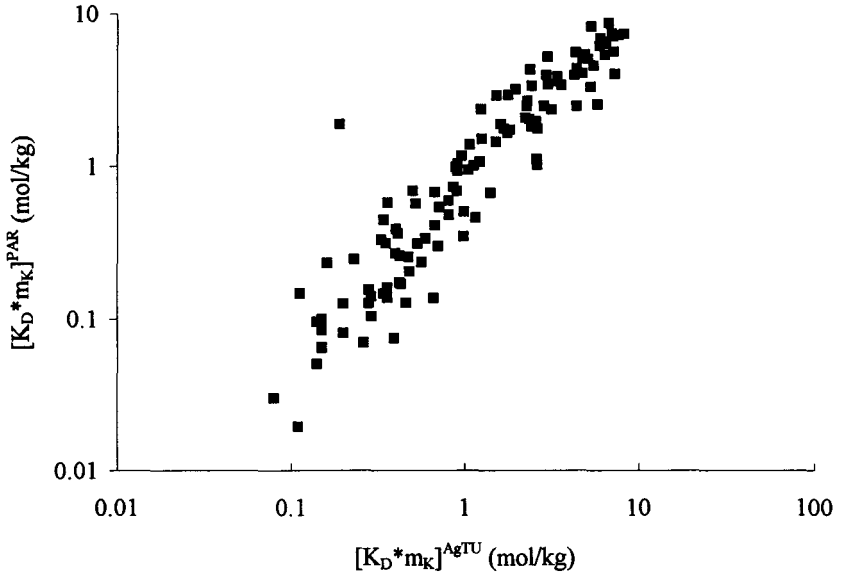

Figure 1: Comparison of $[K_D.m_K]$ values obtained by the AgTU masking technique and the simplified PAR protocol.

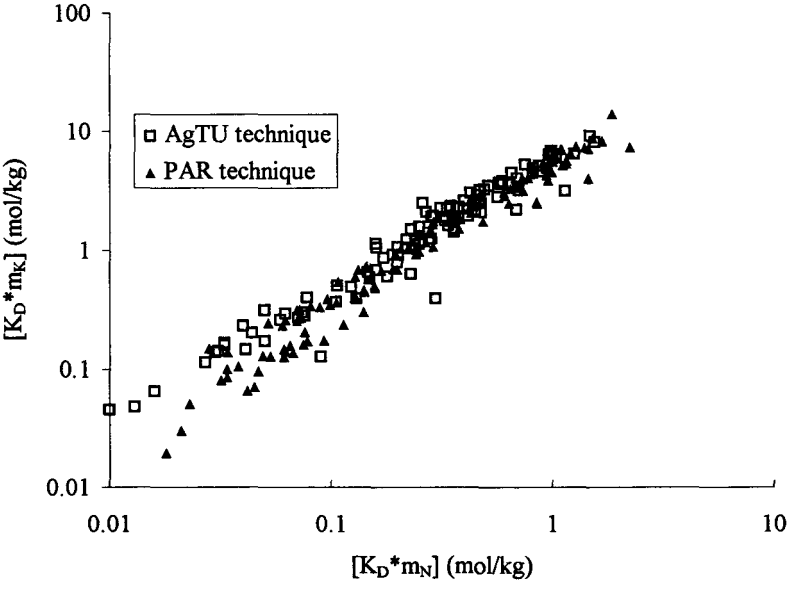

Figure 2: $[K_D.mK]$ values versus $[K_D.mN]$ values for the AgTU masking technique (105 substrates) and the simplified PAR protocol (116 substrates).

Head of project: Prof. R Merckx

1. Objectives for the reporting period

The phytoavailability of ^{137}Cs is analysed. The analysis is based on separately studying plant- and soil related factors which control ^{137}Cs availability in general. The plant related factors studied are the effects of nutrient supply on ^{137}Cs uptake rate, the distribution of ^{137}Cs within the plant and the genotypic effect on ^{137}Cs uptake These factors are studied using solution culture experiments. Soil related factors examined are the transport of ^{137}Cs towards the roots and the effect of fertilisation on ^{137}Cs Activity Concentration (AC) in the rhizosphere. From pot trials and calculations, the role of plant and soil related factors in ^{137}Cs availability is examined.
A large number of solution culture experiments and pot trials have been carried out. Only a selection of the results will be reported here, keeping method description to a minimum Details of experimental methods can be found in the papers of our group (see reference list)

2. Major results obtained

2.1. The effect of nutrient supply on ^{137}Cs uptake rate from solution.

2.1.1 General

The effect of nutrient supply on ^{137}Cs uptake rate is measured to assess the variability of the root uptake parameter with varying soil fertility. Furthermore, the results obtained could suggest the mechanism of ^{137}Cs uptake in the plant, hence allowing to summarise the root kinetics in a meaningful equation, a prerequisite for modeling ^{137}Cs availability in soil

The influence of the solution composition (Ca, Mg, K and NH_4 concentrations) on ^{137}Cs uptake is assessed in expts 1 and 2 The effect of K supply on ^{137}Cs uptake rate was further analysed using a split root experiment with heterogeneous K supply (expt. 3).

2.1 2 Materials and methods

experiment 1

Briefly, spinach (*Spinacia oleracea L*, cv. Subito) was grown in solution culture at 15 nutritional scenario's Total salt concentration was 5.3 meq/L (4 scen.), 10 6 meq/L (8 scen), 12 7 meq/L (2 scen) and 21.2 meq/L (1 scen). Relative concentrations of anions were kept invariant and trace element concentrations (including ^{137}Cs activity in solution) the same throughout The range of cationic concentrations studied were K, 0 53 to 10 4 mM, NH_4, 0 to 8 47 mM; Ca, 0 15 to 5 0 mM, Mg, 0 08 to 2.0 mM. Plants were grown in growth chambers at equal conditions for all scenario's. During plant growth, solution concentrations of K, Ca and Mg were measured and adjusted with

stock solutions to have no more than 20% change of initial values. Water losses in the containers were compensated with deionised water. ^{137}Cs levels in solution were monitored regularly but did not show considerable changes. Results reported here refer to plants harvested at 20 days after sowing except for 1 scenario (21 days)

experiment 2

Spring wheat (*Triticum aestivum* L., cv. Tonic) was grown in solution culture. Treatments were different K concentrations in solution, 25 μM, 50 μM, 250 μM and 1000 μM, added as KNO_3 in a K-free nutrient solution containing all other nutrients in sufficient amounts. Total salt concentration was 10.5 meq/L The solution was spiked with ^{137}Cs at about 5 Bq/mL Plants were grown in eight culture tanks (two for each treatment, 40 L each and 8 plants per tank) which were installed in a growth cabinet. Solution samples were taken daily from day 10 (day 0 is day of sowing) and analysed for ^{137}Cs and K and adjustments of K and ^{137}Cs concentrations were made if changes larger than 10 % of initial concentration were found Lowest K concentration measured was 16 μM for the 25 μM K treatment (day 17) and 42 μM for the 50 μM K treatment. Lowest AC measured were 89 % of initial AC in solution. Plants were harvested at day 18 and their ^{137}Cs γ-activity counted.

experiment 3

In most field conditions, neither ^{137}Cs nor K is evenly distributed over the whole root system of the plant. The impact of these factors is assessed in a solution culture experiment. Spring wheat was grown in complete nutrient solution until day 17 after which the plants were transplanted to a split root system. The composition of the nutrient solution in both root compartments is given in Table 1. The root size in both compartments was about equal. Plant growth conditions were equal to those described above. The treatments were designed to answer the following questions. (i) is uptake of ^{137}Cs in the shoot proportional to the fraction of roots exposed to ^{137}Cs (compare treatment 2 and 5)?; (ii) to what extent is ^{137}Cs uptake and translocation dependent on the K concentration in the ^{137}Cs labeled compartment (compare treatments 1 and 3) or on the K supply in the unlabelled compartment (compare treatment 1 with 2 and 3 with 4)?

2.1.3. Results

experiment 1

The Cs Transfer Factor (TF, the ratio of ^{137}Cs AC in the oven dried plant sample to that in solution) was significantly affected by the solution composition. The TF values cover a range of about 40-120 L/kg Shoot TF's were generally higher than root TF's (both dry weight based), although never more than 1.35 fold (results not shown). No clear correlation could be found between ^{137}Cs TF and the K, NH_4 or $K+NH_4$ concentration (Fig 1) However, ^{137}Cs TF were negatively related to Ca+Mg concentrations in solution. Whether this decrease is due to Ca or Mg cannot be answered here as in most scenarios, Ca and Mg were covaried The negative effect of Ca+Mg concentrations on ^{137}Cs uptake is interpreted from their effect on ^{137}Cs loading in the apoplast of the root cortex. The relationship between the ^{137}Cs TF and the fractional loading of ^{137}Cs in the apoplast, calculated by ion exchange laws, is linear (R^2=0.81, P<0.001, results not shown) for the 15 different solutions studied.

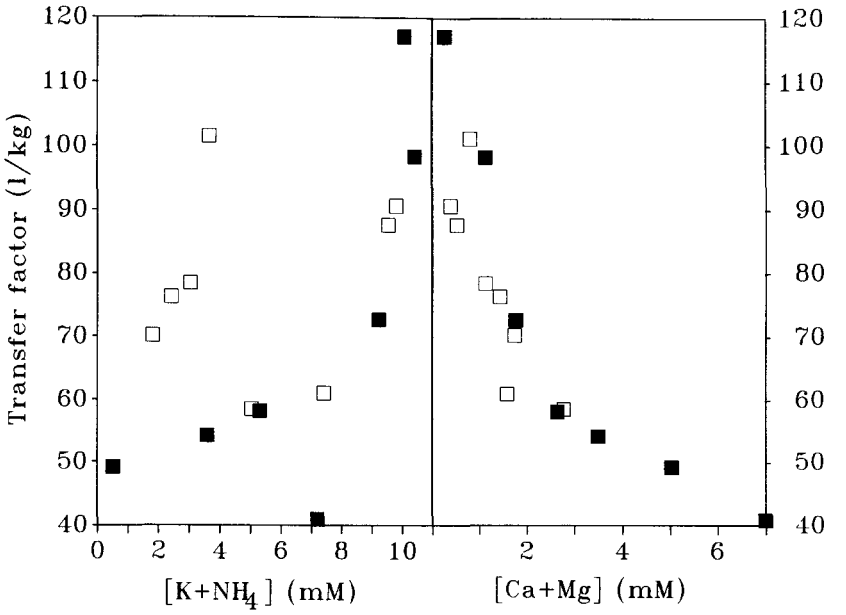

Fig 1 Plot of ^{137}Cs transfer factors (L/kg dry weight) of spinach plants versus $K+NH_4$ and Ca+Mg concentration in nutrient solutions. Open and closed symbols refer to nutrient solutions with and without NH_4

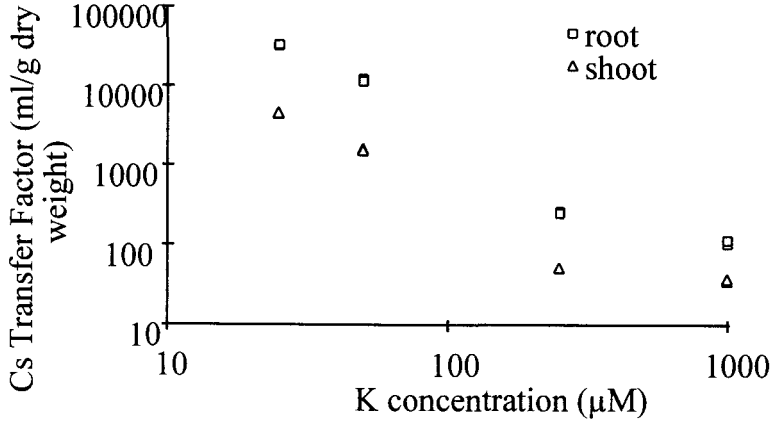

Fig 2. Log-log plot of the ^{137}Cs transfer factor (L/kg dry weight) of shoot and root of 18 day old wheat plants grown at different K concentration in solution. The transfer factor is defined as the ratio of ^{137}Cs AC in plant to that in solution Each symbol represents the observation of one independent replicate.

experiment 2

In contrast to the previous experiment, a strong negative correlation between the ^{137}Cs TF and K concentration was found in expt. 2 (Fig. 2). In between 50 μM K and 250 μM K, ^{137}Cs TF varies more than proportionally to the reciprocal of the K concentration. Since this K concentration effect is larger than the (linear) effect of K concentration on ^{137}Cs desorption from soil, it can be anticipated that K fertilisation can reduce ^{137}Cs uptake from soil, in line with many observations (see expt.6).

The K concentration effect on ^{137}Cs uptake has not been found in spinach in expt. 1 which is most probably *not* related to the plant species used: in expt. 5, the K concentration effect is found for all 4 species used but is almost absent above about 0 5 mM K Apparently, the effect of K supply on ^{137}Cs uptake changes with the K concentration range, the effect being large below about 0.5 mM and becoming absent at higher K concentrations.

experiment 3

The AC in the shoot and root parts of the wheat plants is given in Table 1. Shoot AC's are about proportional to the fraction roots exposed to ^{137}Cs (compare 2 and 5). The external K concentration in the ^{137}Cs labelled root compartment most importantly influences the root AC and, to a smaller extent, the shoot AC (compare 1&2 with 3&4) Reducing the K supply in the unlabeled compartment slightly increased the AC of the root grown in the labeled compartment and marginally affected shoot AC (compare 1 with 2 and 3 with 4).

Table 1. Composition of the solutions in the two root compartments in a split-root design and ^{137}Cs AC in the plant parts after 9 days of growth under the experimental conditions ^{137}Cs activity in solution is given in Bq/mL.

treatment	composition root compartments				^{137}Cs in plant (Bq/g dw)		
	left		right		root		shoot
	K (mM)	^{137}Cs	K (mM)	^{137}Cs	left	right	
1	0.25	10	1	-	3136^{b}	142^{b}	255^{bc}
2	0 25	10	0.25	-	4396^{a}	175^{c}	228^{b}
3	0 25	-	1	10	155^{d}	1167^{b}	241^{c}
4	1	10	1	-	1079^{c}	109^{c}	190^{c}
5	0 25	10	0.25	10	4480^{a}	4760^{a}	625^{a}

2.2 The distribution of ^{137}Cs within the plant.

2.2.1. General

From expts. 2 &5, it has been found that the ^{137}Cs distribution between root and shoot tissue of young plants changes with the K supply, ^{137}Cs becoming preferentially retained in root biomass at reducing K supply As an

example, the ratio of root to shoot levels (dry weight based) in wheat increases from 3 to 7 when K concentration is reduced from 1000 µM to 25 µM. The possible link between K and ^{137}Cs distribution within the plant was assessed in expt. 4 by measuring root to shoot flow of ^{137}Cs and K in the xylem and their shoot-root retranslocation through the phloem.

2.2.2. Materials and methods

The methodology of expt. 4 is fully described elsewhere (Buysse et al., 1995). Briefly, ^{137}Cs and K fluxes are measured based on observed ^{137}Cs/Ca and K/Ca concentration ratio's in collected xylem sap and the shoot accumulation of these elements within a given time interval. Using the assumption that no Ca can be backtranslocated to the roots, xylem fluxes of ^{137}Cs and K and the fraction backtranslocated to the roots can be calculated These fluxes were measured in spinach in two experiments (expt. 4 a and b): in expt. 4 a, ^{137}Cs fluxes were measured after the onset of ^{137}Cs supply at continuous K supply, in expt. 4 b, ^{137}Cs and K fluxes were measured after onset of ^{137}Cs and K supply to previously K starved plants Expt. 4 b also included the effect of different shoot temperatures on distribution. Only the data of the expt. in which root and shoot temperature were equal are represented here.

2 2.3 Results

The most relevant results of expt. 4 are summarised in Table 2. In expt 4 a, ^{137}Cs accumulation rate increased during the 12 h labeling period (details not shown). The percentage ^{137}Cs recirculated increases after the start of labeling, reaching 57 % after 12 h. In expt. 4 b, almost all K translocated to the shoots of previously K stressed plants was retained in the shoot during the first two days after K resupply. In contrast, a high proportion of the ^{137}Cs was backtranslocated to the roots. It is concluded that ^{137}Cs is very mobile within the plant and that no correlation can be found between ^{137}Cs and K fluxes within the plant The physiological interpretation to this is that ^{137}Cs accumulation in the shoot may be limited by ^{137}Cs transport into vacuoles in shoot cells. The different behaviour of ^{137}Cs and K within the plant may explain why ^{137}Cs and K are differently distributed over ears, leaves, stems and roots of solution grown wheat plants (Smolders and Shaw, 1995).

Table 2 Shoot to root recirculation of ^{137}Cs and K in percentage of that transported from root to shoot in the xylem. Measurements are made at different periods after the onset of ^{137}Cs supply to the roots (expt 4 a) or after onset of both ^{137}Cs and K supply to K stressed plants (expt. 4 b). Modified from Buysse et al. 1995.

expt. 4 a		expt. 4 b		
time after labeling (h)	% recirc. of ^{137}Cs	time after labeling (h)	% recirc. of K	% recirc of ^{137}Cs
0-2	22	0-48	2	75
2-4	13	48-96	77	95
4-8	50			
8-12	57			

2.3. Species effect on ^{137}Cs uptake from solution.

2 3.1. Materials and methods

In a solution experiment (expt. 5), seeds of sunflower (*Helianthus annuus* L cv California), clover (*Trifolium repens* L. cv icernat vroege rode), radish (*Raphanus sativus* L. cv Triplo) and maize (*Zea mays* L. cv Caro) were grown at different K concentrations between 0.25 mM and 5.1 mM Total salt concentration was maintained in all treatments at 10 4 meq/L by replacing K salts with Ca and Mg salts All solutions were spiked with ^{137}Cs at 10 Bq/mL. Results refer to plants harvested at day 16 (sunflower and radish), at day 20 (maize) and at day 26 (clover)

2.3.2 Results

The ^{137}Cs AC in the plants is given in Fig 3 Increasing K supply (and decreasing Ca+Mg supply) generally reduced AC's in all plants. However, from about 0.5 mM K, increasing K supply had no or a slight positive effect on plant AC's. Recalling the results of expt. 1, this small increase is most probably due to decreasing Ca+Mg concentrations in solution. Since Ca+Mg concentrations in solution only vary from 2.7 mM to 5.1 mM, the Ca+Mg effect may however be too small to cause a large effect (cf. Fig. 1). The differences in ^{137}Cs AC between species is considerable. The ranking of species with regard to AC however depends on the nutrition

2.4. Potted soil experiments.

2 4.1 General

The combination of soil solution data, kinetic parameters derived in solution culture experiment and soil transport calculations allows to analyse observed ^{137}Cs transfer from soil to plant under controlled conditions.

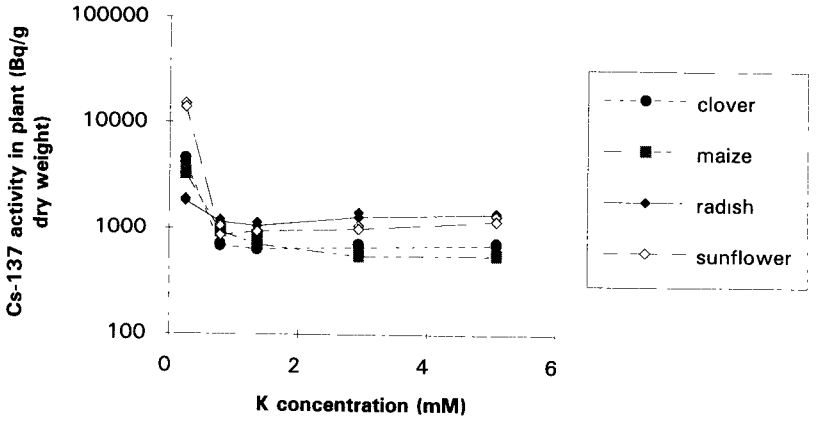

Fig. 3. Semi-log plot of the ^{137}Cs activity in 4 different plants grown in nutrient solution at different K concentration Total salt concentration in solution was maintained by replacing K salts by Ca and Mg salts

In a first experiment (Smolders et al , 1993), spinach and wheat plants were grown up to 24 days in a potted soil (an Ap horizon of a podzol) which was freshly contaminated with ^{137}Cs. The difference in ^{137}Cs AC between the species was small and varied with plant age and size. A proper interpretation of species effect was difficult as ^{137}Cs AC in soil solution was found to decrease during plant growth, probably related to slow adsorption/fixation processes For both plants, the ratio of shoot AC to soil solution AC was well within the range of solution culture TF. This finding indicates that the ^{137}Cs AC in bulk soil solution could be equal to that in the rhizosphere.

In a second experiment, spinach was grown in a potting mixture contaminated with ^{137}Cs. Care was taken that root density was very low in the pot in order to better meet assumptions in soil solute transport calculations. Calculation based on this experiment demonstrate that K around the roots is depleted compared to the bulk soil whereas Ca and ^{137}Cs accumulate (no results shown)

The (indirect) evidence from these two potted soil experiments shows that rhizosphere depletion of ^{137}Cs is limited. For these conditions, the following statement can be made. *^{137}Cs uptake from soil is not controlled by the diffusive flux towards roots but rather by (a) the ^{137}Cs AC in the bulk soil solution and (b) the kinetic parameter of the roots which is under control of the plant (growth rate) and the nutrient supply.*

This general statement was further verified by assessing the effect of K fertilisation on ^{137}Cs uptake from potted soil, further denoted expt.6 The idea behind this test is the following. K addition to a soil increases ^{137}Cs AC in soil solution. If ^{137}Cs uptake is controlled by the diffusive flux towards roots, ^{137}Cs uptake should *increase* upon K

fertilisation. If the opposite effect is found, a strong indication is found the root uptake characteristics control ^{137}Cs uptake from soil, hence supporting the statement given above

2.4 2 Materials and methods

Spring wheat (*Triticum aestivum* L., cv Tonic) was grown in a silt-loam soil sampled in the E horizon of a luvisol under forest. The horizon of this mineral soil was chosen for its low K availability. The soil was amended with lime and phosphor Treatments were three rates of K (0, 1 and 2 mmol K/950 g dry soil, the quantity of soil to fill one pot). K was added as a Cl salt. Plants were grown up to day 16 at equal environmental conditions as in expt 2 and the ^{137}Cs AC measured Soil solution was sampled using a direct centrifugation method and analysed for macronutrients and ^{137}Cs

2.4 3 Results.

Table 3 shows that increasing K supply reduced ^{137}Cs AC in the shoots whereas it increased ^{137}Cs AC in soil solution This result can be explained from the K/^{137}Cs competition for root uptake This is quantified by combining observation from the solution culture (relationship between K concentration and shoot TF, from expt 2) with the solution composition (K and ^{137}Cs concentration) in the rhizosphere. The rhizosphere concentrations of K and ^{137}Cs are derived from soil solute transport calculation which will not be detailed here. The results of this calculation are summarised in Table 3. The K concentrations in the rhizosphere are found to cover the range in which ^{137}Cs TF are sensitively affected (see Fig 2) Therefore, even though the ^{137}Cs AC in the rhizosphere increases 2.7 fold with increasing K application, shoot AC are found to decrease 8 fold and predicted to decrease 18 fold.

The quantitative interpretation of this experiment supports our statement described above.

Table 3 The K and ^{137}Cs concentrations in soil solution at the root surface calculated using a solute transport calculation. From the concentration at root surface and solution culture observations, ^{137}Cs activity in shoots is predicted.

K application (mmol/pot)	average soil solution		soil solution at root surface		^{137}Cs activity in shoot (cpm/g dry weight)	
	K (μM)	^{137}Cs cpm/mL	K (μM)	^{137}Cs cpm/mL	predicted	observed
0	170	4 7	44	2.8	4444	6191
1	420	5.7	354	5.2	278	2765
2	810	7.8	776	7.7	249	755

2.5. Conclusions

Of all plant nutrients, K most importantly controls ^{137}Cs uptake from solution. ^{137}Cs uptake is most drastically affected by K supply below about 0.5 mM K in solution. At higher K concentrations, ^{137}Cs uptake from solution is almost unaffected by the K supply but can be reduced by increasing Ca+Mg supply ^{137}Cs uptake is not only controlled by the K concentration around roots in the ^{137}Cs contaminated root zone but also varies with the K status of the plant which can be affected by the K supply at other parts of the root system or by the K nutritional history of the plant.

The distribution of ^{137}Cs between shoot and root part varies with varying K supply, ^{137}Cs being increasingly retained in the root at decreasing K supply. ^{137}Cs distribution over the plant organs differs from K distribution and short term studies of ion circulation between shoots and roots confirmed a strong difference between these two ions Even though ^{137}Cs circulation within the plant is intensive, net ^{137}Cs uptake in the shoot is proportional to the part of roots exposed to ^{137}Cs.

From three potted soil experiments, evidence is obtained that root uptake characteristics control ^{137}Cs uptake from soil The sensitivity analysis of model calculations given elsewhere in this report (contribution Dr Staunton) confirms this evidence It may therefore be concluded that ^{137}Cs phyotoavailability in not merely a soil chemical characteristic.

The observations that liming and potassium fertilisation reduce ^{137}Cs availability in field grown crops can be explained by the effect of increasing Ca and K concentrations on root uptake characteristics. It can be predicted from our observations that increasing K supply above a certain level will increase ^{137}Cs uptake as K will remobilise ^{137}Cs in soil without further reducing the ^{137}Cs root absorbing power

Publication relevant to this report.

1 Published

Smolders, E., Sweeck L., Buysse, J , Van Den Brande, K. and R. Merckx 1993. Analysis of the genotypic variation in radiocaesium uptake from soil. Plant and Soil, 155/156.431-434.

Buysse, J., Van Den Brande, K. and Merckx, R. 1995. The distribution of radiocesium and potassium in spinach plants grown at different shoot temperatures J Plant. Physiol , 146, 263-267.

Smolders, E and Shaw, G 1995.Changes in radiocaesium uptake and distribution in wheat during plant development: a solution culture study Plant and Soil, in press

2. Submitted and in preparation

Smolders, E., Sweeck, L., Merckx, R. and Cremers, A. Cationic interactions in radiocaesium uptake from solution by spinach. submitted

Smolders, E., Kiebooms, L., Buysse, J. and Merckx, R. ^{137}Cs uptake in spring wheat (*Triticum aestivum* L cv Tonic) at varying K supply:1. the effect in solution culture. submitted.

Smolders, E., Kiebooms, L., Buysse, J. and Merckx, R. ^{137}Cs uptake in spring wheat (*Triticum aestivum* L. cv. Tonic) at varying K supply·2 a potted soil experiment. Submitted

Buysse, J., Van Den Brande, K. and Merckx, R. Genotypic differences in the uptake and distribution of radiocaesium in plants In preparation.

Buysse, J., Smolders, E and Merckx R. The impact of heterogeneously distributed K and ^{137}Cs on the root absorption and distribution of radiocaesium in plants. In preparation.

Head of Project 5: Dr S. Staunton

II. Objectives for the reporting period

1. Development of a mechanistic mathematical model to describe the bioavailability of radiocaesium in soils.
   - definition of geometry, mathematical description of the soil/solution/root system and the boundary conditions
   - development and testing of the model

2 Sensitivity analysis of the model to input parameters

3. Comparison of model simulations with in situ data.
   - conclusions on validity of model
   - conclusions on validity of input parameters
   - indications for the direction of further work

4. Preparation and submission of publications based on experimental studies carried out in the previous reporting period.

III. Progress achieved including publications

A dynamic mechanistic model has been developed and tested. The model simulations suggest that root and shoot recycling play an important role in the cumulative uptake of radiocaesium from soils. They also highlight areas where more research is needed, in particular on the inhibition of root uptake by potassium and similar cations, and the redistribution of absorbed caesium within the plant, which may also be related to the nutritional status of the plants.

Model development

The model has been developed from a previously published model (Kirk & Staunton, *J. Soil Sci.*, **40**, 71-84. There are considerable conceptual changes, which result in a greatly increased mathematical complexity.

The following factors are taken into account:

Uptake by plant roots from the soil solution at the root-solution interface
Movement to the root-solution interface by liquid phase diffusion
Rapid reversible adsorption onto soil constituents
Slow, reversible reaction with the surfaces of soil constituents (ageing or fixation)
Uniformly distributed roots (rooting density may be a function of depth)
Identical roots of finite radius with finite lifetime

A new feature which the model aims to address is the hypothesis that the variation in soil-plant transfer factors between species (or seasonal variations) may arise from differences in root distribution with respect to the depth profile of caesium.

Another important new consideration is that roots do not exploit the same volume of soil over many months or years. The incorporation of root turnover into the model makes significant differences to calculated root uptake.

Detailed description of the model

Model structure

Roots are considered to have a finite lifetime, which is shorter than the total simulation period. Root uptake of caesium during its lifetime depends on the initial caesium distribution between plant, solution, exchangeable and fixed phases. Each successive set of roots finds a different initial caesium distribution. The first step in the model is to run successive simulations with differing initial caesium distributions. Polynomial regressions are then used to fit calculated uptake to initial caesium distribution and root density.

The cumulative uptake is calculated in a second, multi-step stage, as follows:

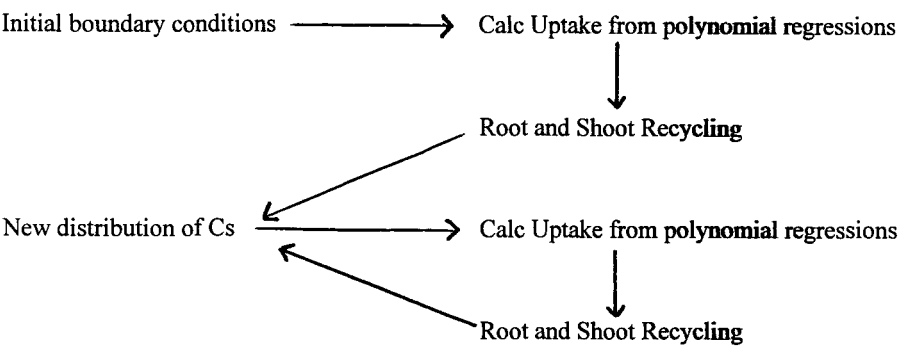

In order to avoid inaccuracy and mathematical instability caused by all roots being replaced simultaneously, roots are divided into classes so that only a fraction (usually 10%) are replaced at any one time.

Soil Chemistry

Caesium exists in the soil system either in solution or in an adsorbed form. Adsorbed caesium exists in two forms; exchangeable (diffusible) which is in rapid equilibrium with the solution phase and fixed. Thus,

$$C_T = \theta C_L + C_s + C_f = C_d + C_f$$

where C_L is Cs in soil solution; C_s is exchangeable Cs; C_d is diffusible Cs; C_f is fixed Cs which are related by the following,

$$\frac{C_L}{C_S} = \frac{1}{B}; \qquad C_d = C_S + C_L\theta \qquad \frac{C_L}{C_d} = \frac{1}{(B+\theta)}$$

Two first order reversible exchange reactions describe the reaction between caesium in solution and in the adsorbed phase. One reaction is instantaneous, and described by a buffer capacity term, B, the other is termed the slow reaction and is described by the rate constant, Km, and the buffer capacity B_2. Thus,

$$\frac{dC_f}{dt} = \frac{Km\theta\ C_d}{(B+\theta)} - \frac{KmC_f}{B_2}$$

Caesium is mobile only in solution, thus the diffusive flux is determined by the effective diffusion coefficient given by which depends on the limiting liquid phase diffusion coefficient, D_L and the liquid phase impedance factor, f_L. The diffusion of caesium is described using cylindrical boundary conditions, as

$$\frac{dC_d}{dt} = \frac{1}{r}\frac{d}{dr}\left(r.\frac{D_L f\theta}{(B+\theta}.\frac{dC_d}{dr}\right) - \frac{dC_f}{dt} \qquad r_a < r < r_b$$

With the following boundary conditions at $r=r_a$ (the root solution interface, and $r=r_b$, the mid-point between adjacent roots,

$$\frac{V_{max}}{Ks.B}C_d = \frac{D_L f\theta}{(B+\theta)}\frac{dC_d}{dr} \qquad r = r_a$$

$$\frac{dC_d}{dt} = 0 \qquad r = r_b$$

Plant Physiology

Roots are considered to be uniformly distributed. They act as uniform cylinders which each exploit cylinders of soil, taking up nutrients, and therefore caesium, from these cylinders. Roots are considered to have a limited lifetime. They do not continue to exploit the same rhizo-cylinders throughout the entire simulation period. At the end of their lifetime roots are assumed to die, and are immediately replaced by the same number of roots. The new roots are in soil which has been averagely depleted by previous roots. There is no concentration gradient.

Root uptake is described by Michalis Menten kinetics. Thus,

$$U = \frac{V_{max}\,[Cs]}{Km + [Cs]} \sim \frac{V_{max}\,[Cs]}{Km}$$

where U is root uptake per unit root length (mol dm^{-1} h^{-1}), Vmax (mol dm^{-1} h^{-1}) and Km (M) have their usual meanings. Total root uptake is the product of root uptake per unit root length and rooting density.

After root uptake, caesium is immediately uniformly distributed throughout the root system and between roots and shoots.

When roots die and are replaced a fraction of caesium in roots may be returned to the soil. Returned Cs enters the soil solution phase. The depth profile of caesium recycling is controlled by root density, not by the soil layer from which caesium was extracted.

Standard Input Parameters

Soil : Volumetric moisture content = 0.3; liquid phase impedance factor = 0.1; exchangeable buffer capacity, $b_1 = 10^2 - 10^4$; fixed phase buffer capacity, $b_2 = b_1$.

Plant : root radius = 0.5 mm; max root density = 1000 dm dm^{-3}; max root depth = 1 m (linear decline with depth); root lifetime = 500 h (50-5000).

Root uptake rate : V_{max} = 3.825 μmol dm^{-2} h^{-1}; Km = 1877 μM (equivalent to 1 mM K considering the data of Shaw & Bell.

Recycling : fraction of plant Cs in root = 0 (0 - 1); fraction of shoot Cs returned to surface layer of soil = 0 (0 - 1).

Radiocaesium : Total amount of radiocaesium = 0.15 pmol/dm2; greatest initial depth of contamination 1.2 dm; initial fraction in fixed phase = 0.

Sensitivity Analysis

Soil Parameters

Figure 1 shows the effect of the buffer capacity of the rapidly equilibrating adsorbed phase, B (equivalent to Kd) on the cumulative transfer factor. This parameter may vary between about 10^2, for organic soils with a low adsorption capacity, to 10^5 for mineral soils with high clay contents, particularly if the clay fraction is dominated by illitic material. In these simulations the slow adsorption reaction has been ignored. It is clear that the value of B has a considerable effect on Uptake. This finding is well known. However the high cumulative uptake over a five year period, and indeed for one year in the case of a poorly buffered soil, is not in agreement with field observed data. One reason is that the root parameters (density, rooting depth and uptake characteristics) are typical of agricultural crops, and not necessarily

of plants generally found on such poor soils. It should also be born in mind that transfer factors measured *in situ* only take shoot concentration into account, whereas the model simulations show transfer to the whole plant. However another important possible cause, which it has not hitherto be possible to take into consideration, is the effect of recycling of both root and shoot material.

Figure 1

Effect of B on the cumulative plant uptake from soil with no root or shoot recycling of absorbed Cs and other input parameters as standard.

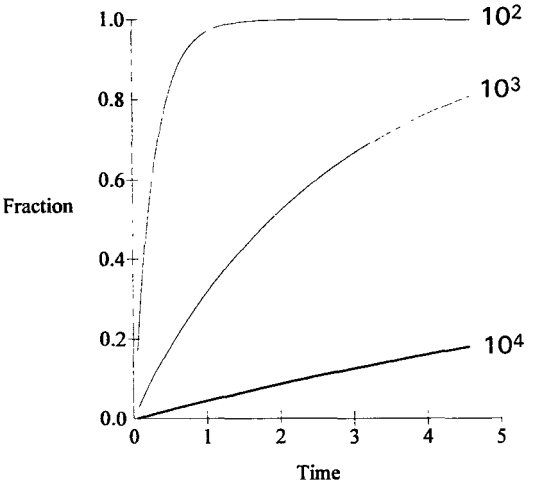

Figure 2 shows the effect of the fraction of plant caesium which is recycled to the soil when roots turnover, R/S. This parameter is a function of the distribution of caesium between roots and shoots and of the proportion of root caesium which is not translocated out of a senescent root. The simulations using input parameters typical of an upland soil are shown. The greater the value of R/S, the lower is the cumulative uptake. However this also introduces considerable changes in the depth profile of caesium. The model predicts that a deeply rooting plant would rapidly transfer down the soil profile (simulations not shown). This is not observed, therefore in reality R/S must be low. This suggests i) that caesium, along with nutrients, is transferred out of a senescent root, and ii) that our assumption that caesium is uniformly distributed throughout the root system is false. Indeed experimental work from Leuven confirms that caesium is not immediately redistributed throughout the entire plant. The distribution of caesium after root uptake depends on the nutrient status of the plant, and is probably also species related.

Figure 2

Effect of root recycling, R/S, on the cumulative plant uptake from soil with a low buffer capacity and no shoot recycling of absorbed Cs and other input parameters as standard.

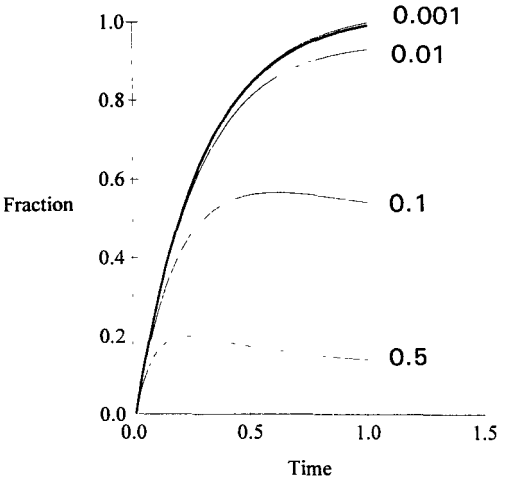

Figure 3 shows the effect of recycling of shoot caesium to the top layer of soil. The greater the extent of shoot recycling, the greater is the proportion of caesium remaining in the soil at any given time. Uptake is quite sensitive to this parameter. Variations in this parameter would result not only from shoot death and decay, but also from grazing and return of caesium via animal urine and faeces. In a completely closed eco-system, a steady state distribution of caesium between soil and plants could be reached and maintained.

Figure 3

Effect of shoot recycling on the cumulative plant uptake from a poorly buffered soil with some root recycling of absorbed Cs (R/S=0.001) and other input parameters as standard.

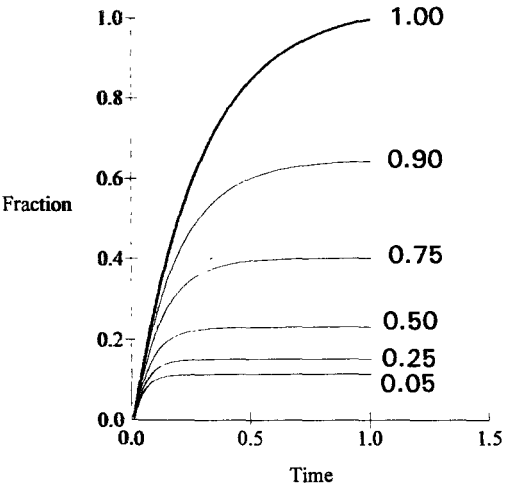

Figure 4 shows the effect of root length, with a constant root depth profile. Uptake is highly sensitive to this parameter. Unfortunately it is experimentally very difficult to obtain accurate values of root length in the field, and rooting patterns in culture solution and in soil are known to be very different. This input parameter is therefore difficult to estimate. However it is probable that differences in root length account for some of the observed differences in Cs transfer factors observed between species.

Figure 4

Effect of maximum root length, with constant rooting depth and a linear decline of root density with depth on the cumulative plant uptake from a poorly buffered soil with some root and shoot recycling of absorbed Cs and other input parameters as standard.

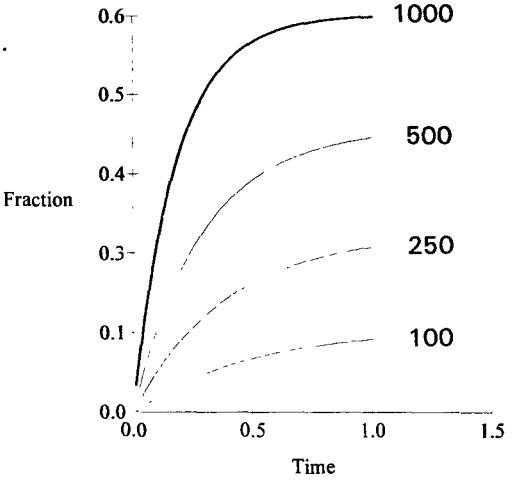

Figure 5 shows the effect of maximum rooting depth, for constant root length. The greater is root depth, the smaller is the root length present in the contaminated soil zone. The model shows that uptake is highly sensitive to the root depth profile, relative the Cs contamination profile. Changes in root depth distribution with age, water supply, or species will cause considerable differences in uptake. Similarly the transfer of Cs down the soil profile over the years will result in a greater proportion of the roots of deeply rooting plants being exposed to Cs. However this effect is not likely to account for major changes in uptake patterns. In this simulation a linear decline of root density with depth was considered. Similar results are obtained with other descriptions of the depth distribution of roots.

Figure 5

Effect of maximum rooting depth, with constant root length on the cumulative plant uptake from poorly buffered soil with someroot and shoot recycling of absorbed Cs and other input parameters as standard.

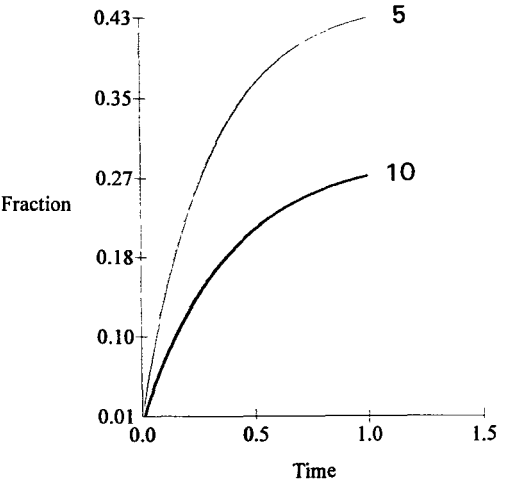

The model predicts low sensitivity to various other, soil-related input parameters such as volumetric moisture content, liquid phase impedance factor, rate of fixation reaction and extent of fixation reaction (B_2). Neither θ nor f_L vary as much as the buffer capacity (K_D); 0.1-0.5 and 0.05-0.3 respectively are realistic ranges. The relative insensitivity to the extent and rate of the fixation reaction is surprising given the amount of work carried out on the determination of the fixation reaction. It is reasonable to suppose that the values of B and B_2 are of the same order of magnitude, therefore $B+ B_2$ will always be very similar to B. Furthermore when the rate of the fixation reaction is relatively high with respect to the uptake period ($month^{-1}$, $week^{-1}$ or day^{-1}) the reaction is quasi-instantaneous. If the reaction rate is very slow, then fixation can have very little effect on the uptake. It should be noted that mathematically it is identical to treat the instantaneous and slow reactions in series or in parallel.

Uptake is also sensitive to root radius (simulations not shown) for constant root length (and not root weight). The finer the roots, the greater the interface with the soil solution and so the greater is uptake. Soil conditions which favour the production of fine roots will thus enhance uptake.

Another important plant input parameter is root lifetime (simulations not shown). The shorter is the average root lifetime, the greater the turnover rate of roots, the more likely is a root to be growing in fresh, undepleted soil. Uptake increases as root lifetime is decreased. This parameter has not previously been considered in radioecological models. Root turnover depends both on the species and on the nutrient status of the plant and is another parameter for which it is difficult to obtain field data.

Figure 6 shows the dependence of uptake on the root uptake parameter. Contrary to previous assumptions, Uptake is sensitive to root uptake parameters; it increases as the K_m decreases and the same effect would be observed if V_{max} were decreased. Uptake at the root-solution interface cannot therefore be assumed to be diffusion controlled.

Figure 6

Effect of the root uptake parameter, Km, corresponding to solution potassium concentrations between 20 μM and 1 mM on the cumulative plant uptake from highly buffered soil with no root or shoot recycling of absorbed Cs and other input parameters as standard.

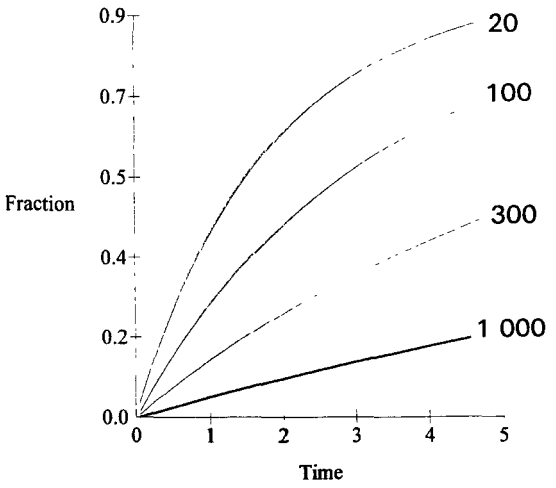

Root uptake approximates to linear uptake, since the concentration of Cs is always much lower than Km. The root uptake coefficient is a function of both Vmax and Km but also the inhibition constants, Ki and the concentration of potential inhibitors of Cs uptake. It seems probable that the major differences in the root uptake coefficient result from differences in potassium concentration at the root interface. These differences arise from the initial potassium status of the soil (organic upland soils have very low K contents) and from depletion by roots over time.

Root uptake parameters have little effect on the predicted uptake in highly buffered soil, where uptake is rapidly limited by diffusion to the root-liquid interface. In contrast, in upland organic soils diffusion in soil is more rapid and so uptake may be sensitive to root uptake rate. Furthermore in these soils potassium content is low, and likely to be further lowered in the rhizosphere by depletion. Both factors contribute to the greater bioavailability of radiocaesium in upland soils.

CONCLUSIONS

A mathematical model containing both classical and innovative features has been developed. The model predictions of uptake agree with observed uptake. The most important soil parameter is the extent of the instantaneous adsorption reaction. The extent and the rate of the slow reaction are of more limited importance. Uptake is sensitive to various plant parameters. Many important input parameters are not specific to radiocaesium bioavailability; root radius, root length and depth distribution. However uptake is also sensitive to uptake rate at the root-solution boundary. Complementary work at KUL indicates that there are important species differences for this factor. Other parameters which had not previously been incorporated in mathematical models, and which have been found to be important are the rate of root turnover, the distribution of caesium within the root system and between roots and shoots and the recycling of caesium contained in roots and in shoots. Considerable further work is required in this field.

Connections between Project 6 and other contractors

Process	Input Parameters	Data Source
Liquid phase diffusion	**D**	Calculated or estimated from readily available data, except for adsorption dependence, see below
Reaction with soil		
* quasi-instantaneous reaction	K_D	NRPB, KUL prediction of K_D from clay mineralogy and content, organic matter content and concentrations in Ca and K
* slow (fixation) reaction	k_+	NRPB, KUL rate and extent of fixation reaction deduced from lysimeter and field data; mechanism investigated under controlled laboratory conditions
Root Uptake		
* root parameters	**r, L, τ**	root radius, density and lifetime Agronomical & Ecological studies
* uptake parameters	V_{max}, **Km**	KUL

Effects likely to be important but not yet taken into account (lack of reliable data or evidence of mechanism)

Rhizosphere effects

* Modification of V_{max}, Km and K_D due to changes in composition of exchange complex and solution	KUL, NRPB
* Microbiological uptake	CNRS
* Microbiological weathering	CNRS
* Root induced weathering	CNRS, INRA

Soil biota

* Worm digestion and Bioperturbation	RIVM

Recycling

* Redistribution within plant	KUL

transfer to edible parts, removal by grazing or harvesting, possible return to soil surface by urine and faeces deposition

retention in roots, recycling to soil at depth on root senescence

List of relevant publications

STAUNTON S. & ROUBAUD M. (1993/94) Measurement of the adsorption of radiocaesium on clays : factors affecting the extrapolation to *in situ* conditions. *Mémoires de la Société Géologique de France* **162**, 269-276.

NYE P.H. & STAUNTON S. (1994) The self-diffusion of phosphate in soil: a two path model to simulate restricted access to exchange sites. *European Journal of Soil Science* **45**, 145-152.

STAUNTON S. (1994) Adsorption of radiocaesium on various soils: interpretation and consequences of the effects of soil:solution ratio and solution composition on the distribution coefficient. *European Journal of Soil Science* **45**, 409-418.

STAUNTON S. & ROUBAUD M. Adsorption of radiocaesium on montmorillonite and illite : Effect of charge compensating cation, ionic strenght, concentration of potassium, caesium and fulvic acid. *submitted*

STAUNTON S. & DARRAH P.R. A mathematical model of root uptake incorporating root turnover, distribution within the plant and recycling of absorbed species. *to be submitted*

STAUNTON S. & DARRAH P.R. On the origin of species related differences in the root uptake caesium from contaminated soil. *to be submitted*

Relevant conference communications

STAUNTON S. (1994) Effect of organic matter on the adsorption of trace amounts of caesium by soil. British Soil Science Society Annual Conference, Silsoe, Bedfordshire, 11-14 April.

STAUNTON S. (1994) On the prediction of the distribution coefficient ^{137}Cs in soils from clay mineralogy. 15th World Congress of Soil Science, Acapulco, Mexico, 10-16 July.

DUMAT C. & STAUNTON S. (1994) Effet de la matière organique sur la capacité de stockage du ^{137}Cs par les argiles. 2emes Journées Nationales des Jeunes Physico-Chimistes, Bordeaux, 18-19 July.

DUMAT C. & STAUNTON S. (1994) Adsorption du ^{137}Cs sur les argiles: effet de la matière organique. Société Française de Chimie, Lyons, 26-30 September.

STAUNTON S. & DARRAH P.R. (1995) Modelling of the bioavailability of radiocaesium in soil systems. 3rd International conference on the Biogeochemistry of Trace Elements "Contaminated Soils", Paris, May 15-19.

STAUNTON S. & LEVACIC P. (1995) The influence of organic matter on the adsorption of radiocaesium by soils. International Conference on "Organo-Mineral Interactions in Sediments and Soils", Newcastle-upon-Tyne, U.K., June 28-29.

DUMAT C. & STAUNTON S. (1995) Influence of humic substances on the capacity of clays to immobilise pollutants: the case of radiocaesium. ECGA Euroclay '95, Leuven, Belgium, August 19-25.

STAUNTON S. (1995) Effect of salt concentration on the adsorption of radiocaesium on clays. ISSALE-95, Valencia, Spain, September 18-25.

I. INTRODUCTION : WHY THE INFLUENCE AND THE ROLE OF MICROBIAL ACTIVITY ON MIGRATION AND BEHAVIOUR OF CS IN SOILS ARE IMPORTANT TO BE STUDIED :

Most of the works of the last decade about the interactions of the radionuclides and more particularly cesium with the constituents of the soils, are dealing mainly with the mineral constituents (Cornell, 1992 ; Wagner and Czurda, 1990), and with its distribution in the soils (Bunzl and al, 1988 ; Davies and Shaw, 1993). The interactions between radionuclides and organic matter are rather little studied (Valcke and Cremers, 1992 ; Bovard et al, 1968 ; Bittel and Lehr, 1968 ; Witkamp, 1968). However in pedological processes, biological mechanisms, that include the role of organic matter and the role of all the soil living community are playing an important role in the biogeochemical cycles : chelation, complexation, migration through a profile, storage in the upper horizons, bioaccumulation by microorganisms, modification of availability for the plant roots... This last point is very important as it takes place at the beginning of the contamination of the food chain in the case of radionuclides. The behaviour of Cs and K can be compared because of their similar characteristics and properties (ionic ray, weight, same chemical group). This allows to make some assumptions about a comparable behaviour in the soil. This can be considered more easily as the biogeochemical cycle of K is well known. For example cesium retained in the clay can be exchanged with K, and so be released in the environment. When cesium is deposited on the surface of the soils, at least 80% can be bound with the mineral constituents, as it has a great affinity for clays as illite and smectite. These binding concerns essentially the FES, Frayed Edges Sites (Cremers, 1988 and 1993) and a little proportion seems to be irreversibly retrogradated. It is why Cs remains in the first centimeters of the soil and seems to have low mobility. For instance 20 and 25% respectively in an alluvial soil and a podzolic soil are concerned by the leaching and for this fraction a great part is retained between 5 and 10 cm (Bovard et al, 1968).

But soils of high organic matter and low clay content present some problems because organic matter can adsorb a great part of the Cs deposited. And even if the proportion of cesium linked to the organic matter is not quantitatively very important in the most case of soils, this fraction represents the more available fraction for the plants, directly or after a first release in particular by the microorganisms and their biological activity. For these reasons it is interesting to present and discuss what we are today knowing about the interactions Cs-organic matter.

For the greatest part Cs linked with the organic matter remains exchangeable but fulvic acids are able to stock some fission products in the B_h horizon of podzolic soils (Bovard et al., 1968). The availability of radionuclides for plants is associated with the degree of their passage in the soil solution, and depends also on the different molecular weight of their water soluble organic compounds (Agapkina, 1991). In some low clay content soils, flux of ammonia through the system of FES (Cremers and al, 1988) could displace some of the sorbed Cs into soil water, and hence into streams (Hilton et al., 1993). At this stage we can suppose that organic matter will be able to form water soluble complexes with cesium.

Birch and Bachofen (1990) are giving examples of the effects of microorganisms on the environmental mobility of radionuclides : complexation with organic compounds of different weight and origin (microbial exudates and constituents), biosorption, bioaccumulation, precipitation. Radiocesium can form complexes with artificial organic components such as valinomycin, nigericin and other similar molecules (Desmet et al., 1991). Cyanoferrate can also form a very strong complexe with Cs (Vreman et al., 1992). West et al. (1987) showed the effect of sulfate reducing bacteria on the ^{137}Cs sorption onto calcium montmorillonite (a potential backfill material). These microorganisms weather the rock material and make the nuclide more mobile, in some cases by up to 2 or 3 orders of magnitude. Differences about Cs mobility between laboratory studies and field assays were noted (Walton and Merrit, 1980) and were there attributed for a great part to the contribution of microorganisms (Champ and Merritt, 1981). Cs present in the mineral fraction can get soluble and mobile again under chemical, physical or biological weathering processes influenced by different characteristics of the soil such as pH, aeration, organic matter/mineral fraction ratio, etc... It is possible that even if a small amount of illite is present in the soil, organic molecules could prevent the development of irreversible sorption (Livens et al., 1991 ; D'Souza et al., 1968).

In a first conclusion of this bibliographic review and discussion, mineral fraction appears preponderant in the behaviour of Cs in the soils but organic matter and microbial activity are able to play an important role in its evolution : temporary linkage, migration, storage, availability, weathering, dissolution, retention, deposit.

To study the role of microorganisms on the behaviour of cesium, different experiments concerning bioleaching, bioaccumulation and biosorption processes have been done. Some have been performed to try to determine the competition between minerals and microorganisms in Cs fixation in presence of very low content. Attempts to approach the speciation have been considered using extractions in order to study the cesium bindings with the mineral and the organic constituents of soils.

II. BIOLEACHING OF CESIUM BY MICROORGANISMS :

Leaching experiments, consisting in semi-continuous flow perfusion devices, were performed in order to determine the possible involvement of soil microorganisms in the dissolution of cesium previously fixed on soil constituents. These experiments corresponded also to an experimental weathering approach of soil constituents bearing cesium. A good adequation between the results obtained with column experiments and fields studies can be awaited because Schimmack and Bunzl (1992) have shown that the presence of a layer of organic material on a mineral soil in column experiments influences the migration of radiocesium in a parabrown earth spruce.

Different analysis were performed (soil extractions and acid titration) in order to complete the results obtained for the bioleaching experiment.

II. A. EXPERIMENTAL DESIGN

II. A. 1. PRINCIPLE :

This study of the leaching of cesium was effected with a semi - continuous flux lixiviation device. Columns of cesium saturated soils were subjected to a defined leaching operation. These columns allowed to work in aerobic conditions and were either inoculated with the endogenous microflora or kept in sterile conditions (without microorganism). The establishement of the balance sheet of the cesium, retained or leached from the columns, would allow to precise the influence of the microorganisms on the biogeochemical behaviour of the cesium.

II. A. 2. MATERIAL :

❖ **Experimental device :**

Figure 1 presents the experimental device used in this experiment. Operating of lixiviation was slow, from 9 to 12 ml per day, at the rate of 6 cycles of one hour every 4 hours using peristaltic pumps (Desaga).

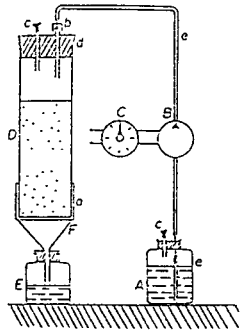

Figure 1 : Semi - continuous flux perfusion device

❖ **Characteristics of selected soils :**

Superficial horizons of two forest soils, one calcimagnesic (rendzine, pH = 7.4) and one brown leached acid soil (pH = 6.4) have been selected for this experiment. The similarities of these soils with those on which were working the others contractants, as their large frequency and distribution around the french nuclear sites, explained the choice. These two soils have been sampled near Nancy (France). The principal characteristics of these soils are presented in table I.

Soils	pH	Organic matter (%)	CEC (meq/100g)
Rendzina	7.4	15	45.5
Orthic luvisol	6.4	5.2	14.5

Table I : Principal characteristics of the horizon A (0-10 cm) of both selected soils.

II. A. 3. PLAN OF THE EXPERIMENT:

Four main treatments are done :

- Treatment I : partially sterilized soil (under U.V.) + percolation with sodium merthiolate 1‰ ($C_9H_9NaO_2SHg$). This treatment allowed to obtain sterile treatment (without microorganism).
- Treatment II : partially sterilized soil (under U.V.) + percolation with distilled water. The aim of this treatment is to quantify in comparison with the treatment I, the desorbing effect of the sodium merthiolate on the cesium, the initial sterility conditions being the same.
- Treatment III : non sterilized soil + percolation with distilled water. Soil organic matter was the only source of energy for the endogenous microflora.
- Treatment IV : non sterilized soil + microbial inoculation (described in *preparation of inoculum)* + percolation with 2% glucose solution. The nutrient medium allowed to increase the microbial activity and so to precise their effect and role on cesium behaviour.

Four columns were used in each experimental treatment giving a total of 32 columns for the experiment. The perfusions were done at 25°C ± 1° in the dark. The leaching experiment was maintained during 114 days. Percolates were regularly collected and after pH measurement they were kept in cold room before different analyses and statistical treatment done on the results concerning solubilized cesium in the percolates of the different treatments.

II. B. RESULTS

II. B. 1. MICROBIAL INOCULATION :

The countings of microorganisms inoculated to the columns are presented in the table 2.

Soils/Media	Medium NA	Medium with Cs
Rendzine	10^7	$6\ 10^6$
Acid brown soil	$6\ 10^7$	$3\ 10^7$

Table 2 : Countings of the microflora inoculated in the experimental design expressed in CFU (Colonies Forming Units)/g soil.

The microbial populations for both soils were essentially composed of bacteria and of some actinomycetes. It is interesting to note that in the medium containing Cs (0.25 mM ; 0.5 mM ; 1 mM), half of the population present in the inoculum was potentially able to acumulate cesium. This result was to be verified in order to ensure that the selective conditions were sufficient.

Figures 2 and 3 represent the cumulated amounts of cesium collected in the percolates during the experiment respectively for the calcimagnesic (rendzina) and leached brown soil.

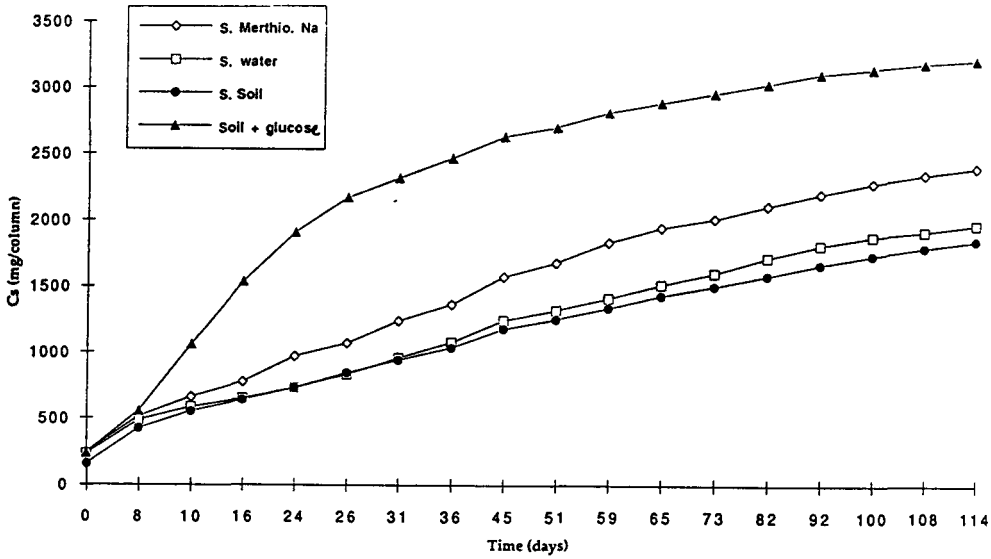

Figure 2 : Cumulated amounts of cesium in the percolates (in mg of Cs/column) for the rendzina

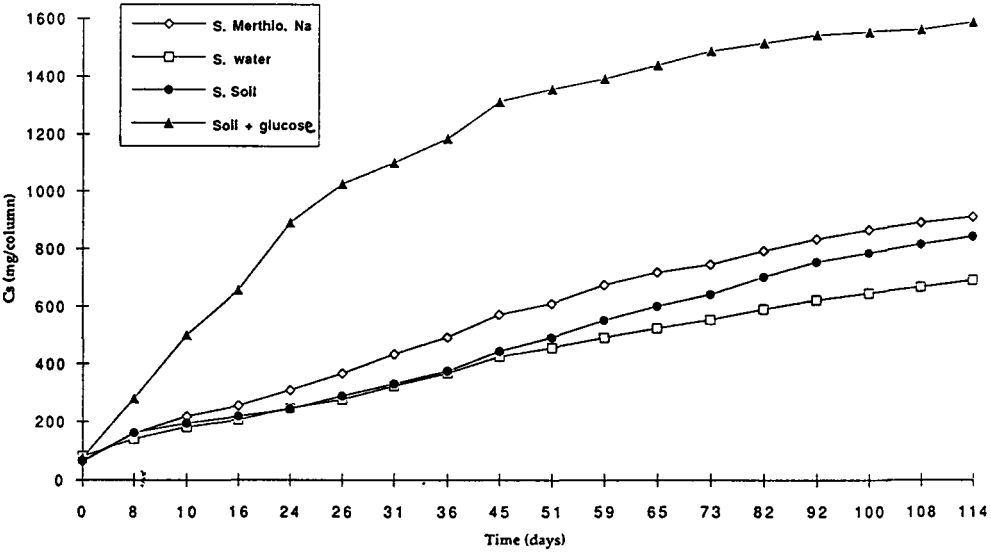

Fig. 3 : Cumulated amounts of cesium in the percolates (in mg of Cs/column) for the brown soil

II. B. 2. EFFECT OF THE SODIUM MERTHIOLATE :

❖ **Microbiological controls :**

Microbiological controls were effected regularly in the percolates and allow to verify the efficiency of the sodium merthiolate as antimicrobial agent. No important bacterial development was noticed in the percolates and more than 3/4 of the leachates in the treatment II remained also sterile.

❖ **Cesium mobility :**

Statistical analyses on the quantities of cesium measured in the percolates show that the sodium of the sodium merthiolate displaced significantly the cesium in comparison to a simple percolation with water during the first 16 days of the experiment. After that, sodium seemed to be no more competitive to the cesium for the exchange sites on which cesium was fixed.

II. B. 3. EFFECT OF THE MICROFLORA :

❖ **Microbiological controls :**

Microbiological countings performed on the general nutrient media (NA) showed an important development of the microflora in the percolates of the treatment IV (inoculated soil + percolation with glucose) in the first 3 weeks of the experiment. After this time, this microbiological activity seemed to decrease. Microbiological activity remained weak in the columns of the treatment III.

❖ **Cesium mobility :**

The results obtained in the treatment III (non sterilized soil + percolation with water) did not show any significative differences for the cesium mobility in both studied soils in comparison with the treatments I and II (see tables in annex I). For both soils the endogenous microflora, which was stimulated by the nutrient medium (treatment IV), increased significantly the cesium mobility during the first 26 days of the experiment. After that, all the leachnig curves converged, without presenting differences between the treatments. It was interesting to note that the kinetics of the treatment IV are similar for both soils.

The desorbing solubilizing effect of microorganisms on the cesium was essentially revealed at the beginning of the experiment. The loss of effectiveness of the microorganisms after these first days would be due to the experimental conditions. Selected leaching rates prevented a uniform and regular water saturation of the columns. However anaerobic conditions could appeared in the middle of the column and so modify and reduce the microbial activity. Others parameters could also interfere : carrying away of the microorganisms from the column, low rates of assimilation of the organic substrates...

For both soils the endogenous microflora, which was stimulated by addition of glucose (treatment IV), increased significantly the cesium mobility during the first 26 days of the experiment, corresponding to an effective activity of the microflora. After this time, the amounts of cesium collected in the leachates every week became similar, without any significant differences between the treatments. It was interesting to note that the kinetics of the treatment IV with a stimulated microbial activity were similar for both soils. In the selected experimental conditions, the microflora of the brown soil seemed to be more efficient to mobilize and solubilize cesium than the microflora of the calcimagnesic soil, as 50% and more than 25% of the initial cesium is solubilized at the end of the experiment respectively for the brown and calcimagnesic soil. But further studies have to be done in particular on the soil constituents, to define their respective role that is certainly important in these types of interactions.

II. B. 4. PH EVOLUTION :

Figures 4 and 5 represent the pH evolution during this experiment. pH decreased simultaneously to an increase of cesium in the leachates of the treatment IV corresponding to an increase and stimulation of microbial activity. This acidification remained during all the experiment and corresponds to the production of acid compounds and protons by the microflora. Such results confirmed again the desorbing - dissolution potential effect of the microflora, that could play a significant role by different metabolites production.

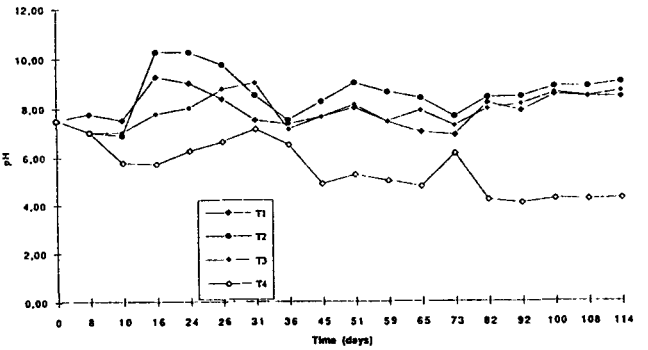

Figure 4 : Evolution of pH for the rendzina

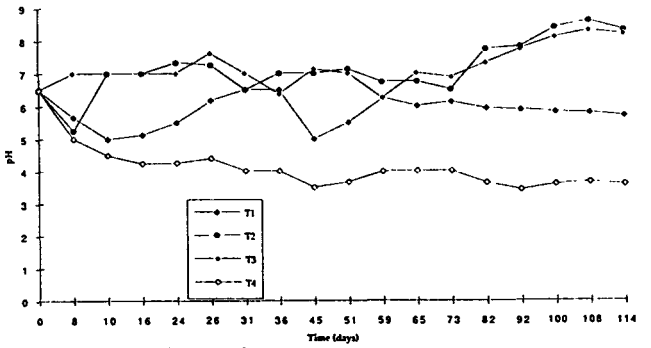

Figure 5 : Evolution of pH for the brown acid soil

II. C. ATTEMPT TO DETERMINE COMPLEXATION ABILITY OF SIMPLE ORGANIC COMPOUNDS : TITRIMETRIC ANALYSES :

II. C. 1. EXPERIMENTAL DESIGN:

Titration studies have been done in order to verify the potentiality of different organic compounds to complexe cesium in solution. The measurement was performed in presence of a constant ionic strength ($NaClO_4$, 0.1 M). The titration of organic compounds, in presence or not of CsCl, was made by NaOH 0.1 N till pH reaches 10.5.

The experiment were performed with oxalic and citric acid in a first time because of their complexing ability and their presence in soil solutions and rhizosphere.

II. C. 2. RESULTS :

No significant differences could be seen between the different titration curves of the three treatments , concluding that both organic acids, citric and oxalic, did not complexe the cesium in these experimental conditions. This result was not surprising, considering the monovalence of the cesium. Nevertheless, it would be interesting to try others organic compounds, less or more complexing, released by the microbial metabolism and soil organic matter fractions (of humic and fulvic acid type).

II. D. ATTEMPT OF CS SPECIATION USING SOILS EXTRACTIONS

In order to know the distribution of the remaining cesium in the soils after leaching, two series of chemical extractions were performed on these soils. Different mineral compounds (salts or acids) in solution and different organic acids of microbial or plant origin were used. Two types of soil samples were used : samples from the previous treatment II of the column leaching experiment (percolation with water on the soil partially sterilized) and IV (percolation of a nutrient (glucose) that had stimulated the endogenous microflora). The extractions were done using usual analytical soil science method.

II. D.1. Extractions with inorganic compounds :

❖ **Design**

4 extractants were used in order to reach different compartments of the remaining cesium :

- NH_4Cl 0.5 M for the exchangeable cesium
- HCL 1N for the cesium not very energetically retained on the soil
- HCL 6N for the cesium strongly retained on the soil
- NaOCl in order to oxidize and solubilize the whole organic matter.

❖ **Results**

• pH obtained : the pH obtained for the different extractions were already the same for the 4 samples of soil : around 0 and 9.5 respectively for the extractions with the hydrochloric acid and NaOCl. For the extraction with NHCL 0.5M, the pH (average of three successive extractions) reached respectively 6.5 and 5.5 for the samples of the rendzina provided by the treatments II and IV, and is around 5 for the samples of the acid soil.

• The production of organic acids by microorganisms in the leaching experiments was certainly responsible of this acidification and consequently of the release of Cs.

Table 3 presents the amounts of cesium expressed in ppm (µg of Cs/g of soil) obtained in the different extractions.

Samples	NH_4Cl	HCL 1N	HCl 6N	NaOCl
Rendzina -Treat. II	5 488	5 123	5 442	5 258
Brown soil - Treat. II	3 171	2 823	2 983	2 912
Rendzina - Treat. IV	4 184	3 375	3 780	4 077
Brown soil - Treat. IV	867	816	1 250	1 302

Table 3 : Amounts of Cs in ppm (µg of Cs/g of soil) measured in the different extractions. (Rendzina = calcimagnesic soil)

The principal results and perspectives of these values were :

- NH_4 seemed to have a great capacity to exchange cesium, as the cesium extracted in both soils was already equal to the cesium extracted with the hydrochloric acid 1N. This result meant that exchange of cesium did not depend on the pH of the extractant, or on the ionic strengh, but on the properties of the cation. Such ions like ammonium certainly influenced the behavior of cesium in the natural soils (as observed or suggested by other authors).

- The total amounts of cesium in the column reached 4 376 and 8 542 µg/g respectively for the brown and calcimagnesic soil for the treatment II. 31 and 36 % of the cesium remaining in the columns respectively for the brown and calcimagnesic soil were not extracted by these chemical solutions. That meant that at least 30 % of the cesium were retrograded (strongly fixed) in the minerals of the soils. But the acid extractions could modify the soil constituents by amorphization so that Cs became less available.

- The differences of the amounts of cesium extracted according to the differents extracts showed, in particular for the acid soil, that in presence of great amounts of cesium, the microorganisms desorbed essentialy the cesium that is not vey energetically retained in the soils.

It would be interesting to extend the action of the microflora and to modify experimental conditions in order to see if microbial weathering processes will be able to reach this "non extracted" cesium in conditions of lower concentrations of cesium.

II. D. 2. EXTRACTIONS WITH ORGANIC ACIDS

The objective of these extractions was to simulate the action of compounds issued from the metabolism of microorganisms in the soils. Several extractants were used according to their complexation potentiality and to their representativity in the soils : acetic acid, malic acid, oxalic acid, citric acid and tartaric acid. All these acid were used at a concentration of 0.1M.

Table 4 gives the amounts of cesium extracted by the different solutions :

Samples	Rendzina Treat. II	Brown Soil Treat. II	Rendzina Treat. IV	Brown Soil Treat. IV
Water	613	214	647	229
Glucose	574	189	687	224
Acetic acid	2 443	1 159	1 513	423
Oxalic acid	3 471	1 823	2 747	677
Tartaric acid	3 492	1 786	2 315	586
Malic acid	2 836	1 679	2 095	540
Citric acid	3 227	1 607	2 203	543

Table 4 : Amounts of cesium in ppm (µg of Cs/g of soil) in the different extractions

The extractions with water and glucose were used as controls. A little part of the remaining cesium was still extracted by them. All the acids had the capacity to extract cesium of the soils even if the amounts are lower than those obtained with the inorganic extractants. Tartaric, oxalic and citric acids seemed to be more efficient than malic and acetic acid.

These results showed that the cesium can be solubilized and bound to natural organic acids of plant and microbial origin. They could certainly play an important role in the migration of cesium in soils.

II. E. CONCLUSION :

Microflora of both soils can increase significantly cesium solubilization retained on the clayed - humic complexe of both soils, when their activity is stimulated by organic energetic nutriments of plant origin. Even if the leaching mechanisms are not yet completely explained, micoorganisms appear to be able to play a major role in the biogeochemical cycle of cesium. This fact has to be taken in account in the previsions of Cs behaviour in soils and in some development of depollution processes.

III. BIOACCUMULATION AND BIOSORPTION OF CESIUM BY A REPRESENTATIVE SOIL MICROORGANISM THE CELLULOLYTIC FUNGUS *TRICHODERMA VIRIDE*

The results presented here are dealing with the direct or non direct involvement of a cellulolytic microflora on the mobility of cesium. Biosorption of cesium by microorganisms is studied in experiments using a fungus, *Trichoderma viride*, the metabolism of which is well known.

III. A. EXPERIMENT WITH SOLUBLE STABLE CS :

III. A. 1. EXPERIMENTAL DESIGN :

The fungus, *Trichoderma viride*, was used as living biomass in suspension maintained as resting cells. It was cultivated in batch in presence of a solution of cesium chloride, and adsorption isotherms were calculated with different amounts of biomass and different amounts of cesium. pH of the initial solutions was near the neutrality. Previous studies showed that 24 hours were sufficient for a good fixation of cesium on the biomass. The following experiments were also performed in 24 h.

III. A. 2. RESULTS :

The following figure 10 gives the balance sheet of the cesium fixation on the fungus in function of different experimental conditions.

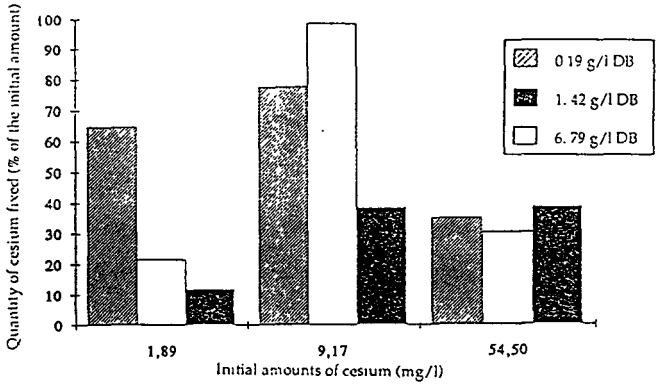

Figure 10 : Balance sheet of cesium fixation by *Trichoderma viride* in function of the initial amount of cesium and of the fungal biomass quantity. (DB = Dry Biomass).

As it is shown in this figure 10, the adsorption capacity of cesium by this soil fungus depended on cesium content and biomass amounts. Cs fixation was relatively higher in presence of low amounts of Cs. The amounts of adsorbed cesium depended on the experimental conditions including pH that control the dissociation of functional group of the microbial cell wall constituents. In the experimental conditions that have been used the higher amounts of Cs fixation were observed with

the medium content of Cs. Almost all Cs present in these conditions was fixed in the devices containing the larger biomass amounts. In these experiments it was important to define by potentiometric methods the exchange and complexing capacity of fungal biomass depending of pH, to determine by isotherms or chromatographic methods the kinetic and capacity of Cs fixation and to get values concerning the saturation conditions.

III. B. EXPERIMENTS IN PRESENCE OF CLAY BEARING CS :

III. B. 1. EXPERIMENTAL DESIGN :

The fungus was cultivated in an original experimental device allowing to separate biomass from the material bearing cesium (kaolinite smectite clay mineral). This device was a reactor presenting two compartments, which are separated by a microporous membran (figure 11). Cesium fixed on the materials (clays) or adsorbed on the fungus was measured without contamination of biomass by mineral particles.

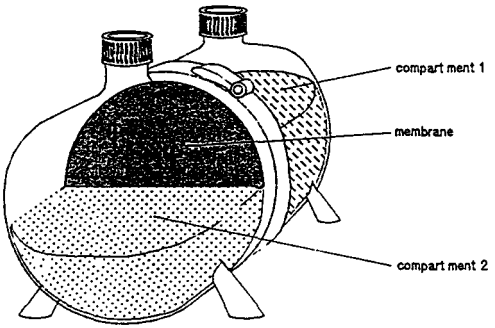

Figure 11 : Bireactor

III. B. 2. RESULTS :

Figure 12 represents the distribution of cesium 8 days after the beginning of the experiment. The percentages were almost the same after 24 h.

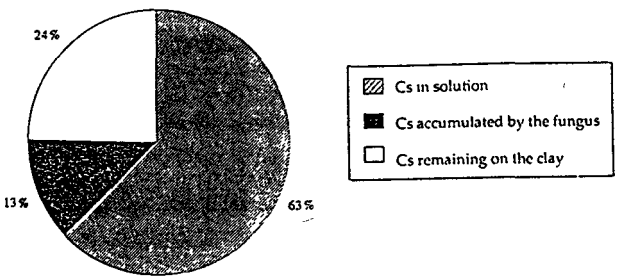

Figure 12 : Balance sheet of cesium distribution after 8 days of incubation.

The material bearing cesium contained no more than 24% of its initial amount. 63 and 13% of the cesium released was found respectively in the solution and in the biomass. Others studies have been performed with other amounts of material and biomass. The conclusion of all these studies was that the percentage of the cesium released is highly correlated to the value of the ratio solid/liquid.

The percentage of dissolved cesium depended of the equilibrium between the soluble form of cesium (Cs^+) and the insoluble form of cesium fixed on the clays. This equilibrium depended also of the conditions of pH, temperature and volumes ratio solid/liquid involved.

When glucose was added to the solution, the biomass increased but seemed to present a lower adsorption capacity than the biomass maintained as resting cells. This result was explained by the fact that as biomass increased the pH decreased, due to the metabolic activity of the fungus. The number of the fixation sites was also decreasing because of the protonation of the functionnal groups concerned by the adsorption that became less available.

III. C. CONCLUSION :

The results presented here show that the fungal living cells present important fixation sites for cesium. In solution, the importance of the cesium fixation on the biomass is highly correlated to the ratio of the initial amounts biomass to the cesium content. In presence of clay material bearing cesium the fungal biomass is able also to adsorb a great quantity of cesium, assuming that efficient conditions are required (in particular great biomass production with relatively low production of acid metabolites).

IV. COMPETITION FOR CESIUM ADSORPTION BETWEEN CLAY MINERAL AND MICROORGANISM IN CONDITIONS OF VERY SMALL CONTENTS OF CESIUM IN THE SOLUTION:

IV. A. PRINCIPLE :

The purpose of this experiment was to study the competition between the fixation of cesium on the clay mineral and the absorption of cesium by microorganisms. Cesium was present in small amounts (80 ppb of cesium). For this we used a solution of ^{137}Cs and a reactor that allowed to follow the distribution of ^{137}Cs between the mineral (smectite-kaolinite, having a large Cs fixation capacity) and the microorganism (the fungus *Trichoderma viride*).

IV. B. EXPERIMENTAL DESIGN :

The fungus was growing in a culture medium in presence of mineral enclosed in a dialysis bag. ^{137}Cs was added to the medium at the concentration of 80 ppb. Cs remaining in solution was daily

measured. Bioaccumulated cesium was measured at the end of the experiment. All these analyses were recorded with a liquid scintillator device.

IV. A. RESULTS :

After 5 days, 82% of the initial cesium remained in solution but respectively 6 and 12% were absorded by the fungus and fixed on the mineral. This result showed that microorganisms were able to absord cesium in presence of mineral even in very low content conditions.

Secondly all the cesium was curiously not fixed on the clay as the same experiment was effected without the fungus, almost all the cesium was fixed on the mineral only after 2 days. These results underlined also a problem of accessibility to the fixation sites and the competition between living organisms such as microbes and clays for Cs fixation.

V. CONCLUSIONS - PERSPECTIVES

All these results show the direct influence of microorganisms on the behaviour of cesium. Bacteria and fungi are able :

(1) to leach cesium that was fixed on minerals and organo-mineral soil constituents

(2) to absorb and adsorb cesium present in solution or fixed on clay mineral presenting a large Cs affinity, and

(3) to compete with clay minerals in the absorption and fixation of cesium even in low concentration in soil solution.

Even if these results need further developments and analysis, they suggest the involvement and efficiency of microorganisms in Cs mobility (solubilisation - accumulation) in field conditions, assuming that their activity will be stimulated by energetic and nutrient supplies of plant and humus origin. Cesium released on or in soils would not be irreversibly retained on the soil clay minerals, as it could be consider only in regard of the affinity of cesium for soil constituents and particularly for the clays *in vitro*. The results of these experiments show that micoorganisms are able to play a role in the biogeochemical cycle of the cesium by different mechanisms of solubilisation and accumulation, weathering of soil minerals and degradation of organic soil constituents. Such consideration has to be taken in account in the estimation of cesium behaviour in the soils, the soil-plant systems, and in the possible development of biodepollution processes. Rhizosphere where symbiotic and non symbiotic microflora play a major role in mineral wheathering and mineral element transfer has to be considered with attention.

The more important perspectives of this work are to verify these first results, but also to introduce the plant factor in order to evaluate the importance of different processes in the behaviour of cesium in soils such as : the weathering of cesium bearing minerals by microorganisms

producing metabolites in the rhizosphere, the modification of absorption of cesium by plants inoculated by symbiotic (mycorrhiza) or non symbiotic microorganisms (rhizobacteria).

These experiments including microorganisms as agents of weathering, as agent of plant growth, as agent of transformation of organic and organo-mineral soil constituents, will define also more precisely the environmental parameters involved in the bioavailability and cycling of cesium in different soils.

VI. RESULTS SUBMITTED TO PUBLICATIONS :

- Spor H., 1994. Contribution to the study of the influence of microorganisms on the mobility of radionucleides fixed in confinement materials of radioactive wastes. Ph D Thesis University Henri Poincaré Nancy I.
- Watteau F. and Berthelin J., 1994. Influence de l'activité microbienne dans la mobilité du césium dans les sols. "Study of the organic matter cycle". 15th meeting of Earth Sciences Nancy, France.
- Watteau F. and Berthelin J. Microbial bioleaching of Cs from calcimagnesic and acid brown soil samples (in preparation).
- Watteau F. and Berthelin J. Biosorption and bioaccumulation of Cs by a soil cellulolytic fungus (in preparation).

VII. BIBLIOGRAPHY

Agapkina, G. I. and F. A. Tikhomirov, 1991. Organic compounds of radionuclides in soil solution and their role in the uptake of elements into plants. Soviet Journal of Ecology, 22, 6, pp. 359-364.

Berthelin J., C. Munier-Lamy and R. Magne, 1988. The involvement of chemoorganotroph microorganisms in the leaching and uptake of uranium and associated metals from different rock materials. In : G. Durand, L. Bobichond, J. Florent (Eds). Proceedings 8th International Biotechniology Symposium. Société Française de Microbiologie. Vol II, pp. 1082-1093.

Berthelin J., C. Leyval and P. de Giudici, 1991. Involvement of roots and rhizosphere microflora in the chemical weathering of soils minerals. In : D. Atkinson (Ed). Plant Root Growth : an ecological perspective. Special Publ. n°10 of the British Ecological Society. Blackwell Scientific Publ. Oxford, pp. 187-200.

Berthelin J.and C. Leyval, 1982. Ability of symbiotic and non-symbiotic rhizospheric microflora of maize (Zea Mays) to weather micas and to promote plant growth and plant nutrition. Plant and Soil, 68, pp. 369-377.

Birch, L. D. and R. Bachofen, 1990. Effects of microorganisms on the mobility of radionuclides. Soil Biochemistry, 6, pp. 483-527.

Bittel R. and J. Lehr, 1968. Quelques aspects qualitatifs de l'influence des matières organiques des sols sur le comportement dans les sols de radioéléments artificiels. Isotopes and radiation in soil organic matter studies, IAEA-SM, pp. 497-513.

Bovard P., A. Grauby and A. Saas, 1968. Effet chelatant de la matière organique et son influence dans la migration des produits de fission dans les sols. Isotopes and radiation in soil organic matter studies, IAEA-SM, pp. 471-495.

Bunzl K., W. Schimmack, K. Kreutzer and R. Schierl, 1989. The migration of fallout ^{134}Cs, ^{137}Cs and ^{106}Ru from Chernobyl and of ^{137}Cs from weapons testing in a forest soil. Z. Pflanzernähr. Bodenk., 152, pp. 39-44.

Champ, D. R., and W. F. Meritt, 1981. Proceedings of Second Annual Conference of Canadian Nuclear Society, pp. 66-69.

Cornell, R. M. , 1992. Adsorption behaviour of cesium on marl. Clays mineral, 27, pp. 363-371.

Cremers A., 1993. Soil pollution and soil protection. International postgrade course, Wageningen HPLO.

Cremers A. , A. Elsen, P. de Preter and A. Maes, 1988. Quantitative analysis of radiocesium retention in soils. Nature, 335, pp. 247-249.

Davies K. S. and G. Shaw, 1993. Fixation of ^{137}Cs by soils and sediments in the Esk Estuary, Cumbria, UK. Science of the Total Environment, 132, 1, pp. 71-92.

Desmet G. M. , L. R. Van Loom and B. J. Howard, 1991. Chemical speciation and bioavailability of elements in the environment and their relevance to radioecology. The Science of the Total Environment, 100, PP. 105-124.

D'Souza T. J. , R. Kirchmann and J. J. Lehr, 1968. Distribution of radiostrontium and radiocesium in the organic and mineral fractions of pasture soils and their subsequent transfer to grasses. Isotopes and radiation in soil organic matter studies, IAEA-SM, pp. 595-604.

Guéniot B., C. Munier-Lamy and J. Berthelin, 1988. Geochemical behaviour of uranium in soils. Part I. Influence of pedogenetic processes on the distribution of uranium in aerated soils. J. Geochem. Expl., 31, pp. 20-37.

Hilton J. , F.R. Livens, P. Spezzano and D. R. P. Leonard, 1993. Retention of radioactive cesium by different soils in the catchment of a small lake. The Science of the Total Environment, 129, PP. 253-266.

Leyval C. and J. Berthelin, 1991. Weathering of a mica by roots and rhizospheric microorganisms of Pine. Soil Sci. Soc. Am. J., 55, pp. 1009-1016.

Livens, F. R. , A. D. Horill and D. L. Singleton, 1991. Distribution of radiocesium in the soil systems of upland areas of Europ. Health Phys., 60, pp. 539-545.

Munier-Lamy C., P. Adrian and J. Berthelin, 1991. Fate of organo-heavy metal compleses of sludges from domestic wastes in soils : a simplified modelization. Toxic. Environ. Chem., 31-32, pp. 527-538.

Munier-Lamy C., P. Adrian, J. Berthelin and J. Rouiller, 1986. Comparison of binding abilities of fulvic and humic acids extracted from recent marine sediments with UO_2^{2+}. Org. Geochem., 9, pp. 285-292.

Papanicolaou E. P. , C. G. Apostolakis, V. Skarlou, C. Nobeli and P. Kritidis, 1992. Ratios of plant to soil concentrations of strontium-85 and their relation to exchangeable bases for soils and crops in Greece. Journal of Agricultural Science, 119, pp. 79-82.

Schimmack, W. and K. Bunzl, 1992. Migration of radiocesium in two forest soils as obtained from field and column investigations. Science of the total environment, 116, 1-2, pp 93-107.

Valcke E. and A. Cremers, 1992. Sorption-desorption dynamics of radiocesium in organic matter soils. Seminar on the dynamic behaviour of radionuclides in forests, Stockholm.

Vreman K., J. van den Hoek and T. D. B. van der Struijs, 1992. Administration of ammonium ferric hexacyanoferrate strongly reduces radiocesium contamination of cows milk. Netherlands milk and dairy journal, 46, 2, pp. 81-88.

Walton, F.B. and W. F. Meritt, 1980. Long term extrapolation of laboratory glass leaching data for the prediction of fission products released under actual groundwater condittions. Scientific Basis for Nuclear Waste Management II, Elsevier, pp. 156-166.

West, J.M., D. G. Haigh, P. J. Hooker and E. J. Rowe, 1987. Radionuclide sorption on Fullers Earth (Calcium Montmorillonite) - the influence of sulphate reducing bacteria. Report of the Brit. Geol. Surv. FLPU 87-7.

Wagner J. F. and K. A. Czurda, 1990. Sorption of radionuclides by tertiary clays. Proceedings of the 9th International Clay Conference, Strasbourg, Sci. Géol., 87, pp. 149-158.

Witkamp M., 1968. External factors influencing mineralisation and immobilization of some radionuclides from free litters. Isotopes and radiation in soil organic matter studies, IAEA-SM, pp. 231-240.

Head of project 7: N.Mocanu

II. Objectives for the reporting period (December 1993-June 1995)

a) To extend studies on the effectiveness of soil-based agrochemical countermeasures in reducing soil-to-plant transfer of radiocaesium and radiostrontium, by enlarging the range of soils and treatments.

b) To introduce in Romania a practical methodology to evaluate, by the means of small scale screening procedures, the effectiveness of different soil-based chemical treatments on radiocontaminated soils (according to the specific land use and management), in the general strategy for the recovery of agricultural lands affected by accidental radioactive releases.

c) To find procedures with potential use as alternative/complementary methods for modified batch equilibrium technique, expanding the scale of investigations on the effectiveness of soil-based chemical countermeasures for radiocontaminated soils.

III. Progress achieved including publications

1. Batch equilibrium experiments

1.1. Preparative stages of experiments

1.1.1. Selection, collection and contamination of soils

After a preliminary investigation on the large variety of soils existing in Romania, especially in southern part which is the most important agricultural area of the country for cereal and vegetable cultures, three soil types were selected, based on their extent and and importance for agricultural use:

- **alluvial soil** (sandy-loamy), usually characterizing floodable meadows placed in immediate vicinity of the rivers; areas with this soil type are largely used in agriculture (cereal and vegetable cultures) having a high fertility and being accessible to irrigation with river water during the rainless summers;
- **brown-reddish forest type soil** (clayey-loamy), an argillaceous soil formed on sandy and loess deposits; usually is recommended for cereal cultures,
- **"green house" soil** (organic), based on old manure, having a high content of organic matter.

The soils used in experiments were collected and contaminated in October 1993. The processing of collected soils has included smashing, drying at ambient temperature (until they got friable state), and separation of gravel and vegetal debris. Forty kilograms of dry alluvial and brown-reddish soils, twenty kilograms of "green house" soil, divided in portions of 1 kg dry soil, were contaminated with $^{137}CsCl$ and $^{90}(Sr+Y)(NO_3)_2$ solutions prepared with rain water collected previously, starting from stock solutions with specific activities of 4.26 MBq/ml for ^{137}Cs and 0.825 MBq/ml for ^{90}Sr. Contamination of small portions of soil has the advantage of a good (uniform) radionuclide distribution in soil, especially when the soils are contaminated manually. Each kilogram of dried soil prepared to be contaminated was spread on a tray as layer of 5 mm thickness. For alluvial and brown-reddish soils, 50 ml of simple rain water and then 150 ml of contaminated rain water (containing ~100 kBq ^{137}Cs and ~10 kBq ^{90}Sr) were sprayed uniformly onto 1 kg soil layer. To contaminate "green house" soil, 200 ml of simple rain water and 300 ml of contaminated rain water (containing ~100 kBq ^{137}Cs and ~10 kBq ^{90}Sr) were used. After contamination, separately for each soil type, the soil portions were put together and mixed in plastic barells doubled inside with a polyethylene bag and provided with a bottom drainage pipe (connected to a plastic flask in which to be released the possible excess of water) The contaminated soils were watered progressively for few days with small amounts of simple rain water so that to achieve a soil moisture in a range placed between field capacity and saturated state. During the whole period of experiments the soil moisture was maintained at a constant level by closing the open end of the plastic bag which doubles inside the wall of the barell used as pot (thus avoiding water loss by evaporation

1.1.2. Physical, chemical and mineralogical analyses

The physical, chemical and mineralogical analyses of the soils prepared for batch equilibrium experiments have included granulometry, organic and mineral mater contents, pH, cation exchange capacity, exchangeable basic cations and H^+, basic cation saturation, ^{137}Cs and ^{90}Sr. The results of analyses are shown in Table 1.

The methods used to determine soil characteristics are standardized methods regularly in use in specialized agricultural chemistry laboratories.

Table 1: Physical, chemical and mineralogical characteristics of alluvial (**A**), brown-reddish forest type (**BRFT**) and "green house" (**GH**) soils collected for experiments.

Parameter	A	BRFT	GH
Texture class	sandy-loamy	clayey-loamy	organic
Organic matter (%)[1]	4.8	3.6	52.4
Mineral matter (%)[1]	95.2	96.4	47.6
Coarse sand (%)[1,2]	6.4	3.2	
Fine sand (%)[1,2]	54.4	32.4	
Silt (%)[1,2]	20.5	30.8	
Clay (%)[1,2]	18.7	33.6	
pH (H_2O)	7.8	7.5	8.5
pH (KCl)	7.2	6.7	7.8
CEC (meq/100 g)[1,3]	16.29	22.25	68.2
Ex.K^+ (meq/100 g)[1]	0.59	0.51	19.17
Ex.Na^+ (meq/100 g)[1]	0.54	0.24	6.05
Ex.Ca^{2+} (meq/100 g)[1]	13.57	18.00	42.98*
Ex.Mg^{2+} (meq/100 g)[1]	1.59	3.12	42.98*
Ex.H^+ (meq/100 g)[1]	-	0.38	-
BCS (%)[4]	100.0	98.3	100.0
^{137}Cs (kBq/kg)	128.4± 7%	125.8± 7%	132.9± 7%
^{90}Sr (kBq/kg)	2.3±10%	1.0±14%	0.5±12%

[1] dry weight; [2]percent of mineral fraction only, [3] cation exchange capacity;
[4] basic cation saturation; * Ex.Ca^{2+} + Ex.Mg^{2+}

1.1.3. Collection of soil solutions

One porous ceramic cup sampler was installed vertically in center of each pot, at a depth of 15 cm. To collect soil water, a negative pressure (40-50 cm of mercury vacuum) was achieved inside the sampler by using a vacuum hand pump. Samples of soil solution were collected periodically to be analyzed separately for checking up the evolution towards the equilibrium state of ^{137}Cs in contaminated soils. After reaching the equilibrium state, soil solutions extracted periodically were bulked together by soil type, later on to be used for batch equilibrium experiments. Collected soil solutions were stored in a refrigerator until required.

1.1.4. Checking up the evolution towards the equilibrium state of ^{137}Cs in contaminated soils

According to literature /1/, for all applied radionuclides to different soils, usually it takes one to three months to reach equilibrium between radionuclide and soil ions. Based on this aspect, it was considered conveniently to check up only the equilibrium state of ^{137}Cs, although the soils had been contaminated both with ^{137}Cs and ^{90}Sr. To check up the equilibration situation of ^{137}Cs in contaminated soils, the soil solutions extracted periodi-cally from each soil type were analyzed for pH, conductivity and ^{137}Cs radioactivity. When the registered activities for ^{137}Cs in soil solutions started to be almost constant, it was considered that equilibrium was attained, so permitting to start batch equilibrium experiments. Additionally, when the equilibrium was attained, the distribution coefficients (K_d) of ^{137}Cs were calculated, knowing ^{137}Cs concentration in the last samples of soil solutions extracted from the three contaminated soils and measuring ^{137}Cs activity in their associated soils. The distribution coefficients were calculated as ratio between the amount of radionuclide per kilogram of dry soil (soil matrix) and the amount of radionuclide per litre of soil solution. The K_d values of ^{137}Cs showed an almost equilibrated state, they being included in K_d ranges for ^{137}Cs at equilibrium found in literature /2/: 22129±42% l/kg for alluvial soil; >57195 l/kg for brown-reddish forest type soil; 38±10% l/kg for "green house" soil.

1.1.5. Selection of fertilisers and application rates

Five fertilisers were selected as potential effective treatments to be applied to soils contaminated with ^{137}Cs and ^{90}Sr for reducing radionuclide transfer from soil to plant. the fertilisers and their application rates in field are as follows: "potassic salt 30%" ,800 kg/ha (~200 kg K); monopotassium phosphate, 700 kg/ha (~200 kg K, ~500 kg PO_4); calcium dihydrogen orthophosphate monohydrate, 7500 kg/h (1200 kg Ca, ~5600 kg PO_4), clover ash, 1200 kg/ha, chicken manure, 1500 kg/ha.

The first four fertilisers were chosen as sources of potasium, calcium and phosphates for soil-plant system, because these ions have been shown to decrease the uptake of radiocaesium and radiostrontium in some

circumstances /3-6/. On the other hand, chicken manure as source of ammonium was chosen because this cation has been to enhance radiocaesium uptake by plants /3-5,7/.
The chemical treatments of soils in batch equilibrium experiments corresponded to the maximum level of standard application rates in field. Due to possible adverse effects, the application of higher rate of fertiliser were avoided

1.2. Sample preparation for modified batch equilibrium technique
As it was shown recently /8/, the use of the modified batch equilibrium technique in studying the effectiveness of soil-based countermeasures in reducing soil-to-plant radionuclide transfer proved to be a handy method for checking up changes in solid-liquid equilibria as response to different chemical treatments of radioactive contaminated soils, by evaluating the radionuclide/stable nutrient analogue ratio in an extract resulted from an equilibrated mixture containing determined amounts of moist soil, its associated soil solution and the treatment.
The batch equilibrium samples were prepared with determined amounts of moist soil, its associated soil solution and the chemical compound of which effect had to be evaluated. The ratios between solid and liquid phases in samples are slightly comparing ratios used in original modified technique /8/. For alluvial and brown-reddish soils the soil matrix:soil solution ratio was 1:2.5 mass/volume, according to the Recommendations of the Committee of International Society for Soil Science (elaborated in 1930) for chemical analyses in soil suspensions. The recommendations (cited by /9/) consider the ratio 1:2.5 as suitable for almost the soils (excepting green house soil for cultures of vegetables where the recommended ratio is 1:5, and soils with an organic content exceeding 30% where the recommended ratio is 1:10). The original modified technique described by /8/ uses 1:5 ratio for all types of soils (considering the mass of moist soil); the technique applied in this study considers the mass of dry soil (according to the above mentioned recommendations.
Appropriate masses of fertiliser were dissolved in soil water previously collected from the appropriate soil in pot. The resulting solution was then mixed with moist soil in a flask in the above mentioned proportions (225 ml solution to the amount of moist soil corresponding to 90 g dry soil, for alluvial and brown-reddish soils; 150 ml solution to the amount of moist soil corresponding to 15 g dry soil, for "green house" soil). Simultaneously, the control samples (without fertiliser) were prepared in the same manner with experimental samples. The prepared flasks were hand shaken for few minutes and left to settle. The mixtures were stored at room temperature and periodically were mechanically shaken. After a 48 hour period elapsed from sample preparation, considered as the end of the necessary time to achieve the equilibrium conditions of the mixture, the samples were centrifuged at 2000 rpm, for 20 minutes. After centrifugation, the supernates were collectedseparately for each sample and filtered through Whatman membrane filters (0.45 μm). Aliquots of 5 ml were were taken for potassium and calcium determinations. The remaining solutions were retained for radiometric analyses

1.3. Chemical and radiometric analyses
The concentrations of potassium and calcium ions in the 5 ml aliquots from control and experimental samples were determined by atomic absorption spectrometry. The remaining filtrate from each sample was evaporated to dryness on a hot plate and the residue dissolved in 20 ml 8M nitric acid (the volume of a scinti vial). Activity concentrations of ^{137}Cs were determined by gamma spectrometry using a Ge-Li detector. Later on, the same sample was prepared for the determination of ^{90}Sr activity concentration, according to the method described by /9/

1.4. Results and discussions

1.4.1. Effects of treatments on ^{137}Cs transfer (Table 2)
1.4.1.1. "Potassic salt 30%" and monopotassium phosphate
Both "potassium salt 30%" and monopotassium phosphate decreased $^{137}Cs/K$ ratios in the liquid extract of the the equilibrated mixtures prepared with alluvial and brown-reddish soils, as resultof different increment factors for potassium and ^{137}Cs, higher for potassium than for ^{137}Cs. The effects of both salts, in terms of reduction factor for $^{137}Cs/K$ ratio, were higher in mixtures prepared with alluvial soil than in samples prepared with brown-reddish soil (possibly, in a correlation with clay content of the soils, lower in alluvial soil: 18.7%, higher in brown-reddish soil: 33.6%0. As it was shown in literature /10/, the soils with a higher content in clays presents a higher fixing capacity for ^{137}Cs and potassium. In the equilibrated mixtures with "green house" soil, the supplementary potassium from fertilisers (not significant, comparing to the initial potassium in soil) practically did not produce any change in $^{137}Cs/K$ ratios, both for "potassic salt 30%" and

monopotassium phosphate. According to literature data /11/, even the initial concentrations of potassium in soil solutions of alluvial and brown-reddish soils (exceeding 0.1 mM/l) are high enough to determine a low uptake efficiency of ^{137}Cs uptake by plant from contaminated soil. The effectiveness of potassium treatments are extremely dependent on the soil type and the availability of potassium before the treatment: the effect is greatest in potassium deficient soils /7,12/. Moreover, the results in this study are in a good agreement with some previous results /13/ evidencing low values of soil-to-plant transfer factors for ^{137}Cs, found in field in brown-reddish forest type soil after the Chernobyl nuclear accident.

Table 2: Effect of "potassic salt 30%" (**K**), monopotassium phosphate (**K+P**), clover ash (**CA**), chicken manure (**CM**) and calcium dihydrogen orthophosphate monohydrate (**Ca+P**) on $^{137}Cs/K$ ratios in liquid phases extracted from equilibrated mixtures of alluvial (**A**), brown-reddish forest type (**BRFT**) and "green house" (**GH**) soils.

Sample	^{137}Cs (Bq/l)	K (mg/l)	$^{137}Cs/K$	Reduction(-) or enhancement(+) factor *
A (control)	17.1± 5%	7.3	2.34	-
A (K)	46.7± 7%	166.9	0.28	-8.4
A (K+P)	40.0± 7%	113.8	0.35	-6.7
BRFT (control)	2.4±17%	8.0	0.30	-
BRFT (K)	3.1±13%	60.7	0.05	-6.0
BRFT(K+P)	3.8±18%	44.0	0.09	-3.3
GH (control)	4790.0± 5%	8350.0	0.57	-
GH (K)	5268.0± 5%	9215.0	0.57	1.0
GH (K+P)	5292.0± 5%	8570.0	0.62	+1.1
A (control)	25.4± 4%	12.4	2.05	-
A (CA)	51.3± 3%	215.4	0.24	-8.5
A (CM)	214.0± 3%	111.9	1.91	-1.1
BRFT (control)	1 9±12%	11 9	0.16	-
BRFT (CA)	2.1±13%	67 4	0.03	-5.3
BRFT (CM)	8.4± 5%	17 4	0.48	+3.0
A (control)	16.2± 3%	165.0	0.0982	-
A (Ca+P)	23.3± 3%	155.0	0.1503	+1.5
BRFT (control)	1 2±17%	137.0	0.0088	-
BRFT (Ca+P)	2.5±15%	87.0	0.0287	+3.3

* Ratio between control and experimental sample (reduction factor) and ratio between experimental sample and control (enhancement factor)

1.4.1.2. Clover ash

Applying the clover ash treatment in mixtures prepared with alluvial and brown-reddish soils, its effect on reducing the soil-to-plant transfer of ^{137}Cs was similar to that observed for "potassic salt 30%", at similar application rates diminishing the values of $^{137}Cs/K$ ratios in liquid extracts of equilibrated mixtures with comparable reduction factors

1.4.1.3. Chicken manure

In liquid extracts from equilibrated mixture with alluvial soil, chicken manure determined a $^{137}Cs/K$ ratio with only 6 8% less than in control sample (practically, non significant). In the mixture prepared with brown-reddish soil, the treatment produced an increase of $^{137}Cs/K$ ratio by an enhancement factor of 3. The high amount of ammonium ion in chicken manure could be responsible for release of ^{137}Cs from soil matrix, at a higher rate than that of potassium.

1.4.1.4. Calcium dihydrogen orthophosphate monohydrate

Adding the fertiliser in mixtures, the treatment enhanced values of $^{137}Cs/K$ quotients in liquid extracts of

samples prepared both with alluvial soil and brown-reddish soil. The enhancement of $^{137}Cs/K$ quotients resulted from increases of ^{137}Cs concentrations accompanied by reductions in potassium concentrations (less for alluvial soil and more for brown-reddish soil).

1.4.2. Effects of treatments on ^{90}Sr transfer (Table 3)

Only "potassic salt 30%", monopotassium phosphate and calcium dihydrogen orthophosphate monohydrate were studied for their potential effectiveness in reducing the soil-to-plant transfer of ^{90}Sr.

Almost the fertilisers diminished the values of $^{90}Sr/Ca$ ratios in liquid phases extracted from equilibrated mixtures, with similar reduction factors ranged between 1 and 2. An exception was the reduction observed in extract from the mixture with brown-reddish soil, where calcium dihydrogen orthophosphate monohydrate reduced the value of $^{90}Sr/Ca$ ratio by a factor of 5.

The modified values of $^{90}Sr/Ca$ quotients (in sense of their reduction) resulted from changes in concentrations with different rates of ^{90}Sr and calcium, detected in liquid extracts from the mixtures at the end of the 48 hour equilibration period

Adding phosphatic fertilisers (K+P and Ca+P) to the soils, that produced in extracts from equilibrated mixtures prepared with alluvial and brown-reddish soils a significant reduction by a factor of about 2 in ^{90}Sr concentrations, probably immobilizing the radionuclide in forms not appearing in liquid extracts, by co-precipitation with insoluble phosphates (according to /14/).

Table 3: Effect of "potassic salt 30%(**K**), monopotassium phosphate (**K+P**) and calcium dihydrogen orthophosphate monohydrate (**Ca+P**) on $^{90}Sr/Ca$ ratios in liquid phases extracted from equilibrated mixtures of alluvial(**A**) and brown-reddish forest type(**BRFT**) soils

Sample	^{90}Sr (Bq/l)	Ca (mg/l)	$^{90}Sr/Ca$	Reduction factor(-) *
A (control)	2262 ± 10%	530	4.3	-
A (K)	2276 ± 10%	619	3.7	-1.2
A (K+P)	1764 ± 10%	495	3.6	-1.2
A (Ca+P)	2193 ± 10%	807	2.7	-1.6
BRFT (control)	1009 ± 10%	203	5.0	-
BRFT (K)	905 ± 10%	313	2.9	-1.7
BRFT (K+P)	459 ± 10%	166	2.8	-1.8
BRFT (Ca+P)	543 ± 10%	528	1.0	-5.0

* Ratio between control and experimental sample

1.5. Conclusions

(i) Potassic fertilisers and clover ash are potentially very effective countermeasures for ^{137}Cs in alluvial and brown-reddish forest type soils, the treatment was practically non significant in "green house" soil, where the initial concentration of potassium was too high

(ii) The effectiveness of "potassic salt 30%" for ^{137}Cs was similar to that of clover ash, both for brown-reddish and alluvial soils

(iii) Chicken manure was ineffective as countermeasure for ^{137}Cs when was applied to alluvial soil and had a harmful effect on brown-redish soil, increasing the value of $^{137}Cs/K$ ratio by a factor of 3.

(iv) Calcium dihydrogen orthophosphate monohydrate had a harmful effect as countermeasure for ^{137}Cs when was applied both to alluvial and brown-reddish soils (more evident at brown-reddish soil).

(v) "Potassic salt 30%", monopotassium phosphate and calcium dihydrogen orthophosphate monohydrate generally had relative low efficiencies as treatments for ^{90}Sr (they decreased the values of $^{90}Sr/Ca$ ratios by a factor less than 2) when they were applied to alluvial and brown-reddish soils; however, calcium dihydrogen orthophosphate monohydrate was an effective countermeasure for ^{90}Sr when was added to brown-reddish soil, reducing the value of $^{90}Sr/Ca$ ratio by a factor of 5.

(vi) "Potassic salt 30%" and monopotassium phosphate can be applied without restrictions, as very effective countermeasures for ^{137}Cs, both to alluvial and brown-reddish soils containing mixed deposits of ^{137}Cs and ^{90}Sr (they have not any harmful effect on soil-to-plant transfer of ^{90}Sr and their effectiveness on reducing the transfer of ^{90}Sr from soil to plant is lower than for ^{137}Cs)

(vii) Calcium dihydrogen orthophosphate monohydrate can be applied as countermeasures to alluvial and brown-reddish soils contaminated only with ^{90}Sr (the treatment is more effective in brown-reddish soil than

in alluvial soil).
(**viii**) Clover ash was assayed only as countermeasure for ^{137}Cs but, taking into account its similar effect with that of "potassic salt 30%" when was applied to brown-reddish and alluvial soils, it is expected not to have any harmful effect on soil-to-plant transfer of ^{90}Sr
(**ix**) The general effect of chicken manure on transfer of ^{137}Cs and ^{90}Sr from soil to plant could be assimilated with the effect of ammonium fertilisers, due to its high concentrations of ammonium ion; although the effect of chicken manure on ^{90}Sr was not studied in this project, based on this assumption it could be expected that chicken manure not to produce any effect (beneficial or harmful), neither on alluvial soil nor in brown-reddish soil, when the soils are contaminated only with ^{90}Sr.

2. Alternative/complementary procedures to evaluate effectiveness of countermeasures for radionuclides in soils

2.1. Plantlet method

The plantlet method of Neubauer and Schneider has been used for many years to check up the soil capacity in providing the necessary potassium for plants in agricultural areas /15/. The method is based on finding that growing up an excessive number of plants on a limited soil nutrient conditions of the method, the plantlets will use mostly or completely the easy available potassium from soil and, occassionally, even a part of the less available forms.
The choice for the plantlet method as an alternative/complementary procedure for the modified batch equilibrium technique to evaluate the effectiveness of potassic fertilisers as countermeasure in reducing the soil-to-plant transfer of radiocaesium relied on the following two supposals:
- the excessive number of plants grown up on a relative small amount of soil contaminated with radiocaesium (simulating the case of normal density of plants cultivated on soils less supplied with available potassium), exhausting quickly the available potassium could complete their need for potassium by extracting available radiocaesium (by virtue of the bio-geo-chemical behaviour of radiocaesium , similar to that of potassium, as chemical analogue);
- adding the potassic fertiliser to a soil containing radiocaesium (which to satisfy the plant need for potassium), its effect on reducing soil-to-plant radiocaesium transfer could be more evidently expressed than in experiments using a "normal" number of plant, since the soil conditions in plantlet method could be considered as "critical" (referring to the limited available potassium resources of soil for the excessive number of plantlets).

2.1.1. Experimental procedure

Portions of 100 g dry soil/sample of alluvial and brown-reddish soils, contaminated in the autumn of 1993 with $^{137}CsCl_2$, were mixed with quartz sand at a ratio of 2:1, in PVC bough pots (11 cm in diameter, 8 cm in height) The main physical, chemical and mineralogical parameters of the soils used for the experiment are shown in Table 1 of this report (at paragraph 1.1.2.). The soil and sand mixture was then covered with a 250 g quartz sand layer, as bed for seeds. In each experimental sample, enough distilled water (~80 ml) containing 160 mg dissolved "potassic salt 30%" as treatment (corresponding to a standard application rate in field of 200 kg K/ha) was added slowly to the surface, to bring the soil mass to field capacity. The control samples were watered only with simple distilled water. Plants were grown in laboratory (~20^{o}C, not exposed directly to the sunlight) for 17 days, during which the samples were brought daily to field capacity of soil. On the 17-th day, the shoots were excised 0 5 cm above the surface of the sand bed. The processing of vegetal mass has included oven drying at 105^{o}C (up to attaining a constant weight) and ashing in a muffle furnace at at a temperature not exceeding 500^{o}C. Vegetal samples were weighed in dried and ashed states. Since the vegetal material had to be measured both for ^{137}Cs (by gamma spectrometry) and potassium (by atomic absorption spectrometry), the ash resulted from each sample was dissolved by a repeated digestion with concentrated HNO_3 and HF. After the last step of digestion the samples were prepared in 8M HNO_3

2.2.1. Results, discussions and conclusions

The experimental results on using the plantlet method to evaluate the effectiveness of "potassic salt 30%" as countermeasure for ^{137}Cs are shown in Tables 4 and 5
The response of applying the fertiliser was materialized in reducing the ^{137}Cs uptake by the wheat plantlets with a factor of 2 37 for those grown on the alluvial soil and a factor of 2.08 for those grown in brown-reddish soil. The decrement of the ^{137}Cs level in plantlets was accompanied by an increase of potassium concentration with a factor of 1.89 in plants grown on alluvial soil, and a factor of 1.73 in plantlets from brown-reddish soil. Corresponding to the changes in opposite directions of ^{137}Cs and potassium

concentrations, $^{137}Cs/K$ quotient decreased by a factor of 4.5 in vegetal samples collected from alluvial soil, and a factor of 3 5 in vegetal samples collected from brown-reddish soil. For the same treatment, the reduction factors of $^{137}Cs/K$ ratios determined in liquid extracts from the mixtures in batch equilibrium experiments were 8 4 for samples prepared with alluvial soil and 6.0 for samples prepared with brown-reddish soil. Both in plantlet method and modified batch equilibrium technique, the values of reduction factor for $^{137}Cs/K$ quotients were lower in samples prepared with brown-reddish soiland higher in samples prepared with alluvial soil: in plantlet method the reduction factor of $^{137}Cs/K$ ratio in plants grown up on brown-reddish soil represents 77.8% of the reduction factor registered in plants grown up on alluvial soil; in modified batch equilibrium technique the reduction factor for $^{137}Cs/K$ quotient found in mixtures prepared with brown-reddish soil represents 71.4% of the reduction factor in samples prepared with alluvial soil.
Based on these findings, it could consider that both methods have comparable sensitivenesses when they are used to evaluate the effectiveness of potassium-based countermeasures in reducing soil-to-plant transfer of radiocaesium.

Table 4: Effect of "potassic salt 30%" on ^{137}Cs transfer from alluvial soil to wheat plants.

Parameter	Control	Experimental
Treatment (mg "potassic salt 30%")	-	160
Dry mass of shoots (g)*	5.368	6.556
Ash mass of shoots (g)*	0.585	0.978
^{137}Cs in shoots (kBq/kg dry mass)	2.437	1.030
Reduction factor for ^{137}Cs	-	2.37
Potassium in shoots (g/kg dry mass)	33 963	64.082
Enhancement factor for potassium	-	1.89
$^{137}Cs/K$ ratio in shoots	0.072	0.016
Reduction factor for $^{137}Cs/K$ ratio	-	4.5

* the values are given for a pool of 4 samples

Table 5: Effect of "potassic salt 30%" on ^{137}Cs transfer from brown-reddish forest type soil to wheat plants.

Parameter	Control	Experimental
Treatment (mg "potassic salt 30%")	-	160
Dry mass of shoots (g)*	5.385	6.685
Ash mass of shoots (g)*	0 573	0.961
^{137}Cs in shoots (kBq/kg dry mass)	1.764	0.847
Reduction factor for ^{137}Cs	-	2.08
Potassium in shoots (g/kg dry mass)	35.666	61.658
Enhancement factor for potassium	-	1.73
$^{137}Cs/K$ ratio in shoots	0.049	0.014
Reduction factor for $^{137}Cs/K$ ratio	-	3.5

* the values are given for a pool of 4 samples

2.2. Speciation experiment

The bio-availability and mobility of radionuclides in soils are markedly influenced by the speciation, namely the chemical and/or physical associations of radionuclides with soil components. It is well known that, with time, deposited radionuclides in soils will be will be subjected to a series of transformation processes (e.g. weathering and incorporation in soil structures) which will influence availability and mobility of radionuclides in soil and, consequently, their transfer in plant. Also, changes in soil chemistry (i.e. changes produced by common agrochemical treatments) can induce modifications in speciation of different elements, including radionuclides and nutrients Getting a better knowledge on speciation of radionuclides and nutrients, that could improve the quality of chemical countermeasures (in terms of application rates, selection and association of treatments) which to be applied to radioactive contaminated soils. A handy method for speciation studies is sequential extraction procedure.

2.2.1. Soils used in experiment

Two mineral soils (loam and sand) and three organic soils (adventurers peat, peat ranker and deep peat),

contaminated with $^{134}CsCl$ over the period March-May 1993, were used to study radionuclide speciation by sequential extraction technique. The physical, chemical and mineralogical properties of experimental soils are given in Table 6. By design, the experimentalsoils cover a wide range of textures, organic matter and mineral contents, cation exchange capacities, potassium concentrations and pH regimes.

Table 6. Physical, chemical and mineralogical characteristics of soils used in speciation experiments.

Parameter	Loam	Sand	Adventurers peat	Peat ranker	Deep peat
Organic matter (%)[1]	8.2	2.7	60.6	77.0	82.3
Mineral matter (%)[1]	91.8	97.3	39.4	23.0	17.7
Coarse sand (%)[1,2]	24	60	5	1	2
Fine sand (%)[1,2]	39	18	6	1	2
Silt (%)[1,2]	18	11	15	10	6
Clay (%)[1,2]	11	9	14	11	8
pH ($CaCl_2$)	6.7	6.8	4.7	3.5	3.9
CEC (meq/100 g)[1,5]	21.4	11.3	83.5	100.0	105.6
Total **K** (mg/kg)[1]	3030	1930	1920	580	450
Ex.**K** (meq/100 g)[1]	1.9	0.6	0 4	0.7	0.6
^{134}Cs (kBq/kg)[1,3]	206	113	407	400	444
^{134}Cs (kBq/kg)[1,4]	99.35	47 32	237.5	198.3	235.4

[1] dry weight; [2] percent of mineral fraction only, [3] initial activity (March-May 1993); [4] activity in March 1995, [5] cation exchange capacity

2.2.2. Sequential extraction procedure

Homogenized soil samples dried at room temperature were weighed (15 g loam, 16 g sand, 12 g peat for each sample) and extracted sequentially according to a scheme developed by Tessier et al./16/, and applied to radionuclides by /17/. Comparing to the method described by /17/, the amounts of soil and reagents were increased proportionally to get larger volumes of extracts with higher activities of ^{134}Cs. The extracted fractions were as follows: water soluble (F1), exchangeable (F2), bound to carbonates (F3), bound to Fe and Mn oxides (F4), bound to organic matter (F5), acid-digestible (F6), and residue (F7, the difference between the total activity in sample and the sum of F1 .F6 fractions

2.2.3. Results, discussions and conclusions

The relative distribution of ^{134}Cs (% of total activity) determined by sequential extraction technique shows large variations in radionuclide distribution both between extracted fractions of each soil and between soil types (Table 7).

Table 7: Relative distribution of ^{134}Cs (% of total activity) in sequential extraction fractions of loam, sand, adventurers peat, peat ranker and deep peat at two years after contamination.

Fraction	Loam	Sand	Adventurers peat	Peat ranker	Deep peat
F1	0.1	0 2	0.005	0.03	0.07
F2	9.9	19.7	0.4	0.2	0.9
F3	1.2	2.6	0.1	0.1	0.2
F4	0.9	2.2	0.09	0.1	0.2
F5	11 3	26.5	0.7	0.7	0.9
F6	41.2	44.9	33.1	42.3	50.8
F7	35.4	3.9	65.6	56.6	46.9

Two years after contamination, in all investigated soils, ^{134}Cs appeared to be strongly associated, mostly with F6 and F7. According to /18/, the strong fixation of ^{134}Cs in soils could be mainly attributed to its association with interlayer exchange sites in clay mineral lattices. This should indicate a rather low transfer of ^{134}Cs from soil to vegetation. Contrasting with concentrations of ^{134}Cs in F6 and F7, those found in F1 (as easily available form for plants) were placed at a very low level (less than 1% of the total activity), especially in peat soils. The concentrations of ^{134}Cs in F1 of loam and sand, somewhat higher than in peat soils, are related to the higher concentrations of ^{134}Cs in exchangeable fraction of mineral soils, comparing to organic soils. The same soils were subject of a previous study on the effectiveness of potassium-based treatments in reducing ^{134}Cs transfer from soil to plant /19/. The effectiveness of potassium treatments, in terms of diminished values of $^{134}Cs/K$ ratios after soil treatment, was higher in organic soils where concentrations of ^{134}Cs in F1 and F2 were at a lower level, comparing to mineral soils. The lower concentrations of ^{134}Cs concentrations found as bound to organic matter in peat soils could be a reflection of the general inability of caesium to form organic complexes /20/ However, the more significant role apparently played by the organic phase in loam and sand (where the concentrations of ^{134}Cs bound to F5 were higher) support the contention that peroxide can attack some mineral surfaces (Schoer, cited by /20/).

3. Publications

Nisbet A F . Mocanu N., Shaw S (1994). Laboratory investigation into the potential effectiveness of soil-based countermeasures for soils contaminated with radiocaesium and radiostrontium. The Science of the Total Environment **149**:145-154.

References

1.IUR(1989) V-th Report of the Working Group on Soil-to-Plant Transfer Factors (Guttannen, Grimselpass, Switzerland, May24-26, 1989), RIVM, Bilthoven, The Netherlands, p.212.

2.Sheppard M.I., Thibault D H.(1990).Default soil solid/liquid partition coefficients, K_ds, for four major soil types. a compendium. Health Physics 59/4:471-482.

3.Jackson W.A., Craig D , Lugo H.M.(1965).Effect of various cations on caesium uptake from soils and clay suspensions. Soil Science 99/5:345-353.

4.Nielsen B., Strandberg M.(1988).A literature study of the behaviour of cesium, strontium and plutonium in the soil-plant ecosystem. Report NEI-DK-107, Riso National Laboratory, Roskilde, Denmark.

5.Arnold R (1990).Methods to reduce agricultural impact subsequent to a nuclear accident. ANS Report No.2387-R1, Epsom, Surrey, UK

6.Alexakhin R M.(1993).Countermeasures in agricultural production as an effective means of mitigating the radiological consequences of the Chernobyl accident. Sci.Total Environ. 137/1-3:9-20.

7.Evans E J., Dekker A.J.(1966) Plant uptake of ^{137}Cs from nine Canadian soils. Can.J.Soil Sci.46:167-176.

8.Nisbet A F , Mocanu N., Shaw S (1994) Laboratory investigation into the potential effectiveness of soil-based countermeasures for soils contaminated with radiocaesium and radiostrontium. Sci Total Environ 149:145-154

9.Metodologie de analiza agrochimica a solurilor in vederea stabilirii necesarului de amendamente si ingrasaminte Vol.1, Partea I, No.13, Cap 3, MAIA-ASAS-ICPA, Bucuresti,1981, pp.24-28.

10. Zhu S., Ghods A , Veselsky J.C., Mirna A., Schelenz R.(1990). Interference of ^{91}Y with the rapid determination of ^{90}Sr originating from the Chernobyl fallout debris. Radiochimica Acta 51:195-198.

11. Shaw G (1993).Blockade by fertilisers of caesium and strontium into crops: effects on the root uptake process. Sci.Total Environ.137/1-3:119-133.

12. Segal M G (1993) Agricultural countermeasures following deposition of radioactivity after a nuclear accident Sci Total Environ 137/1-3:31-48

13. Mocanu N , Galeriu D., Margineanu R., Paunescu N.(1994).^{137}Cs soil-to-plant transfer in field conditions after the Chernobyl nuclear accident J Radioanal Nucl Chem.(Articles) 178/2:253-259.

14. Nisbet A F , Konoplev A V., Shaw G , Lembrechts J.F., Merckx R., Smolders E., Vandecasteele C M., Lonsjo H , Carini F., Burton O (1993) Application of fertilisers and ameliorants to reduce soil to plant transfer of radiocaesium and radiostrontium in the medium to long term: a summary.Sci Total Environ.137/1-3:173-182

15. Bergmann W (1958) Die Ermittlung der Nahrstoftbedurftigkeit des Bodens.In "Handbubuch der Pflanzenphysiologie",Band IV Mineralische Ernahrung der Pflanze (W.Ruhland, Ed.), Springer-Verlag, Berlin, Gottingen, Heidelberg, pp 867-942.

16. Tessier A , Campbell P.G.C., Bisson M (1979) Sequential extraction procedure for the speciation of particulate trace metals Analytical Chemistry 51/7:844-851.

17. Salbu B , Oughton D.H , Ratnikov A V , Zhigareva T.L., Kruglov S.V., Petrov K.V., Grebenshakikova N.V , Firsakova S.K., Astasheva N P , Loshchilov N.A., Hove K., Strand P.(1994). The mobility of ^{137}Cs

and ^{90}Sr in agricultural soils in the Ukraine, Belarus, and Russia, 1991. Health Physics 67/5:518-528.
18. Oughton D., Salbu B , Riise G., Lien H., Ostby G., Noren A.(1992).Radionuclide mobility and bioavailability in Norwegian and Soviet soils Analyst 117:481-486.
19. Nisbet A.F.(1995).Effectiveness of soil-based countermeasures six months and one year after contamination of five diverse soil types with caesium-134 and strontium-90. Contr.Rep. NRPB-M546.
20. Wilkins B.T., Green N., Stewart S.P., Major R.O.(1986).Factors that affect the association ofradionuclides with soil phases. In "Speciation of fission products in the environment"(R.A.Bulman and J.R.Cooper, Eds.), Elsevier Applied Science Publishers, London and New York, pp.101-113.

I. Head of the project of 8: Gy. Szabó

IIa. Objectives for the reporting period (period from 1993 September to 1995 June)

1 To determine the effects of pH and complexing agents on the sorption of radiosilver on soils and artificial soil particles by batch experiment
2. To determine the solid phase speciation of ^{90}Sr, ^{137}Cs, ^{239}Pu and ^{241}Am in soils by extraction method
3 To investigate the effect of time on solid phase speciation of Cs in soils by extraction method

III. Progress achieved including publication

1. Determination of the effects of pH and composition of the aquaous phase on sorption of ^{110m}Ag on soils and artificial soil particles

^{110m}Ag ($t_{1/2}$ 250.4 d) is a little-studied radionuclide that arises as an activation product in nuclear power plants Although it has featured little in studies of environmental pollution from nuclear reactors, it is present in the low level liquid effluents released from some pressurized water reactors under normal operating conditions (1) and has been reported to be 10% of the total gamma radioactivity in some effluents (2) In our investigation on the sorption of radiosilver in soils we have conducted sorption experiments to determine the effects of the pH and the complexing agents on the sorption of radiosilver in soils

1.1 Experimental procedure

Materials and Methods

A chernozem soil was collected from an uncultivated site close to the NPP at Paks in Hungary. Chemically bound humic (**CBHA**) and fulvic acid (**CBFA**) on silica gels were prepared from silica gel (Kieselgel Si-100, 0.063-0.200 mm) The full experimental details of the reaction procedures have been published elsewhere (3). Immobilized Humic Acid Alumina (**IHAl**) was prepared by sorption of humic acid on acid treated alumina (Al_2O_3) at pH 8 5 for 8 h Silica gel was coated with amorphous iron hydroxide (**FeOH**), iron oxide (**FeOX**) and manganese oxide (**MnOX**). The details of the preparation can be found in the literature (4) Removal of the organic content of the soil was carried out by combustion at 540°C (**combusted soil**). The organic content of these solids was determined by thermogravimetric analysis from 200 to 1000°C. The specific surface area of the prepared solids and their parent solid phases were determined by the B.E T method. The ion-binding capacity of the solid phases was determined for Ca(II) and Ag(I).

Investigation of $^{110m}Ag^+$ uptake as a function of time, complexing agents and pH

The uptake of radiosilver onto solid phases was determined by suspending the particles (~ 500 mg) in solutions (20 ml) of either 0.05 M $NaNO_3$ (pH 1-9) or 0.05 M EDTA (pH 3-9) or 1 mM citrate (pH 3-9) to which was added $^{110m}AgNO_3$ (30 kBq; 2.25 x 10^{-6} g; 2.1 x 10^{-8} mol). Aliquots (1 ml) were removed at 1, 5, 10, 30, 60, 120, 240 and 1440 min. for γ-counting.

Characterization of the used solid matters.

The chemical and physical properties of the used sorbents are summarized in Table 1

1.2. Result and discussion

Sorption kinetics of Ag^+ on different solid supports

Kinetic studies are a common prerequisite to equilibrium sorption experiments. By monitoring the distribution ratio (R_d) value as a function of time a 'time invariant' value for R_d is obtained. The uptake of radiosilver from solutions of nitrate (pH 1-9), citrate (pH 3-9) and EDTA (pH 3-9) was studied for contact times varying from 1 min. to 1 day. From an investigation of the obtained data, they are not presented here (4) it can be concluded that after being shaken for 30 min the uptake of Agr was at a maximum of 90% for solids and in each case the equilibrium is reached within 4 h and that there are different sorption rates for all the solid phases

Influence of pH on sorption of radiosilver

In the absence of the humic substance, sorption of Ag^+ by the model mineral phases was strongly dependent

on the pH in $NaNO_3$ solution (Fig. 1). From examination of Fig 1 it is apparent that on silica gel and alumina the uptake of radiosilver is lower than on **FeOX**, **FeOH** and **MnOX**. It can also be seen that the higher the pH the higher the uptake of radiosilver. This effect can be understood because the surface of these sorbents could be negatively or positively charged dependent upon the pH. From a comparison of the uptake of radiosilver by the combusted soil with the uptake by other mineral phases it is evident that the sorption by the combusted soil might be determined by the mixed sorption of **FeOH** and **MnOX**. From Fig 1. it is evident that in the absence of humic substances on the surface of the sorbents and in the absence of a complexing agent in the aqueous phase, the Fe/Mn hydrous oxides control the sorptive behaviour of soils and sediments.

In the presence of humic substances the sorption of radiosilver by model sorbents and soil was not strongly influenced by pH beyond pH 2-3 in $NaNO_3$ solution (Fig. 2) From examination of Fig 2 it is apparent that **CBFA**, **CBHA** and **IHAl** exhibit the sorptive characteristics of **soil** except that they have R_d values which are significantly greater than those of **soil** It can also be seen that the supporting mineral does not influence the sorptive characteristics of the humate components of **CBHA** and **IHAl**. Of note are the slight, but significant, differences in the sorptive characteristics of the immobilized humic and fulvic acids for $^{110m}Ag^{+}$ and also the occurrence of two sorption maxima for **CBHA** and **IHAl**. The lower uptake of radiosilver by **soil** presumably arises from the dissolution of some humic substances from particles of soil and perhaps even competition by other ions. From analysis of Fig 2 it is evident that humic substances represent a significant part of the sorptive sites for radiosilver on soils and sediments

Table 1. Characteristics of used solid sorbent

Sorbent	particle size mm	B E T surface area m^2/g	Humic matter content mg/g	Ca(II) uptake capacity µmol/g	Ag(I) uptake capacity µmol/g	Color
Silica gel	0 063-0 200	320	-	ND	ND	White
Alumina	0.063-0 200	149	-	107	104	White
MnOX	0 063-0 200	5.5	-	13	15	Blackish
FeOX	0 063-0.200	9.3	-	21	24	Reddish
FeOH	0 063-0.200	238	-	106	143	White
combusted soil	0 063-0.200	4 8	-	39	45	Red
Soil	0 063-0.200	65	17 8	117	141	Brownish
CBHA	0 063-0.200	273	18 1	247	271	Brow
CBFA	0 063-0 200	275	19 2	252	264	Orange
IHAl	0 050-0 100	150	16 4	227	238	Brown

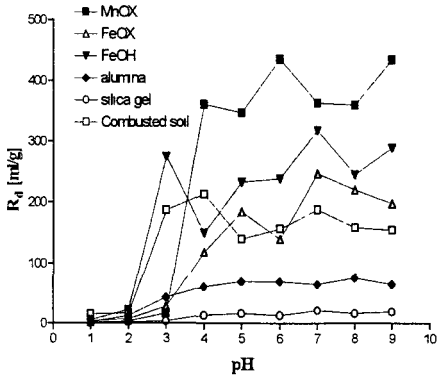

Fig.1. Sorption of ^{110m}Ag by oxide phases from 0 05 M $NaNO_3$

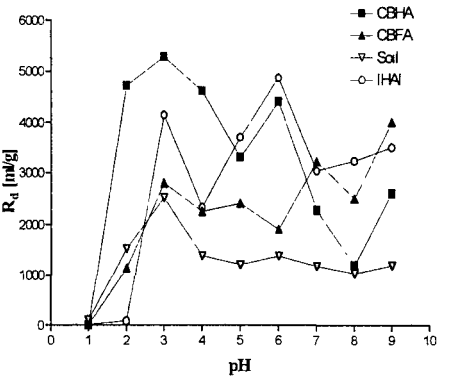

Fig. 2. Sorption of ^{110m}Ag by humate-bearing phases suspended in 0.05 M $NaNO_3$

Effect of EDTA on sorption of Ag^{+}

In the absence of the humic substances, sorption of radiosilver by the model mineral phases was strongly affected by the pH of the solutions of 0 05 M EDTA (Fig 3). It is evident that the higher pHs suppress the sorption of

radiosilver by these phases and presumably this suppression arises from the formation of a stable anionic Ag-EDTA chelate - a value of log 7.32 has been reported for the equilibrium stability constant (5). From Fig. 3. it is evident that in the range pH 6-8, frequently encountered in the environment, only alumina and **combusted soil** could sorb some Ag^+. From the Fig 3., it can be seen that the **Combusted soil** shows a character towards the silver similar to a mixed Fe/Al oxide phase.

In the presence of humic substances, sorption of radiosilver by model sorbents and soil was dependent on pH in EDTA solution (Fig. 4). From examination of Fig. 4 it is apparent that **CBHA, CBFA, IHAl** and natural soil all exhibit similar sorptive properties. It can also be seen that the supporting mineral phase does not influence the sorptive characteristics of **CBHA** and **IHAL**. The sorptive properties of **CBHA** and **CBFA** are largely similar and presumably the lower uptake of radiosilver by **CBFA** arises because Ag-fulvate is less stable than Ag-humate and this is supported by their reported respective equilibrium stability constant values of log 3.62 and 4 51 (6). From Fig. 4 it is evident that the EDTA is a very strong competitor of the metal-binding sites of humic substances for silver To compare the sorption data of silver in nitrate presented in Fig 2. with in EDTA it is apparent that the chelating agent in the same concentration can decrease the distribution ratio of silver ten times on any solid phases, so the strong complexing agents in the environment increase the mobility of silver. Although the man-made ligand EDTA is perhaps an unrepresentative complexing agent to be used in such studies. its use does nevertheless facilitate the demonstration that materials such as **CBHA** and **IHAI** might be used with some confidence to model the sorptive role of naturally occurring humate coatings on soil particles.

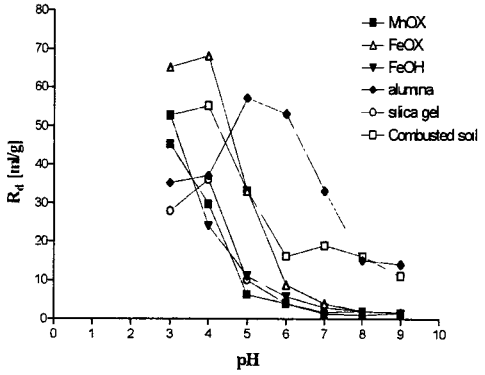

Fig. 3. Sorption of ^{110m}Ag by oxide phases from 0 05 M EDTA

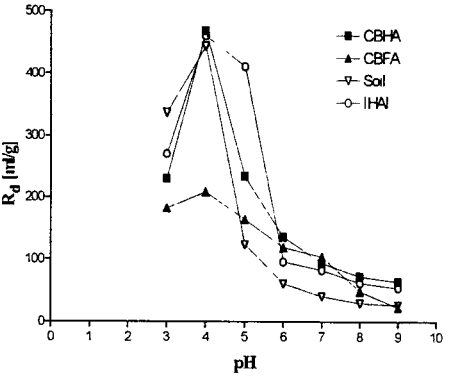

Fig 4 Sorption of ^{110m}Ag by humate-bearing phases suspended in 0.05 M EDTA

Effect of citrate on sorption of $^{110m}Ag(I)$

A comparison of uptake data in nitrate (Fig 1 and 2) with Figs. 5 and 6 shows that the uptake of the radionuclide by **FeOX** and **FeOH** phases is enhanced by citrate. The enhanced uptake of Ag(I) by citrate is possibly determined by surface chelation by a moiety of this multidentate ligand, a phenomenon discussed by Furer and Stumm (7), while Ag(I) is bound another part of the molecule. Our observation that the sorption of Ag(I) by **MnOX** is enhanced in the presence of citrate is similar to the citrate-mediated enhancement of uptake of Ce^{3+} (8), albeit a quite dissimilar cation. Unlike EDTA, citrate is less effective than EDTA at reducing the uptake of $^{110m}Ag(I)$ by **CBHA** and **CBFA** Of particular note, from Fig. 6, is the maximization of uptake of radiosilver by all *humate* coated particles in the presence of citrate over the range pH 5 5 - 7. It is not clear if this maximization of the uptake merely reflects the presence on *humic* substances of binding sites for Ag(I) which have a greater affinity for Ag(I) than that possessed by soluble citrate, or indicates the uptake of a silver citrate complex.

1.3 Conclusion

By using these model substrates and a soil it has been possible to show that humic substances on the surfaces of particles will determine the sorptive properties of soils and sediments for Ag^+ under the conditions which operate in the immediate biosphere. In the absence of humic materials, or at pH 8-9, the sorptive properties of Fe/Mn oxide particles will become more important. The conclusions we have drawn about the association of Ag^+ with humate are supported by the observations of others who have reported a positive correlation between Ag^+ binding in soils and soil organic matter (9, 10).

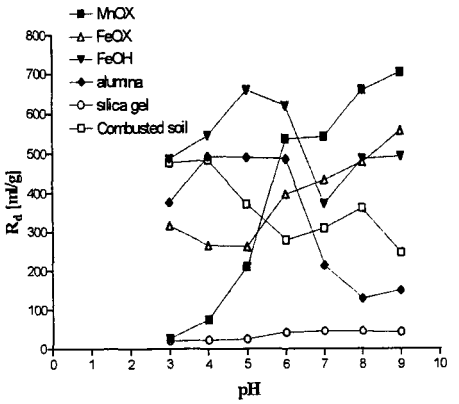

Fig 5. Sorption of ^{110m}Ag by oxide phases from 1 mM citrate solution

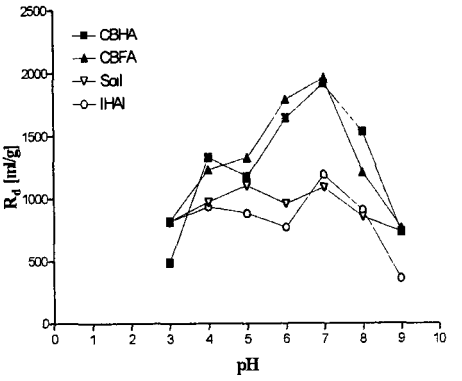

Fig. 6 Sorption of ^{110m}Ag by humate-bearing phases from 1 mM citrate solution

2. Study of physico-chemical forms of ^{90}Sr, ^{137}Cs, ^{239}Pu and ^{241}Am occurrence in soils

Behavior of radionuclides in soils is influenced by their basic chemical characteristics and from this following physico-chemical forms of occurrence in soils as a result of interaction with soil components and soil solution Knowledge about chemical forms and their bounds on soil particles or colloids are important, because of determination of their chemical reactivity, mobility and biological availability Method of fractionation of soils using suitably chosen extraction agents seemed very useful to obtained information about speciation of radionuclides occurrence in soil system. Study of physico-chemical forms of radionuclides in chosen English soils (cooperation with Nisbet, A., NRPB) was the aim of our work. Parallel extraction method was used for determination of speciation of strontium, cesium, plutonium and americium in studied soils.

2.1. Experimental procedure

Soils

Physico-chemical forms of radionuclides occurrence in soils were studied in 3 soil samples sand, loam and agricultural peat The soil samples (radiolabelled in 1984) were obtained from NRPB, dried under laboratory temperature. Basic characteristics and radioactive concentration of samples is shown in Table 2.

Table 2. Physical-chemical characteristics of soils used in the experiment (11)

	Sand	Loam	Peat
Organic (%)	3	8	58
Sand (%)[a]	87	63	26
Silt (%)[a]	5	18	35
Clay (%)[a]	8	11	39
pH ($CaCl_2$)	6.1	7 1	5 5
CEC (meq/100 g)	10	15	133
^{90}Sr (Bq/kg)	1550	1750	6100
^{137}Cs (Bq/kg)	1500	1800	5000
^{239}Pu (Bq/kg)	1100	1400	3850
^{241}Am (Bq/kg)	1300	1400	4300

[a] Percentage of mineral fraction only

Extraction of radionuclides from soils.

Parallel extraction method was used for fractionation of soil components (12). The extraction regimes are listed in Table 3. All soil samples were analyzed in duplicates of 10 g and in general they were suspended in 200 ml of extractant and stirred for 4 h. Solutions were clarified by centrifugation The solutions and the residues radioactivity were measured for cesium and americium by γ-spectrometry, for plutonium by α-spectrometry and for sroncium after chemical separation procedure by beta-counting.

Table 3. Extraction regimes

Extractant	Concentration, pH, temperature	Definition
Ammonium acetate (NH_4Ac)	1 M, pH 7, 23 °C	exchangeable
Ammonium oxalate buffer (NH_4Ox)	0 02 M, pH 3, 23 °C	Bound to Fe and Mn oxides
Sodium hydroxide (NaOH)	0.3 M, 60 °C	Classical humic matter extractant
Trimethyl-chlorosilane/dimethylformamide (TMCS)	60 °C	bound to organic matter

Ultrafiltration to investigate the association of ^{90}Sr, ^{239}Pu and ^{241}Am with humate

The association of ^{90}Sr, ^{239}Pu and ^{241}Am with the fraction isolated by trimethylsilylation (TMCS) of the soils was investigated by ultrafiltartion in CENTRIPLUS™ concentrator obtained from Amicon GMBH 15 ml of extractant containing the humate-nuclide complexes was centrifuged for 8 h in the centriplus concentrators with different cut-off The distribution of radionuclides in the different molecular weight fractions was determined by measuring the activity of the filtrates and the residues

2.2. Results and discussion

It is clear from Figs 7-10 that each radionuclide exhibits a characteristic fractionation profile upon treatment of the soil with the various extracting media

Fig. 7. shows that radiostroncium is weakly bound to soils and extractable with almost all agents used in this study It is apparent that about half of the Sr is bound to organic matter. From the organic matter Sr can be extracted with NH_4Ac From this result it could be concluded that the binding sites for Sr in soil organic matter does not have ability to make strong complexes with Sr and might be restricted to the carboxyl groups of humic matter However in peat soil there is some high stability Sr-humate complexes (about 10-15 %) that cannot be interrupted by NH_4Ac The high solubilization of radiostroncium by NH_4Ac indicates that the Sr is going into the soil solution easily and is available to the plants causing serious radioecological problem

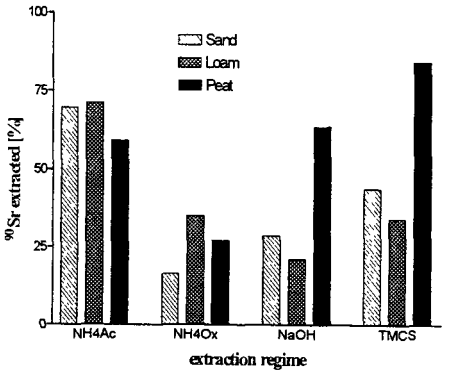

Fig 7. Chemical leaching of ^{90}Sr from soil

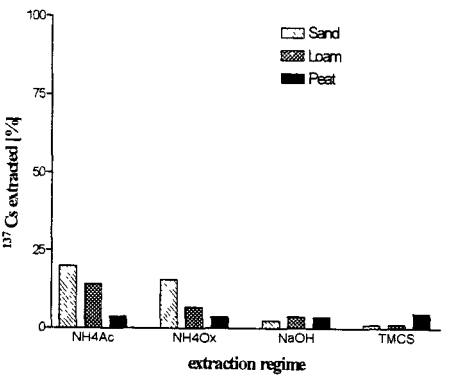

Fig. 8 Chemical leaching of ^{137}Cs from soils

The result of Cs extraction is summarized in Fig. 8. The low solubilization of radiocesium by TMCS and NaOH extractants (1-4 %) indicates that Cs is not bound to the organic matter of soils From the higher amount of cesium extracted with NH_4Ac and NH_4Ox (4-19 %) it can be concluded either some part of the cesium is bound on the exchangeable sites of the soil inorganic phase and available for plans after 11 years of contamination or main part of Cs (80-95 %) is fixed in soils. This fixed part of Cs is unimportant from the radioecology point of view. From the literature data one can conclude that Cs is easily available from soils containing high percentage of organic matter. From the extraction pattern of Cs from soils it is apparent that there is a contradiction with the data available in the literature. Further investigation is needed to find an explanation for this contradiction To summarize, it could be concluded that the main sink for radiocesium in soils is the inorganic phase where the cesium is bound tightly Presumably these binding site are on the clay minerals of soils.

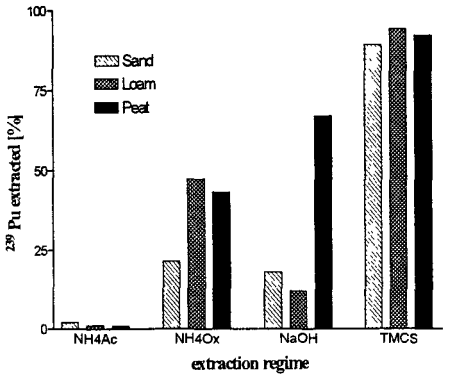

Fig 9 Chemical leaching of ^{239}Pu from soil

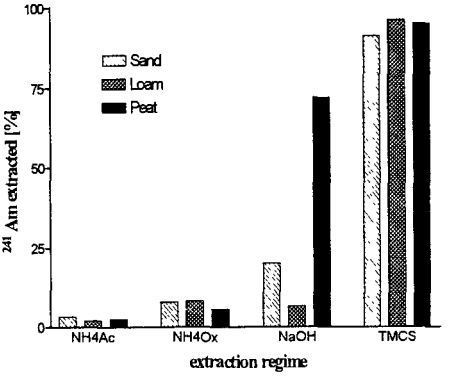

Fig 10. Chemical leaching of ^{241}Am from soils

From an examination of Figs 9. and 10 it is apparent that NH_4Ac solution. a reagent for the extraction of exchangeable fraction of radionuclides, is an ineffective reagents for extraction of Pu and Am It indicates that neither plutonium nor americium is bound by the conventional ion-exchange sites in soils In contrast to this low extractability by NH_4Ac. TMCS was a most effective extractant. The ready extractability of Pu and Am by TMCS (90-96 %) indicates that the main amount of the radionuclides must be present as humate complexes which are inert to competitive cation exchange by NH_4Ac. From the Figs. 9 and 10 it can be seen that NaOH solution. well-established reagent for extraction of humic substances. is an effective reagent for the extraction of these nuclides from peat soil but is weakly effective for the extraction of Pu and Am from sand and loam soils The low extractability of Pu and Am by NaOH from loam and sand soils is noteworthy but no explanation can be offered for the phenomenon From the comparison the extractability of Pu and Am by NH_4Ox it is apparent that NH_4Ox . a reagent to mobilize nuclides from iron and manganese oxides phases of soil by reducing iron and manganese to lower oxidation states. is an effective reagent for extraction of Pu and is weakly effective for extraction of Am If the high extraction of Pu is due to binding of Pu by iron or manganese oxides. we might similarly expect the same for Am. This is not the case and by inference it could be presumed that some part of Pu(IV) oxidation state is changed into Pu(III) by using NH_4Ox solution (pH 3). Further investigation is needed to prove our supposition. From the extraction profile of Pu and Am it could be concluded that Pu and Am are mainly bound by humic substances in soils and are not easily available for plants uptake

It is evident, from Fig. 11, that a substantial amount of radiostroncium extracted in the TMCS extract is associated with high molecular weight humic substances (> 100 kD) in peat soil. distributed about uniformly in loam soil and mainly associated with a low molecular weight (3-10 kD) fraction of humic matter in sand soil From this one could conclude that the organic bound radiostroncium is not available for plant uptake in peat soil. but in sand and loam this fraction of strontium can be uptaken by plan easily.

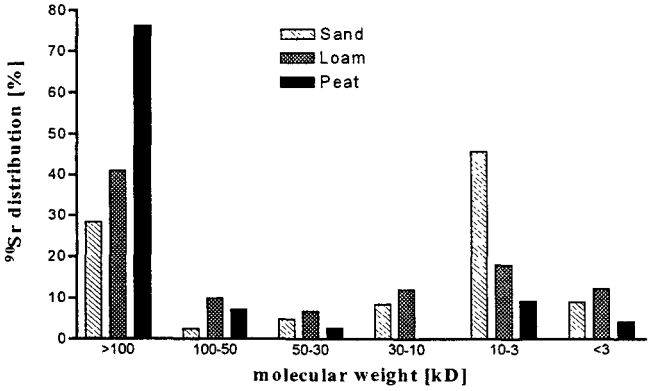

Fig 11 Distribution of ^{90}Sr in different molecular weight humic fraction

From an examination of Figs. 12 and 13 it is apparent that Pu and Am show a similar distribution pattern in the humic fractions in each soil. It also evident that the substantial amount of Pu and Am is bound by high molecular weight (>100 kD) humic substances in peat and loam soils. In contrast to this Pu and Am are bound by a low molecular weight (3-10 kD) humic fraction in sandy soil. From data obtained it could be presumed that Pu and Am is not mobile in soil system The following mobility order for Pu and Am in different type soils can be set up.

sand > loam > peat.

2.3 Conclusion

This study has shown that plutonium and americium are bound nearly 100 % by humic substances in soils From this humate complexes these nuclides could not be mobilized with simple cations. So there is a high possibility that plutonium and americium would not go into the soil solution and they are not available for plant uptake

From the extraction pattern of radiostrontium it can be shown that strontium exits in several sinks in soils and from where it can be mobilized easily by simple cations. This high extractability of radiostrontium indicates that strontium can go into the soil solution, causing serious radioecological problem From the extraction data of radiocesium it could be concluded that the cesium must be bound by the inorganic phase of soils. Presumably these phases are the clay minerals in soils. Low quantity of cesium has been able to be mobilized by simple cations for a long time to make it available for plant uptake

Ultrafiltration has proved to be a promising method for determining the association of radionuclides with different molecular weight humic substances extracted from soils. The results shows that in peat soil strontium, plutonium and americium are bound mainly by high molecular weight humic matter (> 100 kD). In contrast, a large proportion of these nuclides in sand soil is associated with a lower molecular weight humic fraction (3-10 kD) In case of loam soil the plutonium and americium is mainly associated (60-65 %) by a high molecular weight humic fraction and nearly the same proportion of strontium is bound by several different molecular weight humic fraction

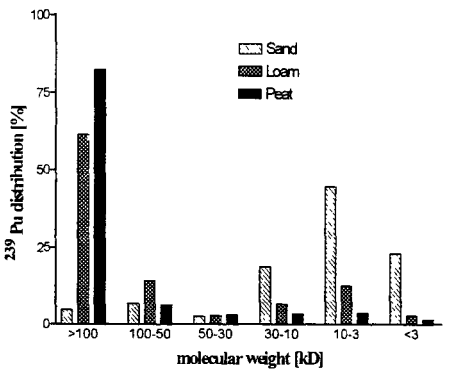

Fig 12. Distribution of ^{239}Pu in different molecular weight humic fraction

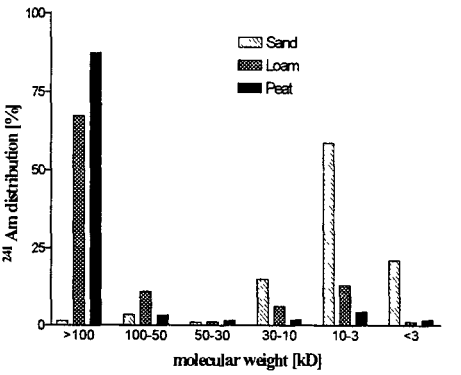

Fig 13 Distribution of ^{241}Am in different molecular weight humic fraction

3. Investigation of the effect of time (years) on the solid phase speciation of radiocesium in soils

It is well known that, with time, radionuclides in soils are subjected to a series of transformation processes which would influence mobility and availability in soils. Studies on the time dependent distribution of radionuclides in soils seem to be necessary. Extraction methods can provide a tool to ascertain the physico-chemical variations of the distribution of radionuclides contaminating soils, subsequently, to be able to predict their future behavior, in terms of migration, bioavailability and plant uptake

This study was undertaken to determine changes in cesium speciation in soil over a 10 year period.

3.1. Experimental procedure

Soils

The changes of physico-chemical forms of radiocesium in soils were studied in 3 soil samples: sand, loam and agricultural peat. The natural soil and the radiolabelled soil samples (radiolabelled in 1984 and 1993) were obtained from NRPB, dried under laboratory temperature. Basic characteristics is shown in Table 2. and radioactive concentration of samples used in the experiment is shown in Table 4.

Radiolabelling of soil samples with ^{134}Cs

Each soil (20 g) was suspended in 200 ml aqueous solution with a concentration of 4 mg/l K^+ and 20 mg/l Ca^{2+} and stirred for 2 days, then the suspension was spiked with 21 kBq ^{134}Cs (6×10^{-8} g; 4.5×10^{-10} mol) After stirring for 3 days, the soils were centrifuged, washed with distilled water and then dried at laboratory temperature. The labeled soil samples was used for extraction study in 1 day after contamination.

Extraction of radionuclides from soils.

Parallel extraction method was used for fractionation of soil components The extraction regimes are listed in Table 3 Another extraction (8 M HNO_3 at room temperature) regime was introduced to determine the residual fraction of cesium All soil samples were analyzed in duplicates using the solid:solvent ratio 1:20 and stirred for 4 h Solutions were clarified by centrifugation. The solutions and the residues radioactivity were measured for cesium by γ-spectrometry

Table 4. The specific activity of soils used in the experiment

	Sand	Loam	Peat
^{137}Cs (Bq/kg) labeled in 1884	1500	1800	5000
^{134}Cs (kBq/kg) labeled in 1993	119	78	251
^{134}Cs (kBq/kg) labeled immediately before introduction of extraction agents	987	1170	1054

3.2 Results and discussion

Table 5 shows ^{134}Cs percentages extracted from soils in 3 different time. In all types of soil the fraction extracted by NH_4Ac (related to exchangeable radiocesium) decreases with time. as well as the percentage of cesium associated with humic substances (TMCS extraction method). which may also be associated to bioavailable cesium (13). This decrease to bioavailable fraction agrees with literature showing a reduction in radiocesium uptake with time (11) Residual fraction. the most significant for radiocesium. as expected for its high affinity to clay minerals (14), increases (decreased extractability with 8 M HNO_3) with time in all types of soil. From an examination of Table 5. it is apparent that the main change in speciation of cesium in soil takes place in 2 year period and there is significant difference only in percentage change of residual fraction between 2 and 11 years Further investigation is needed to determine the change in speciation of radiocesium in a short term.

Table 5. Desorption of radiocesium from soils by extraction method

Soil	Extraction agent	^{134}Cs extracted [%]		
		Immediately after contamination	2 years after contamination	11 years after contamination
SAND	NH_4Ac	40 8	22.3	19.8
	NH_4Ox	38 4	22.4	15.6
	NaOH	1 8	2 1	2 5
	TMCS	3 4	1.7	1.2
	HNO_3	91 2	78.8	68 4
LOAM	NH_4Ac	27.7	16 5	14 1
	NH_4Ox	22.6	6.9	6.9
	NaOH	3 7	3.9	3 8
	TMCS	1 7	1.6	1 2
	HNO_3	88.1	61 2	58.1
PEAT	NH_4Ac	12 8	2 7	3.8
	NH_4Ox	9 8	4 7	3.8
	NaOH	7.8	3.4	3.6
	TMCS	15.6	5.7	4 8
	HNO_3	88.5	27.8	21.2

3.3. Conclusion

An increase with time of residual fraction and a decrease with time of exchangeable (bioavailable) fraction can be observed in all types of soil. The main change in speciation of cesium in soil occurred in 2 years. Further investigation is necessary to determine the parameters (time-scale, ionic strength, other cations etc) that cause this change in speciation of cesium in soil.

4. Publications submitted during reporting period

1 A talajösszetevők hatásának vizsgálata az Ag-110m szorpciójára
Szabó, Gy. , Guczi, J., Valyon, J. & Bulman, R A , *Agrokémia és Talajtan*, in press, in Hungarian
2. Investigation of the sorption characteristics of radiosilver on some natural and artificial soil particles
Szabó, Gy . Guczi, J., Valyon, J & Bulman, R A., *Sci. Total Environm* , in press
3 Investigation of the sorption processes of Ag-110m on various soils
Guczi J & Szabó Gy., 20th Workshop on radiation Protection, 17-19, May 1995, Balatonkenese, Hungary
4 Investigation into the distribution of Sr-90, Cs-137, Pu-239 and Am-241 among soil components
Szabó Gy , Guczi J , Végvári I., Capote C A. & Nisbet A., 20th Workshop on radiation Protection, 17-19. May 1995, Balatonkenese, Hungary
5 Investigation of the sorption processes of Ag-110m on various soils
Guczi J & Szabó Gy , *Isotoptechnika*, submitted in Hungarian
6 Investigation into the distribution of Sr-90, Cs-137, Pu-239 and Am-241 among soil components
Szabó Gy., Guczi J., Végvári I , Capote C A. & Nisbet A , *Isotoptechnika*, submitted in Hungarian

5. Refrences

1 Luykx, F & Fraser, G CEC March 1983
2 Picat, P. Journée scientifique, 20 Juin 1987, CEA Cadarache, Société Françsaise de Radioprotection
3 Bulman, R.A & Szabó, Gy , Investigation of the Interaction of Transuranic Radionuclides with Humic and Fulvic Acids Chemically Immobilized on Silica Gel. Lecture Notes in Earth Science 33. (Eds Allard, B., Boren, H. & Grimvall, A) 329- 339, (1991)
4 Szabó, Gy , Guczi, J., Valyon, J & Bulman, R A., Investigation of the sorption characteristics of radiosilver on some natural and artificial soil particles, *Sci Total Environm.*, in press
5. Sillen, L.E & Martell, A E , Stability Constants of Metal Ion Complexes, Special Publ 17, Chemical Society, London, 1964
6 Sikora,F.J. & Stevenson, F J , Silver complexation by humic substances· conditional stability constants and nature of the reactive sites, *Geoderma*, **42**, 353-363, (1988)
7. Furrer, G & Stumm, W , The coordination chemistry of weathering I Dissolution kinetics of U-Al_2O_3 and BeO, *Geochim. Cosmochim. Acta*, **50**, 1847-1860, (1986)
8 Hasany, S M & Chaudhary, M H , Studies on the adsorptive behaviour of trace amounts of cerium on manganase dioxide from aqueous solutions in the presence of complexing agents, *J Radioanal Nucl Chem. Articles*, **111**, 199-210, (1987)
9 Jones, K.C , Davies, B.E & Peterson, P J , Silver in Welsh soils· physical and chemical distribution studies, *Geoderma*, **37**, 157-163, (1988)
10. Jones, K C & Peterson, P J., The influence of humic and fulvic acid on silver uptake by perennial rye grass, and its contribution to the cycling of silver in soils, *Plant Soil*, **95**, 3-8, (1986)
11. Nisbet, A & Shaw, S., Summary of a 5-year lysimeter study on the time-dependent transfer of Cs-137, Sr-90, Pu-29,240 and Am-241 to crops from three contrasting soil types 1. Transfer to the edible portion, *J. Environ. Radioactivity*, **23**, 1-17, (1994)
12. Szabó, Gy , Wedgwood, A J. & Bulman, R A , Comparison and development of new extraction procedures for Pu-239, Ca, Fe and Cu organic complexes in soil, *J Environ Radioactivity*, **13**, 181-189, (1991)
13 Andolina, J. & Quillite, O , The Transfer of Radionuclides in Natural and Semi-natural Environment, Elsevier Applied Science, London, pp 135-143, (1990)
14. Cremers, A , Elsen, A , De Peter, P & Maes, A , Quantitive analysis of radiocesium retention in soils, *Nature*, **335**, 247-249, (1988)

Final Report
1992 - 1994

Contract: **FI3PCT920022** **Duration: 1.9.92 to 30.9.95** **Sector: A23**

Title: Investigations and modeling of the dynamics of environmental HT/HTO/OBT levels resulting from tritium releases.

1)	Bunnenberg	ZSR, U. Hannover
2)	Belot	CEA, Fontenay aux Roses
3)	Kim	TUM, München
4)	Dertinger	FZK, Karlsruhe
5)	Eikenberg	PSI, Villigen
6)	Uchrin	II.HAS, Budapest
7)	Paunescu	IFIN, Bucharest

I. Summary of Project Global Objectives and Achievements

In order to ensure radiation safety of the public and the environment with regard to releases from major tritium sources, like nuclear fuel reprocessing plants, waste repositories or thermonuclear fusion experiments, the Commission's Radiation Protection Program has financially supported research on the environmental behaviour of tritium and its most common compounds for many years. This has, on one hand, increased our understanding of the physical, chemical and biological processes to an appreciable level. It also has, on the other hand, quite inevitably raised new questions, the importance of which can only roughly be ranked before further knowledge is gained. Unfortunately, this phenomenon, which is quite normal in research work, is often misinterpreted as an argumentation pattern of researchers to prolong work in a familiar field of science.

During the Workshop on Tritium Safety and Environmental Effects, held at Aiken, South Carolina, in 1990 and organized by the Savannah River Laboratories with help of the International Energy Agency, the working group on Environmental Model Validation established a list of processes to be included into accidental tritium transport and dose calculation models and applied rankings with respect to importance, status of modeling and need for experimental data. From this list the participants of this cooperative project have selected two items, which had been characterized by a deficiency of the modeling status compared to the importance and a need for experimental data:

- Tritium reemission from soils and
- Synthesis of tritium into organics.

This has led to the working subtitles of the Contract:

- Experimental investigations and mathematical modeling of tritium reemission from soils after deposition of tritiated hydrogen gas, HT, or tritiated water vapour, HTO, (ZSR and CEA) and
- Elaboration of plant-specific data sets for the production and translocation of organically bound tritium, OBT, in diet-relevant plants (FZK) and associated tritium fractionation processes in the plant/soil system (TUM).

In 1993, the project was extended by a Swiss partner who amended the first item focusing on:

- The effect of rainfall on the infiltration of tritium into soils and on tritium reemission from soil surfaces (PSI).

Under the umbrella of the PECO Programme, two Eastern European institutes joined the Contract by means of Supplementary Agreements in 1994. In both cases, the special features of their contributions are facilities with considerable tritium source terms. Contrary to the studies of selected processes performed by the Western institutions, those laboratories were to evaluate the effects of tritium releases in the various environmental compartments under two different aspects:

- Activity versus distance correlations in the vicinity of a tritium-compound manufacturing facility after 20 years of HT and HTO emissions (II.HAS) and
- Tritium levels in environmental media before and after operation start of a CANDU-type heavy water reactor (IFIN).

While the first subproject aimed at overall (aggregated), long-term consequences of tritium releases into the environment and the deduction of certain aggregated transfer factors, the purpose of the second was the establishment of a data base for the verification of models of tritium processes and pathways in the environment.

Coordination of the project and promotion of the cooperation during the Contract period was performed essentially by means of the Coordination Meetings held in Hannover (1992), Cadarache (1993), Karlsruhe (1994) and Budapest (1995). The actions and decisions of those meetings were documented in Meeting Reports commented and approved by all project partners. The main items at those meetings were the presentations of the individual progress reports, the detailed discussions of the results and their interpretations as well as of the proposals on further procedures in the different projects. Undoubtedly the most efficient was the 4-day meeting hosted by FZK, Karlsruhe, which, in a Workshop on „Radioecological Tritium Modeling", was jointly held with the BIOMOVS II, Special Radionuclides - Tritium, Group. The exceptional merits of this meeting resulted from the discussions on the BIOMOVS presentations about the modeling concepts as well as possible model deficiencies and needs, on one hand, and on the Contract partners's presentations about the experimental generation of data sets for use by the modelers. One of the most beneficial outcomes of these discussions for both, modelers and experimenters, was the cooperative design of special experiments within the scope of the Contract, which exactly meet the needs and boundary conditions of the submodels of existing model codes. Experiments of this kind were performed in the framework of Project 1 and 2 as well as Project 4. The obtained data sets also served as a basis for real scenarios used within the BIOMOVS Group.

Cooperation between the project partners resulted from common interests in certain processes and common or competing experimental methods, combining ZSR, CEA and PSI as well as TUM and FZK, or from the performance of joint field experiments of ZSR, CEA and FZK. Integration of the PECO partners occured quite easily through communication on the development of the individual measuring programs, on the updating of measuring equipment, but most effectively by training of personnel in special analytical techniques. In this context, the training of scientists from IFIN by members of the FZK-group and their analytical lab-intercomparison tests deserve special mentioning. Initially, there had been more PECO applications to the Contract, but the partners agreed to limit the number, in order to ensure the attention needed for fulfilling the aims of PECO.

It can be stated that the four main contractors have fully achieved the initially defined objectives of their projects. The laboratory and small-scale field experiments on tritium reemission

from bare soils have answered the question of the extent of independence of tritium reemission from water evaporation. The importance of this problem had appeared, as tritium reemission is often modeled in terms of water evaporation because of lack of better alternatives, while theoretical considerations and some experimental results had indicated substantial differences between the two processes. The detailed investigations have shown that reemission is largely independent from evaporation and a new separate model has been developed (ZSR). Furthermore, an existing model based on the exchange-velocity concept has proved to reproduce the main physical mechanisms of the process (CEA). One outstanding result is the finding of high initial reemission rates after the deposition of HTO. This has initiated modifications of the broadly accepted UFOTRI code. If those unexpectedly high reemission rates found in the open-air experiments for bare soil also apply for vegetated surfaces, the consequence would be a considerable shift in the dose contributions from inhalation and ingestion. Therefore, ZSR and FZK are planning to continue reemission experiments including vegetation. Upon requests from the modelers, also experiments under extreme climatic conditions are envisaged, to ensure coverage of the whole realistic range of the meteorological parameters involved in the process.

The investigations on tritium fractionation processes in plants and soils have identified a variety of effects resulting from isotopic differences of the two atoms, H and T (TUM), which are usually neglected in natural systems, but more importantly also in the analytical procedures of environmental samples. The dose-relevancy of these studies is introduced by the difference in the radiotoxicity of tritium whether appearing in tissue, ie, tissue water tritium (TWT), or in organic molecules (OBT). This leads to the question, if the value of the specific activity ratio (R-value) of organically bound tritium to tissue water tritium may exceed unity. One important result of this study is the finding that reported values of R>1 may also be a consequence of erroneous analyses of the OBT contents of biological samples, as the analytical procedure itself is subject to isotopic effects, which may increase the error of the total R-value up to 400% depending upon the analytical parameters. In the soil/plant-system the transfer and conversion of tritium from soil-HTO to plant-OBT is associated with a series of physical, chemical and biological isotopic effects, which may, even under equilibrium conditions, cause increases or decreases of the T/H-ratio depending on the process and subcompartment under consideration. It seems that the type of binding of tritium to molecules or solid surfaces is the key to our understanding, whether the T/H-ratio is increased or reduced in the subsequent subcompartment along the tritium pathways. It still needs further research to define, what the maximum increase of the T/H-ratio in the different dose-relevant compartments could be as a consequence of the various isotopic effects. Except for the case of radiation-sensitive molecules, it is doubtful, however, that isotopic effects would increase values of the resulting dose beyond the uncertainty margins of dose prediction models. The statement, that isotopic effects may be at least partly responsible for the observation of higher T/H-ratios in organics of environmental samples compared to those of the ambient water, initiated quite controversial discussions among the project partners. This consequence must be regarded as a theoretical possibility, the actual proof of which is still open.

It is, therefore, of special interest that in the course of the investigations on the production and translocation mechanisms of OBT into diet-relevant plant organs no indication was found for elevated T/H-ratios in OBT-compartments compared to those in the preceding compartments (FZK), thus contradicting the theoretical derivation. The detailed understanding and the high level of modeling capability achieved during these studies is demonstrated, eg, by the good agreement between modeled and measured time courses of the OBT-concentrations in wheat even under water stress conditions. Validation of this model will be a focal point for future work. It became apparent that this high degree of sophistication is necessary to reliably predict the tritium uptake into plants and the subsequent OBT formation and translocation. The ex-

perimental and modeling results also proved to be worth the efforts of studying the dynamics of the metabolic processes, as it provides the possibility to generalise the model for application also to leafy vegetables or pasture grass, which might be consumed at earlier stages of plant development. Verification of this concept of translating metabolic data from one plant species to another will, however, have to be performed by actual measurements, which are, in fact, also planned for the future.

The progress achieved in the investigations on the effects of rainfall on the tritium infiltration into soils and on tritium reemission from soil surfaces has to be viewed under consideration of the fact that the PSI-group had to construct the experimental device almost from zero during the project period including a number of preliminary runs for functional testings. As the experimental system combines unsaturated (upper soil layers) and saturated (ground water) flow, a new model had to be developed to reproduce the measured flow data. As expected, the infiltration rate of tritium into soil increases with increasing rain intensities, and tritium reemission is reduced and delayed by rainfall after HTO deposition. More work is necessary to parameterise and model the processes of concern. They will also have to be verified by respective small-scale field experiments in cooperation with ZSR and FZK.

The PECO-participation in the Contract has been supported by all partners and has been considered successful not only under scientific aspects but also in view of their integration into international project work and project management. It has also provided insight into the expertise and facilities available in those Eastern European institutes as a basis for further information exchange and cooperation. The special interest in the PECO subprojects arose from the existence of a well documented history of tritium release and associated meteorological data, which could serve as a basis to reconstruct long-term release - contamination correlations (II.HAS), an undertaking, which had failed in case of earlier attempts of this kind because of incomplete documentation (eg, in case of military facilities). As expected, the results show a clear correlation between the wind rose and the contamination pattern of the environment around the release point. In the contamination versus distance diagrams even the primary and secondary maxima can be identified, which are attributable to the wet and dry deposition of tritium, respectively. It is those correlations that would deserve more detailed analyses of the long-term effects of the overlapping of the different deposition processes.

It is very unfortunate that only the first part of the project on the evaluation of environmental tritium levels around the Rumanian CANDU-type reactor could be fulfilled (IFIN), as the start of operation had been postponed. However, the Contract phase has been used to its full extent, and an exceptionally detailed program of sample analyses of the pre-operational phase is presented including OBT-values, which are of special dose-relevancy. This actually means a better data base for the background situation than initially expected for the benefit of more reliable interpretations of the activity increases measured after start of operation. Quality control of the values was ensured by the close cooperation especially with FZK and the interlab comparisons.

All Contract partners agreed to undertake any possible attempt towards a continuation of the monitoring program of the Cernavoda area after operation start of the heavy-water reactor, as the resulting data base will be unique in the world and hence an indispensable tool for model calibration and validation. Special features of the site, eg, the unusually high fraction of extremely low wind speeds, which are responsible for high activity concentrations in the near vicinity of the source and which are difficult to predict, should also be used to reduce uncertainty margins of existing model codes. It is quite obvious that making use of this opportunity would also substantially increase public confidence in radiation protection concepts where dose predictions play an important role and that international availability of such data can best be ensured by international cooperation and funding.

Head of project 1: Dr. C. Bunnenberg

II. Objectives for the reporting period

In order to transform the basic physical understanding of the tritium reemission process after HT or HTO deposition into practicable modeling, three main objectives are defined: the experimental confirmation of the theoretical expectation that tritium reemission is essentially independent from soil-water evaporation, the identification and determination of the most important parameter relationships acting on reemission and the incorporation of selected dependencies into a reemission model.

The means to fulfill those tasks within this project are laboratory experiments on reemission under controlled soil physical and meteorological conditions, to quantify fundamental relationships, as well as small-scale field experiments in cooperation with project partners, to verify laboratory findings and to ensure the consideration of naturally occurring variations.

For the modeling task principally two different approaches are envisaged: modification of the reemission module of an existing model code or development of an individual reemission submodel.

III. Progress achieved including publications

1. Methodology

In the laboratory experiments tritium reemission occurs in a device, where the top surface of a soil column is exposed to a defined horizontal air-stream. This arrangement assures variation and control of a great number of meteorological and soil physical parameters, which are expected to affect the reemission process. Before reaching the soil surface the air-stream can be tailored with respect to temperature, humidity, windspeed as well as HT or HTO contents in a fixed-value or variable program. The soil column can be filled with disturbed soil or quasi-undisturbed soil cores taken from the field. The soil physical parameters under consideration are: soil type, soil density and moisture in a homogeneous or stratified fashion. Tritium deposit in the soil column can either be achieved by initiating a real deposition process when introducing HT or HTO into the air-stream, or it can be simulated by labeling the entire soil column or certain soil layers with tritiated water thus producing pre-determined HTO soil profiles.

After a certain phase of pre-conditioning of the tritium-free air-stream, the reemission process is started by removing a shutter between air duct and soil surface. Depending on the windspeed the total air stream or a fraction of it is passed through washing flasks for time intervalls ranging between some minutes or several hours. The reemitted HTO is trapped in initially tritium-free water volumes of the flasks which are analysed by liquid-scintillation counting to yield reemission rates for the respective collection periods. After termination of the experiment, the soil column is disassembled in 5 to 13-mm horizontal layers for determinations of the final profiles of soil HTO and moisture.

The small-scale field experiments have been performed jointly with the CEA/Fontenay aux Roses during the first two years and the FZK/Karlsruhe in the third year. The main features of determining reemission rates in the field are: initiation of an HT or HTO deposition process by flushing HT gas or HTO vapor through an exposure chamber which covers a small soil plot, removal of the chamber to start reemission to the free atmosphere, collection of a fraction of the tritium reemission plume for certain time intervalls with help of an array of air-sampling tubes connected to molecular sieve traps (see Project 2), sampling of soil layers of the exposed soil at the end of the experimental reemission phase. This procedure is very similar to that applied with the laboratory device. However, because of uncertainties of the plume fractions actually collected in case of strongly fluctuating wind directions, the experimental method has been changed. Instead of trapping the plume-HTO, reemission is determined from the analyses of seven identical soil columns, which are exposed to HT or HTO by means of the exposure chamber and which are removed at different times during the reemission phase and disassembled in 5 to 20-mm layers. Considerable effort has been put into the optimization of the soil column disassembling and sample handling procedure, as it needs to be fast, to avoid HTO/H_2O vapor losses, and very precise with respect to the thickness of the soil layers. The new method has the additional advantage of providing starting, end as well as intermediate profiles of HTO and H_2O of the reemitting soils, which is the key to answering the question, to what extent HTO reemission must be considered independent from H_2O evaporation also under field conditions.

2. Results

It follows from theoretical considerations that HTO reemission is only partially comparable to H_2O evaporation from soils, although both processes can be understood as the net effect of a dynamic exchange of molecules between soil and atmosphere. Disregarding isotopic effects, which amount to only a few percent for the temperature and pressure conditions under consideration, the similarities between the two processes are:

- energy requirement for the liquid-to-gas phase transition,
- upward movement in soil in the liquid form for resupply at the soil surface,
- passing of boundary layer resistances at the soil-atmosphere interface.

Hence, the meteorological and soil physical conditions ruling those subprocesses equally apply for HTO reemission and H_2O evaporation. The differences arise from the fact that each type of molecules follows its individual partial vapor pressure gradient, which is the actual driving force for diffusion. Consequently, dissimilarities between reemission and evaporation exist because of differences in the:

- concentrations of HTO and H_2O in the air adjacent to the soil surface,
- HTO and H_2O contents of the uppermost soil layer,
- HTO and H_2O distributions in the soil profile.

As those differences, representing non-equilibrium conditions, are usually prevaling in the natural environment, we can not expect a simple correlation between the two processes.

The effect of differences of the HTO and H_2O concentrations in the air is shown in Fig. 1. The profiles are the result of a laboratory experiment with an initially homogeneously moistened and HTO-labeled soil column exposed to a tritium-free air-stream with a relative humidity of 80%. The profiles clearly show that after the reemission phase the remaining fraction of HTO

is lower than that of soil moisture in all layers, which is also indicated by the reduction of the specific activity. The overall loss of moisture is 15%, while the tritium loss is 30% of its initial value, which means that the HTO reemission rate has been twice the H_2O evaporation rate. It also follows that the specific activity of the evaporating HTO/H_2O mixture has exceeded the specific activity of the top soil water by a factor of 5.

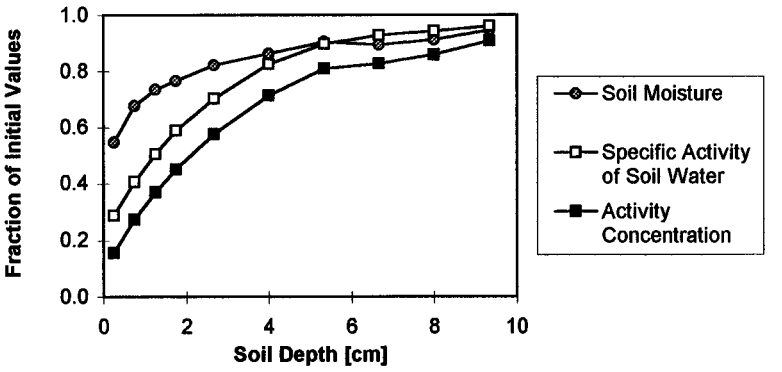

Fig.1: Depth profiles of activity, moisture and specific activity of the soil water after a reemission phase of 5 days into a tritium-free atmosphere with an air humidity of 80%. The soil column was homogeneously moistened and labeled with HTO, initially.

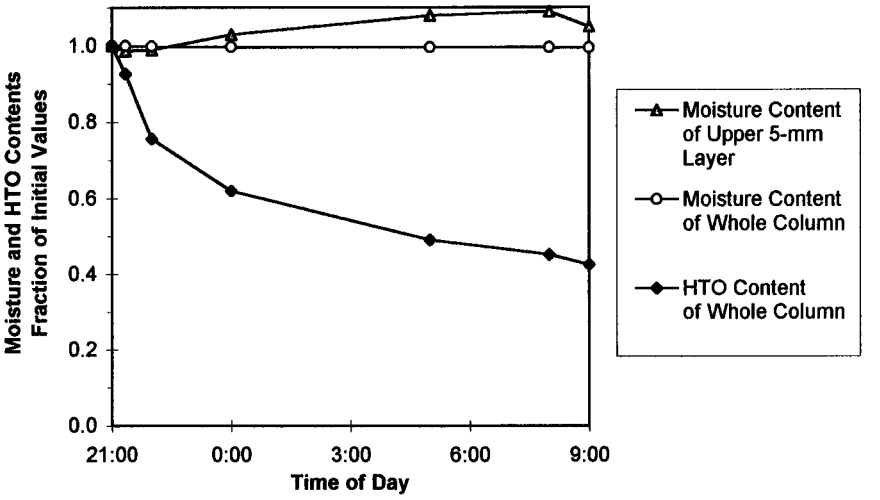

Fig. 2: Time courses of total HTO and moisture contents during a 12-hour reemission phase after a 1-hour HTO deposition at sunset in a field experiment.

The independency of reemission and evaporation also with regard to time courses is demonstrated in Fig. 2 of normalized HTO and H_2O losses determined in a small-scale field experiment, ie, under environmental conditions. While the moisture content of the entire soil

column remains practically constant during the reemission process, more than 50% of the HTO deposit is reemitted during the same 12-hour period. This means that the reemission rate would have been estimated to be nearly zero if strictly coupled to H_2O evaporation. It is interesting to note that the upper 5-mm soil layer has gained moisture during this phase. As the total water content has not changed, this effect must be attributed to upward movement of moisture within the column due to a temperature gradient directed upwards.

After those examples of the independency of HTO reemission and H_2O evaporation, parameters have to be identified, which need to be considered in a pure reemission model. Two very evident examples on the time course of reemission rates in laboratory experiments are given in Fig. 3. In one case the soil column has been homogeneously labeled with HTO, while in the other only a discrete subsurface layer contains HTO, representing a step profile. The reemission rate, defined as the fraction of the momentary HTO content of the soil released to the atmosphere per unit time and expressed in terms of $\%\cdot h^{-1}$, starts with a high value, which decreases with time for the homogeneously labeled column. For the step profile the reemission rate starts from zero, reaches its peak value only after 1.5 days under the constant experimental conditions and decreases thereafter. Those experiments differing only in the HTO profile at the beginning of the reemission phase clearly show that the distribution of the tritium deposit within the soil is an essential parameter in the prediction of initial values and time courses of reemission rates

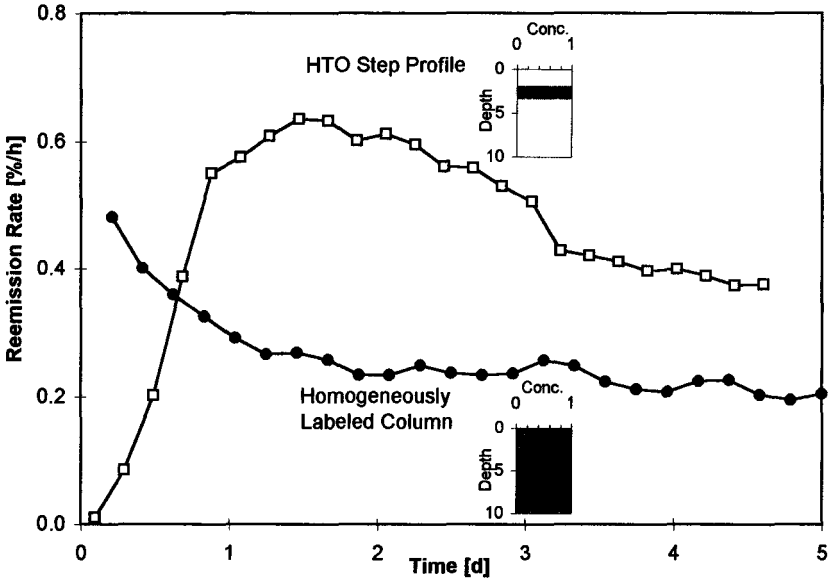

Fig. 3: Time courses of HTO reemission rates from differently labeled soil columns in laboratory experiments.

It is known from several investigations that there are principal differences between the profiles of soil-HTO after HT and HTO deposition processes because of two main reasons: a) the diffusion of HT in soil is much faster than that of HTO, resulting in a deeper penetration of HT

into soils compared to HTO during a given deposition phase, and b) the HT deposition velocity remains constant during the deposition process, whereas the HTO deposition velocity decreases drastically to near zero when the specific activity of top soil moisture has reached equilibrium with that of the air humidity, and further deposition is limited by the slow HTO diffusion into deeper soil layers. The resulting shapes of HT and HTO deposition profiles in soil, which are homogeneous with respect to diffusivities and HT to HTO conversion ability, are shown in Fig. 4 for two deposition durations. The HT deposition profiles are normalized to the top soil value of the 4-hour deposition. They are of exponential shape, represented by a straight line in the semi-log plot. The differences between the 1-hour and the 4-hour profiles is a parallel shifting of the straight lines. The HTO deposition profiles are normalized to an equilibrium value at the soil surface, which remains the same regardless of the deposition duration, and they can be described by an error function. Characterization of those profiles is obvious for the HT case using a scaling length, which denotes the depth at which the HTO concentration is 1/e of that at the soil surface. It is in the range of 2 cm. For the HTO case also a scaling length can be derived, which is, however, time-dependent contrary to the HT case (Fig. 4). After short-term HTO depositions the scaling length is typically below 1 cm. This means that the tritium deposit remains closer to the soil surface after HTO compared to HT deposition and, consequently, is more readily available for reemission. Therefore, it is expected that the initial reemission rate is higher after a deposition process of HTO than after an HT deposition.

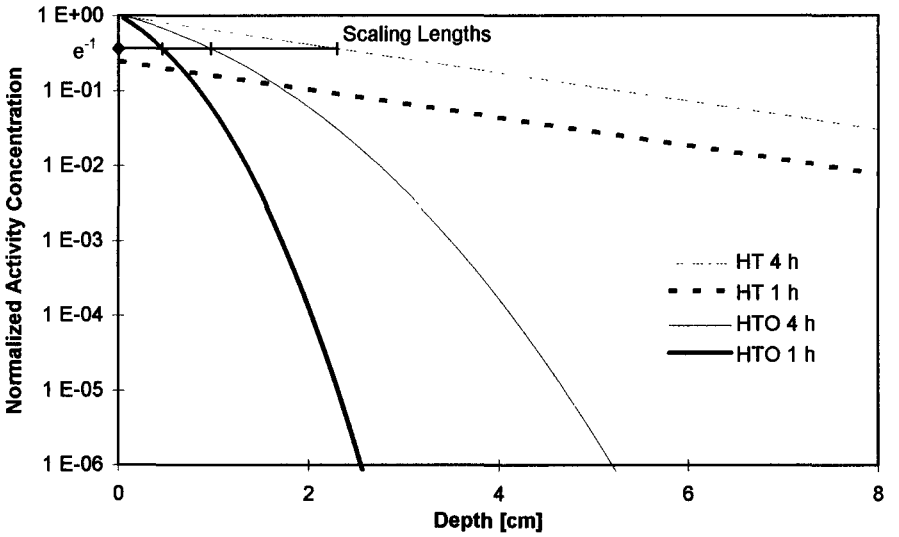

Fig. 4: Principle shapes of HT and HTO deposition profiles after 1 and 4-hour depositions to homogeneous soils. The depth corresponding to a reduction to e^{-1} represents the scaling length of the respective profile.

The examples of two field experiments given in Fig. 5 clearly support this hypothesis. Reemission after HT deposition starts at 18 %·h^{-1} and decreases slowly to 4 %·h^{-1} within a time span of 4.5 hours (Fig. 5A). On the other hand the initial reemission rate after the HTO

deposition experiment is above 45 %·h^{-1}, but decreases rapidly to 10 %·h^{-1} after 4 hours. (Fig. 5B). Also shown in the figures are the potential evaporation rates determined by means of H_2O evaporation losses from an open water surface (evaporation pan). They demonstrate again that especially in the first part of the reemission phase there is no correspondence in the time behaviour of the two types of molecules.

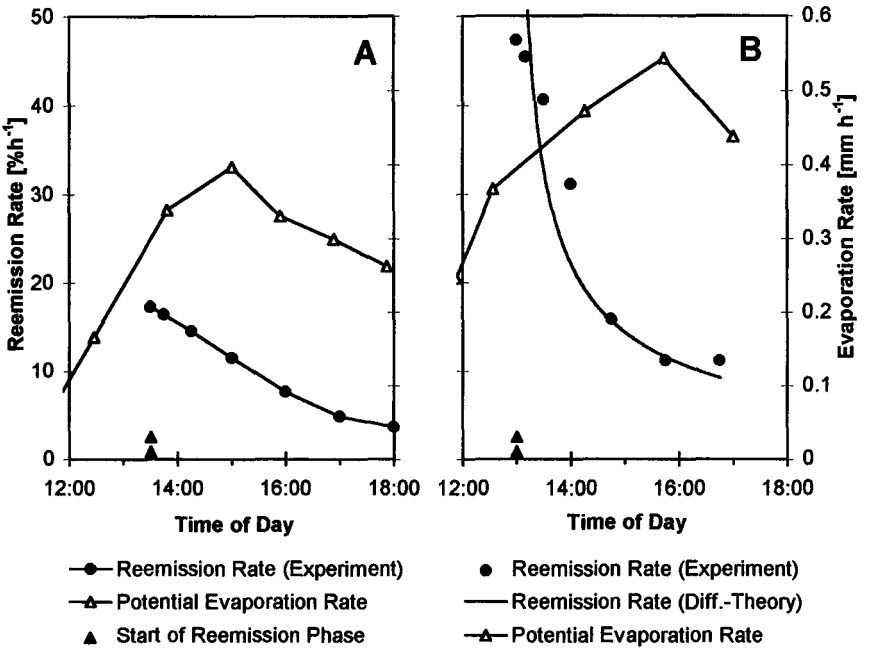

Fig. 5: Time courses of HTO reemission rates (left axes) and potential evaporation rates (right axes) after HT deposition (A) and after HTO deposition (B) under field conditions.

Following the experimental procedure of evaluating reemission rates from successively taken soil profiles, a concept has been developed to mathematically describe time courses of the reemission rate by modeling changes of the soil profiles with time. The theory bases on Garland's effective diffusion coefficient for HTO in soils and is described in detail by Täschner et al., (1995a). The good performance of this diffusion model in comparison with the field measurements after a 4-hour HTO deposition is demonstrated in Fig. 6. The effective diffusion coefficient has been determined using Garland's formula and the environmental conditions of the experiment. The profile at the start of the reemission phase (1-min profile) shows the characteristic shape, as already given in Fig. 4, and it is important to note that also during the reemission process HTO is diffusing into deeper soil layers because of the concentration gradient, while the top layer is losing activity to the atmosphere. More importantly, the model also yields the time course of the reemission rate, which is shown as the theoretical curve in Fig. 5 B, and the agreement between model prediction and measurement is obvious.

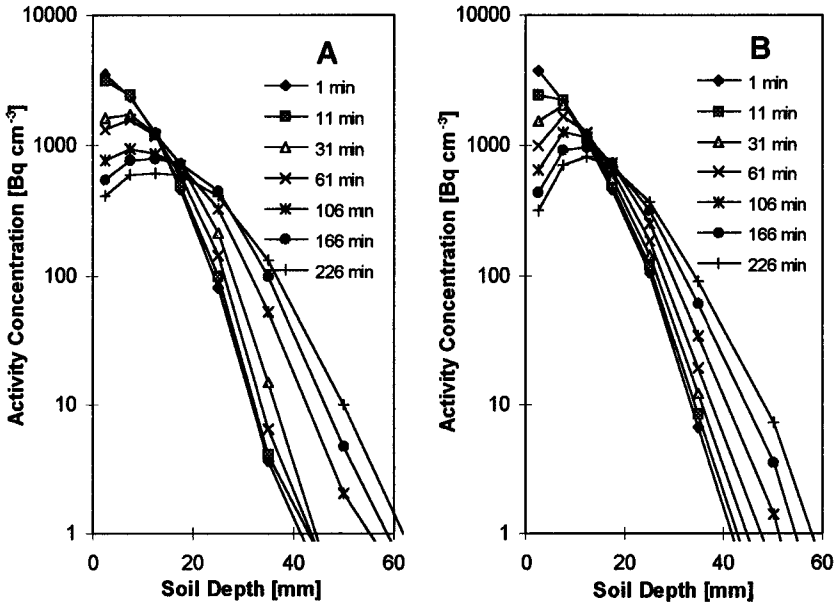

Fig. 6: History of tritium profiles in soil during a reemission phase after a 4-hour HTO deposition under field conditions (A) and a diffusion model simulation (B).

In a final set of field experiments the effect of the time of day has been investigated, and the predictions of the reemission module of the UFOTRI code (FZK) have been validated against the measurements. Fig. 7 shows the results of two reemission phases after 1-hour HTO depositions and reemission starting at sunrise (Fig. 7A) and at sunset (Fig. 7B). In both experiments the same soil type, soil density and initial moisture content has been applied. In both cases wind speeds have been extremely low to absolute calmness during the observed 12-hour reemission periods. Inspite of the pronounced differences of the atmosphere/soil temperature conditions both phases start with the same reemission rate of 28 %·h^{-1} in the first hour. Time-of-day specific deviations of the reemission rates appear only during the subsequent hours leading to total HTO losses of 84 % during the 12-hour day-period after the sunrise and 57 % during the 12-hour night-period after the sunset deposition. Also given in the figures are predictions calculated with help of the UFOTRI model. This code is characterized by the coupling of HTO reemission to H_2O evaporation during daytime, a fixed rate at nighttime and a number of default values including a time constant to account for the decrease of the reemission rate with time. The comparison shows rather poor agreement especially during the first hours of the process. Agreement is improved, however, after modification of the default values (UFOTRI 2).

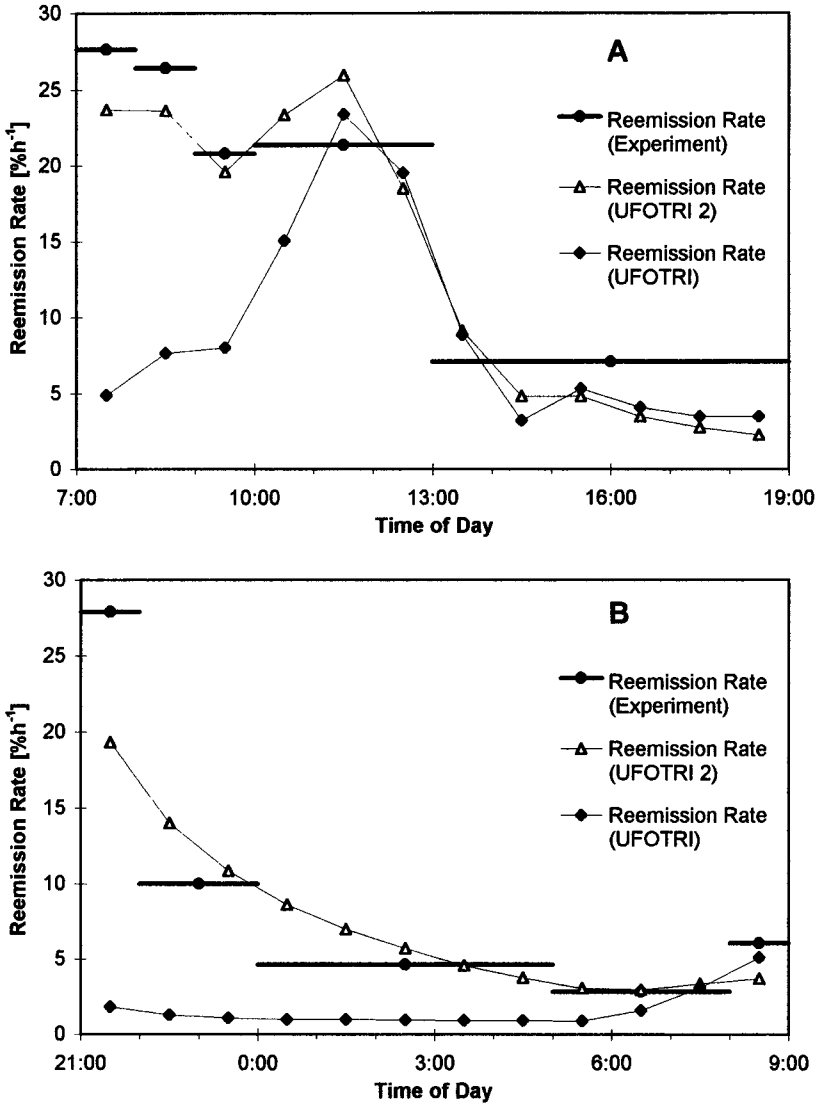

Fig. 7: Time courses of reemision rates measured in the field and modeled with UFOTRI and a modified version (UFOTRI 2) after a 1-hour HTO deposition at sunrise (A) and at sunset (B).

3. Discussion

The investigations have shown that there are principal differences in the behaviour of HTO and H_2O when differing from the soil to the atmospheric compartment. The laboratory experiments have been very helpful with the identification of fundamental parameters acting on HTO reemission because of the high measuring precision achievable in the lab and because of the possibility to extend the processes under concern until the investigated effect is obvious. However, it also turned out necessary to export laboratory precision into the field, in order to study effects under constantly changing environmental conditions. Furthermore, the experimental technique had to be modified substantially, to be able to determine HTO and H_2O movements synchronously under field conditions.

The most important parameters affecting the initial reemission rate and its subsequent time course are the HTO concentration in the surface soil and the distribution profile, respectively. This implies that the type of the depositing tritium compound, HT or HTO, and the duration of the deposition process has to be known. Soil physical conditions, which are equally relevant for the development of the deposition profile and the time course of the reemission rate, seem to be sufficiently characterized by the HT and HTO diffusion coefficients, as has been shown for an HTO deposition case by predicting reemission rates via successive soil profiles with help of a diffusion model. Little attention has been paid to the effect of wind speeds on reemission, as it is expected to equally influence reemission and evaporation. Previous investigations have shown that there is a relationship to the square root of the windspeed.

One of the most interesting results is the finding that the initial reemission rate seems to be independent from the time of day as shown with the sunrise and sunset experiments, while the subsequent rates do reflect the differences of the temperature conditions of the atmosphere-soil system. Retrospectively, this actually follows from the theoretical understanding of the process itself. The upper soil layer with a thickness of a few millimeters is in direct contact with the atmospheric air and reemits HTO within some ten minutes, while the specific activity decreases, as shown in laboratory experiments. Further reemission is depending on resupply from deeper soil layers, which, except for very dry soils, occurs in the liquid form of the HTO/H_2O soil water mixture. This liquid transport is more effective than HTO diffusion within the soil water, and it is essentially controlled by H_2O evaporation from the soil surface. Consequently, a physically-based correlation between HTO reemission and H_2O evaporation is introduced, whenever HTO resupply from deeper soil layers is occurring by liquid transport. It follows from this analysis that the HTO reemission rate has to be modeled independently from evaporation, eg, by the described diffusion model, but may be coupled in a sensible way to H_2O evaporation when liquid resupply dominates.

Another important result is the observation of relatively high initial reemission rates. This is partly due to the high time resolution of the presented studies and partly due to the fact that previously reemission rates and their modeling have been derived mainly from HT deposition experiments, which exhibit lower rates as demonstrated in this study. If the high rates would be confirmed also for vegetated surfaces, the shifting of dose contributions from the different pathways would be considerable as demonstrated in Täschner et al. (1995b). Therefore, modifications of the experimental method are in progress, to include vegetation into the investigations in the future.

4. Publications

M. Täschner, C. Bunnenberg, H. Camus, Y. Belot (1995a):
Investigations and modeling of tritium reemission from soil.
Fifth Topical Meeting on Tritium Technology in Fission, Fusion and Isotopic Applications, 28 May-3 June, 1995, Belgirate, Italy, Fusion Technol., **28**, 3, Part 1, 976 (1995).

M. Täschner, C. Bunnenberg, W. Raskob (1995b)
Measurements and modeling of tritium reemission rates after HTO depositions at sunrise and at sunset.
In preparation for a special issue of the Journal of Environmental Radioactivity.

5. Main contributors to the project

Dr. M. Täschner, Mrs. G. Erb-Bunnenberg, Mr. R. Sachse.

Head of project 2: Dr. Y. Belot

II. Objectives for the reporting period

The purpose of the contract was to study the dynamic behaviour of tritium in the soil-atmosphere system by using small-scale experiments and models in an interactive approach. The ultimate aim was to acquire a better knowledge of the tritium transport in the system and improve the related models. The experimental effort was carried out in close cooperation with the ZSR team (cf. project 1), while the modelling work was run separately but discussed in detail within coordination meetings

III. Progress achieved including publications

1. Tritium-in-soil modelling

The deposition of HTO to the soil surface is described as a diffusion of HTO through the air-soil boundary layer. In the case of HT, the deposition proceeds through the diffusion of HT into the soil interstices and its conversion to HTO at the contact of the soil material. During and after exposure, the HTO deposited in the upper soil layers diffuses downwards and upwards while it evaporates gradually from the soil surface into the atmosphere.

In the following model, the soil is segmented into N horizontal layers, each supposed homogeneous and of uniform moisture. The thickness of each layer is Δz. The layers are connected by transfer coefficients that represent the fraction of radioactivity transferred per unit time between two layers. At the upper boundary of the system, the soil surface is connected to the atmosphere by input fluxes and transfer coefficients. The evolution of the system is described by a set of N simultaneous, first order, linear, ordinary differential equations, that express the change with time of the HTO content of each layer as the difference between inputs and losses. If A_i ($1 \leq i \leq N$) is the tritiated water content of each soil layer expressed in Bq m^{-2}, the differential system reads:

$$dA_1 / dt = V_1 C - (K_1 + L) A_1 + L A_2 + S X_1$$

$$dA_p / dt = L A_{p-1} - 2L A_p + L A_{p+1} + S X_p \quad (2 \leq p \leq N-1)$$

$$dA_N / dt = L A_{N-1} - L A_N + S X_N$$

where X_i (Bq m^{-3}) is the volume concentration of tritium gas in the air phase of each soil layer; C (Bq m^{-3}) the volume concentration of tritiated water in the atmosphere (sometimes negligible); V_1 (m s^{-1}) the velocity of water vapour exchange between the atmosphere and the soil surface; K_1 (s^{-1}) the rate of tritium turnover in the top layer ; L (s^{-1}) the rate of tritium diffusive transport through the soil profile; S (m s^{-1}) the coefficient of the conversion of HT into HTO in each compartment. The subscript 1 refers to the top layer and the subscript N to the bottom layer.
If the air concentration of HT in air is $X_0(t)$ and the scaling length of the distribution of HT in soil is z_e, the distribution of HT in the soil air porosity follows the exponential function:

$$X_i = X_0(t) \exp (- i \Delta z / z_e)$$

The coefficients of the differential system above can be expressed as a function of the soil and atmosphere characteristics by:

$$K_1 = V_1 \rho_s / \theta_w \rho_w \Delta z$$

$$L = D_w / (\Delta z)^2$$

$$S = D_t \Delta z / (z_e)^2$$

where Δz is the space increment; ρ_s the temperature-dependent water vapour concentration in the soil air volume fraction; ρ_w the specific mass of water; θ_w the water volume fraction in soil; D_t and D_w the diffusion coefficients of HT and HTO in soil.

The rationale behind the equation describing the dynamic behaviour of tritium in the top soil layer (i = 1) is worth being detailed. The top layer exchanges HTO with the atmosphere by vapour diffusion through the soil-atmosphere boundary layer; it exchanges also HTO with the soil layer just beneath (i = 2), by liquid / vapour diffusion through the interstices of the soil material. In modelling the soil-atmosphere exchange, one has to take care that the initial distributions of HTO and HHO are not identical and that the movement of each of the two species must be considered separately. The driving force in the movement of HTO between the soil and the atmosphere is the difference between its gas phase concentration in the atmosphere and its gas phase concentration in the air fraction of the soil pores. The difference and then the driving force depend on the concentration of tritium at the very surface of the soil. In consequence, the description of this exchange in a model requires the consideration of very thin layers. Numerical experiments have shown us that the optimum thickness of the layers is $\Delta z = 2$ mm. In case of an explicit calculation scheme the corresponding time step is $\Delta t = 0.1$ h.

2. Experimental vs theoretical data

Experimental methodology

Small-scale field experiments are more flexible and more acceptable by the public than large-scale experiments. They can be performed under a variety of semi-controlled conditions and are well adapted to a study of the tritium transport to and from the soil surface. In the past, a technique was developed which consisted of covering a small area of undisturbed soil by a field chamber, exposing the enclosed soil to some form of tritium, then determining the reemission rate of tritium from the changes in tritiated water vapour content of a measured airstream passing through the chamber. But such closed chambers may alter the environment in ways that may affect the migration of tritiated water in the soil and its exchange with the atmosphere. Thus we planned to use field chambers to expose a small area of soil, and then, following removal of the chamber, to study the reemission of tritium under the actual field conditions prevailing in the open air.

The initial experimental method, used at the beginning of the contract, was based on exposing an undisturbed soil surface, sampling the plume with help of an array of air sampling tubes placed downwind of the contaminated small plot, and finally sampling the soil a few hours after end of exposure. Unfortunately, the reemission rates obtained by this method were not entirely reliable, because of an incomplete sampling of the plume, particularly in case of strongly fluctuating wind direction. Moreover, the vertical distribution of tritium in the soil could only be determined by sampling the soil at the end of the experiment. Therefore it was not possible to follow the evolution of the tritium-in-soil vertical profile during the reemission phase at different times after exposure.

Considering the uncertainties and impossibility to follow the evolution of the tritium distribution in the soil, the procedure was then changed to the one devised by ZSR and described in project 1. The latter procedure consisted of using seven identical soil columns, which were exposed to tritium by means of a field exposure chamber, then after removal of the chamber, were allowed to be in contact with the open air under the same conditions as the natural soil itself. The columns were removed at prescribed times after end of exposure and disassembled into a series of layers. The latter procedure has the disadvantage of using a disturbed soil material, but the huge advantage of allowing to follow the evolution of the tritium-in-soil vertical profile at fixed times after exposure, and also of being more flexible, which is quite useful to evaluate the adequacy of a model to the reality.

Model predictions and experimental results

a) Tritium-in-soil vertical profiles

We were first interested in knowing the difference between the vertical profiles of soil-HTO after an HT or HTO soil exposure. In a first series of experiments carried out in 1993 on two different sites, small plots of natural undisturbed soils were exposed to HT gas during roughly one hour, then the exposure chamber was removed and the exposed plot let in open air conditions. After a few hours, small cores were taken from the contaminated plot and cut into small slices to determine the vertical profile of HTO in soil at end of the experiment.

The distribution of tritium in soil was also calculated using the model described above, and using for the main parameters the following values: $\Delta z = 0.2$ cm; $\Delta t = 0.1$ h and $z_e = 2.3$ cm. The characteristics of the soil and consequently the diffusion coefficients of HT and HTO depend on the water and air volume fractions in the soil, and consequently are different for the two different types of soil considered. The diffusion coefficient of HT is 1.5×10^{-5} and 7.4×10^{-6} $m^2 s^{-1}$ for the sites No.1 and No.2 respectively. The diffusion coefficient of HTO is 2.4×10^{-9} and 1.5×10^{-9} $m^2 s^{-1}$ for the same sites.

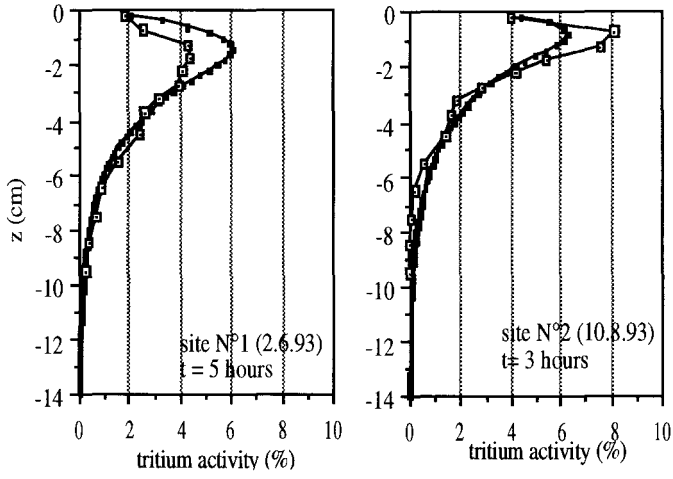

Fig 1 : Activity concentration distribution in soil profiles at time t after exposure The soils have been exposed to HT during about one hour. Each point represents the percentage of total activity present in a 2-mm layer situated at a given depth. The black dots represent the theoretical profiles; the white dots correspond to the experimental data. The soil moisture is roughly 8 % and 21 % for the sites No.1 and No.2.

Fig.1 represents predicted and measured vertical profiles in the two types of undisturbed soil that were exposed to HT during about one hour. The depth of maximum activity and the form of the profiles are correctly predicted. There is only a difference of 20-30 % in the values of the maximal concentrations.

In subsequent experiments that were carried out in 1994 and 1995, the new procedure of soil exposure explained above was applied to small columns of soil. Fig.2 gives the predicted and measured profiles in the case of a soil that has been exposed to HTO during one hour. It appears clearly that the HTO profile has a much smaller extension downward into the soil for

HTO exposure than for HT exposure. This confirms that the tritium deposited onto the soil remains closer to the surface after HTO exposure and is thus more readily available for reemission to the atmosphere (cf. project 1).

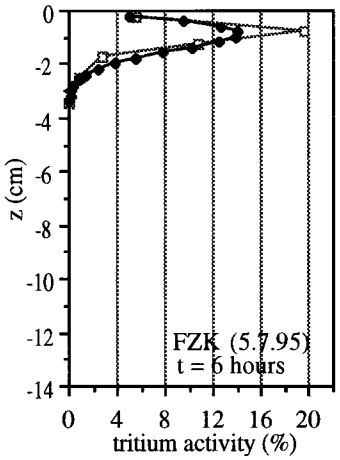

Fig 2: Activity concentration distribution in soil profiles at time t after exposure The soil has been exposed to HTO during one hour. Each point represents the percentage of total activity present in a 2-mm layer situated at a given depth. The black dots represent the theoretical profiles; the white dots correspond to the experimental data. The soil moisture is roughly 22 % .

b) Reemission of tritium from contaminated soils

The second point of interest was the evolution of the total activity of tritium in the soil after end of exposure and the influence of atmospheric conditions on that evolution. Experiments were made in which the same soil material was exposed to HTO during one hour and allowed to reemit tritium into the open air during a number of hours after exposure. By removing soil columns at different times after exposure (cf. methodology), it was possible to follow the decrease of the tritium content of the soil due to the reemission of tritium into the atmosphere. Two different experiments were carried out, one beginning at 6:00 and ending at 19:00 (daytime conditions); the other beginning at 20:00 and ending the day after in the morning at 9:00 (nightime conditions). During the day conditions the wind speed at 2 m was around 1 m s^{-1}, and during night the wind was below 0.2 m s^{-1} so it could not be measured by the classical cup-anemometer used in these experiments. The experimental data obtained are presented in Fig.3.

In parallel, calculations of the soil activity time-evolution were made by using the model presented above. It was first assumed that all the activity that had been deposited during the exposure phase was entirely confined in the top 2-mm layer at the end of exposure, which seems quite plausible if one considers the theoretical deposition and diffusion of tritium at soil surface. The velocity of water vapour exchange at soil surface was evaluated by $V_1 = B\ u_*$, where u_* is the friction velocity that characterizes the turbulent intensity above the soil surface and B a coefficient that can be calculated from the Dipprey and Sabersky formula. The friction velocity u_* in this relation was determined from $u_* = 0.06\ u_2$ where u_2 is the wind velocity that was measured at 2 m above ground level. For the daytime experiment, an average wind speed $u_2 = 0.90$ m s^{-1} and an average soil surface temperature $\theta = 20°C$ were taken as input data. For the nightime experiment, $u_2 = 0.15$ m s^{-1} and $\theta = 12°C$ were taken instead. In both cases, the roughness length was chosen as $z_0 = 0.005$ m.

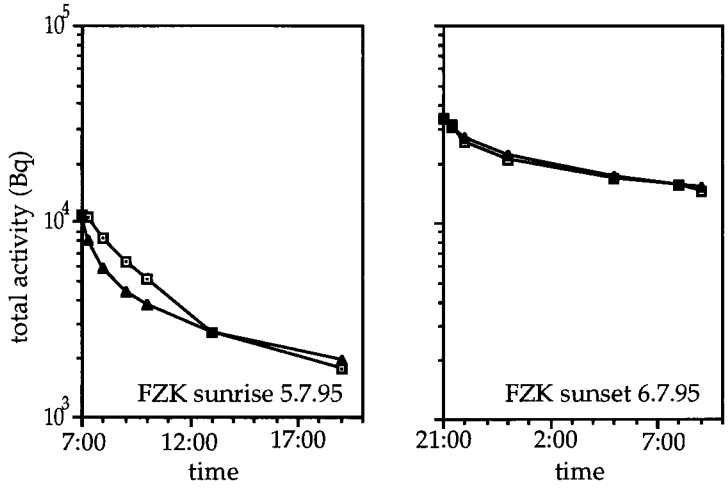

Fig.3: Time-evolution of the tritium activity in soil after deposition of HTO from 6:00 to 7:00 (left) and from 20:00 to 21:00 (right). The initial HTO air concentrations are different. The black triangles and white squares refers respectively to predicted and measured values.

The measured and predicted data are compared in Fig.3. In daytime conditions, there is an overestimation of the tritium loss during the first hours of tritium reemission. This can be explained by the fact that the average wind speed and soil temperature taken throughout computation were higher than the actual values measured in the first hours, thus leading to an overestimation of reemission during that time. At nighttime, the measured and predicted values do not differ when using the average value of wind speed $u_2 = 0.15$ m s^{-1}. This hypothetical value is quite plausible, but cannot be ascertained from measurements since the wind speed was measured by cup anemometers with a lower measurement limit of 0.20 m s^{-1}. It appears nevertheless that the diffusion model used in this work describes correctly the reemission of tritium from a contaminated plot under day and night conditions. The experimental data confirm that an appreciable loss of tritium occurs during nighttime, even if the relative humidity of the atmosphere is 100 % which precludes any ordinary water evaporation from the soil.

3. Discussion and conclusions

The experimental work has first confirmed that, after a short exposure, the thickness of the contaminated layer is smaller for an HTO-exposure than for a HT-exposure, but that anyway the initial vertical extension of this layer is always rather small (a few cm). One consequence is the necessity in the modelling work to consider thin layers of soil. It can be objected that the soil-atmosphere interface is often poorly defined. The surface is not perfectly plane and the structure of the soil material, which is heterogeneous at a small scale, makes difficult to segment the upper part of the soil into very thin layers. But, on the other hand, if we take thick layers, an artifact is introduced in the calculation since the concentration of tritium is automatically considered as uniform throughout each individual layer. This increases artificially the vertical dispersion of tritium and results in a diminution of the HTO concentration at the soil surface and consequently in a diminution of the tritium reemission rate. We need then to consider an ideal homogeneous soil with thin slices of about 2 mm, as was shown in the previous work, being conscious that it is an ideal representation that gives only a probable distribution of tritium in soil. Deviations from the theoretical distribution are to be expected as a function of the local fine structure of the soil material. The choice of the time increment is not always independent of the

vertical space increment; it depends on the calculation scheme that has been adopted and is only a matter of numerical resolution technique.

The initial experiments made in the framework of the present work have also confirmed that the release of HTO from the soil surface proceeds through an interfacial diffusive process and that the reemission is not directly dependent of the ordinary water evaporation rate. The flux of HTO between the soil and the atmosphere can then be expressed by the usual flux-gradient relationship where the mean concentration gradient is replaced by a difference in mean gas-phase concentration between the two adjacent layers, the diffusivity being replaced by an exchange velocity. The difficulty resides in the evaluation of the exchange velocity from friction velocity u_* and roughness length z_0. The existing formulas have never been advanced specifically for the case of air-soil transfer and therefore further research to test their adequacy in this case would be appropriate (see for instance Chamberlain, 1965 and Shepherd, 1974). Furthermore, in calm conditions such as those encountered during night, the friction velocity u_* cannot be determined from standard wind speed measurements.

4. Publications

Täschner M., Bunnenberg C., Camus H. and Belot Y. (1995) "Investigation and modeling of tritium reemission from soil" 5th Topical meeting on Tritium Technology in Fission, Fusion and Isotopic Applications, 28 May - 3 June, 1995, Belgirate, Italy.
Fusion Technology **28**, 976-981: 1995.

5. Main contributors to the project

Dr. H. Camus, Dr S. Raviart., Ms Charlier de Chily

Head of project 3: Dr. M. A. Kim

II. Objectives for the reporting period

In the first period of the contract, an analytical method will be further developed for the accurate determination of the specific activity ratio (R-value) of organically bound tritium (OBT) (exchangeable as well as non-exchangeable) and tissue water tritium (TWT) of some representative biological samples. The experimental R-values as biological tritium fractionation factors will be verified for the dynamic equilibrium state between biotritium and environmental tritium. The R-values will be measured as a function of growth time under constant HTO exposure in a climate chamber specially designed for the purpose.

In the second and third period of the contract, tritium fractionation processes in soils will be studied on the basis of previously developed analytical methods. Distinction will be made between physisorbed tritium in capillary water and chemisorbed tritium associated with soil humus and mineral lattices. The investigation includes identification and quantification of involved isotope effects, e. g. originating from different diffusion or adsorption onto surfaces, which might be inorganics or organics in the solid or the colloidal phase. Other possibilities are isotope effects on water vaporization and on ion-solvation. Model substance / water systems will be compared with different types of real soil / water systems for the purpose.

III. Progress achieved including publications

RESULTS

Tritium fractionation in biological samples [1]

Accurate determina.ion of R values of biosystems

The total R value of a biosystem, defined as the specific activity ratio of total (exchangeable and non-exchangeable) OBT and TWT is inevitably altered through vaporization isotope effects occuring at the separation of the organic and water components. The tritium enriched residual water exchanges with the labile OBT, which remains enriched even after complete tissue water removal. The effect increases with decreasing temperature and has been quantified in our previous work. The error of the total R value may increase up to + 400 % depending upon physical parameters, such as temperature of water vaporization, degree of water removal, water content of the original sample, etc. The minimum attainable error still

amounts to about 15 % in the case that tissue water is completely removed (> 99.9 %) at high temperature, e. g. by azeotropic distillation at 70 °C. This method of water separation has been applied in this work. The analytical isotope effects have been mathematically corrected on the basis of experimentally determined input data for the chosen biosystems, namely barley and maize plants. A similar correction can be performed only for the case of water separation by distillation at constant temperature, accompanied with a constant separation factor. The analytical isotope effects at freeze drying of the biosample, performed at changing temperature and system pressure are unpredictable and therefore not corrigible. Another precaution is a careful elimination of air humidity in contact with the sample in order to avoid isotope dilution by condensation or exchange reactions.

The stable R value of a biosytem, defined as the specific activity ratio of non-exchangeable OBT and TWT, requires the removal of exchangeable OBT through at least two washing procedures with tritium free water and correction for isotope dilution by wash water, physisorbed to the organics.

R value as a biological tritium fractionation factor

The R value of a biosystem does not always correspond to a biological tritium fractionation factor for the equilibrium state between the considered organic and water phases. The equilibrium state can be experimentally achieved by growing the biosystem under constant HTO exposure until constant R values are attained. If this condition is not fulfilled, the R value is a sum of two simultaneously occurring biological effects, namely natural tritium fractionation due to isotope effects on metabolic enzyme reactions, the parameter of interest, and different biokinetics of TWT and OBT. The latter effect reflects the fluctuations of the HTO exposure with a different time delay for the water and the organic components corresponding to their respective biological half lives. This source of error occurs easily if samples are taken from the natural environment.

Fig. 1 compares the accurate biological tritium fractionation factors (percent) for barley and maize. Tritium is discriminated by the transition from tissue water to the plant-organics. The discrimination of OBT is higher in barley (C_3-plant) than in maize (C_4-plant), namely 15.0 % for total OBT and 11.7 % for stable OBT. This is not surprising, since the two plants belong to different metabolic types. They have distinct biochemical and physical regulation mechanisms tending to an optimal compromise between the often contrary requirements of photosynthesis and water balance. The water loss by transpiration is e. g. limited in C_4 plants through closing of the stomata. The accompanying hindrance of CO_2 uptake is compensated

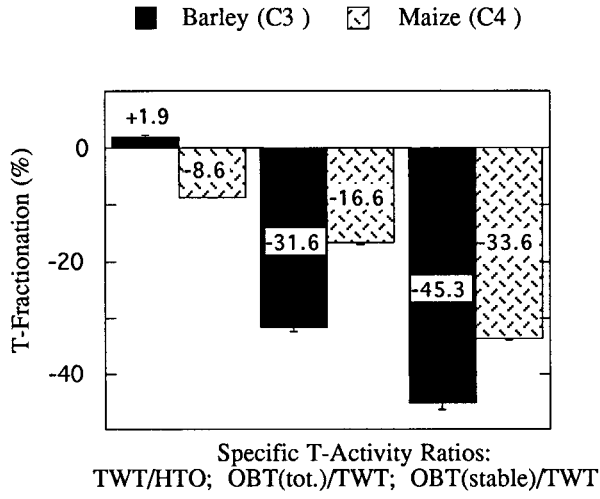

Fig. 1: Comparison of the biological tritium fractionation (%) of barley (C_3-plant)) with that of maize (C_4-plant)

by decreasing the CO_2 consuming photorespiration. It necessitates photosynthetic enzyme systems coupled with isotope effects which are different from that of C_3 plants. Contrary to the OBT, the TWT of barley has a 10.5% higher specific activity than that of maize. The difference seems to be related mainly with physical rather than chemical isotope effects. The higher transpiration rate of C_3 plants as compared with C_4 plants favors tritium enrichment in the tissue water of barley through the vapor pressure isotope effect. The slow transpiration rate of C_4 (desert) plants diminishes the influx of water into plants by viscous flow. It facilitates the exchange reaction of hydrogen between tissue water and atmospheric water, which specific activity is 10 % lower than that of the nutrient solution at 20 °C.

Tritium fractionation in soils [2]

Parametrization of soil-water binding forces

Water molecules at a vapor-liquid interface are attracted upward less strongly than downward which results in a potential energy difference in going from the liquid to the vapor phase. Similarly, soil-water forces cause a potential energy gradient in going from the bulk pore water to within close proximity of solid mineral surfaces. In unsaturated soils these soil-water forces extend to the vapor-liquid interface and influence the escaping tendency of water molecules from the liquid surface. Vapor pressure is therefore a direct measure of the energy status of soil water.

Quantification of soil-bound-water

Tritium enrichment at evaporation of pure water is compared with that of soil water. The former is calculated by the Rayleigh formula, based on the separately determined vaporization isotope effect at 5 °C and 5 mbar. The latter is determined by distilling the super-saturated soil sample, e. g. 20 g of water / 10 g of soil, under the chosen near equilibrium conditions and by measuring the specific tritium activities in fractions of the condensed gasphase. Deviation of the experimental data for soil water from theory for pure water (Rayleigh curve) indicates transition from free water to soil-bound-water in the course of water removal. The results for a model soil from Wulfing (Germany) as a typical example are shown in Fig. 2. They indicate a weight ratio of bound water to dry soil of 0.45. Such determined total bound water may include: (1) physisorbed capillary water, (2) exchangeable bound water, resulting from the exchange of -OT(H) in free water with hydroxyl groups of mineral lattices or humus and (3) very slowly exchangeable hydroxyls Al-O(H)T, Mg-O(H)T in clay micelles.

Differentiation of soil-water binding forms

Soil-bound-water is also detected and differentiated by dehydration kinetics as well as by the conditions of temperature and pressure which are necessary for its conversion to the gas-

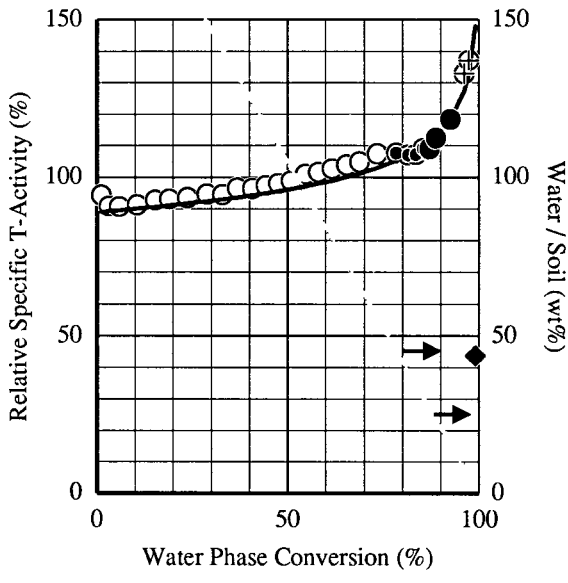

Fig. 2: Specific tritium activity in fractions of the condensed vapor phase at Rayleigh distillation (5°C, 5mbar) with changing water/soil (w/w %) ratio. The values are related to the specific tritium activity of the soil water before distillation. The line (–) is calculated. The markers are measured values: O: free water; ◔, ●: physisorbed waters, differentiable by dehydration kinetics as shown in Fig. 3; ⊕: physisorbed water, vaporized at 45 °C and 10^{-3} mbar; ♦: chemisorbed water after oxidation of the residual dry soil at high temperature (800°C). The model soil is originated from Wulfing (Germany).

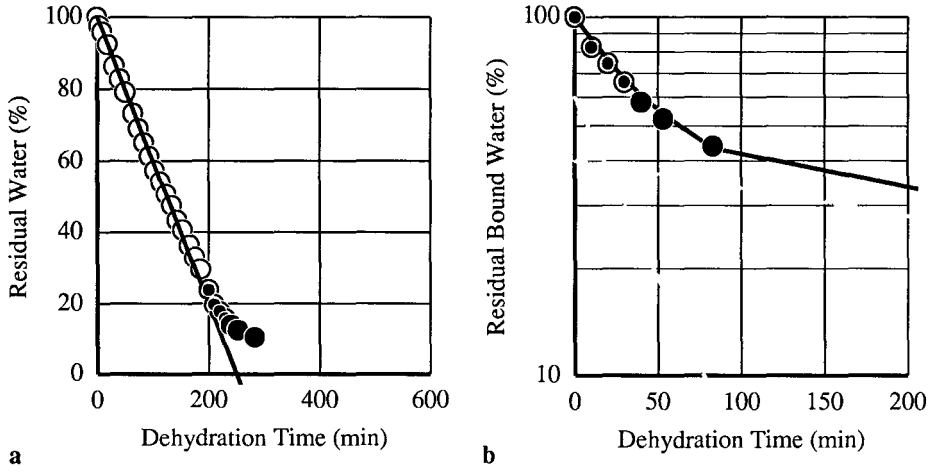

Fig. 3 a,b: Dehydration kinetics (5°C, 5 mbar) of a Wulfing-soil / water mixture. **(a)**: Basis for differentiation of bound water (◉, ●) from free water (O) is the deviation point from linear dehydration kinetics; **(b)**: Physically bound waters with different exponential dehydration kinetics are distinguishable.

phase. Fig. 3 shows the results of the dehydration kinetics at 5°C and 5 mbar for the chosen soil/water sample. Free water is characterized by a linear dehydration curve (Fig. 3a), whereas bound water has an exponential behavior. Two different physically bound waters, corresponding with two exponentials, typical for first order chemical reactions are recognizable (Fig. 3b). A third physisorbed water is separated from the soil sample at 45°C and 10^{-3} mbar. The chemisorbed water, obtained through thermal oxidation (800°C) of the residual dried soil represents a fourth bound water type (the last fraction in Fig. 2).

Soil-water tritium fractionation

The soil-water tritium fractionation factor is defined as the ratio of the specific activity of soil-bound-water and that of free water. The specific activity of each bound-water component is calculated as the ratio of total activity and volume of the corresponding summed fractions. Isotope effects at the separation of the bound-waters are thereby canceled out, if it is assumed that no exchange between the considered components occurs under the chosen water expelling conditions. The vapor pressure isotope effect, accompanying the conversion of the free water into the gasphase, is taken into account by using the specific activity of the last free water fraction as a reference value. Applied to the Wulfing-soil, the tritium fractionation factor for physisorbed water gradually increases with the soil binding

forces from 1.0 to 1.25, indicating tritium enrichment, whereas the value 0.4 for chemisorbed water suggestss tritium dilution. The latter unexpected result is possibly attributable to the very slow exchange rate of tritiated water with the initial soil samples rather than to a real tritium discrimination. A more intensive study is necessary to solve this problem specific for soil samples.

Validation of the results

The above described method for the quantification and differentiation of water bound to solids, as well as the evaluation of the tritium fractionation, accompanying the sorption process, is tested for a model substance. Na-tartrate, with a wellknown amount of bound water, namely 18.5 % of its dry weight, physically sorbed as crystal water, and 9.27%, chemically bound in hydroxyl groups, is chosen for this purpose. The results from the measurement of tritium enrichment at the Rayleigh distillation of a 1.4 M Na-tartrat solution in tritiated water are given in Fig. 4a. Fig. 4b is a large scale presentation, stressing the conversion of the bound water to the gas phase. The possibility of detection of bound water at the deviation point from the theoretical Rayleigh curve valid for pure free water, is clearly demonstrated. Analog to the soil-bound-waters, the bound water of Na-tartrate-dihydrate can be split in three physisorbed and one chemisorbed water. The excellent agreement of the such characterized bound water with the known molecular and crystal structure of Na-tartrate-dihydrate proves the validity of the method. The tritium fractionation factors for the bound waters corresponding with one crystal water and with the Na-tartrate-monohydrate fraction are 0.90 and 1.02, respectively. This result corresponds well with the separately determined tritium partition factors at Na-tartrate crystallization, given elsewhere [2].

Generalization of the results

For answering the question, wether the amount of soil-bound-water and the tritium behavior in it, is generally predictable, three typical soil samples with different characteristics, namely a clayey soil originating from Wulfing (Germany), a silty soil from Cadarache (France) and a sandy soil from Baumannshof (Germany) are compared. The correlation between their particle size distribution and organic carbon content on the one side, and the total bound water content on the other side, is shown in Fig. 5. It is obvious, that the amount of bound water increases proportionally with the percentage of organic carbon in the soil as well as with the relative amount of its small particle fraction (increased soil-surface), e. g. the total soil-bound-water is twice higher in a clayey soil than in a sandy one. Tritium enrichment in the physisorbed water is similar for the three soils and amounts to about 25 % as compared with free water. Although such a degree of tritium fractionation has no immediate consequence for the radiation protection, it can be important at the interpretation of eventual se-

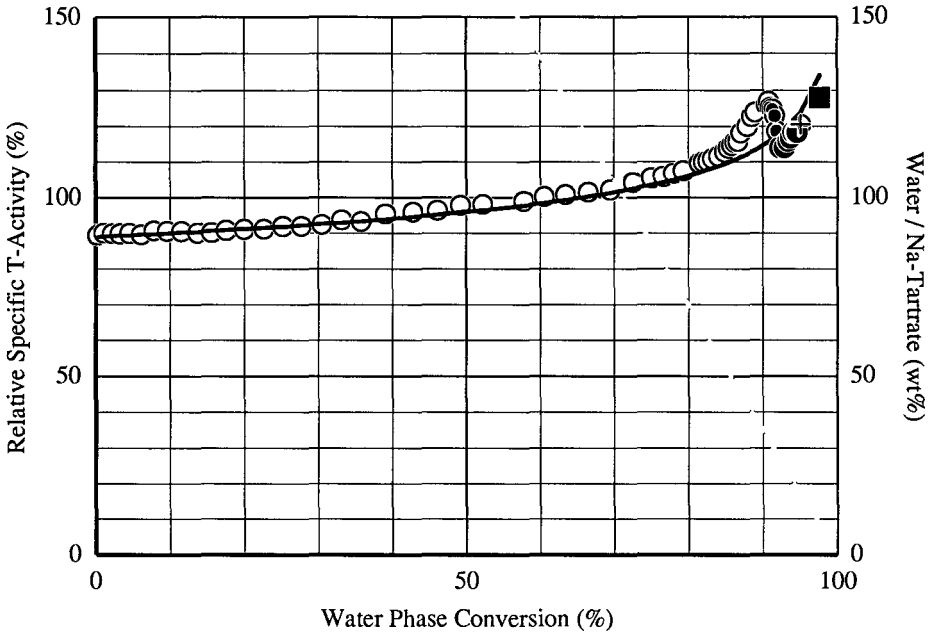

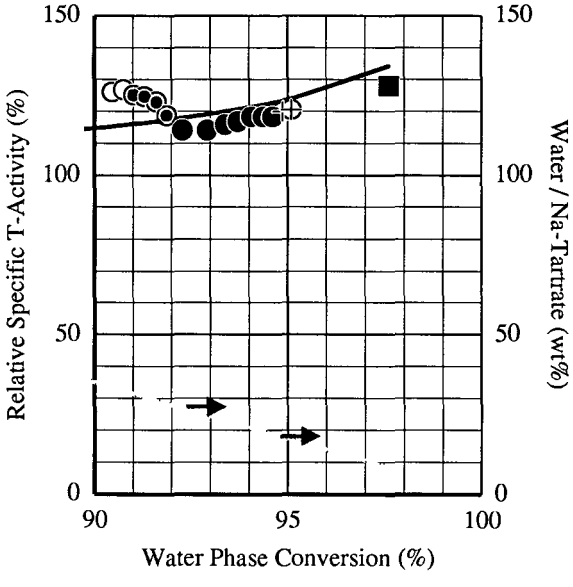

Fig. 4 a,b: Tritium enrichment at Rayleigh distillation (5°C and 5 mbar) of a 1.4 M Na-tartrate solution in tritiated water. The line (–) is calculated. The markers are measured values: O: free water; ◉: physisorbed water, differentiated from free water by dehydration kinetics; ●, ⊕: physisorbed water, vaporized at 10^{-3} mbar, 45°C and 85 °C, respectively; ■: residual fraction, corresponding with Na-tartrate-monohydrate (determined by Karl-Fischer-Titration).

condary effects. For example, the adsorption isotope effect may be one of the intrinsic mechanisms for the often observed higher T/H ratio in the organics of environmental plant samples as compared with that in ambient water [1] since plants mainly rely on bound water. The result further suggests that enrichment in water, bound to solid surfaces, is a general feature. The phenomenon merits a more extensive study for a wide variety of environmental samples, including radiation sensitive materials such as proteins and genetic substances.

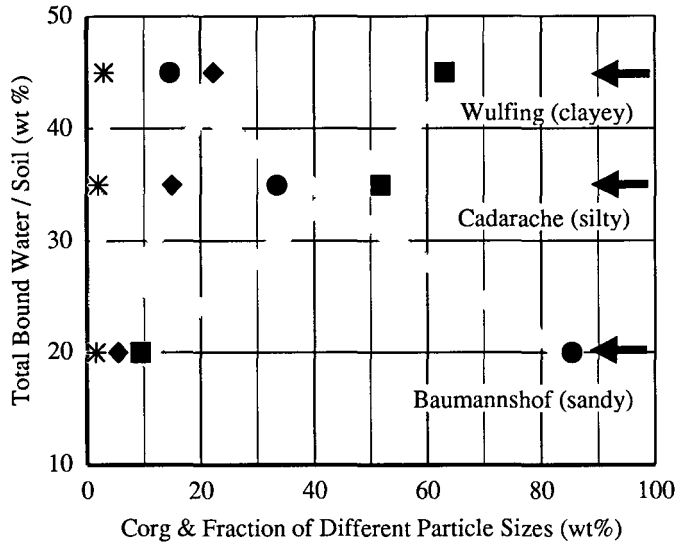

Fig. 5: The relative amount of soil-bound-water as a function of the organic carbon content and of the fraction of different particle sizes: * for the Corg; ♦ for the fraction < 0.002 mm (clay); ■ for the fraction = 0.002-0.06 mm (silt); ● for the fraction = 0.06-2.0 mm (sand) of three typical soils.

SUMMARY AND CONCLUDING REMARKS

Tritium dose estimation necessarily implicates knowledge about fractionation processes in the environment. Since tritium (T) has a higher binding enthalpy as protium (H), isotope effects are expected whenever the hydrogen (H or T) binding state is changed. This occurs as tritium moves from the hydro- and geosphere into the organics of the living cell. Thereby it passes several physical as well as chemical bound states. Free bulk water is transformed into

bound water which is further converted to bioorganic matter. The bound water results from physisorption of free water onto surfaces of inorganic or organic matrices, e. g. soils and biopolymers and from chemisorption of water, mainly as hydroxyls. The further conversion of bound water to the organics occurs through enzymatic reactions.

The presented study, given in detail elsewhere [1, 2, 3], quantifies two kinds of isotope effects: (1) the overall isotope effect at photosynthesis and (2) the isotope effect at the water sorption process. Plants with distinct photosynthetic enzyme systems and soils with different characteristics are chosen for this double purpose. The fractionation factors, defined as the specific activity ratio of the bound tritium component and the free water tritium which are in equilibrium with one another, are measured.

In the first part of the work, much attention is devoted to obtain accurate specific activities which are free from analytical artifacts. The latter easily arise at the separation of free water from the bound tritium component through vaporization isotope effects. In the second part of the study, the importance of the plant sampling time is stressed. The achievement of the dynamic equilibrium between the considered components is confirmed by kinetic experiments. The last part of the work concerns the transition of free water to bound water. Different forms of bound water are characterized on the basis of the measurent of the vapor pressure isotope effect. A simple method that allows the simultaneous determination of the amount and the tritium fractionation factor of bound water is demonstrated and validated by means of model substances such as Na-tartrate-dihydrate.

The results show that tritium is discriminated against protium in photosynthesis and that the degree of discrimination varies with photosynthetic plant type. The net discriminating effect results from a tritium retardation at anabolism which is not completely compensated by tritium enhancement at catabolism, a feature characteristic for any overall anabolic reaction. Opposed to this result, tritium enrichment is found at the equilibrium transition from free water to water in the physisorbed and chemisorbed state involving hydrogen bridges of different strenghts. Since the presented results are not only restricted to soil samples but also include model substances, it is expected that tritium enrichment in the sorbed water state is a phenomenon with broader validity. The analogy between physisorbed soil-water, crystal water in Na-tartrate and conformational water which is required for biological activity of proteins and genetic material is obvious. Hydrogen bridges between OH-, SH-, NH-groups and with physisorbed water , obey the same thermodynamic principles whatever the matrix is. Individual quantification , however, is necessary. Today, tritium dose calculation does not include organically bound tritium under the pretext of tritium discrimination in this binding form. The further investigation of possible tritium enrichment in other binding forms such as in sorbed

water, especially in radiation sensitive material like chromatine, carrying the genetic substance, is an important requirement for a more precise safety assessment of tritium. The present work includes some basic methods which can be applied for this purpose.

REFERENCES

[1] Kim M. A. and Baumgärtner F. (1993) Equilibrium and non-equilibrium partition of tritium between organics and tissue water of different biological systems. *Int. J. Appl. Rad. Isot.* **45**, 353.

[2] Kim M. A. and Baumgärtner F. (1995) Tritium fractionation in anomalous water bound to environmental samples. (submitted to *J. Env. Radioact.).*

[3] Baumgärtner F. and Kim M. A. (1995) Kinetic studies of tritium incorporation in plants. Fifth Topical Meeting on Tritium Technology in Fission, Fusion and Isotopic Applications, Belgirate, May 28- June 3. (*Fusion Technology*, in press).

Head of project 4: Prof.Dr. Dertinger

II. Objectives for the reporting period

- Experimental short term exposures of diet relevant plants (wheat and potatoes) to study
  - the incorporation of tritium from tissue water into organically bound tritium (OBT) in dependence of diurnal variations and of climatic conditions
  - the translocation of OBT to edible plant parts in dependence of the time of exposure
- measurement of growth data and plant physiological parameters in a rural wheat field for model calibration and for model validation in the following year
- development and improvement of a model, which describes the major processes of OBT formation, turnover, translocation, and storage in the grains of wheat plants using only general available meteorological data, such as air temperature, relative air humidity, and the global solar irradiation
- calibration and validation of the model

III. Progress achieved including publications

Work carried out

In the contract period 1992 - 1995, several exposure experiments have been carried out each year during the vegetation period (June, July). The experiments started with potted spring wheat and potatoes, exposed to HTO under laboratory conditions. Since wheat is more important concerning the ingestion dose due to OBT than potatoes it was decided to concentrate the efforts on wheat, in particular winter wheat (*Triticum aestivum*), which is usually cultivated for nutrition in the zone of temperate climate. Because the development of winter wheat in pots was very different compared to growing on the field, some winter wheat plants from the field including roots and surrounding soil were put into pots and exposed in the laboratory. In 1995, winter wheat has been exposed in the field using a special exposure box, but results are not yet available.

Plant physiological data (CO_2 assimilation, transpiration, and stomatal conductance), growth data (dry weights, leaf area index) as well as climatic data (temperature, relative humidity, global irradiation) were continuously measured during the vegetation period at different places:

- experimental field of spring wheat on the FZK area 1993 and 1994
- experimental field of winter wheat on the FZK area 1994 and 1995
- typical field of winter wheat about 30 km from FZK in north-east direction (Weierbach) 1993 and 1994.

The model „Plant-OBT" has been developed in co-operation with Wolfgang Raskob (D.T.I. Dr. Trippe Ingenieurgesellschaft mbH). Since the growth of the plants is one of the fundamental elements of the model, it has been first calibrated with the measured growth data of winter wheat and spring wheat obtained in 1993. Subsequently, the tritium incorporation was calibrated using the results of the exposure experiments in the same year. The validation of growth and tritium incorporation with independent data sets from 1994 is in work.

Experiments

The aerial parts of the potted wheat plants were exposed to atmospheric HTO in the generative phase of development between the beginning of anthesis and beginning of maturity (end of May to early of July). The soil was covered with polyethylene foil to prevent a contamination of the soil.

The exposure box, a transparent glove box of 300 l volume, was installed in a growth chamber with controlled climate. The climate inside was established by continuously passing a stream of climatisized air through the box (10 l/min), providing about one air change every 30 minutes. It was assumed that this air change would replenish the CO_2 which is consumed during the day by photosynthesis of the plants. A fan was installed to prevent gradient build-up and to minimise the leaf boundary layer resistance. Illuminance by fluorescent tubes provided a photosynthetic photon flux density (PPFD) of about 120 µmol m^{-2} s^{-1} inside the box at the height of the flag leaves. For experiments with a more intensive irradiation additional light sources (mercury lamps) have been used providing a PPFD of about 900 µmol m^{-2} s^{-1}. Temperature and relative humidity were 24 - 25°C and 86 - 90 % during exposures under daylight conditions, 16 - 17°C and 86 - 90 % under night conditions.

HTO was introduced into the box as tritiated water vapour by passing a stream of dry air at a constant flow rate through tritiated water of 7 to 16 MBq/ml for 2 hours. The HTO concentration in the box reached 2 - 6 kBq/l of air (100 - 350 kBq/ml of air humidity). Plant samples were taken after the end of HTO dosage, the following day, and then weekly until harvest (40-50 days after anthesis). The tissue water was removed by freeze drying and measured by liquid scintillation spectroscopy (LS 9800, Beckman). The dried plant samples were homogenised and exposed to a stream of wet tritium free air for several days to remove the exchangeable bound tritium. For combustion analysis, an oxidiser 306 (Canberra-Packard) was used. OBT is determined as specific activity in Bq per g dry matter. For comparisons with the TFWT, the specific OBT concentration is converted into the unit Bq per ml of oxidation water, referring to the assumption that 1 g of dry matter yields 0.6 ml oxidation water.

The exchange of CO_2 and water vapour of wheat leaves has been determined using an open gas exchange measuring system (Walz Meß- und Regeltechnik, Effeltrich, Germany). The meteorological data (global solar radiation, air temperature and relative humidity at 1 m height) were continuously recorded during the vegetation periods 1993, 1994 and 1995.

Uptake of atmospheric HTO into TFWT

Table 1 shows the observed concentration ratios between the tissue free water tritium (TFWT) in different plant parts and the air humidity (HTOatm) at the end of the introduction of HTO into the exposure box under conditions of a low PPFD (120 µmol/m²s), high PPFD (900 µ mol/m²s), and night. There was no significant difference in the HTO uptake between spring wheat and winter wheat leaves.

Tab. 1 Comparison of the mean concentration ratios between TFWT and HTOatm observed in wheat plants 2 h after the beginning of the exposure, under different illumination conditions (relative air humidity 86-90 %).

plant parts	concentration ratios TFWT / HTOatm after 2 hours		
	after exposure at 900 µmol/m²s ($x \pm 1\sigma$. n=6)	after exposure at 120 µmol/m²s ($x \pm 1\sigma$. n=3)	after exposure during night ($x \pm 1\sigma$. n=6)
leaves	0.86 ± 0.02	0.75 ± 0.05	0.20 ± 0.07
stems	0.12 ± 0.04	0.10 ±0.04	0.03 ± 0.01
ears	0.22 ± 0.08	0.17 ± 0.07	0.13 ± 0.05

The measurements show that the tritium uptake increases with increasing PPFD in all plant organs. The equilibrium concentration is only reached in the leaves under high light conditions at the end of the 2 hour exposure, indicating that the rate of exchange is not high enough to reach the steady-state in all plant organs within the duration of the experiment. Particularly in night experiments a diminished leaf uptake rate can be observed because of a significant closure of the stomata.

Formation of OBT

While analysing the 1993 experiments, it was recognised, that the measured OBT concentrations in the leaves, observed briefly after the exposure, did not agree with the OBT concentrations predicted by the model. Instead of an expected constant increase the measurements showed a rather high starting point already at the beginning of the experiment and a proportional reduction with decreasing TFWT concentrations. Such a shape of the curve cannot be explained by biological assumptions. It seemed to be attributed to a difficulty in the sample preparation method, e.g. an incomplete removal of the exchangeable tritium from the freeze-dried samples. At the end of exposure, the difference between the TFWT and the OBT concentrations amounts to more than two orders of magnitude. If only less then one percent of the exchangeable tritium, originating from the TFWT, is remaining in the samples, the high OBT concentrations can be explained. This assumption has been confirmed by a more careful removal of the exchangeable tritium of the 1994 samples. For any comparisons, the 1993 measured OBT concentrations of samples from the exposure day have been corrected by a subtraction of 0.75 % of the actual TFWT concentration. This percentage has been assumed by expert judgement.

In order to compare the OBT incorporation under different light conditions and differences in the tritium concentration in the atmosphere, all OBT concentrations (in Bq/ml) have been related to the TFWT concentration in leaves 2 hours after beginning of exposure. This relationship should no be confused with the so-called 'R-value' cited in the literature*.

The courses of the specific activity ratio between OBT and TFWTmax in the 26 hour period after exposure under different light conditions are shown in figure 1 with winter wheat as example. The curves observed with spring wheat are similar. The figures show, that the OBT incorporation is significantly lower under night conditions but the differences between low light and high light conditions are relatively low. This does not agree with the increase of the rate of net photosynthesis with increasing light intensity. In wheat flag leaves, the rate of net photosynthesis is about 4 times higher at 900 $\mu mol/m^2$ s compared to 120 $\mu mol/m^2$ s. The OBT concentration did not increase in this extent. This indicates that the contribution of the photosynthesis to the OBT formation might be less than originally supposed. Another possible reason, in particular for the experiments under high light conditions, may be an impoverishment of CO_2 in the exposure box due to consumption by photosynthesis which has not been measured. The obvious OBT incorporation under night conditions further indicates the significance of other mechanisms of OBT formation than photosynthesis, for instance the reactions of the tricarbonic cycle or other metabolic conversions.

*'R-values' or 'SAR-values' describe specific activity ratios between OBT and TFWT that can be observed in environmental samples under steady-state or supposed steady-state conditions, e.g. an R-value of unity (R=1) means that the ratios between tritium and hydrogen (T/H ratio) in the tissue water equals that in the organic matter.

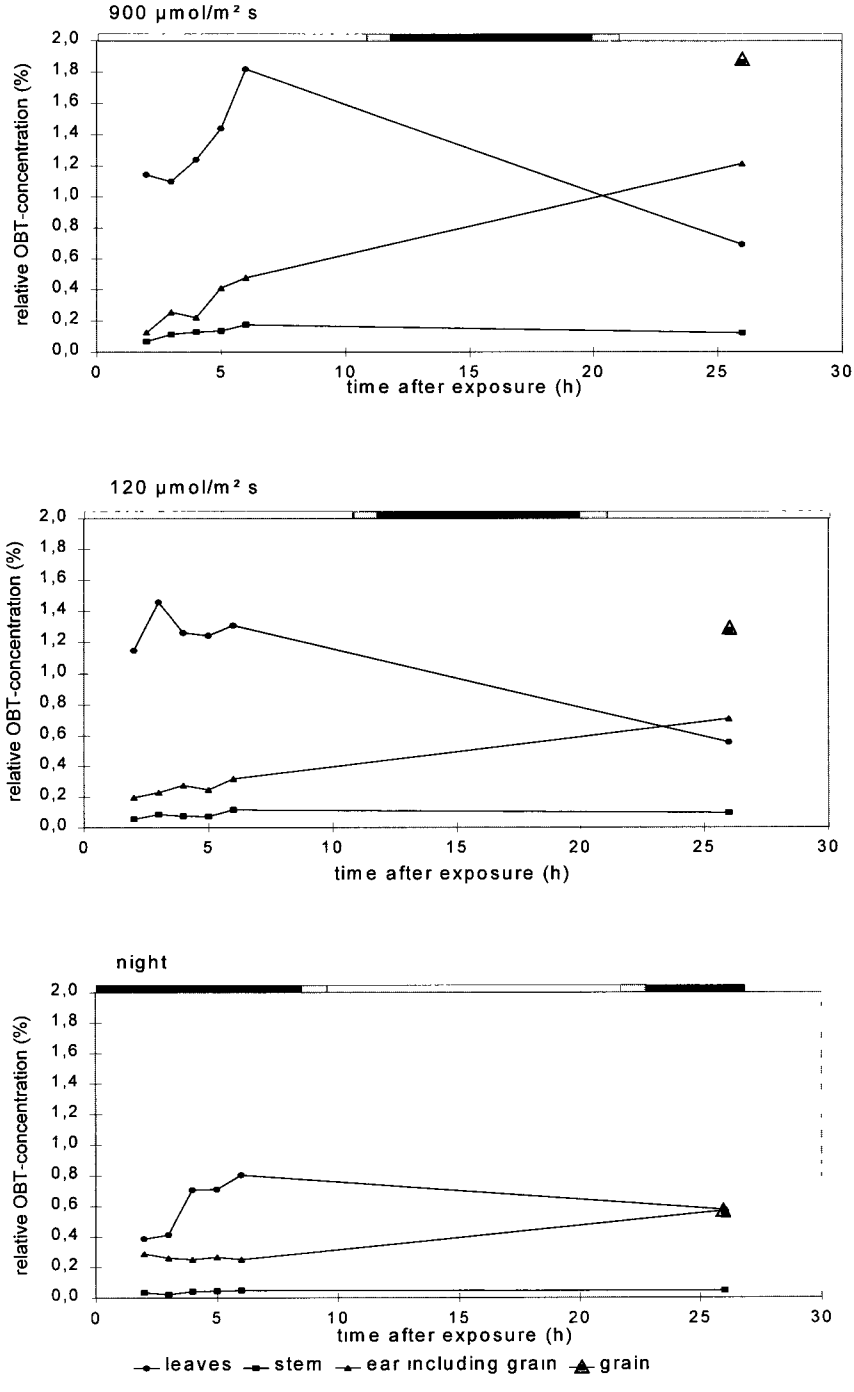

Fig. 1. Course of the relative OBT concentrations (OBT / TFWTmax ·100) in winter wheat exposed 2 hours to HTO at different light conditions.

Translocation of OBT

As a measure for translocation of OBT from leaves to fruits, the translocation index TLI was defined which is the percentage of the OBT concentration in the grains at harvest (Bq/ml) related to the concentration in tissue free water tritium (Bq/ml) 2 hours after start of exposure to HTO. The translocation indices observed in about 23 exposure experiments with spring wheat (17 at 120 µmol/m² s, 2 at 900 µmol/m² s, 4 during night) and 3 experiments with winter wheat (1 at 120 µmol/m² s, 1 at 900 µmol/m² s, 1 during night) at different stages of development after anthesis show that the final OBT concentration in the grain is highly dependent on the time of exposure (table 2) corresponding to physiological understanding. The TLI is lowest when the exposure was at the beginning of the grain filling period. For spring wheat this is the time until about 10 days after start of anthesis (until mid of June). The TLI raised up to 0,9 % when the exposure was during the grain filling period which is 10 - 24 days after start of anthesis (from mid of June to early of July). The TLI decreased when maturity commences in the first part of July.

Table 2: Percentage of OBT concentration in wheat grains at harvest related to the maximum tritium concentration in tissue water of the leaves during exposure to HTO in the generative phase (translocation index).

time of exposure in relation to the stage of development	translocation index (%)
beginning of grain filling period (until mid of June)	0.06 - 0.2
during grain filling period (mid of June until early of July)	0.4 - 0.9
end of grain filling period until harvest (end of July)	0.04 - 0.2

Computer model

The model to describe the major processes of OBT formation, turn-over, translocation, and storage in the grains of wheat plants should use only general available meteorological data, such as air temperature, relative air humidity, and the global solar irradiation. The basic structure of the compartment model 'Plant-OBT' is shown in Fig. 2. It consists of three uniformly constructed subcomponents corresponding to the contributors of assimilates to the grain during the generative phase: ear, leaf, and stem. Their contributions to the formation of organic material respectively of OBT during the grain-filling period have been estimated with 30 % (ear), 60 % (leaf), and 10 % (stem) at the present stage of model development. The transfer processes between the TFWT- and OBT- compartments represent light dependent processes (photosynthesis, photorespiration) as well as reactions which are independent on the light (maintenance respiration and basic metabolism). The rate of photosynthesis depends mainly on the light intensity, the temperature and the leaf resistance. The photorespiration depends on the rate of gross photosynthesis, assuming a constant respiration rate of 36 % of the

actual built up of the organic matter. The rate of maintenance respiration is assumed to be independent on light and temperature and is set to a value of 0.004 per day times the weight of the single parts of the wheat plant. The processes of basic metabolism do not result in changes of weight but only in conversion of different kinds of the organic molecules into other kinds of substances. These turnover processes include isomerisation and hydrolytic splitting reactions, as well as additions of water, which can be accompanied with incorporation's of tritium. Additionally, an isotopic effect due to a discrimination of tritium against hydrogen of 30 % has been taken into account, when tritium from TFWT is converted into OBT.

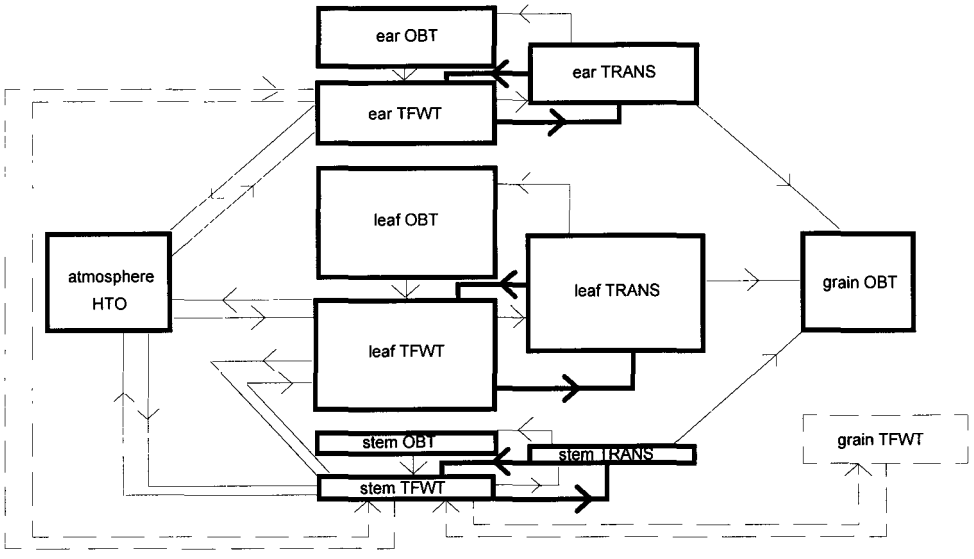

Fig. 2: Diagrammatic layout of the plant-OBT-model. (➔) = metabolic reactions only occurring at light, (→) = metabolic reactions at light and in the dark, (--->) = reactions with very small contribution to the OBT translocation.

The theoretical rate of photosynthetically fixed hydrogen atoms has to be reduced to a certain percentage, because the exchangeable tritium behaves as the tritium in the TFWT and is not stored in the grain. The polymerised assimilates in the form of starch are the intermediately stored products of the photosynthesis in the chloroplasts as well as the finally stored reserve material. Each unit of glucose contains ten hydrogen atoms totally, but only seven hydrogen atoms are covalently bound to the carbon atom and are non-exchangeable. 30 % of the originally incorporated tritium atoms therefore turn into TFWT during metabolism.

In preliminary attempts of calibration it has been assumed that the growth was only dependent on light and temperature and no limitation due to water stress had been taken into account. Gas exchange measurements in the fields, however, show that on warm sunny summer days stomata in the flag leaf close during midday for several hours, even if the water supply from the soil seems to be sufficient (Fig. 3). This is taken into consideration by a depression of transpiration and photosynthesis due to water stress above a solar irradiation of 700 W/m². The simulation of the growth from anthesis to the maturity of the grains at the time of harvest has been successfully on the whole.

In a second step the model 'Plant-OBT' has been fitted due to the uptake of HTO in the atmosphere into TFWT, the incorporation into the organic molecules, the translocation from the chloroplasts of the green parts of the plants, and their storage as starch in the grain. As mentioned above, an accurate and reproducible determination of the OBT concentrations can only be achieved by measuring exclusively the non-exchangeable tritium. A comparison of a simulation run against the observed experimental data is therefore only useful, if the model also produces solely non-exchangeable OBT concentrations.

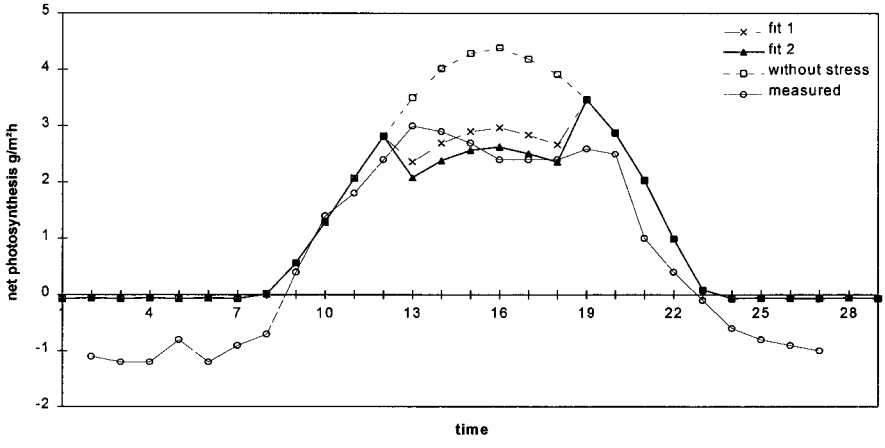

Fig. 3. Observation and modelling of water stress, in July (7/1/93), the rate of the net photosynthesis has been determined by gas exchange measurements in the flag leaf of winter wheat

Simulation of TFWT

The model describes the HTO uptake from the atmosphere by penetration through the stomata until an equilibrium is reached. The equilibrium between the HTO concentrations in the air, the soil, and the TFWT in the leaves depends of the actual relative humidity in the atmosphere, because the ratio between the flux of water from the soil due to transpiration and the flux of water due to gas exchange with the atmosphere is determined by the relative humidity.

In figures 4 and 5 the tritium concentrations of the ears of two experiments are summarised in which the wheat plants have been exposed to tritium under day and night conditions, respectively. The simulation of the TFWT concentrations in the ear show that the model is able to predict satisfactorily the TFWT concentrations within the first 24 h after the exposure as well as the final TFWT concentrations at the time of harvest. The model, however, simulates a much more rapid decline of the TFWT in the ears than observed, but for the OBT formation in the ear this fact is of less interest as long as the highest concentrations after the exposure can be predicted accurately.

Simulation of OBT

Depending on the stage of development a certain amount of the OBT formed in the green parts of the plants is translocated into the ears and is stored almost completely in the grains until the plants are harvested. Only a slight decline of the specific OBT concentrations in the grain are caused by metabolic activities. In the model this amounts in only about 0.01 % per hour. A more effective reduction results from the dilution, as non labelled assimilates are stored during the period following the exposure. In figure 4 the observed and the simulated OBT concentrations in the grains are given from an experiment performed under day conditions. It can be seen that the model is able to describe the course of OBT concentrations in the crop quite well for the whole duration of the experiment.

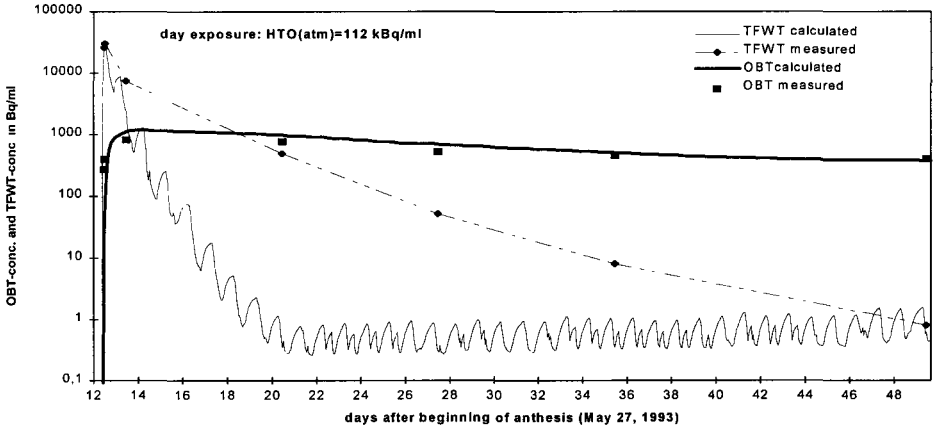

Figure 4: Comparison of measured and calculated concentrations in TFWT and OBT in the ear of spring wheat, which has been exposed 12 days after the beginning of the anthesis for two hours to HTO in the atmosphere (under day conditions with a PPFD of 120 µmol/m² s).

A comparison of observed and calculated OBT concentrations of an experiment performed under night conditions is given in figure 5. The graphs of both experiments, figure 4 (day) as well as figure 5 (night), show at first sight a surprising similarity, however, the most serious difference in both cases is the fact, that the exposure to atmospheric HTO in the night experiment has been nearly 3 times higher (333 kBq/ml of air moisture) than in the day experiment (112 kBq/ml of air moisture). Therefore the initial TFWT concentrations are similar in both experiments. Furthermore, the TFWT concentrations decline relatively slowly during the night and therefore a relatively high TFWT concentration is still present at sunrise. Additionally, the OBT built up due to the basic metabolism appears to differ not significantly from the rate of photosynthesis during the low PPFD conditions. However, the physiological processes are still not fully understood.

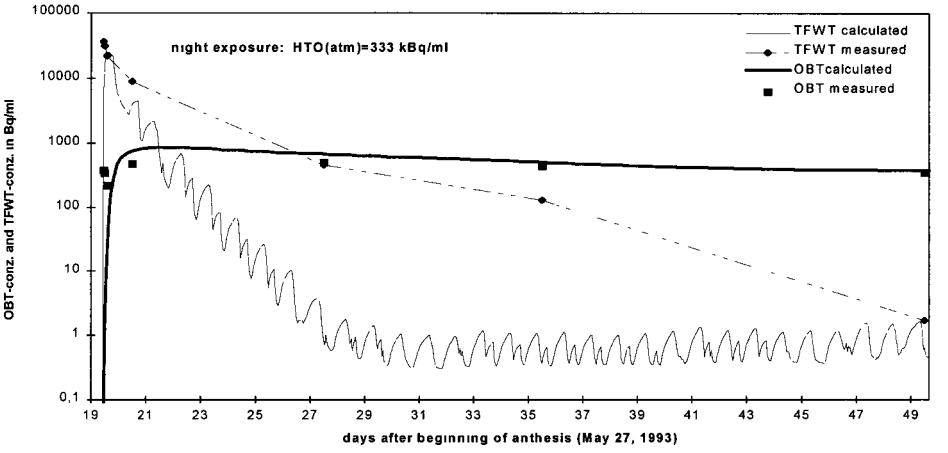

Figure 5: Comparison of measured and calculated concentrations in TFWT and OBT in the ear of spring wheat, which has been exposed 19 days after the beginning of the anthesis for two hours to HTO in the atmosphere (under night conditions)

Conclusions

At the present stage of our work it seems to be possible to predict the final OBT concentrations in the grains following a short-term exposure to atmospheric HTO using only general available meteorological data as input. The metabolic processes converting tissue water tritium (TFWT) into organically bound tritium (OBT) represent light dependent reactions as well as reactions that are independent of light, also occurring during the night. An isotopic discrimination of tritium against hydrogen is included to describe the incorporation into OBT. However, during experimental and modelling work no indications have been found that tritium is enriched or accumulated in the OBT compartments against a concentration gradient.

The plant-OBT model has been fitted with experimental and field data, however, a comprehensive validation of the model with independent data sets is still necessary. From the radiation protection point of view the final OBT concentration at the time of harvest is the most important one, since this is the dominating form of tritium for calculations of the ingestion dose due to wheat consumption. Our intention, however, is not only to predict the final concentration, but also to simulate the dynamics of the metabolic processes even within the first hours after the exposure to tritiated water. This would allow the application of such a model also for dose calculations due to ingestion of leafy vegetable or pasture grass which might be consumed at earlier stages after the tritium releases.

The simulation of OBT concentrations in different plant organs and over the full time span of the plant growth, however, is difficult due to the complex processes in a living plant. At present the amount of available experimental data is highly limited. Additionally some of the data may be erroneous and must be corrected. Therefore further experimental research not only in climate chambers, but also in the field, is recommended to fill the gap in our knowledge on the physiological processes and to complete the modelling of OBT in plants correctly.

Acknowledgements

These investigations have been performed by Silvia Diabaté, Jutta Müller, and Siegfried Strack. The model development was kindly supported by Wolfgang Raskob (D.T.I. Dr. Trippe Ingenieurgesellschaft mbH).

Publications

• Diabaté, S., Strack, S., Studies on Translocation of tritiated assimilates into potatoes and wheat grains. In: *Proceedings* of the International Symposium on Radioecology, chemical speciation - hot particles , Znojmo, CSFR, October 12 - 16 (1992)

• Müller, J., Diabaté, S., Raskob, W., Strack, S., Untersuchungen zum Transport tritiierter Assimilate in Kartoffeln und Weizen, 25. Jahrestagung des Fachverbandes für Strahlenschutz, Sept. 1993, *Proceedings*, 704 - 708 (1993)

• Diabaté, S, Strack, S., Organically Bound Tritium, *Health Physics,* **65** , 698-712 (1993)

• Diabaté, S., Müller, J., Raskob, W., Strack, S., Short term exposure of crop plants to atmospheric tritium. Experimental results and model development. In: Fusion Technolology 1994, *Proceedings* of the 18th SOFT 1994, Karlsruhe, August 22- 26, 1994, eds. Herschbach K., Maurer, W. and Vetter, J.E., 1425 - 1428 (1995)

• Strack, S., Diabaté, S., Müller, J., Raskob, W., Organically bound tritium formation and translocation in crop plants. Modelling and experimental results. Fifth Topical Meeting on Tritium Technology in Fission, Fusion and Isotopic Applications, Belgirate, May 28 - June 3, 1995, *Fusion Technology,* **28**, 951- 956 (1995)

• Diabaté, S. and Strack, S., Zur Aufnahme von Tritium in Weizen. Experimente und Modellrechnungen. *Strahlenschutzpraxis* **3**, 39-44 (1995)

Head of project 5: Dr. J. Eikenberg

II. Objectives for the reporting period

In order to investigate the dominating parameters governing the movement of HTO at the interface of the saturated zone, top soil layer and atmosphere, a flow through Plexiglas apparatus (trough) partially filled with sedimentary material was designed and constructed. The dimensions of 200x80x5 cm (length, height, width) were chosen to give optimum conditions for subsequent two dimensional transport model exercises. Goal of the project is to obtain soil and transport specific parameters such as transmissivity, advection, dispersion, diffusion etc. by analyzing breakthrough curves of HTO entering the saturated zone. Besides the investigation on HTO migration down to the saturated zone, the further goal is to study the reemission rates of evaporated HTO and H_2O from the top soil surface. Here in detail, the effect of later rainfall, following a primary HTO deposition, on the HTO reemission rate is analyzed along with the vertical movement of HTO into the unsaturated zone.

III. Progress achieved including publications

Introduction: After deposition of a tritiated plume downwind of the release location (fusion reactor, fission fuel reprocessing plant) on top surface soil layers, HTO may follow a rather complex migration path at the interface of the atmosphere and top soil sediments. Depending on various meteorological and soil specific parameters additional penetration into deeper zones could also result. To investigate the migration and transport behaviour of non-reemitted HTO, the EC-project was joined in 1993 by this supplementary laboratory and model study on the temporal and spatial movement of HTO into the unsaturated zone as well as its percolation in the sub-surface (saturated) soil environment. The project was then extended to further investigate the HTO and H_2O reemission rates, in particular to study the effect of later rainfalls on soil surface deposited HTO, thereby causing decrease and retardation in reemission rates along with enhanced groundwater infiltration. The transport driving forces are analyzed by fitting the tracer profiles of released HTO using the random-walk transport code MCTAC (modular coupling of transport and chemistry) and describing the hydraulic properties of the system by a two dimensional finite differences flow model over 21 x 17 nodes. In the following the principal parameters of the experimental facilities along with the results of (radio)tracer injection - extraction experiments will be presented.

Experimental device: The full test arrangement (including pumps, analyzers for on-line tracer detection, sensors, data logger connected to a PC, etc.), schematically shown in Fig. 1, was designed similar to that used for the performance of field tracer migration experiments in a planar almost 2-D-shaped shear zone at the Grimesl Test Site, Switzerland. The dimensions of about 200x80x5 cm (length, height, width) of the flow through apparatus were chosen i) to enable tracer breakthrough and reemission experiments to be conducted in reasonable time scales and therefore under stable flow conditions (days to weeks) and ii) to obtain reproducible and consistent breakthrough and reemission profiles for later evaluation of soil and flow specific parameters using the 2-D-transport model code MCTAC (Pfingsten, 1995).

For the first experiments the Plexiglas container was partially filled with mm-sized sand as sediment medium. By continuously pumping water through the apparatus, a groundwater table and flow can be regulated. The length (thickness) of the saturated zone can be varied

using three water extraction valves mounted at different vertical niveaus (Fig.1) and different positions of the end of the extraction line (open water outflow). The water flowing into the system is routed initially into a 3 cm wide storage chamber, mounted in vertical direction, which hence separates a small thin water layer from the soil material. From this water column the water is allowed to enter the saturated zone by passing through about 50 single slits. This enables a continuous horizontal flow towards the water extraction side. Due to this flow direction, the pumping pressure on the left side of the system and the atmospheric pressure conditions on the right (extraction) side, a stationary state of the hydraulic head is obtained, which is an essential criterion for working under proper boundary conditions as required by the transport model code.

After having passed the groundwater through the extraction valves, water samples can be taken at the open outlet for later counting of β-radiation (i.e. ^{3}H analysis) in a liquid scintillation counter (see below). (Radio)tracer injections using HTO and conservatively, i.e. non-reactive, tracers are performed by a dropping system (simulated rainfall) designed for either single (i.e. locally spot-wise) tracer injection or almost homogeneous tracer deposition over the entire surface. This is achieved by using 16 individual valves controlled by a peristaltic pump, which guarantees constant flow distribution into the 16 valves with individual flow rate deviations of less than 5%.

For the reemission experiments air with different moisture concentration can be pumped into the system and subsequently passed through a gas flow meter and a HTO extraction washing system (Fig.2) consisting of three washing flasks connected in sequence. Although typically high gas currents of 10L/min are bubbled through the bottles filled with 200 mL water each, about 90% of the inflowing HTO gas is permanently extracted into the aqueous phase of each bottle. Thus, in total, a 99.9% extraction yield of HTO is obtained. The error introduced by dilution of the water table in the bottles by water vapour from the apparatus can be neglected since a difference in humidity (entering and leaving the system, see below) of typically 40% at a gas flow mentioned above carries about 2g H_2O, when exchanging the bottles every 30 minutes. Assuming all H_2O vapour to be exchanged in the bottle, a difference in concentration of 1% would result for the aqueous phase.

The air entering the system is taken from a compression machine supplied by vapour of the surrounding atmosphere, which reduces (by cooling and condensation) the initially high water vapour humidity to fairly constant values between only 6 and 8% (relative humidity). This additional step was necessary since the relative humidity of the water vapour in the laboratory is highly varying during a full daily cycle in a range between 30 and 80%. Due to this, not ideally reproduced reemission rates were obtained for the first 30-60 minutes after surface HTO deposition during some scoping reemission experiments performed under identical conditions of tracer deposition and wind speed, but that time not dried air was allowed to enter the atmosphere compartment of the system. Meanwhile, the initial humidity can also be increased to still constant values by passing the inlet air over the surface of water columns before pumping it into the atmosphere compartment of the apparatus. In the latter, the humidity typically increases to values about 50%, giving a difference in humidity between inlet and outlet of about 40%. Clearly, the degree of air saturation is also slightly dependent on the level of the unsaturated zone as well as the wind velocity. Since gas flow, temperature and humidity is monitored continuously at the inlet and the outlet of the system, the ratio of reemission rates between H_2O and HTO can be determined. This is of great advantage for later comparison of the reemission rates with those HTO/H_2O reemission rates and HTO soil column profiles obtained by wind tunnel experiments of our EU-partners (Täschner et al., 1993, tritium project 1, this issue).

The data obtained from breakthrough curves of the non-gaseous water tracers (i.e. Na-Fluoresceine, electrical conductivity) entering the saturated zone as well as the reemission rates of evaporated H_2O are measured on-line. These data, along with the results for Tritium, are further processed using standard PC spread sheet programs (Lotus 1-2-3, Excel).

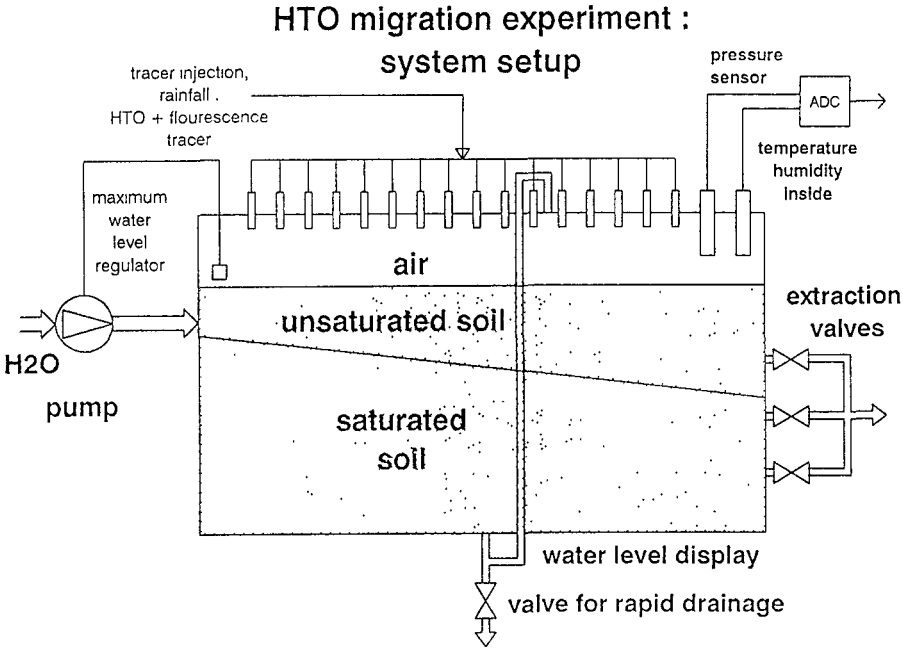

Fig. 1. Schematic diagram showing the vertical cross section of the test setup for the PSI laboratory HTO migration experiment.

The conservatively behaving (see below) substances Na-Fluoresceine and electrical conductivity (caused by injected NaCl solutions) are monitored on-line on the extraction site using a wavelength dispersive fluorescence spectrometer and a conductivity cell, respectively. Detection limits of 0.1 ppb (for Na-Fluoresceine) and 10^{-6} molar NaCl concentrations are obtained. ^{3}H measurement is performed in a Packard low level liquid scintillation analyzer (Model TriCarb 2500 α/β) using 10 mL water samples mixed with 10 mL scintillation liquid „Ultima Gold LLT", which is an environmental completely bio-degradable cocktail. By counting in low level mode, background scatter in the tritium window was reduced to less than 4 counts per minute at a relative counting efficiency of about 30%. Since pure water samples are used with neutral pH, both chemical and color quench is irrelevant and hence a detection limit of about 20 mBq/10mL sample is obtained when counting for about 60 minutes. For injection, tracer concentrations of about 10^{4}Bq (^{3}H), 10 ppm (Na-Fluoresceine) and 1 molar (NaCl) are mixed and prepared in 50mL. Total injected masses typically range between 20 and 40 mL per experiment.

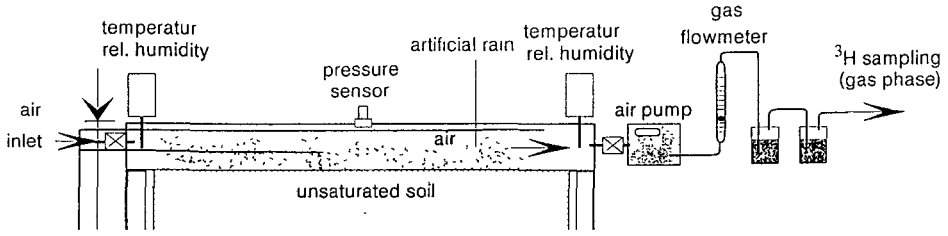

Fig. 2. Schematic diagram (upper section of the apparatus) of the vapor extraction line for the tritium reemission experiments.

Results of the closed system experiments: The first series of migration experiments were carried out as short term pulse injections using the fluorescent dye Na-Fluoresceine (uranine) followed by subsequent extraction of water from the saturated zone and on-line measurement in a flow through fluorescence spectrometer. Since in most types of aquatic environment the dye uranine has been shown to act as conservatively behaving (i.e. non reactive) species, and since in the scoping experiments performed here, the tracer injection was followed by continuous "raining" with tritium free water, complete tracer recoveries and identical breakthrough curves of HTO and the fluorescence dye were expected. This, and furthermore, the reproducibility of the tracer breakthrough curves under identical conditions were indeed experimentally confirmed (Eikenberg and Fiechtner, 1994, Eikenberg et al. 1995). Since in the type of sediment material used (i.e. quartz with almost no sorption capacity for dissociated Na^+), non-reactive behaviour of the NaCl tracer should also show up. Reproducibility and identical tracer breakthrough profiles is indicated in Fig. 3. Therefore, instead of performing rather extensive ^{3}H-tracer experiments necessitating water sampling and subsequent β-measurement in a liquid scintillation counter, these first migration experiments were carried out using the on-line measured tracers (conductivity, fluorescent dye) solely.

To obtain the relevant soil and flow specific parameters such as transmissivity, flow velocity, dispersion lengths etc., various hydrological (flow rate, ratio of the unsaturated to the saturated zone) and meteorological parameters (intensity of rainfall) had to be varied during this test period. Fig. 4 shows the tremendous effect on the shift of tracer breakthrough and mass summation curves when using different levels of the unsaturated zone. It is indicated that with an increasing level of the unsaturated zone a significant peak depression and retardation as well as much longer breakthrough times are obtained. Similar large differences are obtained when using different flow rates in the saturated zone (not shown), clearly indicating that the tracer transport at the interface saturated / non-saturated zone is not dominated by pure advection solely. These types of experiments were completed by variation of the intensity of rainfall (Fig.5) at a height of the unsaturated zone of 22 cm. As shown in this figure, this dimension of the unsaturated zone proved to be sufficient to produce highly different breakthrough curves even at slight differences in rain intensity.

Results of open system experiments: The next series of experiments involved HTO top soil contamination and immediate termination of the water supply from the atmosphere as soon as the tracer has been deposited. With additional variation of the ratio unsaturated to saturated zone, important flow dominating parameters prevailing in the top soil environment will be evaluated. Preceding diffusion experiments conducted via short term tracer deposition without rainfall before and after tracer injection (but without venting) showed a considerable

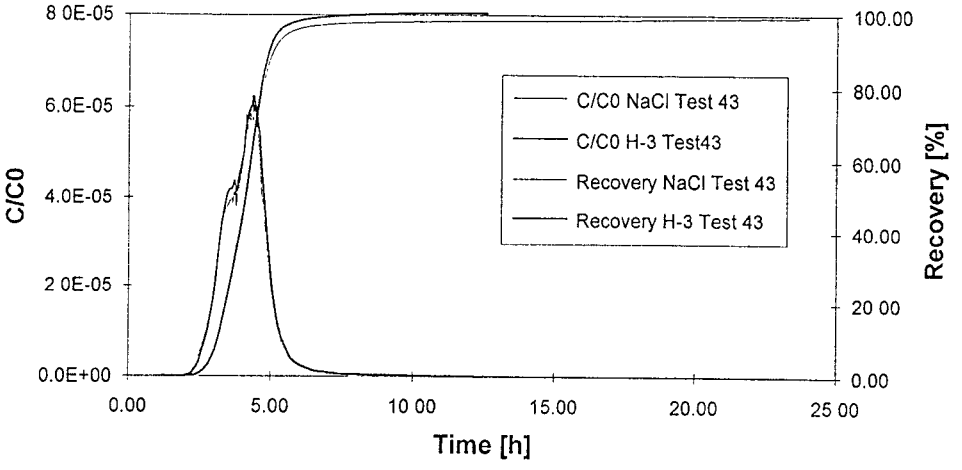

Fig. 3. Tracer breakthrough (measured concentration over the concentration of the injection solution) and recovery curves of simultaneous surface deposited HTO and NaCl tracers followed by continuous rainfall. Under such conditions identical breakthrough profiles are obtained indicating conservative (i.e. non-reactive) behaviour of the salinity.

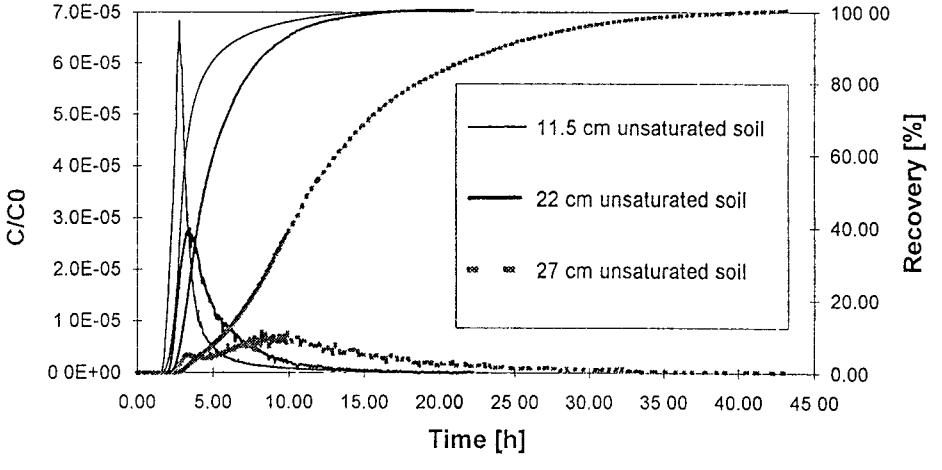

Fig. 4. Breakthrough and recovery curves of Na-Fluoresceine at different ratios of the saturated to the unsaturated zone with heights of 11.5, 22 and 27 cm unsaturated soil.

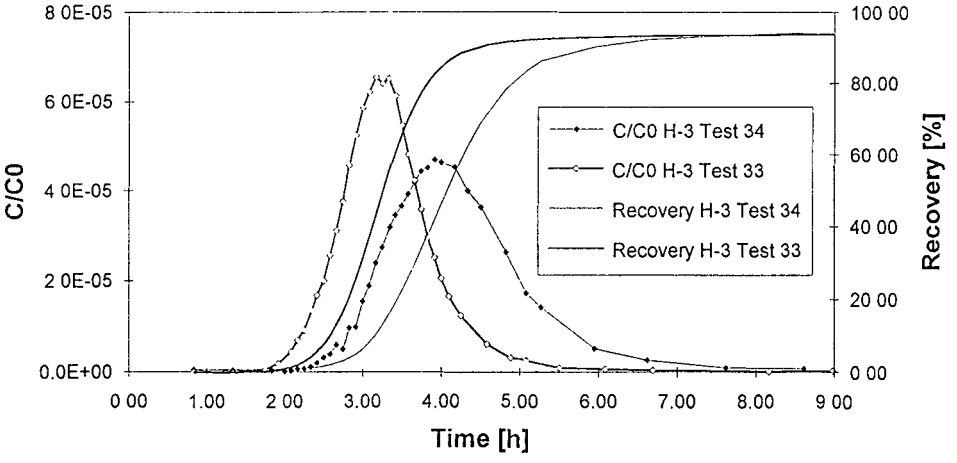

Fig. 5. Breakthrough and recovery curves of HTO obtained under different intensities (10 and 6.5 mL/min) of simulated rainfall.

tracer retardation in the top soil layer (Fig. 6). While in the experiments presented above the tracer pulses ceased within about 1 day (i.e. reaching 100% recovery in that time period), this time only about 30% of the tracers were extracted after one week. To terminate this experiment, rapid washout of the tracer was obtained by starting rainfall again (sharp pulse in Fig. 6, magnification in Fig. 7). The similarity of the tracer breakthrough curves following this manipulation (Fig. 7) indicates that both tracers had gained a similar local diffusion profile in the unsaturated zone.

After having terminated these diffusion experiments, open system experiments under different conditions of top surface contamination (Fig. 8) and different wind flow velocity are carried out. Now the HTO tracer is entering the atmosphere by reemission. By exchanging the atmosphere in the Plexiglas container with air not contaminated with tritium and low water moisture, tritiated water in the system is allowed to evaporate. To obtain the amount of reemitted HTO as a function of time, the gas stream entering the vapor extraction outlet is flushed through a gas washing system in which tritium is fixed by simple exchange between vapor and the aqueous phase (Fig. 2). Clearly, as in the previous tests, the fraction of HTO entering the saturated zone can be monitored simultaneously by collecting water samples for subsequent liquid scintillation counting. Fig. 8 shows two types of reemission experiments with different duration of a HTO wet deposition of 2 and 15 minutes, respectively. While in the first case HTO is deposited initially within the first mm-layers, longer deposition of 15 minutes leads to deeper HTO infiltration. For this reason, HTO reemission in the latter case is significantly retarded (and lower C/C_0-values show up) since those HTO molecules having been transported into deeper layers initially, can evaporate only after having re-migrated (via diffusion) to the surface. After about 1 day both reemission rates are similar shaped since that time diffusion of HTO in the soil layer coupled with capillary transport of water from the deeper zones obviously leaded to similar HTO distributions in the unsaturated zone. Figures 8 and 9 show that the reemission rates of all three reemission experiments presented here do not start with maximum values immediately after HTO deposition. Instead, the reemission rates

exhibit maximum values after about one hour for the 2 minute input experiments (number 73 and 76) and this effect is even more pronounced for experiment 72 (i.e. 15 minute duration of tracer deposition). The reason is that due to the spot-wise water deposition at fixed locations of falling raindrops, HTO deposition does not cover an ideal horizontal layer, but is rather distributed in a cone-shaped geometry. Therefore (immediately after HTO deposition) maximum concentrations of HTO do not occur on the interface of atmosphere and unsaturated zone, but within the first top soil layers. This effect has to be considered seriously by the transport model exercises.

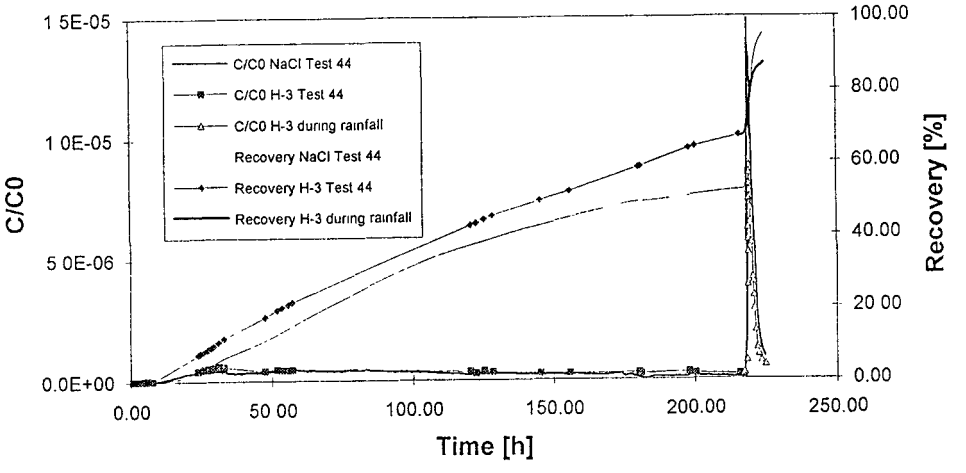

Fig. 6. Breakthrough and recovery curves of HTO and NaCl after wet tracer deposition without further rainfall for 220 hours (followed by rapid tracer washout due to re-starting rainfall). Extremely depressed C/C_0-values due to slow diffusive transport in the unsaturated zone are indicated before the final washout.

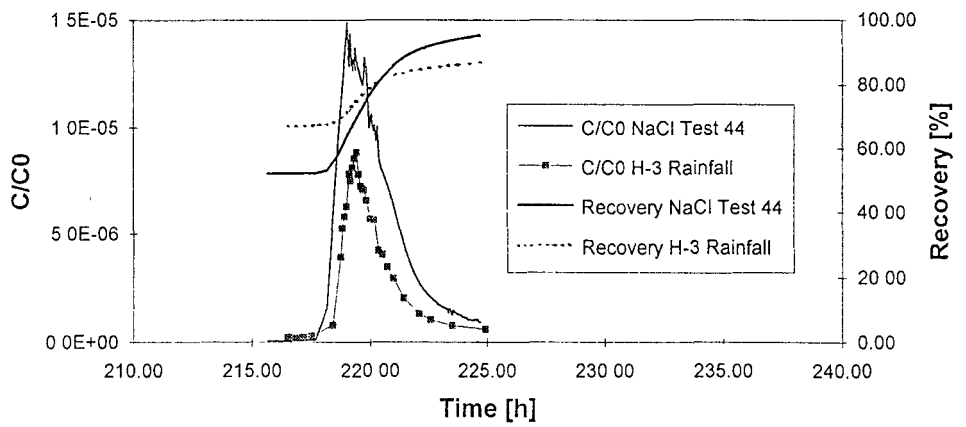

Fig. 7. Magnification of the steep monomodal washout pulses of HTO and NaCl after having re-started rainfall.

The effect of later rainfall on the HTO reemission rate is shown in Fig 9, where the reemission rate strongly decreases immediately after having started a simulated rainfall free of HTO. Since there is a fraction of less mobile tritiated water bound to the soil, the reemission rate does not drop down to zero values initially. This is further supported by the fact, that the simulated rainfall does not homogeneously flush the tritiated water into deeper zones. Therefore plug flow conditions are not obtained, which are, however, also not realistic in a real natural system. The initially strong decrease in the reemission rate can be explained by an initially strong gradient between HTO contaminated water flushed into a deeper zone and rain water in the first top soil layer. This causes an increased diffusive upward transport of higher concentrated HTO per unit of time. After about 5 hours the HTO reemission rate remained (although still slightly decreasing) almost constant, speaking for very little concentration gradients in the unsaturated zone (i.e. almost homogenous distribution of HTO). Fig. 9 also indicates that after about 1 day the reemission rates of both experiments (i.e. without and with later rainfall) have reached an almost similar profile. This is again interpreted as very a similar distribution profile of HTO in the soil after that time.

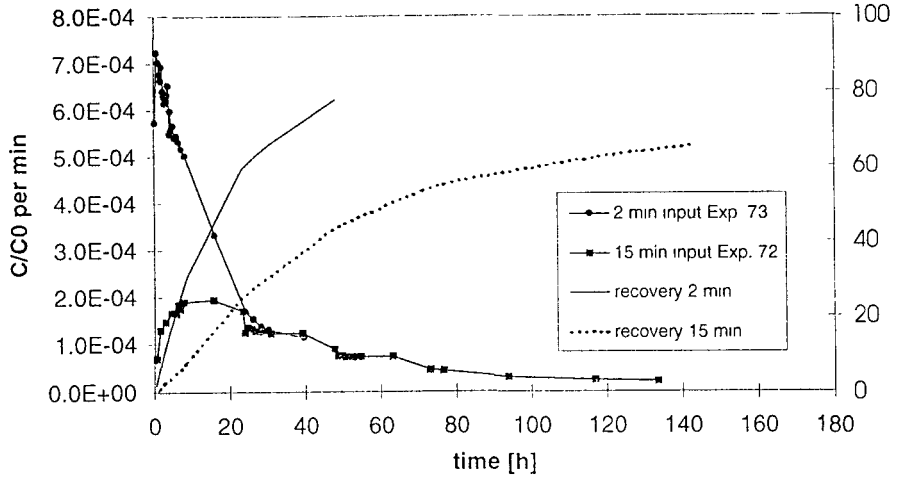

Fig. 8. Reemission profiles of HTO following a 2 minutes short term and extended 15 minutes top surface HTO deposition. Due to deeper infiltration, initial reemission of the extended input is largely depressed, while after ~ 24 hours both reemission curves are similar shaped, indicating similar and low HTO concentration gradients in the unsaturated zone.

Transport model exercises: In order to obtain the major flow governing parameters in both, saturated and unsaturated horizons along with simultaneous reemission into the atmosphere analytical solutions are hardly to apply. Therefore numerical transport model exercises have to be carried out. The two dimensional code used here (MCTAC, Pfingsten 1995) describes particle movement by a random-walk model. Fixed boundary conditions are given by stable inflow and outflow conditions at defined length of the unsaturated zone. Transport processes in the saturated zone are advection, dispersion and diffusion, while rainfall and flow through the unsaturated zone is considered by various source terms at the groundwater surface. Modeling of the hydraulic properties of the flow through system is performed by a two dimensional finite differences flow model based on 21 x 17 nodes. The calculated flow field under steady state hydraulic and flow conditions (i.e. continuous groundwater and surface flow) at fixed height of the unsaturated zone) is depicted in Fig. 10, where the almost

horizontal arrows display the direction and relative velocity of non-reactive species (HTO) in the saturated zone. The increasing velocity in outflow direction is caused by continuous additional water entering the saturated zone from surface infiltration.

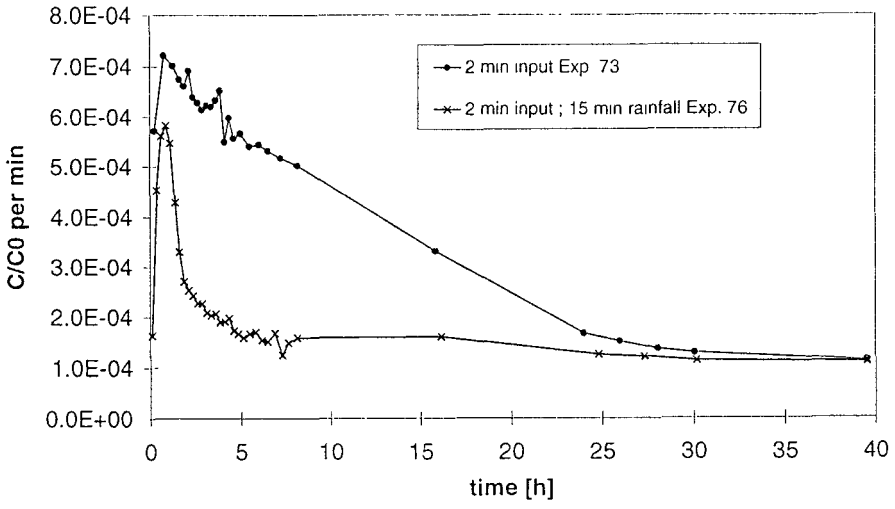

Fig. 9. Reemission profile of HTO following a 2 minutes short term top surface HTO deposition and later deposition of pure H_2O one hour after the radionuclide contamination for a duration length of 15 minutes.

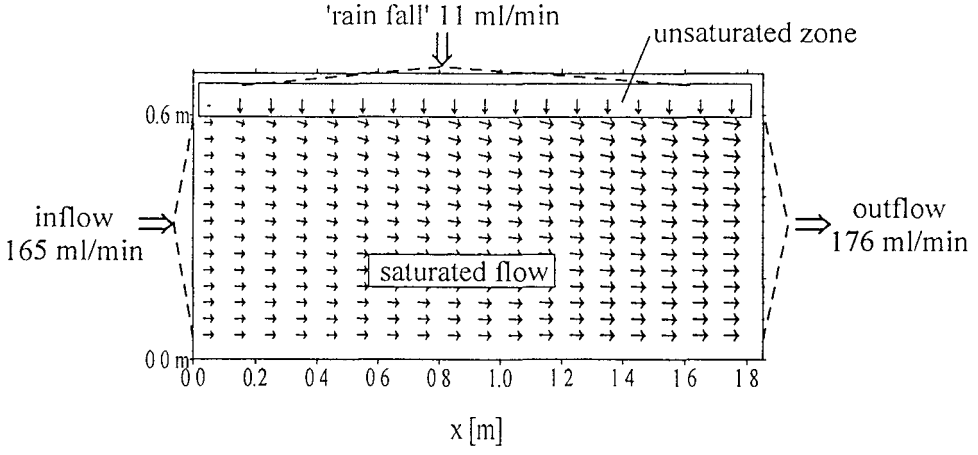

Fig. 10. Schematic illustration of the calculated flow field in the experimental test arrangement for steady state flow conditions with continuous groundwater and surface flow.

Conclusions and future outlook: The dynamics of HTO in top soil layers, following the scenario of a surface contaminated environment from accidental tritium releases, were studied experimentally under controlled laboratory conditions. Preliminary pumping experiments and porosity determinations were conducted for later determination of transmissivity and transfer factors through both the unsaturated as well as saturated zone using the computer code „MCTAC" which is currently extended by implementing time dependent source terms to incorporate unsaturated zone flow with potential evaporation of substances (hydrocarbons, HTO, noble gases etc.) characterized by high vapor pressures. To obtain flow and soil specific transport parameters by later breakthrough curve fitting, several parameters such as flow velocity in the saturated zone, ratio of the unsaturated to the saturated zone and intensity of rainfall were varied. Further experiments focused on pure diffusion and HTO/H_2O reemission experiments with different reemission rates in the atmosphere of the laboratory flow through apparatus due to variation of the time of HTO deposition as well as later rainfalls on the HTO contaminated surface.

The later application of the model exercise to the data set from the experiments is considered to be helpful in understanding and describing the major processes dominating HTO movement at the interface between the atmosphere and the top soil layer. Having determined the key parameters of HTO movement in the different compartments, it is foreseen to perform additional reemission experiments by variation of the length of the unsaturated zone as well as by dry deposition of HTO-vapour on the soil surface.

III. Publications

Eikenberg, J. and Fiechtner, A. (1994) Laboratory investigation on ^3H migration in soils and groundwater. PSI Annual Report 1994, Technical Annex II , 51-54.

Eikenberg, J., Pfingsten, W. and Fiechtner, A. (1995) A laboratory and model study on HTO soil infiltration and atmospheric reemission after surface deposition. In: Tracer Technologies for Hydrological Systems (C. Leibundgut, Ed.) Int. Ass. Hydrol. Sci. Publ. Ser. No. 229 (in press).

Pfingsten, W. (1995) Modular coupling of transport and chemistry. Nagra Technical Report NTB 94-19, National Cooperative for the Disposal of Radioactive Waste, CH-5430 Wettingen, Switzerland (in press).

V. Main contributors to the project

Dr. J. Eikenberg, Dr. W. Pfingsten, Mrs. A. Fiechtner

Head of project 6: Dr. G. Uchrin

Investigators: George Uchrin, Eszter Csaba

II. Objectives for the reporting period

The essential feature of this project is the existence of a tritium source with a well documented history. The records include daily rates of liquid and gaseous tritium releases (more recently also specified by the type of chemical compound), complete meteorological data sets and tritium concentrations in air, soil and vegetation samples taken during the past years. During the running project the collection of environmental tritium levels is being completed by a special sampling program.

It is the aim to evaluate the historic and newly obtained data and to investigate, if there is a correlation between release amounts up to a certain time and the tritium concentrations in environmental samples found at that time.

III. Progress achieved including publications

Introduction

Activity of Tritium Laboratory, Institute of Isotopes, HAS

In the Institute of Isotopes, HAS exists a Tritium Laboratory since early 70's. In the Tritium Laboratory organic compound labeled with tritium were prepared and lighting signs filled with tritium gas were produced.

The amount of the yearly handled tritium is shown in Figure 1. The largest amount of tritium was handled in 1988 and 1989. Since then the tritium handling was decreased significantly from 1992 therefore the releases were also very low.

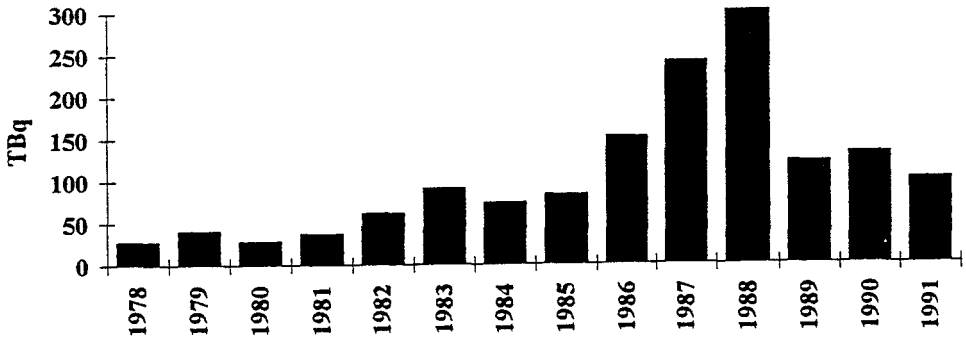

Figure 1. Yearly handled tritium activity

Waste handling

The solid wastes were collected separately and they were buried if their activity was high.

The liquid wastes were collected separately their activity was regularly measured before release and when it was needed dilution was applied. The liquid wastes were discharged through a canal to a natural opened water jump named "Irhas arok " wich ends at Danube river (see Figure8.)

The gaseous effluents were discharged trough a chimney. The height of the release point is 14,5 m from the ground level. The release in this form was not continuous but very often momentary. The regularly control of the released HTO and HT has been started in 1987 and it was finished in 1992. The cumulative activities of released gaseous effluents for 1995 was calculated from the measured tritium release data , see Figure 2.. About 55% of the released tritium was in HT form and 45% of it was in HTO form. The HTO release is divided between the liquid and gaseous effluents, 70 % and 30 % , respectively. The present activity released through gaseous effluents to the environment during the Tritium Laboratoy operation is estimated to be 9 TBq for HTO and 40 TBq for HT, respectively.

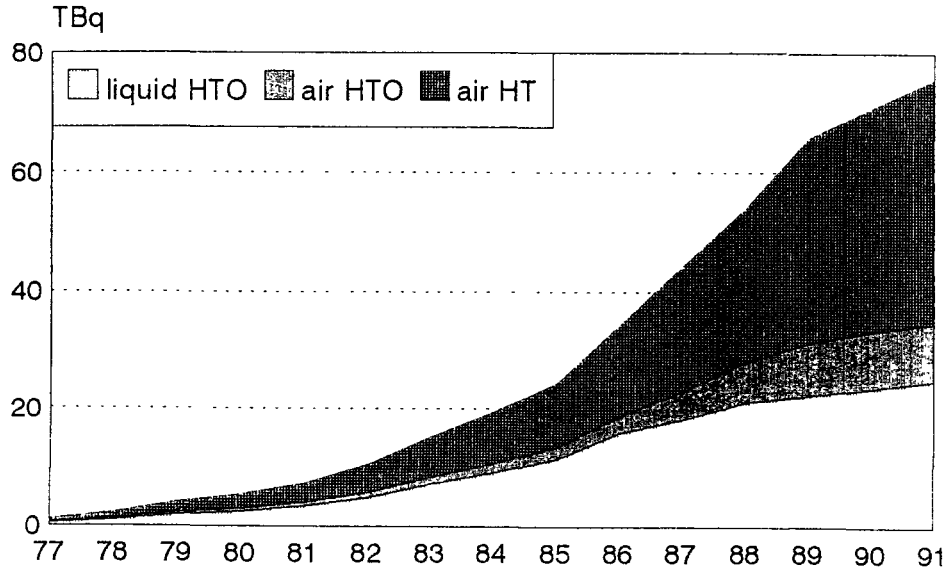

Figure 2. Cumulative activities of released wastes calculated for 1995

Characterization of the release site

The Institute of Isotopes, HAS is located at the border of Budapest city, far from the densely populated area, in the Buda Hills. Its height above the see-level is 430 m. There is a big oak -forest around the institute.

The review and statistical analysis of meerological data have , as a starting point concentrated on the time period between 1987 and 1990, as in this period tritium emissions were highest in the history of the facility. Time bases for averaging of the values are week, month and year, inorder to identify typical variations or similarities.

The climate of the site in concern is typically continental: the average temperature during the summer period is 20-25°C , and in winter it is 0-5°C.; the monthly exposure intensity in summer is equal to 65000 J/cm^2, and in winter is 10000 J/cm^2.; the humidity of the air is 10-12 g/m^3 in summer and 4-5 g/m^3 in winter; the yearly precipitation is about 600mm. The wind speed is about 7-11km/h. The most frequent wind direction was found to be NW (18%), while the least frequent were SE and SW, about 5% each. The yearly averaged "wind rose" based on a five years period is shown in Fig. 3..

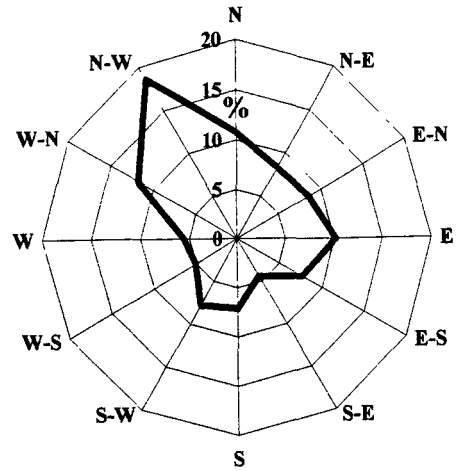

Figure 3. Yearly averaged wind rose at the Institue of Isotopes

We have done the wind statistics of the wind directions for the investigated years was analysed,as an example of a biweekly decomposition is shown in Fig 4.

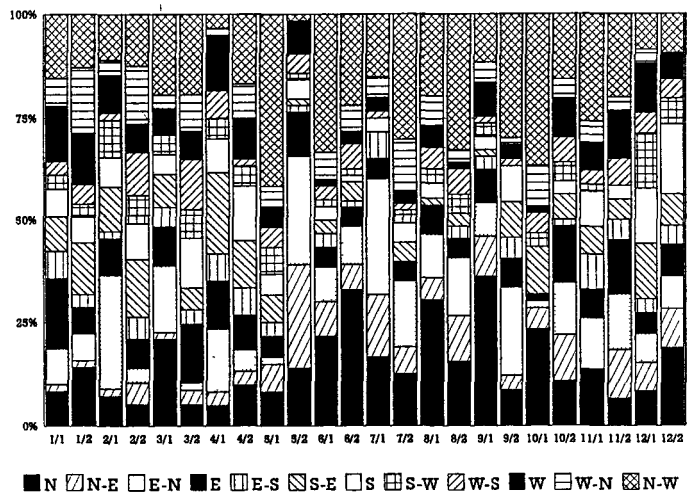

Figure 4. Wind statistics in 1989

The meterological data, first of all the wind statistics were used when integrated dispersions were calculated.

Methods and techniques applied.

LSC measurement

Tritium concentration of water samples was measured by LSC technique, a Packard LS spectrometer Model 1050 and Picofluor LLT scintillation cocktail were used. The sensitivity of our method is equal to 10 TU (or 1,2Bq/l water).

Low level tritium concentrations were determined using electrolytic enrichment, in this case the sensitivity is to 1 TU (or 0,12 Bq/l water).

We have taken part regularly in international intercalibrations devoted to tritium measurements in the latest occasion in November 1994, which was organized by " Bundesanstalt für Gewasserkunde" in Koblenz. Three samples different in concentration were measured our result are shown in the table, below:

code of sample	**T1**	**T2**	**T3**
Institute of Isotopes, HAS	**7,85Bq/l**	**23,4 Bq/l**	**68,8 Bq/l**
Participants mean	**7,25Bq/l**	**21,02Bq/l**	**61,84Bq/l**
Theoretical concentration	**6,81Bq/l**	**21,65Bq/l**	**65,47Bq/l**

HTO/HT air sampling system

In order to measure tritium concentration in the air a differential sampler system has been developed. The main principle of this system is: the moisture of the air is adsorbed on molecular-sieve column,the HT is converted into HTO by a palladium catalyst operating at ambient temperature.The complete conversion is achieved using H_2 as carrier gas produced from a small electrolytic cell. Separation between HTO and HT better than 99%, absorbtion and conversion efficiencies are higher than 99%. The columns of sampler were changed weekly or biweekly. The adsorbed water was desorbed by vacuum distillation and then measured with LSC.

Azeotropic distillation

Azeotropic distillation was applied for preparation of biological and soil samples. The mass of sample prepared depended on its water content. In the case of soil 100 or 200 g sample and 100-150 ml xilol was used and in the case of the grass and "tree" samples these masses are 50-75 g sample and 100 ml Xilol.

HTO/HT concentration in the released air and in the environmental air.

The regular measurement of HTO and HT released by effluents has been started in 1987. Regular monitoring of HT and HTO of the environmental air has been started in 1988 at our Environmental Laboratory which is situating 2.2 km far from the release point in NE direction. Similar monitoring program was initiated at Pestlõrinc at site where the main Meterologycal Station of Hungary is located (20 km far from the capital center) since 1990. The Meteorological Station at Pestlõrinc is located in the E-S direction. The regular monitoring of HT/HTO at Pestlõrinc stopped in 1993 together with the release measurement because of low activities handled in the Tritium Laboratory. This was the time when the Instiute of Isotopes splitted into privat company and research institute.

Using the wind statistics for every sampling period, we calculated the weighed releases which show that how much of the released amount may be expected in the direction of the Environmental Laboratory. With these modification one can derive a better relation between the released amount and the concentration of tritium in the environmental air. Only one representative year are shown from these data. (Fig 5) Results show that in years when the handled tritium activity and releases were the highest the yearly average release rate was about 5-6 GBq/ day for HTO and 25- 30 GBq/day for HT, respectively. The release rate was not steady,it varied according to the works in the Tritium Laboratory. The highest release rate observed was 20-25 GBq/day in the case of HTO and 600 GBq/day in the case of HT (these data are calculated on a biweekly sampling period), respectively. Due to the rather long period of integration in monitoring and in many cases to the short period of release the correlation between releases and environmental tritium concentrations could not be found.

Table 1. contains the data of HTO/HT concentrations measured in the Environmental Laboratory and at the Meterological Station (Pestlõrinc). These data show that the Environmental Laboratory is located in a "contaminated"area, as the average tritium concentrations both for HTO and HT are significantly higher then values observed at the Meterological Station. There is a good correlation between the average HT concentration and the amount of releases, during 1988-89 it was about

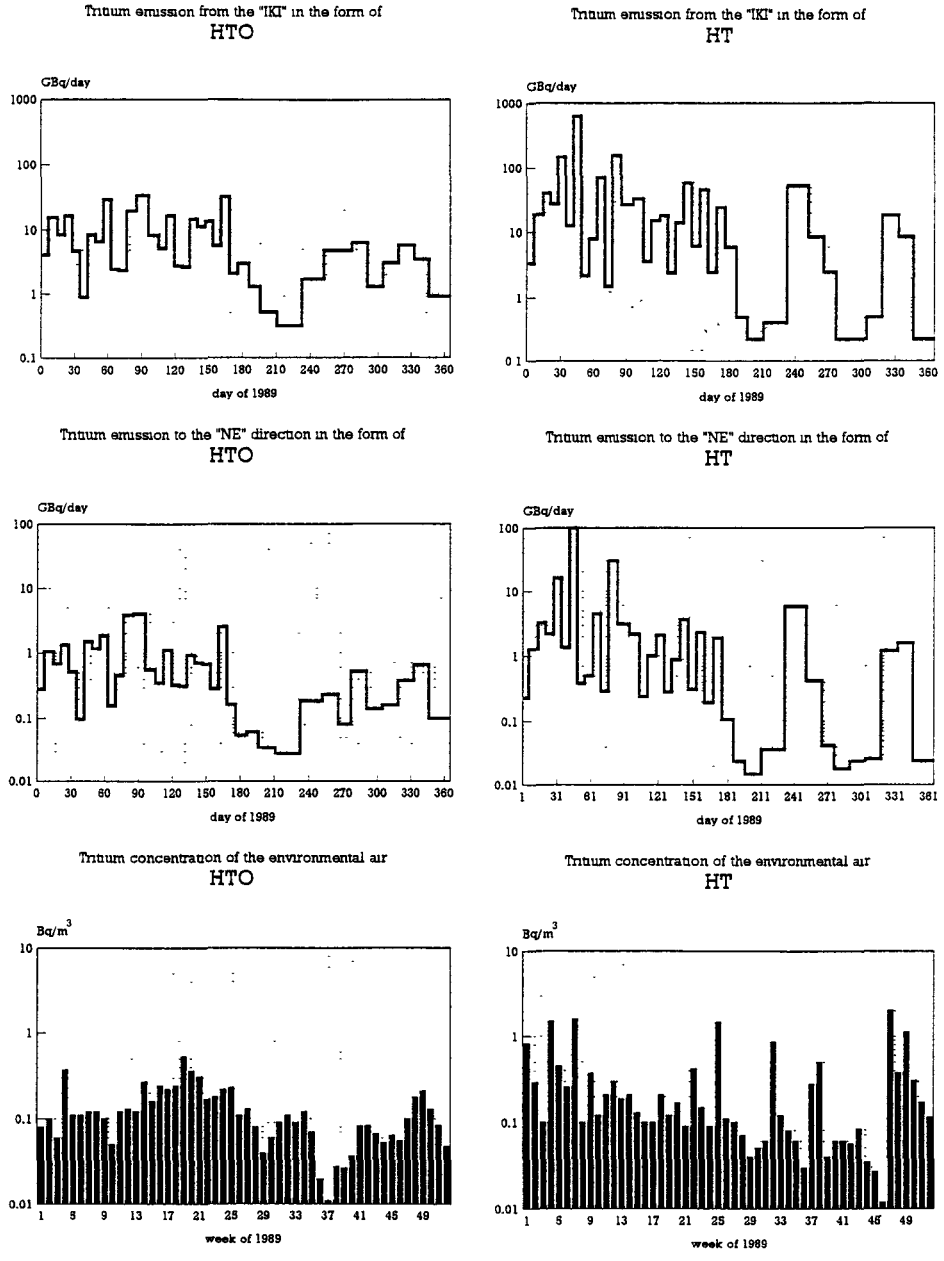

Figure 5. HTO/HT releases and their concentrations in the environmental air 1989

100mBq/m^3 and when the releases decreased the HT concentration also decreased first to 70mBq/m^3 and later to 30 mBq/m^3

Table 1. HTO/HT concentrations mBq/m^3 in the environmental air

	Environmental Laboratory of IKI			Metrological Station Pestlorinc	
	HTO	**HT**		**HTO**	**HT**
Monitoring period	1988-95	1988-95		1990-93	1991-93
Min concentration mBq/m^3	15	12		15	10
Max. concentration mBq/m^3	1500	10000		600	1000
		1988-89	1990-95		
Average concentration mBq/m^3	**50-80**	**~100**	**30-70**	**30-60**	**20-40**

The sensitivity of method applied is 10 mBq/m^3 for HTO and 3 mBq/m^3 for HT,respectively

Environmental biological and soil samples collected during 1994-1995.

In the period of 1993-1995 biological and soil samples were collected around the release point. The investigated area was about one squere kilometer around the tritium source, knowning the wind rose about 100 sampling points were selected from which samples were taken. We collected and measured 170 samples, less than one third of them were soil samples and a little more than two third of them were biological samples. The biological samples included grass samples and so called "tree" samples which means that leaves, fruits, hips from the tree were collected. Table 2. contains the most important data of our samples, and the Figure 6 shows the measured tritium concentrations of the different type of samples. The highest concentrations were found very close to the release point (~100 Bq/kg sample in the case of soil and ~400-500 Bq/kg sample in the case of biological samples) The tritium concentration decreases rapidly by distance and about 500 m far from the release point is mostly less than 50 Bq/kg in the case of biological samples and 10 Bq/kg for soil samples. The tritium concentrations of the water gained from the different samples collected on the same site were very similar (in this case the tritium concentration was expressed in TU) The Figure 7 shows the variation of tritium concentration vs distance from the release point for the highest and lowest wind direction frequency.

Samples were collected in the garden of the Environmental Laboratory of the Institute of Isotopes, too. The tritium concentration of samples taken here were less than 5 Bq/kg for soil, 7 Bq/kg for grass and 3 Bq/kg for tree samples.

From the Figure 8. one can see that the highest contamination is in the direction of the main wind direction (from N-W to S-E) and to the direction of "IRHAS AROK" where the liquid wastes are released.

A rough estimation was done in order to calculate the amount of tritium around the release site within a circle which radius is one km. In the calculation the weighted concentration values, soil water content, wind rose were taken into account and approximately 50 GBq tritium was predicted. It means that about 0,2% of the total releases of HTO was found on the ivestgated territory.

Table 2. Summary of environmental samples analysed for tritium content

Number of sampling sites	**100**
Total number of samples	**170**

Sample characteristics

origin of samples	**Soil**	**Grass**	**Tree**
number of samples	50	40	80
mass of samples (gr)	1000	500	500
depth profil (cm)	surface(0-5cm)		
	5--15		
	15-30		
area (m^2)	0,25		
average water content	5-25 %	65-80 %	50-80 %
sensitivity of methods **	25-5 Bq/kg	2-1,5 Bq/kg	2,5-1,5 Bq/kg

Time periods of sample collection

	1993 Sept.	1994 Aug-Okt	1995 Apr- Jul
number of samples	20	80	70

Distances of sampling sites from the release point

	0-250 m	250-500m	500-2500 m
number of samples	65	55	50

Range of tritium concentrations (Bq/kg sample)

distance from the release point	**Soil**	**Grass**	**Tree**
0-250m	**10-100**	**30-460**	**20-500**
250-500m	**5--50**	**10--300**	**5-250**
500-2500m	**5--70**	**7--40**	**4--40**

*note : tree denotes samples such as leaves of trees andbashes, fruits (apple, rose hip, elder, strawberry..)

** it is calculated on the basis of tritium measurement sensitivity of water content of environmental samples

Soil samples 1994-1995

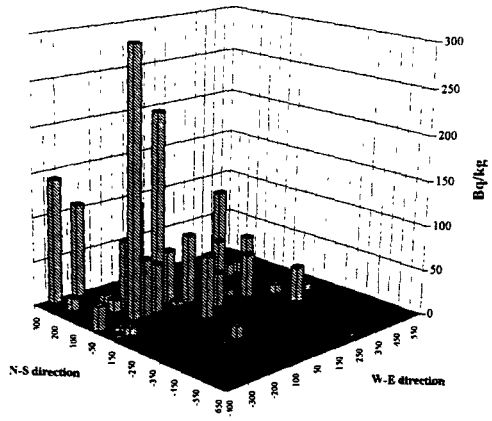

Grass samples 1993-1995

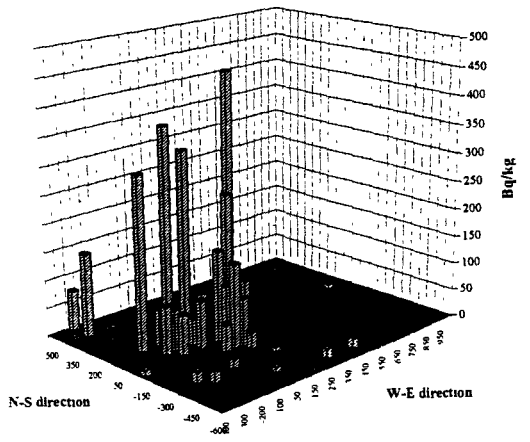

Tree samples 1993-1995

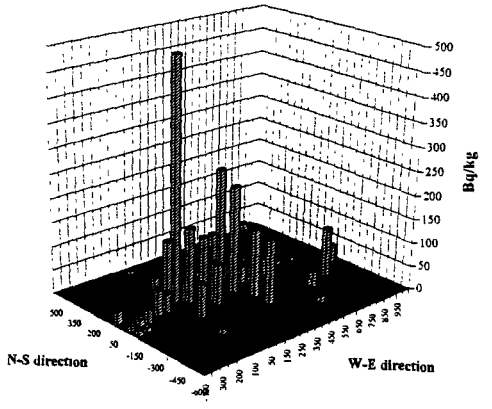

Figure 6. Tritium activity concentration of the environmental samples collected

Some general conclusions

On the basis of regular monitoring of tritium discharges and environmental air samples together with analysis of environmental samples taken around the tritium release point the main conclusions may be summarized are as follow:

i) high rate and long term discharge of tritium did not cause radiologically significant contamination of local area, less than 0.2% of the released activity in HTO form is estimated to be still present in the local environment, the highest tritium concentration of environmental samples does not exceed 500 Bq/kg.

ii) the distribution pattern of tritium concentration around the release point is in agreement with those which may be expected on the basis of integrated release, averaged meteorological data.

iii) dispersion of HTO and HT for a given monitoring site (Environmental Laboratory which is 2.2 km far to the NE direction from the release) are different by a factor of 3, for HT is being higher.

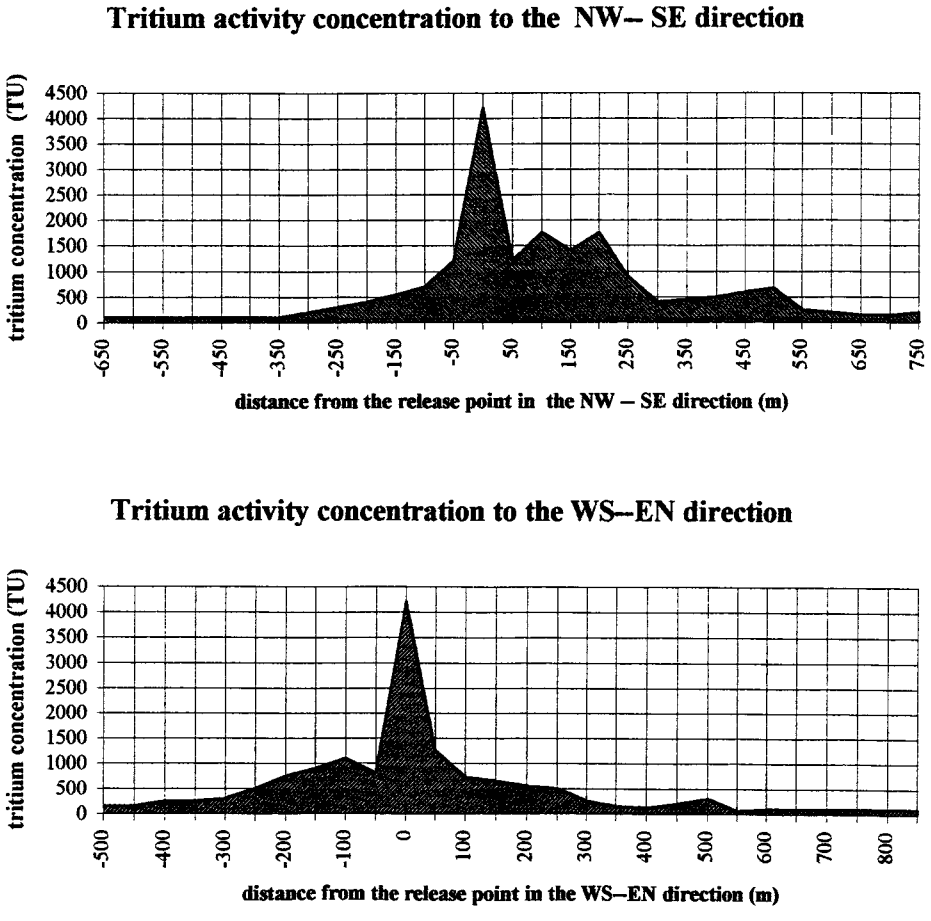

Figure 7 Distribution of the tritium concentration in two wind direction

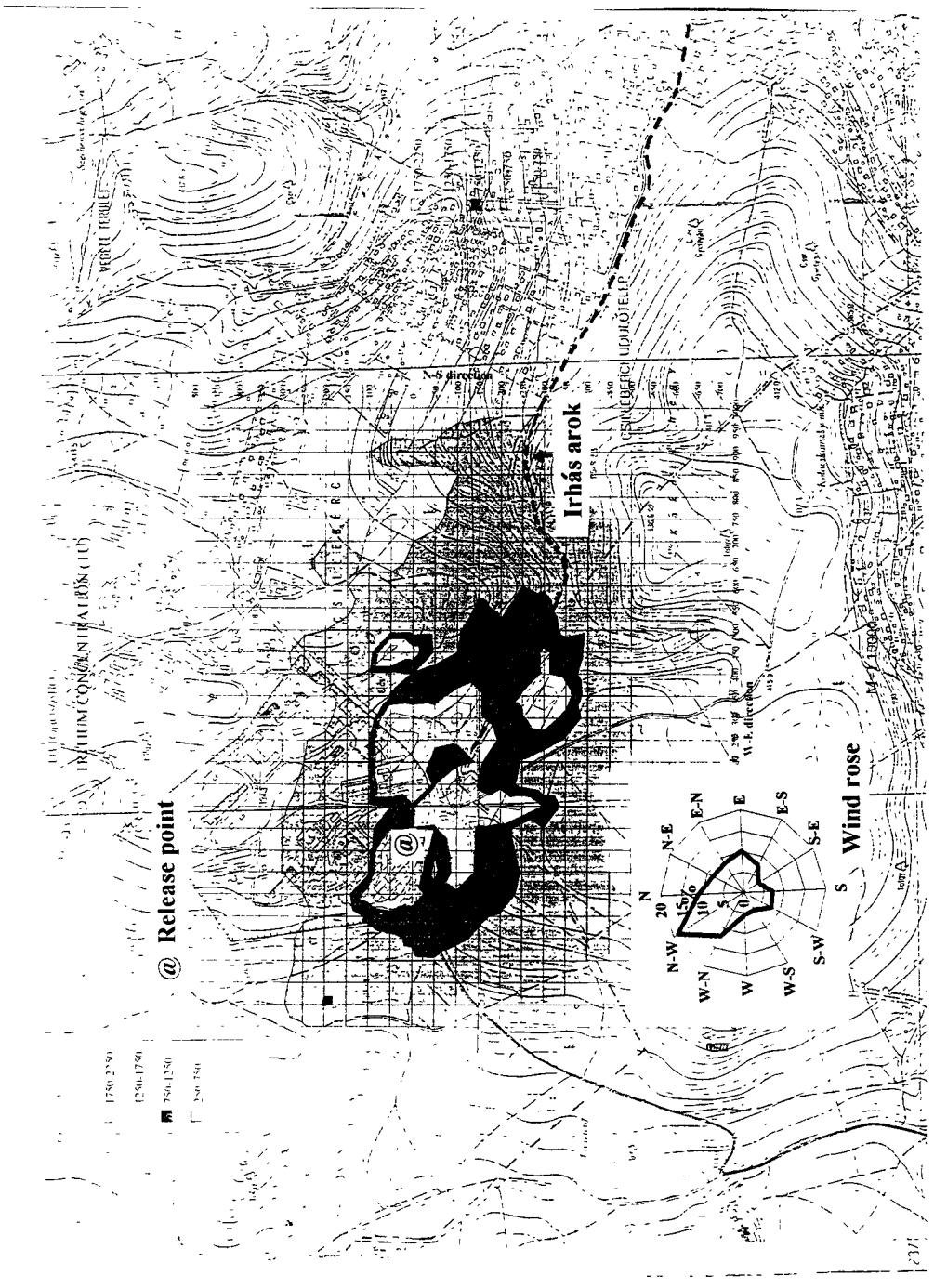

Figure 8. Average tritium concentration (TU) around of the released point in 1994-1995.

Head of project 7: Dr. N. Paunescu

II. Objectives for the reporting period

The lowering of regulatory dose limits and the need for reliable prediction of the risk from tritium exposure have generated an increased interest in environmental tritium modelling.
The commissioning and operation start of a heavy water reactor in a background area is a very good opportunity to study the dynamic of tritium concentration in environmental media and to verify model predictions.
In view of the expected operation start of the Romanian CANDU- type reactor near Cernavoda, in a background area, this project focused on the following objectives during the preoperational phase:
. meteorological and dose relevant characterisation of the reactor site
. upgrade of the analytical and measuring techniques, including the different chemical forms of tritium
. training of the involved personnel
. taking and analysing of background samples;

III. Progress achieved including publications

Characterisation of nuclear power plant site

The site of the Cernavoda nuclear power plant is situated in the SE of Romania, between the Danube River and the Danube - Black Sea Canal . The towns near the nuclear power plant are Cernavoda (2 km, 30000 inhabitants), Medgidia (18 km, 39000 inhabitants) and Fetesti (18 km, 39000 inhabitants) (fig 1). The local climate is prevalent continental and characterised by:
- large temperature differences between winter and summer (68 ^{o}C) ;
- long sunshine duration (2200 hours/year);
- approximate 202 days/year the average temperature more than 30^{o}C;
- reduced rainfall (500 mm/year) compared to the rest of the country.

Air movement is most often following the Danube valley in the N-S direction (fig 1). The prevailing wind directions are as follows: N (10.1 %); WSW (7.9 %); NNW (7.6 %); W (7.3%) (Data of National Institute for Meteorology and Hydrology). There is an unusually high portion of calmness of 25%, with a maximum of 34.2% in September (the definition of calm:wind less than 1m/sec). This is of special importance with respect to the dispersion of the release plume. The close vicinity of the Danube is responsible for the great number of misty days during the cold season.
The agricultural land use is intensive at distances beyond 5 km. Cereals (wheat, rye, maize, barley), fruits (apricot, apples) and grapes are the major agricultural products. Specific animal products of the area are sheep milk and meat, poultry, eggs, fish. The food intake of local population is closes to the typical Romanian diet, with high cereal intake (about 140 kg/year for adult), rich in vegetables and fruits, comparable with mean European habits for dairy products, and slightly less for meat. Comparing to national average, fish consumption is higher and sheep meat and milk shares a larger part of diet.

The routine atmospheric tritium releases from the 3 GWe nuclear power plant site are expected to be about 460 TBq/aGWe and the aqueous releases are estimated to 350 TBq/aGWe, representing a tritium source which is 2 to 3 orders of magnitude more effective than a light water reactor . For the most unfavourable conditions, concentration of HTO in air humidity will be about 400 Bq/L, and the same concentration will be in Canal water and Tibrin lake water. The Cernavoda nuclear power plant will be one of the most important tritium source of Europe.

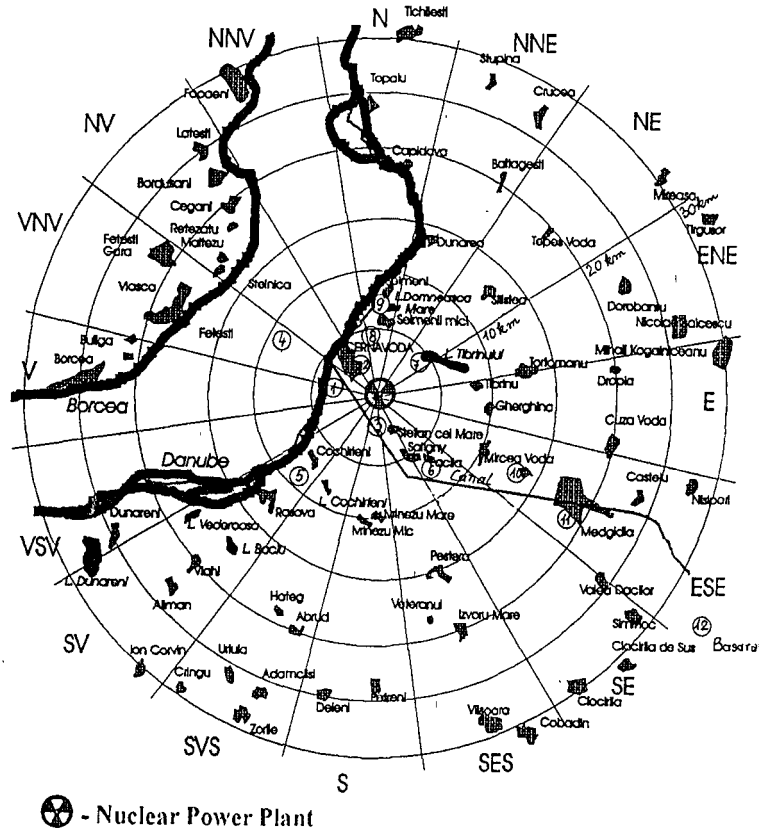

Fig. 1. Cernavoda area

The start of operation has been envisaged for spring 1995, but was postponed, so that project work until now was limited to background measurements of tritium concentration in different kinds of samples:

-air ;
-water from: Danube River, Danube-Black Sea Canal, lakes; drinking and ground water, rain (snow) water ;
-HTO concentration in soil at different depths;
-tissue free water tritium in vegetal and animal foodstuff: cereals (wheat, maize, barley), vegetables (potatoes, tomatoes, cabbage, onion, bean, etc.), fruits, milk, wine.
-organically bound tritium (OBT) in maize grains.
These types of samples are representatives for Cernavoda area and are relevant for human diet.

Equipment and methods

The HTO measurements were carried out in a liquid scintillation analyser TRICARB TR 1600 equipped with High Sensitivity Count Mode feature for increasing the sensitivity by reduction of background without affecting the counting efficiency of the isotope.
Two types of hydrophilic scintillation cocktails with high sample holding capacity were used: Instagel, for water samples and recovered water from molecular sieves, and Pico-Flour^{TM}LLT, for tissue water counting.
For each scintillation cocktail a quench curve was preparated with 10 quench standards in polyethylene vials, in order to determine the counting efficiency. The quench standards, the background and the environmental samples were counted in the same manner. The values of background, counting efficiency and detection limit are shown in the Table 1.

Table 1

Scintillation cocktail	Setting region (KeV)	Water/cocktail (mL)	Background (cpm)	Counting efficiency (%)	Detection limit for 800 min (Bq/L)
Pico-Fluor LLT	0.5-3.5	10/10	3.5	20	2.6
Instagel	0.5-7	8/10	6.5	37	2.4

Two counting vials were prepared for each water sample. After at least two days of storage the samples were measured for 400 - 500 minutes each counting vial.

Tritium in air

Determination of tritium in air concentration was performed by using a sampling system for trapping the atmospheric tritium in the form of water vapours on molecular sieves (Fluka 3A). The sampling system is consisting in: a pump for drawing air at controlled air flow rate, a flowmeter and a sample collector with molecular sieves. The air flow rate is 4 L/min and the collector contains between 100g and 300 g of molecular sieves for retaining the total water vapours contained in 2 to 6 m^3 of air. The adsorbed water is recovered by heating the molecular sieves in a furnace at 300 ^oC connected to a vacuum line and collecting the water sample in a freeze trap (- 60^oC). The recovered water is distilled with $KMnO_4$ and tritium concentration measured with Instagel.
Measurement of HTO concentration were carried out at Basarabi and Cernavoda town sites. The results are presented in Table 2.
The Basarabi site are not in the main wind direction, and after start of nuclear power plant will be a "control" site. Now, is not a difference between the concentration of tritium in these two sites, and tritium concentration is in agreement with the values for background area.

Table 2 HTO concentration in air , in $mBq/m^3 \pm SD$ of counting error

Sampling date	Sampling site	Temperature (^oC)	Relative humidity (%)	Tritium concentration (mBq/m^3)
5.07.1994	Basarabi	31	44	54 ± 15
4.07.1994	Cernavoda	22	70	48 ± 19
14.03.1995	Basarabi	0	100	68 ± 22
27.07.1995	Basarabi	28	55	32 ± 13
26.09. 1995	Cernavoda	18	78	41 ± 18

Tritium in water

Water samples were collected from different sites of interest and aliquots of 50 mL were distilled with $KMnO_4$. The samples were measured in polyethylene vials with Instagel, 500-600 min each vial. The sampling sites are presented in fig 1 and the results in fig 2.

The tritium concentration in surface water is the same like in rain water: most of the values are below the detection limit (2.4 Bq/L), and the maximum is 6.9 Bq/L. The tritium concentration is higher in Danube River (average 4.0 Bq/L) and smaller in drinking water (2.7 Bq/L; for average, we consider the detection limit in the case when the values are below the detection limit).

The tritium concentration in rain and snow water is presented in Table 3

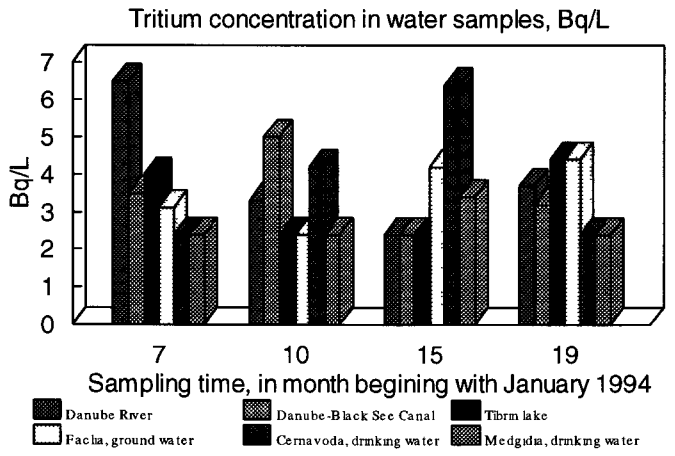

Fig 2 Tritium concentration in water samples from different locations

Table 3 .Tritium concentration in rain or snow water (Bq/L ± SD of counting error)

Sampling period	Bq/L ± SD
May- June 1994	6.9 ± 0.5
Nov. -15 Dec 1994	< 3
15 Dec. 1994-Jan 1995	5.5 ± 0.4
February 1995	3.4 ± 0.3
14 March 1995	4.1 ± 0.3
15-30 March 1995	< 3
April 1995	< 3

Tritium in soil

Soil samples from Basarabi (site 12) were analysed for HTO content. Soil cores of 20 cm length were homogenised and sub samples of 200 g were azeotropic distilled with toluene. The water was distilled and 10 mL with 12 mL of Picofluor LLT scintillation cocktail were measured by Quantulus liquid scintillation analyser. The results are presented in fig 3. The concentration of HTO is low and almost constant from the surface of soil till 150 cm depth. The presence of tritium is due to the atmospheric precipitations., the surface soil concentration of about 4 Bq/L is close with measured rain water.

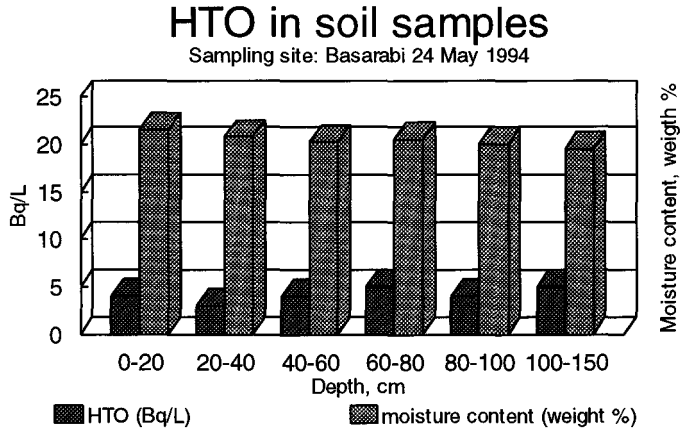

Fig 3 Tritium in soil samples

Tritium in vegetation

The vegetation samples were prepared by azeotropic distillation for determination of tritium water tissue concentration (TFWT). Edible parts of unwashed vegetable samples were used for analysis. All samples were cut and frozen until the preparation time. Tissue water was collected by azeotropic distillation with toluene, from 50-300 g sample. The toluene was tested and found free of tritium. After azeotropic distillation, the water was distilled once or twice and UV spectra recorded in 200-340 nm region. 10 mL of water were mixed with 10 mL Pico-Flour LLT in polyethylene vials. Two counting vials were prepared for each water sample. After at least 2 days of storage (24 hours in the dark at room temperature and 24 hours in the counter) the samples were counted for 400 - 500 minutes each vial.

The water content was determinate by drying the samples in oven, at 102°C and dried untill reaching constant weight. The most important kind of vegetation samples for Cernavoda area and human diet were analysed: cereals, vegetables, fruits, grapes, wine and milk. For each kind of vegetation were analysed many samples (see Table 4), and the TFWT average concentration of vegetation samples are presented in Table 4.
The concentration of TFWT is almost constant in cereal samples analysed, the values ranging between 4.0 and 6.8 Bq/L of tissue water. The TFWT concentrations expressed for fresh weight are 0.74 Bq/kg fw (wheat), 0.79 Bq/kg (barley) and 0.68 Bq/kg (maize).
The TFWT in vegetables ranged between values <2.4 and 8.2 Bq/L (Table 4). These values are in agreement with values for background area from Europe.
Vine leaves, different varieties of grapes and wine were analysed for tritium content. The results are presented also in Table 4. The tritium activity of leaves is higher, in ranged between 3.1 and 8.6 Bq/L, with an average of 5.7 Bq/L. In grapes, the TFWT is generally below the detection limit and in wine the average of HTO is 3.0 Bq/l.
Fig 4 presents the tritium concentrations for soil, rain water and wine-growing produces from Basarabi, the most important wine producer in this area. The tritium concentration is in the same range for all kind of samples.
In addition, several old wine samples were analysed for tritium content at Environmental Research Lab. at AECL Chalk River (manager J. Cornett, group P. Davis, W. Workman, T. Kotzer, R.B. Brown; M. Wood- Health Physics branch). The procedure consist in: ethanol extraction by fractionating distillation, followed by azeotropic distillation of the remaining wine sample. The samples were measured by liquid scintillation analyser (Quantulus) or by He-3 mass spectrometry, if the expected activity was below 10 Bq/L. The results are shown in fig. 5. HTO in wine must be correlated with HTO in precipitations. For the area around Cernavoda, HTO in precipitation was measured from 1980 until 1988. In the limit of experimental errors the wine HTO in 1983, 1986 is close to reported mean activity of HTO in June-October precipitation in the same year. There is no data in Romania for the period 1960-1970 . In respect with HTO in precipitations at Vienna for 1962, the Basarabi wine has 78% and in 1963 45% from the annual mean in Vienna precipitations. The 1963 values seems to low- perhaps the wine have deep roots and have extracted also 1962 water.

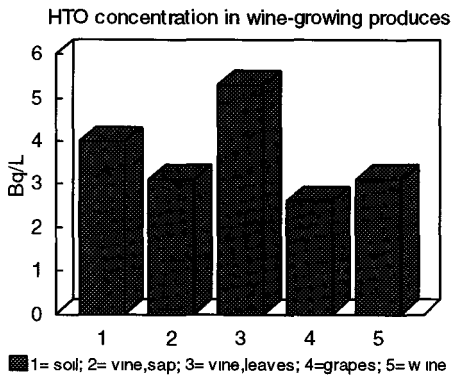

Fig 4.Tritium concentration in wine-growing produces

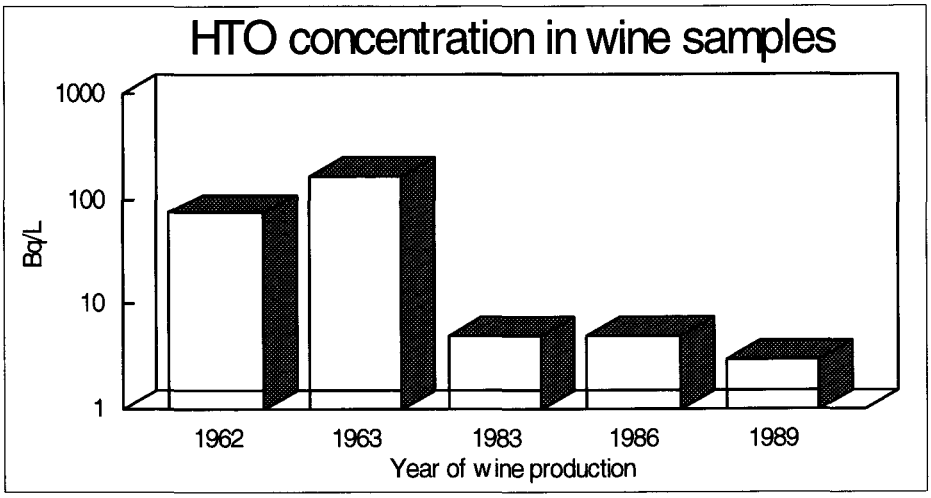

Fig.5. Tritium concentration in old wine samples

Table 4 .TFWT concentration in vegetation samples (Bq/L ± SD)

	Sample	No. analysed samples	Sampling time	Water content (%)	Bq/L ± SD
1	Wheat, leaves	1	14. 3.1995	81.5	3.8 ±0.4
2	Wheat, grains	4	1994	14.3	5.2 ±1.0
3	Barley, grains	3	1994	13.6	5.8 ±1,0
4	Maize, grains	5	1994	11.4	5.9 ±1.1
5	Potatoes	4	1994,1995	76.1	5.5 ±1.3
6	Tomatoes	3	1994,1995	95.1	3.2 ±0.9
7	Onion	3	1995	89.5	<2.7
8	Cabbage	3	1994,1995	91.8	6.3 ±1.5
9	Green pepper	2	1994, 1995	94.7	3.4 ±0.5
10	Aubergine	2	1994,1995	91.7	3.6 ±0.6
11	Bean, pods	2	1994,1995	86.7	4.2 ±0.4
12	Bean, grains	1	1994	8.0	5.7 ±0.6
13	Vegetable marrow	1	1994	94.0	5.0 ±0.4
14	Cucumber	1	1994	95.5	4.0 ±0.4
15	Lettuce	1	1994	96.0	3.4 ±0.3
16	Carrot	1	1994	88.0	4.8 ±0.5
17	Apples	2	1994, 1995	86.2	<3.2
18	Apricots	1	1995	88.2	2.8 ±0.4
19	Clover	1	1994	77.5	3.5 ±0.4
20	Grass	1	1994	70.2	4.3 ±0.4
21	Pine needles	4	1994, 1995	48.4	13.4 ±1.7
22	Milk, cow	3	1994	87.5	<2.6
23	Vine, sap	1	1994	97.0	3.1 ±0.3
24	Vine, leaves	3	1994, 1995	73.0	5.7 ±2.0
25	Grapes	4	1994, 1995	92.5	<2.9
26	Must	1	1994		<2.6
27	Wine	3	1994		<3.0

Two samples of maize grains were analysed for TFWT by freeze-drying and for OBT by plasma-oxidation technique in the laboratory from Forschungszentrun Karlsruhe , HS/US, Germany, by the kindness of Dr. K-G. Langguth and Mr. H. Genzer, and with help of tritium group (Dr. S. Diabate and Dr. S. Strack).
The results are presented in Table 5. The values for TFWT obtained in Germany laboratory (FTU) are in very good agreement with the values obtained in our laboratory (IPNE).

Table 5

Sample	Laboratory	Sampling time	Water content (%)	TFWT (Bq/L±SD)	OBT (Bq/L±SD)	Tritium total (Bq/kg fw)
Maize, grains	IPNE	crop 1994	13.0	5.9 ± 1.5		
Maize, grains	FTU	crop 1994		5.7 ± 1.3	4.2 ± 1.3	2.8 ± 1.3
Pine needles	IPNE	1995	46.7	10.5± 2.0		
Pine needles	FTU	1995		11.2±1.5	6.9 ± 1.6	7.3 ± 1.6

Co-operation and training the personnel

In the frame of this contract N. Paunescu had an working stage in Forschungszentrum Karlsruhe HS/US, tritium group (Dr. S. Diabate , Dr. S. Strack) and participated at the experiment for OBT formation and translocation in wheat and bean after an acute exposure to HTO in air. M. Cotarlea had an working stage in the same laboratory for training the methods for TFWT and OBT determination by different methods (freeze drying, combustion of sample by Packard Oxidiser and Plasma Oxidiser).

Publications

1. *Paunescu N., Cotarlea M., Purghel L., Galeriu D., Mocanu N., Margineanu R.*, -"Method to determine low level of HTO in air", Romanian J. Phys. 40(3), 1995.
2. *Galeriu D.*,-"Transfer parameters for routine release of HTO", report AECL 11052, COG-94--76, 1994

Final Report
1992-1994

Contract: F13P-CT920006 Duration: 1.9.92 to 30.6.95 Sector: A24

Title: Transfer of radionuclides in animal production systems

1)	Howard	ITE
2)	Assimakopoulos	Univ. Ioannina
3)	Crout	Univ. Nottingham
4)	Mayes	Macaulay Land Use Research Institute
5)	Voigt	GSF
6)	Vandecasteele	CEN/SCK Mol
7)	Zelenka	UAB.FAGR (PECO contract)
8)	Hove	AUN
9)	Hinton	PSI

I. Summary of Project Global Objectives and Achievements

The groups' studies have focused on the three radionuclides which are most likely to contaminate animal tissues, and particularly milk, in the event of a nuclear accident; radiocaesium, radiostrontium and radioiodine. The objectives of the programme were:

1. To provide improved information on the behaviour of radionuclides thereby enhancing the ability to predict contamination levels in animal products under different conditions.
2. To determine the true absorption coefficient of mobile radionuclides, in order to provide a physiological parameter which is more mechanistic than transfer factors.
3. To identify and quantify physiological and environmental parameters which affect the transfer of radionuclides to animal products.
4. To identify and test appropriate countermeasures to prevent radiocontamination of animal products.
5. To develop mechanistically based models of the transfer of radiocaesium, radiostrontium and radioiodine to food-producing animals (ruminants and poultry) with the aim of being able to model the effectiveness of countermeasures, stable element status and the influence of physiological parameters.

The programmes' findings are summarized for each radionuclide below.

Radiocaesium

The group recommends a true absorption coefficient value of 0.8 be used for sheep for ionic radiocaesium, or that incorporated into plant material [1,4,6], with reported values range from 0.6 to 1.0. Measurements conducted within this programme suggest that a suitable recommended value for dairy goats would be close to 1 [8]. Measurement of true absorption provides a powerful tool to estimate bioavailability of possible future releases of radiocaesium.

Instead of developing separate models for different ruminants the group has investigated whether it is possible to generalize models of radiocaesium behaviour in ruminants [2]. The model developed by NPL for the transport of trace elements

through animals states that the transfer coefficient *f(k)* to any compartment *k* of an animal is related to the feed-to-blood transfer coefficient *f(blood)* through the simple expression

$$f(k) = a(k)\, f(blood)$$

in which *a(k)* is a constant, independent of animal size or the animal's diet. Consequently if the coefficients *a(k)* are determined, a measurement of *f(blood)* leads to an estimate of the transfer coefficient to any compartment *k* of the animal at equilibrium. Experiments with cows, sheep and goats have been carried out to test this hypothesis. The data were used to calculate the ratios, *a(k)*, in the above equation. The *a(k)* values for each compartment agree within the experimental error for the different sets of animals considered. Therefore, using values of *a(k)*, estimates of tissue contamination can be made from blood sampling alone. However, this is only valid at equilibrium.

Similarly models used within the programme [3], which previously could not be used for sheep of different weights, have been reparameterised so that radiocaesium transfer between compartments is driven by activity concentration rather than total activity. This modification provides a more generally applicable model which can be used to predict radiocaesium transfer in sheep with a wide range of body weights (30-80 kg). However, experiments from the current programme have shown that physiological status and feed intake rates can influence radiocaesium levels within tissues; the model does not yet incorporate these effects [1,4].

During both pregnancy and lactation the transfer of radiocaesium to the muscle of ewes declined in the order:

Barren > ewes bearing single lambs > ewes bearing twin lambs

Differences between animals were greater during lactation, and could be explained by the secretion of radiocaesium in milk. Transfer coefficient to the milk of ewes bearing single lambs were 25% higher than those for ewes bearing twin lambs. However, total outputs were similar due to the higher milk yield of the latter group. After weaning, the transfer of radiocaesium to the muscle of ewes which had had lambs returned to a similar value as that of barren ewes. Radiocaesium transfer to barren ewes receiving a maintenance diet was significantly higher than that of barren ewes receiving a diet which was 50% above maintenance. In a further study the radiocaesium transfer to lambs with a low growth rate (0.01 kg d^{-1}) was shown to be in the order of 1.5 - 2 times higher than that to lambs with a higher rate of growth (0.18 kg d^{-1}). Initial results using ^{35}S to give an estimation of the degree of protein turnover suggest a relationship with radiocaesium uptake. The results also suggest that manipulation of dietary intake rates combined with the feeding of uncontaminated feed could be a more effective countermeasure than the simple provision of uncontaminated feedstuffs.

Further studies have been conducted on various aspects of countermeasure strategies for contaminated animals. The use of stable Cs is not recommended as a countermeasure. Daily administration of stable Cs, at rates of up to 2 g d^{-1}, to lactating goats did not reduce the transfer of radiocaesium to their meat and milk [8]. Consideration has also been given to the potential effects of the presence of AFCF in faeces on soil to plant transfer and possible toxicity [6]. The addition of faeces obtained from a sheep given 2 g d^{-1} AFCF reduced radiocaesium transfer to plants, regardless of whether the radiocaesium was already in the soil, or present in the

faeces. Applying AFCF in faeces at a rate of 1 g m^{-2} decreased the transfer of radiocaesium from soil to plant by a factor 4 to 5. Detrimental effects were only noted at unrealistically high administration rates of AFCF (1 kg m^{-2}) which were probably due to physical inhibition of plant growth. Therefore the addition of AFCF binders to the diet of animals will not only reduce the transfer of radiocaesium to its tissues, but also from soil to vegetation in pastures on which its faeces are deposited.

A mixture of 2% FeHCF and zeolite (RADEKONT) fed to broiler chicken effectively reduced radiocaesium uptake; the effect is probably attributable to the FeHCF in the mixture rather than the zeolite, although this provides a suitable substrate to enable the feeding of small amounts of FeHCF to poultry [7].

Control data for the rate of transfer of radiocaesium to different tissues has been used to develop a model for broiler chickens [3]. Because of the high rates of growth of the birds during the study it was necessary to use activity concentrations rather than total activities to drive transfer between the compartments of the model. When applied to other data the model does not currently accurately describe the data, possibly because of different rates of growth between the studies. During decontamination with uncontaminated feed the activity concentrations decreased rapidly with biological half-lives between 0.6-2d. There are few similar available data for rapidly growing poultry and further work is needed to satisfactorily model radiocaesium transfer to such animals.

Experimental work has been undertaken [5] to investigate the effect of grazing intensity on the soil to plant transfer of radiocaesium to test preliminary model predictions which suggested that more heavily grazed swards would initially have a higher activity than lightly grazed swards, but that in the longer term heavily grazed swards would have a lower radiocaesium activity concentration [3]. The experimental results showed a high variability in vegetation activity concentration and no grazing intensity treatment effects for radiocaesium, or a range of other radionuclides. Nevertheless, the data were used to provide a test of the basic soil and vegetation transfer models, which are linked to our ruminant models. The radiocaesium kinetics of the soils used were measured [3]. Kinetic models were then fitted to the data to provide parameters for the model, where the soil was divided into solution, non-specifically absorbed labile, specifically absorbed labile and non-labile (i.e. fixed) compartments. The results were used to simulate the vegetation activity concentration over the experimental period. The overall pattern of the data appears to be reproduced which is encouraging given that the prediction is based solely on the soil kinetics, and vegetation growth and transpiration estimates made by the model. It does not rely upon empirically derived soil-plant transfer factors.

In farm experiments a 10 fold difference was observed in milk ^{137}Cs activity concentrations (and 2 fold difference in F_m) under two different grazing regimes which could not have been anticipated from the similar ^{137}Cs levels of sampled vegetation. Reasons for the observed difference were not understood, but could have been associated with representativeness of sampling procedures or soil ingestion. Other studies conducted by the group have shown that it is important to calculate soil loadings using the concentrations of the soil tracer and contaminant in the resuspendable particle size fraction of soil, rather than the mean concentrations in unfractionated soil [9]. This is due to (i) the particle size dependence of resuspension, (ii) larger soil particles apparently contributing more to the mass of soil loaded onto

vegetation, and (iii) smaller soil particles apparently contributing more to the contaminant concentration of soil loading. A factor of 10 difference in the soil loading estimate can result if effects due to soil particle size are ignored. Differences in the distribution of the tracer and the contaminant within the various sized soil fractions can bias the soil loading estimate. Knowing if a soil tracer's concentration among particle size fractions is similar to that of a contaminant is fundamental to proper use of the technique. Problems in estimating soil loading are greatest in highly organic soils, which have unusual soil particle size distributions due to a conglomeration of fine particles into larger ones.

Grazing trials in Switzerland showed that soil loadings on pasture grass increased 60% when grazing intensity by sheep increased by a factor of four [9]. Light rains and winds removed soil from ungrazed control plots, but the opposite occurred on grazed pastures — rainfall augmented soil loadings when sheep were present.

To accurately estimate mass loadings onto plants it is necessary to calculate mass loadings using the same soil particle-size distribution as that found adhering to the plant.

However, this is not a simple procedure and for most animal related studies the ultimate aim of measurements of soil adhesion is to be able to predict the likely level of contamination in the tissues of grazing animals. Therefore an alternative approach has been tested which utilizes an *in-vitro* extraction technique to determine the bioavailability of radiocaesium from ingested sources for [1]. There is a relationship between the Ti content of vegetation and the bioavailability of radiocaesium from vegetation indicating a reduced transfer to animals of radiocaesium from vegetation contaminated with adherent soil. Such bioavailability measurements could be employed to provide absorption values for predictive models.

Radioiodine

Experimental data obtained within this programme [6] show a high rate of excretion of radioiodine to faeces for dairy cows, which is consistent with data obtained by other group members [5]. Existing models could not be used to effectively describe this data (r^2=0.14). By the provision of a endogenous faecal excretion pathway the model developed within the programme [3] more accurately predicts radioiodine behaviour within dairy cattle (r^2=0.99).

Significant endogenous excretion of radioiodine (including excretion as inorganic iodine) has been measured for both goats and cows during the programme [1,4,5,6]. Measurements of the true absorption coefficient for radioiodine in ruminants during this programme have consistently shown complete absorption over a range of stable iodine intake rates [1,4]. Therefore, we advise that a true absorption ceofficient of one be assumed for radioiodine in the ruminant gut.

The degree of radioiodine transfer to milk varied considerably between individual goats. Although milk radioiodine levels are generally thought to be correlated to yield, relationships between the activity excreted in milk and milk yield were not strong. In studies using dairy cattle no differences were found in the secretion of radioiodine to milk due to stage of lactation [6]. At low dietary iodine levels, the fraction of radioiodine secreted into milk was higher than that at high stable iodine intakes in dairy cows [6].

The effect of timing of stable iodine dosing on the transfer of radioiodine to milk has been assessed [1,4]. When 1 g of KI was given 12 h before radioiodine contamination the output to milk was reduced more effectively than when the same dose was given 12 h after the radioiodine. In a subsequent study [1,4], dosing of 0.5 g given 6 h prior to radioiodine dosing was, for some animals, as effective as 1 g in the earlier study. In animals of differing stable iodine status no change in the excretion of radioiodine was seen following an administration of 0.5 g KI for goats equilibrated to a high dietary intake. Goats more recently changed from a comparatively low to high dietary stable iodine intake showed a reduced transfer to milk and an increased excretion in urine following administration of 0.5 g KI. An initial saturation of the plasma:milk pathway was observed during all the goat studies following administration of a comparatively large KI dose. The pathway desaturated at differing times dependent upon the animals iodine status.

Previously published models for radioiodine behaviour in ruminants incorporate the effect of stable iodine dosing by reducing thyroid uptake rates, which has the consequence of increasing the proportion of radioiodine which will be secreted into milk. However, such models are not able to predict the subsequent radioiodine output into milk. A revised model for goats has been developed which include a saturation mechanism for the transfer of iodine from ECF to milk [3] and which can, therefore be used to predict the effect of using stable iodine administration as a countermeasure.

The combination of experimental and modelling studies conducted within the programme have increased our understanding of radioiodine metabolism and countermeasures in ruminants leading to models which are better able to predict the effect of possible countermeasures.

Radiostrontium

Measured values of the true absorption coefficient for radiostrontium in lactating goats ranged from 0.074 to 0.43 [1,4,8]. The true absorption of ^{85}Sr was not affected by stable Sr administration. Values of absorption measured for radiostrontium from different plants were similar [6]. Individual measurements for F_m of $^{85}SrCl$ for goat milk ranged from 0.00038 d kg^{-1} to 0.033 d kg^{-1} [1,4,8]. The higher values were obtained from lactating animals which were in negative calcium balance (see figure below). An F_m of 0.041 d kg^{-1} (ie. similar to that expected for ionic radiostrontium) was determined in lactating sheep for ^{90}Sr associated with a soil obtained from the 30 km Chernobyl exclusion zone [2]. It is unlikely that soil:plant transfer values would provide a good indication of the likely differences in availability of radiostrontium associated with different soils if ingested by grazing animals.

Experiments with goats on low calcium intakes showed that the flux of stable Sr relative to intake was higher (equivalent to an A_t of 0.29) than the observed A_t of ^{85}Sr. This was probably due to the negative Ca balance causing Ca and Sr resorption from the bone. When the Ca balance was positive [1,4], a relationship between Ca and Sr absorption was observed. However, in goats with low Ca intakes no significant relationship was observed between Ca and Sr absorption, which may be because Ca absorption was enhanced in all animals. Absorption and transfer of radiostrontium to milk seem therefore to be inversely related to Ca intake, except when Ca is given at intake rates below requirement. However, the partitioning of excretion of Ca and Sr

by milk and urine was found to differ markedly [4,1]. There was also some evidence for time-course differences in Sr and Ca excretion to urine.

Most dynamic food chain models calculate the contamination of animal products using simple transfer coefficients which are assumed to be constant for a particular animal product and isotope. Therefore, there is no allowance for the effect of the animals Ca metabolism. We have shown that there is a wide variation in the observed transfer of radiostrontium to milk, much of which can be attributed to variations in the dietary intake of Ca [1,4,8] (see figure below). A compilation of the literature available for cattle showed an inversely proportional relationship between calcium intake and F_m [1]. Consequently, we have developed a model for radiostrontium transfer in goats which is based upon Ca metabolism, and can therefore simulate the effect on radiostrontium transfer of changes in the animals Ca status [3]. The transfer of radiostrontium in dairy goats has been modeled by assuming that Sr transfer is controlled by the animals Ca metabolism, making allowance for discrimination between the two elements for some processes. Models of radiostrontium transfer which do not consider the Ca status of an animal will only be applicable to particular situations of dietary Ca intake rate. Whilst the model presented provides a useful description of experimental data it should be tested more thoroughly before being used for radiation protection purposes. In particular, attention should be paid to testing the model over a range of dietary Ca intake rates, after the model has been tested further using data generated within the programme.

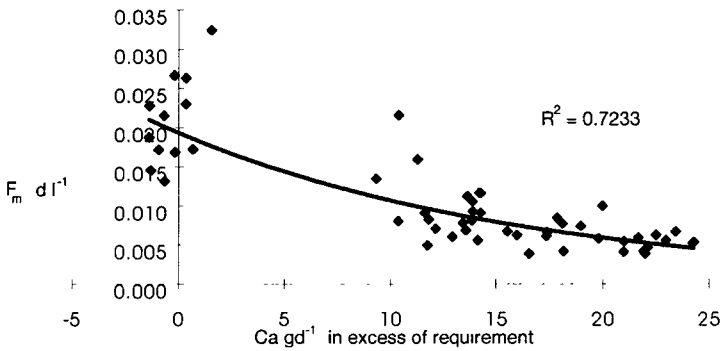

The relationship between radiostrontium F_m and dietary calcium intake in excess of requirement compiled from data collected by MLURI/ITE/AUN.

The revised programme Sr model [3] predicts that administration of Ca to animals contaminated by radiostrontium is a useful countermeasure although its effect will be limited for goats whose Ca intake is greater than approximately 40 g d^{-1}. However, given normal levels of calcium intake this means a reduction of two fold would be possible in many circumstances. In addition to considering the relationship between Ca intake and radiostrontium transfer to milk we have also tested a range of potential Sr binders to test whether they can bind ^{85}Sr, both *in-vitro* and *in-vivo*. Although initial batch sorption experiments with modified smectites (PILCs) showed that these substances had the capacity to bind radiostrontium [2], initial *in-vivo* tests [2,8] showed no reduction in transfer of radiostrontium to milk. The lack of effect was probably due to the slow rate of binding found *in-vivo*. The PILCs were subsequently modified so that the CEC was effectively doubled. The new material (PILCI) had

markedly faster trapping time for both ^{137}Cs and ^{85}Sr *in-vitro*, and *in-vivo* tests of PILCI are planned. Of the other tested compounds, only zeolite A(Na) reduced the transfer of orally administered ^{85}Sr to goat milk in *in-vivo* tests by a factor of 1.6 when given orally at a dose rate of 0.2 - 0.5 g per kg live weight per day.

The efficiency of the tested binders for radiostrontium is currently inferior to that of available Cs-binders. Alternative countermeasures using stable analogues are either ineffective (as we have shown for stable Sr [8]) or will be dependent on the animals current Ca intake compared with Ca requirement. Therefore, there is still a requirement for further research to develop a more efficient Sr-binder.

Overall conclusion

One goal of radiation protection is to predict the risks to humans from ingested radionuclides. Reliable predictions can only be accomplished by understanding the kinetic processes affecting the transfer of radionuclides through the environment. Historically, most predictions have relied on assumptions of equilibrium and did not account for the natural dynamics found in all agricultural systems. Our research has examined processes in the vegetation-herbivore-animal food product pathway under realistic, non-equilibrium conditions. From this we have gained new insights into the mechanisms of radionuclide transfer, and have developed dynamic models that can account for much of the variation inherent in agricultural and semi-natural systems. The models can now be used to more accurately predict impacts of contamination, and help guide effective countermeasures used in radiation protection programmes.

Key conclusions from programme are:

- A true absorption coefficient for plant incorporated radiocaesium of 0.8 is recommended for sheep, although individual values could range from 0.6 to 1.0. Current evidence would suggest that this range is appplicable for other domesticated ruminants.
- Administration of AFCF to animals to reduce their radiocaesium burdens may have the additional benefit of subsequently reducing the soil-plant transfer in pastures on which their faeces is deposited.
- Physiological and dietary status can have a considerable effect on the transfer of radiocaesium to ewes and lambs. Increasing dietary intake rates could be used as a countermeasure.
- Models for of radiocaesium behaviour in sheep have been developed and tested for a variety of situations and breeds. Methods by which such models can be applied to other ruminants have been established.
- Particle size distribution is critical in assessing the importance of soil adhesion.
- The absorption of radioiodine from the gut should be assumed to be complete although endogenous excretion of radioiodine in ruminants can be significantly higher than was previously suggested.
- Current models of radioiodine do not accurately describe the effect of countermeasure doses of stable iodine. Models capable of doing this have been developed.
- Stable iodine used as a countermeasure would be most effective if administered shortly before contamination.
- The transfer of strontium to ruminants is dominated by calcium metabolism and relationships have been shown between Ca intake rate and F_m. Models have been developed to account for the dependence on calcium as existing models were inadequate.
- As yet, no highly effective radiodstrontium binder has been identified and tested in-vivo, and further research is needed. Stable calcium administration would be an effective countermeasure, but its effectiveness will be limited by the animals dietary calcium intake.

Head of Project 1: Dr. Howard

II. Objectives for the reporting period

1. Complete analyses of samples from study conducted to investigate the effect of timing on the effectiveness of stable iodine dosing to reduce radioiodine levels in goat milk.
2. To conduct a study, in collaboration with MLURI, to establish the influence of dietary iodine levels on the effectiveness of stable iodine dosing as a countermeasure to reduce radioiodine transfer to goats milk
3. In collaboration with MLURI complete a series of animal experiments to examine the effect of calcium status on radiostrontium transfer to lactating goats and to supply the data generated to Nottingham University to enable the development of radiostrontium models.
4. To complete a review of factors affecting radiostrontium transfer to ruminants with an emphasis on possible countermeasures.
5. To complete, in collaboration with MLURI, experiments to quantify the effect of different physiological states and feed intakes in sheep on the transfer of ^{137}Cs to muscle.
6. Following on from the results of the previous programme, investigate the use of *in-vitro* bioavailability techniques in soil adhesion studies.
7. To complete the management of the project and collate the final report.

III. Progress achieved including publications

Project staff: N.A. Beresford; C.L. Barnett; B.J. Howard

All animal experiments (1,2,3,5) were conducted jointly with MLURI [4]; the strontium/calcium studies are described in the report from MLURI [4].

1. Factors effecting the use of stable iodine dosing as a countermeasure to reduce radioiodine levels in milk.

a) The effect of timing of an oral dose of stable iodine

Materials and methods

Seven lactating Saanen goats, housed in a group pen, were each orally administered ^{131}I (as iodide). Twelve hours later they were each administered a paper pellet containing 1 g of potassium iodide. After a further 12 h (ie. 24 h after ^{131}I administration) each goat was orally administered ^{125}I (as iodide). Nine control goats received ^{131}I at the same time as the experimental group, but received no stable iodine or ^{125}I. Milk samples were collected from each goat at 6 h intervals from 6-36 h after ^{131}I administration. Thereafter, milking was carried at circa 09:00 and 17:00 h for a total experimental period of 8 days.

The radioiodine level present in the thyroid was determined by live-monitoring at each milking time. A 3" NaI detector, linked to a Canberra Series 20 MCA, was placed firmly on the projection of the thyroid cartilage and the animal immobilised manually. Random checks were made, throughout the study, to ensure that results were reproducible and hence assess whether the detector was being placed in the correct

position on each occasion. The monitor was calibrated, during the course of this project, by comparison with *in-vivo* measurements with levels measured in thyroid samples removed at slaughter.

Feed and selected milk samples were analysed by GSF to determine their stable iodine content [5].

Data generated during the study were supplied, in a suitable form, to Nottingham University [3] to enable model development and testing

Results and discussion

Following administration of KI the ^{131}I activity concentration in the milk of treated goats fell to 30-40 % of control levels. However, by Day 4 levels in the milk of treated animals had increased to those of the controls. A similar pattern and reduction was seen in ^{125}I levels of treated animals. The total excretion of administered ^{131}I into milk over 7 d was significantly lower ($p<0.05$) for treated animals (21%) compared to the controls (34%) (Fig. 1). Output of ^{125}I (17%) over 7 d was significantly lower than that of ^{131}I in the same animals ($p<0.05$). This lower level of excretion was due to ^{125}I having been administered after the KI dose. Therefore, if KI administration were to be used as a countermeasure it would be more effective if given to animals prior to them ingesting contaminated material. The effect of the timing of KI administration is further discussed in the contribution from Crout [3]. The increase in milk radioiodine activity concentrations of treated animals on approximately Day 4 of the study is probably the result of the desaturation of the plasma-milk pathway.

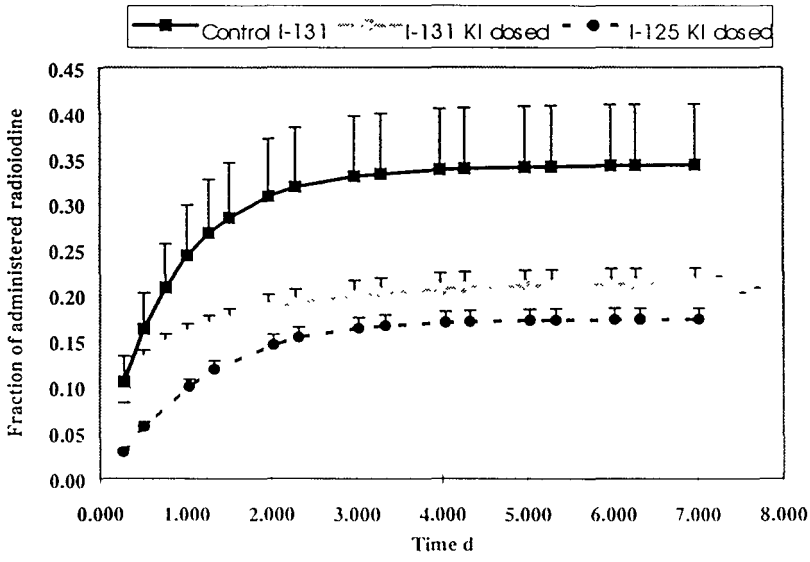

Fig 1. Cumulative outputs of radioiodine into the milk of control and KI dosed animals

Stable iodine levels were measured in the milk of one treated goat throughout the study. The concentration of stable iodide in milk reached a maximum of 20 mg kg^{-1} 12 hours after KI administration. However, levels had returned to those prior to the study (0.17 mg kg^{-1}) within 6 days. The dietary stable iodide intake of the animals was approximately 3 mg d^{-1}.

Further uptake of ^{131}I into the thyroid of treated animals was stopped by the KI administration (Fig. 2). Iodine-125 levels in the thyroid of the treated goats reached a maximum of 34% of control levels, thereafter reducing to 7-8 %. The technique used to monitor the thyroid gave satisfactorily reproducible results (R^2=0.95 for ^{131}I).

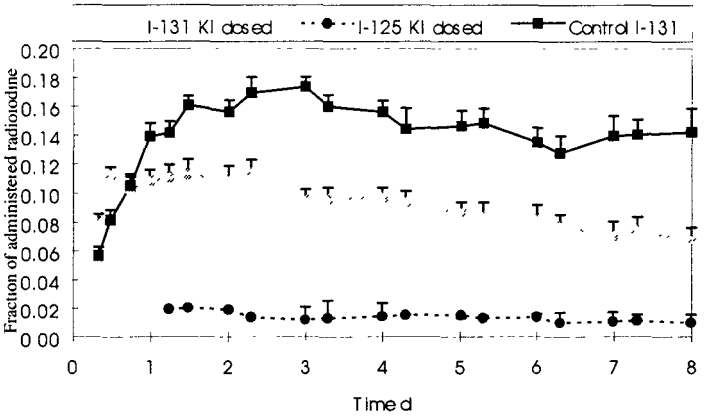

Fig. 2. Changes in the radioiodine content (fraction of administered activity) in the thyroid of the study animals as determined by *in-vivo* monitoring

b) The effect of dietary stable iodine level

Materials and methods

Seventeen lactating Saanen goats were assigned to one of three treatment groups: low dietary iodine (n=6), medium dietary iodine (n=5) and high dietary iodine (n=6). A pellet feed and coarse mix were both obtained from the manufacturers with no added minerals or vitamins. With the exception of iodide the required minerals and vitamins were mixed into the coarse mix. Iodide was added to the coarse mix at different levels for each treatment.

The *low* iodide group were introduced to their diet 34 days prior to the start of the study. The *high* and *medium* goats were on their experimental diet for 12 days before the study. Three hundred grams per day of coarse mix was given to the goats at milking times (circa 09:00 and 17:00 h). The main component of the diet was the pellet feed. The goats were housed in metabolism cages during the course of the study.

The study consisted of two, seven day, periods. At the start of period 1 each goat was given an oral administration of ^{131}I and an intravenous injection of ^{125}I (to enable the estimation of A_0). Milk, faeces and urine sample were collect 6 h, 12 h, 18 h, 24 h and 48 h after radioiodine administration. Thereafter, urine and faeces samples were

collected daily; milk samples were retained separately from morning and afternoon milkings (circa 09:00 and 17:00 h) until Day 5. From Days 5 to 7 morning and afternoon milk collections were bulked prior to samples being retained. Following the collection of Day 7 samples the goats were each orally dosed with 0.5 g of KI contained within a paper pellet. Six hours after this both ^{131}I and ^{125}I were readministered as in period 1. Sampling was conducted at the same intervals as during period 1. The thyroid of each goat was monitored (as described above) on sampling occasions at which a milk sample was retained.

Results

The dietary iodide levels, when measured, were not as had been anticipated. The level of iodide present within the specially prepared *iodine deficient* pelleted diet was similar to that of the normal feed. As a result there was no significant difference in the rate of iodide intakes between the *low* (12.1 mg I d^{-1}) and *medium* (14.4 mg I d^{-1}) treatments. However, the *low* group would have been more equilibrated to their diet than the *medium*. Prior to being introduced to their experimental diets, 34 days before the study, the *low* goats were receiving 13.84 mg I d^{-1} compared with the approximately 4.3 mg I d^{-1} that goats on the *high* and *medium* treatments were receiving until 12 days before the start of the study. The experimental diet of the *high* treatment goats resulted in an iodide intake of 19.3 mg I d^{-1}. All experimental levels of iodide intake would generally be considered to be relatively high (ARC 1980).

Outputs of dietary radioiodine in urine, milk and faeces in the two periods are presented in Table 1. By the end of the first period radioiodine levels in excreta and milk samples were negligible compared with those at the start of period 2; a $T_{1/2}$ value for ^{131}I in milk of about 1 day was determined for all treatments. The ^{131}I activity measured in the thyroid of goats within the *medium* treatment was significantly higher than that measured for *low* treatment goats during period 1. However, no significant increase in the ^{131}I activity measured in the thyroid was detected in period 2 for any treatment group; indicating that the KI had effectively stopped further uptake.

The initial mean activity concentration of ^{131}I in milk samples was reduced for all treatment groups. However, there was considerable variability in the degree of reduction; some individuals within the *low* and *medium* groups showing no effect. Fig. 3 shows the ^{131}I activity concentration in milk during period 1 compared to that during period 2. The saturation of the plasma:milk pathway occurs for approximately 1 day only in the case of the *medium* and *low* treatments. The reduction in ^{131}I levels in milk from the goats on the *high* treatment lasted until after Day 4 by which stage the actual activity concentration values were low. As a result the total ^{131}I output in milk over 5 days was significantly lower ($p<0.05$) in the case of the *high* group.

There were significant increases in the excretion of ^{131}I to urine for the medium and high treatments as a result of the administration of KI.

Discussion

For the *high* treatment group the 0.5 g of KI given 6 h prior to radioiodine contamination reduced the total transfer to milk by about the same degree as the 1 g of KI given 12 h before contamination in the previous study (although the animals would have obviously had a differing stable iodine status. Although at the moment the results from the second study have not been fully interpreted they show the effect of differing stable iodine status on the effectiveness of stable iodine administrations.

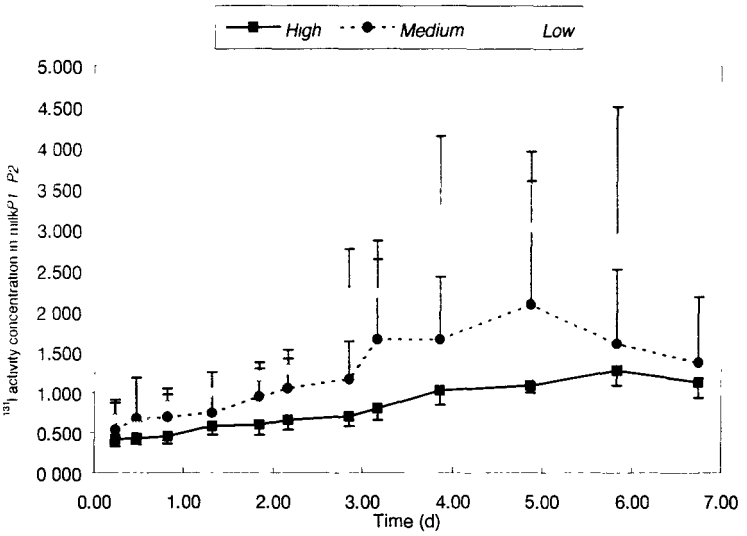

Fig. 3. The ratio of the activity concentration of ^{131}I in milk during period 1 (*P1*) compared with that during period 2 (*P2*).

Table 1. A comparison of the outputs, over 5 days, in milk and excreta of dietary ^{131}I during periods 1 and 2.

		Treatment		
	Period	*High*	*Medium*	*Low*
		% of administered ^{131}I		
Milk	1	51±5.4	40±8.2	68±9.0
	2	22±3.5*	34±7.7	50±5.8
Urine	1	47±3.8	43±6.6	32±5.7
	2	64±7.5*	66±4.6**	52±6.0
Faeces	1	6.5±0.54	9.0±0.15	5.2±1.12
	2	10±1.8*	10±0.7	7.4±2.00

* Comparisons between periods 1 and 2 significantly different at 5 %
** Comparisons between periods 1 and 2 significantly different at 1 %

4. Review of factors affecting radiostrontium transfer to ruminants

The current information on the transfer of radiostrontium to milk was reviewed, and critically evaluated with special emphasis on available countermeasures to reduce radiostrontium contamination of milk. A comprehensive report of the work can be found in Howard et al (1995).

Levels of radiostrontium in milk respond rapidly to those in the diet. The transfer of radiostrontium to milk is determined by calcium intake and status. Under normal ranges of dietary calcium intakes the transfer of radiostrontium to milk is likely to be inversely proportional to that of the dietary calcium intake. Therefore, the usefulness

of conventional transfer coefficients for radiostrontium is limited, and predictions could be misleading. A relationship was noted between calcium intake and radiostrontium transfer to milk, which might allow improved estimation of radiostrontium transfer to milk (Fig. 4].

A similar relationship was found between the transfer of radiostrontium to goats milk and dietary calcium intake in the studies conducted jointly by MLURI and ITE (see reports by [3] and [4]).

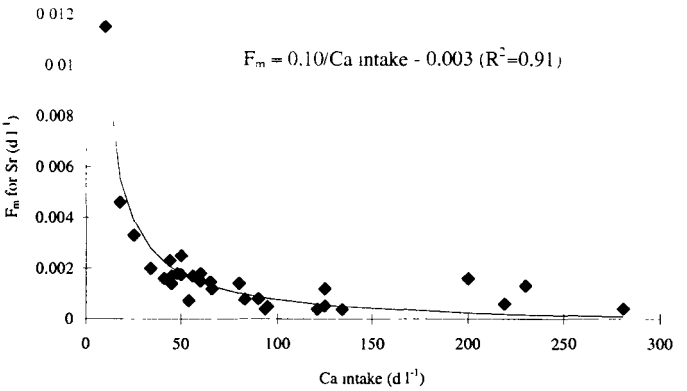

Fig. 4 Relationship between the transfer coefficient for cow milk and the daily calcium intake.

The simplest and most effective countermeasure to reduce radiostrontium activity concentrations in milk is to provide dairy animals with uncontaminated feed, this has the added advantage of being effective for other radionuclides. If the affected area is very large or deposition occurs in late spring it will be difficult to supply uncontaminated fodder to large numbers of dairy animals and the use of alternative countermeasures needs to be considered.

The most practical, simple method of producing fodder or pasture grass with sufficiently low radiostrontium levels would be to apply lime to contaminated soils. The effectiveness of liming will depend on the prevailing calcium status of the soil; since many western European agricultural soils are unlikely to be deficient in calcium the effect of liming may not be high. On organic soils liming may increase plant uptake of radiostrontium, and therefore the effect for major organic soil categories would need to be checked before application. The application of organic matter may also be effective, but the concomitant effect on radiocaesium needs consideration. Removing or diluting the top layer of contaminated soil by surface ploughing should also be considered; skim and burial ploughing may be more effective but would not be possible in most countries as such ploughs are not available.

The use of additives given to ruminants to reduce radiostrontium in milk is an alternative countermeasure, particularly if difficulties are encountered with supplying uncontaminated feedstuffs. Such countermeasures also have the advantage that they are rapidly effective, in contrast to many of the soil-based countermeasures.

Furthermore, countermeasures based on additives are generally easy to administer to dairy animals, which are routinely handled twice daily, and potentially more cost-effective than soil-based treatments. Increasing the calcium intake by a factor of two should decrease radiostrontium levels in milk by a concomitant amount. However, relatively small increases in stable calcium intake are unlikely to achieve a substantial reduction. Other suggested additives to reduce the transfer of radiostrontium to milk are either of limited effectiveness (e.g. clay minerals) or need further investigation (e.g. calcium alginate).

The effectiveness of available countermeasures varies. Radiostrontium activity concentrations decline rapidly in milk when feeding uncontaminated feed, and the rates of loss are determined by the biological half-life of radiostrontium in ruminant milk. Soil treatment can give maximum reduction of ten fold, but a factor of two or three is more common. Feeding dairy cows enhanced levels of Ca will give maximum reduction factors of two to three. Potentially higher reduction factors could be achieved if selective, and appropriate Sr binders were available.

5. The effect of feed intake and physiological status on radiocaesium transfers to sheep tissues

The objectives of this series of experiments were to test whether radiocaesium metabolism differs in adult sheep under different physiological states, and in lambs having different growth rates as a result of different feed intake rates.

The effect of physiological state on radiocaesium uptake by ewes

Materials and methods

Measurement were made for three physiological states:
i) *Pregnancy* - approximately at 4 months into pregnancy, carried out in March/April 1994.
ii) *Lactation* - starting at a maximum of 8 weeks into lactation, carried out in June/July 1994.
iii) *Post weaning* - after separation from lambs, carried out in November 1994.

During each period there were four treatments:
· barren, fed on a normal maintenance level diet (M), n = 6
· barren, fed on a 1.5 x normal maintenance level diet (1.5xM), n = 6
· ewes bearing single lambs, n = 12
· ewes bearing twin lambs, n = 12

The number of lambs carried by each ewe was determined using ultrasonic scanning techniques prior to the allocation of ewes to each treatment. Ewes in the single and twin treatments were fed a maintenance level diet. In each period ewes were orally dosed twice daily with ^{137}Cs for 21 days. The ^{137}Cs level in the muscle of the ewes was measured using *in-vivo* monitoring on days 1, 2, 3, 4, 5, 6, 9, 13, 17 and 21 after ^{137}Cs dosing commenced. To overcome any possible residual ^{137}Cs activity in the sheep, due to previous dosing, for the second and third measurement periods the amount of ^{137}Cs dosed was increased. Ewes were weighed weekly.

During the *lactation* and *post weaning* experiments each ewe was injected with ^{35}S-methionine, before ^{137}Cs dosing commenced. Urine samples were collected at weekly intervals to determine the specific radioactivity of ^{35}S as sulphate. It was hoped that

this would enable us to estimate the rate of protein turnover in the sheep to investigate whether there is a relationship to radiocaesium uptake.

Results

Caesium-137 activity concentrations on Day 21 of each study normalized to the rate of daily intake are shown in Table 2). The transfer of ^{137}Cs to the muscle of the barren ewes was similar in all periods, transfer to the lamb bearing groups changed between periods being lowest during lactation. In both the pregnancy and lactation periods the rate of uptake of ^{137}Cs decreased in the order:

barren (M) > barren (1.5xM) > ewes bearing single lamb > ewes bearing twin lambs.

However, comparisons between 1.5xM ewes and those bearing single lambs, during the pregnancy period, and between the two lactating groups in the second study were not significant ($p>0.05$). The difference between barren and lamb bearing ewes was greater during the lactation period compared with the pregnancy period. This larger difference appears to be due to the excretion of radiocaesium in milk. The transfer of ^{137}Cs was significantly higher ($p<0.05$) to the milk of lambs with single lambs than to that of those with twins. However, as the result of the higher milk yield of the ewes with twins there was no difference in the total ^{137}Cs excretion into milk between the two groups.

Table 2. Caesium-137 activity concentrations on Day 21 of each study normalized to the rate of daily intake

Treatment	Experimental Period (mean±SD)		
	Pregnancy	Lactation	Post-weaning
1M	0.40±0.016	0.37±0.017	0.36±0.019
1.5M	0.33±0.037	0.31±0.057	0.31±0.019
Single lamb	0.30±0.042	0.21±0.022	0.39±0.050
Twin lamb	0.25±0.019	0.18±0.023	0.39±0.039

During the last study period the ^{137}Cs activity of ewes which had borne a lamb was significantly higher ($p<0.05$) than that of ewes within the 1.5xM treatment group. The ^{35}S results have shown no correlation to ^{137}Cs levels in muscle during either of the latter two studies.

The results clearly show that the transfer of radiocaesium to the muscle of ewes varies under differing physiological conditions and on different dietary intake requirements. However, we are currently uncertain as to wether this is as the result of 'physiological changes', or related to treatment differences in feed intake/live weight which have previously been shown to correlate to radiocaesium uptake (Beresford et al 1995).

b) The effect of growth rate on radiocaesium uptake by lambs

Material and methods

The object of this study was to determine if rate of growth influenced the transfer of radiocaesium to lambs. Twenty-four, approximately 6 month-old, lambs were allocated to one of two treatments: *high* growth rate and *low* growth rate. Feeding

levels were set such that the low growth rate group would attain a live-weight gain of 0.05 kg d^{-1} and the high group 0.20 kg d^{-1}.

The lambs were orally dosed, twice daily, with ^{137}Cs for 15 days. The ^{137}Cs level in their muscle was measured using *in-vivo* monitoring on days 1, 2, 3, 4, 5, 6, 7, 9, 11, 13 and 15 after ^{137}Cs dosing commenced. As in the later ewes studies described above each lamb was injected with ^{35}S-methionine, before ^{137}Cs dosing commenced. On Day 15 radiocaesium administration ceased and the lambs within each treatment were reallocated, such that 6 within each treatment were allocated to the other growth rate feeding level and 6 remained on the same feeding level. This resulted in four treatments:

H-H - high growth rate diet in both study periods
H-L - high growth rate in period 1 then reallocated to low growth rate diet
L-L - low growth rate diet in both study periods
L-H- low growth rate in period 1 then reallocated to high growth rate diet

The lambs were then live-monitored over a further 15 day period at the same intervals as before (no radiocaesium was administered). The lambs were weighed at approximately 5 day intervals throughout the study and urine samples (for ^{35}S determinations) were collected on three occasions within each period.

Results and discussion

The mean weight gain of lambs in the *high* treatment during period 1 was 2.75 kg, significantly higher ($p<0.01$) than that of 0.21 kg recorded for the *low* group. The activity concentration in the muscle of lambs achieving the lower growth rate was significantly greater ($p<0.01$) than that of those attaining a higher rate of growth (Fig. 4).

In period 2, the rates of growth of lambs in L-H (3.75 kg over 15 days) and H-H (2.42 kg) were significantly higher ($p<0.05$) than those for the L-L (1.00 kg) and H-L treatments (0.75 kg). Changes in the ^{137}Cs activity concentration measured in the animals muscle (Figure 5) increased in the order:

H-L = H-H < L-L < L-H (comparison being significant at 5%)

Although correlation's between ^{137}Cs and the rate of loss of ^{35}S in urine samples were weak in period 1 the ^{35}S turnover rate by the high group was significantly lower than that by the low group ($p<0.01$). Similarly in period 2 lambs within the L-L group had a significantly higher rate of ^{35}S turnover than those in the L-H and H-H groups. It would therefore appear that there could be a relationship between protein turnover rate (as inferred by ^{35}S turnover rates) and the rate of radiocaesium turnover: animals with a higher rate of protein turnover having a higher rate of radiocaesium turnover.

The considerably greater loss of radiocaesium from the muscle of lambs within the L-H treatment during the second part of the study suggests that manipulation of dietary intake combined with the feeding of uncontaminated feed could be a more useful countermeasure than the simple feeding of uncontaminated feed to a previously contaminated animal.

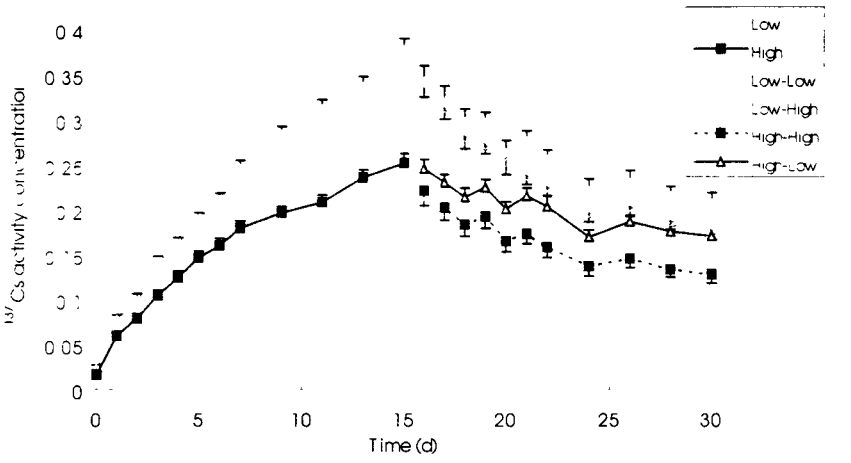

Fig. 5. Changes in the ^{137}Cs activity content (normalised to the daily administration rate) in the muscle of study lambs

6. A method to predict seasonal changes associated with levels of adherent soil on the bioavailability of radiocaesium from pasture grass samples

In the previous programme a number of the collaborating laboratories conducted vegetation and soil sampling over a 12 month period from a range of different pasture types. The aim was to determine the importance of soil adhering to vegetation as a source of radiocaesium to grazing animals. Titanium was used as a marker of soil contamination of vegetation. On a number of sampling occassions the results indicated that more than 100 % of the radiocaesium in vegetation samples was due to soil contamination. It was concluded that this obvious overestimate was due to problems with the sampling protocol adopted (see also the report of [9] from this programme). However, for most animal related studies the ultimate aim of such measurements is to be able to predict the likely level of contamination in the tissues of grazing animals. Therefore an alternative approach has been tested which utilises an *in-vitro* extraction technique (a 2 hour extraction with 0.1M CsCl followed by filtration through a 0.2μ membrane filter) to determine the bioavailability of radiocaesium from ingested sources for absorption in the animal gut developed by ITE/MLURI. Samples collected by ITE from an upland pasture in the UK during the previous programme have been used in this assessment.

Between 35 and 50 % of the ^{137}Cs associated with vegetation samples was extracted during summer months. This compares to a value of approximately 70 % extracted from fresh grass which was comparatively uncontaminated by soil during a previous study. In January to April the amount of radiocaesium extracted fell to between 2 and 14 %. Results indicate a relationship between the Ti content of vegetation and the bioavailability of radiocaesium from vegetation indicating a reduced transfer to animals of radiocaesium from vegetation contaminated with adherent soil.

Publications

Crout, N.M.J., **Beresford, N.A.**, & **Howard, B.J.** 1993. Does soil adhesion matter when predicting radiocaesium transfer to animals? J. Environ. Radioact., 20, 201-212.

Desmet, G.M. & **Howard, B.J.** (eds) 1993. Relative effectiveness of agricultural countermeasures. Sci. Tot. Environ., 137.

Galer, A.M., Crout, N.M.J., **Beresford, N.A., Howard, B.J.**, Mayes, R.W., **Barnett, C.L.**, Eayres, H.F. & Lamb, C.S. 1993. Dynamic radiocaesium distribution in sheep: measurement and modelling. J Environ. Radioact., 20, 35-48.

Hove, K., Strand, P., Voigt, G., Jones, B.-E.V., **Howard, B.J.**, Segal, M.G., Pollaris, K. & Pearce, J. 1993. Countermeasures for reducing radioactive contamination of farm animal products., 261-271.

Howard, B.J. 1993. Management methods of reducing radionuclide contamination of animal food products in semi-natural ecosystems. Sci. Tot. Environ., 137, 249-260.

G. Voigt, **B. J. Howard**, C. Vandecasteele, R. W. Mayes, M. Belli, U. Sansone, G. Stakelum, P. A. Colgan, P. Assimakopoulos, N. M. Crout, B. E. Jones, K. Hove. (1993) Factors affecting radiocaesium transfer to ruminants - Results of a multinational Research group. Proceedings der 25. Jahrestagung des FfS, Publikationsreihe Fortschritte im Strahlenschutz, Band II, 599-604

Wilkins, B.T., **Howard, B.J.,** Desmet, G.M., Alexakhin, R.M. & Maubert, H. 1993. Strategies for the deployment of agricultural countermeasures. Sci. Tot. Environ., 137, 1-8.

Beresford, N.A., Mayes, R.W., Crout, N.M.J., **Howard, B.J.** & Kanyar B. 1994. Dynamic behavior of ^{110m}Ag in sheep tissues. Hlth. Phys. 66, 420-426.

Mayes, R.W., **Beresford, N.A.**, Lamb, C.S., **Barnett, C.L.**, **Howard, B.J.**, Jones, B.-E.V., Eriksson, O. Hove, K., Pedersen, Ø. & Staines, B.W. 1994. Novel approaches to the estimation of intake and bioavailability of radiocaesium in ruminants grazing forested areas. Sci. Tot. Environ. 157, 289-300.

Beresford, N.A., Barnett, C.L., Mayes, R.W., Pollaris, K., Vandecasteele, C.M. & **Howard B.J.** 1995. The use of in-vitro technique to predict the absorption of dietary radiocaesium by sheep. Radiation and Environmental Biophysics, 34, 191-194.

Crout, N.M.J., **Beresford, N.A., Howard, B.J.,** Mayes, R.W., Assimakopoulos, P.A. & Vandecasteele, C.M. In press. The development and testing of a revised dynamic model of radiocaesium to sheep tissues. Radiation & Environmental Biophysics.

Howard, B.J., Voigt, G., Segal, M. G. & Ward, G. M. (submitted)
A review of available countermeasures to reduce radioiodine transfer to milk. Health Physics.

Mayes, R.W., **Beresford, N.A., Howard, B.J.,** Vandecasteele, C.M. & Stakelum G. (submitted July 1995) The use of the true absorption co-efficient of bioavailability of radiocaesium in ruminants. Radiation and Environmental Biophysics.

References

Agricultural Research Council. 1980. The nutrient requirements of livestock. Technical review by an Agricultural Research Council working. Wallingford: C.A.B. International.

Beresford, N.A., Barnett, C.L., Mayes, R.W., Lamb, C.S., Howard, B.J. & Wilson, P.J. 1995. Radiocaesium variability within sheep flocks in the restricted area of Cumbria. Report to The Ministry of Agriculture, Fisheries and Food. TFS Project T07051j1/ MAFF Contract Numbers N2139.2140. Institute of Terrestrial Ecology: Grange-over -Sands.

Howard, B.J., Beresford, N.A., Kennedy,V.H. & Barnett, C.L. 1995. A review of current knowledge of the transfer of radiostrontium to milk and possible countermeasures. Report to The Ministry of Agriculture Fisheries and Food. TFS Project T07051q1/ MAFF Contract Number 1B043. Institute of Terrestrial Ecology: Grange -over-Sands.

Head of Project 2: Prof. Assimakopoulos

II. OBJECTIVES FOR THE REPORTING PERIOD

The objectives for the reporting period were:

1 - Assessment of radiostrontium transfer to sheep's milk due to direct soil ingestion.

2 - Further experimental investigation of the NPL animal model with regard to its applicability to a wide range of ruminants through a unique set of transfer parameters.

3 - Investigation of the effectiveness of modified smectites, particularly Pillared Layered Clays (PILCs), as caesium and strontium binders.

4 - The development of a model for cation exchange processes in PILCs.

III. PROGRESS ACHIEVED INCLUDING PUBLICATIONS

(Assimakopoulos, Pakou, Stamoulis)

1. Soil-to-milk transfer coefficient for ^{90}Sr

In a previous experiment (Sci. Total Environ., 135:13-24) soil ingestion as a source of radiocaesium contamination to ruminants was studied by measuring the transfer coefficient to sheep milk. Eight lactating ewes, housed in individual metabolism cages, were used. Seven grams per day of heavily contaminated sandy topsoil, collected in 1990 from the Chernobyl area, were administered orally to the animals for a period of one week. The daily dose intake in ^{137}Cs was 1,835 Bq d^{-1}. During this contamination period, daily milk production and excreta output were measured. The ewes were monitored for an additional seven day decontamination period, while they fed on uncontaminated feed. Transfer coefficients were obtained through a best fit (minimum χ^2) of the data to predictions of a linear compartment model. The values obtained were $f_m(Cs) = (2.6 \pm 0.7) \times 10^{-2}$ and $f_u(Cs) = (5 \pm 2) \times 10^{-2}$ d kg^{-1} for radiocaesium transport to milk and urine, respectively. These results suggest that soil ingestion can be a major source of radiocontamination for sheep and other free-grazing ruminants.

The samples collected in this experiment were further analyzed during the reporting period with regard to radiostrontium concentrations. Strontium-90 concentration in the soil was measured

as 3031 ± 189 Bq kg^{-1}, which resulted in a daily dose intake of 433 ± 27 Bq d^{-1}. The samples from this experiment were analyzed for strontium-90 concentration and the data were fitted to the NPL animal model. The soil-to-milk ^{90}Sr transfer coefficient obtained from the analysis was $f_m(Sr) = (4.1 \pm 1.6) \times 10^{-2}$ d kg^{-1}. This result indicates that direct soil ingestion is an important pathway for radiostrontium contamination of sheep's milk.

Plasma-tissue transfer of Cs in ruminants

(Assimakopoulos, Pakou, Ioannides, Aslanoglou, Karamanis, Stamoulis)

In two previous publications (Assimakopoulos, *et al.*, 1991; Assimakopoulos, *et al.*, 1993) we presented a general multiple-compartment model for the transport of trace elements through animals. One corollary of this model is that the transfer coefficient *f(k)* to any compartment *k* of an animal (soft tissue, lung, liver, etc.) is related to the feed-to-blood transfer coefficient *f(blood)* through the simple expression

$$f(k) = a(k) f(blood) \qquad (1)$$

in which *a(k)* is a constant, independent of animal size, physiological state of the animal or form of animal diet. Furthermore the coefficients *a(k)* may be expressed in terms of model parameters pertaining to the animal's physiology and should thus exhibit similar values for physiologically similar animals. An immediate consequence of this is that if the coefficients *a(k)* are determined, a measurement of *f(blood)* leads to an estimate of the transfer coefficient to any compartment *k* of the animal.

Two distinct experiments, involving different sets of animals and different feeding regimes, were carried out in order to assess the validity of eqn (1). The first experiment was performed at the Agricultural Research Station of Ioannina and the second in the facilities of the Department of Radiology and Lands Recovery of the Research and Industrial Association (RIA) *Pripyat* within the 30 km zone around the Chernobyl accident site. In both experiments the animals were artificially contaminated through oral administration of a constant daily dose of radiocaesium. In each case the contamination period was sufficiently long for the animals to reach a state of equilibrium with respect to radiocaesium intake.

The number, age and average weight for each group of animals are contained in Table 1. The same Table contains the daily dose of radiocaesium administered to the animals during the study. At the end of the contamination period all animals were sacrificed and samples from ten body compartments for each animal were taken. As indicated in Table 1, a total of 27 animals, grouped according to species, state of lactation and feeding regime, were considered in nine separate groups. Average transfer coefficients for the nine groups of animals as obtained from the data of this study are summarized in Table 2. Each value in Table 2 - with the exception of values in the first and last column - represents an average of measurements on three distinct animals. The data in the first column represent the average from two animals, whereas transfer coefficients for sheep reported in the last column were obtained in a previous study (Assimakopoulos, *et al.*, 1993), in which the animals were fed on hay, heavily contaminated in ^{137}Cs by the Chernobyl fallout.

The data in Table 2 were used to calculate the ratios *a(k)* in eqn (1). All calculations of *a(k)*

Table 1. Animals involved in the studies of radiocaesium transfer to ruminants

Species	No of animals	Age (y)	Average Weight (kg)	Milk production (kg d^{-1})		Feed (kg)		Tracer	Daily dose (kBq d^{-1})
				Start	End	Hay	Concentrate		
Ioannina experiment									
Cows, lactating	2	8-9	670	8 5	2 0	10	5	^{134}Cs, ionic	10
Sheep, lactating	3	5-9	41 5	0 50	0 12	0 6	1	^{134}Cs, ionic	3
Goats lactating	3	5-7	33 5	0.33	0.08	0 6	1	^{134}Cs, ionic	3
Pripyat experiment									
Cows, lactating	3	3-4	420	4 2	3.5	12	2	^{134,137}Cs*	16/444
Cows, non-lactating	3	4	463			12	2	^{134,137}Cs*	16/444
Sheep, lactating	3	2 5	43	0.14	0 11	0 7	0 25	^{134,137}Cs*	0 9/26
Sheep, non-lactating	3	1 5	29			0 7	0 25	^{134,137}Cs*	0 9/26
Goats, lactating	3	2-4	37	0.40	0 24	0.7	0 25	^{134,137}Cs*	0 9/26
Goats, non-lactating	3	2-3	30			0 7	0 25	^{134,137}Cs*	0 9/26

* Incorporated in naturally contaminated hay.

Table 2. Radiocaesium transfer coefficients for cows, goats and sheep. The data represent averages over the sample size in each group of animals. Errors are standard errors.

Compartment	Cows (x 10^{-3} d kg^{-1})			Goats (x 10^{-2} d kg^{-1})			Sheep (x 10^{-2} d kg^{-1})			
	^{134}Cs (ionic,2,L)	^{134,137}Cs (hay,3,L)	^{134,137}Cs (hay,3,NL)	^{134}Cs (ionic,3,L)	^{134,137}Cs (hay,3,L)	^{134,137}Cs (hay,3,NL)	^{134}Cs (ionic,3,L)	^{134,137}Cs (hay,3,L)	^{134,137}Cs (hay,3,NL)	^{137}Cs (hay*,L)
Whole blood	1 4 ± 0 2	1 6 ± 0 2	2 1 ± 0 4	2 5 ± 0.3	3.9 ± 0 4	6 5 ± 0 9	2.7 ± 0 2	2 8 ± 0 3	3 4 ± 0 5	1 4 ± 0 3
Blood cells		1 9 ± 0 2	2 0 ± 0 7		6 1 ± 1.1	7 4 ± 1 2		3 0 ± 0 3	3 9 ± 0 4	
Serum		1 3 ± 0 1	1 8 ± 0 2		3 1 ± 0 3	4 6 ± 0 7		2 7 ± 0 3	3 6 ± 0 5	
Muscle	27 ± 5	21 ± 2	22 ± 2	42 ± 4	72 ± 8	96 ± 11	43 ± 3	70 ± 7	71 ± 9	34 ± 7
Lung	17 ± 5	23 ± 2	24 ± 3	23 ± 6	47 ± 7	55 ± 13	32 ± 3	36 ± 4	45 ± 5	17 ± 3
Liver	20 ± 3	25 ± 2	31 ± 3	23 ±·6	44 ± 7	61 ± 6	47 ± 10	52 ± 5	59 ± 7	18 ± 4
Kidney	26 ± 2	43 ± 4	51 ± 5	59 ± 8	71 ± 11	107 ± 11	78 ± 8	83 ± 8	109 ± 11	36 ± 6
Spleen	21 ± 2	25 ± 2	30 ± 3	35 ± 2	57 ± 6	77 ± 8	46 ± 6	46 ± 5	57 ± 9	23 ± 5
Heart	17 ± 2	27 ± 3	34 ± 4	31 ± 4	52 ± 7	76 ± 8	41 ± 4	49 ± 5	56 ± 7	19 ± 4
Brain	13 ± 4	7 5 ± 0 8	7 8 ± 0 7	19 ± 3	31 ± 3	35 ± 6	25 ± 4	24 ± 3	22 ± 4	15 ± 4
Rumen		23 ± 3	29 ± 3	30 ± 4	48 ± 8	62 ± 11	39 ± 4	51 ± 5	41 ± 9	13 ± 3
Gut		14 ± 1	12 ± 2		53 ± 6	47 ± 12		38 ± 4	30 ± 8	
Fat		2 2 ± 0 4	2 3 ± 0 6	2 7 ± 1 5	12 ± 4	8 0 ± 2 2	1 1 ± 0 3	5 2 ± 2 0	9 5 ± 1,4	0 7 ± 0 7

[a]Assimakopoulos, *et al*., Sci Tot. Environ., 136 (1993) 1-11. The number in the sub-heading of each column denotes the sample size in each group of animals. L = Lactating. NL = Non-lactating.

values were performed by dividing the transfer coefficients in Table 2 by the transfer coefficient to whole blood in the same column. The results are summarized in Table 3.

It is seen in the latter Table that *a(k)* values for each compartment agree within the experimental error for the ten sets of animals considered. Thus average values <*a(k)*> of the ratio

$$a(k) = \frac{f(k)}{f(blood)} \qquad (2)$$

were calculated across each row of Table 3 for the nine compartments k measured here. These values are tabulated in the penultimate column of the Table.

A qualitative inspection of the results in Table 3 shows that all values of the ratios *a(k)*, for all compartments of the animals, are, within experimental error, in agreement with the proposed average values <*a(k)*>. They also agree with values calculated from transfer coefficients found in the literature (last column of Table 3). This result was further verified through a single factor analysis of variance performed on the data.

The results obtained in the present research indicate that although transfer coefficients to the various body compartments of animals may depend strongly on the species, physiological state, or type of feed of the animal (see Table 2), the coefficients *a(k)* in eqn (1) are to a good approximation constants.

The use of Pillared Layered Clays as Cs and Sr adsorbers
(Assimakopoulos, Karamanis, Pakou, Gangas)

A wide class of natural materials, such as various kinds of clays (bentonite, vermiculite,

Table 3 Radiocesium transfer coefficient ratios *f(k)/f(blood)* for cows, goats and sheep. Errors are standard errors.

Compartment	Cows			Goats			Sheep				Average <*a(k)*>	From ref b
	^{134}Cs (ionic,2,L)	$^{134,137}Cs$ (hay,3,L)	$^{134,137}Cs$ (hay,3,NL)	^{134}Cs (ionic,3,L)	$^{134,137}Cs$ (hay,3,L)	$^{134,137}Cs$ (hay,3,NL)	^{134}Cs (ionic,3,L)	$^{134,137}Cs$ (hay,3,L)	$^{134,137}Cs$ (hay,3,NL)	^{137}Cs (hay*,L)		
Muscle	19 ± 5	15 ± 2	12 ± 2	16 ± 3	24 ± 4	21 ± 4	16 ± 3	26 ± 4	20 ± 4	24 ± 7	17 ± 4	28 5
Lung	12 ± 4	17 ± 2	13 ± 2	9 ± 3	15 ± 3	12 ± 3	12 ± 2	14 ± 2	13 ± 2	12 ± 3	13 ± 2	8.5
Liver	14 ± 3	19 ± 3	17 ± 2	9 ± 3	14 ± 3	13 ± 3	17 ± 4	20 ± 3	16 ± 3	13 ± 4	16 ± 3	16 5
Kidney	19 ± 3	32 ± 4	28 ± 4	24 ± 4	23 ± 4	23 ± 5	29 ± 4	31 ± 4	30 ± 5	26 ± 7	26 ± 5	25
Spleen	15 ± 3	18 ± 3	17 ± 2	14 ± 2	19 ± 3	17 ± 3	17 ± 3	17 ± 2	16 ± 3	16 ± 5	17 ± 2	12
Heart	12 ± 2	20 ± 3	19 ± 3	12 ± 2	17 ± 3	17 ± 3	15 ± 2	18 ± 3	16 ± 3	14 ± 4	16 ± 3	
Brain	9 ± 3	6 ± 1	4 ± 1	8 ± 2	10 ± 2	8 ± 2	9 ± 2	9 ± 2	6 ± 1	11 ± 4	6 ± 2	
Rumen		17 ± 3	16 ± 2	12 ± 2	16 ± 3	14 ± 3	14 ± 2	19 ± 3	11 ± 3	9 ± 3	15 ± 3	
Gut		11 ± 2	7 ± 2		17 ± 3	10 ± 3		14 ± 2	8 ± 3		11 ± 3	
Fat		2 ± 1	1 ± 1	1 ± 1	4 ± 1	2 ± 1	1 ± 1	2 ± 1	3 ± 1	1 ± 1	2 ± 1	

[a]Assimakopoulos, *et al*, Sci. Tot Environ., 136 (1993) 1-11. [b]Vandecasteele *et al*, Sci. Total Environ. 85 (1989) 213- 223. The number in the sub-heading of each column denotes the sample size in each group of animals. L = Lactating. NL = Non-lactating

micas, etc.), or industrial products, such as Ammonium Ferric Cyano-Ferrate (AFCF), have been used in the past as effective countermeasures against radiocaesium contamination. However, these materials usually perform very poorly with regard to trapping bivalent cations such as strontium and are thus unable to perform as a general antidote against fallout contamination.

During the reporting period we have been investigating the trapping of both caesium and strontium by Pillared Layered Clays (PILC), a novel class of materials derived from swelling clays. These materials are cation exchangers for mono- as well as for multi-valent cations.

PILCs are usually prepared out from Montmorillonite, a swelling clay mineral found in Bentonite ore. Montmorillonite is a layered clay with a cation exchange capacity (CEC) of about 0.8 mEq g^{-1}. The exchangeable cations in this material are positioned in the space between successive layers. In pure water these layers disassociate to form a clay colloid, whereas in water of about 0.1 N or more, due to the presence of cations in the solution, the layers collapse and remain attached to each other. Thus in an environment like the rumen fluid the clay does not swell and the cation exchangeable positions in the interlayer space are not easily accessible. This makes bentonite much less effective than AFCF with regard to caesium trapping. The situation may be reversed by propping the clay layers apart by nano-size pillars of metal oxide and thus creating a network of pores in the interlayer space. This pillared structure makes the exchangeable cation positions more easily accessible. Indeed the interlayer space in the modified clay presents a specific surface area (SSA) of a few hundred m^2 g^{-1}, i.e. a SSA more that ten times that of the untreated montmorillonite. In addition the new structure is stable with respect to ionic concentration or acidity of the aquatic environment.

The experiments performed during the reporting period were:

A. *In vitro* experiments with PILCs.

Two type of PILCs, coded ATHINA and AZA, were constructed for the purposes of this investigation by STRATON, hi-tech, Ltd. with characteristics shown in Table 4. This materials were further treated in the NPL in order to become Na-saturated. Two isotopes, ^{137}Cs and ^{85}Sr, were used as radiotracers. The kinematics of the exchange processes were studied by placing the material tested in dialysis tube, while batch sorption experiments were also performed. Typical times for the attainment of equilibrium were of the order of a 100 hours.

Table 4. Characteristics of PILC products.

Material	SSA (m^2 g^{-1})	d_{001} (nm)	CEC* (mEq g^{-1})
ATHINA	130	1.3 - 1 8	0 38 ± 0 03
AZA	160	1 82 ± 0.05	0.40 ± 0.03

* Measured by NPL.

RADIOCAESIUM SORPTION

The kinematics of radionuclides - PILC exchange process were investigated for various solution to solid ratios (Fig. 1). As seen in this figure the adsorption process follows a double exponential behaviour involving a fast phase with relaxation time of a few hours and a slow phase of about 100 hours. This indicates the existance of two adsorption processes, probably surface sortpion and interlammelar diffusion. In the case of the 150 mg mass, which presents a high surface area, the surface sortpion process is predominant. As the PILC mass decreases the second process becomes important. Thus, the overall time needed to reach equilibrium is a complicated

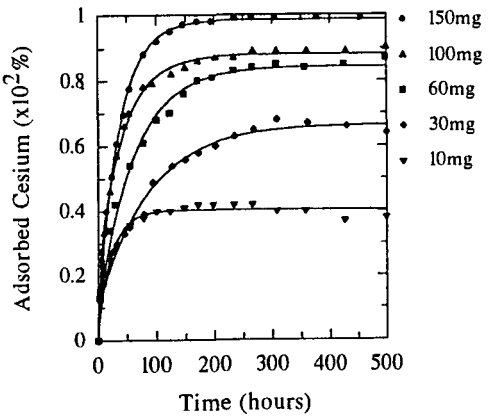

Figure 1. Influence of PILC mass on Cs sorption.

process depending on PILC mass, its granularity and Cs concentration in its environment. The critical mass value for 70% total adsorption was 30 mg. For this mass the two available forms of PILCs (ATHINA and AZA) were compared under various environmental conditions (Table 5). The two types of PILCs had the same sorption properties, with strong preference for Cs adsorption over Na and K. It was also seen that in low pH environment the adsorptive power of PILCs decreases due to the fixation of hydronium ions in the hexagonal cavities of the pillared clays. Finally Na and K ions behaved exactly the same as competitive ions.

The product ATHINA was further

Table 5 Comparison of products ATHINA and AZA under various conditions for 30 mg PILC material in a 200 mL bath containing 1.7 x 10^{-7} M of ^{137}Cs.

Conditions	ATHINA	AZA
^{137}Cs + H^+ pH· 4.0 with HCl	[Cs] 7.5 x 10^{-7} Mol g^{-1} in 22 hours 70 %	[Cs] 7 5 x 10^{-7} Mol g^{-1} in 28 hours 70 %
^{137}Cs + stable Cs (2 x 10^{-4} M) pH 6 0 with CsOH	[Cs] 1 3 x 10^{-4} Mol g^{-1} in 14 hours 70 %	[Cs] 1 6 x 10^{-4} Mol g^{-1} in 14 hours 70 %
^{137}Cs + Na^+ or K^+ (2 x 10^{-4} M) pH 4 0 with NaOH or KOH	[Cs] 8 3 x 10^{-7} Mol g^{-1} in 12 hours 70 %	[Cs] 8 8 x 10^{-7} Mol g^{-1} in 14 hours 70 %

compared to AFCF with regard to caesium uptake under various conditions (Fig. 2). In the presence of competitive cations (Na + K) and for the concentrations employed here, the adsorptive capacity of PILCs is comparable to that of AFCF. In view of AFCF's poor performance for multivalent cations these results were very encouraging to continue the investigastion for radiostrontium adsorption.

RADIOSTRONTIUM SORPTION

All experiments conducted for radiocaesium adsortpion were repeated for radiostrontium (^{85}Sr). Again, there were no remarkable differences in the adsortpion properties of the two PILCs, although AZA was slightly better because of its larger SSA and CEC. Radiostrontium was also adsorbed non linearly with the PILC mass but more rapidly. Indeed, PILCs have negative layer charge and, like clays, they sorb preferentially multivalent ions.

Several other experiments were also performed, such as the study of pH dependence, which revealed that the sorption process takes place for pH > 3.7; the dependence on temperature, with no appreciable effect up to 40 C; the comparison of PILC pretreatment for Na saturation, K

saturation and Ca saturation, with best results for Na saturation. Finally, the rate of strontium adsorption in competition with Na, Na+K, for several ion concentrations and several PILC and AFCF masses, was performed. Some of the results of these experiments are presented in Fig. 3. It is seen in this figure that 30 mg of AFCF stops adsorbing strontium for Na+K concentration of $1x10^{-2}$ M, while 30 mg of AZA adsorbs 50 %.

Thus, in the presence of monovalent counterions, the PILC material adsorbs strontium even in high competitive ion concentrations. The situation becomes more difficult in the presence of bivalent ions and especially Ca which has almost the same chemical behaviour as strontium and is one the main constituents of the rumen liquid. For this reason the selectivity of Sr over Ca was investigated in a series of experiments (Table 6). It was concluded that there is definitely a selectivity of strontium over Na and K and also over calcium but the non linearity did not permit a prediction of the mass needed to have a predetermined Sr sorption. For this reason a non linear cation exchange model was constructed in order to evaluate the selectivity coefficients of Cs and Sr over monovalent and multivalent ions and to predict the caesium and strontium sorption in predefined initial conditions. This model is described at the end of this report. With the help of this model and two further experiments in simulated rumen liquid an *in vivo* experiment was performed in the Agricultural University of Norway to study the sorption properties of PILCs in goats.

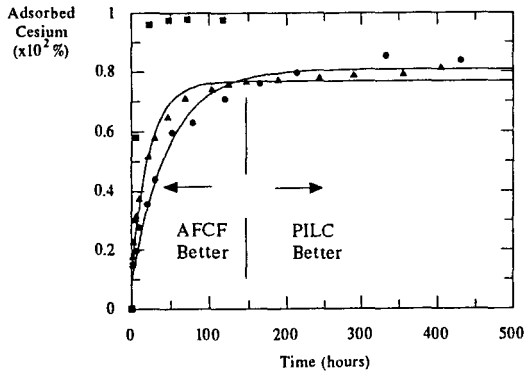

Figure 2. Adsorption characteristics of ATHINA and AFCF in a 200 mL ^{137}Cs (1.7×10^{-11} M) bath under various conditions
(●) ATHINA + Na + K (2×10^{-4} M).
(♦) AFCF + Na + K (2×10^{-4} M).
(■) AFCF - no Na or K in the bath.

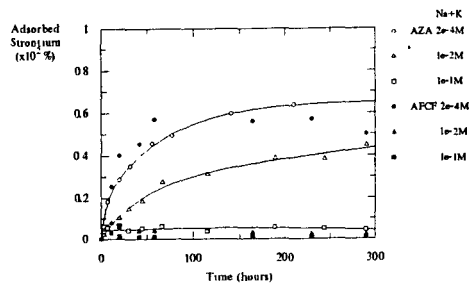

Figure 3 Strontium adsorption by 30 mg AZA and AFCF in competition with Na+K ions in different concentrations Strontium concentration 1.7×10^{-7} M; pH: 6.0

B. *In vivo* testing of PILCs for Sr binding.

The materials used in all the in *vitro* experiments were tested in 4 lactating goats at the Agricultural University of Norway, Department of Animal Science.. For 12 days the goats were given orally 50000 Bq ^{85}Sr to establish eqiulibrium. After 12 days, the four goats were given both ^{85}Sr and PILCs at daily rates of 30, 10, 15 and 10 g PILC, diluted in pure water. Monitoring lasted for 9 further days for the goats receiving 10 and 15 g d^{-1} and 14 days for

Table 6 Percentage strontium absorbed by different PILC masses in the presence of Ca. All measurements were performed in a 200 mL bath with Sr concentration 1.7 x 10^{-7} M.

Mass	Ca concentration (M)		
(mg)	1 x 10^{-4}	4 x 10^{-4}	1 x 10^{-3}
30	25	14	9
60	52	24	12
100	67	36	14
150	77	52	20
500	94	92	64

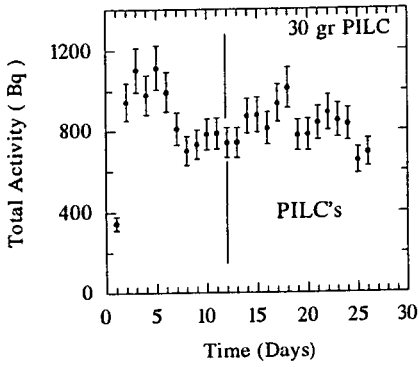

Figure 4. Radiostrontium activity in milk before and after administration of PILC.

the goat receiving 30 g d^{-1}. The milk activity, during the experiment, for the goat receiving 30 g of PILC is presented in Fig. 4. It was concluded that the administration of PILCs had no effect on the activity level in the milk of the animals. Possible reasons for this failure could be the saturation of PILCs with competitive ions and especially Ca, saturation with hydronium ions in the acid part of the digestive tract or the limited time of contact between the material and strontium in the digestive tract. The last reason was thought to be the most important and thus further efforts were concentrated towards improving the material in order to increase its CEC and speed up the process.

C. *In vitro* testing of Improved PILC (PILCI) for Sr and Cs binding.

The CEC of the new improved PILC material (PILCI) and its kinetics are compared to AZA in Table 5 and Fig. 6. It is seen in these data that in the case of PILCI, a few minutes are enough for the attainment of equilibrium, while the amout sorbed is definetely greater than in the case of AZA due to the higher CEC of the new material. The new PILC material was further tested *in vitro* for both Cs and Sr adsorption in rumen liquid taken from slaughtered sheep. The results of these experiments are presented in Table 6 and are very encouraging for perfoming *in vivo* testing of PILCIs for Sr and Cs binding in the near future.

Table 5. CEC of materials AZA and PILCI.

Material	CEC (mEq g^{-1})
AZA	0.57 ± 0 02
PILCI	0 40 ± 0.03

Table 6. Percent caesium and strontium adsorbed in rumen liquid by AZA and PILCI. Rumen cation molarities were measured as Na: 0.07 M; K: 1.73 x 10^{-2} M; Ca· 1.85 x 10^{-3} M; Mg. 3.74 x 10^{-3} M

Material	Mass (g)	Percent sorbed	
		Cs	Sr
AZA	1		8
PILCI	1	37	26
PILCI	3		40

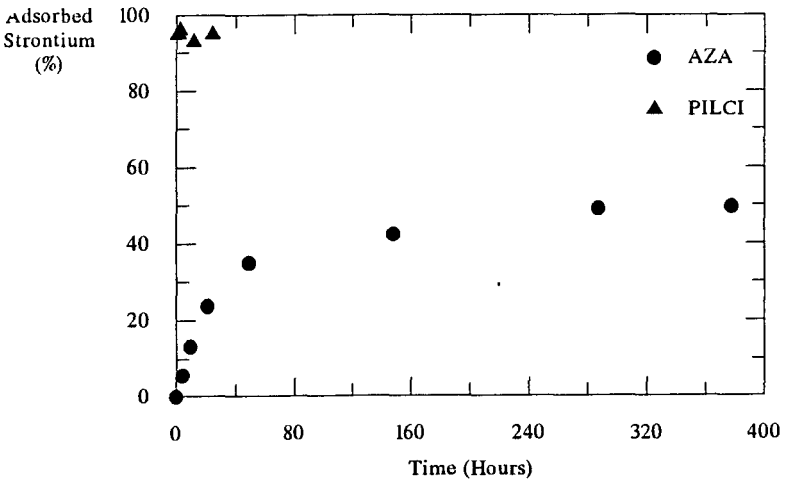

Figure 5 Comparison of AZA and PILCI kinetics. Bath volume 200 mL; Mass of material: 30 mg; Sr concentration: 5 73 x 10^{-8} M.

Modelling of cation exchange processes

(Assimakopoulos, Karamanis)

A model for the description of cation exchange between a solid piece of material and ions in a surrounding bath has been devised. The model considers a piece of material, capable of trapping a total of N_o monovalent cations, totally immersed in a bath containing K distinct species of cations. Let N_{io} be the number of cations i, both in the material and the bath, and at a given time t, N_i the number of cations i in the material. Let further λ_{ij} be the probability for cation i in the material to be replaced by cation j in the bath. Then the rate at which cations j in the bath will replace cations i in the material will be proportional to the respective populations of the two cations, i.e.

$$\lambda_{ij} N_i (N_{jo} - N_j) . \qquad (3)$$

The number of cations i in the material N_i will decrease due to cations j in the bath replacing cations i in the material and will increase due to cations i in the bath replacing cations j in the material. We may thus write

$$\frac{dN_i}{dt} = -\sum_{\substack{j=1 \\ j \neq i}}^{K} \lambda_{ij} N_i (N_{jo} - N_j) + \sum_{\substack{j=1 \\ j \neq i}}^{K} \lambda_{ji} N_j (N_{io} - N_i) \qquad (4)$$

for i = 1,2,...,K. In this model it is further assumed that at any given time all sites available in the material are occupied by a cation, i.e.

$$\sum_{i=1}^{K} N_i = N_o . \qquad (5)$$

This condition is illustrated schematically in Fig. 6.

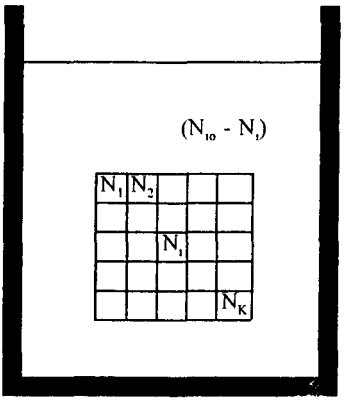

Figure 6 Schematic of the cation exchange model. At any time all sites of the material are occupied by N_1, N_2, .., N_K cations. For each cation species j, the bath population is $(N_{io} - N_j)$.

The system of non-linear differential equations (4) could not be solved analytically. Thus eqns (4) were integrated numerically through the Runge-Kutta method and the results were compared to data obtained from *in vitro* experiments. For this purpose the subroutines which calculated $N_i(t)$ for the population of cation i in the material at time t, were incorporated into the minimization package MINUIT and the probability coefficients λ_{ij} were treated as free parameters. The CEC of the material was also treated as a free parameter. Values of CEC and the coefficients λ_{ij} were determined from the best fit (minimum χ^2) of model predictions to the data. Predictions of the model for a three cation system are compared to data in Fig. 7. In this experiment a 20 mg PILC sample, originally loaded with Na, was immersed in a 200 mL bath of distilled water, which contained 1.7 x 10^{-9} M Cs and 2.0 x 10^{-2} M Na ions. The values of the free parameters obtained from this calculation were

$$CEC = 3.6 \times 10^{-2}$$
$$\lambda_{Na,Cs} = 452$$
$$\lambda_{Cs,Na} = 15$$

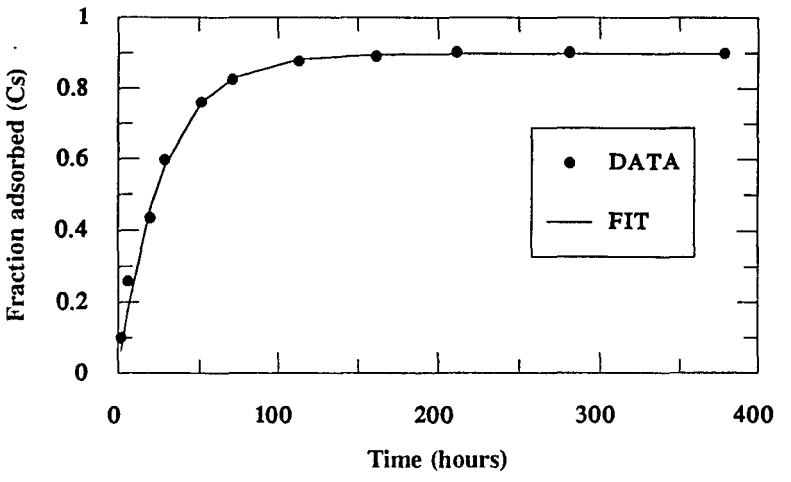

Figure 7. Best fit (minimum χ^2) of model prediction to data for a three cation system.

It is noted that in the framework of the model developed here, the ratio

$$\rho(i/j) = \frac{\lambda_{ij}}{\lambda_{ji}} \qquad (6)$$

which may be termed the **selectivity of *i* over *j***, provides a measure of the efficiency with which the material traps cation *i* over cation *j*. Thus from the results in Fig. 7 it was determined that the particular PILC sample tested in this experiment was highly selective for Cs with

$$\rho(Cs/Na) = 30.$$

Publications

- P.A. Assimakopoulos, K. Divanes, A.A. Pakou, K.C. Stamoulis, A.S. Mantzios and E. Nikolaou, Radiostrontium Transfer to Sheep's Milk as a Result of Soil Ingestion. Sci. Total Environ. 1994, in press.

- P.A. Assimakopoulos, T. Lagoyannis, A.A. Pakou, V. Koutsotolis, A.S. Mantzios and E. Nikolaou, Ratios of Transfer Coefficients for Radiocaesium Transport in Ruminants. Health Physics, 1994, in press.

- D.T. Karamanis, P.A. Assimakopoulos, A.A. Pakou and N.H. Gangas, Sorption of Radiocaesium and Radiostrontium on Pillared Layered Clays (PILCs). International Conference on Separation of Ionic Solutes, Piestani, Slovakia, 15-19 May, 1995.

Head of Project 3: Dr. Crout

II Objectives for the reporting period

1. To test and if necessary extend the sheep radiocaesium model developed previously.
2. To utilise data collected at GSF to model the effect of grazing intensity on radiocaesium dynamics in pasture.
3. To develop a radiostrontium model which accounts for the influence of calcium on radiostrontium transfer.
4. To develop a radioiodine model which accounts for the influence of stable iodine on radioiodine transfer.

An additional objective established during the project was:-

5. To utilise, data collected at Brno to develop a model of radiocaesium dynamics in broiler chickens.

Of these objectives 1, 3 and 4 were considered the most important.

Progress achieved including publications

1. Sheep Radiocaesium Model

The Galer Model

A dynamic simulation model for radiocaesium transfer between sheep tissues ('the Galer model') was developed in a previous contract (Galer et al 1993). The model parameters were estimated by fitting the model to data from a 'calibration' experiment. At the start of this experiment animals were dosed with radiocaesium directly to the rumen and then slaughtered on successive occasions and radiocaesium activities measured in the various compartments. The model accounted for 92.3% of the variation in the data (n=51). The model was used to predict a number of radioecological characteristics of sheep (such as the transfer coefficient and biological half life) and a reasonable level of agreement with literature values was found. However no attempt was made to undertake a detailed validation of the model using data independent of its development.

Following the Chernobyl accident in 1986 there have been a large number of studies investigating the behaviour of radiocaesium in animals, in particular sheep. Therefore it is possible to test the predictions of the Galer model. We found that the Galer model should not be applied to situations where the weights of an animal differ substantially from those in the 'calibration' experiment (mean live weight of 30.5 kg). For example, initial comparisons of the Galer model with data presented by Assimakopoulus et al (1993) for a contamination-decontamination experiment with sheep whose mean live weight was 84 kg showed strong deviations from observation, both in magnitude and dynamic behaviour (Fig 1, discussed below). The Galer model uses compartment activities (i.e. total compartment content, Bq) as the driving variables for transfer in the animal. This simplifies the model and avoids the need to account for a potentially variable body size. However Galer et al (1993) recognised that assuming the models rate coefficients to be constant with varying body size may not be strictly valid.

Revised Model

A revised model has been developed in which radiocaesium transfer between compartments is driven by activity concentration (Bq kg^{-1}) rather than activity (Bq). Although transfers from the extra cellular fluid, kidney, liver, and muscle are driven by concentration we retained the Galer model's approach to drive gut absorption and transfer to excreta by compartment activity (Bq). The model was parameterised using the same data set as that used for the Galer model.

Model Testing Results

To test the reliability of the revised model its predictions have been compared to a range of independent experimental datasets. These experimental results have not been used in the development of the model. It is only possible to summarise the results here.

- **Animals administered a single oral dose.** In this experiment Scottish Blackface sheep (mean live weight, 35 kg) were contaminated by a single oral dose of ionic radiocaesium and slaughtered at subsequent intervals thereafter. A variety of tissues were sampled and excreta collected (Beresford et al 1988). The results are quite showing good agreement between model and experiment (r^2 in the range 0.92 - 0.77)
- **Live monitoring of animals receiving a daily oral dose.** Beresford et al (1995) undertook an experiment to investigate the variation between the radiocaesium transfers of individual sheep (Swaledale and Herdwick breeds). Twenty-two animals (mean live weight, 44kg) were orally dosed twice daily with 16.5 kBq d^{-1} of radiocaesium and their resulting muscle activity concentrations measured by live-monitoring over a 35 day period. A reasonable level of agreement was found (r^2 0.84).
- **Contamination-decontamination experiment.** Assimakopoulos et al (1993) undertook an experiment in which sheep were continuously fed a contaminated diet for a 60 day period and then transferred to an uncontaminated diet. Animals were slaughtered at various intervals and tissues sampled and analysed. The sheep were of the Boutsiko breed which is much larger (mean liveweight in this experiment 84 kg) than the upland breeds (typically 30-40 kg) used for the calibration experiment and some of the other studies presented above. The model predictions were compared with the observed data for muscle, liver and kidney (r^2 in the range 0.92 - 0.65) and the result for muscle is shown in Fig 1. For comparison the corresponding predictions of the Galer model are also shown.
- **Excretions from animals administered a daily oral dose.** Vandecasteele et al (1989) describe an experiment in which lactating ewes (mean live weight 50kg) were orally dosed daily with radiocaesium and radiocaesium excretion measured. An extra term was added to account for lactation so that the model gives a transfer coefficient to milk, equivalent to that observed in the experiment. This has the effect of reducing the predicted radiocaesium output to urine with little effect on output to faeces. The resulting model comparison is shown in Fig. 2. Clearly both comparisons are quite satisfactory, although the urine comparison does not provide as independent a test of the model as the other comparisons above.

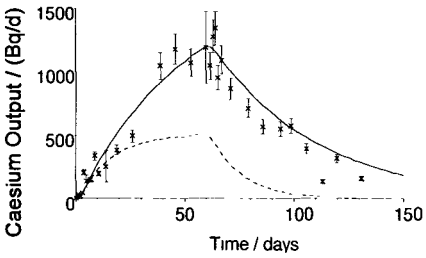

Fig. 1. Revised model predictions (×——) compared to observed muscle activity concentration (Bq kg^{-1}) for the contamination-decontamination data of Assimakopoulos et al (1993). Experimental points are shown as symbols ±sem (replicates=3), model prediction as a continuous curve (r^2=0.92; n=30). For comparison the prediction of the Galer model is shown (- - -).

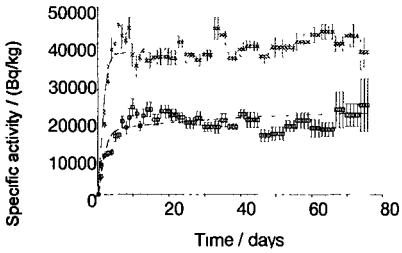

Fig. 2. Model predictions with a lactation correction compared to observed daily radiocaesium output (Bq d^{-1}) to faeces (×—) (r^2=0.75; n=76) and urine (- - -) (r^2=0.71; n=76) for the data of Vandecasteele et al (1989). Experimental points are shown as symbols ±sem (replicates=3), model predictions as continuous curves.

Conclusion

Using the revised model a range of independent dynamic observations of tissue and excreta from different experimental situations have been compared with model predictions. The overall level of agreement is encouraging, r^2 values range from 0.92 (n=30) to 0.65 (n=25). Although some areas of disagreement exist we conclude that the model provides a useful description of radiocaesium transfer in sheep over a wide range of body weights (30 - 80 kg).

Using the same data set for parameterisation a model based on activity concentration rather than activity was found to have more general applicability. For example, the comparisons with the data of Assimakopulos et al (1993) (Fig. 1) could not be reproduced with the model presented by Galer et al (1993). However the predictions of the Galer model for the other experiments described in this paper are similar to those obtained with the new model.

From first principles it might be expected that a concentration based model will be more generally appropriate for the transfer of radionuclides between tissues. The rate of transfer is presumably dependent upon the number of radiocaesium ions arriving at the point of transfer per unit time. In a more concentrated system this rate will be higher, giving rise to differences in the rate of elimination of radiocaesium from an animal (for example, characterised by 'biological half life') attributable to body mass.

The revised model was applied to calculate transfer coefficients (F_m, d kg^{-1}) and biological half lives for adult sheep of 48 kg body mass. The model predicts a biological half life of 20 days which compares with 18 days recommended by Coughtrey (1989) for sheep of the same weight and 17 days reported by Goldman et al (1965). The predicted transfer factor of 0.41 d kg^{-1} compares with observed values of 0.3-0.35 (Pröhl et al 1987) and 0.33 d kg-1 (Voigt et al 1989; Beresford et al 1989). In both cases there is a tendency for the model to overpredict, in the case of the transfer factor this may in part be attributable to experimental values not being measured at a true equilibrium.

2. Grazing Intensity Studies

Experimental work has been undertaken at GSF to investigate the effect of grazing intensity on the soil to plant transfer of radiocaesium. This was to test preliminary model predictions which suggested that shorter swards would initially have a higher activity than tall swards, but in the longer term short swards would have a lower radiocaesium activity concentration. This prediction resulted from assumptions about the translocation of radiocaesium in senescing

leaves and was supported by a field study described by Salt et al (1992). The GSF experimental work has been described elsewhere in this report.

The experimental results showed a high variability in vegetation activity concentration and no grazing intensity treatment effects could be detected. Whether this is because of the experimental variability or because there is no effect is unknown. Nevertheless is was felt that the data could be used to provide a test of the soil and vegetation transfer models.

Soil samples were transferred from GSF to Nottingham so that the radiocaesium kinetics of the soils used could be measured using the techniques described by Absalom et al (in press). This involved the artificial contamination of the soils and subsequent measurement of solution activity concentration over a 3 month period. Kinetic models were then fitted to the data to provide kinetic parameters which could be used in the modelling work. The soil model used described the soil in terms of solution, non-specifically absorbed labile, specifically absorbed labile and non-labile (i.e. fixed) compartments. This approach has been successfully applied to cumbrian soils.

The soil results together with appropriate meteorological data (required to simulate vegetation growth) was used to simulate the vegetation activity concentration over the experimental period. The result for the mineral soil studied is shown below in Fig. 3. The overall pattern of the data appears to be reproduced although because of the high variability this cannot be fully confirmed. It should be noted that the prediction is based solely on the soil kinetics, and vegetation growth and transpiration estimates made by the model. It does not rely upon empirically derived soil-plant transfer factors. Therefore we regard this result as encouraging.

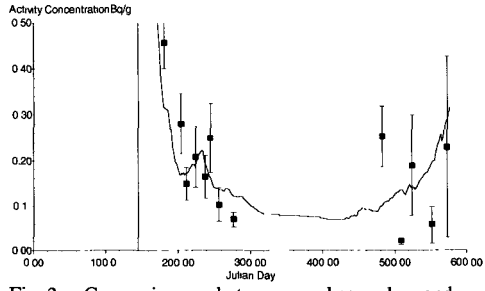

Fig. 3. Comparison between observed and predicted radiocaesium activity concentrations for the mineral soil studies at GSF.

3. Goat Radiostrontium Model

Introduction

Most comprehensive dynamic food chain models, for example PATHWAY and ECOSYS-87 calculate the contamination of animal products using simple transfer coefficients which are assumed to be constant for a particular animal product and isotope. In the case of ECOSYS-87 the value used for the transfer of radiostrontium to goat milk is 0.014 d kg^{-1}, there is no allowance for the effect of the animals Ca metabolism. Experimentally there is a wide variation in the observed transfer of radiostrontium to milk, much of which can be attributed to variations in the dietary intake of Ca (Howard et al 1995). In this project a model for radiostrontium transfer in goats has been developed which is based upon Ca metabolism, and can therefore simulate the effect on radiostrontium transfer of changes in the animals Ca status.

Model Description

The model is primarily a model for the transfer of Ca within the animal, radioisotopes are treated as tracers for Ca, subject to discrimination for transfer between compartments in the case of radiostrontium. The basic Ca model is shown schematically in Fig. 4. The animal is represented as 4 compartments, gastrointestinal tract (GIT), rapidly exchangeable pool (P), slowly exchangeable pool (E), and Bone. The use of the compartments P and E is based upon work by Braithwaite et al (1969). The slowly exchangeable pool (E) is taken to be exchangeable Ca in bone. The compartment Bone represents skeletal Ca and must be included in the model to simulate the resorption of Ca which takes place during lactation (Braithwaite, 1983).

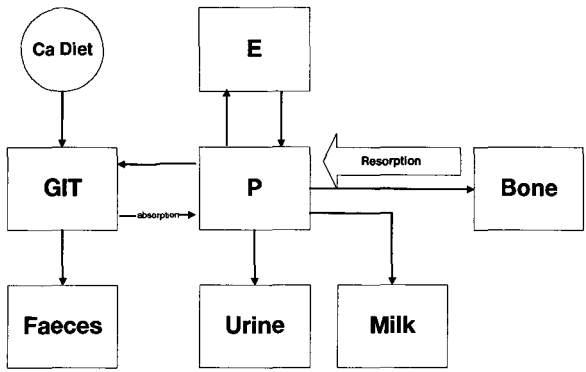

Fig. 4. Schematic Representation of the Calcium Model

Exchanges between compartments P and E are assumed to follow first order kinetics as does the rate of accretion to bone (Braithwaite et al 1969) and excretion to urine. Excretion rate to milk depends upon the milk yield and Ca concentration in milk. Endogenous excretion of Ca to faeces is known to be related to the animals daily intake of feed (Braithwaite 1982). Resorption of Ca from bone is an important part of a lactating animals Ca balance and must be accounted for in the model. Data from Braithwaite et al (1969) has been used to develop a relationship between the bone Ca resorption rate and Ca excretion in milk.

The rate coefficient for transfer from P to bone can be estimated from data presented by Braithwaite et al (1969). The other rate coefficients are unknown and have been estimated by fitting the model to experimental data reported by MLURI [4].

Radiostrontium is simulated by an extension of the Ca model. The stable Ca turnover coefficients described above are utilised, but including discrimination factors for transfers from gut to P; P to faeces; P to milk; and P to urine. Consideration was given to including discrimination factors for transfers between other compartments (such as bone and E) but this was not found to be necessary to obtain a fit with the available data. The values of the discrimination factors are not known and as with the unknown rate coefficients they have been estimated by fitting the model to the experimental data.

Results

The fitted model accounted for 97% (n=64) of the weighted variation in the complete dataset. As an illustration of the comparison between modelled and observed results Fig. 5 shows the excretion of orally administered ^{85}Sr in milk and urine.

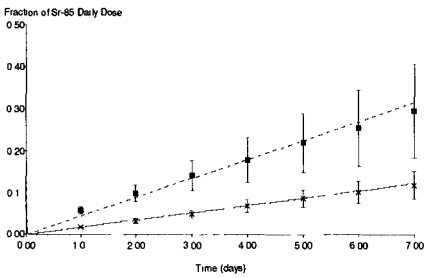

Fig. 5. Modelled and observed cumulative excretion of orally administered Sr-85 to milk (—— ×) and urine (- - - ■). Observed data shown as points ± sem (n=4), model results as a continuous curve.

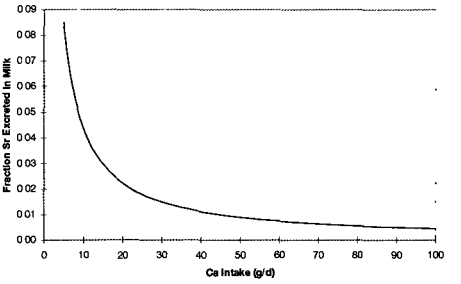

Fig. 6. Fraction of a single oral dose of radiostrontium excreted in milk as a function of dietary Ca intake rate, predicted using the model.

The model was used to simulate the effect of dietary Ca intake rate on the transfer of orally administered radiostrontium to milk. A series of 20 simulations were performed with Ca dietary intake rate ranging from 5 to 100 g d^{-1}. In each case a single oral dose was simulated and the total fraction of the dose excreted in milk after 21 days calculated. The results are shown in Fig. 6. At low Ca intakes absorption is high, resulting in a high transfer of radiostrontium to milk. Clearly ensuring a high Ca intake has potential as a countermeasure for reducing the contamination of milk. This result is similar to that presented by Howard et al (1995) from a review of the available data from 29 studies.

Conclusions

- The transfer of radiostrontium in dairy goats can be modelled by assuming that Sr transfer is controlled by the animals Ca metabolism, making allowance for discrimination between the two elements for some processes.
- Models of radiostrontium transfer which do not consider the Ca status of an animal will only be applicable to particular situations, especially in relation to dietary Ca intake rate.
- Administration of Ca to animals contaminated by radiostrontium is a useful countermeasure although its effect will be limited for animals whose Ca intake is greater than approximately 40 g d^{-1}.
- Whilst the model presented provides a useful description of experimental data it should be tested more thoroughly before being used for radiation protection purposes. In particular attention should be paid to testing the model over a range of dietary Ca intake rates.

4. Cow and Goat Radioiodine Model

Cows

Introduction

In the case of radioiodine transfer within dairy cows, a number of models have been applied although often these are empirically based on analyses of feed and milk concentrations (Kirchner 1994). While useful tools for radiological protection, such models are limited in not considering the details of iodine metabolism within the animal. This is expected to have an important influence on radioiodine transfer because of the important metabolic role of iodine. The metabolically based model presented by Coughtrey & Thorne (1983) is probably the most detailed model available for predicting radioiodine transfer as it considers the influence of stable iodine and thyroid activity.

The Coughtrey model has been applied to experimental data presented by Voigt et al (1994) and alterations to the model are proposed in the light of experimental comparisons.

Coughtrey Model

Coughtrey & Thorne (1983) describe a kinetic model of radioiodine in humans and animals. The structure is the same for all animals considered, and is shown schematically in fig 7. Radioiodine is assumed to be a tracer for stable iodine, and therefore the model primarily considers the dynamics of stable iodine within the animal.

Iodine enters an intake pool, which represents the gut of the animal; this is used to provide a realistic, finite delay component for adsorption which is assumed to be complete. Iodine enters the extra cellular fluid compartment (ECF) as iodide, which is in rapid dynamic exchange with a 'diffusion' compartment representing the remaining tissues of the body. Uptake of iodide occurs from the ECF to the thyroid compartment. Here iodine-based hormones are produced and secreted into the hormone compartment. These are then either excreted directly via the faeces, or broken down to iodide in the diffusion compartment. Losses of iodide occur via urine and milk from the ECF compartment.

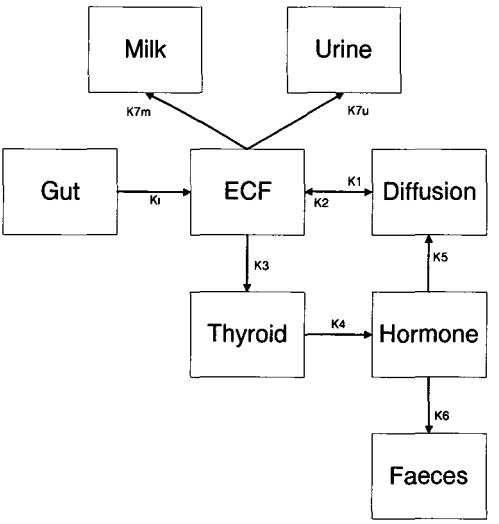

Fig. 7. Schematic representation of the Coughtrey Model for Radioiodine in Cows

The ECF to thyroid rate coefficient is not constant because the uptake of iodine by the thyroid is homeostatically controlled to ensure that the level of iodine-based hormones in the animal remains constant.

Radioiodine is modelled as a tracer within the stable iodine model. The fractional transfer of radioiodine between compartments is simply determined by the fractional transfer of stable iodine.

Experimental Data

The experimental data used in this study has been fully reported by Voigt et al (1994) and will only be outlined here. The objective of the experiment was to investigate the effect of different levels of stable dietary iodine on radioiodine excretion to milk. Three levels of stable dietary iodine were used (71.9, 83.1 and 161.3 mg d^{-1}). For each treatment, 4 cows were given a single oral dose of ^{131}I and the excretions to milk, faeces, and urine measured. No significant differences between the treatments were found, and therefore in the work described here, the data have been combined. All data have been decay-corrected to the time of ^{131}I administration.

Results

The Coughtrey model was run for the experimental situation and the resulting comparisons were very unsatisfactory. An attempt was made to reparameterize the Coughtrey model resulting in improved fit (r^2=0.135), although the agreement for faeces in particular was still not satisfactory. Moreover, the resulting parameters were not physiologically sensible.

Given the high proportion of ^{131}I excreted via faeces in the experimental data, and the model's failure to describe this phenomenon a modification of the model was considered appropriate. A new pathway was included to allow for the endogenous excretion of iodine from the ECF to the faeces (via the lower gut).

This model was fitted to the data and good agreement was obtained (r^2=0.986) (Fig 8).

As an alternative to the ECF-faeces pathway, the possibility of incomplete absorption of iodine in the gut was investigated. This was simulated with an extra compartment representing the lower gut, and the possibility of absorption from this compartment was also considered. Moderate agreement was obtained (r^2=0.696).

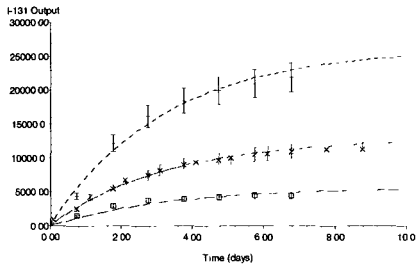

Fig. 8. Model B model predictions compared to the experimental data for accumulated output to milk (× ——), urine (— —), and faeces (+ - - -). Experimental points are shown as symbols ±sem (n=3), model predictions as continuous curves.

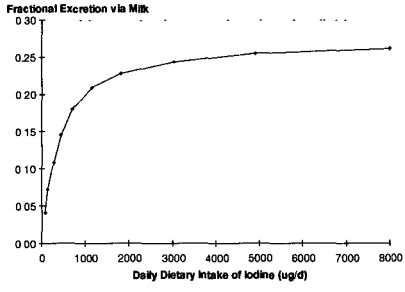

Fig. 9. Predicted relationship between fractional excretion of radioiodine via milk and dietary intake of stable iodine.

Modelling the Influence of Stable Iodine on Radioiodine Output to Milk

The revised model was used to investigate the effect of dietary intake rate of stable iodine on radioiodine transfer to milk. The model was run for 10 rates of stable dietary intake ranging from 100 (which is below the daily requirement for a dairy cow of 400 to 800 μg d^{-1}, (Underwood, 1981)) to 8000 μg d^{-1}. In each case, a single oral dose of radioiodine at t=0 was simulated. The accumulated excretion to milk was calculated and is plotted against dietary intake rate of stable iodine in Fig 9. This shows an increasing proportion of administered radioiodine excreted to milk as the dietary intake of stable iodine increases. Above an intake of

approximately 4000 μg d^{-1}, the proportion excreted to milk plateaus at approximately 25%, which is consistent with the experimental data used to develop the model (Voigt et al 1994) and the results of a previous experiment (Voigt et al 1988).

As modelled, this effect is due to zero order transfer of iodine between the ECF and thyroid compartments. At a low dietary intake of stable iodine, a high proportion of the animals' intake is transferred to the thyroid, ensuring a low concentration of iodine in the ECF and thereby a low transfer to milk. As the dietary intake is increased, the proportion of the daily intake which is transferred to the thyroid falls. This results in a higher concentration of iodide within the ECF and thereby higher transfers to milk.

Conclusions

On the basis of the experimental data used here, it appears that the Coughtrey model is a good prototype for predicting the transfer of radioiodine in cows. However it does require some modification and reparameterization before it can describe the excretion of radioiodine satisfactorily for dairy cows.

The good fit obtained to experimental data with the revised model provides evidence of significant endogenous secretion of iodine from the extra-cellular fluid to the gut and thereby to the faeces. There is further experimental evidence for such a mechanism (Lengeman 1963).

The high dietary intake of stable iodine in the study by Voigt et al (1994) was due to a high level of iodine supplementation in the concentrate used to feed the animals. Animals grazing pasture are likely to have highly variable stable iodine intakes depending upon a range of environmental factors. High dietary supplements of stable iodine in feed may be detrimental from a radiological protection point of view.

While the revised model shows a good agreement with the experimental data, the work described here is best described as model 'calibration'. Further tests of the model against data not used in its development would be required before it can be regarded as reliable. Ideally, this would involve animals whose dietary intake of stable iodine is significantly lower than that used by Voigt et al (1994).

Goats

Introduction

There is a large amount of data available which shows that large doses of stable iodine will reduce the transfer of radioiodine to milk in the case of both cows and goats (Bustad et al 1963; Hill 1966; Lengeman and Swanson 1957). This phenomenon is not accounted for by the Coughtrey model outlined above. Work has been undertaken to apply the Coughtrey model to experimental data for the transfer of radioiodine to goat milk and an extension of the model to account for large doses of stable iodine is proposed.

Model Description

In the Coughtrey model large stable iodine doses will always reduce the thyroid uptake coefficient increasing the amount of iodine in the ECF which means that as a proportion *more* iodine will be secreted into milk. The only way in which a reduction of radio-iodine transfer to milk can be modelled is to include a saturation mechanism for the transfer of milk. To account for this the model has been extended to consider the possibility of a saturating pathway from ECF to milk such that the rate of secretion of iodine (μg d^{-1}) into milk is given by a Michalis-Menten equation.

As for the cow model radioiodine is modelled as a tracer within the stable iodine model. The fractional transfer of radioiodine between compartments is simply determined by the fractional transfer of stable iodine.

The Michalis parameters were estimated by fitting the model to experimental data collected by MLURI/ITE [4,1] which is described elsewhere in this report.

Results

The comparison between modelled and observed excretion of radioiodine to milk is shown in Fig. 10 for the ^{131}I data from the treated and control animals. Overall the model explains 90.2% of the weighted variation in the data ($P<0.001$).

The treated animals were also dosed with ^{125}I at t=24 h and this data is also shown in Fig. 10 together with the corresponding model prediction. The model was not fitted using this data therefore the good comparison provides a measure of confidence in the model. When the ^{125}I data is included the model accounts for 92.3% of the weighted variation in the data.

The model has been used to investigate the dose response of stable iodine in terms of its effect on radio-iodine output to milk. This has been done assuming a single contamination event at t=0 and a simultaneous countermeasure dose of stable iodine. Twenty-five levels of stable dose have been simulated ranging from 0.0 to 5 g. In each case the total fraction of radioiodine excreted in milk was calculated. A daily dietary intake of radioiodine of 3 mg d^{-1} was assumed

The predicted dose response of stable iodine on the excretion of radioiodine in milk is shown in Fig. 11. The greater the administration the greater the reduction in radioiodine excretion to milk. Although there is a continuing reduction at higher stable doses this becomes progressively less and high doses of stable iodine are detrimental to animal health if sustained for any period (ARC 1980). Probably a dose of between 2 to 3 g would be optimal although this should not be regularly administered.

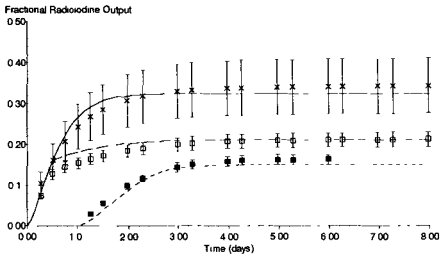

Fig. 10. Model predictions compared to the experimental data for accumulated output to milk for the control group (×——), the dosed group I-131 (— —), and the dosed group I-125 (■ - - -). Experimental points are shown as symbols ±sem (n=6), model predictions as continuous curves.

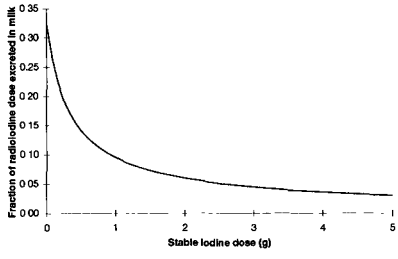

Fig. 11. Variation of the predicted fractional excretion of radioiodine in milk with the amount of stable iodine countermeasure administered. Simulations assume that the radioiodine and stable iodine are simultaneously applied and that the daily dietary intake rate of stable iodine is 3 mg d^{-1}.

Conclusions

The Coughtrey model for radioiodine in goats cannot account for the effect of large countermeasure doses of stable iodine on the transfer of radioiodine to goat milk. Incorporating a saturating pathway from ECF to milk, represented by Michalis-Menten kinetics, enables these effects to be simulated.

The revised model suggests that in the case of dairy goats exposed to a single contamination event a stable iodine dose of 2-3 g will achieve a 85% reduction in radioiodine transfer to milk.

5. Broiler Chicken Radiocaesium Model

Using data collected by Pöschl et al [7] 9in press) above a simple first order kinetic model of radiocaesium transfers in broiler chickens has been developed. The model comprises 7 interconnected compartments described by a set of simultaneous differential equations in which transfers between tissues are driven by radiocaesium concentration in each of the compartments. It is necessary to use concentration (Bq kg^{-1}) rather than amount (Bq) because of the large weight changes during the course of the experiment. The exception to this are transfers from the gut compartment which are driven simply by the amount of radiocaesium present.

Overall the model accounted for 99.7% of the weighted variation in the experimental data. Fits to all individual compartments were good, ranging from r^2 of 0.876 to 0.992. The comparison between the model predictions and observation for the breast compartments is shown in Fig 12.

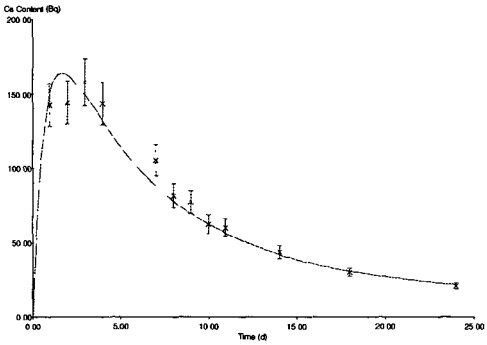

Fig. 12. Comparison between modelled and observed radiocaesium content of the breast compartment (R^2=0.962).

Further work has been undertaken to apply this model to data collected previously by Vandecasteele [6] and Voigt[5]. However significant differences were found. The reasons for these are unclear, the rate of growth differed between the two experiments and this may have been a factor. There may have been differences in breed, or feeding regime. Further experimental work would be required to develop a more generally applicable model.

Publications

Crout, N.M.J., Beresford, N.A., & Howard, B.J. 1993. Does soil adhesion matter when predicting radiocaesium transfer to animals? J. Environ. Radioact., 20, 201-212.

Galer, A.M., **Crout, N.M.J.,** Beresford, N.A., Howard, B.J., Mayes, R.W., Barnett, C.L., Eayres, H.F. & Lamb, C.S. 1993. Dynamic radiocaesium distribution in sheep: measurement and modelling. J. Environ. Radioact., 20, 35-48.

G. Voigt, B. J. Howard, C. Vandecasteele, R. W. Mayes, M. Belli, U. Sansone, G. Stakelum, P. A. Colgan, P. Assimakopoulos, **N. M.J. Crout**, B. E. Jones, K. Hove. 1993. Factors affecting radiocaesium transfer to ruminants - Results of a multinational Research group. Proceedings der 25. Jahrestagung des FfS, Publikationsreihe Fortschritte im Strahlenschutz, Band II, 599-604.

Beresford, N.A., Mayes, R.W., **Crout, N.M.J.**, Howard, B.J. & Kanyar B. 1994. Dynamic behavior of ^{110m}Ag in sheep tissues. Hlth. Phys. 66, 420-426.

Crout, N.M.J & Voigt, G (in press). Modelling Radioiodine Dynamics in Dairy Cows. J. Dairy Science.

Crout N.M.J, Beresford NA, Howard BJ, Mayes RW, Assimakopoulos PA, & Vandecasteele CM (in press). The development and testing of a revised dynamic model of radiocaesium to sheep tissues. Radiation & Environmental Biophysics.

Two further papers are currently being prepared on the models of radioiodine and radiostrontium in goats.

References

ARC, 1980. The nutrient requirements of livestock. CAB, Slough, UK.

Absalom, JP, Young, SD, Crout, NMJ (in press). Radiocaesium Fixation Dynamics: Measurement in Six Cumbrian Soils. J. European Soil Science.

Assimakopoulos PA, Ioannides KG, Pakou AA, Mantzios AS, Pappas CP (1993) Transport of radiocaesium from a sheep's diet to its tissues. Sci Tot Environ., 136: 1-11.

Beresford NA, Barnett CL, Mayes RW, Lamb CS, Howard BJ, Wilson PJ (1995) Radiocaesium variability within sheep flocks in the restricted area of Cumbria. ITE Project Report to the Ministry of Agriculture, Fisheries & Food. Institute of Terrestrial Ecology, Grange-over-Sands, UK.

Beresford NA, Lamb CS, Mayes RW, Howard BJ, Colgrove PJ (1989). The effect of treating pastures with bentonite on the transfer of ^{137}Cs from grazed herbage to sheep. J. Environ. Radioact. 9:251-64.

Beresford NA, Howard BJ, Mayes RW, Lamb CS (1988) Dynamics of radionuclides in sheep tissues. ITE Project Report. Institute of Terrestrial Ecology, Grange-over-Sands, UK.

Braithwaite, GD (1983). Calcium and phosphorus requirements of the ewe during pregnancy and lactation 1. Calcium. Br. J. Nutr. 50:711.

Braithwaite, GD (1982). Endogenous faecal loss of calcium by ruminants. J. Agric. Sci. (Camb.) 99:355.

Braithwaite, GD, Glascock RF, and SH. Riazuddin (1969). Calcium Metabolism in Lactating Ewes. Br. J. Nutr. 23:827.

Bustad, LK, Wood DH, Elefson EE, Ragan HA, and McClellan RO. (1963). I-131 in milk and thyroid of dairy cattle following a single contamination event and prolonged daily administration. Health Physics 9:1231.

Coughtrey PJ (1990) Radioactivity transfer to animal products. ANS 2223-R1. Associated Nuclear Services Ltd., Epsom, UK.

Coughtrey, PJ & Thorne MC. (1983). Radionuclide distribution and transport in terrestrial and aquatic ecosystems. Volume 3. A.A. Balkema, Rotterdam.

Galer AM, Crout NMJ, Beresford NA, Howard BJ, Mayes RW, Barnett CL, Eayres H, Lamb CS (1993) Dynamic radiocaesium distribution in sheep: measurement and modelling. J Environ Radioact. 20: 35-48.

Goldman M, Longhurst WM, Della Rosa RJ, Baker NF, Barnes RD (1965) The comparative metabolism of strontium, calcium, and cesium in deer and sheep. Health Physics 11: 1415-22.

Hill, M. (1966). Uptake and secretion of radioactive material in dairy cows: Effects of radioactive precipitation on beef as well as countermeasures (in German). Arch. Lebensmittelhyg. 17:49.

Howard, BJ, Beresford NA, Kennedy, VH, & Barnett, CL. (1995). A review of current knowledge of the transfer of radiostrontium to milk and possible countermeasures. ITE Project Report. Institute of Terrestrial Ecology, Grange-over-Sands, UK.

Kirchner, G. (1994). Transport of iodine and cesium via the grass-cow-milk pathway after the Chernobyl accident. Health Physics 66:653.

Lengeman, FW (1963). ^{131}I concentrations in blood, milk, urine and faeces of dairy cows following a single dose of radio-iodine. J.Agric. Sci. (Camb.) 61:375.

Lengeman, FW and Swanson EW (1957). A study of the secretion of iodine in milk of dairy cows using oral doses on ^{131}I. J. Dairy Sci. 40:216.

Pöschl M, Borkovec V, Zelenka J. (in press). Dynamic radiocaesium Distribution in Broiler Chickens. Health Phys.

Pröhl G, Müller H, Voigt G, Heinrichs K, Lindner JP, Probstmeier G (1987). Investigations on the transfer of cesium from fodder to animal food products. IUR Workshop on Plant-Animal Transfer of Radionuclides, 19-22 October 1987. Grange-over-Sands, Cumbria,.

Salt CA, Mayes RW & Elston, DA (1992). Effects of season, grazing intensity and diet compostition on the radiocaesium intake by sheep on re-seeded hill pasure. J. Applied Ecology, 29:378-387.

Vandecasteele CM, Van Hees M, Culot JP, Vankerom J (1989). Radiocaesium metabolism in pregnant ewes and their progeny. Sci Tot Environ 85: 212-223.

Voigt, G., Scholtola Ch., Probstmeir G, and Rohrmoser G (1994). Influence of stable iodine on the transfer of ^{131}I into cows' milk. Radiat. Environ. Biophys. 33:243.

Voigt G, Pröhl G, Müller H, Bauer T, Lindner JP, Probstmeier G, Röhrmoser G (1989). Determination of the transfer of cesiumand iodine from feed into domestic animals. Sci. Tot. Environ. 85:329-38.

Voigt, G, Heurids K, Prohl G, and Paretzke HG (1988). Measurements of transfer coefficients for Cs-137, Co-60, Mn-54, Na-22, I-131, and Tc-95m from feed into milk and beef. Radiat. Environ. Biophys. 27:143.12. Underwood, E.J. 1981. The mineral nutrition of livestock. CAB, Slough, UK.

Head of Project 4: Dr. Mayes

II. Objectives for the reporting period

1. To conduct a study, in collaboration with ITE, to establish the influence of dietary iodine levels on the effectiveness of stable iodine dosing as a countermeasure to reduce radioiodine transfer to goats' milk.

2. To quantify plasma turnover rates, metabolic interconversions and routes of excretion of inorganic and organic iodine metabolites in order to improve the effectiveness of prediction models of radioiodine behaviour in lactating goats.

3. In collaboration with ITE, complete a series of animal experiments to examine the effect of calcium status on radiostrontium transfer to lactating goats and to supply the data generated to Nottingham University to enable the development of radiostrontium models.

4. To complete, in collaboration with ITE, experiments to quantify the effect of different physiological states and feed intakes in sheep on the transfer of ^{137}Cs to muscle.

III. Progress achieved including publications

Project staff: R.W. Mayes; C.S. Lamb; P.J. Wilson

Animal experiments comprising objectives 1, 3, and 4 were conducted jointly with ITE [1]. The studies on stable iodine dosing (1) and radiocaesium uptake (4) are described in the report from ITE [1].

2. The behaviour of radioiodine in lactating goats - plasma turnover, metabolic interconversion and routes of excretion of inorganic (iodide) and organic iodine (thyroxine).

Mathematical models have been developed to predict the transfer of radioiodine to the thyroid gland and to milk in farm livestock ingesting ^{131}I following a nuclear accident. In such models assumptions have been made that inorganic iodine (predominantly as iodide) is excreted via the urine and milk and not via the faeces, whereas organic iodine (mainly thyroxine, T4) is exclusively excreted via the faeces, although some conversion to iodide may also occur in the body. Earlier work within this project indicated that in non-lactating sheep about 15% of intravenously-infused [^{131}I]-iodide appeared in the faeces. Although the chemical form of the ^{131}I in the faeces was not known the time scale was such that the contribution from conversion to organic iodine in the thyroid was probably small. It is therefore probable that assumptions made in the models, regarding routes of excretion, are incorrect and thus calls into question the reliability of such models in predicting radioiodine transfers to milk and thyroid following a nuclear accident. The transfer dynamics of radioiodine would be affected by the degree to which organic iodine is recycled by conversion to iodide.

Materials and methods

The routes of excretion of organic iodine (as [^{125}I]-thyroxine) and inorganic iodine (as [^{131}I]-potassium iodide) from blood plasma were compared in lactating dairy goats. In order to quantify the interconversion of the form of iodine between these two blood pools, plasma thyroxine and iodide turnover rates and transfer quotients were estimated by using continuously-infused [^{125}I]-thyroxine and [^{131}I]-iodide as isotopic tracers to evaluate transfers in the following compartmental model:

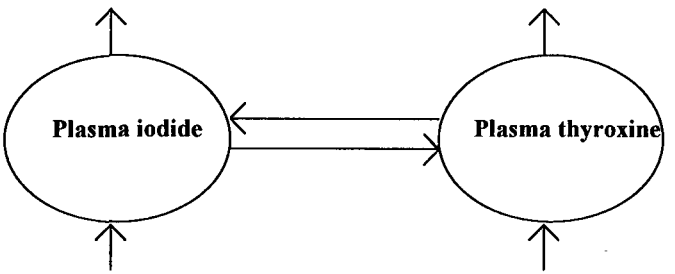

Eight lactating dairy goats which had been maintained on a diet of dried grass pellets and cereal concentrate (of average iodine content) were housed in metabolism cages Following the morning milking on the day after insertion of intravenous jugular catheters, simultaneous jugular infusions of [^{125}I]-thyroxine and [^{131}I]-iodide were commenced. The isotopic tracers, which were dissolved in isotonic saline solution containing blood plasma previously taken from the same animal, were separately infused to each animal via a coaxial catheter over a 10-hour period. Blood samples (10ml) were taken from the uncatheterised jugular vein before the beginning of the tracer infusions and hourly over the last four hours of the infusions. Methylthiouracil was added to plasma samples to minimise deiodination of thyroxine during sample storage and analysis. After the completion of the infusions the jugular catheters were immediately removed and the animals were milked. Throughout the infusion period, and thereafter for seven days, total collections of faeces and urine were made (12-hourly for first two days and then daily); twice daily milk collection and sampling continued over the period of excreta collection.

In order to estimate the specific radioactivities of radioiodine in thyroxine and iodide in plasma (^{125}I and ^{131}I activity per unit amount of thyroxine and iodide) known quantities of carrier thyroxine and iodide were added to plasma samples. After precipitation of the plasma proteins with ethanol/25% ammonia solution (197:3 v/v) plasma extracts were subjected to HPLC analysis to isolate iodide, thyroxine and triiodothyronine (T3). The HPLC column contained an end-capped C8 packing (Lichrocart 5μm) and solvent-programming was used with varying proportions of acetonitrile and aqueous acetic acid (1% w/v). Separate peaks containing iodide, T3 and thyroxine were collected by routing the effluent from the UV detector to a fraction collector. The isolates (5g) were counted on a NaI gamma counter in dual-

channel mode (Canberra Packard Cobra). The concentrations of thyroxine in whole plasma and in relevant fractions after HPLC separation were estimated by an immunoassay technique; iodide concentrations in the same samples were estimated by a continuous-flow (Autoanalyzer) method.

Milk, urine and faeces were analysed for ^{125}I by counting samples in 20ml scintillation vials using a NaI Autogamma counter. Analysis for ^{131}I was carried out with larger samples (740g) using a HpGe gamma detector linked to multichannel analyser (Canberra).

Results and discussion

The turnover rate of thyroxine in plasma in lactating goats, expressed in terms of iodine, was estimated to be 2.31±0.367 mg d^{-1} (mean ± SE). This represented approximately 50% of the daily intake of stable iodine. Since results of stable iodide concentrations in plasma and in the iodide fractions after HPLC separation are still awaited, quantitative estimates of iodide turnover and interconversions are not yet available. However, from the relative activity concentrations of ^{125}I and ^{131}I in the fractions obtained after HPLC separation some assessment of the metabolic behaviour of iodine is possible. The relatively low activity concentrations of [^{131}I]-iodide suggest that the rate of iodide turnover through the blood plasma pool may be substantially higher than that of thyroxine. Throughout the period of intravenous tracer infusion there was negligible incorporation of ^{131}I into plasma thyroxine; this might be expected if iodide (represented by [^{131}I]-iodide), taken up from plasma by the thyroid gland, were substantially diluted by the iodine already present in the thyroid before being incorporated into the thyroid hormones. However, ^{125}I appeared in the plasma iodide pool; [^{125}I]-iodide activity concentrations increased as the intravenous infusion proceeded. By comparing activity concentrations of ^{125}I and ^{131}I in plasma iodide in relation to the respective rates of infusion of the tracers it appears that up to 50% of the iodine from thyroxine may be recycled via plasma iodide. Some ^{125}I also appeared in the T3 fraction of plasma.

In relation to the seven-day period of excreta collection the 10-hour infusions of [^{131}I]-iodide and [^{125}I]-thyroxine can be regarded as being the equivalent of single doses. Changes with time, in the distribution of excreted ^{131}I and ^{125}I via milk, urine and faeces are shown in Figure 1. There were obvious differences in the excretion patterns between the two sources of intravenously administered radioiodine. Whilst existing radioiodine models assume no direct excretion of inorganic iodine via the faeces it is evident that the proportion of excreted ^{131}I appearing in the faeces progressively increased with time after dosing. It is not clear whether this increase is due to conversion of ^{131}I-labelled iodide to organically-bound iodine (as thyroid hormones) prior to faecal excretion; although after the 10-hour tracer infusion evidence of conversion of iodide to thyroxine was not measurable in plasma it is likely that after a longer period of time ^{131}I will appear in plasma thyroxine. However, of the ^{131}I excreted over the first 12h after beginning the tracer infusions, about 6% appeared in the faeces. Considering that this may be an underestimate of the endogenous transfer of ^{131}I to the gut during that time period, because of the time

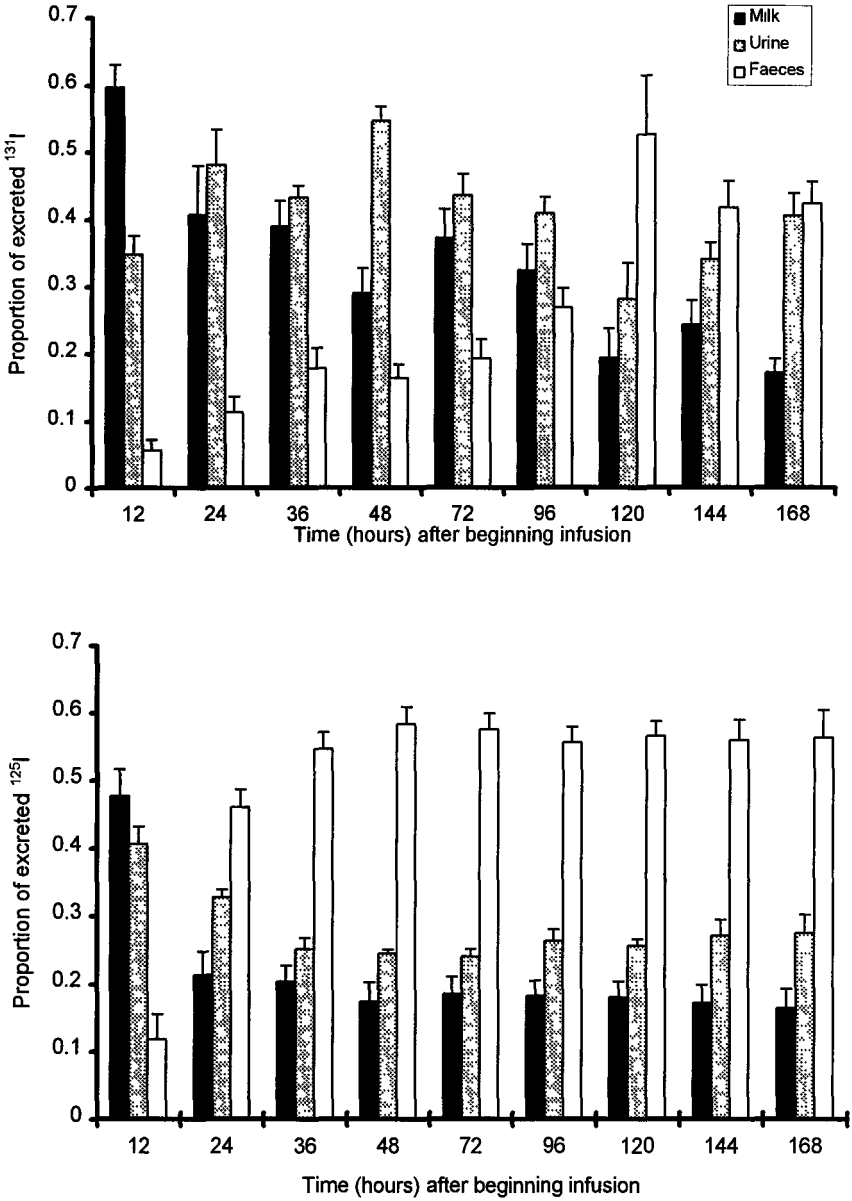

Figure 1. Relative proportions of excreted ^{131}I and ^{125}I appearing in milk, urine and faeces from lactating goats after receiving 10-hour intravenous infusions of [^{131}I]-iodide and [^{125}I]-thyroxine. (mean±SE; n=8).

required for material to pass along the gut, these results show that some inorganic iodine may be excreted via the faeces.

The excretory patterns of ^{125}I, derived from intravenously-administered thyroxine were very different from those resulting from [^{131}I]-iodide. After 36h following the beginning of the tracer infusions the partitioning of excretion via milk, faeces and urine remained constant with about 55% of excreted ^{125}I appearing in the faeces. However, the appearance of ^{125}I in milk and urine does not necessarily indicate that organically-bound iodine can be directly excreted in milk or urine, since there was clear evidence of conversion of thyroxine-iodine to iodide. The predominance of the faecal route for excretion of organic iodine observed in this experiment suggests that the fate of thyroid hormones in the goat are similar to that previously observed in rats, in which there was evidence of excretion into the intestine via the bile and some reabsorption.

The experiment described here can provide data allowing models of radioiodine kinetics in goats to be improved.

3. Effect of calcium status on the behaviour of radiostrontium in lactating goats

As indicated by Nottingham University [3] existing models developed to predict the transfer of radiostrontium to goats' milk take no account of calcium metabolism in the animal despite a considerable wealth of knowledge of the influence of calcium on the behaviour of strontium. The purpose of this work, which was carried out in collaboration with ITE [1], was both to provide data for development of the strontium model for lactating goats conceived by Nottingham University [3] and to examine the effect of the calcium status on radiostrontium behaviour.

Materials and methods

The absorption and dynamic behaviour of calcium and radiostrontium in blood plasma and their excretion via milk, urine and faeces were determined in 11 lactating Saanan goats at four stages of lactation (2, 4, 6 and 8 months after kidding). Intake of calcium relative to calcium requirement, which should have altered calcium status, was modified by maintaining a constant daily intake rate of calcium throughout the period of lactation whilst intakes of other dietary nutrients and milk yield were allowed to decline. The animals were divided into two groups having different fixed levels of calcium intake, such that during the first measurement period the low-calcium group received a barely adequate supply of dietary calcium; thus the high-calcium group during the first period and latterly all animals received calcium at levels in excess of requirements. The basal ration was pelleted dried grass meal; calcium intakes were modified by supplementing with pelleted grass meal containing $CaCO_3$. The animals also received a small fixed quantity of a cereal-based concentrate at milking times 08.00 and 16.00 each day). Except during measurement periods the goats were housed in individual pens. Feeding levels were adjusted at intervals of four weeks.

During measurement period the goats were housed in metabolism cages for two weeks. Radiostrontium (^{85}Sr, as $SrCl_2$ absorbed in paper filters) was orally-administered twice daily throughout each period. On the morning of the fifth day the goats received single intravenous injections of ^{45}Ca and ^{89}Sr (as chloride forms in isotonic saline solution). Blood samples (15ml) were taken 2, 4 and 8h, and thereafter 1, 2, 4 and 6d after the ^{45}Ca and ^{89}Sr injections; the blood was heparinised and centrifuged at 5000*g* to obtain plasma . Daily total collections of milk (combined morning and afternoon milkings), faeces and urine were made for 7d after the intravenous radionuclide administrations. All samples were stored at -20°C prior to analysis. To allow background corrections to be made additional blood, milk and excreta samples were collected prior to intravenous administrations during the second, third and fourth measurement periods. Before the fourth measurement period three animals were removed from the experiment due to ill health.

The activity concentrations of ^{85}Sr in milk, urine and faeces were determined by γ-analysis of thawed samples using HpGe detectors. Due to the presence of ^{85}Sr as a contaminant in administered ^{89}Sr, corrections were made in order to determine the ^{85}Sr in the samples arising from oral dosing. Activity concentrations of ^{45}Ca and ^{89}Sr in plasma, milk, urine and faeces were estimated by β-analysis using liquid scintillation systems; by using triple-channel counting ^{45}Ca and ^{89}Sr could be counted simultaneously, allowing for scintillation arising from the presence of ^{85}Sr.

Blood plasma (3ml) was counted directly in NE260 scintillation fluid (Nuclear Enterprises Ltd, Edinburgh UK)(17ml). Milk (6-9ml) was freeze-dried in scintillation vials, reconstituted in 1.5ml water and four drops concentrated ammonia solution and counted with 19ml NE260 scintillation fluid. Urine (15-20ml) was dried in scintillation vials on a hot plate, acidified with concentrated HNO_3 and evaporated to dryness. The residue was decolourised by repeatedly heating with hydrogen peroxide. The dried residue was reconstituted with 1.5ml water and counted with NE260 scintillant. For ^{45}Ca and ^{89}Sr analysis in faeces mixed oxalates of calcium and strontium were prepared by precipitation from nitric-acid extracts of faecal ash. The ^{45}Ca and ^{89}Sr in the oxalates were determined by suspension counting in Instafluor (Canberra Packard) scintillant containing 4% (w/w) fumed silica (Cab-o-Sil).

Because of large differences in the quenching characteristics for the different sample matrices separate efficiency *vs.* quench relationships were derived for each matrix.

Concentrations of stable Ca and Sr in plasma, milk, urine, faeces and oxalates derived from faecal ash were estimated by atomic absorption spectroscopy; with the exception of plasma which was measured directly, all analysis was carried out on acid digests.

Results and discussion

Mean intakes of dry-matter and calcium, liveweights and milk yields of the two groups of goats over each measurement period are shown in Table 1. At an early stage of the study, mostly prior to the first measurement period, the goats lost considerable amounts of body weight. Because it was apparent that the nutritive value of the basal diet was lower than expected feeding levels, relative to expected milk

yield, were increased for subsequent measurement periods. As a consequence, liveweights were stabilised although milk yields did not decline as rapidly throughout the trial as expected. Calcium intakes were maintained at reasonably constant levels.

For each of the four measurement periods, estimates of the fractions of intravenously-administered ^{45}Ca and ^{89}Sr appearing in milk and excreta for each of the 7d following dosing were obtained, together with changes in ^{45}Ca and ^{89}Sr activity concentrations (relative to dose) in blood plasma.

Table 1. Intakes of dry-matter and calcium, liveweights and milk yields for groups of lactating goats given diets of differing calcium levels.

	Diet	*Measurement period			
		1	2	3	4
Dry-matter intake ($kg\ d^{-1}$)	'Low Ca'	2.44±0.240	2.47±0.128	2.37±0.259	2.59±0.083
	'High Ca'	2.33±0.084	2.24±0.215	2.28±0.282	2.59±0.309
Calcium intake ($g\ d^{-1}$)	'Low Ca'	20.9±1.86	21.1±1.00	21.4±2.07	24.4±2.68
	'High Ca'	28.2±1.10	26.6±3.03	2.68±3.35	27.2±2.58
Liveweight (kg)	'Low Ca'	52.3±3.81	53.1±3.40	52.5±3.21	59.2±0.73
	'High Ca'	53.7±3.72	54.7±3.11	56.7±3.99	57.6±4.61
Milk yield ($kg\ d^{-1}$)	'Low Ca'	2.45±0.346	2.13±0.236	2 31±0.267	2 13±0.062
	'High Ca'	2.44±0.146	2.08±0.274	1.79±0.448	2.26±0.500

* The group on the 'Low Ca' treatment comprised six animals for measurement periods 1 - 3 and three animals for period 4.The 'High Ca' group comprised five animals throughout.

The complete data set was supplied to Nottingham University [3] for developing the strontium model, mentioned elsewhere. Results from the second measurement period, which are typical of all periods, are summarised in Figures 2 and 3. From Figure 2 it is clear that the partitioning of excretion of ^{45}Ca and ^{89}Sr by the various routes, differ markedly. The proportion of the ^{45}Ca dose appearing in milk was greater than that of ^{89}Sr, whereas the proportion of ^{45}Ca excreted in urine was considerably less than ^{89}Sr. There was also evidence of difference in the time-course of excretion of ^{89}Sr in urine compared with ^{45}Ca excretion. However, as Figure 3 shows, the kinetic behaviours of ^{45}Ca and ^{89}Sr in plasma were virtually the same.

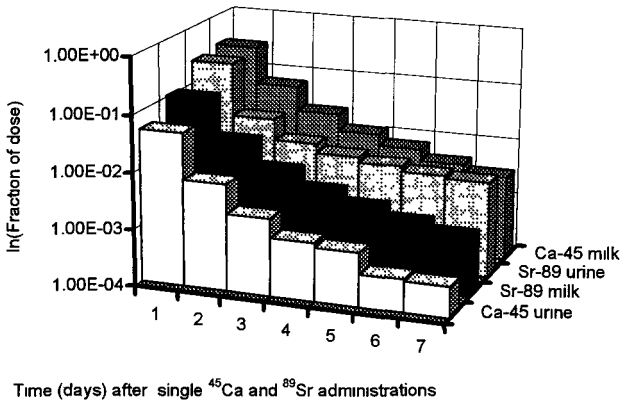

Figure 2. Second measurement period: Outputs of intravenously administered ^{45}Ca and ^{89}Sr in milk and urine of lactating goats expressed as ln(fraction of dose). (mean of 11 goats)

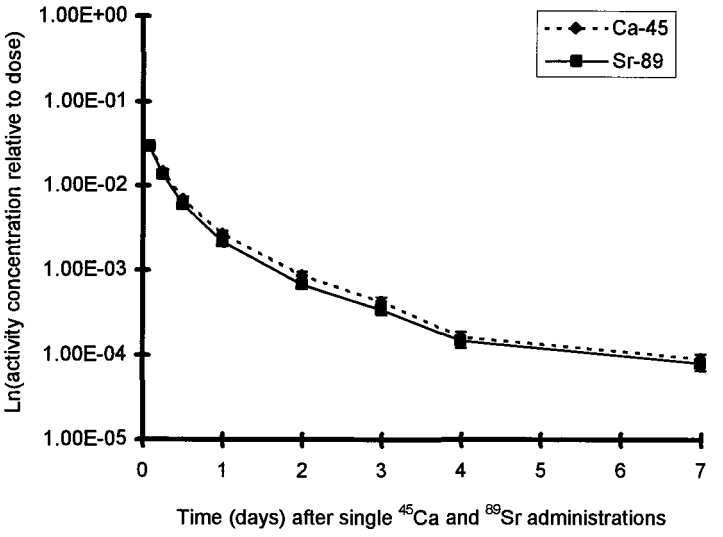

Figure 3. Changes with time in plasma activity concentrations of ^{45}Ca and ^{89}Sr.

Estimates of the true absorption coefficient for orally-administered ^{85}Sr, A_t, estimated by the 'plasma turnover rate' method are summarised in Table 2. Although the differences in A_t measurements between the two dietary Ca level treatments were statistically significant ($P<0.05$), in biological terms, dietary Ca level had a relatively small influence on A_t. Differences between measurement periods were more marked. The relative undernourishment of the goats in early lactation, having lost body weight may explain the higher A_t values observed in the first measurement period compared with the second and third periods. The higher A_t values observed in the fourth measurement period are not easy to explain; on a basis of Ca requirement, A_t values for this period would have been expected to be similar, or slightly lower than the values obtained in the second and third periods.

The transfer of orally-administered ^{85}Sr to milk was estimated as the transfer coefficient, F_m. Although correlation between F_m and A_t was poor, an apparent relationship existed between F_m and calcium intake, when expressed as the intake in excess of requirement. This relationship is shown in Figure 4.

Table 2. Estimates of the true absorption coefficient (A_t) for ^{85}Sr in lactating goats fed at two levels of calcium. (Mean±SE).

Diet	*Measurement period			
	1	2	3	4
'Low Ca'	0.26±0.011	0.13±0.010	0.14±0.009	0.36±0.058
'High Ca'	0.19±0.018	0.12±0.014	0.10±0.007	0.25±0.017

* The group on the 'Low Ca' treatment comprised six animals for measurement periods 1 - 3 and three animals for period 4.The 'High Ca' group comprised five animals throughout.

The results of this study were satisfactory in providing the data necessary for the development of a model to predict the transfer of radiostrontium to goats' milk, based on the dynamic behaviour of calcium (Nottingham University, [3]). However, since the dietary calcium intakes by all of the goats were in excess of requirement, the range of calcium intakes, relative to requirement, was less than intended; therefore, the potential influence of calcium status upon absorption and excretion of radiostrontium at lower dietary calcium intakes remains to be investigated.

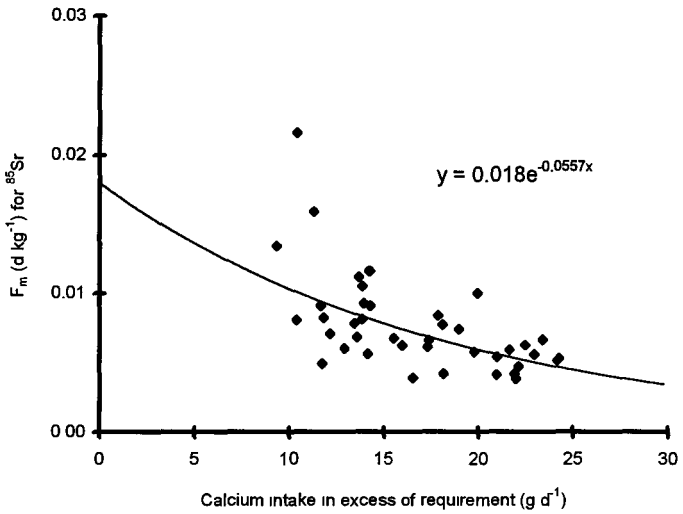

Figure 4. Relationship between estimates of milk transfer coefficient (F_m) for ^{85}Sr and daily intake of calcium, in excess of requirement for lactating goats. Observations (41) from all measurement periods.

Publications

Galer, A.M., Crout, N.M.J., **Beresford, N.A., Howard, B.J.**, Mayes, R.W., **Barnett, C.L.**, Eayres, H.F. & Lamb, C.S. 1993. Dynamic radiocaesium distribution in sheep: measurement and modelling. J. Environ. Radioact., 20, 35-48.

G. Voigt, **B. J. Howard**, C. Vandecasteele, R. W. Mayes, M. Belli, U. Sansone, G. Stakelum, P. A. Colgan, P. Assimakopoulos, N. M. Crout, B. E. Jones, K. Hove. (1993) Factors affecting radiocaesium transfer to ruminants - Results of a multinational Research group. Proceedings der 25. Jahrestagung des FfS, Publikationsreihe Fortschritte im Strahlenschutz, Band II, 599-604

Beresford, N.A., Mayes, R.W., Crout, N.M.J., **Howard, B.J.** & Kanyar B. 1994. Dynamic behavior of ^{110m}Ag in sheep tissues. Hlth. Phys. 66, 420-426.

Mayes, R.W., **Beresford, N.A.**, Lamb, C.S., **Barnett, C.L., Howard, B.J.**, Jones, B.-E.V., Eriksson, O. Hove, K., Pedersen, Ø. & Staines, B.W. 1994. Novel approaches to the estimation of intake and bioavailability of radiocaesium in ruminants grazing forested areas. Sci. Tot. Environ. 157, 289-300.

Beresford, N.A., Barnett, C.L., Mayes, R.W., Pollaris, K., Vandecasteele, C.M. & **Howard B.J.** 1995. The use of in-vitro technique to predict the absorption of dietary radiocaesium by sheep. Radiation and Environmental Biophysics, 34, 191-194.

Crout, N.M.J., **Beresford, N.A., Howard, B.J.,** Mayes, R.W., Assimakopoulos, P.A. & Vandecasteele, C.M. In press. The development and testing of a revised dynamic model of radiocaesium to sheep tissues. Radiation & Environmental Biophysics.

Mayes, R.W., **Beresford, N.A., Howard, B.J.,** Vandecasteele, C.M. & Stakelum G. (submitted July 1995) The use of the true absorption co-efficient of bioavailability of radiocaesium in ruminants. Radiation and Environmental Biophysics.

Head of project 5: Dr. Voigt

II. Objectives for the reporting period

Continuation of the field plot experiments during the 1994 season. Evaluation and interpretation of all data including the studies performed in two farms with different managing systems.

III. Progress achieved including publications

Project staff: G. Voigt; H. Haas; Ch. Schotola; A. Schubert

1. Influence of stable iodine intake on I-131 transfer to cow's milk

The experiments to determine the true absorption of iodine with the two radionuclides ^{131}I and ^{125}I were performed at MLURI/ITE with sheep and goats, and with dairy cows at CEN/SCK. GSF carried out the analysis of stable iodine in feed and milk samples of these experiments by ICP-MS technique. This technique, including the preparation of the samples, has now been successfully adopted by the CEN/SCK group.

The paper by Howard and Voigt et al. giving an overview on the application of countermeasures for radioiodine has been submitted for publication in Health Physics. Together with Nottingham University a publication has been prepared modelling radioiodine dynamics in dairy cows on the basis of experiments of a national funded project; the paper has been accepted in Journal of Dairy Science. The metabolically based model was applied to previously achieved experimental results. It was shown that currently available models need to be modified to satisfactorily describe the measured data for response to stable iodine intake. It was necessary, in particular, to increase significantly the faecal excretion of radioiodine. Applying this modified model to the results describing the influence of stable iodine intake on the transfer of ^{131}I to milk (Voigt et al 1994) we found that increasing dietary intake of stable iodine assympotically increases the proportion of radioiodine excreted via milk. However, the results from the study indicated that stable-iodine administration, as a countermeasure, would have limited effectiveness in Bavaria due to the high level of dietary iodine supplementation.

2. Effect of grazing intensity on radionuclide levels in animals

Field experiments to determine radiocaesium transfer from vegetation to milk under different grazing conditions

For these investigations two farms, located in South-East direction of Munich, were chosen where measurements had previously been performed as a consequence of the Chernobyl accident, and where the farmers were prepared to cooperate.

Farm A (Arnhofen) uses a rotational grazing regime with 4 grazed pastures; this is the most commonly used farm practice in Bavaria. Farm B (Kleinhöhenkirchen) practises a continuous grazing regime with one grazed pasture only. Information on number of animals, areas of the grazed pastures, and deposition densities are given in Table 1. At farm A each dairy cow has a grazing area of almost 2000 m^2, at farm B only about half of this area is is available to each cow. Therefore additional feed was supplied by farmer B originating from other pastures, the ^{137}Cs levels in this feed were below detection limits. At farm A the swards were generally higher than that at farm B although heterogeneous within each pasture. The shorter sward at farm B was more homogenous but with areas of bare soil throughout the pasture.

Table 1 Grazing conditions for dairy cows of farm A and B.

	Farm A	Farm B
Number of animals	45	36
Area of pastures (m^2)	26 150 (A) 29 120 (B) 24 620 (C) 23 080 (D)	36 750 (E)
^{137}Cs in soil (Bq kg^{-1})	27 - 100	45 - 89
^{137}Cs in vegetation (Bq kg^{-1})	0.1 - 30	0.1 - 20

The mean soil activity concentrations of ^{137}Cs were similar for the two farms. However there was considerable variation between soil of the different pasture areas of farm A with values ranging from 27 to 100 Bq kg^{-1} fw with a mean value of 61.1 ± 18.0 Bq kg^{-1} For farm B the values ranged from 45 to 89 Bq kg^{-1} over the whole area with a mean of 67.3 ± 21.9 Bq kg^{-1} (all soil samples taken to a depth of 30 cm). The majority of the ^{137}Cs soil activity (75 %) was still present in the top 10 cm. Soil characteristics of the two farms were generally similar and are given in Table 2.

Table 2 Characteristics of soils in farm A and B

	Farm A	Farm B
Organic matter (%)	10.2	10.5
pH	7.2	5.6
Chalk status	high	average
Phosphate (mg 100 g^{-1})	31	13
Potassium (mg 100 g^{-1})	38	17
Clay (%)	15	22
Silt (%)	41	43
Sand (%)	44	35
CEC (meq 100 g^{-1})*	27.9	32.0

*Cation exchange capacity

The higher chalk, phospate and potassium content in soil at farm A is due to the more intensive fertilization regime used.

In 1993 at farm B bulk milk samples (4 lots of 0.25 l) and vegetation samples (5 replicates, areas of 0.05 m^2 each) were hand clipped once a week as soon as the animals were grazed outdoors (June). Bulk milk samples were taken in farm A in a two day cycle (4 lots of 0.25 l resulting in one liter milk samples to be measured); two replicate vegetation samples (0.23 m^2) were taken from the pasture currently being grazed. Fresh weight of all grass samples was determined immediately after cutting, samples were oven dried in the laboratory (70°C) and weighed; all samples were measured by γ-spectrometry.

The gamma-spectrometric measurements were performed with pure Germanium detectors (25 % efficiency, typical energy resolution 1.9 keV) of 63.5 mm height and 63.5 mm diameter, and with a γ–spectrometry system. Energy and efficiencies were calibrated with standard solutions (PTB, Braunschweig, FRG), the spectra were evaluated by the SPECTRAN F

software programme. Samples were counted in either 1 l Marinelli beakers or 100 g or 30 g PE boxes until the statistical counting errors were less than 5 %.

In order to compare different grazing regimes vegetation and milk activities of farm A and B are shown in Figs. 1 and 2. K-40 activities in milk of both farms were in the same range of 20 to 30 Bq kg^{-1} and in vegetation around 100 ± 10 Bq kg^{-1}. For both milk and soil the ^{40}K values were rather stable, and independent of season and of the different locations.

The movement of animals to the different pastures of farm A applying the rotational grazing regime was not reflected in the milk radiocaesium activity concentrations (Fig. 1). There was a small increase at the end of September due to an unexplained increase in ^{137}Cs activity concentration in pasture grass by a factor of 10.

At farm B a tenfold lower ^{137}Cs activity concentration was observed in milk compared to farm A, even though ^{137}Cs activity concentrations in soil and pasture grass were similar at the two farms (indicating the same transfer rate from soil-plant at both locations). Because animals are forced to graze a smaller area more intensively, activity concentrations can theoretically be decreased by a factor of about 2 to 3 in the grazed plant parts according to the RUINS model [3]. However, this was not observed in vegetation samples measured here.

The additional feeding with uncontaminated feed (estimated to be a maximum of half of the daily intake by the farmer since additional feeding of fresh grass was only provided in the evening), cannot be considered as the only reason for the observed reduction in milk activities of farm B. If we assume that half of the daily intake is due to uncontaminated feed it would account for less than 0.1% of the total ^{137}Cs intake for these cows. The mean daily intake of ^{137}Cs for the cows at each farm was 990 Bq for farm A and 330 Bq for Farm B. Hence ^{137}Cs intake varied by three fold, but milk levels varied ten fold.

The calculated F_m values for farm A and B were 0.006 (0.002-0.009) and 0.003 (0.0009-0.005) d l^{-1} respectively. There is therefore a three-fold difference in the estimated transfer of radiocaesium to milk at the two farms. It is possible that the higher stocking rate at farm B resulted in a higher degree of adherent soil on vegetation (see report by [9]). If so, the estimated radiocaesium intake due to vegetation may be too high. Studies have recently demonstrated that radiocaesium associated with ingested soil has an availability at least 75% lower than radiocaesium incorporated within vegetation. Additionally it is possible that ingested soil may bind radiocaesium originating from vegetation within the gut, making it unavailable for transfer to milk. It is also possible that herbage samples were not representative of material being grazed by the animals. Additionally, because the nature of the grazed swards varied by definition between the two farms the ability to representatively samples vegetation grazed by the two herds may also have differed between the sites. The effect this could have had on estimates of transfer are difficult to predict.

Conclusions

Results of this study demonstrate potential inaccuracies associated with conventional sampling and transfer prediction schemes. It was shown that by just sampling vegetation from grazed pastures and not accounting for differences in farming practices a ten fold discrepancy in the estimation of the transfer of radiocaesium to milk could have been made. In this example all of the difference could not be accounted for by the consideration of additional feedstuffs supplied to the cows.

Since being originally deposited the mobility of radiocaesium originating from Chernobyl has changed. Transfer coefficients for feed-milk had, by 1992, reached values similar to those

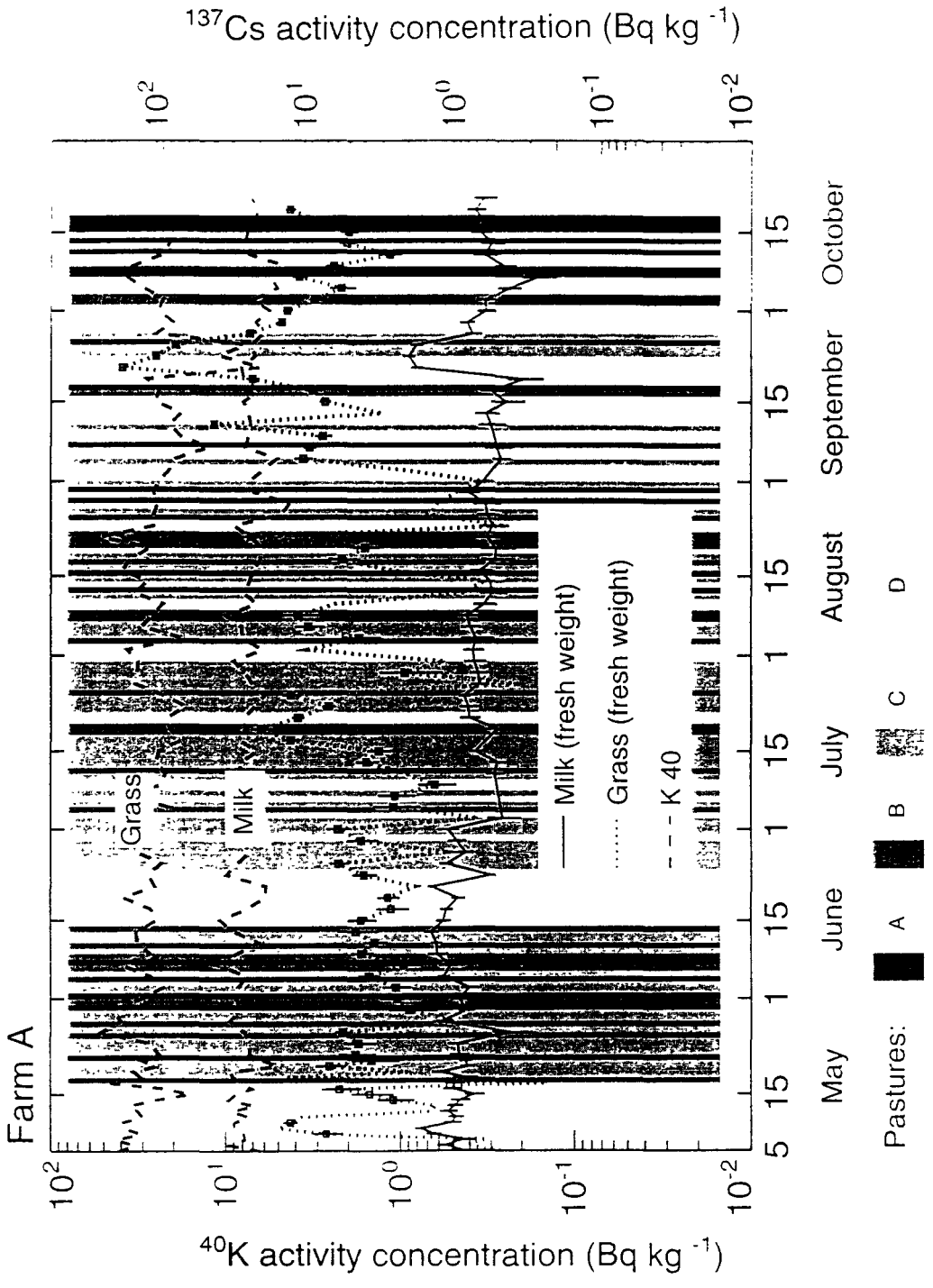

Figure 1. Time dependent activity concentrations of ^{137}Cs and ^{40}K in vegetation and milk samples from farm A

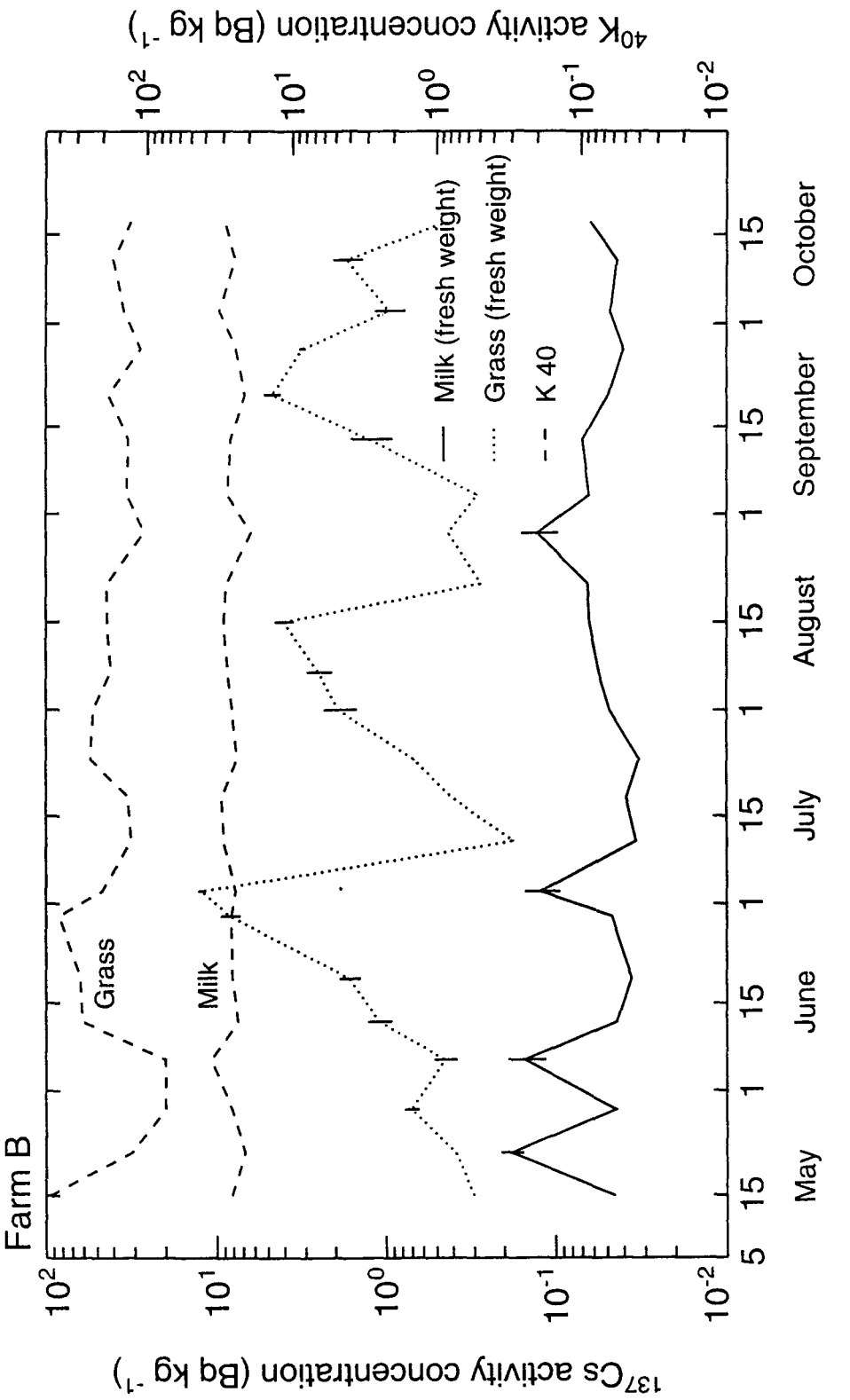

Figure 2. Time dependent activity concentrations of ^{137}Cs and ^{40}K in vegetation and milk samples of farm B

determined for weapon's fallout. In the study reported here grazing intensity/regime was shown to influence ^{137}Cs milk levels relative to ^{137}Cs activity concentrations in sampled vegetation. Under normal agricultural conditions a higher continuous grazing pressure resulted in a lower estimated transfer to milk (by a factor of about 2) than that estimated for rotational grazing. Therefore changing stock density in combination with a continuous grazing regime on a given pasture after a major nuclear accident can be considered as a possible countermeasure which can be easily applied without any additional effort and costs. The results of this study has been submitted for publication in Health Physics.

Simulation of grazing intensity in field plot studies

The experiments above performed at farms are useful for realistic predictions of radiocaesium concentrations in feed of animals under farm conditions. However due to rather high variations in the activities of soils, vegetation and the heterogenity in sward height of the grazed study pastures, these results are difficult to use for models such as RUINS. To acquire more homogenous growth rates, homogenous distribution of radiocontamination and reduce variation, plot experiments were performed to simulate the influence of grazing intensity under more artificial conditions for provision of data to the RUINS model.

In order to detect any weather influences, the weather data such as rainfall, radiation etc. were recorded over the whole experimental procedure. At GSF premises close to the experimental field a weatherstation is located, and therefore data are easily available. No correlation to weather conditions on vegetation activities were found, however of course growing conditions were influenced strongly.

For the simulation experiments the field was subdivided into 30 field plots (aluminum frames) with an area of 1 m^2 each. Two different types of soils (one mineral and one organic soil) with relatively high Chernobyl-^{137}Cs contamination (mineral soil: 144 ± 5.0 Bq kg^{-1} dw, organic soil: 300 ± 10.5 $Bqkg^{-1}$ dw) were received via G. Lindner (Fachhochschule Ravensburg-Weingarten) in January 1993, This soil was chosen because of its high ^{137}Cs content, and because both soils were undisturbed and unfertilized since the Chernobyl accident; the first 15 cms without vegetation were removed and transported to Neuherberg. The soil characteristics are given in Table 4.

Table 4. Characteristics of the soil used in the grazing intensity simulation experiments

	Mineral soil	**Organic soil**
Organic matter (%)	4.1	24.4
pH	6.0	6.3
Chalk status	average	high
Phospate (mg 100 g^{-1})	2	19
Potassium (mg 100 g^{-1})	6	6
Clay (%)	14	11
Silt (%)	33	44
Sand (%)	53	45
CEC (meq 100 g^{-1})*	15.2	54.2

*Cation exchange capacity

After mixing for obtaining a homogeneous distribution the soils were put into 15 aluminum frames each resulting in a volume of about 70 litre soil per m^2. The soil plots were additionally contaminated with an artificial radionuclide mixture. The radionuclides were chosen with regard to their radioecological importance, commercial availability, their γ-

energies (no interference with each other), and because of their short physical half-lives for radiation protection purposes. About 1 litre of the radionuclide mixture containing

^{57}Co (64 kBq L^{-1}), ^{51}Cr (20 kBq L^{-1}), ^{134}Cs (65 kBq L^{-1}), ^{59}Fe (7.1 kBq L^{-1}), ^{85}Sr (55 kBq L^{-1})

was sprayed on the bare soil in each plot two days before seeding *Lolium perenne* (28.5.93), a pasture grass representative for Germany and agricultural use land. Radionuclide activites were calculated on the basis of the sprayed volume/weight and measurement for each individual plot. When the grass has grown to give a closed vegetation cover, it was clipped manually at varying time intervals (generally 2 week intervals depending on weather and growth condition) to obtain three different sward heights (3, 6, and 9 cm) in five replicas each for the two soil types.

Fresh weight of all clipped grass samples was determined immediately after cutting. Samples were oven dried in the laboratory (70^0C) until there was no weight loss, and weighed. All samples were measured by γ-spectrometry already described. Samples were counted in either 1 l Marinelli beakers or 100 g or 30 g PE boxes until the statistical counting errors were less than 5 %. For ^{137}Cs long measuring times were necessary; often the detection limit was reached even after counting for more than 250 000 sec, therefore data for ^{137}Cs are rather uncertain and with high statistical errors.

In Fig. 3 changes with time in the activity concentrations per deposited activity are given for the different radionuclides (given are mean values for 5 replica each, standard variations are not given to enhance the clearness of graphical presentation). It is obvious that freshly deposited radiocaesium is transfered to a higher extent into vegetation compared to aged nuclides. This accounts also for the other radionuclides where activities plateaued at the end of season 1993 and in the next vegetation period 1994. There may be a slight seasonal influence with higher values during summer period (June/July) and in autumn shortly before end of growing (October). The transfer from the two different soil types to vegetation showed little difference for all nuclides with sometimes slightly higher values in the mineral soil, however these were not statistically significant (t-test for mean values) due to a very high variation of the measured values. No effect in activity concentrations in the different sward heights was evident; and to test for a difference further statistical tests were conducted. In conclusion, in some cases there seems to be a slighly higher transfer in lower sward heights; this is the opposite of what was expected in the model by Crout.

C. Salt (Stirling University, UK) has simultaneously performed experiments on the influence of grazing intensity with *Agrostis capillaris* in a national funded project. No influence of the different sward heights could be determined, a finding which is consistent with the field and plot experiments described here.

Nottingham University has undertaken experiments to parameterise the two soils used in this investigation. Both soils showed a rapid fixation to an equilibrium and behaved similarly, predicting similar results for vegetation contaminatian levels at both sites, which was verified by the experimental results. Vegetation data were used by Crout[3] to model grazing intensity.

Conclusions

Under the experimental design used here no effect of grazing intensity on the transfer of radionuclides to vegetation could be found. This is consistent with results of a similar experiment by Salt. Effects of grazing intensity found in the farm-based experiment must be due to sources other than variation in vegetation uptake.

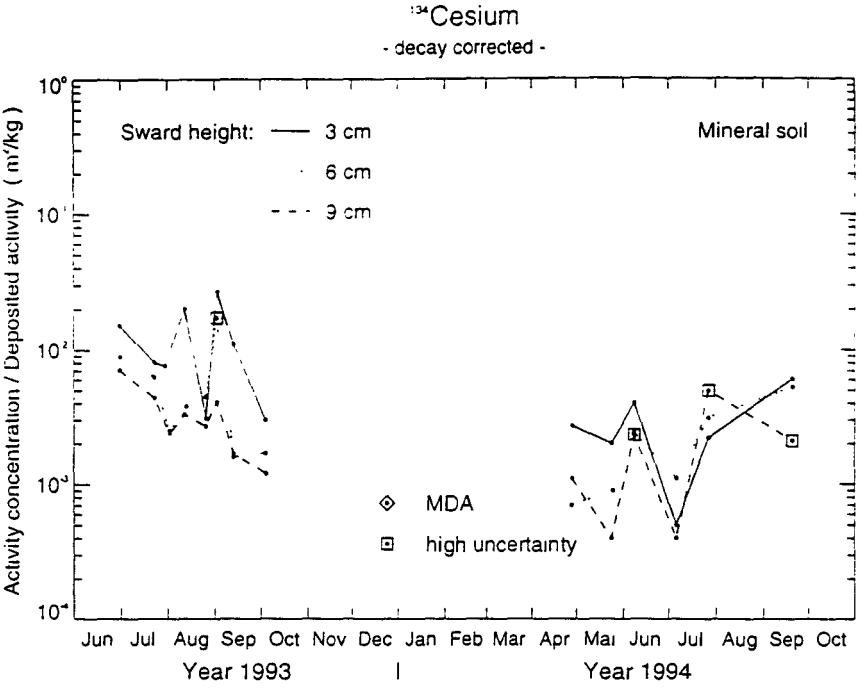

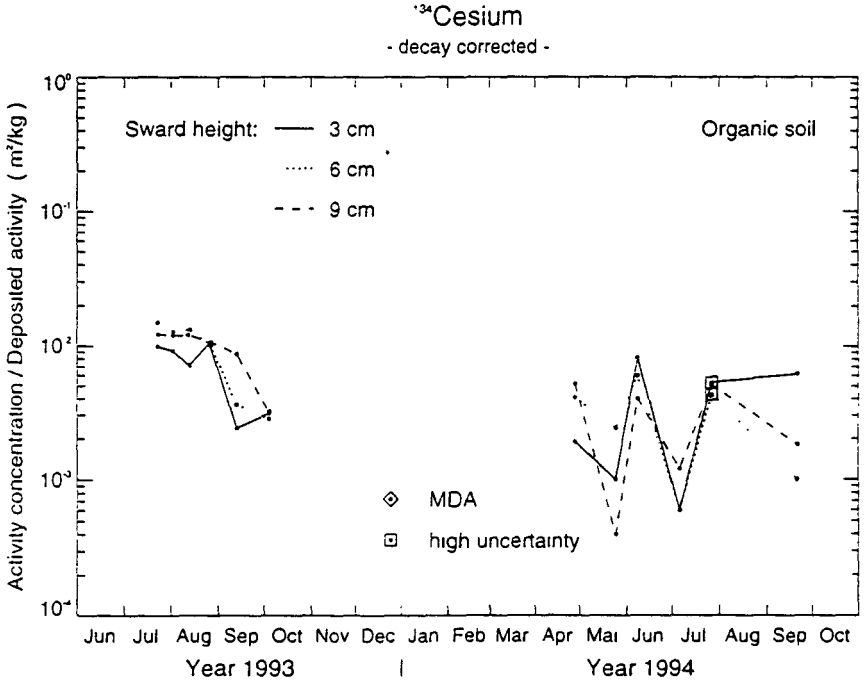

Figure 3a. Time dependent activity concentrations per deposited activity for different radionuclides, two soils and different sward heights for vegetation in plot experiments

(means of 5 replicas, MDA = minimum detectable activity)

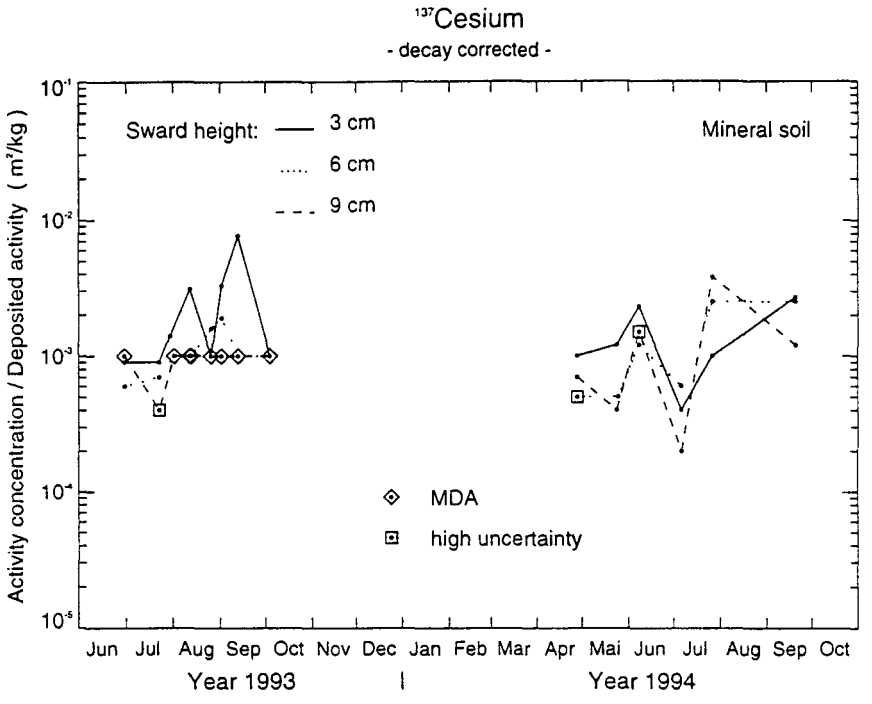
137Cesium
- decay corrected -
Activity concentration / Deposited activity (m²/kg)
Sward height:
3 cm
6 cm
9 cm
Mineral soil
MDA
high uncertainty
Jun Jul Aug Sep Oct Nov Dec Jan Feb Mar Apr Mai Jun Jul Aug Sep Oct
Year 1993
Year 1994

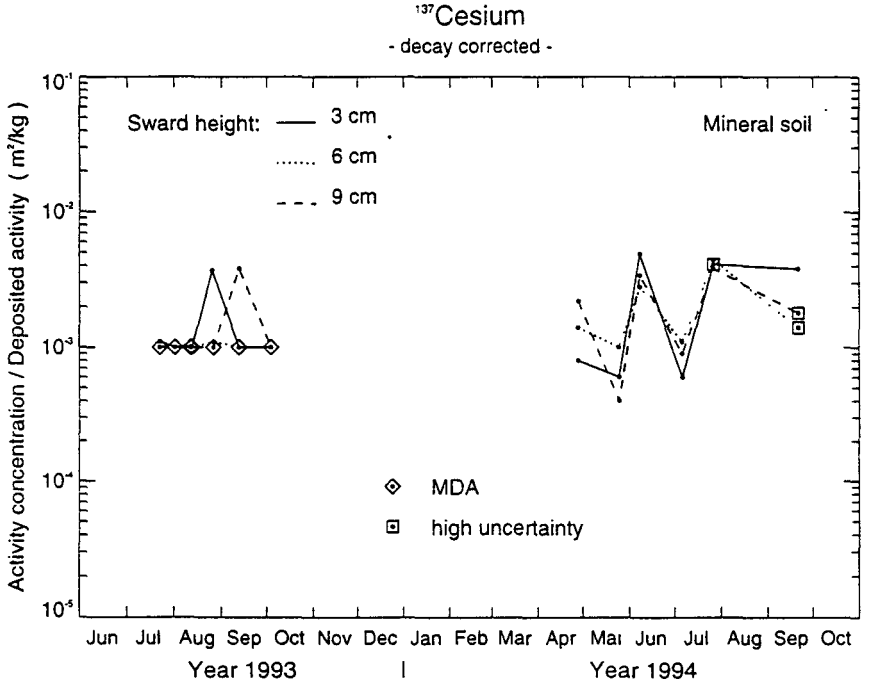
137Cesium
- decay corrected -
Activity concentration / Deposited activity (m²/kg)
Sward height:
3 cm
6 cm
9 cm
Mineral soil
MDA
high uncertainty
Jun Jul Aug Sep Oct Nov Dec Jan Feb Mar Apr Mai Jun Jul Aug Sep Oct
Year 1993
Year 1994

Figure 4b.

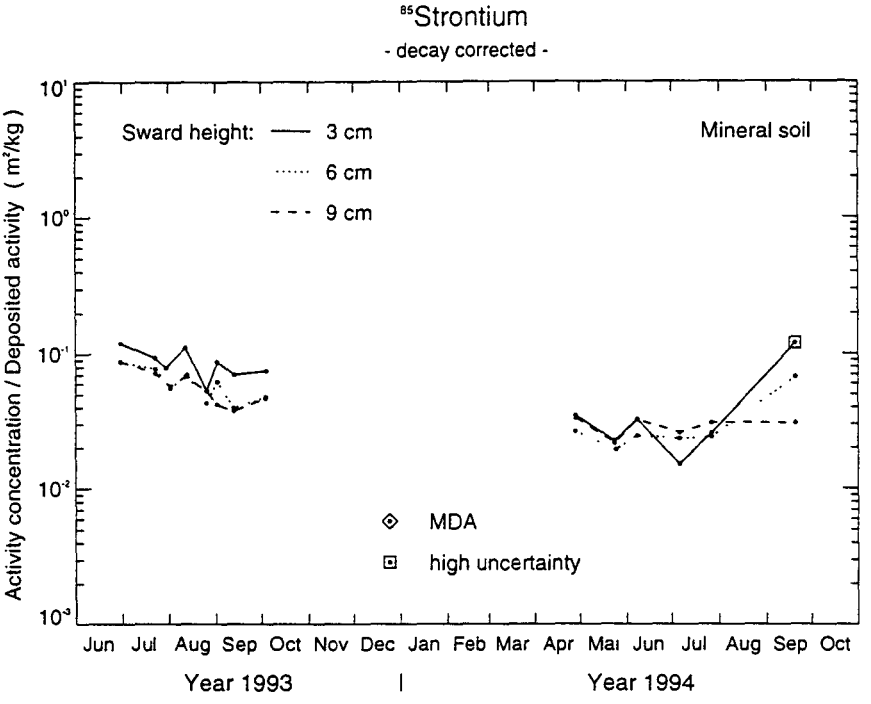
^{85}Strontium
- decay corrected -
Activity concentration / Deposited activity (m²/kg)
Sward height: 3 cm
6 cm
9 cm
Mineral soil
MDA
high uncertainty
Jun Jul Aug Sep Oct Nov Dec Jan Feb Mar Apr Mai Jun Jul Aug Sep Oct
Year 1993
Year 1994

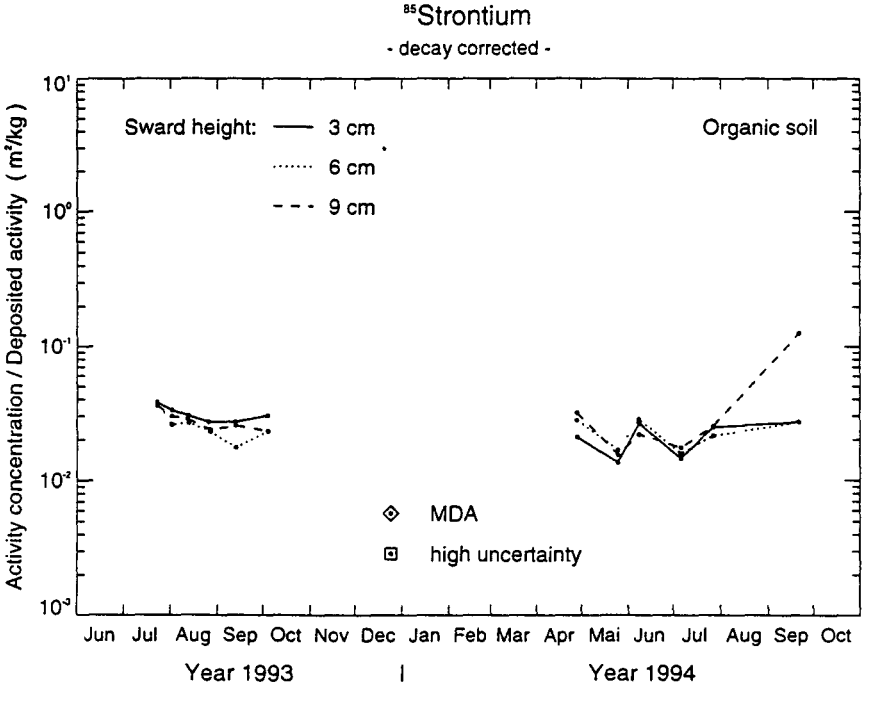
^{85}Strontium
- decay corrected -
Activity concentration / Deposited activity (m²/kg)
Sward height: 3 cm
6 cm
9 cm
Organic soil
MDA
high uncertainty
Jun Jul Aug Sep Oct Nov Dec Jan Feb Mar Apr Mai Jun Jul Aug Sep Oct
Year 1993
Year 1994

Figure 4c.

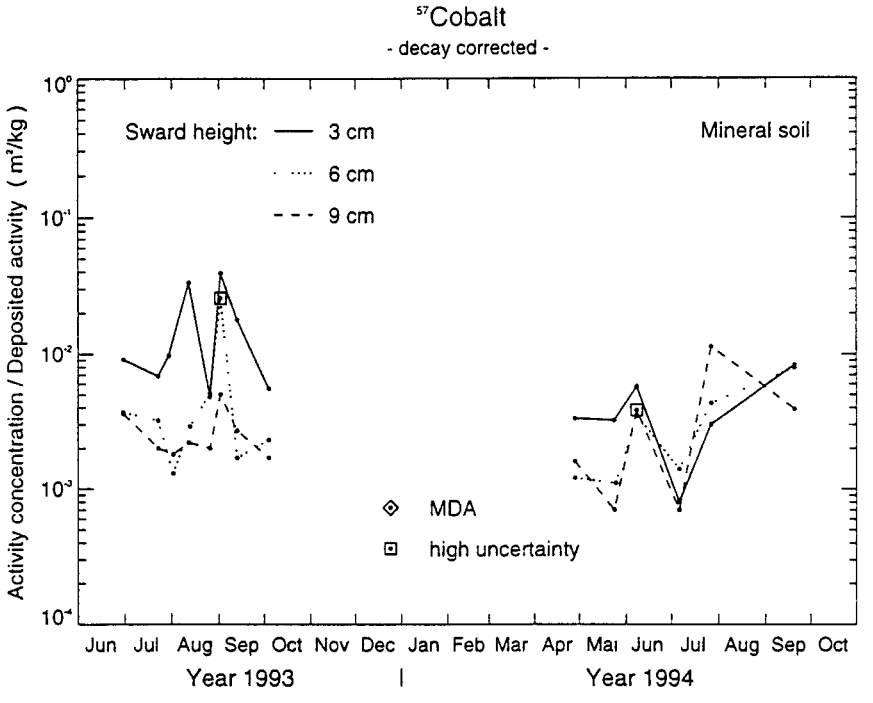
^{57}Cobalt
- decay corrected -
Sward height: 3 cm
6 cm
9 cm
Mineral soil
MDA
high uncertainty
Activity concentration / Deposited activity (m²/kg)
Jun Jul Aug Sep Oct Nov Dec Jan Feb Mar Apr Mai Jun Jul Aug Sep Oct
Year 1993
Year 1994

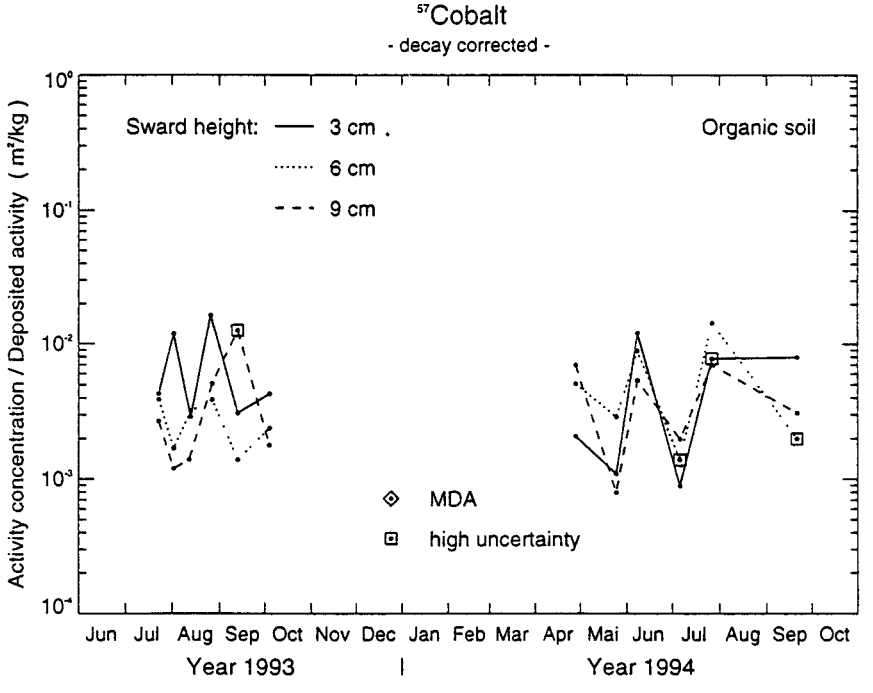
^{57}Cobalt
- decay corrected -
Sward height: 3 cm
6 cm
9 cm
Organic soil
MDA
high uncertainty
Activity concentration / Deposited activity (m²/kg)
Jun Jul Aug Sep Oct Nov Dec Jan Feb Mar Apr Mai Jun Jul Aug Sep Oct
Year 1993
Year 1994

Figure 4d.

Summary of conclusions

- In farm experiments a 10 fold difference was observed in milk ^{137}Cs activity concentrations (and 2 fold difference in F_m) under two different grazing regimes which could not have been anticipated from vegetation sampling alone. Reasons for the observed difference were not understood, but could have been associated with soil ingestion or representativeness of sampling procedures.
- No influence of grazing intensity could be demonstrated in experiments simulating grazing intensity for three different sward heights over two vegetation periods and two different soil types.
- The effectiveness of stable iodine on the transfer of radioiodine to milk was shown to have a limited applicability under current Bavarian farming conditions.

Publications

G. Voigt, B. J. Howard, C. Vandecasteele, R. W. Mayer, M. Belli, U. Sansone, G. Stakelum, P. A. Colgan, P. Assimakopoulos, N. M. Crout, B. E. Jones, K. Hove. (1993)
Factors affecting radiocaesium transfer to ruminants - Results of a multinational Research group. Proceedings der 25. Jahrestagung des FfS, Publikationsreihe Fortschritte im Strahlenschutz, Band II, 599-604

G. Voigt, Chr. Schotola, G. Probstmeier, G. Röhrmoser (1994)
Influence of stable iodine on the transfer of I-131 into cow's milk. J. Radiat. Environ Biophys. 33, 243 - 250.

N. M. J. Crout & **G. Voigt** (in press)
Modelling the dynamics of radioiodine in dairy cows. J. Dairy Science

B.J. Howard, **G. Voigt**, M. G. Segal, G. M. Ward (submitted)
A review of iodine metabolism and available countermeasures to reduce radioiodine transfer to milk. Health Physics.

G. Voigt & H. G. Paretzke (submitted)
Long-term behavior of radiocesium in dairy herds in the years following the Chernobyl accident. Health Physics

Further publications are in progress, a detailed report on the performed experiments is given in a GSF report.

Head of project 6: Dr. Vandecasteele

II. Objectives for the reporting period:

1. Compare intestinal bioavailability of radiostrontium incorporated into plant material (clover) and fed as hay or silage with that of the ionic form by measuring the true absorption coefficient.
2. Determine the effect of lactation stage, stable iodine content in the diet and dosing a prophylactic amount of stable iodine on true absorption and transfer of radioiodine secretion in cow's milk.
3. Investigate possible side-effects arising from the use of manure from animals treated with AFCF on agricultural lands.

III. Progress achieved including publications:

Project Staff : C. Vandecasteele, M. Van Hees

1. Bio-incorporated strontium availability in sheep.

The composition and processing of feed have been reported as one factor which can give rise to different bioavailability of radionuclides ingested by animals. Strontium like calcium, which is strongly bound and complexed with organic matter in the plant, was expected to have different bioavailability depending on its speciation (ionic or organic complex). Therefore, an experiment was conducted to estimate the availability of Sr.

Highly contaminated plant material was produced under greenhouse conditions in PVC trays (100 x 84 x 7 cm) filled with a synthetic, water-retaining polymer (Na polyacrylamide resins, Aquastock ®, Sodetra, France). This substrate has a pure water retention capacity up to 150 times its dry weight and a low exchange capacity and supplies the plants with a suitable foothold. Red clover seeds were sown and grown on these resins swollen with a nutrient solution contaminated with $^{85}SrCl_2$ (740 kBq l^{-1}). The first cut was used for silage production, the second harvest, three weeks later, was oven-dried at 50°C. Larger quantities of uncontaminated clover forage was produced under field conditions and prepared in a similar way.

Twelve ewes of the same age were divided into three groups. The animals, were placed in metabolism cages for 8 days and given a mixture of uncontaminated and ^{85}Sr-contaminated clover, as hay or silage, while the control group was given $^{85}SrCl_2$ solution:

- The first group received biologically incorporated strontium (approximately 94 kBq ^{85}Sr d^{-1}) in clover silage. The highly radioactive plant material (about 50 g wet weight) was given in the morning. The animals then received small amounts of beet pulp and uncontaminated clover silage *ad libitum*.
- The second group was administered biologically incorporated strontium (approximately 66 kBq ^{85}Sr d^{-1}) as clover hay. The contaminated plant material (about 10 g) was given in the morning. The animals then received small amounts of beet pulp and uncontaminated clover hay *ad libitum*.
- The third group was dosed every morning with ionic strontium as $^{85}SrCl_2$ (99 kBq d^{-1}) spiked on beet pulp. Two sheep from this last group were fed uncontaminated clover hay *ad libitum* while the other two were given uncontaminated clover silage.

Simultaneously, all twelve animals were continuously infused a constant rate of isotonic solution with $^{89}SrCl_2$. Faeces and urine (bladder catheter) were collected daily; the animals were sacrificed on the last day when a range of tissue samples were collected. The availability of the ionic and the organic complexed Sr was estimated by comparing the true absorption coefficient for the different feed.

The absorption coefficients were calculated from the integrated excretion activities over the last six to four days (day 3-5 to 8). The two first days were not considered because of the time needed to reach an equilibrium in excretion of the orally and intravenous administered Sr.

The true absorption coefficients were determined using two different methods :

a) True absorption (A_{t1}) estimated from the faecal and urinary excretion ratios, and

b) True absorption (A_{t2}) estimated from the turnover rates through the blood plasma pool or in different organs (bones and muscles).

The apparent absorption (A_a) was estimated from the intake-output.

The values of apparent and true absorption for radiostrontium were at least 4 times less than those that were obtained for radiocaesium in the previous contract period. In contrast with what might be expected from the incorporation of strontium in the plant cell walls, bio-incorporated strontium remained as available for gastro-intestinal uptake as the ionic form. Both of the absorption parameters (A_{t1} and A_{t2}) were similar regardless of the treatments or observation periods considered. Those calculated for the 5-8 days period are illustrated as an example in Fig. 1.

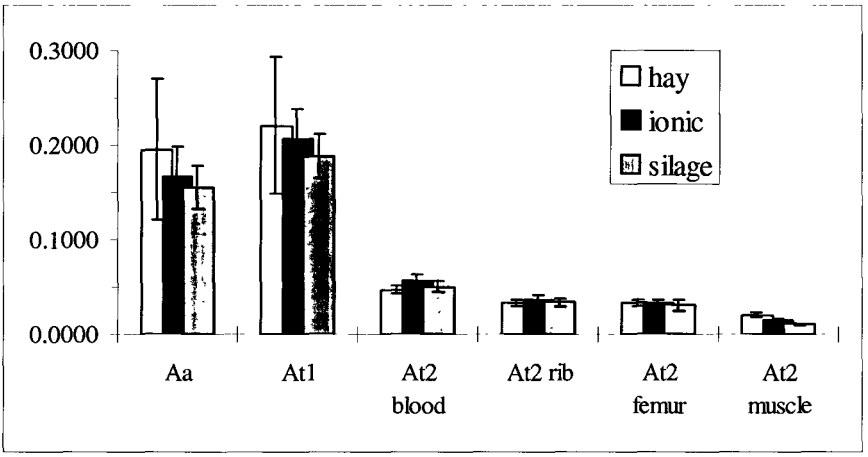

Fig.1. Comparison of apparent and true absorption coefficients for radiostrontium administered to sheep (n=4) as chloride or plant bio-incorporated. (Mean ± SE)

It is concluded that the biologically incorporated strontium, regardless of how the feed was pre-treated, was as available as ionic Sr for gastro-intestinal uptake in sheep. The apparent absorption coefficient (ranging from 16 to 20 %) is comparable to the reported best estimate (Coughtrey et al 1985). On the other hand, the A_a (and A_{t1}) values obtained for sheep in this experiment were more comparable to those reported by AUN for goat and those estimated in the CIS for cows (ECP-2).

The true absorption coefficient (A_{t1}) based on the urine and faeces ratios ranges from 19 to 22 %, and included about 2.5 to 4 % of endogenous excretion. However, the values obtained for A_{t2} were much lower, ranging from 5 to 6 % based on plasma turn-over and from 3 to 4 % taking into account the strontium isotopes ratios in bones (rib or femur). The values obtained from the isotopic ratio in muscles was even lower (1 to 2 %), but the radioactivity levels measured in soft tissues was close to the detection limit and therefore less reliable. The low A_{t2} values compared to the higher ones for A_a and A_{t1} are puzzling and as yet are not explained. These discrepencies between methods of calculation of A_t have not been encountered during studies conducted by ITE/MLURI.

2. True absorption and transfer of iodine to cow's milk.

Project Staff : C. Vandecasteele, M. Van Hees

Experiments at GSF [5] on the influence of the dietary stable iodine level on the secretion of ^{131}I to cow's milk failed to show any effect. The absence of effect of stable I was caused by a rather high level (78 mg d^{-1}, which greatly exceeds the animal requirements) of dietary stable iodine. It was therefore agreed to conduct a new experiment, in which the dietary iodine level was reduced to the lowest achievable amount. A low iodine concentrate (2990±240g I kg^{-1} dw) produced in UK was obtained through MLURI. Provided to cows with the other components of their diet, hay *ad libitum* (3610±170g I kg^{-1} dw) and beet pulp (2490±220g I kg^{-1} dw), the lowest level of dietary iodine was about 4 mg d^{-1}, ranging from 3.80 to 4.23 between cows depending on the individual hay consumption. After a first estimation of the ^{131}I true absorption and transfer to milk at this level, the dietary stable iodine was increased by the addition of stable I as KI to values of 40 and 70 mg d^{-1}. A last experiment tested, at the highest stable dietary iodine level (70 mg d^{-1}), the effect of a large amount of stable iodine (10g) dosed as a countermeasure 6h before contamination.

For all three levels of dietary stable I intake the transfer of radioiodine to milk was measured in cows in peak lactation and late lactation. Six cows, three in peak lactation (about 4 month after the last calving) and three in late lactation (13 month after the last calving) received a single oral dose of ^{131}I, simultaneously with a single intravenous injection of ^{125}I. Samples of milk, faeces, urine and blood collected over 8 days after tracer administration were analysed for radioiodine.

Changes with time in the ^{131}I secretion in milk, related to the amount of radioactivity administered to the animal, are presented in Fig. 2. for the lowest iodine level.

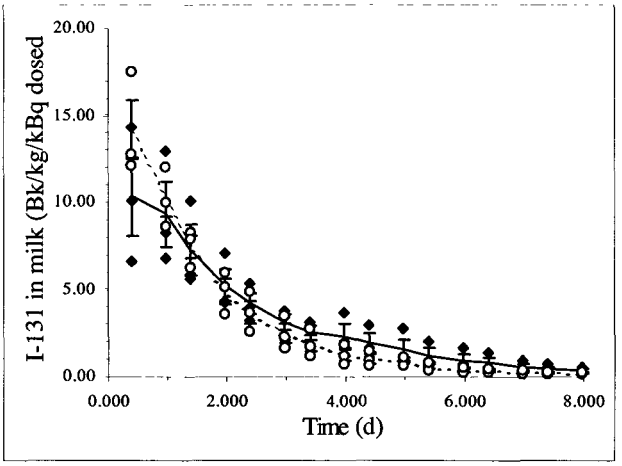

Fig. 2: Change with time of the ^{131}I concentration level in milk from cows in two different lactation stages (full lactation = open circles and dotted line; late lactation = full rhombs and line) fed a low stable iodine diet (about 4 mg d^{-1}). The error bars represent the SE.

Analysis of the initial results indicates no statistical difference in the excretion patterns (distribution within the respective excreted fractions through different paths) and/or rates (half-time) of iodine into blood, milk, urine and faeces (Table 1) that can be related to the stage of lactation. From the results obtained up to now, preliminary conclusions can be made. Increasing the stable dietary iodine tends to reduce the fraction of the ingested radioactive iodine secreted in the milk. Comparison of the excretion pattern of intravenous ^{125}I and oral ^{131}I are not statistically different (Fig. 3).

Table 1: Comparison of the half-time estimates (one compartment) and/or distribution of excreted radioiodine in blood, urine, milk, and faeces of cows in two different lactation stages fed a low iodine diet (4 to 70 mg d^{-1}). Mean ± SE.

Dietary iodine level (mg d^{-1})	Lactation stage	Half-time (d)				Fraction excreted (%)		
		blood	milk	urine	faeces	milk	urine	faeces
4	Late (n=3)	1.89±0.72	1.42±0.17	1.59±0.44	1.53±0.44	32 ± 6	26 ± 10	32 ± 5
4	Full (n=3)	1.96±0.54	1.00±0.06	1.04±0.06	1.12±0.32	37 ± 2	19 ± 1	44 ± 1
40	Late (n=3)	1.93±0.36	1.97±0.16	2.14±0.80	1.84±0.43	29 ± 4	32 ± 6	38 ± 2
40	Full (n=3)	1.12±0.13	1.06±0.13	1.09±0.13	1.08±0.13	31 ± 6	31 ± 7	42 ± 1
70	Late (n=3)	1.82±0.35	1.55±0.14	1.75±0.20	1.54±0.09	18 ± 4	42 ± 4	40 ± 1

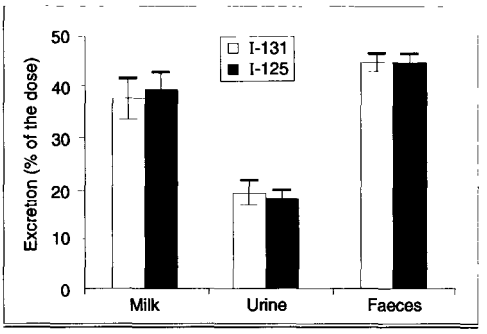

Fig 3. Relative excretion after eight days of intravenous ^{125}I and oral ^{131}I between milk urine and faeces (in % of the administered dose ± SE)

3. Side-effects of AFCF in excretion of animals used to fertilise agricultural lands.

Project Staff : C. Vandecasteele, M. VanHees, S. De Brouwer

The use of Prussian blue compounds to reduce the uptake of radiocaesium in animals may cause environmental side-effects. These molecules cross the GIT unabsorbed, bind caesium atoms ingested with the feed, and are finally excreted together with the faeces. They can thus be deposited directly on the pasture the animals graze or scattered on fields when animal manure is used as a fertiliser. No information has been published regarding possible long-term toxicity of these cyano-compounds in soil and plants. Although these complexes are stable for a limited time in the animal GIT, it is possible that they could be altered by the soil microflora with possible emission of CN^-. Only limited data, obtained in Norway and in CIS, have published on the medium-term availability of radiocaesium associated with the binder, or on the effect of Prussian blue on the radiocaesium already present at the soil level.

Biomass symptoms of toxicity were recorded on soil pots treated with increasing surface deposit of AFCF ranging from 1 - 1000 g m^{-2} (Fig. 4). After 18 successive cuts (over one year), no effects on yield or visual toxicity were observed for concentrations up to 100 g m^{-2}. Only at the very unrealistic application rate of 1 kg m^{-2}, was germination inhibited, probably due to a mechanical action; the few seeds able to germinate on the edges of the pot did not exhibit any toxic symptoms.

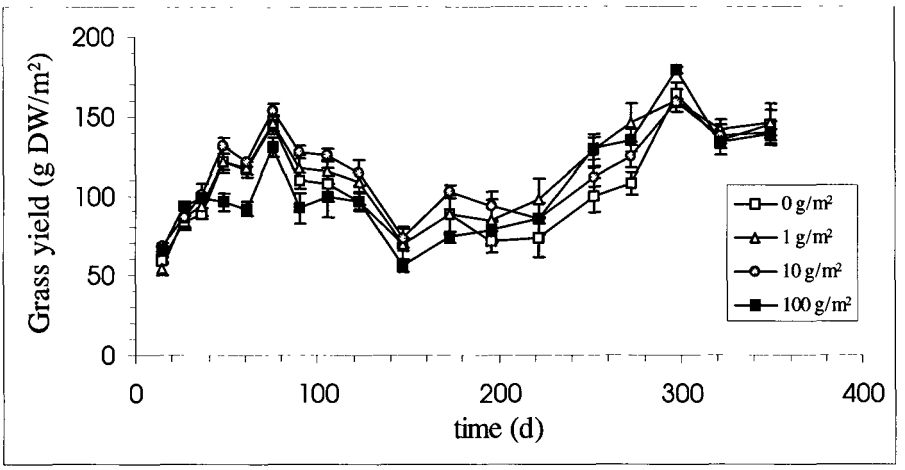

Fig 4. Comparison of the grass yield (relative to the untreated control) in 18 successive cuts on sandy soils spread with increasing amounts of AFCF in water.

Control and ^{137}Cs contaminated faeces, with and without AFCF, were obtained from one sheep: first untreated, then given solely 100 MBq ^{137}Cs d^{-1} and later 60 MBq ^{137}Cs d^{-1} with 2 g d^{-1} AFCF. Faeces were collected during each of these three sucessive phases, and mixed with control and ^{134}Cs contaminated sandy soil. Different combinations were obtained:

- uncontaminated soil with ^{137}Cs contaminated manure (0BC)
- uncontaminated soil with ^{137}Cs contaminated manure from AFCF treated animal (0BP)
- surface ^{134}Cs contaminated soil without manure (0A)
- surface ^{134}Cs contaminated soil with ^{137}Cs contaminated manure (0AC)
- surface ^{134}Cs contaminated soil with ^{137}Cs contaminated manure from AFCF treated animal (0AP)

Moreover, 1 g m^{-2} quantities of AFCF was applied to some treatments (0BC and 0AC) giving supplementary treatments reffered to as IBC and IAC, respectively.

The transfer of the two radionuclides to grass was followed over time indicating changes in their relative bio-availability. The average of the values obtained from the 2nd cut onwards are presented in Figs. 5 and 6 for ^{134}Cs from the soil and ^{137}Cs from the faeces respectively.

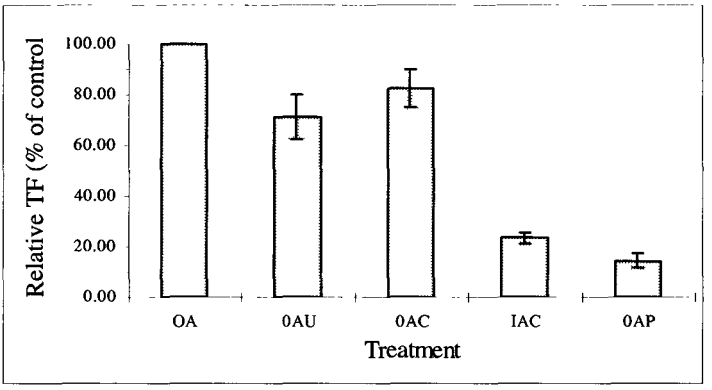

Fig. 5. Influence of the addition of manure from (un-)contaminated animal (with or without AFCF) on the availability of the ^{134}Cs present at the soil surface.

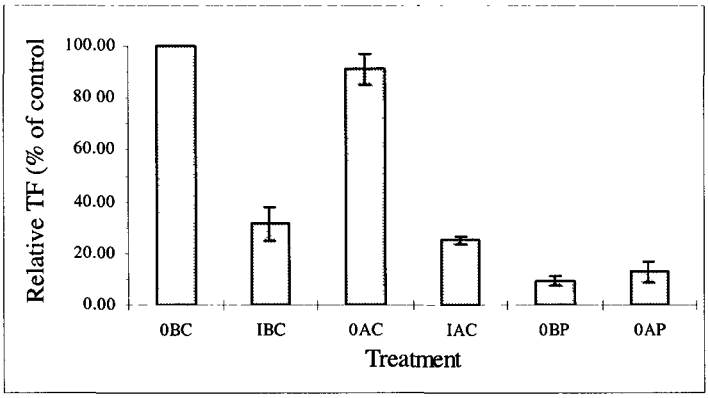

Fig. 6. Relative availability to grass of ^{137}Cs in manure from contaminated animal with or without AFCF applied on uncontaminated and surface contaminated sandy soils.

Results indicated that:

- The addition of organic matter (dry faeces 330 g m^{-2}) reduced radiocaesium transfer to plants, regardless if the radiocaesium was brought with the faeces (^{137}Cs) or was already present in the soil (^{134}Cs).
- Similar reductions in Cs availability to plants was found for AFCF spread on untreated or manured soils contaminated by $^{134}CsCl$ or by ^{137}Cs-contaminated faeces.
- Applying AFCF concentrations at the rate of 1 g m^{-2} decreased the transfer of radiocaesium from soil to plant by a factor 4 to 5.
- The presence of AFCF in the faeces also decreased the availability of ^{134}Cs already present in soil.

Summary of conclusions

- The true absorption of radiostrontium is much less than that of radiocaesium, ranging up to 0.22 in these experiments. Biological incorporation of radiocaesium and radiostrontium into plant tissues (as rye grass or clover) did not affect rates of gut absorption.
- At low dietary iodine levels, the fraction of radioiodine secreted into milk is higher than that at high stable iodine intakes in dairy cows. The true absorption of radioiodine is close to 1, and its behaviour is identical and regardless of whether it is ingested orally or intravenously administered.
- Prussian blue compunds, in particular AFCF, present in manure from treated ruminants, spread over agricultural land is not expected to have detrimental effects for vegetation, with regard to either toxicity or yield. Moreover, it will reduce soil to plant uptake of radiocaesium in the soil.

Publications

G. Voigt, B. J. Howard, **C. Vandecasteele**, R. W. Mayes, M. Belli, U. Sansone, G. Stakelum, P. A. Colgan, P. Assimakopoulos, N. M. Crout, B. E. Jones, K. Hove. (1993) Factors affecting radiocaesium transfer to ruminants - Results of a multinational Research group. Proceedings der 25. Jahrestagung des FfS, Publikationsreihe Fortschritte im Strahlenschutz, Band II, 599-604

Beresford, N.A., Barnett, C.L., Mayes, R.W., **Pollaris, K., Vandecasteele, C.M.** & Howard B.J. 1995. The use of in-vitro technique to predict the absorption of dietary radiocaesium by sheep. Radiation and Environmental Biophysics, 34, 191-194.

Crout, N.M.J., Beresford, N.A., Howard, B.J., Mayes, R.W., Assimakopoulos, P.A. & **Vandecasteele, C.M.** In press. The development and testing of a revised dynamic model of radiocaesium to sheep tissues. Radiation & Environmental Biophysics.

Mayes, R.W., Beresford, N.A., Howard, B.J., **Vandecasteele, C.M.** & Stakelum G. submitted July 1995. The use of the true absorption coefficient of bioavailability of radiocaesium in ruminants. Radiation and Environmental Biophysics.

Vandecasteele, C.M., M. Van Hees., S. De Brouwer & H. Vandenhove. Side-effects caused by manure from ACFC treated animals used to fertilise agricultural lands, submitted to IRPA 96, Vienna 1996.

Vandecasteele, C.M., M. Van Hees.& S. De Brouwer. "Effect of AFCF on the soil-plant transfer of ^{134}Cs". To be presented inVienna May 96

Head of the project 7: Prof. Zelenka

II. Objectives for the reporting period:

1. Carry out experiments to quantify the transfer of radiocaesium to the tissues of broiler chickens.
2. Carry out experiments investigating the effectiveness of the feed additive RADEKONT for reducing radiocaesium uptake in broiler chicken. The variation in effectiveness of RADEKONT for different sources of radiocaesium will be considered by using both ionic and Chernobyl fallout sources. In addition the binding capacity of the components of RADEKONT will be investigated.
3. Develop a model metabolism of radiocaesium in growing chickens in collaboration with Nottingham University, SCK/CEN Mol and GSF Munich.
4. Publish the results of the studies in refereed journals

III. Progress achieved including publications

Project staff: Poschl, M. & Zelenka, J.

1. Transfer of radiocaesium to broiler chicken

The distribution and biological half-live of radiocaesium ^{137}Cs in broiler chicken after tree oral application (in one day) of artificially contaminated feed mixture were studied. There was a rapid retention of the orally administered ^{137}Cs (within a few hours) and also a rapid loss of radiocaesium which varied in different organs (the initial biological half-live was: liver - 0.6d, gut - 0.6d, breast muscle - 2d, leg muscle - 1.2d). One half of the total administered ^{137}Cs activity was excreted from the body within the first day after ^{137}Cs dosing and after 18 days more than 90 % had been excreted. The time-dependent activity concentrations and total activities (expressed as a per cent of the maximum of the activity accumulated) were significantly different in the breast and leg muscle from the second day after application of contaminated feed. The highest accumulation of ^{137}Cs occurred in meat (50% - 90%) but the proportion of total activity in breast and leg muscle varied in the course of the experiment. For the first three days there was a higher portion of ^{137}Cs activity in legs, whereas from the 4th day there was a greater part of total activity in the breast.

This study will be published in Health Physics.

2. Effectiveness of RADEKONT for reducing ^{137}Cs uptake

Experiments were carried out with broiler chickens (breed ISA VEDETTE) kept in metabolic cages, and fed *ad libitum* with a standard feedstuff normally used for broiler chickens in the Czech Republic. Two independent experiments were performed to determine the effectiveness of the additive RADEKONT, comprised of 98% Zeolite with 2% FeHCF immobilized onto the zeolite, as a countermeasure (i) using artificially contaminated feed and (ii) using feed contaminated by the Chernobyl accident.

In experiment 1, ^{137}Cs was orally administered to 14 - 24 day-old chickens twice daily as a $^{137}CsCl$ solution (1 kBq d^{-1}). The influence of RADEKONT on ^{137}Cs transfer was tested by the addition of 0.5 g RADEKONT d^{-1} kg^{-1} of live weight. ^{137}Cs was administered for 10 days, then ceased and the decontamination period was observed for 14 days. Twice weekly in the 24 d experiment, 3 chickens were slaughtered, tissue samples weighed, and ^{137}Cs activity were measured in liver and leg and breast muscles.

In experiment 2, ^{137}Cs activity was administered to 1 - 23 day-old chickens by feeding Durum wheat (49%, ^{137}Cs activity concentration 1,100 Bq kg^{-1}, contaminated by the Chernobyl fallout) to the feed mixture (similar to that of exp. 1). A comparison of RADEKONT and the Zeolite component alone on the transfer of ^{137}Cs from feed to leg and breast muscles was tested using the same experimental procedure as in experiment. 1. Contaminated feed was given for 23 days, and the decline in ^{137}Cs activity in leg and breast muscles was measured for another 14 days. Once a week in the 37d experiment , 3 - 4 animals were slaughtered to measure ^{137}Cs activity in muscles.

Results

Experiment 1.

RADEKONT decreased the retention of ^{137}Cs significantly after 10 d application of artificially contamination (Fig. 1), but the reduction factors for ^{137}Cs activity concentrations in muscles and liver were low, varying from 1.2 - 2.3 over the different fattening periods (Table 1).

Table 1. Reduction factors of ^{137}Cs activity concentrations due to RADEKONT after different fattening period (10d application of artificially contaminated feed to 14d old chickens)

Fattening period (d)	Breast muscle	Leg muscle	Liver
2	2.3	1.5	1.5
4	1.9	1.4	1.3
8	1.3	1.3	1.5
10	1.2	1.3	1.2

- ^{137}Cs activity concentrations increased rapidly over the first two days for all three tissues and then plateaued (Fig. 1).
- The ^{137}Cs total content increased linearly in breast and leg muscles throughout ^{137}Cs application period, whereas in liver it only increased over the first two days.
- The addition of RADEKONT during the decontamination period did not increase the elimination rate of ^{137}Cs (Fig 1.).

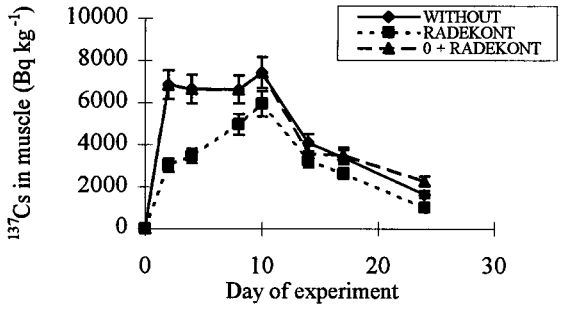

Fig. 1. Comparison of the effect of RADEKONT given during and after ^{137}Cs administration

Experiment 2

RADEKONT significantly decreased the retention of ^{137}Cs by breast and leg muscles from the wheat contaminated by Chernobyl fallout (Fig. 2). Reductions factors for ^{137}Cs activity concentrations and ^{137}Cs total content varied from 1.1 - 3.6 and 1.3. - 5.7 respectively after the different fattening periods (Table 2).

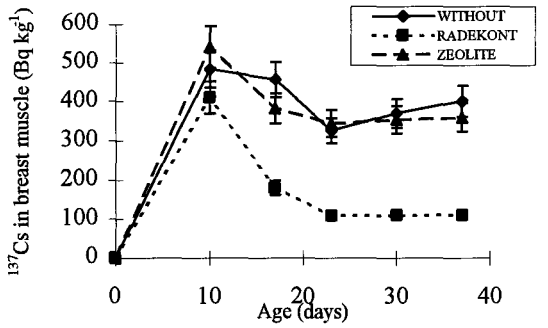

Fig. 2. The effect of RADEKONT and Zeolite on accumulation of ^{137}Cs from contaminted wheat by breast muscle of broiler chickens

Table 2. Caesium-137 activity concentration ratios between meat/feed and reduction factors in concentrations of ^{137}Cs in meat and ^{137}Cs total content in RADEKONT treated animals compared to control animals after different fattening periods

Fattening period days	Concentration ratio meat/feed		Reduction factors ^{137}Cs (Bq kg^{-1})		Total ^{137}Cs content (Bq)	
	Breast	Leg	Breast	Leg	Breast	Leg
10	0.44	0.31	1.2	1.1	1.6	1.3
17	0.41	0.28	2.5	2.4	1.5	1.8
23	0.29	0.32	3.0	3.7	2.8	3.1
37	0.36	0.37	3.6	3.6	5.7	5.2

- The retention of ^{137}Cs was not affected by Zeolite (Fig. 2). Therefore, the effect of RADEKONT is probably due to FeHCF. However, the incorporation of Zeolite to RADEKONT is still recommended since it facilitates the feeding of very small amounts of FeHCF to poultry.
- ^{137}Cs activity concentrations were influenced by the age of the chickens. Muscle ^{137}Cs activity concentrations gradually decreased in the first three weeks of life, and then were stabilized (Fig. 2).

- The total ^{137}Cs content in muscles increased throughout the 37 d contamination period.
- After feeding with uncontaminated feedstuff the rate of decline in radiocaesium activity concentration and total content in muscles was not affected by RADEKONT. Hence it is apparent that potential binding of RADEKONT to endogenously excreted radiocaesium is not important and does not enhance its effectiveness in poultry.

Current results indicate that the timing of application of RADEKONT is important in determining the effectiveness in reducing ^{137}Cs transfer. RADEKONT was most effective after chickens reached an age of 20 d. This may be due to the rapid growth rate of younger birds. The results also demonstrated the importance of starting administering RADEKONT before 20 d of age, because only limited affect was observed when administration of RADEKONT started at 14 d of age.

RADEKONT, as a form of FeHCF immobilized on Zeolite, is recommended as an additive which significantly decreases the uptake of ^{137}Cs in broiler chicken.

3. Modeling the transfer of radiocaesium in growing chicken

The progress of this study, which was conducted in collaboration with Nottingham University, SCK/CEN Mol [6] and GSF Munich [5], has been described in Crouts section of this report [3].

4. Publications

Poschl, M., Borkovec, V., Zelenka, J. & Prochazka, J. (1994). Effect of special modified clinoptilolite as an antidote used for treatment of radiocaesium contaminated broiler chickens. In Book of abstract of XXIVth Annual meeting of European Society for New Methods in Agricultural Research, Varna/Bulgaria, p. 42

Poschl, M., Borkovec, V. & Zelenka J. (in press): Dynamic Radiocaesium Distribution in Broiler Chickens. Health Phys.

Head of Project 8: Prof. Hove

II. Objectives for the reporting period

1. Carry out an experiment to investigate the effect of ^{133}Cs dosing on the transfer of ^{134}Cs to meat and milk.

2. Carry out *in-vivo* testing of the Sr-binding capacity of a variety of substances with the aim of identifying suitable Sr binders for dairy ruminants.

3. Carry out an experiment to test the effect different amounts of stable Sr on the absorption and transfer of radiostrontium to milk in goats given Ca below requirement.

4. Prepare final reports and papers for the studies within the programme.

III. Progress achieved including publications.

Project staff: Hansen, H.S., Tiltnes, M. H., Asper, N. P. & Hove,K.

1. Caesium metabolism study

Stable Caesium analysis

Results for the transfer of ^{134}Cs under varying stable Cs regimes were given in the previous report. Due to problems with accuracy in analysis of stable Cs by atomic absorption, samples have been reanalysed using neutron activation technique, which gave reliable results in the relevant concentration ranges.

Whilst stable Cs was measured satisfactorily in aqueous standard solutions containing small amounts of interfering ions, there were problems in using the atomic absorption method for solutions of biological materials. Aqueous standards for AAS were made in 0.5 N HCl with 500 ppm Rb as RbCl. Attempts to correct for the observed matrix interference in biological samples were unsuccessful. Furthermore, the detection limit increased from 0.054 μg Cs ml^{-1} when aqueous sample solutions were used, to 0.205 μg Cs ml^{-1} with standards in a faeces matrix. Concentrations of stable Cs in environmental samples were then below detection limits hence the atomic absorption method was insufficiently sensitive for our requirements.

Results and discussion

The experimental procedure was described in a previous progress report. Briefly, 28 goats were divided into seven groups and given varying daily supplements of stable Cs (Table 1, mean of 4 goats per group). The effect on absorption and transfer of ^{134}Cs to milk and meat was evaluated.

Table 1. Apparent (A_a) and true absorption (A_t) and transfer coefficients to milk (F_m) and meat (F_f) of ^{134}Cs and stable caesium.

Group	Stable Cs	^{134}Cs				Stable Cs		
		A_a	A_t	F_m	F_f	A_a	A_t	F_f^*
	(mg d^{-1})			(d l^{-1})	(d kg^{-1})			(d kg^{-1})
1	0.11	0.73a	0.99a	0.08ac	0.33	0.66a	1.37a	1.36
2	5.1	0.74a	0.97a	0.09b	0.31	0.82b	0.95b	0.49
3	10	0.74a	1.00a	0 09b	0.25	0.61a	0.77b	0.42
4	50	0.72a	1.06a	0.09b	0.32	0.82b	0.91b	0.03
5	100	0.71a	0.94a	0.11a	0.35	0.85b	0.92b	0.18
6	500	0.75a	1.33b	0.10b	0.32	0.88b	0.92b	0.31
7	2000	0.65b	0.89a	0.11bc	0.40	0.89b	0.92b	0.20

*-Only one animal per group; a,b,c, mean values given different letters are significantly different.

Values of F_m for stable Cs were not estimated for all samples because the milk had deteriorated and could not be reanalysed by neutron activation.

- The data for true absorption of ^{134}Cs were generally at the high end of the previously reported range for sheep.
- Transfer coefficients of ^{134}Cs to meat and milk were generally within the range reported in the literature.
- A_t values for stable ^{134}Cs were somewhat higher and A_a values somewhat lower than those observed for ^{134}Cs.
- The results for F_f values for stable Cs varied greatly between groups. The average of 0.43 was somewhat higher than for ^{134}Cs.
- There was no significant difference in the estimated parameters of Cs transfer that could be related to the increase in stable Cs administration.

The overall conclusion therefore remains that daily oral administration of stable Cs in quantities from less than 1 mg to 2 g does not affect either absorption of ^{134}Cs or transfer of ^{134}Cs to meat and milk. Consequently, stable Cs, administered daily, cannot be used for reduction of radiocaesium transfer to goats and their products.

2. *In vivo* testing of Sr-binders

Possible Sr-binders were tested in lactating goats. Each goat was given ^{85}Sr and the Sr-binder for 14 d and only ^{85}Sr for the following 14 d. The transfer of ^{85}Sr to milk was measured and the reduction factor was estimated (Table 2). Two goats were used to test each amount of the compounds. The binders selected for testing were all synthetic; natural substances have been avoided because of a lack of knowledge regarding their composition.

Table 2. Mean reduction factors for transfer of ^{85}Sr to milk of the tested compounds.

Compound	Sr-binder g d^{-1}	Reduction-factor	Compound	Sr-binder g d^{-1}	Reduction-factor
Humalite	1.0	ns	Zeolite A(Na)	1.0	1.3
Humalite	2.0	ns	Zeolite A(Na)	2.0	1.3
Humalite	4.0	ns	Zeolite A(Na)	4.0	1.3
Sb_2O_5	0.25	ns	Zeolite A(Na)	10.01.6	
Sb_2O_5	1.0	ns	Zeolite A(Na)	30.01.6	
Na-rhodizonate	1.7	ns	Zeolite P(Na)	2.0	ns
K-rhodizonate	1.7	ns	Zeolite P(Na)	10.0ns	
Zeolite A(K)	2.0	ns	Zeolite Y(Na)	2.0	1.4
Zeolite A(Mg)	2.0	1.3	Mordenite	2.0	ns
Zeolite A(Ca)	2.0	ns			

ns = not significant

- Of the tested compounds, only zeolite A(Na) reduced the transfer of orally administered ^{85}Sr to milk.
- A reduction factor of 1.6 was observed when zeolite A(Na) was given at a daily rate of 0.5 g kg^{-1} live weight.

- Zeolite A(Na) may be used as a Sr-binder in lactating ruminants. However, a large amount was administered; 0.5 g kg^{-1} live weight approached the limit of voluntary intake by animals.

The results were presented as a poster at the International Symposium on Environmental Impact of Radioactive Releases, IAEA, Vienna 8-12 May 1995.

3. Absorption and transfer of Sr to milk in goats with negative Ca balance

The experiment was designed to test the effect of oral administration of stable Sr on absorption and transfer of ^{85}Sr, stable Sr and Ca to milk of goats with a high rate of Ca absorption, which was induced by feeding a Ca-deficient diet. The animals were placed in metabolism cages for 3 weeks. Twelve goats were fed a ration containing 3.83 g d^{-1} Ca (50% of recommended Ca intake). The animals were divided into three groups given supplementary stable Sr (as $SrCl_2$) at rates of 0 mg d^{-1}, 330 mg d^{-1} and 1650 mg d^{-1}. The ration contained 14 mg d^{-1} of stable Sr. All animals were fed 57 kBq d^{-1} of ^{85}Sr. Following two weeks of adaptation, the third week was used for measurement of true absorption of Ca, stable Sr and ^{85}Sr using double isotope techniques.

Table 3. Parameters of calcium and strontium absorption and metabolism in experimental goats. (mean ± SD for 4 animals)

Stable Sr	13.5 mg d^{-1}	346 mg d^{-1}	1664 mg d^{-1}
	Mean SD	Mean SD	Mean SD
Apparent absorption			
^{85}Sr	0.25a ± 0.02	0.36b ± 0.07	0.32ab ± 0.04
Stable Sr	0.04a ± 0.08	0.26b ± 0.13	0.30b ± 0.08
Ca	0.28a ± 0.09	0.38ab ± 0.07	0.42b ± 0.05
True absorption of ^{85}Sr	0.17a ± 0.02	0.16a ± 0.09	0.20a ± 0.03
Stable Sr flux through plasma (mg d^{-1})	6.03a ± 0.46	68.81b ± 10.92	474.6c ± 50.3
Ca flux through plasma (g d^{-1})	4.40a ± 1.27	4.54a ± 0.30	3.73a ± 0.86
F_m for ^{85}Sr (d L^{-1})	0.019a ± 0.005	0.019a ± 0.004	0.025b ± 0.006

a,b,c: ean values given different letters are significantly different.

- Calcium balances ranged from -1.4 g d^{-1} to -0.52 g d^{-1}.
- Mean daily flux of Ca from digestive tract and bone through plasma ranged between 3.73 g d^{-1} to 4.54 g d^{-1}. The Ca fluxes were proportional to the net-requirement of Ca and were not affected by administration of stable Sr.
- Mean A_t of ^{85}Sr ranged from 0.17-0.20 for the different stable Sr treatments which was 2-4 times higher than in experiments reported in the literature where Ca was given above maintenance requirement.

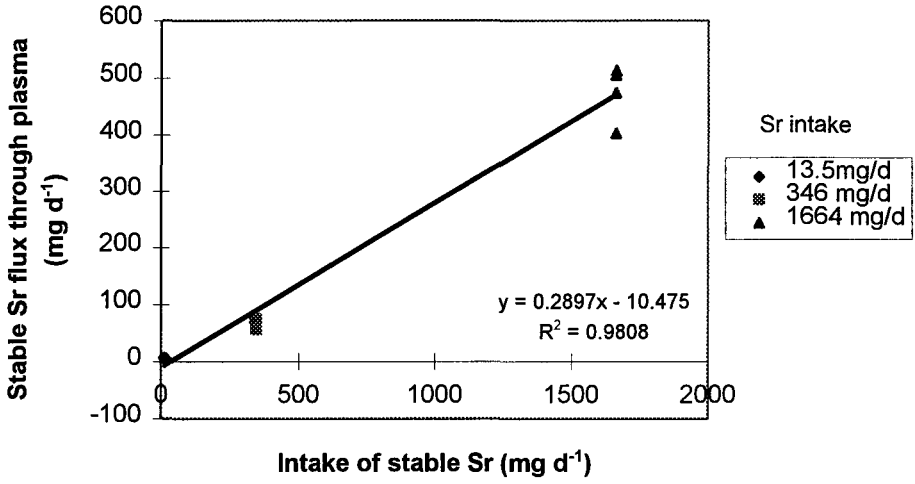

Fig. 1. Flux of stable Sr through plasma as a function of daily intake of stable Sr.

- The flux of stable Sr relative to intake was higher (Fig. 1, equivalent to an A_t of 0.29) than the observed A_t of ^{85}Sr. It is likely that this was due to the negative Ca balance causing Ca and Sr resorption from the bone.
- When the Ca balance is positive, Sr and Ca absorption may vary in similar fashion. However, in the present experiment no significant relationship was observed between Ca and Sr absorption, which may be because Ca absorption was enhanced in all animals.
- True absorption of ^{85}Sr was not affected by stable Sr administration.
- Individual measurements for F_m of ^{85}Sr ranged from 0.012 d l^{-1} to 0.033 d l^{-1} and were positively related to A_t of ^{85}Sr (Fig. 2). Mean F_m values of ^{85}Sr were identical in group 1 and 2 but higher in group 3. Although this difference was statistically significant, the physiological significance is doubtful, since increasing Sr intakes did not affect the Sr absorption parameters.

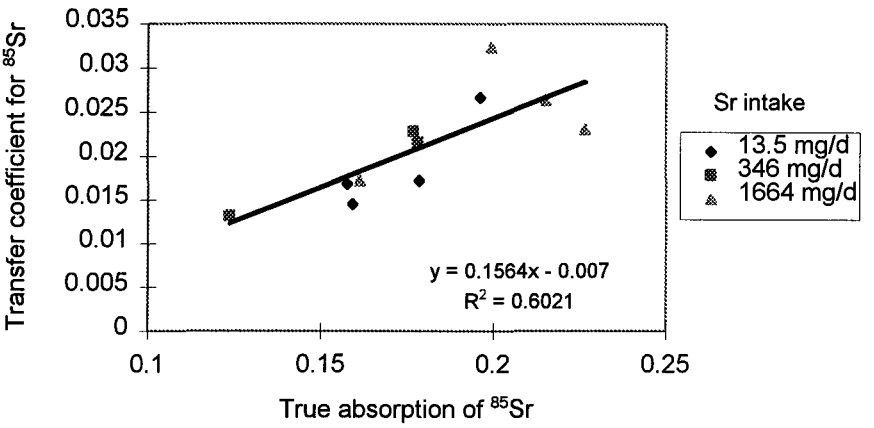

Fig. 2. Transfer coefficient (F_m) of ^{85}Sr in individual goats as a function of true absorption (A_t) of ^{85}Sr

In conclusion, the rate of transfer of orally administered ^{85}Sr to milk was not influenced by increasing intakes of stable Sr. In contrast to situations with Ca sufficiency, differences in Ca absorption did not affect absorption or transfer of ^{85}Sr to milk. In individual goats Sr transfer to milk was proportional to the true absorption of Sr.

Summary of conclusions.

1. Stable Cs administered daily did not reduce the accumulation or transfer of radiocaesium to meat and milk of goats.

2. Zeolite A(Na) acted as an *in vivo* Sr binder in goats. The reduction factor was 1.6 when an oral dose of 0.5 g per kg live weight of zeolite A(Na) was given daily. The efficiency was however inferior to that of available Cs-binders.The search for more efficient Sr-binders should continue.

3. Administration of stable Sr did not affect radiostrontium transfer to goats milk, when Ca absorption was stimulated by a low Ca intake.

4. Publications

G. Voigt, B. J. Howard, C. Vandecasteele, R. W. Mayer, M. Belli, U. Sansone, G. Stakelum, P. A. Colgan, P. Assimakopoulos, N. M. Crout, B. E. Jones, **K. Hove**. (1993) Factors affecting radiocaesium transfer to ruminants - Results of a multinational Research group. Proceedings der 25. Jahrestagung des FfS, Publikationsreihe Fortschritte im Strahlenschutz, Band II, 599-604

Hansen, H. S., Sæther, M., Asper, N. P., Hove, K. (in press) In vivo testing of compounds with possible Sr-binding effects in ruminants. International Symposium on Environmental Impact of Radioactive Releases, IAEA. (abstract).

Hansen, H. S., Tiltnes, M. H., Asper, N. P., Hove, K. Effect of increasing administration of stable Sr on absorption of Sr and Ca and transfer to milk in goats with negative Ca balance. Manuscript 19 pp Will be submitted to J. Dairy Sci.

Head of Project 9: Dr. Hinton

II. Objectives for the reporting period:

1. Conduct a literature review of Ti and Sc uptake by plants to evaluate their suitability as tracers of soil loading onto plants.
2. Determine why some Ti estimates of soil loading, determined by the EC Animal Group during the last contract period, over-predicted the contribution of resuspension to the overall ^{137}Cs contamination of the plant.
3. Determine if grazing density affects soil loading onto pastures.
4. Develop a method to determine the particle size distribution of soil adhering to leaf surfaces.
5. Publish results in refereed journals.

III. Progress made including publications

1. A comparison of techniques used to estimate the amount of resuspended soil on plant surfaces

Project staff: T. G. Hinton, P. Kopp, S. Ibrahim, I. Bubryak, A. Syomov, L. Tobler

The objectives of this study were to compare four common techniques used to estimate soil mass loadings on plant surfaces, and to assess the need to account for particle-size distributions of both the soil tracer and contaminant of concern within the soil. Soil loadings (g soil kg^{-1} dried plant), from split samples collected in a pasture near Chernobyl, were estimated using soil tracers of plutonium analyzed via alpha spectroscopy (mean ± SE; 1.0 ± 0.2), titanium analyzed by ICP (3.6 ± 0.6), and neutron activation analysis for scandium (8.1 ± 1.6), as well as simply washing the soil off the vegetation (34.1 ± 5.6). Differences were significant at $p < 0.001$. We also found that soil loading estimates from any one technique varied by a factor of 10 depending on the soil particle size used in the calculations. This was because soil loadings decreased when smaller-sized soil fractions dominated the resuspension process. However, the percent of the plant's total contamination attributable to soil loading increased with smaller soil particles. Smaller soil particles apparently contribute less to the mass of soil loading (g soil kg^{-1} dry plant), but more to the total plant contamination (Bq) because of the higher concentration of contaminant in the smaller-sized soil fractions. Differences in mass loading estimates due to the technique chosen (a factor of 10), or due to differences in elemental concentration as a result of the soil particle size used in the calculation (also a factor of 10), were greater than the natural variability observed in the field (2.5).

2. Examination of problem soils where soil loading estimates failed

Project Staff: T.G. Hinton; B.J. Howard, B Rafferty

Previous soil loading estimates from specific Ireland and UK soils were too large (Rafferty et al 1994). The contaminant contribution estimated from soil loading was greater than the total ^{137}Cs activity concentrations of the grass. Rafferty et al (1994) concluded that the Ti method for determining soil loading was unreliable and highly variable. Our hypothesis, based on the above. was that the aberrant results may have been due to soil loading estimates being calculated from entire soils, rather than the resuspendable fractions, and that the distribution of ^{137}Cs within the soil fractions may not correspond to the distribution of Ti.

To test this hypothesis we obtained soil and vegetation samples from the same locations in Ireland and the UK, and separated the soil into particle sizes using mechanical sieves and a gravitational settling method. Each soil fraction was analyzed for Ti and ^{137}Cs concentrations. The distribution of both Ti and ^{137}Cs in these soils seems to be atypical. Generally, concentrations of elements, including radionuclides, increased dramatically in the smaller-sized soil fractions. In contrast, ^{137}Cs and Ti distributions from the problem soils of Ireland and the UK are fairly uniform across particle sizes or actually decrease in the smaller-sized fractions. Decreasing or uniform concentrations of Ti among particle sizes, however, would not cause an over-estimate of soil loading compared to an estimate based on a mean concentration in the unfractionated soil. We also have to reject our hypothesis that the soil tracer (Ti) may not be distributed among soil particles in the same way as the contaminant of concern (^{137}Cs). Although the distributions seem unusual because the concentrations do not increase at smaller particle sizes, the distributions of Ti and ^{137}Cs seem fairly similar.

When some of these problem soils were separated into size fractions we found no soil particles less than 8 μm. It is probable that these smaller fractions do exist, but they have conglomerated with organic matter or other particles and behave as if they are of larger size. This may explain the peak observed in the 20 to 38 μm class. We tested this by treating the total soil with H_2O_2 to destroy organic matter, and then fractionated the soil. The distribution of sizes changed, with particle sizes < 8 and 2 υm appearing.

We are not certain if the conglomeration of particles caused the over-estimation of soil loading experienced by Rafferty et al (1994). It is possible that the retention of particles on leaves is particle-size dependent, with smaller clay-sized particles adhering to the leaves more tenaciously than larger ones. If so, then a conglomeration of small particles into larger ones would suggest that the conglomerate particles might have a faster weathering rate and thus decrease soil loading. The influence of the high organic matter, however, needs further investigation. Sheppard and Evenden (1994) studied the adhesion of contaminated soil to skin and found that adhering soil is enriched in contaminant concentration relative to the original soil because of the selective adhesion of finer particles high in organic matter content.

3. Soil Contamination of Plant Surfaces Affected by Grazing Intensity and Rainfall Interactions.

Project staff: T.G. Hinton; J.M. Stoll; L.Tobler

The importance of accounting for soil adhesion on vegetation when predicting the transfer of radionuclides to animals has been identified previously. However, there has been little investigation of the effects of grazing intensity on soil mass loadings. Our hypothesis was that more intensely grazed pastures would have higher soil contamination on the vegetation. We tested this hypothesis by measuring soil loadings on pasture vegetation that had been grazed with various densities of sheep.

Four different grazing densities of sheep were tested against an ungrazed control plot. Grazing blocks were established in a pasture near Kloten, Switzerland. Each block consisted of five fenced grazing plots, corresponding to grazing pressures of 156, 312, 468 and 624 sheep ha^{-1} d^{-1}, plus an ungrazed control. The most severe treatment of our experiment was representative of local grazing practices.

Prior to grazing, each plot was characterized by taking ten vegetation height and 100 point-intercept measurements. The latter were used to estimate the fraction of ground covered by grass, bare soil, rock, and litter. At the end of grazing the same measurements were repeated, and the vegetation was sampled by clipping within three randomly placed 0.25 m^2 frames.

The vegetation was separated into 2 - 10 cm and > 10 cm above ground heights. Scandium was used as a tracer of soil adhesion on vegetation. Pre- and post-grazed vegetation was neutron activated and analyzed for ^{46}Sc. Soil cores were taken within each vegetation sampling frame, frozen, and the upper one cm removed. Soil slices were dried, and the less than 125 μm size fraction was separated by mechanical sifting for subsequent analysis.

Soil loadings (g soil kg^{-1} dry plant) significantly increased with grazing intensity ($p = 0.003$), and then plateaued (Table 1). Differences in soil loadings among grazing treatments depended on which height of pasture was examined. ANOVA revealed that rainfall explained slightly more of the mass loading variation in 2 - 10 cm portion of vegetation ($F = 7.7$, $p = .012$) than did differences due to grazing treatments ($F = 3.4$, $p = 0.031$). In contrast, soil loadings on the upper heights of vegetation were driven strongly by the grazing treatments ($F = 15.7$, $p = 0.0001$) and rainfall had little impact ($F = 3.7$, $p = 0.07$).

Table 1. Results of Bonferoni's comparison of mean soil loadings among treatments (mean ± SE; n = 5). Results are presented for loadings on the entire plant, 2 - 10 cm, and > 10 cm sections. Data are presented on mass and area basis. Within a single column, treatments with the same letters were not statistically different from each other ($p > 0.05$).

Treatment	**g soil (kg dry plant)$^{-1}$**			**g soil (m^2 soil surface)$^{-1}$**	
sheep (ha^{-1} d^{-1})	Total Plant	2-10 cm	>10 cm	2-10 cm	>10 cm
0	7.0 ± 1.1 $_a$	6.1 ± 1.0 $_a$	0.9 ± 0.1 $_a$	1.1 ± 0.3 $_a$	0.3 ± 0.1 $_a$
156	11.0 ± 2.6 $_{a\ b}$	9.1 ± 2.5 $_{a\ b}$	1.6 ± 0.2 $_{a\ b}$	1.6 ± 0.7 $_a$	0.3 ± 0.1 $_a$
312	12.6 ± 1.8 $_{a\ b}$	9.7 ± 1.7 $_{a\ b}$	2.9 ± 0.6 $_{b\ c}$	1.4 ± 0.4 $_a$	0.5 ± 0.2 $_a$
468	18.9 ± 2.8 $_b$	14.4 ± 1.9 $_b$	4.5 ± 1.0	c 1.7 ± 0.5 $_a$	0.4 ± 0.2 $_a$
624	17.5 ± 3.1 $_b$	13.0 ± 3.1 $_{a\ b}$	4.4 ± 0.5	c 1.5 ± 0.5 $_a$	0.4 ± 0.1 $_a$

The influence of rain by itself was marginal ($p = 0.052$), however, both wind and rain were significant components in interaction terms, that is, their influence depended on whether or not sheep were present. When sheep were present, the largest mass loadings occurred when rainfall was greatest (9.7 mm), and an obvious trend of increased soil loadings with increased rainfall was apparent, as long as the rain was greater than 4.9 mm. The opposite occurred in the control plots: soil loadings were the least at maximum rainfall. With light rain (0.3 and 0.8 mm) the addition of sheep had less impact on mass loadings, and results were similar to the control plots. This suggests that the lighter rains washed as much or more soil from the leaves as was being added from the increased grazing pressure.

In our ungrazed control plots rainfall decreased soil loadings. This finding disagrees with Dreicer et al (1984) in which a positive linear relationship was found between soil loadings and the average rainfall intensity. Their rainsplash experiment, however, was conducted on tomato plants in the arid southwestern US, and their plants were surrounded by bare soil. These conditions are in sharp contrast to our grazing experiment, conducted in the lush pastures of central Europe, where vegetative cover was close to 100%.

Increased soil loadings with rain have generally been ascribed to an increase in soil splash from the intensity of the impacting rain drop on bare soil. The feasibility of this occurring in

the dense pastures and light rains encountered in this experiment is slight. Either the importance of rainsplash in conditions typical of central Europe has been previously underestimated, or other mechanisms associated with grazing x rainfall interactions are occurring. This experiment suggests the latter: rainfall decreased soil loadings in our ungrazed control plots, however, when sheep were present the SHEEP X RAIN interaction was the most significant parameter in our model ($F = 13.06$. $p = 0.002$). Thus rainfall's effect on soil loading depended on whether or not sheep were present.

In addition to the physical disturbance caused from the sheep's hooves, it is possible that the sheep's wool became soiled under the moist conditions and contributed to the transfer of contaminated soil to plants. Transfer to the vegetation could occur as animals brush against it. This speculation is reinforced by the observation that soil on the > 10 cm portion of vegetation steadily increased from 13% of the total on the control plots to 25% on the most severely grazed treatment. Thus grazing not only increased soil loadings, but also altered the distribution of soil on the plant surfaces. It is probable, then, that soil loadings would differ in pastures grazed by other types of animals. The obvious morphological and behavioral differences of cattle, for example, as well as differences in the mechanics of their grazing, might cause soil loadings onto vegetation to differ from similar pastures grazed by sheep.

Analysis of variance procedures resulted in an equation that predicts soil mass loadings as a function of grazing intensity, rain and wind speed:

$$\log Y = 0.7 + 0.0006\,(\text{GRAZING}) + 0.038\,(\text{RAIN}) + 0.010\,(\text{WIND})$$

$$\text{SE} = (0.2) \quad (0.0002) \quad (0.001)(0.009)$$

where:

$\log Y$ = log(10) estimate of soil loading (g soil kg^{-1} dry plant)

GRAZING = grazing intensity (number of sheep ha^{-1} d^{-1})

RAIN = total rainfall over 2 d period (mm)

WIND = maximum hourly averaged wind speed over 2 day period ($m\ s^{-1}$)

SE = standard error associated with each parameter

If grazing management was to be used as a tool to reduce contaminant intake due from inadvertent consumption of resuspended soil, the model predicts that, under these experimental conditions, grazing densities would have to be reduced 2.5 times to reduce soil loadings by 50%.

4. Develop a Method to Determine Particle Size Distributions of Soil Adhering to Plant Surfaces

Project Staff: T.G. Hinton, P. Kopp

Recently, the reliability of the titanium method in quantifying soil adhesion's contribution to ^{137}Cs levels in pasture was questioned because the Ti technique greatly over-estimated soil adhesion's contribution (Rafferty et al 1994). They stated that the over-estimation was probably due to the use of bulk soil concentrations in their mass loading calculations, and that the distribution of titanium and ^{137}Cs in the soil may not have been similar. Our data corroborate this by showing the large variations obtained in soil loading estimates due to differences in soil particle size, and the importance of considering the distribution of the tracer and contaminant among the soil fractions.

Undoubtedly, regardless of what technique is used, estimating soil loadings using the total, unfractionated soil invites bias and imprecision. Using the upper 0.5 cm of soil and particle sizes less than 125 μm improves the estimate. Knowing if the tracer's (Ti, Sc, or Pu)

concentration among soil particle sizes is similar to the contaminant of concern also improves the estimation. All of these improvements, however, assume that the distributions within the soil match the distributions actually resuspended and retained on leaf surfaces. To most accurately estimate mass loadings onto plants it will be necessary to calculate mass loadings using the same soil particle-size distribution found adhering to the plant. Such information would allow us to be specific as to the precise soil particle size to use in the mass loading calculations. The accuracy of mass loading estimates could then be improved, and thereby our assessment of contaminant impact to man and the environment.

Particle-size distributions of soil adhering to plants are not currently available. We have been exploring a technique to measure soil particle sizes on plants using a liquid plastic technique originally developed to quantify stable, heavy metal contamination on leaf surfaces (Rentschler 1982). Granulated plastic (Pioloform BL 16, developed by Wacker-Chemie GMBH, Munich, Germany) was mixed with ethanol (18% plastic to 82% ethanol, by weight) to produce a liquid polymer of the desired consistency. The liquid plastic was applied to leaf surfaces, dried to produce a thin film, and meticulously peeled from the leaf using twizzers. The material that was adhering to the leaf becomes embedded in the plastic and was removed when the plastic was peeled off. The thoroughness of this cleaning technique has been confirmed by scanning electron micrographs of leaves to which plastic was applied (Rentschler 1982; Cercasor & Schreiber 1987). After removal of the plastic, the micrographs revealed a clean surface with leaf hairs still intact, compared to a dramatically soiled counter-half that did not receive the cleaning treatment (Rentschler 1982).

We have found the technique to work well for broad-leafed plant species, and have used it to quantify the foliar absorption of resuspended ^{137}Cs (Hinton et al in press). Unfortunately, the technique has not worked on the thin, fragile leaves of pasture grasses. We are now trying ultrasonic washing techniques, followed by filtration of the wash water, and examination of the soil particles using computer-coupled, occular microscopy. The method needs further development because we are uncertain if the small soil particles are being removed by the ultrasonic wash. Confirmation with scanning electron microscopy is planned.

Summary of conclusions

1). *Soil loading estimates depend on the technique used to measure the amount of soil on plant surfaces.* Soil loading estimates using Pu as a soil tracer were significantly lower than estimates from all other techniques. Washing the vegetation resulted in an estimate 30 times greater than that estimated from using Pu, and 10 times greater than that for Ti. Results from Ti and Sc were not significantly different.

2). *It is important to calculate soil loadings using the concentrations of the soil tracer and contaminant in the resuspendable particle size fraction of soil, rather than the mean concentrations in the unfractionated soil.* This is due to (1) the particle size dependence of resuspension, (2) larger soil particles apparently contributing more to the mass of soil loaded onto vegetation, and (3) smaller soil particles apparently contributing more to the contaminant concentration of soil loading. A factor of 10 difference in the soil loading estimate can result if effects due to soil particle size are ignored. Estimating soil loadings using the total, unfractionated soil invites bias and imprecision. Using the upper 0.5 cm of soil and particle sizes less than 0.125 μm improves the estimate.

3). *Differences in the distribution of the tracer and the contaminant within the various sized soil fractions can bias the soil loading estimate.* Knowing if a soil tracer's concentration among particle size fractions is similar to that of a contaminant is fundamental to proper use of the technique.

4). *Soil loading techniques seem to be adequate to estimate the quantity of soil on plant surfaces, but inadequate when extended to estimate the "percent of total plant contamination due to soil loading".* Ratios magnify the inaccuracies of the component variables (Doctor et al 1980). Greater precision is needed in the soil loading estimate before the calculations can be extended to proportioning the sources of contamination using ratios.

5). *Problems in estimating soil loading seem particularly acute in high organic soils.* Such soils seem to have unusual soil particle size distributions due to a conglomeration of fine particles into larger ones. It is possible that high organic matter facilitates resuspension and/or soil adhesion. More work is needed in this area.

6). *Grazing trials in Switzerland showed that soil loadings on pasture grass increased 60% when grazing intensity by sheep increased by a factor of four.* A model was developed that predicts soil loading as a function of grazing density, rainfall and wind speed. If grazing management were to be used as a tool to reduce contaminant intake from inadvertent consumption of resuspended soil by grazing animals, grazing densities would have to be reduced 2.5 times to lower soil loadings by 50%.

7). *Light rains and winds removed soil from ungrazed control plots, but the opposite occurred on grazed pastures — rainfall augmented soil loadings when sheep were present.*

8). *To most accurately estimate mass loadings onto plants it will be necessary to calculate mass loadings using the same soil particle-size distribution found adhering to the plant.* Such information would allow us to define the soil particle size to use in the mass loading calculations. The accuracy of mass loading estimates could then be improved, and thereby our assessment of contaminant impact to man and the environment. Particle-size distributions of soil adhering to plants, however, are not currently available.

5. Publications

Hinton, T.G., Kopp, P., Ibrahim, S., Bubryak, I., Syomov, A. & **Tobler, L.** (1993) Contaminated soil on Chernobyl vegetation. Proceedings of the 26th topical Meeting of the Health Physics Society. Jan 24-28, 1993. Coeurd'Alene, Idaho, USA. pp 407-421.

Hinton, T.G., Kopp, P., Ibrahim, S., Bubryak, I., Syomov, A., **Tobler, L. & Bell, C.** (1995) A comparison of techniques used to estimate the amount of resuspended soil on plant surfaces. Health Physics, 68: 523-531.

Hinton, T.G., Stoll, J. M. & Tobler, L. (1995) Soil contamination of plant surfaces from grazing and rainfall interactions. J. Environ. Radioactivity. (in press).

Hinton, T.G. & Bell, C. Sampling methods and analyses that improve estimates of soil loading onto plants (in preparation).

References

Cercasor, V. & Schreiber H. (1987) Foliar contamination and uptake from aerial sources investigated by INAA and SRFA. J. Radioan. Nucl. Chem. Articles 114,21-27.

Doctor, P.G., Gilbert R.O. & Pinder, J.E. Pinder, III. 1980. An evaluation of the use of ratios in environmental transuranic studies. J. Environ. Qual. 9:539-546.

Dreicer, M., Hakonson, T. E., White, G. C., & Whicker, F. W. (1984). Rainsplash as a mechanism for soil contamination of plant surfaces. Health Physics, 46, 177-187.

Hinton, T. G., McDonald, M.. Ivanov, Y., Arkhipov, N., & Arkhipov A. (in press) Foliar absorption of resuspended ^{137}Cs. J. Environ. Radioactivity.

Rafferty, B., Dawson, D. E. & Colgan, P. A. (1994) Seasonal variation in the transfer of ^{137}Cs and ^{40}K to pasture grass and the ingestion by grazing animals. Sci. Total Environ., 145, 125-134.

Rafferty, B., Dawson, D. E. & Colgan, P. A. (1994) Assessment of the role of soil adhesion in the transfer of ^{137}Cs and ^{40}K to pasture grass. Sci. Total Environ. 145: 135-141.

Rentschler, I. (1982) Einee Mehode zur Trennung abgelagerter und eingebauter Stoffe bei lPflanzenblattern. Naturwissen schaften, 69, 240-241.

Sheppard, S.C., & Evenden W.G. 1994. Contaminant enrichment and properties of soil adhering to skin. J. Environ.Qual.23: 604-613.

Final Report
1992 - 1994

Contract: FI3PCT920016 Duration: 1.9.92 to 30.6.95 Sector: A25

Title: Deposition of radionuclides on tree canopies and their subsequent fate in forest ecosystems - further studies

1) Minski IMPCOL
2) Rauret Fundacio "Bosch i Gimpera"
3) Ronneau Univ. Louvain (UCL) - LLN

I. Summary of Project Global Objectives and Achievements

This project was conceived as an integrated study intended to provide data on aerosol inputs to forest ecosystems and their subsequent fate. The background to the project was, of course, the Chernobyl accident which highlighted the radioecological community' s lack of predictive knowledge with respect to semi-natural ecosystems in general. Forests were identified as a specific type of semi-natural ecosystem for which radioecological data were almost completely absent within the European context.

At the beginning of the project, data on forest ecosystems were beginning to filter from countries of the former Soviet Union. However, these were primarily derived for the Kyshtym accident site and were therefore of little relevance to the contamination scenarios faced in most European forests after the Chernobyl accident. Furthermore, the data that were available from CIS countries were principally concerned with ecosystem transfers of radionuclides following deposition events. Virtually no data were available on the deposition process itself and those data that were available were often contradictory.

Within the sphere of the European Community countries in the aftermath of Chernobyl contamination it was quickly realised that semi-natural ecosystems could contribute to individual and collective doses in a variety of ways not fully appreciated before 1986. In addition to this realisation, the years following the deposition events of 1986 showed that the ecological half lives of radiocaesium contamination (in particular) in semi-natural ecosystems were likely to be significantly longer than previously anticipated. For these reasons the significance of semi-natural ecosystems in assessing individual and collective dose to man became evident with key questions being posed as to the role of specific forest food products in human exposure and the role of particular ecological compartments within the forest in controlling radionuclide persistence within the ecosystem as a whole.

Sensitivity analyses using mathematical models of radionuclide transfers within ecosystems consistently show that the initial inputs to the system in the form of dry and wet deposition events are of major significance. Considering the processes of ecosystem transfer in isolation from atmospheric transport of contamination plumes, it is true to say that deposition processes define the magnitude of the source term within the ecosystem by controlling the input from a given atmospheric concentration in the baoundary layer above. Hence, for successful prediction of dose in the short, medium and long terms it is essential to be able to quantify these deposition processes reliably. The key parameter to be quantified is the deposition velocity, which normalises the deposition flux to the atmospheric concentration of contaminant. Deposition of radionuclides in forest ecosystems occurs largely to the tree canopy itself, although a variety of factors such as tree type and seasonality control the relative interception of the deposit by leaves, needles, twigs and branches of trees. Any radioactive deposit penetrating the canopy will contaminate the underlying leaf litter and understorey plants, thus providing a direct input to the forest floor and its associated vegetation.

In addition to the processes of deposition there are a variety of mechanisms and pathways which will control the fate of the deposit in the short and long term. These include resuspension of the deposit, which is likely to be strongly time dependent, and loss of initial deposit from tree surfaces by weathering. The latter process provides an additional source of input to the litter layer on the forest floor to the extent that after 6 to 12 months following the intial deposition event more than 70% of the radionuclide inventory may reside in the litter layer. A consideration of transport process within and below this layer then becomes essential to the understanding and prediction of radionuclide fate within the forest.

The rate and magnitude of all the above processes briefly outlined above are controlled by the physico-chemical form of the depositing radionuclide(s). The Chernobyl accident, viewed in the context of both near-field and far-field effects, provided a particularly complex and, therefore, problematic situation in that deposits consisted of both sub-micron aerosols and larger 'hot particles'. The latter consisted either of condensed volatile elements such as ruthenium or of discrete fragments of irradiated uranium oxide fuel, together with associated fission and activation products.

All of the processes described above control the physical movement and fate of deposited radionuclides within forests. The global objectives of the three research projects carried out over the last three years have been to quantify these processes within the framework of discrete experimental strategies, bearing in mind the requirement for each process to be considered as part of a continuous chain of transport within the forest. Breaking the global problem down into its component objectives, the partners have studied dry deposition and resuspension at both the canopy scale and the microscale; they have considered losses from the tree canopy to the litter layer; and they have quantified transport rates of particulate sources of radionuclides from leaf litter into the underlying soil horizons. In each of these experimental packages careful attention has been paid to the initial physico-chemical form of the depositing radionuclides, with each group working with carefully characterised particulate sources.

The following sections give full accounts of the achievements and contributions of each group. However, the main achievements can be summarised as follows. Professor Ronneau' s group at Louvain-la-Neuve has developed novel methods for generating uranium based aerosols at high temperatures similar to those experienced within the reactor during the Chernobyl accident. These have been characterised using a variety of physico-chemical methods and have then been used to determine the leachability of individual radionuclides contained within the UO_2 matrix and the flux rates of the aerosol to isolated branches of trees. The Imperial College group, under Miss Minski, has developed a novel low temperature generation technique for uranium-based aerosols which has been used to determine dry deposition velocities within complete model canopies within a wind tunnel. Resuspension, losses due to weathering under ambient conditions and the effects on deposition rates of forest edges have also been investigated and quantified by this group. Professor Rauret' s group, within the University of Barcelona, have used field techniques to determine the rate of vertical transport of thermogenerated aerosols within forest soils in Catalonia. Detailed information on the physico-chemical forms of radiocaesium and radiosilver within these aerosols and their subsequent physico-chemical behaviour is available as a result of this study.

Taken together, the results provided by the three groups over the last three years have significantly advanced our knowledge of the rates of physical transport processes of radionuclides introduced to forest ecosystems in aerosol form. This information is of considerable importance to other groups working within the framework of the European Commission' s Radiation Protection Research and Nuclear Fission Safety Programmes, in which dynamic modelling of radionuclide behaviour and fate within forest ecosystems is currently an urgent priority.

Head of Project 1: Miss M. J. Minski

II. Objectives for the reporting period

The primary objective of our work over the reporting period has been the completion of analyses of dry deposition, resuspension and preliminary field loss experiments. These were carried out during the previous reporting period and involved small scale spruce canopies under well-defined aerodynamic conditions. Additionally two major field experiments have been conducted. The first involved the use of a cascade impactor in conjunction with Scanning Electron Microscopy (SEM) to determine flux rates and size distributions of ambient aerosol depositing to small spruce trees under natural atmospheric conditions. Data from this experiment have been used to validate deposition velocity estimates obtained during wind tunnel studies. The second was a detailed experiment to determine rates of weathering of sub-micron uranium aerosol from the external surfaces of spruce trees exposed to ambient conditions. Finally, a major objective has been the production of a PhD thesis using results gathered over the last three years. Included in this thesis is a synthesis of data from the whole project in the form of a numerical model of canopy deposition, resuspension and loss.

III. Progress achieved including publications

Dry Deposition Studies:

Dry deposition experiments were carried out in the Imperial College wind tunnel using young Norway spruce trees approximately 0.5m in height. The experimental protocols have been fully described by Shaw *et al.* (1994) and Kinnersley *et al.* (1994). In our progress report for 1992 - 1993 (EUR 16003, pp. 471 - 478) we described the development of an aerosol generation technique which allows the production of a stable stream of uranium acetate aerosol of 0.77 - 0.82 μm VMAD. This was used in two detailed dry deposition experiments in which spruce trees were exposed to the aerosol for up to 55 hours at a constant wind speed of 5 m s^{-1}. Deposition fluxes were quantified (by delayed neutron counting of the deposited uranium) to the tree surfaces in 5 discrete horizontal layers. Two groups of deposition velocities were then calculated by normalising aerosol flux to a) the above canopy (boundary layer) air concentration of aerosol and b) the air concentration within the canopy layer under consideration. These two V_g values are referred to as 'normalised' and 'local' V_g, respectively, and are summarised in Table 1.

Table 1: Summary of 'normalised' (V_g1) and 'local' (V_g2) deposition velocities obtained for 0.8μm VMAD uranium aerosol depositing to a Norway spruce canopy in the wind tunnel.

Canopy Layer	V_g1 (± sem)	Total	V_g2 (± sem)	Total
5	0.189 (0.020)		0.400 (0.042)	
4	0.097 (0.016)		0.329 (0.052)	
3	0.069 (0.010)		0.368 (0.056)	
2	0.088 (0.023)		0.754 (0.198)	
1	0.054 (0.009)	0.497	0.733 (0.129)	2.584
Soil under trees	0.0095		0.1739	
Soil between trees	0.0052	0.0147	0.1029	0.2768
Total (canopy)		0.5117		2.8608

'Normalised' V_g exhibits a maximum within the 'flag' layer (ie. the topmost layer) of the canopy with a marked decline as the aerosol penetrates vertically downwards into the canopy. This is shown graphically in Figure 1, which indicates the positions of the 5 canopy layers with respect to the tree itself.

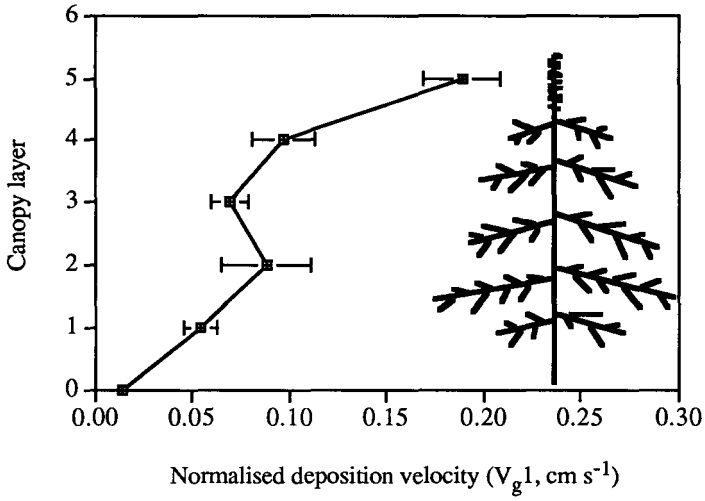

Figure 1: Normalised deposition velocity (±sem) of 0.77-0.82 VMAD uranium particles in 5 layers of a small scale Norway spruce canopy.

Table 1 indicates, however, that 'local' V_g is more constant with respect to canopy height and even shows a slight increase towards the bottom of the canopy. Estimates of 'local' V_g are required by the model described below. 'Normalised' V_g, however, is the more usual way of expressing a deposition velocity and our values of V_g1 are compared below with other values from the literature for both radioactive and non-radioactive aerosols (Tables 2 & 3).

Table 2: Comparison of wind tunnel and field deposition velocities for non-radioactive aerosols from various studies

Reference	canopy type	Aerosol	V_g1 (cm s^{-1})	
			Wind tunnel	Field
Hofken *et al.* (1982)	Spruce	sulphate *		1.5
Hicks *et al.* (1982)	Pine	sulphate *		0.5 - 2.0
Gravenhorst & Höfken (1982)	Spruce	sulphate *		1.3
Dasch (1986)	Pine	sulphate *		0.15 - 0.45
Shanley (1989)	Spruce	sulphate *		0.034 - 0.78
Shaw *et al.* (1994)	Spruce	silica §	1.30	
This study	Spruce	uranium #	0.50	
		ambient †		2.0

* sulphate aerosols in the size range 0.10 - 1.0 μm geometric diameter
§ silica aerosols in the size range 1.30 - 2.30 μm VMAD
# uranium aerosol in the size range 0.77 - 0.82 μm VMAD
† ambient aerosol in the size range 1.50 - 2.50 μm geometric diameter (median aerodynamic diameter (MAD) ~1.0 μm)

Table 3: Field deposition velocities of some Chernobyl derived radionuclides.

Reference	Tree Canopy	Radionuclide*	V_g (cm s^{-1})
Roed (1987)	Spruce	^{134}Cs	0.073
		^{103}Ru	0.28
		^{106}Ru	0.53
Brückmann (1988)	Spruce	^{137}Cs	~ 1
Bunzl *et al.*, (1989)	Spruce	^{134}Cs	> 0.49
		^{106}Ru	> 0.66

* Probable size range of aerosol 0.3 - 1.0 μm (eg. Devell *et al.*, 1986)

The data in tables 2 and 3 show that our wind tunnel estimates of deposition velocity using reduced scale canopies compare favourably with field measurements of V_g of several aerosol types of comparable size ranges. In addition, our studies have provided detailed vertical profiles of V_g which are necessary for the calibration and validation of multi-layered models of aerosol deposition to tree canopies, such as that of Belot *et al.* (1994). As a means of validating our own wind tunnel estimates of V_g we carried out a field experiment using identical spruce trees to the experiments for which wind tunnel measurements had already been made. This involved exposing cleaned surfaces of needles for a fixed period of 10 hours to ambient air. The ambient aerosol flux to the needle surface was then quantified by counting numbers of particles in a defined size class using SEM. Air concentrations in the same size class were evaluated using SEM counting of particles on a filter from a cascade impactor. The resulting V_g of 2.0 cm s^{-1} (Table 2) is at the upper limit of other field determined values, as a result of the relatively large size of the particles collected, though still within the range reported within the literature. Together with our wind tunnel determined values this gives us a useful range of V_g estimates for predicting dry deposition of aerosols in far-field regions of atmospheric plumes emanating from nuclear facilities.

Resuspension Studies:

Detailed resuspension rate estimates for small aerosol particles in forest canopies have not previously been reported in the literature. The results obtained during the course of this study are intended to redress this deficiency using wind tunnel derived measurements of particle fluxes within identical spruce canopies used for the deposition determinations reported above. Pre-contamination of spruce trees with dysprosium labeled silica particles was carried out in a small, enclosed Perspex chamber. After this the trees were arranged to give a uniform canopy and exposed to a 5 ms^{-1} air stream in the wind tunnel. Isokinetic air samples were taken from the 5 layers shown in Figure 1 and aerosol flux rates determined. These were then normalised to the initial contamination of the tree surfaces to give a resuspension rate coefficient (Λ, s^{-1}). Resuspension rates determined in this way are shown in Figure 2, which shows Λ

values plotted on the basis of both canopy layer and time after the initiation of resuspension.

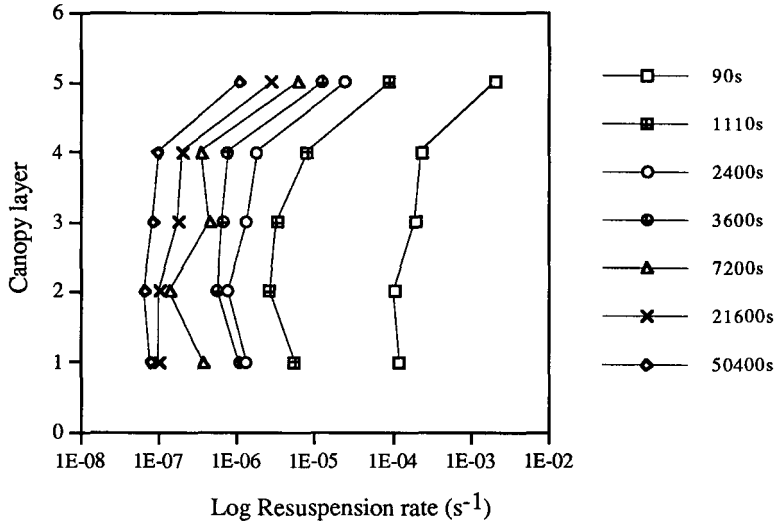

Figure 2: Resuspension rates within small scale Norway spruce canopies plotted with respect to both canopy height (ie. layer) and time after the initiation of resuspension.

Resuspenion rate was markedly greater at the top of the canopy than lower down, although there was a slight upturn in Λ near the base of the canopy. This pattern of resuspension rate reflects the typical distribution of wind velocity within a tree canopy, as previously shown by Kinnersley *et al.* (1994). The declining amplitude of the resuspension rate profile with time is also very marked with Λ being reduced from initial values of between 10^{-3} - 10^{-4} s^{-1} to 10^{-6} - 10^{-7} s^{-1} after 14 hours. When examined more closely this pattern follows the resuspension rate model of Garland (1982) which indicates that Λ varies inversely with time. Summarising Figure 2, the results indicate that resuspension will be greatest at the top of the canopy (where the wind speed is greatest) immediately after deposition of the aerosol. The implication of this result is that 'prompt' resuspension in the hours immediately following a discrete deposition event may be important in a) facilitating a redistribution of the original deposit and b) exposing individuals to an inhalation hazard which is probably diminished rapidly with time.

Field Loss Studies:

After depositing uranium aerosol to spruce trees within the wind tunnel for the purposes of determining deposition velocities a number of trees were transported to the field where they were exposed to ambient atmospheric conditions for 45 days. The concentration of aerosol from each of the five canopy layers identified in Figure 1 was quantified and normalised to the initial concentration to produce the loss curve shown in Figure 3. This is, in fact, a composite plot for all of the canopy layers. When the loss curves for individual layers are plotted there is an indication that as one layer loses

deposit it is transferred to the underlying layer, although it proved impossible to demonstrate this effect with statistical significance.

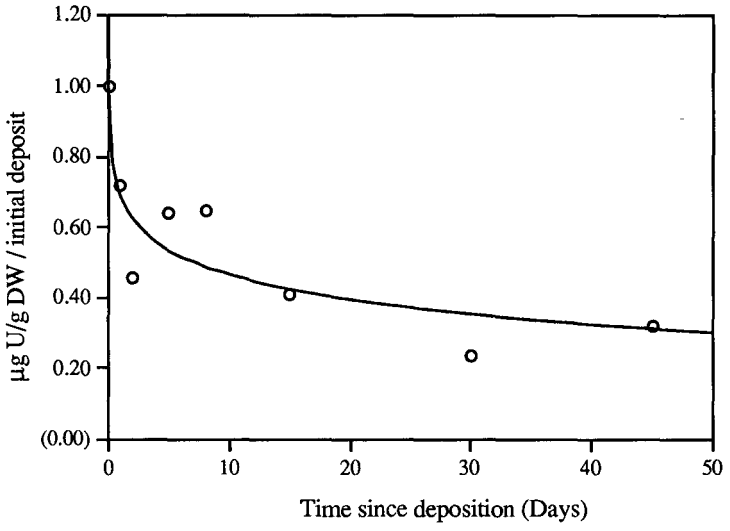

Figure 3: Normalised loss curve for uranium aerosol applied to external surfaces of Norway spruce subsequently exposed to ambient atmospheric conditions.

Table 4: A summary of experimental and field-determined loss rates derived for tree canopies contaminated with a variety of radionuclides.

λ (d^{-1})	$t_{1/2}$ (d)	Author(s)	Notes
0.0061	114	Tikhomirov *et al.* (1993)	Soluble ^{89}Sr, Pine, October
0.0289	24	Tikhomirov *et al.* (1993)	Soluble ^{89}Sr, Pine, June
0.0032	22	Shaw *et al.* (unpublished)	Soluble ^{137}Cs, Spruce, Summer
0.0555	12.5	Shaw *et al.* (unpublished)	Soluble ^{60}Co, Spruce, Summer
0.1386	5	Sombre et al. (1990)	Thermogenerated UO_2 aerosol, Spruce
0.0139	50	Sombre et al. (1990)	Thermogenerated UO_2 aerosol, Spruce
0.0077	90	Bunzl *et al.* (1989)	^{137}Cs, ^{134}Cs, Spruce 0 - 130 days after depn.
0.0030	230	Bunzl *et al.* (1989)	^{137}Cs, ^{134}Cs, Spruce 130 - 600 days after depn.

The half time indicated by Figure 3 is approximately 5 days; however, a single exponential curve could not easily be fitted to the data and a statistical estimate of the loss half time could not, therefore, be achieved. A double exponential curve proved impossible to fit, although from the appearance of the curve it appears that the loss rate was faster immediately after contamination than in the period between 10 and 50 days following contamination. Both Sombre *et al.* (199o) and Bunzl *et al.* (1989) have shown double component losses from aerosols from tree canopies, although the absolute loss rates determined by different workers vary markedly.

Table 4, above, summarises loss half times for tree canopies from various sources. It is evident from this summary that field determinations of Tikhomirov *et al.* and Bunzl *et al.* made after the Kyshtym and Chernobyl accidents, respectively, are longer than the other experimentally based determinations. This may mitigate against the use of experimentally determined field loss rates for tree canopies in modelling the behaviour and fate of radioactive materials deposited to forest ecosystems.

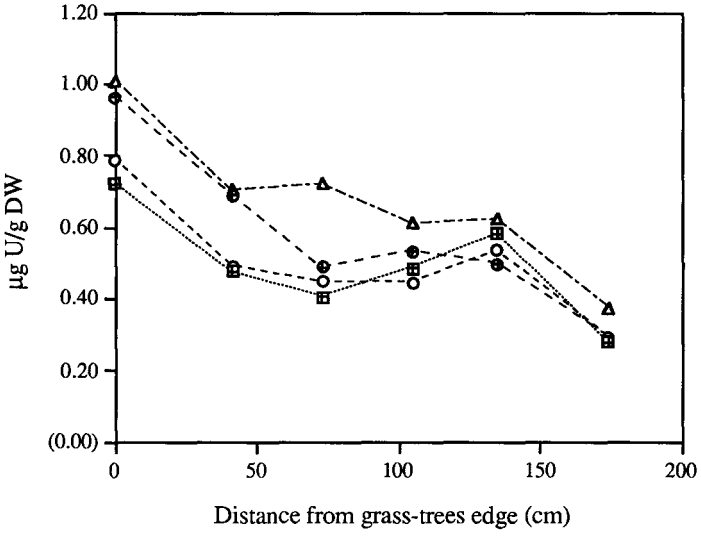

Figure 4: Contamination of Norway spruce trees with uranium aerosol with increasing distance from the grass-tree edge shown diagrammatically in Figure 5.

Aerosol Deposition at a 'Forest' Edge:

The final experiment of the project involved an examination of the possible enhancement of aerosol deposition at the edge of a stand of trees when the wind direction was directly towards the forest edge. Enhanced deposition of ^{90}Sr was observed in the vicinity of the Kyshtym accident, although this effect was rather ambiguous in the forested areas surrounding the Chernobyl nuclear power plant.

Figure 5 shows the layout of an experiment to determine the 'edge effect' on aerosol deposition within the wind tunnel. The inset graphs show the wind velocity profiles measured at the points indicated. The shape of the boundary layer above the grass

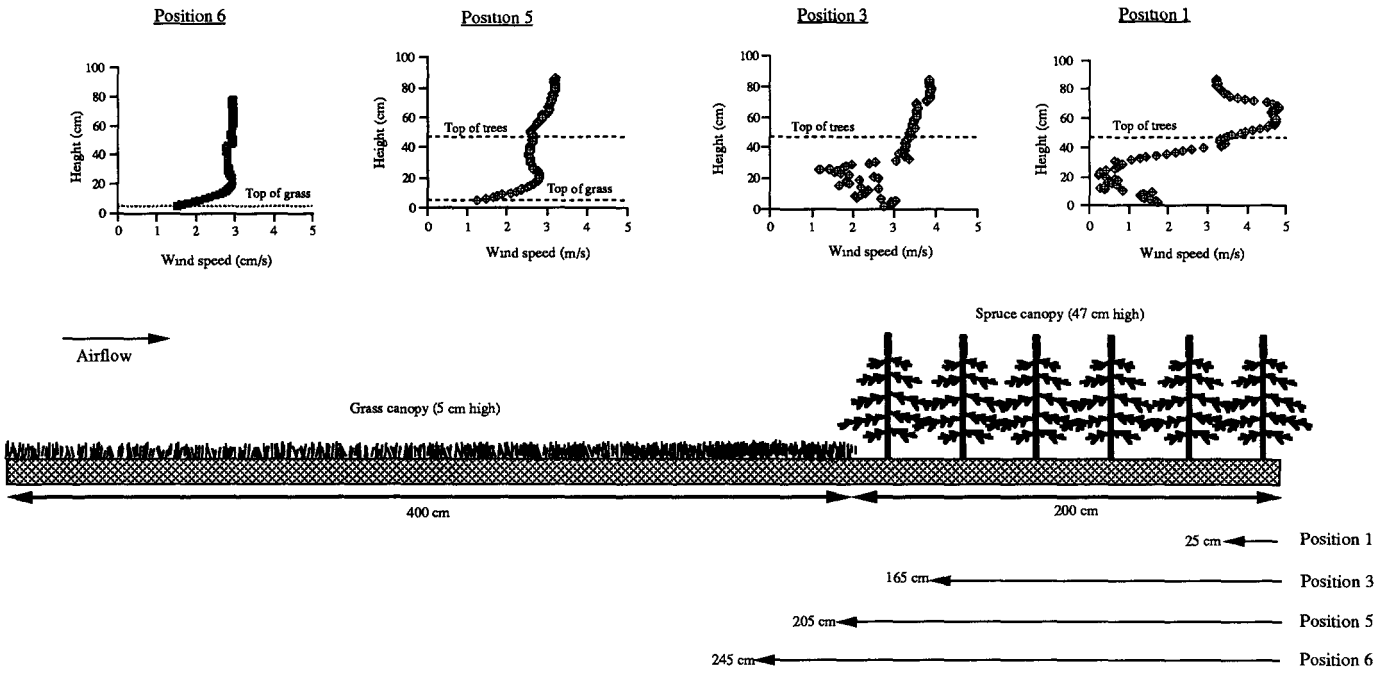

Figure 5: Layout of experiment to determine uranium aerosol deposition at the edge between a grass sward and a tree stand

canopy (position 6) is relatively simple and is confined to less than 20 cm above the grass surface while at position 1 a more complex and deeper boundary layer is evident which is typical of a tree canopy. Between these two positions the boundary layer is subject to rapid deformation and alteration, with a scatter of points in the profile from position 3 indicating an enhencement of turbulence. Figure 4 clearly indicates that this alteration in air-flow resulted in an enhancement of deposition at the edge of the tree stand, thus corroborating results reported from the Kyshtym accident zone (Tikhomirov *et al.*, 1993)

Modelling the Dynamics of Aerosol Behaviour in Tree Canopies:

Figure 6 shows the outline of a dynamic model of aerosol behaviour currently being coded as part of a PhD project on aerosol deposition and fate within tree canopies. The key parameters identified (V_g, Λ and λ) are those which have been determined experimentally during the course of the current project. The model is intended to synthesise each of these measurements within a dynamic framework which may then be used as an input module to a more general model of radionuclide behaviour in forest ecosystems.

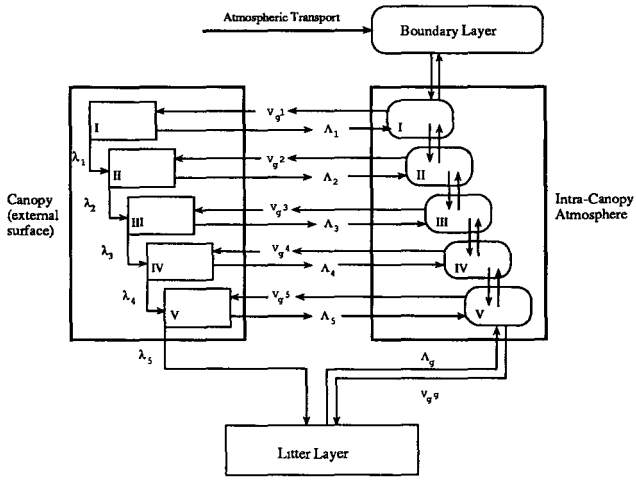

Figure 6: Model Representation of Aerosol Dynamics Within a Multi- Layered Forest Canopy. Key parameters within the model are deposition velocity (V_g), resuspension rate (Λ) and canopy loss rate due to weathering (λ).

Publications Produced During the Project

KINNERSLEY, R., J. G. FARRINGTON-SMITH, G. SHAW, and M. J. MINSKI (1994) Aerodynamic characteristics of model tree canopies in a wind tunnel. Science of the Total Environment, 157, 29 - 33.

KINNERSLEY, R., Z., OULD-DADA & P. JAMES (1994) Production and characterisation of uranium aerosols for use in tracer studies. Presented at the annual conference of the Aerosol Society, University of York, April 1994.

OULD-DADA, Z. (1995) The dynamics of aerosol behaviour and fate within spruce canopies. PhD thesis, Imperial College, University of London, UK. (Submitted November 1995)

SHAW, G., J. G. FARRINGTON-SMITH, R. KINNERSLEY, and M. J. MINSKI (1994) Dry deposition of aerosol particles within model spruce canopies. Science of the Total Environment, 157, 17 - 23.

Publications - In Preparation

KINNERSLEY, R., Z., OULD-DADA & P. JAMES Production and characterisation of uranium aerosols for use in tracer studies. To be submitted to the Journal of Aerosol Science.

OULD-DADA, Z., G. SHAW, R. P. KINNERSLEY & M. J. MINSKI Dry deposition of sub-micron particles to small scale spruce canopies - comparison of wind tunnel measurements with field data. To be submitted to Atmospheric Environment.

OULD-DADA, Z., G. SHAW, R. P. KINNERSLEY & N. MIRZAI-BAGHINI Resuspension and field loss of silica and uranium-based aerosol particles from spruce canopies. To be submitted to Environmental Pollution.

OULD-DADA, Z., G. SHAW & R. P. KINNERSLEY Deposition of sub-micron uranium aerosol at a forest edge - a wind tunnel study. To be submitted to Envionmental Pollution.

Publications - Quoted from Other Sources

BELOT, Y., H. CAMUS, D. GAUTHIER & C. CAPUT (1994) Uptake of small particles by tree canopies. Science of the Total Environment, 157.

BRÜCKMANN, A. (1988) Radionuklidbilanz von 4 Waldoekosystemen nach dem Reaktorunfall in Tschernobyl und eine Bestimmung der trockenen Deposition. Diplomarbeit Forstwissenschaftlicher Fachbereich, Goettingen.

BUNZL, K., W. SCHIMMACK, K. KREUTZER and R. SCHIERL (1989) Interception and retention of Chernobyl-derived ^{137}Cs, ^{134}Cs and ^{106}Ru in a Spruce stand. Science of the Total Environment, 78, 77 - 87.

DASCH J.M. (1986) Measurement of dry deposition to vegetation surfaces. Water, Air and Soil Pollution, 30, 205 - 210.

DEVELL, L., H. TOVEDAL, U., BERGSTRÖM, A. APPELGREN, J. CHYSSLER and L. ANDERSSON (1986) Initial observations of fallout from the reactor accident at Chernobyl. Nature, 321, 192 - 193.

GARLAND, J. A. (1982) Resuspension of particulate material from grass : Experimental programme 1979 - 1980. Harwell report, AERE - R 10106.

GRAVENHORST, G., and K.D. HOFKEN (1982) Concentration of aerosol constituents above and beneath a beach and a spruce forest canopy. In *Deposition of Atmospheric Pollutants* (edited by Georgii H.W. and Pankrath J.), 187 - 190. Reidel, Dordrecht.

HICKS, B.B., M.L. WESELY J.L. DURHAM and M.A. BROWN (1982) Some direct measurements of atmospheric sulfur fluxes over a pine plantation. Atmospheric Environment, 16, 2899 - 2903.

HOFKEN, K.D., F.X. MEIXNER and D.H. EHHALT (1982) Deposition of atmospheric trace constituents onto different natural surfaces. In *Precipitation scavenging, Dry deposition and Resuspension* (edited by Pruppacher H.R., Semonin R.G. and Slinn W.G.N.), 825 - 836 Elsevier, New York.

ROED J. (1987) Dry deposition in rural and in urban areas in Denmark. Radiation Protection Dosimetry, 21, 33 - 36.

SHANLEY J.B. (1989) Field measurements of dry deposition to spruce foliage and petri dishes in the black forest, F.R.G. Atmospheric Environment, 23, 403 - 414.

SOMBRE, L., M. VANOUCHE, Y. THIRY, C. RONNEAU, J. M. LAMBOTTE & C. MYTTENAERE (1990) Transfer of radiocaesium in forest ecosystems resulting from a nuclear accident. In: Desmet, G. M., P. Nassimbeni and M. Belli, Transfer of radionuclides in natural and semi-natural environments. Elsevier Applied Science, London & New York, 1990.

TIKHOMIROV, F. A., A. I. SHCHEGLOV and V. P. SIDOROV (1993) Forest and forestry: radiation protection measures with special reference to the Chernobyl accident zone. Science of the Total Environment, 137, 289 - 305.

Head of the project 2: Dra. Rauret

II Objectives for the reporting period

1st. Comparison between radionuclide behaviour in holm oak leaves contaminated by two different methodologies.
2nd. Global evaluation of radionuclide behaviour in Mediterranean forest soils.
   a) Radionuclide migration in the forest soil
   b) Effect of soil faunal activity in radionuclide migration
   c) Comparison with their chemical homologous (Cs-K)
3nd. Modelling litter decomposition and radionuclides release in Mediterranean conditions.
4rt. Study of the partitioning of radiocaesium in forest soil layers by means of the application of a sequential extraction scheme.
5th. General conclusions and publications.

III Progress achieved including publications

1st. Comparison between radionuclide behaviour in holm oak leaves contaminated by two different synthetic aerosols.

In the 90-92 period, a methodology based on sequential extractions was established to distinguish between the different radionuclide fractions in holm oak leaves (incorporated by direct absorption, removable by rain and retained on surface leaves). To perform this study, holm oak leaves were contaminated by a radioactive aerosol deposited in wet conditions.
Considering that retention and subsequent absorption of radionuclides intercepted by plants not only depend on the type of plant and contact time but also on aerosol physico-chemical properties as well as on the moisture status of leaf epidermis, a similar experiment was designed to be carried out during the 92-94 period using holm oak leaves contaminated by the POLYR aerosol. The solubility of this aerosol is different from the one used in the former period (Wet-Initial), the deposition being in dry conditions (Dry-Polyr). Therefore, a different radionuclide behaviour can be expected.
The two-step scheme applied in the previous period to evaluate radionuclide retention, which uses distilled water and chloroform:hexane (1:2) as extractant reagents, was optimized. The experimental conditions studied were time and speed of shaking as well as volum of extractants.
From the results, two schemes which give complementary information in relation to radionuclide retention may be used. One is defined by a single energetic extraction with water (Scheme A) and the other is defined by a two-step procedure which uses water and chloroform:hexane 1:2 (Scheme B). Since the objective was to study the retention of ^{134}Cs, ^{85}Sr and ^{110m}Ag simultaneously, the best compromise conditions for extraction of individual radionuclide components were chosen. Scheme A allows us to define two fractions: the fraction removed by water, which is related to the total radionuclide content retained on leaf surfaces, and the residual fraction, which is associated with the radionuclide incorporated into the leaves. On the other hand, Scheme B permits to distinguish among three fractions: the fraction removed by water, which is related to radionuclide fraction that is easily leached by rain, the fraction removed by organic solvent, which may be associated with the radionuclide fraction strongly retained on leaf surface and, finally, the residual fraction, which may represent the fraction incorporated into the leaves.
The radionuclide fractionation in holm oak leaves achieved by applying the two schemes are represented in Figure 1. The main conclusions concerning radionuclide extraction are that: the incorporated fraction does not depend on the method used, the fraction retained on leaf surface (fraction extracted with organic solvent) is significant only for ^{85}Sr and ^{10m}Ag, and the fraction easily removed by rain is higher for ^{134}Cs.
Figure 2 compares the fractionation achieved by applying the scheme B in holm oak leaves contaminated using the two different aerosols (Wet-Initial and Dry-Polyr). It can be noticed the clear influence of aerosol and its deposition conditions in subsequent radionuclide behaviour: when POLYR aerosol was used, the fraction of incorporated radionuclide is lower than the one obtained in leaves contaminated by the aerosol used in the 90-92 period.
The leaves contaminated under wet conditions were used for the field incubation study.

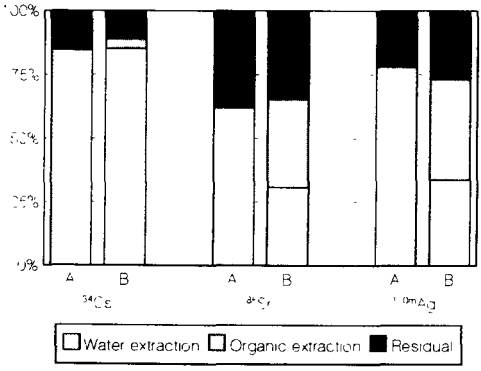

Figure 1. Radionuclide fractionation in holm oak leaves contaminated by dry deposition of the POLYR aerosol by applying schemes A and B.

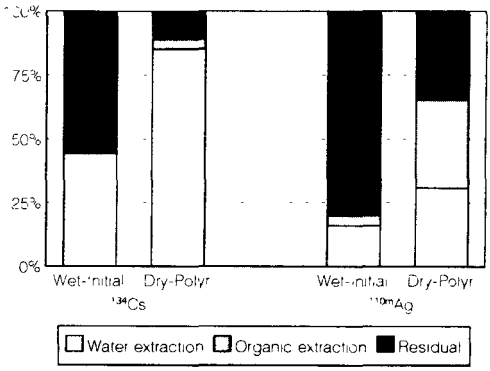

Figure 2. Radionuclide fractionation in holm oak leaves contaminated using the two types of aerosol by applying the scheme B.

2nd. Radionuclide behaviour in Mediterranean forest soils

Experimental design and sampling

^{134}Cs and ^{110m}Ag migration in a Mediterranean forest was estudied in field conditions. Fresh holm oak leaves were exposed to a synthetic aerosol including ^{134}Cs and ^{110m}Ag and were incubated, replacing the original litter layer in the original holm oak forest. The field incubation was carried out in two types of cylinder:

1) Open cylinders (diameter 14 cm), where the contaminated litter lies directly on the superficial F layer and free faunal activity was allowed.
2) Resin cylinder (diameter 11 cm), where a bag containing an exchange cationic resin (Amberlite IR-120 (Styrene-DVB)) was placed between the contaminated green leaves and the F layer in order to avoid the passage of soil fauna from the underlying layers to the L layer and to retain radionuclides migrated within the litter leachates.

Litter decomposition rates in the cylinders were compared with the rates obtained by the classical litter bag technique (20x20cm 2mm mesh size) using non-contaminated green leaves.

44 plots of 0.25 m^2 were installed in the experimental forest. In each plot, an open cylinder, a resin cylinder and a litter bag were incubated (Fig.3).

Over two years (till the end of 1992), nine sample collections were done. At each sampling 4 plots were taken as replicates. For each cylinder the following layers were sampled separately: the remaining litter (L), organic layers (F, H) and mineral soil (A1 (0-2.5 cm depth), A2 (2.5-5 cm depth)).

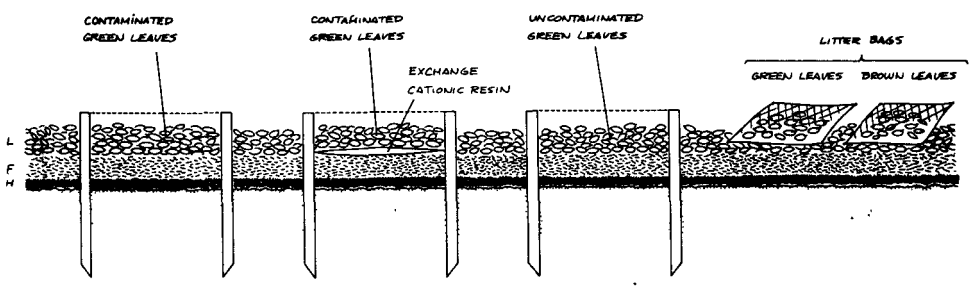

Figure 3. Scheme of one plot.

a) Radionuclide migration in the forest soil

Radionuclide migration in the forest soil profile was studied in the called open cylinders.
Figure 4 shows the distribution of ^{134}Cs among the different layers during the incubation period. The first sampling, 17 days of incubation, accounted for 40% of the release of the initial ^{134}Cs. This figure corresponded with the percentage extracted by water from the original contaminated leaves. Therefore, further ^{134}Cs migration corresponded to the fraction absorbed into the leaves. After 100 days of incubation, 20% of the radiocaesium activity remained in the L layer and at the end of the experiment, 835 days of incubation, 93% of the initial ^{134}Cs has migrated from the L layer. These results are in agreement with the range of Chernobyl radiocaesium distribution found in Mediterranean forests (Roca et al., 1991, Llauradó et al., 1994). The migration profiles in mountain beech forest soils after the Chernobyl event reported by Belli et al. (1990) showed lower migration rates from the L layer compared with the present results.
During the first year, radiocaesium that migrated from the L layer accumulated mainly in the F layer; from this period onwards, a progressive transfer from these layers to the H layer was observed. Migration to the deeper layers ocurred rapidly and very little activity reached the mineral soil after the initial leaching period. At the end of the study, the H layer contained the highest amount of ^{134}Cs. In this kind of layer, an important proportion of radiocaesium remains in available forms and therefore it can be an important source of radiocaesium for root and mycelia uptake.
^{110m}Ag showed similar behaviour but with lower migration rates (Fig.5). The transfer between the forest floor layers was more gradual than for radiocaesium. After 835 days of incubation, 15% of ^{110m}Ag remained in the L layer. ^{110m}Ag migrated from the L layer, like ^{134}Cs, accumulated in F and H layer and very little activity reached the mineral soil.

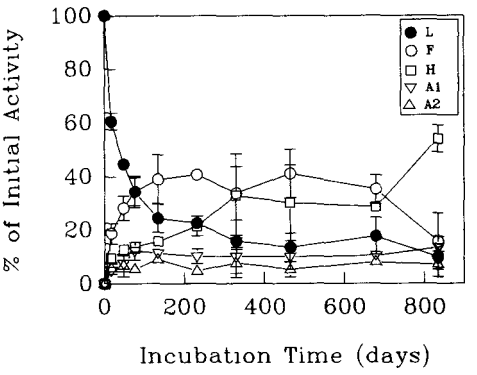

Figure 4. Distribution of ^{134}Cs among the forest floor and top soil layers during the incubation period. Samples from the open cylinders. Mean values and standard errors.

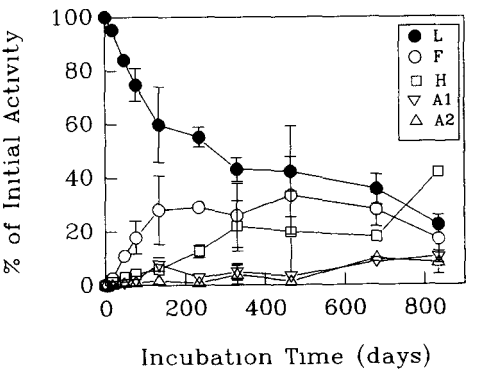

Figure 5. Distribution of ^{110m}Ag among the forest floor and top soil layers during the incubation period. Samples from the open cylinders. Mean values and standard errors.

The relationship between the standing mass of the F layer and radionuclide accumulation in this forest floor can be seen in Figures 6 and 7. These results can be explained as follows:
An initial period of rapid accumulation of radionuclides in F layer as a consequence of initial L layer leaching (50 days). A second period, with both incorporation from L layer and transfer to H layer, related to easily decomposable compounds (600 days). Along this period, the F layer lost about 70% of weight whereas radionuclide content remained constant; during this period, specific radionuclides retention by recalcitrant compounds is suggested. Microorganisms could also play an important role in consuming carbon with subsequent radionuclide inmobilization (Witkamp et al., 1968). Finally, a third period with both carbon and radionuclide mineralization was observed, especially for radiocaesium, towards the end of the incubation period.

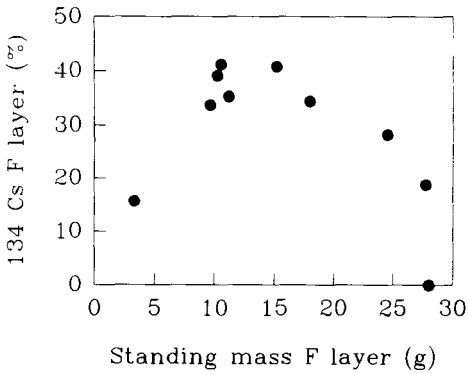

Figure 6. Relationship between the standing mass and ^{134}Cs accumulation in F layer.

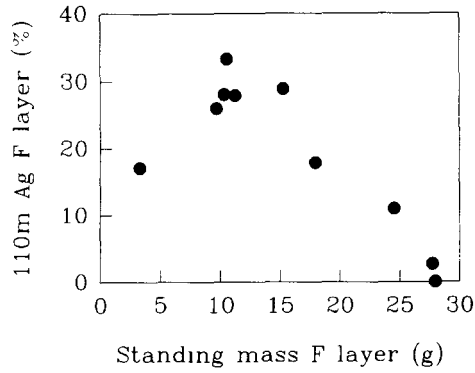

Figure 7. Relationship between the standing mass and ^{110m}Ag accumulation in F layer.

b) Effect of soil faunal activity in radionuclide migration

^{134}Cs migration showed no significant differences between the two types of incubation cylinder (Fig.8), indicating that ^{134}Cs migration was predominantly within the litter leachates.
^{110m}Ag (Fig.9) showed a more clearly differenciated pattern of migration than ^{134}Cs according to the higher absorption into the leaves observed for this radionuclide. This fact facilitated to show macrofaunal activity effects on radionuclide migration allowing to describe the different phases:

1) First period of 50 days when an equivalent proportion to the ^{110m}Ag extracted by water on the original leaves was released in both open and resin cylinders.
2) From that time on and coinciding with the time, when evidence for soil faunal activity appeared in the open cilinder (no evidences in the resin cylinders), the open cylinder lost significantly higher proportion of the initial ^{110m}Ag. Therefore, the difference between the two types of incubation, i.e. 15-20% of the initial ^{110m}Ag activity, is attributed to the effect of litter comminution and transport by soil fauna.
3) These differences disappeared after the first litterfall (around 300 days of incubation, end of spring). The new litter layer completely covered the contaminated litter layer and evidences of soil faunal activity (although less than in open cylinders) also appeared in the resin cylinder. Soil fauna colonized these cylinders laterally and start to fragment the contaminated litter facilitating the progressive leaching of radiosilver incorporated into the leaves.
4) Finally, during the two last samplings, ^{110m}Ag radiosilver release from the remaining litter was significantly higher in the open cylinder. In this period, a particulate transfer of ^{110m}Ag in the open cylinder occurred.

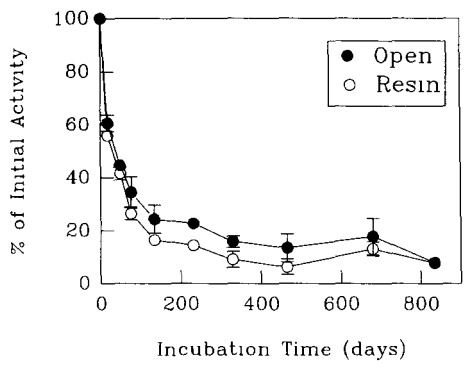

Figure 8. Dynamics of ^{134}Cs release from open and resin cylinders.

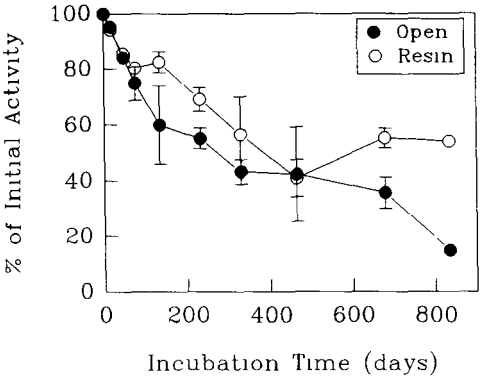

Figure 9. Dynamics of ^{110m}Ag release from open and resin cylinders.

c) Comparison with their chemical homologous: Radiocaesium-potassium.

Potassium release did not show the initial sharp leaching observed for ^{134}Cs (Fig.10). After that period, both elements showed similar mineralization patterns. The interpretation drawn from these observations is as follows:

1) The canopy sampled for contamination was normaly leached for K in field conditions; it is well known that an important proportion of K release by tree canopies come from through fall and stem flow (around 40% in the experimental forest (Lledó, 1990)). Therefore, little external K was available on leaf surfaces.
2) The experimental contaminated holm oak leaves were not exposed to canopy leaching before field incubation. Field data after the Chernobyl accident and experiments with synthetic aerosols (Block & Pimpl, 1990; Sombre et al., 1990) showed that a large part of radiocaesium was rapidly washed off from the canopy.
3) The radiocaesium remaining after the initial superficial leaching, mostly absorbed in the leaves like K, showed similar behaviour than this latter element, in agreement with other authors (Van Voris et al., 1990).

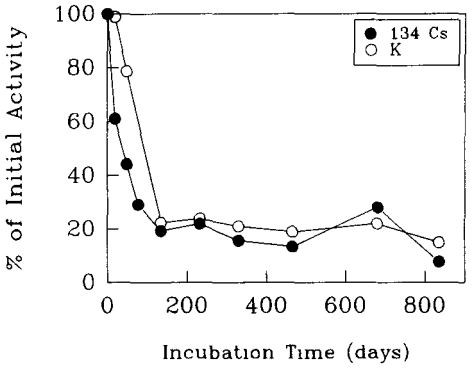

Figure 10. Dynamics of K and ^{134}Cs release from open cylinders.

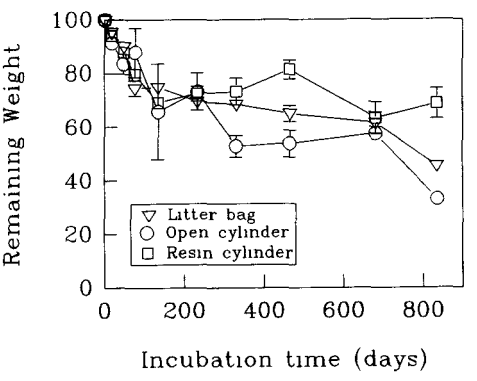

Figure 11. Litter decomposition for the three incubation methods: litter bags, open and resin cylinders.

3rd. Modelling litter decomposition and radionuclides release in Mediterranean conditions.

Figure 11 shows the evolution of litter decomposition, expressed as the remaining weight for the three types of incubation. After 232 days of incubation, significant differences were found among the different incubations. Weight loss increased in the following sequence: resin < litter bag < open cylinder. These differences are explained according to the increasing soil faunal activity from resin to open cilinders. Litter bags represent an intermediate situation, the passage was limited to soil fauna smaller than 2 mm. Therefore soil faunal activity enhanced both radionuclide release and litter decomposition.

Figures 12 and 13 show the relationship between the radionuclide remaining activity and remaining mass of litter layer in the open cylinders. After an initial period, when the leaching of both radionuclides was equivalent to the water extractable fraction of radionuclides obtained by sequential extraction, radionuclides release was dependent on litter decomposition. A positive linear correlation was found between mass loss and radionuclide release after the first leaching period. Regression coefficient was 0.57 for ^{134}Cs and 0.56 for ^{110m}Ag ($p<0.01$). For resin cylinder no significant correlation between remaining activity and remaining mass was found.

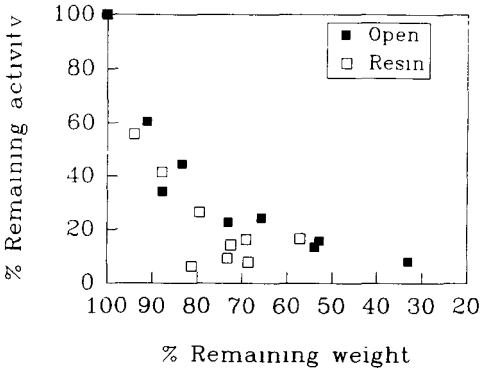

Figure 12. Relationship between ^{134}Cs remaining activity and remaining mass of litter.

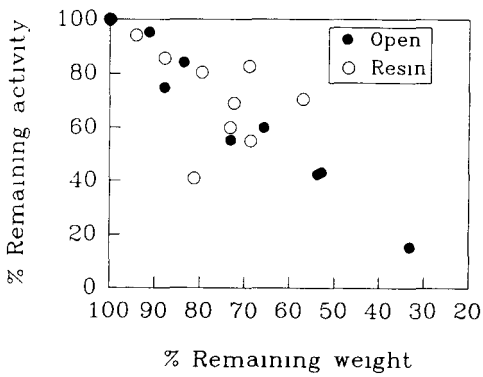

Figure 13. Relationship between ^{110m}Ag remaining activity and remaining mass of litter.

In agreement with these observations, radionuclides released from the litter layer in the open cylinders (Fig.14) followed a double negative exponential function:

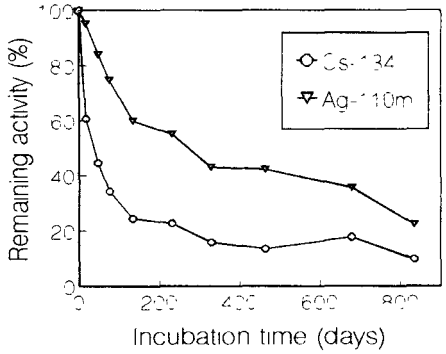

Figure 14. Radionuclides released from the litter layer in the open cylinders.

^{134}Cs: $RA = 66.13 \cdot e^{-0.039\,t} + 32.28 \cdot e^{-0.0015\,t}$

^{110m}Ag: $RA = 29.88 \cdot e^{-0.015\,t} + 71.92 \cdot e^{-0.0014\,t}$

RA: Remaining activity,
t: incubation time (days)

The first part of the exponential, with a higher rate of migration, is attibuted to leaching processes and the second, with a lower rate, is related to decomposition processes associated with litter mass loss. Litter mass loss followed a single negative exponential function:

$RM = 100 \cdot e^{-0.0013\,t}$ (RM: Remaining mass, t: incubation time (days))

As expected by the different solubility of Cs vs. Ag, ^{134}Cs leaching was faster than that of ^{110m}Ag but the release due to decomposition is similar for both radionuclides and their release rate is close to the rate of litter mass loss.

Other studies reported lower release rates for radiocaesium (Belli et al., 1990) and, different release rates depending on plant litters under the same experimental conditions (Clint et al., 1990). The study carried out by Rafferty and Kliashstorin (Raferty et al., 1994) in Chernobyl and Ireland reported that the radiocaesium content in the L layer remained constant during litter decomposition. These results contrast with those obtained in the present work. This could be due to the different nature of litter for both experiments or, more probably in relation to the fact that litter in Chernobyl, in the year that the experiment was carried out, did not received contamination by deposition (in a manner similar to our experiment), but by root absorption which could affect the form of radiocaesium in the leaves (needles in their case). It is well known that during the decomposition

process, the differential release of mineral elements attached to litter depens in great extent on the kind of chemical bounds prevailing for these elements. Therefore radionuclide content in the different pools (labile or recalcitrant) of initial litter could determine further migration as a consequence of differential decomposition rates for these pools.

4rt. Study of the partitioning of radiocaesium in forest soil layers by means of the application of a sequential extraction scheme.

The field experiment showed the accumulation of radionuclides in the H layer after 835 days of incubation. Therefore, organic matter may retain in some way the radionuclides. The sequential extraction scheme applied in this project was designed to study the interactions between the organic matter phases in forest soil layers and radiocaesium, to better understand the role played by these substances in the retention of this radionuclide.

The experimental procedure followed can be summarized as described below:

FRACTION 1: 40 ml/g of NH_4OAc 1 $mol \cdot l^{-1}$ was added to the soil. The suspension was shaken for 16 h at room temperature using an end-over-end shaker.

FRACTION 2: 40 ml/g of $Na_4P_2O_7$ 0.1 $mol \cdot l^{-1}$ was added to the residue and the suspension was shaken for 16 h at room temperature.

FRACTION 3: 40 ml/g of NaOH 0.1 $mol \cdot l^{-1}$ (in N_2 atmosphere) was added to the residue and the suspension was shaken for 16 h at room temperature.

FRACTION 4: (4a) 10 ml/g of H_2O_2 30% (pH 2 with HNO_3) was added to the residue and the suspension was allowed to digest for 2 h at room temperature and for a further 4 h at 85 °C.
(4b) 10 ml/g of H_2O_2 30% (pH 2 with HNO_3) was added to the moist residue and the suspension was allowed to digest for 16 h at 85 °C.
(4c) 50 ml/g of NH_4OAc 1 $mol \cdot l^{-1}$ (pH 2 with HNO_3) was added to the moist residue and the suspension was shaken for 16 h at room temperature, and then, filtered through 0.45 μm membranes.

This scheme allowed the estimation, in an operational way, of the fraction of radionuclide associated with exchangeable sites (Fraction 1), the fraction related to humic and fulvic acids that had not been extracted previously (Fractions 2 and 3), the amount of radionuclide related to passive organic matter like humine or structural components (Fraction 4) and the radionuclide highly fixed to soil mineral matter (residual fraction).
The behaviour of radiocaesium in both H and A layers can be compared in terms of desorption yields after applying the same extractants. Therefore, this scheme was applied to H samples taken from samplings carried out 48, 232, 330 and 820 days after the start of the incubation period, and to A samples from 330 and 820 days.

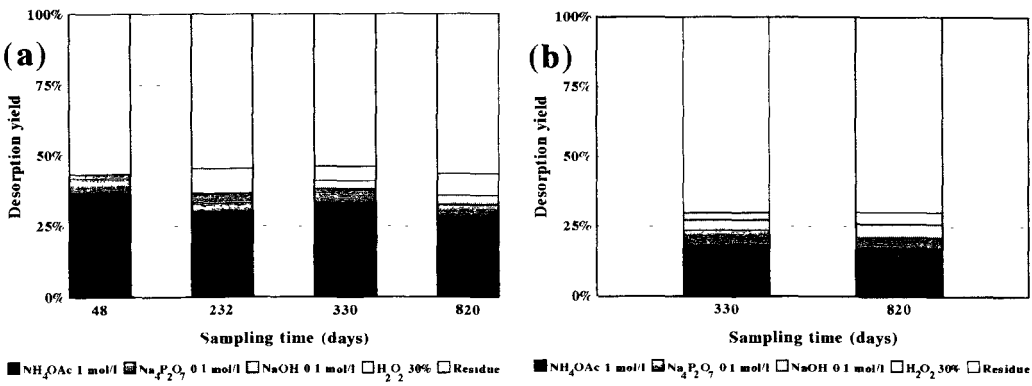

Figure 15. Radiocaesium distributions obtained in H (a) and A (b) layers.

Figure 15 shows ^{134}Cs distributions obtained in H and A samples using the organic scheme. It is important to highlight the rapid fractionation in the samples coming from the first sampling, which is a typical behaviour observed in mineral soils. Moreover, both types of sample showed a similar distribution pattern. In both cases, the residual fraction was the most significant, with an associated radionuclide of about 55% for H samples and 70% for A samples. These different percentages may be explained by the organic matter percentages (42% in H layer; 21% in A layer). The exchangeable fraction, represented by the extraction with NH_4OAc, was higher in H samples: about 30% was desorbed for H samples and 20% for A samples. The intermediate fractions, mostly related to organic matter phases, also had similar low values in both types of sample.
It is difficult to draw conclusions about radionuclide ageing in H and A layers because of the experimental design, since there was a continuous flow of radiocaesium from upper layers, which resulted in an increase in the radionuclide content in the H layer but keeping the distribution pattern quite constant. However, there was a clear difference between the distribution obtained after 48 days of incubation and the final distributions. This fact may be due to a certain ageing; the changes over time of the distributions can be explained because of the association of radiocaesium with structural components, which can be solubilized after an oxidation with hydrogen peroxide.

5th. General conclusions and publications.

From artificially contaminated forest litter with synthetic radioactive aerosols, post-Chernobyl profiles of radiocaesium distribution in the forest floor of Mediterranean forest have been reproduced.
The initial rapid loss from the L-layer corresponded with rapid accumulation in the F layer. This was then followed by a period with progressive transfer to H-layer. After two years the H-layer accumulated the highest amount of radionuclides
Release rates of ^{134}Cs and ^{110m}Ag closely corresponded with litter decomposition rates.
Soil faunal activity enhanced both litter decomposition and radionuclide migration.
Radionuclide release rates followed a double negative exponential function.

$$RA = A \cdot e^{-kl\ t}\ (1) + B \cdot e^{-kd\ t}\ (2)$$

Contamination processes, type of radionuclide and climatic conditions after deposition are the main factors controlling the leaching processes (1). Climate, litter quality and biological activity are the main factors governing decomposition processes.
In F layer, radionuclide retention by recalcitrant compounds is suggested
A review of radiocaesium modelling in forests (Mitteneare et al., 1993) showed the necessity for a better understanding of the role of litter decomposition in radiocaesium cycling, as well as the importance of better identifying the mechanims involved in the biogeochemical processes for caesium availability and uptake in forest soils. In agreement with these ideas our experiment demonstrates that decomposition processes and organic matter dynamics in L and F layer are key factors controlling radionuclides cycling in Mediterranean forest systems.

Publications

Tent, J., Rauret G. 1995. Lixiviation as a tool for radionuclide fractionation in holm oak leaves. J.Radioanal.Nucl.Chem., in press.

Rauret, G., Llauradó M., Tent J., Rigol, A., Alegre L.H., Utrillas, M.J. 1994. Deposition on holm oak leaf surfaces of accidentally released radionuclides. Sci. Tot. Environ., 157: 7-16.

Sauras T., Roca MC., Tent J., Llauradó M., Vidal M., Rauret G., Vallejo VR. 1994. Migration study of radionuclides in a Mediterranean forest soil using synthetic aerosols. Sci. Tot. Environ., 157: 231-238.

Sauras T., Vallejo VR., Tent J., Rauret. 1995. Radionuclide dynamics during litter decomposition in a holm-oak forest. IAEA-SM-339/121.

Rigol, A., Vidal, M., Rauret, G. 1995. Radionuclide fractionation in a forest soil profile. J.Radioanal.Nucl.Chem., in press.

Rigol, A., Vidal, M., Rauret, G. 1995. Capillary Zone Electrophoresis to study humic fraction in organic soilsand its relationship with radiocaesium mobility. J.Radioanal.Nucl.Chem., in press.

LITERATURE CITED

Belli, M., Blasi, M., Borgia, a., Deluisa, a., Menegon, S., Michelutti, G., Nazzi, P., Pividori, G., Sansone, U. "The behaviour of caesium in mountainous soils". Transfer of Radionuclides in Natural and Semi-Natural Environments. (Proc. Int. Workshop. Udine, 1989), (Desmet, G., Nassimbeni, P., Belli, M., Eds.), Elsevier Science Publishers (1990) 143-151.

Block, J. and M. Pimpl, 1990. Cycling of Radiocesium in two forest ecosystems in the State of Rhineland-Palatinate. Proceedings of the Worshop on "Transfer of Radionuclides in Natural and Semi-Natural Environments". ECSC, EEC, EAEC, Elsevier Science Publishers LTD. pp. 450-458.

Clint, G., Harrison, a., Howard, D. " The release of Caesium-137 from plant litters and the effects of microbial axtivity on this process. Transfer of Radionuclides in Natural and Semi-Natural Environments. (Proc. Int. Workshop. Udine, 1989), (Desmet, G., Nassimbeni, P., Belli, M., Eds.), Elsevier Science Publishers (1990) 275-282.

Llauradó, M., Vidal, M., Rauret, G., Roca, M.C., Fons, J., Vallejo, V.R. Radiocaesium behaviour in Mediterranean Conditions. J. Environ. Radioactivity 23 (1994) 81-100.

Lledó, M.J., 1990. Compartimentos y flujos biogeoquímicos en una cuenca de encinar del Monte de Poblet. Ph. D. thesis, University of Alicante.

Mytennaere, C., Shell, W.r., Thiry, Y., Sombre, L., Ronneau, C., Van Der Stegen De Shrieck, J. Modelling of Cs-137 cycling in Forests: recent developments and research needed. Sci. Total Environ. 136 (1993) 77-91.

Rafferty, B., Kliashtorin, a. " The role of decomposition processes in the migration of radiocaesium in forest soils". The behaviour of radionuclides in natural and semi-natural environments. Final report of ECP-5 project (COSU-CT92-0019)(1993).

Roca, M.C., J. Fons-Esteve, V.R. Vallejo, J. Molero and A. Vidal-Quadras, 1991. Radiocaesium dynamics in Mediterranean forest. Fist European Symposium on Terrestrial Ecosystems: Forests and Woodlands. May 20-24, Florence (Italy).

Sombre, L., M. Vanhouche, Y. Thiry, C. Ronneau, J.M. Lambotte and C. Myttenaere, 1990. Transfer of Radiocesium in forest ecosystems resulting from a nuclear accident. Proceedings of the Worshop on "Transfer of Radionuclides in Natural and Semi-Natural Environments". ECSC, EEC, EAEC, Elsevier Science Publishers LTD. pp. 74-83.

Van Voris, P., Cowan, C.E., Cataldo, D.A., Wildung, R.E., Sthugart, H. "Chernobyl case study. Modelling the dynamics of long-term cycling and storage of ^{137}Cs in forested ecosystems", Transfer of Radionuclides in Natural and Semi-Natural Environments. (Proc.Int. Workshop. Udine, 1989), (Desmet, G., Nassimbeni, P., Belli, M., Eds.), Elsevier Science Publishers (1990) 61-73.

Witkamp, M., Barzanasky, B. Microbial immobilization of ^{134}Cs in forest litter. Oikos 19 (1968) 392-395.

Head of project 3: Prof. C. Ronneau

II. Objectives of the reporting period

The present research aims at defining the physico-chemical mechanisms involved in the formation and in the fate of fission products (FP) vehicled by UO_2 particles (aerosols as well as fuel particles) emitted as a consequence of a nuclear accident. These mechanisms determine the physico-chemical forms and, as a consequence, the availability of FP during their subsequent transfer into the environment and to Man. Three stages are considered to be of prime importance for fixing the physico-chemical speciation of radionuclides to be deposited in the environment: (i) the emission stage of FP, as vapours or carried into UO_2 aerosols emitted from reactor fuel at temperatures up to 2500°C; (ii) the maturation stage in which UO_2 aerosols react at intermediate temperatures (700 - 1000°C) with gases and vapours (air, water vapour, CO, CO_2, ...) in the plume of the damaged reactor or inside the reactor confinement; (iii) the deposition stage (onto plant, material and soil surfaces) in which the solubility of the FP plays a key factor in their transfer into the environment.

III. Progress achieved.

GENERAL OVERVIEW

Most of our research has been devoted to the characterisation of FP of radiological interest: mainly radio-cesium, -strontium, -ruthenium and -iodine. Uranium oxide is also of interest because, in many instances, its physico-chemical properties (as vitrified particles) determine the behaviour of the FP it contains.

Our studies have been performed by means of the following techniques:

(i) production of aerosols from UO_2 pellets heated up to temperatures of 2400°C in an electric oven (from an AA spectrometer: see our previous reports for the description of the technique). These aerosols are 'matured' at intermediate temperature: they are then collected by filtration and impaction for further determinations and analyses;

(ii) study of the physico-chemical characteristics of Cs, Sr, I, Ru, ... (as non-radioactive elements) into UO_2 particles (aerosols and reconstituted fuel particles) by means of non-destructive techniques (X-ray induced electron spectroscopy - XPS, R-ray diffraction, Mössbauer spectroscopy, thermogravimetry);

(iii) determination of the solubility of FP from aerosols and fuel particles as a function of time;

(iv) study of microscale deposition behaviour of both radioactive and non radioactive aerosols (0.2 μm MMED) onto plant and material surfaces in wind-tunnels.

Many of these experiments are still in progress: till now, the reproducibility of some experiments has been rather poor. This is attributable to the maturation stage which is difficult to control. This report intends to present the main conclusions to be drawn nowadays as well as some perspectives for further developments.

MAIN RESULTS

UO_2 MATRICES

UO_2 aerosols are emitted by a damaged reactor core together with fuel particles (so called '*hot particles*' or '*hot spots* ') of greater diameter. These aerosols and particles vehicle a broad range of FP of which ultimate fate strongly depends on the properties of the matrix. The very low solubility of UO_2 logically delays the release of the FP. It was therefore interesting to test the solubility of UO_2 particles as aerosols (these aerosols are mainly amorphous as was observed by X-ray diffraction).

On the other hand, the low specific activity of U does not allow to detect minute rates of solubilization. We labelled the UO_2 pellets with ^{160}Tb. A rare earth was

deliberately chosen because of the refractory nature of its oxide, allowing the vitrification of UO_2 - Tb_2O_3 mixtures without any significant loss of radioactivity. By this tagging we were able to detect even very small lixiviation or dissolution rates of UO_2. Figure 1 shows the example of the solubilization rates of UO_2 aerosols (in demineralized water) obtained in two different experiments performed under the same conditions (maturation in argon). The differences of extraction yields are evident, indicating a poor reproducibility. Trends, however, are rather similar: **after a rapid but low solubilization stage** (a few percents), **the lixiviation rate slows down to a pseudo plateau** which is attained in a matter of a few thousand hours.

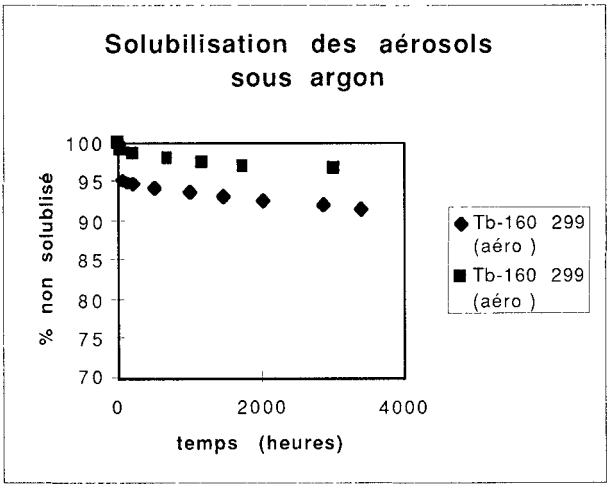

Figure 1. Solubilization rate of aerosols from UO_2 - Tb_2O_3 mixtures heated up to 2300°C. These aerosols have been 'matured' in an inert atmosphere of argon.

The first, rapid solubilization stage is tentatively attributed to the presence of very thin aerosols likely to pass the filters or, more probably, to a rapid lixiviation of the outer surface (stripping) due to particular properties (roughness, brittleness due to the thermal schock, different chemical composition) as compared with the inner part of the particles.

It has to be emphazised that the same trends have been observed with aerosols loaded with more volatile radionuclides: the main difference lies in the lower residual activity remaining in the aerosols (plateau) and in the time constant of the evolution.

RADIOCESIUM IN UO_2 AEROSOLS

Cesium is a volatile element (b.p. 678°C) and, in the case of a reactor accident, its emission yields are high (10-13% of the core inventory were estimated to have been emitted from the reactor at Chernobyl).

In the case of UO_2 doped with 0.3 % (m/m) of Cs, up to 96% of the Cs was emitted after the thermal shock. On the other hand, we were able to observe that **the presence** of a fraction of percent **of Cs into reconstituted UO_2 fuel enhances the emission of aerosols from the fuel.** This is attributable to its volatility which probably increases the mechanical shock suffered by the matrix.

Cs is also very soluble and likely to be easily transfered into trophic chains. However, its inclusion into UO_2 matrices severely reduces its mobility as was demonstrated in earlier experiments.

Furthermore, maturation stages of the aerosols performed under oxidating atmospheres reduces the solubility of Cs. XPS analyses suggest that this could be attributable to **Cs being integrated into poorly soluble uranates as a result of the oxidation of U^{IV} to U^{VI} at the surface of UO_2 particles**. These surface

reactions are certainly a fundamental process during the elaboration of the ultimate forms of aerosols emitted from a damaged reactor. Aerosols matured in inert atmosphere lose up to 95 % of their cesium in water, while they retain 40% of it when matured at 1000°C in an oxidizing atmosphere.

Another interesting feature is that maturation temperature also influences the retention of Cs into the aerosols. This is evidenced by the solubilization curves presented in figure 2.

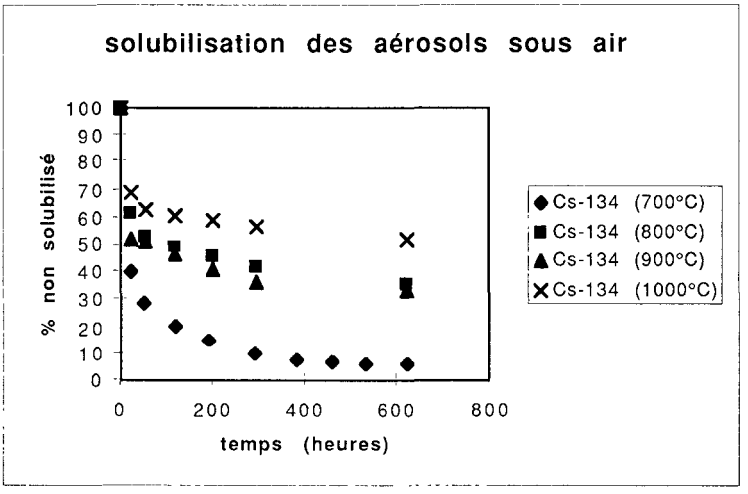

Figure 2. As a function of time, solubilization of Cs from aerosols matured in air at different temperature.

Two trends have to be emphasized:

- there is a **first, rapid solubilization stage** (a few hours) during which 30 to 60 % of the cesium is eliminated; this stage is **followed by a much slower** (pseudo-plateau) **stage,**
- **higher maturation temperatures** significantly reduce **the solubility of cesium.**

This important observation suggests that cesium is carried into UO_2 in two forms: (i) as a condensate onto the surface of the aerosols (readily soluble); (ii) as uranate resulting from the oxidation of U^{IV} (hardly soluble). Cs uranate formation is probably the result of Cs condensing and reacting onto UO_2 aerosol surface. The possible effects of temperature are contradicting: higher temperatures should:

- favour the reactions (oxidation of U^{IV} and diffusion of Cs into the matrix) leading to the retention of Cs, while
- higher temperatures should act as a disadvantage to Cs condensation.

Because of the beneficial role of temperature, it seems that the first hypothesis is prevailing. Experiments have still to validate this point.

RADIO STRONTIUM IN UO_2 AEROSOLS

The element strontium is less volatile than cesium (b.p. Sr: 1384°C - SrO: 3000°C). When introduced into UO_2 pellets (0.3% m/m) and heated to about 2300°C, only 6.5% of Sr is emitted (in Chernobyl, 4.0 % of the core inventory was emitted). However, **when cesium is present, Sr emission yields may amount up to 35%** and this again demonstrates the role of volatile cesium as a disruptive factor of the UO_2 matrix in the process of RN emission.The figures hereunder show the solubilization rate (in %) of Sr carried by aerosols emitted from heated UO_2 pellets. Figure 3 shows the

rates of solubilization from aerosols matured at 700°C under neutral and oxidizing atmospheres.

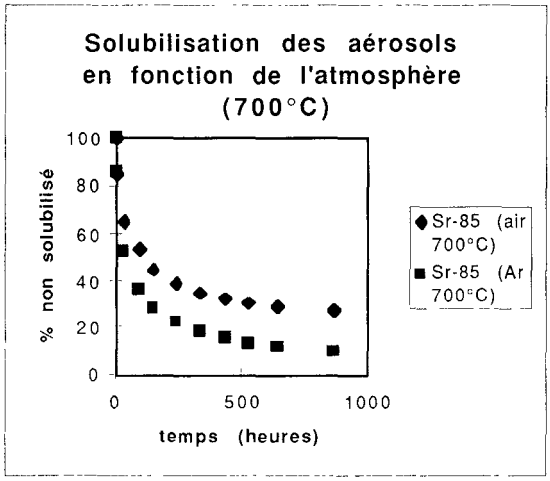

Figure 3. Solubilization rates of Sr from aerosols matured in inert and oxidizing atmospheres.

Once again, **maturation with air enhances retention.** XPS analyses show that uranate is the chemical forms of Sr at the surface of the aerosols. Figure 4 shows the influence of maturation temperature on the dissolution rate of Sr: here again, **temperature enhances retention**.

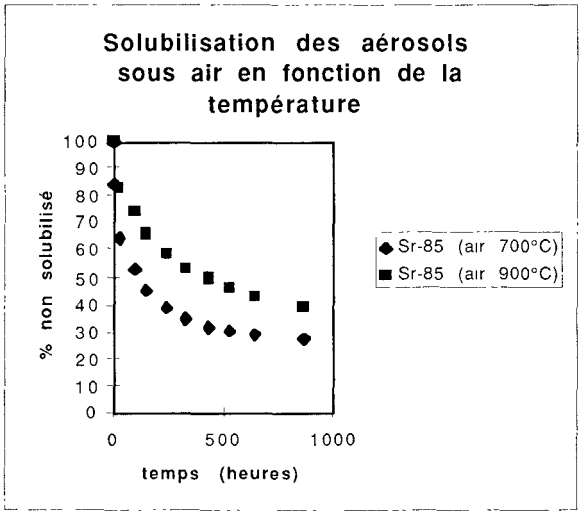

Figure 4. Influence of maturation temperatures on the solubilization of Sr.

RADIORUTHENIUM

Ruthenium is a particular element in the sense that, while being highly refractory (b.p. 3900°C) its higher oxides are volatile. In connection with observations made in

Chernobyl by Dr A. Rimski-Korsakov of the Radium Institute in Saint-Peterburg, we performed a series of experiments in order to reconstitute the particular behaviour of this radionuclide after the accident in Ukraine. As shown in figure 5, the *ratios* $^{103}Ru/^{144}Ce$ observed in air particulates significantly increased *after* the emissions had stopped from the reactor, although the *absolute emission* rates were then, of course, extremely low.

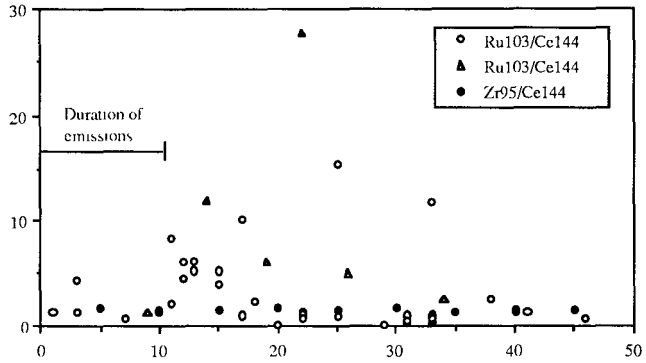

Figure 5. As a function of time after the Chernobyl accident, evolution of the ratios (radio-Ru / radio-Ce) in aerosols.

The following hypothesis was proposed: emissions from the reactor drastically dropped after the 9th day because fission stopped as a consequence of the disruption of the containment vessel and this allowed the nuclear fuel to separate from the graphite moderator. The fuel was put in better contact with the atmosphere and Ru was oxidised giving way to enhanced emissions of its higher oxides as compared with other refractory FP like ^{144}Ce.

We made a laboratory simulation of this by heating UO_2 pellets which contained small amounts of radioactive Ru. These pellets were first heated up to 2300°C in order to simulate the conditions of the reactor accident during the burst stage. Heating sequences were then performed between 500 and 1000°C under oxidizing and inert atmospheres. It was observed that **Ru was emitted at very high yields** when the pellets were heated at 1000°C **in contact with air.**

Temper. °C (for 2h)	Under He	Under air
250	0,005	0,001
500	0,010	0,120
750	0,003	9,40
1000	0,001	44,35
1200	n.d.	42,38
Résidue	100	2,40

Table I. Emission yields of Ru from UO_2 as a function of temperature.

It is of course very important to connect these observations with chemical analyses of the volatile forms of Ru. Two techniques are used: (i) XPS which allows to analyze the surface of the aerosols (note that in these low-temperature experiments, uranium oxide is not emitted), and (ii) Mössbauer spectroscopy.

RuO_2 and RuO_3 have been identified by XPS. Determinations made so far have not been very accurate. Analyses based on Mössbauer spectroscopy are still in progress.

SOLUBILIZATION OF OVEN RESIDUES

After the thermal shock undergone by the UO_2 pellets, the residue left in the oven is supposed to present some similarities with fuel particles which were emitted in significant quantities around the reactor at Chernobyl. It is interesting to analyse the properties of these residues as regards the mobility of the radionuclides they still contain. We do not intend to present all the results obtained so far; suffices it to report the main observations.

Solubilization tests were made on particles sieved to less than 58 μm

I. In the case of pellets tagged with terbium, we noticed that the mobilisation rate is extremely low, of the order of 4.10^{-3} % after 1000 h of contact with water. And this confirms the **great inertness** of this material which could be used to simulate the *hot particles* contaminating the region of Chernobyl.

II. Although Cs content is very low in the oven residue after the thermal shock, it is still possible to dissolve a significant fraction of this element. The **quantity extracted depends on the thermal treatment** imposed to the residue after the thermal shock. Reheating in He (700 -900°C) for a few hours allows to dissolve (after 300 hours) about 40 % of remaining Cs . Reheating in air reduces the solubilization to 10-20 %.

III. After about 400 h of contact with water, UO_2 residues have lost about **0.03 % of residual Sr**. The same pellets, **when having contained Cs, loose about 5 % of the Sr.** Here again we note the disrupting influence of the emission of volatile Cs.

As a general conclusion about the fuel residue, it should be stressed that its chemical and thermal history is important as regards its chemical inertness. The emission of volatile elements such as **Cs probably enhances the porosity** of the UO_2 matrix, allowing a better contact with water. Another explanation could be that the thermal history of both aerosols and fuel residues creates **concentration gradients of FP** into the particles. This phenomenon has been observed in *hot particles* from Chernobyl.

The shape of the time-dependent dissolution curves obtained by us could be explained by such gradients across the aerosols and the particles from the oven residue. Chemico-physical treatment could also be responsible for this kind of evolution. We intend to test these hypotheses by progressive acidic attacks of aerosols and particles surfaces together with non-destructive surface analyses. This kind of study requires that the conditions of elaboration of the samples are clearly defined.

EXPERIMENTS WITH FP FROM ^{235}U

Fission products have been induced in $^{235}UO_2$ samples (about 1 mg) by neutron irradiation. Aerosols were thermo-generated from these samples in the manner described here above. The aerosols were matured in different atmospheres, including methane (1-5 %). The aerosols were sampled for further analyses (solubility, granulometry, deposition behaviour onto spruce twigs and other surfaces). Note that because of the low duration of irradiation (3 x 7 h at 3.10^{11} n/cm^2 s), the production of FP was low and we were not able to detect all of them.

In some experiments, methane was added to the maturation atmospheres, in order to test possible reactions with iodine. The influence of CH_4 is more complex than initially supposed.

The results obtained in the frame of this study are too numerous to be presented in detail: suffices it to present some conclusions to be drawn from the observations:

- I and Ru isotopes behave differently from other fission products and this could be attributed to their higher volatility. In particular, the reactivity of iodine toward deposition surfaces seems to be enhanced when methane is present in the maturation atmosphere,

- some similarities between the behaviour of Cs and I could suggest the formation of CsI although the probability of formation of this compound is extremely low in the present circumstances.

Experiments have also been started in which the FP are put in contacts with different material likely to be present in the confinement of a reactor (steel, concrete, ...). Analyses of deposited elements have to be performed by XPS and Mössbauer sperctroscopy. This part of our project has been provisionally interrupted.

DEPOSITION EXPERIMENTS ONTO PLANT SURFACES

Experiments with inactive ZnO

To the best of our knowledge, the majority of studies devoted to the deposition of particles onto plant material have addressed the macro- to mid-scale transport toward plant cover. By doing so, they were able to stress the very strong positive effect of wind speed and of particles diameter on macro-scale transfer efficiency.

As far as thinner particles are concerned (equivalent aerodynamic diameter - EAD, say, < 0.5 µm), global air movements remain important during the macro-scale atmospheric transfer phase. But the last, micrometer-scale approach stage is primarily determined by diffusion and, in that case, the duration of stay of the particles in the vicinity of receptor surfaces is the main parameter to determine deposition efficiency. Obviously, in that case, wind speed exerts an unfavourable influence. We made observations in a wind-tunnel on the deposition of sub-micrometer particles onto spruce twigs. These experiments were undertaken with a view to understand better the general mechanisms governing the last stage of deposition of air particles onto plants during dry periods. Finally, this study was launched in order to define the transfer parameters of radioactive aerosols to forests ecosystems in the case of a serious nuclear accident.

In a first series of experiments, we determined the relative amount of aerosols captured by whole twigs. Results are expressed in mass percent of zinc retained by the twigs relative to the total mass of zinc which passed through the twigs during the exposure in the tunnel (the surface presented by the plant material to the flux of air was determined from xerox reproductions of the boughs). Figure 6 presents the results of a typical experiment where the fractions of zinc captured by twigs are given as a function of wind speed (fractions are expressed in 10^{-4}, *i.e.* the fraction of aerosols crossing the twigs which has been retained by the plant surfaces: mean of values measured on 10 twigs).

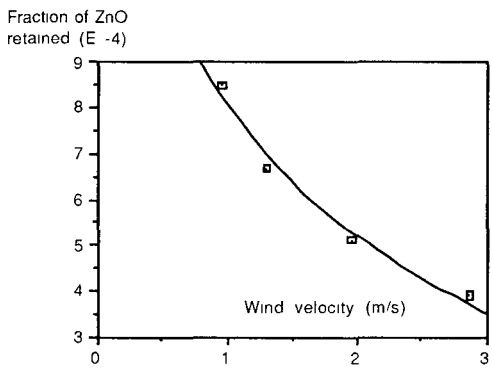

Figure 6. As a function of wind speed, fraction of ZnO aerosols retained by spruce twigs (fractions in 10^{-4}) (median EAD: 0.3 µm, mean concentration in air: 0.30 g/m^3)

Two features are noteworthy: (i) the very low percentage of aerosols retained by the twigs, (ii) the **strong negative influence of wind speed**.

It is interesting to note that small deposition gauges were placed near the twigs. They were made of ordinary filter paper laying in the bottom of a cylindrical plastic cup (diameter: 10 cm - height: 10 cm). Determinations made on these paper surfaces show that deposition rates *increase* with wind speed and this demonstrates that deposition mechanisms are totally different onto both twigs and gauge systems

Moreover, if lowering the speed of air exerts such an influence on deposition, microstuctures of twigs should play a significant role in blocating the movements of air in the very vicinity of the surfaces and deposition rates should very strongly depend upon the location of the surfaces relative to the center of the twigs. Experiments were performed at lower wind speeds, where Zn content was analyzed on twigs separated into three fractions: (i) the branch itself, (ii) the first inner third of the needles, (iii) the two outer thirds of the needles.

Figure 7 presents the results of a typical experiment. The fraction of aerosols deposited is expressed in ppm.m^2/g (mass of Zn deposited onto the unit mass of dried plant material, divided by the total mass of Zn having passed through 1 m^2 during the whole experiment). Obviously, this is a logical way of expressing deposition yields when considering dissociated plant material; it is the *only* way when dealing with whole trees. The influence of decreased wind speed is again confirmed but, more interesting, it appears that, **at lower wind speed, the central parts of the twigs retain more aerosols** than the outer fraction of the needles.

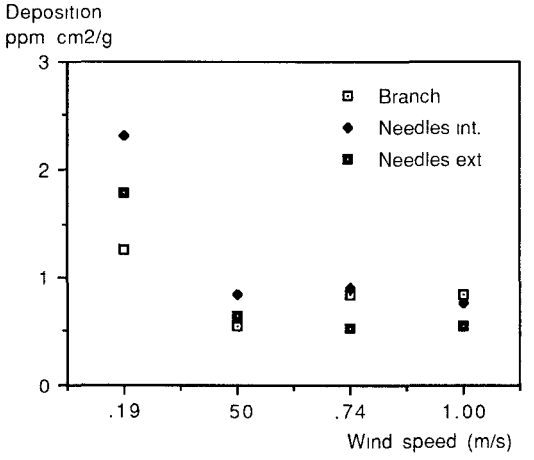

Figure 7. As a function of wind speed, deposition of ZnO aerosols onto different parts of a spruce twig (aerosol median EAD: 0.25 µm - mean concentration in air: 0.33 g/m^3).

It has to be noted that, although the surface presented by the branch itself is relatively low as compared to the surface of the needles, the accumulation of aerosols is far from being negligible. Other experiments performed in the same way have confirmed this wind effect as well as the differential deposition into the twig structure. Experiments are in progress to define deposition patterns inside whole trees. Indeed, wind speed strongly depends on the position taken into consideration into tree canopies. For example, **wind speed may decrease by a factor of 4 across the canopy** of a small tree (diameter: 60 cm).

Deposition experiments with FP from neutron-irradiated $^{235}UO_2$

This part of our programme has been provisionally stopped. A few observations have to be developped in the future: (i) as was previously observed with inactive ZnO aerosols, deposition of FP onto spruce twigs is enhanced at low wind speed (< 0.5 m/s),

(ii) in contrast with ZnO, deposition of radioiodine is enhanced onto the external parts of the needles; deposition yields of other FP have to be ascertained yet; (iii) **deposition of radio-iodine and -ruthenium is about ten times higher** than observed for other radio-nuclides; (iv) deposition onto steel surfaces is very efficient and should be studied from the point of view of the chemical reactions taking place under the influence of temperature and of the atmosphere.

MAIN CONCLUSIONS AND PERSPECTIVES

A few important observations were made during these studies. Let us emphazise the main conclusions to be drawn as well as the perspectives for further research.

A. *The emission of FP from overheated nuclear fuel is strongly dependent upon the presence of volatile elements such as Cs.* This is probably attributable to the emission of vapours which generates a disruption of the UO_2 matrix, probably by creating pores.

B. As a consequence of this increased porosity, *there is an enhancement of the transfer of the FP from the aerosols and from fuel particles into the environment,* when in contact with water.

C. *The influence of volatile elements on the mobilisation of other FP should be systematically tested* with particular attention being paid to:

- the relative mass of Cs being present into the fuel,
- the presence of other volatile elements such as, for example, iodine
- the combination of different volatile elements, for example, Cs and I, with are able to form the relatively volatile compound CsI (b.p. 1280°C).

D. *Chemical speciation should be better defined,* in particular for Ru which can be analysed by two complementary non-destructive methods: XPS and Mössbauer spectroscopy. Other very promising methods such as X-ray fluorescence from synchrotron radiation should be considered.

E. It has been demonstrated that *the influence of the maturation stage of the emission is of utmost importance.* It should be more carefully determined. Work is in progress in order to better control the experimental conditions in the maturation oven and to reduce loss of activity onto the walls of the oven.

F. *Reactions of FP with material surfaces should be better understood.* Reactions with steel is of particular interest because of the possibility of performing Mössbauer spectroscopy on this element. Note that iodine is also in the range of this spectroscopy.

G. Deposition experiments in wind-tunnels will be performed on the basis of what has been observed previously. Radioactive and non-radioactive aerosols will be used with special emphasis on the influence of the chemical nature of their surface (condensed vapours) on deposition yields.

H. A collaboration has been undertaken with specialized laboratories in order *to study the influence of selected micro-organisms on the mobilisation rates of FP* from aerosols and fuel particles produced in our laboratory. These experiments should help to define the behaviour in soils of these particles and eventually lead to suggesting biotechnological remediation techniques.

LIST OF PUBLICATIONS

PRELIMINARY PUBLICATIONS

C. RONNEAU, K. FONSNY and C. MYTTENAERE, "Production of ^{134}Cs thermo-generated aerosols; study of their behaviour after deposition on spruce trees", in "Biological Trace Element Research", R. Zeisler and P.V. Guinn Eds., Humana Press, pp. 243-248 (1990).

A.H. AL RAYYES and C. RONNEAU, "X-Ray photoelectron spectroscopy of cesium uranates, Radiochimica Acta, 54, 189-191 (1991).

PUBLICATIONS MADE DURING THE CONTRACT

A. H. AL RAYYES, C. RONNEAU, J. LADRIERE and D. APERS, "Chemical characterization of UO_2/Fe and Fe/Cs aerosols generated at high temperature", Radiochimica Acta, 56, 47-50 (1992).

A. H. AL RAYYES, C. RONNEAU, W.E. STONE, M.J. GENET, J. LADRIERE and J. CARA, "Radiocaesium in hot particles: solubility vs. chemical speciation, J. Environmental Radioactivity, 21 (1993) 143-151.

C. RONNEAU et J. CARA. "Radioécologie et Chimie", Chimie Nouvelle, vol 12, n° 48 - 12/94

C. RONNEAU, J. CARA and A. RIMSKI-KORSAKOV. "Oxidation-enhanced Emission of Ruthenium from Nuclear Fuel". J. Environ. Radioactivity, 26 (1995) 63-70.

PAPERS SUBMITTED FOR PUBLICATION

J. VAN BEGIN, P. FROMENT, J. CARA and C. RONNEAU, "The influence of cesium in the mobilization of fission products from aerosols and particles emitted by overheated nuclear fuel", to be submitted to 'Radiochimica Acta'.

J. VAN BEGIN, J. CARA and C. RONNEAU, "The influence of maturation stages in the mobility of fission products from aerosols and particles emitted by overheated nuclear fuels", to be submitted to 'Radiochimica Acta'.

Final report
1992–1995

Contract: FI3PCT920050 **Duration: 1.9.92 to 30.6.95** **Sector: A25**

Title: Cycling of cesium 137 and strontium 90 in natural ecosystems

1)	Wirth	BfS
2)	Moberg	SSI
3)	Bergman	FOA
4)	Palo	Swedish Univ. of Agricult. Science Umea
5)	Impens	Faculté Sciences Agronom. Gembloux
6)	Belli	ENEA
7)	Feoli	CETA
8)	Nimis	Univ. Trieste
9)	Antonopoulos-Domis	Univ. Thessaloniki
10)	Pietrzak-Flis	CLRP Warsaw

I. Summary of Project Global Objectives and Achievements

I.1. PROJECT GLOBAL OBJECTIVES

The main objective of the project was to study the cycling of radiocaesium within and between abiotic and biotic forest compartments. On some selected sites, ^{90}Sr was measured additionally. For our investigations different coniferous and deciduous forests were chosen from different climatic zones in Belgium, Germany, Italy, Luxemburg, Sweden, Greece, and Poland. The experimental research emphasizes parameters and mechanisms to understand and to quantify transfer processes of ^{134}Cs, ^{137}Cs, and ^{90}Sr. The investigations of the participating groups cover the following topics:

- analysis of the vertical migration of radiocaesium and radiostrontium in different soil layers,
- influence of soil parameters on the transfer rates from soil to different green understorey plants,
- analysis of uptake mechanisms for caesium in different habitats of mushrooms,
- influence of leaf and needle fall on the cycling of radiocaesium in forests,
- analysis of radiocaesium and potassium concentrations in different components of forest litter (leaves, needles, twigs, and seeds),
- analysis of the retention of radiocaesium and nutrients from leaves and needles,
- influence of different ecological and climatic situations on the amount of leaf and litter production,
- identification of ecological groups of understorey species to detect relations between contamination patterns and ecology,
- seasonal fluctuations of radiocaesium content in these different plant species, and
- dependency of the ecological characterization of forest ecosystems on soil parameters.

I.2. PROJECT GLOBAL ACHIEVEMENTS

I.2.1. Soil

The fate of ^{137}Cs in soil was investigated by different groups.

The vertical distribution of radiocaesium at all sites is similar. In 1994, most of ^{137}Cs is still present in the organic horizons, although the K_d-values for these horizons were significantly lower than for the mineral horizons. The long residence time is probably due to biological fixation by microorganisms and mycelia, which is supported by irradiation experiments with soil performed by the Belgian group.
Long-term observations have been carried out in different forests. To evaluate the time dependence of these data, the German group developed a compartment model, representing the L-, Of-, Oh-, A-, and B-horizons. The dynamic behaviour of ^{137}Cs is described by a set of differential equations. For the German "Hochstadt site", the calculated ecological half-lives increase with soil depth from 2.9 years in the L-horizons, 4.6 years in the Of-horizon, 6.3 years in the Oh-horizon to 8.7 years in the Ah-horizon, suggesting radiocaesium to be bound more efficiently with increasing depth. Surprisingly, the mineral B-horizon is characterized by the lowest half-life of 1.8 years, although clay minerals should prevent migration. The reliability of these results has been demonstrated by comparing the present distribution of ^{137}Cs in soil due to nuclear weapons fallout with the corresponding predicted values.
The Greek group has developed an alternative model for calculating the migration rates of radionuclides in soil, taking into account the transport mechanisms diffusion and convection. Model analysis shows that also a pure diffusion model can provide insight into migration processes, especially in mineral layers. It is amenable to analytic solutions, but cannot always reproduce the experimentally observed profiles.

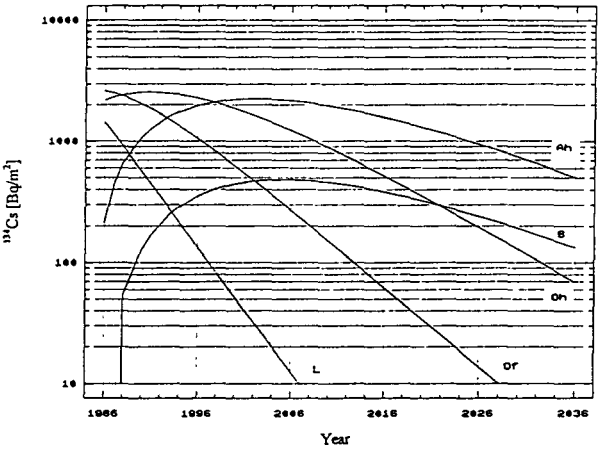

Fig. 1: Time-dependence of ^{134}Cs in different soil horizons of the German sampling site Hochstadt as derived by the compartment model.

The horizontal pattern of radiocaesium is very heterogeneous, since most of the Chernobyl radionuclides were initially retained in the canopy, especially in coniferous forests, and then transferred to ground by different mechanisms like stemflow, wash-out or litterfall. Additionally, horizontal transfer in mycelia and accumulation in fruitbodies might lead to small "hot spots", as demonstrated by the Polish group. Considering these random aspects, soil sampling has to be carried out carefully to get well established mean activities in soil.

The ^{90}Sr activity in the Chernobyl fallout was only about 1% of the Cs-activity. Therefore, the contribution of the Chernobyl fallout has only slightly increased the ^{90}Sr inventory of about 1200 Bq/m^2 originating from nuclear weapons fallout. It is not possible to distinguish between fallout from Chernobyl and nuclear weapons tests. After 30 years of deposition, most of ^{90}Sr is still located in the upper organic horizons, suggesting a low migration rate and a rapid turnover in the forest cycle.

I.2.2. Uptake by plants and mushrooms

The analysis of radionuclide uptake by plants and mushrooms in forest systems is complex, as roots and mycelia are located in different horizons with different ^{137}Cs activities and different soil properties. Symbiosis between mycorrhiza fungi and host plants further complicates the situation. Within this project, relevant parameters for uptake of radiocaesium were analyzed with respect to the amount of transfer.

Fungi

Within this project, different groups confirmed that the mean uptake of ^{137}Cs by symbiots is about 10 times higher than by saprophytes and parasites. The distributions of ^{137}Cs activities of these three different groups overlap. Symbiotic effects should be further investigated. Symbiots supply their hosts with nutrients, i.e. they take up more nutrients than necessary for their own metabolism. During the transfer of caesium into the host cells, discrimination effects might retain ^{137}Cs in the mycelium. This would mean that the ^{137}Cs activity in mushrooms might be an indicator for the intensity of symbiotic exchange.
To understand the different uptake within each group, the locations of the mycelia in different soil horizons as another relevant parameter were investigated by looking at the $^{137}Cs/^{134}Cs$ ratio. The $^{137}Cs/^{134}Cs$ ratio increases with depth, because the amount of radiocaesium due to nuclear weapons fallout is relatively higher in deeper horizons compared to that due to Chernobyl fallout. In two approaches, a static and a dynamic one, the ratios of the two radiocaesium isotopes in fungi and in different soil horizons were compared. Applying this method, the locations of the mycelia were identified for 14 fungi species.

Transfer factors soil/mushrooms were calculated taking into account the specific ^{137}Cs activities of those layers where the mycelia are located. Resulting transfer factors for 14 species vary between 0.4 and 25.8, where the lower values are due to saprophytes and the higher ones to mycorrhiza fungi. Since the migration rates in soil had been derived, it was possible to analyze whether the transfer factors soil/mushrooms depend on time. The results indicate that the transfer factors hardly changed from 1987 until 1994. Differences in mushroom activities were correlated with the increase and decrease of the ^{137}Cs activities in the species-specific mycelium zones. These results are of particular interest regarding long-term considerations. Combining the model for migration

of ^{137}Cs in soil and the results from the transfer factor analysis, long-term contaminations were predicted for the 14 mushroom species whose mycelium locations are known.

Mushrooms were extremly low contaminated with ^{90}Sr. The activities were below 1 Bq/kg FW in all samples from Bavaria. In Sweden, however, the highest specific activity is one order of magnitude higher. Specific differences in accumulation rates were not observed for the investigated mushrooms. Correspondingly, the transfer factors ranged between 0.002 and 0.01.

Understorey vegetation

Clusters of species with different radiocaesium activities were identified on several sampling sites. At Hochstadt, observation of ^{137}Cs showed that the activities in Vaccinium myrtillus are higher by one order of magnitude in comparison to Fragaria vesca. The activities in Rubus fruticosus are between the two other species. In a more systematic approach, studies in a beech stand in Passo Pura revealed that the content of radiocaesium is highest in plants whose root systems occupy the upper soil layer of acidic humus and is lowest in deep rooting megaphorbs of wood clearings.

Besides rooting depth and heterogeneous vertical and horizontal distribution of ^{137}Cs in soil, additional parameters, like potassium concentration in soil and plants as well as organic matter content in soil are important for root uptake. In the upper parts of plants, the ratio $^{137}Cs/^{40}K$ was about the same in stems, leaves, and fruit of one plant. This means that the ^{137}Cs activity is regulated via the K metabolism within plants. A significant increase of the $^{137}Cs/^{40}K$ ratio was observed in some root systems of megaphorbs compared to the upper part of the plant. It seems that plants probably discriminate Cs versus K at root level.

There are still some gaps in the knowledge of discrimination between Cs and K during root uptake, since results were partially contradictory. The Polish results indicate that there is no discrimination between Cs and K during root uptake by Vaccinium myrtillus, Calluna, and grass. In Germany, some fairly good correlations between the uptake of Cs and K were found for dicotyledons, but no correlation at all for grass. Generally, the investigations indicate that vascular plant species occuring in natural forests have different ecological requirements. The concentration of ^{137}Cs in species can be fairly well ordered along a main gradient of increasing content of organic matter and increasingly available potassium in soil.

The activity of ^{90}Sr in understorey vegetation is regulated via the Ca metabolism. Higher activities are found in leaves, where the Ca content is higher than in fruit. The transfer factors range between 0.2 and 1.2, i.e. they are comparable to the ^{137}Cs transfer factors.

Trees

After the Chernobyl fallout, the specific ^{137}Cs activities in coniferous trees have always been significantly higher than in decideous ones growing on the same site. This is likely due to the fact that the crowns of coniferous plants were higher contaminated by direct deposition than crowns of decideous trees, which might lead to a higher "memory effect". On the other hand, the ^{137}Cs activity in Picea abies as well as in Fagus increased by a factor of 2 between Sept. 92 and Sept. 93 on an Italian site. Similar results were obtained in Sweden: In 1994, young trees (Pinus sylvestris) which were not directly contaminated did not show major differences in the ^{137}Cs activities in

needles in comparison to older, directly contaminated ones. Furthermore, the ^{137}Cs concentration was highest in young needles at all investigated sites in Sweden. These findings indicate that root uptake becomes the dominant contamination pathway a few years after deposition. These results agree with Russian studies, which indicate that ^{137}Cs migrated from the canopy to the ground within 2–4 years.

Investigations of the distribution of radiocaesium within trees revealed that current needles and branches are always higher contaminated than older ones. Highest values were found at the top, lowest in needles and branches close to the ground. Considering stems, the bark is always higher contaminated than the trunk, which might be explained by the fact that living cells always show higher nutrient levels than dead ones.

It might also be assumed that some of the originally deposited radiocaesium (direct deposition and stem flow) is still left at the stem surface.

FIGURE 9
Activity concentration of Cs-137 in trees from site H and site L

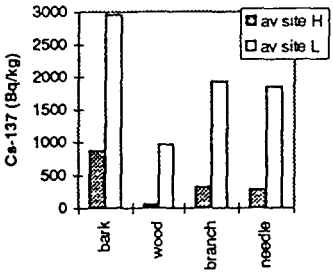

FIGURE 8
Total inventory of Cs-137 in trees from sites H and L

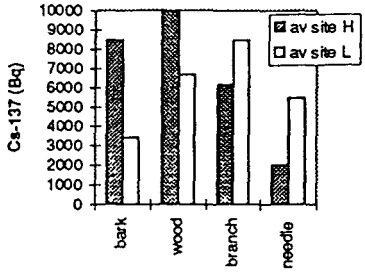

Fig. 2: Distribution of ^{137}Cs within coniferous trees in Sweden.

I.2.3. Transfer of radiocaesium from plant to ground

In an Italian forest, the seasonal amount of litterfall and associated fluxes of radiocaesium onto the forest floor have been assessed. The quantity and type of litter (leaves, needles, twigs) have been analyzed. As expected, the quantities vary as a function of season. In a mixed forest, fagus trees shed their leaves mainly between October and December (about 100 g/m^2). On contrary, the deposition of abies needles is rather constant during the year (about 60 g/m^2). The corresponding annual radiocaesium flux attributed to litter fall was measured to be about 155 $Bq/(m^2 \cdot y)$ on this site, which is about 0.5% of the total inventory. Studies in Swedish boreal forests indicate that the transfer of radiocaesium from vegetation to ground via ingestion of animals amounts to about the same order of magnitude compared to litterfall. In this context, small rodents are of particular interest, because the amount of vegetation they consumed exceeds the annual ingestion of mooses by more than one order of magnitude on average. But according to the oscillation of vole population, actual values will vary from year to year. For the further fate of radionuclides, it would be of interest to compare the bioavailability of ^{137}Cs deposited on soil by litter and via herbivores with respect to plant uptake and migration rates.

I.2.4. Animals

In order to understand the extent of ^{137}Cs variations in mooses and bank voles, radiocaesium was measured in plants and animals from boreal forests. Monte-Carlo simulations of the ^{137}Cs variation in muscles due to consumption habits were carried out. Diet compositions are hard to measure in most situations, since sometimes animals move large distances within a short time. The range of plant species and tissues consumed varies greatly among herbivore species, both seasonally and annually. Even when the composition of diet is known in some detail, significant variations of intake rates and gut absorption due to differences in digestability may still be present.

Fig. 3 shows a Monte-Carlo simulation of the ^{137}Cs activity in muscle tissue generated for 30 individual diets during a 30-year-period. Composition of individual diet was varied by selecting the proportion of bilberry taken randomly from young and old pine forests. The ^{137}Cs activities in bilberries have been measured from 1986 until 1994 and were extrapolated by regression analysis until the year 2016. The amount of ground deposition at the site of collection only explains 5% to 35% of the variability of ^{137}Cs activities in animals.

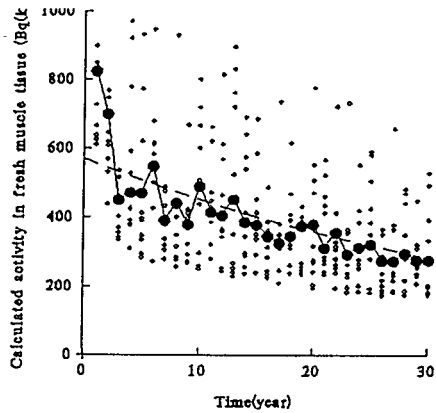

Fig. 3: Monte-Carlo simulation of ^{137}Cs in fresh muscle tissue of herbivore species. Individual data points, mean value, and the function of radioactive decay are shown. For details see text.

Geographical analysis was performed for the radiocaesium distribution in moose populations. In Fig. 4, aggregated transfer coefficients are graphically presented for an area in the country of Västerbotten, covering 52000 km^2. Each pixel in this figure represents an area of 25x25 km^2. Comparison of pattern from 1986 and 1993 suggest that ^{137}Cs transfer is higher in 1993 at levels of deposition over 20 kBq/m^2. Below this ground deposition the uptake is lower in 1993. The reasons for these puzzling results are unclear.

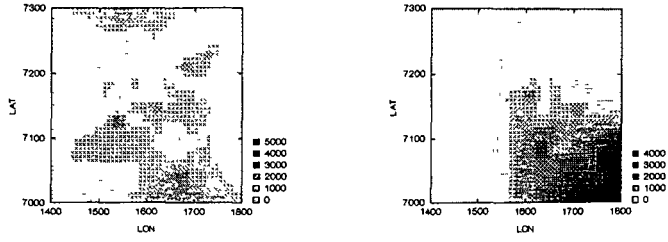

Fig. 4: Aggregated transfer coefficients for moose (left: 1986, right: 1993).

I.2.5. Models of cycling

A site- and system-specific steady-state model was developed for an experimental site located at Tarvisio, Italy. The model is split into two submodels, one for the proper calculation of ^{137}Cs cycling through the compartments and the other to estimate variables and functions related to the uptake of radionuclides and their turnover through the vegetation pathways (foliage production, leaf area, etc.). In comparison with other radioecological models, some new aspects have been included, like vegetation growth by photosynthesis. The model was validated by simulating a deposition event. Thereby the model generally proved to agree well with experimental data for the chosen forest system and the time range considered.

Another explanatory model was developed for a boreal site in Sweden. This model is focussed on redistribution processes in a long-term perspective. In this model, the major regulators of energy flow as well as of ^{137}Cs turnover are related to primary production and its constraints on growth capacity. This approach inherently yields the possibility to describe natural ecosystems from different geographical latitudes via different growth functions. Certain fundamental processes governing the metabolism of living matter in the biotope are also taken into account. The turnover of caesium is described by first order kinetics. The calculated time-dependent change of ^{137}Cs content in perennial vegetation has been compared to that actually observed at different localities with particular focus on bilberry. Fig. 7 shows the change of ^{137}Cs content in the perennial understorey vegetation depending on the age of forest stand and site-specific soil conditions.

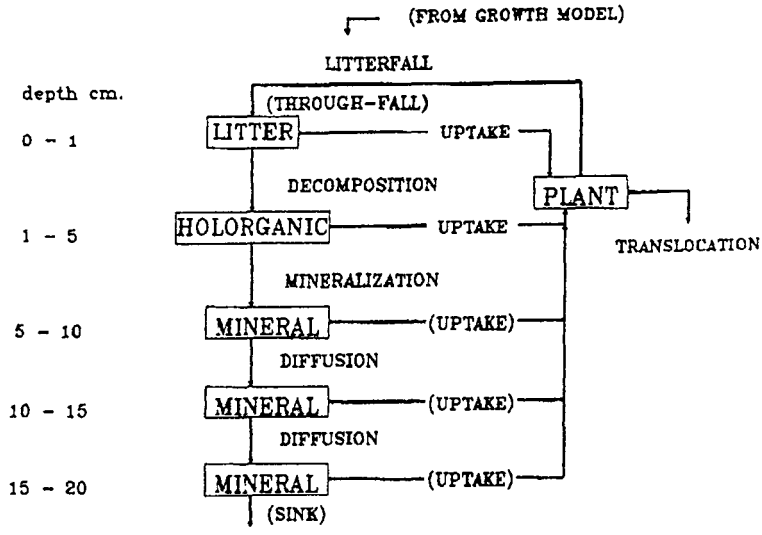

Fig. 5: General structure of the submodel for radiocaesium cycling in different soil compartments at the site Tarvisio, Italy.

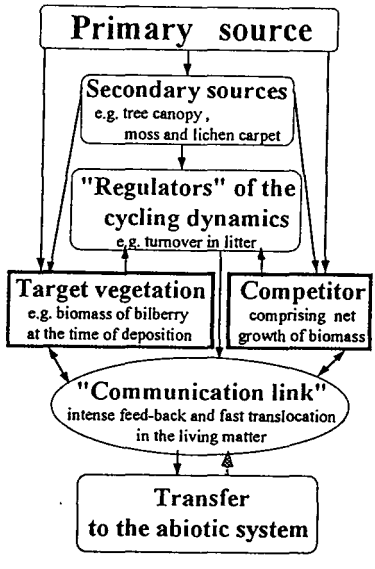

Fig. 6: Principal structure of the forest ecosystem model for boreal sites in Sweden.

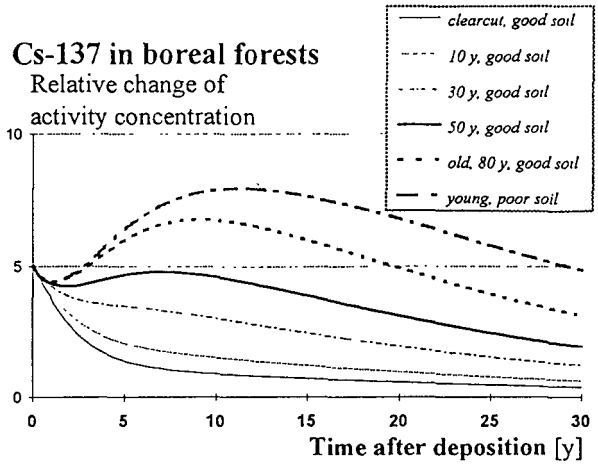

Fig. 7: Change of ^{137}Cs content in the perennial understorey vegetation in boreal forests in Sweden.

I.2.6. Conclusions

The project gave an opportunity to investigate forest sites in Europe systematically and to compare the results from different types of forest grown on different soils under different climatic conditions. Due to this cooperation, the knowledge of basic principles in the behaviour of radionuclides in natural ecosystems was highly improved. Basic mechanisms concerning migration in soils, ^{137}Cs uptake by fungi and plants, transfer to animals and cycling within forest ecosystems are fairly well understood now. Data sets have been obtained, which are useful tools for site-specific long-term prognosis and helpful with respect to recommendations and considerations of countermeasures. In conclusion, the understanding of radionuclides behaviour in forest systems was improved significantly. It should be realized, however, that it is still difficult to define and develop advanced explanatory models which are suitable for forest sites in general. The difficulties are due to the great complexity and wide variations of these systems. To be more successful, more detailed investigations of the peculiarities of soil, plants, and animal species and of corresponding parameters, which have been recognized to be of general importance, are required. The results of this project present a suitable basis for such further investigations.

Head of project 1: Dr. Wirth

II. Objectives for the reporting period

Within this research project the time-dependent behaviour of ^{137}Cs and ^{90}Sr in forest soil and their uptake by fungi and understorey vegetation was investigated. We mainly concentrated on two topics:

a) Quantitative analysis of the time-dependent contamination of fungi by radiocaesium

To solve this task the following strategy was chosen: First, the variation of radiocaesium activity in different soil layers with time was investigated. Secondly, a reliable method to determine the location of the mycelium was developed. Thirdly, species- and site-specific transfer factors were established.

b) Evaluation of transfer factors for the uptake of radionuclides by understorey vegetation

In this context we paid attention especially to the search for common pattern of caesium uptake by different plants.

Both topics a) and b) are particularly important, since the ingestion of contaminated forest products, like berries and mushrooms, is considered as a significant source for the radiation exposure to man.

III. Progress achieved including publications

III.1. SAMPLING SITES

Within this research project two coniferous forest sites in south Bavaria have been investigated continuously, since they represent the most frequent forest types in this region of Germany.
The forest site in the vicinity of Garching/Alz is a mixed coniferous stand with an age of about 120 years. It is composed of 30% Scots pine (Pinus sylvestris) and 70% Norway spruce (Picea abies).
The forest site near the village Hochstadt is characterized by a pure Norway spruce stand aged about 100 years.

The investigated forest soils show characteristic profiles with superficial organic L- and O-horizons, a transitional A organic matter-enriched mineral horizon above the underlying mineral B- and C-horizons. In Garching/Alz, organic horizons are intermixed with mineral horizons due to the activities of the soil fauna. The forest soil at this site consists of pararendsina (German classification) on calcareous gravel, whereas the soil at Hochstadt is a characteristic cambisol on calcareous moraine.

III.2. MIGRATION OF ^{137}Cs AND ^{134}Cs IN UNDISTURBED FOREST SOIL

A compartment model was developed to analyse quantitatively the migration of radionuclides in undisturbed forest soil.

III.2.1. Description of the compartment model

The compartment model consists of five compartments representing the L-, O_f-, O_h-, A_h-, and B-horizons of forest soil. In a first approximation litter fall as source of activity for the L-horizon as well as root uptake by plants as loss of activity in all layers is neglected. Within this model, the dynamics of radioisotopes is given by the following set of differential equations:

$$dL(t)/dt = -\lambda_1 * L(t) \quad (1)$$

$$dO_f(t)/dt = \lambda_1 * L(t) - \lambda_2 * O_f(t) \quad (2)$$

$$dO_h(t)/dt = \lambda_2 * O_f(t) - \lambda_3 * O_h(t) \quad (3)$$

$$dA_h(t)/dt = \lambda_3 * O_h(t) - \lambda_4 * A_h(t) \quad (4)$$

$$dB(t)/dt = \lambda_4 * A_h(t) - \lambda_5 * B(t) \quad (5)$$

L(t), $O_f(t)$, $O_h(t)$, $A_h(t)$, and B(t) are the decay-corrected activities per area of the radionuclide of interest in the L-, O_f-, O_h-, A_h-, and B-horizon, respectively.
This system of coupled differential equations was solved analytically. From the time constants λ_i, an ecological half-life $T_{1/2,i}$ can be calculated for each horizon i via $T_{1/2,i} = \ln 2 / \lambda_i$.

III.2.2. Results and discussion

The compartment model was applied to decay-corrected ^{134}Cs activities measured between 1987 and 1994 in different horizons of a forest site near Hochstadt
From the fitted time constants λ_i, ecological half-lives of ^{134}Cs in different horizons were deduced. The results are summarized in Table 1.

Horizon	L	O_f	O_h	A_h	B
$T_{1/2}$ [y]	2.9 ± 0.6	4.6 ± 0.9	6.3 ± 2 3	8.7 ± 6.5	1.8 ± 0.3

Table 1: Ecological half-lives for ^{134}Cs in different horizons of the Bavarian forest site near Hochstadt.

From top of the forest floor, the resulting ecological half-lives increase with depth from 2.9 years in the L-horizon, 4.6 years in the O_f-horizon, 6.3 years in the O_h-horizon, to 8.7 years in the A_h-horizon, respectively, suggesting the radiocaesium to be bound more efficiently with increasing depth in the organic horizons.
Surprisingly, at Hochstadt the mineral B-horizon is characterized by the lowest half-life of 1.8 years. Although the portion of clay minerals in this horizon is expected to strongly retain radiocaesium, the organic layers seem to bind this isotope even more efficiently. At present, this behaviour is lacking a convincing explanation.
According to the model predictions, half of the initial radiocaesium will have left the upper L-, O_f-, O_h-, A_h-, and B-horizons and will have migrated to deeper layers after about 25 years. The sum of

the initial ^{134}Cs activities in each horizon agrees very well with the total deposition of this radioisotope as given by the German deposition map.
The reliability of these results has been demonstrated by comparing the present distribution of ^{137}Cs in soil due to nuclear weapons fallout with corresponding predictions.

III 3. MYCELIUM LOCATION OF DIFFERENT SPECIES OF FUNGI

Since the different horizons in forest soil usually show different amounts of radiocaesium contamination, the locations of the mycelia essentially influence the magnitude of the specific activities of mushrooms.
Based on the quantitative analysis of the migration of radionuclides in forest soil, a general method to reliably determine the mycelium location for a certain fungi species was developed. Comparing the $^{137}Cs/^{134}Cs$ ratios of mushrooms with those of different soil horizons at the sampling site, information about the mycelium locations was gained. Being well defined within about 10%, the $^{137}Cs/^{134}Cs$ ratio turned out to be very favourable. Furthermore, possible discrimination effects are expected to be minimal for the two caesium isotopes.

III.3.1. Static approach

In the so-called static approach, $^{137}Cs/^{134}Cs$ ratios of different soil horizons, normalized to 1.5.1986 and averaged over the whole period from 1987 to 1994, are compared to the corresponding averaged $^{137}Cs/^{134}Cs$ ratios found in different mushroom species.

Since 1987, ^{137}Cs and ^{134}Cs activities have been measured in about 250 soil samples of the forest site near Hochstadt. The mean $^{137}Cs/^{134}Cs$ ratios for each horizon are summarized in Table 2.

Horizon	n	$^{137}Cs/^{134}Cs$
L	49	1.74 ± 0.06
O_f	66	1.76 ± 0.05
O_h	38	1.89 ± 0.08
A_h	46	2.14 ± 0.23
B	44	2.41 ± 0.46

Table 2: Averaged $^{137}Cs/^{134}Cs$ ratios and corresponding standard deviations in different soil horizons of the sampling site Hochstadt. Data are corrected for 1.5.86 and represent averages over n measurements between 1987 and 1994.

Comparing the $^{137}Cs/^{134}Cs$ ratios of the different soil horizons with those found in fruitbodies of mushrooms gives a first idea in which layer the mycelium of the species investigated might be located. For example, low mean $^{137}Cs/^{134}Cs$ ratios generally indicate the mycelium to inhabit the upper L- or O_f-horizon. The average $^{137}Cs/^{134}Cs$ ratio of 1.82 found in samples of Russula ochroleuca suggests the mycelium to be located in the O_f-/O_h-horizon. An averaged ratio of 2.16 found in samples of Russula cyanoxantha can be explained by a mycelium located in the A_h-horizon. The results for 14 mushroom species are summarized in Table 3.

Species	n	$^{137}Cs/^{134}Cs$	Mycelium location (static approach)	Mycelium location (dynamic approach)
Lepista nebularis	9	1.73 ± 0.12	L/O_f	L/O_f
Collybia maculata	7	1.78 ± 0.10	L/O_f	L/O_f
Collybia butyracea	11	1.81 ± 0.16	O_f/O_h	L/O_f
Xerocomus badius	21	1.79 ± 0.10	L/O_f	O_f/O_h
Russula ochrocleuca	15	1.82 ± 0.08	O_f/O_h	O_f/O_h
Lactarius deterrimus	6	1.83 ± 0.06	O_f/O_h	O_f/O_h
Clitocybe clavipes	8	1.83 ± 0.07	O_f/O_h	O_h
Hydnum repandum	15	1.91 ± 0.12	O_h	O_h
Paxillus atrotomentosus	9	1.92 ± 0.17	O_h	O_h
Lactarius scrobiculatus	8	1.91 ± 0.15	O_h	O_h
Macrolepiota rhacodes	11	1.85 ± 0.18	O_h	O_h
Armillariella spec.	12	1.81 ± 0.18	O_f/O_h	O_h
Sarcodon imbricatus	8	2.06 ± 0.09	O_h/A_h	O_h/A_h
Russula cyanoxantha	7	2.16 ± 0.26	A_h	O_h/A_h

Table 3: Averaged $^{137}Cs/^{134}Cs$ ratios and corresponding standard deviations for different mushroom species of the sampling site Hochstadt. Data are corrected for 1.5.86 and represent averages over n sampling trips between 1987 and 1994. The mycelium location suggested by comparison with Table 2 is given in the fourth column (static approach). For comparison, the mycelium location as deduced from the dynamic approach is shown in the last column Only those species which were found at least in four different years are taken into account.

III.3.2. Dynamic approach

The so-called dynamic approach deals with the comparison of time-dependent $^{137}Cs/^{134}Cs$ ratios in mushrooms and in different soil horizons.

As already described in some detail in the preceding chapter, a compartment model successfully describes the migration of ^{134}Cs in different horizons of the forest site near Hochstadt. Provided the deduced ecological half-lives and thus the migration behaviour of ^{134}Cs and ^{137}Cs are identical, the ratio $^{137}Cs/^{134}Cs$ in different soil layers as function of time can be derived via the compartment model.

If the mycelium of a certain fungi species is located within one soil horizon exclusively, caesium is taken up from this layer only. Therefore, absolute value and time dependence of the $^{137}Cs/^{134}Cs$ ratio found in this species should reflect that of the soil horizon occupied by the mycelium.
Figs. 1 and 2 depict the time-dependent $^{137}Cs/^{134}Cs$ ratios of Russula ochroleuca and Russula cyanoxantha, respectively. These data are compared to the $^{137}Cs/^{134}Cs$ ratios calculated for different soil horizons of the same forest by the compartment model described in the preceding chapter. The ratio of that soil layer corresponding best to the mushroom data is shown as solid line together with the calculated ratios of adjacent soil layers.
The results for 14 mushroom species are also summarized in Table 3.

To give some idea, $^{137}Cs/^{134}Cs$ ratios for two mushroom species are discussed briefly. $^{137}Cs/^{134}Cs$ ratios found in samples of the symbiot Russula ochroleuca, for example, vary between 1.75 and 1.95. These values are typical for the O_f- and O_h-horizon. As mentioned above, distinction between L- and O_f-horizon is difficult in general.
As can be seen from Fig. 2, the $^{137}Cs/^{134}Cs$ ratio of the symbiot Russula cyanoxantha is higher compared to the ratio of the O_h-horizon but lower than that of the A_h-horizon for the whole period of investigation. This indicates that Russula cyanoxantha most probably takes up radiocaesium from both horizons. The experimental data are satisfyingly reproduced, if 40% of radiocaesium found in this species is assumed to be accumulated from the O_h-horizon and 60% from the A_h-horizon.

III.3.3. Comparison of static and dynamic approach

A detailed study of the $^{137}Cs/^{134}Cs$ ratio for 14 mushroom species showed that both approaches yield roughly similar results. The dynamic approach, however, turns out to be more powerful, if a complete time series of contamination data over several years is available and if furthermore the ecosystem investigated is characterized by a considerable dynamic of radiocaesium. In this context considerable dynamic means that ecological half-lives describing the time-dependent behaviour of radiocaesium are similar or smaller than the period of investigation. The static approach suffers mainly from two disadvantages The static approach averages over properties which often appreciably vary with time, thus inherently blurring detailed information and leading to large standard deviations. If on the other hand samples from only one year are considered, the ratios in different horizons do not change considerably with time, but a large number of samples have to be taken with respect to statistical aspects. This, however, is only possible for few species which can be found during the whole growing season.

III.4. EVALUATION OF TRANSFER FACTORS AND PREDICTION OF FUTURE RADIOCAESIUM CONTAMINATION OF DIFFERENT MUSHROOM SPECIES

III.4.1. Evaluation of transfer factors

In radioecology, the uptake of radionuclides from soil to plants resp. mushrooms is commonly expressed by transfer factors according to

$$^{134}Cs_{mushroom} = TF * {}^{134}Cs_{soil}. \quad (6)$$

Here $^{134}Cs_{mushroom}$ and $^{134}Cs_{soil}$ denote the specific activities in Bq/kg DW. Since mushrooms are expected to take up radiocaesium predominantly from those layers where the mycelium is located, appropriate transfer factors, which explicitly take the time dependence of specific activities into account, are defined by:

$$^{134}Cs_{mushroom}(t) = TF * {}^{134}Cs_{horizon}(t) \quad (7)$$

Combining the experimentally determined specific activity $^{134}Cs_{mushroom}(t)$ of a certain mushroom species with the specific activity of those horizons where the mycelium is located, the transfer factor was calculated by a least-squares fit. The results for 14 mushroom species are summarized in Table 5.

Transfer factors for ^{134}Cs turned out to be constant with time within the statistical uncertainties. In general, transfer factors are much lower for saprophytic species compared to symbiotic species. The average transfer factor for six saprophytic species is TF = 1.1 compared to an average transfer factor of TF = 12.9 for seven symbiotic species. The only exception is the saprophyte Clitocybe clavipes which exhibits a rather high transfer factor of TF = 25.8 ± 5.6. This observation is in agreement with other authors who found higher radiocaesium contamination in symbiots compared to saprophytes (Römmelt et al., 1990, Kammerer et al., 1994, Yoshida and Muramatsu, 1994).

Species	Mycelium location	TF
Lepista nebularis	L/O_f	0.7 ± 0.1
Collybia maculata	L/O_f	2.2 ± 0.3
Collybia butyracea	O_f	1.0 ± 0.1
Xerocomus badius	O_f/O_h	12.8 ± 1.1
Russula ochroleuca	O_f/O_h	14.8 ± 1.2
Lactarius deterrimus	O_f/O_h	3.7 ± 1.4
Clitocybe clavipes	O_h	25.8 ± 5.6
Hydnum repandum	O_h	39.0 ± 4.4
Paxillus atrotomentosus	O_h	3.1 ± 1.1
Lactarius scrobiculatus	O_h	2.4 ± 0.5
Macrolepiota rhacodes	O_h	0.5 ± 0.3
Armilariella spec.	O_h	1.4 ± 0.2
Russula cyanoxantha	O_h/A_h	11.6 ± 2.4
Sarcodon imbricatus	O_h/A_h	6.4 ± 1.3

Table 5: Transfer factors for 14 mushroom species evaluated by eq. (7) via a least-squares fit. The second column shows the soil horizon where the mycelium of a certain species is located.

III.4.2. Time-dependent behaviour of radiocaesium contamination in different mushroom species

As already demonstrated, a rather simple compartment model suffices to describe the time-dependent radiocaesium contamination of that soil horizon, in which the mycelium of a certain fungi species is located Additionally taking the site- and species-specific transfer factors into account, the ^{134}Cs contamination of mushrooms with time was calculated. For example, Figs. 3 and 4 depict these results together with the experimentally determined specific activities of Russula ochroleuca and Russula cyanoxantha. These curves should only be considered as a rough estimate of radiocaesium behaviour with time. One should bear in mind that ^{134}Cs activities in fruitbodies of a single species usually vary by a factor of two or even more.

Decreasing contamination

In several species a decrease of radiocaesium with time is obvious from the data or predicted by the analysis of radiocaesium migration in forest soil.
In case of Lepista nebularis and Collybia maculata a decrease of radiocaesium contamination with time is evident even from the measured data, the reason being that the mycelium of both species is located in the L- and/or O_f-horizon. Since ecological half-lives in the L- and O_f-horizon amount to 2.9 and 4.6 years, respectively, a future decrease with half-lives of the same order is expected for both species.
For Colybia butyracea, a decrease in radiocaesium contamination is not obvious from the experimental data. However, since the mycelium is located in the O_f- (or L-) horizon, a decrease with a half-life of about 4.6 years is expected.
As Fig. 3 indicates, Russula ochroleuca shows an interesting behaviour. The $^{137}Cs/^{134}Cs$ ratio increases with time which can not be attributed to one single soil layer. One might speculate that the mycelia of the first fungi samples were predominantly located in the O_f-horizon and those of the later ones in the O_h-horizon, thus leading to the observed decrease of the absolute ^{134}Cs activity.
Due to similar reasons, contamination of Lactarius deterrimus is expected to decrease with an ecological half-life of about 7 years though in this case the scattering of absolute ^{134}Cs activities is large.
In case of Clitocybe clavipes the observed activity decreases even more rapidly than the predicted one.

Constant contamination

The second group of species comprises Hydnum repandum, Paxillus atrotomentosus, Lactarius scrobiculatus, Macrolepiota rhacodes, and Armillariella spec., which are expected to have their mycelia in the O_h-horizon.
For this reason, ^{134}Cs contamination is more or less constant from the Chernobyl accident up to now. According to the results of our compartment model for the O_h-horizon, ^{134}Cs contamination increased by approximately 10% from 1987 to 1991 followed by a decrease of about 5% until 1994. In future, this decrease is expected to continue with an ecological half-life of about 7 years.

Increasing contamination

Two species, Russula cyanoxantha and Sarcodon imbricatus, take up about 40% radiocaesium from the O_h-layer and about 60% from the A_h-horizon. The ^{134}Cs contamination of the latter horizon is characterized by a continuous increase since 1986 due to Chernobyl caesium migrating downwards from the upper layers. Accordingly, for both species an increase of ^{134}Cs contamination

is expectetd to prevail until about 1995 (see also Fig. 4). Contamination has reached its maximum nowadays and starts to diminish It will be reduced to one tenth in about 30 years.

III.5. UNDERSTOREY VEGETATION

Fourteen different green plant species have been sampled during the vegetation period in Hochstadt and Garching/Alz. The radiocaesium activities in plants varied between 10 (berries) and 10000 Bq/kg dry wt. (Ferns), and the potassium concentration between 1 (berries) and 29 g/kg dry wt. (wood-sorrel). The potassium concentration in soil is calculated from ^{40}K activity measurements in soil and varied between 1 and 6 g/kg. The mean caesium activities in soil in Hochstadt and Garching/Alz do not differ, but the activities in some plant species are significantly higher in the samples from Hochstadt, which might be due to the higher contribution of mineral components in the O-horizon in Garching/Alz whereby a part of Cs might be absorbed more strongly and becomes less available for plants. This is indicated by the K_d-values, which are significantly higher in the O_f-horizon in Garching/Alz than in Hochstadt.

Transfer factor soil/plant

The rooting depth, which might be reflected by the $^{137}Cs/^{134}Cs$ ratio, has not yet been analysed. As understorey vegetation takes up most of the nutrients from the O-horizons, the transfer factor is defined as the ratio of caesium activity in plants (Bq/kg dry wt.) to the caesium activity in the O_f- and O_h-horizons (Bq/kg dry wt.). The transfer factors for different plant species taken in Hochstadt and Garching/Alz are shown in Table 6. The values vary between 3.2 for ferns at Hochstadt and 0.01 for berries of Rubus fruticosus on both sampling sites. The transfer factors are significantly higher (Vaccinium myrtillus, Rubus fruticosus) within the standard deviation in Hochstadt compared with Garching/Alz, except Fragaria vesca which shows an inverse behaviour. This might be due to the higher contribution of mineral components in the O-horizon in Garching/Alz whereby a portion of caesium might be absorbed more strongly and therefore becomes less available for plants.

To find out if there is a common pattern of caesium uptake by different plant species, we have tested the relation between radiocaesium in plants and in soils. Assuming a linear approximation, the correlation coefficient (r) is 0.39 for all sampled species, which corresponds with the determination coefficient (r^2) of 0.15. This means that only 15% of the variation of radiocaesium activity in plants can be explained by the caesium concentration in the organic horizon. Analyzing the results from Hochstadt and Garching/Alz separately, the correlations do not improve ($r = 0.36$ for Hochstadt, $r = 0.32$ for Garching/Alz).

Considering the monocots separately, there is absolutely no correlation at all between the activities in soil and in plants ($r < 0$). In this group of "monocotyledons", we have investigated samples of the species Deschampsia flexuosa, Molinia coerulea, Melica nutans, Brachypodium sylvaticu, and Carex. If the monocotyledons are not taken into account, the correlation coefficient increases to 0.51 for the remaining plants. Since the consumption of berries is of interest for the radiation exposure to man, the transfer factor of caesium for bilberries (Vaccinium myrtillus), blackberries (Rubus fruticosus), strawberries (Fragaria vesca), and raspberries (Rubus idaeus) was estimated separately ($r = 0.63$).

Plant type	Part	Site	n	Minimum	Maximum	Mean±S D.
Vaccinium myrtillus	Leaves	Hochstadt	4	1.3	2 1	1.7±0.3
	Leaves	Garching	6	0.30	1.1	0.5±0.3
	Fruit	Garching	1			0.07
Rubus fruticosus	Leaves	Hochstadt	4	0 39	1.5	0.8±0.4
	Leaves	Garching	4	0 04	0.61	0.2±0.2
	Fruit	Hochstadt	1			0.01
	Fruit	Garching	1			0.01
Rubus idaeus	Leaves	Garching	6	0.11	0.50	0.3±0 1
	Fruit	Garching	1			0.006
Fragaria vesca	Leaves	Hochstadt	4	0.10	0.19	0.14±0.03
	Leaves	Garching	3	0.24	0.28	0.26±0.02
	Fruit	Hochstadt	1			0.02
Fern		Hochstadt	4	1.7	4.6	3.2±1.2
		Garching	1			0.19
Euphorbia ssp.		Hochstadt	1			0.34
		Garching	3	0.10	0.32	0.2±0.1
Melampyrum pratense		Hochstadt	1			1.3
		Garching	2	0 80	1.1	1.0±0.2
Oxalis acetosella		Hochstadt	4	0.30	0.70	0.5±0.1
Brachypodium sylvaticu		Garching	3	0.08	0.11	0.10±0.02
Deschampsia flexuosa		Hochstadt	3	0.26	0.97	0.6±0.4
		Garching	5	0.61	1.04	0.8±0.2
Melica nutans		Garching	3	0.22	0.32	0.25±0.06

Table 6: Mean transfer factors and standard deviations for different kinds of plants in Hochstadt and Garching/Alz in 1991.

The ratio of ^{137}Cs /^{40}K is approximately constant in leaves and stems, which suggests the ^{137}Cs activity in plants to be regulated via the ^{40}K metabolism. However, approaches to improve the reliability of prognostic estimates by taking the K level in soil and/or plant into account failed. The correlation coefficients could not be improved compared to those belonging to the transfer factors.

III.6. STRONTIUM-90

The ^{90}Sr activity in the Chernobyl fallout was only about 1% of the Cs-activity. Therefore, the contribution of the Chernobyl fallout has only slightly increased the ^{90}Sr inventory of about 1200 Bq/m^2 originating from nuclear weapons fallout. Obviously, it is not possible to distinguish between Chernobyl- and nuclear weapons fallout. After 30 years of deposition, most of ^{90}Sr is still located in the upper organic horizons, suggesting a low migration rate and a rapid turnover in the forest cycle.

Mushrooms were extremly low contaminated with ^{90}Sr. The activities were below 1 Bq/kg FW in all samples from Bavaria. Specific differences in accumulation rates were not observed

for the investigated mushrooms Correspondingly, the transfer factors ranged between 0.002 and 0.01.

The activity of ^{90}Sr in understorey vegetation is regulated via the Ca metabolism. Higher activities are found in leaves, where the Ca content is higher than in fruits. The transfer factors range between 0.2 and 1.2, i e. they are comparable to the ^{137}Cs transfer factors.

PUBLICATIONS DURING THE RESEARCH PROJECT

Kammerer, L., Hiersche, L., Wirth, E. (1994). Uptake of radiocaesium by different species of mushrooms. J. Environ. Radioactivity 23, 135 - 150.

Rühm, W., Kammerer, L., Hiersche, L., Wirth, E. (1995a). On the mycelium location of different species of fungi. Submitted to Journal of Environmental Radioactivity.

Rühm, W., Kammerer, L., Hiersche, L., Wirth, E. (1995b). Migration of ^{137}Cs and ^{134}Cs in different forest soil layers. Submitted to Journal of Environmental Radioactivity.

Rühm, W., Kammerer, L., Hiersche, L., Wirth, E. (1995c). Future behaviour of radiocaesium in mushrooms. Paper in preparation.

Wirth, E., Hiersche, L., Kammerer, L., Krajewska, G., Krestel, R., Mahler, S., Römmelt, R. (1994). Transfer equations for cesium-137 for coniferous forest understorey plant species. Sci. Tot. Environ. 157, 163 - 170.

REFERENCES

Römmelt, R., Hiersche, L., Schaller, G., Wirth, E. (1990). Influence of soil fungi (basidiomycetes) on the migration of ^{134}Cs + ^{137}Cs and ^{90}Sr in coniferous forest soils. In Proc. CEC Workshop, Transfer of Radionuclides in Natural and Semi-natural Environments, ed. G. Desmet, P. Nassimbeni and M. Belli. Elsevier Applied Science, London, 152 - 160.

Yoshida, S., Muramatsu, Y., Ogawa, M. (1994) Radiocesium concentrations in mushrooms collected in Japan. J. Environ. Radioactivity 22, 141 - 154.

Yoshida, S., Muramatsu, Y. (1994). Accumulation of radiocesium in basidiomycetes collected from Japanese forests. The Science of the Total Environment 157, 197 - 205.

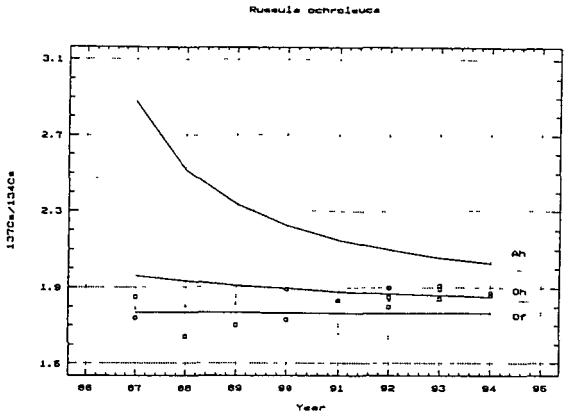

Fig. 1: $^{137}Cs/^{134}Cs$ ratio as function of time in Russula ochroleuca, normalized to 1.5.86. Squares represent the results of fungi measurements. The time-dependent $^{137}Cs/^{134}Cs$ ratios of the O_f-, O_h-, and A_h-horizon, as deduced from our compartment model, are indicated by solid lines for comparison.

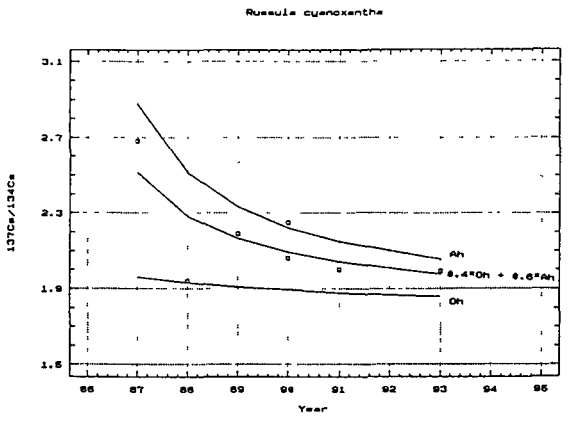

Fig. 2: $^{137}Cs/^{134}Cs$ ratio as function of time in Russula cyanoxantha, normalized to 1.5.86. Squares represent the results of fungi measurements. The time-dependent $^{137}Cs/^{134}Cs$ ratios of the O_h- and A_h-horizon, as deduced from our compartment model, are indicated by solid lines for comparison. Additionally, the calculated $^{137}Cs/^{134}Cs$ ratio assuming 40% radiocaesium uptake from the O_h- and 60% from the A_h-horizon is shown.

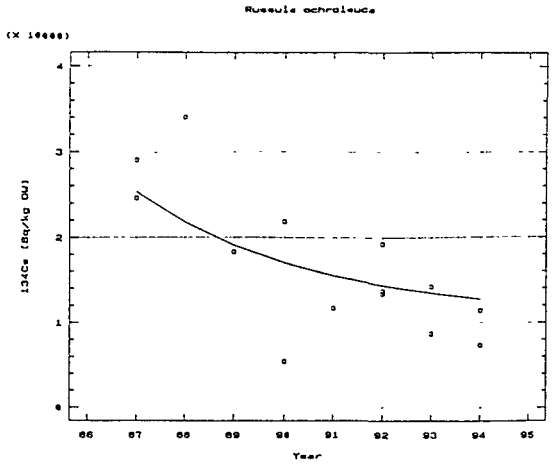

Fig. 3: Specific ^{134}Cs activity in fruitbodies of Russula ochroleuca, expressed in [Bq/kg DW] and normalized to 1.5.86. The solid line represents the time-dependent specific ^{134}Cs activity, also expressed in [Bq/kg DW] and normalized to 1.5.86, as calculated from the time-dependent contamination of the O_f- and O_h-horizon taking a proper transfer factor into account. For details see text.

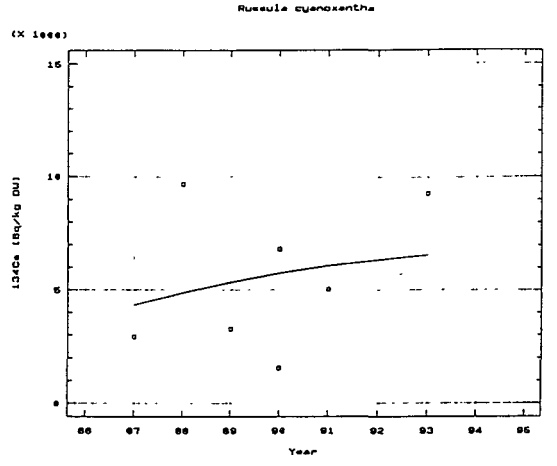

Fig. 4: Specific ^{134}Cs activity in fruitbodies of Russula cyanoxantha, expressed in [Bq/kg DW] and normalized to 1.5.86. The solid line represents the time-dependent specific ^{134}Cs activity, also expressed in [Bq/kg DW] and normalized to 1.5.86, as calculated from the time-dependent contamination of the O_h- (40%) and A_h-horizon (60%) taking a proper transfer factor into account. For details see text.

Head of project 2: Dr. Moberg[1]

II. Objectives for the reporting period

The main objective is to study the behaviour of radiocaesium and radiostrontium in the forest environment. This includes investigations about the influence of forest soil characteristics on the retention and vertical distribution of caesium and strontium in plants and soil, and on the extent of different assimilation processes in trees, primarily pines. Increased knowledge concerning the distribution of caesium and strontium in the different plant-soil compartments in in the long time perspective is needed also for modelling the cycling of radionuclides in the forest environment. The ultimate goal of the research in forest radioecology performed by SSI is to obtain knowledge that can contribute to estimate individual and collective doses from a contaminated forest. That goal is reached by cooperating with other research groups studying for example game animals, and by evaluation of literature data. This report should be seen in that perspective.

III. Progress achieved including publications

The long-term radiological consequences of a radioactive contamination of the forest ecosystem has been clearly demonstrated after the Chernobyl accident. In Sweden large areas of forested land were contaminated by radioactive caesium (Cs-134 and Cs-137). More than nine years after the accident there has been very little decrease in Cs-137 concentrations in some compartments, for example in moose and roe deer which are the two most important game animals in Sweden. Variations in concentrations occur, however, in and between years. Estimates indicate that the ecological half-lives in some cases can be as along as 30 years, i e. equivalent to the physical half-life of Cs-137. The estimated collective dose to the Swedish population from forest products (intake by food products) during the 50 years following the accident is a substantial part of the total internal dose.

In Sweden, the Chernobyl fallout of Sr-90 was around 1% of the Cs-137 fallout in the wet deposition areas in northern Sweden. This is comparable to the fallout of strontium from the atmospheric nuclear weapons tests. At these levels , the radiation dose to man due to radioactive strontium present in the forest ecosystem is very low.

This final report is based mainly on field measurements performed at three sites in Sweden with a Cs-137 deposition, resulting from the Chernobyl accident, between 85 and 220 kBq/m^2 in average. During the reporting period it has been of particular interest to investigate the distribution of radionuclides in the pine trees of the studied area, but extensive measurements have also been performed on mushrooms and other understorey vegetation as well as on soil samples. However, the report is focussed on Scots pine (*Pinus Silvestris* L.) and radiocaesium and summarizes some results obtained so far. Mushroom data have been delivered to a common data base and are evaluated in relation to data from other countries in this project. Some results concerning the transfer and mechanisms of radiocaesium in understorey vegetation has been reported (Guillitte et al 1994).

Material and methods

The three sites selected for the investigation presented in this report and the data characterizing these sites are summarized in table 1.

Table 1 Basic data on the sites Hille, Långsjon and Prylen

PARAMETER	SITE H	SITE L	SITE P
Location	60°48′ N 17°13′ E	60°48′ N 17° E	60°48′ N 17° E
Trees			
Type	*Pinus Sylvestris* L.	*Pinus Sylvestris* L. (60%) *Picea abies* Karst (40%)	*Pinus Sylvestris* L. (90%)
Year of establishment	1930	1977	1988
Site index (H100)	T29	T24	T23
Stems/ha	940	2100	2300
Current annual increment (m^3/ha)	8.2	6	5.5
Understorey vegetation	grass *Pleurozium schreberi* *Dicranium* sp.	grass *Pleurozium schreberi* *Dicranium* sp.	grass *Dicranium* sp.
Soil			
Classification	Podsol	Podsol (watersorted moraine sandy-fine sandy-clay fraction<2%-top soil very rocky)	Podsol (watersorted moraine - sandy-clay fraction<2% top soil very rocky)
Humus type	Mor	Mor	Mor
Humus layer (cm), A_0	2-6	5-10	5-10
Bleached layer (cm), A_1	5-12	7-12	5-9
pH(H_2O), humus	4.3	4.0	4.0
Sampling date	1986, 1990, 1991,1994	1991, 1994	1991, 1994
Estimated deposition (kBq/m^2) Cs-137 aerial survey Cs-137 A_{01} measurement	 >180 90	 30-40 20	 30-40 37

The main sampling for this reporting period took place in the autumn 1991 when four trees (*Pinus Sylvestris* L) were felled at each of three sites (H, L, P). The stands were of different age - 60, 15 and 6 years (1991). In 1994 sampling was performed at site L (branches and needles) and site P (small trees). Soil samples were collected at site H (1986, 1990, and 1991 below fungi only), and sites L (1991) and P (1991). Fungi, appr. 50 species, were collected 1991, 1993 and 1994 at site H. Samples of understorey vegetation (field layer) were collected 1990 at site H. All sampling took place at the same time of the year, in October. More details about the sampling, treatment of samples and measurements can be found in a forthcoming article.

The reported activity concentrations refer, unless otherwise stated, to the sampling date.

Results and discussion

1. Contamination of soil

Three sets of six soil cores were collected at each site. The cores were separated into litter, humus and mineral soil layers. The subsamples from each layer were combined into one sample. Here we report the average values from these three composite samples from each site. The total deposition of radiocaesium, including the radiocaesium from the bomb fallout, was determined from the soil profiles (site H 217 kBq/m^2, site L 115 kBq/m^2, site P 85 kBq/m^2). The remaining fallout from atmospheric bomb tests is less than 2 kBq/m^2.

The depth distributions of Cs-137 in soil in the autumn 1991 are shown in figures 1 and 2. Between 75 and 95% of the activity is recovered in the more or less decomposed organic layer and the eluvial horizons of the mineral soil. At site L, there seems to be a relatively larger amount of radiocaesium in the A1+A2 layers compared to the sites H and P.

FIGURE 1
Distribution of Cs-137 in soil, site H

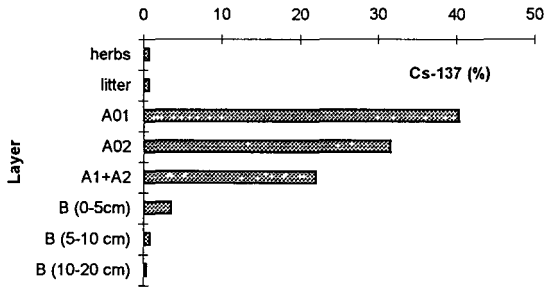

FIGURE 2
Distribution of Cs-137 in soil, site L and site P

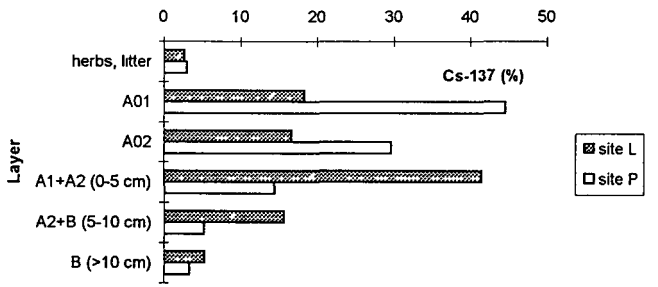

2. Contamination of Scots pine - direct contamination and root uptake

The trees at sites H and L were exposed to direct contamination by wet deposition the last days of April 1986. According to earlier estimates around 80% of the radiocaesium is

intercepted by the canopy initially. Part of the radionuclides will migrate from the canopy to the forest floor. Some of the intercepted activity will be assimilated by the tree and redistributed between its different parts. Our original hypothesis was that the assimilated activity was relatively large, and would dominate over the root uptake for a considerable time period . During the years after the deposition there has been a complete change in the set-up and needles, i.e. all needles subjected to fallout in 1986 have been lost by needle fall. The activities in the tree samples from sites H and L are assumed to be due to a combination of foliar uptake - redistribution by radioactive caesium and by root uptake. The trees at the third site (P) were not exposed to the Chernobyl fallout. They were still in a greenhouse at the time of deposition, and were planted afterwards. They are accordingly very young "trees", but are used in our long time study to follow the root uptake of radiocaesium over a number of years.

3. Comparison with bomb fallout

Melin et al (1994) determined the concentration of Cs-137 in different fractions of Scots pine on samples taken 1980, i.e. these trees were only exposed to the fallout from the nuclear test explosions in the atmosphere. One of the sites (site A in Melin et at, 1994) is judged to be comparable to site H concerning the age of the trees, the type of forest, soil characteristics and climate. Table 2 summarizes the data from site A (nuclear weapons fallout only) and site H (dominated by Chernobyl fallout).

Table 2 Concentrations (Bq/kg) of Cs-137 in Scots pine. Mean and standard deviations of 6 (1980) and 4 (1991) trees, respectively (reference dates 1990, 1991).

Fraction	Zone in canopy	Year of development		Year of development		All	All
		1980	older	1991	older	1980	1991
needles	upper 1/3	51 (3)	16 (3)	590 (183)	187 (68)		
	middle 1/3	31 (4)	12 (1)	499 (221)	169 (68)		
	lower 1/3	29 (9)	14 (3)	389 (82)	213 (111)		
branches	upper 1/3	47 (11)	10 (7)	659 (395)	234 (97)		
	middle 1/3	23 (6)	8 (3)	366 (143)	221 (67)		
	lower 1/3	22 (4)	8 (2)	412 (173)	368 (127)		
stem	bark					15 (5)	634 (145)
	wood					3 (1)	61 (21)

The total average activity in Scots pine (Bq/pine) is 0.8 kBq for the above ground parts for the site A tree, and 25±11 kBq for the site B tree.

For both sites, the concentrations in the current needles and branches are higher than in the older ones, and the highest values are found at the top of the tree (upper 1/3). The concentration of Cs-137 in trees from site H is around 15 (12-19) times higher than those at site A. This is true also for the stemwood. However, for the bark the difference is larger. It has not been possible to measure the radial concentration of radiocaesium in bark, but a probable explanation to the higher concentration is that still much of the originally deposited radiocaesium (direct deposition and stemflow) is left close to the surface of the bark.

As the deposition after the bomb explosions was rather evenly distributed over Sweden, a reasonable assumption is that the concentration of "old" caesium in the trees at site H is approximately the same as at site A That would imply that less than 10% of the Cs-137 concentration in trees at site H is old caesium. (It is difficult to make a reliable estimate of the amount of old caesium from measured concentrations of Cs-134 and known Cs-134/Cs-137 ratio due to the relatively large uncertainties involved in the concentrations of Cs-134 and to the large difference between new and old Cs-137). Considering that the remaining deposition of Cs-137 in 1991 is 100 times higher for the Chernobyl fallout, a first assumption would be that the root uptake of the "new" caesium is still relatively low, especially if a substantial part of the caesium present in the tree is due to the originally intercepted activity. The bioavailable amount of new caesium also depends on the degree of leaching from the needles deposited on the ground. The trees at site H were older at the time of deposition, and the new caesium has been present, and available, in the system for a shorter time period.

A dominating root uptake would lead to a significant increase of Cs activity from the older to the younger needles which may be explained by the phloem mobility of caesium. This fact and the similarities in relative distribution in 1980 and 1991 trees favours the interpretation that root uptake is the major cause for the caesium concentration in the 1991 trees, i.e. already six years after the deposition. Russian s tudies performed around the Kyshtym and Chernobyl sites report a decreasing importance of the initially intercepted radioactivity as a source for contamination of different stand components and the increasing importance of root uptake with time. After a definite time, the main part of radionuclides has migrated from the canopy into the forest litter. This time was found to be 2-4 years and did not depend on soil properties. After 10-15 years there is an equilibrium state where the throughfall losses are being compensated by root uptake. This latter time is dependent on the biological availability of the radionuclide. On the other hand Finnish studies after Chernobyl presumed that the proportion of radiocaesium of soil origin was still very low in conifer needles up to 1991.

4. Root uptake only

The young trees at site P can be used to estimate the root uptake of radioactive caesium as these trees were not subjected to the Chernobyl fallout in 1986. The external contamination is then limited to resuspension, which is considered to be negligable a few years after deposition.

FIGURE 3
Branches and needles from site P

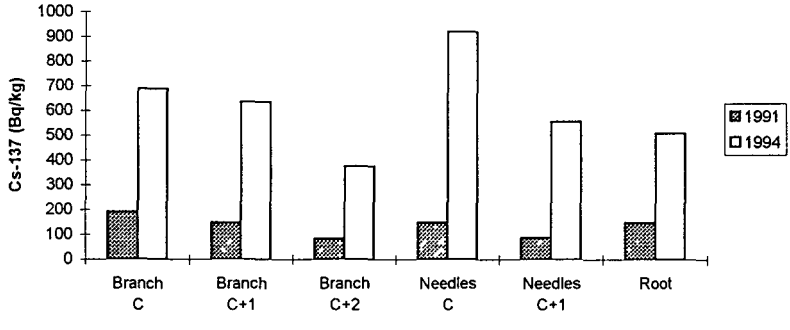

Figure 3 shows the average concentration of Cs-137 in branches and needles from 4 trees (plants) sampled in 1991 (6 years old, planted 1988) and 1994 (9 years old), respectively. During the three years between sampling, the biomass, roots included, has in average increased 14 times, while the activity concentration has increased 5 times. The average concentration in the needles sampled in 1994 is 677 ±172 Bq/kg, or 920±570 for current needles (C-needles) and 556 for the older needles. This can be compared with the concentration in needles from the trees at site L which in 1994 are 637±387, or 1253±243 for the current needles. For site H (61 years old in 1991) the C-needles contained 493 Bq/kg. At all sites the caesium concentrations are higher in the youngest needles, and there is an enhancement of radiocaesium in new shoots in accordance with that expected from pure root uptake.

According to the data presented here, there does not seem to be any major difference in concentration of radioactive caesium in older pines (deposition-assimilation and root uptake) and young pines (root uptake only) The role of soil characteristics as well as the plant physiology in connection with growing is presently investigated

The data show a considerable uptake of radiocaesium by the growing pine (both site P and site L). In the trees at site P, the concentration is as high as (or higher than) in the older trees (sites H and L). This is of special importance, as young pine trees comprise an important food for the moose especially during the late autumn and winter, and therefore can lead to substantial caesium concentrations in moose meat Normally, however, the hunting season in Sweden is before the moose changes its diet and increases the intake of pine, but this has to be further studied.

Even if our results are not conclusive, it is reasonable to assume that a major part of the radioactive caesium trapped in the forest canopy at the time of deposition is transferred to the ground by various processes including needle fall during the first years following the deposition, and that a major part of the radiocaesium in the pine is due to root uptake already a few years after the deposition also in the boreal forest. This is in accordance with certain findings from other vegetational zones.

5 . Distribution of Cs-137 in Scots pine - 6 years after the Chernobyl accident

Trees at sites H and L were both subjected to the Chernobyl fallout. Figure 4 shows the average distribution of radiocaesium in needles from four pines from each site. The distribution in branches are similar.

The concentrations of Cs-137 are generally higher in the trees from site L, and this is particularly the case for the new shoots and those in the top of the tree. In fact, the concentrations are as high as in a pine tree (42 years old 1993) from Russia (Novozybkov) that we have measured (deposition of Cs-137 = 2 MBq/m^2). Caesium, like for example potassium, belongs to the phloem mobile elements, and is assumed to be translocated to active parts of the tree. This may be one explaination to the increasing Cs-137 activities in the younger pine needles, which was observed also by other groups, for example in Finland. Another proposed explanation are the translocation of caesium from older needles to the growing needles during spring. The Finnish group also reports an increase of concentrations of Cs-137 in current needles with time from 1986 to 1991. This is not in agreement with our results (1991 to 1994) from site L (figure 5), but in agreement with the findings from site P. The surprisingly high concentrations of Cs-137 in Scots pine at site L in 1991 have decreased three

FIGURE 4
Needles from site H and site L

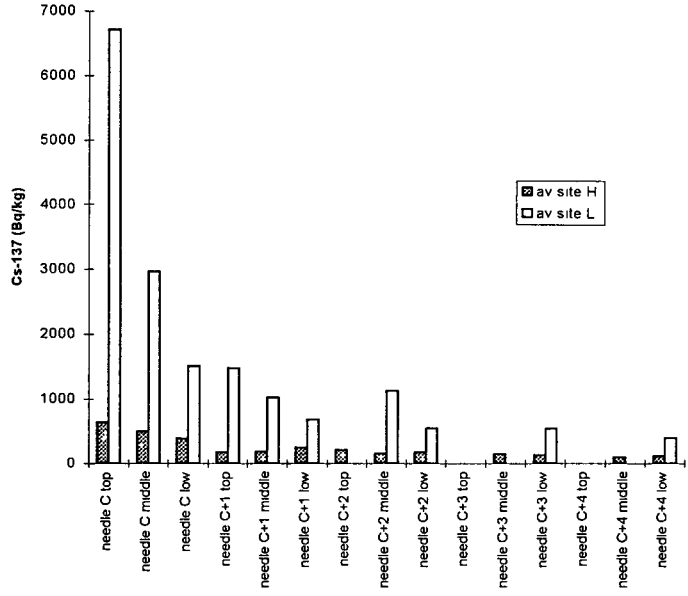

FIGURE 5
Needles from site L - 1991 and 1994

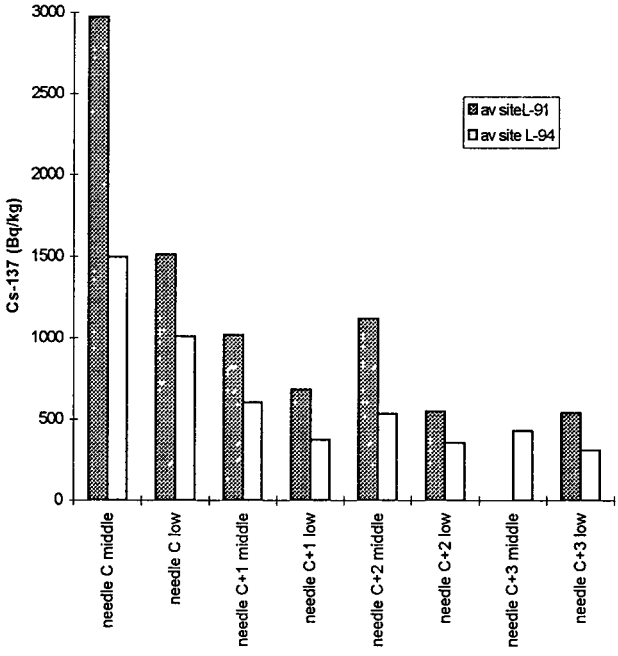

years later (figure 5). The reason for this decrease is not clear but one hypothesis is that it is caused by growth dilution . Our material has not been sufficient to test that. Another factor that can be of importance is the extremely dry summer 1994, just before the samples were taken. These questions are discussed with plant physiologists. The different depth distributions of Cs in the soil (figure 2) with a higher concentration in the A1+A2 horizon, where a large part of the root system is, may also contribute to the higher concentrations at site L.

FIGURE 6
Activity in bark - trees from site H and site L

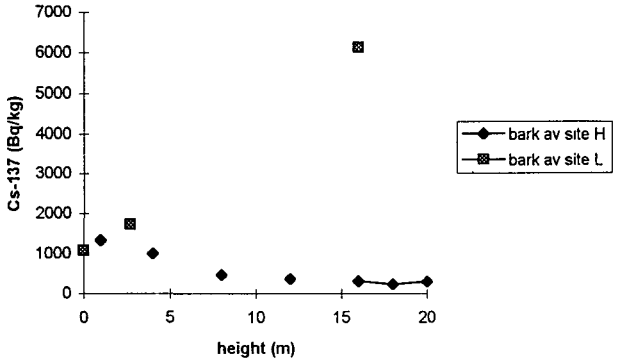

In figures 6 and 7 the average activity concentrations of Cs-137 in bark and stemwood from sites H and L are compared as a function of tree height. The different patterns between the sites is not fully understood. The relatively high concentration of Cs-137 in bark from lower parts of the trees could be due to stemflow. In contrast, the higher concentrations at the top of the trees at site L may be caused by the fact that the bark is much younger and biologically

FIGURE 7
Activity in stemwood - site H and site L

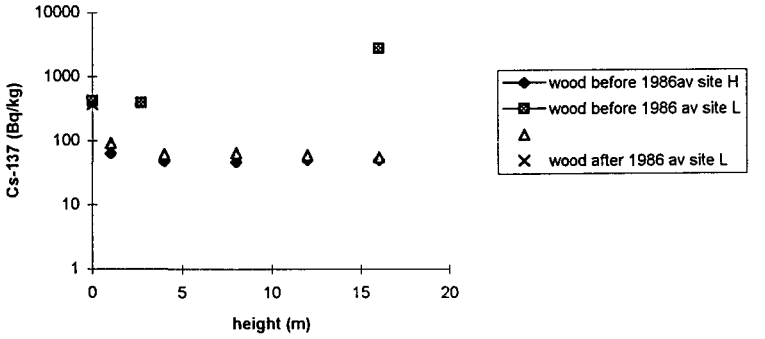

active. The relative distribution of caesium was also measured for wood produced before and after 1986, respectively. For site H, where data exist as a function of height, the concentrations

after 1986 is somewhat higher, 10-40%. There seems to be a smaller difference at the top of the trees. A radial mobility of caesium has been reported in the literature for example for the temporal/radial distribution of bomb fallout in different tree species. For site L data exist only at the tree base. Belgian studies of *Pinus Silvestris* from the Chernobyl area show that alburn is twice as contaminated as duramen. After 1986 the contamination level of the alburn tissues increased with highest values for most recent age ring due to the higher movement of radiocaesium into young tissues

6. Total activity in different parts of Scots pine.

Figure 8 shows the total amount of caesium in different parts of the trees, based on measured concentrations (figure 9) and calculated biomass. Even though the concentrations are much higher at site L, the larger biomass at site H gives a higher total activity.

FIGURE 9
Activity concentration of Cs-137 in trees from site H and site L

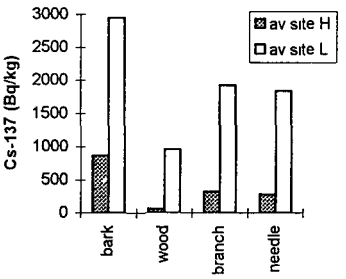

FIGURE 8
Total inventory of Cs-137 in trees from sites H and L

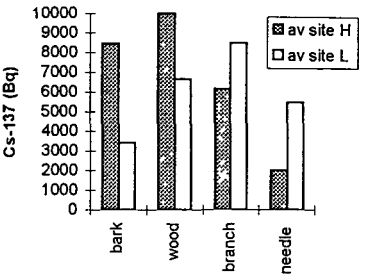

Based on the available information of the three sites it is possible to make an estimate of the amount of Cs-137 present in the above ground parts of the trees in comparison to the total ground deposition. The results are 1% at site H, 4% at site L and at site P only 5 thousands of a per cent in 1991. In 1994 the figure for site P has increased to 0.3%. As a comparison, a rough estimate gives 2% for our Russian trees at Novozybkov. Russian data from a mixed birch-oak-pine show that the Cs-137 in the all overground phytomass has changed from 17.6% in 1986 to 3.3% in 1991 in the Chernobyl zone.

A characterization of the contamination of the understorey vegetation at site H was reported by Guillitte et al (1994). They also estimated that about 40% of the Cs-137 deposited on the ground was retained in the soil microflora particularly by mycelia, while for example 5% were retained in the roots, and less than 1% in the aerial parts of the understorey vegetation.

PUBLICATIONS DURING THE RESEARCH PROJECT

Melin, J., Wallberg, L., and Suomela, J, 1994. Distribution and retention of caesium and strontium in Swedish boreal forest ecosystems. Sci. Total. Environ. 157: 93-105

Moberg, L, Melin, J, and Wallberg, L., 1995. Radiocaesium and radiostrontium in a Swedish pine forest. (manuscript)

(Guillitte, O., Melin, J., and Wallberg, L., 1994. Biological pathways of radionuclides originating from the Chernobyl fallout in a boreal forest ecosystem. Sci. Total Environ. 157:207-215.)

Head of project 3: Dr. Bergman

II. Objectives for the reporting period

To study uptake, turnover and transfer of radionuclides within and between abiotic and biotic compartments of a boreal forest ecosystem in northern Sweden, primarily with the aim to evaluate the time-dependent exposure to man from ^{137}Cs. Our analysis has been focussed on certain processes (soil, vegetation and animal), which are known or expected to affect the distribution and transport of caesium in the system – and ultimately its transfer to man. The possibilities and limitations in extrapolations from the present results to future situations is also considered, particularly with regard to the probable importance of ^{137}Cs intake via forest products as compared to that over meat, milk and milk products from the agricultural area.

In the experimental strategy particular attention has been payed to processes related to (1) soil-water, and (2) soil-plant interactions in a systematic approach to describe the distribution and dynamics of caesium turnover in, as well as loss from, a forest catchment. Systemic effects related to interactions on (3) plant- herbivore levels are to be analysed by the use of input from another of the contractors (T. Palo, SUAS.DWE) participating in this project.

III. Progress achieved including publications

A summary of the main findings from the work - including results appearing in the publications - is given below:

^{137}Cs in the vegetation

The concentration of ^{137}Cs during 1986-1990 has been studied (cf. Nelin and Nylén 1994) based on pooled data from samples in July (*Vaccinium myrtillus*, bilberry twigs; and *Betula pubescens*, birch twigs) and October (bilberry twigs; birch twigs; and *Pinus sylvestris*, pine twigs) in boreal forest biotopes mainly located at the Vindeln experimental forest, 60 km NW of Umeå (64°16'N, 19°48'E). Continued sampling in 1992 of bilberry and birch twigs, and in 1994 of bilberry twigs, complemented with measurements on pre-Chernobyl samples means that at present results are available concerning the ^{137}Cs concentration in samples of perennial vegetation for the period 1985 -1994.

The change in average ^{137}Cs-concentration – based on all regularly used sampling sites at the Vindeln experimental forest – are illustrated for bilberry (fig.1) and birch (fig.2). In bilberry the content in the samples from 1986 is significantly different from that in each of the subsequent years (Tukey $p < 0.001$). For bilberry the ^{137}Cs concentration appears to attain its minimum during 1989/90 (cf. fig.2). In birch , on the other hand, there are no significant differences between the years with exception for the period 1989/90 (the material is pooled over two years due to limited sampling at some sites), where the ^{137}Cs concentration – as in the case of bilberry – is lower than in 1986 (Tukey $p=0.017$).

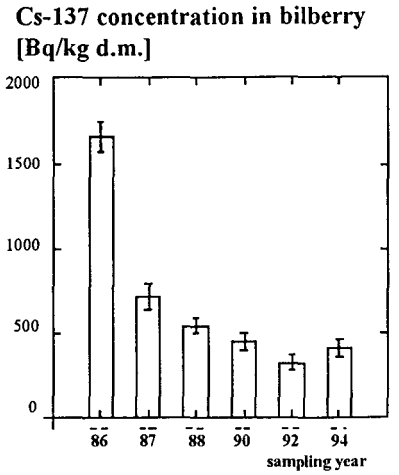

Fig. 1. The concentration (and S.E.) of ^{137}Cs in bilberry. Mean value based on all sampling sites at the Vindeln experimental forest over the period 1986-1994

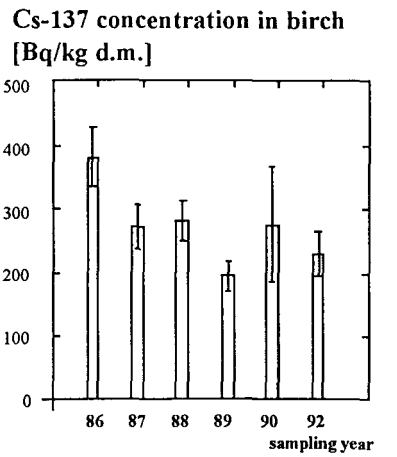

Fig. 2. The concentration (and S.E.) of ^{137}Cs in birch. Mean value based on all sampling sites at the Vindeln experimental forest over the period 1986-1992.

When differentiated in the categories a) bilberry from recently clear-felled areas and young forests, and b) mature forests, some distinctive patterns become evident. During 1986 the concentrations of ^{137}Cs in bilberry are almost similar in the two categories according to figure 3. However, in the following years the change towards lower concentration appears to proceed faster in samples from category a) i.e. the young sites than in category b). From 1987 and onwards the concentration in the young forests is significantly lower than in the mature forests. A further differentiation has been made of category b) to distinguish between the behaviour of ^{137}Cs in mature forest stands where spruce respectively pine predominates. Between these two types of mature coniferous forests there is a significant difference (ANOVA n=92 p=002) with regard to the ^{137}Cs content i bilberry, where bilberry from the pine forests consistently contained higher concentrations of ^{137}Cs than that from the spruce forests. Furthermore, the difference in ^{137}Cs concentration between the two categories was relatively unchanging over the whole time period studied.

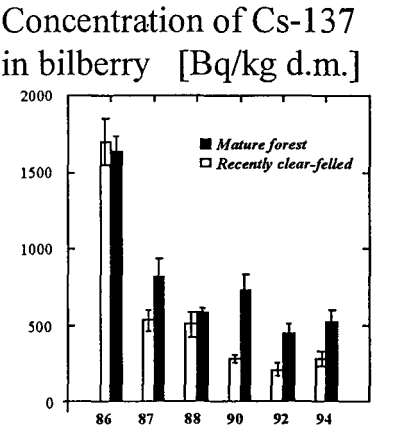

Fig. 3. The concentration (and S.E.) of ^{137}Cs in bilberry. Mean values during the period 1986-1994 for sites at the Vindeln experimental forest belonging to the respective categories *Mature forest* and *Recently clear-felled.*

Influence of herbivory and litterfall on caesium turnover in a forest ecosystem

In comparison to typical levels on the litterfall in boreal forest ecosystems, transfer from vegetation to soil by herbivory (see schematic illustration in figure 4) is relatively important and appears to be within an order of magnitude of litterfall concerning the biomass transfer as an average over many years. Concerning the turnover of Cs-137 in vegetation by herbivory (cf. figure 5), the vole populations in periods of peak biomass density contribute about 30 times as much as the moose population, but relatively little in years when the biomass density is close to the bottom level. In spite of the oscillating population size, the amount of vegetation consumed by small rodents in the forest ecosystem, thus as a long term average, exceeds that consumed by mooses by more than one order of magnitude.

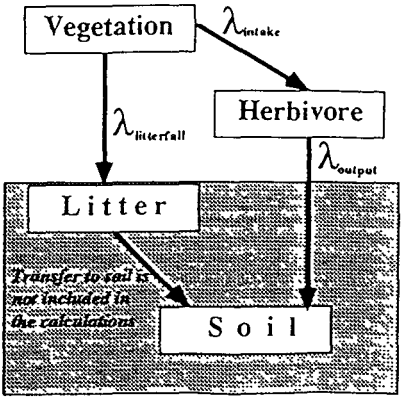

Fig. 4. Schematic illustration of transfer from vegetation by litterfall and herbivory. Basic structure of assessment model [Bergman et al. 1994].

With due regard to generally lower caesium levels in the faded plant components constituting the litterfall, than in the living plant tissue, and an expected high availability of Cs-137 from animal excrements, the importance of feedback from vegetation to soil of radioactive caesium by herbivory might be even higher than apparent from the corresponding transfer of organic matter [Bergman et al . 1994].

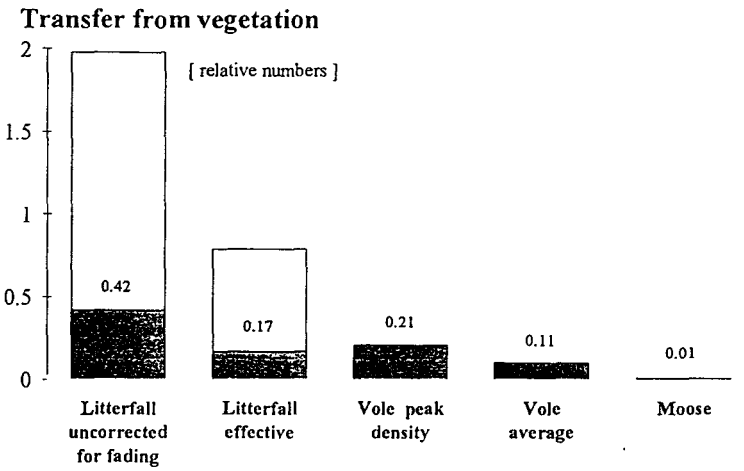

Fig. 5. Transfer of ^{137}Cs by litterfall and herbivory. The estimated ranges of litterfall in the forest biotope are indicated by the light dotted area; "litterfall effective" illustrates the transfer after correction for the level in fresh weight living tissue; "Litterfall uncorrected for fading" for the reduced concentration of ^{137}Cs estimated to remain after fading; "Vole average" refers to the average over a whole population cycle [Bergman et al. 1994].

Theoretical presentation of caesium behaviour in the complex forest ecosystem

The boreal forest ecosystem constitutes an ordered but complex entity. The behaviour of caesium, resulting from the interdependencies and effective interactions within the community, probably cannot be comprehended by constructing a theoretical model based on a detailed pattern of these interrelationships. Theoretical treatments are therefore frequently based on DESCRIPTIVE MODELS These models attempt only to describe a set of observations in mathematical form, for example, by fitting a curve to a set of points. No explanatory mechanism is built into this model, although the model itself may be used to suggest possible mechanisms.

If the emphasis is on attempting to explain observed data in terms of more basic known mechanisms, and on showing the prinicipal trend in the dynamic behaviour e.g. of radioactive caesium in a forest ecosystem, use is made of the EXPLANATORY MODELS. Explanatory models are thus not primarily used to make precise predictions, in contrast to PREDICTIVE MODELS. Models of the latter type, simulating ecological systems, tend to be very complex and generally need to be based on a network including several compartments

Our model (Bergman et al 1993), focused on redistribution processes in a long-term perspective, belongs to the explanatory category. In our model the major regulators of energy flow, as well as of caesium turnover, are related to primary production and its constraints on the growth capacity Certain fundamental physiological processes governing the metabolism of living matter in the biotope are also considered. The principal structure of the model is shown in figure 6.

The model includes qualitatively effects of primary production and growth on turnover of caesium. The dependence on these factors is concluded from the following facts: primary production and its distribution over growth and litterfall constitute major regulators with regard to the dynamics of the redistribution processes of organic matter in the forest. The same conditions should be true for redistribution effects on potassium due to its essential role in the living cell Potassium and caesium are to a high degree exchangeable in active transport over cell membranes in living tissue. Evidently both elements may serve in the same vital processes. Accordingly, as primary production is of importance for the behaviour of potassium in the forest ecosystem, it should be so for caesium too.

The qualitative system structure of processes, interactions and compartments is thus mainly based on physiological characteristics concerning transport of caesium over cell membranes and intracellular distribution, and the apparently conservative conditions prevailing for caesium in boreal ecosystems (Bergman 1994). Also qunatitative estimates have been made from the latter conditions – e.g. the facts that very little of the radioactive caesium deposited over the forest area is lost from the system by run-off, about 90% of the total deposition of ^{137}Cs occurs in the upper organic horizon in podzol areas, and that the availability in the ecosystem, as can be seen from the ^{137}Cs concentration in moose meat, was not

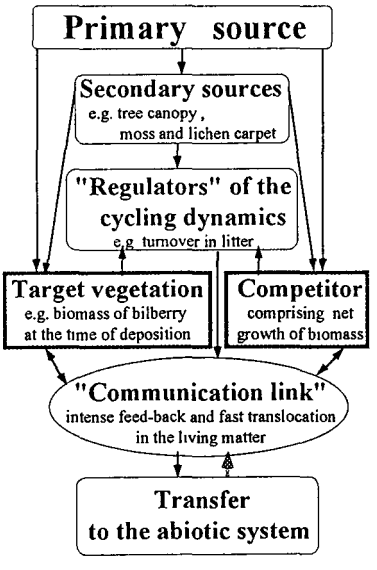

Fig. 6. The principal structure of the forest ecosystem model

significantly different in 1985 (i.e. prior to the Chernobyl accident) compared to the period 1986-1990 (Bergman et al. 1991) .

The theoretical analysis is based on compartment theory and first order kinetics for the turnover of ceasium in the boreal forest. The calculated time dependent change of the Cs-137 content in perennial vegetation has been compared to that actually observed at different local study sites with focus particularly on bilberry.

The primary purpose of applying this model has been to elucidate qualitatively how predictions based primarily on growth and physiological behaviour of caesium corroborate with the main features of the time-dependent change of ^{137}Cs activity according to measurements on perennial vegetation.

Redistribution and transfer processes

Estimated transfer factors (Bergman et al 1993) are based on the actual results for the time-dependent redistribution of ^{137}Cs from secondary sources in a Scots pine canopy by throughfall and needlefall (illustrated in figure 7), in addition to the release to the environment of ^{137}Cs deposited over the moss and lichen carpet. After the Chernobyl accident loss from the system by runoff is less than that due to physical decay –from 1987 and onwards – and therefore disregarded in the model. The model also includes: a "*competitor*" compartment (i.e. indicating the increase in biomass competing for the available caesium) to simulate influence on the redistribution processes of primary production and growth; *target vegetation* (i.e. the biomass of the perennial vegetation under study at the time of deposition); litterfall from this compartment; decomposition in a litter compartment; and exchange of caesium between the vegetation compartments and soil. Se Bergman et al 1993 for detailed list of transfer factors and model parameters.

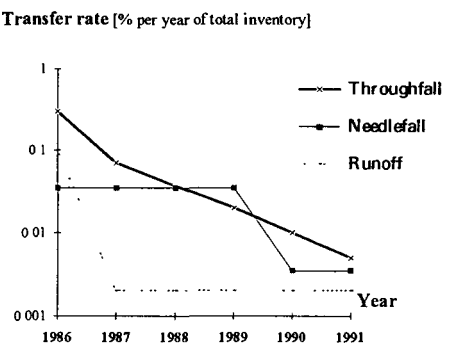

Fig. 7. Rate of ^{137}Cs transfer per year from the canopy and by runoff. The fraction transferred is normalized to the initial deposition (Bergman et al. 1993)

Effects of growth

Both in the context of short and long-term perspectives growth is considered to constitute a major regulator of ceasium redistribution within and between the biotic components of the system. The primary regulators at a particular growing site related to growth are illustrated below. At sites with a poor nutritient state (eg. on peat soil) the net biomass increase is very limited, implying relatively small "dilution" effects on the concentration of ^{137}Cs in the vegetation by redistribuion of some fraction of it to the new biomass. Similarly in an old forest, where the biomass already has approached rather closely to the maxium capacity of the site productivity, further net increase in biomass is limited – i.e. only relatively small changes in the concentration of ^{137}Cs may be expected from growth and subsequent dilution. At sites with good soil conditions possible to support a high biomass, on the other hand, forests at

Primary regulators of the redistribution processes

* **Maximum total biomass at the growing site**
* **Dynamics of age dependent net productivity**
* **Successional stage and age of the growing site**

young stages generally exhibit a fast net increase in biomass, which is expected to influence the concentration of e.g. ^{137}Cs considerably in the vegetation. Growth functions adapted to simulate the dynamics of net growth representative for many sites in the boreal vegetational zones are illustrated in figure 8. Growth of the *competitor* compartment (cf. figure 6) is governed by this time-dependence and scaled to the appropriate level of maximum biomass associated with the soil conditions at the particular sites under study

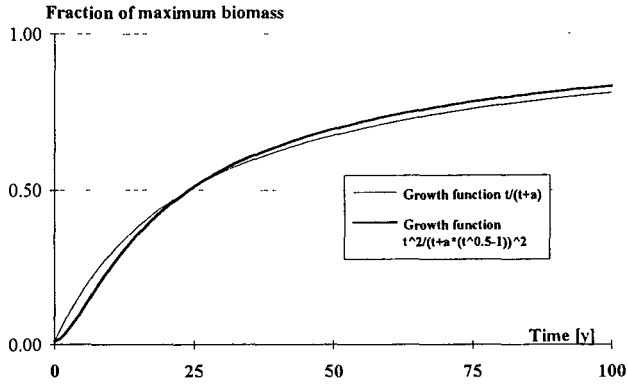

Fig. 8. The growth functions describing the relative net change in total biomass at a growing site as a function of the age of the forest stand. Fifty percent of the total biomass is attained after *a* years.

Model predictions

The behaviour of deposited ^{137}Cs has been simulated using age of the forest at fallout and nutrient state of the growing site as parameters. Interception in the tree canopy has been chosen to be similar to that which resulted after the Chernobyl accident from wet deposition at the study site (Bergman et al 1988, Nylén and Ericsson 1989) and also in coniferous forests at several sites elsewhere in the boreal zones (Bergman1994). Three cases of different surface cover of understorey vegetation, moss and lichens have been considered according to figure 9 to analyse the sensitivity of the dynamics of redistribution processes to the existence of *secondary sources* (such as a moss or lichen carpet), how much of the ground they cover, and the mean residence time for ^{137}Cs there.

Table 2 *Deposition distributed over tree canopy and ground*

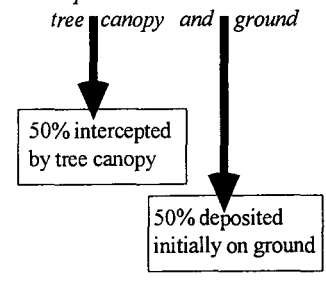

Three alternative cases for surface cover of understorey, moss and lichens

Alt I: *The carpet of moss and lichens covers* **99%**

" II: " " " " " " " **90%**

" III: *The ground cover by moss and lichens is negligible*

Fig. 9 (Cf. Bergman et al. 1993).

Simulations of the change in content of ^{137}Cs in the *target vegetation* according to figure 6 – the target in the present case consists of the biomass of bilberry at the time of fallout – depending on the age of the forest stand, when the deposition takes place, and the site-specific soil condition, are illustrated in figure 10. *Poor soil* corresponds to low productivity (1 kg d.m. of biomass per m^2) generally prevalent on peat soil at bogs in the boreal zones, *good soil* means relatively high productivity (at the level of 20 kg d.m. per m^2). *Clearcut* means new growth at a site where a mature forest stand recently has been clear-felled. Depending on forest practice, we expect a transient phase to occur initially, during which the prerequisites of a sufficiently intact feed-back network may not be satisfied. The re-establishment of a functional complex network, which mainly relies on the recovery of the microbial, mycelial and fine root systems, will probably be fast. This means that the ^{137}Cs content of the perennial vegetation, after a short-lasting transient phase, is expected to undergo the same dynamic stages of redistribution as in the case of a forest exposed to direct deposition – but, of course, only with regard to the recirculated fraction. This assumption is supported by the fact that 3-18 % of the total deposition over a mature forest is contained in the tree biomass over the period from some years to several decades after fallout (Bergman 1994). About two-thirds of this will be removed with the tree trunks, as can be estimated from the internal distribution. Consequently only about 2-12% of the total deposition is lost by that route. This in turn implies that the total inventory of ^{137}Cs will not change considerably as a result of logging.

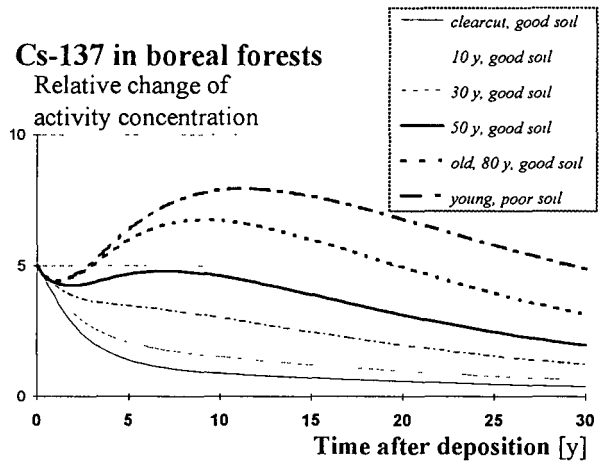

Fig. 10. The change of ^{137}Cs content in the perennial understory vegetation compartment (*Target vegetation* in fig. 6) depending on age of the forest stand at time of fallout and site-specific soil conditions. Moss covers 90% of the ground surface. The mean residence time for Cs in moss and litter is assumed to be respectively 10 and 1 year.

The increased competition for available caesium caused by the addition of new biomass affects the rate of decrease of the ^{137}Cs content in the vegetation. This is indicated by the different dynamics in figure 10 concerning the change of the Cs-137 content in perennial vegetation in the cases with *good soil* as compared to *poor soil*, and younger successional stages as compared to the *old 80 y*.

Besides growth the redistribution is considerably affected by release into circulation from secondary sources such as a moss carpet. The relatively low net biomass increase possible at sites with poor soil or with an old forest means that the dilution effect is rather small while substantial influx may occur from the secondary sources. An implication of these results is thus that the concentration of ^{137}Cs in perennial understorey vegetation will decrease fast in young forests at sites with high primary productivity, while it during an extended period may increase at sites with sufficiently low productivity or old forest.

Comparisons between predicted and measured ^{137}Cs concentrations

The results for bilberry shown in figure 1 are based on pooled data from regular sampling at 10 different sites at the Vindeln experimental forest. At the 10 sampling sites of about one hectare

each, 10 separate subsamples (for statistical assessment of the variability within and between sites) have been taken regularly twice a year (July and October) in the period 1986-1990 (Bergman et al 1991) and continued at a reduced number of sites less frequently till 1994. The sites comprise 3 in mature mesic spruce forests, 4 in dry pine forests, and 4 in young forest at areas, which have been clear-felled within 3-5 years before the Chernobyl accident.

For comparisons of results from the simulations and from measurements the 10 study sites have been categorised according to the site specific factors: age of the forest stand and primary productivity. These factors are of particular importance according to the model. The comparisons in figure 11 test the model predictions against the actual results by specifically focussing on the expected differences in the redistribution dynamics of Cs-137 in the categories (a) young forests or clear-felled areas, and (b) mature coniferous forests (i.e. comprising the pine and mixed coniferous forests at the study sites).

The calculated ratios between the measured concentration in bilberry from category (a) with young forest and from category (b) with mature forest are illustrated in figure 10 for different time periods after the Chernobyl accident: 1) 1986; 2) 1987-1988; and 3) 1989-1990, in comparison to the corresponding ratios according to the model for growing sites with high respectively intermediate primary production.

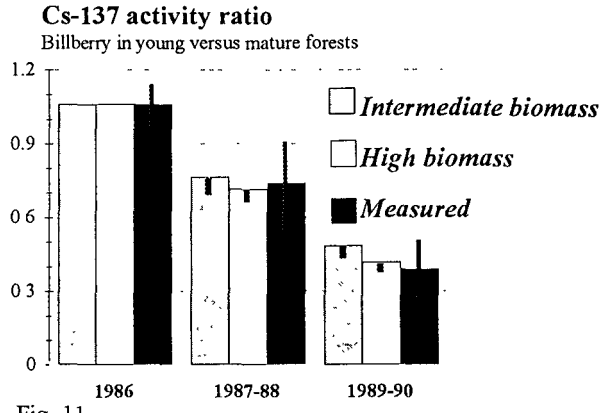

Fig. 11

Ratios between the Cs-137 activity concentration in bilberry in young and mature forests based on measurements, ■, or predictions for cases of high, □, and intermediate, □, biomass. Bars indicate SE for measured data and differences between simulated response in forests which were 3 or 5 years old at the time of fallout.

At the first sampling occasion in July 1986 the Cs-137 concentrations are not significantly different in young- and mature forest areas (Nelin and Nylén 1994). The quotient in figure 11 therefore starts in 1986 at a value close to 1, but decreases significantly over the follwing two periods down to about 1/3. Thus the change towards lower concentrations in bilberry is faster in the young forest or clear cut areas, where the increase in biomass is relatively high, in comparison to that in the mature forest. Concerning the redistribution dynamics for caesium this qualitative dependence on competing biomass is exactly what is predicted by the model. This is apparent from the results in figure 11 of simulations for forests of the same age (3-5 years) for the young and 80 years for the mature stands at fallout at intermediate and good soil conditions, which covers the productivity at the sites in this comparison. The consistency between predicted and measured changes supports our hypothesis about growth as a major regulator of caesium behaviour in the boreal forest.

"Old" ^{137}Cs in different pine stands

Twigs sampled in 1984 from three different pine stands with trees of age 58; 9; or 6 years (see figure 12) indicate that pine trees born before the fifties (i.e. earlier than the start of fallout from nuclear weapons tests) have of the order of 10 times higher levels of Cs-137 in the twigs, as compared to plants of the same size, but less than 10 years of age in 1986. Whether the

difference in concentration of Cs-137 mainly depends on the soil characteristics, on effective retention after deposition directly on old trees, or on cumulative retention as a function of the age of the tree is not clear. In spite of that, it exemplifies that between nearby areas with almost the same deposition of Cs-137 the levels in the vegetation might differ very much in future time. However, the growth at the oldest forest stand had been very low, as indicated by the fact that the pine trees, from which samples were taken, were of the same size (about 2 m) as those at the other two sites with young forest.

In comparison to the results from measurements on the pre- Chernobyl samples of pine twigs from 1984 are presented results in figure 12 for the three simulated cases:

1) fallout on an about 40 year old forest growing on peat soil – i.e. at the period of peak deposition from nuclear weapons tests in the atmosphere during the middle of the sixties – and assumed subsequent sampling 20 years later (i.e. in 1984),
2) fallout in the middle of the sixties on forest growing on good soil, clear-felling about ten years later, new pines planted in 1978, and subsequent sampling 6 years later (1984),
3) similar to case 2 for fallout over forest on "intermediate" soil (productivity 50% of that on "good" soil) and with new plants in 1975 from which samples are taken 9 years later (1984).

The inverse relationship between Cs-137 content in the perennial vegetation and growth capacity (i.e. high content in the vegetation at low net increase of biomass) found at these sites not only agrees with the trend in the predictions made by our model, but fit notably well to the actual levels.

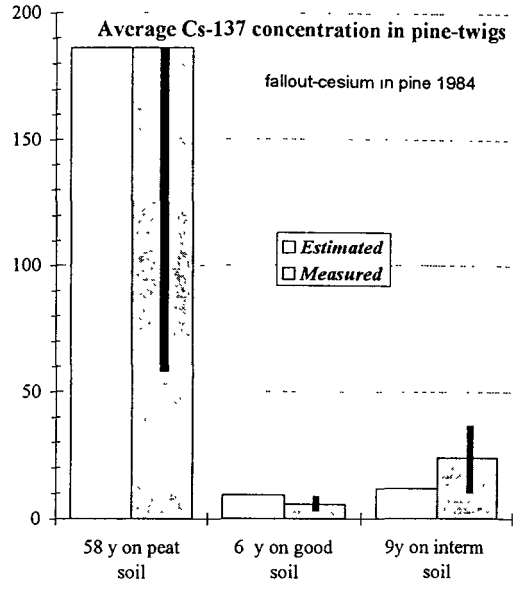

Fig. 12. Measured and calculated activity concentrations of ^{137}Cs in pine twigs in 1984. [Bergman et al. 1993]

The successful correspondence between predicted and measured levels – both in the case of the situation the first five years after the Chernobyl accident (see figure 11) and for the long-term cases (figure 12) associated with fallout from the nuclear weapons tests – strongly supports the general validity of the basic assumption about biomass growth as a governing factor for the redistribution processes in the boreal forest ecosystem.

The contention from these simulations and comparisons is that:

- at the same primary production capacity the decrease in Cs-137 activity concentration in the perennial vegetation is expected to be faster in the young as compared to the mature forest;

- at a particular growing site the rate of decrease of the Cs-137 content in perennial vegetation will be positively related to the local primary productivity (at sufficiently low productivity, e.g. peat soil conditions, decrease may not occur or be extreemely low during several decades).

PUBLICATIONS DURING THE RESEARCH PROJECT

Bergman R, Nylén T, Nelin P and Palo T. 1993. Caesium-137 in a boreal forest ecosystem: Aspects on the long-term behaviour. FOA report C 40284-4.3

Bergman R, Palo T, Nylén T and Nelin P. 1994. Influence by herbivory on caesium turnover in a forest ecosystem. Sci.Total Environ. 157 pp. 301-307.

Bergman R. 1994. The distribution of radioactive caesium in boreal forest ecosystems. In Nordic Radioecology: The transfer of Radionuclides through Nordic Ecosystems to man. (ed. H Dahlgaard) Elsevier Science Publishers, Amsterdam.

Nelin P. and Nylén T. 1994. Factors influencing changes in ^{137}Cs levels with time in boreal-forest plants in Sweden. Sci.Total Environ. 157 pp. 73-81.

REFERENCES

Bergman R, Nylén T, Palo T, Lidström K. 1991. The behaviour of radioactive caesium in a boreal forest ecosystem. In: The Chernobyl fallout in Sweden – Results from a research programme on environmental radiology, Ed. L Moberg the Swedish radiation protection institute). p 425-456.

Head of project 4: Dr. Palo

II. Objectives for the reporting period

The objectives of the project are to improve our understanding of the extent of variation in radiocesium intake in wild animals due to ecological factors. Knowledge of diet composition by wild herbivores is one such factor that is important and insight in animal feeding behaviour will improve our ability to make predictions about contamination levels in animal populations at different seasons, geographical areas and annually. An increased knowledge about radionuclide intake in wild animals would be beneficial to decision makers in their effort to establish guidelines for hunting strategies that limit transfer of radionuclides from game animals to man. Knowledge of animal feeding tactics are important in this respect and necessary for developments of regional and local management plans after accidents and subsequent countermessures that are lenient to the environment. Risk assessment would be considerably improved with the knowledge of underlaying distributions of transfer factors and probability of transfer from vegetation to game.

The aim of the project was measurements of diet composition in moose (Alces alces) and in bank vole (Clethrionomus glareolus), important species in the boreal forest. Comparision between forest types and modelling of time series based on diet selection. Geographical analysis of radiocesium distribution in the moose population was performed.

The use of forest products such as game animals are important commodities for humans. It is estimated that about 100 000 moose and about 150 000 roedeer are shot by the Swedish hunters annually. In addition, some 320 000 hares, 160 000 forest birds are shoot (SCB 1990). The total hunting bag provide about 16x 10^6 kg of meat for consumption by the Swedish human population annually.
In the hunting season of 1986, after the Chernobyl accident, a large number of wild animals were discarded due to elevated levels of ^{137}Cs in their tissues. This caused a pronounced resistance for hunting in areas with high deposition which in turn has led to dramatic increase of deer populations with subsequent damage on vegetation cover. The negative attitude towards hunting in contaminated areas is still prevailing nine years after the accident and levels in game are still high. The consequences caused by the Chernobyl accident on the semi-natural environment and its utility are severe, but could have been substantially reduced with knowledge of variation in diet of wild animal populations and distribution of radionuclides within their feeding areas. There is at present a strong need from decision makers to get accurate predictions about contamination levels in wild animal populations.

III. Progress achieved including publications

Temporal variability in intake

It is difficult to resolve contamination of wild animal populations since many factors besides the amount of deposition affect intake. Diet composition is hard to measure in most situations and animals move over sometimes large distances within a short time span. The range of plant species and plant tissues consumed varies greatly among herbivore species both seasonally and annually (Freeland 1991). Even when the diet is known in some detail, as for most domestic

animals, variation in intake and absorption due to differences in plant quality may still be large (Salt et al. 1994).

Undoubtedly, food is the major transmitter of ^{137}Cs into animals, making diet composition as the most important factor determining the intake of radionuclides by wild animals (Lowe & Horrill 1988; Zach, Hawkins & Mayoh 1989; Lowe & Horrill 1991). Consequently, the variations in dietary composition among individuals and with time, are important factors determining the distribution of radionuclides in animal populations. Most studies on the diet composition of moose have focused on late autumn and winter (Cederlund et al. 1981; Zach et al. 1982, Risenhoover 1989). During this time moose mainly utilise shrubs and trees as their food source (Johansson & Bergström 1991, Palo, Nelin, Nylén & Wickman 1991). Knowledge of the diet at other times of the year, such as in early autumn, and variation between years is poor and presents a problem when considering intake of radionuclides.
It has been shown that quality of major food plants of moose can vary between years and among habitats (Bí & Hjeljord 1991). It is believed that this variation in quality of food plants to a large extent affect feeding patterns and distribution of herbivores in the landscape (Hughes 1993). Despite the logic of this argument few observations exist of herbivores responding to these large scale changes in quality. For example, no significant relationship was found between rainfall pattern and intake of ^{137}Cs in moose (Nelin 1994).
One line of support for changes in diet or habitat is data of the mean activity concentration of ^{137}Cs in the Swedish moose population. Both the mean values (median) and population distributions of ^{137}Cs show unsystematic shifts between years (Palo et al .1991). These changes are puzzling given that the total amount of ^{137}Cs declines as a result of radioactive decay ($T_{1/2}$=30.6 y). We developed a model that takes into account ecological processes such as variation in animal feeding behaviour in an analysis of intake. In this way it might be possible to resolve factors that are important for the intake of ^{137}Cs in free ranging animals. The variation in radionuclide distribution in a population can provide information not only about processes and mechanisms, but also factors underlying individual feeding behaviour (Pinder and Smith 1975).
We have examined how annual variation in diet can explain changes in the ^{137}Cs levels between individuals and between moose populations among years and different environments with same deposition. We use a model in which diet composition varies randomly with time according to a Monte Carlo simulation.

The change of ^{137}Cs content in an animal could be calculated by the equation;

$$d^{137}Cs / dt = \alpha \sum_n p_n \beta_n - \mu k t \qquad (1)$$

Where p_n is the proportion of plant n in the diet, β_n is their activity concentration and α is the daily intake. The body content of ^{137}Cs is lost at rate k where μ is the effect from previous meal. For simplicity we reduced the model to the case where the herbivore's diet is composed of two plant types, B and O. These could be regarded as two types of plants that only differ in initial activity concentrations and that change with different rates with time. One can alternatively consider two types of habitats classified according to high and low deposition and let the animal choose to feed in one of the habitat types in relation to some distribution function of habitat types. Here we consider only the case with two plant types in the diet. the radionuclide concentration (Cs_{conc})in an individual at time t is determined by;

$$Cs_{conc}(t) = \alpha\,(t)\,p + \beta\,(t)\,[1 - p] = p\,[\alpha\,(t) - \beta\,(t)] + \beta\,(t) \qquad (2)$$

where p is the proportion of plant type B in the individual diet and consequently $(1-p)$ is the proportion of the other plant type (O) in the diet. $\alpha(t)$ and $\beta(t)$ denote the functions of annual change in activity concentrations of ^{137}Cs in the different plant types (B and O) as a function of time expressed in Bq/kg. Equation (3) consists of three different processes, firstly, contamination deposited on plant surfaces and that is lost by washout , secondly, a slower overlaid process dependent on the annual fall of plant litter to the ground, and finally, radioactive decay. These processes for a given plant type i are expressed as non–linear equations and the activity concentration of ^{137}Cs (Cs_i) at some time t is given by the equation:

$$Cs_i(t) = \exp\,[-(a_i + b_i) * t] + c_i * \exp\,(-\lambda * t) \qquad (3)$$

where a_i is a specific constant for species i and expresses the rate of loss due to washout of surface contamination by rain , b_i is the amount lost due to litterfall, c_i is the fallout retained in the plant and λ is the physical decay constant. For ^{137}Cs with a half–life of 30 years λ is equal to 0.0231. The species specific constants a_i, b_i and c_i could be determined empirically for each plant type using mean concentration of ^{137}Cs from bilberry (*Vaccinium myrtillus*) and birch (*Betula pubescens*) in September for the year's 1986–1994 (Figure 1).

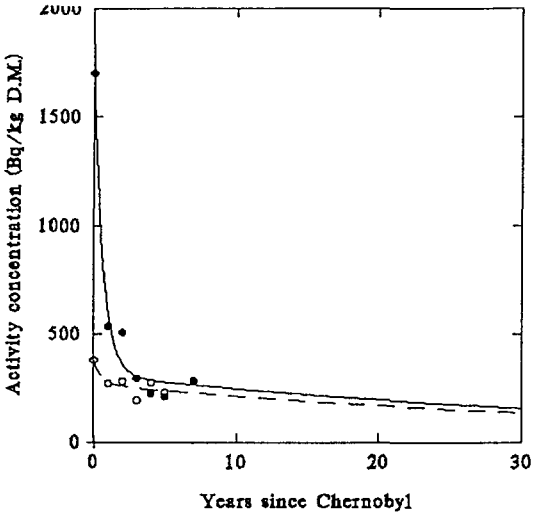

Figure 1. Non–linear regression and interpolation over 30 years of activity concentrations of *Vaccinium myrtillus* and *Betula pubescens*.

Figure 2 shows a Monte Carlo simulation of a time series with thirty individual diets generated by the model during a 30 year period. We varied the individual diet by selecting the proportion (p) of bilberry taken randomly from young and old pine forest in the diet according to an exponential distribution and activity concentrations were calculated for each time step using

equations 2 and 3. Selection of any other distribution function will give a similar result. A non-linear regression of the simulated values to the physical decay equation showed a significant relationship between physical decay and activity concentration but with a low degree of explanation ($Y = \exp^{0.0231 * t}$, $r^2 = 0.486$) (Figure 2).

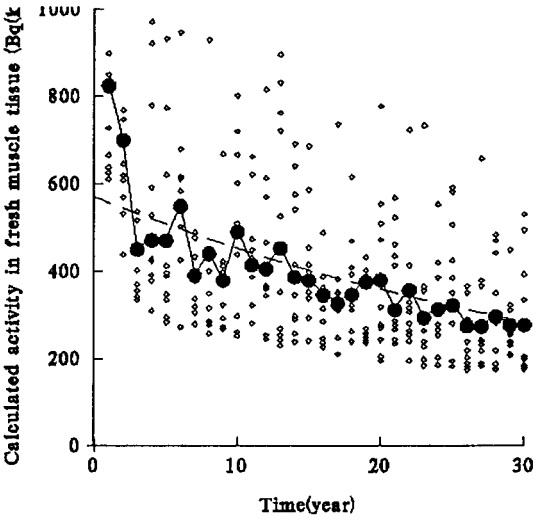

Figure 2. Monte-Carlo simulation of yearly variation in intake of ^{137}Cs over 30 years using data for *Vaccinium myrtillus* in young forest (<10 y) and mature forest (> 50 y). Individual data points, mean value and the function of radioactive decay are shown.

Spatial and temporal variations in transfer of ^{137}Cs to herbivores are common after fallout events. Large variation was observed in caribou (*Rangifer tarandus*) after nuclear bomb testing in the sixthies. Roedeer (*Capreoulus capreoulus*) in Germany and Finland show a yearly variation ranging from 84 to 100 per cent of the mean (Fielitz 1994). For moose in this study, the coefficient of variation range from 60 to 100 per cent between years. Although, deposition is one factor for spatial variability it gives a poor explanation for ^{137}Cs levels observed in herbivores. In the Swedish moose and reindeer, ground deposition at the site of collection explained between 5 to 35 percent of the variability (Palo et al. 1991, Åhman 1994). Nevertheless, amount of deposition within animal's home range nor the size of the home range showed any relationship to individual ^{137}Cs levels in moose (Nelin 1995). Obviously other factors are more important than deposition in explaining variability in animal populations. Although physical decay aggravate ^{137}Cs levels in the animal population with time, this effect is only apparent after several half-life's. Within a period of 30 years, biological factors might be more important for the change in activity concentration in a moose population than physical half-life of ^{137}Cs. As shown in figure 3 the correlation coefficient of physical decay to simulated data in figure (2) increase with time, but physical decay give no significant explanation until after 30 years.

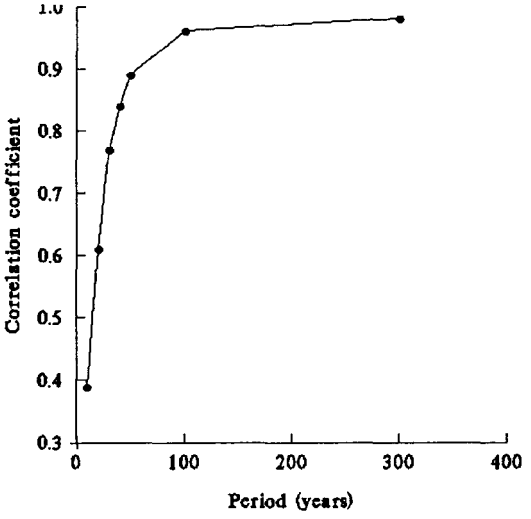

Figure 3. Change in correlation coefficient between radioactive decay and data in figure 2.

Spatial variation

Material from moose was geographically positioned during the sampling in 1986 and 1993. The analysis consist of 409 paired locations for each year. The pixel size is 25x25 km and the analysis was performed in SYSTAT. The area covered is about 52000 km^2 in the county of Västerbotten. Figures 4a and b show the aggregated transfer coefficient (K_{tf}) for 1986 and 1993 respectively. The two years differ significantly in mean K_{tf} with higher value in 1993.

a)

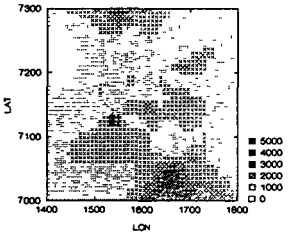

b)

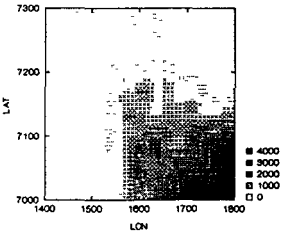

c)

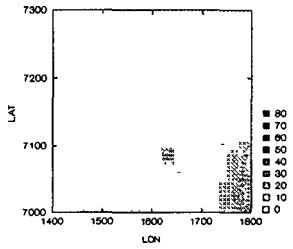

Figure 4 a–c. Aggregated transfer coefficient for moose a) 1986, b) 1993 and c) show the quotient K_{tf} 1986/ K_{tf} 1993.

The quotient in figure 4c show a significant and positivie relationship with ground deposition and suggest that the uptake of ^{137}Cs is higher in 1993 compared to 1986 at level of deposition over 20 KBq/m2. Below this grounddeposition the uptake is lower in 1993 than in 1986. These results are puzzling but might be explained by two possible mechanisms. First, it might be that at low deposition a larger part of the radiocesium is "old" nuclear test fallout that are circulating in the system at a high rate. However, this explanation does not hold in areas with high deposition. An alternative would be that at low deposistion a larger part of the radiocesium has disappeared from the biological matrix, while at higher depositions a larger part is incorporated into living organisms. Thus a logistic function is expected between uptake in plant tissues and deposition rate.

PUBLICATIONS DURING THE RESEARCH PERIOD

Bergman, R., Palo, R.T., Nylen, T. and Nelin, P. 1994. Influence of herbivory on caesium turnover in a forest ecosystem. The Sci.Tot. Environ. 157:310–307.

Nelin, P. 1994. Chernobyl cesium in the Swedish moose population: Effects of age diet and habitat selection. Dissertation, Swedish University of Agricultural Sciences, Umeå, Sweden.

Nelin, P. & Nylen, T. 1994. Factors influencing the change over time in Cs–137 levels in boreal forest plants. J. Sci. Tot. Environ. 157: 73–81.

Nelin, P. 1995. Radiocaesium uptake in moose in relation to home range and habitat composition. J. Environ. Radioactivity 26: 189–203.

Palo, R.T. 1993. Animals and plants as bioindicators of radionuclide contamination in forest ecosystems. In: Use of biomarkers in assessing health and environmental impacts of chemical pollutants, (Ed. C.C. Travis), Plenum Press, New York. 255–263.

Palo, R.T. 1994. Ecological concepts in radioecology. An alternative to Newtonianism. In: Radioecology. Lectures in environmetal radioactivity (ed. E. Holm), pp. 125–136. World Scientific, Singapore.

REFERENCES

Bø, S. & Hjeljord, O. 1991. Do continental moose ranges improve during cloudy summers? Can. J. Zool. 69: 1875–1879.

Belli, M., Sansone, U., Ardiani, R., Scimone, M., Menegon, S. & Parente, G. 1995. The effect of fertilizer applications on ^{137}Cs uptake by different plant species and vegetation types. J. Env. Radioact. 18:75–89.

Belovsky, G. 1984. Herbivore optimal foraging: A comparative test of three models. Am. Nat. 124: 97–115.

Cederlund, G., Ljungqvist, H., Markgren, G. & Stålfelt, F. 1982. Foods of moose and roe deer at Grimsö in central Sweden. Swedish Wildl. Res. 11:171–247.

Danell, K., Nelin, P. & Wickman, G. 1989. 137 Cesium in northern Swedish moose: The first year after the Chernobyl accident. AMBIO 18: 108–111.

Droppo, J.G. 1976. Dry deposition processes on vegetation canopies. In: Atmospheric–surface exchange of particulate and gaseous pollutants (eds. R.J. Engelman and G.A. Schmel), pp. 104–111. US/ERDA Ser. Conf. 740921,1974, Springfield, Va. Natl. Tech. Info. Serv.

Fielitz, U. 1994. Radioaktivität in Wildtieren. Institute für Wildbiologie und Jagdkunde der Universität Göttingen.

Freeland, W. J. 1991. Plant secondary metabolites. Biochemical coevolution with herbivores. In: Plant defences against mammalian herbivory. Eds. R.T. Palo and C.T. Robbins. CRC Press, Boca Raton, Florida. 61–82.

Howard, B. J., Beresford, N. A. & Hove, K. 1991. Transfer of radiocaesium to ruminants in natural and semi–natural ecosystems and appropriate countermeasures. Health Physics 61: 715–725.

Hughes, R. N. 1993. Diet selection. An interdisciplinary approach to foraging behaviour. Blackwell Sci. Publ. Oxford.

Jia, J., Niemelä, P. & Danell, K. 1995. Moose (Alces alces) bite diameter selection in relatin to twig quality on four phenotypes od Scots pine (Pinus sylvestris). Wildlife Biology 1:47–56.

Johansson, K–J & Bergström, R. 1989. Radiocesium from Chernobyl in Swedish moose. Environ. Poll. 61: 249–260.

Kjelle, P. E. 1991. First registration of the Chernobyl accident in the west by the gamma radiation monitoring stations in Sweden. In: The Chernobyl fallout in Sweden. (ed. L. Moberg), pp. 21–28. The Swedish Radiation Protection Institute, Stockholm.

Lowe, V. P. W. & Horrill, A. D. 1988. Ecological half–life of Caesium in Roe Deer (Capreolus capreolus). Environ. Pollut. 54: 81–87.

Lowe, V. P. W. & Horrill, A. D. 1991. Caesium concentration factors in wild herbivores and the fox (Vulpes vulpes). Environ. Pollut. 70: 93–107.

Melin, J. & Wallberg, L. 1991. Distribution and retention of cesium in Swedish boreal forest ecosystems. In: The Chernobyl fallout in Sweden. Ed. L. Moberg. The Swedish Radiation Protection Institute, Stockholm. 467–456.

Palo, R. T., Nelin, P., Nylen, T. & Wickman, G. 1991. Radiocesium levels in Swedish moose in relation to deposition, diet and age. J. Env. Qual. 20:690–695.

Palo, R.T., Danell, K., & Bergström, R. 1992. Digestibility, distribution of phenols, and fiber at different twig diameters of birch in winter. Implications for browsers. Oikos 65: 450–454.

Pinder, J. E. and Smith, M. H. 1975. Frequency distributions of radiocesium concentrations in soil and biota. In Mineral cycling in southeastern ecosystems (eds. F. G. Howell, J. B. Gentry & M. H. Smith), pp. 107–125. Technical Information Center. U.S. Energy Research and Development Administration.

Risenhoover, K. 1989. Composition and quality of moose winter diets in interior Alaska. J. Wildl. Manage. 53: 568–577.

Robbins, C. T. 1983. Wildlife feeding and nutrition. Academic Press, New York.

Salt, C., Mayes R.W., Colgrove, P.M. & Lamb, C.S. 1994. The effect of season and diet composition on the radiocaesium intake by sheep grazing on heather moorland. J. Appl. Ecol.31:125–136.

Stephens, D. W. & Krebs, J. R. 1986. Foraging Theory. Monographs in Behaviour and Ecology (eds. J. R. Krebs & T. Clutton.Brock). Princeton University Press, Princeton.

Zach, R., Hawkins, J. L., & Mayoh, K. R. 1989. Transfer of fallout Cesium–137 and natural Potassium–40 in a boreal environment. J. Environ. Radioactivity 19–45

Zach, R., Chrichton, V. F. J., Steward, J. M. & Mayoh, K. R. 1982. Early winter food habits of Manitoba moose as determined by three rumen analysis methods. Can. J. Zool. 60: 1300–1304.

Åhman, B. & Åhman, G. 1994. Radiocesium in Swedish reindeer after the Chernobyl fallout: seasonal variations and long term decline. Health Phys. 66:503–512.

Head of project 5: Dr. Impens

II. Objectives for the reporting period

The three main objectives were:

1) to assess the effect of canopy on the transfer of radiocaesium from soil to plants;
2) to compare the radiocaesium behaviour in different soil types subjected to the same level of radionuclide deposition;
3) to study the biological retention of radiocaesium in humus and the role of mycorrhizae in soil-plant transfers.

The specific objectives relating to fungi were:

1) to prepare a synthesis of data relating to radiocontamination in wild fungi;
2) to conduct experiments and exchange data/information on fungi and other ecological compartments with various teams;
3) to set up experiments on the transfer of radiocaesium by mycorrhizae.

III. Progress achieved including publications

1. Introduction

In line with our objectives, we continued collecting soil, plant and fungi samples at the sites surveyed before 1992 in the Belgian and Luxembourg Lorraine (Wirth et al, 1992). As explained in an earlier report, this region was selected for two main reasons:

- Luxembourg and southern Belgium of are the most contaminated areas in the Benelux countries (5-10 kBq m^{-2}, compared with an average radiocaesium contamination of about 1-2 kBq m^{-2});
- this region has a wide diversity of soil types (clayey, silty or sandy) over short distances. Radiocaesium transfers can thus be easily compared under similar weather conditions or radionuclide deposition levels.

The main ecological characteristics of the sampling sites are summarised in Table 1.

Table 1 Main ecological characteristics of the sampling sites in Belgium and Luxembourg.

Stations	Canopy	Physiological association	Geology	Soil type	Texture	Humus type
Saint-Leger (BL)	Pine + oak	Luzulo-Quercetum typicum	Sand	Humo-ferric podzol	Sand	Dysmoder
Mersch (LL)	Beech	Melico-Fagetum luzulotosum	Sandstone	Eutric cambisol	Loamy sand	Mesotrophic mull
Arlon (BL)	Beech	Luzulo-Fagetum milietosum	Sand	Eutric luvisol	Light clay	Eumoder
Aubange (BL)	Beech	Melico-Fagetum typicum	Macigno	Calcic cambisol	Clayey sand	Mesotrophic mull
Habay (BL)	Oak	Primulo-Carpinetum filipendulo-aretosum	Marl	Eutric gleyosol	Clay	Calcic hydromull
Florenville (BL)	a.Beech	Melico-Fagetum festucosum	Sandy schist	Dystric cambisol	Clayey loam	Eumoder
	b.Spruce	Melico-Fagetum festucosum	Sandy schist	Dystric cambisol	Clayey loam	Eumoder

BL : Belgian Lorraine

LL : Luxembourg Lorraine

In September 1993, we conducted a joint sampling survey with the Stockholm and Umea teams in the Hille and Vindeln sites in Sweden. In addition to collecting samples for analysis, we also sampled naturally contaminated substrates with a view to culturing mycorrhizae in the laboratory.

During the contract period, we collected 1058 samples, in addition to the 3692 samples already gathered in the 1986-1992 period.

We also participated in three specific workshops on the management and interpretation of fungi databases compiled by the Belgian, German and Italian teams.

2. Material, methods and sampling approach

Benchmark soil, plant and fungi samples are generally collected under the tree canopy at a distance of 1 m from the trunk. This sampling site is the most representative in the western temperate forest. We have shown in previous studies (Guillitte et al, 1990 c, Wirth et al, 1992) that variations in radionuclide deposits are smaller at such sites than at sites close to the trunk or under canopy gaps. When samples are not collected elsewhere, their exact location in relation to the canopy is recorded for the interpretation of results.

Soils are sampled by edaphic horizons using the frame method described by Andolina and Guillitte (1990 b) Each sample usually consists of four individual samples mixed together. Soil sampling takes place in autumn after the leaves have fallen.

Vascular plant samples consist of aerial vegetative parts collected from several plants scattered over the area covered by the benchmark station (± 0.10 ha) or growing around the site where soil samples were taken.

Samples consist of leafy shoots from the current year (geophytes, hemicryptophytes and therophytes) or leaf-bearing branches aged 3-4 years at the most (chamaephytes and phanerophytes). In trees, the bottom branches are sampled, unless otherwise stated. In some cases, samples are subdivided into leaves and branches and/or according to the age of the branch. Because of the low plant density of the understorey vegetation, sampling of underground parts is kept to a minimum to ensure continuous sampling over the years at benchmark stations.

Some herbaceous plants forming thick mats of a single species may be harvested by mowing within the boundary of the frame to assess surface retention. This technique is also commonly used for mosses growing in mats. As far as mosses and lichens are concerned, the whole thallus is collected, with as much as possible of the attached substrate being removed.

Plant sampling usually takes place in summer during the growing period.

In general, fungi samples include several carpophores, harvested using the method used for plants. For each sample, the exact location in relation to the canopy, the maturity stage, the number of carpophores and, for lignicolous fungi, the substrate type are recorded.

Mycorrhizal roots are harvested where they come into direct contact with the carpophores of the presumed mycorrhizal species.

All foreign materials in the samples are removed without using any water, except for underground parts. Samples are weighed either fresh or after freezing, dried in an oven at 105°C and weighed again. They are then ground, wrapped and prepared to fit the volume of the measuring instruments. To this end, samples are often mixed with $CaCO_3$ in powder form.

Gamma-spectrophotometry analyses were performed with a Ge-Li detector in the following laboratories:

- Laboratoire de radioécologie, Faculté des Sciences agronomiques, Gembloux, Belgium;
- IRE, Fleurus, Belgium;
- CEN, Mol, Belgium;
- Laboratoire de physique nucléaire, University of Liège, Belgium;
- Nuclear power station, Tihange, Belgium;
- SCPRI, Le Vesinet, France.

Some of the samples collected in Sweden were analysed by NIRP in Stockholm and by NBC in Umea.

Several inter-calibrations were made from our samples to obtain uniform results.

Chemical analyses using flame spectrophotometry were carried out in our laboratory.

All the the results are expressed at the date of 1.5.1986 to avoid the physical decay of the radionuclides and to facilitate the intercomparisons.

3. Results and discussion

3.1 Soil radiocontamination

3.1.1 Deposits

Table 2 shows the average values of radiocaesium deposits in the holorganic and hemi-organic horizons They are based on the analysis of samples collected in 1986-1989 when caesium migration to mineral horizons was negligible.

Table 2 Mean values of radiocaesium deposits on the ground at sampling sites (in Bq/m^2).

	Mersch Beech	Arlon Beech	St-Léger Pine	Aubange Beech	Habay Oak	Florenville Beech	Florenville Spruce
Cs137 from Chernobyl	3860	3430	3080	3280	2520	2440	2230
Cs134 from Chernobyl	2010	1780	1600	1710	1310	1270	1160
Cs137/Cs134 from Chernobyl	*5870*	*5210*	*4680*	*4990*	*3830*	*3710*	*3390*
Cs137 from bombs	540	550	810	2410	1140	1550	1760
Cs137 Total	*4400*	*3980*	*3890*	*5690*	*3660*	*3990*	*3990*
Cs137/Cs134	*2.19*	*2.24*	*2.43*	*3.33*	*2.79*	*3.14*	*3.44*

Despite the short distances between the benchmark stations, there is a clear SE-NW decreasing gradient in the deposition of radiocaesium from Chernobyl. There can be no comparison of the differences in deposition between stations (values ranging from 3,390 Bq/m² to 5,870 Bq/m²) and within stations under forest cover. For example, in 1990, ^{137}Cs deposits varied from 3,050 to 20,300 Bq/m² in Mersch under beech and from 2,700 to 14,500 Bq/m² in Florenville under spruce.

Previous ^{137}Cs deposits resulting from nuclear tests in the atmosphere and unmapped before the Chernobyl accident were estimated by subtracting the product of ^{134}Cs by 1.92 from the total ^{137}Cs. This value corresponds to the ^{137}Cs/^{134}Cs ratio determined in the air when the radioactive cloud was blown over the region in May 1986. The calculated values are nearly always inversely proportional to the values of the Chernobyl deposits. The highest values in early ^{137}Cs deposits were recorded at the stations with the highest elevation and average annual rainfall. The variation between the other stations can be ascribed to differences in migration towards deeper soil horizons. This topic will be discussed in more depth later.

The inverse relationship between the most recent and the earlier deposits results in a highly variable ^{137}Cs/^{134}Cs ratio between stations. It is easier to separate the calculated ratios of individual soil layers - and therefore to monitor the migration process - at stations with a high ^{137}Cs/^{134}Cs ratio. However, the variation in soil deposits causes the ^{137}Cs/^{134}Cs ratio to vary more substantially, making it harder to compare plants or fungi ratios with the calculated soil ratios when, as is often the case, the different ecological compartments are not sampled within a radius of about 10 m. For instance, a 50% variation from the average value of the radiocaesium deposit from Chernobyl resulted (1) in Florenville, under spruce, in a 17% or 44% change in the ^{137}Cs/^{134}Cs ratio (from 3.44 to 2.97 or 4.95), depending upon whether the variation was positive or negative, and (2) in Mersch, under beech, in a 4% or 12% variation (from 2.19 to 2.10 or 2.46). The variability of the ^{137}Cs/^{134}Cs ratio in the two locations and in the different places in relation to tree trunks is illustrated in Table 3. It is clear that the higher the value of the average ratios the higher their variability.

Table 3 Variation of the $^{137}Cs/^{134}Cs$ ratio measured in holorganic and hemi-organic horizons.

LOCATION	NEAR TRUNK	UNDER CANOPY	UNDER GAP
Ratio in O horizons			
Florenville Spruce	2,44 ± 0,30	2,23 ± 0,38	2,41 ± 0,30
Mersch Beech	1,91 ± 0,21	2,01 ± 0,09	1,97 ± 0,40
Ratio in Ah horizons			
Florenville Spruce	5,40 ± 2,54	4,27 ± 1,36	4,59 ± 2,56
Mersch Beech	2,31 ± 0,21	2,29 ± 0,17	2,36 ± 0,30

3.1.2 Evolution of specific activities

From 1986 to 1994, the specific activity of ^{137}Cs dropped by 80-90% in holorganic horizons (0-horizons) following a conventional exponential decrease (Table 4). In year 1, a reduction of about 40% had already been observed in all the stations surveyed in 1986. However, in 1987-1994, the rate of reduction varied substantially between stations. This variation is attributed to the type of humus and, therefore, to the rate of decomposition of the organic matter at the various stations. During the same period, activity decreased by 80-90% in the 0 horizons of mull humus and by 65-80% in moder humus.

Table 5 shows that, in general, the $^{137}Cs/^{134}Cs$ ratios in the horizons and in the radioactive cloud from Chernobyl are similar and remain fairly constant over time. It is worth noting that the $^{137}Cs/^{134}Cs$ ratio exceeds 1.92 at only three stations - the three with moder or dysmoder humus, indicating the presence of fairly large amounts of caesium originating from the nuclear tests in the atmosphere. Holorganic horizons of mull humus would contain only very low concentrations of caesium, probably bound to slowly decomposing ligneous matter (such as root and branch debris and beechnuts). This could also explain the recent ratio increase in the 0 horizons in Mersch after a large part of the Chernobyl caesium had left these horizons. The substantially higher ratio observed in 1986-1987 in Florenville can be attributed to the partial retention of initial deposits from Chernobyl by the persistent spruce canopy.

Differences in dynamics can be observed between the holorganic horizons at the same station. Table 9 and Figure 1 illustrate the evolution of caesium activity in specific horizons under spruce in Florenville. Whereas the activity decreased exponentially in the Ol horizon, it increased and peaked in 1987-1989 in the Of and Oh horizons, before decreasing exponentially, albeit at a slower rate than in the Ol horizon.

Table 6 shows the evolution of activity in fresh litter (Ol1) which must be compared with the values of canopy contamination (see below). The sharp reduction in activity observed in 1992 was followed by a rise in 1994, particularly at stations with sandy soils. This phenomenon can be attributed to renewed root growth in deeper horizons. The scanty data collected in the OAh horizon at some stations always indicated a very high specific activity.

With regard to hemi-organic horizons (Ah), a gradual increase was observed, with peak values being reached in 1989-1990 (Table 7). A subsequent reduction was noted, possibly the result of sampling artefacts as these horizons do not always have a well-defined lower boundary.

However, at the Saint-Léger station where the sand fraction in soils is the highest, one third of the total deposit was found in deep horizons (down to 1 m depth), which indicates that a massive migration can occur towards the mineral horizons. Conversely, at the Habay station where soils have the highest clay content, there was no activity increase in the mineral horizons and the activity in the Ah horizons was remarkably constant over time

Table 4 Evolution of the O specific activities in ^{137}Cs at the sampling sites.

	Mersch Beech	Arlon Beech	St-Léger Pine	Aubange Beech	Habay Oak	Florenville Beech	Florenville Spruce
O 86	1880	-	1510	-	-	770	-
O 87	1180	1010	900	930	250	445	550
O 88	760	1185	670	1035	-	-	390
O 89	780	665	520	730	-	410	-
O 90	1310	870	1025	650	-	465	475
O 92	320	275	305	480	7	200	200
O 93	-	-	-	-	-	170	210
O 94	160	210	320	250	35	145	180

Table 5 Evolution of the $^{137}Cs/^{134}Cs$ ratio in O horizons at sampling sites. (E = statistical error more than 50%).

	Mersch Beech	Arlon Beech	St-Léger Pine	Aubange Beech	Habay Oak	Florenville Beech	Florenville Spruce
O 86	1.63	1.56	1.86	-	-	2.20	3.20
O 87	1.96	1.56	2.14	1.95	-	2.24	2.68
O 88	1.80	1.82	1.98	1.98	-	-	2.08
O 89	1.76	1.81	1.93	1.82	1.82	2.01	-
O 90	E	E	E	1.93	-	2.11	2.23
O 92	E	E	E	E	E	E	E
O 93	-	-	-	-	-	1.78	2.23
O 94	2.44	E	E	E	E	E	2.23

Table 6 Evolution of the specific activities measured in the soil horizons at Florenville (spruce stand) (The $^{137}Cs/^{134}Cs$ ratio values are given in brackets).

	Mersch Beech	Arlon Beech	St-Léger Pine	Aubange Beech	Habay Oak	Florenville Beech	Florenville Spruce
Oll 86	250	-	590	-	-	130	-
Oll 87	260	160	1060	200	77	80	425
Oll 92	39	12	12	19	7	20	53
Oll 93	-	-	-	-	-	19	55
Oll 94	40	65	98	37	35	25	26

These differences in caesium migration from organic to mineral horizons and the differences within mineral horizons between soils with a high and a low clay content could explain the differences in the activity of the ^{137}Cs originating from nuclear tests in the horizons of these soils. For instance, in the soils of the three stations with the highest sand content and the lowest clay content, the average activity in the humus is about 3 times lower than in the soils at other stations (Table 2).

Although the $^{137}Cs/^{134}Cs$ ratio decreases exponentially (Table 8) over time, as expected, it always remains above 1.92. This seems to indicate that older deposits persisted for a long time and that a major part of the more recent deposits are also likely to be bound for a long time in these

horizons. However, there is some variation in the rate of decrease between stations. The ratio levels off faster in stations with mull humus and a low ^{137}Cs activity in the humus. Conversely, the ratio had not yet stabilised in 1994 in the Ah horizons at the Florenville station, which is characterised by large older deposits and moder humus.

Table 7 Evolution of the Ah specific activities in ^{137}Cs at the sampling sites.

	Mersch Beech	Arlon Beech	St-Léger Pine	Aubange Beech	Habay Oak	Florenville Beech	Florenville Spruce
Ah 86	150	-	70	-	-	240	43
Ah 87	195	155	170	85	120	310	290
Ah 88	285	665	105	115	75	-	285
Ah 89	345	360	155	167	-	430	-
Ah 90	190	810	145	525	64	380	380
Ah 92	180	470	160	260	76	230	240
Ah 93	-	-	-	-	-	260	210
Ah 94	200	300	80	120	67	315	340

Table 8 Evolution of the $^{137}Cs/^{134}Cs$ ratio in Ah horizons at sampling sites. (E = statistical error more than 50%)

	Mersch Beech	Arlon Beech	St-Léger Pine	Aubange Beech	Habay Oak	Florenville Beech	Florenville Spruce
Ah 86	2.83	-	E	-	-	9.50	9.52
Ah 87	2.40	2.61	3.63	8 20	12.20	7.64	5.18
Ah 88	2.11	2.02	3 00	3.85	2.69	-	4.23
Ah 89	2 08	2.20	2.47	3.85	1.86	3.87	-
Ah 90	E	E	E	3.04	2.12	3.06	4.26
Ah 92	E	E	E	E	E	2.72	4.00
Ah 93	-	-	-	-	-	2.41	3.80
Ah 94	2.13	2.29	E	E	E	E	3.52

Table 9 Evolution of the specific activities and deposits measured in the soil horizons at Florenville (spruce stand) (The $^{137}Cs/^{134}Cs$ ratio values are given in brackets).

HORIZONS	1986	1987	1988	1990	1992	1993	1994
Specific activities (Bq/kg D.M.)							
O		550 (2,68)	390 (2,08)	475 (2,23)	197 (2,99)	210 (2,23)	180 (2,23)
Ol	700 (2,04)	530 (2,04)			124	190	73
Ol1		425 (2,01)			53	55	26
Ol2		700 (2,22)			150	260 (1,85)	85
Of+Oh	270 (3,73)	540 (2,75)			240	210 (2,28)	230 (2,62)
Of		465 (2,22)					180
Oh		590 (3,12)					255
Ah	43 (9,52)	290 (5,18)	285 (4,23)	390 (4,26)	236 (4,00)	210 (3,8)	340 (3,52)
B		100 (5,07)		100	70	76 (7,7)	90
C		27			3		
Deposits (Bq/m²)							
O		2190	740	1630	690	580	815
A		1640	2975	4010	2066	1350	615
B		1110			1322	1520	1520
C		570			1322		

As the more mobile ^{137}Cs present in the Chernobyl deposits has the ability to migrate to the deeper mineral horizons, a slight ratio increase can be expected at some stations. Such a rise had already been recorded at the Mersch and Arlon stations, two of the three stations where soils have the lowest clay content.

3.1.3 Partial conclusions

The observed phenomena seem to indicate that two migration patterns come into play:

a) a gravitational mechanism involving free caesium and occurring over a short period of time after its arrival in the individual soil horizons;

b) a biological mechanism occurring over a long period of time and involving complexed caesium and/or caesium bound to minerals, organic matter or their complexes.

In both cases, a distinction needs to be made between their activity in holorganic horizons which involves only the organic component, and their activity in hemi-organic horizons which also involves the mineral component.

In the first case, migration is influenced by several factors:

- rainfall during the period under consideration;
- the complexing or sorption capability of the organic matrix (this matrix depends upon the type of litter - the mineral content differs according to tree species and nature of the subsoil - and, more importantly in our opinion, on the state of decomposition and thickness, which is directly related to the type of humus. The Oh and OAh horizons probably play a major role in caesium retention);
- the binding, complexing or sorption capability of the organo-mineral complex (particularly in the hemi-organic horizon), the texture of the horizon and more importantly its clay and sand content are certainly determining factors.

The same factors apply to the second case, with the exception of rainfall which plays only a secondary and indirect role However, other factors which have to be taken into account are:

- the biological activity in the holorganic horizons, which varies considerably depending upon the type of humus (influence of arthropods and fungi on mull and moder humus, respectively);
- the biological activity in the hemi-organic horizons, which also varies depending upon the type of humus (influence of earthworms and burrowing mammals in addition to arthropods and fungi) and the presence of physical barriers to this activity (such as the presence of gley and rocky soils).

3.2 Soil-fungi transfers

3.2.1 Introduction

Fungi are characterised by the fact that they interface with three different combinations of soil elements:

- soil solution/soil matrix interface (the soil matrix includes the organic matter, organo-mineral complexes and, more rarely, pure mineral particles)
- soil solution/root system interface
- root system/soil matrix interface

The development of a large mycelial net which comes into contact with these interfaces gives us reason to believe that fungi play a major role in the redistribution of caesium, mainly in the organic parts of forest soils.

However, one of the main difficulties in assessing the role of fungi lies in the determination of the exact location of their mycelium. In an attempt to solve this problem, we were amongst the first researchers to suggest (Guillitte et al, 1990 a) the comparative use of the $^{137}Cs/^{134}Cs$ ratios in the carpophores of macromycetes and in soil horizons. This methodology is based on several hypotheses which need to be confirmed, namely that:

a) the mycelium of each species colonises well-defined soil horizons;

b) the mycelium does not make any distinction either between ^{134}Cs and ^{137}Cs or between the ^{137}Cs originating from Chernobyl and that from the nuclear tests;

c) there is no difference between the different types of radiocaesium during their translocation from the mycelium to the carpophores.

In addition to these working hypotheses, several conditions have to be met during deposition:

a) the deposits of the Chernobyl caesium should be large enough to measure ^{134}Cs reliably for several years;

b) the deposits from Chernobyl or from nuclear tests should not be present in excessively large or low quantities such that they can be distinguished from one another;

c) sampling should take place as soon as possible after the latest deposition to preclude the risk of "blending" through vertical redistribution;

d) measurements should be made as early as possible after sampling.

Regarding the first and fourth conditions, our team is at a disadvantage compared with the other teams involved in this study. It was not possible for us to conduct a comparative study of the $^{137}Cs/^{134}Cs$ ratio in the carpophores and soil horizons that were the least contaminated after 1990. However, the ratio remains useful in comparing the most contaminated species in different locations and over time.

On the other hand, our team and the Trieste team had the edge over the other teams with respect to the second and third conditions for many of the stations under study.

We also came across several methodological problems, including the following.

a) because of variable weather conditions from year to year, it was difficult to sample the same species every year;

b) it was difficult to collect soil and carpophore samples at the same time and in the same place (this was achieved only during our sampling trips abroad) while bearing in mind (1) that there is not necessarily a link between where carpophores were picked up and where caesium is being absorbed by the mycelium, and (2) that soil variation is very large, even over short distances (see 3.1.1).

3.2.2 Experimental confirmation of mycelium location

For this purpose, we ranked the $^{137}Cs/^{134}Cs$ ratio of species by station and by year, in decreasing order. We also included their specific activity (Table 10). We used data from stations in Belgium (10), Italy (10) and Germany (3) between 1986 and 1993. Since samples from Italy were homogeneous across stations and years, it was possible to rank each species and represent the

ranking by a percentage in order to calculate the average position of the species (all stations and years), irrespective of the number of species sampled at each station (Table 11). For the Belgian and German stations, it was possible to compare the data relating to fungi with the activities determined in the soil horizons.

Table 11 Mean values and standard deviation of the ranking (in %) of the species grouped according to the $^{137}Cs/^{134}Cs$ ratios determined in fruiting bodies collected at the sampling sites in Italy. The species with the lowest value presented frequently and yearly the lowest ratio at all sampling sites.

SPECIES (BIOLOGICAL BEHAVIOUR)	RANK (expressed in %)
M = mycorrhizal species H = humo-terricolous species L = lignicolous species	
GROUP A	
Laccaria amethystina (M)	24 ± 15
Lactarius blennius (M)	30 ± 10
Russula emetica (M)	31 ± 13
Macrolepiota procera (H)	33 ± 32
Armillariella mellea (L)	34 ± 29
Lactarius gr deliciosus (M)	35 ± 20
Lactarius rubrotinctus (M)	38 ± 10
Hypholoma capnoides (L)	39 ± 29
Lespista spp. (H)	41 ± 25
Russula delica (M)	42 ± 23
GROUP B	
Lactarius pallidus (M)	57 ± 20
Russula fellea (M) *Russula ochroleuca (M)*	60 ± 30
Piptorus betulinus (L)	61 ± 26
Hygrophorus spp. (M)	62 ± 25
Hebeloma sinapizans (M)	63 ± 15
Hypholoma sublateritium ((L)	66 ± 27
Albatrellus ovinus (M)	67 ± 25
GROUP C	
Russula nigricans (M)	75 ± 18
Tricholoma spp. (M)	82 ± 20
Ramaria spp. (M)	86 ± 30
Sarcodon imbricatus	86 ± 21

A number of general observations can be made.

a) The ranks of species from station to station and, particularly, from year to year, did not vary considerably. This observation also applied to the few species that were sampled regularly in the three countries.

b) The variation in the ratios determined in fungi from a given station always diminished over time, irrespective of the station. However, the pattern of this decrease was specific to each station. For the years for which soil data were available, it coincided with the decrease in the ratios determined in the soil horizons at the same stations (for example, see Tables 5 and 8, and Table 10 for comparison) The ratios determined in fungi in Belgium and Italy were generally higher than in Germany because the ratios of the soil deposits from Chernobyl and from nuclear tests were more balanced in the first two countries.

c) In general, when species had had a consistently low ratio since 1986 (group A), their contamination decreased substantially and regularly over time, following the same trend as contamination in the Ol horizons. Conversely, when species had a high initial ratio (group C), this ratio decreased while their contamination was increasing, until recently. The Ah horizons showed a similar trend. Species with an intermediate ratio (group B) were also characterised by decreasing ratios but their contamination was more variable over time. However, a peak was usually observed in 1987-1989, which coincided fairly well with the evolution of these parameters in the Oh horizon. The highest contamination levels in fungi were often found in this category of species.

d) The transfer coefficients calculated on the basis of the activities determined in fungi and in the soil horizon that had a $^{137}Cs/^{134}Cs$ ratio identical to that of carpophores were much less variable from year to year, for a given station, than coefficients calculated on other bases (Guillitte et al, 1990 a)

All these observations support the working hypotheses. If there were any differences between the various types of radiocaesium, the ratio in fungi would probably be lower as we can logically assume that the caesium from Chernobyl is more available. In fact, it was surprising to observe, on several occasions, a sudden drop in the ratio value of species usually characterised by a high ratio and thought to colonise the deepest humus layers and, simultaneously, an increase in their contamination level in the following years, rather than the the opposite trend. It is likely that these species make use of the input of a relatively free and available form of the Chernobyl caesium through the gravitational mechanism suggested earlier.

It is unlikely that there is any distinction between ^{134}Cs and ^{137}Cs from Chernobyl, although several fungi have a ratio much lower than 1.92. However, in most cases, they are also characterised by a low activity which makes the ratio rather unreliable. Furthermore, there could be no consistency of transfer coefficients calculated by the method described if such a distinction existed. Finally, the known biology of fungi matches perfectly the mycelium stratification based on these ratios. Saprophytic species fall mainly into groups A and B, as defined above, while litter-inhabiting species fall into group A. The so-called mycorrhizal species are also present in both groups, but mainly in group B. Obligate mycorrhizal species are found only in groups B and C, but mainly in group C. It is worth noting that the soil layers colonised by the mycelium vary and are known. The mycelium of *Laccaria amethystina* penetrates ever deeper horizons as the invaded tree ages. Variable drought conditions over the years can also influence the depth of the mycelium. At the same station, a species may colonise different soil horizons, depending upon the humus type and, particularly, the thickness of the holorganic horizons. The Habay station is a typical example (Table 12); here, the fungus is found either in the litter or, because of the full decay of holorganic

horizons, in the hemi-organic horizons. It should be noted that the contamination is completely different under such conditions, which highlights the need to know the exact location of the mycelium in order to gain more insight into the transfer of radio-elements.

Table 12 Specific activities in ^{137}Cs and $^{137}Cs/^{134}Cs$ ratio (in brackets) measured in fruiting bodies collected in 1989 from three humus types at Habay.

	OAK STAND		SPRUCE STAND
O-Horizons	ABSENT	PRESENT	PRESENT
Lactarius vellereus	120 (3,06)	--	--
Amanita muscaria	--	--	1230 (3,04)
Xerocomus subtomentosus	--	160 (2,31)	--
Dermocybe cinnamomea	--	--	7990 (2,72)
Laccaria amethystina	--	6520 (2,06)	870 (2,54)
Hygrophorus pustulatus	--	--	2370 (2,37)
Russula sp.	--	--	1950 (2,26)
Lactarius quietus	260 (2,15)	2480 (2,22)	--
Cortinarius anomalus	1020 (2,11)	47270 (2,11)	6720 (2,11)
Laccaria laccata	80 (0,61)	13540 (1,95)	--
Russula nigra	--	360 (2,06)	--
Inocybe geophylla	240 (1,97)	--	--
Xerocomus chrysenteron	--	1030 (1,92)	--
Boletus edulis	100 (1,68)	--	--
Lactarius mitissimus	30 (1,66)	--	--
Lactarius fuscus	60 (1,06)	--	--
Entoloma rhodopolium	730 (0,39)	--	--

3.2.3 Exploitation of results

The results obtained enabled us to undertake a considerable amount of work aimed at determining the transfer coefficient for each species or group of species which were taxonomically or ecophysiologically related. The study carried out on a limited number of species highlighted differences in the order of 10 in the transfer coefficients of carpophores from the same species but collected in entirely different ecological conditions (Habay and Saint-Léger). However, major differences in the transfer coefficient are sometimes observed between species from the same station, or sometimes between carpophores from the same species, whose mycelium colonised entirely different horizons. The difference in the contamination level of 1 to 170 in the *Laccaria laccata* samples collected in Habay on bare soil and on litter (Table 12) can be explained partly by the higher specific activity of holorganic horizons, but mainly by a transfer 30 times larger in these horizons.

The determination of the transfer coefficient is also fraught with methodological problems. For instance, the basis for determining the transfer coefficient will always be biased when using the activity in the Oh and OAh horizons, particularly when they have a large fungal biomass and when our experiments (Guillitte et al, 1994 a) and the measurement of the mycelial activity have led us to believe that we are dealing with a strong biological retention. We also suspect that these horizons act as a reservoir of caesium which is "pumped" by the mycelium and then re-introduced into the upper soil horizons By ensuring the recycling of caesium within

holorganic horizons, the mycelium also slows down its migration towards the mineral horizons (see the experiment conducted jointly with the Umea team).

The comparison of the ratio with the specific activity enables us to identify those species that really accumulate caesium. We have drawn up such a comparative graph on a country-by-country basis for the whole set of data (all stations and years). Figure 2 represents the situation in Italy. Similar graphs were prepared for Belgium and Germany. Concentric distributions, although somewhat offset from the average values, can be observed for the three main biological groups: lignicolous saprophytes or parasites, humo-terricolous saprophytes and the mycorrhizal group (with the largest distribution).

By dividing the graph around the average contamination and $^{137}Cs/^{134}Cs$ ratio values, four areas can be distinguished:

- left, bottom: non- or poorly accumulating species (mainly saprophytes) with a superficial mycelium;
- right, bottom: undoubtedly accumulating species with a superficial mycelium (large majority of mycorrhizal species);
- left, top: non- or poorly accumulating species with a deep mycelium (majority of mycorrhizal species);
- right, top: super-accumulating species with a deep mycelium (exclusively mycorrhizal species).

This type of graph can prove very useful in improving our understanding of contamination trends in fungi. The approach can be applied on a station or year basis and further refined by comparing these values with soil data. In the latter case, the accumulating characteristic can be ranked on a less artificial and more precise basis by using the average ratio values in the benchmark soil horizons.

3.2.4 Partial conclusions

Fungi play an important role in caesium migration. However, there is some confusion as to the exact nature of this role.

They are unrivalled when it comes to decomposing organic matter. In holorganic horizons, particularly in moder or dysmoder humus, they can remobilise and release the caesium immobilised or retained in organic matter, thereby enabling it to migrate towards lower soil layers.

The dense mycelial nets in these horizons can act as radiocaesium filters/traps during the gravitational movements of the soil solution and hence slow down the migration of this element towards deeper layers.

Moreover, fungi can induce horizontal and vertical flows through their structures, mainly to carpophores or to plants that may even reverse the migration trend of caesium.

3.4 Transfers soil/plants through fungi

3.4.1 Indirect influence

The joint experiment carried out in Vindeln in 1993 with the Umea team showed that in the boreal forest a substantial part (up to 75% locally) of the soil caesium is mobilised to carpophores at fruiting time. When decaying, carpophores increase the caesium content in the soil. This phenomenon can influence the pattern of initial deposition, which is related to the type of cover, and may cause unexpected levels of contamination in plants over the years. For instance,

blueberries collected in Vindeln in the vicinity of carpophores had a significantly higher specific activity than those collected further away from carpophores. This clearly illustrates the indirect role fungi can play in the contamination of understorey plants.

3.4.2 Direct influence through ectomycorrhizae

All forest trees are colonised by mycorrhizae, particularly ectomycorrhizae. Mycorrhizae can either stimulate or block the transfer of caesium. To date, no experiment has defined the exact nature of their involvement, but several observations seem to support the hypothesis that mycorrhizae are responsible for an increased transfer of caesium to trees.

a) The experiment conducted with the Stockholm team in 1993 in Hille showed that the contamination in roots colonised by mycorrhizae was significantly higher compared to non-colonised roots.

b) In the old spruce stand at Florenville, the needles of the trees that were directly exposed to the fallout were 3 times less contaminated in 1990 than the needles from young spruces growing at the foot of older trees and never subjected to the direct fallout. Although young spruces tend to grow their roots in more superficial - and therefore more contaminated - soil layers than older trees, we believe that this difference in contamination results from the mycorrhizal association, as nearly all the roots of the young spruces were colonised by mycorrhizae.

c) Table 13 shows the evolution in the contamination level of the tree canopies at the Saint-Léger and Habay stations. The canopies of the beeches at both stations were equally contaminated by the fallout in 1987; however, it is noteworthy that they quickly became decontaminated (95% reduction at Habay; 60% at Saint-Léger). The lower rate of reduction at Saint-Léger can be attributed to a compensation mechanism through root absorption involving mycorrhizae. It also appears that the canopy of pine and oak, which have a deeper root system, is more contaminated than that of beech. There is no doubt that mycorrhizae are largely responsible for this phenomenon Indeed, pine and oak establish a state of mycorrhizal association with many strongly accumulating species (*Lactarius camphoratus, L. theiogalus, Xerocomus badius, Suillus variegatus,* etc.).

Table 13 Evolution of the specific activities in ^{137}Cs in foliage sampled at Saint Léger and Habay.

	Habay Beech	**Saint-Léger Beech**	**Saint-Léger Pine**	**Saint-Léger Oak**
1987	220	260	55	530
1989	19	105	--	--
1990	13	260	300	820
1992	13	100	390	610

3.4.3 Direct action through ericoid mycorrhizae

The contamination level of understorey plants is generally lower than that of fungi. As an example, Table 14 shows the evolution of specific activity in the raspberry bush (*Rubus idaeus*) at our various stations. This plant, which does not enter into any association with mycorrhizae, was only slightly contaminated. Decontamination occured quickly and at a much faster rate than holorganic horizons at all stations. This indicates that the transfer takes place directly from the soil solution to the plant and that the caesium available in the solution decreases faster than other

caesiums. The coefficient factor varies over time, whether it is calculated from the activities in the 0 or Ah horizons, or in the whole humus.

The situation differs for plants in the Ericaceae family (Table 15). They are mycotrophic and are invaded by mycorrhizae. Decontamination in these plants is strongly correlated with that of the holorganic horizons. The transfer factors based on these horizons do not vary much over time. In this case, caesium cannot originate exclusively from the soil solution. Since higher plants are unable to decompose organic matter directly, it follows that symbiotic fungi are involved in the transfer of caesium from the organic matter to the plant.

Table 14 Evolution of the specific activities in ^{137}Cs in *Rubus idaeus* at the sampling sites.

	Mersch Beech	Arlon Beech	St-Léger Pine	Aubange Beech	Habay Oak	Florenville Beech	Florenville Spruce
1987	470	670	--	--	--	--	--
1989	460	610	500	40	23	290	--
1990	260	35	--	60	30	220	200
1992	24	80	120	10	13	80	13
1993	10	26	70	20	40	14	25

Table 15 Evolution of the specific activities in ^{137}Cs in *Calluna vulgaris* and *Vaccinium myrtillus* (in brackets) at the sampling sites.

	Mersch Beech	Arlon Beech	St-Léger Pine	Aubange Beech	Habay Oak	Florenville Beech	Florenville Spruce
1987	--	--	1670	--	--	--	(440)
			(1000)				--
1989	--	(750)	(940)	--	--	(190)	--
1990	--	(260)	1910	--	--	(390)	(350)
			(910)				
1992	--	--	--	--	--	(480)	(300)
1993	--	--	1170	--	--	--	(220)
			(730)				

Table 16 Evolution of the specific activities in ^{137}Cs in *Dryopteris carthusiana* and *Deschampsia flexuosa* (in brackets) at the sampling sites.

	Mersch Beech	Arlon Beech	St-Léger Pine	Aubange Beech	Habay Oak	Florenville Beech	Florenville Spruce
1992	510	360	1310	--	35	430	670
	(780)				(50)		
1993	--	410	1530	--		370	580
(summer)					(40)		
1993	1450	540	2670		10	1010	610
(automn)	(690)			(31)	(90)		

3.4.4 Direct action through endomycorrhizae

Endomycorrhizae are found on any graminous forest species The relatively high contamination level in the wavy hair grass (*Deschampsia flexuosa*) could be explained partly by the presence of endomycorrhizae. The role played by endomycorrhizae was clearly demonstrated by the Trieste team in ferns, particularly *Dryopteris carthusiana*. Our data (Table 16) confirm their observation that contamination is subject to a strong seasonal effect (differences ranging from 1 to 3) and peaks in autumn when mycorrhizae reach their maximum development.

The contamination trend in *D. carthusiana* is similar to that of the Oh or Ah1 horizons (soils with rapidly decaying litter). The maximum retention of caesium in these horizons and their desorption by endomycorrhizal fungi could explain the very high and exceptional constant contamination level in these plants compared with other understorey plants.

4. Conclusion

Our study emphasised that, under similar weather conditions, an identical radiocaesium deposit could result in a wide range of contamination processes of the various ecological compartments, depending upon the type of soil and humus. Fungi appear to be a key element in the migration and transfer of radiocaesium.

Based upon our observations, two broad situations can be defined and related to intermediate situations.

1) Forest soils with mull humus
The decomposition of holorganic horizons occurs rapidly and depends mainly upon the activity of the soil microfauna. The role of the fungi is somewhat negligible, except for the transfer of radionuclides to carpophores or some plants Decontamination takes place quickly in all ecological compartments but the levels of contamination may be very high in the early years, even in the case of fairly thin holorganic horizons. The soil texture (which mainly influences the drainage of underlying mineral horizons), the mineral composition of these horizons and the nature of the vegetation are factors accounting for the differences in caesium availability in this type of humus

   1a Mineral (and hemi-organic) horizons are very clayey.
   Once the organic horizons are decomposed, caesium is strongly fixed The migration towards the deeper soil layers is very slow and involves burrowing animals. There is no risk of contamination of the water table, and transfers to plants remain at a consistently low level.

   1b Mineral horizons are very rich in sand (and poor in clay).
   Once the organic horizons are decomposed, caesium is rapidly leached away. There is a potential contamination risk of the water table but part of the caesium is reabsorbed by the root system. The turnover is therefore higher than in 1a.

2) Forest soils with moder to dysmoder humus
The decomposition of holorganic horizons occurs slowly and depends mainly upon the fungal activity. The role of the fungi in the transfers to most of the plants is probably substantial, particularly for those depending upon the Oh, OAh and even Ah1 horizons. Decontamination takes place slowly. Factors that are alien to the organic horizons (such as type of underlying horizons) continue to influence the transfers from these horizons but to a lesser extent.

   2a Very clayey mineral horizons (see 1a)

2b Very sandy mineral horizons (see 1b)

With regard to longs-term radioprotection, case 2b represents the most dramatic situation. It is also the most difficult case to manage in terms of countermeasures. It is typically found in many podzols in the boreal and continental regions polluted by the Chernobyl fallout. The study of the transfer mechanisms involving fungi under such a situation must be given top priority.

PUBLICATIONS DURING THE RESEARCH PERIOD

GUILLITTE O., TIKHOMIROV F.A., SHAW G., JOHANSON K., DRESSLER A.J. & MELIN J.; 1993. Decontamination methods for reducing radiation doses arising from radioactive contamination of forest ecosystems - a summary of available countermeasures. In Relative Effectiveness of Agricultural Counter-measure Techniques. Sci. Total Environ. 137: 307-314.
GUILLITTE O. & WILLDRODT C.; 1993. An assessment of experimental and potential countermeasures to reduce radionuclide transfers in forest ecosystems. In Relative Effectiveness of Agricultural Counter-measure Techniques. Sci. Total Environ. 137: 273-288.
GUILLITTE O., MELIN J. & WALLBERG L.; 1994 a. Biological pathways of radionuclides originating from the Chernobyl fallout in boreal forest ecosystem. In Radionuclide transfers in forest ecosystems, Sci. Total Environ.157: 207-215.
GUILLITTE O., TIKHOMIROV F.A., SHAW G. & VETROV R.; 1994 b. Principles and Practices of Countermeasures to be Carried Out Following Radioactive Contamination of Forest Areas. In Radionuclide transfers in forest ecosystems, Sci. Total Environ.157:399-406.

REFERENCES

GUILLITTE O., GASIA M.C., LAMBINON J., FRAITURE A , COLARD J. & KIRCHMANN R.; 1987. La radiocontamination des champignons sauvages enBelgique et au Grand-Duché de Luxembourg après l'accident nucléaire de Tchernobyl. Mém.Soc.Roy.Bot.Belg. 9: 79-93.
LAMBINON J., FRAITURE A., GASIA M.C & GUILLITTE O.; 1989. La radiocontamination des champignons sauvages en Wallonie suite à l'accident nucléaire de Tchernobyl. In 4th International Symposium of Radiology, Cadarache, 14-18 March 1988, T2: E37-44.
GUILLITTE O., DE BRABANT B. & GASIA M.C.; 1989. Use of mosses and lichens for valuation of the radioactive fallouts,deposits and flows under forest-cover. Mém.Soc.Roy.Bot.Belg. 12: 89-99.
GUILLITTE O. & FRAITURE A.; 1989. Les polluants dans les champignons. Forêt Wallonne 6: 9-14.
ANDOLINA J. & GUILLITTE O.; 1990 a. Radiocesium availability and retention sites in forest humus. In Transfer of Radionuclides in Natural and Semi-Natural Environment. Ed. Elsevier Appl. Sci., London: 135-142.
ANDOLINA J. & GUILLITTE O.; 1990 b. A methodological approach of soils sampling and analyses in the study of radionuclides transfers in forest ecosystems. In Transfer of Radionuclides in Natural and Semi-Natural Environment. Ed. Elsevier Appl. Sci., London: 161-168.

FRAITURE A., GUILLITTE 0. & LAMBINON J.; 1990. Interest of fungi as bioindicators of the radiocontamination in forest ecosystems. In Transfer of Radionuclides in Natural and Semi-Natural Environment. Ed. Elsevier Appl. Sci., London· 477-484.
GUILLITTE 0., FRAITURE A. & LAMBINON J.; 1990 a Soil-fungi radiocesium transfert in forest ecosystems. In Transfer of Radionuclides in Natural and Semi-Natural Environment. Ed. Elsevier Appl. Sci.,London: 468-476.
GUILLITTE O., KIRCHMANN R., VAN GELDER E. & HURTGEN C.; 1990 b. Radionuclides fallout on lichens and mosses and their leaching by rain in a forest ecosystem. In Transfer of Radionuclides in Natural and Semi- Natural Environment. Ed. Elsevier Appl.Sci., London: 110-117.
GUILLITTE O., KOZIOL M., DEBAUCHE A. & ANDOLINA J.; 1990 c. Plant-cover influence on spatial distribution of radiocaesium deposits in forest ecosystems. In Transfer of Radionuclides in Natural and Semi- Natural Environment. Ed. Elsevier Appl. Sci., London: 441-449.
WIRTH E., GUILLITTE O., NIMIS P.L., MELIN J., BERGMANN R., PALO T. & WICKMANN G.; 1992. Cycling of cesium and strontium in natural ecosystems. CEC Contract N B 17 00016-C (MB), Final report. 226 p.

Table 10 Evolution of the specific activities and $^{137}Cs/^{134}Cs$ ratios (in brackets) in mushrooms collected at Florenville and Mersch.

1986			1987			1988			1989 (91)			1992			1993		
Florenville SPRUCE STAND																	
X.bad	6770	(2,44)	C.ano	24810	(7,69)	B.edu	730	(5,51)	T.fel	4970	(2,90))	R nig	3950	(3,54)	B edu	621	(3,77)
			R.nig	1020	(4,67)	I lan	23550	(3,55)	C bru	10890	(2,64)	I.lan	23560	(3,16)	X.bad	3610	(3,10)
			P.pse	1570	(4,61)	D.cin	19180	(2,84)	X.bad	4520	(2,04)	R.och	6620	(2,90)	C.bru	7510	(2,98)
			I lan	27260	(3,04)	R.och	5730	(2,77)				C.ano	35750	(2,81)	R och	2720	(2,92)
			A.rub	1260	(2,75)	X.sub	1250	(2,77)				C bru	13130	(2,72)			
			T.sej	360	(2,69)	X.bad	12440	(2,33)				L.the	5740	(2,66)			
			P.imp	1430	(2,61)	X.chr	6770	(2,33)				X bad	5890	(2,57)			
			X.bad	9890	(2,51)	L.the	9310	(2,21)				P.inv	7470	(2,26)			
			C.bru	15780	(2,29)							X.sub	400	(0,98)			
			D.cin	28420	(2,24)												
			T.fel	10640	(2,10)												
			C.mac	350	(2,12)												
			C.vib	500	(2,00)												
Florenville BEECH STAND																	
			A.cit	2150	(2,90)	X bad	6820	(2,82)	C.del	1810	(2,65)	T.vir	13580	(7,42)	L.lac	1330	(4,33)
			C.but	670	(1,92)	A.cit	3790	(2,65)	R.och	3120	(2,37)	R.och	2650	(4,36)	R.och	1480	(2,78)
						L.ame	4870	(2,39)				C.ano	23440	(3,60)	C ano	890	(1,50)
						R.och	6050	(2,21)				C.del	3770	(3,20)	L.ame	560	(1,30)
						L.qui	3810	(2,08)				L.ame	8120	(2,92)			
						X.chr	6740	(2,80)				X.bad	4490	(2,83)			
						C.del	3350	(1,63)				A.cit	1980	(2,51)			
												X chr	2320	(2,49)			
												L.lac	3760	(1,66)			
												X.sub	240	(0,61)			
Mersch BEECH STAND																	
R.nig	150	(4,30)	R.nig	1900	(3,14)	B.edu	960	(2,52)				R.nig	4560	(2,75)	L.ame	7990	(2,87)
B.edu	150	(2,67)	X.chr	13860	(2,16)	C ola	31800	(2,07)				R och	10970	(2,74)	H.cru	10870	(2,12)
R.och	2130	(2,19)	S.var	100	(2,10)							L.ame	14160	(2,27)	X.chr	1790	(1,89)
X.chr	5310	(2,16)	A.rub	1200	(2,04)							X.chr	1900	(2,25)			
			L.ame	32060	(1,99)							T.alb	37840	(2,19)			
			L.lac	17570	(1,96)							L.ble	4420	(2,19)			
			T.fel	12310	(1,95)							L.sub	6000	(2,19)			
			H.cru	40760	(1,94)							C.ola	5930	(2,15)			
			C.ola	39760	(1,80)							M pro	50	(0,33)			
			M pro	230	(1,80)												
			T.alb	67210	(1,68)												
			C.per	750	(1,57)												

MYCORRHIZAL SPECIES :

A.cit	*Amanita citrina*
A.rub	*Amanita rubescens*
B.edu	*Boletus edulis*
C.ano	*Cortinarius anomalus*
C.bru	*Cortinarius brunneus*
C.del	*Cortinarius delibutus*
D.cin	*Dermocybe cinnamomea*
H.cru	*Hebeloma crustuliniforme*
I.lan	*Inocybe lanuginosa*
L.ame	*Laccaria amethystina*
L.lac	*Laccaria laccata*
L.ble	*Lactarius blennius*
L.qui	*Lactarius quietus*
L.sub	*Lactarius subdulcis*
L.the	*Lactarius theiogalus*
P.inv	*Paxillus involutus*
P.imp	*Phallus impudicus*
P.pse	*Porphyrellus pseudoscaber*
R.nig	*Russula nigra*
R.och	*Russula ochroleuca*
S.verr	*Scleroderma verrucosum*
T.alb	*Tricholoma album*
T.sej	*Tricholoma sejunctum*
T.vir	*Tricholoma virgatum*
T.fel	*Tylopeus felleus*
X.bad	*Xerocomus badius*
X.sub	*Xerocomus subtomentosus*

SAPROPHYTIC SPECIES :

C.cla	*Clitocybe clavipes*
C.vib	*Clitocybe vibecina*
C.but	*Collybia butyracea*
C.mac	*Collybia maculata*
C.per	*Collybia peronata*
M.pro	*Macrolepiota procera*

Figure 1 Evolution of the specific activities in ^{137}Cs measured in the Ol, Oh+Of and Ah horizons at Florenville (spruce stand).

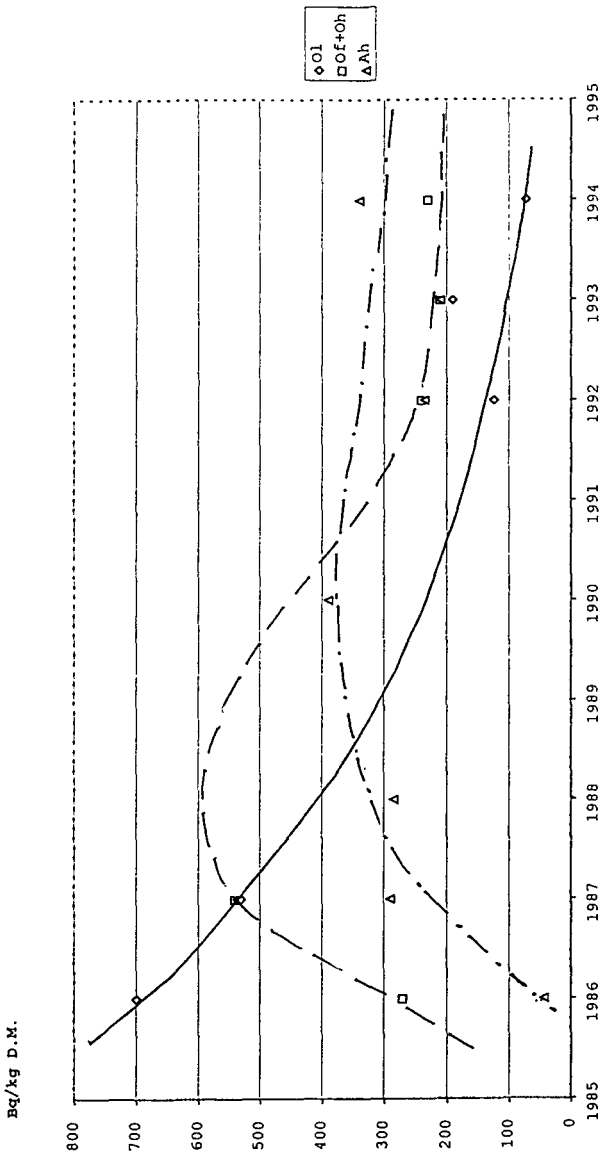

Figure 2 Distribution of the mean specific activity in ^{137}Cs and the mean value of the $^{137}Cs/^{134}Cs$ ratio measured in fruiting bodies of all species collected in north-eastern Italy between 1986 and 1993. 1=mycorrhizal species, 2=humo-terricolous saprophytic species and 4=lignicolous saprophytic or parasitic species.

Head of project 6: Dr. Belli

II. Objectives for the reporting period

The main goals of this project, lasted from January 1993 to June 1995, are:

- the determination of the radiocaesium distribution in different components of litter–fall;
- the assessment of the fluxes of radiocaesium from trees to forest floor attributable to litterfall;
- the determination "in situ" of the release of radiocaesium from decomposing litter.

III. Progress achieved including publications

The analysis of radiocaesium cycling in forest as a whole, involves the determination of caesium distribution in the different components of the forest and the understanding of the caesium transfer processes between the components of these ecosystems. These data will give the basis for the development of a realistc model to assess the long–term behaviour of radionuclides within these systems.

Annual transfer of elements from forest trees to forest floor is mainly attributable to the transfer from canopy to litter via leaf, twig and fruit fall and to the water derived from the interaction of precipitation with the canopy (through–fall and stem–flow). The composition and quantity of litterfall vary according to the type of forest, soil and climate. For a given ecosystem, climatic condition strongly influence radionuclide fluxes. Studies carried out after Chernobyl accident [Bunzl, 1989; Tikhomirov, 1994] have shown that immediately after the accident (about 6 months) leaching of the canopy by rainfall water is the main process of radionuclide transfer from trees to forest floor. In the long term litter–fall represents one of the main process for the turnover of ^{137}Cs in forest.

Re–mobilization of radionuclides from litter is mainly attributable to the leaching of litter material and to the process of litter decomposition. These processes seem key mechanisms in radionuclide cycling in forest floor, because even nine years after deposition the major fraction of radiocaesium deposited in forest is found in the superficial horizons of the forest soil (Of, Oh) [Belli, 1994]. Contrary to the low migration rates in the upper horizons of forest soil, radiocaesium is highly available for plant uptake in these layers.

In the frame of this project, the seasonal amounts of litter material and the associated fluxes of radiocaesium deposited on the forest floor have been assessed. To evaluate which component of the litter gives an higher contribution to the radiocaesium fluxes, litter material was separated in different components (fagus leaves, needles, twigs and fruit).
Remobilization of ^{137}Cs from litter material was studied with litter bags located on the Ol layer of forest floor.

Materials and methods

The experimental site was established in a mixed forest in Tarvisio (Carnic Alps, Eastern part of Italy), located at 870 m above the sea level. The forest is characterised by *Picea excelsa* (77%) and

Fagus sylvatica (17%). The age of the forest ranges from 60 to 100 years. The mean annual rainfall is 1500 mm and the mean temperature is 5°C. The soil is classified as brown earth.
This area received a significant deposition from the Chernobyl accident (about 40kBq m^{-2} of ^{137}Cs).

In an area of about 100x100 m, in which the presence of beech trees is generally higher than spruce trees, 9 sub-areas were selected. In each sub-area one litter, trap with a surface of 1 m^2, was set-up mid-way between trees, and suspended on metal frame. The traps were emptied in April and November of each year and the litter material separated in the different components (leaves, needles, twigs, cones and other components). All litter components have been dried and weighed to determine litter-fall per square meter. The samples were milled for analysis of ^{137}Cs and ^{40}K.

To study the litter decomposition, material from the Ol layer was collected, air dried and mixed. Three sub-samples were taken and analysed to determine ^{137}Cs. The remaining litter material was filled in 54 nylon bags with dimension of 27x40 cm. The mesh size of the nylon net used was 2 mm. The content of the bags were weighed and all the bags installed in Ol layer. The bags were placed horizontally into the litter layer. In each sub-area 6 litter bags were placed. The 6 bags were placed close to each other along a line and a piece of wood secured the border of each bag to the ground. This did not hinder natural deposition of new litter material.
One bag from each sub-area was removed at intervals of two months during the period free from snow cover (from April to October). Any foreign material and invertebrates adhering outside of the bags were brushed away. The bag contents were dried at 105°C and weighed. Each 9 replicate was milled and analysed for ^{137}Cs and ^{40}K.

Five replicates of soil profile were taken seasonally. Soil samples were taken along a soil monolith of surface area of 30x30 cm. The monoliths were divided into three horizons according to their genesis (Ol, Of, Oh) and into three layers (5-10, 10-15 and 15-20). All soil samples were air-dried and sieved to separate the fraction below 2mm. All samples were analysed by gamma spectrometry using HPGe detectors to determine ^{134}Cs, ^{137}Cs and ^{40}K.

Results and Discussions

In table 1 are given the mean values of the litter material collected in the 9 nets, located in the Tarvisio mixed forest. As expected, the quantity and type of litter material deposited on the forest floor vary as a function of seasons; in the mixed forest fagus trees shed their leaves mainly between October and December (about 100 g m^{-2}), on the contrary the deposition of abies needles is rather constant during all the year (about 60 g m^{-2} at each sampling time). The amount of fagus leaves found in November 1992 is not representative, because the nets were placed in the experimental area at the end of October 1992, when the process of leaves shedding was already started.
Table 2 and 3 report ^{137}Cs and ^{40}K concentrations measured seasonally in the different litter components. Abies litter generally show higher values of radiocaesium content than fagus litter. This could be attributable to the fact that:1) fagus tree have had lower interception ability, because they were unfoliated during the deposition; 2) deciduous stand, shedding their leaves each year, then radiocaesium have an ecological half-life shorter than in coniferous stand.

Radiocaesium content in fagus leaves litter and in abies needles litter increase from November 1992 to November 1993. This could be due to the migration of radiocaesium in the root zone (Oh and Ah horizons in which is found about 75% of the radiocaesium content along the soil profile). The analysis of data reported in Table 1-3 show that litter and in particular coniferous litter represents a significative pool of radiocaesium.

To verify the influence of litter storage in the nets (period from litter shedding to litter collection) on radiocaesium and potassium content, fagus leaves have been collected monthly from the trees (Table 4) from May to October 1994. Comparing the data of ^{137}Cs and ^{40}K in living and in dead leaves, it seem that leaching by precipitation during the storage in the nets influence only potassium content. In fact dead leaves collected in November 1993 show quite similar values of radiocaesium as those measured in living material during 1994 (0.100 vs 0.08 Bq g^{-1}).

Radiocaesium fluxes from canopy to forest floor attributable to litter-fall are reported in Table 5. Radiocaesium flux show not only a seasonal pattern attributable to the presence of deciduous trees in the forest studied, but also different values in the same season in different years. In fact higher values are found in May 1994 than in May 1993. This could be due to the higher concentrations measured in needles in 1993, but also to different metereological conditions that can influence the shedding of litter material. The annual radiocaesium flux measured in the Tarvisio mixed forest from November 1992 to November 1993, attributable to litter-fall, is about 155 Bq m^{-2} y^{-1}. Comparing this value with the amount of radiocaesium found along the soil profile, the annual turnover of radiocaesium attributable to litter-fall is 0.5% of radiocaesium in soil.

The results of the experiment carried out with litter bags to study the remobilization of radiocaesium from litter material are given in Table 6. The results achieved show that in the Tarvisio forest 30% of the dry weight is lost in more than 1 year of investigation and radiocaesium content remain quite constant from November 1992 to July 1993. A significant increase in radiocaesium content is observed in October 1993 and in May 1993. Duncan's test was used to compare the weight and the ^{137}Cs content reported in Table 6. The test show that the mean values of the radiocaesium content in the samplings of October 1993 and May 1994 increase significantly ($p<=0.05$). A first analysis of the results suggest an importation of radiocaesium from outside of the litter-bags. This could be attributable to the effect of throughfall, but Sombre, 1994 did not find any difference between litter material in litter bags exposed and not exposed to throughfall water. Other authors found evidence for ^{137}Cs importation to litter bags, and they suggest a link between microbial colonisation and the importation of ^{137}Cs to decomposing litter [Rafferty, in prep.]. Colonisation of Ol material by fungi which have accumulated radiocaesium from Of and Oh horizons, in which the content of radiocaesium have still a maximum, may enhance significantly the radiocaesium content of the Ol material. The mechanism in the more study are necessary on this process because letter layers seem to regulate the cycling of radiocaesium in forest.

PUBLICATIONS DURING THE RESEARCH PROJECT

M.Belli, U.Sansone, S.Menegon, (1994) Behaviour of radiocaesium in a forest in the eastern Italian Alps, Sci. Total Environ., 157, 257-260

REFERENCES

K.Bunzl, W.Schimack, K.Krentzer, R.Schierl, (1989) Interception and retention of Chernobyl-derived ^{134}Cs, ^{137}Cs and ^{106}Ru in spruce stand, Sci. Total Environ., 78, 77-87

L.Sombre, M.Vanhouche, S. de Brouwer, C.Ronneau, J.M. Lambotte, C. Myttenaere, (1994) Long-term radiocaesium behaviour in spruce and oak forests, Sci. Total Environ., 157, 59-71

F.A. Tikhomirov, A.I.Shcheglov, (1994) Main investigation on the forest radioecology in the Kyshtym and Chernobyl accident zones, Sci. Total Environ., 157, 45-57

Table 1. Litter material deposited in the study area from November 1992 to May 1994. All data are referred to dry weight.

Sampling Date	Total ($g\ m^{-2}$)	Fagus leaves ($g\ m^{-2}$)	Fagus twigs ($g\ m^{-2}$)	Fagus other components($g\ m^{-2}$)	Abies needles($g\ m^{-2}$)	Abies twigs ($g\ m^{-2}$)	Abies cones ($g\ m^{-2}$)
26/11/1992	129±18 (n=9)	44±17 (n=3)	9.6±3.7 (n=3)	6.7±1.5 (n=4)	70±30 (n=9)	7.5±1.1 (n=9)	6 (n=1)
21/5/1993	127±47 (n=9)	1.3±0.6 (n=9)	12±12 (n=9)	5.5±5.5 (n=7)	69±34 (n=9)	13±10 (n=9)	2.1±1.9 (n=9)
4/11/1993	315±56 (n=9)	102±33 (n=9)	7±6 (n=9)	-	50±16 (n=9)	15±12 (n=9)	156±180 (n=9)
26/5/1994	254±56 (n=9)	12±2 (n=9)	16±3 (n=6)	-	77±17 (n=9)	32±16 (n=9)	83±50 (n=9)

Table 2. ^{137}Cs and ^{40}K concentrations in fagus litter material collected from November 1992 to May 1994. All data are referred to dry weight.

Sampling Date	Fagus leaves		Fagus twigs	
	^{137}Cs (Bq g^{-1})	^{40}K (Bq g^{-1})	^{137}Cs (Bq g^{-1})	^{40}K (Bq g^{-1})
26/11/1992	0.059±0.014 (n=9)	0.17±0.11 (n=9)	0.07	0.11
21/05/1993	0.25	0.6	0.13	0.07
4/11/1993	0.133±0.05 (n=9)	0.07±0.01 (n=9)	0.055±0.002 (n=2)	0.153±0.007 (n=2)
26/05/1994	–	–	–	–

Table 3. ^{137}Cs and ^{40}K concentrations in abies litter material collected from November 1992 to May 1994. All data are referred to dry weight.

Sampling Date	Abies needles		Abies twigs		Abies cones	
	^{137}Cs (Bq g^{-1})	^{40}K (Bq g^{-1})	^{137}Cs (Bq g^{-1})	^{40}K (Bq g^{-1})	^{137}Cs (Bq g^{-1})	^{40}K (Bq g^{-1})
26/11/1992	0.21±0.02 (n=9)	0.094±0.04 (n=9)	0.77	0.043	–	–
21/05/1993	0.35±0.07 (n=9)	0.094±0.06 (n=9)	0.86	0.17	–	–
4/11/1993	0.54±0.16 (n=9)	0.056±0.01 (n=9)	0.98±0.23 (n=4)	0.07±0.03 (n=4)	0.36±0.26 (n=9)	0.12±0.04 (n=9)
26/05/1994	0.49±0.12 (n=9)	0.057±0.02 (n=9)	0.67±0.14 (n=8)	0.14±0.14 (n=8)	0.20±0.07 (n=9)	0.08±0.02 (n=9)

Table 4. ^{137}Cs and ^{40}K concentrations in fagus leaves collected directely on the trees

Sampling date	^{137}Cs (Bq g^{-1})	^{40}K (Bq g^{-1})
26/05/1994	0.08±0.04 (n=13)	0.34±0.07 (n=13)
12/07/1994	0.09±0.05 (n=14)	0.26±0.06 (n=14)
26/08/1994	0.08±0.06 (n=15)	0.29±0.06 (n=15)
11/10/1994	0.08±0.06 (n=14)	0.32±0.08 (n=14)

Table 5. ^{137}Cs fluxes from canopy to forest floor attributable to litter–fall

Period	^{137}Cs (Bq m^{-2} $month^{-1}$)
October 1992/November 1992	23.7
November 1992/May 1993	6.2
May 1993/November 1993	16.8
November 1993/May 1994	77.3

Table 6. Litter bag experiment . Weight and ^{137}Cs content at different sampling period

Sampling period	Weight (g^{-1})	^{137}Cs (Bq)
November 1992 (t=0)	20±1(a) (n=9)	2.9±0.5 (a) (n=9)
April 1993	14±1(b) (n=9)	2.8±0.6 (a) (n=9)
June 1993	15±1(b) (n=9)	4.9±1.6 (a) (n=9)
July 1993	13±1(b) (n=9)	4.4±1.2 (a) (n=9)
October 1993	14±2(b) (n=9)	11.7±3.2 (b) (n=9)
May 1994	14±2(b) (n=3)	9.5±3.8 (b) (n=3)

(a) (b) $p <= 0.005$

Head of project 7: Prof. Feoli

II. Objectives for the reporting period

The CETA Group, after some years of experimental trials on the radiocaesium circulation in grasslands after the Cernobyl accident (Belli et al., 1990), joined the EC Project "Cycling of caesium and ^{90}Sr in natural ecosystems" in 1993. In the framework of this program, the main objective was to develop a compartment model of radiocaesium cycling in a beech forest of the N–E Italian Alps, in a methodological approach coupling radiological and ecophysiological functions modules. The validation is based on forest soils profile data (since 1987), vegetation growth, foliage activity and litter–bags experiment since 1992. The model output are curves of caesium concentration (in kBq m^{-2}) in each compartment in function of time and different parameters from a deposition event. The whole work has been carried out in close collaboration with the ANPA Group of Rome (former ENEA–DISP), within the activities of the same EC Project.

III. Progress achieved including publications

Data and Methods. The experimental site is located at Tarvisio (Udine, N–E Italy), near the border with Austria and Slovenia, in a mature secondary mixed forest (80 to 100 years) at 870 m a.s.l. The area soils are derived from glacial alluvium, scarcely deep (20–25 cm), with a thin very acid (pH 3 to 4) holorganic layer (5 cm about). The climatic conditions are very continental despite of the altitude. Minimal temperatures reach frequently –20° C during January and February, while in July and August maximal of more than 25° C are not uncommon. The average rainfall is 1400 to 1500 mm per year, the snow cover lasts from November–December to even early May. The forest is composed by dominant red spruce (*Picea abies*) and beech (*Fagus sylvatica*), with a poor understorey of bilberry (*Vaccinium myrtillus*). The area selected for model purposes is a beech stand of about 1 ha. Soil profile samples have been regularly collected since 1987, 2–3 times per year. Since 1992, the experimental design of ANPA with the assistance of ERSA provided a series of 9 conic and linear nets to assess the litter deposition and composition, and 9 series of 6 litter–bags placed near the conic nets, to estimate the litter decomposition rates. The collection of the litter–bags samples starts each year at the end of the snow cover with a frequence of 40–45 days over the whole vegetative season. In spring 1994 new series of litter bags have been placed in the same sites, before the old ones cycle was over. Beyond this, the experimental activity of the CETA Group carried out ecophysiological data sampling during 1993 and 1994. The field collections consisted of repeated all–day recording of photosynthesis and transpiration rates on the beech leaves (with an ADC Infra–Red Gas Analyser), leaf water potential (with a PMS pressure chamber) and soil water content (with a Time–Domain Reflectometry System). These data were structured in a data base and some of them have been used to build up the mathematical functions for the vegetation groth sub–model. Microclimatic data (mainly air temperature, humidity and rainfall) were constantly recorded by two stations placed in the forest and in a near grassland.

Model Assumptions and Constraints The definition of the limits, assumptions and constrains of the model developed may be synthesized in the following points.
(a) The model calculates the circulation of ^{137}Cs between the compartments of a forest system defined by the soil layers and the vegetation of the main component (Beech trees) . The other components (herbs, understory) are neglected because of their scarce mass proportion in the experimental forest stand examined.
(b) The model is strictly site-specific and system-specific. It is not possible to evaluate the performances for other sites (different soil composition or climate) or systems (other forest types) without a new calibration of the variables and parameters involved.
(c) The model takes into account some relevant functions and parameters assumed to be the main ones to drive the fluxes of radionuclides between compartments (decomposition rate, litterfall, etc.). Some of them have experimental basis, whereas some other were used from literature or derived from best-fit of experimental data in a phenomenological viewpoint.
(d) The model does not consider variables or parameters assumed to be not relevant on the dynamics of the whole system, or not controlled by experimental devices (through-fall, stem-flow, interception, etc.). In this sense, the effects of the variables not specifically included can be considered "hidden" by the dynamics of the major variables.
(e) The model is splitted into two sub-models, one for the proper calculation of caesium cycling through the compartments and the other for the estimation of the variables and functions related to the radionuclides uptake and turnover through the vegetation pathways (foliage production, transpiration, leaf area, etc.).
(f) Steady-state is assumed for the forest biomass evolution. This is in accordance with the dynamics of caesium cycling (ecological and radiological half-lives), that are of an order of magnitude considerably lesser than the time span of the forest stages succession in a mature forest.
(g) The output of the model represents dynamical curves of ^{137}Cs content in each compartment versus time ("apparent" concentration, as expressed in kBq m^{-2}), assuming a time step of 1 year.

Model structure (compartments, fluxes). The general structure of the model with the compartments analysed is presented in Fig.1. The major attention was focused on the determination of the soil compartments. Forest soils are stratified in organic and mineral layers, and within the first ones the diversity between litter in different stages of fragmentation and humus fraction is of crucial importance for the caesium distribution and fluxes. In our experimental stand, this is more complicated by the scarce depth of the whole soil system (20-25 cm, with organic layer of about 5 cm) and by the irregular distribution of the soil profiles. The definition of the compartments has been simplified averaging the data of the samples collected during these years in the following way:
(a) layer L (litter, 0-1 cm), including both the "fresh" litter and the litter in the first stages of decomposition;
(b) layer FH (holorganic, 1-5 cm), including both the litter in advanced stage of fragmentation, and the humus fraction;
(c) layer A (1st mineral, 5-10 cm);
(d) layer B (2nd mineral, 10-15 cm);
(e) layer C (3rd mineral, 15-20 cm).
The identification of the soil layers is basically functional, especially for the FH compartment, where the difference between the fragmented litter and the humus fraction is not always easy to detect. The "mineral" layers, where the organic component is still high, are identified by

sand and clay fractions, so that the labels (A, B, C) does not refer to any soil classification. The last compartment (V) refers to the vegetation. Since that only the foliage production is considered for cycling estimation, no other compartments have been included (roots, trunk, etc.)

Underlying processes. As stated before, some main processes have been considered and analysed to define the transfer of caesium through the system compartments. Notwithstanding the overall complexity of the pathways in forest systems, the need of generalization implies a reduction of terms in the sense of the most important variables:

(a) DECOMPOSITION RATE, from litter (L) to holorganic (FH) compartment. According to the general equation of the decomposition (Waring e Schlesinger, 1985):

$$L_t = L_0 e^{-kdt}$$

the constant of decomposition rate (yr^{-1}) is defined as:

$$k = -(1/dt) \ln(L_t/L_0)$$

and has been experimentally calculated from the litter bags data.

(b) "MINERALIZATION" RATE, from holorganic compartment (FH) to the 1st mineral layer (A). Mineralization is the basic process determining the transfer of the elements from the final decomposition stage of the amorphous organic matter (humus) to the mineral horizons. It is assumed here that radiocaesium follows the same pathway of the principal elements, so the term can be defined as improper or "apparent" mineralization. No data being available, the coefficient has been calculated by best-fit from soil data after all the other parameters.

(c) "DIFFUSION" through the mineral compartments (A, B ,C). The diffusion approach is derived from the first Fick's law equation:

$$m/dt = -DA(C_a - C_b)/dx$$

which states that a mass (m) of solute diffuses for a distance dx from one compartment to the adjacent one in the time unit (dt) in function of the surface area (A), the gradient of concentration ($C_a - C_b$) and a proper coefficient of diffusion (D). Since that the concentration of caesium in the compartments is here expressed on area basis and not volume ($kBq\ m^{-2}$), the coefficient D is then expressed in $m\ yr^{-1}$, unlike from the true diffusion coefficient ($m^2\ yr^{-1}$). Also in this case the diffusion can be defined as "apparent". The coefficient has been calculated from experimental soil data by numerical convergence obtained by random iteration technique (Scheid, 1994).

(d) UPTAKE RATE to the plant. It is assumed to be mainly derived from the L and FH compartments, because the biological processes linked to the organic decomposition make radiocaesium more available than in the mineral horizons, where the clay layers immobilize ^{137}Cs for a longer time. The uptake rates, expressed as fractions of caesium passing from the i-

th compartment to vegetation in the time unit (V_L, V_{FH}, yr^{-1}) have been calculated by the equations:

$$C_{wi} = C_{si} / Kd_i$$

$$V_i = C_{wi} WF_i T / X_i$$

The first estimates the concentration of ^{137}Cs in the soil solution for the i–th compartment, based on fitted Kd values based on literature. The second calculates the fraction of caesium (yr^{-1}) uptaken from the i–th compartment by multiplying the concentration of the soil solution with the average water fraction of the i–th compartment on the soil column (WF_i) and the total amount of water transpired by the trees (T, mm yr^{-1}, calculated by the vegetation growth sub–model), divided by the caesium concentration of the i–th soil compartment (X_i). The total uptake per year is then (i=0,1,... n. of compartments):

$$Vj = \sum_i V_i X_i$$

(e) TRANSLOCATION, that is the fraction of caesium uptaken from the soil and transferred from the leaves to the plant body at the end of the vegetative season and before litterfall. The coefficient (yr^{-1}) has been extracted from literature.

(f) TURNOVER, that is the fraction of radiocaesium not translocated and returned to the forest floor by annual litterfall. It is assumed to the depend totally on the litterfall (leaching by through–fall is neglected).

(g) VEGETATION GROWTH. A parallel–running sub–model has been developed based on ecophysiological measurements and assessments, following a guideline carried out by the CETA Group during these last years on grasslands in previous Projects with the ANPA Group (CETA Report, 1992). The underlying assumptions are based on the CO_2 absorption simulated by photosynthesis curves in function of light intensity, and transpiration rates per leaf area in function of temperature. The daily carbon gain produces the dynamic curves of leaf area and leaf dry matter over the whole season, whereas the transpiration rates estimate the total amount of water uptaken by roots. These variables are used to calculate the radiocaesium transferred to the vegetation compartment per year and area basis, the leaf litter production and the leaf litter activity (deposition is deduced as turnover rate independently from litter yield).

Functions and coefficients. Based on the functions and the considerations explained above, the model is summarized by the following systems of equations.

(a) ^{137}Cs circulation sub–model:

$$L_{j+1} = (L_j + Q_j)\, e^{(-k\, dt)} - V_L L_j dt$$

$$F_{j+1} = F_j + (L_j + Q_j)(1 - e^{(-k\, dt)}) - V_{FH} F_j dt - MF_j dt$$

$$A_{j+1} = A_j + MF_j dt - D(A_j - B_j)dt/dx_{AB}$$

$$B_{j+1} = B_j + D(A_j - B_j)dt/dx_{AB} - D(B_j - C_j)dt/dx_{BC}$$

$$C_{j+1} = C_j + D(B_j - C_j)dt/dx_{BC} - D(C_j)dt/dx_C$$

$$V_{j+1} = (V_L L_j + V_{FH} F_j)dt$$

$$Q_{j+1} = V_j(1-R)dt$$

The symbols of the state variables, all expressed in kBq m^{-2}, represent: L, litter compartment (Ol, Of: 0–1 cm); F, holorganic compartment (Of, Oh: 1–5 cm); A, 1st mineral layer (5–10 cm); B, 2nd mineral layer (10–15 cm); C, 3rd mineral layer (15–20 cm); V, vegetation (foliage) compartment; Q, deposition by litterfall. The parameters, all expressed in yr^{-1} (except D, expressed in m yr^{-1}), are: k, litter decomposition rate; D, apparent diffusion coefficient; M, apparent mineralization rate; V_L, uptake rate from litter compartment; V_{FH}, uptake rate from holorganic compartment; R, Translocation rate. The time step assumed (dt) is 1 year, j (0,1,2,...n) is the time from deposition event (years) and dx is the thickness of the mineral layers (m)

(b) Vegetation growth sub–model.
The description of the vegetation sub–model is briefly summarized by the main functions:

$$P_i = [(P_{max}-K_r)(1-\exp(-EQ_i/P_{max}))+K_r]$$

$$TR_i = aT_i + b$$

In the first, the instantaneous photosynthesis rate Pi (micromol CO_2 m^{-2} sec^{-1}) is function of the average light intensity (Q_i) maximum photosynthetic rate (Pmax), respiratory constant (Kr) and quantum efficiency (E) according to a saturation curve. In the second, the instantaneous transpiration rate (mol H_2O m^{-2} sec^{-1}) is a linear function of average temperature (T_i) with empirical coefficients a, b. The integration of the P_i and TR_i values over the whole day give the daily average carbon net gain (dry matter yield) and water balance. Daily temperatures and light intensities are estimated by empirical cosine functions. The vegetation sub–model gives, as average results, a foliage litter production of 0.2 kg m^{-2} yr^{-1} and a transpiration of 400 mm yr^{-1}. These have been used as default values for the model validation runs.

Model validation. In the following examples the model is validated by the simulation of a deposition event following the Cernobyl accident. Three runs have been performed (Fig. 2,3), based on three different scenarios assumed at t=0 simulating the initial distribution of caesium in soil compartments (that is in few days after a wash–out deposition of 25 kBq m^{-2}, average value of the experimental area), expressed as different fractions of the total deposition (TD) in the first soil layers:

(1) L_0 = TD (25 kBq), F_0=0
(2) L_0 = 2/3 of TD (18.75 kBq), F_0= 1/3 of TD (6.25 kBq)
(3) L_0 = 1/2 of TD (12.5 kBq), F_0= 1/2 of TD (12.5 kBq)

Because of wash–out deposition occurred in the period late April–early May 1986, before the beginning of the foliage growth, a complete uptake cycle and litterfall deposition was accounted for also for t=0. The parameters default values are in Tab. 1. The correlation coefficients with the experimental data (Fig.4) show that the first hypothesis is the more reliable (r_1=0.96, r_2=0.89, r_3=0.88), notwithstanding all the coefficients are largely significant over a probability of 99%. This means that, according to the model analysis, it is reasonable to suggest that the whole radioactivity was retained in the first layer after the wash–out deposition. It looks also that the caesium retention is still very high in the holorganic layers nine years after the Cernobyl event. This will probably result into an ecological half–life similar to the radiological half–life. Crucial points of the model actually are the litterfall deposition (data available since 1992 only and maybe over–estimated because not considering leaching by through–fall), and the mineral layers (not always well distinct from the holorganic layer in all the samples), meaning that the parameters related must undergo revision and further analysis.

k	0.37 yr^{-1}
D	0.0093 m yr^{-1}
M	0.043 yr^{-1}
VL	0.011 yr^{-1}
VFH	0.0014 yr^{-1}
R	0.30 yr^{-1}
dt	1 yr
dx	0.05 m
litterfall	0.2 kg m^{-2} yr^{-1}
transpiration	400 mm yr^{-1}

TAB.1. Default values of the parameters for the model validation runs

The model proved generally a good agreement with the experimental data for the system and the time range considered. The future research will be addressed to improve the model analysis through the following steps:
(a) setting–up experimental devices to take into account some relevant parameters actually not under control (stem–flow, through–fall, etc.);
(b) looking for reduction of information redundancy and noise selecting the main variables and parameters accounting for the transfer processes, in order to simplify the model functions;
(c) extending the model analysis to other forest types (conifer, mixed woods, etc.) and the model research to large (regional) areas scale, applying to the transfer dynamics of different forest types in integrated systems (GIS).

PUBLICATIONS DURING THE RESEARCH PROJECT

Ardiani R., Belli M., Feoli E., Sansone U., Scimone M., 1992. Validazione di un modello matematico descrittivo del trasferimento di radiocesio in un sistema agricolo (poster). Symp. of Italian Society of Ecology (SITE), Milano, Sept. 1992.

Belli M., Sansone U., Ardiani R., Feoli E., Scimone M., Menegon S., Parente G., 1995. The effect of fertilizer applications on ^{137}Cs uptake by different plant species and vegetation types. J.Environ.Radioactivity 27:75–89.

Ardiani R., Scimone M., Belli M., Sansone U., Menegon S., 1995. Development of a model of ^{137}Cs cycling in a Beech forest of N–E Italian Alps. Int. Symp. of Environmental Impact of Radioactive Releases. Wien, May 8–12, 1995.

REFERENCES

Belli M. et al., 1990. Radionuclides uptake and mineral fertilization in a grassland of Carnic Alps (NE–Italy). In: Desmet G., Nassimbeni P., Belli M. (eds), Transfer of radionuclides in natural and semi–natural environments: 382–386. Elsevier, London, New York.

CETA, 1992. Messa a punto e validazione di un modello matematico descrittivo del trasferimento di radionuclidi in un sistema agricolo. CETA–ANPA Project Report.

Scheid, F., 1994. Analisi numerica. Schaum, New York.

Waring R.H., Schlesinger W.H., 1985. Forest Ecosystems. Concepts and Management. Academic Press, London.

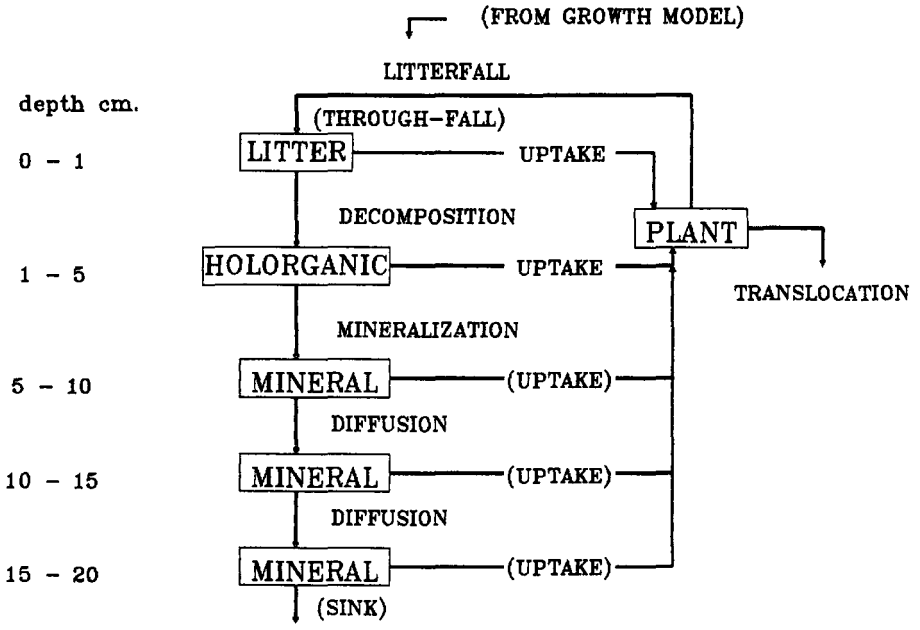

Fig. 1 - General structure of the model. The processes in parenthesis have been neglected.

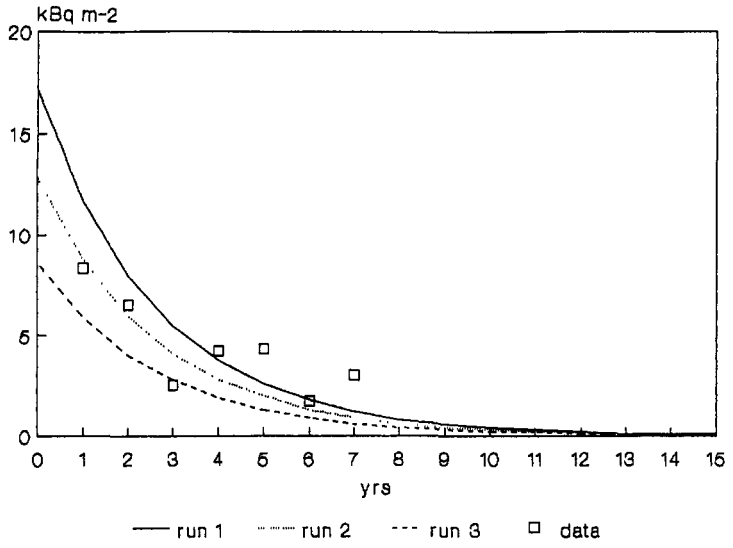

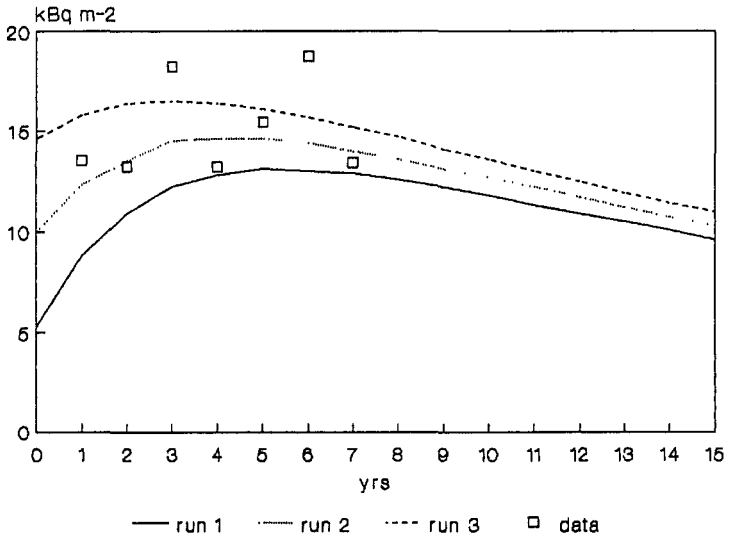

Fig. 2 - Model validation for the litter compartment (above) and the holorganic compartment (below).

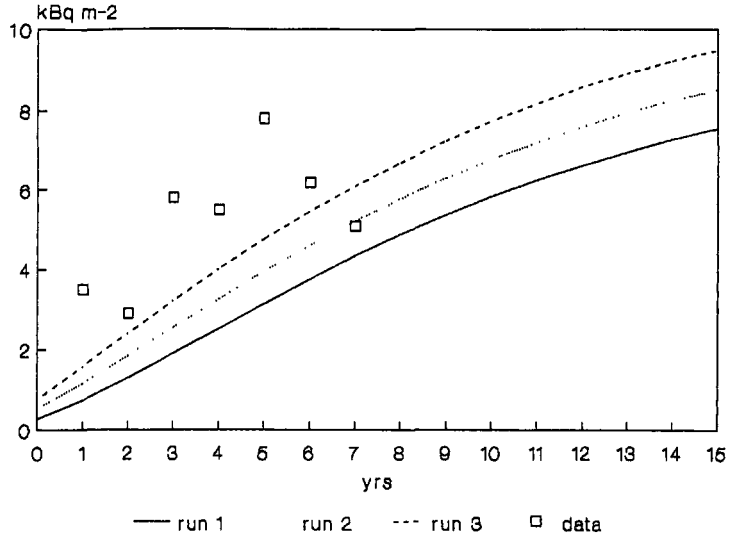

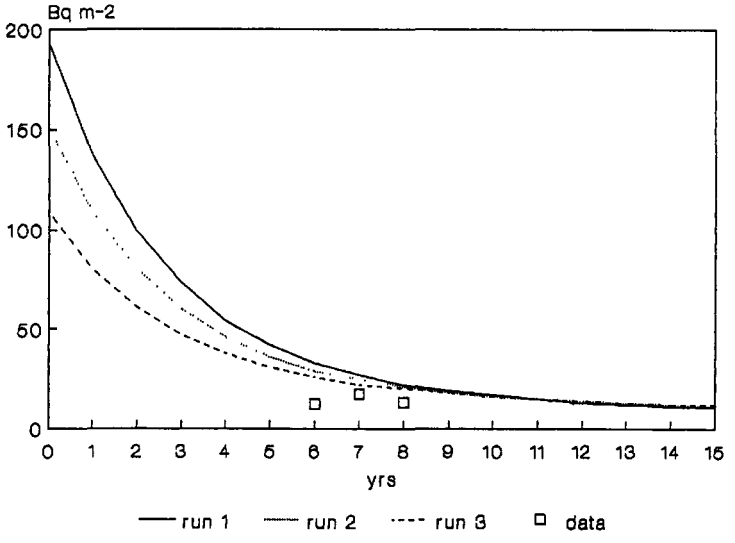

Fig. 3 - Model validation for the whole mineral compartments (above) and the deposition by litterfall (below)

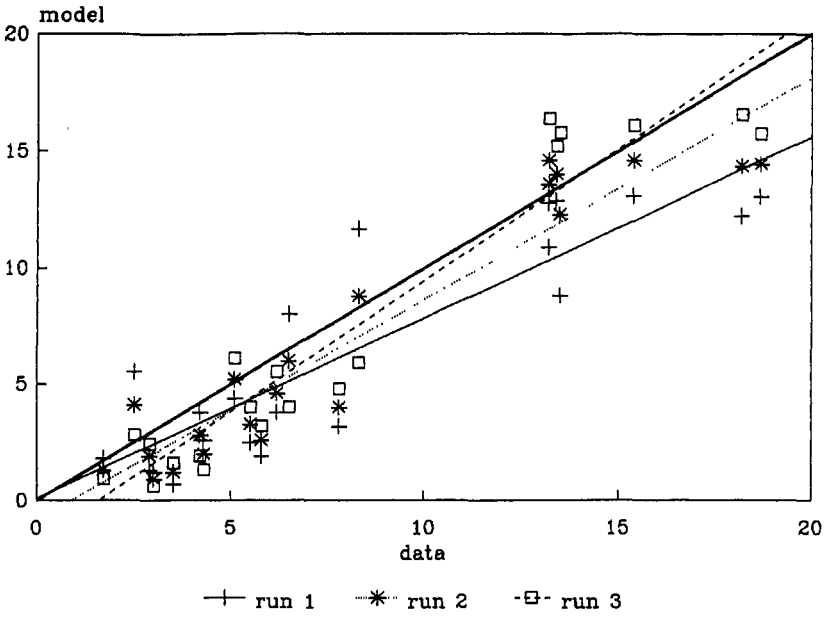

Fig. 4 - Correlations between experimental data and the model simulations. The 1:1 line is also represented.

Head of project 8: Prof. Nimis

II. Objectives for the reporting period

Within the project on the transfer of radionuclides in forest ecosystems, the Trieste group (responsible Prof. P.L. Nimis) was mainly concerned with contamination by radiocesium in lower and higher plants within mountainous forest ecosystems of the eastern Alps. The researches were focused on two main topics:
1) Utilization of biomonitors of radiocontamination for a quick survey of deposition patterns after a strong and sudden deposition event.
2) Study of the contamination patterns in vascular plants within a single forest ecosystem, in order to obtain data for a model of radiocesium transfer within natural forests.

III. Progress achieved including publications

III.1. SURVEY AREA AND SAMPLING STATIONS

The region Friuli-Venezia Giulia in northeastern Italy has been heavily affected by radiodeposition following the Chernobyl accident. The eastern Alps were contaminated mainly by liquid deposition occurring between April, 25 and May, 7, 1986, with total deposition of Cs-137 ranging from less than 2 kBq/m^2 in the lowlands to more than 25 kBq/m^2 in the Carnic and Julian Pre-Alps. The most contaminated parts of the region are mainly covered by forest vegetation: Oak forests prevail in the lower mountainous belt, followed at higher elevations by beech forests, mixed beech-fir stands, and by subalpine, taiga-like forests dominated by larch in the subalpine vegetation belt. Natural, closed *Picea abies* forests of the oroboreal belt are scarcely developed because of the suboceanic character of the climate, although this tree has been largely used for reforestation. Azonal, open woodlands dominated by black pine *(Pinus nigra)*, *Fraxinus ornus* and *Ostrya carpinifolia* are frequent on scree slopes and on alluvial terraces.
The sampling stations are all located within the Friuli-Venezia Giulia region (northeastern Italy). They can be subdivided into two main groups:
1) Main station. This is the station where radiocontamination data have been obtained for vascular plant species, higher fungi, lichens, bryophytes, and soils. The investigation had two main aims: a) to carry out studies on the radiocontamination patterns of vascular plants, including understorey species, b) to carry out preliminary studies on the performance of various plant groups as bioindicators.
The station is located at Passo Pura in the Carnic Alps at 1417 m above sea level. The climate at the station is of suboceanic type, with mean yearly precipitations of ca. 1500 mm with precipitation maxima in May, September and November. About 36 mm of rain fallen in the first 10 days after the Chernobyl accident led to a deposition of radiocesium ranging between 10 and 15 kBq/m^2. The vegetation consists of a mixed beech-fir stand developed on undulating ground on calcareous parent material.
2) Subsidiary stations: These are 36 localities, scattered throughout the entire region, that have been utilized every year, from 1986 to 1991, for sampling mushrooms, with the aim of recording possible time-dependent variations of the contamination of various species and ecological groups. 24 stations have been also utilized for the survey of bryophytes. Most of the

stations are concentrated in the mountains and on the hills, for two main reasons: a) the lowlands have low contamination values, and hence need a lower sampling intensity, b) the surveys were limited to cryptogams occurring in forest vegetation, and the lowlands of Friuli possess only reduced and disturbed fragments of forest.

III.2. BIOINDICATORS OF RADIOCONTAMINATION

In the case of a sudden radiodeposition event, it is important to have a rapid, efficient and cheap method for assessing the main deposition patterns within large areas. Particularly in mountain areas the deposition patterns may be very complicated, due to the rugged geomorphology and to the irregular distribution of precipitations. In such cases, detailed radiodeposition mapping requires a high density of sampling points. Alternatively, it is possible to use different organisms as monitors of radioactive deposition. Within this context an organism is defined as a "biomonitor" when the concentrations of given pollutants within the organism are utilized to reconstruct the deposition patterns of the pollutants (Nimis 1990).
One of the most important advantages of the techniques based on biomonitors is their relatively low cost. This allows to adopt sampling strategies with a relatively high density of sampling points, which, especially in mountain areas, greatly enhances the data quality and permits to draw reliable contamination maps in an easy, cheap and rapid way.
The Trieste group has concentrated the attention on two groups of organisms that could be used as bioaccumulators of radioactive deposition in natural ecosystems: macrofungi and bryophytes. Lichens have been discarded since in Alpine forest ecosystems, contrary to the well-known situation in arctic and boreal environments, they generally have a very low biomass, and rarely form compact carpets on the ground.

III.2.1. Fungi

The study of radiocontamination of mushrooms gives a good example of the progress of radioecology in post-Chernobyl times. The initial high variability in the data has been mostly explained, up to an extent that it is now possible to utilize mushrooms as bioindicators of radioactive deposition over vast areas (Nimis & al. 1986, Haselwandtner & al. 1988).

At the beginnings of our study, the use of macrofungi in biomonitoring studies seemed to be very difficult due to the great variation of contamination values among individuals of different species in the same station, and to the very poor state of knowledge on the physiology and ecology of radionuclide absorption by mushrooms.
The main problems we had to solve at the beginnings of our study were: a) to understand the factors responsible for the high variability of the radiocontamination data among different species of macrofungi collected at the same station, b) to produce a radiocontamination map of macrofungi in northeastern Italy. The solution of point a) was indispensable for solving point b).
A first study, based on measurements of radiocesium in 298 samples belonging to 120 species of mushrooms collected in the 37 subsidiary stations in the fall of 1986 (Nimis & al. 1986) produced the following main results:
1) significant differences in contamination were recorded both among species collected at the same station, and among the average values of each station. The differences among species of the same station depend mainly on the depth of the mycelium in the soil: Contamination is highest in the fungi with superficial mycelium (saprophytic species), lowest in those that are

in symbiosis with deep-rooting deciduous trees (Fig. 1). This is related to the fact that in 1986 most of the radionuclides were concentrated in the upper horizon of the forest soils.
2) The differences among various stations were well correlated with the amount of precipitation in the first 10 days following the Chernobyl accident (Figs. 1 and 2).
The relations between radiocontamination of 4 ecological groups of macrofungi and precipitation are shown in Fig. 1. This relation is non-linear, whereas that relative to the soils of the 37 stations (Fig. 2) is linear, with most of the radiocesium being concentrated in the organic horizon. The reason is probably due to the interception of radionuclides by tree crowns, that is percentually higher in stations with low precipitation values. In these stations most of the radioactivity has been intercepted by the trees and was not available to the macrofungi growing in late summer. The soils were collected in autumn, when all the leaves were fallen, which explains the linear relation between soil contamination and precipitations.
Summarizing, we could demonstrate that the main factors affecting the high variation of radiocontamination data of wild mushrooms were: a) depth of the mycelium, b) precipitation during the 10 days after the Chernobyl accident. Once these factors were understood, it was possible to subdivide the macrofungi in several ecological categories (saprophytes, mycorrhizal etc.) and to use the saprophytic species as biomonitors of radiocontamination. The data spread within each category was much lower than considering all species together, and the data quality was consequently higher (see Nimis 1990).
Three contamination maps of North Eastern Italy have been produced (Nimis & al. 1990): a) a map based on direct contamination data in 1986 (37 sampling stations), b) the same map, with data relative to 1987, c) a map obtained from the precipitation map (135 stations), applying to precipitation data a mathematical function relating precipitation and the radiocontamination of saprophytic fungi. The first two maps have the advantage of being based on direct contamination measurements, the third, based on hypothetical data, has the advantage of having a much larger set of reference points (the 135 meteorological stations). The reliability of these maps has been discussed by Nimis & al. (1990b) on the basis of a fourth map, showing the deviation, point by point, of the data attributed to each point in the two contamination maps concerning mushrooms. Using the reliability map local authorities have a further tool for taking decisions on the measures to be taken in areas that appear to be highly contaminated: If in these areas the reliability of the map is high, restrictive measures will be justified, if it is low they may ask for further studies before taking a decision. The map based on the data of 1986 agrees very well with the estimated deposition of Cs-137 in Friuli-Venezia Giulia published by Velasco & al. (1990). This indicates that mushrooms can be used as very effective monitors of radioactive deposition.
To evaluate cesium migration, the samples have been subdivided into 3 ecological groups, corresponding to different average mycelium depths: Saprophytic fungi with superficial mycelium, mycorrhizal symbionts with shallow rooting trees (conifers) and with deep-rooting (deciduous) trees. Figs. 3 and 4 show a drastic decrease in radiocesium concentrations, from 1986 to the following years, for saprophytic fungi, and an increase for species in mycorrhizal symbiosis with deciduous trees. The figure indicates that already in 1986 there has been a rapid transfer of radiocesium into deeper soil horizons. The comparison of the contamination levels in the four groups with the contamination profiles in soils seems to validate the hypothesis that it is possible to monitor the downward migration of cesium in soils by using macromycetes, since cesium migration differently affects the contamination of the ecological groups. These results also indicate that saprophytic mushrooms can be effectively used as biomonitors over vast areas only a short time after deposition.
The studies carried out on macromycetes allowed to understand the main factors responsible for the high variability of radiological data in these organisms. On this basis, it was possible to

use macrofungi as bioindicators, and to construct deposition maps for a relatively large area; the data on the temporal variation trends in macrofungi can provide the basis for a model on the dynamics of the contamination of edible mushrooms that could be used for health protection purposes in case of other contamination events.

III.2.2. Mosses

In several forest ecosystems, and especially in rainy areas, bryophytes are an important element of the total biomass. The thick carpets of bryophytes covering large parts of the forest floor can intercept a great quantity of the total deposition, slowing down the transfer to soil. Mosses are able to trap and retain a large share of wet radioactive deposition. *Ptilidium cristacastrensis, Pleurozium schreberi* and *Dicranum undulatum* absorb completely more than 1 cm of liquid precipitation in a very short time. Considering also the lower part of the bryophyte mats, constituted of dead leaflets and stems, the absorbing power rises to 3 cm of precipitation.

Particular attention has been devoted to bryophytes in order to: a) evaluate their role in the retention of radionuclides in forest ecosystems; b) develop a standard procedure for utilizing bryophytes as bioindicators of radiocontamination. When growing directly on soil, bryophytes are able to retain a great amount of the total deposition and the transfer to the soil is correspondingly very slow. In ecosystems with an important bryophyte component in the forest floor measurements of radioactivity in the soils (excluding the overlying bryophyte mats) is not a good estimate of total deposition, since most of the radionuclides are retained in the bryophyte mats. If the bryophyte mats are considered as part of the soil, great care should be taken in calculating transfer factors soil–plant, since in most cases bryophyte mats cannot be considered as a part of the soil (no roots of vascular plants are present).
The highest radiocesium concentrations were recorded in Ctenidium carpets collected on horizontal surfaces, and growing directly on calcareous rocks, whose thickness varied between 0.5 and 2 cm. The samples collected just below a trunk showed higher contamination values, probably because of secondary enrichment from stem flow. Otherwise, no statistically significant difference was observed among samples collected in different positions with respect to the tree canopy. These results allowed to set up a standard sampling protocol for using this type of bryophytes as indicators of radioactive deposition. The main recommendations are:
a) the samples should belong to epilithic species; b) the samples must grow on horizontal surfaces; c) the samples must belong to species forming carpets constituted by a lower part, consisting of organic soil, and an upper part, consisting of the living gametophyte; d) the thickness of the samples should range between 0.5 and 2 cm.
A very good correlation between radiocontamination in the bryophytes growing on rock, and in the soils was found, demonstrating the possibility of effectively using bryophytes as biomonitors of radioactive deposition.

III.3. HIGHER PLANTS

III.3.1. Expression of radiocontamination in plants

It is well–known that most of the potassium in plants is free in solution inside the cell or in the apoplastic water. Due to its chemical similarity, this is probably true also for cesium. As, however, the water content of plants is subjected to short–term fluctuations (i.e. after a rainy

period), nowadays most authors use the conventional expression on a dry weight basis. Since the dry weight of plant material is not necessarily correlated with the quantity of plant water, the expression of radiocontamination on a dry weight basis does not reflect with accuracy the actual concentration of radiocesium in the cytoplasm and in the apoplastic water of the plants. This may be of little relevance in radiation protection, but becomes a consistent source of error in radioecology, especially when the following problems are addressed: 1) comparative studies of transfer factors among different species; 2) translocation of radiocesium in different parts of the same plant; 3) study of seasonal fluctuations during the growing season.
Nimis & al. (1988) have discussed this problem, suggesting that, as in the case of potassium, it could be overcome by expressing the radiocesium activities in plants on a water basis, i.e. on the difference between fresh and dry weight. Nimis & al. (1990,1994), studying many species of vascular plants in a complex forest ecosystem in the Carnic Alps, demonstrated that the expression of radiocesium in Bq/l resulted in a much lower degree of infra- and intraspecific variability, and that this allowed to find significant relations with soil features and with the rooting depths of the different plants. The traditional expression on a dry weight basis could easily lead to false interpretations as far as transfer factors soil-to-plant, translocation rates within plants, and seasonal fluctuations in leaves were concerned (Bolognini & Nimis 1995).
As an example, the concentrations of radiocesium and K-40 in different parts of three species of vascular plants of a forest ecosystem (*Fagus sylvatica, Rosa pendulina* and *Picea abies*) are briefly discussed. The data expressed in Bq/kg suggest an "accumulation" of radionuclides in the leaves. However, such an "accumulation" does not depend on physiological mechanisms, but on the expression of the data. When these are expressed in Bq/l, the differences between ligneous and non-ligneous parts of the plants are drastically reduced, and the "accumulation" of radiocesium in certain parts of the plants reflects a very trivial fact, i.e. the relative water content of the plant parts themselves.

III.3.2. Survey of radiocontamination in forest plants

The main aim of the study was to enquire whether it is possible to establish some relations between contamination of the species and their ecology within the forest, in order to provide data for a model of radiocesium absorption patterns. Also the K-40 concentrations have been measured, because of the chemical, and hence physiological, similarities between this element and radiocesium.
The data concern 48 species of vascular plants, collected within an area of 0.3 km^2 in a mixed *Fagus-Abies* forest at the Passo Pura station. Of each species, leaves, stems and hypogeal organs were sampled separately.
The main results may be summarized as follows:
1) The content of radiocesium is highest in plants whose root systems occupy the upper soil layer of acidic humus, is lowest in the deep rooting megaphorbs of the wood clearings. This is due to the unequal distribution of radiocesium in the soil, the highest concentrations being still present in the upper soil horizons, and to the fact that the downward migration of radiocesium in the soils of the clearings is slowed down by the higher contents in clay and by the presence of an almost continuous mat of bryophytes which retained most of the deposition.
2) The K-40 concentration is much less subjected to variations than radiocesium concentrations, and, contrary to the former, seems to be independent from rooting depth.
3) The megaphorbs growing in the clearings of the beech forest tend to retain radiocesium in their root systems. In this case, it appears that the plants are able to discriminate between Cs and K at root level. This fact seems to be a general rule, since the value of the ratio Cs-137/K-40 between roots and leaves is higher than 1 in most species, but is particularly

pronounced in the plants of the clearings. For the moment we have no physiological explanation of this fact, which might be related to the larger atomic weight of Cs, and to an antagonism of Cs and K in the absorption mechanism from the roots.
4) The typical geophytes, trees and shrubs of the beech forest tend to have a higher Cs-137/Cs-134 ratio: This is probably related to the greater depth of their root systems, that can absorb old, pre-Chernobyl cesium that has already migrated into deeper soil horizons. These plants also have a tendency to store old, pre-Chernobyl radiocesium in the roots. This may be due to the fact that several of these plants have hypogeal organs transformed into storage organs.
5) Cs and K seem to have a similar behaviour inside the plants, once passed the root barrier. However, an exception is given by Pteridophytes, which, contrary to all angiosperms, have a clear tendency to accumulate radiocesium in the leaves. Also this fact awaits a causal explanation based on physiological studies.
The results of the analysis allow to simplify the ecosystem for modelling purposes: The 48 species can be reduced to a few groups, each being characterized by a peculiar ecology and by different contamination patterns.

III.3.3. Direct ecological study at microcommunity level

The results presented in the previous paragraphs suggested the possibility of establishing a relation between the ecology of vascular plant species and their radiocesium contents. Based on a study, where the ecology of different species of vascular plants had been characterized directly in the field, the ecological variables with the highest information content were extracted: Organic matter content, K-40 concentrations (i.e. total K), and % of exchangeable K.
The results indicate that:
a) vascular plant species occurring in a natural forest, within a rather narrow area, have different ecological requirements; b) the species can be ordered along a main gradient of increasing organic matter content of the soils, increasing available K and decreasing total K; c) the concentrations of radiocesium in the plants are strongly related with this gradient.
Therefore, the radiocontamination values of plant species seem to be governed mainly by three related factors: 1) organic matter content, 2) available K, and 3) total K content.

III.3.4. Seasonal phenomena

A potential source of variability in radiocesium concentrations in plants are the fluctuations of radionuclides in plant tissue during the growing season. If seasonal variations in cesium uptake among plant species do exist, this must be taken into account by radioecologists, and by those interested in evaluating the radiocesium content of the diet of grazing animals.
We found that many species showed distinct, regular and often very pronounced seasonal rhythms of contamination. The variation in radiocesium concentrations during a growing season and between years, turned out to be so high that transfer factors soil-to-plant would be very different depending on the season or the year, in which the plant material was collected. This indicates that seasonal phenomena may actually be an important source of noise in radioecological studies.
Here, we shall discuss in more detail the results relative to *Dryopteris filix-mas*. Radiocesium concentrations may vary considerably within the same year in plants of the same population, growing in the same environment. The maximum values are much lower in 1992 than in 1993. However, the general trend is similar in both years, with higher values at the beginning and at

the end of the vegetative season, and lower values during summer. Potassium concentrations in plant water were much more stable than those of radiocesium, and with no substantial difference between years. The highest concentrations of both ions were in the fronds, but radiocesium had higher relative concentrations in roots than K–40.
A possible explanation of these fluctuations could be the infection by endomycorrhizal fungi, typical of the roots of *Dryopteris filix–mas*. The seasonal development of mycorrhizal infection in this species was studied in detail by Bouillard (1958): The infection is maximal during winter, starts to decrease as soon as the plant forms the first leaves, disappears almost completely during summer, and rapidly increases again towards the end of the vegetative season. As the mycorrhizal fungi are able to exploit a much larger volume of soil, and since radiocesium distribution along the soil profile shows a pronounced pattern, with higher concentrations in the upper horizons, mycorrhizal fungi could be the main carrier of radiocesium into the plant. This hypothesis is particularly appealing, as it does not require any mechanism of selection between cesium and potassium by the fern. Furthermore, it is supported by the fact that the yearly trend of mycorrhizal infection is similar to that of radiocesium concentrations, and by the higher concentrations of radiocesium with respect to potassium found in roots, where the fungal biomass is highest. Differences between years could be due to different degrees of mycorrhizal infection depending on climatic factors.
Considering that most plants of natural and semi–natural ecosystems are in symbiosis with ecto– and endomycorrhizal fungi, it is possible that a consistent share of the high variability found in radioecological data concerning plants could be due to this phenomenon. Considering the high number of species showing distinct seasonal patterns found in the Passo Pura forest, it is very probable that in natural ecosystems, and especially in forests, mycorrhiza–induced seasonal fluctuations are more the rule than the exception. It follows that transfer factors for the same species growing on the same soil may exhibit a very large variation during the relatively short time of a growing season. This has an important consequence for studies on long–term trends in radiocesium concentrations in plants of natural ecosystems, as great care should be taken of sampling the plants in the same period of the year.

PUBLICATIONS DURING THE RESEARCH PROJECT

Bolognini G. & P.L. Nimis 1995 – Un problema metodologico in radioecologia: l' espressione della radiocontaminazione in piante vascolari. Atti Soc. Ital. Radioecol. (in press).

Giovani C., Bolognini G. & P.L. Nimis 1994 – Bryophytes as indicators of radioactive deposition in northeastern Italy. Sci. Tot. Envir.,157: 35–43.

Nimis P.L., Bolognini G. & C. Giovani 1994 – Radiocontamination patterns of vascular plants in a forest ecosystem. Sci. Tot. Envir.,157:181–188.

REFERENCES

Haselwandtner K., Berreck M., & P. Brunner, 1988 – Fungi as bioindicators of radiocaesium contamination: pre- and post-Chernobyl activities. Trans. Brit. Mycol. Soc., 90, 2: 171–174

Nimis P.L. 1990 – Air quality indicator and indices. The use of plants as bioindicators and biomonitors of air pollution. In: A.G. Colombo & G. Premazzi (eds.); Proc. Workshop on Indicator and Indices, JRC Ispra. EUR 13060 EN: 93–126.

Nimis P.L., Gasparo D., Giovani C. & R. Padovani 1990 – Radiocontamination maps of macrofungi in northeastern Italy following the Chernobyl accident. Gortania,11: 119–126.

Nimis P.L., Giovani C. & R. Padovani 1986 – La contaminazione da Cs–137 nei macromiceti del Friuli–Venezia Giulia nel 1986. Studia Geobot., 6: 3–121.

Nimis P.L., Giovani C. & R. Padovani 1988 – On the ways of expressing radiocaesium contamination in plants for radioecological research. Studia Geobot., 8: 3–12.

Nimis P.L., Tretiach M., Belli M. & U. Sansone 1990 – Individuazione di bioindicatori di radiocontaminazione. Sicur. Prot. Roma, 21: 71–76.

Nimis P.L., Tretiach M., Belli M. & U. Sansone 1990 – The effect of microniches in a natural ecosystem on the radiocontamination of vascular plants. In: Desmet G. & al. (eds.): Transfer of radionuclides in natural and semi–natural environments. Elsevier, London and New York. pp. 84–93.

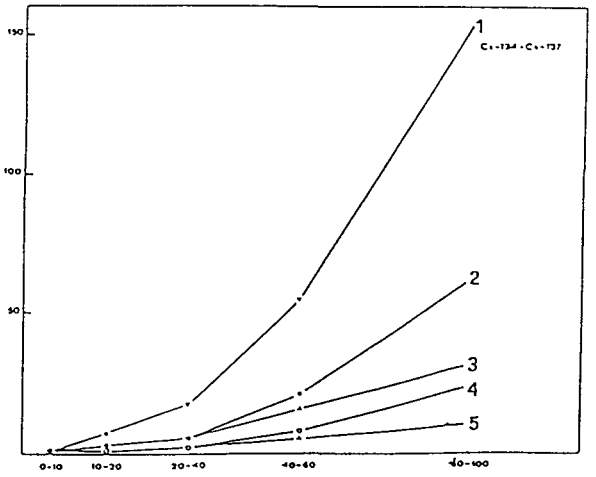

Fig. 1: Relations between radiocontamination of fungi, their ecology, and precipitation in NE Italy four months after the Chernobyl accident. x–axis: radiocesium concentrations (in Bq/kg dry weight) of mushrooms. y–axis: precipitation in mm fallen in the first 10 days after the Chernobyl accident. The 37 sampling stations were grouped into 5 classes, according to precipitation values. The mushrooms were subdivided into the following categories: 1: saprophytic; 2: all species; 3: mycorrhizal with conifers; 4: mycorrhizal with deciduous trees; 5: lignicolous.

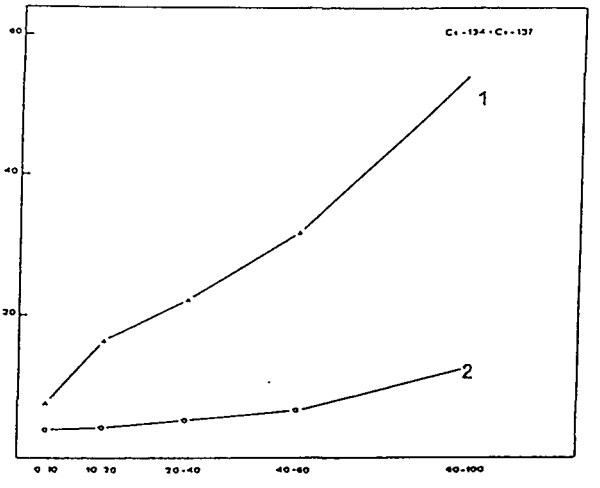

Fig. 2: Relations between precipitation fallen in the first 10 days after the Chernobyl accident (x–axis, in mm), and radiocontamination of soils (y–axis, in kBq/m^2) in NE Italy, measured four months after the accident. The stations were grouped into 5 precipitation classes as in Fig. 1.

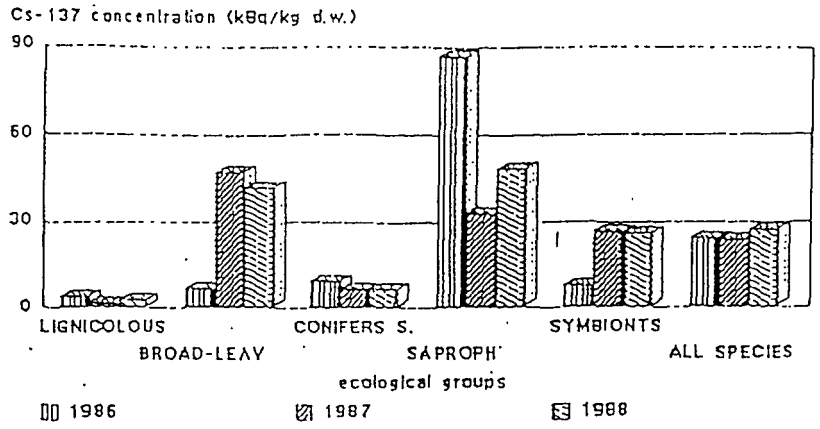

Fig. 3: Trends in the radiocontamination of wild mushrooms by Cs–137 in NE Italy from 1986 to 1988. The mushrooms have been subdivided in several ecological categories: lignicolous, mycorrhizal with broad–leaved trees, mycorrhizal with conifers, saprophytes, all mycorrhizal species, all species.

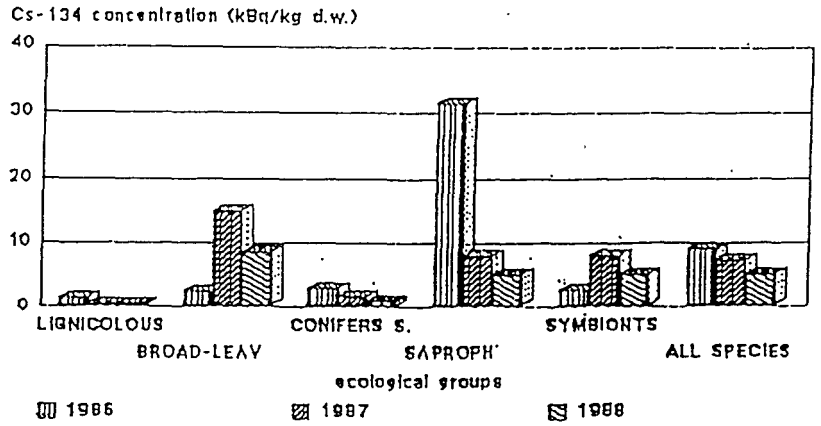

Fig. 4: Trends in the radiocontamination of wild mushrooms by Cs–134 in NE Italy from 1986 to 1988. The mushrooms have been subdivided in several ecological categories: lignicolous, mycorrhizal with broad–leaved trees, mycorrhizal with conifers, saprophytes, all mycorrhizal species, all species.

Head of project 9: Dr. Antonopoulos-Domis

II. Objectives for the reporting period

The objectives were:

- Radiocesium distribution in the different parts of the ecosystem (soil, forest floor, ground vegetation, trees, etc.).
- Radiocesium cycling in the ecosystem.
- Modeling of radiocesium dynamics in the ecosystem.

III. Progress achieved including publications

III.1. Brief (executive) Summary

All objectives described in II above and set out both in our proposal and contract have been achieved with the exception of litter decomposition measurements which are not complete yet.

For the latter more than two years are needed since the relevant decomposition time constant is about three years.

In particular the following were determined experimentally.

(a) Mass per unit area (kg/ha) of different parts of the ecosystem.
(b) Radiocesium distribution in the ecosystem (soil layers, forest floor, ground vegetation, tree parts etc.).
(c) Radiocesium cycling.
(d) In addition (not included in our obligations) the contribution of radiocesium to the total external dose rate and the total external dose rate itself at the forest was determined by in situ γ-spectrometry.

Furthermore:

(e) Cesium migration in soil was modeled by an "equivalent diffusion" model and by a compartment model derived from a diffusion-advection model.
(f) A compartment model of Cesium dynamics in the ecosystem is proposed.

From this work, performed over the last two and a half years, one paper has been submitted so far to the Health Physics.

III.2. Extended summary

MATERIALS AND METHODS

Description of the ecosystem

The research was conducted in the University experimental forest of Taxiarchis Chalkidiki, 50 km from Thessaloniki in Northern Greece. The elevation is 800 m above sea level and the area belong to sub-mediterranean bioclimatic region with 0 to 40 biologically dry days annually. The mean annual temperature is 10.7 °C. The mean temperature of the coldest

month (January) and the warmest (July) are 0.7 °C and 20.5 °C respectively. The mean annual precipitation is 756.2 mm and occurs mostly as rain.

The soils of the area are well drained Acid Brown Forest Soils, developed on mica schists, sandy loams to loams, acid (pH 1.5 to 5.0), 40-60 cm deep, subangural weak to medium structure, moderately well supplied with organic matter and nutrients. The mean soil characteristics are shown in Table 1.

Table 1. Mean soil characteristics

Hor.	Depth	pH	Text.	Org. mat.	N	P Olsen	CEC	exchangable cations			
								Ca	Mg	K	Na
	(cm)			(%)	(%)	(ppm)		me/100g			
$A_{1.1}$	0-6	4.8	SL	7.6	0.18	34	17.1	11.3	1.9	0.5	0.17
A_{12}	6-22	4.5	SL	4.4	0.14	30	16.3	5.9	0.9	0.9	0.17
A_3	22-40	5.0	SL	3.6	0.12	29	13 0	5.7	0.6	0.6	0.15
(B)	40-80	4.7	SL	1.9	0.08	34	8.6	2.8	0.5	0.5	0.17
C_1	>80	-									

Parent materia mica schist for the Quercus ecosystem

The vegetation of the study area is 40 years old coppice stand (under conversion into high forest) of Quercus conferta Kit. The basic stand characteristics are shown in Table 2.

Table 2. Stand Characteristics

Type of ecosystem				Altitude	Site quality	Age of stands
Quercus conferta (Kit.)				850 m	Moderate	42 years old
Breast diam. (cm)	Stems/ha	Basal area (m^2/ha)	Mean height (m)			
<4	498	0.6	3.7			
4-8	955	3.1	8.3			
>8	1231	16.5	12.2			
total	2684	20.2				

The dominant understory species are Pteridium aquelinum, Festuca sp., Cyclaminum persicum, Pactylis glomerata, Brachypodium silvaticum, Luzula forsteri, Rosa sp., Fragaria vesca, Arimonia agrimonoides, etc.

Determination of the mass per unit area (kg/ha) in the different parts of the ecosystem

The various parts of the ecosystem are: above ground biomass, forest floor and soil.

a) Biomass

The above ground tree biomass was separated and measured as foliage, branches of various diameters and trunk wood. Green and dry weights, above stump were determined for 27 Quercus conferta Kit trees in 1983, of 2 to 19 cm diameter at breast height (d) and 2.2 to 14.7 m total height (h). Performing a multiple regression analysis we could estimate the mass of the trunk wood and the mass of the branches taking (d) and (h) as independent parameters.

Measuring the number of trees, the height and diameter of all trees in the experiment plot area (0.2 ha), for the years 1983-1995 the above ground biomass could be estimated For leaf biomass determination, litter fall data was used using standard sampling techniques (litter traps).

b) Forest floor

Forest floor samples were selected with 625 cm^2 (25x25 cm) metal frame (10 cm deep) from 25 randomly distributed locations of the experimental plot. To facilitate sampling the frame was pressed firmly against the forest floor. A sharp knife was used to cut through the organic layers around the edge of the frame and the sample was then carefully removed and placed in plastic bags. Then oven-dried and weighted. Ground vegetation was determined by sampling from 10 randomly distributed locations with 0.5 m^2 metal frame. The value in kg/ha of forest floor used in the present work was deduced from 7 repeated sampling periods at 3-months interval in order to get accurate mean values and seasonal variation.

c) Soil

Soil samples were taken a) according to the different horizons (Ah, $A_{1.1}$, $A_{1.2}$, B) or b) every 5 cm depth. By measuring the bulk density as a function of depth by bulk density meter, the mass of soil per unit area in different depths could be deduced.

Radiocesium Distribution: Sampling Methodology

The radiocesium distribution in the different parts of the ecosystem has been studied for the years 1993-1995. For that, 3 trees were cut down into pieces each time and samples were collected from the different parts of the trees (wood and bark in different heights, branches of different diameters, leaves). The same procedure was repeated 4 times at about 8-months interval. Leaves, as well as samples of forest floor and Ah horizon were collected periodically during this period. Slices (layers) of soil of 5 cm height were collected down to a depth of 40 cm at about 8-months interval from nearly the same location of the experimental plot. The samples were oven-dried for tree samples and air-dried for soil samples in the Forest-Soil laboratory of the Aristotle University of Thessaloniki; ground, passed through a 2 mm sieve (in the case of soil samples) and used for radiocesium counting.

Methodology for radiocesium cycling

For radiocesium cycling in the plot, ten throughfall collectors, five stemflow collectors, ten leaf litter traps and five branch litter traps were installed. Throughfall and rain collector was a 20 cm tunnel mounted 1 m above ground level and drained into a 3 l plastic container. A 0.2 mm mesh nylon filter keep back insects and coarse debris. Stemflow was collected by plastic and polyurethane collars and piped into 20 l polyethylene containers. Leaf litter traps were 0.5 m^2 baskets lined with nylon fabric, while branch litter traps were 4 m^2 plastic sheets fixed on the soil surface. Moreover for radiocesium leaching from forest floor to mineral soil three lysimeters, 0.25 m^2, were located under the forest floor.

Radiocesium determination

Samples were put into cylindrical pots (70 mm diameter, 20 mm high), or in Marinelli beakers and radiocesium content was determined by standard γ-spectroscopy with a high purity Ge detector.

RESULTS AND DISCUSSION

Concentration in the different parts of trees

Table 3 presents the radiocesium activity (Bq/kg) in the different parts of trees for different sampling dates and Table 4 presents measured concentrations in wood and bark along the height of the trees; the particular data presented in this table are those measured from trees sampled on 21-4-94 but are typical of all studied trees.

The following should be noted:

(i) Bark has a relatively large concentration of radiocesium, obviously due to absorption from direct wet deposition of the radioactive cloud from the accident. Most, if not all, of Cesium in the bark is not available for translocation to the biomass of other parts of the tree. In fact stem-flow measurements (see section on cycling) show that this Cesium is bound to the bark. Trunk has relatively small Cesium concentration compared to that of the bark. Cesium is almost uniformly distributed along the height of the tree and, within the experimental error is about the same for all studied trees (Table 4).

(ii) Newly born (smaller than 1 cm) biomass, i.e. leaves and branchletts, has significantly smaller concentrations of Cesium than older biomass, as can be seen in Table 3. This experimental fact suggests that there is a Cesium reservoir in the tree formed by Cesium adsorption during direct, mainly wet, deposition at the year of the accident. In fact for this ecosystem a 6 year study has shown that about 22% of the rain is retained by the trees. Translocation of Cesium from this reservoir must be a significant source of contamination of newly born biomass at least during the first few years following deposition.

Table 3. ^{137}Cs concentration (Bq/kg)

	(8-2-93)	(24-9-93)	(21-4-94)	(1-3-95)
Trunk	11.3 ±3	31 ±10	11 ±3	10 ±4
Bark	127.0 ±17	121 ±50	168 ±79	215 ±137
Branches <1cm	27.0 ±4	45 ±15	27 ±2	20 ±2
Branches 1-3cm	200.0 ±100	123 ±60	32 ±8	87 ±34
Branches 3-6cm	172.0 ±20	77 ±30	67 ±40	97 ±46
Branches >6cm	56.0 ±20	122 ±50	41 ±15	132 ±30

	(29-10-92)	(3-6-93)	(20-10-93)	(21-6-94)
Leaves	88 ±18	56 ±15	35 ±15	36 ±15

	(16-7-94)	(16-9-94)	(5-10-94)	(1-6-95)
Leaves	20 ±5	20 ±6	24 ±8	59 ±10

Table 4. ^{137}Cs concentration (Bq/kg)

	Wood		
	1st tree	2nd tree	3rd tree
Base	-	9	7
1.3 m	10	11	9
2 m	11	13	10
4 m	9	9	13
6 m	14	9	-
8 m	17	10	-
10 m	17	15	-
average	12±3	11±2	11±1

	Bark		
	1st tree	2nd tree	3rd tree
Base	-	85	218
1.3 m	84	87	87
2 m	127	168	158
4 m	92	185	215
6 m	270	388	134
8 m	269	182	132
10 m	136	-	-
average	163±77	182±100	157±47

The same effect has been observed for fruit trees (Antonopoulos-Domis et al. 1990, 1991). However leaves collected in June 1995 from trees planned after the accident, i.e. trees that did not receive direct deposition have Cesium concentration of 44 Bq/kg which is not much smaller than 59 Bq/kg obtained from leaves of old trees collected at the same site and time. This suggests that root uptake is not a negligible mechanism for Cesium contamination of newly born biomass, at least during 1995.

(iii) From the ecosystem compartment model we propose, but not presented here because of text-length limitations, it follows that Cesium content Ln in newly born biomass (leaves etc.) n years following deposition may be expressed by,

$$Ln = c_1 e^{-a_1 n} + c_2 e^{-a_2 n}, \qquad n \geq 1 \tag{1}$$

where the first exponential is due to root uptake and the second exponential is due to translocation from the tree reservoir (dilution). Constants c_1, a_1, c_2 and a_2 may be determined from experimental measurements provided there are such measurements starting the first year following the accident (Antonopoulos-Domis et al. 1991). Unfortunately we started sampling at this site at the end of 1992.

The measured time dependence of Cesium concentration in leaves is not easy to understand. Nevertheless Fig. 1 presents the Cesium concentration (Bq/kg) of leaves collected in October of years 1992 to 1994. It can be seen that the following exponential function fits well the experimental data.

$$Ln = 3944\, e^{-0.65 \cdot n} \tag{2}$$

Comparison of (1) and (2), if the actual situation is well presented by (2), indicates that one of the two mechanisms is now negligible with respect to the other. Measurements over significantly more than three years are needed to clarify the situation and we intend to do that.

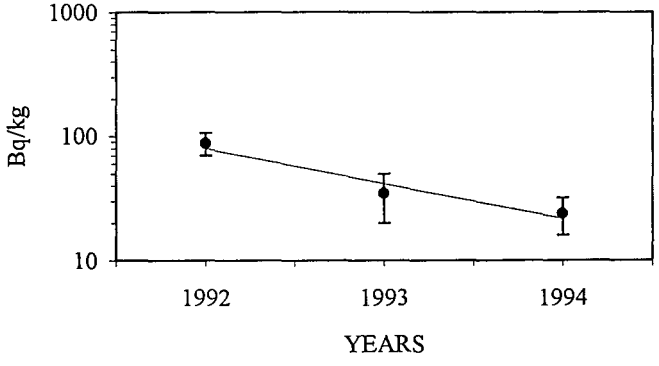

Fig. 1 ^{137}Cs content of leaves collected in October: measurement, function $\mathbf{Ln = 3944\, e^{-0.65 \cdot n}}$

Forest floor and ground vegetation

Table 5 presents Cesium concentration (Bq/kg) in the forest floor and ground vegetation. The following should be noted

(i) samples of forest floor collected in 1982 and 1983, i.e. before the Chernobyl accident, and stored in the Forest-Soil laboratory have ^{137}Cs concentration of 65 Bq/kg and 69 Bq/kg respectively. Clearly this is due to weapons fallout and is less than 3% to 1% of today's concentrations in forest floor.

(ii) Looking at the samples of the same section-1, it can be seen that Cesium in the forest floor appears constant over the years 1992 to 1993. This is consistent with the experimental finding (section on cycling) that the total amount deposited from the above ground biomass per year due to all reasons is 0.18±0.09 MBq/ha.

(iii) As expected Cesium activity in the L layer is one order of magnitude smaller than in the F and H horizons.

(iv) As expected there is a large horizontal variation of Cesium activity in the forest floor even for small distances.

Table 5. ^{137}Cs concentration (Bq/kg)

	1st section					
	(1982)	(1983)	(29-10-92)	(3-6-93)	(21-4-94)	(1-3-95)
Forest floor	65	69	2557	2452	2550	2143

	(1-3-95)		
	1st section	nd section	3rd section
L	350	422	334
F	4615	3445	1842
H	7125	7743	4389
total	3085	5537	2143

Ground vegetation: 28 ± 12 (mean value of 15 measurements)

Radiocesium profile in soil

Soil samples of the horizons and of soil layers of height of 5 cm from 0 to 40 cm depths were taken and the corresponding Cesium distribution (profile) in soil was measured. Six such profiles were taken within a radius of 10 m, over the two year period from 8-2-93 to 1-3-95. There is no trend with time of the variations of the individual profiles; these variations are random and they must be due to horizontal variations and experimental (mainly sampling) errors. It is therefore concluded that the profile is fixed, at least since 1993 when we started measurements at this site. This in turn suggests that most of Cesium is fixed in the soil minerals and free Cesium available for migration is negligible.

The mean activity, over these measurements, and the standard deviation in MBq/ha is included in Table 6. The same are graphically presented in Fig. 2. The profile follows an exponential decrease with depth and seems to level off to a constant value of 1 MBq/ha.

The dashed line connects the experimental values. It is well fitted by the two continuous straight lines: the first representing an exponential function of depth and the second a constant. Bearing in mind the ^{137}Cs found in forest floor samples collected before the Chernobyl accident, it is concluded that the constant value of 1 MBq/ha is due to weapons fallout and not to deposition from the accident. We therefore used, in the migration models that follow, the experimental values from 0 to 20 cm, subtracting 1 MBq/ha.

Table 6. ^{137}Cs distribution

	Kg/ha	^{137}Cs (MBq/ha)	contributio (%)
Soil			
Layer			
Ah	61000 ±8540	128.0 ±59	52.60
0-5	410000 ±65600	57.0 ±25	23.40
5-10	460000 ±92000	12.0 ±6.8	5.00
10-15	525000 ±115500	3.3 ±1.8	1.30
15-20	570000 ±125400	2.0 ±0.2	0.80
20-25	590000 ±135700	1.5 ±1 29	0.53
25-30	630000 ±145000	0.9 ±0.32	0.33
30-35	670000 ±154100	0.6 ±0.23	0.20
35-40	770000 ±177100	0.9 ±0.43	0.20
sub-total		206 ±65	84
Forest floor	13459 ±2422	32.6 ±9	13.40
Gound vegetation	586 ±118	0.016 ±0.007	0.006
Biomass			
trunk	81437 ±9772	1.29 ±0.6	0.53
bark	7868 ±944	1.23 ±0.3	0.50
leaves	3740 ±300	0.16 ±0.08	0.065
branches			
<1 cm	6438 ±1416	0.19 ±0.06	0.078
1-3 cm	10265 ±9772	1.13 ±0.8	0.40
3-6 cm	8996 ±9772	0.90 ±0.5	0.37
>6 cm	9048 ±9772	0.80 ±0.4	0.33
sub-total		5.70 ±1.03	2.27
TOTAL		243.00 ±66	

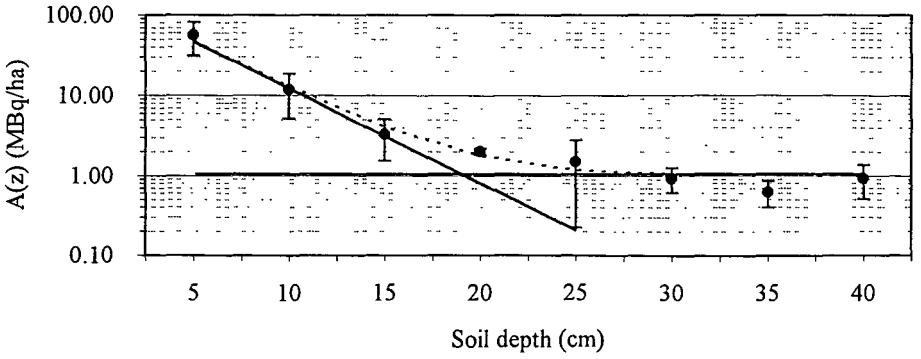

Fig. 2 ^{137}Cs distribution in soil from 0 to 40 cm; • average value, ⊥ standard deviation. Dashed line connects the experimental values. It's well fitted by the sum of the two continuous curves: one exponential and a constant.

Cesium migration in soils may, in general, be modeled by diffusion and advection mechanisms (Antonopoulos-Domis et al. 1995b). However profiles presenting a single exponential decrease with depth, like in the present case, may be modeled by an "equivalent diffusion" model. Such a model is instructive in the sense that, being a meanable in certain cases to analytical solutions, it can give qualitative insight. Furthermore it can provide a single "operative parameter" if one is interested only in the final Cesium profile. In fact the latter is the only interesting one for long term external dose rates. All models discussed here are one dimensional in space, i.e. they depend only on depth z and on time t. We consider two phases of Cesium in soil: (i) free Cesium C(z,t), available for migration, including Cesium adsorbed in microparticles that can migrate and (ii) bound Cesium B(z,t) which is not available for migration. The model equations read:

$$\frac{\partial C}{\partial t} = \frac{\partial}{\partial z}\left(D\frac{\partial C}{\partial z}\right) - kC \tag{3}$$

$$\frac{\partial B}{\partial t} = kC \tag{4}$$

with boundary condition,

$$\left.\frac{\partial C}{\partial z}\right|_{z=0+} = 0 \tag{5}$$

In (3) and (4) the transfer coefficient k accounts for the net transfer from free to bound state. The diffusion coefficient D is in general space dependent, D=D(z), since soil is non-homogeneous.

For a non-homogeneous medium (5) may be solved numerically (Antonopoulos-Domis et al. 1995b). We will however assume that the soil is homogeneous, in order to have

analytical solutions, useful for qualitative discussion. We will first consider the initial condition,

$$C(z,0) = C_o ä(z)$$
$$B(z,0) = 0 \tag{8}$$

where ä(z) is the delta function, i.e. at t=0 there is an infinitesimally thin layer of free Cesium at the soil surface and no bound Cesium anywhere in the soil. In this case (5) has the analytical solution.

$$C(z,t) = \frac{C_o}{2(ðDt)^{1/2}} \exp\left(-\frac{z^2}{4Dt}\right) \exp[-(k+ë)t] \tag{9}$$

Free Cesium decreases, in this case, exponentially with z^2 and not with z. Clearly when free Cesium is significant the profile can not be linear in a semilogarithmic scale. We were not able to find analytical solution of (6), we therefore integrated (6) numerically. We then computed the total T(z,t) Cesium in soil.

$$T(z,t) = C(z,t) + B(z,t) \tag{10}$$

and finally computed the total activity in the soil layers of 5 cm depth. Model parameters D and k may be determined by least squares fit of the measured data. However it can be readily seen from (3) that equilibrium ($\partial C / \partial t = 0$) profile is determined, not by the individual values of D and k, but by the diffusion length L.

$$L = \sqrt{D / k} \tag{11}$$

This is in fact the "operative parameter" determining the eventual profile. By least squares fit to the measured equilibrium profile the diffusion length for this site was found to be L=3.6 cm. Comparison between modeled and measured values is presented in Fig. 3.

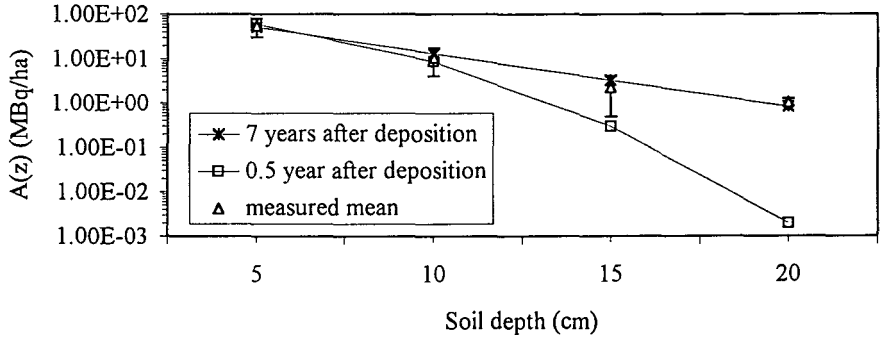

Fig. 3 ^{137}Cs profile in soil. Measured mean and standard deviation.Diffusion model with initial conditions (8): * 7 years after deposition, □ half year after deposition.

It is clear that the model predicts that total Cesium at equilibrium, decreases exponentially with depth z. In the same figure the model prediction of the profile half a year following deposition, i.e. during the transient, is presented. It can be seen that during the transient the profile does not have a single linear slope in semilogarithmic scale. Clearly such a linear slope indicates that the transient is over and Cesium has reached equilibrium in the soil.

A more realistic initial condition is to assume that at time t=0, i.e. immediately after wet deposition, there is Cesium at a small finite depth under the soil surface. The solution to this problem is not presented here. We simply state that the conclusions are identical to those of the previous case.

Although the pure diffusion model, being amenable to analytical solutions, can provide insight to the migration process it nevertheless can not always reproduce the experimentally observed profiles (Antonopoulos-Domis et al. 1995b, 1995c). Starting from the more complete diffusion-advection model a compartment model was derived, and the model parameters determined. We do not present the results here. We simply state that transfer form the forest floor and Ah horizon was also modeled.

Distribution and cycling in the ecosystem

Table 6 presents the measured distribution of mass and of ^{137}Cs in the ecosystem, averaged over the samples of 1993 to 1995. The following should be noted.

(i) A total ^{137}Cs amount of 24.3±6.6 kBq/m^2 is measured in all parts of the ecosystem. Taking into account that ^{137}Cs is mostly due to the Chernobyl this value corresponds to a total deposition of 29 kBq/m^2 at the year of the accident.

(ii) Almost 90% of the radiocesium inventory is still in the upper layers of the soil and the forest floor. In particular 13.4% is in the forest floor, 52.6% in the Ah horizon and 23.4% in the upper 5 cm of the soil.

(iii) Only 2.2% of the radiocesium inventory is in the above ground biomass, bark and trunk have approximately the same amount of radiocesium. Older tree products have significant higher radiocesium amount than newly born biomass, i.e. leaves and branches of diameter less than 1 cm.

From the lysimeters measurements we estimated the Cesium leaching from the forest floor to soil per year to be 0.01 MBq.ha^{-1} y^{-1}, which is negligible in comparison with the 32.6 MBq/ha in the forest floor.

In order to determine the radiocesium cycling in the ecosystem the following observables have been measured. The mean annual throughfall and stemflow in the ecosystem is 5.83 10^6 l/ha and 0.6 10^6 l/ha respectively. The radiocesium concentration in the water from the throughfall and stemflow collectors was below detection limit despite the condensation applied on the samples. The amount of radiocesium on the soil surface coming from the above ground biomass due to stemflow and throughfall is therefore very small, much smaller than 0.003 MBq ha^{-1} y^{-1}.

The mean radiocesium concentration of leaves and branches in the leaf litter traps and branch litter traps is 40.5±11 Bq/kg and 38±10 Bq/kg respectively. Knowing that 3740±300 kg/ha of leaves and 885±100 kg/ha of branches are rejected every year from the trees we can calculate an amount of ^{137}Cs per year on the ground surface due to the rejection of leaves and branches from the trees of 0.15±0.05 MBq/ha and 0.03±0.08 MBq/ha respectively. The total amount of radiocesium deposited from the above ground biomass per year due to all reasons (rejected leaves, deposited branches, stemflow, throughfall) is 0.18±0.09 MBq/ha.

Contribution of radiocesium to external dose rate

We measured the total external dose rate and also the contribution of radocesium to the total external dose rate at the site, by in-situ γ-spectroscopy applying to the γ-spectrum the striping operation and converting the stripped spectrum to incident flux (Antonopoulos-Domis et al. 1995a).

The dose, one meter over the ground, due to ^{137}Cs was found 32.8 nGy/h and this is about 50% of the total dose rate.

PUBLICATIONS DURING THE RESEARCH PROJECT

Antonopoulos-Domis, M.; Clouvas, A.; Xanthos, S.; Alifrangis, D. Radiocesium in a submediteranean semi-natural ecosystem following the Chernobyl accident: measurements and models. (submitted to Health Phys. ; July 1995).

REFERENCES

Antonopoulos-Domis, M.; Clouvas, A.; Gagianas A. Compartment model for long-term contamination prediction in deciduous fruit trees after a nuclear accident. Health Phys. 58,6:737-741; 1990.

Antonopoulos-Domis, M.; Clouvas, A.; Gagianas A. Radiocesium dynamics in fruit trees following the Chernobyl accident. Health Phys. 61,6:837-841; 1991.

Antonopoulos-Domis, M.; Clouvas, A.; Xanthos, S. Pilot survey on the determination by in-situ gamma spectrometry of outdoor and indoor exposure gamma rates in populated areas of Greece due to natural and artificial sources of radiation. Commission of the European Union; Final Report; 1995a.

Antonopoulos-Domis, M; Clouvas, A.; Hiladakis, A.; Kadi, S. Radiocesium distribution in undisturbed soil. measurements and diffusion-advection model. (in press) Health Phys.; 1995b.

Antonopoulos-Domis, M; Clouvas, A.; Marsequerra, M. On the compartmental modeling of caesium migration in soils. (in press) Nuc. Sci. Engng.; 1995c.

Head of project 10: Dr. Pietrzak-Flis

II. Objectives for the reporting period

The objective of the study was:
- to determine the concentration of ^{137}Cs in subsequent horizons of soil,
- to determine concentrations of ^{137}Cs in some species of vascular plants and mushrooms,
- to evaluate transfer factors (TF) from soil to plants,
- to assess an anticipated increase of ^{137}Cs content locally under a mushroom after its decomposition.

III. Progress achieved including publications

1. Introduction

Vertical migration of radiocesium in forest soils was extensively studied after the Chernobyl accident [1-9]. It has been shown that downward migration of radiocesium is slow, and that the major part of this radionuclide is being retained in the organic horizons. In the consequence, radiocesium is still easily available for mushrooms and vascular plants, entering thus into food chains of animals and men.

Transfer of radiocesium from soil to plants depends to a large extent on the concentration of this radionuclide in soil at the depth of the plant roots.

In this work the vertical distribution of radiocesium and potassium was studied in forest soils near Warsaw in Poland. Transfer of ^{137}Cs from soil to mushrooms and vascular plants was determined. The horizons which supply the nutrients were estimated on the basis of the depth of the plants' root.

2. Materials and methods

2.1. Sampling

The study on the behaviour of ^{137}Cs in the forest ecosystem was performed for two locations in the Kampinos National Park, at Truskaw and Palmiry, lying 6 km apart and about 25 km from the center of Warsaw. In the mixed forest at Truskaw there prevail coniferous trees, whereas at Palmiry there grow mainly oaks and hornbeams. In both locations the soil was of the podsol type.

Sampling sites in both locations were about 200 m x 200 m each. Samples of soils and litter, mushrooms and vascular plants were collected from 20 places at Truskaw and 36 places at Palmiry in the period from April through October of 1994. The depth of the root system of the vascular plants was estimated.

Samples of soil with horizons Of through B were taken using a metal frame of 50 cm x 50 cm [10] or a metal tube of 13 cm in diameter (surface area of 133 cm^2). Horizons were separated and analyzed individually. Samples of mushrooms (*Xerocomus badius*) and/or green plants were taken from the same area as the soil samples or in close vicinity. To evaluate an anticipated increase of ^{137}Cs content locally under the mushrooms after their eventual decomposition, there were collected mushrooms and samples of soil from beneath these mushrooms from the surface area of 133 cm^2.

2.2. Sample preparation and analytical methods

Samples of soil were dried at 85°C, sieved through a 2-mm mesh to remove roots of plants and stones, and then homogenized. After such preparation a sub-sample was transferred to a polyethylene beaker for subsequent measurements.

Samples of mushroom fruitbodies and green plants were weighed, dried in an oven at about 100°C and reweighed. Dry plants were ashed at 430°C. The ash was homogenized, weighed and then samples of 10 g or 20 g were placed in a counting beaker. If the amount of ash was smaller than 10 g, the ash was dissolved in mineral acids, diluted with distilled water to the volume of 150 ml and transferred to a counting beaker. Dry mushrooms were wet mineralized with mixture of concentrated nitric and sulphuric acids, then distilled water was added up to the volume of 150 ml, and the solution was placed in a counting beaker.

^{134}Cs, ^{137}Cs and ^{40}K were determined by gamma spectrometry. The gamma spectrometer consisted of a high purity germanium detector with an energy resolution of 1.8 keV for ^{60}Co (1332 keV) and with relative efficiency of 33%. The detector was placed inside a lead shield with walls 10 cm thick which were lined with a 2-mm layer of copper. The detector was connected to a multichannel analyzer, Canberra, Series 90. Calibration of the gamma spectrometer was performed with standard solutions obtained from the US EPA EMSL-LV Laboratory, which covered the range of energy from 81 keV to 2186 keV. Calibration was made for several standard geometries for soil of varying density, for ash from green plants and for 150 ml of the solution from mushrooms and dissolved ash.

Elemental analysis of soil was performed by standard methods.

3. Results

3.1. Characteristics of soil

The following horizons were distinguished: Ol, Of, OhAh (organic horizon intermixed with mineral horizon), Ah 1, Ah 2 and B horizon.

Content of organic matter in soil for the both locations is given in Fig.1. The contents of organic matter for particular horizons at Truskaw and Palmiry are very similar. Higher content was observed only in Of at Truskaw. In OhAh horizon content of organic matter was about four times lower as compared to Of. Other parameters of soil characteristics are given in Table 1. Contents of the essential nutrients (nitrogen, phosphorus, potassium) were similar for both locations. The content of the elements in the OhAh horizon was much lower than in the Of horizon.

3.2. Concentration of radiocesium and K in soils

Concentration of radiocesium was expressed in Bq kg^{-1}_{dw}, whereas its content was given in Bq m^{-2} for the entire horizon. The latter was calculated from the concentration of ^{137}Cs in fresh soil and its weight in the horizon. Potassium was determined from ^{40}K; it was accepted that specific activity of ^{40}K is equal to 31.6 Bq g^{-1} of natural potassium. Table 2 gives mean values of the results from all the samples analyzed separately. Ratios of $^{137}Cs/^{134}Cs$ and $^{137}Cs/K$ in the soil are presented in Table 3.

The total deposition of ^{137}Cs in the soil at Truskaw was slightly higher than that at Palmiry. This radionuclide stayed mainly in the organic horizons Of and OhAh, being about 80% of the total, and almost the same in each of these horizons. Concentration of potassium was in organic horizons lower than that in the mineral horizons, but in the latter horizons it remained at the same level. Correspondingly, the $^{137}Cs/K$ ratios decreased for the subsequent horizons (Table 3).

3.3. Concentration of ^{137}Cs, ^{134}Cs and K in mushrooms and vascular plants

Mean concentrations of the two cesium radionuclides and of potassium in mushrooms

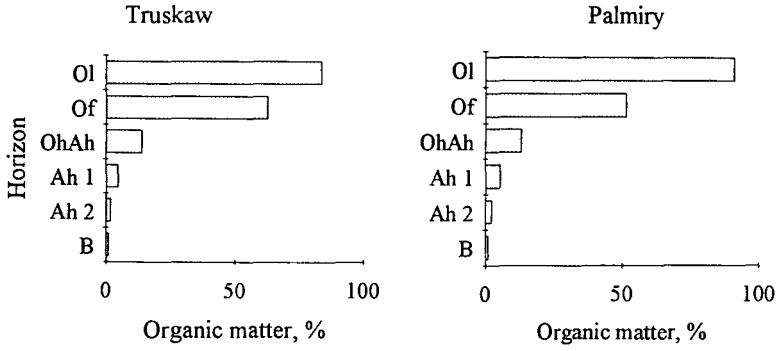

Fig. 1. Content of organic matter in soil horizons

and vascular plants are given in Table 4. As expected, the concentrations of radiocesium in the *Xerocomus badius* and *Paxillus involutus* were considerably higher than in vascular plants. The concentration ratios $^{137}Cs/^{134}Cs$ in mushrooms and *Calluna* were similar to those in the Of horizon, while in the other plants they were higher. The $^{137}Cs/K$ ratios in mushrooms were higher and in *Calluna* almost the same as those in the Of horizon. In case of the other plants the ratios were lower than those in the Of horizon (Table 5).

Table 1. Characteristics of soil at Truskaw and Palmiry

Horizon	C organic %	N %	C/N	K_2O mg/100g	P_2O_5 mg/100g	pH H_2O
			Truskaw			
Ol	48.7±6.6[a]	1.21±0.04	40	68±26	112±9.2	4.3
Of	36.3±4.2	1.09±0.10	33	23±4	78.5±3.6	3.6
OhAh	8.2±2.3	0.26±0.09	32	6.8±1.3	30.4±2.7	3.5
Ah 1	2.8±0.2	0.08±0.01	35	2.1±0.8	22.7±1.9	4.0
Ah 2	1.2±0.1	0.03±0.01	39	2.0±0.4	18.3±2.4	4.0
			Palmiry			
Ol	53.0±0.2	1.45±0.22	37	69±14	127±2.6	4.2
Of	30.0±2.3	0.73±0.05	41	19±3	65.5±7.6	3.7
OhAh	7.7±0.8	0.31±0.05	25	4.3±1.5	26.9±1.7	3.6
Ah 1	3.2±0.2	0.16±0.04	20	2.5±0.7	20.2±1.9	3.6
Ah 2	1.5±0.1	0.05±0.02	30	1.8±0.4	17.5±1.6	3.8

a - standard error of the mean

3.4. Transfer factor soil/plant

For the determination of transfer factors (TF) it is important to know the horizons from which the plant takes nutrients. These horizons may be determined from the $^{137}Cs/^{134}Cs$ ratios in the plant and soil. For identifying the soil layers, from which mushrooms take the nutrients, Guillite et al. [11] and Rühm et al. [12] developed a method based on the estimation

Table 2. Mean ^{137}Cs concentration and ^{137}Cs content in soil horizons at Truskaw and Palmiry in 1994

Horizon	Concentration of ^{137}Cs Bq kg^{-1}_{dw}	Content of ^{137}Cs Bq m^{-2}	Concentration of K g kg^{-1}_{dw}	Percentage of ^{137}Cs content in horizon %
		Truskaw		
Ol	42±17[a]	5.7±3.1	0.9±0 4	0.2
Of	151±67	1363±364	4.7±1.4	41.6
OhAh	71±25	1325±447	6.9±0.8	40.4
Ah 1	25±10	457±169	7.8±0.4	13.9
Ah 2	5.2±4.7	95±38	7.7±0.4	2.9
B	0.8±0.7	32±28	7.5±0.3	1.0
Total		3278±590		
		Palmiry		
Ol	62±26	13±7	1.6±0.6	0.5
Of	143±44	1150±496	4.4±1.0	39.8
OhAh	49±19	1029±440	6.0±0.8	35.6
Ah 1	15±7	475±240	6.4±0.7	16.4
Ah 2	4.5±2.4	179±87	6.3±0.7	6.2
B	1.1±0.4	43±4	6.3±0.7	1.5
Total		2889±711		

a - Standard deviation

Table 3. Average ratios of ^{137}Cs to ^{134}Cs and ^{137}Cs to K concentrations in soil horizons at Truskaw and Palmiry in 1994

	Truskaw		Palmiry	
Horizon	$^{137}Cs/^{134}Cs$	^{137}Cs/ K	$^{137}Cs/^{134}Cs$	^{137}Cs/ K
Of	46±19[a]	35±16	44±12	35±15
OhAh	-	11±5	-	8.2±3.8
Ah 1	-	3.3±1.3	-	2.4±1.1
Ah 2	-	0.7±0.6	-	0.7±0.4
B	-	0.1±0.1	-	0.2±0.1

a - Standard deviation

of the $^{137}Cs/^{134}Cs$ ratio in fruitbodies and in different soil horizons. The soil layer is identified on the assumption that the ratio should be the same as in the fruitbody. Values of the $^{137}Cs/^{134}Cs$ ratios, similar to those for mushrooms (Table 5), were observed for the Of horizon (Table 3), so this horizon was taken for the calculation of TF in the mushroom.

For the location examined, ^{134}Cs was determined only in the Of horizon, because in deeper horizons it was usually below the lower limit of detection, being equal to 0.26Bqkg^{-1}dw (for the measurement time 80,000 s). Therefore, the horizons which supply the nutrients were estimated on the basis of the depth of the plants' root system. In the forest examined, roots of *Calluna* were present in Of horizon, roots of *Vaccinium myrtillus* were seen in Of+OhAh horizons, whereas roots of grass and fern were found to reach the mineral horizons Ah.

Accordingly, for the calculation of TF the mean concentration of ^{137}Cs was taken for the horizons as follow: Of for *Calluna*, Of+OhAh for *Vaccinium myrtillus*, Of+OhAh+Ah for fern and grass. Transfer factors were calculated as a ratio of ^{137}Cs concentration in mushrooms or green plants (Bq kg^{-1}_{dw}) to the ^{137}Cs concentration in the horizons which have been assumed to be the source of this radionuclide. Values of ^{137}Cs concentrations in the mushrooms and plants were taken from Table 4, and the mean ^{137}Cs concentrations for the given horizons were calculated from data in Tables 2.

Table 4. Mean concentration of ^{137}Cs, ^{134}Cs and potassium in mushrooms and green plants at Truskaw and Palmiry in 1994

Plant	^{137}Cs Bq kg^{-1}_{dw}	^{134}Cs Bq kg^{-1}_{dw}	K g kg^{-1}_{dw}	Number of samples
		Truskaw		
Xerocomus badius	2588±1636	58±28	37±11	10
Paxillus involutus	2920±1404	78±43	57±12	9
Calluna	149±56	3.6±1.4	4.4±1.1	7
Grass	63±26	1.1±0.5	10±4	9
		Palmiry		
Xerocomus badius	2434±1081	49±28	39±8	26
Paxillus involutus	3685±1661	97±63	48±15	6
Calluna	176±52	4.0±1.5	5.0±0.9	6
Grass	49±14	1.0±0.5	6.3±2.5	4
Vaccinium myrtillus	92±38	2.0±0.6	4.5±1.1	17
Fern	256±79	4.0±1.1	21±2.4	4

a - Standard deviation

Table 5. Mean concentration ratios of $^{137}Cs/^{134}Cs$ and $^{137}Cs/K$ in mushrooms and vascular plants at Truskaw and Palmiry in 1994

	Truskaw		Palmiry	
Plant	$^{137}Cs/^{134}Cs$	$^{137}Cs/K$	$^{137}Cs/^{134}Cs$	$^{137}Cs/K$
Xerocomus badius	46±15[a]	73±42	53±15	66±30
Paxillus involutus	40±10	53±27	36±6	65±20
Calluna	41±5	34±9	44±8	36±9
Grass	56±13	6.6±1.8	57±10	7.6±0.3
Vaccinium myrtillus	-	-	50±12	21±8
Fern	-	-	64±4	12±3

a - Standard deviation

Calculated values of TF are presented in Table 6. The largest TF occurred for mushrooms, being in the range from 17.0±1.8 to 25.7±4.1. TF for fern was 4.85±1.09, whereas for the other green plants it was close to unity.

Potassium behaves physiologically similarly to cesium, hence it was of intertest to compare ratios of $^{137}Cs/K$ in plants with those in the horizons assumed to be the source of ^{137}Cs and potassium for the plants. Fig. 2 presents $^{137}Cs/K$ ratio in plants as a function of this ratio for the horizons in which the plants' roots were present. It was found, that the average $^{137}Cs/K$ ratio for these horizons was similar to the $^{137}Cs/K$ ratio in a given plant. E.g., for *Calluna*, the $^{137}Cs/K$ ratio was 36 (Table 5) and similar ratio (35) was for the Of horizon (Table 3). For *Vaccinium myrtillus* the ratio was 21 (Table 5); a similar value of $^{137}Cs/K$ was obtained for the average of the Of plus OhAh horizons ((35+8.2)/2=21.6) (Table 3).

Table 5. Mean concentration ratios of $^{137}Cs/^{134}Cs$ and $^{137}Cs/K$ in mushrooms and vascular plants at Truskaw and Palmiry in 1994

Plant	Truskaw		Palmiry	
	$^{137}Cs/^{134}Cs$	$^{137}Cs/K$	$^{137}Cs/^{134}Cs$	$^{137}Cs/K$
Xerocomus badius	46±15[a]	73±42	53±15	66±30
Paxillus involutus	40±10	53±27	36±6	65±20
Calluna	41±5	34±9	44±8	36±9
Grass	56±13	6.6±1.8	57±10	7.6±0.3
Vaccinium myrtillus	-	-	50±12	21±8
Fern	-	-	64±4	12±3

a - Standard deviation

The least squares fit calculations gave the following equation:

$$Y = -4.91 + 1.14x \qquad (1)$$

Where : Y is the $^{137}Cs/K$ ratio in plant, and
x is the $^{137}Cs/K$ ratio in the related horizon of soil

The regression analysis indicates a good correlation between these ratios in the plants and in the horizons. The correlation coefficient r is equal to 0.97. The linear relationship suggest that the plants take cesium and potassium from the indicated horizons. This supports the assumption based on the root's depth.

Similar values of the $^{137}Cs/K$ ratio in plants and soil suggest that ^{137}Cs concentration in plants is proportional to the $^{137}Cs/K$ in soil. Indeed, the results in Fig. 3 manifest a close relationship between these parameters for the plants given. The least squares fit calculations gives the relationship as follows:

$$Y = -4.52 + 4.76x \qquad (2)$$

Where Y is the ^{137}Cs concentration in plant , Bq kg^{-1}_{dw}, and
x is the $^{137}Cs/K$ ratio in the related horizon of soil
Correlation coefficient r = 0.97

This relationship makes it possible to estimate concentration of ^{137}Cs in the given plants on the basis of the soil analysis. Such a relationship has not been observed for fern.

3.5. Local increase of ^{137}Cs content beneath the decomposing mushrooms' fruitbody

Activity concentration of ^{137}Cs in soil strongly differed for the sampling places, even for those lying close to each other. These differences are reflected in the large srandard deviation of the mean values (Table 2). One of the possible reasons of the local increase of the ^{137}Cs content can be the accumulation of this radionuclide in fruitbodies of some species of

mushrooms, and transfer of the radionuclide from the fruitbody to soil as a result of the decomposition of the mushroom

To assess an anticipated increase of the ^{137}Cs content in soil from a decomposing mushroom, the ^{137}Cs content in a mushroom was related to the ^{137}Cs content in the Of

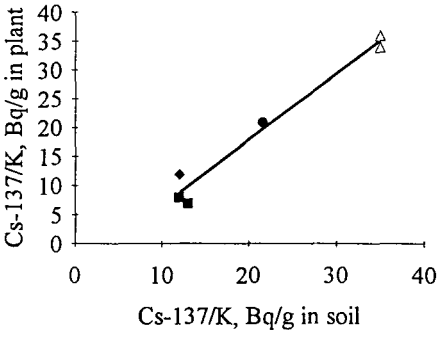

Fig. 2. $^{137}Cs/K$ ratio in plants versus $^{137}Cs/K$ ratio in given horizons
■ Grass, horizons Of through Ah ● *Vaccinium myrtillus*, horizons Of+OhAh
Δ *Calluna*, horizon Of ◆ Fern, horizons Of through Ah

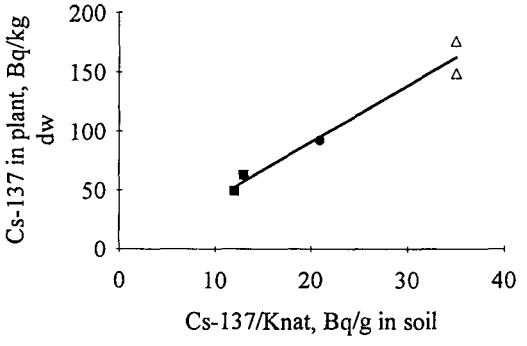

Fig. 3. Concentration of ^{137}Cs in plants as a function of $^{137}Cs/K$ ratio in given horizons
■ Grass, horizons Of through Ah ● *Vaccinium myrtillus*, horizons Of+OhAh
Δ *Calluna*, horizon Of

horizon directly beneath the fruitbody.Table 7 shows the results for 10 sampling points taken at random. The increase of the ^{137}Cs content in the Of horizon amounted from 20% up to 90%, illustrating a possible contribution of the decomposing *Xerocomus badius* to the nonuniform distribution of the radiocesium in the Of horizon.

4. Discussion

Average deposition of ^{137}Cs in the soils from the Kampinos National Park (KNP) near Warsaw was about 3 000 Bq m^{-2}. About 80% of ^{137}Cs was present in the Of and OhAh horizons, being in the OhAh horizon slightly lower than that in the Of horizon. This data indicate a rather slow vertical migration of this radionuclide. After eight years since the Chernobyl accident, ^{137}Cs remained in almost equal amounts in Of and OhAh (in each about 40%), and it penetrated only in about 20% to the deeper mineral horizons. This behaviour of ^{137}Cs is different from that in coniferous forests in South Bavaria [3], where the largest

fraction of ^{137}Cs shifted in the period from 1987 through 1991 to Oh or OhAh and Ah horizons. In KPN content of organic matter in the OhAh horizons amounted to about 14% (Fig 1). Particle size analysis of Of and the OhAh horizons indicated that Of did not contain sand, silt or clay, whereas OhAh horizon contained 3% clay and 5% silt at Truskaw and 5% clay and 4% silt at Palmiry. Cremers et al. [13] found that clay effectively adsorbs cesium, hence the low migration of ^{137}Cs in KPN from OhAh to deeper horizons can be explained by the presence of clay in the OhAh horizons.

Table 6. Transfer factors (TF) from soil to mushrooms and vascular plants

Plant	TF	
	Truskaw	Palmiry
Xerocomus badius	17.1±3.8[a]	17.0±1.8
Paxillus involutus	19.3±3.7	25.7±4.1
Calluna	0.99±0.18	1.23±0.16
Grass	1.00±0.31	0.93±0.28
Vaccinium myrtillus	-	0.96±0.13
Fern	-	4.85±1.09

a - standard error of the mean

Table 7. Content of ^{137}Cs in fruitbodies of *Xerocomus badius* and in Of horizons beneath the mushrooms and the anticipated increase of ^{137}Cs content in the Of horizon of an area of 132.7 cm^2 resulting from the decomposition of the mushrooms

Sampling point	^{137}Cs in mushroom Bq	^{137}Cs in Of horizon Bq	Increase of ^{137}Cs in Of horizon %
1	5.2	14.4	36.1
2	5.8	22.5	25.8
3	13.5	22.5	60.0
4	5.0	14.8	33.8
5	11.8	13.2	89.4
6	4.6	14.6	31.5
7	7.6	23.1	32.9
8	3.5	14.6	24.0
9	4.3	19.7	21.8
10	3.2	14.6	21.9

The high retention of ^{137}Cs in the Of horizons (Table 2) can be attributed to the high content of organic matter (Fig. 1). In the forest environment, organic matter exhibits a high capacity for the cation exchange of the soil, and this favours the retention of radionuclides [14]. Olsen et al. [15] suggest that fungal biomass in soil may be a strong sink for radiocesium. The fungal biomass is mainly situated in the upper part of the organic layer. It absorbs a large part of mineral nutrients, therefore only small amounts of dissolved nutrients remain in the soil. Assuming that accumulation of Cs^+ is the same as K^+, most of radiocesium will be contained in living organisms, mostly in fungi. Olsen et al. [15] estimated, that the radiocesium content in the fungal biomass was at average 32% of the total radiocesium content in the upper part of the organic layer (3-4 cm). Similar content of radiocesium in soil microflora was reported by Guillitte et al. [16]; these authors have found that the microflora, particularly mycelia, could retain up to 40% of the radiocesium.

A large difference in the ^{137}Cs content in the OhAh and Ah1 horizons (Table 2) appears to be typical for podsol. A similarly large decrease in the ^{137}Cs content upon entering

the Ah horizon was earlier found by Kammerer et al [3]. This shows that the migration of ^{137}Cs from the OhAh horizon is very small, demonstrating thus the high retention in the OhAh horizon. A high Cs retention in this horizon was also reported by Sombre et al. [17]

The mineral horizons include radiocesium both from the Chernobyl accident and the nuclear weapon testing, therefore its content cannot be used for the exact evaluation of the migration rate from the organic to mineral horizons. This means that the actual migration of ^{137}Cs to the deeper horizons might be slower than that deduced from the ^{137}Cs content in the mineral horizons.

The evaluated increase of ^{137}Cs in Of horizons beneath the decomposing fruitbodies (Table 7) provides an evidence for a local enrichment of ^{137}Cs. These results support the opinion of Fraiture [18] that decomposed mushrooms can significantly increase the local contamination. This phenomenon can contribute to the horizontal displacement of radiocesium in the soil and to uneven surface contamination.

Different species of the understorey vegetation take nutrients from different soil layers. In this work for particular species, the soil horizons were assessed on the basis of the depth of the rooting system. Those horizons were used to calculate the transfer factors (Table 6). It should be noted that values of TF would be lower if they were calculated for Of only instead of for Of+OhAh or Of+OhAh+Ah.

The correlation between the $^{137}Cs/K$ ratios in the plants and in the horizons with the plants' roots (Fig. 2 and eq. (1)) was high (r=0.97). A much lower correlation for the relation of $^{137}Cs/K$ in plants to that in soil (as eq. 1) was found by Wirth et al [19] for coniferous forest in south Bavaria; the maximum correlation was 0.53 (for leaves of berry plants), whereas for all the plants r was 0.20. The plant-to-soil $^{137}Cs/K$ relation was determined by taking values of ^{137}Cs and ^{40}K from the O-horizons only. In the present work the high correlation was found by taking into account additionally also the Ah horizons, it was justified by the depth of the roots in the forest studied.

The $^{137}Cs/K$ ratios in the plants were very close to those in the soil (Fig. 2). This suggests that there did not occur any noticable discrimination of ^{137}Cs against K in the plants.

PUBLICATIONS DURING THE RESEARCH PROJECT

Z.Pietrzak-Flis, I.Radwan, L.Rosiak, E.Wirth, "Migration of ^{137}Cs in soils and its transfer to mushrooms and vascular plants in mixed forest", submitted for publication in Sci. Total Environ.

REFERENCES

[1]. W.Rühm, L.Kammerer, L.Hiersche, E. Wirth, Migration of ^{137}Cs and ^{134}Cs in different forest soil layers, in preparation.

[2]. R. Römmelt, L.Hiersche, G. Schaller and E. Wirth, Influence of soil fungi (Biasidiomycetes) on the migration of Cs-134+137 and Sr-90 in coniferous forest soils. In: G.Desmet, P.Nassiembeni and M.Belli, (Eds.), Proceedings of the Workshop on Transfer of Radionuclides in Natural and Semi-Natural Environments. Elsevier Applied Science, Barking, UK, 1990, pp. 152-160.

[3]. L. Kammerer, L .Hiersche and E. Wirth, Uptake of radiocaesium by different species of mushrooms, J. Environ. Radioactivity 23 (1994) 135-150.
[4]. K.Bunzl, W. Kracke and W. Schimmack, Vertical migration of plutonium-239+-240, americium-241 and caesium-137 fallout in a forest soil under spruce, Analyst 117 (1992) 469-474.
[5]. M. Belli, U.Sansone, S.Menegon, Behaviour of radiocaesium in a forest in the eastern Italian Alps, Sci. Total Environ., 157 (1994) 257-260.
[6]. W.Schimmack and K. Bunzl, Migration of radiocesium in two forest soils as obtained from field and column investigations, Sci. Total Environ., 116 (1992) 93-107.
[7]. B.H. Fawaris, K.J.Johanson, Radiocesium in soil and plants in a forest in central Sweden, Sci.Total Environ., 157 (1994) 133-138.
[8]. J. Melin and L. Wallberg, Distribution and retention of cesium in Swedish Boreal forest ecosystems. In: Moberg J. (ed): The Chernobyl Fallout in Sweden, Results from a Research Programme on Environmental Radiology. The Swedish Radiation Protection Institute, Stockholm (1991), pp. 467-475.
[9]. J.Andolina and O.Guillitte, Radiocesium availability and retention sites in forest humus. In: G.Desmet, P.Nassiembeni and M.Belli, (Eds.), Proceedings of the Workshop on Transfer of Radionuclides in Natural and Semi-Natural Environments. Elsevier Applied Science, Barking, UK, 1990, pp. 135-142.
[10]. J.Andolina, O.Guillitte, A methodological approach of soils sampling and analyses in the study of radionuclides transfer in forest ecosystens. In: G.Desmet, P.Nassiembeni and M.Belli, (Eds), Proceedings of the Workshop on Transfer of Radionuclides in Natural and Semi-Natural Environments. Elsevier Applied Science, Barking, UK, 1990, pp. 161-168.
[11]. O.Guillitte, A.Fraiture, J.Lambinon, Soil-fungi radiocesium transfers in forest ecosystem. In: G.Desmet, P.Nassiembeni and M.Belli, (Eds.), Proceedings of the Workshop on Transfer of Radionuclides in Natural and Semi-Natural Environments. Elsevier Applied Science, Barking, UK, 1990, pp. 468-476.
[12]. W.Rühm, L.Kammerer, L.Hirsche, E.Wirth, On mycelium location of different species fungi, in preparation.
[13].A.Cremers, A.Elsen, P.DePreter, A.Maas, Quantitative analysis of caesium retention in soils, Nature 335 (1988) 247-249.
[14]. R.G.Menzel, Soil-plant relationships of radioactive elements, Health Phys., 11 (1965) 1325-1332.
[15]. R.A.Olsen, E.Joner, L.R.Bakken, Soil fungi and the fate of radiocaesium in the soil ecosystem - a discussion of possible mechanisms involved in the radiocaesium accumulation in fungi, and the role of fungi as a Cs-sink in the soil. In: G.Desmet, P.Nassiembeni and M.Belli, (Eds.), Proceedings of the Workshop on Transfer of Radionuclides in Natural and Semi-Natural Environments. Elsevier Applied Science, Barking, UK, 1990, pp. 657-663
[16]. O.Gullitte, J.Melin, L.Wallberg, Biological pathways of radionuclides originating from the Chernobyl fallout in a boreal forest ecosystem, Sci. Total Environ., 157 (1994) 207-215.
[17]. L.Sombré, M.Vanhouche, S. de Brouwer, C.Ronneau, J.M. Lambotte, C. Myttenaere, Long-term radiocesium behaviour in spruce and oak forests, Sci. Total Environ., 157 (1994) 59-71.
[18]. A.Fraiture, Introduction to the radioecology of forest ecosystems and survey of radioactive contamination in food products from forests. Commiss. Eur. Comm., Rad. Prot. Rep. 57, pp.103, 1992.
[19]. E.Wirth, L.Hiersche, L. Kammerer. G. Krajewska, R. Krestel, S. Mahler, R. Römmelt,

Transfer equations for cesium-137 for coniferous forest understorey plant species, Sci. Total Environ., 157 (1994) 163-170.

Final Report
1992-1994

Contract: F13P-CT920058 **Duration 1.9.92 - 30.6.95** **Sector: A25**

Title: Radiation Doses and Pathways to Man from Semi-Natural Ecosystems

1.	**McGarry**	**RPII**
2.	**Horrill**	**NERC**
3.	**Nielsen**	**Laboratory at RISO**
4.	**Johanson**	**University of Uppsala**
5.	**Veresogliou**	**University of Thessaloniki**

Summary of Project Global Objectives and Achievements

1. Objectives

Consumption of foodstuffs produced from semi-natural ecosystems contaminated with man-made radioactivity can significantly contribute to the radiation dose of the general population and of critical groups in particular. Because of the long ecological half-life of artificial radioactivity in the natural vegetation and in the animal species which characterise such ecosystems, this dose can be delivered over a period of several decades.

Compared with agricultural ecosystems, there are limited data available on radionuclide cycling in semi-natural ecosystems. In addition, many of the factors controlling radionuclide uptake from these soils are not yet fully understood. This restricts the degree to which radiation doses from semi-natural ecosystems can be evaluated and allows limited predictive capability in the event of future nuclear accidents.

This research programme focuses on evaluating the importance of semi-natural ecosystems as a source of radiation exposure to man. As a first step, the potential pathways of radionuclide transfer to man are identified and prioritised. Previous studies have shown that fungi are an important part of the diet of many farmed and wild animals grazing semi-natural ecosystems and that they are responsible for much of the seasonal and year-to-year variability in the radiocaesium body burden of sheep, reindeer and roe-deer. While the Scandinavian countries are particularly at risk in this regard, increasing afforestation of upland areas in Ireland and the United Kingdom, all of which are extensively grazed by sheep, makes similar studies in these ecosystems important.

A key parameter to be calculated is the ecological half-life, defined as the time taken for the concentration of a radionuclide in an ecosystem to be reduced by half, excluding losses due to radioactive decay. Because this parameter is likely to be different for different semi-natural ecosystems, an understanding of the mechanisms of soil-plant uptake of ^{90}Sr and ^{137}Cs, both in terms of transfer parameters and the interaction with competing ions such as Ca and K respectively, is also necessary.

Once these parameters have been evaluated, there is also a need to determine the consumption rates of the various produce from different semi-natural ecosystem types and subsequently, the radiation doses to both the general population and to critical groups. Work on all these aspects of radioecology has been undertaken in a co-ordinated manner with a high degree of co-operation between participants from Ireland, the U.K., Denmark, Sweden, Greece and Norway. The work programme was designed to maximise the input of participants in areas where they have expertise, over and above that available in the other laboratories. The aim was to provide more accurate estimates of the committed radiation doses from foodstuffs sourced from semi-natural ecosystems and to develop a predictive capability for future accidents.

2. Achievements

2.1 Pathway Studies

2.1.1. Radionuclide Budgets

In order to determine which pathways are of most importance and how the various radionuclides are partitioned within a typical semi-natural ecosystem, all participating laboratories co-operated in a joint study on the inventory and distribution of ^{137}Cs and ^{90}Sr in a semi-natural woodland ecosystem in Sweden. A similar study was also carried out in a Danish pine forest by the Riso National Laboratory.

The total mean content of ^{137}Cs in the system was 54 kBq m^{-2}. Data show that approximately 87% of total fallout is in soils, 5.5% in the bryophyte layer and 7% in the standing biomass of trees. Fungi, understorey vegetation and ruminant populations, which encompass the principal foodstuffs responsible for radiation transfer to man from the system, collectively contained approximately 1% of the total fallout. The low content of radiocaesium in these categories is primarily due to low biomass and patchy distribution. The results for ^{90}Sr demonstrated a significant association with those for ^{137}Cs indicating that they derive mainly from the same source i.e. from the Chernobyl accident. Actual concentrations of ^{137}Cs in individual samples of fungi and ruminants were considerable and frequently exceeded the concentration limit of 1500 Bq kg^{-1} for consumption of wild produce which applies in Sweden. In contrast to the uptake of ^{137}Cs in fungi, the uptake of ^{90}Sr in fungi was found to be 2 to 3 orders of magnitude lower. The data demonstrate that only a small percentage of total fallout enters food produce in this system, that the standing crop of food produce is low, but that it may contain concentrations of radioactivity that give cause for concern. The potential for significant individual dose transfer from the system is primarily limited to critical groups such as hunters, regular consumers of wild produce, and forestry workers.

The data from the Swedish study may be compared with those for a Danish pine forest which received approximately 60 times less fallout from the Chernobyl accident than the Uppsala site. When the concentrations measured in the various compartments are normalised to the soil deposition values, the data show that, in general, transfers in the Swedish forest are higher than transfer in the Danish forest for both ^{137}Cs and ^{90}Sr. This result is consistent with the fact that the radioactive contamination in the Swedish forest was relatively recent (from the Chernobyl

accident in 1986) and thus more available for plant uptake that the contamination in the Danish forest which originates mainly from fallout from atmospheric weapons testing.

2.1.2. Plant Uptake Studies

A study to explain the transfer of radionuclides within semi-natural ecosystems was undertaken at NERC. As part of this work a new ^{137}Cs sequential extraction technique for soils with relatively low radiocaesium contamination has been developed. This procedure is considered to be more representative of field conditions than existing techniques, most of which work with dry soils. The method was subsequently applied to peat samples taken from a range of heather dominated ecosystems grown on organic soils in Scotland, England and Ireland. The results show that, in general, the ^{137}Cs activity concentrations in heather plants are more highly correlated with water extractable ^{137}Cs than with the total ^{137}Cs content of the soil. The ammonium acetate extractable ^{137}Cs is also likely to be a better indicator of ^{137}Cs availability for heather root uptake than the use of traditional transfer factors for organic soils.

Laboratory experiments to investigate the Cs/K and Sr/Ca relationships have been undertaken by the University of Thessaloniki using a range of plant species typical of semi-natural ecosystems. In the experiments the effects of nutrient status, physico-chemical characteristics of the soil and the root distribution of plant species on Cs and Sr uptake were evaluated. The results show that there is a close correlation between Sr and Ca concentrations for different plant species grown on the same soil. The investigators suggest the use of the Ca concentration of plant species as an indicator of the Sr concentration in the same species, as Ca analysis is much simpler and less time consuming than ^{90}Sr analysis. A similar investigation of the relationship between Cs and K concentrations in plant species showed a much less significant correlation and, in some cases, no correlation at all.

The transfer of radionuclides from soils to plants is often defined in terms of transfer factors (T.F.) or transfer coefficients. These terms were originally developed for studies of agricultural ecosystems but have proven to be less appropriate for semi-natural ecosystems. The values of T.F. for Sr were determined for each of the pot experiments described above. The results show a high degree of variation in the T.F.'s determined which raises doubts as to their usefulness in comparing soils according to their ability to supply Sr. A more useful index is the "T.F. for Sr per Ca concentration" which exhibited much less variation among plant species grown in each soil treatment when compared to the traditional T.F. for Sr.

An investigation of the factors affecting Sr uptake from soil to plants showed that C.E.C. and available Ca were the parameters of most importance. The uptake of stable Cs and Sr by plants with the different forms of the elements in the soil was also investigated by means of a pot experiment followed by sequential extraction techniques. The results indicate that the major part of Cs is found in the exchangeable form and in the acid digestible fraction, possibly fixed to clay minerals, causing Cs to be released slowly for plant uptake. Strontium, on the other hand, is found in the exchangeable and soluble form indicating a higher availability.

Methods of characterising and quantifying the available radiocaesium, other than the traditional transfer factors, have been investigated by the RPII. A study of site variability shows that there is less variability in the ^{137}Cs content of Calluna vulgaris Juncus squarrous than of the underlying soils. The use of plant-to-plant ratios instead of the traditional ratio systems also yields better results as these ratios exhibit less variation.

2.1.3 Radiocaesium Transfer to Man

A series of studies of the transfer of radiocaesium from the forest ecosystem to man have been carried out at the University of Uppsala. Experiments investigating the transfer of radiocaesium from soil to various forest plant species show that species related differences are more important factors in determining this transfer than soil related parameters. Particular attention was given to the fungal species as these are known to be significant accumulators of ^{137}Cs. Experiments were conducted which confirm that the major fraction of radiocaesium in soil is located within the fungal compartment of the soil. This finding has implications for the transfer of radiocaesium to man as both moose and roe deer consume wild mushrooms. The seasonal variation of ^{137}Cs concentrations in roe deer have been positively correlated with the mushroom season.

In Sweden, the three main pathways from the forest ecosystem to man are through the consumption of game animals, berries and mushrooms. Using transfer parameters calculated from the studies outlined above, the total time-integrated dose commitment to the Swedish population from forest ecosystems contaminated with fallout from the Chernobyl accident is estimated to be between 5000 and 6000 manSv.

2.2. Ecological Half-life

The effective ecological half-life is a parameter which describes the reduction of contamination with time for an ecosystem compartment or product following a single contamination event. For a radionuclide, this parameter includes both physical decay and the ecological half-life of the corresponding stable element. In calculating collective doses to a population following contamination, effective ecological half life must be included to obtain reliable estimates.

In Ireland, a study of the accumulation and retention of ^{137}Cs in peatland vegetation was carried out between 1989 and 1993 by the RPII. Most species showed a seasonal pattern in ^{137}Cs concentration with higher concentrations in Summer. The calculated effective ecological half-life values ranged from +3 years to -1 year (an increase over time). A similar study of the long term behaviour of radiocaesium in mountain sheep was also undertaken. The calculated effective ecological half-life of ^{137}Cs for ewes and lambs were 7 and 8 years, respectively.

In the Faroe Islands, Riso has been measuring the levels of ^{137}Cs in milk since 1962. Effective half-life calculations for ^{137}Cs derived from weapons tests yield a value of 3 years, while the value for ^{137}Cs derived from the Chernobyl accident is 2 years. This difference in value for ^{137}Cs from different sources has been observed for other ecosystem compartments, but it is expected that, over time, any difference will be eroded as the more recent radiocaesium deposited following the Chernobyl accident becomes fixed to the soil minerals.

The estimated effective ecological half-life for ^{90}Sr in Faroese milk is 4 years. This value may also change (particularly in areas close to the Chernobyl region) if ^{90}Sr, initially deposited as insoluble particles, dissolves and becomes available for plant uptake.

2.3 Dose assessment

As a final step in this project, Riso National Laboratory co-ordinated an assessment of committed average doses to individuals in Denmark, the U.K., Ireland, Greece and Sweden arising from Chernobyl contamination. Each participant was asked to supply data on the consumption rates of food products from semi-natural ecosystems including game, fresh water fish, mushrooms, lamb and mutton. The consumption rates of food products from agricultural environments were also supplied for comparison purposes and for total dose estimations.

These data, together with transfer coefficients, taken from UNSCEAR for food products from agricultural environments or calculated using aggregated transfer factors and effective ecological half-life values for food products from semi-natural environments, were used to determine committed individual average doses. The results show a range in the doses calculated from 0.05 mSv to an average individual in the U.K. to 1.6 mSv to an average individual in Sweden. The relative contribution of food products from semi-natural and agricultural ecosystems to the total dose varies significantly from country to country. In the U.K. and Denmark, food products from semi-natural environments contribute between 10 and 20% of the total dose. In Ireland and Greece, the contributions from both ecosystem types are similar, whereas in Sweden, the doses from foods produced in semi-natural ecosystems are approximately twice those from foods produced in agricultural ecosystems.

Head of Project 1: Dr E McGee and Mr H Synnott

II. Objectives for the reporting period

1. Undertake an investigation of radiocaesium site variability in plants and soils.

2. Continue studies on the utilisation of plant-to-plant ratio systems. Compare and evaluate such a system compared with conventional transfer parameters.

3. Complete a study on the uptake and transfer of ^{137}Cs to flesh, compared with concentrations in faeces and rumen, of individual animals culled from a flock of free-ranging red deer (Cervus elaphus).

4. Complete a study using pollen traps installed on honeybee hives as a means of integrated sampling of peatland vegetation over the forage area of the hive.

5. Undertake a study to determine the effective ecological half-life of ^{137}Cs in peatland soils, vegetation and sheep.

6. Complete the collation of data on an investigation carried out in conjunction with our research partners on the distribution of ^{137}Cs and ^{90}Sr in a forest ecosystem at Uppsala, Sweden.

7. Compile data on foodstuffs consumption from semi-natural ecosystems to be used for committed dose calculations.

8. Determine the uptake of ^{90}Sr to peatland vegetation.

III. Progress achieved including publications

Soil to Plant and Plant to Plant Transfer of ^{137}Cs and ^{40}K.

An investigation of site variability in fallout content of soils and plants sampled from an upland peat site in Ireland was conducted. Sixteen replicate Calluna vulgaris, Juncus squarrosus and soil monoliths were sampled from within a 3600 m^2 area. Plant samples showed less variability in ^{137}Cs content than soils. The coefficient of variation values for ^{137}Cs activity in C.vulgaris and J.squarrosus were 12 and 20% respectively compared to at least 30% for individual soil horizon coefficient of variation values.

The J.squarrosus- C.vulgaris transfer factor (Figure 1) had the least variability (coefficient of variability of 30%) of the ratio data, but this was greater than to the variability shown by the plant and soil data. It is apparent from Figure 2 that a very large number of samples would be required to detect selected between site differences using ratios. This study clearly demonstrated that the most efficient way to detect between site differences in ^{137}Cs content was by plant sampling (especially C.vulgaris sampling). Soil sampling and the use of transfer parameters proved less efficient in this respect.

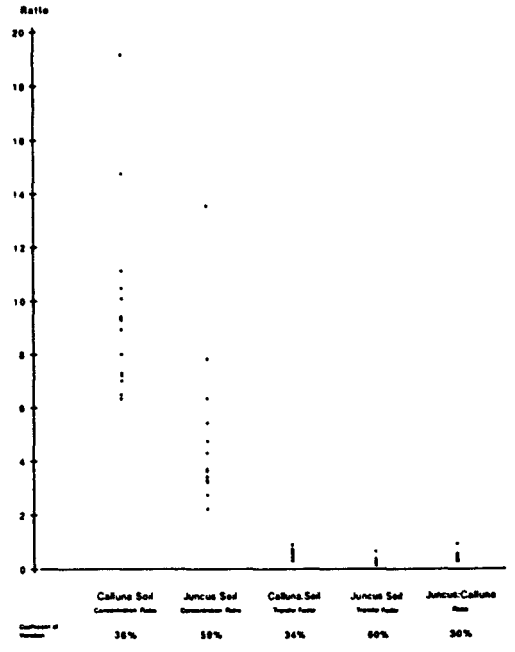

Figure 1 Dot plots of plant-soil concentration ratios, transfer factors, and plant-plant ratios for Calluna (vulgaris) and Juncus (squarrosus) ar each of the sixteen sampling locations. Coefficients of variation associated with each data are also listed.

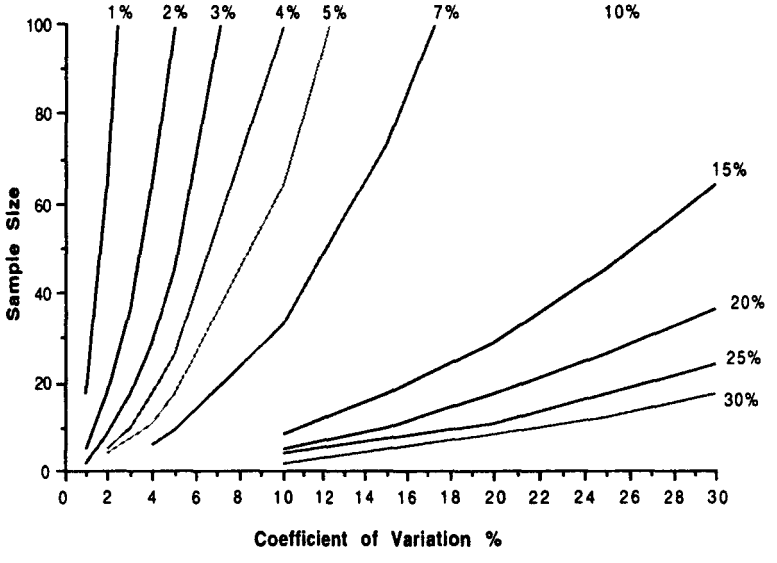

Figure 2 Number of replications needed to detect a given "true" difference between means. Curves illustrate how the required number of samples (y-axis) changes in relation to the coefficient of variation (x-axis) and the desired detection difference (Curves are based on an 80% certainty of detecting a difference between 2 means at the 5% level of significance).

The data set was also used to evaluate the comparative value of plant-to-plant relative to plant-to -soil transfer parameters. Figure 1 illustrates the finding that there was less variability associated with plant-to-plant ratios than with conventional ratio systems at the same site, confirming the validity of the concept. Examination of figure 1 suggests that the greater variability is associated with the Calluna:soil concentration data and a common pitfall associated with the interpretation of ratio data is to quote a range of values and use this range as a measure of data consistency. It is essential to use a statistical measure of variability (coefficient of variation in this example). Consequently it is clear that the greater variability is associated with the Juncus: soil transfer factor.

Data from the above study and data from a similar study of an organic rich forest soil site in Sweden were used to evaluate ratio systems in radioecological studies. Soil and plant ^{137}Cs from sites in both countries approximated the normal distribution. However when the same data are expressed as ratios (concentration ratios and transfer factors) the data was found to be lognormally distributed. The use of parametric statistical analyses are therefore inappropriate and researchers should use distribution free procedures to examine ratio data.

The relationship between plant ^{137}Cs and ^{40}K concentrations and those of corresponding soil substrate was examined. Concentrations of ^{137}Cs in two plant species in Ireland (Figure 3), and a further two species from Sweden (Vaccinium myrtillus and Vaccinium vitis-idaea) showed no evidence of a linear increase in plant concentrations with increasing soil concentrations at each location. Plant concentrations instead tended to remain constant over the observed range of soil concentrations. Two plant species and corresponding soils from Ireland were also analysed for ^{40}K, and these data provided further support for the findings (Figure 4).

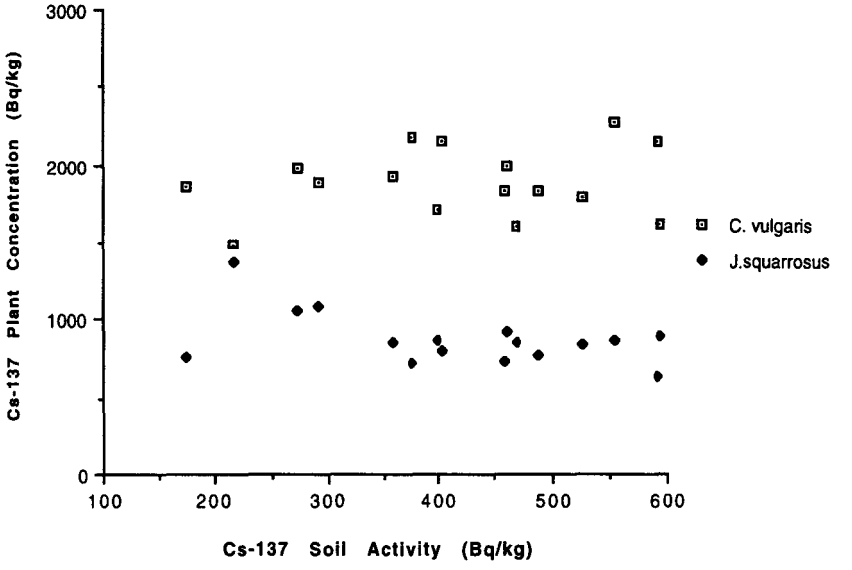

Figure 3 Cs-137 activity concentrations in C.vulgaris and J.squarrosus plotted against activity concentrations in soil samples taken from coincident locations.

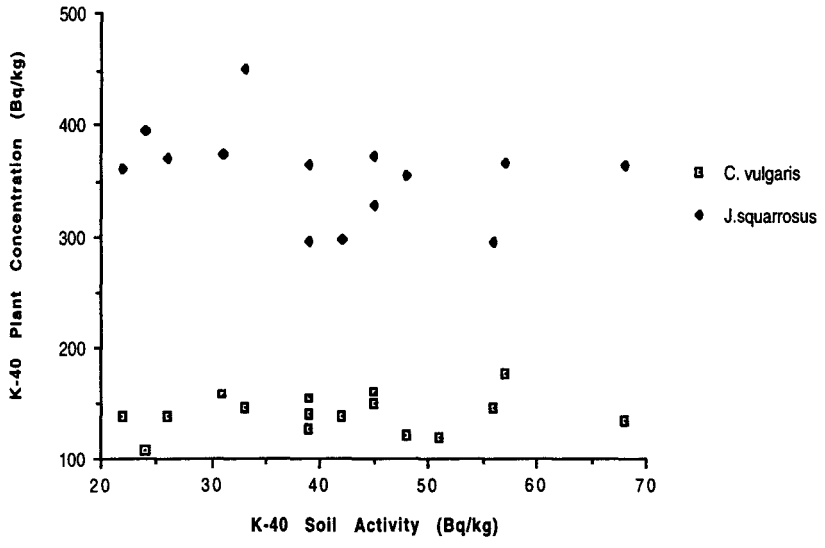

Figure 4 K-40 activity concentrations in C.vulgaris and J.squarrosus plotted against activity concentrations in soil samples taken from coincident locations

Plant-soil concentration ratio data from both countries were observed to decrease with increasing soil concentrations (Figure 5); this decrease was logarithmic in the case of the Irish ^{137}Cs and ^{40}K data. Trends did not change when transfer factors were calculated instead of concentration ratios. The findings of this study provide evidence that supports existing evidence from other researchers that the theory underlying these ratio systems is inherently flawed. Ratio systems of many different types are currently utilised in guidelines used by international radiological protection agencies. It is clear from this study that caution must be exercised in the application of ratios since there is considerable scope for data to be misinterpreted.

The availability of radiocaesium from Chernobyl and nuclear weapons fallout to Irish peatland vegetation was investigated. The percentage contribution of Chernobyl and weapons fallout remained remarkably constant over time in all plants sampled and the data provides evidence that weapons ^{137}Cs is still as available for plant uptake as the more recent Chernobyl deposit, suggesting that progressive fixation of Chernobyl ^{137}Cs in peatland systems seems unlikely. A high soil to plant transfer of ^{137}Cs in peatlands is therefore to be expected for many years.

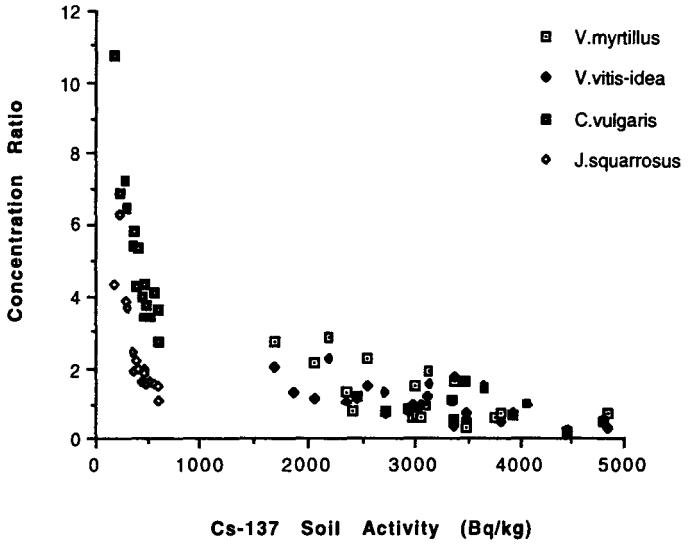

Figure 5 Plot of ^{137}Cs activity concentrations in soil against plant-soil concentration ratio values for C.vulgaris and J.squarrosus from Ireland and V.myrtillus and V.vitis-idaea from Sweden.

Animal Studies.

Forty two red deer (Cervus elaphus) were shot during the 1992 annual cull in Glenveagh National Park, Ireland. Samples of rumen, kidney and faeces were removed from each animal. Kidney samples were used as an estimate of flesh radiocaesium concentrations and the 95% confidence interval for the mean was 203 +/- 12 $Bq.kg^{-1}$. The maximum recorded radiocaesium concentration in kidney was 367 $Bq.kg^{-1}$ (fresh weight).

The altitude of cull, the age and sex of each animal were recorded. Neither age nor sex correlated with concentrations of ^{137}Cs in rumen, kidneys or faeces. Despite the limited altitudinal range of the study and the free ranging behaviour of deer, there was a highly significant positive correlation between rumen, kidney and faecal ^{137}Cs concentrations and the altitude of the cull (Table 1). Potassium-40 concentrations in rumen, kidney and faeces did not correlate with the altitude of cull, age or sex of slaughtered animals.

Significant ^{137}Cs concentration differences were identified in the sequence: rumen < faeces = kidney. Caesium-137 concentrations in rumen, kidney and faeces for individual animals were all significantly correlated (Table 1). Statistical testing showed that the concentration sequence for ^{40}K was: rumen = faeces < kidney; this sequence differs from that of ^{137}Cs. A comparison of ratios test for rumen:faecal ratios demonstrates that significantly more ^{137}Cs is excreted in faeces that is the case for ^{40}K. The concentration of ^{137}Cs excreted in faeces relative to concentrations in forage (rumen) is approximately twice that for ^{40}K.

Table 1 Correlation between the altitude of the cull and the ^{137}Cs content of rumen , kidney and faecal samples of red deer

	Altitude	Kidney	Rumen	Faeces
Altitude	1.00			
Kidney	0.530**	1.00		
Rumen	0.423*	0.769**	1.00	
Faeces	0.489**	0.854**	0.853**	1.00

** $p<0.01$: **$p<0.001$*

Linear regression was applied to investigate the use of faecal ^{137}Cs concentrations to predict flesh concentrations. Linear regression of faecal ^{137}Cs concentrations (y) on kidney concentrations (x) was carried out, the regression equation is:

$$y = -86.90 + 0.97x \ (r^2 = 0.73, F_{1,40} = 107)$$

This equation may be used to predict radiocaesium concentrations in flesh by measurement of faecal concentrations. This is a useful preliminary assessment method, particularly with herds of wild animals that prove difficult to capture for *in-vivo* monitoring.

Bioindicators

A study of the utilisation of honeybee products as a means of quantifying ^{137}Cs concentrations in semi-natural ecosystems has been successfully completed. Bees forage intensively over about 7 km^2 visiting thousands of plants daily in their search for pollen. The study has indicated that the use of honey as an indicator of radiocaesium contamination is unsuitable due to the variety of sources of pollen, nectar and honeydew of which honey is comprised. However pollen collected by honeybees can be used very effectively as a bioindicator of radiocaesium concentrations in vegetation.

By simply fitting a pollen trap to a honeybee hive and identifying the pollen species present , it is possible to produce models for accurate and precise estimation of radiocaesium concentrations in plant species within the forage area. The variability in radiocaesium concentration of a given pollen species is small. An advantage of this method is that it allows a very representative sample to be obtained. In addition, pollen samples represent primary production over a single season. Such time specific sampling is very difficult to achieve by sampling the plant itself, especially in perennial species.

Ecological Half-life of Radiocaesium in Peatland Soils, Peatland Vegetation and Sheep.

A study of the distribution of radiocaesium in adjacent mineral and peat soil was conducted and this facilitated an estimation of short- and long-term losses of ^{137}Cs from the system. Significant depletion of ^{137}Cs, representing 62.5% of the nuclear weapon's fallout and 47% of the Chernobyl deposition, was observed in the peatland soils. These losses were attributed mainly to surface run-off in the months immediately after deposition, and the radioactive half-life in the long-term. This resulted in the calculation of a two compartment decay for ^{137}Cs in peatland soils with effective half-lives of about 8 and 22 years.

An investigation of the accumulation and retention of ^{137}Cs from 1989 to 1993 by peatland vegetation (10 species) from an area of known high radiocaesium transfer to sheep was carried out. All species except V.myrtillus, Eriophorum angustifolium and Sphagnum cuspidatum showed a seasonal pattern in ^{137}Cs concentration. C.vulgaris and Scirpus caespitosus yielded

the highest concentrations (both species in excess of 2000 Bq.kg^{-1}) of ^{137}Cs. Mature C.vulgaris, V.myrtillus, Polytrichum commune, S.cuspidatum and Cladonia impexa exhibited a statistically significant decrease in ^{137}Cs concentration for the study period. These data facilitated preliminary estimates of ^{137}Cs effective ecological half-life that ranged from +3 years for C.impexa to -1 year (an increase over time) for young C.vulgaris shoots.

A long-term study of mountain sheep grazing peatland pasture was carried out from 1989 to 1994. This study enabled the long-term behaviour of radiocaesium in mountain sheep to be evaluated and was of sufficient duration to facilitate the calculation of the effective ecological half-life of ^{134}Cs and ^{137}Cs in both lambs and ewes. Figure 6 shows *in-vivo* radiocaesium concentrations in ewes from June 1989 to September 1994. In general the highest radiocaesium concentrations were observed in summer and lowest concentrations in winter. Similar seasonal patterns of radiocaesium flesh concentrations were found in lambs. Radiocaesium concentrations in flesh for both ewes and lambs show an overall decrease for the study duration. The highest radiocaesium concentration of any single monitoring occasion occurred in autumn and this anomaly was probably due to a greater than average consumption of contaminated fungi at this time. The effective ecological half-life of ^{137}Cs in ewes and lambs for this period was 7 and 8 years respectively

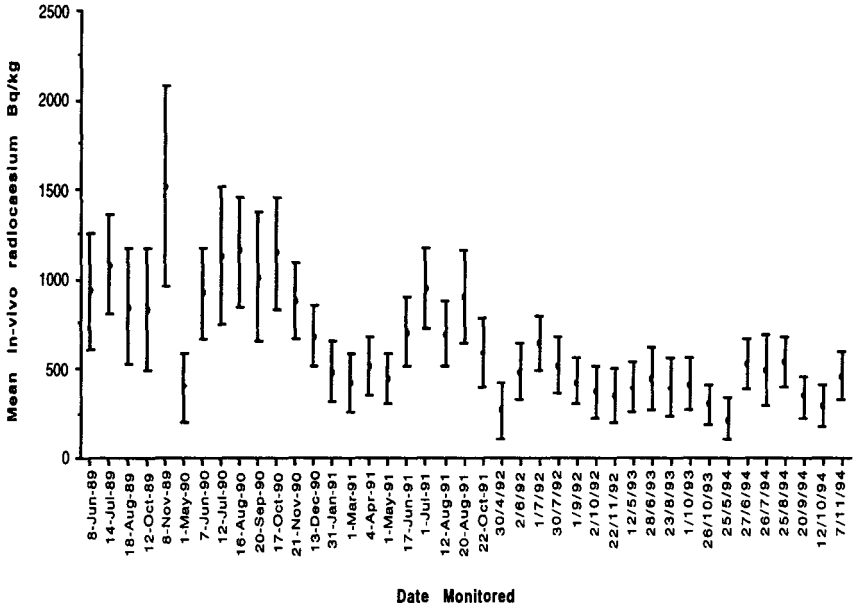

Figure 6 Plot of mean in-vivo radiocaesium concentrations in Irish peatland ewes (error bars represent 1 standard deviation of the mean).

Uppsala forest investigation.

This study details the distribution of the radiocaesium content in the biota of a Swedish Spruce (Picea abies) forest. A 100 x 100 m^2 area of forest area was subdivided into 25 contiguous grid squares of 20 x 20 m^2 using two sets of six lines placed perpendicular to each other . Soils (0-10 cm), bryophytes and understorey vegetation were sampled from a 0.25 m^2 area located at each intersection point (36 in total). Six of the 36 intersections were randomly

chosen and a single monolith was extracted to provide a more detailed examination of radionuclide distribution through the soil profile. All fungi found within the sampling area were sampled and one average sized specimen of Picea abies, Pinus sylvestris and Betula spp. were sampled.

Caesium-137 deposition to 10 cm at the 36 sampling points ranged from 26 kBq.m^{-2} to 61 kBq.m^{-2}. Highest soil ^{137}Cs activity concentrations were found in the 0-5 cm depth profile. Bryophyte cover varied considerably and ^{137}Cs deposition ranged from 0 to 7605 Bq.m^{-2}. Boletus edulis due to it's abundance had the highest ^{137}Cs deposition of 18.5 Bq.m^{-2}, however ^{137}Cs activity concentrations of 162 kBq.kg^{-1} were found in Cortinarius collintus. Understorey vegetation was dominated by V.myrtillus and V.vitis-idaea which had respective mean ^{137}Cs deposition of 181 and 116 Bq.kg^{-1}. All tree samples except P.sylvestris had the same distribution of ^{137}Cs activity concentrations. In all cases twigs had the highest and pre-Chernobyl wood (except P.sylvestris) had the lowest ^{137}Cs activity concentrations.

Table 2 Cs-137 activity in different compartments of the Uppsala experimental forest site.

Compartment	N	Cs-137 Bq.m-2 (1SD)	% of Compartment	% of Total
Soils				
Deposition (0-10cm)	36	41780 (10198)	89.00	
Deposition (10cm - bedrock)		5164*	11.00	
Sub-total		46944		86.75
Bryophytes				
Mixed bryophytes	36	2962 (1914)	100.00	
Sub-total		2962		5.47
Fungi				
Fresh fungi	13	62.98	25.43	
Unidentified fungi	1	184.71	74.57	
Sub-total		247.69		0.46
Understorey				
Vaccinium sp (green)	72	297 (235)	85.89	
Other vegetation	14	48.77	14.11	
Sub-total		345.8		0.64
Trees				
Picea abies	3	2369 (424)	65.51	
Pinus sylvestris	1	957 (67.23)	26.47	
Betula pendula	1	290 (6.87)	8.02	
Sub-total		3616		6.68
Ruminants				
Moose	44	0.16	43.24	
Roedeer	16	0.21	56.76	
Sub-total		0.37		< 0.001
TOTAL INVENTORY			**54116**	

**Estimated from ^{137}Cs in 36 0-10 cm quadrats and including an additional 11 % estimated from soil profile data below 10 cm depth.*

Table 2 details the breakdown of ^{137}Cs within the forest compartment. The total mean content of ^{137}Cs in the system was 54 kBq m^{-2}. Data show that approximately 87% of total fallout is in soils, 5.5% in the bryophyte layer and 7% in standing biomass of trees. Fungi, understorey vegetation and ruminant populations, which encompass the principal foodstuffs responsible for radiation transfer to man from the system, collectively contained approximately 1% of total fallout. The low content of total fallout in these categories is primarily due to low biomass and patchy distribution. Actual concentrations of ^{137}Cs in individual samples of the latter categories were considerable and frequently exceeded the concentration limit of 1500 Bq kg^{-1} for consumption of wild produce in Sweden. The data demonstrate that only a small percentage of total fallout enters food produce in this system, that the standing crop of food produce is low, but may contain concentrations of radioactivity that give cause for concern. The potential for significant individual dose transfers from the system is primarily limited to critical groups such as hunters, regular consumers of wild produce, and forestry workers.

Food Consumption Data

Data on foodstuff production and consumption rates has been compiled for use in the calculation of doses for the ingestion of foodstuffs from semi-natural ecosystems.

Strontium-90 activity concentrations in vegetation.

A preliminary investigation of ^{90}Sr levels in Irish peatland vegetation was carried out. Mean ^{90}Sr activities ranged from 19 Bq.kg^{-1} in C.vulgaris to 60 Bq.kg^{-1} in E.vaginatum (Table 3).

Table 3 Mean ^{90}Sr activity concentrations in a range of vegetation species from a peatland site in Ireland (N represents the number of replicates and s.d. represents one standard deviation of the mean).

Species	N	^{90}Sr Bq.kg^{-1}	s.d.
Calluna vulgaris	3	19	14
Erica tetralix	4	31	6
Scirpus caespitosus	5	26	5
Juncus squarrosus	5	27	9
Eriophorum vaginatum	5	60	25

Publications

McGee, E.J., Synnott, H.J., Keatinge, M. & Colgan, P.A. (1995) The variability in fallout content of soils and plants and the design of optimum field sampling strategies. *Health Physics*, 68(3); 320-327.

McGee, E.J. & McGarry, A. (1994) The uses of bioindicators in radionuclide contamination assessment. International Union of Radioecology, Soil-Plant Group Meeting, Varna Bulgaria, 1994.

McGee, E.J., Synnott, H.J., Keatinge, M. & Colgan, P.A. (1993) Persistence and prediction of radiocaesium levels in animals grazing semi-natural environments. *The Science of the Total Environment*, 138; 91-99.

McGee, E.J., Colgan, P.A. & Synnott, H.J. (1993) A new method for prediction of radiocaesium in vegetation: evidence from Irish uplands. *Journal of Environmental*

Radioactivity, 18; 53-70.

Colgan, P.A., McCann, P., McGee, E.J. & McAulay, R. (1993) Short and long-term losses of ^{137}Cs from peatland soils. *Irish Journal of Agricultural and Food Research*, 32; 37-46.

Colgan, P.A. and Powell, S. (1993) Review of data available on food consumption in Ireland. Internal report to the Environmental radiation advisory committee of the Radiological Protection Institute of Ireland.

McGee, E.J., Synnott, H.J. & Colgan, P.A. (1992) Availability of radiocaesium from Chernobyl and bomb fallout to peatland vegetation in Ireland. International Union of Radioecology, Publication R-921202; 27-29.

McGee, E.J., Pearce, J., Synnott, H.J., McAdam, J.H. and Johnson, A. (IN PREPARATION) The effective half-life of radiocaesium in sheep flocks on montane peatland.

McGee, E.J., Johanson, K.J., Fawaris, B.H., Synnott, H.J., Nielsen, S.P., Horrill, A.D., Kennedy,V.H., Barbayiannis, N., Veresoglou, D.S., Colgan, P.A and McGarry, A. (IN PREPARATION) Chernobyl fallout in a Swedish spruce forest.

Synnott, H.J. and McGee E.J. (IN PREPARATION) The effective half-life of ^{137}Cs in montane peatland vegetation.

McGee, E.J., Synnott, H.J., O'Keeffe, C., Colgan, P.A. (ACCEPTED FOR PUBLICATION) Radionuclide uptake by red deer (*Cervus elaphus*) on mountain grazing. *British Veterinary Journal,*.

McGee, E.J., Johanson, K.J., Synnott, H.J., Keatinge, M. & Colgan, P.A. (ACCEPTED FOR PUBLICATION) An evaluation of the use of ratios in radioecological studies. *Health Physics*.

Head of Project 2: **V H Kennedy & A D Horrill**

II. Objectives for the reporting period.

1. To compare the concentrations and distribution of ^{137}Cs activity and ^{90}Sr activity in two heather dominated semi-natural ecosystems, one growing on a pure peat and one on a peaty podzolic soil.

2. To complete an evaluation of a sequential extraction method for estimating ^{137}Cs bioavailability in organic soils.

3. To apply the sequential extraction method to a range of soils from heather dominated systems and investigate possible relationships between ^{137}Cs concentrations in each sequential extract solution with that in heather growing on the soils.

III. Progress achieved including publications.

Introduction

One of the main objectives of this research was for each group to study ^{137}Cs distribution, and where possible ^{90}Sr distribution, in a semi-natural ecosystem typical of their country. In the UK uplands heather dominated semi-natural ecosystems which cover large tracts of land are grazed by deer, sheep and grouse. Meat from these animals can be important source of food for specific population groups such as game keepers and their families. Data from our study for the Scottish Development Department (SDD) indicated that the ecological half-life of ^{137}Cs in UK heather dominated ecosystems is at least 30 years which is comparable with its physical half-life. The study reported here has three main parts:

1. Strontium-90 analysis of samples from two heather dominated ecosystems, one growing on a pure peat, and one growing on a peaty podzol. The data has been used to compare the distribution of the ^{137}Cs and ^{90}Sr within the two ecosystems.

2. Development of a method to assess ^{137}Cs availability for plant uptake from organic soils.

3. Comparison of the availability of ^{137}Cs for plant uptake from six heather dominated ecosystems in the UK, and three in Ireland using a sequential extraction method.

Samples of UK fungi have been collected and analysed for ^{137}Cs activity concentrations. These data have been supplied to Uppsala University for collation with data from other groups. We have taken part in a collaborative study of a semi-natural woodland at Uppsala. Information on UK dietary habits has also been supplied to Risφ National Laboratory as part of an assessment of the contribution of semi-natural ecosystems to the overall dose to man from European semi-natural ecosytems.

2. ^{137}Cs and ^{90}Sr distribution in two heather dominated semi-natural ecosystems.

Study Areas

Both sites are in the Highland Region of Scotland near Loch Laggan. They are about 1.5 km from each other and each covers an area of about 0.2 hectares. Red deer and sheep range freely over both sites although the heather plants do not appear to be heavily grazed.

The peaty podzol site (National Grid Reference NN 528 915) is situated on a level area of river terrace at an altitude of 305 m. It is a well drained iron humus podzol with an A_o horizon that is approximately 10 cm deep. The podzolic soil supports a dense stand of 15-20 year old heather that covers about 80% of the ground. Associated plant species include the grasses *Deschampsia flexuosa, Festuca ovina and Agrostis vinealis,* and the dicotyledonous herbs *Potentilla erecta* and *Galium saxatile.*

The peat site (National Grid Reference NN 533 902) is on a level area of a west facing slope,at an altitude of 320 m. The peat supports a 25-30 year old heather stand that covers about 65% of the ground. Other ground cover includes about 25% cotton grass *(Eriophorum vaginatum),* associated with cross-leaved heath *(Erica tetralix)*, common cotton grass *(Eriophorum angustifolium)* and heath rush *(Juncus squarrosus).*

The origin of ^{137}Cs and ^{90}Sr in the Loch Laggan area.

Strontium-90 activity at both sites was deposited over a period of 20* years from bomb fallout following atmospheric testing in the 1950s and 1960s. ^{137}Cs activity is dominated by fallout from the Chernobyl accident in 1986 when about 20 kBq m^{-2} ^{137}Cs was deposited at both sites. Thus the time available for redistribution of ^{90}Sr activity and ^{37}Cs activity within the two ecosystems is very different. The samples were taken in June 1989, approximately 30 years after the last ^{90}Sr bomb fallout and 3 years after the fallout from Chernobyl.

Results

Total ^{137}Cs activity concentrations at both sites were an order of magnitude greater than those for ^{90}Sr (Table 1) and a greater proportion of ^{90}Sr activity had penetrated further down the soil profile (Figures 1 and 2). Total inventories for both radionuclides were 30 % higher at the peaty podzol site than at the peat site. This may have been due to uneven deposition in the area or to losses from the peat site due to soil leaching processes. Later samplings, and a lysimeter experiment to study the mobility of ^{137}Cs activity at these two sites confirmed that ^{137}Cs activity is moving more rapidly down the peat soil profile than it is down the peaty podzol profile.

Table 1 Total ^{137}Cs and ^{90}Sr content in plants and the top 0 - 20 cm of the soil profile for two heather dominated ecosystems near Loch Laggan, Scotland (samples collected in June 1989).

Site	^{137}Cs kBq m^{-2}	^{90}Sr kBq m^{-2}
Peaty podzol	17.9	2.4
Pure peat	13.7	1.8

At the peaty podzol site the greatest proportion of ^{137}Cs activity was in the 0 - 5 cm layers of the soil whereas ^{90}Sr activity has penetrated more evenly down the soil profile in the 0 - 10 cm zone (Figure1). Both radionuclides have penetrated at least 15 - 20 cm down the soil profile. Small, but measureable quantities of ^{137}Cs and ^{90}Sr activity were found in the current year's growth of heather. This implies that small amounts of ^{137}Cs and ^{90}Sr in the rooting zone of the peaty podzol are leaching into the soil in a form that is available for plant uptake and/or that translocation of these radionuclides is taking place within the plant.

Figure 1 The distribution of ^{137}Cs and ^{90}Sr in plants and in the top 0 - 20 cm of the soil profile of a heather dominated ecosystem growing on a peaty podzol near Loch Laggan, Scotland (n=3; ± sd).

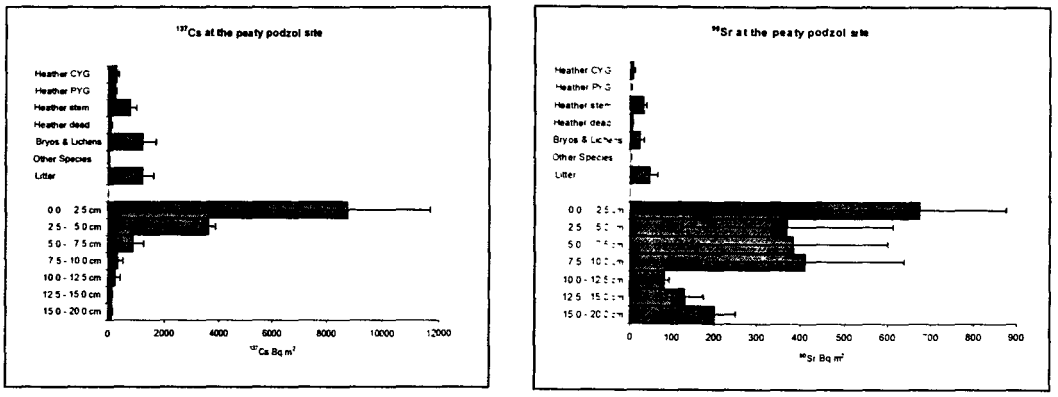

The bryophyte layer and heather plants retained a similar proportion of ^{137}Cs at the peaty podzol site (6.8% and 7.6% respectively). The same is true for ^{90}Sr (1.0% and 1.3 % respectively). The presence of both these radionuclides in the litter layer, 6.8% ^{137}Cs and 2% ^{90}Sr, also supports the hypothesis that both radionuclides are recycling through the soil/plant interface as well as being translocated within heather plants.

Figure 2 The distribution of ^{137}Cs and ^{90}Sr in plants and in the top 0 - 20 cm of the soil profile of a heather dominated ecosystem growing on a pure peat near Loch Laggan, Scotland (n=3; ± sd).

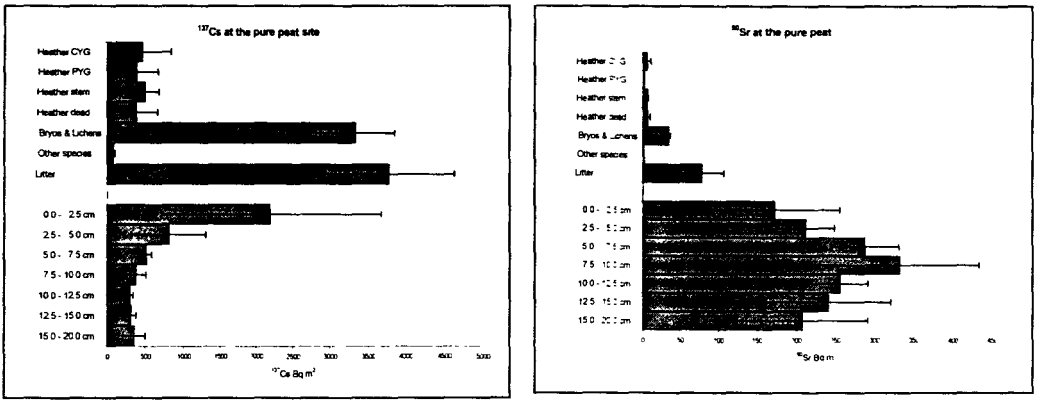

The distribution of ^{137}Cs and ^{90}Sr at the pure peat site was rather different (Figure 2). Approximately 65% of the total ^{137}Cs inventory was still above ground when the samples were taken. Of this, 24% was attributable to the bryophyte layer and 28% in the litter layer. Another 28% was in the 0 - 10 cm rooting zone. Thus approximately 93% of the total ^{137}Cs

inventory at the peat site was still potentially available for re-cycling in the soil plant system three years after the Chernobyl reactor accident. A similar percentage (90%) was found in ground cover and the top 0 - 10 cm of the soil profile at the semi-natural woodland ecosystem near Uppsala, Sweden (sampled August 1992). Although, at the Uppsala site, which received > 50 kBq m^{-2} deposition, the highest proportion of Chernobyl contamination was in the soil rather than in the litter and bryophyte layers. The presence of a significant proportion of ^{137}Cs activity (30%) in the litter layer and heather plants (10%) at the peat site indicates that a greater proportion of ^{137}Cs activity may be available for recyling to plants than at the peaty podzol site.

Strontium-90 activity at the Loch Laggan peat site was more evenly distributed down the soil profile (Figure 2) than at the peaty podzol site (Figure 1), although a similar proportion was found in above ground vegetation at both sites. Given the long period over which the ^{90}Sr has been in the ecosystem, and its distribution down the soil profile (Figures 1 and 2) it is likely that some of the original deposition has penetrated below the 20 cm sampling depth of the soil profile used for this study at both sites. Transfer factors (Tfs; Table 2) indicate that ^{90}Sr at the podzol site is more available for vascular plant uptake than at the peat site whereas they indicate that a similar proportion of ^{137}Cs activity was available for plant uptake at both sites.

Table 2 Transfer factors (Bq kg^{-1} vascular plants/Bq kg^{-1} soil (litter-20 cm)) for ^{137}Cs and ^{90}Sr at both sites.

Soil layer	^{90}Sr		^{137}Cs	
	Peat	**Podzol**	**Peat**	**Podzol**
Litter - 5 cm	0.4	1.4	2.3	2.7
Litter - 10 cm	0.2	1.2	2.3	2.5
Litter - 15 cm	0.1	1.2	2.3	2.4
Litter - 20 cm	0.1	1.1	2.3	2.4

- Total inventories of ^{137}Cs and ^{90}Sr activity in plants and the top 20 cm of the soil at were higher at the peaty podzol site.
- Both ^{137}Cs and ^{90}Sr activity were moving down the soil profile more quickly at the peat site than at the peaty podzol site
- About 95 % of the ^{137}Cs activity at both sites was in plants and the top 10 cm of the soil.
- About 80 % of the ^{90}Sr activity at the peaty podzol site was in plants and the top 10 cm of the soil whereas only 60 % was in these compartments at the peat site.
- The highest proportion of ^{137}Cs and ^{90}Sr activity at the peaty podzol site was in the top 2.5 cms - 50 % and 30 % respectively.
- The highest proportions of ^{137}Cs activity at the peat site were in the litter and bryophyte layers (about 25% each) whereas for ^{90}Sr activity 45 % was found in the 2.5 - 10 cm layers.
- Site differences in radionuclide behaviour are probably attributable to the higher mineral content at the peaty podzol site and topography.
- Small amounts of ^{137}Cs and ^{90}Sr activity are potentially available for entry into human food chains via sheep, deer and grouse grazing heather at both sites.

The ecological half-life of ^{137}Cs in heather dominated ecosystems

Caesium-137 sequential extraction data for both sites (section 3) indicates that ^{137}Cs at the peat site is more available for heather uptake than at the podzol site. This confirms results from an earlier model for the two sites which predicted that ^{137}Cs activity deposited on the peaty podzol is locked up almost immediately (Figure 3) whereas ^{137}Cs activity at the peat site was more mobile and was being progressively leached down the soil profile (Figure 4). ^{137}Cs activity at both sites is slowly declining and has a predicted ecological half-life of about 30 years (ie = to ^{137}Cs physical half-life). The difference between the two sites is probably attributable to the higher mineral content at the peaty podzol site and differences in the topography of the two sites. Thus, ^{137}Cs physical decay as well as organic decomposition rates and mineral decay rates strongly influence the ^{137}Cs ecological half-life in both of these heather dominated ecosystems.

3. Description and evaluation of sequential extraction method

Introduction

When assessing the availability of ^{137}Cs for plant uptake from organic soils it is important to understand how sampling and sample handling techniques can alter the physical and chemical characteristics of soils. Peaty organic soils shrink and harden during drying and are difficult to re-wet evenly during extraction processes. Physical and chemical characteristics of organic soils change as a result of drying, particularly if they are dried at more than 40° C. For example there are likely to be losses of volatile ammonia and small losses of phosphorus, but it is impossible to quantify such losses. It is also difficult to take a 2 - 10 g fresh sample that is truly representative of even 1 m^3 of organic soil.

In an attempt to address some of these problems we have developed a sequential extraction technique that can be used to analyse organic soils with relatively low ^{137}Cs contamination. The method protocol uses 50 g of fresh soil and relies on leaching processes to simulate natural soil leaching processes for the first three extraction stages. However, as with any extraction procedure, it can only give a semi-quantitative estimate of ^{137}Cs availability for plant uptake.

Sampling methods and sample storage

For all UK samples a quadrat of (50 x 50) cm was marked out. All above ground vascular plants were sampled by clipping the plants to ground level, the moss and litter layers were then removed as separate samples. Finally a soil block of (25 x 15 x 10) cm was carefully measured and removed from the centre of the quadrat and split into two layers - 0 - 5 cm and 5 - 10 cm layer. All samples were placed in clearly labelled bags.

On return to Merlewood vegetation and litter samples were sorted into pure samples and weighed. They were then dried at 80° C, for 48 hours, prior to being milled using a 0.7 mm sieve. The soil slices were weighed and halved. One portion was stored at 2° C for sequential extraction. The other portion was broken up by hand and dried at 80° C for 48 hours before being passed through an enclosed 2 mm rotary sieve. Weighed sub-samples of all milled and sieved samples were tubbed for gamma analysis.

Figure 3 Model predictions of ^{137}Cs activity concentrations leached from the soil and in the soil, in heather current years' growth, in sheep and in grouse at the peaty podzol site.

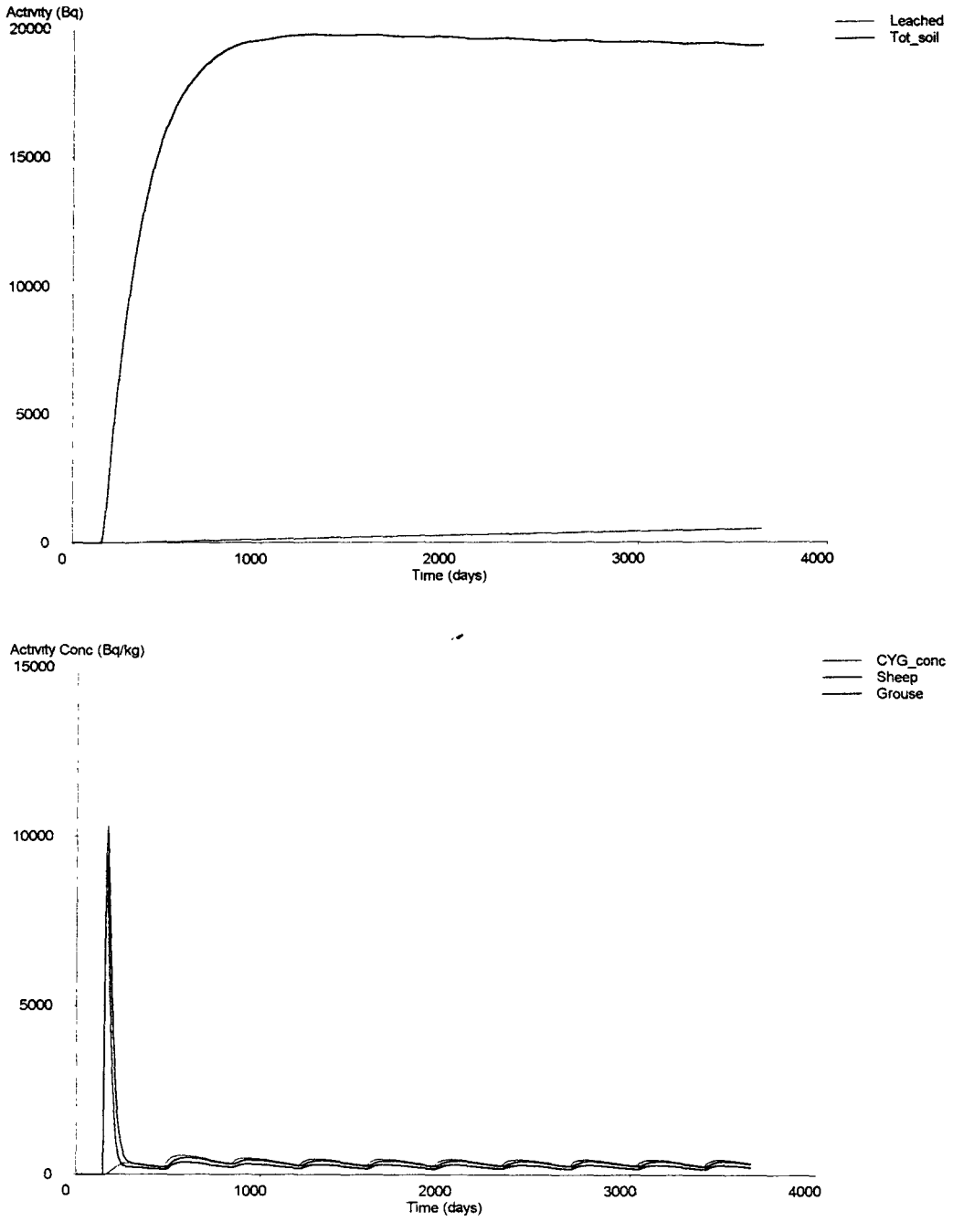

Figure 4 Model predictions of ^{137}Cs activity concentrations leached from the soil and in the soil, in heather current years' growth, in sheep and in grouse at the pure peat site.

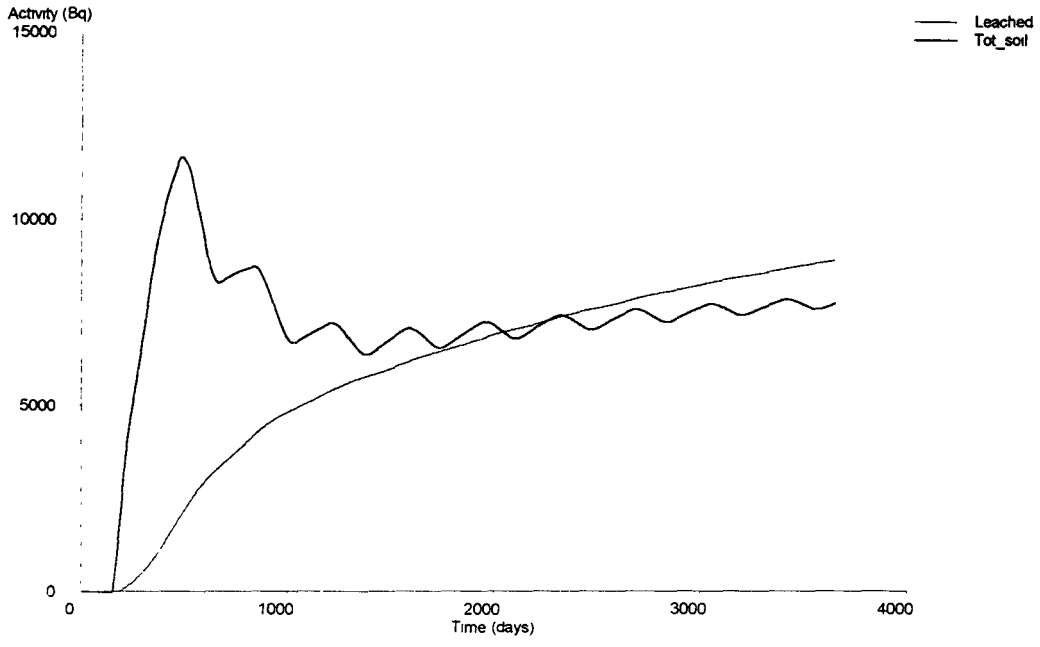

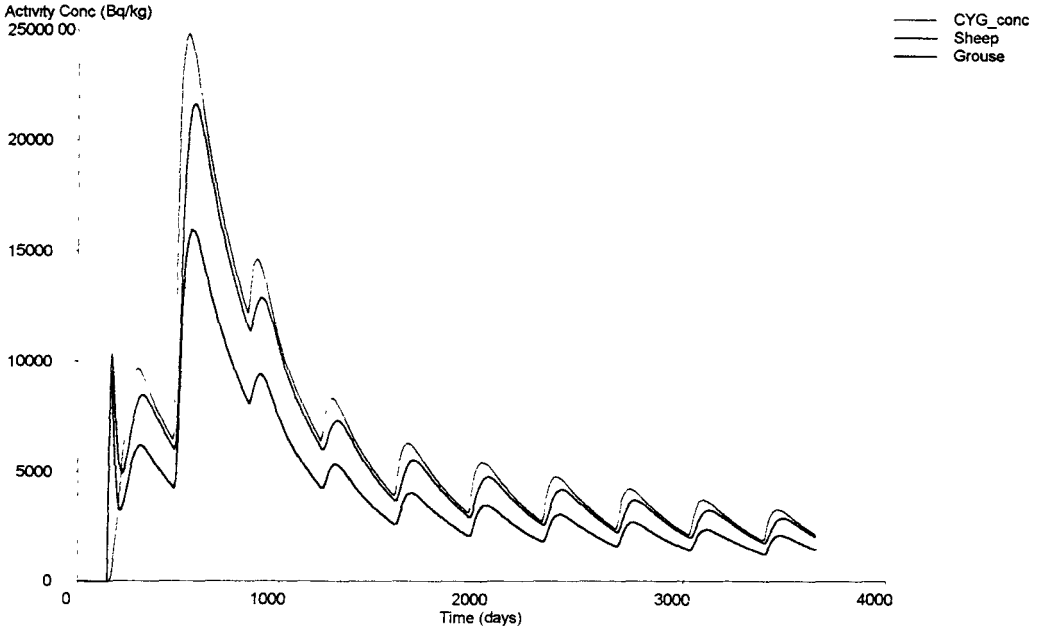

Counting protocols

All samples were counted by high resolution gamma ray spectrometry using hyperpure germanium-lithium (GeLi) detectors with a relative efficiency of 20 -25 %. Calibration was by means of National Physical laboratory certified mixed environmental standards covering the energy range 60 -1836 keV in a matrix appropriate to the sample being measured. Spectral data were analysed using Canberra Apogee software. Counting errors at the 95 % confidence level varied with sample activity and counting time but were within the range 3 - 8 % for standard sample tubs. The accuracy of calibrations was checked against international standards and individual detectors were cross-checked to ensure that their results were comparable.

Conventionally tubbed dried samples were counted for 80,000 seconds (s). Extract solutions that had been evaporated onto petri dishes were counted for 170,000 s. The detection limit for evaporated extract solutions was 0.04 Bq ± 10 - 30 % counting error per petri dish counted for 170,000 s. For evaporated samples of 0.2 Bq and above counting errors were within the range of ± 3 - 8 %.

Method

The main stages of the method are summarised in Table 3. To validate the method for inter site comparison three separate samples were taken from the same sample bags of soil samples from the 0 - 5 cm layer, from Laggan peat site 1, the Laggan podzol site and the Devoke peat site. They were processed using the sequential extraction procedure on separate occasions that were least two weeks apart. Samples taken from three different locations on the same site (0 - 5 cms) at Laggan peat site 1, the Laggan podzol site and the New Galloway peat site were also analysed so that results could be compared and evaluated.

Results and discussion

The first three extraction protocols were designed to simulate soil water leaching processes. 541 filter papers were used to contain the peat samples. They filtered out course and geletinous substances that are unlikely to be available for root uptake and slowed down the rate of water percolation through the soil in an attempt to mimic the effect of compressed, and sometimes waterlogged, lower soil layers. Although 50 g of each sample was weighed for each series of extractions it was difficult to take representative sub-samples because of the physical and biological characteristics of the peat. The peats contained mixtures of organic debris in varying states of decomposition, roots, organic sludge and a small percentage of denser fine mineral particles (Table 4).

Caesium-137 activity concentrations from each stage of the sequential extraction procedure are presented in Figures 5 and 6. ^{137}Cs activity concentrations in both water extractions were at or above the detection limit for the method for the peat sites. This is equivalent to about 1 Bq kg^{-1} (dw) for the four sites. Water extractable ^{137}Cs activity concentrations for the peaty podzol site were similar for extraction 1 but they were at, or below the detection limit for extraction 2.

Data from sequential extractions 1 and 2 show that water extractable ^{137}Cs activity in samples from the same bag can vary as much as water extractable ^{137}Cs activity originating from different soil samples from the same site (Figure 5).

Table 3 The main stages of the sequential extraction method used to extract ^{137}Cs from a range of organic peat soils.

Extraction	Aim	Summary of method
1. Deionised water	1. To isolate the fraction of ^{137}Cs that is readily soluble in water.	1. i. 50 g fresh weight of organic soil ii. Leach with extractant until 500 cm^3 collected iii. Acidify extract solution and evaporate to about 5cm^3 on a hot plate iv Evaporate to dryness in a petri dish with an IR lamp.
2. Deionised water	2. To assess whether initial removal of ^{137}Cs leads to further ^{137}Cs displacement to adsorption sites from which ^{137}Cs can be extracted.	2. i. Leach fresh sample from extraction 1 until 500cm^3 collected. ii As for 1 iii. iii As for 1 iv.
3. Ammonium acetate pH7	3. To assess the bioavailability of ^{137}Cs using an extractant that is widely used to assess nutrient availability for plant uptake (Allen, 1989*).	3 i. Leach fresh sample from extraction 2 until 500cm^3 collected. ii and iii As for extraction 2 iv. Ash extractant residue in beaker at 200° C to remove ammonium acetate crystals.
4. 0.04 M hydroxylamine hydrochloride in 25 % v/v acetic acid	4. To assess the portion of ^{137}Cs associated with easily reducible iron/manganese oxides (5 - 10 years).	4. i. Place peat residue from extraction 3 and filter paper into a beaker. ii. Add 500 cm^3 extractant and mix well. iii. Heat for 6 hours at 80° C in a water bath stirring approximately every 30 minutes. iv Filter extractant into a beaker. v. and vi. As for 1 iii. and 1 iv.
5. 7 M Nitric acid	5. To assess the portion of ^{137}Cs that is acid digestible and may be released slowly during long-term weathering processes (5-15 years in peaty organic soils).	5. i. Place peat residue from extraction 4 and filter papers into a beaker. ii. and iii . As for 4 ii. and 4 iii. iv Filter extract into a beaker using a Buckner flask. v. and vi. As for 1 iii. and 1 iv.
6. Final residue	6. To assess the portion of ^{137}Cs that may be released very slowly during long-term weathering processes (15-30 years in peaty organic soils).	6. i. Place peat residue from extraction 5 and filter papers into a crucible. ii. Evaporate to dryness under an IR lamp. iii. Separate sample residue from filter paper. iv. Transfer sample residue and filter papers to a petri dish (crumble and cut as necessary).

* *Allen, S.E. (ed) 1989, Chemical analysis of ecological materials. Blackwell Scientific Publications: London*

NB It takes approximately two weeks to process three samples through all stages of the sequential extraction excluding counting time.

Table 4 Organic matter and moisture content of the four peats used to validate the sequential extraction method.

Site name	Organic matter content %	Moisture content %
Pure peat 1, Loch Laggan	97.5	70.4
Peaty podzol, Loch Laggan	84.1	67.3
New Galloway peat	95.1	86.3
Devoke peat	95 0	90.5

This variability is probably attributable to ^{137}Cs activity concentrations that are near to the detection limit for the method. Water soluble ^{137}Cs activity is likely to be in a form that is readily absorbed by plant roots alongside the nutrients that they need to sustain growth. Data from both series of samples have demonstrated that it is possible to achieve a semi-quantitative data set for water extractable ^{137}Cs.

Caesium-137 activity concentrations in ammonium acetate pH7 extracts were at least an order of magnitude higher than the water extract residues and were well above the detection limit for the method (Figure 5). Therefore it is not surprising that within bag sample variability was less than variability for samples from different locations on the same site for ammonium acetate pH7 extractsolutions. ^{137}Cs activity extracted by ammonium acetate pH7 is likely to be in a form that is potentially available for plant uptake. However, plant absorption of this fraction is likely to be controlled by root absorption processes rather than by soil cation exchange processes.

Caesium-137 activity extracted by 0.04 M hydroxylamine in 25 % v/v acetic acid (extraction 4) provides an estimate of ^{137}Cs activity that is associated with iron and manganese oxides in the soil. As with extract solutions from extraction 3 ^{137}Cs activity concentrations were above the detection limit for the method (Figure 6). All test soils were found to have higher ^{137}Cs activity concentrations in 0.04 M hydroxylamine extracts than in ammonium acetate pH7 extract solutions except for samples from the Devoke site. As with extraction 3 within bag variability was less than that for different locations from the same site.

Caesium-137 activity extracted by 7 M nitric acid (extraction 5) is probably associated with structural organic matter such as cellulose and lignin. All soils used in this test series had higher ^{137}Cs activities in 7 M nitric acid extracts than in the other extract solutions. As with extract solutions from extractions 3 and 4 there was generally less variability for sample results associated with the same sample bag than for those from different sample locations at the same site (Figure 6).

Caesium-137 activity concentrations in the final sample residues were similar to, or slightly less than those in 7 M nitric acid extract solutions. ^{137}Cs activity in the soil residue is likely to be associated with large fragments of structural organic matter and with the small mineral fraction in these soils.

The reproducibility of results for extractions 3 - 5 and residues for soil sub-samples from the same bag was better than expected for samples that were weighed and extracted several weeks apart.

This seems to indicate that in spite of all the problems associated with selecting representative samples from fresh organic soils this extraction method can provide useful data for assessing the bioavailability of ^{137}Cs activity in organic soils where ^{137}Cs contamination is > 300 Bq kg^{-1}.

- This method was developed because none of the published methods are suitable for use with organic soils with relatively low ^{137}Cs activity concentrations.
- Method protocols have been developed to improve detection limits so that water extractable ^{137}Cs activity can be quantified.
- Reproducible ^{137}Cs activity concentrations have been produced for soil sub-samples analysed at different times.
- Variability between results for samples from different location on the same site is comparable to that found for extractable nutrient elements in organic soils.

4. Sequential extraction results from a range of heather dominated communities.

Introduction.

Samples were taken from a range of heather dominated ecosystems growing on organic soils in Scotland, England and Ireland (Table 5). The aim was to assess whether or not ^{137}Cs activity concentrations attributible to specific components in the soil give a better estimate of plant uptake than traditional transfer factors (Total Bq kg^{-1} in vascular plants/Total Bq kg^{-1} in underlying soils).

Table 5 Heather dominated ecosystem sites used to assess the sequential extraction method as a means of predicting ^{137}Cs bioavailability in organic soils.

Site name	Region	Grid reference	Sampling date	Number of samples
Peaty podzol, Loch Laggan	Highland, Scotland	NN528 915	02-Jun-1994	3
Pure peat 1, Loch Laggan	Highland, Scotland	NN583 902	02-Jun-1994	3
Pure peat 2, Loch Laggan	Highland, Scotland	NN48 86	02-Jun-1994	1
Ben Lawers peat	Tayside, Scotland	NN604383	03-Jun-1994	1
New Galloway peat	Galloway, Scotland	NX384938	21-Oct-1992	3
Devoke peat	Cumbria, England	SD159962	16-Jun-1994	1
Cavan peat	Ulster, Ireland	H128207	30-Jul-1992	3
Mongans peat	Offaly, Ireland	S050070	16-Jul-1992	3
Waterford peat	Munster, Ireland	N052319	10-Jul-1997	3

Results.

Relationships between ^{137}Cs activity extracted at each stage of the procedure are presented in two ways. Firstly as a simple correlation between ^{137}Cs activity concentrations in heather growing on the soil, and ^{137}Cs activity extracted at each stage of the procedure, and then as a cumulative figure derived by sequential addition of ^{137}Cs activity concentrations from each stage (Table 6).

Figure 5 A comparison of variability in ^{137}Cs activity concentrations ± sd extracted by extractions 1 - 3 of the extraction procedure for:

i. different samples from the same site (n=3), and
ii. sub-samples from the same soil sample bags from three different sites.
NB Different scales have been used for each pair of graphs

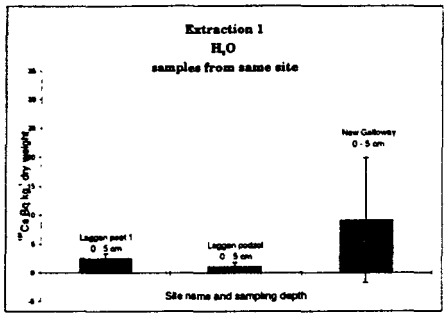

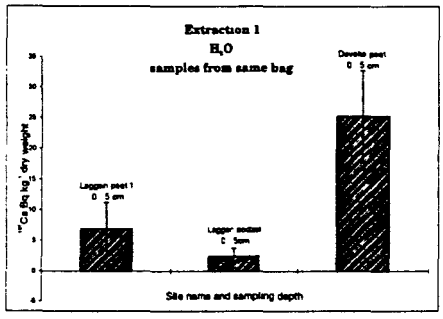

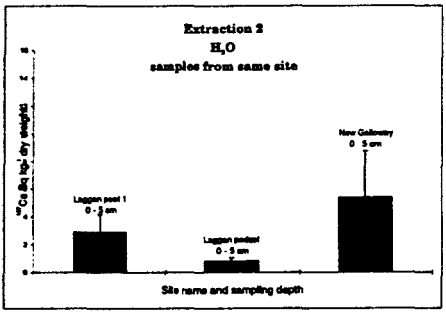

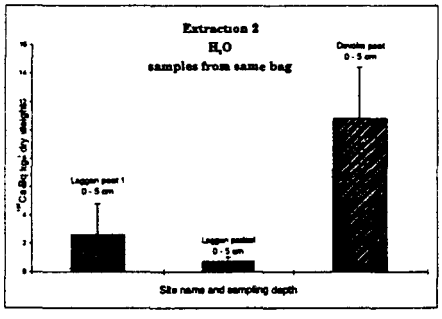

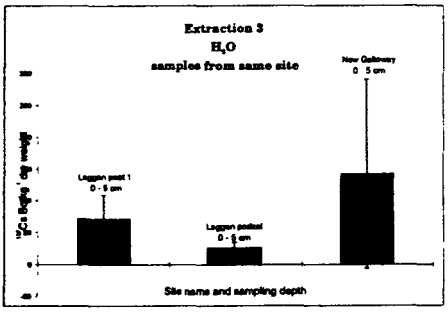

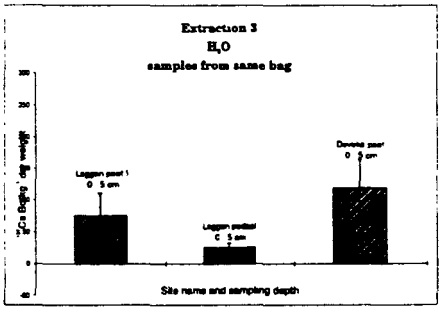

Figure 6 A comparison of variability in ^{137}Cs activity concentrations ± sd extracted by extractions 4 - 5 of the extraction procedure and for the sample residue for

i. for different samples from the same site (n=3), and
ii for sub-samples from the same sample bags for samples from three different site.

NB Different scales have been used for each pair of graphs.

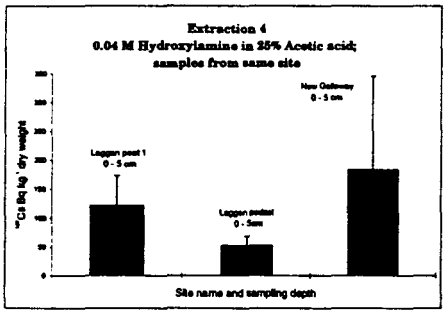

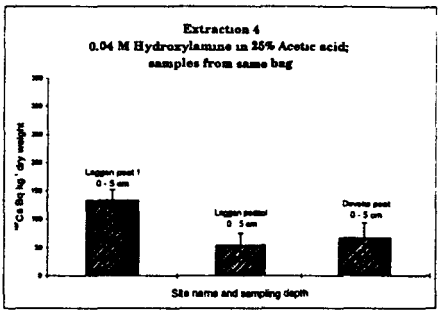

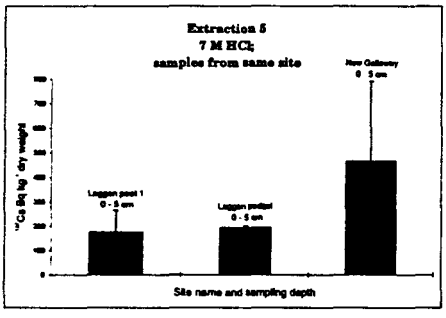

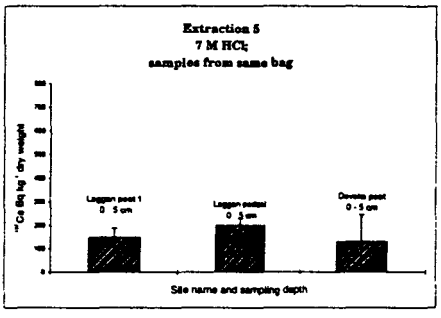

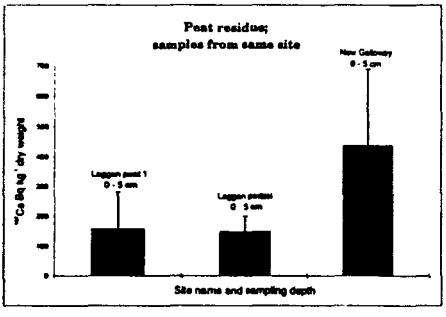

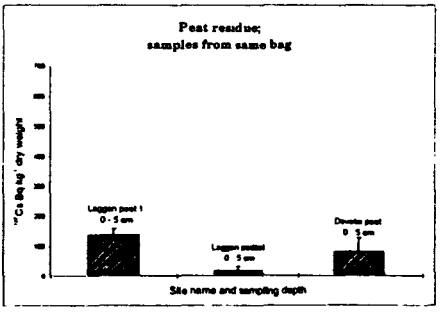

Table 6 Correlation coefficients for ^{137}Cs activity concentrations (Bq kg^{-1} dw) in heather plants and in the soil extract solutions of sub-samples from the underlying soil for 21 paired samples from nine sites in the UK and Ireland

Extractant /soil component	Individual correlation coefficients		Cumulative correlation coefficients	
	21 paired samples (UK & I)	12 paired samples* (UK)	21 paired samples* (UK & I)	12 paired samples (UK)
Water 1	**0.592****	0.565	**0.592****	0.565
Water 2	**0.602****	0.687*	**0.613****	0.602*
Ammonium acetate pH7	0.505*	**0.748****	**0.551****	**0.762****
0.04 M hydroxylamine	0.027	0.469	0.257	0.632
7 M nitric acid	0.286	0.646	0.247	0.663
Residue	0.279	0.638	0.296	0.700
Soil dry weight (used for TFs)		0.406		0.406
	r = > 0.549	r = > 0.708	r = > 0.549	r = > 0.708
	P = 0.01	P = 0.01	P = 0.01	P = 0.01

* *Traditional transfer factor data only available for 12 UK sites at present.*

For 21 paired samples the correlation coefficient for ^{137}Cs activity concentrations extracted by water extracts 1 and 2 from the underlying soil (0 - 10cms) and ^{137}Cs activity concentrations in heather growing on those soils were highly significant (Table 6; r = > 0.569; P = 0.01). Results for ammonium acetate pH7 were also significant (r = > 0.433; P = 0.01). None of the other correlation coefficients in this data set were significant. Cumulative figures show highly significant correlations for the water soluble fractions and for the water plus ammonium acetate fraction (r = > 0.433; P = 0.01) in all cases. These results indicate that even with the high variability inherent in all soil extractions, ^{137}Cs activity concentrations in heather plants are more highly correlated with the water extractable ^{137}Cs, particularly for the cumulative water extractable ^{137}Cs than with the total ^{137}Cs burden in the top 0 - 10 cm of the soil profile which is traditionally use to calculate plant-soil Tfs (Table 6).

As a result of these findings a preliminary trial to remove ^{137}Cs by successive water extractions was set up. Three representative samples of New Galloway peat were extracted using a series of water extractions over a period of 184 days (Figure 5). After seven extractions ^{137}Cs activity leached into water extract solutions was at, or near the detection limit for the method (equivalent to about 20 Bq m^{-2} for New Galloway peat). The peat samples were then allowed to dry out at ambient temperature for 37 days before being extracted using a further series of six water extractions. After the peat had been allowed to dry out ^{137}Cs activity in extract solutions increased to the equivalent of 80 Bq m^2 (dw) before decreasing to the detection limit. A similar phenomenon was observed after peat samples had been stored with field moisture capacity, at 2° C, for 107 days before another series of water extractions were carried out. In this instance the increase was to the equivalent of 50 Bq m^{-2}. These results show that environmental factors such as soil moisture content and soil temperature over time can influence the amount of soluble ^{137}Cs that is leached into soil solution. ^{137}Cs activity concentrations in soil solution are dependent on organic matter and mineral decomposition rates. These rates of solution are not constant and often depend on on other environmental conditions. Environmental changes in soil moisture and soil temperature affect organic decomposition processes and are likely to affect

amounts of soluble ^{137} Cs in soil solution. The impact of these changes on plant uptake will depend on season, and on individual plant growth strategies.

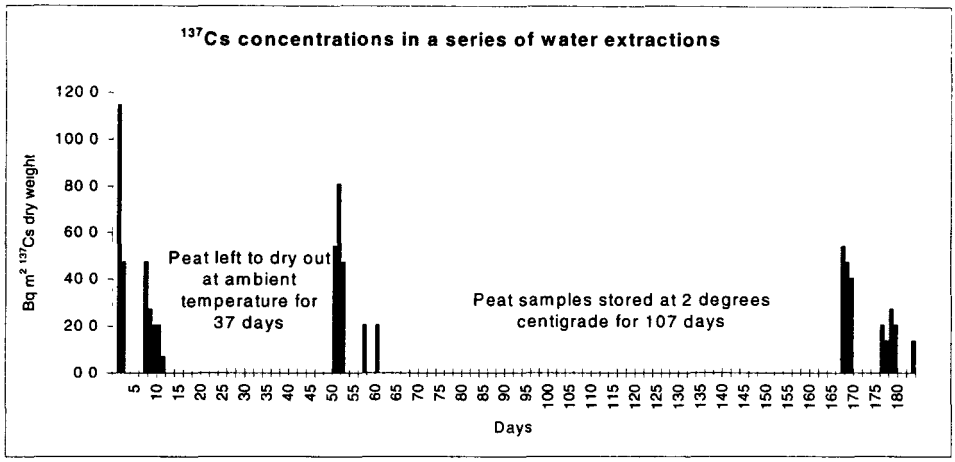

Figure 7 ^{137}Cs activity extracted from sub-samples of New Galloway peat after a series of water extractions over a period of 184 days (n=3)

- ^{137}Cs activity concentrations in heather plants are more highly correlated with water extractable ^{137}Cs than with the total ^{137}Cs soil burden.
- Plant uptake of ammonium acetate pH7 extractable ^{137}Cs is probably controlled by root uptake processes rather than by soil cation exchange processes.
- Water extractable and ammonium acetate extractable ^{137}Cs are likely to be better indicators of ^{137}Cs activity availability for heather root uptake than the use of traditional transfer factors for organic soils.
- Small amounts of ^{137}Cs activity are persistently released into soil water due to cation exchange processes in organic soils.

5. Publications resulting from this research

M^{c}Gee, E.J., Johanson, K.J., Synnott, H.J., Colgan, P.A., Nielsen, S.P., Horrill, A.D., Kennedy, V.H., Barbayiannis, N., Veresoglou, D. and M^{c}Garry, A. (submitted)
Chernobyl fallout in a Swedish spruce forest.
Journal of Ecological Research

Kennedy, V.H., Horrill, A.D. & Singleton, D.L. (in prep)
An evaluation of a ^{137}Cs sequential extraction method for low-level organic soils.

Kennedy, V.H., Horrill, A.D., M^{c}Gee, E. & Singleton, D.L. (in prep)
A comparison of ^{137}Cs availability for heather root uptake from organic soils for nine sites in the UK and Ireland using a sequential extraction method for low-level organic soils.

Head of project 3: Dr. Nielsen

II. Objectives for the reporting period:

The objectives for the reporting period have been 1) to participate in a joint field investigation in a forest area in Uppsala, Sweden, with relatively high Chernobyl radionuclide deposition and carry out ^{90}Sr analyses on samples from this area, 2) to compare data on radiocaesium and radiostrontium in a Danish forest ecosystem with corresponding data from Uppsala, 3) to participate in ^{90}Sr intercomparisons with the other participants, 4) to carry out sampling campaigns in the Faroe Islands and thus continue time series of data on radiocaesium for the determination of ecological half lives, 5) to investigate the availability of ^{90}Sr in samples of soil collected in the zone around Chernobyl, and 6) to prepare the background for an improved assessment of the doses to members of the public in the Member States from radiocaesium in semi-natural ecosystems.

III. Progress achieved including publications

ECOLOGICAL HALF-LIVES

The main objective of radioecological studies of semi-natural ecosystems is to be able to make reliable estimates of radiation doses to man on the short and long term from radioactive contamination in such areas. The experience from the Chernobyl accident has shown that much work is needed in semi-natural ecosystems before this objective is met and that one of the key parameters to be determined is that of the ecological half life.

The effective ecological half life (T_{EE}) is characteristic for the observed rate of reduction of contamination with time from a given compartment of or product from the ecosystem after a single contamination. The effective ecological half life for a radionuclide thus includes both physical decay and the ecological half life. The latter is the parameter characteristic for the rate of removal of the corresponding stable element from the ecosystem. The effective ecological half life is related to the physical half life (T_P) and the ecological half life (T_E) according to:

$$\frac{1}{T_{EE}} = \frac{1}{T_P} + \frac{1}{T_E}.$$

As an illustrative example we may consider calculating collective doses to a population from ingestion of mutton contaminated with ^{137}Cs from an accident involving dispersal of radioactive material. We assume the total annual consumption of mutton in a local population is M (kg y^{-1}), the initial contamination in mutton is C_0 (Bq kg^{-1}) and the effective ecological half life of ^{137}Cs in mutton is T_{EE} (y). The collective dose E (manSv) to the local population is thus given by:

$$E = \frac{C_0 \; T_{EE}}{\ln 2} \cdot M \cdot DF,$$

where DF is the dose factor (Sv Bq^{-1}) for ingestion of ^{137}Cs and ln2 is the natural logarithm of two. The effective ecological half lives are closely associated with radioecological transfer coefficients (UNSCEAR definition). If we consider the example and assume that the accident causes an initial ground contamination of S (Bq m^{-2}), the transfer coefficient P_{23} (Bq y kg^{-1} per Bq m^{-2}) is defined as the ratio of the total time-integrated concentration of ^{137}Cs in mutton to the ground contamination:

$$P_{23} = \frac{C_0 \; T_{EE}}{\ln 2 \; S},$$

and the collective dose may thus alternatively be calculated from:

$$E = S \; P_{23} \; M \; DF.$$

The assumption of a constant ecological half life does not always hold true. The effective ecological half-lives for ^{137}Cs in the environment from the Chernobyl accident observed from 1987 to 1993 are generally shorter than those observed from weapons fallout. However, it is expected that the difference will become insignificant as radiocaesium from the Chernobyl accident with time becomes fixed to the soil minerals. But for ^{90}Sr the reverse process may become important (especially closer to the Chernobyl area) when insoluble strontium with time becomes available for plant uptake.

THE FAROE ISLANDS

Sampling campaigns have been carried out in the Faroe Islands covering soil, water, grass, milk and lamb at a number of locations. The results were used to investigate the behaviour of the Chernobyl radiocaesium relative to that from the weapons fallout. The general trend known from previous results is that the relative reduction with time of the radiocaesium in the Faroese ecosystem from the Chernobyl accident is much faster than that from the weapons fallout. This is apparent from Figure 1 which shows the levels of ^{137}Cs in Faroese milk since 1962. The trend indicates that the rate of reduction with time becomes identical for the two sources of contamination. The effective half life of ^{137}Cs from global fallout was found at 3 years, while ^{137}Cs from Chernobyl decayed with a half life of 2 years. Figure 2 shows the levels of ^{90}Sr in milk where the effective half life has remained at a value of 4 years.

These effective half lives for weapons fallout have been incorporated into transfer coefficients for ^{137}Cs and ^{90}Sr shown in Table 1 which demonstrates the increased sensitivity of the semi-natural Faroese environment to radioactive contamination. The table gives transfer coefficients for a range of foodstuffs including total diet from the Faroe Islands and Denmark. The higher radioecological sensitivity of the Faroese ecosystem is mainly explained by two factors: 1) plant uptake of radionuclides from Faroese soils with high organic content is much higher than from clayish Danish soils, and 2) drinking water in the Faroe Islands is produced from surface water while drinking water in Denmark is derived mainly from ground water. The sensitivity for ^{90}Sr in total diet, however, is found to be larger in Denmark than in the Faroe Islands. This is due to Faroese import of food products important for the ^{90}Sr contribution (milk, bread and potatoes) from Denmark and other countries thus reducing the influence of local food products.

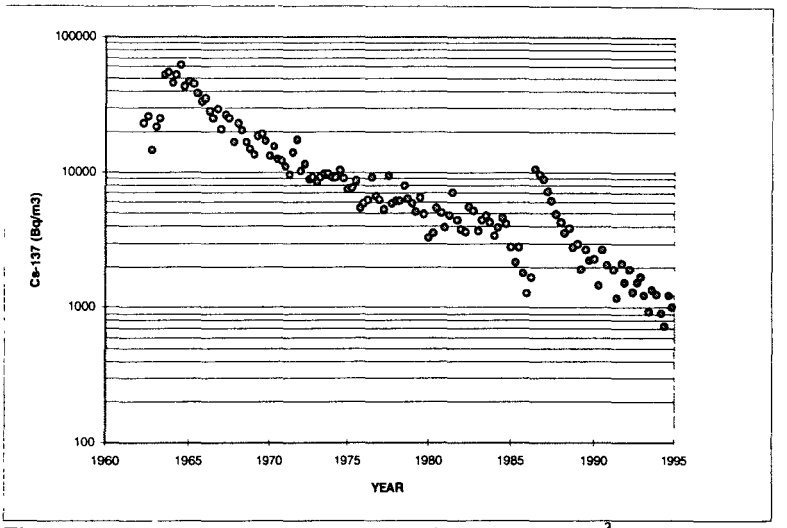

Figure 1. Caesium-137 in Faroese milk, 1962-1994 (Bq m^{-3}).

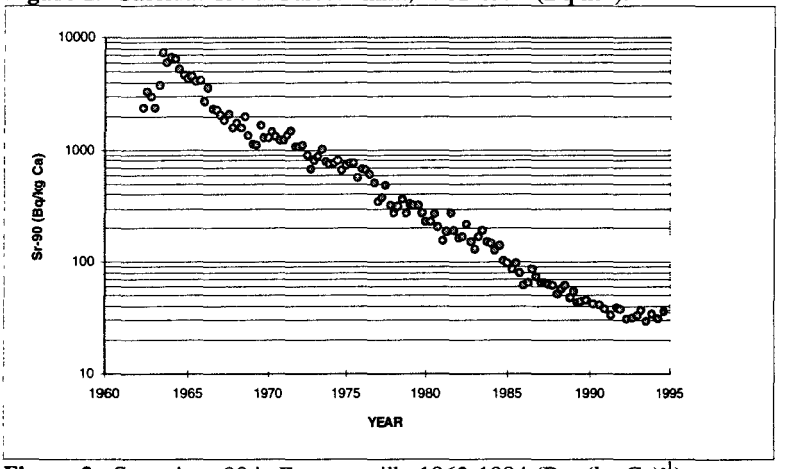

Figure 2. Strontium-90 in Faroese milk, 1962-1994 (Bq (kg Ca)$^{-1}$).

Table 1. Integrated environmental response in Denmark and the Faroe Islands to a contamination of 1 Bq m^{-2}; observations from nuclear weapons fallout.

SAMPLE TYPE		Denmark	Faroe Islands
Drinking water,	Sr-90 (mBq y m^{-3})	9	110
Grass	Sr-90 (mBq y kg^{-1})	38	270
	Cs-137 (mBq y kg^{-1})	24	520
Milk	Sr-90 (mBq y (g Ca)$^{-1}$)	3.3	8.6
	Cs-137 (mBq y (g K)$^{-1}$)	3.4	35
Meat*	Sr-90 (mBq y kg^{-1})	1.4	3.1
	Cs-137 (mBq y kg^{-1})	27	210
Total diet#	Sr-90 (Bq cap^{-1})	3.2	2.2
	Cs-137 (Bq cap^{-1})	5.6	15

* beef and pork in Denmark, lamb in the Faroe Islands

\# including imported food products in the Faroe Islands (e.g. grain, vegetables, fruits)

FOREST ECOSYSTEM STUDIES

An investigation was made in one hectare of Swedish coniferous forest near Uppsala in order to make a detailed study of the inventories of radiocaesium and radiostrontium and to determine the distribution of activity in the different ecosystem sub-compartments. The ^{137}Cs deposition in the area amounts to about 50 kBq m^{-2} originating mainly from the Chernobyl accident in 1986. Sampling was carried out the 28 August 1992.

Risø National Laboratory has carried out ^{90}Sr analyses on samples of soil, vegetation (mosses, lichens, shrubs and fungi) and meat. Most of the radioactivity in the forest ecosystem was found in the soil and the results for ^{137}Cs and ^{90}Sr demonstrate a significant association (correlation coefficient of 0.8) between the two radionuclides indicating that they derive mainly from the same source; the mean activity ratio between ^{90}Sr and ^{137}Cs in the soil is 0.012 ± 12% (1 SE). The data are shown in Figure 3. A comparison between the concentrations of ^{137}Cs and ^{90}Sr in mosses and lichens shown in Figure 4 does not show a strong association between the two radionuclides (correlation coefficient 0.5). However, a regression analysis gives a positive slope which is significantly different from zero ($P<0.01$) indicating that also the levels of ^{90}Sr in vegetation at this location are dominated by the contribution from the Chernobyl accident.

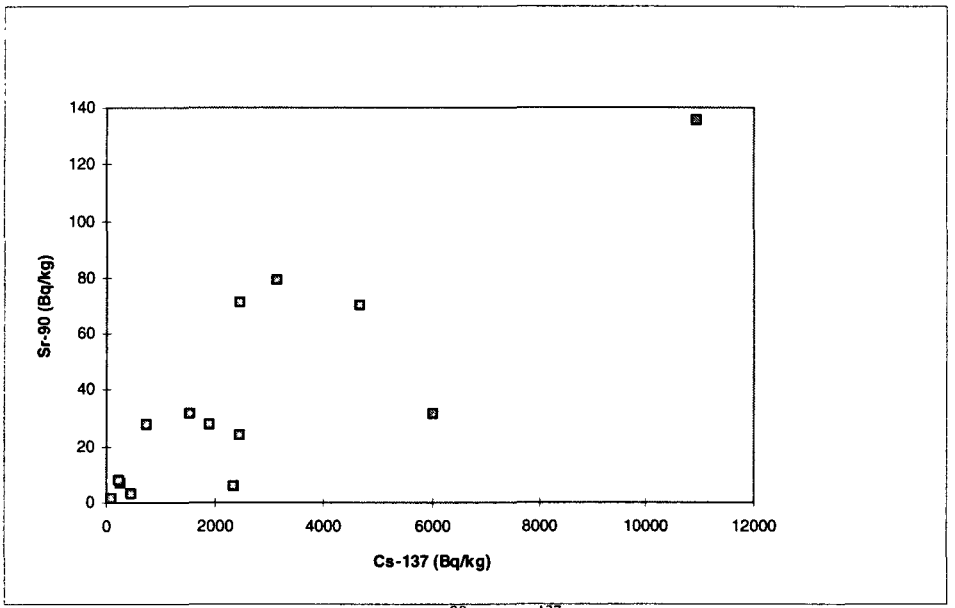

Figure 3. Comparison of concentrations of ^{90}Sr and ^{137}Cs in soil from Uppsala. A correlation coefficient of 0.8 ($P< 0.001$) was found for the data.

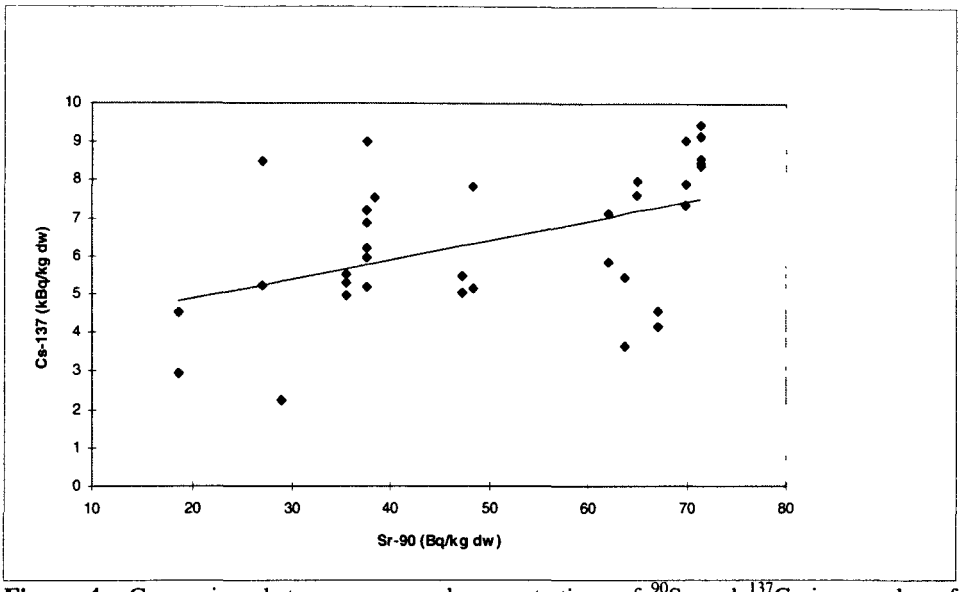

Figure 4. Comparison between measured concentrations of ^{90}Sr and ^{137}Cs in samples of mosses and lichens from Uppsala showing line of regression.

Table 2 summarises the average ^{137}Cs and ^{90}Sr concentrations in the Uppsala forest for the different ecosystem sub-compartments. The highest concentrations of ^{90}Sr were found in shrubs, mosses and lichens, and the uptake of ^{90}Sr in fungi was found to be 2 to 3 orders of magnitude lower than that of ^{137}Cs. Corresponding data are shown from a Danish pine forest in Tisvilde, which received approx. 60 times less fallout from the Chernobyl accident as the Uppsala forest. When the observed concentrations are normalised to the soil depositions, the data show the general tendency that transfers in the Swedish forest are higher than the transfers in the Danish forest. The normalised strontium-90 transfers to vegetation in the Swedish forest range from 2 to 15 times those in the Danish forest, while the normalised ^{137}Cs transfers in the Swedish forest range from 0.6 to 3 times those in the Danish forest. The higher relative transfers in the Swedish forest found in 1992 are consistent with the fact that the radioactive contamination in the Swedish forest was relatively recent (from the Chernobyl accident in 1986) and thus more available for plant uptake than the contamination in the Danish forest which originates mainly from the global fallout which peaked in the 1960's.

Table 2. Average concentrations of ^{90}Sr and ^{137}Cs in sub-compartments of two pine forests in Sweden and Denmark (mean ± 1 SD).

Sample type	SWEDEN, Uppsala		DENMARK, Tisvilde	
	Sr-90	Cs-137	Sr-90	Cs-137
Soil (Bq m^{-2})	720±610	55000±12600	510±360	2600±800
Moss (Bq kg^{-1} dw)	52±15	5900±2000	6.6±2.4	97±14
Lichen (Bq kg^{-1} dw)	27	8500	1.3±0.7	117±46
Shrub (Bq kg^{-1} dw)	34±9	3000	12±2	89±6
Fungi (Bq kg^{-1} dw)	2.4±2.1	54000±44000	0.5±0.3	4200±4500
Tree (Bq kg^{-1} dw)	5.8±2.3	150	2.1±0.9	4.6±1.9
Roe deer (Bq kg^{-1} fw)	0.024±0.007	4200	0.04±0.02	170±160

INTERCOMPARISON OF SR-90 ANALYSES

From the start of the project only two of the participants (RPII and Risø) carried out ^{90}Sr analyses. For intercomparison purposes several samples (dry milk and vegetation) were distributed among the laboratories for both ^{137}Cs and ^{90}Sr analyses. In addition, results from IAEA intercomparison samples were included in the project since these were already available. The results of the ^{90}Sr intercomparison are shown in Table 3. The results are satisfactory considering that ^{90}Sr in the sample IAEA-135 was found to be inhomogeneously distributed.

Table 3. Intercomparison of results from ^{90}Sr analyses showing concentrations (Bq kg^{-1} dw) in IAEA samples in addition to samples derived from this project. Where multiple determinations are made, the table gives mean values ± 1 SD. The IAEA values give the recommended 95% confidence intervals.

Sample	RPII	Risø	IAEA
IAEA-134, Cockle flesh		4.9±0.3	4.1 - 6
IAEA-135, Sediment		117±5	58 - 74
IAEA-373, Grass	1131±35	1390±70	1276 - 1363
IAEA, Soil	94±2	100±5	
RPII, Dried milk	< 3	0.63±0.03	
ITE, Bracken		121	
ITE, Heather		44	

SR-90 AVAILABILITY IN SOILS NEAR CHERNOBYL

The availability of radionuclides in the soil are of importance for the ecological half lives. Part of the ^{90}Sr contamination from the Chernobyl accident were in form of insoluble particles, especially in the zone around Chernobyl. This fraction is not readily determined from standard radiochemical procedures, but requires special radiochemical pre-treatment. Experience from areas in Russia indicates that the ^{90}Sr in these particles with time becomes available for plant uptake. It is therefore important to determine the total ^{90}Sr inventory in the soil.

Soil samples were obtained from three locations: Bourakovka and Novoshepelichi, about 15 km from the Chernobyl nuclear power plant, and from Feofania near Kiev about 114 km from Chernobyl. These samples were subject to standard radiochemical procedures for ^{90}Sr analysis using classical HCl extraction and additionally to total extraction based on oxidative alkaline fusion. Additionally, the ^{137}Cs concentrations were determined in the soil samples. The ^{137}Cs concentrations in the soil were quite different for the three areas. The levels in Feofania ranged from 0.096 to 0.13 kBq kg^{-1} with a mean value of 0.11 Bq kg^{-1}. The levels in Bourakovka ranged from 30 to 140 kBq kg^{-1} with a mean value of 79 kBq kg^{-1}, and the levels in Novoshepelichi ranged from 232 to 1519 kBq kg^{-1} with a mean value of 727 kBq kg^{-1}.

Alkaline fusion gave significantly higer concentrations of ^{90}Sr than HCl extraction for all soil samples. An analysis of variance showed no significant difference between locations of the ratios of ^{90}Sr concentrations from HCl extraction to those from alkaline fusion. The mean ratio was 0.62 ± 0.19 (1 SD, n=22) showing that data on ^{90}Sr contamination near Chernobyl

may be underestimated by about 50% if based on HCl extraction. The results are shown in Figure 5 where regression lines give the mean ratio between ^{90}Sr and ^{137}Cs concentrations to 0.38 ± 0.02 for alkaline fusion and to 0.26 ± 0.02 for HCl extraction. These ratios found in soil samples collected close to Chernobyl are considerably higher than those found in samples from the Nordic countries (range 0.01 to 0.04).

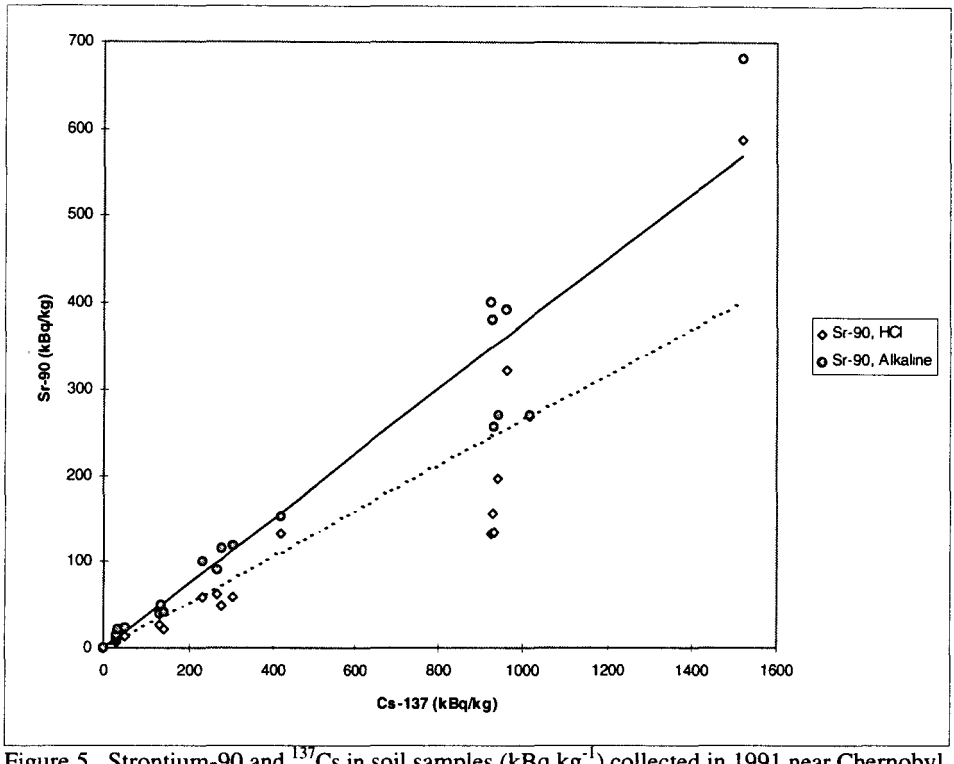

Figure 5. Strontium-90 and ^{137}Cs in soil samples (kBq kg^{-1}) collected in 1991 near Chernobyl. Alkaline fusion (circles and solid line) gave higher concentrations for ^{90}Sr than HCl extraction (diamonds and dashed line).

DOSE FROM CS-137 IN FOOD PRODUCED IN SEMI-NATURAL ENVIRONMENTS

In a previous EC project (Contract B17-044) on the radioecology of semi-natural environments, doses to members of the public from radiocaesium in semi-natural ecosystems were estimated. From this work it became clear that only little information is readily available in the Member States for this assessment and secondly, that there is a high variability between Member States of the relative importance of radiation doses from semi-natural ecosystems. For that purpose a detailed questionnaire was drawn up and circulated to the project participants on consumption rates of the most important food products from semi-natural ecosystems as well as usual food products. The food from semi-natural ecosystems comprise game, fresh water fish, mushroom, lamb and mutton, and usual foods products comprise milk products, grain products, potatoes, vegetables, fruit, beef and pork.

The questionnaire confirmed that official information on consumption of food from semi-natural environments is not available in the Member States, but data were nevetherless gathered from various sources. The results are shown in Table 4 listing for Denmark, Greece, Ireland, Sweden and the United Kingdom average individual rates of consumption of the food products mentioned.

Table 4. Average rates of consumption for adults of food products from agricultural areas and semi-natural environments (kg y^{-1}).

Diet components	Denmark	Greece	Ireland	Sweden	UK
Milk and cheese	173	85	196	171	117
Cereals	80	106	69	74	76
Potatoes, vegetables and fruit	168	311	254	171	215
Beef and pork	55	81	55	20	8
Game	0.2		0.05	2.5	0.02
Fish, freshwater	0.1		1.1	1.1	0.01
Mushrooms	0.05		0	1	0
Lamb and mutton	1	14	9	1	2

In order to illustrate the implication of these assumptions concerning doses from the intake of food from semi-natural environments, calculations were done from these data and relevant transfer coefficients. The coefficients for the transfer of ^{137}Cs from deposition to the usual food products, P_{23} (milk products, grain products, potatoes, vegetables, fruit and meat), were taken from UNSCEAR (1993) emphasizing European climatic conditions. For the food products from the semi-natural environments, the transfer coefficients were calculated based on a few assumptions all of which are listed in Table 5 where all the transfer coefficients, P_{23}, used for the calculations are listed. The transfer coefficients were calculated from assumptions of values of aggregated transfer factors (T_{ag}, Bq kg^{-1} per Bq m^{-2}) and effective ecological half lives, T_{EE}. The aggregated transfer factors and the effective ecological half lives were generally based on data from the northern parts of Europe. The higher sensitivity of seminatural environments are clearly refleced in the higher values of the transfer coefficients for the food products from these environments. Transfer coefficients for game, lamb and mutton are typically one order of magnitude higher than those for beef and pork. The highest transfer coefficients are found for mushrooms and fresh water fish.

Table 5. Transfer coefficients, P_{23}, for the transfer of ^{137}Cs from deposition to the diet (Bq y kg^{-1} per Bq m^{-2}) from UNSCEAR and calculated from aggregated transfer factors, T_{ag}, and effective ecological half lives, T_{EE}.

Diet components	P_{23} (Bq y kg^{-1} per Bq m^{-2})	T_{ag} (m^2 kg^{-1})	T_{EE} (y)
Milk products	0.006		
Grain products	0.027		
Potatoes, vegetables and fruit	0.003		
Beef and pork	0.026		
Game	0.29	0.02	10
Fish, freshwater	1.4	0.2	5
Mushrooms	5.8	0.2	20
Lamb and mutton	0.43	0.03	10

Committed individual average doses (millisieverts) from Chernobyl deposition of ^{137}Cs were calculated for the five countries in Table 6 based on the data in the previous tables and the UNSCEAR deposition data which for ^{137}Cs give average values of 1.3 kBq m^{-2} for Denmark, 4.8 kBq m^{-2} for Greece, 3.3 kBq m^{-2} for Ireland, 9.5 kBq m^{-2} for Sweden and 0.9 kBq m^{-2} for the UK. A dose-per-unit-intake factor of 1.3 10^{-8} Sv Bq^{-1} was used. The results in Table 6 illustrate the variability of the dose committments from ingestion of ^{137}Cs from the Chernobyl accident across two variables: geography and food component. The doses range from a low of 0.05 mSv calculated to an average individual in the United Kingdom to a high of 1.6 mSv calculated to an average individual in Sweden. The relative distributions of doses from the two main groups of food products differ significantly between the countries. Doses from food produced in semi-natural ecosystems in the UK and in Denmark contribute less than doses from agricultural foods. Food from the two types of ecosystems in Greece and Ireland contribute approximately with equal amounts to doses from ingestion, and in Sweden the doses from food produced in semi-natural ecosystems are significantly higher than those from agricultural areas. The relative distributions of the doses from ingestion of ^{137}Cs in food from semi-natural and agricultural ecosystems are shown in Figure 6.

The simplified approach adopted has not made it possible to retain all known ecosystem differences between the countries, but the results illustrate ecosystem features that are important for the transfer of ^{137}Cs to man from ingestion. Further work is needed in order to be able to give reliable quantifications of the doses to man from ingestion of ^{137}Cs in food produced in semi-natural environments. A high priority should be given in the European Community to surveys collecting data on average and maximum rates of human consumption of food from semi-natural environments.

Table 6. Calculated average individual doses (mSv) from consumption of Chernobyl ^{137}Cs in food products from agricultural and semi-natural environments in five European countries.

Dietary components	Denmark	Greece	Ireland	Sweden	UK
Milk products	0.018	0.03	0.050	0.13	0.008
Grain products	0.037	0.18	0.080	0.25	0.024
Potatoes, vegetables and fruit	0.009	0.06	0.033	0.063	0.008
Beef and pork	0.024	0.13	0.061	0.064	0.002
Game	0.001		0.0006	0.09	0.0001
Fish, freshwater	0.002		0.07	0.20	0.0004
Mushrooms	0.005		0	0.71	0
Lamb and mutton	0.007	0.38	0.17	0.05	0.010
Total	0.10	0.78	0.46	1.55	0.05

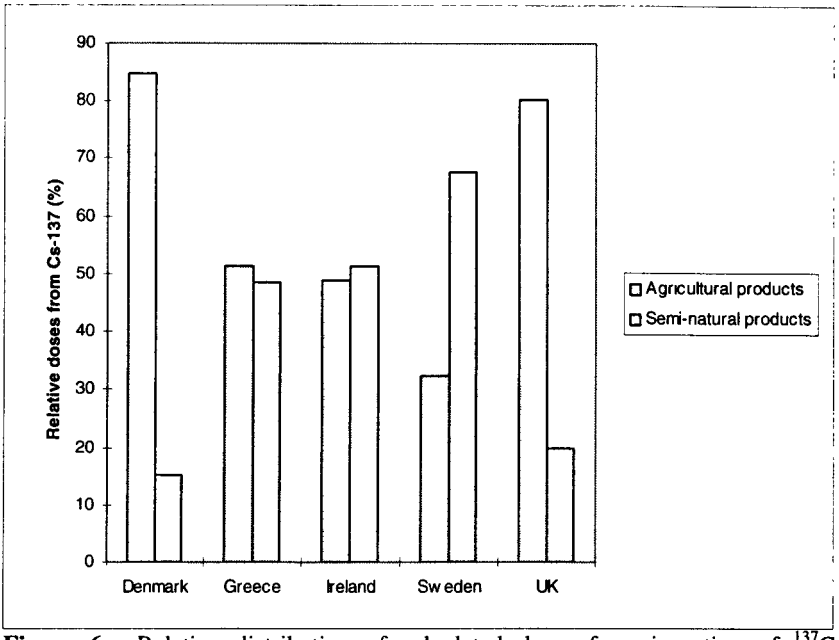

Figure 6. Relative distribution of calculated doses from ingestion of ^{137}Cs from the Chernobyl accident in food produced in agricultural and semi-natural areas in Denmark, Greece, Ireland, Sweden and the UK.

Publications:

McGee, E.J., Johansson, K.J., Synnot, H.J., Colgan, P.A., Nielsen, S.P., Horrill, A.D., Kennedy, V.H., Barbayiannis, N., Veresouglu, D. and McGarry, A. Chernobyl fallout distribution in a Swedish Spruce forest. Submitted.

Head of Project 4: Prof. Karl J.Johanson

II. Objectives of the reporting period

The main objectives of project 4 have been to quantify the transfer of radiocaesium from the forest ecosystem to man and to try to understand the mechansims behind the high transfer of radiocaesium in the forest ecosystems.

III. Progress achieved including publications

1. Soil

Forest soil samples were collected from 22 sites in a coniferous forest and after air drying and milling treated by a sequantial extraction using: F1; water, F2, ammoniumactetat, F3, H_2O_2, F4, nitric acid. The residue after the extraction with nitric acid is called F5. Between 5 and 10% of the total ^{137}Cs activity was found in F1, 10 to 16% in F2, 14 to 16% in F3, 22 to 24% in F4 and 35 to 45% in F5 (Fawaris and Johanson 1995). Obviously there was a large fraction which was heavily bound to soil particles. The soil had a very high fraction of organic matter - the percentage of organic matter in the soil varied from 13 to 93 % with a mean value of 65 %. The correlation between the F1 and F2 fractions and percentage of organic matter was rather good with an equation F1 + F2 = 10.73 + 0.203 * OM %, r^2 = 0.49. The pH of the soils ranged from 3.7 to 5.0.

2. Soil-plant transfer

The transfer coefficients (T.C) (Bq kg^{-1} in dry plant material per Bq m^{-2} in soil) for various forest plants have been determined. The mean TCs for bilberry (n=48), lingonberry (n=31) and heather (n=29) were 0.24, 0.25 and 0.64, respectively. The correlation between TC and various soil parameters were rather poor - the best correlation was found between TC and pH and % organic matter. For bilberry the regression equation was TC = -071 + 0.022 * pH + 0.001 * OM % (r = 0.20, n = 48, $p<0.3$). When using the bilberry soil, lingonberry soil and the heather soil for pot experiments with sheep' fescue as a test plant, the TC for the the three types of soil was rather similar or 0.08, 0.15 and 0.09, respectively. The variation in the TC for field plants could of course be dependent on some biological parameters such as rooting depth or the species of fungi in the mycorrhizae. These results indicate that the species related differences in the capacity to accumulate radiocaesium are more important than the chemical soil parameters such as pH, % organic matter, soluble or total content of potassium and calcium in forest plants at least the dwarf shrubs.

During the period 1986 to 1994 there seems to have been a decrease in the activity concentrations of ^{137}Cs in some plants collected at the same sites (Fawaris, 1995). Bilberry and lingonberry show a marked decrease but heather and Scots pine show a less pronounced decrease.

3. Transfer to berries

The accumulation of radiocaesium in the most common forest berries have been studied (Johanson and Kardell, 1995). The transfer cofficient for bilberry, lingonberry and cloudberry were 0.029, 0.032 and 0.137, respectively. In no case was there good correlation between various soil parameters and TC. During the period 1988 to 1991 no significant decrease of TC could be observed for the three berries studied.

For cranberry, TC were determined both for the radiocaesium derived from the Chernobyl fallout and for the nuclear weapon testing and found to be 0.15 in both cases. These results indicate thus a 30 years effective ecological halflife of radiocaesium in the cranberry ecosystem which is raised bogs in Sweden.

4. Transfer to fungi

The transfer coefficient for many species of fungi are much higher than TC for vascular plants. The mean TC for all species we have sampled is above 1.0. Of these samples, the Cortinarius species usually have the highest TCs and most of the edible species have lower TCs.

In some cases it was possible to find clusters of fruitbodies of a certain species growing in very small areas. In some Cortinarius species and in Suillus variegatus we found that between 15 and 62 % of the total ^{137}Cs inventory in the area below the fruitbodies - between 400 and 625 cm^{-2} - was within the fruitbodies of fungi (Nikolova et al.,1995). We interpret the results that there must be a inflow of ^{137}Cs from the mycelium supporting the fruitbodies. These may give some patchiness of ^{137}Cs distribution in the forest ecosystem.

There have been calculations indicating that most of the ^{137}Cs in the forest soil is located within the mycelium of fungi. These calculations have been based on the assumption that the ^{137}Cs activity concentrations in the fruitbodies are the same as in the mycelium. We have investigated if this is true in Suillus variegatus and Lactarius spp. (Nikolova et al., 1995). The mean ^{137}Cs level in fruitbodies of S. variegatus was 98 kBq kg^{-1} dw compared to 35 kBq kg^{-1} dw in mycorrhizae. Since the S. variegatus mycorrhize is composed of about 50 % fungi and 50 % of roots from the host plant the ^{137}Cs levels in the fungal component of the mycorrhizae would be around 70 Bq kg^{-1} or rather similar to the fruitbodies. The conclusion could thus be that at least in the mycorrhizae there are about the same levels of ^{137}Cs as found in the fruitbodies. This will mean that the major fraction of radiocaesium in soil is located within the fungal compartment of the soil.

5. Soil-plant-game animal

In the central part of Sweden where we have our study area the ^{137}Cs activity concentration in moose muscle has been rather similar from 1986 to 1994 (Johanson and Bergström, 1994). The mean aggregated transfer parameter has been close to 0.02. The effective ecological halflife seems to be close to the physical halflife for ^{137}Cs (30 years). In central Sweden where the hunting season starts in October calves of moose have usually about 10 % higher ^{137}Cs than adults.

The ^{137}Cs levels in roe deer show a very prenounced seasonal variation with a peak value in August, September or October depending on the appearance of mushrooms (Johanson and Bergström, 1994; Karlen et al., 1991). The annual mean aggregated transfer factor is 0.05. During the peak period the mean value of T_{ag} have been between 0.13 and 0.20. The lowest value appears in spring and is around 0.025. One efficient counter measure has been introduced and that is a hunting period of roe buck in May when the ^{137}Cs levels is at the minimum. Compared to roe bucks harvested in the normal roe buck hunting period in August and September the spring values are about 5 times lower.

6. Forest to man transfer

There are three main pathways for transfer of radionuclides from the forest ecosystems to man; game animals, berries and mushrooms. By using the previously presented transfer parameters and the use of an effective ecological halflife of 30 years it is possible to calculate the potential transfer of ^{137}Cs to man (Johanson and Bergström 1994).

For moose we have used an aggregated transfer factor of 0.02 and a mean weight of meat from each harvested moose in Sweden of 100 kg. The number of harvested moose in Sweden is well described in official statistics. The annual potential transfer is between 2 and 2.7 GBq corresponding to between 27 and 35 manSv. The time-integrated transfer is calculated to be 1.5 TBq corresponding to a potential time-integrated dose commitment of 1500 manSv.

For roe deer we used the annual mean aggregated transfer factor of 0.05 and a mean meat weight of 10 kg. During the period 1986 to 1991 there has been a drastic increase of the harvest of roe deer in Sweden from 116 000 to 343 000 mainly due to snow free winters and reduction of the red fox population. The potential annual transfer due to roe deer has been between 600 and 1500 MBq corresponding to 8 to 20 manSv. The potential time integrated dose commitment will be between 300 and 600 manSv depending on the assumption of the harvest of roe deer in future.

Using the transfer coefficients we found for bilberry, lingonberry and cloudberry, the estimated consumption of these berries and assuming an effective ecological halflife of 30 years for ^{137}Cs we calculated the potential transfer to man (Johanson and Kardell 1995). The annual transfer was 1.2 GBq for cloudberry, 0.8 GBq for lingonberry and 0.8 GBq for bilberry. The potential time-integrated cose commitment will be 1500 manSv.

The corresponding calculation for mushrooms cannot easily be calculated due to lack of knowledge about the consumption pattern of mushrooms in Sweden. We know rather well the total amount of mushrooms consumed but not the species used. Since the variation in the ^{137}Cs levels between the various possible edible mushrooms is high we will wait until we know the consumption pattern. Anyhow it seems quite clear that the ^{137}Cs transfer to man by mushrooms is the most important pathway, at least, in Sweden.

Altogether the time-integrated dose commitment due to radiocaesium transfer from forest ecosystems to man in Sweden is at least 5000 to 6000 manSv for the most important pathways.

Publications

1. Karl J.Johanson and R.Bergström, (1994) Radiocaesium transfer to man from moose and roe deer in Sweden. Sci.Total Environ. 157, 309-316.

2. B.Fawaris and K.J.Johanson, (1995) A comparative study on radiocaesium (^{137}Cs) uptake from coniferous forest soil. J.Environ.Radioactivity. In press

3. B.Fawaris and K.J.Johanson, (1995) The influence of potassium, stable caesium and ammonium on uptake of ^{137}Cs from forest soil by sheep's fescue in pot experiment. J.Radioectivity, submitted.

4. B.Fawaris and K.J.Johanson, 1995). Fractionation of caesium (^{137}Cs) in coniferous forest soil in central Sweden. Sci. Total Environ. (in press)

5. B.Fawaris and K.J.JOhanson. 1995, Sorption of ^{137}Cs in zeolite trap from undisurbed forest soil. Sci.Total Environ. In press.

6. K.J.Johanson and L.Kardell. 1995, Radiocaesium in lingonberry, bilberry, cloudberry and cranberry in Sweden. Scand.J.Forest Res. submitted

7. I.Nikolova, K.J.Johanson and A.Dahlberg. (1995), Radiocaesium in fruitbodies and mycorrhizae in ectomycorrhizal fungi. Submitted to J.Environ. Radioactivity.

Main researchers of project 5: Drs D.S. Veresoglou & N. Barbayiannis

II. Objectives for the reporting period

1. To find out if any relationships exist between Sr and Ca or Cs and K concentrations in plant tissues among plant species grown in the same growth medium.

2. The effects of the physicochemical characteristics of the soils and the additions of Ca or K on the uptake of Sr or Cs by plant species.

3. To examine the distribution, with time, of Cs or Sr in shoots, roots, soil solution and in different forms in the soils, using a sequential extraction.

4 To measure ^{137}Cs concentration of mushrooms grown in Greek seminatural ecosystems.

III. Progress achieved including publications

Most of the soils in Greece are inorganic with pH values ranging from 4.5 to 7.5 and with highly variable clay content. However, two areas in Northern Greece have soils with high proportion of organic matter. The first area, the peats of Philippi, is located about 150 km east of Thessaloniki and is characterised by neutral pH and high cation exchange capacity (C.E.C.). The second area, the peats of the former lake Chimaditis, is located about 150 km west of Thessaloniki and is characterised by acid soils and, compared to Philippi peats, by lower values of C.E.C. Most of the soils used in the various pot experiments were taken from various sites of these two areas. Other soils were taken from upland seminatural ecosystems. Although the soils used are not representative of the Greek soils, they were selected with the criterion to vary in the various physicochemical characteristics like pH, organic matter content and C.E.C.

The plant species used were typical grassland species, found also in the North Europe grasslands, and they were selected with criterion to differ in Ca requirements.

In three experiments, pots (1 L volume) were filled with various soils that were different in the various physicochemical characteristics (References 4 & 6). Stable Sr was applied at the rate of 67 mg per pot for three soil treatments, 25 mg per pot for two soil treatments and 50mg per pot for eight soil treatments. In each soil treatment various pasture plant species were grown in monocultures. For either shoots or roots a positive linear relationship was found between Sr and Ca concentrations in different plant species grown in the same soil treatment.

For two years Sr and Cs were injected at depths of 5 and 15 cm in the soil of an upland acid (pH = 4.5) grassland to which a factorial combination of N and P additions had been applied (Reference 3).

For Sr injected at the depth of 5 cm, where the bulk of roots of the various coexisting species was found, the Sr concentration in the aboveground material was positively correlated with the respective Ca concentration at $P = 0.001$ in all nutrient treatments and years. The correlation coefficients were much higher when aboveground material was

harvested a year after Sr injection. When plant material was harvested 24 or 30 days after Sr injection, a proportion of total variation in the correlation between Sr and Ca concentrations must be attributed to differences among species in root activity, since species had already formed their root systems when Sr was injected. For example, with two species having similar Ca requirements and differing in root distribution with depth in soil, the shallow rooted species have higher Sr concentrations than the deep rooted one, because the shallow rooted species have a higher proportion of roots in the soil layer in which Sr was injected. This hypothesis is supported by the higher correlation coefficients between Sr and Ca concentrations when plant material was harvested a year after Sr injection. In this case all species exploited mostly the surface soil layer in the first stages of regrowth during the spring. The close correlation between Sr and Ca concentrations may have practical importance. From the Ca concentration of species it would be possible to find the ranking of species in radioactivity if Sr radionuclides are deposited at any area. It will also be possible to estimate the ^{90}Sr concentration of all species grown in the same medium from the ^{90}Sr concentrations of only two species and all the species Ca concentrations. This is of great importance for ^{90}Sr, since the preparation of samples for ^{90}Sr measurements is laborious and time consuming.

For Cs injected at the depth of 5 cm, the Cs and K concentrations of species in the aboveground material were not related. The significant correlation coefficients in some cases were attributed to *Hypochoeris radicata*. This species had the highest K concentrations. Correlation coefficients were significant only in the treatments in which it had high Cs concentrations.

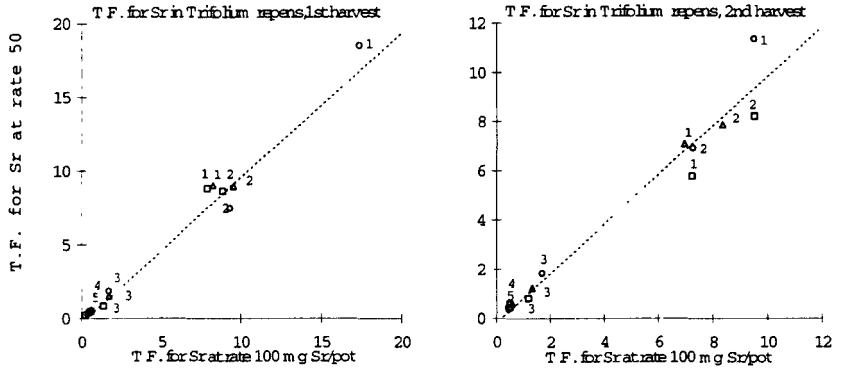

Fig. 1.
T.F. for Sr at the rate of 50 mg per pot plotted against S.F. for Sr at the rate of 100 mg for the 15 soil x liming treatments in a pot (1 L volume) experiment in which *Trifolium repens* was grown and shoots were harvested twice. If T.F. for Sr in the two Sr applications were similar the points would all on the dotted line. O, Δ and refer to 0, 1.43 and 2.86 mg Ca per pot, respectively. Numbers refer to soils. pH and organic matter wererespectively:for soil 1, 5.5 and 1.6, soil 2, 7.2 and 2.8, soil 3, 4.4 and24.1, soil 4, 5.4 and 37.3,soil 5, 7.1 and 30.0.

The values of T.F. for Sr, defined as the ratio of the amount of radionuclide per g of dry plant material and the amount per g dry soil, in the pot experiments were affected by species, soil type and their interaction (References 4 & 6). These values are in agreement with those reported for ^{85}Sr and ^{90}Sr. The quantities of the stable Sr, added to the soil,

were very high in comparison to quantities of radionuclides added to the soil after accidents like Chernobyl in 1986. However, we can use this index because we found a linear relationship between the Sr addition to the soil and Sr uptake by *Trifolium repens* and *Dactylis glomerata* in the range of 0 to 100 mg added Sr per pot in these soils. Furthermore, the T.F. values for Sr in *Trifolium repens* were quite similar between Sr applications of 50 and 100 mg per pot in each of the fifteen soil x Ca addition treatments for every harvest (Reference 8, Fig . 1)

The high variation in the values for T.F. of Sr among species in each soil treatment creates difficulties in comparing soils according to their ability to supply Sr by using this index, if plant species are different in the soils used for comparisons. Since Sr concentrations in shoots and roots are positively related to respective Ca concentrations, T.F. for Sr could be improved for comparative purposes if this index is divided by the shoot (or root) Ca concentration of the respective species in a soil. The usefulness of this index is attributed to the fact that it contains the ratio of Sr to Ca concentration of plants, that would be species independent if plants do not discriminate between Sr and Ca uptake. Although the new index, named "T.F. for Sr per Ca concentration", was also found to be species specific, it exhibited much lower variation among plant species grown in each soil treatment in comparison to T.F. for Sr (References 4 & 6).

Because Sr uptake is very closely tied to Ca uptake, the term strontium- calcium observed ratio (OR), defined as plant-culture solution = (Sr / Ca) in plant /(Sr/ Ca) in culture solution, was introduced. This term was also considered for soil-plant systems by using the extractable Sr/Ca instead of Sr/Ca in the culture solution. Most of the available data suggest that the OR of vegetative tissues are close to 1 and slightly different between species. However, other researchers reported OR values for vegetative tissues of crops much lower than 1. The divergence of OR values from 1 in soil plant systems may be attributed to use of exchangeable Ca and Sr concentrations instead of the respective concentrations in the soil solution.

Shoot (Sr/Ca) was closely and positively related to Sr/Ca of either the extractable form or the soil solution (Reference 6). In all species, the correlation coefficients were significant except in *Agrostis capillaris* when extractable Sr/Ca was used. For any species the values of the correlation coefficients estimated using either the extractable form or the soil solution were quite close because the Sr/Ca ratio in the two forms of soil were closely and positively related. The slope of the linear regression between Sr/Ca in the soil solution and Sr/Ca in the extractable form was 0.85; this indicates that Sr compared to Ca is proportionally less available in the soil solution. For this reason the strontium-calcium OR from soil to plant is expected to be greater when soil solution is used instead of the extractable form. The values of OR shoots-soil solution were affected significantly by soils and species and their interaction. Most of the values for all species except *Agrostis capillaris* falled into a relatively narrow range of 0.8 - 1.5. The respective range for strontium-calcium OR shoots-extractable form was 0.7 - 1.3, if the slope of the linear regression between Sr/Ca in the soil solution and Sr/Ca in the extractable form is taken into account. These values are consistent with most of the reported data.

In agreement with other results reported for Greek inorganic soils, T.F. for Sr was negatively related with extractable Ca (References 2, 4 & 6) C.E.C. and Ca in the nutrient solution (Reference 6). However, it was also related with soil organic matter content but not with soil pH, and extractable Ca and Ca+Mg, expressed as proportion of C.E.C. This

disagreement must be attributed to the soils used. In the inorganic soils used by other researchers in Greece, pH and extractable Ca and Ca+Mg, expressed as proportion of C.E.C., were negatively related to T.F. for Sr simply because these soil properties were highly and positively related to C.E.C. Alternatively, organic matter content in our work was negatively related to T.F. for Sr because it was positively related to C.E.C. It is evident from all reported data that C.E.C. and available Ca are the soil properties which affect Sr uptake.

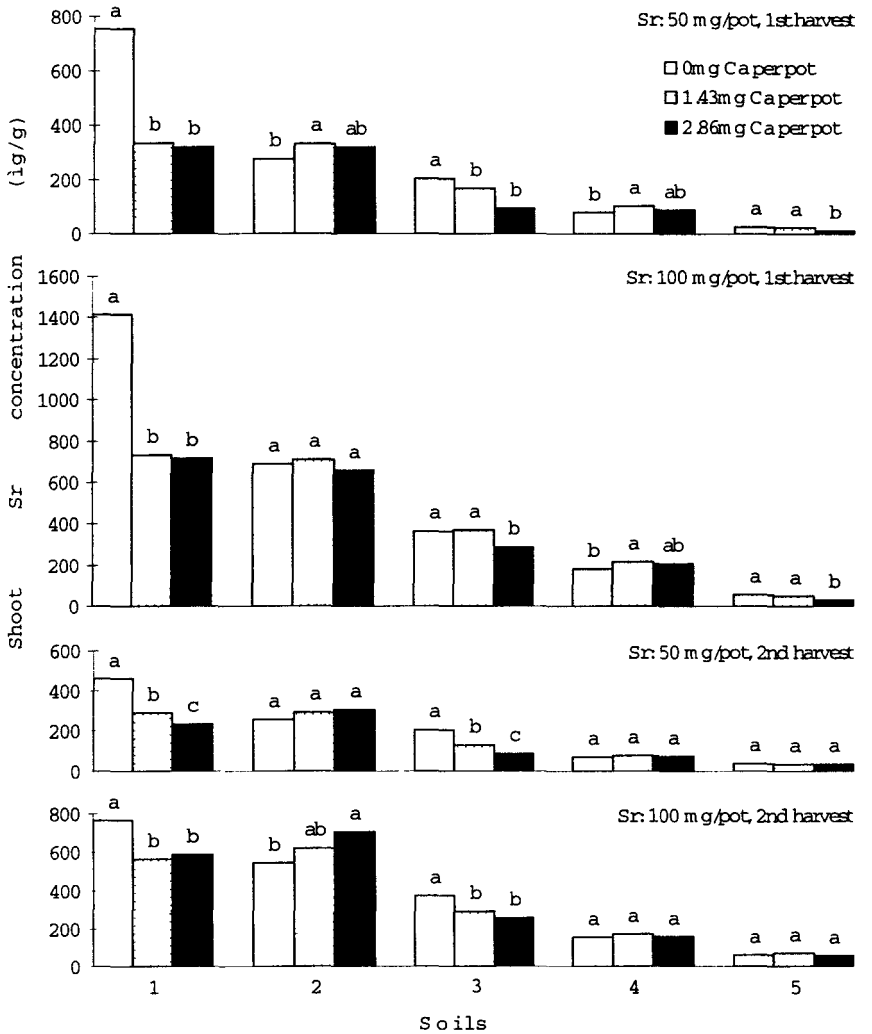

Fig. 2.
Effect of liming on shoot Sr concentrations of Trifolium repens grown in pots (1 L volume) which were filled with the five soils referred to Fig. 1. Within each soil x liming x harvest treatment, means differently superscripted differ at P=0.05. Means are back-transformed from analyses of logarithm-transformed data.

In pot (1 L volume) experiments the effects of liming and K addition to five soils were examined on the uptake of Sr and Cs, respectively, by *Trifolium repens* and *T. subterraneum* (References 8 & 9). Stable Sr and Cs were applied in the rates of 50 and 100 mg per pot

Liming tended to decrease the shoot Sr concentration of *T. repens* when it was grown in the acid inorganic soil 1 (Fig. 2) and the moderate organic soil of Chimaditis (Soil 3) but to increase that of the neutral inorganic soil 2. In the second harvest made, liming did not affect the shoot Sr concentrations of *T. repens* when it was grown in the two other soils. The relationship between shoot Sr concentration (log scale) and extractable Ca was linear negative and highly significant (Fig. 3). When T. subterraneum was sown in the incubated soil for two years x Ca addition treatments, the only significant effect of liming was the decrease of shoot Sr concentrations for plants grown in the soil 3.

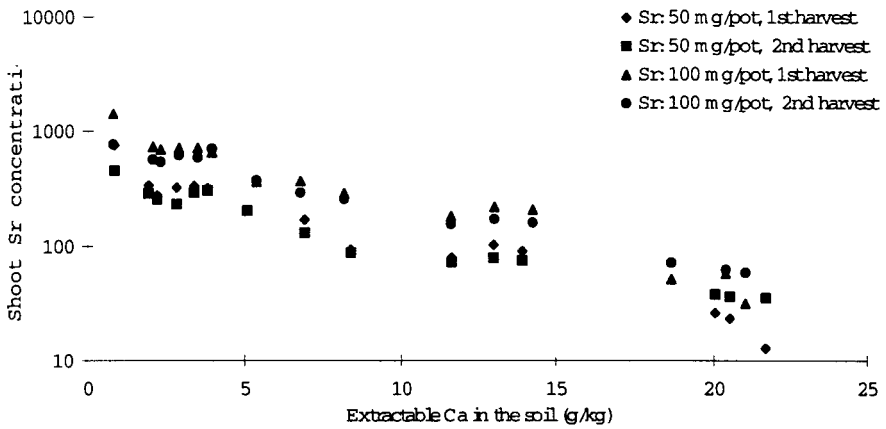

Fig. 3.
Relationship between shoot Sr concentrations of *Trifolium repens* and CH_3COONH_4extractable Ca in the soil for the various soil treatments in which *Trifolium repens* was grown. The experiment was conducted in pots (volume 1 L). Soils and liming treatments are those referred to Fig. 1.

The K addition decreased the shoot Cs concentrations of *T. repens* (Fig. 4). This trend was not, however, so clear in the organic soils 4 and 5, especially in the second harvest. The highest Cs concentrations were observed in the acid organic soils. This was also evident in an experiment in lysimeters in which ^{137}Cs was applied (Table 1) and in experiment with pots (35 L volume) in which stable Cs was applied.

Table 1.
Shoot ^{137}Cs concentrations (Bq/Kg) of *Dactylis glomerata* and *Rumex crispus* grown in lysimeters that were filled with soils taken from six sites of northern Greece. ^{137}Cs was applied in the soil surface and shoots were harvested six months later

Soils			Species	
Location	pH[1]	Organic matter[2] (%)	Dactylis	Rumex
Karantere	7.2	2.8	106	6
Philippi I	5.9	14.0	218	75
Chimaditis	5.4	37.3	885	2733
Paralimni	7.5	5.3	193	50
Philippi II	7.4	8.1	187	70
Philippi III	7.1	30.8	430	584

1 pH was measured in water 1 : 2.5 (w/v).
2 values of organic matter refer to loss after wet oxidation.

A pot experiment using 12 soils and sown with *Dactylis glomerata* was set up in order to relate the uptake of stable Cs and Sr by plants with the different forms of the elements in the soil using a sequential extraction. Also the changes with time on the different forms of the elements were followed with the same sequential extraction procedure.

The pots were harvested every two months and every four months the pots were emptied, a portion of moist soil was removed and used for the sequential extraction. The pots were re-filled and sown again with *Dactylis glomerata*. The sequential extraction included the following steps:

1. Water soluble fraction by centrifuging the moist soil. A portion of the centrifuged soil was air-dried and 2g of soil (on 105° C basis) was used for the following steps:

2. The exchangeable fraction extracted with 0.5M KNO_3

3. The easily reducible fraction with 0.04M NH_2OH*HCl in 25% acetic acid pH 2,

4. The organic fraction with 0.5M NaOH, and

5. The acid digestible fraction with 4M HNO_4

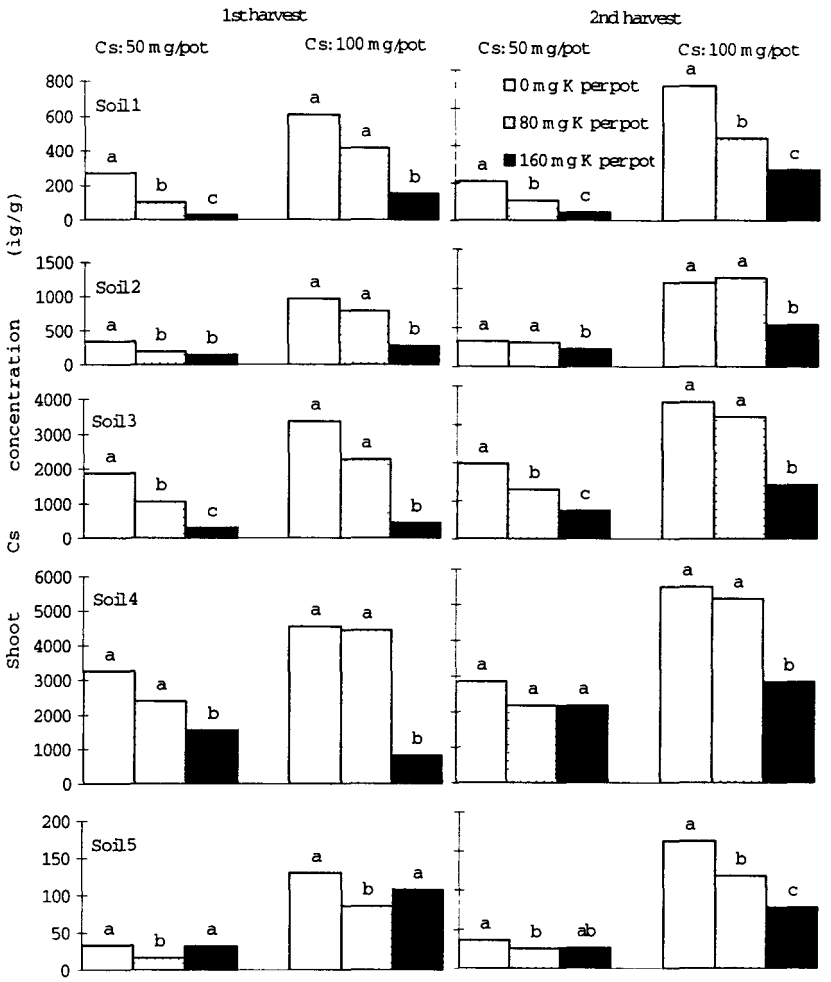

Fig. 4.
Effect of K addition on shoot Cs concentrations of *Trifolium repens* grown in pots (1 L volume)which were filled with the five soils referred to Fig. 1. Within each soil x K addition x harvest treatment, means differently superscripted differ at P=0.05. Means are back-transformed from analyses of logarithm-transformed data.

The results indicate (Table 2), that the major part of Cs is found in the exchangeable form and in the acid digestible fraction possibly fixed in the clay minerals and it seems that Cs is released slowly for plant uptake. On the other hand the major part of Sr is found in the exchangeable and soluble form indicating a higher availability. There was very low variation with time in the different forms of the elements.

Cumulative uptake for Cs showed a negative, statistically significant relationship (r=-0.62, P=0.05), with the acid digestible form indicating that the solid phase controls the supply of element to the plants. For Sr, total uptake was related (r=0.81, P=0.01) with

the soluble form indicating that the main source of Sr for the plants is easily available Sr that moves from the exchange sites to the soil solution. The previous suggestion is supported by the statistically significant relationship (r= 0.78, P=0.01) between clay content and Sr extracted with 0.5M KNO_3.

Table 2: The relative distribution of Cs and Sr in the different forms

	H_2O mg/L	KNO_3 0.5M		NH_2OH*HCl %		NaOH 0.5M		HNO_4 4M	
Soils	Sr	Cs	Sr	Cs	Sr	Cs	Sr	Cs	Sr
Chalkidiki	0.39	39	89	1	0	2	1	57	9
Florina II	0.44	10	98	3	0	3	0	84	2
Drama I	2.15	25	85	2	3	4	2	68	10
Florina V	2.89	55	48	2	26	6	5	37	21
Katerini	1.10	27	82	2	13	2	0	69	5
Florina I	1.45	13	100	4	0	5	0	77	0
Drama II	0.79	11	89	4	1	0	1	85	9
Gianitsa	1.40	8	34	6	36	0	0	84	9
Florina III	0.83	2	81	0	0	0	1	98	18
Kavala	1.62	33	27	12	40	2	2	53	32
Thes/niki	2.02	14	83	1	1	4	0	81	16
Florina IV	3.59	23	67	9	5	5	3	63	24

As co-ordinators, the AUT participated in a joint study on the inventory and distribution of ^{137}Cs and ^{90}Sr in a seminatural woodland ecosystem in Sweden. Full details will be found in the Reference 7 and in other contributions to this report.

Several muushroom species were collected from an upland seminatural ecosystem in northwest Greece and were measured for ^{137}Cs activity by SLU. The concentrations of ^{137}Cs were very low, from 75 to 150 Bq/kg. The low ^{137}Cs concentrations in combination with the low yields of mushrooms in the Greek ecosystems demostrate that the contribution of mushrooms to ^{137}Cs movement through the food chain is negligible in Greek ecosystems

.

Publications

1. Nielsen S. P., A. Aarkrog, P. A. Colgan, E. McGee, H. J. Synnott, K. J. Johansson, A. D. Horrill, V. H. Kennedy & N. Barbayiannis. 1993. An intercomparison of sampling techniques for measurements of radiocaesium in upland pasture and soil. Journal of Radioanalytical and Nuclear Chemistry, Articles 171: 303-317.

2. Veresoglou D.S. 1994. Transfer of radioactive strontium from soil to plants and factors affecting the process. International Conference for Kozlodui held in Drama, Greece.

3. Mamolos A. P., G. K. Elisseou & D. S. Veresoglou. 1995. Depth of root activity of co-existing grasslands species in relation to N and P additions, measured using non-radioactive tracers by the addition of the limiting N and P. Journal of Ecology (in press).

4.. Veresoglou D.S., N. Barbayiannis, G.C. Zalidis, S. Kalpakis & E.A. Batianis. 1995. Transfer factors for Sr as influenced by species Ca uptake and soil Ca availability. Plant and Soil (in press).

5. Veresoglou D. S., J. T. Tsialtas, N. Barbayiannis & G. C. Zalidis. Caesium and strontium uptake by two pasture plant species grown in organic and inorganic soils. Agriculture, Ecosystems & Environment (in press).

6. Veresoglou D.S., N. Barbayiannis, T. Matsi, C Anagnostopoulos & G.C. Zalidis. Shoot Sr concentration in relation to shoot Ca concentration, soil Ca availability and to other properties of soil (submitted in Plant and Soil).

7. McGee E.J., K.J. Johanson, H.J. Synnott, S.P. Nielsen, A.D. Horrill, V.H. Kennedy, N. Barbayiannis, D.S. Veresoglou, A. McGarry & P.A. Colgan. Chernobyl fallout distribution in a Swedish Spruce forest (in preparation).

8. Veresoglou D. S., N. Barbayiannis, J. T. Tsialtas, T. Matsi, A. Sdrakas & C. Anagnostopoulos. Uptake of Sr by Trifolium repens and T. subterraneum as influenced by liming and available Ca in the soil (in preparation).

9. Veresoglou D. S., N. Barbayiannis, T. Matsi, J. T. Tsialtas, A. Sdrakas & C. Anagnostopoulos. Uptake of Cs by Trifolium repens as influenced by K addition (in preparation).

10. Matsi T., N. Barbayiannis & D. S. Veresoglou. The effects of the physicochemical characteristics of the soils and the additions of Ca or K on the uptake of Sr or Cs by plant species (in prerараtion).

Final Report
1992-1994

Contract: F13PCT920013a **Duration: 1.9.92 to 30.6.95** **Sector: A26**

Title: Studies of methods for the rehabilitation of soils and surfaces after a nuclear accident (RESSAC)

1)	Foulquier	CEA - Cadarache
2)	Sandalls	UKAEA
3)	Vandecasteele	CEN/SCK Mol
4)	Vallejo	Fundació "Bosch i Gimpera"
5)	Förstel	KFA Jülich
6)	Gutierrez	CIEMAT
7)	Arapis	Univ. Athens
8)	Kirchman	Faculté Sciences Agronomiques Gembloux

I. Summary of Project Global Objectives and Achievements

1 Global Objectives

The international European research project EURORESSAC is aimed at studying the behaviour of radionuclides likely to be released after a severe accident in a nuclear installation (fusion of the ractor core in a PWR), and their and impact on the agricultural environment.

Such an accidental situation, and the resulting post-accidental contamination of arable land, is simulated in order to study experimentally the behaviour of the most important radionuclides (Cs-137, Sr-90) This simulation is carried out on a realistic scale in the RESSAC facility which includes large lysimeters (using representative European soils) placed under strictly controlled climatic conditions (simulation of original climates in greenhouses), and for a representative source term (aerosols produced by the POLYR facility).

Therefore, the scientific approach considered experimental investigations designed to unravel the fundamental processes governing the behaviour and fate of radionuclides in the environment.

The global objectives were:

- re-create a natural agricultural environment large enough to minimise artefacts (large lysimeters with control of seasonal movements of the water table, simulation of original climates)
- simulate the deposition of fine particles (1μm) of radioactive material, i.e. aerosols (irradiated fuel, POLYR source term) accidentally released from a PWR
- study the mechanisms governing deposition and fixation of radioactive aerosols on soils and plant surfaces (dry deposition, influence of rainfall)
- develop an understanding of the contamination scenario with respect to the agricultural environment (behaviour of Cs and Sr in different soils and crops representative for the European Union)
- study and assess the immediate and potential impact of the contamination to the environment (interception by vegetation, foliar uptake and transfer, translocation within the plants, soil-to-plant transfers, vertical migration in soils).

2 Global Achievements

The choice of soil monoliths, the definition of their associated relevant climatic conditions, the characterisation of their physico-chemistry, and the definition of the crop growth features they could support in the RESSAC facility have first been achieved. Simulations of aerosol-based radioactive contamination have next been carried out in order to investigate various aspects of radioelements interaction with vegetation and soils.

2.1 Characterisation of European field sites

In five countries (B, D, E, F, UK) sampling sites for the soil monolith extraction were characterised by each national team of the RESSAC programme. Over a cycle of at least one entire year soil hydrology data were collected by means of tensiometers and temperature probes installed by the Cadarache team. All national teams provided daily and monthly meteorological data (rainfall, temperature, solar radiation etc.) of the regions covering up to 40 years of observations. The field sites chosen consider the most representative regions and soil types of the European Union (Orthic Podzol, Orthic Luvisol, Brown Earth, Calcaric Fluvisol, Rendzina Cambisol, Fluvisol Arenosol, Calcic Luvisol or *Terra Rossa*).

2.2 Sampling of soil monoliths and preparation of lysimeters

Between May and October 1992 for each soil type selected, six undisturbed monoliths were sampled by the national teams with the technical assistance of France and using a procedure developed by the Cadarache team. The raw monoliths were shipped to Cadarache and transformed into lysimeters by fixing a porous plate in close contact to the lower part of the monolith. A water reservoir beneath the porous plate ensured the seasonal movements of the water table aided by a pump/tensiometer system. By the end of 1992 all lysimeters entered the RESSAC Lysimeter building with the respective original climates.

2.3 Physical and chemical characterisation of soils

An extensive physico-chemical characterisation of the soils of both, the lysimeters and the local field plots, has been carried out (UK- and Gembloux-team) in order to reach a good basic understanding of these soils. The range of physical and chemical properties measured has included the clay fraction , cation exchange capacities (CEC), exchangeable Ca, K, Mg, and X-ray diffraction analysis (illite component). The observed values for the four soils used in the field plots were quite comparable to the respective lysimeter soils.

2.4 Adsorption-desorption capacities of European soils

The Belgian teams of Mol and Gembloux compared the adsorption and desorption behaviour of Cs and Sr applied to the lysimeter soils and the field plots in Mol, either as aerosols or ionic forms. Bare soil surfaces were contaminated with radioactive aerosols generated by the POLYR furnace as well as with ionic forms of radioactive Cs and Sr. Three methods were used to test the availability of radionuclides bound to the soil matrix: a) extraction of interstitial soil water by centrifugation (soluble forms), b) chemical extraction with 1 N Ammonium acetate (potentially available fraction), and c) infinite bath extraction with Prussian Blue (potentially available fraction of Cs). Both forms of caesium, either ionic or as aerosols (POLYR), are readily soluble and behave similarly. Furthermore, a 5 months ageing period showed no significant effect on the behaviour of both Cs forms. Strontium as aerosols (POLYR) is less soluble than in ionic form, but ageing enhanced both, aerosol solubility in interstitial water and its availability, as shown by the increase of the exchangeable fraction of aerosols with time.

2.5 Agricultural programme: comparison of crop growth efficiencies and yields

During two growing seasons the growth and yields of wheat and clover (all countries) and ryegrass (B, UK) were compared between cultures grown on lysimeters in the RESSAC facility and those grown in the field. Collectively, good growth patterns were observed on all lysimeters for wheat, indicating a satisfactory and timely development through the various stages to maturity. Yields of grain and straw were comparable, at the least, or better than in the field for the respective countries. They fell mostly in the range of typical national wheat yields. Differences in absolute values of grain yields could be explained by soil types (fertility) and climates.

2.6 Chemical analysis of crops grown on lysimeters

Multi-element analyses were made for all wheat samples grown on lysimeter soils and on their soil analogues in field plots at Mol (Gembloux). Element analyses of wheat and ryegrass (UK), and wheat and

clover (E), were also performed for the major and minor minerals (N, P, K, Ca, Mg, Na and Fe, Mn, Cu, Zn, Mo, Sr).

In general, the mineral levels were satisfactory. Minor variations and deficiencies of some elements in wheat grains and straw remained within the range of expected values and could be explained by differences in soils constituents and type of climate.

2.7 Generation of radioactive aerosols (POLYR: POllution LYsimeter RESSAC)

The French team at Cadarache which had developed the POLYR-furnace device, was in charge of improving the simulated generation of radioactive aerosols likely to be emitted during a melt-down of the core of a PWR (900MWe). In several test series, the chemical composition (chemical forms and compounds), the physical characteristics (particle size) of the produced aerosols and their solubility in rainwater were determined.

The defined source term used for the contamination of the RESSAC lysimeters consisted of 15 major elements introduced in the crucible including caesium and strontium as radioactive isotopes (Cs-137, Sr-90). The proportions of the various elements reflected the relative abundances of the inventory of a PWR corium. Elemental composition (i.e. global and according to granulometry) of the aerosols produced has been determined, and results are currently being collected. Medium aerosol particle size was about 1 μm and solubility of Cs-compounds in rainwater reached 85 - 95% after only 24 hours. Similar investigations for strontium are still in process. Studies on the solubility of other compounds present in the charge are also being pursued.

2.8 Deposition

Soil-deposition levels of Cs-137 and Sr-90 were measured on bare soils, soil under vegetation, and on smooth filter surfaces (cellulose acetate) under and above crops. On the Spanish calcic luvisol (*Terra Rossa*), slightly more than twice the activity found on the Belgian soil (orthic podzol) could be measured, while on the orthic luvisol of Germany, an intermediate value was determined. On the Belgian lysimeter, activities of Cs and Sr on filters were similar to those found on bare soil and soils under crops. On the calcic luvisol (*Terra Rossa*, E), activity levels of Cs and Sr were about 35% higher than on filters. The relative roughness of the wheat leaf-surface resulted in some 40% higher deposition (Cs and Sr) over that on bare soil surfaces (B). The deposition of Cs-137 and Sr-90 on the soil under crops was reduced to ~20% of the activity levels on bare soils by the higher and more dense vegetation (wheat UK: 55cm; F: 75 and 95cm) on the UK and French lysimeters. In general, Cs and Sr deposition levels on bare soils showed a tendency to augment with the roughness of the exposed soil surface.

Generally, the distribution of the radioactivity was quite heterogeneous over the whole lysimeter surface. In order to better understand this heterogeneity, a cartography of the total radioactivity distribution was carried out on the French lysimeter from Belleville. Deposition levels of Cs and Sr were higher close to the tent walls and opposite to the aerosol inlet.

2.9 Interception

Each lysimeter surface was divided into two parts on which wheat had been sown at two different dates (except for the Belgian one). Therefore, wheat cultures could be contaminated with radioactive aerosols at seven different growth stages and density (soil coverage). These different conditions represented seven scenarios during the wheat growing season covering the period from early growth in spring (three leaves) to nearly maturity (end of flowering).

Interception factors were determined directly after contamination by sampling wheat plants on 10cm squares randomly distributed over the whole lysimeter surface. Interception was found to be directly dependent on the growth stage (size) of the wheat plants reaching nearly 90% (Cs-137 and Sr-90) at maturity (end of flowering, size 95cm). Both radioisotopes present as aerosols behaved similarly and were intercepted nearly at the same degree by wheat plants (Fig. 1).

Interception by ryegrass (UK, height 21cm) was very variable (18-75% Cs-137; 24-43% Sr-90). This was probably due to the difficulty of distinguishing between deposition of both radioisotopes on the mat layer underlying the grass sward and that on the proper soil.

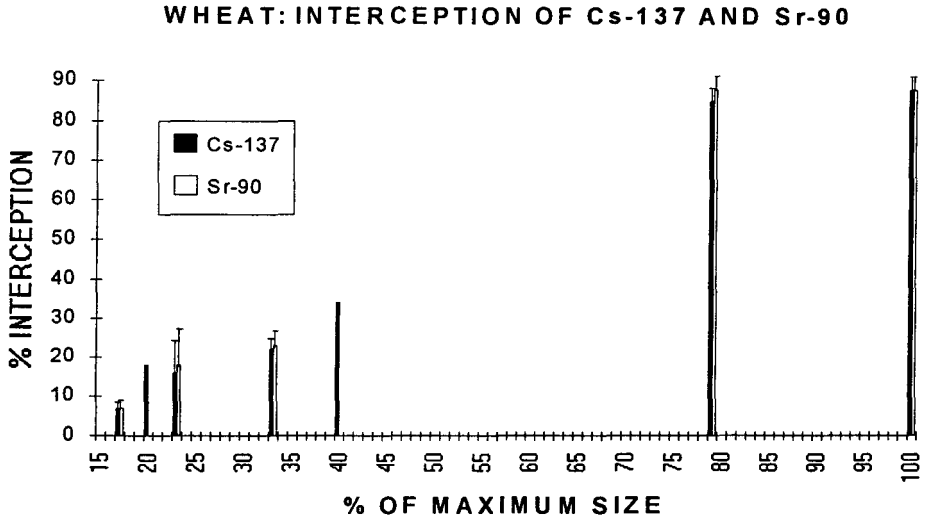

Figure 1: Caesium 137 and strontium 90 interception by wheat cultures contaminated at different stages of development. (Errors not indicated on figure are currently not available)

2.10 Retention

The effect of wash-off and retention after a 10mm rainfall over two hours, six days after contamination, was determined for all growth stages. An overhead irrigation system simulated rainfall as a fine drizzle. One day after application of rainfall 10 wheat plants (as well as leachate) were sampled at random. These samples were compared to similar ones withdrawn before the rain to determine the retention factors.

For younger wheat plants between growth stage 10cm (2-3 leaves unfolded, decimal code 12) and growth stage 55cm (3-4 knots detectable, decimal code 34) the mean percentage of retention was not clearly affected by the plant development. Maximum mean retention values of 59% and 96% were measured for Cs-137 and Sr-90, respectively (Fig. 2).

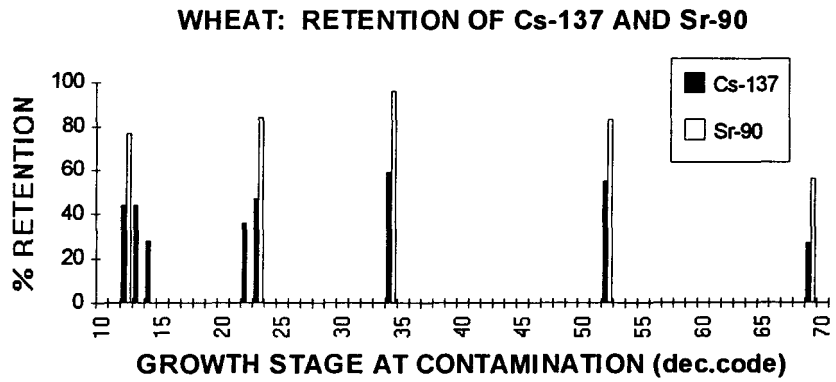

Figure 2: Retention of caesium 137 and strontium 90 by wheat cultures after rain wash off (10mm rain during two hours, six days after contamination) as a function of the growth stage at which contamination took place. (The statistical significance of these data collected from the various partners is still under evaluation).

At older stages of development, the mean retention values exhibited a clearer tendency to decline, both for Cs and Sr. At 75cm of development (ears emergence, decimal code 52), plants retained only 55% and 83% of Cs-137 and Sr-90, respectively. These percentages dropped to 27% (Cs-137) and 56% (Sr-90) for wheat plants close to maturity (95cm, end of flowering, decimal code 69). However, the statistical significance of this trend is not yet established.

These results confirm the poor potential of strontium, as compared to caesium, to be washed off the vegetation by rain. Overall, Cs was washed off the wheat plants almost 2 times more than Sr. Further experiments are required to explain the retention drop when wheat plants are approaching maturity. This may be linked either to changes in the physiological and anatomical status of the superficial leaf cells, or to modifications of the overall canopy surface structure (leaves senescence and litter fall, appearance of ears at the expense of leaves).

2.11 Translocation

WHEAT: After deposition and retention (which has been further reduced by subsequent rainfalls), a certain quantity of the radioisotopes Cs and Sr is taken up and translocated to the various organs of the wheat plant. Translocation factors of Cs in grains of wheat plants grown on two different soils (B, D), where contamination had occurred at nearly the same size (15cm), did not vary considerably and showed comparable values (0.00085; 0.0011) after quite comparable development durations (140; 131 days).

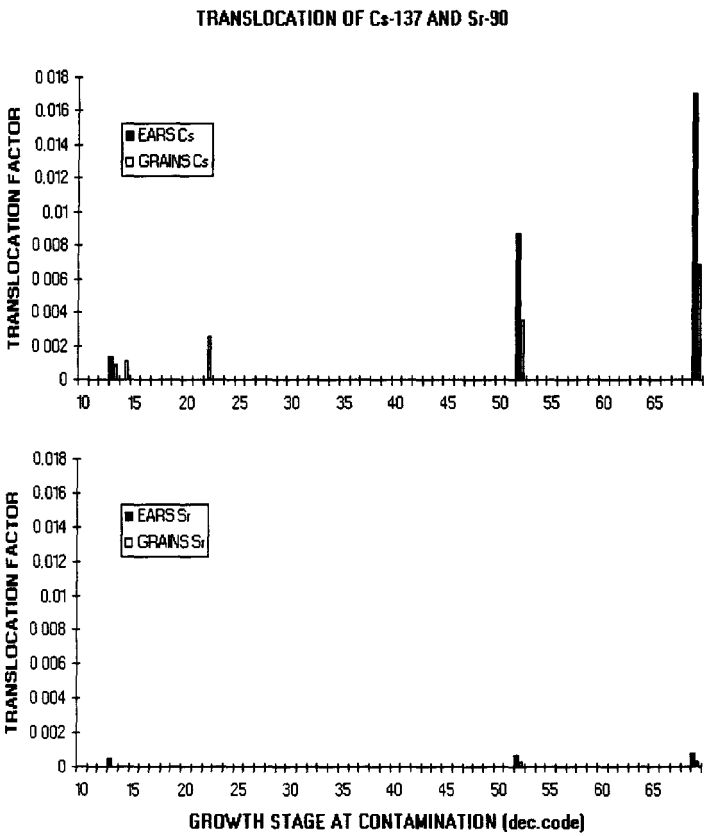

Figure 3: Translocation coefficients of Cs-137 and Sr-90 towards wheat ears and grains for various growth stages at which contamination occurred. (Errors not indicated on figure are still under evaluation).

In general, translocation of caesium to ears and grains increased with contamination occurring at later growth stages. As observed on the Lysimeter from Belleville (F), direct contamination of developed ears

resulted in the highest Cs-137 translocation factors for both, ears and grains. However, caesium translocation factors to grains were found to be 2.5-fold lower than those measured in ears of the same developmental stage (Fig. 3). Sr translocation behaved similarly, but to a much smaller extent than for Cs (maximum translocation about 40 % that of Cs for grains at growth stage 69).

VINE: On the lysimeter from Tricastin (F), part of the leaves and the grapes have been protected during contamination in order to study translocation phenomena. Non-protected leaves lost almost 80% of Cs-137 and 40% of Sr-90 by additional subsequent rainfalls (5 times, 25 mm total) during 20 days. Translocation occurred in masqued leaves already two days after contamination (0.08%) and increased by a factor 7.5-8 for Cs and Sr, respectively on day 30. Translocation of caesium was more pronounced (2.3%) than for strontium (0.8%) considering activities in non-protected leaves. In grapes, translocation after two days was faster than in leaves (Cs: 3%; Sr: 4.4%) with respect to non-protected grapes. After 30 days translocation of Cs-137 exceeded that of Sr-90 by 10 times. The effect of activity loss by rain wash-off in non-protected grapes was partly compensated by the uptake via translocation, as measured in protected grapes. Similar results were obtained in-situ by the Greek team comparing the translocation of soluble Cs-134 in protected and non-protected grapes. In protected grapes, covered with a plastic film, the translocation values of Cs-134 reached only 2.5% that of non-protected ones. These data confirm the findings derived from experiments on the Tricastin lysimeter and demonstrate a nearly identical behaviour of caesium applied either as aerosols or as soluble forms.

2.12 Non-lethal defoliation

The Greek team carried out in-situ experiments testing the efficacy of commercial defoliation products in order to prevent and/or minimise foliar uptake and translocation of radionuclides to grapes and olives. Recommended doses resulted in 80% defoliation in vines while with double doses 100% of vine leaves were shed within 2-3 days. The effect of defoliation was much slower in olive trees resulting in 95 - 100% defoliation with two products, while with a third one only 5% of the leaves could be removed after two weeks. One year after application, 10-40% yield reductions were observed in vines depending on the products used. Respective data for olive trees are still being processed.

2.13 Soil-to-plant transfer

Transfer factors were determined for wheat grown on the Belgian lysimeter (Orthic podzol). After contamination, part of the wheat culture (3 leaves unfolded) was ploughed and the wheat re-sown. Soil-to - plant transfer factors of Cs-137 were similar in wheat grains and ears (0.000445; 0.000538 m^2/kg, respectively). Soil to ears transfer of Sr-90 was 3.5-fold higher than for Cs-137. In barley grown on the lysimeter in the following year, soil-to-plant transfer factors of Cs-137 were reduced by one order of magnitude as compared to what was observed in wheat the preceding year. Repeated conventional ploughing (only several times) reduced Cs and Sr activity levels in the topsoil layer by dilution effect.

- Influence of agricultural practices

Different agricultural practices have been tested in view of reducing the soil-to-plant transfer. These included conventional ploughing and deep placement of contaminated topsoils (B, D), addition of organic matter (cow manure) to the arable soil layer, and mulching (E). Normal ploughing of wheat contaminated at an early growth stage followed by re-sowing, has no effect on Cs- and an adverse effect on Sr-transfer. Caesium activities in straw were reduced by a factor of 3, but strontium activities increased slightly. Addition of cow manure (organic matter) decreased the transfer factor of Cs-137 in barley grains to 17%. In clover, Sr-90 transfer factors could be reduced by a factor of 3, while supply of organic matter had no effect on the Cs transfer. Since the second crop cultures (barley) have been harvested between July and August 1995, only partial results on the soil-to-plant transfers can be reported here. Data on the influence of deep ploughing (D), mulching (E) and different soil types and climates on the soil-to-plant transfer factors in crops are still pursued, and will be presented in the forthcoming common publications.

- Influence of soil type under field condition (field plots Mol)

Soil-to-plant transfer factors of rye-grass and clover grown on four different soils were about 10 times higher in the sandy orthic podzol of Mol than in the three other loamy soils. This is probably due to the higher adsorption and fixation capacity of the three loamy soils (dystric cambisol, calcaric cambisol, orthic luvisol), compared to the orthic podzol of Mol.

Head of project 1 : Dr. Foulquier L., team :

- Lysimeter Experimentation Laboratory : J. Hugon, C. Madoz-Escande, P. Rongier.
- Continental Radioecology Laboratory : F. Bréchignac, C. Colle.
- CCE Representative : E. Schulte.

II - Objectives for the reporting period 1/09/92 to 30/06/95

II.1 Objectives for the period - May 1992 to December 1993

The five objectives for the period considered were :
1.lysimeter sampling in Europe,
2.acquisitions of hydrological and meteorological data at the sampling sites,
3.agronomic program,
4.implementation of an experimental substitution program,
5.completion of the lysimeter building and set-up of experimental facilities.

II.2 Objectives for the period - January 1994 to June 1995

The seven objectives for the period considered were .
1. production and characterisation of radioactive caesium and strontium aerosols,
2. contamination of lysimeters,
3. determination of the aerosol distribution deposit on the soil and vegetation,
4. measurement of the caesium-137 and strontium-90 interception derived from aerosols in relation to the vegetative stage of wheat plants and vines,
5. determination of the foliar deposit retention following washing by rain and measurement of its transfer to the soil,
6.determination of the foliar transfer and the translocation of these isotopes to the various organs of mature plants,
7. soil/plant transfer studies of radionuclides deposited on the soil at the time of contamination.

III - Progress achieved including publications

III.1 Results for the period - May 1992 to December 1993:

1. Lysimeter sampling in Europe

Seven lysimeters were sampled in several countries of the European Community and were installed in the Cadarache "lysimeters" building in greenhouses and subjected to climatic conditions similar to the natural environment from which they came ·

- one lysimeter was sampled in each of the following countries : Germany (Merzenhausen), Belgium (Mol), Spain (Barcelona) and the United Kingdom (Wellesbourne) ; the corresponding soil types being loess (orthic luvisol), podzol (orthic podzol), terra rossa, brown soil, respectively,

- three lysimeters were sampled in France two at Tricastin (the Rhône valley) and one at Belleville (the Loire valley) corresponding to calcareous alluvial soil and sandy alluvial soil (fluvisol podzol), respectively

2. Acquisitions of hydrological and meteorological data at the sampling sites

In conjunction with these samplings, data acquisition facilities were set-up on the sites to obtain data reflecting changes in humidity and temperature gradients in the soils with respect to depth, for an entire year. This data, collected continuously, was used by computer equipment intended for the greenhouse climate control and the hydric-potential of lysimeters

3. Agronomic programme : culture testing in greenhouses and comparison with the field cultures

Spring wheat was sown in 1993 in five lysimeters (Belleville, Spain, Belgium, Germany and United Kingdom) using farming practices specific to each country.

The development of these cultures progressed in a satisfactory manner until grain maturity. The yields obtained on the Belleville lysimeter were comparable with those of field cultures : 62.5 quintals of grains per hectare and 72.2 quintals of straw per hectare.

During the second semester of 1993, clover was sown in lysimeters to be used as a manure crop (providing a supply of nitrogen and improvement of the soil structure). Its incorporation into the soil was completed in late 1993.

4. Implementation of an experimental substitution programme

This programme was designed to compensate for the delay in the construction of the lysimeter building. For the French team, it consisted in testing the performances of the POLYR furnace and to contaminate plants (green beans) and soils (from various lysimeters used in the RESSAC programme) located in a tent (rectangular base : 2.5m x 2.4m) to provide the elements necessary to perform the various substitution programmes of our German, Belgian and Spanish partners. The results of these programmes are indicated in their respective reports. In addition, filters placed in this experimental arrangement allowed the distribution of various caesium and strontium aerosols deposits to be determined and to characterise their solubility.

The charge used for the contamination relative to the substitution programme consisted of 14 elements. Among these elements only caesium and strontium were radioactive (isotopes 134 and 85, respectively).

5. Completion of the lysimeter building and set-up of experimental equipment:

- installation of radiological protection equipment and commissioning of the building following administrative clearances for the handling of radioactive products,
- contamination greenhouse equipment with, among others, the contamination device,
- operational testing of the POLYR furnace : furnace adaptation to improve aerosol emission performances,
- delivery, installation and adjustment of rain simulators on each lysimeter,
- implementation of temperature sensors, tensiometers and the hydric potential control equipment,
- sample preparation and radiochemistry laboratory equipment . set-up of counting devices for the measurement of caesium-137 and strontium-90,
- lysimeter equipment in order to ensure that experiments begin in early 1994, all the devices designed to simulate climatic conditions of lysimeters were tested to guarantee their operational readiness during the experiments.

III.2 Results for the period - January 1994 to June 1995:

1. Production and characterisation of radioactive caesium and strontium aerosols:

The charges used to produce the aerosols designed to contaminate the lysimeters were different from those implemented in the substitution programme of 1/09/93 due to the fact that they contained uranium oxide and the proportions of various elements were in keeping with the relative amounts of elements in the core inventory of a 900 MWe pressurised water reactor. Furthermore, the radioactive isotopes were caesium-137 and strontium-90 (see Table 1).

Chemical and physical aerosols characterisation tests allowed their granulometry characteristics, elementary composition and solubility in rain water to be determined

Size distribution of particles was carried out by Andersen impact separators made up of eight aluminium stages allowing particle diameters between 0.4 and 9µm to be determined.

The various granulometry curves show that the majority of aerosols produced have an average aerodynamic diameter of 1µm

Table 1 - Elements present in the crucible for the 1994 lysimeters contaminations

Elements	Weight of stable elements (mg)	Chemical form of stable elements	Active elements	Activity of elements (MBq)
UO_2	8000	UO_2 depleted to 0,2%		
Fe	2060	Fe		
Cr	620	Cr		
Ni	410	Ni		
Zr	1832	Zr		
Sn	20	Sn		
Ag	190	Ag		
In	36	In		
Cd	12	Cd		
I	15	CsI		
Cs	15	CsI	^{137}Cs*	1480
Te	10	Te		
Sr	24	$SrCO_3$	^{90}Sr**	1480
Ru	19	Ru		
Ce	49	$Ce(NO_3)_3,6H_2O$		

*** introduced in CsCl form**
****introduced in $Sr(NO_3)_2$ form**

The chemical analysis of aerosols will allow the relative importance of the various elements to be established. Analysis are underway.

Rain water solubility tests (identical to those used for the irrigation of lysimeters) of aerosols collected on inert supports at the time of lysimeter contamination showed that the dissolution kinetic of caesium was rapid and that the solubility equilibrium was reached after 24 hours After this time period and following 7 tests, 85 to 95% of caesium were put into solution. Strontium analyses are underway.

2. Contamination of lysimeters

All lysimeters, except the two Tricastin lysimeters, were sown with the same variety of spring wheat ("Arbon" variety) in early 1994. The farming methods and the sowing dates, in particular, were those practised in the country of origin. All lysimeters were irrigated using a rain simulator throughout the cultivation period. The quantities of water delivered monthly matched those of meteorological records corresponding to the zones of lysimeter samplings.

The set-up of cultures began in early January and were spread out until early April and was completed in two periods on each lysimeter (east and west sections) in such way as to have plants at two different vegetative stages at a time of lysimeter contamination.

Contaminations using the POLYR furnace took place on wheat cultures between mid-march and late june 1994 and were successively carried out on the Spanish (22 March), Belgian (14 April), German (19 May), English (14 June) and French (Belleville, 28 June) lysimeters. The Tricastin lysimeter was contaminated 20 September while the grapes were in the "early maturation" stage.

The charge used to generate the aerosols is indicated in Table 1.

3. Determination of the aerosols deposits distribution on the soil and vegetation.

Belleville lysimeter:

At a time of lysimeter contamination, the wheat on the eastern section was in the "late flowering" stage (plant height : 95 cm), while the wheat on the western portion was at the ' early ear appearance' stage (plant height 75 cm) In order to be able to evaluate the aerosol deposits, acetyl cellulose filters were placed horizontally on supports located in the middle of the vegetation at 75 cm, 60 cm and 45 cm height in relation to the soil (Figure 1).The results are given in Table 2 Significant heterogeneity of deposit values can be noticed on both the horizontal and vertical axes

Table 2 - Filter deposit values for caesium-137 in MBq.m^{-2} as per the sampling height in relation to the soil (values given with 10% uncertainty).

Location of sampling points (filters)	caesium-137 (MBq.m^{-2})		
	75 cm	60 cm	45 cm
01	9,18	9,34	7,54
03	4,64	4,84	7,06
05	7,08	5,37	6,65
07	4,91	7,61	8,07
09	6,62	7,03	7,20
11	8,58	9,39	7,55
13	5,60	4,92	5,14
15	8,46	8,47	4,33
17	6,36	4,63	7,03
19	7.63	7,90	10,10
21	6,98	6,28	5,59
23	7,05	7,67	7,80

Similar observations were made for strontium-90. For all filters, the caesium/strontium ratio is 0.73±0.04

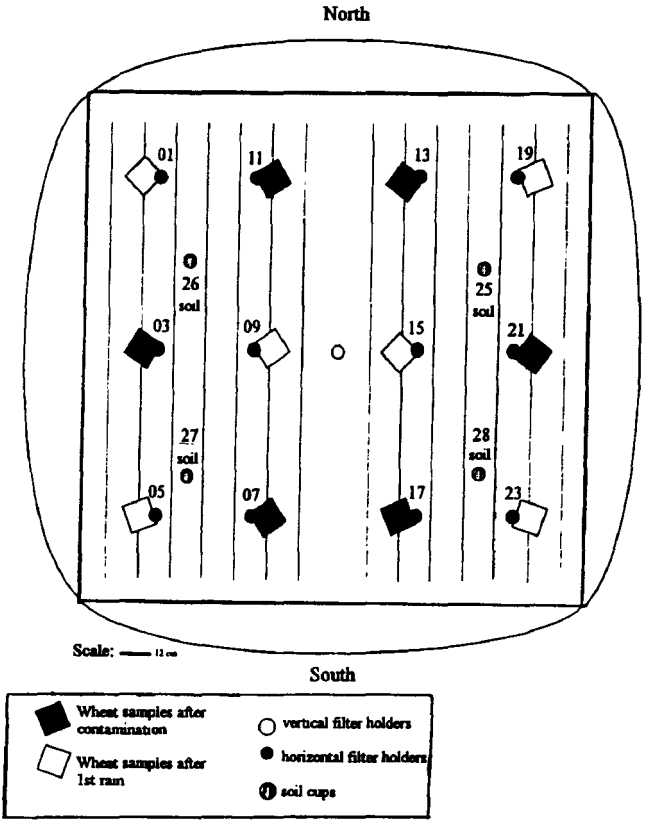

Figure 1- Diagram of locations for the sampling of various samples for the Belleville lysimeter

In order to be able to estimate the deposit on the soil under the vegetation, four cups (diameter 4.9 cm) containing Belleville soil (sieved to 2 mm) were placed on the surface of the lysimeter. The location of these cups is given in Figure 1 The results of the caesium and strontium measurements are provided in Table 3.

Table 3 - Deposit values for caesium-137 and strontium-90 ($MBq.m^{-2}$) on the soil
(measurement uncertainty 10%)

Section	East		West	
Samples	25 soil	28 soil	26 soil	27 soil
Cs-137	13,50	9,97	6,36	10,50
Sr-90	14,70	10,90	7,40	11,7
Cs/Sr	0,92	0,91	0,86	0,90

In view of subsequent aerosol characterisation studies (solubility, extraction tests in the soils...), filters and soil cups were placed on the edges of the lysimeter beyond the vegetation zone (see production and characterisation of aerosols).

The atmospheric concentration measurements during the deposit above the vegetation are indicated in Figure 2. The deposit speed estimation is $3.35.10^{-2}$ $cm.s^{-1}$.

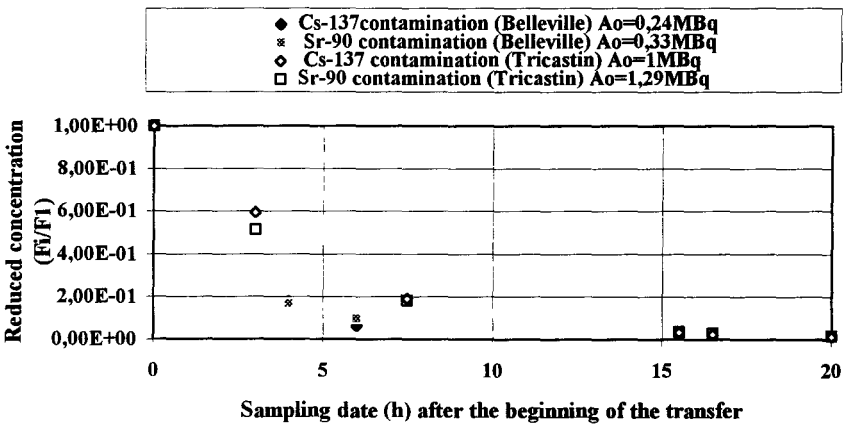

Fig.2. Evolution through time of the relative atmospheric concentration of caesium and strontium above the vegetation on Belleville and Tricastin lysimeters.

Tricastin lysimeter :

The contamination of the first Tricastin lysimeter took place 20/09/94 when grape maturation started. On this lysimeter two vine plants are cultivated.

On one of the two vines, grapes bunches were protected by plastic bags so as to avoid direct aerosols deposits and to evaluate the contamination of the grapes through time resulting from translocation (monitored until harvest).

The other plant was used to determined the washing effect of a rain applied 6 days after contamination. Only a portion of the leaves were protected by plastic bags in order to be able to evaluate the contribution by translocation.

The atmospheric concentration measurements taken during the deposit above the vegetation have given the data shown in Figure 2 and a deposit speed estimation of $1.2.10^{-2}$ $cm.s^{-1}$. The measurement (on an inert support) of soil deposits after contamination was conducted and thereby allowed us to plot the caesium-137 distribution map (Figure 3). The average deposit on these supports is 35 3 ±2.9 $MBq.m^{-2}$ for caesium and 26 7 ±1.4 $MBq.m^{-2}$ for strontium. The caesium/strontium ratio determined from these measurements is 1.32 ±0.03.

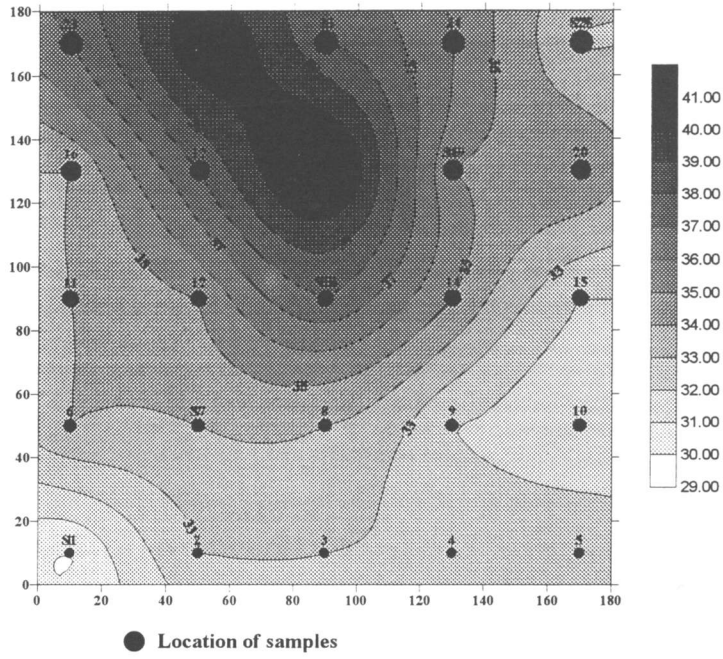

Figure 3 - Distribution of caesium-137 deposits on the soil of the Tricastin lysimeter (MBq. m^{-2})

4. Measurement of caesium-137 and strontium-90 aerosols interception by the cultures.

Belleville lysimeter : wheat culture

Prior to contamination and to be able to determine the interception of radionuclides by the plants, it was necessary to determine the foliar index, i.e. the surface area of leaves capable of receiving deposits. To accomplish this, the number of plants contained in three squares (10cm x 10cm) were counted in each half of the lysimeter so as to determine the average wheat plant surface density. Concurrently, a number of plants equal to the average of that contained in the 10cm x 10cm squares were randomly sampled in each section of the lysimeter. Stems and leaves were sampled from each of the plants then measured before transferring in their image to paper to determine the surface area.

After the contamination and on each half of the lysimeter, three samples corresponding to the wheat plants contained in the 10cm x 10cm squares (see diagram Figure 1) were taken.

The analysis of these samples provided the following results :

- The deposit values of caesium-137 and strontium-90 on the wheat plants were heterogeneous regardless of the vegetative stage of plants.
- The values measured for caesium-137 were between 10 and 85 MBq.m^{-2} of culture for the portion of wheat in the "late flowering" stage and between 17 and 79 MBq.m^{-2} of culture for the portion of wheat in the "early ear appearance" stage.
- On average, the caesium/strontium ratio appears to be similar to that measured in the soil deposit on an inert support (approximately 0.9).

Using the deposit values measured directly on the plants and the soil deposit values measured near these plants, the value of the interception coefficient (I.C.) was evaluated using the following formula :

I.C. = Total deposit per m^2 of vegetation / total deposit per m^2 (soil + vegetation).

For caesium and strontium, the average I.C. is 85 ±3% for wheat in the "early ear appearance" stage, and 88 ±3% for the portion of the wheat in the "late flowering" stage.

For strontium the values are 88% for both sections.

5. Determination of the foliar deposit retention following washing by the rain and measurement of its transfer to the soil

Belleville lysimeter:

Six days after contamination, a rain of 5 mm/h lasting two hours was applied on the entire lysimeter The homogeneity of rain distribution was checked by four rain gauges installed at the same level as the upper portion of the vegetation and in the locations previously occupied by the soil cups (see Figure 1)

Water samples were collected from devices placed under the vegetation at the soil level throughout the entire duration of the rain. Analysis of these samples allowed us to determine the fraction of caesium and strontium derived from the washing of wheat plants and, in the same manner, to estimate the contamination of the soil resulting from this phenomenon.

The average caesium-137 concentrations of these samples were ·

2,160±980 $Bq.ml^{-1}$ under the wheat at the "early ear appearance" stage,

1,310±530 $Bq.ml^{-1}$ under the wheat at the "late flowering" stage,

For strontium-90, the values were ·

626±176 $Bq.ml^{-1}$ under the wheat at the "early ear appearance" stage,

548±160 $Bq.ml^{-1}$ under the wheat at the "late flowering" stage.

The caesium and strontium values show that caesium was washed to a greater extent than strontium

Following the first rain and on each half of the lysimeter, three samples corresponding to the wheat plants contained in the 10cm x 10cm squares (see diagram, Figure 1) were collected.The analysis of these samples provided the following results

The measured caesium-137 values were between 16.2 and 28.7 $MBq.m^{-2}$ of culture for the portion of wheat of the "late flowering" stage and between 16.5 and 26.7 $MBq.m^{-2}$ of culture for the portion of wheat in the "early ear appearance" stage. For strontium-90, the values were between 32.1 and 56.5 $MBq.m^{-2}$ of culture for the portion of wheat in the "late flowering" stage, and 30.4 to 62 5 $MBq.m^{-2}$ of culture for the portion of wheat in the "early ear appearance" stage.

In consideration of the caesium/strontium ratios (0 49 ±0.06), these results show that the caesium was washed to a greater extent than the strontium, which is in keeping with the results of the washing water measurement.

The coefficient of the radioisotopes retention by the vegetation was defined as the fraction of the deposit per square meter of culture not washed by the rain. For the portion of the contaminated wheat ·

- in the "late flowering" stage, this coefficient was: 27% for caesium-137 and 56% for strontium-90,
- in the "early ear appearance" stage, this coefficient was : 55% for caesium-137 and 83% for strontium-90.

Tricastin lysimeter :

The analysis of vine leaves and grape bunches sampled 2 days after contamination provided the results indicated in Tables 4 and 5.

Table 4 - Activities in the covered and uncovered leaves in relation to the time elapsed since contamination ($MBq.kg^{-1}$ fresh)

	Covered leaves			Uncovered leaves		
Time elapsed since contamination (days)	**Cs-137**	**Sr-90**	**Cs/Sr**	**Cs-137**	**Sr-90**	**Cs/Sr**
2	0,34±0,04	0,25±0,02	1,4	408,0±44,0	307±31	1,37
6 (1st rain)						
7 (+1 rain)	0,60±0,07	0,37±0,04	1,6	250,0±25,8	313±31	0,79
20 (+5 rains)	1,27±0,13	2,33±0,23	0,54	88,3±9,3	189±19	0,47
30 (harvest)(+8 rains)	2,86±0,30	1,88±0,19	1,52	122,0±12,7	223±22	0,55

Table 5 - Activities in the covered and uncovered bunches in relation to the time elapsed since the contamination (MBq.kg^{-1} fresh)

	Covered grapes			Uncovered grapes		
Time elapsed since contamination (days)	**Cs-137**	**Sr-90**	**Cs/Sr**	**Cs-137**	**Sr-90**	**Cs/Sr**
2	0,084±0,008	0,081±0,008	1,0	2,73±0,21	1,83±0,18	1,5
6 (1st rain)						
7 (+1 rain)	0,38±0,04	0,088±0,009	4,3	1,77±0,15	1,09±0,10	1,62
20 (+5 rains)	0,90±0,08			1,72±0,14	0,92±0,093	1,87
30 (harvest) (+8 rains)	1,64±0,14	0,123±0,012	13,3	1,97±0,15	1,45±0,14	1,36

Two days after contamination, the contribution due to translocation is already perceptible on the covered portions of the vine

Both vines were subjected to a 5mm.h^{-1} rain for two hours, six days after the contamination The leaves and bunches protected at the time of aerosols deposit remained covered until the harvest. The bags were perforated to allow the free circulation of air.

The analysis results of samples taken 7 days after contamination, i.e. one day after the first rain, are shown in Tables 4 and 5

As for the wheat, the rain provided a much more significant caesium washing effect than for strontium on the leaves subjected to the direct deposit. On the bunches subjected to the direct deposit, the effect was less pronounced, the loss due to the rain being compensated by the contribution by translocation.

6.Determination of the foliar transfer and the translocation of radioisotopes to the different plant organs

Belleville lysimeter :

The wheat reached maturity in late August and harvest took place 6 September 1994. Sampling was conducted by separating the straw from the ears. The ears were processed by removing the grains from the husks (Table 6).

Table 6 - Average caesium-137 and strontium-90 activity of the various components of mature wheat plants in MBq.kg^{-1} dry

		caesium-137	strontium-90	caesium/strontium
grains	**A**	1,91±0,26	0,14±0,01	13,84
	B	0,94±0,30	0,10±0,03	9,12
husks	**A**	1,43±0,26	2,47±0,75	0,58
	B	1,24±0,50	2,41±0,76	0,51
straw	**A**	23,9±5,8	53,2±8,9	0,45
	B	17,1±9,0	40,6±6,0	0,42

A = portion of the lysimeter contaminated at the wheat's "late flowering" stage,
B = portion of the lysimeter contaminated at the "early ear appearance" stage.

It seems that at plant maturity, and for the vegetative stages at the time of contamination, all parts of wheat plants that were contaminated in the "late flowering" stage contain more caesium and strontium than the plant that had been subjected to aerosols deposits at an earlier stage.

As for the grains, in which contamination takes place only by means of translocation (grains protected by the husks at the time of deposit), it appears that the caesium concentration is approximately 10 times higher than strontium

However, for the husks and straw, the contamination of which is essentially due to direct deposit, the strontium activities are greater than those of caesium. This is due to the fact that the successive rains washed caesium to a greater extent than strontium as shown by the Cs/Sr ratios measured in the straw and the husks. These ratios are less than the value of 0 71 measured in the aerosols at the time of contamination

Tricastin lysimeter:

The contamination of leaves and grape bunches by translocation were monitored through time : the samples were taken 2, 7, 20 and 30 days (harvest) after contamination. The results are given in Tables 4 and 5

Figure 5 indicates the changes through time on the various components of grape bunches protected from direct deposit and the relative mass distributions of caesium-137 and strontium-90.

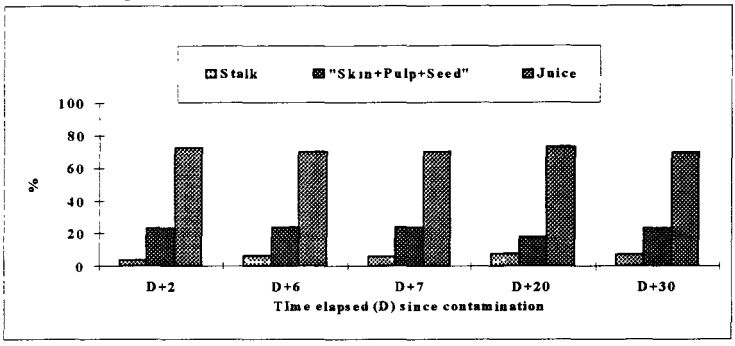

Figure 5.a) - Changes through time in the relative mass distribution of various grape bunch components protected from direct deposit

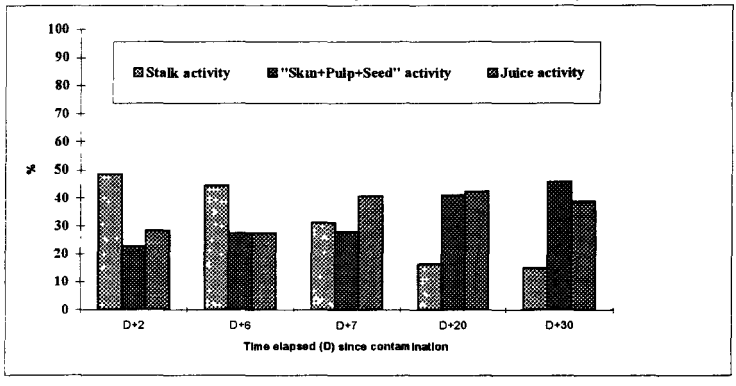

Figure 5.b) - Changes through time in the distribution of caesium-137 in various grape bunch components protected from direct deposit

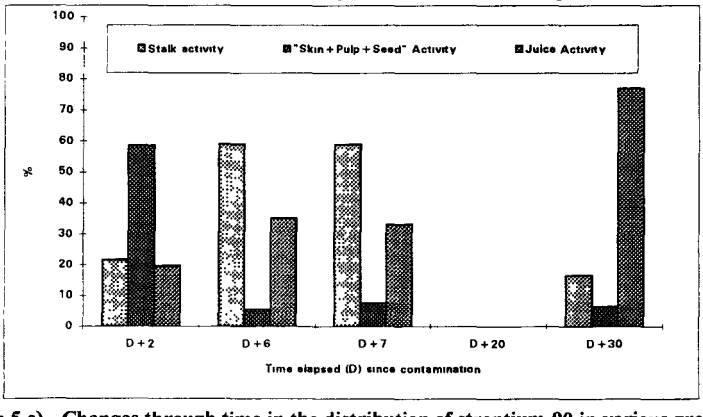

Figure 5.c) - Changes through time in the distribution of strontium-90 in various grape bunch components protected from direct deposit

7. *Soil-plant transfer studies of radionuclides deposited on soils at the time of contaminations*

Belleville lysimeter:

1) After the wheat harvest and just before ploughing, a sample was taken of fresh wheat regrowth (i.e. 5 months after contamination). Analyses of samples provided the following results:

$(3.09\pm0.43).10^{-5}$ Bq.kg^{-1} dry for caesium-137,
$(2.06\pm0.20).10^{-5}$ Bq.kg^{-1} dry for strontium-90.

2) Cartography analysis was performed before ploughing using a probe (total γ) placed 10 cm above the soil. Measurements were taken on a 20cm x 20cm grid. The results of this measurement are shown on Figure. 6.

Three fourths of the lysimeter was ploughed. The south-east quarter was left fallow in view of subsequent studies concerning the migration of radioelements into the soil. On the north-east quarter, the straw harvested (corresponding to the harvest on this portion of the lysimeter), was incorporated into the soil.

Cartography analysis, in the same conditions as mentioned above, was then undertaken. The results of this measurement are shown in Figure 7. Comparison of Figures 6 and 7 shows that ploughing reduced the distribution heterogeneity of radionuclides in the soil which was determined at the time of a contamination.

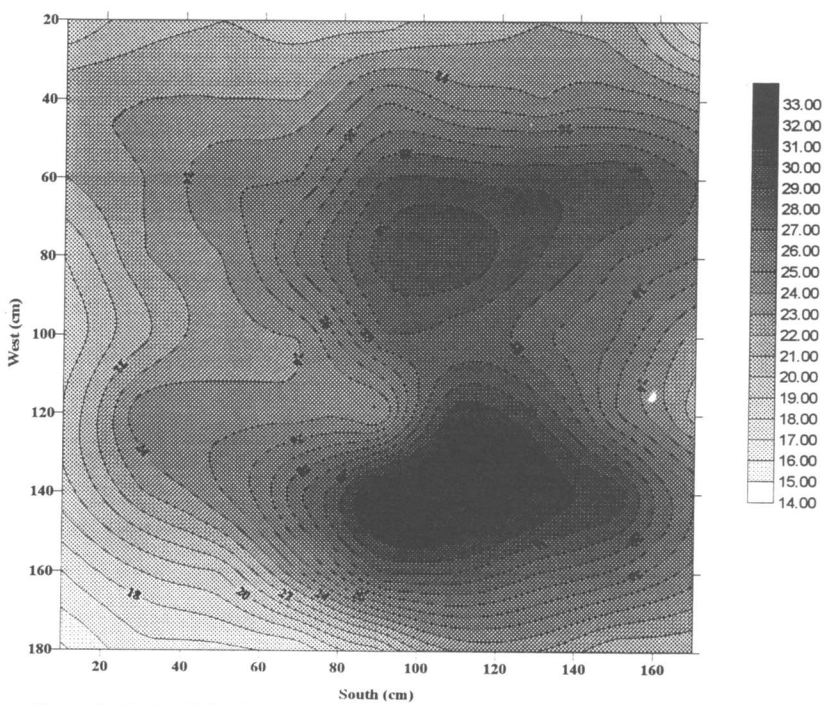

Figure 6 - Belleville lysimeter. γ measurement performed 25/11/94 before ploughing. The probe is 10 cm above the soil. Values are in counts.second^{-1}

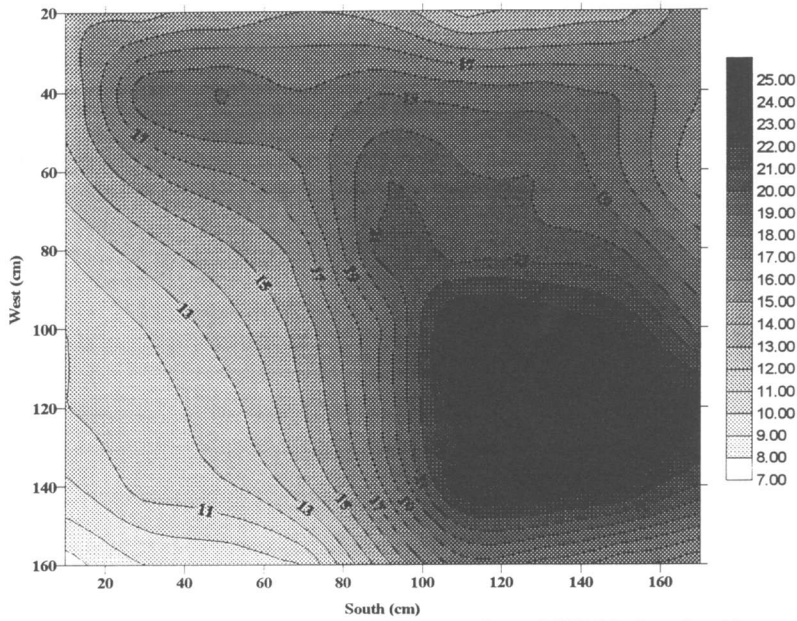

Figure 7 - Belleville lysimeter. γ measurement performed 5/12/95 after ploughing. The probe is 10 cm above the soil. Values are in counts.second^{-1}.

3.) Following ploughing, winter barley ("Orblonde") was sown on the south-west quarter.In mid-February 1995 spring wheat was sown on the entire north half on the lysimeter. In May 1995, samples of wheat (at the "4-5 leaf" stage) and barley (at the "mid-tillering" stage) were collected. Measurements provided the following results.

Table 7 - Caesium-137 and strontium-90 activity of wheat and barley samples. Values given in kBq.kg^{-1} (uncertainty 10%)

	caesium-137	strontium-90	Cs/Sr
Plot sown with barley	24,6±2,6	562,7±55,2	0,044
Plot sown with wheat	33,95±3,7	670,7±67,1	0,051
Plot sown with wheat with incorporated straw	20,85±2,43	275,1±27,7	0,076

Concurrently, soil samples, six from the plot sown with wheat and two from the plot sown with barley were taken and analysed. These samples were located at the centre of plots forming a triangle. The results of caesium-137 measurements provided :

Table 8 - Caesium-137 activity of soil samples taken from wheat and barley plots. Values given in kBq.kg^{-1} (uncertainty 10%)

Samples	B1	B2	B3
Plot sown with barley	22,1		11,2
Plot sown with wheat	131,3	57,45	351,8
Plot sown with wheat with incorporated straw	74,3	58,2	641,5

These results are in keeping with the measurements conducted in total γ after ploughing (see Figure 7), i.e. more activity in the northern portion of the lysimeter, the weakest being found at the barley culture location.

Head of project 2: Dr. Sandalls

(UK Team: Steve Baker, John Branson, Ken Nicholson, John Sandalls and Allen Stacey)

II OBJECTIVES FOR THE REPORTING PERIOD

1 OBJECTIVES FOR THE PERIOD MAY 1992 TO AUGUST 1993

These were as follows:

(i) to extract a soil monolith from a suitable location in the United Kingdom to the specification of the EUROSOIL-RESSAC project, and install it as a lysimeter at the RESSAC facility at CE Cadarache.

(ii) to install and maintain an AXONE data acquisition unit at the original location of the monolith and establish a telemetric link with the RESSAC facility at CE Cadarache.

(iii) to design and implement a technical programme regarding the use of the lysimeters within the RESSAC facility.

A further objective arose in June 1993 when the technical programme had to be postponed for one year, while construction work at the RESSAC facility was completed. This objective was:

(iv) to design and implement a substitution programme of work for the lysimeters.

2 OBJECTIVES FOR THE PERIOD SEPTEMBER 1993 TO JULY 1994

These were as follows:

(i) to complete the substitution programme for the UK lysimeter.

(ii) to re-commence the original technical programme for the UK lysimeter.

3 OBJECTIVES FOR THE PERIOD AUGUST 1994 TO JUNE 1995

These were as follows:

(i) to complete the analysis, for Sr-90 and Cs-137, of selected samples taken post-contamination and post-rainfall from the UK lysimeter.

(ii) to collate and interpret data obtained from analysis of selected samples taken from the UK lysimeter to gain information on interception factors for grass and wheat, retention and wash-off after rainfall, soil-splash and soil to plant transfer, for Sr-90 and Cs-137.

(iii) to harvest the wheat crop at maturity and determine the distribution of Sr-90 and Cs-137 in grain and straw.

III PROGRESS ACHIEVED

1 1992/93 PROGRAMME

1.1 Extraction of UK Soil Monolith

The UK soil monolith was extracted from a site at the scientific institute of Horticulture Research International (HRI), Wellesbourne, Warwickshire in central England. The site provided a soil which has been well characterised over a period of some twenty years. The soil is a Brown Earth of the Wick series and had recently been used for production of arable crops The sampling location at HRI Wellesbourne also allowed provision of amenities such as electricity and communications, these were utilised during excavation of the monolith and were required to operate the AXONE unit. Excavation of the soil monolith, using the technique adopted for the RESSAC programme, took place over 10 days in September 1992 The monolith was then transported in a steel tank for installation in the RESSAC facility at CE Cadarache.

The AXONE data acquisition unit was installed and commissioned at HRI during December 1992. This unit would provide data for soil temperature and moisture to help recreate natural conditions within the lysimeter installed in the RESSAC facility. These data were collected via telemetric link by colleagues at RESSAC. Long -term monthly averages of climatic data for the HRI site, such as rainfall, air temperature and humidity, were also to be used to recreate the local climate within the RESSAC facility.

1.2 Technical Programme of Work for the UK lysimeter

Following a meeting of all partners (from Belgium, France, Germany, Spain and United Kingdom) of the EUROSOIL-RESSAC programme in December 1992, a technical programme was designed for the lysimeters of each partner. A schedule of crop-cultivation, crop contamination by radioactive aerosol using the POLYR facility, soil and crop sampling and crop harvesting was drawn up.

Each lysimeter surface was divided into two halves. Wheat (var. Arbon standard to all lysimeters) as sown on the western half (part B) of the UK lysimeter in March 1993; ryegrass (var Morenne) was sown on the eastern half (part A). The application of fertiliser and pesticides followed a treatment protocol for the UK lysimeter. Wheat was sown at different times on each lysimeter to produce crops at different growth stages at the time of contamination, scheduled for May 1993 for the UK lysimeter. The UK programme provided an exception in that grass instead of wheat was sown on the second half of the lysimeter, reflecting better agricultural practices, i.e. the use of pasture land, within the UK.

The postponement of the technical programme (see 1. above) led to a substitution programme. The ryegrass was cut at intervals during the summer and both crops were harvested from the UK lysimeter in August 1993 as part of the substitution programme (see 1.3). After harvesting of the wheat, clover (var. Alejandria, standard to all lysimeters) was sown on part A, to be cultivated as a green manure until re-commencement of the original programme in 1994

1.3 Substitution Programme for the UK lysimeter intended for 1993/94

In June 1993, each partner devised a substitution programme of work for their lysimeter to complement the original technical programme. The main areas of the UK programme involved:

(a) completion of the analysis of soils from each of the six lysimeters for physical and chemical properties;
(b) a characterisation of crops harvested from the UK lysimeter in August 1993;
(c) the establishment of a 'parallel' field plot at HRI Wellesbourne to compare crops grown in the field with those from the UK lysimeter in the RESSAC facility;
(d) tracer experiments with soluble forms of Sr-90 and Cs-137 to provide information on their interception and retention by wheat and ryegrass. The solutions of Sr-90 and Cs-137 would provide 'worst case' conditions with 100% bioavailability of the radionuclides. These data would then be compared with results from the original programme of crop contamination by the POLYR aerosol.

2 1993/94 PROGRAMME

2.1 COMPLETION OF THE SUBSTITUTION PROGRAMME

2.1.1 Physical and chemical analysis of soils from the six EUROSOIL-RESSAC lysimeters

In December 1993, a report of the analysis of soil samples from each of the six lysimeters was sent to each partner. The analysis was carried out by the Soil Survey and Land Research Centre at Silsoe in the UK. A range of physical and chemical properties were measured to characterise the soils to be used in the EUROSOIL-RESSAC programme. These properties included:

particle size distribution, organic carbon, cation exchange capacity, exchangeable and total cations, extractable and fixed ammonium, calcium carbonate and clay mineralogy.

2.1.2 Characterisation of crops harvested from the UK lysimeter in August 1993

Samples of ryegrass, wheat grain and straw were harvested from the UK lysimeter in August 1993. The wheat crop yield was evaluated for comparison with those from the other lysimeters In addition, a multi-element analysis of the UK crops was made. Results for the essential major and minor elements are shown in Table 1 and some are compared with typical values obtained from a databank of the Agricultural Development and Advisory Service (ADAS) in the UK. In general, the mineral levels were satisfactory but some deficiencies were found for trace elements. e.g. Mn concentrations in the wheat grain and straw were only around 20% of the typical value, while Fe concentrations reached only 50-60% of expected values.

TABLE 1 Elemental analysis of wheat and ryegrass crops grown on the UK lysimeter at Cadarache during 1993

Crop	Yield Dry Weight (g)	% Organic N	% P	% K	% SO_4-S	% Ca	% Mg	% Na
Wheat Grain	510	2.6 (1.5-2.5)	0.49	0.41	0.18	0.05 (0.2-0.4)	0.16 (0.11)	0.007 (0 14)
Wheat Straw	632	0 8 (0 5)	0 16 (0.07)	4.2	0.18	0.83 (0.15)	0.15 (0 11)	0.041 (0.14)
Ryegrass	-	2.6 (2-3)	0.72 (0.3)	4 7	0.35	0.85 (0 5)	0.29 (0.15)	0.081 (0.1-0.2)
Concentration of element (ppm)								
		Zn	B	Mn	Fe	Mo	Cu	Sr
Wheat Grain	-	19.9 (16)	nd	10 5 (58)	29.4 (62)	0.04	0.37 (8)	0.64
Wheat Straw	-	16.5	5 0	9.9 (40)	90.1 (148)	0.48	1 1 (3)	17.7
Ryegrass	-	28.9	11.0	27.9 (20-30)	134.0 (180-350)	4.5	2.4 (6-15)	15.0

Figures in parentheses are typical values obtained from Agricultural Development and Advisory Service (ADAS) data bank.

2.1.3 Establishment of a field plot at HRI Wellesbourne

In August 1993, a field plot was established at HRI Wellesbourne, near the site of the source of the UK soil monolith Ryegrass and clover were cultivated simultaneously with those on the UK lysimeter. The area of the field plot was identical to that of the lysimeter surface. The clover crops were harvested in January/February 1994 (prior to sowing of the wheat crop for re-commencement of the original programme), with the ryegrass periodically cut between August 1993 and May 1994. All samples were oven dried and yields recorded for the respective growth periods. These are given below:

Crop	Yield (g dry weight/m^2)	
	Wellesbourne	UK Lysimeter
Ryegrass	127	619
Clover	34	330

The yield of ryegrass from the UK lysimeter was around 5-fold greater than that from the field plot at Wellesbourne. The ryegrass in the field was only becoming established during August/September 1993, whereas that on the lysimeter was well established so the comparison is not ideal. The clover yield at Cadarache was about 10-fold that obtained under field conditions. Also, a comparison can be made of the yields of the wheat crop at Cadarache in 1993 (699 g dry weight of ears, 632 g of straw) with that of the crop produced at Wellesbourne in 1994 (394 g ears, 216 g straw). A 2 to 3-fold increase in yield of wheat grown under greenhouse conditions is observed. These differences reflect the differences between the actual and artificial climates and soil conditions prevailing at the two locations, despite attempts to reproduce the field climate within the RESSAC greenhouse.

2.1.4 Application of soluble forms of Sr-90 and Cs-137 to wheat and ryegrass

In July 1993, four small lysimeters of dimensions 60 cm x 60 cm x 40 cm were installed in a greenhouse at Harwell Laboratory. Each was filled to 30 cm depth with the UK soil type obtained from HRI Wellesbourne. Wheat and ryegrass crops were cultivated in the lysimeters (Nos. 1 & 2 for wheat, 3 & 4 for ryegrass). Varieties of crop, sowing rates and fertiliser application were identical to those used on the UK lysimeter at Cadarache. Irrigation was by hand according to long-term average rainfall data for Wellesbourne.

Just before the wheat crops flowered, soluble forms of Sr-90 (as nitrate) and Cs-137 (as chloride) were sprayed onto the four lysimeters to achieve contamination levels of 1 kBq/m^2 Sr-90 and 10 kBq/m^2 Cs-137. The spray was applied evenly by hand over each crop over 2 minutes. The average height of the wheat crop was 60 cm, with 'boots' being visibly swollen on the least advanced plants and the emergence of inflorescence was 75% complete for the more advanced plants. The decimal code for the growth stage of the wheat was 45 to 57. The grass crop averaged 20 cm height.

24 hours after contamination, half of the wheat from No.1 lysimeter and all grass from No.3 lysimeter were harvested. Two soil cores (11.4 cm^2) were taken from each of these lysimeters to 1 cm depth. One week after contamination, 10 mm of rainfall was applied to all four lysimeters. 24 hours later, the second half of wheat from lysimeter No.1 and all grass on No.4 were harvested The mature wheat crop from lysimeter No.2 was harvested in March 1994, processed and stored.

All crop samples were oven-dried at 105°C and ashed at 370°C. Soil samples were dried and ground. All samples were analysed by γ-spectrometry for Cs-137, followed by radiochemical separation and β-counting for Sr-90. From the analytical results obtained, interception and retention factors for Sr-90 and Cs-137 applied as a solution to wheat and ryegrass have been derived and are listed in Table 2.

TABLE 2 Interception and retention factors for Sr-90 and Cs-137 applied in solution to wheat and ryegrass

	Interception Factor (f)	Absorption Coefficient μ (m^2/kg)	Retention Factor
Sr-90 applied to wheat	0.53	2 3	0 80
Cs-137 applied to wheat	0 64	3.1	0.86
Sr-90 applied to ryegrass	0.29	3 4	0 58
Cs-137 applied to rye grass	0 37	4.6	0.64

The interception factor, f, is defined as the fraction of applied activity initially retained on crop.

$$f = \frac{Bq / m^2 \text{ (crop)}}{Bq / m^2 \text{ (crop)} + Bq / m^2 \text{ (soil)}}$$

The absorption coefficient is calculated from $1-f = \exp(-\mu B)$, where B is the biomass of the crop per unit area , kg (dry weight)/m^2 (Chamberlain, 1970).

The retention factor is defined as the fraction of material remaining on the crop after rainfall

$$\text{Retention factor} = \frac{\text{Activity in crop after rainfall (kBq / kg dry crop)}}{\text{Activity in crop before rainfall (kBq / kg dry crop)}}$$

The interception factors, f, for both Sr-90 and Cs-137 applied in ionic form as a solution to the wheat are comparable. i.e. 0 53 and 0.64 respectively This is also true for the ryegrass, i.e. 0.29 and 0.37 respectively. Clearly, a difference exists for interception of the radionuclides in the spray droplets between the two crops, although it must be noted that interception is dependent on aerodynamic effects and would be likely to differ according to meteorological conditions anyhow. The values for μ in Table 2 agree with literature values reviewed by Chamberlain and Garland (1991), although they might be expected to vary according to environmental conditions.

80% of the applied Sr-90 activity initially intercepted was retained by wheat after 10 mm of rainfall was applied a week after contamination, with 86% of Cs-137 retained. More activity was washed off the ryegrass, only 58% of Sr-90 and 64% of Cs-137 that were initially intercepted were retained in this case.

References: Chamberlain, A C (1970). Interception and retention of radioactive aerosols by vegetation. Atmos. Environ. 4,57-58.

Chamberlain, A C and Garland, J A (1991). Interception of radioactive fallout by vegetation. AEA Technology Report R-13826, HMSO, London.

2.2 RE-COMMENCEMENT OF THE ORIGINAL TECHNICAL PROGRAMME

Upon completion of the RESSAC facility at Cadarache, the original technical programme was re-commenced in early 1994. In March 1994, wheat was again sown on part B of the UK lysimeter, with the established ryegrass crop present on part A. The UK lysimeter was scheduled for contamination in June 1994.

2.2.1 Pre-contamination work on the UK lysimeter

Before contamination, the lysimeter surface was marked along its four sides at 10 cm intervals to provide a reference grid square system of the surface. This would allow the exact position of any sample taken from the lysimeter to be recorded.

Seven individual wheat plants were sampled randomly from the lysimeter. These were processed according to a method recommended by the Belgian team for Leaf Area Index (LAI) measurements. Images of the plant fractions obtained have been analysed by the conventional gravimetric method and by computer-aided Image Analysis at the University of Barcelona. The upper surface area of each plant, as measured by both methods, is listed in Table 3. In general, there was a good agreement between the measurements made by both techniques. Excepting the data for sample UKW7 (Table 3), plant fresh weight correlated well with surface area, $r = 0.965$, $p < 0\ 01$ The average height of the wheat crop prior to contamination was 55 cm, the grass height averaged 21 cm.

TABLE 3 Measurement of the upper surface area of wheat plants before contamination of the UK lysimeter

Sample Code	Fresh Weight (g)	Dry Weight (g)	Plant surface area (cm^2)*	
			gravimetric method	by image analysis
UKW1	16.13	1.71	470	477 (413)
UKW2	12.02	0 86	368	365 (337)
UKW3	15.27	1.62	463	473 (426)
UKW4	16.44	1.41	522	559 (503)
UKW5	10.39	0.88	349	345 (296)
UKW6	18 38	1.82	-	608 (525)
UKW7	20.24	0.54	279	286 (258)

*area is of stem + leaves (upper surface only).
Figures in parentheses are of leaves only.

Several interceptors were placed on and around the lysimeter At crop canopy level, 12 pairs of cellulose acetate filter papers of 47 mm diameter (6 on part A, 6 on part B), mounted on steel wire frames, were positioned to monitor the deposition of the POLYR aerosol. Also, five 5 cm diameter Petri dishes containing 5 g of 2 mm sieved lysimeter soil were placed on the soil surface within the wheat crop. A plan of the lysimeter surface, showing positions of the interceptors, is illustrated in Figure 1. Analysis of the interceptors allows the spatial distribution of the deposited aerosol to be determined.

Contamination of the UK lysimeter by the POLYR generated aerosol took place on 14 June 1994 following a protocol used for previous contaminations of the Spanish, Belgian and German lysimeters. The charge in the POLYR furnace consisted of some 14 elements, UO_2, and some 1840 MBq each of Sr-90 and Cs-137. One micron (1 μm) particulate material was formed in the contaminating aerosol.

2.2.2 Post-contamination sampling on the UK lysimeter

Three days after contamination, all interceptors were removed from the lysimeter. Five 10 cm x 10 cm squares of grass cut back to the grassy mat layer (measuring some 1-2 cm) above the soil surface were sampled randomly. Due to the poor physical state of the wheat crop (much of it had fallen over), 20 relatively upright wheat plants were selected and sampled. Six soil cores (5 cm diameter) were randomly sampled from the wheat area and one core was taken from each of the grass sampling areas to 5 cm depth.

2.2.3 Application of first rainfall post-contamination

To measure the amount and spatial distribution of the rainfall over the lysimeter surface, five plastic cups (70 mm diameter) and one rain gauge were placed in wire supports on each half of the lysimeter. In addition, four rainsplash samplers were placed on each half: each consisted of a strip of Whatman 41 filter paper measuring 1.5 cm x 20 cm supported on a wire frame

Six days after contamination, 10 mm rainfall was applied over some four hours to the lysimeter This was achieved by the overhead irrigation system that simulated rainfall as a fine drizzle. One day after application of rainfall various samples were taken All rainwater collection

vessels were removed and their contents transferred to plastic bottles. The rainsplash samplers were collected. Ten suitable wheat plants were sampled and a further five grass samples were taken at random. Three soil cores were taken from three of the areas of grass just sampled.

2.2.4 Sample preparation and analysis

All radioactively contaminated samples were transferred from the RESSAC greenhouse to the laboratory following a protocol recommended by the French team. The subsequent preparation, conditioning and analysis for Sr-90 and Cs-137 of all samples taken also followed protocols. A selected number of each type of sample taken, i.e. grass, wheat, soil, filter paper and rainwater were analysed for Cs-137 and Sr-90.

3 1994/95 PROGRAMME

Since the contamination and application of the first rainfall, irrigation of the lysimeter by the automated overhead irrigation system has been carried out by the RESSAC team at Cadarache, according to long-term monthly averages for the Wellesbourne site.

3.1 Further post-contamination sampling of crops from the UK lysimeter

The whole of the ryegrass area was harvested at intervals since contamination took place; grass was cut back to 3 to 5 cm in July, August and November 1994. Samples were taken by the UK team in August and the French team on the other occasions. Unfortunately, the November sample was lost. Analysis of these samples was intended to provide information on the soil-to-plant transfer of Sr-90 and Cs-137 from the aerosol deposited to the lysimeter surface, since all growth had occurred post-contamination and had not been exposed to direct contamination.

In August, the majority of the wheat crop had either died or was not mature. Some new tillers had emerged since contamination and were still immature. Consequently, only 14 mature tillers from three suitable sampling locations were sampled at this time. These would have been exposed to the deposited aerosol. Analysis of selected samples of grain, chaff and straw for Sr-90 and Cs-137 was made (section 3.3.8).

Harvesting of the mature wheat crop was delayed until February 1995. However, sufficient wheat remained for sampling and the grain was analysed for Sr-90 and Cs-137. It was likely that any Sr-90 or Cs-137 present in the grain would have been translocated within the wheat plants since these plants had not been exposed to direct contamination by the deposited aerosol.

3.2 Completion of analysis of selected samples for Sr-90 and Cs-137

During August 1994 and February 1995, the analysis of selected samples of all types originating from the UK lysimeter since contamination was completed. Due to constraints on time and on analytical resources only a proportion of all samples taken could be analysed: not all samples analysed for Cs-137 could be analysed for Sr-90 due to such constraints. Samples were selected for analysis to try and gain sufficient information on the fate of Sr-90 and Cs-137 deposited during contamination of the lysimeter.

3.3 RESULTS FROM MEASUREMENTS MADE ON UK LYSIMETER

3.3.1 Measurement of deposition of Sr-90 and Cs-137 during contamination

Deposition of Sr-90 and Cs-137 to the UK lysimeter during contamination was measured by analysis of the interceptors present (section 2.2.1). All 12 upper filter papers and 4 lower filter papers were counted for Cs-137, with 8 upper and 3 lower analysed for Sr-90 All 5 soils in

Petri dishes were analysed for Cs-137 only. Analytical uncertainties for both Sr-90 and Cs-137 were around 10%.

Deposition of Sr-90 and Cs-137 was in the following ranges:

Filters above grass:	Sr-90: 4.1-11.5 MBq/m^2	Cs-137: 5 7-8 9 MBq/m^2
Filters above wheat:	Sr-90: 3.9-12.3 MBq/m^2	Cs-137: 3.3-10 5 MBq/m^2
Soil in Petri dishes in wheat crop (part B):		Cs-137: 5.9-7 9 MBq/m^2

Average deposition of Sr-90 and Cs-137 is shown in Figure 2. The measurements indicate a degree of non-uniformity in the deposition of the aerosol, however average values are very similar for the two halves of the lysimeter as measured by the filter papers. Also, there is good agreement with the average deposition of Cs-137 to the soil/Petri dish interceptors. Cs-137 and Sr-90 activity on the lower filter papers (section 2.2.1) whose exposed surface faced downwards was only around 5% of that present on the upper filters.

Cs-137/Sr-90 ratios measured on the upper filter papers ranged from 0.55 to 2.1 (mean 1.07) on the grass half and from 0.78 to 0.84 (mean 0.82) for the wheat half. These ratios were similar on the corresponding lower filters, i.e 0.84 and 0.75 respectively.

3.3.2 Interception of Sr-90 and Cs-137 in aerosol deposited to ryegrass

The prevailing conditions during contamination of the crops were unrealistic to determine interception factors representative of natural environmental conditions. The lysimeter was fumigated rather than subjected to a wind driven deposition The experiment did not simulate the turbulent eddies that would be present in a natural environment. Therefore the following results obtained for interception factors must be treated with caution.

From analysis of the grass and corresponding soil cores sampled post-contamination (section 2 2.2), the fraction of deposited radionuclide initially retained by the grass, or interception factor f (described in 2.1.4), has been derived for Cs-137. These results are listed in Table 4 with more limited data for Sr-90.

TABLE 4 Interception of Sr-90 and Cs-137 in deposited aerosol by ryegrass.

SAMPLE CODE	Cs-137 (MBq/m^2)		Sr-90 (MBq/m^2)		Interception Factor f	
	on grass	on soil	on grass	on soil	Cs-137	Sr-90
UKG3	7.75	35.0	13.6	44.0	0.18	0.24
UKG4	15 8	15.1	-	18.3	0.51	-
UKG5	12.3	13.4	-	-	0 48	-
UKG6	23 0	7.50	43.4	-	0 75	-
UKG7	15.9	13.1	26.2	34.8	0.55	0.43

Note: sampling area of grass samples was 0.01m^2 and soil 0 00196m^2.

Between 18% and 75% of deposited Cs-137 was intercepted and retained by ryegrass. In deriving these values for f, it must be recognised that the Cs-137 activity measured on the soil includes that in the mat layer that is underlying the grass sward. Actual deposition to the bare soil surface will be less but was difficult to measure under the circumstances (although measured Cs-137 deposition to the soil surface under the wheat crop was found to be 2 to 3-fold less than that on the soil cores taken from under the grass). If this is the case , f values will be increased The data for Sr-90 are limited due to time constraints on analysis and are more

unreliable than the Cs-137 data due to analytical errors. Cs-137/Sr-90 ratios recorded in the grass (mean = 0 57) and soil cores (mean = 0.66), are low in comparison to those in the deposited aerosol measured using the interceptors.

Using a mean f value of 0.49 for Cs-137, and a measured mean biomass value, B, of 0.053 kg/m^2, a mean absorption coefficient, μ, of 12.7 m^2/kg is derived (see section 2.1.4). This value is rather high when compared with literature values from field experiments (Chamberlain & Garland, 1991). This perhaps reflects the unnatural experimental conditions.

3.3.3 Interception of aerosol by wheat

Due to the poor physical state of the wheat crop at the time of contamination, it is doubtful whether any useful information on the interception of the contaminating aerosol by wheat can be obtained. LAI measurements could not be completed, as the area of soil covered by the plants sampled (section 2.2.1) for this purpose could not be determined, due to the fallen wheat plants.

An average value for the surface area of the wheat plants, at contamination, has been derived (section 2.2.1). However, use of this parameter only, to determine an interception factor, rather than LAI measurements, would lead to an overestimation of the interception factor.

3.3.4 Retention of Sr-90 and Cs-137 by ryegrass and wheat after first rainfall

Calculation of the retention of Sr-90 and Cs-137 after rainfall is described in 2.1.4. Concentrations of Cs-137 in ryegrass after contamination ranged from 215 MBq/kg to 359 MBq/kg, averaging 274 MBq/kg. After 10 mm of rainfall, concentrations were in the range 56 to 148 MBq/kg, averaging 99 6 MBq/kg. Therefore, an average of only 36% of Cs-137 initially retained by the ryegrass remained after the first rainfall.

Corresponding average Sr-90 concentrations were 514 and 259 MBq/kg before and after rainfall respectively; 50% of Sr-90 initially present in the grass was retained after exposure to 10 mm rainfall applied as a fine drizzle over 4 hours.

The mean Cs-137/Sr-90 ratios in grass were 0.53 and 0.38 prior to and after rainfall respectively. These are notably different to the ratio measured in the aerosol during contamination, i.e. 0.95 This suggests either that there are relatively high errors in the sample analysis (probably in the recovery of Sr-90) or there has been a difference in the loss of Sr-90 and Cs-137 from the vegetation.

Measurement of Cs-137 activity in soil cores sampled from the ryegrass area post-rainfall (mean = 14 MBq/m^2) were similar to the pre-rainfall average of 16.8 MBq/m^2. Yet an average of some 8 MBq/m^2 was estimated to be removed from grass after rainfall, presumably washed to the soil surface. This imbalance may be attributed to some difference in the way the samples were taken pre- and post-rainfall, i e. perhaps more grassy mat above the actual soil surface was present on those sampled pre-rainfall; this matter could have contained a considerable amount of Cs-137

For wheat plants, concentrations of Cs-137 were between 10.1 and 295 MBq/kg (average = 147 MBq/kg) pre-rainfall and 22.8 to 198 MBq/kg (average = 87.2 MBq/kg) post-rainfall. On average, 59% of Cs-137 activity present was retained by wheat plants after 10 mm of rainfall.

For Sr-90, a retention factor of 0 96 was calculated Only pre-rainfall and 4 post-rainfall samples were analysed for Sr-90 and concentrations were quite variable, i.e. 80.5-346 and 91.6-315 MBq/kg, respectively An attempt was made to sample post-rainfall plants adjacent to those sampled pre-rainfall to try to minimise possible effects of a non-uniform aerosol deposit,

nevertheless the concentrations of both Sr-90 and Cs-137 in the wheat plants did vary considerably. Had more wheat plants been analysed for Sr-90 perhaps the retention factor for Sr-90 would be determined with a greater degree of certainty.

The average Cs-137/Sr-90 ratio in wheat plants was reduced from 0.86 to 0 60 after rainfall, which again implies that there may be a difference in the loss of Sr-90 and Cs-137 from the material present on the vegetation Analytical uncertainties may also be responsible, to some extent.

These retention factors may be compared to those derived in 2 1.4 for soluble forms of Sr-90 and Cs-137 sprayed on ryegrass and wheat. For wheat, these were 0.80 and 0.86 for Sr-90 and Cs-137, respectively, and for ryegrass these were 0.58 (Sr-90) and 0 64 (Cs-137). Again, higher retention was observed for wheat compared to ryegrass and with the exception of Sr-90 on wheat, the radionuclides in soluble form were better retained after rainfall compared with the particulate material deposited after contamination by the POLYR aerosol. The soluble forms of these radionuclides are more bioavailable than in the particulate material, hence the greater retention. It should be noted that rainfall amounts applied were the same but the duration and means by which it was applied differed in the two studies

3.3.5 Analysis of rainwater collected during first rainfall application

An attempt has been made to equate Cs-137 activity measured in collected rainwater with losses from grass and wheat plants after rainfall. Cs-137 levels in rainwater collected from the grass area of the lysimeter represented only 10% of that calculated to be removed from ryegrass in terms of MBq/m^2. Better results were estimated for the wheat. Average Cs-137 activity on the surface of the wheat plants was calculated to be 3.89 MBq/m^2 and 1.86 MBq/m^2 before and after rainfall respectively. Converting average Cs-137 concentrations (MBq/l) in collected rainwater to MBq/m^2 from knowledge of the area of the collection vessels led to an estimate of 1 4 MBq/m^2 for Cs-137 wash-off by rainwater. This accounts for 70% of Cs-137 measured to have been removed from the wheat plants by rainfall, i.e. 2.03 MBq/m^2. No corresponding Sr-90 measurements were made.

3.3.6 Rainsplash measurements

To try and identify possible contributions from soil-splash to Cs-137 activity present on vegetation after application of rainfall, 4 rainsplash samplers (described in 2.2.3) were placed on either half of the lysimeter The Cs-137 activity measured on selected samplers is illustrated in Figure 3 Each filter had an area of 7.5 cm^2. Very little Cs-137 was present on these samplers and activities measured were quite variable. On each sampler, highest Cs-137 activity was not always on the portion of filter paper closest to the ground (Figure 3), although relatively high analytical and experimental errors must be noted. It must be added that activity on these samplers could have originated from splash from vegetation or soil. Visual inspection of the filters nearest the soil surface did not indicate the presence of soil particles.

3.3.7 Temporal changes in radionuclide concentrations in ryegrass

Figure 4 shows the temporal change in average concentrations of Sr-90 and Cs-137 in ryegrass samples taken since contamination of the lysimeter (see section 3.1). In August 1994, radionuclide concentrations were two orders of magnitude lower than those immediately after contamination of the vegetation in June. Soil-to-plant transfer (including root uptake and the effects of resuspension) may contribute to concentrations measured in July and August, which might include some residual effects of the initial contamination. Rainfall applied to the lysimeter in July (48 mm) and August (66 mm) will probably have washed off some surface deposits, although exact resuspension and wash-off contributions are unknown

From average concentrations of radionuclides measured in soil after contamination (0-5 cm depth),i.e. 0.65 and 0 49 MBq/kg for Sr-90 and Cs-137, respectively, transfer factors have been derived and are shown below. These values are still high, even in August, compared to average soil-to-plant transfer factors quoted by the International Union of Radioecologists (IUR), i.e. 0.20 and 0.12 for Sr-90 and Cs-137 in ryegrass respectively. This indicates that resuspension of deposited material and the retention of initially deposited materials rather than soil-to-plant transfer, are probably the sources of contamination.

Rye grass sampled in	Transfer Factor	
	Sr-90	Cs-137
July 1994	13.5	10.8
August 1994	2.3	2.2

$$\text{Transfer Factor} = \frac{\text{Concentration in rye grass (MBq / kg)}}{\text{Concentration in soil (0 - 5 cm) (MBq / kg)}}$$

The average Cs-137/Sr-90 ratios in grass were. 0.61 and 0.71 in July and August respectively. Allowing for analytical uncertainties this is fairly constant, although it is less than that measured in the original deposited material

3.3.8 Sr-90 and Cs-137 in mature wheat harvested from the UK lysimeter

The range of concentrations of Sr-90 and Cs-137 measured in the mature wheat tillers sampled in August 1994, together with those in grain sampled in February 1995 are listed in Table 5.

TABLE 5 Concentrations of Sr-90 and Cs-137 in mature wheat

	Radionuclide Concentration (MBq/kg dry weight)			
Sampled in August 1994	Sr-90	Mean	Cs-137	Mean
Wheat grain	0.0186	-	0 587	-
Wheat chaff	0 207	-	1.49-2.30	1.76
Wheat straw	3.1 - 222	107	2.96-69.2	20.8
Sampled in February 1995				
Wheat grain	0.007-0.0118	0.009	0.361-0.587	0.376

From the data for the August sample, the relative distribution of activity in the three parts of the plants analysed is recorded. Cs-137 concentrations exceed those for Sr-90 in the grain and chaff, yet the mean Sr-90 concentration was 5 times greater than that for Cs-137. Analytical uncertainties (only one grain sample could be analysed from the August sample) or differences in the transfer of Sr-90 and Cs-137 from plant to grain may account for the difference in Sr-90 and Cs-137 activities in grain and chaff

Cs-137 concentrations in the wheat tillers sampled after the first rainfall in June 1994 were in the range 10.1 to 295 MBq/kg (mean = 147 MBq/kg). These may be compared with those sampled in August 1994 (Table 5); the average concentration was 7-fold greater in June which gives some indication of the loss of Cs-137 that has occurred during the two months The difference may also be due to the emergence of tillers post-contamination which were not

subjected to direct contamination by the aerosol. These tillers would probably have been contaminated by particulate resuspended from the older portion of the wheat crop.

Comparing the grain sampled in August and February, little difference in either Sr-90 or Cs-137 concentrations were recorded. This is perhaps surprising since much of the grain sampled in February was thought to have originated from tillers that emerged and developed after contamination with the aerosol. Analysis of the wheat straw harvested In February for comparison with that sampled in August may have confirmed this, however due to time constraints this could not be performed.

A coefficient of transfer for the radionuclides deposited to wheat defined by:

$$\frac{\text{Activity in grain (MBq / kg}}{\text{Activity deposited to soil (MBq / m}^2\text{)}}$$

has been derived based on average Cs-137 and Sr-90 activities in grain and soil. For the August grain these are 0.094 m^2/kg for Cs-137 and 0.0009 m^2/kg for Sr-90; in February 1995 these were 0.060 and 0.0004 m^2/kg for Cs-137 and Sr-90 respectively.

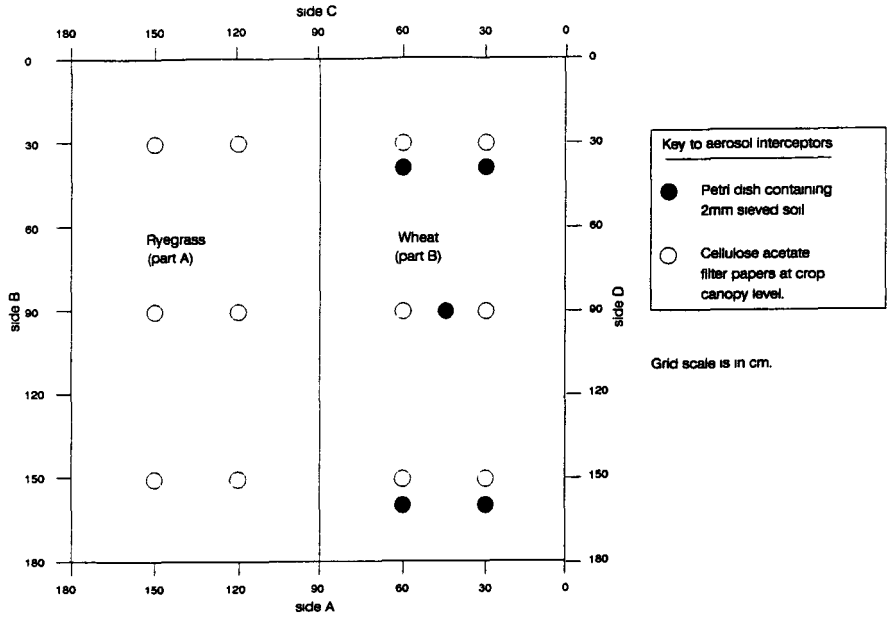

Figure 1 Plan View of Surface of UK Lysimeter Before Contamination by the POLYR aerosol.

Figure 2

Average Deposition of Sr-90 and Cs-137 to UK Lysimeter During Contamination by POLYR Generated Aerosol.

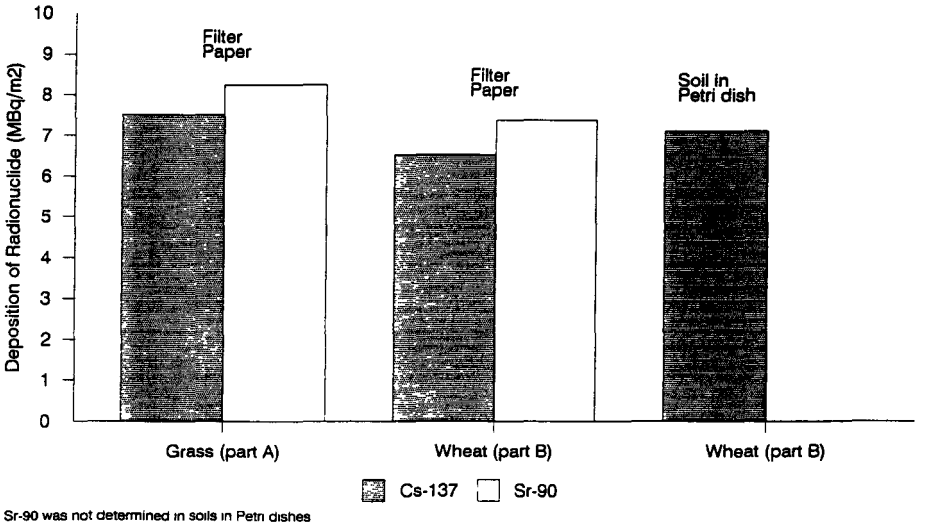

Sr-90 was not determined in soils in Petri dishes

Figure 3 Cs-137 Activity on Rainsplash Measurement Filters

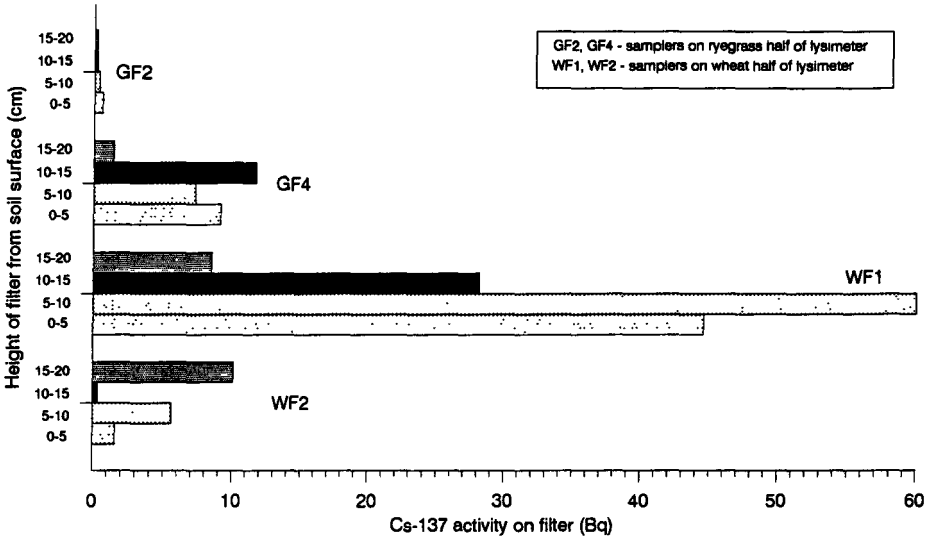

Figure 4 Temporal Changes in Average Sr-90 and Cs-137 Concentrations in Ryegrass.

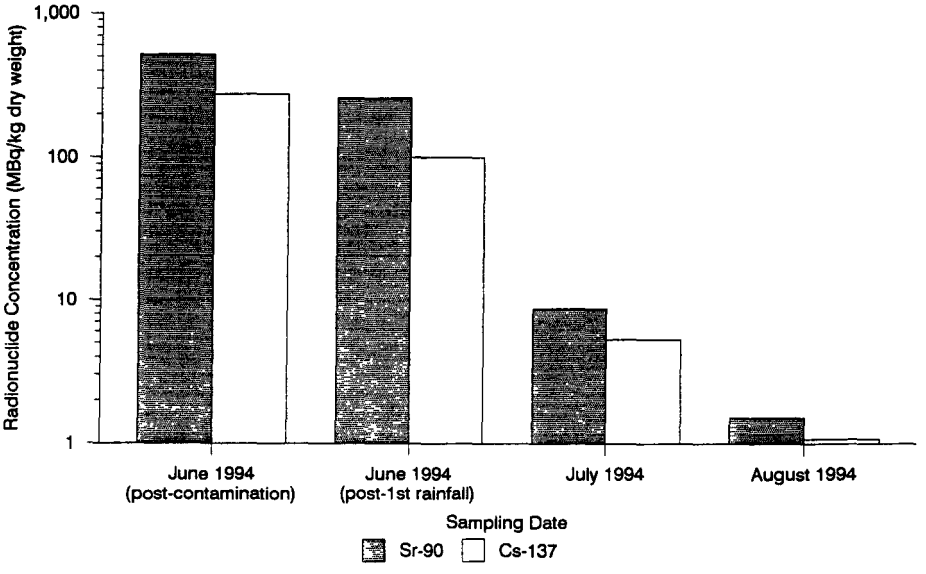

Head of project 3: Dr. Vandecasteele

II. Objectives for the reporting period

These were as follows:

Agriculture. - comparison of growth of wheat, barley and rye-grass grown on the RESSAC lysimeter and field plots (growth pattern, yield and nutritional status: in collaboration with FSAGx)

Radioecology: - interception of Cs and Sr by young wheat plants (early tillering, 3 leaves)
- wash-down effect of application of first rain one week after contamination
- translocation of Cs and Sr in wheat (straw, ears)
- countermeasure: ploughing under of wheat on one half of the lysimeter surface and re-sowing wheat on one half and rye-grass on the second half of the ploughed part
- comparison of soil-to-plant transfer of Cs and Sr in wheat and grass on ploughed area
- gather preliminary information on the behaviour of aerosol and ionic radiocesium and radiostrontium in the selected European soils (substitution programme)
- to provide data on the soil to plant transfer in plants grown at the experimental site in Mol, which will be compared to the values obtained under controlled conditions at Cadarache

III. Progress achieved including publications

1. Preparation activities and preliminary tests (programme 1992-1993)

A whole range of preparation and preliminary activities was carried out during the period 1991-1993, part of which form part of the Substitution Programme agreed for the year 1993

1.1. Field studies in European sites foreseen for lysimeter sampling (1992)

The SCK/CEN was asked to provide a typical sandy podzol. In order to reproduce in the RESSAC greenhouse at Cadarche climatic conditions as comparable as possible to those that are specific for the region where the monolith originates form, several relevant parameters were measured over more than one year, from winter 91 until winter 92. Therefore, the zone of the monolith was instrumented with tensiometers and temperature sensors at different depths until 1.2 m below the ground level (AXONE data acquisition unit). The collected data were transferred to the CEA Cadarache (by modem). In addition, other climatic data (air temperature and humidity, rain frequency and intensity, sunshine frequency and intensity) were measured locally or obtained from the national meteorological stations network. All the data were transmitted to the RESSAC staff at Cadarache.

1.2. Lysimeter sampling and installation (1992)

In spring 1992, the place for the monolith extraction was prepared. A preliminary test was conducted to observe the stability of a large sand block surrounded by trenches, especially the hold of the angles. These observations led to some modifications of the extraction procedure of the monolith (which was originally described for more compact loamy-clayey soils). One week prior to excavation, the soil water table was lowered by pumping around the place of the lysimeter extraction. The excavation and sampling of the monolith was succesfully performed during the third week of August 1992. After conditioning, the lysimeter was transported by truck to Cadarache to be installed in the RESSAC greenhouse (November - December 1992) During meetings with all participants, general agreements were made on prophylactic and fertilization plans to be followed and on the optimization of the growth conditions in the lysimeters.

1.3. Substitution programme (1993)

Due to delays in the installation of the required equipment in the RESSAC greenhouse, the contamination which was foreseen for 1993 was postponed by one year and a substitution programme was planned. In agreement with the CEC representatives, it was decided to make use of the uncontaminated material present in the lysimeter to check for the realism of the growth conditions

recreated in the greenhouse by measuring the production yield and plant mineral content and to gather preliminary information of the adsorption and desorption behaviour of aerosol radiocesium and -strontium in the European soils selected.

1.3.1. Check for the realism of the growth conditions (1993)

In the beginning of 1993, the Belgian lysimeter installed in the RESSAC greenhouse was divided into two equal parts by a stainless steel oriented north-south and sown in lines with spring wheat (Triticum aestivum L., var. Arbon). In August 1993, the plants were harvested from each half of the lysimeters, line per line, and separated into straw and ears. The mean germination was about 90% for the two half plots. It was somewhat higher in the western part (93%) than in the eastern part (87%). The production yield obtained for the whole surface indicated a very good productivity (5.9 tons Fresh Weight/ha for grain and 7.2 tons F.W./ha for straw), i.e. more than what can be expected in the field. This may be due to the better climatic conditions in the lysimeter building at Cadarache, since the instrumental equipment fails to fully generate the colder temperatures recorded for the Mol podzol soil (particularly in winter, spring and autumn). The production was also higher in the western part of the lysimeter than in the eastern part (by 33% for straw and 7% for grain). The relative values between the production of grain and the total production indicate that the western part shows a relative higher yield of straw (18%). This may be due to the localisation of the aeration system in the greenhouse, combined with a heterogeneous circulation of air. The higher humidity (48% versus 32% humidity for the eastern part) may partly explain this higher production.

Samples of the vegetation of all lysimeters (including those at the field site in SCK/CEN, Mol) were prepared for further analysis of their major mineral content (measurements performed by FSAGx, Gembloux; see their report) For the Mol podzol soil, K, Ca, Mg and Na concentrations in both grains and straw were comparable for the experimental site at SCK/CEN (Mol) and in the greenhouse at Cadarache. P and N contents were significantly higher in plants grown on the experimental site at Mol than those grown in Cadarache.

1.3.2. Study of the adsorption and desorption behaviour of aerosol and ionic radiocesium and -strontium in the selected European soils (1993)

In September 1993, 300 g (air dried) of the 6 soils in the RESSAC greenhouse and the 4 ones present at Mol were exposed to Cs-134 and Sr-85 aerosols generated by the POLYR furnace. At the same time, paper filters were exposed in the contamination chamber to study the spatial variation of the deposit.

A comparison between the average deposition on the filters with that on the ten soils showed that soils tend to be systematically more contaminated than paper filters. The ratios between the deposition (Bq/m^2) on soils and filters were 1.37 ± (Standard Error) 0.10 for Cs and 1 16 ± 0.05 for Sr. This observation can be related to the higher roughness of soils compared to the filters. Large differences between the soil types could be observed, depending on the smoothness of the surface presented to the deposition. The bare soils from Jülich and Tricastin, for example, trapped 80% more Cs and 40% more Sr per unit area than the filters, while the Terra Rossa from Spain showed the same deposition as the filters. The difference observed between the two isotopes is probably due to different physico-chemical properties of the aerosol particles they are associated with.

Batch experiments were performed in order to gain more information on the Cs and Sr adsorption and desorption capacity in each soil type after contamination by the POLYR aerosols or by ionic forms (spraying with a contaminated aqueous solution of chloride forms of ^{137}Cs and ^{85}Sr). Three methods were used to test the availability of deposited radionuclides:

a) physical extraction (by centrifugation; 20000g) of the interstitial soil water ("soluble forms").

Kd-values for Cs ranged in all soils between 10^4 and 10^5 dm^3/kg, except for sandy ones showing a value of $10^3 dm^3/kg$, regardless of the source term and ageing. For ionic Sr the Kd values ranged between 12 and 34 dm^3/kg. Sr as aerosols was less available than as ionic form (higher Kd values). Ageing of the samples (5 months) augmented soluble forms of aerosol Sr in interstitial soil waters (close to ionic Sr)

b) chemical extraction with 1 N NH_4Ac ("potentially available fraction"):

Between 15% and 35% (loamy soils) and 50% (sandy soil) of Cs could be extracted, with slightly higher extraction yields for ionic Cs. No significant effects were observed after five months of ageing. The extraction yield of Sr was clearly influenced by the source term. 50% to 80% for the ionic forms

and 11% to 35% for the aerosols. After five months of ageing, the extractable fraction of the aerosol form increased, for most soils by a factor of two.

c) infinite bath extraction (Prussian Blue) ("potentially available fraction of Cs"):

This method, specific for Cs, confirms the trends and conclusions drawn for (b).

As a conclusion, it can be stated that Cs as aerosols (POLYR) and as ionic forms is readily soluble and both species behave similar. Sr as aerosols (POLYR) is less soluble than as chloride form but ageing results in higher solubility and availability.

2. Study of the transfer of deposited radionuclides, including the effect of some countermeasures (programme 1994-1995): lysimeter at Cadarache

The experimental programme initially foreseen for 1993 was carried out in 1994. Spring wheat (var. Arbon) was sown again and exposed to the deposition of radioactive aerosols at a given development state.

2.1. Contamination and subsequent characterization (april 1994)

The Belgian lysimeter (podzol) was contaminated on April 14, 1994, when the wheat was in the 3 leaves vegetation stage The plants were about 15 cm high and the green biomass was 0 0169 ± (S.E.) 0.001 kg DW/m² (covering some 20 % of the soil surface). The Leaf Area Index, defined as the ratio of *total* leaf surface (m²) and total soil surface (m²) was 0.31 ± 0.02. Deposition levels were measured on filters (ground level and vegetation level), soil (between rows and under crops) and on the crop itself. 7 days after the contamination, the first rain (10 mm) was applied and contamination levels on the different materials were measured again. The green biomass at this moment was 0.0172 ± 0.001 kg DW/m².

Results of these measurements are presented in table 1. Deviations with respect to average values were about 10-15% for most measurements. It should be stressed that activity levels on crops, expressed as Bq/m², are calculated as the activities intercepted by the total amount of (green) biomass (Bq/kg dry material) standing on 1 m² total surface (Bq/kg dry material divided by kg dry material/m²).

Table 1: Results on deposition levels (Bq/m²) in the Belgian lysimeter (contamination 14/04/94); D and R refer to deposition levels before and after rainfall, respectively, F = filter at ground level; FH = filter at vegetation level; S = soil between rows; SUC = soil under crop; C = crop; *RW = concentration of Cs and Sr in rain water intercepted under plants (in Bq/liter!)* Standard errors are given in parentheses. I.F. refers to the Interception Factor and was calculated with respect to the different substrates measured after deposition. Sr/Cs refers to the Sr to Cs ratio in the different substrates.

material	Cs-137 Bq/m²	Sr-90 Bq/m²	Sr/Cs	I.F. Cs	I.F. Sr	Sr/Cs
DF	1.33(0.05)E7	2.02(0.06)E7	1.56(0.04)	0.155	0.186	1.20
DFH	9.74(0.33)E6	1.71(0.13)E6	1.66(0.02)	0.213	0.220	1.03
DS	1 26(0.03)E7	2.05(0.02)E7	1.65(0.01)	0.165	0.184	1.12
DSUC	1.16(0 11)E7	1.72(0.16)E7	1.51(0 08)	0.178	0.219	1.23
DC	2.07(0 15)E6	3 76(0 33)E6	1.66(0.01)			
RS	1.41(0.02)E7	2.17(0 12)E7	1.62(0.13)			
RSUC	1.37(0.10)E7	2 05(0 18)E7	1 51(0 09)			
RC	9.04(0.53)E5	1.79(0.22)E6	2 00(0.31)			
RW	*1.19(0.21)E4*	*3.05(0.42)E3*	*0 22(0.02)*			

The deposition was not homogeneous throughout the lysimeter surface: differences up to about 60% were observed, although in general differences were smaller (±15%) This rather heterogenous deposition results in rather high variations (standard errors) of the activity levels measured in the different samples taken, as can be seen in the following tables (tables 2 to 5) The interception by crops was some 5% higher on the eastern part of the lysimeter, while contamination levels on filters and soil surfaces were some 5% higher on the western part of the lysimeter Furthermore, different deposition levels were observed for the different materials. The highest deposition was measured on the filters at

ground level, the lowest on the filters at the vegetation level. Soil deposition levels between rows were very similar to those of the filters at the ground levels. Soil deposition levels under crops were only slightly lower than between rows, which is evidently related to the small coverage by the crop at this growth stage (some 20%) Accordingly, the deposition on the crop (Bq/m²) was about 5-6 times lower than the deposition on filters and soils (Bq/m²).

Interception Factors - calculated as the ratio of Bq/m² (crop) and Bq/m² (total deposition) - were somewhat higher for Sr than for Cs **[0.16-0.21 (Cs) and 0.18-0.22 (Sr)]**, indicating a stronger retention of Sr than Cs. Interception factors agree very well with the fraction of soil surface which is covered by plants (some 20%; this value differs strongly from the *LAI value* defined above, which considers *the total leaf surface of all leaves*). This agreement is very likely due to the absence of turbulences during the time of deposition, as a result of which the results obtained for interception factors are not representative for those to be expected in natural environmental conditions (wind driven deposition).

Cs activities in the wash-off water were higher than Sr activities (Sr/Cs ratio 0.22), again showing that Sr is stronger retained than Cs (after rainfall, the Sr/Cs ratio on the wheat plants had slighly increased to 2.00).

Retention Factors - defined as the ratio of Bq/kg dry crop after and before rainfall - are **0.44 (Cs) and 0.48 (Sr). Thus, <u>at this stage of 3 leaves</u>, sprinkling with uncontaminated water very shortly after contamination of the crops can leach a considerable fraction (> 50%) of the activity initially deposited.** The increase of contamination of soils is higher for Cs than for Sr (due to its higher leaching succeptibility), but remains rather low (which was expected in view of the low interception by plants).

2.2. Countermeasure: conventional ploughing and re-sowing with spring-wheat and rye-grass

2.2.1. Agricultural aspects

After the second sampling, the eastern half of the lysimeter was ploughed (in fact: digging by spade), as a countermeasure, and rye-grass (Lolium perenne L , part C, north-east) and spring wheat (var. Arbon; part B, south-east) were sown each on a half of the ploughed part. Conventional ploughing as a countermeasure aims to reduce the external irradiation dose and to prevent resuspension effects, by diluting the deposited activity in the (30 cm) ploughing layer. At this early stage of growing (3 leaves), re-sowing of wheat is still possible and therefore tested as a countermeasure. Re-sowing with rye-grass is a countermeasure which principally aims at reducing the resuspension risks (permanent pasture). Spring wheat was sampled in June 1994 and harvested in August 1994. At this moment, soil cores (1-6 cm depth) were taken in order to analyze the radioactivity profile in the soil. Rye-grass was periodically cut between June 1994 and July 1995

2.2.2. Spring wheat (1994)

With 4360 kg grains/ha (F.W) and 3908 kg straw+chaff/ha (F.W.), the 1994 yield of spring wheat is much lower than the 1993 yield (5900 and 7200 kg/ha respectively) but comparable to the yield normally observed for this type of soil (4000-5000 kg grains/ha). The lower straw yield is partly due to the use of a "shortening agens" which is applied in order to prevent the fall of the wheat at higher vegetation stages. The wheat in part A was allowed to stand longer than that of part B (which was resown after contamination). Therefore, the wheat in part A contains a higher weight % stems and a lower weight % leaves than that in part B.

In case of direct (foliar) contamination, the **Translocation Factor** is defined as the ratio of Bq/m² at time t>0 and Bq/m² at the time of deposition (assuming that only a negligible fraction of the activity in the crop is due to root uptake; <u>table 2</u>) These results warrant various comments. In both cases, only a very small fraction of the activity initially deposited on the wheat plants (3 leaves vegetation stage) is finally retained by the plant (0.5% and 2.6% for Cs and Sr, respectively). However, Cs and Sr appear to behave differently. For cesium, the total activity in the crop continues to decrease [1 0% (June) and 0 5% (August) of the initial activity] and a small translocation from the straw to the ears is observed during this period [2833 Bq/m² in August versus 2055 Bq/m² in June). For strontium, the total activity in the crop increases [1.3% (June) and 2.6% (August) of the initial activity]. This indicates that strontium is also taken up indirectly by those roots which are close to the soil surface. So, the assumption of a negligible contribution by root uptake does not apply for strontium, and hence the calculated Translocation Factors for Sr is not useful.

The different behaviour of Cs and Sr reflects their different behaviour in the soil. Cs is characterized by a specific and only partially reversible adsorption on micaceous minerals (although poorly present in this sandy podzol: 7.3% illite/smectite interstratified). Consequently, Cs deposited on the soil becomes rather strongly adsorbed on the solid phase, rendering it less available for uptake and vertical migration. Sr, on the other hand, is characterized by a straightforward ion exchange reaction involving the regular ion exchange sites (also poorly present in this sandy podzol: Cation Exchange Capacity = 0.12 Eq/kg). Therefore, Sr is more available for root uptake and more succeptible to vertical migration (towards the surroundings of the upper roots). The higher vertical migration of Sr versus Cs can also be deduced from the analysis of the activity levels in the soil (table 5; only 1 measurement available). For the activities in the 0 to -1 cm layer (part A), a Sr/Cs ratio of 1.20 is found, while the Sr/Cs ratio at the time of deposition was 1 65 (table 1).
The decrease of the yield of straw (August versus June) is due to the decrease of the mass of leaves (the mass of straw increased from 0.181 kg (June) to 0 233 (August) kg DW/m²

Table 2: Yields (kg dry weight/m²), specific activities (Bq/m² dry material) and translocation data for spring wheat grown on part A (foliar contamination) of the Belgian lysimeter at Cadarache (standard errors in parentheses)

date of sampling	organ	yield (kg DW/m²)	^{137}Cs (Bq/m²)	Translocation Factor Cs	^{90}Sr (Bq/m²)	Translocation Factor Sr
140494	total plant	0.017	2 07(0.15)E6		3.76(0.33)E6	
210694	ears	0.060	2055 (657)	9.9 E-4	1810 (245)	4.8 E-4
210694	straw	0 292	17830 (3212)	8.6 E-3	47703 (3347)	1.3 E-2
300894	grains	0.334	1767 (360)	8.5 E-4	*11905 (643)*	*3.2 E-3*
300894	chaff	0 092	1066 (108)	5.2 E-4	*(grains+chaff)*	
300894	straw	0.262	7070 (515)	3.4 E-3	87055 (4420)	2.3 E-2

Table 3 Yields (kg dry weight/ha), specific activities (Bq/kg dry material) and transfer factor data (m²/kg) for spring wheat (var. Arbon) grown on the Belgian lysimeter (standard errors in parentheses)

Organ	yield (kg DW/ha)	^{137}Cs Bq/kg	TF ^{137}Cs (m²/kg)	^{90}Sr Bq/kg	TF ^{90}Sr (m²/kg)	Sr/Cs ratio
			part A (foliar contamination)			
grains	3338	5293 (1078)*	n.a.	d.n.a.	n.a	d.n.a.
chaff	920	11594 (117)*	n a.	d.n.a.	n.a.	d.n.a.
ears	4258	8697 (1100)	n.a.	27960 (1514)	n.a.	3.2
stem	2332	21188 (1799)	n.a.	259541 (7560)	n.a.	12.3
leaves	288	73921 (4279)	n.a.	921193 (92709)	n.a	12.5
straw	2620	26988 (1964)	n.a.	332323 (3459)	n.a.	12 3
total plant	6878	15658 (1393)	n.a.	143750 (2271)	n.a.	9.2
			part B (root uptake)			
grains	3212	5611 (2784)	4 45(2.21)E-4	d.n.a.	d.n.a.	d.n.a.
chaff	887	13329 (5889)	8.10(4 67)E-4	d.n.a.	d.n.a.	d.n a.
ears	4099	6778 (3745)	5.38(2.97)E-4	37881 (18300)	1.85(0.73)E-3	5.6
stem	1764	8419 (2767)	6 68(2.20)E-4	245936 (49179)	1.20(0.20)E-2	29.2
leaves	620	22252 (9135)	1.77(0 73)E-3	947464 (66543)	4.62(0.27)E-2	42.6
straw	2384	9940 (3419)	9 54(3.45)E-4	428333 (43841)	2.09(0.21)E-2	4 3
total plant	6483	8713 (3961)	6 92(3 14)E-4	187048 (33848)	9.12(1.65)E-3	21.5

* results not validated yet by IPSN/DPEI/LMRE; d n a. = data not available yet, n.a. = not applicable

Table 3 gives a summary on specific activities (Bq/kg) and transfer factors (TF, only applicable in case of root uptake) calculated for the different organs and for the total plant. Transfer factors were

calculated as the ratio of Bq/kg dry material (grain, chaff, ears .) and Bq/m² initially deposited activity on the soil (table 1) Particularly for part B (root uptake), Standard Errors are very high (reflecting differences of a factor 3 to 5 for the different replicates). This is principally the result of the heterogeneous activity profile in the ploughed soil layer, which on its turn may be a result of the way of ploughing (digging by spade). These variations are confirmed by analysis of Cs and Sr activities in the soil (table 5).

Because of these high standard errors, it is difficult to make statistically significant statements about the effect of conventional ploughing as a countermeasure. Considering the average data, a reduction by a factor of 2 of the Cs activity in the total plant is observed, but this reduction stems from a reduction of the activity in the straw Conventional ploughing does not affect the Cs activities in the grain. For Sr, there seems to be an increase of the activity, both in the ears and in the straw. This is of course due to the high availability and hence high transfer of Sr in this poor sandy soil. Similar results have been reported for the Terra Rossa soil by the Spanisch team. **As far as the grains are concerned, conventional ploughing at this vegetation stage of 3 leaves has no (Cs) or an adverse (Sr) effect on the activities in the grains.**

TF's (m²/kg) are in general one order of magnitude higher for strontium than for cesium. This is of course due to the difference in adsorption behaviour of both radionuclides in the soil, which was already discussed. The high soil-to-plant transfer of Sr is also reflected in the Sr/Cs ratio in the plants or plant organs. Immediately after contamination (april 14, 1994), the Sr/Cs ratio on the plants was 1.66, and 7 days later, after the first rain, 2.00. At the end of the growth, Sr/Cs ratios for the total plant had increased to 9.2 (foliar contamination) and 21.5 (root uptake).

2.2.3. Rye-grass (1994-1995; part C)

The production of rye-grass seems to be higher in the lysimeter at Cadarache than in the field This difference reflects the difference between the actual and artificial climates and soil conditions prevailing at the two locations, despite attempts to reproduce the field climate within the RESSAC greenhouse (table 4).

Table 4: Yields (kg fresh weight/ha), dry weight (%), specific activities (Bq/kg dry material), transfer factor data (m²/kg) and Sr/Cs ratio for rye-grass grown on the Belgian lysimeter at Cadarache and at the experimental site in Mol (standard errors in parentheses)

date of sampling	kg/ha FW	DW %	^{137}Cs Bq/kg	TF ^{137}Cs (m²/kg)	^{90}Sr Bq/kg	TF ^{90}Sr (m²/kg)	Sr/Cs ratio
Cadarache							
210694	5886	11.0	57056(20875)	4.53(1.66)E-3	729246(179080)	3.56(0.87)E-2	13
110794	7426	10.5	33670 (794)	2.67(0.06)E-3	n.d.	n.d.	n.d.
260794	6556	12.2	17053 (300)	1.35(0.02)E-3	n.d.	n.d.	n.d.
110894	4219	11.7	15607 (664)	1 24(0.05)E-3	n.d.	n.d.	n.d
300894	2849	16.8	23305 (4167)	1.85(0.33)E-3	520151 (95098)	2.54(0.46)E-2	22
041094	5180	16 1	14533 (953)	1 15(0 08)E-3	n.d.	n.d.	n.d.
100395	2154	28 2	11331 (2020)	0 90(0 16)E-3	d.n.a	d.n.a.	d.n a
050595	9216	18.7	4181 (856)	3 32(0 68)E-4*	d.n.a.	d.n.a	d.n.a
050795	3943	25.4	4161 (1409)	3 30(0 79)E-4*	d.n.a.	d.n.a	d.n.a
Mol (4 plots)							
041094	1913 (741)	16 8(0 9)	163 (26)	3 39(0.54)E-4	2880 (309)	8.73(0 94)E-3	18
060495	6073 (577)	17.8(0.5)	84 (3)	1 74(0 07)E-4	2459 (420)	7.45(1.27)E-3	29
110595	14040 (438)	18.7(0.2)	267 (6)	5 57(0.12)E-4	d.n.a.	d.n a.	d.n.a.
300695	9349 (559)	26.2(0 6)	d.n.a	d.n.a	d n a.	d n a.	d.n.a.

* results not validated yet by IPSN/DPEI/LMRE; d n a. = data not available yet,
n a. = not applicable, n.d. = not determined

The low yield and transfer factors observed for the experimental site in Mol in October 1994 is probably due to the fact that the rye-grass in the field was only becoming well-established in spring 1995. Only for May 1995, when the rye-grass in Mol was well established, Cs transfer factors measured at Mol and at Cadarache coincide.
The transfer of Cs towards rye-grass has decreased with a factor of 10 over the 12 months period studied. This decrease is of course due to the effect of ageing which is well-known for the cesium sorption on illite containing soils. Also Sr root-uptake has decreased (by some 35%) in the first months after the contamination, but it is not clear yet whether this decrease will continue. According to the literature data Sr availability and uptake is expected to remain high, since for Sr no specific adsorption reactions are known. Furthermore, it is seen that Transfer Factors for Sr are ten about times higher than for Cs, a value which is also proposed by the International Union of Radioecologists (IUR).
It may be of interest to calculate the total Cs activity withdrawn by ryegrass versus spring wheat. The total Cs activity withdrawn by spring wheat (harvested on 30/08/94), is 53 MBq/ha (i.e. 18, 12 and 24 MBq/ha for grains, chaff and straw, respectively). For ryegrass, this is 96 MBq/ha (until 30/08/94, i.e. the date of the harvest of spring wheat) and 126 MBq/ha (until 05/07/95, i.e. the last measurement). Thus, **during the same period (until 30/08/94), the export of Cs activity by ryegrass is almost twice as much that of spring wheat.**

2.2.4. Contamination of soils

The soil cores sampled in August 1994 were analyzed for the Cs or Sr activity in the upper 1 cm (= 0 to -1 cm) and one lower 1 cm layer (≈ -6 to -7 cm) of the core. Results are presented in table 5 For part A (direct contamination, not ploughed), both Cs and Sr are nearly quantitatively present in the upper 1 cm layer, and the Cs contamination is similar for the different samples. The Sr/Cs ratio is 1 20, which is lower than the value measured at the time of the deposition (1 65; table 1). This lower value points to a higher vertical Sr migration. For parts B and C (one ploughing treatment), Cs and Sr activities vary considerably both vertically and horizontally (i.e. for Cs between samples), which is due to the way of ploughing (digging by spade). These spacial variations may explain the variations observed for Cs and Sr activity in plant material.

Table 5: Cs and Sr activities (Bq/kg dry soil) in the Belgian lysimeter (August 1994)

sub-plot	treatment	depth	sample	^{137}Cs (Bq/kg)	^{90}Sr (Bq/kg)
part A	no ploughing	0 to -1 cm	1	961	1156
	"	"	2	855	n.d.
	"	"	3	904	n.d.
	"	-6 to -7 cm	1	0.93	5.97
	"	"	2	5.01	n.d.
	"	"	3	1.01	n d.
part B	1x ploughing	0 to -1 cm	1	6.17	10.94
	"	"	2	9 46	n.d.
	"	-6 to -7 cm	1	0.07	0.14
	"	"	2	0.17	n.d.
part C	1x ploughing	0 to -1 cm	1	14 98	28.26
	"	"	2	19.71	n.d.
	"	-6 to -7 cm	1	511	442
	"		2	24.55	n.d.

2.3. Further post-contamination sampling of the Belgian lysimeter

2.3.1. Agricultural aspects

After the August harvest, part A (western part) was diveded in part A (south-west) and part D (north-west), part D receiving an extra fertilization of 40 tons/ha of cow manure (the composition of which is, unfortunately, unknown). All areas (except part C with rye-grass) were ploughed (A and D for the first time, B for the second time) and clover (Trifolium pratense L., var Alejandria) was sown as an

intermediate culture to be used as green manure. Clover was sampled in October 1994 (2x1dm²) and was digged into the soil for parts A and D (2nd ploughing), after which winter barley (Hordeum vulgare L., var. Orblonde) was sown. Unlike part A, part D was extra fertilized with 900 kg/ha Thomaskali (8% P_2O_5, 15% K_2O, 6% MgO). In March 1995, clover on part B was digged into the soil (3rd ploughing) and spring wheat (var. Arbon) was sown. Winter barley and spring wheat were harvested in July and August 1995, respectively.

2.3.2. Clover (1994)

Yields obtained for clover are rather similar for the three different sub-plots (table 6). The values obtained at the experimental site in Mol are not representative due to the very dry summer of 1994 (see section 3.3.2.). Transfer factors for Cs and Sr are higher for the lysimeter in Cadarache than for the experimental plots.

For part A and D, both Cs and Sr concentrations in the plant show high spacial variations, which again point to the heterogeneous Cs and Sr activity profile in the arable soil layer caused by ploughing with a spade. For part B, which was ploughed two times before the clover sowing, spacial variations are much smaller, pointing to a less heterogeneous profile of the Cs and Sr activity in the arable soil layer after a second ploughing treatment. For Cs, data for part A and D are similar, indicating that the cow manure added on part D has no effect on the Cs uptake in clover. Cs uptake in part B is lower as compared to parts A and D, which may be caused by the increasing dilution (and specific adsorption) of Cs in the soil profile with more ploughing treatments. Sr concentrations in the clover are almost three times higher in part A (which was not fertilized with cow manure) as compared to part D, the reason herefore likely being an increased complexation with the organic matter in the cow manure. Sr concentrations in part B are about 50 % lower than in part A, which again may be due to the dilution of the Sr activity in the soil profile.

Table 6. Yields (kg/ha), dry weight (%), specific activities (Bq/kg dry material), transfer factor data (m²/kg) and Sr/Cs ratio for clover grown on the Belgian lysimeter at Cadarache and at the experimental site in Mol (standard errors in parentheses)

sub-plot or treatment	kg/ha wet	DW %	^{137}Cs Bq/kg	TF ^{137}Cs (m²/kg)	^{90}Sr Bq/kg	TF ^{90}Sr (m²/kg)	Sr/Cs ratio
			Cadarache				
partA	1943 (383)	13.8	28771 (7540)	2.28(0.60)E-3	3255737 (525173)	1.59(0.26)E-1	113
partD	1700 (315)	12.2	27436 (6718)	2.18(0.53)E-3	1216389 (302603)	5.93(1.48)E-2	44
partB	1598 (223)	14.9	20978 (1900)	1.66(0.15)E-3	2047510 (215196)	9.99(1.05)E-2	98
			Mol (4 plots)				
not-ploughed	1188 (632)	19.7 (0.4)	1216 (283)	2.53(0.59)E-3	10404 (532)	3 15(0.16)E-2	9
ploughed	1023 (205)	19.0 (0.1)	437 (34)	9 11(0.70)E-4	12614 (2804)	3.82(0.85)E-3	29

d n.a. = data not available yet

2.3.3. Winter barley (1995)

There is a significant difference in the yield of winter barley grown on part A and D: 5272 (part A) versus 4462 (part B) kg/ha grains (Fresh Weight), and 5594 (part A) versus 11629 (part D) kg/ha straw + chaff. However, winter barley in part D was not fully mature (part D lies close to the only concrete wall in the lysimeter building), which may explain the lower yield of grains. Harvest at complete maturity would probably have resulted in higher yield of grain in part D, but this was not possible for practical reasons. Anyhow, the higher yield of straw and chaff in part D may be directly the result of the extra fertilisation with cow manure and Thomaskali (see 2.3.1.). The crop material was processed in order to measure Cs and Sr activities in the different plant parts. Until now, only a few samples have been measured (table 7) but data are not validated yet by IPSN/DPEI/LMRE. From the results, it is

seen that extra fertilisation (part D) has no significant effect on the Cs content in the different plant organs

Table 7: Yields (kg dry weight/ha), specific activities (Bq/kg dry material) and transfer factor data (m^2/kg) of winter barley (var Orblonde) grown on the Belgian lysimeter (not validated data; standard errors in parentheses)

Organ	Yield kg DW/ha	^{137}Cs Bq/kg	TF ^{137}Cs (m^2/kg)	^{90}Sr Bq/kg	TF ^{90}Sr (m^2/kg)	Sr/Cs ratio
			part A			
grains	4620	2083 (657)	1 65(0.52)E-4	d.n.a.	d.n a.	d.n.a.
chaff	800	6531 (1742)	5 18(1.34)E-4	d.n.a.	d.n.a.	d.n.a.
straw	2870	4145 (1494)	3.29(1.19)E-4	d.n a.	d.n.a.	d.n.a.
			part D			
grains	3170	1740 (142)	1 38(0.11)E-4	d.n a.	d n.a.	d n.a.
chaff	1210	4061 (612)	3.22(0 49)E-4	d.n a.	d.n a.	d.n.a.
straw	4790	4811 (464)	3 82(0.37)E-4	d.n.a.	d.n.a.	d.n.a.

d.n.a. = data not available yet

2.3.4. Spring Wheat (1995)

The 1995 yield of spring wheat was rather low: 3182 kg/ha grains FW and 3529 kg/ha straw and chaff This may be due to the fact that spring wheat was cultivated during three succeeding years on part C This is reflected by the rather small germination (about 70%). Spring wheat was processed in order to measure Cs and Sr activities in the different plant parts (straw, chaff and grain) but data are not available yet

3. Study of the transfer of deposited radionuclides, including the effect of some countermeasures (programme 1994-1995): experimental site at MOL (in collaboration with FSA,Gembloux)

3.1. Preparative work

At the experimental site of the SCK/CEN in Mol, field plots of the same dimension (4m^2) as the RESSAC lysimeters have been installed The arable fertile layer (30 cm) of the original podzol soil was replaced with that of four different soil types from the surroundings of the Belgian sites Tihange, Chooz, and of Mol. The pedological characteristics of the three additional soil types to the already existing Mol podzol lysimeter (orthic podzol) are comparable to two French and the German lysimeter soil present in the RESSAC building.

1 dystric cambisol (comparable to acidid cambisol from Flamanville); "sol brun acide, Chooz"
1 calcaric cambisol (comparable to calcaric fluvisol fro Tricastin); "sol brun calcaire, Tihange South"
1 orthic luvisol (comparable to orthic luvisol from Jülich); "sol brun lessivé, Tihange North"

A sample of each soil type was taken for granulometry analysis and thorough physico-chemical characterization (FSAGx, see their report). In spring 1994, all plots were sown with spring wheat (var. Arbon).

As it was not possible to contaminate these plots directly with radioactive dry aerosols generated by POLYR, it was firstly decided to apply the POLYR aerosol as a wet deposit, after recovering the radioactive particles from the first pocket around the furnace. Wash-off of radioactive aerosols trapped on the POLYR furnace pocket yielded in very low percentage i e. less than 3.5 % Therefore, it was decided to recover those particles deposited beside the furnace, trapping them in a receptable containing a few centimetres of water. During the contamination of the Belgian lysimeter in Cadarache, 1.635 liters of contaminated water were collected, containing 3.16 E7 Bq Cs-137 and 2.14 E7 Bq Sr-90.

3.2. Contamination and agricultural practices

On 4/07/94, the 16 field plots were contaminated, each with 100 ml of the contaminated solution, resulting in contamination levels of 0.48 MBq/m^2 Cs-137 and 0 33 MBq/m^2 Sr-90 (Sr/Cs ratio = 0 69)

Since the wheat culture on the lysimeters was grown too high to ensure a homogeneous contamination, the contamination took place directly on the soil, after wheat harvesting and ploughing. Afterwards, one half of each plot was ploughed again, and rye-grass was sown on one half (part B) of the ploughed part, while clover was sown on the rests of the plots (part C+A+D). Because of the very dry summer of 1994, we observed a very bad growth for the two crops. Therefore, clover and rye-grass were sown again in september 1994 (without ploughing manipulations).

Table 8 Yields (kg fresh weight/ha), dry weight (%) and transfer factor data (m^2/kg) for rye-grass and clover grown on the field plots at the experimental site in Mol (standard errors in parentheses); transfer factors are calculated as the ratio of Bq/kg dry material and Bq/m^2 total deposition.

date or treatment	kg/ha FW	dry weight %	TF ^{137}Cs (m^2/kg)	TF ^{90}Sr (m^2/kg)	Sr/Cs ratio
		RYE-GRASS			
		≈Flamanville			
041094	4215 (1256)	16 5 (0 5)	1 09(0.25)E-4	3 88(0.03)E-3	24
101194	957 (137)	12.8 (0 3)	n.d.	n.d.	
060495	11028 (576)	16.0 (0.2)	3.81(0.54)E-5	3.13(0.39)E-3	56
110595	18804 (634)	18.3 (0.2)	2.56(0.57)E-5	d.n.a.	
300695	9405 (355)	26.3 (0 4)	d.n.a.	d.n.a.	
		≈Jülich			
041094	3335 (1354)	16 6 (0.7)	1.39(0.14)E-4	3.33(1.39)E-3	17
101194	891 (249)	12.9 (0.4)	n.d.	n.d.	
060495	8588 (1415)	16 2 (0.3)	3.46(0.57)E-5	5.92(1.29)E-3	118
110595	17771 (1090)	18.0 (0.2)	1.74(0 07)E-5	d.n.a.	
300695	10860 (457)	24 6 (0.6)	d.n.a.	d.n.a.	
		Mol			
041094	1913 (741)	16.8 (0.8)	3.39(0 54)E-4	8 73(0.94)E-3	18
101194	727 (139)	12.7 (0 2)	n.d.	n.d.	
060495	6073 (577)	17.8 (0.5)	1 74(0.07)E-4	7.45(1.27)E-3	29
110595	14040 (438)	18.7 (0 2)	5 57(0.12)E-4	d.n.a.	
300695	9349 (559)	26.2 (0 6)	d.n.a.	d.n.a.	
		≈Tricastin			
041094	3231 (1250)	17.3 (0 8)	1.78(0.37)E-4	5.75(2.62)E-3	22
101194	822 (225)	14.1 (1.1)	n.d.	n.d.	
060495	8040 (827)	17.0 (0 2)	3 67(0.15)E-5	2.95(0.49)E-3	55
110595	16615 (1130)	18.1 (0 5)	2 10(0.14)E-5	d.n.a.	
300695	9954 (763)	27.3 (0 5)	d n.a.	d.n.a.	
		CLOVER			
		≈Flamanville			
not-ploughed	387 (-)	18.6 (--)	-	1.92(-----)E-2	-
ploughed	8117 (3785)	17.7 (0.6)	1 75(0 19)E-4	1.16(0.14)E-2	46
		≈Jülich			
not-ploughed	-	-	-	-	-
ploughed	4303 (4019)	18.5 (0.8)	2.46(0.62)E-4	1 18(0 15)E-2	33
		Mol			
not-ploughed	1188 (632)	19.7 (0 4)	2.53(0.59)E-3	3.15(0.16)E-2	8 6
ploughed	1023 (205)	19 0 (0.1)	9.11(0 70)E-4	3.82(0 85)E-2	29
		≈Tricastin			
not-ploughed	1513 (320)	18.6 (0 2)	8 49(0.46)E-4	9.58(1.18)E-3	7 8
ploughed	4634 (3437)	18.8 (1 0)	2.65(0 75)E-4	8.86(0.83)E-3	18

d.n.a. = data not available yet; n d. = not determined

In October, crops were harvested (rye-grass also in november 1994) All parts of the plots, except the part with rye-grass, were ploughed and winter barley (var Orblonde) was sown on parts A and D (only once ploughed) Part D (two times ploughed) was sown with spring wheat (var. Arbon) in april 1995

Winter barley and spring wheat were harvested in July and August, respectively. The crops are now being processed for analysis of yield and Cs and Sr activities.
So far, very few data have been obtained from the crops grown in these field plots. Results are summarized in table 8. From these results, it is seen that the Cs transfer to rye-grass and clover is about a factor of 3 to 5 higher in the Mol podzol as compared to the other soils, which could be expected in view of the lower specific sorption properties for cesium generally observed for this type of soil. For Sr, transfer factors are similar for the 4 soils, which also could be expected in view of their similar Cation Exchange Capacities. Furthermore, it is seen that ploughing reduces the Cs transfer factors for clover, which is a "shallow rooting" crop, by a factor of about 3. Ploughing, however, does not reduce the Sr transfer factors in these soils. These different effects are directly linked with the different soil chemical behaviour of both radionuclides (specific and but partially reversible cesium adsorption versus non-specific and almost completely reversible strontium adsorption). Similar results have been observed for the spring wheat grown in the Belgian lysimeter in Cadarache (section 3.2.2)
The results obtained for the Mol podzol were also given in the tables 4 and 6, for comparison with the results obtained on the Belgian lysimeter at Cadarache

4. General conclusions

4.1. Comparison of the yield of wheat grown in the lysimeter and at the field plots (Mol)

In the first year, the yield obtained in the lysimeter at Cadarache was higher than in the field, most probably due to the better climatic conditions prevailing in the lysimeter (higher temperatures, i e. the equipment fails to impose the climatic conditions recorded for this soil). Moreover, a spacial variation of the yield is observed for the wheat in the lysimeter, which is probably linked with the presence of a concrete wall at one side of the lysimeter, and the presence of aeration systems (resulting in different "micro-climates").

4.2. Adsorption and desorption behaviour of aerosol versus ionic form of Cs and Sr

Cs as aerosol (POLYR) and in ionic form is readily soluble and both species behave similar. Sr as aerosol (POLYR) is less soluble than as chloride form but ageing results in higher solubility and availability All soils show a rather similar adsorption and desorption behaviour for Cs, exept the podzol from Mol, which shows a lower Cs adsorption and desorption capacity. For Sr, all soils behave rather similarly (i.e. low adsorption and desorption capacity).

4.3. Interception by spring wheat at the 3 leaves vegetation stage

For this scenario, with no or very little turbulence during the deposition - and therefore not representative for natural environmental conditions - , the interception of aerosol Cs and Sr is directly related with the percentage coverage of the soil by the plant (about 20 %). 10 mm rain applied 7 days after contamination removed about 50 % of the activity initially present. Therefore, sprinkling with non-contaminated water very shortly after deposition may be an effective countermeasure (at this vegetation stage of 3 leaves). The bivalent Sr is stronger retained than the monovalent Cs.
At harvest, only about 0.5 % of the cesium initially intercepted is retained by the plant (with a small translocation occurring from the straw towards the grains). It is unlikely that Cs, which is still present at the soil surface (no ploughing), is taken up by the roots. For strontium, specific activities (Bq/kg dry material) are higher at harvest (August) than in June, indicating that Sr - which is more succeptible to leaching than Cs - is also taken up by the roots (beside translocation after foliar contamination). At harvest, 2.6% of the Sr activity initially deposited is found in the total plant.

4.4. Ploughing and re-sowing spring wheat and rye-grass as a countermeasure

Conventional ploughing at this vegetation stage of 3 leaves, followed by re-sowing, has no (Cs) or an adverse (Sr) effect on the activities in the grains Cs activities in straw are reduced by a factor of 3, but Sr activities have slightly increased (by a factor of 1.3). Considering however the higher irradiation doses and the risks of resuspension, ploughing of the contaminated surface may be considered as a countermeasure (eventually to be postponed till after the harvest).
During the same period (from 14/04/94 to 30/08/94, i.e. harvest of spring wheat), the withdrawal of Cs activity by rye-grass (MBq/ha) was almost twice as high as the value calculated for spring wheat.

4.5. Further post-contamination sampling of the Belgian lysimeter

Addition of cow manure (containing organic material) decreased the Sr transfer to clover with a factor of 3, but had no effect on the Cs transfer. The transfer of both isotopes decreases as the number of ploughing treatments increases, indicating that this is due to the increasing dilution of the Cs and Sr activity in the soil profile. So, the effect of conventional ploughing in order to dilute the Cs and Sr activity in the 30 cm zone seems to reach a maximum effect only after several ploughing treatments.
Addition of cow manure and Thomaskali results in higher yields of winter barley, but it has no influence on the transfer of both Cs and Sr towards the plant

4.6. Comparable field study at the experimental site in Mol

In most cases, yields recorded at the experimental field plots in Mol are lower than yields measured in the lysimeter in Cadarache. This clearly demonstrates the difference between the actual and the artificial climates and soil conditions prevailing at the two locations, despite attempts to reproduce the field climate within the RESSAC greenhouse. Furthermore, it is seen again that conventional ploughing reduces the transfer of Cs (no data available yet on Sr).
Finally, it is seen that the Cs transfer is about 10 times higher in the sandy Mol podzol than in the 3 other loamy soils. This is most likely due to the higher adsorption and fixation potential of these 3 soils, compared to the Mol podzol (conclusion from the substitution programme). Since the adsorption and desorption characteristics of Cs and Sr in the different soils proves to be important in regard to the soil to plant transfer, a detailed study of these soil characteristics will be subject of the proposal for the 1996 programme.

3.5. Publications

Since it was agreed to write some joint publications once all the results are available, no publications have been written so far by the Radio-ecology Laboratory of SCK/CEN Mol.

Head of Project. 4: Dr. V.R. Vallejo. Universidad de Barcelona.

II Objectives for the reporting period.

Global objectives

The general aim of this research was the study of the fluxes of radionuclides in a Mediterranean agricultural ecosystem contaminated by condensed particles, in the framework of a NPP accident The main objectives for the first phase were to adjust the greenhouse installations to close to real field conditions, to test its performance by simultaneous cropping in the field and in the lysimeter, and to establish comparisons between the soil types and climates selected. The main experiments were conducted maintaining the same crop for all lysimeters; the research was focused in analysing radionuclide interception by vegetation, foliar uptake, effect of the first rainfall after contamination and radionuclide root absorption at different stages of plant growth comparing two agricultural techniques, conventional ploughing and mulching.

Specific objectives.

The specific objectives for the University of Barcelona group in the reporting period 1992-95 are described as follows:

A) Installation.

1st. Crop comparisons between the lysimeter from Spain in Cadarache and the real field conditions in Spain: Monitoring the phenological development of the crops during their growth and evaluation of crop production at harvesting (1993-95)

B) Exploratory pot studies.

2nd. In pot experiments, evaluation of the effectiveness of *'deep-placement* and *conventional ploughing* as countermeasures after deposition of radionuclides on the soil surface, paying special attention to the role of the root distribution with respect to the radionuclides location in the soil profile (1993-94).

C) Lysimeter studies.

3rd Study of the deposit homogeneity and plant interception after contamination at two different stages of plant growth (1994).
4th. Study of the foliar uptake after contamination and effect of the first rainfall (1994).
5th Radionuclide content in soil solution and exchangeable form (1994).
6th. Radionuclide accumulation at the first harvest after contamination (1994).
7th ^{137}Cs and ^{90}Sr root absorption at different plant growth stages (1995).

To achieve these objectives, the activities that follow were performed in collaboration with CIEMAT

III Progress achieved including publications.

A) Installation.

1st. Crop comparisons between the lysimeter in Cadarache and the real field conditions in Spain (1993-95).

The control system of the climatic conditions in the greenhouse of the RESSAC building has been tested through the growth characteristics of the crops cultivated simultaneously in the lysimeter and in the real field in Barcelona, using the same cultural practices. Careful monitoring of phenological development of plants in the lysimeter and real field was carried out. At harvesting, production analysis was carried out at both sites. Also, a detailed chemical analysis for wheat and clover cultivated in 1993 was carried out. The crops and cropping period are described as follows, and the main characteristics at harvesting are summarised in *Table I.*

1993 Wheat: Part A (East): January-July.
Part B (West) February-July.
Clover: Part A, B July-December.
1994 Wheat: Part A (East): January-July.
Part B (West): March-July.
1995 Barley: Part A (East)-Mulching, Part B (West)-Ploughing: October 94-July 95

Table I. Comparisons of crop production data between the lysimeter in Cadarache and Experimental Fields in Barcelona.

	Wheat 1993		Wheat 1994		Barley 1995	
(Data per m^2).	Part A (East)	Part B (West)	Part A (East)	Part B (West)	Part A (East) *Mulching*	Part B (West) *Ploughing*
Spanish lysimeter.						
Total weight (g of d.w)	2437 7	1553 7	558 7	791 5	773 6	1342.7
Total weight of grain (g of d.w)	941 1	629 6	159.0	226 8	399.5	704 3
Total weight of straw (g of d.w)	1496 5	924 1	399 7	564.7	374 1	638 4
Number of ears	552 5	429 6	454 2	472 0		
Total number of grains	15179 0	10581 5	4367 8	6685 4		
Grains/ears	27 5	24 6	9 6	14 2		
Experimental Fields (Barcelona).						
Total weight (g. of d.w)	749 0	535 0	662.5	721 3	420.4	716 7
Total weight of grain (g of d w)	287 0	207 8	192.4	201.1	111 5	223.9
Total weight of straw (g of d w)	462 0	327.3	470 2	520 2	308 9	492 8
Number of ears.	329 3	276 8	421 2	412 5	213.2	310 8
Total number of grains.	7285 0	5275 5	7670 2	7978 5	3223 7	6480 0
Grains/ears	22 1	19 1	18 2	19 3	15 1	20 9

The climatic greenhouse conditions in Cadarache (lower temperature and irradiation and a regular irrigation) performed during the year 1993 could be the reason for the crop vegetative stage prolongation with respect to the more stressed real conditions in Barcelona. This may have resulted in the higher production was obtained in the lysimeter with respect to the real crop in Barcelona. The production in field conditions in Barcelona (2870 kg grain/ha) was a medium-low value for dry farming in Mediterranean zone versus the extremely high production in the greenhouse conditions in Cadarache (9411 kg grain/ha) For the period 1994 differences between the crop in the lysimeter and in the real field conditions in Barcelona were lower than for 1993 in agreement with the regulations of the climatic conditions in the greenhouse In 1995, the extraordinary dry and hot conditions in the early summer produced an anormally poor grain filling of barley in the experimental fields of Barcelona as compared with the average conditions reproduced in the greenhouse. As is often the case, the first year of application of no-tillage (with mulching) produced a reduction of the crop yield.

Detailed chemical analysis of wheat and clover samples.

The chemical analysis were performed by IPC technique in the Spectroscopy Service of the University of Barcelona. Differences observed in macronutrients (P,K) between lysimeter and field crops, these differences are attributed to somewhat different growing conditions in climate which caused a delay in the maturation of wheat in the greenhouse. Other differences may probably be related to the quality of the rainfall-irrigation water (Ca, Mg, Na, Sr) A disparity has been observed for Al and Fe in the wheat straw samples which could be due to contamination from soil particles in the samples from Barcelona. Comparing part A and B, the global trends of wheat straw analysis from field conditions showed higher concentration values in part B. This fact could be the result of the different growth degree of maturation of each part at harvesting.

B) Exploratory pot studies.

2nd. Evaluation of the effectiveness of *deep-placement* and *conventional ploughing* as countermeasures (1993-94).

1. Experimental design and sampling. Study of root distribution.

Sunflower plants (*Helianthus annuus* var. Tesoro) were cultivated in the same soil of the lysimeter. A total soil surface of 1.6 m^2 (volume of 29.95 dm^3), previously sieved at 2 mm., was contaminated by the POLYR device, being the initial activity deposited: 1.46 $MBq.m^{-2}$ and 0.17 $MBq.m^{-2}$ for ^{85}Sr and ^{134}Cs respectively. The contaminated surface was homogenised in the total soil volume. The final values of soil concentration obtained were 4.58 $Bq.g^{-1}$ for ^{134}Cs and 54.08 $Bq.g^{-1}$ for ^{85}Sr. The total soil volume was distributed in equal parts in each of the 16 experimental pots. 4 treatments were compared (4 replicates per treatment):

Three of the treatments consisted in placing a 1cm thick layer of contaminated soil at different depths.

1st. - At soil surface Treatment S.
2nd. - At 15 cm depth. Treatment 15.
3rd. - At 30 cm depth. Treatment 30

The fourth treatment consisted in mixing the contaminated soil through the upper 15 cm of soil, being the final concentration after mixing 0.43 $Bq.g^{-1}$ for ^{134}Cs and 5.73 $Bq.g^{-1}$ for ^{85}Sr.

4th. - Simulation of conventional ploughing. Treatment M.

The entire experiment was carried out in duplicate (two series): one in a greenhouse in Cadarache, and the second series in real field conditions in Barcelona. In each series, three samplings were performed at different stages of plant growth. At each sampling time, four replicates of groups of leaves were separated by growth stage: leaves in expansion and fully expanded (*See Table I in CIEMAT report*). Root mass distribution at depth was determined through root sampling by drilling in parallel not contaminated pots (*Figures 1a, 1b*). ^{134}Cs contamination was in many cases under the detection limit, in theses cases, was considered the half of the detection limit value with a standard error of the 100%.

2. Results and discussion.

Leaves and root biomass (*Figures 1a, 1b*) showed higher values for the 2nd. series than for 1st., which could be explained by the different climatic conditions of the greenhouse of Cadarache (lower temperature and irradiation) where the 1st. series was carried out in comparison with real conditions in the Experimental Fields of Barcelona. In both series, the leaves-root ratio obtained is considered in the normal range for this plant. The higher root mass was measured between 5 to 15 cm depth, being its higher growth between 2nd. and 3rd. samplings in coincidence with the development of the groups L3 and L4 of leaves.

2.1Temporal changes in the radionuclide absorption.

First Series:
For ^{85}Sr, considering in each sampling the group of most recently expanded leaves, a displacement in the absorption has been observed (*Fig 2a: 1A, 1B. 1C*) in relation to the root growth. At the initial stages of growth for group L1 (*Table II*), the maximum absorption appears in the treatment S (*Fig. 2a: 1A*) and the lowest in 30. In the second sampling, and regarding the group L2, these values tend to converge (*Fig. 2a: 1B*). At the third sampling, (*Fig. 2a 1C*), the absorption of the groups L3 and L4 of the 30 treatment are higher than the groups L3 and L4 of the S treatment, thus confirming the displacement of the absorption root area.

Second Series:
For ^{85}Sr, the absorption was higher than the first series in relation to the higher root mass obtained, as well as similar displacement in the absorption in relation to the root growth. Maximum absorption of group L1 in the first sampling, and the groups L2, L3 and L4 tend to converge at the second and third sampling (*Fig. 2b: A, B, C*)

2.2 Comparison between treatments.

Considering final absorption in each treatment, an inverse relation between ^{85}Sr and ^{134}Cs absorption in both series has been observed, which could indicate a different root absorption model for both radionuclides, and greater susceptibility of ^{134}Cs to clay fixation than ^{85}Sr [1,2]

Table II. Comparisons between treatments of ^{85}Sr and ^{134}Cs concentration in leaves (in Bq/g of d.w).

First Series

Treatment	^{85}Sr (Bq/g)	(Std)	^{134}Cs (Bq/g)	(Std)
S	6,427	0,384	0,030	0,013
15	8,173	0,482	0,030	0,014
30	10,431	0,168	0,014	0,003
M	7,843	0,645	0,023	0,007

Second Series

^{85}Sr (Bq/g)	(Std)	^{134}Cs	(Std)
8,253	2,734	0,010	0,003
4,444	2,620	0,014	0,009
4,412	3,219	0,027	0,005
5,755	1,911	0,011	0,004

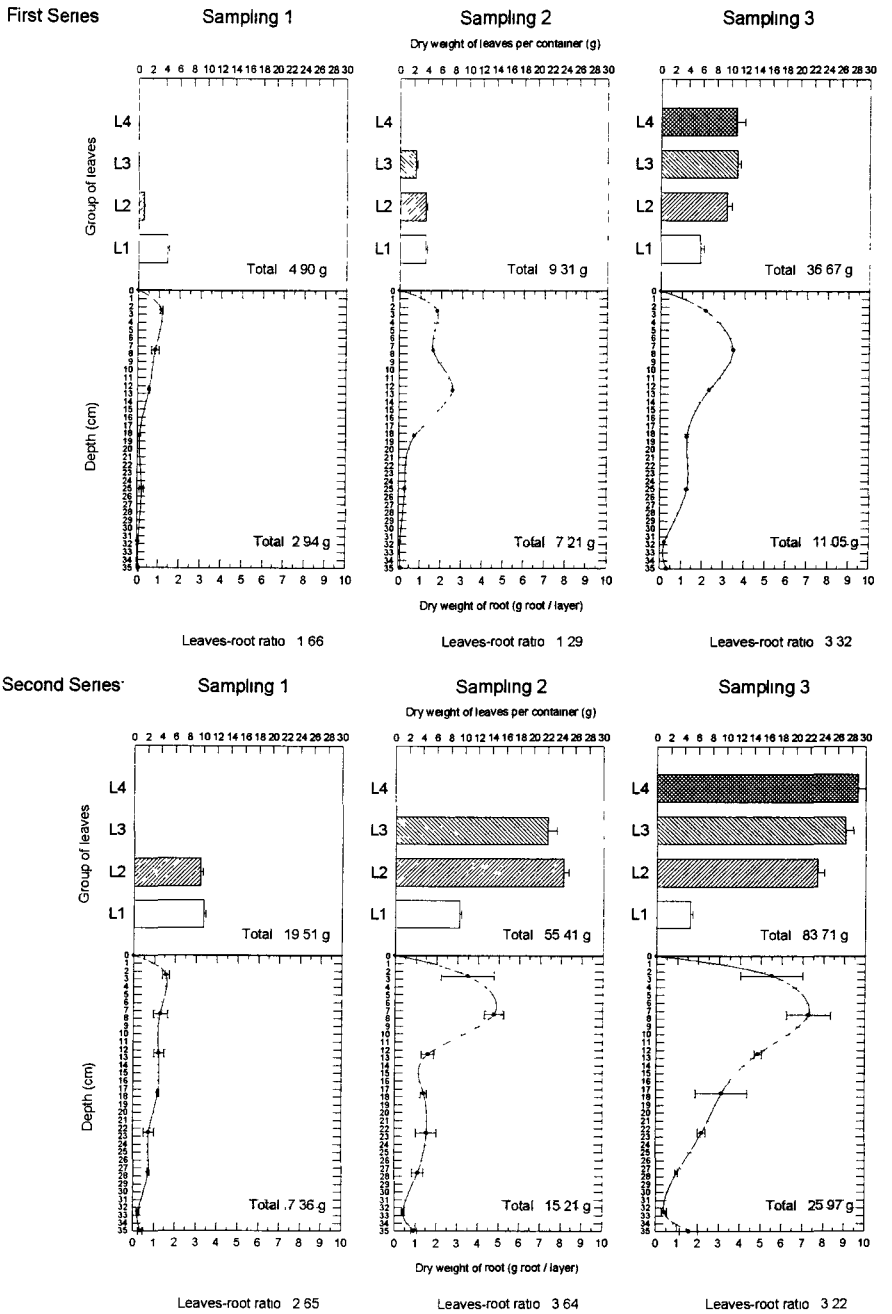

Figures 1a, 1b Plant growth dynamics. The dry weight of each group of leaves and the root growth pattern with depth (g. of dry weight) is shown for each series of experiments and sampling times.

First Series.

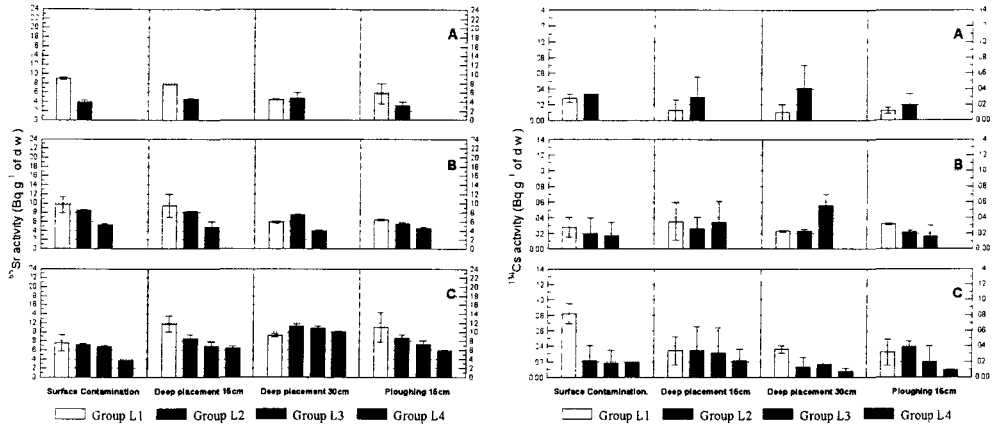

Second Series.

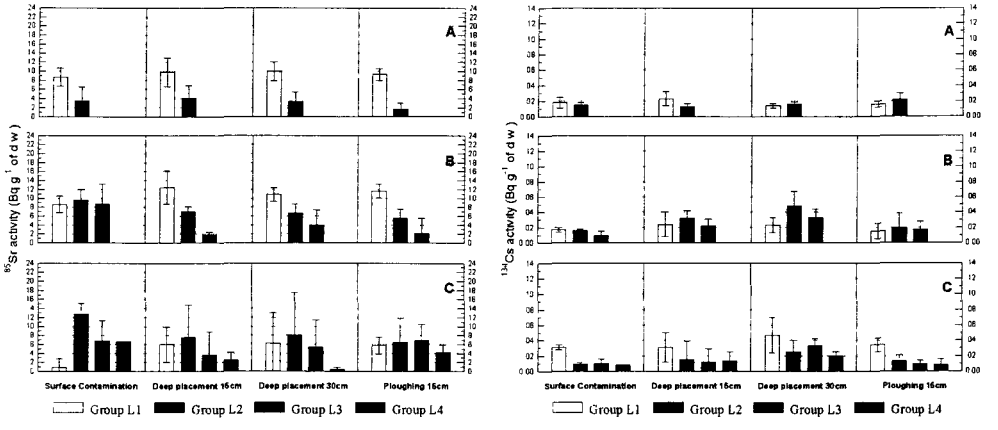

Figures 2a, 2b Temporal changes of ^{85}Sr and ^{134}Cs absorption in plant for the two series of experiments (3 sampling per series : A, B, C), and considering different groups of leaves (L1, L2, L3, L4) (Part of the L1 leaves were senescent at the third sampling time).

C) Lysimeter studies.

3rd. Study of the deposit homogeneity and plant interception after contamination at two different stages of plant growth (1994).

1 Experimental design.

To carry out this experiment, the lysimeter was divided in two parts: part A (East) and B (West). Wheat seeds were sown first in part A, and 30 days later in part B, in order to obtain two different stages of plant growth at the time of contamination (part A: beginning of shooting and part B: beginning of tillering)

Before contamination the Leaf Area Index (LAI) was calculated by sampling plants in part A and B and measuring their leaf area by image analysis. To calculate the percentage of soil surface covered by the crop at the moment of the contamination, the vertical projection of the lysimeter surface was obtained with photographs made perpendicular to the soil.

Two days after contamination, the following samples were collected:

- Filters (8 in each side of the lysimeter) and sieved soil in petri dishes (located beside the filters) distributed in inter-row position, to evaluate the homogeneity of the aerosol deposit over the lysimeter surface.
- Wheat plants (5 replicates of 10 x 10 cm of surface) randomly distributed in each side of the lysimeter in order to evaluate the interception of the aerosol by vegetation.
- Six soil samples per side: 3 in the squares previously sampled for plants, and 3 between the plant rows.

2 Results and discussion.

2.1 Crop interception.

At the moment of the contamination, owing to the different growth stages, significant differences in LAI between A and B were observed (*Table III*), this is likely to have caused the higher interception of the deposit for the crop in the part A than in B.

Table III. Comparisons of the growth stage, dry weight and L.A.I. between the part A and B of the lysimeter

	Growth stage.	**Dry weight (g plant/m^2 soil)**	**L.A.I (m^2 plant/m^2 soil)**
Part A	Beginning of shooting 20 cm high. (8 leaves)	33.81	1.08
Part B	Beginning of tillering 10 cm high. (3 leaves)	11.37	0.28

Considering the vertical projection of the lysimeter surface, the 49 51% of the total soil surface in the part A has been covered by the crop respect to the 13.84% observed in part B (*Figure 3*), which correlated highly with the calculated L.A.I. (r^2=0.99)

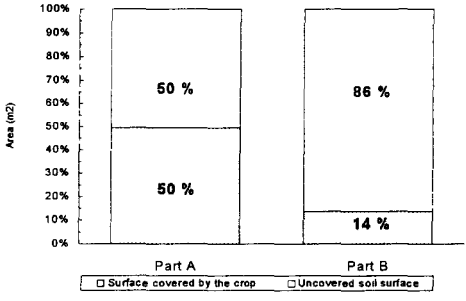

Figure 3. Percentage of area covered by the crop and uncovered in the Part A and B of the lysimeter at the moment of contamination

2.2 Deposit.

No significant differences were observed between filter paper and sieved soil in petri dishes. The standard deviations obtained in filters and soil deposit showed that the soil surface deposit has been relatively homogeneous in the whole lysimeter. Considering both filter paper and soil samples not significant differences existed between part A and B (*Table IV*). In particular, the not significant differences of activity between the soil samples taken from inter-row positions and the soil samples taken beside plants in both part A and B, showed that the different growth stage in both parts was not enough to produce differences between inter-row and plant row positions. The higher activity in the soil with respect to that measured on the filter could be explained by the higher rugosity of the soil surface.

Table IV. Comparisons of ^{137}Cs and ^{90}Sr activities in filters, soil samples and plant samples between part A and B. (mean values (s.d.))

	Filters (Bq.m^{-2})		Soil samples (Bq.m^{-2})		Plant (Bq. plant .m^{-2} soil)	
	A	B	A	B	A	B
^{137}Cs	2.99E+07 (2.49E+06)	2.92E+07 (1.64E+06)	4 12E+07 (3 46E+06)	3.47E+07 (5.13E+6)	1.13E+7 (1.06E+06)	2.61E+06 (6.00E+04)
^{90}Sr	3.05E+07 (2.02E+06)	3 18E+07 (1 88E+06)	4 24E+07 (8 20E+06)	3.45E+07 (7.05E+06)	1 23E+07 (4.80E+05)	2.71E+06 (2.50E+05)

Analysing the data of the deposit in the crop-soil system in Part A and B (*Figure 4*), the higher crop development in part A produced an increased deposition of radionuclides in absolute terms for the soil-crop system. Within that, the proportion of crop interception was related to the stage of crop growth.

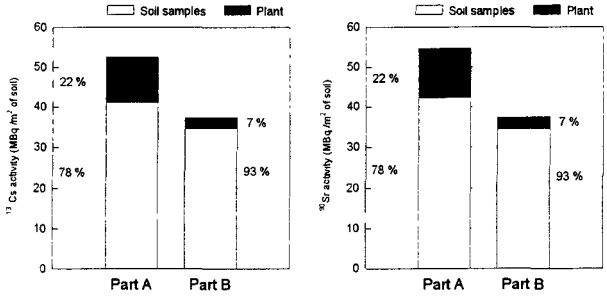

Figure 4. Comparisons between Part A and B of ^{137}Cs and ^{90}Sr deposit in the soil and plant

4th. Study of the foliar uptake after contamination and effect of the first rainfall (1994).

To compare the foliar uptake of radionuclides after the contamination and just after the first rainfall, a study has been carried out based on a sequential extraction scheme (methodology developed in TARRAS Project) using water and organic solvent, in order to determine the proportion of the radionuclides rapidly incorporated into the plant, the proportion retained by the cuticle and the proportion which could be leached off by the rain. The measurements of the Spanish lysimeter samples was carried out by the Department of "Química Analítica" of the Barcelona University with the method developed by this Department.

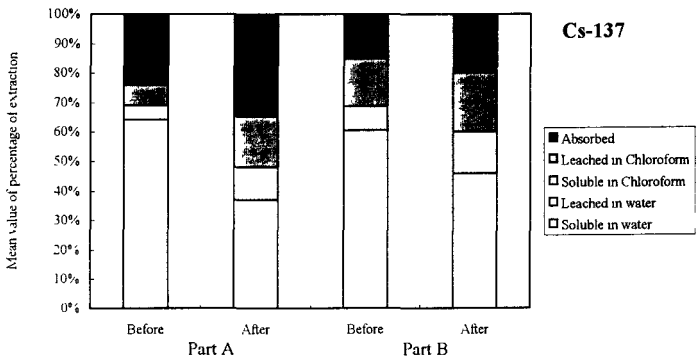

Figure 5 Extraction percentage of ^{137}Cs in wheat plants, before and after rainfall.

Just after the aerosol deposition, the water soluble fraction accounted for about 60% of the total ^{137}Cs intercepted by the canopy. The irrigation simulated a medium intensity rainfall of 10 mm during about 2 hours common in spring time After the first rainfall, a decrease in the total activity was observed: approximately 50-55% of ^{137}Cs and 20% of ^{90}Sr was leached. If we assume that all the leached ^{137}Cs came from the water soluble fraction defined by the sequential extraction, and recalculate the redistribution of the fractions refered to percentage, the remaining water soluble fraction should be 17%

and the absorbed fraction 54% in part A These estimations differ from the actual percentage obtained for these performed in the plants collected after the first rainfall which gave a 36% for water soluble and 36% for absorbed. The rest of the fractions, linked to the cuticule, did not change. Therefore, the first rainfall produced ^{137}Cs leaching from the initially absorbed fraction that has been transformed into the water soluble as defined by the extraction procedure. Similar results are obtained in part B. These results confirm the high mobility of ^{137}Cs within the plant.

5th. Radionuclide content in soil solution and exchangeable form (1994).

Radionuclides in soil solution were extracted by centrifugation (30 bar) from fresh soil at field moisture conditions water content. Exchangeable radionuclides were extracted with sodium acetate 1N in a soil-reactant suspension 1 10. Soil sampling was carried out at the first harvest (July 1994).

Table V. Radionuclide content (Bq/m^2) in soil solution and exchangeable complex.

Rdn.	Total	Exchangeable	in solution	% Exchangeable	% in solution
^{137}Cs	4 29E+07 (1.56E+07)	3.44E+05 (1.29E+05)	642.5 (92)	0.8	0.0076
^{90}Sr	4 93E+07 (1.18E+07)	1.84E+07 (0 66E+07)	38089 (7629)	36.9	0 39

The percentage of actually available radionuclides is very low with respect to the total. ^{90}Sr remains around 55 times more available than ^{137}Cs, both in the soil solution and exchangeable complex, showing similar results than other studies[3].

6th. Radionuclide accumulation at the first harvest after contamination (1994).

The activity was always higher in part A than in part B according to the highest deposition intercepted in part A. According with others authors[4,5], at harvesting time only the quantity that remained in plants was 0.3% in part A and 0 5% in part B, for ^{137}Cs and 1.0% (part A) and 1.8% (part B) for ^{90}Sr of the total activity initially intercepted.

The ^{90}Sr seems to show greater relative retention by the plants (according to the observed lower leaching than ^{137}Cs). The activity in chaff and grain must be explained by root uptake, due to the low Sr mobility into the plant. For ^{137}Cs, the retranslocation could explain part of the activity found in chaff and grain. The higher ^{137}Cs activity in grain than in chaff pointed out the role of sink played by the fruits.

The $^{137}Cs/^{90}Sr$ ratio in the straw showed the different leaching pattern for the two radionuclides studied which indicated again the lower Cs retention than Sr. In chaff, the $^{137}Cs/^{90}Sr$ ratio was around 5 times higher than in the straw, showing the highest ^{137}Cs mobility into the plant. In part A, where the intercepted activity was higher, the grain showed a $^{137}Cs/^{90}Sr$ ratio 2 times that of the chaff. This fact again confirm the role of the grain as a sink for radiocaesium[6].

Table VI. Radionuclide accumulation at harvest in part A and B (straw, grain and chaff (mean±s d)).

		^{137}Cs Bq/m^2	^{90}Sr Bq/m^2	$^{137}Cs/^{90}Sr$
Part A	Straw	39397 ±11660	119153±36499	0.33
	Grain	5768± 1468	1446± 405	3 99
	Chaff	2265± 721	1158± 800	1.95
Part B	Straw	13107± 6854	48105± 7511	0.27
	Grain	926± 69	776± 133	1.21
	Chaff	605± 164	402± 247	1 50

In conclusion, for similar deposition of ^{137}Cs and ^{90}Sr, leaching was much more important for Cs and root uptake was much higher for ^{90}Sr owing to its higher soil availability. As a result of these processes and to the different mobility of Cs and Sr within the plant, straw contamination at harvesting was very high for ^{90}Sr.

In the grain, ^{90}Sr accumulation followed approximatively the same trend as for straw In contrast, for ^{137}Cs the grain accumulation was much more dependent on the direct crop interception of the deposition, that is on the growth stage of the crop at contamination. The different behaviour of both radionuclides agrees with their mobility in the plant and in the soil.

7th. ^{137}Cs and ^{90}Sr in the root absorption at different plant growth stages (1995).

To develop this task four samplings in different plant growth stages for each treatment were carried out in 1995:

- Part A: mulch without tillage (uncontaminated straw from Barcelona).
- Part B: conventional ploughing

From the results of the 1st. (tillering) and the 2nd. (shooting) sampling of part B (conventional ploughing), it is observed different ^{90}Sr vs. ^{137}Cs plant accumulation in agreement with their comparative concentration in soil solution

Different dynamics of accumulation for both radionuclides has been observed. ^{90}Sr dynamic accumulation in plant is related to biomass accumulation (mass flow root uptake), and ^{137}Cs presented higher absorption at the early growth stages and declining root uptake at shooting (*Figures 6a, 6b*).[3,7].

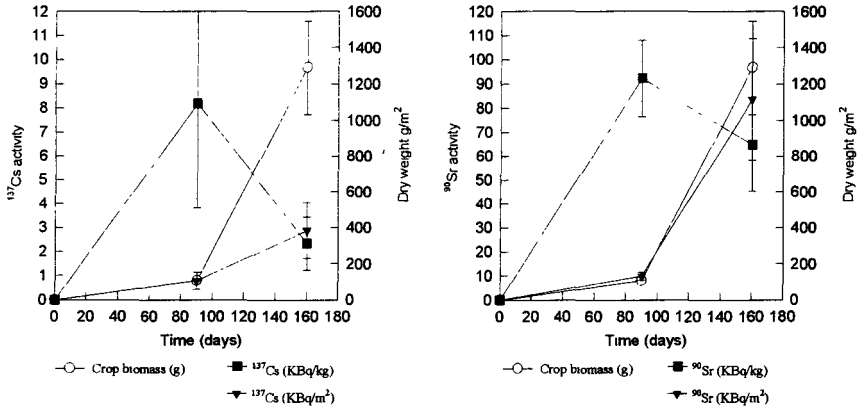

Figures 6a, 6b. Crop biomass accumulation and dynamics of ^{137}Cs and ^{90}Sr absorption of the crop in conventional ploughing treatment.

References.

1 Cremers, A., Elsen, A., De Preter, P. & Maes, A. (1988). Quantitative analysis of radiocaesium retention in soils. Nature, 335(6187), 247-9

2 Brouwer, E., Baeyenes, B., Maes, A. & Cremers, A. (1983). Caesium and rubidium ion equilibria in illite clay. J. Phys. Chem., 87(7), 1213-19

3 Roca, M. C. & Vallejo, V R. (1995). Effect of Soil Potassium and Calcium on Caesium and Strontium Uptake by Plants Roots. J. Environ. Radioactivity. Vol. 28. No. 2, pp. 141-159.

4 Frissel, M. J. (1992). Thirty years soil-to-plant transfer of Cs-137 and Sr-90. A comparison of "old" data, IUR data and Russian, White Russian and Ukranian data. Proc. Int. Symp. Radioecology. Chemical Speciation-Hot Particles. CEC, IUR, SCR, Brussels, Belgium.

5 Coughtrey, P. J, & Thorne, M. C. (1983). Caesium. In Radionuclide Distribution and Transport y Terrestrial and Aquatic Ecosystems. A Critical Review of Data. Vol. 1, Chapt. 7, de. A. A. Balkema, ECSC, EEC, Rotterdam, The Netherlands.

6 Shaw, G., Minski, M.J., Bell, J. N. B. (1992). Retention, loss and translocation of radionuclides applied to foliar surface of wheat. Environm. Exp. Bot. Vol 32. pp. 391.401.

7 Marschner, H. (ed.) (1986). Mineral Nutrition of Higher Plants. Academic Press, Belfast, UK.

Publications.

García, F., Millán, R., Tapia, L., Romero, L., Gutierrez, J., Vallejo, V.R. *Efecto de la dilución y localización en profundidad de ^{134}Cs y ^{85}Sr en el suelo sobre su absorción por la planta.* Communication in: XX Reunión Anual de la Sociedad Nuclear Española. Córdoba 1994.

García, F., Millán, R., Tapia, L., Romero, J., Vallejo, V.R. *Study of the effectiveness of deep-placement and conventional ploughing as countermeasures, regarding the role of the root distribution with respect to the ^{85}Sr and ^{134}Cs location in the soil profile.* Communication in: International Symposium on Environmental Impact of Radioactive Releases. IAEA. Vienna, 1995.

Head of the project 5: Dr. Förstel Forschungszentrum Jülich

II. Objectives for the reporting period:

The substitution programme achieved a first impression of interception, weathering and leaf adsorption of aerosols. It has been demonstrated that the aerosols were tightly deposited to the plant surface. This experience improved the study of the pathway of aerosol contamination in the RESSAC greenhouse, observing interception and wash-off. The effect of precipitation some time after contamination was studied comparing different developmental stages on the different lysimeters. The extension of the lysimeters allowed a direct comparison of different crops and agricultural treatments according to realistic cultivation. The standing crop of grass and wheat has been harvested. As countermeasures normal and deep placement are recently applied to test simply achieving techniques. Additionally experimental techniques to test the homogeneity of deposition and the subsequent distribution of radioactivity in the soil were tested.

III. Progress achieved including publications:

1. Substitution programme

For the substitution programme a set of 16 lysimeters of 0.25 m^2 surface area were filled with well-mixed plough-layer from a parabraunerde out of the vicinity of Jülich (Merzenhausen). Half of them was exposed to aerosols produced by the POLYR furnace, the other half was contaminated by spraying the radionuclide containing solution on top of the canopy. According to the late time in growth season, only bush beans (*Vicia fabae*) could fit the climatic conditions in Jülich.

Each group of lysimeters was equally divided into two growth stages representing different leaf area index and standing crop. To restrict handling of contaminated plant material the correlation between fresh weight and leaf area was measured and then consequently applied. This technique was adopted in 1994 for the RESSAC experiments, too. Part of the lysimeters of both forms of radionuclide application were exposed to natural rain to study the wash-off effect, especially for freshly deposited material.

To get more experience two important aspects which had to determine further planning and handling were tested: The tightness of the binding of radioactive aerosol particles to the leaf surface and the effects of weathering (resuspension and wash-off directly after contamination respectively).

As a general experience the binding of the aerosols was more tight than expected. Resuspension can be neglected, even under extreme conditions. The 8 lysimeters exposed in Cadarache to POLYR aerosols were immediately after contamination loaded on a truck and transported overnight to Julich, for at that time in Cadarache no facilities to handle the material were available. It was an important experience for us that despite of vigorous shaking during the transport the paper cover around the material did not receive any contamination. The only doubt remained from the fact that under the cover the humidity was kept near to saturation Later results from depositions of aerosols in the LEL confirm these observations.

The wash-off was studied by exposing the lysimeters successively to rain. For rain cannot be expected in a regular manner the wash-off was simulated by a threefold washing procedure: The plant material was dipped into 200 ml of water, was left there under shaking and was transferred to the next water container after exactly one minute stay. This procedure was

repeated three times for each sample. This procedure was adopted from Cadarache. The advantage is that under intensive mixing a tixotropic gel is formed which can be easily handled, traps aerosols particles inside and achieves a constant geometry for counting.

For **strontium** at the first day after exposure, i.e. the first opportunity directly after the exposure tent has been opened, 84 % of the nuclide could not be removed, the following day 87 %. According to that result in each fraction of the removal procedure 4 and 6 % of the contamination were detected. No clear tendency between the subsequent fractions of the extracting liquid could be seen

The according data for **caesium** are: At the first day 72 % of the radioactivity are not removable, at the following day 90 %. The different solubility, higher for caesium compared to strontium, can be seen from fractionation during the washing procedure: The yields on the first and on the following day in subsequent fractions were :

-yields of washing after the first day:

first fraction	23 %
second fraction	3 %
third fraction	2 %

- corresponding data for the subsequent day.

first fraction	6 %
second fraction	2 %
third fraction	2 %

These data indicate a rapid uptake of caesium out of the aerosol particles into the interior of the plant biomass, according to the chemical behaviour of that element.

During deposition within the aerosol particles both elements are not fractionated, for that process is a pure physically driven one. But thereafter physiologically governed differences begin to play their role. Caesium as an analogue of potassium will be taken up and translocated more quickly compared to strontium as an analogue of calcium. Calcium has a limited mobility within the plant.

The substitution experiment was a preparation for the final and more sophisticated exposure. It suffered from some technical preparations. The tent enclosing the experimental set of plants was situated very closely above the canopy. Therefore, the activity deposited at the plant surfaces differs usually by a factor of 2.

2. LEL-Experiments

2.1 Deposition

In the RESSAC-experiments, in order to test the hypothesis that the initial aerosol deposition onto a plant surface does not differ from the deposition onto a inert surface, pure physically defined surfaces of different structure (soil, filter paper) were exposed at different orientations to the gravitational axis (horizontal, vertical, upper and lower surface). A kind of octogonal frame was positioned above the crops and above bare areas.

The effect of interception of aerosols by plants can be studied only immediately following the radionuclide deposition. In our case very early stages of development were exposed, covering only some percent of the soil. In addition to wheat which has small leaves, a broad leaf plant (kohlrabi, a kind of cabbage) was cultivated in one third of the lysimeter.

The development of the wheat was retarded by several treatments and technical necessities, e.g. the contamination itself. During some days the lysimeter is kept in a part of the greenhouse where only a very reduced portion of sunlight is available. Plant physiology has thus been disturbed.

Due to slower plant development than scheduled, the activity deposited onto the soil surface was uniform for the smaller wheat stage (EC 14, i.e. description of the stage of development in the decimal code) and the kohlrabi. Only for the higher wheat (EC 22) it differed slightly. Hopefully the data of the other groups allow complementary calculations.

The amount of radioactivity deposited was calculated from soil samples obtained with the help of different techniques: filter paper, soil cores and soil exposed in Petri dishes. No significant differences could be seen (30 MBq m^{-2} ^{137}Cs), except for those Petri dishes which partially were covered by kohlrabi leaves (25 MBq m^{-2} ^{137}Cs). The variation within the subplots of the lysimeter was low (1-10%), and lowest on bare soil (<7%; Figure 1).

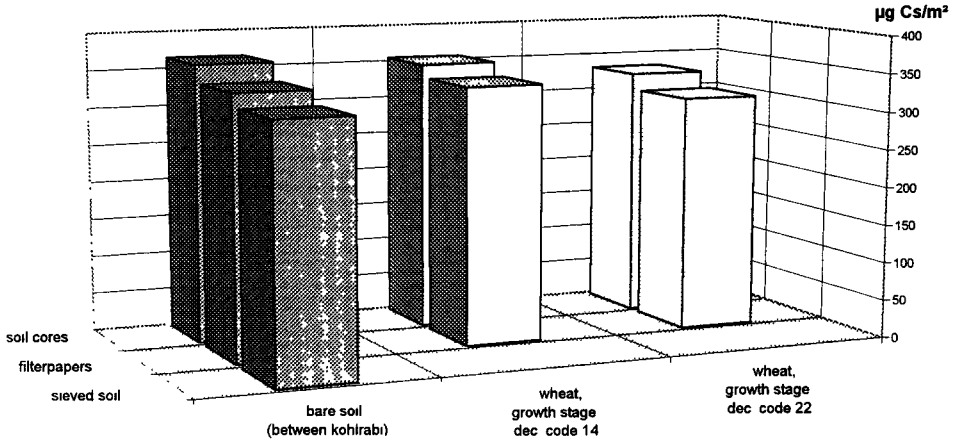

Figure 1: Contamination of the soil surface under vegetation as measured by different techniques

2.2 Interception and weathering

The more standing biomass was on the plot (growth stages), the less aerosols were deposited on the soil. In contrast to this, the intercepted fraction increased with the biomass (Table 3). Percentages of intercepted aerosols were 6% in kohlrabi plants and 18% and 34% in wheat at growth stage EC14 and EC22, respectively.

From the subsequent weathering one calculates a 19 day mean radioecological half-life of caesium on wheat, mainly on leaves. Table 1 reports the results from weathering after deposition of the aerosols.

Table 1: MBq Cs on plants /m² soil surface

	May 24 1994	May 25 1994	June 8 1994
kohlrabi	2,1	0,68	0,14
wheat EC 14	6,7	1,9	1,1
wheat EC 22	15,1	5,5	2,8

2.3 Translocation

The final yields of biomass are shown in Table 2.

Table 2: Yields of wheat 1994

	Plot 1		Plot 2	
Plant Fraction	FW [dt/ha]	H_2O [%]	FW [dt/ha]	H_2O [%]
grain	91	11%	55	10%
straw+chaff	64		34	

The transfer of caesium and strontium to the grain is shown in Figure 2. The later growth-stage had a higher translocation of caesium. The strontium found in the grain is probably due to root uptake of the nuclide deposited on the soil, for the translocation of strontium within the plant is very low. Analogue to calcium it does not move from one tissue to another.

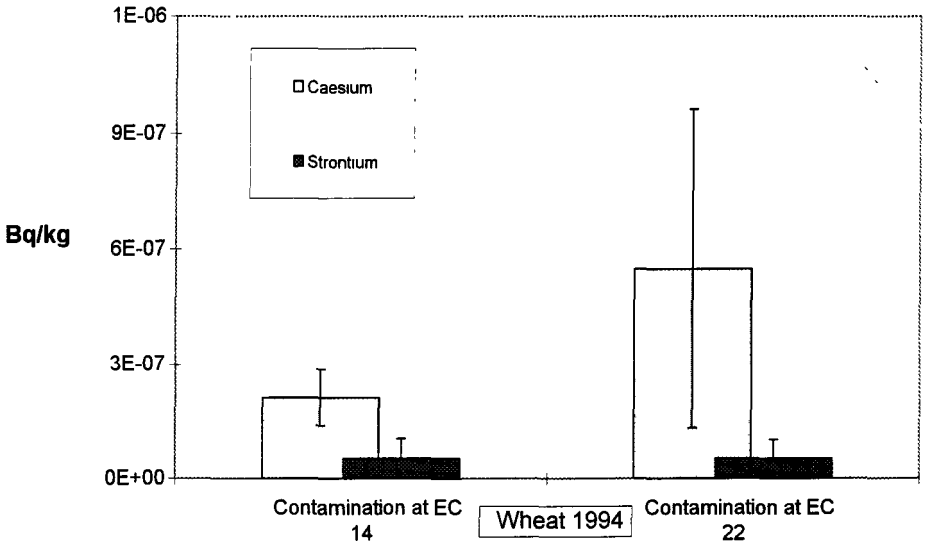

Figure 2: Wheat: Concentration of 137-Cs and 90-Sr in grains (translocation and root uptake)

Table 3 reports the portion of caesium translocated from the radioactivity deposited on the plants and on the soil to the grain, Fig. 2 the actually measured radioactivity in the grain.

Table 3: After deposition on leaf surface translocated caesium to the wheat grain (%)

	dry matter (g/m^2)	leaf area index	Cs-deposition (MBq/m^2)	% interception by plants	TF as % of intercepted Cs translocated to grain	Cs translocated to grain / Cs deposited on soil (in %)
Kohlrabi	5,3	0,176	2,1	6		
EC 14	15	0,762	6,74	18	0,11	0,0198
EC 22	37	1,44	15,1	34	0,25	0,085

2.4 Countermeasures

In autumn 1994, "skim and burial ploughing" was applied on one of the former wheat plots. This meant to skim off the contaminated layer of 0-5 cm, and to place it underneath the plough layer (deeper than 30 cm) The other former wheat plot was ploughed as in common agricultural practice. In order to obtain a well defined profile, the plough layer was skimmed off in two sections (0-15 cm and 15-30 cm), each one coarsely mixed and their sequence inverted when filling in again. The contaminated soil is now located, coarsely mixed, in 15-30 cm depth. After these two treatments, both plots were sown with winter barley.

In parallel with tillage, soil water was labelled at 15 cm depth by applying D_2O (deuterated water). Analysis of soil and plants should clarify water movement in the soil and allow

determination of the active rooting zone. The water was extracted from soil samples by cryodistillation under vacuum to obtain a water sample free from the radioactivity added. The samples were measured in Jülich by mass spectrometry after reduction of water to hydrogen gas The method is usually applied to natural variations of isotopes (SIRA· stable isotope ratio mass spectrometry). Therefore the D-data are reported as deviations from the natural concentrations expressed in millesimal, i.e. °/oo (natural concentration 0.015 atom-%). A deviation of 1 ‰ is an increase of the natural concentration by 0 000015 atom-%, therefore large numbers result from labelling with water highly enriched in D Such water highly enriched in D usually is applied to ensure longer observation periods for most of the labelling is lost by the water uptake of roots.

Due to the limited counting capacities, only results of caesium measurements are yet available now Further data are processed continuously. Moreover, the harvest in July is not included in the financially supported period. That's why only a part of the final results can be presented now.

Water movement in the soil seems to have gone downwards as expected from natural conditions and soil type, but upwards too (Figure 3). This unexpected high upward water movement during winter is probably due to the artificial greenhouse conditions, where the topsoil dried out too fast. Together with the French team, measuring devices have now been set up for verification.

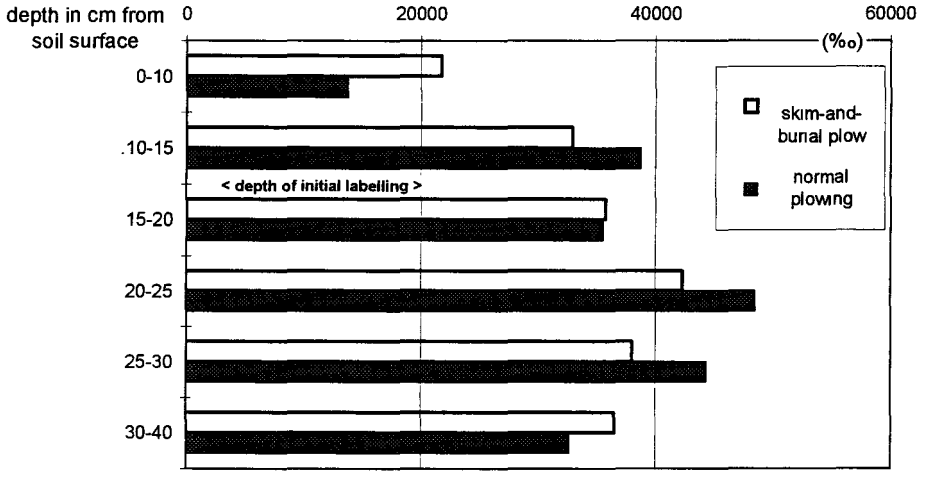

Figure 3: Spreading of soil water 4 months after labelling (Deuterium) applied in 15 cm depth.

Barley development on both plots was parallel (Figure 4). Uptake kinetics of Cs-137 have been measured, taking plant samples (five repetitions) of three plants each. Standard deviation was very high. This could be due to small-scale heterogeneous distribution in the soil, to be shown in soil autoradiographies soon.

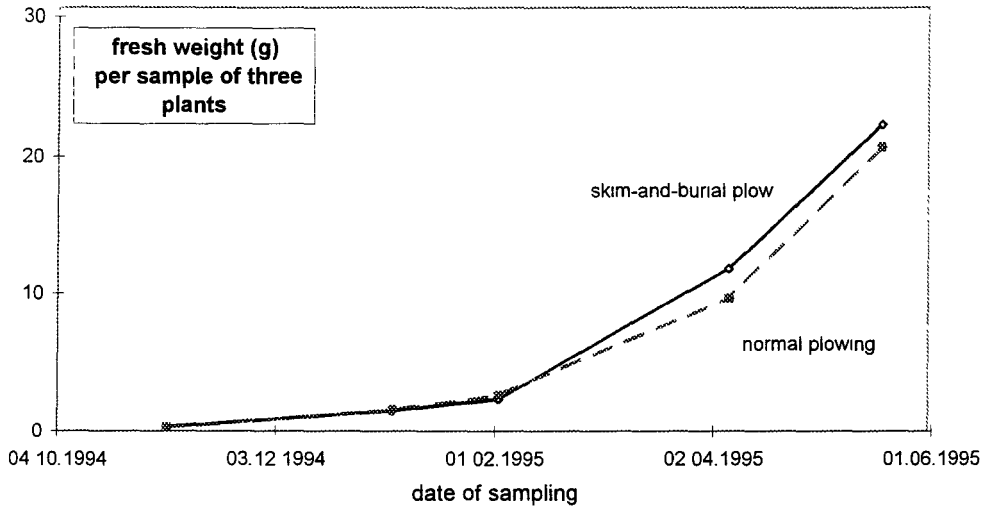

Figure 4: Plant development on both barley plots

Deep placement seems to enhance caesium uptake instead of reducing it, however, this trend may not be statistically significant. Possible reasons will be discussed as soon as harvest results (bigger sample size) confirm (or not) this observation (Figure 5).

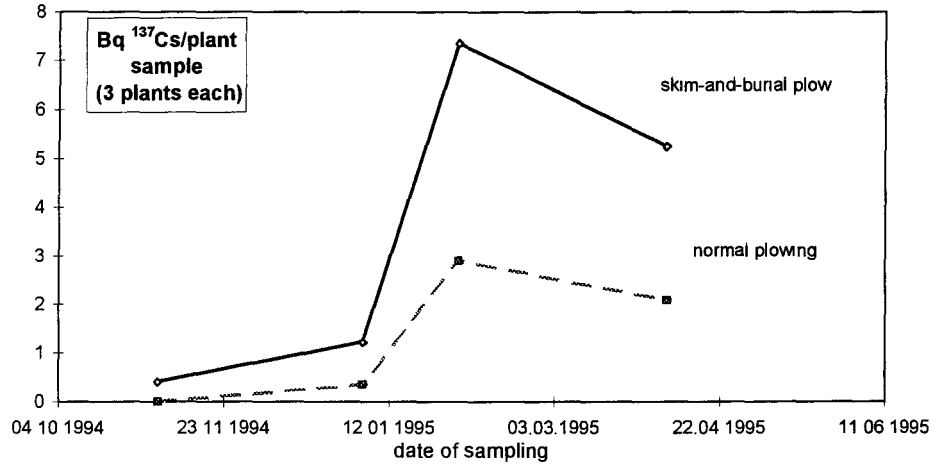

Figure 5: Kinetics of ^{137}Cs content in barley on both plots

Publications

As soon as further measurements of samples will be available, results will be processed and be published as agreed.

Head of Project 6: Dr. J. Gutierrez

II. Objectives for the reporting period.

1st Selection of the area to extract the monolith: Soil and climate characterization of the site.
- Soil characterization of *Terra rossa* soil: profile description and analysis.
- Research climatic data from the field station, installation and measurements by tensiometers and temperature sensors at differents depths of soil and digitalization of the data.
- Monolith sampling and installation of the lysimeter in the Cadarache-RESSAC building.

2nd. Intercomparison exercise.

3rd. Pot experiments (substitution programme), evaluation of the effectiveness of *deep-placement* and *conventional ploughing* as countermeasures, paying special attention to the role of the root distribution with respect to the radionuclides location in the soil profile.

4th. Determination of the wash-off and rainsplash after the first rainfall.

5th. Study of radionuclide migration in the soil profile.

6th. At harvesting, determination of the radionuclide translocation to grain, chaff and straw.

7th. Evaluation of the effect of mulching and ploughing in the final soil to plant transfer factor.

III. Progress achieved including publications.

1st. Selection of the area to extract the monolith: Soil and climate characterization of the site.

Selection of the site Field prospection.

The site has been selected taking into account the following criteria:
- Soil type, to match with the general features of *Terra rossa*.
- The agricultural relevance of the soil unit in the Mediterranean countries.
- The availability of technical facilities such as meteorological station, known land use history, protection, access and the feasibility to extract a big soil monolith.

Soil characterization: profile description and analysis.

From a general prospection of the Experimental Fields (Institute of Botany, Universidad de Barcelona) by means of hand auger, the specific area for the extraction of the monolith was delimited avoiding disturbances other than the common agricultural practices.

Classification: *Calcic Palexeralf* (Soil Taxonomy). *Calcic Luvisol* (FAO-Unesco, 1988)
Present vegetation: Herbaceous community managed as fallow

Research of climatic data from the conventional weather stations and digitalization of the data.

The climatic features for the area of Barcelona have been described from the metereological records The main parameters digitalized (*Figures. 1, 2, 3)*.

Installation of tensiometers and temperature sensors for differents depths of soil.

8 tensiometers and temperature sensors have been installed at 4 differents levels (30, 60, 90 and 120 cm.) with 2 replicates for each depth, producing a preliminar record of the hydric potential of the soil (*Figures. 4, 5, 6, 7*) and temperatures (*Figures. 8, 9, 10, 11*).

Monolith sampling and installation of the lysimeter in the Cadarache-RESSAC building.

During the period 12-20/October/1992, the Spanish monolith was extracted from the Experimental Fields of the Barcelona University preserving its structure and surface vegetation according to the procedure from C.E.N in Cadarache. The dimensions are 3.24m^2 of surface and 1.4m depth After its transport to Cadarache, the porous ground plate was installed and the lysimeter was placed into the RESSAC building during the first week of December 1992.

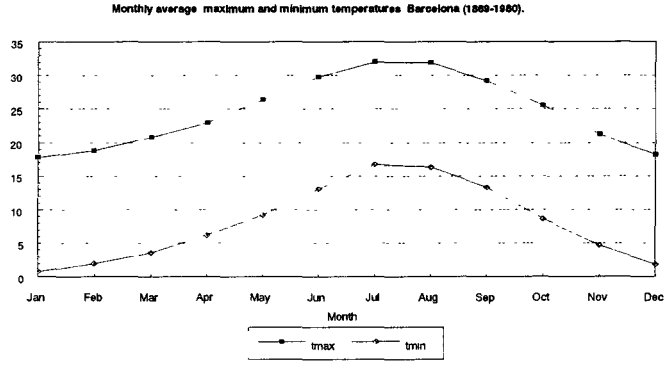

Figure 1

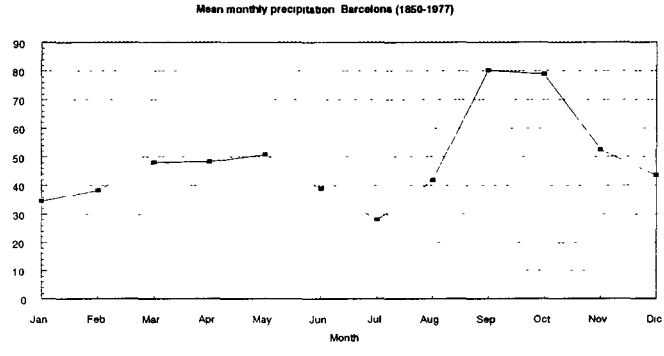

Figure 2

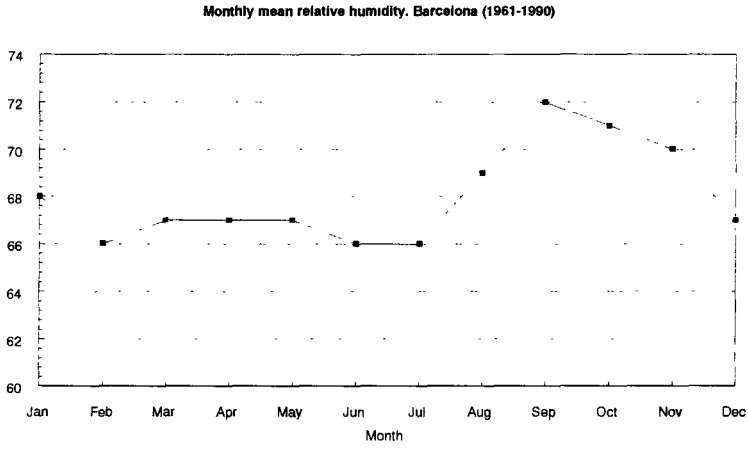

Figure 3

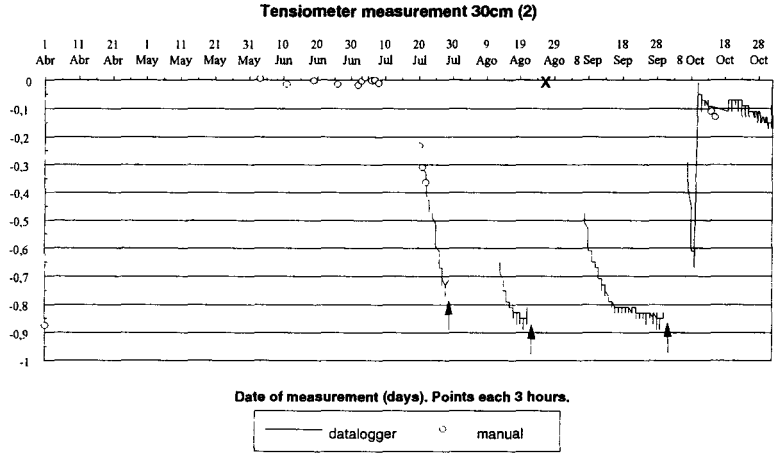

Figure 4.

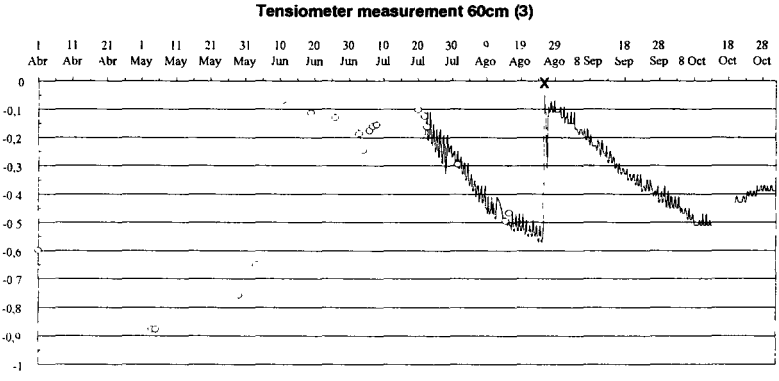

Figure 5

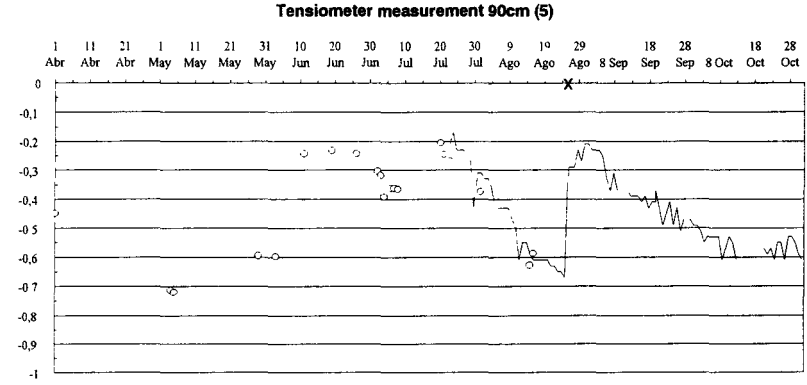

Figure 6.

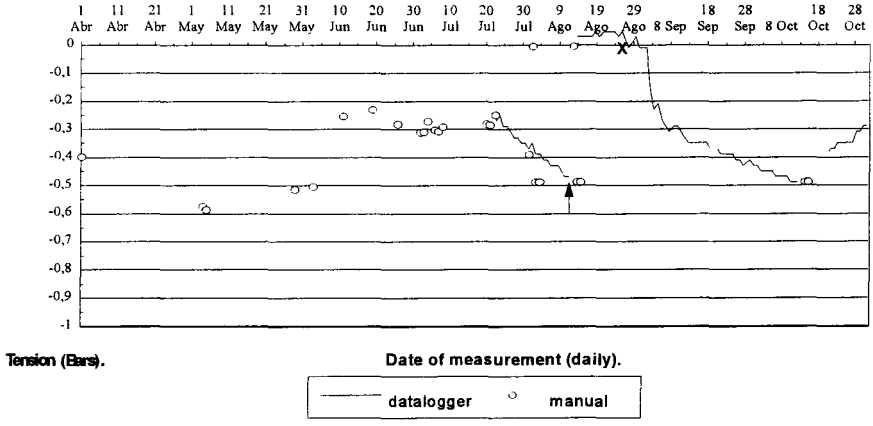

Figure 7 The symbol X is an accidental irrigation point. The vertical arrow indicate a tensiometer column's break

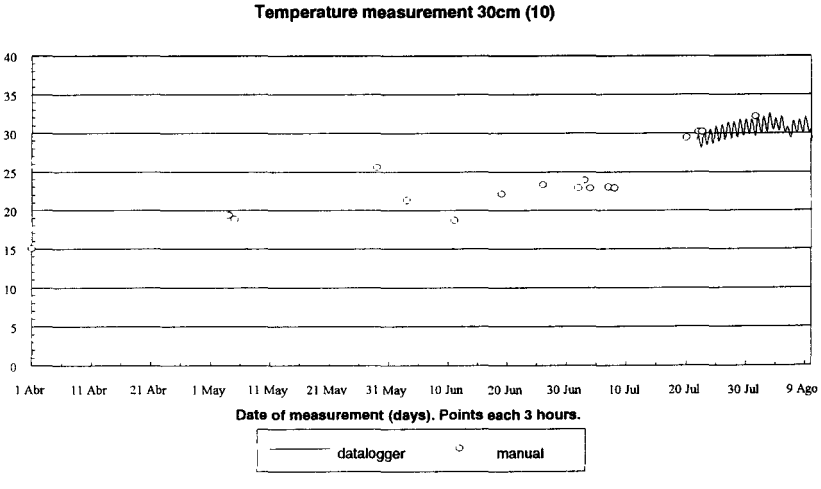

Figure 8.

Temperature measurement 60cm (12)

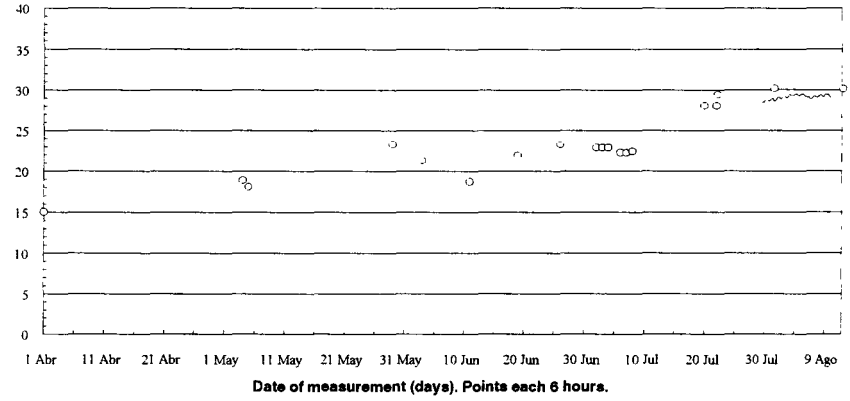

Figure 9.

Temperature measurement 90cm (14)

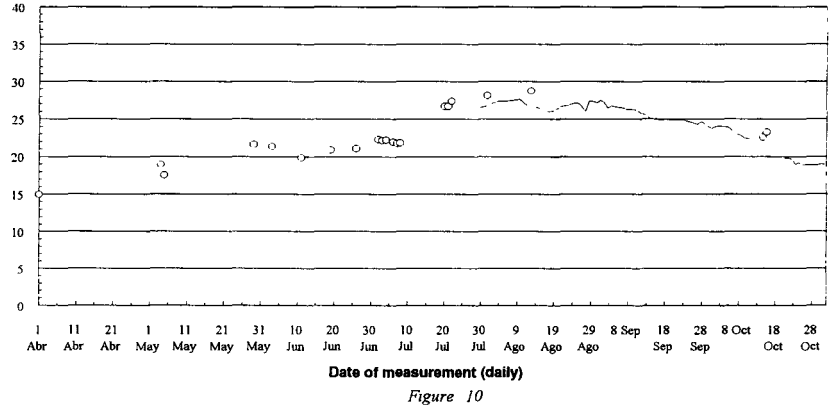

Figure 10

Temperature measurement 120cm (16)

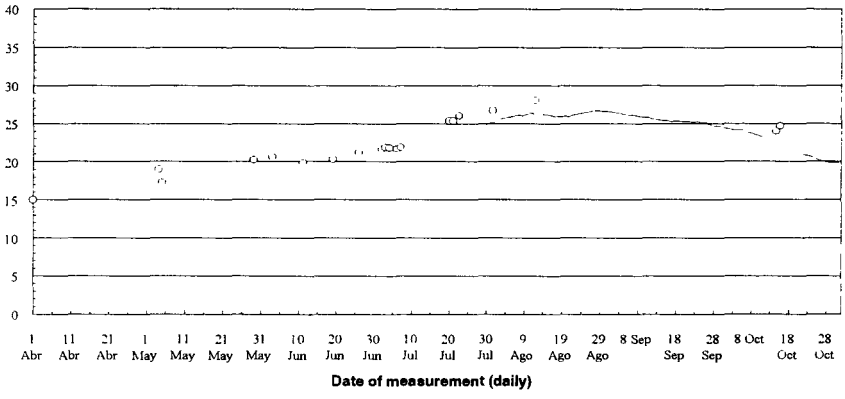

Figure 11

2nd. Intercomparison exercise.

To ensure the validity of all the radionuclide measurements performed during this project, it was decided to carry out an intercomparison exercise between all the participants. The samples to be measured were prepared at Cadarache and latter distributed, three of them were artificially contamined with ^{85}Sr, ^{134}Cs (plant material, soil attack and soil) and the other sample was a lichen from Chernobyl. Samples were analized at CIEMAT, the ^{90}Sr analysis were performed according to the CIEMAT/IMA radiochemical procedure[1], gamma measurements were performed in an hiperpure Ge n-type detector, the results obtained are presented below.

Soil + γ emitter S (Bq/g)	**Plant + γ emitter V (Bq/g)**	**Lichen Chernobyl L (Bq/g)**	**HNO_3 Soil attack A (Bq/ml)**
250.± 16.(Cs-134)	22.7 ± 1.4 (Cs-134)	20.8 ± 1.1 (Cs-134)	0.93 ± (Cs-134)
5 4 ± 0.4 (Sr-85)	111 0 ± 6.6 (Sr-85)	367 ± 16 (Cs-137)	4 65 ± 0.2 (Sr-90)
		60.6 ± 1.2 (Sr-90)	

The data were in good agreement with the ones provided by Cadarache

3rd. Pot experiments, evaluation of the effectiveness of *deep-placement* and *conventional ploughing* as countermeasures.

Experimental design and sampling. Radiochemical analysis.

Sunflower plants (*Helianthus annuus* var. Tesoro) were cultivated in *Terra rossa* soil. A total soil surface of 1.6 m^2 (volume of 29.95 dm^3), previously sieved at 2 mm., was contaminated by the POLYR device, being the initial activity deposited: 1.46 $MBq.m^{-2}$ and 0.17 $MBq.m^{-2}$ for ^{85}Sr and ^{134}Cs respectively The contaminated surface was homogenized in the total soil volume. The final values of soil concentration obtained were 4.58 $Bq.g^{-1}$ for ^{134}Cs and 54 08 $Bq.g^{-1}$ for ^{85}Sr. The total soil volume was distributed in equal parts in each of the 16 experimental pots. 4 treatments were compared (4 replicates per treatment).

Three of the treatments consisted in placing a 1cm thick layer of contaminated soil at different depths.

1st.- At soil surface. Treatment S.
2nd.- At 15 cm. depth. Treatment 15
3rd - At 30 cm. depth. Treatment 30.

The fourth treatment consisted in mixing the contaminated soil through the upper 15 cm. of soil, being the final concentration 0.43 $Bq.g^{-1}$ for 134Cs and 5 73 $Bq.g^{-1}$ for ^{85}Sr.

4th.- Simulation of conventional ploughing. Treatment M.

The entire experiment was carried out in duplicates (two series): one in a greenhouse in Cadarache, and the second series in real field conditions in Barcelona. In each series, three samplings were performed at different stages of plant growth At each sampling time, groups of leaves were separated by growth stage (*Table I*) The samples were dried during 24h. at

60°C and grounded at Cadarache. ^{134}Cs and ^{85}Sr activities were measured by gamma spectrometry in a intrinsic Ge n-type detector at CIEMAT

Sampling	Group L1	Group L2	Group L3	Group L4
1st. (A) 26/10/93	1st..2nd.3rd pair	4th..5th. pair		
2nd. (B) 5/11/93	1st..2nd.3rd pair	4th .5th. pair	6th..7th. pair	
3rd. (C) 15/11/93	1st..2nd.3rd pair	4th..5th. pair	6th..7th. pair	8th..9th. pair

Leaves in expansion. Fully expanded leaves.

Table I. Pairs of leaves and their stage of growth for each sampling.

Temporal changes in the radionuclide absorption.

For ^{85}Sr, considering in each sampling the group of last expanded leaves, a displacement in the absorption has been observed (*Figures 12A, 12B, 12C*) in relation to the root growth. At the initial stages of growth for group L1 (*Table I*), the maximum absorption appears in the treatment S (9.01 Bq.g^{-1}) (*Figure 12A*) and the lowest in 30 (3 54 Bq.g^{-1}). In the second sampling, and regarding the group L2, these values tend to converge (S: 8.42 Bq g^{-1}, 15: 8.19 Bq.g^{-1} and 30: 7.40 Bq.g^{-1}) (*Figure 12B*). At the third sampling, (*Figure 12C*), the absorption of the groups L3 and L4 of the 30 treatment (10 81 and 10.01 Bq.g^{-1} respectively) are higher than the groups L3 and L4 of the S treatment (6 82 and 3.74 Bq.g^{-1} respectively), confirming the displacement of the absorbing root area to lower depth levels.

Figures 12 and 13, show the different behavior observed in the ^{134}Cs and ^{85}Sr absorption in relation to the plant vegetative stage and the root mass profile in depth (*Figure 14*).

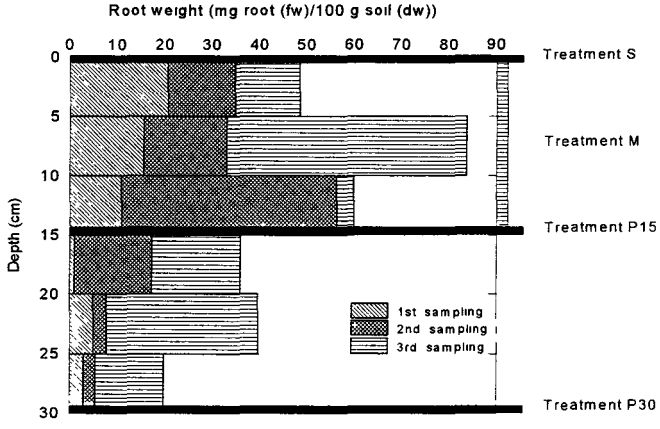

Figure 14. Evolution of the root development in depth towards the placement of the contaminated layers (S, 15, 30 and M treatments)

Activity in plant

The ^{134}Cs concentration in total plant was two orders of magnitude lower than for ^{85}Sr (*Table II*). Considering the lower concentration of ^{134}Cs in the soil respect to the ^{85}Sr, the net ^{134}Cs activity in plant was one order of magnitude lower than for ^{85}Sr This fact could be explained for the greater fixation of ^{134}Cs in the *Terra rossa* soil.

Figure 12.

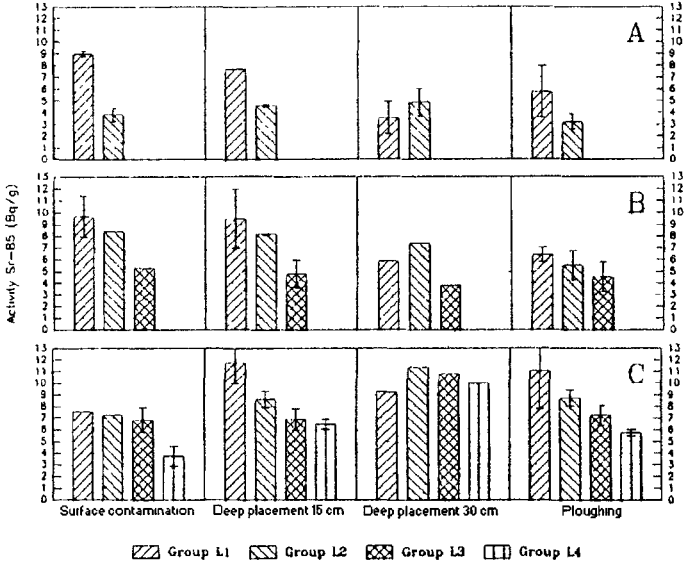

Figure 13.

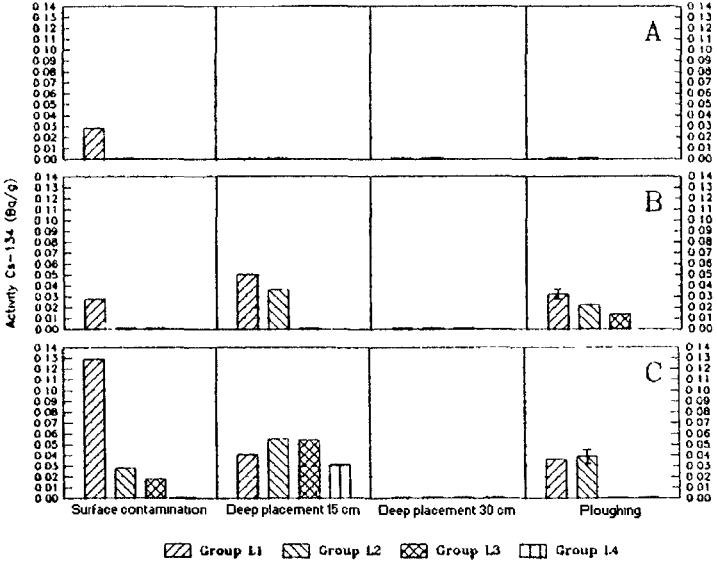

Figures 12, 13. Temporal changes of ^{85}Sr and ^{134}Cs absorption in plant leaves for the 3 samplings (A, B, C), and considering different groups of leaves (L1, L2, L3, L4).

Considering the final activity values in total plant (*Table II*). ^{85}Sr showed a maximum absorption in the 15 and 30 treatments, less in M, and minimum in the treatment S. For ^{134}Cs, the absorption in M is lower than in S and 15 treatments, indicating that the dilution has affected the ^{134}Cs absorption. For ^{85}Sr, the dilution effect has not been observed. In the 30 treatment, no measurable ^{134}Cs absorption was observed, in contrast with the high ^{85}Sr absorption and the mass root accumulated at this depth (*Figure 14*). The non measurable ^{134}Cs absorption only in the 30 treatment, could indicate that other factors than ^{134}Cs soil fixation were involved.

The final absorption of ^{85}Sr was not affected by conventional ploughing, whereas it was for ^{134}Cs (*Table II*). Therefore, conventional ploughing was effective to reduce ^{134}Cs transfer to the crop, being negligible for ^{85}Sr.

	^{85}Sr ($Bq.g^{-1}$) (dw)	^{134}Cs ($Bq.g^{-1}$) (dw)
Treatment S (Surface contamination).	6.19 ± 0.31	0 050
Treatment 15 (deep placement 15 cm.).	8 20 ± 0.70	0.048
Treatment 30 (deep placement 30 cm.).	10.43	LLD
Treatment M (Conventional ploughing).	7.82 ± 0.81	0.035

Table II. Final ^{85}Sr and ^{134}Cs activity per treatment in total plant. (mean value ± sd where enough replicates were available)

Lysimeter contamination

The contamination of the Spanish lysimeter was performed the 03/22/94, the radioactive aerosol (containing ^{90}Sr and ^{137}Cs isotopes) was produced by the POLYR system[2] . The lysimeter was divided into two halves (A and B) with different growth stages (tillering and shooting respectively) of crop (*Triticum aestivum* v Arbon) The deposit was found to be homogeneus (eight filters were randomly located in the surface, and samples of soil and plants were collected from A and B sides). The first rainfall was simulated one week after the contamination (10mm. during 1h. 20'), 5 collecting bottles were randomly placed in both sides of the lysimeter to evaluate the homogeneity.

4th. Determination of the wash-off and rainsplash after the first rainfall.

To evaluate the effect of rainfall in the existing vegetation, 5 plant samples (from a $100cm^2$ surface) were collected in both sides. ^{90}Sr analysis were performed by the crown-ether method[3] and ^{137}Cs was measured in a Ge detector at LEL-Cadarache.
Due to the inhomogeneous distribution of the rainfall found in the lixiviation water (Fig.15), the results of wash-off in plants have been considered over the whole lysimeter. Higher levels of wash-off were observed for ^{137}Cs than for ^{90}Sr (*Table III*) in both growth stages.

	Side A		Side B	
	Before	**After**	**Before**	**After**
^{137}Cs	3 32E+8 (3.11E+07)	1.46E+08 (5.32E+07)	2.30E+08 (8.73E+06)	1 09E+08 (2.01E+07)
^{90}Sr	3.61E+08 (1.14E+05)	2.80E+8 (6 08E+7)	2.35E+08 (2.20E+05)	1 97E+08 (8 89E+06)

Table III. Comparisons of ^{137}Cs and ^{90}Sr activities in plants between part A and B of the lysimeter before and after first rainfall. (mean values (s.d.)).

Data obtained show that the activity ratio in plant between part A and B is 5 times higher in A than in B for both radionuclides, due to the different growth stage, and this ratio remains constant after the wash-off. The ^{137}Cs wash-off is similar in part A than B, 56% and 52% respectively, that means a high reduction of the direct contamination in plant after rain. This reduction is not so efficient for ^{90}Sr (23% in part A and 16% in part B), the lower washing effect is also observed in the water of lixiviation. It can be said that the radiological consequences of direct contamination in plant are higher in the case of strontium

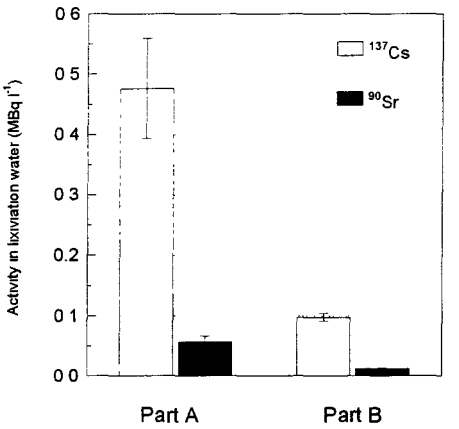

Figure. 15. ^{137}Cs and ^{90}Sr activity in the water of lixiviation. Comparison between part A and B of the lysimeter.

5th. Study of radionuclide migration in the soil profile.

The study of the radionuclide migration in soil is being performed by periodical collection of soil cores (5 cm diameter), which are divided in 0-2.5 cm, 2.5-5 cm and 5-10 cm sections. At the present time, first samples are being collected, wich will be processed shortly.

6th. At harvesting, determination of the radionuclide concentration in grain, chaff and straw.

Two crops have been cultivated wheat (v. Arbon) January to July 1994, and barley (v Orblonde) October 1994 and January 1995 (part A of the lysimeter) to July 1995. At harvest (July-94) wheat samples have been collected from part A and B of the lysimeter, totalling :
- Straw : 24 samples (^{137}Cs analysis) and 12 samples (^{90}Sr analysis)
- Grain : 12 samples (^{137}Cs analysis) and 6 samples (^{90}Sr analysis)
- Chaff 12 samples (^{137}Cs analysis) and 6 samples (^{90}Sr analysis)

The results of the measurements are being processed and evaluated.

Samples from barley harvest will be collected in July-95 it is foreseen to obtain the same number as in the wheat harvest

7th. Evaluation of the effect of mulching and ploughing in the final soil to plant transfer factor

The samples are also being processed, and results will be evaluated later.

Publications.

García, F., Millán, R., Tapia, L., Romero, L., Gutierrez, J., Vallejo, V.R. *Efecto de la dilución y localización en profundidad de ^{134}Cs y ^{85}Sr en el suelo sobre su absorción por la planta.* In: XX Reunión Anual de la Sociedad Nuclear Española. Córdoba 1994.

García, F , Millán, R., Tapia, L., Romero, J., Vallejo, V.R. *Study of the effectiveness of deep-placement and conventional ploughing as countermeasures, regarding the role of the root distribution with respect to the ^{85}Sr and ^{134}Cs location in the soil profile.* In: International Symposium on Environmental Impact of Radioactive Releases. IAEA. Vienna, 1995.

References.

(1) - "Procedimiento para la determinación de ^{89}Sr y ^{90}Sr en suelos y sedimentos". CIEMAT/IMA/UCRE/07-09

(2) - Madoz-Escande, C., Real, J , Fenerstein, J., Hamoniaux, M., Rouxel, M. "Aeropolyr" Caractérisation d'émission d'aérosols lors de tirs "Polyr". CEA Cadarache (France), (Rapport intern). 1993

(3) - J. Tormos, A. Jouve, D. Revy, R Milan-Gomez, R. Zanon, M.J. Erario "A rapid Method for Determining Strontium-90 in Contaminated Samples of Soil and Plant" J Environ. Radioactivity, Vol.27, nº 3, pp.193-206, 1995.

Head of project 7: Dr. Gerasimos ARAPIS

Title: Efficacy of the "non-lethal defoliation" and ecotoxicological impact of the countermeasures used for the recovery of agricultural areas.

II. Objectives for the reporting period.

The main objective of this sub project was the study of the possibility to use the "non-lethal defoliation" as countermeasure to minimise the foliar uptake of radionuclides by the vine and the olive tree. In this work is also included the study of radioactivity translocation to the wine and to the olives, as a function of the defoliation degree achieved by the application of different defoliation products and doses.

A secondary objective of this sub project was to evaluate the secondary effects, especially the ecotoxicological impact of the chemicals involved in the application of this countermeasure.

III. Progress achieved including publications.

Related to the main objective of our sub project which was the investigation of the defoliation efficacy of some agrochemical products, a comparative study of products was conducted on the basis of their specific action and their easy availability at the specialised market. The following three products were selected: Basta, Harvade and Reglon (trade names). The defoliation efficacy of the above products was tested in vine and olive tree using two different doses per product.

Related to the above-mentioned aim, which was the study of caesium uptake by crops (vine and olive tree) and its translocation to fruits (grapes and olives), *in-situ* experiments were carried out during two growth seasons in order to study the foliar uptake of Cs-134 (dry deposition) by the vine (this work was made in collaboration with the CEN of Cadarache - France) and by the olive tree grown in productive agricultural fields in Spata, Attika - Greece. The translocation of Cs-134 to the grapes and to the olives was also investigated.

Related to the secondary objective of our sub project, which was the ecotoxicological impact of the above mentioned three agrochemical products, a comparative study was carried out based on the crops yield.

Some final observation can be made only in November 1995 because this sub project suffered form late financing in July 1993 (14 months delay).

1. Results

1.1 Products selection

In order to study the efficacy of "non-lethal defoliation", we selected three agrochemical products: Two herbicides (Basta and Reglon) and one growth regulator (Harvade). The characteristics of these products are as follow:

Trade name	Basta	Harvade	Reglon
Common name:	Glufosinate-ammonium	Dimethipin	Diquat
Active ingredient:	20%	60%	20%
Presentation form.	Liquid solution	Suspension concentrate	Aqueous solution
Used doses:	25 ml/l 50 ml/l	2 ml/l (+4 ml/l Catapult) 4 ml/l (+4 ml/l Catapult)	10 ml/l 20 ml/l
Producer:	HOECHST AG (Germany)	UNIROYAL CHEM. (U.S A.)	ZENECA (G.B.)

1.2 Defoliation efficacy

VINE

The recommended commercial doses of Harvade 60% F L. (2 ml/l) and Basta 20% S.L. (25 ml/l) are capable of defoliating up to 80% of the crop. Double doses of these products resulted in approximately total defoliation. In both cases defoliation was fast (approx. 2-3 days) and also non-lethal. It was observed that the defoliation efficacy of Harvade seems higher compared to Basta.

OLIVE TREE

The different physiology of olive tree resulted in slow defoliation action of the three products. The efficacy of Basta 20 S.L. and of Reglon A S. was great after 1 or 2 weeks (85%-100% of defoliation). However, the used doses of Harvade 60% FL defoliated only 5% of the olive tree. Table 1 shows the kinetics of defoliation efficacy of the used products for the olive tree.

Table 1
Defoliation efficacy of the applied agrochemical products on the olive tree

PRODUCT	DOSE	PERCENTAGE OF DEFOLIATION			
		24 HOURS	2 DAYS	1 WEEK	2 WEEKS
Harvade	2 ml/l	3%	5%	5%	5%
	4 ml/l	4%	5%	5%	5%
Basta	25 ml/l	5%	10%	85%	90%
	50 ml/l	6%	12%	90%	95%
Reglon	10 ml/l	10%	40%	90%	95%
	20 ml/l	30%	50%	99%	100%

1.3 Uptake and translocation of radionuclides

In-situ experiments were carried out in order to study the interception and foliar uptake of Cs-134 by the vine and the olive tree. The obtained results are briefly presented below.

VINE

Deposition: 93,5 KBq/m2

Foliar concentration: 55,3 KBq/Kg

Grapes: 11,6 KBq/Kg

Grapes protected. (covered by plastic film) 0,3 KBq/Kg

Next grapes production

Our results related to the first productive period of vine following the radio contamination, showed that the contamination of new grapes production is very slight. Also, they did not show significant difference in caesium translocation to the new grapes grown on defoliated and on non-defoliated plants.

Table 2
Level of contamination of a new production of grapes from defoliated and non-defoliated vines.

Grapes of next year (Harvade):	0.006 KBq/Kg
Grapes of next year (non treated):	0.006 KBq/Kg

OLIVE TREE

Deposition:	215 KBq/m2
Leaves:	318 KBq/Kg
Olives:	17 KBq/Kg
Edible part of olives:	23 KBq/Kg
Nucleus (without cleaning)	9.6 KBq/Kg

New olives production

The estimation of the contamination level of a new olive production will be possible next winter because of the fact that the first production of olives following the Cs-contamination of olive-trees is expected to start in November 1995.

1.4 "Non-lethal defoliation" as countermeasure

The study of the possibility to use the "non-lethal defoliation" as countermeasure to minimise the translocation of Cs-134 from vine to grapes was made measuring the radio contamination of grapes. a) from non-defoliated vines and b) from defoliated vines.
Table 3 shows that "non lethal defoliation" could decrease the grapes contamination by a factor of approximately two.

Table 3
Decrease of grapes radio-contamination using the "non-lethal defoliation"

Grapes contamination from non-defoliated vines (Control A)	11,6 KBq / Êg
Grapes contamination from partially defoliated vines	5,5 KBq / Êg
Contamination of protected (covered by plastic film) grapes from non-defoliated vines (Control B)	0,3 KBq / Êg
Contamination of protected (covered by plastic film) grapes from defoliated vines	0.15 KBq / Êg

1.5 Ecotoxicological impact

The ecotoxicological impact of the used products was analysed on the basis of the productivity of vine in our agricultural field. The obtained results show that the impact on the yield, one year after the application of the defoliant, appears to be stronger for Harvade (approximately 40% yield reduction was observed) than for Basta (10% yield reduction). The physiological state of the vines appeared excellent for Basta, one year after its application. The vines, however, treated with Harvade, were slower in reverting to their original state.

In November 1995 it will be possible to do similar observations for olive-trees because in that period the first new olive-production will be produced.

2. Publication

G. Arapis (1995) Reduction of radiocontamination of agricultural crops by the method of "non-lethal defoliation". 4th International Conference on Environmental Science and Technology, Lesbos-Greece, 4-7 September 1995.

3. Summary

The aim of this study was to investigate the possibility of using "non-lethal defoliation" as countermeasure to mitigate the foliar uptake of radionuclides by the leaves. We experimented on vines and on olive-trees, in productive agricultural fields in Spata, Attica. Studies of radionuclides interception and translocation were performed by using Cs-134 as marker. The deposition of Cs-134 was dry. As defoliation products were used Basta, Harvade and Reglon. Our data showed that the recommended commercial doses of these chemicals result in defoliating up to 80-100% of the plants. A reduction of radioactivity translocation to grapes as a function of the defoliation degree was observed. The efficacy of Harvade to defoliate vine seems higher, than that of Basta. One year after application of the defoliant the observed yield reduction was approximately 40% for Harvade and 10% for Basta. As a result the vines treated with Basta appeared to be in excellent physiological state, whereas those treated with Harvade were slower in reverting to their original state. However, the defoliation efficacy of Harvade is very slight for olive-trees. In this case Reglon seems to be the more efficacious defoliant among the three used agrochemical products.

Head of Project 8: Dr. R. Kirchmann

II Objectives for the reporting period

In the previous contract period (1989 - 1991), a survey on agricultural production and a classification of the relevant soils around Belgian NPP was achieved, leading to the identification of the critical transfer pathways of radionuclides of importance in the long term.

For the present research project, a comparison of the radionuclide transfer data obtained in the lysimeters of the RESSAC facility in Cadarache (controlled conditions) and in field plots (natural conditions) was planned, in order to check to which extent they could differ, after application of the same experimental protocol.

III Progress achieved including publications

3.1 Preliminary work (1993)

In March 1993, 3 soil types, identified during the previous contract period as representative of the surroundings of Belgian nuclear power plants, were selected in cultivated fields:

- one dystric cambisol ("sol brun acide" /"sol limoneux caillouteux")

- one calcaric cambisol ("sol brun calcaire"/"sol à charge calcaire")

- one orthic luvisol ("sol brun lessivé"/"sol limoneux")

From the pedological point of view, these are quite comparable, respectively, to the acidic cambisol of Flamanville, the calcaric fluvisol of Tricastin and the orthic luvisol from Germany (KFA Jülich) that were settled in the lysimeters at Cadarache.

The radioecology section of the CEN/SCK Mol had also foreseen to reproduce on its field plots occupied by orthic podzols ("podzols"/"sol sableux") the lysimeter experiment carried out at Cadarache.

For this reason, after agreement with the CEN/SCK Mol, the research work was performed in close cooperation between both Institutes, from 1993 to 1995.

This allowed to apply the same experimental work on 4 soil types in field conditions.

The superficial disturbed layers (0-30cm) of the 3 above-mentioned soil types were thus sampled "in situ" and transferred onto the top of the soil substrate (sand) of the Mol experimental fields, where application of high levels of radioactivity is authorised. There, they were placed into plots (12/soil type) surrounded by concrete plates to reach a 35 cm deep layer.This area was fenced in order to protect the plots from damages by rabbits The experimental plots (4 m^2 each) were sown at the end of April with spring wheat (Triticum aestivum L., var. Arbon), the same variety as the one sown on the lysimeters at Cadarache

The 4 soil types were submitted to pedological analysis in order to verify their characteristics. The main parameters are summarised in the following tables:

	pH		$CaCO_3$	C	Cationic exchange Capacity - pH 7 (meq/100g)					N
	H2O	KCl	%	%	CEC	Ca++	Mg++	K+	Na+	%
Sol Sableux (FAO Orthic podzol)	5 9	4 5	-	4 7	11.0	5.07	0.28	0.13	0 02	0 25
Sol Limoneux-caillouteux (FAO : Dystric cambisol)	7 8	7 2	0 3	1.4	10.6	10 43	0 78	0.56	0 05	0 14
Sol Limoneux (FAO · orthic luvisol)	7 4	6 7	-	1 2	13 2	10.83	0.82	0.79	0.05	0.12
Sol à charge calcaire (FAO Calcaric cambisol)	8.0	7 5	8 0	1 2	12 2	16 22	0.74	0 64	0 04	0 13

	CLAY	SILT				SAND					
Texture (µm)	0-2	2-10	10-20	20-50	Total	50-100	100-200	200-500	500-1000	1000-2000	Total
Sol sableux	3.3	2 2	1 7	5 1	9.0	13.4	48 9	23 3	1.8	0.3	87.7
Sol limoneux-caillouteux	15 3	13.5	8 6	13 7	65.8	7 0	0.8	2.0	4 9	4 2	18 9
Sol limoneux	17.3	12.9	14 7	47.1	74.7	6.5	0 6	0 3	0 3	0.3	8.0
Sol à charge calcaire	21 6	9 6	15.6	36 6	61 8	11.7	3.0	0.8	0 5	0.6	16 6

In this first experimental year, the wheat had to be contaminated during the early vegetative growth phase.

After contamination, one half of the plot area had to be ploughed down as a countermeasure, sown again, with the cereal on one half of the ploughed area and grass on the second half. This protocol had to provide data, in different soil conditions, on the transferability of directly deposited radionuclides to grain and grass, and on the effectiveness of normal ploughing on the contamination of these cultures.

Due to unforeseen circumstances at the RESSAC facility in Cadarache, it was impossible to perform in 1993 the planned experiments that were thus postponed for one year.

It was nevertheless commonly decided to carry out a substitution programme, based for FSA Gembloux, on 3 objectives.

1) Verification of the growth pattern, yield and nutritional status of spring wheat grown on different European soil types in the RESSAC lysimeters and that grown on similar soil types under field conditions.

The plants were harvested at maturity in the experimental plots of Mol and the lysimeters of Cadarache, and straw and grain samples were taken for stable nutrients analysis

The results obtained are summarised in the following table:

Lysimeters			D M (%)	Major components in wheat					
				K (% D.M.)	Ca (% D.M.)	Mg (% D.M.)	Na mg/KgDM	P (% D M.)	N (% D.M.)
Sol sableux		S	94 3	1 47	0.454	0 075	50	0.231	2 2
		G	90.8	0 73	0.049	0 120	<5	0 375	2 7
Sol limoneux-caillouteux		-	-	-	-	-	-	-	-
Sol limoneux		S	94 1	1 47	0.394	0 070	56	0.287	2.0
		G	92.6	0 70	0 037	0 124	<5	0 396	2.8
Brun calcaire		S	92 0	1 60	0 382	0 074	90	0 224	1 6
		G	92.1	0 92	0 084	0 143	74	0 432	2 8
Belleville	E		93 4	1.49	0 452	0.078	98	0 053	0 3
		G	92 3	0 42	0.031	0 092	<5	0 204	1 6
	W	S	93.1	1 73	0.554	0 087	104	0 111	0 4
		G	92.1	0 42	0.049	0 097	15	0.146	2.1
Wellesbourne		S	92.8	3 75	0.806	0 148	269	0.095	0.9
		G	92 9	0 38	0.033	0 115	<5	0 323	2.5
Mol		S	92 6	1.71	0 452	0 055	159	0 017	0.3
		G	89 5	0 33	0.027	0 061	<5	0.191	1.5
Terra rossa	E	S	92 9	2.68	0.774	0 179	189	0 101	0 7
		G	93 8	0.40	0 029	0.095	11	0 303	2 1
	W	S	92.9	2.39	0.552	0.095	163	0 059	0 5
		G	93 9	0.40	0.038	0.090	<5	0 257	1 9
Jülich		S	92.5	3 08	0 720	0 117	151	0 031	0.5
		G	90.2	0 36	0.028	0.085	<5	0 250	2.3
Mean			93.06	2 14	0.55	0.10	132.90	0 12	0 94
ST DEV		S	0.67	0 76	0 15	0.04	63.45	0 09	0 69
Mean			92 02	0.51	0 04	0 10	-	0 29	2.23
ST DEV		G	1 38	0 19	0 02	0.02	-	0 09	0.45

Legend : S=straw G=grain W (E)=Western (Eastern) part of the lysimeter

As far as K is concerned, it appeared that the highest straw concentrations were found in the samples collected at Cadarache (*Terra Rossa*, Jülich and Wellesbourne) while for grain, the highest concentrations were found in the samples collected at Mol.

For the Ca content, the same statements were also true for straw, but no more for grain.

For Mg, it was very surprising that for the *Terra Rossa*, Jülich and Wellesbourne soils, the concentrations were more important in straw than in the grain.

If no direct correlation could be made between the mineral status of the soil (exch. K/Ca) and the mineral content of the plants, the highest K and Ca concentrations in the straw were found on samples collected on soils with the highest CEC, and the highest Ca concentrations in the grain were found on samples collected on soils with the highest amount of exch. Ca .

2) Determination by X-ray diffraction of mineral characteristics of the soils

Applying X-ray diffraction to soils, both gathered at Mol and at Cadarache, allowed to complete by qualitative investigations the information that were previously obtained by usual pedochemical determinations.

The first step was a X-ray diffraction analysis on the raw soil samples.

Besides the identification of quartz, feldspaths, micas, clay minerals, it allowed to identify the presence of calcite in 4 soil types (1 from the experimental plots at Mol (calcaric cambisol) and 3 at Cadarache (Belleville, Tricastin, *Terra Rossa*)). The second step concerned only the clay fraction (<2μm) of the soil.

The diffractograms obtained allowed to identify the minerals found in the clay fraction such as chlorites, illites, kaolinites, vermiculites.

One peculiarity of the results obtained is that lime was found only in the clay fraction of Tricastin soil. No lime was found in the clay fraction of Belleville, nor of the *Terra Rossa* nor of the calcaric cambisol from Mol plots.

Another pecularity is that vermiculite (a clay mineral of the 2/1 type) was found only in the *Terra Rossa*, the Jülich and the Wellesbourne soils, which could partly explain the higher K, Ca, Mg concentrations obtained in the straw grown on these soils.

3) Realisation of tests on the adsorption and desorption capacity of soils after contamination by radiocaesium and radiostrontium.

The sorption and desorption capacity of the different Belgian soils was studied in batch experiments using two source terms (ionic/aerosol) and different extraction techniques: centrifugation, NH4Cl 1N and infinite bath (ion exchange resins + Prussian blue). Following a contamination by aerosols (POLYR) and soluble forms of Cs executed in September 1993, the ^{134}Cs soil concentrations obtained in 0.12 m^2 trays reached 64.8 ± 8.6 and 64.5 ± 8.3 Bq/g for aerosols and ionic forms, respectively. For ^{85}Sr, the concentrations reached 257.8 ± 23 1 and 355 5 ± 47.2 Bq/g for aerosols and ionic forms, respectively. This work was performed at the CEN Mol which reported, for extraction with NH4CI, an identical solubility of ^{134}Cs released as aerosols or ionic forms and an effect of the source term on the extractability of ^{85}Sr.

Moreover, for ^{85}Sr, one observed that the percentage of extraction was 2 to 3 times less important for aerosol than for ionic forms, and that the soil type did not influence the ratio of the percentage of extraction (0.36 ± 0.040).

3.2 Field plots experiments (1994-1995)

3.2.1 1994

In April 1994, spring wheat (Triticum aestivum L., var. Arbon), the same variety as the one sown on the lysimeters at Cadarache, was sown like in 1993, in 48 plots.

After the harvest (July 1994), plots were contaminated with ^{137}Cs and ^{90}Sr recovered from the tank located under the POLYR furnace, after the contamination of the Belgian lysimeter on April 14th, 1994.

On July 4th, 1994, activities of 0.48 MBq/m^2 ^{137}CS and 0.33 MBq/m^2 ^{90}Sr were applied as a wet deposition (after wash-off of the radioactive particles on the furnace pocket) on 16 plots, which were divided in 4 parts (ABCD) of 1 m^2 each.

Afterwards, one half of each plot (parts B+C) was ploughed, and rye grass (Lolium perenne L.) was sown on one fourth of the plots (part B) while clover (Trifoliurn pratense L.) was sown on the rest of the plots (parts A+C+D).

Because of the extremely dry weather, a weak growing was observed for both crops (see the yields in CEN/SCK Mol report), which still allowed a harvest in October.

In November 1994, rye grass and clover were harvested again.

Samples were also prepared for the determination of their ^{90}Sr content.

Parts A+C+D were ploughed afterwards and winter barley (Hordeum vulgare L., var. Orblonde) was sown (parts A+D).

Results obtained for caesium and strontium

The results obtained for rye-grass and clover collected in October 1994 are summarised in the following table (^{137}Cs transfer factors expressed as the ratio of Bq/kg D.M. and Bq/m^2 total deposition):

^{137}Cs TF (m²/Kg) E-4	Rye grass m±σ	Clover (ploughed) m±σ	Clover (unploughed) m±σ
Sableux (Orthic podzol) (=MOL)	3.4±1.1 (11 5)	9.1±1.0	25.3±10.2
Limoneux-caillouteux (Dystric cambisol)	1.1±0.5	1 8±0.4	/
Limoneux (orthic luvisol) (=JULICH)	1 4±0 3	2.5±1 1	/
à charge calcaire (Calcaric cambisol) (=TRICASTIN)	1 4±0 2	2 7±1 5	8 5±0 6

The corresponding results for ^{90}Sr are summarised in the following table (^{90}Sr transfer factors expressed as the ratio of Bq/kg D.M. and Bq/m^2 total deposition):

^{90}Sr TF (m²/Kg) E-3	Rye grass m±σ	Clover (ploughed) m±σ	Clover (unploughed) m±σ
Sableux (Orthic podzol) (=MOL)	8.7±1 6 (8/1994 25 4)	38 2±12.0	31 5±3.2
Limoneux-caillouteux (Dystric cambisol)	3 9±0 05	11 6±2 0	/
Limoneux (orthic luvisol) (=JULICH)	3 3±2 0	11.8±2 7	/
à charge calcaire (Calcaric cambisol) (=TRICASTIN)	5 7±3.7	6 9±1 5	9 6±1 7

Comments for caesium

Unexpected hot and dry weather conditions during the Summer prevented the collection of a sufficient number of samples for each crop which would enable a complete statistical analysis. However, some comments can be made:

Rye grass

- The observed concentrations as a function of the different soil types are of the same order of magnitude.
- The vegetation developed on the orthic podzol does not behave like on the other soil types: it appears to be 2-3 times more contaminated than on the others.

The comparison of the results obtained at Cadarache (Mol lysimeter) and in the field plots shows that the T.F. are higher in the lysimeter at Cadarache (factor 3).

Clover

The vegetation developed on the podzol appears again the most contaminated one, for ploughed plots like unploughed plots. The influence of ploughing reduces the transfer of ^{137}Cs by a factor of about 3 (between 2.4 and 3.9).

Comments for strontium

For rye grass, the general comments made for caesium can be applied to strontium. For clover, the effect of ploughing on the reduction of root uptake is not so well marked. Obviously, the observed ^{90}Sr transfer factors appeared to be of one order of magnitude higher than for ^{137}Cs, which was expected.

Again, the comparison of the results obtained at Cadarache (Mol lysimeter) and in the field plots shows that the T.F. are higher in the lysimeter at Cadarache (factor 3).

3.2.2 1995

The winter barley sown in 1994 was harvested in Summer 1995. Spring wheat was sown in April 1995 (part C) and was also harvested in Summer 1995. In 1995, rye grass was first harvested in April and May for which results are reported below.

Results obtained for caesium and strontium

^{137}Cs and ^{90}Sr results related to the spring wheat and the winter barley contaminations are still being processed.

The following table shows the time evolution (1994-1995) of the ^{137}Cs transfer factor (expressed as the ratio of Bq/kg D.M. and Bq/m2 total deposition) to rye grass:

^{137}Cs T F (m²/Kg) .E-4	November 1994	April 1995	May 1995
Sableux (Orthic podzol) (=MOL)	/	1.7±0.1 (9.0)	5 6±0.3
Limoneux-caillouteux (Dystric cambisol)	0 8±0 4	0.4±0 1	0 3±0 1
Limoneux (orthic luvisol) (=JULICH)	1 1±0 4	0 3±0 1	0 2±0.01
à charge calcaire (Calcaric cambisol) (=TRICASTIN)	1 3±0.2	0.4±0.1	0.2±0 03

The corresponding (available) results for ^{90}Sr are summarised in the following table (^{90}Sr transfer factors expressed as the ratio of Bq/kg D.M. and Bq/m^2 total deposition)

^{90}Sr T.F (m²/Kg) .E-3	November 1994	April 1995	May 1995
Sableux (Orthic podzol) (=MOL)	N.A	7 5±2.6	N.A
Limoneux-caillouteux (Dystric cambisol)	N.A.	3 1±0.8	N.A.
Limoneux (orthic luvisol) (=JULICH)	N.A.	5.9±2 6	N.A.
à charge calcaire (Calcaric cambisol) (=TRICASTIN)	N A.	3.0±0 08	N.A.

legend : N.A = Not yet available

Comments for caesium and strontium

In April and May 1995, like in October 1994, the samples collected on the orthic podzol were again the most contaminated ones, and no significant differences appeared between the ^{137}Cs T.F obtained on the other soil types, neither in November nor in the following harvests.

From October 1994 to May 1995, the ^{137}Cs uptake by rye grass decreased gradually, due to the sorption/fixation processes in the clay fraction of the soils (which is not expected for ^{90}Sr). One has to notice an exception to this rule: on the podzol, where the clay content is the lowest, root uptake of ^{137}Cs dropped from October 1994 to April 1995, but increased in May 1995

In April 1995, the ratio of the ^{137}Cs T.F.'s at Cadarache and in the field plots at Mol is about 5 Regarding the rye grass contamination by strontium, the highest levels were again observed on the podzol.

The obtained ^{137}Cs and ^{90}Sr T.F. to rye grass, spring wheat and winter barley will have to be compared with those obtained in the lysimeters at Cadarache (Mol, Jülich, Flamanville).

Final Report
1992-1994

Contract: F13PCT920049 **Duration: 1.9.92 to 30.6.95** **Sector: A26**

Title: Transfer of accidentally released radionuclides in agricultural systems.

1)	Cancio	CIEMAT
2)	Real	IPSN
3)	Rauret	Fundació "Bosch i Gimpera"

I. Summary of Project Global Objetives and Achievements

The experiences following the Chernobyl accident in 1986 emphasized the need to improve the quantification of several processes and parameters in the transfer of radionuclides along the food chain. The use of reliable parameters and accurate descriptions of processes are essential for pre-accident assessment modelling and for the implementation of protective measures designed to mitigate the radiological consequences of an eventual accident. Therefore, the aim of the TARRAS project, implemented in two consecutive periods (90-92 and 92-95) was to contribute to the realibility of radiological assessment parameters and to establish scientific bases to be used in the design of post-accident actions.

The main aim of the period 92-95 was to complete all the knowledge deduced from the achievements of the former period using a different aerosol and different crops. Then, the objectives of the project dealt with the following aspects: i) characterization of a synthetic, radioactive aerosol which simulated an accidental source term of a PWR reactor; ii) the study of the physical and chemical processes involved in its behaviour after deposition on some Common European soil-crop systems; iii) derivation of relevant transfer factors.

The radioactive POLYR aerosol was used in this period (the same facility as for the RESSAC project) , which contained three radioelements, ^{134}Cs, ^{85}Sr and ^{110m}Ag. Its chemical and physical properties as well as deposition conditions were different from that used in the 1990-1992 period.

The crops selected were lettuce (Lactuca sativa), as a representative of directly consumed crop, which in addition allowed the comparison between the two aerosols of the two periods as it was also studied in the former period, pea plant (Pisum sativa), as a vegetable with fruit, and alfalfa (Medicago sativa), as a typical perennial crop used for animal feeding. Two types of soil were used as in the former period, a sandy and a sandy-loam soil.

A number of experiments were performed in order to study the following aspects:

-Aerosol characterization.
-Aerosol interception by different types of crop.
-Direct absorption of radionuclides deposited on different plants (lettuce, pea plants

and alfalfa).

-Loss of radionuclides from lettuce and pea plants by leaching.
-Evaluation of root uptake and retranslocation to fruit of radionuclides deposited o pea plants.
-Study of the dynamics of soil-to-plant radionuclide transfer using a perennial crop (alfalfa).
-Study of radionuclide partitioning in soils as well as their distribution in depth.

Aerosol characterization.

Firstly, it was demonstrated the homogeneity of the aerosol deposition. The diameter of the particles of the POLYR aerosol ranged from 0.6 μm to 1.3 μm. In addition, the study of the aerosol solubility showed that radiocaesium was 100% soluble, radiostrontium 40% and radiosilver only a 10%.

Aerosol interception by different types of crop.

An experiment in which the aerosol deposition took place on mature plants allowed the calculation of interception factors (R). These ranged from 0.4 to 0.8 for the three types of crop. Similar values were found for lettuces and alfalfa since lettuces had a high foliar effective surface and alfalfa covered the total surface.

Yield factors (Y) and R/Y rates were also calculated for the three crops. These were grown under high density conditions to obtain enough weight to work with, although it did not reflect the usual field agricultural practices. Nevertheless, the R/Y rates found for mature lettuces were similar to the values observed in field conditions.

Direct absorption of radionuclides deposited on different plants (lettuce, pea plants and alfalfa).

To study the foliar uptake of radionuclides deposited on leaf surfaces a sequential extraction scheme was designed. This scheme uses water, to wash the non-adhered aerosol in order to evaluate the fraction potentially removed by rain or irrigation, and chloroform, to solubilize cuticle waxes in order to evaluate the fraction adhered. The residual fraction may be associated with directly absorbed radionuclide into leaf. Furthermore, it is possible to distinguish between particulate (>0.45 um) and soluble (<0.45 um) forms by filtration.

From the application of this scheme it was observed a large difference in the direct absorption of ^{134}Cs depending on the plant studied: 85% for lettuce, 28% for alfalfa, 23% for steams and leaves of pea plants and 42% for pea pods. These results may be related to the different thickness and hydrophobic properties of the cuticles of each crop. A similar behaviour pattern was observed for ^{85}Sr comparing lettuce and pea plants, direct absorption being around 50%. With respect to pea pods and alfalfa, direct absorption was around 30%.

In relation to the radionuclide absorption in lettuces from the two aerosols no significant differences were found for the three radionuclides.

Loss of radionuclides from lettuce and pea plants by leaching. Washout factor

To study the dynamics of the loss of radionuclide retained on lettuces and pea plants, after an aerosol deposition on mature plants, 5 manual sprinklings were carried out with distilled water along a period of 16 days simulating a light rain event.

For pea plants, the leaching effect decreased according to the following order: Cs >> Sr = Ag. This behaviour was in agreement with the predictions of the sequential extraction scheme described in the previous section. For lettuces, the leaching effect was quite similar for the three radionuclides.

The washout factor was calculated as the daily loss of activity from the surface of the plant due to irrigation. To quantify the growth dilution and other kind of effects, these losses of activity of the plant have been studied with a drop by drop irrigation experiment. So, to obtain the washout factor, these effects were removed from the total losses

The washout factor was higher for pea plants than for lettuce, probably due to differences in the shape of leaves and also in cuticle characteristics. The hydrophobic pattern of leaf surface of pea plant avoided the radionuclide absorption and consequently facilitated the washout effect.

Evaluation of root uptake and translocation to fruit of radionuclides deposited on pea plants.

In order to ascertain the role of root growth on radionuclides root uptake an experiment with pea plants sown in contaminated soil was performed.

The ^{85}Sr and ^{110m}Ag concentration in plants increased over time independently of root surface changes. In the case of ^{134}Cs the activity concentration showed a similar pattern to root surface changes over time. These results could be related to the root absorption mechanism. For radiocaesium, root interception seemed to be relevant (probably due to its rapid soil immobilization), added to the mass flow absorption mechanism. For radiostrontium and radiosilver the root absorption mechanism could be also by mass flow but their lower mobility into the plant could lead to an accumulation in plant and, consequently, and increase of these two radionuclides over time.

Another experiment was designed to distinguish between root uptake and retranslocation, by means of contamination of pea plants in covered and non-covered soils. It was observed that translocation depended upon each radionuclide: for ^{134}Cs was higher than for the other radionuclides, and it concentrated in fruits with respect to ^{85}Sr and ^{110m}Ag.

For pea plants, ^{85}Sr was the radionuclide with the highest transfer factor soil to plant in both soils. Furthermore, root uptake increased with plant growth, which was in a clear contrast with the pattern found for lettuces, in which the activity concentration diminished with plant growth.

A mobility factro for each radionuclide has been defined as the fraction extracted with Cl_2Mg. This factor has been used to calculate the soil to plant transfer factor considering the

mobile activity fraction in soil. Larger values of transfer factor are obtained for ^{134}Cs due to its very higher retention rate and the available activity for plant is very small.

Study of the dynamics of soil-to-plant radionuclide transfer using a perennial crop (alfalfa).

To study the dynamics of soil-to-plant radionuclide transfer, an experiment using alfalfa was designed, in which different cuts were performed consecutively according to growth pattern.

Radiostrontium was the radionuclide with the highest transfer: this was constant during the period studied. On the other hand, radiocaesium uptake decreased with time and radiosilver showed a first period with an increasing uptake, followed by a rapid decrease.

Study of radionuclide migration in soils as well as their distribution in depth.

Single and sequential extractions were tested as predictive tools of radionuclide mobility. The sequential scheme allowed the estimation of the radionuclide associated with exchangeable sites, the fraction desorbed in an acidic pH, that extracted after using reducing and oxidizing reagents and the fraction of radionuclide highly fixed to soil. Therefore, the information deduced from these desorption experiments could be compared with that coming from transfer and migration.

Vertical migration pattern was quite similar in both soils, but clearly higher for ^{85}Sr than for ^{134}Cs in both soils, this latter mostly remaining in the top 4-cm, 9 months after the depostion.

From the desorption studies it was deduced that ^{134}Cs was the most fixed radionuclide in sandy soils, ^{85}Sr being the most mobile. In sandy-loam soil, the conclusions depended upon the extractant used. ^{85}Sr seemed to be again the most mobile, although the relative order between ^{110m}Ag and ^{134}Cs changed with the extractant reagent applied.

The quantification of the radionuclide exchangeable fraction was highly dependent on the extractant reagent used. Among the extractants studied, NH_4Cl better explained vertical migration, whereas $MgCl_2$ better explained the relative transfer.

Conclusions

The POLYR aerosol simulated a condensed deposition, as it can be found in far-distance scenarios from a nuclear accidental source in a PWR reactor.

Different pathways in plant contamination (direct foliar absorption, root uptake, retranslocation) were quantified and evaluated. The TARRAS project succeeded in explaining which are some of the parameters that may be of paramount importance in the behaviour of radionuclides in the soil-plant system after a radioactive aerosol deposition. Factors such as interception, washout and foliar absorption have been observed to depend hardly on the type of culture due to the cuticles composition and the shape of the plants. Under this project three

types of cultures have been contaminated and values for each of the previous paramaters, as well as for the root uptake, have been derived.

It is pointed out that speciation of radionuclides is an important factor for plant contamination. The soil to plant transfer factor varies for a factor of 6 for ^{134}Cs, depending if mobility fraction is taken into account.

Head of Project: Dr. Cancio

II Objetives for the Reporting period

- Study of plant aerosol interception and comparison of dry and wet aerosol deposition for both sources used (wet deposition for 90-92 period and POLYR, dry deposition for 92-95 period).

- Translocation of radioactivity from surface contamination to the edible part of pea plants.

- Study of the radioactivity losses due to irrigation water for lettuce and pea plants.

- Study of the radioactivity distribution in with depth soils.

- Soil to plant transfer factors for the three selected crops.

III Progress achieved including publications

Analysis of plant deposition

A. Study of plant aerosol interception

The interception factor for dry deposition on the plant is defined as the fraction of the deposited activity retained by crops on their surface.

The interception factor (R), the yield factor (Y) and the rate R/Y have been calculated for lettuce, peas and alfalfa. The interception factor obtained for lettuce and alfalfa are similar (ranges between 0.80 to 0.98), although the yield of both crops is very different. In both cases the surface was covered and this is the reason for those high interception factors.

In the case of alfalfa, comparing the yield of crop with the one in the agricultural usual practices, the difference is significant and lower in our experiment. In this experiment the yield factor is derived from the 20 cm height of plant and in the usual practice the plant is cut much higher (near twice). The interception for the plant at 20 cm and the ones at 8 cm were very similar (Table1).

The rate R/Y is very different for each crop, due to the importance of the total surface areaof the crop and available for the deposition respect to the yield of the crop.

Plant	Yield Factor Y (kg f.w. m^{-2})	Interception Factor R			R/Y		
		Cs-134	Ag-110m	Sr-85	Cs-134	Ag-110m	Sr-85
Mature Lettuce	2.73	0.81	0.98	0.98	0.30	0.36	0.36
Fruited Peas	0.25	0.39	0.51	0.46	1.57	2.07	1.86
Flowering Peas	0.22	0.43	0.58	0.49	1.98	2.64	2.25
Alfalfa 20 cm	0.85	0.83	0.81	0.80	0.97	0.96	0.94
Alfalfa 8 cm	----	0.77	0.70	0.72	----	----	----

Table 1.- Yield (Y), interception (R) factors and R/Y rate.

Mature lettuces were cultivated, as in the previous phase (Ref 1.), to be able to compare the behaviour of both aerosols, wet and dry (POPLYR). Comparing the results for the mature lettuce with the ones for the previous TARRAS phase (90-92) and with the literature (R/Y=0.3 Ref 2), it can be seen that although the yield factor in this case is a little lower and there are some differences in the interception, the rate R/Y, that is generally used in modelling, remains very similar in both cases. The differences in the yield factor may be due to the greenhouse agricultural conditions.

In the case of green peas, the results for R/Y for both growing stages ranges from 1.57 to 2.64. As the flowering plant and the fruited one had very similar size, there are no significant differences between their yield factors and the interception factors.

B. Translocation inside the plant

The translocation factor inside the plant may be defined as the fraction of activity in the edible part (fruit) to the total initial activity in the plant. These factors are shown in Table 2 for green peas.

	Ag-110 m	Cs-134	Sr-85
1 Irrigation	2.20E-05	4.40E-04	----------
3 Irrigations	----------	7.95E-03	1.50E-04
5 Irrigations	3.09E-05	1.02E-02	3.63E-05
Drop by drop	1.54E-04	1.47E-02	2.56E-05

Table 2.- Translocation factors for green peas (fruit)
Cs-134 shows higher mobility and it clearly increases during the experimentation period

(about 15 days). Sr-85 and Ag-110m have similar behaviour and no time evolution can be observed.

An experiment was designed with the crop contaminated at the flowering stage and with the soil covered not to take into account the root uptake. Measurements of activity in leaves and stems, pod and fruits have been made. After contamination marks were made to see the new growing parts of the plants. Samples of the initial old parts and the new ones were taken and measured separately. Table 3 shows the percentages of activity in them.

	Leaves and Stems			Pod			Fruit		
	Ag-110m	Cs-134	Sr-85	Ag-110m	Cs-134	Sr-85	Ag-110m	Cs-134	Sr-85
0 day									
Old	100	100	100	-----	-----	------	-----	-----	-----
New	-----	-----	-----	-----	-----	------	-----	-----	-----
18 days									
Old	93.6	87.3	93.3	2.5	3.6	2.7	0.005	1.24	0.007
New	3.9	7.9	3.9	-----	-----	-----	-----	-----	-----
41 days									
Old	93.7	79.9	81.1	1.5	3.2	1.4	0 .004	0.93	0.004
New	4.6	14.4	4.3	0.2	2.9	0.2	0.001	2.70	0.020

Table 3.- Percentajes of activity in the green peas plants

For all the radionuclides, most of the activity remains in the old fraction of leaves and stems. Cs-134 percentages in pods and fruit are higher, which suggests that this is the most mobile radionuclide within the plant. Ag-110m and Sr-85 have similar distributions within the plants.

The percentge of activity in the fruit of the young part of the plant (0.001% for Ag-110m, 2.7% for Cs-134 and 0.02% for Sr-85) are substantially higher than the values reached in the old parts of the plant (0.004, 0.93 and 0.004% respectively). This may be explained because the young part needs a higher amount of nutrients and so there is higher transfer of elements. Again, the higher mobility of Cs-134 is clearly shown. In the literature similar behaviour for these radionuclides have been observed (Ref 2).

In order to compare the behaviour of the two types of aerosols, lettuces were grown to a mature stage and sequential extraction schemes were applied (see participant 3). In these cases similar behaviour of the radionuclides can be observed within the plants for the two aerosols used. Cs-134 is readily incorporated in lettuce and stays in water soluble form; Strontium and Silver penetrate less than Caesium. In the experiment 2 with the POLYR, the absorption of the radionuclides was obseved to increase during the studied period (16 days). For Cs-134 the percentages of the absorved fraction by the plant goes from 85 to 95%. At the end of the experiment the percentage of Ag-110m and Sr-85 in the absorbed fraction increased to about 50%

Clear differences can be observed depending on the type of crop. In the case of Cs-134,

the fraction absorved is about the 80% for lettuce, around 30% for alfalfa, 25% for stems and leaves of green peas and 45% for pods. This is due to the differences in the properties of the cuticles of the plants.

C. Washout

The washout factor may be defined as the daily loss of activity from the surface of the plant due to irrigation.

One experiment has been designed, with green peas and lettuce to highlight the effect of irrigation on the loss of activity by plants. From the total amount of plant, one part was irrigated with a drop by drop system; and for the other part, spraying irrigation was used to simulate natural precipitation. The growth dilution and other kind of effect have been taken into account in studing the loss of activity of the plants with drop by drop irrigation. One, three and five spraying irrigations have been applied both to fruited green peas and lettuce.

For the lettuce plants, the results can be compared with those of the previous phase (TARRAS 90-92). Table 4 shows the washout factor for the lettuce and green peas. The washout factor decreases with time as the radionuclides are being incorporated inside the plant. Cs-134, Ag-110m and Sr-85 have very similar behaviour in the case of washout.

	Lettuces			*Green Peas*		
	Ag-110m	**Cs-134**	**Sr-85**	**Ag-110m**	**Cs-134**	**Sr-85**
1 Irrigation	3.5E-01	3.0E-01	3.9E-01	5.2E-01	6.5E-01	5.4E-01
3 Irrigations	4.6E-02	4.8E-02	4.9E-02	7.9E-02	1.1E-01	8.2E-02
5 Irrigations	6.3E-03	5.1E-03	6.6E-03	3.7E-02	4.4E-02	2.6E-02

Table 4.- Washout factor (d^{-1})

The washout factor is higher for green peas than for lettuce, due to differences in the structure of the plants. The lettuce has a compact structure, and its own leaves can retain the irrigation water, while for the green peas, the activity that goes in the irrigation water can drop easily to the soil.

D. Effect of plant growing and harvesting

The experiment 4 was designed with alfalfa a typical crop for animal feed and which allows several harvestings along the year. The period of study was 201 days, with 6 cuts. The plants were harvested at a height between 20 to 25 cm. The contamination was done with the plants at three heights: very near from the soil surface, previously cut to 8 cm and with 25 cm (no cut).

Cut	Date of Sample	Type of Plant	Ag-110m	Cs-134	Sr-85
1	12-4-94	25 cm	1.6E+06	1.3E+06	3.0E+06
	10-5-94	8 cm	1.8E+06	1.2E+06	3.2E+06
	20-5-94	2 cm	9.0E+04	2.3E+05	2.7E+05
2	20-5-94	25 cm	3.8E+04	1.5E+05	1.4E+05
	16-6-94	8 cm	3.9E+04	1.1E+05	1.5E+05
	16-6-94	2 cm	1.2E+05	1.6E+05	3.5E+05
3	16-6-94	25 cm	1.0E+05	1.5E+05	2.9E+05
	19-7-94	8 cm	1.0E+05	6.0E+04	1.5E+05
	19-7-94	2 cm	6.4E+03	8.1E+04	2.7E+05
4	19-7-94	25 cm	3.3E+03	3.8E+04	1.6E+05
	31-8-94	8 cm	6.4E+03	1.7E+04	1.6E+05
	31-8-97	2 cm	1.5E+04	1.8E+04	1.4E+05
5	31-8-94	25 cm	4.0E+03	8.5E+03	1.1E+05
	13-10-94	8 cm	1.2E+03	1.5E+04	1.4E+05
	13-10-94	2 cm	1.9E+03	1.8E+04	2.5E+05
6	13-10-94	25 cm	8.7E+02	8.3E+03	1.7E+05
	28-11-94	8 cm	9.7E+03	2.5E+04	2.0E+05
	28-11-94	2 cm	1.7E+04	4.2E+04	2.8E+05
7	28-11-94	25 cm	3.7E+04	2.0E+04	2.8E+05

Table 5.- Activity in alfalfa (three types of samples) (Bqkg-1 d.w.)

The sampling of the plant with 25 cm was done the day after the contamination; the other plants, contaminated with 8 and 2 cm, were sampled after one month when they reached about 25 cm. As commented about the interception factors, the activity in the plants at 25 cm is very similar to the activity in the first samples of the plants at 8 cm.

The three heights of the plants show the same behaviour for each radionuclide. The concentration in plant of Cs-134 decreases rapidly until the fourth cut, after this one, the concentration remains quite constant. The concentration of Ag-110m decreases between the first and the second cut, afterwards it increases and from the third cut it a reaches very low and quite constant concentration. Sr-85 does not present this type of decrease, although the high deviation of the values it can be seen that the concentration ranges between a narrower interval (see figure 5, paticipant 3).

This behaviour can be due to the mobility of the contaminants in the soil and to the need of radionuclides by the plants. The level of Sr-85 in plant stays stable due to the lower rate of fixation in soil, whereas the Cs-134 in soils is less available for the plants.

Analysis of soil contamination

E. Soil to plant transfer

E1. Soil migration

Two types of soils were used to follow the migration of the isotopes with soil depth. At the end of the experiment 1 three samples were taken for the total depth of soil, the samples were taken in three layer of 2cm with depths from 0-2 cm, 2-4 cm, 4-6 cm and the other from 6 to 14 cm (bottom of the lysimeter).

As expected, the retention in the first layer is higher in sandy-loam soil for the three radionuclides, the values in this case range from 98% for Ag-110m and Cs-134 to 93% for Sr-85. For the french soil, retention values range, from 92% for Cs-134 to 70% for Sr-85. These results agree with the post-Chernobyl measurements (Figures 1 and 2).

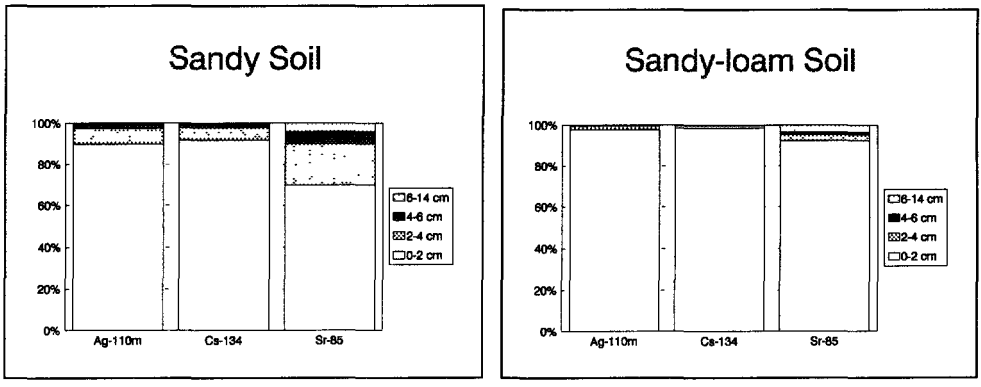

Figures 1 and 2.- Percentages of the total activity in soil that remains in each layer two months after contamination.

For both types of soil, Sr-85 is more mobile than the other radionuclides, and this effect is more important for sandy soil. In general, the radionuclides remain in layers 1 and 2.

In the experiment with a new aerosol (POLYR) the behaviour of the radionuclides in soil seems similar to the first period aerosol (90-92). In both cases the Sr-85 is the radionuclide most mobile, Cs-134 and Ag-110m show similar distributions for each type of soil.

Sandy-loam and sandy bare soils were contaminated during experiment 4 to study the migration of the radionuclides through the profile. Samples were taken 3 and 9 months later, with depths of 0-2 cm, 2-4 cm, 4-6 cm and 6-10 cm. During this period manual irrigation was

undertaken. Results of the measurements are shown in table 6.

	Ag-110m		Cs-134		Sr-85	
	Sandy loam	Sandy	Sandy loam	Sandy	Sandy loam	Sandy
3 Months						
0-2 cm	37.77	61.32	70.31	80.47	40.92	33.00
2-4 cm	23.89	28.02	14.96	15.26	24.01	25.15
4-6 cm	27.47	8.40	11.12	3.27	22.66	15.75
6-10 cm	10.87	2.26	3.61	1.00	12.41	26.10
9 Months						
0-2 cm	51.17	56.30	60.49	65.31	32.27	31.28
2-4 cm	26.00	21.14	21.43	18.99	23.17	20.31
4-6 cm	12.88	14.30	11.56	11.71	18.13	16.34
6-10 cm	9.95	8.27	6.52	4.00	26.43	32.06

Table 6.- Percentage of activity in soils profiles

The migration in soils is higher for the three radionuclides that in the other experiment, especially for Sr and Ag. This is due to the manual irrigation effect. Both soil types show similar behaviour for the radionuclides, for all the cases except Ag-110m and 3 months after the contamination.

E. Soil to Plant transfer factor

The soil to plant transfer factor (TFsp) is defined as the ratio of plant activity (fresh weight) to soil activity (dry weight). The soil activity is mainly present in the first two layers, however for TFsp calculation, 14 cm deep soil samples have been taken, this soil depth is more accurate because mature plant roots reach the bottom.

Three experiements were designed with green peas and alfalfa to study this factor. Values of TFsp parameters are shown in Table 7 and 8.

Growing stages	Soil	Ag-110m	Cs-134	Sr-85

Young plant	Sandy-loam	0.002 ± 0.001	0.002 ± 0.001	0.017 ± 0.014
	Sandy	0.006 ± 0.003	0.015 ± 0.022	0.340 ± 0.455
Flowering plant	Sandy-loam	0.003 ± 0.004	0.003 ± 0.006	0.032 ± 0.052
	Sandy	0.014 ± 0.021	0.024 ± 0.037	0.843 ± 2.074
Fruited plant	Sandy-loam	0.011 ± 0.014	0.013 ± 0.010	0.078 ± 0.128
	Sandy	0.042 ± 0.076	0.029 ± 0.027	2.504 ± 1.722
Pod and fruit	Sandy-loam	0.026 ± 0.034	0.004 ± 0.004	0.029 ± 0.047
	Sandy	0.028 ± 0.053	0 031 ± 0.013	1.245 ± 0.168

Table 7.- Soil to plant transfer factors for green peas (Bq kg^{-1} f.w) (Bq kg^{-1} d.w)$^{-1}$

For green peas, the radionuclide most transferred for both soils is the Sr-85. The root uptake of activity increases when the plant grows. Transfer to the fruit has also been calculated (Table7). Differences with the previous similar experiments with lettuce have been observed, in this case working with peas, the specific activity increases with the growth of the plant biomass while in the experiments with lettuce the activity decreased with plant growth.

Experiment 4 was designed to study the root uptake for alfalfa. Results are shown in table 8. The soil to plant transfer factors are calculated substraing the surface contamination of the plants, intercepted from deposition, so they are values derived, not directly from measurements.

The TFsp are given for the seven cuts of the plant. As with the contamination of plants, explained in previous paragraphs, the root uptake by the plant clearly decreases for Cs-134, and remains quite constant for Sr-85.

All the soil to plant transfer factors given for the second cut show high values, probably due to the activity from direct deposition that still remains until this time. Therefore these TFsp are not really representive of the soil to plant transfer of activity.

Type of plant	Cut	Ag-110m	Cs-134	Sr-85
20 cm	2	0.57 ± 0.49	2.57 ± 0.75	0.97 ± 0.54
	3	1.53 ± 1.06	2.40 ± 0.95	1.93 ± 3.00
	4	0.05 ± 0.31	0.60 ± 0.44	1.07 ± 1.32
	5	0.10 ± 0.36	0.33 ± 0.41	1.62 ± 1.81
	6	0.01 ± 0.15	0.15 ± 0.18	1.19 ± 1.74
	7	0.97 ± 1.13	0.62 ± 0.82	3.50 ± 6.59
8 cm	2	0.51 ± 1.15	1.69 ± 1.51	0.98 ± 2.98
	3	0.12 ± 0.41	0.80 ± 0.52	0.82 ± 1.33
	4	0.18 ± 0.60	0.45 ± 0.68	1.86 ± 1.98
	5	0.02 ± 0.27	0.25 ± 0.36	0.97 ± 3.04
	6	10.6 ± 0.55	0.60 ± 0.60	1.74 ± 4.54
2 cm	2	0.76 ± 1.17	1.27 ± 1.15	1.17 ± 2.47
	3	0.03 ± 0.19	0.59 ± 0.31	0.76 ± 0.71
	4	0.18 ± 0.50	0.26 ± 0.56	0.87 ± 1.39
	5	0.02 ± 0.19	0.18 ± 0.24	1.01 ± 2.01
	6	0.15 ± 0.46	0.44 ± 0.51	1.24 ± 3.79

Table 8.- Soil to plant transfer factors for alfalfa (Bq Kg^{-1} f.w) (Bq kg^{-1} d.w)$^{-1}$

A mobility factor for each radionuclide is defined as the rate between the easily extracted soil activity and the total activity (Table 9). The easily extracted phase is considered as the fraction extracted with Cl_2Mg (1M) (see participant 3).

Sandy soil			Sandy-loam soil		
Ag-110m	Cs-134	Sr-85	Ag-110m	Cs-134	Sr-85
0.412	0.125	0.597	0.061	0.034	0.452

Table 9.- Mobility factors

These factors have been used to calculate the soil to plant transfer factors considering the movable activity fraction in soil. Larger values are obtained for Cs-134 due to its higher retention rate and the available activity for plants is very small. This effect is clearly seen for sandy-loam soil. For Sr-85 it is less obvious because the fixation in soils is lower (Figures 3 and 4).

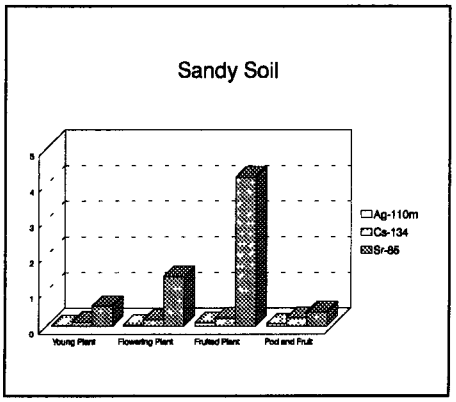

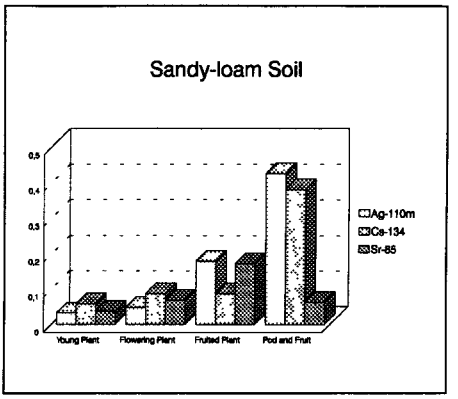

Figures 3 and 4. Soil to plant transfer factors with the mobility factor.

REFERENCES

1- Transfer of Accidentally Released Radionuclides in Agricultural System (TARRAS) Final Report. June 1992. Contract Nº Bi7-046. Sector A26.

2- Methodology for Assessing the Radiological Consequences of Routine Released of Radionuclides to the Environment. Report by the National Radiological Protection Board UK. Preprint, Radiation Protection 72 (XI-5026-94-EN) 1994.

PUBLICATIONS

G. Rauret, D. Cancio, J. Real, V.R. Vallejo. "Transfer of Simulated Accidentally Released Aerosol in Soil-plant Transfer System: Design and First Results". J. Environ. Radiactivity (in press)

B. Robles, D. Cancio, I. Simón. "Resultados experimentales sobre la transferencia de radionúclidos depositados sobre cultivos" Proceeding of V Congreso Nacional de la Sociedad Española de Protección Radiológica. Santiago de Compostela, 26-29 Abril 1994.

M.C. Roca, V.R. Vallejo, G. Rauret, M. Vidal, J. Real and D. Cancio. "Cs-134, Sr-85 and Ag-110m Transfer in Different Soil-plant System (TARRAS Project)". Proceeding of the International Sysposium on Environmental Impact of Radioactive Releases. Vienna 8-12 May 1995.

Head of Project 2: Dra. J. Real

II - Objectives for the Reporting Period

- Producing and characterizing radioactive aerosols representative of an accidental source term using the same facility as for the RESSAC project, i.e. the POLYR furnace,
- Performing four tests involving contamination of pea, lettuce and alfalfa cultures at various stages of vegetative development,
- Monitoring the cultures in our greenhouses.

III - Progress Achieved Including Publications

A - Characteristics of the Source Term Used

A.1 - Characteristics of the POLYR Furnace

The POLYR furnace is an induction furnace. Inside it a graphite crucible contains the mixture to be studied (load). Maximum temperatures may exceed 2850°C (fusion of UO_2). The crucible is covered with an envelope heated to 80°C containing steam which simulates the reactor containment. The aerosols produced remain in this enclosure for 30 minutes before being transferred. During this time the chemical reactions that would occur in the reactor building take place. In particular these include particle coalescence.

Next the aerosols are transferred into a second Terphan pocket connected to the first by a junction which is also made of Terphan (see Figure 1). The transfer takes place by increasing the volume of the lysimeter pocket. This creates a pressure drop which draws in approximately 1.5 m^3 from the furnace enclosure containing the aerosols.

Figure 1 - Diagram Showing the Contamination Apparatus

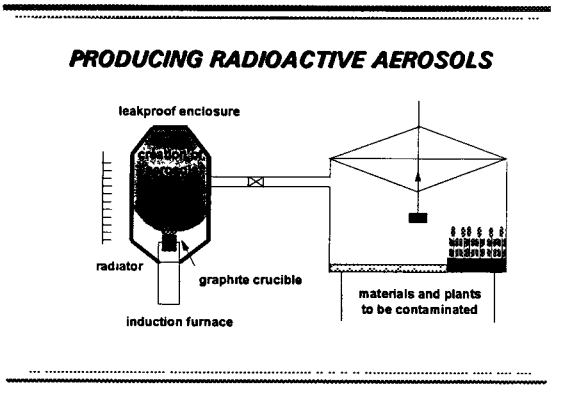

A.2 - Load Characteristics

The load comprises a mixture of 14 representative elements:
- structure and control rod materials: Fe, Cr, Ni, Ag, In, Cd.
- fission products: I, Cs, Sr, Te, Ru, Ce.
- sheaths: Zr and Sn

Uranium (representing the fuel) is not included in the load as its presence distorts the measurements.

The 14 elements are used in the chemical form shown in Table 1 below.

The three radioelements included and studied are ^{134}Cs, ^{85}Sr and ^{110m}Ag. Their respectice activity levels are provided in Chapter 1V B.

Table 1 - Definition of the Standard Load in the POLYR Furnace Crucible

			simplify heart inventory		load POLYR	
Element	atomic mass	origin	representative elements	total mass (kg)	Chemical form in the crucible	Mass of compound in the crucible (mg)
U	238.03	fuel	U	70520.0		
I	126.904		I + Br	11.7	I	140
Cs	132.905		Cs + Rb	148.4	Cs_2CO_3	212
Te	127.6	fission	Te + Sb + Se	25.6	Te	60
Sr	87.62	products	Sr+Mo+Tc+Ba	30.70	$SrCO_3$	188
Ru	101.107		Ru + Rh	19.24	Ru	440
Ce	140.12		La + Ce +Y	49.77	$Ce(NO_3)_3,6H_2O$	62
Zr	91.22	sheaths	Zr	1832.65	Zr	4200
Sn	118.69		Sn	20.23	Sn	470
Ag	107.87	rod	Ag	190.32	Ag	444
In	114.82	controls	In	36.00	In	28
Cd	112.4		Cd	12.37	Cd	73
Fe	55.847		Fe	2060.00	Fe	2000
Cr	51.996	structure	Cr	620.00	Cr	560
Ni	58.71		Ni	410.00	Ni	400
				123 518.5		9277

A.3 Aerosol Characteristics

A large number of analyses and measurements were carried out to characterize the aerosols.

A.3.1. Physical Characteristics

The particle size distribution curve was plotted for the aerosols. The measurements were taken using Andersen impactors standardized for this type of measurement. The cutoff diameter for these impactors ranges from 0.4 to 9 μm. Figure 2 below indicates the impact rates for five tests. They are expressed as cumulative percentages versus the particle diameter in microns. The D50 reading (the diameter corresponding to the 50% impact rate) provides the average diameter of the particles. It will be noted that this varies between 0.6 and 1.3 μ. The D25-D75 diameter range varies between 0.4 and 1.8 μ.

Figure 2: Particle Size Distribution Curve for Aerosols Produced Using the POLYR Furnace

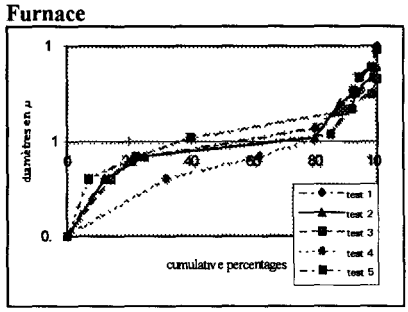

A.3.2. Chemical Characteristics

ICP/MS mass spectrometry was used to provide a global analysis of the chemical composition of the aerosols. The aerosol samples analyzed were taken from the impactor plates after pumping the air contained in the enclosure. Table 2 below indicates the filter efficiency levels for tests carried out between 1990 and 1991. The / sign indicates that the element could not be measured.

The chemical species were determined using X-ray diffraction. This method differentiates between the crystalline phases. These measurements provided identification of non-oxidized metal silver, metal Sr which rapidly transforms into $Sr(OH)_2$ in contact with air, and metal Cs which also transforms rapidly into caesium hydroxide.

Table 2 - Chemical Composition of the Aerosols Measured Using ICP/MS

Efficiency levels observed by measuring aerosols deposited on the impactor plates. The levels for each element are expressed as aerosol mass / mass placed in the crucible.

ELEM.	PREVIOUS FIGURE Average 88/89	EFFICIENCY LEVEL OBTAINED in 1990 and 1991 (%)				AVERAGE X (%)	STANDARD DEVIATION σ	σ/X 100 (%)
		02/90	03/90	05/90	01/91			
Fe	0.25	0.27	/	0.1	0.63	0.31	0.19	61
Zr	0.02	0.016	/	/	0.017	0.018	0 002	9.5
Cr	0.25	0.32	/	0.2	0.66	0.36	0.18	50
Ni	0.25	0 11	/	0.023	0.37	0 19	0.13	68
Ag	10	5.4	/	8.3	22.6	11.6	6.6	57
In	30	27.7	/	46 6	26 4	32 7	8.1	25
Sn	10	4 12	/	2 5	12	7.2	4	55
Cd	20	24 4	/	32 6	23 7	25.2	4.6	18
I	2	0.75	/	19 1	8.3	7.5	7.3	97
Ce	0 24	0.064	/	/	0.09	0.08	0 09	112.5
Cs	20	25	24	30	24.1	24.6	3.2	13
Sr	5	7 2	16	9 9	10 1	9.6	3.7	38.5
Te	10	21 4	/	/	24.4	18 6	6.2	33
Ru	0.016	0 012	/	/	0 09	0.04	0.04	100

ELEM · Elements

A.3.3. Aerosol solubility in rainwater:

Figure 3 below indicates the dissolving kinetics of aerosols in rainwater. The results are very similar about the four tests represented in this figure. We notice the rapidity of dissolving kinetics. The caesium is soluble per 100%, the strontium per 40% and the silver per 10%.

Figure 3: dissolving kinetics of aerosols in rainwater (4 tests):

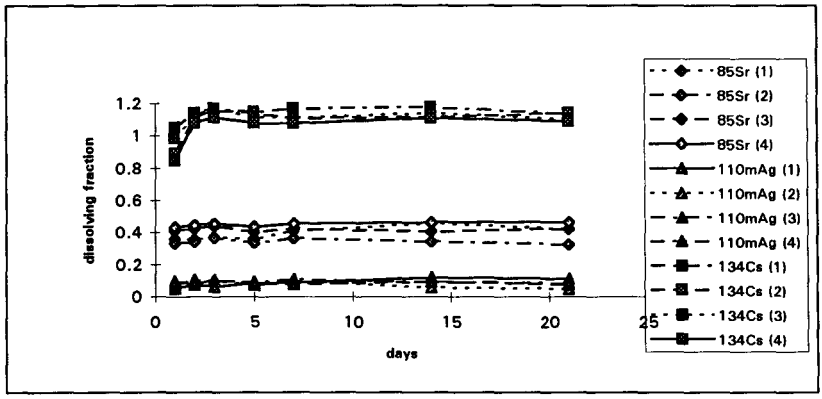

A.3.4. Comparison between aerosols produced for atomic absorption furnace and POLYR furnace:

The aerosols produced for POLYR furnace present a average diameter higher (0.6 to 1.3 μm), because the maturation time in enclosure furnace is larger. The relative size for elements represented in POLYR aerosols is different, this last allow less Fe, Cr, Ni, Sr but more In, Sn, Cd, I, Cs and Te. The POLYR aerosols more approximate the accidentals aerosols.

B - Experimental Conditions

Four contamination tests were carried out using ^{134}caesium, ^{85}strontium and ^{110m}silver as the radioelements included in the load as defined above.
The initial activity levels were 5.3×10^7 Bq for caesium, 1.8×10^8 Bq for strontium and 3.5×10^7 Bq for silver.
During contamination cellulose acetate filters are installed evenly over the surface of the enclosure containing the vegetables. These filters are then measured using γ spectrometry to check the deposited activity level and its uniformity across the enclosure.
Table 4 indicates the radioactive characteristics of the filters for the four tests involved.

Table 4 - Filter Characteristics

	Activity levels in Becquerels par m2				
		test 1(11/92)	test 2 (05/93)	test 3 (12/93)	test 4 (04/94)
average	^{85}Sr	1465069	423032	643326	1065750
	^{110m}Ag	554537	195408	201145	782076
	^{134}Cs	343058	97910	99531	490040
standard dev.	^{85}Sr	131023	109548	108405	333036
	^{110m}Ag	44091	51200	33676	230575
	^{134}Cs	34577	24134	23033	173806
max. level	^{85}Sr	1743878	771939	844388	2058673
	^{110m}Ag	658673	357143	253061	1418367
	^{134}Cs	426531	166837	143878	1010204

During the four tests various plants were contaminated :

-first test, 4 m^2 of young pea plants
-second test 4 m^2 pea plants in the mature stage and lettuce
-third test 4 m^2 flowering peas
-fourth test 6 m^2 alfalfa cultures at various stages of vegetative development.

Publication:

G. Rauret, D. Cancio, J. Real and V.R. Vallejo. "A radioactive aerosol to study radionuclide transfer in soil plant system." This publication is currently being prepared for possible inclusion in the "Journal of Environmental Radioactivity".

Head of project 3: Dra. Rauret

II. Objectives for the reporting period.

1st. Study of the direct absorption of radionuclides deposited by dry deposition on different plants (lettuce, pea plants and lucerne).
2nd. Effect of aerosol type and conditions of its deposition in leaves absorption.
3rd. Loss of radionuclides from lettuce and pea plants by leaching.
4th. Evaluation of root uptake and retranslocation to fruit of radionuclides deposited on pea plants.
5th. Study of the dynamics of soil-to-plant radionuclide transfer, using a crop of continuous growth (lucerne).
6th. Study of the radionuclide partitioning in soils as well as their distribution in depth.
7th. Conclusions.

III. Progress achieved including publications.

1st. Study of the direct absorption of radionuclides deposited by dry deposition on different plants (lettuce, pea plants and lucerne).

The study of the direct absorption of radionuclides is of extreme importance in directly consumed crops, as lettuce plants. By contrast, it is also interesting to use vegetables which edible part is the fruit like pea plants, to analyze the contamination in pods and fruits. In addition, the third plant studied is lucerne since is a typical culture used for animal feeding.
To study plant-radionuclide interactions, a two-step sequential extraction procedure was established and applied to lettuce, pea plants, pea pod and lucerne, which had been contaminated using POLYR aerosol.
The extraction scheme uses distilled water, to wash the non-adhered aerosol in order to evaluate the fraction potentially removed by rain or irrigation, and chloroform, to solubilize cuticle waxes in order to evaluate the fraction adhered. The residual fraction after these two extractions may be associated with directly absorbed radionuclide into leaf. Furthermore, it is possible to distinguish between particulate (>0.45 μm) and soluble (<0.45 μm) forms by filtration.
To study the dynamics of radionuclide retention-absorption in lettuce and pea plants extractions were performed 3 and 16 days after contamination. Considering that the soil was covered at the moment of plant contamination and, that drip irrigation was applied during the studied period, neither loss of activity in plants nor root uptake were taken into account. For lucerne, extractions were performed 1 day after contamination.
Figure 1 represents ^{134}Cs and ^{85}Sr mean activity percentages in each fraction obtained from the extraction procedure. Results of ^{110m}Ag are not given due to their similarity with those of ^{85}Sr. The 'retranslocated fraction', included in pea pods distribution, is defined from fruit activity. It can be noticed that:

- There was a large difference in the direct absorption of ^{134}Cs depending on the plant studied: 85% ± 5% for lettuce, 28% ± 5% for lucerne, 23% ± 5% for stems and leaves of pea plants and 42% ± 8% for pea pods. These results may be related to the different thickness and hydrophobic properties of the cuticles of each plant.
  Direct absorption in lettuces slightly increased with time: from 85% ± 5% to a 95% ± 1%. This increase is more significant for pea pods, since percentage activity is two-fold the initial, considering both residual and retranslocated fractions. These results point out the relevance of retranslocation to fruit of radionuclides initially absorbed by leaves and/or by pods, even only few days after contamination.
- A similar behaviour was observed for ^{85}Sr between lettuce and pea plants. Direct absorption is around 50% (48% ± 2% and 50% ± 13%, respectively), whereas a 30% is retained by cuticle (26% ± 3% and 33% ± 7%, respectively). There was not a significant variation with time of these values. With respect to pea pods, direct absorption was slightly lower (28% ± 5%) and a 39% ± 4% was retained by the cuticle. There was not a change with time in direct absorption in any of the cases studied. The absorption for lucerne was 29% ± 5% and cuticle retention 13% ± 5%.

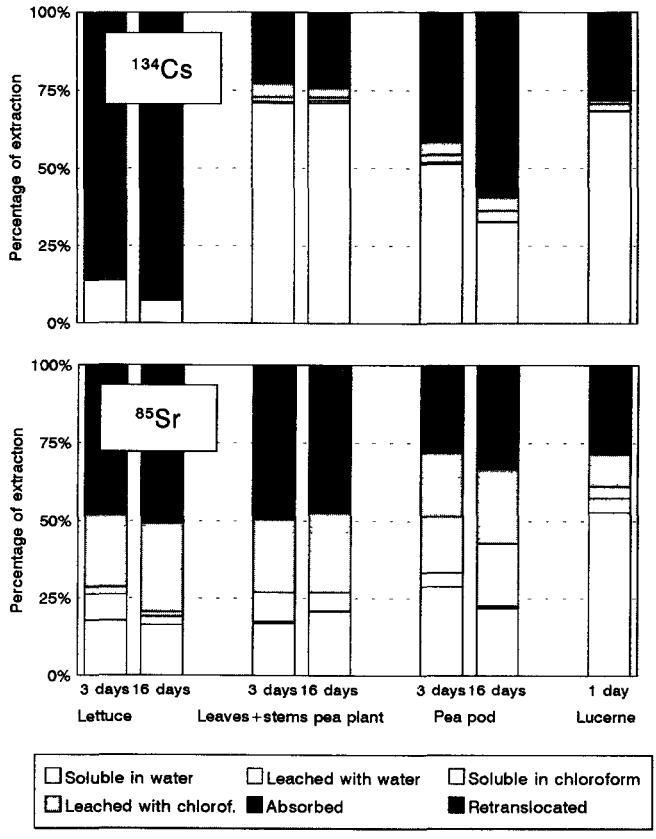

Figure 1. Mean activity percentages for ^{134}Cs and ^{85}Sr in each fraction obtained from the extraction procedure applied to lettuce, leaves + stems of pea plants, pea pods and lucerne.

2nd. Comparison between the solubility of two types of intercepted aerosol in a soil-plant system, by means of sequential extractions.

In TARRAS project, two types of aerosol, with different chemical and physical properties as well as deposition conditions, have been used. Wet deposited (90-92 period) and dry deposited aerosols (POLYR aerosol used in 92-94 period) were intercepted by the same plant.
Considering that retention and subsequent absorption of radionuclides intercepted by plants will depend on both aerosol properties and physico-chemical interactions with plant surfaces, the two-step sequential extraction procedure decribed previously, which studies plant-radionuclide interactions, was applied to lettuces which had been contaminated by the two types of aerosol mentioned above.
If a 'total particulate fraction' is defined as the sum of water and chloroform particulate fractions, it can be seen for ^{134}Cs and ^{110m}Ag, that this fraction was similar independently of the aerosol it came from: about 2% for ^{134}Cs and 40% for ^{110m}Ag. However, significant differences were found for ^{85}Sr: the value was of 7% ± 2% for ^{85}Sr coming from wet deposited aerosol, whereas for dry deposited aerosol, the value increased up to 32% ± 5%.
Despite the differences found in the 'total particulate fraction' for ^{85}Sr, depending on the aerosol used, it can be observed similar direct absorption values in lettuce plants for all the radionuclides studied.

3rd. Loss of radionuclides from lettuce and pea plants by leaching.

Due to the fact that the loss of some leaf nutrients by leaching may be a significant process, a similar behaviour for some radionuclides can be expected.
To be able to study the dynamics of this process in lettuces and pea plants, 5 manual sprinklings were carried out with distilled water along a period of 16 days, using 1.2 mm in each irrigation to simulate a light rain event. The crop density was 24 lettuces and 64 pea plants per m^{-2}. Irrigation water was collected and its activity determined. From these values and final plant activities, it was possible to calculate the percentage of activity leached during the experiment.
Figures 3 and 4 represent the percentage of accumulative sum of leached radionuclide activity after 1, 2, 3, 4 and 5 sprinklings for pea plants and lettuces. The sum of water soluble and particulate fractions (E), derived from the application of the sequential extraction scheme, is also represented.
It can be concluded that:

- For pea plants, the leaching effect decreased according to the following sequence: Cs ➤ Sr ≈ Ag. This behaviour is in agreement with the predictions of the sequential extraction scheme.
- For lettuces, the leaching effect was quite similar for the three radionuclides. However, for ^{86}Sr, water extraction (E) was more efficient than the actual leaching process whereas for ^{134}Cs, an opposite behaviour was observed.

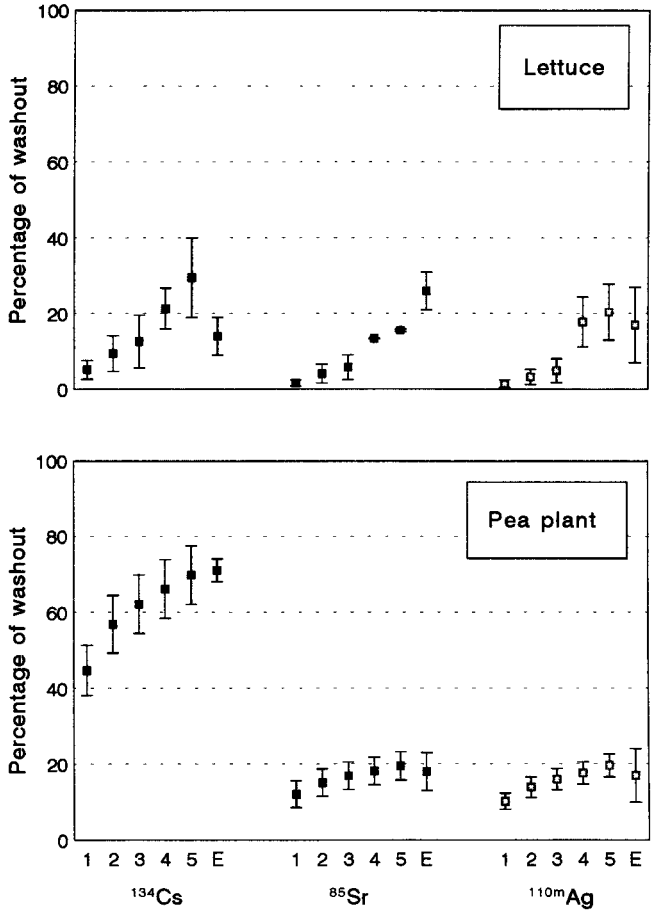

Figure 2. Percentage of accumulative sum of leached radionuclide activity after 1, 2, 3, 4 and 5 sprinklings and water extraction (E), for lettuce and pea plants.

4th. Evaluation of root uptake and retranslocation to fruit of radionuclides deposited on pea plants.

An experimental design with pea plants sowed in contaminated soil, was performed in order to ascertain the role of root growth on radionuclides root uptake.
The plant activity concentration of ^{85}Sr and ^{110m}Ag increased over time independently of root surface changes, whereas in the case of ^{134}Cs the activity concentration showed a similar pattern than root surface changes over time (Figure 3). These results could be related to the root absorption mechanism .For Cs, root interception seems to be relevant (probably due to his rapid soil inmobilization), added to the mass flow absorption mechanisme (passive). For ^{85}Sr and ^{110m}Ag, the root absorption mechanism could be also by mass flow but, their lower mobility into the plant could lead to an accumulation in plant and, consequently, and increase of this two radionuclides over time.
At the same time, non root interception effect could be observed, probably due to their higher soil mobility.

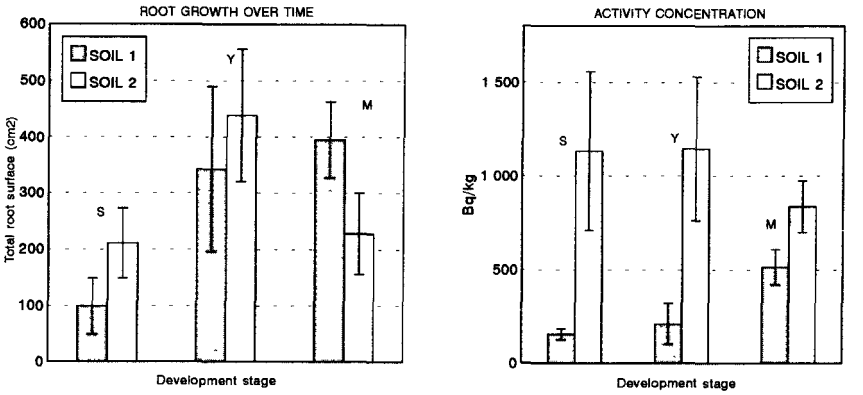

Figure 3. Total root surface at diferent growth stages and B) ^{134}Cs activity concentration in plant at different growth stages (S:seedling, Y:young plant, M:mature plant).

When studying radionuclide activity in fruits, it is important to be able to distinguish between root uptake and retranslocation, in order to ascertain the relative importance of each process for different radionuclides.
An experiment was designed to distinguish between root uptake and retranslocation, by means of contamination of pea plants in covered and non-covered soils. The activity of leaves + stems, pea pods and fruits, grown from directly and/or non-directly plant parts contaminated in covered soils, comes from retranslocation, whereas in non-covered soil, activity originates from both root uptake and retranslocation. Two samplings were carried out: 20 days (a) and 42 days (b) after contamination.

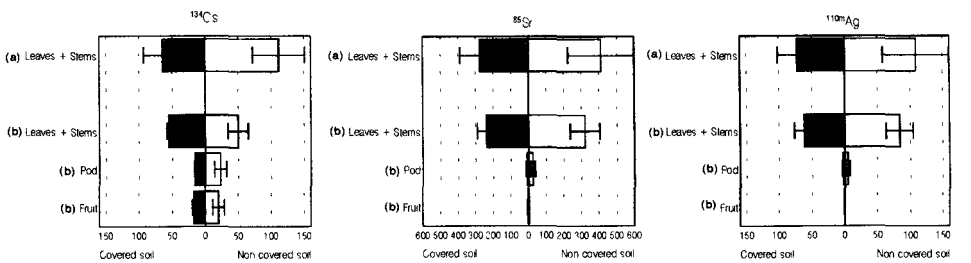

Figure 4. Activity concentrations of non-directly contaminated plant parts grown in covered and non-covered soils, for both samplings: 20 days (a) and 42 days (b) after contamination.

Figure 4 shows the activity concentrations of non-directly contaminated plant parts grown in covered and non-covered soils, for both samplings. It can be observed that:

- In leaves and stems, 20 days after contamination, concentrations of the three radionuclides were higher in non-covered than in covered soil. This fact showed the role of root uptake.
- In non-covered soil, the plant ^{134}Cs concentration decreased with time. This fact can be explained by the roots growing down and far from the highest contaminated layers of the soil. This behaviour was not observed for the other radionuclides, probably due to their higher soil migration rates.
- Non significant differences with time were observed of the plant activity concentration growing in covered soil, showing that the retranslocation kept constant along the period studied.

Table 1 shows radionuclide activity concentration ratios in leaves and stems, pea pods and fruits, in both covered and non-covered soils. It can be concluded that:

- The retranslocation depends on each radionuclide: for ^{134}Cs is higher than for the other radionuclides, and it concentrates in fruits with respect to ^{85}Sr and ^{110m}Ag.
- For covered soils, the ratio Sr/Ag keeps constant in the different parts of the plant. However, in non-covered soils, it can be noticed an increase of Sr/Ag ratios in fruits, due to ^{85}Sr root uptake. The decrease with time of Cs/Sr ratios in fruits, in non-covered soils, corroborates the significant contribution of ^{85}Sr root uptake and its character of non-mobile cation into the plant.

Table 1. Radionuclide activity concentration ratios (standard deviation is given into brackets) in leaves and stems, pea pods and fruits, in covered and non covered soil (n.s.: no samples; *: one replicate).

Sampling description	Leaves + stems			Pods			Fruits		
	Cs/Sr	Cs/Ag	Sr/Ag	Cs/Sr	Cs/Ag	Sr/Ag	Cs/Sr	Cs/Ag	Sr/Ag
Initial	0.17 (0.01)	0.67 (0.03)	3.81 (0.07)						
Covered soil - 20 days after contamination Plant parts directly contaminated	0.16 (0.01)	0.59 (0.03)	3.76 (0.07)	0.18 (0.01)	0.70 (0.06)	3.95 (0.11)	6.48 (6.66)	28 (22)	2.88 (2.02)
Covered soil - 20 days after contamination Plant parts non-directly contaminated	0.23 (0.01)	0.96 (0 44)	4.15 (2.04)	n.s.	n.s.	n.s.	n.s.	n.s.	n.s.
Covered soil - 42 days after contamination Plant parts directly contaminated	0.15 (0.01)	0.59 (0.05)	3 94 (1E-3)	n.s.	n.s.	n.s.	n.s.	n.s.	n.s.
Covered soil - 42 days after contamination Plant parts non-directly contaminated	0.24 (0.04)	0.92 (0.17)	3.86 (0.09)	1.72 (0.76)	8.05 (4.56)	4.54 (0.64)	14.8 (15.9)	19.7* -	4.83* -
Non covered soil - 20 days after contamination Plant parts directly contaminated	0.13 (0.02)	0 47 (0.06)	3.72 (0.19)	0.18 (0 02)	0.73 (0.09)	4.04 (0.06)	24.0 (4.7)	90.3 (28.6)	4.10 (1.07)
Non covered soil - 20 days after contamination Plant parts non-directly contaminated	0.28 (0.04)	1.06 (0.16)	3.78 (0.08)	n.s.	n.s.	n.s.	n.s.	n.s.	n.s.
Non covered soil - 42 days after contamination Plant parts directly contaminated	0.16 (0.02)	0.60 (0.07)	3 66 (0.02)	0.15 (0.04)	0.61 (0.16)	3.95 (0.08)	14.4 (0.9)	84.0 (17.4)	5.91 (1.64)
Non covered soil - 42 days after contamination Plant parts non-directly contaminated	0.16 (0.05)	0.61 (0 19)	3.81 (0 12)	1.16 (0.69)	7 53 (4.60)	6.43 (2.82)	10.1 (6.6)	60 6 (29.0)	7.94 (2.46)

5th. Study of the dynamics of soil-to-plant radionuclide transfer, using a perennial crop (lucerne).

To study the dynamics of soil-to-plant radionuclide transfer, an experience using lucerne was designed. During the period studied (201 days), 6 cuts were performed consecutively according to growth pattern (when plants height was about 25 cm).
Radionuclides showed a different behaviour depending on their migration pattern and aging. Radiostrontium was the highest absorbed with a constant transfer rate during the period studied. Whereas, radiocaesium uptake decreased with time and radiosilver showed a first period (66 days-2cuts) with an increasing uptake followed by a rapid decrease. These results pointed out that in this case, the radionuclide aging increased in this order: Ag > Cs >> Sr.
A similar behaviour was observed when the aerosol was deposited on plants with different heights. Figure 5 shows the mean activity concentration in plants collected in each cut (except the values corresponding to the plants directly contaminated).

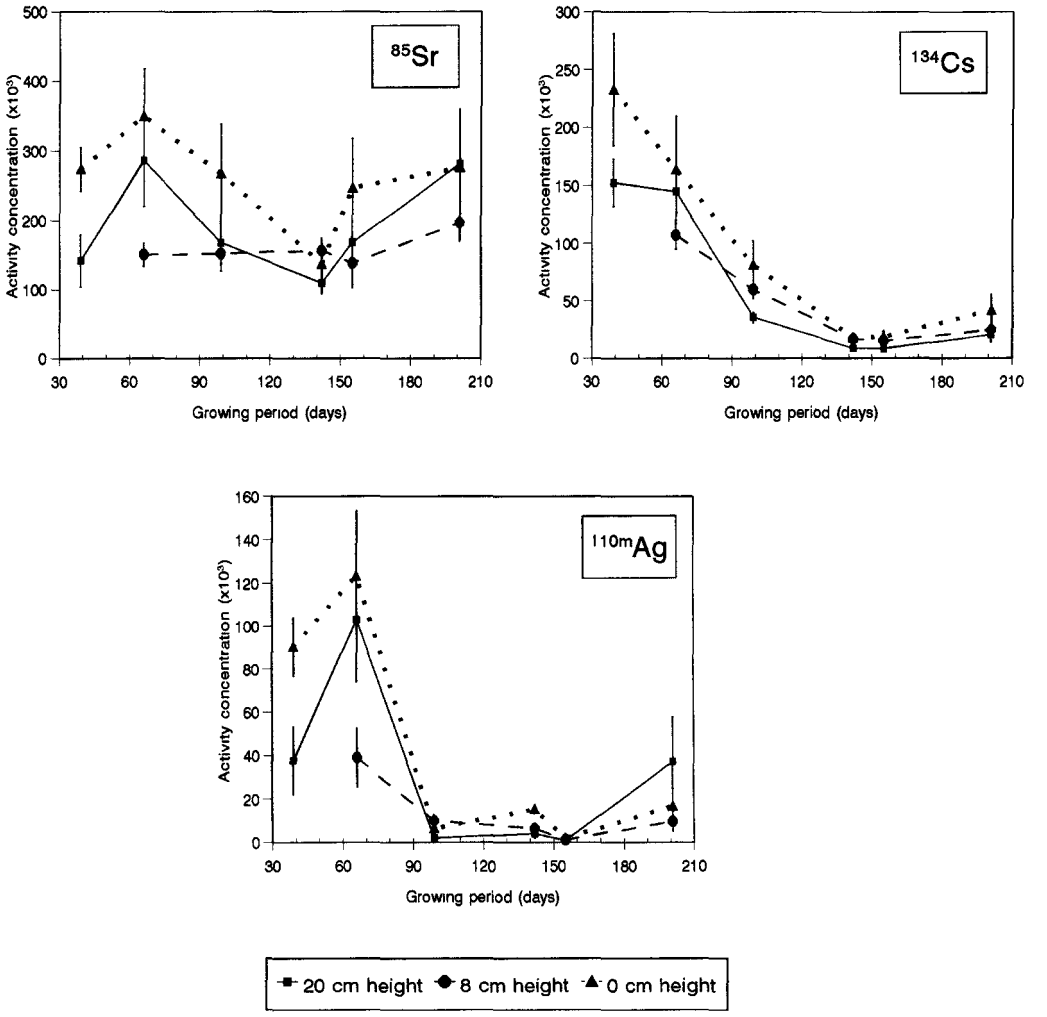

Figure 5. Mean activity concentration in plants (Bq/kg(dw)) and standard error (n = 4) collected in each cut (except the values corresponding to the plants directly contaminated).

The ratio Sr/Cs in plants at the different cuts it showed an increase with time. If we consider only the first cut and compare its Sr/Cs ratio with that of aerosol deposited, higher Cs uptake than of Sr was observed (Table 2). These results show that initially, the order of radionuclide uptake was Cs > Sr, but this relative behaviour was progressively reversed probably due to the higher Sr migration and a lower Sr immobilization (aging) than Cs.

From the high Cs mobility into the plant it can be expected a retranslocation of this radionuclide from the leaves directly contaminated to the roots and consequently, a decrease in the Sr/Cs ratio in the following cut respect to the Sr/Cs ratio in the same cut of plants non-directly contaminated. The values obtained for each case (0.92 ± 0.33 and 1.26 ± 0.28, respectively) showed this tendency but no statistical differences were observed.

Table 2. Sr/Cs ratio in plants at diferents cuts.

Plant height at contamination time	20 cm	8 cm	0 cm
Directly contaminated	2.28 ± 0.02	2.79 ± 0.23	-
1st. cut	0.92 ± 0.33	1.41 ± 0.19	1.26 ± 0.28
2nd. cut	1.60 ± 1.02	2.55 ± 0.63	2.39 ± 0.74
3rd. cut	4.54 ± 1.88	10.91 ± 4.51	3.61 ± 2.20
4th. cut	13.34 ± 3.35	15.46 ± 9.20	8.10 ± 1.97
5th. cut	18.91 ± 5.39	10.97 ± 4.72	13.36 ± 2.72
6th. cut	13.73 ± 2.02	-	7.50 ± 2.57

6th. Study of the radionuclide partitioning in soils as well as their distribution in depth.

In the TARRAS project, two different soils - a sandy-loam and a sandy soil, fully described in previous reports (final report 90-92) -, were used in a serie of experiments in order to ascertain the influence of the type of soil in radionuclide behaviour, especially with respect to radionuclide mobility (vertical migration and transfer) in the soil-plant system.

Single and sequential extractions were tested as predictive tools of radionuclide mobility, paying especial attention to the exchangeable fraction. The sequential extraction scheme allowed, in an operational way and by the application of increasingly stronger reagents, the estimation of the fraction of radionuclide associated with exchangeable sites (by using H_2O + $MgCl_2$ or NH_4Cl or KCl), the fraction desorbed in a acidic pH (extraction with HOAc), the fraction of radionuclide extracted after the use of reducing and oxidizing reagents ($NH_2OH \cdot HCl$ and H_2O_2) and, finally, the fraction of radionuclide highly fixed to soil mineral matter (residual fraction). Therefore, the information deduced from the desorption experiments could be compared with that coming from transfer and migration.

Figure 6 is an example of the different radionuclide distribution that were obtained in both soils, in samples taken the day after aerosol deposition. In this example, exchangeable fraction was estimated with NH_4Cl. As can be seen, radionuclide partitioning depended on both radionuclide and type of soil.

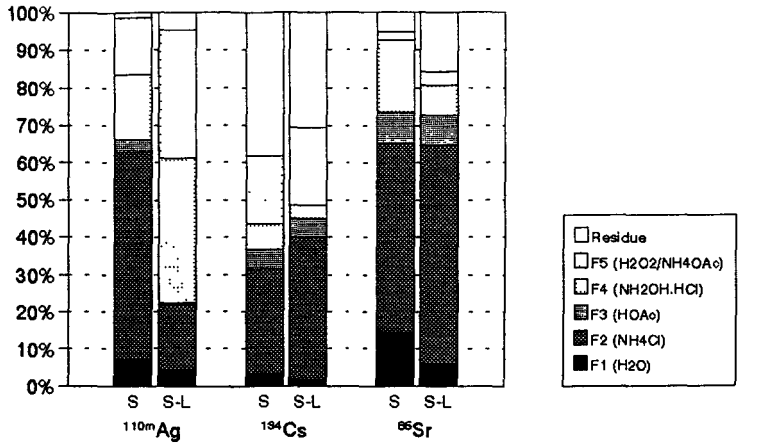

Figure 6. Radionuclide distribution in sandy-loam and sandy soils, after the application of the sequential extraction scheme.

In sandy soils, ^{134}Cs was the most fixed radionuclide, whereas ^{85}Sr seemed to be the most mobile. ^{110m}Ag showed an intermediate behaviour, with a low residual fraction, an intermediate exchangeable fraction and a significant fraction desorbed with oxidizing agents. The distributions obtained in the sandy-loam soil were similar for ^{134}Cs and ^{85}Sr, although the residual fraction was slightly higher for ^{85}Sr and lower for ^{134}Cs. ^{110m}Ag was clearly different and a significant decrease in the exchangeable fraction of ^{110m}Ag.

Figure 7 summarizes the estimation of the radionuclide exchangeable fraction, depending of the extractant reagents used in its quantification. It is important to highlight that the prediction of the mobility of radionuclides mainly depended on the extractant used and that changes of this fraction had a significant effect in the final distribution, although the residual fractions were similar for all cases. ^{85}Sr seemed to be the most mobile radionuclide in both soils, especially in the sandy-loam soil, although, depending on the extractant, in the sandy soil its mobility could be quite similar to that of ^{110m}Ag. The predictions for ^{134}Cs largely depended on the extractant. $MgCl_2$ predicted a lower mobility in the sandy-loam soil, NH_4Cl the reverse behaviour, whereas KCl levelled out the behaviour of ^{134}Cs in both soils. Therefore, in the sandy-loam soil, the prediction of the relative mobility Cs/Ag varied according the extractant used.

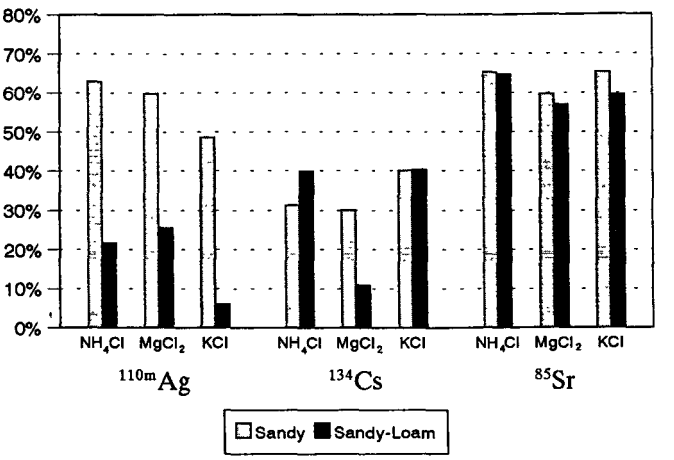

Figure 7. Estimation of the radionuclide exchangeable fraction.

The results of the quantification of the exchangeable fraction can be compared with those from vertical migration. Figure 8 shows the results of ^{134}Cs and ^{85}Sr migration, 3 and 9 months after the aerosol deposition. 3 months after, ^{85}Sr migration was higher than that of ^{134}Cs, as expected from its higher exchangeable fraction.

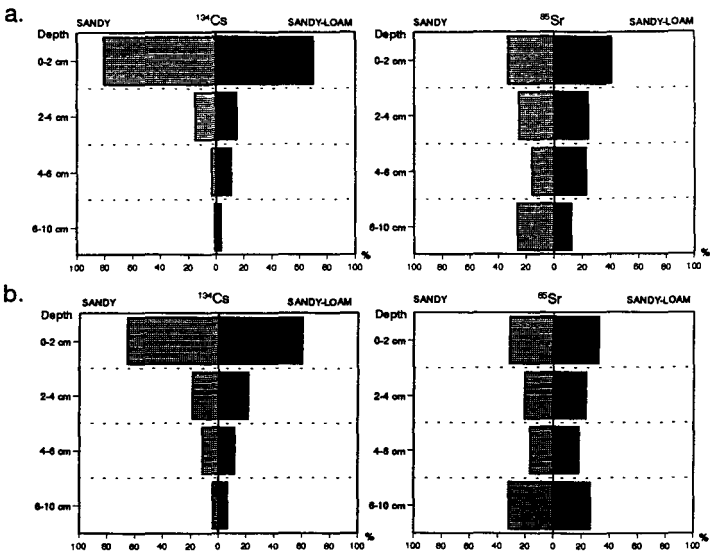

Figure 8. ^{134}Cs and ^{85}Sr distribution in the sandy-loam and sandy soil profiles, after 3 (a) and 9 (b) months after aerosol deposition.

Vertical migration pattern was quite similar in both soils, although higher for ^{134}Cs in sandy-loam soil and lower for ^{85}Sr in sandy soil. These results were in agreement with desorption results using NH_4Cl. 9 months after the aerosol deposition the radionuclide distributions in the soil profile were more similar.

Finally, when comparing the soil-to-plant transfer, it was clear the higher values found in sandy soil. This fact was nicely predicted for ^{134}Cs by using $MgCl_2$, in contrast with what can be deduced with the other reagents. In any case, neither extractant distinguished enough the different transfer found for ^{85}Sr in both soils, clearly indicating that other factors besides the quantification of the exchangeable fraction, should be considered in the transfer predictions.

7th. Conclusions

- The different experimental aerosols, differing in particle size and composition, did not affect the direct absorption into lettuce leaves of ^{134}Cs, ^{85}Sr and ^{110m}Ag.

- Cuticle leaves, with respect to their thickness and hydrophobic pattern, play a key role in direct absorption of ^{134}Cs, whereas for ^{110m}Ag and ^{85}Sr no effect is noticed.

- Retention of canopy deposition depended a great deal on crop type, probably in relation to the leaf surface characteristics. Pea plants showed a higher ^{134}Cs leaching rates than lettuces, probably due to differences in leaf surface characteristics.

- Sequential extraction procedure is useful to predict the retention and washout of radionuclides deposited on leaf surfaces.

- ^{134}Cs concentrates in fruit with respect to ^{85}Sr and ^{110m}Ag.

- Soil migration rates and downward growth of roots influence plant root uptake. The mechanism governing Cs and Sr root uptake is mass flow, but for Cs the root interception plays a key role in his uptake due to the low mobility of this radionuclide in soil.

- For lucerne, Cs root uptake decreased by a factor of 10 along the season. This decrease is related to Cs soil aging and it would be different depending on soil characteristics. The Sr root uptake was constant along the period studied because the Sr aging in the soil used was insignificant.

- The quantification of the radionuclide exchangeable fraction is highly dependent on the extractant reagent used and it is unsufficient to predict radionuclide mobility, especially with respect to the soil-to-plant transfer. Among the extractants studied, NH_4Cl better predicted vertical migration, whereas $MgCl_2$ better explained the relative transfer, which depended on type of soil and radionuclide.

Publications

1) M. Vidal and G. Rauret. "Two approaches for sequential extraction of radionuclides in soils: batch and column methods". *Int. J. Environ. Anal. Chem.*, 51 (1993) 85-95.
2) M. Vidal and G. Rauret. "A sequential extraction scheme to ascertain the role of organic matter in radionuclide retention in Mediterranean soils". *J. Radioanal. Nucl. Chem.*, 173 (1993) 79-86.
3) M. Vidal, J. Tent, M. Llauradó and G. Rauret. "Study of the evolution of radionuclide distribution in soils using sequential extractions schemes". *J. Radioecology*, 1 (1993) 49-55.
4) J. Tent, M. Vidal, M. Llauradó, G. Rauret, J. Real and P. Mischler. "Sequential extraction as a tool to study foliar uptake of radionuclides". *J. Radioanal Nucl. Chem.*, 173 (1993) 377-385.
5) G. Rauret, D. Cancio, J. Real and V.R. Vallejo. "Transfer of simulated accidentally released aerosol in soil-plant systems: design and first results". *J. Environ. Radioactivity* (in press).
6) M.C. Roca and V.R. Vallejo. "Effect of soil potassium and calcium in caesium and strontium root uptake'. *J. Environ. Radioactivity* (in press).
7) M. Vidal and G. Rauret. "Prediction capacity of a sequential extraction scheme". *J. Radioanal. Nucl. Chem.*, 181 (1994) 85-95.
8) M. Vidal and G. Rauret. "Use of sequential extractions to study radionuclide behaviour in mineral and organic soils". *Química Analítica*, 14 (1995) 102-107.
9) M.C. Roca, V.R. Vallejo, G. Rauret, M. Vidal, J. Real and D. Cancio. "^{134}Cs, ^{85}Sr and ^{110m}Ag transfer in different soil-plant systems (TARRAS project)". Proceedings of the International Symposium on Enviromental Impact of Radioactive Releases, Viena 8-12 May, 1995.
10) M. Roig, M. Vidal and G. Rauret. "Radionuclide behaviour in agricultural soils: a qualitative approach". Proceedings of the International Symposium on Enviromental Impact of Radioactive Releases, Viena 8-12 May, 1995.

Final report
1992 - 1994

Contract : FI3P-CT30071 **Duration 1.1.93 to 30.6.95** **Sector : A26**

Title : Influence of food-processing techniques on the level of radionuclides in foodstuffs.

1)	C.Colle	C.E.A./ I.P.S.N.
2)	K. W. Nicholson [1]	A.E.A. Technology
3)	A. Grandison	Department of Food Science and Technology University of Reading

I. Summary of Project Global Objectives and Achievements

The global objectives are to determine the extent of radionuclide transfer through the food chain to man as modified by food processing methods.

An initial collaborative research program [2] between the participants has demonstrated that food processing can either decrease or increase the radionuclide concentrations in the final products.

In order to complement the basic data, some specific topics were studied, namely, a) the fate of radionuclides in recycled by-products, b) the effect of food processing on removing silver and ruthenium deposited to foliage of leafy vegetables, c) the influence of the species variety on the retention of cesium, strontium and potassium during processing for canned vegetables, and d) the removal of actinides during canning of vegetables.

The main part of the project was devoted to more detailed examination of basic processes in studying modifications to traditional processing techniques : a) additives, b) peeling, blanching or canning processes, c) time of storage, that may result in maximum removal of cesium, strontium, potassium, cobalt, ruthenium, from canned vegetables.

Within this scope, the following results [3] were obtained :

---

[1] Dr. Nicholson replaces Dr. Cawse who has retired

[2] CEC "TARRAS" project 1990-1992

[3] Conventionally, results are presented as :

Retention factor : $Bq.kg^{-1}$ (or $\mu g.g^{-1}$) of processed food divided by $Bq.kg^{-1}$ (or $\mu g.g^{-1}$) of raw food, $\mathbf{R_d}$: relative to dry weight, $\mathbf{R_w}$: relative to fresh weight.

Mass retention factor : kg of processed food divided by kg of raw food, **Rm** : relative to dry weight , $\mathbf{Rm_w}$: relative to fresh weight.

Residual activity (total recovery) : total Bq (or μg) of processed food divided by total Bq (or μg) of raw food, $\mathbf{Rt} = R_d \cdot Rm = R_w \cdot Rm_w$

Complement to basic data

a) The assessment of the fate of some radionuclides in factory by-products and wastes from food processing intended for animal feed showed that by-products are a significant secondary contamination pathway through animal foods.

Information on the fate of "waste" material produced during the processing of oilseed, wheat and sugar beet was obtained by University of Reading, through collecting statistical information in the United Kingdom. Some industrial samples of the raw materials used and by-products produced in industrial processes were analysed for cesium, strontium and potassium by A.E.A. and by I.P.S.N..

The results show that levels of these elements are significantly elevated in wastes used as animal feed, suggesting that important quantities of ^{90}Sr and ^{137}Cs could hence enter the human food chain.

b) The influence of cooking (as in domestic preparation) on the removal of ^{103}Ru and ^{110m}Ag deposited to mature foliage of cabbage, cauliflower and spinach was investigated by A.E.A. Cooking leaves one day after deposition resulted in a significant decrease of activity : for ^{103}Ru, losses of between 22 % and 38 % were recorded ; for ^{110m}Ag, losses ranging from 10 % (spinach) to 63 % (cauliflower) were measured.

c) Two varieties, each of carrots, peas and potatoes, were cultivated by A.E.A. in a region having relatively high soil concentrations of ^{90}Sr and ^{137}Cs, for processing (canning) in the pilot plant facilities at Reading.

Considering the two varieties of each vegetable, analysis by A.E.A. showed that there is little, if any, difference in the loss of radionuclides or nutrients during canning. However, comparison with previous results (1990/91) highlights the fact that reductions in the radionuclide content of vegetables by a particular food processing technique can be highly variable.

d) The actinides removal during canning of vegetables was investigated by I.P.S.N. through experimental processing of green beans, contaminated in the laboratory by root uptake of ^{239}Pu and ^{241}Am.

The removal of ^{239}Pu during canning of green beans was about 40%, mainly due to the removal of stems.

Effect of modifications to processing techniques

The main topics to be examined were the influence of different processing technologies and additives on the radionuclide content of vegetables after canning plant products which had been contaminated by indirect transfer (internal contamination).

Parallel and complementary experiments were carried out by the three participants,

- either with vegetable crops cultivated by A.E.A. in some field plots established near Sellafield Works, for processing in the pilot plant facilities at Reading, and analysing for cesium, strontium and potassium by A.E.A.,

- or, by I.P.S.N., with vegetables contaminated in the Cadarache facilities, processed and analysed for ^{134}Cs, ^{85}Sr, ^{57}Co and ^{106}Ru, in the laboratory.

Parameters tested by I.P.S.N. were essentially the influence of the currently used additives (or process additives) added to the brine of canned vegetables (green beans, carrots, tomatoes), and the effect of pH variation of the brine. Additional experiments also investigated the effects of the time of storage, and different processing techniques (blanching and peeling).

A.E.A. and the University of Reading examined the effects of : a) increasing the potassium content of the blanching and/or canning solutions, b) varying blanching regimes used prior to dehydration, and c) the duration of storage time on the retention of ^{90}Sr and ^{137}Cs of canned vegetables (carrots, peas and potatoes).

The results obtained in these various experiments show that, in general, no significant change in the retention of radionuclides contents of vegetables was recorded when modifying the above mentionned parameters :

The retention of radionuclides by canned vegetables did not exhibit any significant change when the storage time varied from 4 weeks to 4 months.

Variations in the blanching regime used prior to processing vegetables did not greatly affect the retention of radionuclides.

There was no significant trend in the retention of radionuclides when the composition of blanching and/or canning solutions of canned vegetables was modified by a wide range of additives or by pH variation.

PROJECT 1 : DR. C. COLLE / S. ROUSSEL-DEBET

II. Objectives for the reporting period (January 93 to June 95)

The objectives were to improve our knowledge of the behaviour of radionuclides during food processing, with emphasis on :

- the fate of some radionuclides that enter factory by-products intended for animal feed,
- the influence of different canning technologies including the effect of additives on the radionuclide content of vegetables artificially contaminated by ^{57}Co, ^{85}Sr, ^{106}Ru and ^{134}Cs,
- the effect of canning on the actinide content of processed vegetables.

III. Progress achieved including publications

a) Use of by-products for industrial fodder production

Quantitative data concerning the use of industrially produced by-products in rearing feed show that more than 5 million tons of feedstock is used in France for animal fodder; about 30% are produced by cereals milling and more than 10% comes from sugar refining.
Radioactive measurements (gamma Ge spectrometry) of industrial samples from cereals milling and from sugar refining show (Table 1) that retention factors of ^{40}K in by-products vary from 2,7 to 3,5 (cereals) and are lower for sugar beet chips (R_w=0,2), 80% of potassium being retained in raw sugar, and consequently in molasses. This indicates that the fraction of radioactivity removed during processing will be re-incorporated in the food chain through animal feeding.

Table 1 : Retention factors [a] for by-products from measurements of industrial samples.

	Mass retention Rm_w	R_w	
		^{40}K	^{137}Cs
Rice (by-products)	0,30	2,7	3,0
Durum wheat (offal)	0,23	2,9	1,4
Soft wheat (offal)	0,23	3,5	1,5
Sugar beet			
chips	0,83	0,2	[b]
raw sugar	0,17	6,0	

[a] Relative to fresh weight, see § I ; one sample for each product, the error of measurement is 5 % (2σ).

[b] Below detection limits

b) Effect of different parameters on the radionuclide content of canned vegetables

- **Preliminary experiments**

The laboratory study of canning vegetables contaminated by soil-to-plant transfer requires large quantities of contaminated soils to obtain enough activity in raw products. Therefore, in order to produce contaminated vegetables, we cultivated them on nutritive solutions. When the vegetables were mature, their non-edible parts (roots of beans and tomatoes, leaves of carrots) were dipped in artificially contaminated solutions, for 48 h, with no direct radioactive contamination of the edible

parts. The vegetables were then harvested and processed normally. The first step was to compare the results of a classical process (canning) with two different contaminating procedures. Table 2 shows that there is no difference on the final result between the two methods.

Table 2 : Retention factors R_w [a], for the two different methods of plants contamination.

		^{57}Co		^{134}Cs		^{85}Sr	
		b	c	b	c	b	c
Green bean	raw → blanched	0,85	0,85	0,79	0,74	0,86	0,67
	raw → canned	0,31	0,37	0,24	0,31	0,46	0,37
Carrot	peeled→ canned	0,16	0,14	0,18	0,15		
	raw → canned	0,06	0,08	0,06	0,05		

[a] Relative to fresh weight, see § I , one sample for each treatment ; the error of measurement (2σ) is 5 % for Cs and Co and 7 % for Sr.

[b] Plants grown on contaminated soil.

[c] Contamination of non edible parts by dipping in a radioactive solution for 48 hours.

Thereafter, the following experiments used vegetables contaminated by radioactive solutions.
The activity levels of raw products were about 20 000 ± 600 Bq. kg^{-1} . For these experiments, (Figure 1) activity was measured on wet (acid) mineralized samples by using a gamma-Ge detector. Experiments with ^{57}Co, ^{106}Ru and ^{134}Cs, on the one hand, and ^{85}Sr, on the other hand, were made separately because of the interference of gamma emission from ^{106}Ru and ^{85}Sr.

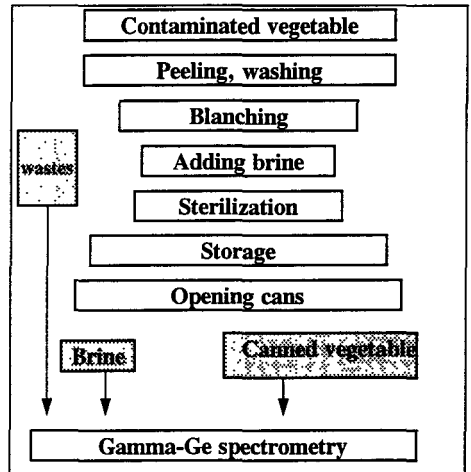

Figure 1 : General method for experimental tests.

- **Effect of blanching methods**

Contaminated carrots were processed as indicated in Table 3. Manual peeling of roots eliminated 70 to 80 % of the total activity. Of the different blanching methods used, boiling in soft water for 5 minutes is more effective in decreasing the activity of processed vegetables than using water vapour (or no blanching at all).

Table 3 : Effect of different treatments applied on peeled carrots.

Treatment	Brine [a]	Storage (month)	Residual activity [b] ^{57}Co	^{106}Ru	^{134}Cs
boiling in water 5mn	NaCl 2%	1	17	< 12	21
vapor 5mn	NaCl 2%	1	32	49	28
vapor 5mn + boiling in water 30mn	NaCl 0,3%	1	30	53	25
no blanching	NaCl 2%	1	28	(60)	23
no blanching	NaCl 2%	2	29	(53)	24

[a] Added before sterilization (30 minutes).

[b] Total Bq in processed food / total Bq of peeled carrots, in %; one sample for each treatment ; the error of measurement (2σ) is 5 % for Cs and Co, and 15% for Ru.

- **Effect of peeling**

Artificially contaminated carrots have been canned (blanching + sterilization) after either no peeling, peeling manually or chemically - by dipping two minutes in hot KOH 1N -. Results (Table 4 and Figure 2) show that the retention decreases in the following order : no peeling > manual peeling > chemical peeling for the radionuclides ^{57}Co, ^{103}Ru, ^{134}Cs. This may be due to two factors : elimination of relatively higher contaminated parts (peel), and partial destruction of cells by the potassium hydroxide treatment.

Table 4 : Retention factors [a] for canned carrots,depending on the processing technique.

	no peeling			manual peeling			chemical peeling [b]		
Rm_w	0,98			0,58			0,61		
	^{57}Co	^{106}Ru	^{134}Cs	^{57}Co	^{106}Ru	^{134}Cs	^{57}Co	^{1063}Ru	^{134}Cs
R_w	0,47	0,62	0,45	0,42	0,69	0,27	0,29	0,50	0,15

[a] Relative to fresh weight, see § I ; one sample for each treatment ; the error of measurement (2σ) is 5 % for Cs and Co and 15 % for Ru.

[b] Dipping for 2 minutes in hot KOH 1 N.

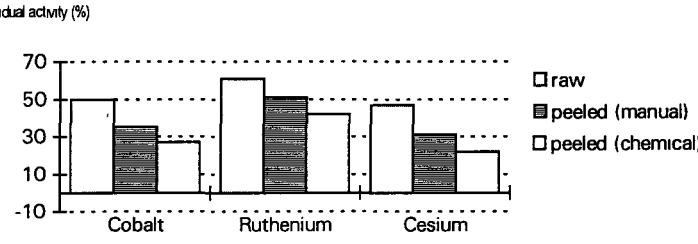

Figure 2 : Activity in canned carrots, in percent of the total activity (brine+treated vegetable) of the can contents.

One sample for each tratment ; the error of measurement (2σ) is 5 % for Cs and Co and 15 % for Ru.

- **Effect of time of storage**

Artificially contaminated green beans were canned and the storage time was increased from 1 to 4 months. As shown in Figure 3, there is no noticeable effect of storage time on the retention of radionuclides.

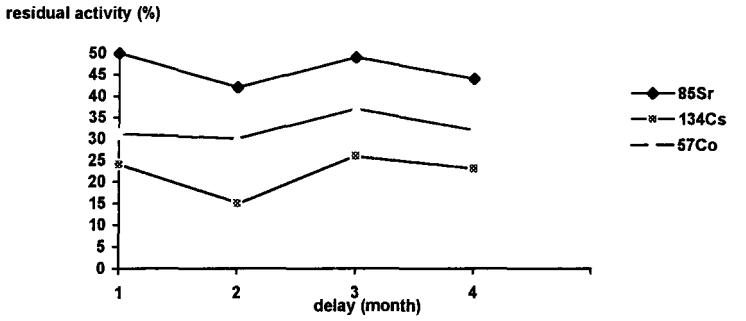

Figure 3 : Effect of storage time before opening the cans, on the residual activity Rt (100 x Bq in processed food relative to Bq in raw product) of canned green beans.

One sample for each time ; the error of measurement (2σ) is 5 % for Cs and Co and 7 % for Sr.

- **Effect of pH-variation of canning brine**

The aim was to determinate if a modification of the pH of the brine (introduced in cans before sterilization) had an effect on the final vegetable radioactivity content. Contaminated green beans were blanched and canned with soft water (final pH of brine when opening the cans = 5,5), and with water buffered with a mixture of 0,5 M citric acid + 0,5 M sodium phosphate from pH = 2 to pH = 9. Retention factors, R_w , were plotted (Figure 4) ; there was no significant effect of pH for cesium or cobalt, but there was a slight increase of R_w for ^{85}Sr when pH >7, presumably due to strontium phosphate precipitation.

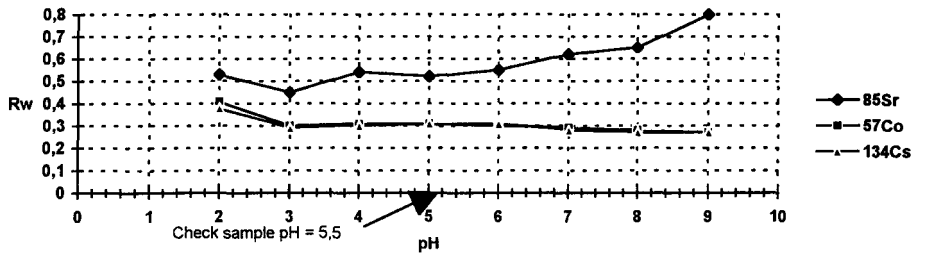

Figure 4 : Effect of modifications of pH of juices for canned contaminated green beans on the retention factor R_w.

One sample for each pH ; the error of measurement (2σ) is 5 % for Cs and Co and 7 % for Sr.

- **Effect of additives**

Green beans, carrots and tomatoes, which were artificially contaminated with ^{57}Co, ^{85}Sr, ^{134}Cs and ^{106}Ru have been canned. The effect of the chemical composition of the canning brine on the final radioactivity content of canned vegetables was studied. Juices which were tested were solutions of sodium chloride, citric acid, potassium citrate, tartric acid and calcium chloride, which are all

additives authorized in the Community food industries. Data are summarized in Table 4 and have been analysed, when possible, by Student's τ - test, although the number of replicates was very low.

Table 4 : Effect of additives on the retention factors [a] of dipped canned vegetables

	Retention factors R_w [b]				statistical test [c]					
						u				τ
	^{57}Co	^{106}Ru	^{134}Cs	^{85}Sr	n	Co	Ru	Cs	Sr	95%
Green bean										
water	0,46 ± 0,040	0,55 ± 0,050	0,40 ± 0,020	0,46 ± 0,016	6					
sodium chloride 2 %	0,51 ± 0,025	0,58 ± 0,040	0,41 ± 0,012	**0,38 ± 0,013**	4	0,40	0,70	1,00	**2,30**	2,26
sodium chloride 4%	0,43 ± 0,043	0,52 ± 0,070	**0,30 ± 0,020**		2	0,76	0,70	**2,61**		2,37
citric acid 1 %	0,43 ± 0,017	0,60 ± 0,034	0,36 ± 0,009		2	0,90	1,10	1,90		2,37
citric acid 0,5%	*0,42 ± 0,042*	*0,56 ± 0,08*	*0,37 ± 0,020*		1					
citric acid 0,1 %	0,44 ± 0,018	0,54 ± 0,031	0,37 ± 0,009		2	0,60	0,30	1,50		2,37
potassium citrate 1 %	0,37 ± 0,018	0,51 ± 0,035	0,35 ± 0,010		2	2,00	0,90	2,10		2,37
potassium citrate 0,1 %	*0,41 ± 0,041*	*0,44 ± 0,060*	*0,40 ± 0,020*		1					
tartric acid 1%	*0,45 ± 0,045*	*0,60 ± 0,080*	*0,37 ± 0,020*		1					
tartnc acid 0,5%	*0,46 ± 0,047*	*0,59 ± 0,080*	*0,39 ± 0,020*		1					
Carrot										
water	0,45 ± 0,040	0,56 ± 0,090	0,33 ± 0,030	0,78 ± 0,080	4					
sodium chloride 2%	0,39 ± 0,019	0,59 ± 0,041	0,26 ± 0,008	0,72 ± 0,036	2	1,50	0,50	1,90	0,9	2,57
sodium chloride 4%	*0,41 ± 0,040*	*0,43 ± 0,060*	*0,30 ± 0,020*	*0,66 ± 0,067*	1					
citric acid 1 %	0,46 ± 0,023	0,60 ± 0,053	0,34 ± 0,010	0,80 ± 0,040	2	0,30	0,60	0,50	0,3	2,57
citric acid 0,1 %	0,43 ± 0,021	0,68 ± 0,061	0,36 ± 0,011	0,76 ± 0,038	2	0,60	1,30	1,20	0,3	2,57
potassium citrate 1 %	0,37 ± 0,018	0,50 ± 0,045	0,34 ± 0,010	0,69 ± 0,034	2	1,70	0,70	0,50	1,1	2,57
potassium citrate 0,1 %	0,42 ± 0,021	0,64 ± 0,057	0,35 ± 0,010	0,79 ± 0,039	2	0,90	1,00	0,90	0,2	2,57
Whole tomato										
water	0,53 ± 0,026	0,60 ± 0,053	0,53 ± 0,016		2					
sodium chloride 2%	0,51 ± 0,025	0,61 ± 0,054	0,50 ± 0,015		2	0,45	0,11	0,98		3,18
citric acid 1%	0,63 ± 0,031	0,68 ± 0,061	0,61 ± 0,018		2	1,34	0,76	1,48		3,18
citric acid 1%+sodium chloride 1%	*0,38 ± 0,039*	*0,48 ± 0,090*	*0,21 ± 0,010*		1					
calcium chloride 1%	0,63 ± 0,031	0,71 ± 0,063	0,62 ± 0,018		2	1,34	0,95	1,52		3,18
calcium chloride 1% +sodium chloride 1%	*0,61 ± 0,060*	*0,68 ± 0,120*	*0,62 ± 0,040*		1					
Tomato without core										
water	0,44 ± 0,044	0,50 ± 0,090	0,49 ± 0,030		2					
sodium chloride 2%	*0,48 ± 0,047*	*0,54 ± 0,100*	*0,45 ± 0,030*		1					
citric acid 1%	*0,45 ± 0,044*	*0,45 ± 0,080*	*0,45 ± 0,031*		1					
citric acid 1% + sodium chloride 1%	*0,33 ± 0,030*	*0,33 ± 0,060*	*0,30 ± 0,020*		1					
calcium chloride 0,5%	*0,44 ± 0,043*	*0,53 ± 0,110*	*0,38 ± 0,020*		1					
calcium chloride 1% + sodium chlonde 1%	*0,42 ± 0,040*	*0,42 ± 0,081*	*0,39 ± 0,020*		1					

[a] $Bq.kg^{-1}$ of canned vegetables by $Bq.kg^{-1}$ of raw vegetables, relative to fresh weight

[b] Mean and uncertainty (2 σ) of the n replicates . For single samples (n = 1), value and measurement error (2 σ).

[c] τ (Student) - test, with the assumption (verified for the gross samples) of a normal distribution, n is the number of repetitions, x_1 and x_2 are data for samples treated with soft water or with an additive,

$$u = \frac{\overline{x_1} - \overline{x_2}}{\sqrt{\frac{\sigma_1^2}{n_1^2} + \frac{\sigma_2^2}{n_2^2}}}$$

; when $|u| > \tau\,95\%$, the probability that the mean $\overline{x1} = \overline{x2}$ is less than 5%

These results show that the modification of the chemical composition of the brine, relative to pure water, has a slight but non significant effect on the retention factor, except in the case of canning green beans, for cesium with sodium chloride 2 % and for strontium with sodium chloride 4 %. In these later cases, the effect is then a reduction of the retention factor by about 0,1. Therefore this is probably not significant compared to the the whole canning process technologies.

c) Effect of canning on the actinide content of processed vegetables.

Green beans which had been contaminated by ^{239}Pu (approximately 50 $Bq.kg^{-1}$, fresh weight) were canned in the laboratory, and the activities of the different fractions, before and after canning, were measured by low level alpha spectrometry, after radiochemical extraction. The activity distribution associated with the process and the retention factors are indicated Table 5. The data show that canning leads to a noticeable decrease in the final product, mainly by elimination of the most contaminated parts (stems are 3,7 times more contaminated than the edible part of the beans, data not shown).
Similar experiments were performed with ^{241}Am, but the results are not yet available.

Table 5 : Data [a] for ^{239}Pu in canned beans.

a) Activity distribution in percent of the total activity of the raw vegetable

Canned bean	57,5 ± 4,0
Juice	16,0 ± 2,7
Blanching water	1,6 ± 0,9
Stem	24,9 ± 1,5

b) Retention factors (relative to fresh weight)

	Rm_w	R_w
whole → canned	0,99	0,58 ± 0,08
whole→ trimmed	0,92	0,82 ± 0,02
whole→ blanched	0,93	0,79 ± 0,03
trimmed → blanched	1,01	0,97 ± 0,01
trimmed→ canned	0,92	0,82 ± 0,04
blanched→ canned	0,93	0,79 ± 0,06

[a] Mean and uncertainty (2σ) of three replicates.

PROJECT 2: MR S J BAKER/DR K W NICHOLSON

II. Objectives for the reporting period

From initial studies made within the TARRAS project in 1990/91, it was clear that food processing can either decrease or increase the radionuclide concentrations in the final products. A more detailed examination of basic processes was required to explore ways to reduce radionuclide concentrations in foodstuffs. The main topics to be examined were the influence of different processing technologies and of additives on the radionuclide content of vegetables. An assessment of the fate of some radionuclides that enter factory by-products intended for animal feed was also to be made.

During 1993/94, vegetable crops were cultivated in a region having relatively high soil concentrations of Sr-90 and Cs-137, for processing in the pilot plant facilities at the Department of Food Science and Technology, University of Reading. The objective was to examine the effect of increasing the potassium content of the blanching and/or canning solutions used in the canning of carrots, peas and potatoes, as a means of reducing the radionuclide content of these foods.

In addition, the influence of food processing (as in domestic culinary preparation) on the removal of Ru-103 and Ag-110m deposited to mature leafy vegetables was investigated. Mature crops of cabbage, cauliflower and spinach were contaminated by the application of soluble radiotracers of Ru-103 and Ag-110m. Retention of Ru-103 and Ag-110m after cooking of these leafy vegetables was measured.

The third part of the 1993/94 programme of work concerned the fate of radionuclides in by-products and wastes from industrial food processing. Information on the fate of "waste" material produced during the processing of oilseed wheat and sugar beet was obtained by Reading University. Using this information, together with the results of analysis of the raw materials used and by-products produced in industrial processes, for stable Sr and Cs, a semi-quantitative inventory of the annual loss of food solids, and hence potential Sr-90 and Cs-137 losses, has now been derived (see Project 3).

In 1994/95, the studies were extended to investigate further processing techniques and their effects in reducing the radionuclide content of vegetables. The objectives were:

(i) to investigate the effect of varying blanching regimes used prior to dehydration on the radionuclide content of vegetables,

(ii) to investigate the effect of the duration of storage time of canned vegetables on their retention of radionuclides,

(iii) to examine the importance of variety of vegetable used for canning on the retention of radionuclides.

III. Progress achieved including publications

1993/94 Programme.

A. The effect of increasing the potassium content of blanching and/or canning solutions on the radionuclide content of canned vegetables.

Carrots, peas and potatoes were canned using six processing treatments using pilot plant facilities at Reading University. The potassium concentration of the blanching and/or canning solution was varied in each treatment. These treatments were:

Treatment	Blanching Solution	Canning Solution
I	Soft H_2O	2% NaCl
II	Soft H_2O	1% NaCl, 1% KCl
III	Soft H_2O	2% KCl
IV	1% KCl	2% NaCl
V	2% KCl	2% NaCl
VI	2% KCl	2% KCl

Food processing retention factors for K-40, Sr-90, Cs-137 and their stable elements were derived from concentrations in raw and processed foods for each vegetable for all six processing treatments. Retention factors are defined as follows:

$$R_d = \frac{\text{Concentration (Bq/kg or } \mu g/g) \text{ in dry processed food}}{\text{Concentration (Bq/kg or } \mu g/g) \text{ in dry raw food}}$$

$$R_w = \frac{\text{Concentration (Bq/kg or } \mu g/g) \text{ in fresh processed food}}{\text{Concentration (Bq/kg or } \mu g/g) \text{ in fresh raw food}}$$

$$R_m = \frac{\text{Total dry weight of processed vegetable}}{\text{Total dry weight of raw vegetable}}$$, i.e. dry matter retention factor.

Retention factor based on total recovery of activity, $R_t = R_d \times R_m$.

Retention factors derived on a fresh weight basis (R_w) were reported in September 1994 for all vegetables processed using treatments I to VI. Now, dry matter retention factors, R_m , have been calculated allowing the parameter, R_t , to be derived. R_t takes into account losses of vegetable material during processing thus allowing the total recovery of radionuclide in food after processing to be calculated.

Figures 1a to 1c show R_t for the three radionuclides and their stable elements for carrots, peas and potatoes canned under treatments I to III. The potassium concentration of the canning solution was increased from 0% to 2% while the blanching solution was soft water in each case. No significant increases or decreases in R_t were seen for strontium or caesium. The increase in concentration of KCl in the canning solutions of treatments I, II and III is reflected in the increase in R_t for potassium.

The effect of increasing the potassium content of the blanching solution, whilst keeping the same 2% NaCl canning solution (treatments IV, V and VI) was also investigated (Figures 2a to 2c). Again, for all three vegetables no significant trend in the variation of processing retention factor (R_t) for strontium and caesium with potassium content of the blanching

solution was found. Increased R_t values for potassium were recorded for all vegetables canned under treatment VI, where a 2% KCl blanching solution was used.

B. The influence of food processing on removal of radionuclides deposited to foliage of mature leafy vegetables.

Mature crops of cabbage, cauliflower and spinach were contaminated by the application of solutions of Ru-103 (as chloro-complexes of ruthenium) and Ag-110m (as nitrate). Approximately 1.1 kBq of each nuclide was applied by spray to cabbage and cauliflower, with 2 kBq of each applied to the spinach.

All vegetables were processed one day after contamination. Each was prepared as for domestic use and boiled for 10 minutes. The cooked vegetables were drained, oven-dried and ashed at 380°C prior to analysis by γ-spectrometry. Also, the cooking waters were concentrated and analysed to allow losses of Ru-103 and Ag-110m during cooking to be determined.

Retention factors for Ru-103 and Ag-110m after cooking of leafy vegetables are presented in Table 1. Retention factors are as defined in part A above.

TABLE 1. Retention factors for Ru-103 and Ag-110m after boiling leafy vegetables.

Vegetable	Radionuclide	Retention Factor			
		R_d	R_w	R_m	R_t
Cabbage	Ru-103	0.76	0.59	0.87	0.66
	Ag-110m	0.92	0.71		0.80
Cauliflower	Ru-103	0.83	0.61	0.75	0.62
	Ag-110m	0.50	0.37		0.37
Spinach	Ru-103	0.83	0.54	0.94	0.78
	Ag-110m	0.96	0.62		0.90

The parameter R_t takes into account losses of vegetable material during cooking (such losses are measured by the dry matter retention factor, R_m). For Ru-103 losses of between 22% and 38% were recorded after the cooking of cabbage, cauliflower and spinach; for Ag-110m losses ranging from 10% for spinach to 63% for cauliflower were measured.

1994/95 Programme.

In 1994, further crops of carrots, peas and potatoes were cultivated by AEA Technology at the same sites used in 1993. These are close to the Sellafield nuclear fuel reprocessing facility in Cumbria, north-west England. This region has a relatively high concentration of Cs-137 in soil owing to fallout from the Chernobyl accident, nuclear weapons testing and historical releases from Sellafield. Concentrations of Sr-90 were of the order of 10 Bq/kg dry soil and 40 Bq/kg for Cs-137 at the cultivation sites in 1993. Varieties of vegetables were selected according to their use by the food processing industry in Great Britain.

Two varieties of each of carrots (Narman and Chantenay Supreme), peas (Bunting and Maro) and potatoes (Maris Peer and Romano) were grown for the dehydration and canning studies.

Crops were harvested between August and October 1994. Raw and processed foods were produced using facilities at the Department of Food Science and Technology, University of

Reading. Details of processing methods used for vegetables in the dehydration and canning studies are described in Project 3, by Reading University.

Raw and processed samples were oven-dried at 105°C and ashed at 370°C for analysis of radionuclides; by radiochemical separation followed by β-counting for Sr-90 and γ-spectrometry for K-40 and Cs-137. A sub-sample of around 50g of dry material was ground in an agate ball-mill for measurement of stable elements. The ground material was ashed at 450°C and the residue dissolved in nitric acid. ICP-MS was used to measure Cs and ICP-AES for K, Sr. Ca, Mg, P and S were also analysed by ICP-AES in some raw and canned vegetables.

The uncertainties in the analysis for Cs-137 ranged from 12 to 106% (average uncertainty was 44%) where results were above the limit of detection (0.1 Bq/kg dry weight); for Sr-90 uncertainties ranged from 2 to 22% average uncertainty 9%; the average uncertainty for K-40 was 10%. For stable element analysis, the results significantly above the limit of detection (LOD) have an uncertainty of ± 20%.

A. The effect of varying the blanching regime used in the dehydration of peas and potatoes on their radionuclide content.

The pea variety, Maro, was used in the dehydration study. This variety had been used in initial studies in 1990/91. Three different blanching regimes were used prior to dehydration. The peas were blanched in (I) boiling water for 2 minutes; (II) steam at atmospheric pressure for 2 minutes; (III) boiling water for 5 minutes.

Concentrations of Sr-90 ranged from 0.96 to 1.2 Bq/kg dry weight in the raw and processed crops. Cs-137 concentrations were below limits of detection (<0.1 Bq/kg dry weight).K-40 concentrations were in the range 248-272 Bq/kg dry weight. Corresponding stable element concentrations were: Sr 4.5-5.1 μg/g dry weight, K 6400-14000 μg/g. Cs concentrations were below limits of detection, i.e. <0.01 μg/g.

Food processing retention factors for Sr-90, K-40 and their stable elements have been derived for the three blanching/dehydration processes used and are listed in Table 2a. Retention factors for Cs-137 and stable Cs could not be derived.

TABLE 2a Retention factors for Sr-90, K-40 and their stable elements for different blanching processes prior to the dehydration of peas.

Blanching Process	Dry Matter Retention Factor R_m	Retention Factor			
			R_d	R_w	R_t
I	1.02	Sr-90	0.83	2.2	0.85
		Stable Sr	0.98	2.7	1.0
		K-40	1.0	2.7	1.0
		Stable K	0.46	1.2	0.47
II	1.02	Sr-90	0.80	2.1	0.82
		Stable Sr	0.96	2.6	0.98
		K-40	0.94	2.5	0.96
		Stable K	0.61	1.6	0.62
III	0.97	Sr-90	0.92	2.3	0.89
		Stable Sr	0.88	2.3	0.85
		K-40	0.97	2.5	0.94
		Stable K	0.79	2.1	0.77

Retention factors derived on a fresh weight basis (R_w) show elevated values, i.e. in excess of unity, because activity concentrations are increased in the dehydrated product. Values for R_t are shown in Figure 3a for the three different blanching processes used in the dehydration of the peas. R_t values for Maro peas dehydrated using similar processing techniques in an initial study undertaken in 1990/91 are also shown. These values are similar for both strontium and potassium to those measured in the current programme. No significant differences in R_t were recorded for either strontium or potassium using the three blanching processes. Therefore it appears that variations in how the peas were blanched before dehydration do not greatly affect the retention of Sr-90 and K-40.

In the 1990/91 programme, where a variety of processing methods were used (e.g. canning, dehydration, boiling, baking, crisp production) on several vegetables, retention of Cs-137 and K-40 by processed foods were highly significantly correlated. Thus K-40 provides a useful indicator for likely Cs-137 behaviour in the absence of retention factors for caesium in this study.

The variety Romano was used for dehydration of potato, which also was used in initial studies in 1990/91. The three blanching regimes used prior to dehydration of potato were blanching in boiling water for (I) 1, (II) 4 and (III) 10 minutes. The mashed potato was then drum-dried (see Project 3).

Concentrations of Sr-90 were in the range 0.22-0.37 Bq/kg dry weight in the raw and processed crops. Cs-137 concentrations, as for the peas, were below limits of detection (<1 Bq/kg dry weight), therefore its retention during processing could not be measured. K-40 concentrations ranged from 280 to 363 Bq/kg dry weight. Stable element concentrations were in the ranges: 0.63 to 1.8 μg/g dry weight for Sr, 9800-12000 μg/g for K, and 0.019-0.026 μg/g for Cs in the processed potato. However, the concentration of Cs in the unprocessed potato was <0.01 μg/g.

Retention factors for strontium and potassium recorded for potato using the three blanching/dehydration processes are listed in Table 2b. These have been derived on both a dry and fresh weight basis. R_t values could not be derived since losses of dried potato from the drum drier, and hence R_m values, were impossible to measure.

TABLE 2b Retention factors for Sr-90, K-40 and their stable elements for different blanching processes prior to the dehydration of potatoes.

Blanching Process		Retention Factor	
		R_d	R_w
I	Sr-90	1.3	4.5
	Stable Sr	0.51	1.8
	K-40	1.3	4.4
	Stable K	1.2	4.2
II	Sr-90	1.7	5.7
	Stable Sr	0.43	1.4
	K-40	1.1	3.7
	Stable K	1.2	4.0
III	Sr-90	1.1	3.8
	Stable Sr	0.35	1.2
	K-40	0.97	3.5
	Stable K	0.98	3.5

R_d values for stable Cs were >2 with corresponding R_w values >9 for all processes. Values for R_d are shown in Figure 3b for the three different blanching processes used in the dehydration of the potatoes. R_d values for Romano potatoes dehydrated using similar processing techniques in an initial study undertaken in 1990/91 are also shown for comparison; these are similar to those found in the present study. Taking into account uncertainties in analytical results from which R_d values are calculated, no significant decreases or increases in retention factors for strontium or potassium were found when the blanching time was increased prior to dehydration of the potatoes.

B. The effect of duration of storage time of canned vegetables on their retention of radionuclides.

Carrots (var. Narman), peas (var. Bunting) and potatoes (var. Maris Peer) were canned and stored for 4, 16 and 32 weeks. Concentrations of K-40, Sr-90 and Cs-137 and their stable elements were determined upon opening of the canned vegetables and their retention as a function of storage time was investigated.

Concentrations (Bq/kg or μg/g dry weight) of K-40, Sr-90, K and Sr in the raw and canned vegetables were in the following ranges:

	K-40	K	Sr-90	Sr
Carrots:	151-236	4300-8000	0.52-5.6	9.2-23
Peas:	240-282	6300-13000	0.21-0.98	2.1-3.5
Potatoes:	207-329	6400-12000	0.007-0.41	0.55-1.8

Many analytical results for Cs-137 were around or below the limit of detection (0.1Bq/kg), with the majority of stable Cs results also below the limit of detection (<0.01 μg/g). Therefore, the retention of caesium in vegetables after processing could not be determined with any confidence.

Retention factors, derived on both a dry and fresh weight basis, for potassium and strontium for canned vegetables after storage times of 4, 16 and 32 weeks are listed in Table 3. Dry matter retention factors (R_m) are also listed. Corresponding retention factors (R_t), derived from $R_d \times R_m$ are shown in Figures 4a, 4b and 4c for carrots, peas and potatoes respectively.

An increasing or decreasing trend in R_t with storage time is only apparent for Sr-90. However, closer inspection of the data throws doubt on the significance of these trends. For carrots, an apparent increase in R_t with time is caused by the low value for R_t obtained after 4 weeks storage (Figure 4a). A low result for the Sr-90 concentration was recorded for this sample, i.e. 0.52 Bq/kg dry weight which was an order of magnitude lower than those measured in the raw and other canned carrots. This outlying result thus gives the impression of an increase in the retention of Sr-90 with increasing storage time of canned carrots. Corresponding R_t values for stable Sr were more constant, although unusually high, in the range 1.9-2.5.

For canned peas, the retention of Sr-90 appears to decrease with an increase in storage time, although no such trend is observed for stable Sr (Figure 4b). In the case of canned potatoes, a low R_t value was recorded after 32 weeks storage (Figure 4c). The low concentration of Sr-90 measured in this potato sample (0.007 Bq/kg dry weight) is responsible; other Sr-90 concentrations in potato were in the range 0.21-0.41 Bq/kg.

In the absence of measurements for Cs-137, the K-40 data can be used as an indicator of the retention of Cs-137 after processing. No significant change in the retention of potassium by canned carrots, peas and potatoes was recorded as a function of storage time.

TABLE 3. Food processing retention factors for potassium and strontium for canned vegetables as a function of storage time.

Vegetable and storage time	Retention Factor								
	R_d				R_w				R_m
	K-40	K	Sr-90	Sr	K-40	K	Sr-90	Sr	
CARROT									
4 weeks	0.72	0.54	0.09	2.4	0.58	0.43	0.07	2.0	0.74
16 weeks	0.64	0.61	0.84	2.0	0.46	0.49	0.58	1.6	0.70
32 weeks	0.67	0.74	1.0	2.5	0.46	0.52	0.71	1.8	0.66
PEA									
4 weeks	0.91	0.48	0.83	0.69	0.66	0.35	0.59	0.50	0.99
16 weeks	0.89	0.60	0.65	0.60	0.61	0.41	0.44	0.42	1.0
32 weeks	0.85	0.69	0.21	0.71	0.56	0.45	0.15	0.50	1.0
POTATO									
4 weeks	0.64	0.53	0.73	0.42	0.56	0.46	0.67	0.25	0.92
16 weeks	0.63	0.53	0.51	0.32	0.57	0.48	0.44	0.25	0.96
32 weeks	0.84	0.58	0.02	0.31	0.72	0.50	0.01	0.25	0.88

C. The influence of variety of vegetable used for canning on the retention of radionuclides during processing.

Two varieties of each of carrots (Narman and Chantenay Supreme), peas (Bunting and Maro) and potatoes (Maris Peer and Romano) were canned and stored for four weeks. Concentrations of K-40, Sr-90 and Cs-137 and their stable elements were determined in the raw and canned vegetables from which retention factors were derived for the different varieties of vegetables. The retention of Ca, Mg, P and S after canning was also measured.

In addition, the dry matter, total ash, total N, water soluble carbohydrate and starch content of each variety of the raw and canned vegetables was measured by Reading University (see Project 3). Possible links between losses of these parameters (and Ca, Mg, P and S) with losses of Sr-90 and Cs-137 were to be examined.

Concentrations of radionuclides (Bq/kg dry weight) and stable elements (μg/g dry weight) in raw and canned vegetables were in the following ranges:

	K-40	K	Sr-90	Sr
Carrots:	151-308	4300-9700	0.52-5.6	9.2-23
Peas:	194-282	6300-14000	0.81-1.2	2.4-5.1
Potatoes:	194-329	5800-12000	0.21-0.41	0.76-2.0
	Ca	Mg	P	S
Carrots:	3000-3900	730-920	2000-2600	900-1100
Peas:	930-1500	1300-1600	4200-4400	240-700
Potatoes:	210-230	330-590	1400-2000	500-670

Again, analytical results for Cs-137 and stable Cs were mainly below limits of detection and losses in vegetables during canning could not be determined.

Retention factors for potassium, strontium, Ca, Mg, P and S derived for the two varieties of each of carrots, peas and potatoes are listed in Table 4.

TABLE 4. Food processing retention factors for potassium, strontium, Ca, Mg, P and S for different varieties of carrots, peas and potatoes after canning.

Retention Factor	Carrot		Pea		Potato	
	Narman	Chantenay Supreme	Bunting	Maro	Maris Peer	Romano
R_d						
K-40	0.72	0.63	0.91	0.73	0.64	0.67
K	0.54	0.58	0.48	0.57	0.53	0.58
Sr-90	0.09	0.73	0.83	0.57	0.73	0.95
Sr	2.4	2.2	0.69	0.65	0.42	1.1
Ca	1.2	1.3	0.78	0.80	0.96	0.91
Mg	0.96	1.2	0.81	0.88	0.70	0.75
P	0.88	0.83	0.95	1.0	0.78	0.80
S	1.0	0.98	0.40	0.67	0.85	0.85
R_w						
K-40	0.58	0.47	0.66	0.55	0.56	0.50
K	0.43	0.42	0.35	0.43	0.46	0.43
Sr-90	0.07	0.53	0.59	0.42	0.67	0.67
Sr	2.0	1.6	0.50	0.50	0.25	0.80
Ca	0.93	0.95	0.55	0.60	0.82	0.68
Mg	0.77	0.85	0.58	0.66	0.61	0.55
P	0.71	0.61	0.68	0.77	0.67	0.59
S	0.80	0.71	0.29	0.50	0.73	0.63
R_m	0.74	0.82	0.99	1.0	0.92	0.86

Corresponding values for R_t, have been derived (R_d x R_m), and are plotted as the percentage retention of element after canning in Figures 5a to 5c for carrots, peas and potatoes respectively. In these figures, a comparison of the retention of radionuclide or stable element after canning between the two varieties used of each vegetable type is shown by plotting percentage retention for one vegetable variety against the other. Similarly, the retention of total N, water-soluble carbohydrate and starch (derived from measurements made by Reading University, project 3) for the two varieties of carrots (Figure 5a), peas (Figure 5b) and potatoes (Figure 5c) are also compared. The line drawn on each figure is representative of the case when percentage retention is equal for both vegetable varieties.

There are some differences in losses of these parameters between vegetable type, e.g. less P is lost from peas (0-6%) than from carrots (32-35%) or potatoes (28-31%). However, in considering the two varieties of each vegetable, there is little if any significant difference in the loss of radionuclides or nutrients during canning, i.e. most points do not deviate greatly from the line indicating equal retention by the two varieties of vegetable (Figures 5a to 5c). Outlying points, e.g. for Sr-90 and starch (Figure 5a), are due to relatively low values derived for R_t for the Narman and Chantenay varieties respectively: unusually low concentrations were measured in the canned produce. Differences between the retention of K-40 and Sr-90 and their respective stable elements, e.g. exhibited by potassium in peas (Figure 5b) and strontium in potato are probably caused by analytical uncertainties.

Values of R_t for canned peas obtained in initial studies during 1990/91 (shown below) confirm that losses of radionuclides from vegetables during processing do not appear to differ significantly despite differences in the varieties of vegetables processed.

Pea variety	Retention Factor (R_t)				
	K-40	K	Sr-90	Sr	Cs-137
Bunting	0.26	0.24	0.85	0.43	0.36
Maro	0.23	0.18	0.75	0.62	<0.2

However, the above R_t values for canned peas are different to those measured during the 1994/95 programme. Similar differences are also observed for canned carrots and potatoes. This highlights the fact that reductions in the radionuclide content of vegetables by a particular food processing technique can be highly variable.

Figure 1a

Food Processing Retention Factors (Rt)
For K-40, Sr-90, Cs-137 And Their Stable Elements
For Carrots Canned Using Different Canning Solutions.

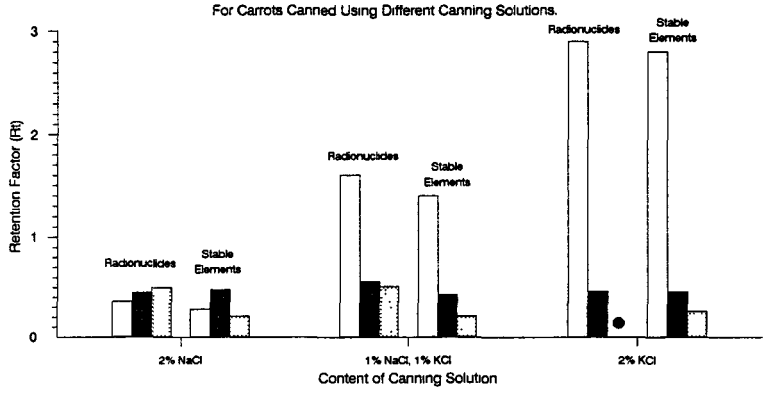

Carrots in all three canning treatments were blanched in soft water

K Sr Cs Rt for Cs-137 not derived

Figure 1b

Food Processing Retention Factors (Rt)
For K-40, Sr-90, Cs-137 And Their Stable Elements
For Peas Canned Using Different Canning Solutions.

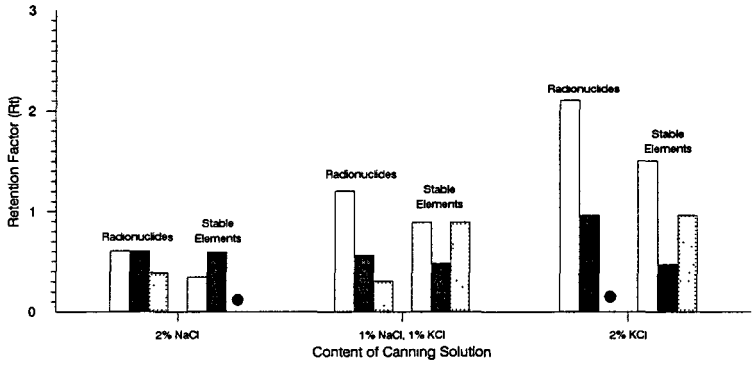

Peas in all three canning treatments were blanched in soft water

K Sr Cs Rt for Cs not derived

Figure 1c

Food Processing Retention Factors (Rt)
For K-40, Sr-90, Cs-137 And Their Stable Elements
For Potatoes Canned Using Different Canning Solutions

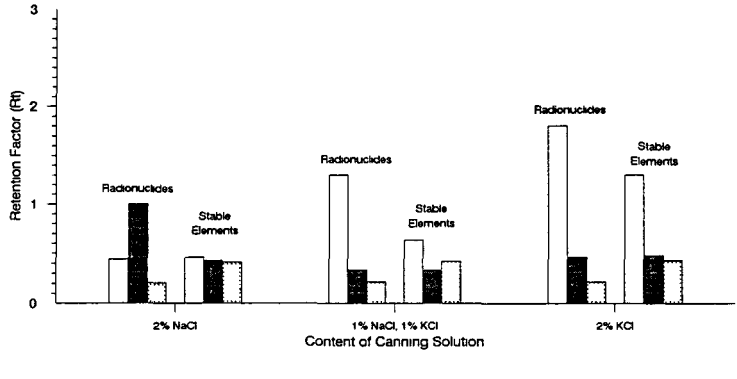

Potatoes in all three canning treatments were blanched in soft water

K Sr Cs

Figure 2a

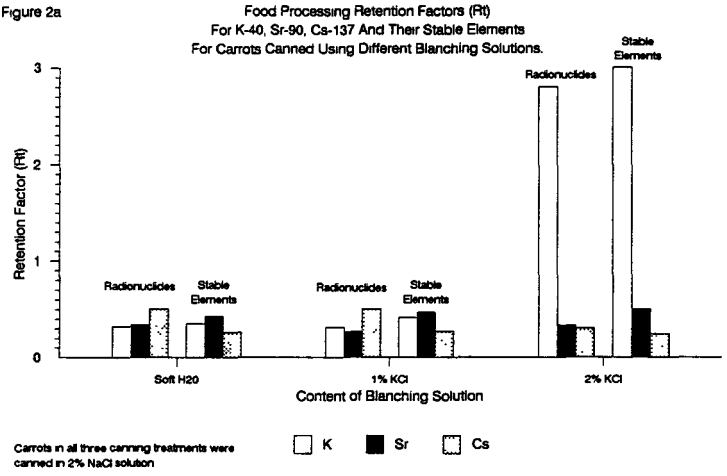

Figure 2b

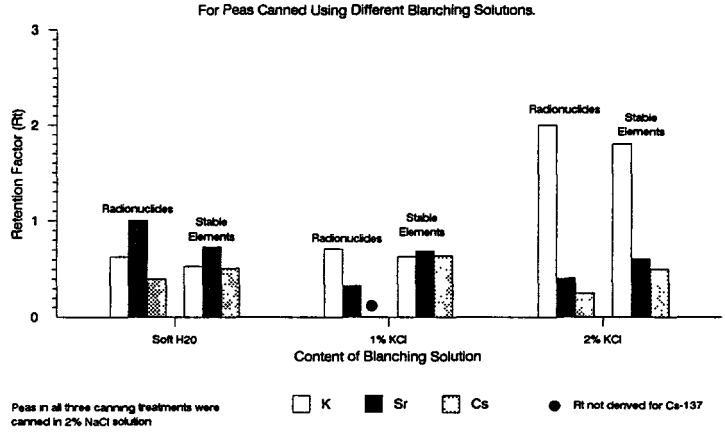

Figure 2c

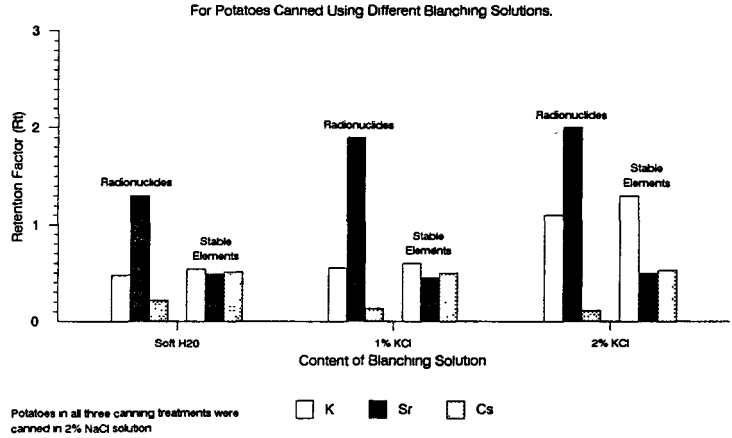

Figure 3a

Food Processing Retention Factors (Rt)
For K-40, Sr-90 and Their Stable Elements
For Peas Using Different Blanching Processes Before Dehydration.

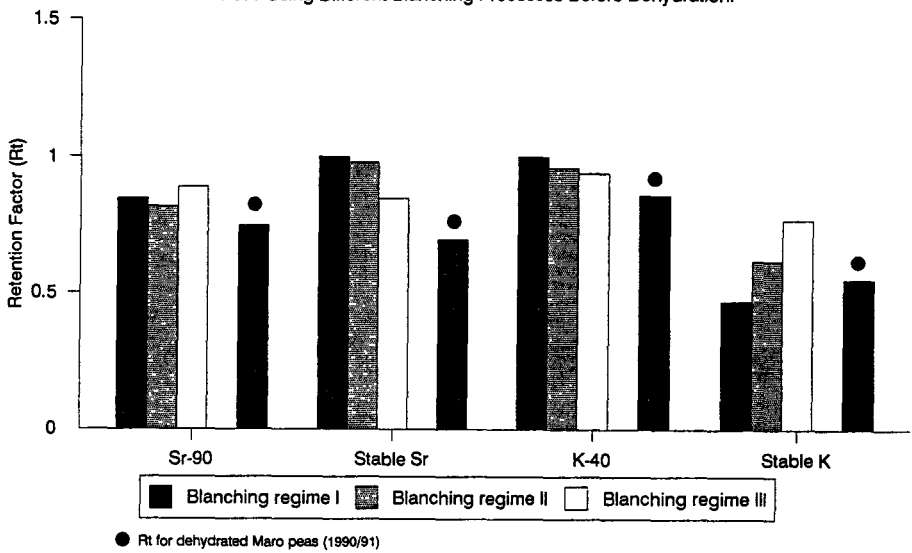

Figure 3b

Food Processing Retention Factors (Rd) Derived From
Dry Weight Concentrations For K-40, Sr-90 and Their Stable Elements
For Potatoes Using Different Blanching Processes Before Dehydration.

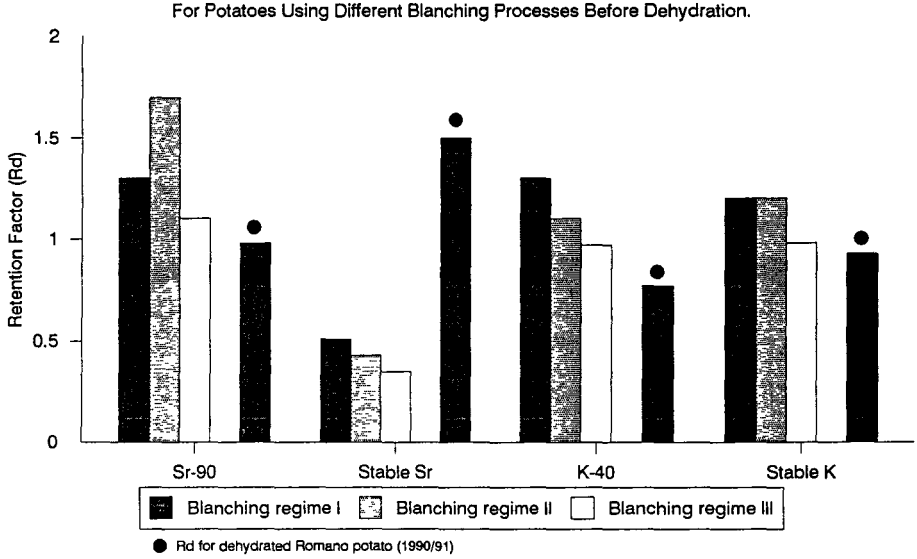

Figure 4a

Food Processing Retention Factor (Rt) For Potassium and Strontium For Canned Carrots as a Function of Storage Time.

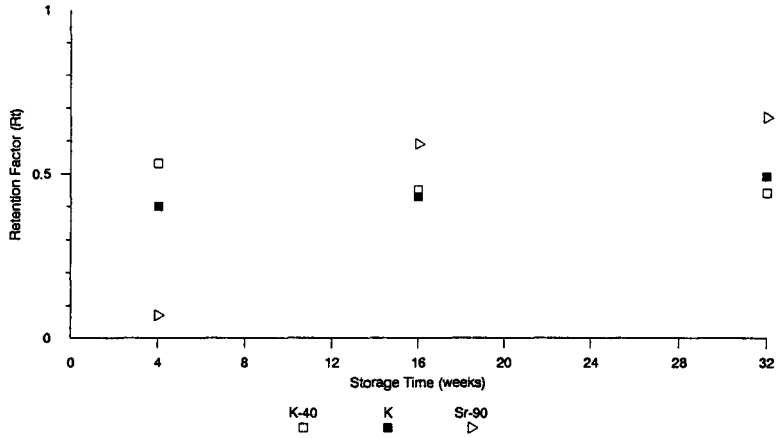

Figure 4b

Food Processing Retention Factor (Rt) For Potassium and Strontium For Canned Peas as a Function of Storage Time

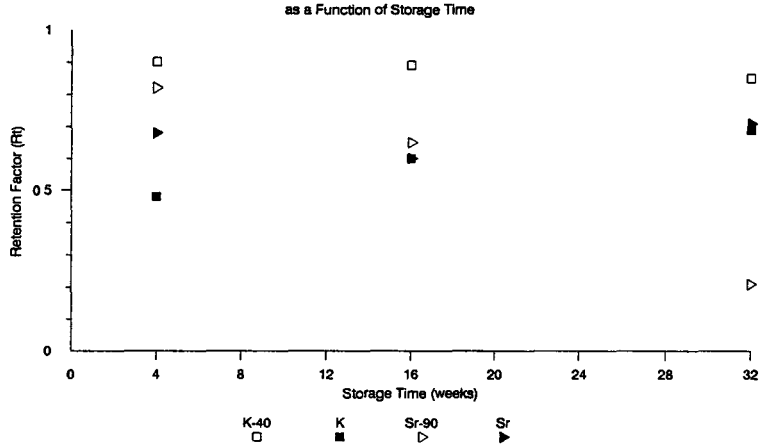

Figure 4c

Food Processing Retention Factor (Rt) For Potassium and Strontium For Canned Potatoes as a Function of Storage Time

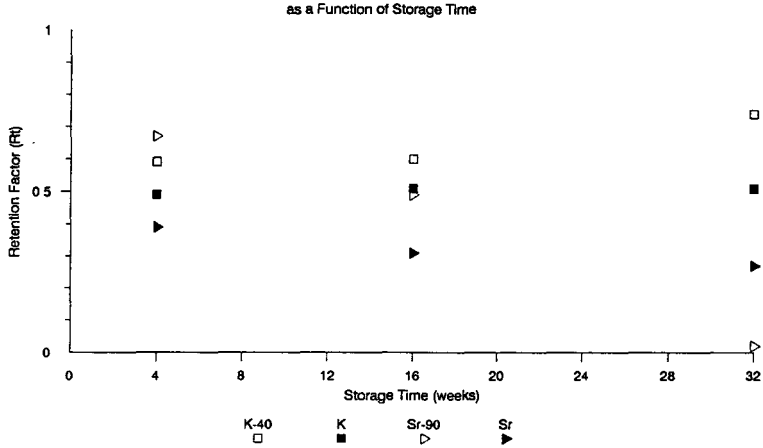

Figure 5a

Comparison of the Retention (Rt) of Potassium, Strontium, Macronutrients, Carbohydrate and Starch Between Two Varieties of Carrot After Canning

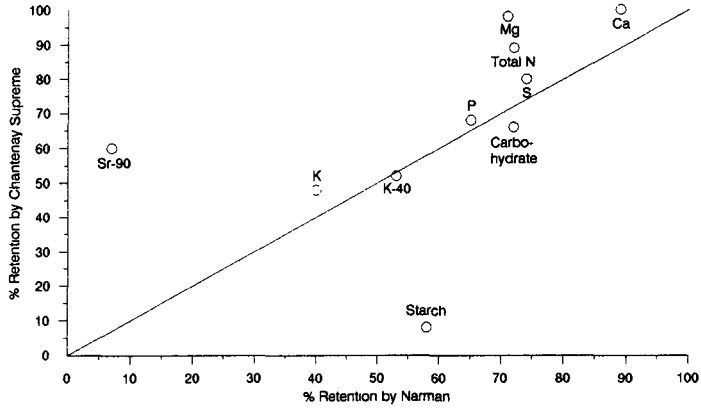

Figure 5b

Comparison of the Retention (Rt) of Potassium, Strontium, Macronutrients, Carbohydrate and Starch Between Two Varieties of Pea After Canning

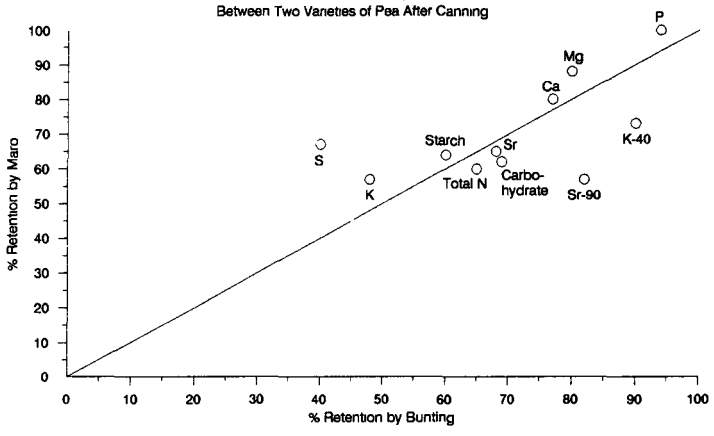

Figure 5c

Comparison of the Retention (Rt) of Potassium, Strontium, Macronutrients, Carbohydrate and Starch Between Two Varieties of Potato After Canning

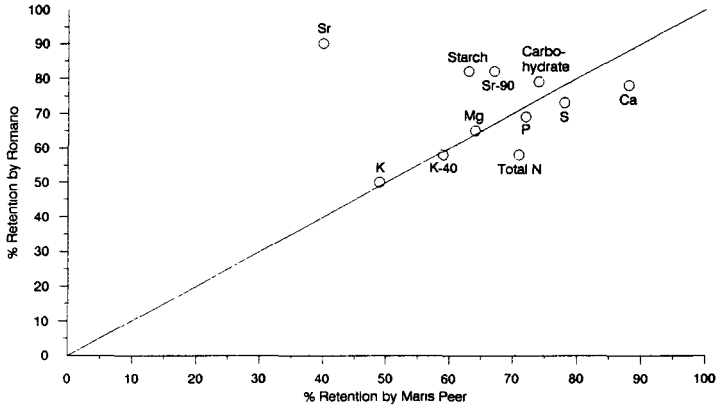

PROJECT 3: DR A S GRANDISON

II. Objectives for the reporting period

A. The influence of processing methods and additives on radionuclide concentrations in foods

It was clear from the initial studies made within the CEC "TARRAS" project in 1990 / 1991 that food processing can either decrease or increase the radionuclide concentrations in the final products. A more detailed examination of basic processing technologies was needed to explore ways to reduce radionuclide concentration in foodstuffs and to identify procedures that will enhance losses of activity from the final products intended for human consumption.

The objectives were as follows:

i) to determine any differences in radionuclide content in canned vegetables caused by varying the composition of blanching and/or canning solutions.

ii) to determine how the length of storage affects radionuclide content in canned vegetables.

iii) to determine whether the retention of radionuclides differs for different varieties of vegetables during canning

iv) to determine the effect of different blanching treatments on the radionuclide content of dehydrated vegetables.

B. The influence of food processing on removal of radionuclides deposited to foliage of mature leafy vegetables

This work was carried out entirely by AEA Technology and is reported in Project 2.

C. The fate of radionuclides in by-products and wastes from food processing.

Research carried out within the "TARRAS" project suggested that substantial quantities of radioisotopes removed during industrial food processing will be found in by-products and factory wastes, and may subsequently be recycled, mainly by their uses for animal feed.

A further objective was to compile information on the fate of "waste" material produced during processing of oilseeds, wheat and sugar beet. In addition, samples of raw materials and products were obtained from industrial processes for analysis of stable Sr, K and Cs (by AEA) such that a semi-quantitative inventory of losses of food solids, and hence potential Sr-90, K-40 and Cs-137 could be derived.

III. Progress achieved including publications

A. THE INFLUENCE OF PROCESSING METHODS AND ADDITIVES ON RADIONUCLIDE CONCENTRATIONS IN FOOD

The general processing methods for canning (parts i to iii) were as follows:

FIG 1. FLOW DIAGRAM FOR CANNING OF POTATOES

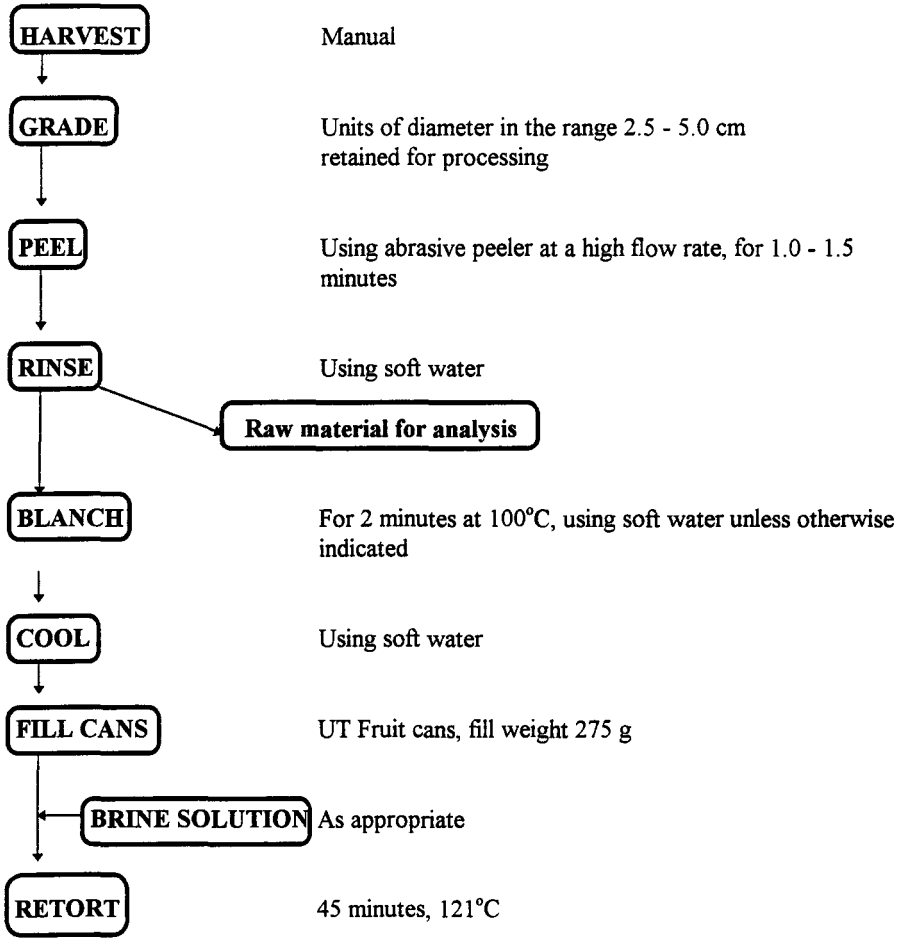

FIG 2. FLOW DIAGRAM FOR CANNING OF PEAS

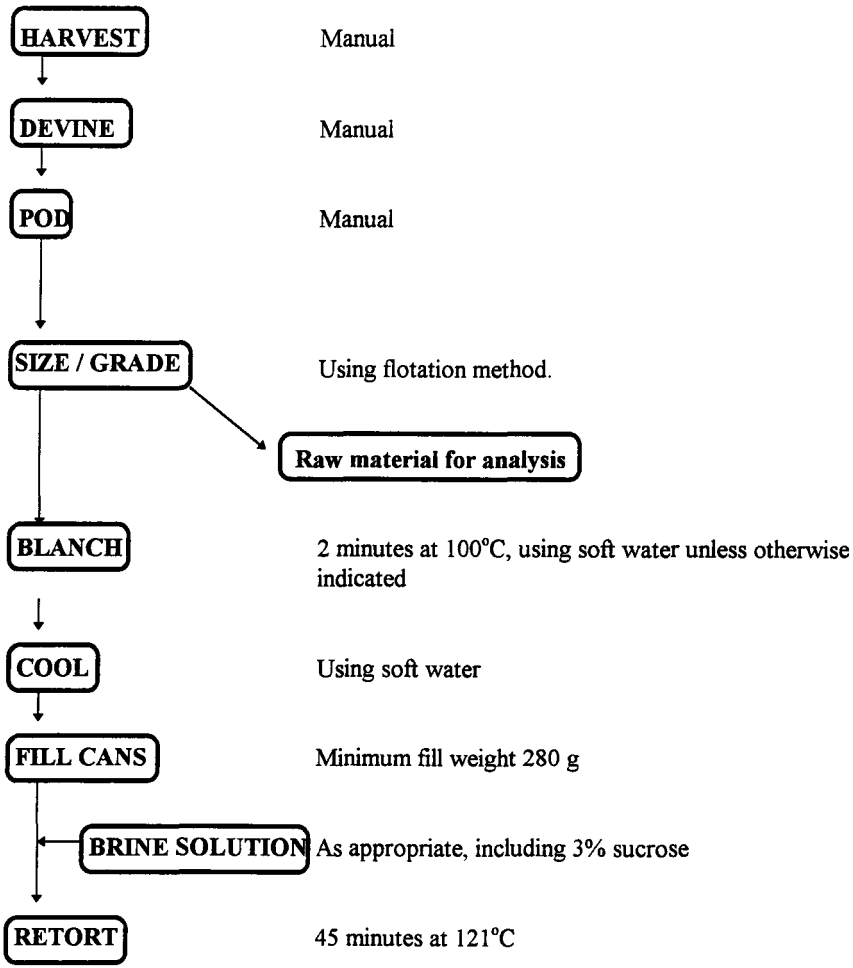

FIG 3. FLOW DIAGRAM FOR CANNING OF CARROTS

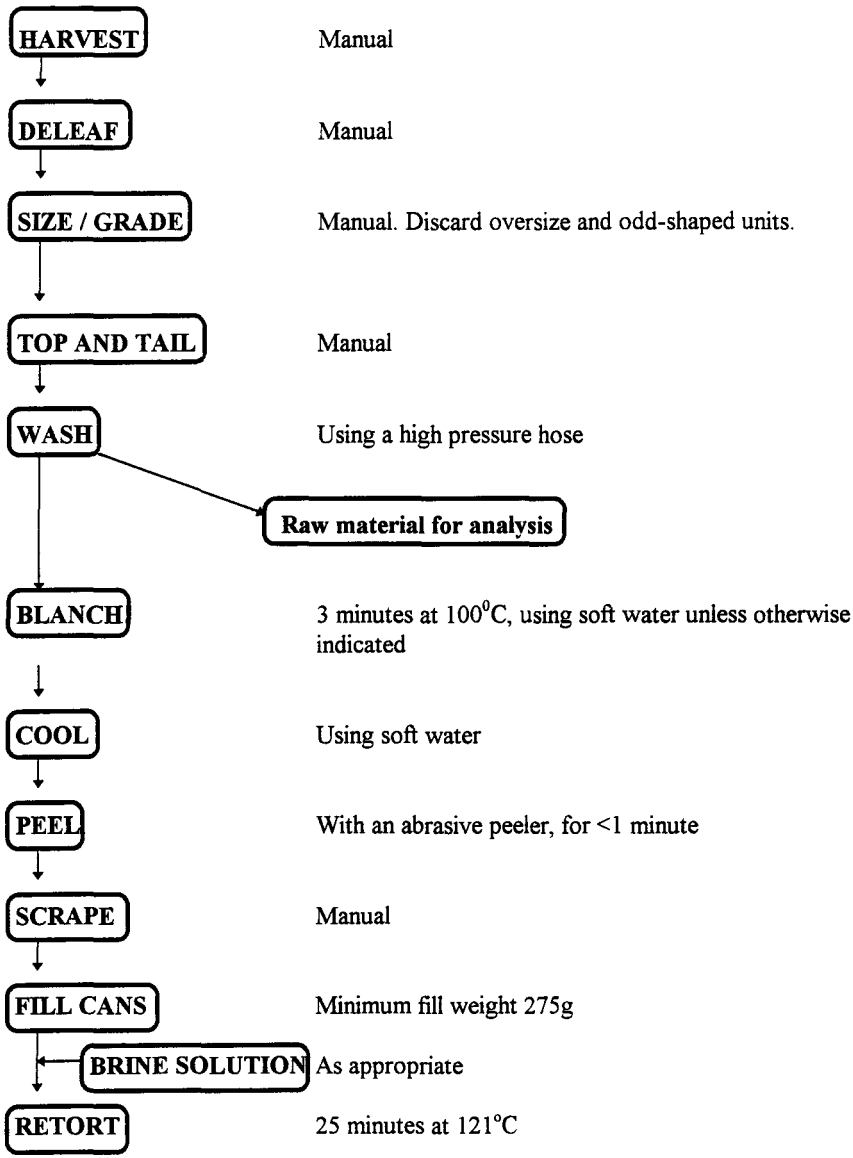

i) The effect of increasing the potassium content of blanching and/or canning solutions on the radionuclide content of canned vegetables

The raw materials under test were produced in regions of Great Britain having relatively high concentrations of Sr-90 and Cs-137 as shown by Harwell environmental surveys. Peas (Bunting variety), potatoes (Maris Peer) and carrots (Narman) were processed by blanching and canning, stored for 1 month, and subsequently analysed, along with raw vegetables, for radioactive and stable Sr, Cs and K as described in Project 2. The natural radioactivity due to K-40 was measured in the course of gamma spectrometry for the determination of Cs-137, since this radionuclide is a valuable indicator of radiocaesium removal. The effect of increasing the potassium content of blanching and/or canning solutions was examined as a means of reducing Cs-137 retention factors in food.

The vegetables were processed under the following conditions:

Table 1. Canning and Blanching Treatments used

		CANNING SOLUTION		
		2% NaCl	1% NaCl / 1% KCl	2% KCl
BLANCHING SOLUTION	Soft water	I	II	III
	1% KCl	IV		
	2% KCl	V		VI

Potatoes, peas and carrots were canned as illustrated in Figs 1-3.

Each process led to gains due to blanching and losses due to peeling and other operations as follows:

Potatoes:

Quantity of raw material	10.1 kg
Peeling losses	46%
Blanching gain	0%
Total loss	46%

Peas

Quantity of raw material	25.8 kg
Sorting / Grading losses	4.7%
Blanching gain	2.4%
Total loss (not including podding)	2.3%

Carrots

Quantity of raw material	56.4 kg
Topping / Tailing losses	14 5%
Blanching gain	7.8%
Peeling losses	33.3%
Total loss	40 0%

The results for radionuclide concentrations and retention factors are presented and discussed in Project 2. It was concluded that increasing the potassium content of the blanching or canning solutions with peas, potatoes or carrots, led to no significant changes in the retention factors for strontium and caesium. Increased R_t values for potassium were recorded when KCl was included in either blanching or canning waters.

ii) The effect of duration of storage of canned vegetables on retention of radionuclides

One variety of each vegetable was chosen for use in the storage trials to determine whether time of storage affects radionuclide retention by canned vegetables. As before, the raw materials under test were produced in regions having relatively high concentrations of Sr-90 and Cs-137 as shown by Harwell environmental surveys. 24 cans each of Maris Peer potatoes and Bunting peas were produced along with 48 cans of Narman carrots and sent to AEA for analysis at 1, 4 and 8 months.

The vegetables were processed using the methods already illustrated (Figs 1-3) and stored at ambient temperature. The brine solution used was 2% NaCl (with 3% sucrose added for peas) and the vegetables were blanched in boiling soft water for 2 minutes.

Samples of the vegetables were chemically analysed when fresh and after 1 month of storage and the results are discussed in part iii.

Retention factors for K-40, Sr-90 and Cs-137, and their stable elements, are presented and discussed in section 2. The data generally suggest that there were no significant changes in retention of these elements in canned potatoes, carrots or peas during storage.

iii) The influence of variety of vegetable used for canning on the retention of radionuclides during processing

To determine the effects of varietal differences on radionuclide retention, two varieties of each of the three test vegetables (produced in an area known to have relatively high concentrations of Sr-90 and Cs-137) were processed and canned as illustrated earlier (Figs 1-3). The samples were blanched in boiling soft water for 2 minutes and the canning solution was 2% NaCl (plus 3% sugar in the case of peas).

The raw materials and processed samples (4 weeks after canning) were analysed chemically and the results are presented in Table 2. There were some differences in composition between varieties of the same vegetables. The starch and total ash contents of Maro peas were greater than the Bunting variety. Chantnay carrots contained higher levels

of starch, total nitrogen and total ash, and less water soluble carbohydrate than the Narman variety.

In all samples the dry matter content was considerably lower in the canned products than the raw materials, which reflected the weight gained due to uptake of water from the canning solutions. The total ash content increased in all cases; this was due to the uptake of minerals from the processing solutions. Starch percentages decreased in all cases due to migration into the canning and, possibly, blanching solutions. This was particularly marked with Chantnay carrots.

Retention factors for radionuclides and a range of stable elements for the different varieties are presented and discussed in project 2. While there were some differences in retention between vegetable types, there was little, if any, significant difference in retention between vegetable varieties.

TABLE 2. Chemical analysis of vegetable samples

(Dry matter values are expressed as g/100g, other results are expressed as % of dry matter. The values shown are means of duplicate analysis of 2 subsamples)

Vegetable / Variety	Fresh / Canned	Dry Matter	Total Ash	Total N	Water Soluble carbohydrate	Starch
POTATO						
Maris Peer	**Fresh**	26.6	2.45	1.03	8.79	66.7
	Canned	20.2	5.66	0.96	8.64	55.4
Romano	**Fresh**	23.2	2.85	1.24	9.17	66.4
	Canned	19.9	6.58	0.84	8.42	62.8
PEA						
Maro	**Fresh**	39.8	4.88	3.84	9.17	37.2
	Canned	28.1	6.49	3.5	8.86	31.8
Bunting	**Fresh**	37.6	3.78	3.89	9.77	30.1
	Canned	24.6	4.96	3.57	9.35	29.4
CARROT						
Narman	**Fresh**	11.5	5.37	0.72	80.9	1.94
	Canned	8.24	13.1	0.76	82.5	1.57
Chantnay	**Fresh**	11.3	7.03	0 95	72.7	5.25
	Canned	9.12	13.2	0 77	80.9	0.54

iv) The effect of varying the blanching regime used in the dehydration of peas and potatoes on their radionuclide content

Three different blanching regimes were used for each of the samples prior to dehydration as follows:

Maro peas
i) 2 minutes in boiling water (38.8%)
ii) 2 minutes in steam at atmospheric pressure (38.5%)
iii) 5 minutes in boiling water (37.0%)

The figures shown in brackets are the percentage yields after dehydration.

The dehydration process used is illustrated below:

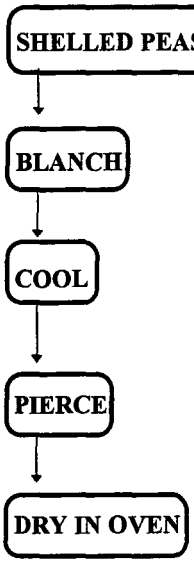

Manual

As described above

Individually pierce using needles

Conventional oven on trays at 55°C for 48 hours (69% moisture removed)

Romano potatoes
i) 1 minute in boiling water (94.8%)
ii) 4 minutes in boiling water (89 0%)
iii) 10 minutes in boiling water (95.7%)

The figures in brackets are the dry matter contents of the dehydrated products. Yields after processing were impossible to calculate due to varying losses of product in the drum drier.

The dehydration process used is illustrated below·

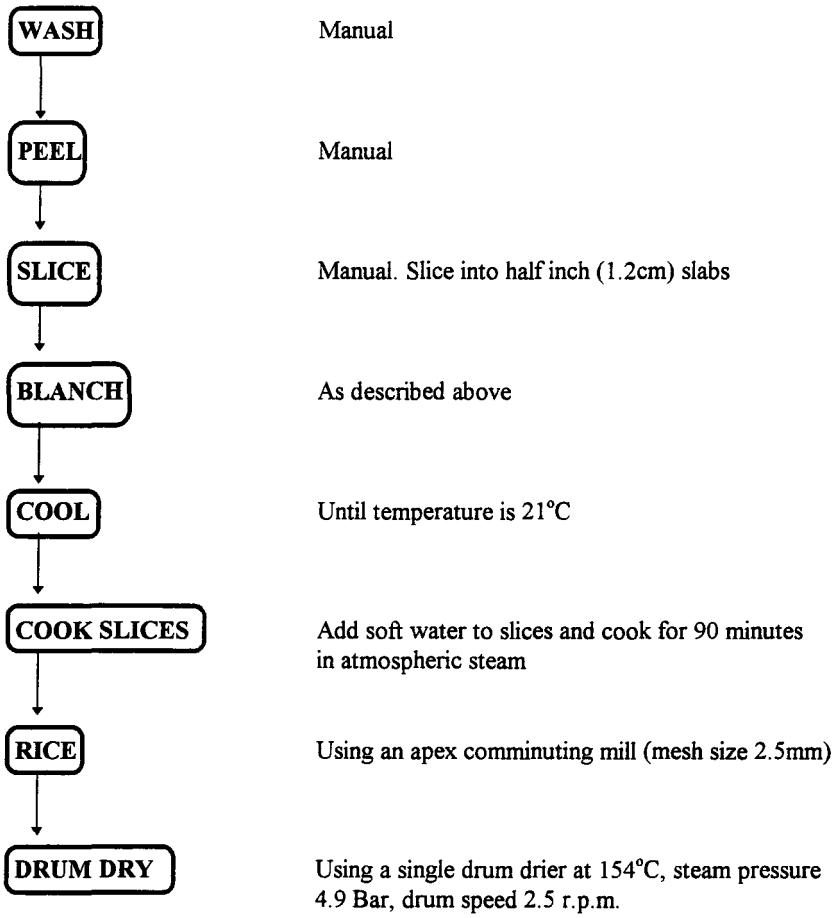

Radionuclide contents and retention factors of the products are presented and discussed in Project 2. In summary, no differences in retention of Sr-90, K-40 or their stable elements, could be detected between the different blanching methods for either peas or potatoes. Cs-137 levels were below the limit for detection in either vegetable, and stable Cs levels were below the limit for detection in peas or processed potatoes, and thus could not be derived.

C THE FATE OF RADIONUCLIDES IN BY-PRODUCTS AND WASTES FROM FOOD PROCESSING

Research carried out within the CEC "TARRAS" programme showed that substantial quantities of radionuclides that are removed by processing will be found in by-products and/or factory wastes. A majority of these by-products are recycled mainly as animal feed, but the importance of this transfer pathway to animals and, eventually, man is not known.

Information on the processing of sugar beet, potatoes, oilseed rape and wheat in the United Kingdom has been compiled with particular reference to the production of wastes used in animal food. Summaries are given in Figs 4-7.

Levels of stable potassium, strontium and caesium were measured in samples obtained from food factories, of raw materials and some by-products, are presented in Table 3.

In the production of sugar, feed pellets are one of the three main by-products (Fig 4) and, levels of the stable elements are elevated significantly in this by-product compared with the raw material (Table 3). In the case of potassium, the level in the pellets was 15 times that found in the raw beet; for strontium the level is over 60 times and for caesium the level is more than 360 times that found in the raw material. Clearly this data suggests that Sr-90 and Cs-137 would be highly concentrated in this by-product. Unfortunately it was impossible to obtain samples of by-products A and C for analysis, so an accurate estimate of total potential contamination via sugar by-products cannot be made, but it is clear that significant quantities of radionuclides could enter the human food chain by this route.

In the production of rapeseed the levels of stable elements found in raw material and meal are approximately the same (Table 3). It was demonstrated in the 1990/91 TARRAS study that retention of Sr and Cs in rapeseed oil for human consumption was extremely low and it must be assumed that Sr-90 and Cs-137 entering the human food chain from rapeseed would be through animal feed. Fig 5 shows that considerable quantities of meal as well as some unprocessed rapeseed are used as animal feed.

Levels of K, Sr and Cs were similar in flour and unprocessed wheat (Table 3). This is in contrast to the data from the 1990/91 TARRAS study which indicated much lower retention factors for K-40, Sr-90 and Cs-137 in flour produced from two varieties of wheat. However the high levels of the three elements in the feed pellets produced from wheat (Table 3), and the large quantities of wheatfeed used in the UK (Fig 6) suggest that considerable quantities of Sr-90 and Cs-137 could enter the human food chain from contaminated wheat via the animal feed route.

Potato production in the UK is outlined in Fig 7. It is apparent that potato by-products are not used as animal feed in the UK, although approximately 10% of the potato crop is used as feed in the form of whole potatoes. It can therefore be assumed that radionuclide contamination of human food from potatoes via the animal feed route would be quite low.

It was impossible to obtain samples of feed by-products from the dairy industry due to the sensitive nature of the subject and therefore no analysis was possible for milk products.

FIG 4. COMMERCIAL PROCESSING OF SUGAR BEET IN THE UK

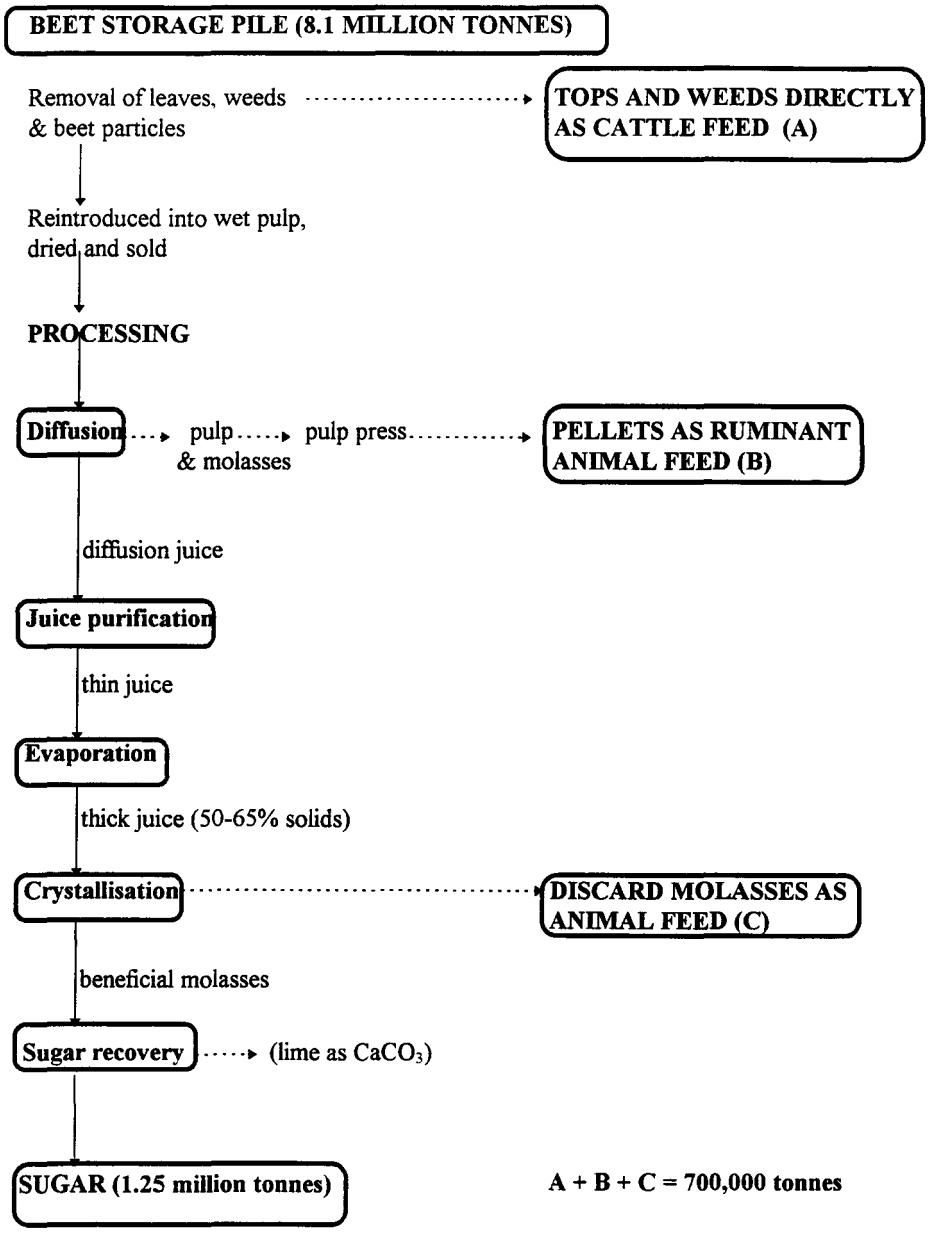

FIG 5. COMMERCIAL PROCESSING OF OILSEED RAPE IN THE UK

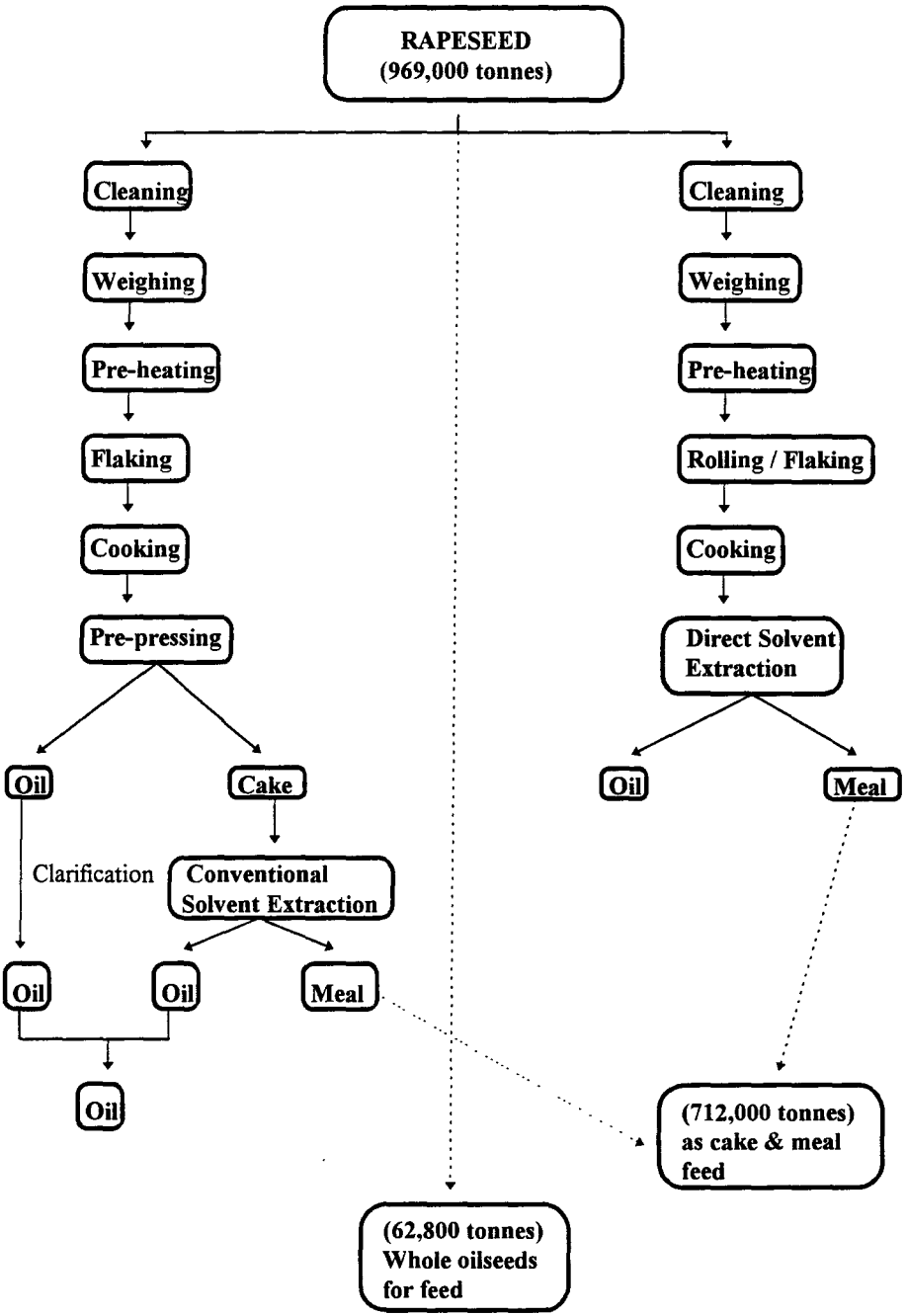

FIG 6. COMMERCIAL PROCESSING OF WHEAT IN THE UK

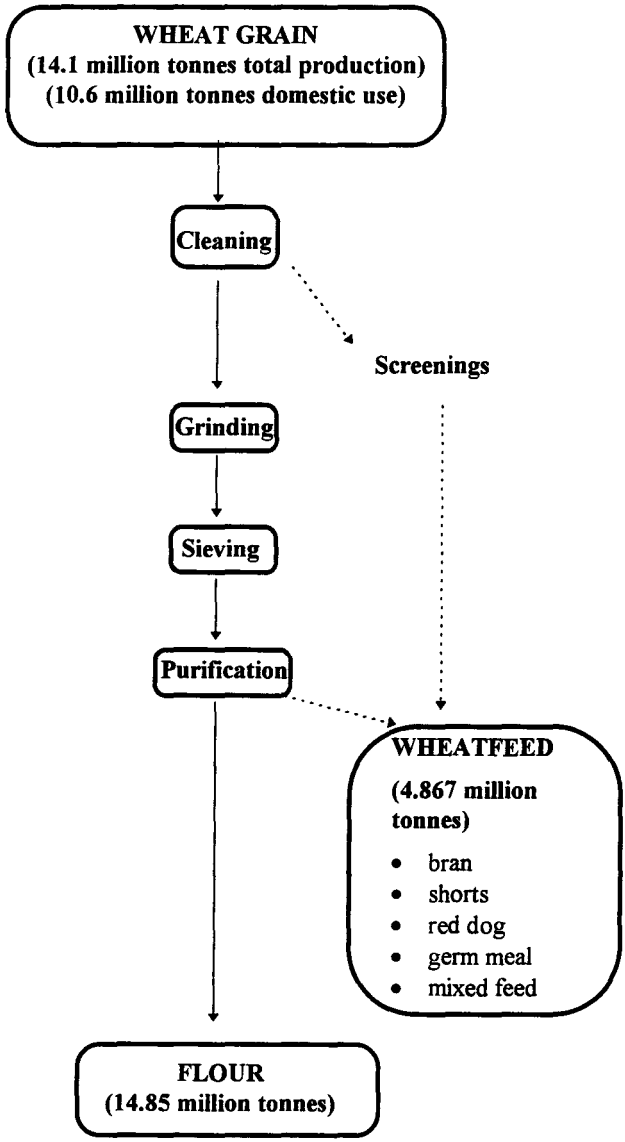

Seed = 312,000 tonnes

Other uses and waste = 775,000 tonnes

FIG 7. COMMERCIAL PRODUCTION OF POTATO IN THE UK

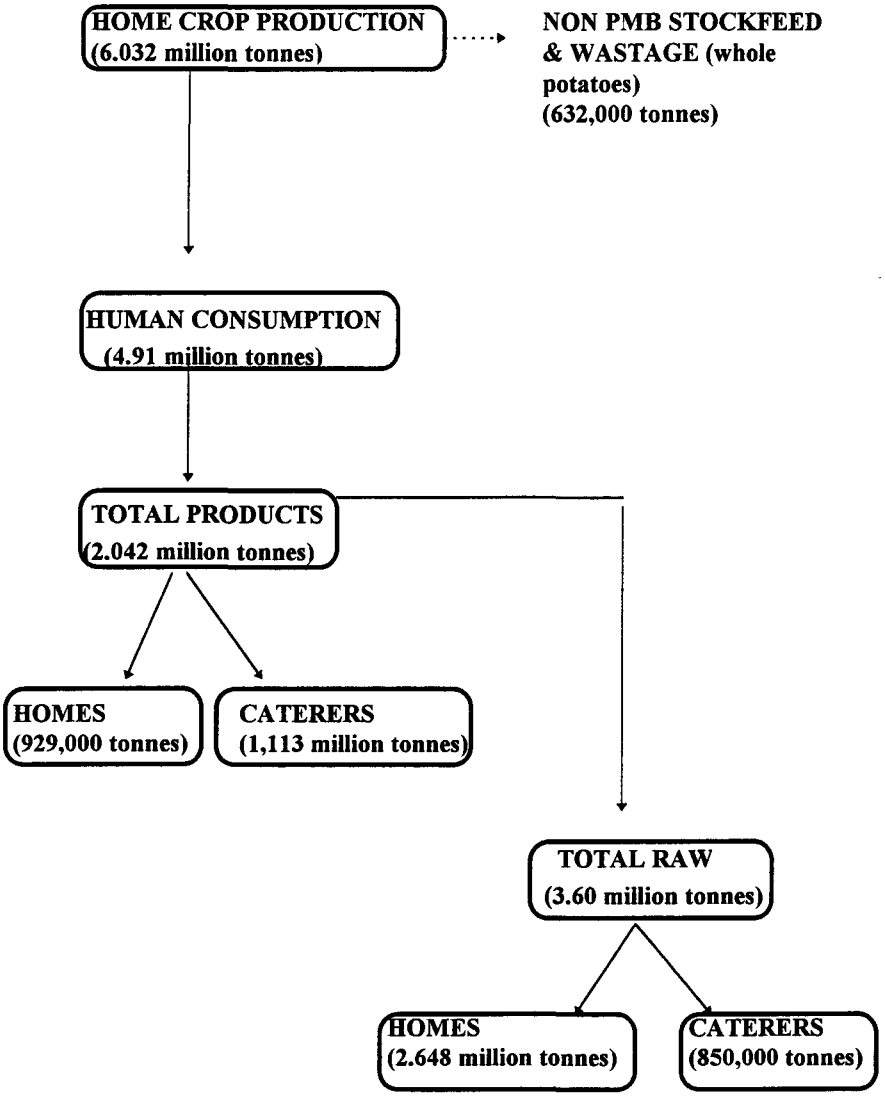

TABLE 3 Stable potassium, strontium and caesium levels (dry weight basis) of raw materials and some by-products obtained from food factories.

	K (mg/g)	Sr (μg/g)	Cs (μg/g)
Sugar Beet			
Raw material	**9.5**	**7.2**	**0.002**
Pellets	**140**	**460**	**0.72**
Rapeseed			
Raw material	**162**	**330**	**0.49**
Meal	**150**	**210**	**0.51**
Wheat			
Raw material	**5.4**	**1.8**	**0.003**
Flour	**3.4**	**2.5**	**0.008**
Pellets	**150**	**70**	**0.19**

The Community Research and Development Information Service

Your European R&D Information Source

CORDIS represents a central source of information crucial for any organisation - be it industry, small and medium-sized enterprises, research organisations or universities - wishing to participate in the exploitation of research results, participate in EU funded science and technology programmes and/or seek partnerships.

CORDIS makes information available to the public through a collection of databases. The databases cover research programmes and projects from their preparatory stages through to their execution and final publication of results. A daily news service provides up-to-date information on EU research activities including calls for proposals, events, publications and tenders as well as progress and results of research and development programmes. A partner search facility allows users to register their own details on the database as well as search for potential partners. Other databases cover Commission documents, contact information and relevant publications as well as acronyms and abbreviations.

By becoming a user of CORDIS you have the possibility to:

- Identify opportunities to manufacture and market new products
- Identify partnerships for research and development
- Identify major players in research projects
- Review research completed and in progress in areas of your interest

The databases - nine in total - are accessible on-line free of charge. As a user-friendly aid for on-line searching, Watch-CORDIS, a Windows-based interface, is available on request. The databases are also available on a CD-ROM. The current databases are:

News (English, German and French version) - Results -
Partners - Projects - Programmes - Publications -
Acronyms - Comdocuments - Contacts

CORDIS on World Wide Web

The CORDIS service was extended in September 1994 to include the CORDIS World Wide Web (WWW) server on Internet. This service provides information on CORDIS and the CORDIS databases, various software products, which can be downloaded (including the above mentioned Watch-CORDIS) and the possibility of downloading full text documents including the work programmes and information packages for all the research programmes in the Fourth Framework and calls for proposals.

The CORDIS WWW service can be accessed on the Internet using browser software (e.g. Netscape) and the address is: http://www.cordis.lu/

The CORDIS News database can be accessed through the WWW.

Contact details for further Information

If you would like further information on the CORDIS services, publications and products, please contact the CORDIS Help Desk :

CORDIS Customer Service
B.P. 2373
L-1023 Luxembourg

Telephone: +352-401162-240
Fax: +352-401162-248
E-mail: helpdesk@cordis.lu
WWW: http://www.cordis.lu/

Europäische Kommission
European Commission
Commission européenne

EUR 16769
Nuclear fission safety programme 1992-94
Radiation protection research action
(Volume 1)

Luxembourg: Office des publications officielles des Communautés européennes

1997 — XXIV, 1684 pp., num. tab., fig. — 16.2 x 22.9 cm

ISBN (Volume 1) 92-827-7983-1
ISBN (Volume 2) 92-827-7984-X
ISBN (Volume 3) 92-827-7985-8
ISBN (Volumes 1, 2 and 3) 92-827-7982-3

Preis in Luxemburg (ohne MwSt.):
Price (excluding VAT) in Luxembourg: ECU 194 (Volumes 1, 2 and 3)
Prix au Luxembourg (TVA exclue):

The final report of the 1992-94 period of the radiation protection programme outlines the research work carried out during the whole contractual period under all contracts between the European Commission and research groups in the Member States. More than 450 scientists collaborated on this programme. Results of more than 500 projects are reported. They are grouped into three sectors:

1. Human exposure to radiation and radioactivity, which includes:
   1.1. Measurement of radiation dose and its interpretation
   1.2. Transfer and behaviour of radionuclides in the environment
2. Consequences of radiation exposure to Man; assessment, prevention and treatment, which includes:
   2.1. Stochastic effects of radiation
   2.2. Non-stochastic effects of radiation
   2.3. Radiation effects on the developing organism
3. Risks and management of exposure, which includes:
   3.1. Assessment of human exposure and risks
   3.2. Optimization and management of radiation protection

Within the framework programme, the aim of this scientific research is to improve the conditions of life with respect to work and protection of man and his environment and to assure safe production of energy, i.e.:

(i) to improve methods necessary to protect workers and the population by updating the scientific basis for appropriate standards;
(ii) to prevent and counteract harmful effects of radiation;
(iii) to assess radiation risks and provide methods to cope with the consequences of radiation accidents.

Venta • Salg • Verkauf • Πωλήσεις • Sales • Vente • Vendita • Verkoop • Venda • Myynti • Försäljning

BELGIQUE/BELGIE

Moniteur belge/Belgisch Staatsblad
Rue de Louvain 40-42/Leuvenseweg 40-42
B-1000 Bruxelles/Brussel
Tél (32-2) 552 22 11
Fax (32-2) 511 01 84

Jean De Lannoy
Avenue du Roi 202/Koningslaan 202
B-1060 Bruxelles/Brussel
Tél (32-2) 538 51 69
Fax (32-2) 538 08 41
E-mail jean de lannoy@infoboard be
URL http://www jean-de-lannoy be

Librairie européenne/Europese Boekhandel
Rue de la Loi 244/Wetstraat 244
B-1040 Bruxelles/Brussel
Tél (32-2) 295 26 39
Fax (32-2) 735 08 60

DANMARK

J. H Schultz Information A/S
Herstedvang 10-12
DK-2620 Albertslund
Tlf (45) 43 63 23 00
Fax (45) 43 63 19 69
E-mail schultz@schultz dk
URL http://www schultz dk

DEUTSCHLAND

Bundesanzeiger Verlag
Breite Straße 78-80
Postfach 10 05 34
D-50667 Köln
Tel (49-221) 20 29-0
Fax (49-221) 202 92 78
E-mail vertneb@bundesanzeiger de
URL http://www bundesanzeiger de

ΕΛΛΑΔΑ/GREECE

G. C. Eleftheroudakis SA
International Bookstore
Panepistimiou 17
GR-10564 Athina
Tel (30-1) 331 41 80/1/2/3
Fax (30-1) 323 98 21
E-mail elebooks@netor gr

ESPAÑA

Mundi Prensa Libros, SA
Castelló, 37
E-28001 Madrid
Tel (34-1) 431 33 99
Fax (34-1) 575 39 98
E-mail librena@mundiprensa.es
URL http://www mundiprensa es

Boletín Oficial del Estado
Trafalgar, 27
E-28010 Madrid
Tel (34-1) 538 21 11 (Libros)/
384 17 15 (Suscripciones)
Fax (34-1) 538 21 21 (Libros)/
384 17 14 (Suscripciones)
E-mail webmaster@boe es
URL http://www boe es

FRANCE

Journal officiel
Service des publications des CE
26, rue Desaix
F-75727 Paris Cedex 15
Tel (33) 140 58 77 01/31
Fax (33) 140 58 77 00

IRELAND

Government Supplies Agency
Publications Section
4-5 Harcourt Road
Dublin 2
Tel (353-1) 661 31 11
Fax (353-1) 475 27 60

ITALIA

Licosa SpA
Via Duca di Calabria, 1/1
Casella postale 552
I-50125 Firenze
Tel (39-55) 64 54 15
Fax (39-55) 64 12 57
E-mail licosa@ftbcc it
URL http://www ftbcc it/licosa

LUXEMBOURG

Messageries du livre SARL
5, rue Raiffeisen
L-2411 Luxembourg
Tel (352) 40 10 20
Fax (352) 49 06 61
E-mail mdl@pt lu

Abonnements

Messageries Paul Kraus
11, rue Christophe Plantin
L-2339 Luxembourg
Tél (352) 49 98 88-8
Fax (352) 49 98 88-444
E-mail mpk@pt lu
URL http://www mpk lu

NEDERLAND

SDU Servicecentrum Uitgevers
Externe Fondsen
Postbus 20014
2500 EA Den Haag
Tel (31-70) 378 98 80
Fax (31-70) 378 97 83
E-mail sdu@sdu nl
URL http://www sdu nl

ÖSTERREICH

Manz'sche Verlags- und Universitatsbuchhandlung GmbH
Siebenbrunnengasse 21
Postfach 1
A-1050 Wien
Tel (43-1) 53 16 13 34/40
Fax (43-1) 53 16 13 39
E-mail auslieferung@manz co at
URL http://www austria EU net 81/manz

PORTUGAL

Imprensa Nacional-Casa da Moeda, EP
Rua Marquês de Sá da Bandeira, 16 A
P-1050 Lisboa Codex
Tel (351-1) 353 03 99
Fax (351-1) 353 02 94, 384 01 32

Distribuidora de Livros Bertrand Ld.ª
Rua das Terras dos Vales, 4/A
Apartado 60037
P-2701 Amadora Codex
Tel (351-1) 495 90 50, 495 87 87
Fax (351-1) 496 02 55

SUOMI/FINLAND

Akateeminen Kirjakauppa/Akademiska Bokhandeln
Pohjoisesplanadi 39/
Norra esplanaden 39
PL/PB 128
FIN-00101 Helsinki/Helsingfors
P /fin (358-9) 121 41
F /fax (358-9) 121 44 35
E-mail akatilaus@stockmann mailnet fi
URL http://booknet cultnet fi/aka/index htm

SVERIGE

BTJ AB
Traktorvagen 11
S-221 82 Lund
Tfn (46-46) 18 00 00
Fax (46-46) 30 79 47
E-post btjeu-pub@btj se
URL http://www btj se/media/eu

UNITED KINGDOM

The Stationery Office Ltd International Sales Agency
51 Nine Elms Lane
London SW8 5DR
Tel (44-171) 873 90 90
Fax (44-171) 873 84 63
E-mail ipll speed@theso co uk
URL http://www the-stationery-office co uk

ISLAND

Bokabud Larusar Blondal
Skolavördustig, 2
IS-101 Reykjavik
Tel (354) 551 56 50
Fax (354) 552 55 60

NORGE

NIC Info A/S
Ostenjoveien 18
Boks 6512 Etterstad
N-0606 Oslo
Tel (47-22) 97 45 00
Fax (47-22) 97 45 45

SCHWEIZ/SUISSE/SVIZZERA

OSEC
Stampfenbachstraße 85
CH-8035 Zurich
Tel (41-1) 365 53 15
Fax (41-1) 365 54 11
E-mail uleimbacher@osec ch
URL http://www osec ch

BÅLGARIJA

Europress-Euromedia Ltd
59, Bld Vitosha
BG-1000 Sofia
Tel (359-2) 980 37 66
Fax (359-2) 980 42 30

ČESKÁ REPUBLIKA

NIS CR — prodejna
Konviktská 5
CZ-113 57 Praha 1
Tel (420-2) 24 22 94 33, 24 23 09 07
Fax (420-2) 24 22 94 33
E-mail nkposp@dec nis cz
URL http://www nis cz

CYPRUS

Cyprus Chamber of Commerce & Industry
Griva-Digeni 38 & Deligiorgi 3
Mail orders
PO Box 1455
CY-1509 Nicosia
Tel (357-2) 44 95 00, 46 23 12
Fax (357-2) 36 10 44
E-mail cy1691_eic_cyprus@vans infonet com

MAGYARORSZÁG

Euro Info Service
Europa Haz
Margitsziget
PO Box 475
H-1396 Budapest 62
Tel (36-1) 111 60 61, 111 62 16
Fax (36-1) 302 50 35
E-mail euroinfo@mail matav hu
URL http://www euroinfo hu/index htm

MALTA

Miller Distributors Ltd
Malta International Airport
PO Box 25
LQA 05 Malta
Tel (356) 66 44 88
Fax (356) 67 67 99

POLSKA

Ars Polona
Krakowskie Przedmiescie 7
Skr pocztowa 1001
PL-00-950 Warszawa
Tel (48-22) 826 12 01
Fax (48-22) 826 62 40, 826 53 34, 826 86 73
E-mail ars_pol@bevy hsn com pl

ROMÂNIA

Euromedia
Str G-ral Berthelot Nr 41
RO-70749 Bucuresti
Tél (40-1) 210 44 01, 614 06 64
Fax (40-1) 210 44 01, 312 96 46

SLOVAKIA

Slovak Centre of Scientific and Technical Information
Namestie slobody 19
SK-81223 Bratislava 1
Tel (421-7) 531 83 64
Fax (421-7) 531 83 64
E-mail europ@tbb1 sltk stuba sk

SLOVENIA

Gospodarski Vestnik
Zalozniska skupina d d
Dunajska cesta 5
SLO-1000 Ljubljana
Tel (386) 611 33 03 54
Fax (386) 611 33 91 28
E-mail belicd@gvestnik si
URL http://www gvestnik si

TÜRKIYE

Dünya Infotel AS
Istiklâl Cad No 469
TR-80050 Tünel-Istanbul
Tel (90-212) 251 91 96
Fax (90-212) 251 91 97

AUSTRALIA

Hunter Publications
PO Box 404
3167 Abbotsford, Victoria
Tel (61-3) 94 17 53 61
Fax (61-3) 94 19 71 54

CANADA

Subscriptions only/Uniquement abonnements

Renouf Publishing Co Ltd
5369 Chemin Canotek Road Unit 1
K1J 9J3 Ottawa, Ontario
Tel (1-613) 745 26 65
Fax (1-613) 745 76 60
E-mail renouf@fox nstn ca
URL http://www renoufbooks com

EGYPT

The Middle East Observer
41, Sherif Street
Cairo
Tel (20-2) 393 97 32
Fax (20-2) 393 97 32

HRVATSKA

Mediatrade Ltd
Pavla Hatza 1
HR-10000 Zagreb
Tel (385-1) 43 03 92
Fax (385-1) 43 03 92

INDIA

EBIC India
3rd Floor, Y B Chavan Centre
Gen J Bhosale Marg
400 021 Mumbai
Tel (91-22) 282 60 64
Fax (91-22) 285 45 64
E-mail ebic@giasbm01 vsnl net in

ISRAËL

ROY International
17, Shimon Hatarssi Street
PO Box 13056
61130 Tel Aviv
Tel (972-3) 546 14 23
Fax (972-3) 546 14 42
E-mail royil@netvision net il

Sub-agent for the Palestinian Authority

Index Information Services
PO Box 19502
Jerusalem
Tel (972-2) 627 16 34
Fax (972-2) 627 12 19

JAPAN

PSI-Japan
Asahi Sanbancho Plaza #206
7-1 Sanbancho, Chiyoda-ku
Tokyo 102
Tel (81-3) 32 34 69 21
Fax (81-3) 32 34 69 15
E-mail psijapan@gol com
URL http://www psi-japan com

MALAYSIA

EBIC Malaysia
Level 7, Wisma Hong Leong
18 Jalan Perak
50450 Kuala Lumpur
Tel (60-3) 262 62 98
Fax (60-3) 262 61 98
E-mail ebic-kl@mol net my

PHILIPPINES

EBIC Philippines
19th Floor, PS Bank Tower Sen
Gil J Puyat Ave cor Tindalo St
Makati City
Metro Manilla
Tel (63-2) 759 66 80
Fax (63-2) 759 66 90
E-mail eccpcom@globe com ph

RUSSIA

CCEC
60-letiya Oktyabrya Av 9
117312 Moscow
Tel (70-95) 135 52 27
Fax (70-95) 135 52 27

SOUTH AFRICA

Safto
5th Floor Export House,
CNR Maude & West Streets
PO Box 782 706
2146 Sandton
Tel (27-11) 883 37 37
Fax (27-11) 883 65 69

SOUTH KOREA

Kyowa Book Company
1 Fl Phyung Hwa Bldg
411-2 Hap Jeong Dong, Mapo Ku
121-220 Seoul
Tel (82-2) 322 67 80/1
Fax (82-2) 322 67 82
E-mail kyowa2@ktnet co kr

THAILANDE

EBIC Thailand
Vanissa Building 8th Floor
29 Soi Chidlom
Ploenchit
10330 Bangkok
Tel (66-2) 655 06 27
Fax (66-2) 655 06 28
E-mail ebicbkk@ksc15 th com

UNITED STATES OF AMERICA

Bernan Associates
4611-F Assembly Drive
MD20706 Lanham
Tel (800) 274 44 47 (toll free telephone)
Fax (800) 865 34 50 (toll free fax)
E-mail query@bernan com
URL http://www bernan com

ANDERE LANDER/OTHER COUNTRIES/ AUTRES PAYS

Bitte wenden Sie sich an ein Buro Ihrer Wahl / Please contact the sales office of your choice / Veuillez vous adresser au bureau de vente de votre choix

NB Country order EU, EFTA, EU applicant countries, others

NOTICE TO THE READER

Information on European Commission publications in the areas of research and innovation can be obtained from:

- **CORDIS, the Community R&D Information Service**

  For more information, contact:
  CORDIS Customer Service, BP 2373, L-1023 Luxembourg
  Tel. (352) 40 11 62-240, Fax (352) 40 11 62-248, e-mail: helpdesk@cordis.lu
  or visit the website at http://www.cordis.lu/

- **euro abstracts**

  The European Commission's periodical on research publications, issued every two months. For a subscription (1 year: ECU 65) please write to the sales office in your country.

Preis in Luxemburg (ohne MwSt.):
Price (excluding VAT) in Luxembourg: ECU 194 (Volumes 1, 2 and 3)
Prix au Luxembourg (TVA exclue):

AMT FÜR AMTLICHE VERÖFFENTLICHUNGEN
DER EUROPÄISCHEN GEMEINSCHAFTEN
OFFICE FOR OFFICIAL PUBLICATIONS
OF THE EUROPEAN COMMUNITIES
OFFICE DES PUBLICATIONS OFFICIELLES
DES COMMUNAUTÉS EUROPÉENNES
L-2985 Luxembourg

ISBN 92-827-7983-1

15

CG-NA-16769-3A-C